

AD A 088889

**LEVEL**

B.S.

**Proceedings of the  
NATO Advanced Study Institute  
on Atmospheric Ozone:  
Its Variation and Human Influences,**

Aldeia das Acoteias,  
Algarve, Portugal,

**October 1-13, 1979,**

11 May 80

12 9926

with the support of the  
U.S. Federal Aviation Administration  
and with the help of the  
Meteorological and Geophysical  
Institute of Portugal

DTIC  
COLLECTED  
SEP 1980

10  
**Marcel/Nicolet, Director  
Arthur C./Aikin, Editor**

U.S. Department of Transportation  
Federal Aviation Administration  
Office of Environment and Energy  
High Altitude Pollution Program  
Washington, D.C. 20591



This document has been approved  
for public release and sale; its  
distribution is unlimited.

DDC FILE COPY

442037

80 9 8 137

**Best  
Available  
Copy**



1. Report No. FAA-EE-80-20 ✓		2. Government Accession No. AD-A088 889		3. Recipient's Catalog No.	
4. Title and Subtitle Proceedings of the NATO Advanced Study Institute on Atmospheric Ozone: Its Variation and Human Influences		5. Report Date May 1980		6. Performing Organization Code	
		8. Performing Organization Report No. 411034			
7. Author(s) Marcel Nicolet, Director Arthur C. Aikin, Editor		10. Work Unit No. (TRAIS)		11. Contract or Grant No. AIA/CA-18	
9. Performing Organization Name and Address NATO Advanced Study Institutes Programme 1110 Brussels, Belgium		13. Type of Report and Period Covered Conference Proceedings October 1-13, 1979			
		14. Sponsoring Agency Code			
12. Sponsoring Agency Name and Address U.S. Department of Transportation, Federal Aviation Administration, Office of Environment and Energy, High Altitude Pollution Program Washington, D.C. 20591					
15. Supplementary Notes					
16. Abstract <p>This volume contains the proceedings of a North Atlantic Treaty Organization Advanced Study Institute on Atmospheric Ozone and its Human Influences. The conference was held at Aldeia das Acoteias, Portugal in October 1979. Included are papers from speakers who were invited to review the current state of knowledge for different aspects of the ozone problem. Selected short contributions of new results by other conference attendees are also given. Topics covered include solar flux and its changes, ozone observations and the theories of spatial and temporal distribution of ozone. Natural and man made trace gases which may influence atmospheric ozone are also discussed.</p>					
17. Key Words Atmospheric Ozone, Man's Impact on the Stratosphere			18. Distribution Statement This document is available to the public through the National Technical Information Service, Springfield, Virginia 22161		
19. Security Classif. (of this report) Unclassified		20. Security Classif. (of this page) Unclassified		21. No. of Pages 1008	
				22. Price	

## P R E F A C E

Fifty years ago, the first international conference on atmospheric ozone was held in Paris under the title "Meeting on Ozone and Atmospheric absorption". At that meeting 27 papers and notes were presented and subsequently published in Gerlands Beiträge zur Geophysik, 24, 1-77, 1929. Among these, for example, was a report by G.M.B. Dobson on the first detailed ozone observations involving latitudinal and seasonal variations and a comparison between night and day total ozone content by D. Chalonge and P. Götz. Also included were works on the ozone absorption cross-sections by R. Ladenburg, by D. Lambrey and D. Chalonge and by C. Fabry. The climatological problem and atmospheric ozone by A. Angström and the relationship between ozone and the tropospheric motions by V. Bjerkness outlined these aspects of the studies. And, finally, the first note on the ozone theory by S. Chapman appeared in this publication.

In October 1979, the same problems, with the important additions of the budget of various trace constituents which are both naturally and industrially produced and of the stratospheric ozone models, have been discussed at Aldeia das Açoteias, Algarve, Portugal by more than 100 scientists. The NATO Advanced Study Institute on "Atmospheric Ozone : its variation and human influences" has had the privilege of assembling, during a two week interval, lecturers, students and observers, for the discussion of all aspects of relevant atmospheric ozone problems, which are of current great scientific and practical interest.

The material presented and discussed at this Ozone Institute are published in this special volume thanks to the generous help of the US Federal Aviation Administration. The collaboration between the lecturers and the various participants is reported in the various texts dealing with their specific subjects. It must be added that, due to various circumstances, the few speakers who were not able to attend the Institute have supplied the texts of their lectures which are reproduced in these Proceedings. In addition, a few papers with the new results have been included.

I would like to add, that, in addition to the NATO funds, several people came to the Institute with the support of their Institution, that the support of the FAA has provided the opportunity to many US scientists to participate in the Institute. Also that funds for several individuals were supplied by the NASA Upper Atmospheric Research Program.

Finally, I would like to thank for their friendly and helpful collaboration the members of the Organizing Committee : J. Blamont, T. Donahue, D. Ehhalt, R. Murgatroyd and H. Schiff, and also the Chairmen of the sessions : H. Dütsch, R. Hudson, F. Kaufman, J. London, F.S. Rowland and S. Tilford. A special note of thanks is made to A. Aikin who has kindly agreed to help in the publication of this volume.

Marcel NICOLET.

Accession For	
NTIS GRA&I	<input checked="checked" type="checkbox"/>
DDC TAB	<input type="checkbox"/>
Unannounced	<input type="checkbox"/>
Justification	
By _____	
Distribution/	
Availability Codes	
Dist	Avail and/or special
A	

# TABLE OF CONTENTS

		<u>PAGE</u>
Preface	Marcel Nicolet	i
The First Years of the Study of Atmospheric Ozone	Marcel Nicolet	1
Vertical Ozone Distribution and Tropospheric Ozone	H. U. Dutsch	7
The Observed Distribution and Variations of Total Ozone	Julius London	31
Spatial and Temporal Variability of Ozone as Seen from Space	Donald F. Heath	45
Ozone Distributions by Infrared Limb Scanning: Preliminary Results from the LRIR	John C. Gille	103
Ozone Results from Indian Stations Using Dobson Instruments	D. K. Chakrabarty and Purobi Chakrabarty	123
Hydrogen and Carbon Compounds in the Stratosphere	D. H. Ehhalt and A. Tonniben	129
The Homogeneous Chemistry of Formaldehyde Generation and Destruction within the Atmosphere	Jack G. Calvert	153
Ethane and Ethylene Behavior in the Atmosphere	A. C. Aikin, J. R. Herman, and E. J. Maier	191
Atmospheric Halocarbons: Measurements and Analyses of Selected Trace Gases	R. A. Rasmussen and M. A. K. Khalil	209
Free Radicals in the Earth's Stratosphere: A Review of Recent Results	J. G. Anderson	233
Observations of Odd Nitrogen Compounds in the Stratosphere	D. G. Murcray	253
Nitric Oxide in the Upper Stratosphere and Mesosphere	William Swider	263
Measurements of Stratospheric Bromine	W. A. Sedlacek, A. L. Lazrus, and B. W. Gandrud	273
The Photochemistry of Tropospheric Iodine	W. L. Chameides and D. D. Davis	281
Sources and Sinks of Stratospheric Water Vapor	Hugh W. Ellsaesser	283
The Atmospheric CH <sub>4</sub> Budget	Thomas M. Donahue	301

# TABLE OF CONTENTS (CONT.)

		<u>PAGE</u>
The Atmospheric H <sub>2</sub> Cycle	U. Schmidt, G. Kulesa, and E. P. Roth	307
Sources and Sinks for Carbon Monoxide	Jennifer A. Logan	323
Sources and Sinks for Nitrous Oxide	Michael B. McElroy	345
The Problem of Atmospheric Methyl Chloride	Andrew J. Watson, J. E. Lovelock, and D. H. Stedman	365
Release of Industrial Halocarbons and Tropospheric Budget	J. P. Jesson	373
Elementary Atmospheric Reactions: Labo- ratory Measurements and Their Interpretation	Frederick Kaufman	397
Laboratory Studies of Reactions of Odd Hydrogen Species of Atmospheric Interest	Carleton J. Howard	409
Laboratory Studies of Halogen Compounds of Atmospheric Interest	R. T. Watson	429
Temperature Dependent Absorption Cross Sections for Formaldehyde (CH <sub>2</sub> O): The Effect of Formaldehyde on Stratospheric Chlorine Chemistry	A. M. Bass, L. C. Glasgow, C. Miller, J. P. Jesson, and D. L. Filkin	467
Absolute Rate of the Reaction OH + H <sub>2</sub> CO at Stratospheric Temperatures	L. J. Stief, D. F. Nava, W. A. Payne, and J. V. Michael	479
Kinetic Studies of Atmospheric Free Radicals	J. P. Burrows, R. A. Cox, and M. C. Addison	483
EPR Kinetic Study of the Reactions of H <sub>2</sub> CO with F, Cl and Br Atoms and ClO Radical	G. LeBras, R. Foon, G. Poulet, and J. Combourieu	497
Oxidation of the CH <sub>3</sub> Radical and Some Halomethyl and Haloethyl Radicals of Atmospheric Interest	R. Simonaitis	501
Stratospheric Ion Chemistry Related to Neutral Trace Composition	Eldon E. Ferguson	517
Observation of the Solar Ultraviolet Radiation	Paul C. Simon	529
Influence of Diffuse Solar Radiation on Stratospheric Chemistry	G. Fiocco	555
Laboratory Measurements of Absorption Cross Sections	Mario J. Molina	589

# TABLE OF CONTENTS (CONT.)

		<u>PAGE</u>
O( <sup>1</sup> D) Quantum Yields from O <sub>3</sub> Photodissociation and O( <sup>1</sup> D) Reactions with Atmospheric Constituents	Geert Karel Moortgat	599
The Mesospheric and Stratospheric Absorption of the Solar Ultraviolet Radiation	Marcel Nicolet	647
An Introduction to Studies of the General Characteristics of the Stratosphere and Mesosphere	R. J. Murgatroyd	689
Radiative Energy Sources and Sinks in the Stratosphere and Mesosphere	Julius London	703
Dynamical Processes in the Stratosphere: Wave Motion	Alan O'Neill	723
Stratospheric Sudden Warmings	Alan O'Neill	739
One-Dimensional Coupled Transport and Chemical Kinetics Models of the Stratosphere	Julius S. Chang and Donald J. Wuebbles	749
On Eddy Diffusion Coefficients	Guy Brasseur	767
Transport Processes	J. A. Pyle and C. F. Rogers	815
The Chemical Equations of Stratospheric and Mesospheric Ozone	Marcel Nicolet	823
Uncertainty and Sensitivity Studies of Stratospheric Photochemistry	R. S. Stolarski	865
Three-Dimensional Models and Their Application to the Ozone Problem	D. M. Cunnold, F. N. Alyea, and R. G. Prinn	877
Modeling Tropospheric N <sub>2</sub> O	Hiram Levy II and J. D. Mahlman	893
Effect of Past Atmospheric Nuclear Explosions on Total Ozone	Ernest Bauer	909
Effects on Atmospheric Ozone of Emissions from Cruise Aircraft: History and Current Status	R. C. Oliver	921
Summary of the U. S. National Academy of Sciences Report: Stratospheric Ozone Depletion by Halocarbons: Chemistry and Transport	H. I. Schiff	967
High Altitude Pollution Program of the U. S. Federal Aviation Administration	N. Sundararaman	977

TABLE OF CONTENTS (CONT.)

	<u>PAGE</u>
NASA's Atmospheric Research Program	983
Summary of the Commission of the European Communities Report: Chlorofluorocarbons and Their Effect on Stratospheric Ozone	985
List of Participants	987
Author Index	997

## THE FIRST YEARS OF THE STUDY OF ATMOSPHERIC OZONE

by Marcel NICOLET

Royal Meteorological Institute  
3 Avenue Circulaire, 1180 BRUSSELS - Belgium

### 1. Historical aspects

The problem of atmospheric ozone has been studied by many scientists since the suggestion made by Schoenbein (1840 a,b) of the existence of an atmospheric constituent having a particular odor (from the Greek, ozein = to smell). In a letter to Arago, Schoenbein (1840a) wrote as follows : "Since I am fairly sure that the source of the odor must belong to the same category of substances as chlorine and bromine, that is the elementary halogens, I propose to call it ozone. As I am convinced that this substance is always freed in noticeable amounts during thunderstorms, I intend to carry out a series of experiments this year designed to demonstrate the presence of ozone in our atmosphere". (translation)

The exact origin of ozone was deduced by de la Rive (1845) when it was produced in an electrical discharge through pure oxygen. In a letter to Arago, de la Rive (1845) wrote as follows : "We have passed through a tube a flow of perfectly pure and perfectly dry oxygen;... Hence the ozone can only originate in the oxygen and, in order to generate it, the simplest and most direct method is to discharge a series of electric sparks through the oxygen". (translation)

Ozone was chemically proven to exist in the troposphere, at ground level, by Houzeau (1858). However, the first chemical identification was made more than a hundred years ago, by Soret (1863, 1865) who, in a Research Note entitled : "Sur les relations volumétriques de l'ozone", wrote : "Many chemists and physicists admit that ordinary oxygen in the gaseous state is formed by the combination of two atoms and constitutes an oxide of oxygen  $OO$ . Looked at from this point of view, assuming that ozone is an allotropic form of oxygen, we must conclude that the ozone molecule results from a different arrangement of atoms... One could, for example, imagine that one molecule of ozone is composed of three atoms  $OOO$ , constituting a dioxide of oxygen". (translation)

The first clear spectroscopic detection of ozone (Chappuis band), related to the atmosphere, was made by Chappuis (1880 - 1882). In a Research Note entitled "Sur le spectre d'absorption de l'ozone", Chappuis (1880) wrote : "The absorption spectrum of ozonized oxygen, produced by an electric current and observed using a spectroscope with one or two prisms, shows eleven dark clearly defined bands in the ordinary visible part of the spectrum. I have made a map of these bands and have compared it with those of the telluric bands". (translation)

During the same period, Hartley (1881 a) detected, in the laboratory, the strong ultraviolet spectrum of ozone (Hartley band) below 300 nm. Hartley wrote : "Being much engaged in the examination of organic substances, I delayed the experiments on ozone, until the announcement of the liquefaction of this remarkable body by Messrs Hautefeuille and Chappuis (Compt. Rend. 91, 522, 1880) attracted my attention once more on the subject". The first photograph taken showed a broad absorption-band, stretching from wavelengths of about 285 to 233 millionths mm". The mean wavelength of the rays intercepted by ozone is 256 millionths mm".

At the same time, Hartley (1881 b) identified the atmospheric limit of the solar spectrum due to ozone as detected by Cornu (1878). The conclusions reached by Hartley (1881 b) were "that : (1) ozone is a normal constituent of the higher atmosphere, (2) it is in larger proportion there than near the earth's surface, (3) the quantity of atmospheric ozone is quite sufficient to account for the limitation of the solar spectrum in the ultraviolet region; without taking into account the possible absorption caused by the great thickness of oxygen and nitrogen". However, Hartley (1881 b) added an erroneous fourth conclusion "that the blue tint of the atmosphere is due to ozone".

As far as the Huggins bands at wavelengths greater than 310 nm are concerned, they were detected by Huggins and Huggins (1890) as a new group of lines in the photographic spectrum of Sirius and, finally, identified by Fowler and Strutt (1917) as absorption bands of atmospheric ozone.

Before the first world war, the quantitative analysis of atmospheric ozone was made only by chemical methods at ground level. Among various methods, the process introduced by Levy (1898) at Montsouris (Paris) was in use for 30 years; from 1877 to 1907. In this method the ozone was collected daily over an interval of 24 hours and its quantity was estimated by a very elaborate technique. But it must be conceded that such observations, even if they are examples of accurate work, cannot lead to the true proportion of ozone present in the air, due to the difficulty of separating the chemical action of ozone from that of other oxidizing constituents. Nevertheless, it is interesting to note the average values deduced of  $2.5 \times 10^{11}$  and  $1.5 \times 10^{11}$   $\text{cm}^{-3}$   $\text{O}_3$  molecules at the maximum in summer (June - July) and at the minimum value in winter (December - January); respectively. The average annual values between 1877 and 1896 vary between  $5 \times 10^{10}$   $\text{cm}^{-3}$  in 1880 and  $5 \times 10^{11}$   $\text{cm}^{-3}$  in 1895. These figures, given month after month for an interval of 30 years in the "Annuaire de l'Observatoire de Montsouris", cannot be accepted as indicating absolute values of the ozone concentration but they can lead to useful comparisons. In any case, they remind us that, in 1865, the French National Academy of Sciences had appointed a special commission of 9 members in order to reduce the number of theoretical, experimental and observational papers on ozone and to receive recommendations and comments before their publication. After one hundred years, such a commission could work, perhaps, on a planetary scale !

## 2. The period of pioneers of spectroscopic observations.

The first quantitative analysis was made by Fabry and Buisson (1921 a,b) in 1920 at Marseille, in a study of the ultraviolet absorption of solar radiation in the Hartley and Huggins bands. This led to the first absolute determination of the total atmospheric content with an average value of 0.3 cm (STP) and irregular variations between 0.285 cm and 0.335 cm from 21 May to 23 June.

The ozone problem in its more general aspects was really developed after the first world war. This can be seen from the publication by Fabry (1929) of 27 papers presented at a meeting in Paris which was, as a matter of fact, the first international conference on atmospheric ozone. At the same meeting at which, as a result of this observational work, Dobson introduced the real meteorological significance (figs 1, 2 and 3) of atmospheric ozone (Dobson and Harrison, 1926; Dobson et al., 1927, 1929. Chalonge and Götz (1929) had shown that their daytime and nighttime observations, by spectroscopic methods, did not detect any variation in the total content of atmospheric ozone.

The first theoretical approach was also given at this Paris Conference (May 1929) by Chapman (1929, 1930) who had introduced the first atmospheric analysis of the ozone problem. However, in 1929, it was not yet possible to reach a general understanding since the ozone peak (Cabannes and Dufay, 1925, 1927; Götz and Dobson, 1928, 1929) had been misplaced at an average height of about 45 km.

The first data on the vertical distribution of stratospheric ozone were obtained by an indirect method introduced by Götz (1931) during his various observations at Spitzbergen. It is called the Umkehrmethod and was further developed by Götz et al. (1934). The principal results



# NICOLET

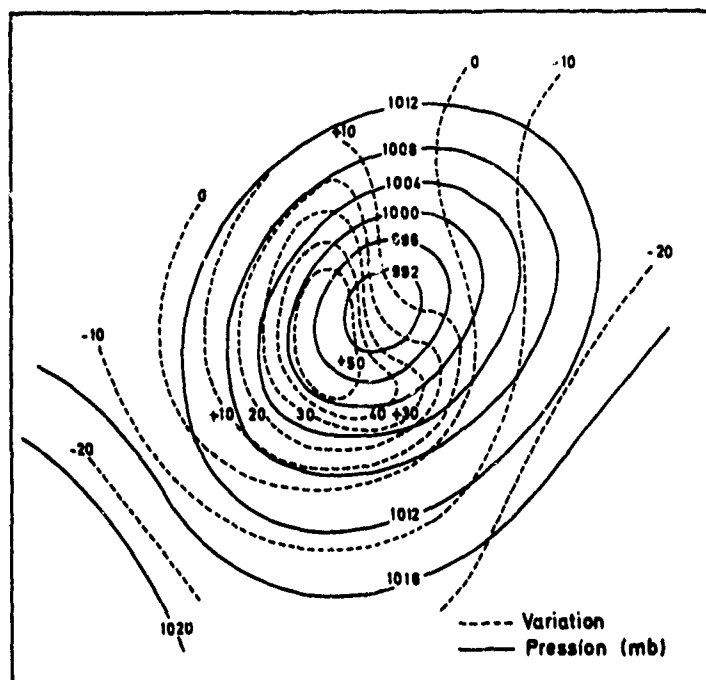


Figure 1.- Typical distribution of increases of total ozone (unit = 0.001 cm at STP) in a low-pressure system as presented by Dobson(1929)

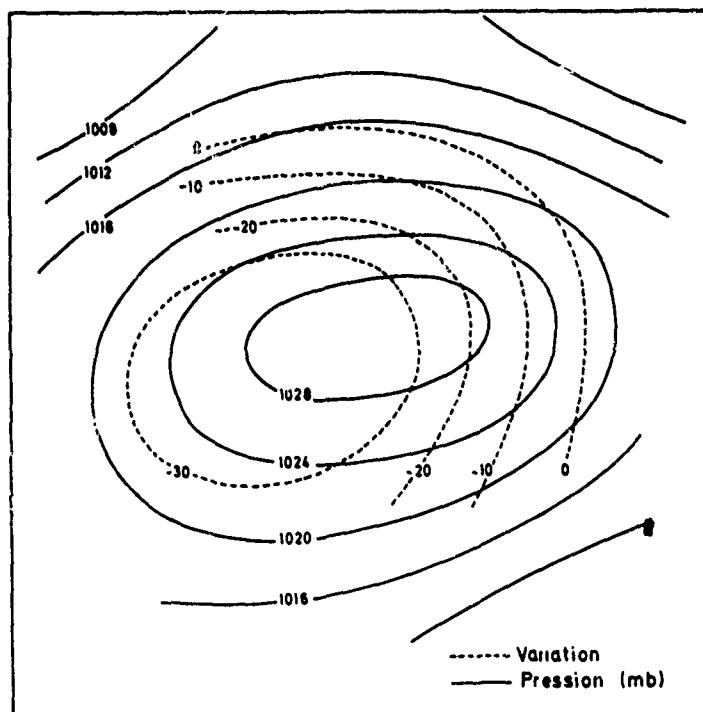
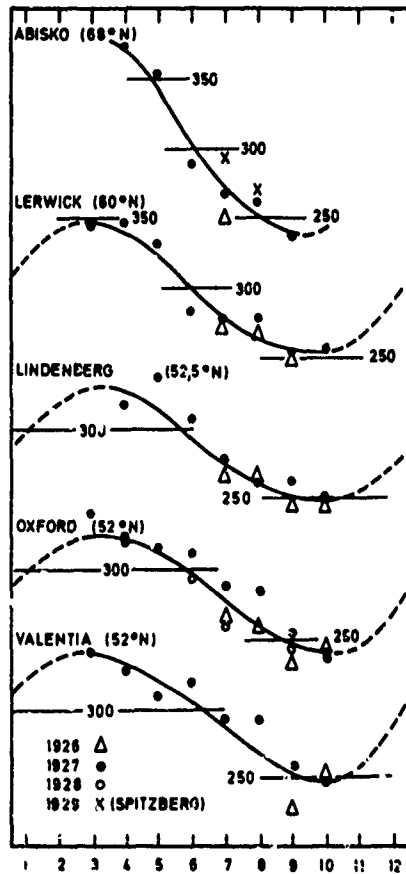
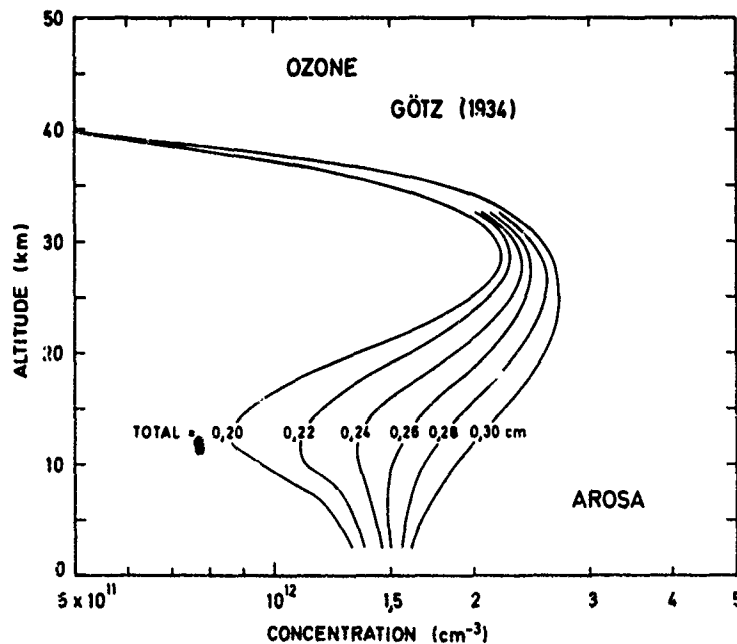


Figure 2.- Typical distribution of decreases of total ozone (unit = 0.001 cm at STP) in a high-pressure system as presented by Dobson(1929)

# NICQLET



**Figure 3.-** Seasonal variation of total ozone (unit = 0.001 cm at STP) as detected by Dobson (1929) fifty years ago. Absolute values correspond to the first calibration.



**Figure 4.-** First determinations of the vertical distribution of stratospheric ozone with the Umkehr method by Götz et al. (1934) where the principal variations occur below the concentration peak.

(Fig. 4) showed that the average height is only of the order of 25 km and that the main changes in ozone content appear to be centered between 10 and 20 km, a fact of real meteorological significance. Since 1965, the use of chemical instruments became the basis for the analysis of meridional cross sections of the vertical ozone distribution.

Today, the rocket observations and the continuous survey by satellites are leading to a detailed and continuous analysis on a planetary scale.

#### REFERENCES

- CABANNES, J. et J. DUFAY, Mesure de l'altitude de la couche d'ozone dans l'atmosphère, C. R. Acad. Sc. Paris, 181, 302, 1925.
- CABANNES, J. et J. DUFAY, Mesure de l'altitude et de l'épaisseur de la couche d'ozone dans l'atmosphère, J. Phys. Rad., 6e sér., 8, 125, 1927
- CHALONGE, D. et F. W. P. GÖTZ, Mesures diurnes et nocturnes de la quantité d'ozone contenue dans la haute atmosphère, C. R. Acad. Sc. Paris, 189, 704, 1929a
- CHALONGE, D. et F. W. P. GÖTZ, Comparaison entre les teneurs en ozone de la haute atmosphère pendant le jour et pendant la nuit, Gerlands Beitr. Geophys., 24, 20, 1929b
- CHAPMAN, S., On the variations of ozone in the upper atmosphere, Gerlands Beitr. Geophys., 24, 66, 1929
- CHAPMAN, S., A theory of upper atmospheric ozone, Mem. Roy. Meteorol. Soc., 3, 103, 1930
- CHAPPUIS, J., Sur le spectre d'absorption de l'ozone, C. R. Acad. Sc. Paris, 91, 985, 1880
- CHAPPUIS, J., Sur les spectres d'absorption de l'ozone et de l'acide pernitrique, J. Phys., Paris, 2e série, 1, 494, 1882
- de la RIVE, M., Sur l'ozone, C. R. Acad. Sc. Paris, 20, 1291, 1845
- DOBSON, G. M. B., Atmospheric ozone, Gerlands Beitr. Geophys., 24, 8, 1929
- DOBSON, G. M. B. and D. N. HARRISON, Measurements of the amount of ozone in the earth's atmosphere and its relation to other geophysical conditions, Part. 1, Proc. Roy. Soc. London, A110, 660, 1926
- DOBSON, G. M. B., D. N. HARRISON and J. LAWRENCE, Measurements of the amount of ozone in the earth's atmosphere and its relation to other geophysical conditions, Part II, Proc. Roy. Soc. London, A114, 524, 1927
- DOBSON, G. M. B., D. N. HARRISON and J. LAWRENCE, Measurements of the amount of ozone in the earth's atmosphere and its relation to other geophysical conditions, Part III, Proc. Roy. Soc. London, A122, 456, 1929
- FABRY, C. Rapport de la réunion de l'ozone et de l'absorption atmosphérique, Gerlands Beitr. Geophys., 24, 1, 1929
- FABRY, C. et H. BUISSON, Etude de l'extrémité ultraviolette du spectre solaire, J. Phys., Paris, 6e série, 2, 197, 1921a
- FABRY, C. and H. BUISSON, A study of the ultra-violet end of the solar spectrum, Astrophys. J., 54, 297, 1921b
- FOWLER, A. and R. J. STRUTT, Absorption bands of atmospheric ozone in the spectra of sun and stars, Proc. Roy. Soc., London, A93, 577, 1917
- GÖTZ, F. W. P., Zum Strahlungsklima des Spitzbergensommers. Strahlungs- und Ozonmessungen in der Königsbucht 1929, Gerlands Beitr. Geophys., 31, 119, 1931
- GÖTZ, F. W. P. and G. M. B. DOBSON, Observations of the height of the ozone in the upper atmosphere, Proc. Roy. Soc. London, A120, 251, 1928 and A125, 292, 1929
- GÖTZ, F. W. P., A. R. MEETHAM and G. M. B. DOBSON, The vertical distribution of ozone in the atmosphere, Proc. Roy. Soc. London, A145, 416, 1934
- HARTLEY, W. N., On the absorption spectrum of ozone, J. Chem. Soc., 39, 57, 1881a

NICOLET

HARTLEY, W. N., On the absorption of solar rays by atmospheric ozone, J. Chem. Soc., 39, 111, 1881b

HOUZEAU, A., Preuve de la présence dans l'atmosphère d'un nouveau principe gazeux, l'oxygène naissant, C. R. Acad. Sc. Paris, 46, 89, 1858

HUGGINS, W. and Mrs HUGGINS, On a new group of lines in the photographic spectrum of Sirius, Proc. Roy. Soc. London, 48, 216, 1890

LEVY, A., Vingt années d'observations ozonométriques, Ciel et Terre, 19, 291, 1898

SCHOENBEIN, C. F., Recherches sur la nature de l'odeur qui se manifeste dans certaines réactions chimiques, C. R. Acad. Sc. Paris, 10, 706, 1840a

SCHOENBEIN, C. F., Beobachtungen über den bei der Elektrolyse des Wassers und dem Ausströmen der gewöhnlichen Elektrizität aus Spitzen sich entwickelnden Geruch, Ann. Phys. Chem., 50, 616, 1840b

## VERTICAL OZONE DISTRIBUTION AND TROPOSPHERIC OZONE

H.U. Dütsch

Laboratory for Atmospheric Physics ETH, Hönggerberg HPP, 8093 Zurich,  
Switzerland

### Abstract

The methods for measuring the vertical ozone distribution (excluding satellite techniques) are discussed. The Götz-Umkehr method is the only remaining indirect method; its main importance lies in the information obtained on the ozone content of the upper stratosphere. The bulk of the direct sounding has been made with electrochemical instruments which have a somewhat reduced accuracy close to their ceiling in the middle stratosphere. The available material is rather inhomogeneous and the spatial distribution quite inadequate, especially in the tropics and in the Southern Hemisphere. The implications on stratospheric transport processes given by the seasonal variation of the world wide vertical distribution obtained from the available material, mainly soundings, is discussed. The information on ozone in the troposphere is rather less reliable than in the stratosphere. The ozone concentration at ground level sites is strongly influenced by local conditions and can therefore only with great care be used for extrapolations to the free troposphere. Improved measurements are of special importance considering the present uncertainties about the contribution of tropospheric photochemical processes to the overall ozone budget.

### A. THE NEED FOR OBSERVATIONS OF THE VERTICAL DISTRIBUTION

Quantitative studies with Chapman's photochemical theory (1930) - now often called the classical theory - done during the 1940s revealed grave inconsistencies between observed and theoretical total ozone values with respect to the dependence on latitude and season (fig. 1) - while on the other hand the total world-wide ozone burden was reasonably well reproduced considering the accuracy of the reaction rate constants then available (this discrepancy was later by no means removed by the advent of the modern photochemical theory). An explanation of the dilemma was given by assuming that due to the rapid downward increase of the photochemical relaxation time from hours and days in the upper stratosphere to years below 20 km the ozone distribution in the lower stratosphere was predominantly determined by transport through the stratospheric general circulation. In order to prove this hypothesis it became necessary to obtain reliable world-wide data on the vertical distribution of ozone, for showing that the discrepancy between theory and observations was located at those levels where the relaxation time was large, i.e. in the lower stratosphere (see fig. 2). Further it was of importance for the understanding of stratospheric energetics to have a reliable knowledge of the heat source provided by the UV-absorption

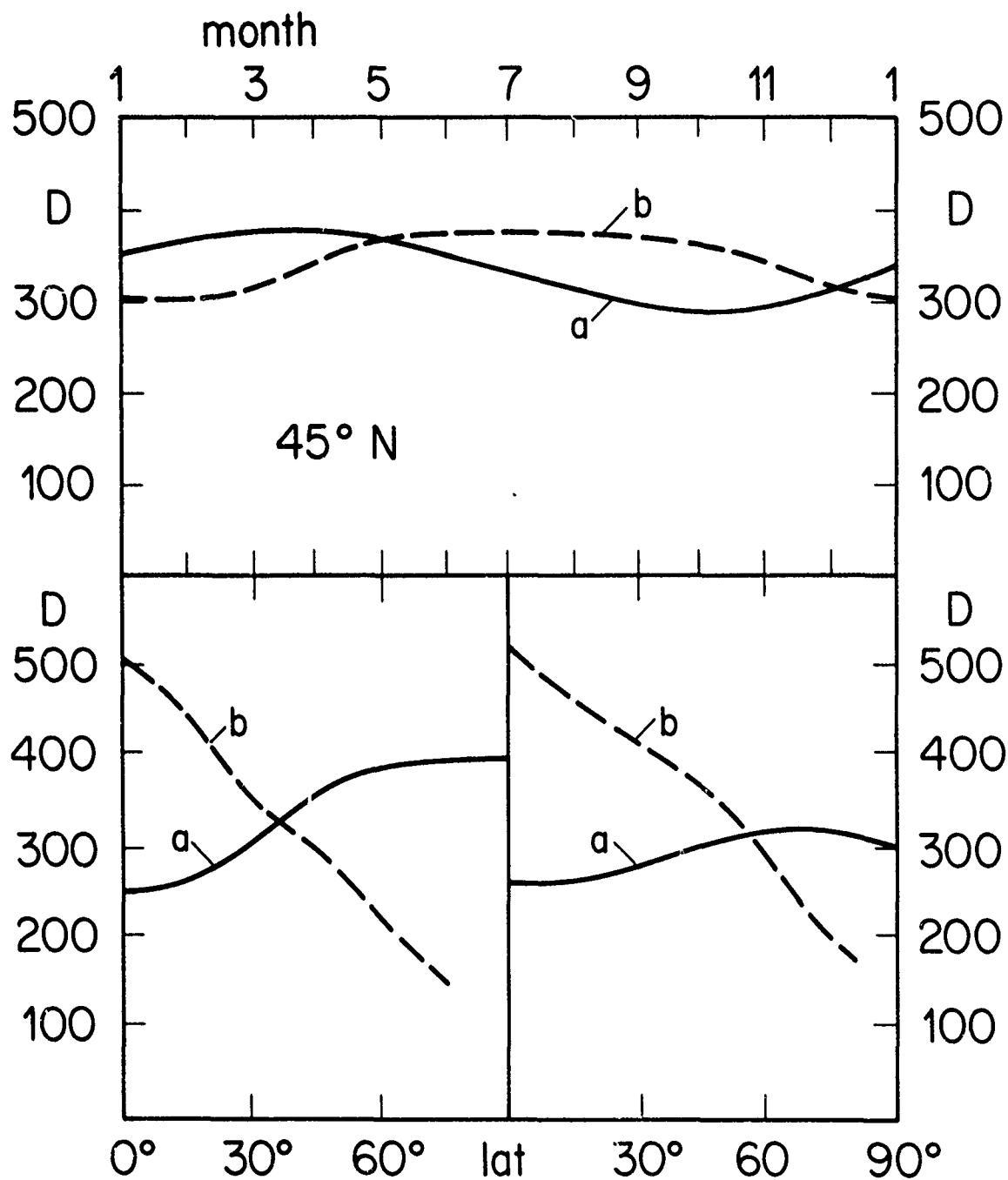


Fig. 1. Contradiction between observed total ozone distribution and the values deduced from the photochemical theory with respect to season (top) and latitude (bottom, left: late winter, right: late summer).

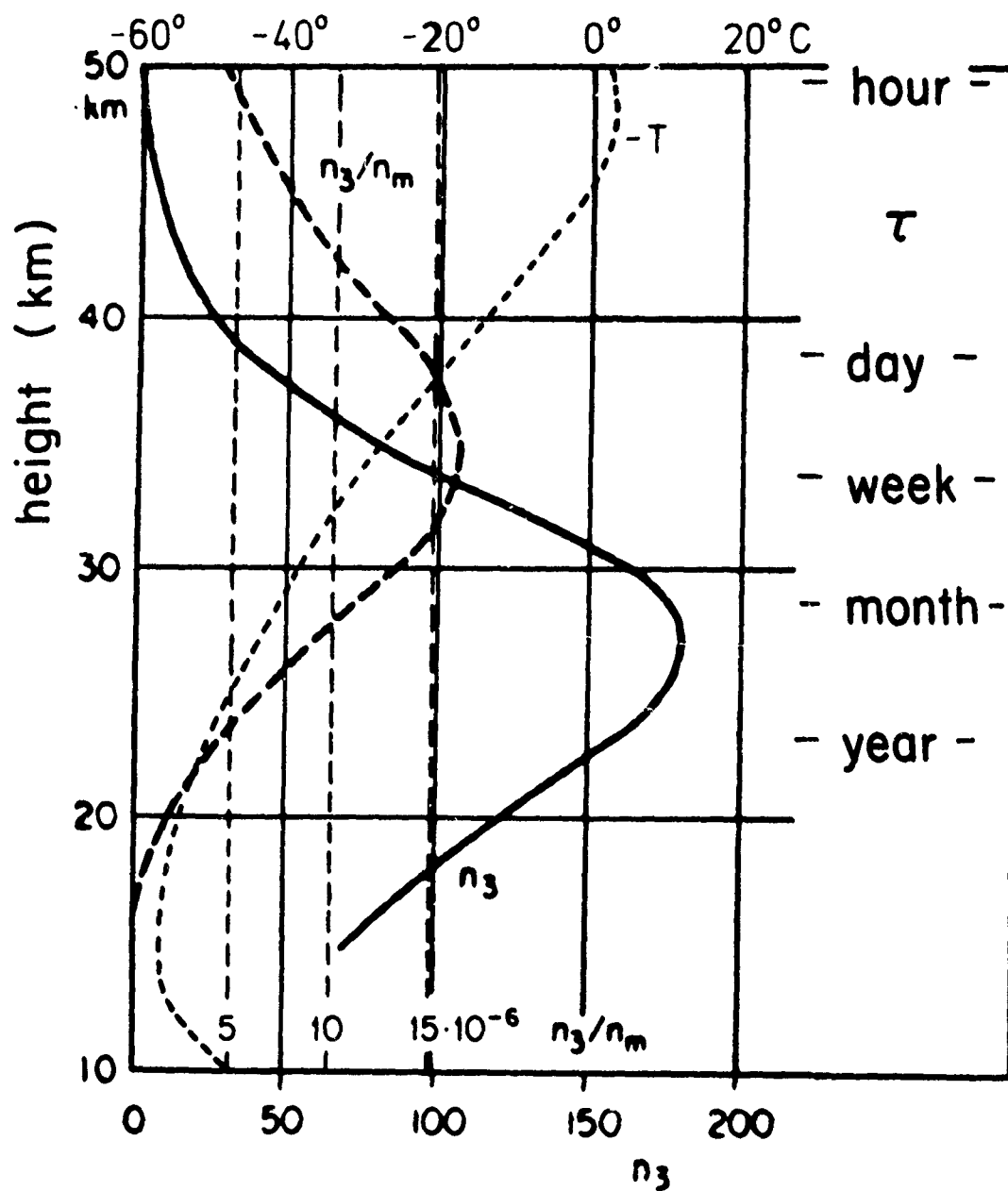
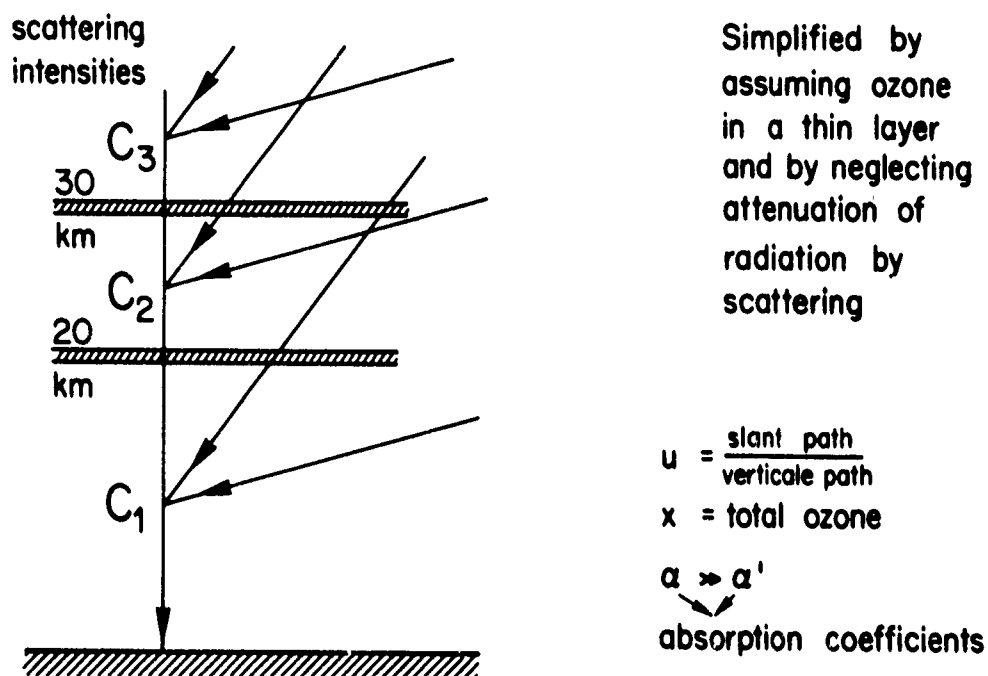


Fig. 2. Vertical ozone distribution ( $45^{\circ}$ , summer) computed from the Chapman theory (partial pressure:  $n_3$ , mixing ratio in ppmV:  $n_3/n_m$ ) and temperature distribution. On the right hand side relaxation time  $\tau$  for summer conditions.



$$C_1 = 0.95 C, \quad C_2 = 0.04 C, \quad C_3 = 0.01 C$$

$$R_{20} = \frac{I}{I'} = \frac{\overbrace{C_1 e^{-\alpha x \mu}}^A + \overbrace{(C_2 + C_3) e^{-\alpha x}}^B}{\underbrace{C_1' e^{-\alpha' x \mu}}_C + \underbrace{(C_2' + C_3') e^{-\alpha' x}}_D}$$

$$R_{30} = \frac{I}{I'} = \frac{\overbrace{(C_1 + C_2) e^{-\alpha x \mu}}^A + \overbrace{C_3 e^{-\alpha x}}^B}{\underbrace{(C_1' + C_2') e^{-\alpha' x \mu}}_C + \underbrace{C_3' e^{-\alpha' x}}_D}$$

first  $A \gg B, \quad C \gg D$

then  $A \ll B, \quad D \gg C - \text{Umkehr}$

Fig. 3. Schematic explanation of the Umkehr effect.



## DUTSCH

by the ozone layer - again this information can only be fully obtained on the basis of the vertical distribution. Although the first useful determinations of the vertical ozone distribution by indirect (Götz-Umkehr, 1934) and direct methods (Regener's (1934) balloon spectrograph) were obtained soon after the development of Chapman's theory it was not until the late 50s and the early 60s that the techniques for obtaining comparable world wide data were fully developed - largely on the basis of the impetus given by the JGY (1957/58).

### B. METHODS FOR MEASURING THE VERTICAL DISTRIBUTION

Both direct and indirect methods gave early indications of the vertical distribution and both are still being used to yield the information presently needed in connection with the problem of a possible anthropogenic threat to the ozone layer.

#### 1) Indirect methods

Although several methods permitting information to be obtained on the vertical ozone distribution were developed (measurements of absorption and emission in the infrared (9.6  $\mu$  band of ozone) (Vigroux, 1969), spectral measurements (in the visible) of the eclipsed moon etc.) only the initial one, relying on stray light measurements on the zenith sky in the UV, the so called Umkehr method, first detected by Götz and put into use jointly with Dobson and Meetham (1934), is still largely applied.

As shown in figs. 3 and 4, the reversal of the trend with decreasing sun height of the (logarithmic) intensity ratio of two ultraviolet wavelengths (measured with the Dobson spectrophotometer) is produced by the ozone maximum in the stratosphere and depends on both altitude and intensity of that layer. As we do not deal with a sharp layer but with a continuous and rather diffuse distribution, the evaluation is complex and routine use of the method became only possible through the development of objective computer methods (Dütsch, 1959; Mateer and Dütsch, 1964). The observed Umkehr curve is compared with theoretically computed standard curves (fig. 4) and the vertical ozone distribution is deduced by adjusting the initially assumed standard distribution layerwise until best fit with the observed curve is obtained. An Umkehr curve together with the concurrently measured total amount (direct sun observation) provides in fact only 4-5 bits of independent information. Trying to use only these five bits to distribute the ozone into as many preassumed very broad layers (10 km wide) would, however, introduce too much subjective forcing into the solution. In practice therefore 12 points from the observed curve are used to distribute the ozone into nine layers bounded by the pressure ratio 2:1. (As an exception at the bottom a layer of double thickness represents the troposphere and at the top it is - due to the lack of more information - assumed that 2/3 of the ozone remaining above layer 8 is concentrated in a layer 9 having the same vertical extent as layers 2-8.)

The mathematical overdetermination (12 points for 9 layers) - which is needed because of a number of inherent problems - means that an exact fit between observed and varied standard curve cannot be obtained, indicating a remaining uncertainty and at the same time a considerable smearing of the solution. It is in principle not possible to resolve by the indirect method the strong secondary maxima often observed in the lower stratosphere by direct soundings (fig. 5) and even the main maximum is considerably smeared out (fig. 6).

The main reason for the continued use of the indirect method even after direct soundings became routine, lies - apart from its relative inexpensiveness - in the fact that it gives information on the upper stratosphere, i.e. on a level which is of particular interest in connection with possible influences of solar

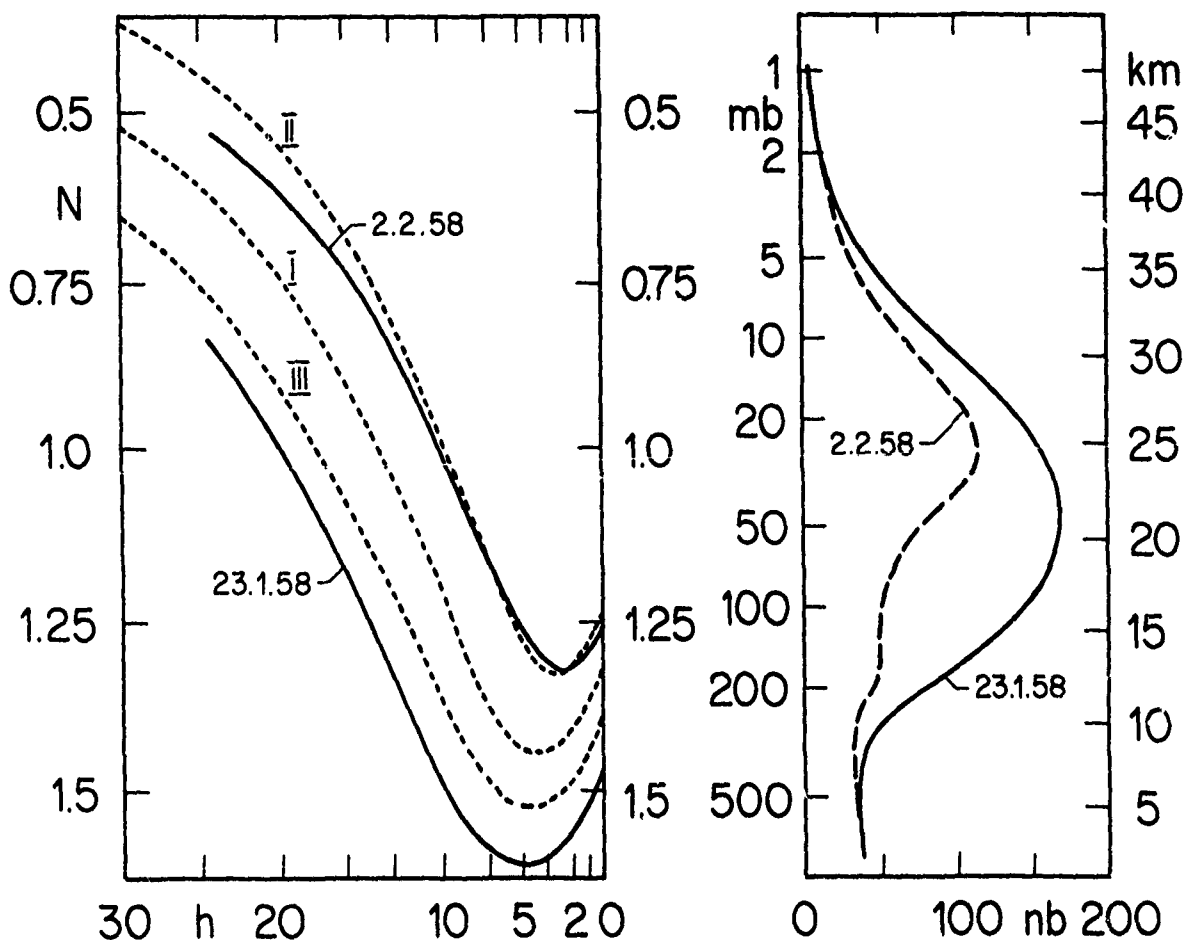


Fig. 4. The three standard Umkehr curves (corresponding to total amounts of 341 D (I), 254 D (II) and 423 D (III) compared with two observed curves (left side) and the corresponding solutions (obtained by subjective smoothing of the objectively computed block distributions, right side).

activity on ozone (fig. 16) and in which also the strongest influence of CFMs on the ozone layer is expected.

In connection with the search for long-term periodicities or trends by the Umkehr method, some further remarks are appropriate. Although the usefulness of the Umkehr method has certainly been much improved by introducing a uniform world wide standard evaluation scheme - which also contains corrections for multiple scattering - nevertheless a number of problems remain - apart from the smearing mentioned above - which could produce misleading conclusions.

It has been pointed out that stratospheric dust layers due to a volcanic eruption could considerably disturb the Umkehr curve and thereby simulate ozone values too low in the upper stratosphere (DeLuisi, 1979). Further, Umkehr observations need 3-4 hours of clear sky - which in many climates is a rare event - therefore the means obtained for the vertical distribution are even more biased towards fair weather situations as this is the case with respect to the total amount. Although this bias is presumably less important in studying

DUTSCH

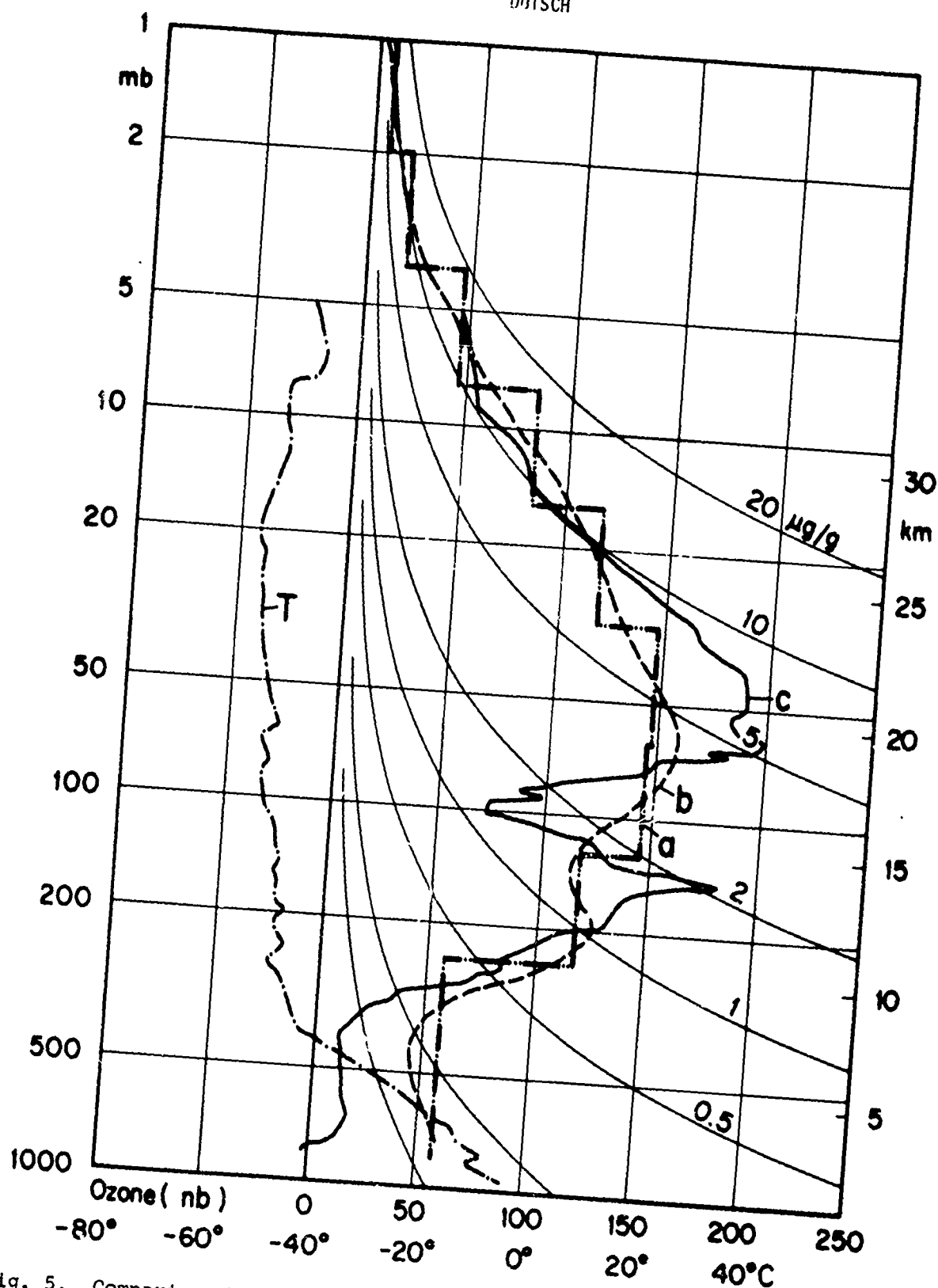


Fig. 5. Comparison between vertical ozone distribution obtained by the Umkehr method (block distribution, curve a and subjectively smoothed distribution, curve b) with concurrent results of a direct sounding with an electrochemical instrument (curve c); temperature (T) is also shown.

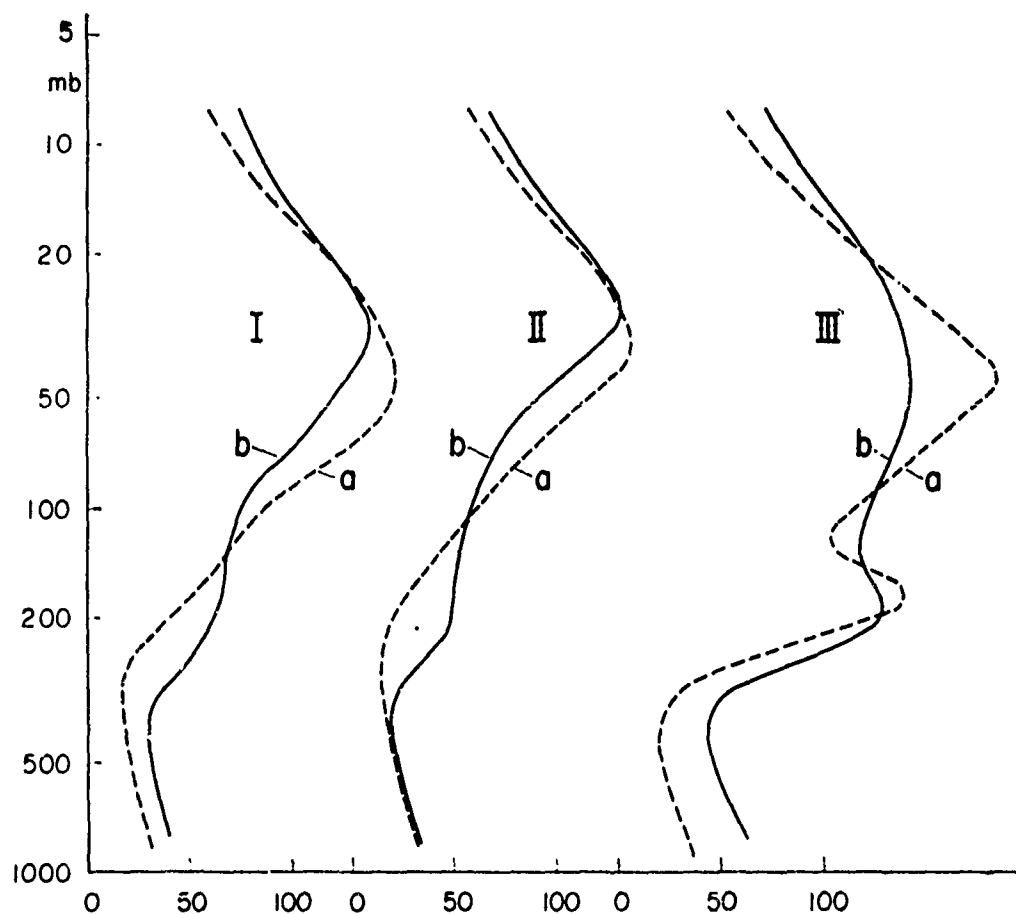


Fig. 6. Comparison of mean values of the vertical ozone distribution for different values of the total amount (standard curves I, II and III) obtained from the Umkehr method (b) and from concurrent direct soundings with an electrochemical instrument (a) (Dütsch and Ling, 1969).

the upper stratosphere, the number of single observations in monthly means can be reduced to a dangerously low level. It must be realised that the accuracy of a single Umkehr observation is always questionable for the following reasons: apart from the temperature influence on the absorption coefficients which must necessarily be neglected in the evaluation, but which is not too important except may be in cases of sudden stratospheric warmings, and apart from the influence of clouds below the horizon (at very low sun), it is mainly the possible change of the ozone distribution during the time of the observation which can lead to erroneous solutions because the evaluation method basically assumes no variation during that time. It is for these reasons that even for research on long-time variations, especially in the upper stratosphere, a minimum of 8-10 single distributions per month should be obtained. A considerable part of the (more rapid) fluctuations in the 20 year Umkehr series over Arosa (fig. 16) may be due to the fact that this goal could not always be reached.

## 2) Direct observations

### a) Optical

Optical instruments were the first ones to be used for direct measurements of the vertical ozone distribution and also the first to provide a longer series of such observations after the spectrograph (to be recovered!) had been replaced by a filter instrument (in order to provide easy telemetering, i.e. to build an ozone sonde) (Kulke and Paetzold, 1957). Nevertheless it has contributed comparatively little to our present knowledge of the world-wide vertical ozone distribution mainly for two reasons: The conversion from spectrograph to filter instrument led to some reduction in the accuracy of the single observation; this results, because the method is a differential one, in a certain smearing of the obtained vertical distribution. Although the vertical resolution stays far better than that obtained from the indirect Umkehr method, faulty distributions could already be produced by slight disturbances due to haze layers and much more by clouds in the lower part of the atmosphere. In addition, these instruments stayed comparatively heavy and expensive.

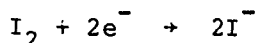
### b) Chemical

Therefore after the breakthrough in miniaturizing chemical instruments had been made around 1960 (Brewer and Milford, 1960; Regener, 1964), this type provided practically all the information on which our present knowledge of the world wide vertical ozone distribution is based. While the Brewer electrochemical instrument and other sensors of this type, developed later, have an instrumental relaxation time of 20-30 seconds and thus provide some smearing over layers between 100 and 200 m thick - which is for many purposes rather an advantage than a disadvantage - Regener's chemiluminescent type gives instantaneous values. Although this latter instrument, which measures the light produced by ozone flowing over the luminescent surface with a photomultiplier, was the first to be used in a routine network (1963-1965) over the North American continent (Hering and Borden, 1965/1967) and also has the advantage of not being confined to pressure levels below the triple point of the liquid solution (i.e. above about 35 km) it was later largely abandoned due to problems with the stability of the luminescent disk. The chemiluminescent sensor has still been in use for turbulent flow studies near ground where rapid response is essential and the calibration easily controlled, and for application in rocket soundings (Hilsenrath, 1969) where only a dry chemical or an optical method is applicable. A gas phase chemiluminescent instrument (ethylene type) has recently been built in France but was so far only used for special studies aiming at a high vertical resolution and another chemiluminescent sonde using the reaction of NO with O<sub>3</sub> had its first flights in the US during the last 12 months (Kley, personal communication). Thus the information assembled during the last 15 years on the vertical ozone distribution was to a large extent obtained with the Brewer electrochemical instrument, built in a number of versions and by other electrochemical sensors later developed by Komhyr (1969) (concentration cell), and in Japan (Kobayashi and Toyama, 1966) (Carbon-iodine sonde).

All of them use the basic KI-ozone reaction:



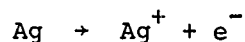
and in all cases the iodine is reconverted to the ion at a platinum cathode:



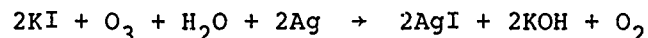
The anodic reactions, however, which must avoid a reformation of iodine in the

## DUTSCH

cell, are different from each other in the 3 cases. The Brewer sonde uses a silver anode, the reformation of  $I_2$  is then prevented by the insolubility of  $AgI$ ; the anodic reaction is



and the total process can be written as



All instruments use a small battery powered pump to provide a calibrated air flow; this allows the ozone partial pressure to be deduced in a simple way from the current which is flowing through the cell. This information is telemetered to the ground alternatingly with meteorological data either by an attached radio sonde or by the instrument's own transmitter. The whole package weighs only about 2 kg and can thus easily be flown by a normal high altitude radio sonde balloon.

The electrochemical instruments need to be kept very clean in order to avoid a loss in ozone response especially in the troposphere. Slight changes in the geometry of the sensor can also lead to a reduced sensitivity. In order to eliminate this latter error, it has become customary to correct the raw data by multiplying them with a constant factor in such a way that the sum of the integrated total supplemented by the ozone above burst level equals the total amount simultaneously observed with the Dobson instrument. The intercomparisons of sondes at Hohenpeissenberg (Attmannspacher and Dütsch, 1970) have shown that this "one factor" method works quite satisfactorily.

The sounding altitude is limited by the boiling of the solution at and above the triple point (6.1 mb) which leads to rapid freezing at about 35 km. The reliability of the sounding decreases anyhow rapidly above 10 mb; the necessary correction for decreasing pump efficiency at low pressures (applied before the one factor correction) which varies in fact from instrument to instrument but cannot be specifically determined for each of them, reaches considerable values in the middle stratosphere; in addition small errors in pressure determination become important at that level. With respect to the climatological mean values discussed in the following section a reduced reliability has thus to be expected in the troposphere (due to poisoning effects) and above 10 mb; the latter deterioration is also due to the rapid drop in the number of available soundings with altitude above that level. The precision of the sounding within the main ozone layer should on the basis of the one factor correction not be much less than that of the Dobson instrument, i.e.  $\pm 4-5\%$  instead of  $\pm 2-3\%$ ; the absolute accuracy is basically tied to that of the Dobson and by this to the set of absorption coefficients used with that instrument.

## C. RESULTS

### 1) Ozone climatology

For preparing a world wide ozone climatology we presently dispose of about 8000 soundings. This set is, however, rather inhomogeneous; the sounding periods and the number of soundings obtained vary drastically from one station to another; the soundings made with the chemiluminescent sonde may not be fully comparable with the bulk obtained with the electrochemical instrument. The geographical distribution of the data is extremely irregular with a strong concentration on northern mid-latitudes. The coverage in the tropics and over most of the Southern hemisphere is very poor; there are, however, data available from the Antarctic (most of them obtained with the chemiluminescent sonde).

While it is possible to construct a rather reliable global climatology for the

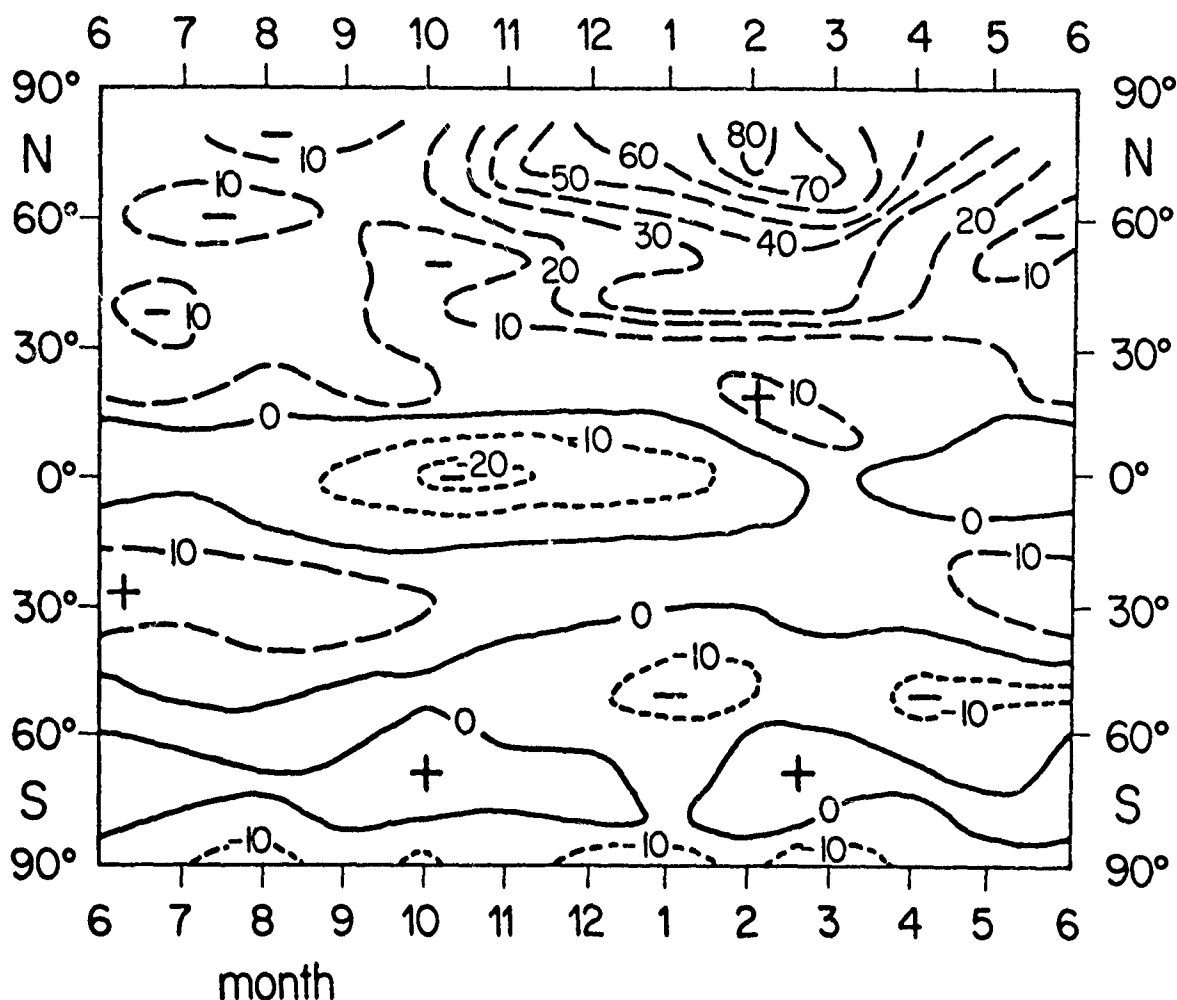


Fig. 7. Difference between latitudinal mean total ozone obtained from the available soundings and the corresponding value derived from the observations of the Dobson network, due to the irregular distribution of sounding stations.

ozone total amount there are not enough data available to do the same for the vertical distribution; even the evaluation of latitudinal mean values involves considerable interpolation and smoothing. The bias of the observational sites towards upper air trough positions (Dütsch, 1978) presents a considerable problem in the Northern hemisphere (fig. 7) and one must try to eliminate its influence by data adjustment using the correlation between vertical distribution and total amount (fig. 8) which is, however, not well enough known for all latitudes. The uncertainty in the world wide data discussed below is thus considerably higher than that of the climatology of a well kept single station in the network.

The mean vertical ozone distributions at different latitudes show the expected behaviour: Strong increase with latitude (more pronounced in spring than in fall) in the lower stratosphere up to about 23 km (as a consequence of transport processes) and poleward decrease (more pronounced in fall) in the middle stratosphere under the prevailing influence of photochemical processes (fig. 9).

Meridional cross sections (fig. 10) demonstrate clearly the importance of the

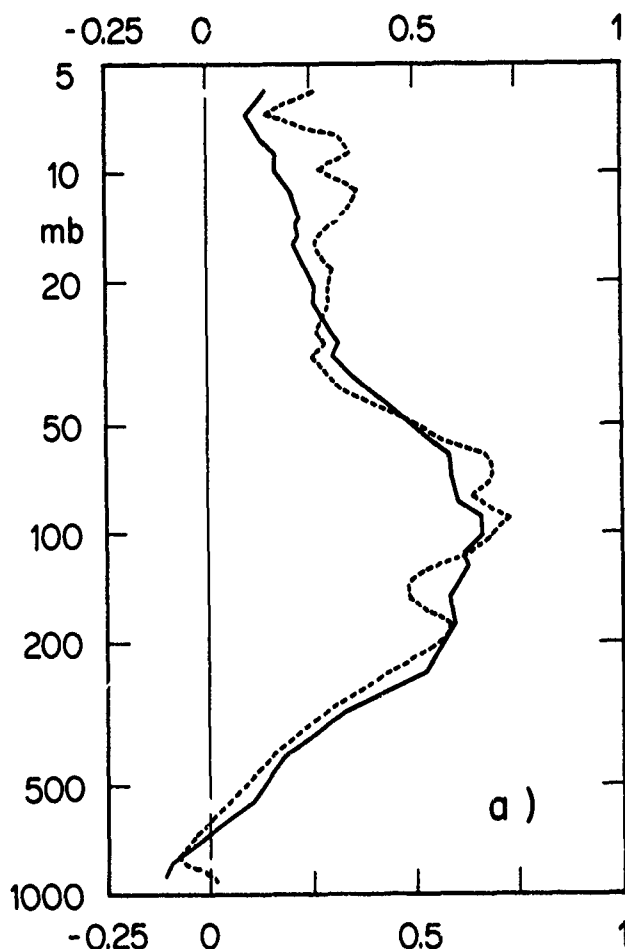


Fig. 8. Correlation between ozone partial pressure at different altitudes and the total amount obtained from 11 years of soundings at Payerne (seasonal variation removed); full line: for single observations; dashed line: for monthly means.

high reaching tropical troposphere with its low ozone content for the small total ozone values observed at low latitudes. Due to strong vertical mixing up to a relatively high altitude, we find at the tropical tropopause the lowest ozone concentrations observed anywhere below 40 km, almost at a level where in the Arctic the world wide maxima are observed. The layer of maximum ozone concentration has its highest elevation close to the equator and is more strongly sloping toward higher latitudes in winter and spring than in summer and fall.

In contrast to this the mixing ratio maximum has over the tropics its lowest position (due to the very steep vertical gradient between 20 and 30 km observed at these latitudes) (fig. 11). The upward slope toward high latitudes of the maximum layer seems more pronounced in the Southern Hemisphere especially in fall and winter; it must, however, be realized that the ozone distribution at high levels shown here is largely deduced from preliminary satellite data and from a rather unsatisfactory coverage by Umkehr observations including extrapolation across the polar night terminator (Umkehr information in fact ends at  $20^{\circ}$  latitude from the terminator and satellite data (BUV) presumably lose accuracy approaching the terminator).

In order to discuss transport processes and also for the purpose of quantitative combination of observations and photochemical theory for computing ozone flux



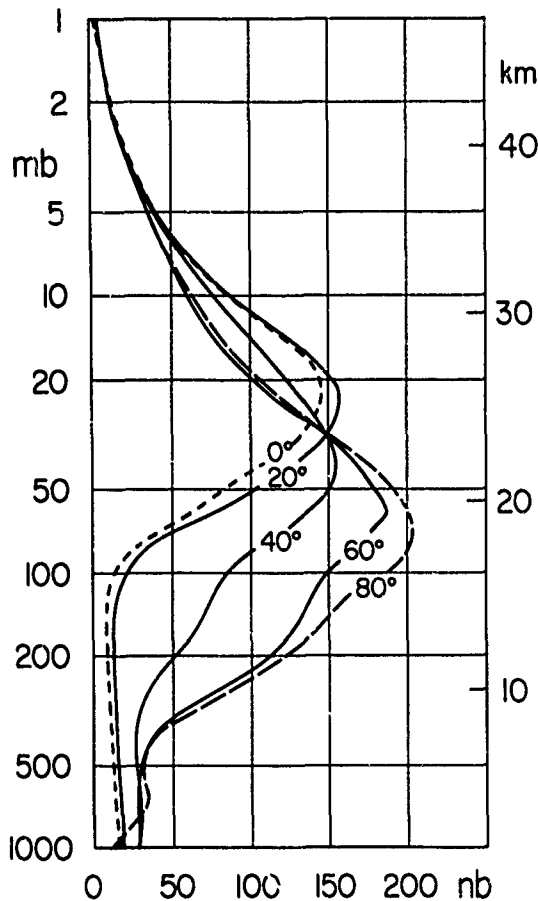


Fig. 9a

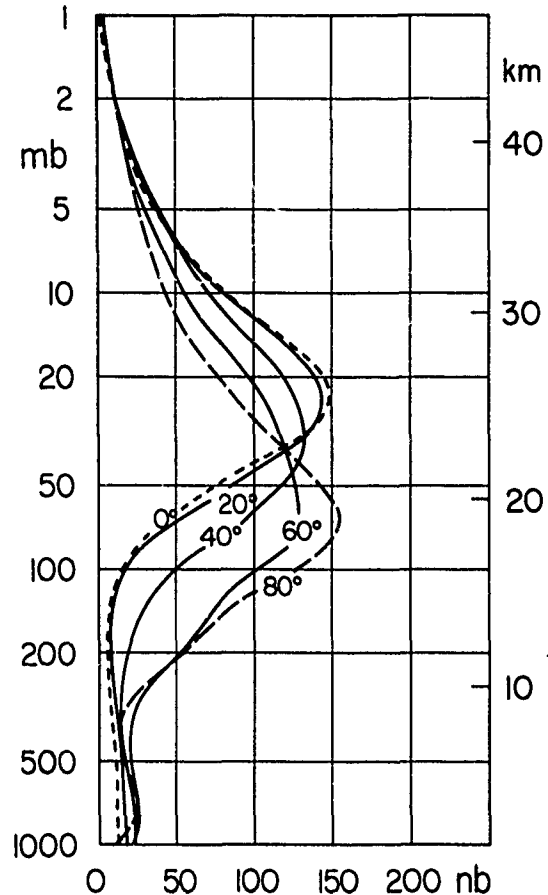


Fig. 9b

Mean vertical distribution at different latitudes. a: April, b: October.

divergences (Dütsch, 1977), the representation of the ozone variation with latitude and season on constant pressure levels is presumably the most appropriate technique (fig. 12); in this case the same isolines (with different labels) may represent partial pressure and mixing ratio.

The transition from the photochemically dominated state in the middle stratosphere to a distribution completely determined by transport just above the (mid-latitude) tropopause and its dependence on season as well as the differences between the two hemispheres are easily seen from the sequence of figs. 12c through h.

In the middle stratosphere (11 and 22 mb) a clear tropical maximum is the main feature (its seasonal variation may, however, be simulated by the lack of data); while an extension of high values into the Arctic already shows up at the end of winter, a corresponding feature is practically missing in the Antarctic (there is a slight indication of it but much later, at the end of spring). From 25 km down to the 20 km level we find a successive transition towards an equatorial minimum and a polar maximum. Again that maximum appears at considerably greater heights and is more strongly developed in the Arctic than in the Antarctic; it also appears two months later in the latter region. The seasonal

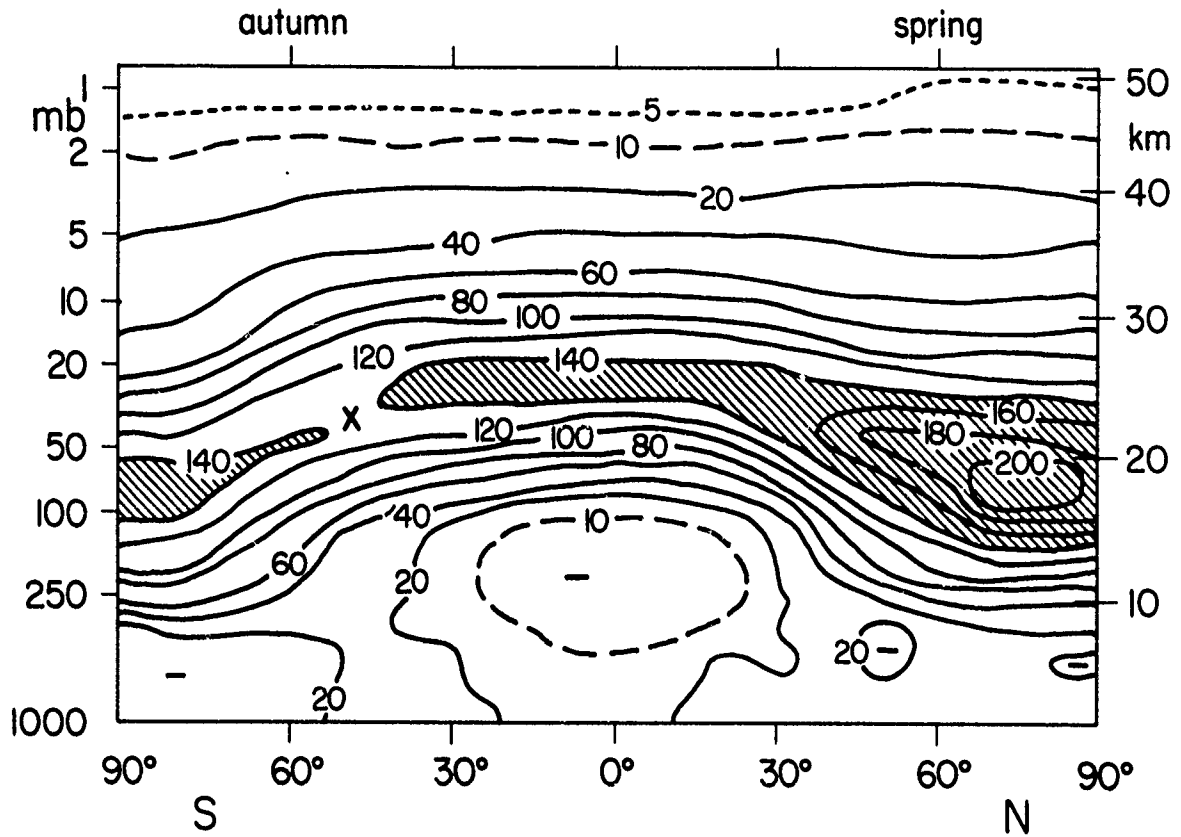


Fig. 10. Meridional cross section of ozone partial pressure (nb) in February.

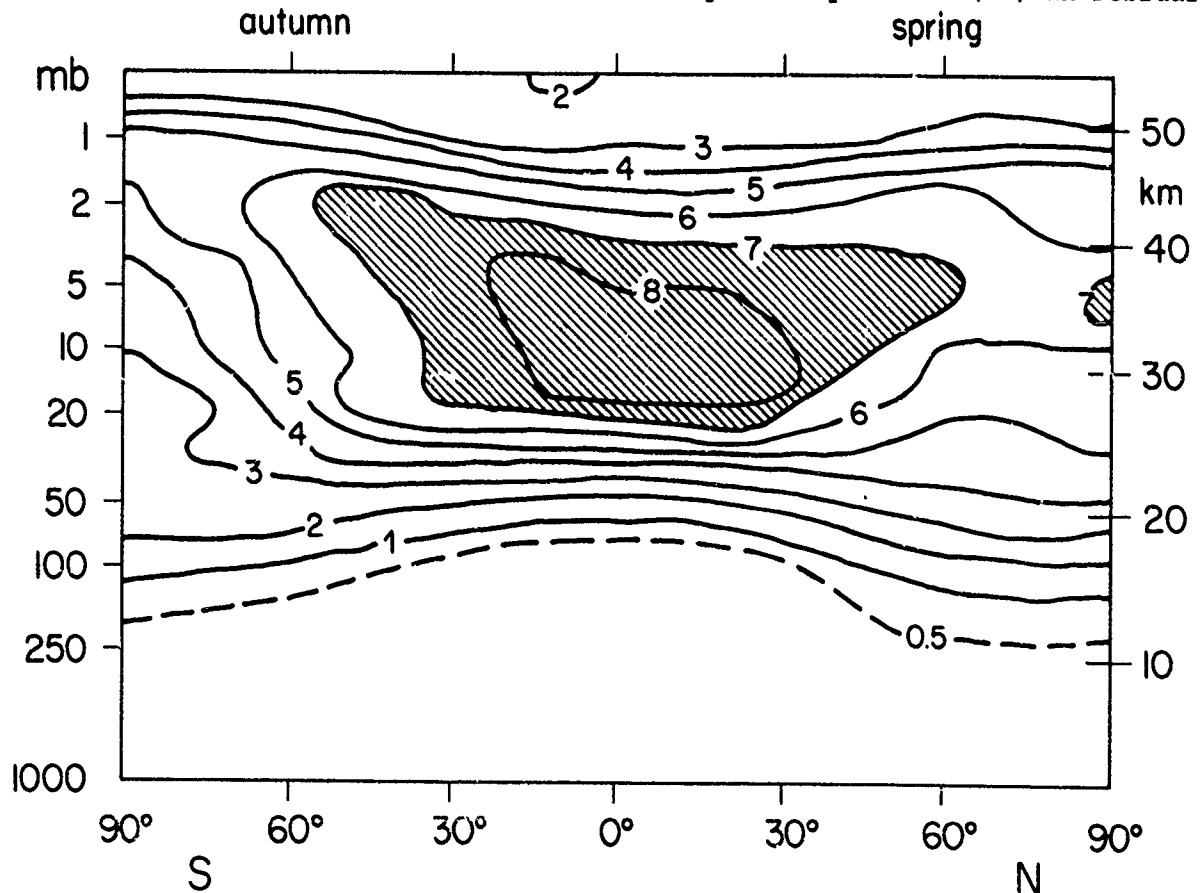


Fig. 11. Meridional cross section of ozone/air mixing ratio (ppmV) in April.

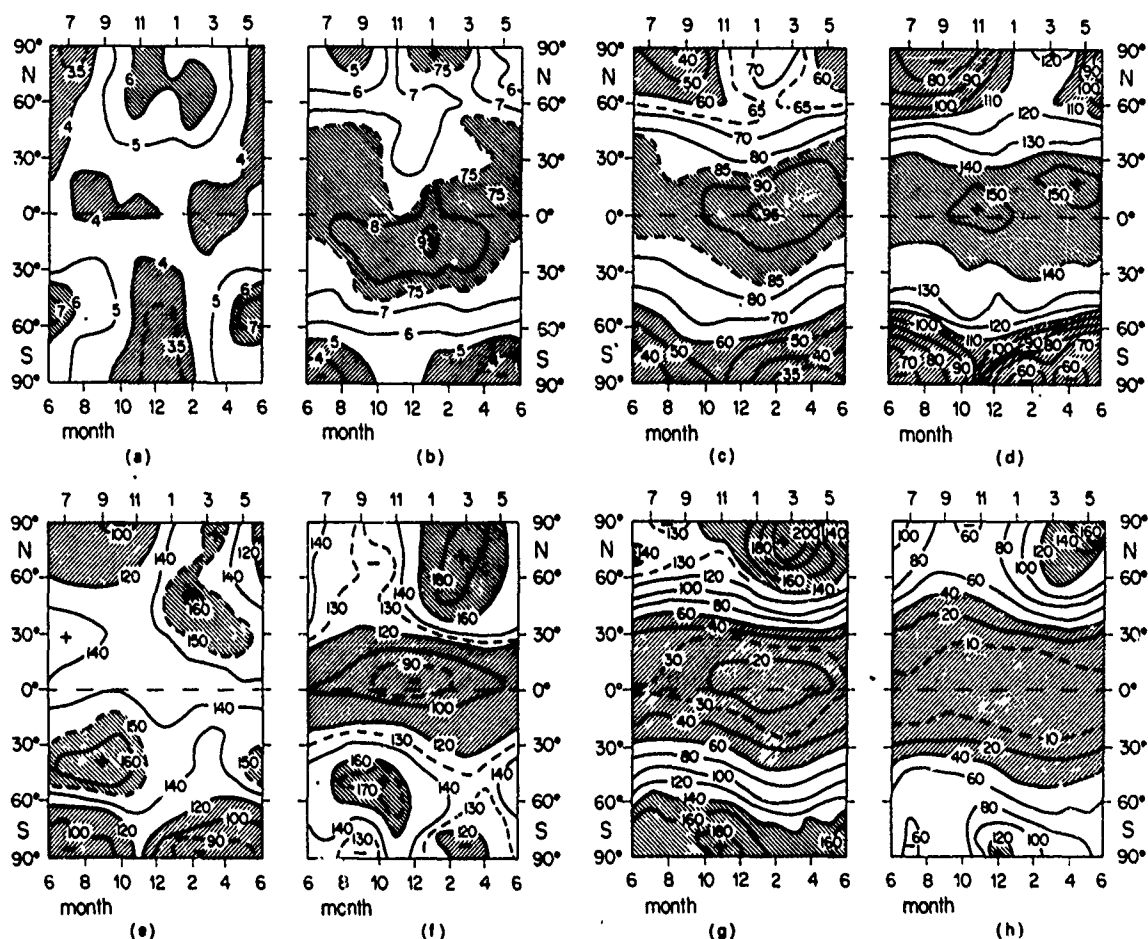


Fig. 12. Global ozone distribution at different levels: a (1.4 mb) and b (3.9 mb): isoline of ozone/air mixing ratio in ppmV; c (11 mb), d (22 mb), e (31 mb), f (44 mb), g (88 mb) and h (176 mb): isolines of partial pressure in  $r'$  (figs. 9-12 are from [Dütsch, 1978]).

variation is thus much stronger in Northern than in Southern high latitudes: while through the cold season the poleward ozone flux produced by the general circulation goes into the Arctic it ends in Southern mid-latitudes and reaches the Antarctic only in connection with the final stratospheric warming in late spring, i.e. at a time when above equilibrium ozone is - except in the lowest stratosphere - relatively rapidly destroyed by photochemical processes.

While the reversal of the latitudinal and seasonal dependence of ozone distribution between the middle and the lower stratosphere is due to the transition from the dominance of photochemical to that of transport processes a similar variation from the middle to the upper stratosphere is in full agreement with the prediction of the photochemical theory. (Note that in figs. 12a and b, ozone isolines are for convenience labelled in mixing ratio terms, rather than as partial pressure). Whether the differences in position of the winter maximum at the 46 km level between the 2 hemispheres is real and still shows a difference in transport at that elevation or whether it is simulated by the unsatisfactory data base as discussed above remains to be seen.

# DUTSCH

## 2) Irregular variations of the vertical ozone distribution

### a) Variations in connection with weather

The dominance of transport processes leads to rapid day-to-day fluctuations of the vertical ozone distribution especially in middle latitudes where we have the best observational coverage. They are as to be expected strongest in the lower stratosphere but may extend into the middle stratosphere in connection with sudden stratospheric warmings. They can also produce very irregular vertical profiles with strong secondary maxima at lower elevations. Figs. 13a and b show the possible changes within a day or even within a few hours. Horizontal transport and vertical motion are equally important in producing such rapid variations. The day-to-day variations are largest in the neighbourhood of 100 mb (as in fig. 13a) and they become, as also shown there, small above the level of the ozone maximum (where the influence of the normal tropospheric weather systems is damped out). However, under the influence of the flow conditions connected with sudden stratospheric warmings, strong ozone fluctuation may also occur in the middle stratosphere (fig. 14).

Longer scale persistent deviations from normal weather patterns often lead to considerable variations in the vertical ozone distribution from one year to the next, again most strongly in the lower stratosphere (fig. 15). At the level of the ozone maximum a biennial variation becomes evident, high values being in phase with stratospheric easterlies at the 20 mb level which, following Reed (1965), are connected with the strengthening of the stratospheric extension of

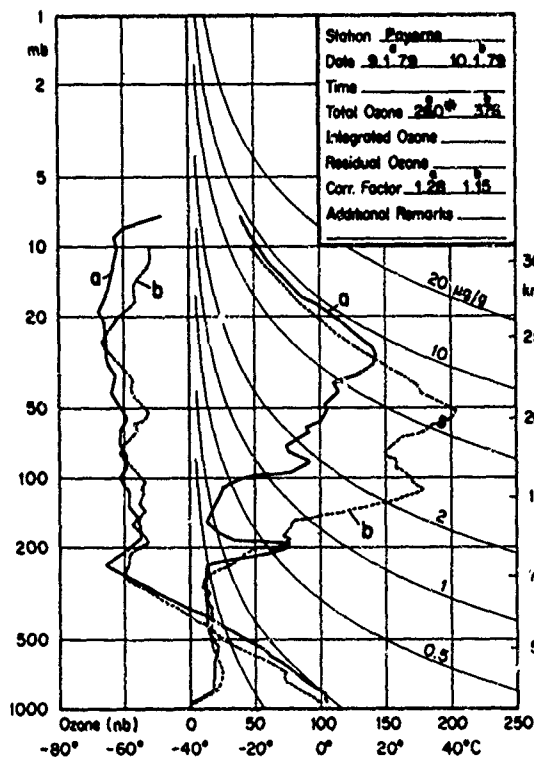


Fig. 13a. Change of vertical ozone distribution within one day.

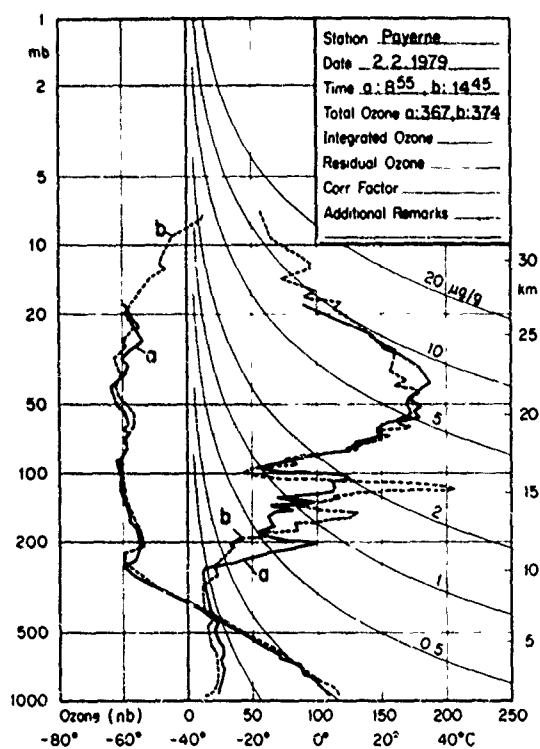


Fig. 13b. Change of vertical ozone distribution within 6 hours.

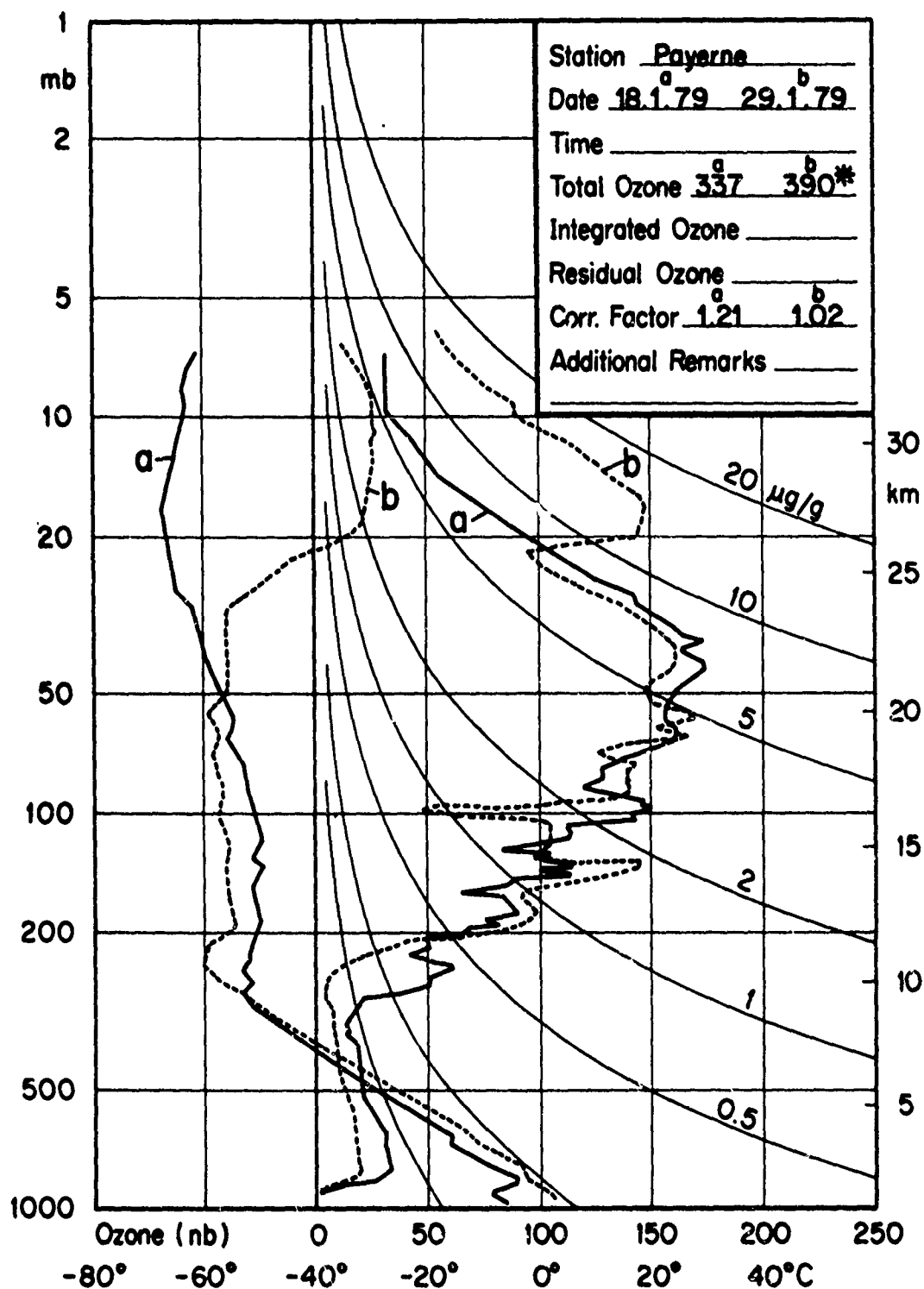


Fig. 14. Large changes in ozone content of the middle stratosphere in connection with a sudden warming.

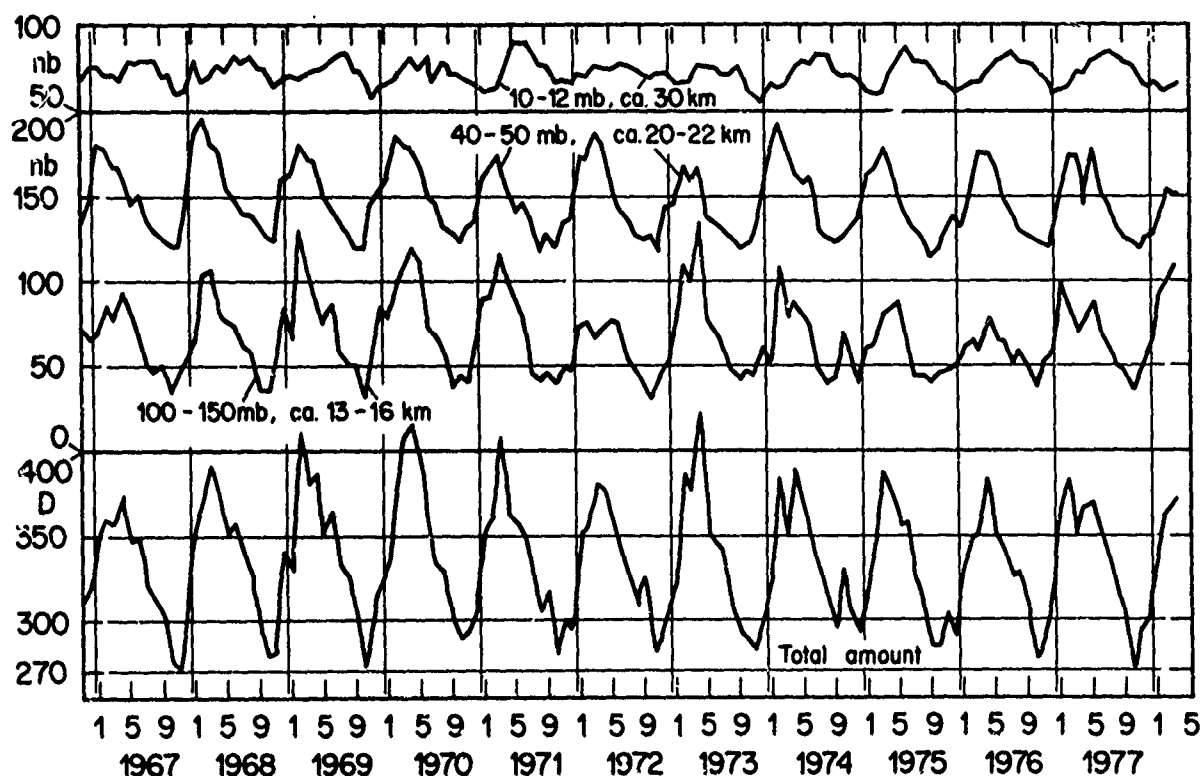


Fig. 15 Year-to-year differences in the seasonal variation of ozone in different layers over Payerne (from (Dütsch, 1979)).

the Hadley cell. This feature, which was also found for total ozone when the whole polar cap north of  $40^{\circ}$  lat. was considered (Züllig, 1973), is, however, not seen in the single station's total amount because it is there overshadowed by the larger fluctuations which are, as already mentioned, produced by the smaller scale circulation anomalies tied to tropospheric weather patterns.

### b) Longer term periodicities and trends

Especially in connection with possible anthropogenic influences on the ozone layer, the search for trends has become an intriguing problem, one reason being that it might be quite difficult to distinguish small possible man-made trends from natural long term variations which undoubtedly exist (one possible reason being slow variations in the intensity of the stratospheric branch of the Hadley cell or changes possibly introduced by solar activity).

The sounding material is certainly inadequate to look for world wide trends of ozone at different levels for the reasons discussed earlier, while in single station observations it is difficult to eliminate the so-called meteorological noise especially in the lower part of the layer. The 11 year series at Payerne, Switzerland, indicates a small downward trend between about the 30 and 70 mb level; however, from the present material it is difficult to distinguish it from a possible near 11 year periodicity.

The most intriguing long term periodicities are indicated by the Umkehr observations at Arosa (smoothed by a filter) for the upper stratosphere (fig. 16)

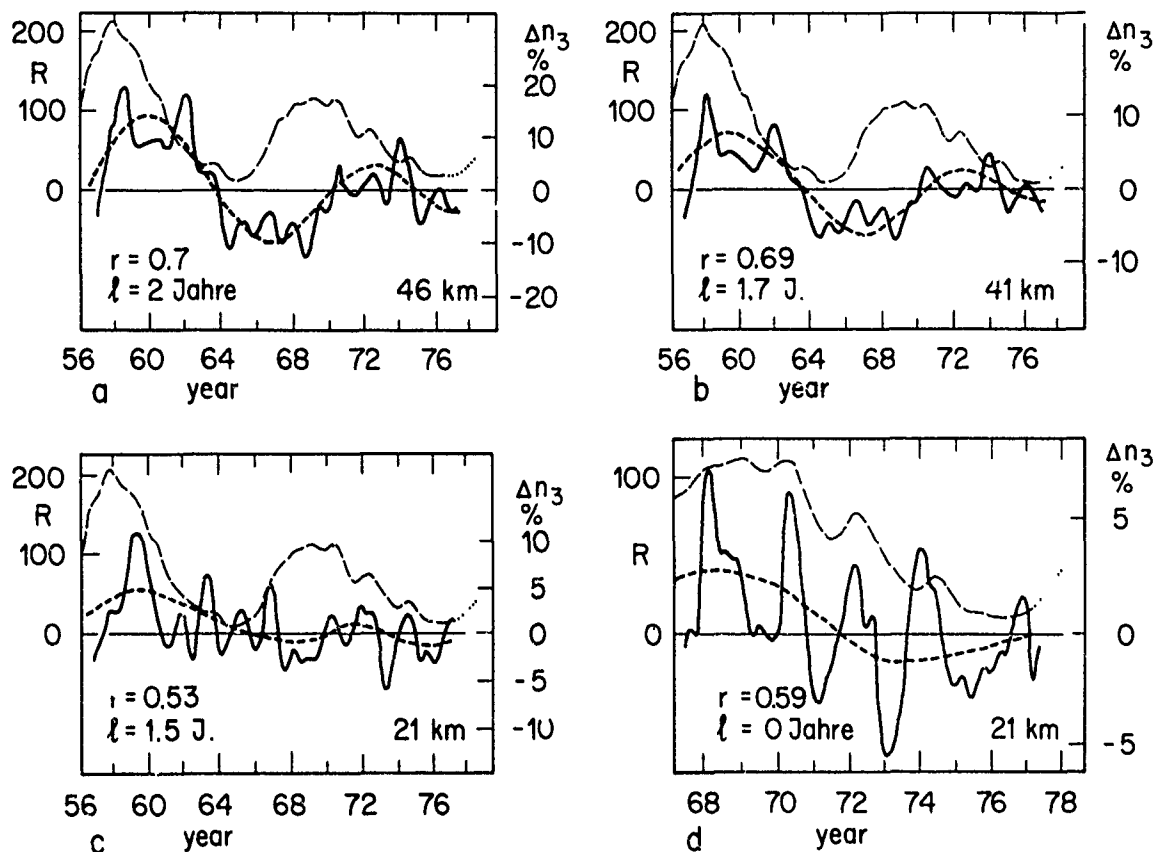


Fig. 16. Ozone variation at different levels (monthly mean values, seasonal variation removed, smoothed by a filter) compared with the sunspot cycle (smoothed by the same filter). Short dashed curve: ozone variation after further subjective smoothing. a - c: from Umkehr measurements at Arosa (Switzerland), d: from soundings over Payerne (Switzerland).

which show a correlation of 0.7 with sunspots with a phase shift of about 2 years (Dütsch, 1979). However, the total observational period is too short to prove any physical link (especially as it is somewhat difficult to explain the phase shift theoretically). Even the apparent superimposed downward trend is hardly significant.

#### D. TROPOSPHERIC OZONE

According to the classical (Chapman) photochemistry ozone was in the troposphere completely passive; it was inserted through the tropopause and mixed downward to be finally destroyed at the ground by contact with various substances, mainly organic material. Thus the ground was a sink the magnitude of which was identical with the influx through the tropopause. Its study was of some interest in connection with the global ozone budget.

At least 20 years ago it became clear that in the polluted air of certain big cities, having in addition specific meteorological conditions, ozone was produced by a complex reaction system between a number of trace substances (smog situation). However, due to the small area involved, that contribution seemed to have no global significance. On the basis of the modern photochemical theory,

#### DUTSCH

however, which was developed during the past 15 years, ozone is not inert even in the clean troposphere. Production or destruction is basically possible through the  $\text{HO}_x\text{-NO}_x\text{-CH}_4$ -oxydation chain-photochemistry. Although the hypothesis of near-photochemical equilibrium in the lowest layers (Chameidas and Walker, 1973) seems hardly tenable on the basis of the available observations, a non-negligible contribution from photochemical processes cannot be ruled out. This together with the alarming spread of at least smog-like conditions over much larger areas of the industrialized world than was initially realized, has generated a need for more observational information on tropospheric ozone.

Initially commercial instrumentation was mainly produced for measurements under smog conditions where, due to the high ozone values, a relatively low sensitivity was acceptable. For the more general purpose of the studies indicated above higher sensitivity (down to 1-2 nb) and also improved accuracy is wanted.

In principle the same sensors as used for measuring the vertical distribution, i.e. the electrochemical type, could be used; however, they would have to be converted for continuous automatic and unattended service during periods of days to a week. On the one hand, these sensors are not fully ozone specific under polluted air conditions; on the other hand poisoning by reducing substances (especially  $\text{SO}_2$ ) may become a problem (especially in stagnant air winter situations) and may require the use of filters.

Some ozone specific instruments have been built lately, one applying gas phase chemiluminescence (on ethylene basis); with the aid of modern electronics it has also become possible to directly use the UV-absorption of ozone with a path length of only 20 cm for the required sensitivity. While these new instruments are largely used in monitoring surface ozone (and also for measurements from aircraft), the cheaper electrochemical cells are suited for field experiments with many stations, provided the necessary calibration and checking technique is available either with the above mentioned instruments or with well calibrated and stable ozone generators. Surface ozone data are strongly locally influenced because of the variable chemical effectiveness of the ground destruction, but even more due to the local circulation as will be shown below by two examples. One must therefore be very careful when deriving even the ozone concentration in the boundary layer from surface measurements. Mountain stations are better suited but even there care must be taken. Further there is a variation with season and from station to station in the small positive vertical gradient of the mixing ratio, making inference of free-atmospheric ozone from ground based measurements difficult. Our knowledge of the global ozone distribution in the troposphere is therefore still largely based on the same soundings which provide the stratospheric picture. Because of the larger relative error in the tropospheric part of the measurement - within a series of observations and from one station to another - our knowledge is by no means satisfactory.

From the present material it seems that the tropospheric ozone content is lower in the Southern hemisphere than in the North (fig. 10). Although this result is in agreement with surface observation (Fabian and Pruchniewicz, 1977), it is still open to question due to the scarcity of observations in the Southern Hemisphere. The differences might be due to the unequal influx through the tropopause as a consequence of the difference in the general circulation between the two hemispheres. On the other hand the available information points to lower surface destruction over the vast water bodies of the Southern hemisphere. If there should be a considerable photochemical contribution to the tropospheric budget, it might be lower in the Southern hemisphere due to its lower CO content. Obviously better observational evidence is urgently needed.

On the basis of the present observations, one must infer that the influx of stratospheric air into the troposphere is not a smooth, continuous process but rather occurs in single discrete intrusions which are sometimes caught by



# DUTSCH

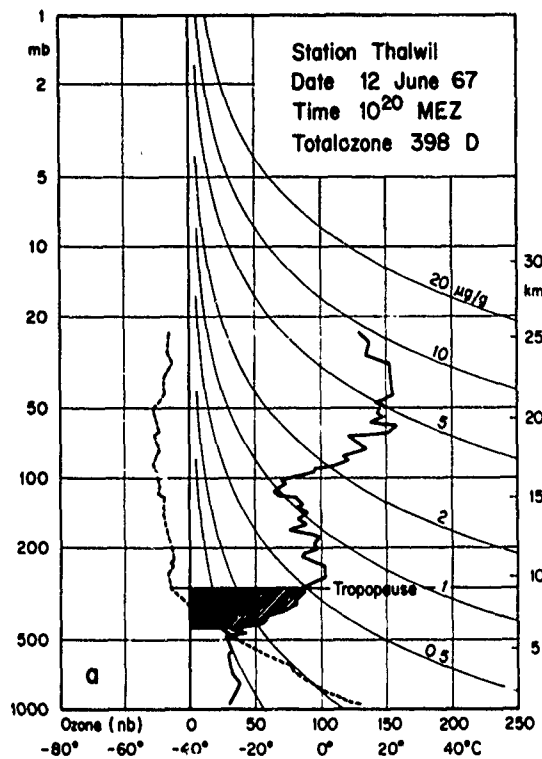


Fig. 17a. High ozone below the tropopause shows the stratospheric origin of that airparcel; the vertical temperature gradient has already been converted to tropospheric values by vertical divergence (horizontal convergence).

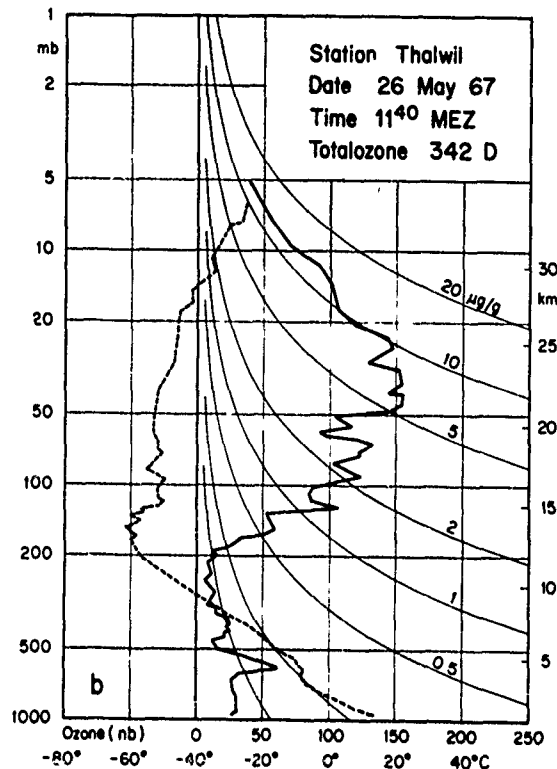


Fig. 17b. High ozone values in the middle stratosphere show the intrusion of stratospheric air down to this level.

soundings either at the moment of the transfer (fig. 17a) or later when the ozone rich parcel has already reached lower levels and is locally disconnected from the stratosphere (fig. 17b). Synoptic studies (Piaget, 1971) or more directly measurements (Danielson and Mohnen, 1977) from airplanes have shown that strong intrusions predominantly occur in the jet stream region in connection with developing disturbances.

The strong influence of local conditions, especially topography, on surface ozone (or ozone in the boundary layer) and particularly its daily variations and also on the intensity of ground destruction will be illustrated by two examples:

Fig. 18 shows the variation with daytime of ozone up to 1000 m above ground in a rather wide valley near Zurich bounded by chains of hills topping the river by about 400 to 500 m (mean values from 7 days - light wind fair weather conditions, i.e. minimal advection, obtained with the Brewer-Mast ozone sonde carried by a tethered balloon) (Dütsch, Graber and Broder, 1978). Clearly the night-time loss due to ground destruction and inhibition of replacement by vertical turbulent transport reaches above 500 m. From this a flux into the ground of at least  $10^{12}$  molecules  $\text{cm}^{-2}\text{sec}^{-1}$  is computed which is an order of magnitude higher than the normally assumed destruction rate. Part of this is certainly due to the fact that the mean afternoon mixing ratio values in the whole boundary layer are

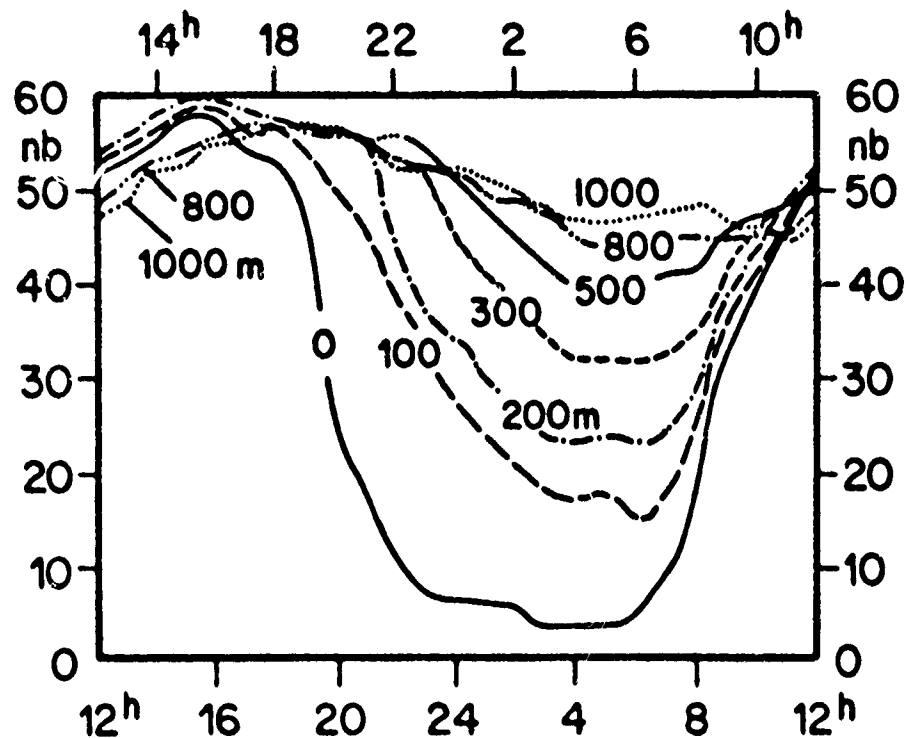


Fig. 18. Night time destruction of ozone in hilly country in summer.

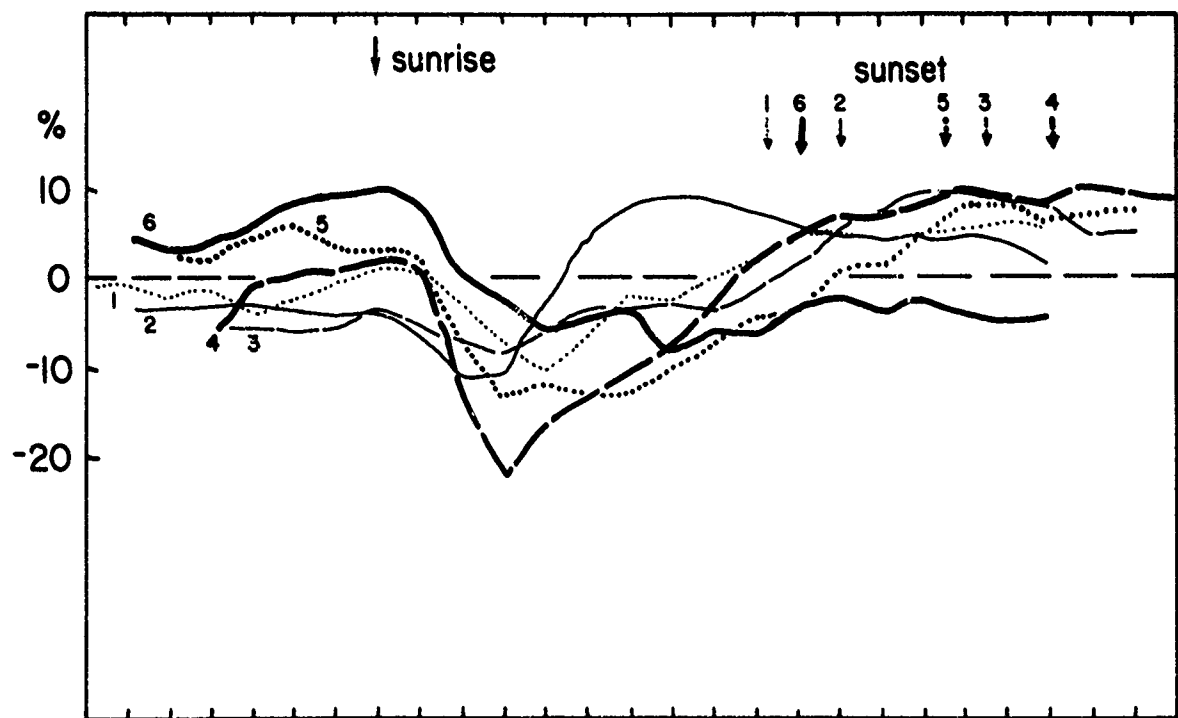


Fig. 19. Bimonthly means of the daily ozone variation on a hill top near Arosa in different seasons. The 6 curves are plotted such that astronomical sunrise coincides for all of them (fair weather days only).

# DUTSCH

about 60 ppb and thus a factor of 1.5 higher than background values at this latitude due to the smog influence of the nearby city of Zurich. The main reason for the high reaching ozone loss must be the influence of the local circulation (downslope motion along the hillsides and rising motion over the open valley at night) which brings more ozone into contact with the ground.

The continuous measurements on a hill top near Arosa, Switzerland, at 2000 m.s.l., surrounded, however, by higher mountains, show a very different daily variation (fig. 19). The range (being season dependent) is much less than in the low country and also the phase quite different. Maximum values are reached at night, the ozone concentration starts decreasing one hour after local sunrise to a minimum which is reached after about three hours; the recovery phase varies with season. The night time maximum is produced by the descending branch of the valley/mountain wind system; soon after sunrise the upslope motion along the sunexposed hillside brings air with low ozone content to the observing site; later in the day increasing vertical exchange starts compensating or overcompensating this continuing effect.

These are just two examples demonstrating the enormous differences in local effects on ozone concentration which make it rather difficult to determine representative values for the sink at the surface. Both cases are easily explainable without local photochemistry, but they cannot rule out a contribution from it. Also they show how problematic it can be to deduce the mean ozone content of the lower troposphere from surface observations.

## REFERENCES

- Attmannspacher, W. and H.U. Dütsch, International ozone sonde intercomparison at the observatory Hohenpeissenberg, Ber. Deutsch. Wetterdienst, 16.120, 1970.
- Brewer, A.W. and J.R. Milford, The Oxford-Kew ozone sonde, Proc. Roy. Soc., London, A 256, 470, 1960.
- Chameides, W. and J.G.G. Walker, A photochemical theory of tropospheric ozone, J. Geophys. Res. 78, 8751, 1973.
- Chapman, S., A theory of upper atmospheric ozone, Mem. Roy. Met. Soc. 46.3, 103, 1930.
- Danielson, E.E. and V.A. Moanen, Project duststorm report: Ozone transport, in situ measurement and meteorological analyses of tropopause folding, J. Geophys. Res. 82, 5867, 1977.
- DeLuise, J.J., Umkehr vertical ozone profile errors caused by the presence of stratospheric aerosol, J. Geophys. Res. 84, 1766, 1979.
- Dütsch, H.U., Vertical ozone distribution from Umkehr observations, Arch. Meteorol. Geophys. Biokl. A, 11, 240, 1959.
- Dütsch, H.U., Computation of world wide ozone flux divergence between 10 and 30 km combining a photochemical model with the observed ozone distribution. Proc. Joint Symp. Atmosph. Ozone, Dresden 1976, Berlin 1977.
- Dütsch, H.U., Vertical ozone distribution on a global scale, Pure appl. Geophys. 116, 511, 1978.
- Dütsch, H.U., W. Graber and B. Broder, Bedeutung der Lokalzirkulation in hügeligem Gelände für die Bodenzerstörung des Ozons, Proc. Int. Tagung alpine Meteorol., Grindelwald, 2, 31, 1978.
- Dütsch, H.U., The search for solar cycle ozone relationships, J. Atmos. and Terrest. Phys., 41, 771, 1979.
- Dütsch, H.U., Regular ozone soundings at the aerological station of the Swiss Meteorological Office at Payerne, Switzerland 1972-1976, LAPETH-16, 239 pp, Zürich, 1979.
- Fabian, P. and P.G. Pruchniewicz, Meridional distribution of ozone in the troposphere and its seasonal variations, J. Geophys. Res. 82, 2063, 1977.
- Götz, F.W.P., A.R. Meetham and G.M.B. Dobson, The vertical distribution of ozone in the atmosphere, Proc. Roy. Soc. A 145, 416, 1934.

# DUTSCH

- Hering, W.S. and Th. R. Borden, Ozone sonde observations over North America, Vol. 1-4, Air Force Cambridge Res. Lab. 1965-1967.
- Hilsenrath, E., L. Seiden und Ph. Goodman, An ozone measurement in the mesosphere and stratosphere by means of a rocket sonde, J. Geophys. Res. 74, 6873, 1969.
- Kley, D., Personal communication.
- Kobayashi, J. and Y. Toyama, On various methods of measuring the vertical distribution of atmospheric ozone, Pap. Meteor. Geophys. 17.2, 113, 1966.
- Komhyr, W.D., Electrochemical concentration cell for gas analysis, Ann. Geophys. 25, 221, 1969.
- Kulcke, W. and H.K. Paetzold, Über eine Radiosonde der vertikalen Ozonverteilung, Ann. Meteorol. 8.40, 47, 1957.
- Mateer, C.L. and H.U. Dütsch, Uniform evaluation of Umkehr observations from the world ozone network. Part I. Proposed standard Umkehr evaluation technique, NCAR, Boulder, 1964.
- Piaget, A., Utilisation de l'ozone atmosphérique comme traceur des échanges entre la troposphère et la stratosphère, Veröff. SMZ 21, 71 pp, 1971.
- Reed, R.J., The present status of the 26 months oscillation. Bull. Am. Meteor. Soc. 46, 374, 1965.
- Regener, E. and V.H. Regener, Aufnahme des ultravioletten Sonnenspektrums in der Stratosphäre und vertikale Ozonverteilung, Phys. Z. 35, 788, 1934.
- Regener, V.H., Measurements of ozone with the chemiluminescent method, J. Geophys. Res. 69, 3795, 1964.
- Vigroux, E., Distribution de l'ozone atmosphérique d'après les observations en émission et en absorption de la bande 9.6  $\mu$ , Ann. Géophys. 25, 193, 1969.
- Züllig, W., Beziehung zwischen der Intensität des stratosphärischen Polar-nachtwirbels und dem Ozongehalt der Winterhemisphäre, LAPETH-7, Zürich, 1973.

## THE OBSERVED DISTRIBUTION AND

### VARIATIONS OF TOTAL OZONE

Julius London

Dept. of Astro-Geophysics, University of Colorado  
Boulder, Colorado

#### Abstract

The global distribution of total ozone, as observed at ground based stations during the 20 year period 1958-1977, and the statistical characteristics of the ozone distributions are presented and discussed. Long period variations in the Northern and Southern Hemispheres significantly differed during this period. Comparison of the observed seasonal and year to year variations over a two year period, as determined from ground based stations and derived from satellite radiance data, show good agreement. However, the satellite derived total ozone amounts were, on the average, about 5 percent lower than those derived from ground based observations.

**INTRODUCTION:** A vertical air column above the earth's surface contains, on the average, approximately  $8 \times 10^{18}$  ozone molecules per square centimeter. This is equivalent to an ozone depth of about 0.3 cm at standard temperature and pressure (STP) (300 m-atm cm). The total ozone amount varies geographically, principally with latitude, and seasonally. In addition, there are significant variations associated with meteorological parameters, notably stratospheric pressure and temperature patterns, and possibly with solar activity. Long period total ozone changes, over a few years or more, are largely unexplained. They are thought to be related to climatic variations of the large scale circulation systems in the stratosphere but they may also be influenced by aspects of the "eleven-year" solar cycle or by variations in the concentration of other atmospheric trace constituents.

Typical variations of total ozone for different time periods have been discussed by Dütsch, (1974), and others. For Arosa, Switzerland, total ozone can change by as much as 70 m-atm cm during a single day and, during the winter or spring, the day to day range within a single month can be as high as 250 m-atm cm. The month to month change, and the inter-annual variation for the month of February at Arosa is about 100 m-atm cm (Dütsch, 1974). In general, it has been shown that the annual range of observed total ozone has significant geographic variation and is somewhat larger in the Northern than the Southern Hemisphere (London et al., 1976).

The ozone concentration also varies with height. It is a maximum in the middle stratosphere (20-25 km) and variations in total ozone largely reflect variations of the ozone concentration at these heights. The average amount of ozone above different heights in the atmosphere as a percentage of the total amount above the surface is shown in Fig. 1. On the average about 60 percent of the total ozone amount is found in the stratospheric layer 15-30 km. The depth and height of this layer varies somewhat with location and season. It is lower and thicker at high

# LONDON

latitudes during the winter/spring than at tropical latitudes during all seasons (London and Angell, 1979).

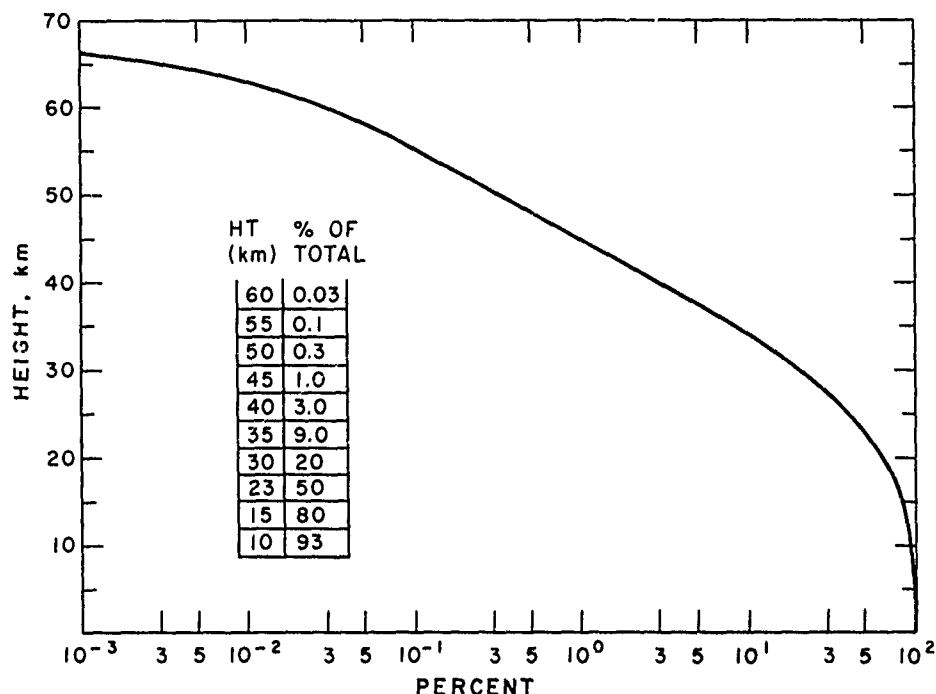


Fig. 1 The amount above different heights in the atmosphere expressed as a percentage of the total amount above the surface (based on average conditions).

It is well established that the ozone concentration is nearly in photochemical equilibrium at heights above about 30 km. Below 30 km the photochemical relaxation time for ozone is longer than the relaxation time due to stratospheric transport processes. (see for instance, Park and London, 1974; Crutzen and Ehhalt, 1977). The photochemical relaxation time,  $T_{ph}$ , for ozone in an oxygen-hydrogen-nitrogen-chlorine system and for ozone transport due to various scales of atmospheric motion,  $T_{tr}$ , are shown in Fig. 2, for average condition. Since most of the ozone is found at levels below about 30 km, total ozone variations are strongly influenced by variations of the lower and middle stratospheric circulation.

**METHODS OF OBSERVATION:** Total ozone is determined from ground based observations by measurement of the absorption of solar radiation, or radiation from some other external light source. The first observations of the total amount of ozone were made in the United States in the early 1900's by use of measurements of solar radiance in the Huggins ozone absorption bands (440-760nm). Subsequent measurements were made in the Hartley-Huggins bands (300-360nm). The present standard method for ground based observations is adapted from a technique first suggested by Fabry and Buisson (1921) and put into practical operation by Dobson in 1924. This method uses a spectrophotometer universally called the Dobson Spectrophotometer (Dobson, 1957).

The Dobson Spectrophotometer is a double monochromator used to determine the total amount of ozone in an atmospheric column from the observing site up to the external light source (usually the sun). Measurements are made of the relative radiance of sunlight or skylight at two different wavelengths in the Huggins ozone absorption bands after the radiation has undergone extinction due to absorption and scattering. In practice it is usual to take the observations on double pairs of wavelengths (referred to as A/D pairs) to minimize errors due to atmospheric aerosol scattering effects. There are many other sources of error in the 'Dobson' measurements. These include the use of incorrect or inappropriate absorption cross sections in evalu-

# LONDON

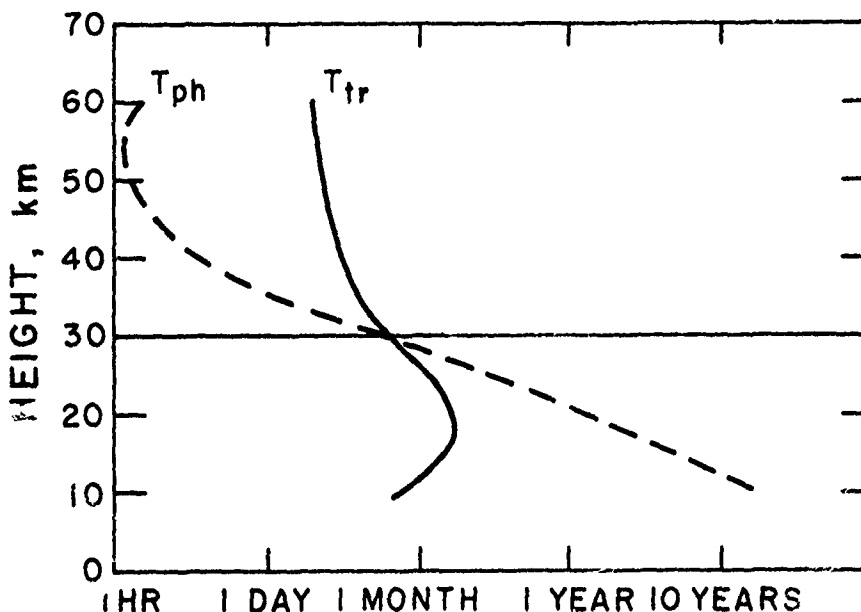


Fig. 2 Characteristic relaxation time for ozone due to photochemistry ( $T_{ph}$ ) and transport ( $T_{tr}$ ) (After Park and London 1974; Crutzen and Ehhalt, 1977).

ating the observations; possible variations in the assumed constant extraterrestrial solar irradiance; extraneous internal light scattering, etc. In addition, Dobson observations are not fully automatic and calibration procedures are not completely controlled. For a well maintained and operated instrument, A/D direct sun observations yield a measurement precision of about  $\pm 1.5$  percent. For the average of the observations taken over the Dobson network, the precision is probably  $\pm 3$  percent (Hudson and Reed, 1979). The Dobson Spectrophotometer has been adopted as the standard by the World Meteorological Organization for the International Ozone Network.

A second ozone observing instrument, the M-83, has been developed in the USSR and has been in use since 1957 (see for instance, Gushchin, 1977). The M-83 is an optical filter photometer that measures the solar radiance received by the instrument in three broad spectral intervals in the ultraviolet and visible regions after that radiation has passed through a set of interference filters. The M-83 is less accurate than the Dobson Spectrophotometer and has an average precision of the order of  $\pm 5$  percent (Gushchin, 1977). Total ozone observations using the M-83 are made chiefly in the USSR and Eastern European countries.

Recent comparison of ozone measurements with a well calibrated Dobson Spectrophotometer and an improved M-83 filter ozonometer (Kovalev et al., 1978) indicated that, on the average, the M-83 observations yielded ozone amounts about 3 percent lower than those determined from the Dobson instrument. It may be that the higher values given by the Dobson observations are associated with inappropriate absorption coefficients used in A/D observations, as recently suggested by Komhyr (1979). A few other instruments, similar to the Dobson or the M-83, have been used from time to time in the ozone network. A more detailed discussion of the major characteristics of these two instruments and their modifications is given by London and Angell (1979).

# LONDON

THE DISTRIBUTION AND LONG TERM VARIATIONS OF TOTAL OZONE: Although some routine total ozone observations have been made since about 1925, there were only a few stations taking regular measurements prior to the IGY (July 1957). The number of observing stations throughout the world significantly increased after 1957. During the 1930's and 1940's there were 3-5 stations at which total ozone observations were taken more or less routinely. These stations were located in the Northern Hemisphere and not all were operative during the same time periods. In the 1950's the number of stations increased from 8 in 1950 to almost 40 at the start of the IGY including 3 stations in the Southern Hemisphere.

The yearly variation of the number of stations reporting ozone observations in the period 1958-1977 is shown in Fig. 3. A significant increase in reporting stations occurred just prior to the IQSY 1964/1965. It should be noted that during the entire 20 year period about 2/3 of all observing stations in the Northern Hemisphere were in the latitude belt 30°N to 60°N. In the Southern Hemisphere before 1963, half of the operative stations were at latitudes poleward of 50°S. After 1963, however, most of the stations were at lower latitudes. This difference in the location of the observing stations in the Southern Hemisphere probably accounts for the apparent long term ozone decrease indicated in Fig. 10. Most of the stations in the Northern Hemisphere and almost all in the Southern Hemisphere took their observations on the Dobson Spectrophotometer.

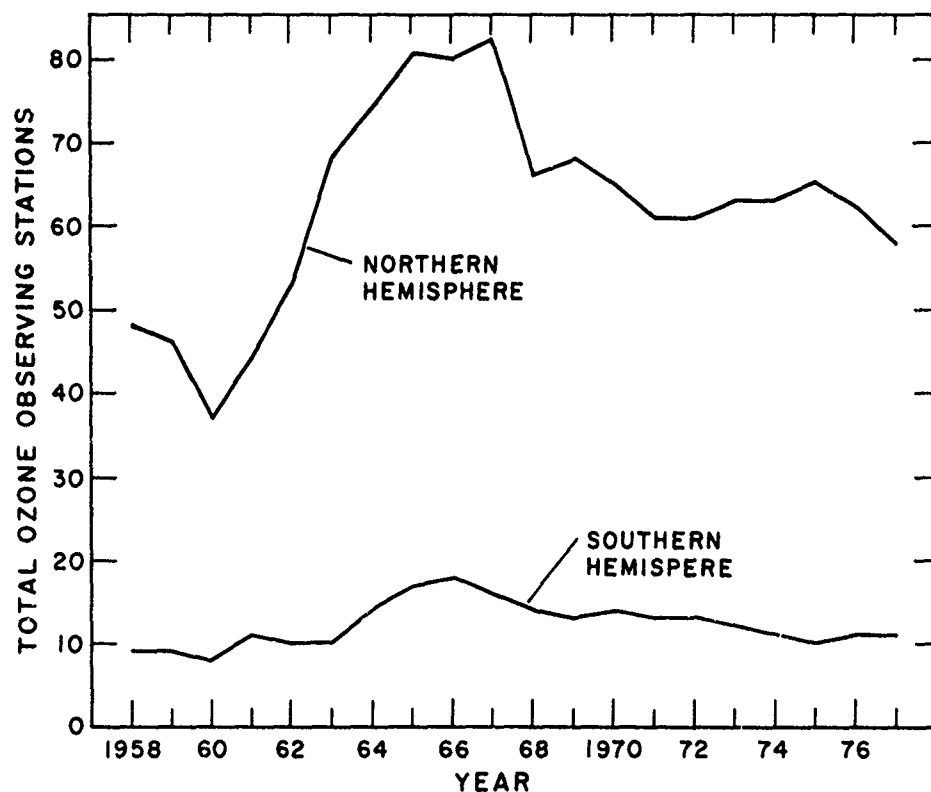


Fig. 3 Total number of stations reporting ozone observations given for each year in the period 1958-1977. Approximately 2/3 of all Northern Hemisphere observing stations were located between 30°N and 60°N.

The average observed global distribution of total ozone for the 20 year period (1958-1977) is shown in Fig. 4. The filled circles indicate Dobson observations, the open circles indicate other types (generally M-83). Underlined circles indicate stations for which there were observations in 1977. Very few stations have observations for the entire 20 year period. The data used for the analysis shown in Fig. 4 are not homogeneous in time nor uniformly distributed



# LONDON

over the globe. Nevertheless, the ozone distribution as shown is probably representative of the long term global average.

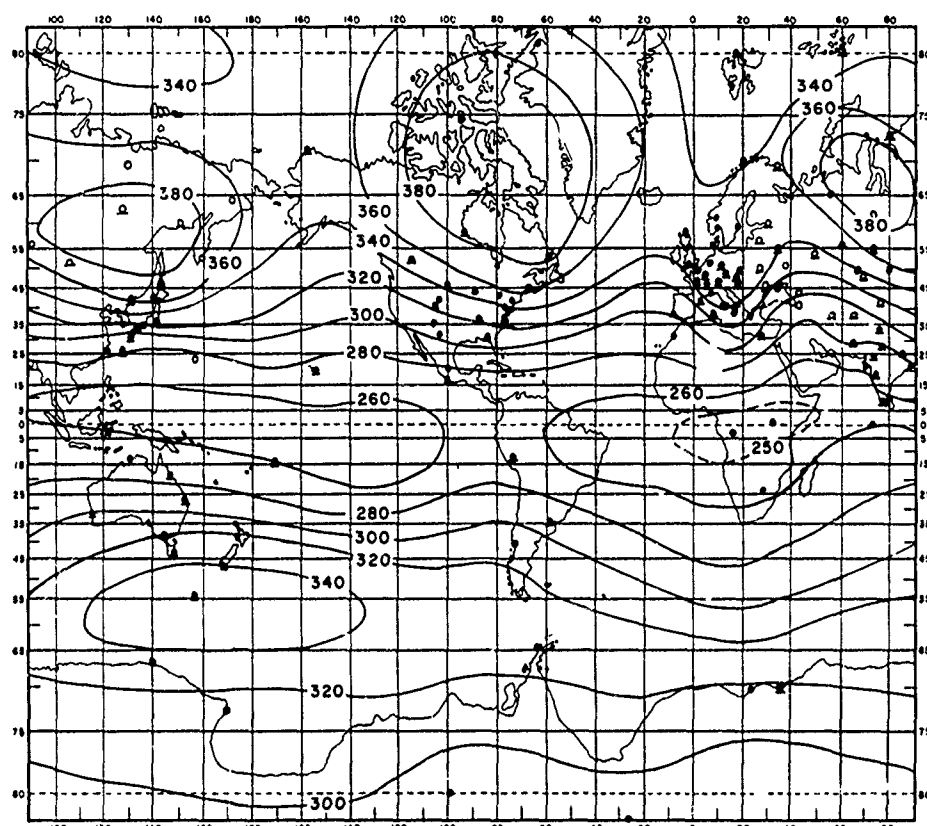


Fig. 4 The average global distribution of total ozone for the period 1958-1977 (Units: m-atm cm). ● = Dobson stations; ○ = other (generally M-83); Underline indicates current observations (1977).

The broad scale features of the average ozone distribution are quite well known and have been discussed elsewhere (see, for instance, London, 1978). Total ozone is a minimum in equatorial regions and increases poleward in both hemispheres to a maximum at subpolar latitudes. The high latitude maximum results from transport of ozone from the primary region of production in the equatorial upper stratosphere to the lower and middle stratosphere in polar regions where it is relatively inert photochemically. The ozone maximum at high latitudes is stronger in the Northern than Southern Hemisphere. This results from the stronger horizontal mixing in the Northern Hemisphere stratosphere, a consequence of the hemispheric difference in land/ocean distribution. Some longitude variations are also indicated as shown in Fig. 4. Little can be said about the large scale geographic distribution of ozone in the Southern Hemisphere where most of the observations are concentrated in the general region of the Australian Continent.

The long-term (20 year) average latitude-time ozone variation is shown in Fig. 5. Minimum ozone occurs in equatorial regions during all seasons. The high latitude maximum in the Northern Hemisphere (about 460 m-atm cm) is found in late March and early April at about 70°N-75°N. The maximum in the Southern Hemisphere is not as pronounced (400 m-atm cm), and is present at a somewhat lower latitude (50°S-60°S). Also, it occurs at a later time in the

# LONDON

Spring (October/November). This Hemispheric difference, as mentioned earlier, is due to the difference in Stratospheric circulation pattern of the two hemispheres.

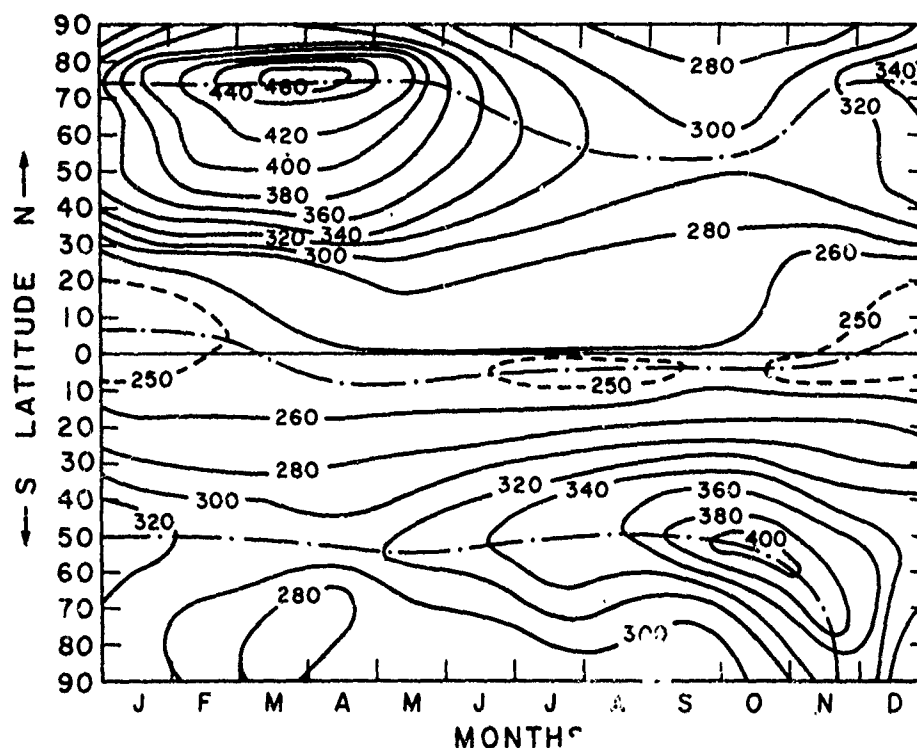


Fig. 5 Latitude-season cross section of total ozone from station data for the period 1958-1977. (Units: m-atm cm). Dashed-dot curves show axes of maxima and minimum ozone.

Curves of the hemispheric average annual variation of total ozone as shown in Fig. 6 are nearly opposite in phase but the amplitude of the Northern Hemisphere variation is the larger. Consequently, the annual global variation shows a major maximum in late April and a second, smaller maximum, in October. The long term average total ozone is about 2 percent higher in the Northern than the Southern Hemisphere, an effect of the stronger poleward ozone transport in the Northern Hemisphere.

LONDON

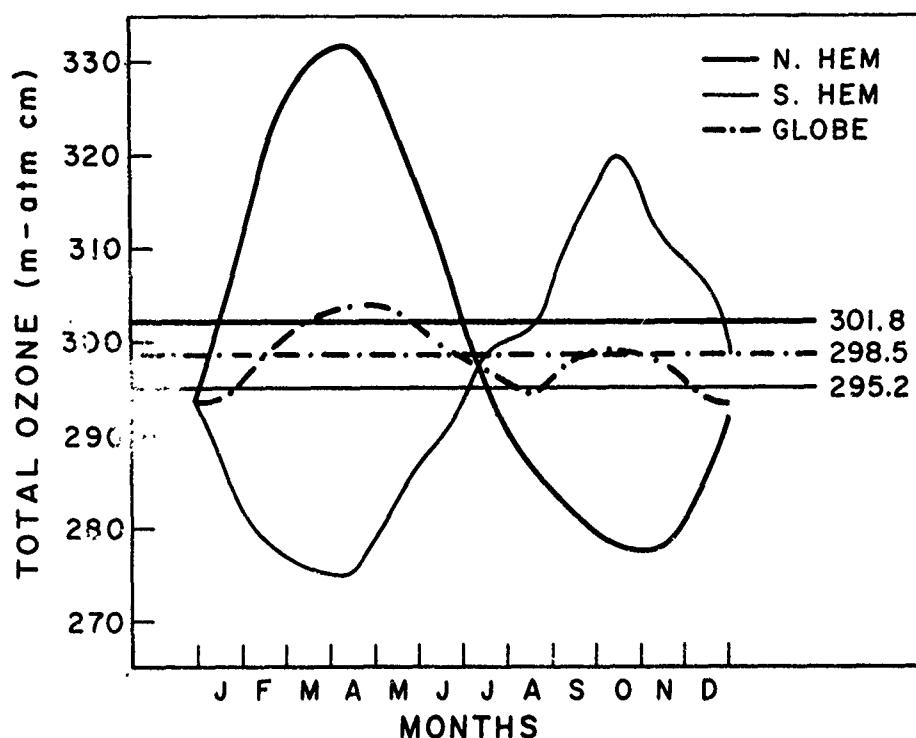


Fig. 6 Average annual variation of total ozone for the period 1958-1977. Straight lines represent long term hemispheric and global averages.

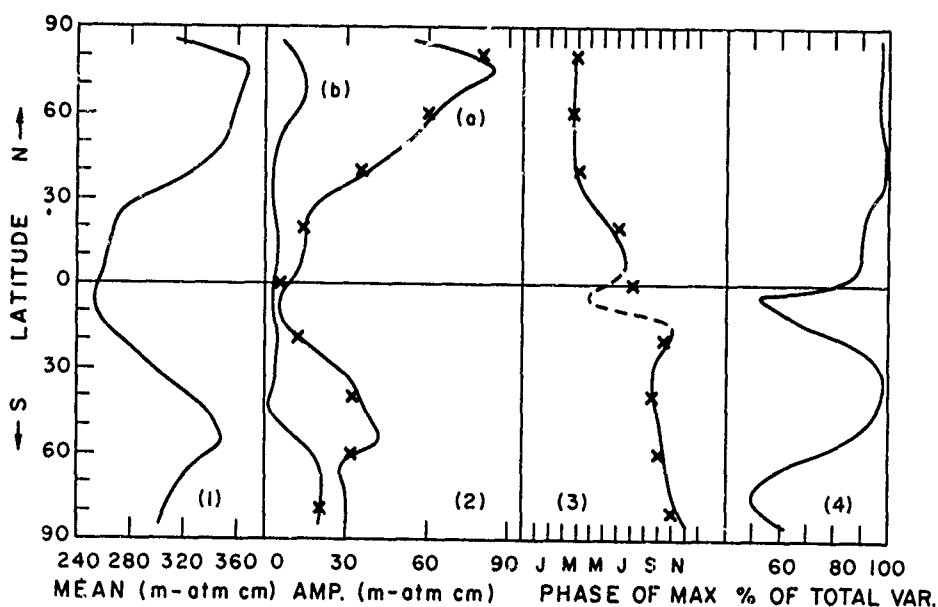


Fig. 7 Latitudinal dependence of the harmonic components of the mean annual total ozone variation.

1. Long term mean
2. Amplitude of the first (a) and second (b) harmonics
3. Phase of maximum of the first harmonic
4. Percent of total variance due to the first harmonic

The seasonal variation of total ozone has a strong latitude dependence. Harmonic analyses giving the phase and amplitude of the 1st and 2nd harmonic of the annual variation along with the long term mean and the percent of total variance due to the 1st harmonic are given in Fig. 7. The results are based on analyses of mean monthly observed station data as averaged for 10° latitude belts. The annual variation is dominant at all latitudes poleward of 20° and is particularly pronounced in the Northern Hemisphere. The phase of maximum for the annual variation is delayed somewhat with decreasing latitude in the Northern Hemisphere (March to July) and then is delayed further to November at high latitudes of the Southern Hemisphere. The crosses shown on the diagram correspond to the amplitude and phase of the 1st harmonic for an average of 2 years of total ozone data as derived from satellite (NIMBUS 4) observations (Hudson and Reed, 1979). Ground based and satellite derived 1st harmonic parameters are in very good agreement. The slight discrepancy near the equator is certainly due to the limited amount of station data in that region. The available data, however, indicate a pronounced semi-annual variation of total ozone in the tropics similar to that found for stratospheric winds (Hudson and Reed, 1979).

**VARIANCE OF TOTAL OZONE:** The variance of mean monthly total ozone has a seasonal and latitudinal dependence (see, for instance, London and Angell, 1979). The variance, as calculated for individual representative station data, increases with latitude and has a maximum during the winter and a minimum during the summer months. This pattern is similar for both hemispheres, but the winter values for the Northern Hemisphere are generally larger than analogous values at the same latitudes in the Southern Hemisphere. These differences result from the seasonal and hemispheric differences in stratospheric circulation characteristics.

The long-term annual averaged monthly mean standard deviation of total ozone is shown in Fig. 8 as calculated for all stations having at least 10 years of complete data during the period 1958-1977. The data are shown for those stations using a Dobson Spectrophotometer (dot) and others taking observations with the M-83 filter instrument (crosses). A smooth free hand curve has been drawn approximating the Dobson derived measurements. The standard deviations of the ozone data determined from M-83 observations are larger by a factor of about 3 than the Dobson observed values and seem to show a negative latitudinal dependence (if any). This large variation involving the filter observations has already been noted in comparison with satellite measurements (Miller et al., 1978). Improvements of the M-83 ozonemeter (Gushchin et al. 1976) should reduce part of this apparent discrepancy in the International Ozone Observing Network.

The statistical characteristics of the ozone variations are not constant with time. The standard deviation of the mean monthly total ozone amounts as computed for 5 year intervals is given in Fig. 9 for representative stations in sub-tropical and middle latitudes. Values of  $\sigma = \pm 10$ , and  $\sigma = \pm 15$  m-atm cm for the sub-tropics and mid-latitudes represent normalized variations of about 3.5 percent and 4.5 percent respectively. The Oxford and Arosa curves as well as those for Caribou and Bismark are quite similar, particularly after 1965, indicating perhaps a similar response to variations in stratospheric transport patterns. Before 1965, the European (Oxford and Arosa) and North American (Caribou and Bismark) curves are opposite in phase.

Three of the sub-tropical stations also show similar variability patterns for the 5 year intervals starting with the period centered at 1965. Again, however, before 1965, the patterns are somewhat different. Note also that although Tateno and Aspendale are at about the same latitude, Tateno shows an intermediate variance pattern between those for the sub-tropics and mid-latitudes, Aspendale, of course shows smaller values typical of the Southern Hemisphere. It cannot be generally assumed that the statistical characteristics of the ozone variations at one station, or for one interval of time, are representative for the hemisphere or globe as a whole.

# LONDON

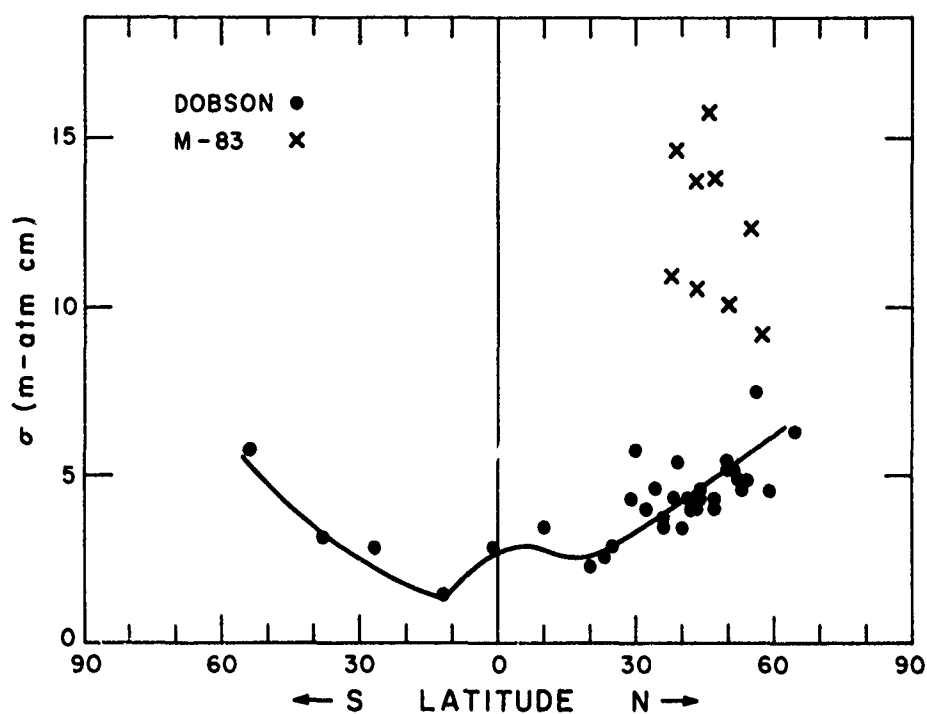


Fig. 8 Latitude variation of the average long term monthly mean standard deviation of total ozone for Dobson and M-83 observing stations.

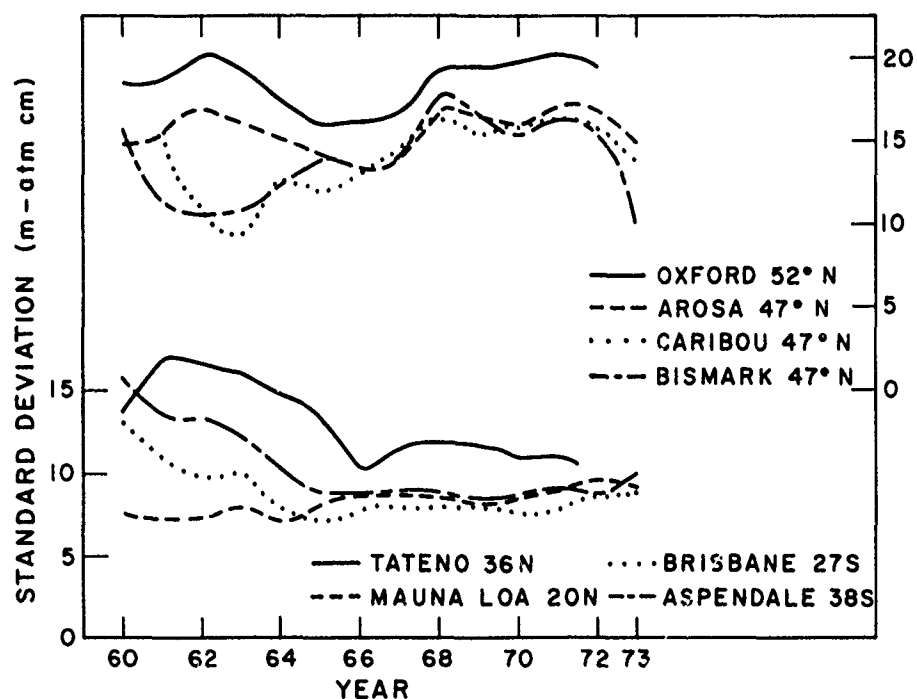


Fig. 9 Time variations of the standard deviation of mean monthly total ozone calculated for running 5-year periods (60 values each) for representative sub-tropical and mid-latitude stations. All observations using Dobson Spectrophotometer.

## LONDON

**LONG TERM VARIATIONS:** Progress has been made in recent years in documenting and explaining ozone variations associated with particular meteorological events. For example, it is known that large increases of total ozone, resulting from increased ozone concentrations in the lower stratosphere, accompany the occurrence of high latitude winter "stratosphere warmings". The ozone increase is a consequence of the strong downward vertical motion found in the region of the warming (see, for instance, Miller et al., 1977). There is also some indication of a quasi-biennial oscillation in total ozone and in the ozone concentration in the middle stratosphere (20-25 km) but the geographic pattern of this oscillation is unclear. Also, some studies have shown that observed station and hemispheric year-to-year changes may be associated with variations in the large scale patterns of the stratospheric circulation (see, for instance Rosen et al., 1976; Newell and Wu, 1978). Strong evidence, however, is lacking for other geophysically related changes in the ozone distribution. The documentation of a solar induced perturbation in total ozone is rather inconsistent and the supporting data for such a relation involving stratospheric ozone is far from compelling. We do not yet know what specific atmospheric parameters are related to long period ozone changes nor how these are related.

The annual variation of total ozone for the Northern and Southern Hemispheres for the period 1958-1977 is given in Fig. 10. Also shown in Fig. 10 are the mean values for each hemisphere for the entire 20-year period with an average of approximately 2 percent more ozone indicated for the Northern Hemisphere. The larger ozone amount shown for the Southern Hemisphere during the period before 1963 probably results from the biased distribution of reporting stations. Independent information derived from satellite observations verify the hemispheric differences shown in Fig. 10 for the early 1970's.

During the mid 1960's there was a sharp increase in total ozone in the Northern Hemisphere and a subsequent slight decrease in the 1970's. Apparently no such dramatic change took place in the Southern Hemisphere. As mentioned earlier, there was a substantial decrease in the mean latitude of observing stations in the Southern Hemisphere after 1963 which was the principal reason for the indicated slight ozone decrease after that time. Note that there is no obvious long period ozone change in the Southern Hemisphere after about 1964. Thus, for the entire period shown, there seems to have been approximately a 5 percent increase in the ozone amount in the Northern Hemisphere and about a 2 percent decrease (if any) in the Southern Hemisphere. If the two curves are reasonably representative of the hemispheric conditions, it is difficult to reconcile the hemispheric differences in the long period changes with any direct solar cycle influence on the total ozone variation.

Detailed analysis shows that these long period variations are not geographically uniform. Nevertheless, an ozone increase seemed to have occurred at all latitudes in the Northern Hemisphere during the 1960's (London and Oltmans, 1979). The largest concentration of ozone stations is in the latitude belt 30°N-60°N. The long term ozone variation for that region is the same as the hemispheric pattern. That is, there is a significant ozone increase (8 to 10 percent) in the latter half of the 1960 decade. It is thus unlikely that the apparent hemispheric increase is merely a result of a peculiar geographic distribution of observing stations. The basic cause of this increase, however, has not yet been established.

**COMPARISON OF GROUND BASED AND SATELLITE OBSERVED TOTAL OZONE:** Because of their relatively long history, ground based ozone measurements can be used to determine the climatological characteristics of the ozone distribution. However, as pointed out above, one of the problems involved in the use of station observations in analysis of zonal or hemispheric average variations is that of the geographic representativeness of the data. There is a reasonably well documented relationship between meteorological and total ozone patterns such that average total ozone is higher in regions of pressure troughs. As a result, year-to-year or longer period average zonal variations may simply be a reflection of sampling biases associated with longitude shifts in the positions of large scale planetary waves. These possible biases can be tested, in part, by comparison of the ground based ozone measurements with these determined from global satellite observations.

Total ozone data as derived from two different measurement techniques on the NIMBUS-4 satellite are available for such a comparison. The two data sets were based on observations using the Infrared Interferometer Spectrometer (IRIS) and the Back Scattered Ultraviolet (BUV) instrument. They cover the period April 1970-January 1971 (IRIS) and April 1970-April 1972 (BUV). (Additional BUV total ozone data for the period May 1972-November 1972 have recently been made available but have not been used for the present analysis). The mean monthly variation of

# LONDON

total ozone as measured from ground based stations and determined from IRIS and BUV observations is given in Figs. 11 and 12 for the Northern Hemisphere and Southern Hemisphere respectively. The dominant feature of each curve is the pronounced seasonal variation. For both hemispheres the IRIS and BUV curves (with instruments on the same satellite and taking nearly synchronous observations during the daytime) give higher and lower ozone values, respectively, than the ground based ozone data. The average difference between the ground based and the BUV data is about 5 percent.

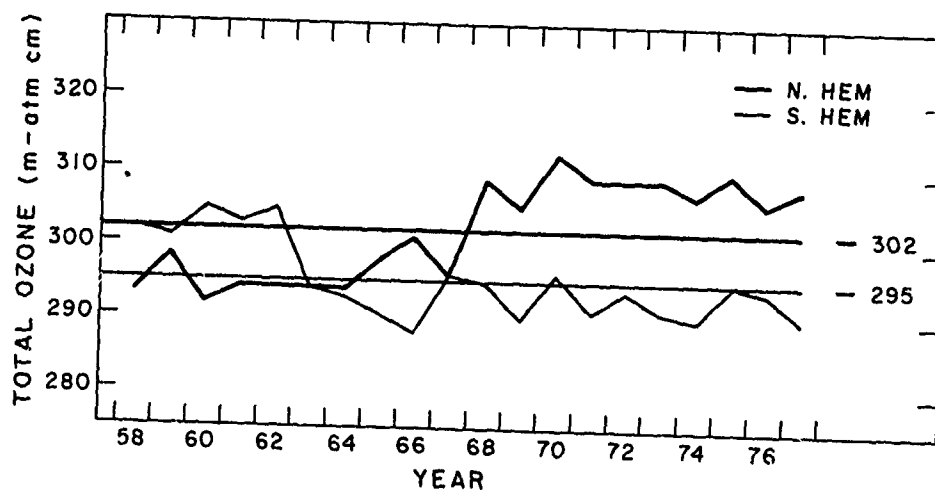


Fig. 10 Long term variation of total ozone for the period 1958-1977 from station observations. Straight lines are the long term hemispheric averages.

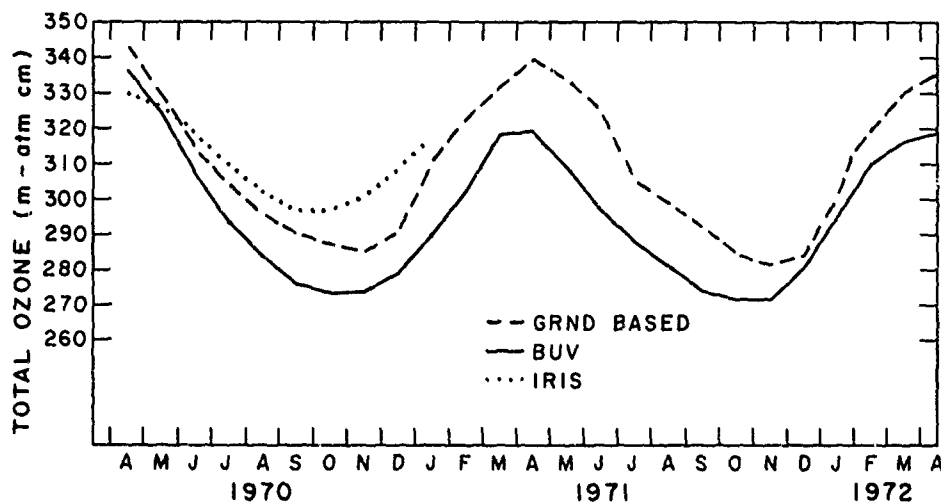


Fig. 11 Monthly average of total ozone for the period April 1970-April 1972, Northern Hemisphere

# LONDON

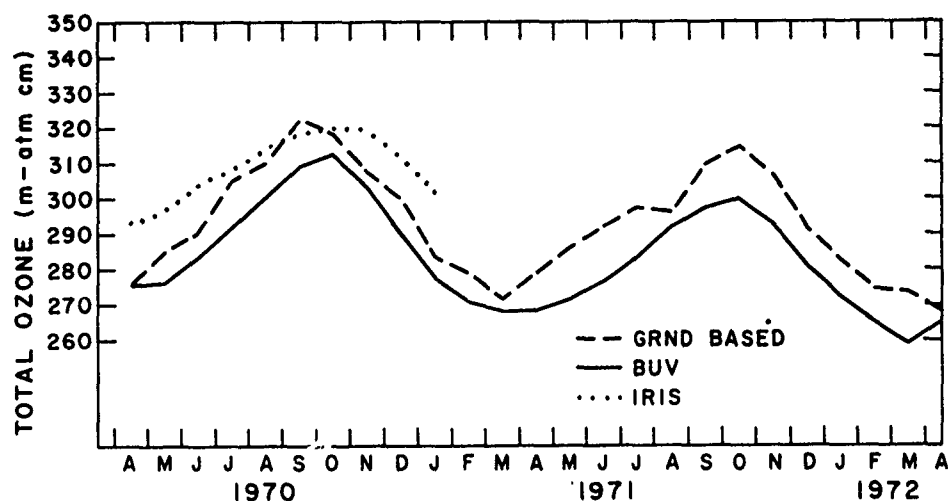


Fig. 12 Monthly average of total ozone for the period April 1970-April 1972, Southern Hemisphere.

It is of particular interest to compare the year-to-year changes as determined from the ground based and BUUV observations. For this comparison we take the period April 1970 to March 1971 as the 1st year; April 1971 to March 1972 as the 2nd year. In addition to hemispheric values, we include a comparison for a Northern Hemisphere mid-latitude belt (40°N-50°N) where there is a relatively large number of ground based stations but where ozone and meteorological variations are also quite large. The year-to-year changes are shown in Table 1.

Table 1 A comparison of year-to-year changes of total ozone as determined from BUUV and ground based station data. (Units: m-atm cm)

		1970-71	1971-72	Difference
NH	BUV	296.8	294.3	-2.5
	Ground based	309.5	308.2	-1.3
SH	BUV	288.7	280.2	-8.5
	Ground based	295.8	291.8	-4.0
40°N-50°N	BUV	340.4	331.6	-8.8
	Ground based	348.9	342.8	-6.1

The year-to-year ozone changes as determined from each set of observations for the two hemispheres have the same sign and are approximately of the same value. The discrepancy in the amount of the change, as indicated for the two observing systems, is larger for the Southern Hemisphere as would be expected because of the sparseness of the observing stations in that hemisphere. Note that for the two years both observing systems show larger ozone amounts in the Northern Hemisphere by about 3-5 percent.



# LONDON

The results for 40°N-50°N are consistent with those derived from the hemispheric data: there is an ozone decrease in each case and the amount of the decreases are about the same. No particular significance is attached to the sign of the one year-to-year change shown in Table 1. However, these results do indicate that the broad pattern of long term ozone variations indicated by ground based total ozone observations reflect real changes and are probably not due to unrepresentative distribution of the observing stations. It is still necessary to determine the reasons for these variations.

ACKNOWLEDGEMENTS: I would like to acknowledge the important technical assistance provided by Rose Gustafson, Mahnaz Matahari and Irene Rodríguez V. in the preparation of the manuscript. The work discussed here was supported by the National Aeronautics and Space Administration under research grant NSG 5153.

## REFERENCES:

- Crutzen, P.J., and D.H. Ehhalt, Effects of nitrogen fertilizers and combustion on the stratospheric ozone layer, *Ambio*, 6, 112-117, 1977.
- Dobson, G.M.B., Observers handbook for the ozone spectrophotometer, *Ann, IGU*, V, 46-89, Pergamon Press, New York, 1957.
- Dütsch, H.U., Ozone distribution in the atmosphere, *Can. J. Chem.*, 52, 1491-1504, 1974.
- Fabry, C. and M. Buisson, Etude de L'extrémité Ultraviolet du Spectre Solaire, *J. Phys. Rad.*, 2, 197-226, 1921.
- Gushchin, G.P., K.I. Romashkina, and A.M. Shalamyanskii, Experience in measurement of total ozone content with the updated M-83 ozonometer at Voeikovo in 1971-1974, *Trudy GGO*, 106-120, 1976.
- Gushchin, G.P., On the technique for measuring of atmospheric ozone at the world network of stations, *Proceedings Joint Symposium on Atmospheric Ozone*, Dresden, I, 135-147, Berlin, 1977.
- Hudson, R.D. and E.I. Reed, The stratosphere: Present and Future, NASA Reference Publication 1049, 1979.
- Komhyr, W.D., Dobson spectrophotometer systematic total ozone measurement error, in press, 1979.
- Kovalev, V.A., K.I. Romashkina, and A.A. Eliseev, Comparison of instruments for measurement of total atmospheric ozone content at the Mauna Loa background station, *Meteorologiya i Gidrologiya*, 110-113, 1978.
- London, J., R.D. Bojkov, S. Oltmans, and J.I. Kelley, Atlas of the global distribution of total ozone, July 1957-June 1967, National Center for Atmospheric Research, 1976.
- London, J. and S. Oltmans, The global distribution of long-term total ozone variations during the period 1957-1975, *PAGEOPH*, 117, (1978/79). 345-354, 1979.
- Miller, A.J., B. Körtz, R.M. Nagatani and J.D. Laver, Variations in the 100 mb height fields as indicator of long-term trends of total ozone at individual sampling sites, *Conference on Meteorology of Upper Atmosphere*, AMS, 25-27, 1978, Boston, Mass., 1978.
- Miller, A.J., R.M. Nagatani, K.B. Labitzke, E. Klinder, K. Rose and D.F. Heath, Stratospheric ozone transport during the mid-winter warming of December 1970-January 1971, *Proceedings Joint Symposium on Atmospheric Ozone*, Dresden, II, 135-148, Berlin, 1977.
- Newell, R.E., and M-F. Wu, A pilot study of concomitant changes in total ozone and atmospheric general circulation, *Quart. J. Roy. Meteorol. Soc.*, 104, 999-1003, 1978.
- Park, J.H. and J. London, Ozone photochemistry and Radiative heating of the middle atmosphere, *J. Atmos. Sci.*, 31, 1898-1916, 1974.

LONDON

Rosen, R. D., M-F Wu and J.P. Peixoto, Observational study of the interannual variability in certain features of the general circulation, *J. Geophys. Res.*, 81, 6383-6389, 1976.

## SPATIAL AND TEMPORAL VARIABILITY OF OZONE AS SEEN FROM SPACE

Donald F. Heath

National Aeronautics and Space Administration  
Laboratory for Planetary Atmospheres  
Goddard Space Flight Center  
Greenbelt, Maryland 20771

### ABSTRACT

The ozone data which have been produced by BUV type instruments on Nimbus 4 and 7 have been used to investigate the scales of spatial and temporal variability of stratospheric ozone over the period from 1970-1979. Generally periodicities or changes in atmospheric structure over meteorological and short-term climate time scales are seen in the ozone data. These changes in ozone reflecting its natural variability may be much larger and in an opposite sense from those predicted by current photochemical modeling of the effects of anthropogenic constituents on the stratospheric ozone. The available evidence on the natural variability of stratospheric ozone indicates that a much improved understanding is needed of this natural variability and the processes which produce it before one can hope to detect changes due to anthropogenic constituents from observations.

INTRODUCTION: That atmospheric ozone is a highly variable quantity both spatially and temporally has been known for years, e.g., the review by Dutsch (1971). Knowledge of the vertical distribution of ozone on a global scale from combined satellite and non-satellite observations has been described recently by Dutsch (1978). Prior to the 1970's little emphasis was placed on the determination of long term trends resulting from the influence of anthropogenic constituents. The current need for the early detection of trends resulting from anthropogenic constituents is well documented in other sections of these proceedings. It is the purpose of this paper to describe some aspects of the spatial and temporal variability of atmospheric ozone which have been derived from satellite-borne instruments. These aspects of the global scale natural variability must be considered in an evaluation of global trends in ozone burdens associated with the introduction of anthropogenic constituents into the stratosphere.

A listing of satellite borne sensors or systems utilizing satellites is contained in Table 1, and a listing of currently available ozone data sets is given for both satellite and non-satellite sources (Hilsenrath, 1979) is given in Table 2.

SPATIAL SCALES OF TOTAL OZONE: An example of the spatial inhomogeneity in a global total ozone field is shown in the false color photograph of figure 1 which was derived from the Total Ozone Mapping Spectrometer (TOMS) on Nimbus-7 on November 24, 1978. Measurements of terrestrial albedo in the 312.5-380 nm region from a cross-track spatial scanner are used to infer the total field. The inversion of the ultraviolet albedo to infer total ozone has been described by Mateer et al., (1971) and the instrument by Heath et al., (1975). The black and red colors indicate low total ozone values while blue and white are high values. The scale

TABLE 1  
Satellite Systems Used to Infer Ozone Remotely

Satellite	System	Type	Spectral Region	Ozone	Coverage	Dates	References
Echo I	filter, phot.	solar-limb occultation	590, 529 nm	Profile	17N	Dec. 1960	Venkateswaran et al. (1961)
U.S.A.F.	filter phot.	solar occ.	260 nm	Profile	33S-13S	July 1962	Rawcliffe et al. (1963)
Ariel 2	spectrometer, phot.	solar occ.	200-400 nm	Profile	50S-50N	April, May, Aug, 1964	Miller and Stewart (1965)
COSMOS	spectrometer	nadir	225-307 nm	Profile	60S-60N	April 1965	Iozenas et al. (1969)
COSMOS	spectrometer	nadir	250-330 nm	Profile Total	60S-60N	June 1966	Iozenas et al. (1969)
1966-111B	spectrometer	nadir	175-310 nm	Profile	80S-80N	1966	Elliott et al. (1967)
OGO-4	spectrometer	nadir	110-340 nm	Profile	80S-80N	Sept. 1967 Jan. 1969	Anderson et al. (1969)
Nimbus-3	interferometer (IRIS)	nadir	9.6 $\mu$ m	Total	80S-80N	April-July 1969	Hanel et al. (1970)
Nimbus-4	spectrometer (BUV)	nadir	255-339.8 nm	Profile/ Total	80S-80N	Apr. 1970 July 1977	Heath et al. (1975)
Nimbus-4	interferometer (IRIS)	nadir	9.6 $\mu$ m	Total	80S-80N	Apr. 1970 Jan. 1971	Prabhakara et al. (1976)
Nimbus-6	photometer (LRIR)	Limb	9.6 $\mu$ m	Profile	80S-80N	June 75-Jan. 76	Gille (1979)
AE-5	spectrometer (BUV)	nadir	255-339.8 nm	Profile/ Total	20S-20N	Nov. 1975	Heath (1980)
DMSP (USAF)	photometer (MFR)	nadir scanner	9.6 $\mu$ m	Total	Global	Mar. 1977- July 1977-Feb. 1980	Lovill et al. (1978)
"	"	"	"	"	"	July 1978-Jan. 1980	
"	"	"	"	"	"	June 1979-Dec. 1979	

HEATH

TABLE I (Continued)

Satellite Systems Used to Infer Ozone Remotely

<u>Satellite</u>	<u>System</u>	<u>Type</u>	<u>Spectral Region</u>	<u>Ozone</u>	<u>Coverage</u>	<u>Dates</u>	<u>References</u>
Meteor {GDR-USSR}	interferometer	nadir	9.6 $\mu$ m	Total			
Meteor (GDR-USSR)	interferometer	nadir	9.6 $\mu$ m	Total			
Nimbus-7	spectrometer (SBUV)	nadir	160-400 nm	Profile/ Total	80S-80N	Oct. 1978	Heath et al. (1975)
Nimbus-7	spectrometer (TOMS)	nadir (spatial)	312.5-339.8 nm	Total	Global	Oct. 1978	Heath et al. (1975)
Nimbus-7	photometer (LIMS)	limb	9.6 $\mu$ m	Profile	80S-80N	Oct. 1978-May 1979	Gille (1979)
TIROS-N	photometer (HIRS II)	nadir spatial	9.6 $\mu$ m	Total	Global	Nov. 1978-	
A.E.M.-B	spectrometer (SAGE)	limb, solar occ.				Jan. 1979	McCormick

HEATH

## HEATH

TABLE 2

### Availability of Ozone Data Sets \*

#### Non Satellite

Dobson - Total Ozone		1950 -
Umkehr - Ozone Profiles	0-50 km	1950 -
Balloon Ozonesondes	0-30 km	1965 -

Archived in World Ozone Data Center (WODC) AES/Canada  
Published in standard format and on tape  
Approximately 1 year lag time

#### Rocket Soundings Profiles 20-55 km

Operating: 1976 -  
Regular monthly soundings from VA and Canada  
Data publish in NASA quarterly reports  
Plan to archive in World Ozone Data Center  
Two year lag, decreasing to 6 months lag

#### NASA Satellites

IRIS Nimbus-3 (3 months), Nimbus-4 (9 months)      Total Ozone  
• Operation: 1969-1971  
• Radiances archived in NSSDC  
• Total ozone retrievals available on tape from principal investigator  
• Initial scientific analysis complete

BUV Nimbus 4      Total ozone and profiles 30-50 km  
• Operation: 1970-1977  
• All data being reprocessed and validated  
• Validated total ozone, 1970-1972, in NSSDC  
• Ozone profiles, 1970-1972 in preparation  
• All data for 1970-1977 archived in NSSDC by October 1979  
• Plan to archive in World Ozone Data Center (WODC)  
• Scientific analysis beginning

LRIR Nimbus-6      Ozone profiles 20-50 km  
• Operation: June 1975-Jan. 1976  
• Data being reprocessed, validated and completed by CY1980  
• Archived at NCAR and available by special arrangement with principal investigator  
• Plan to archive in NSSDC  
• Scientific analysis beginning

# HEATH

TABLE 2 (continued)

## BUV on Atmospheric Explorer-5 Total ozone and profiles 30-50 km

- Operation: 1974-1976
- Radiances available on dedicated computer, some processed to ozone values
- No operational data processing, no validation
- Plan to reprocess and validate total ozone, not funded
- Initial scientific analysis complete

## SBUV/TOMS/LIMS Nimbus-7 Total ozone and profiles to 50 km

- Operation: 1978 -
- Plan to operate, process and validate for 3 years
- Operational processing is not yet accomplished
- NET validation and initial investigations
- Plan to archive in NSSDC with 1 year or less lag time

## SAGE/AEM Ozone profiles to 15-50 km

- Operation: 1979 -
- Plan to operate and process data for two years
- Science team to validate and perform initial investigation
- Begin archiving in NSSDC and WODC 6 months after launch and 2 month lag thereafter

## Non-NASA Satellites

### HIRS TIROS-N Total ozone

- Operation: 1978 -
- Regression coefficients being established, complete in 6 months
- Plan to process and validate operationally by NOAA/NESS and NMC
- Plan to archive in National Climate Center and possibly WODC

### MFR DMSP Total ozone

- Operation: 1977 - (4 systems flown)
- Data processed and validated by Lawrence Livermore Laboratory
- (Accessibility)

\* Compiled by E. Hilsenrath

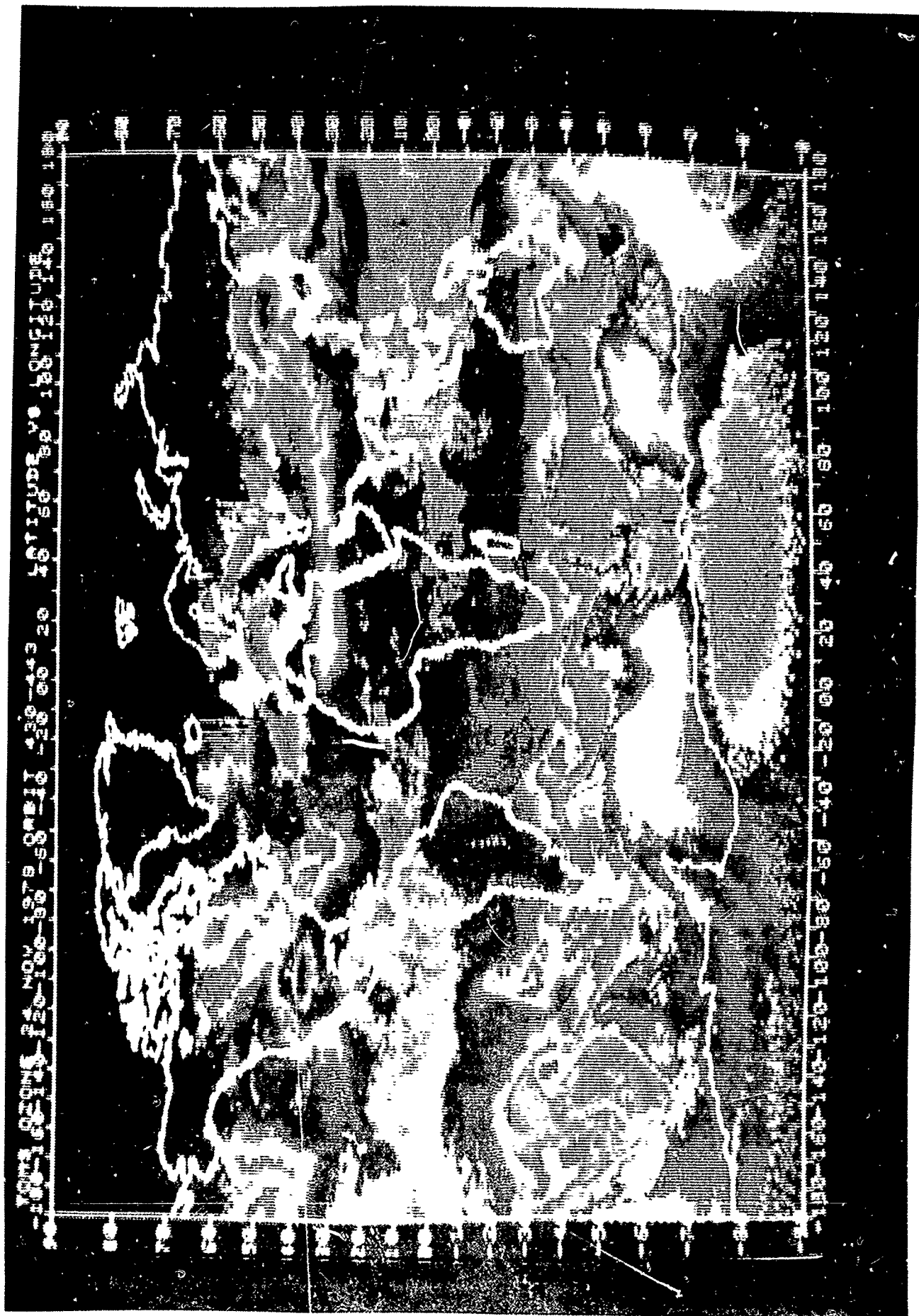


Figure 1: False color photograph of total ozone field derived from the TOMS instrument on November 24, 1978.



goes from 0.24 atm-cm (black) through mid-scale values indicated by yellow and green to 0.415 atm-cm (white).

This figure shows the well known equatorial low values with rather steep latitudinal gradients as one moves southward. A general high is evidenced in the tropics over and east of the African continent with the displacement of the minimum southward. Northward from the tropics one can see surprisingly deep lows centered over the middle United States, over the Atlantic Ocean north of Spain and over the Pacific Ocean east of China. In the vicinity of the northern terminator one can begin to see evidence of the high latitude buildup of total ozone which leads to the well known spring maximum.

In the Southern Hemisphere south of Australia one finds the highest values of total ozone on this particular day which seem to indicate a wave number three pattern centered about the pole.

A sequence of TOMS images on successive days shows continual motion and evolving changes in shape. It is well known that the large scale patterns in total ozone are well correlated with the 100 and 300 mb height fields.

These inferred ozone fields indicate more structure than is found in meteorological charts. At this time the causal mechanisms leading to the observed structure are unknown. Furthermore there is no known reason to doubt the authenticity of the structure depicted in the global field.

**SOLAR RADIATION AND ITS VARIABILITY:** The slowly varying spatial and temporal components of the global scale ozone fields certainly represent a complex superposition of effects due to a variable solar input to the terrestrial-atmosphere system whether it be due to variations in the earth's orbital parameters with respect to the sun or the intrinsic variability of the sun itself. This section presents some recent observations of the uv spectral irradiance of the sun from 160-400 nm which were obtained with the Solar Backscattered Ultraviolet (SBUV) experiment. The SBUV was launched aboard Nimbus-7 in October 1978 and appears to be the only experiment which has obtained measurements of the uv solar flux and its variability in the wavelength region which is either absorbed in the mesosphere, stratosphere, and troposphere or penetrates to the ground.

Since the photochemistry of atmospheric ozone and its transport within the middle atmosphere is driven by the temperature gradients resulting from the absorption of ultraviolet solar radiation, some recent results on the intrinsic variability of the sun are described in this section.

A crude representation of the time scales of uv solar flux temporal variability with wavelength is depicted in figure 2 along with the wavelength regions which are absorbed in the middle atmosphere.

Only two regions of the electromagnetic spectrum of the sun are absorbed in the middle atmosphere which are capable of producing significant changes in the photochemistry and atmospheric heating of the region. One region is centered around the soft x-ray region and extends up to wavelengths of several tenths of a nanometer and the other spans the region from 170-300 nm with the latter representing the largest energy input into this atmospheric region.

To date no conclusive evidence has been obtained on the effect of optical solar flares on stratospheric ozone although some evidence has been presented by Heath (1978) for a reduction of upper stratospheric ozone of about 10 percent as a consequence of the intense x-ray flare on August 7, 1972, but the reality of this effect is in question due to the difficulty in subtracting out effects on the instrument due to high energy trapped particle radiation of the radiation belts.

While doubt exists as to the effect of electromagnetic radiation from intense solar flares on stratospheric ozone, no doubt exists as to the effect of high energy proton streams which entered the polar cap region of the stratosphere from the August 4 solar proton event. These observations have been described by Heath et al., (1977).

# EVIDENCE FOR VARIATIONS IN RADIATIVE OUTPUT OF SUN

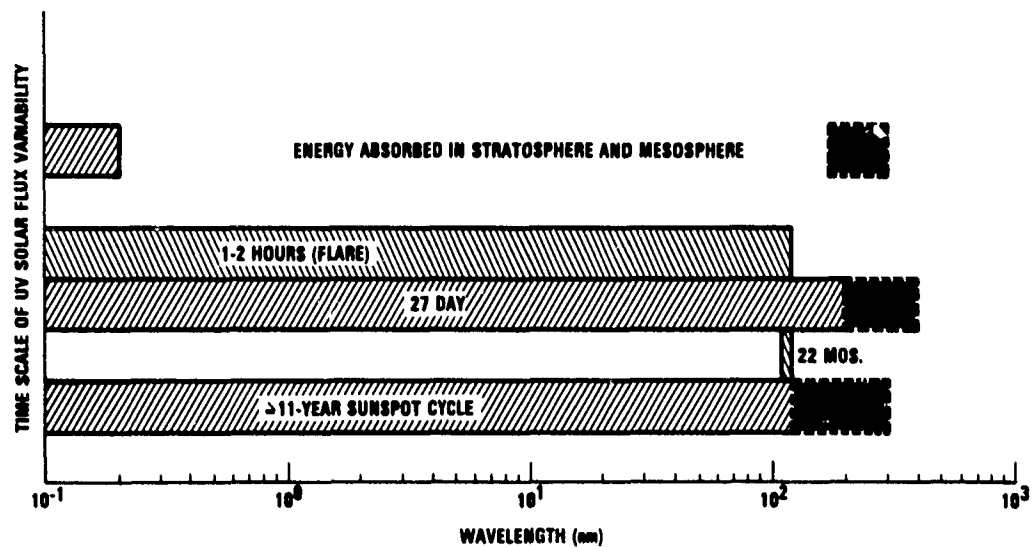


Figure 2: Wavelength dependence of UV solar flux variability for different temporal periods of variability. Top portion represents band of wavelengths which are absorbed in the stratosphere and mesosphere.

# EVIDENCE FOR VARIATIONS IN RADIATIVE OUTPUT OF SUN

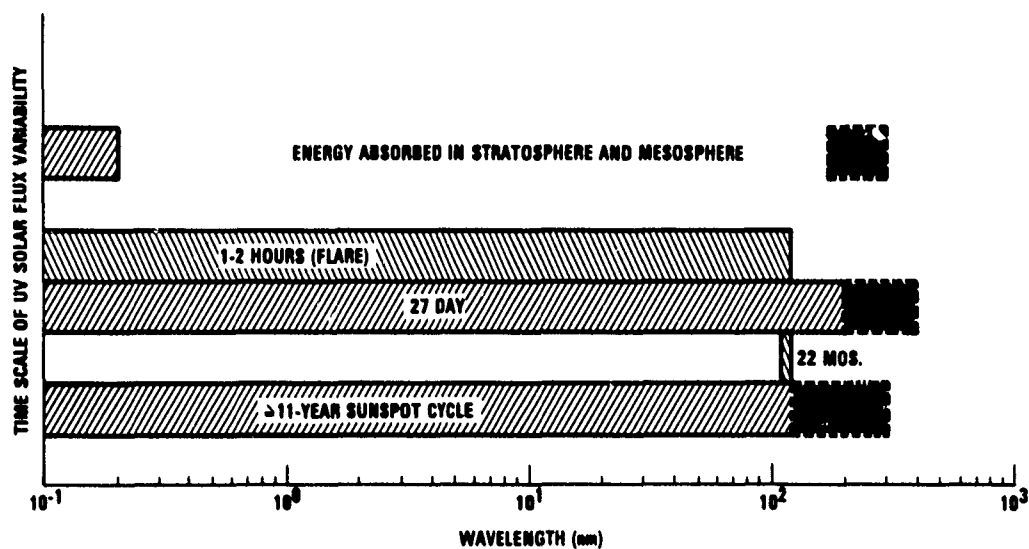


Figure 2: Wavelength dependence of UV solar flux variability for different temporal periods of variability. Top portion represents band of wavelengths which are absorbed in the stratosphere and mesosphere.

## HEATH

TABLE 3 - SOLAR SPECTRAL IRRADIANCE W/cm<sup>3</sup>

Wavelength Range (nm)		D. &P.	H. &S.	S. &S.	B.	EUVS*	SBUV
FROM	TO						
165	166	0.42	0.33	0.278		0.56	0.337
170	171	0.73	0.55	0.411		0.72	0.602
175	176	1.02	0.70	0.853	0.859	0.88	0.918
180	181	1.4	1.24	1.69	1.56	1.6	1.54
185	186	2.0	1.31	2.04	1.89		1.92
190	191	3.1	2.3	3.06	3.07		3.18
195	196	4.8		4.34	4.32		5.00
200	201	7.1		6.19	5.92		6.66
205	206	10.7	Broadfoot	8.89	9.18		9.79
210	211	37.2	39.2				25.0
215	216	48.3	47.3				34.8
220	221	61.1	52.1				45.0
225	226	66.5	60.9				50.5
230	231	68.3	65.3				47.8
235	236	67.3	62.1				46.0
240	241	50.7	49.9				37.7
245	246	60.1	58.9				47.8
250	251	68.5	61.8				56.1
255	256	99.8	101.6				71.6
260	261	107	96				84.3
265	266	292	288				245
270	271	302	283				262
275	276	212	245				168
280	281	121	175				95.3
285	286	183	295				173
290	291	623	611				594
295	296	585	593				546
299	300	496	434				440
300	310		L. &N.	Arvesen	T.		571
310	320			592	603		702
320	330			729	704		866
330	340			878	975		972
340	350			1020	1080		966
350	360			997	1070		999
360	370			1020	1080		1130
370	380			1050	1130		1150
380	390			1040	1160		1010
390	400			945	1100		1160
				1130	1210		

\* : 2.5 nm interval

D. &amp;P. : Dcnnelly and Pope, 1973, NOAA Technical Report, ERL 276-SEL25

H. &amp;S. : Heroux and Swirbalus, 1976, J.G.R. 81, 46

S. &amp;S. : Samain and Simon, 1976, Solar Phys., 49, 33

B. : Brueckner et al., 1976, Ap. J., 209, 935

Broadfoot : Broadfoot, 1972, Ap. O., 173, 681

L. &amp;N. : Labs and Neckel, 1970, Solar Phys. 15, 79

Arvesen : Arvesen et al., 1969, Appl. Optics, 8, 2215

T. : Thekaekara et al., 1969, Appl. Optics, 8, 1713

EUVS : Hinteregger, 1979, Private Communication

A graphical presentation of the ultraviolet solar spectral irradiance for November 7, 1978 is given in figure 3. The spectra are recorded with a 1.0 nm spectral band pass at 0.2 nm intervals from 160-400 nm. The transition from a spectrum dominated by strong Fraunhofer line absorption at long wavelengths down to the aluminum ionization limit just below 210 nm is clearly evident. At wavelengths shorter than 210 nm and down to 160 nm there is a gradual transition from absorption to emission features superimposed on the solar continuum.

A comparison of these observations of solar spectral irradiance recorded for November 7, 1978 with previous observations of others is given in Table 3. Below 210 nm strong evidence from several sources indicates a variation in the solar output which appears to be in phase with the sunspot cycle in that the solar flux has increased as the sunspot number increases. Above 210 nm the solar flux appears to behave quite differently. A comparison of the solar flux measured by Broadfoot (1972) in June 1970 is significantly higher than that observed with the SBUV experiment in November 1978.

During solar cycle 20 Heath and Thekaekara (1978) indicated a significant long term variability which appeared to be in phase with the sunspot numbers from 170 to 300 nm. If the observations are correct it would appear that the solar spectrum from 160-210 nm follows an in-phase relation with the 11 year sunspot cycle whereas the region above 210 nm is following the 22 year magnetic cycle. It should be emphasized that even though the low spectral irradiance values between 210-250 nm appear to be corroborated by Mount and Rottman (1980). This suggested behavior above 200 nm is far from being proven conclusively.

Simon in this volume has already discussed the evidence for solar variability associated with active regions moving at the rate associated in the 27-day solar rotational period. The SBUV experiment on Nimbus 7 confirms his conclusions as well as providing conclusive evidence that the solar flux is also varying in the region of 210-400 nm at the solar rotational rate.

The observations on the magnitude and variability of the ultraviolet solar spectral irradiance in the 160-400 nm region are discussed in detail in a paper by Heath and Parks (1980).

An apparent 22 month variation in H. Lyman alpha (indicated in figure 2) was reported by Heath (1973) from broad-band photometer observations however no evidence was seen with any of the other photometer channels at longer wavelengths.

**HIGH ENERGY SOLAR PARTICLE EFFECTS:** The only solar induced short-term variations in the vertical distribution of ozone which have been observed from satellites apart from diurnal effects are those due to high energy particle events on the sun such as the one of August 4, 1972. These effects have been described by Heath et al., (1977).

The largest solar proton event for the last 25 years which occurred late on day 217 (August 4, 1972). The effect of this event on stratospheric ozone is shown in figure 4. It produced an abrupt decrease in the ozone above 4 mbar in the latitude zone of 75-80°N. This geodetic latitude zone lies wholly within the oval of the polar cap. The latitude zone from 55-65°N shows an abrupt decrease followed by a fairly rapid recovery which is probably due to the advection of modified air from the source region (symmetric in geomagnetic coordinates) by zonal winds (symmetric in geodetic coordinates). Thereafter the trend is dominated by the typical seasonal behavior for this region. The normal seasonal behavior for 3 years other than 1972 is shown in figure 5. Clearly the ozone cavity formed within the polar cap is a long lasting phenomena.

The gradual rise to a peak in ozone in the tropics around day 207 with a subsequent decline thereafter does not appear to be related to the solar proton event but rather to a Southern Hemisphere stratosphere warming (Labitzke, 1974) which has associated with it a stratospheric cooling in the tropics which produces an increase in ozone in regions which are dominated by photochemistry.

The question of long term modulation of solar ozone fields by high energy particles which can produce effects in the polar stratosphere is being pursued with the combined ozone data sets from the BUV type instruments which were flown on the polar orbiting Nimbus 4 in 1970 and Nimbus 7 in 1978.

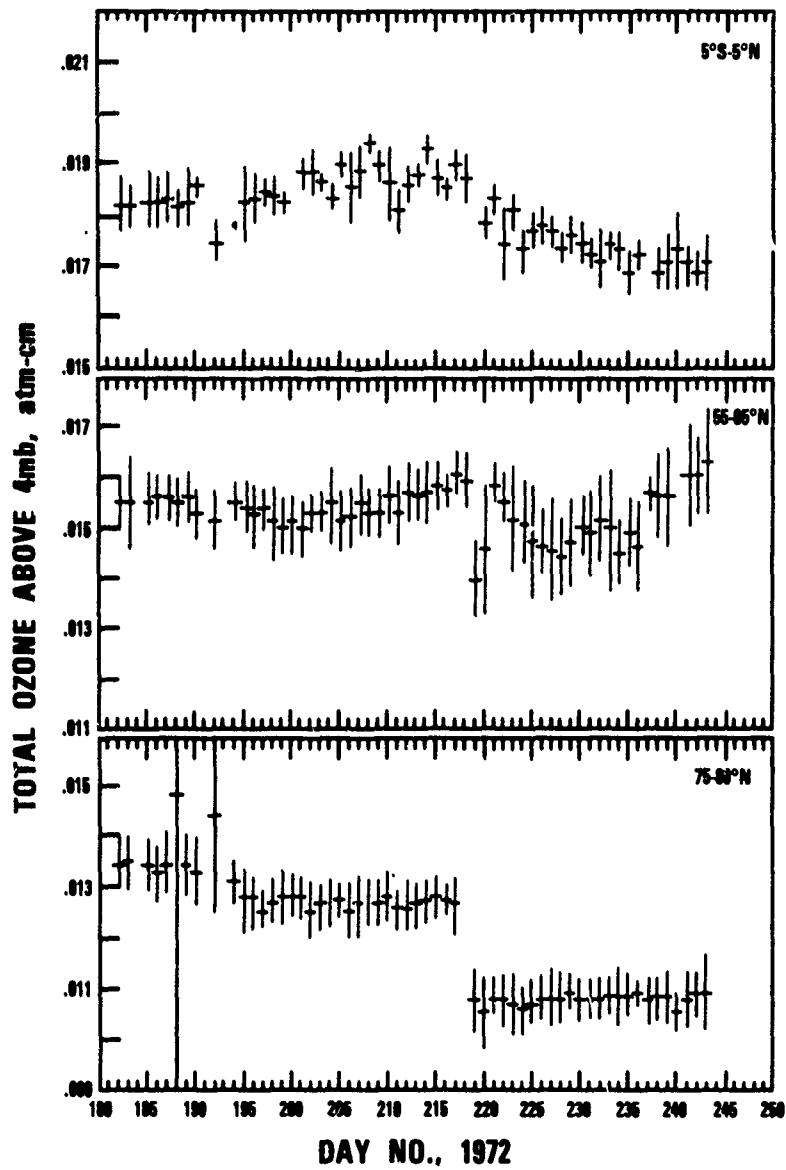
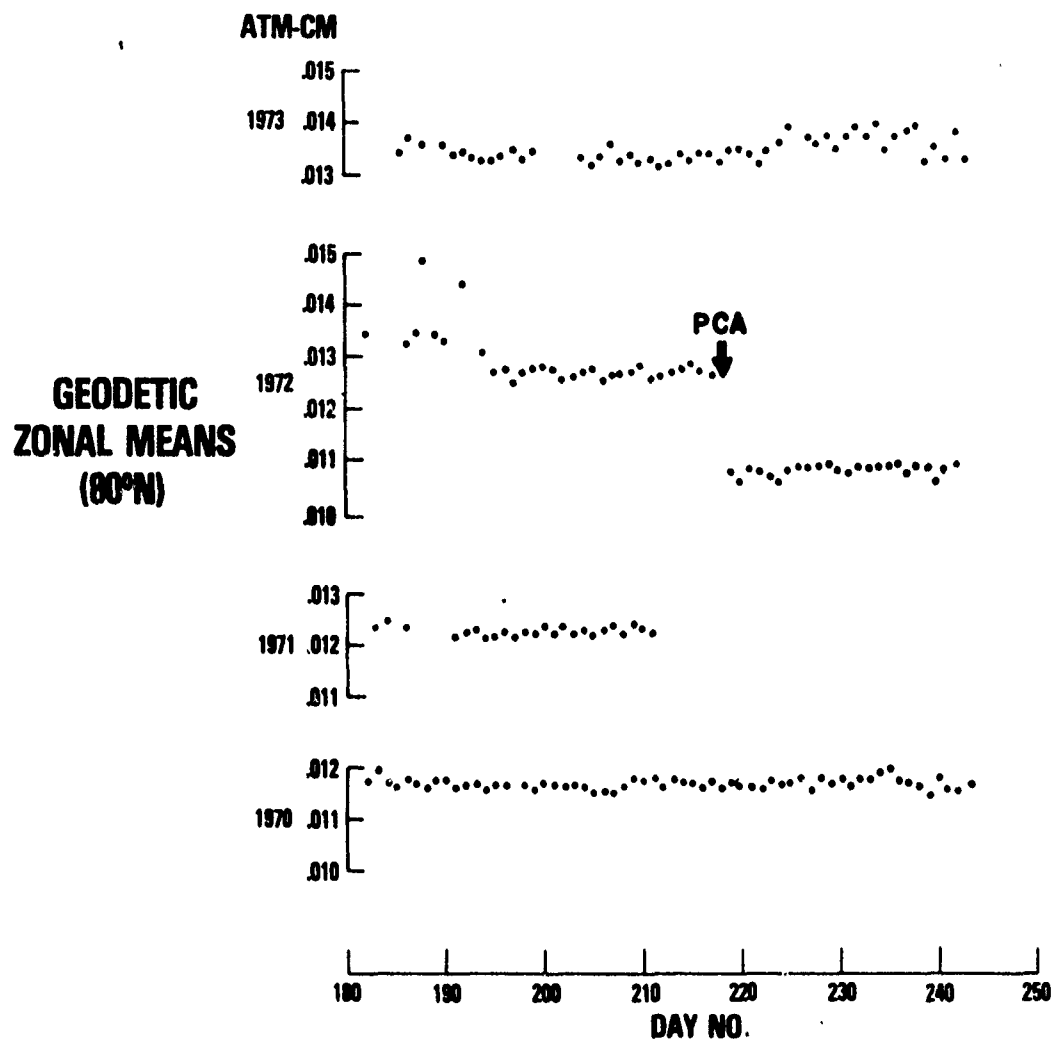


Figure 4: Zonally averaged total ozone above the 4-mbar pressure surface for equatorial (top) and mid (middle) and high latitudes (bottom) during July and August 1972. The solar proton event occurred on August 4, (day 217).

## PCA EVENT DETECTED BY NIMBUS-4



## COMPARISON OF OZONE AMOUNT (ABOVE 4mb), 1970-1973

Figure 5: Seasonal behavior of seasonally averaged total ozone above the 4-mbar pressure surface for July and August for years 1970-1973 derived from an early analysis of Nimbus-4 BUUV data.

## HEATH

**OZONE-TEMPERATURE RELATIONSHIP:** The importance of temperature in the determination of photochemical equilibrium concentrations in ozone in the upper stratosphere is well known. An example of the relationship between the ozone mixing ratio at 60°N derived from the BUV experiment on Nimbus 4 and the stratospheric 2-mbar temperature derived from the Selective Chopper Radiometer (SCR) experiment (Barnett 1974) over a period of 1 year has been published by Krueger et al., (1979) and is reproduced here in figure 6. This relationship between ozone and temperature illustrates the importance of knowing temperature structure of the stratosphere on a global basis along with ozone. They found the ozone mixing ratio ( $r_3$ ) in  $\mu\text{g/g}$  related to the temperature by the equation

$$r_3 = 0.072 \exp (1062/T)$$

With a correlation coefficient of 0.991. This relationship was observed to hold except during the period of the January 1971 stratospheric warming.

Since the temperature structure of the stratosphere on a year to year basis is highly variable, e.g., Labitzke (1978) the requirement that one know the absolute temperature structure of the stratosphere to within 1-2K or to be able to detect and map temperature changes of this magnitude in the stratosphere over decades does seem to pose a serious experimental problem.

**CLIMATOLOGICAL VARIATIONS OF OZONE:** Seasonal variations in total ozone have been derived from the BUV experiment on Nimbus 4 by Hilsenrath et al., (1979) for a 2 year period from April 1970 to April 1972. A time-latitude cross section of total ozone for this period is shown in figure 7 with 20 Dobson Unit (DU) contours. In this figure one can easily see the interhemispheric differences in the seasonal trends which center around the spring maximum and the fall minimum.

In the northern hemisphere the spring maximum occurs in late March with a high degree of simultaneity at the different latitudes. At polar latitudes the spring maximum north of 70° decreases from 500 DU in 1970 to 460 DU in 1971 and 440 DU in 1972.

The behavior in the southern hemisphere is quite different in that the maximum occurs at 50°S in September and is considerably lower in magnitude (380 DU) than its northern counterpart. The coherence of the maximum amplitude with latitude is not followed either in that the high latitude maximum peaks about 1 month later than at mid-latitudes. McInturff (1978) has suggested that the poleward transport of ozone may be delayed due either to the weakness of stratospheric warmings or the resistance to breakdown of the southern hemisphere polar vortex.

The observed interhemispheric differences may be related to the strength of the eddy processes associated with the intense planetary waves. Miller et al., (1978) have reported a strong negative correlation of total ozone departures from the latitudinal zonal mean with departures of the height from the 100 mbar level from its corresponding zonal mean in the same zone. This analysis would seem to indicate evidence for the importance of synoptic scale waves in the poleward transport of ozone.

A harmonic analysis has been applied by Hilsenrath et al., (1979) to daily zonal means of total ozone which has been smoothed with a binomial filter with a 10-day half width. The results of this analysis on the 2 year data base yielded the results shown in figure 8 which gives the amplitude of the first harmonic in the Fourier expansion and its corresponding percent of variance as functions of latitude. From this analysis it is clearly evident there are significant interhemispheric differences in the amplitudes of the annual waves. Note that a shift in the minimum amplitude southward of about 10° corresponds to a shift southward of a similar amount in the peak amplitude in the southern hemisphere.

A similar analysis is shown for the semi-annual wave in figure 9. At high latitudes in the southern hemisphere the semi-annual component appears to be important. The full importance at latitudes beyond 70° may be questionable since during the winter time the inference of total ozone presently is terminated at solar zenith angles beyond 83°. In the absence of high latitude ozone data, values from lower latitude zones for which data do exist are extrapolated. A discussion of the extrapolation is described by Heath et al., (1980).



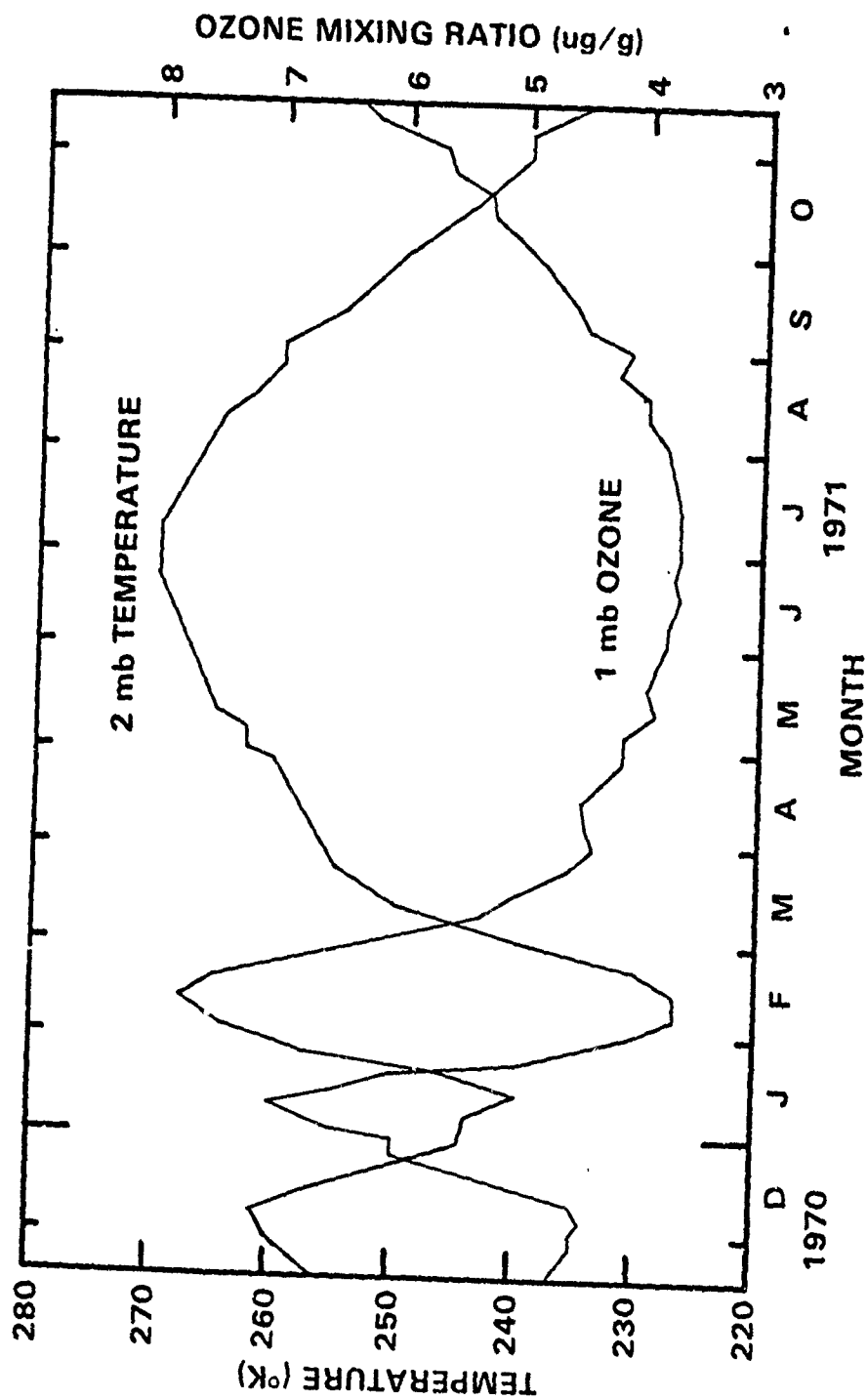


Figure 6: Zonally averaged ( $60^\circ\text{N}$ ) 2-mbar temperature from the SCR experiment and 1-mbar zone mixing ratio from the BUV experiment on Nimbus-4.

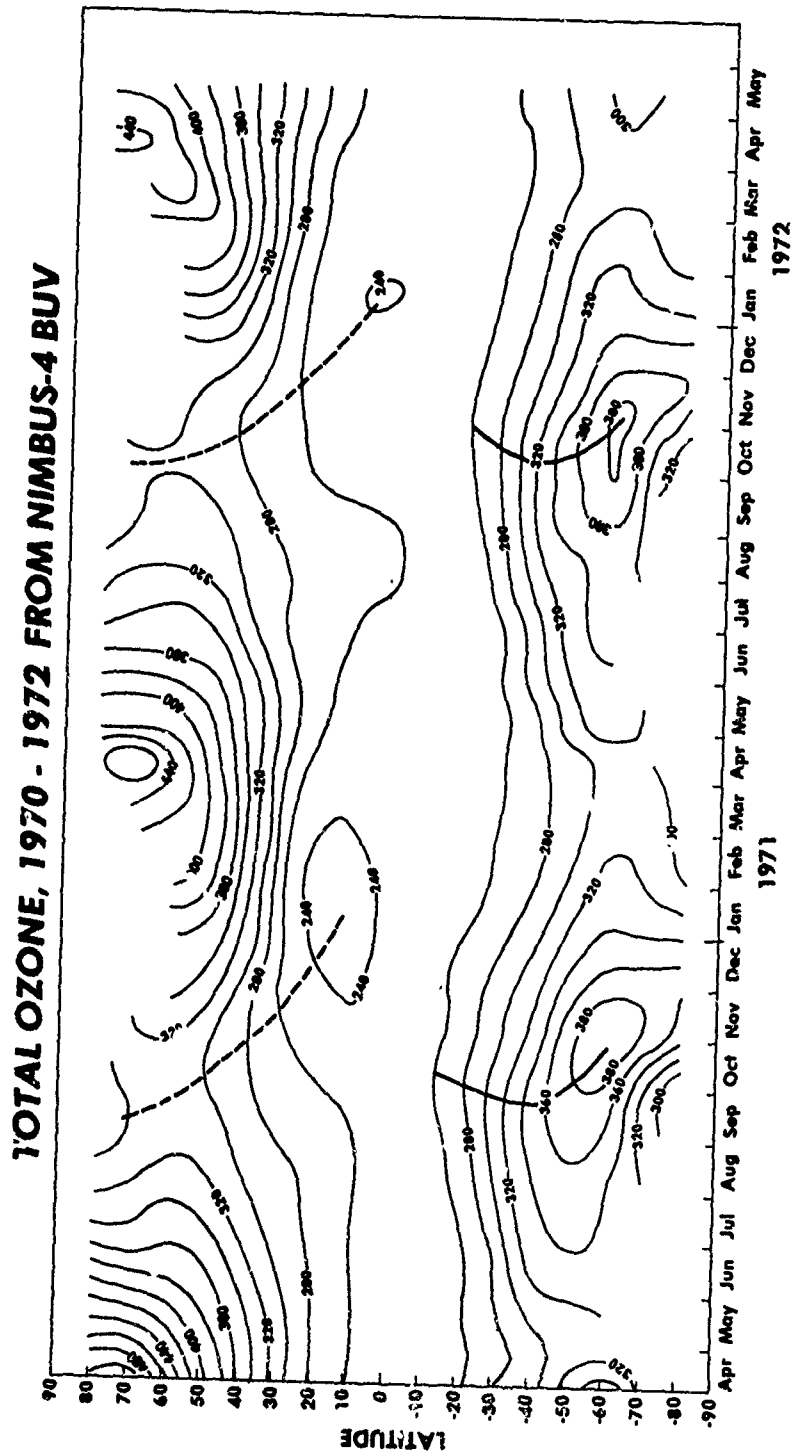


Figure 7: Time-latitude cross-section of total ozone for the period of April 1970 through May 1972 derived from daily zonal means in  $10^\circ$  latitude bands. The contour increment is 20-DU from Hilsenrath et al., (1979).

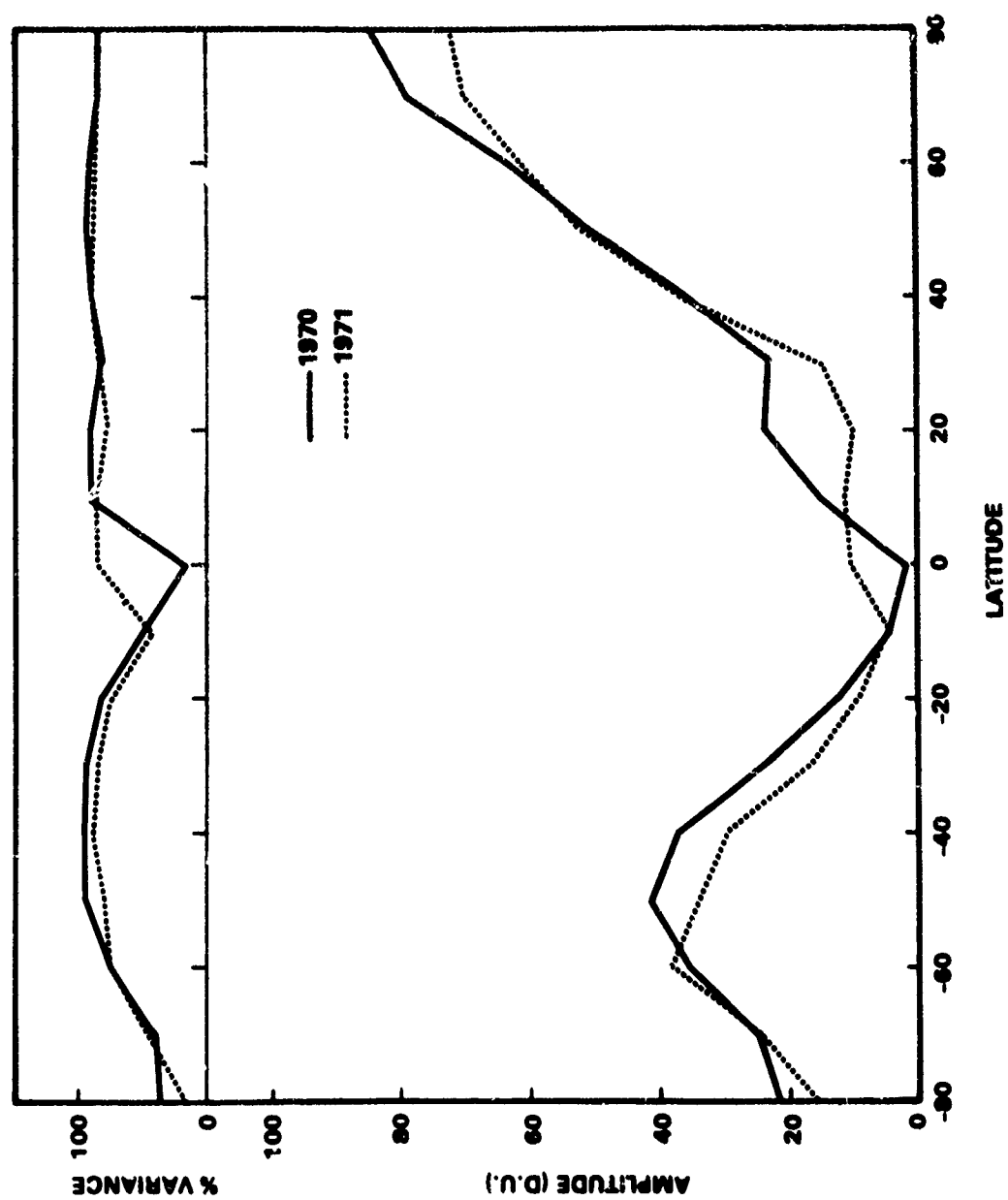


Figure 8: Amplitude of the annual wave in total ozone (bottom) and variance of 1st harmonic (top) derived from the first and second year of BUV total ozone data from Hilsenrath et al., (1979).

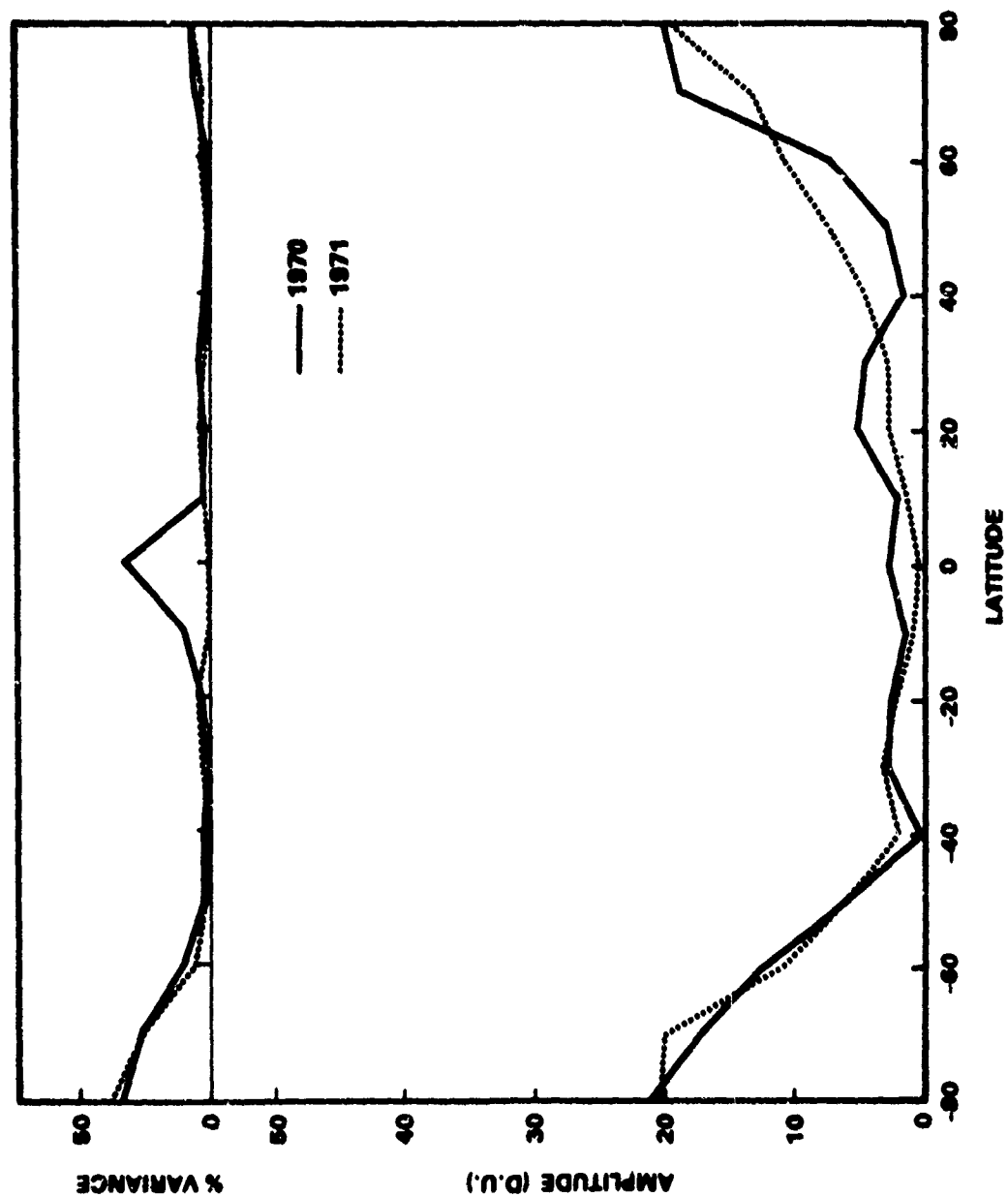


Figure 9: Amplitude of the semi-annual wave in total ozone (bottom) and variance of first harmonic (top) derived from the first and second year of BUV total ozone data from Hilsenrath et al., (1979).

## HEATH

At this time the complex relationships which take place between total ozone, temperature, and winds are not known sufficiently well to explain the semi-annual wave in total ozone. An analysis of the time of maxima of the semi-annual wave at low latitudes shows that they coincide with the maxima of the annual waves in the two hemispheres; hence it has been concluded by Hilsenrath et al., (1979) that the occurrence of the semi-annual wave in total ozone in the tropics is related to the annual waves in the two hemispheres.

The previous section described the global scale behavior in terms of the behavior of the latitudinal zonal means. This section describes the interhemispheric differences in terms of the spatial distribution of total ozone, mass mixing ratio cross sections as a function of height, latitude and total ozone. These data are shown for the months of June, September, and December in 1970 and March in 1971.

Monthly mean total ozone values from the UV experiment were objectively analyzed on the basis of the standard NMC grid (Miller et al., 1979). The data presented in this section represent a part of an ozone climatology being developed jointly by NASA, NOAA and the Free University of Berlin (Heath 1980a). Monthly mean total ozone maps for June 1970 are shown in figures 10 and 11 for the Northern and Southern Hemispheres respectively. The corresponding monthly height latitude mixing ratio cross sections and the latitudinal zonal mean are shown in figures 12 and 13.

In the Northern Hemisphere a high of 400 DU centered over the Aleutian Islands and a low over Northern Europe dominate the high level fields. The steepest latitudinal gradients are concentrated between 30-50° latitude from the Aleutian high westward to the western coast of Africa.

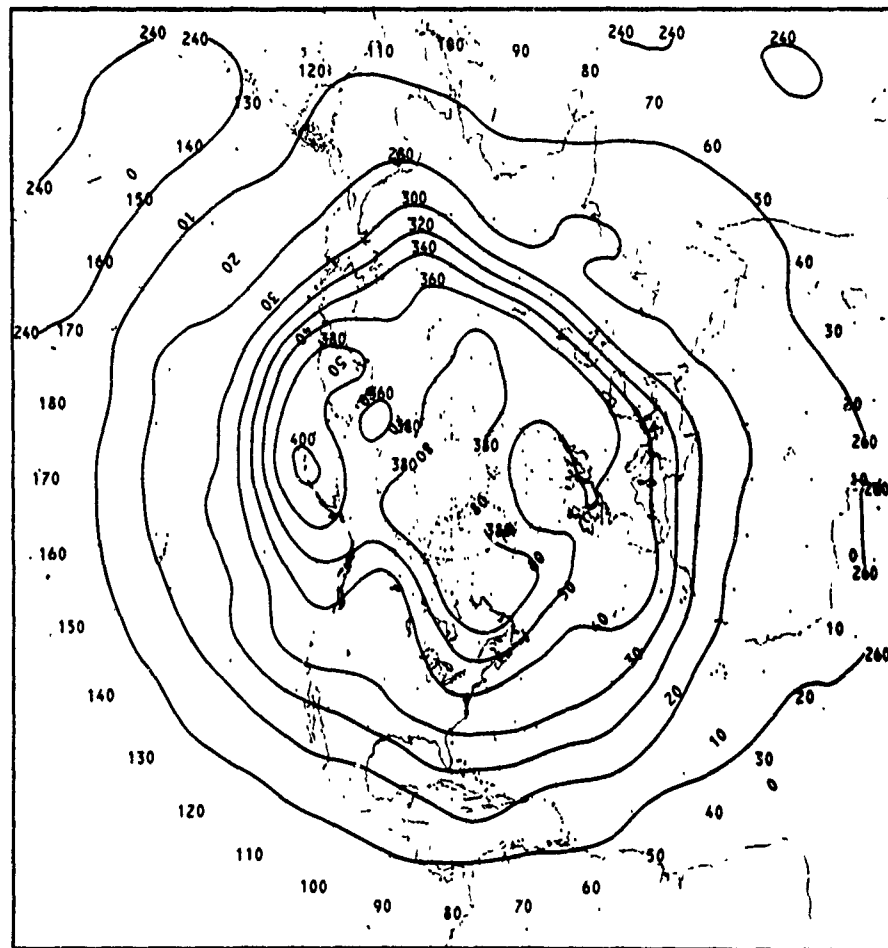
At this point the ozone gradients weaken by diverging northward and southward. The map for June shows the southern hemisphere winter. The principal high is located southwest of Australia. Even though this represents winter, the ozone isolines are nearly zonally symmetric about the pole and the planetary wave patterns are weaker than those for the northern hemisphere summer.

The height-latitude mixing ratio contours for June are given in figure 12. The mixing ratio maximum is centered approximately over the subsolar point in the Northern Hemisphere. There is a secondary maximum at mid to high latitudes in the Southern Hemisphere which is centered over the total ozone maximum at 50°S shown in figure 13. There is an extensive high in the middle stratosphere which extends from 20°S to 40°N. This is probably the result of solar control of the photochemical region. In the upper stratosphere the mixing ratio isolines slope downward in altitude from the southern winter pole to the northern summer pole. In the intervening months between June and September (figure 13) the poleward latitudinal gradients weaken in Northern Hemisphere and strengthen in the Southern Hemisphere. By August the southern maximum at 50°S exceeds that in the northern hemisphere at 60°N. During this 3 month period the tropical minimum has remained centered about 5°S.

The month of September represents the time of the ozone fall minimum in the Northern Hemisphere (figure 14) and the spring maximum in the Southern Hemisphere (figure 15). In the Northern Hemisphere the latitudinal gradients are quite weak. There is some evidence of a wave number 2 at latitudes with one maxima centered over Siberia and the other centered over Greenland.

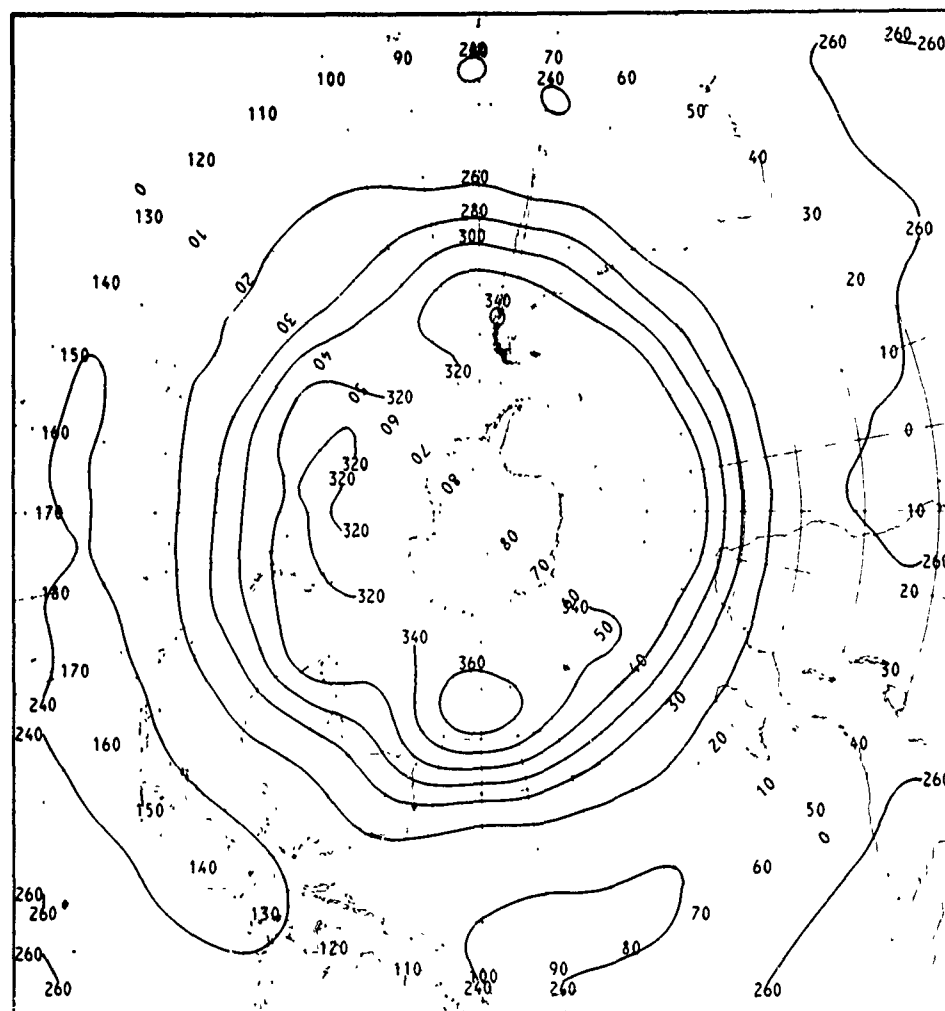
In the Southern Hemisphere there is an intense wave number 1 pattern with its maximum centered south of the east coast of Australia and just off shore of Antarctica. The steepest ozone latitudinal gradients lie between Antarctica and the middle of Australia. The height-latitude mixing ratio cross section is shown in figure 16. The maximum lies nearly centered about the equator but projects slightly more into the northern hemisphere. The steepest vertical gradients lie between 4 and 1.5 mbar in the tropics. At high latitudes in both hemispheres the mixing ratio is nearly constant between 20 and 2.5 mbar.

The monthly latitudinal zonal mean of total ozone for the months of September-November are given in figure 17. During September the Southern Hemisphere maximum is located at 50°S and gradually moves southward to its maximum at 60°S during October and November. In the northern hemisphere the high latitude gradients increase while the tropical minimum broadens. During this period the amplitude of the maximum remains essentially constant.



U.S. JUNE, 1970, MEAN MONTHLY TOTAL OZONE (DOBSON UNITS)

Figure 10: Monthly mean total ozone for the Northern Hemisphere (June 1970) from an analysis of Nimbus-4 BUV data. Contour intervals are 10 DU.



S.H. JUNE, 1970, MEAN MONTHLY TOTAL OZONE (DOBSON UNITS)

Figure 11: Monthly mean total ozone for the Southern Hemisphere (June 1970), from an analysis of Nimbus-4 BUV data. Contour intervals are 10 DU.

6/70

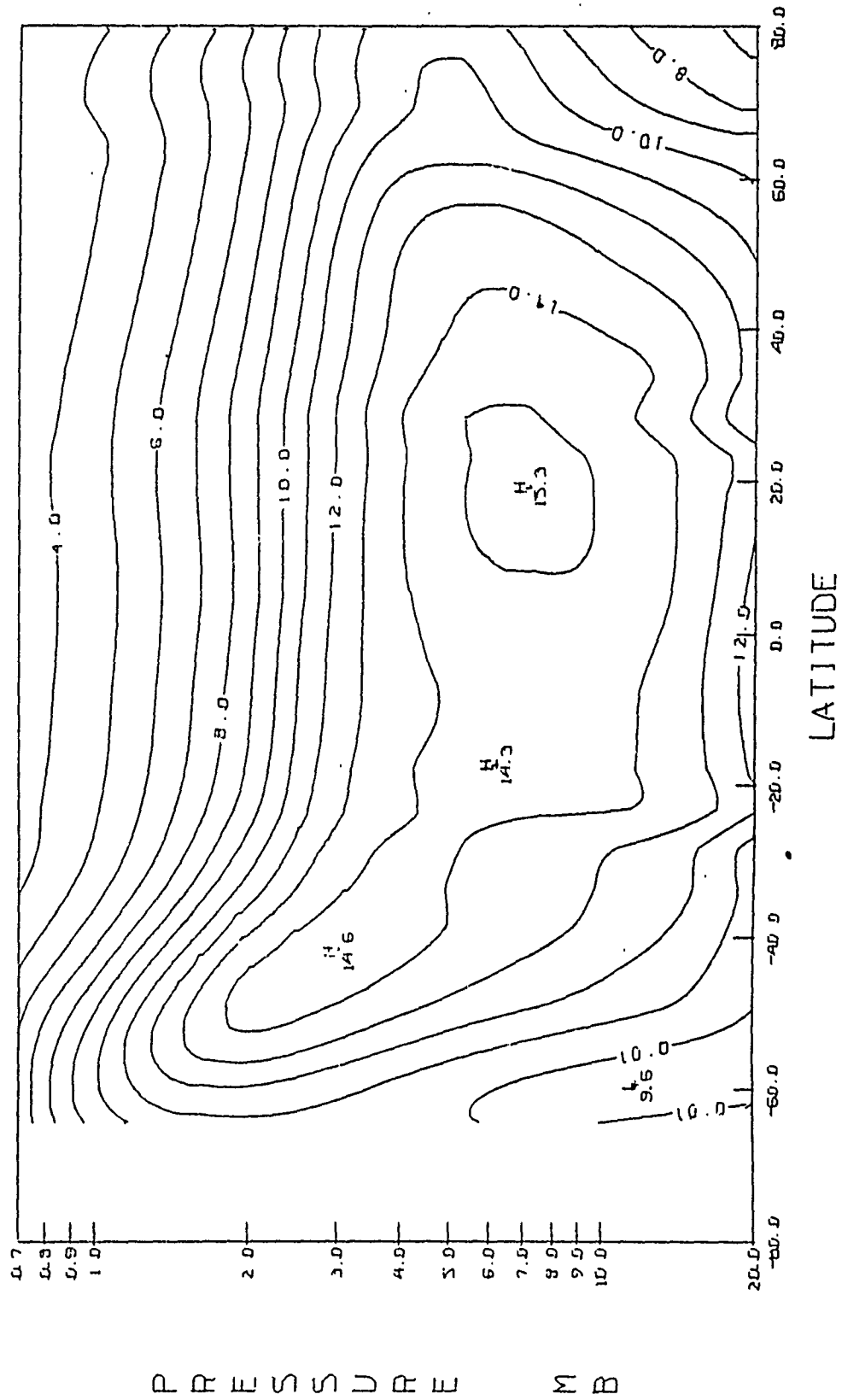


Figure 12: Monthly mean height-latitude cross-section of ozone mass mixing ratio ( $\mu\text{g/g}$ ) for June 1970 from an analysis of Nimbus-4 BUV data. Contour intervals are 1.0  $\mu\text{g/g}$ .



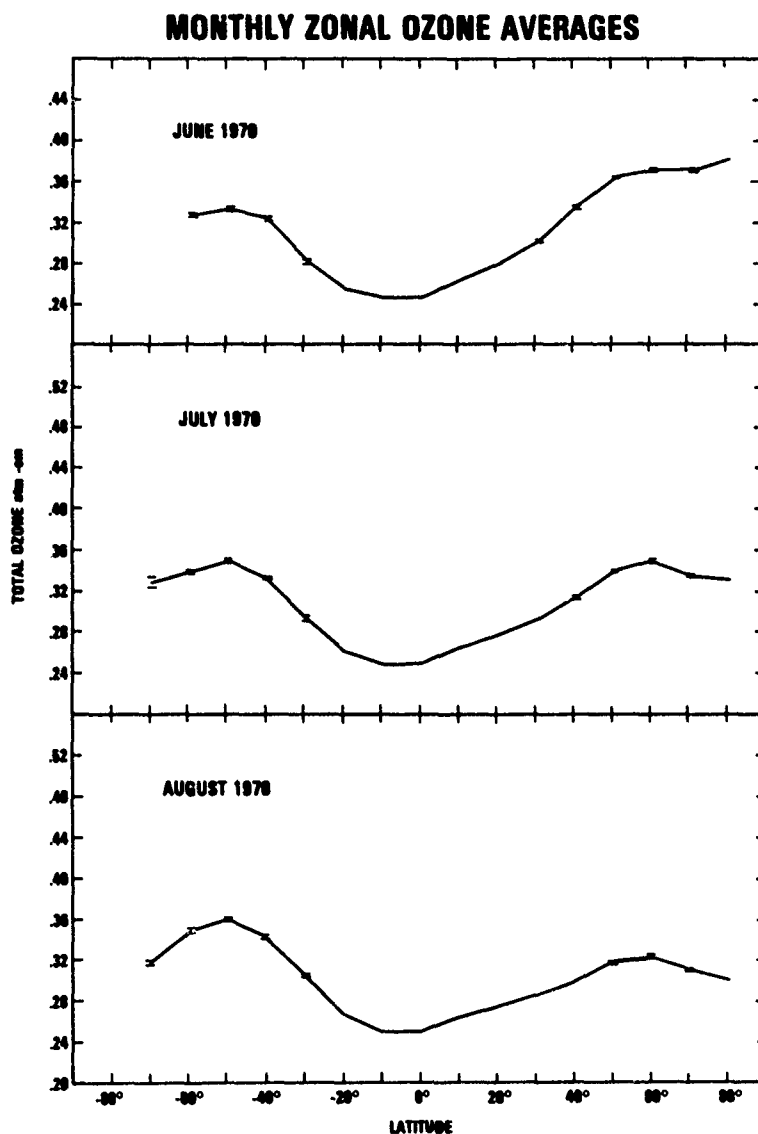
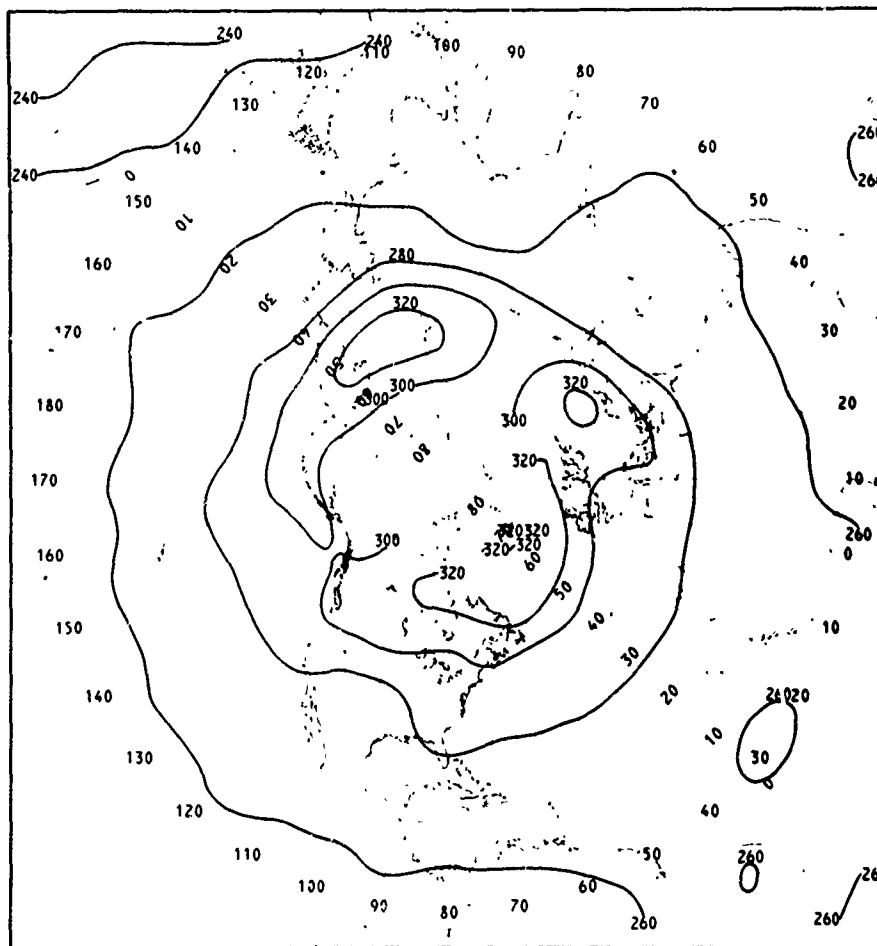
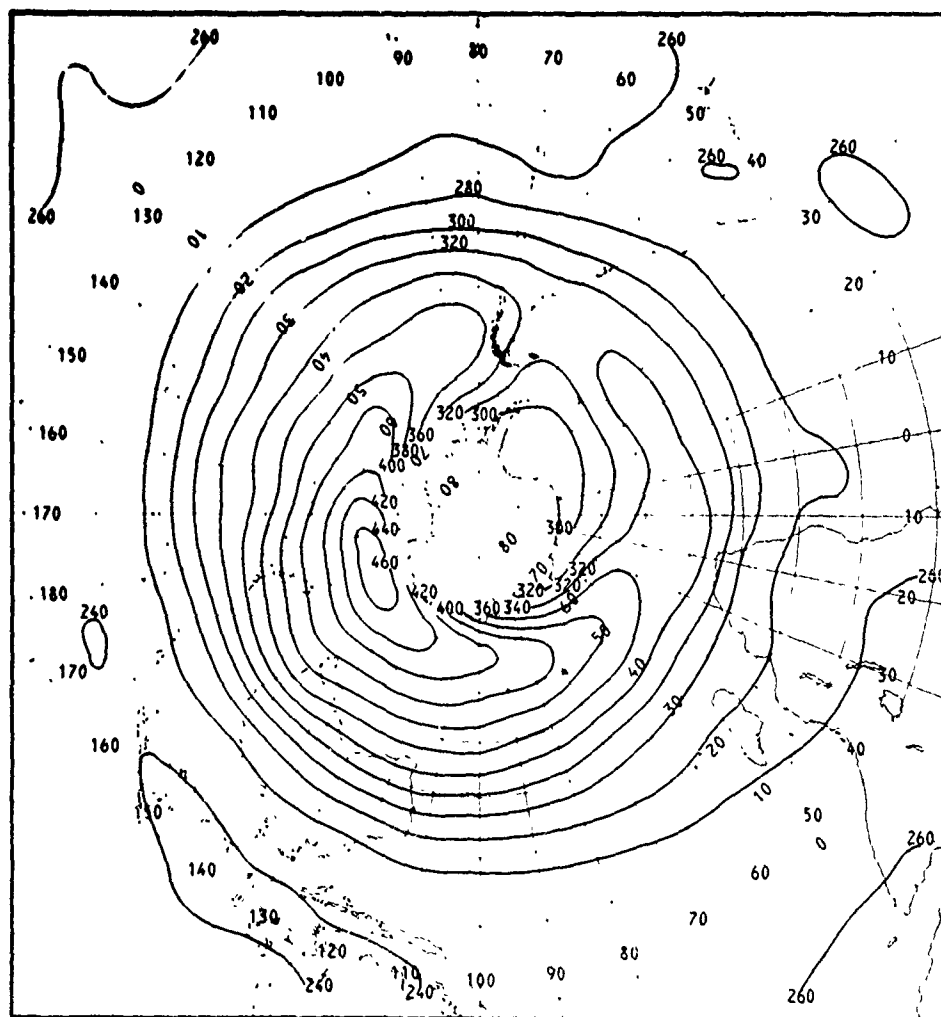


Figure 13: Total ozone monthly zonal means for June, July, and August 1970 derived from an analysis of daily zonal means in 10° latitude from Nimbus-4 BUV data.



N.H. SEPTEMBER, 1970, MEAN MONTHLY TOTAL OZONE (DOBSON UNITS)

Figure 14: Monthly mean total ozone for the Northern Hemisphere, September 1970 from an analysis of Nimbus-4 BUUV data. Contour intervals are 10-DU.



S.H. SEPTEMBER, 1970, MEAN MONTHLY TOTAL OZONE (DOBSON UNITS)

Figure 15: Monthly mean total ozone for the Southern Hemisphere during September 1970 from an analysis of Nimbus-4 BUUV data. Contour intervals are 10-DU.

Q U E S T I O N                      A N S W E R

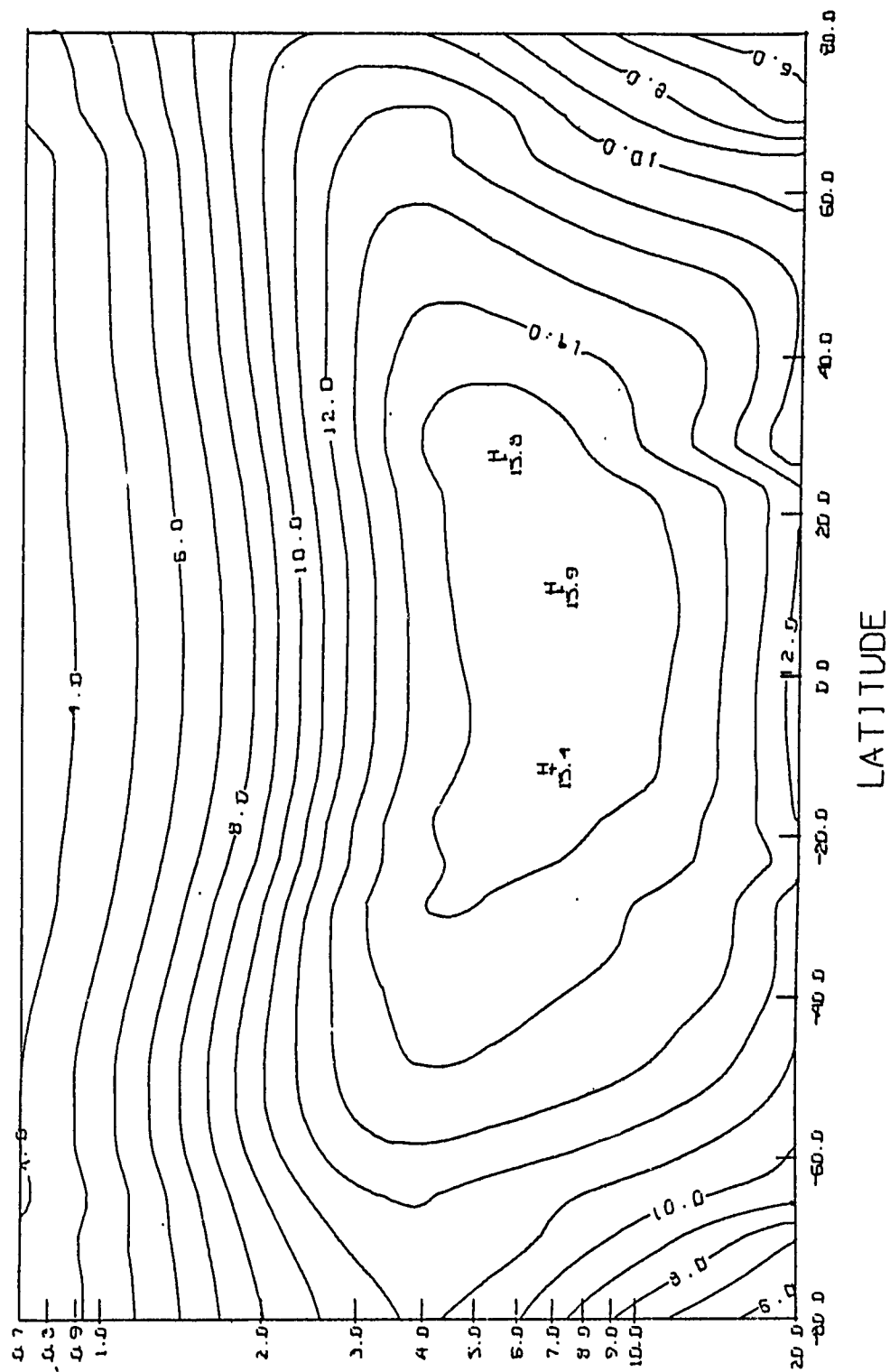


Figure 16: Monthly mean height-latitude cross-section of ozone mass mixing ratio ( $\mu\text{g/g}$ ) for September 1970 from an analysis of Nimbus-4 BUV data. Contour intervals are  $1.0 \mu\text{g/g}$ .

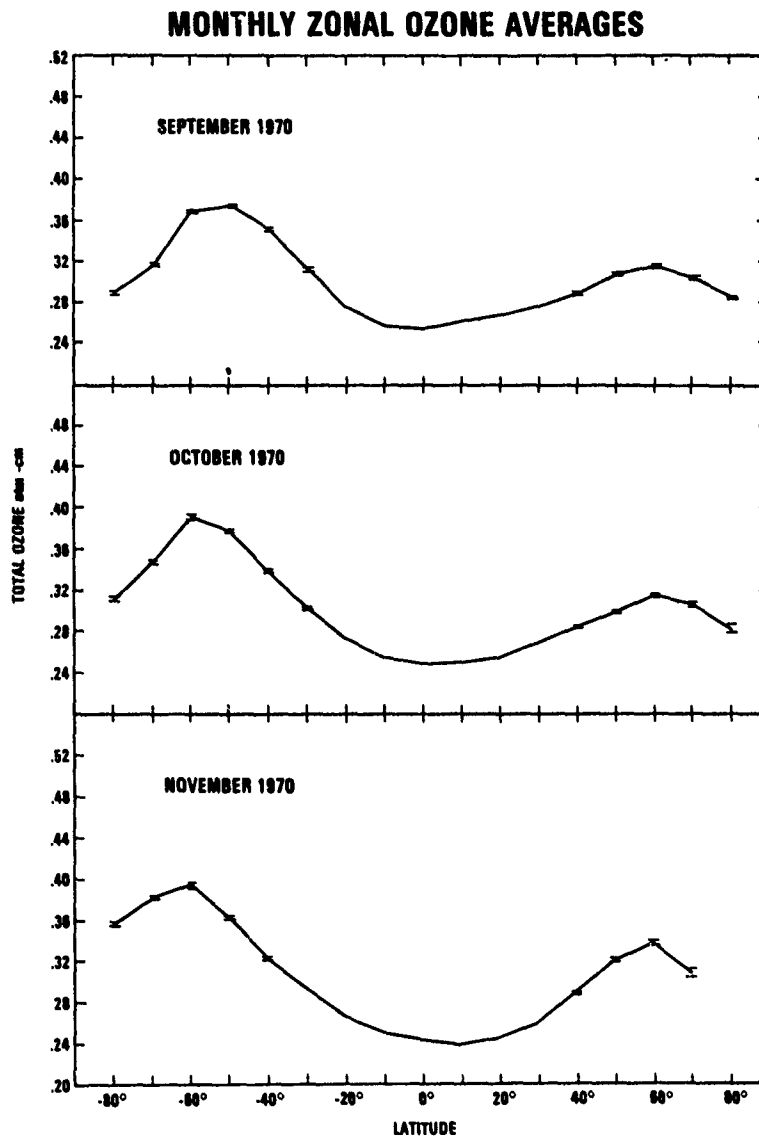


Figure 17: Total ozone monthly zonal means for September, October, and November 1970 derived from an analysis of daily zonal means in 10° latitude bands from the Nimbus-4 BIV data.

The ozone distribution during the Northern Hemisphere winter (December) is shown in figure 18. The most notable feature is the very intense wave number 1 pattern whose maximum is located over Siberia. This spatial distribution marks the period just prior to the intense stratospheric warming of January 1970. The corresponding low is located southeast of Greenland and west of the coast of England. The steepness of the ozone gradients extending southward from the Siberian high nearly equal those observed during the March spring maximum in the Northern Hemisphere. In moving around the latitude circle of  $50^{\circ}\text{N}$  one encounters a maximum of 420 DU and a minimum of 300 DU. This variation of maximum to minimum is slightly greater than that encountered during the spring maximum in the northern hemisphere.

During the southern hemisphere summer (December) one sees in figure 19 a rather weak high over a section of the Antarctic coast between Africa and Australia. Moving northward one encounters a wavenumber 4 or 5 pattern just south of Australia. The planetary waves in December bear some resemblance to those observed during the month of June during the same calendar year. The monthly mean height-latitude mixing ratio cross section for December (figure 20) has roughly the same characteristics as a mirror image of the one for June except that the tropical maximum is not shifted as much towards the subsolar point in the southern hemisphere. Another difference can be noted in that the winter season, high latitude, upper stratospheric is not as intense as that observed in the southern hemisphere in June.

A significant difference is observed between the winter hemispheres. In December (figure 21) the total ozone minimum is located at  $20^{\circ}\text{N}$  and is displaced significantly further from the tropics than the corresponding situation in June when the tropical minimum is located at  $5^{\circ}\text{S}$  in figure 12. Whereas the high latitude maxima are nearly equal in December, ozone in the Northern Hemisphere is beginning to build up in preparation for the spring maximum.

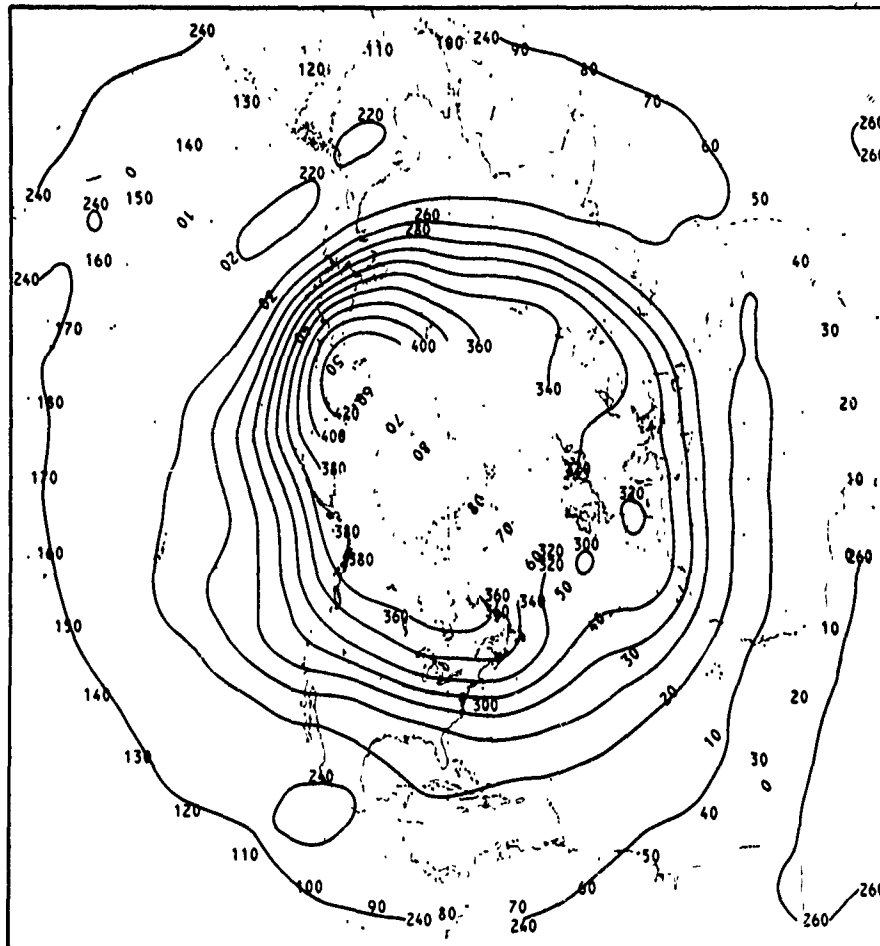
March, the time of the spring maximum in the Northern Hemisphere (figure 22) is dominated by a wavenumber 3 pattern with intense ozone ridges extending southward along the east coast of the United States, Central Europe, and Siberia. The ridges over the North America and Central Europe are separated by a deep trough which extends northward between Greenland and the west coast of Europe. The ozone gradients during the Northern Hemisphere spring greatly exceed those of the Southern Hemisphere spring maximum in September. It is quite obvious that there are major interhemispheric differences.

The Southern Hemisphere in March (figure 23) shows a weak wave number two pattern just off the coast of Antarctica and as one moves northward it develops into a wavenumber 4 pattern just south of Australia.

The height-latitude mixing ratio cross section for March (figure 24) shows an intense cell of maximum ozone centered about  $5^{\circ}\text{S}$  latitude. Above 3 mbar the cross section is reasonably symmetric about the tropics for the two hemispheres. The steepest mixing ratio gradients with respect to altitude are observed in the tropics above 4 mbar. The minimum altitude mixing ratio gradients are observed in the polar regions in the altitude range of 20-4 mb.

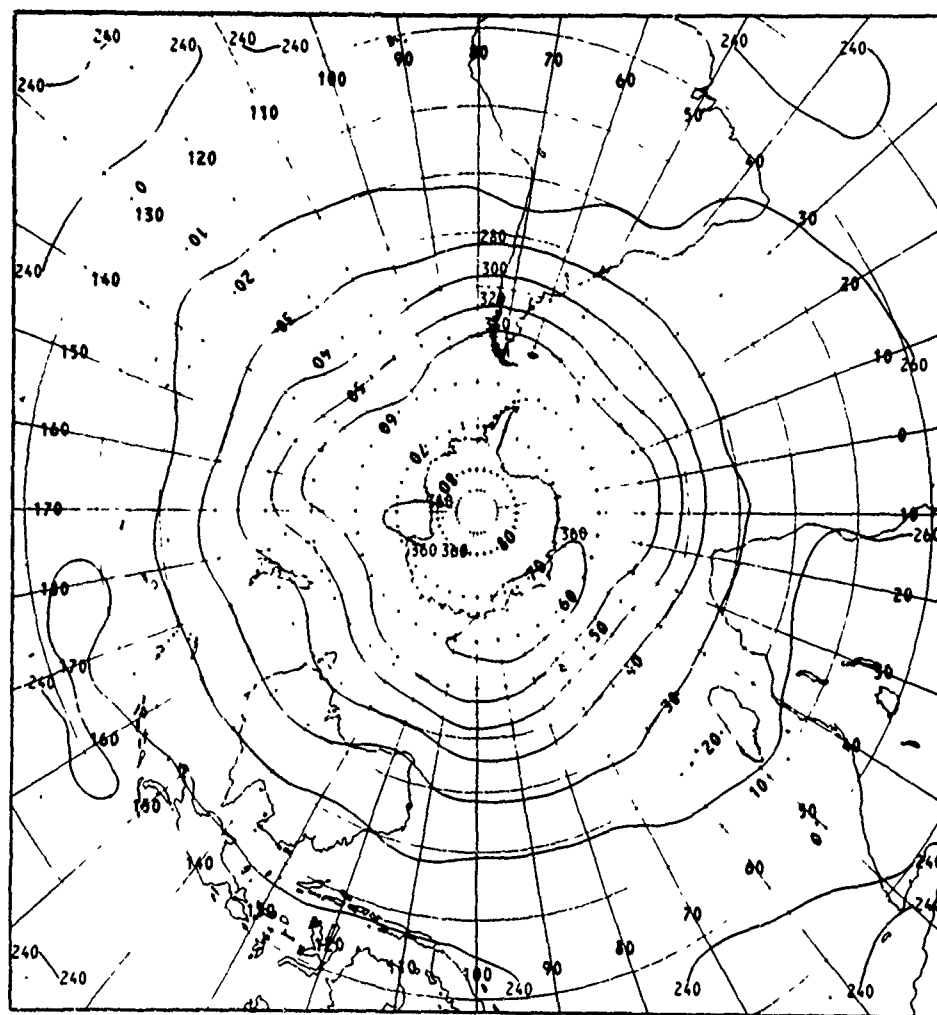
The latitudinal zonal means for March, April, and May in figure 25 show some very interesting interhemispheric differences. All three months exhibit a small maximum in the vicinity of the equator. Small minima are observed on either side of the equatorial maximum at  $20^{\circ}\text{S}$  and  $10^{\circ}\text{N}$ . This same feature is evident in figure 21 which gives the zonal means for December to February. It is not present in the proceeding 6 months of June-November. In a later section evidence will be presented which indicates that it may be associated with the quasi-biennial oscillation in ozone.

LONG TERM VARIATIONS IN TOTAL OZONE: In attempts to determine the long term changes in the global ozone data it is important to recognize that the measurements may be biased by a slowly changing instrument sensitivity resulting from long term operation in the harsh environment of space. It should be emphasized that the ozone quantities inferred from the observations with the BUV instrument are derived from first principles and are not in any way normalized against any of the ground truth systems. A complete description of the BUV system and its uses and limitations for ozone monitoring is given by Heath (1980b). Furthermore it has been assumed that the sun has remained constant over the 7 years of operation in processing Nimbus-4 BUV data.



N.H., DECEMBER, 1970, MEAN MONTHLY TOTAL OZONE (DOBSON UNITS)

Figure 18: Monthly mean total ozone for the Northern Hemisphere for December 1970 from an analysis of Nimbus-4 BUV data. Contour intervals are 10 DU.



S.H. DECEMBER, 1970. MEAN MONTHLY TOTAL OZONE (DOBSON UNITS)

Figure 19: Monthly mean total ozone for the Southern Hemisphere for December 1970 from an analysis of Nimbus-4 BUV data. Contour intervals are 10-DU.



12/70

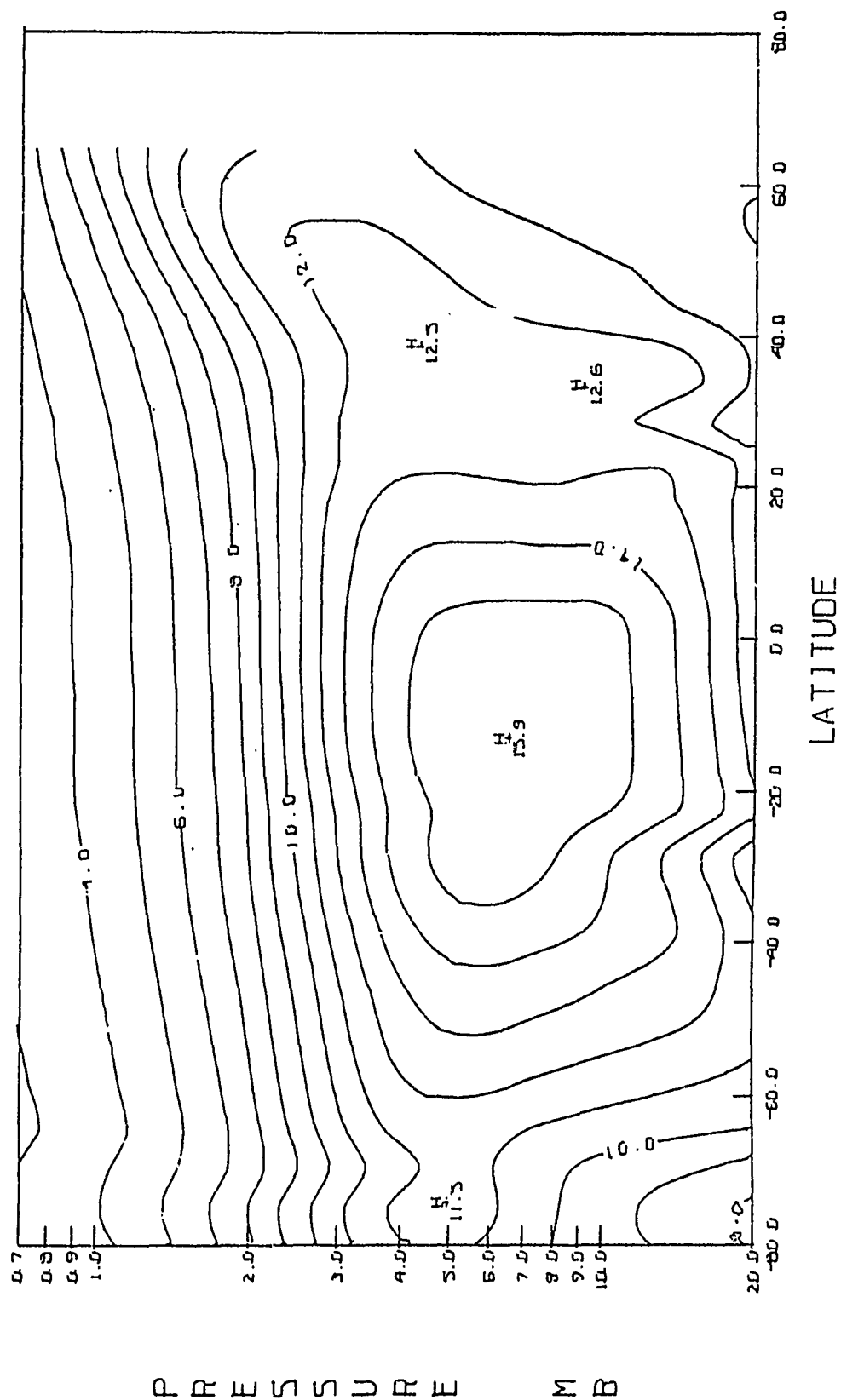


Figure 20: Monthly mean height-latitude cross-sections of ozone mass mixing ratio ( $\mu\text{g/g}$ ) for December 1970 for an analysis of Nimbus-4 BUV data. Contour intervals are 1.0  $\mu\text{g/g}$ .

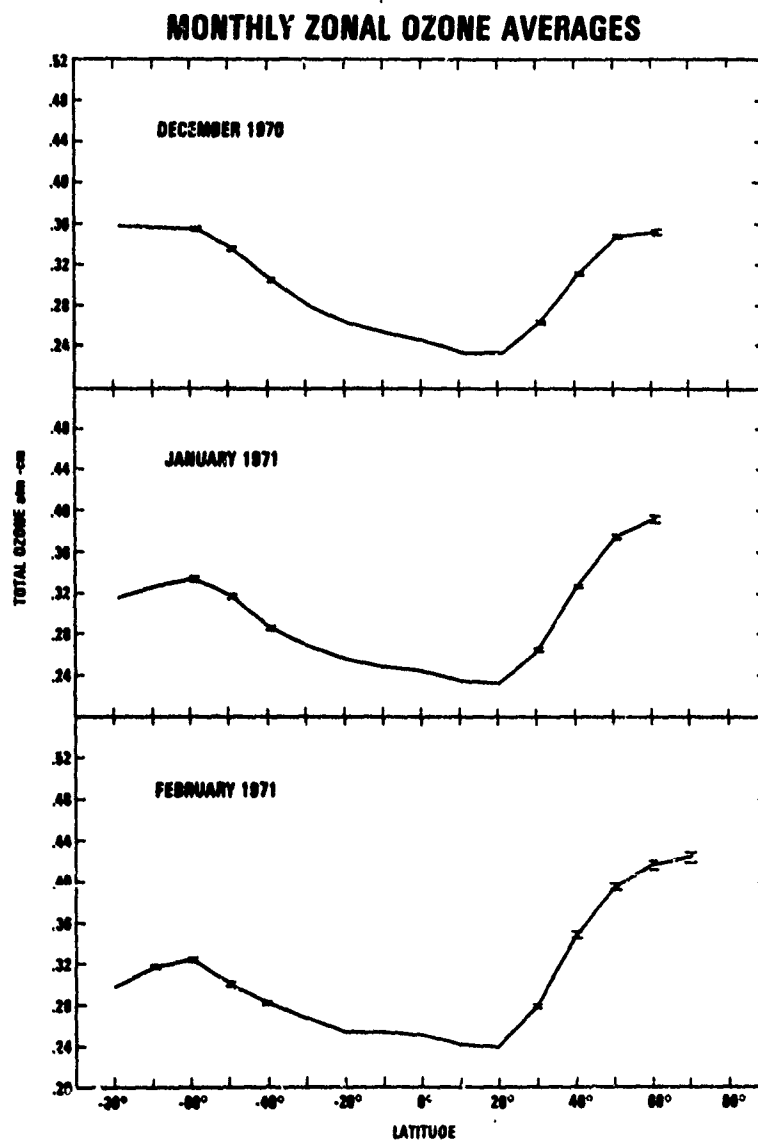
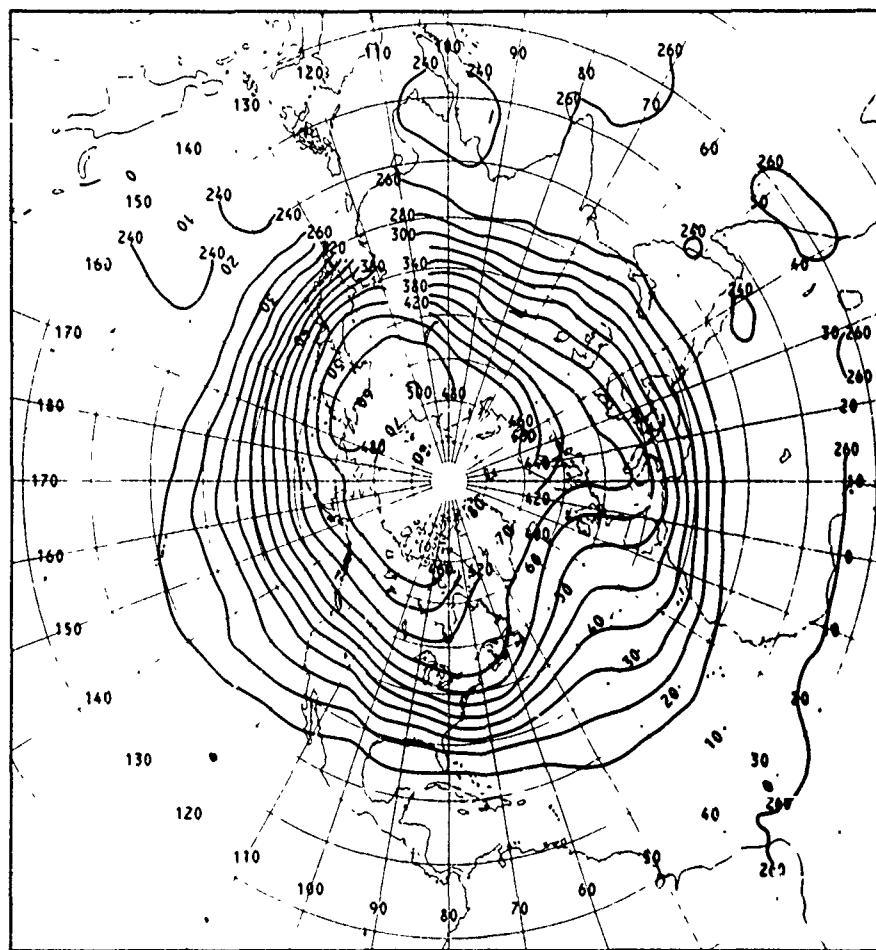
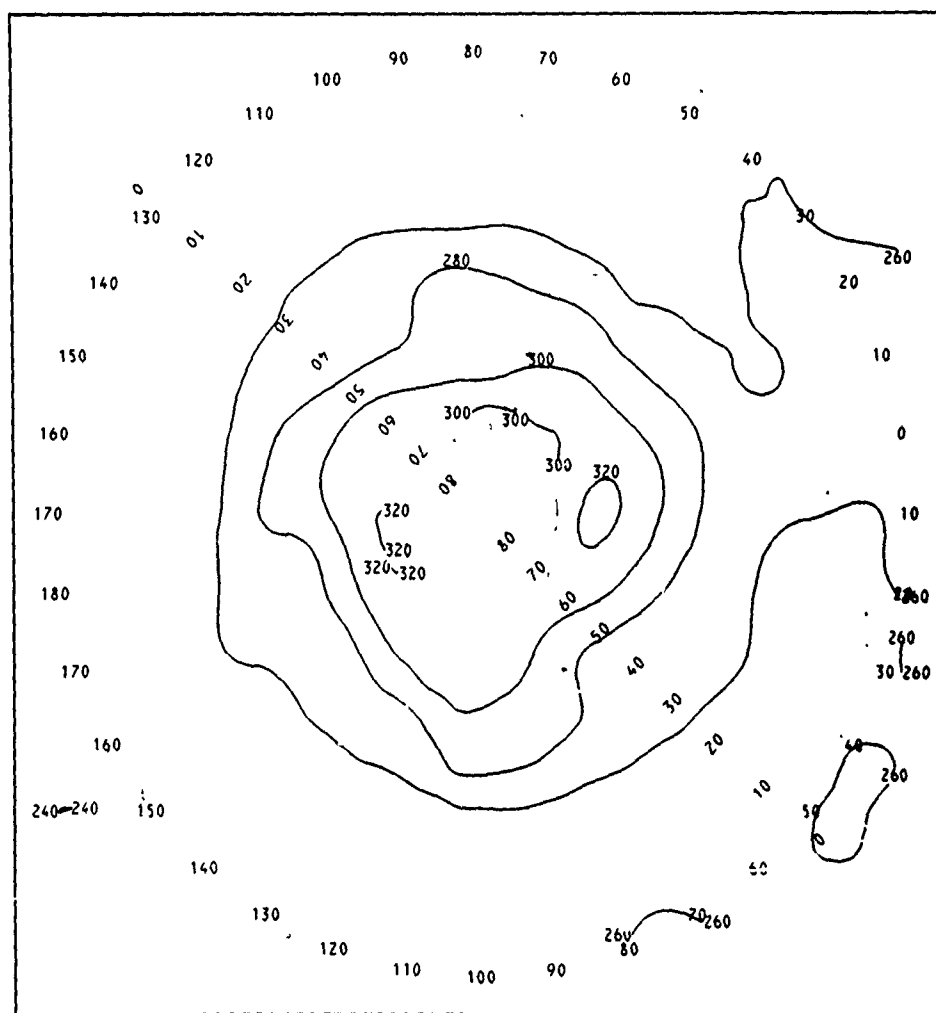


Figure 21: Total ozone monthly zonal means for December 1970, and January and February 1971 derived from an analysis of daily zonal means in 10° latitude bands from Nimbus-4 BUUV data.



11 MARCH, 1971. MEAN MONTHLY TOTAL OZONE (DOBSON UNITS)

Figure 22: Monthly mean total ozone for the Northern Hemisphere for March 1971 from an analysis of Nimbus-4 UV data. Contour intervals are 10 DU.



S H MARCH, 1971, MEAN MONTHLY TOTAL OZONE (DOBSON UNITS)

Figure 23: Monthly mean total ozone for the Southern Hemisphere for March 1971 from an analysis of Nimbus-4 BUUV data. Contour intervals are 10-DU.

3/71

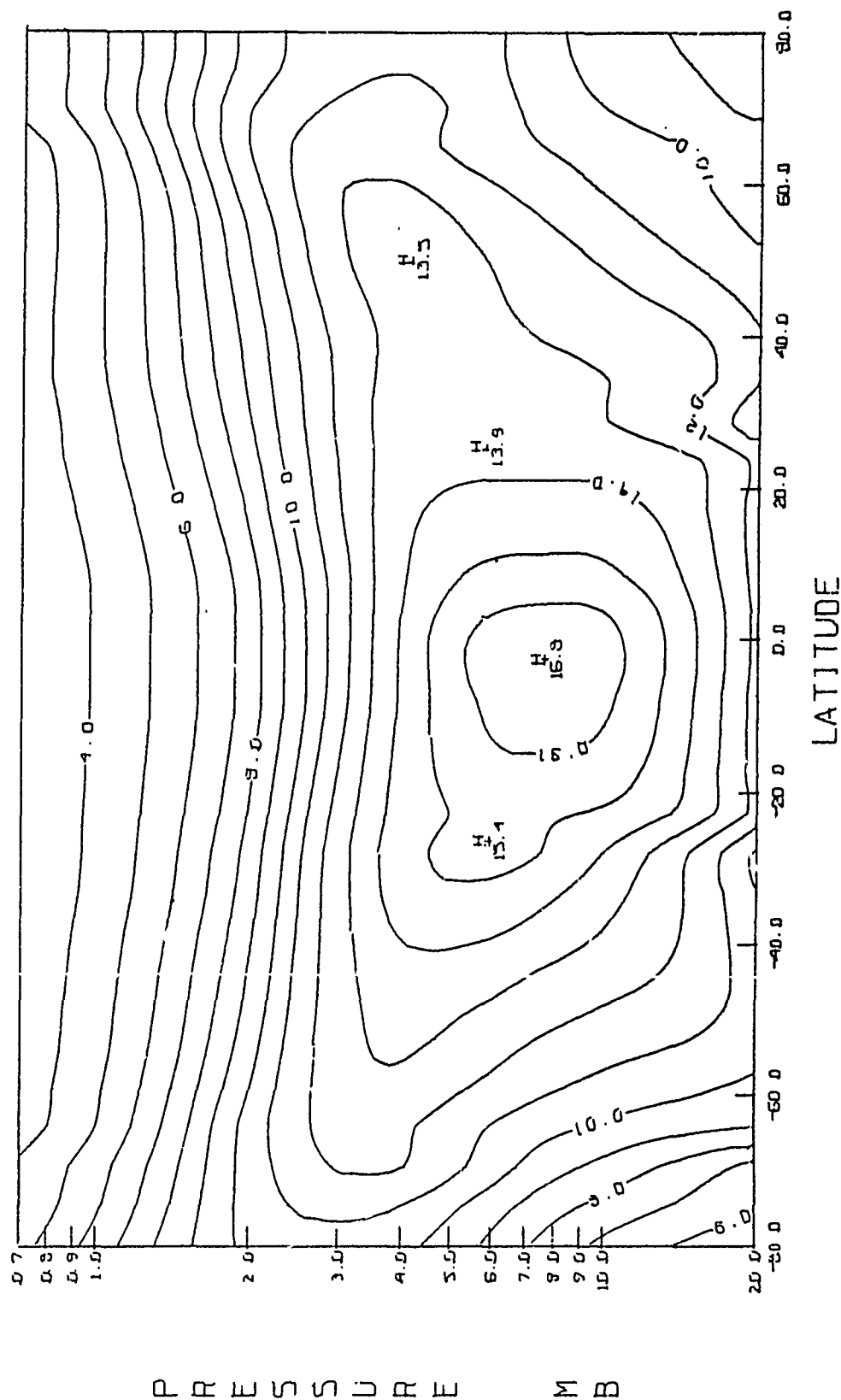


Figure 24: Monthly mean height-latitude cross-sections of ozone mass mixing ratio ( $\mu\text{g/g}$ ) for March 1971 from an analysis of Nimbus-4 BUV data. Contour intervals are 1.0  $\mu\text{g/g}$ .

## MONTHLY ZONAL OZONE AVERAGES

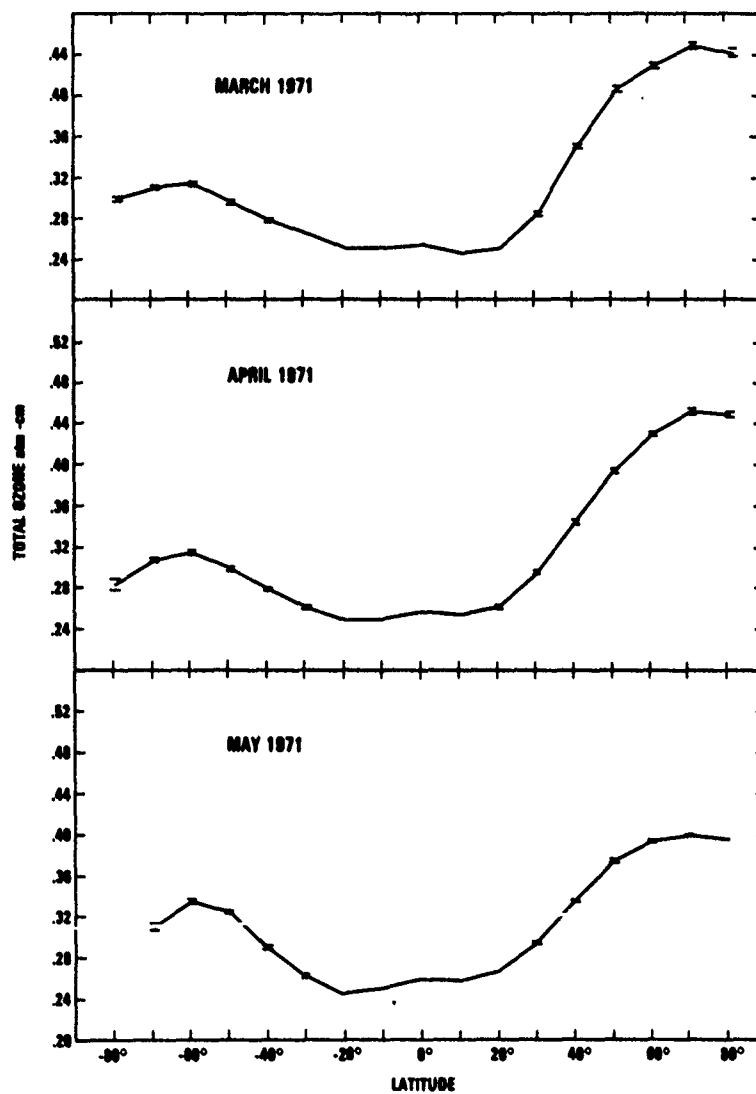


Figure 25: Total ozone monthly zonal means for March, April and May 1971 derived from an analysis of daily zonal means in 10° latitude bands from Nimbus-4 BUUV data.

The observed biases between the BUV and the ground based systems of the international ozone network are given in Table 4. All data (both satellite and Dobson) meeting the collocation criteria for AD-direct Sun wavelength pair (00 code) observations with the center of the BUV field of view passing within  $2^\circ$  of the ground station on the same day were used. No attempt has been made to remove the individual station biases from the intercomparisons given in table 4. In later years unfortunately the BUV operational time was reduced due to power limitations on board the spacecraft. This is the reason why only 125 comparisons were possible in 1977 in contrast to the 1305 which were made in 1971. The annual observed biases between the Dobson and the M-83 ground based systems are shown in figure 26. The annual mean of the Zurich sunspot number is plotted on an inverted scale in the upper portion of this figure. It is important to realize that all three systems use different wavelengths and none of them incorporate any correction for possible changes in the solar spectral irradiance with time. There is little doubt that the sensitivity of the BUV instrument is changing slowly with time as a function of wavelength.

The question as to whether the annual bias between the Dobson and BUV is decreasing in later years after 1975 is not clear and may be due to non-uniform sampling of Dobson stations with different biases.

Before the 7 year record of ozone data derived from the BUV experiment is discussed it is worthwhile to intercompare the ozone data derived from the improved BUV instrument called the Solar Backscattered Ultraviolet (SBUV) experiment which was launched aboard Nimbus 7 in 1978.

In this section the initial 3 month period of data from the SBUV experiment on Nimbus 7 is compared with the corresponding 3 month data set from the BUV experiment on Nimbus 4 8 years earlier. The systematic bias between the BUV type instruments on Nimbus 4 and 7 is given in Table 5. During 1970 and 1971 the bias or observed difference in total ozone measured when the satellite passed within  $2^\circ$  of the Dobson station and the corresponding total ozone amount reported by the Dobson station on that day remained essentially constant. The bias observed during the 3 month period between 1971 and 1972 seems to have undergone a step change of about 8.3 DU. The reason for this apparent change is unknown. The SBUV experiment on Nimbus 7 has a significantly lower bias of 3.2 DU against the Dobson network. Thus it would appear that the long term time dependent changes in the bias between the BUV instrument and the Dobson network are real.

The comparison which is shown in figure 27 gives the monthly latitudinal zonal mean data for November for the period of 1970-1976 and 1978. Some of the most significant interannual differences are seen in the Southern Hemisphere and poleward of  $40^\circ$ . The Southern Hemisphere high latitude ozone indicates significant interannual variability which is well outside the standard error of measurement which is indicated by the height of the data points. The November 1978 latitudinal distribution derived from the SBUV instrument on Nimbus 7 is very similar to that observed for the years of 1970-1972 and 1974. Significant differences can be seen in the tropics and Northern Hemisphere. Tropical ozone is significantly higher in 1978 and 1975 than in the other years. Furthermore the poleward gradient in the Northern Hemisphere is significantly less in 1978 and 1973 than in the other years. The evaluation and analysis of long term changes in atmospheric ozone will have to consider whether these interannual variations represent atmospheric noise or whether they are the result of long period atmospheric oscillations.

A sample of daily interannual variations in global ozone burdens is shown in figure 28. The extrapolation to the pole is being made by a technique described earlier. The daily global means of ozone are shown for a 3 month period beginning in November for the years 1970, 1971, 1975 and 1978. During 1972, 1973, 1974 and 1976 there were too many data gaps to derive a good global burden over the entire 3 month period. For the years 1970, 1971, and 1978 where the global coverage was very good the standard errors are quite similar at around 0.6 percent of the mean. Several interesting features can be seen in this figure. It is very obvious that there are significant variations in the interannual global variations. During the period beginning in 1970 the distribution over the 3 months was relatively smooth and decreasing monotonically whereas the other periods seem to show global oscillations with periods of 30 to 40 days. In 1978 there appears to be long period variation of about 70 days. These global variations appear to be well outside the experimental error. At this time it is not possible to state whether these variations are really global oscillations or random fluctuations.

TABLE 4  
DOBSON INTERPOLATED BUUV OZONE COMPARISON DATA

YEAR	TOTAL POINTS	AVE. BUUV OZONE (D.U. UNITS)	AVE. DOBSON OZONE (D.U. UNITS)	AVE. OZONE DIFFERENCE (D.U. UNITS)	AVE. DIFF. ST. DEVIATION
1970	1272	315.9	327.1	11.2	17.34
1971	1305	310.5	321.0	10.6	18.01
1972	1009	320.7	335.0	14.3	17.77
1973	403	314.0	333.7	19.8	17.90
1974	415	301.0	322.3	21.3	15.72
1975	344	300.4	322.0	21.5	19.79
1976	309	298.4	316.3	17.9	14.02
1977	125	345.2	358.7	13.5	17.92

Wavelength Weather Code = 00

Sum Weight  $\geq .50$



TABLE 5

SATELLITE BUV, SBUV - DOBSON NETWORK BIAS  
 BUV - DOBSON (DU)

<u>YEAR</u>	<u>NOVEMBER</u>	<u>DECEMBER</u>	<u>JANUARY</u>	<u>3-MONTH AVERAGE</u>
1970	-9.2	-8.5	-6.3	-8.0
1971	-11.7	-7.0	-10.2	-9.6
1972	-18.1	-10.4	-20.1	-16.2
1973	-15.5	-27.3	-11.5	-18.1
1974	-16.9	-16.9	-20.3	-17.9
1975	-17.1	-18.0	-14.1	-16.4
1976	-19.7	-15.5	-15.7	-17.0

SBUV - BUV (DU)

1978	-5.2	-2.7	-1.6	-3.2
------	------	------	------	------

# HEATH

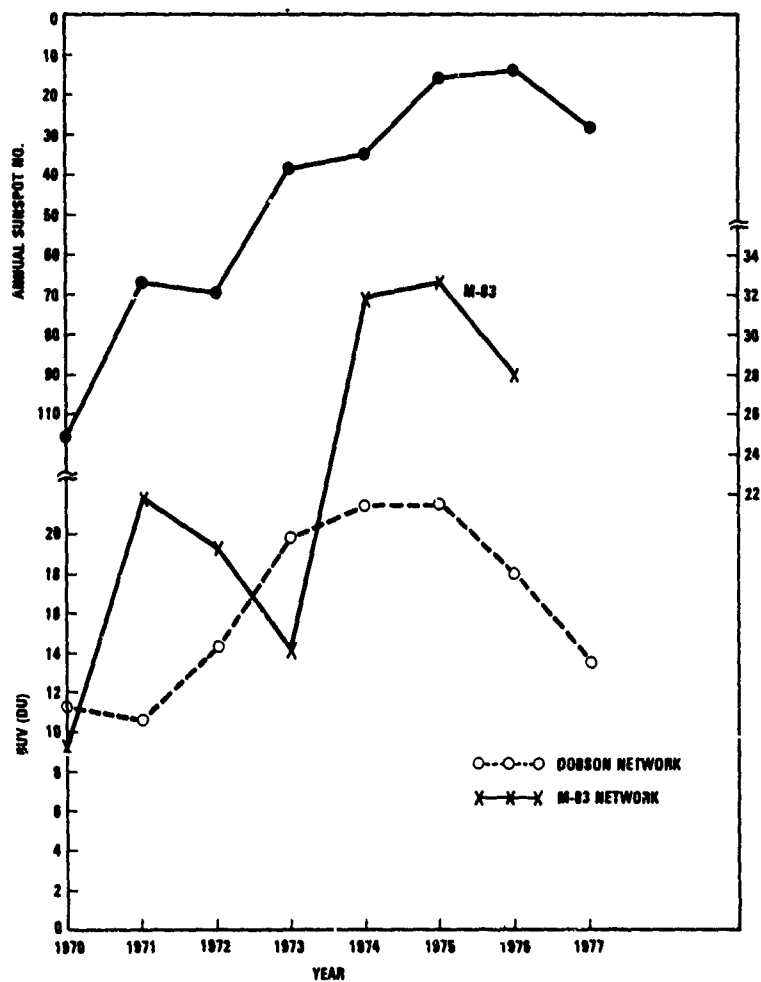


Figure 26: Annual total ozone bias (Dobson or M-83 total - UV total) for years 1970-1977 (bottom figures) and annual mean sunspot number on an inverted scale.

## VARIATION WITH LATITUDE OF MEAN NOVEMBER OZONE

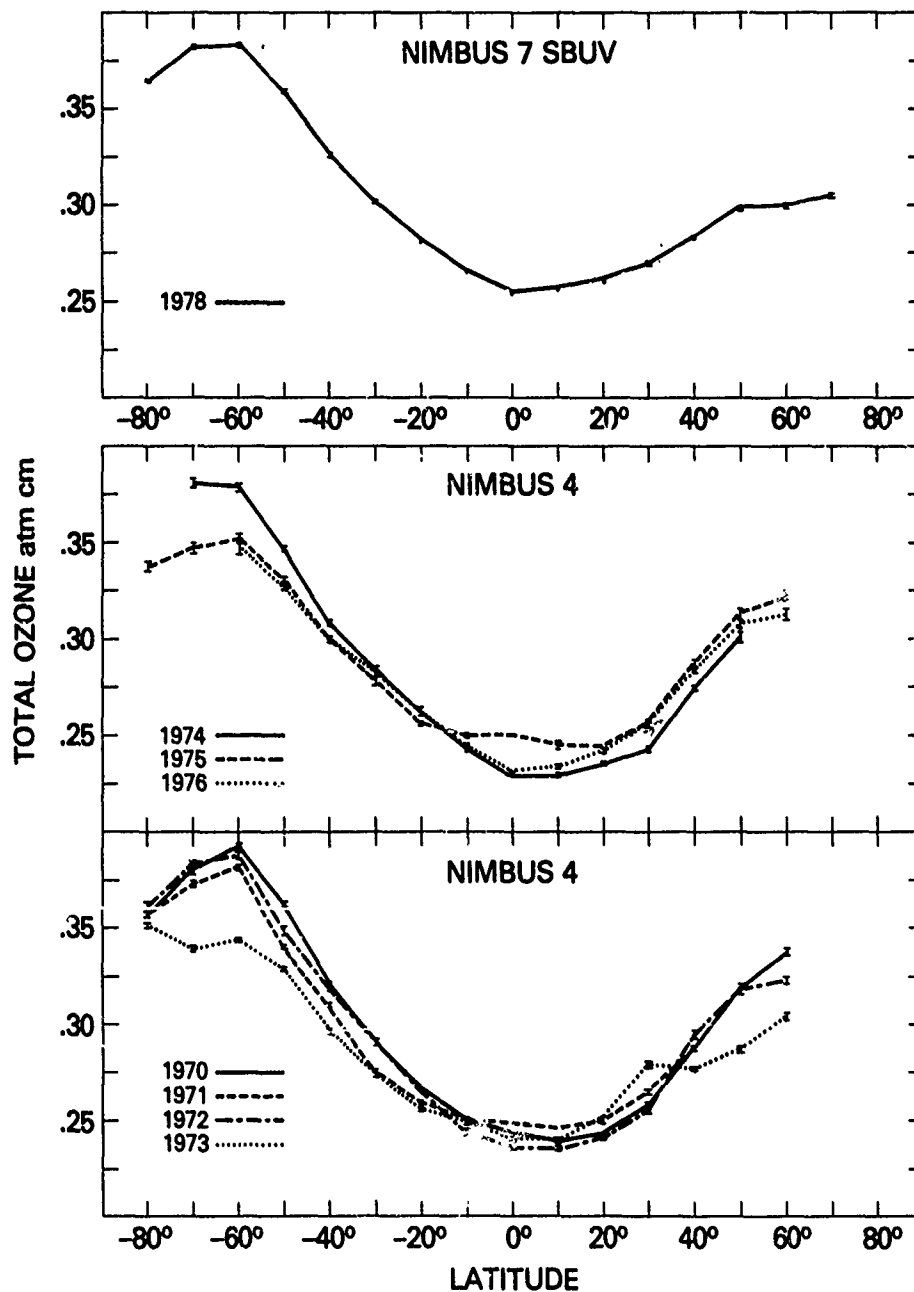


Figure 27: Total ozone monthly zonal means from the Nimbus-4 BUUV for November 1970-1976 and the Nimbus-7 SBUV for 1978.

HEATH

# GLOBAL TOTAL OZONE

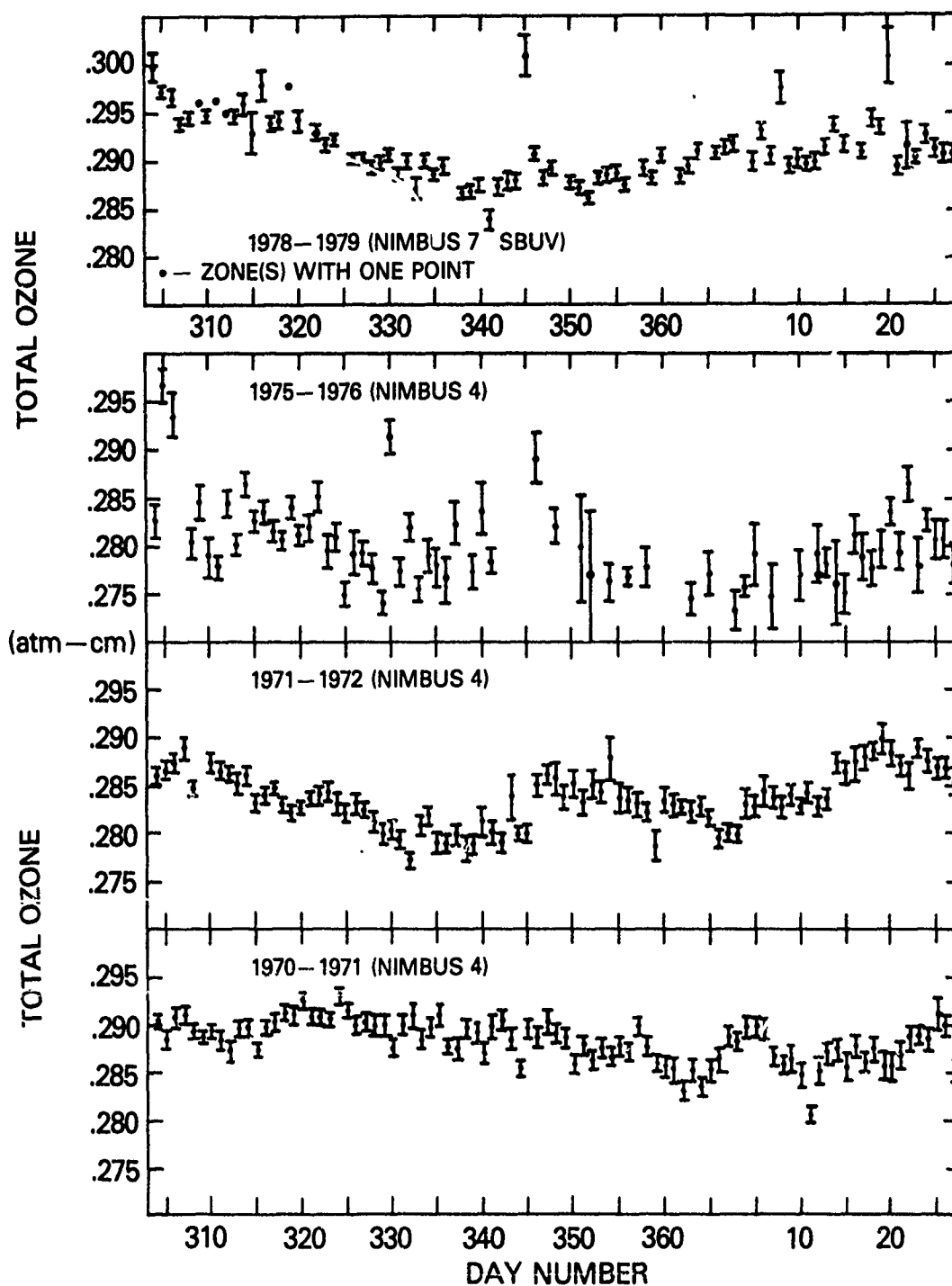


Figure 28: Daily global total ozone for November, December and January from the Nimbus-4 BUUV for years beginning in 1970, 1971 and 1975 and the Nimbus-7 SBUV in 1978.

## HEATH

It should be noted that the global burdens are quite similar over an 8 year period. A comparison of monthly mean global and hemispheric burdens is given in table 6 for November, December and January for the periods beginning in 1970 and 1978. The fourth column gives the net change over the 8 year period. The fifth column gives the difference in the measurement bias between the SBUV instrument on Nimbus 7 (1978-79) and the BUV instrument on Nimbus 4 (1970-1971) as given by the Dobson network. This bias was not used to derive the global and hemispheric burdens given in Table 6. It should be emphasized that all ozone measurements from the BUV and SBUV experiments given in the paper are derived from the instrument pre-flight spectroradiometric calibration and direct observations of the Earth-Sun system.

The 3 month average of the satellite measurements indicate that the ozone has decreased in the northern hemisphere by 0.9 DU or about 0.3 percent, increased in the southern hemisphere by 2.4 percent for a net increase in the global burden of 1.0 percent between the 3 month period in 1970-1971 and that in 1978-1979. The most accurate determination of long term changes quite likely will come from the intercomparison of satellite observations taken early during their respective lifetimes before long term instrument changes in the form of degradation or drift in sensitivity become important.

A summary of annual latitudinal zonal means of total ozone derived from the BUV experiment on Nimbus 4 is given in Table 6 for the years 1970-1977. Note that the observations for the year 1970 begin in mid April and in 1977 they terminate in July. A very interesting feature of the interannual variability which can be seen in the tropics is the shift in latitude of the ozone minimum. During even years it is located on the equator and during the odd years it is located at 10°S. If one analyzes the equatorial ozone data one would see a biennial oscillation because of a minimum which shifts in latitude with positive latitudinal gradients poleward.

The suggested quasi-biennial oscillation is shown in figure 29 which gives the weekly mean total ozone in a 10° latitude band centered on the equator after the mean annual wave has been subtracted. A detailed discussion of the quasi-biennial oscillations in total ozone will be treated in a paper to be published at a later date.

LONG TERM VARIATIONS IN GLOBAL OZONE: An analysis of the long term changes in total ozone inferred from the ground-based ozone network has been given by London and Kelley (1974). Observations derived from the network for the 13-year period from July 1957 to July 1970 were analyzed into monthly maps. Grid point values for 10° of latitude and 20° of longitude were used to derive global trends. The analysis observed that ozone increased over the 13 year period at rates of 7.5 percent per decade in the Northern Hemisphere and 2.5 percent per decade in the Southern Hemisphere. Their analysis also indicated that there was a change in slope of the trend lines which is particularly noticeable for the Northern Hemisphere. The Northern Hemisphere during the period from August 1957 to March 1961 shows a linear trend of -4.7 percent per decade and +11.3 percent for April 1961 through May 1970. In the Southern Hemisphere ozone exhibited trends of +2.5 percent per decade for August 1957 through September 1961 and -1.1 percent per decade for October 1961 through May 1970.

An analysis of global trends has been made by Angell and Korshover (1979) using selected stations of the international ozone network from 1958 through 1977. They found a world decrease of 2 percent between 1958 and 1962, a subsequent increase of about 4 percent for 1961 to 1970 and a slight decrease of about 0.8 percent between 1970 to 1973. For the next couple of years the world ozone remained essentially constant and then increased slightly by about 0.2 percent to 1977. This period overlaps the period of record of the measurements by the BUV instrument on Nimbus 4 and these satellite measurements will be discussed in the following section.

Long term seasonal and interannual variations in total ozone which have been derived from the BUV experiment for the Southern Hemisphere are shown in figure 30. Maxima are observed in October and minima in April. The most prominent feature is the large amplitude annual variation of about 40 DU. Apart from the general downward trend one can see an apparent modulation of the minimum and peak amplitudes during the odd numbered years. An exception to this is the Southern Hemisphere fall minimum in April 1975. The interannual variation of the amplitude of the Southern Hemisphere annual wave appears to be related to the quasibiennial oscillation in total ozone shown in figure 29 when the tropical maximum in total ozone is observed in the odd numbered years which implies that on ozone buildup in the tropics is associated with the weakening of the Southern Hemisphere annual wave.

TABLE 6  
COMPARISON O<sub>3</sub> MONTHLY MEAN GLOBAL AND HEMISPHERIC OZONE BURDENS

	NOVEMBER			SBUV-BUV BIAS ACCORDING DOBSON NET.
	78	70	(78-70)	
NORTH H.	275.1 DU	275.5 DU	-0.4 DU	
SOUTH H.	311.6	304.6	+7	
GLOBE	293.2	290.0	+3.2	
	DECEMBER			11.2
NORTH H.	279.6	282.8	-3.2	
SOUTH H.	298.5	292.3	+6.2	
GLOBE	288.7	287.6	+1.2	
	JANUARY			
	79	71	(79-71)	
NORTH H.	296.5	295.6	+0.9	7.9
SOUTH H.	287.4	279.4	+8.0	
GLOBE	291.9	287.5	+4.4	
	AVERAGE			
NH	283.7	284.6	-0.9 DU	+7.7 DU
SH	299.2	292.1	+7.1	
GLOBE	291.3	288.4	+2.9	

Table 7  
YEARLY LATITUDINAL MEAN  
TOTAL  $O_3$

	70	71	72	73	74	75	76	77
-80	.3308	.3168	.3072	.3120	.3132	.3384	.2931	.2582
-70	.3375	.3314	.3200	.3208	.3438	.3306	.3009	.3275
-60	.3519	.3466	.3358	.3375	.3439	.3370	.3204	.3243
-50	.3465	.3293	.3281	.3298	.3308	.3163	.3073	.3061
-40	.3231	.3019	.3064	.3059	.3030	.2883	.2824	.2830
-30	.2903	.2730	.2795	.2758	.2763	.2646	.2646	.2624
-20	.2631	.2526	.2554	.2546	.2535	.2457	.2526	.2401
-10	.2499	.2508	.2456	.2482	.2404	.2417	.2442	.2300
0	.2478	.2545	.2435	.2497	.2345	.2441	.2397	.2233
+10	.2545	.2519	.2503	.2506	.2415	.2421	.2406	.2303
+20	.2644	.2558	.2622	.2590	.2546	.2474	.2513	.2513
+30	.2840	.2782	.2851	.2836	.2737	.2699	.2739	.2907
+40	.3123	.3127	.3165	.3055	.3056	.3106	.3123	.3544
+50	.3391	.3447	.3456	.3306	.3400	.3514	.3461	.4014
+60	.3534	.3575	.3593	.3486	.3459	.3609	.3592	.4286
+70	.3544	.3615	.3579	.3516	.3570	.3765	.3805	.4468
+80	.3596	.3511	.3512	.3492	(?)	.3843	.4119	.4442

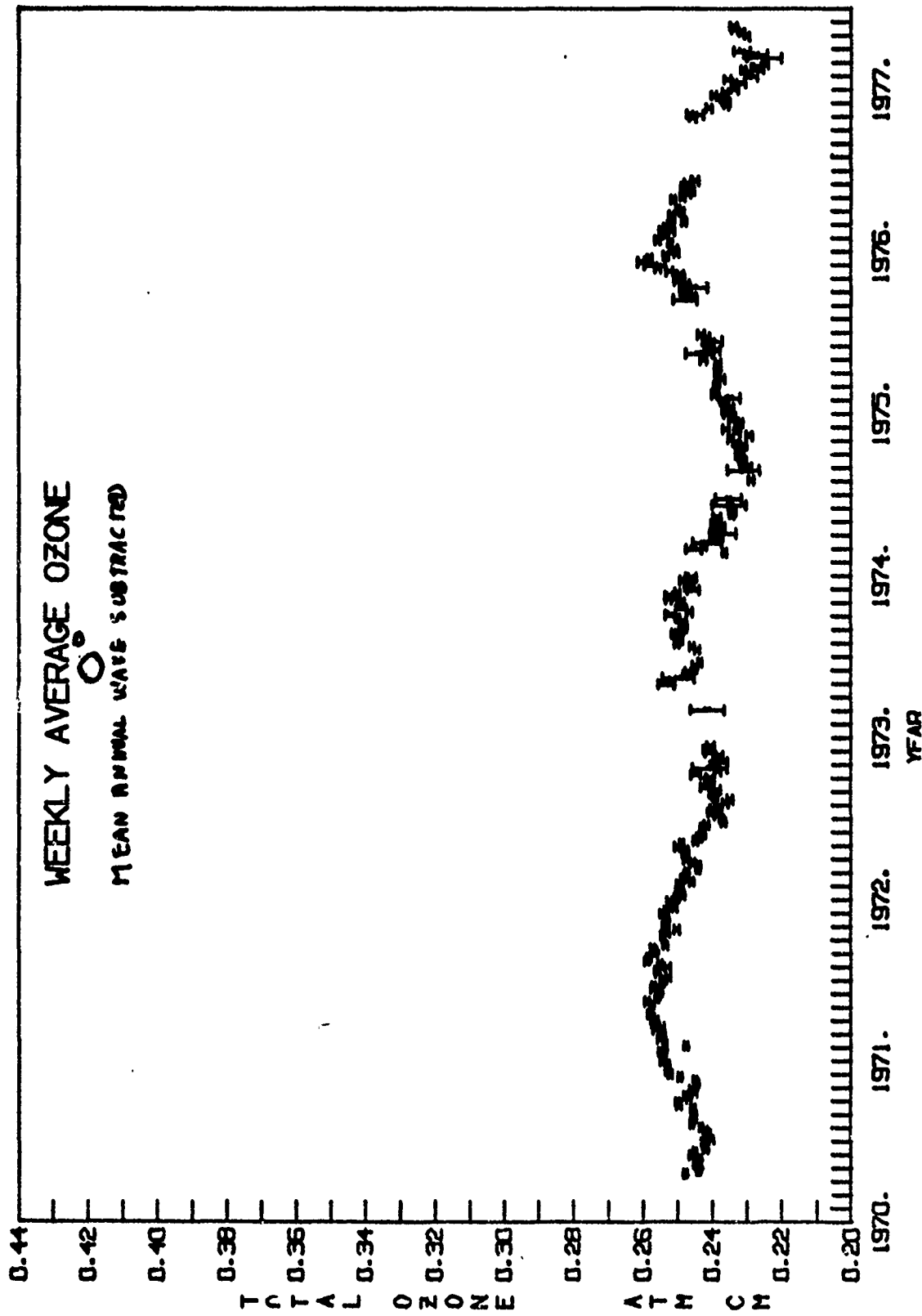


Figure 29: Weekly average total ozone in a 10° latitude band centered at the equator from the BUV experiment on Nimbus-4. The mean annual wave has been subtracted.



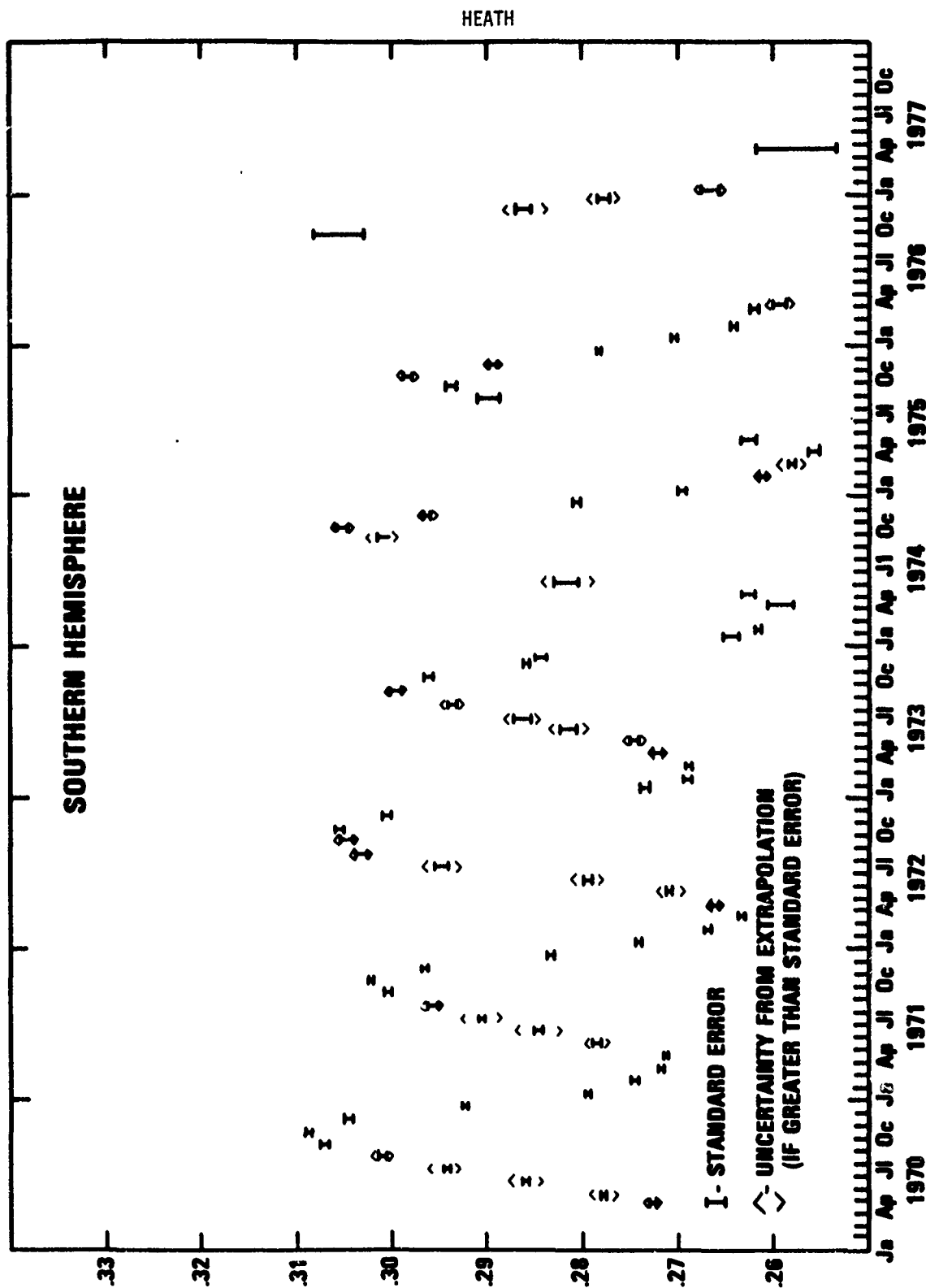


Figure 30: Monthly average total ozone in the Southern Hemisphere derived from the Nimbus-4 BUV experiment. Daily zonal means in 10° latitude bands were averaged and area weighted to form a hemispheric mean.

After removal of the annual wave by the technique described by Hilsenrath et al., (1979) one is left with the resulting trend curve for the Southern Hemisphere shown in figure 31. The assumption that the trend is linear leads to a rate of decrease of 7 percent per decade. This is significantly different from the rate of change inferred by London and Kelley for the 1960's which showed ozone increasing at the rate of 2.5 percent per decade between 1957 and 1970. Note however that they did infer a turn around and a subsequent decrease of 1.1 percent per decade between 1961 and 1970. Taken at face value this would seem to indicate that the rate of decrease is increasing with time after 1961.

Ozone behavior in the Northern Hemisphere is distinctly different in behavior from that observed in the Southern Hemisphere. Maxima tend to occur in April and minima in October which is 6 months out of phase in the Southern Hemisphere. Annual variations in the Northern Hemisphere are shown in figure 32. The most noticeable hemispheric differences are that in the Northern Hemisphere that the amplitude of the annual wave is of the order of 50 DU and that there is no apparent biennial modulation of the maxima and minima. The nature of the trend is shown in figure 33 after removal of the annual wave. The decadal linear trend is -2.6 percent. The most noticeable residual appears to be a semi-annual component which peaks at the time of the Northern and Southern Hemisphere maxima around April and October.

The interannual variations in the global total ozone burden is shown in figure 33. Even though both hemispheres are included the annual wave in the Northern Hemisphere clearly dominates the seasonal variations where the amplitude is of the order of 13 DU with maxima occurring around April and minima around January. The interhemispheric differences in the amplitude of the annual wave are responsible for the sawtooth waveform. Removal of the annual wave leads to the global trend shown in figure 34. Apart from the decreasing trend from 1970 onward, one is left with a residual semi-annual component analogous to that shown for the Northern Hemisphere. The linear rate of decrease is 2.6 percent per decade.

An analysis of ground based determinations of total ozone indicated a world wide decrease of about 0.8 percent between 1970 and 1973. During this period the BUV Nimbus 4 observations indicate an ozone decrease of 2.5 percent. Beyond 1973 ground based data indicate a lower rate of decrease or no decrease at all for several years and a possible increase of 0.2 percent by 1977. The corresponding satellite data indicate a continuing rate of decrease of about 0.2 percent/year up through 1977. The reasons for the differences between the trends derived from ground based and satellite data are not known at this time.

Part of the reason for the previously discussed discrepancies in derived global trend in total ozone may be due to the non-uniform spacing in latitude of the station of the international ground based network. The latitude dependence of the derived trend for the Nimbus 4 BUV observations is shown in figure 35. Whereas the most stable latitudes appear to be in the vicinity of 70°S and 20°-50°N, the greatest rate of decrease appears to be confined to the regions 10°N and 60°S and poleward of 70°N.

Another reason for this discrepancy in the trends may be due to the time dependent bias between the Dobson and the BUV measurements which is given in Table 4 and is shown in the lower part of figure 36.

**SUMMARY AND CONCLUSIONS:** The satellite derived ozone data discussed in the previous sections have shown spatial and temporal variabilities which have ranged from over distances of tens of km to the global scale and periods from a day to a period close to an 11 year solar cycle. In most instances periods of temporal variability correspond to well known meteorological and short term climatic periods. Ozone variations over these periods have been observed in both total ozone burdens and in the vertical profiles.

The close relationship between ozone and temperature variability indicate that the problem of determining the effect of anthropogenic constituents on stratospheric ozone on a global scale is far more complex than has heretofore been recognized. If the analyses by Angell and Korshover (1978) which indicated decreasing stratospheric temperatures in the Western Hemisphere equatorial region from 1970 through 1976 is correct for the 26-55 km altitude region there should be a significant increase of upper stratospheric ozone due to the temperature dependence of the ozone photochemistry. The indicated temperature decrease is of the order of 6°K in the 46-55 km region over the 6 year period Quiroz (1979) has found an apparent in-phase relationship between the sunspot numbers of cycle 20 and stratospheric temperatures at 35 to

## HEATH

50 km from an analysis of temperature data from seven rocketsonde stations in the latitude region from 8°S to 64°N. The amplitude of the variation is about 4K.

A preliminary analysis by Heath et al., (1980c) of ozone profile data for November, December and January from the Nimbus 4 BUUV experiment in 1970-1971 and from the Nimbus 7 SBUV experiment in 1978-1979 indicates that there has been a substantial increase in ozone in the upper stratosphere. This analysis is too preliminary to discuss in any detail at this time. Nevertheless evidence is mounting which indicates that both ozone total amounts and the vertical distributions are changing by amounts which are many times larger and in an opposite sense from that predicted for modifications due to the introduction of anthropogenic constituents into the stratosphere. Clearly if an early detection of ozone depletion due to anthropogenic constituents is desired one must first understand the processes which drive the natural variability of atmospheric ozone on a global scale.

Major factors which are limiting our understanding of the natural variability of ozone over periods beyond a year are lack of knowledge of the absolute temperature structure of stratosphere to within 1K over several decades, the temporal variability of the absolute solar flux over the wavelength range from 180-350 nm to 5%, and insufficient numbers of high quality Umkehr and rocketsondes measurements of ozone profiles to provide for a good statistical intercomparison between the satellite based observations and the corresponding "truth" data. Until one understands the processes which determine natural variability of ozone such quantities as temperature and UV solar flux which control the ozone photochemistry, it is unlikely that a meaningful assessment can be made of ozone depletion due to anthropogenic constituents from atmospheric measurements. One would do well to consider the evidence of the variability of the short-term climatic record, e.g., see the recent work by Pittock et al., (1978) in order to realize what time scales of natural variability may be present in the ozone data record which is being used to infer trends.

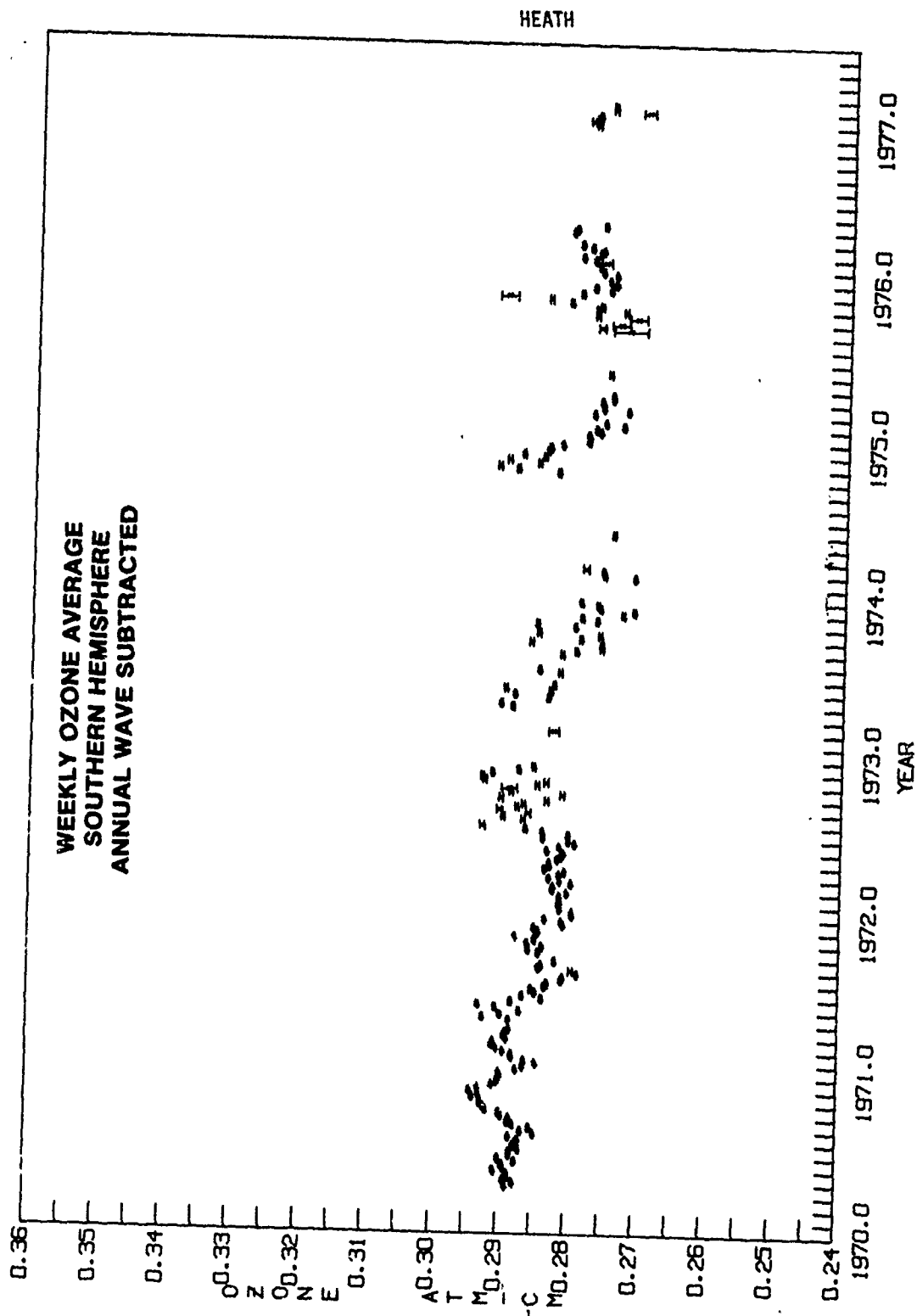


Figure 31: Weekly average total ozone in the Southern Hemisphere with annual wave subtracted from the Nimbus-4 data.

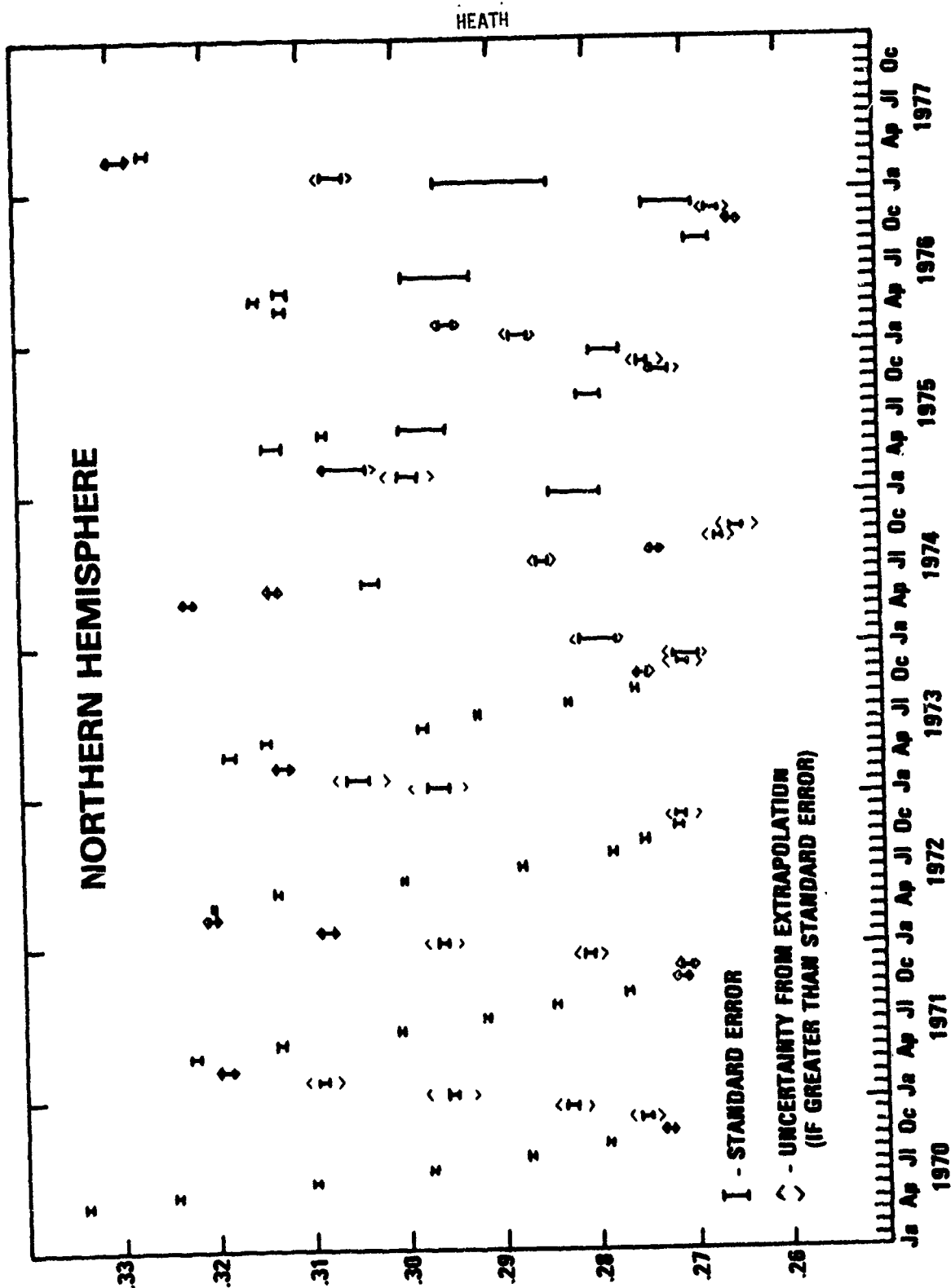


Figure 32: Monthly average total ozone in the Northern Hemisphere derived from the BUV experiment on Nimbus-4. Daily zonal means in 10° latitude bands were averaged and area weighted to form a hemispheric mean.

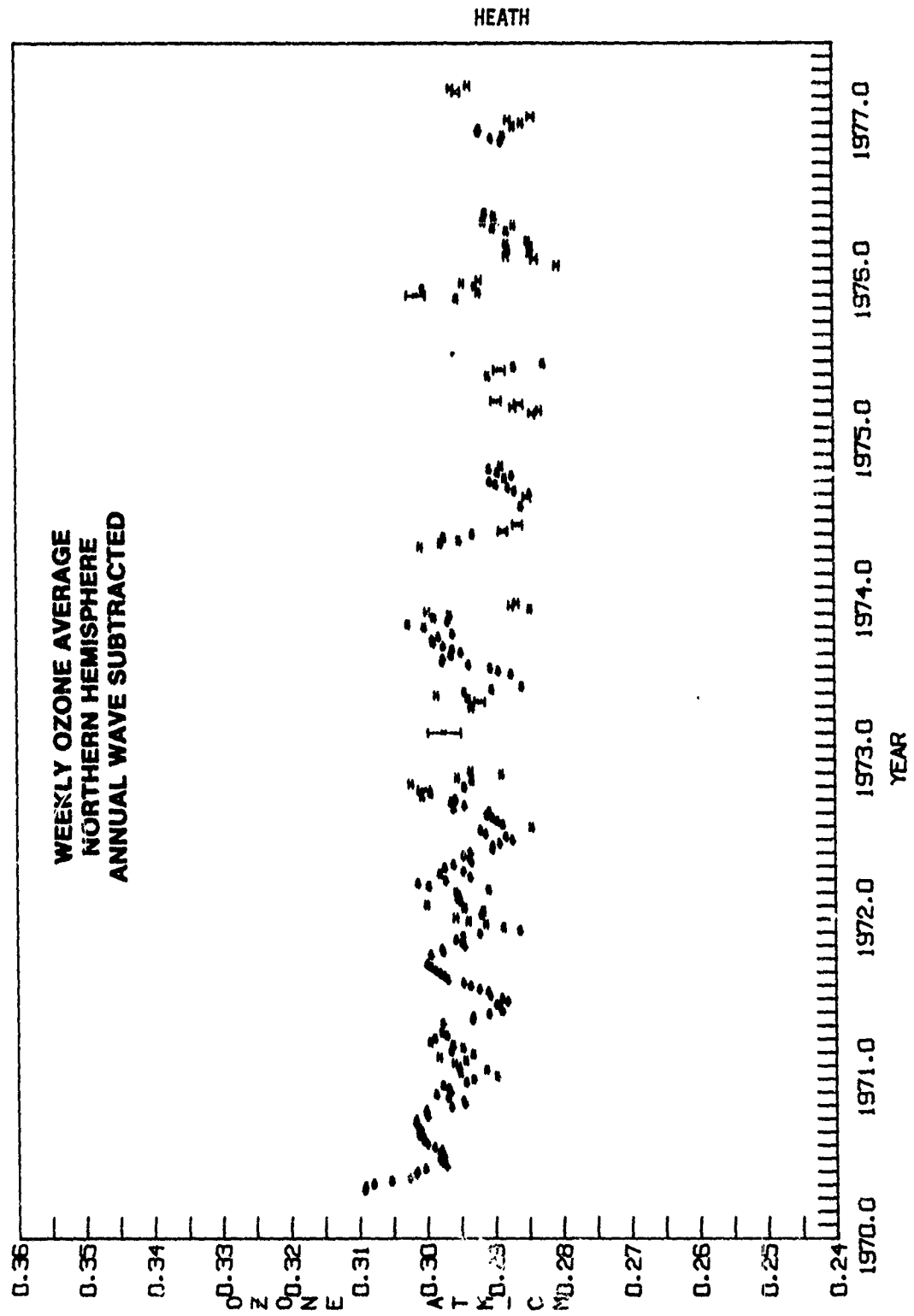


Figure 33: Weekly average total ozone in the Northern Hemisphere with the annual wave subtracted from the Nimbus-4 BUV data.

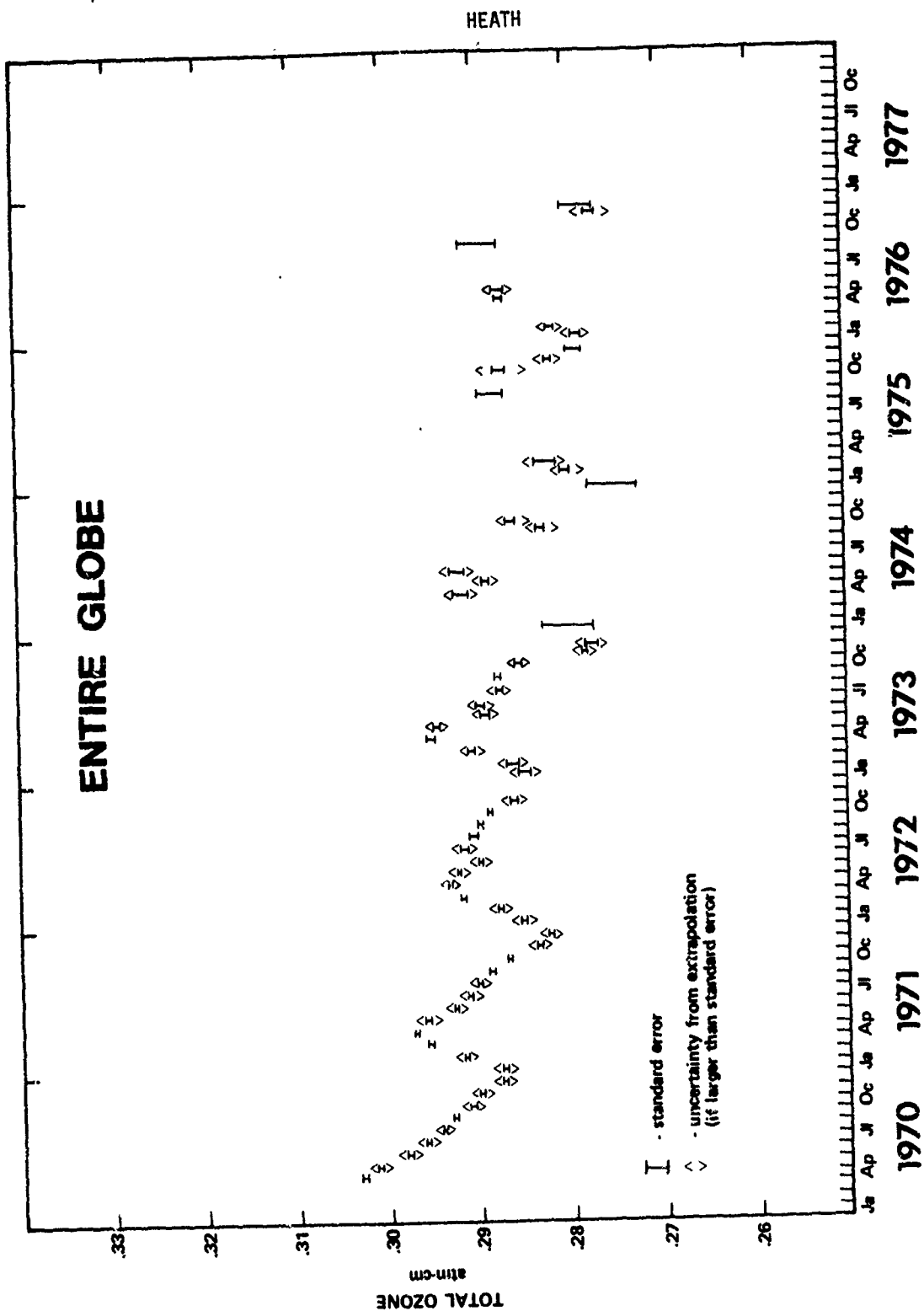


Figure 34: Monthly average total ozone for the globe derived from the Nimbus-4 BUV experiment. Daily zonal means in 10° latitude bands were averaged and area weighted to form a global mean

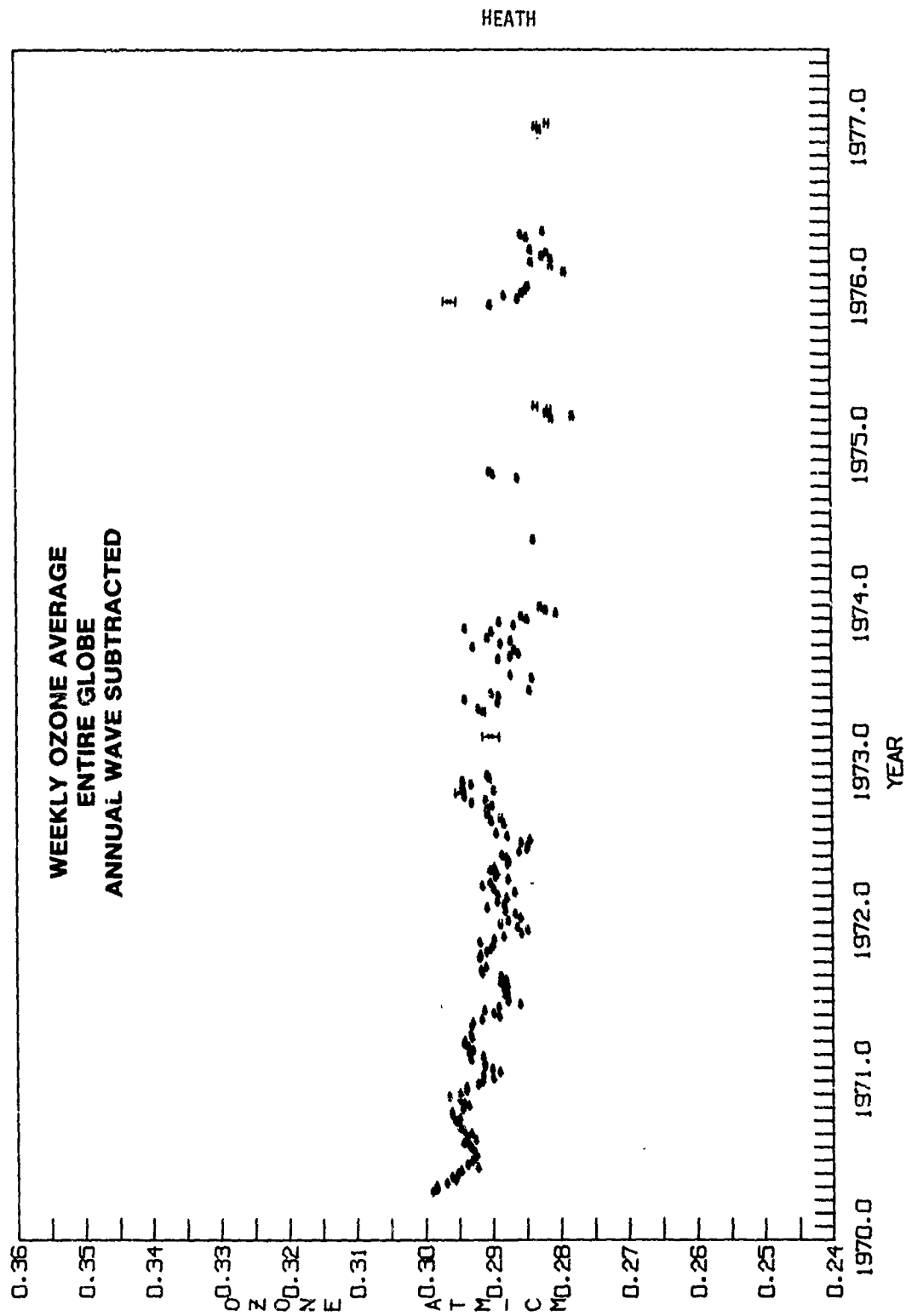


Figure 35: Weekly average total ozone for the world with the annual wave subtracted from the Nimbus-4 BUV data.



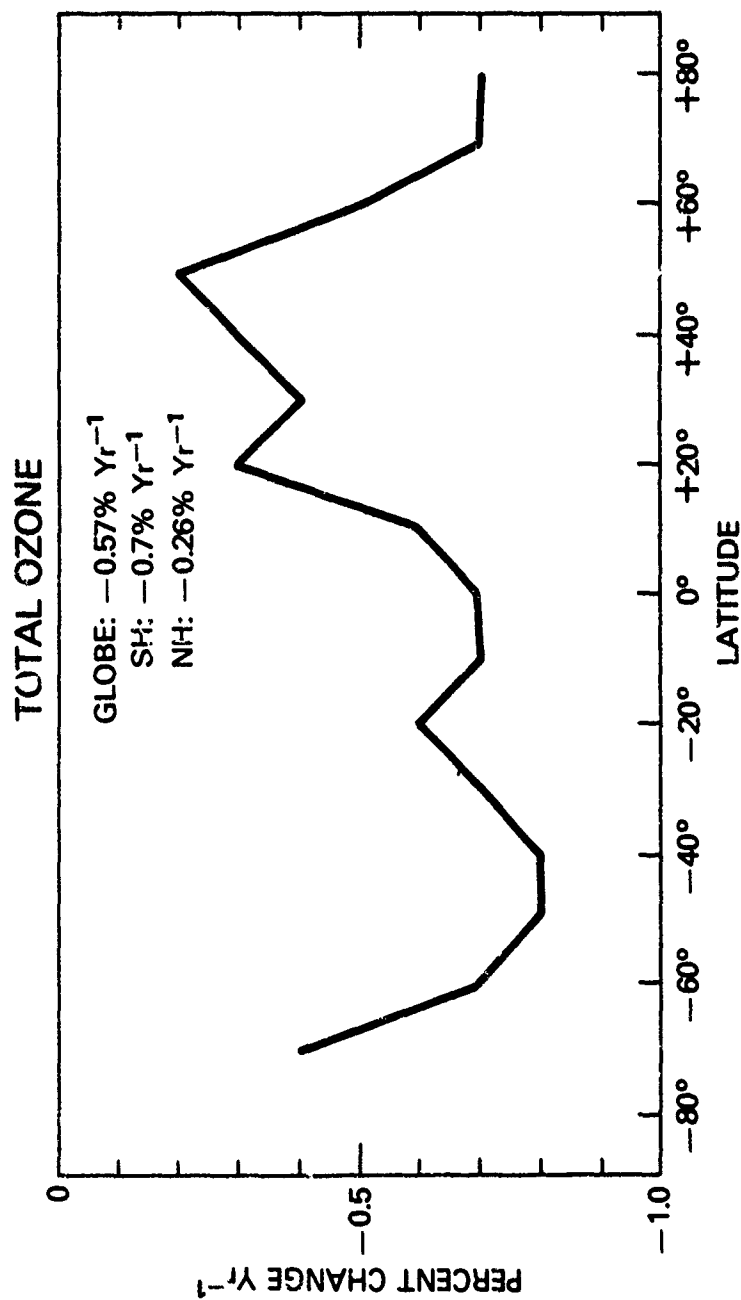


Figure 36: Yearly percent change in total ozone assuming a linear trend for the Nimbus-4 BUV data. No correction is made for the time dependent bias between the Dobson network and coincident BUV measurements.

## HEATH

## REFERENCES

- Angell, J. K., and J. Korshover (private communication) 1979.
- Angell, J. K. and J. Korshover, Recent rocketsonde-derived temperature variations in the Western Hemisphere, *J. Atmos. Sci.*, **35**, 1758-1764, 1978.
- Arvesen, J. C., R. N. Griffin, Jr., and B. D. Pearson, Jr., Determination of extraterrestrial solar spectral irradiance from a research aircraft, *Appl. Opt.*, **8**, 2215-2232, 1969.
- Barnett, J. J., J. T. Houghton, and J. A. Pyle, The temperature dependence of the ozone concentration near the stratopause, *Quart. J. R. Met. Soc.*, **101**, 245-257, 1975.
- Broadfoot, A. L., The solar spectrum 2100-3200Å, *Ap. J.*, **173**, 681-689, 1972.
- Brueckner, G. E., J.-D.F. Kjeldseth, O. Moe and M. E. Van Hoosier, Absolute solar ultraviolet intensities and their variations with solar activity, I. The wavelength region 1750-2100Å, *Ap. J.*, **209**, 935-944, 1976.
- Donnelly, R. F. and J. H. Pope, NOAA Technical Report ERL 276-SEL 25, U.S. Government Printing Office, Washington, DC.
- Dutsch, H. U., Photochemistry of atmospheric ozone, *Advances in Geophysics*, Vol. **15**, Ed. Landsberg and Van Mieghem, Academic Press, New York, USA, 1971.
- Dutsch, H. U., Vertical ozone distribution on a global scale, *Pure Appl. Geophys.*, **116**, 511-529, 1978.
- Gille, J. C., P. L. Bailey, and J. M. Russell III, Temperature and composition measurements from the LRIR and LIMS experiments on Nimbus 6 and 7, *Phil. Trans. R. Soc. Lond, A* **296**, 205-218, 1980.
- Heath, D. F., unpublished work, 1978.
- Heath, D. F., A. J. Krueger, H. A. Roeder and B. D. Henderson, The solar backscatter ultraviolet and total ozone mapping spectrometer (SBUV/TOMS) for Nimbus G, *Optical Eng.*, **14**, 323-331, 1975.
- Heath, D. F., A. J. Krueger and P. J. Crutzen, Solar proton event: Influence on stratospheric ozone, *Science*, **197**, 886-889, 1977.
- Heath, D. F. and H. Parks, The magnitude and variability of the solar flux from 160-400 nm during the period of maximum of cycle 21 (to be published), 1980
- Heath, D. F., Space observations of the variability of solar irradiance in the near and far ultraviolet, *J. Geophys. Res.*, **78**, 2779-2792, 1973.
- Heath, D. F., B. M. Schlesinger and E. Hilsenrath, Changes in the global ozone budget derived from the BUV experiment on Nimbus-4 and the SBUV experiment on Nimbus-7 (to be published), 1980
- Heath, D. F., A. J. Miller, K. L. Labitzke and E. Hilsenrath, Global ozone climatology derived from the BUV experiment on Nimbus 4, 1970-1977 (to be published), 1980a.
- Heath, D. F., Ozone measurements from space with the BUV experiment on Nimbus-4 and the SBUV experiment on Nimbus-7, (to be published) 1980b.
- Heroux, L. and R. A. Swirbalus, Full-disk solar fluxes between 1230 and 1940Å, *J. Geophys. Res.*, **81**, 436-440, 1976.
- Hilsenrath, E., (private communication) 1979.
- Hilsenrath, E., D. F. Heath and B. M. Schlesinger, Seasonal and interannual variations in total ozone revealed by the Nimbus 4 backscattered ultraviolet experiment, *J. Geophys. Res.*, **84**, 6969-6979, 1979.
- Hinteregger, H. F., (private communication), 1979.
- Krueger, A. J., B. W. Guether, A. J. Fleig, D. F. Heath, E. Hilsenrath, R. McPeters and C. Prabakhara, Satellite ozone measurements, *Phil. Trans. R. Soc. Lond A*, 191-204, 1979.
- Labitzke, K., *J. Geophys. Res.*, **79**, 2171, 1974.
- Labitzke, K., On the different behavior of the zonal harmonic height waves 1 and 2 during the Winters 1970/71 and 1971/72, *Mon. Wea. Rev.*, **106**, 1704-1713, 1978.
- Labs, D. and H. Neckel, Transformation of the absolute solar radiation data into the International practical temperature scale of 1968, *Solar Phys.*, **15**, 79-87, 1970.
- London, J. and J. Kelley, Global trends in total atmospheric ozone, *Science*, **184**, 987-989, 1974.
- Mateer, C. L., D. F. Heath and A. J. Krueger, Estimation of total ozone from satellite measurements of backscattered ultraviolet radiances, *J. Atmos. Sci.*, **28**, 1307-1311, 1971.
- McInturff, R. M. (Ed.), Stratospheric warmings: Synoptic, dynamic and general circulation aspects, NASA Ref. Pub. 1017, 1978.
- Miller, A. J., B. Korty, E. Hilsenrath, A. J. Fleig and D. F. Heath, Verification of Nimbus-4 BUV ozone data and requirements for operational satellite monitoring, Symposium on the Geophysical Aspects and Consequences of Changes in the Composition of the Stratosphere, Toronto, Canada, June 26-30, 1978, pap. 511, WMO, Geneva, 1978.

# HEATH

- Miller, A. J., E. Korty, and D. F. Heath, Comparison of Backscattered ultraviolet and ground-based total ozone fields for December 1970, PAGEOPH, 117, 355-360, 1979.
- Pittock, A. B., Ed. L. A. Frokes, Jenssen, J. A. Peterson, and J. W. Zillman, Climate change and variability, a Southern perspective, Cambridge University Press, 1978.
- Quiroz, R. S., Stratospheric temperatures during solar cycle 20, J. Geophys. Res., 84, 2415-2420, 1979.
- Samain, D. and P. C. Simon, Solar flux determination in the spectral range 150-210 nm, Solar Phys., 49, 33-41, 1976.
- Thekaekara, M. P., R. Krueger, and C. H. Duncan, Solar irradiance measurements from a research aircraft, Appl. Opt., 8, 1713-1732, 1969.

## OZONE DISTRIBUTIONS BY INFRARED LIMB SCANNING:

### PRELIMINARY RESULTS FROM THE LRIR

John C. Gille

National Center for Atmospheric Research  
P. O. Box 3000, Boulder, Colorado 80307, USA

#### Abstract

The Limb Radiance Inversion Radiometer (LRIR) experiment on the Nimbus 6 spacecraft and the data resulting from it are briefly described. Results of a preliminary inversion of Northern Hemisphere measurements for November and December 1975 are objectively analyzed, and several different depictions of the ozone distribution are presented. The monthly mean latitude-altitude cross sections show contours of higher concentration extending upward and poleward. The mean maps at a sequence of altitudes show different features, reflecting the varying processes which control ozone at different altitudes. At upper levels temperature variations are highly anticorrelated with ozone patterns. The distribution of zonal wave number amplitude is considerably different for the two months. The LRIR mesospheric values agree with models and most other measurements, but not the OAO-3 results. Future limb scanning measurements are also described.

**INFRARED LIMB SCANNING:** In this discussion, infrared limb scanning means the technique of scanning across a planet's limb, or horizon, as seen from a spacecraft, with an infrared radiometer. The geometry is illustrated in Figure 1. By measuring the emission from atmospheric gases in wide spectral bands as a function of altitude, information can be obtained regarding the distribution of temperature and atmospheric composition from the upper troposphere into the mesosphere.

The advantages of the limb scanning technique for research on middle atmosphere chemistry and dynamics are considerable [Gille and House, 1971]. The geometry allows an inherent high vertical resolution, since the radiation received comes from a layer that is only about 4 km thick [Gille and Bailey, 1977]. The long, nearly horizontal paths through the atmosphere contain large amounts of the emitting gases, allowing sensitivity to low concentrations, and the ability to sound the atmosphere to high altitudes. The received signals all originate in the atmosphere, and are seen against the cold, dark background of space. By measuring infrared emission, data can be obtained at all local times, on both the day and night sides of the planet limited only by the orbital and instrument characteristics. As indicated above, it is possible to measure the temperatures and a large number of trace constituents over a wide altitude region with a single instrument.

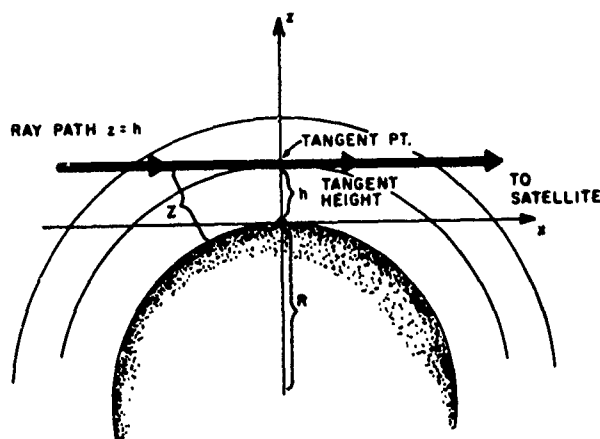


Figure 1. The geometry of limb scanning (from Gille and House, 1971).

The drawbacks of the technique are that clouds along the ray path preclude regular sensing below the upper troposphere. To take advantage of the inherent high vertical resolution of the geometry, the radiometer must have narrow fields-of-view. In order to measure the resulting small signals with a high signal-to-noise ratio, the detectors must be cooled. In instruments flown to date, the cooling has been provided by a subliming mass of solid methane. Seven months of cooler (and experiment) lifetime have been obtained with this technique. Future possibilities for extending experiment lifetime will be discussed below.

**THE LRIR INSTRUMENT:** The first limb scanning radiometer to fly on a satellite was the Limb Radiance Inversion Radiometer (LRIR), launched on the Nimbus 6 satellite in June, 1975. The instrumentation is described in Gille et al, [1975], and more succinctly by Gille et al, [1980c].

A scanning mirror directed radiance from various positions on the earth's limb through the radiometer optics and filters to the cold detectors. A mask was used to limit the vertical size of the fields-of-view to 2 km. Filters to define the region of spectral response were mounted on the mask. The resulting instrument parameters are presented in Table 1.

Table 1					
Characteristics of LRIR Channels					
Channel	Purpose	Band Pass 50% Relative Response Points ( $\text{cm}^{-1}$ )	Field-of-view at Limb (km)		Noise Equivalent Radiance ( $\text{watts/m}^2\text{-sr}$ )
			Vertical	Horizontal	
1	$\text{NCO}_2$	649-672 $\text{cm}^{-1}$	2.0	20	0.0023
2	$\text{WCO}_2$	592-700 $\text{cm}^{-1}$	2.0	20	0.0040
3	$\text{O}_3$	984-1169 $\text{cm}^{-1}$	2.0	20	0.011
4	$\text{H}_2\text{O}$	412-446 $\text{cm}^{-1}$	2.5	25	0.008

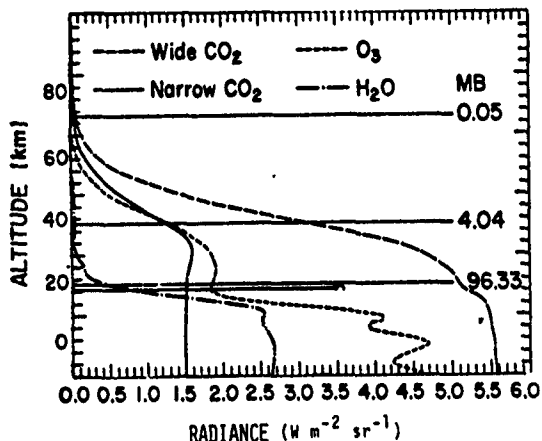


Figure 2. Limb radiances measured by the LRIR. The altitude scale and the pressure levels are derived. Line marked with C is determined cloud top altitude.

A set of radiance scans are shown in Figure 2. Comparison of the signals with the noise values from Table 1 shows the high signal-to-noise which is available in these channels. It is clear that information is recoverable over a wide altitude range. It is also very easy to see the large and varying signal due to clouds at the lower altitudes (higher pressures), especially in the more transparent ozone and water vapor channels. As noted above, these set the lower limits to useful information recovery. Note that the altitude scale and pressure levels are derived in the inversion. The radiation is actually measured on an angular scale which contains only relative altitude information; it is not known at what level in the atmosphere the radiometer is looking. As we shall see below, even if the geometric altitude were known, this would not be enough. The pressure, or density at a level is a much more important piece of information.

The water vapor channel proved to have a higher noise level than expected, and also was not able to be calibrated as well as the other channels. No information from this channel will be discussed here.

**INVERSION OF RADIOMETRIC MEASUREMENTS:** If the state of the atmosphere is known, the equation of radiative transfer can be used to calculate the outgoing radiance. This is referred to as the forward problem. The expression by which the outgoing radiance in a channel can formally be calculated is given by

$$I(h)\Delta\nu = \int_{\Delta\nu}^1 \int_0^1 B_\nu[T(s)]\phi(\nu) d\tau_\nu(h, s) d\nu \quad (1)$$

where  $I$  is the radiance measured when looking at level  $h$  in the atmosphere,  $B$  is the Planck function, which depends upon temperature  $T$ ,  $\phi(\nu)$  is the relative spectral response of the channel, and  $\tau(h, s)$  is the transmittance from the point  $s$  to the satellite along a ray path whose lowest point is  $h$ , and  $\nu$  is the frequency.

The inverse problem in radiative transfer is one in which measurements of outgoing radiance are interpreted to provide information about atmospheric quantities. There is a large and complex literature in this area, so this problem will not be discussed in any detail here. The overall strategy is to use a gas for which the mixing ratio is known, in this case carbon dioxide, and calculate the transmittance. With these transmittances and the measured radiances, one can determine the Planck function as a function of pressure and thus the vertical temperature structure in the atmosphere.

Then, knowing the temperature, the Planck function can be calculated for the ozone channel and used with the measurements of ozone radiance to determine the transmittance. The transmittance depends upon the ozone mixing ratio in a known way, which allows the ozone distribution to be inferred.

The temperature problem is highly nonlinear, since the carbon dioxide concentration depends upon atmospheric pressure, which depends upon the temperature through the hydrostatic equation. The approach to solving this problem was described by Gille and House [1971], who showed how measurements in two channels for which  $\text{CO}_2$  has different opacities could be used to determine the temperature as a function of pressure, and therefore avoid the uncertainty of knowing where the radiometer is looking. The original technique for determining the ozone distribution is described in House and Gille [1980].

These studies employed an iterative method for solving the radiative transfer equation which was very time-consuming on the computer. While it served to explore the problem, it was too slow for operational use on large volumes of data. A newer technique is described by Bailey and Gille [1978], and Bailey and Gille (in preparation). In this approach, a fast nonlinear method is used to obtain an initial solution with low vertical resolution. The final profile is obtained through the application of a second, linear corrector.

One of the interesting features is that, since the information is obtained in a spatial scan, spatial filtering and deconvolution may be used to reduce the noise, and to improve the vertical resolution lost by the finite field-of-view [Gille and Bailey, 1978].

**PRECISION AND ACCURACY OF OZONE PROFILES:** It is necessary to know something of the characteristics of the individual ozone profiles, before considering the hemispherical distributions derived from them. The solid line in Figure 3a shows an LRIR ozone retrieval, presented in parts per million by volume (ppmV), equivalent to number of ozone molecules per million air molecules. The LRIR profile extends from 15-68 km altitude (100-.08 mb), and shows sensitivity to rapid vertical variations.

Gille et al, [1980b] have pointed out that it is necessary to know the precision as well as the accuracy of the profiles. Here the precision or repeatability of the ozone determinations is defined as the standard deviation of the indicated values when many determinations are made of the same profile. This is fairly readily determined for a satellite instrument if it is possible to find a region of the globe where the atmosphere is uniform over a distance in which these determinations are made. The standard deviation about the mean of the determinations is then an estimate of the precision. The repeatability of the LRIR ozone retrievals is shown as a function of altitude by the dashed line in Figure 3b. It varies from 0.1-0.4 ppmV. These values are averages of several determinations for different latitudes and seasons. As implied above, they include not only the effects of instrument noise and random variations in the inversion algorithm, but also real variations in the atmosphere over the region selected.

The accuracy is much more difficult to determine. There are no internationally recognized standards for ozone measurements in the stratosphere. About the best that can be done is to show the relationship between the remote measurements and the measurements obtained by in-situ techniques which employ different principles, and therefore have different systematic errors. To cover the altitude range of interest, it was necessary to compare with rocket-borne ozone measurements. There were only four such comparison situations, in which the satellite overpass was within 2 degrees great circle distance and 3 hours in time of the rocket sounding. Two were with Krueger optical sensors [Krueger, 1973] and two were with Hilsenrath chemiluminescent rocketsondes [Hilsenrath and Kirschner, 1980]. Two of these comparisons are shown in Figure 3a; they show reasonably good overall agreement between the LRIR and rocket determinations. Mean differences (rocket minus LRIR) for all four comparisons are given by the solid line in Figure 3b. The error bars indicate the standard deviation of that mean. Below 30 km, the rocket values are greater by up to ~ 1 ppmV. This difference is statistically significant. The cause is not understood at this time; it may be due to the rocket instruments, or a systematic effect in the inter-

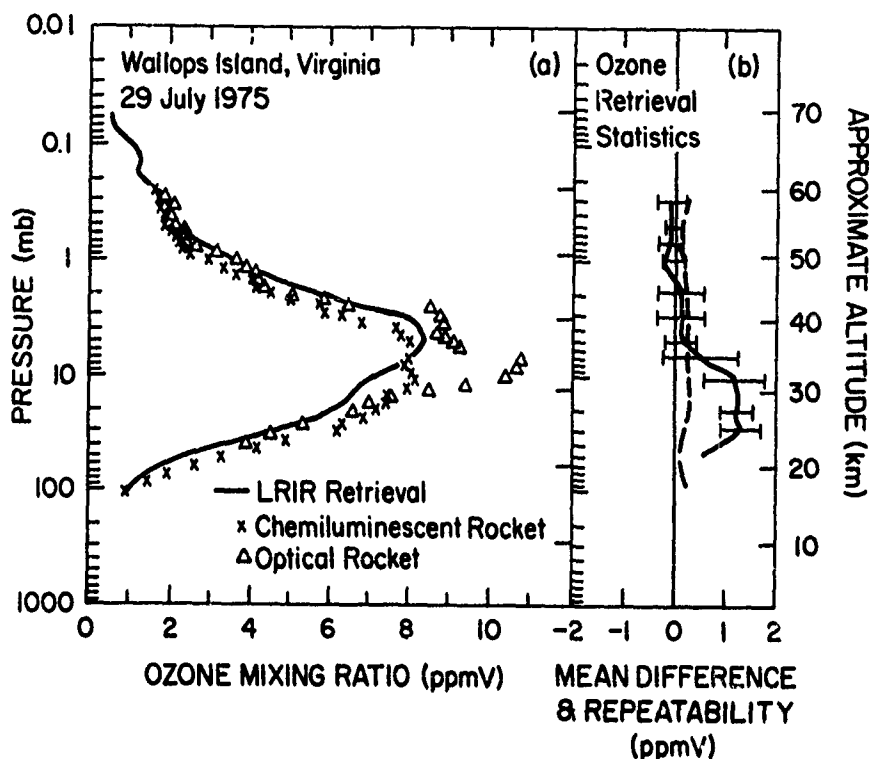


Figure 3. Results of comparisons among LRIR ozone determinations and rocketsondes. a: 29 July determinations at Wallops Island. b: Dashed line, repeatability of LRIR ozone determinations; solid line, mean difference, rocket minus LRIR, for four comparisons. Bars show standard deviation of the mean difference. (From Gille et al., 1980b.)

pretation of the satellite data. The source of this difference is still under study. More importantly, it is quite clear that there is no significant difference between the rockets and the LRIR above about 30 km.

It should be emphasized that there has been no normalization or adjustment of LRIR values to get this agreement.

These results have been based on a "final" inversion algorithm. At this time, the only data for which objectively analyzed distributions are available were obtained using an earlier inversion scheme. The data presented below are labelled as preliminary for this reason. The earlier results are not as good below 50 mb, nor above 1 mb, as the "final" inversion. Between 50 mb and 1 mb the differences between the two retrievals are expected to be small.



## GILLE

**OBJECTIVE ANALYSIS:** The results of inverting the LRIR data are a series of temperature and ozone retrievals along the orbit for the period of the instrument operation. It is necessary to convert these serial retrievals into the maps and cross sections which are discussed below. A technique suggested by Rodgers [1977] has been studied and adapted by Kohri [1980] and Kohri et al, [1977, also in preparation].

In this approach, the observations at a latitude circle are used to improve an estimate of the Fourier coefficients describing the variation of the field around that latitude circle. The data are treated as a time series, and a Kalman filter is used to produce a time series of the Fourier coefficients. This approach is applied to the data in both forward and backward time directions. At each stage an estimate of the uncertainty of the estimated coefficients is also obtained. The forward and backward estimates may then be combined according to their inverse variances to produce the final estimate of the coefficients at any time. Perhaps the most important outcome is that the data, which are taken at different times (asynoptically in meteorological terms), may be combined to produce a synchronous or synoptic estimate. The data coverage is sufficient to allow estimation of 7 or 8 waves around the latitude circle. However, the amplitude even for the 6 wave pattern (referred to as zonal wave number 6 or wave 6) is generally quite small, and in the results that follow only wave numbers 1-6 are included.

Inverted data were obtained every 4 degrees of latitude, from 64°S to 84°N. At each of those latitude circles, the wave number coefficients were determined in the manner described, and stored once each day, at 1200 UT. To make a map, these coefficients are used to calculate ozone mixing ratios at a set of grid points, which is then contoured.

An example of such a map on a polar stereographic projection for Day 317 (November 12) is shown in Figure 4. This is the ozone distribution on the 1 mb surface. There is considerable variation from low to high latitudes, and as a function of longitude on this surface for this day. The temperature map (Figure 5) for the same situation shows many of the same features. However, where there is high temperature, there tends to be low ozone, and vice versa. This is an example of the out-of-phase variation between temperature and ozone mixing ratio which is predicted by photochemical theory. It arises because of the temperature dependence of the reaction rates for ozone production and destruction. How far down does this extend? The ozone map at 5 mb would again show a great deal of variability across the field. An examination of a temperature map at this level would also show variations of temperature, but they would not correlate well in position with the ozone, and do not exhibit the photochemical out-of-phase relationship.

A way to get a more quantitative picture of this effect is to follow the approach used by Hartmann and Garcia [1979] in a heuristic model. They calculated the phases of wave number 1 for temperature and ozone as functions of altitude. The level at which temperature becomes  $\sim 180^\circ$  out of phase with the ozone is the base of the region of photochemical domination of the ozone distribution. The ozone and temperature phases observed by LRIR at 60°N are shown in Figure 6 [from Gille et al, 1980c]. It can clearly be seen that the photochemistry is exerting a major control above 2 mb. The results of applying this approach at a number of latitudes show that photochemical control extends to lower altitudes at low latitudes, and rises with increasing latitude. This is not unexpected, in view of the deeper penetration of solar radiation at low latitudes, and the weaker atmospheric motions.

This phase relationship between temperature, geopotential, and ozone is important for understanding the observed ozone distributions in terms of both chemistry and dynamics.

## OZONE MIXING RATIO (PPMV)

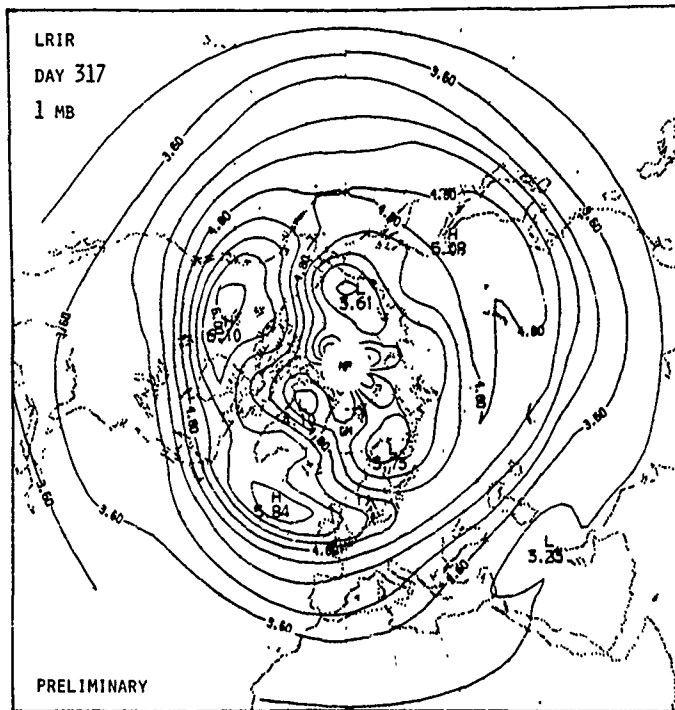


Figure 4. Preliminary Northern hemisphere ozone mixing ratio (ppmV) on the 1 mb surface ( $\sim 48$  km) on 12 November 1975.

## TEMPERATURE (K)

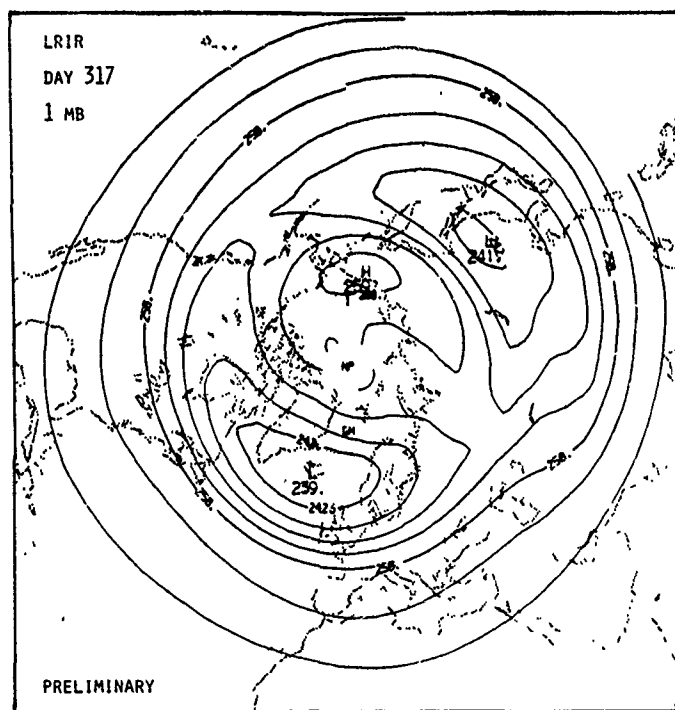


Figure 5. Preliminary Northern hemisphere temperature (K) on the 1 mb surface ( $\sim 48$  km) on 12 November 1975.

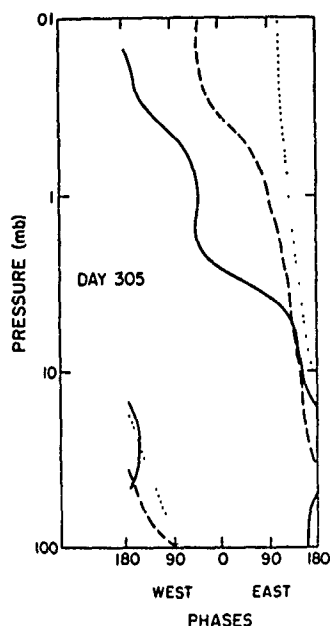


Figure 6. Phases of wave number one in temperature (dashed line), ozone mixing ratio (solid line) and geopotential height (dotted line) as a function of altitude on 1 November 1975. According to Hartmann and Garcia (1979), the in-phase relationship between ozone mixing ratio and geopotential indicates dynamical control, while an out-of-phase relationship between ozone and temperature signifies photochemical control (from Gille et al., 1980c).

**CROSS SECTIONS OF OZONE AND ITS VARIATIONS:** There are many ways of looking at the four-dimensional fields of ozone. These include latitude-altitude cross-sections of zonally averaged ozone or related quantities, maps on pressure surfaces, and decomposition of the fields into waves around latitude circles. Ozone distributions are presented below in each of these ways.

Figure 7 shows the mean ozone cross-section for November 1975. At lower altitudes (higher pressures) the values are fairly constant with latitude. Similarly, at upper altitudes there is little dependence upon latitude. However, in the middle there is an interesting region in which high ozone concentrations extend upward and poleward. This effect may be due to transports or to the temperature effects alluded to earlier. The cross-section for December is shown in Figure 8. The overall picture is quite similar, but there are some changes. The region of 6 ppmV is not as large nor does it extend as far poleward. Similarly, the region of 7 ppmV is much smaller.

An immediate question concerns the day to day variability over this monthly period. How steady is the cross section? It is possible to take the daily values and compute the standard deviation at each altitude/latitude point. Such values are shown for November in Figure 9. The feature that stands out is that the variation is rather small at high and low pressures, being of the order of 2% in both of those regions. However, at the edges of the region of high concentration the variations are of the order of 5% (e.g., 52°N). This variation becomes even larger in December, when the variations reach 10% near the stratopause at 52°. This variability is presumably due in part to the temperature variability, through its effect on the photochemistry, on the varying strength of the meridional circulations, seasonal changes, and changes in insolation.

GILLE

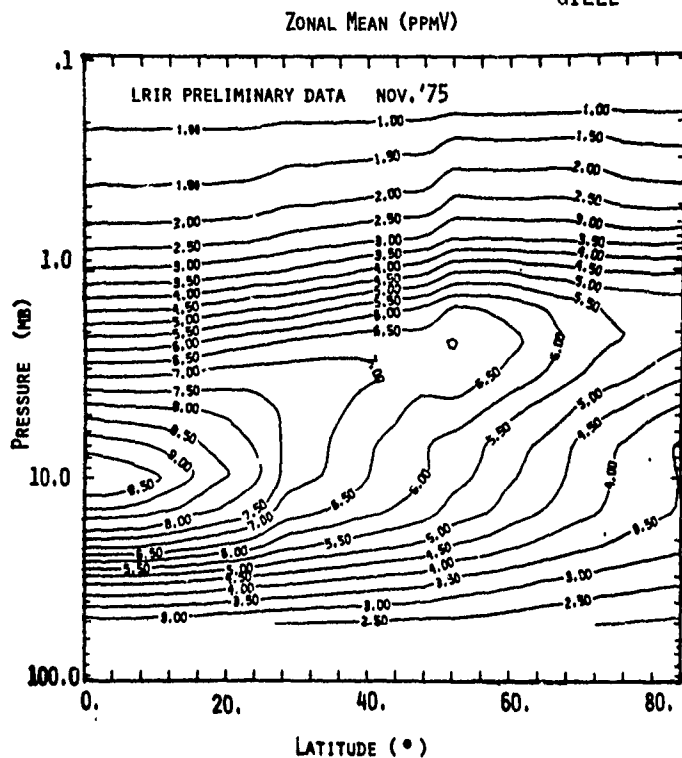


Figure 7. Preliminary mean cross-section of ozone mixing ratio (ppmV) for November 1975.

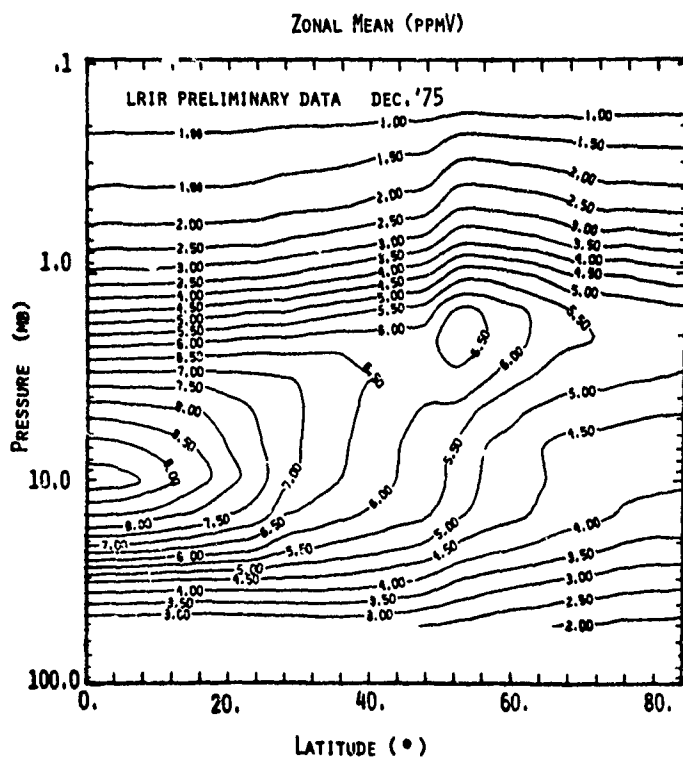


Figure 8. Preliminary mean cross-section of ozone mixing ratio (ppmV) for December 1975.

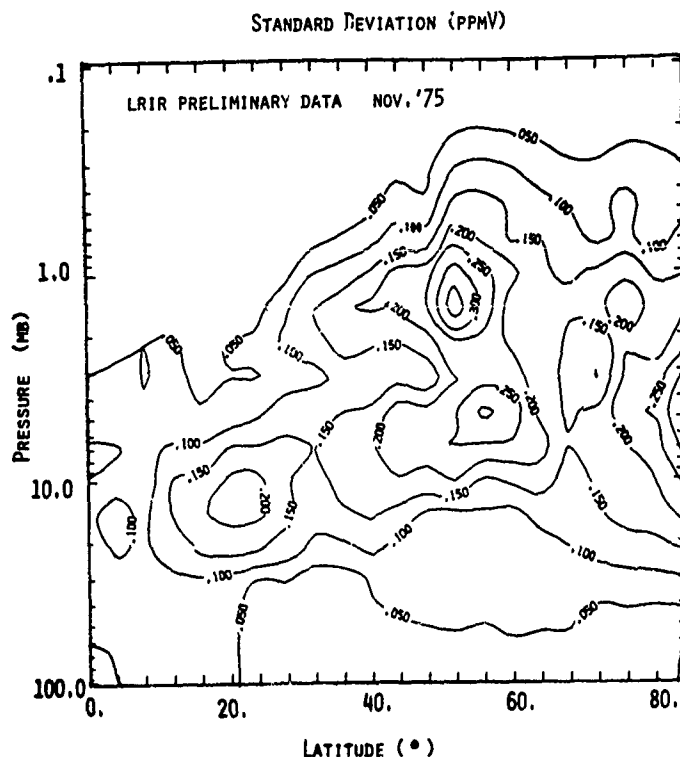


Figure 9. Standard deviation of preliminary mean cross-section of ozone mixing ratio (ppmV) for November 1975.

**MONTHLY MEAN MAPS:** Turning next to the distribution of ozone on pressure surfaces, Figure 10 presents the mean map for December on the 30 mb surface, at about 24 km altitude, which shows closed, nearly circular isolines around the pole. Their elongated or elliptical shape tends to be aligned toward 70°E. The mean distribution shows no very strong zonal asymmetries. Consistent with the cross-section, the mean mixing ratio decreases toward the pole. The November plot, which is not shown, is very similar. The ozone isolines on the 10 mb surface (Figure 11), located at about 31 km altitude, are similar to those at 30 mb. There is an extension of low values over the Pacific Ocean region. Once again the change from high mixing ratios at low latitudes to lower mixing ratios over the poles is apparent. The main difference between November and December is the 1/2 ppmV higher value over the pole in December than in November. The field becomes somewhat less regular at 3 mb, or approximately 40 km, as shown in Figure 12. The contours for the most part are elongated, closed circles, centered on the pole, and oriented along the line about 30°E. However, isolated regions of high ozone appear at this level, as well as the extension of low values over the North Pacific. Now there is an increase of the value over the pole from 4.5 ppmV in November to 5.5 ppmV in December. Otherwise, the flatness of the field is quite similar.

The cross-section at 1 mb indicated a very slight region of high ozone about 55° latitude, but otherwise rather little variation along this surface. This is borne out by the 1 mb map, shown in Figure 13. The mixing ratio increases from 3.3 ppmV at low latitudes to a high of 5.8 ppmV, and then decreases to 4.2 ppmV in the polar region. The band of high values, however, actually consists of three rather separated maxima. One is located over central Asia, one over the Yukon region, and one over Scotland. These appear to be due at least in part to standing regions of low temperature. There is an indication of greater variability at latitudes greater than 60°. Again the November map is quite similar to December.

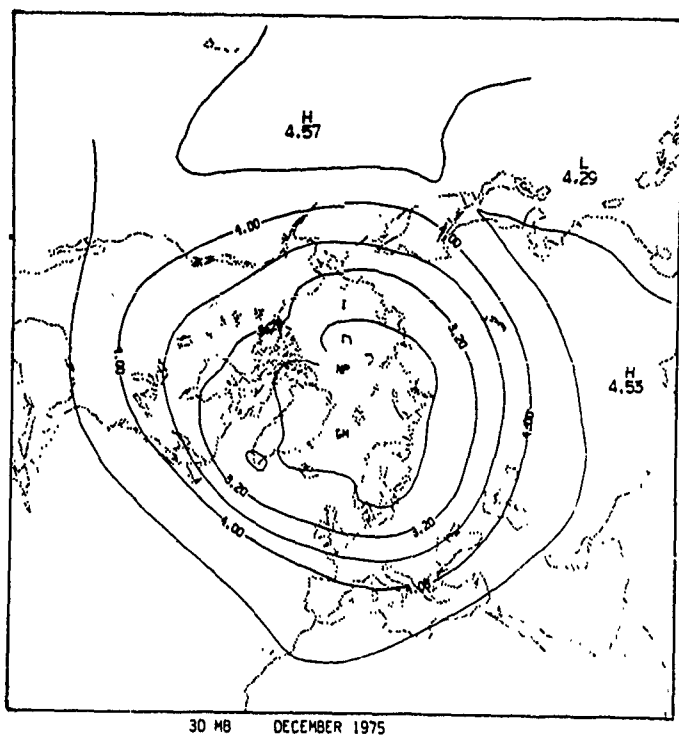


Figure 10. Preliminary mean Northern hemisphere ozone mixing ratio (ppmV) on the 30 mb surface for December 1975.

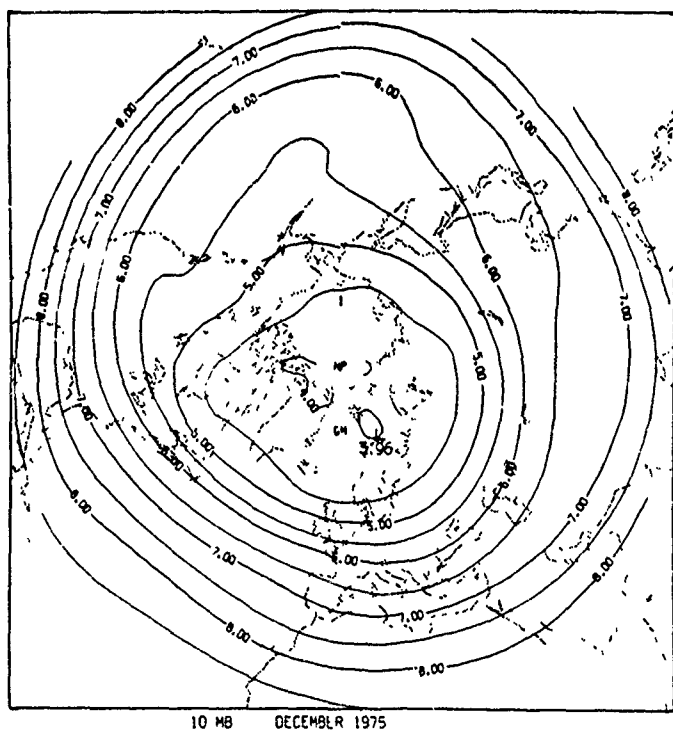


Figure 11. Preliminary mean Northern hemisphere ozone mixing ratio (ppmV) on the 10 mb surface for December 1975.

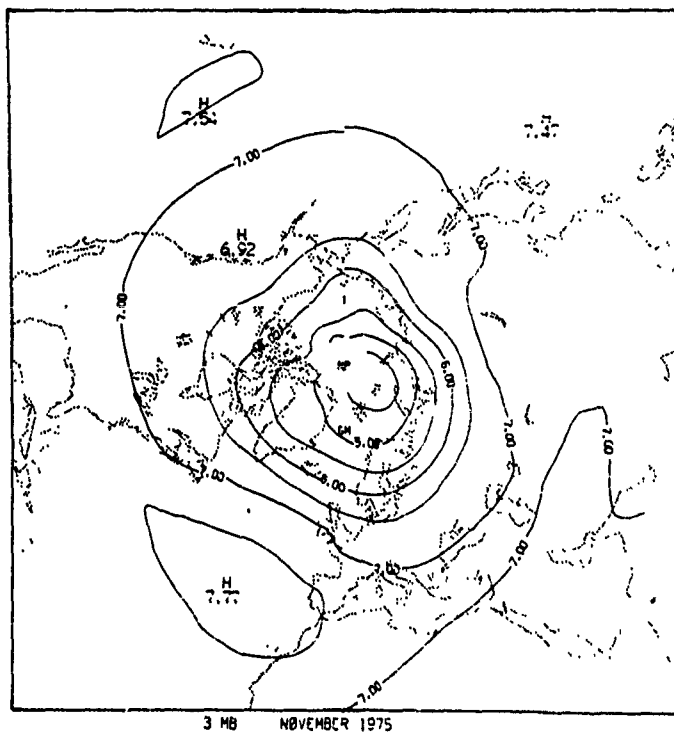


Figure 12. Preliminary mean Northern hemisphere ozone mixing ratio (ppmV) on the 3 mb surface for December 1975.

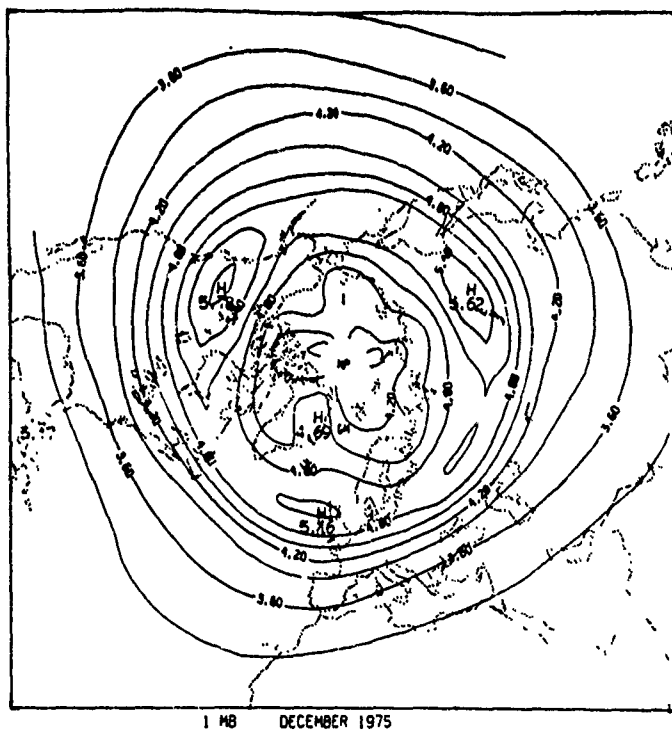


Figure 13. Preliminary mean Northern hemisphere ozone mixing ratio (ppmV) on the 1 mb surface for December 1975.

## GILLE

Many of the same features seen at 1 mb can also be seen at .4 mb (55 km, not shown). The mean mixing ratio increases from low latitude to a region of maximum values around 52°, and then drops back to lower values over the pole. The band of high values is characterized again by three centers of high mixing ratio, located in much the same places as at 1 mb. The isolines show more longitudinal variability than was seen at lower altitudes.

The field at .2 mb (60 km, not shown) is again similar to that at .4 mb, and is even flatter by .1 mb (64 km). The field shows very little in the way of longitudinal variation in these levels. It should be noted that the way these plots have been done will suppress any diurnal variations.

**LONGITUDINAL VARIATION DUE TO STANDING WAVES:** As noted above, the analysis being employed results in a daily value for the amplitude of longitudinal waves from 1 to 6. We can look at the mean value of these amplitudes for a month to learn something about the mean longitudinal distribution of ozone. Figure 14 shows the mean amplitude of wave number 1 for November. The maximum amplitude occurs at high latitude, around 72°, and at about 5 mb. At this level, it is about 12% of the amplitude of the mean zonal cross-section. The wave amplitude becomes very small at high altitudes, as we might expect from photochemical considerations. It is also rather small at low altitudes, presumably as most of the wave structure at those altitudes is transient, and removed by the process of taking the monthly average.

The situation shown for December in Figure 15 is radically different. Now the maximum amplitude occurs at low latitudes, 32°, and at around 10 mb. Here it is about 10% of the zonal mean amount. There is considerably more wave 1 amplitude in the lower stratosphere at midlatitudes than in the previous month, but the overall distribution is quite similar.

The maximum amplitude for wave number 2 (not shown) is only about half the wave 1 amplitude, and for November occurs in two locations, at the lower and upper edges of the region of maximum mixing ratio at latitudes around 40-44°. The amplitude in these regions is about 5% of the mean value. The situation in December is somewhat different. Again, the maximum values are at 44°, but there is only a single maximum, centered in a region of high ozone concentration around 5 mb. At this level it amounts to about 7% of the mean contribution.

The wave patterns are thus seen to be one of the more highly variable and less stable features of the ozone distribution. This is not too surprising, since these are presumably driven by dynamical phenomena which are expected to be characterized by more variability. The maxima occur in the region in which dynamics are expected to play a major role in the ozone distribution. It is interesting that the variations are as small as they are compared to the mean distribution, and confirms the impressions from the maps, that throughout the stratosphere the ozone distribution was characterized by relatively small longitudinal variation.

**MESOSPHERIC OZONE:** Mesospheric ozone has not been subject to frequent measurement. Perhaps the most complete set of measurements are those of Hays and Roble [1973], who interpreted measurements of stellar occultation to obtain ozone distributions up to 100 km. More recently, Reigler et al. [1976, 1977] have obtained occultation measurements using the Copernicus telescope on OAO-3. Their first set of observations was taken when LRIR was operating, allowing a comparison between the two determinations, [Gille et al., 1980a]. Copernicus observations were made in the tropics at midnight, while LRIR soundings occur at a local time of 10:30 p.m. Unfortunately the LRIR was not operating on July 26, when the Copernicus observations were made. The closest in time were on the preceding day, 25 July, in the same longitudinal range.

Figure 16 shows the results of this comparison. The solid line shows the LRIR retrieval closest to the minimum altitude reached by the occultation. The bars indicate the repeatability of the LRIR results. Other lines indicate the range of values obtained on nearby orbits. The LRIR results all cluster closely around a fairly well defined profile, in agreement with other determinations.



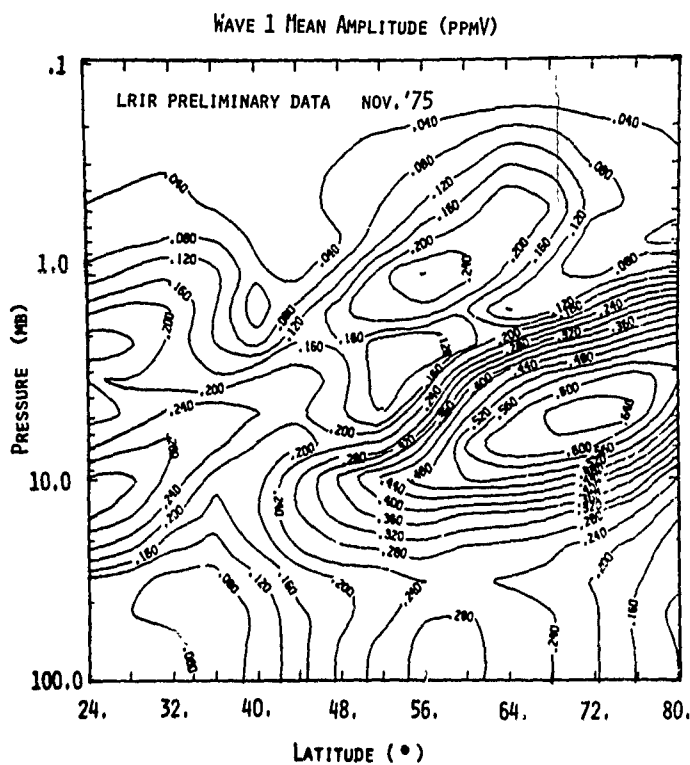


Figure 14. Mean amplitude of wave number one in ozone mixing ratio (ppmV) for November 1975.

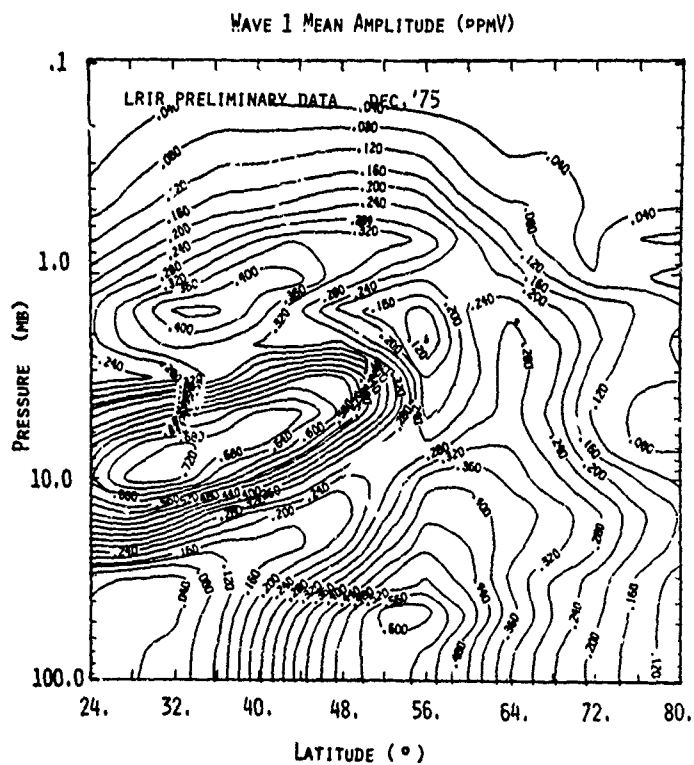


Figure 15. Mean amplitude of wave number one in ozone mixing ratio (ppmV) for December 1975.

The Copernicus values are characterized by moderate spread, but can be seen to be almost a factor of 3 higher than the LRIR values in the lower regions. The reason for the difference is not understood.

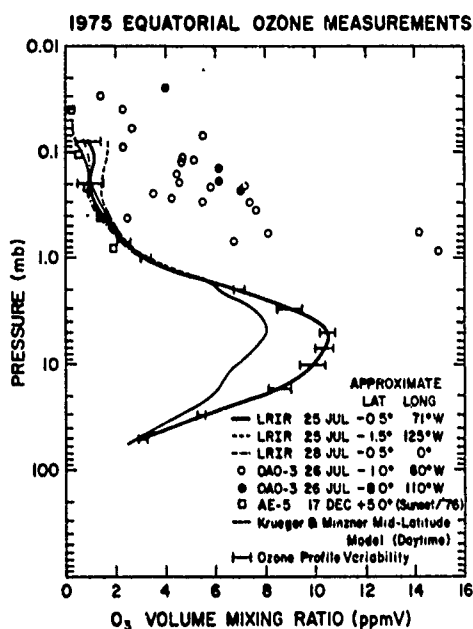


Figure 16. Comparison among OAO-3 ozone mixing ratios (circles), nearby LRIR observations on the previous day, and other determinations. (From Gille et al., 1980a.)

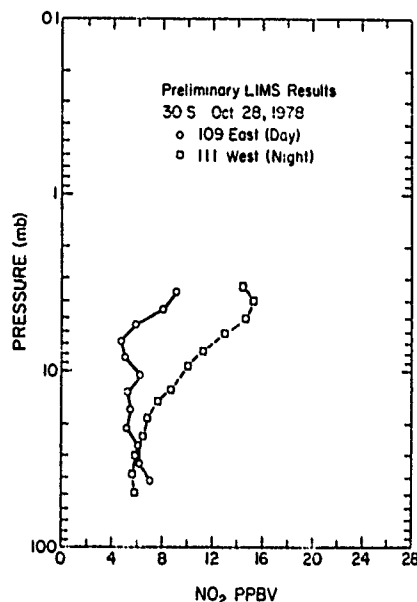


Figure 17. Preliminary LIMS determinations of  $\text{NO}_2$ , showing the expected day-night difference. (From Gille et al., 1980c.)

**FUTURE DEVELOPMENTS:** The LRIR data presented here are preliminary. The most immediate development to be anticipated is the reduction of all seven months of the LRIR temperature and ozone data. These will then be analyzed, and maps of the type presented above prepared. Statistics on the mean ozone distribution and its variations will be prepared for the LRIR period--June 1975-January 1976. These data will also cover the southern hemisphere (to 64°S). The picture they provide will be more detailed than what has been available to date; in particular they will more clearly show the ozone variations, and how they develop over the entire globe.

The Limb Infrared Monitor of the Stratosphere (LIMS) was launched on Nimbus-7 in October 1978 and operated until the beginning of June 1979. It has been described by Russell and Gille [1978] and Gille et al. [1980c]. It was a limb-scanning instrument very similar to the LRIR, but had a changed channel for  $\text{H}_2\text{O}$ , and added channels for the measurement of  $\text{NO}_2$  and  $\text{HNO}_3$ . The noise level in the ozone channel is about a factor of three lower than for LRIR, which should allow confident ozone measurements to a somewhat higher altitude than those presented here. Preliminary results have been presented by Gille et al. [1980c].

As an example, two  $\text{NO}_2$  profiles are shown in Figure 17. They show, as expected, an increase from day to night, as NO is oxidized to  $\text{NO}_2$ . The factor of two increase is about what is predicted. Once more, later retrievals will extend to higher altitudes. The  $\text{HNO}_3$

and  $\text{NO}_2$  retrievals are the first demonstration of the capability of measuring constituents in the parts-per-billion range from a satellite.

These results are not presented with any suggestion they constitute final results. They are meant to show that the LIMS operated very well in orbit, and that the data appear capable of providing the kind of information that was expected when the experiment was planned. There is still considerable work required to understand the actual functioning of the instrument in orbit, to complete the algorithms for the optimal extraction of information from the data, its verification, and its presentation to the community of users. It is now planned for these data to be made public beginning in early 1981.

In the longer range future, the Solar Mesosphere Explorer (SME), a small satellite, will be launched in the fall of 1981. One of the instruments will be an infrared limb scanner which will measure temperature, ozone, and water vapor. The detectors will be radiatively cooled, giving it a long lifetime. This will circumvent the 7 month limit on experiment lifetime exhibited by the Nimbus instruments mentioned above.

The SME is described by Thomas et al. [1980]. Its objectives are to study the photochemistry of the mesosphere, and the response of mesospheric ozone to solar phenomena and other natural variability. In addition, a great deal should be learned about stratospheric ozone,  $\text{NO}_2$ , and related chemistry.

NASA is considering an Upper Atmosphere Research Satellite (UARS). It is hoped that a limb scanner whose capabilities are at least as good as those described here, and perhaps orders of magnitude better, will fly on that satellite. This will be discussed later in this institute.

Finally, mention should be made of the Cryogenic Limb-scanning Interferometer and Radiometer (CLIR). As the name implies, this is a combination of interferometer-spectrometer and radiometer, in which not only detectors but also the optics and telescope through which it looks at the atmosphere are cooled to cryogenic temperatures. This reduces the noise level, and allows measureable signals to be obtained up into the thermosphere. With the high resolution spectrometer, it will be possible to measure lines of many trace gases and radicals, and determine their global distribution. Initial deployment is planned for the Space Shuttle, although it is possible that an instrument may be placed in a free flyer later on. An indication of the species which may be measurable is shown in Figure 18. Information on the distribution of these species should add immeasurably to our ability to understand the photochemistry of the middle atmosphere, and perhaps create new challenges for chemical modellers.

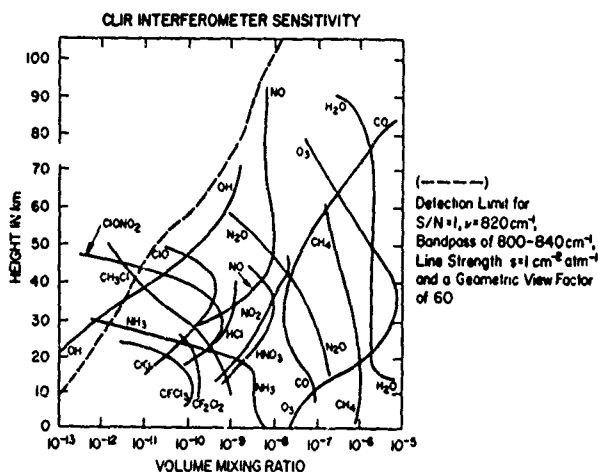


Figure 18. Vertical profiles of a number of constituents which may be measurable with the CLIR.

**CONCLUSIONS:** The data shown have indicated the wide range of conditions under which the ozone distribution exists and is maintained at different altitudes and different regions of the globe for two winter months. In the lower and middle stratosphere, the ozone distribution can be rather complex, reflecting the atmospheric motions and the small scales still present from waves propagating upward from the troposphere. At higher levels, the ozone distribution becomes more zonal and simple, as the higher zonal wave numbers are attenuated. Only the largest scales are present. There follows a transition zone, into a region in which the ozone distribution is governed by photochemistry, shown by an inverse temperature dependence. Finally, there is a region in which the ozone distribution is rather flat.

Considering the temporal variation, the fields are qualitatively very similar in the two month period presented here. Quantitatively, there is somewhat greater pole to equator contrast in December than in November at the lowest levels, but there are smaller ozone mixing ratios in the cross-section indicated during December.

The most variable aspects of the ozone distribution appear to be the wave amplitudes and locations of their maxima. While the amplitude of wave 1 increases only slightly from November to December, its location changes from 72°N to 30°N, and it shifts downward slightly in altitude. Wave 2 changes from a distribution with two major peaks to one with one major peak, at about the same latitude, and 30% greater peak amplitude.

These data are just beginning to be carefully studied. It is premature to draw too many conclusions, especially at the highest and lowest levels, in view of their preliminary nature. However, it is clear that these limb scanning data provide a wealth of detail on ozone phenomena which will allow closer studies of atmospheric phenomena and more stringent tests of theoretical prediction than has been possible before. It will be of special interest to see how similar these months are when compared to the same months in 1978 as determined from LIMS.

**ACKNOWLEDGMENTS:** The long and careful work of Paul L. Bailey, William J. Kohri, Stanley C. Nolte, Gail P. Anderson and Verrill Rinehart in the reduction, inversion and mapping of the data is gratefully acknowledged. Special thanks are due to GPA for helpful comments on the manuscript and extensive assistance in its preparation.

This work was sponsored in part by NASA under Work Order S 40135B. The National Center for Atmospheric Research is sponsored by the National Science Foundation.

REFERENCES

- Bailey, P. L. and J. C. Gille, An Approximate Method for Non-linear Inversion of Limb Radiance Observations, in Remote Sensing of the Atmosphere: Inversion Methods and Applications, edited by A. L. Fymat and U. E. Zuev, pp. 115-122, Elsevier Scientific Publishing Co., Amsterdam, 1978.
- Gille, J. C., G. P. Anderson, and P. L. Bailey, Comparison of Near Coincident LRIR and OAO-3 Measurements of Equatorial Night Ozone Profiles, in preparation, 1980a.
- Gille, J. C. and P. L. Bailey, Inversion of Infrared Limb Emission Measurements for Temperature and Trace Gas Concentrations, in Inversion Methods in Atmospheric Remote Sounding, edited by A. Deepak, pp. 195-213, Academic Press, New York, 1977.
- Gille, J. C. and P. L. Bailey, Information Content and Results of Non-linear Inversion of Nimbus 6 Limb Radiance Inversion Radiometer Data, in Remote Sensing of the Atmosphere: Inversion Methods and Applications, edited by A. L. Fymat and U. E. Zuev, pp. 107-113, Elsevier Scientific Publishing Co., Amsterdam, 1978.
- Gille, J. C., P. L. Bailey, R. A. Craig, F. B. House, and G. P. Anderson, Sounding of the Stratosphere and Mesosphere by Infrared Limb Scanning from Space, Science, in press, 1980b.
- Gille, J. C., P. L. Bailey, F. B. House, R. A. Craig, and J. R. Thomas, The Limb Radiance Inversion Radiometer (LRIR) Experiment, in Nimbus 6 Users' Guide, edited by J. E. Sissala, pp. 141-161, NASA Goddard Space Flight Center, Greenbelt, Md., 1975.
- Gille, J. C., P. L. Bailey, and J. M. Russell III, Temperature and Composition Measurements from the LRIR and LIMS Experiments on Nimbus 6 and 7, Philosophical Transactions of the Royal Society, London, in press, 1980c.
- Gille, J. C. and F. B. House, On the Inversion of Limb Radiance Measurements I: Temperature and Thickness, Journal of Atmospheric Science, 28, 1427-1442, 1971.
- Hartmann, D. L. and R. R. Garcia, A Mechanistic Model of Ozone Transport by Planetary Waves in the stratosphere, Journal of Atmospheric Science, 36, pp. 350-364, 1979.
- Hays, P. L. and R. G. Roble, Observations of Mesospheric Ozone at Low Latitudes, Planetary and Space Science, 21, 273, 1973.
- Hilsenrath, E. and D. T. Kirschner, A Rocket Ozonesonde for Atmospheric Research and Satellite Intercomparisons, Reviews of Scientific Instruments, in press, 1980.
- House, F. B. and J. C. Gille, On the Inversion of Limb Radiance Measurements II: Ozone and Water Vapor, Journal of Geophysical Research, in press, 1980.
- Kohri, W. J., Ph.D. Thesis, Drexel University, Philadelphia, Pa., 1980.
- Kohri, W. J., J. C. Gille and P. L. Bailey, Mapping of the LRIR Data by Sequential Estimation of Fourier Coefficients, in Collection of Extended Summaries of Contributions Presented at Joint Assembly Seattle, Washington, IAGA/IAMAP, edited by A. D. Belmont, NCAR, Boulder, Co., 1977.
- Krueger, A. J., The Mean Ozone Distribution from Several Series of Rocket Soundings to 52 km at Latitudes from 58°S to 64°N, Pure and Applied Geophysics, 106-108, 1272-1280, 1973.

GILLE

Reigler, G. R., S. K. Atreya, T. M. Donahue, S. C. Liu, B. Wasser, and J. F. Drake, U.V. Stellar Occultation Measurements of Nighttime Equatorial Ozone, Geophysical Research Letters, 4, 145-148, 1977.

Reigler, G. R., J. F. Drake, S. C. Liu, and R. J. Cicerone, Stellar Occultation Measurements of Atmospheric Ozone and Chlorine from OAO-3, Journal of Geophysical Research, 81, 4997-5001, 1976.

Rodgers, C. D., Statistical Principles of Inversion Theory, in Inversion Methods in Atmospheric Remote Sounding, edited by A. Deepak, pp. 117-138, Academic Press, N.Y., 1977.

Russell, J. M. III and J. C. Gille, The Limb Infrared Monitor of the Stratosphere (LIMS) Experiment, in The Nimbus 7 Users' Guide, edited by C. R. Madrid, pp. 71-103, NASA Goddard Space Flight Center, Greenbelt, Md., 1978.

Thomas, G. E., C. A. Barth, E. R. Hansen, C. W. Hord, G. M. Lawrence, G. H. Mount, G. J. Rottman, D. W. Rusch, A. I. Stewart, R. J. Thomas, J. London, P. L. Bailey, P. J. Crutzen, R. E. Dickinson, J. C. Gille, S. C. Liu, J. F. Noxon, C. B. Farmer, Scientific Objectives of the Solar Mesosphere Explorer Mission, Pure and Applied Geophysics, in press, 1980.

## OZONE RESULTS FROM INDIAN STATIONS USING DOBSON INSTRUMENTS

D.K. Chakrabarty and Purobi Chakrabarty

Physical Research Laboratory, Ahmedabad 380009, India.

### Abstract

A number of Dobson instruments has been operating at different locations of India, some of them from as early as 1952. An examination of the monthly average of the data collected by these instruments has been made in this paper. It is found that a marked seasonal variation exists with a maximum around May and a minimum around winter at the following locations: Kodaikanal ( $10^{\circ}\text{N}$ ), Dum Dum ( $22^{\circ}\text{N}$ ), Ahmedabad ( $23^{\circ}\text{N}$ ), Varanasi ( $25^{\circ}\text{N}$ ) and New Delhi ( $28^{\circ}\text{N}$ ). At Srinagar ( $34^{\circ}\text{N}$ ), however, the trend of the variation is opposite to that mentioned above. When a mass plot of F10.7, the solar flux at 10.7 cm wavelength, versus total ozone is made, it is found that total ozone remains constant upto a solar activity level of F10.7  $\approx$  150, beyond which, it starts decreasing. The same trend is also seen in a plot in which seasonal effect is eliminated. The amplitudes of these variations, both, seasonal and solar activity are found to be minimum at Kodaikanal and maximum at Srinagar.

**INTRODUCTION:** An intriguing question which the present day atmospheric scientists are facing is whether or not the human activities such as the operation of supersonic aircrafts, nuclear weapon tests, release of chlorofluoromethane from aerosol sprays and refrigerating systems and increased application of nitrogen fertilizers could deplete the amount of ozone in the atmosphere. Since this minor atmospheric constituent provides a shield to the biological life from the harmful solar radiation and also controls the climate of the earth, considerable attention has been paid to it in the recent years. While Crutzen (1974) and Molina and Rowland (1974) have shown that the ozone content of our atmosphere is indeed on the decline, the others like Fabian (1977), Ellsaesser (1978) find that it could be the other way round. Their approach is numerical model calculation study by solving all the relevant photo-chemical equation, either by incorporating or without incorporating the transport processes. One could also study this problem by examining the large amount of ozone data collected at several stations all over the world. The instrument which has been mostly used and for a considerable period of time is Dobson Spectrophotometer. A set of such instruments has been operating at more than 60 stations of the world and some of them from as early as 1930. Several studies have been made by using

the data recorded by these instruments (i.e. Hill and Sheldon 1975, Angell and Korshover 1973). These include correlation of ozone trends with volcanic eruptions, equatorial wind, sunspot activity and solar flux at 10.7 cm wavelength. Some of these studies have revealed long-term variations of total ozone of the order of 11 years. But, controversy exists as to whether these variations are due to changes in the solar activity level. Recently, however, Keating (1978), using the Nimbus 4 data of April 1970 to January 1971, has shown that the global monthly averaged ozone variation is in phase with the monthly averaged solar flux variations at 10.7 cm wavelength. Natural variations of ozone content both short term and long term, are to be taken into consideration before trying to isolate the effects of anthropogenic species on the ozone amount. For that, the type and the extent of these variations must be known. Till now, informations on these aspects are far from definitive. In order to obtain an understanding as well as the trend of the behaviour of global ozone, more work is necessary. In this study, we have used the total ozone values collected by Dobson Spectrophotometers at several places in India to examine the behaviour of total ozone with solar activity and season over the Indian subcontinent.

**BASIC DATA USED:** The basic data for this study consists of monthly averaged values of total ozone for 6 stations of India spreading over a latitudinal span of  $10^{\circ}$  to  $34^{\circ}$ . These are Kodaikanal ( $10^{\circ}14'N$ ,  $77^{\circ}28'E$ ), Dum Dum ( $22^{\circ}39'N$ ,  $88^{\circ}27'E$ ), Ahmedabad ( $23^{\circ}01'N$ ,  $72^{\circ}39'E$ ), Varanasi ( $25^{\circ}27'N$ ,  $82^{\circ}52'E$ ), New Delhi ( $28^{\circ}38'N$ ,  $77^{\circ}13'E$ ) and Srinagar ( $34^{\circ}05'N$ ,  $74^{\circ}50'E$ ). We have used the data from the dates as early as available (from January 1952 for some stations) upto the beginning of 1978. The monthly averaged values of total ozone are based on about 6 observations per day and then all are averaged over the entire month. There may be subjective error as well as error due to instrumental uncertainties in the data of different places. No attempt has been made to synthesise them. We have assumed that these uncertainties will be lessened while taking the average of large number of scattered values for the entire month and have used these values as available from the bulletins of "Ozone Data for the World".

**RESULTS:** Figure 1 represents the mean monthly total ozone values of six Indian stations as available till date. An examination of this figure shows

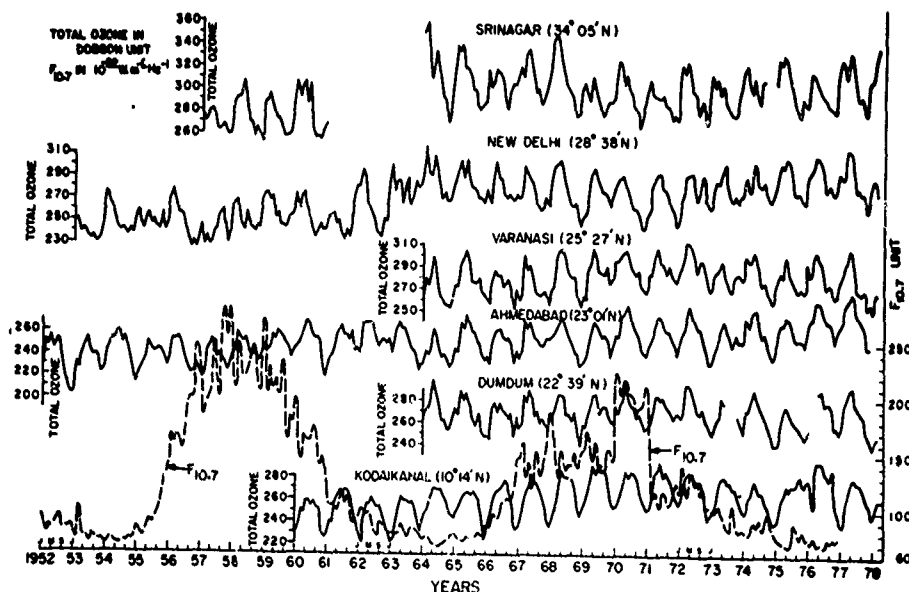


Fig.1 Monthly averaged values (—) of total ozone for 6 stations of India. The F10.7 values (---) for the same period are also shown.



that for all stations from Kodaikanal to New Delhi i.e. for a latitude zone of  $10$  to  $28^{\circ}\text{N}$ , the ozone content is maximum around May and minimum in the winter. For Srinagar, however, (latitude greater than  $30^{\circ}$ ), this is the other way round. Also, one finds that the amplitude of variation increases as the latitude increases. In Figure 1,  $F_{10.7}$ , the solar flux values at  $10.7$  cm wavelength are also plotted for the same period for which the ozone values are shown. It can be seen from this figure that the variation of  $\bar{O}_3$ , the total ozone amount is not always in phase with the variation of  $F_{10.7}$ . Also, there is no clear cut indication of either an increase or a decrease of  $\bar{O}_3$  with time.

To examine, closely, the variation of  $\bar{O}_3$  with solar activity, a plot of  $F_{10.7}$  against  $\bar{O}_3$  has been made. This is shown in Figure 2. Since, the data for New Delhi, Ahmedabad and Srinagar are for a longer period of time, values of these stations are only plotted. It is seen from this figure that  $\bar{O}_3$  remains constant upto  $F_{10.7} \approx 150$ , after which it starts decreasing. The magnitude of change in  $\bar{O}_3$  from maximum to minimum level of solar activity is more at Srinagar ( $34^{\circ}05'\text{N}$ ) than at Ahmedabad ( $23^{\circ}01'\text{N}$ ). In this plot, we

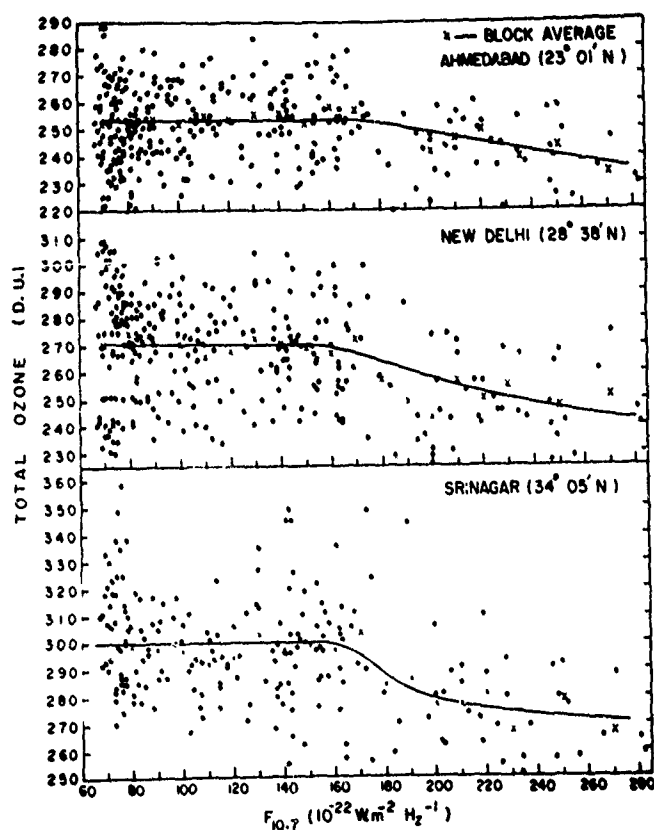


Fig.2 Plot of  $\bar{O}_3$  against  $F_{10.7}$  for 3 stations of India.

have not considered the effect of seasonal variation. Actually, the data points are so random, that we feel that in taking the block average, this effect will be eliminated. In addition, if only one season is chosen, in that case, the number of data points will become less. This can be seen in Figure 3 where a plot of similar type of Figure 2 has, in fact, been made for the May-June months. Here, again, a trend of decrease of  $\bar{O}_3$  after  $F_{10.7} \approx 150$  is noticed. In another attempt to remove the seasonal effect, a plot of  $(\bar{O}_3)_i - (\bar{O}_3)_j$  against  $(F_{10.7})_i - (F_{10.7})_j$  has been made (shown in Figure 4) where  $i$  stands for the months January, February etc. and

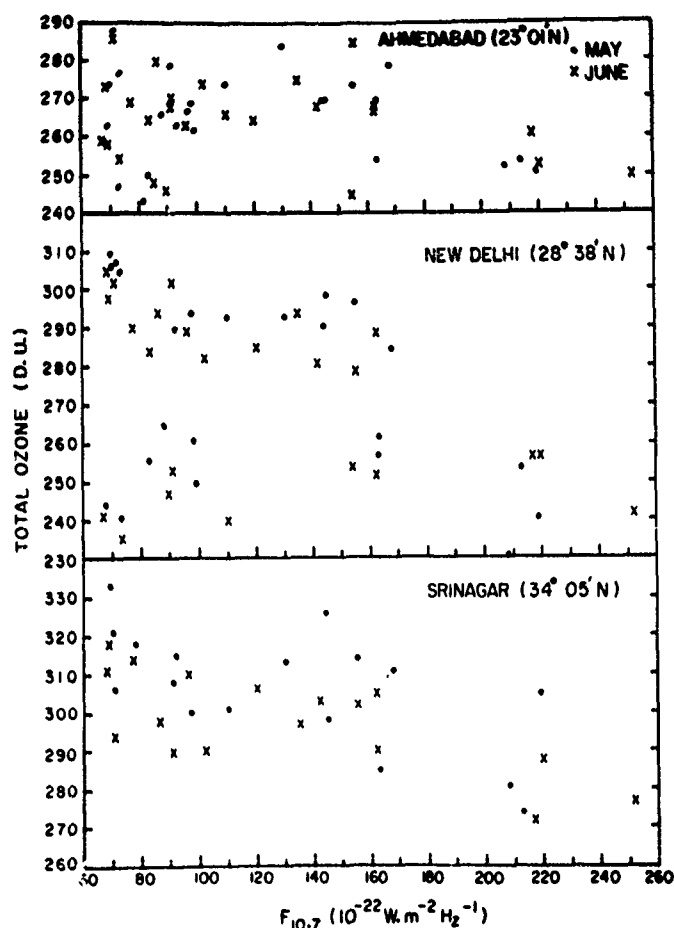


Fig.3 Plot of  $\bar{O}_3$  against  $F_{10.7}$  for 3 stations of India for May and June.

$(\bar{O}_3)_i$  and  $(F_{10.7})_i$  are the average values of  $\bar{O}_3$  and  $F_{10.7}$  for the month  $i$  of all the years considered. Here also, it is seen that upto certain level of solar activity  $\bar{O}_3$  remains constant, after which it starts decreasing.

The variation of  $\bar{O}_3$  of the type mentioned above is difficult to explain at the present stage of our knowledge. Both galactic cosmic rays and solar UV radiations could play dominant role for such type of variation. Ruderman and Chamberlin (1975) have suggested that during solar minimum condition, there is an increase in the low energy cosmic rays in the earth's atmosphere which will increase  $NO_x$  and decrease  $O_3$ . Accordingly, an increase in  $\bar{O}_3$  is expected during high solar activity period, which is not found in this study. At the time of proton events, however, when there is an increase of ionization, a decrease in  $\bar{O}_3$  has been noticed. It may be worth mentioning here, that during low solar activity, ion production rate due to cosmic rays in the stratosphere is much higher than that at high solar activity (approximately double at 36 km, see Heaps, 1978).

Evidence of solar UV variability has recently been reviewed by Heath and Thekaekara (1976). They find substantial variation in solar UV near  $2.2\mu m$  over 11 years cycle with the largest variation at the shortest wavelength. It may be noted that the impact of different regions of UV on different species is different. While the region less than  $0.2050\mu m$  dissociates  $O_2$  and about  $2450 - 3980 nm$  dissociates  $NO_2$  molecules (both the processes try to increase  $O_3$ ), the entire UV region dissociates  $O_3$  molecules (try to

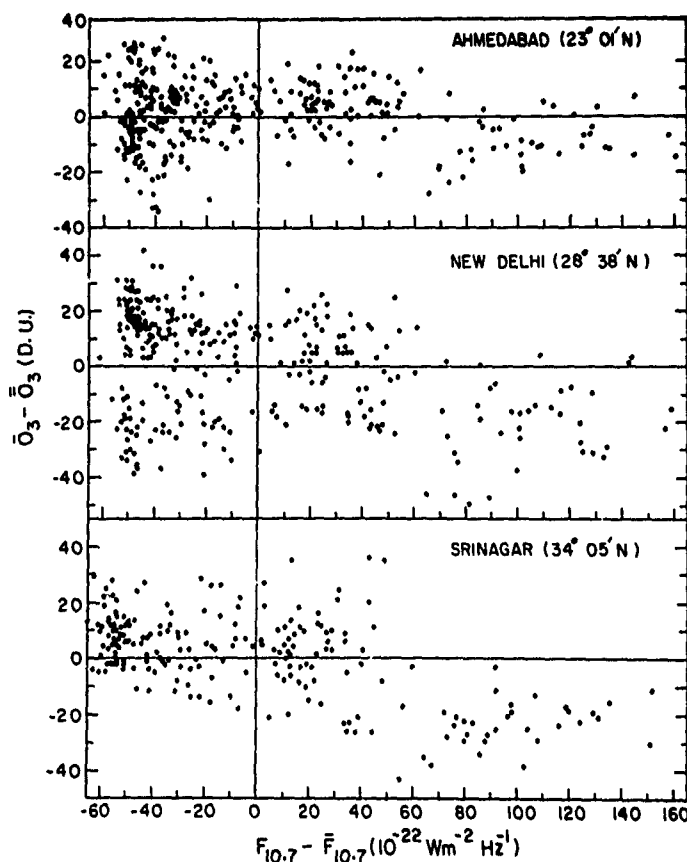


Fig.4 Plot of  $(\bar{O}_3 - \bar{O}_3)$  against  $(F_{10.7} - \bar{F}_{10.7})$  for 3 stations of India.

decrease  $O_3$ ). It is likely that as the solar activity level increases, the dissociation rate of  $O_3$  increases by a magnitude greater than the dissociation rates of  $O_2$  and  $NO_x$ . To confirm this, reliable information on the variation of different parts of UV with solar activity is required.

ACKNOWLEDGEMENT: We are grateful to Prof.K.R. Ramanathan without whom this work would not have been possible. We thank Mrs.S. Jani for providing useful information for this work. We also thank Prof.J. London for his useful comments and suggestions. One of the authors (P.C.) acknowledges the Council of Scientific and Industrial Research, New Delhi for financial support.

#### REFERENCES

- Angell, J. K. and J. Korshover, Quasi-biennial and long-term fluctuations in total ozone, *Mon. Weath Rev.*, **101**, 426, 1973.
- Crutzen, P. J., Estimates of possible variations in total ozone due to natural causes and human activities, *Ambio*, **3**, 201, 1974.
- Ellsaesser, H. W., Ozone destruction by catalysis: credibility of the threat, *Atmos. Environment*, **12**, 1849, 1978.
- Fabian, P., Ozone increase from Concorde operations? *Nature*, **272**, 306, 1978.
- Heaps, M.G., Parametrization of the cosmic ray ion-pair production rate above 18 km, *Planet. Space Sci.*, **26**, 513, 1978.
- Heath, D. and M. Thekaekara, *NASA TM-X-71172*, 1976.
- Hill, W. J. and P. N. Sheldon, Statistical modeling of total ozone measurements with an example using data from Arosa, Switzerland, *Geophys. Res. Lett.*, **2**, 541, 1975.

CHAKRABARTY and CHAKRABARTY

- Keating, G. M., Relation between monthly variations of global ozone and solar activity, Nature, 274, 873, 1978.
- Molina, M. J. and F. S. Rowland, Stratospheric sink for chlorofluoromethanes: chlorine catalyzed destruction of ozone, Nature, 249, 810, 1974.
- Ruderman, M.A. and J. W. Chamberlain, Origin of the sunspot modulation of ozone: its implications for stratospheric NO injection, Planet. Space Sci., 23, 247, 1975.

## HYDROGEN AND CARBON COMPOUNDS IN THE STRATOSPHERE

D.H. Ehhalt and A. Tönnissen

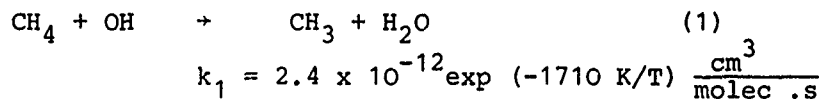
Institute for atmospheric chemistry,  
Kernforschungsanlage Jülich, Postfach 1913, D-5170 Jülich

The stratospheric chemistry of the hydrogen and carbon compounds,  $\text{H}_2\text{O}$ ,  $\text{H}_2$ ,  $\text{CH}_4$ ,  $\text{CH}_2\text{O}$ ,  $\text{CO}$ , and  $\text{CO}_2$  is described. It is shown, how these species are coupled through the oxidation of  $\text{CH}_4$ . Model predicted vertical mixing ratio profiles are compared to experimental data whose latitudinal dependence is also represented when available. For  $\text{CH}_4$  and  $\text{H}_2$  the vertical profiles of the measured mixing ratio vary systematically with latitude, a fact which appears to be mainly connected with the stratospheric Hadley circulation. As in the troposphere, stratospheric  $\text{CO}_2$  concentrations are increasing - at a rate of  $1.4 \pm 0.2$  ppm/year.

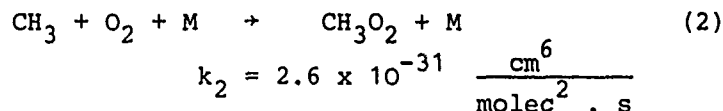
1. INTRODUCTION: Much of the chemistry in the stratosphere depends on gases which originate at the earth's surface, are long-lived in the troposphere, and can therefore reach the stratosphere in significant amounts. In the case of stratospheric hydrogen and carbon compounds the major source gases are  $\text{H}_2\text{O}$ ,  $\text{H}_2$ ,  $\text{CH}_4$ ,  $\text{CO}$ , and  $\text{CO}_2$ . Some of these gases have a direct impact on the stratosphere. For example  $\text{CO}_2$  and  $\text{H}_2\text{O}$  - except for  $\text{O}_3$  - are the most important infrared absorbing gases in the stratosphere, and therefore control the infrared cooling and the temperature of the stratosphere. Others interact through their chemical products. In this way the hydrogen compounds become important. They serve as the source of the  $\text{HO}_x$  radicals in the stratosphere which together with  $\text{NO}_x$  and  $\text{Cl}_x$  provide the major pathways of catalytic destruction of stratospheric  $\text{O}_3$ .  $\text{HO}_x$ , and also the long-lived hydrogen compounds  $\text{CH}_4$ ,  $\text{H}_2$ , provide the major loss reactions for stratospheric  $\text{NO}_x$  and  $\text{Cl}_x$ . Moreover, the carbon and hydrogen compounds are coupled: During the oxidation of  $\text{CH}_4$ ,  $\text{H}_2$ , and  $\text{CO}$  are produced as intermediates, the final reaction products being  $\text{H}_2\text{O}$  and  $\text{CO}_2$ . Besides being required as basic input data, measurements of the stratospheric distributions of these trace gases can be used for the validation of models of stratospheric chemistry, particularly if the measurements are made simultaneously. This coupling also provides the rationale for discussing these gases jointly.

To better understand the relations between the vertical distributions of the various hydrogen and carbon compounds, we will first discuss the present views on stratospheric  $\text{CH}_4$  oxidation and show the resulting theoretical profiles of  $\text{CH}_4$ ,  $\text{CH}_2\text{O}$ ,  $\text{CO}$ , and  $\text{H}_2$ . Then we will introduce the experimental data for comparison.

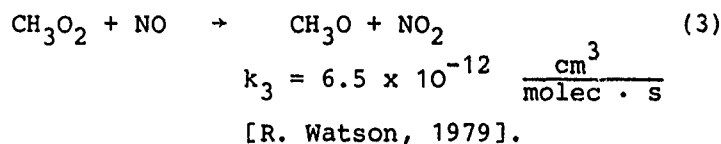
2. THE STRATOSPHERIC OXIDATION OF  $\text{CH}_4$ : The oxidation of  $\text{CH}_4$  is initiated mainly by reaction with the OH radical



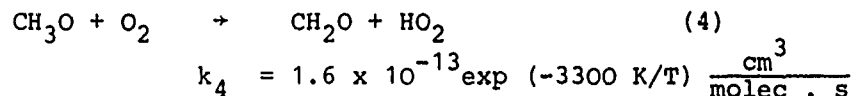
which is immediately followed by



(These and the following rate coefficients are taken from the compilation of Hampson and Garvin [1978], unless otherwise specified). The methylperoxy radical,  $\text{CH}_3\text{O}_2$ , has several reaction channels, the most important is

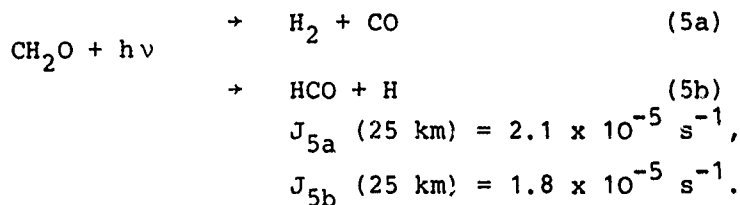


The methoxy radical reacts with  $\text{O}_2$

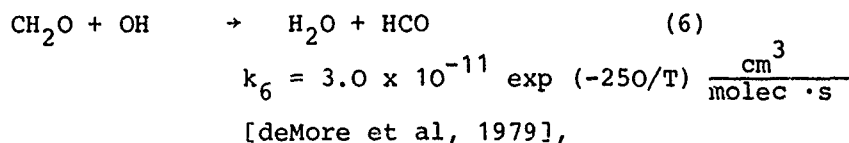


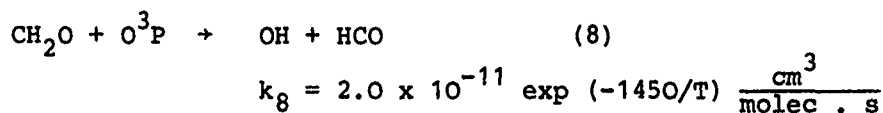
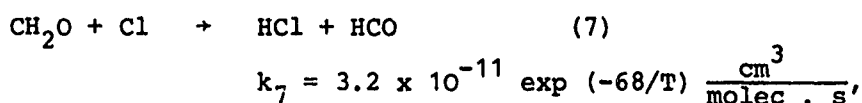
to form formaldehyde,  $\text{CH}_2\text{O}$ , the first intermediate of the  $\text{CH}_4$  oxidation sequence long-lived enough to be measurable.

$\text{CH}_2\text{O}$  is photolyzed into two channels

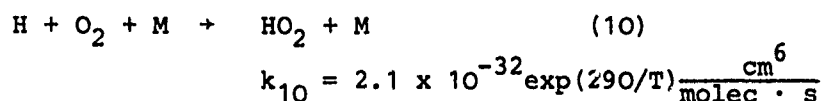
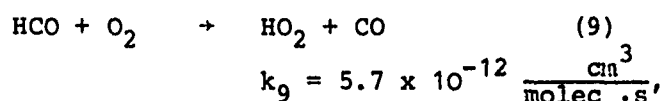


At 25 km the so-called molecular channel, yielding  $\text{H}_2$  and  $\text{CO}$ , is still the more important one ( $J$  represents the photodissociation coefficient.). (5a) is the reaction which provides the coupling between the  $\text{CH}_4$ ,  $\text{CO}$  and  $\text{H}_2$  cycle.  $\text{CH}_2\text{O}$  can further react through the following channels:

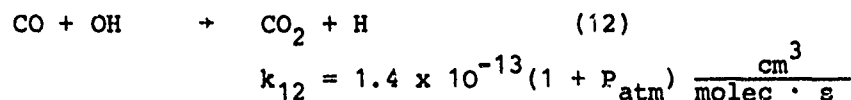
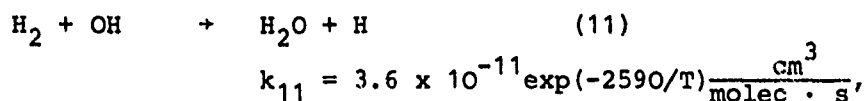




Both HCO and H react further:



to form  $\text{HO}_2$ . Thus the oxidation of  $\text{CH}_4$  leads to a conversion of the OH to the  $\text{HO}_2$  radical, which proceeds with a gain in the number of  $\text{HO}_x$  radicals mainly because of (5b). The long-lived products  $\text{H}_2$  and CO are eventually also oxidized - mainly by reaction with OH



to form  $\text{CO}_2$  and  $\text{H}_2\text{O}$ , the final, most stable products in the stratosphere.

To illustrate the oxidation sequence of  $\text{CH}_4$ , and the importance of the various parallel channels in the reactions (1)-(12) in a more quantitative way, the respective rates are shown in a fluxdiagram (figure 1), which depicts the situation at 25 km altitude. The numbers are calculated using a one dimensional steady state model of stratospheric chemistry [Röth et al, 1979]. Figure 1 shows that at 25 km altitude  $2 \times 10^3$   $\text{CH}_4$  molecules react with OH to form  $\text{CH}_3$ . This amounts to about 70 % of the total  $\text{CH}_4$  destruction rate, because already at 25 km sizable fractions of  $\text{CH}_4$  react with excited atomic oxygen, O D, or with chlorine atoms to form  $\text{CH}_3$ . A small fraction of the  $\text{CH}_4$ , less than 2 %, reacts with O D to form  $\text{CH}_2\text{O}$  and  $\text{H}_2$  directly. It should be noted that the total reaction rate of  $\text{CH}_4$  as well as the contribution from the various reaction channels change with altitude. In particular the fraction of  $\text{CH}_4$  reacting with O D increases significantly with altitude because the O D concentration increases more rapidly than OH or Cl.

A possible branching into several channels is also indicated for  $\text{CH}_3\text{O}_2$ . The present model calculations treat only the reaction of  $\text{CH}_3\text{O}_2$  with NO. However reactions of  $\text{CH}_3\text{O}_2$  with O and  $\text{O}_3$  are expected to be important too.

Unfortunately the respective reaction rate coefficients have not yet been measured. Their inclusion would reduce the calculated steady state concentration of  $\text{CH}_3\text{O}_2$ . Most important for our present considerations are the various channels of the  $\text{CH}_2\text{O}$  reactions. At 25 km altitude and below, reaction with atomic oxygen and chlorine are relatively unimportant. The destruction is dominated by the reaction with OH, 36 %, and by photolysis through the channels (5a), 34 %, and (5b), 27 %. The calculated importance of the various channels has recently been changed significantly due to new measurements of quantum yield for (5a) and (5b) [Moortgat and Warneck, 1979] and the UV absorption cross section of  $\text{CH}_2\text{O}$  [Bass et al, 1979].

Adding up all the channels shows that for each  $\text{CH}_4$  molecule destroyed one  $\text{CH}_2\text{O}$  molecule and eventually one  $\text{CO}$  molecule is formed. This is not true for  $\text{H}_2$ . Only 0.36  $\text{H}_2$  molecules are formed for one  $\text{CH}_4$  molecule destroyed i.e. only 18 % of the hydrogen atoms in  $\text{CH}_4$  are converted to  $\text{H}_2$ . The others form  $\text{H}_2\text{O}$  either directly as in reaction (1) or after having passed through a  $\text{HO}_2$  radical as in reaction (4). The fraction of  $\text{H}_2$  formed becomes even

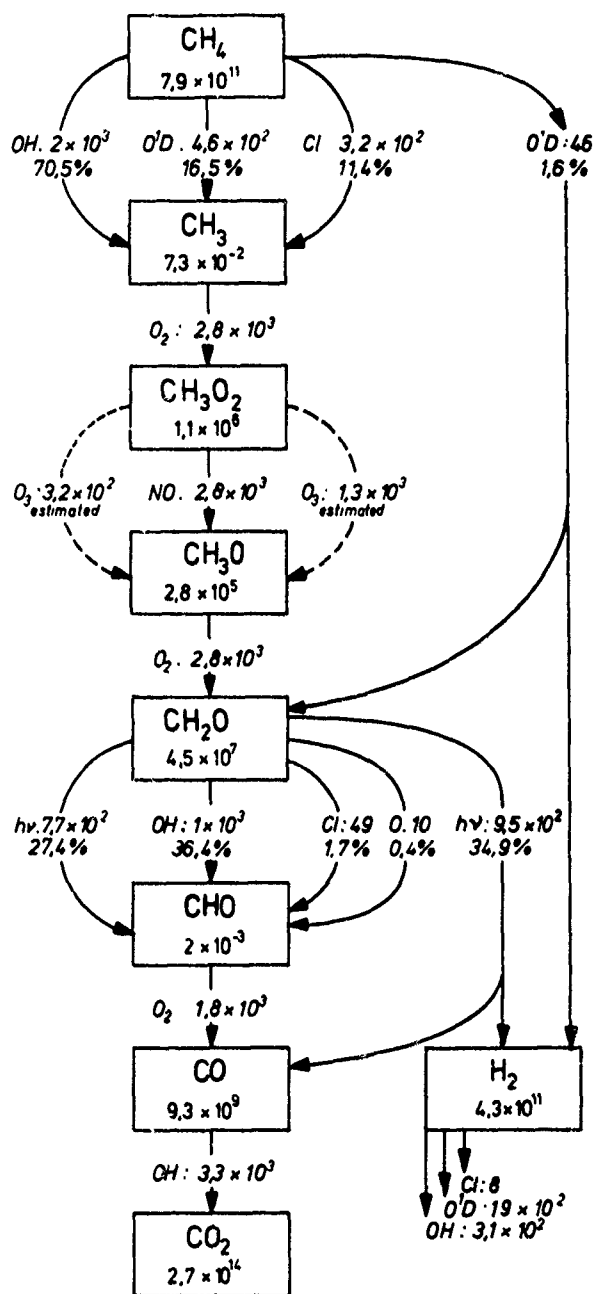


Fig. 1: Methane oxidation scheme.

Concentrations and fluxes are given for 25 km. The numbers in the boxes denote concentrations in  $\text{molec}/\text{cm}^3$ ; fluxes (slanted numbers) are in  $\text{molec}/(\text{cm}^3 \cdot \text{s})$ , the fraction (in %) of a particular destruction channel is also indicated.

Concentration for other involved species are:

O : $8 \times 10^6 \text{ cm}^{-3}$	O <sup>1</sup> D: $4.5 \text{ cm}^{-3}$
OH: $2.3 \times 10^8 \text{ cm}^{-3}$	Cl : $1.6 \times 10^4 \text{ cm}^{-3}$
NO: $3.7 \times 10^8 \text{ cm}^{-3}$	



smaller for higher altitudes; mainly because of the increase in OH concentration with altitude the reaction of  $\text{CH}_2\text{O}$  with OH becomes favored over the photolysis. It is also seen from the production, resp. destruction rates of  $\text{H}_2$  and CO that the stratosphere at 25 km altitude must act as a net source for  $\text{H}_2$  and a net sink for CO. The excess is balanced by the vertical eddy transport. In any case  $\text{H}_2$  and CO are produced in significant quantities within the stratosphere besides being imported from the troposphere below. Finally we can estimate the chemical lifetimes of all species by dividing their calculated concentrations by the calculated destruction rates. At 25 km altitude the more abundant species have lifetimes of  $\tau(\text{CH}_2\text{O}) = 4.4$  hours,  $\tau(\text{CO}) = 33.4$  days,  $\tau(\text{CH}_4) = 9$  years and  $\tau(\text{H}_2) = 26.8$  years.

The chemical lifetimes decrease considerably with increasing altitude because the concentrations of the main reaction partners OH, Cl, O<sup>1</sup>D increase with altitude and also because the reaction rate coefficients generally rise with the increase in temperature at higher altitudes. Figure 2 shows the altitude dependence of the chemical lifetimes of CO,  $\text{CH}_4$  and  $\text{H}_2$ .

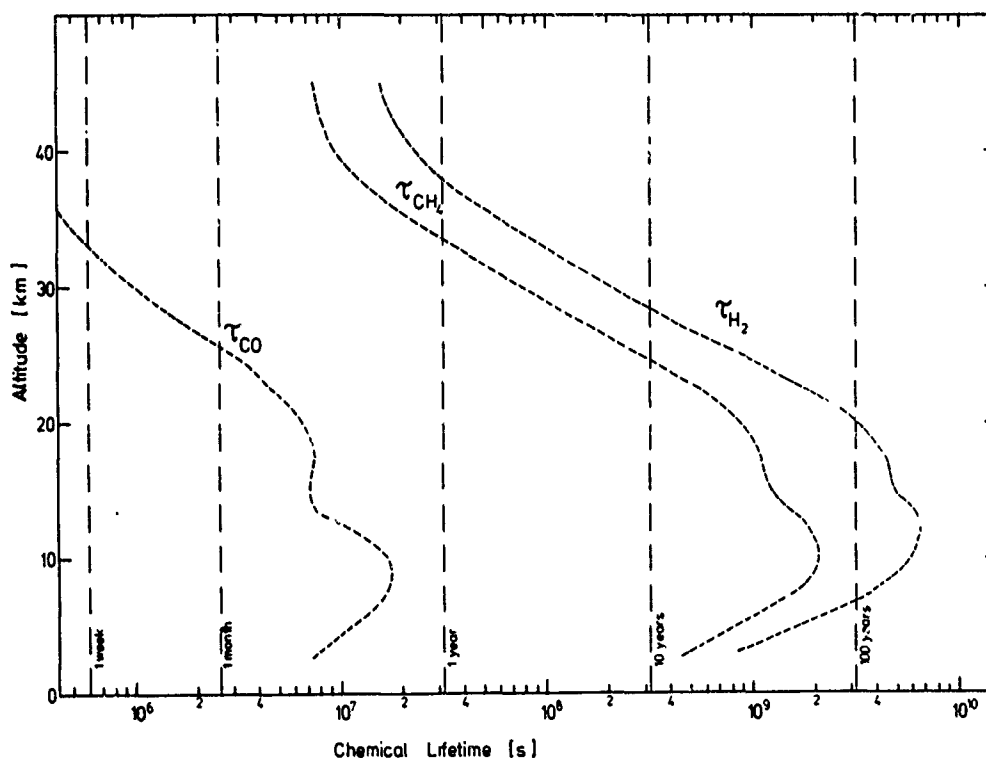


Fig. 2: Altitude dependence of chemical lifetimes of CO,  $\text{CH}_4$  and  $\text{H}_2$ .

### 3. THEORETICAL PROFILES OF $\text{CH}_4$ , $\text{H}_2$ , $\text{CO}$ , AND $\text{CH}_2\text{O}$ IN THE STRATOSPHERE:

Modern one dimensional models fully incorporate the  $\text{CH}_4$  oxidation scheme as indicated in figure 1. They are therefore capable of predicting the stratospheric profiles of  $\text{CH}_4$  and its reaction products. The KFA model, used to calculate the profiles shown in the following, is a one dimensional steady state model [R8th et al, 1979]. It uses the rate coefficients recommended by Hampson and Garvin [1978], includes a simplified treatment of multiple scattering and albedo [Isaksen et al, 1977], and uses a k-profile which has been described by Ehhalt et al [1975]. This profile is identical to that used more recently by Crutzen et al [1977]. The calculations have been updated using the  $\text{CH}_2\text{O}$  absorption spectrum reported by Bass et al [1979] at this meeting. The profiles are evaluated for  $30^\circ \text{N}$  latitude and equinox conditions.

#### $\text{CH}_4$

Figure 3 shows the  $\text{CH}_4$  profile. The  $\text{CH}_4$  mixing ratio decreases everywhere in the atmosphere. Yet, although most of the  $\text{CH}_4$  destruction takes place in the troposphere (also by reaction (1)-(12)), the tropospheric gradient is extremely weak owing to the fast vertical mixing of the troposphere. The largest gradient is observed in the lowest stratosphere despite the slow chemical destruction there (cf. fig. 2). However, this is the region with the slowest vertical transport resulting in the largest concentration gradients. Because of the relatively long chemical lifetime of  $\text{CH}_4$  in the lower stratosphere the calculated  $\text{CH}_4$  profile is quite sensitive to the choice of the k-profile used to parameterize the vertical transport. Comparison of the measured with the calculated  $\text{CH}_4$  profile has been used to tune the k-profile [Wofsy and McElroy, 1973; Ehhalt et al, 1975]. Thus the good agreement of the calculated  $\text{CH}_4$  profile with the experimental data shown below is not surprising.

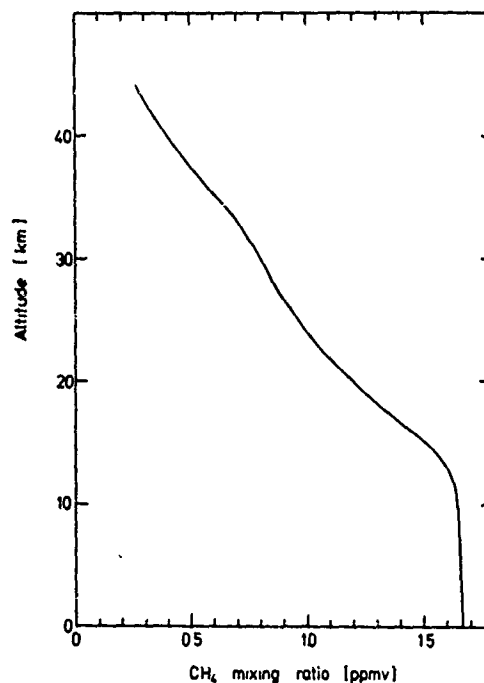


Fig. 3: Vertical profile of the  $\text{CH}_4$  mixing ratio, calculated with 1-D-model at  $30^\circ \text{N}$  under equinox conditions.

## H<sub>2</sub>

The calculated H<sub>2</sub> profile is shown in figure 4. The H<sub>2</sub> mixing ratio exhibits a slight decrease in the lower stratosphere beginning at about 15 km altitude. Nevertheless H<sub>2</sub> is produced from CH<sub>4</sub> throughout the entire stratosphere. This can be seen from a comparison with the dashed profile in which the H<sub>2</sub> produced from CH<sub>4</sub> is "switched off". Without the presence of CH<sub>4</sub> the stratospheric H<sub>2</sub> mixing ratio is significantly lower. It is, however, not reduced to zero. This is due to the fact that H<sub>2</sub> is transported upward from the troposphere, and transported downward from the upper stratosphere and mesosphere where it is produced from



in the upper stratosphere. The required H-atoms originate from reaction (12) and from the photolysis of H<sub>2</sub>O. This additional source expresses itself in the increase in the H<sub>2</sub> mixing ratio in the upper stratosphere. To demonstrate that increased levels of CH<sub>4</sub> would lead to increased H<sub>2</sub> concentrations, the H<sub>2</sub> profile was also calculated for a CH<sub>4</sub> profile with a fixed mixing ratio of 1.6 ppm (right hand curve).

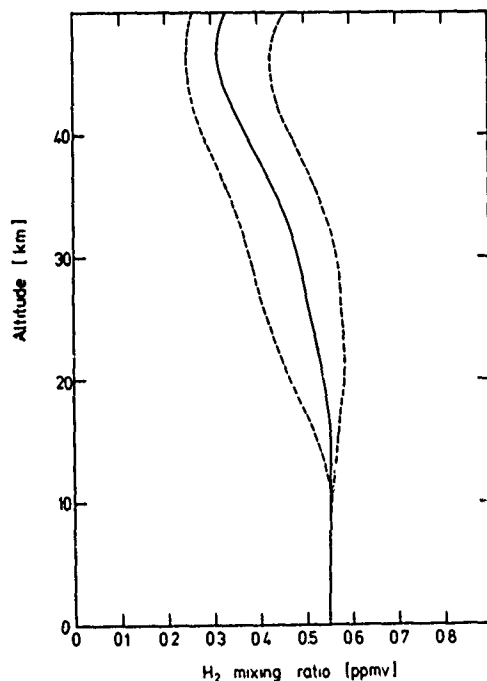


Fig. 4: Vertical profile of the H<sub>2</sub> mixing ratio. The dashed curves show the profiles with no CH<sub>4</sub> present (left) and with a fixed CH<sub>4</sub> mixing ratio of 1.6 ppmv (right hand curve). All profiles were calculated with a 1-D-model at 30° N under equinox conditions.

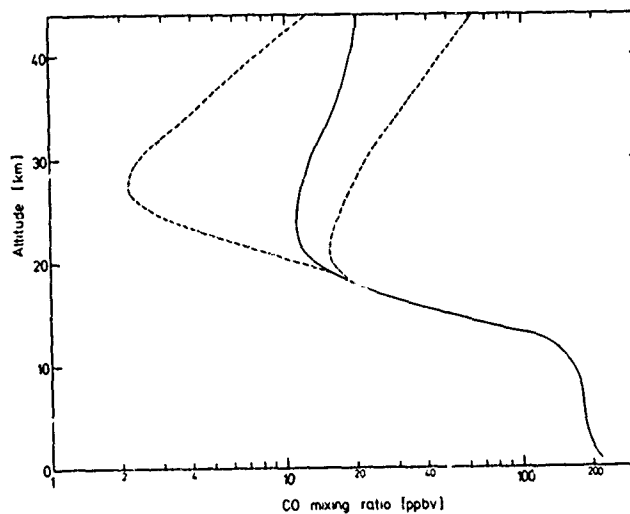


Fig. 5: Vertical Profile of the CO mixing ratio. The dashed curves show the CO profiles with no CH<sub>4</sub> present and with a fixed CH<sub>4</sub> mixing ratio of 1.6 ppmv. All profiles were calculated with a 1-D-model at 30° N under equinox conditions.

# CO

The corresponding CO profiles are shown in figure 5. Because of faster chemical destruction, the stratospheric CO concentration is more dependent on the local production of CO from CH<sub>4</sub> oxidation and less on the CO import from the troposphere and mesosphere. Its mixing ratio therefore responds much more strongly to the changes in CH<sub>4</sub> input. As is seen from the increase in the CO mixing ratio in the upper stratosphere, CO also has a mesospheric source independent from CH<sub>4</sub>. This is due to the photolysis of CO<sub>2</sub>.

# CH<sub>2</sub>O

In the hope that reliable measurements of CH<sub>2</sub>O will become available in the near future, the calculated vertical profile of the CH<sub>2</sub>O mixing ratio is shown in figure 6. The CH<sub>2</sub>O mixing ratio decreases very rapidly with altitude in the troposphere. This essentially reflects the decrease in the production rate of CH<sub>2</sub>O which is rate-limited by reaction (1). With increased O<sub>3</sub> levels in the lower stratosphere the OH concentration increases rapidly with altitude and so does the CH<sub>2</sub>O production rate. The stratospheric CH<sub>2</sub>O mixing ratio follows this increase in production, because the destruction of CH<sub>2</sub>O in the lower stratosphere is essentially due to photolysis (cf. figure 1) which increases very little with altitude. Destruction by OH provides only 20 % of the total loss. Thus the CH<sub>2</sub>O mixing ratio profile in the lowest stratosphere essentially reflects the profile of the OH mixing ratio. To highlight this point we briefly consider the local CH<sub>2</sub>O balance equation. It is given by

$$\frac{\partial \text{CH}_2\text{O}}{\partial t} = \text{div } j + P - D \quad (14)$$

The local change in time of the CH<sub>2</sub>O concentration is balanced by the divergence in CH<sub>2</sub>O flux,  $j$ , the production,  $P$ , and the destruction,  $D$ . It turns out that equation (14) can be simplified considerably. CH<sub>2</sub>O has a lifetime of about 8 hours in the lower stratosphere during day light, which means that it will exhibit only a weak diurnal variation in concentration. Consequently the time derivative of the concentration is expected to be small. In addition the divergence of the vertical

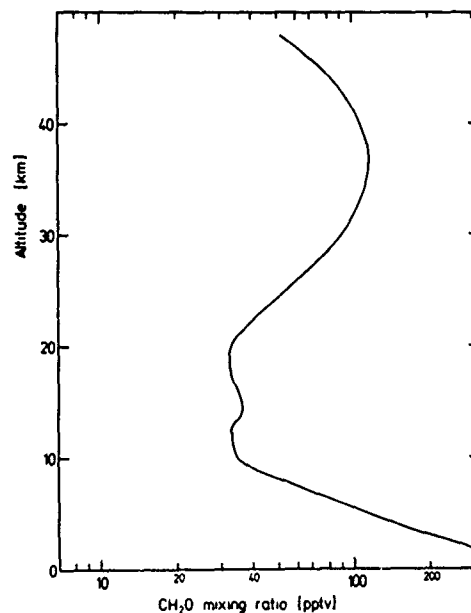


Fig. 6: Vertical profile of the CH<sub>2</sub>O mixing ratio calculated with 1-D-model at 30° N under equinox conditions.

flux is quite small, a factor of 1000 smaller than P or D, and can also be neglected. Furthermore in the lower stratosphere the concentration of Cl atoms and O D atoms are very small. Thus P and D are given in good approximation by

$$P \approx k_1 [\text{OH}] [\text{CH}_4] \quad (15)$$

$$D \approx (J_{5a} + J_{5b}) [\text{CH}_2\text{O}] + k_6 [\text{OH}] [\text{CH}_2\text{O}] \quad (16)$$

Equating the remaining terms of the balance equation (14), i.e. P and D, and rearranging the terms one obtains

$$[\text{OH}] = \frac{(J_{5a} + J_{5b}) [\text{CH}_2\text{O}]}{k_1 [\text{CH}_4] - k_6 [\text{CH}_2\text{O}]} \quad (17)$$

which shows the essential proportionality between OH and  $\text{CH}_2\text{O}$  concentration (the second term in the denominator is much smaller than the first one). Assuming the current view of  $\text{CH}_4$  oxidation chemistry, equation (17) also shows that the OH profile in the upper troposphere and lower stratosphere can be derived from a simultaneous measurement of  $\text{CH}_2\text{O}$ ,  $\text{CH}_4$  and preferably also  $J_{5a}$  and  $J_{5b}$ . The measurement of  $\text{CH}_2\text{O}$  in that altitude range and comparison with calculation will provide the simplest test available to check the validity of the  $\text{CH}_4$  oxidation scheme. At all other altitudes,  $\text{CH}_2\text{O}$  production and destruction are either complicated by the presence of Cl and O atoms as in the middle and upper stratosphere, or by the presence of non-methane hydrocarbons, washout and heterogeneous processes as in the lower troposphere.

## $\text{H}_2\text{O}$

The vertical profile of  $\text{H}_2\text{O}$  in the stratosphere can be derived very simply. The derivation rests on the H mass balance which requires that in a one dimensional steady state model the sum of all H compounds, essentially  $\text{H}_2\text{O}$ ,  $\text{CH}_4$ ,  $\text{H}_2$ , - weighted properly - has to be constant at all altitudes. Thus the  $\text{H}_2\text{O}$  profile in the stratosphere is given by the  $\text{H}_2\text{O}$  mixing ratio at the tropopause, usually 3 ppm, plus the deficit in the  $\text{CH}_4$  and  $\text{H}_2$  mixing ratios with respect to the values at the tropopause. This results in an increase in  $\text{H}_2\text{O}$  mixing ratio with altitude of essentially twice the magnitude of the decrease in the  $\text{CH}_4$  mixing ratio, since the  $\text{H}_2$  profile is comparatively constant with altitude.

**4. EXPERIMENTAL PROFILES OF  $\text{CH}_4$ ,  $\text{CH}_2\text{O}$ ,  $\text{H}_2$ ,  $\text{H}_2\text{O}$ , CO AND  $\text{CO}_2$  IN THE STRATOSPHERE:** In the following the data published since 1975 will be reviewed. Much of these data were measured using cryogenic sampling which offers the advantage of simultaneous determination of three or more species of the hydrogen and carbon compounds. This allows explanation of some of the fine structure observed in the profiles. The measured data will be compared with the calculated profiles shown in the previous paragraph. Such a comparison has its limitations because the profiles calculated from a 1 D steady state model represent an average situation - averaged in a somewhat ill-defined way over time, latitude and longitude - whereas the measurements present individual profiles subject sometimes to large fluctuations resulting from the instantaneous flow pattern in the stratosphere. Nevertheless it is of great interest to see, how far one dimensional model calculations can be used to explain the measured profiles.

## $\text{CH}_4$

$\text{CH}_4$  is probably the best studied trace gas among the hydrogen and carbon compounds. Vertical profiles have been obtained at several latitudes, and they are sufficiently numerous to warrant a representation divided into separate latitude belts (figure 7). As expected from the fact that

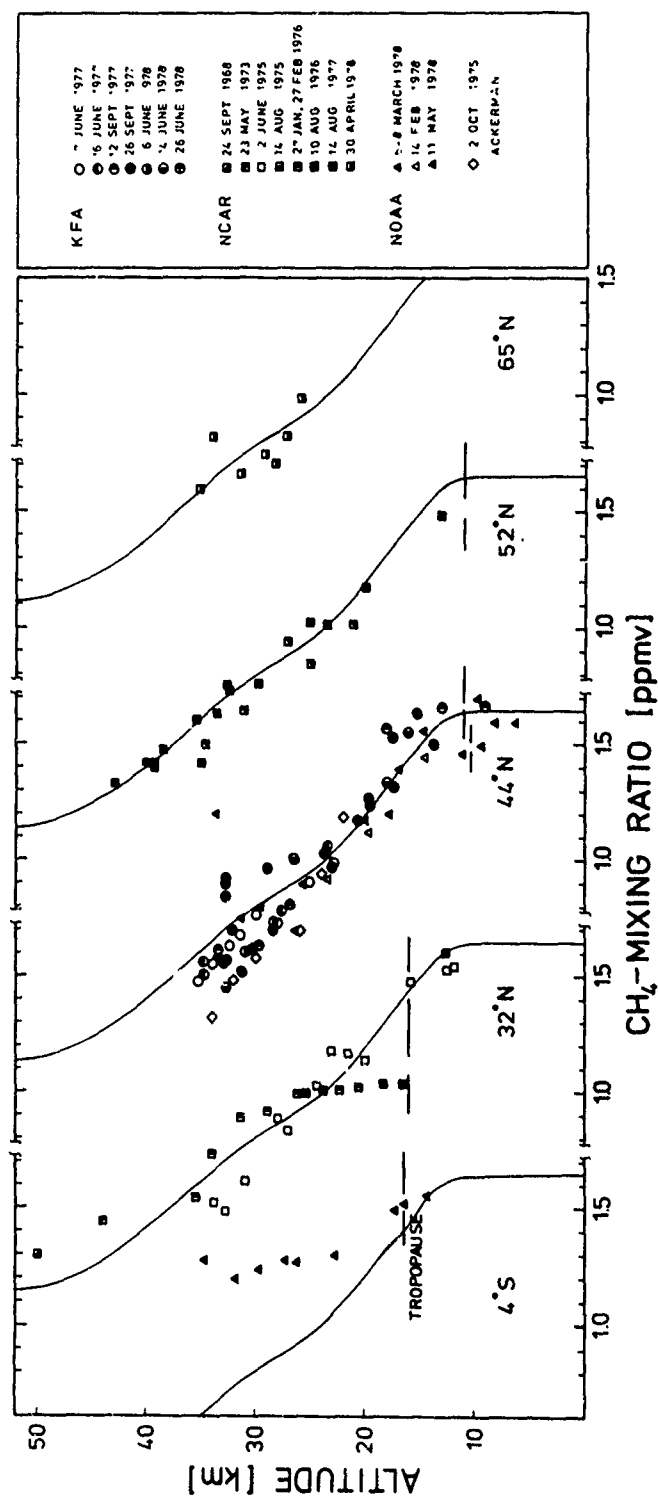


Fig. 7: Experimental data of the CH<sub>4</sub> mixing ratio at several latitudes. For comparison the model profile for 30° N is superposed at any latitude. NCAR-profiles are reported by Heidt et al [1979], NOAA-profiles by Bush et al [1978], KFA-profiles are published by Fabian et al [1978, 1979] (see also text).

CH<sub>4</sub> is destroyed everywhere in the stratosphere, the mixing ratio profiles show a vertical decrease at all latitudes beginning at the local tropopause. The structure of the decrease, however, varies considerably with latitude. The most conspicuous feature is the weak vertical decrease at tropical latitudes. Unfortunately this is so far documented only by one single profile measured over Brazil by Bush et al [1978]. But profiles of N<sub>2</sub>O and CF<sub>2</sub>Cl<sub>2</sub> over Panama and Brazil by Goldan et al [1979] also clearly show that long-lived trace gases in the tropical stratosphere exhibit a significantly weaker vertical decrease - at least during the months January through March. This signifies a considerably stronger upward transport (probably by mean motions) than at mid and high latitudes. At first glance the profiles at the other latitudes seem to agree reasonably well with each other and the calculated comparison profile. But on closer inspection one detects significant differences. The profiles at 32°N collected by Heidt et al [1979] over Palestine, Texas, show a steep decrease at or just below the tropopause, a - sometimes deep - layer of constant mixing ratio in the lower stratosphere, and a steep decrease above. This behavior is quite common, apparently occurring in all seasons. It has been found in a number of profiles collected prior to 1975 and has been commented on previously [Ehhalt and Heidt, 1973a, 1973b; Ehhalt et al, 1975]. The peculiar form of the CH<sub>4</sub> profiles at 32°N latitude can be explained on the basis of the stratospheric Hadley circulation. The sinking poleward motion of the Hadley cell displaces air from the tropical mid stratosphere into the lower stratosphere at 30°N latitude. As long as this air preserves its identity: weak vertical gradient and medium mixing ratio, it will create a layer with a weak gradient and a relatively low CH<sub>4</sub> mixing ratio in the lower stratosphere. At the same time the sinking motion confines the transition between the high tropospheric CH<sub>4</sub> mixing ratio and the lower CH<sub>4</sub> mixing ratio in the stratosphere layer to a shallow zone, thereby compressing the gradient into a steep decrease at the tropopause. Similarly the steeper gradient above the layer is caused by the transition from tropical air with relatively high mixing ratios at these altitudes to air from higher latitudes with lower mixing ratios. This explanation of the structure of the CH<sub>4</sub> profile at 32°N latitude requires that the tropical air can maintain its characteristic CH<sub>4</sub> mixing ratio during its quasi horizontal transport northward. This requires in turn long chemical lifetimes of CH<sub>4</sub> in the lower stratosphere, a condition which is fulfilled (see figure 2).

The CH<sub>4</sub> profiles over 44°N latitude were collected over Wyoming by Bush et al [1978] using grab sampling, and over Southern France by Fabian et al [1979] using cryogenic collection (see also Ehhalt [1978]). Also shown is a profile by Ackerman et al [1977] obtained over Southern France by infrared spectroscopy. These profiles show a different behavior. The decrease above the tropopause (around 10 - 11 km altitude) begins very weakly. In most circumstances tropospheric concentrations prevail to 16 and even 18 km altitude. This fact is probably connected with the frequently observed minima in O<sub>3</sub> concentration a few kilometers above the tropopause of the midlatitudes (c.f. Hering and Borden [1965]). It points to incorporation of tropospheric air into the lower, extratropical stratosphere during the process of tropopause folding (c.f. Hudson [1979]). Above 18 km altitude a more or less linear decrease is generally observed. However in a few instances profiles with distinct layers of nearly constant mixing are also observed at 44°N, for example, the one over Southern France on 26. September 1977, which resembles quite closely some of the profiles found earlier over Palestine, Texas, 32°N (c.f. Ehhalt et al [1975]).

The  $\text{CH}_4$  profiles at  $52^\circ \text{N}$  were obtained over Yorkton, Canada, by Heidt et al [1979]. As far as the data go, they show a linear decrease with altitude starting at the tropopause. Unfortunately all these profiles were taken in August and do not provide seasonal coverage. However, one flight collected over Fairbanks, Alaska,  $65^\circ \text{N}$  on 30. April 1978 shows essentially the same gradient.

It is obvious from figure 7 that the stratospheric distribution of  $\text{CH}_4$  also depends on latitude. The different features seem to be caused by mean vertical and quasi horizontal motions which are beyond the scope of a one dimensional model. However, when combined into a global average profile, the data of figure 7 can be described quite well by a one dimensional model: Apart from its incapability of describing the two dimensional features a one dimensional model seems to explain the globally averaged, stratospheric decrease of  $\text{CH}_4$  quite well.

### $\text{CH}_2\text{O}$

There is only one observation of stratospheric  $\text{CH}_2\text{O}$ . It is a high resolution infrared absorption measurement of the total overburden from the ground [Barbe et al, 1979]. The obtained column density was  $5 \times 10^{15}$  molecules/ $\text{cm}^2$  with an estimated error of a factor of 2. From the observed line shape and a theoretical profile of  $\text{CH}_2\text{O}$  in the troposphere the authors deduced a  $\text{CH}_2\text{O}$  concentration profile which is shown in figure 8. (Incidentally this profile implies a column density of about  $2 \times 10^{15}$  molecules/ $\text{cm}^2$  and is thus not consistent with the value given above.) The experimental  $\text{CH}_2\text{O}$  profile is compared to a theoretical profile corresponding to the  $\text{CH}_2\text{O}$  mixing ratio profile in figure 6. The form of the experimental profile in the stratosphere depends strongly on the author's assumption of a concentration of  $2 \times 10^6$  molecules/ $\text{cm}^3$  at 15 km and may not be correct. However, the overburden above 10 km deduced from the experimental profile in figure 8,  $1.5 \times 10^{14}$  molecules/ $\text{cm}^2$ , agrees within the error limits given by the authors with that from the theoretical profile.

### $\text{H}_2$

The most recent stratospheric measurements of molecular hydrogen,  $\text{H}_2$ , are summarized in figure 9. There are vertical profiles available at three latitudes, but - in contrast to  $\text{CH}_4$  -  $\text{H}_2$  shows little vertical, and even less latitudinal variation. The data at  $44^\circ \text{N}$ , over Southern France, are the only ones which show a clear decrease with altitude - from 0.55 ppm at the tropopause to 0.45 ppm at 35 km altitude [Ehhalt, 1978; Fabian et al, 1979]. A similar trend although with a much larger scatter can be deduced from the data at  $52^\circ \text{N}$  over Yorkton, Canada [Heidt et al, 1979]. No such trend is found for the data at  $32^\circ \text{N}$  over Palestine, Texas [Heidt et al, 1979], on the contrary, in the lower stratosphere the  $\text{H}_2$  mixing ratio from both flights seem to show a slight increase, a fact which had also been noted in previous profiles and led to an average profile with a slight maximum just below 30 km altitude [Ehhalt et al, 1977].

It should be noted, that the absolute calibration of NCAR's measurement is about 10 % lower than ours (KFA), a fact which is also indicated by the data in the upper troposphere and lower stratosphere (figure 9). For proper comparison NCAR's data should have been shifted by 0.05 ppm to higher values, emphasizing a maximum around 30 km altitude at  $32^\circ \text{N}$  lati-



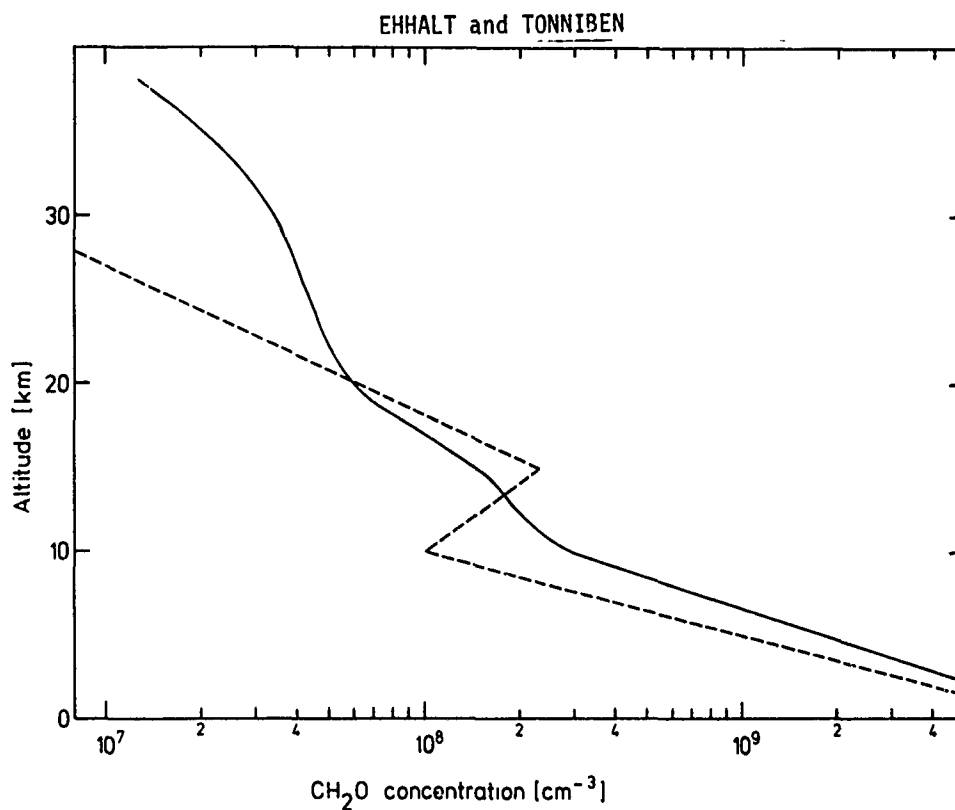


Fig. 8: Experimental and calculated  $\text{CH}_2\text{O}$  concentration profile. The experimental values (dashed curve) are taken from Barbe et al [1979], the theoretical profile corresponds to the mixing ratio profile in fig. 6.

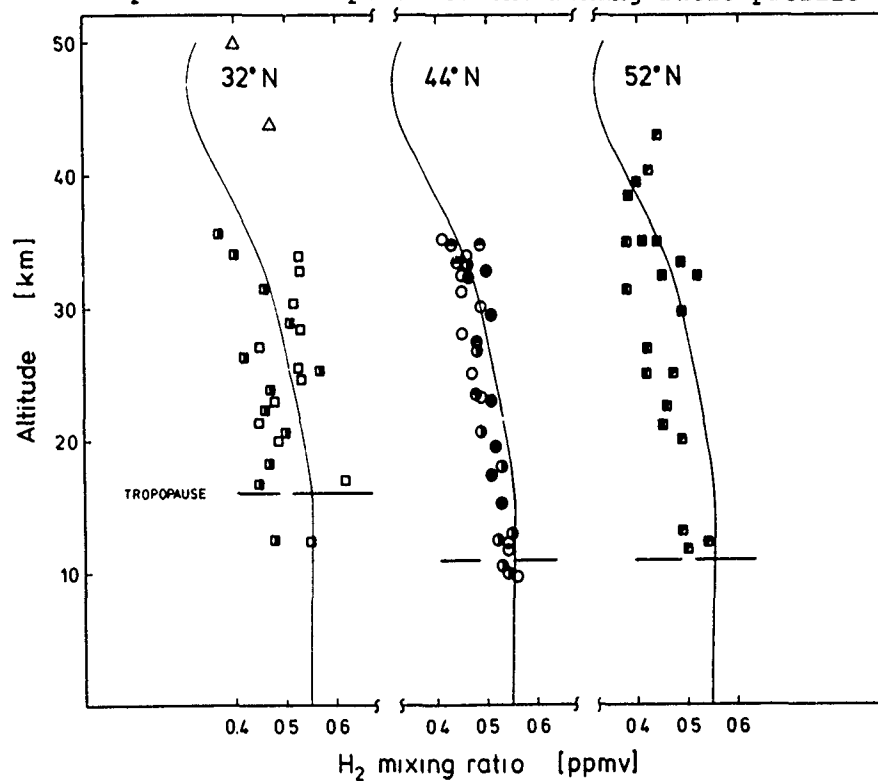


Fig. 9: Vertical profiles of the  $\text{H}_2$  mixing ratio in the stratosphere at several latitudes. Data sources and symbols as in fig. 7.

tude and bringing the data at  $52^{\circ}$  N into better agreement with those at  $44^{\circ}$  N latitude. The larger scatter in the recent data as well as in the previous data make the conclusion of a  $H_2$  maximum somewhat ambiguous. However, slightly increased levels of  $H_2$  at around 30 km altitude at  $32^{\circ}$  N are not unexpected: As it is seen from figure 7, the  $CH_4$  levels around 30 km altitude above  $32^{\circ}$  N are generally elevated above the global average values, possibly due to quasi horizontal advection of tropical air by the Hadley circulation. It is further seen in a qualitative way from figure 4 that elevated levels of stratospheric  $CH_4$  could lead to increased  $H_2$  concentrations. The increase in  $H_2$  concentration will also depend on the time for which the elevated  $CH_4$  levels in the stratosphere are maintained above a given altitude to let the  $H_2$  grow in. Because of the long chemical lifetime of  $H_2$  in the stratosphere this time has to be in the order of one year to produce a measurable increase. Since the travel time of equatorial air arriving at  $30^{\circ}$  N may vary widely, this would also explain some of the scatter found in the stratospheric  $H_2$  concentration over Palestine, Texas,  $32^{\circ}$  N. It should be noted that in those events, during which layers of elevated  $CH_4$  mixing ratios were found over Southern France,  $44^{\circ}$  N, the  $H_2$  mixing ratios around 30 km altitude were also increased. The profile from 26. September 1977 is such an example. As pointed out in the discussion of figure 7 it has significantly higher  $CH_4$ -mixing ratios above 30 km altitude, and figure 9 shows that the corresponding  $H_2$  mixing ratios are increased above the average as well. We may therefore conclude that the observed latitudinal differences in the  $H_2$ -distribution, although quite small, are nevertheless real and connected with the latitudinal variation of the  $CH_4$  profiles. The description of  $H_2$  by one dimensional models seems satisfactory.

### $H_2O$

$H_2O$  is one of the most abundant and most important trace gases in the stratosphere. Yet the measurement of stratospheric  $H_2O$  is still a somewhat controversial subject: Large temporal and spatial variations have been observed, and it is still not clear how much of this variability has been instrumental scatter and how much represents true fluctuations in stratospheric water vapor. Part of the difficulties arises from the fact that a variety of techniques can be and have been used to measure stratospheric water vapor, each one having its own distinct analytical and interpretational problems, so that systematic errors are likely to contribute to the observed scatter.

The techniques employed so far and the measurements obtained from them have been critically reviewed by Harries [1976] and Penndorf [1978]. Such critical analysis is way beyond the scope of the present paper. Thus in contrast to the previous paragraphs in which it was attempted to represent all available data, we will restrict the discussion of  $H_2O$  here to measurements obtained by cryogenic collection [Pollock et al., 1979].

Figure 10 combines the vertical profiles of the water vapor mixing ratio over Yorkton, Sask.,  $55^{\circ}$  N, and Fairbanks, Alaska,  $65^{\circ}$  N. For comparison an average profile of the water vapor mixing ratio over Washington, D.C.,  $39^{\circ}$  N, is included representing the median values for the period 1964-1973 [Mastenbrook, 1974]. The data from  $55^{\circ}$  N and  $65^{\circ}$  N cluster rather closely around Mastenbrook's profile or around its extrapolation to higher altitudes. However they indicate the vertical increase much more clearly than Mastenbrook's data. The highest sample from the Yorkton flight shows a rather high mixing ratio which may be due to contamination. Otherwise the scatter of the data as well as their measurement error is rather small.

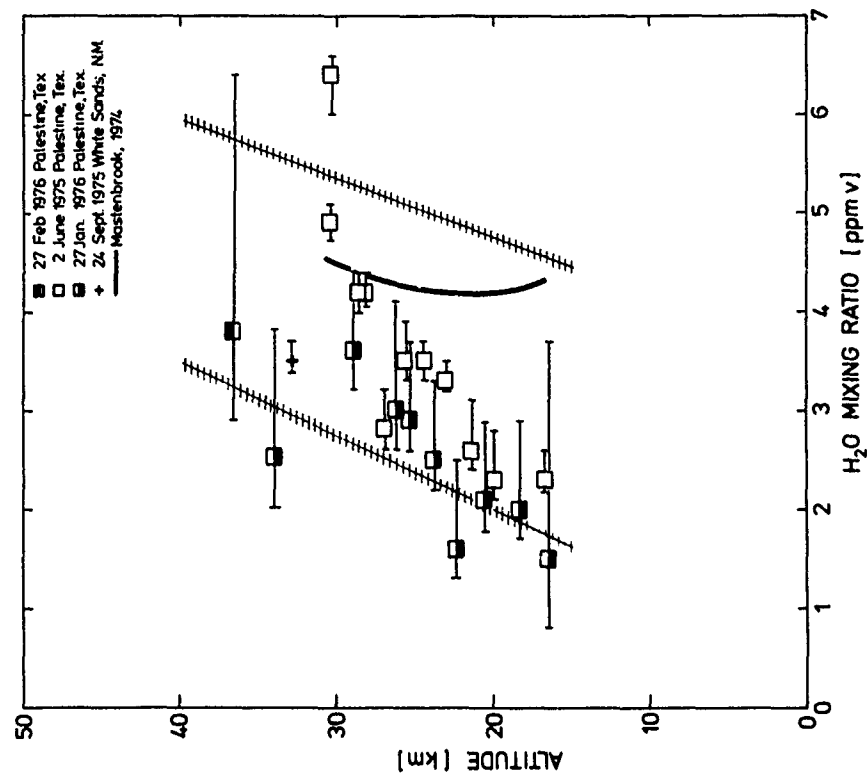


Fig. 10: Vertical profiles of water vapor mixing ratio at higher latitudes. Hatched lines indicate the smoothed variance of individual measurements reported by Harries [1976]. Data points are from Pollock et al [1979].

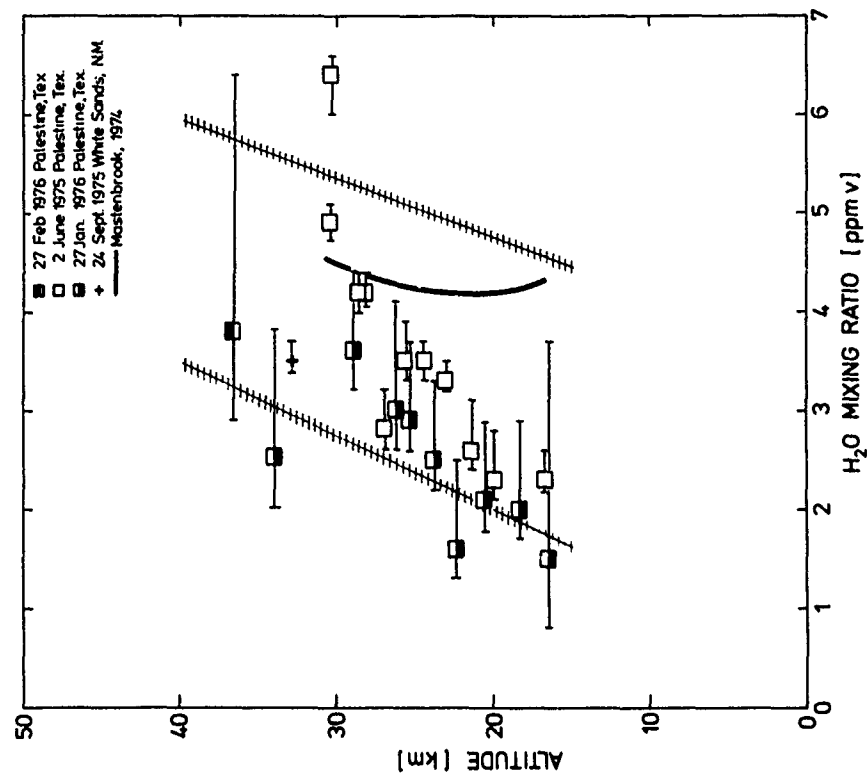


Fig. 11: Vertical profiles of water vapor mixing ratio at 32° N latitude. Hatched lines as in figure 10. Data points are taken from Pollock et al [1979].

Figure 11 combines the water vapor data obtained over Palestine, Texas, and White Sands, N.M., both at  $32^{\circ}$  N. There the measurement errors are larger, especially those from the flight on 27. Jan. 1976. These data were collected during the earlier flights, when experimental procedures were not yet optimized. Still, the error of most measurements and the scatter in the experimental data are quite reasonable. The data over  $32^{\circ}$  N exhibit significantly lower water vapor mixing ratios in the lower stratosphere between 16 and 25 km altitude than Mastenbrooks average profile over Washington, D.C., or the data at higher latitudes.

The profiles at  $32^{\circ}$  N also show a steeper increase in the water vapor mixing ratio with altitude, than those at higher latitudes, and therefore, at about 30 km altitude they reach concentrations similar to those found for the higher latitude profiles. Unfortunately, there are only a few published profiles available for comparison covering the same altitude range at  $32^{\circ}$  N. These tend to show a similar steep increase in the lower stratosphere [Burkert et al, 1974; c.f. Harries, 1976]. Most recently 1978 Gille and Russell [quoted in UAP-Bulletin, June 1979] measured a profile over Palestine, Texas, which does show an even steeper increase than the ones reported here with similar low mixing ratios in the lowest stratosphere. If shown to be a persistent feature at these latitudes, the low concentrations at 15 to 20 km altitude and  $32^{\circ}$  N would point to a strong latitudinal variation in stratospheric water vapor. Horizontal aircraft flights in the lower stratosphere by Kuhn [1975] and Hilsenrath et al [1977] did not show mixing ratios at  $30^{\circ}$  N as low as those found here, nor did they reproduce the latitudinal pattern suggested by the present measurements, although strong latitudinal variations were observed. McKinnon and Moorewood [1970] reported low mixing ratios between 17 and 19 km at all latitudes with much less variation. Their data have minima around  $30^{\circ}$  latitude and would agree better with present measurements.

The main advantage of the cryogenic collection technique is the fact that it allows the simultaneous measurements of all major hydrogen compounds:  $H_2O$ ,  $CH_4$ , and  $H_2$ . This we can use to test one of the assumption implicit in 1-D-modelling namely that the sum of all hydrogen compounds must be constant with altitude.

Any strong deviation of the measured averages for total hydrogen from vertical constancy would point to the existence of atmospheric transport processes which do not average out to give a simple  $k_z$  parameterization of vertical transport. This would indicate a basic inability of 1-D-models to describe global averages properly. The vertical profiles of the total hydrogen mixing ratio ( $1 \times H_2O$ ,  $2 \times CH_4$ ,  $1 \times H_2$ ) corresponding to the  $H_2O$  profiles are shown in figure 12. The first impression from the data is that of little vertical or horizontal variation, especially when the error bars are considered. The increase of the water vapor mixing ratio seen in figures 10 and 11 appears to be virtually compensated by the decrease in  $CH_4$  concentration with altitude. From the average of the present data we would conclude that the vertical increase in stratospheric  $H_2O$  can be essentially explained by the stratospheric oxidation of  $CH_4$  to  $H_2O$ .

Still there is some fine structure left in the vertical profiles of total hydrogen with fluctuations or possible trends around 1 ppm, part of which seems to be significant and could be real. Such fluctuations will require further explanation. Additional processes are also required for some of the published profiles. Even among the most recent data there are profiles with a vertical increase in  $H_2O$  mixing ratio far too steep to be explained only by the oxidation of  $CH_4$  [c.f. UAP-Bulletin, 79-3]. To explain those profiles or others which show maxima at intermediate altitudes,

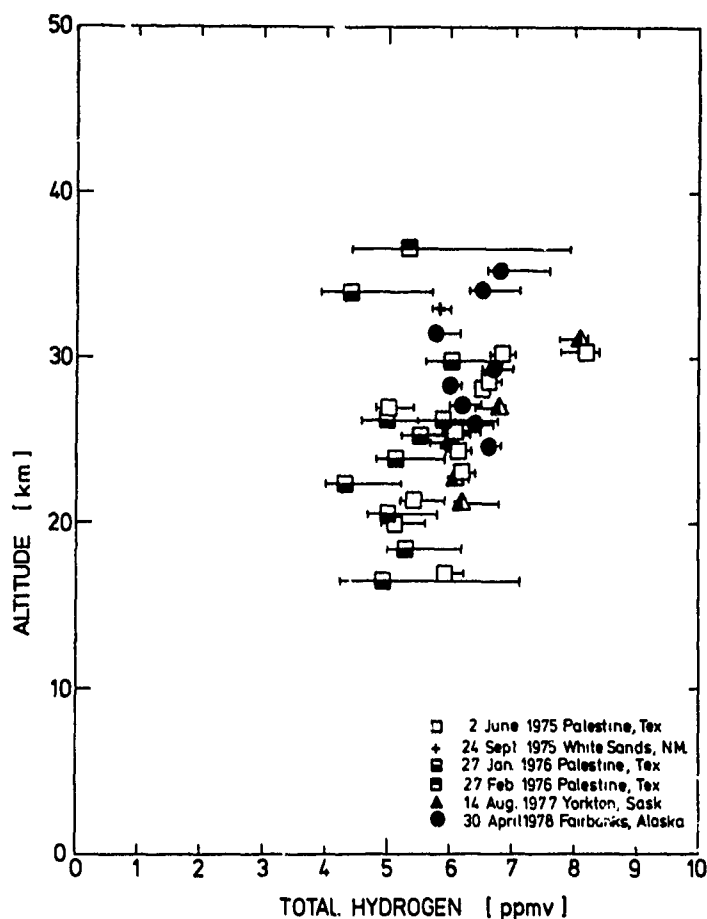


Fig. 12: Total hydrogen content in the stratosphere (data source as in figures 10 and 11).

further mechanisms have definitely to be invoked. There are a number of processes and parameters governing the transport of  $H_2O$  into the stratosphere [Elsaesser, 1974] which can cause such fluctuations. One of the most important ones is the tropopause temperature at the site of upward transport. There are temporal (short-term, seasonal and secular) and spatial variations in the altitude and temperature of the tropical tropopause. A change of only  $4^\circ C$  around  $-80^\circ C$ , the average tropopause temperature in the tropics, causes a change in saturation pressure of a factor of 2, enough to cause substantial fluctuations in the  $H_2O$  mixing ratio of the air transmitted through the tropopause. Such fluctuations with different vertical length scales and amplitudes up to a few ppm can superimpose on the general increase of the  $H_2O$  mixing ratio based on  $CH_4$  oxidation. It may sometimes strengthen it, sometimes weaken or even invert it. Most recent measurements are within the bounds of possible fluctuations. However because of the observed and quite possibly natural fluctuations it is still difficult to establish a mean vertical profile and latitudinal dependences.

#### CO

Only few data exist on the stratospheric distribution of CO. The more recent data are summarized in figure 13. Unfortunately, most measurements obtained by cryogenic collection have been troubled by contamination which rendered the samples collected at higher altitudes useless. The CO contamination occurred during collection, apparently through reaction of stratospheric  $O_3$  with hydrocarbons absorbed on the inner walls of the

inlet line. The cryogenic measurements above 20 km altitude showed widely scattered CO mixing ratios increasing with altitude to about 200 ppb at 30 km [Ehhalt, 1978; Fabian et al, 1979]; they are omitted from figure 13. The cryogenic samples collected below 20 km altitude are essentially free of contamination due to the continued flushing of the inlet line during descent, and lower  $O_3$  but higher CO concentrations at lower altitudes. These data show a strong decrease in the CO mixing ratio in the upper troposphere and lower stratosphere reaching about 10 ppb around 20 km altitude, about 10 km above the tropopause. In the altitude range between 20 and 35 km the only data published recently are those of Farmer et al [1979]. The profile shows a more or less constant mixing ratio of 10 ppb. There is some evidence of an increase in the CO mixing ratio in the upper stratosphere based on one sample collected cryogenically between 40 and 50 km altitude by a rocket [Ehhalt et al, 1975]. Owing to the large size of this sample, 300 l STP, and the short collection time, 10 sec, the sample should be essentially free of contamination. Considering the differences in tropopause altitude the experimental data are reasonably well described by the calculated profile.

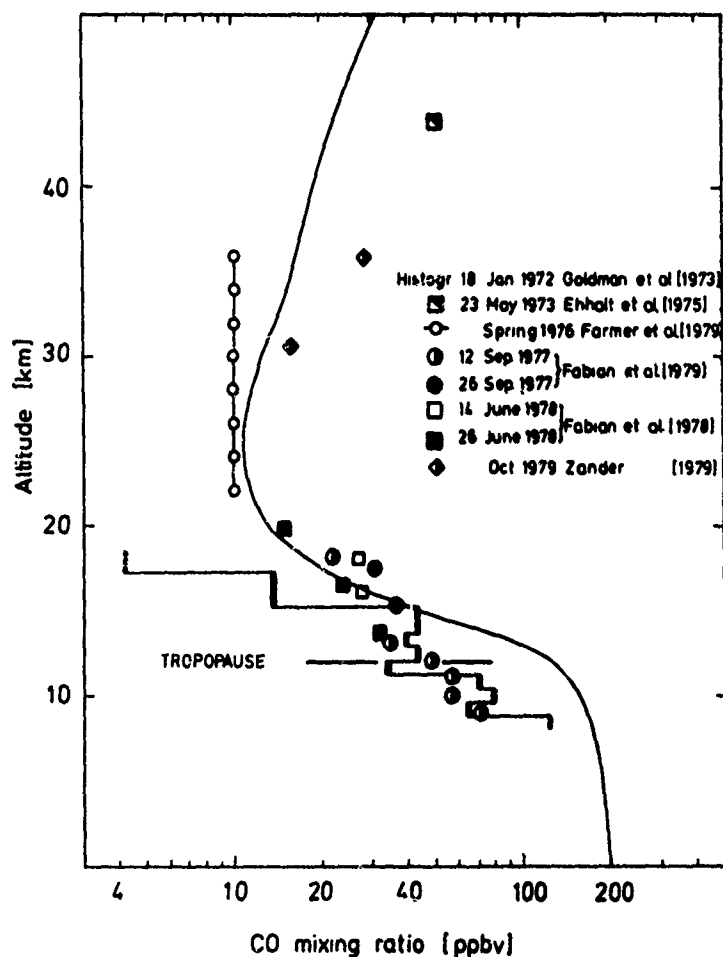


Fig. 13: Vertical profiles of the CO mixing ratio in the stratosphere. Data from Farmer et al and Goldman et al were measured by IR spectroscopy, other data were obtained by cryogenic sampling.

CO<sub>2</sub>

Except for its photolysis in the upper stratosphere to yield CO, CO<sub>2</sub> is of little importance for the stratospheric chemistry. However, because of its absorption of infrared radiation, it is quite important for the stratospheric radiation balance. For the same reason it is important for the measurement of stratospheric temperature from satellites. The radiance utilized by satellite borne instruments to monitor stratospheric temperature comes from CO<sub>2</sub>. The retrieval of a stratospheric temperature profile requires the knowledge of the stratospheric CO<sub>2</sub> profile. This is usually assumed to be constant with altitude. However any error in the CO<sub>2</sub> concentration propagates into the retrieved temperature, an error of 1 % in the CO<sub>2</sub> concentration at a given altitude will cause an error of 0.5 % to 1 %, or 1 to 2 K, in the retrieved temperature at that altitude [Gille, private communication]. Thus it seems very important to know the stratospheric CO<sub>2</sub> distribution with good precision. Yet CO<sub>2</sub> is probably the trace gas most neglected by in situ sampling, although it can be measured with relative ease and high precision by gas chromatography. Figure 14 summarizes the available measurements [c.f. Volz et al, 1979]. The data show considerable scatter, part of which is due, however, to the secular increase

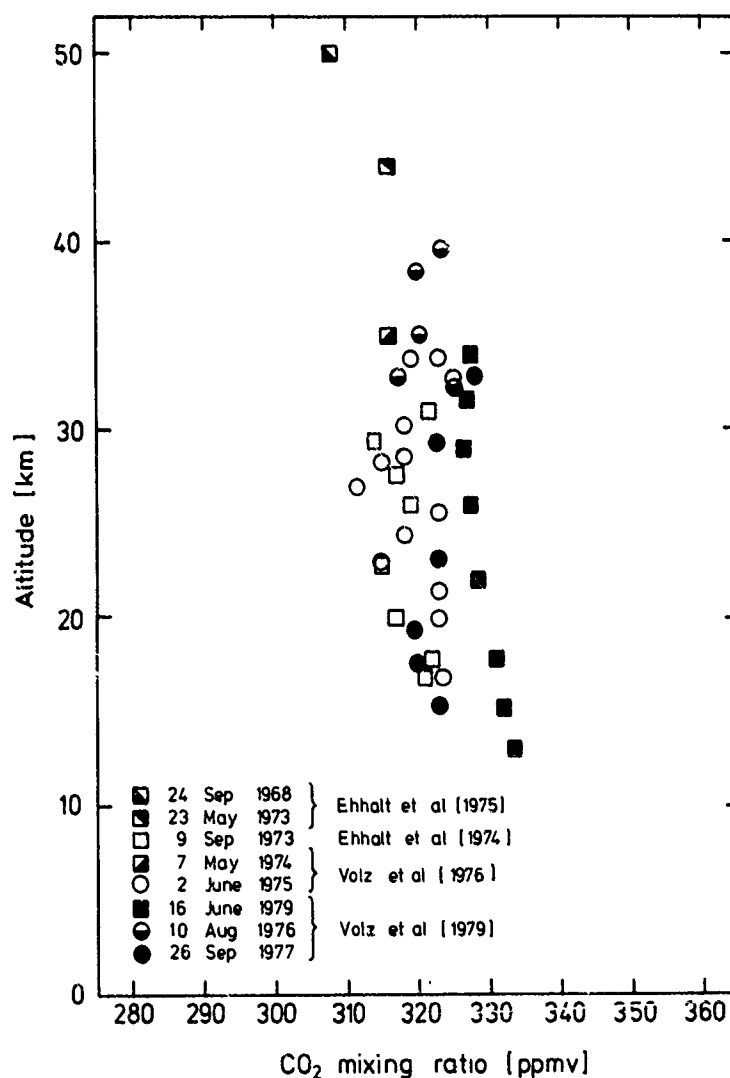


Fig. 14: Vertical profiles of the CO<sub>2</sub> mixing ratio in the stratosphere.

in atmospheric  $\text{CO}_2$  concentration between the rather widely spaced sampling dates. Another part is due to the fact that the earlier  $\text{CO}_2$  measurements had  $1\sigma$  errors above 1 %. On the average the  $\text{CO}_2$  mixing ratio is constant with altitude over the observed altitude range.

However individual profiles can show deviations from uniform mixing. The most recent profile from 16. June 1979 over Southern France shows a more or less steady decrease in  $\text{CO}_2$  mixing ratio from 333 ppm at the tropopause to 326 ppm at 32 km altitude which - in view of the high precision of about  $\pm 1$  ppm with which these measurements were made - is considered real. To bring out the long term increase on the  $\text{CO}_2$ , which fossil fuel burning causes also in the stratosphere, the altitude averaged concentrations from these flights are plotted against time in figure 15. Only samples above 20 km altitude were included in the averages to remove any influence from tropospheric air. The data exhibit a clear increase with a rate of about  $1.4 \pm 0.2$  ppm per year, which is close to the one observed in the troposphere over the past decade.

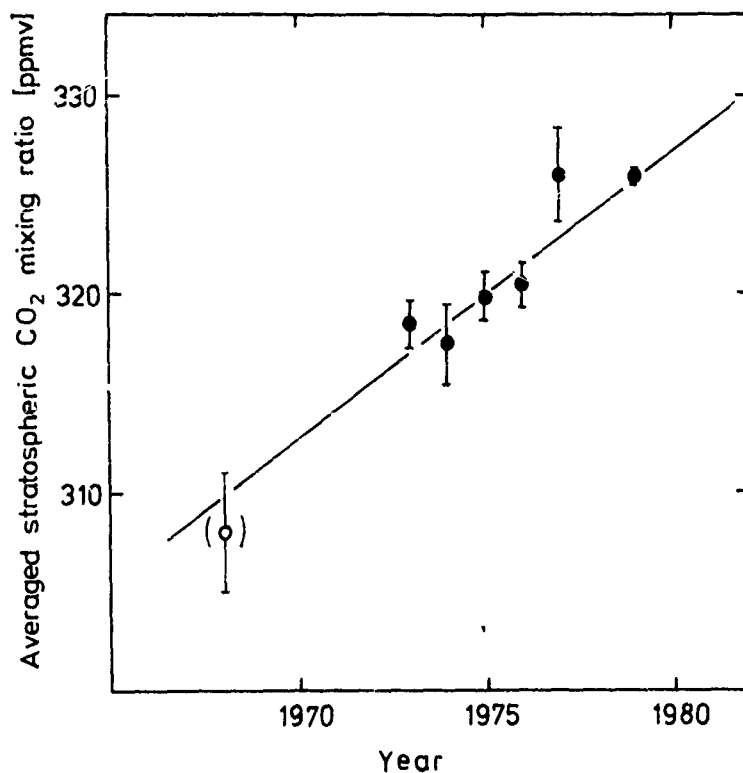


Fig. 15: The secular increase of the stratospheric  $\text{CO}_2$  mixing ratio. O: Single rocket sample; ●: av of balloon profiles. The rocket sample was not included in the regression analysis.



5. CONCLUSION: The comparison in the previous paragraphs show that, as far as the hydrogen and carbon compounds are concerned, one dimensional models provide an adequate description of the globally averaged vertical distribution; for the averages the differences between experimental data and theoretical profiles remain generally below 20 %. With the advance of more data from different latitudes and in different seasons, however, it becomes clear that significant, for  $\text{CH}_4$  or  $\text{H}_2\text{O}$  even large, differences may exist between the concentrations at different latitudes which 1-D-models will not be able to describe. The present rather incomplete data sets seem to indicate that these differences are mainly connected with the stratospheric branch of the tropical Hadley cell, which as a matter of principle cannot be treated in the 1 D models.

# REFERENCES

- Ackerman, M., D. Frimout, and C. Müller, Stratospheric  $\text{CH}_4$ ,  $\text{HCl}$ , and  $\text{ClO}$  and the Chlorine-Ozone Cycle, Nature, 269, 226, 1977.
- Barbe, A., P. Marché, C. Secroun, P. Jouve, Measurements of Tropospheric and Stratospheric  $\text{H}_2\text{CO}$  by an Infrared High Resolution Technique, Geophysical Research Letters, 6, 463, 1979.
- Bass, A.M., L.C. Glasgow, C. Miller, J.P. Jesson, D.L. Filkin, Temperature Dependent Absorption Cross Sections for Formaldehyde ( $\text{CH}_2\text{O}$ ): The Effect of Formaldehyde on Stratospheric Chlorine Chemistry, submitted to Planetary and Space Science, 1979.
- Burkert, P., D. Rabus, H.J. Bolle, Stratospheric Water Vapor and Methane Profiles, in: IAMAP, p. 267, International Association of Atmospheric Physics, Melbourne, Australia, 1974.
- Bush, Y.A., A.L. Schmeltekopf, F.C. Fehsenfeld, D.L. Albritton, J.R. McAfee, P.D. Goldan, E.E. Ferguson, Stratospheric Measurements of Methane at Several Latitudes, Geophysical Research Letters, 5, 1027, 1978.
- Crutzen, P.J., I.S.A. Isaksen, J.R. McAfee, The Impact of the Chlorocarbon Industry on the Ozone Layer, Journal of Geophysical Research, 83, 345, 1978.
- DeMore, W.B., L.J. Stief, F. Kaufman, D.M. Goldan, R.F. Hampson, M.J. Kurylo, J.J. Margitan, M.J. Molina, R.T. Watson (ed.), Chemical Kinetic and Photochemical Data for Use in Stratospheric Modelling, JPL 79-27, 1979.
- Ehhalt, D.H., L.E. Heidt, The Concentration of Molecular  $\text{H}_2$  and  $\text{CH}_4$  in the Stratosphere, Pageoph, 106-108, 1352, 1973a.
- Ehhalt, D.H., L.E. Heidt, Vertical Profiles of  $\text{CH}_4$  in the Troposphere and Stratosphere, Journal of Geophysical Research, 78, 5265, 1973b.
- Ehhalt, D.H., L.E. Heidt, R.H. Lueb, E.A. Martell, Concentrations of  $\text{CH}_4$ ,  $\text{CO}$ ,  $\text{CO}_2$ ,  $\text{H}_2$ ,  $\text{H}_2\text{O}$ , and  $\text{N}_2\text{O}$  in the Upper Stratosphere, Journal of the Atmospheric Sciences, 32, 163, 1975a.
- Ehhalt, D.H., L.E. Heidt, R.H. Lueb, W. Polluck, The Vertical Distribution of Trace Gases in the Stratosphere, Pageoph, 113, 389, 1975b.
- Ehhalt, D.H., In Situ Measurements of Stratospheric Trace Constituents, Reviews of Geophysics and Space Physics, 16, 217, 1978.
- Elsaesser, H.W., Water Budget of the Stratosphere, Proc. III. Conf. Climatic Impact Assessment Program, 26. Febr. - 1. March 1974, Cambridge, Mass. DOT-TSC-OST-14-15.
- Fabian, P., R. Borchers, K.H. Weilers, U. Schmidt, A. Volz, D.H. Ehhalt, W. Seiler, F. Müller, The Vertical Distribution of  $\text{H}_2$ ,  $\text{CH}_4$ ,  $\text{CO}$ ,  $\text{N}_2\text{O}$ ,  $\text{CFCl}_3$  and  $\text{CF}_2\text{Cl}_2$ , II. Proceedings of the Second Meeting of the CEC Study Groups, Brüssels, 1978.
- Fabian, P., R. Borchers, K.H. Weiler, U. Schmidt, A. Volz, D.H. Ehhalt, W. Seiler, F. Müller, Simultaneously Measured Vertical Profiles of  $\text{H}_2$ ,  $\text{CH}_4$ ,  $\text{CO}$ ,  $\text{N}_2\text{O}$ ,  $\text{CFCl}_3$  and  $\text{CF}_2\text{Cl}_2$  in the Midlatitude Stratosphere and Troposphere, Journal of Geophysical Research, 84, 3149, 1979.

- Farmer, C.B., O.F. Raper, B.D. Robbins, R.A. Toth, C. Müller, Simultaneous Spectroscopic Measurements of Stratospheric Species:  $O_3$ ,  $CH_4$ ,  $CO$ ,  $CO_2$ ,  $N_2O$ ,  $H_2O$ ,  $HCl$  and  $HF$  at Northern and Southern Midlatitudes, submitted to Journal of Geophysical Research, 1979.
- Gille, J., Private Communication, 1979.
- Goldan, P.D., W.G. Kuster, D.L. Albritton, A.L. Schmeltekopf, Stratospheric  $CFCl_3$ ,  $CF_2Cl_2$  and  $N_2O$  Height Profile Measurements at Several Latitudes, submitted to Journal of Geophysical Research, 1979.
- Goldman, A., D.G. Murcray, F.H. Murcray, W.J. Williams, J.N. Brooks, C.M. Bradford, Vertical Distribution of  $CO$  in the Atmosphere, Journal of Geophysical Research, 78, 5273, 1973.
- Hampson, R.F., D. Garvin (ed.), Reaction Rate and Photochemical Data for Atmospheric Chemistry 1977, NBS-SP-513, 1978.
- Harries, J.E., Distribution of Water Vapor in the Stratosphere, Reviews of Geophysics and Space Physics, 14, 565, 1976.
- Heidt, L.E., quoted in: R.L. Hudson (ed.), The Stratosphere: Present and Future, NASA Reference Publication, 1979.
- Heidt, L.E., W.A. Pollock, R.A. Lueb, and J.P. Krasnec, Vertical Distributions of Stratospheric Trace Gases at Northern Latitudes, presented at the Symposium on the Budget and Cycles of Trace Gases and Aerosols in the Atmosphere, by the Commission on Atmospheric Chemistry and Global Pollution, 12-18 August 1979, Boulder, Colorado.
- Hering, W.S., T.R. Borden jr., Ozone Sonde Observations over Northern America, AFRCL-64-30, I/II/III, 1965.
- Hilsenrath, E., B. Guenther, P. Dunn, Water Vapor in the Lower Stratosphere Measured from Aircraft Flight, Journal of Geophysical Research, 82, 5453, 1977.
- Hudson, R.L. (ed.), The Stratosphere: Present and Future, NASA Reference Publication, 1979.
- Isaksen, I.S.A., K.H. Midtbø, J. Sunde, P.J. Crutzen, A Simplified Method to Include Molecular Scattering and Reflection in Calculations of Photon Fluxes and Photodissociation Rates, Geophysica Norvegica, 31, 11, 1977.
- Kuhn, P.M., L.P. Stevens, M.S. Lojko, Latitudinal Profiles of Stratospheric Water Vapor, Geophysical Research Letters, 2, 227, 1975.
- Mastenbrook, H.J., Water Vapor Measurements in the Lower Stratosphere, Canadian Journal of Chemistry, 52, 1527, 1974.
- McKinnon, D., and H.W. Moorewood, Water Vapor Distribution in the Lower Stratosphere over North and South America, Journal of the Atmospheric Sciences, 27, 483, 1970.
- Moortgat, G.K., P. Warneck,  $CO$  and  $H_2$  Quantum Yields in the Photo-decomposition of Formaldehyde in Air, Journal of Chemical Physics, 70, 3639, 1979.
- Penndorf, R., Analysis of Ozone and Water Vapor Field Measurement Data, US Dept. Transport, Federal Aviation Administration Rept. No FAA-EE-78-29, 1978.
- Pollock, W., L.E. Heidt, R. Lueb, D.H. Ehhalt, Measurement of Stratospheric Water Vapor by Cryogenic Collection, submitted to Journal of Geophysical Research, 1979.
- Röth, E.P., A. Tönnißen, Th. Janssen-Schmidt, Report from Study-Group III (Modelling) on the Ozone Depletion Problem, Commission of the European Communities, to be published, 1979.
- Upper Atmospheric Bulletin 79-3, 1979, FAA, Washington
- Volz, A., D.H. Ehhalt, L.E. Heidt, W. Pollock, Vertical Profiles of  $CH_4$ ,  $CO$  and  $CO_2$  in the Stratosphere, Proceedings of the Joint Symposium on Atmospheric Ozone, Aug. 1976, Dresden GDR, Vol. II, 219, 1977.
- Volz, A., D.H. Ehhalt, F.J. Johnen, A. Khedim, U. Schmidt, L.E. Heidt, Vertical Profiles of  $CFCl_3$ ,  $CF_2Cl_2$ ,  $N_2O$ ,  $CH_4$  and  $CO_2$  in the Stratosphere, WMO-Symposium on the Geophysical Aspects and Consequences of Changes in the Composition of the Stratosphere, 12-18 August, 1979, Boulder, Colorado.

- Watson, R., Laboratory Studies of the Oxidation of  $\text{CH}_3$  Radicals of Stratospheric Interest, Nato Advanced Study Institute, Atmospheric Ozone, Aldeia das Acoteias, Portugal, 2-13 Oct. 1979.
- Wofsy, S.C., M.B. McElroy, On Vertical Mixing in the Upper Stratosphere and Lower Mesosphere, Journal of Geophysical Research, 18, 2619, 1973.
- Zander, R., Complementary Aspects of Ground Based and Balloon Borne Spectroscopic Measurements of Minor Telluric Species: Applications to HF, HCl,  $\text{CH}_3\text{Cl}$  etc., MPAAE-Workshop on Stratospheric Trace Gas Measurements, Bad Lauterberg, FRG, 22-24 Oct. 1979.

# THE HOMOGENEOUS CHEMISTRY OF FORMALDEHYDE GENERATION

## AND DESTRUCTION WITHIN THE ATMOSPHERE

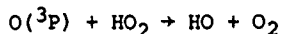
Jack G. Calvert

Chemistry Department, The Ohio State University, Columbus,  
Ohio, U.S.A., 43210

### Abstract

The available information related to the formation and decay reactions of formaldehyde in the atmosphere has been reviewed. A critical evaluation of the many published studies of the primary photodecomposition reactions I and II, has led to new recommended values for the primary quantum efficiencies,  $\phi_I$  and  $\phi_{II}$ , as a function of wavelength and altitude (pressure):  $\text{CH}_2\text{O} + h\nu \rightarrow \text{H} + \text{HCO}$  (I);  $\text{CH}_2\text{O} + h\nu \rightarrow \text{H}_2 + \text{CO}$  (II). These data were combined with recently determined ultraviolet cross sections for  $\text{CH}_2\text{O}$  [Bass et al., 1979] and actinic irradiances to estimate first order photolytic rate constants  $J_I$  and  $J_{II}$  applicable to the lower atmosphere and at different altitudes within the 5-55 km range. A current best estimate of the theoretical formaldehyde concentration-altitude profile in the atmosphere was derived using these new data and other recent rate constant estimates. Several photochemical and rate parameters involving  $\text{CH}_2\text{O}$  were identified for further study in order to provide a quantitative description of the role of formaldehyde in atmospheric chemistry.

I. INTRODUCTION: There are several important aspects of the atmospheric chemistry of formaldehyde which have been identified in recent years. In the polluted urban atmosphere formaldehyde and other aldehydes are expected to have a major influence on the rate of photochemical smog generation [Demerjian et al., 1974]. The higher concentrations of the aldehydes ( $\text{CH}_2\text{O}$ ,  $\text{CH}_3\text{CHO}$ , etc.) present initially in the polluted air decrease the induction period observed for ozone, peroxyacetyl nitrate and other product formation and increase the final concentrations of these irritants in sunlight-irradiated smog mixtures [Jeffries and Kamens, 1977; Pitts et al., 1976]. Throughout the upper and lower atmosphere formaldehyde is a major source of both molecular hydrogen and carbon monoxide [Levy, 1973]. Furthermore, the reactions of formaldehyde within the atmosphere provide a significant fraction of the  $\text{HO}_2$  radicals which are generated at some altitudes. Of course the  $\text{HO}_2$  radical is one of the important species which controls the "odd oxygen",  $\text{O}(^3\text{P})$ ,  $\text{O}_3$ ,  $\text{O}(^1\text{D})$ , levels in the atmosphere through its reactions with  $\text{O}_3$  and  $\text{O}(^3\text{P})$ -atoms:



In this work we will review the chemistry of formaldehyde and identify remaining areas of uncertainty which must be removed to achieve a quantitative understanding of the roles of formaldehyde in atmospheric chemistry.

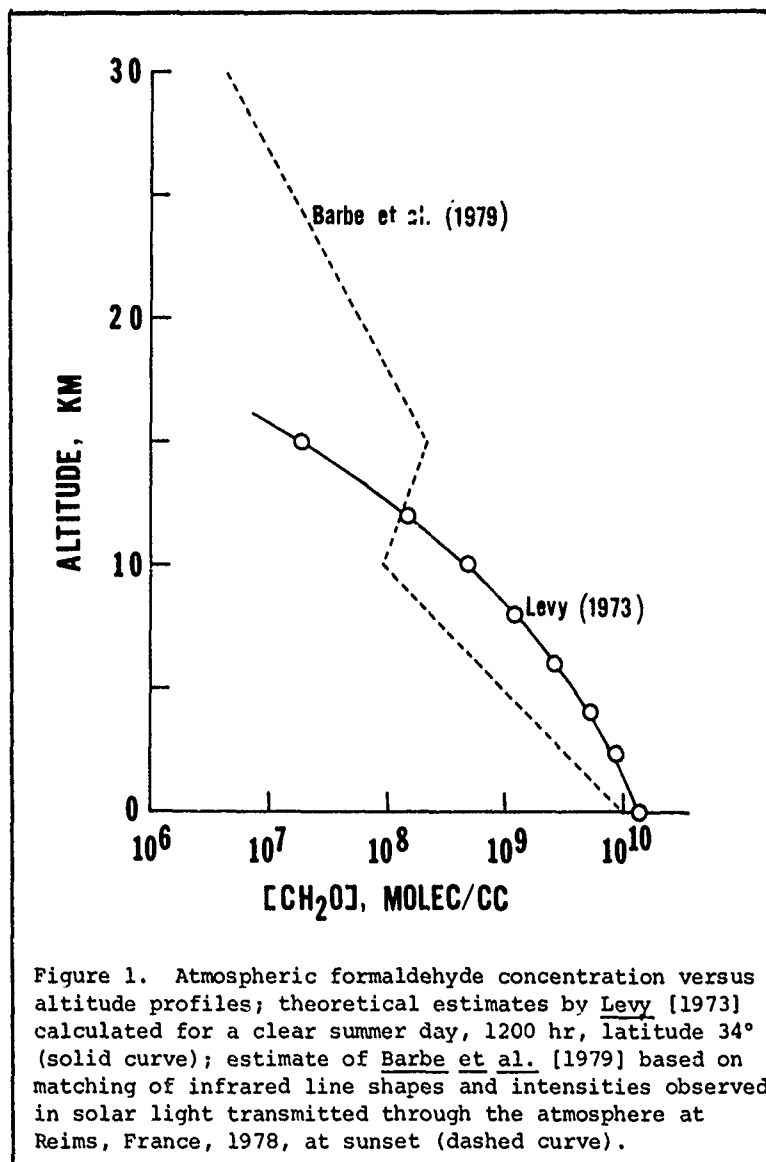
**II. THE AMBIENT LEVELS OF FORMALDEHYDE:** Formaldehyde ( $\text{CH}_2\text{O}$ ) is a truly ubiquitous compound in nature. It has been observed in the lower atmosphere, both in remote regions of the earth as well as in the highly polluted urban areas. It is even an identified constituent of interstellar space [Snyder et al., 1969; Rank et al., 1971]. Ambient clean air measurements made throughout the world show small quantities of aldehydes, presumably largely formaldehyde, to be present: Panama, <0.2 to 2.7 ppb [Lodge et al., 1966]; Antarctica, <0.5 to 10 ppb [Fischer et al., 1968]; Amazon Basin, 1.0 to 6.0 ppb [Pate et al., 1970]; rural Illinois and Missouri, 1.0 to 2.0 ppb [Breeding et al., 1973]. Formaldehyde levels measured in maritime air at Dagebüll, Germany were about 0.2 ppb [Platt et al., 1979]. Thus it appears that background concentrations of aldehydes in sunlight-irradiated ambient clean air are commonly of the order of 1-2 ppb over land masses and somewhat less (about 0.2 ppb) over the seas. This difference appears to result from the somewhat more efficient removal of  $\text{CH}_2\text{O}$  by dissolution in surface waters than by the solid surfaces of the land masses. It is interesting to note that Galbally [1972] has suggested that the photodecomposition of  $\text{CH}_2\text{O}$  ( $\text{CH}_2\text{O} + h\nu \rightarrow \text{H}_2 + \text{CO}$ ) in surface ocean waters and in rain water may be the origin of the CO supersaturation which has been observed in these systems [Swinerton et al., 1970; Seiler and Junge, 1970].

In polluted urban air aldehyde concentrations are typically higher than those found in clean, remote regions of the earth. For example, the following concentrations of total aliphatic aldehydes (24 hr, annual averages) were reported in several cities in the United States [referenced by Jeffries and Kamens, 1978]: Cincinnati, Ohio (1973), 11.7 ppb; Houston, Texas (1974), 7.8 ppb; St. Paul, Minnesota (1974), 11.7 ppb. A large fraction (some 30-75%) of the aliphatic aldehydes formed in the urban atmosphere is commonly formaldehyde, although acetaldehyde and the higher aliphatic aldehydes as well as acrolein and aromatic aldehydes are present by virtue of the unique hydrocarbon sources which are found in the polluted urban atmosphere [Altshuller and McPherson, 1963]. The formaldehyde and total aldehyde levels in a poorly ventilated urban atmosphere commonly show diurnal variations which are characteristic of ozone and many other products of photochemical smog. However this may not be the case in relatively clean atmospheres; thus Platt et al. [1979] found no strong daily variations of formaldehyde concentrations under stable weather conditions in the lower atmosphere near the outskirts of the small town of Jülich, West Germany. On rare occasions the maximum levels of aldehydes have been observed to rise during the day to over 100 ppb in highly polluted areas such as Los Angeles, California.

In most of the studies of aldehyde concentrations in the lower atmosphere somewhat indirect chemical methods of analysis have been employed. The formaldehyde or the higher aldehydes were converted to visible light-absorbing chemical derivatives and the amounts then determined by visible absorption spectrometry. These methods are generally sound, but possible interferences can create problems. It warms the heart of a doubting physical chemist to see that less ambiguous, direct spectroscopic methods of identification of formaldehyde in ambient air are now being employed. Recently Tuazon et al. [1978] have followed directly formaldehyde concentrations in ambient air at Riverside, California through the use of long-path, Fourier transform infrared spectroscopy. During one day (October 14, 1977) formaldehyde concentrations were observed to rise to 40 ppb at the 1700 hr. Recently Platt et al. [1979] have utilized the characteristic ultraviolet absorption of  $\text{CH}_2\text{O}$  at three strong bands near 3261, 3297, and 3309 Å together with long path lengths (5-10 km) within the atmosphere to follow  $\text{CH}_2\text{O}$  concentrations near ground level at several sites in Germany. In Jülich the average  $\text{CH}_2\text{O}$  concentration was about 2 ppb with peak values as high as 6.5 ppb.

The first direct spectroscopic detection of formaldehyde in the clean upper atmosphere was reported recently by Barbe et al. [1979]. In observations made from ground level in Reims, France (altitude 83 m) the absorptions due to six strong  $\text{CH}_2\text{O}$  infrared lines were observed in solar light transmitted through the clean atmosphere at sunset during November and December, 1978. From the shapes of the two absorption lines at 2806.858 and 2869.871  $\text{cm}^{-1}$  and suitable reference to theoretical  $\text{CH}_2\text{O}$  concentration-altitude profiles, the column concentrations and the approximate atmospheric distribution of  $\text{CH}_2\text{O}$  as a function of altitude were estimated. These data are reproduced as the dashed curve in Figure 1. They suggest that formaldehyde levels decrease from the maximum at ground level, near  $10^{10}$  molec  $\text{cm}^{-3}$  (0.4 ppb) to about  $10^7$  molec  $\text{cm}^{-3}$  (0.02 ppb) near 26 km altitude, with a concentration buldge near 15 km.

Levy [1973] published the first theoretical estimates of the vertical profile of  $\text{CH}_2\text{O}$  in the atmosphere from a somewhat abbreviated chemical reaction sequence and the older rate and photo-



chemical data then available to him. This profile calculated for a summer noon at 34° N latitude is shown also in Figure 1 as the solid line. Although the concentration buldge in the stratosphere which is suggested from the limited data of Barbe et al. is not predicted, the magnitudes of the  $[\text{CH}_2\text{O}]$  at various altitudes are in qualitative accord. Obviously many more accurate experimental measurements of the  $\text{CH}_2\text{O}$  concentrations, both made directly at given altitudes and as total column densities, are required as well as more sophisticated theoretical estimates in order to make any definitive test of the proposed formaldehyde formation and decay mechanisms in the atmosphere.

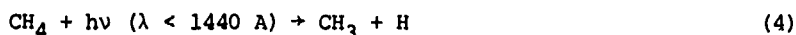
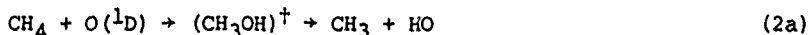
It is the hope of the present author to provide a review and evaluation of the present rate constant and photochemical information which is required to make accurate theoretical estimates of the  $[\text{CH}_2\text{O}]$ -altitude profiles and to identify seemingly important information which is not available today. We will confine most of our considerations to the relatively clean atmosphere, recognizing however that formaldehyde source terms involving many different hydrocarbon impurities are expected to be very important in the lower troposphere near urban areas. We will consider first some of the most important formaldehyde generating reactions which must occur in the atmosphere. Then the removal mechanisms will be discussed--those involving intermediate species in the atmosphere and the photochemical pathways. Finally we will attempt to gauge the relative significance of the various processes which control formaldehyde levels in each region of the atmosphere and derive a current best theoretical estimate of the  $\text{CH}_2\text{O}$  concentration-

altitude profile.

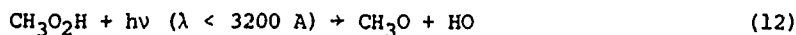
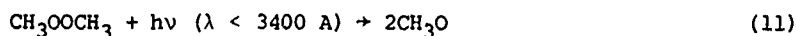
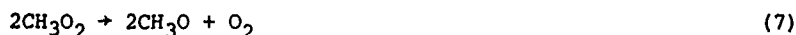
III. THE CHEMICAL REACTIONS GENERATING FORMALDEHYDE WITHIN THE ATMOSPHERE: The incomplete oxidation of methane ( $\text{CH}_4$ ) and other hydrocarbons present in the atmosphere generates formaldehyde among many other products. Of course methane is the dominant hydrocarbon component in the air. Because of its relatively low reactivity with HO-radicals,  $\text{O}(^3\text{P})$ -atoms, and ozone molecules, it survives to populate even the upper atmosphere, although at a mixing ratio greatly reduced from that near ground level (1.6 ppm). Many of the higher molecular weight hydrocarbons have relatively short half-lives (of the order of hours or days) in the sunlight-irradiated troposphere, so they are expected to be only minor constituents of the upper atmosphere to which transport times are long.

Recently interest has developed in the possible role of hydrocarbons other than methane in the stratospheric chemistry. The best candidate for the possible significant participation is the ethane ( $\text{C}_2\text{H}_6$ ) molecule which is the second least reactive alkane toward the HO-radical. Indeed Singh et al. [1979] have observed from their analyses of the atmosphere near ground level that the concentration of  $\text{C}_2\text{H}_6$  in the northern hemisphere is relatively uniform, approaching 2 ppb at the northern midlatitudes but dropping off to about 1 ppb near the equator. The first vertical distributions of ethane and acetylene ( $\text{C}_2\text{H}_2$ ) which extend into the lower stratosphere have been reported recently by Cronn and Robinson [1979]. The average upper tropospheric concentrations (between 6 and 11 km, near  $37^\circ\text{N}$ ,  $123^\circ\text{W}$ ) were 1.0 ppb for ethane and 0.23 ppb for acetylene. Although there are detectable quantities of both ethane and acetylene in the lower stratosphere, a significant drop in their mixing ratios occurs above the tropopause; here ethane levels ranged from about 0.1 to 0.75 ppb while acetylene values were somewhat less (0 to 0.1 ppb).

The major atmospheric reactions of methane which lead ultimately to formaldehyde have been considered by many workers; for examples and references to the earlier literature see: McEwan and Phillips [1975], Heicklen [1976], and Stief et al. [1978]. The reactions are the following:



Most of the methyl radicals ( $\text{CH}_3$ ) formed in these reactions will react ultimately within the atmosphere to generate formaldehyde. The principal reactions are the following:



If one follows through the sequence of reactions (5) through (13) he will note that a major

# CALVERT

portion of the methane which takes part in reactions (1), (2), (3), and (4) will lead to CH<sub>2</sub>O. The rate limiting steps for this transformation are reactions (1) through (4). In Table I current best estimates of the rate constants for these key reactions are summarized. The

Table I

Summary of Current Best Estimates of the Rate Constants for Several Reactions of Importance in Formaldehyde Generation Within the Atmosphere<sup>a</sup>

Reaction	Recommended Rate Constant, cc molec <sup>-1</sup> sec <sup>-1</sup>
(1) CH <sub>4</sub> + HO → CH <sub>3</sub> + H <sub>2</sub> O	2.4 × 10 <sup>-12</sup> e <sup>-(1710 ± 200)/T</sup>
(2a) CH <sub>4</sub> + O( <sup>1</sup> D) → CH <sub>3</sub> + HO	1.3 × 10 <sup>-10</sup>
(2b) CH <sub>4</sub> + O( <sup>1</sup> D) → CH <sub>2</sub> O + H <sub>2</sub>	0.14 × 10 <sup>-10</sup>
(3) CH <sub>4</sub> + Cl → CH <sub>3</sub> + HCl	9.9 × 10 <sup>-12</sup> e <sup>-(1359 ± 150)/T</sup>

<sup>a</sup>Recommendation of NASA Panel for Data Evaluation [1979].

effective first order rate constants for methane photolysis which apply for the solar radiation at various altitudes, latitudes, and seasons have been estimated and published by Nicolet [1971].

It is instructive to note the relative significance of the reactions leading to CH<sub>2</sub>O formation at various altitudes. This can be seen from the data shown in Table II. The generation of

Table II

The Relative Significance of the Formaldehyde Formation Reactions from Methane as a Function of Altitude (1200 hr, 30°N, solar equinox)<sup>a</sup>

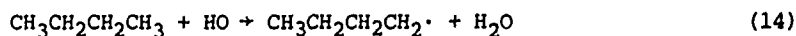
	(A) CH <sub>4</sub> + HO → CH <sub>3</sub> + H <sub>2</sub> O			
	(B) CH <sub>4</sub> + O( <sup>1</sup> D) → CH <sub>3</sub> + HO → CH <sub>2</sub> O + H <sub>2</sub>			
	(C) CH <sub>4</sub> + Cl → CH <sub>3</sub> + HCl			
	(D) CH <sub>4</sub> + hν → CH <sub>3</sub> + H CH <sub>3</sub> + O <sub>2</sub> → CH <sub>3</sub> O <sub>2</sub> → CH <sub>2</sub> O			
Altitude, km	Rate of Reaction, molec cc <sup>-1</sup> sec <sup>-1</sup> × 10 <sup>-3</sup>			
	A	B	C	D
10	45.6	0.089	0.65	0
20	7.6	0.73	1.00	0
30	4.9	2.5	0.75	0
40	3.7	2.8	0.82	0
50	0.65	0.50	0.15	0
60	0.017	0.015	----	0
70	0.001	0.001	----	0.041
80	0	0	----	0.020
90	0	0	----	0.0008

<sup>a</sup>The 10-50 km rates are from Wuebbles [1979]; the 60-90 km rates were calculated using data of Nicolet [1979].



$\text{CH}_2\text{O}$  through HO-radical attack on  $\text{CH}_4$  is a dominant pathway throughout most of the atmosphere. The  $\text{O}(^1\text{D})$  and Cl-atom reactions with  $\text{CH}_4$  become significant sources of  $\text{CH}_2\text{O}$  from 20 to 50 km altitudes. The methane photodecomposition by light absorption at wavelengths less than 1440 Å becomes the major source of  $\text{CH}_3$  and ultimately  $\text{CH}_2\text{O}$  formation at 70 km and above. The  $\text{O}(^1\text{D})$  and Cl-atom reactions with  $\text{CH}_4$  were not included in the first theoretical  $\text{CH}_2\text{O}$  concentration-altitude profile calculations of Levy in 1973. Incorporation of these pathways into his reaction scheme leads to somewhat higher  $\text{CH}_2\text{O}$  levels within the 20-40 km region, in better accord with the approximate profile derived from the experimental  $\text{CH}_2\text{O}$  infrared band shapes by Barbe *et al.* [1979]; see Figure 1.

In the lower atmosphere where the higher hydrocarbons can be a significant reactant, additional large sources of formaldehyde and other aldehydes exist. Also the direct emission of aldehydes to the atmosphere may occur from the incomplete combustion of hydrocarbon fuels in internal combustion engines and other sources. In illustration of the nature of the chemical pathways which generate aldehydes in the polluted lower troposphere, consider the decay of n-butane ( $\text{n-C}_4\text{H}_{10}$ ), a typical impurity alkane. The dominant removal mechanism in the lower atmosphere involves the attack of the HO-radical on the hydrocarbon:



Reaction (15) occurs about 3.5-times faster than (14) at 298 K. However even the slower of these reactions has a rate constant about 200-times that for the analogous reaction (1) involving methane. The reaction sequence which follows (14) generates  $\text{CH}_2\text{O}$  and every other possible straight chain aldehyde containing 4-carbon atoms or less. This is shown in schematic form in Figure 2 where the aldehyde products are highlighted in boxes. Some other reactions of the alkylperoxy ( $\text{RO}_2$ ), alkoxy ( $\text{RO}$ ), and acylperoxy ( $\text{RCOO}_2$ ) radicals not shown in Figure 2 compete with those given here, but the aldehyde forming reactions are expected to dominate in the polluted atmosphere. A similar set of reactions occurs following reaction (15) in which formaldehyde, acetaldehyde ( $\text{CH}_3\text{CHO}$ ), propionaldehyde ( $\text{CH}_3\text{CH}_2\text{CHO}$ ), and methyl ethyl ketone ( $\text{CH}_3\text{COCH}_2\text{CH}_3$ ) are the expected products; a further discussion of these and other examples is given by Demerjian *et al.* [1974]. Indeed most of the impurity alkane, alkene, and aromatic hydrocarbon molecules present in the troposphere, both from anthropogenic and natural sources, can lead to formaldehyde and the higher aldehydes through their reactions with HO-radicals as well as ozone and  $\text{O}(^3\text{P})$ -atoms in the lower atmosphere.

The half-lives of the reactive higher alkanes are relatively short in the polluted lower troposphere, of the order of 10 hr. The highly reactive alkenes have much shorter half-lives, about an hour or so, in the polluted troposphere. In the clean lower troposphere where an average concentration of HO-radicals may be of the order of  $10^6 \text{ molec cc}^{-1}$ , the half-life of n-butane is about 70 hr in contrast to that of  $\text{CH}_4$  which is about 2.5 yr. If the levels of reactive hydrocarbons such as n-butane climb above the 0.5 ppb level in the natural lower troposphere, then the contribution of these compounds to the formation of  $\text{CH}_2\text{O}$ ,  $\text{CH}_3\text{CHO}$ , and the higher aldehydes and ketones will become significant; at these levels they will contribute more than 10% of the total aldehyde formation in the troposphere.

The decomposition of the ethane molecule in the troposphere is of special interest in atmospheric chemistry in view of its seemingly significant concentration here. It is anticipated that ethane will be removed largely by attack of the HO-radical:

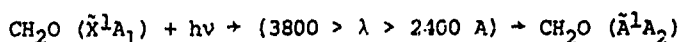


The ethyl radical ( $\text{C}_2\text{H}_5$ ) will react largely to generate acetaldehyde ( $\text{CH}_3\text{CHO}$ ), formaldehyde, and other products as shown schematically in the lower left of Figure 2; the reactive peroxy radicals,  $\text{CH}_3\text{O}_2$ ,  $\text{CH}_3\text{COO}_2$ , and  $\text{HO}_2$  which form in the photooxidation of the  $\text{CH}_3\text{CHO}$  molecules can in theory influence the ultimate ozone level of the stratosphere provided that sufficient  $\text{C}_2\text{H}_6$  enters the stratosphere. The aldehyde generation rate which we anticipate from the relatively unreactive ethane molecule, observed recently at the 1 ppb level in the troposphere, should amount to only a few percent of the rate of formaldehyde formation from methane. However if the atmospheric burden of ethane and the other non-methane hydrocarbons increases dramatically from anthropogenic sources in the years ahead, then the potential influence of these hydrocarbons on the chemistry of the troposphere and the lower stratosphere will become of concern.



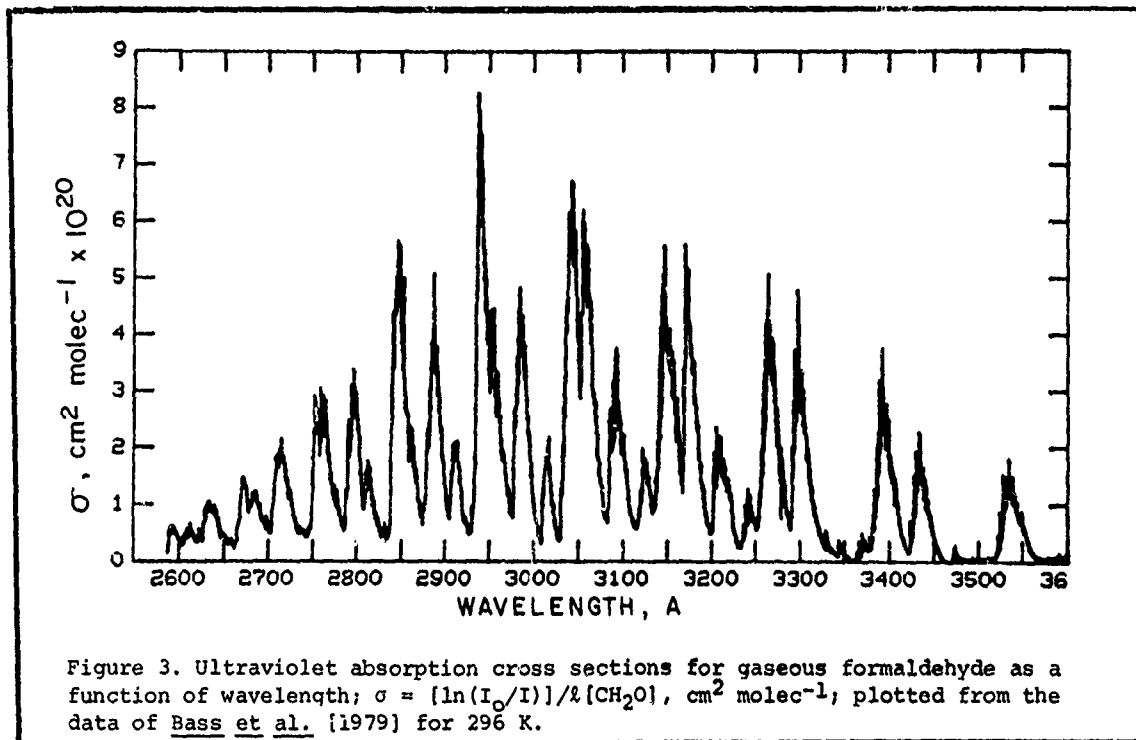
IV. THE CHEMICAL MECHANISMS FOR FORMALDEHYDE REMOVAL IN THE ATMOSPHERE: The buildup of formaldehyde in the atmosphere is suppressed by several natural removal processes. Many of the chemical steps are seemingly well understood, while other chemical and physical processes remain speculative. The action of sunlight on formaldehyde results in its photodecomposition. Also the reaction of the reactive transient species present in the atmosphere, HO, HO<sub>2</sub>, O(<sup>3</sup>P), NO<sub>3</sub>, Cl, etc., may result in the chemical destruction of CH<sub>2</sub>O and the generation of HO<sub>2</sub> radicals. In this section we will review first the current information related to the photochemical reaction pathways of CH<sub>2</sub>O.

IV-A. The Photochemical Processes in CH<sub>2</sub>O: 1) Spectroscopic and Theoretical Evidence of Their Nature. The light absorption which corresponds to the first allowed electronic transition in CH<sub>2</sub>O extends from wavelengths less than 3800 Å to about 2400 Å. Recent cross section measurements for this band made by Bass et al. [1979] are shown in Figure 3. These should replace the use of the earlier data observed using a lower resolution instrument and temperatures near 348 K [Calvert and Pitts, 1966]. There is, of course, a significant overlap of this absorption region with the solar distribution within the atmosphere which may allow sunlight to excite formaldehyde to the  $\tilde{A}^1A_2$  state:



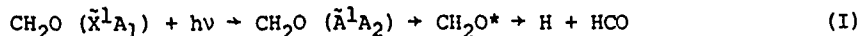
The excitation involves a weakly allowed  $n \rightarrow \pi^*$  electronic transition in which an electron in a non-bonding (n) orbital on oxygen is promoted to the antibonding  $\pi^*$  orbital associated with the carbon-oxygen double bond of formaldehyde. For a further quantitative description of this excitation process see: Harding and Goddard [1975]; Langhoff et al. [1977]. Detailed analyses of the spectral features of this CH<sub>2</sub>O absorption have been made in several studies, and the nature of the vibronic transitions involved appears to be well established; see Brand [1956]; Robinson and DiGiorgio [1958]; Callomon and Innes [1963]; Parkin [1965]; Herzberg [1967]; Job et al. [1969]; Sethuraman et al. [1970].

Formaldehyde shows strong absorption bands at wavelengths below 1770 Å which have been associated with upper excited states of  $1A_1$ ,  $1B_1$ , and  $1B_2$  symmetries in which  $\sigma \rightarrow \pi^*$  and  $\pi \rightarrow \pi^*$  transitions and various Rydberg transitions are involved; see Mentall et al. [1971] and Langhoff et al. [1977]. The onset of photoionization accompanies absorption of light of wavelengths less than 1140 Å. The photochemistry of CH<sub>2</sub>O excited within this short wavelength region is important only in the higher reaches of the atmosphere and in interstellar space,



and we will not consider it further in this work.

The radiative decay of  $\text{CH}_2\text{O}$  excited within the 3800-2400 Å band is relatively unimportant even at low pressures where collisional quenching processes are not significant. The quantum yields of fluorescence are small, a maximum of only a few percent at the longest wavelengths of absorbed light [Yeung and Moore, 1973, 1974; Miller and Lee, 1975]. Indeed the photodecomposition of excited formaldehyde appears to occur with near perfect efficiency for excitation over most of the absorption band. A variety of studies extending over more than forty years show that the photodecomposition of formaldehyde may occur by the two reactions I and II:



Here the excited molecule of undesignated state ( $\text{CH}_2\text{O}^*$ ) represents the  $\tilde{\text{A}}^1\text{A}_2$ ,  $\tilde{\text{a}}^3\text{A}_2$  or a vibrationally excited  $\tilde{\text{X}}^1\text{A}_1$  ground state of  $\text{CH}_2\text{O}$ , and the same state need not be common to both I and II.

The energy relationships between the various low-lying electronic states of  $\text{CH}_2\text{O}$  and the products of I and II and other dissociation products are summarized in Figure 4. The minimum energy required for process I has been the subject of much controversy in the years past. Recent results are shown in Table III. A value consistent with these results is  $\Delta H^\circ_{298} = 87 \pm 2 \text{ kcal mole}^{-1}$  for the reaction  $\text{CH}_2\text{O} \rightarrow \text{H} + \text{HCO}$ . Thus there is sufficient energy per quantum to promote process I for  $\text{CH}_2\text{O}$  absorption at all wavelengths shorter than about  $3287 \pm 75 \text{ Å}$ . The thermal decomposition reaction analogous to II,  $\text{CH}_2\text{O} \rightarrow \text{H}_2 + \text{CO}$ , is slightly exothermic with  $\Delta H^\circ_{298} = -0.5 \pm 0.1 \text{ kcal mole}^{-1}$ . The energy per quantum at wavelengths below 2757 Å is sufficient to promote the fragmentation of both of the C-H bonds in  $\text{CH}_2\text{O}$ ,  $\text{CH}_2\text{O} \rightarrow 2\text{H} + \text{CO}$ ;  $\Delta H^\circ_{298} = 103.7 \pm 0.1 \text{ kcal mole}^{-1}$ .

The nature of the states of  $\text{CH}_2\text{O}$  involved in the primary photodecomposition reactions I and II is not fully proven although this has been considered by many investigators; for example, see the recent reviews of Lee [1977], Avouris et al. [1977], Van Dijk et al. [1978], Kemper et al.

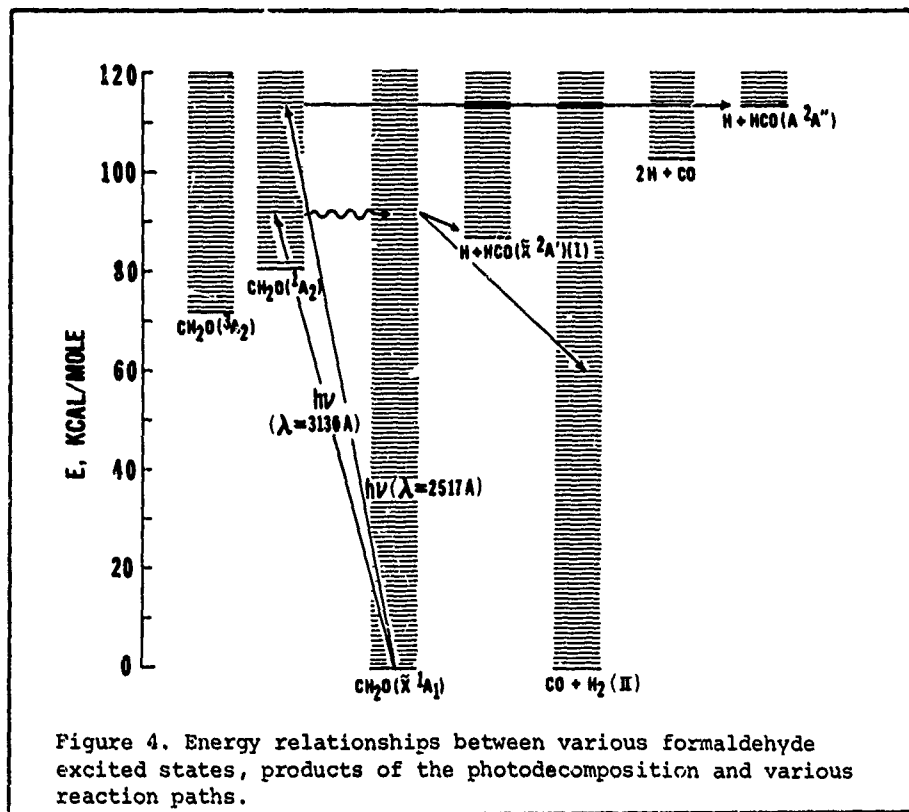


Figure 4. Energy relationships between various formaldehyde excited states, products of the photodecomposition and various reaction paths.

Table III  
Recent Estimates of  $\Delta H^\circ_{298}$  for the Reaction:  $\text{CH}_2\text{O} \rightarrow \text{H} + \text{HCO}$

$\Delta H^\circ_{298}$ , kcal mole <sup>-1</sup>	Method	Reference
87 ± 1	Kinetic data	Walsh, Benson [1966]
88.0 ± 1.6 } 88.3 ± 1.4 }	Photoionization	Warneck [1971] Warneck [1974]
88.5 ± 0.9	Thermal data	Fletcher, Pilcher [1970]
88.8 ± 1.0	Chemiluminescence	Becker et al. [1977]
86.6 } 84.8 ± 0.3 }	Photodissociation limit	Lewis et al. [1976] Horowitz, Calvert [1978] Clark et al. [1978]

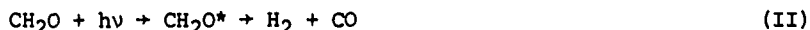
[1978], Goddard and Schaefer [1979], Weisshaar and Moore [1979], and Miller [1979]. The free radical dissociation I from the excited singlet state ( $\tilde{A}^1A_2$ ) correlates with the formation of an H-atom and an electronically excited HCO ( $^2A''$ ) radical; see Figure 4. Energy considerations rule out the significant occurrence of this process at wavelengths larger than 2517 Å. Dissociation by process I through the triplet state ( $\tilde{a}^3A_2$ ) does correlate with ground state H and HCO products, but in this case there is a small energy barrier for dissociation which is anticipated theoretically [Hayes and Morokuma, 1972]. The dissociation from high vibrational levels of the ground electronic state of  $\text{CH}_2\text{O}$  also correlates with the ground state H and HCO products.

A definitive experimental proof of the precursor state to process I is not now at hand, but some interesting experiments which bear on the problem have been reported. Thus Solomon et al. [1971] photolyzed  $\text{CH}_2\text{O}$  under collision-free conditions at low pressures using linearly polarized light from the full spectrum of either mercury or mercury-xenon lamps. The walls of their spherical cell were coated with a tellurium mirror which reacted with H-atoms (and possibly HCO radicals) formed in I. They concluded from the known orientation of the transition electric dipole of  $\text{CH}_2\text{O}$  (in the molecular plane, perpendicular to the C-O bond) and the anisotropy of the tellurium mirror removal that the dominant pathway for the departing H-atom in process I occurs in the direction perpendicular to the molecular plane. In both the triplet and ground state dissociations of  $\text{CH}_2\text{O}$  in process I the expulsion of the H-atom is anticipated to be in a direction perpendicular to the molecular plane. The results require that an extremely rapid photodissociation occur which is faster than the time required for molecular rotation. Solomon et al. [1971] concluded that the  $^1A_2 \rightsquigarrow ^3A_2$  reaction would not occur in this time frame, but the internal conversion,  $^1A_2 \rightsquigarrow \tilde{X}^1A_1(v)$  and dissociation of the vibrationally rich  $\tilde{X}^1A_1(v)$  molecule may be the origin of the effect. These results of Solomon et al. are somewhat surprising in view of the significant delay observed in the appearance of CO product from process II following  $\text{CH}_2\text{O}$  excitation at 3371 Å [Houston and Moore, 1976]. Obviously Solomon et al. would not have observed anisotropy of the mirror removal if such a delay were present in the free radical product formation in their experiments. Presumably the short wavelengths which were absorbed preceding process I in their experiments led to highly excited  $\text{CH}_2\text{O}$  molecules of very short lifetimes which account for this difference. Since the wavelength range responsible for the effects seen by Solomon et al. was not defined, conclusions derived from the experiment may not be relevant to the primary processes which occur at the longer wavelengths.

Recently Tang et al. [1977] have helped elucidate the nature of the state responsible for I in a series of rather ingenious experiments. They studied the effects of rotational state dependence on the quantum yields of fluorescence and H-atom formation both within and outside of the region of strong singlet-triplet perturbations observed in the Zeeman spectrum of  $\text{CH}_2\text{O}$  [Brand and Stevens, 1973]. The quantum yield of H-atom formation was essentially constant for the various rotational levels studied, while the fluorescence quantum yield showed some strong variations within the same band. An analysis of these results suggested that the triplet state ( $\tilde{a}^3A_2$ ) must have a minor or negligible role in the photochemical mechanism for the  $2^4_1$  level of the  $\tilde{A}^1A_2$  state excited at 3260 Å, and the  $\tilde{A}^1A_2 \rightsquigarrow \tilde{X}^1A_1(v)$  internal conversion preceding I is probably the most important pathway for its radiationless decay, at least within the limited vibronic range studied here.

There has been both theoretical [Lucchese and Schaefer, 1978; Kemper et al., 1978; Goddard and Schaefer, 1979] and experimental evidence [Sodeau and Lee, 1978; Diem and Lee, 1979] which suggests that the formaldehyde isomer, hydroxymethylene (HOCH) may be an intermediate in the  $\tilde{A}^1A_2 \rightsquigarrow \tilde{X}^1A_1(v)$  conversion in  $CH_2O$  photolysis which precedes dissociation. This possibility was apparently first considered by Houston and Moore [1976] in their attempts to rationalize the delay in the appearance of dissociation products following  $\tilde{A}^1A_2$  disappearance. Theoretical calculations predict that the ground state of the trans-HOCH species lies at an energy about 53 kcal mole<sup>-1</sup> above the  $CH_2O(\tilde{X}^1A_1)$  ground state. The experimental evidence for the involvement of the HOCH molecule in  $CH_2O$  photodissociation is not unambiguous at this time, and acceptance of this interesting hypothesis and further speculation on the mechanistic details of primary process I in  $CH_2O$  photolysis should await further definitive experimentation.

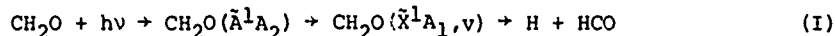
Theoretical studies show that the primary process II probably occurs from the vibrationally excited ground state of  $CH_2O$ ; see Jaffee et al. [1974], Gillispie and Lim [1976], Goddard and Schaefer [1979], Weisshaar and Moore [1979], and Miller [1979].



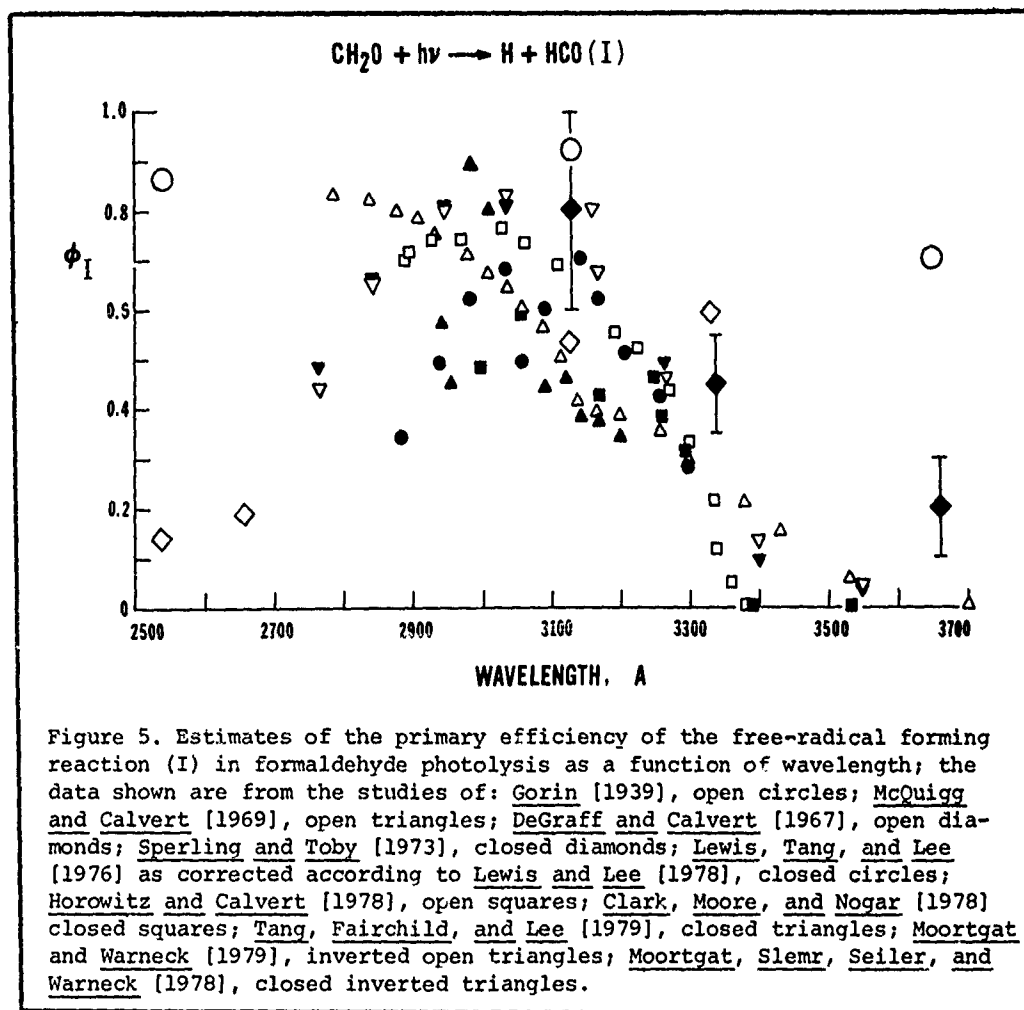
The  $^1A_2$  and  $^3A_2$  states which correlate with excited states of CO and  $H_2$ , increase in energies substantially as the molecule begins to dissociate. At no geometry examined by Jaffee et al. did this energy come close to the potential energy surface of the  $\tilde{X}^1A_1$  ground state. Therefore they concluded that it is unlikely that the  $CH_2O$  molecule partially dissociates on the  $^1A_2$  or  $^3A_2$  surfaces and then crosses over to the  $\tilde{X}^1A_1$  state to reach the ground state products. Only one pathway for II was found to exist within the calculated energy regime of  $CH_2O$  (<5 eV): a planar asymmetric path on the ground state potential energy surface. It appears to be well accepted today that process II does occur from the vibrationally excited ground state molecule following internal conversion from the excited  $^1A_2$  state. However Jaffee et al. point out that the interesting theoretical problem remains as to how vibrational energy of the hot molecule on the  $\tilde{X}^1A_1$  surface is converted from the initially large excess in the out-of-plane bending and C-O stretching modes into the energy of the reaction coordinate for II, a mixture mainly of C-H stretching and asymmetric bending modes.

It is interesting to note that Miller and Lee [1974] observed that the equivalent of process II occurred when the  $CH_2O(\tilde{a}^3A_2)$  species was generated from triplet benzene ( $^3B_{1u}$ ) by energy transfer. They estimated that the maximum overlap for energy transfer probably occurs at about 78 kcal mole<sup>-1</sup> in this case. Thus only a negligible fraction of the  $CH_2O(^3A_2)$  molecules formed initially is expected to have the  $87 \pm 2$  kcal mole<sup>-1</sup> necessary for the occurrence of process I. However CO and  $H_2$  were formed, presumably through the molecular decomposition II. This implies that the  $CH_2O(^3A_2)$  molecules underwent an intersystem crossing:  $^3A_2 \rightsquigarrow \tilde{X}^1A_1(v)$ . Furthermore Miller and Lee noted that a hot ground state molecule could be produced in the direct photolysis of  $CH_2O$  by an efficient, yet undetected  $^1A_2 \rightsquigarrow ^3A_2$  intersystem crossing combined with the observed  $^3A_2 \rightsquigarrow \tilde{X}^1A_1(v)$  intersystem crossing. Thus the commonly employed  $^1A_2 \rightsquigarrow \tilde{X}^1A_1(v)$  internal conversion mechanism for  $CH_2O$  photodecomposition is not unique, since the radical-forming process I may occur not only from the high vibrational levels of the ground state but from the hot triplet state by way of the sequence:  $CH_2O(\tilde{A}^1A_2) \rightsquigarrow CH_2O(\tilde{a}^3A_2) \rightsquigarrow CH_2O(\tilde{X}^1A_1, v) \rightarrow H + HCO$ . However the more recent work of Tang and Lee [1977] shows that the  $^1A_2 \rightsquigarrow \tilde{X}^1A_1(v) \rightarrow H + HCO$  pathway is favored; see the preceding discussion.

IV-A-2. The Quantum Efficiencies of the Primary Photodecomposition Modes in  $CH_2O$ . The primary quantum efficiencies  $\phi_I$  and  $\phi_{II}$  for the primary processes I and II, respectively, have been estimated in many studies through the application of a variety of experimental techniques.



Rather great inconsistencies exist between the various estimates. Those for  $\phi_I$  can be compared in Figure 5. Although a general trend toward increasing  $\phi_I$  values at the shorter wavelengths is discernable here, it is evident that there are major problems which result in the very great scatter of these data. A brief review of the methods used to arrive at these estimates should be made here, before we derive from them a recommended set of  $\phi_I$  and  $\phi_{II}$ .



values for our use in describing the photochemistry of  $\text{CH}_2\text{O}$  in the atmosphere.

The early studies were not designed to yield quantitative estimates of  $\phi_{\text{I}}$  and  $\phi_{\text{II}}$  although trends in the wavelength dependence of I and II were shown. Thus McQuigg and Calvert [1969] flash photolyzed pure  $\text{CH}_2\text{O}$ ,  $\text{CD}_2\text{O}$ , and  $\text{CHDO}$  and mixtures of  $\text{CD}_2\text{O}$  and  $\text{CH}_2\text{O}$ . In their experiments a series of filters were added in successive experiments to restrict the excitation region to longer and longer wavelengths. They observed that the yield of CO and  $\text{H}_2$  products was directly proportional to the number of quanta absorbed in each wavelength region and correctly assumed that  $\phi_{\text{I}} + \phi_{\text{II}} \approx 1.0$  over most of the first absorption region of  $\text{CH}_2\text{O}$ . From the distribution of  $\text{H}_2$ , HD, and  $\text{D}_2$  in the products of the  $\text{CH}_2\text{O}$ - $\text{CD}_2\text{O}$  mixture photolyses and an assumed D- and H-atom scrambling mechanism they derived the approximate wavelength dependence of  $\phi_{\text{I}}$  and  $\phi_{\text{II}}$ . These estimates for  $\phi_{\text{I}}$  are shown as open triangles in Figure 5. The limited wavelength resolution which is a necessary consequence of this method prevents the derivation of highly accurate quantum yield values from this work.

Sperling and Toby [1973] have determined the quantum yields of CO and  $\text{H}_2$  in  $\text{CH}_2\text{O}$  photolyses at 80 and 120°C, at various pressures, and absorbed light intensities in bands near 3130, 3340, and 3660 A. They have assumed that all possible H-H, H-HCO, and HCO-HCO reactions occur and derived from complex steady state relations the expected theoretical form of  $\phi_{\text{H}_2}$  and  $\phi_{\text{CO}}$  variations with  $[\text{CH}_2\text{O}]$ , absorbed light intensity, and  $\phi_{\text{I}}$  and  $\phi_{\text{II}}$ . From the low pressure data the limiting values of  $\phi_{\text{H}_2}$  and  $\phi_{\text{CO}}$  at zero light intensity were determined. Although the data were not sufficient to define all of the necessary rate parameters involved in their expressions, through various simplifying assumptions they arrived at estimates of  $\phi_{\text{I}}$  and  $\phi_{\text{II}}$ . These  $\phi_{\text{I}}$  values are given as the darkened diamonds in Figure 5. The data show the same trend of quantum yields with wavelength which was observed by McQuigg and Calvert, but again they are only of qualitative value. The very indirect method employed here insures that the results are

subject to uncertainties much greater than the authors' large error bars shown on these points in Figure 5.

IV-A-2a. Radical Inhibition Studies. Many of the quantitative methods which have been employed in the estimation of the primary quantum yields depend upon the capture of H-atoms and possibly HCO radicals through the addition of various molecular species to the CH<sub>2</sub>O photolysis mixture. It is obvious that if one can suppress the H<sub>2</sub>-forming reactions involving the H and HCO species which may follow I, then the quantum yield of H<sub>2</sub> formed in the mixture can be attributed to the occurrence of primary process II:



Now if the added free radical trap does not perturb the excited molecule precursors of I and II, and the sum of the quantum yields of I and II are known in the absence of added trapping gas, then  $\phi_{\text{I}}$  can be found readily by difference:  $\phi_{\text{I}} = \phi_{\text{total}} - \phi_{\text{II}}$ .

It is fortunate for the users of this method that the total primary quantum yield of CH<sub>2</sub>O photodecomposition ( $\phi_{\text{I}} + \phi_{\text{II}}$ ) can be determined readily. First it has been observed by many workers that within the 2900-3350 Å region CH<sub>2</sub>O photolyses near room temperature give  $\phi_{\text{H}_2} = \phi_{\text{CO}} = 1.0$  within the experimental error; see for example Horowitz and Calvert [1978]; Clark et al. [1978]; Moortgat et al. [1978, 1979]. For experiments at wavelengths greater than 3360 Å the  $\phi_{\text{H}_2} = \phi_{\text{CO}} < 1.0$ , and these quantum yields are decreased by added unreactive gases. The most significant quenching occurs in CH<sub>2</sub>O excited at the longest absorbed wavelengths (3353-3550 Å). In order to interpret these total product quantum yields in terms of the occurrence of processes I and II, the nature of the H and HCO-radical reactions which occur following process I must be established. It is generally agreed today that the reactions (16) and (17) are the major fates of these species:



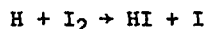
The significance of the alternative channels such as (18) and (19) involving the HCO radicals is not supported by the experimental facts:



Reaction (18) cannot be important here since no (HCO)<sub>2</sub> product is observed. However the chemiluminescence resulting from excited (HCO)<sub>2</sub> observed in CH<sub>2</sub>O photolysis by Hartley [1967] suggests that (18) must occur to some small extent. Conceivably the association of HCO radicals does occur here, but if so the vibrationally-rich glyoxal molecule formed initially (excitation >72 kcal mole<sup>-1</sup>) must rearrange quickly to CH<sub>2</sub>O and CO products; note that this is the dominant photodecomposition path observed for glyoxal molecules photoexcited in the 3130 and 3660 Å regions: (HCO)<sub>2</sub> + hν → CH<sub>2</sub>O + CO (Calvert and Layne [1953]; Parmenter [1964]). Reaction (19) is unimportant also since its occurrence would lead to  $\phi_{\text{H}_2}$  and  $\phi_{\text{CO}}$  values above unity, assuming  $\phi_{\text{I}} + \phi_{\text{II}} = 1.0$ . Horowitz and Calvert [1978] found  $\phi_{\text{CO}} = \phi_{\text{H}_2} = 1.10 \pm 0.08$  in their 3130 Å CH<sub>2</sub>O photolyses and originally interpreted this as indicating the minor occurrence of (19). From subsequent studies at other wavelengths where they found  $\phi_{\text{H}_2} = \phi_{\text{CO}} = 1.0$  within the error limits, they concluded that  $k_{19}/k_{17}$  must be near zero. In experiments at room temperature, the decomposition of the HCO radical (HCO + M → H + CO + M) is also unimportant; see Horowitz and Calvert [1978]. Thus we see from the simple mechanism of CH<sub>2</sub>O photolysis that  $\phi_{\text{I}} + \phi_{\text{II}} = \phi_{\text{H}_2} = \phi_{\text{CO}}$  for experiments near room temperature.

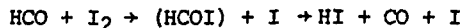
The first radical inhibition experiments designed to estimate the primary quantum yields of CH<sub>2</sub>O were carried out many years ago by Gorin [1939]. He photolyzed formaldehyde-iodine mixtures at 100°C. Presumably the quantum yields of HI reflected the occurrence of reaction (20) which followed I:





(20)

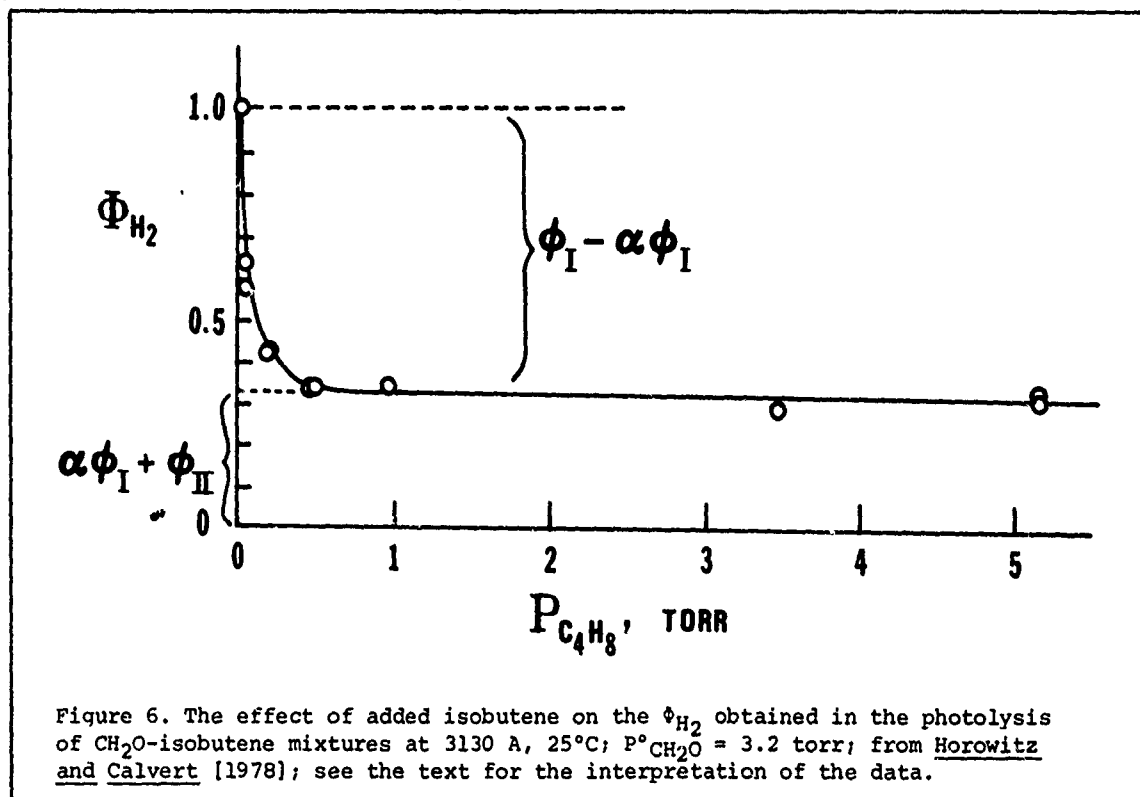
The unquenchable  $\text{H}_2$  quantum yield was taken as a measure of  $\phi_{\text{II}}$ . Gorin's estimates of  $\phi_{\text{I}}$  are given as open circles in the summary of data shown in Figure 5. The results are not reliable for several reasons. Thus, unknown to Gorin, the  $\text{HCO}$  radicals as well as the  $\text{H}$ -atoms react with iodine to lead to  $\text{HI}$ ; see Walsh and Benson [1966] and Calvert and Pitts [1966].



(21)

Furthermore it is also possible that the thermal reactions between  $\text{I}_2$  and  $\text{CH}_2\text{O}$  may have been significant at the  $100^\circ\text{C}$  temperature employed by Gorin. However the largest problem associated with these older measurements arises with the analytical procedures employed for  $\text{HI}$  analysis by Gorin. These have been found to be unreliable in subsequent aldehyde-iodine photolyses of the Blacet group; for early examples see Blacet and Loeffler [1942] and Blacet and Heldman [1942]. In addition there is good evidence that acetone and acetaldehyde molecules excited at 3130 Å are deactivated by iodine through some undefined energy-transfer mechanism [Noyes, 1951; Pitts and Blacet, 1952]. Similar interactions with excited  $\text{CH}_2\text{O}$  may exist. Thus we conclude that the iodine-inhibited  $\text{CH}_2\text{O}$  photolyses at  $100^\circ\text{C}$  are not well suited to the determination of  $\phi_{\text{I}}$  and  $\phi_{\text{II}}$ . In the unlikely event that none of these potential experimental problems existed in Gorin's study, then in terms of our present understanding of the mechanism of  $\text{HI}$  formation, we must divide his  $\phi_{\text{HI}}$  values by two in order to get  $\phi_{\text{I}}$  estimates. When we apply this correction, we find the unreasonably high value for  $\phi_{\text{I}} = 0.37$  at 3660 Å. It is highly likely that inadvertent complications do exist in the  $\text{CH}_2\text{O}$ - $\text{I}_2$  system, and further attempted use of these data is unwarranted.

Several investigators have employed the alkenes as  $\text{H}$ -atom traps in  $\text{CH}_2\text{O}$  photolyses and taken the quantum yield of hydrogen as a measure of  $\phi_{\text{II}}$  [DeGraff and Calvert, 1967; Horowitz and Calvert, 1978; Moortgat et al., 1978; Moortgat and Warneck, 1979]. In this case the  $\text{H}$ -atoms are removed largely by the reaction of addition to the alkene double bond. We may illustrate the data treatment from these alkene-formaldehyde mixtures using the data of Horowitz and Calvert [1978]; see Figure 6. It can be seen that as increasing pressures of isobutene were added in successive  $\text{CH}_2\text{O}$ -isobutene mixture photolyses at 3130 Å, the quantum yield of hydrogen product approached a limiting value. The suppression of  $\text{H}_2$  formation results largely from the capture of  $\text{H}$ -atoms in this case through the addition reaction (22); the rate of the  $\text{H}$ -atom



abstraction reaction 23 is much lower, although the absolute value of the  $k_{23}/k_{22}$  ratio is still somewhat uncertain.



In theory the limiting  $\phi_{\text{H}_2}$  value observed at high isobutene added pressures should equal  $\alpha\phi_{\text{I}} + \phi_{\text{II}}$ , where  $\alpha$  is the rate constant ratio  $k_{23}/(k_{22} + k_{23})$ . The difference between the uninhibited  $\phi_{\text{H}_2}$  and the limiting  $\phi_{\text{H}_2}$  value is related to  $\phi_{\text{I}} - \alpha\phi_{\text{I}}$ . Thus an evaluation of the rate constant ratio  $\alpha$  is necessary in order to derive  $\phi_{\text{I}}$  and  $\phi_{\text{II}}$  estimates from these data. Measurements of Jennings and Cvetanovic [1961] gave the estimates:  $k_{23}/k_{22} = 0.020$  and  $0.017$  (error limits not reported), while Wooley and Cvetanovic [1969] found  $k_{23}/k_{22} = 0.032 \pm 0.028$  or  $k_{23}/(k_{22} + k_{23}) = \alpha = 0.031 \pm 0.028$ . We feel these estimates are upper limits to the actual values. In these studies the  $\text{Hg}(^3\text{P}_1)$ -butane reaction and the  $\text{H}_2\text{S}$  photolysis at 2490 Å, respectively, were the sources of H-atoms. It is difficult to exclude hot H-atoms effects, particularly in the  $\text{H}_2\text{S}$  photolysis experiments where H-atom translational energies may be as high as 22 kcal mole<sup>-1</sup>. If as seems likely to us, non-thermalized H-atoms are present, then reaction (23) with its significant energy barrier would be favored, while the highly exothermic addition reaction (22) would be somewhat less favored than with thermal H-atoms. Potential error in their  $k_{23}/k_{22}$  estimates is also noted in the discussion of Wooley and Cvetanovic. They used the same procedures to find the extent of the analogous H-atom addition and abstraction reactions with the simplest alkene, ethylene ( $\text{C}_2\text{H}_4$ ). Here the ratio of constants for abstraction to that for addition was found to be  $0.067 \pm 0.003$ . However in this case, the authors correctly state that other evidence points to a value very near zero; they feel the  $\text{C}_2\text{H}_4$  result must be regarded as an artifact of the extrapolation procedure involved in the method. Indeed the values of  $k_{23}/k_{22}$  involving isobutene were derived by the same extrapolation procedure, and, in our opinion, they are also equal to zero within the experimental error of the method. This conclusion is supported by the findings of DeGraff and Calvert [1966]; very small ratios of HD to  $\text{H}_2$  were found in the  $\text{C}_3\text{H}_6$ -inhibited photolyses of  $\text{CH}_2\text{O}$ - $\text{CD}_2\text{O}$  mixtures at 3130 Å. They estimated that the error in  $\phi_{\text{II}}$  estimates for  $\text{CH}_2\text{O}$  due to incomplete scavenging of H-atoms by addition to  $\text{C}_3\text{H}_6$  must be less than 3-5%. In the studies of the Calvert group the ratio  $\alpha$  has been taken as zero. Moortgat and Warneck [1979] have accepted the Wooley and Cvetanovic estimates as correct and have used these to adjust their own  $\text{C}_3\text{H}_6$ - $\text{CH}_2\text{O}$  data and the Horowitz and Calvert isobutene- $\text{CH}_2\text{O}$  data. Although the correction to the isobutene- $\text{CH}_2\text{O}$  data is very small, that for the  $\text{C}_3\text{H}_6$ - $\text{CH}_2\text{O}$  data is not trivial. Accepting the Horowitz and Calvert assumption of  $\alpha = 0$ , or some other finite value,  $\phi_{\text{I}}$  and  $\phi_{\text{II}}$  may be derived readily from the limiting  $\phi_{\text{H}_2}$  data as indicated graphically in Figure 6.

In the first alkene- $\text{CH}_2\text{O}$  photolysis study of DeGraff and Calvert [1966], propylene ( $\text{C}_3\text{H}_6$ ) was used as the H-atom trap. They made a rather detailed study of the effects of temperature, concentration of added  $\text{C}_3\text{H}_6$  and neopentane in experiments at only one wavelength, 3130 Å. Here the average limiting  $\phi_{\text{H}_2}$  value at high  $[\text{C}_3\text{H}_6]$  was used to derive  $\phi_{\text{II}} \approx 0.47$  and hence  $\phi_{\text{I}} = 1 - \phi_{\text{II}} \approx 0.53$ ; this is somewhat lower but in qualitative accord with the other more recent data summarized in Figure 5. The technique was extended to photolyses at other wavelengths in regions near 3340, 2654, and 2537 Å. These data, shown as open diamonds in Figure 5, suggested that  $\phi_{\text{I}}$  decreased and  $\phi_{\text{II}}$  increased progressively in photolyses at the shorter wavelengths, a conclusion inconsistent with the extrapolation of the trend observed by McQuigg and Calvert [1969] and others in more recent work at the longer wavelength region, 3600-3000 Å. However both the recent data of Horowitz and Calvert [1978] and Moortgat and Warneck [1979] show a decrease in  $\phi_{\text{I}}$  with decreasing wavelength does occur at wavelengths beyond 3000 Å. Thus the trend first observed by DeGraff and Calvert and later discounted by the Calvert group may be correct. However in view of the very limited data obtained at the wavelengths other than 3130 Å, no great confidence can be placed in these findings.

Horowitz and Calvert [1978] made a rather extensive series of studies of  $\text{CH}_2\text{O}$  photodecomposition using a variety of radical quenching agents. The results from the isobutene- $\text{CH}_2\text{O}$  mixture photolyses appeared to be the simplest and the most readily interpretable. These were used to derive the  $\phi_{\text{I}}$  data shown as the open squares in Figure 5. The kinetics of the observed H-atom quenching reflected the occurrence of the two competing reactions for H-atoms in this system:





The large ratio of the rate constants which the data support,  $k_{16}/k_{22} = 43 \pm 4$ , allowed effective quenching of the H-atoms with relatively small ratios of  $\text{C}_4\text{H}_8$  to  $\text{CH}_2\text{O}$ . Values of  $\phi_{\text{II}}$  and  $\phi_{\text{I}}$  could be calculated from the measured quantum yields of hydrogen in pure  $\text{CH}_2\text{O}$  ( $\phi_{\text{H}_2}^0$ ) and in  $\text{CH}_2\text{O}$ -isobutene mixtures ( $\phi_{\text{H}_2}^i$ ) using the relations (24) and (25) to correct for the small extent of incomplete quenching:

$$\phi_{\text{I}} = (\phi_{\text{H}_2}^0 - \phi_{\text{H}_2}^i) \left\{ 1 + \frac{P_{\text{CH}_2\text{O}}}{43P_{\text{C}_4\text{H}_8}} \right\} \quad (24)$$

$$\phi_{\text{II}} = \phi_{\text{H}_2}^0 - \phi_{\text{I}} = \phi_{\text{H}_2}^i \left\{ 1 + \frac{P_{\text{CH}_2\text{O}}}{43P_{\text{C}_4\text{H}_8}} \right\} - \phi_{\text{H}_2}^0 \frac{P_{\text{CH}_2\text{O}}}{43P_{\text{C}_4\text{H}_8}} \quad (25)$$

The results obtained from this system were in excellent accord with those found using other quenching gases [Horowitz and Calvert, 1978], and we feel confident that they are reasonably accurate.

Moortgat et al. [1978] studied  $\text{C}_3\text{H}_6$ - $\text{CH}_2\text{O}$  mixture photolyses in 1 atmosphere of added  $\text{N}_2$  and at a series of different wavelengths; the  $\phi_{\text{I}}$  estimates which they derived are given as closed inverted triangles in Figure 5. These conditions are more representative of those present in the lower atmosphere than in previous work and the results are considered reliable. However the small correction applied for the H-atom abstraction reaction for  $\text{C}_3\text{H}_6$  which the authors employed seems of dubious validity to the present author.

Nitric oxide is very reactive toward atoms and free radicals and it has been used also in the study of primary processes I and II. Clark et al. [1978] have carried out the most extensive study of this system. Following process I in experiments with NO added, the reactions (26) and (27) are expected to occur in strong competition with (16) and (17) which dominate in the absence of NO.



Clark et al. concluded that II and (27) were the only significant reactions leading to CO and  $\text{H}_2$  for their conditions ( $P_{\text{NO}} \geq 1$  torr;  $P_{\text{CH}_2\text{O}} = 5$  or 10 torr). They noted that  $\phi_{\text{I}}$  should be given by the simple relation (28):

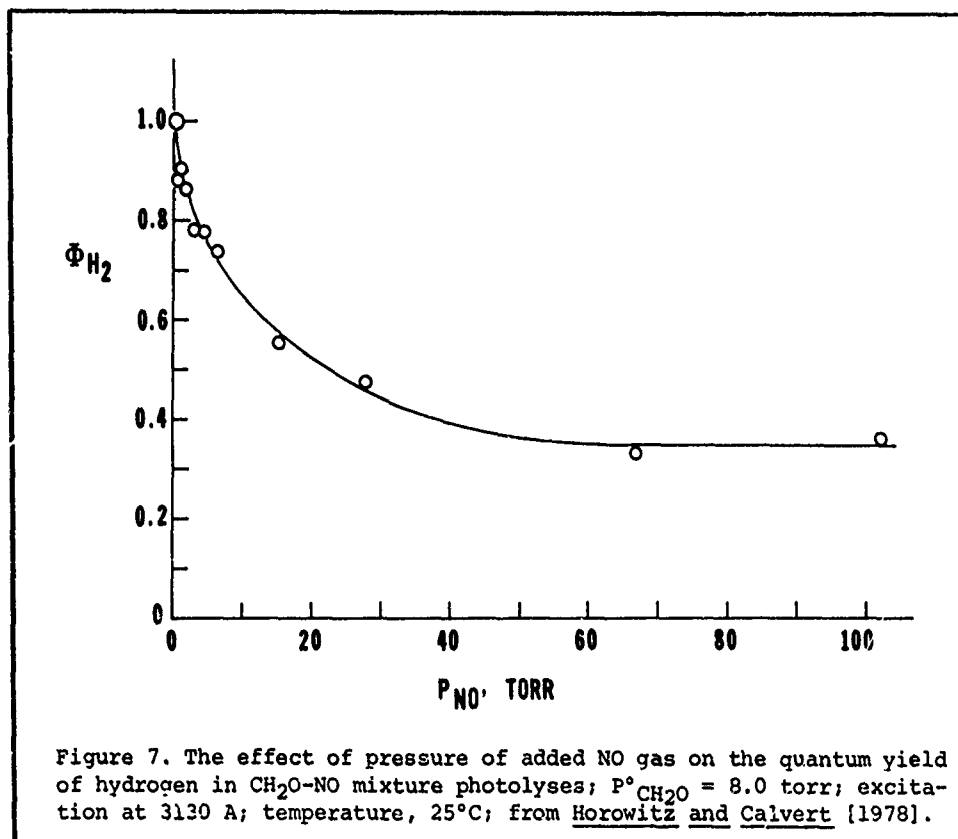
$$\phi_{\text{I}} = \phi_{\text{CO}} - \phi_{\text{H}_2} \quad (28)$$

In fact relation (28) should hold regardless of the completeness of removal of H-atoms in (26), provided that all HCO radicals react in (27). However if this mechanism alone were operative than  $\phi_{\text{CO}} - \phi_{\text{H}_2}$  should be independent of the pressure of added NO, once enough NO is added to make the reaction (27) dominate over (17). This expectation was not realized by Clark et al.; they found that  $\phi_{\text{CO}} - \phi_{\text{H}_2}$  increased significantly when  $P_{\text{NO}}$  was increased from 2 to 50 torr. Thus at 2991 Å the quantum yield difference increased from 0.48 to 0.70 with NO increase from 2 to 50 torr. They speculated that this effect may have originated from an excited  $\text{CH}_2\text{O}$  molecule reaction with NO:  $\text{CH}_2\text{O}^* + \text{NO} \rightarrow \text{HCO} + \text{HNO}$ . Thus to avoid possible complications from such a reaction they used only the results of experiments at low NO pressures in the estimation of the  $\phi_{\text{I}}$  values they report. These are shown as the darkened squares in Figure 5. A somewhat related effect of NO in  $\text{CH}_2\text{O}$  photolysis has been reported by Houston and Moore [1976]. They found that the presence of NO in  $\text{CH}_2\text{O}$  photolysis at 3055 Å increased the rate of formation of vibrationally excited  $\text{CO}(v=1)$  product. One of their alternative

rationales for this effect was that excited  $\text{CH}_2\text{O-NO}$  interactions enhanced the molecular mode II of formaldehyde decomposition. However if this were the case then  $\phi_{\text{CO}} - \phi_{\text{H}_2}$  would decrease with increasing NO, contrary to the findings of Clark et al.

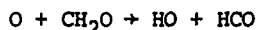
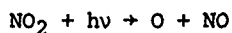
Horowitz and Calvert [1978] have also studied the  $\text{CH}_2\text{O-NO}$  system at 3130 Å, and their findings add some further insight into the interpretation of the quantum yield results from the  $\text{CH}_2\text{O-NO}$  mixture photolyses. The results from a series of experiments with 8 torr of  $\text{CH}_2\text{O}$  and at varied NO pressures are shown in Figure 7. The variation of  $\phi_{\text{H}_2}$  with  $P_{\text{NO}}$  appears to be a normal inhibition curve with  $\phi_{\text{H}_2}$  decreasing to a limiting value at high NO pressures; there is no evidence here of an excited molecule-NO reaction. From the published rate constants for the reactions (26), (27), and (17) Horowitz and Calvert estimated that nearly all of the HCO radicals should react with NO for their light intensities when only about 0.5 torr of NO was added. However if the unknown value for  $k_{26}$  with  $\text{M} = \text{CH}_2\text{O}$  is only about 10-times that which was measured for  $\text{M} = \text{H}_2$ , then less than 15% of the H-atoms will react with NO present at the 0.5 torr level. More than 85% will still react to form  $\text{H}_2$  through reaction (16). They noted that the limiting  $\phi_{\text{H}_2}$  found at high NO ( $0.34 \pm 0.02$ ) was equal within the error limits to that found in experiments with added isobutene ( $0.31 \pm 0.02$ ). Thus they suggested that the limiting  $\phi_{\text{H}_2}$  found by Clark et al. in their experiments with 50 torr of added NO should provide good estimates of  $\phi_{\text{II}}$  as well. These values checked well with the Horowitz and Calvert estimates using the isobutene- $\text{CH}_2\text{O}$  photolyses. Apparently this interpretation of the rate data of Clark et al. was also adopted by Moortgat and Warneck [1979].

It is somewhat surprising that the  $\phi_{\text{CO}} - \phi_{\text{H}_2}$  values from the  $\text{NO-CH}_2\text{O}$  experiments of Clark et al. at the shorter wavelengths do not give  $\phi_{\text{I}}$  estimates in accord with the limiting  $\phi_{\text{H}_2}$  values at high NO where one expects  $\phi_{\text{I}} = 1 - \phi_{\text{H}_2}$ . In fact the  $\text{CH}_2\text{O-NO}$  data of Horowitz and Calvert at 3130 Å do give such consistent estimates for experiments at low NO. As we indicated previously, relation (28) should hold even at low NO pressures as long as nearly all HCO radicals are removed in reaction (27). This should be the case for NO pressures above about 0.5 torr for the conditions used by Horowitz and Calvert. Their data for low NO give  $\phi_{\text{CO}} - \phi_{\text{H}_2} = \phi_{\text{I}} = 0.724$  ( $\text{CH}_2\text{O}$ , 3 torr) and 0.717 ( $\text{CH}_2\text{O}$ , 8 torr). These estimates do compare reasonably well with  $\phi_{\text{I}} = 0.68$  derived from the  $\text{CH}_2\text{O-isobutene}$  mixtures. Horowitz and Calvert also confirmed the observation of Clark et al. that  $\phi_{\text{CO}} - \phi_{\text{H}_2}$  increased with increasing NO pressure. They



# CALVERT

reported that  $\text{NO}_2$  as well as  $\text{N}_2\text{O}$  products were formed in this system at high NO pressures and concluded that additional reactions may provide other as yet unexplained sources of CO for these conditions. Conceivably reactions initiated by the  $\text{NO}_2$  product photolysis such as the following may lead to the new sources of CO in the high NO mixtures:



In any case uncertainties in the interpretation of the  $\text{CH}_2\text{O}$ -NO data remain. The use of the estimates of  $\phi_I$  made by Clark et al. from the low pressure NO experiments and relation (28) is open to serious question at this time.

The most important and useful data for the atmospheric scientist related to formaldehyde photo-decomposition which one might hope to derive are the wavelength dependence of  $\phi_I$  and  $\phi_{II}$  measured directly in air at the pressures and temperatures which are characteristic of the different atmospheric regions. In this sense the recent studies of Moortgat et al. [1979] are most pertinent. They have photolyzed low concentrations of  $\text{CH}_2\text{O}$  (15-133 ppm) in air at various pressures and determined  $\phi_{\text{CO}}$  and  $\phi_{\text{H}_2}$  at several wavelengths. The important key to the success of their experiments was the development of the reliable and sensitive analytical techniques which allowed the determination of very small amounts of  $\text{H}_2$  and CO in the large excess of air [Seiler and Junge, 1967]. It was anticipated from the results of earlier product rate studies of formaldehyde photooxidation in air at 1 atmosphere pressure [Bufalini et al., 1972] that the H and HCO products of primary process I would react largely by the following mechanism:



If only these reactions are important then from  $\phi_{\text{H}_2}$  and  $\phi_{\text{CO}}$  measurements  $\phi_I$  and  $\phi_{II}$  can be estimated readily:  $\phi_{II} = \phi_{\text{H}_2}$ ;  $\phi_I = \phi_{\text{CO}} - \phi_{\text{H}_2}$ . At least to a first approximation the seeming simplicity of the system is realized, and the estimates of  $\phi_I$  and  $\phi_{II}$  have been obtained by Moortgat et al. [1978, 1979] using this very direct method. The  $\phi_I$  data points are given in Figure 5 as inverted triangles. The results agree within the experimental error with those found in  $\text{CH}_2\text{O}$ ,  $\text{C}_3\text{H}_8$ ,  $\text{N}_2$  mixture photolyses by Moortgat et al. [1978] and  $\text{CH}_2\text{O}$ -isobutene photolyses by Horowitz and Calvert [1978].

However there are some possible complications in the estimation of  $\phi_I$  and  $\phi_{II}$  using  $\text{O}_2$  as the free radical trap. It is possible that molecular oxygen may quench electronically excited  $\text{CH}_2\text{O}$  molecules in a fashion analogous to that observed for excited acetone ( $\text{CH}_3\text{COCH}_3$ ) in  $\text{O}_2$ -containing mixtures [Srinivasan and Noyes, 1960]. Indeed this is the claim of Morrison and Heicklen [1979] who recently reported results of their photooxidation of  $\text{CH}_2\text{O}$ . They concluded that  $\phi_{\text{H}_2}$  and  $\phi_{\text{CO}}$  values were quenched to zero when pressures of added  $\text{O}_2$  were greater than 100 torr. Presumably  $\phi_{\text{HCO}_2\text{H}}$  approached a value of 2 for these conditions. Their interpretation that  $\text{CH}_2\text{O}$  photolysis involves either a triplet  $\text{CH}_2\text{O}$  or HCOH biradical reaction with oxygen as the source of formic acid ( $\text{HCO}_2\text{H}$ ) is not supported by other work. It is probable that the reactions observed by Su et al. [1979] better describe the Morrison and Heicklen results and unrecognized analytical difficulties of estimating  $\text{H}_2$  and CO products in the large excess of  $\text{O}_2$  were present in this work. Yet other complications may exist in the experiments of Moortgat et al. Thus Horowitz, Su, and Calvert [1978] attempted to use small amounts of  $\text{O}_2$  to quench the H and HCO free radical reactions in  $\text{CH}_2\text{O}$ - $\text{O}_2$  mixture photolyses at 3130 Å and 25°C. However they found that even small amounts of added  $\text{O}_2$  (0.02-0.05 torr) to 8 torr of  $\text{CH}_2\text{O}$  led to a marked increase in the quantum yields of  $\text{H}_2$  and CO, and formic acid also appeared as a product for these conditions. The  $\phi_{\text{H}_2}$  value jumped from 1.0 in the absence of  $\text{O}_2$  to a value greater than 4 when 0.02-0.05 torr of  $\text{O}_2$  was added. They postulated a series of chain reactions initiated by a reaction of  $\text{HO}_2$  addition to  $\text{CH}_2\text{O}$  in order to rationalize their results. The

exact nature of the reaction mechanism remained unclear, but it was well established that at relatively low added pressures,  $O_2$  is not a good reagent to capture the free radical products of primary process I. The gas chromatographic method employed by Horowitz and Calvert did not allow additions of  $O_2$  over 8 torr. However in experiments with  $CO_2$  additions up to 300 torr in the  $CH_2O-O_2$  mixtures,  $\phi_{H_2}$  remained high (about 4). When small amounts of isobutene (2 torr) were added to a mixture of  $CH_2O$  (8 torr) and  $O_2$  (1 torr) the  $\phi_{H_2}$  value dropped to 0.33, nearly equal to the value found by Horowitz and Calvert for  $CH_2O$ -isobutene photolyses (0.32). In view of the Moortgat et al. results using large pressures of air, it is evident that the capture of H-atoms by  $O_2$  can be effective in reaction (29) provided the  $O_2$  and M concentrations are sufficiently high. Furthermore the good agreement between the  $O_2$ -free  $CH_2O-C_4H_8$  mixture photolyses of Horowitz and Calvert and the  $CH_2O-O_2$  mixture photolyses of Moortgat et al. shows that CO and  $H_2$  product quenching by  $O_2$  is unimportant.

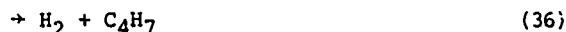
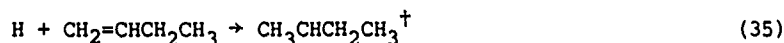
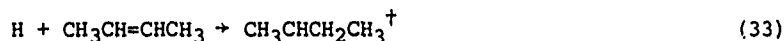
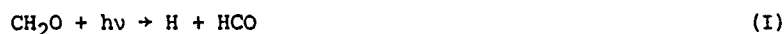
Houston and Moore [1976] also found some unusual effects in  $CH_2O-O_2$  mixture photolyses. The addition of small amounts of  $O_2$  in the photolysis of  $CH_2O$  at 3050 Å increased markedly the yield of both vibrationally excited CO ( $v = 1$ ) and vibrationally relaxed CO ( $v = 0$ ). The Horowitz and Calvert observation of  $\phi_{H_2}$  equality in the photolysis of  $CH_2O-O_2-C_4H_8$  and  $CH_2O-C_4H_8$  mixtures proves that the effect of  $O_2$  is not attributable to interactions between  $O_2$  and vibrationally excited  $CH_2O$  molecules. This was one of the alternatives considered by Houston and Moore. However the effect is more likely the trivial result of the occurrence of the exothermic reaction (32) in the  $O_2$ -containing mixtures:



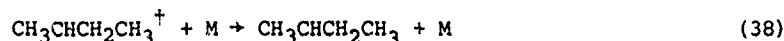
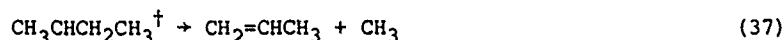
When CO ( $v = 0$ ) is the product in (32),  $\Delta H \approx 30 \text{ kcal mole}^{-1}$ . Since the CO ( $v = 0$ ) to CO ( $v = 1$ ) excitation involves only  $6.2 \text{ kcal mole}^{-1}$ , reaction (32) is readily possible.

Recent studies by Su et al. [1979] which we will consider in a later section give some important further insight into the nature of the chain photooxidation mechanism of  $CH_2O$ . It is sufficient to note here that the reaction which initiates formic acid formation is  $HO_2$  addition to  $CH_2O$ . The chain is short for photolyses of  $CH_2O$  in the ppm range in air, but it could be significant for 100 ppm of  $CH_2O$  in air at 1 atm pressure. It seems probable to the author that  $HCO_2H$  was a minor undetected product in the experiments of Moortgat et al. [1979]. However unless this product interferes in some way with the CO and  $H_2$  analyses, which seems unlikely to us, the primary quantum yield estimates of Moortgat et al. should be reliable.

IV-A-2b. Estimation of  $\phi_I$  Values by H-Atom Chemical Counting Methods. Lee and co-workers have designed some ingenious and rather direct methods to monitor the quantum efficiency of process I in  $CH_2O$  photolysis. Although these are only applicable to measurements in the very low pressure regime, they provide compelling evidence of the extent of occurrence of I for these conditions. In the first of these methods Lewis et al. [1976, 1978] have photolyzed  $CH_2O$ -cis-2-butene and  $CH_2O$ -1-butene mixtures at pressures below 1 torr. The method depends upon the fact that H-atoms formed in primary process I may react by addition to the alkene in reactions (33) and (35) to form vibrationally-rich sec-butyl radicals:



A small fraction of the H-atoms react to abstract in (34) and (36). The hot sec-butyl radicals may either fragment to form propylene in (37) or be stabilized by collision in (38):



For these conditions and the simple mechanism outlined one expects the measured  $\phi_{C_3H_6}$  values

to be a predictable function of the pressure,  $1 - \alpha$ , the fraction of the H-atoms which add to the butene ( $k_{33}/(k_{33} + k_{34})$  or  $k_{35}/(k_{35} + k_{36})$ ), and the desired  $\phi_I$  value:

$$\frac{1}{\phi_{C_3H_6}} = \frac{1}{(1 - \alpha)\phi_I} + \frac{k_{38}[M]}{k_{37}} \quad (39)$$

Thus an extrapolation of  $1/\phi_{C_3H_6}$  versus  $[M]$  plot to zero  $[M]$  should provide  $1/(1 - \alpha)\phi_I$  as an intercept. The experimental data appear to follow well the form of relation (39). The choice of  $\alpha$  was derived from the estimates of Wooley and Cvetanovic [1969]. As we have discussed earlier there is considerable uncertainty associated with these estimates. Furthermore at the very low pressures which apply to the extrapolation of the  $\phi_{C_3H_6}$  data, hot H-atom effects may enhance the occurrence of reactions (34) or (36) over (35) and (37) and alter the value of  $\alpha$  from that observed at the higher pressures by Wooley and Cvetanovic. The  $1 - \alpha$  terms used by Lewis et al. amount to 9 and 14% increases in the  $\phi_{C_3H_6}$  limiting values to derive  $\phi_I$  from the cis-2-butene and 1-butene experiments, respectively. The  $\phi_I$  values calculated from these experiments are shown as darkened circles in Figure 5. These estimates from the longer wavelengths are in reasonable accord with the results from the most extensive studies employing very different techniques [Horowitz and Calvert, 1978; Moortgat et al., 1979]. However at the shorter wavelengths the  $\phi_I$  values are significantly lower. If  $1 - \alpha$  decreases for H-atoms of increased translational energy, as seems likely to this author, then the  $\phi_I$  results from the shorter wavelengths may be underestimated. The data treatment which involves the extrapolation of the kinetic data to zero pressure certainly accentuates any hot atom effects which may be present. In view of the complexity of the system and the necessary uncertainties in the data treatment, the absolute values of  $\phi_I$  may have somewhat greater uncertainties than those derived in the less direct methods.

The Lee group [Lewis et al., 1976; Tang et al., 1979] has designed another interesting and rather direct method of  $\phi_I$  determination. This is based upon the relative intensities of chemiluminescence of electronically excited  $HNO(\tilde{A}^1A'')$  formed by the recombination of H and NO in photolyzed  $CH_2O$ -NO mixtures at low pressures. Following process I, only the H-atom product may lead in part to the excited HNO species:



The exothermicity of reaction (27),  $\Delta H = -34 \text{ kcal mole}^{-1}$ , is not sufficient to populate the  $HNO(\tilde{A}^1A'')$  excited state.

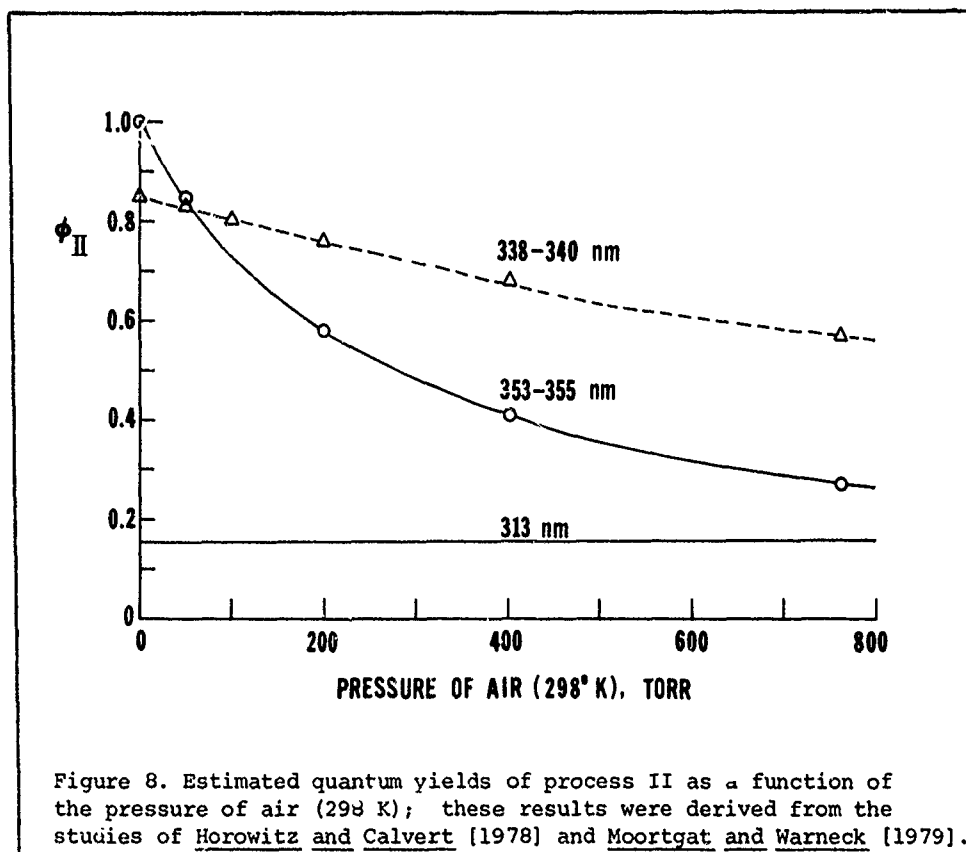


At the low pressures which must be employed in these studies, the fraction of H-atoms formed in I which eventually react in (40) and subsequently emit measurable light in (41) is expected to be a complex function of the concentrations of NO,  $CH_2O$ , and the third body M. Thus absolute measurements of  $\phi_I$  from these studies cannot be made readily. Relative values of  $\phi_I$  at various wavelengths have been measured. Tang et al. [1979] have calibrated them accepting  $\phi_I = 0.68$  at 3035 Å as estimated by Lewis and Lee [1978] using the H-atom capture by butene and the sec-butyl radical fragmentation reaction just considered. The data from this system are shown as darkened triangles in Figure 5. These estimates are reasonably consistent with other estimates from recent studies at the longer wavelengths. They are somewhat lower at the shorter wavelengths. Again it is possible that hot H-atom effects are significant in this system. The increased translational energy of the H-atom product of I at the shorter wavelengths may lower the efficiency of capture of the H-atoms by NO for a given pressure. Lee and co-workers feel that effects due to non-thermally equilibrated H-atoms are unimportant here. It is difficult to prove either position from the present data. Certainly these results support the general features of the  $\phi_I$  dependence derived by other methods and do give further rather direct evidence of the relative efficiency of H-atom involvement in  $CH_2O$  photolysis.

IV-A-2c. The Pressure Dependence of the Primary Processes I and II. All of the present data for  $CH_2O$  photolyses at wavelengths below 3300 Å suggest that  $\phi_I + \phi_{II} = 1.0$  and  $\phi_I$  and  $\phi_{II}$  are insensitive to added  $CO_2$  (up to 400 torr) [Horowitz and Calvert, 1978], and  $N_2$  or air

(up to 1 atm) [Moortgat and Warneck, 1979]. However the quantum yields of CO and H<sub>2</sub> are reduced somewhat with added gases in experiments at  $\lambda > 3300 \text{ \AA}$ ; for example see Sperling and Toby [1973]; Horowitz and Calvert [1978]; Moortgat and Warneck [1979]; and Clark et al. [1978]. It is not clear whether this effect results from a lowered efficiency of process I as well as process II. Some indication can be had from the data of Horowitz and Calvert derived from 3300  $\text{\AA}$  experiments. The  $\phi_{\text{H}_2}$  value obtained in CH<sub>2</sub>O-isobutene mixtures in the absence of CO<sub>2</sub> was 0.660. This was lowered somewhat for photolyses at near identical CH<sub>2</sub>O and isobutene pressures but with CO<sub>2</sub> added:  $\phi_{\text{H}_2} = 0.564 \pm 0.018$  for  $P_{\text{CO}_2} = 318 \pm 2$  torr. Similar CH<sub>2</sub>O photolyses in the absence of isobutene gave  $\phi_{\text{H}_2}$  (and its equal,  $\phi_{\text{I}} + \phi_{\text{II}}$ ) = 1.0 in the absence of CO<sub>2</sub> and 0.905 with 305 torr of CO<sub>2</sub> added. If both  $\phi_{\text{I}}$  and  $\phi_{\text{II}}$  were quenched equally by CO<sub>2</sub> addition we would expect  $\phi_{\text{H}_2}$  in CH<sub>2</sub>O-CO<sub>2</sub> mixtures to be lowered to  $(0.564 \pm 0.018)/0.660 = 0.85 \pm 0.03$ . If only  $\phi_{\text{II}}$  were lowered by CO<sub>2</sub> addition then we expect  $\phi_{\text{H}_2} = 0.34 + (0.564 \pm 0.018) = 0.904 \pm 0.018$ . Obviously the experimental value observed here for the CH<sub>2</sub>O-CO<sub>2</sub> mixture,  $\phi_{\text{H}_2} = 0.905$ , suggests the latter alternative is more nearly correct. The accuracy of the data don't allow a firm conclusion, but it appears likely that the quenching of process II is the dominant origin of the added gas quenching for 3300  $\text{\AA}$  photolyses. If process I and II both occur from vibrationally excited levels of the ground state, then the observed  $\lambda$ -dependence of  $\phi_{\text{I}}$  and  $\phi_{\text{II}}$  suggests that the higher levels available to the molecule excited at the shorter wavelengths of light favor I; the lower states favor II. In line with this hypothesis one would expect that the lifetime of the higher levels toward dissociation would be shorter than those of the lower levels, and hence the process II pathway would be more sensitive to quenching effects.

A much more dramatic quenching of  $\phi_{\text{H}_2}$  and  $\phi_{\text{CO}}$  occurs in CH<sub>2</sub>O photolyses in the 3380  $\text{\AA}$  and 3550  $\text{\AA}$  regions. Horowitz and Calvert [1978] concluded that process II is the only significant decomposition mode for these wavelength regions. With this view the quenching in these cases is clearly an effect of lowering  $\phi_{\text{II}}$ . The limited data derived by Moortgat and Warneck [1979] for the quenching of excited CH<sub>2</sub>O by air, coupled with the  $\phi_{\text{II}}$  estimates for these wavelengths by Horowitz and Calvert [1978] have been used to derive the rough estimates of  $\phi_{\text{II}}$  as a function of air pressure shown in Figure 8. We will use these data in arriving at estimates of  $\phi_{\text{II}}$  which should apply at the lowered pressures of the upper atmosphere.

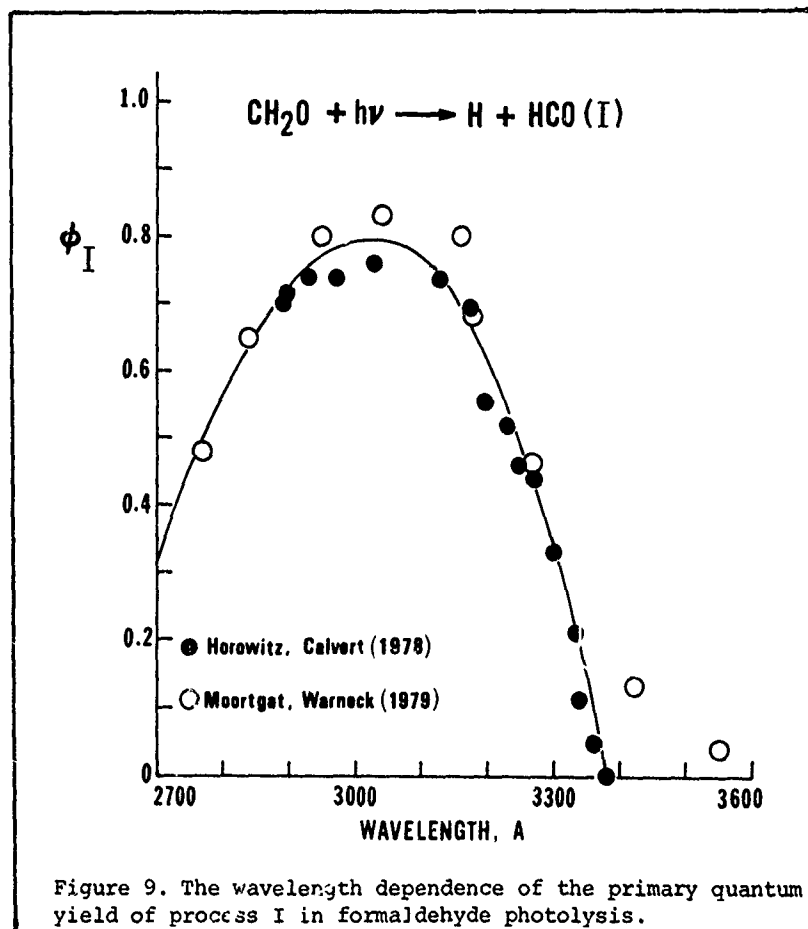


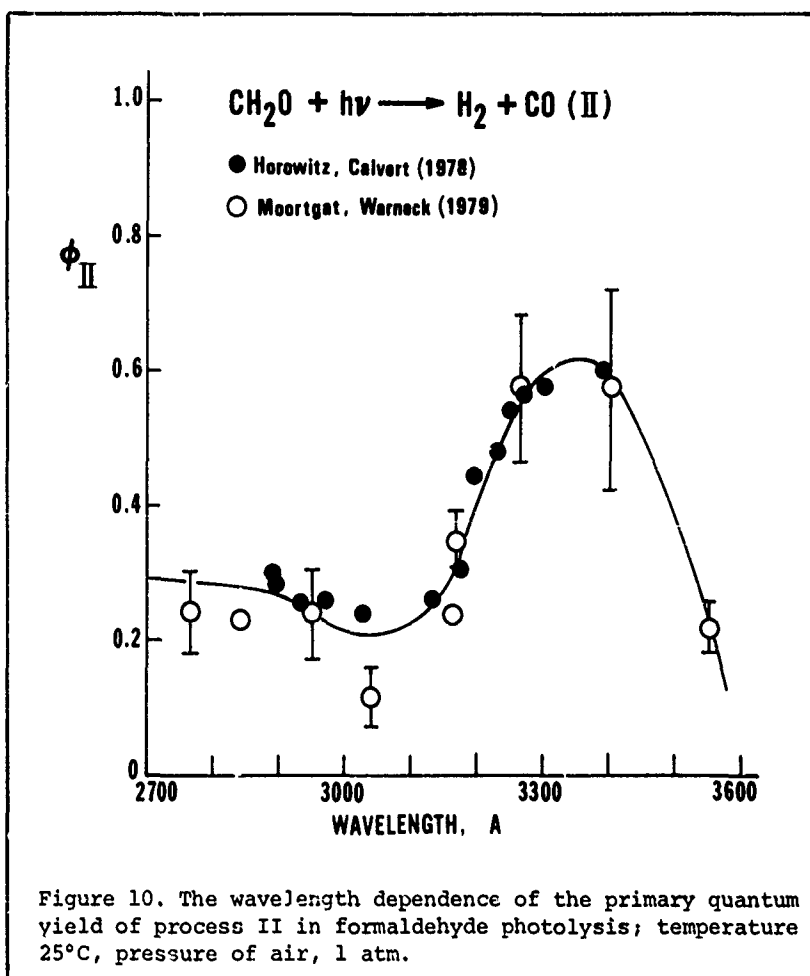


# CALVERT

IV-A-2d. The Effect of Temperature on  $\phi_I$  and  $\phi_{II}$ . No extensive study of the effect of temperature on the primary quantum yields has been made. However there are limited data available which bear on this problem. DeGraff and Calvert [1967] found that the limiting quantum yield of hydrogen in the  $C_3H_6$ -inhibited  $CH_2O$  photolyses was the same in experiments at 91° and 129°C. Obviously the partitioning of 3130 Å excited  $CH_2O$  molecules between fragmentation by I and II is not very sensitive to temperature. Since all  $CH_2O$  molecules excited at 3130 Å decompose by either I or II, and the quantum energy is well in excess of the threshold for both processes, it is not surprising that there is little effect seen at this wavelength. One would expect temperature effects to be more significant at the longer wavelengths near the onset of these processes. Very little data are available from this wavelength region. The product function  $F_I$  observed in  $CH_2O$ - $CD_2O$  flash photolyses by McQuigg and Calvert [1969], which is proportional to the quantum yield of products, increased from  $0.32 \pm 0.03$  at 60°C to  $0.34 \pm 0.08$  at 80°C and  $0.38 \pm 0.08$  at 100°C for exciting light in the range from 3300 to 3530 Å. This may suggest a small increase in the primary process II with temperature or it may be the trivial result of an increased light absorption of  $CH_2O$  with temperature. Obviously we need more extensive data at the lower atmospheric temperatures (176-298 K) to test properly for the possible significance of  $\phi_I$  and  $\phi_{II}$  variations with temperature.

IV-A-2e. Recommended  $\phi_I$  and  $\phi_{II}$  Estimates for Use in the Lower Troposphere. The rather extensive quantum yield data of Horowitz and Calvert [1978] and Moortgat et al. [1978, 1979] form the basis for our estimations. These data are shown in Figures 9 and 10. Although the results from many other studies provide useful information related to  $\phi_I$  and  $\phi_{II}$ , these are considered to be less accurate but consistent with the data chosen in most cases. Their use in any averaging procedure would not improve the precision or the reliability of the results in our opinion. In deriving the solid lines which show reasonable fits to the two sets of data we have excluded the higher values for  $\phi_I$  observed by Moortgat and Warneck for wavelengths greater than 3400 Å. The apparent inefficiency of the total decay which these curves suggest for  $\lambda < 2900$  Å ( $\phi_I + \phi_{II} < 1.0$ ) is not yet well established by the limited data.





IV-A-2f. The First Order Photolysis Constants for  $\text{CH}_2\text{O}$  Photochemical Decay in the Lower Troposphere. We have employed the  $\phi_{\text{I}}$  and  $\phi_{\text{II}}$  estimates of Figures 9 and 10, the new  $\text{CH}_2\text{O}$  absorption data of Bass et al. [1979] for 296 K, and the recent theoretical actinic flux estimates of Demerjian et al. [1979] for ground level (using best estimate surface albedos), to derive the photochemical rate parameters for the lower troposphere. Quantum yield and extinction data were averaged over each 5 nm bandwidth in calculating the product terms included in the summation of each constant:  $J_{\text{I}} = \sum (\phi_{\text{I}})_{\lambda} \sigma_{\lambda} q_{\lambda}$ . These  $J_{\text{I}}$  and  $J_{\text{II}}$  estimates and the total  $\text{CH}_2\text{O}$  decay constant ( $J_{\text{I}} + J_{\text{II}}$ ) are shown in Figure 11. Note as well in Figure 12 that the fraction of the photodecomposed formaldehyde which decays in the lower troposphere by the free radical pathway,  $J_{\text{I}}/(J_{\text{I}} + J_{\text{II}})$ , is a strong function of the solar zenith angle,  $\chi$ ; it increases from 27% at  $\chi = 86^\circ$  to about 44% for an overhead sun. The magnitudes of the new estimates for  $J_{\text{I}}$  and  $J_{\text{II}}$  are significantly lower than those published previously [Calvert et al., 1972; Demerjian et al., 1979]. The older estimates were based upon the less well resolved spectral data obtained in experiments at about 75°C and less accurate  $\phi_{\text{I}}$  and  $\phi_{\text{II}}$  information then available. The present estimates should be more reliable.

IV-A-2g. The First Order Photolysis Constants for  $\text{CH}_2\text{O}$  Photochemical Decay in the Upper Atmosphere. Our knowledge of the pressure and temperature dependence of  $\phi_{\text{I}}$  and  $\phi_{\text{II}}$  at the long wavelengths and the actual values of these quantum yields for wavelengths below 2800 Å is now very limited. Thus accurate estimates for  $J_{\text{I}}$  and  $J_{\text{II}}$  for the upper atmosphere are not now possible. However we may derive "best" current estimates of  $\phi_{\text{I}}$  and  $\phi_{\text{II}}$  which should be useful on the short time scale for upper atmosphere calculations. We have extended the wavelength range of quantum yield estimates to 2537 Å using the data of DeGraff and Calvert [1967] for 2654 and 2537 Å, and the assumption that  $\phi_{\text{I}} + \phi_{\text{II}} = 1.0$  over the entire short wavelength range. These data form a consistent smooth extension to the short wavelength data points of

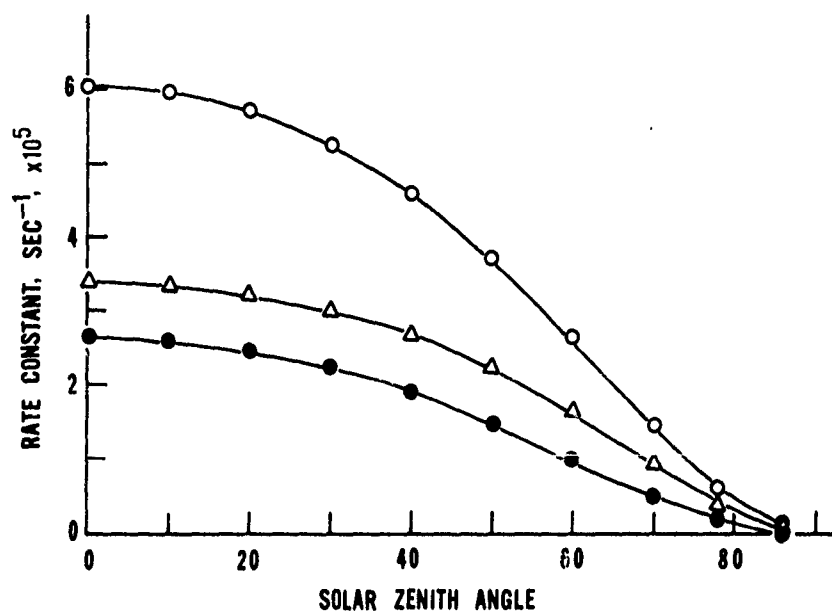


Figure 11. Theoretical first order decay constants for the photo-decomposition of formaldehyde by primary processes I and II in the lower troposphere as a function of solar zenith angle;  $J_I$ , closed circles;  $J_{II}$ , triangles;  $J_I + J_{II}$ , open circles.

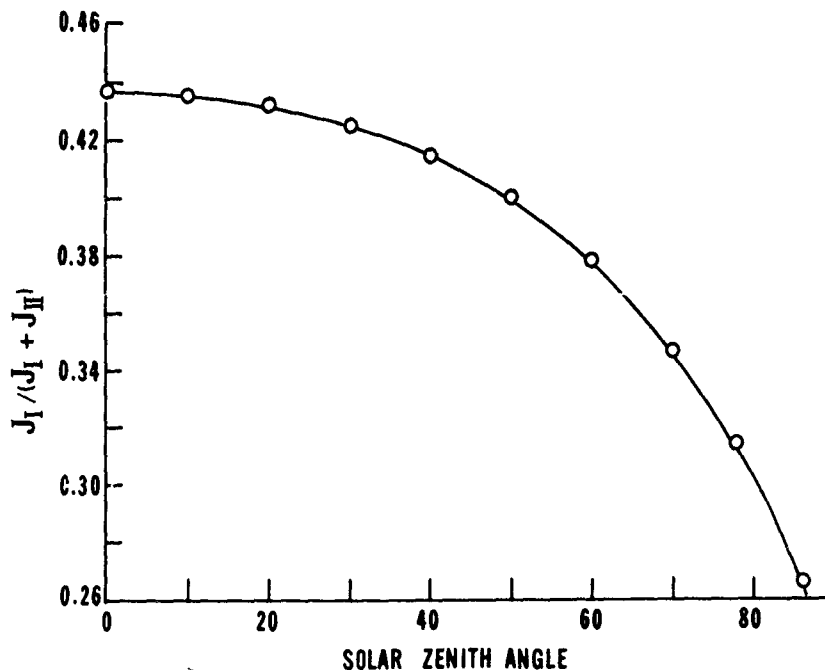


Figure 12. Theoretical fraction of the total formaldehyde photo-decomposition which is expected to occur by the free radical path I in the lower troposphere as a function of the solar zenith angle.

Moortgat and Warneck, but their reliability is not great. The pressure dependence shown in Figure 8 for 298 K was assumed to hold for the conditions of equal  $[M]$  at the low temperatures of the upper atmosphere in deriving preliminary estimates of  $\phi_{II}$ . The approximate  $\phi_I$  and  $\phi_{II}$  estimates made in this fashion are summarized in Table IV. In Part (a) of this Table the data apply to the lower troposphere for both  $\phi_I$  and  $\phi_{II}$ ; the  $\phi_I$  values are pressure insensitive and apply to all altitudes; the  $\phi_{II}$  values for  $\lambda > 3350$  Å (marked with an asterisk in part (a)) are pressure sensitive, and these are shown for various altitudes in part (b) of the Table IV. The solar irradiance data compiled for use in the Lawrence Livermore Laboratory, kinetic-transport 1D atmospheric model (including multiple scattering, 30% surface albedo) were coupled with the quantum yield data derived here and the cross section estimates of Bass et al. [1979] at 223 K to estimate  $J_I$  and  $J_{II}$  values. These estimates derived for various altitudes and times during the day are summarized in Figure 13; they apply in theory to 30°N latitude at the solar equinox. However they should be qualitatively useful for other latitudes as well if the same solar zenith angle is maintained in the calculations; for the 30°N latitude and solar equinox for which these calculations apply, the solar zenith angle (degrees),  $\chi \approx 64, 41, 30, 41, \text{ and } 64$  correspond to the times, 0800, 1000, 1200, 1400, and 1600 hr, respectively. Of course the  $J_I$  and  $J_{II}$  values for 1400 and 1600 hrs are the same as those for 1000 and 0800 hr, respectively, in Figure 13. These estimates must be considered present "best" estimates which will require adjustment when the appropriate more extensive data on the primary process quantum yield dependence on temperature and pressure become available.

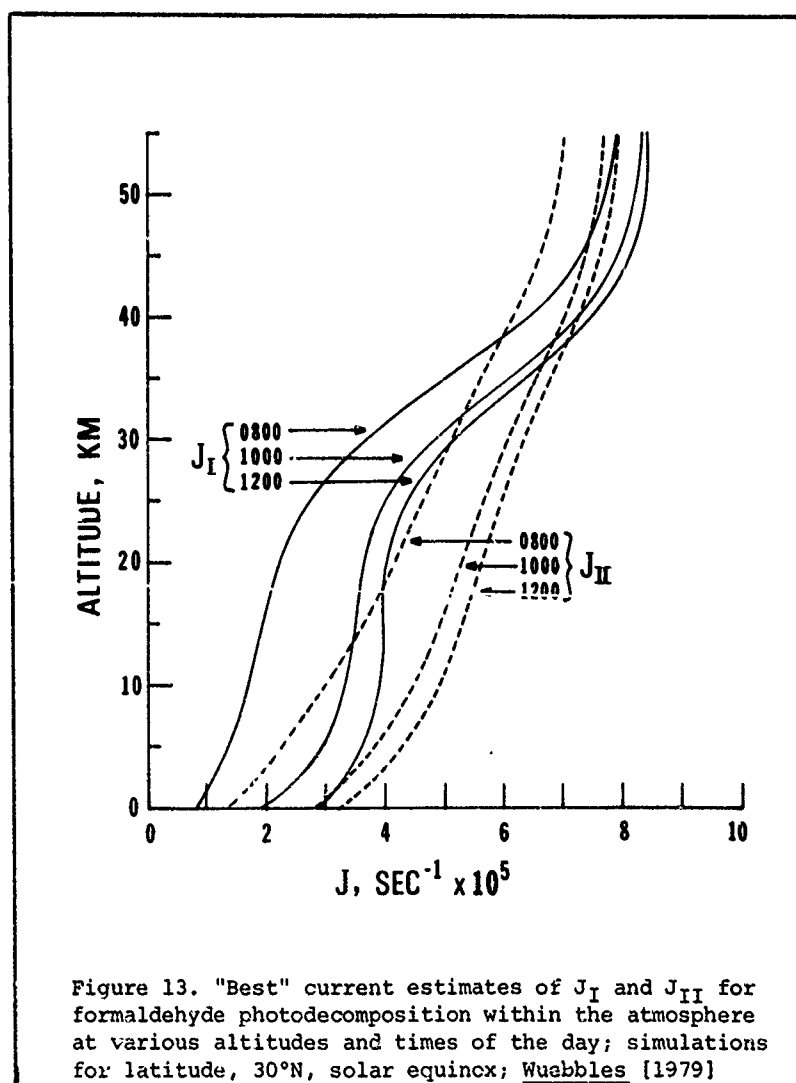


Figure 13. "Best" current estimates of  $J_I$  and  $J_{II}$  for formaldehyde photodecomposition within the atmosphere at various altitudes and times of the day; simulations for latitude, 30°N, solar equinox; Wuabbles [1979]

# CALVERT

Table IV

Approximate  $\phi_I$  and  $\phi_{II}$  Estimates Recommended for Use in the Simulation of  $\text{CH}_2\text{O}$  Photodecomposition

Part (a): Values marked\* are pressure (altitude) dependent; see part (b)

$\lambda, \text{\AA}$	$\phi_I$	$\phi_{II}$	$\lambda, \text{\AA}$	$\phi_I$	$\phi_{II}$	$\lambda, \text{\AA}$	$\phi_I$	$\phi_{II}$
2500	0.14	0.86	2870	0.68	0.32	3250	0.49	0.51
2510	0.14	0.86	2880	0.70	0.30	3260	0.46	0.54
2520	0.14	0.86	2890	0.71	0.29	3270	0.43	0.55
2530	0.14	0.86	2900	0.72	0.28	3280	0.39	0.57
2540	0.14	0.86	2910	0.73	0.27	3290	0.36	0.58
2550	0.14	0.86	2920	0.75	0.25	3300	0.33	0.59
2560	0.14	0.86	2930	0.76	0.24	3310	0.29	0.60
2570	0.14	0.86	2940	0.76	0.24	3320	0.25	0.61
2580	0.15	0.85	2950	0.77	0.23	3330	0.21	0.62
2590	0.15	0.85	2960	0.78	0.22	3340	0.17	0.62
2600	0.15	0.85	2970	0.79	0.21	3350	0.13	0.62*
2610	0.15	0.85	2980	0.79	0.21	3360	0.083	0.62*
2620	0.16	0.84	2990	0.79	0.21	3370	0.038	0.62*
2630	0.16	0.84	3000	0.80	0.20	3380	0.00	0.61*
2640	0.17	0.83	3010	0.80	0.20	3390	0.00	0.61*
2650	0.19	0.81	3020	0.80	0.20	3400	0.00	0.60*
2660	0.20	0.80	3030	0.80	0.20	3410	0.00	0.59*
2670	0.23	0.77	3040	0.80	0.20	3420	0.00	0.57*
2680	0.26	0.74	3050	0.79	0.21	3430	0.00	0.56*
2690	0.28	0.72	3060	0.79	0.21	3440	0.00	0.54*
2700	0.31	0.69	3070	0.79	0.21	3450	0.00	0.52*
2710	0.34	0.66	3080	0.78	0.22	3460	0.00	0.50*
2720	0.37	0.63	3090	0.77	0.23	3470	0.00	0.47*
2730	0.39	0.61	3100	0.76	0.24	3480	0.00	0.45*
2740	0.42	0.58	3110	0.75	0.25	3490	0.00	0.42*
2750	0.44	0.56	3120	0.74	0.26	3500	0.00	0.39*
2760	0.47	0.53	3130	0.73	0.27	3510	0.00	0.36*
2770	0.49	0.51	3140	0.72	0.28	3520	0.00	0.33*
2780	0.51	0.49	3150	0.70	0.30	3530	0.00	0.30*
2790	0.54	0.46	3160	0.69	0.31	3540	0.00	0.26*
2800	0.56	0.44	3170	0.67	0.33	3550	0.00	0.23*
2810	0.58	0.42	3180	0.65	0.35	3560	0.00	0.20*
2820	0.60	0.40	3190	0.63	0.37	3570	0.00	0.16*
2830	0.62	0.38	3200	0.61	0.39	3580	0.00	0.13*
2840	0.63	0.37	3210	0.59	0.41	3590	0.00	0.10*
2850	0.65	0.35	3220	0.57	0.43	3600	0.00	0.063*
2860	0.67	0.33	3230	0.54	0.46	3610	0.00	0.00*
			3240	0.51	0.49			

Part (b):  $\phi_{II}$  Values

Altitude; km	Wavelength Range, $\text{\AA}$			
	3350-3400	3400-3450	3450-3500	3500-3550
0	0.61	0.56	0.46	0.31
5	0.65	0.61	0.54	0.37
10	0.73	0.68	0.64	0.52
15	0.78	0.76	0.74	0.67
20	0.82	0.82	0.82	0.82
25	0.83	0.86	0.89	0.92
30	0.84	0.88	0.93	0.97
35	0.85	0.89	0.94	0.98
40	0.85	0.90	0.94	0.99
45	0.85	0.90	0.95	1.00
50	0.85	0.90	0.95	1.00
55	0.85	0.90	0.95	1.00

# CALVERT

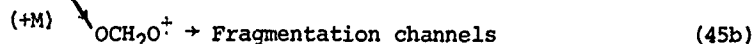
IV-B. THE CHEMICAL REACTIONS WHICH REMOVE FORMALDEHYDE IN THE ATMOSPHERE: Many of the reactive species which are present in the sunlight-irradiated atmosphere do react with formaldehyde: HO, O(<sup>3</sup>P), HO<sub>2</sub>, NO<sub>3</sub>, Cl, and O<sub>3</sub>. A summary of the most recently published second order rate constants for these reactions is given in Table V.

Table V		
Bimolecular Rate Constants for the Reactions of Reactive Atmospheric Species with Formaldehyde		
Species	k, cc molec <sup>-1</sup> sec <sup>-1</sup> (298 K)	Reference
a) HO	(1.4 ± 0.35) × 10 <sup>-11</sup>	Morris, Niki [1971]
	(1.5 ± 0.1) × 10 <sup>-11</sup>	Niki, et al. [1978]
	(0.65 ± 0.15) × 10 <sup>-11</sup>	Smith [1978]
	(0.94 ± 0.10) × 10 <sup>-11</sup>	Atkinson, Pitts [1978]
	(0.99 ± 0.11) × 10 <sup>-11</sup>	Stief et al. [1979]
Recommended value, independent of temperature (228-362 K):		
	(1.05 ± 0.22) × 10 <sup>-11</sup>	Stief et al. [1979]
b) O( <sup>3</sup> P)	(1.5 ± 0.5) × 10 <sup>-13</sup>	Herron, Penzhorn [1969]
	(1.5 ± 0.2) × 10 <sup>-13</sup>	Mack, Thrush [1973]
	1.64 × 10 <sup>-13</sup>	Niki et al. [1969]
	(1.50 ± 0.10) × 10 <sup>-13</sup>	Klemm et al. [1979]
	(1.61 ± 0.17) × 10 <sup>-13</sup>	Klemm [1979]
	(1.9 ± 0.4) × 10 <sup>-13</sup>	Chang, Barker [1979]
Recommended value (250-500 K):		Klemm [1979]
	(2.78 ± 0.32) × 10 <sup>-11</sup> e <sup>-(3030 ± 80 cal mole<sup>-1</sup>)/RT</sup>	
c) NO <sub>3</sub>	~1.2 × 10 <sup>-15</sup> (assumed equal to that measured for CH <sub>3</sub> CHO)	Morris, Niki [1974]
d) HO <sub>2</sub>	~1.0 × 10 <sup>-14</sup> (air, 1 atm)	Su et al. [1979]
e) O <sub>3</sub>	<2.1 × 10 <sup>-24</sup>	Braslavski, Heicklen [1976]
f) Cl	7.8 × 10 <sup>-11</sup>	Niki et al. [1978]
	(7.5 ± 0.9) × 10 <sup>-11</sup>	Stief et al. [1978]
Recommended value (200-500 K):		
	(7.48 ± 0.50) × 10 <sup>-11</sup>	Michael et al. [1979]

If these rate constants are used together with estimates of the concentrations of the reactive intermediates within the upper atmosphere, it becomes evident that only the HO, O(<sup>3</sup>P), Cl, and HO<sub>2</sub> radical reactions will remove CH<sub>2</sub>O at any significant rate within the atmosphere. Thus we may confine our attention to these reactions.

The majority of experimental evidence suggests that the HO-radical, NO<sub>3</sub>, and Cl-atom attack on CH<sub>2</sub>O are typical H-atom abstraction reactions. Although the O(<sup>3</sup>P)-CH<sub>2</sub>O reaction has been considered to have the same abstraction mechanism, recent studies of Chang and Barker [1979] suggest that (45a) may not be the exclusive reaction channel; some addition of O(<sup>3</sup>P) to the CH<sub>2</sub>O molecule may occur forming OCH<sub>2</sub>O and leading to its subsequent fragmentation products:



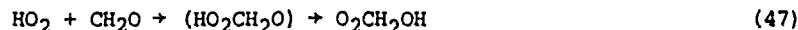


The most recent kinetic data demand that following the generation of the HCO radical in the primary photodecomposition of CH<sub>2</sub>O in process I or in reactions (42) to (45), the reaction (30) rather than (46) must dominate, even in the lower atmosphere where the concentration of the third body M is a maximum [Su et al., 1979]:

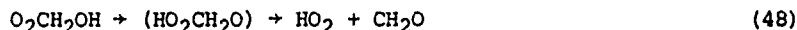


Reaction (46) has been considered to be a logical step in a reaction sequence which would lead ultimately to the formic acid product which is observed in Cl<sub>2</sub>, CH<sub>2</sub>O, O<sub>2</sub> mixture photolyses [Osif and Heicklen, 1976; Niki et al., 1977]. However the relative unimportance of CO<sub>2</sub> [Horowitz and Calvert, 1978; Su et al., 1979] and peroxyformic acid product formation [Osif and Heicklen, 1976; Niki et al., 1977] in CH<sub>2</sub>O photooxidation, and the second order kinetics of the HCO-O<sub>2</sub> reaction observed in gaseous mixtures up to 1 atm pressure [Washida et al., 1974; Shibuya et al., 1977; Reilly et al., 1978] point to the probable unimportance of reaction (46) compared to (30). The recent results of Su et al. [1979] confirm this conclusion and offer new kinetic information on the favored routes (other than (46)) to formic acid formation in CH<sub>2</sub>O photooxidation; see the following discussion.

The HO<sub>2</sub>-CH<sub>2</sub>O reaction observed at relatively low temperatures of the atmosphere is not one of H-atom abstraction. Recent studies of Su et al. [1979] show that HO<sub>2</sub>-radical addition to CH<sub>2</sub>O is the major elementary step:



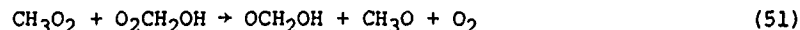
However the reverse of this reaction occurs as well with  $k_{48} \approx 1.5 \text{ sec}^{-1}$  (25°C, 700 Torr air), and the removal of a CH<sub>2</sub>O molecule need not result with each occurrence of (47).



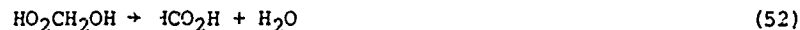
In laboratory studies the O<sub>2</sub>CH<sub>2</sub>OH radical has been shown to react by two pathways; either it disproportionates with HO<sub>2</sub> radicals in (49) or with other O<sub>2</sub>CH<sub>2</sub>OH radicals in (50):



It is likely that the O<sub>2</sub>CH<sub>2</sub>OH radicals may also disproportionate with CH<sub>3</sub>O<sub>2</sub> radicals under atmospheric conditions:



The new HO<sub>2</sub>CH<sub>2</sub>OH species formed in (49) has been characterized and its reactions followed by Fourier transform infrared spectroscopy. It gives formic acid in laboratory experiments through the overall reaction (52) which may be initiated by light and wall-catalyzed reactions:



This species when formed in the atmosphere will probably be destroyed through a rapid photo-decomposition which should parallel that for CH<sub>3</sub>O<sub>2</sub>H:



The OCH<sub>2</sub>OH radical product of (50), (51), and (53) is expected to react rapidly with O<sub>2</sub> in a fashion similar to the related CH<sub>3</sub>O radical, forming formic acid and an HO<sub>2</sub>-radical:



# CALVERT

Note that the reaction sequence initiated by the HO<sub>2</sub> addition to CH<sub>2</sub>O in (47) may result in the regeneration of HO<sub>2</sub> radicals; thus there is a chain mechanism, carried by the HO<sub>2</sub> radical, forming HCO<sub>2</sub>H in the formaldehyde photooxidation. The extent to which this may occur in the atmosphere has not been determined to date.

The rate constants for the HO<sub>2</sub>-addition reaction (47) and its reverse (48) have been estimated only in experiments near 25°C. These data provide an estimate for the equilibrium constant: K<sub>47</sub> = 6.7 x 10<sup>-15</sup> cc molec<sup>-1</sup> (25°C).



For the purposes of our considerations here we may use the thermochemical kinetic methods of Benson [1976] to estimate the approximate temperature dependence of this equilibrium constant. This procedure gives:

$$K_{47} = 3.25 \times 10^{-27} e^{16.8(\text{kcal mole}^{-1})/K} \text{ cc molec}^{-1}$$

We may use these data to estimate the approximate rate of CH<sub>2</sub>O removal by the HO<sub>2</sub> radical. Let us assume that equilibrium is reached in the HO<sub>2</sub>-CH<sub>2</sub>O-O<sub>2</sub>CH<sub>2</sub>OH radical system in the atmosphere and that the major removal path for O<sub>2</sub>CH<sub>2</sub>OH is reaction with the abundant HO<sub>2</sub> species. We shall take k<sub>49</sub> = 2.0 x 10<sup>-12</sup> cc molec<sup>-1</sup> sec<sup>-1</sup>, independent of temperature. We will assume further that CH<sub>2</sub>O is not regenerated from the HO<sub>2</sub>CH<sub>2</sub>OH product once it is formed, but the decay of this molecule proceeds to form HCO<sub>2</sub>H as outlined above. From these assumptions we would expect the rate of CH<sub>2</sub>O removal by HO<sub>2</sub> reactions to be given approximately by relation (55):

$$-d[\text{CH}_2\text{O}]/dt = [\text{HO}_2]^2 [\text{CH}_2\text{O}] K_{47} k_{49} \quad (55)$$

The relative significance of the various homogeneous removal paths for formaldehyde in the atmosphere can be compared in Table VI; these data were calculated for the 1200 hr (noon) at 30°N latitude and solar equinox using the Livermore 1D atmospheric model [Wuebbles, 1979]; the present CH<sub>2</sub>O quantum yield data and absorption cross section data were incorporated.

Table VI

Comparison of the Theoretical CH<sub>2</sub>O Removal Rates in the Atmosphere as a Function of Altitude; 1200 hr, 30°N, Solar Equinox [Wuebbles, 1979]

- A) HO + CH<sub>2</sub>O → H<sub>2</sub>O + HCO
- B) O(<sup>3</sup>P) + CH<sub>2</sub>O → HO + HCO  
→ OCH<sub>2</sub>O<sup>+</sup> + Products
- C) Cl + CH<sub>2</sub>O → HCl + HCO
- D) HO<sub>2</sub> + CH<sub>2</sub>O ⇌ O<sub>2</sub>CH<sub>2</sub>OH → Products
- E) CH<sub>2</sub>O + hν → HCO + H
- F) CH<sub>2</sub>O + hν → H<sub>2</sub> + CO

Altitude, km	Rate Reaction/[CH <sub>2</sub> O], sec <sup>-1</sup> x 10 <sup>4</sup>					
	A	B	C	D	E	F
a	0.93	0.00	0.02	0.000	0.28	0.34
5	0.28	0.00	0.00	0.001	0.36	0.44
10	0.30	0.00	0.00	0.042	0.39	0.49
15	0.40	0.00	0.00	0.010	0.40	0.53
20	0.35	0.00	0.01	0.004	0.41	0.57
25	0.58	0.00	0.02	0.005	0.44	0.60
30	1.32	0.03	0.07	0.003	0.52	0.64
35	2.52	0.17	0.19	0.001	0.64	0.68
40	3.77	0.95	0.35	0.000	0.75	0.73
45	3.42	3.52	0.36	0.000	0.82	0.77
50	2.16	5.59	0.23	0.000	0.84	0.79
55	1.37	5.79	0.14	0.000	0.85	0.79

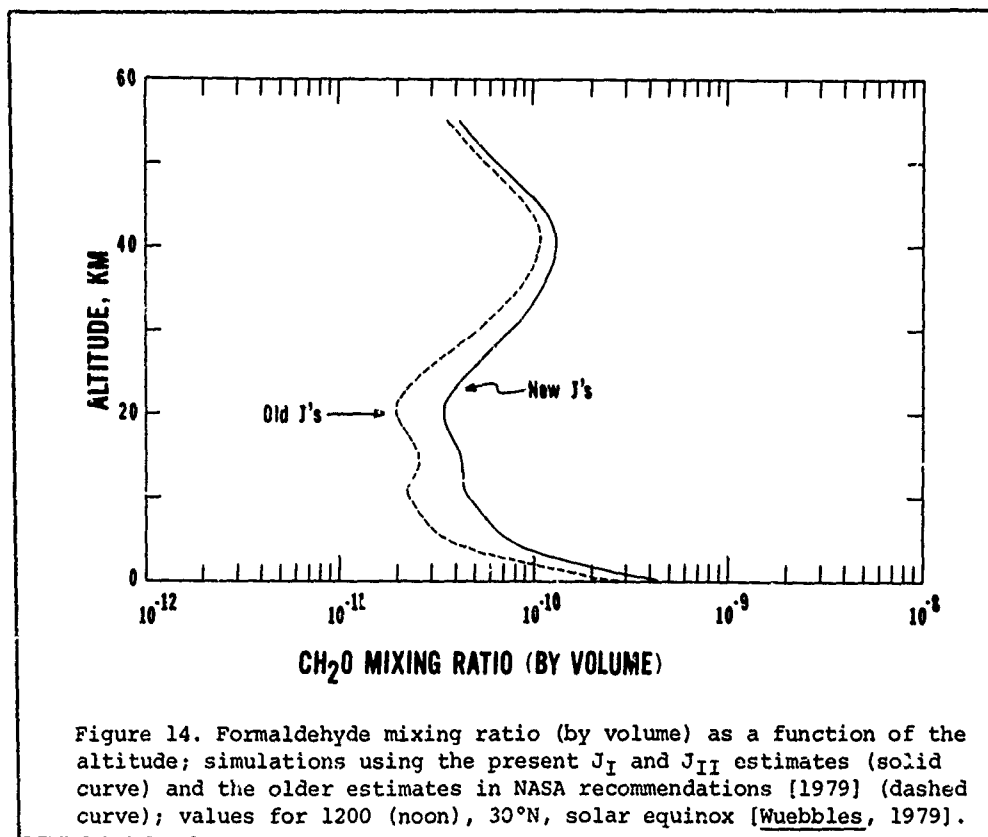
<sup>a</sup> Atmosphere in a remote region, away from urban sources.



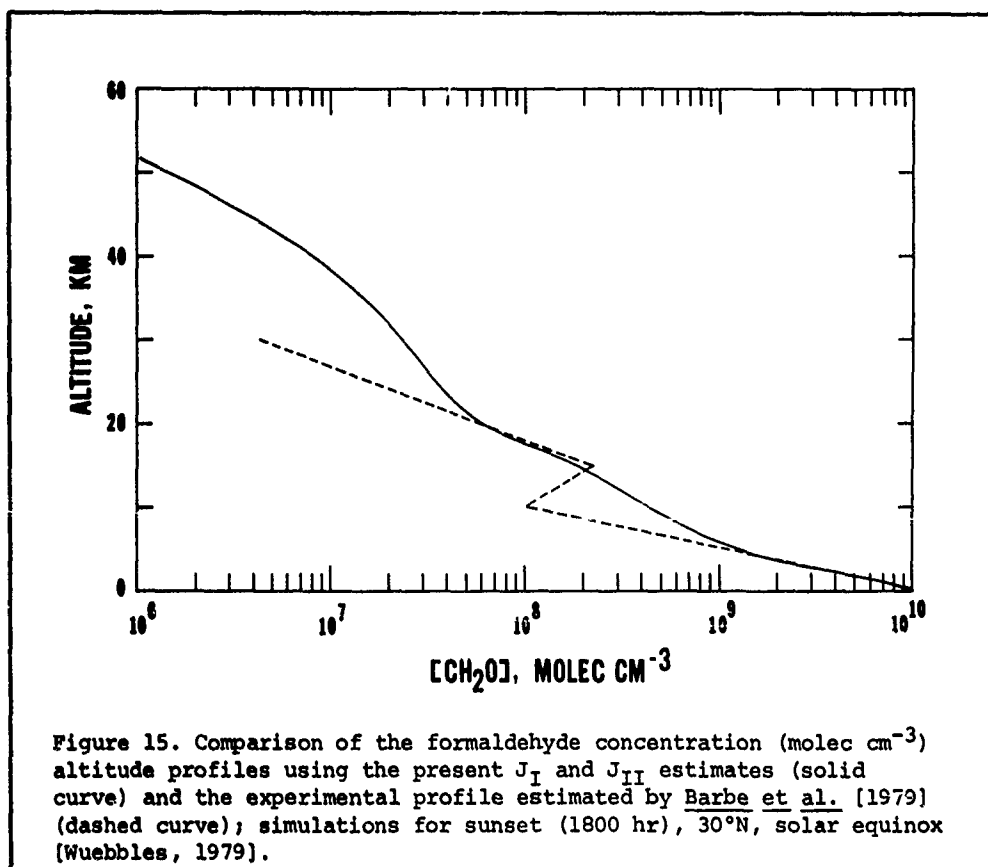
# CALVERT

(In all of these simulations the chlorofluorocarbon input was modeled from the known emissions for the 28 years up to January, 1978.) It is apparent from the rate data of Table VI that the attack of HO-radicals on CH<sub>2</sub>O (route A) and the photochemical decay (E and F) are the major CH<sub>2</sub>O loss reactions up to about 30 km altitude. The fraction of the CH<sub>2</sub>O decay which results from O(<sup>3</sup>P) attack (route B) continues to grow at elevations above 30 km, and this is the dominant decay path in the 45-55 km region. It is interesting to find that the relatively minor Cl-atom constituent of the atmosphere accounts for a finite fraction of the CH<sub>2</sub>O decay (maximum of 5.3% at 40 km). Stief et al. [1978] have considered the effect of this reaction on stratospheric ozone perturbations recently. The estimated contribution from the HO<sub>2</sub>-CH<sub>2</sub>O reaction to the removal of CH<sub>2</sub>O is small at all altitudes, accounting for a maximum of about 3% of the total at 10 km. However direct experimental determinations of the rate constants for reactions (47) and (48) at the lower temperature and pressures of the upper atmosphere are required before any definitive conclusion about the potential significance of this pathway is warranted. The combined CH<sub>2</sub>O removal processes lead to a relatively short lifetime for CH<sub>2</sub>O in the atmosphere. For the 1200 hr, 30°N, solar equinox conditions which apply for the data of Table VI, the lifetime of CH<sub>2</sub>O decreases from about 2.6 hr in the troposphere at 5 km, to about 0.3 hr at 55 km altitude.

Theoretical estimates of the CH<sub>2</sub>O mixing ratio-altitude profile can be made using the current "best" estimates of the photochemical data selected in this study [Wuebbles, 1979]. These are shown in Figure 14 where they may be compared with the profile based upon the older J<sub>I</sub> and J<sub>II</sub> estimates which NASA has recommended for atmospheric use until recently. We may compare the



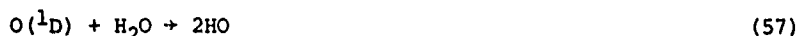
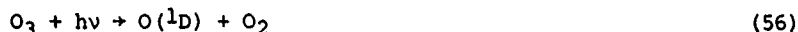
current best estimates of the theoretical CH<sub>2</sub>O concentration-altitude profile in Figure 15 with the experimental profile of Barbe et al. [1979]. In this case we have used the atmospheric simulation data for the sunset hour (1800 hr) 30°N, solar equinox to allow a somewhat more realistic match of the conditions present in the measurements of Barbe et al. which were made at sunset. A reasonable agreement between theory and experiment is seen, although the experi-



mental determinations are not precise enough to establish any detail. The theoretical diurnal variation of  $[CH_2O]$  which is anticipated in theory at several altitudes at 30°N, solar equinox, is shown in Figure 16. It is interesting to note that although the  $[CH_2O]$  usually increases somewhat during the daylight hours, the opposite change is predicted for the 50 km altitude. Obviously more extensive and accurate experimental profiles of  $[CH_2O]$  versus altitude are required to test the accuracy of the theoretical expectations based upon the present  $CH_2O$  photochemical and kinetic data.

The computer simulations allow us to see clearly the relative importance of formaldehyde chemistry in several key processes in the atmosphere. One such observation is worthwhile here in that it bears directly on the ozone levels in the stratosphere. The "odd oxygen", the sum of  $[O_3]$ ,  $[O(^3P)]$ , and  $[O(^1D)]$ , is generated largely by  $O_2$  photolysis and is destroyed mainly by four reaction cycles involving the  $O_x$ ,  $HO_x$ ,  $NO_x$ , and  $ClO_x$  species; see Luther et al. [1979] for a recent consideration of the theoretical ozone perturbations in terms of these cycles. We have plotted in Figure 17 the rate (diurnal average) of "odd oxygen" destruction by the various cycles using the present  $CH_2O$  photochemical data in atmospheric simulations [Wuebbles, 1979]. It is clear that the  $HO_x$  cycle of reactions is most significant to the "odd oxygen" loss rate below 15 km altitude, and it remains important, although somewhat less important than the  $ClO_x$  cycle, in the 15-30 km altitude,  $O_3$ -rich region of the stratosphere.

The major primary photochemical sources of the  $HO_x$  radicals in the atmosphere are: (1)  $HO$ -radical formation in the reaction (57) which follows  $O(^1D)$  generation by  $O_3$  photolysis a small fraction of the time; and (2)  $HO_2$ -radical formation in (29) and (30) following formaldehyde photolysis in (I):



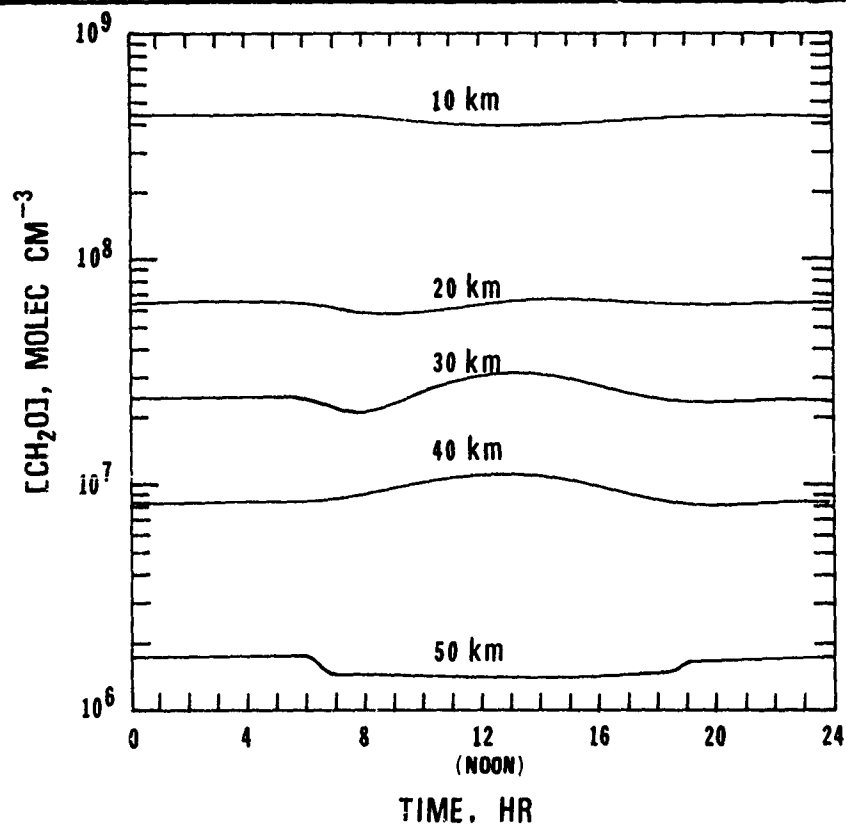


Figure 16. Theoretical diurnal variation of the formaldehyde concentration at several altitudes; simulations for 30°N, solar equinox [Wuebbles, 1979].

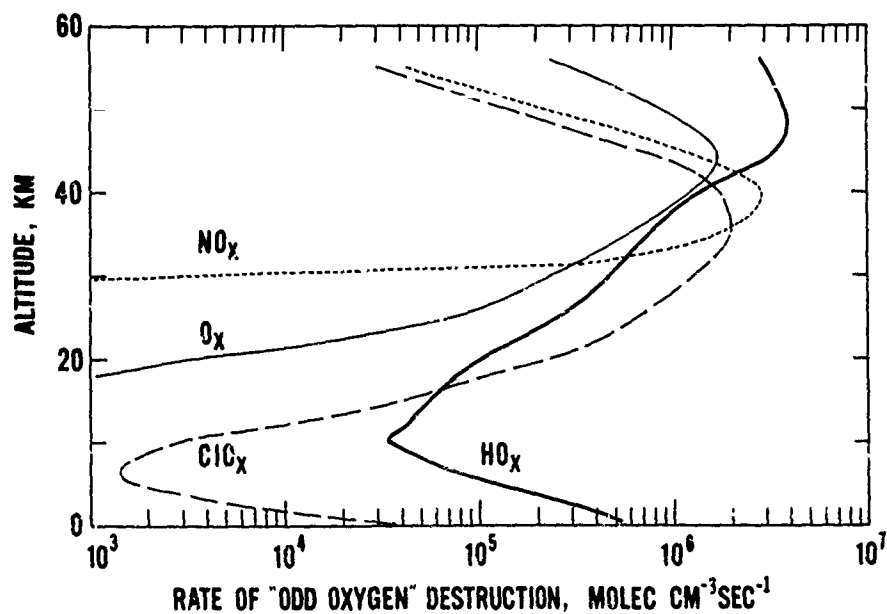
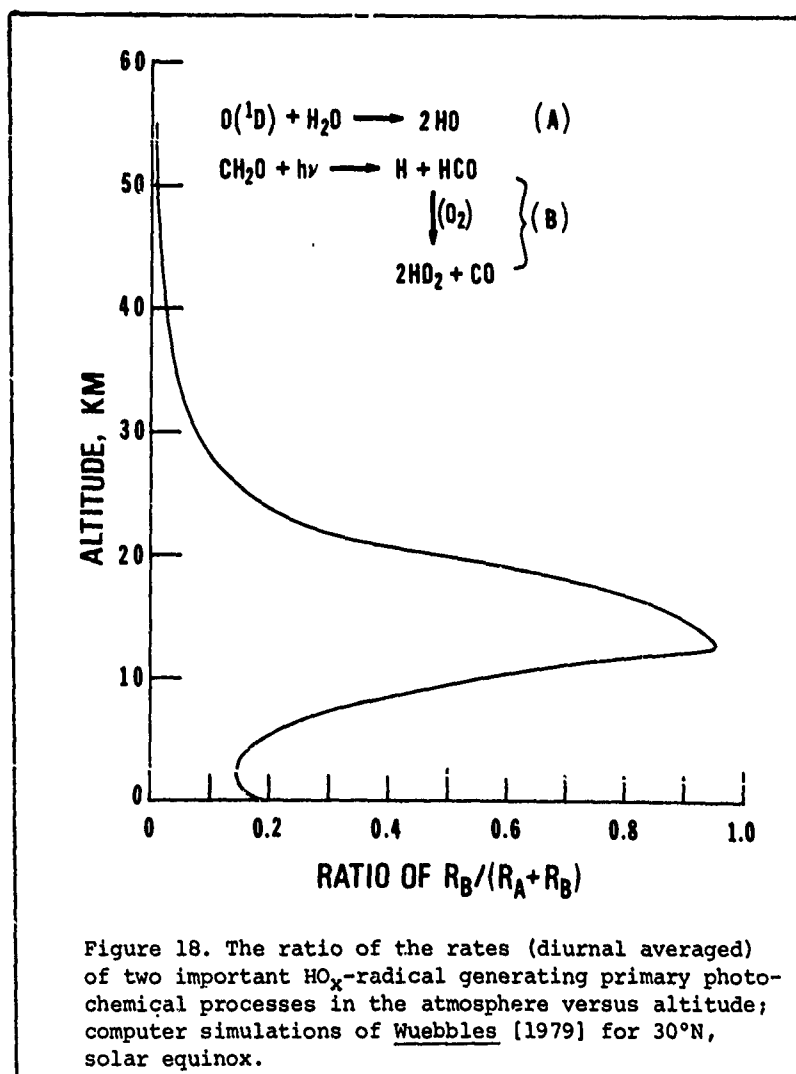


Figure 17. Comparison of the rates of "odd oxygen" destruction by reaction cycles involving various classes of reactive species versus altitude; rates are diurnal averages for 30°N, solar equinox; Wuebbles [1979].

# CALVERT



In Figure 18 one can compare the theoretical rates of these two important processes (diurnal averages). Note that  $\text{HO}_x$  ( $\text{HO}_2$ ) radical generation is very significant through formaldehyde photolysis in the lower stratosphere following the  $\text{CH}_4$  oxidation steps which we considered in section III. Hence it can be seen at least qualitatively that the chemistry and photochemistry of the formaldehyde molecule are important among the many other processes which control the ozone levels in the atmosphere. This chemistry must be well understood if we are to predict successfully the effect of perturbations on the ozone levels in the stratosphere.



V. RECOMMENDATIONS FOR FURTHER STUDIES OF  $\text{CH}_2\text{O}$  AND ITS RELATED ATMOSPHERIC COMPOUNDS: Although the broad outlines of the pathways of formaldehyde generation and decay reactions within the atmosphere appear well established, certain key information related to these processes is still required in order that one may calculate rates of the photochemical and chemical processes for  $\text{CH}_2\text{O}$  in the atmosphere with some confidence and to allow a quantitative test of current theory. We suggest the following critical areas for further study:

- 1) Establish accurate  $\text{CH}_2\text{O}$  concentration profiles by both column density measurements and direct, unambiguous measurements at selected altitudes within the troposphere and the stratosphere. These measurements should be made at various latitudes, solar zenith angles, and

## CALVERT

seasons during daylight and nighttime hours.

2) Detect acetaldehyde and determine its vertical profile in the troposphere and stratosphere to help establish the potential role of ethane oxidation in the atmospheric chemistry.

3) Determine the relative importance of the abstraction and addition channels of the  $O(^3P)-CH_2O$  reaction as a function of temperature and pressure in the range of their atmospheric variations. If the addition step is important as Chang and Barker [1979] now believe, then the simulations of  $CH_2O$  reaction pathways will require suitable modification from the presently adopted calculations which neglect this channel.

4) Determine the forward and reverse rate constants for the  $HO_2-CH_2O$  addition reaction over the range of atmospheric temperatures and pressures. The potential involvement of the newly identified species,  $HO_2CH_2OH$ , formic acid, and the free radicals,  $O_2CH_2OH$  and  $OCH_2OH$ , in atmospheric chemistry cannot be adequately assessed from the present limited data.

5) Detect formic acid in the clean atmosphere and establish its vertical concentration profile. The relatively unreactive nature of the  $HCO_2H$  molecule compared to  $CH_2O$  toward photochemical decay and attack by the reactive atmospheric species,  $HO$ ,  $Cl$ ,  $O(^3P)$ , suggests that its build-up may occur in the atmosphere to detectable levels.

6) Estimate  $\phi_I$  and  $\phi_{II}$  for  $CH_2O$  photolyses at the short wavelength end of  $CH_2O$  absorption, 2400-2800 Å. Also establish the temperature and pressure dependence of  $\phi_{II}$  at selected wavelengths within the long wavelength range of formaldehyde's absorption band (3350-3600 Å). The questionable accuracy of the limited data for this region demands that further studies be made to quantify the  $J_I$  and  $J_{II}$  values for  $CH_2O$ .

**ACKNOWLEDGMENT:** The author is grateful to the Environmental Protection Agency which supported this work under its research grant R-806479-01; the pre-reprints of current work provided by Drs. John Barker, Arnold Bass, Dieter Ehhalt, Bruce Klemm, Geert Moortgat, and Marcel Nicolet are appreciated, as is the help of William Stockwell with spectral data treatment, and Dr. Fu Su in the preparation of the figures. The author owes a special thanks to Donald J. Wuebbles for his atmospheric simulations made using the Lawrence Livermore Laboratory, 1D atmospheric kinetic-transport model with incorporation of the present  $CH_2O$  data derived in this work, and to Arnold M. Bass for the use of his new  $CH_2O$  cross section data before publication.

## REFERENCES

- Altshuler, A. F., and S. P. McPherson, Spectrophotometric Analysis of Aldehydes in Los Angeles Atmosphere, J. Air Poll. Control Assoc., **13**, 109-111, 1963.
- Atkinson, R., and J. N. Pitts, Jr., Kinetics of the Reactions of the OH Radical with HCHO and  $CH_3CHO$  over the Temperature Range 299-426°K, J. Chem. Phys., **68**, 3581-3584, 1978.
- Avouris, P., W. M. Gelbart, and M. A. El-Sayed, Nonradiative Electronic Relaxation under Collision-Free Conditions, Chem. Rev., **77**, 793-833, 1977.
- Barbe, A., P. Marché, C. Secroun, and P. Jouve, Measurements of Tropospheric and Stratospheric  $H_2CO$  by an Infrared High Resolution Technique, Geophys. Res. Lett., **6**, 463-465, 1979.
- Bass, A. M., L. C. Glasgow, C. Miller, J. P. Jesson, and D. L. Filkin, Temperature Dependent Absorption Cross-Sections for Formaldehyde ( $CH_2O$ ): The Effect of Formaldehyde on Stratospheric Chlorine Chemistry, paper posted at NATO Advanced Institute on Atmospheric Ozone, Portugal, Oct., 1979; to appear Planetary Space Sci., 1980.
- Becker, K. H., H. Lippmann, and U. Schurath, Schwingungs-Rotations-Anregung von  $OH(X^2\Pi)$ -Radicalen durch die Reaction  $O + HCO \rightarrow OH(v) + CO$ , Ber. Bunsenges Phys. Chem., **81**, 567-572, 1977.
- Benson, S. W., Thermochemical Kinetics, 2nd Ed., John Wiley, New York, 1976.
- Blacet, F. E., and J. D. Heldman, The Photolysis of Aliphatic Aldehydes. X. Acetaldehyde and Iodine Mixtures, J. Amer. Chem. Soc., **64**, 889-893, 1942.
- Blacet, F. E., and D. E. Loeffler, The Photolysis of Aliphatic Aldehydes. XI. Acetaldehyde and Iodine Mixtures, J. Amer. Chem. Soc., **64**, 893-896, 1942.
- Brand, J. C. D., The Electronic Spectrum of Formaldehyde, J. Chem. Soc., **1956**, 858-872.
- Brand, J. C. D., and C. G. Stevens, Analysis of Some Singlet-Triplet Perturbations in  $1A_2$  State of Formaldehyde, J. Chem. Phys., **58**, 3331-3338, 1973.
- Braslavsky, S., and J. Heicklen, The Gas Phase Reaction of  $O_3$  with  $H_2CO$ , Int. J. Chem. Kinet.,

# CALVERT

- 8, 801-808, 1976.
- Breeding, R. J., J. P. Lodge, Jr., J. B. Pate, D. C. Sheesley, H. B. Klonis, B. Fogle, J. A. Anderson, T. R. Englert, P. Haagenson, R. B. McBeth, A. L. Morris, R. Pogue, and A. F. Wartburg, Background Trace Gas Concentrations in the Central United States, J. Geophys. Res., **78**, 7057-7064, 1973.
- Bufalini, J. J., B. W. Gay, Jr., and K. L. Brubaker, Hydrogen Peroxide Formation from Formaldehyde Photooxidation and Its Presence in Urban Atmospheres, Environ. Sci. Technol., **6**, 816-821, 1972.
- Callomon, J. H., and K. K. Innes, Magnetic Dipole Transition in the Electronic Spectrum of Formaldehyde, J. Molec. Spectrosc., **10**, 166-181, 1963.
- Calvert, J. G., and G. S. Layne, The Photolysis of Glyoxal Vapor at Wavelength 3130 Å, J. Amer. Chem. Soc., **75**, 856-859, 1953.
- Calvert, J. G., and J. N. Pitts, Jr., Photochemistry, John Wiley, New York, 1966.
- Calvert, J. G., J. A. Kerr, K. L. Demerjian, and R. D. McQuigg, Photolysis of Formaldehyde as an H-Atom Source in the Lower Troposphere, Sci., **175**, 751, 1972.
- Chang, J. S., and J. R. Barker, Reaction Rate and Products for the Reaction  $O(^3P) + H_2CO$ , J. Phys. Chem., submitted, 1979.
- Clark, J. H., C. B. Moore, and N. S. Nogar, The Photochemistry of Formaldehyde: Absolute Quantum Yields, Radical Reactions, and NO Reactions, J. Chem. Phys., **68**, 1264-1271, 1978.
- Cronn, D., and E. Robinson, Tropospheric and Lower Stratospheric Vertical Profiles of Ethane and Acetylene, Geophys. Res. Lett., **6**, 641-644, 1979.
- DeGraff, B. A., and J. G. Calvert, A Study of the Primary Processes in  $CH_2O$  and  $CD_2O$  Photolysis, J. Amer. Chem. Soc., **89**, 2247-2253, 1967.
- Demerjian, K. L., J. A. Kerr, and J. G. Calvert, The Mechanism of Photochemical Smog Formation, Adv. Environ. Sci. Technol., **4**, 1-262, 1974.
- Demerjian, K. L., K. L. Schere, and J. T. Peterson, Theoretical Estimates of Actinic (Spherically Integrated) Flux and the Photolytic Rate Constants of Atmospheric Species in the Lower Troposphere, Adv. Environ. Sci. Technol., 1979, in press.
- Diem, M., and E. K. C. Lee, The Role of the Cage Dimer of Formaldehyde in the Photolysis of Formaldehyde: Argon Matrix at 12 K, Chem. Phys., **41**, 373-377, 1979.
- Fischer, W. H., J. P. Lodge, Jr., A. F. Wartburg, and J. B. Pate, Estimation of Some Atmospheric Trace Gases in Antarctica, Environ. Sci. Technol., **2**, 464-466, 1968.
- Fletcher, R. A., and G. Pilcher, Measurements of Heats of Combustion by Flame Calorimetry, Part 6.--Formaldehyde, Glyoxal, Trans. Faraday Soc., **66**, 794-799, 1970.
- Galbally, I. E., Production of Carbon Monoxide in Rain Water, J. Geophys. Res., **77**, 7129-7132, 1972.
- Gillispie, G. D., and E. C. Lim, Small Molecule Photochemistry. Theory and Application to Formaldehyde, J. Phys. Chem., **80**, 2166, 1976.
- Goddard, J. D., and H. F. Schaefer, III, The Photodissociation of Formaldehyde: Potential Energy Surface Features, J. Chem. Phys., **70**, 5117-5134, 1979.
- Gorin, E., Photolysis of Aldehydes and Ketones in the Presence of Iodine Vapor, J. Chem. Phys., **7**, 256-264, 1939.
- Harding, L. B., and W. A. Goddard III, The Generalized Valence Bond Description of Low-Lying States of Formaldehyde, J. Amer. Chem. Soc., **97**, 6293-6299, 1975.
- Hartley, D. B., Chemiluminescence Recombination of Formyl Radicals, Chem. Comm., 1967, 1281-1282.
- Hayes, D. M., and K. Morokuma, Theoretical Studies of Carbonyl Photochemistry. I. Ab Initio Potential Energy Surfaces for Photodissociation  $H_2CO^* \rightarrow H + HCO$ , Chem. Phys. Lett., **12**, 539-542, 1972.
- Heicklen, J., Atmospheric Chemistry, Academic Press, New York, 1976.
- Herron, J. T., and R. D. Penzhorn, Mass Spectrometric Study of the Reactions of Atomic Oxygen with Ethylene and Formaldehyde, J. Phys. Chem., **73**, 191-196, 1969.
- Herzberg, G., Electronic Spectra of Polyatomic Molecules, Van Nostrand, Princeton, N. J., 1967.
- Horowitz, A., and J. G. Calvert, The Quantum Efficiency of the Primary Processes in Formaldehyde Photolysis at 3130 Å and 25°C, Int. J. Chem. Kinet., **10**, 713-732, 1978.
- Horowitz, A., and J. G. Calvert, Wavelength Dependence of the Quantum Efficiencies of the Primary Processes in Formaldehyde Photolysis at 25°C, Int. J. Chem. Kinet., **10**, 805-819, 1978.
- Horowitz, A., F. Su, and J. G. Calvert, Unusual  $H_2$ -Forming Chain Reaction in the 3130 Å Photolysis of Formaldehyde-Oxygen Mixtures at 25°C, Int. J. Chem. Kinet., **10**, 1099-1117, 1978.
- Houston, P. L., and C. B. Moore, Formaldehyde Photochemistry: Appearance Rate, Vibrational Relaxation, and Energy Distribution of the CO Product, J. Chem. Phys., **65**, 757-770, 1976.

# CALVERT

- Jaffee, R. L., D. M. Hayes, and K. Morokuma, Photodissociation of Formaldehyde: Potential Energy Surfaces for  $\text{H}_2\text{CO}^* \rightarrow \text{H}_2 + \text{CO}$ , J. Chem. Phys., **60**, 5108-5109, 1974.
- Jeffries, H. E., and R. M. Kamens, Progress Report, Outdoor Simulation of Air Pollution Control Strategies, U.S. Environmental Protection Agency Grant 800916, 1977.
- Jeffries, H. E., and R. M. Kamens, A Critical Review of Ambient Air Aldehyde Measurement Methods and an Analysis of Houston Aldehyde Data; Part II; An Analysis of Houston Aldehyde Data and Comparison with Cincinnati and St. Paul Data; report prepared for Houston Area Oxidant Study, 1978; the Cincinnati data were derived by the authors from the original data in Air Quality Data Ohio Counties-Hamilton, Clermont, Butler, and Warren, published by the City of Cincinnati and the Southwest Ohio Air Pollution Control District; the original data from Houston were from the Texas Air Control Board and the City of Houston; the St. Paul data were from the Minnesota Pollution Control Agency, Division of Air Quality.
- Jennings, K. R., and R. J. Cvetanovic, Addition of Hydrogen to Olefins, J. Chem. Phys., **35**, 1233-1240, 1961.
- Job, V. A., V. Sethuraman, and K. K. Innes, The  $3500 \text{ \AA } ^1\text{A}_2 \rightarrow \tilde{\text{X}}^1\text{A}_1$  Transition of Formaldehyde- $\text{D}_2$  and HD; Vibrational and Rotational Analyses, J. Molec. Spectrosc., **30**, 365-426, 1969.
- Kemper, M. J. H., J. M. F. van Dijk, and H. M. Buck, Ab Initio Calculation of the Photochemistry of Formaldehyde. The Search for a Hydroxycarbene Intermediate, J. Amer. Chem. Soc., **100**, 7841-7845, 1978.
- Klemm, R. B., E. G. Skulnick, and J. V. Michael, J. Chem. Phys., submitted for publication, 1979.
- Klemm, R. B., Absolute Rate Parameters for the Reactions of Formaldehyde with O-Atoms and H-Atoms over the Temperature Range 250-500 K, J. Chem. Phys., **71**, 1987-1993, 1979.
- Langhoff, P. W., S. R. Langhoff, and C. T. Corcoran, Photoabsorption of Formaldehyde, J. Chem. Phys., **67**, 1722-1731, 1977.
- Lee, E. K. C., Laser Photochemistry of Selected Vibronic and Rotational States, Accounts Chem. Res., **10**, 319-326, 1977.
- Lewis, R. S., K. Y. Tang, and E. K. C. Lee, Photoexcited Chemiluminescence Spectroscopy: Detection of Hydrogen Atoms Produced from the Single Vibronic Level Photolysis of Formaldehyde ( $\text{A}^1\text{A}_2$ ), J. Chem. Phys., **65**, 2910-2911, 1976.
- Lewis, R. S., and E. K. C. Lee, Photolysis of Formaldehyde-Butene Mixtures at Low Pressures. Quantum Yields of Radical Decomposition Processes in Formaldehyde, J. Phys. Chem., **82**, 249-254, 1978.
- Levy, H., II, Tropospheric Budgets for Methane, Carbon Monoxide, and Related Species, J. Geophys. Res., **78**, 5325-5332, 1973.
- Lodge, J. P., Jr., and J. B. Pate, Atmospheric Gases and Particulates in Panama, Sci., **153**, 408-410, 1966.
- Lucchese, R. R., and H. F. Schaefer, Metal Carbene Complexes and the Possible Role of Hydroxycarbene in Formaldehyde Laser Photochemistry, J. Amer. Chem. Soc., **100**, 298-299, 1978.
- Luther, F. M., J. S. Chang, W. H. Duewer, J. E. Penner, R. L. Tarp, and D. J. Wuebbles, Potential Environmental Effects of Aircraft Emissions, University of California Lawrence Livermore Laboratory Report 52861, 1979.
- Mack, G. P. R., and B. A. Thrush, Reaction of Oxygen Atoms with Carbonyl Compounds. Part I. Formaldehyde, J. Chem. Soc., Faraday I, **69**, 208-215, 1973.
- McEwan, J., and L. F. Phillips, Chemistry of the Atmosphere, John Wiley, New York, 1975.
- McQuigg, R. D., and J. G. Calvert, The Photodecomposition of  $\text{CH}_2\text{O}$ ,  $\text{CD}_2\text{O}$ ,  $\text{CHDO}$ , and  $\text{CH}_2\text{O}-\text{CD}_2\text{O}$  Mixtures at Xenon Flash Lamp Intensities, J. Amer. Chem. Soc., **91**, 1590-1599, 1969.
- Mentall, J. E., E. P. Gentieu, M. Kraus, and D. Neuman, Photoionization and Absorption Spectrum of Formaldehyde in the Vacuum Ultraviolet, J. Chem. Phys., **55**, 5471-5479, 1971.
- Michael, J. V., D. F. Nava, W. A. Payne, and L. J. Stief, Rate Constant for the Reaction of Atomic Chlorine with Formaldehyde, J. Chem. Phys., **70**, 1147-1150, 1979.
- Miller, R. G., and E. K. C. Lee, Intersystem Crossing of Triplet Formaldehyde, Chem. Phys. Lett., **27**, 475-478, 1974.
- Miller, R. G., and E. K. C. Lee, Single Vibronic Level Photochemistry of Formaldehyde ( $\text{H}_2\text{CO}$ ,  $\text{A}^1\text{A}_2$ ): Radiative and Non-Radiative Transitions, Chem. Phys. Lett., **33**, 104-107, 1975.
- Miller, W. H., Tunneling Corrections to Unimolecular Rate Constants, with Application to Formaldehyde, J. Amer. Chem. Soc., **101**, 6810-6814, 1979.
- Moortgat, G. K., F. Slemr, W. Seiler, and P. Warneck, Photolysis of Formaldehyde: Relative Quantum Yields of  $\text{H}_2$  and CO in the Wavelength Range 270-360 nm, Chem. Phys. Lett., **54**, 444-447, 1978.
- Moortgat, G. K., and P. Warneck, CO and  $\text{H}_2$  Quantum Yields in the Photodecomposition of Formaldehyde in Air, J. Chem. Phys., **70**, 3639-3651, 1979.
- Morris, E. D., Jr., and H. Niki, Mass Spectrometric Study of the Reaction of Hydroxyl Radical

- with Formaldehyde, J. Chem. Phys., **55**, 1991-1992, 1971.
- Morris, E. D., Jr., and H. Niki, Reaction of the Nitrate Radical with Acetaldehyde and Propylene, J. Phys. Chem., **78**, 1337-1338, 1974.
- Morrison, B. M., Jr., and J. Heicklen, The Photooxidation of  $\text{CH}_2\text{O}$  at 3130 Å in the Absence and Presence of NO, J. Photochem., **11**, 183-196, 1979.
- NASA Panel for Data Evaluation, Chemical Kinetic and Photochemical Data for Use in Stratospheric Modelling, Evaluation Number 2, Jet Propulsion Laboratory Publication, 79-27, April 15, 1979.
- Nicolet, M., Aeronomic Reactions of Hydrogen and Ozone, in Mesospheric Models and Related Experiments, G. Fiocco, Ed., Reidel Publ., Dordrecht, Holland, p. 1, 1971.
- Nicolet, M., private communication to the author, 1979.
- Niki, H., E. E. Daby, and B. Weinstock, unpublished data reported in the 12th Symposium (International) on Combustion, p. 277, The Combustion Institute, 1969.
- Niki, H., P. Maker, C. Savage, and L. Breitenbach, Abstracts 173rd American Chemical Society Meeting, New Orleans, La., March 20-25, 1977.
- Niki, H., P. D. Maker, C. M. Savage, and L. P. Breitenbach, The Relative Rate Constants for the Reaction of Hydroxyl Radical with Aldehydes, J. Phys. Chem., **82**, 132-134, 1978.
- Niki, H., P. D. Maker, L. P. Breitenbach, and C. M. Savage, FTIR Studies of the Kinetics and Mechanism for the Reaction of Cl Atom with Formaldehyde, Chem. Phys. Lett., **57**, 596-599, 1978.
- Noyes, W. A., Jr., Free Radicals, Activated Molecules, and Wall Effects in Photochemical Systems, J. Phys. & Colloid Chem., **55**, 925-938, 1951.
- Osif, T. L., and J. Heicklen, Oxidation of HCO Radicals, J. Phys. Chem., **80**, 1526-1531, 1976.
- Parkin, J. E., Band Contour Analyses of the Spectra of Asymmetric Rotor Molecules. Part 1. Calculation of Asymmetric Rotor Contours; the 3500 Å System of Formaldehyde, J. Molec. Spectrosc., **15**, 483-501, 1965.
- Parmenter, C. S., Primary Photochemical Processes in Glyoxal at 4358 Å, J. Chem. Phys., **41**, 658-665, 1964.
- Pate, J. G., L. R. M. Pitombo, A. F. Wartburg, D. C. Sheesley, M. D. LaHue, and J. P. Lodge, Jr., Atmospheric Sampling (Chemical) in Amazonas, 5, Gases, Paper presented at Symposium on Environment in Amazonia, April 4, 1970, Instituto Nacional de Pesquisas da Amazonia, Manaus, Brazil.
- Pitts, J. N., Jr., and F. E. Blacet, Vapor Phase Photolysis of Acetone-Iodine Mixtures, J. Amer. Chem. Soc., **74**, 455-457, 1952.
- Pitts, J. N., Jr., A. M. Winer, K. R. Darnall, G. J. Doyle, and J. M. McAfee, Chemical Consequences of Air Quality Standards of Control of Implementation Programs: Roles of Hydrocarbons, Oxides of Nitrogen, and Aged Smog in the Production of Photochemical Oxidant, Final Report to California Air Resources Board, Contract No. 4-214, May, 1976.
- Platt, U., D. Perner, and H. W. Pätz, Simultaneous Measurement of Atmospheric  $\text{CH}_2\text{O}$ ,  $\text{O}_3$ , and  $\text{NO}_2$  by Differential Optical Absorption, J. Geophys. Res., in press, 1979.
- Rank, D. M., C. H. Townes, and W. J. Welch, Interstellar Molecules and Dense Clouds, Sci., **174**, 1083-1101, 1971.
- Reilly, J. P., J. H. Clark, C. B. Moore, and G. C. Pimentel, HCO Production, Vibrational Relaxation, Chemical Kinetics, and Spectroscopy Following Laser Excitation of Formaldehyde, J. Chem. Phys., **69**, 4381-4394, 1978.
- Robinson, G. W., and V. E. DiGiorgio, The Nature of Formaldehyde in Its Low-Lying Excited States, Can. J. Chem., **36**, 31-38, 1958.
- Seiler, W., and C. Junge, Entwicklung eines Messverfahrens zur Bestimmung kleiner Mengen Kohlenoxid (CO), Meteorol. Rundsch., **20**, 175-176, 1967.
- Seiler, W., and C. E. Junge, Carbon Monoxide in the Atmosphere, J. Geophys. Res., **75**, 2217-2226, 1970.
- Sethuraman, V., V. A. Job, and K. K. Innes, The 3500 Å  $1A_2-1A_1$  Transition of Formaldehyde- $\text{H}_2$ ,  $\text{D}_2$ , and HD; Analysis of Coriolis and Fermi Perturbations, J. Molec. Spectrosc., **33**, 189-243, 1970.
- Shibuya, K., T. Ebata, K. Obi, and T. Tanaka, Rate Constant Measurements for the Reactions of HCO with NO and  $\text{O}_2$  in the Gas Phase, J. Phys. Chem., **81**, 2292-2294, 1977.
- Singh, H. G., L. J. Salas, H. Shigeishi, and E. Scribner, Atmospheric Halocarbons, Hydrocarbons, and Sulfur Hexafluoride: Global Distribution, Sources, and Sinks, Sci., **203**, 899-903, 1979.
- Smith, R. H., Rate Constant and Activation Energy for the Gaseous Reaction between Hydroxyl and Formaldehyde, Int. J. Chem. Kinet., **10**, 519-528, 1978.
- Snyder, L. E., D. Buhl, B. Zuckerman, and P. Palmer, Microwave Detection of Interstellar Formaldehyde, Phys. Rev. Lett., **22**, 679-681, 1969.
- Solomon, J., C. Jonah, P. Chandra, and R. Bersohn, Photolysis Mapping Studies of Aliphatic Carbonyl Compounds, J. Chem. Phys., **55**, 1908-1914, 1971.



# CALVERT

- Sodeau, J. R., and E. K. C. Lee, Intermediacy of Hydroxymethylene (HCOH) in the Low Temperature Matrix Photochemistry of Formaldehyde, Chem. Phys. Lett., 57, 71-74, 1978.
- Sperling, H. P., and S. Toby, The Photodecomposition of Gaseous Formaldehyde, Can. J. Chem., 51, 471-475, 1973.
- Srinivasan, R., and W. A. Noyes, Jr., Photochemical Production of Acetone-O<sup>18</sup> in the System Acetone:O<sub>2</sub><sup>18</sup> at 3130 Å, J. Amer. Chem. Soc., 82, 5591-5593, 1960.
- Stief, L. J., J. V. Michael, W. A. Payne, D. F. Nava, D. M. Butler, R. S. Stolarski, The Reaction Cl + H<sub>2</sub>CO → HCl + HCO: Decreased Sensitivity of Stratospheric Ozone to Chlorine Perturbations, Geophys. Res. Lett., 5, 829-831, 1978.
- Stief, L. J., D. F. Nava, W. A. Payne, and J. V. Michael, Rate Constant for the Reaction of Hydroxyl Radical with Formaldehyde over the Temperature Range 228-362 K, paper posted at the NATO Advanced Study Institute on Atmospheric Ozone, Portugal, Oct., 1979.
- Su, F., J. G. Calvert, J. H. Shaw, H. Niki, P. D. Maker, C. M. Savage, and L. D. Breitenbach, Spectroscopic and Kinetic Studies of a New Metastable Species in the Photooxidation of Gaseous Formaldehyde, Chem. Phys. Lett., 65, 221-225, 1979.
- Su, F., J. G. Calvert, and J. H. Shaw, The Mechanism of the Photooxidation of Gaseous Formaldehyde, J. Phys. Chem., 1979, in press.
- Swinnerton, J. W., V. J. Linnenbom, and R. A. Lamontagne, The Ocean: A Natural Source of Carbon Monoxide, Sci., 167, 984-986, 1970.
- Tanq, K. Y., P. W. Fairchild, and E. K. C. Lee, A Photochemical Study of Rotational State Dependence of Laser Excitation of Formaldehyde (A<sup>1</sup>A<sub>2</sub>). I. Coriolis and Singlet-Triplet Perturbation, J. Chem. Phys., 66, 3303-3305, 1977.
- Tanq, K. Y., P. W. Fairchild, and E. K. C. Lee, Laser-Induced Photodecomposition of Formaldehyde (A<sup>1</sup>A<sub>2</sub>) from Its Single Vibronic Levels. Determination of the Quantum Yield of H-Atom by HNO\* (A<sup>1</sup>A") Chemiluminescence, J. Phys. Chem., 83, 569-573, 1979.
- Tuazon, E. C., R. A. Graham, A. M. Winer, R. R. Easton, J. N. Pitts, Jr., and P. L. Hanst, A Kilometer Pathlength Fourier-Transform Infrared System, Atm. Environ., 12, 865-875, 1978.
- Tuazon, E. C., A. M. Winer, R. A. Graham, and J. N. Pitts, Jr., Adv. Environ. Sci. Technol., 10, 1979, in press.
- Van Dijk, J. M. F., M. J. H. Kemper, J. H. M. Kerp, and H. M. Buck, Ab Initio CI Calculation of the Radiationless Transition of the <sup>1</sup>(nπ\*) State of Formaldehyde, J. Chem. Phys., 69, 2462-2473, 1978.
- Walsh, R., and S. W. Benson, Kinetics and Mechanism of the Gas Phase Reaction between Iodine and Formaldehyde and the Carbon-Hydrogen Bond Strength in Formaldehyde, J. Amer. Chem. Soc., 88, 4570-4575, 1966.
- Warneck, P., Photoionisation von Methanol und Formaldehyd, Z. Naturforsch., 26A, 2047-2057, 1971.
- Warneck, P., Heat of Formation of the HCO Radical, Z. Naturforsch., 29A, 350-351, 1974.
- Washida, N., R. I. Martinez, and K. D. Bayes, The Oxidation of Formyl Radicals, Z. Naturforsch., A29, 251-255, 1974.
- Weisshaar, J. C., and C. B. Moore, Collisionless Nonradiative Decay Rates of Single Rotational Levels of S<sub>1</sub> Formaldehyde, J. Chem. Phys., 70, 5135-5146, 1979.
- Woolley, G. R., and R. J. Cvetanovic, Production of Hydrogen-Atoms by Photolysis of H<sub>2</sub>S and the Rates of Their Addition to Olefins, J. Chem. Phys., 10, 4697-4704, 1969.
- Wuebbles, D. J., private communication to the author; simulations using the Lawrence Livermore Laboratory 1D Atmospheric Model with the present quantum yield and rate constant estimates.
- Yeung, E. S., and C. B. Moore, Photochemistry of Simple Vibronic Levels of Formaldehyde, J. Chem. Phys., 58, 3988-3998, 1973.
- Yeung, E. S., and C. B. Moore, Predissociation Model for Formaldehyde, J. Chem. Phys., 60, 2139-2147, 1974.

## ETHANE AND ETHYLENE BEHAVIOR IN THE ATMOSPHERE

A. C. Aikin, J. R. Herman and E. J. Maier

National Aeronautics and Space Administration  
Laboratory for Planetary Atmospheres  
Goddard Space Flight Center  
Greenbelt, MD 20771

### ABSTRACT

Observations of the  $C_2$  hydrocarbons, ethane,  $C_2H_6$ , ethylene,  $C_2H_4$ , and acetylene,  $C_2H_2$ , have been reported throughout the troposphere. Of these, ethane and acetylene have sufficiently long chemical lifetimes to allow significant concentrations to be transported to the stratosphere. The short chemical lifetime of ethylene should confine it within the troposphere except where it arises as the chemical product of a stratospheric reaction.

A detailed study of ethane and ethylene photochemistry is presented for the troposphere and stratosphere. It is shown that the loss of ethane is controlled by OH in the troposphere and by Cl in the stratosphere. The rapid stratospheric decrease in the mixing ratio of  $C_2H_6$  is an indirect measure of the atmospheric Cl content near the troposphere. The oxidation chain starting from  $C_2H_6$  leads to the production of acetaldehyde and formaldehyde and in turn to CO,  $H_2$ ,  $C_2H_4$ , and other species in parallel to the methane oxidation chain. In the troposphere,  $C_2H_4$  concentrations are dominated by ground sources giving rise to measured concentrations of 0.1 ppb. Ambient  $C_2H_6$  (1 ppb) leads to a tropospheric formaldehyde production rate that is a few percent of that arising from methane oxidation and 3 percent of total column formaldehyde.

**Introduction:** Ethane,  $C_2H_6$ , accounts for between 75 and 85% of the  $C_2H_x$  hydrocarbons, including ethylene,  $C_2H_4$ , and acetylene  $C_2H_2$ , observed in the troposphere and lower stratosphere. Typical northern hemisphere concentrations are  $C_2H_6$ , 820 ppt,  $C_2H_4$ , 150 ppt and  $C_2H_2$ , 115 ppt. (Rasmussen, 1979). Because of ethane's relatively long tropospheric lifetime, 29 days at the ground to 231 days at 10 km, it is transported from the troposphere, where it is destroyed by OH, into the stratosphere, where the distribution is controlled by reaction with atomic chlorine, (Chameides and Cicerone, 1978). Measurements of the altitude distribution of  $C_2H_6$  can provide an indirect measure of the OH and Cl distribution in the lower stratosphere.

The breakdown of ethane leads to the production of formaldehyde, acetaldehyde, other compounds and ultimately CO. Since ethane represents the major compound of the  $C_2$ - $H_x$  hydrocarbons, it is instructive to investigate the detailed photochemistry of ethane at its present concentration to assess its influence on tropospheric ozone. Ethylene will also be considered. However, it is far less abundant in the atmosphere and reacts rapidly with OH preventing it from reaching the stratosphere. It will be shown that while  $C_2H_6$  enters the stratosphere the bulk of the photochemical products are produced in the troposphere. Available data on the latitudinal and altitude variation of ethane are compared with theory.

Sources: Although several sources of atmospheric ethane have been suggested, the major contributor has not been identified. Natural sources include volcanoes (Stoiber et al., 1971), vegetation (Graedel, 1979), and natural gas (Grenda and Goldstein, 1977). Synthetic fuel production and petroleum refining operations are known anthropogenic sources. Ethane concentration in the northern hemisphere is found to be twice that of the southern. Singh (1979) attributes this difference to additional sources in the northern hemisphere that may be either natural or anthropogenic.

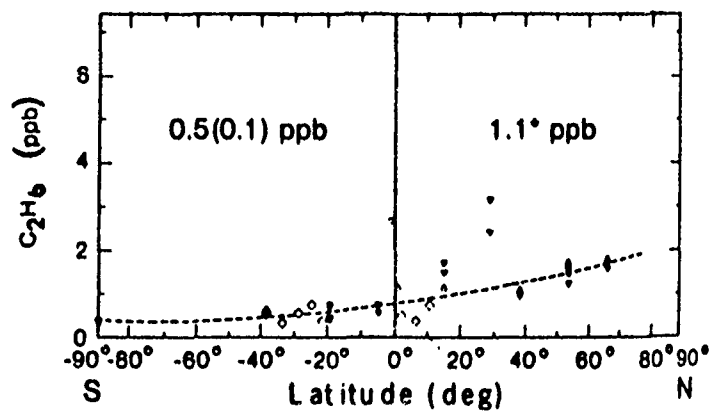
**Tropospheric Distribution of Ethane:** Tropospheric distribution measurements of ethane have been carried out as a function of latitude near the Earth's surface and as a function of altitude to the tropopause. Figure 1a illustrates the latitude data of Singh (1979) for low altitudes near the Earth's surface. In the southern hemisphere the distribution is fairly uniform at 0.5 ppb. The average value in the northern hemisphere is 1 to 2 ppb with 3 to 5 ppb over the continental United States. Singh (1979) estimates the global source strength at between  $3$  to  $5 \times 10^{12}$  gm yr<sup>-1</sup>. The most complete data set on the tropospheric latitudinal and altitude distribution has been obtained by Rasmussen (1979). Surface concentrations of C<sub>2</sub>H<sub>6</sub> are greater over land than the oceans, exhibiting values as large as 1 to 2 ppb compared to 850 ppb over the Pacific Ocean. Several aircraft flights were conducted, which show a factor of 2 more C<sub>2</sub>H<sub>6</sub> in the northern hemisphere than the southern. Some of these data are summarized in figure 1b.

Measurements of the altitude distribution of the C<sub>2</sub>H<sub>6</sub> mixing ratio show a rapid decrease starting in the vicinity of the tropopause (Cronn and Robinson, 1979). A comparison of these data with calculated altitude distributions of C<sub>2</sub>H<sub>6</sub> is shown in Figure 2. Theoretical curves apply to the cases 1) where both Cl and OH attack C<sub>2</sub>H<sub>6</sub> and 2) where only OH is responsible. If the free chlorine distribution is less than the distribution given in Table I, then C<sub>2</sub>H<sub>6</sub> will exhibit larger concentrations in the stratosphere. As shown in Figure 2 there is not sufficient data available above the tropopause to estimate the importance of Cl in establishing the altitude distribution of ethane. Figure 3 compares the loss of C<sub>2</sub>H<sub>6</sub> by OH and Cl, for the rates of reaction given in Table II. While tropopause height, eddy diffusion rates, and water vapor are important in determining the altitude distribution of OH, the extreme sensitivity of C<sub>2</sub>H<sub>6</sub> to Cl allows stratospheric the altitude distribution of C<sub>2</sub>H<sub>6</sub> to serve as a measure of the Cl concentration. Its distribution is also a consistency test of chlorine photochemistry in an altitude regime not presently accessible to experimental techniques that measure Cl directly.

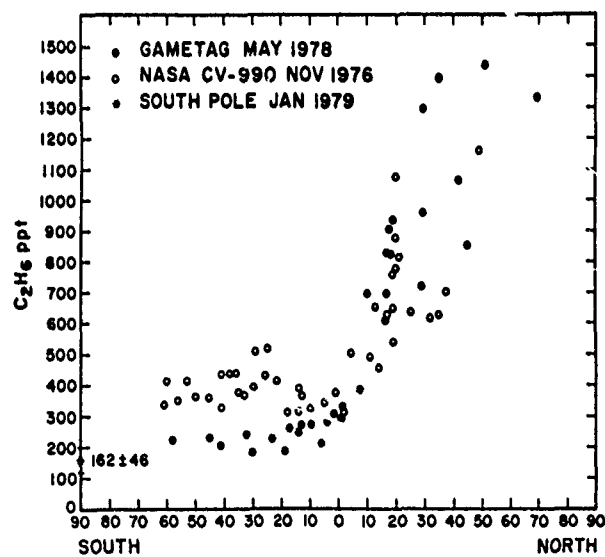
TABLE I

Atmospheric Parameters Used in the Calculation

Altitude (km)	H <sub>2</sub> O ppm	OH cm <sup>-3</sup>	Cl cm <sup>-3</sup>	T°K
0	$2.25 \times 10^3$	$1.7 \times 10^6$	--	265
5	$4.3 \times 10^2$	$5 \times 10^5$	$6.6 \times 10$	256
10	$4.6 \times 10$	3.8	$8.1 \times 10$	229
15	3.7	6.8	$6 \times 10^2$	213
20	4.1	$1.6 \times 10^6$	$1.2 \times 10^4$	212
25	4.7	2.5	$1.5 \times 10^4$	219
30	5.1	3.6	$3.8 \times 10^5$	232
35	5.4	6.3	$1.0 \times 10^5$	245
40	5.6	$1.1 \times 10^7$	$2.2 \times 10^5$	246



a



b

Figure 1. Latitudinal variation of ethane concentration a) data of Singh (1979), b) results due to Rasmussen (1979).

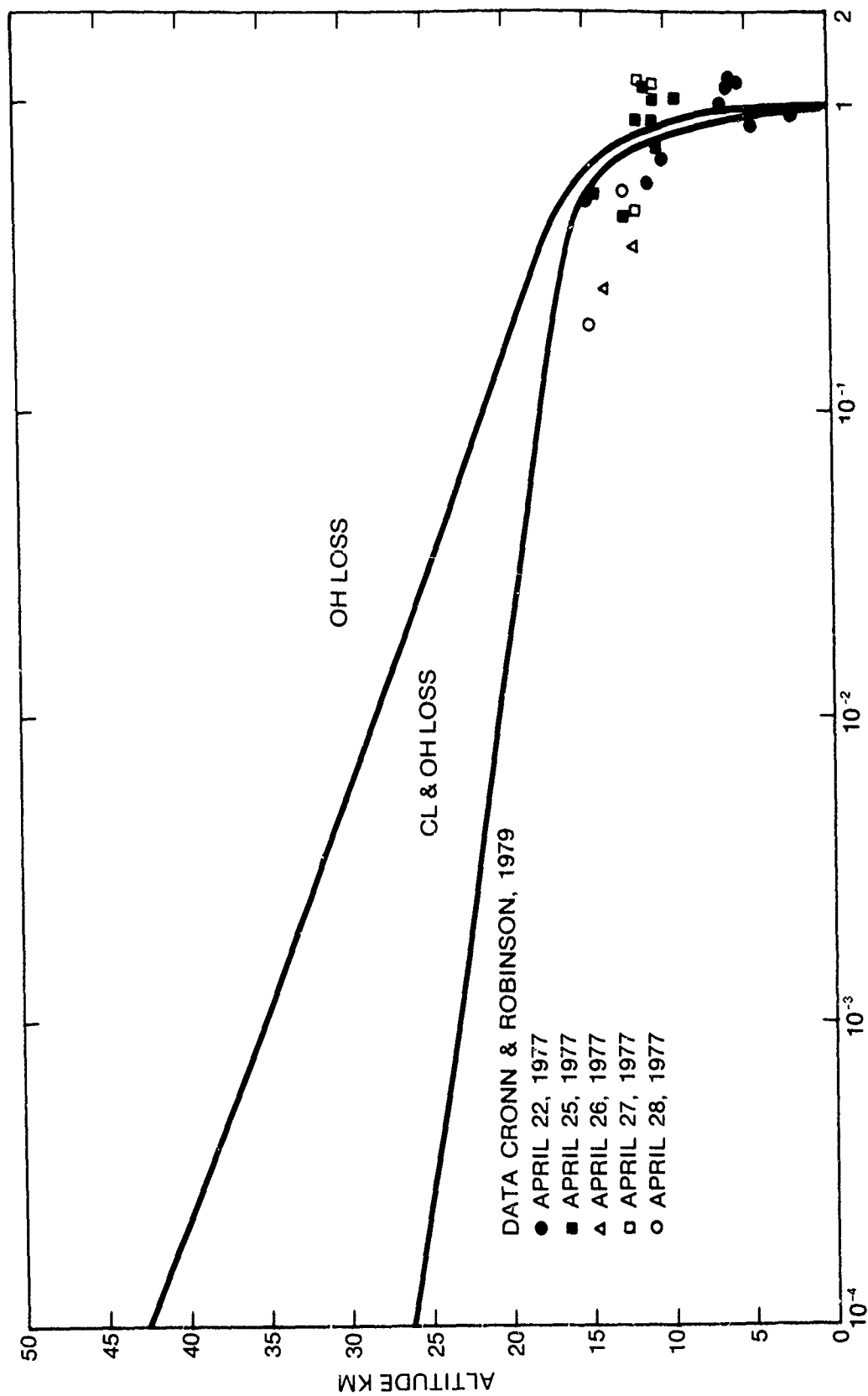


Figure 2. Measured altitude distribution of ethane compared with computed value. For the lower curve C<sub>2</sub>H<sub>6</sub> reacts with Cl as well as OH. In the upper curve loss due to Cl is omitted.

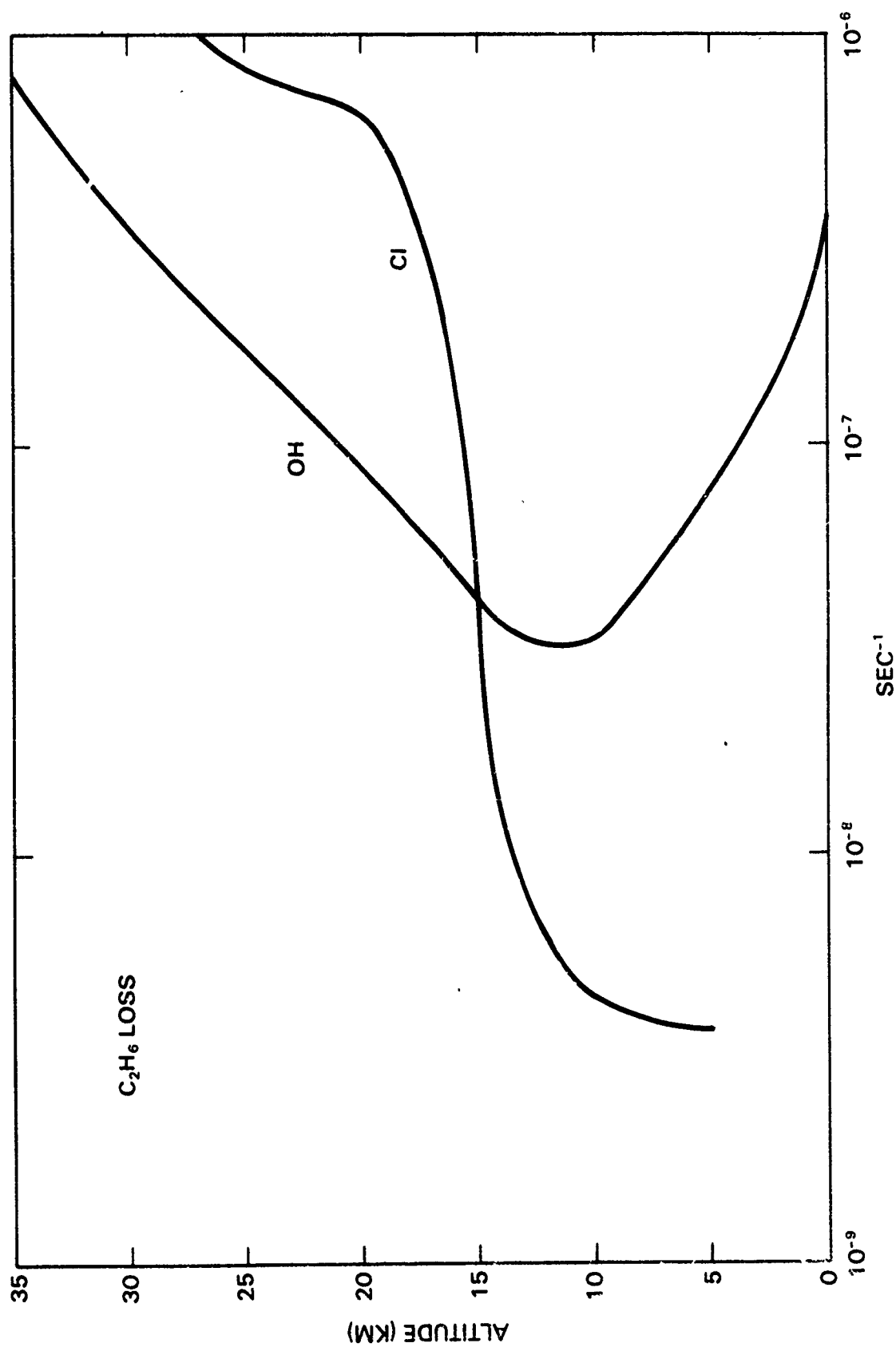


Figure 3. Loss rates of  $C_2H_6$  due to  $OH$  and  $Cl$  plotted as a function of altitude.

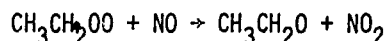
Ethane Photochemistry: The ethane reaction chain is shown in Figure 4 and the details of the reactions are given in Table II. In the figure heavy lines indicate the primary chemical paths taken during oxidation. Also shown in this figure are the numerical production and diffusion rates ( $\text{cm}^3 \text{sec}^{-1}$ ) which result from solution of a time-dependent one dimensional photochemical model of the troposphere and stratosphere. Details of the model are discussed in the next section. Figures for production, loss and diffusion of each species are shown for steady-state conditions at 5 km.

Photodissociation of  $\text{C}_2\text{H}_6$  occurs only for wavelengths shorter than 1500 Å and thus can be ignored as a loss process for  $\text{C}_2\text{H}_6$  in the lower stratosphere. As noted earlier, the leading loss processes for  $\text{C}_2\text{H}_6$  are reaction with OH and Cl to form  $\text{CH}_3\text{CH}_2$ . Once formed ethyl,  $\text{CH}_3\text{CH}_2$ , reacts strongly with  $\text{O}_2$  to form the peroxide. Dingley and Calvert (1963) have found some evidence for the formation of ethylene by the reaction



Baldwin et al. (1976) have reevaluated earlier data to estimate the rate for the reaction at 713°K. Evidence that the reaction occurs at lower temperatures is found in the fact that the reaction is employed in room temperature chemical kinetics studies as a means of generating  $\text{HO}_2$ , (Howard, 1979). We estimate that the reaction accounts for between 10 and 50% of the  $\text{CH}_3\text{CH}_2$  loss with  $\text{O}_2$ . In the extreme case illustrated here where (1) represents 50% of the loss, the quantity of  $\text{C}_2\text{H}_4$  produced is less than the  $\text{C}_2\text{H}_4$  occurring naturally. Nevertheless the breakdown of ethane is one method of producing ethylene throughout the atmosphere.

Loss of  $\text{CH}_3\text{CH}_2\text{OO}$  can occur thru combination with  $\text{HO}_2$  and  $\text{NO}$ .



The NO reaction rate has been measured in the laboratory by Adachi and Bosco (1979) for a lower limit of  $2.7 \times 10^{-12} \text{cm}^3 \text{sec}^{-1}$ . Earlier estimates give rates as high as  $8 \times 10^{-12} \text{cm}^3 \text{sec}^{-1}$ . However, possible experiment contamination suggests that even the lower limit of Adachi and Bosco is too large. For this reason the lower value given in Table II should be adopted. Using this rate of  $2.7 \times 10^{-12} \text{cm}^3 \text{sec}^{-1}$  the reaction with  $\text{HO}_2$  dominates over NO in the troposphere while in the stratosphere the NO reaction is more important. The chemical path arising in the troposphere is very sensitive to the amount of tropospheric NO so that industrialized areas can be quite different from average global conditions.

The  $\text{CH}_3\text{CH}_2\text{OOH}$  is subject to photodissociation at wavelengths less than 4500 Å giving rise to  $\text{CH}_3\text{CH}_2\text{O}$ . Reactions with other species such as  $\text{NO}_2$  are unspecified at present but may be important. Once formed  $\text{CH}_3\text{CH}_2\text{O}$  reacts with  $\text{O}_2$  to form acetaldehyde,  $\text{CH}_3\text{CHO}$ , or spontaneously decomposes (Demerjian et al., 1974). The main loss of  $\text{CH}_3\text{CH}_2\text{O}$  above 15 km is due to spontaneous decomposition, while below 15 km altitude the reaction with  $\text{O}_2$  dominates. The concentration of acetaldehyde is limited by photodissociation and the reaction with OH. The most recent study of the  $\text{CH}_3\text{CHO}$ -OH reaction has been a temperature dependence study yielding the value in Table II. (Atkinson and Pitts, 1978). The photodecomposition of acetaldehyde occurs for wavelengths shorter than 3400 Å and is therefore significant throughout the troposphere. Nearly equal amounts of methyl and formyl radicals are produced in the photodissociation process. However, as seen in Figure 4, the most effective loss is by reaction with OH. The formation rate of  $\text{CH}_3\text{COO}_2$  by addition of  $\text{O}_2$  to  $\text{CH}_3\text{CO}$  is adopted from Gradel, (1979), and probably represents the bimolecular high pressure limit. The destruction of  $\text{CH}_3\text{COO}_2$  involves NO and  $\text{NO}_2$ . Nitrogen dioxide leads to the production of peroxyacetylnitrate, the component of smog known as PAN. Nitric oxide leads to the formation of  $\text{CH}_3$  from  $\text{CH}_3\text{COO}_2$ . This step is followed by interaction of  $\text{CH}_3$  with  $\text{O}_2$  to form  $\text{CH}_3\text{O}_2$ . Reaction of  $\text{CH}_3\text{O}_2$  with NO forms  $\text{CH}_3\text{O}$  which in the presence of  $\text{O}_2$  forms  $\text{CH}_2\text{O}$ . The products of formaldehyde photodissociation are H and CHO,  $\text{H}_2$  and CO; see for example Calvert these Proceedings. The production of CO is predominant at wavelengths longer than 3300 Å. In summary tropospheric CO production from ethane occurs by the following sequence:

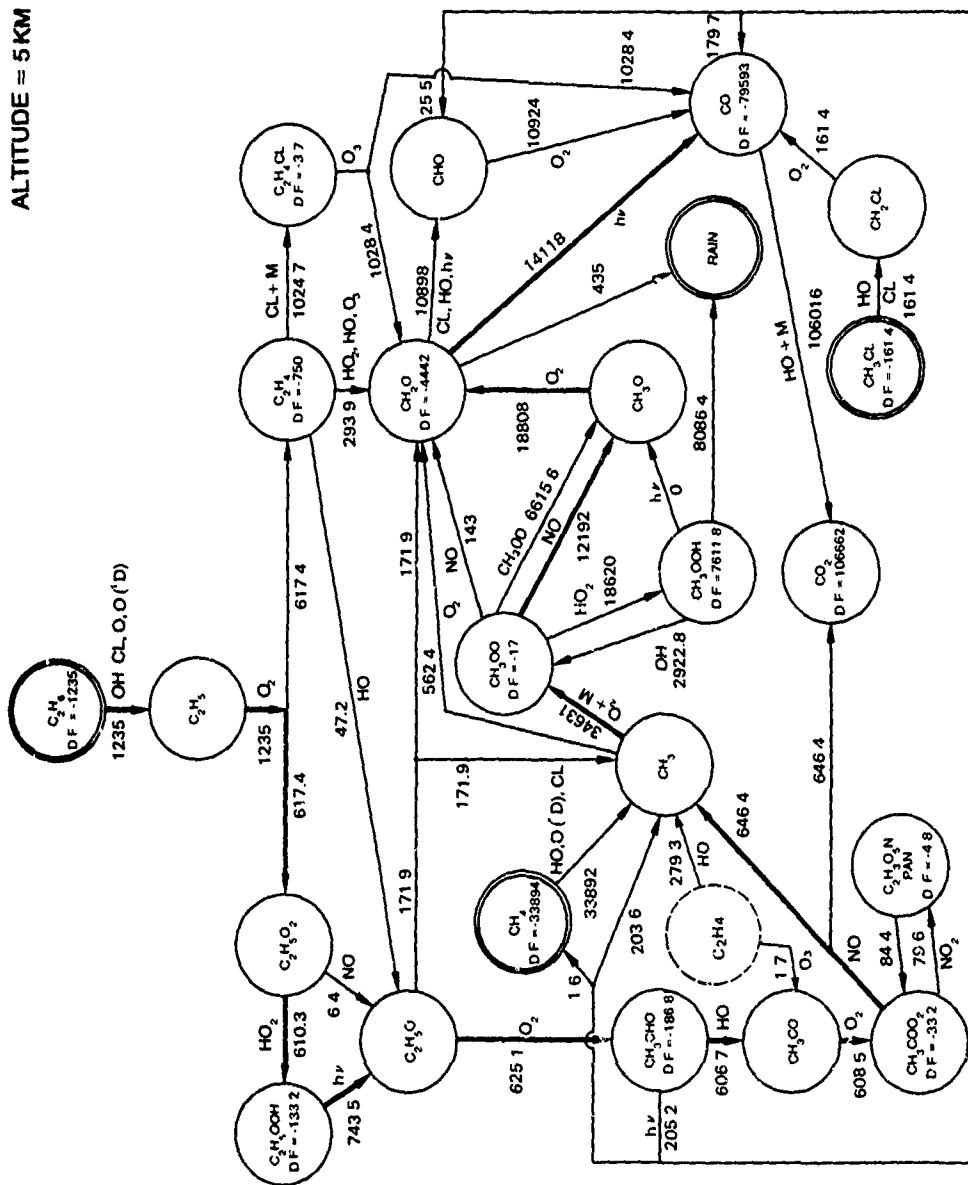
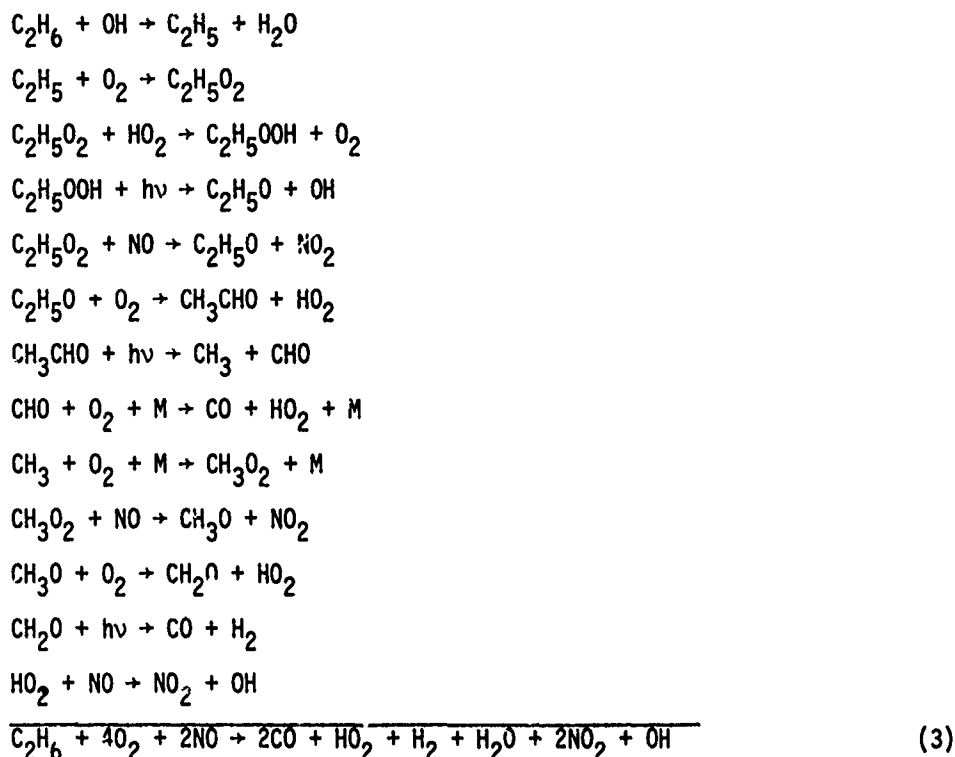


**Figure 4.** The ethane and methane reaction chain.





Ozone is produced by the above sequence with the additional reactions

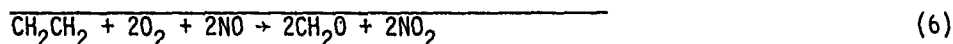
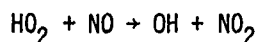
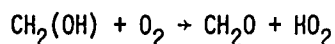
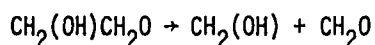
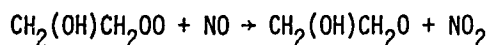
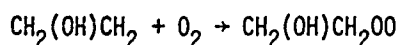
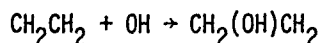


The concentration of ozone can be reduced by the sequence involving CO



Nitric oxide is very important in the ethane process and controls CO and O<sub>3</sub> production from ethane and other nonmethane hydrocarbons.

Ethylene Photochemistry: Atmospheric measurements indicate that 0.1 ppb C<sub>2</sub>H<sub>4</sub> is present in the troposphere, (Rasmussen, 1979). This cannot be accounted for by production from ethane, but must arise either from ground-level sources or as the result of oxidation of more complex hydrocarbons. Kinetic studies, (Howard, 1976; and Meagher and Heicklen, 1976) indicate that OH reacts rapidly with CH<sub>2</sub>CH<sub>2</sub>. The reaction will be an adduct. Details of the reaction sequence in the presence of O<sub>2</sub> and NO have received considerable attention by Demerjian et al. (1974) and most recently Niki et al. (1978). Laboratory results by the Niki group show the formation of 2 formaldehyde molecules for each molecule of C<sub>2</sub>H<sub>4</sub> destroyed. The sequence of reactions is



This is the main reaction sequence although small quantities of other products such as formic acid have been observed but these are negligible in comparison with formaldehyde (Niki et al. 1978). Reaction rates for this sequence are not available so the sequence will be treated here as if  $\text{C}_2\text{H}_5\text{O}$  is formed in step one of (6) together with some direct formation of  $\text{CH}_2\text{O}$ .

There have been extensive studies of ozone reacting with ethylene, (Herron and Huie, 1977; Kühne, 1976). The rate is only  $1.6 \times 10^{-19} \text{ cm}^3 \text{ sec}^{-1}$  and the products are uncertain. Reaction with  $\text{O}_3$  is negligible in comparison with OH. A similar situation exists with regard to  $\text{HO}_2$ , (Lloyd, 1974). Reaction of  $\text{CH}_2\text{CH}_2$  with Cl is fast and pressure dependent (Lee and Rowland, 1977). Loss to chloring will be the same order as that due to OH if the concentration is  $10^3 \text{ cm}^{-3}$  and Cl is  $10^3 \text{ cm}^{-3}$ . The product of the reaction is an adduct  $\text{C}_2\text{H}_4\text{Cl}$ . This molecule may be lost by reactions with  $\text{O}_2$  or  $\text{O}_3$  by reactions analogous with other chlorinated species as discussed by Gay et al. (1975).

**Solution of the Chemical Equations:** The hydrocarbon photochemical reactions for the ethane cycle have been added to the stratosphere-troposphere model developed by Herman (1979a and 1979b). The full set of chemical equations described in Herman (1979b) has been included along with tropospheric rainout terms for  $\text{CH}_2\text{O}$ ,  $\text{CH}_3\text{OOH}$ ,  $\text{HCl}$ ,  $\text{ClNO}_2$ ,  $\text{HO}_2\text{NO}_2$ ,  $\text{HNO}_3$ ,  $\text{H}_2\text{O}_2$ , and gas phase  $\text{H}_2\text{O}$ . Solutions were obtained for steady state conditions using diurnally averaged solar fluxes and chemical production and loss rates appropriate to equinox and 30 degrees north latitude. The mid-latitude water vapor measurements of Kley et al. (1979) were considered as well as other measurements to obtain the water vapor profile on which the OH distribution is based. Table I summarizes some of the species altitude distributions. Formaldehyde photodissociation is calculated using the results of Bass (see Jesson and Bass this Proceedings). The flux of NO is adjusted so that the NO concentration near the surface is 3 pptV in agreement with recent measurements by McFarland et al. (1979).

#### Results of the Computation: 1. Altitude Distribution of the Products

Figure 5 gives ethane and product concentrations as a function of altitude for an upward flux of ethane assumed to have a near ground level concentration of 1 part per billion in agreement with observations. In addition an upward flux of ethylene equivalent to 0.1 ppb is assumed. This concentration is consistent with measurements (Rasmussen, 1980). Products of the photochemistry include  $\text{CH}_3\text{CHO}$ ,  $\text{CH}_3\text{COO}_2$ ,  $\text{CH}_3\text{CH}_2\text{OO}$ , and PAN. The concentrations of these species are at least one order of magnitude less than the parent ethane. Production of such compounds from ethane photochemistry indicates that similar species will be generated during the oxidation of other hydrocarbons. Our results show that the compound PAN is generated throughout the troposphere and lower stratosphere. This gas has a long lifetime against photolysis and rainout. Crutzen (1979) has suggested that PAN may serve as a sink for  $\text{NO}_x$ . The quantity of PAN produced from ethane is a small fraction of the ethane concentration. As with the other species generated during oxidation the actual amount expected in the atmosphere will be much larger since other hydrocarbons are also oxidized. It is possible that some of the products such as acetaldehyde may be affected by rainout.

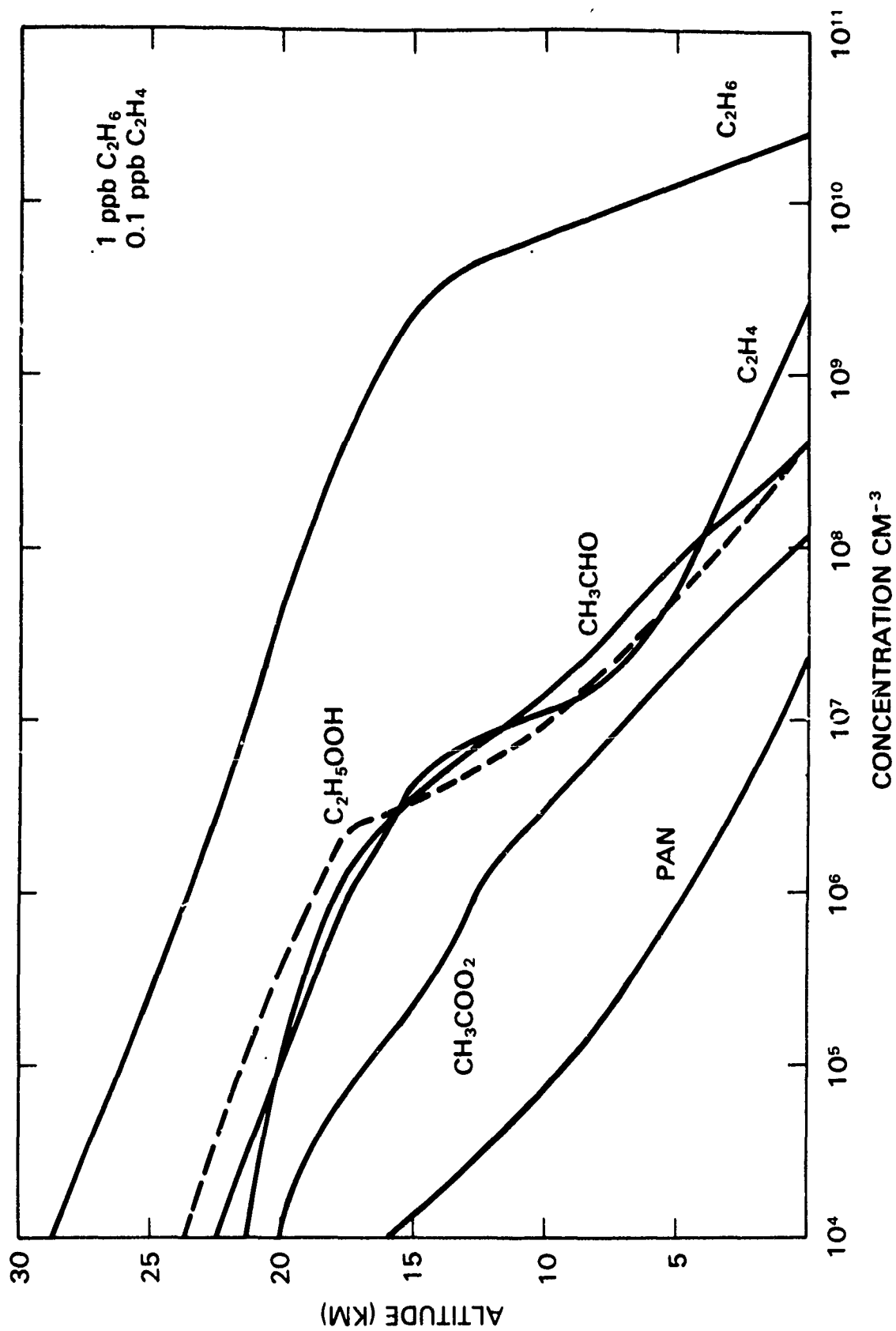


Figure 5. Concentration versus altitude for ethane and ethylene oxidation products

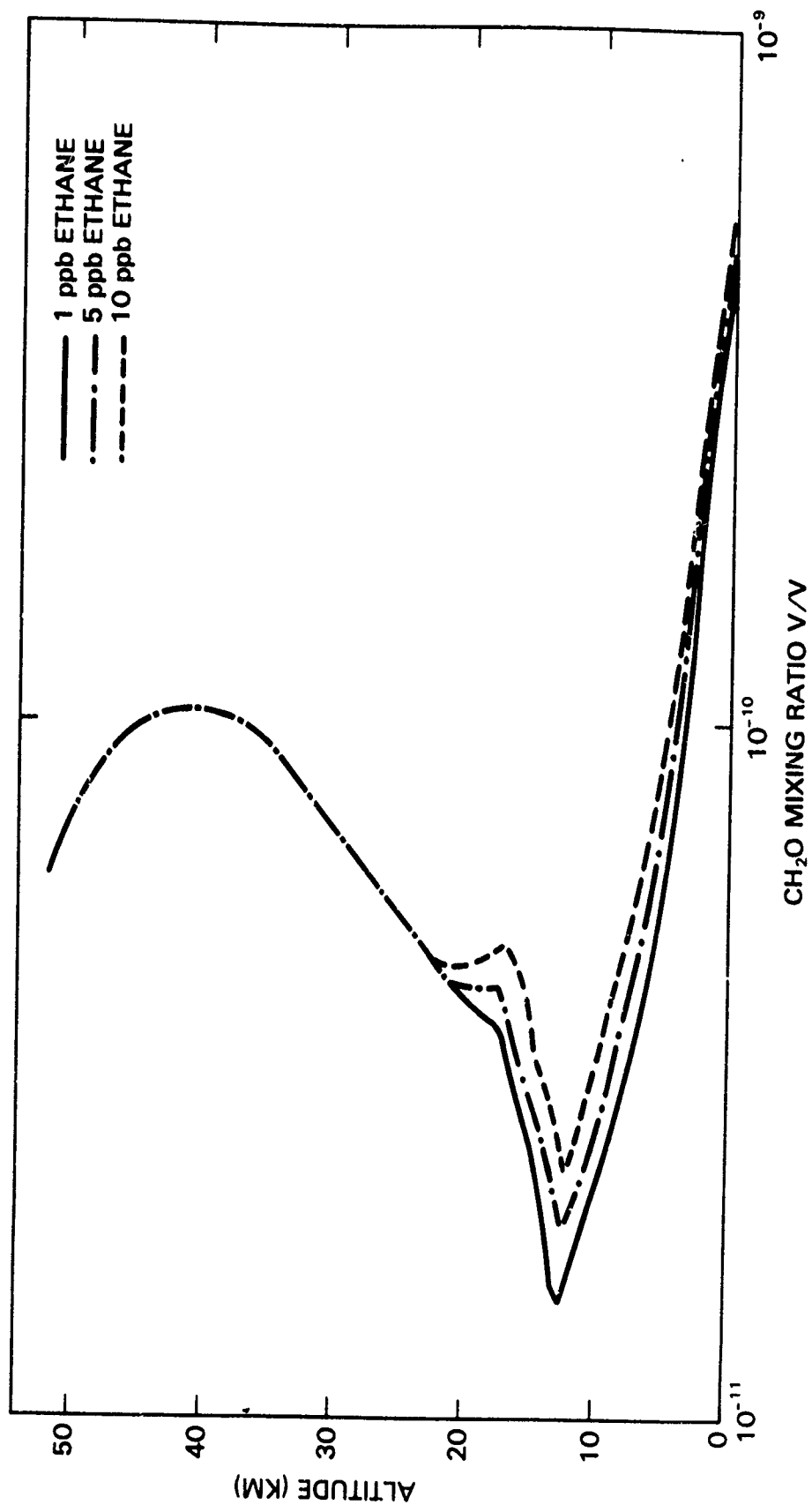


Figure 6. Distribution of formaldehyde.

## 2. The Formaldehyde Distribution

Formaldehyde in the troposphere and stratosphere is normally considered to arise from methane oxidation, principally by the following steps:



However, as is shown in Figure 4, several of the steps in the hydrocarbon oxidation process also lead to formaldehyde production. For 1 ppb ethane the column concentration of  $\text{CH}_2\text{O}$  is modified by about 3%. This modification increases with  $\text{C}_2\text{H}_6$  concentration. Figure 6 illustrates the formaldehyde distribution for 1 ppb  $\text{C}_2\text{H}_6$  and 0.1 ppb  $\text{C}_2\text{H}_4$ . Also illustrated are the effects of increasing the ethane concentration. At 10 ppb ethane is the dominant tropospheric source of formaldehyde. Even for concentrations as low as 1 ppb the  $\text{CH}_2\text{O}$  concentration is enhanced by 3% relative to methane as the sole oxidation source. Formaldehyde production from ethane is negligible throughout most of the stratosphere.

## 3. Influence on the Ozone and Carbon Monoxide Content

Calculations were carried out for ethane concentrations as large as 10 ppb. While ozone concentration increases with increasing ethane concentration the influence on column ozone is minimal. Tropospheric ozone is observed to increase, but this increase is limited to less than 10% of the tropospheric ozone content. Since other hydrocarbon cycles will similarly influence ozone, tropospheric ozone models should include hydrocarbon cycles even in clean air situations.

Zimmerman et al. (1978) have estimated that heavy hydrocarbons from vegetation in the form of terpenes and other constituents should contribute substantially to the CO content of the terrestrial atmosphere. The present detailed calculations on the  $\text{C}_2$  hydrocarbons support this result.

**Conclusions:** Present concentrations of ethane and ethylene contribute to the tropospheric budgets of formaldehyde, ozone and carbon monoxide. The contribution is limited to less than 10%. The current influence of these gases on the total column content of ozone and carbon monoxide is negligible.

Ethylene reacts rapidly with OH and is not expected to be found in concentrations greater than 1 ppt above 5 km. Ethane is sufficiently unreactive that it can penetrate the stratosphere. Its distribution is controlled by the OH and Cl radical concentrations at the tropopause and in the lower stratosphere. As such ethane serves as a tracer and allows an independent estimate of Cl and OH in the lower stratosphere.

The tropospheric formaldehyde distribution is a sensitive indicator of hydrocarbon and methane oxidation. Although carbon monoxide production is related to the breakdown of formaldehyde, carbon monoxide may have quite different distribution due to sources other than hydrocarbon oxidation. Since formaldehyde is a very sensitive indicator of hydrocarbon oxidation, it should be measured in conjunction with ozone and carbon monoxide studies of the troposphere.

AIKIN, HERMAN, and MAIER  
REFERENCES

- Adachi, H. and N. Bosco, Kinetic spectroscopy study of the reaction of  $C_2H_5O_2$  with NO, Chem. Phys. Lett., **64**, 431-434, 1977.
- Atkinson, R., B.J. Finlayson and J.N. Pitts, Photoionization mass spectrometer studies of gas phase ozone-olefin reactions, J. Am. Chem. Soc., **95**, 7592-7599, 1973.
- Atkinson, R., Perry, R.A., and Pitts, J.N., Jr., Rate constants for the reaction of OH radicals with ethylene over the temperature range 299-425°K, J. Chem. Phys., **66**, 1197-1201, 1977.
- Atkinson, R. and J.N. Pitts, Jr., Absolute rate constants for the reaction of  $O(^3P)$  atoms with a series of olefins over the temperature range 298-439°K, J. Chem. Phys., **67**, 38-43, 1977.
- Atkinson, R. and J.N. Pitts, Jr., Kinetics of the OH radical with HCHO and  $CH_3CHO$  over the temperature range 299-426°K, J. Chem. Phys., **60**, 3581-3584, 1978.
- Back, R.A. and D.W.L. Griffiths, Flash Photolysis of Ethylene, J. Chem. Phys., **46**, 4839-4843, 1967.
- Baldwin, R.R., C.J. Clench and R.W. Walker, Reactions of iso-propyl radicals with oxygen, hydrogen and deuterium, Far. Trans. T. J. Chem. Soc., **74**, 1715-1722, 1976.
- Calvert, J.G., The homogeneous chemistry of formaldehyde generation and destruction within the atmosphere, Proceedings of the NATO Advanced Study Institute on Atmospheric Ozone, 1980.
- Chameides, W.L. and R.J. Cicerone, Effects of nonmethane hydrocarbons in the atmosphere, J. Geophys. Res., **83**, 947-952, 1973.
- Chang, J.S. and J.R. Barker, Reaction rate and products for the reaction  $O(^3P) + H_2CO$ , J. Phys. Chem., **83**, 3059-3064, 1979.
- Cronn, D. and E. Robinson, Tropospheric and lower stratospheric vertical profiles of ethane and acetylene, Geophys. Res. Lett., **6**, 641-644, 1979.
- Crutzen, P. J., The role of NO and  $NO_2$  in the chemistry of the troposphere and stratosphere, Ann. Rev. Earth Planet. Sci., **443-472**, 1979.
- Davis, D.D., S. Fischer, R. Schiff, R.T. Watson, and W. Bollinger, A kinetic study of the reaction of OH radicals with two  $C_2$  hydrocarbons  $C_2H_4$  and  $C_2H_2$ , J. Chem. Phys., **63**, 1707-1712, 1975.
- Demerjian, K.L., J.A. Kerr and J.G. Calvert, The mechanism of photochemical smog formation, Advan. Environ. Sci. Technol., **4**, 1-262, 1974.
- Dingley, D.P. and J.G. Calvert, A study of the ethyl-oxygen reaction by flash photolysis, J. Am. Chem. Soc., **85**, 856-861, 1963.
- Gay, Jr., B.W., P.L. Hanst, J.J. Bufalini and R.C. Noonan, Atmospheric oxidation of chlorinated ethylenes, Environ. Sci. and Tech., **10**, 58-67, 1975.
- Graedel, T.E., L.A. Farrow, and T.A. Weber, Urban kinetic chemical calculations with altered source conditions, Atmos. Envir., **12**, 1403-1412, 1978.
- Graedel, T.E., The kinetic photochemistry of the marine atmosphere, J. Geophys. Res., **84**, 273-286, 1979.
- Graedel, T.E., Urban precursors and their photochemical products, in Man's Impact on the Troposphere, NASA Ref. Publication 1022, p. 149, 1978.
- Graedel, T.E., Terpenoids in the atmosphere, Rev. Geophys. and Space Physics, **17**, 937-947, 1979.
- Grenda, R.N. and H.W. Goldstein, Nonurban measurements of methane and ethane under varying atmospheric conditions, J. Geophys. Res., **82**, 5923-5927, 1977.
- Hameed, S., J. P. Pinto and R. W. Stewart, Sensitivity of the predicted CO-OH- $CH_4$  perturbation to tropospheric  $NO_x$  concentration, J. Geophys. Res., **84**, 763-768, 1979.
- Hampson, R.F. and D. Garvin, Reactions rate and photochemical data for atmospheric chemistry-1977, NBS Special Publication 513, May 1978.
- Hendry, D.G. and R.A. Kenley, Generation of peroxy radicals from peroxy nitration ( $RO_2NO$ ); Decomposition of peroxy-acyl nitrates, J. Amer. Chem. Soc., **99**, 3198-3199, 1977.
- Herman, J.R., The response of stratospheric constituents to a solar eclipse, sunrise and sunset, J. Geophys. Res., **84**, 3701-3710, 1979.
- Herman, J.R., The problem of nighttime stratospheric  $NO_3$ , J. Geophys. Res., **84**, 6336-6338, 1979.
- Herron, J.T. and R.E. Huie, Stopped-flow studies of the mechanisms of ozone-alkene reactions in the gas phase ethylene, J. Am. Chem. Soc., **99**, 5430-5435, 1975.

- Horowitz, A., and J.G. Calvert, Wavelength dependence of the quantum efficiencies of the primary processes in formaldehyde photolysis at 25°C, Int. J. Chem. Kinet., **10**, 805-819, 1978.
- Howard, C.J. and K.M. Evenson, Rate constants for the reactions of OH with ethane and some halogen substituted ethanes at 296K, J. Chem. Phys., **64**, 4303-4306, 1976.
- Howard, C.J., Rate constants for the gas-phase reactions of OH radicals with ethylene and halogenated ethylene compounds, J. Chem. Phys., **65**, 4771-4777, 1976.
- Hudson, R.D., Editor, The Stratosphere: Present and Future, National Aeronautics and Space Administration, Reference Publication, 1979.
- Japan, S.M., C.H. Wu and H. Niki, Rate constants for the reaction of ozone with olefins in the gas phase, J. Phys. Chem., **78**, 2318-2320, 1974.
- Kelly, N. and J. Heicklen, The rate coefficient for the reaction of  $\text{CH}_3\text{O}$  with  $\text{CH}_3\text{CHO}$  at 25°C, J. Photochem., **8**, 83-88, 1978.
- Kley, D., E.J. Stone, W.R. Henderson et al., In situ measurements of the mixing ratio of water vapor in the stratosphere, J. Atmos. Sci., **36**, 2513-2524, 1979.
- Kühne, H., S. Vaccani, T.K. Ha, A. Bauder and Hs. H. Günthard, Infrared-matrix and microwave spectroscopy of the ethylene-ozone gas-phase reaction, Chem. Phys. Lett., **38**, 449-455, 1976.
- Lee, F.S.C. and F.S. Rowland, Thermal chlorine 38 atom reactions with ethylene, J. Phys. Chem., **81**, 1235-1239, 1977.
- Lee, F.S.C. and F.S. Rowland, The reaction of chlorine atoms with acetylene and its possible stratospheric significance, J. Phys. Chem., **81**, 684-685, 1977.
- Leighton, P.A., Photochemistry of Air Pollution, Academic Press, New York, 1961.
- Lloyd, A.C., Evaluated and estimated kinetic data for gas phase reactions of the hydroperoxyl radical, Int. J. Chem. Kinetics, **6**, 169-228, 1974.
- Lloyd, A.C., Tropospheric chemistry of aldehydes, in Chemical Kinetics Data Needs for Modeling the Lower Troposphere, Ed. J.T. Herron and R.E. Huie, NBS Special Publication 557, August 1979.
- McFarland, M., D. Kley, J.W. Drummond, A.L. Schmeldekopf and R.H. Winkler, Nitric oxide measurements in the equatorial pacific region, Geophys. Res. Lett., **6**, 605-608, 1979.
- Meagher, J.F. and J. Heicklen, Reaction of HO with  $\text{C}_2\text{H}_4$ , J. Phys. Chem., **80**, 1645-1652, 1976.
- Morris, E.D., Jr., D.H. Stedman and H. Niki, Mass Spectrometric Study of the Reactions of the Hydroxyl Radical with Ethylene Propylene and Acetaldehyde J. Am. Chem. Soc., **93**, 3570-3572, 1971.
- Morris, E.D., Jr. and H. Niki, Reaction of the nitrate radical with acetaldehyde and propylene, J. Phys. Chem., **78**, 1337-1338, 1974.
- McNesby, J.R. and H. Okabe, Vacuum ultraviolet photochemistry in Advances in Photochemistry, Vol. 3, p. 157-240, Ed. W.A. Noyes, G.S. Hammond and J.N. Pitts, Interscience Publishers, New York, 1964.
- Niki, H., P.D. Maker, C.M. Savage, and L.P. Breitenbach, Mechanism for hydroxyl radical initiated oxidation of olefin-nitric oxide mixtures in parts per million concentrations, J. Phys. Chem., **82**, 135-137, 1978.
- Penner, J.E., M.B. McElroy and S.C. Wofsy, Sources and sinks for atmospheric  $\text{H}_2$ : A current analysis with projections for the influence of anthropogenic activity, Planet. Space Sci., **25**, 521-540, 1977.
- Rasmussen, R.J., private communication, 1979.
- Singh, H.B., L.J. Sales, H. Shigeishi and E. Scribner, Atmospheric halocarbons, hydrocarbons and sulfur hexafluoride: global distribution sources and sinks, Science, **203**, 899-903, 1979.
- Seiler, W., The cycle of carbon monoxide in the atmosphere, Proceedings ICESA, Inst. of Electr. and Electronic Engrs., New York, 1976.
- Stevens, D.J. and L.D. Spicer, Kinetics and mechanism of recoil chlorine atom reactions with ethylene, J. Phys. Chem., **81**, 1217-1222, 1977.
- Stief, L.J., J.V. Michael, W.A. Payne, D.F. Nava, D.M. Butler, and R.S. Stolarski, The reaction of  $\text{Cl} + \text{H}_2\text{CO} \rightarrow \text{HCl} + \text{HCO}$  decreased sensitivity of stratospheric ozone to chlorine perturbations, Geophys. Res. Lett., **5**, 829-831, 1978.
- Stoiber, R.E., Leggett, D.C., T.F. Jenkins, R.P. Murrmann, and W.I. Rose, Jr., Organic compounds in volcanic gas from Santiageuto volcano, Guatemala, Geolog. Soc. of Am. Bul., **82**, 2299-2302, 1971.
- Watson, R.J., Rate constants for reactions of  $\text{ClO}_x$  of atmospheric interest, J. Phys. Chem. Ref. Data, **6**, 871-918, 1977.

AIKIN, HERMAN, and MAIER

- Moortgat, G.K., and P. Warneck, CO and H<sub>2</sub> quantum yields in the photodecomposition of formaldehyde in air, J. Chem. Phys., 70, 3639-3651, 1979.
- Weaver, J. Meagher, and J. Heicklen, Photo-oxidation of CH<sub>3</sub>CHO vapor at 3130Å, J. Photochem., 6, 111, 1976/77.
- Zimmerman, P.R., R.B. Chatfield, J. Fisherman, P.J. Crutzen and P.L. Hast, Estimates on the production of CO and H<sub>2</sub> from the oxidation of hydrocarbon emissions from vegetation, Geophys. Res. Lett., 5, 679-682, 1978.



TABLE II

## ETHANE CYCLE REACTIONS AND RATES

REACTION	RATE CONSTANT	REFERENCE
$C_2H_6 + h\nu \rightarrow C_2H_4 + H_2$	$\lambda < 1500\text{\AA}$	1
$C_2H_6 + h\nu \rightarrow C_2H_5 + H$	$\lambda > 1250\text{\AA}$	
$C_2H_6 + h\nu \rightarrow CH_4 + CH_2$	$\lambda < 1250\text{\AA}$	
$C + C_2H_6 \rightarrow CH_3CH_2 + HC$	$7.3E-11 \cdot \exp(-61/T)$	
$HO + C_2H_6 \rightarrow CH_3CH_2 + H_2O$	$1.9E-11 \cdot \exp(-1230/T)$	
$O(^1D) + C_2H_6 \rightarrow CH_3CH_2 + HO$	$3.0E-10$	5
$CH_3CH_2 + HO \rightarrow CH_2CH_2 + H_2O$	$1.9E-11 \cdot \exp(-1230/T)$	6
$CH_3CH_2 + O_2 \xrightarrow{M} CH_3CH_2OO$	$6.8E-12^*$	7
$CH_3CH_2 + O_2 \rightarrow CH_2CH_2 + HO_2$	$5.0E-14$	8
$CH_3CH_2OO + NO \rightarrow CH_3CH_2O + NO_2$	$3.2E-13$	9
$CH_3CH_2OO + HO_2 \rightarrow CH_3CH_2OOH + O_2$	$2.5E-12$	10
$CH_3CH_2O + NO \rightarrow CH_2CH_2O + HNO$	$2.7E-14$	7
$CH_3CH_2O + NO \xrightarrow{M} CH_3CH_2ONO$	$1.35E-13^*$	7
$CH_3CH_2O \rightarrow CH_2O + CH_3$	$3.3E1$	7
$CH_2CH_2 + h\nu \rightarrow C_2H_2 + H_2$	$1550\text{\AA} < 1970\text{\AA}$	11
$CH_3CH_2 + h\nu \rightarrow CH_2CH_2 + H$		11
$O + CH_2CH_2 \rightarrow CH_3 + CHO$	$5.5E-12 \exp(-565/T)$	12
$HO + CH_2CH_2 \rightarrow CH_2O + CH_3$	$2.2E-12 \cdot \exp(385/T)$	4
$CH_2CH_2 + HO \rightarrow CH_2(OH)CH_2$	$1.7E-12$	13
$CH_2CH_2 + O_3 \rightarrow CH_3CO + HO_2$	$1.6E-19$	14
$CH_2CH_2 + O_3 \rightarrow CH_2O + O + HCOOH$	$1.0E-19$	14
$HCOOH + Cl \rightarrow HCl + COOH$	$1.0E-10$	Estimate

$\text{COOH} + \text{CO}_2 + \text{H}$	$2.0\text{E}1$	Estimate
$\text{CH}_3\text{CH}_2\text{ONO} + h\nu \rightarrow \text{CH}_3\text{CH}_2\text{O} + \text{NO}$	$\lambda < 4100\text{\AA}$	10
$\text{CH}_3\text{CH}_2\text{OOH} + h\nu \rightarrow \text{CH}_3\text{CH}_2\text{O} + \text{HO}$	$\lambda < 4500\text{\AA}$	15
$\text{CH}_3\text{CHO} + h\nu \rightarrow \text{CH}_3 + \text{CHO}$	$\lambda < 3400\text{\AA}$	7
$\text{CH}_3\text{CHO} + \text{HO} \rightarrow \text{CH}_3\text{CO} + \text{H}_2\text{O}$	$6.9\text{E}-12\text{EXP}(255/\text{T})$	16
$\text{CH}_3\text{CHO} + \text{NO}_3 \rightarrow \text{CH}_3\text{CO} + \text{HNO}_3$	$1.2\text{E}-15$	17
$\text{CH}_3\text{CHO} + \text{O} \rightarrow \text{CH}_3\text{CO} + \text{HO}$	$3.2\text{E}-13$	18
$\text{CH}_3\text{CHO} + \text{HO}_2 \rightarrow \text{CH}_3\text{CO} + \text{H}_2\text{O}_2$	$7.4\text{E}-18$	Estimate
$\text{CH}_3\text{CHO} + \text{CH}_3\text{O} \rightarrow \text{CH}_3\text{OH} + \text{CH}_3\text{CO}$	$5.0\text{E}-16$	19
$\text{CH}_2\text{O} + h\nu \rightarrow \text{HCO} + \text{H}$	$\lambda < 3400\text{\AA}$	20
$\text{CH}_2\text{O} + h\nu \rightarrow \text{CO} + \text{H}_2$	$\lambda < 3600\text{\AA}$	
$\text{CH}_2\text{O} + \text{HO} \rightarrow \text{H}_2\text{O} + \text{CHO}$	$1.0\text{E}-11$	21
$\text{CH}_2\text{O} + \text{O} \rightarrow \text{HO} + \text{CHO}$	$3.2\text{E}-11\text{EXP}(-1550/\text{T})$	21
$\text{CH}_3\text{CO} + \text{O}_2 \xrightarrow{\text{M}} \text{CH}_3\text{COOO}_2$	$6.7\text{E}-12^*$	22
$\text{CH}_3\text{COO}_2 + \text{NO}_2 \rightarrow \text{CH}_3\text{COO}_2\text{NO}_2$	$3.0\text{E}-13^*$	7
$\text{CH}_3\text{COO}_2 + \text{NO} \rightarrow \text{CH}_3 + \text{CO}_2 + \text{NO}_2$	$3.3\text{E}-12$	19
$\text{CH}_3\text{COO}_2\text{NO}_2 \rightarrow \text{CH}_3\text{COO}_2 + \text{NO}_2$	$1\text{E}-4$	23
$\text{CH}_3\text{COO}_2\text{NO}_2 \rightarrow \text{CH}_3\text{COO}_2 + \text{NO}_2$	$\lambda < 3000\text{\AA}$	24
$\text{CH}_3\text{COO} \rightarrow \text{CH}_3 + \text{CO}_2$	$9.3\text{E}3$	7

AIKIN, HERMAN, and MAIER

Notation - Equations  $\text{CH}_3\text{CH}_3$   $\text{C}_2\text{H}_6$ ;  $1.0\text{E}-12 \equiv 1.0 \times 10^{-12}$ . Units for 2 body reactions are  $\text{cm}^3\text{sec}^{-1}$ , for 3 body reactions  $\text{cm}^6\text{sec}^{-1}$  and for J second $^{-1}$ . \*Assumed to be the bimolecular high pressure limit.

References:

1. McNesby and Okabe, 1964. 2. Watson, 1977. 3. Howard and Evenson, 1976. 4. Atkinson et al., 1977. 5. Hampson and Garvin, 1978. 6. Dingley and Calvert, 1963. 7. Demejian et al., 1974. 8. Baldwin et al., 1976. 9. Adachi and Bosco, 1979. 10. Leighton, 1961. 11. Back and Griffiths, 1967. 12. Atkinson and Pitts, 1977. 13. Davis et al., 1975. 14. Estimate based on Herron and Huie, 1977. Kühne, 1976 and Atkinson et al., 1973. 15. Graëde et al., 1978. 16. Morris et al., 1971. 17. Morris and Niki, 1974. 18. Hendry and Mabey, 1973, Lloyd, 1979. 19. Kelley and Heicklen, 1978. 20. Horowitz and Calvert, 1978; Moortgat and Warneck, 1979, Calvert, 1980. 21. Hudson, 1979. 22. Graedel, 1979. 23. Hendry and Kenly, 1977. 24. Leighton, 1961.

# ATMOSPHERIC HALOCARBONS: MEASUREMENTS AND ANALYSES OF

## SELECTED TRACE GASES

R. A. Rasmussen  
M. A. K. Khalil  
Department of Environmental Science  
Oregon Graduate Center  
19600 N. W. Walker Road  
Beaverton, Oregon 97006

### Abstract

The atmospheric distributions of several trace gases are reviewed. Observational data on  $N_2O$ ,  $CFC1_3$  (F-11),  $CF_2Cl_2$  (F-12),  $CCl_4$ ,  $CH_3Cl$ ,  $CF_4$  (F-14),  $CO$ ,  $CH_4$ , and some  $C_2$  light hydrocarbons are included. Our data base on  $CH_3CCl_3$  is emphasized. In general the observations reported here include measurements in both the northern and southern hemispheres- and the differences of concentrations between the upper troposphere and the lower stratosphere. Accuracy, precision, stability, and related experimental topics are also discussed. A budget analysis of  $CH_3CCl_3$ , based on the data reported here, is reviewed. Some of our recent results on  $CHFCl_2$  (F-21) and  $CHF_2Cl$  (F-22) are discussed.

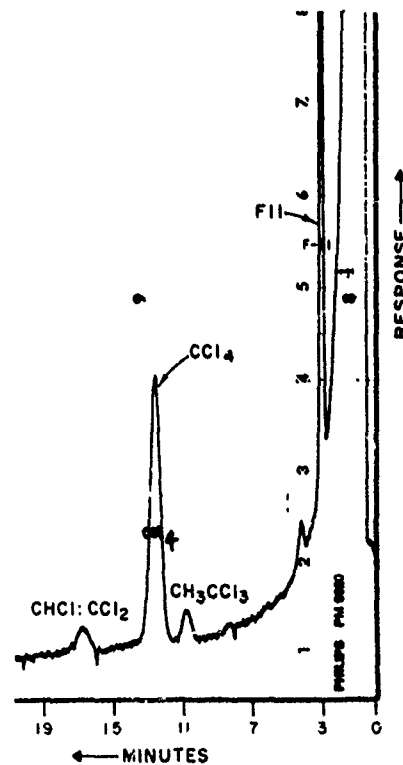
I. INTRODUCTION: Considerable attention has been focused upon the stratospheric ozone layer and the atmospheric chemical cycles involved in its production and destruction over the past decade. The interest arose when Crutzen [1970] proposed the theory that nitrogen oxides represent the most important sink for stratospheric ozone and Johnston [1971] suggested that the exhaust from supersonic aircraft could seriously disturb the steady-state concentration of ozone in the lower stratosphere. These hypotheses prompted the United States Department of Transportation to sponsor the Climatic Impact Assessment Program (CIAP) which initiated a dramatic increase in our knowledge of atmospheric chemistry. More recently, Molina and Rowland [1974] proposed in their classic paper that chlorine atoms formed, in the stratosphere, by the photolysis of chlorofluoromethanes [ $CFC1_3$  (F11) and  $CF_2Cl_2$  (F12)] could also act catalytically to reduce the steady-state stratospheric ozone concentration. Subsequently, Crutzen et al. [1978] pointed out that other relatively long-lived anthropogenic chlorocarbons such as  $CCl_4$  and  $CH_3CCl_3$  represent a serious threat to the ozone layer. This is particularly so if tropospheric  $HO$  radical concentrations are as low as recent estimates indicate [Love- lock, 1977; Singh, 1977; and Neely and Plonka, 1978]. In addition Crutzen [1974] and McElroy [1976] have examined the possible effect of anthropogenic nitrogen fixation on atmospheric nitrous oxide ( $N_2O$ ) levels. Since  $N_2O$  is the principal source of the nitrogen oxides in the stratosphere [McElroy and McConrell, 1971], an increase in the  $N_2O$  concentration in the troposphere would result in a proportional decrease in stratospheric ozone.

Theoretical model calculations are required in all of these predictions and therefore are subject to great uncertainties because of the simplifications inherent in formulating models as well as insufficient data on atmospheric concentrations and reaction rate constants for many of the trace species involved. In order for the models to be tested and improved, measurements must be made of the spatial and temporal variations in the atmospheric distribution of these trace gases. Accordingly our laboratory has specialized over the past five years in measuring the global distribution of  $N_2O$ ,  $F12$ ,  $F11$ ,  $CH_3CCl_3$ ,  $CCl_4$ ,  $CH_3Cl$ , and more recently  $CHFC1_2$  ( $F21$ ),  $CHF_2Cl$  ( $F22$ ),  $CF_4$  ( $F14$ ),  $C_2$  light hydrocarbons,  $CH_4$  and  $CO$  in the troposphere and lower stratosphere. All of these trace gases play important roles in the general problem of understanding the environmental and ecological damage that trace gases of anthropogenic origin may cause in the future. The measurements have been made in several ways, direct analysis using instruments operated *in situ* at field stations, on-board ships at sea, on aircraft in flight; or on discrete samples collected in the field and returned to our laboratory for analysis.

This paper is a survey of some of the results we have obtained in our laboratory. In the next Section (II) we discuss the development and the state of experimental techniques in measurements of atmospheric trace gases. In Section III we review the observational data on the concentrations of various atmospheric trace gases. Finally, in Section IV some selected trace gases, particularly  $CH_3CCl_3$ , are isolated for theoretical analyses of their tropospheric behaviour. In writing this paper we have kept two broad objectives in mind. First, we want to convey the observational data on several trace gases of current interest. In this context, we also discuss the methods used to collect and analyze air samples and provide estimates of the accuracy and precision of the data. Second, we offer a broad perspective on the various states in putting together a more complete picture of an atmospheric trace gas.

II. INSTRUMENTATION: Since the first atmospheric measurements of  $SF_6$  and  $F-11$  made by Lovelock [1971] using the electron capture detector, the majority of halocarbon analyses have been made using the EC/GC method. Professor Lovelock's pioneering work was done with EC/GC systems that he personally constructed and operated essentially at room temperature. The quality of these analyses for direct measurement of  $F11$  and  $CCl_4$  in ambient air is shown in Figure II.1. These low temperature EC/GC conditions are well suited for strongly electron-capturing species like  $F11$  and  $CCl_4$  but not for less efficient species like  $F12$ ,  $CH_3Cl$ ,  $CH_3CCl_3$  and  $N_2O$ .

FIGURE II.1. Direct analysis of 5 ml of clean air with a "suitcase" EC/GC built by J. E. Lovelock. Oven and EC detector temperature  $41^\circ C$ .



Subsequently, Rasmussen et al. [1976] and others using commercially constructed EC/GC instruments found they could optimize the response of the EC detector for  $N_2O$  and other halocarbons by operating the detector at temperatures between  $250$  and  $350^\circ C$ . An analysis of samples containing  $F12$ ,  $F11$ ,  $F113$ ,  $CHCl_3$ ,  $CH_3CCl_3$ ,  $CCl_4$  and  $C_2HCl_3$  using an ECD at  $350^\circ C$  is shown in Figure II.2.

Further improvements in the stability of the ECD at temperatures of 325 to 375°C have made it possible to reduce/signal noise even further and increase the response of  $\text{CH}_3\text{CCl}_3$  to where the minimum detection limit is 5 pptv in a 5 ml air sample and precision of analysis at the 100 to 150 pptv level is ~1%.

FIGURE II.2. Automated direct analysis of 5 ml of clean Alaskan air with Perkin Elmer 3920-B EC/GC and Hewlett-Packard 3388A data processor. Microprocessor in HP 3388A controls all functions of loading, injection, auto zero attenuation change and peak height and peak area calculations. Oven 68°C, EC detector at 350°C. TCE ( $\text{C}_2\text{HCl}_3$ ) is believed to be present in sample because of long-distance transport from Europe over the polar region related to arctic haze phenomenon.

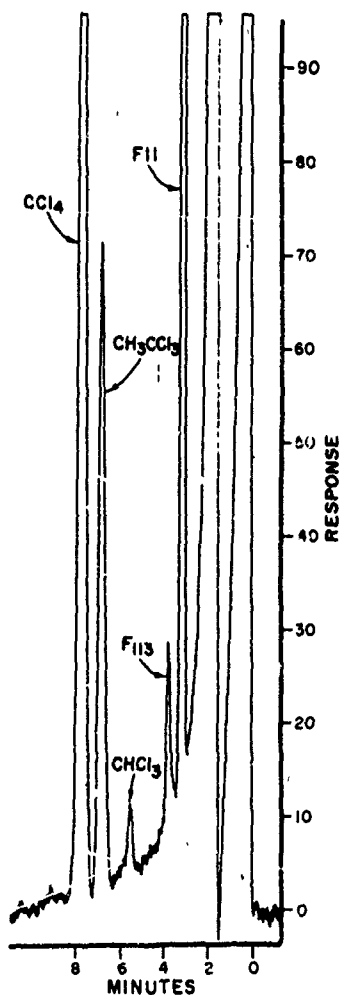
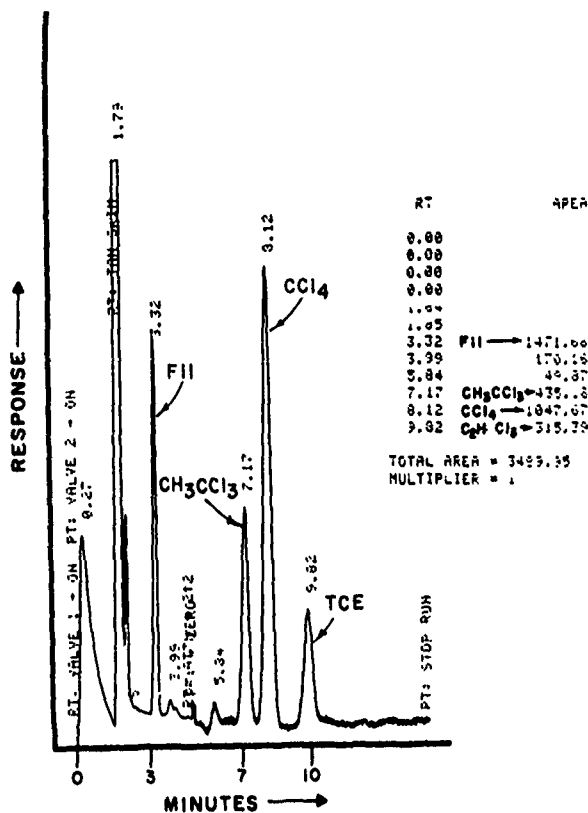


Figure II.3 shows an analysis of  $\text{CH}_3\text{CCl}_3$  at maximum usable sensitivity for routine analysis. Presently our routine analyses are recorded and electronically integrated using a Hewlett-Packard 5840 or 3388 data system.

FIGURE II.3. Direct analysis, manual operation using a P.E. 3920 B EC/GC. Calibration standard using cryogenically collected clean air sample. An analysis of 5 ml air sample,  $\text{CH}_3\text{CCl}_3$  at maximum usable sensitivity for routine analysis.  $\text{CH}_3\text{CCl}_3$  concentration 134 pptv.

# RASMUSSEN and KHALIL

The precision of analysis and absolute accuracy of the halocarbon measurements at the parts per trillion level ( $10^{-12}$  v/v) have been a continuing concern of both the analysts who have made the measurements and the modelers who depended upon these data for use in their more theoretical interpretations and calculations of environmental and ecological perturbations expected in the future. Over the years the sensitivity and electronic stability of the EC/GC instruments as well as the durability and performance of the gas chromatographic columns have improved. In Table II.1 are listed our present state-of-the-art precision of measurement of the halocarbons and related compounds at ambient levels typical of the mid-latitudes in the northern hemisphere. The standard deviation of the concentrations demonstrates the atmospheric variability about the mean on a monthly basis.

TABLE II.1

## PRECISION AND ACCURACY OF HALOCARBON MEASUREMENTS

COMPOUND	CONCENTRATION <sup>†</sup>	PRECISION OF ANALYSIS			ABSOLUTE* ACCURACY
		<sup>‡</sup> MANUAL	ELECTRONIC	INTEGRATED	
N <sub>2</sub> O	330 ±3 PPBV	<1%	<1%	<.6%	±4 - 5%
F12	282±15 PPTV	<1%	<1%	<1.5%	±10%
F11	170±10 PPTV	<1%	<1%	<1.7%	±5%
F113	25 ±5 PPTV	<5%			±25%
CH <sub>3</sub> CCl <sub>3</sub>	135±20 PPTV	<5%	<3%	<4.5%	±10%
CCl <sub>4</sub>	145 ±7 PPTV	<3%	<1%	<3.0%	±20%
CO	147±48 PPBV	<2%			±10%
CH <sub>4</sub>	1.63±.02 PPMV	<1%			±5%

† FALL, 1978, VALUES AT CAPE MEARES, OREGON.

\* ESTIMATED ABSOLUTE ACCURACY.

‡ MANUAL MEASUREMENT OF PEAK HEIGHTS WITH RULER  
ELECTRONIC MEASUREMENT OF PEAK HEIGHTS WITH HP3388A  
INTEGRATED AREAS MEASURED WITH HP3398A

The precision of analysis was determined in three ways. The first was a manual measurement of peak heights of the respective species in mm. The second method was an automated electronic measurement of peak heights. The comparison of peak heights was selected because it provides a more accurate and reproducible measurement of the response than does the integration of peak areas. This is due in part to the small area counts determined for some of the peaks like CH<sub>3</sub>CCl<sub>3</sub> and the almost identical chromatograms obtained isothermally with baseline resolution. It should be noted that the precision of analysis using peak areas increases dramatically at higher concentrations because of the much larger peak areas. However, at the parts per trillion levels typically measured in ambient air the peak areas for F12, CH<sub>3</sub>CCl<sub>3</sub> and CCl<sub>4</sub> are less than 1000 counts. Third, the precision of analyses for the same chromatograms obtained by electronically integrating the peak areas (third column, Table II.1) is obviously lower. These data represent 10 replicate analyses on the same sample. The absolute accuracy to which the concentrations are believed to be known is an estimate of our confidence in the correctness of its primary standards first developed in 1975 and subsequently reproduced in 1977.

In 1975 it became obvious that comparison of the halocarbon measurements, published by the dozen or more laboratories that were active in fluorocarbon analyses, had become very difficult because of the lack of a standard reference gas. Recognizing this problem in early 1976, a small informal interlaboratory comparison was conducted by Rasmussen et al. [1976]. This work led to the convening of a workshop on Halocarbon Analyses and Measurement Tech-

# RASMUSSEN and KHALIL

nique held in Boulder, Colorado, on March 25-26, 1976. A recommendation from the participants was that further collaborative tests should be conducted to continue to evaluate the state of the art of such measurements. The results from the first study conducted after the workshop were published in 1978 [Rasmussen, 1978; and Rasmussen and Pierotti, 1978]. In this paper we report briefly the results of our earlier and recent laboratory halocarbon intercomparisons. Over the years the participants in the study have represented a wide range of scientific interests and capabilities. The data in Table II.2 are presented in summary form for the purpose of comparing the results in the respective exchanges between 1976 and 1979. The mean values obtained from the independent analysis of the samples submitted to each participant represent a consensus value calculated from the respondents' results. Obviously the standard deviation around the mean value is quite large compared to accuracy to which the submitted value was known.

TABLE II.2.

## SUMMARY RESULTS INTERLABORATORY COMPARISON

		N <sub>2</sub> O PPB	F12 PPT	F11 PPT	CH <sub>3</sub> CCl <sub>3</sub> PPT
1976 FINAL RESULTS					
SUBMITTED	$\bar{x}$	--	230	137	101
N = 12	$\%$	--	3	2	3
INDEPENDENT	$\bar{x}$	--	230	132	93
N = 6-12	$\%$	--	19	16	12
1977 FINAL RESULTS					
SUBMITTED	$\bar{x}$	329	250	150	104
N = 17	$\%$	0.6	2	1	4
INDEPENDENT	$\bar{x}$	324	253	140	88
N = 9-16	$\%$	3	17	11	39
1979 SET A PRELIMINARY RESULTS AS OF OCTOBER 1, 1979					
SUBMITTED	$\bar{x}$	335	298	175	137
N = 12	$\%$	0.2	0.6	0.6	2
INDEPENDENT	$\bar{x}$	322	281	156	108
N = 7-12	$\%$	3	6	20	26
1979 SET B PRELIMINARY RESULTS AS OF OCTOBER 1, 1979					
SUBMITTED	$\bar{x}$	225	104	68	51
N = 12	$\%$	4	6	4	5
INDEPENDENT	$\bar{x}$	214	115	64	41
N = 6-12	$\%$	18	5	13	25

Overall the results indicate that significant systematic errors exist in the results reported by the various laboratories. A casual look at the data would suggest that the differences between laboratories have not decreased appreciably over the past 4 years. However, focusing on the results from individual laboratories that have previously calibrated with the authors or have derived their calibration standards from the authors' primary standards indicates that precise replicate measurements on F11 and F12 can be obtained with an agreement of  $\pm 4\%$  or better between these laboratories. Fraser [1979] has obtained similar results from circulating the same calibration tank of known halocarbon concentrations between several laboratories whose primary calibration standard is related to the authors' calibration stan-



## RASMUSSEN and KHALIL

dards. However, the agreement does not mean that the absolute concentrations of these halocarbons or  $N_2O$  are known with the same certainty. One of the improvements in the exchanges conducted in 1979 was the post-analysis of the samples at the Oregon Graduate Center (OGC) to verify that the concentrations submitted did not differ from those returned. The results indicate no changes in the halocarbon and  $N_2O$  concentrations. Since October the work was expanded to 25 laboratories. The results of this comparison are now nearing completion. An in-depth analysis of these data will be published elsewhere.

The last subject to be discussed in this section is the collection and sample analyses methods used in our laboratory over the past decade of trace gas analyses. An important point throughout the following discussion is that we have conducted the analyses in the field whenever it has been possible or practical. In many cases the analyses were made on the samples shortly after collection in the field and later again at the home laboratory. In this way species that are not ideally stable for delayed laboratory analyses are better quantified and characterized. However,  $N_2O$  and the halocarbons (except  $CCl_4$ ) are exceptionally stable in the collection vessels we have used. This is shown by the data in Table II.3. The data represent three different high pressure (@400 psi) cryogenic air samples of 1000 liters (STP) prepared in 1978 on the Oregon Coast at OGC's Cape Meares clean air station. The samples have been intermittently analyzed to determine if any significant changes were occurring with time. The same stability has been observed in 40 of these types of cryogenically prepared air samples. The observed differences of 1 to 2 parts per trillion are most likely due to analytical precision rather than real changes in  $N_2O$  and the halocarbons. The stability of other trace gases in these large volume high pressure samples has also been studied and found to be acceptable. At low pressures, <40 psi, wall losses of  $CCl_4$  occur, however, the  $N_2O$ , F12, F11 and  $CH_3CCl_3$  concentrations remain stable even after several months.

The containers currently used in the field are thin-walled stainless steel high pressure sampling vessels, with internal volumes of 0.8, 1.6 and 35.7 liters (STP). These vessels have been internally electropolished using the SUMMA® process, which produces an extremely inert, passive surface. The passivation is done at the Oregon Graduate Center, and the surface finish obtained is equal to or better than that specified by NASA (specification for the Apollo program). The combination of the inert internal surface of the canisters and the large volume (or mass) to surface ratio of the samples has given us excellent stability for trace gases, even for CO at the sub-100 ppb level, over the past several years.

Preparing the stainless steel canisters used to collect and store cryogenic air samples, and verifying that they are free of contamination and adsorption problems has become a specialty of our laboratory. All of the containers are tested, and the integrity of gas mixtures stored in them is verified before they are used in the field. One simple test we use to determine if any contamination is occurring from surface desorption involves filling the vessels with zero air (prepared at OGC) containing less than 1 ppt halocarbons and less than 1 ppb CO and hydrocarbons, and holding them at 80°C for 72 hours. If the tank has been properly prepared, no significant increase in the concentration of trace gases in the vessels is observed. If any increase occurs, then the vessels are put through the preparation procedures again, until no increase is observed. It is especially noteworthy that the vessels in use at this time are of all welded stainless steel construction, with no Teflon® pipe thread tape, and the valves are Nupro SS 1/4" H4 bellow seal types. A diagram of the 0.8 liter air sampling bottle is shown in Figure II.4. The bottle has been designed to provide a flow-through purge of the vessel before pressurization. This enables the bottle to be thoroughly flushed and the walls equilibrated with the trace gases in the air being sampled. All of the low pressure (<40 psig) air samples are collected using a Metal Bellows Corp. Model MB-158 pump.

Our alternate air sampling system that does not use a pump is a method of cryogenically collecting air samples of 50 and 1000 liters (STP). In its simplest form, the cryogenic collection system is driven by the liquefaction of ambient air inside a container immersed in liquid nitrogen ( $LN_2$ , -196°C). The liquid air (LA, -193°C), which is collected, is then allowed to come to room temperature, after the sampling valve of the container has been closed. The final sample pressure in the container is a function of the total volume of ambient air collected and the fixed volume of the sample container. The whole-air liquefaction process is 100% efficient and requires no pumps, thereby eliminating the major source of contamination in most sampling techniques. The condensation of the air inside the sampling vessel provides the partial vacuum necessary to drive the system. The only practical limit on the amount of air which can be collected by this method is the pressure limitations of the sampling vessels

TABLE II.3.

## HALOCARBON STABILITY IN CRYOGENIC AIR SAMPLES

Calib. No.	Event	Analyzed	F11 ppt $\bar{x}$	$\sigma$	F12 ppt $\bar{x}$	$\sigma$	CH <sub>3</sub> CCl <sub>3</sub> ppt $\bar{x}$	$\sigma$	CCl <sub>4</sub> ppt $\bar{x}$	$\sigma$	N <sub>2</sub> O ppb $\bar{x}$	$\sigma$
Sample (1)	Original	04/09/78	167.4	1.39	280.8	2.87	162.8	2.52	143.2	1.48	335.2	1.80
	Rechecked	12/06/78	164.8	1.72	280.0	1.67	166.0	4.5	142.5	0.84	333.5	2.12
	Rechecked	04/10/79	167.5	0.8	281.3	2.0	164.7	2.2	145.7	1.2	335.5	0.5
	Rechecked	02/01/80	166.8	0.4	279.0	0.6	164.5	0.8	145.8	0.4	334.8	0.4
Sample (2)	Original	04/09/78	168.5	0.65	285.3	2.92	134.5	2.85	146.8	1.49	332.8	1.55
	Rechecked	12/04/78	169.2	0.75	282.8	1.09	128.3	1.21	146.2	0.75	332.3	1.21
	Rechecked	04/11/79	168.0	0.0	283.2	1.0	129.2	0.8	144.2	1.0	333.3	0.5
	Rechecked	01/30/80	168.7	0.5	284.2	0.8	129.7	0.5	143.2	1.5	333.8	0.8
Sample (3)	Original	04/09/78	168.5	0.96	281.5	1.22	148.9	2.79	146.8	1.93	335.4	1.35
	Rechecked	01/24/79	167.5	0.55	282.0	0.63	149.0	1.26	146.0	1.10	335.0	0.0
	Rechecked	04/24/79	167.8	0.4	283.0	1.3	150.7	0.8	146.3	0.5	333.3	1.2
	Rechecked	08/29/79	167.2	1.2	282.0	1.1	148.7	0.8	145.7	1.4	334.3	0.5
	Rechecked	02/05/80	168.0	0.6	284.5	0.5	148.3	1.4	145.5	0.5	334.5	0.5

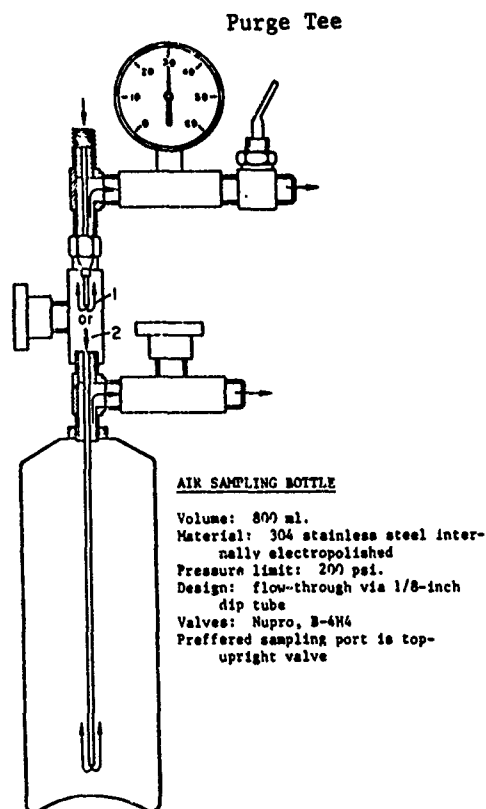
Number of analyses: a minimum of 6.

when the liquid air comes to room temperature. For more details the reader may consult the paper published in 1972 describing the original system [Rasmussen, 1972].

The primary use of the samples collected in the past was for measurements of F11, F12, CH<sub>3</sub>CCl<sub>3</sub>, CCl<sub>4</sub> and N<sub>2</sub>O. However, the large volumes collected also enable the analyses of CO, CH<sub>4</sub>, C<sub>2</sub>H<sub>6</sub>, C<sub>2</sub>H<sub>4</sub>, C<sub>2</sub>H<sub>2</sub>, CH<sub>3</sub>Cl, CH<sub>3</sub>Br, CH<sub>3</sub>I, CHCl<sub>3</sub>, CHCl=CCl<sub>2</sub>, CCl<sub>2</sub>=CCl<sub>2</sub>, COS and CS<sub>2</sub>, among other compounds. These types of samples have also enabled us to verify the ubiquitous presence of CF<sub>4</sub> and F21 (a proposed degradation product of F11) in the earth's atmosphere, and discover the existence of two compounds, C<sub>2</sub>F<sub>6</sub> and CF<sub>3</sub>Cl, which had never been measured in the atmosphere previously. Recently we have used the last remaining cryogenic sample from the South Pole for January 1979 to measure the F22 concentration for that period. This data point has been very useful in constructing a latitudinal profile as well as establishing a reference point for further corroboration.

Enrichment, fractionation and other sample concentration and transfer techniques all have to be modified and tested for operation under the intended field laboratory conditions. Special sample preparation techniques are usually needed

FIGURE II.4.  
Air Sampling Bottle



if the in situ analyses are to be accomplished successfully. At present our methods include removing the oxygen and nitrogen from the samples by vacuum methods, isothermal distillations at  $-78^{\circ}\text{C}$  in dry ice-acetone baths, matrix isolation on cold-finger traps, and enrichment of the trace gases of interest on solid adsorbents.

In summary, the collection and storage system is rugged, safe, extremely simple to operate and proven in the field under a variety of conditions. Development of the system for returning to the laboratory the air samples as liquid air offers an exciting challenge and hope for measuring an entirely new list of trace gas species in the atmosphere.

Immediately upon arriving at our OGC laboratory the samples are analyzed routinely for  $\text{N}_2\text{O}$ ,  $\text{F12}$ ,  $\text{F11}$ ,  $\text{CH}_3\text{CCl}_3$  and  $\text{CCl}_4$ . These measurements are made to establish that the samples show no adverse effects due to contamination ( $\text{F11}$  and  $\text{CH}_3\text{CCl}_3$  are the best indices) or wall adsorption ( $\text{CCl}_4$  is a very sensitive indicator). The routine analyses for  $\text{N}_2\text{O}$ ,  $\text{F12}$ ,  $\text{F11}$ ,  $\text{CH}_3\text{CCl}_3$  and  $\text{CCl}_4$  are made on a Perkin-Elmer 3920B dual EC/GC. One channel uses a  $10' \times \frac{1}{4}"$  (o.d.) column packed with 10% SP2100 (80-100 mesh), while the second channel uses a  $10' \times \frac{1}{8}"$  (o.d.) column packed with Porasil B (80-100 mesh). The oven temperature is  $70^{\circ}\text{C}$ , the temperature of the electron capture detectors is  $350^{\circ}\text{C}$ , with a standing current of 3.5 nA, and the carrier gas is 95%Ar/5% $\text{CH}_4$ . The temperature stability of the electron capture detectors has been improved by the use of a special ice-point temperature reference cell, which minimizes problems caused by changes in the ambient temperature. Chromatograms showing the performance of these EC/GC systems are shown in Figures II.1, II.2 and II.3.

Measurement of the other species usually requires other analytical instruments. Both electron capture-gas chromatography and gas chromatography-mass spectrometry are used to measure these compounds. While all of the species we are interested in can be measured using GC/MS, it is not practical to use this instrument for all of the measurements. Its primary use is to measure those species which cannot be measured using EC/GC, such as  $\text{CF}_4$ ,  $\text{C}_2\text{F}_6$ ,  $\text{CF}_3\text{Cl}$  and  $\text{F21}$  ( $\text{CHFCl}_2$ ). It is also used to search the samples for new species which have not previously been measured in the atmosphere, as we did for  $\text{CF}_4$ ,  $\text{C}_2\text{F}_6$  and  $\text{CF}_3\text{Cl}$ . GC/MS analyses are also used to verify the identification of those species which are readily measured by EC/GC, such as  $\text{F22}$ ,  $\text{F113}$ ,  $\text{F114}$ ,  $\text{CH}_3\text{CCl}_3$ ,  $\text{CH}_2\text{Cl}_2$ ,  $\text{CHCl}_3$ ,  $\text{CHCl}=\text{CCl}_2$ ,  $\text{CCl}_2=\text{CCl}_2$ , etc., and to augment the flame-photometric-detector GC analyses of  $\text{COS}$  and  $\text{CS}_2$ . A major emphasis of our EC/GC analysis methodology is in the use of subambient temperature programmed analyses using fused silica capillary column and in the use of  $\text{O}_2$ -doped carrier gases which selectively enhance the response of the ECD to weakly electron-capturing species like  $\text{CH}_3\text{Cl}$  and  $\text{F22}$  [Rasmussen et al., 1980; Rasmussen and Khalil, 1980].

III. OBSERVATIONAL RESULTS: Over the past several years our laboratory has made a number of extensive high altitude aircraft flights, especially in the northern hemisphere. The flight profiles have been obtained mainly over the western part of the United States, Canada and Alaska. In addition, one of the Lear-jet flights traversed the Pacific Ocean from  $80^{\circ}\text{N}$  to  $59^{\circ}\text{S}$  in the summer of 1976. From these and related data obtained at ground level sites in remote parts of the world it has been possible to determine the observed concentration distributions of selected trace gases in the upper troposphere and the lower stratosphere. A synopsis of these types of data is given in Table III.1. The concentrations listed for the lower troposphere represent our measurements as of May 1979. Again the data are skewed for samples obtained over the Pacific Ocean at mid-latitudes of  $45^{\circ}\text{N}$  (Cape Meares, Oregon) and  $43^{\circ}\text{S}$  (Cape Grim, Tasmania). Nevertheless, the data for the conservative species like the fluorocarbons are typical of the observed concentrations at even higher latitudes as we have not measured any appreciable changes at  $90^{\circ}\text{S}$  or  $65^{\circ}$ - $70^{\circ}\text{N}$  from their respective mid-latitude values at the longitudes we have worked. This is not the situation for more reactive species like  $\text{CO}$ ,  $\text{CH}_3\text{Br}$ ,  $\text{CH}_3\text{I}$  and the  $\text{C}_2$  hydrocarbons. The methyl halogen values are reasonably well characterized, especially  $\text{CH}_3\text{Cl}$ . No significant inter-hemispheric difference for this species has been observed, although much higher concentrations in the boundary layer over equatorial oceans were observed in the GAMETAG flights [Rasmussen et al., 1980]. The work on  $\text{CH}_3\text{Br}$  and  $\text{CH}_3\text{I}$  is still preliminary. Similarly the work we are doing on  $\text{COS}$  and  $\text{CS}_2$  is preliminary, as GC/FPD atmospheric measurements made on these species in 1970-73 are being compared with current GC/MS and GC/FPD data. Much of our work on  $\text{COS}$  and  $\text{CS}_2$  has also been concerned with their respective concentrations in a variety of volcanic emissions.

The measurement of  $\text{CF}_4$  was previously reported [Rasmussen et al., 1979]. Since this early work, it has been measured again several times by Drs. Penkett and Prosser at A.E.R.E. Har-

# RASMUSSEN and KHALIL

LOWER TROPOSPHERE      UPPER TROPOSPHERE      LOWER STRATOSPHERE  
SPECIES      N.H.      S.H.      CONCENTRATION EXPECTED

N <sub>2</sub> O	332 PPB	331 PPB	NC	
F12	303 PPT	275	-1 TO 2%	-5 TO 8%
F11	178	159	-1 TO 2	-5 TO 10
CH <sub>3</sub> CCl <sub>3</sub>	135	97	-1 TO 3	-5 TO 20
CCl <sub>4</sub>	143	141	-1 TO 3	-5 TO 10
CF <sub>4</sub>	65 PPT	65 PPT	NC	NC
CF <sub>3</sub> Cl	3	3	NC	NC
C <sub>2</sub> F <sub>6</sub>	3	3	NC	NC
CO	145 PPB	45 PPB	-1 TO 5%	-25 TO 50%
CH <sub>4</sub>	1595 PPB	1510 PPB	-1 TO 2	-2 TO 3
C <sub>2</sub> H <sub>2</sub>	90 TO 180 PPT	0 - 25 PPT	60 - 120 PPT	50 PPT
C <sub>2</sub> H <sub>4</sub>	160	30 - 130	80 - 150 PPT	--
C <sub>2</sub> H <sub>6</sub>	800 - 1000	150 - 350	670 - 1100 PPT	300 PPT
CH <sub>3</sub> Cl	630 PPT	630 PPT	-2 TO 10%	-5 TO 25%
CH <sub>3</sub> Br	~ 5	~ 5	-5 TO 25	-50%
CH <sub>3</sub> I	< 5	< 5	--	--
COS	500 PPT	400-600 PPT	NC	-10 TO 30%
CS <sub>2</sub>	70	50	--	--
CHFCl <sub>2</sub>	2 PPT	<1 PPT	--	--
CHF <sub>2</sub> Cl	45	40	-1 TO 3%	-5 TO 15%

TABLE III.1  
TRACE GAS CONCENTRATIONS RELEVANT TO  
CONCORDE AIR SAMPLING PROGRAM

Table III.2  
MEASUREMENTS OF CFC1<sub>3</sub>, CCl<sub>2</sub>F<sub>2</sub>,  
CH<sub>3</sub>CCl<sub>3</sub>, CCl<sub>4</sub> AND N<sub>2</sub>O

		PACIFIC NORTHWEST CONCENTRATION PPTV	ANTARCTICA CONCENTRATION PPTV	RATIO N/S
JANUARY 1975	F11	125	90	1.39
	CCl <sub>4</sub>	130	120	1.08
	CH <sub>3</sub> CCl <sub>3</sub>	90	54	1.67
JANUARY 1976	F12	228	195	1.17
	F11	138	113 (109)*	1.22
	CCl <sub>4</sub>	133	121	1.10
	CH <sub>3</sub> CCl <sub>3</sub>	98	57	1.72
JANUARY 1977	F12	251	216	1.16
	F11	154	127 (128)*	1.21
	CCl <sub>4</sub>	144	128	1.13
	CH <sub>3</sub> CCl <sub>3</sub>	107	70	1.53
	N <sub>2</sub> O	330 PPBV	330 PPBV	1.00
JANUARY 1978	F12	280	244	1.15
	F11	166	145 (149)*	1.14
	CCl <sub>4</sub>	154	123	1.25
	CH <sub>3</sub> CCl <sub>3</sub>	117	85	1.38
	N <sub>2</sub> O	332 PPBV	331 PPBV	1.00
JANUARY 1979	F12	300	260	1.15
	F11	173	154	1.12
	CCl <sub>4</sub>	140	135	1.04
	CH <sub>3</sub> CCl <sub>3</sub>	135	95	1.42
	N <sub>2</sub> O	332 PPBV	332 PPBV	1.00
JANUARY 1980	CH <sub>3</sub> CCl <sub>3</sub> †	103	157	1.52

\* TASMANIA DATA; † PRELIMINARY DATA

well, and its atmospheric concentration reaffirmed. The identification of  $\text{CF}_3\text{Cl}$  and  $\text{C}_2\text{F}_6$  at the few parts per trillion level was made during these subsequent  $\text{CF}_4$  studies. Because all three of these species are inert and ubiquitously distributed in the atmosphere, no measurable changes of mixing ratios are expected with height in the vertical profiles obtained from our high altitude aircraft flights.

The results obtained for  $\text{CO}$ ,  $\text{C}_2\text{H}_2$ ,  $\text{C}_2\text{H}_4$  and  $\text{C}_2\text{H}_6$  are much more variable both seasonally and latitudinally than the other species. This most probably reflects their reaction with tropospheric HO radicals. Accordingly, the values listed in Table III.1 provide a range rather than a mean value. More recently we have measured F21 and F22 in conjunction with Drs. Penkett and Prosser. Currently the global distribution of F22 is being rigorously studied using an  $\text{O}_2$ -doped EC/GC method. This technique in conjunction with a freezeout concentration procedure of 100 ml samples is needed in order to measure it because of its very weak response to the ECD. A chromatogram of the co-analysis of F11 with F22,  $\text{CH}_3\text{Cl}$  and F113 is shown in Figure III.1. An advantage of the co-measurement of F11 is that it provides an internal standard against which one can judge the efficiency of the cryotrapping procedure. In addition, valuable information on  $\text{CH}_3\text{Cl}$  and F113 are obtained.

In comparison with this portfolio of observed lower tropospheric concentrations it has been possible to determine the percent decrease for each of these species in samples collected in the upper troposphere and lower stratosphere. It is too early to discuss these high altitude data in detail as they are at present being evaluated in the current Concorde program. However, it is appropriate to present the observed percent decrease in species concentration measured to date.

A detailed description of the halocarbons pattern of annual increase and the changing ratios from year to year between the South Pole in Antarctica and the Pacific northwest is given in Table III.2. The data cover a period of 5 years and represent the longest data record of this kind. Also the results are internally consistent, having been determined by the same method of analysis and referenced to the same primary calibration standards throughout the study. The values represent the concentrations determined for January of each year and are not integrated annual means. The results have already been used by a number of modelers for estimating atmospheric lifetimes and global budgets of the halocarbons [Chang and Penner, 1978; Fink and Klaes, 1978; Meakin et al., 1978]. In the next section we present our own analysis of the data and its relevance to interpreting global atmospheric processes. The only drawback to applying these models to the data is the fact that five years of data are barely enough to begin to show any statistically significant results, particularly since we are only able to obtain data from Antarctica during one time of the year: the austral summer. Therefore, making halocarbon measurements in Antarctica for the next few years is very important, and we expect to continue the program.

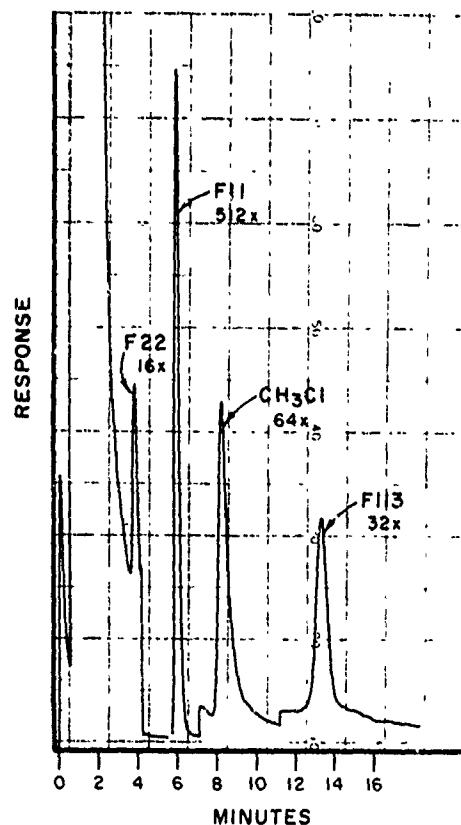


FIGURE III.1. Freezeout analysis of 100 ml of clean air from Cape Meares, Oregon, with  $\text{O}_2$ -doped (0.3%)  $\text{N}_2$  carrier gas. Oven  $60^\circ\text{C}$ , EC detector  $350^\circ\text{C}$ . Precision of analysis: F22  $\pm 5\%$  @40 ppt; F11  $\pm 0.5\%$  @170 ppt;  $\text{CH}_3\text{Cl}$   $\pm 2\%$  @600 ppt; F113  $\pm 3\%$  @15 ppt.

Between 1976 and 1978 our laboratory participated in several ocean cruises and aircraft flights measuring the latitudinal distribution of several trace gases. These measurements give almost continuous data on the ground level mixing ratio of a trace gas as a function of latitude. Similar measurements have also been reported by Singh et al. [1979] for F11, F12,  $\text{CH}_3\text{CCl}_3$  and several other trace gases. Makide and Rowland [1979] have reported  $\text{CH}_3\text{CCl}_3$  measurements from 25 ground-based locations, most of which were at  $\phi > +\pi/6$  radians and  $\phi < -\pi/6$  radians. It has become customary to report the results of such observations with a third order polynomial in latitude so that the mixing ratio at any latitude  $\phi$  is given by:

$$\xi(\phi) = A_0 + A_1\phi + A_2\phi^2 + A_3\phi^3 \quad (3.1)$$

One of the principal reasons for obtaining a function like (3.1) is to be able to compute global and hemispherical averages.

In Figure III.2, our measurements of  $\text{CH}_3\text{CCl}_3$  during 1976, 1977 and 1978 are illustrated.

Measurements of several other trace gases were also made, but these are not illustrated here. The coefficients of the third order polynomials given by eqn. (3.1) are listed in Table III.3. These correspond to Figure III.2 for  $\text{CH}_3\text{CCl}_3$ .

In principle, it is possible to use these data to obtain the ambient concentration of the appropriate trace gas at any latitude, to obtain a measure of increasing atmospheric burden or to determine lifetimes. However, these particular data may require some further interpretation before they can serve these purposes.

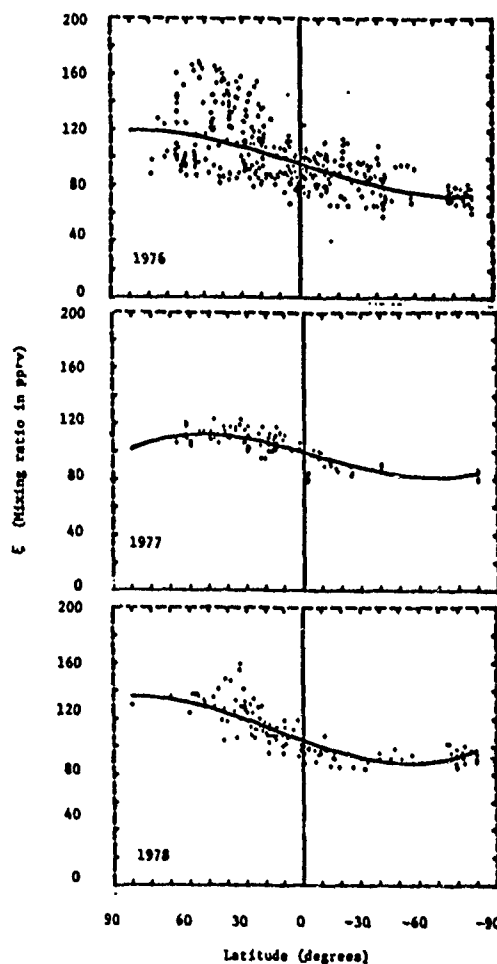


TABLE III.3

POLYNOMIAL DESCRIPTION OF GLOBAL OBSERVATIONAL DATA

		$A_0$	$A_1$	$A_2$	$A_3$
1976	$\text{CH}_3\text{CCl}_3$	96.0	0.421	$4.10 \times 10^{-5}$	$-2.93 \times 10^{-5}$
	F11	130.8	0.102	$4.31 \times 10^{-4}$	$-3.26 \times 10^{-6}$
	F12	221.0	0.223	$1.28 \times 10^{-3}$	$-7.49 \times 10^{-6}$
1977	$\text{CH}_3\text{CCl}_3$	99.6	0.362	$-8.04 \times 10^{-5}$	$-3.30 \times 10^{-5}$
	F11	149.1	0.145	$3.30 \times 10^{-5}$	$-1.38 \times 10^{-5}$
	F12	249.0	0.200	$5.94 \times 10^{-4}$	$7.46 \times 10^{-6}$
1978	$\text{CH}_3\text{CCl}_3$	104.5	0.479	$-1.45 \times 10^{-3}$	$-3.28 \times 10^{-5}$
	F11	155.9	0.304	$6.21 \times 10^{-4}$	$-3.37 \times 10^{-5}$
	F22	261.6	0.343	$1.14 \times 10^{-3}$	$-4.40 \times 10^{-5}$

NOTE THAT  $\phi$  IS IN DEGREES. FOR INTEGRATION  $A_1$  SHOULD BE CONVERTED TO THE APPROPRIATE UNITS IN RADIANS.

FIGURE III.2. Global measurements of  $\text{CH}_3\text{CCl}_3$  for 1976, 1977, 1978.

IV. THEORETICAL ANALYSES: REVIEW OF SELECTED RESULTS. Theoretical analyses using simple models are discussed in this section. These analyses are designed to consider the global sources, sinks and distributions of selected trace gases to explain their tropospheric behaviour.

(a) Methylchloroform ( $\text{CH}_3\text{CCl}_3$ ): Methylchloroform in the atmosphere is believed to be entirely man-made. A relatively large amount of observation data is available on its tropospheric distribution. We have, however, isolated one set of data for further analysis because of its internal consistency and because it covers a long period of time over which measurements have been made. These data represent measurements of  $\text{CH}_3\text{CCl}_3$  in ambient air at two locations on the earth's surface. One location is the U.S. Pacific northwest (Washington and Oregon) at about  $45^\circ\text{N}$  latitude and the other is the south pole ( $90^\circ\text{S}$  latitude). The results of measurements at the beginning of each year are given in Table III.2. They cover five years. This measurement program is continuing.

In addition to several years of observational data on global concentrations, accurate industrial emissions estimates for  $\text{CH}_3\text{CCl}_3$  are also available [Neely and Plonka, 1978]. The lifetime is the variable which ties together the emissions estimates and the atmospheric burden. The lifetime and the mechanisms responsible for the destruction of a trace gas determine the potential dangers of continuing and increasing global emissions. Long-lived trace gases often pose greater dangers to the future environment. The specific dangers depend on the physical properties of the trace gas. For  $\text{CH}_3\text{CCl}_3$  and several other trace gases of anthropogenic origin, the dangers to the global environment include the adverse consequences of stratospheric ozone depletion and the enhancement of the atmospheric greenhouse effect.

To deduce the lifetime of  $\text{CH}_3\text{CCl}_3$  we used a hemispherically averaged mass balance equation given by:

$$\frac{d}{dt} \xi_n = S_n - \eta_n \xi_n - \eta_T (\xi_n - \xi_s) \quad (4.1)$$

$$\frac{d}{dt} \xi_s = S_s - \eta_s \xi_s + \eta_T (\xi_n - \xi_s); \quad \eta = 1/\tau \quad (4.2)$$

This theory is appropriate for the long time series of data shown in Table III.2. In eqns. (4.1) and (4.2)  $\xi_n$  and  $\xi_s$  are the average northern and southern hemisphere concentrations,  $\eta_n$  and  $\eta_s$  are the reciprocals of the average lifetimes,  $\tau_n$  and  $\tau_s$ , of  $\text{CH}_3\text{CCl}_3$  in the two hemispheres, and  $\eta_T$  represents the reciprocal of the average effective interhemispheric exchange time.  $S_n$  and  $S_s$  are the global emissions (say in pptv per year) at a given time. It is generally believed that  $S_s \approx 0$ , but even if it is between 5 and 10% of the total global emissions, this approximation ( $S_s = 0$ ) does not lead to significantly different results. Next, we have to convert measurements into  $\xi_n$  and  $\xi_s$ . The source term,  $S_n$ , is determined from independent estimates of global industrial emissions [Neely and Plonka, 1978]. The value of  $\eta_T$  also has to be specified [see for example Newell et al., 1969]. There are several ways by which one can derive the appropriate lifetimes which would balance the emissions data on the one hand and the observed concentrations on the other. One simple way to accomplish this is to simply integrate both sides of eqns. (4.1) and (4.2), resulting in the following equations:

$$\tau_n = [\xi_{n*}] / [S_{n*} - \Delta\xi_n - \eta_T \delta\xi_*]; \quad \tau_s = [\xi_{s*}] / [\eta_T \delta\xi_* - \Delta\xi_s] \quad (4.3)$$

$$\delta\xi_* = \xi_{n*} - \xi_{s*}; \quad \tau = [\xi_{n*} + \xi_{s*}] / [\eta_n \xi_{n*} + \eta_s \xi_{s*}] \quad (4.4)$$

The symbols used in these equations (4.3) and (4.4) are defined as follows:  $S_{n*}$  are the total emissions from the time measurements began (zero) to the time when the last measurements of concentration were made (time = T).  $\xi_{n*}$  and  $\xi_{s*}$  are defined by  $\xi_* = \int_0^T \xi(t) dt$  and  $\Delta\xi_n = \xi_n(T) - \xi_n(0)$ ,  $\Delta\xi_s = \xi_s(T) - \xi_s(0)$ . The rest of the symbols are the same as before. Eqn. (4.4) for  $\tau$  represents the composite global lifetime. In order to obtain numerical results

for  $\tau_n$  and  $\tau_s$ , the measured concentrations shown in Table III.2 must be converted to  $\xi_n$  and  $\xi_s$ . There are two considerations: (1) the concentration of  $\text{CH}_3\text{CCl}_3$  declines with decreasing latitude in the northern hemisphere and continues to decline for latitudes up to  $\sim 30^\circ\text{S}$ . More detailed measurements of  $\text{C}^{13}\text{CCl}_3$  support the following function:

$$\xi(\phi) = \begin{cases} a & -\pi/2 \leq \phi < -\phi_0 \\ \frac{1}{2}(a+b) + (\frac{1}{2})[(b-a)/\phi_0]\phi & -\phi_0 \leq \phi \leq \phi_0 \\ b & \phi_0 < \phi \leq \pi/2 \end{cases} \quad (4.5)$$

where (a) is given by the measurements at the south pole and (b) by the measurements at the Pacific northwest site. Consequently,

$$\xi'_n = b - \frac{1}{2}(b-a)(1 - \cos \phi_0)/\phi_0; \quad \xi'_s = a + \frac{1}{2}(b-a)(1 - \cos \phi_0)\phi_0. \quad (4.6); (4.7)$$

$\phi_0$  is about  $\pi/6$  radians. (2) The decline of the  $\text{CH}_3\text{CCl}_3$  mixing ratio above the tropopause must also be taken into account. This is accomplished by assuming that  $\xi_n = \alpha_n \xi'_n$  and  $\xi_s = \alpha_s \xi'_s$  where  $\alpha_n \approx (N_T/N_\infty)[1 + \xi_n(N_S/N_T)]$   $\xi_n = \xi_{un}/\xi_{Tn}$  ( $N_T$  and  $N_S$  are the number of molecules of air in the troposphere and the stratosphere respectively,  $N_\infty = N_S + N_T$ ,  $\xi_{un}$ ,  $\xi_{Tn}$  are the northern hemisphere mean mixing ratios in the stratosphere and the troposphere respectively.) The equations for  $\alpha_s$  are analogous. Since detailed measurements of  $\text{CH}_3\text{CCl}_3$  have not been made in the stratosphere, it is difficult to estimate  $\alpha_n$  and  $\alpha_s$  accurately. Fortunately, the  $\alpha$ 's are not very sensitive to uncertainties in  $\xi$ , reflecting the fact that the stratospheric burden of  $\text{CH}_3\text{CCl}_3$  (total number of molecules) is small compared to the tropospheric burden. The details of the equations (4.5)-(4.7) as well as the equations for  $\alpha$  are discussed by Khalil [1979]. The reader is no doubt aware that the translation of the ground level observational data into hemispheric (or global) burdens includes uncertainties from each of the two considerations discussed above. Still we believe that ignoring these factors is worse. With all these assumptions, the results of the calculations may be summarized as shown in Table IV.1.

TABLE IV.1.  $\text{CH}_3\text{CCl}_3$  Lifetimes in a Hemispherically Averaged Theory

$\tau_T$ (yrs)	1	1.2	1.4
$\tau$ (yrs)	8.5	8.5	8.5
$\tau_n$ (yrs)	27	12.3	8.9
$\tau_s$ (yrs)	4.4	6	8

In Table IV.1  $\xi$  is assumed to be 0.25. The results of the calculations indicate that an interhemispheric exchange time  $\tau_T = 1$  yr is very unlikely because it predicts a difference between  $\tau_n$  and  $\tau_s$  which cannot be explained by our current knowledge of the sources and sinks of  $\text{CH}_3\text{CCl}_3$ .  $\tau_T = 1.2$  or  $1.4$  yrs are both reasonable and relatively small compared to previous estimates [see for example: Chang and Penner, 1978, where  $\tau_T$  was found to be 1.8 years using some of the same  $\text{CH}_3\text{CCl}_3$  data]. If  $\tau_T$  is taken to be 1.4 years, then the lifetime of  $\text{CH}_3\text{CCl}_3$  is approximately the same in both hemispheres. If  $\tau_T = 1.2$  years, the lifetime of  $\text{CH}_3\text{CCl}_3$  is twice as large in the northern hemisphere compared to the lifetime in the southern hemisphere. At this time we tend to favour the case where  $\tau_T = 1.2$  yrs. Current measurements indicate that the concentration of CO is higher in the northern hemisphere than in the southern hemisphere. This in turn implies that the average HO density is larger in the southern hemisphere since in the troposphere CO is believed to control HO densities. Since the dominant destruction mechanism for  $\text{CH}_3\text{CCl}_3$  in the troposphere is its reaction with HO radicals, it follows that  $\tau_n$  should be larger than  $\tau_s$ .

Meteorological studies of mass transport across the equator have been used to estimate the interhemispheric exchange time to be about 1 yr. [Newell et al., 1969]. If one believes that the interhemispheric transport is fast ( $\sim 1$  yr), then the results of Table IV.1 can be interpreted to favour  $\tau_n > \tau_s$ .



Equations (4.4) and (4.5) are a particularly simple set of solutions for the mass balance equation. Another approach for estimating lifetimes based on eqns. (4.1) and (4.2) is to write their solutions and try various lifetimes to see which one reproduces the observed  $\xi_n$  and  $\xi_s$  the best. The solutions are written as:

$$\underline{\xi} = [P^{-1} \exp(-\Lambda t)P] \underline{\xi}_0 + P^{-1} \exp(-\Lambda t) \int_0^t \exp(\Lambda t') P \underline{S}(t') dt' \quad (4.8)$$

$$\Lambda = P Q P^{-1} = \begin{bmatrix} \lambda_1 & 0 \\ 0 & \lambda_2 \end{bmatrix} \quad (4.9)$$

$$\underline{\xi} = \begin{bmatrix} \xi_n \\ \xi_s \end{bmatrix}; \quad \Omega = \begin{bmatrix} (\eta_n + \eta_T) & -\eta_T \\ -\eta_T & (\eta_s + \eta_T) \end{bmatrix} \quad (4.10)$$

The matrix  $P$  is defined by eqn. (4.9).  $\lambda_1$  and  $\lambda_2$  are the eigenvalues of  $\Omega$ . The results of the calculations are shown in Figure IV.1. The upper curves are for  $(\tau_n, \tau_s, \tau_T) = (16, 8, 1.2)$  and the lower curves are for  $(\tau_n, \tau_s, \tau_T) = (8, 4, 1.2)$ . The best agreement with observations is obtained by assuming  $(\tau_n, \tau_s, \tau_T) = (12, 6, 1.2)$  which agrees with the estimates of lifetimes based on equations (4.3) and (4.4).

The observational data given in Table III.2 imply that the global lifetime of  $\text{CH}_3\text{CCl}_3$  is about 8-9 years. Again, there are uncertainties involved in both measurements and the models adopted here. Absolute accuracies of both the measurements and the emissions data are important. Assuming that the measurements represent mixing ratios which are consistently high by 10% compared to true ambient concentrations, and at the same time emissions estimates are consistently low by 15%, yields 6 years as the global lifetime for  $\text{CH}_3\text{CCl}_3$ . We, therefore, expect that  $\tau(\text{CH}_3\text{CCl}_3)$  is between 6-10 yrs, and most likely to be about 9 yrs.

The data shown in Table III.1 led us to consider the emissions estimates more carefully. Figure IV.2 shows the  $\ln$  of emissions estimates as a function of time. A least squares fit through the points between the years from 1963 to 1978 implies that

$$S_0 = a \exp(bt) \quad (4.11)$$

where  $b = 0.153$  per year. Such a function has been used in earlier budget calculations for  $\text{CH}_3\text{CCl}_3$  with  $b = 0.15-0.16/\text{yr}$ . [See Chang and Penner, 1978, and references in their paper.] These emissions data were reported by Neely and Plonka [1978] and updated by Neely and Farber [1979] (980 million lbs. emitted in 1977 and 1100 million lbs. in 1978). One would expect that the global burden (or globally averaged mixing ratio) should have increased at about the same rate as the emissions (i.e., 15-16% per year, exponentially) during the years our measurements were made (1975-1979). The data in Table III.1, however, indicate a lower global average rate of increase or about

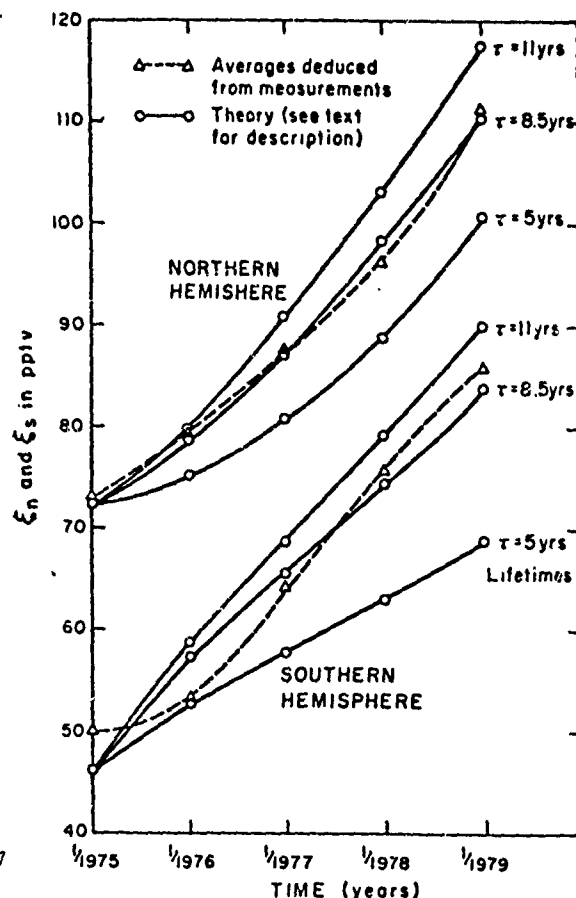


FIGURE IV.1. Predictions of hemispherically averaged mass balance equation and measured concentrations of  $\text{CH}_3\text{CCl}_3$ .

12% per year (exponentially). Furthermore, based on the mass balance equations (for example, eqns. (4.1) and (4.2)), the ratio of northern to southern hemisphere concentrations (denoted  $R_0$ ) should be constant. Once again, the observation data in Table III.1 indicate sizeable fluctuations in  $R_0$ . Looking at the emissions estimates more carefully (Figure IV.2) reveals sizeable fluctuation in the emissions function,  $S(t)$ , away from a pure exponential given by eqn. (4.11). We propose that these fluctuations in the emissions are responsible for the lower rate of increase ( $\sim 12\%/yr$ ) in the atmospheric burden and the variations of  $R_0$ , during the years when observations were made (1975-1979). Both the rate of increase  $(1/\xi)(d\xi/dt)$  and  $R_0$  are ratios of concentrations, so that absolute accuracy of measurements is relatively unimportant in observing their changes with time. The effects of source fluctuations are quantified next.

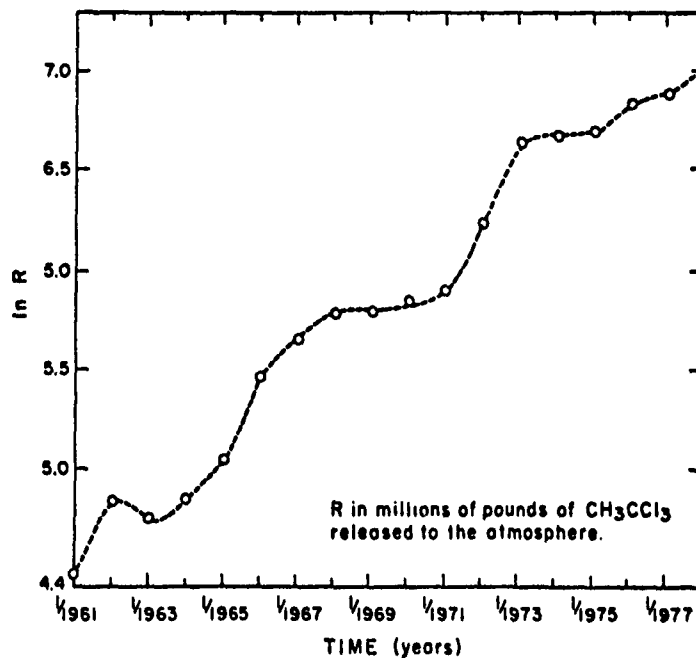


FIGURE IV.2. Time variation of global  $\text{CH}_3\text{CCl}_3$  emissions (1961-1978).

First, we derive an expression for the emissions function,  $S(t)$ , which more accurately represents the estimates of Neely and Plonka [1978]. Let us designate the "true" emissions function by  $S(t)$  which we assume to be given by the estimates shown in Figure IV.2. The deviations of  $S(t)$  from a pure exponential may be isolated by defining a function  $\Delta_1(t)$ :

$$\tilde{\Delta}_1(t) = [S(t)/S_0(t)] - 1 \quad (4.12)$$

(where  $S_0(t)$  is given by eqn. (4.11)). In Figure IV.3 the triangles ( $\Delta$ ) represent  $\tilde{\Delta}_1(t)$ .

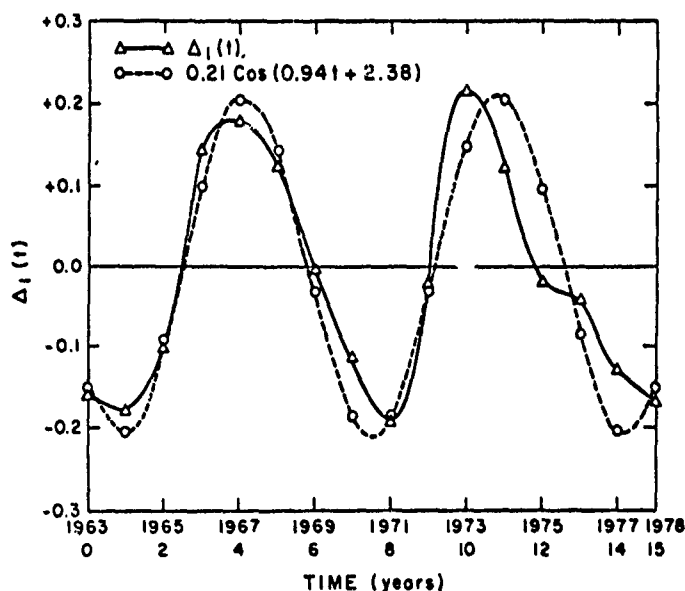


FIGURE IV.3. The  $\Delta_1$  cycle in the global emissions of methylchloroform.

Next we describe the  $\tilde{\Delta}_1(t)$  by a model cyclic function  $\Delta_1(t)$

$$\Delta_1(t) = \alpha \cos (\omega t + \phi) \quad (4.13)$$

where  $\alpha$ ,  $\omega$  and  $\phi$  are determined from the true emissions function  $S(t)$ . Instead of using  $S_0$  (eqn. 4.13) as an estimate of  $S(t)$ , we can now use  $S_1(t)$  given by

$$S_1(t) = a \exp (bt) [1 + \alpha \cos (\omega t + \phi)] \quad (4.14)$$

$S_1(t)$  is more accurate at describing the emissions estimates than  $S_0(t)$ . We can define a new function,  $\tilde{\Delta}_2(t)$  by:

$$\tilde{\Delta}_2(t) = [S(t) - S_1(t)]/S_0(t) \quad (4.15)$$

The  $\Delta_1(t)$  represents the difference between the "true" emissions function and our model function  $S_1(t)$ . Figure IV.4 illustrates  $\tilde{\Delta}_2(t)$ .

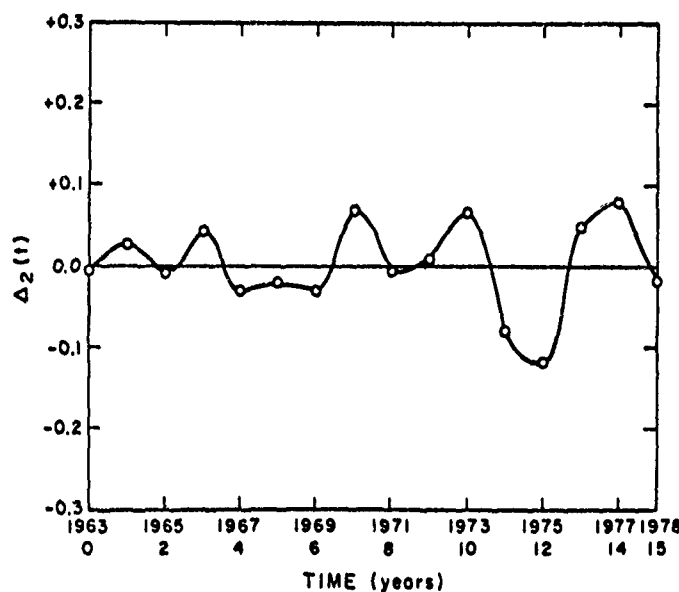


FIGURE IV.4. The  $\Delta_2$  cycle in the global emissions of methylchloroform.

The function  $\tilde{\Delta}_2(t)$  can be represented by another cyclic function given by

$$\Delta_2(t) = [\alpha_* + \tilde{\alpha}_* \cos (\omega_* t + \phi)] H(t - T) \quad (4.16)$$

where  $\alpha_*$ ,  $\tilde{\alpha}_*$ ,  $\omega_*$  and  $\phi_*$  are all determined from the true emissions estimates.  $H(t - T) = 0$  for  $t < T$  and 1 for  $t \geq T$ ,  $T$  is at 1972. Before 1972,  $\tilde{\Delta}_2(t)$  has insignificant magnitude. This process of defining residuals can be continued but in the case of  $\text{CH}_3\text{CCl}_3$ ,  $\Delta_2(t)$  is sufficiently accurate. This method is analogous to obtaining a Fourier spectrum of the residual  $\Delta_1(t)$ . Finally, we may write our model for the emissions function as:

$$S(t) \approx S_2(t) = a \exp (bt) [1 + \Delta_1 + \Delta_2] \quad (4.17)$$

A rough estimate of the goodness of fit of the various model functions,  $S_0$ ,  $S_1$  and  $S_2$  can be made by computing their mean deviations from the true emissions function:

$$\delta_k = \frac{1}{N+1} \sum_{i=0}^N |S(t_i) - S_k(t_i)| \quad (4.18)$$

where  $k = 0, 1$  or  $2$ . The results are:  $\delta_0 = 0.12$ ,  $\delta_1 = 0.04$  and  $\delta_2 = 0.012$ . Thus, a simple exponential model deviates from the true source function by about 12% on the average. This deviation is considerably reduced by including the cycles  $\Delta_1$  and  $\Delta_2$ .

The numerical values of  $\alpha$ ,  $\omega$ ,  $\phi$ ,  $\tilde{\alpha}_*$ ,  $\omega_*$ ,  $\phi_*$ ,  $a$  and  $b$  are 0.22, 0.94 radians/yr, 1.91 radians, 0.12, 1.57 rad/yr, 4.3 rad, 121 pptv and 0.153/yr respectively. The  $\Delta_2$ -cycle has a relatively small effect on predicted global burdens and changes of  $R_0$ . It will not be considered further, although it is included in the numerical results reported here.

The global mass balance equation using (4.17) for the source function can be solved explicitly. For the case of a globally averaged theory the mass balance equation and the solution using eqn. (4.17) (with  $\Delta_2 \rightarrow 0$ ) are:

$$\frac{d\xi}{dt} = s - \eta\xi \quad (4.19)$$

$$\xi = \xi_0 e^{-\eta t} + [a/(b+\eta)] [\exp(bt) - \exp(-\eta t)] + [\omega\alpha a]/[\omega^2 + (b+\eta)^2] \cdot \{\exp(bt)f(\phi+\omega t) - \exp(-\eta t)f(\phi)\} \quad (4.20)$$

$$f(x) = \sin x + [(b+\eta)/\omega] \cos x \quad (4.21)$$

Figure IV.5 shows the results of the calculations. Clearly, if the cycles in the emissions are not included, the predicted increase in the global burden ( $\sim 15\%$  per yr) is higher than estimates of global burdens based on the observations (Table III.2). Inclusion of the  $\Delta_1$  and  $\Delta_2$  cycles yields the average predicted increase in global burdens of 12.5% per yr, which is very close to the observed increase. It should be noted that even though emissions increased exponentially at about 15-16% per year over a 16-year period, the atmospheric burden rose by only 12% per year over the 5 years of measurements. This difference between the rate of increase in emissions and the rate of increase of the global burden can be explained by the cyclic fluctuations of the source function given by  $\Delta_1$  and  $\Delta_2$ .

Can these fluctuations (eqn. 4.17) of the emissions also explain the changes in  $R_0$  (ratio of northern to southern hemisphere concentrations)? Calculations show that the ups and downs of the emissions occurred at just the right times to predict the ups and downs of the observed values of  $R_0$ . Furthermore, the magnitude of the fluctuations of  $R_0$  from its mean value is in quantitative agreement with the predicted values.

The theory described by eqns. (4.1) and (4.2) with  $S_n(t) = a \exp(bt)[1 + \Delta_1 + \Delta_2]$  predicted  $R_0$  is in agreement with observations. Here we report the results of a four-box theory, where each hemisphere is subdivided into two pieces of approximately equal atmospheric masses. In general the equation predicting  $R_0$  is (after many years of emissions):

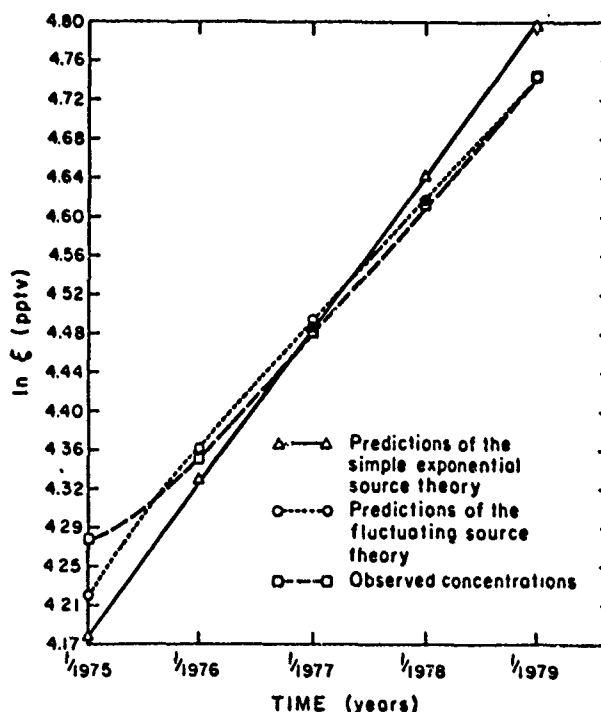


FIGURE IV.5. A comparison of observed concentrations of  $\text{CH}_3\text{CCl}_3$  with two theories.

$$R_o \approx \bar{R}_o \left[ \frac{1 + a_o \sin(\omega t + \phi) + a_1 \cos(\omega t + \phi)}{1 + b_o \sin(\omega t + \phi) + b_1 \cos(\omega t + \phi)} \right] \quad (4.22)$$

where only the  $\Delta_1$  cycle has been included. Theories with different numbers of boxes predict different values for  $\bar{R}_o$ ,  $a_o$ ,  $a_1$ ,  $b_o$ , and  $b_1$ . When the fluctuations of the source function are ignored,  $R = \bar{R}$  (a constant in time). The mass balance equations are:

$$\frac{d\xi}{dt} = \underline{S}(t) - M \underline{\xi}(t) \quad (4.23)$$

$$M = \begin{bmatrix} (\eta + \eta_T + \eta_o) & -\eta_T & -\eta_o & 0 \\ -\eta_T & (\eta + \eta_T + \eta_o) & 0 & -\eta_o \\ -\eta_o & 0 & (\eta + \eta_o) & 0 \\ 0 & -\eta_o & 0 & (\eta + \eta_o) \end{bmatrix} \quad (4.24)$$

$$\underline{\xi} = P^{-1} \exp(-\Lambda t) \int_0^t \exp(\Lambda t') P \underline{S}(t') dt' \quad (4.25)$$

$$R_o = \xi_3 / \xi_4 \quad (4.26)$$

Eqn. (4.26) is of the form (4.22) where  $R_o$ ,  $a_o$ ,  $a_1$ ,  $b_o$  and  $b_1$  are complicated functions of  $\eta$ ,  $\eta_T$ ,  $\eta$ ,  $\omega$ ,  $\phi$  and  $b$ . The exact equations will not be reproduced here, but the results are shown in Figure IV.7. These calculations included the  $\Delta_2$ -cycle as well. The two curves in Figure IV.7 reflect slightly different choices of transport times within each hemisphere. In this figure  $\eta = 0.12/\text{yr}$ ,  $\bar{\eta} = 0.08/\text{yr}$ ,  $\eta_o = 5/\text{yr}$  (curve 1),  $\eta_o = 4/\text{yr}$  (curve 2),  $\eta_T = 1.14/\text{yr}$ , 80% of the sources are in the northernmost box (3) and the rest in boxes 1 and 2. These  $\eta$ 's may be converted to the more familiar  $\tau$ 's by  $\eta = 1/\tau$ . For example,  $\eta_o = 5/\text{yr}$  means that  $\tau_o = 2.4$  months, implying relatively fast transport within the hemisphere. The rise and fall of  $R_o$  (as well as atmospheric burdens) are out of phase with the rises and falls of the emissions function, reflecting the delay caused by transport.

Summary: We chose a set of observational data on  $\text{CH}_3\text{CCl}_3$  concentrations spanning the last five years. These data are most consistent with an average lifetime of  $\text{CH}_3\text{CCl}_3$  of 8-9 years, but lifetimes as low as 6 years and as high as 10 years are not excluded. The description of  $\text{CH}_3\text{CCl}_3$  global emissions requires the inclusion of cyclic terms. This complex behaviour of the year to year changes in total emissions explains two salient features in our observational data, namely the rate of increase of the

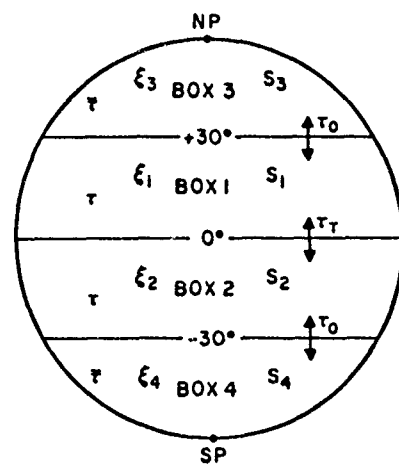


FIGURE IV.6. A picture of the four-box theory.

global atmospheric burden of  $\text{CH}_3\text{CCl}_3$  and the changes in the ratio of northern hemisphere to southern hemisphere concentrations. The emissions estimates and observational data are therefore in close agreement. (See also Khalil & Rasmussen, 1980.)

Using the results on lifetimes we have estimated that in 20 years  $\text{CH}_3\text{CCl}_3$  tropospheric concentrations could rise to high levels, depending on the emissions patterns. If emissions don't increase above the 1978 levels,  $\xi_n$  and  $\xi_s$  could reach 215 and 180 pptv respectively in 20 years. If emissions rise at an annual exponential rate of 8% per year,  $\xi_n$  and  $\xi_s$  would reach 685 and 530 pptv in 20 years. (Recall that over the past 16 years the average increase in emissions has been about 16% per year.) Finally, if emissions keep increasing until they reach twice the current (1978) yearly emissions -- and then stay at that level, the eventual tropospheric concentrations will be ~450 and 380 pptv in the northern and southern hemispheres respectively. It appears that substantially higher tropospheric concentrations can be expected in the future. These higher expected tropospheric concentrations may be used to estimate the magnitude of ozone depletion which  $\text{CH}_3\text{CCl}_3$  is capable of causing in the future.

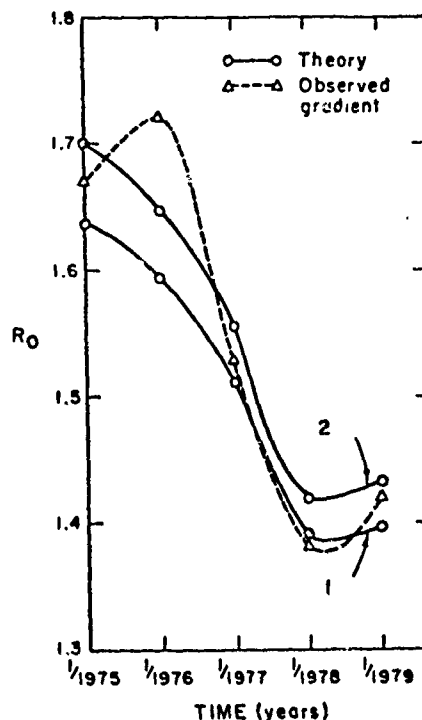


FIGURE IV.7. The observed methylchloroform gradient and the four-box theory with the  $\Delta_1$  and  $\Delta_2$  cycles.

(b)  $\text{CHClF}$  (F-22) and  $\text{CHCl}_2\text{F}$  (F-21): There are several reasons for studying F-21 and F-22 in the atmosphere, even though these compounds are present in very low concentrations. Laboratory studies of Ausloos et al. [1977] indicated that F-11 may be transformed to F-21 in the presence of sand and u.v. light. A similar transformation may also be possible for F-12 to F-22. In the environment, these processes may occur in dust storms, on deserts, or on other surfaces. If these transformations are significant on the global scale, they would provide a tropospheric sink for F-11 and F-12, thus reducing their potential for destroying stratospheric ozone or accumulating in the atmosphere to the levels currently expected. There are two other reasons why atmospheric studies of F-22 are important. F-22 is an anthropogenic emission being a refrigerant which has been produced in increasing quantities since the early 1950's. It has a relatively long lifetime, probably around 20 years. Therefore, it could play a role in the destruction of the ozone layer, similar to F-11 and F-12 -- certainly not at this time, but perhaps in the future if its emissions increase considerably [see the NAS 1979 report]. The atmospheric burden of  $\text{CH}_3\text{CCl}_3$  has been used to calculate global hydroxyl radical (HO) abundances [Lovelock, 1977; Singh, 1977; Neely and Plonka, 1978]. Any similar compound whose source strength (global emission, per unit time) are well known, and whose primary tropospheric sink is reaction with HO radicals, can be used for such calculation (provided also that the compound has an intermediate lifetime and concentrations low enough so as not to disturb the steady state HO concentration). F-22 could have played this role of providing independent estimates of HO abundance. As we will soon discuss, this possibility could not be realized.

Next we discuss our current results obtained in collaboration with Drs. Penkett and Prosser at A.E.R.E. Harwell (UK). GC/MS measurements of F-21 indicate that its atmospheric concentrations are very small -- the average being between 1 and 2 pptv. Even if all of this F-21 is a product of F-11 degradation, the conclusion is that such a transformation is not a significant tropospheric sink of F-11 [Penkett et al., 1980]. In arriving at this conclusion the average atmospheric lifetime of F-21 was taken to be 2-3 years.

Current measurements of F-22 revealed a completely different picture. The global average tropospheric concentration was calculated from the observational data between latitudes --  $-90^\circ$  to  $+50^\circ$ , and turned out to be about 47 pptv. We matched this number with the concen-

tration expected from anthropogenic release [McCarthy et al., 1977; Alexander Grant & Co., 1979]. Even if the lifetime of F-22 is infinite, so that all the F-22 ever released is still in the atmosphere, the average concentrations at the time of measurement should have been about 35 pptv. This leads to two broad alternatives for explaining the difference. First, it is possible that the observations and calculations of the atmospheric burden are inaccurate. Second, it is possible that there are other sources of F-22. In this case, the sources could be natural emissions, transformation of F-12 to F-22, indirect industrial emissions (not related to the production and use of F-22), or due to underestimates of direct anthropogenic emissions. Although either alternative poses fascinating challenges, it is not possible to independently calculate H<sub>0</sub> abundances from the current F-22 observations.

Next we will amplify the alternatives for explaining the observed F-22 concentrations as discussed above. If the high global average we have calculated is due to inaccuracies in the measurements and the model used to obtain a global average, then no resolution of the apparent excess of the F-22 global burden is possible without further experimental work. Additional measurements, some with GC/EC techniques (see Figure III.) are underway and work on determining absolute accuracy is also continuing. It may well be that there are other sources which contribute F-22 to the atmosphere. The ones we have mentioned are reasonable possibilities. Stoiber et al [1971] reported observing both F-21 and F-22 in volcanic emissions [see also Graedel, 1978] -- such a natural source is possible. Rasmussen [1979 unpublished data] observed enhanced F-21 and F-22 in plumes of aluminum manufacturing plants. If either or both these processes contribute to the global burden, they should be emitting about 12 - 20 billion grams per year to account for the excess. (Contrast this with direct anthropogenic emissions of F-22 in 1977 which are estimated to have been about 58 billion grams, NAS [1979]). In case the excess is due entirely to the transformation of F-12, the global lifetime of F-12 due to this process alone would have to be 80-130 years. Thus, a slow, probably currently undetectable, conversion of F-12 is sufficient. The reasons why such a small conversion of F-12 suffices to explain the excess are that F-12 has been emitted in very large quantities, and the F-22 formed lingers in the atmosphere because of its relatively long lifetime. Finally, there is margin for error in the release estimates. Unlike F-11 and F-12, the ratio of total F-22 released to F-22 produced is small (R/P, F-22 ~ 41%; R/P, F-11 and F-12 ~ 85%; McCarthy et al., [1977]). Certainly, more than enough F-22 has been produced to account for the excess. Further discussion of F-22 is included in the paper of Rasmussen et al. [1980].

The reader should be aware that the results on F-22 are preliminary and that we don't yet have an adequate grasp of its sources, sinks, and lifetimes. On the other hand, continuing studies of F-22 in the atmosphere offer promise of a deeper understanding of atmospheric chemistry.

(c) CFC1<sub>3</sub> (F-11) and CCl<sub>2</sub>F<sub>2</sub> (F-12); The time series data given in Table III.2 was analyzed by the techniques discussed earlier for CH<sub>3</sub>CCl<sub>3</sub> (eqns. (4.1) and (4.2)). It was assumed that emissions have not increased since 1975 and that  $\tau_n = \tau_s$  (the lifetimes in the two hemispheres are the same).

In the analysis of F-11 and F-12 by this method there appears to be little justification in trying to deduce the absolute lifetime. Again, this is because both are long-lived, and it is not possible to decide between the bunched up theoretically predicted lines for all lifetimes > ~30 years. Figure IV.8 shows the results of the calculations. The dashed lines represent the mean northern and southern hemisphere mixing ratios of F-11. The lower cross-hatched regions represent the expected concentrations if the lifetime was 10 years. The upper cross-hatched region represents the expected concentrations if the lifetime was 20 years. The lower limits of each region are for the best estimate of the emissions currently available. The upper limits of each region are the expected concentrations if the true source was in reality 20% higher than the initial estimate. It is apparent that even if there were sizeable errors in the source strength, a lifetime of less than or equal to 20 years it not consistent with the measured concentrations. When eqns. (4.3) and (4.4) were applied to the data, it turned out that  $\tau_{F-11} \sim 50$  years and  $\tau_{F-12} \sim 70$  years.

There are other techniques also available for the analysis of the lifetimes of F-11 and F-12. These generally require a more detailed data base than is available for analysis in this section. It is anticipated that the Atmospheric Lifetime Experiment (ALE) will make significant progress towards determining the lifetimes of F-11 and F-12 [Cunnold et al., 1978].

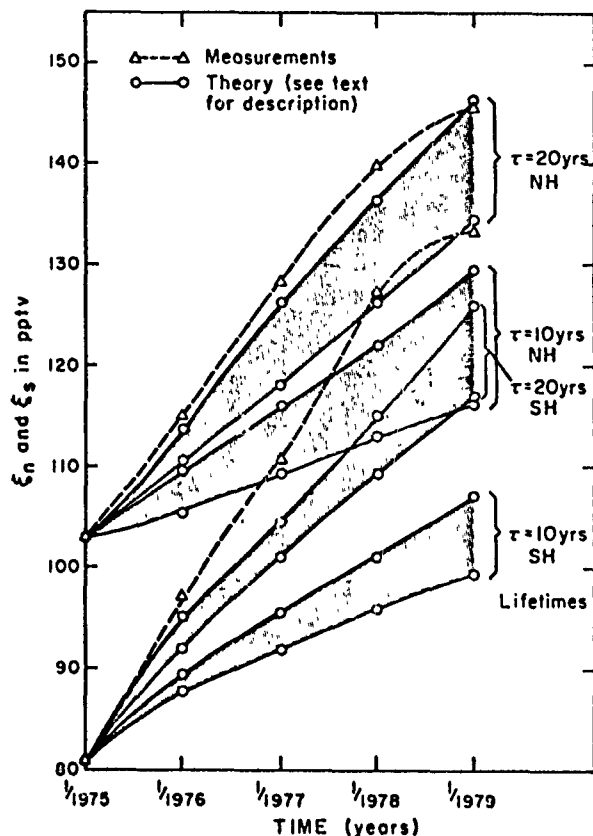


FIGURE IV.8. Comparison of measurements and theory for F-11.

V. SUMMARY AND CONCLUSIONS: Global atmospheric trace gas measurements have been made by Rasmussen and his research group, for nearly a decade now. In this paper some results of the recent measurements program have been reported. One set of data on  $\text{CH}_3\text{CCl}_3$ ,  $\text{CCl}_4$ ,  $\text{CFC}_1_3$  (F-11) and  $\text{CF}_2\text{Cl}_2$  (F-12) from early 1975 to 1979 is included

In planning the measurements, considerable effort has been directed towards keeping the precision and accuracy within the limits required to establish lifetimes, and understand the salient sources and sinks. Absolute accuracy and a sufficient number of globally distributed measurements are important in establishing global burdens, which can, in turn, be used in standard budget analyses. The longer the lifetime of a trace gas is, the more susceptible to error the lifetime calculation is due to inaccuracies in the global burden. For example, in the case of F-11, if the estimated burden is too high by 10%, the calculated lifetime will be about 60% higher than the true lifetime. To avoid some of these difficulties, computed lifetimes may be based on a trend analysis. In this case apart from global coverage, which is always needed, very precise measurements are necessary. The stringent demands on precision and accuracy require continued periodic interlaboratory comparisons with all the research groups involved in the atmospheric measurements of the trace gases with long or intermediate lifetimes. Lumping data, from different observers, without careful consideration of accuracy or systematic biases between laboratories, can wash out important real features of the atmospheric behaviour of a trace gas. The larger data base obtained this way often gives only an illusion of greater reliability.

In this paper we isolated a self-consistent set of data on  $\text{CH}_3\text{CCl}_3$  and analyzed it to quantitatively study the sources and sinks of  $\text{CH}_3\text{CCl}_3$ . Based on the analysis in Section IV an atmospheric lifetime of 8-9 years appears to be most consistent with observation, though the calculation is subject to errors in absolute accuracy. A 12% per year observed global growth rate (since 1975) in concentrations and fluctuations of the ratio of northern to southern hemisphere concentrations are also consistent with the emissions history of  $\text{CH}_3\text{CCl}_3$ . Analysis of recent data on F-21 and F-22 indicates that even if their presence in the atmosphere is partly due to transformations of F-11 and F-12 respectively, such transformations are not



a significant tropospheric sink of F-11 and F-12. Currently, data support this conclusion more strongly for F-11 and for F-12.

In the last couple of years, a very large number of atmospheric measurements have been made, both at our laboratory and by other groups. We expect that many current issues will be resolved when these data become available for general use in the next year or two.

**Acknowledgements:** This work was supported in part by the following grants: Department of Transportation High Altitude Pollution Program, Contract #79WA-4285; National Science Foundation Grants #ATM78 09711, DPP77-23468; National Aeronautical and Space Administration NSG #7457; and the Chemical Manufacturers Association; and PPG Industries.

# REFERENCES:

- Alexander Grant & Co., 1978 World Production and Sales of Fluorocarbons FC-11, FC-12 and FC-22, Reports to the Manufacturing Chemists Association, 1979.
- Rasmussen, P., R.E. Rebbert, L.C. Glasgow, Photodecomposition of Chloromethanes Adsorbed on Silica Surfaces, J. Res. NBS, **82**, 1, 1977.
- Chang, J. S., and J. E. Penner, Analysis of Global Budgets of Halocarbons, Atmospheric Environment, **12**, 1867-1873, 1978.
- Crutzen, P. J., I. S. A. Isaksen, and J. R. McAfee, The Impact of the Chlorocarbon Industry on the Ozone Layer, J. Geophys. Res., **83**, 345-363, 1978.
- Crutzen, P. J., The Influence of Nitrogen Oxides on the Atmospheric Ozone Content, Quart. J. Roy. Met. Soc., **96**, 320, 1970.
- Crutzen, P. J., Estimates of Possible Variations in Total Ozone Due to Natural Causes and Human Activities, Ambio, **3**, 301-310, 1974.
- Cunnold, D., F. Alyea, and R. Prinn, A Methodology for Determining the Atmospheric Lifetimes of Fluorocarbons, J. Geophys. Res., **83**, 5493-5500, 1978.
- Fink, H. J., and O. Klaes, Global Distribution of Fluorocarbons, Ber. Bunsenges Phys. Chem., **82**, 1147-1150, 1978.
- Fraser, P. J., Baseline Atmospheric Halocarbon Measurements: An Interlaboratory Calibration Comparison, CSIRO preprint, 1979.
- Graedel, T. E., Chemical Compounds in the Atmosphere (Academic Press, N. Y., 1978).
- Johnston, H. S., Reduction of Stratospheric Ozone by Nitrogen Oxide Catalysts from Supersonic Transport Exhaust, Science **173**, 517, 1971.
- Khalil, M. A. K., Topics in the Behaviour of Atmospheric Trace Gases (Doctoral Dissertation, Oregon Graduate Center, Beaverton, Oregon, 1979).
- Khalil, M. A. K., and R. A. Rasmussen, Methylchloroform ( $\text{CH}_3\text{CCl}_3$ ): Accumulation in the Earth's Atmosphere, submitted to Science, 1980.
- Lovelock, J. E., Atmospheric Fluorine Compounds as Indicators of Air Movements, Nature, **230**, 379, 1971.
- Lovelock, J. E., Methyl Chloroform in the Troposphere as an Indicator of OH Radical Abundance, Nature, **267**, 32, 1977.
- Makide, Y., and F. S. Rowland, Tropospheric Concentrations of Methylchloroform,  $\text{CH}_3\text{CCl}_3$ , in January 1978, and Estimates of Its Atmospheric Residence Time. Paper presented before the Division of Environmental Chemistry, American Chemical Society, Honolulu, Hawaii, April 1-6, 1979.
- McCarthy, R. L., F. A. Bower, and J. P. Jesson, The Fluorocarbon-Ozone Theory-I: Production and Release - World Production and Release of  $\text{CCl}_3\text{F}$  and  $\text{CCl}_2\text{F}_2$  (Fluorocarbons 11 and 12) Through 1975, Atmospheric Environment, **11**, 491-497, 1977.
- McElroy, M. B., and J. C. McConnell, Nitrous Oxide: A Natural Source of Stratospheric NO, J. Atmos. Sci., **28**, 1095, 1971.
- McElroy, M. B., Chemical Processes in the Solar System: A Kinetic Perspective, in MTP International Review of Science (ed. D. Herschbach, Butterworths, London, 1976).
- Meakin, P., P. S. Gumerman, L. C. Glasgow, and J. P. Jesson, The Fluorocarbon-Ozone Theory - III. Atmospheric Environment, **12**, 1271-1285, 1978.
- Molina, M. J., and F. S. Rowland, Stratospheric Sink for Chlorofluoromethanes: Chlorine Atom-Catalysed Destruction of Ozone, Nature, **249**, 810-812, 1974.
- NAS, Stratospheric Ozone Depletion by Halocarbons: Chemistry and Transport (National Academy of Sciences, Washington, D. C., 1979).
- Neely, W. B., and J. H. Plonka, Estimation of Time Averaged Hydroxyl Radical Concentration in the Troposphere, Env. Sci. & Tech., **12**, 317-321, 1978.

- Neely, W. B., and H. Farber, 1977 and 1978 emissions estimates for methylchloroform, personal communication, 1979.
- Newell, R. E., D. G. Vincent, and J. W. Kidson, Interhemispheric Mass Exchange from Meteorological and Trace Substance Observations, Tellus, 21, 641-647, 1969.
- Penkett, S. A., N. J. D. Prosser, R. A. Rasmussen, and M. A. K. Khalil, Measurements of  $\text{CHFC}_2$  (Freon 21) in Background Tropospheric Air, submitted to Nature, 1980.
- Rasmussen, R. A., A Quantitative Cryogenic Sampler - Design and Operation, American Laboratory 4, 19-27, 1972.
- Rasmussen, R. A., D. Pierotti, and J. Krasner, Analysis of Halocarbons in the Atmosphere: Report of a Workshop. Presented at the 69th Annual Meeting of the Air Pollution Control Association, Paper No. 76-15.1, 1976.
- Rasmussen, R. A., J. Krasner, and D. Pierotti,  $\text{N}_2\text{O}$  Analysis in the Atmosphere via Electron Capture-Gas Chromatography, Geophys. Res. Lett., 3, 615-618, 1976.
- Rasmussen, R. A., Interlaboratory Comparisons of Fluorocarbon Measurements, Atmospheric Environment, 12, 2505-2508, 1978.
- Rasmussen, R. A., and D. Pierotti, Interlaboratory Calibration of Atmospheric Nitrous Oxide Measurements, Geophys. Res. Lett., 5, 353-355, 1978.
- Rasmussen, R. A., S. A. Penkett, and N. Prosser, Measurement of Carbon Tetrafluoride in the Atmosphere, Nature, 227, 549-551, 1979.
- Rasmussen, R. A., L. E. Rasmussen, M. A. K. Khalil, and R. W. Dalluge, Concentration Distribution of Methyl Chloride ( $\text{CH}_3\text{Cl}$ ) in the Atmosphere. Submitted to J. Geophys. Res., 1980.
- Rasmussen, R. A., M. A. K. Khalil, S. A. Penkett, and N. J. D. Prosser,  $\text{CHClF}_2$  (F-22) in the Earth's Atmosphere. Submitted to Geophys. Res. Lett., 1980.
- Singh, H. B., Atmospheric Halocarbons: Evidence in Favor of Reduced Hydroxyl Radical Concentrations in the Troposphere, Geophys. Res. Lett., 4, 1977.
- Singh, H. B., L. J. Salas, H. Shigeishi, and E. Scribner, Atmospheric Halocarbons, Hydrocarbons and Sulfur Hexafluoride: Global Distributions, Sources and Sinks, Science, 203, 899-903, 1979.
- Stoiber, R. E., D. C. Leggett, T. F. Jenkins, R. P. Murrmann, and W. I. Rose, Organic Compounds in Volcanic Gas from Santiaguito Volcano, Guatemala, Geol. Soc. Amer. Bull., 82, 2299-2302, 1971.

# FREE RADICALS IN THE EARTH'S STRATOSPHERE:

## A REVIEW OF RECENT RESULTS

J. G. Anderson  
Center for Earth and Planetary Physics  
and  
Department of Chemistry  
Harvard University

### ABSTRACT

Recent observations of four free radical systems are reviewed:  $O_x$ ,  $HO_x$ ,  $ClO_x$  and  $NO_x$ . Although significant variability is observed among the six available atomic oxygen observations, the mean of the observations agrees well with the calculated distribution. The  $[O(^3P)]/[O_3]$  ratio determined from a simultaneous in situ observation is found to match the steady state ratio within the uncertainty of the experiment. Perhydroxyl, observed on three occasions, is found to exceed the calculated distribution by a factor of two in the middle stratosphere but observed variability requires an extended data base to establish or refute the discrepancy in the mean. Hydroxyl observations in the stratosphere are compared with mesospheric observations and with ground based total column absorption measurements. Agreement among the observational techniques and with calculations of this pivotal radical are encouraging. Observations of  $ClO$  show an emerging trend which defines an envelope within which a significant majority of the  $ClO$  observations fall which exhibits a decrease with altitude markedly greater than that predicted by current models. In addition several clear departures from the "envelope" are noted. Measurements of  $NO$ , both in situ and remote, are briefly discussed. Finally, three simultaneous observations of  $O(^3P)$ ,  $O_3$ ,  $HO_2$ ,  $NO$ , and  $ClO$  are used to appraise the rate of odd oxygen destruction throughout the middle and upper stratosphere.

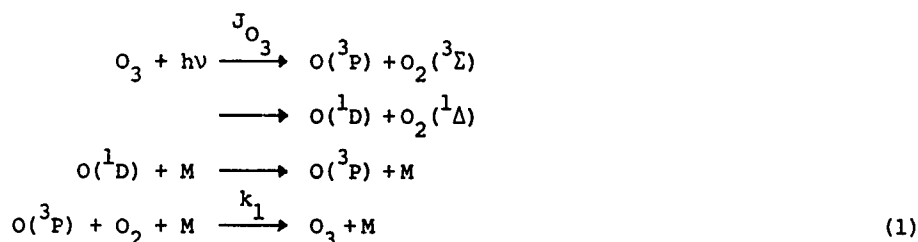
### I. INTRODUCTION

The sections which follow review briefly the contents of four papers which discuss recent results of in situ measurements of  $O(^3P)$ ,  $O_3$ ,  $OH$ ,  $HO_2$ ,  $ClO$  and  $NO$  in the earth's stratosphere. Observations of  $O(^3P)$  and or a simultaneous  $O(^3P)$ - $O_3$  measurement [see Anderson et al. 1980a for details] are discussed in Section II.A. The  $HO_x$  radicals [see Anderson et al. 1980b] are reviewed in II.B and  $ClO_x$  [Anderson et al. 1980c] observations are discussed in II.C. A review of  $NO$  observations and a review of the odd oxygen destruction rate based on simultaneously observed  $O(^3P)$ ,  $O_3$ ,  $HO_2$ ,  $ClO$  and  $NO$  [Anderson et al. 1980d] are treated in II.D and II.F, respectively.

### II. A REVIEW OF RECENT RESULTS

**II.A. ATOMIC OXYGEN AND OZONE:** Atomic oxygen is of particular interest to the photochemistry of stratospheric ozone because, first, it is believed to be in strict photochemical steady state with ozone through the rapid exchange reactions

ANDERSON



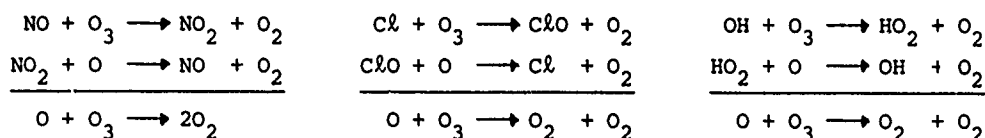
such that the ratio

$$[\text{O}(^3\text{P})]/[\text{O}_3] = \frac{J_{\text{O}_3}}{k_1 [\text{M}] [\text{O}_2]}$$

should be obeyed throughout the stratosphere. Second, atomic oxygen is the reactive partner with ozone in the direct recombination step



which establishes the rate of odd oxygen destruction apart from any free radical catalyzed recombination and third, atomic oxygen is the odd oxygen reactant in the slowest (i.e., rate determining) reaction in the major catalytic cycles



and thus knowledge of its concentration within any volume element is essential in the determination of the rate of destruction of  $\text{O}_x = \text{O}(^3\text{P}) + \text{O}_3$  within that volume.

There are six observations of  $\text{O}(^3\text{P})$  in the stratosphere, all obtained using balloon borne, parachute descent, in situ atomic resonance fluorescence, the results of which are shown in figure 1. Experimental accuracy is  $\pm 30$  percent and experimental precision  $\pm 10$  percent for each measurement.

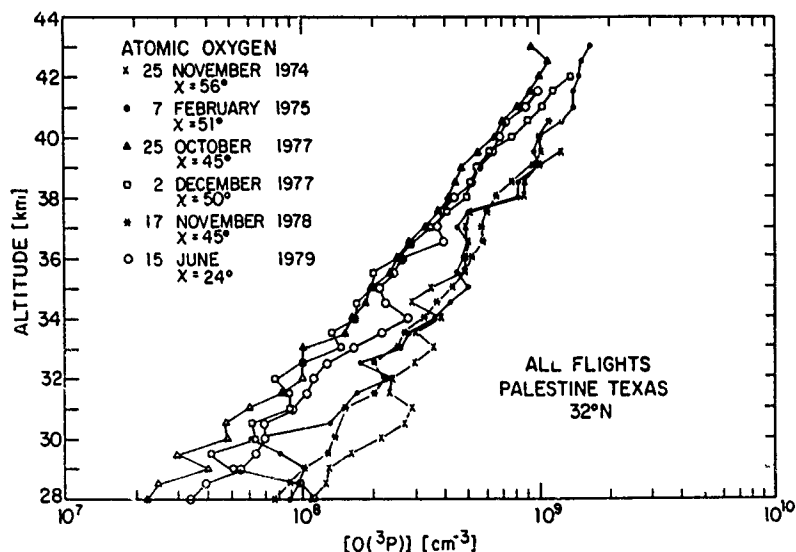


Figure 1. Observed concentration of  $\text{O}(^3\text{P})$  between 28 and 43 km in the stratosphere. All data determined in situ using atomic resonance fluorescence.

Several points are readily apparent from the figure. First, there is both local structure within and absolute displacement among observed distributions which exceed respectively the precision and accuracy of the measurements. It should also be noted that the local structure does not consistently appear. For example, the profiles observed on 25 October 1977 and 2 December 1977 display a small degree of local structure, typically less than  $\pm 20$  percent variation over an interval of  $\pm 1$  km above  $\sim 34$  km. Below that altitude significantly greater local structure is apparent, though seldom more than  $\pm 50\%$ . On the other hand, the remaining four observations exhibit at least one example of major (factor of two) variation over a  $\pm 2$  km interval with an increasing structural development below the 33-35 km interval. Although this local structure makes a detailed profile-by-profile comparison with modeled distributions difficult, a comparison between the mean of the observed  $O(^3P)$  distribution and the calculated atomic oxygen distribution [Logan et al., 1979] is illustrative and is shown in figure 2.

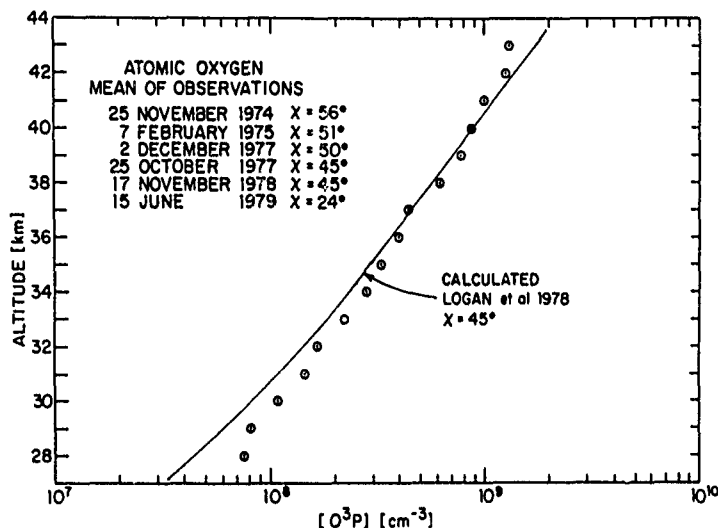


Figure 2. Comparison between the mean of the in situ  $[O(^3P)]$  observations and the calculated distribution of Logan et al. (1979).

The difference between the observed and predicted distribution is within the experimental uncertainty between 30 and 43 km, below which the observed concentration is measurably greater than the calculated amount.

A modified Dasibi instrument [see Robbins and Carnes, 1978] was used to observe ozone simultaneously with  $O(^3P)$  in an experiment in which both instruments were mounted  $\sim 1$  meter apart on the descent platform. The results of that observation, which encompass the altitude interval 28-42 km, are shown in figure 3. Observations were made with a solar zenith angle of  $50^\circ$  at Palestine, Texas  $32^\circ N$  latitude on 2 December 1977.

The atomic oxygen-ozone ratio was determined from those observations for each 0.5 km interval and the results are compared in figure 4 with the calculated ratio from the diurnal model of Logan et al., 1978, for a solar zenith angle of  $50^\circ$ . The accuracy of the  $[O(^3P)]$  and  $[O_3]$  observations are  $\pm 25\%$ .

An inspection of figure 4 indicates that with the exception of the two lowest points at 28 km, the calculated and observed ratio lies well within the experimental uncertainty. Although obviously a single observation cannot be offered as proof, the measurement strongly suggests that O and  $O_3$  are in photochemical steady state and that the photodissociation of  $O_3$  and the three body recombination, reaction (1), dominate the exchange between the major odd

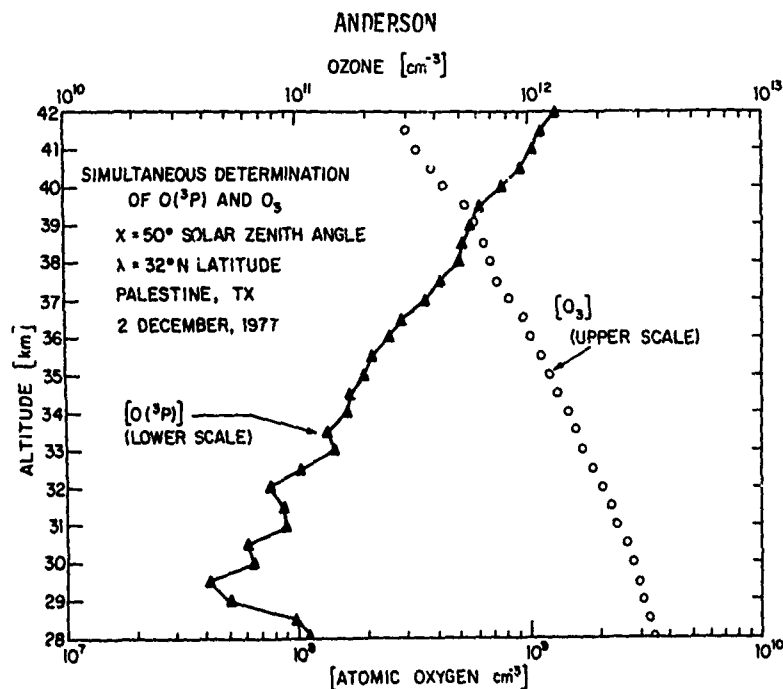


Figure 3. Observed concentration of  $O(^3P)$  and  $O_3$  determined simultaneously within the same volume element of the stratosphere.

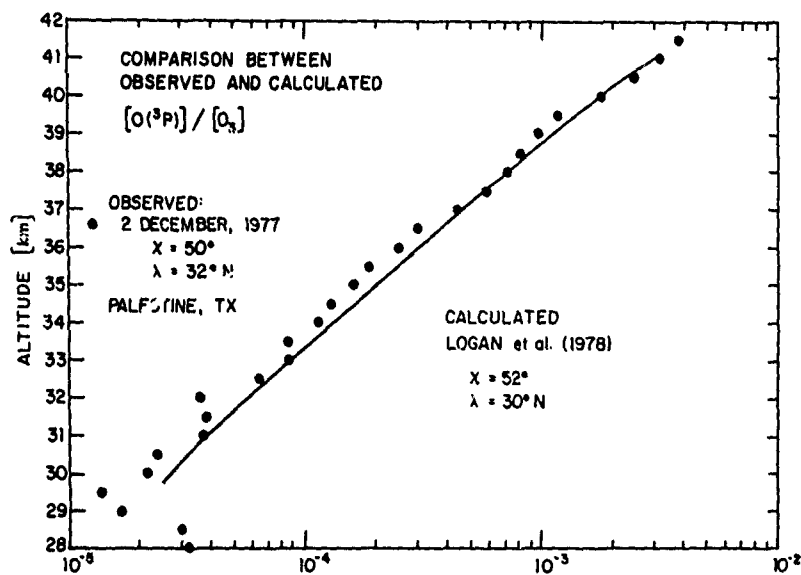


Figure 4. Comparison between observed and calculated ratio of  $[O(^3P)]$  to  $[O_3]$  from the simultaneous observation of both.

oxygen species. Perhaps of greater importance, however, is the fact that observed in situ ozone concentrations can now be used to determine with considerable confidence the atomic oxygen concentration within a given volume element and likewise observed  $[O(^3P)]$  can be used to establish  $[O_3]$ .

**II.B. THE FREE RADICALS OF HYDROGEN:** Two major oxygen-hydrogen free radicals, OH and HO<sub>2</sub>, occupy important but significantly different positions within the current framework of stratospheric photochemistry. Results of recent *in situ* observations of each are discussed in this section, beginning with the perhydroxyl radical.

### 1. HO<sub>2</sub>

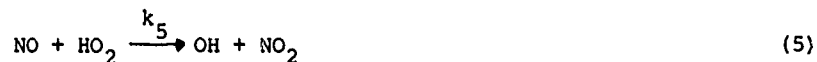
During the past three years the perhydroxyl radical, first introduced into the photochemistry of planetary atmospheres by Bates and Nicholet (1950), has assumed a prominent position among the major free radicals which govern chemical transformations in the troposphere and stratosphere of the Earth. A major factor contributing to this renewed interest is that the kinetic behavior of HO<sub>2</sub> with a number of aeronomically interesting reactants has been accurately defined for the first time [see for example, Howard and Evenson, 1977; Zahniser and Howard, 1978]. Based upon the interpretation of these laboratory results [see for example Crutzen and Howard, 1978, Turco et al., 1978; Whitten et al., 1978; Luther and Duewer, 1978; Rundel et al., 1978; Wofsy, 1978; Logan et al., 1978; Johnston and Podolske, 1978] it is now believed that the HO<sub>2</sub> radical limits the rate of closure of the homogeneous gas phase catalysis cycles



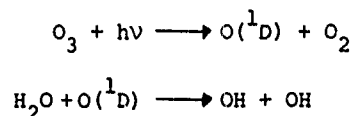
and



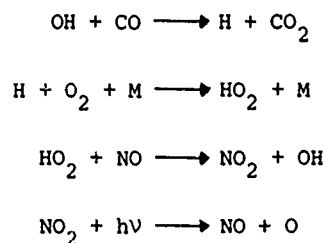
and thus dictates the rate of ozone destruction by  $\text{HO}_x \equiv \text{H} + \text{OH} + \text{HO}_2$  in the stratosphere. In addition, perhydroxyl provides the major link between the NO<sub>x</sub> and HO<sub>x</sub> radicals through the reaction



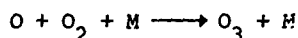
which in turn controls the ratio of HO<sub>2</sub> to OH in the lower stratosphere. In the troposphere, the HO<sub>2</sub> concentration controls the proportion of free radicals, produced by the reaction pair



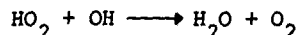
which lead to the reformation of ozone through the reaction sequence



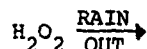
# ANDERSON



In addition HO<sub>2</sub> limits the rate of HO<sub>x</sub> recombination via



in the stratosphere and by



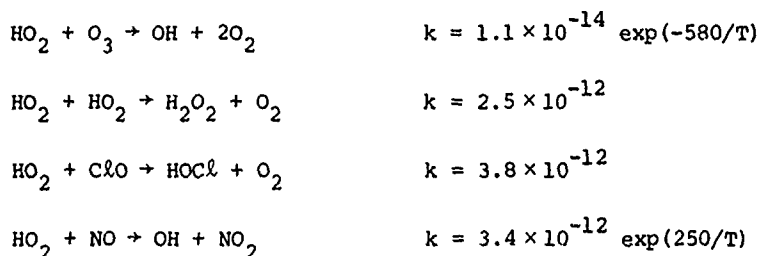
in the troposphere.

Although perhydroxyl is believed to directly control the rate of odd oxygen ( $O_x = O(^3P) + O(^1D) + O_3$ ) destruction only in the lower stratosphere, the importance of HO<sub>2</sub> for predicting changes in the integrated ozone column density resulting from the injection of NO<sub>x</sub> into the lower stratosphere was clearly revealed when a major revision in the reaction rate constant,  $k_5$ , by Howard and Evenson (1977) altered significantly the predicted response of the column integrated ozone concentration to a limited fleet of low altitude (18 km) SST's. The major cause for this dramatic response was that HO<sub>2</sub> controls the rate of odd oxygen recombination in a region (15-22 km) which contains a significant fraction of total stratospheric ozone and any process which alters the calculated ratio of HO<sub>2</sub> to OH in favor of the latter will decrease the rate of O<sub>x</sub> recombination. There are of course other processes linking the HO<sub>x</sub>, NO<sub>x</sub>, ClO<sub>x</sub>, and O<sub>x</sub> radicals which alter this interpretation at other altitudes but it is clear that a thorough understanding of the distribution and chemical behavior of this radical must precede our understanding of the photochemistry of the troposphere and stratosphere.

The results of three midday, in situ observations of HO<sub>2</sub> are discussed which encompass the altitude interval between 27 and 41 km in the Earth's atmosphere. Results are interpreted in terms of recent model calculations and are compared with a recent cryogenic matrix isolation measurement by Mihelcic (1978). For a description of the experimental technique see Anderson et al., 1980b.

**RESULTS AND CONCLUSIONS.** Table 1 presents the location, flight date, solar zenith angle, instrument sensitivity, C<sub>OH</sub>, observed count rate, ΔS<sub>HO<sub>2</sub></sub>, perhydroxyl mixing ratio, [HO<sub>2</sub>]/[N<sub>2</sub> + O<sub>2</sub>], and detection threshold for the three HO<sub>2</sub> experiments performed to date. All observations were made with the same instrument which, in each case, operated as described in Anderson et al., 1980b. All flights were made close to local noon, the progression in solar zenith angle reflects changes in solar declination. Experimental uncertainties are ± 35% and each reported data point represents the mean determined over ± 2 km of the listed median altitude.

A comparison of observed mixing ratios in table 1 indicates that significant variability in the HO<sub>2</sub> mixing ratio was observed. Note however that in the vicinity of 30 km and below, the variability is of marginal statistical significance. Figure 5 displays, as a shaded zone, the range of observed HO<sub>2</sub> mixing ratios listed in table 1 and compares the mean of the three observations with the calculated HO<sub>2</sub> mixing ratio using the model described in Logan et al., (1978) with the most recent reaction rate constants [see the review by DeMore, 1979] for





LAUNCH DATE	SOLAR ZENITH ANGLE	INSTRUMENT SENSITIVITY $C_{OH}$	OBSERVED DATA							
			ALTITUDE (km)	37	35	33	31	29		
9-20-77	41°	$1.9 \times 10^{-6}$ (ct/sec)/3 (mole/cm <sup>3</sup> )	OBSERVED RESONANCE FLUORESCENCE AS $HO_2$	17	9	13	8	2		
			$HO_2$ MIXING RATIO [ $HO_2$ ]/[M]	$7.1 \times 10^{-10}$	$1.84 \times 10^{-10}$	$8.5 \times 10^{-11}$	$<8 \times 10^{-11}$	$<7 \times 10^{-11}$		
			DETECTION THRESHOLD	$1.1 \times 10^{-10}$	$8.2 \times 10^{-11}$	$7.0 \times 10^{-11}$	$7.6 \times 10^{-11}$	$6.4 \times 10^{-11}$		
			ALTITUDE (km)	37	35	33	31	29		
10-25-77	45°	$9.0 \times 10^{-7}$	OBSERVED RESONANCE FLUORESCENCE AS $HO_2$	3	3	9	5	--		
			$HO_2$ MIXING RATIO [ $HO_2$ ]/[M]	$3.6 \times 10^{-10}$	$3.7 \times 10^{-10}$	$6.9 \times 10^{-10}$	$2.1 \times 10^{-10}$	$<1.0 \times 10^{-10}$		
			DETECTION THRESHOLD	$1.6 \times 10^{-10}$	$1.5 \times 10^{-10}$	$1.5 \times 10^{-10}$	$1.0 \times 10^{-10}$	$1.0 \times 10^{-10}$		
			ALTITUDE (km)	37	35	33	31	29		
12-2-77	50°	$2.3 \times 10^{-6}$	OBSERVED RESONANCE FLUORESCENCE AS $HO_2$	33	25	20	22	16		
			$HO_2$ MIXING RATIO [ $HO_2$ ]/[M]	$3.4 \times 10^{-10}$	$2.3 \times 10^{-10}$	$4.2 \times 10^{-10}$	$3.4 \times 10^{-10}$	$1.7 \times 10^{-10}$		
			DETECTION THRESHOLD	$8.1 \times 10^{-11}$	$6.0 \times 10^{-11}$	$4.6 \times 10^{-11}$	$8.8 \times 10^{-11}$	$8.7 \times 10^{-11}$		
			ALTITUDE (km)	37	35	33	31	29		

Table 1. Summary of experimental parameters for the  $HO_2$  observations.

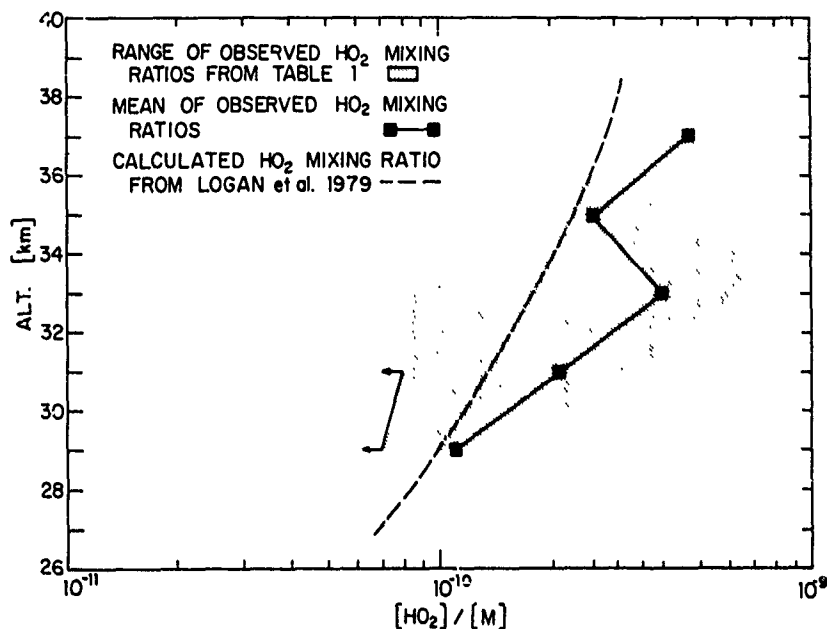


Figure 5. A comparison between the mean of the three  $\text{HO}_2$  observations, tabulated on the previous page, and the recently calculated distribution of  $\text{HO}_2$  by Logan et al. (1979).

A detailed discussion of  $\text{HO}_x$ - $\text{H}_2\text{O}$  photochemistry is at present impossible given the limited number of  $\text{HO}_2$  observations and the observed variability of stratospheric water vapor [Kley et al., 1979]. However, an inspection of figure 5 reveals, first, that the calculated distribution of  $\text{HO}_2$  in the mid-stratosphere falls within a factor of two of the mean of the observed distribution with the latter falling consistently above the former. Second, these data provide for the first time the information necessary to determine the rate of odd oxygen destruction by hydrogen free radicals in the middle and upper stratosphere when taken in combination with *in situ* observations of  $\text{O}(^3\text{P})$ . This determination proceeds as follows: Knowledge of  $k_2$ ,  $k_3$ ,  $k_4$ ,  $[\text{OH}]$ ,  $[\text{O}_3]$ ,  $[\text{O}(^3\text{P})]$ , and  $[\text{HO}_2]$  demonstrates (see the discussion by Johnston and Podolske, 1978) that the reaction pairs (2)-(3), and (2)-(4) are the dominant catalytic cycles in the  $\text{HO}_x$  system and that  $k_3[\text{HO}_2][\text{O}] < k_2[\text{OH}][\text{O}_3]$  and  $k_4[\text{HO}_2][\text{O}_3] < k_2[\text{OH}][\text{O}_3]$  throughout the region encompassed by the  $\text{HO}_2$  observations. Thus the rate at which the  $\text{O}_2$  bond is reformed by hydrogen catalyzed recombination of odd oxygen is  $2k_3[\text{HO}_2][\text{O}] + k_4[\text{HO}_2][\text{O}_3]$ .

Mihelcic et al., (1978) have reported an observation of  $\text{HO}_2$  using EPR detection in a cryogenic matrix isolation experiment. The sample was collected on 8/8/76, 53°N latitude, 31.8 km altitude between 6:40 and 9:00 AM for which they reported an  $\text{HO}_2$  mixing ratio of  $1.0 \times 10^{-10}$  with a factor of three (3) uncertainty. If these results are converted to midday values for comparison with our results, using a diurnal calculation [Logan et al., 1978] to determine the  $\text{HO}_2$  concentration ratio between the appropriate solar zenith angles, one infers a mixing ratio of  $2.2 \times 10^{-10}$  from that observation, in substantial agreement with the mean reported here.

Hydroxyl, while not believed to be a rate controlling free radical in the destruction of odd oxygen in the stratosphere, is nevertheless responsible for the partitioning of chlorine between its free radical forms,  $\text{ClO}_x = \text{Cl} + \text{ClO}$ , and its more stable "reservoir" form  $\text{HCl}$  and for the partitioning of the nitrogen-oxygen compounds  $\text{NO} + \text{NO}_2 + \text{HNO}_3$  between the catalytically active form  $\text{NO} + \text{NO}_2$  and the reservoir  $\text{HNO}_3$  term.

# ANDERSON

Four *in situ* observations of OH have been made in the stratosphere, the results of which are displayed in figure 6 in terms of the volume mixing ratio between 29 and 42 km.

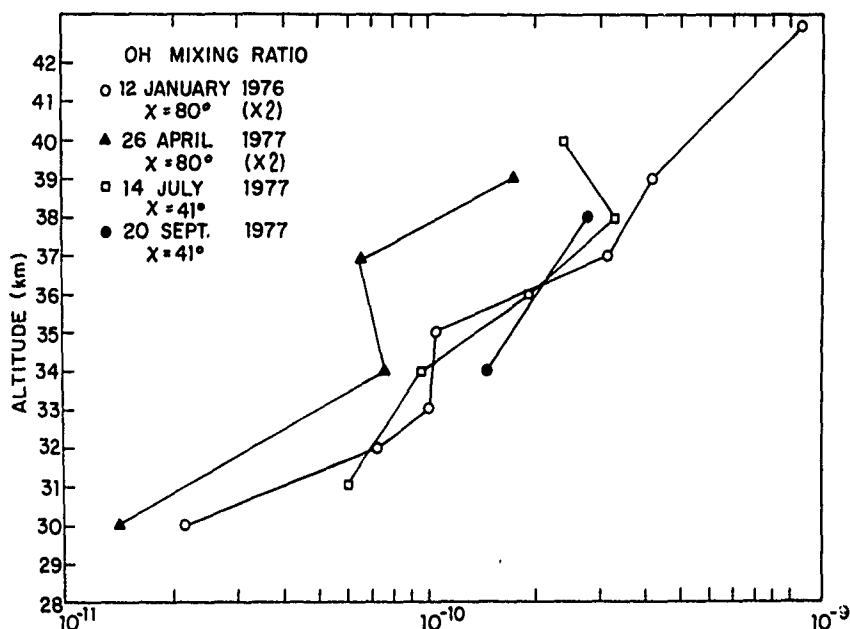


Figure 6. Summary of the available *in situ* observations of OH in the earth's stratosphere taken by balloon-borne molecular resonance fluorescence methods.

The upper altitude limit is established by the peak balloon altitude and the lower altitude limit by a combination of OH[A<sup>2</sup>Σ] collisional quenching by O<sub>2</sub>/N<sub>2</sub> and Rayleigh scatter from the lamp beam [see Anderson et al., 1980b] which reduces the signal to noise ratio to less than 2/1 below 28 km. The extension of those observations to the tropopause is an important gap in our knowledge.

Figure 7 joins the "band" of stratospheric OH observations shown in figure 6 with the mesospheric rocket-borne solar induced fluorescence measurements [Anderson 1971, 1975] and compares those combined results, which encompass the altitude interval for 29 to 70 km, with the range of calculated distributions from 5 models (NASA/GSFC, NOAA, HARVARD, LAWRENCE LIVERMORE, RDA) all of which used the most recent gas phase kinetic rate constants [see DeMore et al., 1979].

Considering the importance OH has for the partitioning of chlorine and nitrogen radicals, this agreement between calculated and observed OH is of major importance. Throughout the stratosphere, the observations bound the calculated distribution although the significant variability, noted in figure 7, is of course not reproduced in a given model calculation. In addition, an important test of the absolute calibration of the *in situ* observations is afforded by comparing the integrated *in situ* observations between 30 and 70 km, which contain the preponderance of atmospheric OH, with the ground based total OH column density determined by Burnett and Burnett (1979), who find an integrated column concentration of OH between  $4 - 9 \times 10^{13} \text{ cm}^{-2}$  for the integrated *in situ* results. That comparison is also indicated in figure 7. Thus both the *in situ* and the total integrated column measurements report a variability in total OH column (corrected to midday steady state conditions) of a factor of 2.

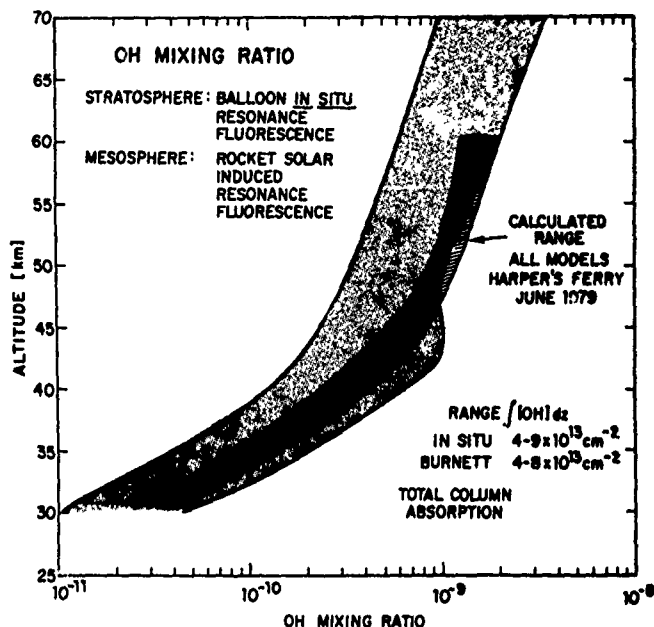
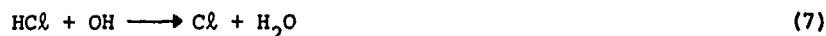
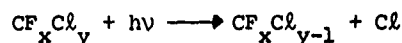


Figure 7. Comparison between the band of observed OH mixing ratio in the stratosphere and mesosphere and the range of calculated hydroxyl mixing ratios. Also indicated is the range of observed OH total column measurements of Burnett and Burnett (1979).

**II.C. THE FREE RADICALS OF CHLORINE:** The chlorine radicals Cl and ClO have drawn wide attention since the Rowland-Molina hypothesis that fluorocarbon release at the surface must lead to ozone depletion in the stratosphere through the reaction sequence



where steps (8) and (9) lead to the gas phase catalytic recombination of  $\text{O}_3$  and  $\text{O}$ . Figure 8 summarizes current stratospheric observations of "free" chlorine.

There are currently 11 in situ, midday, vertical soundings of ClO in the stratosphere (10 are displayed in figure 8, one more obtained on 9/26/79 falls within the envelope defined by the 8 observations) and one post-sunset ( $\chi = 95^\circ$ ) remote sensing laser heterodyne absorption measurements by Menzies (1978). Two observations of atomic chlorine are available. These observations are compared with the most recent calculations from the NASA/GSFC, LL, HARVARD, NOAA and RDA models displayed as a shaded region for both Cl and ClO. In the vicinity of 40 km, the calculated and observed profiles overlap, but there is a clear divergence with decreasing altitude such that at 25 km the observed ClO concentration extends from a factor of two to a factor ten below the calculated distribution. It is perhaps more instructive to consider the comparison between the mean of the ClO observations and a single model which is done in figure 9 using the Logan et al., 1978 model with the most recent  $\text{HO}_x$  reaction rate constants listed above. The comparison demonstrates that the difference between the mean of

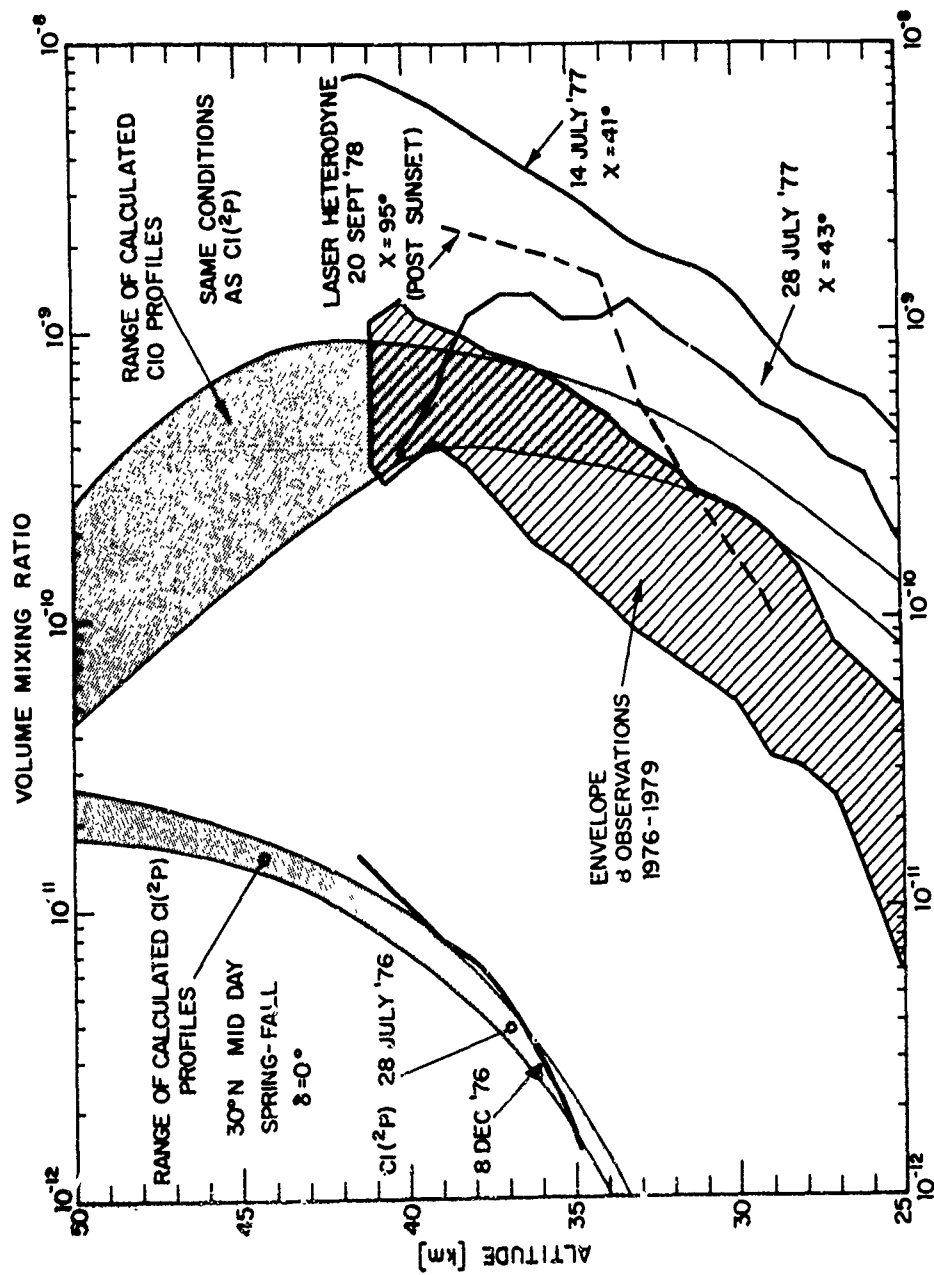


Figure 8. Summary of observed  $C1O$  and  $C1O_2$  observations and the comparison with the calculated distribution.

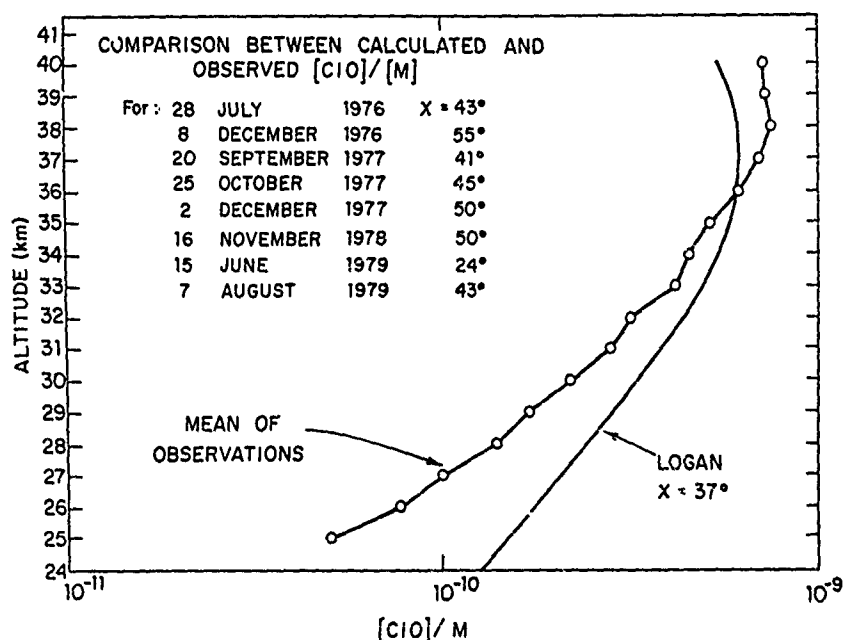


Figure 9. Comparison between calculated and observed  $[C_2O]/[M]$  excluding the 7/14/77 observations of  $[C_2O]$  and using the most recent model of Logan et al. (1979).

the observed  $C_2O$  and the calculated distribution is approximately a factor of 4 at 25 km—a major discrepancy. This discrepancy may result either from improper partitioning between  $C_2O_x = C_2 + C_2O$  and the main  $C_2$  reservoir  $HCl$  or from the improper distribution with altitude of  $HCl$ . A comparison between calculated and observed  $HCl$ , however, implies that  $[HCl]$  is in fact properly distributed with altitude and that the fault lies in the ratio of  $[C_2O]$  to  $[HCl]$ . That ratio is believed to be controlled by reactions 6-10 alone such that in steady state

$$\frac{[C_2O]}{[HCl]} = \frac{[C_2]}{[HCl]} \frac{[C_2O]}{[C_2]} = \frac{k_7 [OH]}{k_6 [CH_4]} \left\{ \frac{k_8 [O_3]}{k_9 [O] + k_{10} [NO]} \right\}$$

Below 35 km, however, reaction (10) is the dominant term in the denominator so

$$[C_2O]/[HCl] \approx \frac{k_7 [OH]}{k_6 [CH_4]} \frac{k_8 [O_3]}{k_{10} [NO]}$$

Since there are a large number of observations of  $[CH_4]$  and  $[O_3]$  in the 25-30 km altitude region which are in close agreement with the modeled distribution and since the observed  $[NO]$  profiles are equal to or less than the modeled distribution, the principle candidate for the incorrect  $[C_2O]/[HCl]$  distribution must be the  $OH$  concentration below 30 km. This emphasizes once again how critical the lower stratosphere  $OH$  data are.

A breakdown of the individual  $C_2O$  profiles is shown in figure 10 demonstrating that while the eight observations which define the envelope are distributed throughout the interval and the mixing ratio gradients are nearly identical in all cases, there remains significant local structure over a vertical scale  $\pm 2$  km. The observation of 7/28/76 is distinctly separated from the envelope but is in fact the only profile which fits the calculated distribution using 8 ppm  $H_2O$  throughout the stratosphere [see Logan et al., 1978]. The observation of 7/14/77 on the other hand cannot be accepted within our current global and time average

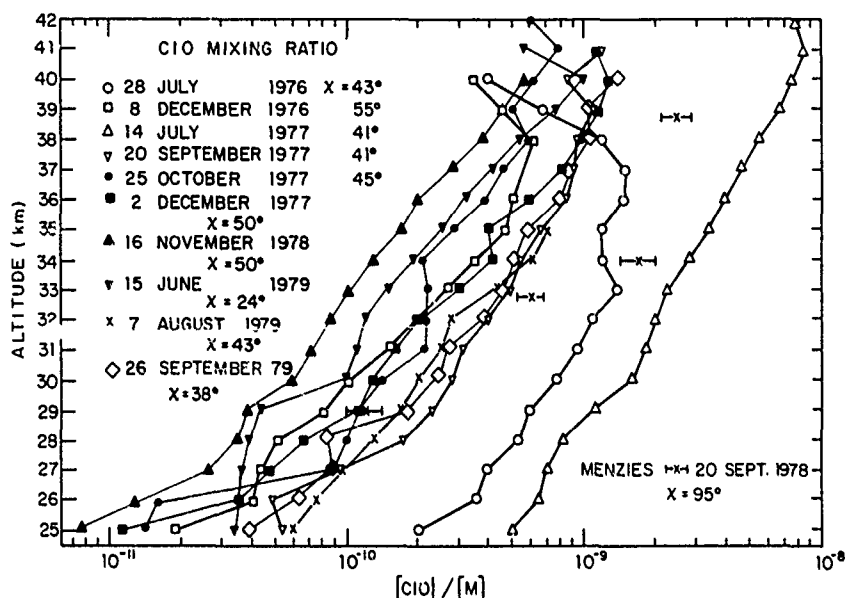


Figure 10. Detailed summary of the ClO observations available at the time of writing.

formulation of stratospheric chlorine photochemistry and can only be explained in terms of a local enhancement in total chlorine. That the 7/14/77 observation has little relationship to the normal distribution of ClO in the stratosphere there can be little doubt. The point of concern with respect to that observation is that O<sub>3</sub> and OH were observed simultaneously with ClO on that flight indicating that [O<sub>3</sub>] did not adjust (downward) to the presence of amplified ClO in a region of the atmosphere which reaches photochemical steady state within a few hours. The simultaneity of the observation and the simplicity of the photochemistry in the 40 km region severely limits the number of possible conclusions to the three: (a) the [ClO] and/or [O<sub>3</sub>] observation was wrong, (b) [O<sub>3</sub>] was not in steady state when the observation was made (i.e., the observed ClO<sub>x</sub> was injected into the stratosphere in a period short compared with the chemical response time of [O<sub>3</sub>]) or (c) there is an odd oxygen production term proportional to ClO<sub>x</sub> which is not included in our current formulation of chlorine-ozone photochemistry.

**II.D. NITROGEN-OXYGEN RADICALS: OBSERVATIONS OF NITRIC OXIDE.** Molecular resonance fluorescence in the  $\gamma$  band system of NO( $A^2\Sigma-X^2\Pi$ ) affords a method for detecting nitric oxide using the same flight hardware which is used for O(<sup>3</sup>P), OH, ClO etc., although the resonance lamp for NO is not as satisfactory for fluorescence as its counterpart for the other experiments. Results obtained with this technique are summarized in figure 11 by comparison with other observations of stratospheric NO, both in situ and remote.

In situ resonance fluorescence measurements of [NO] agree best with the remote IR emission measurements of Drummond and Jarnot, both with respect to absolute concentration and vertical distribution. Although nitric oxide is not the rate limiting nitrogen free radical, its stratospheric concentration is of particular interest because in the altitude region between 40 and 45 kilometers, the sum  $[NO] + [NO_2] + [HNO] \approx [NO]$  is a crucial measure of the active nitrogen compounds throughout the stratosphere above ~20 km. The observed NO distribution shown in figure 11 indicates [NO] ranges between 7 and 14 ppb, measurably below the calculated [NO] distribution (see R.D. Hudson, 1979). However, both the IR emission data and the resonance fluorescence observations define the high edge of the observed distribution--this point must be clarified in the near future.

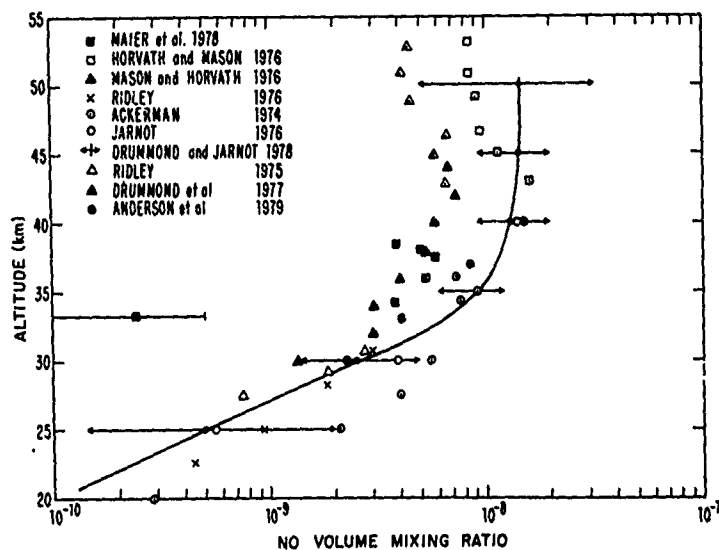


Figure 11. Summary of NO measurements throughout the 20-55 km altitude interval.

II.E. SIMULTANEOUS OBSERVATIONS OF  $O(^3P)$ ,  $HO_2$ ,  $ClO$ , NO and  $O_3$ : DO THE RATES OF ODD OXYGEN PRODUCTION AND DESTRUCTION BALANCE? A necessary step for correctly predicting trends in the concentration of stratospheric ozone is a correct formulation of the continuity equation for odd oxygen

$$\frac{d[O_x]}{dt} = \frac{d([O] + [O_3])}{dt} = P_{O_x} - L_{O_x} + \nabla \cdot \phi \quad (11)$$

where  $[O]$  and  $[O_3]$  are respectively the concentration of atomic oxygen and ozone,  $P_{O_x}$  and  $L_{O_x}$  are the rates of photochemical production and destruction of odd oxygen and  $\nabla \cdot \phi$  the flux divergence of  $O_x$  for the volume element under consideration. While  $[O_x]$  is controlled both by the general circulation of the atmosphere and by local photochemistry, throughout a major segment of the stratosphere  $P_{O_x}$  and  $L_{O_x}$  exceed  $\nabla \cdot \phi$  by orders of magnitude and thus equation (1) reduces to

$$\frac{d[O_x]}{dt} = P_{O_x} - L_{O_x}$$

In addition, in this region of the stratosphere,  $O_x$  achieves a photochemical steady state,  $(|P_{O_x} - L_{O_x}|)/P_{O_x} \ll 1$ , in a period short compared with the time required to transport a given volume element of the stratosphere to a location characterized by a measurably different radiation field, and thus

$$\frac{d[O_x]}{dt} = P_{O_x} - L_{O_x} \approx 0 \quad (12)$$

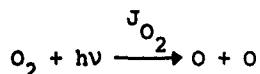
In order to test, with a tractable number of simultaneous observations, whether our current understanding of stratospheric ozone photochemistry yields a complete formulation of  $P_{O_x}$  and  $L_{O_x}$ , it is first necessary to define the photolytic and thermal reactions which constitute the rate limiting steps in  $P_{O_x}$  and  $L_{O_x}$ . A careful consideration of this point appears in a recent article by Johnston and Podolske (1978) which demonstrates, after elimination of null



or "do nothing" cycles, that between 25 and 45 km

$$P_{O_x} = 2J_{O_2} [O_2]$$

where  $J_{O_2}$  is the photodissociation rate of  $O_2$



and

$$L_{O_x} = 2k_{14} [O_3] [O(^3P)] + 2k_{15} [NO_2] [O(^3P)] + 2k_9 [ClO] [O(^3P)] \\ + 2k_3 [HO_2] [O(^3P)] + 2k_4 [HO_2] [O_3] \quad (13)$$

where the reaction rate constants refer to the bimolecular reactions



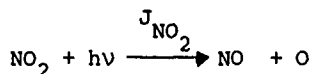
Second, it is necessary to test, with a set of simultaneous in situ observations of  $O_3$ ,  $O(^3P)$ ,  $NO_2$ ,  $ClO$ ,  $HO_2$ , and  $J_{O_2}$  taken within the same volume element of dimension less than that of the local variability<sup>2</sup> of those species, whether

$$J_{O_2} [O_2] - [O(^3P)] \{k_3 [O_3] + k_4 [NO_2] + k_5 [ClO] + k_6 [HO_2]\} - k_7 [O_3] [HO_2] \quad (16)$$

is less than, equal to or greater than zero throughout the altitude interval for which condition 12 holds. Third, the partial derivative of  $[O_x]$  with respect to each of those rate limiting free radicals must be established through studies of the covariance between  $[O_x]$  and the rate limiting radicals  $[HO_2]$ ,  $[NO_2]$ , and  $[ClO]$ . This approach becomes particularly simple for the case of large fluctuations in  $ClO$ ,  $NO_2$ ,  $HO_2$ , etc. in contrast to the difficulty encountered when one attempts to "verify models" by comparing inherently variable observations of the real atmosphere with the invariant stratosphere described by current one- and two-dimensional computer models.

The discussion presents the results of three sets of simultaneous in situ observations of  $NO$ ,  $HO_2$ ,  $ClO$ ,  $O(^3P)$ , and  $O_3$  between 25 and 45 km in the earth's atmosphere and takes, therefore, a first step toward testing whether the rate of odd oxygen production and destruction balance in the middle stratosphere. For detailed discussion see Anderson et al. (1980d).

RESULTS. Since nitric oxide is not the rate limiting free radical in the major  $\text{NO}_x$  catalytic cycle, the concentration of the rate limiting radical,  $[\text{NO}_2]$ , must first be determined from observed  $[\text{NO}]$ , assuming the reactions



control the interconversion of these two constituents. The ratio

$$[\text{NO}_2]/[\text{NO}] = \frac{k_{17}[\text{O}_3] + k_{10}[\text{ClO}]}{J_{\text{NO}_2} + k_{15}[\text{O}(^3\text{P})]} \quad (18)$$

is determined from observed values of  $[\text{O}_3]$ ,  $[\text{ClO}]$  and  $[\text{O}(^3\text{P})]$  for each altitude. Rate constants are taken from the recent review by DeMore (1979). Since it is decidedly easier to demonstrate that reaction (15) is rate limiting in the  $\text{NO}_x$  catalytic cycle, (since  $k_{10}[\text{NO}][\text{O}_3] \approx J_{\text{NO}_2}[\text{NO}_2] \gg k_4[\text{NO}_2][\text{O}]$  in this region of the atmosphere), than to demonstrate that our understanding of the photochemistry linking NO and  $\text{NO}_2$  is complete, the insertion into  $L_{\text{O}_x}$  of  $[\text{NO}_2]$  calculated from observed  $[\text{NO}]$  via (18) weakens the approach.

Before comparing the instantaneously observed rate of destruction

$$L_{\text{O}_x} = 2k_{14}[\text{O}_3][\text{O}(^3\text{P})] + 2k_{15}[\text{NO}_2][\text{O}(^3\text{P})] + 2k_9[\text{ClO}][\text{O}(^3\text{P})] + 2k_3[\text{HO}_2][\text{O}(^3\text{P})] + 2k_4[\text{HO}_2][\text{O}_3]$$

with the rate of production  $P_{\text{O}_x} = 2J_{\text{O}_2}[\text{O}_2]$  it is necessary to take into account the slightly different time dependence of each term in  $L_{\text{O}_x}$  and  $P_{\text{O}_x}$  over the course of a diurnal cycle resulting from the difference in the wavelength dependence of  $J_{\text{O}_2}$  and  $J_{\text{O}_3}$  and to the rate of build-up and decay of  $\text{HO}_2$ ,  $\text{ClO}$  and  $\text{NO}_2$  at sunrise and sunset. The asymmetry in  $\text{NO}_2$  resulting from the formation of  $\text{N}_2\text{O}_5$  is also significant. This adjustment was done to first order by dividing the day into 24 equal segments, taking mean values for  $[J_{\text{O}_2}]$ ,  $[\text{O}(^3\text{P})]$ ,  $[\text{HO}_2]$ ,  $[\text{NO}_2]$  and  $[\text{ClO}]$  within each segment and then scaling the quantities

$$\frac{\int_{24 \text{ hr}} k[\text{NO}_2][\text{O}] dt}{\int_{24 \text{ hr}} J_{\text{O}_2}[\text{O}_2] dt}, \quad \frac{\int_{24 \text{ hr}} k[\text{ClO}][\text{O}] dt}{\int_{24 \text{ hr}} J_{\text{O}_2}[\text{O}_2] dt},$$

etc. at each altitude to the ratio of observed and calculated radical concentrations at the particular solar zenith angle corresponding to the observation.

This analysis results in the partitioning of odd oxygen loss rates, normalized to the rate of production,  $2J_{\text{O}_2}[\text{O}_2]$ , for each free radical family at each altitude between 25 and 41 km which are displayed in table 2.

ANDERSON

That tabulation is shown in table 2 with the model values for  $[\text{NO}_2]$  at 27 and 25 km inserted for completeness and to show the difference between observed and calculated  $\text{NO}_x$  destruction and similarly for  $[\text{HO}_2]$  at 38 and 41 km and at 25 km.

PARTITIONING OF ODD OXYGEN  
DESTRUCTION RATES FROM MEAN  
OF SIMULTANEOUS OBSERVATIONS ON  
9-20-77 10-25-77 12-2-77  
NORMALIZED TO  $J_{\text{O}_2}[\text{O}_2]$

ALTITUDE	$k[\text{O}_3][\text{O}]$	$k[\text{NO}_2][\text{O}]$	$k[\text{ClO}][\text{O}]$	$k[\text{HO}_2][\text{O}]$	$k[\text{HO}_2][\text{O}_2]$	SUM
43	—	—	—	—	—	—
40	0.12	0.36	0.53	0.15*	0.0*	1.17
39	0.14	0.49	0.41	0.13*	0.0*	1.17
37	0.13	0.52	0.27	0.10	0.01	1.03
35	0.10	0.51	0.15	0.07	0.01	0.84
33	0.07	0.37	0.10	0.08	0.06	0.68
31	0.08	0.39	0.08	0.06	0.06	0.71
29	0.09	0.39	0.08	0.04	0.09	0.70
27	0.10	0.73*	0.09	0.05	0.13	1.10
25	0.11	0.37*	0.06	0.03	0.22	0.80

Table 2. Partitioning of the odd oxygen destruction rates normalized to the  $\text{O}_2$  photodissociation rate  $J_{\text{O}_2}[\text{O}_2]$  displayed as a function of altitude from 25 to 41 km. Rate limiting steps determined from the mean of 3 flights which determined simultaneously the concentration of  $\text{O}(^3\text{P})$ ,  $\text{O}_3$ ,  $\text{HO}_2$ ,  $\text{ClO}$  and  $\text{NO}$ . See text for the determination of  $[\text{NO}_2]$  from  $[\text{NO}]$ . Quantities which are indicated by the asterisk exceed the altitude bounds of the observation. Calculated values from Logan et al. (1978) are inserted for  $\text{NO}_2$  at 25 and 27 km and for  $\text{HO}_2$  at 25, 41 and 43 km.

## REFERENCES

- Ackerman, M., J.C. Fontanella, D. Frimout, A. Girard, N. Louisnard, C. Muller, Simultaneous Measurements of NO and NO<sub>2</sub> in the Stratosphere, Planet Space Sci., **23**, 651, 1975.
- Anderson, J.G., Rocket Measurement of OH in the Mesosphere, J. Geophys. Res., **76**, 7820, 1971.
- Anderson, J.G., The Measurement of Atomic Oxygen and Hydroxyl in the Stratosphere. Proceedings of the 4<sup>th</sup> Conference on the Climatic Impact Assessment Program DOT-TSC-OST-75-38 pages 458-464, 1975.
- Anderson, J.G., The Absolute Concentration of OH(X<sup>2</sup>Π) in the Earth's Stratosphere, Geophys. Res. Lett., **3**, 165, 1976.
- Anderson, J.G., D.E. Robbins, J. Carnes, Simultaneously Observed O(<sup>3</sup>P) and O<sub>3</sub> in the Stratosphere: Do the Observed and Calculated [O(<sup>3</sup>P)]/[O<sub>3</sub>] Ratios Agree? Geophys. Res. Lett., submitted, 1980a.
- Anderson, J.G., H.J. Grassl, R.E. Shetter, J.J. Margitan, In Situ Measurements of HO<sub>2</sub> in the Earth's Stratosphere, Geophys. Res. Lett., submitted, 1980b.
- Anderson, J.G., E. Weinstock, J.P. Phillips, ClO in the Stratosphere: A Brief Review, Geophys. Res. Lett., submitted, 1980c.
- Anderson, J.G., H. J. Grassl, R.E. Shetter, J.J. Margitan, NO, HO<sub>2</sub>, ClO and O(<sup>3</sup>P) in the Earth's Stratosphere: Do the Rates of Odd Oxygen Production and Destruction Balance? Journal Atmos. Science, submitted, 1980d.
- Burnett, C.R., and E.B. Burnett, Measurements of the Vertical Abundance of Hydroxyl (OH) in the Earth's Atmosphere, Manuscript, 1979.
- Crutzen, P.J., C. J. Howard, The Effect of the HO<sub>2</sub> + NO Reaction Rate Constant on One-Dimensional Model Calculations of Stratospheric Ozone Perturbations, Pageoph, **116**, 497, 1978.
- DeMore, W.B., ed. for Review Committee, L.J. Stief, F. Kaufman, D.M. Golden, R.F. Hampson, M.J. Kurylo, J.J. Margitan, M.J. Molina, R.T. Watson, Chemical Kinetic and Photochemical Data for use in Stratospheric Modelling, JPL Publication, 79-27, 1979.
- Drummond, J.R., J.M. Rosen, D.J. Hoffman, Balloon Borne Chemiluminescent Measurements of NO to 40 km, Nature, **265**, 319, 1977.
- Drummond, J.R., and R.F. Jarnot, Infrared Measurements of Stratospheric Composition II, Simultaneous NO and NO<sub>2</sub> Measurements, Proc. Roy. Soc., London, Sec. A, **364**, 237, 1978.
- Horvath, J.J., C.J. Mason, Nitric Oxide Mixing Ratios Near the Stratopause Measured by a Rocket-Borne Chemiluminescent Detector, Geophys. Res. Lett., **5**, 1023, 1978.
- Howard, C.J., and K. Evenson, Kinetics of the Reaction of HO<sub>2</sub> with NO, Geophys. Res. Lett., **4**, 437, 1977.
- Hudson, R.D., ed., The Stratosphere: Present and Future, NASA Reference Publication #1049, December 1979.
- Johnston, H.S., and J. Podolske, Interpretation of Stratospheric Chemistry, Rev. of Geophys. and Space Physics, **16**, 491, 1978.
- Kley, D., E.J. Stone, R.W. Henderson, J.W. Drummond, W.J. Harrop, A.L. Schmeltekopf, T.L. Thompson, submitted to J. Geophys. Res., 1979.
- Logan, J.A., M.J. Prather, S.C. Wofsy, M.B. McElroy, Atmospheric Chemistry: Response to Human Influence, Phil. Trans. Roy. Soc. London, **290**, 187, 1978.
- Logan, J.A., M.J. Prather, S.C. Wofsy, and M.B. McElroy, Same Calculation as Logan et al. [1978] with the following revised reaction rate constants.
- |  |                                      |
|--|--------------------------------------|
| HO <sub>2</sub> + O <sub>3</sub> → OH + 2O <sub>2</sub>                            | 1.40 × 10 <sup>-14</sup> exp(-580/T) |
| HO <sub>2</sub> + HO <sub>2</sub> → H <sub>2</sub> O <sub>2</sub> + O <sub>2</sub> | 3.0 × 10 <sup>-12</sup>              |
| HO <sub>2</sub> + ClO →  | 4.5 × 10 <sup>-12</sup>              |
| HO <sub>2</sub> + NO → OH + NO <sub>2</sub>  | 3.3 × 10 <sup>-12</sup> exp(255/T)   |
- Maier, E.J., A.C. Aikin, J.E. Ainsworth, Stratospheric Nitric Oxide and Ozone Measurements Using Photoionization Mass Spectroscopy and U.V. Absorption, Geophys. Res. Lett., **5**, 37, 1978.
- Mason, C.J., and J.J. Horvath, The Direct Measurement of Nitric Oxide Concentration in the Upper Atmosphere by a Rocket Borne Chemiluminescent Detector, Geophys. Res. Lett., **3**, 391, 1976.
- Menzies, R.T., Remote Measurement of ClO in the Stratosphere, Geophys. Res. Lett., **6**, 151, 1979.

# ANDERSON

- Mihelcic, D., D.H. Ehhalt, C.F. Kulesa, J. Komfass, M. Trainer, U. Schmidt, H. Rohrs, Measurements of Free Radicals in the Atmosphere by Matrix Isolation and Electron Paramagnetic Resonance, Pageoph, 116, 530, 1978.
- Ridley, B.A., J.T. Bruin, H.I. Schiff, J.C. McConnell, Altitude Profile and Sunset Decay Measurements of Stratospheric Nitric Oxide, Atmosphere, 14, 180, 1976.
- Ridley, B.A., H.I. Schiff, A. Shaw, J. R. Megill, In Situ Measurements of Stratospheric Nitric Oxide Using a Balloon-Borne Chemiluminescent Instrument, J. Geophys. Res., 80, 1925, 1975.
- Robbins, D.E. and J. Carnes, WMO. Conference Proceedings, June 1978, Toronto.
- Rundel, R.D., D.M. Butler, R.S. Stolarski, Uncertainty Propagation in a Stratospheric Model, 1. Development of a Concise Stratospheric Model, J. Geophys. Res., 83, 3063, 1978.
- Turco, R.P., R.C. Whitten, I.G. Poppoff, L.A. Capone, SST'S, Nitrogen Fertilizers and Stratospheric Ozone, Nature, 276, 805, 1978.
- Whitten, R.C., W.J. Borucki, L.A. Capone, R.P. Turco, The Effect of the Reaction  $\text{HO}_2 + \text{OH} \rightarrow \text{OH} + 2\text{O}_2$  on Stratospheric Ozone, Nature, 275, 523, 1978.
- Wofsy, S.C., Temporal and Latitude Variations of Stratospheric Trace Gases: A Critical Comparison Between Theory and Experiment, J. Geophys. Res., 83, 364, 1978.
- Zahniser, M., C.J. Howard, Paper presented at WMO Symposium on Ozone, Toronto, June 1978.

## OBSERVATIONS OF ODD NITROGEN COMPOUNDS IN THE STRATOSPHERE

D.G. Murcray

Department of Physics, University of Denver, Denver, Colorado, 80208

**Abstract.** Current photochemical model studies of the stratospheric ozone layer indicate that the oxides of nitrogen play a significant role in determining the ozone concentration. Information concerning the presence and altitude distribution of the odd nitrogen compounds is therefore of great interest in the study of the stratospheric ozone layer. Measurements have been made of NO, NO<sub>2</sub>, HNO<sub>3</sub> by several techniques. Summaries of these measurements are presented. NO<sub>3</sub> and ClONO<sub>2</sub> have been measured by a single technique and the limited data base for these species is discussed. Upper limits based on infrared solar and atmospheric emission spectra are given for N<sub>2</sub>O<sub>5</sub> and HO<sub>2</sub>NO<sub>2</sub>.

### INTRODUCTION

During a balloon flight performed on December 7, 1967 we recorded infrared solar spectra from 30 km at sunset. The spectral region covered during this flight was from 1000 cm<sup>-1</sup> to 1800 cm<sup>-1</sup>. Upon detailed examination, it became evident that absorption features due to HNO<sub>3</sub> and NO<sub>2</sub> were present in these spectra. Analysis of the spectra also indicated that both constituents were present in the stratosphere and that their concentration decreased very rapidly in the lower stratosphere close to the tropopause. The maximum mixing ratio for both species was on the order of 10 ppbv.

When reported, these results attracted very little attention among the photochemists studying the ozone layer because they felt that HNO<sub>3</sub> and NO<sub>2</sub> were present at too low a concentration to be important in ozone photochemistry. Only after Crutzen (1971) and Johnston (1971) pointed out the catalytic destruction of ozone by NO, did interest in the presence of these species in the stratosphere and their role in the photochemistry of stratospheric ozone increase.

The controversy concerning possible environmental effects of the SST increased the interest in the ozone layer and added to the overall interest in the presence of nitrogen compounds in the stratosphere. Studies undertaken as a result of the controversy (the Department of Transportation Climatic Impact Assessment Program) indicated that odd nitrogen compounds play a significant role in the photochemistry of the ozone layer. These model calculations indicate that the following nitrogen compounds are predicted to play a significant role in the photochemistry of the stratospheric ozone layer: NO, NO<sub>2</sub>, HNO<sub>3</sub>, N<sub>2</sub>O<sub>5</sub>, HO<sub>2</sub>NO<sub>2</sub>, NO<sub>3</sub> and ClONO<sub>2</sub>. (ClONO<sub>2</sub> is included in the list as the result of the more recent concern over the possible catalytic effect of ClO - due to the use of chlorofluoromethanes - on the ozone layer.) Our present state of knowledge concerning the photochemistry of the ozone layer is treated in other sections of this volume. The current status of the observation of these constituents is reviewed below.

## CURRENT MEASUREMENT STATUS

NO: As noted above, the controversy over the possible environmental effects of the SST coupled with the catalytic effect of NO, as noted by Crutzen (1971) and Johnston (1971), led to this species being a major concern of CIAP program. As a result, a number of investigators designed and constructed systems to measure NO from aircraft and balloons.

The most successful technique for in situ measurement of NO, at least from the standpoint of the number of measurements made, is the NO/O<sub>3</sub> chemiluminescence technique. This technique was developed initially for balloon use by Ridley et al., (1974), and for aircraft use by Loewenstein and Savag  (1975). The instrumentation uses ozone introduced into a suitable reaction chamber to convert ambient NO into excited NO<sub>2</sub>. The amount of NO<sub>2</sub> created is monitored (using a suitable photomultiplier detection system) by measuring the NO<sub>2</sub> emission. Ridley et al., (1976) have made a number of balloon-borne measurements of the NO altitude distribution at several geographic locations using this technique. Loewenstein et al., (1975, 1978) have made extensive surveys of the geographic variability of NO at selected altitudes using the instrument mounted in the U-2 aircraft.

NO is a moderately strong infrared absorber and two infrared techniques have been used to obtain data on its stratospheric distribution. One technique is the study of infrared solar spectra obtained at large solar zenith angles covering the 5.3  $\mu$ m spectral region where NO has its strongest band. Ackerman et al., (1974) have used this technique from balloons and Farmer (1974) and Girard et al., (1977) have used it from aircraft. One problem with this technique is that the absorptions are so weak that data can only be obtained at large solar zenith angles, at which time NO is being rapidly converted to NO<sub>2</sub>. This results in a significant analysis problem when attempting to derive profile data from successive spectral scans obtained at zenith angles greater than 90°. Another problem is the interference with the NO absorption features by features due to solar CO and absorptions due to minor atmospheric species (CO, CO<sub>2</sub>, O<sub>3</sub>, H<sub>2</sub>O, N<sub>2</sub>O, CH<sub>4</sub>). High spectral resolution is required to isolate the NO absorption features. Recent results obtained at higher resolution than with the early studies indicate that the lines used in those analyses were blended at the resolution achieved in the early work. It is also possible to use the NO absorption for an in situ measurement of NO by using the absorption over a short atmospheric path at balloon altitude. Since the absorption will be weak even at high resolution, this measurement requires a very sensitive technique for measuring the small absorption. This sensitivity was achieved by Patel et al., (1974) using a special laser-detector combination and resulted in an in situ measurement of NO at 30 km.

NO has also been measured using photoionization mass spectrometry (Aiken et al., 1978). The chemiluminescent technique has also been used for a rocket-borne instrument (Mason et al., 1976), to obtain data in the NO distribution in the upper stratosphere.

Figure 1 summarizes the results obtained to date. For comparison purposes only the data obtained at midlatitudes are presented in this figure. The latitudinal and seasonal variability of NO have only been studied by Loewenstein et al., (1975, 1978) using the U-2 instrumentation. These data show increased NO amounts in the summer in the 30°N to 45°N latitude region. The summer values appear to be a factor of three higher above 50°N.

NO<sub>2</sub>: As noted above, NO<sub>2</sub> was first detected in the stratosphere using infrared solar spectra obtained from a balloon covering the 6.3  $\mu$ m region. Solar spectra continue to be the major measurement technique for obtaining data concerning concentration of NO<sub>2</sub> in the stratosphere; however, the majority of the recent measurements comes from studies using the absorption due to NO<sub>2</sub> in the 4400 Angstrom region rather than the infrared. The NO<sub>2</sub> band in the 6.3  $\mu$ m region is a strong band and, although it is overlapped by the 6.3  $\mu$ m H<sub>2</sub>O band, the water lines are separated enough that a number of NO<sub>2</sub> lines are not blended in the stratosphere. While strong, the band still requires the enhanced optical path associated with large solar zenith angles in order to get measurable absorptions. The visible region has the benefit that, by studying the spectrum of the zenith sky at solar zenith angles greater than 90°, one can get the advantage of the large optical path from ground based measurements.

Balloon based measurements of the visible NO<sub>2</sub> absorptions have been made by Goldman et al., (1978) and Kerr et al., (1976). Noxon (1979), has made extensive ground based measurements using this region. Infrared absorption measurements have been made from balloons by

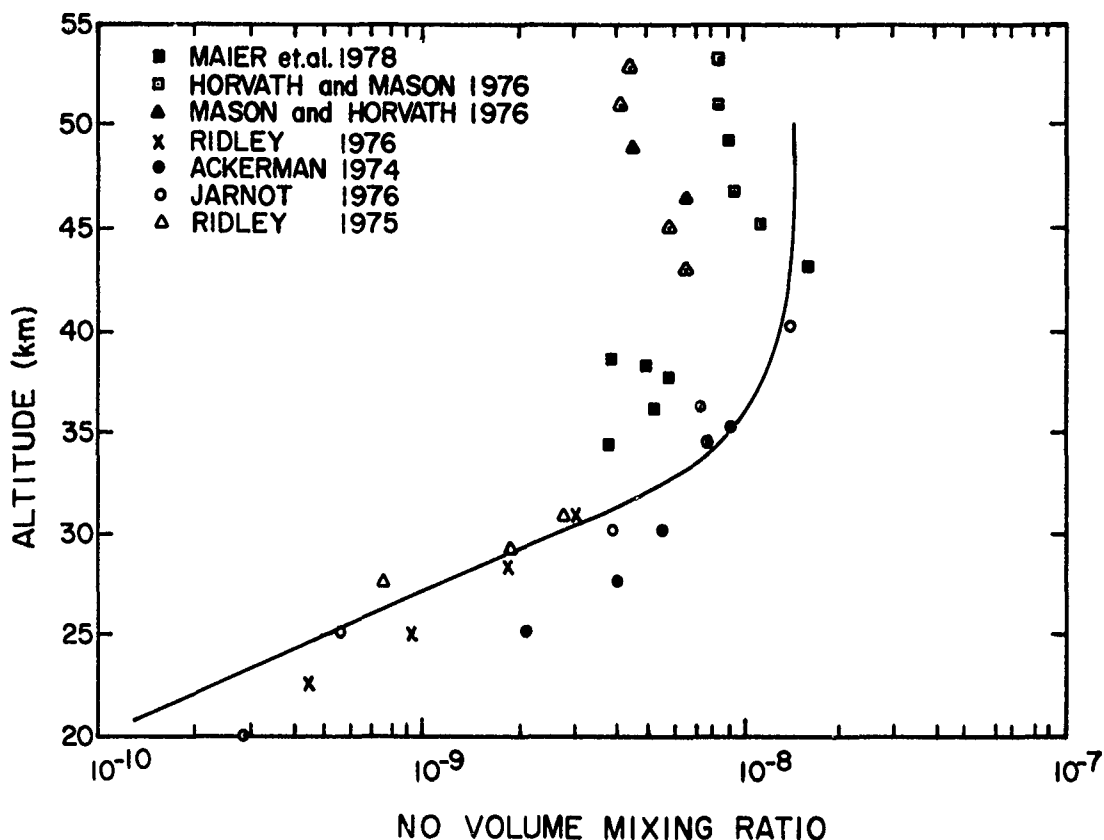


Fig. 1. Nitric oxide mixing ratio profiles as measured by several investigators.

Murcray (1970, 1974), Fontanella et al., (1975), Ackerman et al., (1975), and from aircraft by Girard et al. (1977), and Mankin (1978). Profiles for the midlatitude distribution of  $\text{NO}_2$  are given in Figure 2. Over the range for which the IR and visible results overlap, the agreement is reasonable. Variation of  $\text{NO}_2$  column density with latitude has been studied by Noxon using the ground based measuring technique. One of his major findings is the occurrence of a sharp decline in the column abundance around  $50^\circ$  latitude in the winter hemisphere when there is a strong polar vortex. He also finds less total column of  $\text{NO}_2$  in the equatorial regions than at the midlatitudes.

For species with infrared absorptions there exists the possibility of obtaining data on their distribution by measuring atmospheric emissions. Since atmospheric emission is a weak infrared source such measurements require great sensitivity or relatively broad spectral intervals. Various techniques have been employed for trying to achieve spectral resolution combined with large spectral regions. These generally use an absorption cell containing a sample of the gas of interest. In order to enhance the signal due to the constituent of interest these techniques use some method of modulating that signal. The most successful modulation technique is that of pressure modulation. Unfortunately, in almost all cases, the chopping gives rise to signals from species other than the one of interest and these signals have to be removed in the analysis. This results in the possibility of large systematic errors which are difficult to eliminate. Because the one  $\text{NO}_2$  profile obtained with this technique published to date (Jarnot, 1976), differs significantly from those obtained by other techniques, the data are suspect. Broad band filter measurements have been used for satellite measurements. (Gille et al., 1979.) Here again the emission due to  $\text{H}_2\text{O}$  must be properly removed from the signals. The results obtained with the satellite instruments are currently being analyzed and at this time it is uncertain how accurately the  $\text{NO}_2$  amounts can be determined from the data.



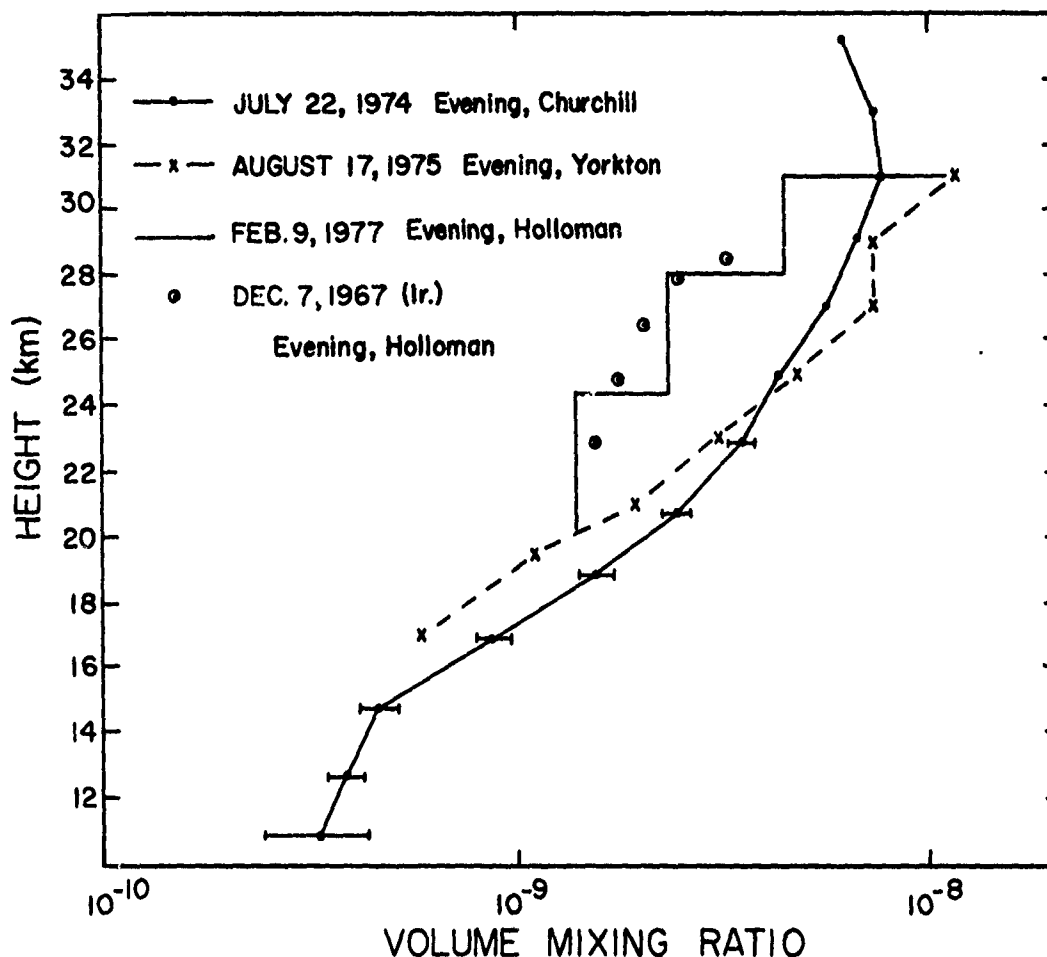


Fig. 2. Nitrogen dioxide mixing ratio profile as observed by two groups. The Canadian results were obtained by Kerr et al., (1977), and the Holloman results by Goldman et al., (1978).

HNO<sub>3</sub>: The compound was first detected in the stratosphere (Murcray et al., 1968) using infrared solar spectra covering the 7.5  $\mu$ m spectral region. Subsequent balloon flight data confirmed the initial identification by observing spectral features due to the species in the 5.8  $\mu$ m region and also in the 11.2  $\mu$ m region. The absorption at 11.2  $\mu$ m occurs in a spectral region where, particularly at the higher altitudes, there is very little interference by other atmospheric constituents. This lack of interference makes it possible to use the atmospheric emission technique employing low resolution instruments. The sensitivity required can be reduced by utilizing the geometric advantage of viewing close to the limb. When they provide adequate information about the constituent of interest, atmospheric emission measurements have significant advantages over the solar occultation technique. Since the 11  $\mu$ m HNO<sub>3</sub> emission satisfies this criteria, most of the data concerning the distribution of HNO<sub>3</sub> in the stratosphere have been obtained using the atmospheric emission technique.

On the basis of the initial identification of HNO<sub>3</sub> as a stratospheric constituent, Lazrus was able to show that the nitrate portion of stratospheric aerosols collected on his aerosol filters was due to the reaction of stratospheric HNO<sub>3</sub> with the filters, rather than nitrate in the aerosol. He used the filters to obtain data concerning the distribution of HNO<sub>3</sub> (Lazrus et al., 1974). By properly treating his filters he has been able to use the technique for obtaining data on other stratospheric constituents. While no direct comparison has been made between the two techniques, comparisons of profiles obtained at the same geographic location indicate that the filter technique yields lower HNO<sub>3</sub> mixing ratios than the atmospheric emission method.

HNO<sub>3</sub> data have been obtained using the atmospheric emission technique from balloons, high flying aircraft, and satellites. Figure 3 gives an altitude profile of HNO<sub>3</sub> obtained from atmospheric emission spectra which were acquired with a balloon-borne spectrometer system. The occurrence of the peak mixing ratio in the altitude region between 20 and 25 km and the

rapid decrease in ratio above 30 km are features that are typical of all  $\text{HNO}_3$  profiles. If this profile is compared with other profiles obtained at the same geographic location, the results will quite often be different. The large variability in  $\text{HNO}_3$  mixing ratio observed at a given altitude reflects the fact that through much of its altitude range  $\text{HNO}_3$  has a relatively long lifetime. Thus, the observed concentration is a function of the atmospheric motion particularly in the region below 30 km. As a result, the measurements show large variability and this is reflected in Figure 4 which indicates the range of mixing ratio versus altitude observed at midlatitude. The region below the peak of the altitude profile and above the tropopause exhibits great variability, reflecting the extent to which mixing is occurring between the stratosphere and the troposphere.

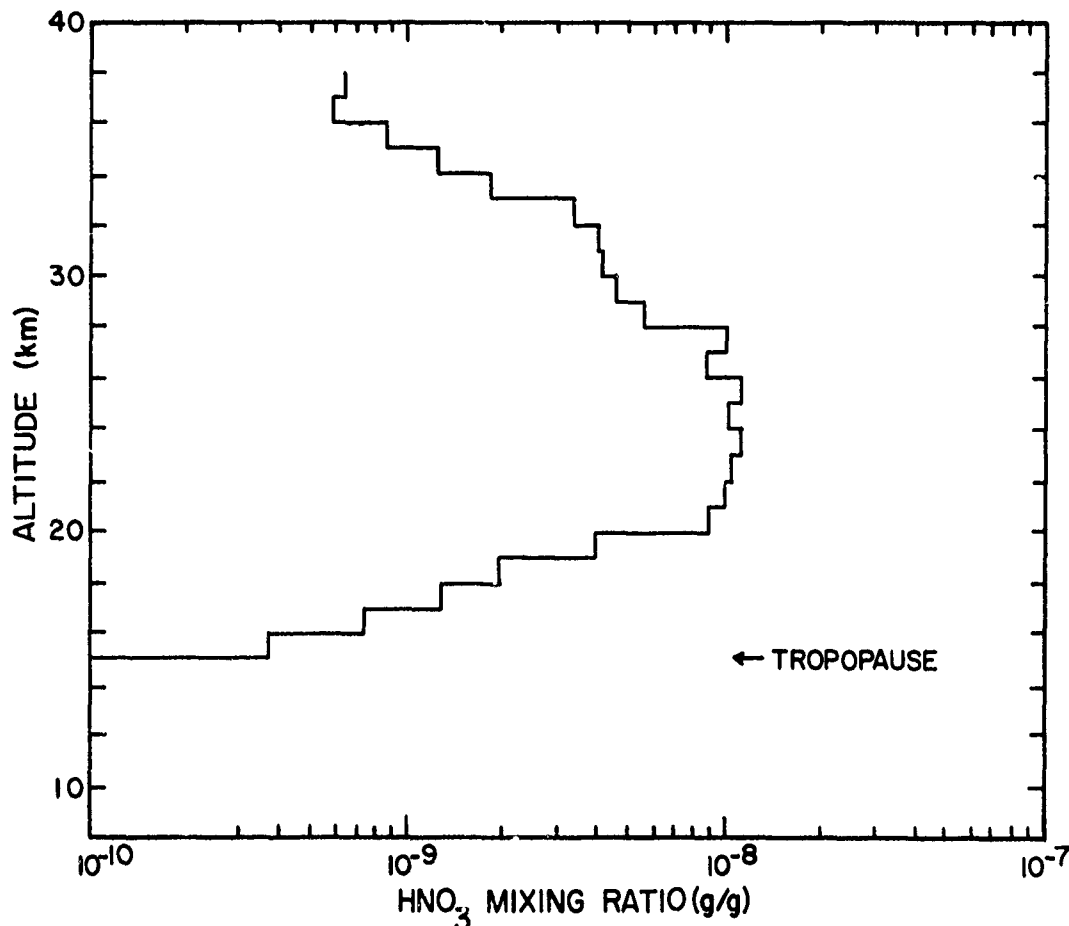


Fig. 3.  $\text{HNO}_3$  profile observed at Holloman AFB 27 June 1974. Measurements were made using the atmospheric emission technique, Murcray et al.

As mentioned, measurements of  $\text{HNO}_3$  altitude profiles have been made using balloon-borne instruments over a wide range of latitudes and several seasons.  $\text{HNO}_3$  overburden data have also been obtained from aircraft over a large range in latitude. These measurements indicate a definite seasonal and latitudinal variation in the  $\text{HNO}_3$  profiles. The latitudinal variability is shown in Figure 5 which gives the  $\text{HNO}_3$  column amount above 15 km as observed with an emission spectrometer flown on a WB 57 (Murcray et al., 1975).

The change in slope between the winter and summer hemispheres is believed to reflect a definite seasonal variability of the  $\text{HNO}_3$  profile. Part of the increase in the column amount above the aircraft is associated with the change in height of the tropopause with latitude. The lowering of the tropopause as the latitude increases results in the peak of the  $\text{HNO}_3$  layer occurring at lower altitude, resulting in a large  $\text{HNO}_3$  column amount.

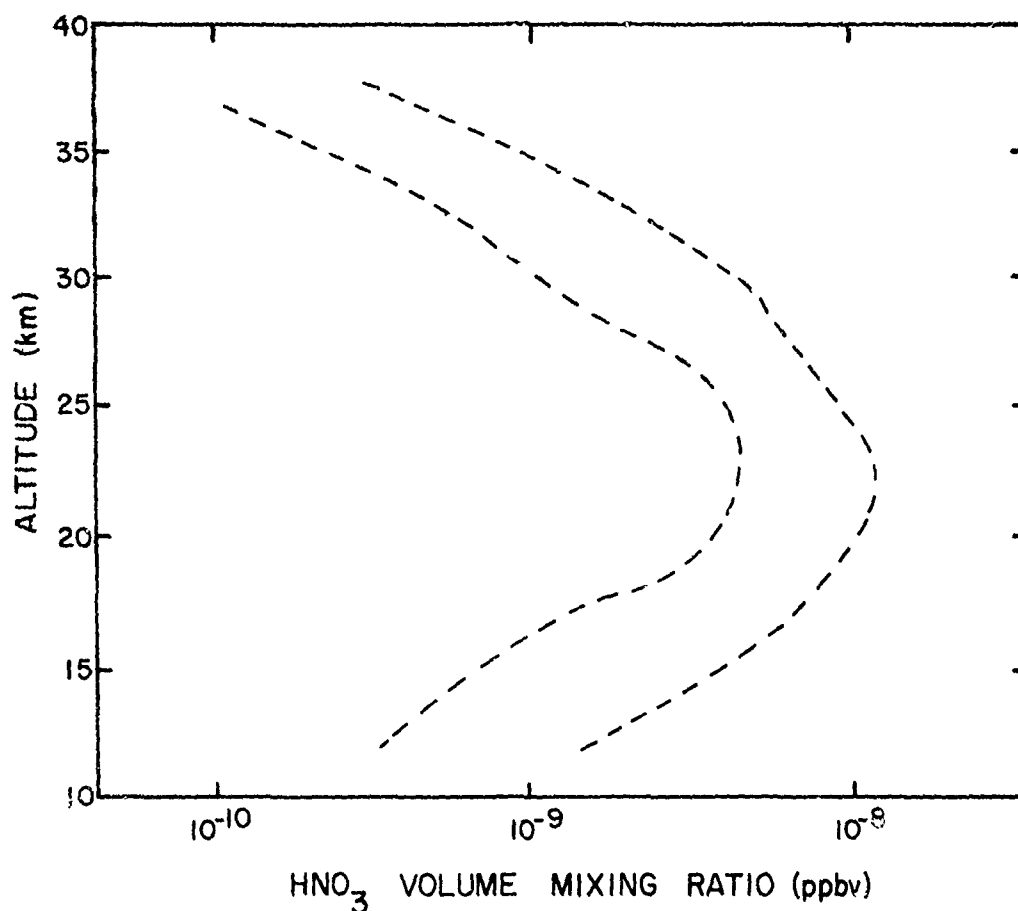


Fig. 4. Range of  $\text{HNO}_3$  mixing ratios observed at midlatitudes.

$\text{N}_2\text{O}_5$ : Modeling studies based on current chemical and photochemical reaction rates predict that  $\text{N}_2\text{O}_5$  should be present in the stratosphere at concentrations approaching that of  $\text{HNO}_3$  at 30 km.  $\text{N}_2\text{O}_5$  has a strong infrared absorption band in the  $8\text{ }\mu\text{m}$  region. Under fairly good resolution the absorption fails to show any rotational structure, exhibiting instead a relatively broad absorption. Infrared solar spectra obtained with moderate resolution (Murcray et al., 1969) have been examined by King et al., (1976), and no indication of any absorption due to  $\text{N}_2\text{O}_5$  was found.  $\text{N}_2\text{O}_5$  exhibits a strong diurnal variation with a minimum concentration occurring at sunset; thus, the upper limit based on sunset solar spectra does not contradict the modeling results. The concentration of  $\text{N}_2\text{O}_5$  should peak just before sunrise. Attempts to observe features due to  $\text{N}_2\text{O}_5$  in atmospheric emission spectra obtained from U-2 altitudes just before sunrise show no indication of emission attributable to this compound (Murcray et al., 1978). The detection limit imposed by these observations contradicts the model results and is a cause of concern.

$\text{HO}_2\text{NO}_2$ : Studies of photochemical smog showed that  $\text{HO}_2\text{NO}_2$  might be an important constituent in the photochemistry of the ozone layer. Addressing the question of the role of  $\text{HO}_2\text{NO}_2$  in stratospheric ozone photochemistry, Jesson et al., (1977) showed that under the assumptions they made in modeling the problem,  $\text{HO}_2\text{NO}_2$  should have a mixing ratio in the 25 km region that was close to  $\text{HNO}_3$ .  $\text{HO}_2\text{NO}_2$  has an absorptor feature at  $803\text{ cm}^{-1}$  which is comparable in strength to the  $\text{HNO}_3$  absorption at  $895\text{ cm}^{-1}$ . Atmospheric emission spectra taken from 36 km viewing the limb, as obtained by Murcray et al., (1978) show the  $\text{HNO}_3$  emission at a signal to noise ratio of at least 100, but fail to show any emission feature at  $803\text{ cm}^{-1}$  due  $\text{HO}_2\text{NO}_2$ . Thus the  $\text{HO}_2\text{NO}_2$  ratio must be at least an order of magnitude below that of  $\text{HNO}_3$  around 25 km. This result is contrary to the model results.

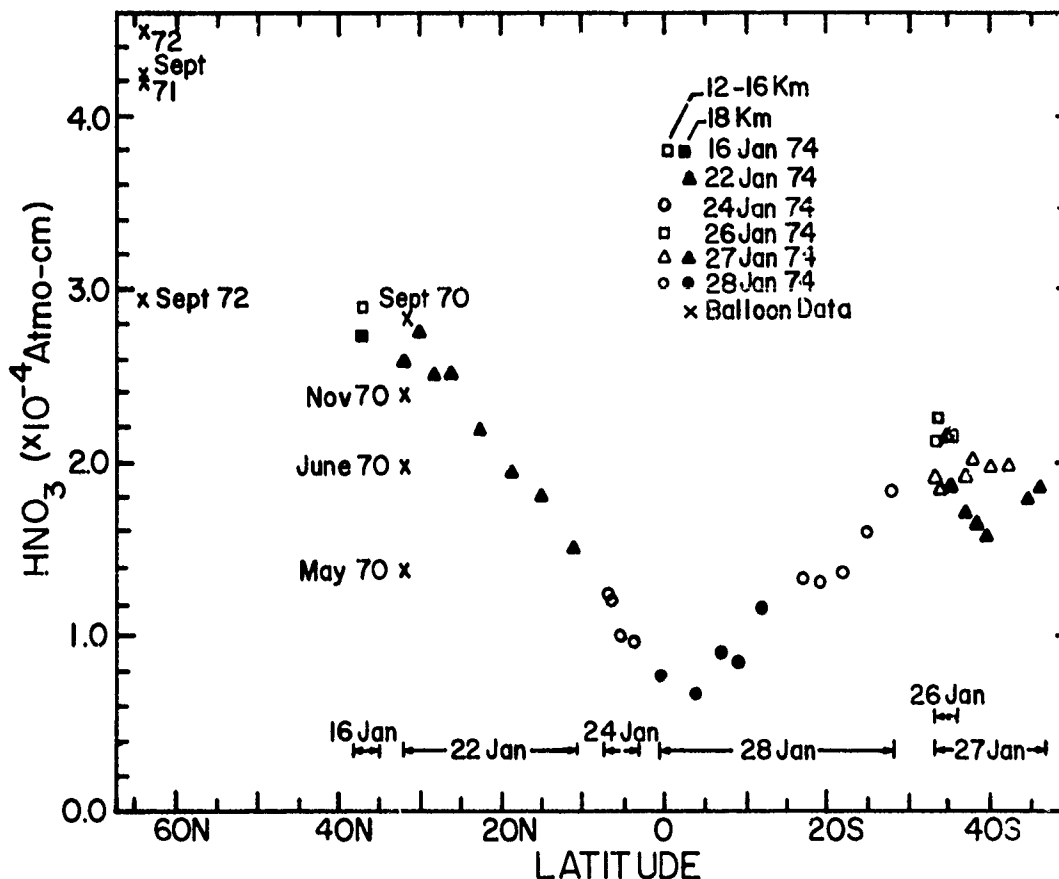


Fig. 5. Latitudinal variation of  $\text{HNO}_3$  column density as observed from the WB57 Aircraft by Murcray et al.

$\text{NO}_3$ : Noxon et al., (1978) have reported observations of an absorption feature at 6620 Angstrom in lunar spectra obtained at large zenith angles. They attribute the observed absorption to the presence of  $\text{NO}_3$  in the stratosphere. Subsequent observations indicate a possible seasonal effect with the  $\text{NO}_3$  decreasing below the detection limit during the summer. No data concerning any possible latitudinal variability have been obtained at this time.

$\text{ClONO}_2$ : Rowland et al., (1976) suggested that the reaction  $\text{ClO} + \text{NO}_2 + \text{M} \rightarrow \text{ClONO}_2 + \text{M}$  might be rapid enough to be significant in the stratospheric chemistry. Subsequent laboratory studies showed that the reaction was significant and  $\text{ClONO}_2$  should be present in the stratosphere in the several hundred ppt range.  $\text{ClONO}_2$  is a moderately strong infrared absorber with bands occurring in the  $780 \text{ cm}^{-1}$ ,  $1292 \text{ cm}^{-1}$ , and  $1728 \text{ cm}^{-1}$  region. Infrared solar spectra obtained from balloons during sunset covering the  $780 \text{ cm}^{-1}$  and  $1292 \text{ cm}^{-1}$  regions have been examined for indications of absorption due to  $\text{ClONO}_2$ . The  $780 \text{ cm}^{-1}$  was examined first since spectra were available covering that region at the time that Rowland put forth the hypothesis. At the resolution achieved in those spectra no absorption due to  $\text{ClONO}_2$  could be observed and thus only an upper limit for  $\text{ClONO}_2$  could be determined. During a subsequent flight  $1292 \text{ cm}^{-1}$  spectra covering the region was obtained at a resolution of  $0.15 \text{ cm}^{-1}$ . These spectra exhibited a small absorption which was tentatively identified as being due to  $\text{ClONO}_2$  and yielded a mixing ratio for the compound of 2 ppbv at 26 km. Spectra covering the region at a resolution of  $0.015 \text{ cm}^{-1}$  were obtained during a balloon flight made October 27, 1978. At this resolution it is possible to identify a broad absorption due to  $\text{ClONO}_2$  and to determine an altitude profile for the compound. The profile is shown in Figure 6, (Murcray et al., 1979).

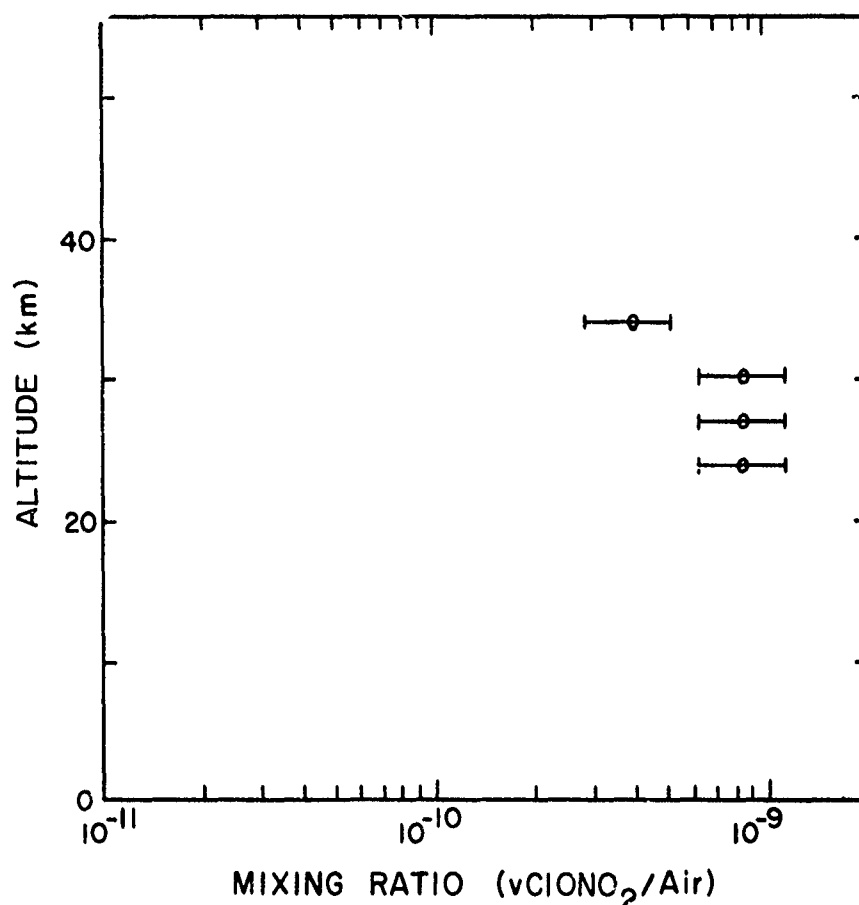


Fig. 6. Chlorine nitrate mixing ratio profile observed at sunset at Holloman AFB on October 29, 1978 by Murcray et al., (1979).

#### SUMMARY AND CONCLUSIONS

In the discussion above I have attempted to summarize the current measurement status of the various odd nitrogen species involved in the photochemistry of the stratospheric ozone layer. The summary is intended to be illustrative rather than exhaustive, and the results obtained by some investigators have not been included. Since the majority of the measurements have been made at midlatitude (~30°N), the discussion has emphasized these results. Therefore, I have included only selected higher latitude profiles obtained by investigators as part of a coordinated effort under project Stratoprobe.

Examination of the results obtained to date reveals a large variability in the observations, which in many cases was not expected. This has led to considerable discussion among investigators concerning the absolute accuracy of various techniques and adequacy of the various data bases, as well as the basic question of why the variability is present. It also pointed out the need for simultaneous measurements of compounds closely related chemically. It is easy to state the requirement, but difficult to implement the measurements since, in many cases, quite different techniques are used. When coordinated measurements are made, as in project Stratoprobe, they may lead to additional questions since quite often the results are not in good agreement with the theory.

Also notable in the above discussion is the small amount of data available for many of the species--despite the fact that, in some cases, such a need has existed for nearly ten years. It is apparent that additional measurements of many of these constituents are necessary, particularly if they can be made simultaneously with those of other constituents of the same family.

- Ackerman, M., D. Frimout, C. Muller, D. Nevejans, J.C. Fontanella, A. Girard, L. Gramont and N. Louisnard, Recent stratospheric spectra of NO and NO<sub>2</sub>, Can. J. Chem., 52, 1532-1535, 1974.
- Ackerman, J., J.C. Fontanella, D. Frimout, A. Girard, N. Louisnard and C. Muller, Simultaneous measurements of NO and NO<sub>2</sub> in the stratosphere, Planet. Space. Sci., 23, 651, 1975.
- Aiken, A.C. and E.J.R. Maier, A balloon-borne photoionization mass spectrometer for measurement of stratospheric gases, Rev. Sci. Instr., 49, 1034, 1978.
- Crutzen, P.J., Ozone production notes in an oxygen-hydrogen-nitrogen oxide atmosphere, Journal of Geophysical Research, 76, 7311, 1971.
- Farmer, C.B., Infrared measurements of stratospheric composition, Can. J. Chem., 52, 1544-1559, 1974.
- Fontanella, J.C., A. Girard, L. Gramont, and N. Louisnard, Vertical distribution of NO, NO<sub>2</sub>, and HNO<sub>3</sub> as derived from stratospheric absorption infrared spectra, Applied Optics, 14, 825, 1975.
- Gille, J.C., P.L. Bailey, and J.M. Russell, III, Temperature and composition measurements from the LRIR and LIMS experiments on Nimbus-6 and -7, Proc. of the Roy. Meteorol. Soc., Lon., in press, 1979.
- Girard, A., J.C. Fontanella, R. Giraudet, and N. Louisnard, Simultaneous measurements of nitrogen dioxide and nitric acid in the lower stratosphere, J. de Chimie Physique, 74, 7-8, 809, 1977.
- Goldman, A., F.G. Fernald, W.J. Williams, and D.G. Murcray, Vertical distribution of NO<sub>2</sub> in the stratosphere as determined from balloon measurements of solar spectra in the 4500 Å region, Geophys. Res. Lett., 5, 257, 1978.
- Jarnot, R.F., Radiometric measurements of atmospheric minor constituents, D. Phil. Thesis, Oxford University, 1976.
- Jeseon, J.P., L.C. Glasgow, D.L. Filkin, and C. Miller, The stratospheric abundance of peroxy-nitric acid, G.R.L., 4, 513-516, 1977.
- Johnston, H.S., Reduction of stratospheric ozone by nitrogen oxide catalysts from SST exhaust, Science, 173, 517, 1971.
- Kerr, J.B., and C.T. McElroy, Measurement of stratospheric nitrogen dioxide from the AES stratospheric balloon program, Atmosphere, 14, 166, 1976.
- King, P., I.R. McKinnon, J.G. Mathieson, and I.R. Wilson, Upper limit to stratospheric N<sub>2</sub>O<sub>5</sub> abundance, J. Atmos. Sci., 33, 1657, 1976.
- Lazrus, A.L., and B.W. Gandrud, Distribution of stratospheric nitric acid vapor, J. Atmos. Sci., 31, 1102-1108, 1974b.
- Loewenstein, M., W.S. Borucki, H.T. Savage, J.G. Borucki, and R.C. Whitten, Geographical variations of NO and O<sub>3</sub> in the lower stratosphere, J. Geophys. Res., 83, 1875, 1978.
- Loewenstein, M., and H.F. Savage, Latitudinal measurements of NO and O<sub>3</sub> in the lower stratosphere from 5° to 82° North, G.R.L., 2, 448-450, 1975.
- Mankin, W.G., and M.T. Coffey, Airborne fourier transform spectroscopy, Topical Meeting on Atmospheric Spectroscopy, Keystone, Colorado, August 30 - September 1, 1978.
- Mason, C.J. and J.S. Horvath, The direct measurement of nitric oxide concentration in the upper atmosphere by a rocket-borne chemiluminescent detector, G.R.L., 3, 391, 1976.
- Murcray, D.G., D.B. Barker, J.N. Brooks, A. Goldman and W.J. Williams, Seasonal and latitudinal variation of the stratospheric concentration of HNO<sub>3</sub>, G.R.L., 2, 223-225, 1975.
- Murcray, D.G., A. Goldman, F.H. Murcray, F.J. Murcray, W.J. Williams, Stratospheric distribution of ClONO<sub>2</sub>, G.R.L., 6, 857-859, 1979.
- Murcray, D.G., T.G. Kyle, F.H. Murcray, W.J. Williams, Nitric acid and nitric oxide in the lower stratosphere, Nature, 218, 78-79, 1968.
- Murcray, D.G., F.H. Murcray, W.J. Williams, T.G. Kyle, and A. Goldman, Variation of the infrared solar spectrum between 700 cm<sup>-1</sup> and 2240 cm<sup>-1</sup> with altitude, Applied Optics, 8, 2519, 1969.
- Murcray, D.G., W.J. Williams, D.B. Barker, A. Goldman, C. Bradford, and G. Cook, Measurements of constituents of interest in the photochemistry of the ozone layer using infrared techniques. WMO Symposium on the Geophysical Aspects and Consequences of Changes in the Composition of the Stratosphere, Toronto, 26-30 June 1978.
- Noxon, J.F., Stratospheric NO<sub>2</sub> II: global behavior, J. Geophys. Res., in press, 1979.
- Noxon, J.F., R.B. Norton, and W.R. Henderson, Observation of atmospheric NO<sub>3</sub>, G.R.L., 5, 675-678, 1978.
- Patel, C.K.N., E.G. Burkhardt and C.A. Lambelt, Spectroscopic measurement of stratospheric nitric oxide and water vapor, Science, 184, 1172, 1974.
- Ridley, B.A., J.T. Bruin, H.I. Schiff and J.C. McConnell, Altitude profile and sunset decay measurements of stratospheric nitric oxide, Atmosphere, 14, 180-188, 1976.

MURCRAY

- Ridley, B.A., H.I. Schiff, A.W. Shaw, L. Bates, C. Howlett, H. LeVaux, C.R. Megill, T.E. Ashenfelfen, Measurements of nitric oxide in the stratosphere between 17.4 and 22.9 km, Nature, 245, 310, 1974.
- Rowland, F.S., J.E. Spencer, and M.J. Molina, Stratospheric formation and photolysis of chlorine nitrate, J. Phys. Chem., 80, 2711-2713, 1976.

# NITRIC OXIDE IN THE UPPER STRATOSPHERE AND MESOSPHERE

William Swider

Air Force Geophysics Laboratory, Hanscom AFB, MA 01731

## Abstract

The distribution of nitric oxide in the mesosphere and upper stratosphere is reviewed. Although nitric oxide is recognized as being of great significance to D-region formation in the upper mesosphere and ozone destruction in the upper stratosphere, little information is available concerning the vertical height distribution of this gas at these altitudes. There is no major NO production mechanism in these regions. Sources for NO exist in the lower thermosphere/E-region and the lower stratosphere. Hence, the vertical distribution of nitric oxide is thought to be strongly controlled by eddy diffusion at upper stratosphere and mesosphere heights. Nitric oxide profiles obtained from gamma band and chemiluminescent techniques are compiled along with profiles deduced from ionospheric composition measurements. Other data, including satellite results for upper boundary (near 100 km) trends, are considered briefly. The greater preponderance of mesospheric nitric oxide at polar latitudes in winter is attributed to a lower diurnally integrated photodissociation rate. Except perhaps for winter high-latitude conditions, nitric oxide appears to attain a local minimum near 80 km. A mean mid-latitude NO profile is presented. It is suggested that the 1-0 gamma band scattering factor may vary somewhat with solar activity.

INTRODUCTION: Historically, Nicolet [1945] first suggested that NO might play a role in the atmosphere. In particular, he suggested that the quiet D-region might have its origin in the ionization of NO by the strong solar line, HLy $\alpha$ , which penetrates into the upper mesosphere because of an atmospheric window in O<sub>2</sub> near 122 nm. Many years passed before the appropriate experiments could be performed. Finally, Jursa et al., [1959], with a rocket-borne absorption spectroscopic technique, reported that they were unable to observe a 10<sup>16</sup> cm<sup>-2</sup> column of NO, a detectable limit, and suggested that the column concentration was likely less than 10<sup>15</sup> cm<sup>-2</sup>, with, therefore, NO concentrations of not more than 10<sup>8</sup> cm<sup>-3</sup> at altitudes of 63 to 87 km. A few years later, Barth [1964] measured 1.7 x 10<sup>14</sup> cm<sup>-2</sup> for column NO above 85 km through successful application of a scanning ultraviolet spectrometer. At the end of the decade, Crutzen [1970] introduced the idea that nitric oxide might catalytically reduce atmospheric ozone to some extent.

However, significant nitric oxide may be, the determination of the distribution of this minor constituent has been difficult, especially in the upper stratosphere and lower mesosphere, regions inaccessible to balloons and satellites, except by remote sensing. Hence, our knowledge of the distribution of NO at 40-100 km relies heavily on models. Since little production or loss of nitric oxide occurs in the 40-100 km height interval, its profile is strongly determined by transport (eddy diffusion) processes. The main loss of NO in this region is by means of the process NO + N → N<sub>2</sub> + O, which is slow because both reactants are minor atmospheric species. Brasseur and Nicolet [1973] found that the major stratospheric production of NO, N<sub>2</sub>O + O(<sup>1</sup>D) → NO + N, decreases with altitude, being between 45 and 0.9 cm<sup>-3</sup> s<sup>-1</sup> at 40 km for a solar zenith angle of 60°, decreasing to between 1.0 and 2 x 10<sup>-2</sup> at 50 km depending upon seasonal and latitudinal conditions. Above this altitude NO is produced only as a result of the ionization of the atmosphere by cosmic rays, except for



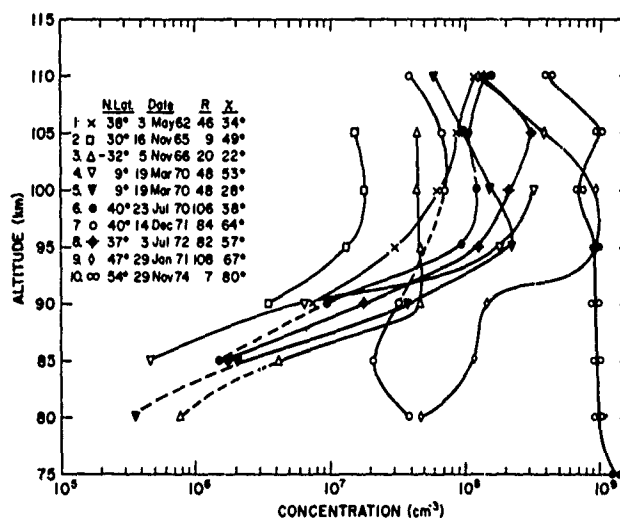
special events like an SPE. The NO production rate resulting from cosmic ray ionization is essentially equal to the ion production rate, and by 60 km a rate of only  $1.4 \times 10^{-2}$  to  $1.1 \times 10^{-1} \text{ cm}^{-3} \text{ s}^{-1}$ , depending upon latitude, is attained (Brasseur and Nicolet [1973]). Above this height, X-rays and especially with E-region heights, EUV radiation, eventually lead to NO formation (e.g. Strobel [1971]; Kondo [1977]).

In this paper we survey the available data concerning NO at 40-100 km. Various problems/concepts concerning the NO distributions at these altitudes are discussed.

#### NITRIC OXIDE DISTRIBUTIONS IN THE UPPER MESOSPHERE AND LOWER THERMOSPHERE

a. Ionic Data: The chemistry of  $\text{NO}^+$  ions is very simple in the upper mesosphere/lower thermosphere where  $\text{N}_2^+ + \text{O} \rightarrow \text{NO}^+ + \text{N}$  is unimportant as compared to  $\text{N}_2^+ + \text{O}_2 \rightarrow \text{O}_2^+ + \text{N}_2$  and where  $\text{NO}^+$  is lost only by recombining with electrons,  $\text{NO}^+$  being generated by the process  $\text{O}_2^+ + \text{NO} \rightarrow \text{NO}^+ + \text{O}_2$  and by direct ionization of NO by  $\text{H Ly}\alpha$  at 121.6 nm. This simple chemistry enables NO profiles to be determined from the analysis of daytime ion composition profiles. Ten such profiles ascertained by Swider [1978] are shown in Figure 1.

Fig. 1 Nitric oxide distributions determined from ion composition experiments for the quiet daytime D-region [from Swider 1978]. The latitudes, dates, sunspot numbers and solar zenith angles are as indicated.

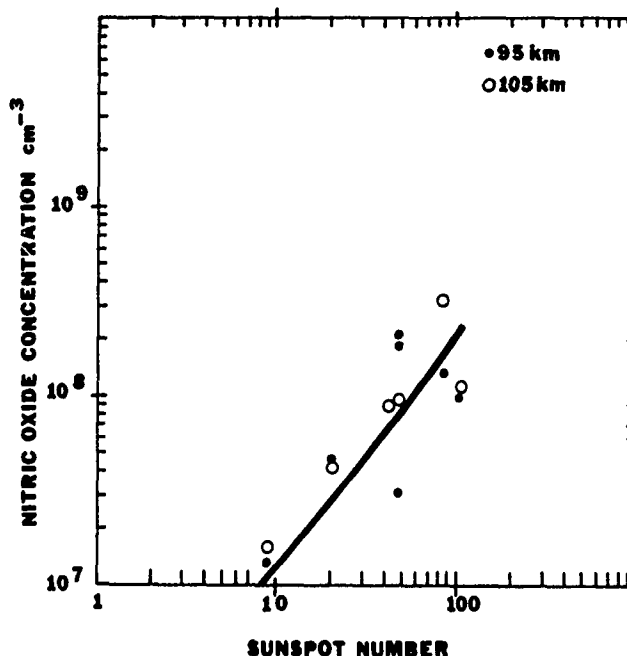


Ignoring the winter, high latitude profiles (7, 9 and 10) for the moment, a striking feature of the remaining profiles is the rather sharp gradient in the nitric oxide concentration below 90 km. This strong NO gradient suggests that vertical transport, as represented by an eddy diffusion term, would require a coefficient near the minimum one chosen by Brasseur and Nicolet [1973], cf. Hunten and Strobel [1974]. The ionospheric requirement of decreasing NO with decreasing altitude near 85-90 km has long been recognized (e.g. Nicolet [1965]; Keneshea et al., [1970]; Swider [1972]). The sharp gradient in NO shown in Figure 1 is certainly compatible with a similar well known gradient in electron concentration profiles for these heights Mechtley et al., [1972].

There is no clear latitudinal pattern associated with the non-winter profiles shown in Figure 1. However, as Golshan and Sechrist [1975] found in their study of NO deduced from ionic composition measurements in the E-region, there seems to be a dependence on solar activity. In Figure 2, nitric oxide is plotted versus sunspot number for two altitudes, 95 and 105 km. The straight line is an "eyeball" fit to the scattered data. (A more careful analysis probably would not yield much better results, but would indicate the degree of reliability.) The trend should not be too surprising, however, since EUV and X-ray radiation do increase with solar activity and odd nitrogen formation above 80 km originates in conjunction with the atmospheric absorption of these radiations. On the other hand, the curve is strongly dependent on the one low sunspot number result.

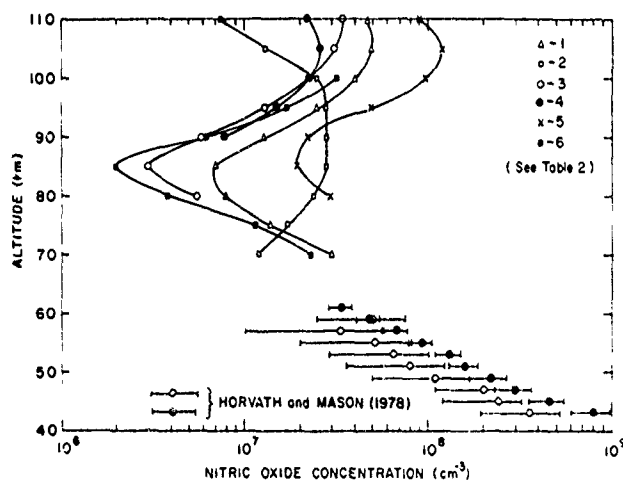
b. Gamma Band Data: Barth [1964] first observed nitric oxide in the high atmosphere, specifically, the upper mesosphere and lower thermosphere. His measurements were based upon the fluorescence of the gamma bands of NO in sunlight, the 1-0 band at 215.5 nm being

Fig. 2 Nitric oxide concentrations versus sunspot number for the indicated altitudes, based on the seven non-winter profiles shown in the previous figure.



the strongest feature. Several other nitric oxide profiles have been published since Barth [1964],[1966a] presented his original profile, not including three subsequent rocket observations of the NO  $\gamma$  - bands Barth,[1966b] for which profiles have never been presented. Table 1 lists the information pertinent to the results obtained by other investigators. The actual data for the six profiles listed (Meira's two profiles being combined) are shown in Figure 3. The first three profiles have been corrected in terms of a specific fluorescence rate of  $7.7 \times 10^{-6} \text{ s}^{-1}$  for the 1-0 gamma band of NO Barth[1966b]; Cravens [1977].

Fig. 3 Nitric oxide concentrations in the mesosphere. Details regarding the upper ( $\gamma$ -band derived) profiles are given in Table 1. The lower profiles are discussed in the text.



Comparison of the data suggests that Rayleigh scattering may not have been subtracted properly from Tisone's [1973] results. The results of Barth [1966a] are omitted because the same remark may apply to his data below 90 km. The largest nitric oxide concentrations are those of Witt et al., [1976] for which the latitude and sunspot number are also the highest among the six profiles. (Witt and Stegman [1977] have reported an even greater NO peak

# SWIDER

concentration, about  $1.5 \times 10^9 \text{ cm}^{-3}$  at 102 km, for a midnight flight on 7 March 1975 at  $67^\circ\text{N}$  as based on the continuum emission from  $\text{NO} + \text{O} \rightarrow \text{NO}_2 + \text{hv}$ .) Meira's [1971] profiles were obtained during D-region winter anomaly conditions (Geller and Sechrist [1971]). The three profiles numbered 3, 4 and 6 in Figure 3, all associated with Tohmatsu, are all very similar despite somewhat different conditions (Table 1). A plot of the 95 km data for the six profiles versus sunspot number would yield a mean slope about one-half that for the ion-based data (Figure 2).

Table 1

## Rocket-borne References for $\gamma$ -Band NO Data

#	Reference	Date	R	Kp	$\chi$	Lat. ( $^\circ\text{N}$ )
1.	<u>Meira</u> [1971]	1/31/69	95	2-	$63^\circ$	38
		2/6/69	101	2°	$64^\circ$	38
2.	<u>Tisone</u> [1973]	5/26/71	35	2°	$90^\circ(\text{AM})$	22
3.	<u>Tohmatsu and Iwagami</u> [1975]	8/19/73	7	1-	$90^\circ(\text{PM})$	31
4.	<u>Tohmatsu and Iwagami</u> [1976]	3/26/76	42	4	$82^\circ(\text{AM})$	9
5.	<u>Witt et al.</u> [1976]	6/8/68	119	2+	$87^\circ(\text{PM})$	69
6.	<u>Baker et al.</u> [1977]	10/4/73	50	1°	$93^\circ(\text{PM})$	32

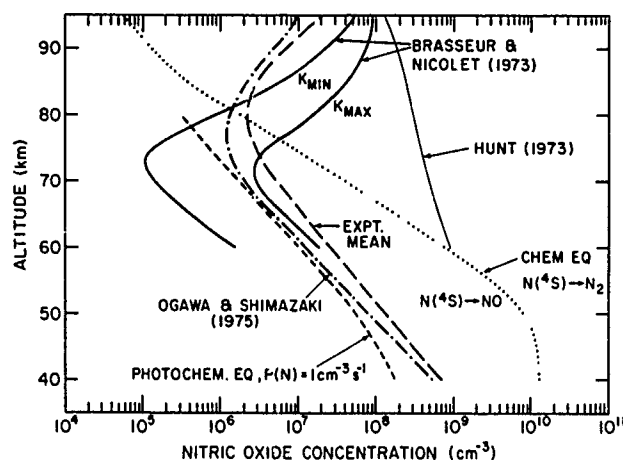
c. Low Altitude Results: Measurements by Horvath and Mason [1978] are shown also in Figure 3. Their results are the only ones available for the low mesosphere and upper stratosphere and unfortunately their work may have been discontinued. They used rocket-borne chemiluminescent detectors, making observations on 9 April 1975 (open circles) and 19 March 1976 near 1400 hours local time. Both rockets were launched from Wallops Island, Virginia. Their results are compatible with a balloon-borne measurement by Drummond et al. [1977], a  $6.5 \pm 2.0$  ppbv mixing ratio attained at peak altitudes, 40-45 km. Maier et al. [1978] reported a similar mixing ratio for 37.5 km,  $5.7 \pm 0.35$  ppbv using a balloon-borne photoionization mass spectrometer; the peak value they encountered between 29.8 km and 38.4 km. In general, various balloon observations of nitric oxide show a rise in its mixing ratio with altitude from less than 1 ppb below 20 km to  $\sim 5$  ppb near 35 km. (A summary of these measurements is given in Figure 2 of Maier et al. [1978]).

Pontano and Hale [1970] obtained measurements of an ionizable constituent with a mixing ratio of  $2 \times 10^{-8} - 4 \times 10^{-8}$  in the same altitude region as Horvath and Mason [1978]. The measurements were accomplished by using a flashing H $\gamma$  lamp in post-sunset (at altitude) flights. This is certainly a less direct way of deducing NO as compared to Horvath and Mason [1978] yet these mixing ratios are not vastly different than those of the latter, whose mixing ratios for their second flight ranged from about  $10^{-8}$  near 45 km to  $6 \times 10^{-9}$  at 60 km. However, other constituents may have been ionized besides NO in the flashing lamp experiment.

d. Global Information: The enormous global coverage capabilities of satellites have provided much information about NO at the 105 km level from observation of sunlight scattered by the (1,0) gamma band of NO. In general, NO concentrations at this altitude are about  $2 \times 10^{-7} \text{ cm}^{-3}$  worldwide for quiet conditions whereas for even moderate levels of magnetic activity, [NO] increases with latitude (Cravens et al. [1979]). Peak concentrations of nitric oxide near 105 km, as deduced from nighttime auroral ion composition measurements using rockets, have been found to range from  $10^8$  to  $10^9 \text{ cm}^{-3}$  (Swider and Narcisi [1977]). Satellite  $\gamma$ -band information appears to give a somewhat smaller increase in NO (3-4x) for auroral latitudes as compared with mid-latitudes (Rush and Barth [1975]). However, since the satellite data is an average over a much larger volume than rocket data ( $\text{km}^2$  vs  $\text{m}^3$ ), these differences are not necessarily incompatible.

NITRIC OXIDE MODELS: In Figure 4, the curve EXPT.MEAN is our best reasonable match of the nitric oxide profiles illustrated in Figure 3. The theoretical distribution of Ogawa and Shimazaki [1975] is their steady-state Model B with efficiencies of 0.5:1.0 or 1.0:0.5 for the relative formation  $\text{N}(^2\text{D})/\text{N}(^4\text{S})$  in photodissociation processes and chemical reactions,

Fig. 4 Theoretical profiles for nitric oxide in the upper atmosphere compared with a mean experimental profile derived from the data in the previous figure.



respectively, with a mean solar zenith angle of  $67.5^\circ$ . Below 70 km, efficiency ratio choices are not important except for highly disturbed ionospheric conditions. The  $K_{MAX}$  model of Brasseur and Nicolet [1973] fit the experimental mean curve very well below 70 km, above this height, the poorer fit is due largely to their choice of  $10^8 \text{ cm}^{-3}$  for NO at the upper boundary (100 km) of the model. The computed profile of Kondo [1977] is not shown. It is in good agreement with the experimental mean curve but his model has a lower boundary of 70 km. It should be noted that the NO photodissociation rates in these models are all somewhat high because  $J_\infty(\text{NO})$  is now given as about  $4 \times 10^{-6} \text{ s}^{-1}$  Frederick and Hudson [1979] and  $5 \times 10^{-6} \text{ s}^{-1}$  Nicolet and Cieslik [1979] as compared to  $1.5 \times 10^{-5} \text{ s}^{-1}$  Cieslik and Nicolet [1973].

The nitric oxide profile of Hunt [1973] is displayed even though his application of a rather low,  $J_\infty(\text{NO}) \approx 10^{-6} \text{ s}^{-1}$ , photodissociation coefficient gives an NO distribution at considerable variance with the mean. (He acknowledged that a higher rate might be applicable.) His model, as we shall discuss later, might be roughly appropriate, at times, to winter conditions.

The lower straight portion (40–65 km) of the experimental mean curve has a constant scale height of 6.3 km, suggestive of a photochemical and/or mixing distribution. We know the latter type distribution is more appropriate and observe that  $H_p$ , the pressure scale height of the U.S. Standard Atmosphere [1976], decreases slowly from 7.4 km at 40 km to 7.0 km at 65 km, with  $H_p = 6.2 \text{ km}$  at 75 km.

The simplest chemical distribution, considered as perhaps appropriate two decades ago, may be ascertained from the equations

$$(1) \quad \text{N} + \text{O}_2 \rightarrow \text{NO} + \text{O}, \quad k_1 = 2.4 \times 10^{-11} e^{-3975/T}$$

$$(2) \quad \text{N} + \text{NO} \rightarrow \text{N}_2 + \text{O}, \quad k_2 = 1.5 \times 10^{-12} T^{1/2}$$

which may be solved for NO, yielding the dotted line distribution in Figure 4 labeled "CHEM.EQ.". Although inappropriate as an NO distribution, this curve, as indicated, represents a dividing line between whether ground state atomic nitrogen,  $\text{N}(^4\text{S})$ , is converted into NO via  $\text{O}_2$ , or reacts with NO to destroy odd nitrogen by producing  $\text{N}_2$ . Above 80 km, we see that  $\text{N}(^2\text{D})$ , which reacts rapidly with  $\text{O}_2$  to form NO, must be produced at a much more significant rate than  $\text{N}(^4\text{S})$  since the experimental curve shows considerable excess NO over the CHEM.EQ. distribution, transport considerations notwithstanding.

If the process

$$(3) \quad \text{NO} + h\nu \rightarrow \text{N} + \text{O}$$

is included with the above set, no equilibrium solution is obtainable except  $NO = 0$ . However, a photochemical equilibrium solution is possible (Brasseur and Nicolet [1973]) if a source of nitrogen atoms,  $P(N)$ , is included, as, for example, those generated in the dissociation of  $N_2$  by cosmic rays. We have determined a solution,

$$(4) \quad [NO] = \frac{-k_2 P(N) + \sqrt{[k_2 P(N)]^2 + 8 k_1 k_2 J_{NO} [O_2] P(N)}}{4 k_2 J_{NO}}$$

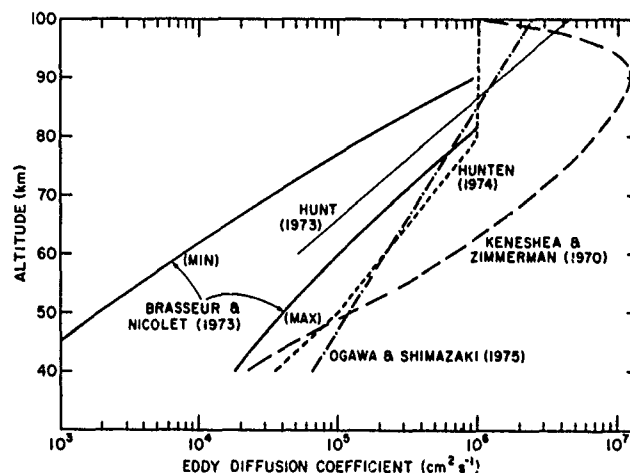
which may be simplified ( $Z \lesssim 80$  km) to

$$(5) \quad [NO] \approx \frac{\sqrt{k_1 [O_2] P(N)}}{2 k_2 J_{NO}}$$

where  $[O_2]$  is the molecular oxygen concentration. The solution of this equation is depicted as a dashed line in Figure 4 for  $P(N) = 1 \text{ cm}^{-3} \text{ s}^{-1}$ . Although this distribution is not substantially different from the experimental results for  $Z \lesssim 70$  km, the choice  $P(N) = 1 \text{ cm}^{-3} \text{ s}^{-1}$  is rather large and inappropriate, therefore, for normal, quiet conditions. However, this result may be feasible for short time periods during SPE (PCA) and REP conditions, when even  $P(N) \gg 1$  is possible. Note that formula (4) may then be more appropriate.

Since  $P(N) \ll 1$  normally for  $40 \lesssim Z \lesssim 80$  km, transport, in the form of the vertical eddy diffusion coefficient,  $K_e$  in the 1-D models, has a major role in the distribution of NO at these altitudes. In Figure 5, a variety of  $K_e$  profiles is given. There is certainly no unanimous choice, but most workers assume profiles lying between the extreme variations

Fig. 5 Selected profiles of the 1-D eddy diffusion coefficient.

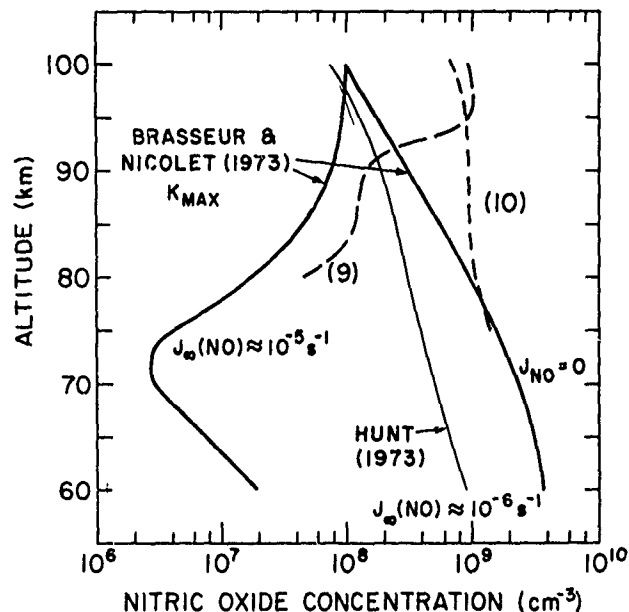


given by the minimum profile of Brasseur and Nicolet [1973] and the profile of Zimmerman (cited by Keneshea and Zimmerman [1970]). Not only is there no unique profile, but seasonal and latitudinal variations may be operative which cannot be appreciated in terms of basically global 1-D models. Ultimately, 3-D models may be required since satellite observations show that near 105 km, the world-wide NO distribution is fairly inhomogeneous, Cravens and Stewart [1978]. Winds likely are an important factor in this inhomogeneity. In any case, it should be appreciated that the choice of  $K_e$  is not inconsequential to the derived NO profile and arbitrary adjustments can be made to a certain extent in order to improve model-data agreement, an agreement which may thus be somewhat artificial and better reside in the adjustment of one or more other parameters, such as the average solar flux.

In considering solar flux levels, we present two NO distributions by Brasseur and Nicolet [1973] and one by Hunt [1973] in Figure 6 along with two profiles (Figure 1) determined by

Swider [1978] from ion composition data for high latitude winter conditions. We see that these excessive NO profiles may be acceptable in terms of a lesser NO photodissociation rate for wintertime at high latitudes. (It should be appreciated that "winter" applies to the months about solstice, i.e. November, December, January and February, rather than the calendar definition.) The higher levels of NO near 100 km are presumably associated with auroral production mechanisms for odd nitrogen. Brasseur and Nicolet [1973] choose  $10^8$   $\text{cm}^{-3}$  for the 100 km upper boundary of their (non-auroral) model.

Fig. 6 Model nitric oxide profiles for three different photodissociation levels of NO compared with two high-latitude winter profiles from Figure 1.



Energetic particles penetrate into the D-region during relativistic electron particle (REP) events and polar cap absorption (PCA)/solar proton events (SPE). Certain of these latter events are both of sufficient intensity and enough energy (for penetration) to significantly increase  $\text{NO}_x$  in the upper stratosphere (Crutzen et al., [1975]). Heath et al., [1977] have, in fact, observed a roughly 20% decrease in the  $\text{O}_3$  content above the 4 mb level for the August 1972 SPE, the largest event on record, in rough qualitative agreement with theory. But a detailed time history calculation of the problem should be undertaken including the important changes in chemistry which have occurred since that analysis.

In a more typical SPE, little ionization is generated in the stratosphere. Weeks et al. [1972] found  $\text{O}_3$  decreased in the mesosphere during the November 2-5, 1969, SPE. Swider and Keneshea ([1973]; see also Swider et al. [1978]) found that this increase could be attributable to  $\text{HO}_x$  concentrations enhanced by ionic processes, if the key reaction  $\text{OH} + \text{HO}_2 \rightarrow \text{H}_2\text{O} + \text{O}_2$  were near  $2 \times 10^{-11}$   $\text{cm}^3/\text{s}$  rather than the nearly order of magnitude higher rate coefficient measured by one group. The increase in mesosphere  $\text{NO}_x$  for this event was found to be small, having negligible impact on mesospheric ozone.

**DISCUSSION AND CONCLUSIONS:** There are very few measured nitric oxide profiles available for the mesosphere and upper stratosphere considering that important latitudinal and seasonal variations may exist. Rocket-borne measurements of the  $\gamma$ -band system of nitric oxide yield NO profiles for the upper mesosphere which generally appear to show a minimum concentration value near 85 km (Figure 3). It seems odd that the minimum occurs here for all profiles, except one, regardless of the concentration values. The precision of the correction for Rayleigh scattering may be involved. In presenting a mean experimental NO profile in Figure 4, we lowered the NO to 80 km, in order to be better reconciled with the data for NO in the low mesosphere/upper stratosphere.

Nitric oxide concentrations derived from ionic composition measurements in the upper mesosphere (Figure 1) are similar to the  $\gamma$ -band results except that they generally run higher than the  $\gamma$ -band results. Thus, at 100 km, the mean  $\gamma$ -band result is about  $4.5 \times 10^7 \text{ cm}^{-3}$  or  $2.5 \times 10^7 \text{ cm}^{-3}$  if the high latitude ( $69^\circ\text{N}$ ) winter result is ignored. In comparison, the ionic data yields a mean value of  $1.2 \times 10^8 \text{ cm}^{-3}$  which would have been more compatible with a lower value for the 1-0 fluorescent g- factor.

There is still some uncertainty in the atomic factors for g(1-0). Cravens [1977] suggests  $7.2$  or  $7.7 \times 10^{-6} \text{ s}^{-1}$  depending upon whether experimental or theoretical branching ratios are adopted. There does not appear to have been any discussion of whether the solar flux at 215.5 nm changes to any significant extent. Barth [1966b] assumed  $5.23 \times 10^{11} \text{ photons cm}^{-2} \text{ A}^{-1} \text{ s}^{-1}$  in determining  $7.7 \times 10^{-6} \text{ s}^{-1}$  for g(1-0). However, a factor as great as 2 may be involved although a lower factor is likely (Callis and Nealy [1978]; Penner and Chang [1978]). A change in the solar flux does not clarify why, as noted earlier, the NO profiles determined from  $\gamma$ -band observations have a solar variability half as great as that of the ion-composition derived NO profiles. In fact, a solar variable g(1-0) would make the problem worse since it could imply that  $\gamma$ -band observations of an increase in NO with solar activity might be false, and attributable only to the increase in the solar flux factor for g(1-0).

At 90 km, both sets of data are compatible with a mean NO concentration of about  $10^7 \text{ cm}^{-3}$ , ignoring the high latitude winter ionic data results. In fact, a median value of  $8 \times 10^6 \text{ cm}^{-3}$  might be even more appropriate. However, the ion composition based data suggest that the eddy diffusion coefficient at 80 - 100 km is close to the minimum  $K_e$  profile of Brasseur and Nicolet [1973]. This is not true of the winter profiles, where a greater eddy coefficient may be required. However, the excessive NO associated with these high latitude winter profiles undoubtedly results, at least in part, from the much lower diurnal photodissociation rate for NO (Figure 6).

Except maybe for very low magnetic activity, there appears to be more NO in the high latitude upper mesosphere. How much of this NO can be transported towards lower latitudes must be investigated carefully. The auroral zones occupy only a small portion of the earth's surface, as can be seen from Table 2. Transport into the mid-latitude region seems feasible, but must be patchy since transport is into a zone of larger area. It is unlikely that any significant amount of NO could be transported by winds into the tropical or even sub-tropical zones. Photodissociation of NO as it is transported equator-ward will help in its destruction since some of the atomic nitrogen generated will react with NO via  $\text{NO} + \text{N} \rightarrow \text{N}_2 + \text{O}$ , as opposed to recreating NO via  $\text{N} + \text{O}_2 \rightarrow \text{NO} + \text{O}$ , a slow process in the upper atmosphere (Figure 4).

Table 2

Area of the Earth in  $10^\circ$  Intervals

Interval (degrees)	Area (%)
0-10	17.36
10-20	16.84
20-30	15.80
30-40	14.28
40-50	13.32
50-60	10.00
60-70	7.37
70-80	4.51
80-90	1.52

For altitudes in the lower mesosphere/upper stratosphere, there is very little data, mainly the results of Horvath and Mason [1978]. There is probably no strong variation in nitric oxide at these altitudes for low and mid-latitudes. However, at high latitudes, there may be important differences. Darkness, especially for high latitude winter, prevents  $\text{NO}_2$  photodissociation from counteracting  $\text{NO} + \text{O}_3 \rightarrow \text{NO}_2 + \text{O}_2$ . Significant conversion to  $\text{NO}_2$  occurs up to roughly 60 km for even normal nighttime conditions.

In conclusion, we recommend a best (median) value of  $8 \times 10^6 \text{ cm}^{-3}$  for NO at 90 km and  $(5+3) \times 10^7 \text{ cm}^{-3}$  at 100 km exclusive of high latitudes ( $>40^\circ$ ) and especially winter high latitudes. Near 40 km, a daytime mixing ratio of  $(8+2) \times 10^{-9}$  appears to be appropriate with probably similar limitations.

#### REFERENCES

- Baker, K.D., A.F. Nagy, R.O. Olsen, E.S. Oran, J. Randhawa, D.F. Strobel and T. Tohmatsu, Measurement of the nitric oxide altitude distribution in the mid-latitude mesosphere, J. Geophys. Res., **82**, 3281-3286, 1977.
- Barth, C.A., Rocket measurement of the nitric oxide dayglow, J. Geophys. Res., **69**, 3301-3303, 1964.
- Barth, C.A., Rocket measurement of nitric oxide in the upper atmosphere, Planet. Space Sci., **14**, 623-630, 1966a.
- Barth, C.A., Nitric oxide in the upper atmosphere, Ann. Geophys., **22**, 198-207, 1966b.
- Brasseur, G. and M. Nicolet, Chemospheric processes of nitric oxide in the mesosphere and stratosphere, Planet. Space Sci., **21**, 939-961, 1973.
- Callis, L.B. and J.E. Nealy, Solar UV variability and its effect on stratospheric thermal structure and trace constituents, Geophys. Res. Lett., **5**, 249-252, 1978.
- Cravens, T.E., Nitric oxide gamma band emission rate factor, Planet. Space Sci., **25**, 369-372, 1977.
- Cravens, T.E. and A.I. Stewart, Global morphology of nitric oxide in the lower E-region, J. Geophys. Res., **83**, 2446-2452, 1978.
- Cravens, T.E., J.C. Gerard and A.I. Stewart, The latitudinal gradient of nitric oxide in the thermosphere, J. Geophys. Res., **84**, 2675-2680, 1979.
- Crutzen, P.J., The influence of nitrogen oxides on the atmospheric ozone content, Quart. J. Roy. Meteorol. Soc., **96**, 320-325, 1970.
- Crutzen, P.J., I.S.A. Isaken and G.C. Reid, Solar Proton events: stratospheric sources of nitric oxide, Science, **189**, 457-459, 1975.
- Frummond, J.W., J.M. Rosen and D.J. Hofmann, Balloon-borne chemiluminescent measurement of NO to 45 km, Nature, **265**, 319-320, 1977.
- Frederick, J.E. and R.D. Hudson, Predissociation of nitric oxide in the mesosphere and stratosphere, J. Atmos. Sci., **36**, 737-745, 1979.
- Golshan, N., and C.F. Sechrist, Jr., Seasonal and solar cycle variation of E-region nitric oxide, Radio Sci., **10**, 305-315, 1975.
- Heath, D.F., A.J. Krueger, and P.J. Crutzen, Solar Proton event: influence on stratospheric ozone, Science, **197**, 886-889, 1977.
- Horvath, J.J. and C.J. Mason, Nitric oxide mixing ratios near the stratopause measured by a rocket-borne chemiluminescent detector, Geophys. Res. Lett., **5**, 1023-1026, 1978.
- Hunt, B.G., A generalized aeronomic model of the mesosphere and lower thermosphere including ionospheric processes, J. Atmos. Terr. Phys., **35**, 1755-1798, 1973.
- Hunten, D.M., Vertical transport in atmospheres, pp. 59-72 in Atmospheres of Earth and the Planets, B.M. McCormac (Ed.), D. Reidel Publ. Co., Dordrecht-Holland, 1975.
- Hunten, D.M. and D.F. Strobel, Production and escape of terrestrial hydrogen, J. Atmos. Sci., **31**, 305-317, 1974.
- Jursa, A.S., Y. Tanaka and F. LeBlanc, Nitric oxide and molecular oxygen in the earth's upper atmosphere, Planet. Space Sci., **1**, 161-172, 1959.
- Keneshea, T.J. and S.P. Zimmerman, The effect of mixing upon atomic and molecular oxygen in the 70-170 km region of the atmosphere, J. Atmos. Sci., **27**, 831-840, 1970.
- Kondo, Y., A theoretical study of the variations of  $\text{NO}_x$  abundance in the upper atmosphere, (Ph.D. Dissertation) Proc. Res. Inst. of Atmospheric Sciences, Nagoya Univ., **24A**, January, 1977.
- Maier, E.J., A.C. Aiken and J.E. Ainsworth, Stratospheric nitric oxide and ozone measurements using photoionization mass spectrometry and UV absorption, Geophys. Res. Lett., **5**, 37-40, 1978.
- Mechtley, E.A., S.A. Bowhill and L.G. Smith, Changes of lower ionosphere electron concentrations with solar activity, J. Atmos. Terr. Phys., **34**, 1899-1907, 1972.
- Meira, L.G., Jr., Rocket measurements of upper atmospheric nitric oxide and their consequence to the lower ionosphere, J. Geophys. Res., **76**, 202-212, 1971.
- Nicolet, M., Contribution à l'étude de la structure de l'ionosphère, Inst. Roy. Met. Belgique, Mém. **19**, 74-236, 1945.
- Nicolet, M., Ionospheric processes and nitric oxide, J. Geophys. Res., **70**, 691-701, 1965.
- Nicolet, M., and S. Cieslik, The photodissociation of nitric oxide in the mesosphere and stratosphere, submitted to Planet. Space Sci., 1979.



- Ogawa, T. and T. Shimazaki, Diurnal variations of odd nitrogen and ionic densities in the mesosphere and lower thermosphere: simultaneous solution of photochemical-diffusive equations, J. Geophys. Res., 80, 3945-3960, 1975.
- Penner, J.E. and J.S. Chang, Possible variations in atmospheric ozone related to the eleven-year solar cycle, Geophys. Res. Lett., 5, 817-820, 1978.
- Pontano, B.A., and L.C. Fale, Measurements of an ionizable constituent of the low ionosphere using a Lyman-alpha source and blunt probe, Space Res., 10, 208-214, 1970.
- Rusch, D.W. and C.A. Barth, Satellite measurements of nitric oxide in the polar regions, J. Geophys. Res., 80, 3719-3721, 1975.
- Strobel, D.F., Diurnal variation of nitric oxide in the upper atmosphere, J. Geophys. Res., 76, 2441-2452, 1971.
- Swider, W., Reply, J. Geophys. Res., 77, 2000-2003, 1972.
- Swider, W., Daytime nitric oxide at the base of the thermosphere, J. Geophys. Res., 83, 4407-4410, 1978.
- Swider, W. and T.J. Keneshea, Decrease of ozone and atomic oxygen in the lower mesosphere during a PCA event, Planet. Space Sci., 21, 1969-1973, 1973.
- Swider, W., and R.S. Narcisi, Auroral E-region: ion composition and nitric oxide, Planet. Space Sci., 25, 103-116, 1977.
- Swider, W., T.J. Keneshea, and C.I. Foley, An SPE-disturbed D-region model, Planet. Space Sci., 26, 883-892, 1978.
- Tisone, G.C., Measurements of NO densities during sunrise at Kauai, J. Geophys. Res., 78, 746-750, 1973.
- Tohmatsu, T. and N. Iwagami, Measurement of nitric oxide distribution in the upper atmosphere, Space Res., 15, 241-245, 1975.
- Tohmatsu, T. and N. Iwagami, Measurement of nitric oxide abundance in the equatorial upper atmosphere, J. Geomag. Geo-elect., 28, 343-358, 1976.
- Weeks, L.H., R.S. Ciukay and J.R. Corbin, Ozone measurements in the mesosphere during the solar proton event of 2 November 1969, J. Atmos. Sci., 29, 1138-1142, 1972.
- Witt, G., J.E. Dye and N. Wilhelm, Rocket-borne measurements of scattered sunlight in the mesosphere, J. Atmos. Terr. Phys., 38, 223-238, 1976.
- Witt, G. and J. Stegman, Optical observation of enhanced nitric oxide abundance in the lower ionosphere following extended auroral activity, Space Res., 17, 285, 1977.

## MEASUREMENTS OF STRATOSPHERIC BROMINE

W. A. Sedlacek

Los Alamos Scientific Laboratory  
Los Alamos, New Mexico 87545

A. L. Lazrus and B. W. Gandrud

National Center for Atmospheric Research\*  
Boulder, Colorado 80307

### ABSTRACT

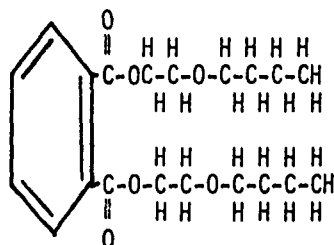
Acidic bromine containing molecules in the stratosphere were sampled using tetrabutyl ammonium hydroxide impregnated filters. Sampling was accomplished using WB-57F aircraft and high altitude balloons spanning latitudes from the equator to 75° N and altitudes up to 36.6 km. Analytical results are reported for four years of measurements and for laboratory simulations to determine filter collection efficiencies of a number of brominated species. Volume mixing ratios in air of the collected bromine species average about 10 ppbv in the stratosphere. Seasonal and latitudinal variability seems to be small.

In the late 1960's and early 1970's neutron activation analysis by Shedlovsky and by Sedlacek, of IPC filter papers collected on WB-57F aircraft flights [Cadle 1972] [Sedlacek 1973], revealed the presence of trace amounts of bromine and iodine in the lower stratosphere, but chlorine was not observed. Shortly thereafter a series of simultaneous collections with two different samplers using the same filter material, but different air velocities through the filter, gave the same sulfate concentration (particulate phase), but different nitric acid concentrations (vapor phase) [Sedlacek 1973]. Apparently the vapor phase was also collected on the filter, but at less than 100% efficiency. A 100% efficient vapor phase filter-sampling technique would have the very great advantage of being able to extract a particular species from an extremely large amount of air and thereby make possible measurements of very small traces of gas species. Therefore Lazrus et al [1975, 1976, and 1977] [Bonelli 1978] developed a method of impregnating the filters with a high molecular weight base to efficiently collect acidic vapor species. Very shortly thereafter Rowland and Molina [1975] published their classical paper suggesting the impact of chlorofluoromethanes on the stratospheric ozone layer. Wofsy et al [1975] also presented a model for the impact of the observed bromine on the ozone layer. Wofsy concluded that bromine was about five times as effective as chlorine for the catalytic destruction of ozone, but that since its concentration was about fifty times lower, bromine's impact on the ozone was small compared to that of chlorine. At that time the National Aeronautics and Space Administration (NASA) provided funding to make measurements of the spatial and temporal distributions of inorganic acidic chlorine species in the lower stratosphere using

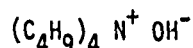
the filter technique. Since the bromine analysis came right along with the chlorine analysis, a data base for bromine concentrations was also established. Now Yung et al [1979] have put forth a model in which a synergistic relationship in the heterochemistry of the chlorine and bromine cycles causes a considerable enhancement in the catalytic destruction of ozone.

The sampling program was "piggybacked" on the regular flights of the Energy Research and Development Agency Projects "Airstream" and "Ashcan". Project Airstream utilizes the WB-57F aircraft to collect samples each April, July, and October. Samples are collected at four altitudes between 40,000 and 63,000 ft for each 3° of latitudinal span from the equator to 75° N. Project "Ashcan" utilizes high altitude balloons to collect samples at 70,000, 80,000, and 90,000 ft altitudes. Samples are collected each January, April, July, and October over Holloman Air Force Base in New Mexico; and also from Fairbanks, Alaska, and Panama on the April cycle. NASA funding provided balloons for additional flights at 105,000- and 120,000-ft altitudes on each cycle during the halogen measurement program.

The filter used is IPC 1478, which is a loose mat of cellulose fibers from cotton linters. The fibers have a cross section that is oval with about a 50  $\mu\text{m}$  major axis and a 30  $\mu\text{m}$  minor axis. Pressure drop across the filter is only a few inches of water even at very high face velocities. At face velocities greater than about 2000 ft/min particulates down to less than 0.05  $\mu\text{m}$  diameter collect with approximately 100% efficiency. The fibers are covered with a high molecular weight oil, kronisol, to prevent particles from being knocked off the filter after their initial collection. Kronisol is bis butoxy ethyl phthalate:



Prior to use each filter is washed repeatedly with deionized water until all soluble materials are leached out [Gandrud et al 1972]. After washing and drying, a highly purified alcohol solution of the high molecular weight base, tetrabutyl ammonium hydroxide (TBAH):

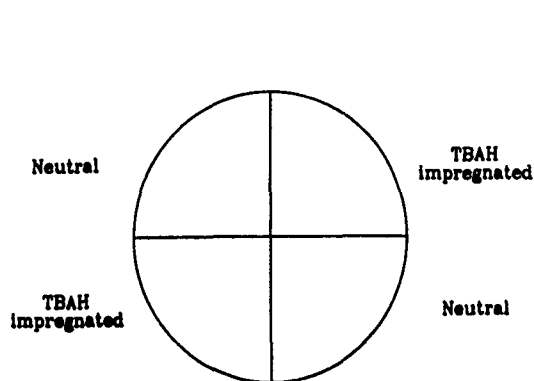


is sprayed on the filter. TBAH is a solid at room temperature and the resulting coating on the filter is probably a very fine coating of TBAH particles imbedded in the kronisol layer on the filter fibers. This provides a highly absorptive surface for acidic vapors in a most favorable geometry for exposure to the air passing through the filter.

The WB-57F aircraft-sampling system provides the capability for collecting up to 12 samples per flight by sequentially inserting filters into the sampler duct from a "record changer" type cartridge. Blanks for the entire sampling and analysis scheme are obtained by closing the sampler door and sequencing to the next filter immediately after opening the sampler door. The aircraft sampler duct is not symmetrical and hence a non-uniform deposition pattern of collection on the filter results. This has been adequately compensated for by segmenting the filter into quadrants with strips of "silastic" and combining opposite sections when the filters are cut for analysis. By coating two opposite quadrants with TBAH and leaving the other two neutral, as illustrated in Figure 1, both a neutral and a base impregnated collection are made on each filter.

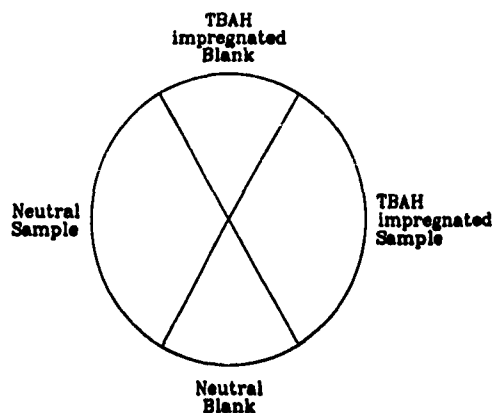
Air mass sampled is calculated based on instrumented calibrations of the sampler as a function of observed altitude, air speed, and temperature.

For the balloon flights, asymmetry of the sampler is not a problem, but only one filter can be used per sampler. The segmenting used is illustrated in Figure 2. The blank sections are masked off during sampling in order to provide a total sampling and analysis system blank.



Aircraft Sampler Filter

Figure 1.



Balloon Sampler Filter

Figure 2.

Two types of samplers are used on the balloons. For samples up to 90,000 ft a "direct flow sampler", DFS, is used in which a fan draws the air through the filter. At altitudes above 90,000 ft an "air ejector sampler", AES, is used in which an air ejector pump with a high velocity jet of  $N_2$  into a venturi is used to draw the air through the filter. Both samplers use a "PR-3" fan-type flowmeter to continuously measure the air mass being sampled. Both samplers have ducting to carry the exhaust air away from the sampler.

After the filters are returned to the laboratory, they are cut into the various neutral, TBAH-impregnated, and blank segments and sealed in ultraclean plastic bags to be extracted with deionized water. Aliquots are used to analyze colorimetrically for  $SO_4$ ,  $HNO_3$ ,  $NH_4$ ,  $Na$ , and  $Cl^-$ . Another aliquot is analyzed by neutron activation analysis for chlorine, bromine, and iodine.

The analysis scheme used is:

9-min irradiation  $\longrightarrow$  3-min delay  $\longrightarrow$  10-min gamma count (clock time)

The gamma rays emitted from atoms rendered radioactive by neutron absorption, are counted as a function of energy using a pulse height analyzer with the detector system diagrammed in Figure 3.

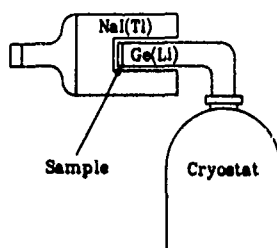
Anticoincident Compton Suppression  
Gamma Counting System

Figure 3.

The  $Ge(Li)$  signal is analyzed in anticoincidence with the  $NaI(Tl)$  signal so that whenever a gamma ray undergoes Compton scattering in the  $Ge(Li)$  detector and part of the energy is deposited in the  $NaI$  detector, the pulse height analyzer does not count that pulse. This results in suppression of the Compton continuum in the gamma ray spectrum by about a factor of 5 to 10 (dependent on the gamma energy) and enhances the sensitivity for low gamma-ray energy, single gamma emitting isotopes such as  $^{80}Br$ . The gamma energies used in the analysis are:

Isotope	$\gamma$ counted	$t_{1/2}$
$^{80}\text{Br}$	617 keV	4.5 hr
$^{38}\text{Cl}$	1642 keV	37.18 min
$^{75}\text{Ge}$	265 keV	79.0 min

The  $^{75}\text{Ge}$  comes from germanium which is added as a trace spike to each sample to act as an internal monitor for irradiation flux, counting geometry and counter deadtime. Samples are directly compared to standards (having similar ranges of concentrations to the samples) irradiated and gamma counted under the same analytical scheme, to calculate the concentrations of the various halogens.

These results are of course only indicative of the total amount of each halogen collected by the filter and do not tell us what chemical state existed in the atmosphere. In order to interpret the measured concentrations, a series of laboratory simulations were attempted to determine which chemical species were collected and at what efficiency. These simulations were conducted at relative humidities, temperatures, and air velocities through the filters that are comparable to typical mid-latitude balloon flight conditions. However, Ar carrier gas was used and the bromine concentrations were approximately one order of magnitude higher than typical ambient conditions. The bromine was injected into the carrier gas by passing the carrier gas stream through glass wool on which bromine had been absorbed and allowing it to saturate in bromine at the melting temperature of methanol. When  $\cdot\text{Br}$  was tested, it was produced in a microwave discharge a few inches before the carrier gas stream reached the filter. To test for  $\cdot\text{BrO}$ , excess  $\text{O}_3$  was mixed into the  $\cdot\text{Br}$ -Ar system about six inches (10 to 15 milliseconds) before the filter. The presence of  $\cdot\text{Br}$  was confirmed by observing their recombination fluorescence. The presence of  $\cdot\text{BrO}$  was assumed. The results of these tests are listed in Table I.

Table I

Filter Collection Efficiency Test		
Species	TBAH impregnated	Neutral
$\text{CH}_3\text{Br}$	0 %	0%
$\text{Br}_2$	>96%	0%
HBr	100%	0%
$\cdot\text{Br}$	>96%	73%
$\cdot\text{BrO}^*$	85%	50%
particulate	100%	100%

\*  $\cdot\text{Br}$  and  $\text{Br}_2$  also present and we do not know whether  $\cdot\text{BrO}$  recombined before reaching filter.

By looking at these results in series, we can "bootstrap" ourselves into some understanding of the species which will collect on the filter as follows:

- 1) From the  $\text{CH}_3\text{Br}$  results we presume that none of any organic bromine will collect.
- 2)  $\text{Br}_2$  collects only on the TBAH filter at 100% efficiency.
- 3) HBr collects only on the TBAH filter at 100% efficiency.
- 4)  $\cdot\text{Br}$  collects on the TBAH filter at about 100% efficiency, since any recombination to  $\text{Br}_2$  or formation of HBr would also be collected totally, overall 100% efficiency is observed and the presence of  $\cdot\text{Br}$  was confirmed.  $\cdot\text{Br}$  or ( $\cdot\text{HOBr}$  or  $\cdot\text{H}_2\text{OBr}$ ) also collect at least partially on neutral filters.
- 5)  $\cdot\text{BrO}$  collection efficiency is unknown, since recombination to form  $\text{Br}_2$ ,  $\cdot\text{Br}$  and/or HBr would produce some collection of bromine on the filter. The decrease in collection efficiency from that observed for  $\cdot\text{Br}$ , HBr, and  $\text{Br}_2$  may indicate that  $\cdot\text{BrO}$  is not trapped very well by the filter.

- 6) All particulates are known from laboratory testing to be collected at about 100% efficiency down to particle diameters much less than  $0.1 \mu\text{m}$ .

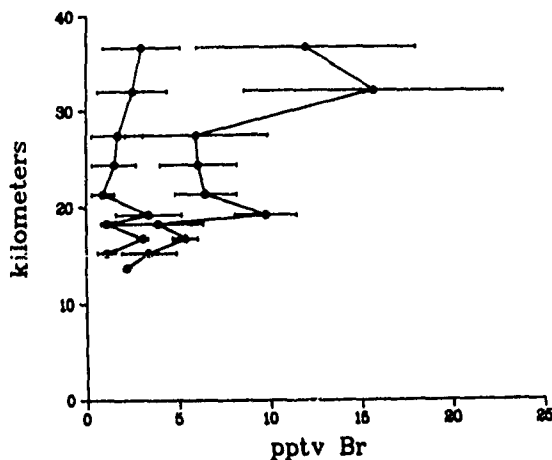
Similar test on chlorine nitrate by Bonelli et al [1979] suggest that  $\text{BrNO}_3$  would also be collected with a very high efficiency.

Based on these results, we feel that the bromine found on the neutral filter probably represents the partial collection of  $\text{Br}$  rather than particulates containing bromine.

Figure 4 shows vertical profiles with one sigma error bars for the average of all data at  $33^\circ \text{N}$ . The left line is for the neutral filters and the right line is for the TBAH impregnated filters.

Vertical profiles of average bromine concentrations measured at  $33^\circ \text{N}$ . Neutral filter is the left line and TBAH impregnated filter is the right line. Error bars are  $\pm 1$  sigma.

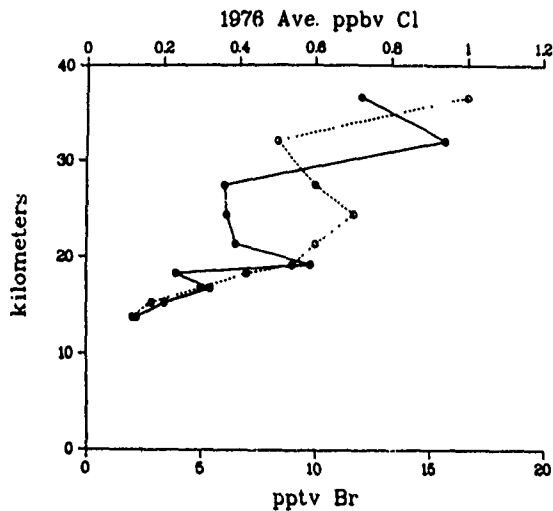
Figure 4.



One area of concern observed in this data is the decrease in bromine concentration between 20 and 30 km. Coincidentally these three altitudes are those sampled by the balloon borne direct flow sampler, while those above are collected with the air ejector sampler and those below with the aircraft sampler. However, Figure 5 which compares chlorine data and bromine data taken from the very same filters and analysis, indicates a similar decrease for chlorine, but at a different altitude. Therefore, we feel that these features of the vertical profiles are related to the chemistry of the sampler collection efficiency rather than to the different types of samplers.

Comparison of chlorine (dashed line) and bromine (solid line)  
Vertical profiles

Figure 5.



If all inorganic bromine species were collected, one would expect the vertical profile to continually increase with altitude until the mixing ratio reached the total bromine mixing ratio and then remain constant with increasing altitude. The observed profiles are logical only if some species are not collected by the filter. We believe that most probably  $\text{BrO}$  is not collected or only partially collected. We will be attempting to test the filter collection efficiencies for these species in the near future using a mass spectrometer, so that individual species can be sensed.

Table II lists a summary of data to date from  $33^\circ \text{N}$  taken over nearly a four-year span. The average for each altitude over the available data  $\pm 1 \sigma$  is tabulated in the right column. Two points, July 75 at 13.7 km and July 77 at 36.6 km, seem very high and are excluded from the average. Each data point is regarded as being accurate to better than  $\pm 25\%$ . The counting statistics of the analysis are better than  $\pm 10\%$  for  $^{81}\text{Br}$  except the very lowest values, and the calibration of the air flow through the sampler is about a  $\pm 15\%$  value. Table III compares two-years data as a function of latitude. There are three very high values reported, all at 36.6 km. At this time we do not know of any system malfunction which can explain the very high concentrations. The corresponding chlorine values were reasonable in all but one of the cases where bromine was very high. There were also a few cases where chlorine was somewhat unreasonably high, but bromine concentrations seemed consistent with the rest of the bromine data. This leads us to believe that neither sample contamination nor sampler malfunction was the source of the high bromine concentrations. All of the very high bromine values except one occur on the 36.6 km balloon flights (the 13.7 km high value may have been in tropospheric air). We did experience considerable difficulty flying 36.6 km balloon flights successfully, but when they did fly the equipment worked satisfactorily. On the other hand, where there is a high bromine concentration at 36.6 km, it seems to occur at either the very high latitude or the very low latitude with a more modest concentration at the corresponding mid-latitude. Table III also shows that the samples of 32.0 km and lower give a similar high, low, high pattern as a function of latitude. The integrating and averaging nature of the filter sampler should also make it less susceptible to influence by a very localized injection of extraneous material from a source such as a rocket, meteor, or aircraft trail than a measurement by a direct measuring instrument. Hence, despite some reservations about these few very high values, in the spirit of scientific honesty, we report them here.

Table II

Table 1.

Vertical Profiles of Bromine Measurements at  $33^\circ \text{N}$   
Concentrations  $\times 10^{12}$  by volume, for TBAH  
Impregnated filters with valves for neutral filters beneath in ( ).

Altitude	Nov. 74	April 75	July 75	Oct. 75	Feb. 76	April 76	Aug. 76	Nov. 76	April 77	July 77	Ave $\pm 1\sigma$
36.58 km						5.4 (2.1)	10.0 (5.2)	13.2 (3.7)	19.6 (3.0)	86.5 (12.9)	12.0 $\pm$ 6.0 (3.0 $\pm$ 2.1)
32.00					29.0 (1.3)	13.0 (5.3)	15.7 (4.6)	11.0 (1.5)	8.8 (0.9)	16.6 (1.5)	15.7 $\pm$ 7.1 (2.5 $\pm$ 1.9)
27.43		6.6 (3.2)	7.0 (1.1)	5.6 (2.8)	4.3 (0.2)	4.2 (1.0)	7.2 (1.2)	1.1 (0.1)	3.3 (1.0)	15.1 (4.3)	6.0 $\pm$ 3.9 (1.7 $\pm$ 1.4)
24.38		6.6 (0.1)	10.5 (0.1)		4.4 (3.5)	4.7 (1.8)	5.5 (0.7)	6.1 (1.5)	3.8 (0.3)	7.3 (2.4)	6.1 $\pm$ 2.1 (1.5 $\pm$ 1.2)
21.34		8.7 (0.8)	8.8 (0.8)	4.6 (0.7)	7.4 (1.6)	5.4 (1.3)	6.2 (1.3)		6.7 (0.1)	4.2 (0.3)	6.5 $\pm$ 1.7 (0.9 $\pm$ 0.6)
19.20						12.1 (4.5)	8.1 (1.4)		9.4 (4.4)	9.4	9.8 $\pm$ 1.7 (3.4 $\pm$ 1.8)
18.29	3.1			5.7 (0.9)	2.1 (1.3)						3.9 $\pm$ 2.5 (1.1 $\pm$ 0.3)
16.76						6.0 (2.8)	6.1 (3.0)		5.0 (3.4)	4.6	5.4 $\pm$ 0.7 (3.1 $\pm$ 0.3)
15.24	1.3		2.3 (0.6)		6.2 (0.8)	3.2	3.7 (1.7)		2.7 (1.4)	2.1	3.4 $\pm$ 1.5 (1.1 $\pm$ 0.5)
13.72			64.6 (0.5)			2.3 (1.2)			2.4	2.0	2.2 $\pm$ 0.2
12.19					1.6 (0.9)						

Table III

Vertical Profiles of Bromine Measurements at 65°N, 33°N & 9°N Concentrations $\times 10^{12}$ by volume, for TBAH impregnated filters with valves for neutral filters beneath in ( ).						
Altitude	April 76			April 77		
	66°N	33°N	9°N	66°N	33°N	9°N
36.58 km	133.1 (11.8)	5.4 (2.1)		233.0 (25.5)	19.6 (3.0)	88.7* (48.5)
32.00	15.0 (5.0)	13.0 (5.3)		23.4 (1.8)	8.8 (0.9)	18.4† (0.3)
27.43	5.9 (2.5)	4.2 (1.0)	5.7 (2.4)	5.8 (1.4)	3.3 (1.0)	
24.38	5.4 (1.5)	4.7 (1.8)	5.3 (2.5)	6.2 (0.7)	3.8 (0.3)	6.8
21.34	6.2 (1.3)	5.4 (1.3)	3.7 (1.8)	5.6	6.7 (0.1)	4.4 (5.8)
19.20	11.1 (4.3)	12.1 (4.5)	6.8 (2.9)	9.6	9.4 (4.4)	3.1
18.29			5.9 (2.5)			
16.76	6.6 (3.7)	6.0 (2.8)	3.5 (1.8)	5.2	5.0 (3.4)	3.8
15.24	5.3 (2.8)		1.8 (0.7)	2.6	2.7 (1.4)	2.4
13.72		(1.2)			2.4	1.0
12.19	3.6 (2.0)			2.8		
* Sampler damage on recovery						
† Sampler hung in tree for 2 days before recovery						

An overall look at the data of Tables II and III shows a rather strong indication (ignoring the few very high values), that for the species collected on the filter the upper limit on total bromine should be about 20 parts per trillion by volume. At the aircraft sampling altitudes, below 20 km, there are also measurements spanning about each 3° of latitude from the equator to 75° N at each altitude for April 76, April 77, and July 77. These data are very consistent with and strongly support the latitudinal pattern illustrated by the data of Table III. The data are undoubtedly influenced to some extent by seasonal variation in the photochemistry since they probably do not represent total bromine, which most likely is the principal cause of the somewhat large  $\pm \sigma$  values shown in Figure 4 and Table II. However, within these variations, no large seasonal or temporal trend is apparent.

We hope to be able to make at least a measurement of a 33° N vertical profile once a year to assess any possible trend in stratospheric bromine. We are also currently using a charcoal trap technique (in collaboration with Walter Berg of the National Center for Atmospheric Research) to measure total halogens. The well purified activated charcoal traps all halogen species both organic and inorganic which are analyzed by neutron activation analysis directly on the charcoal. Only a couple of flights have been flown to date, but a total bromine about 40 pptv is indicated. Use of the charcoal sampling technique and the TBAH filter technique together, coupled with better understanding of the chemical species selectivity of the filters should greatly enhance our understanding of atmospheric halogen chemistry. One of the remaining mysteries is in what chemical form is bromine transported to the stratosphere. Rasmussen finds only 5 pptv of methyl bromine. What other species provide the additional 35 pptv?



REFERENCES

- Bonelli, J. E., A. L. Lazrus, and B. W. Gandrud, Stratospheric Trace Gas Sampling with Chemical Absorption Filters, Atmos. Tech., 9, 8-13, 1978.
- Bonelli, J. E., J. P. Greenberg, A. L. Lazrus, J. E. Spencer, and W. A. Sedlacek, Laboratory Simulation of Impregnated Filter Collection of Stratospheric Hydrogen Chloride and Chlorine Nitrate, Atmos. Environ., 12, 1591-1594, 1978.
- Cadle, R. D., Composition of the Stratospheric "Sulfate Layer", CIAP Survey Conf., February 1972, DOT-TSC-OST-72-13, 130-139, 1972.
- Gandrud, B. W. and A. L. Lazrus, Design of System for Removing Water-Soluble Materials from IPC-1478 Filter Paper, Envir. Sci. and Tech., 6, 455-457, 1972.
- Lazrus, A. L., B. W. Gandrud, R. N. Woodard, and W. A. Sedlacek, Stratospheric Halogen Measurements, Geophys. Res. Lett., 2, 439-441, 1975.
- Lazrus, A. L., B. W. Gandrud, R. N. Woodard, and W. A. Sedlacek, Direct Measurements of Stratospheric Chlorine and Bromine, J. Geophys. Res., 81, 1067-1070, 1976.
- Lazrus, A. L., B. W. Gandrud, J. Greenberg, J. Bonelli, E. Mroz, and W. A. Sedlacek, Midlatitude Season Measurements of Stratospheric Acidic Chloride Vapor, Geophys. Res. Lett., 4, 587-589, 1977.
- Rowland, F. S. and M. J. Molina, Chlorofluoromethanes in the Environment, Rev. Geophys. Space Phys., 13, 1-36, 1975.
- Sedlacek, W. A., Letter Report for DOT/AEC Contract DOT-AS-20055 Task 5 on Results of June 1973 Project Airstream Sampling, Dec. 28, 1973.
- Sedlacek, W. A., Letter Report for DOT/AEC Contract DOT-AS-20055 Task 5 on Results of Sampler Calibration Flight August 1973, Dec. 28, 1973.
- Wofsy, S. C., M. B. McElroy, and Y. S. Yung, The Chemistry of Atmospheric Bromine, Geophys. Res. Lett., 2, 215-218, 1975.
- Yung, Y. L. and R. Watson, to be published, 1979.

# THE PHOTOCHEMISTRY OF TROPOSPHERIC IODINE

W. L. Chameides\* and D. D. Davis\*\*

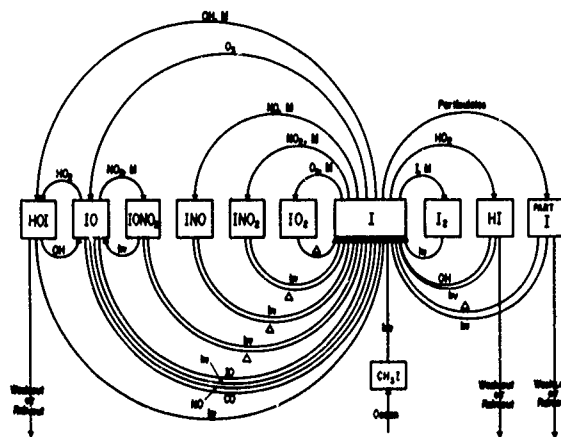
\*Dept. of Physics, Univ. of Florida, Gainesville 32611

\*\*School of Geophysical Sciences, Georgia Inst. of Tech., Atlanta 30332

## Abstract

A detailed study of the photochemistry of iodine and its oxides indicates that iodine species may play an important, but heretofore ignored, role in the tropospheric photochemical system. Methyl iodide, often observed in the marine troposphere with an average concentration of 5-10 ppt (v/v), is photolyzed and thereby produces I atoms. Chemical interactions with  $O_3$ ,  $H_xO_y$ , and  $NO_x$  cause I to be converted to other inorganic compounds such as IO, HOI,  $IONO_2$ , and  $I_2$ . The production of these species and their subsequent recycling back to I can lead to the catalytic removal of tropospheric  $O_3$ , the enhancement of the  $NO_2/NO$  ratio, and an increase in the local OH abundance by conversion of  $HO_2$  to OH. Ultimately, tropospheric inorganic iodine (IX) is removed by heterogeneous processes. Calculations using a numerical model to simulate tropospheric photochemistry indicate that iodine may have a strong impact upon the atmospheric  $O_3$ - $NO_x$ - $H_xO_y$  system. The magnitude of these effects is dependent upon the value of several uncertain rate constants and the primary source distributions of  $CH_3I$  and other organic and inorganic iodine compounds.

A Possible Chemical Scheme for Iodine in the Tropospheric Marine Boundary Layer



## SOURCES AND SINKS OF STRATOSPHERIC WATER VAPOR\*

Hugh W. Ellsaesser

Lawrence Livermore Laboratory, University of California  
Livermore, California 94550 U.S.A.

### Abstract

Herein is presented a tutorial review of our understanding of stratospheric  $H_2O$  and the processes controlling it. Paradoxes posed by currently available observational data are cited and suggestions made as to how they might be resolved.

Such resolution appears to require:

- 1) That the bulk of our current data provides unrepresentative and misleading vertical and latitudinal  $H_2O$  gradients immediately downstream from the tropical tropopause.
- 2) That there exist within the troposphere a mechanism different from or in addition to the tropical tropopause cold trap for drying air to the mixing ratios found in the lower stratosphere.

Satisfaction of these requirements will reconcile much heretofore puzzling observational data and will obviate the necessity for a stratospheric sink for  $H_2O$ .

**INTRODUCTION:** When the Meteorological Research Flights (MRF-see Cluley and Oliver [1978]) for measuring stratospheric humidity with a frost point hydrometer began in the 1940's, they found  $H_2O$  mixing ratios of 2 to 3 ppm corresponding to relative humidities of only a few percent. As this extreme aridity was confirmed by additional flights, Brewer and Dobson [Dobson et al., 1946; Brewer, 1949] hypothesized that all air entering the stratosphere did so via the tropical tropopause where it was freeze dried sufficiently to produce the low mixing ratios consistently observed in the lower stratosphere. In the polar regions where tropopause temperatures were warm enough to permit diffusive upward transport of air of much greater moisture content, such transport was prevented by the subsidence of the return Hadley flow.

Others tried by a variety of techniques to measure the humidity of the stratosphere. The results were widely varying and gave rise to a controversy between those who defended a "dry" stratosphere and those who claimed that the mixing ratio increased significantly with height. This controversy was summarized by Gutnick [1961] in a paper entitled "How dry is the sky?" Sissenwine et al., [1972] wrote a sequel entitled "How dry is the sky?"

\*This report contains more detail than could be presented orally and some of the new ideas have been developed beyond the stage they had reached at the time of presentation.

# ELLSAESSER

A decade later and the SST." As you will note below, this controversy is still not laid to rest. Due to the tremendous drop in  $H_2O$  mixing ratio between the surface and the stratosphere, balloon lofted platforms and instruments provided many opportunities for contamination. This became very obvious when data recorded on descent were compared with that recorded during the ascent portion of a flight; mixing ratios were generally much lower on descent and the difference increased with altitude [Mastenbrook, 1965]. The contamination problem was also discussed by Zander [1966, 1973].

In the early 1960's Mastenbrook, [1968, 1971, 1974a, b] began a series of balloon soundings with a frost point hygrometer, using data only from the descent portions of the flights. These included two soundings from Thule, a year of soundings from Trinidad and a continuing series from Washington, D.C. These gave a median mixing ratio of  $\sim 2.6$  ppm, confirming the low humidities found by the MRF and showing remarkably little variation with latitude, altitude and flight to flight. Most other observational programs consisted of short data records and frequent modifications in equipment and/or technique which didn't allow accumulation of sufficient homogeneous data to permit estimation of repeatability and reliability. Both the MRF and the Mastenbrook flights, on the other hand, have been sufficiently extensive and consistent as to more or less gain acceptance as a standard against which other soundings are judged. For these reasons and because their observations were consistent with the Brewer-Dobson hypothesis for the consistent aridity of the stratosphere, observations of stratospheric  $H_2O$  departing significantly from the mean Mastenbrook profile have in general been disregarded as at least unsupported.

If we accept the Brewer-Dobson hypothesis, then all air entering the stratosphere should be freeze dried to the saturation mixing ratio of the tropical tropopause. This has generally been assumed to have an average temperature of  $-80^\circ C$  and an average pressure of 100 mb - corresponding to a saturation mixing ratio of  $\sim 3.4$  ppm. However, when I attempted to develop an  $H_2O$  budget for the stratosphere for CIAP [Ellsaesser, 1974], I was immediately struck by the question; how can the lower stratosphere maintain a mixing ratio of  $\sim 2.6$  ppm if all the air entering through the tropical tropopause is freeze dried to only 3.4 ppm? This appeared to require a stratospheric sink for  $H_2O$ .

At that time, other than the return flow of the Hadley circulation (which presumably consisted of air with a mixing ratio of  $\sim 2.6$  ppm), the only  $H_2O$  sinks which had been proposed were planetary escape of hydrogen [Brinkman, 1969] and the  $H_2O$  incorporated into the  $H_2SO_4$  particles of the Junge layer [Grams and Fiocco, 1967]. These were too small by 4 and 2 orders of magnitude respectively. It occurred to me that the low temperatures developing around 25 to 30 km in the winter polar vortices might be cold enough to form ice crystals or cirrus cloud which might precipitate into the troposphere before reevaporation. A paper by Newell called my attention to the fact that stratospheric cirrostratus had been observed during at least 3 separate winters in Antarctica [Liljequist, 1956]. At about this time I learned that Stanford [1973] had independently proposed that the Antarctic winter vortex might act as a freeze-dry sink for the stratosphere.

Figures 1, 2, and 3 show meridional profiles of winter temperature for the northern and southern hemispheres and the annual cycles of temperature at the 100- and 50-mb levels. The temperature distributions shown in these Figs are consistent with saturation mixing ratios  $\leq 10$  ppm from 22 to 30 km over the Arctic pole and  $\leq 3$  ppm from 16 to 24 km over the Antarctic pole. These are only marginally of the required coldness for an effective sink even over Antarctica. The two latitudinal profiles of stratospheric  $H_2O$  available in 1974 (curves of McKinnon and Morewood [1970] and Kuhn and Stearns [1973] of Fig. 8) indicated a maximum near the equator and a minimum at the southernmost observation point.

I pointed out that these data were consistent with an Antarctic winter freeze-dry sink sufficient to remove the approximately  $3 \times 10^8$  tonnes  $H_2O$ /yr apparently required to balance the stratospheric  $H_2O$  budget. No one, including myself, has been particularly happy with this proposal. But neither has any one yet come up with a more satisfactory resolution of this apparent paradox.

But this is not the end of our paradox. By current understanding air entering the stratosphere contains  $\sim 1.6$  ppmv of  $CH_4$  which, if completely oxidized would add 2 ppm to

to follow that the ITCZ should be strongest and produce the most precipitation when it is in the southern hemisphere, i.e. during Dec-Feb. The available data rather strongly imply that the ITCZ is strongest and produces the most visible cloud and precipitation in Jun-Aug when it is in the northern hemisphere. This is not conclusive, of course, since the convection could be confined to fewer but deeper cells in the southern hemisphere, but why it should behave differently in this respect is not at all clear.

The strength of the Hadley flux through the tropopause has been estimated from atmospheric models, from vertical velocities computed from radiosonde data, from vertical velocities required to balance radiational heating of the tropical tropopause, from the mass of the stratosphere divided by its mean residence time and from the 6 month change in mass of the stratosphere indicated by the tropopause positions in Fig. 6. The latter value applies only to the northern hemisphere, of course. The derived estimates range from  $1.5$  to  $9.2 \times 10^{14}$  tonnes/yr [Elsaesser, 1974 Robinson, 1978]. The preferred estimate, based on a stratospheric mass of  $6.7 \times 10^{14}$  tonnes/yr divided by a mass weighted mean stratospheric residence time of 2 years, is  $3.3 \times 10^{14}$  tonnes/yr [Elsaesser, 1974]. The hemispheric asymmetries in the Hadley cells, tropical tropopauses, stratospheric ozone [London, 1975] and tropospheric tritium [Schell et al., 1974] all suggest that this flux is not evenly divided and that significantly more than half of it returns to the troposphere of the northern hemisphere.

**THE H<sub>2</sub>O BUDGET OF THE STRATOSPHERE:** The above flux rate corresponds to a mean vertical velocity spanning  $22.5^\circ$  of latitude on either side of the equator of  $0.03$  cm/sec. If this flux of air enters the stratosphere with a mixing ratio of  $3.4$  ppm and leaves with a mixing ratio of  $2.6$  ppm, we have  $11.3 \times 10^8$  tonnes H<sub>2</sub>O/yr entering the stratosphere and  $8.6 \times 10^8$  tonnes/yr returning to the troposphere leaving  $2.7 \times 10^8$  tonnes/yr unaccounted for. And we have not yet accounted for the H<sub>2</sub>O presumably generated by oxidation of CH<sub>4</sub> within the stratosphere. According to a recent calculation by the LLL 1-D model this produces another  $1.8 \times 10^8$  tonnes H<sub>2</sub>O/yr making a total of  $4.5 \times 10^8$  tonnes/yr which apparently vanishes without a trace.

**THE OBSERVATIONS:** Now let's take a look at the observations of H<sub>2</sub>O in the stratosphere. Figs. 7, 8 and 9 show summaries of observations of stratospheric H<sub>2</sub>O mixing ratio. The observations taken prior to 1976 have been reviewed by Mastenbrook [1974b], Harries [1976] and Penndorf [1978], all of whom arrived at conclusions quite similar to the following:

- a. The data support a northern mid-latitude constant mixing ratio from the tropopause to about 30 km with a mean value (Circa 1968) of  $\sim 2.6 \pm 0.6$  ppm with some evidence of an increase at higher levels. While the data fairly consistently indicate a slight decrease above the tropopause to a minimum around 19-20 km and an increase above this level, it is difficult to argue that the instrumental accuracy is sufficient to resolve such structure.
- b. While nearly every relevant data set suggests latitudinal gradients with a maximum near the equator there remains the fact that most soundings, even in the tropics, reveal a decrease in mixing ratio in the first km or so above the tropopause. Due to the great height of the tropopause in the tropics and the ceiling of most aircraft, observations near the equator may simply reflect this vertical gradient or may actually represent some tropospheric air.
- c. All relevant northern hemisphere data sets indicate or support an annual cycle below 20 km, amounting to 10 to 15% in the lower stratosphere and decreasing with altitude. In mid-latitudes the maximum occurs around November at the base of the stratosphere and lags with altitude. Thus the cycle and phase are consistent with a maximum influx of H<sub>2</sub>O in late summer at the time of the lowest and warmest tropical tropopause. However, Hyson [1978] failed to find an annual cycle over Longreach, Australia from 1973 to 1976.
- d. The MRF data reevaluated by Cluley and Oliver [1978] and the Mastenbrook series over Washington, D.C. (see Penndorf [1978]) support an upward trend from 1954 to 1973 of  $\sim 0.86$  ppm/decade and a steeper decrease thereafter about twice as fast. See Fig. 9.

There is additional evidence of long period cycles in stratospheric H<sub>2</sub>O. Fig. 10 shows the year to year distribution of northern hemisphere sightings of nacreous clouds as compiled by Stanford and Davis [1974]. Nacreous clouds occur in high latitudes in winter at altitudes of 20 to 30 km. They are presumed to be due to condensed ice crystals

resulting from local cooling to the ambient frost-point. The 26-year gap in the sightings from 1895 to 1923, confirmed by Stormer [1929], appears to suggest long period cycles in stratospheric mixing ratios exceeding anything that might have occurred since observations were begun in the 1940's.

A summary of recent soundings of stratospheric and mesospheric  $H_2O$  appears in Figs. 11 and 12. These represent new instruments and techniques and some feel that the fairly consistent suggestion of an increase in mixing ratio with height above 20 km may be real. If the trend suggested by Fig. 9 is correct, the recent drop in stratospheric mixing ratio should make any contribution from oxidation of  $CH_4$  more apparent since 1975 than at anytime since the beginning of the Mastenbrook series. On the other hand it should be noted that the temporal and spatial variability suggested by Figs. 11 and 12 is well outside anything we would expect from the Mastenbrook series or our current understanding of the stratosphere. Several of the soundings show increases with height greater than the maximum 2 ppm expected from complete oxidation of  $CH_4$ . Accordingly it appears prudent to echo Gutnick's [1961] comment of nearly 20 years ago: "lack of a tenable explanation of the various conflicting reports on stratospheric humidity casts doubt on the accuracy of part or all of the data." It should also be noted that the Jan. 1979 sounding reported at this institute by D. Kley, aside from fine-scale variations, only increased from  $\sim 2.3$  ppm at 12 km to  $\sim 2.6$  ppm at 32 km.

DISCUSSION: How do we reconcile the apparent inconsistencies in the  $H_2O$  budget of the stratosphere? To fit the available data we need to increase the sinks or decrease the sources. The sinks so far proposed include: the "cold finger" of overshooting thunderstorms of Johnston and Solomon [1979]; Antarctic winter freeze-out of Stanford [1973] and Ellsaesser [1974]; the Junge layer of  $H_2SO_4$  particles;  $H_2O$  bound in  $HNO_3$  and  $HCl$  and planetary escape of hydrogen. The more certain of these are too small by 2 or more orders of magnitude and both overshooting thunderstorms and Antarctic winter freeze-out appear highly uncertain. But can we reduce the sources? I believe we can. Other than the increases with altitude above 20 km which frequently exceed  $CH_4$  oxidation, the principal sources of our difficulty have been the apparent poleward and upward directed  $H_2O$  gradients immediately downstream from the major source - the tropical tropopause. But remember that all the observations suggesting these gradients were taken over continents. In fact, most of them were taken near the downwind boundaries of continents. If we make the quite reasonable assumption that  $H_2O$  carried to the stratosphere by penetrations of the tropical tropopause by convective clouds will be concentrated in such locations, then the gradients we are seeing would be due to essentially point sources, i.e. they would not be representative of zonal mean gradients as they have been interpreted to be.

If these gradients do disappear in valid zonal mean data, the requirement for a stratospheric sink is reduced to that required to account for the  $H_2O$  from oxidation of  $CH_4$ , i.e. approximately  $1.8 \times 10^6$  tonnes/yr. Here again a resolution may be in sight. With a yearly troposphere-to-stratosphere Hadley flux of  $3.3 \times 10^{14}$  tonnes of air/yr, an excess in mixing ratio of only 0.55 ppm in the return flow over that in the entering flow would be sufficient to balance the budget. As pointed out by Cluley and Oliver [1978] and Penndorf [1978], and as is clearly evident in Fig. 9, the MRF measurements over the British Isles are consistently  $\sim 0.5$  ppm higher than those of Mastenbrook over Washington, D.C. Penndorf [1978] noted that this difference appears to exceed the estimated systematic errors of 8-10% and may be real. That the difference should be so near the required magnitude may indeed be fortuitous! However, the equatorward gradient is supported by the northern hemisphere data of McKinnon and Morewood [1970] shown in Fig. 9. This solution to our problem would also vindicate Kley's [1979] proposal that above the "hygropause" (level of minimum mixing ratio near 60 mb) there is an equatorward directed gradient and that above this level the downwelling return Hadley flow in high latitudes carries more  $H_2O$  than the low latitude upwelling branch of the Hadley flow.

At present the above proposals can only be regarded as ad hoc solutions designed to fit specially selected data. For example the last one would require that Harries' [1973] data in Fig. 9 be in error (or unrepresentative) by a factor of 2 and that all of the profiles in Fig. 8 (except McKinnon and Morewood's [1970]) be in error (or unrepresentative) and in

particular that the latitudinal gradient implied by Mastenbrook's soundings from Trinidad, Washington, D.C. and Tule also be in error (or unrepresentative). While such a circumstance is clearly possible for each individual data set, to expect all of them to be off in the same sense is asking a lot. But the above proposals do point a way out of our current paradoxes and establish the types of observational data required for their confirmation or refutation. Thus they should advance our understanding of the stratosphere if only by the elimination of some of the currently available possibilities.

However, I believe we have an additional problem. As Robinson [1978] recently pointed out, if we visualize the Hadley circulation as a large scale mean motion, then the tropical updraft should give rise to a widespread layer of thick cloud as the tropospheric air is being freeze-dried in passing upward to and through the tropical tropopause. Such clouds are rarely if ever observed. In fact, Robinson [1978] noted that most soundings (those on so-called 'dry' days) show, even in the tropics, that "humidity at points as much as 100 mb below the tropopause is less than saturation humidity at [the overlying] tropopause temperature. On the 'wet' days humidity corresponds to saturation at [the] tropopause temperature, about  $6 \times 10^{-6}$  and is reasonably constant up to pressures as much as 60 mb below the tropopause pressure." Robinson [1978] concluded that Kuhn's data from the NASA 1977 ITCZ Experiment [Poppoff et al., 1979] appear to imply stratospheric injection by a structure made up of relatively humid ( $\sim 6$  ppm) and dry ( $\sim 3$  ppm) air columns in close juxtaposition extending over the pressure range 200 to 60 mb. The soundings on the 'wet' days appear to conform to the requirement for freeze-drying to the tropopause temperature in the deep cloud of cumulus towers and are surrounded by descending air with mixing ratio typical of the stratosphere, i.e.  $\sim 3$  ppm. He observed: "Most of the tropical observations, if considered from the point of view of humidity alone, suggest that stratospheric air is entering the troposphere in the tropics, but other tracers, particularly ozone, show no evidence of this."

From Robinson's [1978] observations it would be tempting to conclude that all air enters the stratosphere through cumulus penetrations of the tropical tropopause and that these cumuli are surrounded by subsiding air producing a dry layer sometimes extending from the tropopause down to 200 mb. However, if this were true and the mixing ratios conformed to those so far reported in the vicinity of tropopause penetrations we would still need a stratospheric sink to get rid of the excess water. An even stronger objection is the apparent rarity of tropopause penetrations. Holton, Director of the NASA 1977 ITCZ Experiment, strongly supported the belief that the entire upward flux of the Hadley cell is concentrated in cumulonimbus towers in the troposphere. But with regard to the stratosphere he wrote [Poppoff et al., 1979]: "However, observations indicate that relatively few tropical cumulonimbus actually penetrate the tropopause. Very few clouds actually overshoot their levels of neutral buoyancy sufficiently to penetrate the high tropical tropopause. In addition it is by no means clear that those few clouds that do penetrate the tropopause actually mix tropospheric air into the stratosphere. Rather, it is likely that the overshooting cells as they collapse due to negative buoyancy actually entrain stratospheric air which is then mixed into the troposphere."

From these observations it would appear that the aridity of the stratosphere is not controlled by freeze-drying at the tropical tropopause after all. The specific observations suggesting this conclusion are as follows:

- 1) As pointed out by Robinson [1978], freeze-drying requires a deep layer of cloud, either the widespread deep cirrus of a mean up draft or the hot towers of cumulus convection surrounded by subsidence. Observational data support neither in sufficient quantity to maintain the Hadley flow to the stratosphere.
- 2) Available observations indicate that when convective clouds do penetrate the tropical tropopause they produce mixing ratios  $\geq 6$  ppm rather than  $\leq 3$  ppm. This point is also made by Danielson's comment in the NASA 1977 ITCZ Experiment: "Kuhn's stratospheric water vapor measurements indicate large, day-to-day temperature variations which are positively correlated with easterly waves. Thus, the moist stratosphere appears to be directly related to the highest coldest clouds. These results are inconsistent with the hypothesis that the dry stratosphere is produced by vapor in equilibrium with cirrus from cumulonimbus clouds" [Poppoff et al., 1979].
- 3) As emphasized by Robinson [1978], mixing ratios typical of the stratosphere ( $\leq 3$  ppm) are observed to extend as much as 100 mb beneath the tropical tropopause in clearly tropospheric air. If correct, these seem to demonstrate that tropospheric air is not only

dried before it cools to the temperature of the tropical tropopause but that it is also dried more than it would have been by simple freeze-drying to the ambient tropopause temperature.

This analysis appears to have led to an even bigger dilemma than the one with which I started. As of now I have only two suggestions as to how this dilemma might be resolved.

- 1) There remains the possibility that all or most of the Hadley flux to the stratosphere is restricted to geographical areas and seasons in which the tropical tropopause is colder than  $-80^{\circ}\text{C}$ . This could include the period Dec-Feb when the ITCZ is in the southern hemisphere and the tropical tropopause is highest and coldest ( $\sim 80$  mb and  $-84^{\circ}\text{C}$ ). It might also include the period Jun-Aug when the Indian monsoon is pushing against the Himalayas and this area experiences its highest and coldest tropopause, although the temperature of  $-75^{\circ}\text{C}$  indicated by Sastry and Narasimham [1966] does not appear cold enough. These are the periods and areas in which the Hadley cells achieve their maximum intensity. Also Doppl's [1979] recent downward revision of the total radiative heating rates at the tropical tropopause makes an impulsive, as opposed to a steady, Hadley flux to the stratosphere somewhat more palatable. Even if this were sufficient to explain the sustained aridity of the stratosphere it would leave unexplained the apparent widespread occurrence of mixing ratios  $\leq 3$  ppm in the upper tropical troposphere.
- 2) The other possibility pushes even farther into the unknown. We know that cirrus clouds, particularly the so-called mare's tails, provide a mechanism for condensing  $\text{H}_2\text{O}$  from upper levels of the troposphere and, through gravitational sedimentation and re-evaporation, transporting it to a lower level. I pose the following as a question rather than as a theory: Is it possible that in the temperature range of  $-50$  to  $-80^{\circ}\text{C}$  at pressures below 200 mb there exist seeding agents, possibly including cirrus crystals themselves, which are capable of collecting water vapor from what we now consider to be unsaturated air until the  $\text{H}_2\text{O}$  mixing ratio is reduced to the range of 2-3 ppm? This is reaching but it is the type of phenomena which appears to be required to reconcile our present observational data. If such were found to be true it would open up a whole new pathway for transport of air from the troposphere to the stratosphere i.e. through the jet stream gap between the polar and tropical tropopauses. While many have proposed such a route, most have rejected it because it appeared to provide no means for maintaining the aridity of the stratosphere. However, if the aridity is produced in the troposphere this objection goes away and a great deal of observational data suddenly becomes understandable. For example several authors have noticed the frequent occurrence poleward of  $30^{\circ}$  of a minimum in the vertical profile of  $\text{O}_3$  at a height of about 15 km which strongly suggests that tropospheric air regularly enters the stratosphere through the tropopause gap [Dobson, 1973]. Mastenbrook [1974b] included one of his Washington, D.C. soundings to "illustrate the frequent occurrence of pronounced ozone structure and the absence of pronounced water vapor structure in the altitude layer between the polar and equatorial tropopauses (in this case April 25, 1968 between 300 mb and 85 mb)." "In the multiple tropopause region," he reported, "an ozone peak just above the polar tropopause is overlaid by a layer low in ozone which is more characteristic of tropospheric air. The water vapor mixing ratio for the ozone poor layer does not differ noticeably from the overlying stratospheric air above the tropical tropopause." Mastenbrook [1974b] also cited Helliwell's [1960] description of flights which traveled north below the tropical tropopause and entered the stratosphere above the polar tropopause; these found that the frost point of air in the multiple tropopause region was not noticeably different from that of stratospheric air to the north.

At present I am not much happier with these suggestions than with my earlier suggestion [Ellsaesser, 1974] that Antarctic winter freeze-out removes  $3$  to  $4.5 \times 10^8$  tonnes of  $\text{H}_2\text{O}/\text{yr}$  from the stratosphere. However, no more palatable way has yet occurred to me for reconciling the apparent paradoxes posed by our current observational data on stratospheric  $\text{H}_2\text{O}$ .

**ACKNOWLEDGEMENTS:** This work was performed under the auspices of the U.S. Department of Energy by the Lawrence Livermore Laboratory under contract No. W-7405-Eng-48 with support by the High Altitude Pollution Program of the Department of Transportation, Federal Aviation Administration. Deep appreciation is expressed to Marcel Nicolet for the tendering of an expense-paid invitation to attend this NATO Advanced Study Institute on Stratospheric Ozone which made the above support possible.



## REFERENCES

- Ackerman, M., "Stratospheric Water Vapor from High Resolution Infrared Spectra," Plan. Space Sci., 22, 1265, 1974.
- Arnold, A. and D. Krankowsky, "Water Vapour Concentrations at the Mesopause," Nature, 268, 218, 1977.
- Bertaux, J.-L. and A. Delannoy, "Vertical Distribution of  $H_2O$  in the Stratosphere as Determined by UV Fluorescence In-situ Measurements," Geophys. Res. Lett., 5, 1017, 1978.
- Brewer, A. W., "Evidence for a World Circulation Provided by Measurements of Helium and Water Vapour Distribution in the Stratosphere," Quart. J. Roy. Met. Soc., 75, 351-363, 1949.
- Brewer, A. W. and K. P. B. Thomson, "A Radiometer-sonde for Observing Stratospheric Emission due to Water Vapour in its Rotational Band," Quart. J. Roy. Met. Soc., 98, 187-192, 1972.
- Brinkman, R. T., "Dissociation of Water Vapor and Evolution of Oxygen in the Terrestrial Atmosphere," J. Geophys. Res., 74(23), 5355-5368, 1969.
- Burkert, P., D. Rabus and H. J. Bolle, "Stratospheric Water Vapour and Methane Profiles," pp 267-274 in Vol I, Proc Intl Conf on Structure, Composition and Gen Cir of the Upper and Lower Atmos and Possible Anthropogenic Perturbations, Jan. 14-25, 1974, Melbourne, Australia, 1974.
- Busoletti, E. and J. P. Baluteau, "Determination of  $H_2O/O_2$  Stratospheric Mixing Ratio from High resolution Spectra in the Far Infrared," Infrared Phys., 14, 293, 1974.
- Chaloner, C. P., J. R. Drummond, J. T. Houghton, R. F. Jarnot and H. K. Roscoe, "Stratospheric Measurements of  $H_2O$  and the Diurnal Change of NO and  $NO_2$ ," Nature, 258, 696-697, 1975.
- Chaloner, C. P., J. R. Drummond, J. T. Houghton, R. F. Jarnot and H. R. Roscoe, "Infra-red Measurements of Stratospheric Composition I. The Balloon Instrument and Water Vapour Measurements," Proc. Roy. Soc. London, A364, 145-159, 1978.
- Cluley, A. P. and M. J. Oliver, "Aircraft Measurements of Humidity in the Lower Stratosphere Over Southern England, 1972-76," Quart. J. Roy. Met. Soc., 104, 511-526, 1978.
- Danielson, E. F., "Transport by Mean and Turbulent Motions," pp. 6-1 to 5-137 in CIAP Monograph 1, DOT-TST-75-51, U.S. Department of Transportation, Washington, D.C., 1975.
- De Jonckheere, C. G., "A Measurement of the Mixing Ratio of Water Vapour from 15 to 45 km," Quart. J. Roy. Met. Soc., 101, 217-226, 1975.
- Dobson, G. M. B., "The Laminated Structure of the Ozone in the Atmosphere," Quart. J. Roy. Met. Soc., 99, 599-607, 1973.
- Dobson, G. M. B., A. W. Brewer and B. Cwilog, "Meteorology of the Lower Stratosphere," Proc. Roy. Soc. London, A185, 144-147, 1946.
- Dopplick, T. G., "Radiative Heating of the Global Atmosphere: Corrigendum," J. Atmos. Sci., 36, 1812-1817, 1979.
- Dutsch, H. U., "The Present Status of Ozone Research: Photochemistry and Observations," Proc. 2nd CIAP Conf., pp 106-113, DOT-TSC-OST-73-4, NTIS, Springfield, VA, 1973.
- Ellsaesser, H. W., "Water Budget of the Stratosphere," in Proc. 3rd CIAP Conf., pp 273-283, DOT-TSC-OST-74-15, NTIS, Springfield, VA., 1974.
- Evans, W. F. J., "Rocket Measurements of Water Vapour in the Stratosphere," pp 249-256 in Vol I, Proc. Intl. Conf. on Structure, Composition and Gen. Cir. of the Upper and Lower Atmos. and Possible Anthropogenic Perturbations, Jan. 14-25, 1974, Melbourne, Australia, 1974.
- Farmer, C. B., "Infrared Measurements of Stratospheric Composition," Can. J. Chem., 52, 1544-1559, 1974.
- Grams, G. and G. Fiocco, "Stratospheric Aerosol Layer During 1964 and 1965," J. Geophys. Res., 72(14), 3523-3542, 1967.
- Gutnick, M., "How Dry is the Sky?," J. Geophys. Res., 66(9), 2867-2871, 1961.
- Harries, J. E., "Measurements of Stratospheric Water Vapor using Infrared Techniques," J. Atmos. Sci., 30, 1691-1698, 1973.
- Harries, J. E., "The Distribution of Water Vapor in the Stratosphere," Rev. Geophys. Space Phys., 14, 565-575, 1976.
- Helliwell, N. C., "Airborne Measurements of the Latitudinal Variation of Frost-Point Temperature and Wind," Scientific Paper No. 1, Air Ministry, Meteorological Office, London, 1960.
- Hilsenrath, E., B. Guenther and P. Dunn, "Water Vapor in the Lower Stratosphere Measured From Aircraft Flight," J. Geophys. Res., 82, 5453-5458, 1977.

- Hyson, P., "Recent Measurements of Stratospheric Water Vapour Over Australia," pp 257-267 in Vol I, Proc. Intl. Conf. on Structure, Composition and Gen. Cir. of the Upper and Lower Atmos. and Possible Anthropogenic Perturbations, Jan. 14-25, 1974, Melbourne, Australia, 1974.
- Hyson, P., "Stratospheric Water Vapour Measurements Over Australia 1973-1976," Quart. J. Roy. Met. Soc., 104, 225-228, 1978.
- Johnston, H. S. and S. Solomon, "Thunderstorms as Possible Micrometeorological Sink for Stratospheric Water," J. Geophys. Res., 84(C6), 3155-3158, 1979.
- Kennedy, J. S. and W. Nordberg, "Circulation Features of the Stratosphere Derived from Radiometric Temperature Measurements with the TIROS VII Satellite," J. Atmos. Sci., 24(6), 711-719, 1967.
- Kley, D., "The Budget of Stratospheric Water Vapor," Position paper for NASA Stratospheric Workshop, Harper's Ferry, W.V., June 4-8, 1979, NOAA Aeronomy Laboratory, Boulder, CO., 1979.
- Kley, D., E. J. Stone, W. R. Henderson, J. W. Drummond, W. J. Harrop, A. L. Schmeltekopf and T. L. Thompson, "In Situ Measurements of the Mixing Ratio of Water Vapor in the Stratosphere," J. Atmos. Sci., 36, 2513-2524, 1979.
- Kochanski, A., "Cross Sections of the Mean Zonal Flow and Temperature Along 80°W," J. Meteor., 12(2), 95-106, 1955.
- Kuhn, P.M., L. P. Stearns and M. S. Lojko, "Latitudinal Profiles and Stratospheric Water Vapor," Geophys. Res. Letts., 2, 227-230, 1975.
- Kuhn, P. M. and L. P. Stearns, "Interim Letter Report No. 10 for Period 1 Dec-1 May 1973," for the Climatic Impact Assessment Program, U.S. Department of Transportation, NOAA, Boulder, CO., 1973.
- Labitzke, K. and H. van Loon, "The Stratosphere in the Southern Hemisphere," Meteor. Monogr., 13, 113-138, 1972.
- Liljequist, G. H., Norwegian - British - Swedish Antarctic Expedition, 1949-52, Scientific Results, Vol II, Parts 1 and 2, Norsk Polarinstitut, Oslo, 1956.
- London, J., "The Global Distribution and Variations of Atmospheric Ozone," AD/A-019 501, University of Colorado, Boulder, CO., 1975.
- Louis, J. F., Ph.D. Thesis, Astro-Geophysics Department, University of Colorado, Boulder, CO., 1974.
- Louisnard, N., A. Girard and G. Eichen, "Mesures du Profile Vertical de Concentration de la Vapeur d'eau Stratospherique," C. R. Acad. Sciences, 290, Ser. B, p. 385, Paris 1980 and (private communication, 1979).
- Martell, E. A. and D. H. Ehhalt, "Hydrogen and Carbon Compounds in the Upper Stratosphere and Lower Mesosphere," pp. 223-232 in Vol I, Proc. Intl. Conf. on Structure, Composition and Gen. Cir. of the Upper and Lower Atmos. and Possibly Anthropogenic Perturbations, Jan. 14-25, 1974, Melbourne, Australia, 1974.
- Mastenbrook, H. J., "Frost-Point Hygrometer Measurements in the Stratosphere and the Problem of Moisture Contamination," pp. 480-485 in Humidity and Moisture Measurement Control in Science and Industry, Vol. 2, Reinhold, NY, 1965.
- Mastenbrook, H. J., "Water Vapor Distribution in the Stratosphere and High Troposphere," J. Atmos. Sci., 25(2), 299-311, 1968.
- Mastenbrook, H. J., "The Variability of Water Vapor in the Stratosphere," J. Atmos. Sci., 28, 1495-1501, 1971.
- Mastenbrook, H. J., "Water Vapor Measurements in the Lower Stratosphere," Can. J. Chem., 52, 1527-1531, 1974a.
- Mastenbrook, H. J., "Stratospheric Water Vapor Distribution and Variability," pp 233-248 in Vol I, Proc. Intl. Conf. on Structure, Composition and Gen. Cir. of the Upper and Lower Atmos. and Possible Anthropogenic Perturbations, Jan. 14-25, 1974, Melbourne, Australia, 1974b.
- McKinnon, D. and H. W. Morewood, "Water Vapor Distribution in the Lower Stratosphere Over North and South America," J. Atmos. Sci., 27, 483-493, 1970.
- Murcray, D. G., et al. (10 authors), "Recent Results of Stratospheric Trace Gas Measurements from Balloon-Borne Spectrometers," Proc. 3rd CIAP Conf., DOT-TSC-OST-74-15, pp 184-192, 1974.
- Murgatroyd, R. J., P. Goldsmith and W. E. H. Hollings, "Some Recent Measurements of Humidity from Aircraft up to Heights of about 50,000 feet Over Southern England," Quart. J. Roy. Met. Soc., 81, 533-537, 1955.

ELLSAESSER

- Murgatroyd, R. J., "Ozone and Water Vapour in the Upper Troposphere and Lower Stratosphere, Meteorological Aspects of Atmospheric Radioactivity," Tech. Note 68, W. Bleaker (ed.), pp 68-94, WMO, Geneva, 1965.
- Newell, R. E., J. W. Kidson, D. E. Vincent and G. J. Boer, The General Circulation of the Tropical Atmosphere, Vol. I, The MIT Press, Cambridge, MA., 1972.
- Newell, R. E., G. J. Boer and J. W. Kidson, "Application of Tropical General Circulation Statistics to the Cycles of Carbon Monoxide, Water and Sulphate," (paper presented at GACGP Symposium on Trace Gases, Mainz, Germany, April 2-5, 1973).
- Patel, C. K. N., E. G. Burkhardt and C. A. Lambert, "Spectroscopic Measurements of Stratospheric Nitric Oxide and Water Vapor," Science, 184, 1173-1176, 1974.
- Penndorf, R., "Analysis of Ozone and Water Vapor Field Measurement Data," Report No. FAA-EE-78-29, NTIS, Springfield, VA., 1978.
- Poppoff, I. G., W. A. Page and A. P. Margozi, 1977 Intertropical Convergence Zone Experiment, NASA Tech. Memo. 78577, Ames Res. Center, Moffett Field, CA., 1979.
- Prabhakara, C. and E. B. Rodgers, "Study of the Lower Stratospheric Thermal Structure and Total Ozone from NIMBUS-4 IRIS," NASA Tech. Note D-8134, GSFC, Greenbelt, MD., 1976.
- Radford, H. E., M. M. Litvak, C. A. Gottlieb, E. W. Gottlieb, S. K. Rosenthal and A. E. Lilley, "Mesospheric Water Vapor Observed from Ground-Based Microwave Absorption," J. Geophys. Res., 82, 472-478, 1977.
- Reed, R. J. and C. L. Vlcek, "The Annual Temperature Variation in the Lower Tropical Stratosphere," J. Atmos. Sci., 26(1), 163-167, 1969.
- Robinson, G. D., "Water Vapour in the Lower Stratosphere," EOS, 59(12), 1085, 1978 (Abstract).
- Rogers, J. W., A. T. Stair, T. C. Degges, C. L. Wyatt and D. J. Baker, "Rocketborne Measurements of Mesospheric H<sub>2</sub>O in the Auroral Zone," Geophys. Res. Letts., 4, 366-368, 1977.
- Sastry, P. S. N. and A. L. Narasimham, "Some Characteristics of Tropopause Over India," Ind. J. Meteor. Geophys., 17(4), 567-572, 1966.
- Schell, W. R., G. Sauzay and B. R. Payne, "World Distribution of Environmental Tritium," pp 325- , in Physical Behavior of Radioactive Contaminants in the Atmosphere, IAEA-SM-181/34, IAEA, Vienna, 1974.
- Sissenwine, N., A. J. Kantor and D. D. Grantham, "How Dry is the Sky? A Decade Later and the SST," A. F. Surveys in Geophysics, No. 240, AFCRL-72-0294, 1972.
- Sissenwine, N., D. D. Grantham and H. A. Samela, "Mid-Latitude Humidity to 32 km," J. Atmos. Sci., 30, 1129-1140, 1968.
- Stanford, J. L., "Possible Sink for Stratospheric Water Vapor at the Winter Antarctic Pole," J. Atmos. Sci., 30, 1431-1436, 1973.
- Stanford, J. L. and J. S. Davis, "A Century of Stratospheric Cloud Reports: 1870-1972," Bull. Am. Meteor. Soc., 55(3), 213-219, 1974.
- Stormer, C., "Remarkable Clouds at High Altitudes," Nature, 123, 260-261, 1929.
- Swann, N. R., M. J. Bangham and J. E. Harries, "Measurements of Stratospheric Water Vapour Using a Far Infrared Radiometer," National Physics Laboratory, U.K. (to be submitted to Appl. Optics).
- Waters, J. W., J. J. Gustincic, R. V. Kakar, A. R. Kerr, H. R. Roscoe and P. N. Swanson, NASA Report TMX-73630, NTIS, Springfield, VA., 1977.
- Weickmann, H., C. C. Van Valin and J. M. Anderson, "Review of Natural Sources and Sinks of Stratospheric Water Vapor," in CIAP Monograph 3, pp 7-4 to 7-12, DOT-TST-75-53, NTIS, Springfield, VA., 1975.
- Williamson, E. J. and J. T. Houghton, "Radiometric Measurements of Emission from Stratospheric Water Vapour," Quart. J. Roy. Met. Soc., 91, 330-338, 1966.
- Zander, R., "Water Vapor Above 25 km Altitude," PAGEOPH, 106-108, 1346-1351, 1973.
- Zander, R., "Moisture Contamination at Altitude by Balloon and Associated Equipment," J. Geophys. Res., 71(15), 2775-3778, 1966.

NOTICE

This report was prepared as an account of work sponsored by the United States Government. Neither the United States nor the United States Department of Energy, nor any of their employees, nor any of their contractors, subcontractors, or their employees, makes any warranty, express or implied, or assumes any legal liability or responsibility for the accuracy, completeness or usefulness of any information, apparatus, product or process disclosed, or represents that its use would not infringe privately-owned rights

Reference to a company or product name does not imply approval or recommendation of the product by the University of California or the U.S. Department of Energy to the exclusion of others that may be suitable

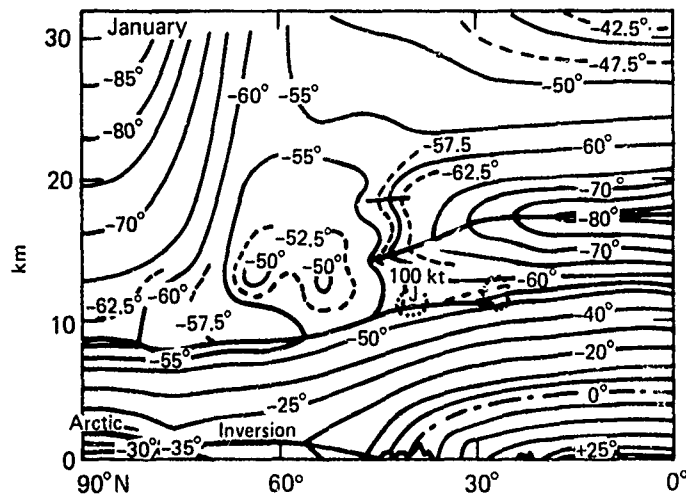


Figure 1. Northern hemisphere meridional section of 1948-1951 mean January temperature in °C along 80°W from Kochanski [1955].

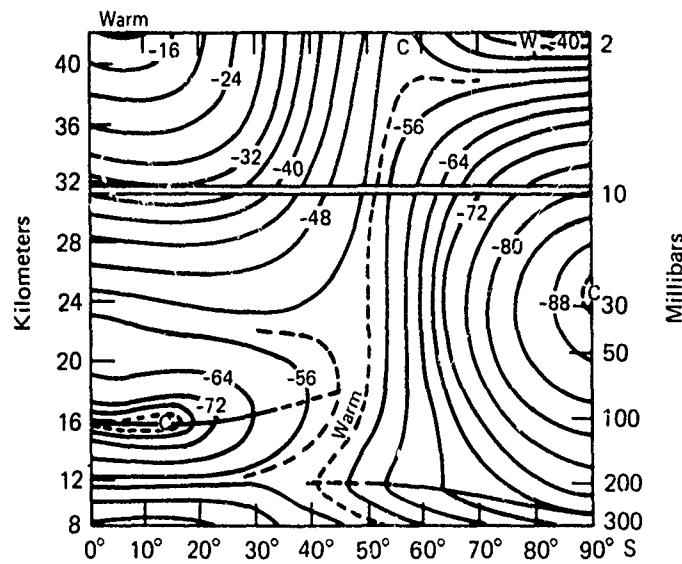


Figure 2. Southern hemisphere meridional section of mean winter temperature (June-July) in °C along 180°E composited from radiosondes and satellites by Labitzke and van Loon [1972].

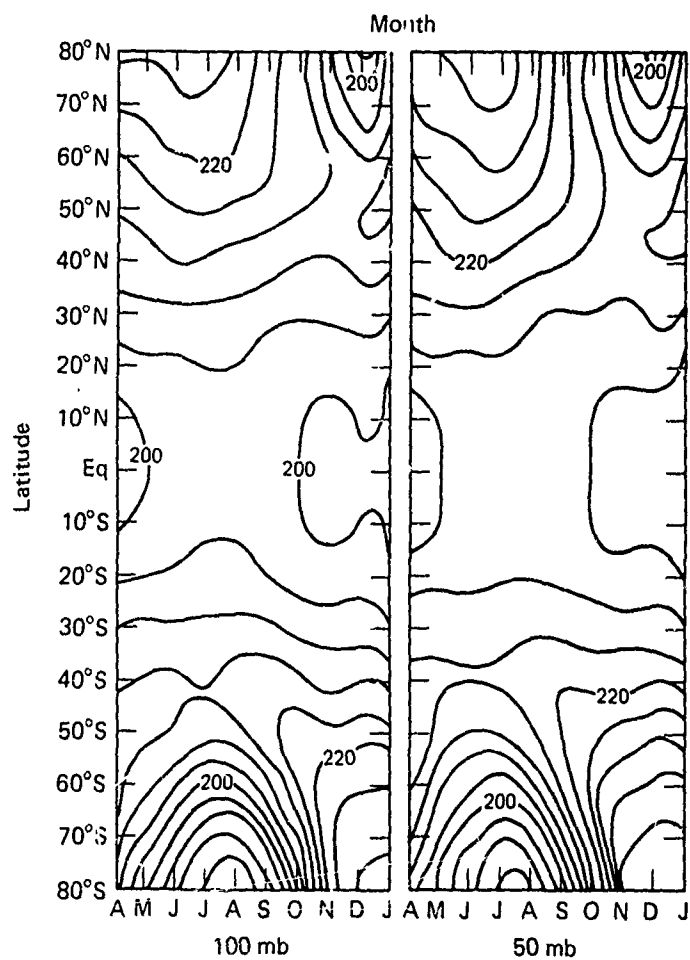


Figure 3. Zonal average 100- and 50-mb temperatures derived from Nimbus-4 IRIS measurements for April 1970 through January 1971 by Prabhakara and Rodgers [1976]. Contour interval 4 K.

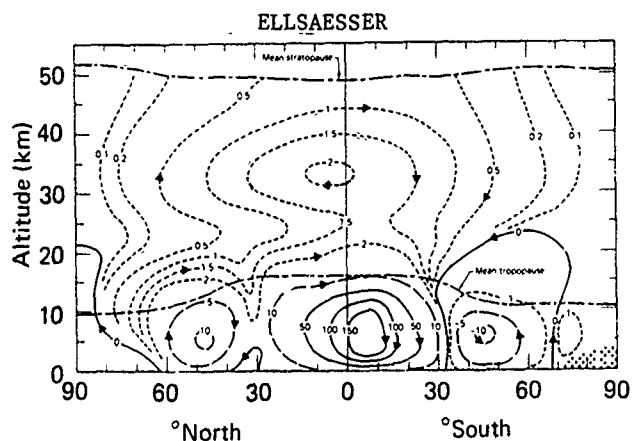


Figure 4. Streamlines ( $10^9$  Kg/sec) of mean meridional circulation for Jun-Aug composited from data of Newell et al. [1972] and Louis [1974]. From Danielson [1975].

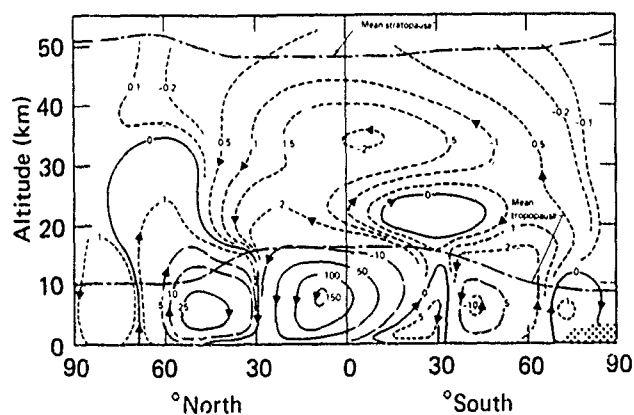


Figure 5. Streamlines ( $10^9$  Kg/sec) of mean meridional circulation for Dec-Feb composited from data of Newell et al. [1972] and Louis [1974]. From Danielson [1975].

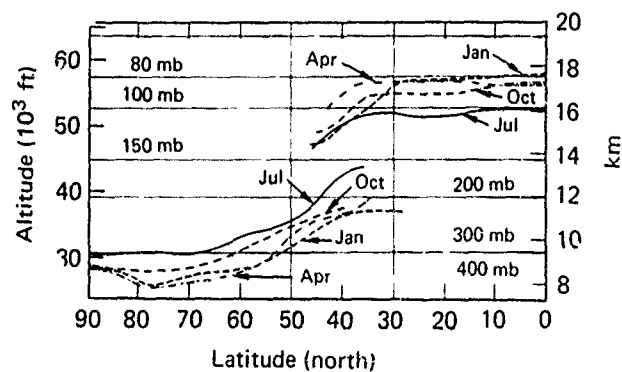


Figure 6. 1948-1951 mean heights of the northern hemisphere tropopauses along  $80^\circ\text{W}$  for months of Jan., Apr., Jul. and Oct. from Kochanski [1955].

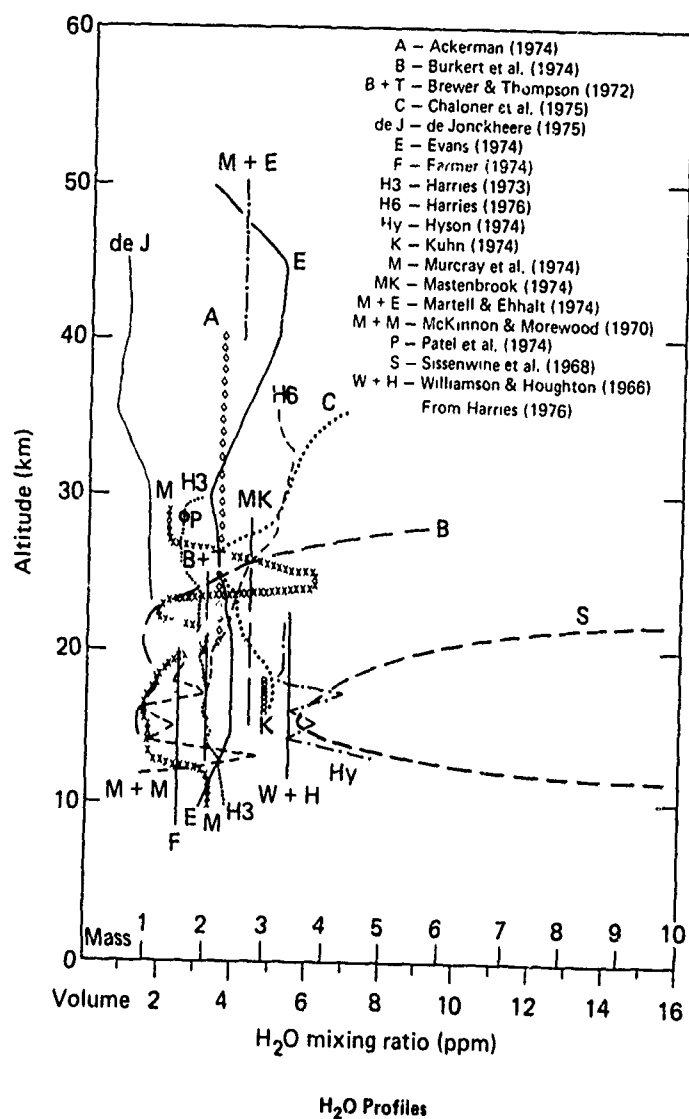


Figure 7. Summary of observations of vertical profiles of stratospheric H<sub>2</sub>O compiled by Harries [1976].

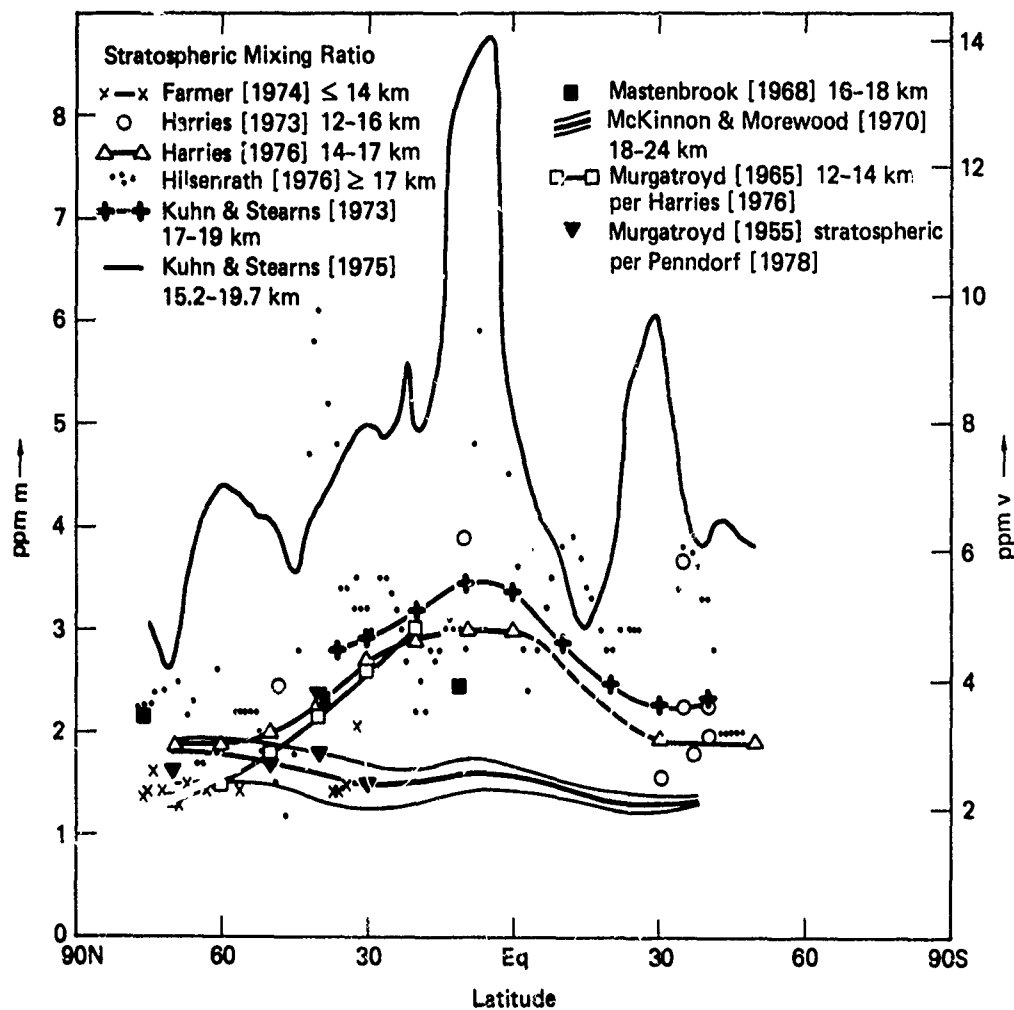


Figure 8. Summary of observations of the latitudinal gradient in stratospheric  $\text{H}_2\text{O}$ . Data sources identified by references.



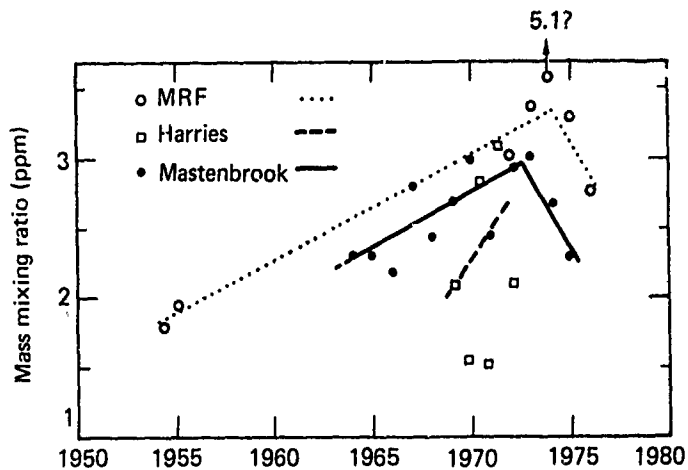


Figure 9. Long term trend in stratospheric mixing ratio as indicated by data of MRF [Cluley and Oliver, 1978], Mastenbrook [Penndorf, 1978] and Harries [1973].

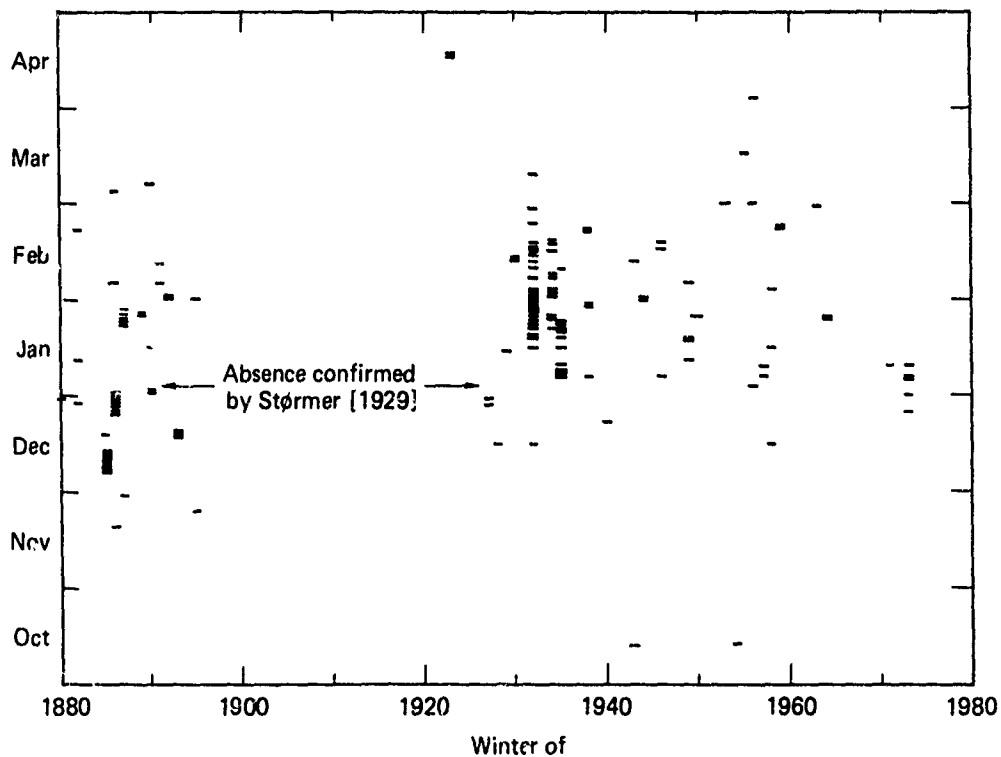


Figure 10. Map of northern hemisphere sighting of nacreous clouds compiled by Stanford and Davis [1974].

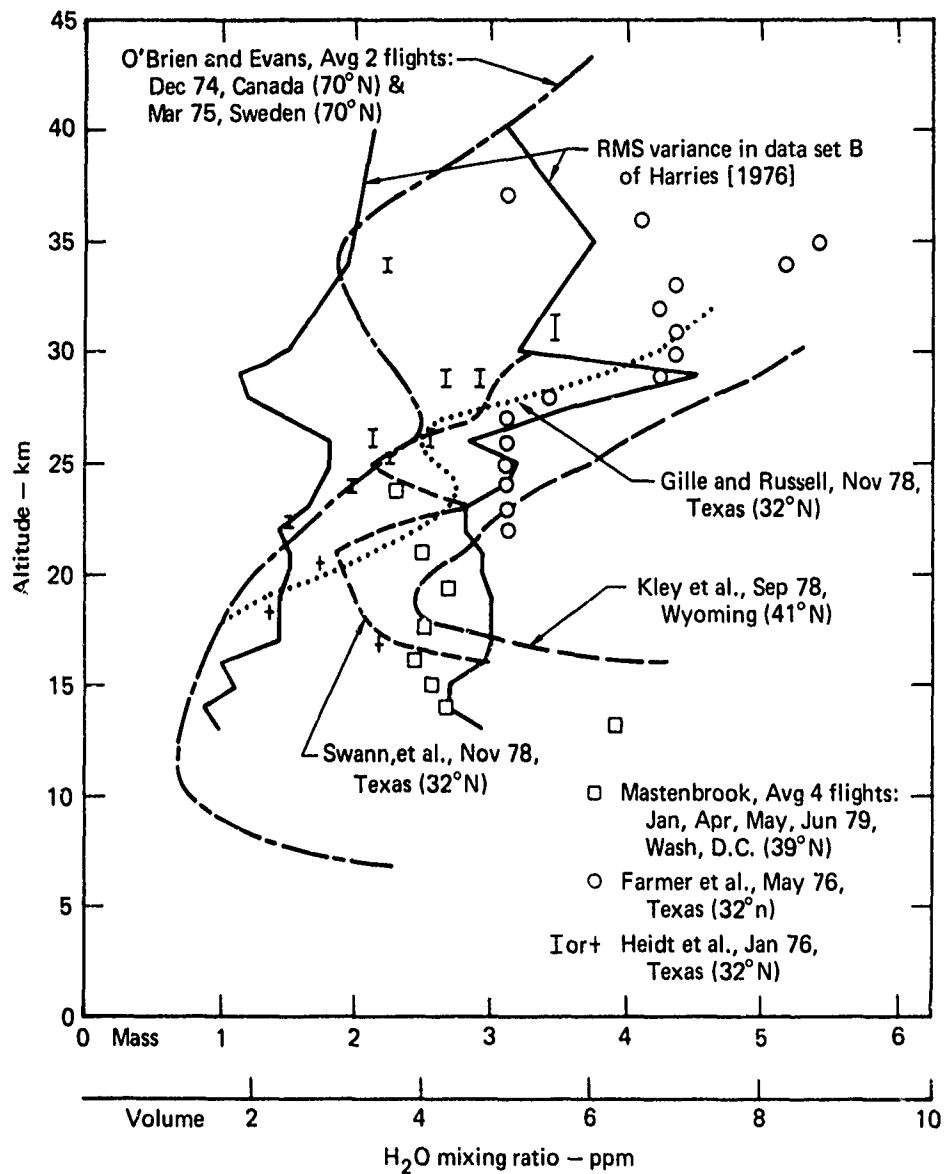


Figure 11. Summary of recent stratospheric H<sub>2</sub>O soundings from the DOT HAPP Bulletin for June 1979.

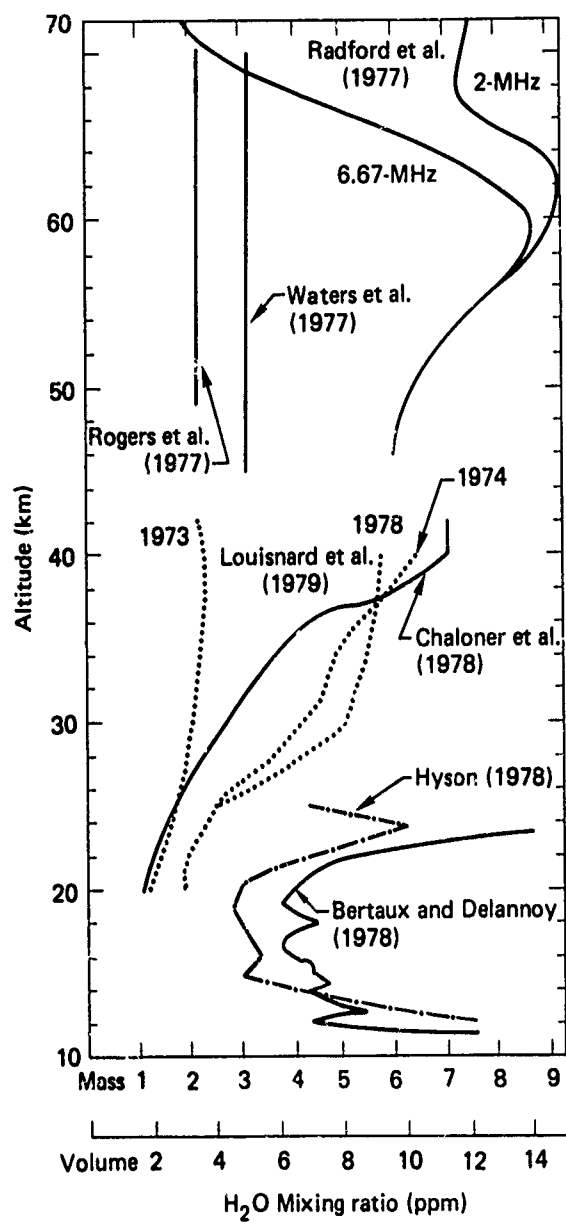


Figure 12. Summary of recent soundings of stratospheric and mesospheric H<sub>2</sub>O not included in Figure 11.

## THE ATMOSPHERIC CH<sub>4</sub> BUDGET

Thomas M. Donahue

Department of Atmospheric and Oceanic Science  
The University of Michigan, Ann Arbor, MI USA

### Abstract

Measurements of the tropospheric methane concentration are discussed. Estimates of the strength of various methane sources - natural wetlands, rice paddies, ruminants, anthropogenic and lithospheric - are presented. These allow limits to be placed on the tropospheric lifetime of CH<sub>4</sub> of 5 to 13 years. In turn, these estimates put limits on the allowable concentration of tropospheric OH which reacts with CH<sub>4</sub> to provide the principal tropospheric sink. The range of OH concentrations implied at the Earth's surface is 1.7 to 0.7 x 10<sup>6</sup> cm<sup>-3</sup>. Present estimates of CH<sub>4</sub> source strengths are very uncertain and a serious effort to improve this state of affairs is in order.

**INTRODUCTION** It is a fascinating thermodynamic anomaly that a gas as reactive as methane can exist in concentrations greater than 1 ppm in a highly oxidizing atmosphere such as that of the Earth. The departure from thermodynamic equilibrium is some 50 orders of magnitude, as Watson, Lovelock and Margulis (1978) have emphasized. This is a very interesting fact in itself and it can lead one to some fascinating cybernetic speculation. Furthermore, as Ehalt (1980) discusses elsewhere in this volume the presence of methane in the atmosphere is very important to the chemistry of the stratosphere since it is the principal source of hydrogen compounds and radicals in the upper atmosphere. It is, therefore, of interest to consider what is the state of our knowledge about the sources and sinks of methane in the biosphere and the atmosphere.

**TROPOSPHERE METHANE CONCENTRATION** There is little in the present review that has not been presented in the excellent article by Ehalt and Schmidt (1978). The review will begin by assessing the present state of information relative to the global methane inventory. CH<sub>4</sub> was first detected in the atmosphere spectroscopically by Migeotte (1948) shortly after World War II when he measured the concentration by volume to be 2 ppm. Subsequently, there have been published the following results where N. and S. refer respectively to northern and southern hemispheres

# NONAHUE

Ehalt and Heidt	(1973)		1.60 ppm v/v
Heidt and Krasnec	(1978)		1.63
Ehalt	(1978)	N.	1.74
		S.	1.56
		Mean	1.65
Singh, et al.	(1978)	N.	1.43±0.06
		S.	1.39±0.05
Mayer, et a.	(1978)	N.	1.58
		S.	1.47
Rasmussen	(1980)		1.63±0.02

For the purposes of this review it will be assumed that the tropospheric concentration is 1.6 ppm v/v. A 10% excess of methane in the northern hemisphere appears to be real. Having established the amount of CH<sub>4</sub> present in the atmosphere, it is next necessary to undertake the far more difficult task of conducting an inventory of sources. To the extent that this exercise is successful, it will be possible to make quantitative statements concerning the tropospheric lifetime of methane. The lifetime can then be compared with the lifetime predicted by an evaluation of the loss processes which are transport into the stratosphere and reaction with tropospheric OH. It will turn out that there is a large uncertainty in the source strength matched by an equally large uncertainty in the tropospheric burden of OH. Thus, at the present time, it is difficult to use good data concerning the strength of source or sink of CH<sub>4</sub> to put limits on the other.

**METHANE SOURCES: BIOGENIC** Because of its high energy content and complex structure, methane is difficult to produce by gas phase reactions in the atmosphere. Thus, it is no surprise to find that the CH<sub>4</sub> in the atmosphere is produced by reactions in the biosphere or in the lithosphere. A comparison of the ratio of <sup>14</sup>C to <sup>12</sup>C in atmospheric CH<sub>4</sub> with that in fresh wood by Libby (1973) showed that at least 80% of the methane in the air is of recent biological origin. Some of the remaining 20% might also be fresh CH<sub>4</sub> because the samples used were collected in urban areas. There is an unknown contribution of CH<sub>4</sub> in these samples from industrial sources in which the carbon would have originated from fossil fuels poor in <sup>14</sup>C. Thus, 80% is an upper limit to the biogenic source. (Meaningful repetition of this experiment is prevented because of the contamination of atmospheric <sup>14</sup>CH<sub>4</sub> by nuclear weapons tests.)

Much of natural biogenic methane production can be attributed to the activity of anaerobic bacteria, such as Methanobacterium, Methanococcus and Methanosarcina. Accordingly source regions tend to be alkaline, high temperature anoxic domains rich in organic matter such as peat bogs, swamps, marshes, sediments in ponds less than 10m in depth, rice paddies and the rumen of animals such as cattle, sheep and camels.

Quantitative studies of methane fluxes from wetlands are practically non-existent. Baker-Blocker, et al., (1977) during the months from May through October in 1975, have measured the flux from 4 ponds in southern Michigan of average depth about 1 meter and a pH of 8. Fluxes were measured that ranged from 9 x 10<sup>-6</sup> to 10<sup>-4</sup> g cm<sup>-2</sup> d<sup>-1</sup>. The wild scatter plot of data was "fitted" to a curve expressing the flux as a function of the ambient air temperature T in °K

$$\phi = 4.6 \times 10^{-5} - 5.6 \times 10^{-6}T + 2.6 \times 10^{-7}T^2 \text{ g cm}^{-2} \text{ d}^{-1}$$

Using this formula and knowledge of local temperature variations, these investigations characterized the fluxes from 4 major wet-land sources as follows:

	g m <sup>-2</sup> yr <sup>-1</sup>	g yr <sup>-1</sup>
The Sudd	400	60 x 10 <sup>12</sup>
The Everglades	170	4.0 x 10 <sup>12</sup>
Ugandan Swamps	230	2.2 x 10 <sup>12</sup>
The Pripet Marshes	40	1.9 x 10 <sup>12</sup>
		<hr/>
		68 x 10 <sup>12</sup>

Extrapolating these results to all natural wetlands in the form of swamps, marshes and ponds can be accomplished by estimating their average temperature to be  $15^{\circ}\text{C}$ , their area to be  $2.5 \times 10^{12} \text{ m}^2$  and, allowing for the scatter in the data of Baker-Blocker, a flux between 50 and  $100 \text{ g m}^{-2} \text{ yr}^{-1}$ . The result is for natural wetlands a source strength of  $200 - 300 \text{ g yr}^{-1}$ .

Rice paddies represent a large man-made biogenic source. Koyama (1965) from Japanese paddy soils estimated the average  $\text{CH}_4$  production in Japan to be  $80 \text{ g m}^{-2} \text{ yr}^{-1}$  or  $2.3 \times 10^{12} \text{ g yr}^{-1}$ . In extrapolating to the rest of the world he apparently took into account temperature variability and the fact that most paddies are waterlogged throughout the year rather than only 4 months as in the case in Japan to estimate a global rate of  $1.90 \times 10^{12} \text{ g yr}^{-1}$ . Because of the increase in the area of paddy fields since 1963 this source strength would grow to about  $280 \text{ g yr}^{-1}$  at present. Rather arbitrarily attaching the same kind of uncertainty to this estimate that applies to the natural wetlands estimate one can put the rice paddy source between  $140$  and  $280 \text{ g yr}^{-1}$ .

By enteric fermentation a cow is known to produce 200 g of methane per day on a diet of at least 10 kg of plant matter. Similar data are available for other domestic ruminants leading to an estimate of  $100 \times 10^{12} \text{ g yr}^{-1}$  of methane production. To account for the methane generation by wild herbivores it can be assumed that they are as efficient as cattle in converting plant matter to methane ( $2 \times 10^{-2} \text{ g CH}_4/\text{g food}$ ), use an estimate that  $1.1 \times 10^{16} \text{ g}$  of dry plants are eaten every year by herbivores of all kinds and produce an estimate of  $220 \times 10^{12} \text{ g yr}^{-1}$  of  $\text{CH}_4$  production. Hence, the enteric fermentation source can be taken to lie between  $100$  and  $220 \text{ g yr}^{-1}$ .

Other biogenic sources include wet tundra and the margins of lakes and oceans. A crude attempt to characterize these puts their contribution at  $3$  to  $50 \times 10^{12} \text{ g yr}^{-1}$ .

Adding the natural wetland, rice paddy, ruminant, and miscellaneous upper and lower source limits results in a biogenic source estimate of between  $440$  and  $850 \times 10^{12} \text{ g yr}^{-1}$ .

METHANE SOURCES: NONBIOGENIC The principal anthropogenic sources of methane appear to be the consequence of coal mining and industrial activity. These account for between  $16$  and  $50 \times 10^{12} \text{ g yr}^{-1}$ .

On the other hand, the  $^{14}\text{C}$  analyses already discussed allow as much as 20% of the  $\text{CH}_4$  in the atmosphere to contain fossil carbon. Such  $\text{CH}_4$  would certainly have to be ascribed to non-biogenic release mechanisms. It would imply a source of 25% as strong as the biogenic source yielding  $110$  to  $210 \times 10^{12} \text{ g yr}^{-1}$ .

The latter figures are, however, upper limits since the air samples on which they are based may be contaminated. Thus, the upper and lower limits to non-biogenic source have to be put at  $16$  and  $210 \times 10^{12} \text{ g yr}^{-1}$ .

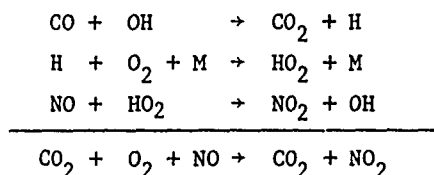
Altogether the biogenic, anthropogenic and other sources of  $\text{CH}_4$  then total between  $450$  and  $1100 \times 10^{12} \text{ g yr}^{-1}$ .

TROPOSPHERIC LIFETIME: About 10% of the  $\text{CH}_4$  injected into the atmosphere makes its way into the stratosphere. Hence a tropospheric sink must be found for  $400$  to  $1000 \times 10^{12} \text{ g yr}^{-1}$  of  $\text{CH}_4$  or between  $0.9 \times 10^{11} \text{ molecules cm}^{-2} \text{ s}^{-1}$  and  $2.3 \times 10^{11} \text{ molecules cm}^{-2} \text{ s}^{-1}$ . Since the atmospheric burden of 1.6 ppm amounts to  $4.6 \times 10^{15} \text{ gm}$  or  $3.8 \times 10^{19} \text{ molecules cm}^{-2}$ , the tropospheric lifetime of these molecules must lie between  $4.2$  and  $1.7 \times 10^8 \text{ sec}$  or  $13$  and  $5 \text{ years}$ .

TROPOSPHERIC SINK: OH Now that a range of lifetimes for tropospheric methane has been set by comparing the methane inventory with the extremes of source strengths it is necessary to determine whether this range of lifetimes is consistent with the known tropospheric sinks of  $\text{CH}_4$ . The only important sink known is gas phase reaction of  $\text{CH}_4$  with OH



The principal source of OH is reaction of water vapor with  $\text{O}(^1\text{D})$  resulting from ozone photolysis. The resulting OH can become involved in a  $\text{HO}_x$  cycle



or in terminating steps other than reaction with  $\text{CH}_4$ . If the methane density is taken as known, the lifetime limits set by the source inventory impose a requirement on the tropospheric OH density. It is necessary that

$$1.7 \times 10^8 \text{ s} \leq \int k(T) [\text{CH}_4] [\text{OH}] dz \leq 4.2 \times 10^8 \text{ s}$$

This immediately implies for the surface density of OH a permitted range

$$0.7 \times 10^6 \text{ cm}^{-3} \leq [\text{OH}]_0 \leq 1.7 \times 10^6 \text{ cm}^{-3}$$

Reported measurements of tropospheric OH densities have shown a downward trend during the past several years from values far exceeding  $10^6 \text{ cm}^{-3}$  to levels considerably below  $10^6 \text{ cm}^{-3}$ . For example

$30 \times 10^6 - 60 \times 10^6 \text{ cm}^{-3}$	Wang, et al., (1975)
$<4 \times 10^6 - 7 \times 10^6 \text{ cm}^{-3}$	Perner, et al., (1976)
$0.2 - 0.5 \times 10^6 \text{ cm}^{-3}$	Singh (1979)
$0.5 \times 10^6 \text{ cm}^{-3}$	Wang (1979)

From this discussion, it should be apparent that more extensive studies of methane sources are in order. None of the important inventories is in good shape. Particular attention needs to be paid to extending the work of Baker-Blocker, et al., (1977). A study restricted to 4 shallow ponds in southern Michigan during one summer is certainly a shaky base on which to extrapolate to a global wetland source strength. In particular the effects of water composition with depth on the transformation of  $\text{CH}_4$  as it tries to make its way from bottom sediments to the water surface need to be assessed. Rice paddy studies in the field are needed to supplement Koyama's laboratory work. A resolution of the uncertainty introduced in the census of non-biogenic sources by the fossil  $^{14}\text{C}$  problem is needed. Finally, consensus on the tropospheric OH budget would be welcome. Nevertheless, it is gratifying although perhaps fortuitous that the present evaluation of  $\text{CH}_4$  sources and concentration implies an OH tropospheric concentration in the neighborhood of  $10^6 \text{ cm}^{-3}$  which is about where current measurements are putting it.

ACKNOWLEDGEMENTS: This work was supported by NASA's Upper Atmospheric Research Program.

#### REFERENCES

- Baker-Blocker, A., T. M. Donahue, K. H. Mancy, Methane Flux From Wetlands Areas, *Tellus*, 29, 245, 1977.  
 Ehalt, D. H., The  $\text{CH}_4$  Concentration Over Ocean and its Possible Variation with Latitude, *Tellus*, 30, 169, 1978.  
 Ehalt, D. H., U. Schmidt, Sources and Sinks of Atmospheric Methane, *Pageoph.*, 116, 432, 1978.

- Heidt, L. E., J. P. Krasnec, Tropospheric Distributions of CO, CH<sub>4</sub>, CO<sub>2</sub> and N<sub>2</sub>O in the Northern and Southern Hemispheres, EOS, 59, 1077, 1978.
- Heidt, L. E., W. H. Pollock, Measurements of N<sub>2</sub>O, CH<sub>4</sub>, H<sub>2</sub>, CO and CO<sub>2</sub> in the non urban troposphere, Proceedings Symposium II The Non-Urban Tropospheric Composition, Hollywood, FL, 1976.
- Koyama, T., Gaseous Metabolism in Lake Sediments and Paddy Soils, J. Geophys. Res., 68, 3971, 1963.
- Perner, D., D. H. Ehalt, et al., OH-radicals in the Lower Troposphere, Geophys. Res. Lett., 3, 466, 1976.
- Rasmussen, R. A., These proceedings, 1980.
- Singh, H. B., Atmospheric Halocarbons: Evidence in Favor of Reduced Hydroxyl Radical Concentration in the Troposphere, Geophys. Res. Lett., 4, 101, 1977.
- Singh, H. B., L. J. Salas, H. Shigeishi, E. Scribner, Global Distribution of Selected Halocarbons, SF<sub>6</sub> and N<sub>2</sub>O, E.P.A. Grant 600/3-78-100, Research Triangle Park, N.C. 27711, 1978.
- Wang, C. C., Private Communication, 1979.
- Wang, C. C., L. I. Davis, et al., Hydroxyl Radical Concentrations Measured in Ambient Air, Science, 189, 797, 1975.
- Watson, A., J. E. Lovelock, L. Margulis, Methanogenesis, Fires and Regulation of Atmospheric Oxygen, Biosystems, 10, 293, 1978.



## THE ATMOSPHERIC H<sub>2</sub> CYCLE

U. Schmidt, G. Kullessa

Kernforschungsanlage Jülich GmbH  
Institut für Chemie III: Atmosphärische Chemie  
D-5170 Jülich, FRG

E.P. Röth

Universität Essen - Gesamthochschule  
Institut für Physikalische Chemie, D-4300 Essen, FRG

The tropospheric H<sub>2</sub> mixing ratio averages 0.56 ppmv. A small difference of about 4 % is observed between both hemispheres. The total global amount of H<sub>2</sub> in the atmosphere is  $200 \times 10^{12}$  g, two thirds of which comes from natural sources. The various known processes, which produce and destruct H<sub>2</sub>, are discussed and the tropospheric residence time is estimated to be about 3 years.

1. INTRODUCTION: The presence of molecular hydrogen in the atmosphere has been recognized since the beginning of this century. The first reliable measurements, which were made by Schuftan [see Paneth, 1937], showed a mixing ratio of 0.5 ppmv (parts per million by volume). However, the fate, the sources and sinks as well as the global distribution remained largely speculative until recently. A first attempt at estimating the sources and sinks of tropospheric H<sub>2</sub> was made by Schmidt [1974] on the basis of comprehensive measurements in atmospheric air and identification of important production and destruction processes. These investigations showed, that H<sub>2</sub> is well mixed throughout the troposphere and that there are rather strong sources, which enable H<sub>2</sub> to build up to a relatively large mixing ratio in the ppmv-range. Both these observations indicated that the tropospheric lifetime of H<sub>2</sub> should be relatively long, i.e.  $\geq$  one year.

Investigations of the cycle of atmospheric H<sub>2</sub> will not only provide information about the trace gas itself but is also of further interest in atmospheric chemistry. It is well established that H<sub>2</sub> and CO are important, rather longlived, intermediate products of the chemical oxidation of atmospheric CH<sub>4</sub>. Chemical processes in the atmosphere serve as the predominant sink for CH<sub>4</sub> (and CO) and as relatively important sources for CO and H<sub>2</sub>. Therefore, they are coupling the cycles of these three trace gases, and investigations of the H<sub>2</sub> cycle may also provide some valuable information on the cycles of CO and CH<sub>4</sub>.

In the stratosphere H<sub>2</sub> - besides H<sub>2</sub>O and CH<sub>4</sub> - serves as a source of OH and HO<sub>2</sub> radicals, which are very important for chemical processes in that altitude region. The chemical lifetime of H<sub>2</sub> is about 100 years in the lower stratosphere and therefore H<sub>2</sub> mixing ratios depend very sensitively on transport. The same holds for CH<sub>4</sub>, which provides the only other H<sub>2</sub>-source in the stratosphere. Therefore, the stratospheric H<sub>2</sub> distribution serves as a valuable check of model calculations of at-

mospheric chemistry and, together with simultaneous  $\text{CH}_4$  measurements, it may provide information on stratospheric transport processes. In this paper we summarize the available information on the cycle of  $\text{H}_2$  in the troposphere and stratosphere. The major aspects of the distribution, sources and sinks of this trace gas will be reviewed. For more detailed information the reader is referred to the quoted literature. We have updated previous estimates where new information has become available during recent years.

2. ATMOSPHERIC MEASUREMENTS: The first published series of measurements [Paneth, 1937; Glueckauf and Kitt, 1957] showed that  $\text{H}_2$  mixing ratios in ambient air averaged around 0.5 ppmv. Higher values with large variations occurred in polluted areas.

However, our knowledge about tropospheric levels of the  $\text{H}_2$  mixing ratio remained rather sparse until 1972. Available data were compiled by Schmidt [1974]. Since that time background measurements of the tropospheric  $\text{H}_2$  mixing ratio have been reported by various investigators. Published data are summarized in Table 1. They show the troposphere to be rather well mixed vertically as well as horizontally.

Table 1 Tropospheric $\text{H}_2$ measurements reported since 1974					
Time	Location	Altitude [km]	Number of samples	average mixing ratio (ppmv)	Reference
1966 - 1975	North America 26°N-42°N	1.5 - 13.1	~ 350	$0.503 \pm 0.010$	<u>Ehhalt et al</u> [1977]
1973	North Atlantic 18°N-50°N	surface	cont	$0.582 \pm 0.018$	<u>Schmidt</u> [1978]
1974	Northern Hemisphere 67°N-10°N	6.5 - tropopause	cont	$0.561 \pm 0.012$	<u>Schmidt</u> [1978]
1974	Southern Hemisphere 5°N-53°S	6.5 - tropopause	cont	$0.554 \pm 0.014$	<u>Schmidt</u> [1978]
1974	North America 30°N-34°N	1.0 - 13.1	78	$0.512 \pm 0.059$	<u>Heidt and Pollock</u> [1976]
1976	Europe 50°N-60°N	1.0 - 12.5	64	$0.51 \pm 0.02$	<u>Seiler et al</u> [1978]
1977	North Atlantic 36°N-18°N	surface	98	$0.65 \pm 0.02$	<u>Herr and Barger</u> [1978]
1977	Europe 42°N-45°N	2.8 - 13.0	24	$0.54 \pm 0.02$	<u>Fabian et al</u> [1979a]
cont = continuous registration					

Differences between individual data sets predominately originate from the fact that the absolute calibration employed at the different laboratories did not agree.

Results obtained during continuous registrations in both hemispheres indicated that there exists a small but significant interhemispheric difference of the  $H_2$  mixing ratio, which is about 5.8 % in surface air and 1.5 % in the upper troposphere. If roughly twice the weight is attached to the surface values to account for the vertical density profile in the atmosphere, the average hemispheric difference amounts to 4.4 %. The average mixing ratio in the southern and northern hemisphere is 0.552 ppmv and 0.576 ppmv, respectively [Schmidt, 1978]. Thus for an averaged height of the tropopause of 13 km (165 mb-level) the total mass of  $H_2$  present in the northern and southern troposphere is  $M_n = 87.2 \times 10^{12}$  g and  $M_s = 83.5 \times 10^{12}$  g, respectively. Correspondingly, the total abundance of  $H_2$  is  $170 \times 10^{12}$  g in the troposphere and  $30 \times 10^{12}$  g in the stratosphere and mesosphere.

Available data on the vertical distribution of  $H_2$  in the troposphere generally do not exhibit significant vertical gradients. However, a number of profiles from distinct regions indicated the existence of sources (reported by Ehhalt et al [1977] for the East Pacific) or sinks (reported by Schmidt [1978] for high northern latitudes) at the surface.

The first data for the stratosphere were reported by Ehhalt and Heidt [1973]. They were derived from samples, which had been collected during balloon flights employing a grab sampling system. Measurements since 1973 employed cryogenic sampling techniques [Lueb et al, 1975]. Data obtained during stratospheric balloon flights, performed over Palestine, Texas, USA ( $32^\circ$  N), Parana ( $32^\circ$  S) and over Southern France ( $44^\circ$  N) were published by Ehhalt et al [1974, 1975a], Schmidt et al [1977], and Fabian et al [1979], respectively.

The only data for the upper stratosphere ( $> 40$  km) have been derived from two samples, which had been collected over New Mexico ( $31^\circ$  N) in the upper stratosphere by means of a rocket-borne cryocondenser [Scholz et al, 1970; Ehhalt et al, 1975b]. Published data on stratospheric  $H_2$ , which are based on cryogenic samples collected at different latitudes are plotted in Figure 1.

Data for  $32^\circ$  N and  $44^\circ$  N are plotted separately. A comparison of both data sets shows that  $H_2$  mixing ratios slightly decreasing with height (5 ppbv/km) are observed at  $44^\circ$  N, whereas no average vertical gradient is visible for  $32^\circ$  N. Some individual profiles from  $32^\circ$  N do display maxima of the  $H_2$  mixing ratio [Ehhalt et al, 1975a] and in this case  $CH_4$  profiles derived from the same samples show a rather pronounced stepwise decrease of the  $CH_4$  mixing ratio. A similar feature has also been observed during a recent balloon flight at  $44^\circ$  N [Fabian et al, 1979b]. It might reflect the presence of air, which was transported to higher latitudes from the equatorial region after it had been injected into the stratosphere through the tropical tropopause [Ehhalt and Toenissen, 1979]. This is due to the fact that vertical transport is much stronger at tropical regions than at higher latitudes, a feature which has been also demonstrated for  $CH_4$  [Bush et al, 1978] and  $N_2O$  [Schmeltekopf et al, 1977].

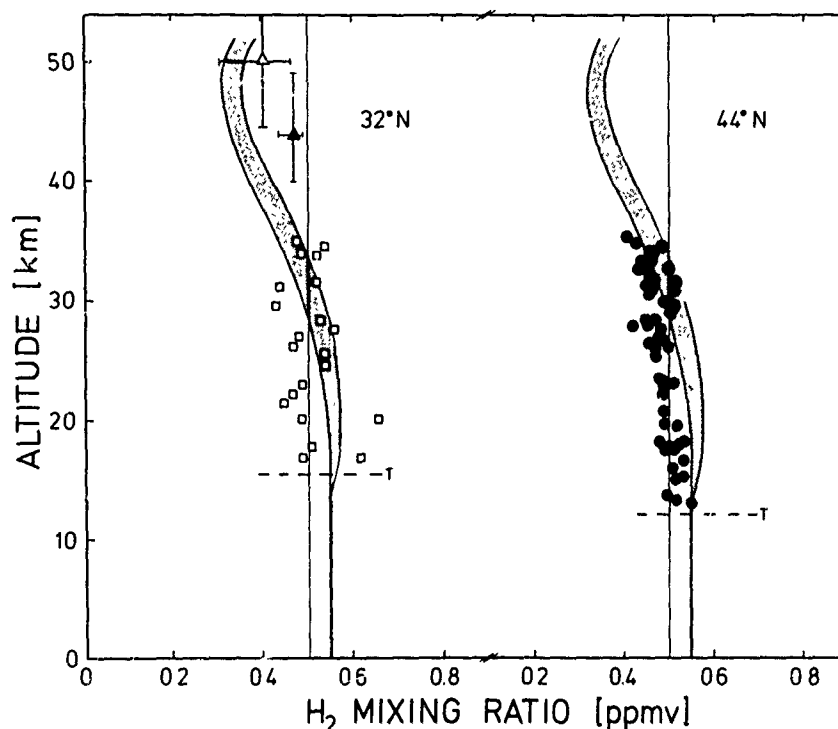


Fig. 1: Stratospheric measurements of the  $H_2$  mixing ratio. Two samples had been collected during rocket flights:  $\Delta$  Scholz et al [1970]  $\blacktriangle$  Ehhalt et al [1975b]. The other data are from balloon flights:  $\square$  Ehhalt et al [1977];  $\bullet$  Fabian et al [1979a]; T = average tropopause. The shaded area gives the vertical  $H_2$  distribution as calculated with the KFA-1-D Model. The upper limit represents the  $H_2$  profile which is based on the absorption cross sections for  $CH_2O$  photolysis given by Calvert et al [1972]. The profile, which is given as the lower limit is based on net quantum yields for  $CH_2O$  photolysis reported by Moortgat and Warneck [1979].

3. SOURCES OF ATMOSPHERIC  $H_2$ : All data on tropospheric  $H_2$  mixing ratios reported to date show a uniform distribution in unpolluted areas and rather low natural variations of only a few percent (Tab. 1).

The observed tropospheric difference may be caused by additional sources in the northern hemisphere and/or additional sinks in the southern hemisphere. However, only the first suggestion is valid as will be seen from the following discussion of sources and sinks.

a) NATURAL SOURCES: A large variety of microbial species is able to produce  $H_2$  - under anaerobic conditions - [see e.g. Schlegel, 1974], however, because it is a favoured energy donor for microorganisms,  $H_2$  is quickly used up in anaerobic and, even more, in aerobic environments. The oldest estimate for a natural  $H_2$ -source is that of the microbial production in paddy soils. Koyama [1963] determined the  $H_2$  to  $CH_4$  ratio in different biogenic gases, which were produced during incubation experiments with a number of Japanese paddy soils. The average value of this ratio was found to be  $(5.6 \pm 2.9) \times 10^{-4}$ . Applying this value to Kojama's estimate of the  $CH_4$  productivity of paddy soils -  $80 \text{ g } CH_4/m^2/yr$  - we estimate the global

H<sub>2</sub>-production from the global area of paddy soils -  $1.43 \times 10^6$  km<sup>2</sup> in 1977  
[United Nations FAO, 1977] - to be

$$P_{NP} = (2+1) \times 10^{10} \text{ g/yr}$$

or an annual production of about 0.1 ‰ of the atmospheric H<sub>2</sub> abundance.

However, this estimate certainly will not represent natural conditions. Since Kojama used closed incubators during the experiments, which were run over several weeks, a significant fraction of the H<sub>2</sub> gas produced might have been used up by bacteria. The same conditions exist in the natural environment but it depends on a variety of biological and physical factors if the H<sub>2</sub> produced in subsurface layers eventually may reach the atmosphere. This source, however, appears to be negligible, unless further measurements in natural environments would result in net production rates that are at least higher by one order of magnitude than those derived from Kojama's laboratory experiments.

Ocean surface waters, which were found to be supersaturated with respect to H<sub>2</sub>, might act as another natural source, which according to area would be twice that strong in the southern than in the northern hemisphere. Available data on dissolved H<sub>2</sub> in ocean surface waters are rather sparse. Tab. 2 gives a compilation. For comparison a body of water at 20°C and 35 ‰ salinity, which is in equilibrium with background air (0.56 ppmv H<sub>2</sub>), would contain 8.5 nl H<sub>2</sub> (STP)/l H<sub>2</sub>O.

Table 2: H<sub>2</sub>-content of ocean surface waters

Location	Number of samples	H <sub>2</sub> -content (nl H <sub>2</sub> (STP)/l H <sub>2</sub> O)	Reference
South Pacific	16	80 - 1620	<u>Williams and Bainbridge [1973]</u>
North Atlantic	cont	8 - 50	<u>Seiler and Schmidt [1974]</u>
South Atlantic	cont	18 - 57	<u>Seiler and Schmidt [1974]</u>
North Atlantic	46	4 - 73	<u>Herr and Barger [1978]</u>
cont = continuous analysis			

The very first measurements were performed by Williams and Bainbridge [1973], who admitted that the magnitude of their H<sub>2</sub> values is questionable.

The other data are in reasonable agreement. The average H<sub>2</sub> content as derived from the original data for the different cruises is 27 nl H<sub>2</sub>/l H<sub>2</sub>O corresponding to about 300 ‰ supersaturation. By extrapolating this value to the global ocean surface the oceanic H<sub>2</sub> production can be estimated by applying the thin film model [see e.g. Bröecker and Peng, 1974]. According to this model the net flux of gas, J, is given by

$$J = \frac{D}{2} \rho (C - \beta \text{ mP}) \quad \text{g/cm}^2/\text{s}$$

SCHMIDT, KULESSA, and ROTH

where  $D$  is the diffusion coefficient of  $H_2$  in water at  $20^\circ C$ :  
 $D = 4 \times 10^{-5} \text{ cm}^2/\text{s}$ ;  $\rho$  is the density of  $H_2$ ;  $\approx 8.3 \times 10^{-5} \text{ g/cm}^3$ ;  $C$  is the average content of  $H_2$  in the mixed layer:  $\approx 27.0 \text{ nl } H_2/\text{l } H_2O$ ;  $\beta$  is the Bunsen solubility coefficient for  $H_2$  at  $20^\circ C$ :  $\approx 0.0154 \text{ cm}^3 H_2/\text{cm}^3 H_2O$ . at for 35 ‰ salinity [Schmidt, 1979];  $m$  is the average  $H_2$  mixing ratio in surface air:  $\approx 0.56 \text{ ppmv}$  and  $P$  is the atmospheric pressure in atm. The most variable parameter is  $z$ , the thickness of the laminar boundary layer  $\approx 36 \times 10^{-4} \text{ cm}$  [Peng et al, 1979]. Using these numbers we obtain an average net flux of  $J = 16.8 \times 10^{15} \text{ g } H_2/\text{cm}^2/\text{s}$ . The total area of the oceans is  $3.6 \times 10^{18} \text{ cm}^2$ . Thus, due to an uncertainty factor of two, which accounts for an error in the estimate for  $z$ , the global flux of  $H_2$  release from the surface of the oceans into the atmosphere ranges from  $1.0 \times 10^{12}$  to  $4.0 \times 10^{12} \text{ g/yr}$ , with an average of

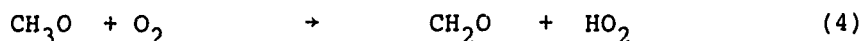
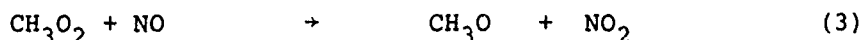
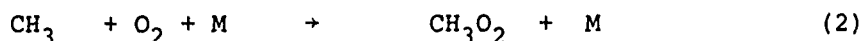
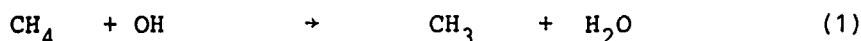
$$P_{NO} = 2.0 \times 10^{12} \text{ g/yr.}$$

Some information is available for other possible natural  $H_2$  sources. Geothermal steam generally contains a few percent of  $H_2$  [see e.g. Walker, 1977], but extremely high concentrations up to 45 % were reported for distinct areas [Arnarson, 1974]. The global  $H_2$  release by volcanoes was estimated to be about  $2 \times 10^{10} \text{ g/yr}$  [Walker, 1977]. Biogenic gases, which are produced in waterlogged soils or in very productive sediments, [see e.g. Cloud et al, 1958] may eventually reach the atmosphere, if these habitats are covered by rather shallow water layers. Such areas might release significant amounts into the atmosphere, at least on a local or regional scale. However any quantitative estimate would be speculative. We believe that the value of

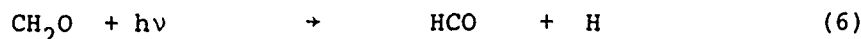
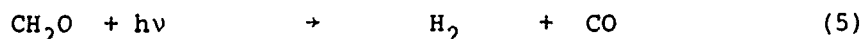
$$P_N = 5 \times 10^{12} \text{ g/yr}$$

is the upper limit of the total global production of all natural sources.

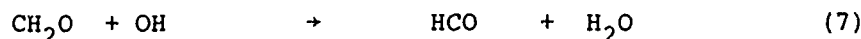
b) PHOTOCHEMICAL PRODUCTION: Photochemical oxidation of  $CH_4$  provides a source of tropospheric  $H_2$ . Levy [1971] proposed a reaction path, which is now well accepted, although there is still some uncertainty about additional reaction pathways.



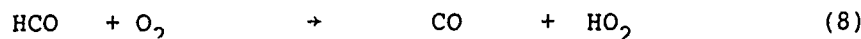
Formaldehyde is removed through photolysis



or by reaction with OH radicals



which is the main destruction process in the lower troposphere. Since HCO reacts with  $O_2$ ,



these chain reactions lead to the production of one CO molecule for each  $\text{CH}_4$  molecule consumed. The loss rates for tropospheric  $\text{CH}_2\text{O}$  due to reaction (5), (6), (7) are plotted in Fig. 2. They have been calculated on the basis of net quantum yields measured by Moortgat and Warneck [1979] for (5) and (6) and the rate constant for (7) given by Morris and Niki [1971].

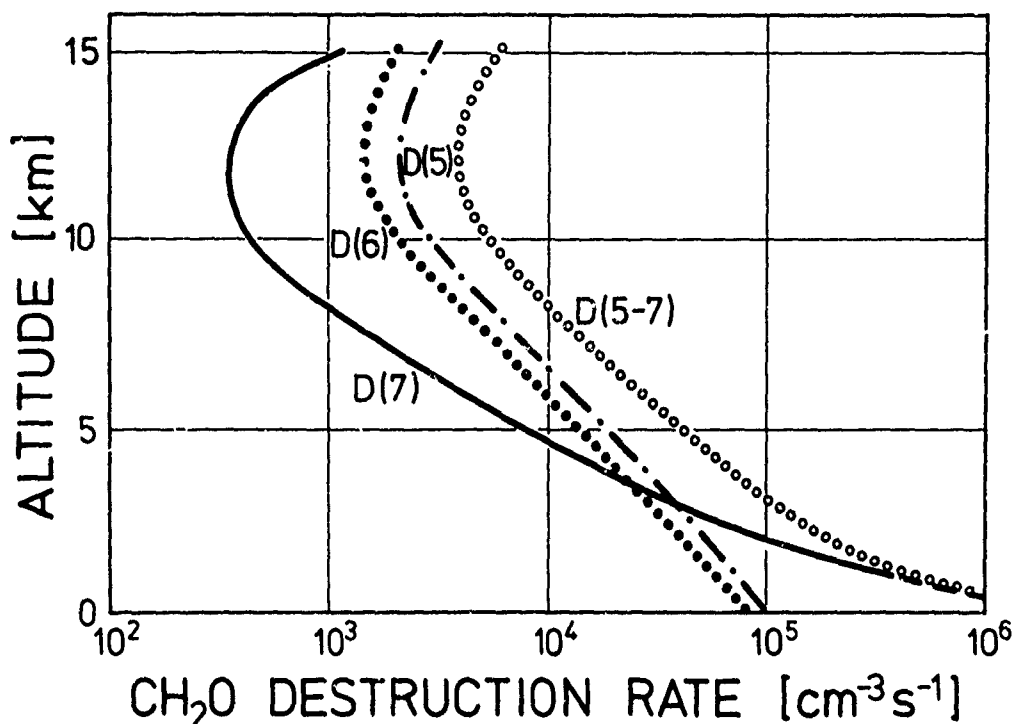


Fig. 2:  $\text{CH}_2\text{O}$  destruction rates for the main tropospheric removal processes:

- D (5):  $\text{CH}_2\text{O} + h\nu \rightarrow \text{H}_2 + \text{CO}$
- ..... D (6):  $\text{CH}_2\text{O} + h\nu \rightarrow \text{HCO} + \text{H}$
- D (7):  $\text{CH}_2\text{O} + \text{OH} \rightarrow \text{HCO} + \text{H}_2\text{O}$

ooooo D (5-7): The total  $\text{CH}_2\text{O}$  loss rate. It is equal to the destruction rate for  $\text{CH}_4$ :  $D(\text{CH}_4)$  if photochemical equilibrium is assumed.

Reaction (5) is the photochemical process in the troposphere, which acts as a source of  $\text{H}_2$ . It accounts for about 20 % of the total photochemical  $\text{CH}_2\text{O}$  removal. Integrating with height we obtain a column loss of about  $3 \times 10^{10}$   $\text{CH}_2\text{O}$  molecules/ $\text{cm}^2/\text{s}$  due to reaction (5). Extrapolating the equivalent column production for  $\text{H}_2$  to the global troposphere we obtain an estimate for the annual  $\text{H}_2$  production from methane to be

$$P_c = 16.0 \times 10^{12} \text{ gH}_2/\text{yr.}$$

For this estimate we used the tropospheric OH-profile as calculated by the KFA 1-D model. The average tropospheric OH-concentration derived from this profile is  $9.5 \times 10^5$  molecules  $\text{cm}^{-3}$ . Based on a study of the  $^{12}\text{CO}$  and  $^{14}\text{CO}$  cycle, Volz et al [1979] derived an average tropospheric OH concentration of  $6.5 \pm 2.5 \times 10^5$   $\text{cm}^{-3}$ . Adopting this range of OH-concentrations the

above estimate should represent the upper limit of this  $H_2$  source. A value of  $10.7 \times 10^{12}$  g  $H_2$ /yr corresponds to the lower limit of the  $OH$ -concentration,  $4 \times 10^5$  cm<sup>-3</sup>. Therefore our best estimate for  $H_2$  production through photochemical oxidation of methane is ranging from  $10.7 \times 10^{12}$  to  $16.0 \times 10^{12}$  g/yr and averages

$$P_{C_1} = 13.1 \times 10^{12} \text{ g/yr.}$$

This source is almost equally distributed between both hemispheres since there exist only small interhemispheric differences in the average  $CH_4$  mixing ratio [Ehhalt, 1978], and the average tropospheric  $OH$ -concentration appears to be almost the same in both hemispheres [see e.g. Wofsy, 1976; Volz et al, 1979] although there are strong daily as well as seasonal variations.

The photochemical model suggests an average tropospheric  $CH_2O$  mixing ratio of about 0.1 ppbv. However  $CH_4$  oxidation is not the only source of formaldehyde in the atmosphere. Zimmermann et al [1978] discussed the possibility of photochemical conversion of terpenes and isoprenes into  $CH_2O$ , and they estimated an additional  $H_2$  production of

$$P_{C_2} = (10 - 35) \times 10^{12} \text{ g/yr}$$

which could be even higher than the effect of  $CH_4$  oxidation. Other potential sources for  $CH_2O$  are exhaust gases, and incomplete combustion processes. First measurements of  $CH_2O$  mixing ratios in background surface air range from 0.2 to 0.6 ppbv [Platt et al, 1979], values which are in harmony with model calculations assuming  $CH_4$  as the only source of  $CH_2O$ . Better estimates of the photochemical  $H_2$  source will only be possible if tropospheric profiles of the  $CH_2O$  mixing ratio are available.

c) ANTHROPOGENIC PRODUCTION: Numerous measurements have shown that the  $H_2$  mixing ratio in tropospheric air is affected by pollution sources.  $H_2$  is an important product of incomplete combustion and various industrial processes. Quantitative estimates are only available for  $H_2$  emission from automobile exhaust gases, which may contain up to several percent of  $H_2$  (by volume). However the percentage varies according to engine operating conditions. Actually the  $H_2$  concentration with respect to CO obeys the water gas equilibrium



Typical temperatures in the internal combustion engine range between 1500 K and 1700 K [see e.g. D'Alleva and Lovell, 1936] and accordingly one should expect a yield for  $H_2$  equal to about 40 % that for CO. In fact experimental results show such  $H_2$ /CO ratios [c.f. Hurn, 1962; Patterson et al, 1972]. A different approach was made by Schmidt [1974], who studied the excess quantities of CO and  $H_2$  during simultaneous measurements in urban air at Mainz and found a ratio of 0.43. In a similar study, Zankl [1976] observed CO and  $H_2$  mixing ratio at different areas in Germany and derived ratios of  $0.60 \pm 0.20$ , indicating that there should exist other anthropogenic  $H_2$  sources, which show higher  $H_2$  contents relative to CO than observed in automobile exhaust gases.

Absolute  $H_2$  emission factor are not available. However, adopting the above ratios we may derive a reasonable estimate relative to the rather well known CO production by anthropogenic combustion processes. This source was estimated by Logan [1979] to range from 400 to  $1000 \times 10^{12}$  g/yr, the pro-



bable average being  $500 \times 10^{12}$  g<sub>2</sub>CO/yr. The corresponding H<sub>2</sub> production is between  $11.5 \times 10^{12}$  and  $57.1 \times 10^{12}$  g/yr with an average of

$$P_A = 21.4 \times 10^{12} \text{ g/yr.}$$

This annual production is equal to 13 % of the tropospheric H<sub>2</sub> reservoir and due to the population distribution at least 85 % of this source is in the northern hemisphere.

There are other industrial processes which might act as H<sub>2</sub> sources. About  $30 \times 10^{12}$  g H<sub>2</sub> are annually produced for industrial uses such as petroleum refining, ammonia synthesis, methanol synthesis. Most of this production is used up at the same place, only 7 % are delivered as "merchant" hydrogen [Brewer, 1978]. We believe that due to economical and safety regulation leakage or loss of H<sub>2</sub> will not exceed 5 % of the industrial production. Therefore the H<sub>2</sub> release from these activities most probably is negligible on a global basis.

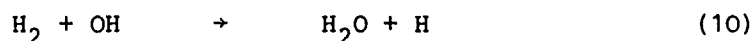
Other potential anthropogenic and natural sources are woodburning, bush fires or waste burning. Crutzen et al [1979] measured excess H<sub>2</sub> in two fire plumes and by comparison with excess CO<sub>2</sub> they derived an annual H<sub>2</sub> production from biomass burning of  $(9 - 21) \times 10^{12}$  g/yr with an average of

$$P_B = 15.0 \times 10^{12} \text{ g/yr.}$$

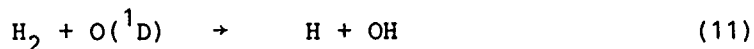
If the strength of this source will be confirmed by further measurements this process has to be considered a rather important contribution to the H<sub>2</sub> budget.

4. SINKS OF TROPOSPHERIC H<sub>2</sub>: The historical record of H<sub>2</sub> measurements in background air indicates that the H<sub>2</sub> mixing ratio has remained constant with time [Schmidt, 1974]. Assuming the H<sub>2</sub> cycle to be in a steady state, the sources must be balanced by equivalent sinks. Since the oceans act as a source for H<sub>2</sub>, consumption of H<sub>2</sub> must occur by chemical destruction within the atmosphere and/or other destruction processes at the earth surface.

a) CHEMICAL DESTRUCTION: The dominant chemical reaction, which consumes H<sub>2</sub> is attack by OH radicals.



The reaction with excited atomic oxygen (O<sup>1</sup>D) is of minor importance in the stratosphere.



Due to these removal processes the H<sub>2</sub> mixing ratio in the stratosphere decreases with height. However, since CH<sub>4</sub> is also photochemically destroyed in the stratosphere, part of the destruction is matched by H<sub>2</sub> production from CH<sub>4</sub>, which is demonstrated by the vertical H<sub>2</sub> distribution (Fig. 1). It is CH<sub>4</sub> oxidation, which maintains the H<sub>2</sub> level at 0.4 to 0.5 ppmv in the lower stratosphere. Without this chemical process, the H<sub>2</sub> mixing ratio at 40 km altitude would be lower by about a factor of two. The net sink is represented by the vertical gradient of the H<sub>2</sub> mixing ratio in the stratosphere (Fig. 1). Its strength may be calculated from the H<sub>2</sub> flux into the lower stratosphere.

The main process is upward eddy diffusion, driven by the gradient of the H<sub>2</sub> mixing ratio within the tropopause region. Available measurements show that the decrease is about 5 ppbv/km or even less (Fig. 2). The vertical flux due to turbulent eddy diffusion is given by

$$F = - \rho K_z \frac{\partial M}{\partial z}$$

where  $\rho$  is the density ( $\text{g/cm}^3$ );  $K_z$  is the vertical eddy diffusion coefficient ( $\text{cm}^2/\text{s}$ ) and  $\frac{\partial M}{\partial z}$  is the gradient of the  $\text{H}_2$  mixing ratio at the tropopause. The hemispherically averaged height of the tropopause is  $13 \text{ km}$  ( $\rho = 2.7 \times 10^{-4} \text{ g/cm}^3$ ). For values of  $K_z$  ranging from  $3 \times 10^3$  to  $10^4 \text{ cm}^2/\text{s}$  and using the  $\text{H}_2$  gradient of  $5 \text{ ppbv/km} = 3.6 \times 10^{-15} \text{ g H}_2/\text{g air/cm}$  as an upper limit for the global average, the global flux of  $\text{H}_2$  is calculated to range within

$$D_S = (0.6 - 1.6) \times 10^{12} \text{ g/yr.}$$

This is only about 1 % of the tropospheric  $\text{H}_2$  abundance.

In the troposphere reaction (10) acts as a more efficient removal process. The loss rate for this reaction is plotted in Fig. 3 using the recommended reaction rate coefficient as compiled by Baulch et al [1972] and the OH-profile predicted by the KFA 1-D-model (see above). Integrating over the whole troposphere (0 - 13 km) we obtain a column loss rate between  $1.9 \times 10^{10}$  and  $4.4 \times 10^{10} \text{ molecules/cm}^2/\text{s}$  for average tropospheric OH-concentrations between  $4 \times 10^6$  and  $9 \times 10^6$  respectively. The corresponding annual  $\text{H}_2$  destruction due to this reaction is between  $10.0 \times 10^{12}$  and  $23.7 \times 10^{12} \text{ g/yr}$  and the average is

$$D_C = 16.3 \times 10^{12} \text{ g/yr.}$$

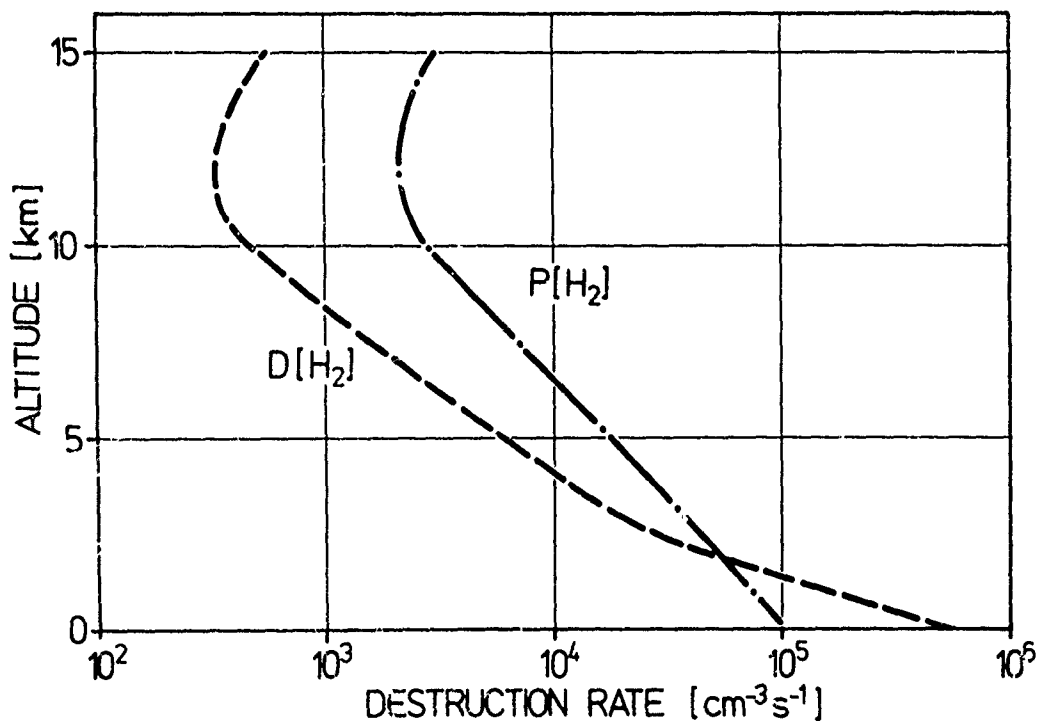
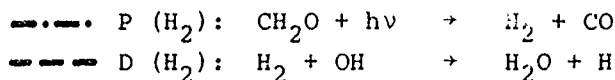


Fig. 3: Photochemical production and removal rates for  $\text{H}_2$ .



Thus, the average tropospheric chemical  $H_2$  sink is stronger than the  $H_2$  production from  $CH_4$  ( $131 \times 10^{12}$  g/yr). This is due to the fact that below 2 km altitude the destruction rates strongly exceed production rates (Fig. 3).

b) CONSUMPTION AT THE SOIL SURFACE: Photochemical reactions destroy only about 25 % of the known sources. Consequently there must exist other sinks at the earth surface. Indeed, based on both laboratory and field experiments, a variety of different natural soils have been proved to act as very effective sinks. Ehhalt [1973] reported a deposition velocity of about 0.1 cm/s, based on a laboratory test employing several natural soils. Both laboratory tests and field experiments on the  $H_2$  uptake were reported by Liebl and Seiler [1975]. The average deposition velocity derived from their data is  $(6.7 \pm 2.1) \times 10^{-2}$  cm/s. The experiments included measurements over natural soil with and without vegetation. For distinct soils the deposition velocity was found to increase with increasing temperatures at the soil surface. Other soils showed an almost constant  $H_2$  uptake over the temperature range from  $5^\circ - 30^\circ$  C. The rather rapid uptake at the soil surface is due to microbial consumption, predominantly by "Knallgas" bacteria. These species are widespread in natural soils and their ability to oxidize molecular hydrogen does not change much, even for a wide range of environmental conditions (temperature, pH, humidity).

So far estimates of the  $H_2$  uptake have been based on only these data. By extrapolating the average deposition velocity to the global land surface but neglecting areas covered with ice, rocks and deserts, a global  $H_2$  sink of about  $(110 \pm 30) \times 10^{12}$  g/yr was estimated [Schmidt, 1975; Liebl and Seiler, 1975].

Recent measurements of the  $H_2$  deposition velocity for various natural soils, which have been performed at this laboratory, showed significantly lower values for several soils with different types of vegetation. Values comparable to the average reported by Liebl and Seiler [1975] have been observed only for forest soils, those for cultivated land with crops sometimes appeared to be lower by a factor of ten. Table 3 gives a summary of the results of field experiments available so far.

Table 3: $H_2$ uptake by various natural soils			
Ecosystem	Deposition velocity $\times 10^{-2}$ [cm/s]	Soil Temperature [ $^\circ$ C]	Reference
Forest	6.5 - 11.5	5.0 - 13.0	a)
	2.1 - 8.0	14.0 - 20.0	b)
Grassland	4.2 - 7.2	3.0 - 11.0	a)
	0.4 - 2.2	11.0 - 17.0	b)
Cultivated land	2.2 - 8.4	3.0 - 27.0	a)
	0.3 - 3.6	8.0 - 26.0	b)
a) from <u>Liebl and Seiler</u> [1975]			
b) <u>Schmidt and Kulessa</u> , to be published			

Considering the importance of  $H_2$  uptake by soils as a global  $H_2$  sink this data base still appears to be too limited in order to provide a reliable

Table 4: Global estimates of the H<sub>2</sub> uptake by various ecosystems

Ecosystem type	Area <sup>*)</sup> x10 <sup>6</sup> km <sup>2</sup>	Deposition velocity [cm/s]	Activity factor K	Comments	H <sub>2</sub> uptake x12 g/yr
Tropical forest	14.5	0.070 ± 0.030	0.1 - 0.2	estimated for reduced bacteria population and high water content	0.9 - 4.6
Temperate forest	6.0	0.070 ± 0.030	1.0		3.8 - 9.5
Boreal forest	10.5	0.070 ± 0.030	0.5	6 months covered with snow	3.3 - 8.3
Woodland and Shrubland	4.5	0.070 ± 0.030	1.0		2.8 - 7.1
Grassland and Savanna	35.0	0.040 ± 0.030	1.0		2.8 - 38.7
Tundra	9.5	0.040 ± 0.030	0.33	activity during only 4 summer months	0.5 - 3.4
Desert scrub	21.0	0.040 ± 0.030	1.0		3.3 - 23.2
Cultivated land	16.0	0.030 ± 0.020	1.0		2.5 - 12.6
Total	117.0				19.9 - 107.4
<sup>*)</sup> from Ajtay et al [1979]					

estimate. However, we feel that previous estimates have been too high and can be improved by applying average deposition velocities from Table 3 to calculate the  $H_2$  uptake by the main types of ecosystems. A first attempt is given in Table 4. About 80 % of the continental surface are assumed to contribute to the  $H_2$  removal. The total  $H_2$  consumption ranges from  $19.9 \times 10^{12}$  to  $107.4 \times 10^{12}$  g/yr and the average is

$$D_s = 60 \times 10^{12} \text{ g/yr.}$$

Due to the distribution of land and sea, the major consumption occurs in the northern hemisphere. The strength of this sink may still be over-estimated. Our measurements indicated that the deposition velocity depends strongly on the water content of the soil. The uptake rate is strongly reduced due to decreased ventilation of wet soils, and this effect was generally observed after rain falls, when all pores at the surface are flushed with water. This feature was well recognized by Liebl and Seiler [1975], however it was neglected in previous estimates. Ventilation is also reduced in case of very dense vegetation. Since at present the data base is still too small, our estimate is based only on the range of available values of the deposition velocity for three types of vegetation (Table 3). However, we tried to account for the effects of water content by applying an activity factor for some of the ecosystems, listed in Table 4.

Table 5: Tropospheric budget of $H_2$			
Sources [ $\times 10^{12}$ g/yr]	Global	Northern Hemisphere	Southern Hemisphere
Natural (oceans, volcanoes)	2.0 - 5.0	1.2 - 3.0	0.8 - 2.0
Photochemical			
$CH_4$ oxidation*	10.8 - 16.0	5.4 - 8.0	5.4 - 8.0
oxidation of terpenes and isoprenes (§)	10.0 - 35.0	6.0 - 20.0	4.0 - 15.0
Anthropogenic			
automobiles	11.5 - 57.1	9.8 - 48.5	1.7 - 8.6
industry	-	-	-
biomass burning (§§)	9.0 - 21.0	4.5 - 10.5	4.5 - 10.5
Total sources	43.3 - 134.1	26.9 - 90.0	16.4 - 44.1
Sinks [ $\times 10^{12}$ g/yr]			
Photochemical			
Stratosphere	0.6 - 1.6	0.3 - 0.8	0.3 - 0.8
Troposphere*	10.0 - 23.7	5.0 - 11.8	5.0 - 11.9
Soil surface	19.9 - 107.4	12.9 - 69.6	7.0 - 37.8
Total sinks	30.5 - 132.7	18.2 - 82.2	12.3 - 50.5
Average mixing ratio [ppmv]	0.560	0.575	0.550
Abundance [ $10^{12}$ g]	170.7	87.2	83.5
* average tropospheric OH-concentration $(6.5 \pm 2.5) \times 10^6 \text{ cm}^{-3}$ Volz et al [1979]			
§ Zimmermann et al [1978]			
§§ Crutzen et al [1979]			

5. THE TROPOSPHERIC  $H_2$ -BUDGET: Table 5 lists the estimates of all sources and sinks. It also gives some information on the distribution of the different sources and sinks between both hemispheres. As discussed before, the observation of higher  $H_2$  mixing ratios points to the presence of either a production process dominating in the northern hemisphere or a consumption process, which is larger in the southern hemisphere.  $H_2$  production by combustion is the only source which is distributed in this way. Photochemistry provides net  $H_2$  production, which appears to be equally distributed.

Moreover, the dominant sink at the soil surface is even larger in the northern than in the southern hemisphere. Therefore we must conclude that anthropogenic combustion is an important contribution to the global budget. So far other sources, which could maintain the interhemispheric difference of the  $H_2$  mixing ratio have not been clearly identified.  $H_2$  production from isoprenes as suggested by [Zimmermann et al, 1978] should dominate in the tropical regions and seems to be equally distributed between both hemispheres. A similar production from terpenes, however, - though still more speculative - would dominate in the northern hemisphere.

The total tropospheric sources and sinks amount to  $(43.3-134.1) \times 10^{12}$  g  $H_2$ /yr and  $(30.5-132.7) \times 10^{12}$  g  $H_2$ /yr respectively. The average annual production of  $71.2 \times 10^{12}$  g  $H_2$  compares to an average consumption of 63.6 g  $H_2$ /yr. This agreement is probably coincidental since the uncertainties of the individual estimates are large. Much better information is needed about possible natural  $H_2$  sources, such as photochemical  $H_2$  production from hydrocarbons (isoprenes etc.), and  $H_2$  emissions from biomass burning and especially about the sink of the soil surface. Assuming the  $H_2$  cycle to be in a steady state, a tropospheric residence time of about 3 years with an uncertainty factor of two is obtained.

#### REFERENCES

- Ajtay, G.L., P. Ketner, and P. Duvigneaud, Terrestrial primary production and phytomass, in: The Global Carbon Cycle - SCOPE 13 [B. Bolin, E.T. Degens, S. Kempe, P. Ketner, Eds.] J. Wiley & Sons, Chichester, p. 129-182, 1979.
- Arnorsson, S., The composition of thermal fluids in Iceland and geological features related to the thermal activity, in: Geodynamics of Iceland and the North Atlantic Area [Ed. Kristjansson], p. 307-323., D. Reidel Publ. Company, Dordrecht, 1974.
- Baulch, D.L., D.D. Drysdale, D.G. Horne, and A.C. Lloyd, in "Evaluated Kinetic Data for High Temperature Reactions, Vol. 1: Homogeneous Gas Phase Reactions of the  $H_2$ - $O_2$  System" Butterworths, London, Great Britain, 1972.
- Brewer, G.D., Some environmental and safety aspects of using hydrogen as a fuel, International Journal of Hydrogen Energy, 3, 461-474, 1978.
- Broecker, W.S., and T.-H. Peng, Gas exchange rates between air and sea, Tellus, 26, 21-35, 1974.
- Bush, J.A., A.L. Schmeltekopf, F.C. Fehsenfeld, D.L. Albritton, J.R. McAfee, P.D. Goldan, E.E. Ferguson, Stratospheric measurements of methane at several latitudes, Geophysical Research Letters, 5, 1027-1029, 1978.
- Calvert, J.G., J.A. Kerr, K.L. Demerjian, and R.D. McQuigg, Photolysis of formaldehyde as a hydrogen atom source in the lower atmosphere, Science, 175, 751-752, 1972.
- Cloud, P.E., I. Friedman, F.D. Sisler, and V.H. Dibeler, Microbiological fractionation of the hydrogen isotopes, Science, 127, 1394-1395, 1958.
- Crutzen, P.J., L.E. Heidt, J.P. Krasnec, W.H. Pollock, W. Seiler, Biomass burning as a source of the atmospheric gases  $CO$ ,  $H_2$ ,  $N_2O$ ,  $NO$ ,  $CH_3Cl$ , and  $COS$ , Nature, 282, 253-256, 1979.
- D'Alleva, B.A., and W.G. Lovell, Relation of exhaust gas composition to air fuel ratio, Society of Automotive Engineers Journal, 38, 90-98, 116, 1936.

- Ehhalt, D.H., On the uptake of tritium by soil water and groundwater, Water Resources Res., 9, 1073-1074, 1973.
- Ehhalt, D.H., The  $\text{CH}_4$  concentration over the ocean and its possible variation with latitude Tellus, 30, 169-176, 1978.
- Ehhalt, D.H. and L.E. Heidt, The concentration of molecular  $\text{H}_2$  and  $\text{CH}_4$  in the stratosphere, Pageoph, 106-108, 1352-1360, 1973.
- Ehhalt, D.H., L.E. Heidt, R.H. Lueb, and N. Roper, Vertical profiles of  $\text{CH}_4$ ,  $\text{H}_2$ ,  $\text{CO}$ ,  $\text{N}_2\text{O}$  and  $\text{CO}_2$  in the stratosphere, Proceedings of the "Third Conference on CIAP", Febr. 1974, U.S. Department of Transportation, p. 153-160, 1974.
- Ehhalt, D.H., L.E. Heidt, R.H. Lueb, and W. Pollock, The vertical distribution of trace gases in the stratosphere, Pageoph, 113, 389-402, 1975a.
- Ehhalt, D.H., L.E. Heidt, R.H. Lueb, and E.A. Martell, Concentrations of  $\text{CH}_4$ ,  $\text{CO}$ ,  $\text{CO}_2$ ,  $\text{H}_2$ ,  $\text{H}_2\text{O}$  and  $\text{N}_2\text{O}$  in the upper stratosphere, Journal of the Atmospheric Sciences, 32, 163-169, 1975b.
- Ehhalt, D.H., U. Schmidt, and L.E. Heidt, Vertical profiles of molecular hydrogen in the troposphere and the stratosphere, Journal of Geophysical Research, 5907-5911, 1977.
- Ehhalt, D.H., and A. Toenissen, Hydrogen and carbon compounds in the stratosphere, Proceedings of the NATO Study Institute on Ozone, Aldeias das Acoteias, Portugal, 2.-12. October 1979, U.S. Federal Aviation Administration, Washington, D.C., in press.
- Fabian, P., R. Borchers, K.H. Weiler, U. Schmidt, A. Volz, D.H. Ehhalt, W. Seiler, and F. Müller, Simultaneously measured vertical profiles of  $\text{H}_2$ ,  $\text{CH}_4$ ,  $\text{CO}$ ,  $\text{N}_2\text{O}$ ,  $\text{CFCl}_3$  and  $\text{CR}_2\text{Cl}_2$  in the midlatitude stratosphere and troposphere, Journal of Geophysical Research, 84, 3149-3154, 1979a.
- Fabian, P., R. Borchers, U. Schmidt, A. Khedim, F.J. Johnen, A. Volz, W. Seiler, The vertical distribution of stable trace gases at midlatitudes, to be submitted to Geophysical Research Letters, 1979.
- Friedman, I., and T.G. Scholz, Isotopic composition of atmospheric hydrogen 1967-1969, Journal of Geophysical Research, 79, 785-788, 1974.
- Glueckauf, E., and G.P. Kitt, The hydrogen content of atmospheric air at ground level, Quarterly Journal of the Royal Meteorological Society, 83, 522-528, 1957.
- Heidt, L.E., and W.H. Pollock, Measurements of  $\text{N}_2\text{O}$ ,  $\text{CH}_4$ ,  $\text{H}_2$ ,  $\text{CO}$  and  $\text{CO}_2$  in the non-urban troposphere, Proceedings of the AGU/AMS Symposium on "The Non-Urban Tropospheric composition", November 10-12, Hollywood, Florida, USA, 1976.
- Herr, F.L., and W.B. Barger, Molecular hydrogen in the near-surface atmosphere and dissolved in waters of the tropical North Atlantic, Journal of Geophysical Research, 83, 6199-6205, 1978.
- Hurn, R.W., Comprehensive analyses of automotive exhausts, Archives of Environmental Health, 5, 78-82, 1962.
- Kojama, T., Gaseous metabolism in lake sediments and paddy soils and the production of atmospheric methane and hydrogen, Journal of Geophysical Research, 68, 3971-3973, 1963.
- Levy, H., Normal atmosphere: Large radical and formaldehyde concentrations predicted, Science, 173, 141, 1971.
- Liebl, K.-H., and W. Seiler,  $\text{CO}$  and  $\text{H}_2$  destruction at the soil surface, in "Microbial Production and Utilization of Gases" (H.G. Schlegel, G. Gottschalk, N. Pfennig, Eds.) Akademie der Wissenschaften, Göttingen, FRG, p. 215-230, 1976.
- Logan, J.A., Sources and sinks of carbon monoxide, paper presented at the NATO Study Institute on Ozone, Aldeias das Acoteias, Portugal, 2.-12. October 1979.
- Lueb, R.A., D.H. Ehhalt, and L.E. Heidt, Balloonborne low temperature air sampler, Review of Scientific Instruments, 46, 702-705, 1975.
- Moortgat, G.K., and P. Warneck,  $\text{CO}$  and  $\text{H}_2$  quantum yields in the photodecomposition of formaldehyde in air, Journal of Chemical Physics, 70, 3639-3651, 1979.

- Morris, E.D., and H. Niki, Mass spectrometric study of reaction of hydroxyl radical with formaldehyde, Journal of Chemical Physics, 55, 1991-1992, 1971.
- Paneth, F.A., The chemical composition of the atmosphere, Quarterly Journal of the Royal Meteorological Society, 63, 433-438, 1937.
- Patterson, D.J., R.H. Kadlec, B. Carnahan, H.A. Lord, J.J. Martin, W. Mirshy, and E. Sondreal, - Kinetics of Oxidation and Quenching of Combustibles in Exhaust Systems of Gasoline Engines, Final Report, Environmental Protection Agency, Contract CPA-22-69-51-HEW, 1972.
- Peng, T.H., W.S. Broecker, G.G. Mathieu, Y.-H. Li, A.E. Bainbridge, Radon evasion rates in the Atlantic and Pacific Oceans as determined during the Geosecs program, Journal of Geophysical Research, 84, 2471-2486, 1979.
- Platt, U., D. Perner, and H.W. Pätz, Simultaneous measurement of atmospheric  $\text{CH}_2\text{O}$ ,  $\text{NO}_2$ , and  $\text{O}_3$  by differential optical absorption, Journal of Geophysical Research, 84, 6329-6335, 1979.
- Schlegel, H.G., Production, modification, and consumption of atmospheric trace gases by microorganisms, Tellus, 26, 11-20, 1974.
- Schmeltekopf, A.L., D.L. Albritton, P.J. Crutzen, P.D. Goldan, W.J. Harrop, W.R. Henderson, J.R. McAfee, M. McFarland, H.I. Schiff, T.L. Thompson, D.L. Hofmann, N.T. Kjöme, Stratospheric nitrous oxide altitude profiles at various latitudes, Journal of the Atmospheric Sciences, 34, 729-736, 1977.
- Schmidt, U., Molecular hydrogen in the atmosphere, Tellus, 26, 78-90, 1974  
Errata: Tellus, 27, 93-94, 1975.
- Schmidt, U., The latitudinal and vertical distribution of molecular hydrogen in the troposphere, Journal of Geophysical Research, 83, 941-946, 1978.
- Schmidt, U., The solubility of carbon monoxide and hydrogen in water and sea water at partial pressures of about  $10^{-5}$  atmospheres, Tellus, 31, 68-74, 1979.
- Schmidt, U., D.H. Ehhalt, and L.E. Heidt, The vertical distribution of molecular hydrogen in the troposphere and stratosphere, Proceedings of the "Joint Symposium on Atmospheric Ozone", Dresden, August 1976, 227-239, 1976.
- Scholz, T.G., D.H. Ehhalt, L.E. Heidt, and E.A. Martell, Water vapor, molecular hydrogen, methane, and tritium concentrations near the stratosphere, Journal of Geophysical Research, 75, 3049-3054, 1970.
- Seiler, W., and U. Schmidt, Dissolved nonconservative gases and seawater, in "The Sea", Vol. 5 (E.D. Goldberg, editor) 219-243, John Wiley & Sons, Inc. New York, 1974.
- Seiler, W., F. Müller, and H. Oeser, Vertical distribution of chlorofluoromethanes in the upper troposphere and lower stratosphere, Pageoph, 116, 554-566, 1978.
- United Nations Food and Agricultural Organisation, Production Yearbook, Vol. 31, Rome, Italy, 1977.
- Volz, A., D.H. Ehhalt, R.G. Derwent, A. Khedim, Messung von atmosphärischem  $\text{CO}$ : eine Methode zur Bestimmung der troposphärischen OH Radikalkonzentration, Report Jül 1604, KFA Jülich, FRG, 136 p., 1979.
- Walker, J.C.G., Evolution of the atmosphere, Macmillan Publishing Co, Inc. 318 p., 1977.
- Williams, R.T., and A.E. Bainbridge, Dissolved  $\text{CO}$ ,  $\text{CH}_4$  and  $\text{H}_2$  in the southern ocean, Journal of Geophysical Research, 78, 2691-2694, 1973.
- Wofsy, S.C., Interactions of  $\text{CH}_4$  and  $\text{CO}$  in the Earth's atmosphere, Ann. Rev. Earth Planet. Sci., 4, 441-469, 1976.
- Zankl, H., Bestimmung der anthropogenen Produktion von  $\text{CO}$  und  $\text{H}_2$  mittels Feldmessungen im Raum Mainz und München, Master Thesis, University of Mainz, Dep. of Physics, 1976.
- Zimmermann, P.R., R.B. Chatfield, J. Fishman, P.J. Crutzen, and P.L. Hanst, Estimates on the production of  $\text{CO}$  and  $\text{H}_2$  from the oxidation of hydrocarbon emissions from vegetation, Geophysical Research Letters, 5, 679-682, 1978.



## SOURCES AND SINKS FOR CARBON MONOXIDE

Jennifer A. Logan

Center for Earth and Planetary Physics  
Harvard University, Cambridge, Massachusetts 02138.

### Abstract

Sources, sinks and observational data for carbon monoxide are reviewed. The magnitude of the photochemical sink for CO by reaction with OH is derived from a model for the troposphere which is in reasonable accord with the budget for  $\text{CH}_3\text{CCl}_3$  (Logan et al., 1980). The major sources for CO are oxidation of methane and other naturally occurring hydrocarbons, fossil fuel combustion, and burning associated with agriculture in the tropics. Difficulties associated with quantification of these sources are discussed.

**INTRODUCTION:** Carbon monoxide was first detected in the Earth's atmosphere by Migeotte (1949) who identified CO infrared absorption lines in the solar spectrum. Bates and Witherspoon (1952) proposed that combustion of fossil fuels provides an important source of atmospheric CO, but they were unable to identify a significant removal mechanism for the gas. They combined their estimate for the anthropogenic source with Migeotte's observations to infer an atmospheric residence time of a few years. Weinstock (1969) derived a much shorter residence time, 0.1 yr, based on limited measurements of the  $\text{C}^{14}$  content of CO (MacKay et al., 1963) and a calculation of the cosmogenic source of  $\text{C}^{14}\text{O}$ . Weinstock's calculation implied that the unknown sink for atmospheric CO should be much larger than that derived by Bates and Witherspoon, and indicated that large unknown sources of CO must exist in order to maintain the observed CO concentration.

Reaction with tropospheric hydroxyl radicals



was soon recognized as the unknown sink for CO. Levy (1971) presented a simple model of tropospheric photochemistry, which predicted that the concentration of OH radicals near the ground should be of order  $10^6 \text{cm}^{-3}$ . He also pointed out that the oxidation of atmospheric methane is initiated by reaction with OH



with subsequent production of formaldehyde. McConnell et al. (1971) proposed that photo-oxidation of formaldehyde, in turn, provides a source of CO poten-

tially large enough to balance the global budget of CO.

By the mid 1970's it was recognized that methane oxidation and fossil fuel combustion provide major sources of CO, and that reaction with OH and uptake by soil (Seiler, 1974) are important removal mechanisms. Seiler (1974, 1976) and Wofsy (1976) give excellent reviews of the atmospheric cycle of CO, from somewhat different perspectives, as it was understood at that time. This paper focuses on developments since 1976.

The magnitude of the photochemical sink for CO has been the subject of considerable controversy. Observational data for OH are sparse. The global distribution of OH is not presently known with precision adequate to define the rate at which CO is removed from the atmosphere by reaction (2). Consequently, estimates of the global sink for CO are based on OH distributions calculated by photochemical models. Analysis of data for atmospheric methylchloroform ( $\text{CH}_3\text{CCl}_3$ ) has been proposed as a test of these models. This compound is used extensively as a solvent, has no known natural sources, and its release rate to the atmosphere has been estimated from data provided by the chemical industry (Neely and Plonka, 1978). Methylchloroform is removed from the atmosphere primarily by reaction with tropospheric OH. To the extent that the source is determined, measurements of atmospheric  $\text{CH}_3\text{CCl}_3$  may be used to check calculations for the global distribution of OH. Preliminary studies (Singh, 1977; Lovelock, 1977) suggest that early photochemical models (e.g. Levy, 1972; Wofsy et al., 1972; Crutzen, 1974) overestimated the concentration of OH by a factor of 2-5. This paper summarizes a recent model for OH in the troposphere (Logan et al., 1980) which is in reasonable accord with the observational data for  $\text{CH}_3\text{CCl}_3$ . The model is used to estimate the magnitude and distribution of the photochemical sink for CO.

Oxidation of non-methane hydrocarbons has long been considered as a possible source of CO (cf. Robinson and Robbins, 1969; Wofsy et al., 1972). Significant quantities of isoprene and terpenes are emitted by vegetation (Rasmussen, 1970; Went, 1960; Zimmerman et al., 1978) but it is very difficult to quantify the global emission rates. Moreover, the atmospheric degradation mechanisms for these compounds are not well understood, especially the role of gas to particle conversion. Problems associated with estimating the source of CO from oxidation of these compounds will be highlighted in the discussion below.

It is difficult also to quantify rates for production of CO associated with burning of vegetation. Fire is used extensively for land clearance, particularly in the tropics, and the areas and quantities of vegetation burned annually are highly uncertain. Biomass burning represents another potentially large source of CO (Crutzen et al., 1979).

This paper presents current estimates for sources of CO, and emphasizes where new data would help to reduce existing uncertainties.

The next section summarizes tropospheric photochemistry, emphasizing recent kinetic data. The atmospheric model is described briefly in Section 3, which includes also a review of observational data for CO. The global budget for CO is presented in Section 4. Conclusions and recommendations for further work are given in Section 5.

**TROPOSPHERIC CHEMISTRY.** The chemistry of OH is linked directly to the chemistry of H,  $\text{HO}_2$  and  $\text{H}_2\text{O}_2$ , as illustrated in Figure 1. It is convenient to consider the species OH, H,  $\text{HO}_2$ , and  $\text{H}_2\text{O}_2$  as a family, odd hydrogen. Hydroxyl radicals are produced by photolysis of ozone



followed by



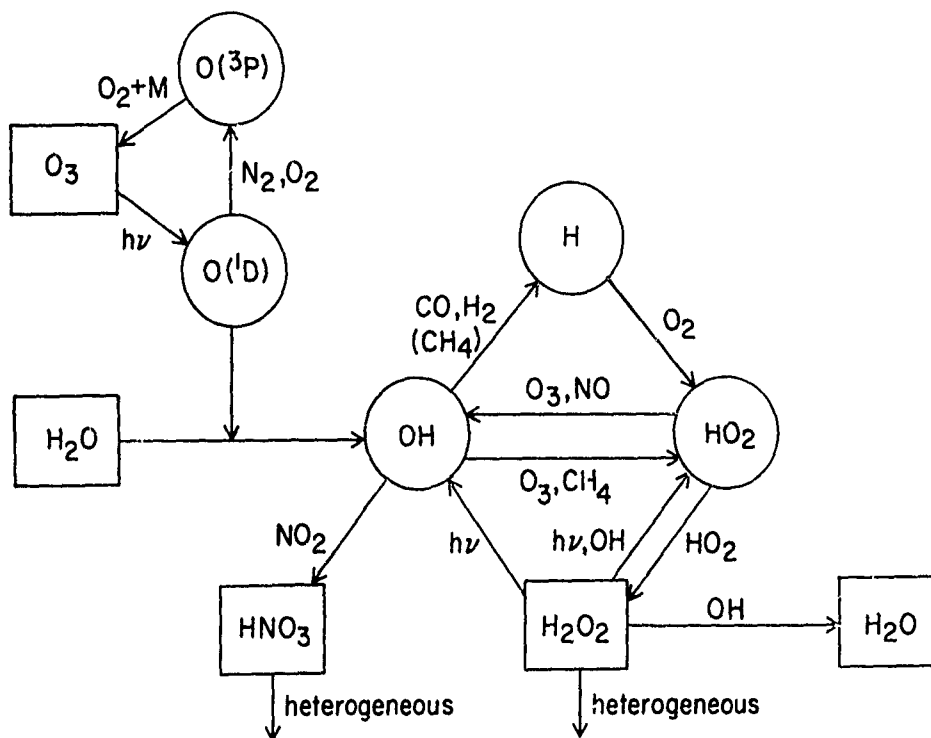
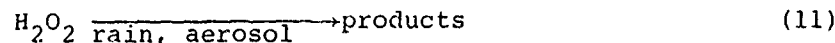


Figure 1. The major chemical reactions affecting odd hydrogen ( $OH$ ,  $H$ ,  $HO_2$ ,  $H_2O_2$ ) in the troposphere are illustrated schematically.

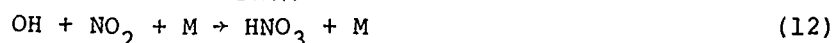
Reaction (4) provides the major source of odd hydrogen in the troposphere. The  $OH$  radical reacts either with  $CO$  or  $CH_4$ ,



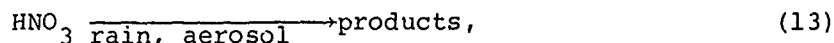
Reaction (1) dominates (2), particularly in the northern hemisphere where  $CO$  concentrations are relatively high. Subsequent chemistry of the odd hydrogen species involves



Odd hydrogen is conserved in reactions (1) and (5)-(9). Two molecules of odd hydrogen are lost in each of reaction (10) and (11). Together with



and



reactions (10) and (11) constitute the dominant sinks for tropospheric odd hydrogen. Loss of odd H proceeds mainly by (11) when the concentration of NO is less than about 200 ppt. Reaction (13) is important for higher concentration of NO.

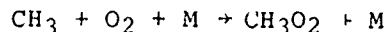
The relative quantum yield of  $\text{O}(^1\text{D})$  from ozone photolysis near 310 nm is fairly well determined as a function of wavelength and temperature (Lin and DeMore, 1973; Moortgat and Kudzus, 1978; Brock and Watson, 1980). However, the absolute quantum yield is uncertain. The experimental results of Amimoto et al. (1978) and Kajimoto and Cvetanovic (1979) imply a quantum yield of unity near 300 nm, while the work of Fairchild et al. (1978) and Sparks et al. (1979) gives a value of 0.9. Since the production rate of OH (reaction (4)) is proportional to the  $\text{O}(^1\text{D})$  concentration, it is important that this issue is resolved. The OH production rate depends also on the ratio of the rate for reaction of  $\text{O}(^1\text{D})$  with  $\text{H}_2\text{O}$  as compared to the total rate for quenching by  $\text{N}_2$  and  $\text{O}_2$ . Lee and Slanger (1979) have recently confirmed the measurements by Streit et al. (1976) of these rate constants.

The OH concentration depends critically on the rate constants for reactions (1) and (2). The rate for reaction (1) depends on pressure (Biermann et al., 1978) and the rate constant for this process at 1 bar of air is about a factor of two larger than the low pressure limit. This important effect was unknown prior to 1977.

Reactions (6) and (7), which cycle  $\text{HO}_2$  to OH, may play an important role in determining the OH concentration. The rate constant for reaction of NO with  $\text{HO}_2$  is larger (Howard, 1979) than values accepted prior to 1976 by a factor of 40, which ensures more efficient regeneration of OH from  $\text{HO}_2$  at any given concentration of NO. Impact of this change on model results is offset in part by recent observations (McFarland et al., 1979; Noxon, 1978) indicating that concentrations of NO in the clean troposphere are considerably lower than values suggested earlier by Robinson and Robbins (1969). Regeneration of OH by reaction of  $\text{HO}_2$  with NO (reaction (7)) is more important than cycling by reaction with  $\text{O}_3$  (reaction (6)) if the concentration ratio  $[\text{NO}]/[\text{O}_3]$  exceeds  $2 \times 10^{-4}$ . In the tropics reaction (7) will be more important than (6) if [NO] exceeds 4 ppt. A somewhat greater concentration of NO, about 8 ppt, is required to ensure dominance of (7) at higher latitudes, due to the larger concentration of tropospheric ozone at higher latitudes.

The concentration of OH is independent of [NO] for concentration of NO below about 10 ppt and is an increasing function of [NO] for [NO] between 10 ppt and 500 ppt (cf. Weinstock et al., 1979; Hameed et al., 1979, and Fishman et al., 1979). The concentration of OH decreases as a function of [NO] above 1 ppb, behavior which reflects the increasing importance of reaction (13) as a loss process for odd hydrogen.

The photochemical source of CO resulting from oxidation of atmospheric  $\text{CH}_4$  depends on details of the oxidation mechanism, which is shown schematically in Figure 2 (Levy, 1971; Wofsy et al., 1972). Reaction (2) is followed by



with  $\text{CH}_3\text{O}_2$  removed by reaction with NO,  $\text{HO}_2$  or  $\text{CH}_3\text{O}_2$ . Kinetic data has become available only recently for some of these processes. The rate constant for reaction of  $\text{CH}_3\text{O}_2$  with NO has been measured by several groups (Plumb et al., 1979; Adachi and Basco, 1979; Cox and Tyndall, 1979; Simonaitis and

Heicklen, 1979) and is similar to that for the analogous reaction (7). Preliminary work by Cox and Tyndall (1979) suggests that the rate constants for reactions of  $\text{CH}_3\text{O}_2$  with  $\text{NO}$  and  $\text{HO}_2$  may be comparable, whereas the rate constant for the self-reaction of  $\text{CH}_3\text{O}_2$  is considerably smaller (Parkes, 1977).

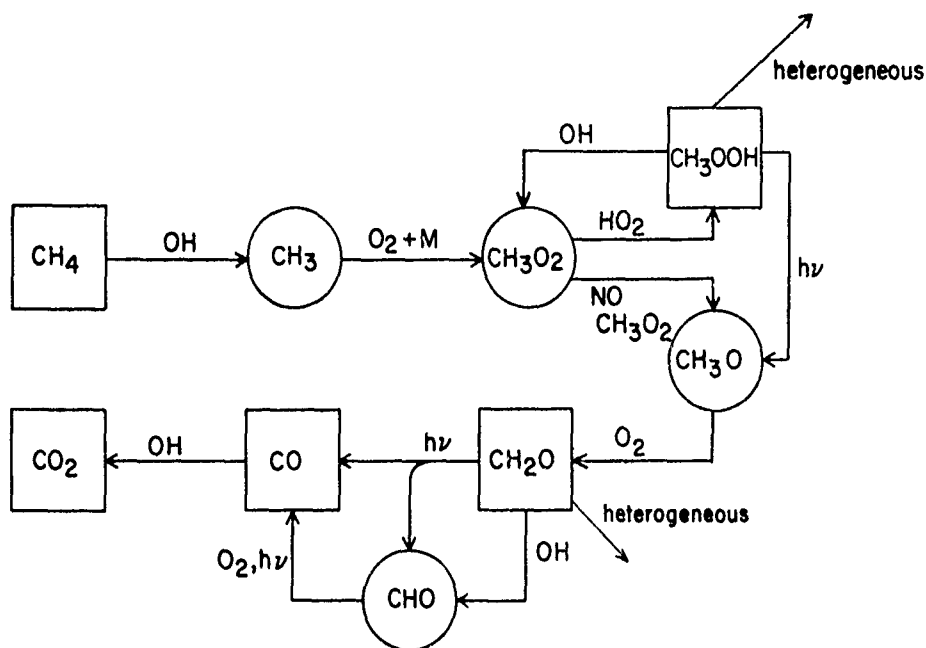


Figure 2. The atmospheric oxidation of  $\text{CH}_4$  is illustrated schematically.

The yield of  $\text{CO}$  from  $\text{CH}_4$  oxidation should be close to unity unless significant quantities of intermediates such as  $\text{CH}_3\text{OOH}$  or  $\text{H}_2\text{CO}$  are removed heterogeneously. The formation rate of  $\text{CH}_3\text{OOH}$  depends on the relative importance of the  $\text{CH}_3\text{O}_2$  reactions discussed above. Concentrations of  $\text{HO}_2$  and  $\text{CH}_3\text{O}_2$  are available only from model calculations, which give values of a few parts in  $10^{12}$  (ppt) (Logan et al., 1980). It seems more likely that  $\text{CH}_3\text{OOH}$  should be formed over the oceans, where measurements indicate exceedingly low  $\text{NO}$  concentrations (McFarland et al., 1979). Reaction of  $\text{CH}_3\text{O}_2$  with  $\text{NO}$  should dominate over land where  $\text{NO}$  concentrations are usually larger than 50 ppt (Bush et al., 1979; Kelly and Stedman, 1979). Since the lifetime of  $\text{CH}_3\text{OOH}$  against photolysis (Molina and Arguello, 1979) and reaction with  $\text{OH}$  is a few days, heterogeneous loss could be significant. Hydroperoxides undergo a  $\text{Fe}^{2+}$ -catalyzed and sometimes base-catalyzed decomposition, but the  $\text{C-O}$  bond remains intact (Hiatt, 1971). Destruction of  $\text{CH}_3\text{OOH}$  by reaction on the surface of aerosols is a possibility and is considered in the estimation of the  $\text{CO}$  yield from  $\text{CH}_4$ . It should be noted that formaldehyde and methanol are likely products of heterogeneous decomposition. Rainout of  $\text{CH}_3\text{OOH}$  is included in the model.

Photolysis of  $\text{CH}_2\text{O}$  is much more rapid than that of  $\text{CH}_3\text{OOH}$  (Bass et al., 1980). Recent observations of the formaldehyde concentrations in aerosols (Klippel and Warneck, 1979) and in rainwater over the Pacific Ocean (Zafariou et al., 1980) imply that heterogeneous loss of formaldehyde should be negligible, relative to photochemical loss. These observations suggest also that heterogeneous loss of  $\text{CH}_3\text{OOH}$  may be minor (Wofsy et al., 1972).

Oxidation of methane could provide either a small source or a small sink for odd hydrogen in the troposphere. It is likely to represent a source of odd H where NO is abundant, and may introduce a sink where NO is low and  $\text{CH}_3\text{OOH}$  formation is favored.

The photochemistry of the troposphere described in Figures 1 and 2 provides important chemical sources and sinks for ozone. This topic is discussed in detail in a recent paper by Fishman et al. (1979).

**MODEL CALCULATIONS:** This section describes a recent model of the troposphere (Logan et al., 1980) which was used to calculate the concentration of OH as a function of latitude and time, and hence the photochemical sink for CO. Global distributions of CO,  $\text{CH}_4$ ,  $\text{H}_2\text{O}$ ,  $\text{O}_3$  and  $\text{HNO}_3$  were prescribed in this model, based on the observational data reviewed below.

A summary of observations for tropospheric CO is given in Table 1 and Figure 3. The majority of these observations were taken over the ocean, either from ships or from aircraft. Most of the measurements should represent conditions in the clean troposphere remote from sources. However, all the surface measurements at northern mid-latitudes are from the North Atlantic region, and are almost certainly influenced by industrial and biogenic sources on the North American continent. The influence of sources is also apparent in the vertical soundings over Europe, which show considerable variability, as is shown in Figure 4.

TABLE 1: Observational Data for Carbon Monoxide

Reference	Date	Latitude	Location	Symbol
<u>Surface Measurements</u>				
Robinson & Robbins 1969	Nov.-Dec. 67	37°N-37°S	Pacific	▲
Seiler & Schmidt 1974	April-May 69	60°N-10°S	Atlantic	△
" "	Nov. 71	50°N-30°S	Atlantic	+
" "	Mar. 72	50°N-60°S	Atlantic	○
Wilkness et al. 1973	Nov.-Dec. 72	30°N-77°S	Pacific	●
Heidt et al. 1979	May 78	30°N-60°S	Pacific	
<u>Mid-troposphere Measurements</u>				
Junge et al. 1971	Jan.-April 68	80°N-40°N	Pacific	X
"	Nov. 68	85°N-26°S	Atlantic	○
Seiler & Schmidt 1974	Nov. 71	50°N-20°S	Atlantic	—
" "	Mar. 72	30°N-20°S	Atlantic	----
Seiler 1976	July-Aug. 74	65°N-56°S	East & West American coasts	●
Heidt & Krasnec 1978	May 78	30°N-60°S	Pacific	

The measurements in Figure 3 indicate that the northern hemisphere contains about 1.5-2 times as much CO as the southern hemisphere. It is more difficult to determine from the somewhat limited data base if CO varies with longitude. None of the measurements from the southern Pacific and Atlantic were taken during the same time period. Seiler (1976) found no difference in the CO mixing ratio in the upper troposphere above the west and east coasts of America.

Wilkness et al. (1973) reported considerably lower values than Heidt and Krasnec (1978) for CO in surface air over the South Pacific, but the

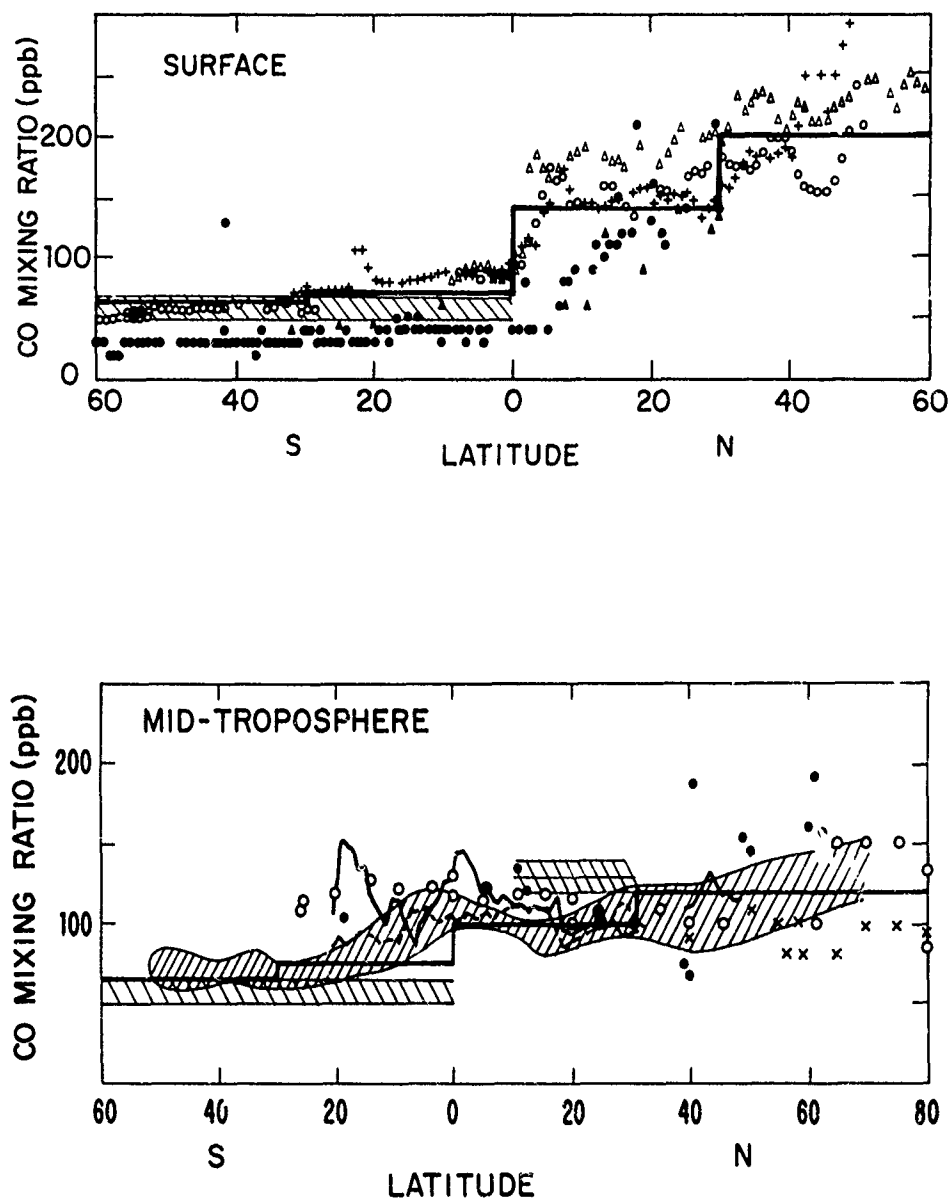


Figure 3. Observational data for carbon monoxide near the surface and in the mid-troposphere are shown. The symbols are explained in Table 1. The heavy lines show the values for CO used in the model of Logan et al. (1980).

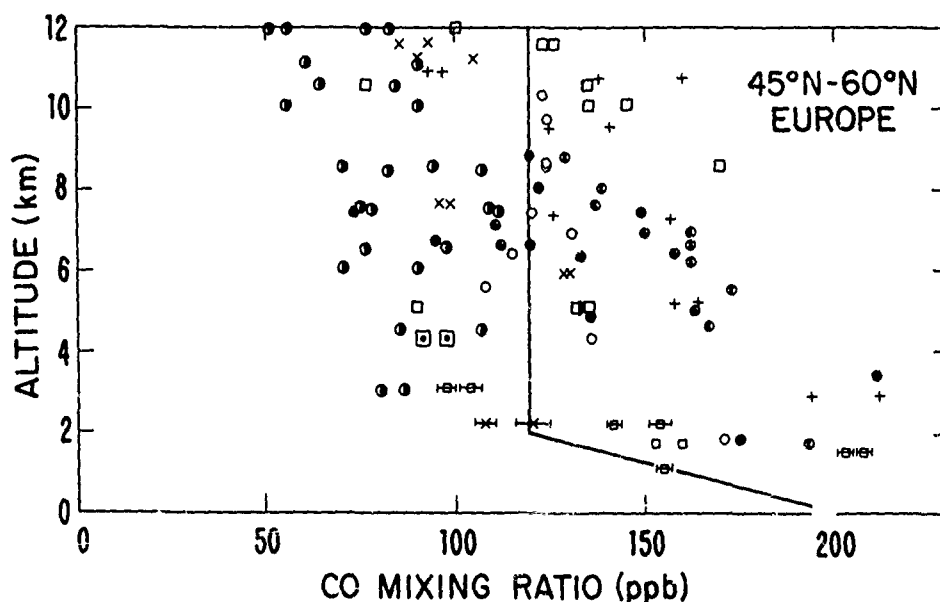


Figure 4. Tropospheric profiles for CO are shown. The individual symbols represent data from separate flights over Europe, and are from Seiler et al. (1978) and Fabian et al. (1979). The solid line shows the profile used in the model of Logan et al. (1980) at northern mid-latitudes.

observations were made in summer and winter, respectively, 6 years apart. Measurements at Mauna Loa Observatory in Hawaii ( $19.5^{\circ}\text{N}$ ) (Seiler et al., 1976) suggest that CO may exhibit a seasonal variation, with highest concentrations in winter, lowest in summer. This behavior may reflect prevailing wind patterns, as well as seasonal variations in the sources of CO or in the concentration of OH. The seasonal variation of  $^{14}\text{CO}$  has been measured, in Europe (Volz et al., 1980). Minimum values are found in summer, a trend which correlates with the expected seasonal variation in the concentration of OH.

The CO model for the southern hemisphere was based on the measurements of Seiler (1976) over the coasts of S. America, and those of Heidt and Krasnec (1978) over the central Pacific Ocean. The CO mixing ratio showed little gradient with altitude south of  $20^{\circ}\text{S}$  during these expeditions. There is clearly appreciable uncertainty, perhaps 20-30%, in the model for CO. Temporal variations are not well known, and there is a need for data from northern locations other than the Atlantic. It should be noted, however, that in the model the magnitude of the photochemical sink for CO is relatively insensitive to uncertainties in the CO concentration. Since reaction with CO is the major sink for tropospheric OH, calculated concentrations of OH and CO tend to be inversely related.

The latitudinal distribution of  $\text{CH}_4$  was derived from the data of Seiler et al. (1979), Fabian et al. (1978) and Ehhalt (1978). Profiles for water vapor were obtained from Oort and Rasmussen (1971) and Mastenbrook (1966, 1968). Ozone distributions were derived from observations reported by Chatfield and Harrison (1977), Dutsch and Ling (1973), Attmanspacher and Hartmannsgruber (1976), Pittcock (1977) and Fishman et al. (1979) as described in detail in Logan et al. (1980). Total ozone columns were taken from Dutsch (1974) and nitric acid



profiles from Huebert and Lazrus (1980).

Measurements of NO in the clean troposphere are sparse. McFarland et al. (1979) found concentrations of NO of about 3 ppt in surface air over the central Pacific Ocean. Schiff et al. (1979) recently reported mixing ratios of 30-40 ppt both in and above the boundary layer over the Pacific Ocean, and slightly higher values (40-60 ppt) in "clean" air over North America. However, the authors emphasized that these values are upper limits. Measurements of NO in continental air, in Colorado and Wyoming, range from 20 ppt to more than 1 ppb (Drummond, 1977; Bush et al., 1979). The high values are associated with advection of urban pollutants. These data suggest that the concentration of NO in continental air should lie in the range 20-100 ppt, and measurements by Noxon (1978) of the integrated column of tropospheric NO<sub>2</sub> are consistent with these low values.

In the model calculations, the NO<sub>x</sub> mixing ratio at the surface was specified, and a mid-tropospheric source of NO was included. This source is intended to simulate input of NO from lightning (Noxon, 1978) as well as production from precursor molecules such as NH<sub>3</sub> (McConnell, 1973) or peroxyacetyl nitrate (Crutzen, 1979). The surface NO<sub>x</sub> mixing ratio was taken to be 10 ppt over the oceans, 100 ppt over land.

Model atmospheres were taken from the U.S. Standard Atmosphere Supplement (1966). Concentrations of OH were calculated by solving time dependent continuity equations, as described by Logan et al. (1978) and Wofsy (1978). The chemical model is described in these papers and the rate constants recommended by NASA (1979) were used. The model incorporates diurnal variation of insolation and includes the effects of clouds and aerosols. The method of calculation is described in detail in Logan et al. (1980).

The model was used to examine the sensitivity of computed OH concentrations to uncertainties in input parameters. As discussed above, considerable uncertainty is attached to the NO distribution. Larger concentrations of NO result in more efficient regeneration of OH from HO<sub>2</sub> radicals by reaction (7) and hence larger concentrations in OH. Uncertainties in NO introduce an uncertainty in the photochemical loss for CO of about 30% (Logan et al., 1980).

Heterogeneous decomposition of H<sub>2</sub>O<sub>2</sub> is a major loss process for odd hydrogen. In the lower troposphere, peroxide lifetimes of a few hours to a few days are possible, depending on whether attachment to aerosols or rainout is the dominant loss process. This range of H<sub>2</sub>O<sub>2</sub> lifetimes introduces an uncertainty in the OH concentration and in the sink for CO of about 20%.

**THE BUDGET FOR CARBON MONOXIDE:** Hydroxyl radical profiles were calculated as functions of altitude, time and season for latitudes 15° and 45° in each hemisphere. Profiles of OH calculated for use in budget estimates are shown in Figure 5, and are intended to simulate average tropical and mid-latitude conditions. The results reflect an average over diurnal, seasonal, and cloud-related changes in insolation, and are taken from Logan et al. (1980). The lack of a significant interhemispheric asymmetry in the OH profiles reflects the lower ozone concentrations in the southern versus the northern hemisphere. The model assumes that concentrations of NO are higher over land than over the oceans. The areas of land and ocean in each latitude region were taken into account in estimating the photochemical loss rate for CO,

$$\text{Loss (CO)} = \int_0^{t=1 \text{ year}} dt \int \int \int_0^\infty k_1 [\text{OH}] [\text{CO}] dz dx dy.$$

The loss of CO in the stratosphere was estimated from the observational data for CO in the lower stratosphere (Seiler and Warneck, 1972; Seiler, 1974; Fabian et al., 1979; Pratt and Falconer, 1979) and the upper troposphere and from the model of Logan et al. (1978).

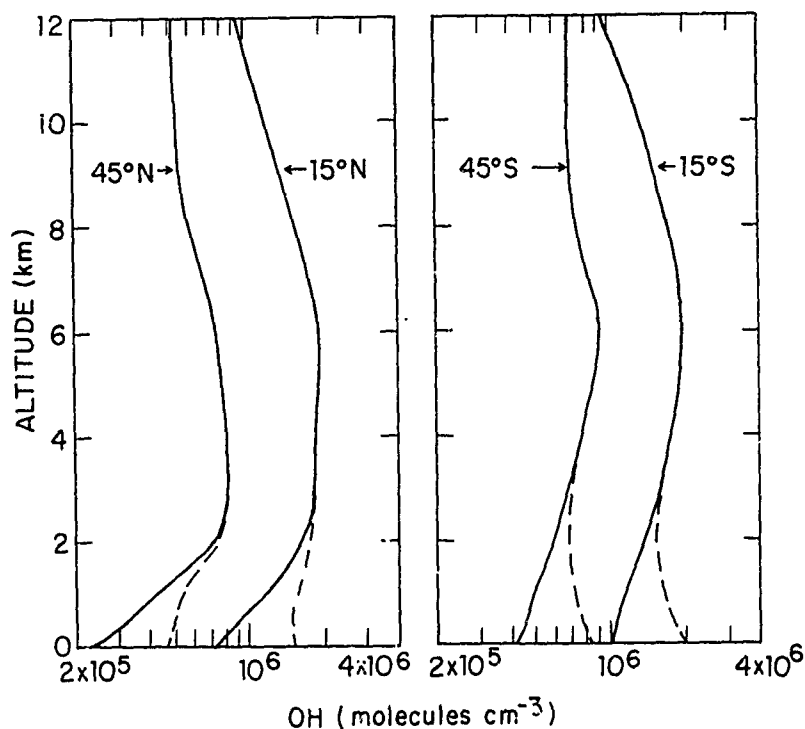


Figure 5. Profiles for OH in the troposphere which were used in the budget calculations are shown. Hydroxyl concentrations were calculated from a model in which the profiles of CO, CH<sub>4</sub>, H<sub>2</sub>O, O<sub>3</sub> and HNO<sub>3</sub> were fixed at mean mid-latitude and tropical conditions for each season and hemisphere. The diurnal variation of insolation and the effects of clouds and aerosols were included. The profiles shown are the mean of the diurnally averaged concentrations for the four seasons. The solid curves are assumed to represent marine air; the model included an NO<sub>x</sub> profile of 10 ppt below 6 km. The dashed curves were taken to represent continental air; the model included an NO<sub>x</sub> mixing ratio of 100 ppt at the ground.

Analysis of the budget for CH<sub>3</sub>CCl<sub>3</sub> was used as a test of the model for OH. The concentration of CH<sub>3</sub>CCl<sub>3</sub> was calculated as a function of time and latitude region using a simple model. The troposphere was divided into four zones of equal area with boundaries at 30°N, 0° and 30°S, and exchange between zones parametrized by a time constant for transfer across each boundary, 0.2, 0.6, and 0.2 years, respectively (Logan et al., 1980). Industrial emissions of CH<sub>3</sub>CCl<sub>3</sub> at northern mid-latitudes (Neely and Plonka, 1978), OH profiles (given in Figure 5), and the OH + CH<sub>3</sub>CCl<sub>3</sub> rate constant (Kurylo et al., 1979; Jeong and Kaufman, 1979) were specified, and the CH<sub>3</sub>CCl<sub>3</sub> concentrations were calculated.

Comparison of the box model results with the observational data for CH<sub>3</sub>CCl<sub>3</sub> (e.g. Lovelock, 1977; Rasmussen, private communication; Rowland, private communication) indicates that computed OH concentrations may be too high by about 30%, and are unlikely to be too low. There is, however, a large spread in

the observational data. The model results agree best with the data of Lovelock and Rowland. The analysis of the  $\text{CH}_3\text{CCl}_3$  budget, and sources of uncertainties in the model for OH are discussed in more detail in Logan et al. (1980).

The analysis discussed above suggests that concentrations of OH, and hence the magnitude of the photochemical sink for CO may be determined to better than a factor of 2. The model results of Logan et al. (1980) imply photochemical sinks for CO in the northern and southern hemispheres of  $1.8 \times 10^{15} \text{ gm yr}^{-1}$  and  $1.2 \times 10^{15} \text{ gm yr}^{-1}$ , respectively. About 95% of the photochemical loss for CO occurs in the troposphere.

Biological activity in the soil also provides a small net sink for CO as discussed by Seiler (1974). Liebl and Seiler (1976) measured deposition velocities for CO over soils in the range  $0.02$  to  $0.07 \text{ cm sec}^{-1}$ , with a median value of  $0.04 \text{ cm sec}^{-1}$ . This value, and the data for CO given in Figure 3 may be used to calculate a net sink for CO due to uptake by soils of magnitude  $2.5 \times 10^{14} \text{ gm yr}^{-1}$ , of which about 80% should occur in the northern hemisphere. This estimate is similar to those given in Liebl and Seiler (1976) and Seiler (1976). Nozhevnikova and Turganov (1979) given an excellent review of microbiological processes involving CO.

The world's oceans are believed to represent a small net source of CO. Measurements of depth profiles of dissolved CO in the surface waters of the oceans (Linnenbom et al., 1973; Seiler, 1974), and a simple model for diffusion through the ocean surface (Broeker and Peng, 1974) were used to estimate a source of magnitude  $4 \times 10^{13} \text{ gm CO yr}^{-1}$  (Seiler, 1976).

Reaction with OH is the major tropospheric sink for both CO and  $\text{CH}_4$ . The fraction of atmospheric CO derived from  $\text{CH}_4$  oxidation is almost independent of the OH concentration, and depends primarily on the relative rate constants for reactions (1) and (2). Methane oxidation could account for as much as 25% of the global source for CO, if aerosol loss of  $\text{CH}_3\text{OOH}$  is omitted. The analysis of Logan et al. (1980) implies sources for CO from  $\text{CH}_4$  of  $4.0 \times 10^{14} \text{ gm yr}^{-1}$  and  $3.8 \times 10^{14} \text{ gm yr}^{-1}$  in the northern and southern hemispheres, respectively. Inclusion of an aerosol loss process for  $\text{CH}_3\text{OOH}$  comparable to that adopted for  $\text{H}_2\text{O}_2$  reduces the source of CO from oxidation of  $\text{CH}_4$  by about 15%. The formation rate of  $\text{CH}_3\text{OOH}$  depends on the NO mixing ratio, and should be significant over the oceans and perhaps in the upper troposphere.

The sources of CO from fossil fuel combustion and industrial activities were estimated by Jaffe (1973). He used emission factors published by the U.S. Environmental Protection Agency (EPA) and information describing world usage of coal and oil to derive a global emission rate for CO of  $3.6 \times 10^{14} \text{ gm yr}^{-1}$  for 1970. This estimate was revised upward by Seiler (1974) to  $6.4 \times 10^{14} \text{ gm yr}^{-1}$  to take into account increases in fuel use, estimates of CO emissions in Germany, and processes which he felt were omitted from Jaffe's study. Seiler and Zankl (1976) measured the CO distribution over Munich and used the CO data and the horizontal wind speed to calculate the CO production rate within the area. The emission rate was comparable to that estimated from fuel usage and CO emission factors.

We used updated emission factors for the U.S. and F.R.G. in conjunction with statistics for fossil fuel consumption, fuel use patterns for coal, oil and natural gas, and industrial production of various commodities to estimate a source of CO of magnitude  $4.5 \times 10^{14} \text{ gm in 1976}$ , as given in Table 2 (Logan et al., 1980). Automobiles account for about half of the source of CO from fossil fuels. The partial implementation of vehicle exhaust emission standards in the U.S. and Western Europe was reflected in reduced emission factors for these areas ( $180$ - $320 \text{ gm CO per liter fuel}$ ) and it was assumed that emission rates outside these countries were similar to those in the U.S. prior to regulation of exhaust emissions ( $360 \text{ gm CO per liter of fuel}$ ). The largest industrial source of CO is the iron and steel industry, and it is important

to note that the U.S. and F.R.G. account for only 23% of total steel production (U.N., 1978b). Clearly there is a need for emission data from other countries where different industrial practices and air quality standards prevail.

TABLE 2: CO Emissions ( $10^{12}$  gm yr<sup>-1</sup>)<sup>a</sup>

	<u>Europe</u>	<u>N. America</u>	<u>Rest of the World</u>	<u>Total</u>
Combustion: coal <sup>b</sup>	24	1	23	48
lignite	3	-	-	3
gas	0.3	0.2	0.1	0.6
oil	4.6	2.2	3.7	11
Total Combustion	32	3.4	27	62
Transportation <sup>c</sup>	71	94	66	233
Sub Total	103	97	93	295
Industrial Processes	46	36	48	130
Waste Disposal <sup>d</sup>	6	3	11	20
TOTAL	155	137	152	445

<sup>a</sup>These estimates are derived from statistics for global fossil fuel consumption (U.N., 1978a), fuel use patterns (O.E.C.D., 1976) and emission factors for the U.S. (EPA, 1977, 1978a) and F.R.G. (Welzel and Davids, 1978). The uncertainty in the transportation source is considered to be about 30%, and in all other sources, about a factor of two.

<sup>b</sup>This source results from the use of coal in residential heating.

<sup>c</sup>The total includes a source of CO from aviation of  $1.6 \times 10^{12}$  gm. (Broderick, private communication).

<sup>d</sup>Estimate, based on limited data for the U.S. (EPA, 1977), and world population figures.

Atmospheric oxidation of anthropogenic hydrocarbons provides a small source of CO as shown in Table 3. Vehicle exhaust emissions and evaporation of fuels and solvents are the two largest sources of these hydrocarbons. Emission data for the U.S. (EPA, 1978b, c) were used to estimate the global source of hydrocarbons, and we assumed that 50% of the carbon could be photochemically converted to CO.

In many parts of the world, combustion of wood provides the major source of energy. About 1.5 billion people use between 0.1 and 2.0 tons of firewood per capita per year (Eckholm, 1979; Openshaw, 1974; Revelle and Monk, 1977). United Nations statistics for fuel wood usage ( $8.5 \times 10^{14}$  gm yr<sup>-1</sup>; FAO, 1979) and the emission factor for combustion of wood in an open fire (60 gm CO per kg of wood; EPA, 1977) may be used to estimate a CO source of magnitude  $5 \times 10^{13}$  gm yr<sup>-1</sup> from the burning of firewood.

Estimates for the source of CO from biomass burning depend on a product of three factors, the area of land burned per unit time, the quantity of fuel

TABLE 3: Global CO Budget ( $10^{12}$  gm CO yr $^{-1}$ )

Sources	Total	N.H.	S.H.
Fossil fuel use	450 (400-1000)	425	25
Oxidation of anthropo- genic hydrocarbons	90 (0-180)	85	5
Wood fuel	51 (17-150)	33	17
Forest and woodland clearing	380 (80-1200)	260	120
Burning of pasture	200 (50-600)	100	100
Forest wildfires	25 (8-75)	22	3
Ocean	40 (20-80)	13	27
Emissions by plants	70 (21-210)	50	20
Oxidation of isoprene and terpenes	560 (190-1700)	380	180
Methane oxidation	780 $\pm$ 350	400	380
<b>TOTAL</b>	<b>2650</b> <b>(1500-6000)</b>	<b>1770</b>	<b>880</b>
<hr/>			
Sinks	Total	N.H.	S.H.
Soil uptake	250	210	40
Photochemistry	3100 (2000-4000)	1850	1250
<b>TOTAL</b>	<b>3350</b>	<b>2060</b>	<b>1290</b>

consumed per unit area and the production of CO per unit fuel. The estimates given below are taken from the recent analysis of Logan et al. (1980). Direct measurements of CO from wild forest fires have been obtained only recently, by Crutzen et al. (1979), whose data imply a CO yield of 130 kg CO per ton of fuel burned. The EPA give a value of 70 kg CO ton $^{-1}$ , based on measurements of CO from experimental, controlled fires (EPA, 1977). In the present work a compromise value of 100 kg CO ton $^{-1}$  was used. Reasonably accurate data are available for the extent of forest fires in the U.S., Canada and Australia, which contain about 25% of the world's forests (Persson, 1974). About 0.4% of the forests of these countries are burned each year, and about 30 tons of fuel per hectare are consumed by fire (Yamate, 1975; EPA, 1977). These data, and the estimates by Persson (1974) of the area of the world's forests may be used to estimate a CO source from forest wild fires of  $2.5 \times 10^{13}$  gm yr $^{-1}$ . There is clearly a large uncertainty (at least a factor of 3) attached to this estimate, given the limited information available about fire in the world's forests (Persson, 1974; Yamate, 1975).

It is even more difficult to assess the source of CO from deliberate burning of forests and woodland. Seiler and Junge (1970) reported elevated concentrations of CO in the mid-troposphere when flying over extensive bush fires in Africa. Shifting cultivation is the major form of agriculture in the tropics of Africa and in regions of Latin America and South East Asia. Fire is used to clear forest, woods, or savanna so that crops may be grown, and is used extensively to maintain pastures for grazing (Nye and Greenland, 1960; Gourou, 1966; Spencer, 1966; Webster and Wilson, 1967; Watters, 1971; Ruthenberg, 1976). It is very difficult to obtain data for the amount or type of land cleared annually in different regions, although there exist very detailed accounts of the agricultural practices of a few communities. The available data suggest that between 0.05 to 0.28 ha of land is cleared each year for each person subsisting by shifting cultivation, with a median value of 0.15 ha per person per year. This information, in combination with statistical data for the agricultural population of individual countries (FAO, 1978) and maps showing the extent of shifting cultivation (Whittlesey, 1937; Grigg, 1974), may be used to estimate the total area of land cleared for agriculture in the tropics. The biomass consumed per area burned may be estimated from the mean standing biomass and annual productivity of different types of vegetation (Whittaker and Likens, 1975; Bourliere and Hadley, 1970; Murphy, 1975).

The CO sources from clearance of forest and woodland for crops and from burning of pasture land were estimated to be  $3.8 \times 10^{14}$  and  $2.0 \times 10^{14}$  gm CO yr<sup>-1</sup>, respectively (Logan et al., 1980). The total source of CO from biomass burning given in Table 3,  $6.6 \times 10^{14}$  gm yr<sup>-1</sup>, is similar to that given recently by Crutz et al. (1979),  $8.4 \times 10^{14}$  gm yr<sup>-1</sup>, although individual sources differ by as much as a factor of 2. It is important to emphasize the limited data base from which these estimates were derived. They must be considered highly uncertain, but they indicate the type of data needed to make such an estimate.

Early studies of the influence of carbon monoxide on green plants showed that they could both produce and consume the gas (Wilks, 1959; Bidwell and Fraser, 1972). Recent laboratory and field experiments demonstrated that higher plants act as a net source of CO at ambient CO concentrations (Seiler and Geihl, 1977; Bauer et al., 1979). The CO production rate per unit leaf surface area was measured as a function of light intensity and season for four plant species, and reached a maximum of  $4.4 \times 10^{-12}$  gm cm<sup>-2</sup>s<sup>-1</sup> at noon in summer. Bauer et al. (1979) used these results and average values for global leaf surface area and light intensity to estimate a source of CO from plants of  $7 \times 10^{13}$  gm yr<sup>-1</sup>. This estimate is uncertain to at least a factor of two.

Oxidation of hydrocarbons emitted by plants may provide a significantly larger source of CO. Went (1960) estimated that plants release  $1.8 \times 10^{14}$  gm organic material each year, and he proposed that atmospheric oxidation of the volatile plant emissions is responsible for the blue haze observed over vegetated areas in summer. Rasmussen and Went (1965), using gas chromatography, tentatively identified the volatiles from intact plants as isoprene and terpenes, including  $\alpha$ - and  $\beta$ -pinene, limonene and myrcene.

Isoprene (2 methyl-1, 3-butadiene, C<sub>5</sub>H<sub>8</sub>) is a major component of the volatile emissions of many plant species (Sanadze, 1963; Rasmussen, 1970). Two recent estimates for the global source of isoprene are  $3.5 \times 10^{14}$  gm C yr<sup>-1</sup> (Zimmerman et al., 1978) and  $5 \times 10^{14}$  gm C yr<sup>-1</sup> (Rasmussen, private communication), but the authors emphasize that these values are extrapolations of limited data and are uncertain by at least a factor of 3. The estimates are based on field investigations of emission rates of plants growing in the U.S. The estimated source of terpenes is similar to that for isoprene (Zimmerman et al., 1978). Observational data for isoprene and the terpenes are sparse. Isoprene mixing ratios as high as 2 ppb were observed in forests in the U.S. (Rasmussen, 1970; Robinson, 1978), while terpene mixing ratios have been measured in the range 10 ppt to 1 ppb (Holdren et al., 1979).

The fate of these hydrocarbons in the atmosphere is not well defined, but it seems likely that oxidation of isoprene should lead to production of between one and three molecules of CO. Isoprene is likely to be removed by reaction with OH or with O<sub>3</sub>, and laboratory studies of similar reactions indicate that CO should be produced (Niki et al., 1978; Cox et al., 1979; Zimmerman et al., 1978). Gas to particle conversion is likely to be a significant sink for the carbon present in the larger, more complex terpenes, as discussed by Went (1960) and Schuetzle and Rasmussen (1978). Graedel (1979) recently reviewed possible atmospheric oxidation schemes for the terpenes, and emphasized current uncertainties. Quantitative estimates for the source of CO from oxidation of isoprene and terpenes are limited by uncertainty in the CO yield and by lack of reliable data for the total biospheric sources of the hydrocarbons.

If we assume that the global sources of isoprene and the terpenes are each about  $4 \times 10^{14}$  gm yr<sup>-1</sup>, and that 2 molecules of CO are derived from each hydrocarbon precursor, the source of CO is estimated to be  $5.6 \times 10^{14}$  gm CO yr<sup>-1</sup>. As indicated by the discussion above, the magnitude of this source is not at all well determined, and is uncertain by about a factor of 5. Given the potentially large role of these hydrocarbons in the CO budget, field and laboratory studies of their emission rates and oxidation mechanisms are clearly required.

**CONCLUSIONS:** The summary of the budget for carbon monoxide given in Table 3 indicates that the global source strength for the gas is about  $3 \times 10^{15}$  gm CO yr<sup>-1</sup>. Over one third of the total sources might be termed "anthropogenic" with human related emissions dominated by fossil fuel use in the industrial nations at northern mid-latitudes and by agricultural burning in the developing countries in the tropics. Quantification of the source of CO from biomass burning will remain a problem until more reliable estimates can be made of the areas of forest and grassland involved, the mass of material consumed by fire and the CO emission factors. It may be possible to extract information from future satellite surveys of tropical regions to determine the extent of annual burning. More in-situ measurements of CO in the vicinity of fires should clarify the yield of the gas in combustion. Two natural processes, oxidation of CH<sub>4</sub> and oxidation of higher hydrocarbons, are among the largest sources of CO. Field measurements of background concentrations and emission rates of isoprene and terpenes are needed. These should be made in different vegetation zones, especially in the tropics, as functions of time, season, light intensity and plant species. Laboratory studies designed to elucidate the atmospheric oxidation mechanisms of these compounds (including CH<sub>4</sub>) are clearly desirable. In particular the roles of heterogeneous chemistry and gas to particle conversion need to be understood.

Precise definition of the photochemical sink for CO requires either measurement of the global distribution of OH or verification of photochemical models of the troposphere or both. The discussion of tropospheric chemistry given earlier indicates that the concentration of the OH radical depends on many factors, including location, time of day, background gas concentrations and cloudiness. It is unlikely, therefore, that the global OH distribution can be determined experimentally in the near future. However, simultaneous measurements of OH, H<sub>2</sub>O, O<sub>3</sub>, CO, CH<sub>4</sub>, NO, NO<sub>2</sub> and insolation may be used to verify details of photochemical models. Analysis of the budgets of trace gases like CH<sub>3</sub>CCl<sub>3</sub>, whose source and distribution with latitude may be accurately determined, provide a means for testing models which attempt to integrate over variable atmospheric conditions. Measurements of CH<sub>3</sub>CCl<sub>3</sub> in remote locations should continue and current calibration and sampling problems must be resolved (NASA, 1979).

Although CO has been measured at various times and places for more than a decade, only the gross features of its distribution with latitude, altitude and season are determined. The gas should be measured regularly at several remote locations so that its seasonal variation may be understood. Since there are

significant anthropogenic sources of CO, it is important to establish if the concentration is increasing with time. Changes in CO would cause changes in OH with potential for feedback on other aspects of atmospheric chemistry, including changes in photochemical sources of ozone in the troposphere (Logan et al., 1978). The concentration of CH<sub>4</sub> would also be affected, which would influence stratospheric chlorine chemistry (Sze, 1977; Chamedies et al., 1977).

**ACKNOWLEDGEMENTS:** This work was supported by the National Science Foundation and the National Aeronautic and Space Administration under contracts NSF-ATM79-13251 and NASA-NSG-2031, respectively. The author acknowledges useful discussions with S.C. Wofsy, M.J. Prather and M.B. McElroy.



## References

- Adachi, H., N. Basco, Kinetic Spectroscopy Study of the Reaction of  $\text{CH}_3\text{O}_2$  with NO, Chem. Phys. Lett., **63**, 490-492, 1979.
- Amimoto, S.T., A.P. Force, J.R. Wiesenfeld, Ozone Photochemistry: Production and Deactivation of  $\text{O}(^2\text{D}_2)$  Following Photolysis at 248 nm, Chem. Phys. Lett., **60**, 40-43, 1978.
- Attmannspacher, W., R. Hartmannsgruber, Some Results of 6 Years (1967-1972) of Regular Ozone Soundings at the Meteorological Observatory Hohenpeissenberg, FRG, Beitrage Zur Phys. der Atmos., **49**, 18-33, 1976.
- Bass, A.M., L.C. Glasgow, C. Miller, J.P. Jesson, D.L. Filkin, Temperature Dependent Absorption Cross-Sections for Formaldehyde: the Effect of Formaldehyde on Stratospheric Chlorine Chemistry, submitted for publication, 1979.
- Bates, D.R., A.E. Witherspoon, The Photochemistry of Some Minor Constituents of the Earth's Atmosphere ( $\text{CO}_2$ , CO,  $\text{CH}_4$ ,  $\text{N}_2\text{O}$ ), Mon. Not. R. Astron. Soc., **112**, 101-124, 1952.
- Bauer, K., W. Seiler, H. Giehl, CO Production by Higher Plants, Zeitschrift fur Pflanzenphysiologie, **94**, 219-230, 1979.
- Bidwell, R.G.S., D.E. Fraser, Carbon Monoxide Uptake and Metabolism by Leaves, Can. J. Bot., **50**, 1435-1439, 1972.
- Biermann, H.W., C. Zetzsch, F. Stuhl, On the Pressure Dependence of the Reaction of HO and CO, Ber. Bunsenges Phys. Chem., **82**, 633-639, 1978.
- Bourliere, F., M. Hadley, The Ecology of Tropical Savannas, Ann. Rev. Ecol. and Sys., **1**, 125-152, 1970.
- Brock, J.C., R.T. Watson, Laser Flash Photolysis of Ozone:  $\text{O}(^1\text{D})$  Quantum Yields in the Fall-Off Region, accepted for publication in Chem. Phys., 1980.
- Broeker, W.S., T.-H. Peng, Gas Exchange Rates Between Air and Sea, Tellus, **26**, 21-34, 1974.
- Bush, Y.A., D. Parrish, F.C. Fehsenfeld, Measurements of Trace Gases in the Troposphere, paper presented at CACGP Symposium on the Budgets and Cycles of Trace Gases in the Atmosphere, August 12-18, 1979, Boulder, Colorado.
- Chameides, W.L., S.C. Liu, R.J. Cicerone, Possible Variations in Atmospheric Methane, J. Geophys. Res., **82**, 1795-1798, 1977.
- Chatfield, R., H. Harrison, Tropospheric Ozone: 2. Variations Along a Meridional Band, J. Geophys. Res., **82**, 5969-5976, 1977.
- Cox, R.A., R.G. Derwent, M.R. Williams, Atmospheric Photo-oxidation Reactions: Rates, Reactivity and Mechanism for Reaction of Organic Compounds With FO Radicals, accepted for publication in Env. Sci. and Tech., 1979.
- Cox, R.A., G.S. Tyndall, Rate Constants for the Reactions of  $\text{CH}_3\text{O}_2$  in the gas Phase, Chem. Phys. Lett., **65**, 357-360, 1979.
- Crutzen, P.J., Photochemical Reactions Initiated by and Influencing Ozone in Unpolluted Tropospheric Air, Tellus, **26**, 47-57, 1974.
- Crutzen, P.J., The Role of NO and  $\text{NO}_2$  in the Chemistry of the Troposphere and Stratosphere, Ann. Rev. Earth Planet. Sci., **7**, 443-472, 1979.
- Crutzen, P.J., L.E. Heidt, J.P. Krasnek, W.H. Pollack, W. Seiler, Biomass Burning as a Source of Atmospheric Gases CO,  $\text{H}_2$ ,  $\text{N}_2\text{O}$ , NO,  $\text{CH}_3\text{Cl}$ , and COS, Nature, **282**, 253-256, 1979.
- Drummond, J.W., Atmospheric Measurements of Nitric Oxide Using a Chemiluminescent Detector, Ph.D. Thesis, Univ. of Wyoming, 1977.
- Dütsch, H., The Ozone Distribution in the Atmosphere, Can. J. Chem., **52**, 1491-1504, 1974.
- Dütsch, H., C.C. Ling, Six Years of Regular Ozone Soundings Over Switzerland, Pure & Appl. Geophys., **106-108**, 1151-1168, 1973.
- Eckholm, E., Planting for the Future: Forestry for Human Needs, Worldwatch Paper No. 26, Worldwatch Institute, Washington, D.C. 1979.
- Ehhalt, D.H., The  $\text{CH}_4$  Concentration Over the Ocean and Its Possible Variations With Latitude, Tellus, **30**, 169-176, 1978.
- Environmental Protection Agency, Compilation of Air Pollution Emission Factors, Publication AP-42, 3rd Edition, 1977.
- Environmental Protection Agency, Mobile Source Emission Factors, Publication EPA-400/9-78-006, 1978a.

- Environmental Protection Agency, 1974 National Emissions Report: National Emissions Data System of the Aerometric and Emissions Reporting System, Publication EPA-450/2-78-026, 1978b.
- Environmental Protection Agency, National Air Quality, Monitoring and Emissions Trends Report, Publication EPA-450/2-78-052, 1978c.
- Fabian, P., R. Borchers, K.H. Weiler, U. Schmidt, A. Volz, D.H. Ehhalt, W. Seiler, F. Muller, Simultaneously Measured Vertical Profiles of  $H_2$ ,  $CH_4$ ,  $CO$ ,  $N_2O$ ,  $CFCl_3$ , and  $CF_2Cl_2$  in the Midlatitude Stratosphere and Troposphere, J. Geophys. Res., **84**, 3149-3154, 1979.
- Fairchild, C.E., E.J. Stone, G.M. Lawrence, Photofragment Spectroscopy of Ozone in the UV Region 270-310 nm and at 600 nm, J. Chem. Phys., **69**, 3632-3638, 1978.
- Fishman, J., S. Solomon, P.J. Crutzen, Observational and Theoretical Evidence in Support of a Significant In-Situ Photochemical Source of Tropospheric Ozone, Tellus, **31**, 432-446, 1979.
- Food and Agricultural Organization, Production Yearbook, 1977, Food and Agricultural Organization, United Nations, 1978.
- Food and Agricultural Organization, Yearbook of Forest Product Statistics 1966-1977, Food and Agricultural Organization Forestry Series, United Nations, 1979.
- Gourou, P., The Tropical World (4th Edition), Wiley, New York, 1966.
- Graedel, T.E., Terpenoids in the Atmosphere, Rev. Geophys. Space Phys., **17**, 937-947, 1979.
- Grigg, D.B., The Agricultural Systems of the World, Cambridge University Press, 1974.
- Hameed, S., J.P. Pinto, R.W. Stewart, Sensitivity of the Predicted  $CO-OH-CH_4$  Perturbation to Tropospheric  $NO_x$  Concentrations, J. Geophys. Res., **84**, 763-768, 1979.
- Heidt, L.E., J.P. Krasnec, Tropospheric Distributions of  $CO$ ,  $CH_4$ ,  $CO_2$ , and  $N_2O$  in the Northern and Southern Hemispheres, EOS Trans., **59**, 1077, 1978.
- Holdren, M.W., H.H. Westberg, P.R. Zimmerman, Analysis of Monoterpene Hydrocarbons in Rural Atmospheres, J. Geophys. Res., **84**, 5083-5088, 1979.
- Howard, C.J., Temperature Dependence of the Reaction  $HO_2 + NO \rightarrow OH + NO_2$ , J. Chem. Phys., **71**, 2352-2359, 1979.
- Huebert, B.J., A.L. Lazrus, Tropospheric Gas Phase and Particulate Nitrate Measurements, submitted to J. Geophys. Res., 1980.
- Jaffe, L. S., Carbon Monoxide in the Biosphere: Sources, Distribution, and Concentration, J. Geophys. Res., **78**, 5293-5305, 1973.
- Jeong, K.-M., F. Kaufman, Rates of the Reactions of 1,1,1 Trichloroethane and 1,1,2-Trichloroethane with OH, Geophys. Res. Lett., **6**, 757-759, 1979.
- Junge, C., W. Seiler, P. Warneck, The Atmospheric  $^{12}CO$  and  $^{14}CO$  Budget, J. Geophys. Res., **76**, 2866-2879, 1971.
- Kajimoto, O., R.J. Cvetanovic, Absolute Quantum Yield of  $O(^1D)$  in the Photolysis of Ozone in the Hartley Band, Int. J. Chem. Kin., **11**, 605-612, 1979.
- Kelly, T.J., D.H. Stedman, Measurements of Trace Nitrogen Species at a Remote Mountain Site, Paper presented at CACGP Symposium on the Budgets and Cycles of Traces Gases in the Atmosphere, August 12-18, 1979, Boulder, Colorado.
- Klippel, W., P. Warneck, Formaldehyde in Rain Water and on the Atmospheric Aerosol, Geophys. Res. Lett., **5**, 177-179, 1978.
- Kurylo, M.J., P.C. Anderson, O. Klais, A Flash Photolysis Resonance Fluorescence Investigation of the Reaction  $OH + CH_3CCl_3 \rightarrow H_2O + CH_2CCl_3$ , Geophys. Res. Lett., **6**, 760-762, 1979.
- Lee, L.C., T.G. Slanger, Atmospheric OH Production: The  $O(^1D) + H_2O$  Reaction Rate, Geophys. Res. Lett., **6**, 165-166, 1979.
- Levy, H., II, Normal Atmosphere: Large Radical and Formaldehyde Concentrations Predicted, Science, **173**, 141-143.
- Levy, H., II, Photochemistry of the Lower Troposphere, Planet. Space Sci., **20**, 919-935, 1972.
- Liebl, K.H., W. Seiler,  $CO$  and  $H_2$  Destruction at the Soil Surface, in Microbial Production and Utilization of Gases, ed. H.G. Schlegel, G. Gottschalk, N. Pfennig, 215-230, 1976.
- Lin, C.L., W.B. DeMore, J. Photochem., **2**, 161-164, 1973.
- Linnenbom, V.J., J.W. Swinnerton, R.A. Lamontagne, The Ocean as a Source of

- Atmospheric CO, J. Geophys. Res., 78, 5833-5840, 1973.
- Logan, J.A., M. Prather, S. Wofsy, M. McElroy, unpublished manuscript, 1980.
- Logan, J.A., M.J. Prather, S.C. Wofsy, M.B. McElroy, Atmospheric Chemistry: Response to Human Influence, Phil. Trans. Roy. Soc., 290, 187-234, 1978.
- Lovelock, J.E., Methylchloroform in the Troposphere as an Indicator of OH Radical Abundance, Nature, 267, 32, 1977.
- McConnell, J.C., Atmospheric Ammonia, J. Geophys. Res., 78, 7812-7821, 1973.
- McConnell, J.C., M.B. McElroy, S.C. Wofsy, Natural Sources of Atmospheric CO, Nature, 233, 187-188, 1971.
- McFarland, M., D. Kley, J.W. Drummond, A.L. Schmeltekopf, R.H. Winkler, Nitric Oxide Measurements in the Equatorial Pacific Region, Geophys. Res. Lett., 6, 605-608, 1979.
- MacKay, C., M. Pandow, R. Wolfgang, On the Chemistry of Natural Radiocarbon, J. Geophys. Res., 68, 3929-3931, 1963.
- Mastenbrook, H.J., Water Vapor Observations at Low Middle and High Latitudes During 1964-1965, Naval Research Laboratory Report 6447, Washington, D.C., 1966.
- Mastenbrook, H.J., Water Vapor Distribution in the Stratosphere and High Troposphere, J. Atmos. Sci., 25, 299-311, 1968.
- Migeotte, M.V., The Fundamental Band of Carbon Monoxide at  $4.7\mu$  in the Solar Spectrum, Phys. Rev., 75, 1108-1109, 1949.
- Molina, M.J., G. Arguello, Ultraviolet Absorption Spectrum of Methyl Hydroperoxide Vapour, Geophys. Res. Lett., 6, 953-955, 1979.
- Moortgat, G.K., E. Kudzus, Mathematical Expression for the O('D) Quantum Yields from the O<sub>3</sub> Photolysis as a Function of Temperature (230-320K) and Wavelength (295-320 nm), Geophys. Res. Lett., 5, 191-196, 1978.
- National Aeronautics and Space Administration, The Stratosphere: Present and Future, NASA Reference Publication 1049, 1979.
- Neely, W.B., J.H. Plonka, Estimation of the Time-Averaged Hydroxyl Radical Concentration in the Troposphere, Environ. Sci. Tech., 12, 317-321, 1978.
- Niki, H., P.D. Makar, C.M. Savage, L.P. Breitenbach, Mechanism for Hydroxyl Radical Initiated Oxidation of Olefin-Nitric Oxide Mixtures in Parts Per Million Concentrations, J. Phys. Chem., 82, 135-137, 1978.
- Noxon, J.F., Tropospheric NO<sub>2</sub>, J. Geophys. Res., 83, 3051-3057, 1978.
- Nozhevnikova, A.N., L.N. Yurganov, Microbial Aspects of Regulating the Carbon Monoxide Content in the Earth's Atmosphere, Ch. 5 in Advances in Microbial Ecology, 2, ed. M. Alexander, Plenum Press, New York, 1978.
- Nye, P.H., D.J. Greenland, The Soil under Shifting Cultivation, Technical Communication No. 51, Commonwealth Bureau of Soils, England, 1960.
- Organization for Economic Cooperation and Development, Energy Statistics 1973-1975, Paris, 1976.
- Oort, A.H., E.M. Rasmusen, Atmospheric Circulation Statistics, National Oceanic and Atmospheric Administration Professional Paper 5, 1971.
- Openshaw, K., Wood Fuels the Developing World, New Scientist, 61, 271-272, 1974.
- Parkes, D.A., The Oxidation of Methyl Radicals at Room Temperature, Int. J. Chem. Kin., 9, 451-469, 1977.
- Persson, Reider, World Forest Resources, Dept. of Forestry Survey, Research Notes No. 17, Royal College of Forestry, Stockholm, 1974.
- Pittock, A.B., Climatology of the Vertical Distribution of Ozone Over Aspendale (38°S, 145°E), Quart. J. Roy. Met. Soc., 103, 575-584, 1977.
- Plumb, I.C., K.R. Ryan, J.R. Steven, M.F.R. Mulcahy, Kinetics of the reaction of CH<sub>3</sub>O<sub>2</sub> with NO, Chem. Phys. Lett., 63, 255-258, 1979.
- Pratt, R., P. Falconer, Circumpolar Measurements of Ozone Particles and Carbon Monoxide From a Commercial Airliner, J. Geophys. Res., 84, 7875-7882, 1979.
- Rasmusen, R.A., Isoprene: Identified As a Forest Type Emission to the Atmosphere, Env. Sci. & Tech., 4, 667-671, 1970.
- Rasmusen, R.A., F.W. Went, Volatile Organic Material of Plant Origin in the Atmosphere, Proc. Nat. Acad. Sciences, 53, 215-220, 1965.
- Reiter, E.R., Stratospheric-Tropospheric Exchange Processes, Rev. Geophys. Space Phys., 13, 459-474, 1975.
- Revelle, R., W. Munk, The Carbon Dioxide Cycle and the Biosphere, Energy and Climate, National Academy of Sciences, 1977.

- Robinson, E., Hydrocarbons in the Atmosphere, Pure & Appl. Geophys., 116, 372-384, 1978.
- Robinson, E., R.C. Robbins, Sources, Abundance and Fate of Gaseous Atmospheric Pollutants, Res. Proj. PR-6755, Supplemental Report, Stanford Research Institute, Menlo Park, Calif., 1969.
- Ruthenberg, H., Farming Systems in the Tropics, Clarendon Press, Oxford, Eng. 1976.
- Sanadze, G.A., On the condition of Evolution of the Diene  $C_5H_8$  (Isoprene) From Leaves, Fiziol. Rast., 11, 42-45 (English), 1963.
- Schiff, H.I., A. Pepper, B.A. Ridley, Tropospheric NO Measurements up to 7 km, J. Geophys. Res., 86, 7895-7897, 1979.
- Schuetzle, D., R.A. Rasmussen, The Molecular Composition of Secondary Aerosol Particles Formed from Terpenes, J. Air Pollut. Control. Assn., 28, 236-240, 1978.
- Seiler, W., The Cycle of Atmospheric CO, Tellus, 26, 118-135, 1976.
- Seiler, W., The Cycle of Carbon Monoxide in the Atmosphere, Proceedings of the ICESA Conference, 2, published by I.E.E.E., New York, 35/4/1-9, 1976.
- Seiler, W., H. Giehl, Influence of Plants on the Atmospheric Carbon Monoxide, Geophys. Res. Lett., 4, 329-332, 1977.
- Seiler, W., H. Giehl, H. Ellis, A Method for Monitoring of Background CO and First Results of Continuous CO Registrations on Mauna Loa Observatory, WMO Special Envir. Rept. No. 10, 31-39, 1976.
- Seiler, W., C. Junge, Carbon Monoxide in the Atmosphere, J. Geophys. Res., 75, 2217-2225, 1970.
- Seiler, W., F. Muller, H. Oeser, Vertical Distribution of Chlorofluoromethanes in the Upper Troposphere and Lower Stratosphere, Pure and Appl. Geophys., 116, 554-566, 1978.
- Seiler, W., U. Schmidt, New Aspects of CO and  $H_2$  Cycles in the Atmosphere, Proc. Int. Conf. on Structure, Composition, General Circulation of Upper and Lower Atmospheres and Possible Anthropogenic Perturbations, IAMAP, 192-222, 1974.
- Seiler, W., P. Warneck, Decrease of the Carbon-Monoxide Mixing Ratio at the Tropopause, J. Geophys. Res., 77, 3204-3214, 1972.
- Seiler, W., H. Zankl, Man's Impact on the Atmospheric CO Cycle, 2nd Symposium on Environmental Biogeochemistry, April 8-12th, 1975, Proc. Published by Ann Arbor Science, 1976.
- Simonaitis, R., J. Heicklen, The Mechanism of  $SO_2$  Oxidation by  $CH_3O_2$  Radicals: Rate Coefficients for the Reactions of  $CH_3O_2$  with  $SO_2$  and NO, Chem. Phys. Lett., 65, 361-365, 1979.
- Singh, H.B., Atmospheric Hydrocarbons: Evidence in Favor of Reduced Average Hydroxyl Radical Concentration in the Troposphere, Geophys. Res. Lett., 4, 101-104, 1977.
- Sparks, K.S., L. Carson, K. Shobatake, M.L. Kowalczyk, Y.T. Lee, Dynamics of Photodissociation of  $O_3$ , Paper presented at 7th Int. Symposium on Molecular Beams, Riva del Garda, Italy, May 28-June 1, 1979.
- Spencer, J.E., Shifting Cultivation in Southeastern Asia, Univ. of Calif. Publications in Geography, 19, Univ. Calif. Press, Berkeley, 1966.
- Streit, G.E., C.J. Howard, A.L. Schmeltekopf, J.A. Davidson, H.I. Schiff, Temperature Dependence of  $O(^1D)$  Rate Constants for Reactions With  $O_2$ ,  $N_2$ ,  $CO_2$ ,  $O_3$ , and  $H_2O$ , J. Chem. Phys., 65, 4761-4764, 1976.
- Sze, N.D., Anthropogenic CO Emissions: Implications for Atmospheric CO-OH- $CH_4$  Cycle, Science, 195, 673-675, 1977.
- United Nations, World Energy Supplies 1973-1976, Statistical Papers, Series J, No. 21, United Nations, New York, 1978a.
- United Nations, Yearbook of Industrial Statistics, 1976, United Nations, New York, 1978b.
- United States Government Printing Office, United States Standard Atmosphere Supplement, 1966.
- Volz, A., D.H. Ehhalt, R.G. Derwent, Seasonal and Latitudinal Variation of  $^{14}CO$  and the Tropospheric Concentration of OH Radicals, Manuscript in preparation.
- Watters, R.F., Shifting Cultivation in Latin America, Food and Agricultural Organization Paper No. 17, 1971.

- Webster, C.C., P.N. Wilson, Agriculture in the Tropics, Longmans, 1967.
- Weinstock, B., Carbon Monoxide: Residence Time in the Atmosphere, Science, 166, 224-225, 1969.
- Weinstock, B., H. Niki, T.Y. Chang, Chemical Factors Affecting the Hydroxyl Radical Concentration in the Troposphere, Adv. in Environ. Sci. Tech., in press, 1979.
- Welzel, K., P. Davids, Die Kohlenmonoxide Emissionen in der Bundes Republik Deutschland in den Jahren 1965, 1970, 1973 und 1974, Rat von Sachverständigen für Umweltfragen, 317, 1978.
- Went, F.W., Organic Matter in the Atmosphere, and its Possible Relation to Petroleum Formation, Proc. Nat. Acad. Sci., 46, 212-221, 1960.
- Whittaker, R.H., G.E. Likens, The Biosphere and Man, Ch. 15 in Primary Productivity of the Biosphere, ed. H. Lieth, R.H. Whittaker, 305-331, Springer Verlag, New York, 1975.
- Whittlesey, D., Fixation of Shifting Cultivation, Econ. Geog., 13, 139-154, 1937.
- Wilkness, D.E., R.A. Lamontagne, R.E. Larson, J.W. Swinnerton, C.R. Dickson, T. Thompson, Atmospheric Trace Gases in the Southern Hemisphere, Nature, 245, 45-57.
- Wilks, S.S., Carbon Monoxide in Green Plants, Science, 129, 964-966, 1959.
- Wofsy, S.C., Interactions of CH<sub>4</sub> and CO in the Earth's Atmosphere, Ann. Rev. of Earth & Planet. Sci., 4, 441-469, 1976.
- Wofsy, S.C., Temporal and Latitudinal Variations of Stratospheric Trace Gases: A Critical Comparison Between Theory and Experiment, J. Geophys. Res., 83, 364-378, 1978.
- Wofsy, S.C., J.C. McConnell, M.B. McElroy, Atmospheric CH<sub>4</sub>, CO and CO<sub>2</sub>, J. Geophys. Res., 77, 4477-4493, 1972.
- Yamate, G., State of the Art Report on Atmospheric Aspects of Forest Fires, ITT Research Institute Report No. C8269-2, 1975.
- Zafariou, O.C., J. Alford, M. Herrerra, G. Peltzer, A.M. Thompson, R.B. Gagosian, S.C. Liu, Formaldehyde in Remote Marine Air and Rain: Flux Measurements and Estimates, Submitted for publication to Geophys. Res. Lett., 1980.
- Zimmerman, P.R., R.B. Chatfield, J. Fishman, P.J. Crutzen, and P.L. Hanst, Estimates on the Production of CO and H<sub>2</sub> from the Oxidation of Hydrocarbon Emissions from Vegetation, Geophys. Res. Lett., 5, 679-682, 1978.

## SOURCES AND SINKS FOR NITROUS OXIDE

Michael B. McElroy

Center for Earth and Planetary Physics  
Harvard University, Cambridge, Massachusetts 02138

### Abstract

Factors which influence the budget of atmospheric  $N_2O$  are discussed. The ocean is shown to provide a source of less than  $10^7$  tons  $N\ yr^{-1}$ , most probably less than  $4 \times 10^6$  tons  $N\ yr^{-1}$ . The bulk of oceanic production is attributed to nitrification and nitrification may be important also for soils. The global source of  $N_2O$  could be as large as  $5 \times 10^7$  tons  $yr^{-1}$  but is probably closer to  $1 \times 10^7$  tons  $N\ yr^{-1}$ . Human activity, associated particularly with combustion and with production of food and disposal of organic wastes, could lead to a significant rise in  $N_2O$  and there are indications that such an increase may have been detected by Weiss (1979), Rasmussen (1979) and Goldan et al. (1980).

INTRODUCTION: Nitrous oxide is the twelfth most abundant constituent of the atmosphere, or the eighth most abundant if we exclude the noble gases Ar, Ne, He, and Kr. It accounts for about  $4 \times 10^{-7}$  of the total nitrogen of the atmosphere, contributing approximately  $1.5 \times 10^9$  tons N to a reservoir of  $3.9 \times 10^{15}$  tons N. It is removed, according to present ideas, mainly by photolysis,



at wavelengths below  $2400\text{\AA}$ , with additional loss due to



and



Reactions (1)-(3) account for a sink of atmospheric  $N_2O$  equivalent to  $1.1 \times 10^7$  tons  $N\ yr^{-1}$ , with approximately 87% of the loss due to (1). If we define a lifetime  $\tau(\text{yr})$  for  $N_2O$  by the relation

$$\tau = \frac{N}{L} \quad (4)$$

where  $N$  denotes the abundance of the gas in the atmosphere (tons  $N$ ), with  $L$  the rate at which it is removed (tons  $N \text{ yr}^{-1}$ ), we may conclude immediately that  $\tau$  cannot exceed 135 years. The rate for production of  $N_2O$  must be at least as large, in steady state, as the rate at which the gas is consumed by (1)-(3). It follows that global production of  $N_2O$  must equal or exceed  $1.1 \times 10^7$  tons  $N \text{ yr}^{-1}$ . According to present ideas most of this source can be attributed to reactions mediated by the biosphere.

The role of the biosphere as a source for  $N_2O$  was recognized first by Bates and Witherspoon (1952). Bates and Hays (1967) reported an initial attempt to compute the variation of  $N_2O$  with altitude. Crutzen (1971), McElroy and McConnell (1971) and Nicolet and Vergison (1971) discussed the importance of (3) as a source for stratospheric  $NO$ , while Crutzen (1970) and Johnston (1971) drew attention to the role which  $NO$  might play in the chemistry of stratospheric  $O_3$ . Nitric oxide acts as a catalyst for recombination of odd oxygen, through



followed by



Thus a change in  $N_2O$  could lead to a change in  $NO$ , with consequent impact on  $O_3$  (Crutzen, 1974; McElroy, 1974). McElroy (1974, 1976a) and McElroy et al. (1977) argued that stress on the nitrogen cycle imposed by agriculture could cause the concentration of  $N_2O$  to double in less than 100 years. The significance of the agricultural influence for global nitrogen was discussed earlier by Delwiche (1970).

Nitrogen is essential for life. Yet, in the form in which it may be utilized by the biosphere, it is in remarkably limited supply. Before the element can be incorporated into the tissue of living organisms it must be fixed, i.e. it must be transformed from the relatively abundant though inert form  $N_2$  to more useful compounds such as  $NH_4^+$  and  $NO_3^-$ . Nitrogen is fixed in nature by lightning, by blue-green algae and by bacteria functioning either alone or in symbiotic association with certain plants, notably legumes. Man contributes to the pool of fixed nitrogen in a number of ways. Fixation by biological processes in land devoted to agriculture, crops and pasture, accounts for  $9 \times 10^7$  tons  $N \text{ yr}^{-1}$  (Burns and Hardy, 1975) and there are reasons to believe that biological fixation was much less effective for these lands in the pre-industrial pre-agricultural era, about  $6 \times 10^7$  tons  $N \text{ yr}^{-1}$ . The larger rate in the present system may be attributed mainly to cultivation of legumes. Fixation of nitrogen by the biosphere as a whole occurs at a rate of about  $1.4 \times 10^8$  tons  $N \text{ yr}^{-1}$  (Burns and Hardy, 1975). Manufacture of chemical fertilizer and combustion of fossil fuel provide additional sources of magnitude  $4.2 \times 10^7$  and  $2.3 \times 10^7$  tons  $N \text{ yr}^{-1}$ , respectively (Logan et al., 1978). We estimate a globally integrated source for fixed nitrogen of about  $2.2 \times 10^8$  tons  $N \text{ yr}^{-1}$ . It appears that as much as 40% of this source may be attributed either directly or indirectly to the activity of man.

The concerns raised by Crutzen (1974) and McElroy (1974) reflect a recognition that the human influence on nitrogen is growing and likely before long to dominate at least the source side of the budget for fixed nitrogen. The conclusions reached by McElroy (1974, 1976a,b) and McElroy et al. (1977) regarding  $N_2O$  assume that the nitrogen cycle should adjust relatively rapidly to additional input, that a significant fraction of the extra nitrogen should be returned to the atmosphere as either  $N_2$  or  $N_2O$  on a time scale of less than 100 years.

According to present views, fixation of nitrogen is balanced by denitrification, a term used to describe the production of nitrogen gas during bacterially mediated reduction of nitrite and nitrate. As we shall see, most of the world's fixed nitrogen resides in the ocean, as nitrate. Assessment of the human influence on  $N_2O$  requires therefore a relatively complete model for global nitrogen. This paper offers a brief account of research intended to define at least the elements of such a model. We begin with a discussion of the nitrogen cycle.

**THE NITROGEN CYCLE.** Major components of the nitrogen cycle are illustrated in Figure 1. Fixation takes place mainly on land, according to present ideas, and the nitrogen economy of the ocean is maintained primarily by transfer from the land-based biosphere with perhaps a small contribution from lightning. Transfer may occur in either of two ways. The first involves transport of nitrate and dissolved organic material by rivers. The second involves air-borne transport of gaseous forms of fixed nitrogen, including  $NH_3$ ,  $NO$ ,  $NO_2$ ,  $HNO_3$  and PAN (peroxyacetyl nitrate).

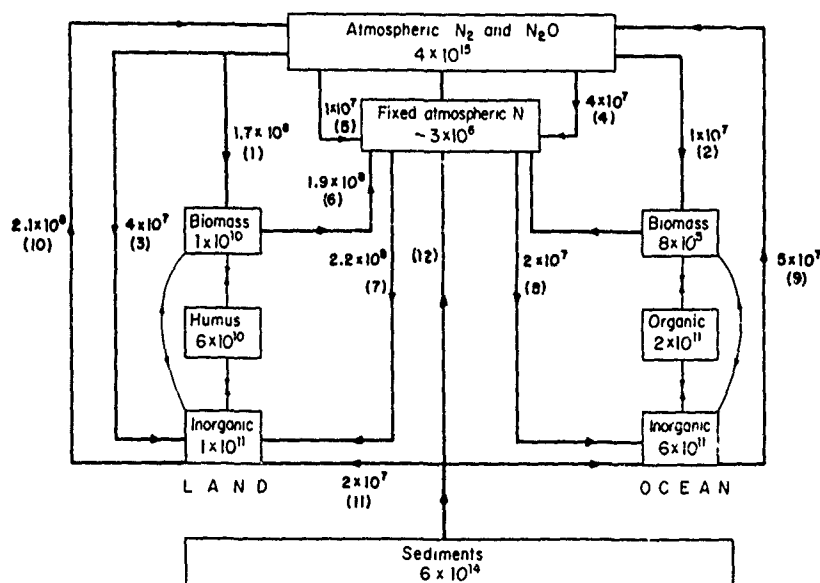


Figure 1. Representation of the nitrogen cycle. Numbers in rectangular boxes give the abundance of N measured in metric tons. Transfer rates are given in tons per year, and the numbers in parentheses define the transfer reactions as follows: (1) land biological fixation; (2) marine biological fixation; (3) fixation in chemical fertilizer; (4) fixation due to combustion; (5) fixation due to lightning; (6) transfer due to volatilization of  $NH_3$ ; (7) transfer due to rain over land; (8) transfer due to rain over sea; (9) marine denitrification; (10) land denitrification; (11) transfer from land to sea in river run-off; (12) transfer due to raising of sediments, with a comparable amount due to deposition (from McElroy, 1976a).



Ammonia arises due to volatilization of  $\text{NH}_4^+$  under alkaline conditions,



It is oxidized in the atmosphere, where it may play an important role in the budget of tropospheric  $\text{NO}_x$ . The biosphere provides additional sources of NO and  $\text{NO}_2$ , while  $\text{HNO}_3$  and PAN are formed mainly by photochemical reactions.

Fixed nitrogen is removed from the atmosphere by rain and by heterogeneous reactions at the surface. The data in Figure 1 imply that rates for transfer of fixed N from land to ocean by rivers and air are similar, about  $2 \times 10^7$  tons  $\text{N yr}^{-1}$ . It is obvious however that neither rate is defined to better than about a factor of 3. It may be possible indeed to place more realistic constraints on the oceanic source for fixed N from analysis of the oceanic sink. It appears that denitrification is confined to a relatively small number of sites in the ocean, primarily those associated with regions of upwelling. The Eastern Tropical Pacific is particularly important and could account for more than half of the total sink for oceanic N. Elkins (1978) estimates a sink of about  $2 \times 10^7$  tons  $\text{N yr}^{-1}$  for waters off Peru, while Codispoti and Richards (1976) report loss of similar magnitude from the North Tropical Pacific.

The ocean contains a vast quantity of fixed nitrogen, enough to satisfy needs of the global biosphere for more than 5000 years. Most of this nitrogen resides in the deep ocean, below the thermocline. Deep waters exchange however with surface waters in a time of order  $10^3$  years, with corresponding transfer of nitrogen. Upper layers of the ocean benefit from a source of nitrogen of magnitude  $6 \times 10^8$  tons  $\text{yr}^{-1}$ , approximately 10 times the supply from fertilizer and combustion, or 30 times the input from rivers. The fate of this nitrogen is obviously a matter of some importance. It could dominate the budget of atmospheric  $\text{N}_2\text{O}$  even if the fraction of N transformed to  $\text{N}_2\text{O}$  were as small as 2%.

Early measurements and analysis by Hahn (1974, 1975) appeared to indicate that the ocean should play a dominant role for  $\text{N}_2\text{O}$ . He estimated a flux of  $\text{N}_2\text{O}$  from the world's oceans to the atmosphere of magnitude  $8.5 \times 10^7$  tons  $\text{N yr}^{-1}$ . His estimate was based however on a rather difficult extrapolation of data from the North Atlantic. Hahn used measurements carried out in late spring and summer, during the years 1969-1971. Data were obtained for some 42 stations, and included a few measurements of the concentration of  $\text{N}_2\text{O}$  to depths of about 3000 m. Surface waters were analysed for  $\text{N}_2\text{O}$  at 33 distinct locations. Analysis of these data indicated that shallow waters of the North Atlantic were apparently supersaturated in  $\text{N}_2\text{O}$  by about 24% over the period covered by the observations. Largest supersaturations, exceeding 75%, were detected in warm waters at  $0.6^\circ\text{N}$  latitude and at  $25.6^\circ\text{N}$ . An average of all of the surface data obtained at latitudes higher than  $37^\circ\text{N}$ , some 29 samples, showed supersaturation by about 13%, a rather small value when one considers the uncertainty in Hahn's measurements (about 10%), inaccuracies in then available data for the solubility of  $\text{N}_2\text{O}$  in sea water (about 5%), and complications due to physical effects (entrainment of bubbles, warming of surface waters, etc.) which might influence the concentration of dissolved gas (see McElroy et al., 1976).

Analysis of data from latitudes below  $37^\circ\text{N}$ , four measurements, indicated supersaturation by about 80% and Hahn's estimate for the flux of  $\text{N}_2\text{O}$  from the world's oceans to the atmosphere was based on an assumption that these data might be considered representative, i.e. that surface waters of the ocean could be characterized on a global scale by a supersaturation of 80%. It is obvious, however, that one could arrive at much smaller estimates for the flux of  $\text{N}_2\text{O}$  if one were to use Hahn's high latitude measurements rather than his low latitude data as a basis for extrapolation. Hahn thought that his estimate for the global flux should be accurate to within an order of magnitude,

$2.9 \times 10^7$  to  $2.9 \times 10^8$  tons  $\text{N yr}^{-1}$ . Hahn and Junge (1977), allowing for variations in the rate of gas transfer due to changes in wind speed, lowered their estimate for the most probable flux to  $4.8 \times 10^7$  tons  $\text{N yr}^{-1}$ , quoting a range of values from  $2.9 \times 10^7$  to  $7.6 \times 10^7$  tons  $\text{N yr}^{-1}$ . Yoshinari (1976) on the other hand concluded that the open ocean was at most a small source of  $\text{N}_2\text{O}$ , favoring a flux of about  $10^6$  tons  $\text{N yr}^{-1}$ . By far the most extensive set of oceanic surface measurements are those by Weiss (1979). His data cover cruise tracks in excess of 60,000 km. He finds a mean supersaturation of 4%, from which he estimates a flux of about  $4 \times 10^6$  tons  $\text{N yr}^{-1}$ . We regard this as the best current estimate for the marine source. The net source could indeed be smaller, in that physical effects could account for at least some of the excess  $\text{N}_2\text{O}$  seen by Weiss (1979).

One might hope using surface measurements of dissolved gas to define the magnitude of the oceanic source of atmospheric  $\text{N}_2\text{O}$  to within perhaps a factor of 2. Weiss's work makes a significant contribution towards this goal. It is imperative however that we go further. We must strive to develop an understanding of the nature and function of the chemical and biological reactions which determine the source of  $\text{N}_2\text{O}$  from a variety of natural systems. It is obvious that we have much to learn in this respect from oceanic measurements of  $\text{N}_2\text{O}$  and related species such as  $\text{O}_2$ ,  $\text{NH}_4^+$ ,  $\text{NO}_2^-$ ,  $\text{NO}_3^-$ , and  $\text{PO}_4^{3-}$ .

Figure 2 shows a selection of data reported by Elkins et al. (1978) for  $\text{N}_2\text{O}$ ,  $\text{NO}_3^-$  and  $\text{PO}_4^{3-}$  in the Central Pacific. Data were collected between 2 and 18 December 1977 on the Norpax Leg II cruise of the RV Kana Keoki. Samples were taken to depths of 1000 m every degree of latitude along the  $150^\circ\text{W}$  meridian between  $17^\circ\text{S}$  and  $20^\circ\text{N}$ . The cruise provided measurements of  $\text{O}_2$ ,  $\text{NO}_2^-$ ,  $\text{NH}_4^+$ ,  $\text{SiO}_2$ , temperature and salinity, in addition to  $\text{N}_2\text{O}$ ,  $\text{NO}_3^-$  and  $\text{PO}_4^{3-}$  (Elkins, 1978).

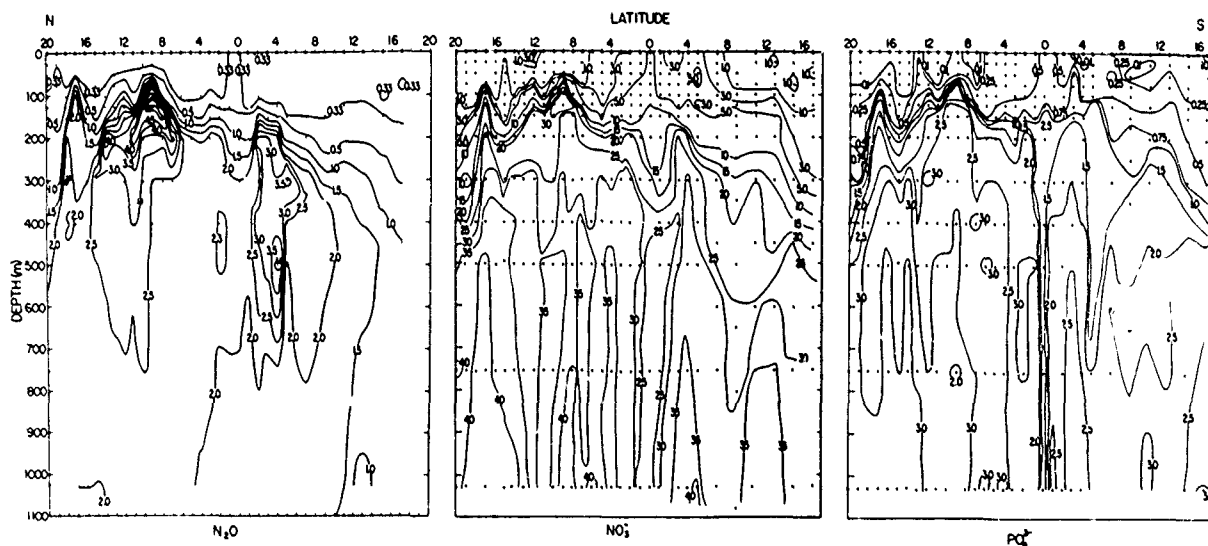


Figure 2. Cross sections for (a)  $\text{N}_2\text{O}$  ( $\mu\text{g l}^{-1}$ ); (b)  $\text{NO}_3^-$  and (c)  $\text{PO}_4^{3-}$  ( $\mu\text{g-atm l}^{-1}$ ) along the  $150^\circ\text{W}$  meridian in the tropical Central Pacific Ocean. Experimental precision is better than 3% for  $\text{N}_2\text{O}$  and  $0.1 \mu\text{g-atm l}^{-1}$  for  $\text{NO}_3^-$  and  $\text{PO}_4^{3-}$  (from Elkins et al., 1978).

Cross sectional contours for the various species measured in the Central Pacific exhibit a number of similar structures. Highest concentrations of  $\text{N}_2\text{O}$  were observed at  $9^\circ\text{N}$  at 120 m in an intense feature associated most

probably with upwelling in the north tropical convergence zone. Structure analogous to that seen for  $N_2O$  is apparent also in contours for temperature,  $O_2$ ,  $NO_3^-$ ,  $NO_2^-$ , and  $PO_4^{3-}$ , and similar behavior was observed at  $17^\circ N$  (128 m) and  $4^\circ S$  (502 m). Highest concentrations of  $N_2O$  are associated with regions of low  $O_2$ , as shown in Figure 3.

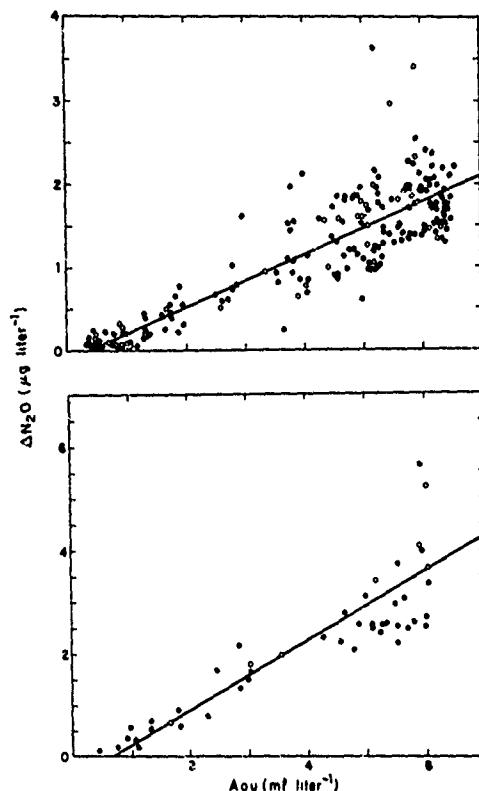
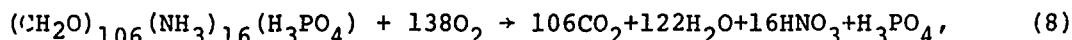


Figure 3.  $N_2O$  observations (Fig.2) expressed as excess  $N_2O$  plotted against apparent oxygen utilization. Most of the data are shown in (a) but data from the active regions at  $17^\circ$ ,  $13-8^\circ N$ , and  $2-4^\circ S$  are plotted separately in (b). The straight lines are least-squares fits, which yield r.m.s. deviations of  $0.37$  and  $0.6 \mu g \text{ l}^{-1}$  for (a) and (b) respectively. Data points from the mixed layer ( $AOU \text{ } 0.3 \text{ ml l}^{-1}$ ) are not included. The measured concentration of atmospheric  $N_2O$  was 291 parts per  $10^9$  (by volume) (p.p.b.) (from Elkins et al., 1978).

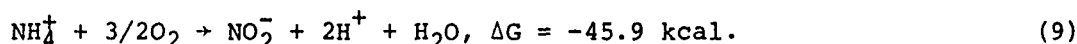
Figure 3 shows the relationship between  $\Delta N_2O$  and  $\Delta O_2$ , where  $\Delta X$  defines the excess of  $X$  with respect to the atmosphere, assuming equilibrium at the local temperature and salinity. The quantity of  $\Delta N_2O$  provides a measure of the net amount of  $N_2O$  which accumulated in the water mass since last contact with the atmosphere. By the same token  $-\Delta O_2$ , the apparent oxygen utilization or AOU, measures the quantity of oxygen consumed over the same period due to oxidation of organic matter. Figure 3 is limited to data taken from regions below the photic zone. Information from active regions at  $17^\circ N$ ,  $8^\circ-13^\circ N$  (above 200 m) and  $2^\circ-4^\circ S$  (above 500 m) are shown separately in Figure 3b. The apparently linear nature of the relationship between  $\Delta N_2O$  and  $-\Delta O_2$  as shown in Figure 3 suggests that production of  $N_2O$  may be associated in some

way with the oxidation of organic material. Elkins et al. (1978) argued that oxidation of ammonium and amino nitrogen, nitrification, could represent a dominant source for marine  $N_2O$ , as suggested elsewhere by Hahn (1974, 1975), Yoshinari (1976) and Cohen and Gordon (1978). If we assume that the C:N:P ratios in marine organic material are similar to values quoted by Redfield et al. (1963), and if we represent the stoichiometry of decay by



then the data in Figure 3 may be used to obtain a corresponding yield for  $N_2O$ . Elkins et al. (1978) estimate that on average 1 molecule of  $N_2O$  is formed for every 709 molecules of  $NH_3$  which undergo oxidation. Interpretation of the marine data in terms of a source due to nitrification finds support in recent laboratory studies of nitrifying organisms carried out by Goreau et al. (1980).

Goreau et al. studied a number of organisms, including Nitrosococcus oceanus, an ammonium oxidizing bacterium isolated from open waters of the Atlantic Ocean near Barbados (Watson, 1965). *N. oceanus* is an aerobic chemoautotroph which satisfies its energy requirements through the overall reaction



A 0.5 ml inoculum ( $\sim 10^7$  cells) was obtained by centrifuging a sample derived from an actively growing culture. The inoculum was introduced into a 550 ml distillation flask containing 300 ml of an autoclaved buffered growth medium. The apparatus provided continuous equilibration of the medium with a slow flow ( $\sim 0.14 \text{ cm}^3 \text{ sec}^{-1}$ ) of  $N_2O$ -free synthetic air, with an arrangement similar to that described by Barbaree and Payne (1967). The head space of the distillation flask was exhausted directly to the sample loop of an electron capture gas chromatograph and samples of medium were withdrawn periodically through a 3-way port allowing analysis for  $NO_2^-$  in addition to  $N_2O$ .

Experiments were carried out in triplicate over a period of 8 days, with results shown in Figure 4. A fourth flask, treated with  $HgCl_2$  served as a sterile control. Live flasks showed consistent and smooth production of  $NO_2^-$  and  $N_2O$  following onset of exponential growth after about 24 hours. The parallel behavior of  $NO_2^-$  and  $N_2O$  shown in Figure 4 implies that production of  $N_2O$  represents a relatively constant fraction of nitrogen oxidized, at least during the period of growth. These data imply a yield for  $N_2O$ , defined as the number of moles of N appearing as  $N_2O$  associated with production of one mole of  $NO_2^-$ , of  $2.1 (\pm 0.3) \times 10^{-3}$ . By way of comparison, results from the Central Pacific imply a yield of  $2.8 (\pm 0.3) \times 10^{-3}$ , while data from the Atlantic (Yoshinari, 1976; Cohen and Gordon, 1978) give  $2 \times 10^{-3}$ , in obviously excellent agreement with the laboratory value.

It is possible now to place an upper limit on the magnitude of the source of  $N_2O$  which might arise due to marine nitrification. We obtain a limit of  $10^7$  tons N  $yr^{-1}$  for  $N_2O$ , assuming a C:N ratio of 6.6 for the marine biosphere (Redfield et al., 1963) together with a rate for fixation of carbon of  $2 \times 10^{10}$  tons C  $yr^{-1}$  (Koblentz-Mishke et al., 1970; Whitaker and Likens, 1973). Evidently the source could be much smaller if growth of phytoplankton were to occur using reduced rather than oxidized forms of nitrogen.

It appears that denitrification may represent a sink rather than source for marine  $N_2O$ . Figure 5 shows vertical profiles for  $N_2O$ ,  $O_3$ ,  $NO_3^-$ ,  $NO_2^-$  and  $NH_4^+$  from a representative station in the upwelling region off the coast of Peru. Data were taken from the R.V. Knorr between March 20 and 31, 1978 (Elkins et al., 1978). The dashed line illustrates concentrations of  $N_2O$  expected on the basis of the empirical relation between  $\Delta N_2O$  and  $\Delta O_2$  suggested by results from the Central Pacific. The empirical formula provides good agreement with  $N_2O$  measurements below 300 m, and is in accord also with measurements between

30 and 50 m. A major discrepancy exists, however, between 100 and 300 m where concentrations of  $O_2$  lie below  $0.1 \text{ ml l}^{-1}$ . Concentrations of  $N_2O$  observed in this region are undersaturated with respect to the atmosphere, providing clear evidence for a local sink.

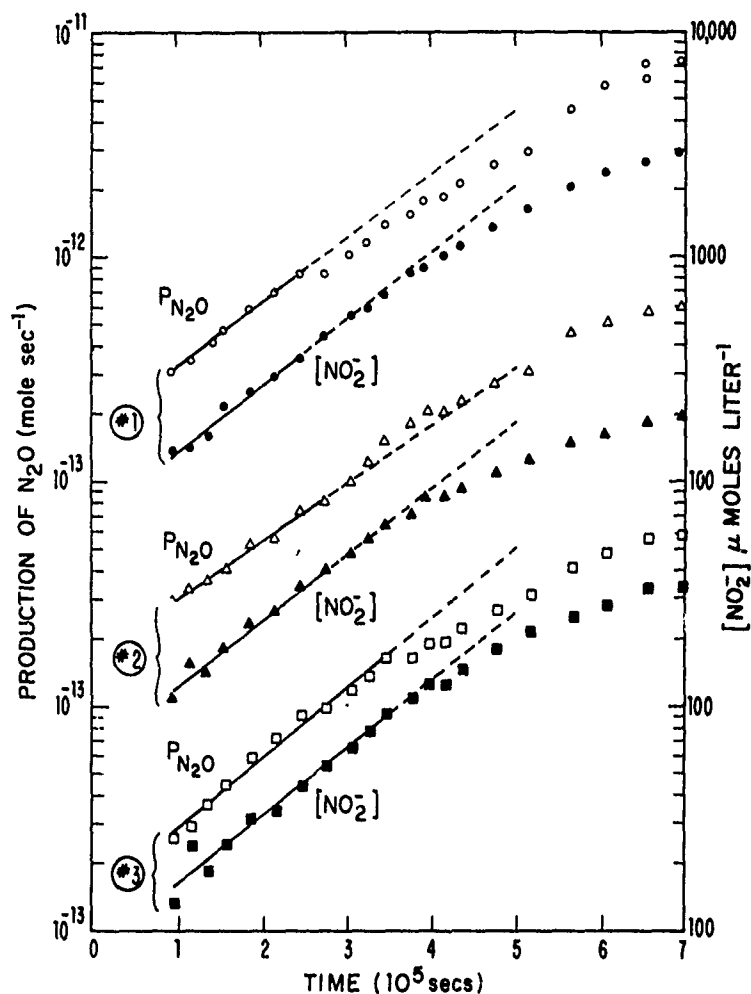


Figure 4. Production rates for  $N_2O$  (moles/sec) and concentrations of dissolved  $NO_2^-$  ( $\mu\text{M liter}^{-1}$ ) as functions of time after inoculation. Results for sequential flasks have been displaced by one decade for ease of presentation. The solid lines represent least-squares fits of the form  $\ln x = \Gamma t + \ln A$  with estimated standard errors of slopes ( $\Gamma$ ) smaller than  $\pm 10\%$  in all cases. Curves were fitted to the exponential portion of the logistic growth curve. Note that the production rate for  $NO_2^-$  parallels that for  $N_2O$  over the time period  $1-4 \times 10^5$  secs after inoculation. The flux of  $N_2O$  is measured with a precision of about  $10^{-13}$  moles/sec. (from Goreau et al., 1980).

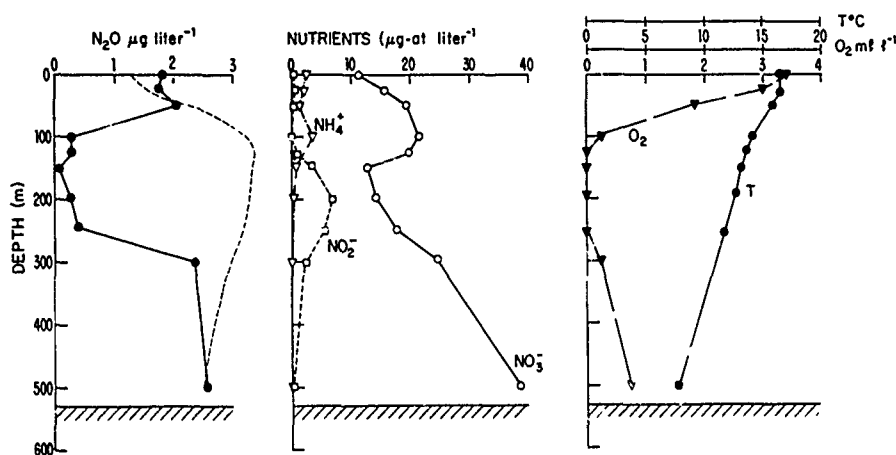
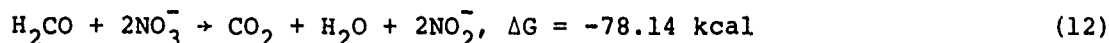
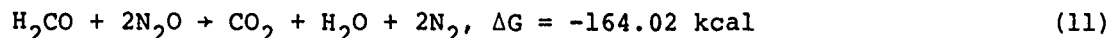
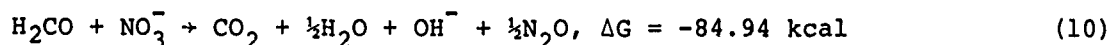
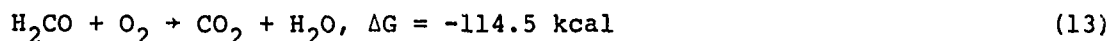


Figure 5. Depth profiles for  $N_2O$ , mineral nitrogen, oxygen and temperature for a station at  $15^{\circ}10.6'S$ ,  $75^{\circ}35.5'W$ , in the region of Peruvian upwelling. The dashed line represents the relationship  $N_2O = -0.46 + 0.180 + 0.027T$  AOU (from Elkins et al., 1978).

Denitrification involves reduction of nitrogen and there are several important paths which may be summarized as follows:

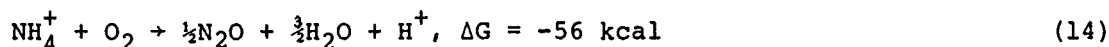


Note that respiration of  $N_2O$  is relatively efficient. It competes favorably, at least from an energetic viewpoint, with



It appears therefore that the bulk of  $N_2O$  formed in (10) may be consumed in (11). Elkins (1978) estimates a net source for atmospheric  $N_2O$  from waters off Peru of only  $3.5 \times 10^4$  tons  $N \text{ yr}^{-1}$ , suggesting that these waters, surface area  $8500 \text{ km}^2$ , play a minor role for  $N_2O$ . Loss of nitrogen as  $N_2$  is much larger, as much as  $2.5 \times 10^7$  tons  $N \text{ yr}^{-1}$  as noted earlier.

In summary, it appears that the bulk of oceanic  $N_2O$  is formed by nitrification,



rather than denitrification. The net globally integrated source lies probably between  $1$  and  $5 \times 10^6$  tons  $N \text{ yr}^{-1}$  and is surely less than  $10^7$  tons  $N \text{ yr}^{-1}$ , in conflict with much higher values given by Hahn (1974, 1975) and Hahn and Junge (1977). The earlier conclusions were based on extrapolation from an exceedingly limited data base and are superseded by more recent work drawing on more extensive measurements, combined with improved appreciation of the marine nitrogen cycle. The ocean can account for at most 50% of the net quantity of  $N_2O$  consumed by the stratosphere. It remains to define the magnitude and nature of the land based source. Measurements of the spatial and temporal variation of  $N_2O$  in the air can make an important contribution

in this regard.

MAGNITUDE OF THE GLOBAL SOURCE FOR ATMOSPHERIC  $N_2O$ : Stratospheric photolysis and reaction with  $O(^1D)$  constitute the most important identified sinks for atmospheric  $N_2O$ . They account for removal of  $1.1 \times 10^7$  tons  $N \text{ yr}^{-1}$  and allow us to set an upper limit of 135 years on the lifetime for atmospheric  $N_2O$ . We know that denitrification can provide an important sink for  $N_2O$  in limited regions of the ocean (Elkins et al., 1978; Cohen, 1978). It is likely, however, that most of the  $N_2O$  consumed in anoxic waters is produced in situ. As a consequence these systems represent at most a small sink for atmospheric  $N_2O$ , except under rather special circumstances where waters low in  $N_2O$  reach the surface. Several such systems were discussed by Kaplan et al. (1978) and Elkins et al. (1978). Their significance for  $N_2O$  on a global scale is unclear however.

Land-based sources of  $N_2O$  could be quite large. Breitenbeck et al. (1980) found surprisingly high fluxes of  $N_2O$  from unfertilized soils in Iowa, emissions at a rate of  $330 \text{ g N hectare}^{-1}$  over a 96 day period, and Goreau (1979) observed releases of similar magnitude from undisturbed forest soils in New England. If we assume that the Iowa results are representative, we may infer a global source of  $N_2O$  from soils of magnitude  $1.9 \times 10^7$  tons  $N \text{ yr}^{-1}$ , more than enough to account for the quantity of  $N_2O$  consumed in the stratosphere. Breitenbeck et al. (1980) observed a significant enhancement in production of  $N_2O$  following application of fertilizer, as much as a factor of 14 over 25 days after treatment with  $250 \text{ kg N hectare}^{-1}$  as ammonium sulfate. The total quantity of fertilizer nitrogen converted to  $N_2O$  over a period of 96 days was relatively small, however, in the range of 0.11 to 0.18% of the amount applied.

Observations defining the level and variability of the concentration of an atmospheric gas may be used to obtain valuable information on the magnitude and spatial distribution of its source and/or sink. The problem was discussed extensively by Junge (1974) and by Hahn and Junge (1977). Variations in global  $N_2O$  satisfy the equation

$$\frac{dM}{dt} = P - L \quad (15)$$

where  $M$  measures abundance (tons  $N$ ), and  $P$  and  $L$  are production and loss rates (tons  $N \text{ yr}^{-1}$ ) respectively. An average of (15) with respect to time over an adequately long interval  $\tau$  gives

$$\bar{P} = \bar{L} = \bar{M} T^{-1} \quad (16)$$

where

$$\bar{X} = \frac{1}{\tau} \int_c^\tau X(t) dt. \quad (17)$$

Equation (16) serves to define the residence time or turnover time  $T$ , a concept of particular use when the source and sink are reasonably steady. In this case

$$|P - L| \ll \bar{L} = \bar{M} T^{-1} \quad (18)$$

and (15) and (18) may be combined to yield

$$T \ll \frac{\bar{M}}{|\Delta M|} \Delta t \quad (19)$$

where  $\Delta t$  denotes a time interval short compared to  $T$ .

More generally, the concentration of a gas is expected to show maximum variability when  $T$  is short or where measurements are carried out in the vicinity

of either a strong source or sink. Junge (1974) argued that the mean standard deviation,  $\bar{\sigma}_d$ , of concentrations measured at a remote station should vary inversely with  $T$ . He showed that results for a variety of tropospheric gases satisfy the simple relation

$$\bar{\sigma}_d T = 0.14 \quad (20)$$

where  $\bar{\sigma}_d$  is expressed as a percentage and  $T$  is measured in years. Measurements of atmospheric  $N_2O$  available in 1976 were reviewed by Hahn and Junge (1977). They noted that standard deviations of individual data sets ranged from 9.6% (Schutz et al., 1970) to less than 0.5% (Craig et al., 1976), a spread which, according to (20), would permit lifetimes for  $N_2O$  as short as 1.5 years or longer than 28 years. Corresponding values for production and loss of  $N_2O$  could be as large as  $10^9$  tons  $N \text{ yr}^{-1}$ , or as small as  $10^7$  tons  $N \text{ yr}^{-1}$ , the limiting magnitude of the flux required to supply the stratosphere.

There are difficulties associated with the use of (20) as a quantitative device for determination of  $T$ . It is not easy to distinguish between intrinsic, atmospheric, and extrinsic, instrumental, sources of variability. The observed residual standard deviation must include inherently unknown contributions from random measurement errors. These errors may be minimized with experience, as shown by Goldan et al. (1978). One is tempted therefore to adopt as superior the set of data characterized by the smallest mean standard deviation of measurement. Laurels in this case would appear to belong to Craig et al. (1976). If the sweepstakes are restricted, however, to work documented in the literature, the spoils should be shared by Rasmussen et al. (1976), Pierotti and Rasmussen (1977), and Goldan et al. (1980). Their results, interpreted using (20), suggest a lifetime for  $N_2O$  in excess of 15 years. It would follow that the average value of the global source for  $N_2O$  should lie between  $10^7$  and  $10^8$  tons  $N \text{ yr}^{-1}$ .

Hahn and Junge (1977) favored a range of lifetimes between 4 and 12 years with a preferred value of 8 years. They attached relatively little weight to the measurements of Craig et al. (1976), but were influenced to a considerable extent by results obtained by Schutz et al. (1970) and Goody (1969) between 1966 and 1969. These data have particular significance in that they show evidence for a simultaneous rise in concentrations of  $N_2O$  measured in Milton, Massachusetts, U.S.A. and in Mainz and Schauinsland, West Germany. Concentrations of  $N_2O$  appeared to increase by about 15% over approximately a 3 month period between January and March 1968. If we assume that the rise encompassed half of the northern hemisphere, a reasonable assumption given the spatial separation of Boston and Mainz, we would need to account for an impulsive source of  $N_2O$  of magnitude  $5-6 \times 10^7$  tons  $N$ , quite a demanding task as we shall see when we attempt to identify the nature and location of the extra source.

One might hypothesize that the rise in  $N_2O$  observed in Boston and Mainz resulted from a temporary increase in the rate for production of  $N_2O$  from soils in North America. We would require in this case additional production of about  $2 \times 10^{11}$  molecules  $\text{cm}^{-2} \text{ sec}^{-1}$  averaged over the continent, approximately 10 times the flux observed from unfertilized soils in Iowa by Breitenbeck et al. (1980). It would seem unlikely that the enhanced flux should extend over the entire continent. If we assume that it emanated from 10% of the land area we would require production of  $2 \times 10^{12}$  molecules  $\text{cm}^{-2} \text{ sec}^{-1}$ , larger by almost a factor of 50 than the highest fluxes observed from heavily fertilized plots by Breitenbeck et al. (1980) and McKenney and Wade (1978). It would seem most improbable that this situation should prevail over 10% of the land area of the North American continent for as long as 3 months during the winter of 1968.

The ocean contains a relatively large concentration of  $N_2O$ , as much as  $5 \times 10^8$  tons  $N$  if we scale to global dimensions using data presented by Elkins et al. (1978). Most of this  $N_2O$  resides at depth, below the permanent thermocline. The quantity presented above the thermocline is relatively small, of order



$10^7$  tons N. It is difficult to imagine circumstances under which as much as  $5 \times 10^7$  tons N of preformed oceanic  $N_2O$  could be released to the atmosphere. It would appear to require a climatic perturbation of global scale and there is no evidence for such an event in either 1967 or 1968.

Perturbations might arise on a more localized scale and it is of interest to speculate on ways through which they might affect  $N_2O$ . As noted earlier, denitrification is confined to a relatively small number of sites in the ocean. Upwelling regions in the Eastern Tropical Pacific account for as much as 90% of the net global sink for marine nitrogen and there are reasons to believe that the loss rate might vary in time (Codispoti, 1980), perhaps in response to change in local oceanic dynamics. According to present understanding, denitrification involves sequential reduction of nitrogen from  $NO_3^-$  to  $NO_2^-$ , to  $N_2O$ , thence to  $N_2$ , and it may be estimated from studies of the nitrogen budget of the Eastern Tropical Pacific (Codispoti and Richards, 1976; Elkins, 1978) that denitrification provides a source of approximately  $4 \times 10^7$  tons  $N\ yr^{-1}$  as  $N_2$ , with similar production of  $N_2O$ . Most of the  $N_2O$  formed during denitrification is cycled to  $N_2$  and rates for production and loss of  $N_2O$  are in approximate balance. Such was the case at least for the Peruvian system sampled by Elkins et al. (1978) in March 1978. The fraction of  $N_2O$  molecules formed by denitrification which escaped to the atmosphere at that time was exceptionally small, of order  $10^{-3}$ . We need to develop a better understanding of the processes which determine the magnitude of the atmospheric yield.

The dependence of yield on the strength of upwelling is a matter of particular concern. One cannot on the basis of present knowledge rule out the possibility that the yield might approach unity under some conditions. The concentration of  $N_2O$  present in waters off Peru was quite variable as shown in Figure 5. Concentrations measured by Elkins (1978) ranged from as high as  $6\ \mu g\ liter^{-1}$  to less than  $0.02\ \mu g\ liter^{-1}$ . We need to understand the factors which regulate this variability. The rise in atmospheric  $N_2O$  seen by Goody (1969) and Schutz et al. (1970) could be attributed to transient production by the Eastern Tropical Pacific. The yield of atmospheric  $N_2O$  could be especially high if the rate of upwelling were particularly large or variable. We need further observations to elucidate the longer term contributions which oceanic upwelling systems might make to the budget of atmospheric  $N_2O$ . The source from the Peruvian system was relatively modest during March 1978 but might have been much higher in the past.

In summary, with the possible exception of measurements by Goody (1969) and Schutz et al. (1970), the atmospheric evidence seems to point to a relatively long lifetime for  $N_2O$ , more than 28 years (Craig et al., 1976) and perhaps as long as 135 years. The behavior observed in 1967-1968 should not be used to estimate a lifetime. Based on the more recent observations (see excellent account in NASA, 1979), we conclude, either that the 1967-1968 results are spurious, or that they reflect a transient, in which case one should not expect (18) to hold and estimates for the lifetime of  $N_2O$  based on (19) have dubious validity. The available data, taken as a whole, suggest a time averaged source for atmospheric  $N_2O$  in the range  $1-2 \times 10^7$  tons  $N\ yr^{-1}$ . We reach this conclusion from two points of view. First, it is difficult to account for a sink of  $N_2O$  much larger than that which arises in the stratosphere,  $10^7$  tons  $N\ yr^{-1}$ . Second and equally binding, studies of a variety of different media, including soils and both fresh and salt water systems, indicate that the source is unlikely to exceed  $2 \times 10^7$  tons  $N\ yr^{-1}$ .

**ANTHROPOGENIC EFFECTS ON  $N_2O$ :** Human activity can affect  $N_2O$  in a number of ways, some direct, others indirect. Stress on the nitrogen cycle associated with production of food and the disposal of waste could be important, as discussed by Crutzen (1974, 1976), McElroy (1974, 1976a,b), McElroy et al. (1977), Sze and Rice (1976), Liu et al. (1976, 1977), Johnston (1977), Hahn and Junge (1977) and Crutzen and Ehhalt (1977). Combustion of fossil fuel can provide a direct source of  $N_2O$  as discussed by Pierotti and Rasmussen

(1976) and Weiss and Craig (1976), and can also have an indirect influence as described by McElroy (1976a) and McElroy et al. (1977). Comprehensive assessment of the cumulative human influence on  $N_2O$  is difficult, perhaps even impossible. We begin with a treatment of nitrogen involved in the agriculture-food-waste chain. A schematic view of the agriculture-food-waste chain is shown in Figure 6.

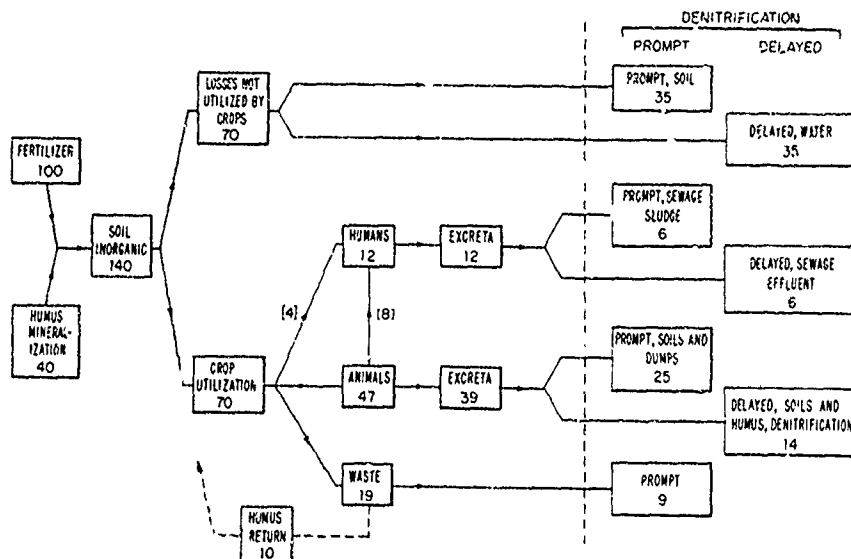


Figure 6. Transfer of nitrogen in the agricultural food chain (arbitrary units), adapted from data given by the National Academy of Sciences (1972). The relative contributions of soil nitrogen and fertilizer are intended to model average conditions in the United States. Notation is such that humans are assumed to satisfy their N requirement of 12 units, with 4 derived from crops, 8 from animals (from McElroy et al., 1977).

The nitrogen content of soils in a natural ecosystem will tend to approach equilibrium, if the environmental conditions remain constant for a sufficiently prolonged time period. The equilibrium state may be influenced by the nature of the vegetative cover, by physical conditions in the soil, by microbial activity and by climate. Nitrogen may be lost from the system by denitrification, as  $N_2$  and  $N_2O$ . It may be dissipated during nitrification, as  $N_2O$ , and may undergo additional loss due to volatilization of compounds such as  $NH_3$ ,  $NO$  and  $NO_2$ . It may be removed from soils also by erosion and leaching. In equilibrium loss would be balanced by in situ fixation and by supply of fixed nitrogen compounds in rain.

Cropping will tend to disturb the local equilibrium. The nitrogen content of the medium will decline as the soil is cultivated. The decline may be minimized to some extent by periodic applications of chemical fertilizer, or if the farmer should choose to plant the land with legumes. There is little doubt though that traditional farm practices will tend to lower the reserve of soil nitrogen, at least in the early stages of agricultural development. The nitrogen content of soils in the North Central United States decreased rapidly during the first 10-20 years of cultivation, with 25% of the total soil reservoir depleted during the first 20 years, 10% lost in the

subsequent 20 years and about 7% lost between the 40th and 60th years (Jenny, 1941). Similar results under a variety of conditions were reported by Haas, Evans and Miles (1957) for the Great Plains, by White, Holben and Richer (1945) for the Jordan Soil Fertility Plots in Pennsylvania, by Bracken and Greaves (1941) for semi-arid regions of Utah, by Giddens and Garman (1942) for Georgia, and by Smith, Thompson, Collier and Hervey (1954) for the black-land soils of Texas. Agricultural soils of the United States lost approximately  $1.6 \times 10^9$  tons of fixed nitrogen, out of an initial reservoir of about  $4 \times 10^9$  tons in a fifty year period following the first large scale development of the Midwest (Jenny, 1941; Council on Agricultural Science and Technology, 1976). It is clear from these data that the nitrogen content of soils may be altered by agricultural practice on a relatively short time scale, less than 50 years. The system will adjust to a new equilibrium state, in which fertilizer and various fixing organisms can balance the loss of nitrogen extracted in crops and lost by denitrification, leaching and erosion. It appears, for the United States at least, that this new equilibrium configuration is one in which the nitrogen content of soil is reduced to approximately 50% of its initial value.

Approximately 50% of the total nitrogen made available in agricultural soils, i.e. the sum of the contributions from humus mineralization and fertilizer, may be taken up by the growing crop, according to data summarized by the Committee on Nitrate Accumulation (1972). Some 25% of the plant nitrogen may be lost due to a combination of factors, including drought, hail, fire, insects, plant pathogens, failure to harvest, processing wastes and spoilage. About 35% of the initial mineral supply is fed to livestock, and some 15% of this ultimately reaches the human consumer as meat, poultry, and dairy products such as milk and cheese. Plant sources - fruits, vegetables, potatoes, flour, etc. - account for somewhat less than 30% of the daily nitrogen requirements of people in the United States, though meat and animal products may be emphasized to a lesser extent elsewhere. These considerations provide a basis for the results shown in Figure 6. Note that approximately 30% of the total nitrogen involved in agriculture appears ultimately as animal waste and we have little quantitative information on the fate of this nitrogen. Approximately 10% appears as human waste which may pass through a sewage treatment plant, undergoing substantial chemical modification before it is returned to the environment. Nitrogen is converted most commonly to inorganic form, either  $\text{NH}_4^+$  or  $\text{NO}_3^-$ , and relatively little is lost during treatment. Effects of processed waste on receiving systems may be quite large, however, as we shall illustrate now for the Potomac Estuary near Washington, D.C.

The Potomac is under stress due to input of sewage effluent from treatment plants near Washington, D.C. The river receives approximately 90% of its sewage load ( $\sim 3.5 \times 10^4$  kg  $\text{NH}_4^+\text{-N}$  day $^{-1}$ ) over a short distance, 17-23 km below the head of the estuary at Chain Bridge. Concentrations of  $\text{NH}_4^+$  and  $\text{NO}_3^-$  often exceed 1 mg N liter $^{-1}$  in the river, with concentrations of  $\text{PO}_4^{3-}$  as high as 0.8 mg P liter $^{-1}$ . The Blue Plains treatment plant, located 18.3 km below Chain Bridge, provides the largest input of sewage, processing waste from a population of about 2.3 million people ( $\sim 70\%$  of the population of the drainage basin). The principal form of nitrogen released from Blue Plains is  $\text{NH}_4^+$ , on average about  $1.8 \times 10^4$  kg N day $^{-1}$ . Phosphorus is removed with relatively high efficiency (70%) during treatment, and release rates for P have decreased from about  $1.1 \times 10^4$  kg P day $^{-1}$  in 1970 to about  $2 \times 10^3$  kg P day $^{-1}$  in 1979.

Sewage nitrogen undergoes a series of complex transformations in the Potomac. Ammonium is oxidized (nitrified) by bacteria, first to nitrite, then to nitrate. Both ammonium and nitrate may be taken up by phytoplankton, with ammonium released to the water as the plankton decompose. In addition to loss due to algal uptake, nitrate is transported out of the estuary and may be removed also by denitrification. Rates for these various processes appear to vary markedly from year to year, and even week to week, as discussed by

Elkins et al. (1980).

We sampled the Potomac Estuary at frequent intervals since July 1977 (Kaplan et al., 1978; McElroy et al., 1978; Elkins et al., 1980). Measurements have emphasized a section of the river between National Airport (11 km below Chain Bridge) and Quantico, Virginia (61 km). Results for a typical run are shown in Figure 7. Note the evidence for sequential oxidation of nitrogen from  $\text{NH}_4^+$  to  $\text{NO}_2^-$  to  $\text{NO}_3^-$ . Concentrations of  $\text{N}_2\text{O}$  are relatively high throughout the river and data such as shown here may be used to estimate a yield for production of  $\text{N}_2\text{O}$  associated with disposal of human waste. Detailed analyses (McElroy et al., 1978; Elkins et al., 1980) suggest that between 0.3 and 5% of the nitrogen supplied to the river by sewage treatment plants is converted promptly to  $\text{N}_2\text{C}$  and released to the atmosphere. The yield shows considerable variability in both space and time, and there are indications that it may be much higher when the concentration of dissolved  $\text{O}_2$  is low. The trend is consistent with behavior observed in the laboratory for nitrifying bacteria by Goreau et al. (1980). They found yields as high as 10% at concentrations of  $\text{O}_2$  near  $0.2 \text{ mg l}^{-1}$  and one is tempted to conclude that nitrification may

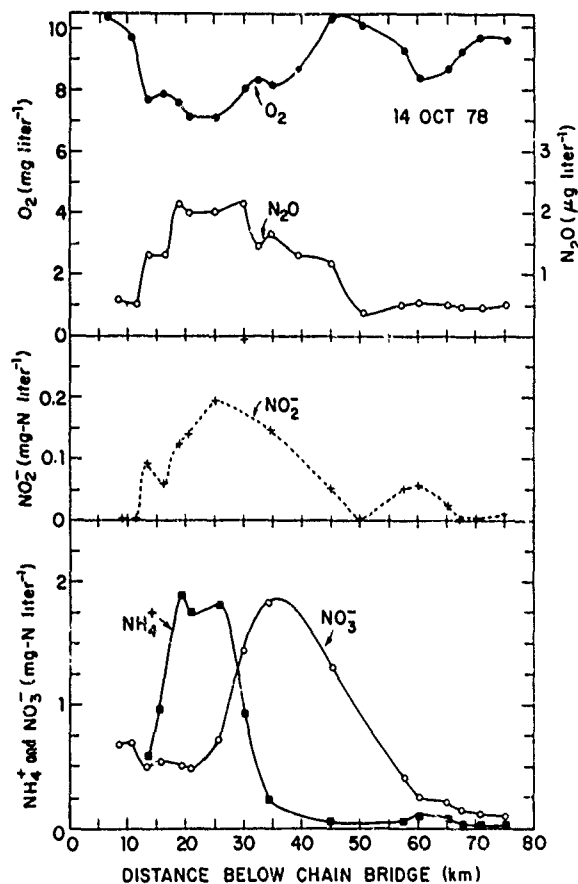


Figure 7. The distribution of dissolved species in the Potomac on 14 October 1978. Note the efficient oxidation of  $\text{NH}_4^+$  to  $\text{NO}_2^-$  and  $\text{NO}_3^-$ , and the association of maxima for  $\text{N}_2\text{O}$  and  $\text{NO}_2^-$ . Water temperatures were between 15 and 18°C. The river flow at Little Falls dam was approximately  $50 \text{ m}^3 \text{ sec}^{-1}$  (from Elkins, 1978).

represent the dominant source for  $N_2O$  in the Potomac. We may anticipate in this case that the yield for  $N_2O$  should increase in a non-linear fashion in response to change in  $O_2$  at low concentrations of  $O_2$ . To the extent that human activity leads to concentration of organic waste, favoring occurrence of low oxygen conditions, we might expect production of  $N_2O$  from waste disposal to rise at a rate faster than population. With a yield of 1%, the present population,  $4 \times 10^9$  persons consuming approximately 5 kg N per person per year, would account for direct production of  $N_2O$  of magnitude  $2 \times 10^5$  tons  $N\ yr^{-1}$ . If we adopt a similar yield for decomposition of organic waste produced by domesticated animals, we might expect additional production of  $6 \times 10^5$  tons  $N\ yr^{-1}$ , corresponding to a net source of approximately  $10^6$  tons  $N\ yr^{-1}$ . Experience with the Potomac suggests that the global source of  $N_2O$  associated with decomposition of organic waste should lie in the range  $0.3-5 \times 10^6$  tons  $N\ yr^{-1}$ . It may be expected to increase by at least 50% over the next 20 years as world population expands to its expected value of  $6.5 \times 10^9$  persons in the year 2000. The source of  $N_2O$  from waste disposal could be as large as  $1.3 \times 10^7$  tons  $N\ yr^{-1}$  in 2000, comparable in magnitude to the present stratospheric sink, if the yield for conversion of  $N_2O$  were 10%, the value observed for nitrification at low oxygen by Goreau et al. (1980).

We might arrive at an estimate for the anthropogenic source of  $N_2O$  from a rather different point of view, focusing attention on the human contribution to fixation, postulating that the nitrogen cycle is in an approximately steady state as regards  $N_2O$ . We estimated earlier that nitrogen was fixed globally at a rate of about  $2.2 \times 10^8$  tons  $N\ yr^{-1}$ , with approximately 40% of this source attributable either directly or indirectly to man. If we assume that the stratosphere is the dominant sink for  $N_2O$ , we may conclude that fixed nitrogen is converted to  $N_2O$  with an efficiency of about 5%, i.e. an input of fixed nitrogen of  $2.2 \times 10^8$  tons  $N\ yr^{-1}$  supplies an output of  $N_2O$  of  $1.1 \times 10^7$  tons  $N\ yr^{-1}$ . The anthropogenic contribution should be about  $4 \times 10^6$  tons  $N\ yr^{-1}$  in this case and would be expected to grow to more than  $1 \times 10^7$  tons  $N\ yr^{-1}$  by the year 2000 if demand for fixed nitrogen should follow the pattern suggested by McElroy et al. (1977). The source of  $N_2O$  would be even larger if the yield were to increase in the non-linear fashion discussed earlier.

It is of interest to note that these rather different approaches lead to quite similar estimates for the anthropogenic source of  $N_2O$ . The weight of the evidence suggests a contemporary anthropogenic source in the range  $1-4 \times 10^6$  tons  $N\ yr^{-1}$  and there are reasons to believe that the anthropogenic contribution may grow by at least a factor of 2 over the next 20 years. The fluxes of  $N_2O$  quoted here reflect perturbations to the biosphere caused by enhanced and accelerated cycling of fixed N. The net anthropogenic source of  $N_2O$  must allow in addition for direct production of  $N_2O$  associated with combustion of fossil fuel.

Pierotti and Rasmussen (1976) and Weiss and Craig (1976) measured concentrations of  $N_2O$  in the range 3.1 to 37.6 ppm in stack gases of a number of power plants in the Western United States. Largest concentrations of  $N_2O$  were observed for oil and coal fired plants, with somewhat smaller yields from plants fueled by natural gas. Weiss and Craig (1976) estimated a global source of  $N_2O$  from combustion of  $1.6 \times 10^6$  tons  $N\ yr^{-1}$  in 1976. They emphasized that the combustion source was growing at a rate of 3.5% per year. It is obviously of some importance to clarify the mechanism for production of  $N_2O$  in power plants. It is likely that reactions such as



should play a role, and there may be a trade-off in operational conditions between production of  $NO_x$  and  $N_2O$ . Excess concentrations of  $N_2O$  were observed also in exhaust gases of automobiles equipped with specific types of catalytic converters (Pierotti and Rasmussen, 1976; Cicerone, 1976). The source from

automobiles is likely, however, to be small compared to production by power plants.

CONCLUDING REMARKS: Our understanding of atmospheric  $N_2O$  has improved considerably over the past 5 years. There was at that time controversy concerning the role of the ocean, the lifetime of  $N_2O$ , and the impact of human activity. Uncertainty remains. It is clear, however, that we can reject at least some of the more extreme possibilities considered by Hahn (1974, 1975) and Hahn and Junge (1977). The ocean is at most a small source of  $N_2O$ , less than  $4 \times 10^6$  tons  $N \text{ yr}^{-1}$ . The lifetime for atmospheric  $N_2O$  is long, surely more than 15 years and probably close to 135 years, the limit which would apply if photolysis in the stratosphere were the dominant sink.

There is evidence for a rise in  $N_2O$ . Craig et al. (1976) concluded that the concentration over the Pacific Ocean increased by about 1.5%, 4 ppb, between 1965 and 1975. Weiss (1979) observed an increase of 0.17% per year, or 0.5 ppb per year, between 1977 and 1979. Measurements by Goldan et al. (1980) between 1976 and 1979 could be interpreted to indicate a rise of 1% per year, though these authors were careful to state their results in terms of an upper limit to the rise equal to 2% per year. Rasmussen (1979) reported an increase similar to that seen by Weiss (1979) and Goldan et al. (1980). It is difficult to escape the conclusion that the concentration of  $N_2O$  has risen from about 293 ppb in 1965 to about 301 ppb in 1980. Approximately half of this rise may be attributed to direct sources of  $N_2O$  due to combustion of fossil fuels in power plants. The balance, approximately  $2 \times 10^7$  tons  $N \text{ yr}^{-1}$ , may be attributed to enhanced production by the biosphere. The additional biospheric source represents approximately 4% of the quantity of N applied as chemical fertilizer over the same period.

We have every reason to expect anthropogenic sources of N to rise above  $3 \times 10^8$  tons  $N \text{ yr}^{-1}$  in the early part of the next century (McElroy et al., 1977). Production of  $N_2O$  should exceed  $1.2 \times 10^7$  tons  $N \text{ yr}^{-1}$  and could be as large as  $3 \times 10^7$  tons  $N \text{ yr}^{-1}$ . We see no reason, therefore, to back off from our initial concern (McElroy, 1976a), that the concentration of  $N_2O$  could double in less than 100 years. The rise in  $N_2O$  observed over the past 15 years is similar on a relative basis to that seen for  $CO_2$  (NASA, 1979).

ACKNOWLEDGEMENTS: I am indebted to S.C. Wofsy for helpful discussions and to F. Forrestel Zingale for patient expertise during preparation of the manuscript. This work was supported by NSF grant DEB79-20282 and NASA contract NASW 2952.

## REFERENCES

- Barbaree, J.M. and W.J. Payne, Products of Denitrification by a Marine Bacterium as Revealed by Gas Chromatography, Mar. Biol., 1, 136, 1967.
- Bates, D.R. and P.B. Hays, Atmospheric Nitrous Oxide, Planet. Space Sci., 15, 189, 1967.
- Bates, D.R. and A.E. Witherspoon, The Photochemistry of Some Minor Constituents of the Earth's Atmosphere, Mon. Not. R. Astronom. Soc., 112, 101, 1952.
- Bracken, A.F. and J.E. Greaves, Losses of Nitrogen and Organic Matter from Dry-Farm Soils, Soil Sci., 51, 1, 1941.
- Breitenbeck, G.A., A.M. Blackmer, and J.M. Bremner, Effects of Different Nitrogen Fertilizers on Emission of Nitrous Oxide from Soil, J. Geophys. Res., 7, 85, 1980.
- Burns, R.C. and R.W.F. Hardy, Nitrogen Fixation in Bacteria and Higher Plants, New York: Springer-Verlag, 1975.
- Cicerone, R., private communication, 1976.
- Codispoti, L.A., Denitrification in the Eastern Tropical North Pacific Ocean, Ph.D. Thesis, 1973.
- Codispoti, L.A. and F.A. Richards, An Analysis of the Horizontal Regime of Denitrification in the Eastern Tropical North Pacific, Limnol. Oceanogr., 21, 379, 1976.
- Cohen, Y., Consumption of Dissolved Nitrous Oxide in an Anoxic Basin, Saanich Inlet, British Columbia, Nature, 272, 235, 1978.
- Cohen, Y. and L.I. Gordon, Nitrous Oxide in the Oxygen Minimum of the Eastern Tropical North Pacific: Evidence for Its Consumption During Denitrification and Possible Mechanisms for its Production, Deep-Sea Res., 25, 509, 1978.
- Committee on Nitrate Accumulation 1972, Accumulation of Nitrate, Washington, D.C., National Academy of Sciences.
- Council for Agricultural Science and Technology, Effect of Increased Nitrogen Fixation on Stratospheric Ozone, Department of Agronomy, Iowa State Univ., Ames, Iowa, 1976.
- Craig, H., R.F. Weiss, and W.L. Dowd, paper presented at AGU Symposium on The Terrestrial Nitrogen Cycle and Possible Atmospheric Effects, Spring, 1976.
- Crutzen, P.J., The Influence of Nitrogen Oxides on the Atmospheric Ozone Content, Q.J.R. Met. Soc., 96, 320, 1970.
- Crutzen, P.J., Ozone Production rates in an Oxygen-Hydrogen-Nitrogen Atmosphere, J. Geophys. Res., 76, 7311, 1971.
- Crutzen, P.J., Estimates of Possible Variations in Total Ozone Due to Natural Causes and Human Activities, Ambio, 3, 201, 1974.
- Crutzen, P.J. and D.H. Ehhalt, Effects of Nitrogen Fertilizers and Combustion on the Stratospheric Ozone Layer, Ambio, 6, 112, 1977.
- Delwiche, C.C., The Nitrogen Cycle, Scient. Am., 223, 137, 1970.
- Elkins, J.W., Aquatic Sources and Sinks for Nitrous Oxide, Ph.D. Thesis, 1978.
- Elkins, J.W., S.C. Wofsy, M.B. McElroy, C.E. Kolb, and W.A. Kaplan, Aquatic Sources and Sinks for Nitrous Oxide, Nature, 275, 602, 1978.
- Elkins, J.W., S.C. Wofsy, M.B. McElroy, and W.A. Kaplan, Nitrification and Production of N<sub>2</sub>O in the Potomac: Evidence for Variability, in press, 1980.
- Giddens, J. and W.H. Garman, Some Effects of Cultivation on the Piedmont soils of Georgia, Soil Sci. Am. Proc., 6, 439, 1942.
- Goldan, P.D., W.C. Kuster, D.L. Albritton, and A.L. Schmeltekopf, Stratospheric CHCl<sub>3</sub>, CF<sub>2</sub>Cl<sub>2</sub>, and N<sub>2</sub>O Height Profile Measurements at Several Latitudes, J. Geophys. Res., 85, 413, 1980.
- Goody, R.M., Time Variations in Atmospheric N<sub>2</sub>O in Eastern Massachusetts, Planet. Space Sci., 17, 1319, 1969.
- Goreau, T.J., private communication, 1979.
- Goreau, T.J., W.A. Kaplan, S.C. Wofsy, M.B. McElroy, F.W. Valois, and S.W. Watson, Laboratory Studies on the Nitrifying Bacterium *Nitrosococcus Oceanus*: Implications for Marine and Atmospheric N<sub>2</sub>O, in press, 1980.
- Haas, H.J., C.E. Evans, and E.F. Miles, Nitrogen and Carbon Changes in Great Plains soils as influenced by cropping and soil treatments, U.S.D.A. Tech. Bull., 1164, 1, 1957.
- Hahn, J., The North Atlantic Ocean as a Source of Atmospheric N<sub>2</sub>O, Tellus, 26, 160, 1974.

- Hahn, J., N<sub>2</sub>O Measurements in the Northeast Atlantic Ocean: Meteor Forsch-  
Ergebnisse, Reich A, 16, 1, 1975.
- Hahn, J. and C. Junge, Atmospheric Nitrous Oxide: A Critical Review, Z.  
Naturf., 32a, 190, 1977.
- Jenny, H., Factors of Soil Formation, New York: McGraw Hill, 1941.
- Johnston, H.S., Reduction of Stratospheric Ozone by Nitrogen Oxide Catalysts  
from SST Exhaust, Science, 173, 517, 1971.
- Johnston, H.S., Analysis of the Independent Variables in the Perturbation of  
Stratospheric Ozone by Nitrogen Fertilizers, J. Geophys. Res., 82, 1767,  
1977.
- Junge, C.E., Residence Time and Variability of Tropospheric Trace Gases,  
Tellus, 26, 477, 1974.
- Kaplan, W.A., J.W. Elkins, C.E. Kolb, M.B. McElroy, S.C. Wofsy, and A.P. Duran,  
Nitrous Oxide in Fresh Water Systems: An Estimate for the Yield of Atmo-  
spheric N<sub>2</sub>O associated with the disposal of human waste, Pure Appl. Geophys.  
116, 423, 1978.
- Koblentz-Mishke, O.J., V.V. Volkovinsky, and J.G. Kabanova, in Scientific  
Exploration of the South Pacific, ed. Wooster, W.S., 183, 1970.
- Liu, S.C., T.M. Donahue, R.J. Cicerone, and W.L. Chameides, Effect of  
Water Vapor on the Destruction of Ozone in the Stratosphere Perturbed by  
Cl<sub>x</sub> or NO<sub>x</sub> Pollutants, J. Geophys. Res., 81, 3111, 1976.
- Liu, S.C., R.J. Cicerone, T.M. Donahue, Sources and Sinks of Atmospheric N<sub>2</sub>O  
and the Possible Ozone Reduction Due to Industrial Fixed Nitrogen Fertiliz-  
ers, Tellus, 29, 251, 1977.
- Logan, J.A., M.J. Prather, S.C. Wofsy, and M.B. McElroy, Atmospheric Chemistry:  
Response to Human Influence, Phil. Trans. Roy. Soc. London, Ser. A., 290,  
187, 1978.
- McElroy, M.B., Testimony Presented to the Committee on Interstate and Foreign  
Commerce, U.S. House of Representatives, Washington, D.C., 11 Dec. 1974.
- McElroy, M.B., Chemical Processes in the Solar System: A Kinetic Perspective,  
M.T.P. International Review of Science, ser. 2, 9, ed. D. Herschbach,  
London: Butterworths, 1976a.
- McElroy, M.B., Man's Impact on the Global Environment: Some Recent Problems  
in Atmospheric Pollution, Atomic Processes and Applications, ed. P.G. Burke  
and B.L. Moiseiwitsch, Amsterdam: North Holland Pub. Co., 1976b.
- McElroy, M.B. and J.C. McConnell, Nitrous Oxide: A Natural Source of Strato-  
spheric NO, J. Atmos. Sci., 28, 1095, 1971.
- McElroy, M.B., S.C. Wofsy, and Y.L. Yung, The Nitrogen Cycle: Perturbations  
Due to Man and Their Impact on Atmospheric N<sub>2</sub>O and O<sub>3</sub>, Phil. Trans. R. Soc.  
Lond., B277, 159, 1977.
- McKenney, D.J. and D.L. Wade, Rates of Evolution from N-Fertilized Soil,  
Geophys. Res. Lett., 5, 777, 1978.
- National Aeronautics and Space Administration, The Stratosphere: Present and  
Future, Reference Publication 1049, 1979.
- Nicolet, M. and A. Vergison, L'Oxyde Azoteux dans la Stratosphere, Aeron.  
Acta, 90, 1, 1971.
- Pierotti, D. and R.A. Rasmussen, Combustion as a Source of Nitrous Oxide in  
the Atmosphere, Geophys. Res. Lett., 3, 265, 1976.
- Pierotti, D. and R.A. Rasmussen, The Atmospheric Distribution of Nitrous Oxide,  
J. Geophys. Res., 82, 5823, 1977.
- Rasmussen, R.A., quoted in The Stratosphere: Present and Future, NASA Ref-  
erence Publication 1049, 1979.
- Rasmussen, R.A., D. Pierotti, J. Krasnec, and B. Halter, Report on the Cruise  
of the Alpha Helix Research Vessel, March 5 to 20, 1976, N.S.F. Grant No.  
OCE 75 04688 AO3, 1976.
- Redfield, A.C., B.H. Ketchum, and F.A. Richards, The Sea, vol. II, 26, New York,  
Wiley-Interscience, 1963.
- Schutz, K., C. Junge, R. Beck and B. Albrecht, Studies of Atmospheric N<sub>2</sub>O, J.  
Geophys. Res., 75, 2230, 1970.
- Smith, R.M., D.O. Thompson, J.W. Collier, R.J. Hervey, Soil Organic Matter,  
Crop Yields, and Land Use in the Texas Blackland, Soil Sci., 77, 377, 1954.
- Sze, N.D. and H. Rice, Nitrogen Cycle Factors Contributing to N<sub>2</sub>O Production  
From Fertilizers, Geophys. Res. Lett., 3, 343, 1976.



- Watson, S.W., Characteristics of a Marine Nitrifying Bacterium, Nitrosocystis oceanus sp.n., Limnol. Oceanog. Suppl., 10, R274, 1965.
- Weiss, R., results quoted in The Stratosphere: Present and Future, NASA Reference Publication 1049, 1979.
- Weiss, R. and H. Craig, Production of Atmospheric Nitrous Oxide by Combustion, Geophys. Res. Lett., 3, 751, 1976.
- White, J.W., F.J. Holben, and A.C. Richer, Maintenance Level of Nitrogen and Organic Matter in Grassland and Cultivate Soils Over Periods of 54 and 72 Years, J. Am. Soc. Agron., 37, 21, 1945.
- Whittaker, R.J. and G.E. Likens, The Biosphere and Man, Primary Productivity of the Biosphere, H. Lieth and R.H. Whittaker, eds., New York: Springer-Verlag, 1975.
- Yoshinari, T., Nitrous Oxide in the Sea, Mar. Chem., 4, 189, 1976.

# THE PROBLEM OF ATMOSPHERIC METHYL CHLORIDE

Andrew J. Watson,\* James E. Lovelock<sup>†</sup> and D. H. Stedman\*

\* Dept. of Atmospheric and Oceanic Science  
University of Michigan  
Ann Arbor, MI 48109

<sup>†</sup> Dept. of Cybernetics  
University of Reading  
Reading, U. K.

## ABSTRACT

Methyl chloride is the most abundant halocarbon in the atmosphere and the only chlorocarbon with at least one proven natural source. We review atmospheric measurements of  $\text{CH}_3\text{Cl}$  to date and estimate the magnitude of possible sources and sinks. The major sink is reaction with tropospheric hydroxyl radicals; the major source is the oceans, but other non-negligible contributions may come from the combustion of vegetation, urban pollution and possibly, certain species of wood moulds. The global source is estimated to be  $1.6\text{--}9.6\text{mt yr}^{-1}$ . Methyl chloride is not sensitively detected by present measurement techniques and this has restricted the collection of data. We report here a method by which the sensitivity of measurements may be increased to a level similar to that of the other major halocarbons.

Methyl chloride is the most abundant halocarbon in the atmosphere. Of these halocarbons present in 'large' concentrations (>10ppt) it is the only one with at least one indisputably non-anthropogenic source. It is possible, therefore, that in the undisturbed stratosphere, methyl chloride would be the only significant source of chlorine. For this reason alone it is worthy of study by atmospheric scientists. In addition, its role as the only biologically produced chlorine species in the atmosphere makes it of interest to biogeochemists.

In this paper we shall review present knowledge of atmospheric methyl chloride--measurements to date, sources and sinks. We shall show that the magnitude of the sources and sinks are comparable but that there remain large uncertainties in the global budget so that further research is still required.

First, to remind us of the significance of methyl chloride to stratospheric ozone, Table 1 shows the relative impact on the ozone column density of the four major chlorocarbons, both at present and in a projected steady state. The figures are derived from the published work of Crutzen *et al.* (1978) and the  $\Delta O_3$  values are rather lower than most models currently predict. As can be seen, methyl chloride is still the major source of stratospheric chlorine, though it is unlikely to remain so.

TABLE 1. MAJOR ATMOSPHERIC CHLOROCARBONS, C 1976

TROPOSPHERIC CONCENTRATION (PPT)		Cl FLUX TO STRATOSPHERE CM <sup>-2</sup> S <sup>-1</sup>	$\Delta O_3$ %	$\Delta O_3$ STEADY STATE 1975 EMISSION
CH <sub>3</sub> Cl	610	8 x 10 <sup>6</sup>	1	1
CCl <sub>2</sub> F <sub>2</sub>	220	6.4 x 10 <sup>6</sup>	0.8	3.3
CCl <sub>3</sub> F	120			3.6
CCl <sub>4</sub>	120	4 x 10 <sup>6</sup>	0.5	1
COMPUTED FROM INFORMATION IN CRUTZEN <i>ET AL.</i> (1978)				

MEASUREMENTS OF TROPOSPHERIC MeCl: Table 2 summarizes tropospheric measurements to date. Methyl chloride was first detected by Grimsrud and Rasmussen in 1975. They used a technique of cryoconcentration followed by GC/MS. Shortly afterwards Lovelock reported measurements by direct analysis of air using electron capture detection, which is also the method used by Singh. The recent measurements by the authors employed a technique of chemical conversion.

It is interesting to note that these measurements show rather wide disagreement both as to the mean atmospheric concentration and the variability. This is in part due to the difficulty of the analysis: direct detection of ambient methyl chloride requires much greater care than does detection of the other major halocarbons because the electron capture detector is some two orders of magnitude less sensitive to CH<sub>3</sub>Cl. Detection limits for the above measurements were 50ppt (Lovelock, 1975) and 200ppt (Singh *et al.*, 1978a). A proportion of the variability in these measurements is, therefore, instrumental in origin and not a real feature of the atmosphere.

TABLE 2. MEASUREMENTS OF TROPOSPHERIC METHYL CHLORIDE

	MEAN (STD DEV) PPT	LOCATION	NO. MEASUREMENTS	DATE
GRIMSRUD AND RASMUSSEN	530 (30)	WASHINGTON STATE	--	1975
LOVELOCK	1140 (500)	WILTSHIRE, ENGLAND	8	1975
LOVELOCK AND WATSON	2100 (1000)	KENYA	6	1976
SINGH <u>ET AL.</u>	733 (134)	CALIFORNIA	39	1977
SINGH <u>ET AL.</u>	613 (98)	GLOBAL	~90	1977
AUTHORS	632 (150)	MICHIGAN COLORADO	25	1979

Our knowledge of the global distribution is due to Singh's recent measurements. These show that methyl chloride concentrations exhibit very little variation with latitude. He found a mean of 611ppt in the Northern Hemisphere and 613 in the Southern. The lack of an interhemisphere gradient is one line of evidence which indicates that the developed countries are not major sources of the gas; the residence time of methyl chloride is of the same order as the time for interhemispheric exchange of air so that a sizeable gradient would exist if the sources were not evenly distributed between North and South.

SINKS: The major sink for  $\text{CH}_3\text{Cl}$  in the atmosphere is reaction with tropospheric hydroxyl radicals. The rate constant has been measured by several groups and has been evaluated (NASA, 1977) at  $2.2 \times 10^{-11} \exp(-1142/T)$ , possible error is  $\pm 25\%$ . The major difficulty in quantifying the sink, therefore, stems from the present uncertainty in tropospheric average OH concentration. Table 3 shows calculated residence times and sink strengths for 'low' and 'high' hydroxyl concentrations ( $3 \times 10^5$  and  $2 \times 10^6 \text{ cm}^{-3}$  respectively). We have used a tropospheric average concentration of 612ppt reported by Singh et al. (1978b) to calculate sink strengths. The magnitude of the stratospheric sink is also shown; at most it amounts to less than 10% of the total.

TABLE 3. RESIDENCE TIMES AND SINKS OF ATMOSPHERIC METHYL CHLORIDE

	RESIDENCE TIME (YR)	GLOBAL SINK RATE (MT YR <sup>-1</sup> )
STRATOSPHERE		~0.1
TROPOSPHERE $\Delta$ ( $[\text{OH}] = 2 \times 10^6 \text{ cm}^{-3}$ )	0.65	7.9
TROPOSPHERE ( $[\text{OH}] = 3 \times 10^5 \text{ cm}^{-3}$ )	4.3	1.2

SOURCES: So far four potential sources of methyl chloride have been identified; production by microbes, urban sources, the combustion of vegetation and the sea. Below, we summarize knowledge on each.

A) MICROBES: As far as we know, the only organisms which have been shown to directly metabolize methyl chloride are some six species of wood mould of the genus *fomes*, as reported by Cowan *et al.* (1973). These authors state that the organisms produced 'substantial quantities' but do not specify exactly how much. These fungi are quite common, but in the absence of further information little can be done to further quantify the microbial source. In the limiting case, if all dead wood were decomposed by these species and all the chlorine it contained were converted to methyl chloride, this source would generate a flux of many tens of megatons per annum. The limiting case is clearly, therefore, a gross overestimate of the true source because such a flux is inconsistent with the known sinks. Until more information is obtained we can be no more specific.

B) URBAN SOURCES: Direct industrial emission of methyl chloride is thought to be small. For example, total production in 1973 was 0.35 mt but little of this was released to the atmosphere. However, measurements made by Singh *et al.* (1978a) have led him to suggest that a significant urban source does exist. The concentration at urban monitoring sites was found to be consistently high; in Riverside, California for example, it was twice the background level. A number of secondary processes could be responsible for this enhancement. The burning of PVC waste has been suggested as a source of  $\text{CH}_3\text{Cl}$ . Palmer, (1976) estimated a U. S. production from this source of  $0.08 \text{ mt yr}^{-1}$ ; he assumed arbitrarily that 10% of the chlorine in PVC was converted to methyl chloride. Singh has suggested that automobile exhausts may be a source. The possibility that heterogeneous reactions occurring on the surface of smog particles may form methyl chloride also needs investigation.

A very rough idea of the magnitude of all these sources can be obtained by comparing the enhancement of methyl chloride concentrations with those of fluorocarbons in urban air masses. Singh's data show that at Riverside, the sum of the average concentrations of F11 and F12 in 1977 was 1010ppt which was about 650ppt above the Northern hemisphere background. Methyl chloride was enhanced on average by 750ppt, suggesting that the rate of urban methyl chloride emission was about 750/650 or 1.15 times the rate of freon emission by volume. If we multiply the global freon emission by this ratio, we find an urban methyl chloride source of about  $0.3 \text{ mt yr}^{-1}$ . This estimate is, of course, liable to wide errors, at least a factor of two. It indicates, however, that this source may make up quite a significant portion of the global budget, perhaps 10% or more.

C) COMBUSTION OF VEGETATION: The smoldering combustion of vegetation produces methyl chloride. Flaming combustion probably does not, because methyl chloride is thermally labile and tends to decompose at temperatures much in excess of  $300^\circ\text{C}$ . The yield of methyl chloride from a fire is thus sensitively dependent on the temperature of combustion. An upper limit on this yield is provided by the analysis of tobacco smoke by Chopra and Sherman (1972). They found that about 2000  $\mu\text{g}$  of the gas were evolved per gram of cigarette tobacco burned. They noted that other workers found less methyl chloride depending on the technique used to 'smoke' the cigarettes. In these experiments, methyl chloride emission accounted for most of the chlorine lost by the tobacco on ashing.

Crutzen *et al.* (1979) have recently addressed the problem of the impact of biomass burning on the atmosphere. They have estimated the total mass of vegetation burned per annum to be about 8000mt dry weight, a good proportion of which is due to fires in tropical and subtropical forest and grassland. They also made measurements of various gases including methyl chloride in the plumes of some temperate zone fires. From their experiments they found that 75mg of  $\text{CH}_3\text{Cl}$  were produced per gram of material burned--only about 4% of the yield in tobacco smoke. It seems likely either that only a very small proportion of the fuel in these fires burned by smoldering combustion or possibly that the chlorine content of tobacco is unusually high.

Batchelder and Hirt (1966) state that tropical forest is burned only with difficulty because of the high moisture content of the wood; if this is the case one might expect the yield of methyl chloride from fires in tropical forest to exceed that reported by Crutzen, because the wet fuel would promote smoldering rather than flaming combustion. The very high concentrations of methyl chloride in air found by Lovelock and Watson in 1976 were measured during a season of intense forest clearance and may reflect the combustion source. An investigation of tropical forest fires now being carried out by the NCAR group should help resolve this matter. For the present, we suggest that the figure of 0.4mt per year which Crutzen *et al.* estimate for the global yield of methyl chloride from biomass burning is probably a lower limit. One megaton per year seems a reasonable upper bound.

D) MARINE SOURCE: Table 4 summarizes all the measurements of methyl chloride in seawater so far published. The concentration is highly variable, indicating that some process generates methyl chloride in comparatively localized source regions.

TABLE 4. METHYL CHLORIDE IN SURFACE SEAWATER

INVESTIGATOR	DATE	LOCATION	CONCENTRATION NG LITER <sup>-1</sup>
LOVELOCK	1975	ENGLISH COAST	15
LOVELOCK	1975	ENG. COAST	12.3
LOVELOCK	1975	ENG. COAST	43
SINGH <u>ET AL.</u>	1977	SOUTH PACIFIC	34.5
SINGH <u>ET AL.</u>	1977	SOUTH PACIFIC	85.8
SINGH <u>ET AL.</u>	1977	SOUTH PACIFIC	21.2
SINGH <u>ET AL.</u>	1977	SOUTH PACIFIC	1.4
SINGH <u>ET AL.</u>	1977	SOUTH PACIFIC	12.5
SINGH <u>ET AL.</u>	1977	SOUTH PACIFIC	5.3
MEAN CONCENTRATION			<u>25.7</u>

The flux of a gas from the sea to the air can be estimated from the stagnant-film model of gaseous exchange (Liss and Slater, 1974; Broecker and Peng, 1976). The equation for the flux  $F$  is

$$F = D/Z (C_{\text{sea}} - C_{\text{air}}/H)$$

where

$D$  is the diffusion coefficient of the gas in solution.  
 $D_{\text{CH}_3\text{Cl}} = 1.5 \times 10^{-5} \text{ cm}^2 \text{ s}^{-1}$

$Z$  is the thickness of a 'stagnant film' at the sea surface, and equals  $50 \pm 30 \text{ } \mu\text{m}$ .

$C_{\text{sea}}$  and  $C_{\text{air}}$  are the ocean and atmospheric concentrations of the gas and

$H$  is the partition coefficient.

...ation data for methyl chloride in seawater is representative of all the world's oceans, we obtain a value of  $8.2 \text{ mt yr}^{-1}$  as the most likely value of the global marine source. The possible error is again wide due to the uncertainty in  $Z$ , the stagnant film thickness. Singh, using a low diffusion coefficient and a high film thickness, obtained a value of  $3 \text{ mt yr}^{-1}$ .

What generates the methyl chloride in seawater? Zafiriou (1975) has described one process by which  $\text{CH}_3\text{Cl}$  is produced from methyl iodide and chloride ions, summarized in fig. 1. The methyl iodide is in turn given off by certain marine algae. He found that the reaction



will occur in surface seawater at a rate such that the lifetime of methyl iodide against conversion to methyl chloride is one month or longer depending on the temperature.

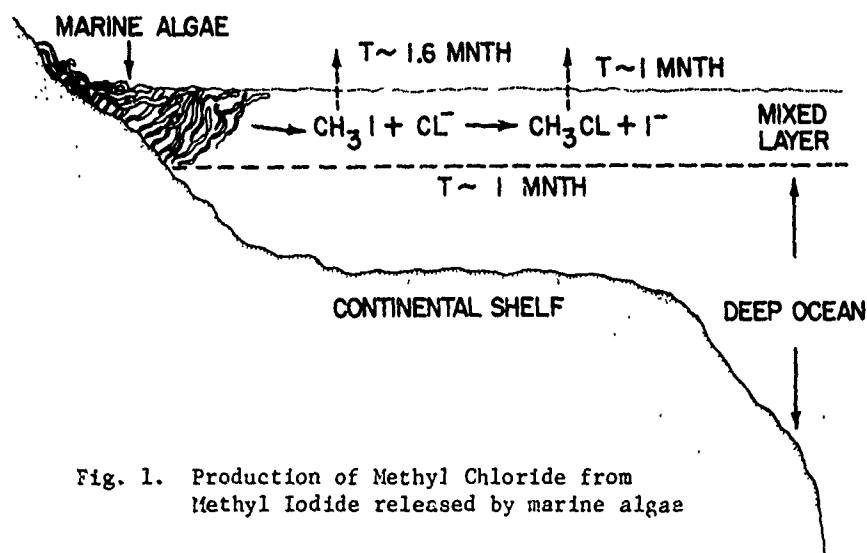


Fig. 1. Production of Methyl Chloride from Methyl Iodide released by marine algae

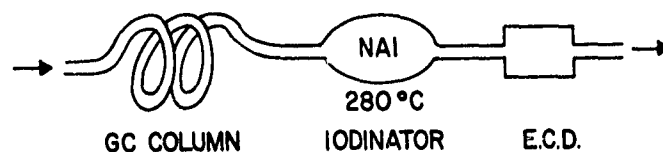
Like methyl chloride,  $\text{CH}_3\text{I}$  will also flux into the atmosphere at a rate which can be calculated from the stagnant film model. From a knowledge of the volume of the ocean's mixed layer one can calculate its lifetime in the sea before exchange into the atmosphere. This turns out to be ~1.6 months, so that the rate at which methyl iodide enters the atmosphere is very comparable to the rate at which it reacts to form methyl chloride, and we should expect the marine flux to the atmosphere of the two compounds to be similar. The marine flux of methyl iodide may be estimated from its observed atmospheric concentration (2.2ppt, Singh *et al.*, 1978b) and its lifetime against photolysis (about 6 days according to Zafiriou, 1974) to be about  $2.8 \text{ mt yr}^{-1}$ . If the marine methyl chloride flux were equal (in volume) to the methyl iodide flux, its strength would be about  $1 \text{ mt yr}^{-1}$ . This is quite considerably less than the value of  $8.2 \text{ mt yr}^{-1}$  calculated directly from the measurements of seawater concentration. Perhaps there is another marine source of  $\text{MeCl}$ , or perhaps the measurements of seawater concentration so far made are not representative of the oceans as a whole. This second possibility seems quite likely, since most of the measurements were made either at the coast or (in the case of Singh's data) in the Pacific's south equatorial current, which transports water rapidly from the continental margins to the open Pacific. Many of the algae which may be expected to metabolize methyl iodide are photosynthesizing bottom-dwellers, and so are confined to shallow waters. Continental water may therefore, be enriched in both methyl chloride and iodide. It is interesting to note that these algae, some of which concentrate large amounts of iodine from seawater, (*Laminaria*, the giant kelp, contains 0.2% by weight of iodine), evolved some 400 million years ago. Halocarbons have presumably been trace components of the atmosphere since this time. Chlorine-catalysed destruction of ozone is not a new invention!

To conclude our discussion of sources, Table 5 summarizes our estimates of the various contributions to atmospheric methyl chloride. On the basis of the above discussion, we have estimated the marine source to lie between 1 and 8  $\text{mt yr}^{-1}$ ; the lower figure is derived by equating the  $\text{CH}_3\text{I}$  and the  $\text{CH}_3\text{Cl}$  sources while the upper is calculated from the measurements of seawater concentration and the stagnant film model. The marine source dominates but it is clear that further measurements of seawater concentration and flux rates are required to more precisely define this source.

TABLE 5. SOURCES OF METHYL CHLORIDE

SOURCE	STRENGTH, $\text{MT YR}^{-1}$
MICROBES	?
URBAN ANTHROPOGENIC	0.15 - 0.6
COMBUSTION OF VEGETATION	0.4 - 1
MARINE	1 - 8
TOTAL	1.6 - 9.6

**NEW MEASUREMENTS:** The difficulty of ambient methyl chloride analysis has meant that the data base has been limited up till now. Our most recent measurements have been made by a technique of Selective Electron Capture Sensitization (SECS) which increases the sensitivity with which methyl chloride is detected to a level comparable with that of the other major halocarbons. The effluent from the GC column is passed through a reactor heated to about  $280^\circ\text{C}$  and packed with sodium iodide crystals. Methyl chloride in the sample is converted to methyl iodide by reaction with the sodium iodide, with about 80% efficiency (fig. 2). The sensitivity of the electron capture detector is one to two orders of magnitude greater toward methyl iodide than towards methyl chloride, so that a greatly increased signal is observed. We hope that the improved measurements made possible by this technique will prove valuable in solving the remaining problems associated with atmospheric methyl chloride.



ANALYSIS OF AMBIENT METHYL CHLORIDE BY  
IODINATION AND ELECTRON CAPTURE DETECTION

#### REFERENCES

- Batchelder, R. B., and H. F. Hirt, Fire in tropical forests and grasslands, U. S. Army Natick Laboratories document no. 67-41-ES, Natick, MA., 1966.
- Broecker, W. S. and T. H. Peng, Gas exchange rates between air and sea, *Tellus*, **26**, 39-40, 1976.
- Chopra, N. M., and L. R. Sherman, Systematic studies of the breakdown of p. p', DDT in tobacco smokes; investigations into the presence of methyl chloride, dichloromethane and chloroform in tobacco smoke, *Anal. Chem.*, **44**, 1036-1038, 1972.



- Cowan, M. I., A. T. Glen, S. A. Hutchinson, M. E. Maccartney, J. M. Mackintosh, and A. M. Moss, Production of volatile metabolites by species of fomes, Trans. Br. Mycol. Soc., 60, 347-360, 1973.
- Crutzen, P. J., I. S. A. Isaksen, and J. R. McAfee, The impact of the chlorocarbon industry on the ozone layer., J. Geophys. Res., 83, 345-363, 1978.
- Crutzen, P. S., L. E. Heidt, J. P. Krasnec, W. H. Potlock, and W. Seiler, Biomass burning as a source of the atmospheric gases CO, H<sub>2</sub>, N<sub>2</sub>O, CH<sub>3</sub>Cl, and COS, in press, Nature, 1979.
- Grimsrud, E. P., and R. A. Rasmussen, Survey and analysis of halocarbons in the air by gas chromatography/mass spectrometry, Atmos. Environ., 9, 1014-1017, 1975.
- Liss, P. S., and P. G. Slater, Flux of gases across the air-sea interface, Nature, 247, 181-184, 1974.
- Lovelock, J. E., Natural halocarbons in the air and in the sea, Nature, 256, 193-194, 1975.
- National Aeronautics and Space Administration, Chlorofluoromethanes and the stratosphere, Ed. R. D. Hudson, NASA Reference Pub. no. 1010, 1977.
- Palmer, T. Y., Combustion sources of atmospheric chlorine, Nature, 263, 44-46, 1976.
- Singh, H. B., L. J. Salas, H. Shieyeishi, and A. H. Smith, Fate of halogenated compounds in the atmosphere; interim report, Publication E. P. A.-600/3-78-017, Environmental Protection Agency, Research Triangle Park, NC, 1978a.
- Singh, H. B., L. J. Salas, H. Shiegeishi, and E. Scribner, Global distribution of selected halocarbons, hydrocarbons, SF<sub>6</sub> and N<sub>2</sub>O, Publication E. P. A.-600/3-78/100, Environmental Protection Agency, Research Triangle Park, NC, 1978b.
- Zafiriou, O. C., Photochemistry of halogens in the marine atmosphere, J. Geophys. Res., 79, 2730-2732, 1974.
- Zafiriou, O. C., Reaction of methyl halides with seawater and marine aerosols, J. Mar. Res., 33, 75-81, 1975.

## RELEASE OF INDUSTRIAL HALOCARBONS AND TROPOSPHERIC BUDGET

J. P. Jesson

Central Research and Development Department  
E. I. du Pont de Nemours and Company  
Experimental Station  
Wilmington, Delaware 19898

### Abstract

This paper presents summary information on the production and release of industrially produced chlorine compounds. Four of these compounds ( $\text{CCl}_3\text{F}$ ,  $\text{CF}_2\text{Cl}_2$ ,  $\text{CCl}_4$ , and  $\text{CH}_3\text{CCl}_3$ ) are present in tropospheric air in concentrations greater than 50 ppt, and must be considered when assessing the impact of chlorine on stratospheric ozone. Phenomenological methods for determining the lifetimes of these chlorine compounds in the troposphere are discussed. Sources of uncertainty in the approaches are considered. It is concluded that current measurements do not allow reliable estimates of the tropospheric lifetimes for  $\text{CCl}_3\text{F}$ ,  $\text{CCl}_2\text{F}_2$ , and  $\text{CCl}_4$ . Lifetimes in the range 10- $\infty$  years can be accommodated by the data. A number of possible tropospheric degradation processes are considered explicitly -: attack by hydroxyl radicals on  $\text{CH}_3\text{CCl}_3$ , decomposition of  $\text{CCl}_3\text{F}$  and  $\text{CCl}_2\text{F}_2$  on the surface of sand particles, and dissolution of  $\text{CCl}_4$  in sea water. It is concluded that the tropospheric lifetime of  $\text{CH}_3\text{CCl}_3$  is probably less than 10 years. The contribution of  $\text{CCl}_3\text{F}$ ,  $\text{CCl}_2\text{F}_2$ ,  $\text{CCl}_4$ ,  $\text{CH}_2\text{Cl}_2$ , and  $\text{CH}_3\text{CCl}_3$  to the stratospheric odd chlorine burden is estimated to be 2 ppb.

**INTRODUCTION:** A primary prerequisite for understanding the possible impact of commercially produced halocarbons on atmospheric chemistry is a detailed knowledge of the types of compounds produced, the quantities in which they are produced, and the rate at which they are released to the atmosphere.

To assess the impact of the chlorocarbons released, on stratospheric ozone, we need to know not only the individual release figures for each chlorocarbon, but also the fraction of the chlorocarbon which reaches the stratosphere. This fraction may be different for each chlorocarbon and is determined by the possibility of removal processes in the troposphere. If there are no effective removal processes, the fraction is 1.

This paper presents an assessment of the quantities of industrial chlorocarbons released to date and their tropospheric budgets.

**HALOCARBON SOURCES:** The Halocarbon Industry - Overall Production and Release

The quantities of the major halocarbons produced in 1973 are given in Table 1 [Little, 1975], [Manufacturing Chemists Association Fluorocarbon Technical Panel, 1978, 1979], Figures

TABLE 1

## QUANTITIES OF PRINCIPAL HALOCARBONS PRODUCED IN 1973

(10<sup>3</sup> metric tons)

Compound	U.S. Production <sup>1</sup>	World Production <sup>1,2</sup>
CFCl <sub>3</sub>	150	354
CF <sub>2</sub> Cl <sub>2</sub>	220	447
CHClF <sub>2</sub>	60	78
CCl <sub>4</sub>	470	950
CH <sub>3</sub> CCl <sub>3</sub>	250	420
CHCl <sub>3</sub>	115	225
C <sub>2</sub> H <sub>5</sub> Cl	300	550
CH <sub>2</sub> ClCH <sub>2</sub> Cl	4224	12,000
CH <sub>3</sub> Cl	247	400
CH <sub>2</sub> Cl <sub>2</sub>	236	425
CCl <sub>2</sub> :CCl <sub>2</sub>	321	750
CCl <sub>2</sub> :CClH	205	700
CH <sub>2</sub> :CHCl	2432	7100

1. [Little, 1975]

2. [Manufacturing Chemists Association Fluorocarbon Technical Panel, 1978, 1979].

for production tend to be very accurate (+5%) for the United States since they are available through United States Tariff Commission reports. World production figures are in general less accurate. For the particular cases of CCl<sub>3</sub>F and CCl<sub>2</sub>F<sub>2</sub> (FC-11 and FC-12) a concerted effort by the major manufacturers has produced accurate (<+5%) worldwide production figures [McCarthy, et al, 1977], [Manufacturing Chemists Association Fluorocarbon Technical Panel, 1979].

Atmospheric release is much more difficult to determine and must be assessed for each material on the basis of use. Assessments of this type have been carried out for the halocarbon industry [Little, 1975], [Manufacturing Chemists Association Fluorocarbon Technical Panel, 1978, 1979], [Bauer, 1978], [Galbally, 1976], [McConnell and Schiff, 1978]. The results for 1973 are given in Table 2. It can be seen that during 1973, for most compounds, about half the release was in the United States. Note also that in the cases of CCl<sub>4</sub> and CH<sub>3</sub>CCl<sub>3</sub> there are several estimates which differ significantly.

The compounds in Table 2 may be divided into two categories - (i) those that are produced in large quantities and at the same time are expected to have a relatively long lifetime in the troposphere (>5 years half-life) and (ii) those which are produced in relatively small amounts and/or are expected to have relatively short tropospheric lifetimes. The distinction is important since it is only if a compound is produced in large quantities and is relatively long lived in the troposphere that significant quantities can survive to reach the stratosphere. Production and release of compounds in category (i) will be considered in more detail later in this paper. [It should be noted that the natural product CH<sub>3</sub>Cl is a partial exception to this classification: the biosphere produces an enormous flux of this compound and, even though it is thought to have a comparatively short tropospheric lifetime (~1 yr), CH<sub>3</sub>Cl represents a significant source of stratospheric chlorine.]

We conclude the present section by examining the factors which allow us to divide the industrial halocarbons into the two categories. One factor which will assure a relatively short lifetime in the lower atmosphere is high water solubility. Thus, large amounts of HCl, inorganic halides, and molecular chlorine are produced commercially. Although they are, in general, intermediates in manufacturing processes and therefore are largely converted to other chemicals instead of being released to the atmosphere, some undoubtedly escape. They have not been included in Tables 1 and 2 because they are highly water soluble and, under

TABLE 2

## ESTIMATED RELEASE OF PRINCIPAL HALOCARBONS IN 1973

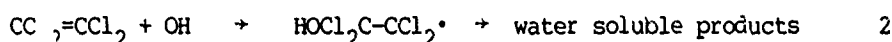
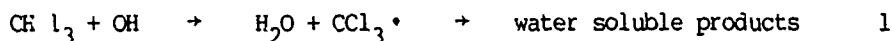
(10<sup>3</sup> metric tons)

Compound	U.S. Release <sup>1</sup>	World Release <sup>1-5</sup>
CFC1 <sub>3</sub>	127	290
CF <sub>2</sub> Cl <sub>2</sub>	178	386
CHClF <sub>2</sub>	28	36
CCl <sub>4</sub>	21	42
		61
		90
CH <sub>3</sub> CCl <sub>3</sub>	195	324
		387
		423
CHCl <sub>3</sub>	6.2	12.4
C <sub>2</sub> H <sub>5</sub> Cl	8.0	14.6
CH <sub>2</sub> ClCH <sub>2</sub> Cl	199	565
CH <sub>3</sub> Cl	4.8	7.9
CH <sub>2</sub> Cl <sub>2</sub>	197	346
CCl <sub>2</sub> :CCl <sub>2</sub>	272	609
CCl <sub>2</sub> :CClH	194	648
CH <sub>2</sub> :CHCl	89	352

1. [Little, 1975]
2. [Manufacturing Chemists Association Fluorocarbon Technical Panel, 1979]
3. [Bauer, 1978]
4. [Galbally, 1976]
5. [McConnell and Schiff, 1978]

normal circumstances, are prevented from reaching the stratosphere by washout in rain water. [It might be noted however, that, particularly in the case of naturally produced soluble halogen containing compounds (e.g. HCl from volcanoes) and in the case of salt in sea water, one can conceive of bulk processes (volcanic eruption, violent storms) transporting soluble material to the stratosphere directly. This type of activity must be considered in attempts to establish a total chlorine budget for the stratosphere.] In the normal troposphere, the concentration of water soluble halogen compounds drops off very rapidly with altitude.

Organic halocarbons such as those listed in Tables 1 and 2 have very low water solubility and are not subject to efficient rainout. Some of them can, however, react with other trace species in the troposphere. The end products of these interactions are usually water soluble so that, if the conversion of the chlorocarbon to the soluble form is sufficiently rapid, only a small fraction of the chlorine content of the compound will reach the stratosphere. Examples of this type of process are reaction of compounds containing C-H or C=C functions with hydroxyl radicals (Eqns. 1, 2)



Fully halogenated compounds such as CCl<sub>3</sub>F or CCl<sub>4</sub> do not undergo rapid reaction with trace species such as OH. They are, therefore, relatively long lived in the troposphere and appreciable fractions survive to reach the stratosphere.

We may now divide the compounds in Table 2 into the two categories. In harmony with the above discussion  $\text{CH}_2\text{Cl}_2$ ,  $\text{CHCl}_3$ ,  $\text{CCl}_2=\text{CCl}_2$ , and  $\text{CHCl}=\text{CCl}_2$ , are found in the troposphere in concentrations  $< 30 \text{ ppt}$  (relative to a total of  $> 300 \text{ ppt}$  for  $\text{CCl}_3\text{F}$  and  $\text{CCl}_2\text{F}_2$ ). The only halocarbons found in amounts  $> 50 \text{ ppt}$  are  $\text{CCl}_3\text{F}$ ,  $\text{CCl}_2\text{F}_2$ ,  $\text{CCl}_4$ ,  $\text{CH}_3\text{CCl}_3$ , and  $\text{CH}_3\text{Cl}$ . These are considered in more detail in the following sections.

Detection of  $\text{CH}_2\text{ClCH}_2\text{Cl}$  in the atmosphere has not been reported in the literature. Singh [1979] indicates that it is difficult to detect by gas chromatography since it elutes close to the  $\text{CCl}_3\text{CH}_3$  peak, and has much lower intrinsic sensitivity in electron capture detection. Reaction with  $\text{OH}$  appears to be an order of magnitude faster than for  $\text{CCl}_3\text{CH}_3$  [Howard and Evenson, 1976]. This, combined with the comparable release rates for the two compounds given in Table 2 suggests that  $\text{CH}_2\text{ClCH}_2\text{Cl}$  will not be an important source of stratospheric odd chlorine.

#### Long Lived Halocarbons - Production and Release

##### $\text{CCl}_3\text{F}$ and $\text{CCl}_2\text{F}_2$

Accurate data for the production and release to the atmosphere of  $\text{CCl}_3\text{F}$  and  $\text{CCl}_2\text{F}_2$  have been obtained through a survey of the manufacturers carried out by independent examiners. The totals to the end of 1975 have been published [McCarthy, et al., 1977]. Totals to the end of 1978 are available [Manufacturing Chemists Association Fluorocarbon Technical Panel, 1979] and annual updates are planned. Release to the atmosphere is estimated as being close to 85% of the amount produced at any given time; this value was obtained by breaking down sales in terms of end use (refrigeration, aerosols, closed cell foam, etc.) and combining it with a release pattern for each application. For instance, the  $\text{CCl}_2\text{F}_2$  in domestic refrigerators is released slowly, whereas aerosol propellants are released quickly.

Total world release to the atmosphere by the end of 1978 was  $3.73 \times 10^9$  kilograms of  $\text{CCl}_3\text{F}$  and  $5.48 \times 10^9$  kilograms of  $\text{CCl}_2\text{F}_2$  [Manufacturing Chemists Association Fluorocarbon Technical Panel, 1979]. Overall estimates of release to the atmosphere are probably accurate to  $\pm 5\%$ . World production and release of  $\text{CCl}_3\text{F}$  and  $\text{CCl}_2\text{F}_2$  on a year by year basis to the end of 1978 are given in Table 3. The exponential growth in  $\text{CCl}_3\text{F}$  and  $\text{CCl}_2\text{F}_2$  release to the end of 1974 is illustrated in Figure 1 for  $\text{CCl}_3\text{F}$ . Since 1973 the release has been relatively constant.

##### $\text{CHClF}_2$

Other fluorocarbons  $\text{CHF}_2\text{Cl}$  (FC-22),  $\text{CFCl}_2\text{CF}_2\text{Cl}$  (FC-113), and  $\text{CF}_2\text{ClCF}_2\text{Cl}$  (FC-114) are produced in much smaller amounts. Of these  $\text{CHF}_2\text{Cl}$  occurs in the largest volume, world production through the end of 1977 for uses other than as an intermediate in the production of other chemicals being  $\sim 1000$  metric kilotons [Manufacturing Chemists Association Fluorocarbon Technical Panel, 1978] ( $\sim 1/10$ th the combined  $\text{CCl}_3\text{F}$  and  $\text{CCl}_2\text{F}_2$  production). Additionally, as discussed below,  $\text{CHClF}_2$  is subject to attack by hydroxyl radicals which gives an approximate upper limit to its tropospheric lifetime. World Production and Release of FC-22 on a year by year basis to the end of 1977 is given in Table 4.

##### $\text{CCl}_4$

$\text{CCl}_4$  is currently manufactured largely as an intermediate for the production of  $\text{CCl}_3\text{F}$  and  $\text{CCl}_2\text{F}_2$ . In this application it is not released to the atmosphere in significant amounts. The use of  $\text{CCl}_4$  for other purposes (solvent applications, fire extinguishing applications, use as a fumigating agent, etc.) has declined significantly since the nineteen fifties.

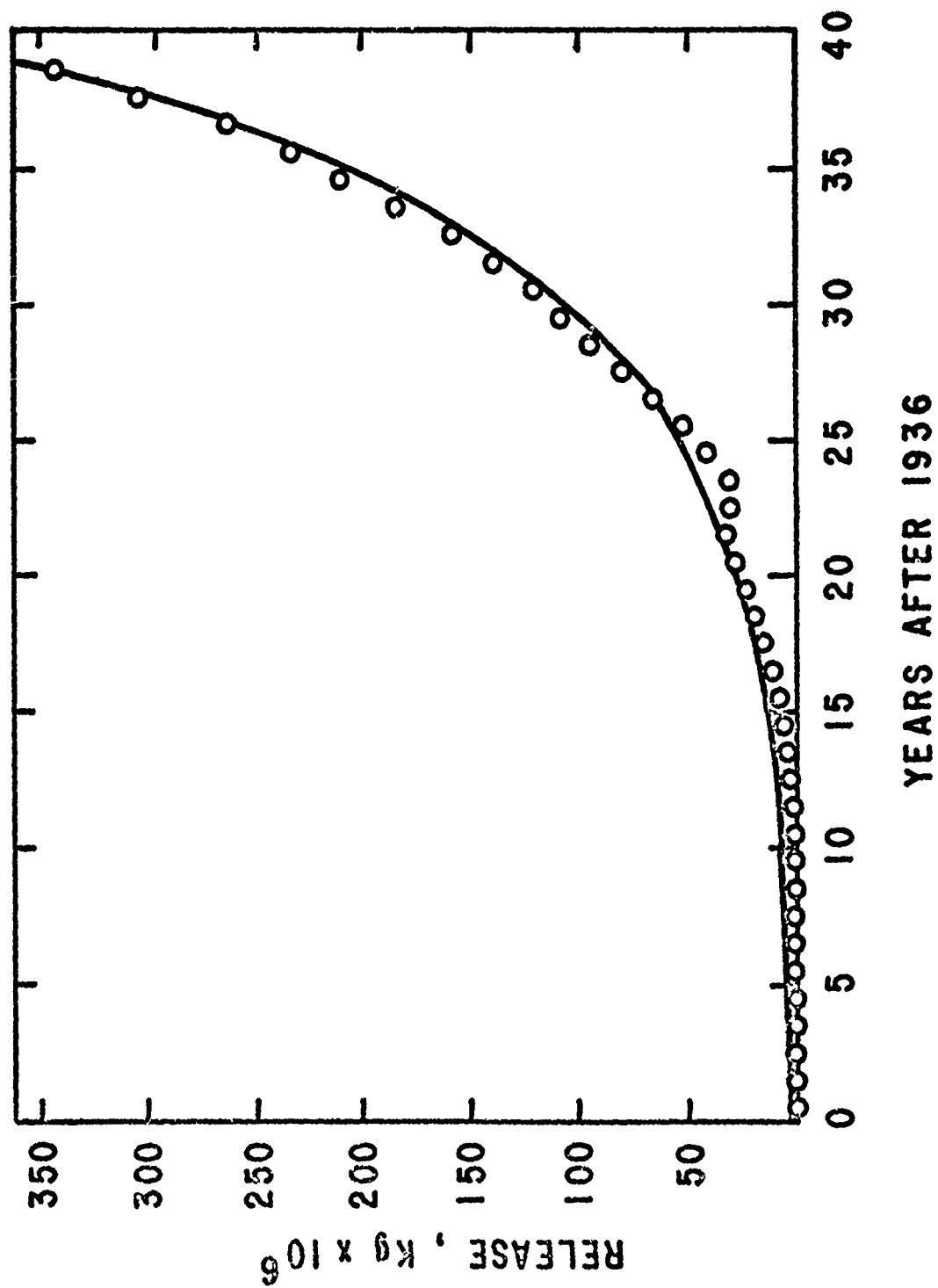
Values for production and atmospheric emissions through 1976 are given in Table 5. The estimates are from several sources and show considerable scatter (release in recent years is only a small fraction of total production and could, therefore, be subject to large errors. Total worldwide production is also somewhat uncertain).

The estimates of Galbally (1976) assume that the only significant production between 1914 and 1955 was in the USA, UK, France, and Germany. Estimates for later dates include Japan and European countries. No data are available for the USSR and China. The emissions estimates were obtained by subtracting  $\text{CCl}_4$  production used as a feedstock and assuming 90% of the remainder is lost to the atmosphere. Linear interpolation was used to obtain estimates for those years where no production and usage figures were available. An uncertainty figure of  $\pm 30\%$  was given for the final estimates [Galbally, 1976].

TABLE 3  
CFC1<sub>3</sub> AND CF<sub>2</sub>Cl<sub>2</sub> PRODUCTION AND RELEASE SUMMARY - WORLD TOTAL 2,4  
(10<sup>3</sup> metric tons)

CFC1 <sub>3</sub>				CF <sub>2</sub> Cl <sub>2</sub>			
YEAR	ANNUAL		CUMULATIVE	YEAR	ANNUAL		CUMULATIVE
	PRODUCTION	RELEASED			PRODUCTION	RELEASED	
1931	0	0	0	1931	.5	.0	.5
1932	0	0	0	1932	.1	.0	.6
1933	0	0	0	1933	.3	.1	.9
1934	0	0	0	1934	.7	.2	1.6
1935	0	0	0	1935	1.0	.4	2.6
1936	.1	0	2	1936	1.7	.6	4.3
1937	.1	0	3	1937	3.1	.9	7.4
1938	.1	.1	4	1938	2.8	1.3	10.2
1939	.1	.1	5	1939	3.9	1.7	14.1
1940	.2	.1	7	1940	4.5	2.3	18.6
1941	.3	.1	10	1941	6.3	2.9	24.9
1942	.3	.2	13	1942	5.9	3.5	30.8
1943	.4	.2	17	1943	8.2	4.7	39.0
1944	.4	.3	21	1944	16.7	6.1	55.7
1945	.7	.6	28	1945	20.1	11.9	75.8
1946	1.3	1.2	31	1946	20.1	19.0	94.8
1947	3.0	2.3	34	1947	24.8	22.2	119.6
1948	4.5	3.7	39	1948	26.1	24.2	145.7
1949	6.6	5.4	45	1949	34.6	27.1	180.3
1950	9.1	7.5	54	1950	36.2	30.2	216.5
1951	13.6	10.8	68	1951	37.2	31.5	253.7
1952	17.3	14.7	85	1952	46.5	35.5	300.2
1953	20.9	18.3	106	1953	49.1	40.3	349.3
1954	26.3	22.6	132	1954	57.6	45.2	406.9
1955	33.9	28.2	166	1955	68.7	52.6	475.6
1956	39.7	31.6	206	1956	74.2	59.8	545.4
1957	49.7	29.7	255	1957	73.4	62.6	618.0
1958	35.6	30.3	291	1958	87.6	69.6	705.6
1959	60.5	51.2	351	1959	99.4	83.2	795.0
1960	78.1	64.1	429	1960	108.5	93.2	883.5
1961	93.3	78.5	522	1961	128.1	107.1	991.6
1962	111.1	93.2	633	1962	146.4	125.8	1117.4
1963	122.8	106.3	755	1963	170.1	146.6	1288.0
1964	141.0	119.0	896	1964	190.1	165.6	1478.6
1965	159.8	135.1	1055	1965	216.2	184.3	1662.9
1966	184.8	154.6	1240	1966	242.8	208.3	1870.9
1967	219.8	180.2	1459	1967	278.8	238.0	2108.9
1968	241.1	205.1	1660	1968	311.4	270.0	2378.9
1969	266.6	225.4	1926	1969	336.9	296.2	2675.2
1970	310.5	253.8	2236	1970	360.5	319.1	2985.7
1971	354.3	290.6	2630	1971	401.7	348.3	3318.1
1972	377.6	320.9	3008	1972	447.5	386.2	3719.7
1973	322.5	312.4	3320	1973	473.6	420.3	4167.2
1974	349.9	303.6	3669	1974	419.7	412.6	4586.9
1975	330.7	305.6	4012	1975	449.8	396.3	5000.5
1976	307.9	283.6	4319	1976	401.2	340.9	5410.4
1977				1977			5934.7
1978				1978			6335.9

Figure 1. Plot of release versus time for  $\text{CCl}_3\text{F}$  from 1936-1974 together with an exponential fit (solid curve).



JESSON  
TABLE 4

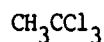
CHClF<sub>2</sub> PRODUCTION<sup>a</sup> AND RELEASE - WORLD TOTAL

(10<sup>3</sup> metric tons)

Year	Annual Production	Released <sup>b</sup>	Cumulative Production	Released <sup>b</sup>
1943	0.1		0.1	
1944	0.1		0.2	
1945	0.1		0.3	
1946	0.1		0.4	
1947	0.1	0.0	0.5	
1948	0.2	0.0	0.7	
1949	0.3	0.1	1.0	0.1
1950	0.8	0.1	1.8	0.2
1951	1.0	0.2	2.8	0.4
1952	1.6	0.3	4.4	0.7
1953	2.2	0.4	6.6	1.1
1954	2.9	0.6	9.5	1.7
1955	3.7	0.8	13.2	2.5
1956	6.1	1.2	19.3	3.7
1957	6.3	1.1	25.6	4.8
1958	7.6	1.4	33.2	6.2
1959	11.2	2.7	44.4	8.9
1960	12.1	3.3	56.5	12.2
1961	12.1	3.6	68.6	15.8
1962	15.4	4.6	84.0	20.4
1963	17.6	5.6	101.6	26.0
1964	22.4	6.8	124.0	32.8
1965	25.0	8.1	149.0	40.9
1966	31.5	9.8	180.5	50.7
1967	37.3	12.3	217.8	63.0
1968	46.0	16.4	263.8	79.4
1969	56.1	20.4	319.9	99.8
1970	59.5	23.6	379.4	123.4
1971	65.4	26.6	444.8	150.0
1972	71.6	31.7	516.4	181.7
1973	78.7	36.8	595.1	218.5
1974	90.2	42.9	685.3	261.4
1975	76.0	48.6	761.3	310.0
1976	94.2	60.3	855.5	370.3
1977	101.9	65.2	957.4	435.5

<sup>a</sup>The amounts exclude production as an intermediate for chemical or plastic production.

<sup>b</sup>Release obtained using scaling factors from Table 7 of [McCarthy, et al., 1977]. 1975 factor was used for 1976 and 1977 also.



Production and release figures for methyl chloroform through 1978 are given in Table 6. [Neely and Plonka, 1978], [Neely, 1979].



TABLE 5

PRODUCTION AND RELEASE RATES OF CARBON TETRACHLORIDE THROUGH 1976 ( $10^3$  metric tons)

Year	U.S. Production		U.S. Production not used		World Production		World Emissions	
	for FC-11 & FC-12 manufacture		for FC-11 & FC-12 manufacture		not used for FC-11 & FC-12 manufacture		Annual <sup>d</sup>	
	Annual	Cumulative from 1923 <sup>a</sup>	Annual	Cumulative from 1948 <sup>b</sup>	Annual <sup>c</sup>	Annual	Annual	Annual
1934	21	145			30	30	27	31
1939	41	316			51	51	46	54
1941	55	417			69	69	62	63
1943	79	562			99	99	89	75
1945	87	744			108	108	97	76
1946	67	812			82	82	74	75
1947	90	902			113	113	102	73
1948	97	999	63	63				
1950	98	1187	49	163	109	98	88	62
1955	130	1752	49	402	145	67	60	52
1956	137	1889	48	450	156	67	60	-
1957	144	2033	47	497	170	66	59	-
1958	142	2175	40	537	171	60	54	-
1959	167	2341	45	582	206	64	58	-
1960	169	2510	36	618	216	61	55	50
1961	174	2684	28	646	229	55	50	-
1962	219	2903	36	682	297	59	53	-
1963	235	3139	39	721	-	-	-	-
1964	243	3382	36	757	-	-	-	-
1965	269	3651	26	783	408	69	62	62
1966	294	3944	42	825	-	-	-	45
1967	323	4268	52	878	-	-	-	72
1968	346	4614	54	932	-	-	-	-
1969	400	5014	67	999	-	-	-	89
1970	458	5473	118	1117	-	-	-	93
1971	457	5930	102	1219	-	-	-	114
1972	451	6382	46	1265	-	-	-	123
1973	475	6858			904	87	78	96
1974	459	7317			998	100	78	79
1975					1014		90	53
1976					907		-	-
					857		-	-

JESSON

<sup>a</sup> Cumulative production prior to 1923 is estimated to be ~50 metric kilotons. [U.S. International Trade Commission Reports.]

<sup>b</sup> Cumulative production not including use in fluorocarbon manufacture, prior to 1948 is estimated to be ~900 metric kilotons. [U.S. International Trade Commission Reports.]

<sup>c</sup> [Galbally, 1976].

<sup>d</sup> [Galbally, 1976], [Singh, et al., 1976], [Parry, 1977].

## JESSON

TABLE 6

## PRODUCTION AND RELEASE RATES OF METHYL CHLOROFORM THROUGH 1978

(10<sup>3</sup> metric tons)

Year	Annual		Cumulative	
	Production	Release	Production	Release
1951	.14	.14	.14	.14
1952	.26	.23	.40	.36
1953	.98	.95	1.38	1.32
1954	2.9	2.7	4.28	4.04
1955	8.4	8.0	12.7	12.0
1956	13.8	12.4	26.5	24.4
1957	20.6	19.6	47.1	44.0
1958	21.8	20.7	68.9	65.8
1959	31.9	30.3	100	95
1960	38	36.1	139	131
1961	40.0	38.0	179	169
1962	59.4	56.2	238	225
1963	58	50.8	296	276
1964	64.4	56.7	361	333
1965	82.5	73.0	443	406
1966	116	109	559	515
1967	146	131	705	645
1968	158	145	863	790
1969	168	148	1031	939
1970	181	155	1212	1093
1971	191	167	1403	126
1972	267	230	1670	1490
1973	350	340	2020	1831
1974	389	363	2409	2194
1975	374	365	2783	2558
1976	438	416	3221	2974
1977	444	422	3665	3396
1978	438	473	4163	3869

TROPOSPHERIC CONCENTRATIONS: On release the chlorocarbons enter the troposphere, are transported upwards slowly, cross the tropopause (~15 km) and enter the stratosphere (~15-50 km). Any processes which degrade the chlorocarbons in the troposphere will diminish the fraction which survives to reach the stratosphere. We define a lifetime for any particular removal process as the time required for that process to reduce a given chlorocarbon concentration to 1/e of its original value.

The measured tropospheric concentrations for a variety of chlorocarbons at the end of 1977 [Singh, et al., 1976, 1979] and during 1977 [Rasmussen, 1979] are given respectively in Tables 7 and 8. As anticipated from the earlier discussion, the compounds can be divided into two categories, those with average tropospheric concentrations >90 ppt (CCl<sub>3</sub>F, CCl<sub>2</sub>F<sub>2</sub>, CCl<sub>4</sub>, CH<sub>3</sub>CCl<sub>3</sub>, CH<sub>3</sub>Cl) and those with average concentrations <40 ppt. In the following subsections we consider each of the compounds in the first category individually with the exception of the natural product CH<sub>3</sub>Cl.

CCl<sub>3</sub>F

It is still not known whether there are processes in the troposphere which destroy CCl<sub>3</sub>F at a rate sufficiently fast to compete with photolysis in the stratosphere as a removal process. One way to check this point is to compare the amount of CCl<sub>3</sub>F and CCl<sub>2</sub>F<sub>2</sub> known to have been released to the atmosphere with the amount found to be present by direct measurements.

TABLE 7

## BACKGROUND CONCENTRATIONS OF HALOCARBONS

AT THE END OF 1977

Compound	Concentration (ppt)		
	N. Hemisphere Average	S. Hemisphere Average	Global Average
$\text{CCl}_2\text{F}_2$ (FC12)	230	210	220
$\text{CCl}_3\text{F}$ (FC11)	133	119	126
$\text{CCl}_2\text{FCClF}_2$ (FC113)	19	18	18
$\text{CClF}_2\text{CClF}_2$ (FC114)	12	10	11
$\text{CHCl}_2\text{F}$ (FC21)	5	4	4
$\text{CCl}_4$	122	119	120
$\text{CH}_3\text{CCl}_3$	113	75	94
$\text{CH}_2\text{Cl}_2$	611	615	613
$\text{CH}_3\text{I}$	2	2	2
$\text{CHCl}_3$	14	< 3	8
$\text{CH}_2\text{Cl}_2$	44	20	32
$\text{C}_2\text{HCl}_3$	16	< 3	8
$\text{C}_2\text{Cl}_4$	40	12	26

TABLE 8

## ATMOSPHERIC HALOCARBON CONCENTRATIONS (ppt) (1976-1978)

		1976	1977	1978
$\text{CCl}_2\text{F}_2$	North	230	258	271
	South	217	246	258
	Average	223	252	264
$\text{CCl}_3\text{F}$	North	134	154	164
	South	127	148	151
	Average	130	151	157
$\text{CH}_3\text{CCl}_3$	North	108	108	119
	South	84	91	94
	Average	96	99	106
$\text{CCl}_4$	North	131	137	137
	South	124	131	135
	Average	127	134	136

Estimation of the FC11 Tropospheric Lifetime from a Determination of the Atmospheric Burden

There have been extensive measurements of  $\text{CCl}_3\text{F}$  over a period of eight years. Most of these measurements have been carried out at mid-latitude locations in the Northern hemisphere. Whatever the latitude, several criteria have to be satisfied to allow a meaningful comparison between measured values and the amount released [Meakin, et al., 1978], (a) the measurements must represent background concentrations at the latitude of measurement. This is particularly difficult in the northern hemisphere because of proximity to the sources of release, (b) the measurements must be accurately calibrated on an absolute scale, (c) since the background concentration varies as a function of latitude, any given set of measurements must be converted to a global average, using latitude correction factors, before it is possible to compare the measurements with the results of a 1-D modelling calculation, (d) since calculated concentrations for a particular release scenario are sensitive to the

vertical transport the eddy diffusion scheme must be chosen correctly, (e) since the calculated concentrations depend on the source strength, the release figures must be accurately known, (f) a 2-D model is desirable for proper interpretation of the data. We consider each of these factors in turn.

(a) Background Concentrations: Measurements by Singh, et al., (1978, 1979), Rasmussen (1979), and by Pack, et al., (1977) show that local variability is small at remote points in the Southern Hemisphere (i.e. points well removed from sources of release). These measurements may reasonably be assumed to represent background concentrations at the respective locations. Measurements by Singh, et al., (1978, 1979) and by Rasmussen, (1979) at relatively remote locations in the Northern Hemisphere suggest that Northern Hemisphere background concentrations are less than 20% greater than the Southern Hemisphere background. The South/North ratios of ~0.5 found by Pack, et al., (1977) between Capetown (35°S) and Adrigole (51°N) suggest that a significant contribution to the Adrigole measurements is arising from local sources (vide infra).

It appears that with careful selection of a number of locations and repeated measurement over a significant period of time, reliable samplings of background air could be obtained.

(b) Absolute Calibration: In determining tropospheric lifetimes for fluorocarbons from a comparison of the burden calculated from release and that found from measurement the greatest difficulties are presented by the absolute calibration problem. The results of an interlaboratory calibration exercise for  $\text{CCl}_3\text{F}$  (Rasmussen, 1978) involving 16 blind determinations are given in Table 9. The extremes of the range, for a single standard sample, were 120 and 176 ppt, and, although 8 of the measurements were within 6 ppt of the nominal value (150 ppt), 5 of the measurements were at the 120 ppt extreme (20% below the nominal value). Corresponding data for  $\text{FCl}_2$ ,  $\text{CH}_2\text{CCl}_3$ , and  $\text{CCl}_4$  intercalibrations are also given in Table 9. Here the results were even less satisfactory. The highest  $\text{FCl}_2$  value was 45% above the standard, the highest  $\text{CCl}_4$  value was 114% above the standard, and the highest  $\text{CH}_2\text{CCl}_3$  value was 30% above the standard. The overall scatter was worse for these three cases than for  $\text{FCl}_2$ . Additionally, comparison of the data in Tables 7 and 8 shows that Rasmussen, (1978) finds a global  $\text{FCl}_2$  concentration of 151 ppt for 1977 while Singh, et al., 1978, 1979 find a value of 126 ppt for the end of 1977. Clearly both numbers cannot be correct. The difference is 20% and is equal to the calculated difference between an infinite tropospheric lifetime and a lifetime of less than 30 years.

A further comparison, which is critical to the discussion of interhemispheric gradients which follows, is between the sets of southern hemisphere data for 1976 - Lovelock found 85-95 ppt  $\text{FCl}_2$  at Capetown in mid 1976 (consistent with many earlier measurements taken at this location over a period of 4 years, see Meakin, et al., (1978)) while Rasmussen, (1979) reports a southern hemisphere value for 1976 of 127 ppt. The difference is 40% and corresponds to the calculated difference between an infinite tropospheric lifetime and one of less than 20 years. Since there is comparatively little difficulty in sampling background air in the southern hemisphere, the differences noted must be due to problems of absolute calibration. It is this problem, and not the question of interhemispheric gradients, which leads to large differences in tropospheric lifetimes calculated from the data of Rasmussen, Lovelock, and Singh.

(c) Latitude Distributions: There is a higher concentration of fluorocarbons in the Northern Hemisphere (where they are released) than in the Southern Hemisphere. Measurements of Singh, et al., 1978, 1979 and of Rasmussen, (1979) show that currently, for background air, the difference between the two hemispheres is less than 20%. These results appeared to be in conflict with the earlier data obtained by Lovelock, et al., (1973) on a voyage of the Shackleton from the north to the south and back in 1971-2 (Figure 2). A least squares fit to these data has been used to generate empirical latitude conversion factors (Meakin, et al., 1978).

A set of theoretical curves for  $\text{CCl}_3\text{F}$  concentrations, calculated as a function of tropospheric lifetime, is compared with the data of Pack, et al. (1977) in Figure 3. The data were adjusted for latitude using the empirical conversion factors from the Shackleton voyage (Jesson, et al., 1977). The data, which were collected in both the Northern and Southern Hemispheres over a period of five years, lie between the 15 and 20 year lifetime curves. The fact that the Northern and Southern data, after adjustment for latitude, lie close together, is an indication of the internal consistency of the procedure. In all cases

the relatively slow Hungen diffusion profile was chosen. Faster diffusion would have lead to longer estimated tropospheric lifetimes.

TABLE 9

## HALOCARBON RESULTS RETURNED FROM PARTICIPATING LABORATORIES\*

Sample No.	FC-12 (ppt v/v)	FC-11 (ppt v/v)	CH <sub>2</sub> CCl <sub>3</sub> (ppt v/v)	CCl <sub>4</sub> (ppt v/v)
1	243 2.8%	145 3.3%		
2	246 1.6%	136 9.3%	97	167
3	223 10.8%	120 20.0%		
4	250 0%	148 1.3%	100	144
5		145 3.3%		
6	227 9.2%	149 0.7%		130
7	246 1.6%	150 0%	112	105
8	322 28.8%	176 17.3%		
9	250 0%	120 20.0%	80	120
10	362 44.8%	150 0%	103	108
11	249 0%	141 6.0%	130	71
12		156 4.0%	37	126
13	224 10.4%	124 17.3%	106	122
14		145 3.3%		
15	243 2.8%	123 18.0%		
16	204 18.4%	120 20.0%	30	321

\*The % figures are percent difference from the submitted value.

The Rasmussen data would lead to a much longer tropospheric lifetime (close to infinite) based on a similar calculation.

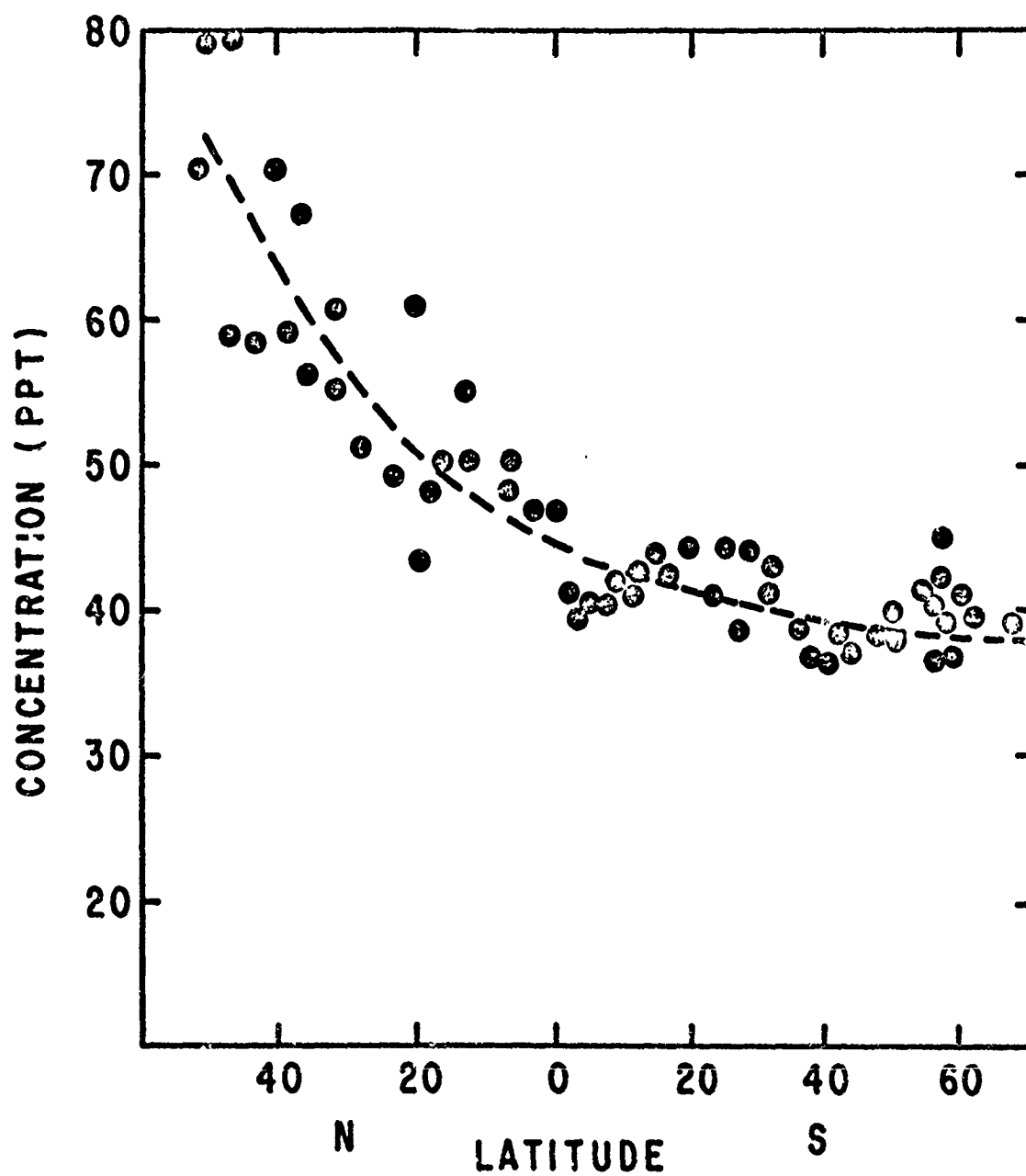
We now try to identify the source of this discrepancy. The National Academy of Sciences report (NAS, 1976) suggested that the Lovelock data for 1971-72 might be less reliable than his more recent data. This explanation is not viable. Table 1 of Jesson, et al., 1977 summarizes the Lovelock Northern and Southern Hemisphere data from 1970 to the end of 1975. From this, one can estimate a South/North ratio for 35°S to 51°N for each of the years as shown below:

1971	0.48
1972	0.53
1974	0.51
1975	0.54

The actual value used (Jesson, et al., 1977) from the full data set of the 1971-72 cruise corresponds to a ratio for 35°S to 51°N of 0.54, exactly the 1975 spot value.

JESSON

Figure 2.  $\text{CCl}_4\text{F}$  concentrations as a function of latitude measured on a cruise of the Shackleton in 1971-2. The dotted curve is a polynomial fit.



Another factor which has been suggested is that the decrease in the rate of annual increase of fluorocarbon production in recent years accounts in part for the discrepancy (Cunnold, et al., 1978). The Lovelock data (for 1976) shows a continuation in the Southern hemisphere trend with a value of 85-95 ppt for mid-1976 and little change in the South/North ratio. This suggests that changes in production levels were not of major importance up to mid 1976. The Lovelock Southern Hemisphere data from the end of 1971 to mid-1976 are plotted in Figure 4 and show a smooth trend.

We are left with the conclusion that the North/South ratios found by Lovelock and by Rasmussen and Singh are real (apart possibly from an absolute calibration problem). Cunnold, et al., 1978 have pointed out two factors which could make the data compatible: (a) higher fluorocarbon concentrations over the Atlantic relative to the Pacific due to proximity to sources of fluorocarbons released in the United States and Europe, (b) the fact that exchange between the hemispheres occurs mainly in the upper troposphere. They analyzed the problem on the basis of an 8 box model (4 latitudinally x 2 vertically). In the lower troposphere at mid-latitudes in the Northern hemisphere, they calculate a concentration 1.14 times the global average. For the lower troposphere at mid-latitudes in the Southern Hemisphere, the calculated value is 0.93 times the global average leading to a surface South/North ratio of 0.82. They estimate the ratio could be as low as 0.50 when proximity to sources in the North is taken into account. The corresponding value in the upper troposphere is 0.89 with a mid-latitude southern hemisphere value in the upper troposphere 0.94 times the global average.

This analysis provides the most reasonable explanation for the observed distributions. If it is correct, it leads to the conclusion that the Lovelock southern data (lower troposphere) at any given time should correspond to the global mean concentration multiplied by a factor of the order 0.93, while the Rasmussen southern data (upper troposphere) should correspond to the global mean concentration multiplied by a factor of the order 0.94. In other words, at any given time the two sets of data should agree in the southern hemisphere, with the Lovelock data being higher than the Rasmussen data in the northern hemisphere due both to proximity to sources of release and to the tropospheric circulation patterns. From Figure 4 we get a southern value of 85-95 ppt for Lovelock for mid-1976. This translates into an approximate global mean of  $90/0.93 = 97$  ppt which corresponds to a tropospheric lifetime of between 15 and 20 years, assuming the Hunten profile. In other words, if the Lovelock Northern data are high for the reasons outlined by Cunnold, et al. (1978) the reanalysis leads to a shorter tropospheric lifetime.

On the other hand, the Rasmussen Southern Hemisphere data (also shown in Figure 4) give values of ~120 ppt for 1976 leading to a global estimate of 128 ppt and a lifetime of ~50 years for the Hunten profile.

On the basis of the analysis given above, the Lovelock and Rasmussen data should agree in the Southern hemisphere, while the Lovelock data should be much higher than the Rasmussen data in the Northern Hemisphere. What has been consistently found is approximate agreement between the two groups in the North and much higher values for Rasmussen than Lovelock in the South.

Assuming the analysis of Cunnold, et al. (1978) is correct, there is a systematic absolute calibration difference between the Lovelock and Rasmussen groups with the Rasmussen data being uniformly higher. The Singh data lie between the other two sets (see Tables 7 and 8 and Figure 4).

(d) Eddy Diffusion: In trying to establish tropospheric lifetimes from global fluorocarbon burdens, the stratospheric photolytic sink must be properly taken into account. The effectiveness of this sink is quite sensitive to the rate of transport to the stratosphere (Meakin, et al., 1978).

For example, if the hypothetical global average concentration of  $\text{FC11}$  in mid 1975 was 80 ppt, the tropospheric lifetime, assuming a Hunten diffusion profile would be 12 years. The corresponding lifetimes for a range of other diffusion profiles (Meakin, et al., 1978) would be Crutzen III, 15 y; Chang I, 16 y; Chang II, 16 y; McElroy, 18y; Crutzen II, 22 y. Thus, within a range of commonly treated diffusion profiles, the estimated tropospheric lifetimes can vary by a factor of close to two.

JESSON

Figure 3. A comparison of  $\text{CCl}_3\text{F}$  mixing ratios in the troposphere calculated for tropospheric lifetimes of  $\infty$ , 50, 30, 20, 15, 10, and 7 years with the measurements of Lovelock.

▲ Data from exponential least squares fit to all Bowerchalke and Adrigole data (51°N) adjusted for latitude. ● Southern Hemisphere data adjusted for latitude.

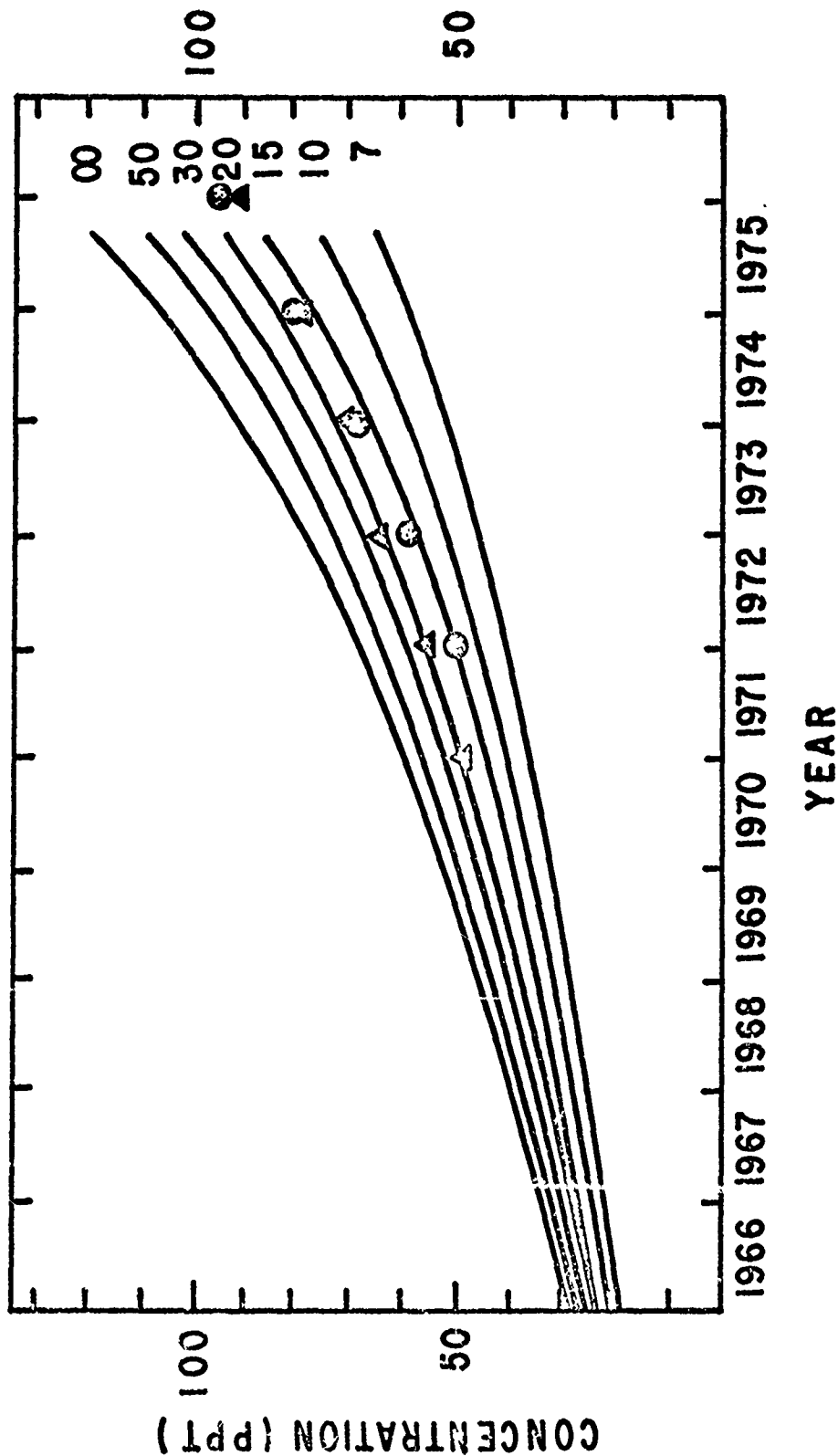
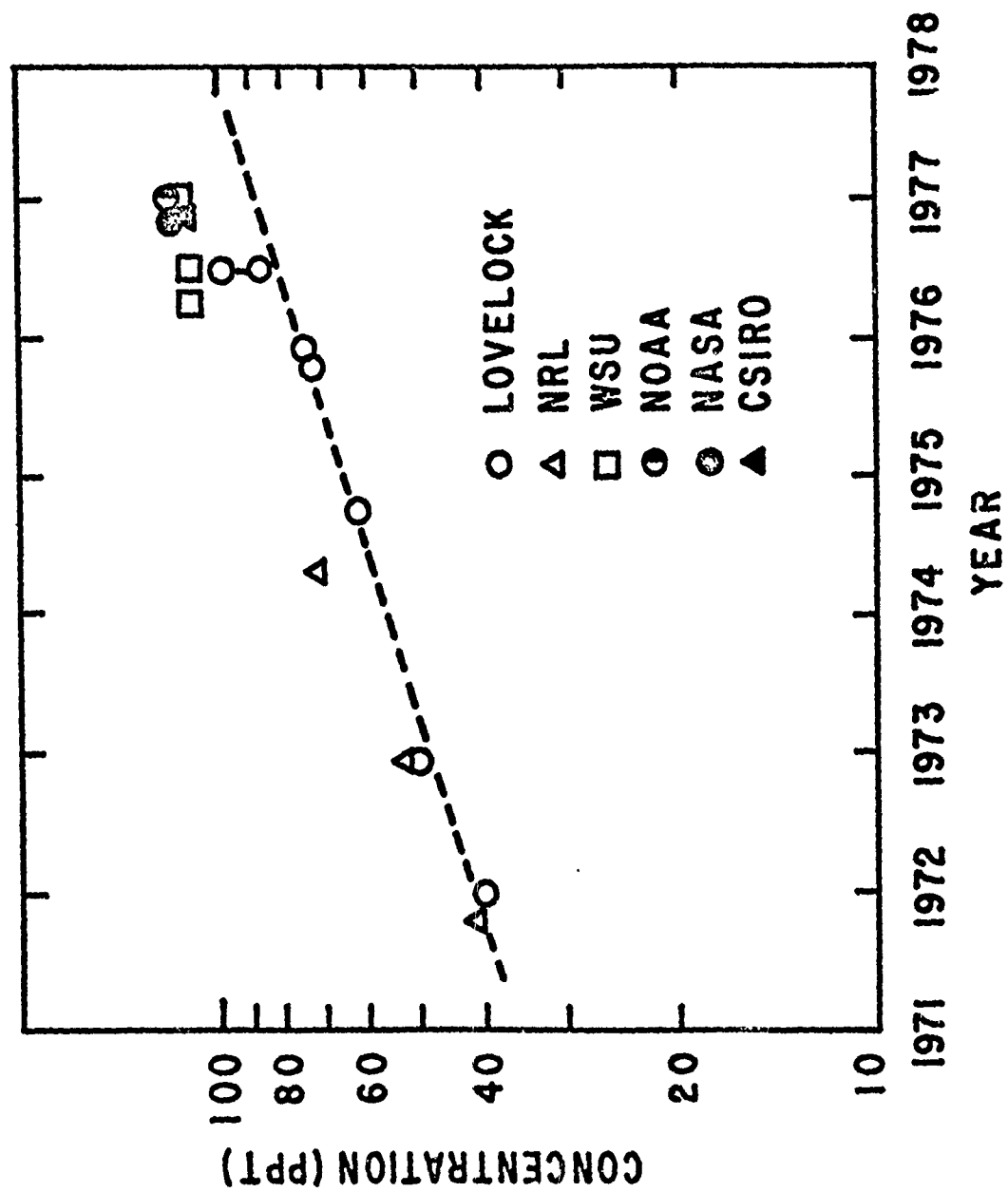




Figure 4. Southern Hemisphere  $\text{CCl}_3\text{F}$  concentrations versus time. The straight line is the data of Lovelock (1971-1976).



#### JESSON

The accuracy with which transport of fluorocarbons to the stratosphere must be specified places a significant limitation on the accuracy with which tropospheric lifetimes can be calculated from global burdens.

(e) Release: Figures for fluorocarbon release are now believed to be accurate to  $\pm 5\%$ . This is one of the smaller uncertainties in the problem but must be allowed for in comparing measurements and theory.

(f) 2-D Modelling: With the current emphasis on the development of 2-D models, it should be possible to empirically describe the transport in a much more realistic fashion. Interhemispheric gradients would be expected to be correctly reproduced as well as seasonal effects. Use of a 2-D model with a convincing description of transport and proper inclusion of the photolytic sink would appear to be necessary for a sound evaluation of tropospheric lifetimes from global burdens. Such models will soon be available.

The combination of problems listed above, relative to estimation of tropospheric lifetimes from global burdens, make it unlikely that the approach will prove satisfactory in the immediate future.

#### Estimation of the FC11 Tropospheric Lifetime from the Rate of Increase of Atmospheric Concentration with Time

The difficulties associated with the determination of tropospheric lifetimes from absolute atmospheric burdens, have lead to the examination of alternative approaches. The most promising of these is to determine lifetimes from trends in concentration as a function of time (Cunnold, et al, 1978). Although fluorocarbon growth rate differences for different tropospheric lifetimes are small ( $< 3\%$  between an infinite and a 10 y lifetime), the approach has the advantage that it is largely independent of absolute calibration, detailed release history, and eddy diffusion scheme. Moreover, a single station year to year trend is likely to be not much different from the global average trend.

In assessing the quantitative aspects of the trend approach, Cunnold et al. (1978) estimated that the yearly fluorocarbon production figures are subject to a random error of  $\pm 5\%$  and a systematic error of  $\pm 5\%$ . An additional  $\pm 5\%$  systematic error was assumed in the yearly release figures.

Instrumental uncertainties were estimated to give  $2\sigma$  errors of  $\pm 10\%$  for systematic effects and  $\pm 5\%$  for random effects.

Variability arising from single station observations was assessed as  $\pm 10\%$  for systematic and  $\pm 20\%$  for random errors.

While the global burden approach is subject in general to both the systematic and random errors, the trend analysis approach is primarily sensitive to random errors.

It was assumed that a sufficient number of observations would be made to eliminate instrument precision problems and that repeated calibrations would allow for any long term drift. Additionally, it was assumed that seasonal variations were either repeatable or small. (Seasonal variations appear to be very small in the Southern Hemisphere.)

Using the above criteria, it was calculated that, for a network of four stations spaced around the globe, it would be possible to establish a 10 y tropospheric lifetime from observations over a period of 3 y and a 20 y lifetime from observations over a period of 5 y ( $2\sigma$  confidence limits) assuming relatively constant production and release.

A network of four fluorocarbon measuring stations has been established under the auspices of the Manufacturing Chemists Association to acquire long term fluorocarbon growth trend data with the specific objective of establishing fluorocarbon tropospheric lifetimes. The network has been operational since mid 1978.

CCl<sub>2</sub>F<sub>2</sub>

Measured atmospheric concentrations for CCl<sub>2</sub>F<sub>2</sub> are given in Tables 7 and 8. Most of the detailed discussion of concentrations and lifetimes has been focussed on CCl<sub>3</sub>F since there are a much larger number of CCl<sub>3</sub>F measurements over a longer period of time. However, all the considerations in the previous section apply essentially unchanged, to CCl<sub>2</sub>F<sub>2</sub>.

Other Fluorocarbons

Table 7 gives global average concentrations for CCl<sub>2</sub>FCClF<sub>2</sub> (FC113) at 18 ppt, CClF<sub>2</sub>CClF<sub>2</sub> (FC114) at 11 ppt, and CHCl<sub>2</sub>F (FC21) at 4 ppt. Based on production, CHClF<sub>2</sub> (FC22) might be expected to be the most abundant fluorocarbon after FC11 and FC12. However, it is subject to attack by OH and, additionally, it is difficult to detect by electron capture gas chromatography. No reliable estimates of the atmospheric concentration of FC22 are available.

Of the three other fluorocarbons which were detected, FC113 and FC114 are produced industrially. Presumably their concentrations can be roughly accounted for on the basis of historical release. FC21, on the other hand, is not produced commercially and total release from industrial sources could account for only 0.03 ppt (Glasgow, et al, 1978).

FC21 has now been detected by a number of groups [Singh (1978)], [Cronn (1978)], [Rasmussen (1978)], [Bruner (1979)] and has been unambiguously identified using gas chromatography/mass spectrometry [Bruner (1979)].

It has been suggested that FC21 may arise from Teflon®, [poly(tetrafluoroethylene)], off gassing in the measuring equipment. This seems unlikely on the basis of the following studies: FC21 is still detected in Teflon® free equipment (Rasmussen 1978); no increase in FC21 is observed when the off gas from large amounts of finely divided Teflon® are sampled (Rasmussen 1978); there is no indication in the manufacture, chemistry, or industrial experience with Teflon® that FC21 is a contaminant (Glasgow, et al., 1978).

Ausloos, et al. (1977) have observed the formation of CHCl<sub>2</sub>F following irradiation of CCl<sub>3</sub>F with near u.v. light (300<λ<400nm) in the presence of sand. Although the size of this effect, in terms of a possible tropospheric sink, has not been determined, it does provide direct evidence for conversion of CFCl<sub>3</sub> into CHFC1<sub>2</sub>. Thus, if FC21 is a real atmospheric constituent, its most likely source is as a degradation product of FC11.

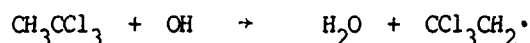
An alternative explanation is that FC21 arises from decomposition of FC11 on the chromatographic columns, or from degradation of stored FC11 standards. Either of these explanations would raise questions about the accuracy of current FC11 measurements.

CCl<sub>4</sub>

Tables 7 and 8 give measured atmospheric concentrations for CCl<sub>4</sub>. Unlike the fluorocarbons, CCl<sub>4</sub> is very uniformly distributed, presumably because the growth of emissions over the last decade has been relatively small. It is difficult to determine, because of uncertainties in the release figures for CCl<sub>4</sub>, whether all of the current atmospheric burden is of industrial origin. The observation of elevated CCl<sub>4</sub> concentrations in urban areas is evidence for continued industrial emission [Singh, et al. 1977] as is the observation of a continued growth rate of ~2%/y in the atmospheric background concentration [Singh, et al. (1979)]. The ocean appears to be a somewhat more efficient sink for CCl<sub>4</sub> than for CCl<sub>3</sub>F (vide infra).

CH<sub>3</sub>CCl<sub>3</sub>

CH<sub>3</sub>CCl<sub>3</sub> is the only industrial halocarbon found in concentrations >50 ppt which is subject to attack by tropospheric OH at a significant rate.



For this reason, most of the studies of the tropospheric concentration of CH<sub>3</sub>CCl<sub>3</sub> have been used as an indirect route to determining the average tropospheric OH concentration.

# JESSON

Singh has noted a fairly sharp change in the latitude gradient for  $\text{CH}_3\text{CCl}_3$  between  $20^\circ\text{N}$  and  $20^\circ\text{S}$  and suggests that this is due to the fact that this is the region of highest tropospheric OH concentration and of highest tropospheric temperature. Singh, et al. 1979 find the average concentration in the northern hemisphere to be 113 ppt and in the southern hemisphere 75 ppt for late 1977 (Table 7). The much larger interhemispheric difference (50%) than is observed for background FCl1 and FCl2 (<20%), is clearly suggestive of a latitude dependent removal mechanism. In this regard it must be noted, however, that the interhemispheric difference found by Rasmussen (1979) for  $\text{CH}_3\text{CCl}_3$  is much smaller (Table 8, 24%).

The tropospheric lifetimes and average tropospheric OH levels estimated in a variety of studies are given in Table 10.

TABLE 10

ESTIMATIONS OF THE TROPOSPHERIC LIFETIME,  $\tau$ , OF  $\text{CH}_3\text{CCl}_3$  AND OF THE  
AVERAGE TROPOSPHERIC OH CONCENTRATION, C, BY A VARIETY OF AUTHORS

$\tau \text{ CH}_3\text{CCl}_3 \text{ (y)}$	$C_{\text{OH}} \text{ (radicals/cc)}$	Reference
7.2	$4(+2) \times 10^5$	Singh (1977a)
5-10	$< 7 \times 10^5$	Lovelock (1977)
8-11	$4.1 \times 10^5$	Singh (1977b)
8		McConnell and Schiff (1978)
12		Chang and Penner (1978)
3.3	$1 \times 10^6$	Neely and Plonka (1978)
1.4		NAS (1976)
10		Crutzen and Fishman (1977)

While there is a grouping of many of the estimates for the tropospheric lifetime around 8 y and while the estimated average tropospheric OH concentrations ( $\sim 5 \times 10^5$  molecules/cc) suggest a lower tropospheric OH concentration than is given by most 1-D models, it is clear that the quantitative aspects of the situation are even less satisfactory than for FCl1. We briefly examine the same factors for  $\text{CH}_3\text{CCl}_3$  that we considered for FCl1 earlier in this paper.

## Background Concentrations

As for FCl1 it should be possible to obtain background readings if sufficient samplings are taken in well chosen areas. Comparison of Tables 7 and 8, however, suggests that this may be a problem with current measurements. The results in Table 7 show an interhemispheric difference of 50% while those in Table 8 show an interhemispheric difference of 18% for the same year.

## Absolute Calibration

The results in Table 9 show this to be a bigger problem for  $\text{CCl}_3\text{CH}_3$  than for FCl1, the values span the range +30% to -70% from the submitted value of 100.

## Latitude Distributions

As noted under (1) above there are large differences in the measured latitude distribution.

## Transport

To properly model the  $\text{CH}_3\text{CCl}_3$  situation, a 2-D model is required which generates realistic relative OH distributions as a function of latitude, properly simulates interhemispheric mixing and latitudinal temperature gradients, and properly includes the stratospheric sink.

## JESSON

### Release

The results in Table 2 show that, unlike the FC11 situation, estimates of  $\text{CH}_3\text{CCl}_3$  release differ appreciably (the highest value is 30% greater than the lowest value).

### Rate of Reaction with OH

There is some disagreement between currently available measurements of the rate of reaction of  $\text{CH}_3\text{CCl}_3$  with OH.

It is clear that the cumulative effect of the uncertainties listed above leads to large uncertainties in both the estimated tropospheric lifetime for  $\text{CH}_3\text{CCl}_3$  and the estimated tropospheric OH concentration.

### Removal Mechanisms for Chlorocarbons in the Troposphere

Inactive removal processes become significant when their rate approaches or exceeds the overall rate of removal via stratospheric photolysis. That removal however, is a slow process, and therefore other processes need not be very fast to be important. In the case of  $\text{CH}_3\text{CCl}_3$ , removal by OH is clearly a process which competes effectively with stratospheric photolysis (vide supra).

In the case of fully halogenated hydrocarbons, processes of comparable efficiency have not been established to date. The National Academy of Sciences [NAS (1976)] identified three inactive removal processes for FC11 and FC12 which they believed warranted more study -- solution in surface waters (estimated lower limit on removal time  $\sim 100$  y) ion molecule reactions (1000 y) and photodissociation in the troposphere (500 y). As they stand, none of these is likely to present significant competition to stratospheric photolysis.

Singh has investigated the possibility that the ocean might act as a sink for  $\text{CCl}_4$ . He estimates this sink to be about half as effective as the stratospheric photolysis sink. This leads to residence times in the 25-40 y range (Singh, et al. 1979).

A sink of possible interest for FC11 and FC12 which has been suggested since the 1976 National Academy of Sciences report is photodecomposition on the surface of sand particles (Ausloos, et al. 1977). Irradiation of  $\text{CCl}_4$ ,  $\text{CCl}_3\text{F}$ , and  $\text{CCl}_2\text{F}_2$  in the presence of  $\text{C}_2\text{H}_6$  in vessels containing silica sand results in the formation of chlorine containing products. The formation of these compounds occurs at wavelengths extending to 400 nm i.e. at wavelengths where the solar radiation penetrates to the earth's surface. Because of the detection method used, the experiments described above could not be conducted under an oxygen atmosphere. More recent developments of the approach have allowed experiments to be conducted in the presence of oxygen. It was speculated that oxygen might poison the sand surface and therefore reduce the decomposition efficiency. Results of the new experiments (Rebbert 1978) in fact show that the apparent efficiency is increased by about a factor of 40. Additionally earlier work by Lovelock has suggested that  $\text{CCl}_4$  concentrations in the atmosphere are diminished in the vicinity of large bodies of windblown sand (Lovelock 1976). The question of photodecomposition of FC11 and FC12 on airborne and surface sand (and other surfaces) clearly merits further study. However, to date, no reliable quantitative estimate of the possible size of the effect is available.

### Chlorocarbon Contributions to the Stratospheric Chlorine Burden

Concentration vs. altitude profiles for the chlorocarbons currently included in 1-D models of the atmosphere are shown in Figure 5. The contributions of each of these compounds to stratospheric odd chlorine is given in Table 11. It can be seen that the total odd chlorine contribution from these sources is  $\sim 2$  ppb. Clearly, if the high concentrations found for ClO in the stratosphere on some flights are correct, there must be other sources of stratospheric chlorine yet to be included in the models.

## JESSON

TABLE 11

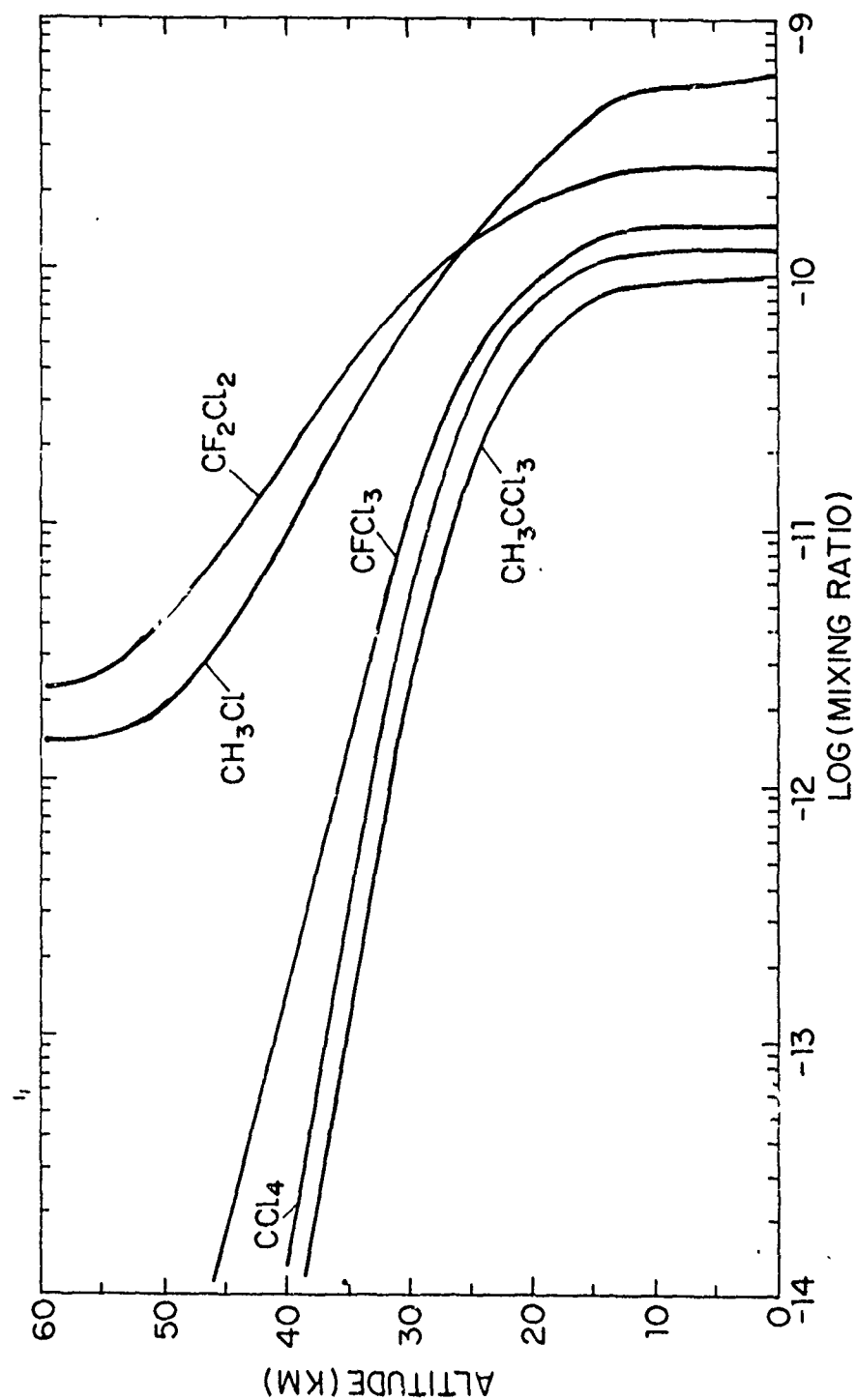
CHLORINE CONTRIBUTIONS OF VARIOUS  
CHLORINE COMPOUNDS TO STRATOSPHERIC CLX (ppb)

$\text{CH}_3\text{Cl}$	0.56
$\text{CCl}_4$	0.50
$\text{CH}_3\text{CCl}_3$	0.29
$\text{HCl}$	0.16
$\text{CCl}_3\text{F}$	0.62
$\text{CCl}_2\text{F}_2$	
	<hr/> 2.13

Summary

- Production and Release for a variety of chlorocarbons are now reasonably well characterized. In particular production and release of  $\text{CCl}_3\text{F}$  and  $\text{CCl}_2\text{F}_2$  are probably known to better than  $\pm 5\%$ .
- Most chlorocarbons which are produced industrially in significant quantities have been detected in the troposphere. The major contributors are  $\text{CCl}_3\text{F}$ ,  $\text{CCl}_2\text{F}_2$ ,  $\text{CCl}_4$ , and  $\text{CH}_3\text{CCl}_3$ .
- Attempts to determine a tropospheric lifetime for  $\text{CCl}_3\text{F}$  using the atmospheric burden approach remain unsatisfactory largely because of the problem of absolute calibration. Lifetimes of  $10^{-\infty}$  y can be accommodated by the data.
- Estimation of tropospheric lifetimes using growth of concentration with time appear promising. A network of four stations has been in operation for about a year. Preliminary conclusions should be available in about 3 years.
- Global distributions of fluorocarbons suggests rapid interhemispheric mixing ( $\sim 1.5$  y). Background concentrations in the northern hemisphere are probably less than 20% above those in the southern hemisphere.
- Carbon tetrachloride appears to be largely of industrial origin.
- The current best estimate for the residence time of  $\text{CH}_3\text{CCl}_3$  is  $\sim 8$  years. The number has a substantial uncertainty range.
- Photolysis of  $\text{FC11}$  on sand surfaces can occur with wavelengths of radiation available in the troposphere. Quantitative estimates of the size of this effect are not yet available.
- The detection of  $\text{FC21}$  by a number of workers suggests either a tropospheric sink for  $\text{FC11}$  or decomposition of  $\text{FC11}$  in the chromatographic equipment.
- The contribution of known chlorocarbons to the stratospheric chlorine burden, based on conventional diffusion approximations, is less than 2.5 ppb.

Figure 5. Vertical concentration profiles for the chlorocarbons currently included in 1-D models of the atmosphere.



## REFERENCES

- Ausloos, P., R. E. Rebbert, and L. C. Glasgow, Journal of Research, National Bureau of Standards, **82**, 1, 1977.
- Bauer, E., A Catalog of Perturbing Influences on Stratospheric Ozone, Institute of Defense Analysis Paper P 1340, September 1978.
- Bruner, F., (private communication, 1979).
- Chang, J. S., and J. E. Penner, Atmospheric Environment **12**, 1867, 1978.
- Cronn, D. R., American Chemical Society Fall Meeting, Miami Beach 1978.
- Crutzen, P. and J. Fishman, Geophysical Research Letters, **4**, 321 1977.
- Cunnold, D. M., F. N. Alyea, and R. G. Prinn, A Methodology for Determining the Atmospheric Lifetime of Fluorocarbons (preprint 1978).
- Galbally, I. E., "Man-Made Carbon Tetrachloride in the Atmosphere," Science, **193**, 573, 1976.
- Glasgow, L. C., J. P. Jesson, and R. B. Ward, Urban Non-Urban Relationships of Halocarbons..., Atmospheric Environment, **12**, 962, 1978.
- Howard, C. J., and K. M. Evenson, Rate Constants for the Reactions of OH with Ethane and Halogen Substituted Ethanes at 296°K, Journal of Chemical Physics, **64**, 4303, 1976.
- Jesson, J. P., P. Meakin, and L. C. Glasgow, The Fluorocarbon-Ozone Theory II. Tropospheric Lifetimes - An Estimate of the Tropospheric Lifetime of  $\text{CCl}_3\text{F}$ , Atmospheric Environment, **11**, 499, 1977.
- Little, A. D., Inc. Preliminary Economic Impact Assessment of Possible Regulatory Action to Control Atmospheric Emissions of Selected Halocarbons, Prepared for the Environmental Protection Agency, publication number EPA-450/3-75-073, 1975.
- Lovelock, J. E., R. J. Maggs, and R. J. Wade, Halogenated Hydrocarbons in and over the Atlantic, Nature, **241**, 194, 1973.
- Lovelock, J. E., presented at the Third European Geophysical Society Meeting, Amsterdam, September 1976.
- Lovelock, J. E., Nature, **267**, 32, 1977.
- Manufacturing Chemists Association Fluorocarbon Technical Panel: 1977 World Production and Sales of Fluorocarbon 22, June 28, 1978.
- Manufacturing Chemists Association Fluorocarbon Technical Panel: World Production and Release of Chlorofluorocarbons 11 and 12 Through 1978, August 6, 1979.
- McCarthy, R. L., F. A. Bower, and J. P. Jesson, The Fluorocarbon-Ozone Theory I: Production and Release. World Production and Release of  $\text{CCl}_3\text{F}$  and  $\text{CCl}_2\text{F}_2$  (Fluorocarbons 11 and 12) through 1975, Atmospheric Environment, **11**, 491-497, 1977.
- McConnell, J. C., and H. I. Schiff, "Methyl Chloroform: Impact on Stratospheric Ozone," Science, **199**, 174, 1978.
- Meakin, P., P. S. Gumerman, L. C. Glasgow, and J. P. Jesson, The Fluorocarbon-Ozone Theory III. Fluorocarbon Mixing and Photolysis. The Effects of Eddy Diffusion and Tropospheric Lifetime on  $\text{CCl}_3\text{F}$  and  $\text{CCl}_2\text{F}_2$  Tropospheric Mixing Ratios, Atmospheric Environment, **12**, 1271, 1978.
- NAS (1976) Halocarbons: Effect on Stratospheric Ozone, National Academy of Sciences, Washington, DC.
- Neely, W. B., and J. H. Plonka, "Estimation of Time Averaged Hydroxyl Radical Concentration in the Troposphere." Environmental Science and Technology, **12**, 317, 1978.
- Neely, W. B., (private communication 1979).
- Pack, D. H., J. E. Lovelock, G. Cotton, and C. Curthoys, "Halocarbon Behavior from a Long Time Series," Atmospheric Environment, **11**, 329, 1977.
- Parry, H. D., "Ozone Depletion by Chlorofluoromethanes? Yet Another Look." Journal of Applied Meteorology, **16**, 1137, 1977.
- Rasmussen, R. A., Interlaboratory Comparison of Fluorocarbon Measurements, Atmospheric Environment, **12**, 2505, 1978.
- Rasmussen, R. A., American Chemical Society Fall Meeting, Miami Beach, 1978.
- Rasmussen, R. A., (private communication 1979).
- Rebbert, R. E., WMO Symposium, Toronto, Canada, June 1978.
- Singh, H. B., D. P. Fowler, and T. O. Peyton, "Atmospheric Carbon Tetrachloride: Another Man-Made Pollutant." Science, **192**, 1231, 1976.
- Singh, H. B., L. Salas, H. Shigeishi, and A. H. Smith, "Atmospheric Fates of Halogenated Compounds: Second Year (Phase I) Summary Report," EPA Grant R-80380202, SRI Project 4487, Stanford Research Institute, Menlo Park, California, 1977.
- Singh, H. B., Geophysical Research Letters, **4**, 101, 1977a.
- Singh, H. B., Geophysical Research Letters, **4**, 453, 1977b.



JESSON

- Singh, H. B., L. J. Salas, H. Shigeishi, and E. Scribner, "Global Distribution of Selected Halocarbons, Hydrocarbons, SF<sub>6</sub>, and N<sub>2</sub>O" (Publ. EPA - 600/3-78-100 Environmental Protection Agency, Research Triangle Park, North Carolina 1978.)
- Singh, H. B., American Chemical Society Fall Meeting, Miami Beach, 1978.
- Singh, H. B., L. J. Salas, H. Shigeishi, and E. Scribner, "Atmospheric Halocarbons, Hydrocarbons, and Sulfur Hexafluoride: Global Distributions, Sources, and Sinks." Science, 203, 899, 1979.
- Singh, H. B. (private communication, 1979).

# ELEMENTARY ATMOSPHERIC REACTIONS: LABORATORY MEASUREMENTS

## AND THEIR INTERPRETATION

Frederick Kaufman

Department of Chemistry, University of Pittsburgh,  
Pittsburgh, PA 15260

### Abstract

Recent progress in laboratory studies of elementary reactions has made possible the fairly accurate measurement of many dozens of atom and radical reaction rate constants, particularly those involved in the catalytic removal of stratospheric ozone. The present status of the principal experimental methods, discharge-flow and flash photolysis, is described and compared. Advances, limitations, and future needs are assessed. The role of theory in the evaluation of experimental results and in a priori prediction of rate parameters is examined. Following the classification of elementary steps as direct-mode, complex-mode, and bond-forming, a recent example of experimental and theoretical studies from the author's laboratory is presented: The reactions of OH with methane and with six Cl- and F-substituted methanes are measured, their rate parameters analyzed and compared with transition state theory calculations by the method of thermochemical kinetics.

INTRODUCTION: Mature branches of physical science are characterized by an active interplay between inductive, i.e. observational, experimental, and deductive, i.e. theoretical descriptions of the phenomena under investigation. Atmospheric science provides excellent examples of this interplay. Because it is an interdisciplinary field that includes parts of radiation physics, photochemistry and chemical kinetics, meteorology and atmospheric transport, and mathematical modeling, the interactions are particularly rich and varied. Atmospheric observations call for theoretical models; these, in turn, call for laboratory measurements whose understanding requires insight into the theories of chemical kinetics, spectroscopy, molecular structure, and so on.

If there is a single thread that goes through this paper's discussion, it is this growing need for collaboration among the experimentalists and theorists of the disciplines involved. In that sense, I am apprehensive about what I view to be a temporary lull in the theory and modeling effort. One-dimensional models appear to have converged on their terminal state of usefulness and sophistication, while higher dimensional models are not yet far enough advanced to be of predictive value. This weakens the link between observation and analysis and inhibits progress towards a more quantitative understanding of the atmosphere and of its response to perturbation.

We need not repeat here the account of the rapid proliferation of the minimal set of chemical and photochemical processes needed to understand the workings of the stratosphere, from two species, O and O<sub>3</sub>, and four reactions of the Chapman pure oxygen model to the 30-40 species and 100-150 reactions of present-day models. Much of the theoretical side of this progress is due to the work of the three giants, Chapman, Bates, and Nicolet, and we are fortunate, indeed, to have Professor Nicolet as the convenor, director, and guiding spirit of the NATO Advanced Study Institute of whose proceedings this paper is a part. Let us not forget that it was the fruitful interactions between aeronomers and physical chemists that have catalyzed this phenomenal recent growth.

As a chemical kineticist, I welcome the incentive provided by the needs of atmospheric chemistry for measuring rate parameters of single-step, elementary reactions. This field, too long overshadowed by single-collision, molecular dynamics is again coming into its own. It is fortunate, furthermore, that these needs for rate constants with some state-specificity for atmospheric applications are perfectly met by the experimental techniques to be discussed here. Rate constants are measured under such conditions that rapidly relaxed degrees of freedom (translation, rotation) remain equilibrated, whereas metastable degrees of freedom (some vibrations or electronic excitations) are unrelaxed, i.e. are monitored as separate species. These are, of course, the conditions applicable to the troposphere and stratosphere where reactions take place in a bath gas of N<sub>2</sub> and O<sub>2</sub> that maintains thermal equilibrium. This obviates the necessity of measuring detailed state-to-state rate parameter. In the following sections of this paper, these experimental methods will first be examined and assessed, our theoretical understanding of measured rate parameters will next be summarized, and an example of our own recent work will lastly be presented that tests this interplay of experiment and theory on a set of seven closely related OH-radical reactions.

**REVIEW OF LABORATORY METHODS:** This paper is restricted to the kinetics of chemical reactions, i.e. excludes photochemical measurements such as absorption coefficients and quantum yields. It also omits the discussion of many useful techniques, e.g. molecular modulation, classical photochemistry, etc., because of their lack of specificity or sensitivity, in spite of their usefulness. It is thus restricted to the two major methods responsible for a large fraction of recent results: discharge-flow (DF) and flash photolysis (FP). These have been assessed and compared recently [Howard, 1979; Michael and Lee, 1979]. The DF method is operated in steady-state in a cylindrical flow tube and is therefore beset with the complexities arising from the interplay of transport (diffusive and convective) and chemical reaction. Exact or approximate solutions of the transport equation including radial and axial diffusion, plug flow or laminar flow, and surface removal of reactive species, have been worked out for many cases [Kaufman, 1961; Walker, 1961; Ferguson, et al., 1969; Poirier and Carr, 1971; Brown, 1978]. The analysis is simple when surface removal is either very inefficient or highly efficient, and when the convective flow regime is well characterized, i.e. as in plug flow where  $v(r) = \text{constant}$  or in laminar flow where  $v = v_0 (1 - (\frac{r}{r_0})^2)$ . The method's difficulties are usually connected with one or more of the following points: a. The surface reactivity is not well characterized or it is dependent in poorly known ways on the concentration of reactant species; b. the flow velocity profile is not known or it is affected by the mixing of added gases; c. the mixing of reactants is not sufficiently fast or complete, especially at higher pressures; d. the detection method and geometry are poorly controlled.

Figure 1 shows the diagram of an apparatus used in our laboratory in the study of a number of Cl- and ClO-reactions using resonance fluorescence detection of Cl at 134.7 nm as a diagnostic [Zahniser, et al., 1976; Zahniser and Kaufman, 1977; Zahniser, et al., 1978]. It uses a 2.54 cm diameter flow tube fitted with various easily replaceable sections, the reaction region up to 50 cm upstream of the detection cell is capable of being controlled at constant temperature from near 77 K to 500 K. Reactants are added through a movable injector tube. Surface reactions of atoms or radicals are inhibited by coatings of phosphoric acid, fluorocarbon waxes, or teflon. In favorable cases [Zahniser, et al., 1978] random errors of pseudo-first-order atom. concentration decays are in the 2 to 3% range (single standard deviation) and second-order rate constants are accurate to 10-15% including estimates of systematic errors. A detection limit of 10<sup>8</sup> to 10<sup>9</sup> cm<sup>-3</sup> is obtained yet improvements of geometrical factors in larger flow tubes with better collection efficiency can reduce these limits by three orders of magnitude [Anderson, 1978].

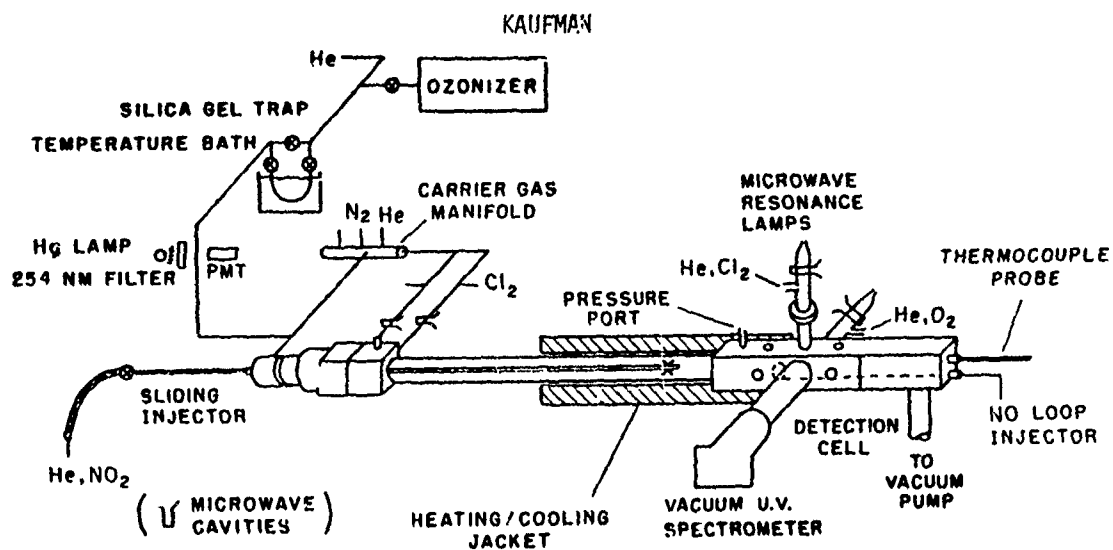


Figure 1

The addition of laser fluorescence detection using a tunable dye laser with frequency doubling and narrowing options (Chromatix, CMX-4), as shown in Figure 2, increases the versatility of the system by allowing the simultaneous measurement of atoms and radicals,

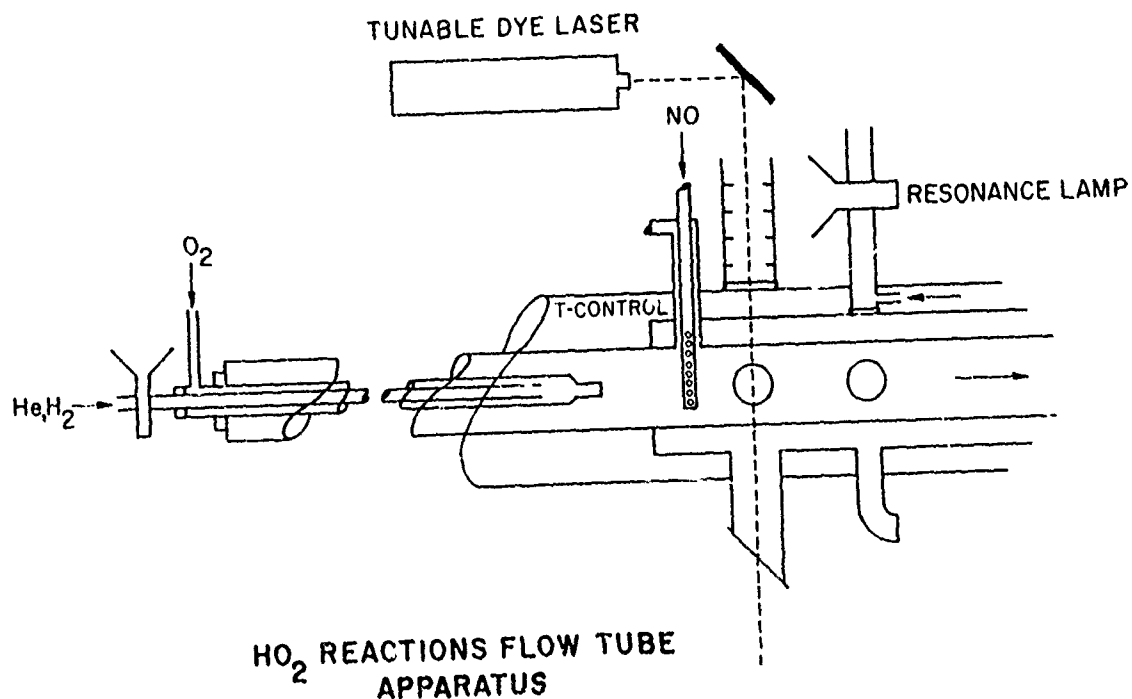


Figure 2

## KAUFMAN

and reduces the detection limit by two or more orders of magnitude. This apparatus was used for the measurement of the rate of the  $\text{HO}_2 + \text{ClO}$  reaction in our laboratory. The importance of measuring as many of the reactive species as possible cannot be overestimated. Discharge sources produce a variety of atom and radical species, sometimes from impurity precursors and their concentrations should be monitored to insure compatibility with the proposed reaction scheme. Figure 2 also shows a nested sliding injector consisting of two concentric tubes. This arrangement allows the generation reaction  $\text{H} + \text{O}_2 + \text{M} \rightarrow \text{HO}_2 + \text{M}$  to go essentially to completion in the larger injector tube at higher than flow tube pressure before this gas stream is mixed with that in the main tube where  $\text{ClO}$  is generated upstream by the  $\text{Cl} + \text{O}_3$  reaction. This example underscores the versatility of the method: two different radicals are produced separately by microwave discharges plus post-discharge reactions, one of them in a sliding injector tube. They are brought together rapidly, and one or more reactant or product species are monitored as function of variable reaction time.

The technique's potential disadvantages are also apparent: mixing problems; surface effects, particularly those introduced by the sliding injector; control of flow parameters such as development of laminar flow; and limitation of available pressure range (usually  $\leq 10$  torr) because of slower mixing and diffusion. Still, the advantage of versatility outweighs the disadvantages. It must be said, however, that the recent advances in the use of DF have been primarily concerned with the detection problem and have done little to improve the pressing transport, mixing, and surface problems.

Figure 3 shows the application of the powerful laser magnetic resonance technique (LMR) as pioneered by Howard at the Boulder NOAA laboratories. Especially for  $\text{HO}_2$  detection,

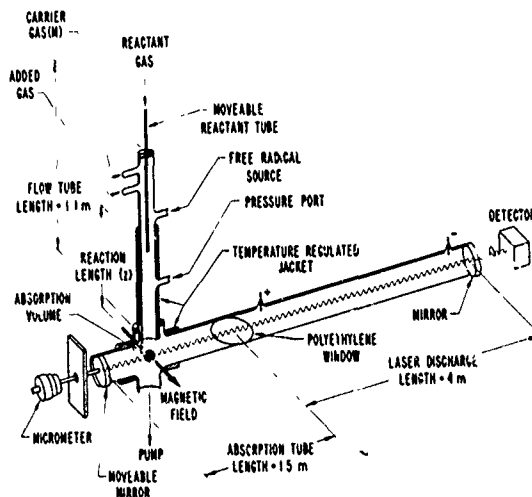


Figure 3

but also for  $\text{ClO}$ ,  $\text{CH}_3\text{O}$ , and other radicals, the method's sensitivity and directness far outperforms others. As can be seen in Figure 3, the LMR part of the apparatus dwarfs the DF part, and although this introduces problems connected with the large LMR detection cell and its flow/concentration patterns, the technique has provided spectacularly successful results for a variety of  $\text{HO}_x$  and  $\text{ClO}_x$  reactions as is described in Howard's paper in these Proceedings.

Mass spectrometric (MS) detection has been used in DF experiments for many years. It has the major advantage of very wide applicability and is deserving of more extensive use. A recent DF/MS apparatus of Watson at the Jet Propulsion Laboratory is shown in Figure 4. The combination of molecular beam sampling and time-of-flight techniques to provide discrimination between different molecular precursors of a given mass ion peak makes MS the

## KAUFMAN

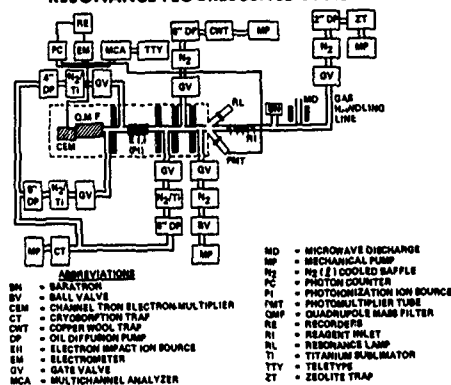
DISCHARGE FLOW - MASS SPECTROMETRIC/  
RESONANCE FLOURESCENCE SYSTEM

Figure 4

preferred method for reactions of polyatomic radicals whose optical spectra are weak and diffuse. The minor disadvantages of discrimination in the ion detection system and of mass spectrum overlap can be overcome through judicious use of chemical information (titration reactions). The additional use of resonance fluorescence in the JPL apparatus makes this a very versatile system, particularly well suited for studies of larger radicals as described by Watson in a paper of this volume.

The flash photolysis (FP) method has its roots in the pioneering work of Norrish and Porter [1949]. The combination with vacuum u.v. resonance fluorescence detection by Braun and Lenzi [1967] marked the beginning of its modern use in atom/radical reaction kinetics. In its basic configuration, a photolysis flash produces the atom or radical species in a gas mixture that contains both the atom precursor and the other reactant species. With the resonance lamp operating continuously, a time-resolved fluorescence signal is obtained, but since there is usually insufficient signal from a single flash, the experiment is carried out repetitively, and the signal is summed in the multiscaling mode until satisfactory statistics are obtained. A useful recent modification by Watson at JPL, shown in Figure 5, incorporates resonance absorption rather than fluorescence which makes absolute concentration measurements more accessible but requires long path

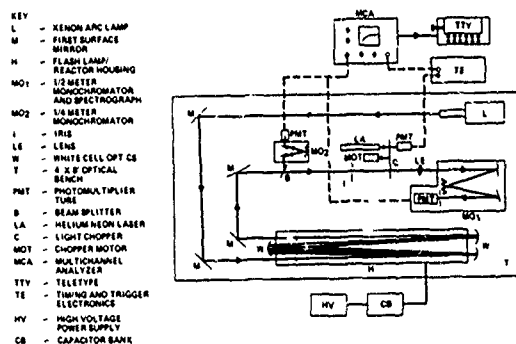
SCHEMATIC DIAGRAM OF FLASH PHOTOLYSIS/UV  
ABSORPTION APPARATUS

Figure 5

length and therefore includes a multiple path absorption cell. Another recent apparatus, Figure 6, uses laser flash photolysis to generate radical species and resonance fluorescence to monitor their concentration.

## LASER FLASH PHOTOLYSIS SYSTEM

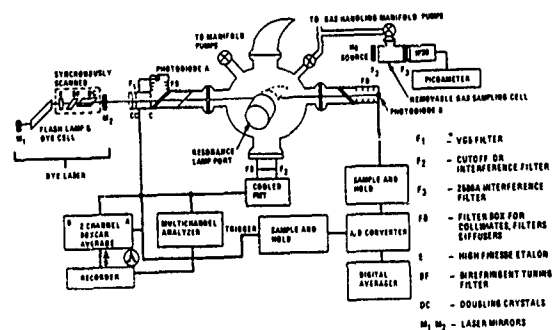


Figure 6

The substantial advantages of FP over DF, where applicable, are clear: real time measurements, little affected by transport problems, absence of surface effects, and possible use over wide pressure ranges. Deviations from ideal behavior must be considered, such as diffusion effects at low pressure, spatially inhomogeneous radical generation, "hot" radical effects due to excess initial translational energy, limitation on the nature and concentration of inert gas molecules because of interference with the flash and/or resonance line detection radiation. Still, these complications can often be avoided or taken into account, and the FP method, whose inherent accuracy roughly equals that of DF, is the method of choice when applicable. However, its range of applicability is far narrower than that of DF, and the latter technique will thus necessarily find greater use in the future. The generation of radicals by photolysis is a much more restrictive process requiring not only a strong radiative transition to a cleanly dissociative excited state, but requiring also sufficiently low absorption by all other reactant species. Thus, both the generation and detection methods of DF are more varied and plentiful. Furthermore, different reactive species may be prepared in separate parts of the flow system, each on a 1-100 millisecond timescale, and brought together rapidly in a desired reaction.

Lastly, a short list of experimental research aims for the near term: Work is needed on several aspects of the DF technique. Surface materials or coatings of reproducibly low activity for radical removal over wide temperature ranges need to be developed. Better flow characterization, both experimental and theoretical, is required, leading to application at higher pressures ( $\sim 10$  to 100 torr), and coupled with laser fluorescence or mass spectrometric detection. With those improvements and with the introduction of new radical generation techniques such as laser multiphoton dissociation, the DF method will be able to supply most of the required reaction rate information.

REVIEW OF REACTION RATE THEORY: This subject is surely much too large to be treated in all but the briefest manner in this section. The intent is clear: Our experimental methods provide us with rate constants of thermal, elementary reactions for a surprisingly large and rapidly growing number of systems, many of them in the field of stratospheric ozone photochemistry. How may we best correlate this body of information, check its reasonableness, and extend it to include a priori prediction of new parameters? We begin by looking for a reasonable classification scheme grounded in the fundamental properties of the reaction process.

The desired scheme is twofold: it first subdivides reactions into two classes, I. metathesis reactions, wherein atoms or groups are exchanged in the course of a process that consists of the more or less simultaneous breaking and forming of chemical bonds; and II. bond forming (or breaking) reactions in which two species come together (or one breaks apart), i.e. recombination (or decomposition). The first class, metathesis, is further subdivided into two groups, I.a. direct-mode reactions where the half-reacted

# KAUFMAN

intermediate, the transition state, is likely to be well defined and to represent a local maximum of the system's internal energy at the top of its activation barrier; and I.b. complex-mode reactions where a bound, energy-rich adduct is first formed whose subsequent decomposition produces the reaction products.

For very simple systems, e.g. the  $H + H_2$  exchange reaction and its isotopic variants, a vast amount of theoretical work has been done on all its classical, semi-classical, and quantum mechanical aspects, using a variety of semi-empirical and *ab initio* potential energy surfaces. Unfortunately, although these calculations are valuable in checking the accuracy of semi-empirical theories for that simple process, they cannot be extended to the reactions of interest here, and we must fall back on the predictions of transition state theory as developed by Eyring [Glasstone, Laidler, and Eyring, 1941] and applied to a large number of systems by Benson [1976] and Golden [1979]. Since this approach presupposes some knowledge of the properties of the transition state through its assumed geometry and vibration frequencies, it will be most clearly applicable to class I.a. above. The next section of this paper describes experimental results and calculations of seven reactions that fall into this category. Class I.a. will therefore not be discussed further except to say that it should provide the most useful examples for the needed interplay of experiment and theory.

Class I.b. reactions are much less amenable to simple predictions than their direct-mode counterparts. They consist essentially of a sequence of two processes: the formation of an intermediate complex and its exothermic decomposition into products. Two complications arise: there may be small activation barriers in the entrance and exit channels of the complex; and if the entrance barrier is small or zero and the complex is strongly bound ( $\gtrsim 20$  kcal mole<sup>-1</sup>), there may not exist a unique transition-state geometry, i.e. a wide range of geometrical arrangements may be allowable in the formation of the complex. This may result in abnormally large rate constants compared to the predictions of simple transition-state theory. Golden [1979] has directed attention to the mechanistic aspects of such complex-mode reactions and to the conditions under which they may exhibit unusual pressure and temperature effects such as the negative temperature coefficient of the  $ClO + NO$  reaction. It would seem that future progress will be slower for this class of reactions than for the other two, because they are inherently complicated processes. In each example, it will be necessary, first, to understand the thermochemistry of the complex and then to estimate the range of allowed structures for its entrance channels. This may be akin to the models used for bond-forming reactions that are described next.

Class II, bond forming or breaking reactions are very different in principle from I.a. and I.b., because they are of necessity many-step processes. They consist of the formation of an energy-rich adduct and of its collisional step-wise de-excitation by energy transfer. The internal clock of the overall process is the lifetime of the energy-rich adduct towards re-dissociation,  $\tau_E$ . This lifetime is strongly dependent on the adduct's excess energy in accordance with RRKM theory. When the collisional energy transfer lifetime,  $\tau_C$ , is much longer than the re-dissociation lifetime,  $\tau_C \gg \tau_E$ , i.e. at low pressure, energy transfer is rate-controlling, and in the opposite case, at high pressure, when  $\tau_E \gg \tau_C$ , the recombination is rate-controlling. Under stratospheric conditions, for atom or small radical recombination reactions, one is usually closer to the low than to the high pressure limit, and one needs to understand the step-wise energy transfer process.

Troe [1977a, 1977b, 1979] has treated all aspects of this problem in a useful, semi-empirical manner. Starting with detailed information on the thermochemistry of the reaction, the structural and spectroscopic properties of the product, its vibrational state density, and the Lennard-Jones collision frequency, the "strong collision" rate constant is calculated where deactivation to the ground vibrational state is assumed to occur with every collision. A collision efficiency factor,  $\beta_C$ , is then introduced, related to  $\langle \Delta E \rangle$ , the average energy transferred per collision (including up and down transitions in energy).  $\beta_C / (1 - \beta_C^{1/2}) \approx \langle \Delta E \rangle / kT$  has been shown to hold approximately in the solution of the master equation for energy transfer with an exponential model for the transition probability [Troe, 1977a]. Values of  $\beta_C$  have been experimentally obtained from studies of unimolecular reactions with added inert gases [Tardy and Rabinovitch, 1977] and span a fairly small range from about 0.1 to 1 at 200 to 500 K. For important stratospheric



recombination reactions, Golden has obtained  $\beta_c$  and  $\langle \Delta E \rangle$  values from the comparison of calculated "strong collision" rate constants with experimentally measured ones [JPL Publication 79-27].

The "fall-off" region of recombination (or dissociation) reactions is that pressure regime in which the inequalities between  $\tau_E$  and  $\tau_C$  no longer hold and in which both the formation and the energy transfer rates enter into the rate of the overall process. Simple, empirical interpolation formulas have been worked out [Troe, 1979] that provide a smooth transition from the low pressure rate constant,  $k_0$ , to the high pressure  $k_\infty$  as function of pressure in terms of a single, empirical parameter. The high pressure rate constant can be obtained fairly easily in those cases where the critical configuration is well defined, e.g. in elimination reactions, using transition state theory. For simple bond-forming reactions, the transition state is not as easily defined. Quack and Troe [1977] have suggested an empirical interpolation between the known reactant and product states in their adiabatic channel model to identify and calculate the needed transition state properties. For atmospheric reaction applications, particularly for the stratosphere, accurate estimates of  $k_\infty$  are not needed. In concluding this brief discussion of semi-empirical rate theory, I want to stress the need for new and better theoretical approaches. If, for example, potential energy surfaces could be estimated with reasonable accuracy, classical trajectory calculations would provide reliable rate parameters for many reactions. The reader interested in the present renaissance of the kinetics of thermal, elementary reactions would be well advised to examine the first issue of Vol. 83 of J. Phys. Chem., January 11, 1979, which is devoted to papers of a symposium held at the National Bureau of Standards entitled "Current Status of Kinetics of Elementary Gas Reactions: Predictive Power of Theory and Accuracy of Measurement."

THE KINETICS OF SEVEN OH + SUBSTITUTED METHANE REACTIONS: A TEST OF TRANSITION STATE THEORY: Methane and several Cl-substituted methanes are present in the natural atmosphere or are released in large quantities by man. Their principal removal mechanism begins with their reaction with OH. For  $\text{CH}_4$ , the subsequent reactions produce ozone and more  $\text{HO}_x$  in the troposphere and are a substantial source of water in the stratosphere. For those halocarbons whose atmospheric release is mainly anthropogenic, and whose release rate and atmospheric concentration are both known, the average OH concentration can be determined if their OH reaction rate constants are also known. Since  $\text{HO}_x$  are key catalyst species in the troposphere and stratosphere whose reactions control atmospheric photochemistry, such indirect concentration measurements are valuable.

Although many OH-reaction rate constants have been measured using direct as well as indirect methods, there is a need for strictly comparable data covering a sufficiently wide temperature range so that one might derive rate parameters for a series of reactions and compare them with theoretical predictions. Mr. K-M. Jeong of this laboratory has carried out such experiments and calculations whose results will be published elsewhere in detail but are presented here in brief summary. They are in somewhat preliminary form, i.e. some experimental and theoretical checks are still in progress, and they should be viewed here in a methodological sense rather than as fully confirmed findings.

Experimentally, the DF/resonance fluorescence method was used in a 2.54 cm i.d., 1.5 m long flow tube with movable injector tube, OH generation by  $\text{H} + \text{NO}_2 \rightarrow \text{OH} + \text{NO}$ , detection by resonance fluorescence at 309 nm, and usable temperature range from about 250 to 480 K, as described in previous papers [Jeong and Kaufman, 1979; Chang and Kaufman, 1977]. Pseudo-first-order decays of [OH] as function of injector-to-detector distance provide rate constants,  $k^I \equiv k[\text{RH}]$ , where [RH] is the halocarbon concentration which is effectively constant because  $[\text{RH}] \gg [\text{OH}]$ . Plots of  $k^I$  vs. [RH] then give the desired bimolecular rate constant,  $k$ , as their slope. Because of possible surface reaction effects, least squares fits to the slopes of these plots were used to obtain  $k$  rather than average values of  $k^I/[\text{RH}]$ , because the latter forces the line to go through the origin and fails to account for surface effects. Plots with unusually large intercepts for  $[\text{RH}] = 0$  were rejected, since they indicated surface contamination.

Figure 7 shows the Arrhenius diagrams for the seven reactions. For the slowest reactant,  $\text{CHF}_3$ , only a smaller temperature range, 387 to 480 K, was accessible. The other six plots

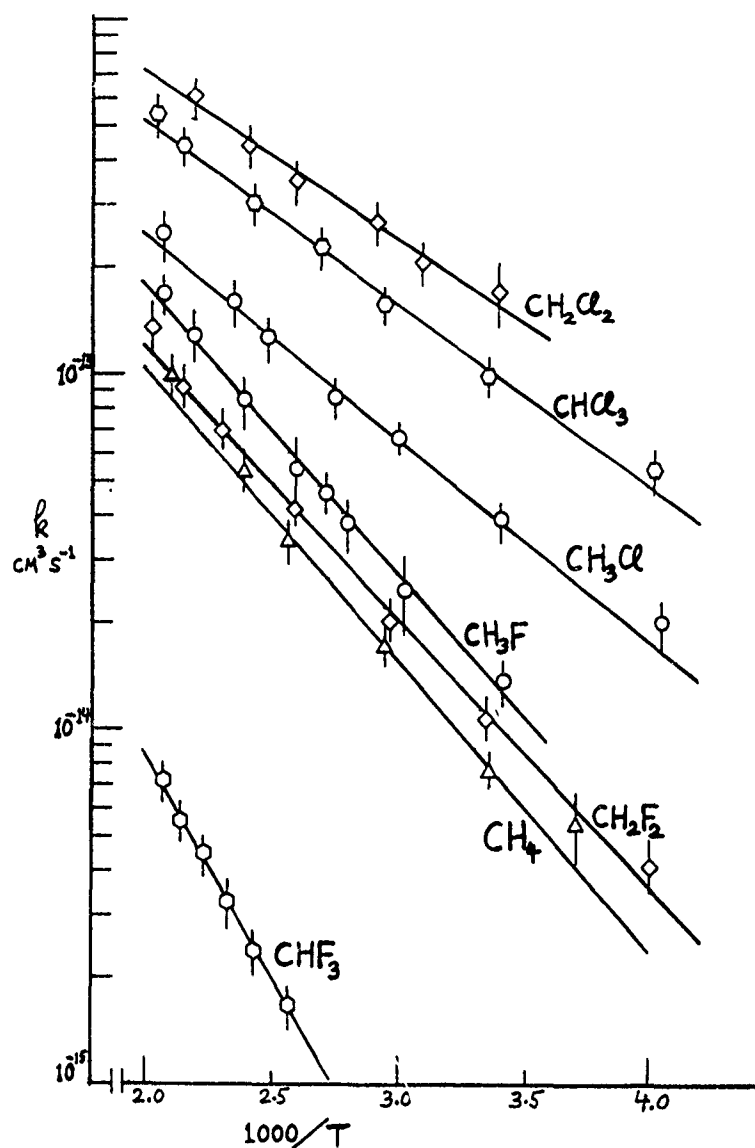


Figure 7

show curvature and are best fitted by a value of  $n \approx 2.0$  in the three-parameter expression  $k = BT^n \exp(-E'/RT)$ . For comparison with theory, the simple two-parameter expression,  $A \exp(-E/RT)$ , was used since the probable errors of  $B$ ,  $n$ , and  $E'$  in the three-parameter expressions were very large. Nevertheless,  $A$  and  $E$  must be viewed as being temperature dependent and may be adjusted for comparison with theoretical estimates using  $n = 2.0$ . The reported values of  $A$  and  $E$  were obtained from least square fits of  $\ln k$  vs.  $1/T$  in which the standard deviation of each  $k$  was the square root of the sum of the squares of its experimental, random error, and its estimated systematic error based on uncertainties in the primary measurements of flows, pressure, temperature, and physical dimensions. The details of this procedure and the comparison with other published results will be given elsewhere. While the agreement with other groups is quite good at 298 K or at other temperatures, usually to better than  $\pm 20\%$ , the same cannot be said for the  $A$ -values, as, for example, for  $\text{OH} + \text{CH}_4$  where the recommended value of  $2.4 \times 10^{-12} \text{ cm}^3 \text{ s}^{-1}$  [JPL Publication 79-27] is much lower (and the recommended value of  $E$  is also lower) than our finding of  $5.6 \times 10^{-12} \text{ cm}^3 \text{ s}^{-1}$ .

## KAUFMAN

The theoretical calculation of these Arrhenius A-values uses the thermodynamic form of transition state theory as developed by Benson [1976], i.e.  $A = e^2 k T h^{-1} \exp(\Delta S^\ddagger/R)$  where  $\Delta S^\ddagger = \Delta S^\ddagger_p + R \ln R'T$ ,  $\Delta S^\ddagger_p$  is the activation entropy for standard states of 1 atm, and the change of molecules in the reaction is  $1 - 2 = -1$ . The known  $\Delta S^\ddagger$  of a model reaction is used as a starting point, and its value is then corrected for mass, electron spin, external rotation, internal rotation, symmetry, and vibration frequencies of the transition state whose geometry is assumed on the basis of chemical knowledge. For the parent reaction,  $\text{CH}_4 + \text{OH} \rightarrow \text{H}_3\text{C}-\text{H}-\text{OH} \rightarrow \text{CH}_3 + \text{H}_2\text{O}$ , for example, methanol,  $\text{CH}_3\text{OH}$ , is used as that starting point and two different geometries are tried for the transition state: one with a linear  $\text{C}-\text{H}-\text{OH}$  approach and the other with OH approaching  $30^\circ$  off the linear extension of the C-H bond.

The many, somewhat arbitrary details of these calculations and the likely limits of their correctness cannot be presented here. Suffice it to say that the "bent" transition state appears to give predictions closer to the experimental values and that many but not all of the arbitrary assignments of geometry or frequencies have fairly small effects on the calculated result. Two further complications arise: (1) For the halogen-substituted methanes, the model compounds, chloro- or fluoro alcohols, do not exist, and their entropy must therefore be estimated in various ways, e.g. by adding to the known entropy of the corresponding fluorine compound the difference between  $S_{\text{CH}_3\text{OH}}$  and  $S_{\text{CH}_3\text{F}}$ ; and (2) A tunneling correction should be applied, since the reactions involve the transfer of a light particle across a small potential barrier of magnitude 2 to 6 kcal/mole. The simplest but probably unrealistic way to introduce tunneling corrections is to calculate one-dimensional barrier penetration factors [Johnston, 1966]. Because quantum mechanical tunneling increases with decreasing temperature, this has the effect of lowering both A and E compared to a classical calculation. For the range of experimental E's and likely transition state geometries, one-dimensional penetration factors using a fitted Eckart potential would lower the A's by 40 to 60%, but in view of the existing uncertainties and the recent suggestion [Marcus and Coltrin, 1977] that tunneling occurs near the vibrational end points rather than through the middle of the barrier, these corrections are not included here. They should be kept in mind in the sense that too high a theoretical A-value is more reasonable than too low a value when compared with experiment.

The experimental and theoretical results, both of which are to be considered preliminary, are presented in Table 1. Since the Arrhenius plots are curved (all but the  $\text{CHF}_3$  plot

Table 1

Reactant	Temperature Range	$E^{\text{exp}}$ kcal/mole	$A^{\text{exp}}$	$A_{300}^{\text{exp}}$ $10^{-12} \text{ cm}^3 \text{ s}^{-1}$	$A_{300}^{\text{theor}}$ linear	$A_{300}^{\text{theor}}$ bent	$\frac{A_{\text{bent}}^{\text{theor}}}{A^{\text{exp}}}$
$\text{CH}_4$	269-473	3.9	$5.6 \pm 1.5$	4.2	4.4	7.7	1.8
$\text{CH}_3\text{Cl}$	247-483	2.6	$3.5 \pm 0.6$	2.3	2.0	5.7	2.5
$\text{CH}_2\text{Cl}$	295-455	2.2	$6.4 \pm 1.4$	4.4	0.86	2.1	0.48
$\text{CHCl}_3$	249-487	2.4	$5.7 \pm 0.8$	3.8	0.31	0.93	0.24
$\text{CH}_3\text{F}$	292-480	3.8	$8.2 \pm 1.3$	5.4	1.8	4.4	0.81
$\text{CH}_2\text{F}_2$	250-492	3.5	$4.4 \pm 0.7$	3.5	0.69	1.8	0.51
$\text{CHF}_3$	387-480	5.8	$3.0 \pm 0.6$	1.4	0.26	0.72	0.51

whose temperature range is the smallest), and since the experimental temperatures extend much farther above than below 300 K, the experimental A's are corrected to give  $A_{300}^{\text{exp}}$  either by the three-parameter expression,  $A_{300} = B (300 e)^n$ , or by  $A_{300} = A (300/T_m)^n$ , where  $T_m$  is the average temperature of the experimental range. It is interesting to note that the theoretical temperature dependence of A which consists of the direct proportionality to T

# KAUFMAN

plus specific heat effects on  $\Delta S^\ddagger$  amounts to an effective  $n$  of 1.9 to 2.7 for the seven reactions over the ranges 300 to 400 to 500 K, in very good agreement with experiment.

An examination of the seven  $A_{300}^{\text{exp}}$  and  $A_{300}^{\text{theor}}$  for trends within each group and for cross comparison provides the following observations: The simple notion of a geometrical factor, i.e. 4 vs. 3 vs. 2 vs. 1 available reaction sites (hydrogens) in each series, is borne out by detailed transition state theory, but with considerable amplification, i.e. factors of 8 and 11 rather than 4 in the Cl- and F-series, respectively. This is due to a balance of at least three effects: the entropy change of the model reaction which was estimated by three different methods and which produces a larger than statistical effect; the external rotation of the transition state which has a decreasing effect on the entropy change with increasing halogen substitution; and the vibrational entropy effects of the transition state which increase  $\Delta S^\ddagger$  (and  $A$ ) with increasing halogen substitution.

The comparison of the experimental and theoretical A-factors is disappointing. As the last column of Table 1 shows, the  $A^{\text{theor}}/A^{\text{exp}}$  ratio ranges from 2.5 (for  $\text{CH}_3\text{Cl}$ ) to 0.24 (for  $\text{CHCl}_3$ ), and although the average value of that ratio fortuitously equals 1.0, the theoretical prediction of decreasing A-factors with increasing halogen substitution is not borne out by experiment. These discrepancies are much smaller in the F-series, where the A-ratio goes from 1.8 to 0.51, i.e. where all A's are (barely) within a factor of two of theory, than in the Cl-series where the ratio spans a full order of magnitude. It is possible, of course, that a somewhat different choice of the transition state geometry and of its calculated entropy will decrease these differences, that tunneling corrections will have a systematic effect, albeit not a very large one, and, finally, that further experimental checks may uncover systematic errors. The latter point is particularly difficult to rule out, since small systematic changes in the  $k$ 's lead to much larger changes in the A's. However, barring any major modifications in the results, one would be led to postulate correction terms that increase the transition state entropy in the order  $\text{Cl} > \text{F} > \text{H}$ . In spite of the poor prediction of the substituent effects in the two series studied here, it is reassuring to find good agreement regarding the magnitude of the A-factor. One may hope, therefore, that further experimental and theoretical work on series of related reactions will result in improvements of the predictive power of transition state theory.

ACKNOWLEDGMENTS: This work was supported by NASA under Grant No. 39-011-161.

## REFERENCES

- Anderson, J. G., The Detection of Atoms and Diatomic Radicals in the Earth's Stratosphere, Atmospheric Technology, **9**, 55, 1979.
- Benson, S. W., Thermochemical Kinetics, Second Edition, Wiley, NY, 1976.
- Braun, W. and M. Lenzi, Resonance Fluorescence Method for Kinetics of Atomic Reactions. Reactions of Atomic Hydrogen with Olefins, Faraday Discussions, **44**, 252, 1967.
- Brown, R. L., Tubular Flow Reactors with First-Order Kinetics, J. Res. Natl. Bur. Standard, **83**, 1, 1978.
- Chang, J.-S. and F. Kaufman, Kinetics of the Reactions of Hydroxyl Radicals with Some Halocarbons:  $\text{CHFCl}_2$ ,  $\text{CHF}_2\text{Cl}$ ,  $\text{CH}_3\text{CCl}_3$ ,  $\text{C}_2\text{HCl}_3$ , and  $\text{C}_2\text{Cl}_4$ , J. Chem. Phys., **66**, 4989, 1977.
- Ferguson, E. E., F. C. Fehsenfeld, and A. L. Schmeltekopf, Flowing Afterglow Measurements of Ion-neutral Reactions, Adv. At. Mol. Phys., **5**, 1, 1969.
- Glasstone, S., K. J. Laidler, and H. Eyring, The Theory of Rate Processes, McGraw-Hill, NY, 1941.
- Golden, D. M., Experimental and Theoretical Examples of the Value and Limitations of Transition State Theory, J. Phys. Chem., **83**, 108, 1979.
- Howard, C. J., Kinetic Measurements Using Flow Tubes, J. Phys. Chem., **83**, 3, 1979.
- JPL Publication 79-27, NASA Jet Propulsion Laboratory, 1979.
- Jeong, K.-M. and F. Kaufman, Rates of the Reactions of 1,1,1-Trichloroethane (Methyl Chloroform) and 1,1,2-Trichloroethane with OH, Geophys. Res. Lett., **6**, 757, 1979.
- Johnston, H. S., Gas Phase Reaction Rate Theory, Ronald Press, NY, p. 44, 1966.
- Kaufman, F., Reactions of Oxygen Atoms, Progr. React. Kin., **1**, 3, 1961.
- Marcus, R. A. and M. E. Coltrin, A New Tunneling Path for Reactions Such as  $\text{H} + \text{H}_2 \rightarrow \text{H}_2 + \text{H}$ , J. Chem. Phys., **67**, 2609, 1977.
- Michael, J. V. and J. H. Lee, Rate Constant Measurements at Constant Temperature by the Flash Photolysis-Resonance Fluorescence Technique and Recombination-Dissociation Theory for  $\text{NO}_2$  and  $\text{NOCl}$ , J. Phys. Chem., **83**, 10, 1979.

# KAUFMAN

- Norrish, R. G. W. and G. Porter, Chemical Reactions Produced by Very High Light Intensity, Nature (London), 164, 658, 1949.
- Poirier, R. V. and R. W. Carr, Jr., The Use of Tubular Flow Reactors for Kinetic Studies Over Extended Pressure Ranges, J. Phys. Chem., 75, 1593, 1971.
- Quack, M. and J. Troe, Unimolecular Processes V: Maximum Free Energy Criterion for the High Pressure Limit of Dissociation Reactions, Ber. Bunsenges. Phys. Chem., 81, 329, 1977.
- Tardy, D. C. and B. S. Rabinovitch, Intermolecular Vibrational Energy Transfer in Thermal Unimolecular Systems, Chem. Rev., 77, 369, 1977.
- Troe, J., Theory of Thermal Unimolecular Reactions at Low Pressures. I. Solutions of the Master Equation, J. Chem. Phys., 66, 4745, 1977.
- Troe, J., Theory of Thermal Unimolecular Reactions at Low Pressures. II. Strong Collision Rate Constants. Applications, J. Chem. Phys., 66, 4758, 1977.
- Troe, J., Predictive Possibilities of Unimolecular Rate Theory, J. Phys. Chem., 83, 114, 1979.
- Walker, R. E., Chemical Reaction and Diffusion in a Catalytic Tube Reactor, Phys. Fluids, 4, 1211, 1961.
- Zahniser, M. S., F. Kaufman, and J. G. Anderson, Kinetics of the Reaction  $\text{Cl} + \text{O}_3 \rightarrow \text{ClO} + \text{O}_2$ , Chem. Phys. Lett., 37, 226, 1976.
- Zahniser, M. S. and F. Kaufman, Kinetics of the Reactions of  $\text{ClO}$  with  $\text{O}$  and with  $\text{NO}$ , J. Chem. Phys., 66, 3673, 1977.
- Zahniser, M. S. B. M. Berquist, and F. Kaufman, Kinetics of the Reaction  $\text{Cl} + \text{CH}_4 \rightarrow \text{CH}_3 + \text{HCl}$  from 200 to 500 K, Intl. J. Chem. Kin., 10, 15, 1978.

# LABORATORY STUDIES OF REACTIONS OF ODD HYDROGEN SPECIES OF ATMOSPHERIC INTEREST

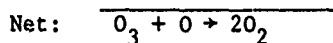
Carleton J. Howard

National Oceanic and Atmospheric Administration, Aeronomy Laboratory, Boulder CO 80303 USA

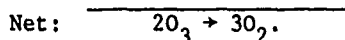
## Abstract

This paper describes some important aspects of the chemistry of odd hydrogen radicals (H, OH, and HO<sub>2</sub>) in the atmosphere. The major emphasis is given to describing recent developments in laboratory studies of the reactions of these species. Some important new measurements include studies of the reactions of OH with O and H<sub>2</sub>O<sub>2</sub> and the reactions of HO<sub>2</sub> with O, OH, HO<sub>2</sub>, and ClO. Some of the implications of these results are also discussed.

INTRODUCTION: The odd hydrogen radical family, H, OH, and HO<sub>2</sub>, plays a dominant role in the chemistry of the atmosphere. In the stratosphere the radicals OH and HO<sub>2</sub> help to regulate the ozone concentration through cycles such as



and



The sequence (1) + (2) is most important in the upper stratosphere, above about 30 km, where the oxygen atom concentration is sufficiently high to drive this cycle and similar catalytic cycles involving Cl and ClO or NO and NO<sub>2</sub>. Reactions (1) + (3), on the other hand, dominate ozone destruction in the lower stratosphere, below about 25 km, where the decreasing oxygen atom concentration reduces the effectiveness of the chlorine and nitrogen oxide cycles.

Some general features of atmospheric odd hydrogen chemistry will be described with reference to Fig. 1. In discussing this chemistry it is helpful to divide the reactions into the three categories that chemists use to describe radical reactions. These are initiation, propagation, and termination.

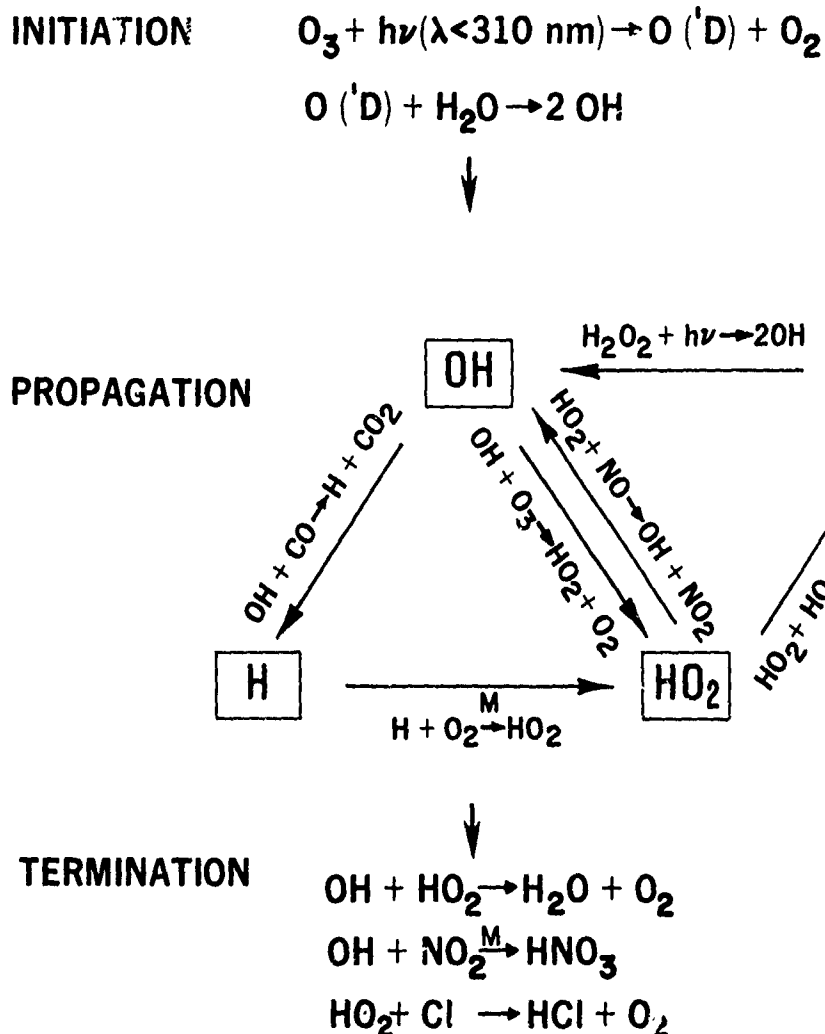


Figure 1. Diagram showing examples of some important reactions in the atmospheric chemistry of the odd hydrogen family.

In the atmosphere the most important initiation processes are photolytic reactions. The production of  $\text{O} (^1\text{D})$  by the photolysis of ozone in the Hartley band is particularly important in the generation of radicals below about 50 km altitude. The  $\text{O} (^1\text{D})$  reacts with nearly all atmospheric polyatomic molecules to form radical products. Thus stable molecules such as  $\text{H}_2\text{O}$ ,  $\text{CH}_4$ , and  $\text{H}_2$  are converted to OH by collisions with  $\text{O} (^1\text{D})$ . Some molecules that are formed by radical reactions in the atmosphere are photolyzed to regenerate radicals, e.g.,



and



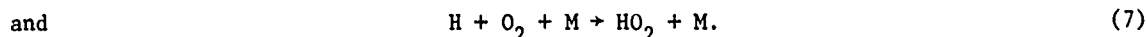
The propagation reactions are characterized by having radical reactants and products. Some examples of these reactions are also shown in Figure 1. The relative concentrations of the three odd hydrogen species H, OH, and  $\text{HO}_2$  are controlled by propagation reactions.  $\text{H}_2\text{O}_2$  is included on this figure because its most important loss process is photolysis to form hydroxyl

# HOWARD

radicals,  $J(\text{H}_2\text{O}_2) \approx 5 \times 10^{-6} \text{ s}^{-1}$ . Some typical stratospheric concentrations for H, OH,  $\text{HO}_2$ , and  $\text{H}_2\text{O}_2$  calculated by Liu (1979) using a one-dimensional model are shown in Table 1. Although

Table 1. Typical daytime average concentrations of odd hydrogen species in the atmosphere (molecules $\text{cm}^{-3}$ ) [Liu, 1979]			
	Altitude		
Species	15 km	35 km	50 km
H	0.13	$3 \times 10^2$	$4 \times 10^5$
OH	$3 \times 10^6$	$2 \times 10^7$	$2 \times 10^7$
$\text{HO}_2$	$2 \times 10^7$	$3 \times 10^7$	$2 \times 10^7$
$\text{H}_2\text{O}_2$	$6 \times 10^7$	$2 \times 10^7$	$5 \times 10^6$

the calculated concentrations show variation with altitude, the daytime averages for OH,  $\text{HO}_2$ , and  $\text{H}_2\text{O}_2$  generally fall between  $10^6$  to  $10^8$  molecules  $\text{cm}^{-3}$  and about  $10^7$  molecules  $\text{cm}^{-3}$  is a useful average value to remember. Hydrogen atoms, on the other hand increase dramatically in concentration with increasing altitude in response to the two reactions that dominate its chemistry:



At higher altitudes the [O] increases and forms more H via Reaction (6) while the  $[\text{O}_2]$  and [M] decrease lowering the rate of (7). Several other important propagation reactions are shown in Figure 1. Typical stratospheric models include about 50 such reactions.

The termination reactions are crucial to the reaction scheme because they destroy radicals and limit the concentrations of the radicals. These are reactions of two radicals that form non-radical products. The termination reactions may involve two identical radicals, e.g.,



or different types, often from different families, e.g.,



Reaction (9) is also a good example of how the odd hydrogen family interacts with radicals from other families, namely the nitrogen oxides ( $\text{NO}_x = \text{NO}$  and  $\text{NO}_2$ ) or chlorine ( $\text{Cl}_x = \text{Cl}$  and  $\text{ClO}$ ).

The key reactions that couple these families are



for the nitrogen oxide family and



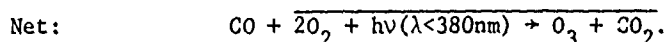
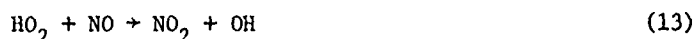
for the chlorine family. Thus the dominant effect of odd hydrogen radicals on the role of  $\text{NO}_x$  is to convert the ozone destroying radicals to inactive  $\text{HNO}_3$ . Conversely, the most important<sup>x</sup> interaction of the hydroxyl radical with chlorine species is to convert inactive chlorine, HCl, to the catalytic species Cl. From this simple analysis, one may predict the way that changes in odd hydrogen reaction rate data will affect model calculations of ozone depletion by stratospheric releases of nitrogen oxides or chlorine. For example, if a change in data lowers the concentration of odd hydrogen radicals, specifically OH,  $\text{NO}_2$  concentrations will increase and



# HOWARD

the  $\text{NO}_x$  cycle will remove more ozone. On the other hand, the balance between  $\text{Cl}_x$  and  $\text{HCl}$  will be shifted toward  $\text{HCl}$  and the impact of chlorine will be decreased.

Although most emphasis is put on the radical reaction cycles that remove ozone, there is an important cycle through which odd hydrogen and  $\text{NO}_x$  radicals combine to produce ozone. This sequence is important in the troposphere and lower stratosphere where ozone production by direct  $\text{O}_2$  photolysis is negligible



The cycle requires CO which is formed by combustion, in the atmospheric oxidation of hydrocarbons, and by biological activity (Zimmerman et al., 1978, Logan, 1979). Since  $\text{O}_2$  must be dissociated to form ozone, a key step is Reaction (7), the formation of the  $\text{HO}_2$  radical, which has a weakened O-O bond.

In the troposphere odd hydrogen radicals, particularly OH, play another important role, they initiate the oxidation of most of the natural and anthropogenic chemicals that are released into the atmosphere. Hydrocarbons, CO,  $\text{H}_2\text{S}$ ,  $\text{SO}_2$ ,  $\text{CH}_3\text{Cl}$ ,  $\text{CH}_3\text{CCl}_3$  and  $\text{NO}_2$  are just a few examples of compounds that are removed by reaction with OH radicals. Also the selection of alternatives for the inert fluorocarbons  $\text{CF}_2\text{Cl}_2$  and  $\text{CFCl}_3$  will be based upon their reactivity with OH and removal in the troposphere.

A variety of different laboratory methods are used to study the kinetics of odd hydrogen species. Details about these techniques are given by Kaufman (1979), so only a brief summary of the basic methods is shown in Table 2. The emphasis of this paper is on direct kinetic studies so various competitive schemes are not described. When applied carefully, these indirect studies can provide valuable and accurate data, however, as a rule direct pseudo-first-order studies are more reliable. Only three different detection schemes are now commonly applied to study odd hydrogen chemistry: 1. resonance absorption, 2. resonance fluorescence, and 3. laser magnetic resonance (LMR). Resonance absorption has the advantages of not being as pressure sensitive as the other two methods and of providing measurements of absolute concentrations. Its disadvantages are that it requires a long path length for high sensitivity, a severe limitation with flow systems, and when detecting polyatomic molecules there are often interfering absorptions, e.g.,  $\text{H}_2\text{O}_2$  absorbs in the same region as  $\text{HO}_2$ . Resonance fluorescence is a very powerful method for detecting species with bound excited states and with short radiative lifetimes ( $\tau \lesssim 10^{-6}\text{s}$ ). Our knowledge of the chemistry of H and OH has been expanded tremendously in the last decade because of the application of resonance fluorescence. The limitations of this method are that the fluorescence is quenched by collisional deactivation of the excited species at high pressures and that some molecules, e.g.,  $\text{HO}_2$  and  $\text{ClO}$ , predissociate and do not yield significant fluorescence radiation. LMR is a very sensitive method for detecting paramagnetic molecules such as OH and  $\text{HO}_2$  but becomes insensitive at pressures above about 20 torr and has a slow response so it is limited to use with steady state methods such as the flow system.

There are two basic kinetic methods. These are the flow system, which is used at low pressures ( $p < 10$  torr), and pulsed systems. The pulsed systems include flash photolysis, modulated molecular absorption, and pulsed radiolysis methods. The first two are operated over a wide range of pressures from about 10 torr to over an atmosphere.

## HOWARD

Table 2. Methods for laboratory studies of odd hydrogen radical kinetics		
Detection Method	Kinetic Method	Approximate Sensitivity (molecules cm <sup>-3</sup> )
	<u>H Atoms</u>	
Resonance Fluorescence	Flow system	10 <sup>8</sup>
	Pulsed system	
	<u>OH Radicals</u>	
Resonance Absorption	Flow system	10 <sup>12</sup>
	Pulsed system	10 <sup>10</sup>
Resonance Fluorescence	Flow system	10 <sup>9</sup> - 10 <sup>6</sup>
	Pulsed system	
Laser Magnetic Resonance	Flow system	10 <sup>6</sup>
	<u>HO<sub>2</sub> Radicals</u>	
UV Absorption	Pulsed system	10 <sup>12</sup>
Laser Magnetic Resonance	Flow system	4 × 10 <sup>8</sup>

The last column in Table 2 gives the approximate sensitivity that is obtained for each combination of detection and kinetic methods. The minimum sensitivity required for most pseudo-first-order studies is about 10<sup>10</sup> molecules cm<sup>-3</sup>.

In the following sections some results of recent studies of atmospheric odd hydrogen chemistry are discussed. Most of this work is taken from prepublication reports and, therefore, is subject to revision. The object of discussing these data is to point out some significant changes in kinetic data, some new interpretations of reaction mechanisms and some possible implications to atmospheric chemistry.

REACTIONS OF H: The reaction of atomic hydrogen with ozone was the object of a study by Finlayson-Pitts and Kleindienst (1979) who reported a quantitative analysis of the products of the reaction. Using a flow system containing mixtures of H and O<sub>3</sub> they directly observed the formation of significant quantities of O and indirectly detected HO<sub>2</sub> by conversion to OH with NO.



They reported  $k_{16b}/(k_{16a} + k_{16b}) \approx 0.2 - 0.3$ .

In a recent study (Howard and Finlayson-Pitts, 1979) a LMR system was used to quantitatively detect the OH and HO<sub>2</sub> products of Reaction (16). In this work, no evidence of (16b) was observed, and we conclude that  $k_{16b}/(k_{16a} + k_{16b}) \lesssim 0.03$ . It is not clear why this result differs so greatly from that of Finlayson-Pitts and Kleindienst but one possible explanation is that their the flow tube surface was treated with a halocarbon wax to inhibit deactivation of the vibrationally excited OH from (16a). Under the higher radical concentration conditions of

their experiment, some of the vibrationally excited product may have reacted with ozone forming the detected O and HO<sub>2</sub> products.

REACTIONS OF OH: The reaction of OH with O is similar to Reaction (2) because it is important in the upper stratosphere as a mechanism for recombining odd oxygen.



An error in  $k_6$  or in its temperature dependence could explain the discrepancy between observed and model calculated ozone concentrations in the upper stratosphere and mesosphere (Logan et al., 1978).

Lewis and Watson (1979) have used a discharge flow system with resonance fluorescence detection to measure  $k_6$  over the temperature range from 220 to 500 K. Their results are shown in Figure 2 along with the previous measurements of Breen and Glass (1970) and Westenberg et al. (1970).

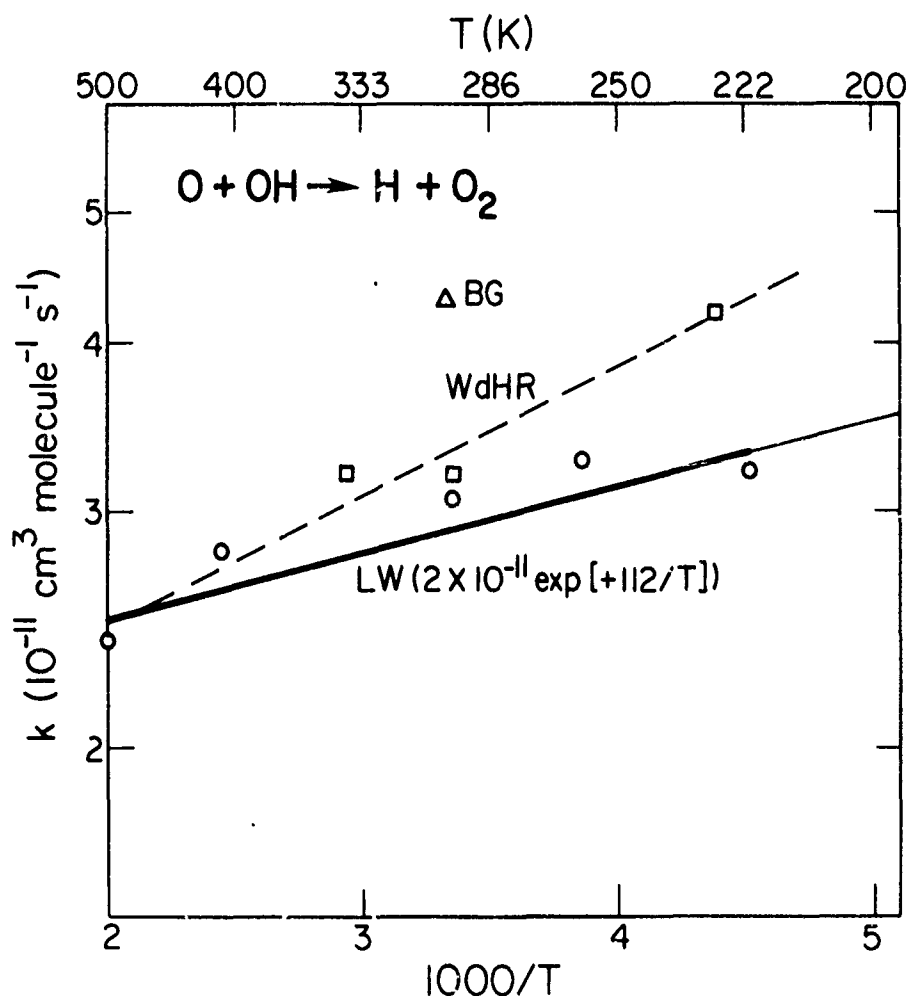


Figure 2. Summary of recent measurements of the rate constant for the O + OH reaction.  $\Delta$  = (Breen and Glass, 1970),  $\square$  = (Westenberg et al., 1970), and  $\circ$  = (Lewis and Watson, 1979).

# HOWARD

The solid line represents the fit given by Lewis and Watson,  $k_6 = 2 \times 10^{-11} \exp(112/T) \text{ cm}^3 \text{ molecule}^{-1} \text{ s}^{-1}$ . Although Westenberg et al. measured  $k_6$  at 228, 298, and 340 K and observed some variation (indicated by my dashed line in Figure 2), they reported a single average value for all of their measurements,  $3.3 \times 10^{-11} \text{ cm}^3 \text{ molecule}^{-1} \text{ s}^{-1}$ . The new result from Lewis and Watson is about 40% lower than the present recommendation,  $4 \times 10^{-11} \text{ cm}^3 \text{ molecule}^{-1} \text{ s}^{-1}$  (JPL, 1979) at 298 K.

The reaction of OH with  $\text{H}_2\text{O}_2$  is important for several reasons



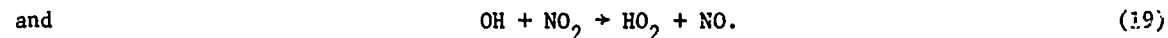
It has been used as a reference reaction in the studies of Burrows et al. (1977, 1979a) and is the basis for their measurements of the rate constants of several important  $\text{HO}_2$  reactions.

Reaction (17) is also of potential importance in the troposphere and lower stratosphere where it is a sink for odd hydrogen radicals when combined with the  $\text{H}_2\text{O}_2$  source reaction (8).

Reaction (8) will be discussed later, but new measurements indicating it has a strong negative temperature dependence ( $T^{-4}$ ) enhances the efficiency of the sequence (8) + (17). There are two new studies of  $k_{17}$  for which the preliminary results are shown in Figure 3. Reimann et al. (1979) (RSK) and Keyser (1979) used resonance fluorescence detection of OH with a discharge flow system to obtain excellent agreement at 296 K,  $k_{17} = 1.6 \times 10^{-12} \text{ cm}^3 \text{ molecule}^{-1} \text{ s}^{-1}$ . This is about two times larger than the accepted value based upon the measurements of Greiner (1968), Hack et al. (1975) (HHW), and Harris and Pitts (1979) (HP). Both of the new measurements have attempted to demonstrate that heterogeneous reactions are not occurring. Reimann et al. have used different surface coatings and Keyser has changed the flow tube diameter by about a factor of four. Unfortunately there are no measurements in the critical region below room temperature, but an extrapolation of the data of Reimann et al. to stratospheric temperatures gives values of  $k_{17}$  that are 3 to 5 times higher than current recommendations (JPL, 1979). This may have a significant effect in model calculations, acting to lower the calculated odd hydrogen radical concentrations.

REACTIONS OF  $\text{HO}_2$ : Some of the most exciting new developments in the kinetics of atmospheric reactions involve the  $\text{HO}_2$  radical. This is the result of the large number of laboratories applying different methods to study  $\text{HO}_2$  chemistry. Some of the conclusions of these new studies are described in this final section.

The thermochemistry of  $\text{HO}_2$  was the subject of a recent study (Howard, 1979a). The goal of this work was to determine the heat of formation,  $\Delta H_f^\circ$ , of the  $\text{HO}_2$  radical and the method was to use LMR detection to measure the temperature dependence of the reactions



From measurements of  $k_{18}$  and  $k_{19}$  over the range from about 500 to 1200 K, we obtain the equilibrium constant,  $K = k_{18}/k_{19}$ . The equilibrium constant can be combined with thermochemical data, heats of formation and standard entropies, for OH, NO, and  $\text{NO}_2$  to obtain  $\Delta H_f^\circ(\text{HO}_2)$ . This and several bond dissociation energies that can be derived from the  $\Delta H_f^\circ(\text{HO}_2)$  are shown in Table 3. The standard entropy of  $\text{HO}_2$  is also given because this has been recalculated using new spectroscopic data and is significantly different from the value given in thermochemical data sources.

Hack et al. (1979a) have measured the overall rate constant for the reactions

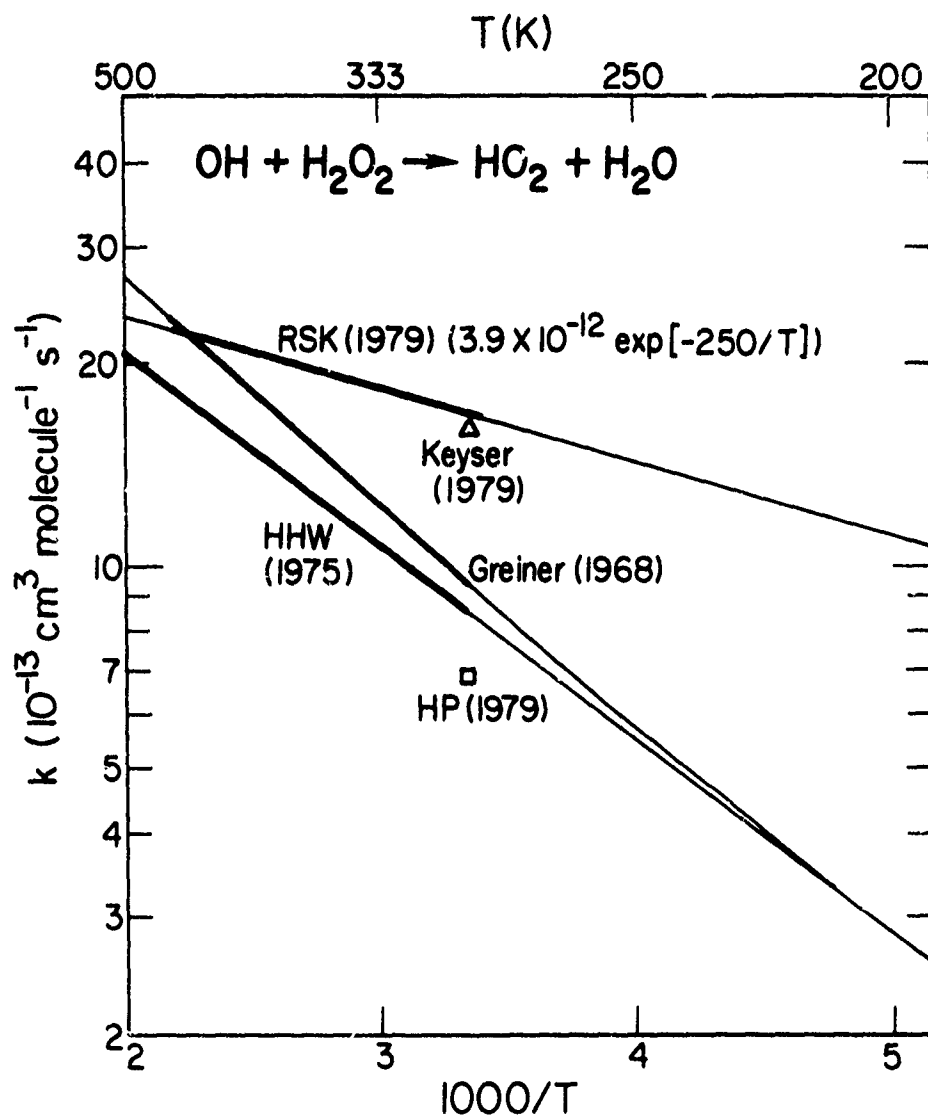


Figure 3. Summary of recent measurements of the rate constant for the  $\text{OH} + \text{H}_2\text{O}_2$  reaction. RSK = (Reimann et al., 1979), HHW = (Hack et al., 1975), HP = (Harris and Pitts, 1979). The heavy lines indicate the temperature range of the measurements.



and the branching ratios for each channel (Hack et al. 1978a). They report  $k_{20} = (4.7 \pm 1) \times 10^{-11} \text{ cm}^3 \text{ molecule}^{-1} \text{ s}^{-1}$ ,  $k_{20a}/k_{20} = 0.69$ ,  $k_{20b}/k_{20} = 0.02$  and  $k_{20c}/k_{20} = 0.29$  from measurements using flow systems with LMR and EPR detection at 293 K. Pagsberg et al. (1979) have estimated  $k_{20a} = 3.3 \times 10^{-11}$  from measurements of OH formation and decay rates in a pulse

## HOWARD

Table 3. HO<sub>2</sub> Thermochemistry.

$$\Delta H_{f298}^{\circ}(\text{HO}_2) = 2.5 \pm 1 \text{ kcal mol}^{-1}$$

$$D(\text{H-O}_2) = 49.6 \text{ kcal mol}^{-1}$$

$$D(\text{HO-O}) = 66.4 \text{ kcal mol}^{-1}$$

$$D(\text{H-O}_2\text{H}) = 87.1 \text{ kcal mol}^{-1}$$

$$S_{298}^{\circ}(\text{HO}_2) = 54.73 \text{ cal deg}^{-1} \text{ mol}^{-1}$$

radiolysis experiment containing about 1 atm of argon at 349 K. These two measurements are in excellent agreement.

There are two new studies of the reaction of O atoms with HO<sub>2</sub>.



The data on this reaction is summarized in Table 4. The first measurement of  $k_{21}$  was reported

Table 4. Summary of Measurements of the Rate Constants for HO <sub>2</sub> + O.				
$k_{21} (10^{-11} \text{ cm}^3 \text{ molecule}^{-1} \text{ s}^{-1})$	T(K)	p(torr)	Reference	
3.5 ± 1	293	2-3	<u>Burrows et al.</u> [1977]	
3.1 ± 1.0	298	2-3	<u>Burrows et al.</u> [1979a]	
4.0 ± 0.8	298	1200	<u>Lii et al.</u> [1979a]	
3.3 ± 1	298	0.8-8	<u>Hack et al.</u> [1979b]	

by Burrows et al. (1977, 1979a) who used a flow system and LMR detection of HO<sub>2</sub>. The new studies were made by Lii et al. (1979a) using uv absorption detection of HO<sub>2</sub> in a pulse radiolysis system and by Hack et al. (1979b) using LMR detection of HO<sub>2</sub> and ESR detection of O in a flow system. The agreement among the three different investigations is excellent and gives no indication of any pressure dependence for Reaction (21).

One of the most interesting and most frequently studied reactions of HO<sub>2</sub> is the disproportionation reaction:



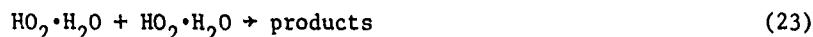
In a sense this is the most easily studied HO<sub>2</sub> reaction because high HO<sub>2</sub> concentrations are used. Reaction (8) is important in atmospheric chemistry as a termination reaction and is the most frequently used reference reaction in indirect, competitive type measurements of HO<sub>2</sub> kinetics.

The first direct measurement of  $k_8$  was reported by Foner and Hudson (1962) who used a low

# HOWARD

pressure flow system with mass spectrometric detection of  $\text{HO}_2$  to obtain  $k_8 = 3 \times 10^{-12} \text{ cm}^3 \text{ molecule}^{-1} \text{ s}^{-1}$ . Ten years later, measurements of  $k_8$  were reported by Paukert and Johnston (1972),  $k_8 = 3.6 \times 10^{-12} \text{ cm}^3 \text{ molecule}^{-1} \text{ s}^{-1}$ , and Hochanadel et al. (1972),  $k_8 = 9.5 \times 10^{-12}$ .

Part of the discrepancy between these two measurements results from differences in the measured  $\text{HO}_2$  absorption cross section, the value measured by Hochanadel et al. being about 1.5 times larger than the value reported by Paukert and Johnston,  $\sigma(210\text{nm}) = 4.5 \times 10^{-18} \text{ cm}^2$ . The remaining factor of 2 discrepancy between the measurements was explained by Hamilton (1975) who demonstrated that water vapor, which was present in the Hochanadel et al. apparatus, accelerates Reaction (8). He reported  $k_8 = 3.2 \times 10^{-12} \text{ cm}^3 \text{ molecule}^{-1} \text{ s}^{-1}$  in the absence of  $\text{H}_2\text{O}$  and  $k_8 = 6.4 \times 10^{-12}$  with 15 torr of  $\text{H}_2\text{O}$  added. In an extensive second study (Hamilton and Lii, 1977) a kinetic model was proposed to explain the observed enhancement by  $\text{H}_2\text{O}$ :



Measurements were made at  $T \approx 295 \text{ K}$  and at total pressures of about two atmospheres, with varied concentrations of  $\text{H}_2\text{O}$ , 0-15 torr. Reaction (21) was assumed to be in equilibrium. The equilibrium constant  $K_{21}$  and other kinetic parameters for this model can be obtained by fitting observed  $\text{HO}_2$  decay rates at different water vapor concentrations to the rate equation:

$$\begin{aligned} - \frac{d([\text{HO}_2] + [\text{HO}_2 \cdot \text{H}_2\text{O}])}{dt} &= 2k_8[\text{HO}_2]^2 + 2k_{22}[\text{HO}_2][\text{HO}_2 \cdot \text{H}_2\text{O}] + 2k_{23}[\text{HO}_2 \cdot \text{H}_2\text{O}]^2 \\ &= 2 \frac{k_8 + k_{22}K_{21}[\text{H}_2\text{O}] + k_{23}K_{21}^2[\text{H}_2\text{O}]^2}{(1 + K_{21}[\text{H}_2\text{O}])^2} ([\text{HO}_2] + [\text{HO}_2 \cdot \text{H}_2\text{O}])^2 \end{aligned} \quad (24)$$

It was assumed that the absorption cross section of  $\text{HO}_2$  is not changed by association with water molecules. They reported  $K_{21} = (2-63) \times 10^{-20} \text{ cm}^3 \text{ molecule}^{-1}$  and  $k_{22}/k_8 \approx 6$ .

The next major breakthrough in the study of Reaction (8) came from work by Cox (1978) and Cox and Burrows (1979) who reported the first studies of its temperature and pressure dependence. They reported that  $k_8$  decreases with pressure below  $\approx 25$  torr, and that the high pressure rate constant has a strong negative temperature dependence,  $k_8 = (3.8 \pm 1.4) \times 10^{-14} \exp\{(1250 \pm 200)/T\} \text{ cm}^3 \text{ molecule}^{-1} \text{ s}^{-1}$   $273 < T < 338 \text{ K}$ . The negative activation energy was also found by Lii et al. (1979b, 1979c):  $k_8 = (1.14 \pm 0.16) \times 10^{-13} \exp\{(1057 \pm 45)/T\} \text{ cm}^3 \text{ molecule}^{-1} \text{ s}^{-1}$ ,  $k_{22} = 7.3 k_8$ ,  $k_{23} = 44 k_8$ , and  $K_{21} = 2.1 \times 10^{-26} \exp(+9700/RT) \text{ cm}^3 \text{ molecule}^{-1}$  for  $276 < T < 400 \text{ K}$  and  $p \approx 1200$  torr.

A very significant and startling finding was made by Thrush and Wilkinson (1979) who measured  $k_8$  at low pressures,  $2 < p < 4$  torr. Their data are shown in Figure 4, where the measured rate constant is plotted vs  $[M]$ , the concentration of the buffer gas, i.e., total pressure. A line through their measurements extrapolates to  $k_8 \approx 0$  at  $[M] = 0$ . The termolecular rate constant given by my line through their data is  $k = 4.4 \times 10^{-30} \text{ cm}^6 \text{ molecule}^{-2} \text{ s}^{-1}$ , which is very large, e.g., about 4 times the rate constant for  $\text{OH} + \text{NO}_2 + \text{H}_2$  at 298 K. This result helps to form a consistent, albeit extraordinary, picture of Reaction (8). It involves an association mechanism. The conclusion reached in most of the recent studies is that the primary product is  $\text{H}_2\text{O}_4$ . Patrick and Pilling (1979) have reported a tentative identification by uv absorption of a long lived ( $\tau \approx 8\text{s}$ )  $\text{H}_2\text{O}_4$  intermediate at  $T \approx 298 \text{ K}$  and  $P \approx 1 \text{ atm}$ . This adduct must be strongly bound,

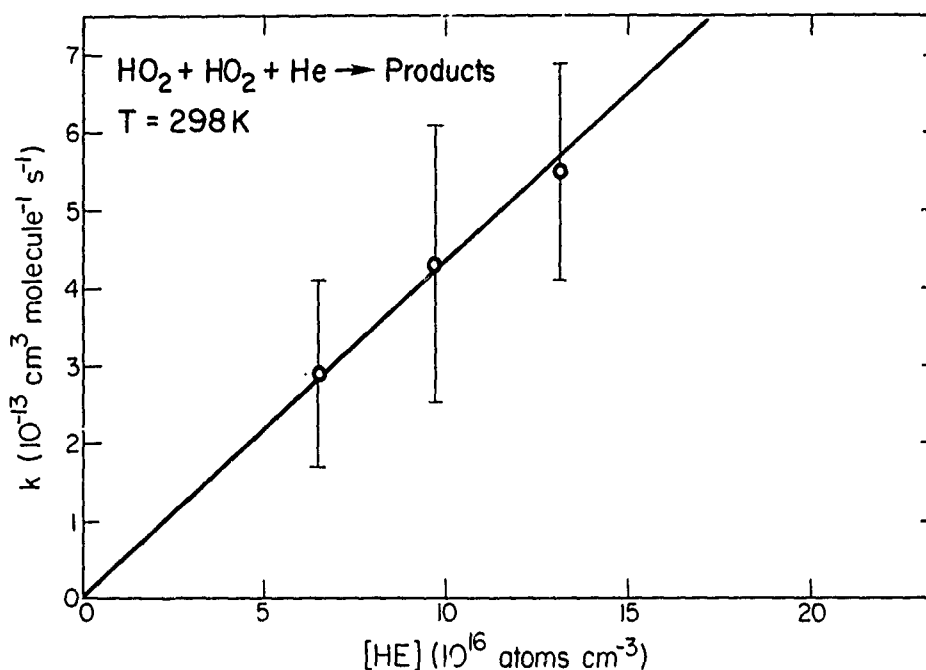


Figure 4. Data from Thrush and Wilkinson, (1979) on the reaction HO<sub>2</sub> + HO<sub>2</sub> at low pressures. Error bars indicate their estimated accuracy limits.

$D(\text{HO}_2\text{-HO}_2) \approx 15\text{-}25 \text{ kcal mol}^{-1}$ , to explain its rapid formation rate and stability. Nangia and Benson (1979) estimate the  $\Delta H_{f298}^\circ$  for the chain structured compound HOOOOH to be  $\approx 1 \text{ kcal mol}^{-1}$ , which combined with  $\Delta H_{f298}^\circ(\text{HO}_2) \approx 2.5 \text{ kcal mol}^{-1}$ , yields  $D(\text{HOO-OOH}) \approx 4 \text{ kcal mol}^{-1}$ . One also has a problem of drawing a reasonable intermediate structure for the chain molecule that would readily rearrange to give H<sub>2</sub>O<sub>2</sub> + O<sub>2</sub> products. To conserve spin the O<sub>2</sub> product must be in a singlet state and the  $a^1\Delta_g$  state is energetically accessible,

In view of the strong hydrogen bond between HO<sub>2</sub> and H<sub>2</sub>O,  $D(\text{HO}_2\text{-H}_2\text{O}) \approx 9 \text{ kcal mol}^{-1}$ , one might expect that HO<sub>2</sub>, which has a larger dipole moment than H<sub>2</sub>O ( $\mu_D = 2.1$  and  $1.85$  Debye, respectively), may also hydrogen bond to a second HO<sub>2</sub>. A cyclic structure with a pair of hydrogen bonds is also possible. However, it is not obvious how this H<sub>2</sub>O<sub>4</sub> complex is converted to the final products. Hamilton and Lii (1977) found very large isotope effects when D was substituted for H in both the HO<sub>2</sub> and H<sub>2</sub>O. Although these results are not subject to an unambiguous interpretation, it is very interesting that  $k_8(\text{HO}_2)/k_8(\text{DO}_2) \approx 2.8$ . This factor seems too large for a mechanism in which the only limiting step is the formation of the H<sub>2</sub>O<sub>4</sub> complex, but implies an additional critical step involving an H atom transfer. This conclusion is not consistent with the formation of a very long lived H<sub>2</sub>O<sub>4</sub> molecule but indicates that the stabilized or partially stabilized H<sub>2</sub>O<sub>4</sub> must decompose to products with a short lifetime.

There are few measurements of the products of Reaction 8. Hochanadel et al. (1972) collected and measured the amount of H<sub>2</sub>O<sub>2</sub> formed to calculate the HO<sub>2</sub> absorption cross section. The high value derived for their cross section indicates that only about 70% of the HO<sub>2</sub> reactant is accounted for as H<sub>2</sub>O<sub>2</sub> product. Similarly, Cox and Burrows (1979) find less than stoichiometric



# HOWARD

amounts of  $\text{H}_2\text{O}_2$ , typically, 60-90% in the absence of  $\text{H}_2\text{O}$  and somewhat less when  $\text{H}_2\text{O}$  is present. However, both studies used relatively small reactors, with large surface area to volume ratios, Hochanadel et al. used a 10 mm id tube and Cox and Burrows used 26 and 40 mm id vessels, so there may have been significant heterogeneous decomposition of the  $\text{H}_2\text{O}_2$  product. A study by Su et al. (1979a) using long path Fourier transform ir spectroscopy probably gives the best data on the yield of  $\text{H}_2\text{O}_2$  from Reaction (8). They used a very large reactor, 305 mm id and relatively simple photochemistry: (a)  $\text{Cl}_2 + h\nu \rightarrow 2 \text{Cl}$ , (b)  $\text{Cl} + \text{H}_2 \rightarrow \text{HCl} + \text{H}$ , (c)  $\text{H} + \text{O}_2 + \text{M} \rightarrow \text{HO}_2 + \text{M}$ , (d)  $\text{HO}_2 + \text{HO}_2 \rightarrow \text{H}_2\text{O}_2 + \text{O}_2$ . From measurements of the amounts of HCl and  $\text{H}_2\text{O}_2$  products in the reactor, their data indicated a yield of  $\text{H}_2\text{O}_2$  from (8) of about  $97 \pm 12\%$  at  $p \approx 700$  torr and  $T = 298$  K. Accurate measurements of the products of Reaction (8) are as important as measurements of the rate constant. Clearly, more work is needed to determine both the rate coefficients and the products as a function of temperature, pressure, and  $[\text{H}_2\text{O}]$ . Possible products from the  $\text{HO}_2 + \text{HO}_2$  reaction and the corresponding overall reaction enthalpy changes are: (a)  $\text{H}_2\text{O}_2 + \text{O}_2$  ( $-37.6 \text{ kcal mol}^{-1}$ ), (b)  $\text{H}_2\text{O} + \text{O}_3$  ( $-28.7 \text{ kcal mol}^{-1}$ ), (c)  $\text{H}_2\text{O} + \text{O}_2 + \text{O}$  ( $-3.2 \text{ kcal mol}^{-1}$ ),  $\text{O}_2$  (d) and  $\text{H}_2 + 2\text{O}_2$  ( $-5 \text{ kcal mol}^{-1}$ ).  $\text{H}_2\text{O}_4$  may also decompose back to  $2\text{HO}_2$  molecules.

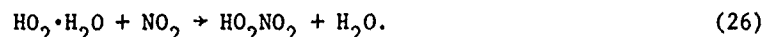
There are some interesting implications of the measurements of Lii et al. (1979c) on the thermochemistry of the  $\text{HO}_2$  complexes with  $\text{H}_2\text{O}$  and  $\text{NH}_3$ . If the product of the reaction of  $\text{HO}_2$  with  $\text{HO}_2 \cdot \text{H}_2\text{O}$  (or  $\text{HO}_2 \cdot \text{NH}_3$ ) is  $\text{H}_2\text{O}_4$ , then  $D(\text{HO}_2 - \text{HO}_2) \geq D(\text{HO}_2 - \text{H}_2\text{O} \text{ or } \text{NH}_3) \approx 10 \text{ kcal mol}^{-1}$ . If the product of the reaction of  $2 \text{HO}_2 \cdot \text{H}_2\text{O}$  or  $2\text{HO}_2 \cdot \text{NH}_3$  is  $\text{H}_2\text{O}_4$ , then  $D(\text{HO}_2 - \text{HO}_2) \geq 2D(\text{HO}_2 - \text{H}_2\text{O} \text{ or } \text{NH}_3) \approx 20 \text{ kcal mol}^{-1}$ . Decomposition of a strongly bound and stabilized  $\text{H}_2\text{O}_4$  complex of this type is endothermic for product channels (c) and (d) above.

There is now overwhelming evidence that Reaction (8) occurs by an association mechanism involving an  $\text{H}_2\text{O}_4$  intermediate. The negative temperature dependence, the pressure dependence, and the enhancement of reactivity by polar molecules (a chapcrone mechanism) are all harmonious. It seems, however, at high temperatures in combustion systems the mechanism must be a direct H atom transfer. The largest rate constant for that mechanism at 298K that is consistent with the Thrush and Wilkinson (1979) data is about  $2 \text{ or } 3 \times 10^{-13} \text{ cm}^3 \text{ molecule}^{-1} \text{ s}^{-1}$ .

The complexed  $\text{HO}_2$  radical,  $\text{HO}_2 \cdot \text{H}_2\text{O}$ , first proposed by Hamilton (1975) may be important in other atmospheric reactions. Using the equilibrium constant given by Lii et al. (1979c) with  $\text{H}_2\text{O}$  concentration and temperature profiles found in the U.S. Standard Atmosphere, 1976, the ratio  $[\text{HO}_2 \cdot \text{H}_2\text{O}]/[\text{HO}_2]$  has been calculated for several altitudes in the troposphere and lower stratosphere and these are shown in Table 5. Although the equilibrium constant is not measured accurately, it is clear that a significant fraction of the  $\text{HO}_2$  molecules in the lower atmosphere may be complexed with water (Hamilton and Lii, 1977). If the extent of complexing is 10% as shown in Table 5, then probably only association or recombination reaction (8) will be affected. For example, the formation of peroxyntiric acid



may be enhanced by the reaction



The  $\text{HO}_2 \cdot \text{H}_2\text{O}$  complex may modify some reactions, for example,



is only moderately exothermic  $\Delta H_r^\circ \approx -7 \text{ kcal mol}^{-1}$ , therefore the analogous reaction of  $\text{HO}_2 \cdot \text{H}_2\text{O}$  is 2 to 3  $\text{kcal mol}^{-1}$  endothermic. A possible new path for this reaction is

Table 5. Estimated Fraction of HO<sub>2</sub> Molecules Associated with H<sub>2</sub>O at Different Altitudes in the Atmosphere.

Altitude (km)	T (°K)	[H <sub>2</sub> O] (10 <sup>16</sup> molecule cm <sup>-3</sup> )	K <sup>a</sup> (10 <sup>-18</sup> cm <sup>3</sup> molecule <sup>-1</sup> )	Fraction [HO <sub>2</sub> ·H <sub>2</sub> O]/[HO <sub>2</sub> ]
0	288	19	0.48	0.092
1	282	14	0.69	0.097
2	275	9.6	1.1	0.10
4	262	3.5	2.6	0.091
6	249	1.2	6.9	0.082
8	236	0.38	20	0.077
10	223	0.060	68	0.041
12	217	0.012	120	0.015
14	217	0.0025	120	0.0031

(a)  $K = \frac{[\text{HO}_2 \cdot \text{H}_2\text{O}]}{[\text{HO}_2][\text{H}_2\text{O}]} = 2.1 \times 10^{-26} \exp(9700/RT)$  [Lii et al. 1979c].



However, this will probably not change the overall chemistry because HO<sub>2</sub>NO will decompose into OH and NO<sub>2</sub> (Howard, 1979b).

Another reaction that may be affected by the HO<sub>2</sub>·H<sub>2</sub>O complex is



This reaction is a very important termination reaction for the odd hydrogen radicals and is probably the source of the largest known uncertainty in stratospheric modelling. Measurements of  $k_{29}$  are summarized in Table 6. All of the measurements were made at temperatures near 300 K so the differences cannot be explained by a temperature effect. The value of Hochanadel et al. (1972) probably should be divided by 1.5 to account for the error in the HO<sub>2</sub> absorption cross section. The measurements seem to fit into two categories: low rate constants at low pressure (2-4 torr) and high rate constants at high pressure (~1 atm). In his second study of  $k_{29}$ , DeMore (1979) noted this trend and also provided evidence that there may be an enhancement by H<sub>2</sub>O vapor. From the data in Table 6 one predicts an increase in  $k_{29}$  from about  $3 \times 10^{-11}$  at low pressure to about  $15$  or  $20 \times 10^{-11}$  at high pressure. Unlike  $k_8$ ,  $k_{29}$  does not extrapolate to zero at  $P = 0$ , because OH is always reactive toward weakly bound H atoms. Although the pressure dependent component of (29) is still speculative, it is interesting to note that the expected intermediate H<sub>2</sub>O<sub>3</sub>(HO<sub>2</sub>OH) is much more stable than the H<sub>2</sub>O<sub>4</sub> analog. Nangia and Benson

Table 6. Summary of data on the OH + HO<sub>2</sub> reaction.

$k_{29}(10^{-11} \text{ cm}^3 \text{ molecule}^{-1} \text{ s}^{-1})$	T(K)	P(torr)	Reference
$20 \pm 3$	298	760	Hochanadel et al. [1972]
$\sim 16$	298	700	DeMore and Tschuikow-Roux [1974]
$5.1 \pm 1.6$	293	2-3	Burrows et al. [1977]
$\leq 2-3$	295	2-4	Chang and Kaufman [1978]
$3 \pm 1$	293	2	Hack et al. [1978b]
12 - 20	298	755	DeMore [1979]
$10 \pm 1.3$	308	1200	Lii et al. [1979d]

(1979) estimate the  $\Delta H_{f298}^\circ(\text{H}_2\text{O}_3) \approx -15.7 \text{ kcal mol}^{-1}$ , therefore,  $D(\text{HO}_2\text{-OH}) \approx 28 \text{ kcal mol}^{-1}$ . A recombination reaction between OH and HO<sub>2</sub> is similar to the OH + OH reaction (which also has a fast bimolecular component) forming H<sub>2</sub>O<sub>2</sub>,  $k(\text{OH}+\text{OH}+\text{N}_2) \approx 7 \times 10^{-31} \text{ cm}^6 \text{ molecule}^{-2} \text{ s}^{-1}$ . In order to explain the difference between the low and high pressure values of  $k_{29}$  ( $\Delta k \approx 10^{-10} \text{ cm}^3 \text{ molecule}^{-1} \text{ s}^{-1}$ ), the termolecular rate constant must be about  $4 \times 10^{-30} \text{ cm}^6 \text{ molecule}^{-2} \text{ s}^{-1}$ . This estimate neglects fall-off effects and is still very large. If there is a pressure dependent reaction of that magnitude, it is a challenge to kinetic theory to explain it. The H<sub>2</sub>O<sub>3</sub> molecule will probably redissociate into OH and HO<sub>2</sub>. In this case it will only act as a temporary reservoir for OH and HO<sub>2</sub> radicals. At low temperature it may survive long enough to react with OH or photolyse.

There are no data on the temperature dependence of the OH + HO<sub>2</sub> reaction. The direct abstraction reaction probably has little or no temperature dependence, while a termolecular reaction is expected to follow the usual  $T^{-n}$  ( $n = 3$  to  $4$ ) dependence.

The final discussion of the chemistry of the HO<sub>2</sub> radical concerns the reaction

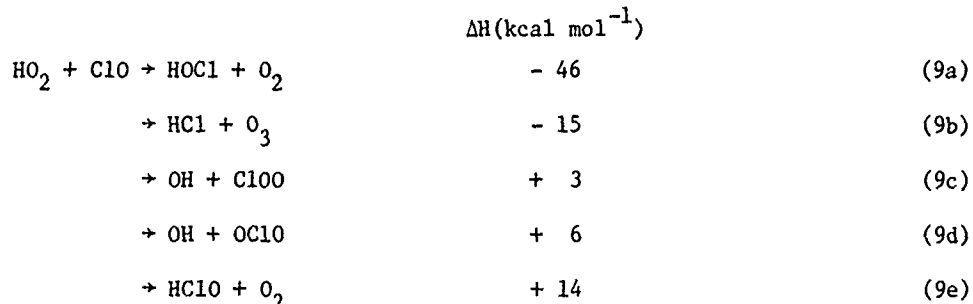


Table 7 is a summary of room temperature measurements of  $k_0$ . It can be seen that the agreement is fairly good, especially considering the difficulty of measuring the rate constant for the reaction of two transient radicals. The recent measurement of Burrows et al. (1979b) indicates that there are probably no unusual pressure effects at 298 K. Unfortunately, the temperature behavior of Reaction (9) is not as simple. Figure 5 shows the measurements of Stimpfle et al. (1979) in Arrhenius form for the range  $235 < T < 393 \text{ K}$ . To fit the data within the precision of each point as shown with the dashed line requires a four parameter equation:

Table 7. Summary of measurements of the  $\text{HO}_2 + \text{ClO}$  rate constant at 298K.

$k_9 (10^{-12} \text{ cm}^3 \text{ s}^{-1})$	P(torr)	Method	Reference
$6.3 \pm 1.3$	0.8 - 3.4	LMR-Flow System	<u>Stimpfle et al.</u> [1979]
$4.5 \pm 0.9$	2 - 6	Mass Spec.-Flow System	<u>Leck et al.</u> [1979]
$3.8 \pm 0.5$	2 - 3	Res. Fluoresc.-Flow System	<u>Reimann and Kaufman</u> [1978]
$5.4^{+4}_{-2}$	$\sim 760$	Molecular Modulation	<u>Burrows et al.</u> [1979b]

$$k_9 = 3.3 \times 10^{-11} \exp(-850/T) + 4.5 \times 10^{-12} (T/300)^{-3.7}.$$

We have interpreted this unusual temperature dependence as an indication that two different mechanisms may be occurring. It is possible that both give the same product but it would be more interesting if they did not. Leck et al. (1979) first detected a product of the reaction using a mass spectrometer. They found large amounts of  $\text{HOCl}$  and report an upper limit of 2% for production of  $\text{HCl} + \text{O}_3$  via (9b). Leu (1979) also used a mass spectrometer to set the limits,  $k_{9b}/k_9 \leq 1.5\%$  at 298 K and  $\leq 3\%$  at 248 K. These findings are very important because a determination of the products of (9) defines the role the reaction plays in stratospheric chemistry. If  $\text{HOCl}$  is the only product, then Reaction (9a) will contribute to the chlorine catalyzed destruction of ozone as seen by the reaction sequence



On the other hand, if  $\text{HCl}$  is a product, Reaction (9b) provides a path for converting the most abundant atmospheric chlorine radical,  $\text{ClO}$ , directly to the inactive form  $\text{HCl}$ . A one-dimensional model calculation by Liu (1979) predicts about a three-fold decrease in the effect of CFM's on stratospheric ozone when  $k_{9b}/k_9 = 0.1$ . It is obvious that an accurate determination of the product of (9) is needed before the role of the reaction can be assessed.

In addition to the results described above, there are new measurements of several other  $\text{HO}_2$  reactions. These are shown in Table 8. This table is presented to provide access to the recent literature related to  $\text{HO}_2$  and to demonstrate the rapid growth in our knowledge of  $\text{HO}_2$  kinetics. One should consult the original papers for details of the measurement methods and references to earlier studies. Although great advances have been made in the study of atmospheric  $\text{HO}_2$  kinetics, it is clear that a great deal of work remains to be done.

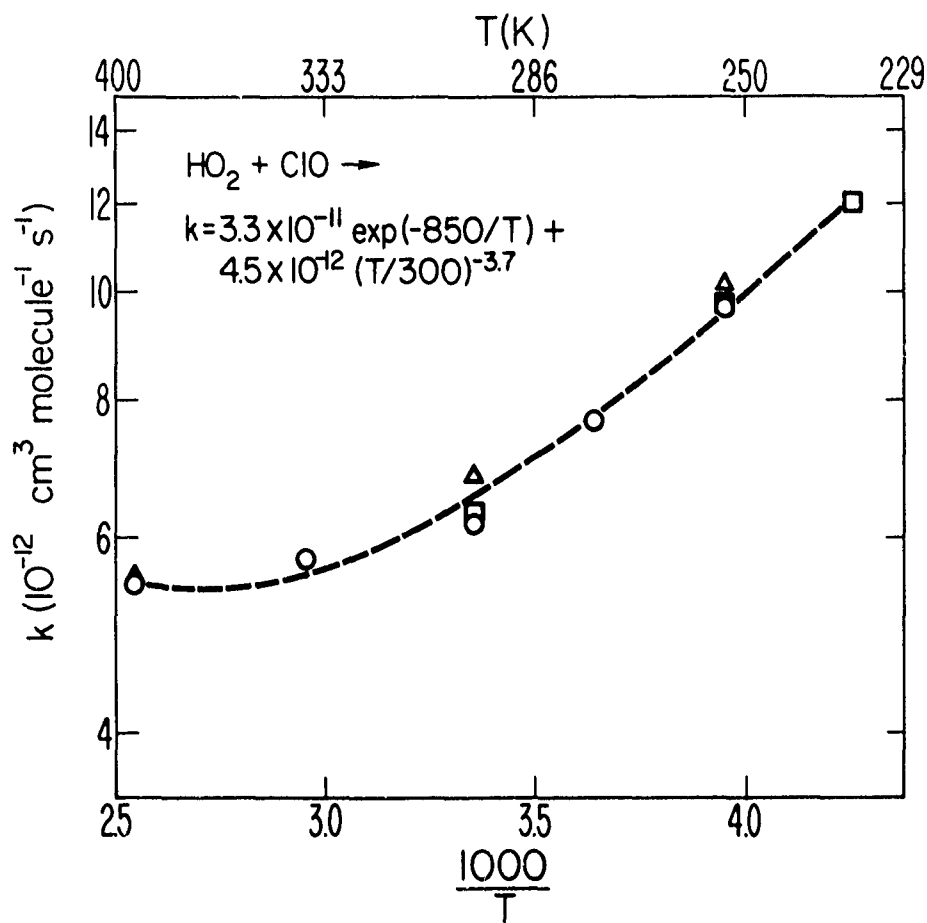


Figure 5. Data from Stimpfle et al., (1979) on the reaction  $\text{HO}_2 + \text{ClO}$ . The different symbols indicate the diameter of the flow tube:  $\Delta = 14.0$  mm,  $\circ = 25.4$  mm, and  $\square = 36.7$  mm id. The line is the fit given by the equation  $k = 3.3 \times 10^{-11} \exp(-850/T) + 4.5 \times 10^{-12} (T/300)^{-3.7} \text{ cm}^3 \text{ molecule}^{-1} \text{ s}^{-1}$ .

Table 8. Summary of recent measurements of miscellaneous HO<sub>2</sub> reactions.

Reactant	k (cm <sup>3</sup> molecule <sup>-1</sup> s <sup>-1</sup> )	T (K)	P (torr)	Reference
NO	$(3.3 \pm 0.7) \times 10^{-12} \exp\{(254 \pm 50)/T\}$	232-403	1-3	<u>Howard, 1979b</u>
	$(5.7^{+5.6}_{-4.0}) \times 10^{-12} \exp\{(130 \pm 270)/T\}$	270-425	2.5-5	<u>Leu, 1979b</u>
	$(8.2 \pm 2.4) \times 10^{-12}$	298	0.8-3	<u>Burrows et al., 1979a</u>
CO	$< 4 \times 10^{-17}$	304	3	<u>Howard, 1979b</u>
	$\leq 2 \times 10^{-17}$	298	$\sim 2$	<u>Burrows et al., 1979a</u>
	$\leq 2 \times 10^{-19}$	300	667	<u>Graham et al., 1979</u>
N <sub>2</sub> O	$< 5 \times 10^{-17}$	300-394	3	<u>Howard, 1979b</u>
	$< 2 \times 10^{-20}$	300	702	<u>Graham et al., 1979</u>
NO <sub>2</sub> +M (M=N <sub>2</sub> +O <sub>2</sub> ) (k is pressure dependent)	$(2-9) \times 10^{-13}$	283.5	40-600	<u>Cox and Patrick, 1979</u>
SO <sub>2</sub>	$\leq 2 \times 10^{-17}$	298	3	<u>Burrows et al., 1979a</u>
	$\leq 1 \times 10^{-18}$	300	750	<u>Graham et al., 1979</u>
NH	$7 \times 10^{-11}$	349	$\sim 760$	<u>Pagsberg et al., 1979</u>
NH <sub>2</sub>	$2.7 \times 10^{-11}$	349	$\sim 760$	<u>Pagsberg et al., 1979</u>
Cl	$(4.1 \pm 1.4) \times 10^{-11}$	298	$\sim 2$	<u>Burrows et al., 1979a</u>
O <sub>3</sub>	$(1.4 \pm 0.4) \times 10^{-14} \exp\{-(580 \pm 100)/T\}$	245-365	1.5-4	<u>Zahniser and Howard, 1979</u>
	$1.2 \times 10^{-14} \exp(-600/T)$	231-334	$\sim 750$	<u>DeMore, 1979</u>
Cl <sub>2</sub> O	$< 3 \times 10^{-15}$	298	$\sim 2$	<u>Stimpfle et al., 1979</u>
Cl <sub>2</sub>	$< 8 \times 10^{-16}$	298	$\sim 2$	<u>Stimpfle et al., 1979</u>
CH <sub>2</sub> O	$\approx 1 \times 10^{-14}$	298	700	<u>Su et al., 1979b</u>
trans-2-butene	$\leq 4 \times 10^{-18}$	300	755	<u>Graham et al., 1979</u>
2,3-dimethyl-2-butene	$\leq 4 \times 10^{-17}$	300	755	<u>Graham et al., 1979</u>

## REFERENCES

- Breen, J. E. and G. P. Glass, Rate of some hydroxyl radical reactions, J. Chem. Phys. **52**, 1082-6, 1970.
- Burrows, J. P., G. W. Harris, and B. A. Thrush, Rates of reaction of  $\text{HO}_2$  with HO and O studied by laser magnetic resonance, Nature **267**, 234-5, 1977.
- Burrows, J. P., D. I. Cliff, G. W. Harris, B. A. Thrush, and J. P. T. Wilkinson, Atmospheric reactions of the  $\text{HO}_2$  radical studied by laser magnetic resonance spectroscopy, Proc. Roy. Soc. (London), in press, 1979a.
- Burrows, J. P., R. A. Cox, and M. C. Addison, Kinetic studies of atmospheric free radicals, poster paper presented at this NATO Institute, 1979b.
- Chang, J. S. and F. Kaufman, Upper bound and probable value of the rate constant of the reaction  $\text{OH} + \text{HO}_2 \rightarrow \text{H}_2\text{O} + \text{O}_2$ , J. Phys. Chem. **82**, 1683-7, 1978.
- Cox, R. A., Kinetics of  $\text{HO}_2$  radical reactions of atmospheric interest, paper presented at the WMO Symposium on the Geophysical Aspects and Consequences of Changes in the Composition of the Stratosphere, Toronto, Canada, June 26-30, 1978.
- Cox, R. A. and J. P. Burrows, Kinetics and mechanism of the disproportionation of  $\text{HO}_2$  in the Gas Phase, J. Phys. Chem. **83**, 2560-8, 1979.
- DeMore, W.B. and E. Tschuikov-Roux, Temperature dependence of the reactions of OH and  $\text{HO}_2$  with  $\text{O}_3$ , J. Phys. Chem. **78**, 1447-51, 1974.
- DeMore, W. B., Reaction of  $\text{HO}_2$  with  $\text{O}_3$  and the effect of water vapor on  $\text{HO}_2$  kinetics, J. Phys. Chem. **83**, 1113-8, 1979.
- Finlayson-Pitts, B. J. and T. E. Kleindienst, The reaction of hydrogen atoms with ozone: Evidence for a second reaction path producing  $\text{HO}_2$  and  $\text{O}(\text{P})$ , J. Chem. Phys. **70**, 4804-6, 1979.
- Foner, S. N. and R. L. Hudson, Mass spectrometry of inorganic free radicals, Advances in Chemistry Series No. 36, Free Radicals in Inorganic Chemistry 34-49, 1962.
- Greiner, N. R., Hydroxyl radical kinetics by kinetic spectroscopy. III. Reactions with  $\text{H}_2\text{O}_2$  in the range 300-458 K, J. Phys. Chem. **72**, 406-10, 1968.
- Hack, W., K. Hoyer mann, and H. Gg. Wagner, The reaction  $\text{NO} + \text{HO}_2 \rightarrow \text{NO}_2 + \text{OH}$  with OH +  $\text{H}_2\text{O}_2 \rightarrow \text{HO}_2 + \text{H}_2\text{O}$  as an  $\text{HO}_2$  source, Int. J. Chem. Kinet. (Symposium 1), 329-39, 1975.
- Hack, W., H. Gg. Wagner, and K. Hoyer mann, Reactions of H with  $\text{HO}_2$  I. Determination of specific rate constants for the reaction channels, Ber. Bunsenges. Phys. Chem. **82**, 713-9, 1978a.
- Hack, W., A. W. Preuss, and H. Gg. Wagner, Measurement of the rate constant of the reaction of OH and  $\text{HO}_2$  radicals with laser magnetic resonance, Ber Bunsenges Phys. Chem. **82**, 1167-1, 1978b.
- Hack, W., A. W. Preuss, H. Gg. Wagner, and K. Hoyer mann, Reactions of H with  $\text{HO}_2$  II. Determination of the overall rate constant, Ber. Bunsenges. Phys. Chem. **83**, 212-7, 1979a.
- Hack, W., A. W. Preuss, F. Temps, and H. Gg. Wagner, The reaction  $\text{O} + \text{HO}_2 \rightarrow \text{OH} + \text{O}_2$  studied with a LMR-ESR-spectrometer, Ber. Bunsenges. Phys. Chem. in press, 1979b.
- Hamilton, Jr., E. J., Water vapor dependence of the kinetics of the self-reaction of  $\text{HO}_2$  in the gas phase, J. Chem. Phys. **63**, 3682-3, 1975.
- Hamilton, Jr., E. J. and R.-R. Li, Dependence on  $\text{H}_2\text{O}$  and on  $\text{NH}_3$  of the kinetics of the self-reaction of  $\text{HO}_2$  in the gas phase formation of  $\text{HO}_2 \cdot \text{H}_2\text{O}$  and  $\text{HO}_2 \cdot \text{NH}_3$  complexes, Int. J. Chem. Kinet. **9**, 875-885, 1977.
- Harris, G.W. and J. N. Pitts, Jr., Rate constant for the reaction of OH radicals with hydrogen peroxide at 298 K, J. Chem. Phys. **70**, 2581-2, 1979.
- Hochanadel, C. J., J. A. Ghormley, and P. J. Ogren, Absorption spectrum and reaction kinetics of the  $\text{HO}_2$  radical in the gas phase, J. Chem. Phys. **56**, 4426-32, 1972.
- Howard, C. J., Kinetic study of the equilibrium  $\text{HO}_2 + \text{NO} \rightleftharpoons \text{OH} + \text{NO}_2$  and the heat of formation of  $\text{HO}_2$ , to be published, 1979a.
- Howard, C. J., Temperature dependence of the reaction  $\text{HO}_2 + \text{NO} \rightarrow \text{OH} + \text{NO}_2$ , J. Chem. Phys. **71**, 2352-9, 1979b.
- Howard, C. J. and B. J. Finlayson-Pitts, Yields of  $\text{HO}_2$  in the reaction of hydrogen atoms with ozone, J. Chem. Phys., 1979.
- JPL Publication 79-27, Chemical kinetic and photochemical data for use in stratospheric modelling, 1979.
- Kaufman, F., Elementary Atmospheric Reactions: Laboratory Measurements and Their Interpretation, this volume, 1979.
- Keysor, L. F., private communication, 1979.
- Leck, T. J., J. E. Cook, and J. W. Birks, Studies of reactions of importance in the stratosphere. III. Rate constant and products of the reaction between ClO and  $\text{HO}_2$  radicals at 298 K, J. Chem. Phys., in press 1979.

- Leu, M.-T, Product distribution for the reaction of  $\text{HO}_2$  with  $\text{ClO}$ , poster paper presented at this NATO Institute, 1979a.
- Leu, M.-T., Rate constant for the reaction  $\text{HO}_2 + \text{NO} \rightarrow \text{OH} + \text{NO}_2$ , J. Chem. Phys. **70**, 1662-6, 1979b.
- Lewis, R. and R. T. Watson, private communication, 1979.
- Lii, R.-R., M. C. Sauer, Jr., S. Gordon, Rate constant of the reaction of  $\text{O}(^3\text{P})$  with  $\text{HO}_2$ , J. Phys. Chem. in press 1979a.
- Lii, R.-R., R. A. Gorse, Jr., M. C. Sauer, Jr., and S. Gordon, Negative activation energy for the self-reaction of  $\text{HO}_2$  in the gas phase, J. Phys. Chem. **83**, 1803-4, 1979b.
- Lii, R.-R., R. A. Gorse, Jr., M. C. Sauer, Jr., and S. Gordon, Temperature dependence of the gas phase disproportionation of  $\text{HO}_2$  in the presence of  $\text{H}_2\text{O}$  and  $\text{NH}_3$ , J. Phys. Chem. (in press), 1979c.
- Lii, R.-R., R. A. Gorse, Jr., M. C. Sauer, Jr., and S. Gordon, Rate constant for the reaction of  $\text{OH}$  with  $\text{HO}_2$ , J. Phys. Chem., in press, 1979d.
- Liu, S. C., private communication, 1979.
- Logan, J. A., M. J. Prather, S. C. Wofsy, and M. B. McElroy, Atmospheric chemistry: response to human influence, Philos. Trans. Roy. Soc. (London) **290**, 187-234, 1978.
- Logan, J. A., Sources and Sinks of Carbon Monoxide, this volume, 1979.
- Nangia, P. S. and S. W. Benson, Thermochemistry of organic polyoxides and their free radicals, J. Phys. Chem. **83**, 1138-42, 1979.
- Pagsberg, P. B., J. Eriksen, and H. C. Christensen, Pulse radiolysis of gaseous ammonia oxygen mixtures, J. Phys. Chem. **83**, 582-90, 1979.
- Paukert, T. T. and H. S. Johnston, Spectra and kinetics of the hydroperoxyl free radical in the gas phase, J. Chem. Phys. **56**, 2824-38, 1972.
- Patrick, R. and M. J. Pilling, Flash photolysis studies of the disproportionation of  $\text{HO}_2$  radicals in the gas phase, poster paper presented at this NATO Institute, 1979.
- Reimann, B. and F. Kaufman, Rate constant for the reaction  $\text{HO}_2 + \text{ClO} \rightarrow \text{HOCl} + \text{O}_2$ , J. Chem. Phys. **69** 2925-6, 1978.
- Reimann, B., U. C. Sridharan, and F. Kaufman, private communication, 1979.
- Stimpfle, R. M., R. A. Perry, and C. J. Howard, Temperature dependence of the reaction of  $\text{ClO}$  and  $\text{HO}_2$  radicals, J. Chem. Phys. **71**, 15 December issue, 1979.
- Su, F., J. G. Calvert, C. R. Lindley, W. M. Uselman, and J. H. Shaw, A Fourier transform infrared kinetic study of  $\text{HOCl}$  and its absolute integrated infrared band intensities, J. Phys. Chem. **83**, 912-20, 1979a.
- Su, F., J. G. Calvert, J. H. Shaw, H. Niki, P. D. Maker, C. M. Savage, and L. D. Breitenbach, Spectroscopic and kinetic studies of a new metastable species in the photooxidation of gaseous formaldehyde, Chem. Phys. Letters **65**, 221-5, 1979b.
- Thrush, B. A. and J. P. T. Wilkinson, Pressure dependence of the rate of reaction between  $\text{HO}_2$  radicals, Chem. Phys. Letters, in press, 1979.
- U.S. Standard Atmosphere, 1976, NOAA-S/T 76-1562.
- Westenberg, A. A., N. deHaas, and J. M. Roscoe, Radical reactions in an electron spin resonance cavity homogeneous reactor, J. Phys. Chem. **74**, 3431-8, 1970.
- Zahniser, M. S. and C. J. Howard, Kinetic studies of the reaction of  $\text{HO}_2$  with ozone, to be published, 1979.
- Zimmerman, P. R., R. B. Chatfield, J. Fishman, P. J. Crutzen, and P. L. Hanst, Estimates of the production of  $\text{CO}$  and  $\text{H}_2$  from the oxidation of hydrocarbon emissions from vegetation, Geophys. Res. Letters **5**, 679-82, 1978.



## LABORATORY STUDIES OF HALOGEN COMPOUNDS OF ATMOSPHERIC INTEREST

R. T. Watson

Jet Propulsion Laboratory, 4800 Oak Grove Drive, Pasadena, CA 91103 USA

### Abstract

Laboratory studies of homogeneous gas phase reactions involving halogen containing species, that are important in either photochemically controlling the production and loss of odd oxygen in the stratosphere, or in the interpretation of field measurement data, are discussed. The reactivities and the reliability of the kinetic data base of each of the halogen analogs (X, XO, HX, XONO<sub>2</sub>, etc., where X = F, Cl, Br and I) are discussed and intercompared. Emphasis will be placed on discussing both the reaction rate coefficients, and the mechanistic details of those reactions of current interest, e.g., Cl + CH<sub>4</sub>, Cl + HO<sub>2</sub>, ClO + OH, ClO + HO<sub>2</sub>, ClO + NO<sub>2</sub> + M, BrO + NO<sub>2</sub> + M, ClO + BrO, and BrO + BrO.

INTRODUCTION: There are well known sources for all the halogens (F, Cl, Br and I) in the earth's atmosphere, and organic and inorganic forms of each of the halogens have been monitored either in the troposphere or stratosphere in concentrations such that an understanding of their photochemistry is required. Most of the recent interest has centered around the role of chlorine in perturbing the total integrated column content, and the vertical distribution of ozone in the stratosphere (NAS, 1976; NASA, 1977; NAS, 1979; NASA, 1979). This is due to the significant magnitude of natural (CH<sub>3</sub>Cl) and man-made (e.g., CFC<sub>2</sub>, CF<sub>2</sub>Cl<sub>2</sub>, CCl<sub>4</sub> and CH<sub>3</sub>CCl<sub>3</sub>) sources of chlorine coupled with their ability to be converted in the stratosphere into inorganic forms, (Cl, ClO, HOCl, ClONO<sub>2</sub>, etc.) which can participate in efficient catalytic cycles which destroy odd oxygen. Although there are significant sources of fluorine (e.g., CFC<sub>2</sub>, CF<sub>2</sub>Cl<sub>2</sub> and CF<sub>4</sub>), there has been less interest in the photochemistry of the inorganic forms due to the low efficiency with which it is presently predicted to catalytically remove odd oxygen. However, recent measurements of the concentration of HF and total inorganic fluorine in the stratosphere disagree with current photochemical models (NASA, 1979). This may stimulate renewed interest in the photochemistry of the organic and inorganic forms of fluorine in order to explain the apparent discrepancy. It has been suggested by Yung et al. (1980) that low concentrations of bromine (~ 20 pptv)

can result in the efficient removal of odd oxygen in the lower stratosphere ( $< 25$  km) via a catalytic cycle involving not only bromine but also chlorine. The key issues in evaluating the potential importance of bromine in the stratosphere are understanding the sources (e.g.,  $\text{CH}_3\text{Br}$ ,  $\text{CF}_3\text{Br}$ , etc.) and budget of bromine, the photochemistry of bromine, the chemical composition of the lower stratosphere, and how dynamical processes affect the latter. In addition, there has been the recent suggestion by Chameides and Davis (1980) that iodine compounds may play a role in controlling tropospheric ozone in the planetary boundary layer in remote areas, one source of the iodine being  $\text{CH}_3\text{I}$ .

The major theme of this paper is to discuss the similarities and dissimilarities of the chemical reactivities of the different types of halogen species (i.e.,  $\text{X}$ ,  $\text{XO}$ ,  $\text{XOO}$ ,  $\text{OXO}$ ,  $\text{HX}$ ,  $\text{HOX}$ ,  $\text{XONO}_2$ , etc.) from one member of the halogen family to another. The different reactivities will be discussed in terms of the influence they have on the partitioning within a family, and the catalytic efficiency of the family for ozone destruction. Within the context of the above theme the following topics will be discussed:

- (i) Reactions which control the  $[\text{X}]:[\text{HX}]$  ratio.
- (ii) Reactions of  $\text{XO}$  radicals which produce  $\text{HX}$ .
- (iii) Reactions which control the  $[\text{X}]:[\text{XO}]$  ratio.
- (iv) Temporary reservoirs,

Figure 1 shows a general reaction scheme for the halogen family. The figure does not show

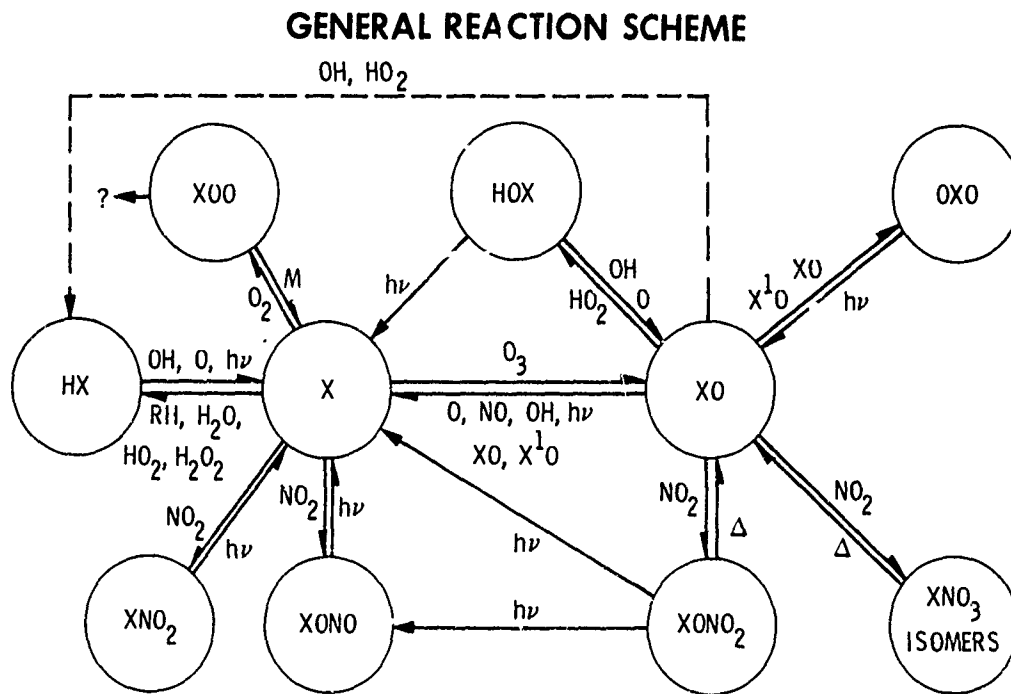
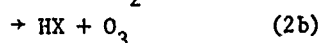
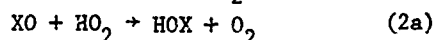
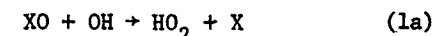


Figure 1. General reaction scheme showing the key reactions involved in the atmospheric photochemistry of inorganic halogens.  $\text{X} \equiv \text{F}, \text{Cl}, \text{Br}, \text{I}$ .

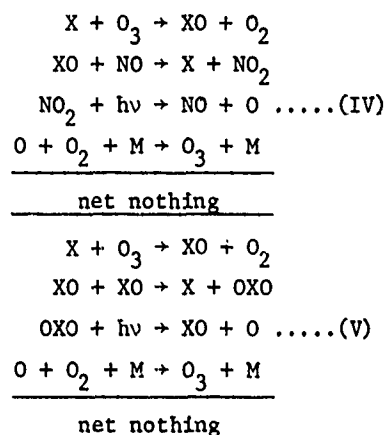
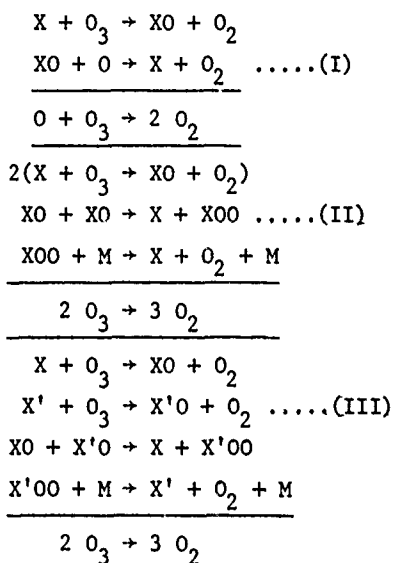
the organic precursors of the inorganic species as the degradation mechanisms of the pre-

cursors will not be discussed in this paper. New features of this general reaction scheme include possible direct linking reactions between XO and HX, i.e. (reactions (1b) and (2b)):

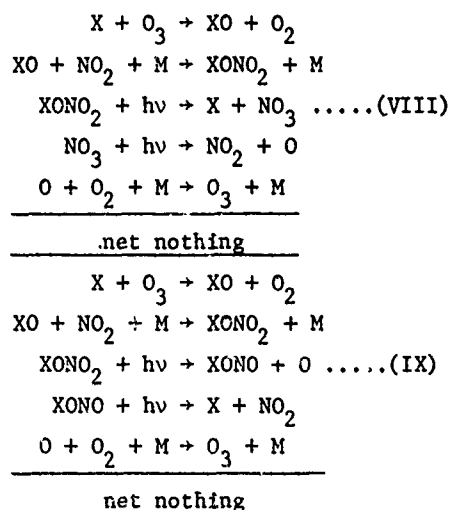
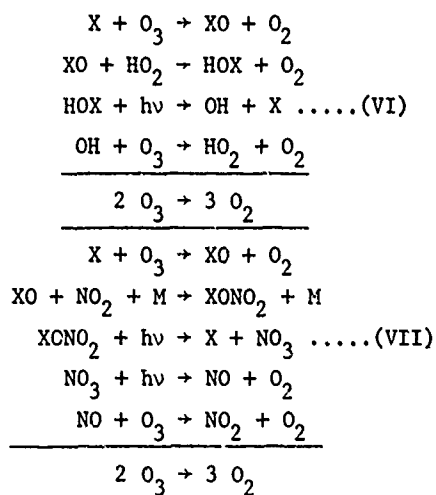


These particular reactions will be discussed in some detail later. There will be little discussion of the  $\text{XNO}_2$  and  $\text{XONO}$  species as the present kinetic and photochemical data base suggests that these species play only a minor role in the photochemistry of the halogen families. Each of the other species, and the reactions which control the partitioning will be discussed.

Prior to discussing specific chemical reactions, catalytic cycles involving both radicals and temporary reservoirs will be reviewed. Those involving radicals can be written:



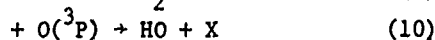
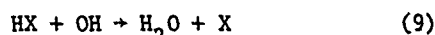
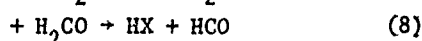
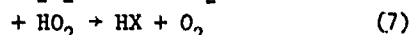
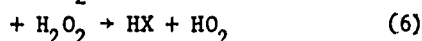
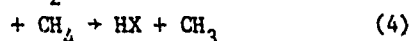
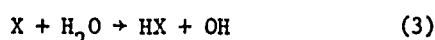
Those involving temporary reservoirs can be written:



The importance of these cycles will be discussed as the key reactions are

reviewed. The only comment to be made at this state concerns the role of species such as HOX and XONO<sub>2</sub> which are commonly referred to as temporary reservoirs. The term "temporary reservoir" has normally implied that such a species would partially inhibit the catalytic efficiency of either chlorine or bromine for destroying odd oxygen by lowering the concentration of radical species. However, whether a temporary reservoir such as HOX or XONO<sub>2</sub> acts to increase or decrease the catalytic efficiency of ClX, BrX or IX depends upon the magnitude of the rate determining processes of the catalytic cycles that involve these species, i.e., cycles (VI) and (VII). Each cycle which destroys odd oxygen involves the XO radical in the rate determining process (this assumes a high value for J(HOX) which is currently accepted (NASA, 1979)). Consequently, the reactions responsible for governing the photochemical partitioning will now be discussed.

REACTIONS WHICH CONTROL THE [X]:[HX] RATIO: The X:HX ratio is controlled by the following reactions:



The [X]:[HX] ratio can simply be expressed:

$$\frac{[X]}{[HX]} = \frac{k_9[OH] + k_{10}[O(^3P)] + k_{11}[O(^1D)] + J_a}{k_3[H_2O] + k_4[CH_4] + k_5[H_2] + k_6[H_2O_2] + k_7[HO_2] + k_8[H_2CO]}$$

A detailed discussion of each of these rate processes will not be forthcoming as most of them have been evaluated in great detail in several recent reviews (Watson, 1977; JPL, 1979; NASA, 1979; CODATA, 1980). The CODATA review tabulates and discusses all recent studies of every reaction. A few general comments can be made at this state which will highlight the major differences between the halogen families, and then a few of the reactions will be discussed in detail. Whereas atomic fluorine reacts rapidly ( $> 10^{-11} \text{ cm}^3 \text{ molecule}^{-1} \text{ s}^{-1}$ ) with all hydrogen containing molecules including H<sub>2</sub>O, the other halogens react more slowly with all hydrogen containing molecules except possibly the HO<sub>2</sub> radical (indeed many reactions, especially those of bromine and iodine, are endothermic and thus negligibly slow). Table I tabulates the heats of reaction, and the rate constants for the X + RH reactions. Reactions such as Cl + H<sub>2</sub>O, Br + CH<sub>4</sub>, etc. which are very endothermic are not included in Table I. Combining the rate constants in Table I with the concentrations of RH molecules in the stratosphere it can be shown that the rate of formation of HX, i.e. d[HX]/dt are in the sequence: d[HF]/dt >> d[HCl]/dt > d[HBr]/dt ≥ d[HI]/dt. Due to the high bond strength in HF, HF once formed is unreactive towards OH and O(^3P) and can only be photodissociated by light of wavelengths shorter than 165 nm (Safary et al. 1951). The other HX molecules are all reactive

TABLE I. Heats of Reaction and Rate Constant for X + RH Reactions

Reaction	$\Delta H_{298}^{\circ}$ (kcal mol <sup>-1</sup> )	$k$ (cm <sup>3</sup> molecule <sup>-1</sup> s <sup>-1</sup> )	Reference
F + H <sub>2</sub> O → HF + OH	- 17.2	$2.0 \times 10^{-10} \exp(-620/T)$	CODATA, 1980
+ CH <sub>4</sub> → HF + CH <sub>3</sub>	- 33.2	$3.0 \times 10^{-10} \exp(-400/T)$	"
+ H <sub>2</sub> → HF + H	- 32.2	$2.2 \times 10^{-11} \exp(-200/T)$	"
+ HNO <sub>3</sub> → HF + NO <sub>3</sub>	- 35.1	$> 10^{-11}$	estimate
+ H <sub>2</sub> O <sub>2</sub> → HF + HO <sub>2</sub>	- 49.2	$> 10^{-11}$	"
+ H <sub>2</sub> CO → HF + HCO	- 49.4	$6.6 \times 10^{-11}$	Le Bras et al. 1979
+ HO <sub>2</sub> → HF + O <sub>2</sub>	- 86.8	$> 10^{-11}$	estimate
Cl + CH <sub>4</sub> → HCl + CH <sub>3</sub>	+ 1.6	$9.9 \times 10^{-12} \exp(-1360/T)$	CODATA, 1980
+ H <sub>2</sub> → HCl + H	+ 1.1	$4.7 \times 10^{-11} \exp(-2340/T)$	"
+ HNO <sub>3</sub> → HCl + NO <sub>3</sub>	+ 2.0	$< 7 \times 10^{-15}$	"
+ H <sub>2</sub> O <sub>2</sub> → HCl + HO <sub>2</sub>	- 17.9	$1.0 \times 10^{-11} \exp(-980/T)$	"
+ H <sub>2</sub> CO → HCl + HCO	- 16.1	$7.9 \times 10^{-11} \exp(-34/T)$	"
+ HO <sub>2</sub> → HCl + O <sub>2</sub>	51.6	$4.1 \times 10^{-11}$	"
+ C <sub>2</sub> H <sub>6</sub> → HCl + C <sub>2</sub> H <sub>5</sub>	- 5.3	$7.7 \times 10^{-11} \exp(-90/T)$	"
Br + H <sub>2</sub> O <sub>2</sub> → HBr + HO <sub>2</sub>	- 2.4	$< 2 \times 10^{-15}$	Lau, 1980a
+ H <sub>2</sub> CO → HBr + HCO	- 0.5	$4.7 \times 10^{-12}$	Le Bras et al. 1979
+ HO <sub>2</sub> → HBr + O <sub>2</sub>	- 36.1	$1 \times 10^{-11}$	estimate
I + HO <sub>2</sub> → HI + O <sub>2</sub>	- 21.7	$\sim 1 \times 10^{-11}$	"

towards OH, and to a lesser extent O(<sup>3</sup>P), thus leading to the regeneration of X atoms.

Table II tabulates the heats of reaction, and the rate constants for the HX + OH, O<sup>3</sup>P and

TABLE II

Heats of Reaction and Rate Constants for HX Removal Processes

Reaction	Heat of Reaction (298K)	$k$ (cm <sup>3</sup> molecule <sup>-1</sup> s <sup>-1</sup> )	Reference
HF + OH → H <sub>2</sub> O + F	+17.2	-	-
+ O( <sup>3</sup> P) → OH + F	+34.1	-	-
+ O( <sup>1</sup> D) → OH + F	-11.3	$\sim 1 \times 10^{-10}$	estimate
HCl + OH → H <sub>2</sub> O + Cl	-16.1	$3.0 \times 10^{-12} \exp(-425/T)$	CODATA, 1980
+ O( <sup>3</sup> P) → OH + Cl	+0.8	$1.1 \times 10^{-11} \exp(-3370/T)$	"
+ O( <sup>1</sup> D) → OH + Cl	-44.5	$1.4 \times 10^{-10}$	Davidson et al., 1977
HBr + OH → H <sub>2</sub> O + Br	-31.7	$8.5 \times 10^{-12}$	CODATA, 1980
+ O( <sup>3</sup> P) → OH + Br	-14.8	$7.0 \times 10^{-12} \exp(-1560/T)$	"
+ O( <sup>1</sup> D) → OH + Br	-60.1	$> 1 \times 10^{-10}$	estimate
HI + OH → H <sub>2</sub> O + I	-48.0	$1.3 \times 10^{-11}$	Takacs and Glass, 1973
+ O( <sup>3</sup> P) → OH + I	-31.0	$\sim 1 \times 10^{-11} \exp(-1000/T)$	estimate
+ O( <sup>1</sup> D) → OH + I	-76.3	$> 1 \times 10^{-10}$	"

<sup>1</sup>D reactions. The combination of the high reactivity of atomic F towards RH molecules, and the unreactivity of HF, results in a low [F]/[HF] ratio which is in sharp contrast to the Cl<sub>2</sub>,

Br and I analogs which have much higher  $[X]/[HX]$  ratios. Ultimately this results in Cl, Br and I being more efficient in catalytically destroying odd oxygen.

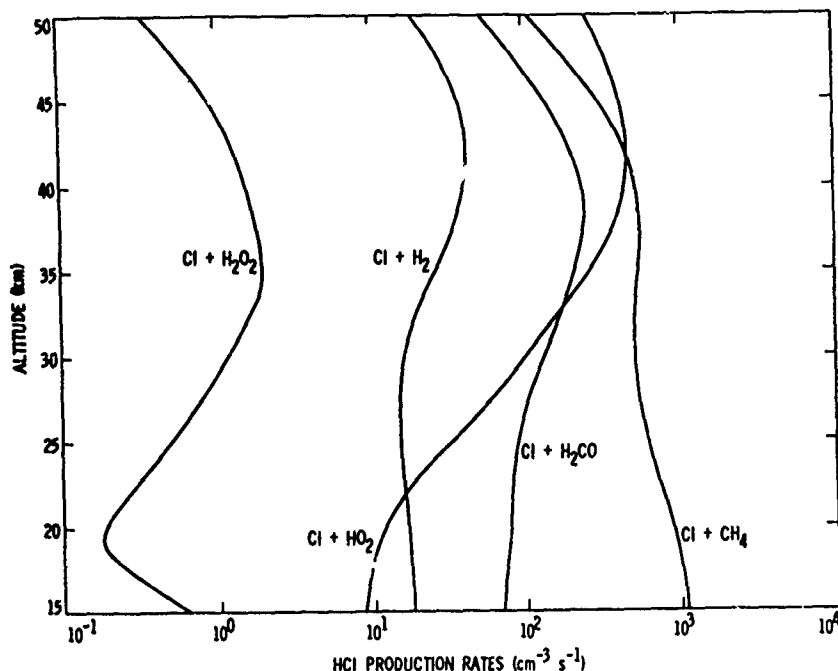
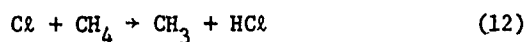


Figure 2a. HCl production rates as a function of altitude in the stratosphere due to atomic chlorine reactions.

Figure 2a shows the rates of HCl formation as a function of altitude and illustrates how the dominant Cl atom reactions are with  $\text{CH}_4$ ,  $\text{H}_2\text{CO}$  and  $\text{HO}_2$ . The  $\text{Cl} + \text{CH}_4$  and  $\text{Cl} + \text{HO}_2$  reactions are discussed, but not the  $\text{Cl} + \text{H}_2\text{CO}$  reaction as it is thought to be well defined. There have been numerous studies of the  $\text{Cl} + \text{CH}_4$  reaction:



using a variety of techniques, e.g., discharge flow-resonance fluorescence, (Michael and Lee, 1977; Zahniser et al. 1978; Keyser, 1978); discharge flow-mass spectrometry (Lin et al. 1978); flash photolysis-resonance fluorescence (Watson et al. 1976; Whytock et al. 1977; Manning and Kurylo, 1977); and competitive chlorinations (Lin et al; Pritchard et al. 1954; Knox and Nelson, 1959; Knox, 1955; Pritchard et al. 1955). Overall the recent results (those studies referenced above) are in good agreement above  $\sim 235\text{K}$ . However, at temperatures below  $235\text{K}$ , the agreement becomes less acceptable with the measured values appearing to depend upon the kinetic technique used to study the reaction. Figure 3 shows the results obtained for the  $\text{Cl} + \text{CH}_4$  rate constant (only those studies which are thought to be free from significant error are shown). It can be seen that at  $\sim 215\text{K}$ , a temperature relevant to the lower stratosphere, there is a wide spread in the values of  $k_{12}$  in contrast to the situation at  $235\text{K}$  and  $298\text{K}$ . The results from a recent laser flash photolysis-resonance fluorescence study (Ravishankara and Wine, 1980) may possibly lend an explanation for the disagreement at low

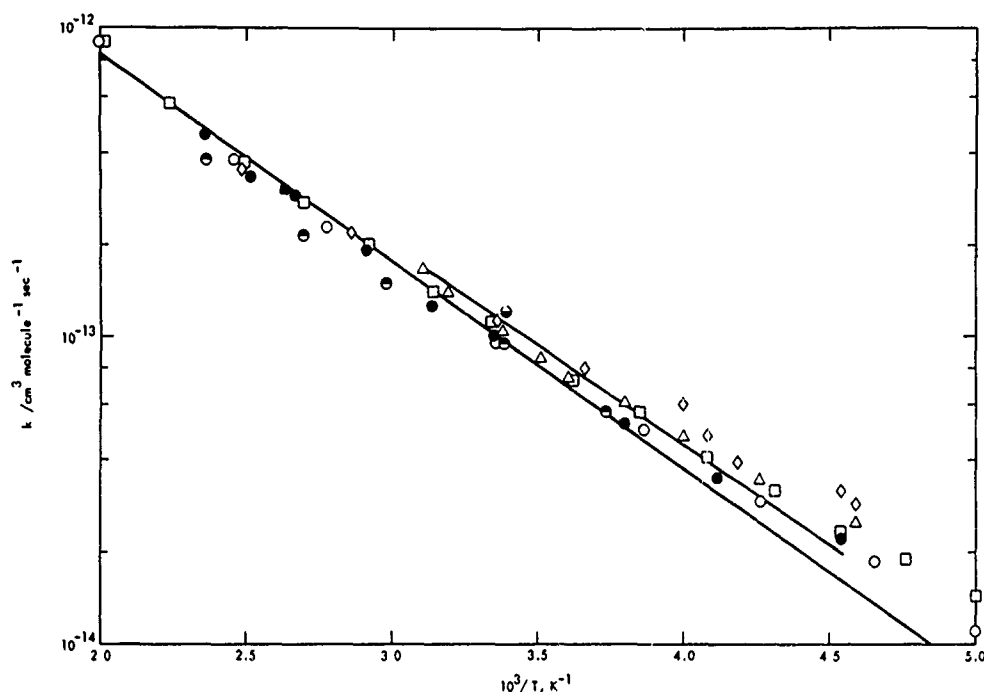


Figure 3. The  $\text{Cl}_2 + \text{CH}_4 + \text{HCl} + \text{CH}_3$  reaction. Summary Arrhenius plot. The symbols are as follows:  $\bullet$ , Keyser (1978);  $\circ$ , Zahniser et al. (1978);  $\square$ , Whytock et al. (1977) and Michael and Lee (1977);  $\diamond$ , Watson et al. (1976), corrected for 25 ppm of ethane;  $\Delta$ , Manning and Kurylo (1977);  $\ominus$ , Lin et al. (1978); —, competitive chlorination results of Lin et al. (1978) which are relative to  $\text{Cl}_2 + \text{C}_2\text{H}_6$ . Upper line used Manning and Kurylo's (1977) value of  $k(\text{Cl}_2 + \text{C}_2\text{H}_6)$ , lower line used Lewis et al.'s (1980) value of  $k(\text{Cl}_2 + \text{C}_2\text{H}_6)$ .

temperatures. A possible explanation for the disagreement is based upon the assumption that the  $^2\text{P}_{1/2}$  and  $^2\text{P}_{3/2}$  states of atomic chlorine react at substantially different rates, and that a disequilibrium can exist in some of the experimental studies. Figure 4 is an energy level diagram which shows how the  $^2\text{P}_{3/2}$  reaction is  $\sim 1 \text{ kcal mol}^{-1}$  endothermic, while the  $^2\text{P}_{1/2}$  reaction is  $\sim 1\text{--}1/2 \text{ kcal mol}^{-1}$  exothermic. Figure 5 shows a plot of the pseudo-first-order rate constant versus methane concentration at temperatures of 221K and 231K. It can be seen that for  $\text{He}/\text{Cl}_2/\text{CH}_4$  mixtures there is a discontinuity in the slope with the slope decreasing at high  $\text{CH}_4$  concentrations. The data collected using  $\text{He}/\text{Cl}_2/\text{CH}_4/\text{CCl}_4$  and  $\text{Ar}/\text{Cl}_2/\text{CH}_4$  reaction mixtures was observed to fit on the extrapolated line obtained using  $\text{He}/\text{Cl}_2/\text{CH}_4$  mixtures at low  $\text{CH}_4$  concentrations. Figure 6 shows an Arrhenius plot of the data from which it can be seen that at temperatures at and below 241K that two different values of the rate constant were determined depending upon the reaction mixture used. Values of the rate constant obtained using  $\text{He}/\text{Cl}_2/\text{CH}_4$  mixtures at high  $\text{CH}_4$  concentrations were lower than those obtained using  $\text{Ar}/\text{Cl}_2/\text{CH}_4$  or  $\text{He}/\text{Cl}_2/\text{CH}_4/\text{CCl}_4$  mixtures. At low  $\text{CH}_4$  concentrations and at temperatures above 241K, the rate constants were independent of the composition of the reaction mixtures. The sequence of reactions taking place can be written:

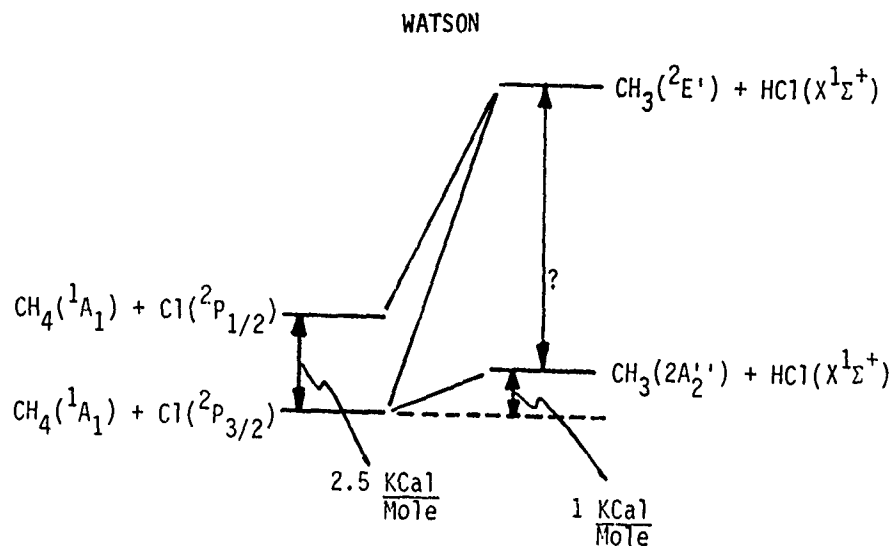


Figure 4. Adiabatic correlation diagram for the reaction  $\text{Cl}(^2\text{P}) + \text{CH}_4 \rightarrow \text{CH}_3 + \text{HCl}$ .

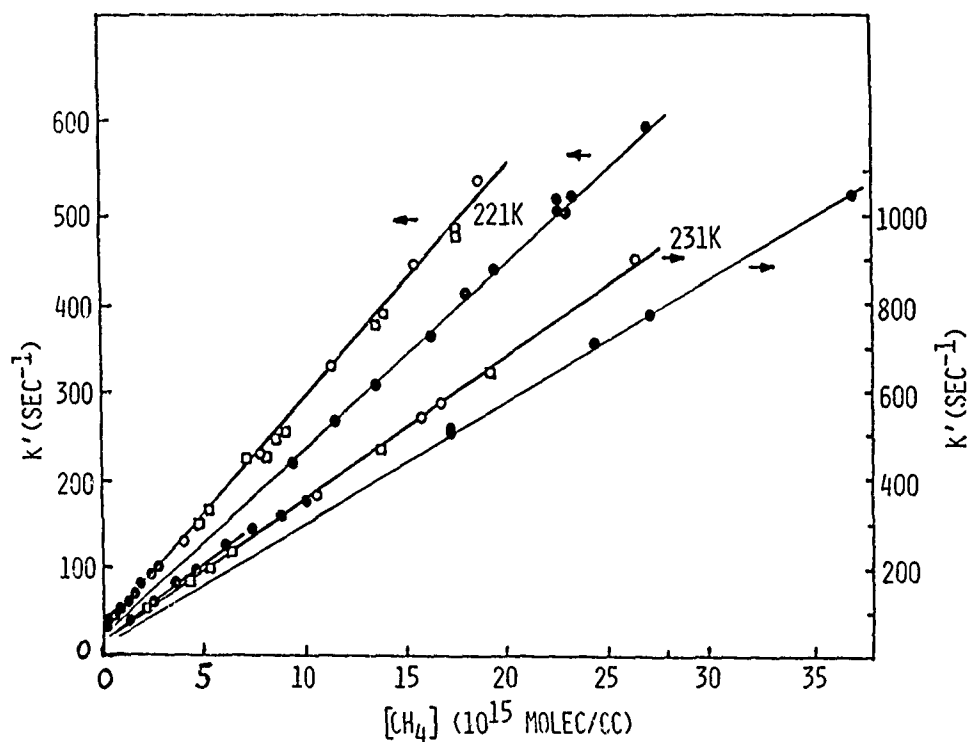


Figure 5. The  $\text{Cl}(^2\text{P}) + \text{CH}_4 \rightarrow \text{HCl} + \text{CH}_3$  reaction. Plots of pseudo-first order rate constant vs. methane concentration for  $T = 221$ , and  $231\text{K}$ . Data obtained with  $\text{He}/\text{Cl}_2/\text{CH}_4$  reaction mixtures at intermediate methane concentrations gave non-exponential decays. Since accurate pseudo-first order rate constants could not be deduced from this data, the results are not plotted. ●:  $\text{He}/\text{Cl}_2/\text{CH}_4$  reaction mixtures; □:  $\text{He}/\text{Cl}_2/\text{CCl}_4/\text{CH}_4$  reaction mixtures; ○:  $\text{Ar}/\text{Cl}_2/\text{CH}_4$  reaction mixtures.



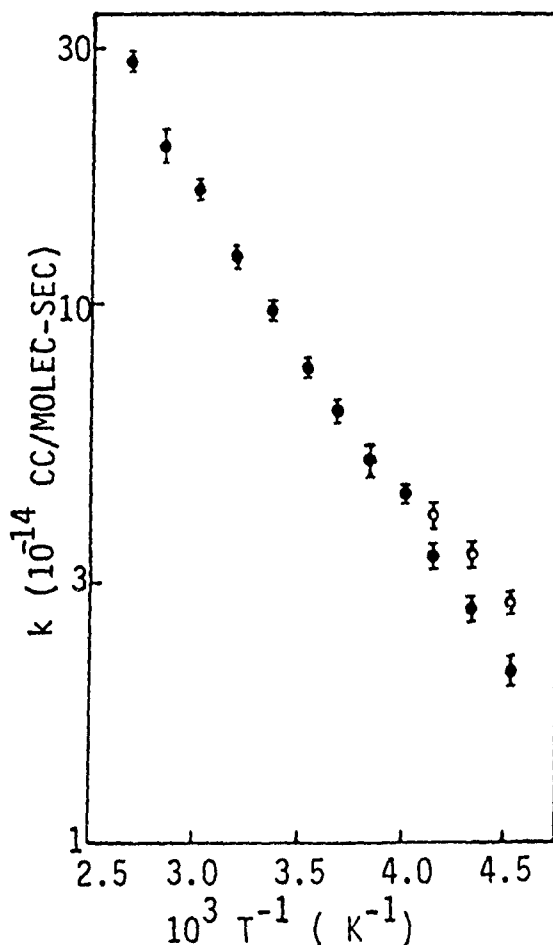
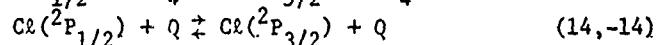
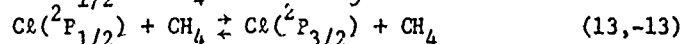
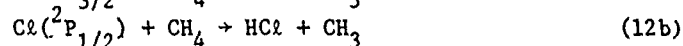
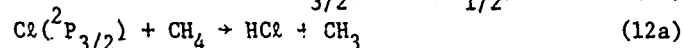
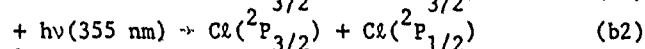
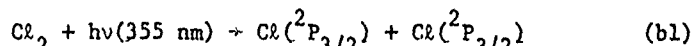


Figure 6. Arrhenius plot for the reaction  $Cl(^2P) + CH_4 \rightarrow CH_3 + HCl$ . At low temperatures, where the rate constant is found to depend upon the methane concentration:  $\bullet$ , high  $[CH_4]$ ;  $\circ$ , low  $[CH_4] \equiv$  high  $[CH_4]$  in the presence of Ar or  $CCl_4$ . This data was obtained with  $Cl_2/CH_4/He$  reaction mixtures at a total pressure of 50 torr. Error bars are  $2\sigma$  and refer to precision only.



where Q represents quenching gases, i.e., He, Ar,  $CCl_4$  or  $Cl_2$ . The above mechanism correctly assumes that there are no complicating reactions such as  $CH_3 + Cl_2 \rightarrow CH_3Cl + Cl$  under the experimental conditions used in their study. Values for  $k_{14}$  were obtained from the recent work of Fletcher and Husain (1977, 1978) and were combined with calculated equilibrium constants to obtain values for  $k_{-14}$ . A speculative interpretation of the observations was forwarded which can simply be summarized as follows. If the  $Cl(^2P_{1/2})$  atom reacts much more rapidly with  $CH_4$  than does the  $Cl(^2P_{3/2})$  atom, especially at low temperatures, then at high  $CH_4$  concentrations the  $Cl(^2P_{1/2})$  atom concentration may be depopulated relative to its equilibrium value if the reaction mixture does not contain a gas which can rapidly repopulate the  $^2P_{1/2}$  state. Therefore, it is speculated that in  $He/Cl_2/CH_4$  mixtures at high  $CH_4$  concentrations the He is unable to repopulate the  $^2P_{1/2}$  state at a rate equal to the depopulation

# WATSON

by reaction with  $\text{CH}_4$ . However, in the presence of Ar or  $\text{CCl}_4$  it is argued that these gases can maintain an equilibrated mixture of  $^2\text{P}_{1/2}$  and  $^2\text{P}_{3/2}$  states. Once the  $^2\text{P}_{1/2}$  state has been depopulated in the  $\text{He}/\text{Cl}_2/\text{CH}_4$  system it is assumed that the slower rate is mainly attributed to the reaction of the  $^2\text{P}_{3/2}$  state. The authors speculate that this difference in reactivity between the two spin states of atomic chlorine may account for the differences in the rate constants reported at low temperatures from one technique to another. They argue that the low values reported in the discharge flow-resonance fluorescence studies are due to a rapid depopulation of the  $^2\text{P}_{1/2}$  state, and that at  $\sim 1$  torr of He that state cannot be re-equilibrated. A comment that should be made is that the walls of the flow system would have been expected to have acted as an efficient equilibrator of the two-spin states. The results of the earlier flash photolysis resonance fluorescence studies were all in good agreement with each other and with the recent results of Ravishankara and Wine. This is compatible with the hypothesis of Ravishankara and Wine as the earlier FP/RF studies all used an efficient electronic equilibrator in their reaction mixture, e.g. Watson et al. used  $\text{CCl}_4$  as the atomic chlorine precursor. The authors also speculated that the competitive chlorination studies may have also underestimated the  $\text{Cl} + \text{CH}_4$  rate constant at low temperatures due to a non-equilibrium distribution of  $^2\text{P}$  states in atomic chlorine. In these studies the bath gas was  $\text{CH}_4$  itself, and unfortunately the value of  $k_{13}$  has not been determined. Consequently, it is not possible at present to analyse these studies further. In conclusion it should be stated that the discrepancies between the various values of the  $\text{Cl} + \text{CH}_4$  rate constant at low temperatures may possibly be explained by postulating a non-equilibrium distribution of spin states. However, the message is that when laboratory kinetic studies are performed it is essential to ensure that the distribution of states, whether they be electronic, vibrational, or rotational, is equilibrated (or at least known). An interesting question is: "If the hypothesis is correct, then why do the two  $^2\text{P}$  spin states of Cl react differently - Energetics of spin considerations?"

The second major channel for production of  $\text{HCl}$  from atomic chlorine at and above 35 km is the  $\text{Cl} + \text{HO}_2$  reaction:



There is a second possible reaction pathway which does not form  $\text{HCl}$ :



To date, there have been no direct studies of this reaction, only relative determinations. Several different kinetic techniques have been used, i.e., discharge flow-laser magnetic resonance (Burrows et al. 1979a); discharge flow-mass spectrometry (Leu and DeMore, 1976; Poulet et al. 1978); molecular modulation-ultraviolet absorption (Cox, 1980); and a complex static system (Cox and Derwent, 1977), to determine the rate constant for  $\text{Cl} + \text{HO}_2$  relative to another "hopefully" well-known rate constant. Table III shows the studies performed to date. As can be seen, the majority of studies used the  $\text{Cl} + \text{H}_2\text{O}_2$  reaction as a standard. Consequently, before evaluating the reliability of the  $\text{Cl} + \text{HO}_2$  studies, a review of the  $\text{Cl} + \text{H}_2\text{O}_2$ , and to a lesser extent, a review of the  $\text{Cl} + \text{H}_2$  reaction is needed.

TABLE III

Summary of Measurements of  $\text{Cl} + \text{HO}_2$  at  $\sim 298\text{K}$ 

$k(10^{-11} \text{ cm}^3 \text{ molecule}^{-1} \text{ s}^{-1})$	Ref. Reaction	$k(\text{Cl} + \text{HO}_2)/k_{\text{ref.}}$	Reference
$2.1 \pm 3.2$ $-1.3$	$\text{Cl} + \text{H}_2\text{O}_2$	48 (a)	<u>Leu and DeMore</u> , 1976
$2.5 \pm 1.0$	Complex	-	<u>Cox and Darwent</u> , 1977
$7.3 \pm 1.9$	$\text{Cl} + \text{H}_2\text{O}_2$	$170 \pm 45$ (a)	<u>Poulet et al.</u> , 1978
$4.5 \pm 0.5$	$\text{Cl} + \text{H}_2\text{O}_2$	$104 \pm 12$ (a)	<u>Burrows et al.</u> , 1979a
$6.8 \pm 3.4$	$\text{Cl} + \text{H}_2$	$\sim 3.7 \times 10^3$ (b,c)	<u>Cox</u> , 1980

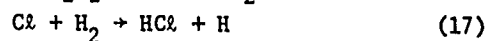
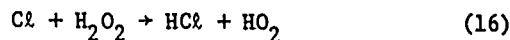
(a)  $k_{\text{ref}} = 4.3 \times 10^{-13} \text{ cm}^3 \text{ molecule}^{-1} \text{ s}^{-1}$  (CODATA).(b)  $k_{\text{ref}} = 9.9 \times 10^{-12} \exp(-1360/T) \text{ cm}^3 \text{ molecule}^{-1} \text{ s}^{-1}$  (CODATA).(c)  $k(\text{Cl} + \text{HO}_2)/k(\text{Cl} + \text{H}_2)$  reported to be  $3.0 \pm 5.1 \exp(+ (2120 \pm 370)/T)$  from 274-338K.

Figure 7 shows all the experimental data associated with the  $\text{Cl} + \text{H}_2\text{O}_2$  reaction. There is

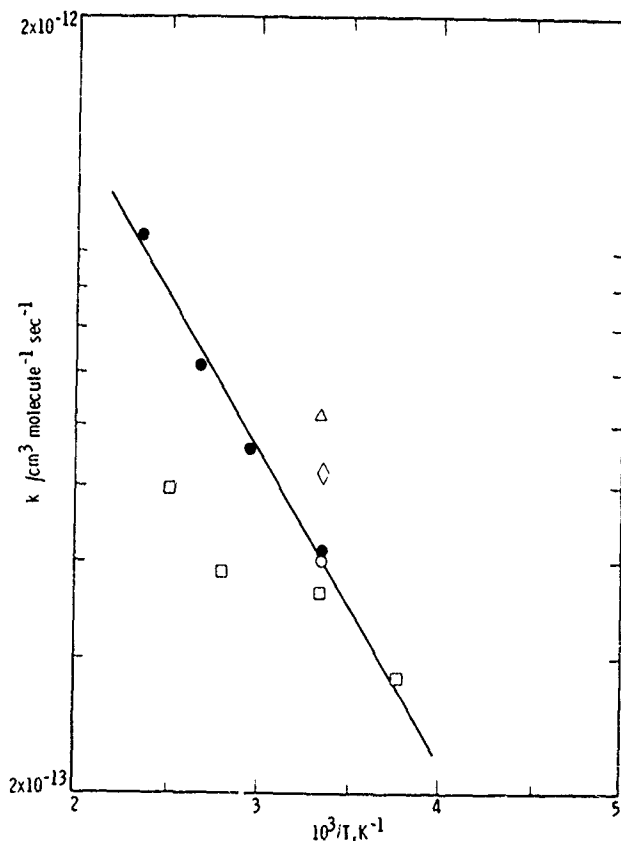
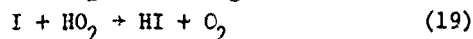
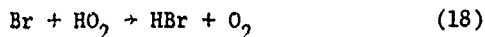


Figure 7. The  $\text{Cl} + \text{H}_2\text{O}_2 \rightarrow \text{HCl} + \text{HO}_2$  reaction. Summary Arrhenius plot. The symbols are as follows:  
 ●, Keyser (1980);  
 □, Michael et al. (1977); ◇, Watson et al. (1976); Δ, Leu and DeMore (1976); ○, Poulet et al. (1978).

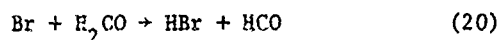
# WATSON

good agreement within the stated uncertainties at 298K and from this data an evaluated value of  $4.3 \times 10^{-13} \text{ cm}^3 \text{ molecule}^{-1} \text{ s}^{-1}$  can be derived. From Figure 7 it can be seen that the temperature dependences reported by Keyser (1980) and Michael et al. (1977) are in poor agreement. The expression reported by Keyser is to be preferred. The pre-exponential A-factor reported by Keyser is in accord with that expected based on theoretical grounds for a hydrogen atom abstraction reaction, whereas that reported by Michael et al. is much lower than would be expected for such a process. It can be seen from Figure 7 that at and below 298K the values reported in these two studies are in good agreement. The disagreement at higher temperatures could possibly be due to heterogeneous decomposition of  $\text{H}_2\text{O}_2$  in the study of Michael et al. The other reaction used as a standard was the  $\text{Cl} + \text{H}_2$  reaction. The rate constant for this reaction has been studied both directly, and indirectly (i.e. by calculating it from experimental values of  $k_{-17}(\text{H} + \text{HCl})$  and the thermodynamic equilibrium constant). Most of the  $\text{H} + \text{HCl}$  studies are thought to be in error due to complicating secondary processes, both homogeneous and heterogeneous, and the 298K data for the  $\text{Cl} + \text{H}_2$  studies is more sparse than would be imagined. Recent evaluations differ on their recommendation for  $k_{17}(\text{Cl} + \text{H}_2)$  at 298K. The NASA panel for data evaluation recommended a value of  $1.6 \times 10^{-14} \text{ cm}^3 \text{ molecule}^{-1} \text{ s}^{-1}$  in contrast to the value of  $1.8 \times 10^{-14} \text{ cm}^3 \text{ molecule}^{-1} \text{ s}^{-1}$  preferred by the CODATA task group for chemical kinetics. Data considered in both of these evaluations was reported by Watson et al. (1975), Lee et al. (1977), Westenberg and deHaas (1968) and Benson et al. (1969). The values of  $k_{15}(\text{Cl} + \text{HO}_2)/k_{16}(\text{Cl} + \text{H}_2\text{O}_2)$  reported by Leu and DeMore, Poulet et al., and Burrows et al. are in poor agreement. The discrepancy between the two mass-spectrometric results may be attributed to inaccurate estimates of the mass spectrometric sensitivity for  $\text{HO}_2$  in one or both studies. When a value of  $4.3 \times 10^{-13} \text{ cm}^3 \text{ molecule}^{-1} \text{ s}^{-1}$  is used for  $k_{16}(\text{Cl} + \text{H}_2\text{O}_2)$  the values of  $k_{15}(\text{Cl} + \text{HO}_2)$  range from  $(2.1-7.3) \times 10^{-11} \text{ cm}^3 \text{ molecule}^{-1} \text{ s}^{-1}$ . The value derived by Cox, using the  $\text{Cl} + \text{H}_2$  reaction as a standard was  $(6.8 \pm 50\%) \times 10^{-11} \text{ cm}^3 \text{ molecule}^{-1} \text{ s}^{-1}$  (relative to the CODATA value for  $k_{17}$ ). The earlier work of Cox and Derwent is rather more complex but the results fit within the range of values derived by the slightly more direct studies. Obviously more data is required, preferably using a pseudo-first-order technique ( $[\text{Cl}]_0 \gg [\text{HO}_2]_0$ ) where values for absolute  $\text{HO}_2$  concentrations and reference rate coefficients are not needed. The mechanism for this reaction will be discussed later (at present assumed to predominantly produce  $\text{HCl} + \text{O}_2$ ). The rate of production of  $\text{HCl}$ , and hence the  $[\text{Cl}]:[\text{HCl}]$  ratio, is quite sensitive to this rate constant.

The kinetic data base for Br and I atom reactions with RH molecules is sparse. As shown in Table I there are only three Br atom reactions and one I atom reaction which are exothermic to form  $\text{HBr}$  and  $\text{HI}$ , respectively. The dominant reactions are:



and possibly:



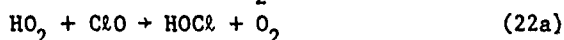
The values of  $k_{18}$  and  $k_{19}$  can only be estimated as there is no experimental data. Consequently, studies of these reactions are urgently required. A provisional value of  $1.6 \times 10^{-12} \text{ cm}^3 \text{ molecule}^{-1} \text{ s}^{-1}$  has been determined for  $k_{20}$  at 298K by Le Bras et al. (1979).

# WATSON

REACTIONS OF XO RADICALS WHICH PRODUCE HX: At present there are no reactions in the photochemical models which directly connect HX to XO. All reaction schemes presently connect HX to XO via the X atom. Let us consider the case for chlorine. Due to the high  $[ClO]/[Cl]$  ratios ( $4.2 \times 10^3$  (20km) -  $1.3 \times 10^2$  (40km)) which are predicted from the photochemical models a much slower first order rate constant ( $k[\text{reagent}]$ ) for a reaction directly converting  $ClO$  into  $HCl$  can be important relative to a reaction converting  $Cl$  into  $HCl$ :

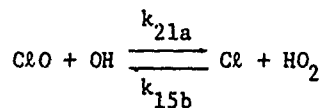
$$d[HCl]/dt = k[Cl][A] + k'[ClO][B].$$

For the magnitudes of  $k[Cl][A]$  and  $k'[ClO][B]$  to be comparable the value of  $k[A]$  must far exceed  $k'[B]$  due to the high  $[ClO]/[Cl]$  ratio. Reactions which may possibly provide a direct  $HCl:ClO$  link which are at present being studied include:



The situation in the  $BrX$  and  $IX$  systems is somewhat similar, but in these systems the  $[XO]/[X]$  ratio is less than in the  $ClX$  case.

The  $ClO + OH$  reaction has recently been studied by Leu and Lin (1979) using the discharge flow technique coupled to both resonance fluorescence (for  $OH$ ) and mass spectrometric (for  $ClO$ ) detection systems. A total rate constant,  $k_{21} = (k_{21a} + k_{21b})$  of  $9.1 \times 10^{-12} \text{ cm}^3 \text{ molecule}^{-1} \text{ s}^{-1}$  was determined by monitoring the rate of removal of  $OH$  radicals in the presence of an excess concentration of  $ClO$  radicals. By monitoring the production of  $HO_2$  radicals (this was achieved by the somewhat indirect technique of converting the  $HO_2$  radicals into  $OH$  radicals via the  $NO + HO_2 \rightarrow OH + NO_2$  reaction upon addition of a large concentration of  $NO$ ) the authors were able to place a lower limit of 65% on the total reaction which took place via channel (a). Indeed, the experimental data could not provide any evidence for channel (b) at all. If channel (b) was as high as 35% of the total reaction, i.e.,  $k_{21b} = 3.2 \times 10^{-12} \text{ cm}^3 \text{ molecule}^{-1} \text{ s}^{-1}$ , then it would be a major channel for the formation of  $HCl$  throughout the stratosphere (see Figure 2b). Consequently, additional work is required so that the overall rate constant is confirmed and the branching ratio of  $k_{21b}/k_{21}$  is more accurately determined. Obviously, these studies are required over a range of temperature (200-270K). At present there is one other experimental study which pertains to this topic, and that is the study of Burrows et al. (1979a) where an upper limit of  $< 3 \times 10^{-13} \text{ cm}^3 \text{ molecule}^{-1} \text{ s}^{-1}$  was placed on  $k_{15b}(Cl + HO_2 \rightarrow OH + ClO)$ :



Therefore, combining Leu and Lin's lower limit of  $5.9 \times 10^{-12} \text{ cm}^3 \text{ molecule}^{-1} \text{ s}^{-1}$  with Burrows et al. upper limit of  $3 \times 10^{-13} \text{ cm}^3 \text{ molecule}^{-1} \text{ s}^{-1}$  for  $k_{15b}$  results in a lower limit of 20 for the equilibrium constant,  $K_{eq} = k_{21a}/k_{15b}$ . Using the CODATA recommended values for  $\Delta H_{f298}^{\circ}(ClO, OH \text{ and } Cl)$ , and for  $S_{298}^{\circ}(ClO, OH, Cl, \text{ and } HO_2)$  a value of  $\leq 1.8 \text{ kcal mol}^{-1}$  can

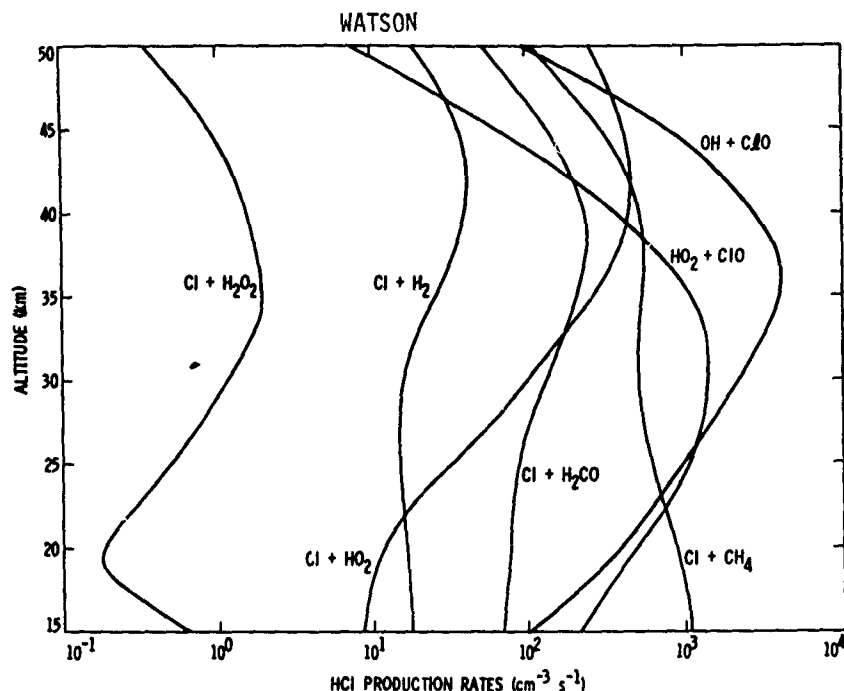
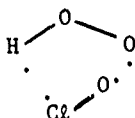


Figure 2b. HCl production rates as a function of altitude in the stratosphere. The production rates shown for the OH + C<sub>2</sub>O reaction assumed the upper limit for  $k_{21b}$ , i.e.  $3.2 \times 10^{-12} \text{ cm}^3 \text{ molecule}^{-1} \text{ s}^{-1}$ . The production rates shown for the HO<sub>2</sub> + C<sub>2</sub>O reaction assumed  $k_{22b}$  to be 3% (upper limit) of the total rate constant reported by Stimpfle et al. (1979), i.e.  $k_{22} = 3.3 \times 10^{-11} \exp(-850/T) + 4.5 \times 10^{-12} (T/300)^{-3.7}$ .

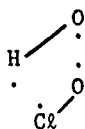
be calculated for  $\Delta H_{298}^{\circ} \text{HO}_2$ . This contrasts to a value reported by Howard (1979a) (see following paper entitled "Laboratory Studies of Reactions of Odd Hydrogen Species of Atmospheric Interest") of  $2.5 \pm 1.0 \text{ kcal mol}^{-1}$  for  $\Delta H_{f298}^{\circ} \text{HO}_2$ . The point to be noted is that the values used for  $k_{21a}$  and  $k_{15b}$  are lower and upper limits, respectively. The value of  $k_{21a}$  could be as high as  $9.1 \times 10^{-12} \text{ cm}^3 \text{ molecule}^{-1} \text{ s}^{-1}$ , while  $k_{15b}$  could be any value lower than  $3 \times 10^{-13} \text{ cm}^3 \text{ molecule}^{-1} \text{ s}^{-1}$  as the authors stated that there was no evidence at all (based on production of OH radicals) for the existence of reaction (15b). A change of  $1 \text{ kcal mol}^{-1}$  in the value of  $\Delta G$  at 298K requires a change of a factor of 5.4 in  $K_{eq}$  at 298K. Consequently, at present it is difficult to state that the three reported parameters ( $k_{21a}(\text{C}_2\text{O} + \text{OH})$ ;  $k_{15b}(\text{Cl} + \text{HO}_2)$ , and  $\Delta H_{f298}^{\circ}(\text{HO}_2)$ ) are either consistent or inconsistent within their stated uncertainties.

The other reaction presently being studied which may directly link C<sub>2</sub>O to HCl is the C<sub>2</sub>O + HO<sub>2</sub> reaction. There will be very little discussion of the four studies which have measured the rate constant for this reaction as this topic is covered in some detail in Howard (1979b). However, the importance of this reaction as a direct link between C<sub>2</sub>O and HCl will be emphasized. The results of the four studies of this reaction are in reasonable agreement, three using the low pressure discharge flow technique (Reimann and Kaufman, 1978; Leck et al. 1979; and Stimpfle et al. 1979) and one using the molecular modulation technique at one atmosphere total pressure (Burrows et al. 1979b). The average of these four determinations of  $k_{22}$  at 298K is  $5.0 \times 10^{-12} \text{ cm}^3 \text{ molecule}^{-1} \text{ s}^{-1}$ , and Stimpfle et al. have reported that the rate constant increases as the temperature is reduced below 298K (see the following paper by Howard). There have been two studies which have attempted to determine the branching ratio

for this reaction (Leck et al., and Leu, 1979). In each case the approach used was to monitor the production of ozone mass spectrometrically, and in each case it was reported that the amount of ozone produced was below the detection limits of the systems i.e.  $\sim 10^9 \text{ cm}^{-3}$ . By combining the upper limit for  $[\text{O}_3]_{\text{produced}}$  with  $[\text{HO}_2]_{\text{removed}}$  values for  $k_{22b}/k_{22}$  of  $< 2\%$  at 298K (Leck et al.), and  $< 1.5\%$  at 298K, and  $< 3.0\%$  at 248K (Leu) have been reported. From these studies an upper limit of  $\leq 10^{-13} \text{ cm}^3 \text{ molecule}^{-1} \text{ s}^{-1}$  can be placed on  $k_{22b}$  at 298K. However, even such a slow reaction would be of enormous importance, and could be the major production channel for HCl between 20 and 40 km (fig. 2b). Consequently, more work is required to both accurately measure the branching ratio, and to reduce the uncertainty in  $k_{22}$ . Although it should not be difficult to improve upon the quoted  $\text{O}_3$  detection limits by at least one order of magnitude with an improved mass spectrometric system, it may prove difficult to detect small concentrations of HCl. On the question of rapid reactions with "complex" transition states little will be said at this juncture. Howard (1979a) discusses the  $\text{HO}_2 + \text{ClO}$  reaction and the likelihood of a five member ring,



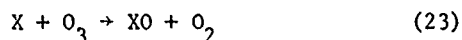
and the probability of a four member ring in the  $\text{OH} + \text{ClO}$  reaction,



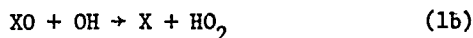
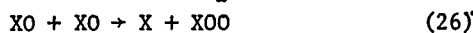
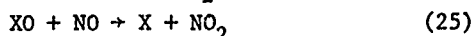
cannot be ruled out. As will be discussed later the experimental data supports such a four-center mechanism in the  $\text{ClO} + \text{ClO}$  and  $\text{BrO} + \text{BrO}$  reactions, i.e.  $\text{XO} + \text{XO} \rightarrow \text{X}_2 + \text{O}_2$ .

To summarize this section on X to HX and XO to HX it should be stated that while there are suggestions that reactions such as  $\text{XO} + \text{HO}$ , and  $\text{XO} + \text{HO}_2$  may play a significant role, there is a dire need for accurate rate data with a special emphasis on the product distribution as a function of temperature. There is no data on the reactions of BrO and IO with OH and  $\text{HO}_2$  but these would, of course, be quite important, especially as the only reactions of I and Br which are thought to form HI and HBr are with  $\text{HO}_2$ , and in the case of Br, possibly with  $\text{H}_2\text{CO}$  and  $\text{H}_2\text{O}_2$ . These reactions would be quite challenging as the  $\text{BrO} + \text{BrO}$  and  $\text{IO} + \text{IO}$  reactions are quite rapid (discussed later) and would prevent the simple use of pseudo-first order conditions as used in the  $\text{ClO} + \text{OH}$  and  $\text{ClO} + \text{HO}_2$  reactions. The  $\text{FO} + \text{OH}$  and  $\text{FO} + \text{HO}_2$  reactions would not be expected to be as important due to the rapidity of the  $\text{F} + \text{H}_2\text{O}$ ,  $\text{F} + \text{CH}_4$ , and  $\text{F} + \text{H}_2$  reactions coupled with the high mixing ratios of these hydrogen containing species in the stratosphere.

REACTIONS WHICH CONTROL THE [X]:[XO] RATIO: The X:XO ratio is controlled by the following reactions:



## WATSON



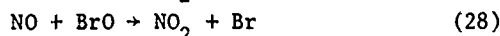
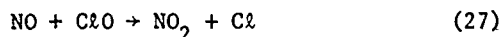
The X:XO ratio can be expressed:

$$\frac{[\text{X}]}{[\text{XO}]} = \frac{k_{24}[\text{O}] + k_{25}[\text{NO}] + k_{1b}[\text{OH}] + J_c}{k_{23}[\text{O}_3]}$$

Although this expression was derived by neglecting the  $\text{XO} + \text{XO}$  (26) reaction it does not lead to any significant error. Because the XO radical participates in each of the rate determining reactions of the catalytic cycles which result in the destruction of odd oxygen, shown earlier, reactions such as (25) and (c) which reduce the fraction of the inorganic halogen in the form of XO are obviously important in controlling the efficiency of the halogen in destroying odd oxygen. In contrast, reactions such as (24) and (26) are the rate limiting reactions in those cycles which catalytically destroy odd oxygen. Little will be said about reactions (24) and (26) except to note that the rate constant for the  $\text{O} + \text{ClO}$  reaction is reasonably well established (better than 25%) whereas the  $\text{O} + \text{BrO}$  rate constant is poorly defined ( $\pm$  factor of 3) and the  $\text{O} + \text{FO}$  and  $\text{O} + \text{IO}$  reactions have never been studied. The rate constants for all four reactions are expected to be quite similar, i.e.  $k_{24} \approx 5 \times 10^{-11} \text{ cm}^3 \text{ molecule}^{-1} \text{ s}^{-1}$  ( $\pm$  factor of 2). Whereas the photolysis of  $\text{ClO}$  is completely unimportant in controlling the  $[\text{ClO}]/[\text{Cl}]$  ratio, the photolysis of  $\text{BrO}$  and  $\text{IO}$  is very important in controlling the  $[\text{BrO}]/[\text{Br}]$  and  $[\text{IO}]/[\text{I}]$  ratios, respectively. Unfortunately the absorption cross-section data for  $\text{BrO}$  and  $\text{IO}$  is marginal at best. The  $\text{XO} + \text{NO}$  and  $\text{XO} + \text{XO}$  reactions will now be discussed.

XO + NO: Watson et al. (1979) have shown how the  $\text{BrO} + \text{NO}$  reaction is important in controlling the  $[\text{BrO}]/[\text{Br}]$  and  $[\text{BrO}]/[\text{HBr}]$  ratios in the stratosphere, but does not affect the catalytic efficiency of  $\text{BrX}$  in ozone destruction. This is in sharp contrast to the situation in the  $\text{ClX}$  system where the  $\text{NO} + \text{ClO}$  reaction controls not only the  $[\text{ClO}]/[\text{Cl}]$  and  $[\text{ClO}]/[\text{HCl}]$  ratios, but also the catalytic efficiency of  $\text{ClX}$  in ozone destruction. This difference arises because, (a)  $\text{BrO}$  is the dominant form of  $\text{BrX}$  whereas  $\text{HCl}$  and  $\text{ClONO}_2$  are the dominant forms of  $\text{ClX}$ , and (b) the only important process which converts  $\text{ClO}$  to  $\text{Cl}$  below 32 km is the  $\text{NO} + \text{ClO}$  reaction, whereas the photolysis rate of  $\text{BrO}$  is comparable to the rate of the  $\text{NO} + \text{BrO}$  reaction. The role of the  $\text{IO} + \text{NO}$  reaction in the  $\text{IX}$  system is similar to that of the  $\text{BrO} + \text{NO}$  reaction in the  $\text{BrX}$  system.

Of the four halogen oxide radicals only  $\text{ClO}$  and  $\text{BrO}$  have been studied with  $\text{NO}$ :



However, the reactivity of  $\text{FO}$  and  $\text{IO}$  with  $\text{NO}$  is expected to be quite similar to the reactivity of  $\text{ClO}$  and  $\text{BrO}$  with  $\text{NO}$ , i.e.  $k \approx 2 \times 10^{-11} \text{ cm}^3 \text{ molecule}^{-1} \text{ s}^{-1}$ . The  $\text{NO} + \text{ClO}$  and  $\text{NO} + \text{BrO}$  reactions are both characteristic of a growing number of rapid ( $k > 10^{-11} \text{ cm}^3 \text{ molecule}^{-1} \text{ s}^{-1}$ )



## WATSON

bimolecular reactions involving atoms and radicals, e.g.  $O(^3P) + NO_2$  (Bemand et al. 1974),  $NO + HO_2$  (Leu, 1979b; Howard, 1979b),  $O + OH$  (Lewis and Watson, 1980),  $O + ClO$  (Zahniser and Kaufman, 1977) and  $BrO + BrO$  (Sander and Watson, 1980b) that exhibit a negative temperature dependence of the rate constant. Several different hypothesis have been proposed to account for this behavior including a temperature dependent A-factor (Bemand et al.), metastable complex formation (Singleton and Cvetanovic, 1976; Leu and DeMore, 1978), and dependence of the collision cross-section on reactant energy (Davis et al. 1976; Jaffe, 1978). Alternatively, the observed dependence is small enough to be due to systematic experimental error in several cases. The  $NO + ClO$  and  $NO + BrO$  reactions have been the subject of several studies, the results of which are shown in Table IV. In most cases it

TABLE IV

Summary of measurements of  $NO + ClO$  and  $NO + BrO$ 

$k/cm^3 \text{ molecule}^{-1} s^{-1}$	Temp./K	Reference
(A) $NO + ClO \rightarrow NO_2 + Cl$		
$(1.7 \pm 0.2) \times 10^{-11}$	298	Clyne and Watson, 1974b
$1.4 \times 10^{-11} \exp(+216 \pm 200/T)$	230-295	Zahniser and Kaufman, 1977
$(2.2 \pm 0.4) \times 10^{-11}$	293	
$5.72 \times 10^{-12} \exp(+296 \pm 20/T)$	227-415	Leu and DeMore, 1978
$(1.53 \pm 0.11) \times 10^{-11}$	299	
$(1.75 \pm 0.15) \times 10^{-11}$	298	Ray and Watson, 1980
$(1.58 \pm 0.16) \times 10^{-11}$	298	Clyne and MacRoberts, 1980
(b) $NO + BrO \rightarrow NO_2 + Br$		
$(2.2 \pm 0.4) \times 10^{-11}$	298	Clyne and Watson, 1975
$7.11 \times 10^{-12} \exp(+296 \pm 10/T)$	230-425	Leu, 1979a
$(1.89 \pm 0.16) \times 10^{-11}$	298	
$1.28 \times 10^{-11} \exp(+181 \pm 46/T)$	224-396	Watson et al., 1979
$(2.15 \pm 0.25) \times 10^{-11}$	298	
$(2.32 \pm 0.16) \times 10^{-11}$	298	Ray and Watson, 1980

(a) Zahniser and Kaufman determined  $k(NO + ClO)$  relative to  $k(Cl + O_3)$ . They reported a value of  $0.32 \exp(+373 \pm 75/T)$  for  $k(NO + ClO)/k(Cl + O_3)$ . The value of  $k(NO + ClO)$  shown in the table combines their ratio with the CODATA value for  $k(Cl + O_3)$ . Alternate expressions can be derived for  $k(NO + ClO)$  by substituting other values for  $k(Cl + O_3)$ .

can be seen that the rate constant data for both  $ClO$  and  $BrO$  is in excellent agreement at both 298K and as a function of temperature. In the  $NO + ClO$  system the weight of evidence now suggests that the value reported by Zahniser and Kaufman (1977) at 298K is high by  $\sim 30\%$  with the preferred value being  $\sim 1.65 \times 10^{-11} \text{ cm}^3 \text{ molecule}^{-1} s^{-1}$ . The only example of a study of an  $XO + NO$  reaction ( $X = OH, Cl, Br$ ) which was not performed using the low pressure discharge flow technique was the flash photolysis-ultraviolet absorption study of  $NO + BrO$  by Watson et al. (1979). This was performed to test for any pressure dependence in the rate constant which might be expected if the reaction proceeded through a metastable complex which could be stabilized. Figure 8 shows a plot of  $k'_{28} (-d \ln [BrO]/dt)$  as a function of  $[NO]$  at several different total pressures. It can be seen that the reaction rate constant exhibits no pressure dependence in agreement with the RRK calculations of Watson et al. (1979) which suggest that even if the metastable complex formation mechanism is correct then a pressure

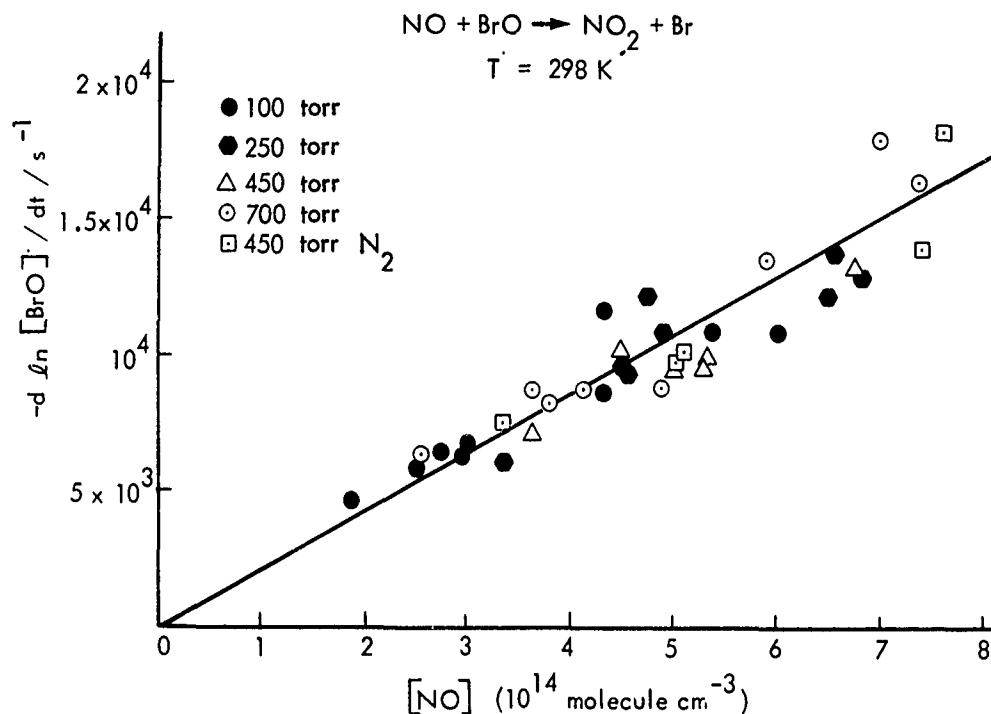
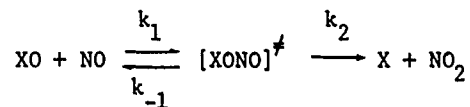


Figure 8. The reaction  $\text{NO} + \text{BrO} \rightarrow \text{NO}_2 + \text{Br}$ . Variation of the pseudo-first-order rate constant,  $-\text{d} \ln [\text{BrO}] / \text{d}t$  (corrected for NO removal), with  $[\text{NO}]$  at 298 K and total pressures from 100 to 700 torr of He.

effect on  $k_{28}$  would not be observed until the total pressure exceeds 10–20 atmospheres (or  $\sim 5$  atmospheres in the  $\text{ClO} + \text{NO}$  system). Figure 9 shows the small but statistically significant negative temperature dependence of  $k_{28}$ . At present it is not clear if any of the proposed hypotheses which attempt to explain the negative temperature dependences of these rapid bimolecular reactions is correct as each has difficulty in explaining all the experimental observations. The metastable complex can be schematically represented as:



A vibrationally "hot" XONO radical is formed which may either decompose to products or reactants. Steady state analysis of this mechanism yields an observed rate constant of the form:

$$k_{\text{obs}} = \frac{k_1 k_2}{k_{-1} + k_2}$$

The negative temperature dependence of  $k_{\text{obs}}$  requires that  $k_{-1}$  be more strongly temperature dependent than  $k_2$  and comparable in magnitude. Following the arguments of Lin and DeMore, the RRK theory gives the unimolecular rate expressions for  $k_{-1}$  and  $k_2$  in the form:

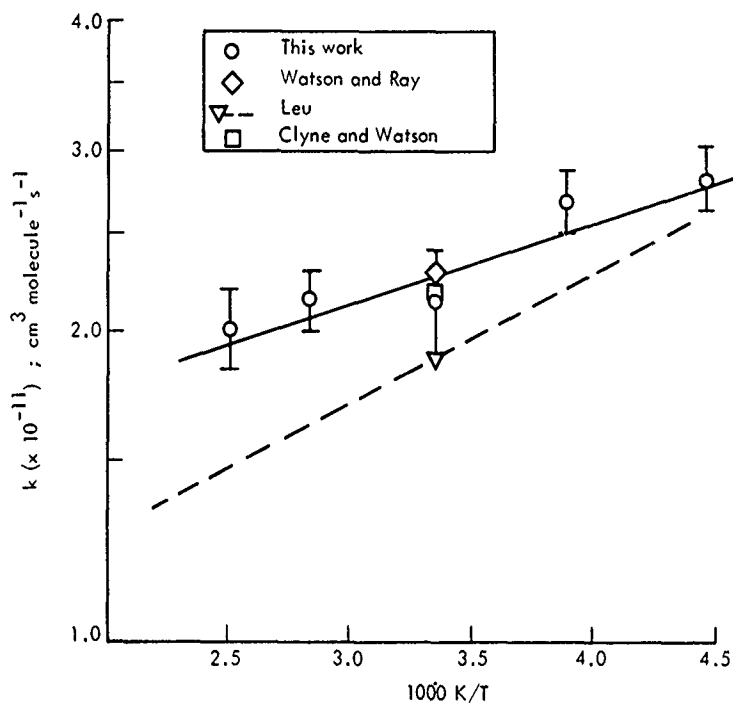


Figure 9. Arrhenius plot for the  $\text{NO} + \text{BrO} \rightarrow \text{NO}_2 + \text{Br}$  reaction: o, Watson et al. (1979);  $\nabla$ , --, Leu (1979);  $\diamond$ , Ray and Watson, 1979;  $\square$ , Clyne and Watson, 1975.

$$k = A \left( \frac{E^* - E_c}{E^*} \right)^{s-1}$$

where  $E^*$  is the total excitation energy,  $E_c$  is the threshold energy of the reaction, and  $s$  is the effective number of oscillators. The quantity  $(E^* - E_c)$  is determined mainly by the exothermicity of the overall reaction for  $k_2$ , but mainly by thermal energy for  $k_{-1}$  ( $\sim 2 \text{ kcal mol}^{-1}$ ), hence  $k_{-1}$  will be much more temperature dependent than  $k_2$ . The ratio,  $k_2/k_{-1}$ , can be written:

$$\frac{k_2}{k_{-1}} = \left( \frac{A_2}{A_{-1}} \frac{E^* - E_c(2)}{E^* - E_c(-1)} \right)^{s-1}$$

The range of possible values for  $s$  is 1-6 with a most probable value of  $\sim 3$  (the effective number of oscillators is normally  $\sim$  half the total number of oscillators). For each of the  $\text{XO} + \text{NO}$  reactions, where  $\text{X} \equiv$  halogen, the values of  $s$  would be expected to be comparable in magnitude. Therefore, for the values of  $k_2$  and  $k_{-1}$  to be comparable, and assuming the value of  $s$  is 3, requires the ratio of  $A_2/A_{-1}$  to be in the range 30-200 (varies between the chemical systems due to the differences in the exothermicities). In the  $\text{NO} + \text{HO}_2$  reaction the value of  $s_{\text{effective}}$  would be expected to be higher than in the analogous halogen reactions thus

# WATSON

requiring a higher value for  $A_2/A_{-1}$ . Consequently it is difficult to believe that the metastable complex formation hypothesis would predict that the magnitude of the temperature dependences of the  $\text{NO} + \text{HO}_2$ ,  $\text{NO} + \text{ClO}$  and  $\text{NO} + \text{BrO}$  reactions would be comparable, i.e.  $E/R \approx 200 \pm 100$  or  $n \approx -(0.75 \pm 0.25)$  where  $k = AT^n$ , or that the values of  $A_2$  and  $A_{-1}$  could differ by as much as a factor of 100 or greater considering the relatively small differences in the two transition states, especially in the case of the  $\text{NO} + \text{HO}_2$  reaction.

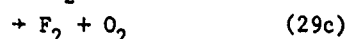
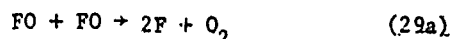
An alternate hypothesis is that of a temperature dependent A-factor. According to Absolute Rate Theory, the A-factor for a bimolecular reaction such as  $\text{NO} + \text{XO} \rightarrow \text{XONO}^\ddagger \rightarrow \text{NO}_2 + \text{X}$  is given by:

$$A = \frac{kT}{h} \frac{q_{\text{XONO}}^\ddagger}{q_{\text{XO}} q_{\text{NO}}}$$

where  $q$  is a composite partition function. When NO reacts with XO to form a nonlinear  $\text{XONO}^\ddagger$  activated complex, the product of  $kT/h$ , and the electronic, rotational and translational functions varies with  $T^{-1}$ . Watson et al. evaluated the temperature dependence of the vibrational partition function ratio for the  $\text{NO} + \text{ClO}$  reaction using  $\text{ClONO}$  as the model for the complex. They reported that from 200-400K the vibrational partition function ratio can be fit to a  $T^x$  dependence with a value of 0.78 for  $x$ . The temperature dependence of the complete A factor with the  $T^{-1}$  term included is therefore  $T^{-0.22}$ . This calculation used the vibrational frequencies derived from infrared spectra which probably leads to underestimate in the value of  $x$  as the frequencies of the  $\text{ClONO}^\ddagger$  complex are likely to be lower than that of  $\text{ClONO}$ . Therefore this would reduce the magnitude of the "predicted" negative temperature dependence to less than  $T^{-0.22}$  which would be significantly less than the experimentally observed temperature dependence. Similarly, the A-factor for the  $\text{NO} + \text{BrO}$  reaction would be expected to have a zero or small positive temperature dependence due to the lower frequency vibrations expected for  $\text{BrONO}^\ddagger$ , in contrast to the  $T^{-1.0}$  and  $T^{-0.6}$  dependences observed.

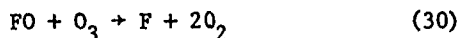
XO + XO: The  $\text{FO} + \text{FO}$  and  $\text{ClO} + \text{ClO}$  reactions are currently thought to be unimportant processes in stratospheric photochemistry due to the low (predicted) concentrations of FO and the slow  $\text{ClO} + \text{ClO}$  rate constant. In contrast, the  $\text{BrO} + \text{ClO}$  (via cycle III) and to a lesser extent the  $\text{BrO} + \text{BrO}$  (via cycle II) reactions may play a major role in stratospheric photochemistry if the mixing ratio of inorganic bromine is greater than 20 ppt, and the  $\text{IO} + \text{IO}$  (via cycle II) reaction is thought to play an important role in tropospheric boundary layer ozone photochemistry. These four  $\text{XO} + \text{XO}$  reactions will be briefly discussed.

The  $\text{FO} + \text{FO}$  reaction has been the subject of two discharge flow-mass spectrometric studies at 298K (Clyne and Watson, 1974a; Wagner et al. 1972), with the reported rate constants only being in fair agreement, i.e.  $8.5 \times 10^{-12} \text{ cm}^3 \text{ molecule}^{-1} \text{ s}^{-1}$  and  $3.3 \times 10^{-11} \text{ cm}^3 \text{ molecule}^{-1} \text{ s}^{-1}$ , respectively. From the data of Wagner et al. it can be seen that the dominant reaction channel is that producing  $2\text{F} + \text{O}_2$ :



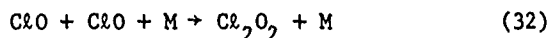
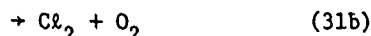
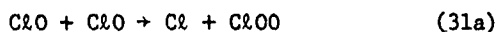
# WATSON

However, their data base is not adequate to conclude that it is the only process. Starrico et al. (1962) measured quantum yields for ozone destruction in  $F_2/O_3$  mixtures, and attributed the high values,  $\sim 4600$  to be due to rapid regeneration of atomic fluorine via the  $FO + O_3$  reaction:



However, their results are probably also consistent with the chain propagation process being reaction (29a).

The  $ClO + ClO$  reaction has been the subject of numerous kinetic studies using a wide variety of techniques including discharge flow-ultraviolet absorption (Clyne and Coxon, 1966; Clyne and Coxon, 1968; Clyne and White, 1971; and Walker, 1972); discharge flow-mass spectrometry/resonance absorption (Clyne et al. 1975); flash photolysis-ultraviolet absorption (Basco and Dogra, 1971a, b; Basco and Hunt, 1979); molecular modulation-ultraviolet absorption (Johnston et al. 1969; Cox et al. 1979; Cox and Derwent, 1979). However, the exact mechanism and the rate constants of the different reaction channels are still not considered to be well established. As the reaction is of little importance in stratospheric chemistry the mechanism and rate constants will not be discussed in detail. The mechanism is currently (Basco and Hunt, and Cox and coworkers) thought to consist of concurrent bimolecular and termolecular channels:



The value of  $k_{31} (= k_{31a} + k_{31b} + k_{31c})$  reported from the low pressure discharge flow studies is  $\sim 2.5 \times 10^{-14} \text{ cm}^3 \text{ molecule}^{-1} \text{ s}^{-1}$  at  $\sim 298K$ , whereas the value of  $k_{31}$  reported from the flash photolysis and molecular modulation studies is a factor of  $\sim 2$  lower, i.e.  $k_{31} \approx 1.2 \times 10^{-14} \text{ cm}^3 \text{ molecule}^{-1} \text{ s}^{-1}$  ( $k$  defined as:  $k = -d[ClO]^2/dt$ ). From the discharge flow studies of Clyne and co-workers it has been estimated that  $k_{31a}$  is at least equal to  $k_{31b}$ , and may possibly be much greater, however, the data base is inadequate to draw any final conclusions due to the complexity of the overall reaction system. The value of  $k_{31c}$  was reported to be  $\leq 3.2 \times 10^{-15} \text{ cm}^3 \text{ molecule}^{-1} \text{ s}^{-1}$  (Clyne et al.), i.e.  $\sim 10-15\%$  of the total reaction pathway at 298K. Cox and Derwent reported  $k_{31a} : k_{31b} : k_{31c}$  to be 0.35 : 0.49 : 0.16, while Wongdontri-Stuper et al. (1979) from some  $Cl_2$  photosensitized decomposition studies of  $O_3$  at  $\sim 298K$  reported  $k_{31a} : k_{31b} : k_{31c}$  to be 0.63 : 0.34 : 0.032. Similar quantum yield studies by Lin et al. (1975) have yielded somewhat comparable results, and have showed that the ratio of the rate constants was independent of total pressure. It can therefore be seen that there seems to be a consensus of opinion that  $k_{31}$  lies in the range  $1.0-2.5 \times 10^{-14} \text{ cm}^3 \text{ molecule}^{-1} \text{ s}^{-1}$ , and that channels (a) and (b) are both important, with channel (c) being a minor pathway. The recent high pressure results of Cox and co-workers, and Basco and Hunt provide evidence for reactions (32) and (-32). Values for  $k_{32}(298K)$  in the range  $(5-30) \times 10^{-33} \text{ cm}^6 \text{ molecule}^{-2} \text{ s}^{-1}$  were reported, the value being dependent upon the identity of the

third body. These values are somewhat lower than those reported by Johnston et al. where  $k_{32}$  was reported to range from  $\sim 40\text{--}60 \times 10^{-33} \text{ cm}^6 \text{ molecule}^{-1} \text{ s}^{-1}$  at 298K.

Clyne and co-workers have reported values for the overall activation energy ( $E_{31a} + E_{31b}$ ) ranging from 2.3–2.6 kcal mol<sup>-1</sup> in the low pressure regime. The only high pressure temperature dependent study was performed by Porter and Wright (1953) who reported the rate constant to be independent of temperature. This difference may well be attributed to a change in reaction mechanism, i.e. at low pressures the bimolecular routes dominate, while at high pressures the third order reaction dominates. Clyne and co-workers reported linear Arrhenius behavior from 273–710K which is possibly surprising as the two channels (31a) and (31b) might be expected to exhibit different temperature dependences.

Figure 10 shows how the quantum yield for ozone destruction is strongly temperature dependent

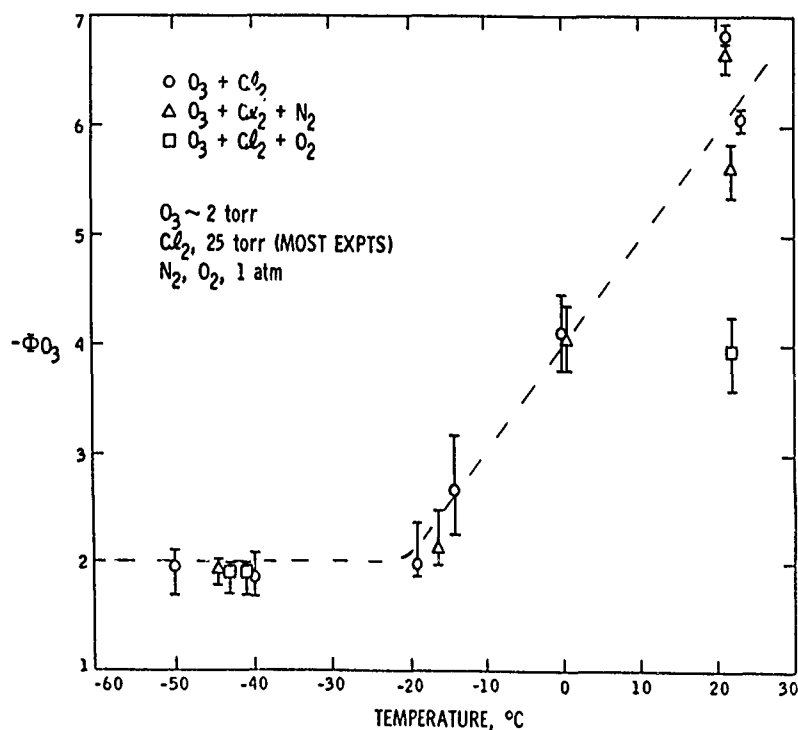


Figure 10. Quantum yield for  $O_3$  destruction,  $-\Phi(O_3)$ , as a function of temperature in the  $CCl_2$  photosensitized decomposition of  $O_3$ . Data of Lin et al.<sup>3</sup> (1975).

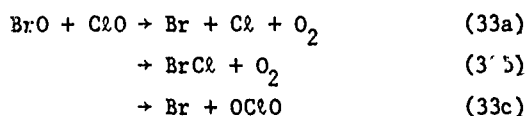
with the value of  $-\Phi(O_3)$  decreasing from a value of  $\sim 6$  at 298K to a value of 2 at and below 245K. A quantum yield of 6 requires  $k_{31a} : k_{31b}$  to be  $\sim 2 : 1$ , while a quantum yield of 2 requires  $k_{31a} : k_{31b}$  to be  $< 1 : 10$ . For the ratio of  $k_{31a}$  to  $k_{31b}$  to change by a factor of  $\geq 20$  from 298K to 245K would require an activation energy difference of  $\geq 9 \text{ kcal mol}^{-1}$ . This is totally unreasonable in view of the overall activation energy of  $\sim 2.5 \text{ kcal mol}^{-1}$  reported by Clyne and co-workers for  $k_{31a} + 31b$ . If the change in quantum yield cannot be wholly attributed to a change in the  $k_{31a} : k_{31b}$  ratio then an alternate explanation is required. One possibility is that the bimolecular reactions are unimportant at low temperatures due to the increased stability of  $CCl_2O_2$ . Based on the values of  $k_{32}$  reported by Basco and Hunt, and Cox and co-workers, the third order reaction becomes the dominant pathway for removal of  $CClOat$  and above 30 torr total pressure ( $T \leq 298K$ ). At 298K and 760 torr the lifetime of  $CCl_2O_2$  is

# WATSON

$\sim 13\text{ms}$  (assuming  $k_{-32}$  is  $\sim 3 \times 10^{-18} \text{ cm}^3 \text{ molecule}^{-1} \text{ s}^{-1}$  - based on the values of  $k_{32}$  and  $K_{\text{eq}}$  reported by Cox and co-workers, and Basco and Hunt), whereas at 245K and 760 torr the lifetime of  $\text{Cl}_2\text{O}_2$  is  $> 6\text{s}$  (assuming that the activation energy for thermal decomposition is  $\geq 16.5 \text{ kcal mol}^{-1}$  which is the  $\text{ClO-OC}\ell$  bond strength reported by Basco and Hunt). Consequently, it is possible that the reason  $-\phi(\text{O}_3)$  decreases to a value of 2 at and below 245K is that the  $\text{ClO}$  is rapidly removed via reaction (32) to produce  $\text{Cl}_2\text{O}_2$  which is in turn removed heterogeneously, thus preventing  $\text{Cl}_2\text{O}_2$  from establishing an equilibrium with  $\text{ClO}$ . The time required for diffusion to the reactor walls in the studies of Lin et al. (1975) is  $\sim 1\text{-}2\text{s}$  at 760 torr. Consequently the lifetime of  $\text{Cl}_2\text{O}_2$  is comparable to, or greater than, the diffusion time to the reactor walls at  $\leq 245\text{K}$ , but is much shorter than the diffusion time at 298K. Therefore, no significant wall loss of  $\text{Cl}_2\text{O}_2$  would be expected at 298K, but might be at 245K. This explanation is more tenable than that of a difference in the activation energies of reactions (31a) and (31b) of  $\geq 9 \text{ kcal mol}^{-1}$ . Obviously the decrease in  $-\phi(\text{O}_3)$  with decreasing temperature is probably due to some change in the ratio of  $k_{31a} : k_{31b}$  in conjunction with loss of  $\text{ClO}$  via  $\text{Cl}_2\text{O}_2$  on the reactor walls.

To conclude the discussion on the  $\text{ClO} + \text{ClO}$  reaction it can be stated that while it now appears that most of the features are reasonably understood at 298K, there is still uncertainty as to the temperature dependence of the branching ratio of reaction (31) and the temperature dependence of reaction (32). In addition, the effect observed due to the presence of  $\text{O}_2$  in the  $\text{Cl}_2$  photosensitized decomposition studies of  $\text{O}_3$ , i.e. a lowering of  $-\phi(\text{O}_3)$  (shown in figure 10), is still not understood, although several hypothesis have been forwarded including complex formation,  $\text{ClO} \cdot \text{O}_2$  (Prasad and Adams, 1980).

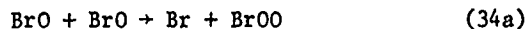
The  $\text{BrO} + \text{ClO}$  reaction has been the subject of one discharge flow-mass spectrometric study (Clyne and Watson, 1977), and one flash photolysis-ultraviolet absorption study (Basco and Dogra, 1971c). The reaction has three possible channels:



The overall rate constants reported in the two studies are in poor agreement with values of  $2.5 \times 10^{-12} \text{ cm}^3 \text{ molecule}^{-1} \text{ s}^{-1}$  (Basco and Dogra) and  $1.34 \times 10^{-11} \text{ cm}^3 \text{ molecule}^{-1} \text{ s}^{-1}$  (Clyne and Watson) being reported at  $\sim 298\text{K}$ . Clyne and Watson have shown that the data of Basco and Dogra should be rejected due to an erroneous analysis of the kinetic data. Clyne and Watson measured  $k_{33c}$  and the sum of  $k_{33a} + k_{33b}$  separately. Even though the results obtained in their study could not be used to differentiate between channels (a) and (b), by analogy with  $\text{FO} + \text{FO}$ ,  $\text{BrO} + \text{BrO}$ , and  $\text{ClO} + \text{ClO}$  (where it has been demonstrated that the atomic channel dominates) it can be assumed that channel (a) predominates over channel (b). However, even if channel (b) were important, it would have the same effect as channel (a) in the stratosphere due to the rapid rate at which  $\text{BrCl}$  would be photodissociated. Channel (a) almost certainly proceeds via either  $\text{Br} + \text{ClOO}$  or  $\text{Cl} + \text{BrOO}$ . However, both of these channels are equivalent in the atmosphere as the  $\text{XOO}$  peroxy radicals will rapidly dissociate into  $\text{X} + \text{O}_2$ . Clyne and Watson reported that  $k_{33a} + k_{33b} = k_{33c} = (6.7 \pm 1.0) \times 10^{-12} \text{ cm}^3 \text{ molecule}^{-1} \text{ s}^{-1}$ . The temp-

erature dependence for such processes is expected to be small, e.g.  $\text{BrO} + \text{BrO}$ , but has yet to be studied. It is quite possible that the branching ratio is somewhat temperature dependent as the individual channels may have small but opposite temperature dependences.

The  $\text{BrO} + \text{BrO}$  reaction has been the subject of numerous kinetic studies using a wide variety of techniques including discharge flow-ultraviolet absorption (Clyne and Cruse, 1970a), discharge flow-mass spectrometry (Clyne and Watson, 1975), and flash photolysis-ultraviolet absorption (Basco and Dogra, 1971c; Sander and Watson, 1980b). Unfortunately there is a wide spread in the values of the rate constant at 298K, i.e.  $(2.1-10.5) \times 10^{-12} \text{ cm}^3 \text{ molecule}^{-1} \text{ s}^{-1}$  ( $k = d[\text{BrO}]^2/dt$ ), and as a function of temperature, i.e.  $E/R = (450 \text{ to } -244\text{K})$ . The reaction has two possible bimolecular channels:



As three of the studies monitored the  $\text{BrO}$  concentration using ultraviolet absorption spectrometry knowledge of  $\sigma$  was required to determine  $k_{34}$ . Although the magnitude of  $\sigma$  is dependent upon the particular transition used in the  $A + X$  system, and instrumental parameters such as spectral band width, the large differences in the reported values of  $\sigma$  can probably be attributed to errors in the earlier studies (Clyne and Cruse, and Basco and Dogra). The results of the mass-spectrometric study of Clyne and Watson ( $k_{34} = 6.34 \times 10^{-12} \text{ cm}^3 \text{ molecule}^{-1} \text{ s}^{-1}$ ) and the flash photolysis study of Sander and Watson ( $k_{34} = 4.8 \times 10^{-12} \text{ cm}^3 \text{ molecule}^{-1} \text{ s}^{-1}$ ) are in good agreement at 298K, leading to a preferred value of  $5.6 \times 10^{-12} \text{ cm}^3 \text{ molecule}^{-1} \text{ s}^{-1}$ . From the values of  $k_{34}$  reported in these two studies it can be stated that the  $\text{BrO} + \text{BrO}$  reaction exhibits no pressure dependence in the range 1-600 torr. As noted earlier there is a discrepancy in the reported values of  $E/R$ . Although the study of Sander and Watson ( $E/R = -244\text{K}$ ) is to be preferred over that of Clyne and Cruse ( $E/R = 450\text{K}$ ), additional studies are required to resolve this discrepancy preferably using a technique other than ultraviolet absorption so that  $\sigma$  is not required.

Sander and Watson determined the branching ratio  $k_{34a}/k_{34}$ , at 298K using two approaches. One required knowledge of  $\sigma$ , the other was independent of  $\sigma$ . The first approach monitored the amount of ozone removed ( $\Delta\text{O}_3$ ) as a function of initial  $\text{BrO}$  concentration ( $[\text{BrO}]_0$ ) in a system with a large excess concentration of ozone. This is a simple variation of the standard  $\text{X}_2/\text{O}_3$  photosensitized decomposition studies of  $\text{O}_3$ . A value of  $0.81 \pm 0.03$  was reported for  $k_{34a}/k_{34}$  which is equivalent to a quantum yield for ozone destruction ( $-\phi(\text{O}_3) = \text{number of ozone molecules destroyed per photon absorbed}$ ) of  $\sim 12$ . The alternate approach was to monitor the time dependence of the  $\text{BrO}$  concentration in a  $\text{Br}_2/\text{O}_3$  system in both (a) an excess of atomic bromine; and (b) an excess of  $\text{O}_3$ . In case (a) the  $\text{BrO}$  decayed by both channels, (34a) and (34b), while in case (b) the  $\text{BrO}$  only decayed by channel (34b) as the atomic bromine formed in (34a) regenerated  $\text{BrO}$  radicals via the  $\text{Br} + \text{O}_3$  reaction. Figure 11 shows two typical  $\text{BrO}$  decay plots from which the branching ratio of the reaction can be derived from the ratios of the slopes. A value of  $0.84 \pm 0.03$  was determined for  $k_{34a}/k_{34}$ . The latter approach was preferred as the result is independent of  $\sigma$ . These values for the branching ratio at 298K are consistent with the estimate of 0.8-0.9 reported by Cruse (1971). To date there has been



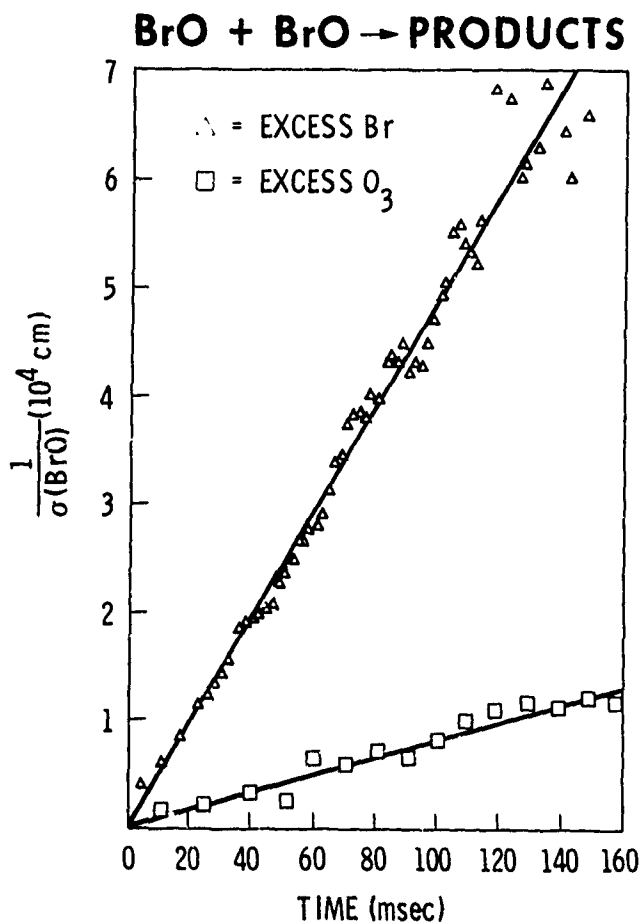


Figure 11. Second-order decay plots of BrO radicals in Br<sub>2</sub> - O<sub>3</sub> - He mixtures with excess atomic bromine (△) and excess O<sub>3</sub> (□).

no attempt to study the temperature dependence of the branching ratio.

There has only been one discharge flow-ultraviolet absorption study of the IO + IO reaction (Clyne and Cruse 1970b):



A value of  $1.2 \times 10^6 \text{ cm s}^{-1}$  was reported for  $k/\sigma$  at 298K. Unfortunately Clyne and Cruse were unable to determine  $\sigma$ . If  $\sigma$  is estimated to be similar to that of BrO, i.e.  $\sim 10^{-17} \text{ cm}^2 \text{ molecule}^{-1}$ , then an estimate of  $\sim 1 \times 10^{-11} \text{ cm}^3 \text{ molecule}^{-1} \text{ s}^{-1}$  is obtained for  $k_{35}$ .

Table V summarizes the pertinent features of the XO + XO reactions.

#### TEMPORARY RESERVOIRS:

**HOX:** A temporary reservoir which will not be discussed in detail is HOX as the subject is covered in detail by Howard (1979a). The only source of HOX considered in the models at present is the XO + HO<sub>2</sub> reaction (2a), although there are two other possible sources, i.e., XO + H<sub>2</sub>CO → HOX + HCO, and XONO<sub>2</sub> + surface (hydration) → HOX + HNO<sub>3</sub>. The former is probably negligibly slow as are all other hydrogen abstraction reactions by XO (except radical-radical

TABLE V  
XO + XO → Products

Reaction	$k_{298}(\text{cm}^3 \text{ molecule}^{-1} \text{ s}^{-1})^*$	Comments
FO + FO	$\sim 10^{-11}$	> 95% atom regeneration
ClO + ClO	$\sim 2 \times 10^{-14}$	~ 50% atom regeneration ~ 10% OClO formation ~ possible dimer formation (third-body effect) ~ temperature dependence (positive)
BrO + BrO	$\sim 5 \times 10^{-12}$	~ 85% atom regeneration ~ small negative temperature dependence (no third-order effects)
IO + IO	$\sim 5 \times 10^{-12}$	Probably similar to BrO + BrO
BrO + ClO	$\sim 10^{-11}$	50% atom regeneration 50% OClO formation

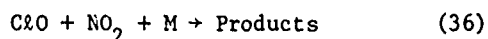
$$^* -d[XO]/dt = k[XO]^2.$$

reactions), and there is no experimental data on the latter heterogeneous process. One aspect of the XO + HO<sub>2</sub> reaction has already been discussed, i.e., the formation of O<sub>3</sub> and Hx via reaction (2b). That reaction acts to suppress the catalytic efficiency of the halogens to destroy odd oxygen. Reaction 2a can act to either inhibit or increase, through cycle VI, the catalytic efficiency of the halogens. The role depends on the J value of HOX and on the photolysis mechanism:

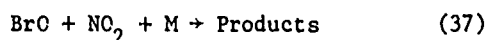


The only XO + HO<sub>2</sub> reaction studied to date is the ClO + HO<sub>2</sub> reaction. The BrO and IO analogs could be quite important in their respective systems, unfortunately neither of these reactions have yet been studied, and both are likely to prove to be quite difficult.

XONO<sub>2</sub>: The other temporary reservoir, which will be discussed in detail is XONO<sub>2</sub>. As shown earlier this molecule can participate in both net destruction (cycle VII) and net nothing (cycles VIII and IV) cycles depending upon the photolysis mechanism for XONO<sub>2</sub> (possibly discussed by Molina, 1979). Whereas there have been several kinetic studies of the ClO + NO<sub>2</sub> + M reaction:



as a function of temperature, there has been only one study of the BrO + NO<sub>2</sub> + M reaction at 298K;



and none of the IO + NO<sub>2</sub> + M and FO + NO<sub>2</sub> + M reactions. The ClO + NO<sub>2</sub> + M reaction has been

measured both in its third-order kinetic region (1 to 7 torr total pressure) by Zahniser et al. (1977), Birks et al. (1977), Leu et al. (1977) and Stimpfle et al. (private communication), and in the fall-off region between second- and third-order kinetics (25 to 600 torr total pressure) by Knauth (1978), Cox and Lewis (1979), and Handwerk and Zellner (1978). Sander et al. (1980) studied the  $\text{BrO} + \text{NO}_2 + \text{M}$  reaction at 298K in both the third-order kinetic region (1.5-6 torr total pressure) and in the fall-off region between second- and third-order kinetics (50-700 torr total pressure).

Discrepancies exist between rate measurements of  $k_{36}(\text{C}_2\text{O} + \text{NO}_2 + \text{M})$  obtained by observing the overall rate of decay of  $\text{C}_2\text{O}$  as in the discharge flow (Zahniser et al.; Birks et al.; Leu et al.; and Stimpfle et al.), flash photolysis (Handwerk and Zellner) and molecular modulation (Cox and Lewis) studies, and a technique based on the thermal decomposition of chlorine nitrate (Knauth) leading to speculation by Knauth, and Chang et al. (1979) that there is more than one primary process leading to several different isomers of  $\text{C}_2\text{NO}_3$  being formed (discussed later). The low pressure discharge flow results are all in good agreement ( $\pm 15\%$ ) at 298K with values for  $k_0$  (third-order rate constant) of  $1.8 \times 10^{-31} \text{ cm}^6 \text{ molecule}^{-2} \text{ s}^{-1}$  ( $\text{M} = \text{N}_2$ ) and  $1.0 \times 10^{-31} \text{ cm}^6 \text{ molecule}^{-2} \text{ s}^{-1}$  ( $\text{M} = \text{He}$ ). There is also good agreement on the temperature dependence of this reaction with a value of  $-3.0$  for  $n$  between 250 and 400K ( $k = \text{AT}^n$ ). Alternatively the temperature dependence can be expressed in the standard, but less satisfactory, Arrhenius form with a value for  $E/R$  of  $\sim 1050\text{K}$ . Cox and Lewis studied this reaction between 20 and 600 torr ( $\text{M} = \text{N}_2$ ) and noted fall-off from third-order kinetic behavior over this pressure range, i.e. the third-order rate constant at 600 torr was a factor of 1.6 less than the third-order rate constant at 25 torr. Cox and Lewis's third-order rate constant at 25 torr is in excellent agreement with the third-order rate constants determined in the discharge flow studies, i.e. both at 298K and as a function of temperature. Handwerk and Zellner's value of  $(3 \pm 1) \times 10^{-12} \text{ cm}^3 \text{ molecule}^{-1} \text{ s}^{-1}$  for  $k_{36}$  at 625 torr of  $\text{N}_2$  and 298K is only just, within the stated experimental uncertainties, in agreement with Cox and Lewis's value of  $(2.0 \pm 0.2) \times 10^{-12} \text{ cm}^3 \text{ molecule}^{-1} \text{ s}^{-1}$  at 600 torr of  $\text{N}_2$ . The value of Handwerk and Zellner translates into a third order rate constant of  $1.5 \times 10^{-31} \text{ cm}^6 \text{ molecule}^{-2} \text{ s}^{-1}$  which would, if correct, surprisingly suggest little or no fall-off from third order behavior by 625 torr of  $\text{N}_2$ . The value of  $k_{36}(\text{C}_2\text{O} + \text{NO}_2 + \text{M})$  reported by Knauth at 298K, and its temperature dependence are both lower than in other studies. The value of  $k_0$  at 298K is a factor of  $\sim 3$  lower, and the value of  $n$  was reported to be  $-2.4$ . Knauth also reported little fall-off, ( $< 5\%$ ) at pressures up to 210 torr of  $\text{N}_2$ , with the fall-off increasing to 20% at 350 torr. This is much less fall-off than that reported by Cox and Lewis.

The low pressure discharge flow-mass spectrometric values for  $k_0(\text{BrO} + \text{NO}_2 + \text{M})$  reported by Sander et al. are  $2.33 \times 10^{-31} \text{ cm}^6 \text{ molecule}^{-2} \text{ s}^{-1}$  ( $\text{M} = \text{He}$ ) and  $5.41 \times 10^{-31} \text{ cm}^6 \text{ molecule}^{-2} \text{ s}^{-1}$  ( $\text{M} = \text{N}_2$ ) at 298K. Figure 12 shows that the reaction is in the third-order kinetic region below 6 torr total pressure. These results indicate that the third-order rate constants for  $\text{BrO} + \text{NO}_2 + \text{M}$  are factors of 2.4 ( $\text{M} = \text{He}$ ) and 3.0 ( $\text{M} = \text{N}_2$ ) greater than the  $\text{C}_2\text{O} + \text{NO}_2 + \text{M}$  third-order rate constants at 298K. The flash photolysis results of Sander et al. show that there is significant fall-off from pure third-order kinetic behavior between 50 and 700 torr of  $\text{N}_2$ .

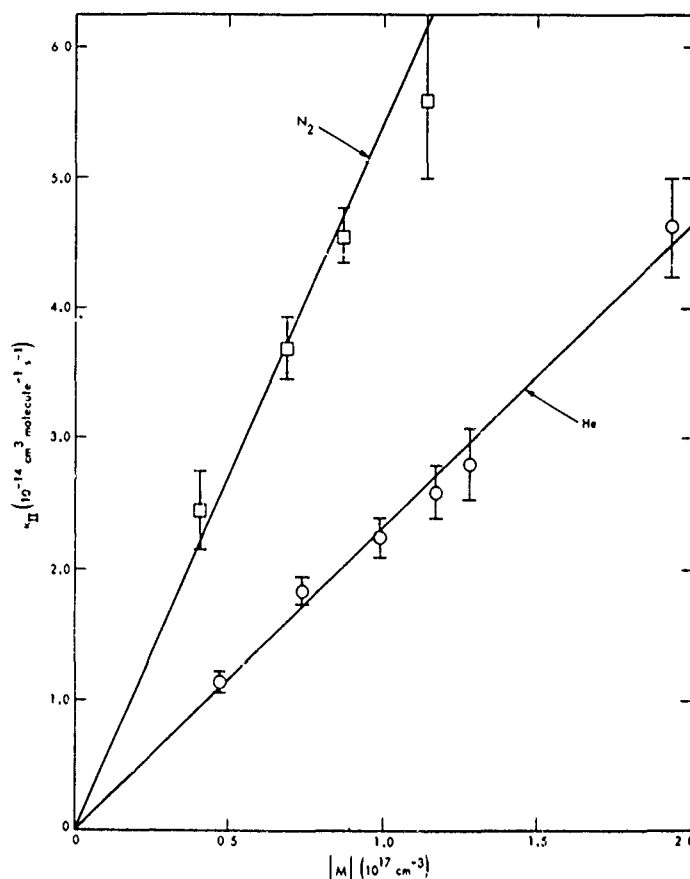
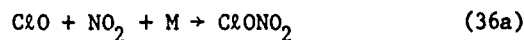


Figure 12. The  $\text{BrO} + \text{NO}_2 + \text{M} \rightarrow \text{BrONO}_2 + \text{M}$  reaction. Variation of the effective bimolecular rate constant as a function of  $[\text{M}]$  at 298K.

at 298K (Figure 13). In fact there is fall-off from third-order kinetic behavior between the low pressure discharge flow regime and 50 torr (lowest pressure used in the flash photolysis study). The value of  $k_{37}(\text{BrO} + \text{NO}_2 + \text{M})$  at 600 torr is a factor of 4.1 less than the extrapolated third-order rate constant determined in the discharge flow studies. Therefore, these results suggest that the extent of fall-off in the  $\text{BrO} + \text{NO}_2 + \text{M}$  system is greater than that in the  $\text{ClO} + \text{NO}_2 + \text{M}$  system.

As stated earlier it has been suggested that more than one isomer of  $\text{ClNO}_3$  may be formed in the  $\text{ClO} + \text{NO}_2 + \text{M}$  reaction:



Besides the experimental data of Knauth which possibly suggests the formation of two or more isomers of  $\text{ClNO}_3$ , some unpublished experimental data of Molina et al. (1980), has been interpreted in this vein. Molina et al. have noted different rates of removal of  $\text{ClO}$  depending upon the  $\text{ClO}$  precursor ( $\text{Cl}_2\text{O}$  or  $\text{OC}(\text{Cl})\text{O}$ ). This has been interpreted as being due to partial

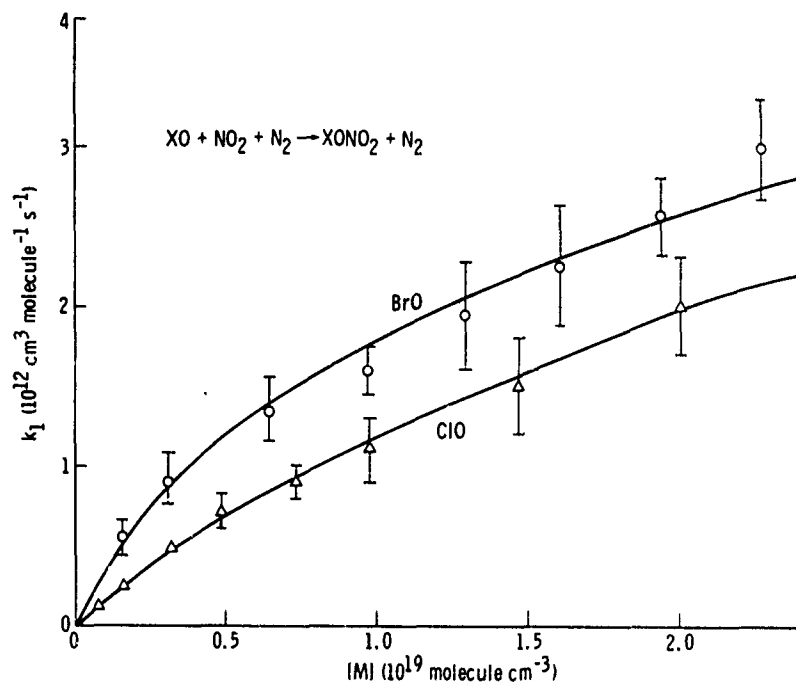
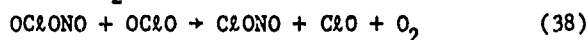
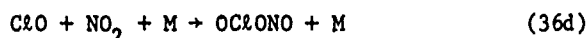


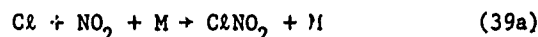
Figure 13. Variation of the effective bimolecular rate constant for the reaction  $XO + NO_2 + N_2 \rightarrow XONO_2 + N_2$  for  $X = Br$  (Sander et al. 1980) and  $Cl$  (Cox and Lewis, 1979).

reformation of  $ClO$  in the  $OClO$  system. One such possibility is:



The above reactions would occur in conjunction with reaction (36a) and result in the removal of  $ClO$  via reactions (36a) and (36d) and the production of  $ClO$  via reaction (38). Significant reformation of  $ClO$  requires that the value of  $k_{38}$  is  $\sim 2 \times 10^{-14} \text{ cm}^3 \text{ molecule}^{-1} \text{ s}^{-1}$ . Molina et al. also observed, using IR absorption, that  $[ClONO_2]_{\text{produced}}/[ClO]_{\text{removed}}$  was significantly less than unity ( $\sim 1/3$ ) again indicating multiple reaction pathways.

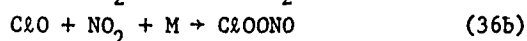
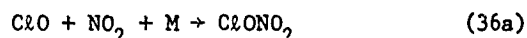
The reaction between atomic chlorine and nitrogen dioxide has been shown by Niki et al. (1978) to produce two isomers:



Although the most thermodynamically stable product is  $ClNO_2$ , the product  $ClONO$  is produced with a rate constant  $\geq 4$  times greater than that for  $ClNO_2$ . Chang et al. calculated the low-pressure limiting rate constants for the two channels of reaction 39 using a model developed by Troe (1977). In this method the low pressure limiting rate constant,  $k_o$ , is defined:

$$k_o = k_o^{SC} \times \beta$$

where  $k_o^{sc}$  is the strong collision rate constant, and  $\beta$  is an efficiency parameter ( $0 < \beta < 1$ ) which provides a measure of energy transfer. To calculate  $k_o^{sc}$  knowledge of the thermochemistry and the structures of the molecules involved is required. Chang et al. calculated the ratio of  $k_{39a}$  to  $k_{39b}$  to be 1:4 in a given buffer gas, which is in excellent agreement with the experimental observations of Niki et al. In this calculation the major uncertainty in calculating the strong collision rate constants was due to experimental uncertainties in the thermochemistry (i.e.  $\Delta H_f^\circ$  C $\ell$ ONO) and not in the geometry and molecular parameters (i.e. vibrational frequencies) of the products (C $\ell$ NO $_2$  and C $\ell$ ONO). Chang et al. then used the same approach to calculate the strong collision rate constants for the following pair of reactions involving C $\ell$ O and NO $_2$ :

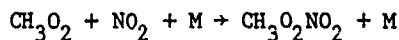


The molecular parameters for C $\ell$ OONO were estimated, consequently it was necessary to calculate the strong collision rate constants for several combinations of  $\Delta H(\pm 2 \text{ kcal mol}^{-1})$  and  $\Delta S(\pm 2 \text{ eu})$ . Chang et al. concluded that reaction 36a may be the only pathway but this requires rather high values of  $\beta$  (i.e. 0.61 (N $_2$ ) and 0.24 (He)) and an error in one of the following measurements: the recombination rate constant (36a), the decomposition rate constant ( $-36a$ ), or the thermochemical data. The calculations were also consistent with the possibility that two isomers of C $\ell$ NO $_3$  are formed. This could explain the discrepancy between the experiments of Knauth and coworkers who studied the thermal decomposition of C $\ell$ ONO $_2$  and those where the recombination rate constant was studied. Chang et al.'s calculations show that an isomer such as C $\ell$ OONO with an O-O bond energy of  $21 \pm 2 \text{ kcal mol}^{-1}$  will explain the experimental discrepancies. Obviously a similar calculation can be performed assuming that product to be OC $\ell$ ONO. At present it is not possible to be sure where the source of error is, but further studies are required to test for the possibility of separate reaction pathways producing two or more distinct isomers of C $\ell$ NO $_3$ . Although several groups have searched for isomers of C $\ell$ NO $_3$ , none have yet been identified. If they are formed, then studies of their absorption spectra and photolytic decomposition products would be required. The studies of Sander et al. were not capable of distinguishing whether there was more than one reaction pathway in the BrO + NO $_2$  + M system producing different isomeric forms of BrNO $_3$ .

As stated earlier, both the C $\ell$ O + NO $_2$  + M and BrO + NO $_2$  + M reactions exhibit fall-off from third order kinetic behavior at pressures in excess of  $\sim 50$  torr. The rate constant data obtained for both BrO + NO $_2$  + M and to a lesser extent C $\ell$ O + NO $_2$  + M (M = N $_2$ ) shows significant deviations from Lindemann-type behavior. Recent work by Troe (1979) and Luther and Troe (1978) has shown that the three-parameter equation,

$$k([M], T) = \frac{k_o(T)[M]}{1 + \frac{k_o(T)[M]}{k_\infty(T)}} F_c \{1 + [\log_{10}(k_o(T)[M]/k_\infty(T))]\}^{-1} \quad (A)$$

which contains a correction to the usual Lindemann expression, can be used to fit rate constant fall-off curves. The details of this procedure as applied to the reaction



have been described previously by Sander and Watson (1980a). The parameters derived from nonlinear least squares curve fitting of the data shown in figure 13 for  $\text{M} = \text{N}_2$  to eqn. (A) were:  $k_0 = (4.5 \pm 1.5) \times 10^{-31} \text{ cm}^6 \text{ molecule}^{-2} \text{ s}^{-1}$ ,  $k_\infty = (1.05 \pm 0.15) \times 10^{-11} \text{ cm}^3 \text{ molecule}^{-1} \text{ s}^{-1}$  and  $F_c = 0.53 \pm 0.10$  for  $\text{BrO} + \text{NO}_2 + \text{M}$ , and  $k_0 = (1.7 \pm 0.1) \times 10^{-31} \text{ cm}^6 \text{ molecule}^{-2} \text{ s}^{-1}$ ,  $k_\infty = (2.0^{+0.5}_{-1.0}) \times 10^{-11} \text{ cm}^3 \text{ molecule}^{-1} \text{ s}^{-1}$  and  $F_c = 0.52^{+0.2}_{-0.1}$  for  $\text{C}_2\text{O} + \text{NO}_2 + \text{M}$  (data of Cox and Lewis). The uncertainties represent the variation in the fitted parameters obtained when the mean-squared error is allowed to increase by  $\sim 10$ -20% from its minimum value. The low-pressure limiting rate constants,  $k_0$ , for  $\text{BrO} + \text{NO}_2 + \text{M}$  and  $\text{C}_2\text{O} + \text{NO}_2 + \text{M}$  obtained by curve fitting the high pressure data are in excellent agreement with the experimental values of  $k_0$  determined in the discharge flow studies, i.e.  $k_0 = (5.4 \pm 0.6) \times 10^{-31} \text{ cm}^6 \text{ molecule}^{-2} \text{ s}^{-1}$  and  $(1.8 \pm 0.2) \times 10^{-31} \text{ cm}^6 \text{ molecule}^{-2} \text{ s}^{-1}$  for  $\text{BrO} + \text{NO}_2 + \text{M}$  and  $\text{C}_2\text{O} + \text{NO}_2 + \text{M}$  respectively, where  $\text{M} = \text{N}_2$ .

Luther and Troe have shown how to estimate the broadening factor ( $F_c$ ) at the point where  $k_0[\text{M}] = k_\infty$ , from structural information about the product of an addition reaction. The broadening factor is the product of a strong collision factor,  $F_c^{\text{sc}}$ , and a correction factor for weak-collision effects,  $F_c^{\text{wc}}$ , i.e.

$$F_c = F_c^{\text{sc}} \times F_c^{\text{wc}}$$

where  $F_c^{\text{wc}} = \beta_c^{0.14}$ .  $F_c^{\text{sc}}$  is a function of the parameters  $S_k$  and  $B_k$ , given by:

$$S_k \approx S_{\text{eff}} + 1 \text{ or } S_{\text{eff}} + 2$$

$$B_k = \frac{(S_k - 1)}{S - 1} \frac{(E_0 + a(E_0)E_z)}{kT}$$

where  $S_{\text{eff}}$  = effective number of transition-state oscillators

$$= - \frac{1}{T} \frac{\partial \ln Q_V}{\partial (1/T)}$$

$E_0$  = critical energy for the decomposition of the adduct

$E_z$  = adduct vibrational zero-point energy

$a(E_0)$  = Whitten-Rabinovitch factor

$Q_V$  = vibrational partition function

$S$  = number of internal degrees of freedom

Values of  $F_c^{\text{sc}}$  as a function of  $S_k$  and  $B_k$  are tabulated in Luther and Troe's paper. The fundamental vibrational frequencies of  $\text{BrONO}_2$  and  $\text{C}_2\text{ONO}_2$  are required to evaluate  $Q_V$ . These were obtained from the infrared spectral measurements of Shimanouchi (1977) for  $\text{C}_2\text{ONO}_2$  and of Spencer and Rowland (1978) for  $\text{BrONO}_2$  (the low-frequency bands of  $\text{BrONO}_2$  which could not be observed were estimated using the frequencies of  $\text{C}_2\text{ONO}_2$  and  $\text{FONO}_2$  as models). Values of  $(0.49 \pm 0.11)$  and  $(0.54 \pm 0.11)$  were calculated for  $F_c^{\text{sc}}$  for the  $\text{BrO}$  and  $\text{C}_2\text{O}$  reactions respectively.  $\beta_c$  has been estimated (NASA, 1979) to be in the range 0.2-0.4 for similar reactions

when  $M = N_2$  giving  $F_c^{WC} = 0.84 \pm 0.03$ . Consequently, values of  $0.41 \pm 0.11$  (BrO) and  $0.45 \pm 0.11$  (ClO) for  $F_c$  result. These  $F_c$  values are in good agreement with those determined by fitting the data of Sander et al. (BrO) and Cox and Lewis (ClO). Obviously this agreement would have to be considered to be fortuitous if there were more than one reaction pathway as each pathway would have its own set of values for  $k_o$ ,  $k_\infty$  and  $F_c$ . Linear isomers of  $ClNO_3$ , e.g.  $ClOONO$  would have some lower frequency modes than  $ClONO_2$  resulting in a slightly lower predicted value for  $F_c$ . At present no attempt has been made to analyze either Cox and Lewis's ClO or Sander et al.'s BrO data into two separate components for different reaction pathways.

To conclude this section on  $XO + NO_2 + M$  it should be stated that the IO and FO reactions have yet to be studied, the BrO reaction has only been studied at 298K, there is controversy as to whether these reactions have multiple pathways, and the extent of fall-off from pure third order behavior between 1 and 760 torr is not well established in the ClO system.

**SUMMARY:** While the kinetic data base is in good shape for a large number of chlorine reactions, it is in rather poor shape for the fluorine, bromine, and iodine analogs. Fortunately, many of the unknown rate constants, e.g.  $IO + NO$  and  $IO + O$ , can be estimated to within a factor of 2-3. It is clear that more emphasis must be placed on understanding the mechanistic details of the reactions, i.e. the product distribution as a function of temperature and pressure. This is amply demonstrated for reactions such as  $XO + NO_2 + M$ ,  $XO + OH$ , and  $XO + HO_2$  where the role of these reactions in atmospheric photochemistry is totally dependent upon their product distribution.

#### REFERENCES

- Basco, N., and S. K. Dogra, Reactions of halogen oxides studied by flash photolysis. I. The flash photolysis of chlorine dioxide, *Proc. R. Soc. A*, **323**, 29-68, 1971a.
- Basco, N., and S. K. Dogra, Reactions of halogen oxides studied by flash photolysis. II. The flash photolysis of chlorine monoxide and of the ClO free radical, *Proc. R. Soc. A*, **323**, 401-415, 1971b.
- Basco, N., and S. K. Dogra, Reactions of halogen oxides studied by flash photolysis. III. The production and reactions of BrO and ClO radicals in the halogen-sensitized decomposition of chlorine dioxide, *Proc. R. Soc. A*, **323**, 417-429, 1971c.
- Basco, N., and J. E. Hunt, Mutual combination of ClO radicals, *Int. J. Chem. Kinet.* **11**, 649-664, 1979.
- Bemand, P. P., M. A. A. Clyne, and R. T. Watson, Atomic resonance fluorescence and mass spectrometry for measurements of the rate constants for elementary reactions:  $O(^3P_j) + NO_2 \rightarrow NO + O_2$  and  $NO + O_3 \rightarrow NO_2 + O_2$ , *J. Chem. Soc., Faraday Trans. II*, **70**, 564-576, 1974.
- Benson, S. W., F. R. Cruickshank, and R. Shaw, Iodine monochloride as a thermal source of chlorine atoms: The reaction of chlorine atoms with hydrogen, *Int. J. Chem. Kinet.* **1**, 29-43, 1969.
- Birks, J. W., B. Shoemaker, T. J. Leck, R. A. Borders, and L. J. Hart, Studies of reactions of importance in the stratosphere. II. Reactions involving chlorine nitrate and chlorine dioxide, *J. Chem. Phys.* **66**, 4591-4599, 1977.



- Burrows, J. P., D. I. Cliff, G. W. Harris, B. A. Thrush, and J. P. T. Wilkinson, Atmospheric reactions of the  $\text{HO}_2$  radical studied by laser magnetic resonance spectroscopy, Proc. R. Soc. Lond. A **368**, 463-481, 1979a.
- Burrows, J. P., R. A. Cox and M. C. Addison, Kinetic studies of atmospheric free radicals, poster paper presented at this NATO Institute, 1979b.
- Chameides, W. M., and D. D. Davis, Iodine: its possible role in tropospheric photochemistry, submitted to J. Geophys. Rev. 1980.
- Chang, J. S., A. C. Baldwin, and D. M. Golden, An explanation of the preferential formation of less stable isomers in three-body reactions:  $\text{Cl} + \text{NO}_2 + \text{M}$ ;  $\text{ClO} + \text{NO}_2 + \text{M}$ , J. Chem. Phys. **71**, 2021-2024, 1979.
- Clyne, M. A. A., and J. A. Coxon, Kinetic studies of oxy-halogen radical systems, Proc. R. Soc. A **303**, 207-231, 1968.
- Clyne, M. A. A., and J. A. Coxon, Reactions of chlorine oxide radicals. Part 1. Reaction kinetics of the  $\text{ClO}$  radicals, Trans. Faraday Soc. **62**, 1175-1189, 1966.
- Clyne, M. A. A., and H. W. Cruse, Rates of elementary reactions involving the  $\text{BrO}(\text{X}^2\Pi)$  and  $\text{IO}(\text{X}^2\Pi)$  radicals. Part 1- Formation and decay of the  $\text{BrO}$  radicals, Trans. Faraday Soc. **66**, 2214-2226, 1970a.
- Clyne, M. A. A., and H. W. Cruse, Rates of elementary reactions involving the  $\text{BrO}(\text{X}^2\Pi)$  and  $\text{IO}(\text{X}^2\Pi)$  radicals. Part 2- Reactions of  $\text{BrO}$  and  $\text{IO}$  radicals, Trans. Faraday Soc. **66**, 2227-2236, 1970b.
- Clyne, M. A. A., and A. J. MacRobert, Kinetic studies of free radical reactions by mass spectrometry. Part I- Reactions of  $\text{SO} + \text{NO}_2$  and  $\text{ClO} + \text{NO}$ , Int. J. Chem. Kinet. In press, 1980.
- Clyne, M. A. A., and R. T. Watson, Kinetic studies of diatomic free radicals using mass spectrometry, Part 1- System description and applications to F atoms and  $\text{FO}$  radicals, J. Chem. Soc., Faraday Trans. I, **70**, 1109-1123, 1974a.
- Clyne, M. A. A., and R. T. Watson, Kinetic studies of diatomic free radicals using mass spectrometry. Part 2- Rapid bimolecular reactions involving the  $\text{ClO X}^2\Pi$  radical, J. Chem. Soc., Faraday Trans. I, **70**, 2250-2259, 1974b.
- Clyne, M. A. A., and R. T. Watson, Kinetic studies of diatomic free radicals using mass spectrometry. Part 3- Elementary reactions involving  $\text{BrO X}^2\Pi$  radicals, J. Chem. Soc., Faraday Trans. I, **71**, 336-350, 1975.
- Clyne, M. A. A., and R. T. Watson, Kinetic studies of diatomic free radicals using mass spectrometry. Part 4- The  $\text{Br} + \text{OClO}$  and  $\text{BrO} + \text{ClO}$  reactions, J. Chem. Soc., Faraday Trans. I, **73**, 1169-1187, 1977.
- Clyne, M. A. A., and I. F. White, Reactions of chlorine oxide radicals. Part 3- Kinetics of the decay reaction of the  $\text{ClO}(\text{X}^2\Pi)$  radical, Trans. Faraday Soc. **67**, 2068-2076, 1971.
- Clyne, M. A. A., D. McKenny, and R. T. Watson, Reactions of chlorine oxide radicals. Part 5- The reaction  $2\text{ClO}(\text{X}^2\Pi) \rightarrow \text{products}$ , J. Chem. Soc., Faraday Trans. I, **71**, 322-335, 1975.
- CODATA Bulletin Number 33, Evaluated kinetic and photochemical data for atmospheric chemistry.
- CODATA Task Group on Chemical Kinetics, D. L. Baulch, R. A. Cox, R. F. Hampson, Jr., J. A. Kerr Chairman, J. Troe, and R. T. Watson, In press. J. Phys. Chem. Ref. Data, 1980.

- Cox, R. A., Kinetics of the reaction of  $\text{Cl} + \text{HO}_2 \rightarrow \text{HCl} + \text{O}_2$  using molecular modulation spectrometry, Int. J. Chem. Kinet. In press, 1980.
- Cox, R. A., and R. G. Derwent, Kinetics of chlorine oxide radical reactions using modulated photolysis. Part 1. Disproportionation of  $\text{ClO}$  in the  $\text{Cl}_2$  photosensitized decomposition of ozone, J. Chem. Soc., Faraday Trans. I, **75**, 1635-1647, 1979.
- Cox, R. A., and R. G. Derwent, Kinetics of the chlorine-photo-sensitized oxidation of hydrogen at 1 atmosphere pressure, 306K, J. Chem. Soc., Faraday Trans. I, **73**, 272-283, 1977.
- Cox, R. A., and R. Lewis, Kinetics of chlorine oxide radical reactions using modulated photolysis, J. Chem. Soc., Faraday Trans. I, **75**, 2649-2661, 1979.
- Cox, R. A., R. G. Derwent, A. E. Eggleton, and H. J. Reid, Kinetics of chlorine oxide radicals using modulated photolysis. Part 2-  $\text{ClO}$  and  $\text{ClOO}$  radical kinetics in the photolysis of  $\text{Cl}_2 + \text{O}_2 + \text{N}_2$  mixtures, J. Chem. Soc. Faraday Trans. I, **75**, 1648-1666, 1979.
- Cruse, H. W., Ph.D. Thesis, Queen Mary College, London University, 1971.
- Davidson, J. A., H. I. Schiff, G. Streit, J. R. McAfee, A. L. Schmeltekopf, and C. J. Howard, Temperature dependence of  $\text{O}(^1\text{D})$  rate constants for reactions with  $\text{N}_2\text{O}$ ,  $\text{H}_2$ ,  $\text{CH}_4$ ,  $\text{HCl}$  and  $\text{NH}_3$ , J. Chem. Phys. **67**, 5021-5025, 1977.
- Davis, D. D., R. E. Huie, and J. Herron, Direct rate measurements showing negative temperature dependence for reaction of atomic oxygen with cis-2-butene and tetramethylethylene, J. Chem. Phys. **59**, 628-634, 1976.
- Fletcher, I. S., and D. Husain, The collisional behavior of  $\text{Cl}(3p^5(^2\text{P}_{1/2}))$  by time-resolved attenuation of atomic resonance radiation in the vacuum ultraviolet, Chem. Phys. Lett. **49**, 516-519, 1977.
- Fletcher, I. S., and D. Husain, Collisional quenching of  $\text{Cl}(3p^5(^2\text{P}_{1/2}))$  by noble gases, J. Chem. Soc., Faraday Trans. II, **74**, 203-212, 1978.
- Handwerk, and R. Zellner, quoted in, Zellner, R., Recombination reactions in atmospheric chemistry, Ber. Bunsenges. Phys. Chem. **82**, 1172-1179, 1978.
- Howard, C. J., Laboratory studies of reactions of odd hydrogen species of atmospheric interest, This NATO meeting, Portugal 1979a.
- Howard, C. J., Temperature dependence of the reaction  $\text{HO}_2 + \text{NO} \rightarrow \text{OH} + \text{NO}_2$ , J. Chem. Phys. **71**, 2352-2359, 1979b.
- Jaffe, R. L., Can a bimolecular gas phase reaction have a negative activation energy? 175th National meeting of the American Chemical Society, Anaheim, California, 1978.
- JPL 79-27, Chemical kinetic and photochemical data for use in stratospheric modelling. Evaluation Number 2. NASA Panel for Data Evaluation, W. B. DeMore, L. J. Stief, M. J. Kurylo, R. F. Hamson, Jr., J. Margitan, M. J. Molina, D. Golden, and R. T. Watson, 1979.
- Johnston, H. S., E. D. Morris, Jr., and J. Van den Bogaerde, Molecular modulation kinetic spectrometry.  $\text{ClOO}$  and  $\text{ClO}$  radicals in the photolysis of chlorine in oxygen, J. Am. Chem. Soc. **91**, 7712-7727, 1969.
- Keyser, L. F., Absolute rate and temperature dependence of the reaction between  $\text{Cl}(^2\text{P})$  atoms and methane, J. Chem. Phys. **69**, 214-218, 1978.
- Keyser, L. F., Absolute rate constant of the reaction between  $\text{Cl}(^2\text{P})$  atoms and hydrogen peroxide from 298-424K, J. Phys. Chem. **84**, 11-14, 1980.

- Knauth, H. D., Über den thermischen zerfall von  $\text{ClONO}_2$  in gegenwart von NO,  $\text{ClNO}$  and  $\text{N}_2$ , Ber. Bunsenges. Phys. Chem. **82**, 212-216, 1978.
- Knox, J. H., Applications of gas phase partition chromatography to competitive chlorination reactions, Chem. and Ind. 1631-1632, 1955.
- Knox, J. H., and R. L. Nelson, Competitive chlorination reactions in the gas phase: Hydrogen and  $\text{C}_1\text{-C}_5$  saturated hydrocarbons, Trans. Faraday Soc. **55**, 937-946, 1959.
- LeBras, G., R. Foon, G. Poulet, and J. J. Combourieu, EPR kinetic study of the reactions of  $\text{H}_2\text{CO}$  with F, Cl, and Br atoms and ClO radical, This NATO meeting, Portugal, 1979.
- Leck, T. J., J. E. Cook, and J. W. Birks, Studies of reactions of importance in the stratosphere. III. Rate constant and products of the reaction between ClO and  $\text{HO}_2$  radicals at 298K, J. Chem. Phys. In press, 1979.
- Lee, J. H., J. V. Michael, W. A. Payne, L. J. Stief, and D. A. Whytock, Absolute rate of the reaction of  $\text{Cl}(^2\text{P})$  with molecular hydrogen from 200-500K, J. Chem. Soc., Faraday Trans. 1. **73**, 1530-1536, 1977.
- Leu, M. T., Rate constant for the reaction  $\text{BrO} + \text{NO} \rightarrow \text{Br} + \text{NO}_2$ , Chem. Phys. Lett. **61**, 275-279, 1979a.
- Leu, M. T., Rate constant for the reaction  $\text{HO}_2 + \text{NO} \rightarrow \text{OH} + \text{NO}_2$ , J. Chem. Phys. **70**, 1662-1666, 1979b.
- Leu, M. T., Upper limits for the rate constant for the reaction  $\text{Br} + \text{H}_2\text{O}_2 \rightarrow \text{HBr} + \text{HO}_2$ , Chem. Phys. Lett. **69**, 37-39, 1980a.
- Leu, M. T., Product distribution for the reaction of  $\text{HO}_2$  with ClO, Geophys. Res. Lett. Jan. issue, 1980b.
- Leu, M. T., and W. B. DeMore, Rate constants at 295K for the reactions of atomic chlorine with  $\text{H}_2\text{O}_2$ ,  $\text{HO}_2$ ,  $\text{O}_3$ ,  $\text{CH}_4$  and  $\text{HNO}_3$ , Chem. Phys. Lett. **41**, 121-124, 1976.
- Leu, M. T., and W. B. DeMore, Rate constant for the reaction  $\text{ClO} + \text{NO} \rightarrow \text{Cl} + \text{NO}_2$ , J. Phys. Chem. **82**, 2049-2052, 1978.
- Leu, M. T., and C. L. Lin, Rate constants for the reactions of OH with ClO,  $\text{Cl}_2$  and  $\text{Cl}_2\text{O}$  at 298K, Geophys. Res. Lett. **6**, 425-428, 1979.
- Leu, M. T., C. L. Lin, and W. B. DeMore, Rate constant for formation of chlorine nitrate by the reaction  $\text{ClO} + \text{NO}_2 + \text{M}$ , J. Phys. Chem. **81**, 190-195, 1977.
- Lewis, R. S., and R. T. Watson, Temperature dependence of the reaction  $\text{O}(^3\text{P}) + \text{OH}(^2\text{H}) \rightarrow \text{O}_2 + \text{H}$ , submitted to J. Phys. Chem. 1980.
- Lewis, R. S., S. P. Sander, S. G. Wagner, and R. T. Watson, Temperature dependent rate constants for the reaction of ground state atomic chlorine with simple alkanes, J. Phys. Chem. In press, 1980.
- Lin, C. L., S. Jaffe, and W. B. DeMore, Photochemistry of chlorine-ozone mixtures, American Chemical Society, 169th National meeting, Philadelphia, April, 1975.
- Lin, C. L., M. T. Leu, and W. B. DeMore, Rate constant for the reaction of atomic chlorine with methane, J. Phys. Chem. **82**, 1772-1777, 1978.
- Luther, K., and J. Troe, Weak collision effects in dissociation reactions at high temperatures, 17th International Symposium on Combustion, Leeds, August, 1978.

- Manning, R. G., and M. J. Kurylo, Flash photolysis resonance fluorescence investigation of the temperature dependencies of the reaction of  $\text{Cl}(^2\text{P})$  atoms with  $\text{CH}_4$ ,  $\text{CH}_3\text{Cl}$ ,  $\text{CH}_3\text{F}$ ,  $\text{CF}_3\text{F}$ , and  $\text{C}_2\text{H}_6$ , J. Phys. Chem. **81**, 291-296, 1977.
- Michael, J. V., and J. H. Lee, Selected rate constants for H, O, N, and Cl atoms with substrates at room temperatures, Chem. Phys. Lett. **51**, 303-306, 1977.
- Michael, J. V., D. A. Whytock, J. H. Lee, W. A. Payne, and L. J. Stief, Absolute rate constant for the reaction of atomic chlorine with hydrogen peroxide over the temperature range 265-400K, J. Chem. Phys. **67**, 3533-3536, 1977.
- Molina, M. J., Laboratory measurements of absorption cross-sections. This NATO meeting, Portugal, 1979.
- Molina, M. J., L. T. Molina, and T. Ishawata, Kinetics of the  $\text{ClO} + \text{NO}_2 + \text{M}$  reaction. Manuscript in preparation, 1980.
- NASA RP-1010, Chlorofluoromethanes and the stratosphere, ed. R. D. Hudson, 1977.
- NASA RP-1049, The stratosphere present and future, eds. R. D. Hudson and E. I. Reed, 1979.
- NATIONAL ACADEMY OF SCIENCES, HALOCARBONS: Effects on stratospheric ozone, National Academy of Sciences, Washington, D.C., 1976.
- NATIONAL ACADEMY OF SCIENCES, Stratospheric ozone depletion by halocarbons: Chemistry and Transport, National Academy of Sciences, Washington, D.C., 1979.
- Niki, H., P. D. Maker, C. M. Savage, and L. P. Breitenbach, Fourier transform IR spectroscopic observation of chlorine nitrite,  $\text{ClONO}$ , formed via  $\text{Cl} + \text{NO}_2 (+\text{M}) \rightarrow \text{ClONO} (+\text{M})$ , Chem. Phys. Lett. **59**, 78-79, 1978.
- Poulet, G., G. LeBras, and J. Combourieu, Elementary reactions of Cl and ClO radicals with hydrogenated species of stratospheric interest, WMO Symposium, Toronto, June, Proceedings 289-293, 1978.
- Prasad, S. S., and W. M. Adams, Asymmetrical  $\text{ClO}_3$ : Its possible formation from ClO and  $\text{O}_2$  and its possible reactions, J. Photochem. In press, 1980.
- Pritchard, H. O., J. B. Pyke, and A. F. Trotman-Dickenson, A method for the study of chlorine atom reactions. The reaction  $\text{Cl} + \text{CH}_4 \rightarrow \text{CH}_3 + \text{HCl}$ , J. Am. Chem. Soc. **76**, 1201-1202, 1954.
- Pritchard, H. O., J. B. Pyke, and A. F. Trotman-Dickenson, The study of chlorine atom reactions in the gas phase, J. Am. Chem. Soc. **77**, 2629-2633, 1955.
- Porter, G., and F. J. Wright, Studies of free radical reactivity by the methods of flash photolysis. The photochemical reaction between chlorine and oxygen, Disc. Faraday Soc. **14**, 23-34, 1953.
- Ravishankara, A. R., and P. H. Wine, A laser flash photolysis-resonance fluorescence kinetics study of the reaction  $\text{Cl}(^2\text{P}) + \text{CH}_4 \rightarrow \text{CH}_3 + \text{HCl}$ , J. Chem. Phys. **72**, 25-30, 1980.
- Ray, G. W., and R. T. Watson, A kinetics study of the reaction  $\text{NO} + \text{XO} \rightarrow \text{NO}_2 + \text{X}$  at 298K, manuscript in preparation, 1980.
- Reimann, B., and F. Kaufman, Rate constant for the reaction  $\text{HO}_2 + \text{ClO} \rightarrow \text{HOCl} + \text{O}_2$ , J. Chem. Phys. **69**, 2925-2926, 1978.
- Safary, E., J. Romand and B. Vodar, Ultraviolet absorption spectrum of gaseous hydrogen fluoride, J. Chem. Phys. **19**, 379-380, 1951.

# WATSON

- Sander, S. P., G. W. Ray, and R. T. Watson, A pressure dependence kinetics study of the formation of bromine nitrate at 298K, submitted, J. Phys. Chem. 1980.
- Sander, S. P., and R. T. Watson, Kinetic studies of the reactions of  $\text{CH}_3\text{O}_2$  with  $\text{NO}$ ,  $\text{NO}_2$  and  $\text{CH}_3\text{O}_2$  at 298K, J. Phys. Chem. In press, 1980a.
- Sander, S. P., and R. T. Watson, Rates and mechanism of the disproportionation of  $\text{BrO}$  radicals, submitted to J. Phys. Chem. 1980b.
- Schimanouchi, T., Tables of molecular vibrational frequencies. Consolidated volume II, J. Phys. Chem. Ref. Data, 6, 993-1102, 1977.
- Singleton, D. L., and R. J. Cvetanovic, Temperature dependence of the reactions of oxygen atoms with olefins, J. Am. Chem. Soc. 98, 6812-6819, 1976.
- Spencer, J. E., and F. S. Rowland, Bromine nitrate and its stratospheric significance, J. Phys. Chem. 82, 7-10, 1978.
- Staricco, E. H., J. E. Sicre, and H. J. Schumacher, Die photochemische reaktion zwischen fluor and ozon, Z. Phys. Chemie, N.F. 31, 385-396, 1962.
- Stimpfle, R. M., R. A. Perry, and C. J. Howard, Temperature Dependence of the reaction of  $\text{C}\dot{\text{O}}$  and  $\text{HO}_2$  radicals, J. Chem. Phys. 71, 5183-5190, 1979.
- Takacs, G. A., and G. P. Glass, Reactions of hydroxyl radicals with some hydrogen halides, J. Phys. Chem. 77, 1948-1951, 1973.
- Troe, J., Predictive possibilities of unimolecular rate theory, J. Phys. Chem. 83, 114-126, 1979.
- Troe, J., Theory of thermal unimolecular reactions at low pressures - II. Strong collision rate constants. Applications. J. Chem. Phys. 66, 4758-4775, 1977.
- Wagner, H. Gg., C. Zetzsch, and J. Warnatz, Gas phase preparation of  $\text{OF}$  radicals by reaction of fluorine atoms with ozone, Ber. Bunsenges. Phys. Chem. 76, 526-530, 1972.
- Walker, R. F., Ph.D. Thesis, University of London, Queen Mary College (1972).
- Watson, R. T., Rate constants for reactions of  $\text{C}\dot{\text{O}}$  of atmospheric interest, J. Phys. Chem. Ref. Data 6, 871-918, 1977.
- Watson, R. T., G. Machado, S. Fischer, and D. D. Davis, A temperature dependence kinetics study of the reaction of  $\text{Cl}(\text{}^2\text{P}_{3/2})$  with  $\text{O}_3$ ,  $\text{CH}_4$  and  $\text{d}_2\text{O}_2$ , J. Chem. Phys. 65, 2126-2138, 1976.
- Watson, R. T., E. S. Machado, R. L. Schiff, S. Fischer, and D. D. Davis, Chlorine atom reactions of atmospheric importance, Proceedings of the fourth conference on the climatic assessment program, Cambridge, Mass. February 1975. DOT-TSC-OST-75-38, 372-390, 1975.
- Watson, R. T., S. P. Sander, and Y. L. Yung, Pressure and temperature dependence kinetics study of the  $\text{NO} + \text{BrO} \rightarrow \text{NO}_2 + \text{Br}$  reaction. Implications for stratospheric bromine photochemistry, J. Phys. Chem. 83, 2936-2944, 1979.
- Westenberg, A. A., and N. de Haas, Atom-molecule kinetics using ESR detection. IV. Results for  $\text{Cl} + \text{H}_2 \rightleftharpoons \text{HCl} + \text{H}$  in both directions, J. Chem. Phys. 48, 4405-4415, 1968.
- Whytock, D. A., J. H. Lee, J. V. Michael, W. A. Payne, and L. J. Stief, Absolute rate of the reaction of  $\text{Cl}(\text{}^2\text{P})$  with Methane from 200-500K, J. Chem. Phys. 66, 2690-2695, 1977.
- Wongdontri-Stuper, W., R. K. M. Jayanty, R. Simonaitis, and J. Heicklen, The  $\text{Cl}_2$  photo-sensitized decomposition of  $\text{O}_3$ : The reactions of  $\text{C}\dot{\text{O}}$  and  $\text{OC}\dot{\text{O}}$  with  $\text{O}_3$ , J. Photochem. 10, 163-186, 1979.

WATSON

Yung, Y. L., P. J. Pinto, R. T. Watson, and S. P. Sander, Atmospheric bromine and ozone perturbations in the lower stratosphere, J. Atmos. Sci. February issue, 1980.

Zahniser, M. S., B. M. Berquist, and F. Kaufman, Kinetics of the reaction of  $\text{Cl} + \text{CH}_4 \rightarrow \text{CH}_3 + \text{HCl}$  from 200 to 500K, Int. J. Chem. Kinet. 10, 15-29, 1978.

Zahniser, M. S., J. S. Chang, and F. Kaufman, Chlorine nitrate: Kinetics of formation by  $\text{ClO} + \text{NO}_2 + \text{M}$  and of reaction with OH, J. Chem. Phys. 67, 997-1003, 1977.

Zahniser, M. S., and F. Kaufman, Kinetics of the reactions of  $\text{ClO}$  with O and with NO, J. Chem. Phys. 66, 3673-3681, 1977.

TEMPERATURE DEPENDENT ABSORPTION CROSS SECTIONS FOR FORMALDEHYDE (CH<sub>2</sub>O):

THE EFFECT OF FORMALDEHYDE ON STRATOSPHERIC CHLORINE CHEMISTRY

A. M. Bass

National Bureau of Standards  
Washington, DC

and

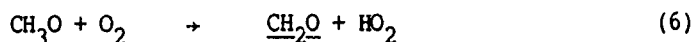
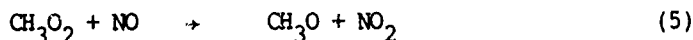
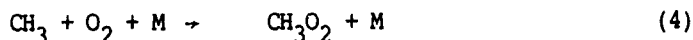
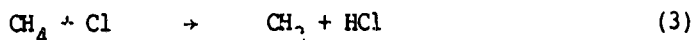
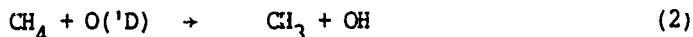
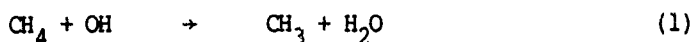
L. C. Glasgow, C. Millier, J. P. Jesson, and D. L. Filkin

Central Research and Development Department  
and Engineering Department  
E. I. du Pont de Nemours and Company  
Experimental Station  
Wilmington, DE 19898

ABSTRACT

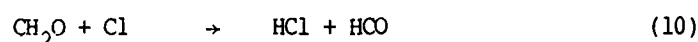
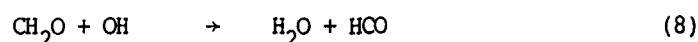
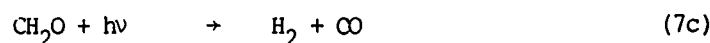
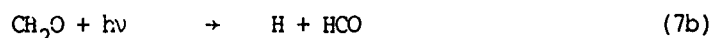
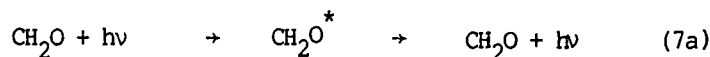
New measurements are reported of the absorption cross sections of formaldehyde at 296°K and 223°K. These measurements are significantly lower than those reported in the earlier literature at ca. 353°K. The implications of the lower absorption cross sections for stratospheric chlorine chemistry are considered using a one dimensional atmospheric model. A slight modification to ClX partitioning is predicted for the new cross sections, with only a small effect on estimated chlorine-catalyzed ozone perturbations.

INTRODUCTION: Formaldehyde (CH<sub>2</sub>O) is produced in the atmosphere as a product of hydrocarbon oxidation. Although the detailed mechanism of the oxidation process is not known with great certainty, current theoretical models include reaction schemes such as the following for methane:



It is quite possible that there are other species of importance to atmospheric hydrocarbon oxidation chemistry, such as CH<sub>3</sub>OOH, CH<sub>3</sub>O<sub>2</sub>NO<sub>2</sub>, CH<sub>3</sub>OH, which are not included in the above mechanism (NASA, 1977).

CH<sub>2</sub>O, once formed, may react further according to the reactions:



New data on the quantum yields of reactions 7a-7c and reactions 8-10 have recently become available (see DeMore, *et al.*, 1979).

In this paper we report new measurements for the photoabsorption cross sections of CH<sub>2</sub>O at 296°K and 223°K. A one dimensional model of atmospheric chemistry and transport (Miller, *et al.*, 1979) is used to assess the impact of changes in the CH<sub>2</sub>O photolysis behavior with specific reference to stratospheric chlorine chemistry. A comparison is made with an earlier modelling study (Stief, *et al.*, 1978) and consequences of ozone perturbations by chlorofluoromethanes are discussed.

**EXPERIMENTAL:** CH<sub>2</sub>O was prepared by gently heating a mixture of phosphorus pentoxide (J. T. Baker) and paraformaldehyde (Fisher) to about 100°C in a glass vacuum system. CH<sub>2</sub>O was purified by vacuum distillation and stored in the dark at 77°K until required. Infrared and gas chromatographic analyses indicated no detectable impurities implying a purity of >99.9%. CH<sub>2</sub>O sample pressures were measured in an MKS capacitance manometer to an accuracy of 3% or better. Sample pressures were typically in the range of 0.5 to 5 Torr. All runs included the addition of helium (Linde UHP) to bring the total pressure in the cell to 100 Torr.

The apparatus used for measuring CH<sub>2</sub>O absorption cross sections has been described previously (Bass and Laufer, 1973; Bass, Ledford, and Laufer, 1976). The basic elements of the system are a hydrogen light source dispersed by a 0.75 m Ebert grating monochromator, beam splitter, and absorption cell. Photomultiplier tubes view the light both before and after passing through the absorption cell. The absorption cell has a variable path length accomplished through multiple reflection MgF<sub>2</sub> coated aluminum mirrors. The cell wall temperatures can be varied between -100°C and 350°C by means of a methanol circulation system. All interior surfaces with the exception of the mirrors are Teflon® coated.

**CH<sub>2</sub>O ABSORPTION SPECTRUM:** The spectroscopy of CH<sub>2</sub>O has been reviewed recently (Moule and Walsh, 1975). Photodissociation in the atmosphere is due to the transition  $\tilde{A} \leftarrow \tilde{A}_1 (n, \pi^*)$  which gives rise to sharply featured absorption in the near ultraviolet beginning about 353 nm and extending to ~235 nm. The spectrum shows complex vibrational-rotational structure; individual lines are quite narrow being limited only by Doppler line broadening. The resolution employed in the present work (0.05 nm) can resolve only the envelopes of the vibronic bands. However, this is more than sufficient since for the purposes of atmospheric modeling, absorption cross sections are typically averaged over 2.5 to 5.0 nm intervals. Implicit in this treatment is the reasonable assumption that the integrated absorbance is independent of instrumental resolution.

**RESULTS AND DISCUSSION:** Figure 1 shows the averaged cross section data for all runs (upper trace = 296°K, lower trace = 223°K). No effects of helium pressure (0-600 Torr) or CH<sub>2</sub>O pressure (1-10 Torr) on the derived cross sections were observed. The main effect of lower temperature is a decrease in absorption strength on the red side of the main absorption features.

Table I gives the measured CH<sub>2</sub>O cross sections at 296°K and 223°K averaged over the wavelength intervals used in the model calculations (Miller, *et al.*, 1978, 1979). Table II gives the absorption cross sections at both temperatures averaged over 10 nm intervals for comparison with the data of Calvert, *et al.*, (1972) obtained at ca. 353°K. The data of Calvert, *et al.*, is that currently recommended for atmospheric modeling (Hampson and Garvin,



Figure 1. Averaged cross section data for all runs (upper trace = 296°K, lower trace = 223°K).

A. 2500-3100 $\text{\AA}$   
B. 3100-3600 $\text{\AA}$

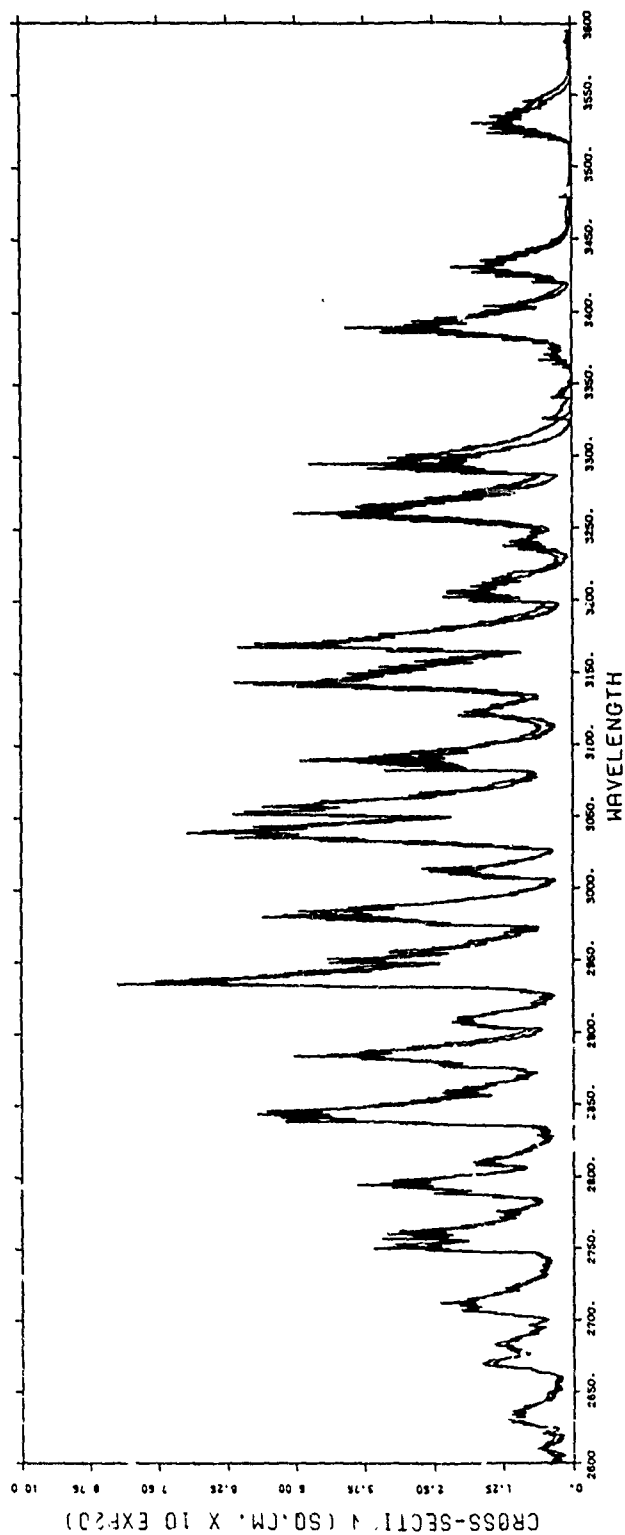


TABLE I  
CROSS SECTIONS OF CH<sub>2</sub>O AVERAGED OVER THE WAVELENGTH  
INTERVALS USED IN THE MODEL CALCULATIONS

Wavelength Bin	Wavelength Interval	$\sigma_{\text{Ave}}(296^\circ\text{K}) \times 10^{21}$ (cm <sup>2</sup> )	$\sigma_{\text{Ave}}(223^\circ\text{K}) \times 10^{21}$ (cm <sup>2</sup> )
68	355±2.5	5.5	4.4
69	350±2.5	1.1	1.0
70	345±2.5	5.5	5.0
71	340±2.5	11.8	11.0
72	335±2.5	1.6	1.2
73	330±2.5	15.3	9.7
74	325±2.5	16.3	13.6
75	320±2.5	14.4	12.2
76	315±2.5	27.9	27.1
77	310±2.5	15.1	15.5
78	305.25±2.25	39.5	36.0
79	300.75±2.25	13.8	14.7
80	296.3±2.2	28.5	26.8
81	292.0±2.1	22.3	21.3
82	287.8±2.1	20.6	19.4
83	283.7±2.0	22.2	22.5
84	279.75±1.95	15.8	16.6
85	275.9±1.9	16.2	17.8
86	272.15±1.85	11.5	11.4
87	268.5±1.8	9.6	9.8
88	264.95±1.75	5.6	5.5
89	261.45±1.75	5.1	4.4

TABLE II  
CROSS SECTIONS OF CH<sub>2</sub>O COMPARED WITH PREVIOUS WORK

Wavelength Interval	Calvert 353°Kx10 <sup>21</sup> (cm <sup>2</sup> )	This work 296°Kx10 <sup>21</sup> (cm <sup>2</sup> )	This work 223°Kx10 <sup>21</sup> (cm <sup>2</sup> )
360±5	1.8		
350±5	8.4	3.2	2.9
340±5	19.7	8.8	8.2
330±5	23.6	14.8	10.7
320±5	23.4	16.4	14.7
310±5	31.4	22.5	21.9
300±5	32.5	24.1	23.4
290±5	31.8	23.7	22.0
280±5	--	18.4	19.7
270±5	--	9.3	9.4

TABLE III  
SPECIES SLATE FOR MODEL CALCULATIONS

Fixed Species: N<sub>2</sub>, O<sub>2</sub>, CO<sub>2</sub>

Assumed In Photochemical Equilibrium:

O('D), H, N, CH<sub>3</sub>O, HCO

Fully Active Species: H<sub>2</sub>O\*, CH<sub>4</sub>, H<sub>2</sub>, O(<sup>3</sup>P), O<sub>3</sub>, NO, NO<sub>2</sub>,  
HNO<sub>3</sub>, N<sub>2</sub>O, NO<sub>3</sub>, N<sub>2</sub>O<sub>5</sub>, H<sub>2</sub>O<sub>2</sub>, OH, HO<sub>2</sub>,  
CFCl<sub>3</sub>, CF<sub>2</sub>Cl<sub>2</sub>, HCl, ClO, Cl, HOCl,  
CCl<sub>4</sub>, CH<sub>3</sub>Cl, CH<sub>3</sub>CCl<sub>3</sub>, CO, ClONO<sub>2</sub>,  
CH<sub>3</sub>O<sub>2</sub>, CH<sub>2</sub>O, CH<sub>3</sub>O<sub>2</sub>H

\*Active above tropopause (15 km) only.

1978). Use of the low temperature cross sections leads to somewhat greater photochemical lifetimes than implied by the 353°K cross sections.

A one dimensional model of atmospheric chemistry and transport was used to calculate vertical mixing ratio profiles for the atmospheric trace constituents (Miller, *et al.*, 1978, 1979). The formaldehyde chemistry, as well as other photochemical reaction rates in the model, are taken from DeMore, *et al.* (1979). The species slate for the calculations is summarized in Table III. Table IV gives those few reactions and rates present in the model that were not included in DeMore, *et al.*, (1979). The lower CH<sub>2</sub>O cross sections reported here for 223°K lead to a significant increase in the calculated CH<sub>2</sub>O mixing ratios, as shown in Figure 2. The theoretical curve for the 353°K cross-section is similar to that given by Stief, *et al.* (1978), who calculated a peak mixing ratio at 40 km of  $0.85 \times 10^{-10}$ . The peak mixing ratio from the curve for the 223°K cross section is  $1.1 \times 10^{-10}$  i.e. an increase in peak mixing ratio of 35% relative to the earlier results. The largest effects are in the lower stratosphere where the contribution of Reaction 8 to CH<sub>2</sub>O destruction is smallest.

The new CH<sub>2</sub>O cross sections also produce minor changes in the calculated mixing ratio profiles for other species. For example, in the ClX family, an increase of 4% in the HCl mixing ratio is calculated at 28 km, while corresponding decreases of this same order are estimated for the other chlorine species ClONO<sub>2</sub>, HOCl, ClO, and Cl. These small revisions to the partitioning of the ClX family are found to have only a slight influence on calculated ozone perturbations due to chlorofluoromethanes (less than a factor of 1.02 reduction in sensitivity).

Figure 3 shows the 24 hr. average rate of CH<sub>2</sub>O destruction due to reactions 7, 8, 9, and 10 as a function of altitude for a 1.5 ppb ClX background and the new low temperature cross sections. Photodissociation is the major sink below 30 km. Above this altitude reactions with OH and O become dominant loss mechanisms for CH<sub>2</sub>O.

The main termination reaction for Cl chain reactions in current atmospheric chemistry models is reaction (3). The relative importance of the reaction of Cl with CH<sub>2</sub>O in terminating Cl chains is conveniently expressed as the ratio

$$R = \frac{k_{10} (\text{CH}_2\text{O})}{k_3 (\text{CH}_4)}$$

For example, if  $R = 1.0$  at a given altitude, then CH<sub>2</sub>O is as important as CH<sub>4</sub> in removing Cl (at that altitude).

Figure 4 shows the 24 hr. average rate of HCl production for various Cl reactions as a function of altitude.  $R$  varies from 0.1 at 45 km to 0.4 at 40 km. Reaction 10 is the second most important source of HCl below 30 km.

It should be noted that, unlike most other H atom abstraction reactions of ClO, the reaction of ClO with CH<sub>2</sub>O is exothermic by nearly 18 kcal.



If the rate of reaction 11 is  $10^{-13} \text{ cm}^3 \text{ molecule}^{-1} \text{ sec}^{-1}$  or greater it could be an important source of HOCl (Glasgow, *et al.*, 1979).

**NON-METHANE HYDROCARBONS:** Current models assume that methane is the only hydrocarbon reaching the stratosphere in significant quantities. However, it is well known that the biosphere produces large amounts of non-methane hydrocarbon (Zimmerman, *et al.*, 1978). Although most of these are expected to be removed by reaction with hydroxyl radicals in the troposphere, (Chameides and Cicerone, 1978), to the extent which they reach the stratosphere they constitute an additional source of CH<sub>2</sub>O.

TABLE IV  
MODEL REACTIONS NOT INCLUDED IN DEMORE, ET AL., 1979

Reaction	Rate *	Reference
$\text{NO} + \text{NO}_3 \rightarrow 2\text{NO}_2$	$1.9 \times 10^{-11}$	Garvin and Hampson (1978)
$\text{NO}_2 + \text{O} \xrightarrow{\text{M}} \text{NO}_3$	$1 \times 10^{-31}$	"
$\text{NO}_2 + \text{NO}_3 \rightarrow \text{NO} + \text{O}_2 + \text{NO}_2$	$2.3 \times 10^{-13} \text{e}^{-1000/\text{T}}$	"
$\text{NO}_2 + \text{NO}_3 \xrightarrow{\text{M}} \text{N}_2\text{O}_5$	$\frac{3.5 \times 10^{-30}}{(1+3.17 \times 10^{-8} \text{e}^{-500/\text{T}_\text{M}^{0.5}})}$	**
$\text{N}_2\text{O}_5 \xrightarrow{\text{M}} \text{NO}_2 + \text{NO}_3$	$\frac{2.9 \times 10^{-3} \text{e}^{-1180/\text{T}}}{(1+3.17 \times 10^{-8} \text{e}^{-500/\text{T}_\text{M}^{0.5}})}$	**
$\text{N}_2\text{O}_5 + \text{H}_2\text{O} \rightarrow 2\text{HNO}_3$	$1 \times 10^{-20}$	
$\text{HO}_2 + \text{H} \rightarrow \text{H}_2 + \text{O}_2$	$4.2 \times 10^{-11} \text{e}^{-350/\text{T}}$	"
$\text{HO}_2 + \text{H} \rightarrow 2\text{OH}$	$4.2 \times 10^{-11} \text{e}^{-950/\text{T}}$	"
$\text{CH}_3\text{O}_2 + \text{CH}_3\text{O}_2 \rightarrow 2\text{CH}_3\text{O} + \text{O}_2$	$4 \times 10^{-13}$	"
$\text{Cl} + \text{OH} \rightarrow \text{O} + \text{HCl}$	$1 \times 10^{-11} \text{e}^{-2970/\text{T}}$	"
$\text{CO}_2 + \text{h}\nu \rightarrow \text{CO} + \text{O}$	Photolytic Cross Sections	Hudson and Kieffer (1975)
$\text{Cl} + \text{HOCl} \rightarrow \text{HCl} + \text{ClO}$	$1.7 \times 10^{-12} \text{e}^{-384/\text{T}}$	Estimate

\*Units are  $\text{sec}^{-1}$  for 1st order reactions,  $\text{cm}^3 \text{ molecules}^{-1} \text{ sec}^{-1}$  for second order reactions, and  $\text{cm}^6 \text{ molecules}^{-2} \text{ sec}^{-1}$  for 3rd order reactions.

\*\*Analytical Fit.

Figure 2. Effect of new absorption cross sections on the calculated  $\text{CH}_2\text{O}$  mixing ratio as a function of altitude.

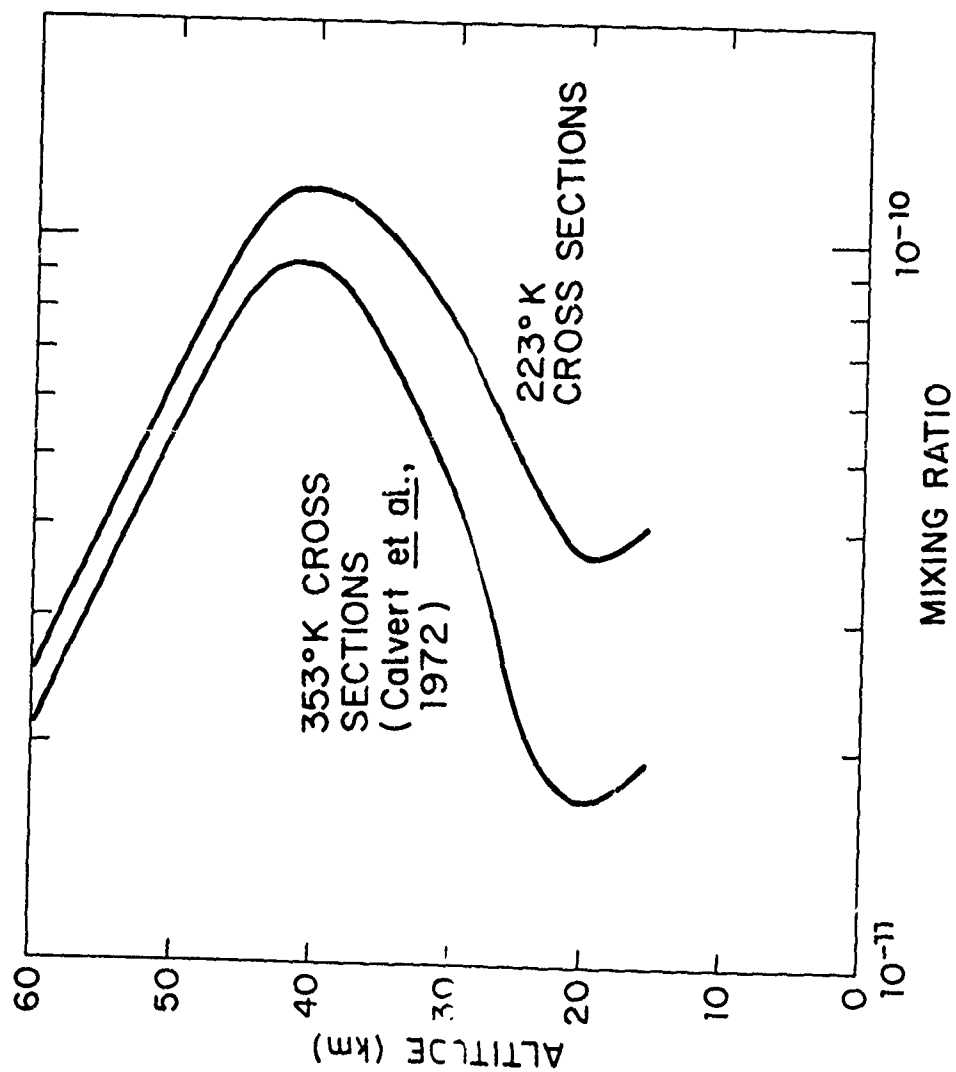


Figure 3. Contributions to destruction rates for  $\text{CH}_2\text{O}$  by various reactions, as a function of altitude (24 hr. average).

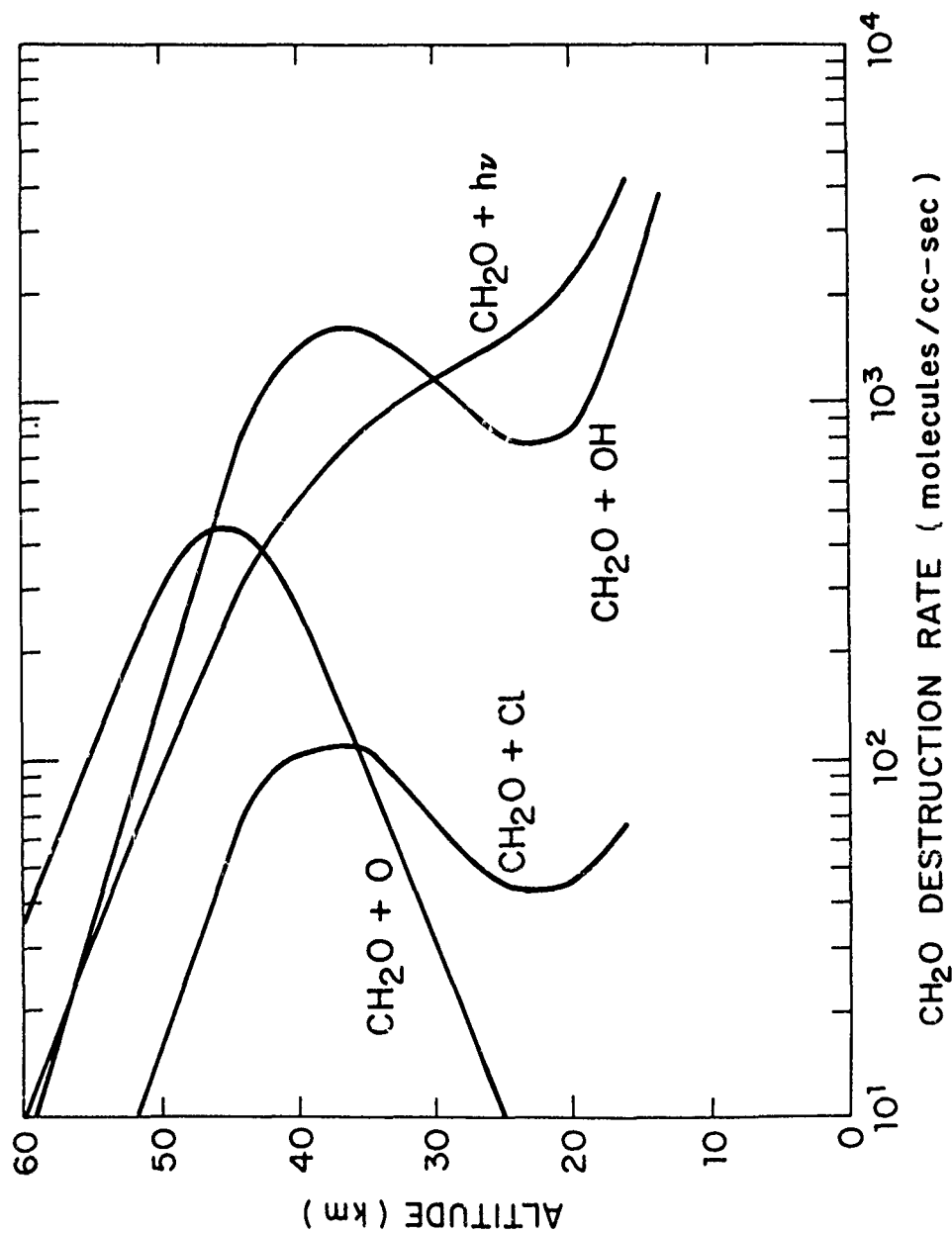
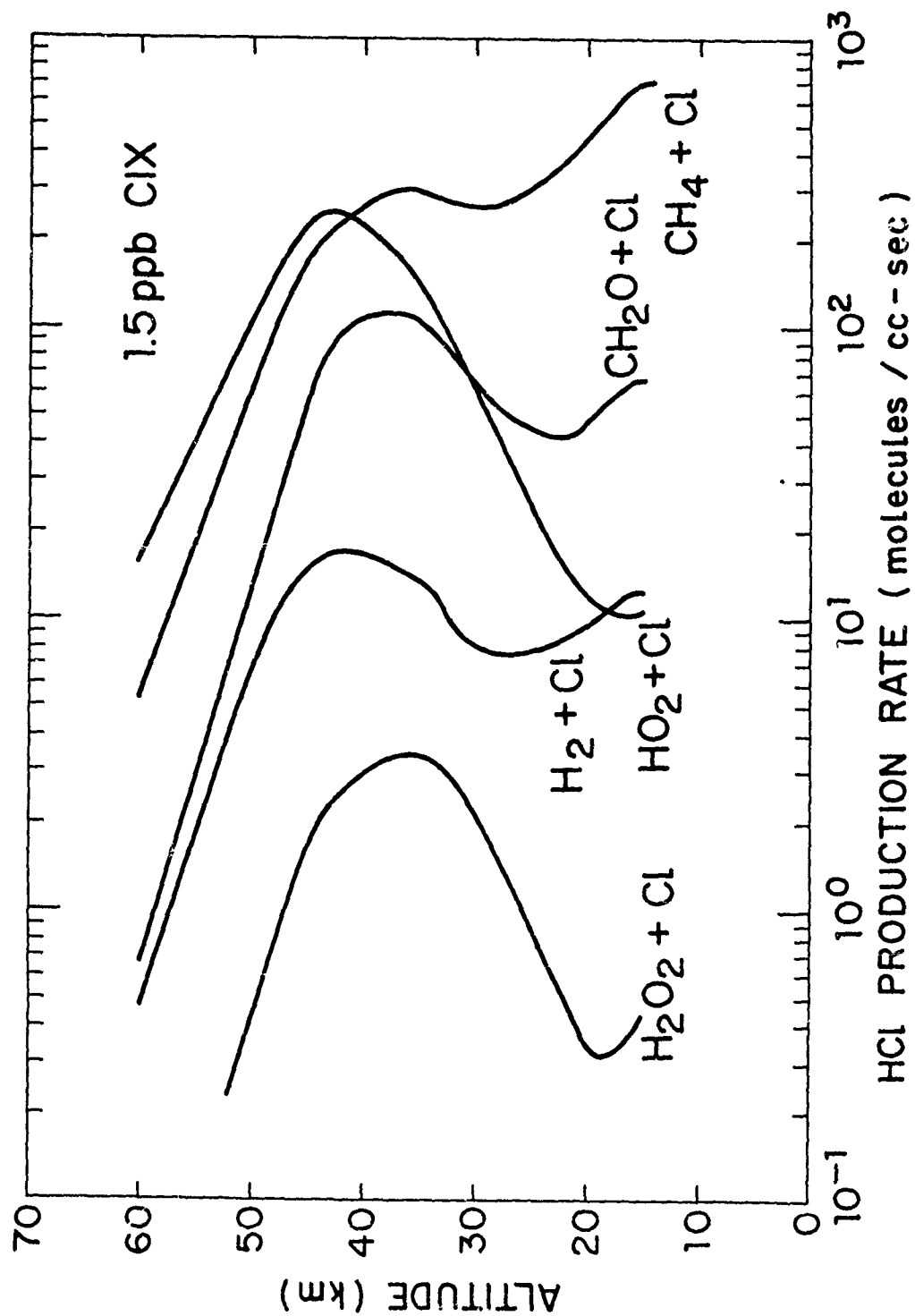


Figure 4. Contributions to rate of HCl production by various Cl reactions, as a function of altitude (24 hr. average).





References

- Bass, A. M. and A. H. Laufer, (1973/74). J. Photochem. 2, 465.  
Bass, A. M., A. E. Ledford, Jr., and A. H. Laufer, (1976). J. Res. Nat. Bur. Stds. 80A, 143.  
Calvert, J. G., J. A. Kerr, K. L. Demerjian, and R. D. McQuigg, (1972). Science 175, 751.  
Chameides, W. L. and R. J. Cicerone, (1978). J. Geophys. Res. 83, 947.  
DeMore, W. B., L. J. Stief, F. Kaufman, D. M. Golden, R. F. Hampson, M. J. Kurylo, J. J. Margitan, M. J. Molina, and R. T. Watson, (1979). NASA Panel for Data Evaluation, JPL Publication 79-27.  
Glasgow, L. C., J. P. Jesson, D. L. Filkin, and C. Miller, (1979). Planet. Space Sci. 27, 1047.  
Hampson, R. F. and D. Garvin, eds. (1978). Nat. Bur. Stds. NBS-SP-513.  
Hudson, R. D. and L. J. Kieffer, (1975). CIAP Monograph 1, 5-156 - 5-194.  
Miller, C., P. Meakin, R. G. E. Franks, and J. P. Jesson, (1978). Atmospheric Environment 12, 2481.  
Miller, C., D. L. Filkin, and J. P. Jesson, (1979). Atmospheric Environment 13, 381.  
Moule, D. C. and A. D. Walsh, (1975). Chem. Rev. 75, 67.  
NASA Reference Publication 1010, Hudson, R. D. (1977). Chlorofluoromethanes and the Stratosphere.  
Stief, L. J., J. V. Michael, W. A. Payne, D. F. Nawa, D. M. Butler, and R. S. Stolarski, (1978). Geophys. Res. Lett. 5, 829.  
Zimmerman, P. R., R. B. Chatfield, J. Fishman, P. J. Crutzen, and P. L. Hanst, (1978). Geophys. Res. Lett. 5, 679.

# ABSOLUTE RATE OF THE REACTION $\text{OH} + \text{H}_2\text{CO}$

## AT STRATOSPHERIC TEMPERATURES

L. J. Stief, D. F. Nava, W. A. Payne and J. V. Michael

NASA/Goddard Space Flight Center  
Greenbelt, Maryland 20771

### Abstract

Absolute rate constants for the reaction  $\text{OH} + \text{H}_2\text{CO}$  have been measured over the temperature range 228 to 362 K using the flash photolysis-resonance fluorescence technique. The reaction is temperature independent over this range, the best representation being  $k_1 = (1.05 \pm 0.11) \times 10^{-11} \text{ cm}^3 \text{ molecule}^{-1} \text{ s}^{-1}$ .

Formaldehyde ( $\text{H}_2\text{CO}$ ) is a product of the oxidation of methane in the upper atmosphere. It is removed by photolysis and by reaction with OH, O and Cl, the first two processes being dominant [Stief et al., 1978]. There have been no direct measurements of the absolute rate for  $\text{OH} + \text{H}_2\text{CO}$  at stratospheric temperatures. The only measurements of the absolute rate constant as a function of temperature are those of Atkinson and Pitts [1978] who studied the reaction between 299 and 426 K using the flash photolysis-resonance fluorescence (FP-RF) technique. Room temperature measurements of the absolute rate constant include those of Herron and Penzhorn [1969] (who obtained only a lower limit) and Morris and Niki [1971a]. Both studies employed the discharge flow-mass spectrometric (DF-MS) technique with OH in excess. Relative rate constant measurements at 300 K have been made by Morris and Niki [1971b] using the DF-MS technique and by Niki et al. [1978] using Fourier Transform Infra-Red Spectroscopy, the reference reactions being  $\text{OH} + \text{C}_3\text{H}_6$  and  $\text{OH} + \text{C}_2\text{H}_4$  respectively. Finally, Smith [1978] has reported measurements between 268 and 334 K of the rate constant for  $\text{OH} + \text{H}_2\text{CO}$  relative to that for  $\text{OH} + \text{OH}$  using the DF-MS technique. This is the only study of the reaction below room temperature but its utility is considerably reduced by the fact that the rate parameters of the reference reaction,  $\text{OH} + \text{OH}$ , are far more uncertain than those for  $\text{OH} + \text{H}_2\text{CO}$  itself.

In the work summarized here, absolute rate constants have been determined for the reaction



from 228 to 362 K using the FP-RF technique. The apparatus has been described in detail previously [Klemm and Stief, 1974]. Specific modifications of the apparatus and techniques for monitoring OH will be given in a fuller report on these experiments [Stief et al., 1980]. A very brief summary will suffice here. OH radicals were produced by flash photolysis of  $\text{H}_2\text{O}$  and detected as a function of time via resonance fluorescence in the region of the 306 nm  $\text{A}^2\Sigma^+ \rightarrow \text{X}^2\Pi$  transition. OH resonance radiation was produced by flowing Ar saturated with water vapor through a microwave discharge lamp.

Under the pseudo-first-order conditions employed, i.e.,  $[H_2CO] \gg [OH]$ , the decay of OH radicals may be represented by

$$\ln[OH] = -k_{\text{observed}} t + \ln[OH]_0 \quad (2)$$

where the observed pseudo-first-order rate constant is given by

$$k_{\text{observed}} = k_1 [H_2CO] + k_d \quad (3)$$

The diffusion correction  $k_d$  was determined independently by flash photolysis of Ar + H<sub>2</sub>O mixtures. Plots of  $\ln[OH]$  vs. time were linear as required by equation (2) and  $k_{\text{observed}}$  was obtained from such plots using linear least squares analysis. Values of  $k_1$  were calculated from  $k_{\text{observed}}$  according to equation (3). Experiments were performed at  $T = 228, 257, 298$  and  $362$  K. At each temperature, experiments were performed with variations in total pressure,  $[H_2CO]$  and flash intensity. The results are summarized in Table I.

Temperature (K)	Number of experiments	$k \times 10^{11}$ (cm <sup>3</sup> molecule <sup>-1</sup> s <sup>-1</sup> )
228	14	$1.12 \pm 0.10$
257	12	$1.03 \pm 0.09$
298	25	$0.99 \pm 0.11$
362	20	$1.05 \pm 0.15$

The error limits are one standard deviation values. The results show that the reaction is temperature independent for  $228 \leq T \leq 362$  K. The best representation for this temperature range is  $k_1 = (1.05 \pm 0.11) \times 10^{-11}$  cm<sup>3</sup> molecule<sup>-1</sup> s<sup>-1</sup>, where the error is given as two standard deviations to more accurately represent the uncertainty in the results for each of the four temperatures.

The value of  $k_1$  measured in the present study at 298 K is consistent with the lower limit  $k_1 \geq 0.7 \times 10^{-11}$  cm<sup>3</sup> molecule<sup>-1</sup> s<sup>-1</sup> of Herron and Penzhorn [1969] and, within the stated uncertainty, the absolute measurement of Morris and Niki [1971a] who reported  $k_1 = (1.4 \pm 0.35) \times 10^{-11}$  cm<sup>3</sup> molecule<sup>-1</sup> s<sup>-1</sup>. The relative values of Morris and Niki [1971b],  $k_1 = (1.5 \pm 0.15) \times 10^{-11}$  cm<sup>3</sup> molecule<sup>-1</sup> s<sup>-1</sup>, and of Niki et al. [1978],  $k_1 = (1.5 \pm 0.1) \times 10^{-11}$  cm<sup>3</sup> molecule<sup>-1</sup> s<sup>-1</sup> do not agree with the present results within the uncertainty limits.

The present results are in excellent agreement with the results of Atkinson and Pitts [1978] who obtained  $k_1$  values of  $(0.94 \pm 0.10) \times 10^{-11}$ ,  $(0.94 \pm 0.10) \times 10^{-11}$  and  $(1.03 \pm 0.11) \times 10^{-11}$  (all in units cm<sup>3</sup> molecule<sup>-1</sup> s<sup>-1</sup>) at temperatures of 299, 356 and 426 K respectively. Although these three values differ amongst themselves by less than 10%, Atkinson and Pitts [1978] preferred to represent their data by the temperature dependent expression:

$$k_1 = 1.25 \times 10^{-11} \exp - (88 \pm 150/T) \text{ cm}^3 \text{ molecule}^{-1} \text{ s}^{-1} \quad (4)$$

At 228 K, which corresponds to an altitude of 25 km, this underestimates our average value by about 20%. A more serious discrepancy results from the relative data of Smith [1978] whose results between 268 and 334 K may be represented by

$$k_1 = 6 \times 10^{-11} \exp(-635 \pm 250/T) \text{ cm}^3 \text{ molecule}^{-1} \text{ s}^{-1} \quad (5)$$

Extrapolation to 228 K gives a value about three times lower than we observe. Thus for modeling of the stratosphere, the average of our results and those of Atkinson and Pitts gives a recommended [NASA, 1979] value of  $k_1 = (1.01 \pm 0.10) \times 10^{-11}$  cm<sup>3</sup> molecule<sup>-1</sup> s<sup>-1</sup> independent of temperature from 228 to 426 K.

## REFERENCES

- Atkinson, R. and J. N. Pitts, Jr., Kinetics of the Reactions of the OH Radical with HCHO and CH<sub>3</sub>CHO over the Temperature Range 299-426°K, J. Chem. Phys., **68**, 3581, 1978.
- Herron, J. T. and R. D. Penzhorn, Mass Spectrometric Study of the Reaction of Atomic Oxygen with Ethylene and Formaldehyde, J. Phys. Chem., **78**, 191, 1969.
- Klemm, R. B. and L. J. Stief, Absolute Rate Parameters for the Reaction of Ground State Atomic Oxygen with Carbonyl Sulfide, J. Chem. Phys., **61**, 4900, 1974.
- Morris, E. D., Jr., and H. Niki, Mass spectrometric Study of the Reaction of Hydroxyl Radical with Formaldehyde, J. Chem. Phys., **55**, 1991, 1971a.
- Morris, E. D., Jr., and H. Niki, Reactivity of Hydroxyl Radicals with Olefins, J. Phys. Chem., **75**, 3640, 1971b.
- National Aeronautics and Space Administration, The Stratosphere: Present and Future, NASA Reference Publication 1049, 1979.
- Niki, H., P. D. Maker, C. M. Savage, and L. P. Breitenbach, Relative Rate Constants for the Reaction of Hydroxyl Radical with Aldehydes, J. Phys. Chem., **82**, 132, 1978.
- Smith, R. H., Rate Constant and Activation Energy for the Gaseous Reaction between Hydroxyl and Formaldehyde, Int. J. Chem. Kinet., **10**, 519, 1978.
- Stief, L. J., J. V. Michael, W. A. Payne, D. F. Nava, D. M. Butler and R. S. Stolarski, The Reaction  $\text{Cl} + \text{H}_2\text{CO} \rightarrow \text{HCl} + \text{HCO}$ : Decreased Sensitivity of Stratospheric Ozone to Chlorine Perturbations, Geophys. Res. Lett., **5**, 829, 1978.
- Stief, L. J., D. F. Nava, W. A. Payne and J. V. Michael, Rate Constant for the Reaction of Hydroxyl Radical with Formaldehyde over the Temperature Range 228-362°K, to be submitted to J. Chem. Phys., 1980.

# KINETIC STUDIES OF ATMOSPHERIC FREE RADICALS

J. P. Burrows

R. A. Cox

Environmental and Medical Sciences Division  
AERE, Harwell, Didcot, Oxfordshire, UK

M. C. Addison

Department of Physical Chemistry,  
University of Edinburgh

## Abstract

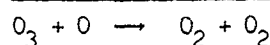
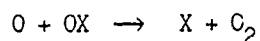
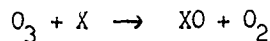
Results are presented here of some recent investigations into the reactions



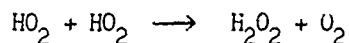
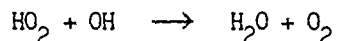
Rate coefficients have been obtained and a mechanism suggested for reaction (1).

**INTRODUCTION:** In recent years considerable concern has been generated by the potential depletion of atmospheric ozone by anthropogenic pollution. The ozone layer in the stratosphere shields the earth's surface from U.V.-B. radiation and by absorbing this energy heats the stratosphere. In order to assess accurately the potential environmental hazards created by pollutants such as, the exhaust emissions from high flying aircraft, the release of fluorocarbon compounds, and the use of nitrate fertilisers, it is necessary to understand in detail the chemistry of the atmosphere. Interest in these problems has emphasised the need for laboratory investigations of the gas phase reactions of atmospheric constituents.

In the stratosphere the concentration of odd oxygen species ( $\text{O}$  and  $\text{O}_3$ ) are predominantly controlled by destruction cycles, e.g.



Cycles have been identified for  $\text{HO}_x$  species [Nicolet and Bates, 1950],  $\text{NO}_x$  species [Crutzen 1970, Johnston 1970] and  $\text{ClO}_x$  species [Molina and Rowland 1974, Stolarski and Cicerone, 1974]. Two species which play an important role in determining stratospheric ozone abundance, are  $\text{HO}_2$  and  $\text{ClO}$ .  $\text{HO}_2$  is involved in the catalytic removal of odd oxygen both directly and indirectly through its control of the reactive species  $\text{OH}$  via its reactions with  $\text{NO}$ ,  $\text{O}$  and  $\text{H}$ . The major loss processes for  $\text{HO}_x$  species from the stratosphere are thought to be



$\text{ClO}$  also takes part in the catalytic removal of odd oxygen species in the stratosphere. Its reactions with other species are of interest as potential loss processes for  $\text{ClO}_x$  from the upper atmosphere.

**EXPERIMENTAL:** Experiments were undertaken using a molecular modulation spectrometer (MMS) shown in figure 1 [R.A.Cox et al 1979]. The square wave light source was provided by up to 6 fluorescent blacklights mounted radially around the jacketed pyrex reaction vessel which was 120 cm long and had 2.5 cm diameter quartz windows at each end. Absorption was monitored in the long axis of the cell on a collimated beam from a deuterium lamp (Manufacturers Supply Ltd). The modulated absorption was measured as separate in phase and in quadrature components using the digital lock in detector.

The  $\text{HO}_2$  radical was monitored at 220 nm with a spectral slit width of 1.1 nm. At this wavelength the absorption cross sections of  $\text{ClO}$ ,  $\text{Cl}_2\text{O}$  [Watson 1977] and  $\text{HOCl}$  [Molina 1978] are relatively low and do not cause serious interference. At the monitoring wavelength for  $\text{ClO}$  277.2 nm, appreciable absorption due to  $\text{Cl}_2\text{O}$  occurs, it was therefore necessary to use a differential technique to monitor  $\text{ClO}$  in the 11-0 band without interference from underlying continuous absorptions [Cox and Derwent 1979]. The differential detector signals were interfaced with digital lock in through a differential Electrometer Amplifier (Keithley 6010). The device was calibrated using known concentrations of  $\text{ClO}$  produced in the photolysis of  $\text{Cl}_2\text{-O}_2$  mixtures [Cox and Derwent 1979]. The signal to noise ratio for detection of modulated signals with the differential system was approximately a factor of three smaller than the direct monitoring arrangement; this gave a lower precision of measurement for  $\text{ClO}$  than for  $\text{HO}_2$ , but this was offset by the advantage of specificity.

Experiments were performed both in a stopped flow and a flowing manner. Gas flows were measured using calibrated rotameters and the gases were mixed prior to entry into the reaction vessel.  $\text{H}_2$  cylinder grade,  $\text{N}_2$  white spot grade,  $\text{Cl}_2$  5% in  $\text{N}_2$  high purity and  $\text{O}_2$  Breathing grade were supplied by EOC; the  $\text{O}_2$  was further purified by passage through a convertor containing hot Cu turnings to remove any hydrocarbon impurities and then dried by passing through a molecular sieve. The  $\text{Cl}_2\text{O}$  was prepared continuously by passing  $\text{Cl}_2$  in  $\text{N}_2$  over yellow  $\text{HgO}$ .

The rate of photochemical decomposition of  $\text{Cl}_2$  in the experiments was determined by measuring the rate of decay of  $\text{Cl}_2$  in  $\text{Cl}_2\text{-H}_2\text{-O}_2$  mixtures [Cox and Derwent 1977]. The photolysis rate of  $\text{Cl}_2\text{O}$  was determined by comparison of the overlap of the absorption spectra of  $\text{Cl}_2$  and  $\text{Cl}_2\text{O}$  as a function of the output intensity of the lamps [Cox and Lewis 1979] and yielded  $0\text{Cl}_2\text{O} + 0.2\ 0\text{Cl}_2$ . The kinetic treatment of the data obtained from an MMS experiment has been described elsewhere [Cox et al 1979]. For an absorbing species, e.g. radical R, the in-phase counting rate P and the in quadrature counting rate Q are given by

$$P = C\sigma l \left[ \int_0^{\tau/2} {}^2[R](t)dt - \int_{\tau/2}^{\tau} [R](t)dt \right] \quad (i)$$

$$Q = C\sigma l \left[ \int_{\tau/4}^{3\tau/4} [R](t)dt - \int_{3\tau/4}^{\tau} [R](t)dt \right] \quad (ii)$$

where C is a calibration factor,  $\sigma$  is the absorption coefficient, l the length of the vessel, and  $\tau$  the period of photolysis. The differential equations for radical removal by a 2nd order process are

$$\frac{d[R]}{dt} = 2\theta - 2\delta[R]^2 \quad \text{for lights on}$$

$$\frac{d[R]}{dt} = -2\delta[R]^2 \quad \text{for lights off}$$

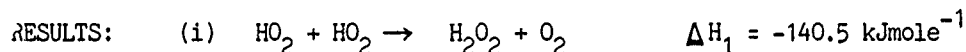
where  $2\theta$  is the rate of production of radicals and  $2\delta$  is the overall second order decay coefficient. As  $\tau \rightarrow \infty$ , the in-phase count rate approaches a limiting value given by

$$A_0 = \frac{\sigma}{2} \left( \frac{\theta}{\delta} \right)^{\frac{1}{2}}$$

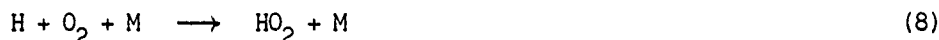
and the period  $\tau_0$  when  $P$  is equal to  $\theta$  is given by

$$\tau_0 = \frac{2.2}{(\theta\delta)^{\frac{1}{2}}}$$

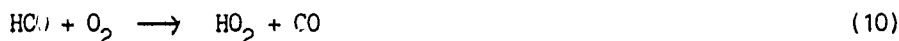
For first order behaviour another exact solution is obtained [Cox and Lewis 1979] but for mixed order kinetic behaviour numerical analysis is required by computer.



A detailed description of the investigation of this reaction exists elsewhere [Cox and Burrows 1979]. Radicals were produced by the photolysis of  $\text{Cl}_2$ , either in the presence of excess  $\text{H}_2$  and  $\text{O}_2$ :



or in the presence of excess HCHO and  $\text{O}_2$ :



Provided the concentration of  $\text{H}_2$  is high enough to eliminate Cl atom reactions competing with (7), then the simple mechanism involving (1), (6), (7) and (8) dominates. At low pressure this is no longer true and reaction (8) is much slower, therefore for total pressures < 25 torr, the HCHO system was used.

The kinetic behaviour of  $\text{HO}_2$  in the  $\text{Cl}_2\text{-O}_2\text{-H}_2$  system at high pressure was investigated, by measurement of the in-phase and in-quadrature absorption at 220 nm, as a function of photolysis period. A range of  $\text{HO}_2$  generation rates was obtained by varying the concentration of  $\text{Cl}_2$  and the number of photolysis lamps. The data for total pressures near 760 torr and at 298 K are plotted in figure (2). The data were well fitted with a pair of second order curves except at very long photolysis periods, when a systematic departure from the model was present. The rate coefficient for  $\text{HO}_2$  recombination from these curves is

$$k_{\text{HO}_2 + \text{HO}_2} = (2.3 \pm 0.3) \times 10^{-12} \text{ cm}^3 \text{ molecule}^{-1} \text{ s}^{-1} \text{ at } 298 \text{ K}$$

and the corresponding absorption cross section for  $\text{HO}_2$  at 220 nm is

$$\sigma = (3.5 \pm 0.4) \times 10^{-18} \text{ cm}^2 \text{ molecule}^{-1}$$

The pressure dependence of  $\text{HO}_2 + \text{HCHO}$  was investigated by performing experiments at 347 and 25 torr in the  $\text{H}_2\text{-O}_2\text{-Cl}_2$  system and at 25, 10, 5.3 and 3.0 torr in the  $\text{HCHO-O}_2\text{-Cl}_2$  system. On reduction of the total pressure below 25 torr in the HCHO mixture, kinetic changes were observed in the  $\text{HO}_2$  behaviour. There appeared to be some first order process competing with  $\text{HO}_2$  disproportionation. This could possibly be due to



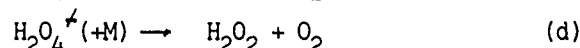
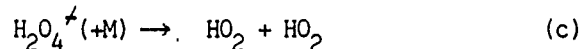
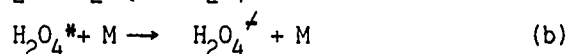
[Niki et al 1979] or perhaps wall loss. Although the accessible conditions did not allow an unambiguous direct measurement of  $k_1$  at these low pressures it could be estimated by fitting pairs of values of  $k_1^I$  and  $k_1$  to the data obtained, (here  $k_1^I$  is the effective first order rate coefficient for  $\text{HO}_2$  loss). It is concluded that there is a fall-off in  $k_1$  at pressures of 10 torr and below in agreement with a recent observation [Burrows et al 1979].

The effect of temperature on  $k_1$  was investigated over the range 273–339 K using total pressures of 760 torr ( $\text{H}_2 - \text{O}_2 - \text{Cl}_2$ ) and 10 torr ( $\text{HCHO} - \text{O}_2 - \text{Cl}_2$ ):

$$\begin{aligned} \text{at } 760 \text{ torr} \quad k_1 &= (3.8 \pm 1.4) \times 10^{-14} \exp \left( \frac{1245 \pm 185}{T} \right) \text{cm}^3 \text{molecule}^{-1} \text{s}^{-1} \\ \text{at } 10 \text{ torr} \quad k_1 &= (2.7 \pm 0.4) \times 10^{-13} \exp \left( \frac{581 \pm 44}{T} \right) \text{cm}^3 \text{molecule}^{-1} \text{s}^{-1} \end{aligned}$$

The effect of water vapour on the modulated absorption at 220 nm was investigated. The results obtained were in general agreement with a recent work [Hamilton 1975] that the apparent 2nd order  $\text{HO}_2$  decay constant was increased by the presence of a few torr of  $\text{H}_2\text{O}$ .

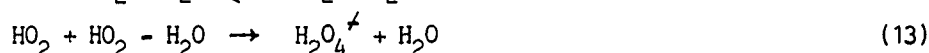
It is clear that an elementary H atom stripping reaction as suggested previously [Hockanadel et al 1972, Paukert and Johnston 1972] is inconsistent with the observed temperature and pressure dependence. The results suggest the formation of an  $\text{H}_2\text{O}_4$  intermediate. One simple mechanism which possibly explains the observed phenomena is



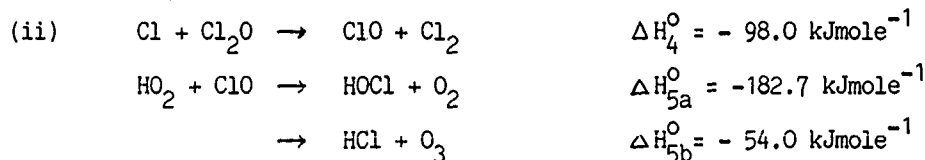
The observed rate of reaction is given by

$$\frac{d[\text{H}_2\text{O}_2]}{dt} = \frac{k_a [\text{HO}_2]^2}{((k_{-a}/k_b[\text{M}]) + 1)} \times \frac{1}{((k_c/k_d) + 1)} = k_1 [\text{HO}_2]^2$$

This model indicates that the overall second order rate constant is composed of two parts one of which will decrease with a fall in pressure, the other which implies a negative activation energy provided  $k_{-a}/k_b \gg 1$  and  $E_c > E_d$ . A possible explanation of the effect of water vapour on the kinetic behaviour of  $\text{HO}_2$  is through the reactions:



Further work is necessary to confirm these suggestions and to establish the existence of the proposed  $\text{H}_2\text{O}_4^{\ddagger}$  intermediate.



The above reactions were investigated by studying the kinetic behaviour of  $\text{HO}_2$  and  $\text{ClO}$  in flowing mixtures of  $\text{H}_2$ ,  $\text{N}_2$ ,  $\text{O}_2$ ,  $\text{Cl}_2$  and  $\text{Cl}_2\text{O}$ , typical concentrations being  $1.8 \times 10^{19} \text{ cm}^{-3}$ ,  $1.3 \times 10^{18} \text{ cm}^{-3}$ ,  $4.0 \times 10^{18} \text{ cm}^{-3}$ ,  $1.0 \times 10^{16} \text{ cm}^{-3}$  and  $2.0 \times 10^{15} \text{ cm}^{-3}$  respectively. The approach adopted to produce  $\text{HO}_2$  in the presence of  $\text{ClO}$  was to allow reaction (4) to compete with reaction (6) for  $\text{Cl}$  atoms:

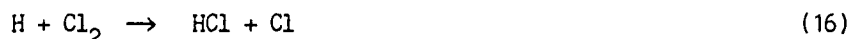






The  $\text{HO}_2$  and  $\text{ClO}$  then decay via reactions (1), (2) and (5) reaction (3) being assumed to be in equilibrium with (-3). For a fixed period  $\tau$  of 4s, the in phase and in quadrature signals for  $\text{HO}_2$  at 220 nm and  $\text{ClO}$  at 277 nm were observed as a function of the ratio  $[\text{H}_2]/[\text{Cl}_2\text{O}]$ . The in quadrature signals due to  $\text{ClO}$  were observed to decrease relative to the in phase signals as the  $[\text{H}_2]/[\text{Cl}_2\text{O}]$  ratio increased. This reflected the decreasing lifetime of  $\text{ClO}$  as the fast reaction (5) started to compete against the slow disproportionation reaction (2). The  $\text{HO}_2$  signals appeared to behave in the manner expected for competition between reactions (1) and (5), and (4) and (7). However at high  $[\text{Cl}_2\text{O}]$  the absorption at 220 nm was complicated by the presence of another absorbing species kinetically similar to  $\text{ClO}$ , which is tentatively assigned as  $\text{Cl}_2\text{O}_2$ .

Experimentally it was observed that the concentration modulation and 'lifetime' of  $\text{ClO}$ , as measured from  $\tau_0$ , was a sharp function of the ratio  $[\text{H}_2]/[\text{Cl}_2\text{O}]$  in the region where reactions (4) and (7) were apparently competitive. This allowed a determination of the ratio  $k_4/k_7$  using computer simulation of the experimental observations for different values of this ratio. In addition to the reactions (1) to (8), the chemical scheme also involved the following reactions:



The best fit of the experimental observations (see Fig.(3)) was obtained with the following ratio:

$$\frac{k_4}{k_7} = (6.9 \pm 0.3) \times 10^3$$

This fit was independent of the value chosen for  $k_2$  over the range  $(3-6) \times 10^{-12} \text{ cm}^3 \text{ molecule}^{-1} \text{ s}^{-1}$ . Using the mean of four recent 298 K values for  $k_7$ ,  $1.5 \times 10^{-14} \text{ cm}^3 \text{ molecule}^{-1} \text{ s}^{-1}$  [Watson et al 1979, Lee et al 1977, Ambidge et al 1976, Davis et al 1970], the value obtained for the rate coefficient of reaction (4) is

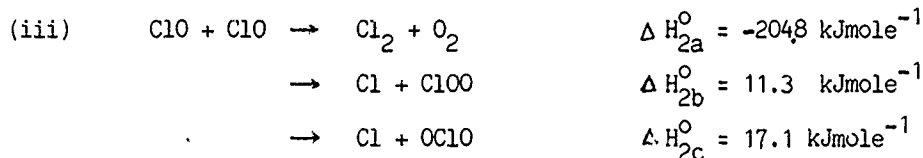
$$k_4 = (1.0 \pm 0.33) \times 10^{-10} \text{ cm}^3 \text{ molecule}^{-1} \text{ s}^{-1} \text{ at } 298 \text{ K}$$

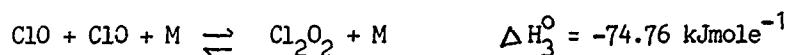
This is over two orders of magnitude greater than the value reported previously [Basco and Dogra 1971], but in excellent agreement with a recent direct measurement of  $9.8 \times 10^{-11} \text{ cm}^3 \text{ molecule}^{-1} \text{ s}^{-1}$  [Watson 1979]. For the simulation,  $k_1$  was taken from the previous section,  $k_8$   $k_{16}$  were taken from a recent review of reaction rate data [Hampson and Garvin 1977],  $k_2$  was taken as the measured overall decay coefficient for  $\text{ClO}$  when  $\text{Cl}_2\text{O}$  is in excess, ( $5.6 \times 10^{-15} \text{ cm}^3 \text{ molecule}^{-1} \text{ s}^{-1}$ ), and  $k_{15}$  was taken from recent measurements [Burrows et al 1979, Cox 1979].

The measurement of  $k_5$  was achieved from observation of the  $\text{ClO}$  and  $\text{HO}_2$  absorption components in phase and in quadrature as a function of photolysis period. The ratio  $[\text{H}_2]/[\text{Cl}_2]$  was fixed at a value corresponding to a slight excess of  $\text{HO}_2$  over  $\text{ClO}$ , so that  $\text{ClO}$  kinetics were dominated by reaction (5) and  $\text{HO}_2$  by reactions (1) and (5). Computer simulation was used to predict the experimental results, using  $k_5$  in the range  $3-10 \times 10^{12} \text{ cm}^3 \text{ molecule}^{-1} \text{ s}^{-1}$ . A least squares method was used to determine the best fit (see fig.(4)) which gave the result:

$$k_5 = (5.4 \pm 4.0 \text{ } ^{-2.0}) \times 10^{-12} \text{ cm}^3 \text{ molecule}^{-1} \text{ s}^{-1} \text{ at } 298 \text{ K}$$

This value, which was obtained at a total pressure of 760 torr should be compared with recent measurements, [Kaufman and Reiman 1978], [Birks, J. 1978] and [Stimple et al 1979].





Reactions (2) and (3) were studied by modulated photolysis of mixtures of  $\text{Cl}_2 - \text{O}_2$  and  $\text{Cl}_2 - \text{Cl}_2\text{O} - \text{O}_2$  over the temperature range 278–346 K. ClO concentration changes were obtained by monitoring the absorption at 277 nm in a differential manner both using the lock-in detector and also, in the  $\text{Cl}_2\text{O}$  mixtures, by direct observation of the absorption using low frequency photolysis ( $\tau = 40$  s). A preliminary analysis of the data has been undertaken, the results of which are presented here.

For mixtures of 3.5 torr of  $\text{Cl}_2$  in 45 torr of  $\text{O}_2$ , the period  $\tau$  and photolysis intensity were varied. Second order kinetic behaviour for the ClO concentration was observed over the temperature range stated. The reaction mechanism proposed for this system [Cox et al 1979] is .



Since reactions (18) and (19) remove Cl atoms from the system the overall second order rate coefficient  $k_{2nd}$  is given by

$$k_{2nd} = k_3[M] + k_{2a} + k_{2b} + k_{2c}$$

The experiments yield a value for  $k_{2nd}$  of (see Fig.(5))

$$k_{2nd} = (1.4 \pm 0.5) \times 10^{-13} \exp\left(-\frac{251 \pm 150}{T}\right) \text{ cm}^3 \text{ molecule}^{-1} \text{ s}^{-1}$$

Using the values obtained from a previous investigation [Cox et al 1979] then

$$k_3 = (1.4 \pm 1.0) \times 10^{-33} \exp\left(-\frac{100 \pm 150}{T}\right) \text{ cm}^3 \text{ molecule}^{-1} \text{ s}^{-1}$$

In the  $\text{Cl}_2 - \text{Cl}_2\text{O} - \text{O}_2$  system deviation from second order behaviour was observed for the ClO below 333 K. This is probably due to the  $\text{Cl}_2\text{O}_2$  behaviour since its stability increases as the temperature decreases. The quantum yield of  $\text{Cl}_2\text{O}$  molecules reacted per  $\text{Cl}_2$  molecule absorbing a photon is defined by the equation

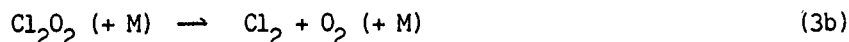
$$\Phi = \sum_{n=0}^{\infty} \alpha^n$$

$$\Phi = (1 - \alpha)^{-1}$$

where  $\alpha$  is the ratio of branching to terminating steps, for reaction 2 in the system.  $\Phi$  was observed as a function of temperature and the results obtained were in agreement with a previous study of the  $\text{Cl}_2 - \text{O}_3$  system [Cox and Derwent 1979]. The data indicates the presence of a non-radical (terminating) route (2a) as well as radical (branching) routes (2b) and (2c) for the ClO disproportionation reaction.

An alternative explanation of the kinetic behaviour of ClO in the  $\text{Cl}_2 - \text{Cl}_2\text{O} - \text{O}_2$  mixture is that

termination, instead of occurring via reaction (2a), may proceed through the unimolecular decay of  $\text{Cl}_2\text{O}_2$ :



This behaviour would be similar to that of  $\text{H}_2\text{O}_4^*$  postulated in section (i). At present experimentation is continuing in an effort to establish whether or not (3b) is the dominant step in the system.

#### ACKNOWLEDGEMENTS:

The authors wish to thank Dr. R.G. Derwent for discussions about the chemistry, and for assistance with the computer modelling. This work has been supported by the Department of the Environment.

#### REFERENCES:

- Ambidge, P.F., Bradley, J.N., Whytock, D.A., J.Chem.Soc.Faraday Trans.I, 72, 2143, (1976).  
 Basco, N., Dogra, S.K., Proc.Roy.Soc.A., 323, 401 (1971)  
 Basco, N., Hunt, J.E., Int.J.Chem.Kinetics, 11, 649 (1979)  
 Birks, J., WMO meeting (1978).  
 Burrows, J.P., Harris, G.W., Cliff, D., Wilkinson, J., Thrush, B.A., Proc.Roy.Soc.A., in press (1979).  
 Calvert, J.G., Fu Su, Lindley, C.R., Uselman, W.M., Shaw, J.H., J.Phys.Chem., 83, 912 (1979)  
 Cox, R.A., submitted to Int.J.Chem.Kinetics, (1979).  
 Cox, R.A., Burrows, J.P., J.Phys.Chem., in press (1979)  
 Cox, R.A., Derwent, R.G., J.Chem.Soc.Faraday Trans.I, 73, 272 (1977)  
 Cox, R.A., Derwent, R.G., J.Chem.Soc.Faraday Trans.I, 75, 1635 (1979)  
 Cox, R.A., Derwent, R.G., Eggleton, A.E.J., Reid, H.J., J.Chem.Soc.Faraday Trans.I, 75, 1648 (1979)  
 Cox, R.A., Lewis, R., J.Chem.Soc.Faraday Trans.I, in press (1979)  
 Crutzen, P. Q.J.R.Met.Soc., 96, 320 (1970)  
 Davis, D.D., Braun, W., Bass, A., Int.J.Chem.Kinetics, 2, 101 (1970)  
 Hamilton, E.J., J.Chem.Phys., 63, 3682 (1975)  
 Hampson, R.F., Garvin, D. "Reaction Rate and Photochemical Data for Atmospheric - 1977" NBS Special Publication, 513  
 Hochanadel, C.J., Ghormley, J., Ogren, P.T., J.Chem.Phys., 56, 4426 (1972)  
 Johnston, H., Science, 173, 517 (1971)  
 Kaufman, F., Reiman, B., J.Chem.Phys., 69, 2925 (1978)  
 Lee, J.H., Michael, J.V., Payne, W.A., Stief, L.J., Whytock, D.A., J.Chem.Soc.Faraday Trans.I, 73, 1530 (1977)  
 Molina, M.J., Rowland, F.S. Nature, 249, 810 (1974)  
 Molina, L.T., Molina, L.J., J.Phys.Chem., 82, 2410 (1978)  
 Nicolet, M., Bates, D., J.G.R., 55, 301 (1950)  
 Niki, H., Maker, T.D., Savage, C.M., Fu Su, Calvert, J.G., Shaw, J.H., Chem.Phys.Lett., 65, 221 (1979)  
 Paukert, T.T., Johnston, H., J.Chem.Phys., 56, 2824 (1972)  
 Stimple, R.M., Perry, R.A., Howard, C.J., J.Chem.Phys. in press (1979)  
 Stolarski, R.S., Cicerone, R., Can.J.Chem., 52, 1610 (1974)  
 Watson, R.T., J.Phys.Chem.Ref.Data, 871 (1977)  
 Watson, R.T., private communication (1979)  
 Watson, R.T., Machado, E.S., Schiff, R.L., Fischer, S., Davis, D.D., in preparation (1979)

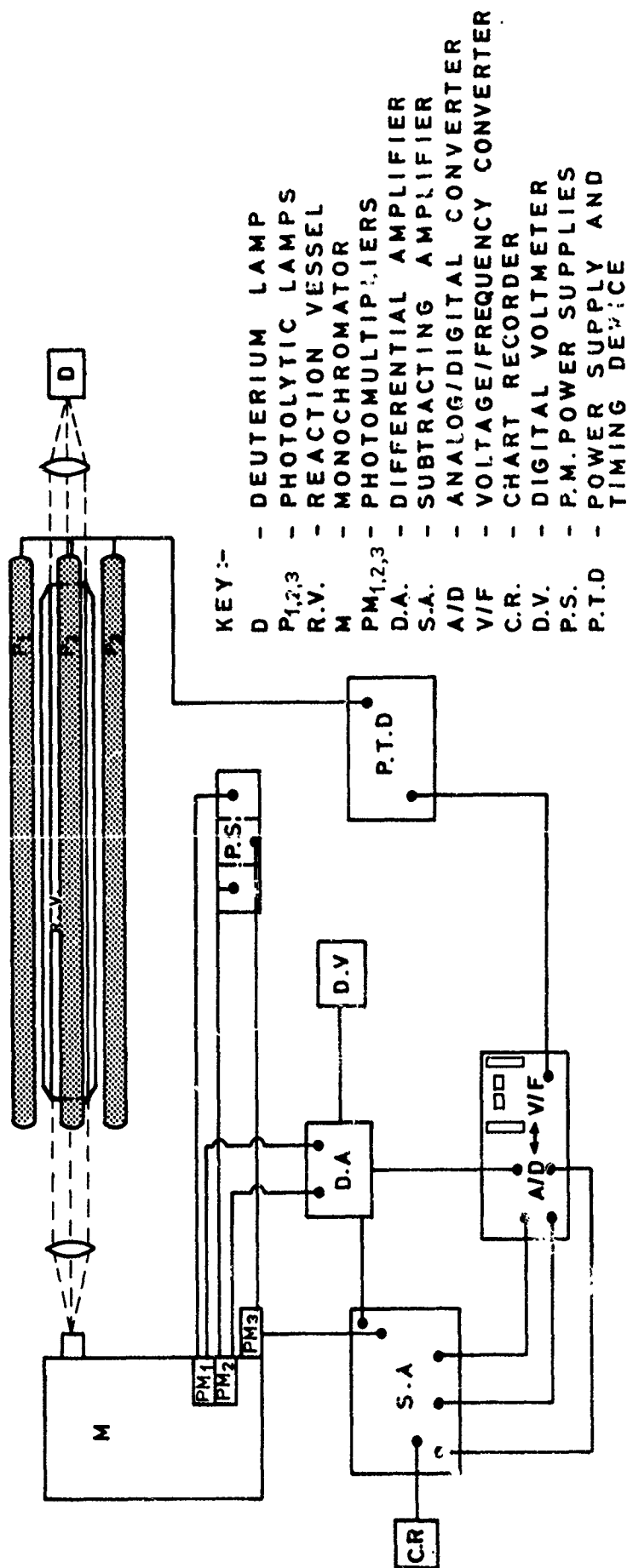
Fig.1 Schematic of Molecular Modulation Apparatus.

Fig.2 Plot of reduced in phase (open points) and in quadrature (closed points) absorption data versus reduced photolysis period for  $H_2-O_2-Cl_2$  mixtures at 298 K and 1 atm pressure.

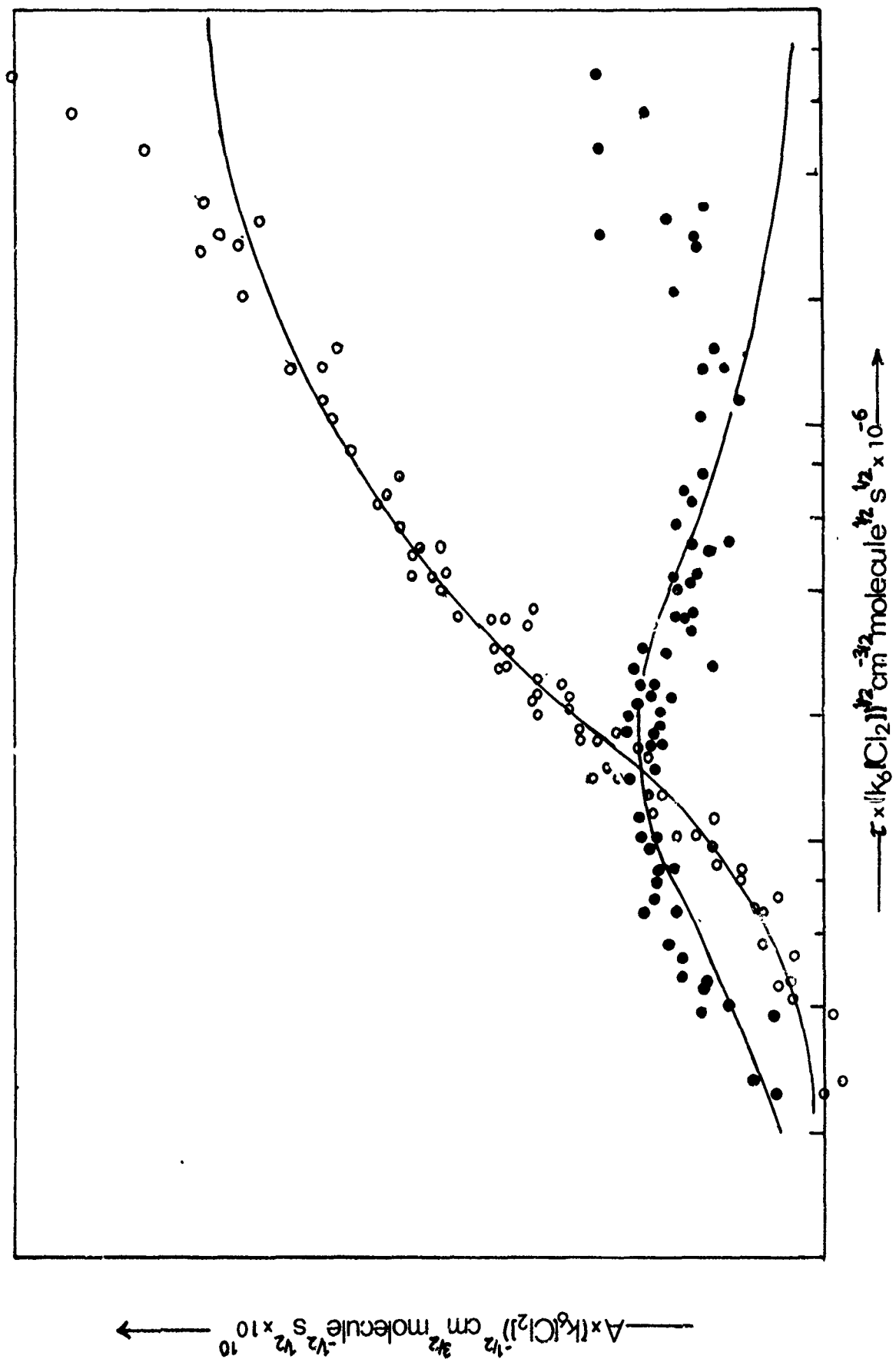
Fig.3 Experimental Data and computer fit for  $k_{Cl+Cl_2O}$ . The experimentally determined  $[H_2]/[Cl_2O]$  ratio is represented by the shaded area. The dotted line <sup>666</sup> represents computer model with  $k_{Cl+Cl_2O}$  varying. The bold line represents the computer fit with  $k_{HO_2+ClO}$  varying.

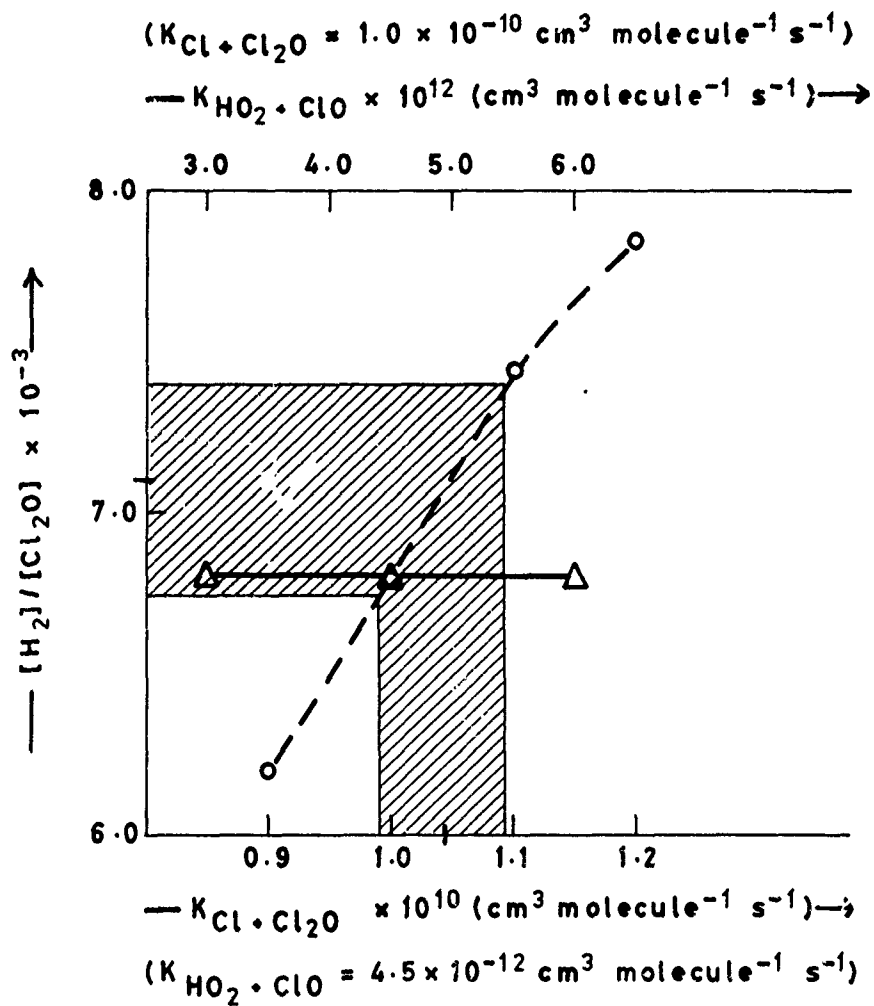
Fig.4 Least squares fit for  $ClO$  and  $HO_2$  absorptions to  $k_{HO_2+ClO}$ .

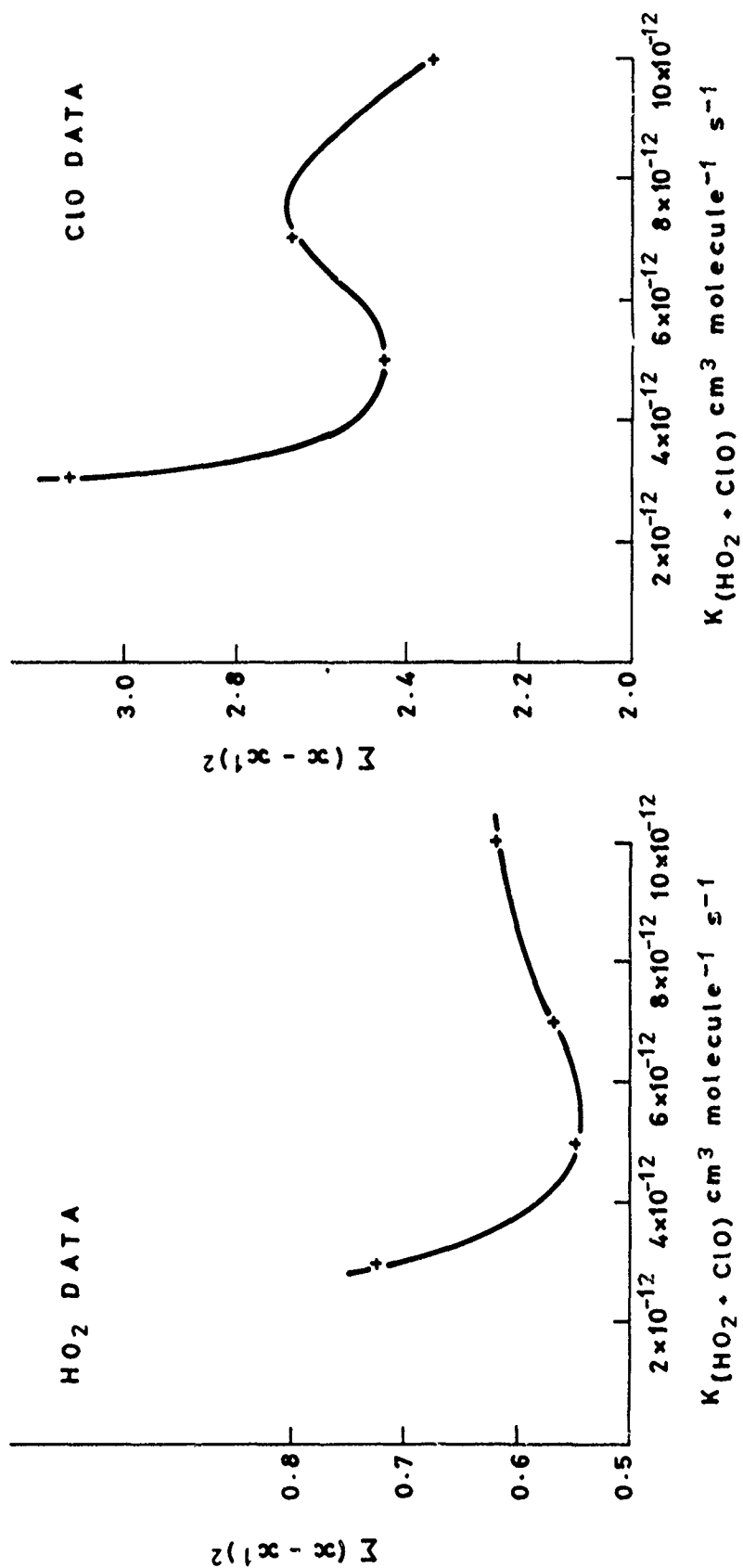
Fig.5 Plot of  $K_{ClO+ClO}$  versus  $T^{-1}$ . Open points are  $K$  derived from  $A_0$  and  $\tau_0$  for  $Cl_2-O_2$  mixtures. The closed points show the deviation from 2nd order kinetic behaviour (■  $k$  derived from  $A_0$ , ●  $k$  derived from  $\tau_0$ ) for the  $Cl_2-Cl_2O-O_2$  mixtures.



MOLECULAR MODULATION SPECTROMETER

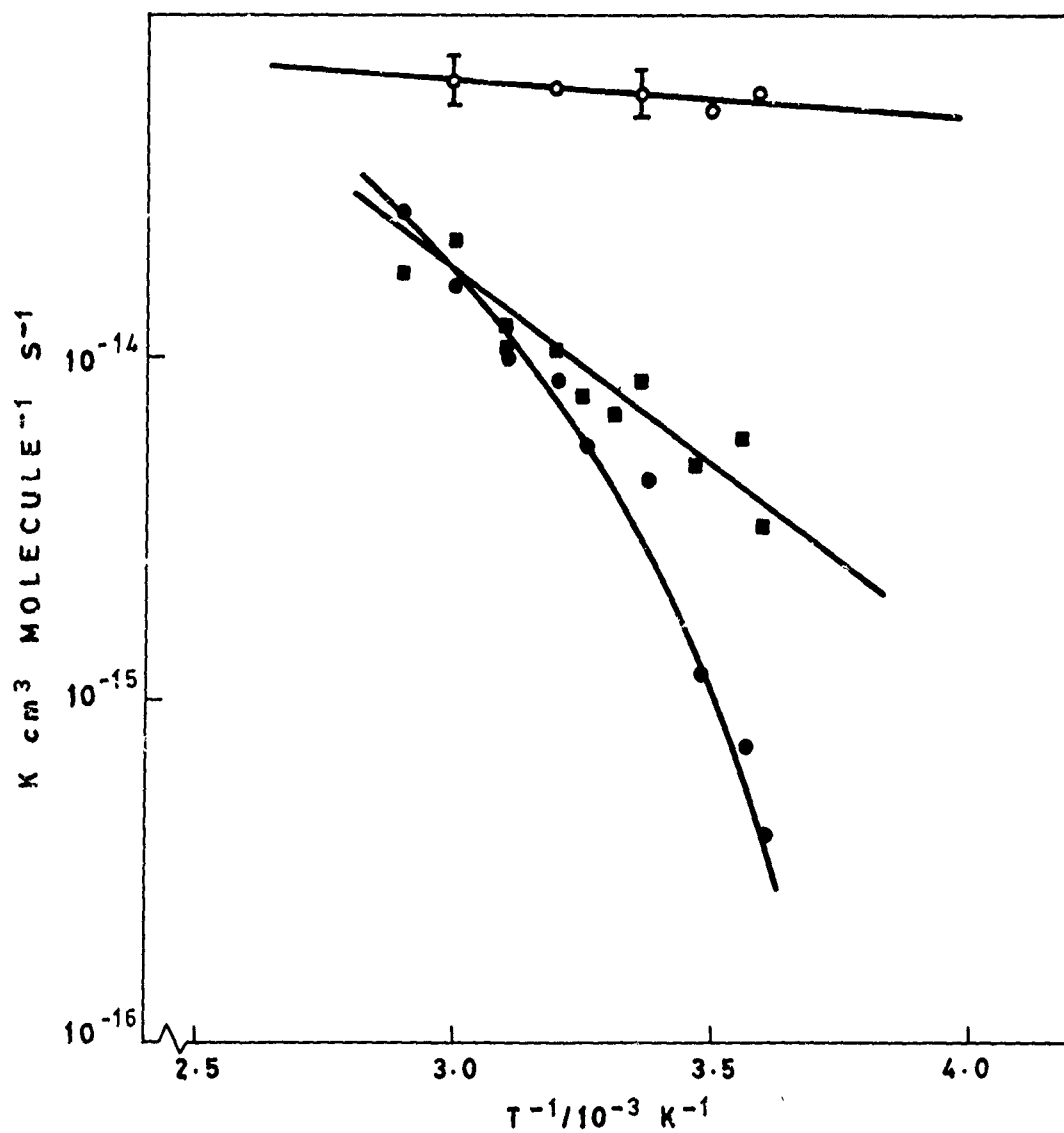






LEAST SQUARES FIT FOR  $\text{K HO}_2 + \text{ClO}$





LOG  $k_{\text{clo}} + \text{clo}$  vs.  $T^{-1}$

# EPR KINETIC STUDY OF THE REACTIONS OF $\text{H}_2\text{CO}$ WITH F,

## Cl AND Br ATOMS AND ClO RADICAL

G. Le Bras, R. Foon\*, G. Poulet and J. Combourieu

Centre de Recherches sur la Chimie de la Combustion et des Hautes Températures, CNRS et Université d'Orléans, 45045-Orléans-Cedex. France.

\* Present address: School of Chemistry, University of New South Wales, P.O.Box 1, Kensington 2033, N.S.W. Australia.

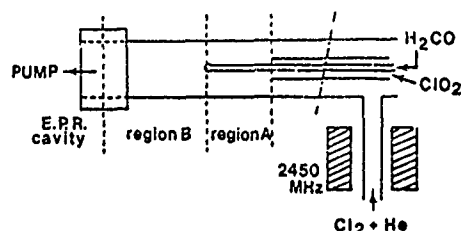
### Abstract

The reactions of  $\text{H}_2\text{CO}$  with F, Cl, Br and ClO were studied using the discharge flow reactor-EPR technique. The rate constants were measured at room temperature and the stratospheric implication of the data is discussed. No reactivity was observed for the reaction between ClO and  $\text{H}_2\text{CO}$  at room temperature but evidence was shown for the reaction of ClO with HCO.

**INTRODUCTION:** The rate constants for many reactions of Cl atoms and ClO radicals have been measured recently in relation with the possible ozone depletion in the stratosphere due to the catalytic cycle of ClO [Rowland and Molina, 1975]. Formaldehyde has been identified recently as a stratospheric species [Barbe et al. 1979]. This confirms the previous assumption that this molecule could be present in the earth's atmosphere as a product of the oxidation mechanism of methane. Some atmospheric calculations [Stief et al., 1978] have shown that the reaction of Cl atoms with  $\text{H}_2\text{CO}$  should be added to the list of the main sink reactions considered until now for stratospheric chlorine atoms. Three kinetic measurements of this reaction have been recently published [Niki et al., 1978; Michael et al., 1979; Anderson and Kurylc, 1979]. No kinetic work had yet been published for the other reactions presented here. The reaction of Br atoms with  $\text{H}_2\text{CO}$ , which is nearly thermoneutral, may be a sink for stratospheric bromine. Although the effects of bromine compounds on the ozone layer seem presently to be less important than the effects of chlorofluoromethanes [Wofsy et al. 1975], no efficient sink reaction has been previously found for Br atoms. The reaction of F atoms with  $\text{H}_2\text{CO}$  has been studied as a possible source of HCO radicals, which may be of atmospheric interest. And the reaction of ClO radicals with  $\text{H}_2\text{CO}$  which is about 11 kcal exothermic, could be expected to be a sink for ClO in the fast catalytic cycle of  $\text{ClO}_x$ . These results have been published, or submitted for publication: reactions of F, Cl and Br with  $\text{H}_2\text{CO}$  [Foon et al., 1979; Le Bras et al., 1979], reaction of ClO with  $\text{H}_2\text{CO}$  [Poulet et al., 1979].

**EXPERIMENTAL:** The apparatus used for this work has been described previously [Le Bras and Combourieu, 1978]. Briefly, all measurements were made in a discharge-flow system using an E.P.R. spectrometer (Varian E 12) for the observation of atoms and free radicals. The quartz flow tube was 60 cm in length and 2.2 cm inside diameter. In a side tube, coated with  $\text{H}_3\text{PO}_4$ , halogen atoms were produced by a micro-

wave discharge in  $F_2$ ,  $Cl_2$  or  $Br_2$ , highly diluted in a helium carrier.  $ClO$  radicals were produced by admitting  $ClO_2$  into the flow tube using a double introduction:



$Cl$  atoms were rapidly converted into  $ClO$  radicals in the A region of the reactor from the fast reaction  $Cl + ClO_2 \rightarrow 2 ClO$ .

$H_2CO$  was prepared by pyrolysis of paraformaldehyde, as described by Spence and Wild [1935], and was admitted through the moveable injector. Flow rates of  $H_2CO$  were obtained from the increase of pressure in a known volume. The  $F_2$ ,  $Cl_2$  and  $Br_2$  flowrates were calibrated by measuring the pressure drop, at constant volume and temperature, with a pressure transducer (Membravac C. Sogev). The total pressure in the reactor was measured in the middle of the reaction zone with a high precision MacLeod gauge. Pressure ranges were 0.6 - 0.7 Torr for the reactions of  $F$ ,  $Cl$  and  $Br$  atoms and 1-3 Torr for the reaction of  $ClO$  radicals. All experiments were carried out at 298 K.

Kinetics were obtained under pseudo first order conditions using a large excess of  $H_2CO$  over  $F$ ,  $Cl$ ,  $Br$  or  $ClO$ . The rate constants were measured by observing the decay of these species, versus reaction times. Concentrations were obtained from the analysis of the E.P.R. lines, respectively observed for a microwave frequency of 9.325 GHz at the following magnetic fields:  $F$  (5451.5 Gauss),  $Cl$  (4819 Gauss),  $Br$  (4150 Gauss) and  $ClO$  (8330 Gauss: center of the spectrum = 3 groups of 4 lines).

Absolute concentrations were calculated using the method of first moments and the transition probabilities given for  $F$ ,  $Cl$ ,  $Br$  and  $O_2$  previously reported by Westenberg [1973].  $ClO$  concentrations were deduced from the measurement of  $Cl$  concentrations,  $ClO_2$  being flowed in excess over  $Cl$  atoms. In some cases,  $ClO$  concentrations were calculated by titration methods using the fast reactions of  $Cl$  atoms with  $ClO_2$  or  $H_2CO$ .

RESULTS: In the kinetic studies of reactions of  $X$  atoms ( $X = F$ ,  $Cl$ ,  $Br$ ) with  $H_2CO$ , the rate constants,  $k_1$ , were obtained from the slope of the straight lines which verified the pseudo first order law:  $-d \ln |X|/dt = k_1 |H_2CO|_0$

The results are summarized in the following table:

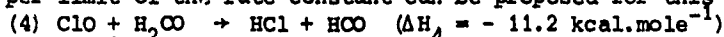
REACTION	$\Delta H$ (kcal mole <sup>-1</sup> )	$k_1$ at 298 K (cm <sup>3</sup> molecule <sup>-1</sup> s <sup>-1</sup> )	Number of experiments
(1) $F + H_2CO \rightarrow HF + HCO$	- 48.7	$(6.6 \pm 1.1) 10^{-11}$	28
(2) $Cl + H_2CO \rightarrow HCl + HCO$	- 13.9	$(4.7 \pm 1.0) 10^{-11}$	26
(3) $Br + H_2CO \rightarrow HBr + HCO$	- 0.4	$(1.6 \pm 0.3) 10^{-12}$	15

Reaction enthalpies  $\Delta H$  are calculated from thermochemical data given by Benson [1976]. The uncertainties in the values of the rate constants represent the standard deviation of  $k_1$ . Reaction rates have been corrected from the axial diffusion in the measurements of  $k_1$  (correction < 11%) and  $k_2$  (correction < 5%). The lowest atomic concentrations observable

(corresponding for a signal-to-noise ratio of 10) were successively  $2.5 \cdot 10^{11}$ ,  $2.0 \cdot 10^{11}$  and  $5.0 \cdot 10^{11} \text{ cm}^{-3}$  for F, Cl and Br atoms.  $\text{H}_2\text{CO}$  concentrations ranged from 2.36 to  $15.4 \cdot 10^{12} \text{ cm}^{-3}$  for reaction (1), from 1.64 to  $22.0 \cdot 10^{12} \text{ cm}^{-3}$  for reaction (2) and from 1.41 to  $15.8 \cdot 10^{13} \text{ cm}^{-3}$  for reaction (3).

Secondary reactions of halogen atoms were kept negligible in these experiments. Stoichiometry measurements have been done for reactions (1) and (2) when F and Cl were used in excess over  $\text{H}_2\text{CO}$ . A value of the stoichiometry near 2 was obtained in each reaction, as was expected from the secondary steps  $\text{F} + \text{HCO} \rightarrow \text{HF} + \text{CO}$  (2') and  $\text{Cl} + \text{HCO} \rightarrow \text{HCl} + \text{CO}$  (3') which are highly exothermic ( $\Delta H_2 = -119.1 \text{ kcal.mole}^{-1}$  and  $\Delta H_3 = -86.3 \text{ kcal.mole}^{-1}$ ).

For the reaction of ClO with  $\text{H}_2\text{CO}$  at the highest  $\text{H}_2\text{CO}$  concentrations used ( $5 \cdot 10^{14} \text{ cm}^{-3}$ ), no consumption of ClO could be observed for reaction times up to  $10^{-1} \text{ s}$ . Consequently, only an upper limit of the rate constant can be proposed for this reaction at 298 K:



$$k_4 < 1 \cdot 10^{-15} \text{ cm}^3 \text{ molecule}^{-1} \text{ s}^{-1}$$

An interesting observation, which has been made during these experiments, is to be reported: a decrease of ClO concentration was qualitatively observed in the presence of  $\text{H}_2\text{CO}$  when  $\text{ClO}_2$  was no longer in excess over Cl in the conversion zone (A). In this case,  $\text{ClO}_2$  being entirely consumed by Cl, excess Cl atoms could rapidly react with the  $\text{H}_2\text{CO}$  following reaction (2):  $\text{Cl} + \text{H}_2\text{CO} \rightarrow \text{HCl} + \text{HCO}$ . Thus, the decrease of ClO concentration which was observed in the main region (B) of the reactor suggests that the following reaction occurred in our system:  $\text{ClO} + \text{HCO} \rightarrow \text{ClOH} + \text{CO}$ . This reaction is about 81.6 kcal./mol. exothermic.

#### DISCUSSION: STRATOSPHERIC IMPLICATIONS:

Reaction (1)  $\text{F} + \text{H}_2\text{CO} \rightarrow \text{HF} + \text{HCO}$ : this reaction which has no direct impact on stratospheric chemistry appears to be a suitable source of HCO radicals. These radicals, which were effectively detected by the E.P.R. technique used in the present study, may be produced in flow systems in future kinetic work of stratospheric interest.

Reaction (2)  $\text{Cl} + \text{H}_2\text{CO} \rightarrow \text{HCl} + \text{HCO}$ : although the value of  $k_2$  obtained in this work is somewhat lower than the values obtained by other authors using photolytic techniques [Niki et al., 1978; Michael et al., 1979; Anderson and Kurylo, 1979], the present determination of  $k_2$  confirms the possible stratospheric effect of reaction (2), which has been previously discussed [Stief et al., 1978].

Reaction (3)  $\text{Br} + \text{H}_2\text{CO} \rightarrow \text{HBr} + \text{HCO}$ : as Br atoms are unreactive with the major stratospheric hydrogenated species (excepted probably with  $\text{HO}_2$ ), this reaction might be a sink, at least temporarily, for Br atoms issuing from the photolysis of brominated compounds in the stratosphere. The influence of this reaction depends on stratospheric  $\text{H}_2\text{CO}$  concentrations and on the rate of the reaction  $\text{Br} + \text{HO}_2$ , which is presently unknown.

Reaction (4)  $\text{ClO} + \text{H}_2\text{CO} \rightarrow \text{ClOH} + \text{HCO}$ : although this reaction is exothermic, the lack of reactivity observed at room temperature between ClO and  $\text{H}_2\text{CO}$  makes this reaction inefficient in trapping stratospheric ClO radicals. This result confirms the non-reactivity generally observed between ClO and hydrogenated molecules [Watson, 1977]. Against, the preliminary observation of some reactivity between ClO and HCO radicals at 298 K agrees with previous works which have shown that ClO reacts with free radicals ( $\text{O}_2\text{OH}$ ,  $\text{HO}_2$ , ...). However this reaction seems to be negligible in stratospheric chemistry compared to the  $\text{ClO} + \text{HO}_2$  reaction as a result of the probably low HCO concentrations, due to the fast reaction between HCO and  $\text{O}_2$ .

REFERENCES

- Anderson, P.C. and M.J. Kurylo, Rate constant measurements for the reaction  $\text{Cl} + \text{CH}_2\text{O} \rightarrow \text{HCl} + \text{CHO}$ . Implications regarding the removal of stratospheric chlorine, J. Phys. Chem., **83**, 2055, 1979.
- Barbe, A., P. Marche, C. Secroun, and P. Jouve, Measurements of tropospheric and stratospheric  $\text{H}_2\text{CO}$  by an infrared high resolution technique, Geophys. Res. Lett., **6**, 463, 1979.
- Benson, S.W., Thermochemical Kinetics, John Wiley, 1976.
- Foon, R., G. LeBras, and J. Combourieu, Etude cinetique par resonance paramagnetique electronique de la reaction des atoms de chlore avec le formaldehyde, C.R. Acad. Sci. Paris, **288c**, 241, 1979.
- LeBras, G. and J. Combourieu, EPR kinetic study of the reaction of  $\text{CF}_3\text{Br}$  with H atoms and OH radicals, Int. J. Chem. Kin., **10**, 1205, 1978.
- LeBras, G., R. Foon, and J. Combourieu, Submitted for publication.
- Michael, J.V., O.F. Nava, W.A. Payne, and L.J. Stief, Rate constant for the reaction of atomic chlorine with formaldehyde from 200 to 500 K, J. Chem. Phys., **70**, 1147, 1979.
- Niki, H., P.D. Maker, L.D. Breitenbach, and C.M. Savage, FTIR studies of the kinetics and mechanism for the reaction of Cl atom with formaldehyde, Chem. Phys. Lett., **57**, 596, 1978.
- Poulet, G., G. LeBras, and J. Combourieu, Submitted for publication.
- Rowland, F.S., and M.J. Molina, Chlorofluoromethanes in the environment, Rev. Geophys. and Space Phys., **13**, 1, 1975.
- Spence, R. and W. Wild, The preparation of liquid monomeric formaldehyde, J. Chem. Soc. London, 338, 1935.
- Stief, L.J., J.V. Michael, O.F. Nava, and W.A. Payne, Geophys. Res. Lett. The reaction  $\text{Cl} + \text{H}_2\text{CO} \rightarrow \text{HCl} + \text{HCO}$ : decreased sensitivity of stratospheric ozone to chlorine perturbations.
- Watson, R.J., Rate constants for reaction of  $\text{ClO}_x$  of atmospheric interest, J. Phys. Chem. Ref. Data, **6**, 871, 1977.
- Westenberg, A.A., Use of ESR for the quantitative determination of gas phase atom and radical concentrations, Programs in Reaction Kinetics, **7**, 24, 1973.
- Wofsy, S.C., M.B. McElroy, and Y.L. Yung, The chemistry of atmospheric bromine, Geophys. Res. Lett., **2**, 215, 1975.

OXIDATION OF THE CH<sub>3</sub> RADICAL AND SOME HALOMETHYL  
AND HALOETHYL RADICALS OF ATMOSPHERIC INTEREST

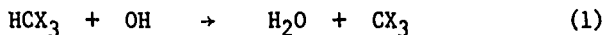
R. Simonaitis

Department of Chemistry and Ionosphere Research Laboratory  
The Pennsylvania State University  
University Park, Pennsylvania 16802 USA

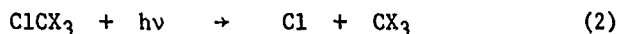
Abstract

The atmospheric oxidation pathways of the residual radicals which are produced from CH<sub>4</sub>, CH<sub>3</sub>Cl, CFCl<sub>3</sub>, CF<sub>2</sub>Cl<sub>2</sub>, CCl<sub>4</sub> and CH<sub>3</sub>CCl<sub>3</sub> either by photodecomposition or by reaction with hydroxyl radicals are discussed. A brief review is given of selected reactions in the oxidation chains of these radicals.

I. INTRODUCTION: CH<sub>4</sub>, CCl<sub>4</sub>, CFCl<sub>3</sub>, CF<sub>2</sub>Cl<sub>2</sub>, CH<sub>3</sub>Cl, and potentially CH<sub>3</sub>CCl<sub>3</sub> are the most important organic, either natural or man made, minor constituents of the earth's atmosphere which affect, or may affect in the future, the stratospheric O<sub>3</sub> budget. In the atmosphere these molecules are oxidized to CO<sub>2</sub>, H<sub>2</sub>O, HF and HCl. The oxidation is initiated by reaction with OH (CH<sub>4</sub>, CH<sub>3</sub>Cl)



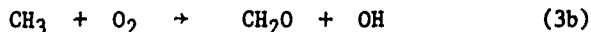
or by photolysis (CH<sub>3</sub>Cl, CFCl<sub>3</sub>, CF<sub>2</sub>Cl<sub>2</sub>)



where X represents H, Cl, or F atoms. Analogous reactions occur for CH<sub>3</sub>CCl<sub>3</sub> leading to the radicals CH<sub>3</sub>CCl<sub>2</sub> and CCl<sub>3</sub>CH<sub>2</sub>. The CX<sub>3</sub> radicals produced in reactions (1) and (2) are oxidized via a series of complex reactions leading to the formation of a variety of other radicals, additional free Cl atoms, F atoms and molecules, depending upon the particular radical in question, before the production of the final oxidation products.

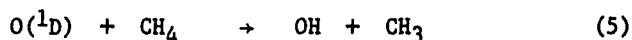
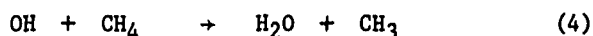
The purpose of the present brief review is to summarize the atmospheric oxidation pathways of the CX<sub>3</sub> (CX<sub>3</sub> = CH<sub>3</sub>, CH<sub>2</sub>Cl, CFCl<sub>2</sub>, CF<sub>2</sub>Cl) CH<sub>3</sub>CCl<sub>2</sub> and CCl<sub>3</sub>CH<sub>2</sub> radicals and to review the present status of laboratory studies of the selected reactions involved. I will not discuss the above initiation reactions and CH<sub>2</sub>O chemistry, since this has been done by others in this volume. A recent excellent review, NASA [1979] evaluated reactions important in stratospheric chemistry, including many reactions pertinent to the CH<sub>4</sub> oxidation chain. Therefore, those reactions will not be reviewed in detail here except where new information is available.

II. THE  $\text{CH}_3$  RADICAL OXIDATION CHAIN: Bates and Witherspoon, [1952] were the first to discuss the atmospheric methane cycle. They correctly recognized that the atmospheric sink for  $\text{CH}_4$  would lead to the production of  $\text{CH}_3$  radicals that would be oxidized to  $\text{CH}_2\text{O}$ . However, due to a lack of good kinetic data, they incorrectly concluded that the main sink for  $\text{CH}_4$  would be the reaction with  $\text{HO}_2$  radicals and that  $\text{CH}_2\text{O}$  would be produced from the two body reaction



which is now known to be incorrect.

It was nearly twenty years later, when better kinetic data became available, that the main features of atmospheric  $\text{CH}_4$  chemistry were correctly described. [Levy, 1971, 1972, 1973; Nicolet, 1970, 1971, 1972; McConnel et al., 1971; Wofsy et al., 1972; Crutzen, 1973] The role of OH and  $\text{O}(^1\text{D})$  as sinks for  $\text{CH}_4$  were recognized



and most of the detailed chemistry of the subsequent  $\text{CH}_3$  oxidation delineated.

Oxidation of atmospheric  $\text{CH}_3$  has many important consequences for atmospheric chemistry. Its atmospheric oxidation pathways are shown in Figure 1 [Levy, 1973; Nicolet, 1972; Isaksen and Crutzen, 1977; Crutzen et al., 1978],

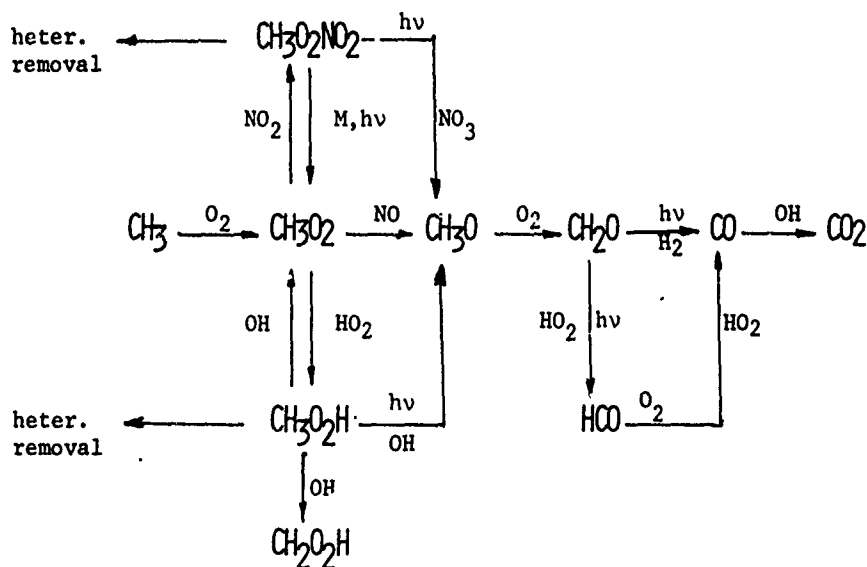
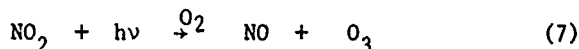
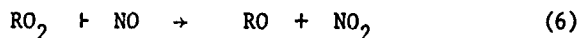
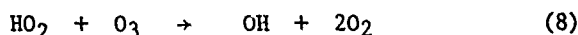


Figure 1. Atmospheric oxidation pathways of the  $\text{CH}_3$  radical

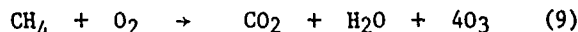
Depending upon which pathways are dominant,  $\text{CH}_3$  oxidation can, among other effects, be a source of atmospheric  $\text{CO}$ ,  $\text{H}_2$  and  $\text{H}_2\text{O}$ , a source or sink of odd hydrogen,  $\text{HO}_x$ , a source of  $\text{O}_3$  via the sequence



or a sink of  $O_3$  via the reaction



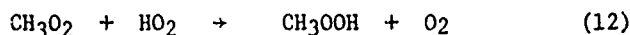
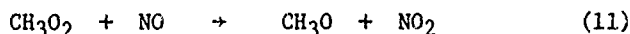
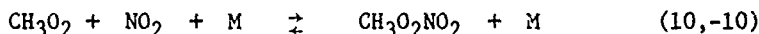
As an illustration of  $HO_x$ , CO and  $O_3$  production, several of the pathways shown in Figure 1 may be considered. For each  $CH_3$  oxidized, the pathway  $CH_3O_2 + NO$ ,  $CH_2O \rightarrow CHO$  leads to the production of three  $HO_x$  (two  $HO_x$  for each  $CH_4$  oxidized), four  $O_3$  (since four peroxy radicals are produced for each  $CH_3$  oxidized, assuming that all the peroxy radicals react with NO), and one CO. The net reaction for  $O_3$  production in this case is



The pathway  $CH_3O_2 \rightarrow CH_3OOH \rightarrow CH_2O \rightarrow HCO$  still leads to three  $HO_x$ , one CO, but only two  $O_3$  (since there is a net gain of only two peroxy radicals for each  $CH_3$  oxidized). Other pathways depicted in Figure 1 have different consequences. When NO is not present,  $O_3$  production does not occur; instead it is destroyed by reaction (8).

In the troposphere and stratosphere,  $CH_3$  radicals react only with  $O_2$  to produce  $CH_3O_2$ . In the stratosphere,  $CH_3O_2$  reacts predominantly with NO along the pathway leading to  $CH_2O$ , since  $[NO] > [HO_2]$ . A small fraction ( $\sim 10\%$ ), however, may react with  $HO_2$  to produce  $CH_3OOH$ , which may lead to  $[CH_3OOH] \sim (1-10) \times 10^7 \text{ cm}^{-3}$  between 15-20 km, if the removal rates are the same as for  $H_2O_2$ .

In the stratosphere  $CH_3O_2$  will also react with  $NO_2$  to produce  $CH_3O_2NO_2$ , which is likely to be rapidly photodissociated. The atmospheric lifetimes of  $CH_3O_2NO_2$  is determined by the reactions (assuming that the photodissociation products are  $CH_3O_2 + NO_2$ )



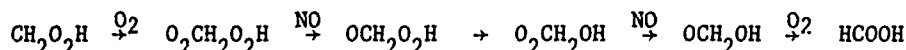
and its concentration is determined by the rate of  $CH_4$  oxidation and the above reactions leading to  $CH_3O_2NO_2$  formation and loss. Approximate calculations ( $J\{CH_3O_2NO_2\}$  and  $k_{-10}$  are not known precisely at this time, but  $J\{CH_3O_2NO_2\} \approx J\{ClONO_2\}$  and  $k_{-10} \approx 1 \times 10^{16} \exp(-23000/RT) \text{ cm}^3 \text{ sec}^{-1}$  at  $\sim 1$  atm pressure are reasonable approximations) indicate that  $[CH_3O_2NO_2]$  is not more than  $\sim 1 \times 10^8 \text{ cm}^{-3}$  at  $\sim 20$  km and it decreases rapidly with altitude. Therefore, no very significant effects due to  $CH_3O_2NO_2$  formation in the stratosphere are expected. If the photolysis products are  $CH_3O + NO_3$  instead of  $CH_3O_2 + NO_2$ , then  $[CH_3O_2NO_2]$  would be even lower, but  $HO_x$  and  $O_3$  production from  $CH_3$  oxidation would be the same.

In the troposphere, the NO concentration is very low,  $< 10 \text{ ppt}$ , [McFarland et al., 1979]; consequently, the pathway leading to  $CH_3OOH$  could be an important loss process for  $CH_3O_2$ . It is important to establish the fate of  $CH_3OOH$  in the troposphere, since as we have seen, the various loss processes have a significant impact upon  $HO_x$  and CO production. Recent measurements of the absorption cross sections of  $CH_3OOH$  by Cox and Tyndall, [1979] indicate that photolytic removal dominates removal by OH; however, heterogeneous removal may also be important, since its rate is not known [Isaksen and Crutzen, 1977]. In the troposphere  $CH_3O_2NO_2$  will be formed, since  $NO_2$  has a fractional abundance of  $\sim 10^{-10}$  [Noxon, 1975]. Based on the reaction scheme given above, reasonable estimates lead to  $CH_3O_2NO_2$  lifetimes of minutes to several hours in the lower troposphere, and days to several weeks in the upper troposphere, with a concentration of the order of  $1 \times 10^{10} \text{ cm}^{-3}$ . Loss of  $CH_3O_2NO_2$  via heterogeneous processes could constitute a sink for  $CH_3O_2$  and  $NO_2$ .



# SIMONAITIS

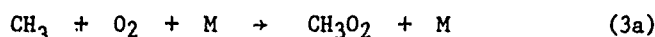
The  $\text{CH}_3\text{O}$  radical will almost certainly react exclusively with  $\text{O}_2$  in both the troposphere and stratosphere, unless the indirectly measured rate coefficient for the reaction of  $\text{CH}_3\text{O}$  with  $\text{O}_2$  is significantly in error (several orders of magnitude at stratospheric temperatures). It is not known whether the  $\text{CH}_2\text{O}_2\text{H}$  radical will be formed in the atmosphere. If it is formed, it may react in the presence of  $\text{NO}$  via the sequence leading to formic acid.



The isomerization  $\text{OCH}_2\text{O}_2\text{H} \rightarrow \text{O}_2\text{CH}_2\text{OH}$  has been suggested by Su et al., [1979] and the radical  $\text{OCH}_2\text{OH}$  is known to react with  $\text{O}_2$  to produce  $\text{HCOOH}$  [Niki et al., 1979]. This scheme is interesting because the further oxidation of  $\text{HCOOH}$  may lead to  $\text{CO}_2$  instead of  $\text{CO}$ .

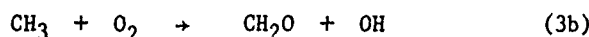
## II.1. Review of laboratory measurements

$\text{CH}_3 + \text{O}_2$ : There are no new measurements of the three body reaction



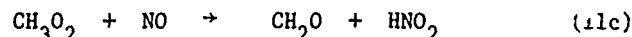
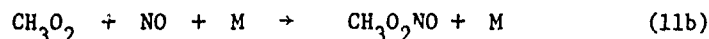
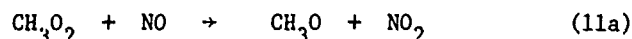
since the recent NASA evaluation [NASA, 1979]. The exact value of the rate coefficient for this reaction is not very important, since there are no competing reactions for the  $\text{CH}_3$  radical.

A slow two body reaction



$k_{3b} = 10^{-12.54 \pm 0.35} \exp(-900 \pm 250/T) \text{ cm}^3\text{sec}^{-1}$  has been reported [Washida and Bayes, 1976], but others have not observed this reaction [Golden et al., 1973; Basco et al., 1972; Klais et al., 1979]. In any case, the two body reaction, even with the above value for  $k_{3b}$ , is too slow to be of any importance in the troposphere or stratosphere.

$\text{CH}_3\text{O}_2 + \text{NO}$ : There are three possible channels for the reaction of  $\text{CH}_3\text{O}_2$  with  $\text{NO}$



Contrary to Spicer et al., [1973] who found channel (11a) to be unimportant, Simonaitis and Heicklen, [1974], and Pate et al., [1974] using competitive kinetics-product analysis methods, determined that reaction (11) goes by way of channel (11a)  $80 \pm 15\%$  and  $100\%$ , respectively.

Recently, numerous direct studies of the total rate coefficient for the reaction, using a variety of techniques, have been reported and they are summarized in Table 1. The reported measurements fall into two groups. The lower values must be rejected, however, because in the study by Adachi and Basco [1979] absorption due to the product  $\text{CH}_3\text{ONO}$  probably interfered in the measurement of  $\text{CH}_3\text{O}_2$  by absorption [Sander and Watson, 1979], and the study by Simonaitis and Heicklen is indirect and of low sensitivity. Of the remaining measurements, those by Sander and Watson and by Ravishankara et al., [1979] are preferred. The temporal variation of the reactant  $\text{CH}_3\text{O}_2$  in the former study and of the product  $\text{NO}_2$  in the

## SIMONAITIS

TABLE I

Rate Coefficients for the Reaction  $\text{CH}_3\text{O}_2 + \text{NO} \rightarrow \text{CH}_3\text{O} + \text{NO}_2$ 

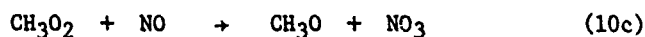
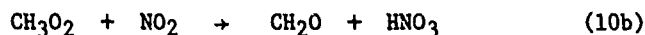
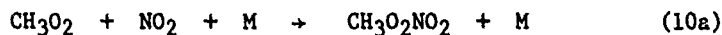
Method <sup>a</sup>	Source of $\text{CH}_3\text{O}_2$	T, K	P, Torr	$10^{12}k, \text{cm}^3\text{sec}^{-1}$	Reference
DF-MS	$\text{O} + \text{C}_2\text{H}_4$	$295 \pm 2$	2-3 (Ar)	$8.0 \pm 2.0$	<u>Plumb, Ryan, Steven and Mulcahy [1979]</u>
FP-UV	AM / $\text{O}_2$	296	75-100 (Ar)	3.0	<u>Adachi and Basco [1979]</u>
Competition <sup>b</sup> with $\text{SO}_2$	AM / $\text{O}_2$	296	700 ( $\text{N}_2$ )	$3^{+2}_{-1}$	<u>Simonaitis and Heicklen [1979]</u>
FP-UV	AM / $\text{O}_2$ $\text{Cl}_2/\text{CH}_4/\text{O}_2$	296	75-700 (He)	$7.1 \pm 1.4$	<u>Sander and Watson [1979]</u>
Mol.-Mod.	AM / $\text{O}_2$	298	540 ( $\text{N}_2$ ) 50 (Ar + $\text{CH}_4$ )	$6.5 \pm 2.0$	<u>Cox and Tyndall [1979]</u>
LFP- $\text{NO}_2$ fluorescence	$\text{Cl}_2/\text{CH}_4/\text{O}_2$	296	-----	$7.5 \pm 1.2$	<u>Ravishankara, Eisele and Wine [1979]</u>

a. DF-MS, discharge flow, mass spectrometric detection of  $\text{CH}_3\text{O}_2$ ; FP-UV, flash photolysis, detection of  $\text{CH}_3\text{O}_2$  by uv absorption; Mol. Mod., molecular modulation  $\text{CH}_3\text{O}_2$  detection by uv absorption LFP- $\text{NO}_2$  fluorescence, laser flash photolysis,  $\text{NO}_2$  detection by laser induced  $\text{NO}_2$  fluorescence.

b.  $k_{\text{SO}_2} = 8.2 \times 10^{-15} \text{ cm}^3\text{sec}^{-1}$  [Sanhueza, Simonaitis, and Heicklen, 1979]

second study were monitored directly with no interference from products in simple, well characterized chemical systems leading to simple pseudo first order kinetics. The molecular modulation technique employed by Cox and Tyndall [1979] is complex. In order to obtain values of  $k_{11}$ , a complex curve fitting procedure, with  $k_{11}$ ,  $k_{10}$  and  $[\text{CH}_3\text{O}_2]$  as parameters, was used. Knowledge of the photolysis rate and corrections due to light absorption by the products and the reaction of  $\text{CH}_3\text{O}_2 + \text{NO}_2$  was required. In the study by Plumb et al., [1979],  $\text{CH}_3\text{O}_2$  decay under pseudo first order conditions was monitored using its mass peak at  $m/e = 47$ . Although the analysis necessary to obtain  $k_{11}$  is direct, the results depend upon the correctness of the complex chemistry in their system.

$\text{CH}_3\text{O}_2 + \text{NO}_2$ : There are three possible channels for the reaction of  $\text{CH}_3\text{O}_2$  with  $\text{NO}_2$



The first evidence that  $\text{CH}_3\text{O}_2$  radicals react with  $\text{NO}_2$  was provided by Spicer et al., [1973]. They photolysed azomethane in the presence of  $\text{O}_2$  and  $\text{NO}_2$  at room temperature and 150 Torr total pressure (mostly  $\text{N}_2$ ) and observed the formation of  $\text{CH}_3\text{ONO}_2$  as a product. Based on complex arguments, they concluded that reaction (10a) was the dominant (75%) channel, but, that since  $\text{HCOOH}$  was also produced, channel (10b) was also important (25%). Simonaitis and Heicklen, [1974] photolysed  $\text{N}_2\text{O}$  in the presence of  $\text{CH}_4/\text{O}_2/\text{NO}_2$  mixtures and concluded that

## SIMONAITIS

channel (10a) was dominant, but a contribution due to channel (10b) could not be excluded. Spectroscopic evidence for the formation of  $\text{CH}_3\text{O}_2\text{NO}_2$  was obtained by Niki et al., [1978]. They photolysed  $\text{Cl}_2$  in the presence of  $\text{CH}_3\text{OOH}/\text{NO}_2$  mixtures and observed the formation of characteristic infrared bands using Fourier transform infrared spectroscopy.

Recently, two direct kinetic studies of the reaction have been reported. Sander and Watson, [1979], measured  $k_{10}$  over a wide range of pressures using a flash photolysis - u.v. absorption technique (FP-UV). They flash photolysed mixtures of  $(\text{CH}_3)_2\text{N}_2/\text{O}_2/\text{NO}_2$  or  $\text{Cl}_2/\text{CH}_4/\text{O}_2/\text{NO}_2$  and monitored  $\text{CH}_3\text{O}_2$  disappearance using u.v. absorption near 270 nm. They found reaction (10) to be in the fall-off regime and were able to fit their data to Troe's formula [NASA, 1979, and references cited therein], with  $F_c = 0.4$ ,  $k_0 = (2.33 \pm 1.08) \times 10^{-30} (\text{N}_2) \text{ cm}^3 \text{ sec}^{-1}$  and  $k_\infty = (8.0 \pm 1) \times 10^{-12} \text{ cm}^3 \text{ sec}^{-1}$ . The pressure dependent value of  $k_{10}$  may be computed from

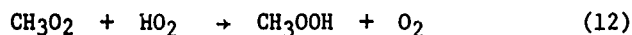
$$k(z) = k(m, T) = \frac{k_0(T) [M]}{1 + k_0(T) [M] / k_\infty(T)} F_c \{1 + [\log_{10} (k_0(T) M / k_\infty(T))]\}^{-1}$$

where  $k_0(T) = k_0(300) [T/300]^{-n}$  and  $k_\infty(T) = k_\infty(300) [T/300]^{-m}$  with  $m = 4 \pm 2$ .

Cox and Tyndall, [1979] determined  $k_{10} = 1.6 \pm 0.3 \times 10^{-12} \text{ cm}^3 \text{ sec}^{-1}$  and  $k_{10} = 1.2 \times 10^{-12} \text{ cm}^3 \text{ sec}^{-1}$  at a total pressure of 540 Torr  $\text{N}_2$  and 50 Torr ( $\text{Ar} + \text{CH}_4$ ), respectively, and 298K using molecular modulation spectrometry. The value at 540 total pressure is a factor of 2.5 below the value measured by Sander and Watson and the reported pressure dependence is significantly weaker than what might be expected from theory. Complications in this method arise from the indirect complex analysis necessary to extract  $k_{10}$  using curve fitting with  $(\text{CH}_3\text{O}_2)$  and  $k_{10}$  as parameters and due to light absorption by the products (see also comments for the  $\text{CH}_3\text{O}_2 + \text{NO}$  reaction). Thus, for the present, the values reported by Sander and Watson are preferable. It is interesting to compare the relative value  $k_{11}/k_{10} = 2.2$  at 700 Torr (mostly  $\text{CH}_4$ ) measured by Simonaitis and Heicklen [1974] with the value  $k_{11}/k_{10} = 1.8$  ( $\text{N}_2 = 700$  Torr) calculated from Sander and Watson's data; the agreement is good.

The observed pressure dependence of  $k_{10}$  indicates that reaction (3a) is dominant. However, a minor contribution due to channel (10b), in which the products  $\text{CH}_2\text{O}$  and  $\text{HNO}_3$  are produced from an activated  $\text{CH}_3\text{O}_2\text{NO}_2^*$ , cannot be completely ruled out without a direct determination of the products. Channel (10b), even if minor, could be important since it would act as a sink for  $\text{NO}_2$  due to the stability of  $\text{HNO}_3$ .

$\text{CH}_3\text{O}_2 + \text{HO}_2$ : There is only one measurement of the rate coefficient for the reaction



Cox and Tyndall, [1979], determined that  $k_{12} = (7.7)^{+18.4}_{-5.4} \times 10^{-11} \exp (1296 \pm 364/T) \text{ cm}^3 \text{ sec}^{-1}$  over the range 275 - 338°K using molecular modulation spectrometry.  $\text{CH}_3\text{O}_2$  and  $\text{HO}_2$  were produced by the photolysis of  $\text{Cl}_2$  in the presence of  $\text{CH}_4/\text{H}_2/\text{O}_2$  mixtures and their concentrations were measured by absorption at 250 nm and 210 nm, respectively. This surprisingly large value makes reaction (12) very important, particularly in the troposphere. Additional work is needed to confirm the above value for  $k_{12}$  at atmospheric pressures and humidity conditions.

$\text{CH}_3\text{O} + \text{O}_2$ : There are no direct measurements of reaction (13)

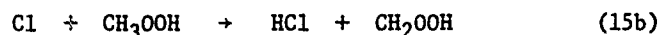
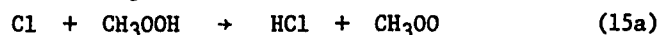
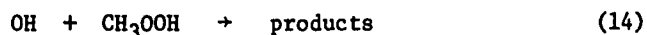


However, several relative measurements have been reported. The NASA evaluation [NASA, 1979], recommends  $k_{13} = 5 \times 10^{-13} \exp (-2000/T) \text{ cm}^3 \text{ sec}^{-1}$  based upon the work of Barker et al., [1977]. The only new measurement, since the NASA evaluation, is that by Batt and Robinson, [1977]. They obtained  $k_{13} = 1.67 \times 10^{-12} \exp (-2400 + 550/T) \text{ cm}^3 \text{ sec}^{-1}$  based upon  $k =$

## SIMONAITIS

$1.3 \times 10^{-11} \text{ cm}^{-3} \text{ sec}^{-1}$  for the reaction  $\text{CH}_3\text{O} + \text{NO}_2 \rightarrow \text{CH}_3\text{ONO}_2$ . This value for  $k_{11}$  gives a slightly higher A factor and a somewhat higher E value than the value recommended by the NASA evaluation, but it is consistent with that value in view of the limited temperature range used.

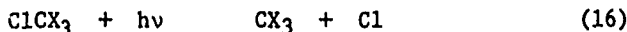
CH<sub>3</sub>OOH chemistry: There are no measurements of rate coefficients for the reactions



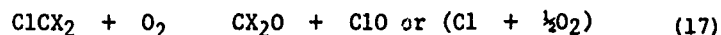
The products of reaction (14) are not known. Reaction (15a) is an important channel of reaction (15) [Niki et al., 1978], but a minor contribution due to channel (15b) cannot be excluded. It has been suggested that reaction (15a) may contribute to HCl formation in the stratosphere, if  $k_{15a}$  is similar to that for  $\text{Cl} + \text{CH}_3\text{OH}$ , i.e.,  $6 \times 10^{-11} \text{ cm}^{-3} \text{ sec}^{-1}$  [Michael et al., 1979]. However, since the dominant products of reaction (15) are due to an H atom abstraction from the OH group, it is likely that  $k_{15}$  is much smaller and closer to the value for  $\text{Cl} + \text{H}_2\text{O}_2$ . Detailed studies of the mechanism and kinetics of reactions (14) and (15) are important.

The absorption spectrum of CH<sub>3</sub>OOH has been recently measured [Cox and Tyndall, 1979] over the range of 210 - 280 nm. The spectrum is very similar to that for H<sub>2</sub>O<sub>2</sub>. Therefore, the spectrum of H<sub>2</sub>O<sub>2</sub> can be used as a reasonable model for the CH<sub>3</sub>OOH spectrum over a wider range of wavelengths.

III. THE OXIDATION CHAIN OF SOME HALOMETHYL AND HALOETHYL RADICALS: Molina and Rowland, [1974], recognized that "Freons", particularly CFC1<sub>3</sub> and CF<sub>2</sub>Cl<sub>2</sub>, may be significant sources of stratospheric odd chlorine, ClO<sub>x</sub>, which could catalyze the destruction of stratospheric O<sub>3</sub> via the now notorious ClO<sub>x</sub> cycle, first identified by Stolarski and Cicerone, [1974]. Soon after the Molina and Rowland's hypothesis, it became apparent that other halocarbons may also be significant sources of ClO<sub>x</sub>. The most important of these are CH<sub>3</sub>Cl, the most abundant natural ClO<sub>x</sub> source, and anthropogenic CH<sub>3</sub>CCl<sub>3</sub> and CCl<sub>4</sub>. It was initially suspected and later proved that photolysis of the perhalomethanes releases a chlorine atom with  $\phi = 1$  [Jayanty et al., 1975; Rebert and Ausloos, 1975; Milstein and Rowland, 1975].



However, it was uncertain whether all the remaining Cl atoms in the CX<sub>3</sub> fragment would be released [Molina and Rowland, 1975]. From laboratory work, it was learned that the oxidation of halomethyl radicals leads to the production of carbonyl halides, CX<sub>2</sub>O [Heicklen, 1968].



Therefore, it was assumed that one additional Cl atom is released in the oxidation step and additional Cl atoms could be released from photolysis and oxidation of the CX<sub>2</sub>O molecules (CCl<sub>2</sub>O, CFC1O), at a rate which depends upon their stratospheric stability. Milstein and Rowland [1975] showed that the photooxidation of CF<sub>2</sub>Cl<sub>2</sub> under laboratory conditions leads to the production of CF<sub>2</sub>O with  $\phi = 1$  and thus  $\phi_{\text{ClO}_x} = 2$ . This was taken as proof that both Cl atoms of CF<sub>2</sub>Cl<sub>2</sub> are released in the atmosphere.<sup>x</sup> However, under atmospheric conditions, at least in principle, the oxidation could lead to other products which may delay the release of the remaining Cl atom. In order to determine the rate of release of the remaining chlorine atoms from the CX<sub>3</sub> fragment, as well as other potential effects, it is important to be aware of the various intermediates produced from the CX<sub>3</sub> fragment oxidation and their atmospheric lifetimes. A fairly detailed knowledge, therefore, of their atmospheric oxidation chemistry is desirable.

## SIMONAITIS

The atmospheric oxidation pathways of the CX<sub>3</sub> radicals (CCl<sub>3</sub>, CFC1<sub>2</sub>, CF<sub>2</sub>Cl, CH<sub>2</sub>Cl) are shown in Figure 2.

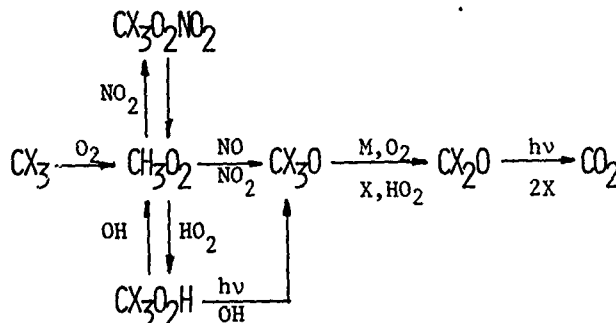


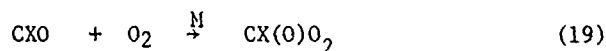
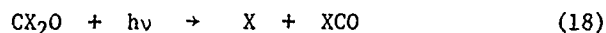
Figure 2. Oxidation pathways of CX<sub>3</sub>, (CCl<sub>3</sub>, CFC1<sub>2</sub>, CF<sub>2</sub>Cl, CH<sub>2</sub>Cl).

Analogous pathways will occur for the radicals CX<sub>3</sub>CX<sub>2</sub> (CX<sub>3</sub>CX<sub>2</sub> ≡ CH<sub>3</sub>CCl<sub>2</sub> and CCl<sub>3</sub>CH<sub>2</sub>) derived from CH<sub>3</sub>CCl<sub>3</sub> except that CX<sub>2</sub>O for these radicals is CH<sub>3</sub>C(O)Cl and CCl<sub>3</sub>CHO, respectively, and the oxidation of CH<sub>3</sub>CCl<sub>2</sub> may also lead to CH<sub>2</sub>CCl<sub>2</sub>. The diagram is based upon the present understanding of the oxidation chemistry of haloalkyl radicals. For many of the reactions, rate coefficients are not available, but this is not critical for stratospheric modeling because, except for molecules of the type CX<sub>2</sub>O, the intermediates have short lifetimes and are primarily of interest as sources of atmospheric ClO<sub>x</sub>.

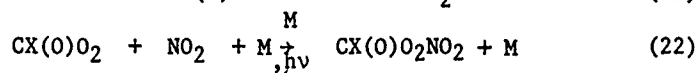
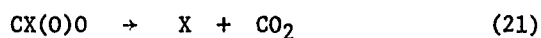
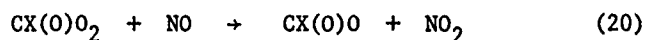
The oxidation of CX<sub>3</sub> and CX<sub>3</sub>CX<sub>2</sub> proceeds in a manner very similar to the oxidation of CH<sub>3</sub>. In the atmosphere, the CX<sub>3</sub> and CX<sub>3</sub>CX<sub>2</sub> radicals except possibly CH<sub>3</sub>CCl<sub>2</sub> (see below) react with O<sub>2</sub> immediately to give the peroxy radicals as the exclusive products. In the stratosphere, the peroxy radical will react along three main pathways: with NO<sub>2</sub>, NO and HO<sub>2</sub>. The reaction pathways with NO and NO<sub>2</sub> dominate, but a small fraction, depending upon the rate coefficients and atmospheric conditions, may react with HO<sub>2</sub> to form the peroxides CX<sub>3</sub>O<sub>2</sub>H, which will likely be predominantly photodissociated to CX<sub>3</sub>O + OH with a rate similar to that for H<sub>2</sub>O<sub>2</sub>. In the troposphere the pathway leading to the peroxides may be important since the background NO concentrations may be low.

The peroxy nitrates CX<sub>3</sub>O<sub>2</sub>NO<sub>2</sub> and CX<sub>3</sub>CX<sub>2</sub>O<sub>2</sub>NO<sub>2</sub> are produced by the reaction of CX<sub>3</sub>O<sub>2</sub> and CX<sub>3</sub>CX<sub>2</sub>O<sub>2</sub> with NO<sub>2</sub>. Simonaitis and Heicklen, [1979] and Niki et al., [1979] observed CFC1<sub>2</sub>O<sub>2</sub>NO<sub>2</sub> and CCl<sub>3</sub>O<sub>2</sub>NO<sub>2</sub> formation in laboratory measurements and it is likely that the other nitrates also exist. However, in the stratosphere they are rapidly photodissociated [Morel et al., 1979]. Approximate calculations indicate that CFC1<sub>2</sub>O<sub>2</sub>NO<sub>2</sub> will have a stratospheric lifetime of no more than a few days, and number densities of the order of 10<sup>5</sup> - 10<sup>6</sup> cm<sup>-3</sup> in the 20 - 30 km altitude range. Therefore, the nitrates are not likely to play a role in stratospheric chemistry, but a more detailed analysis for the nitrates produced from CH<sub>3</sub>Cl and CH<sub>3</sub>CCl<sub>3</sub> near the tropopause is needed.

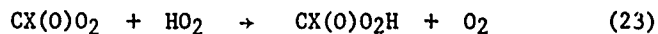
The CX<sub>3</sub>O radical produced from CX<sub>3</sub>O<sub>2</sub> either ejects a Cl atom (if there are at least two halogen atoms on the radical carbon), or an H atom transfer to O<sub>2</sub> takes place leading to CX<sub>2</sub>O. CCl<sub>2</sub>O, CFC1O, CF<sub>2</sub>O, and CHClO produced from CCl<sub>4</sub>, CFC1<sub>3</sub>, CF<sub>2</sub>Cl<sub>2</sub> and CH<sub>3</sub>Cl, respectively, will be photolysed leading to the production of halogen atoms and CO<sub>2</sub> via the sequence (NO, NO<sub>2</sub> present) [e.g. Niki et al., 1979; Spence et al., 1978].



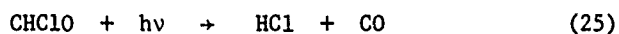
## SIMONAITIS



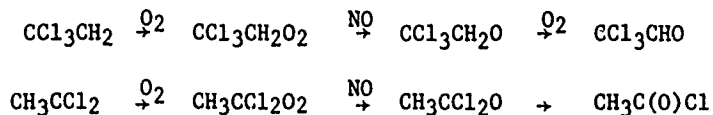
By analogy, with other peroxy radicals, the reactions



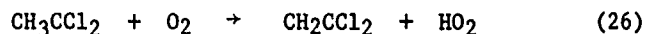
may also occur. The photochemistry of  $\text{CHClO}$  has not yet been studied; its photolysis may lead to  $\text{HCl}$  production.



In the case of  $\text{CH}_3\text{CCl}_2$  and  $\text{CCl}_3\text{CH}_2$ , produced from  $\text{CH}_3\text{CCl}_3$ , the oxidation in the presence of  $\text{NO}$  will lead to  $\text{CH}_3\text{C(O)Cl}$ , and possibly trichloroacetaldehyde,  $\text{CCl}_3\text{CHO}$ , respectively.



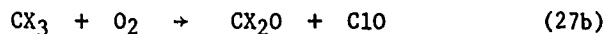
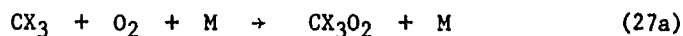
$\text{CH}_3\text{CCl}_2$  may also, by analogy with  $\text{C}_2\text{H}_5$  [Howard, 1977], react with  $\text{O}_2$  in a two body reaction



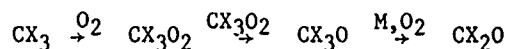
In each case, the further atmospheric chemistry of  $\text{CCl}_3\text{CHO}$ ,  $\text{CH}_3\text{C(O)Cl}$  and  $\text{CH}_2\text{CCl}_2$  needs to be considered. The likely photoproducts from  $\text{CCl}_3\text{CHO}$  and  $\text{CH}_3\text{C(O)Cl}$  are  $\text{CCl}_3 + \text{CHO}$ , and  $\text{Cl} + \text{CH}_3\text{C(O)}$  or  $\text{CH}_3 + \text{C(O)Cl}$ , respectively. Evidently, photolysis of  $\text{CH}_3\text{C(O)Cl}$  does not produce  $\text{CH}_3\text{Cl}$  at lower temperatures, [Majer and Robb, 1968].

### III. 1. Brief review of laboratory studies

$\text{CX}_3 + \text{O}_2$ ,  $\text{CX}_3\text{O}_2$  and  $\text{CX}_3\text{O}$  radicals: There are two possible channels for the reaction of chlorofluoromethyl and chloromethyl radicals with  $\text{O}_2$



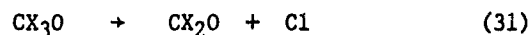
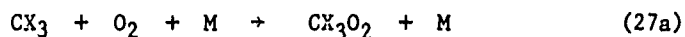
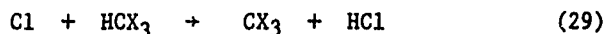
Numerous studies of the oxidation of these radicals under laboratory conditions in which only  $\text{O}_2$  is present show that the product is always a carbonyl halide  $\text{CX}_2\text{O}$ , [Heicklen, 1968; Sanhueza, 1977; Jayanty et al., 1975, Sanhueza and Heicklen, 1975; Spence et al., 1976].  $\text{CX}_2\text{O}$  may be produced by either the reaction sequence



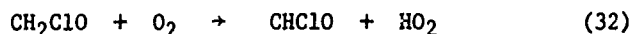
or by reaction (27b). However, overwhelming kinetic and spectroscopic evidence indicates that the reaction proceeds via reaction (27a).

Gillespie et al., [1977], produced  $\text{CCl}_3$  by flash photolysis of  $\text{CCl}_3\text{Br}$  in the presence of  $\text{O}_2$ . They looked for  $\text{ClO}$  formation by absorption, but none due to reaction (27b) could be detected at a total pressure of  $\sim 20$  Torr. Niki et al., [1979], photolysed  $\text{Cl}_2$  in the presence of  $\text{HCX}_3$  ( $\text{CX}_3 = \text{CCl}_3, \text{CFCl}_2$  and  $\text{CF}_2\text{Cl}$ )/ $\text{O}_2/\text{NO}_2$  mixtures. Using Fourier transform infrared spectroscopy, they observed the formation of peroxy nitrates  $\text{CX}_3\text{O}_2\text{NO}_2$ , which require  $\text{CX}_3\text{O}_2$  as an intermediate. Cooper et al., [1979], produced  $\text{CCl}_3$  and  $\text{CF}_3$  in the presence of  $\text{O}_2$  by the pulse radiolysis of  $\text{CCl}_4$  and  $\text{CF}_3\text{Cl}$ , respectively, and observed absorption due to  $\text{CCl}_3\text{O}_2$  and  $\text{CF}_3\text{O}_2$  radicals. From measurement of the  $\text{CX}_3\text{O}_2$  growth profiles, the limiting high pressure rate coefficients  $k_{27}(\text{CCl}_3) = (5.15 \pm 0.5) \times 10^{-12} \text{ cm}^3\text{sec}^{-1}$  and  $k_{27}(\text{CF}_3) = (1.00 \pm 0.3) \times 10^{-12} \text{ cm}^3\text{sec}^{-1}$  were determined.

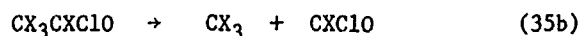
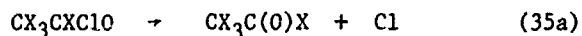
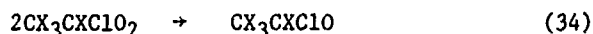
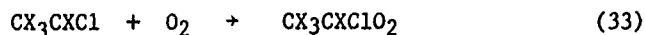
There have been no direct studies of the reactions of halomethoxy radicals.  $\text{Cl}_2$  photosensitized halomethane oxidation studies show that carbonyl halides are formed in a long chain process in the case of halomethyl radicals containing more than one halogen and at least one chlorine atom ( $\text{CCl}_3, \text{CFCl}_2, \text{CF}_2\text{Cl}$ , etc.) [Sanhueza and Heicklen, 1975; Sanhueza, 1977; Simonaitis et al., 1979]. For this type of radical the mechanism is



On the other hand, the oxidation of the  $\text{CH}_2\text{Cl}$  radical leads to the production of  $\text{HCClO}$  in a non chain process. Therefore,  $\text{CH}_2\text{ClO}$  is stable and reacts with  $\text{O}_2$  in the same manner as the  $\text{CH}_3\text{O}$  radical [Sanhueza and Heicklen, 1975]

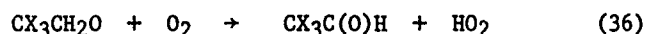


$\text{CX}_3\text{CX}_2 + \text{O}_2$ ,  $\text{CX}_3\text{CX}_2\text{O}_2$  and  $\text{CX}_3\text{CX}_2\text{O}$  radicals: The oxidation reactions of many haloethyl radicals (not including  $\text{CH}_3\text{CCl}_2$  and  $\text{CCl}_3\text{CH}_2$ ) were reviewed by Sanhueza et al., [1976]. More recently Spence and Hanst, [1978], studied the oxidation of many haloethyl radicals, including  $\text{CH}_3\text{CCl}_2$  and  $\text{CCl}_3\text{CH}_2$ , derived from haloethanes by H atom abstraction with Cl atoms in the ppm range in the presence of 1 atm air using FTIR spectrometry. In general, two types of major products were observed: acid halides or carbonyl halides derived from C-C bond cleavage. The following general mechanism has been proposed for radicals of the type  $\text{CX}_3\text{CXCl}$  [Bertrand et al., 1971; Sanhueza et al., 1976].

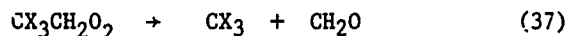


The relative importance of the two types of products depends in general upon the relative bond strengths  $\text{D}(\text{C}-\text{C})$  and  $\text{D}(\text{C}-\text{Cl})$ , where  $\text{D}(\text{C}-\text{Cl})$  refers to the Cl atom attached to the oxygen bearing carbon of the ethoxy radical [Bertrand et al., 1971]. Presumably, for radicals of the type  $\text{CX}_3\text{CH}_2$ , the reaction

## SIMONAITIS

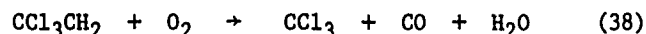


may compete with reaction (35b) since the C-C bond cleavage reaction

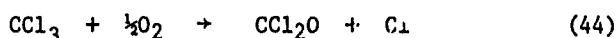
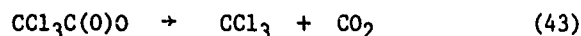
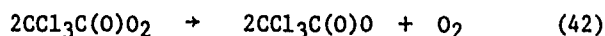
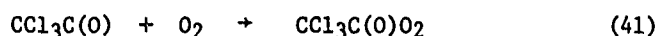
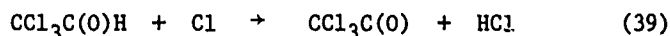


is endothermic [Bertrand et al., 1971]. However, the acetaldehydes have not been observed as products.

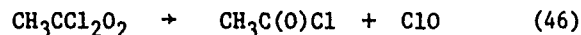
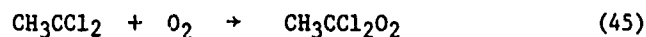
For  $\text{CCl}_3\text{CH}_2$  and  $\text{CH}_3\text{CCl}_2$  radicals, Spence and Hanst observed the major products to be  $\text{CCl}_2\text{O}$ , CO, and some  $\text{CO}_2$ , and  $\text{CH}_3\text{C(O)Cl}$ , respectively. For the  $\text{CCl}_3\text{CH}_2$  radical, they suggested the reaction



The mechanism given above for other haloalkyl radicals seems more likely, however, since considerable rearrangement would have to occur for  $\text{H}_2\text{O}$  elimination from the  $\text{CCl}_3\text{CH}_2\text{O}_2$  adduct. Presumably,  $\text{CCl}_3\text{C(O)H}$  is not observed as a product because it is destroyed by secondary reactions, as suggested by Spence and Hanst for some other aldehydes,

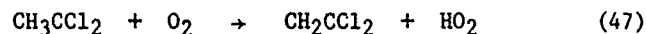


leading to  $\text{CCl}_2\text{O}$ , CO and  $\text{CO}_2$  as products. For the formation of  $\text{CH}_3\text{C(O)Cl}$  from the oxidation of the  $\text{CH}_3\text{CCl}_2$  radical and other radicals of a similar structure, Spence and Hanst suggested the sequence



This scheme, however, appears to be in conflict with the photooxidation studies in which product formation occurs via long chains when this type of a radical is involved [Bertrand et al., 1971; Sanhueza et al., 1976], since the ClO radical cannot act as an effective chain carrier. Therefore, the sequence via the ethoxy radical must be preferred.

In addition to the pressure dependent channel leading to the peroxide radical, haloethyl radicals containing H atoms on the carbon atom adjacent to the radical carbon may react with  $\text{O}_2$  to produce an ethylene by a reaction analogous to the reaction of  $\text{C}_2\text{H}_5$  radicals with  $\text{O}_2$  [Howard, 1977]. For the  $\text{CH}_3\text{CCl}_2$  radical, the reaction

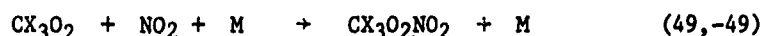
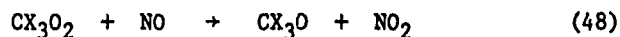




## SIMONAITIS

May occur in competition with the pressure dependent channel.

CX<sub>3</sub>O<sub>2</sub> + NO, NO<sub>2</sub>, the thermal decomposition of peroxy nitrates: By analogy with the reactions of HO<sub>2</sub> and CH<sub>3</sub>O<sub>2</sub> radicals with NO and NO<sub>2</sub>, it is expected that halomethyl and other peroxy radicals would react with NO and NO<sub>2</sub> by analogous reactions



Simonaitis et al., [1979], using the methods developed by Simonaitis and Heicklen, [1976], for the first observation of HNO<sub>4</sub> formation from the HO<sub>2</sub> + NO<sub>2</sub> reaction, photolysed Cl<sub>2</sub> in the presence of HCCl<sub>3</sub> and HCFC1<sub>2</sub> (HCX<sub>3</sub>), and O<sub>2</sub>, NO and NO<sub>2</sub> at ~1 atm total pressure and monitored the NO to NO<sub>2</sub> conversion by measuring the NO removal quantum yield. Reaction (48) (CX<sub>3</sub> = CCl<sub>3</sub> and CFC1<sub>2</sub>) accounts for the NO to NO<sub>2</sub> conversion and reaction (49) accounts for the inhibition of the NO oxidation by NO<sub>2</sub>. The occurrence of the reverse of reaction (49) at or near room temperature was shown by the fact that NO to NO<sub>2</sub> conversion continues after cessation of irradiation, because CX<sub>3</sub>O<sub>2</sub>NO<sub>2</sub> acts as a source of CX<sub>3</sub>O<sub>2</sub> radicals. Independently, Niki et al., [1979], obtained infrared evidence for the formation of peroxy nitrates derived from CCl<sub>3</sub>, CFC1<sub>2</sub> and CF<sub>2</sub>Cl radicals.

Table II summarizes the kinetic data for the reactions of CCl<sub>3</sub>O<sub>2</sub> and CFC1<sub>2</sub> radicals with NO and NO<sub>2</sub> and, for comparison, includes data for some other peroxy radicals.

Table II

Rate Coefficients for the Reaction of Peroxy Radicals with NO and NO<sub>2</sub>  
and the Thermal Decomposition of Peroxynitrates

Peroxy Radical	T, K	P, Torr	k <sub>49</sub> /k <sub>48</sub>	10 <sup>-16</sup> A <sub>-49</sub> , s <sup>-1</sup>	E <sub>-49</sub> /R, K	References
CCl <sub>3</sub> O <sub>2</sub>	268-298	700(CH <sub>4</sub> )	0.68	1.4	11500±600	<u>Simonaitis et al.</u> , [1979]
CFC1 <sub>2</sub> O <sub>2</sub>	286-305	700(CH <sub>4</sub> )	0.58	3.9	12300±600	<u>Simonaitis et al.</u> , [1979]
CH <sub>3</sub> O <sub>2</sub>	296	700(N <sub>2</sub> )	0.56	---	-----	<u>Sander and Watson</u> , [1979]
C <sub>3</sub> H <sub>7</sub> O <sub>2</sub>	289-296	700(Air)	----	0.05	9900	<u>Edney et al.</u> , [1979]
C <sub>3</sub> H <sub>7</sub> O <sub>2</sub>	289-296	700(Air)	----	---	10800 <sup>a</sup>	<u>Edney et al.</u> , [1979]
ClC(O)O <sub>2</sub>	293-300	700(Air)	----	6.3	13900	<u>Spence et al.</u> , [1978]

a. Calculated assuming A = 1 x 10<sup>16</sup> s<sup>-1</sup>.

b. Calculated from the absolute values.

The ratio  $k_{49}/k_{48}$  and the A values indicate that the reactions of the halomethyl radicals are within a factor of two of their high pressure limit and the values are close to those for the  $\text{CH}_3\text{O}_2 + \text{NO}_2$  reaction discussed previously. The reported A factor for  $\text{C}_3\text{H}_7\text{O}_2\text{NO}_2$  decomposition appears to be too low compared to other peroxy nitrates. A value of  $\sim 1 \times 10^{16}$  seconds<sup>-1</sup> is more reasonable; with this value of A,  $E/R = 10800 \text{ K}$  is obtained. Therefore, it is likely that the thermal decomposition reactions of alkyl and haloalkyl peroxy nitrates have A factors of  $\sim 1 \times 10^{16}$  seconds<sup>-1</sup> and  $E/R = (11600 \pm 700)\text{K}$ , near atmospheric pressure. The pressure fall-off behavior of halomethyl and haloethyl peroxy radical reactions with  $\text{NO}_2$  may, therefore, be approximated by the equation given previously for  $\text{CH}_3\text{O}_2 + \text{NO}_2$ . The pressure fall-off of  $k_{49}$  may be estimated from the estimated value at atmospheric pressure and from the pressure fall-off characteristics given for the  $\text{CH}_3\text{O}_2 + \text{NO}_2$  reaction.

#### ACKNOWLEDGMENT:

I wish to express my appreciation to Professor M. Nicolet for suggesting the topic of this review and for many enlightening conversations. I also thank Drs. R. T. Watson, A. R. Ravishankara and R. A. Cox for allowing me access to their data prior to publication. Financial assistance by the Atmospheric Sciences Section of the National Science Foundation through grant No. 78-16832 is acknowledged.

#### REFERENCES:

- Adachi, H. and N. Basco, Kinetic spectroscopy study of the reaction of  $\text{CH}_3\text{O}_2$  with NO, *Chem. Phys. Lett.*, **63**, 490, 1979.
- Barker, J. R., S. W. Benson and D. M. Golden, Decomposition of dimethyl peroxide and the rate constant for  $\text{CH}_3\text{O} + \text{O}_2 \rightarrow \text{CH}_2\text{O} + \text{HO}_2$ , *Int. J. Chem. Kinetics*, **9**, 31, 1977.
- Basco, N., D. G. L. James and F. C. James, A quantitative study of alkyl radical reactions by kinetic spectroscopy, II. Combination of the acetyl radical with the oxygen molecule, *Int. J. Chem. Kinetics*, **4**, 29, 1972.
- Bates, D. R., and A. Witherspoon, Photochemistry of minor constituents of the earth's atmosphere, *Astr. Soc.*, **112**, 101, 1952.
- Batt, L., and G. N. Robinson, Reaction of  $\text{CH}_3\text{O}$  with  $\text{O}_2$ . I. Using dimethyl Peroxide as a Thermal Source of  $\text{CH}_3\text{O}$ , *Int. J. Chem. Kinetics*, **11**, 1046, 1979.
- Bertrand, L., L. Exsteen-Meyers, J. A. Franklin and G. Hubrechts, Chlorine photosensitized oxidations of chloroethanes and chloroethylenes in the gas phase, *Int. J. Chem. Kinetics*, **3**, 89, 1971.
- Cooper, R., J. B. Cumming, S. Gordon and W. A. Mulac, The reaction of the halomethyl radicals  $\text{CCl}_3$  and  $\text{CF}_3$  with oxygen, *Int. J. Radiat. Phys. Chem.*, to be published.
- Cox, R. A. and G. Tyndall, Rate constants for the reactions of  $\text{CH}_3\text{O}_2$  in the gas phase, *Chem. Phys. Lett.*, **65**, 397, 1979.
- Cox, R. A. and G. Tyndall, Rate constants for the reactions of  $\text{CH}_3\text{O}_2$  with  $\text{HO}_2$ , NO and  $\text{NO}_2$  using molecular modulation spectrometry, *J. Chem. Soc., Faraday II*, accepted for publication, 1979.
- Crutzen, P. J., A discussion of the chemistry of some minor constituents in the stratosphere and troposphere, *Pure. App. Geophys.*, **106**, 1385, 1973.
- Crutzen, P. J., I. S. A. Isaksen and J. R. McAfee, The impact of the chlorocarbon industry on the  $\text{O}_3$  layer, *J. Geophys. Res.*, **83**, 345, 1978.
- Gillespie, H. M., J. Garraway and R. J. Donovan, Reaction of  $\text{O}(^1\text{D})$  with halomethanes, *J. Photochem.*, **7**, 29, 1977.
- Golden, D. M., G. N. Spokes and S. W. Benson, Very low pressure pyrolysis (VLPP); A versatile kinetic tool, *Angew. Chem. (int. Ed.)*, **12**, 534, 1973.
- Heicklen, J., Gas phase oxidation of perhalocarbons in *Advances in Photochemistry*, Vol. 7, edited by J. N. Pitts, Jr., G. S. Hammond and W. A. Noyes, pp. 57 - 148, Interscience, New York, 1969.
- Howard, C. J., The kinetics of the reaction of  $\text{HO}_2$  with  $\text{NO}_2$ , *J. Chem. Phys.*, **67**, 5258, 1977.
- Isaksen, I. S. A., and P. J. Crutzen, Uncertainties in calculated radical densities in the troposphere and stratosphere, *Geophys. Res. Norway*, **31**, 1, 1977.
- Jayanty, R. K. M., R. Simonaitis, and J. Heicklen, The photolysis of chlorofluoromethanes in the presence of  $\text{O}_2$  or  $\text{O}_3$  at 213.9 nm and their reactions with  $\text{O}(^1\text{D})$ , *J. Photochem.*, **4**, 381, 1975.

- Klais, O., P. C. Anderson, A. H. Laufer and M. J. Kurylo, The upper limit for the rate constant of the bimolecular reaction  $\text{CH}_3 + \text{O}_2 \rightarrow \text{OH} + \text{CH}_2\text{O}$  at  $368^\circ$ , Chem. Phys. Lett., 60, 898, 1979.
- Levy, H., Normal atmosphere, large radical and formaldehyde concentrations predicted, Science, 173, 141, 1971.
- Levy, H., Photochemistry of the lower troposphere, Planet. Space Sci., 20, 919, 1972.
- Levy, H., Photochemistry of minor constituents in the troposphere, Planet. Space Sci., 21, 575, 1973.
- Majer, J. R., and J. C. Robb, Photolysis of acetyl chloride, J. Chem. Soc., B, 447, 1968.
- McConnell, J. C., E. B. McElroy and S. C. Wofsy, Natural sources of atmospheric CO, Nature, 233, 187, 1971.
- McFarland, M., D. Kley, J. W. Drummond, L. A. Schmeltekopf, and R. H. Winkler, Nitric oxide measurements in the equatorial pacific region, Geophys. Res. Lett., 6, 685, 1979.
- Michael, J. V., D. F. Nava, W. A. Payne and L. J. Stief, Rate constants for the reaction of atomic chlorine with methanol and dimethyl ether from 200 - 500K, J. Chem. Phys., 70, 3652, 1979.
- Milstein, R. and F. S. Rowland, Quantum yield for the photolysis of  $\text{CF}_2\text{Cl}_2$  in  $\text{O}_2$ , J. Phys. Chem., 79, 669, 1975.
- Molina, M. J., and F. S. Rowland, Stratospheric sink for chlorofluoromethanes: Chlorine atom destruction of stratospheric ozone, Nature, 249, 810, 1974a.
- Molina, M. J., and F. S. Rowland, Chlorofluoromethanes in the environment, Rev. Geophys. and Space Phys., 13, 1, 1975.
- Morel, O., R. Simonaitis and J. Heicklen, The ultraviolet absorption spectra of  $\text{CCl}_3\text{O}_2\text{NO}_2$  and  $\text{CFC}_2\text{O}_2\text{NO}_2$ , to be published, 1980.
- National Aeronautics and Space Administration, Chemical kinetic and photochemical data for use in stratospheric modelling, JPL publication 79-27, 1979.
- Nicolet, M., Ozone and hydrogen reactions, Ann. Geophys., 26, 531, 1970.
- Nicolet, M., Un regard sur la stratosphere, Aeronomica Acta, A-91, 1971.
- Nicolet, M., in Mesospheric Models and Related Experiments, p 1-51, D. Reidel, Dordrecht, 1971.
- Nicolet, M., Aeronomic chemistry in the stratosphere, Planet. Space Sci., 20, 1671, 1972.
- Niki, H., P. D. Maker, C. M. Savage and L. P. Breitenbach, FTIR spectroscopic observation of peroxyalkyl nitrates formed via  $\text{RO}_2 + \text{NO}_2 \rightarrow \text{RO}_2\text{NO}_2$ , Chem. Phys. Lett., 55, 289, 1978.
- Niki, H., P. D. Maker, C. M. Savage and L. P. Breitenbach, Mechanism for hydroxyl radical initiated oxidation of olefin-nitric oxide mixtures in parts per million concentrations, J. Phys. Chem., 82, 135, 1978.
- Niki, H., P. D. Maker, C. M. Savage, and L. P. Breitenbach, FTIR spectroscopic observation of haloalkyl peroxy nitrates formed via  $\text{ROO} + \text{NO}_2 \rightarrow \text{ROONO}_2$  ( $\text{R} = \text{CCl}_3$ ,  $\text{CFC}_2$  and  $\text{CF}_2\text{Cl}$ ) J. Chem. Phys. Lett., 61, 100, 1979.
- Noxon, J. F., Nitrogen dioxide in the stratosphere and troposphere measured by ground based absorption spectroscopy, Science, 189, 547, 1975.
- Pate, C. T., B. J. Finlayson and J. N. Pitts, Jr., A long path infrared study of the reaction of methylperoxy free radicals with nitric oxide, J. Amer. Chem. Soc., 96, 6554, 1974.
- Plumb, I. C., K. R. Ryan, J. R. Steven and M. F. R. Mulcahy, Kinetics of the reaction of  $\text{CH}_3\text{O}_2$  with NO, Chem. Phys. Lett., 63, 255, 1979.
- Ravishankara, A. R., F. L. Eisele, and S. P. H. Wine, A study of the reaction of the  $\text{CH}_3\text{O}_2$  radical with NO, Private Comm., 1979.
- Rebber, R. and P. J. Ausloos, Photodecomposition of  $\text{CFC}_2\text{Cl}_2$  and  $\text{CF}_2\text{Cl}_2$ , J. Photochem., 4, 419, 1975.
- Sander, S. P. and R. T. Watson, Reactions of the  $\text{CH}_3\text{O}_2$  radical, To be submitted to J. Phys. Chem., 1979.
- Sanhueza, E. and J. Heicklen, Chlorine atom sensitized oxidation of dichloromethane and chloromethane J. Phys. Chem., 79, 7, 1975.
- Sanhueza, E., I. C. Hisatsune, and J. Heicklen, Oxidation of haloethylenes, Chem. Rev., 76, 801, 1976.
- Sanhueza, E., The chlorine atom sensitized oxidation of  $\text{HCCl}_3$ ,  $\text{HCF}_2\text{Cl}$  and  $\text{HCF}_3$ , J. of Photochem., 7, 325, 1977.

# SIMONAITIS

- Sanhueza, E., R. Simonaitis and J. Heicklen, The reaction of  $\text{CH}_3\text{O}_2$  with  $\text{SO}_2$ , Int. J. Chem. Kinetics, 11, 907, 1979.
- Simonaitis, R. and J. Heicklen, The reaction of  $\text{CH}_3\text{O}_2$  with NO and  $\text{NO}_2$ , J. Phys. Chem., 78, 2417, 1974.
- Simonaitis, R. and J. Heicklen, The reaction of  $\text{HO}_2$  with NO and  $\text{NO}_2$  and of OH with NO, J. Phys. Chem., 80, 1, 1976.
- Simonaitis, R. and J. Heicklen, The reactions of  $\text{CCl}_3\text{O}_2$  with NO and  $\text{NO}_2$  and the thermal decomposition of  $\text{CCl}_3\text{O}_2\text{NO}_2$ , Chem. Phys. Lett., 62, 473, 1979.
- Simonaitis, R., S. Glavas and J. Heicklen, The reactions of  $\text{CCl}_2\text{FO}_2$  with NO and  $\text{NO}_2$  and the thermal decomposition of  $\text{CFCl}_2\text{O}_2\text{NO}_2$ , Geophys. Res. Lett., 6, 385, 1979.
- Simonaitis, R. and J. Heicklen, Mechanism of the reaction of  $\text{CH}_3\text{O}_2$  with  $\text{SO}_2$  and the reaction of  $\text{CH}_3\text{O}_2$  with NO, J. Chem. Phys. Lett., 65, 361, 1979.
- Spence, J. W., E. O. Edney and P. J. Hanst, Peroxychloroformyl nitrate: Synthesis and thermal stability, Chem. Phys. Lett., 56, 478, 1978.
- Spence, J. W., P. L. Hanst, and B. W. Gay, Jr., Atmospheric oxidation of methyl chloride methylene chloride and chloroform, J. Air Poll. Control Assoc., 26, 994, 1976.
- Spence, J. W. and P. L. Hanst, Oxidation of chlorinated ethanes, J. Air Poll. Control Assoc., 28, 250, 1978.
- Spicer, C. W., A. Villa, H. A. Wiebe, and J. Heicklen, Reactions of the methylperoxy radical with nitric oxide and nitrogen dioxide, J. Amer. Chem. Soc., 95, 15, 1973.
- Stolarski, R. S. and R. J. Cicerone, Stratospheric chlorine: A possible sink for ozone, Can. J. Chem., 52, 1610, 1974.
- Su, F., J. G. Calvert, J. H. Shaw, H. Niki, P. D. Maker, C. M. Savage and L. D. Breitenbach, Spectroscopic and kinetic studies of new metastable species in the photooxidation of gaseous formaldehyde, Chem. Phys. Lett., 65, 221, 1979.
- Washida, N. and K. D. Bayes, The reaction of methyl radicals with atomic and molecular oxygen, Int. J. Chem. Kinetics, 8, 777, 1976.
- Wofsy, S. C., J. C. McConnell and M. B. McElroy, Atmospheric  $\text{CH}_4$ , CO and  $\text{CO}_2$ , J. Geophys. Res., 77, 4477, 1972.

## STRATOSPHERIC ION CHEMISTRY RELATED TO NEUTRAL TRACE COMPOSITION

Eldon E. Ferguson

National Oceanic and Atmospheric Administration Aeronomy Laboratory, Boulder CO 80303 USA

### Abstract

The positive and negative ion chemistry of the stratosphere is treated as an extension of D-region ionospheric chemistry. A number of laboratory measurements concerning the reactions of stratospheric ions with trace stratospheric neutrals have been carried out to facilitate this extension. Recent stratospheric ion composition measurements by Arnold and coworkers at Heidelberg, combined with laboratory reaction rate and equilibrium constant data, allow a very sensitive determination of neutral molecule concentrations in the  $10^{-12}$  mixing ratio range. Upper limits of  $\sim 10^5$  molecules  $\text{cm}^{-3}$  of  $\text{NH}_3$ ,  $\text{CH}_3\text{OH}$ ,  $\text{NaOH}$  and  $\text{KOH}$  above 40 km are inferred. An  $\text{NaOH}$  concentration of  $\sim 10^5$   $\text{cm}^{-3}$  near 38 km has been inferred from the measured positive ion composition. An  $\text{H}_2\text{SO}_4$  concentration of  $1.7 \times 10^5$   $\text{cm}^{-3}$  and an  $\text{HNO}_3$  mixing ratio of 1 ppbv have been determined at 30.5 km by Arnold and coworkers from their negative ion observations. The association of large positive ion and negative ion clusters is likely to play a role in gas-to-particle conversion in the stratosphere.

**INTRODUCTION:** A very sensitive modern technique for trace gas analysis is called chemical ionization mass spectrometry. The method utilizes the tendency for the composition of ionized gas mixtures to evolve rapidly toward the most stable ions. Certain energetically favored species can be detected extremely sensitively with this technique. Species may be energetically favored for charge accumulation by virtue of low ionization potentials, large electron affinities, or large proton affinities.

The natural ion chemistry of the earth's atmosphere also provides a sensitive method of detection of certain trace neutral species, in the part per trillion or lower range in the stratosphere. The problem which has prevented utilization of atmospheric ion chemistry for this purpose has been the lack of measurements of stratospheric ion composition. This difficult technological problem is now beginning to yield to the efforts of Arnold and his colleagues at Heidelberg and Arijs at Brussels. I will describe the current status of minor stratospheric composition measurements deduced from these first stratospheric-ion composition measurements.

Historically, this application of ion chemistry has been used before in atmospheric chemistry. There have been a number of papers in which the neutral  $\text{NO}$  concentration in the E-region has been deduced from the ratio of  $\text{NO}^+$  to  $\text{O}_2^+$  concentrations,  $\text{NO}^+$  production being dominated by



In addition to the utility of ion composition measurements as a tool for measuring trace neutral concentrations, the possibility of ion reactions as a significant source or sink of stratospheric neutral species is a matter of recurring concern and the possibility of ion-induced nucleation is relevant to aerosol formation.

Our approach to understanding stratospheric ion chemistry is to extend the well-studied (although not necessarily well-understood) D-region ion chemistry downwards. The D-region already represents relatively high pressure ion chemistry where three-body reactions, reactions with trace species, and negative ion reactions are important. The extension to the stratosphere is largely a matter of considering the role of additional species that may become involved in the ion chemistry.

**STRATOSPHERIC POSITIVE ION CHEMISTRY:** A useful guiding principle in atmospheric ion chemistry follows from thermochemistry. Only neutral species that have exothermic reaction channels with atmospheric ions need to be considered. This severely restricts the possibilities.

There are two times scales of concern. There is a relatively short time scale for production of the terminal D-region proton hydrate (PH) ions,  $\text{H}^+(\text{H}_2\text{O})_n$ , of the order of milliseconds in the stratosphere. In order to interrupt the relatively fast PH production from primary  $\text{O}_2^+$  ions, a reactive species would need to have a relatively large concentration, of the order of that of  $\text{H}_2\text{O}$  with which it must compete, i.e., of the order of ppm.

The only species present in the stratosphere at concentrations comparable to  $\text{H}_2\text{O}$  are  $\text{CO}_2$ ,  $\text{CH}_4$  and  $\text{O}_3$ .  $\text{CO}_2$  does not have exothermic reactions with  $\text{O}_2^+$  or  $\text{O}_2^+\cdot\text{H}_2\text{O}$ . The switching-reaction,  $\text{O}_4^+ + \text{CO}_2 \rightarrow \text{CO}_4^+ + \text{O}_2$  is nearly thermoneutral,  $\Delta H = -0.3 (\pm 1.0) \text{ kcal mol}^{-1}$ ,  $\Delta S = 4.3 (\pm 2.6) \text{ eu}$  (Dotan, et al., 1978), and the large  $\text{O}_2/\text{CO}_2$  ratio thus keeps the  $\text{O}_4^+/\text{CO}_4^+$  ratio large.  $\text{CO}_4^+$  would not in any case have an significant effect since the reaction



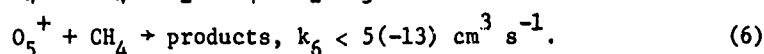
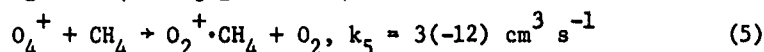
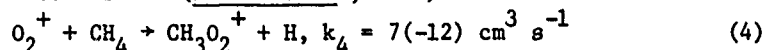
is rapid. Therefore  $\text{CO}_2$  does not interfere with the production of  $\text{H}^+(\text{H}_2\text{O})_n$  clusters.

Ozone reacts rapidly with  $\text{O}_4^+$  to produce  $\text{O}_5^+$  (Dotan et al., 1978), but this has no effect since

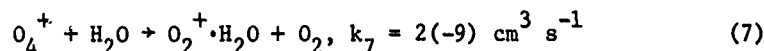


is rapid,  $k_3 = 1.2(-9) \text{ cm}^3 \text{ s}^{-1}$ .  $\text{O}_5^+$  has probably been observed in the D-region by Arnold and his colleagues, although a mass  $80^+$  ion was not so identified by them.

Methane does not react rapidly with  $\text{O}_2^+$ ,  $\text{O}_4^+$ , or  $\text{O}_5^+$  and hence also has no direct effect on stratospheric ion chemistry. The reactions are (Dotan et al., 1978)



Reaction (5) is not competitive with



and in any case the reaction

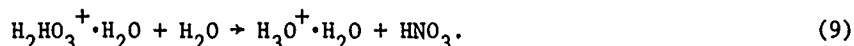


would undoubtedly be fast.

Therefore we conclude that PH's will be produced in the stratosphere (and in the troposphere) just as they are in the D-region. The question then arises as to whether these ions will

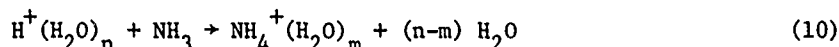
further react in the stratosphere. The time scale for this to occur, our second time scale, is the lifetime of ions in the stratosphere. The lifetime is determined by positive ion-negative ion recombination (Smith and Church, 1977). This varies with altitude of course but is of the order of  $10^4$  seconds. This means that species in much smaller concentrations than water must be considered. Species with concentrations down to about  $(10^{-9} \text{ cm}^3 \text{ s}^{-1} \times 10^4 \text{ s})^{-1} \approx 10^5 \text{ cm}^{-3}$  could produce detectable ions. Few of the part-per-trillion atmosphere species are reliably measured, indeed many remain to be identified. These will include radicals and species whose thermochemistry is not established. A promising goal is to deduce certain atmospheric concentrations in this range by ion composition measurements, a goal just now starting to be realized, largely as a result of the Heidelberg measurements.

Two species known to react exothermically with PH's and to exist in ppb concentrations are  $\text{HNO}_3$  (Fehsenfeld et al., 1975) and  $\text{N}_2\text{O}_5$ , the anhydride of  $\text{HNO}_3$  (Davidson et al., 1978). However, as shown in Fig. 1, their reactions lead only "do nothing" cycles, producing  $\text{NO}_2^+$  hydrates which reconvert to PH's and  $\text{HNO}_3$  by the reaction

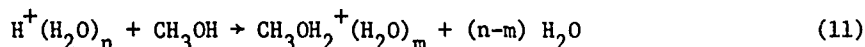


$\text{H}_2\text{NO}_3^+$ , protonated nitric acid, is chemically equivalent to  $\text{NO}_2^+ \cdot \text{H}_2\text{O}$ , hydrated  $\text{NO}_2^+$ .

Two species which react irreversibly with PH's are  $\text{NH}_3$  (Fehsenfeld and Ferguson, 1973) and  $\text{CH}_3\text{OH}$  (Fehsenfeld et al., 1978)



where  $k_{10} \sim 2(-9) \text{ cm}^3 \text{ s}^{-1}$  for  $n = 0-4$ , and



where  $k_{11} \sim 2(-9) \text{ cm}^3 \text{ s}^{-1}$  for  $n = 0-4$ . Reactions (10) and (11) are typical of exothermic proton transfer reactions for small molecules, occurring on essentially all collisions.

$\text{NH}_4^+$  and  $\text{CH}_3\text{OH}_2^+$  hydrates are not observed by Arnold et al. (1978) above 40 km and therefore  $\text{NH}_3$  and  $\text{CH}_3\text{OH}$  must have concentrations less than  $10^5 \text{ cm}^{-3}$  in this altitude range. This is to be expected for  $\text{NH}_3$ , whose source is at the earth's surface and which is soluble and presumably washed out of the troposphere and removed by reaction with OH.  $\text{CH}_3\text{OH}$  on the other hand is produced in the stratosphere by methane oxidation, the details of which are insufficiently well known to establish the concentration even crudely. The determination that  $\text{CH}_3\text{OH} \sim 10^5 \text{ cm}^{-3}$  is therefore significant.

Other species which are expected to occur in the stratosphere as a consequence of methane oxidation are  $\text{CH}_3\text{O}_2$  and  $\text{CH}_3\text{OOH}$ . We estimate, although it is quite uncertain, that the proton affinities of these species are not sufficiently greater than water to accept protons from PH's in the stratosphere. It has been shown that formaldehyde,  $\text{H}_2\text{CO}$ , which has a proton affinity  $4.3 \text{ kcal mol}^{-1}$  greater than water, cannot play a significant role in stratospheric ion chemistry because hydration stabilizes PH's relative to protonated formaldehyde (Fehsenfeld et al., 1978). The experimental observations of Arnold show that PH's dominate the positive ion composition above  $\approx 40$  km, indicating that there are no species above this altitude that perturb the normal PH-dominated ion chemistry. The only utility for the positive ion chemistry above  $\approx 40$  km is then to place upper limits on species which would have altered the terminal ions if they had been present, examples being the  $\text{NH}_3$  and  $\text{CH}_3\text{OH}$  cited above.

Below 40 km Arnold et al. (1977, 1978) and Arijs et al. (1978) discovered a conversion of PH's to a different set of ions which have subsequently been identified by Ferguson (1978) as protonated sodium hydroxide clusters,  $\text{NaOH}_2^+ \cdot n\text{H}_2\text{O} \cdot \text{NaOH}$ . The sodium deposited by meteor ablation to form the well-known sodium layer around 90 km has been shown by Liu and Reid (1979) to lead

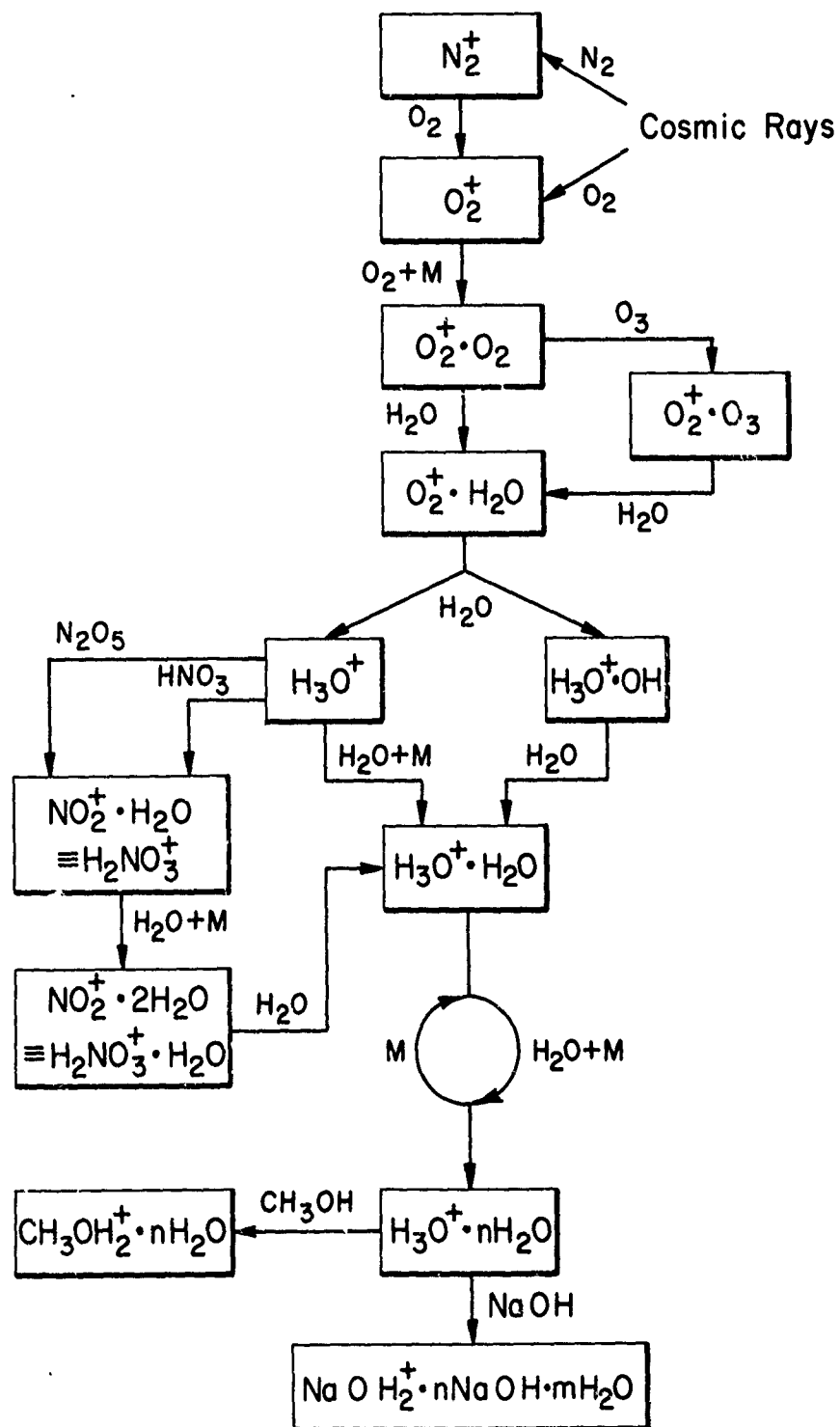


Figure 1. Stratospheric positive ion chemistry reaction scheme.



to  $10^5 \text{ Na}_x \text{ molecules cm}^{-3}$  near 40 km for a one-dimensional model calculation, adopting a sufficient flux of sodium atoms into the atmosphere ( $5 \times 10^5 - 5 \times 10^6 \text{ cm}^{-2} \text{ s}^{-1}$ ) to yield the observed sodium layer and assuming the  $\text{Na}_x$  sink is below 40 km (Fig. 2). Assuming a reason-

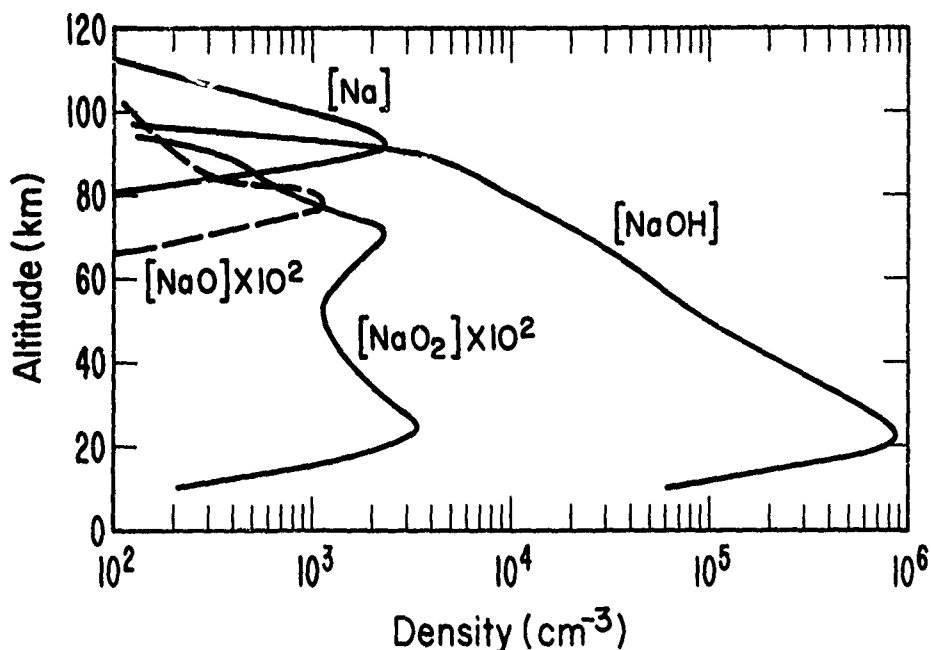
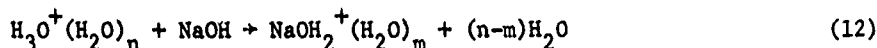
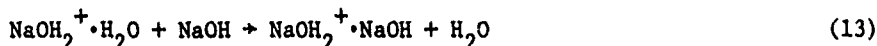


Figure 2.  $\text{Na}_x$  altitude profiles (Liu and Reid, 1979).

able (but unmeasured) neutral reaction kinetic scheme leads to conversion of the sodium species largely to NaOH below the sodium layer. The reactions



are so exothermic with the large proton affinity of  $\text{NaOH} = 248 \text{ kcal mol}^{-1}$  (Kearle, 1977), that there is little question that reaction (12) is fast. The dipole moment of NaOH (unmeasured) is so large that neutral NaOH molecules will readily displace  $\text{H}_2\text{O}$  molecules in clusters,



Recent laboratory measurements in the NOAA Aeronomy Laboratory have shown that water displaces  $\text{HNO}_3$  and  $\text{HCl}$  molecules clustered to sodium ions, exothermically and rapidly. This means that neither  $\text{HNO}_3$  or  $\text{HCl}$  would destroy  $\text{Na}^+ \cdot \text{H}_2\text{O} = \text{NaOH}_2^+$  ions. It also implies that sodium the form of  $\text{NaNO}_3$  or  $\text{NaCl}$  in the atmosphere would be incorporated into the ion chemistry as protonated sodium hydroxide (or hydrated  $\text{Na}^+$ ) ions.

Potassium hydroxide has an even greater proton affinity than sodium hydroxide,  $265 \text{ kcal mol}^{-1}$ . The failure to observe  $\text{KOH}_2^+$  clusters implies a  $\text{KOH}$  concentration less than  $10^5 \text{ cm}^{-3}$  at 40 km, which is consistent with the calculation of Liu and Reid and the relative meteoritic abundances,  $\text{Na/K} \sim 13$ .

# FERGUSON

The abundances of Si, Mg and Fe on the other hand are 20, 18 and 15 times greater than that of sodium while S, Ca, Al and Ni are all comparable to or greater than Na. However the energetics of the positive ion chemistry of these species are probably unfavorable, essentially as a consequence of their larger ionization potentials, Mg may be an exception to this.  $\text{MgOH}^+$  ions would have the same mass as  $\text{NaOH}_2^+$ . At present one cannot be certain that the observed ions are  $\text{NaOH}_2^+$  and not  $\text{MgOH}^+$  ions but the 10 and 11% mass 25 and 26 Mg isotopes will allow a resolution of this uncertainty when improved mass spectra are obtained in the stratosphere.

The Mg situation merits a more detailed consideration. According to the calculations of Liu and Reid, and the Mg/Na ratio of 18, there should be greater than  $10^5 \text{ cm}^{-3}$  Mg molecules in some form throughout the stratosphere and the D-region. The failure to observe Mg containing ions in the PH dominated stratosphere and the D-region implies either that the Mg is tied up in compounds with proton affinities not very much greater than that of water,  $170 \text{ kcal mol}^{-1}$  (Kearle, 1977) or that the atmospheric abundance is lower than expected on cosmic abundance arguments. Liu and Reid expect the dominant form of Mg to be MgOH. This is less certain than in the case of Na, however, since the Mg reaction analogous to the reaction of  $\text{NaO}_2$  with OH to give NaOH, assumed to be fast by Liu and Reid, may be endothermic. The reaction of  $\text{MgO}_2$  with H to give MgOH is probably endothermic while it may be exothermic in the case of Na and is assumed to be quite fast by Liu and Reid ( $7 \times 10^{-12} \text{ cm}^3 \text{ s}^{-1}$ ). The thermochemistry of Mg compounds is quite deficient for present purposes, the heat of formation of MgOH has a  $\pm 20 \text{ kcal mol}^{-1}$  uncertainty and that of  $\text{MgOH}^+$  a  $\pm 40 \text{ kcal mol}^{-1}$  uncertainty (JANAF, 1970).

We estimate the proton affinity of MgOH to be  $185 \pm 30 \text{ kcal mol}^{-1}$  and that of MgO to be  $225 \pm 40 \text{ kcal mol}^{-1}$ . Any species with a proton affinity less than about  $175 \text{ kcal mol}^{-1}$  is unlikely to strip protons from water in the atmosphere, as we have shown specifically for formaldehyde which has a proton affinity about  $4 \text{ kcal mol}^{-1}$  greater than  $\text{H}_2\text{O}$  (Fehsenfeld et al., 1978). The observations of Arnold seem to tell us that whatever Mg compounds exist above  $\sim 40 \text{ km}$  do not have proton affinities larger than  $\sim 175 \text{ kcal mol}^{-1}$ . Perhaps  $\text{Mg(OH)}_2$  or more stable Mg Compounds with lower proton affinities occur.

Below  $\sim 40 \text{ km}$ , where the NaOH concentration is sufficiently large, we can obtain no evidence concerning Mg compounds because then ions would be destroyed by NaOH in any case,



or



At altitudes below  $40 \text{ km}$ , the metal compound concentrations are increasing so that at low enough altitude, perhaps  $\sim 30 \text{ km}$ , the KOH concentration may be great enough to convert  $\text{NaOH}_2^+$  clusters to  $\text{KOH}_2^+$  clusters. Measurements at the lower altitudes remain to be carried out but are now becoming feasible. The largest uncertainty in this connection is the altitude at which the metal compounds are removed to form aerosols. In this connection the possibility exists of getting a handle on gas-to-particle conversion processes by careful ion composition measurements lower in the stratosphere. For example one might be able to determine the relative rates of removal of NaOH and KOH.

The factor-of-five seasonal variation in Na reported by Megie et al., (1978) with a winter maximum, implies a seasonal variation in the stratospheric NaOH concentration such that the altitude of conversion of PH's to NPH's might show a slight seasonal variation. This effect will be largely attenuated by the long diffusion time from  $90 \text{ km}$  to  $40 \text{ km}$ , which is comparable to or longer than one year.

The present state of stratospheric positive ion chemistry carries the implication that concentrations of the order of  $10^7 \text{ cm}^{-3}$  of MgO, FeO, and SiO, or the hydroxides may be present

in the stratosphere. Since these species could participate in catalytic odd-oxygen destruction, they may be of some importance. Aiken (1979) has suggested that CaOH may provide a stratospheric ionization source due to its photoionization by  $\lambda$  2100 Å photons (5.9 eV). This is based on speculative photoionization cross-sections and neutral chemistry.

Sulfuric acid, which has been found to occur in the stratosphere from the negative ion composition as we shall discuss below, does not appear likely to impact on the positive ion chemistry. The proton affinity of  $\text{H}_2\text{SO}_4$  ( $172 \pm 2 \text{ kcal mol}^{-1}$ , Smith and Munson, 1978) only slightly exceeds that of  $\text{H}_2\text{O}$  ( $170 \text{ kcal mol}^{-1}$ ) and  $\text{H}_3\text{O}^+ \cdot (\text{H}_2\text{O})_n$  ions with  $n = 1, 2, 3$  are found to react only slowly with  $\text{H}_2\text{SO}_4$ ,  $k < 6 \times 10^{-12} \text{ cm}^3 \text{ s}^{-1}$ , and the sulfuric acid concentration is too low for this to be significant (Viggiano et al., 1979). Protonated sulfuric acid would in any case proton transfer rapidly with NaOH.

**STRATOSPHERIC NEGATIVE ION CHEMISTRY:** We pursue the stratospheric negative ion chemistry in the same way as the positive ion chemistry, as an extension of the much-studied D-region. For the D-region we have developed a detailed laboratory reaction rate scheme over the last  $\sim 15$  years which leads to  $\text{NO}_3^-$  terminal ions. The  $\text{NO}_3^-$  ions will of course hydrate and cluster in the atmosphere. The first question we ask is whether  $\text{NO}_3^-$  will also be produced in the stratosphere. The answer appears to be yes, as indicated by the scheme shown in Fig. 3. The D-

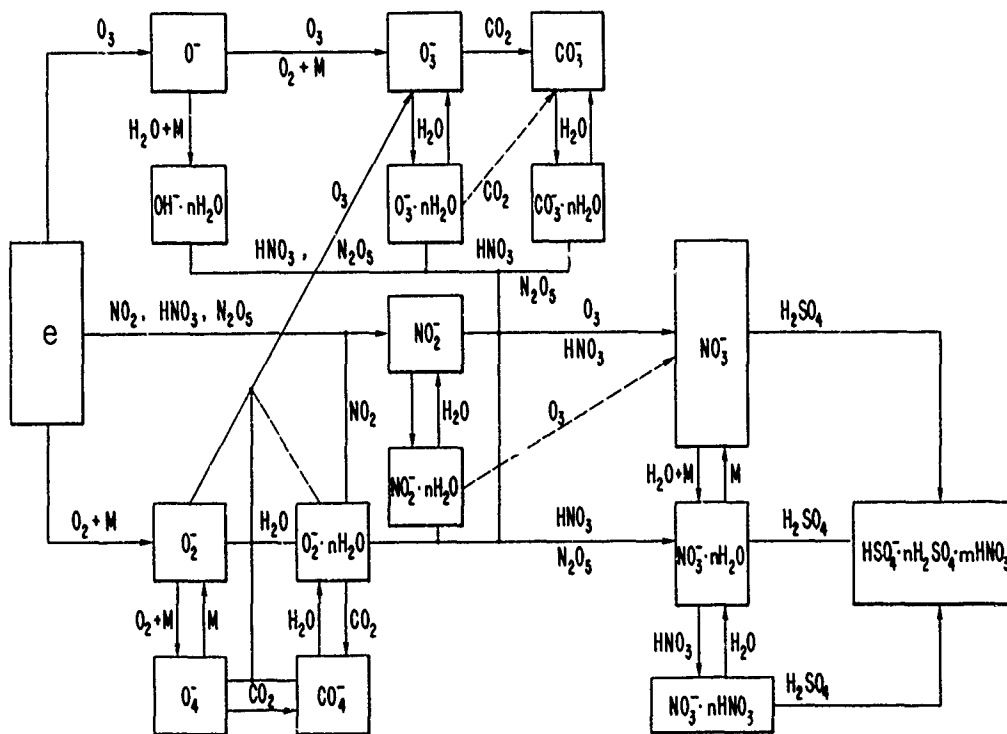


Figure 3. Stratospheric negative ion chemistry reaction scheme.

region reactions for  $\text{NO}_3^-$  production are reinforced by additional reactions in the stratosphere. The  $\text{NO}_2^-$  ion for example can be produced directly by charge-transfer of  $\text{O}_2^-$  with  $\text{NO}_2$ , circumventing the more circuitous D-region route.  $\text{NO}_3^-$  can be produced directly by reaction of

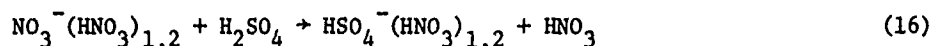
FERGUSON

almost any atmospheric negative ion,  $O^-$ ,  $O_2^-$ ,  $O_3^-$ ,  $NO_2^-$ , and  $Cl^-$ , with either  $HNO_3$  (Fehsenfeld et al., 1975) or  $N_2O_5$  (Davidson et al., 1978). Thus it appears almost certain that  $NO_3^-$  ions will be produced in the stratosphere.

$HNO_3$  molecules readily replace  $H_2O$  molecules clustered to negative ions, with equilibrium constants exceeding  $10^5$  so that in the stratosphere, where  $[H_2O]/[HNO_3]$  is only  $\sim 10^3$ ,  $HNO_3$  will effectively displace the water molecules in hydrated negative ions.

The second question is whether the  $NO_3^-(HNO_3)_n$  cluster ions then further react in their lifetime. The first stratospheric negative ion composition measurements have recently been reported by Arnold and Henschen (1978) who found a series of masses at  $\sim 35$  km that can be interpreted as  $NO_3^-(HNO_3)_{1,2}$ ,  $HSO_4^-(HNO_3)_{1,2}$ ,  $HSO_4^-(H_2SO_4)_{1,2}$ , and  $HSO_4^- \cdot H_2SO_4 \cdot HNO_3$ .

Viggiano et al. (1979) have found that  $NO_3^-(HNO_3)_{1,2}$  reacts rapidly with  $H_2SO_4$ ,



$k_{16} \sim 10^{-9} \text{ cm}^3 \text{ s}^{-1}$ . Fehsenfeld et al. (1975) found earlier that  $HNO_3$  strongly displaces  $H_2O$  clustered to negative ions. The observations of Arnold and Henschen are consistent with the production of  $NO_3^-(HNO_3)$  by the known ion chemistry of Fig. 3 followed by reaction (16) with sulfuric acid vapor. Since both  $NO_3^-$  and  $HSO_4^-$  ion cores were observed, the  $H_2SO_4$  concentration must lie in the range of  $10^5$  molecules  $\text{cm}^{-3}$ . A much larger concentration would have removed the  $NO_3^-$  ions altogether and a much lower concentration would not have introduced a detectable concentration of  $HSO_4^-$  ions. Subsequently Arnold and Fabian (1980) have analyzed their ion composition measurements in detail to deduce a sulfuric acid vapor concentration of  $1.7 \times 10^5 \text{ cm}^{-3}$  at 36.5 km over southwestern France in November 1977 with a temperature of 227 K. This is a volume mixing ratio of 1.7 pptv. The uncertainty is estimated to be a factor of 3, due to uncertainties in reaction rates, ion-ion recombination rates, positive ion concentration and relative negative ion concentrations. Turco et al. (1979) have developed a sulfur species model recently which has 2 orders of magnitude more  $H_2SO_4$  at 35 km than this. The studies of Viggiano et al. also establish a lower limit on the electron affinity of  $HSO_4^-$  of 4.5 eV. No atmospheric species other than  $H_2SO_4$  that can react with  $NO_3^-$  has yet been identified.

It is interesting to note that the observed  $H_2SO_4$  concentration at 36.5 km can be adequately supplied by the atmospheric meteor ablation influx. The meteoritic or cosmic S/Na ratio is about 4 and scaling the total Na in Fig. 2 by this factor gives substantially more than is observed by Arnold and Fabian. This raises the interesting possibility that the  $H_2SO_4$  observed at this altitude may be originating from the meteor ablation altitudes above rather than from tropospheric sulfur compounds. Perhaps the tropospheric sulfur compounds are removed heterogeneously below 36 km.

From the ratio of  $NO_3^-(HNO_3)_2/NO_3^-(HNO_3)$  ions, Arnold et al. (1980) have deduced a nitric acid mixing ratio of  $\sim 1$  ppbv at 36.5 km in the same experiments in which the sulfuric acid determination was made. These cluster ions are in a near equilibrium and the laboratory equilibrium constants are used to deduce the  $HNO_3$  concentration.

ION REACTIONS AS STRATOSPHERIC NEUTRAL SOURCES AND SINKS: Ion-molecule reactions produce and destroy neutral molecules. The numbers involved are rather small to be of concern in stratospheric photochemistry but this is a matter for continuing consideration as our knowledge of both the ion chemistry and stratospheric composition increase.

Galactic cosmic rays dominate the ionization in the stratosphere. This ionization is a function of latitude and time, increasing with geomagnetic latitude and with solar sunspot minimum conditions (Neher, 1967). Under disturbed solar conditions the ionization rate can increase by orders of magnitude at high latitude (Fig. 4). Crutzen et al. (1975) calculated that during

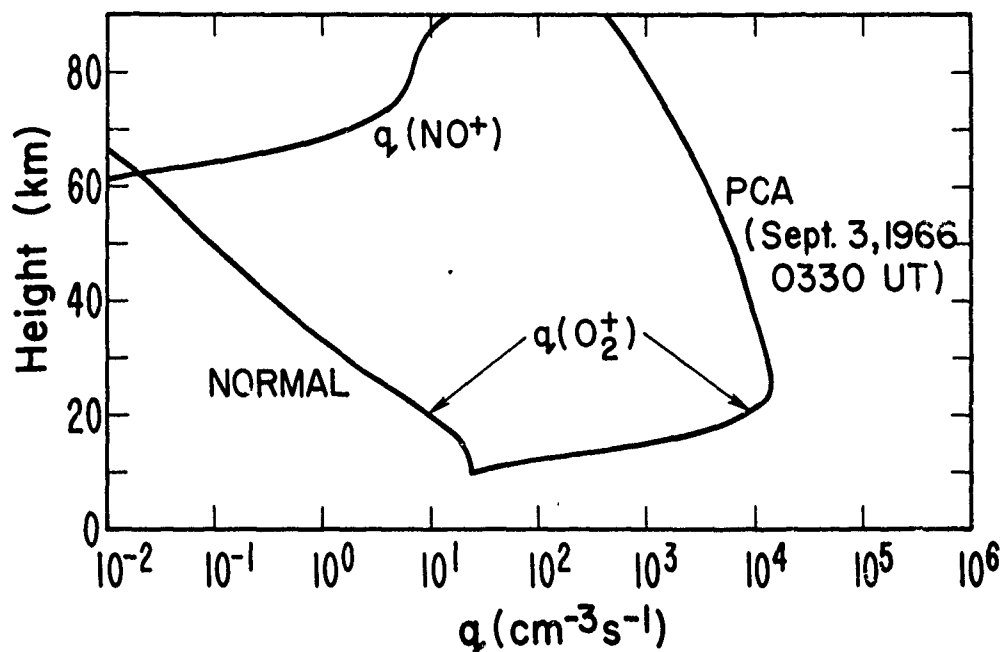
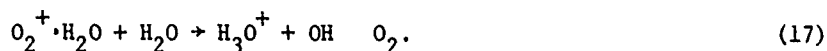


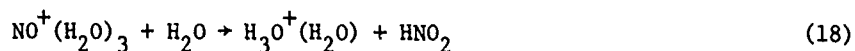
Figure 4. Ion production rate at the peak of the solar-proton event of September 1966 compared with undisturbed rates (Reid, 1979).

several large solar proton events (1960, 1966, 1972) the production of stratospheric NO was comparable to or larger than the total average annual production of NO by galactic cosmic rays. The August 1972 event led to a detected ozone decrease at high latitude and high altitude. The NO production is a consequence of both ionization and dissociation processes and is not precisely ion chemistry in the sense of this discussion.

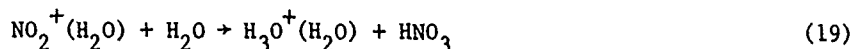
In the normal stratospheric ion chemistry,  $O_2^+$  is the major ion produced, either directly or by charge-transfer with  $N_2^+$ . Almost every  $O_2$  ionization will lead to an OH molecule production in the  $O_2^+$  deionization step,



Each  $NO^+$  ion produced will lead to a nitrous acid molecule by



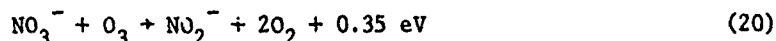
and each  $NO_2^+$  ion to a nitric acid molecule by



The number of  $NO^+$  and  $NO_2^+$  ions produced in the stratosphere however is quite negligible. The rate of OH production by (17) is negligible.

The number of ion pairs produced by galactic cosmic rays is less than  $10 \text{ cm}^{-3} \text{ s}^{-1}$  in the equatorial stratosphere, less than  $15 \text{ cm}^{-3} \text{ s}^{-1}$  at  $30^\circ$  and less than  $40 \text{ cm}^{-3} \text{ s}^{-1}$  at high latitude (Neher, 1967; Reid, 1979). This is not a significant production rate for most neutral atmospheric species. For example, the species in the ppb concentration range would need to have lifetimes as long as years in order for a production rate (= loss rate) as small as  $10 \text{ cm}^{-3} \text{ s}^{-1}$  to be significant. There are few stratospheric species with photolysis rates this low. In the ppt range on the other hand, a lifetime would only need to be a day for a  $10 \text{ cm}^{-3} \text{ s}^{-1}$  rate to be significant.

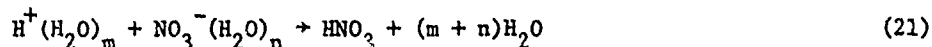
There have been a few suggestions of stratospheric neutral species destruction by ion molecule reactions. Ruderman et al. (1976) suggested that the reaction



might account for a reported solar cycle variation in stratospheric ozone; however, Fehsenfeld et al. found the rate constant for (20) to be much too low,  $k_{20} < 10^{-13} \text{ cm}^3 \text{ s}^{-1}$ .

The possibility that the stratospheric concentrations of critical species which are derived from the troposphere might be controlled by tropospheric ion chemistry has been considered. Fehsenfeld et al. (1976b), showed that the critical stratospheric species  $\text{CFCl}_3$  and  $\text{CF}_2\text{Cl}_2$  are not significantly removed in the troposphere by ions. It has also been shown that  $\text{N}_2\text{O}$  is not significantly removed in the troposphere by ion reactions before diffusing into the stratosphere (Fehsenfeld and Ferguson, 1976). It was also shown that the reactive chlorine species  $\text{Cl}$ ,  $\text{HCl}$ , and  $\text{ClO}$  are not removed in the stratosphere by ion-molecule reactions (Fehsenfeld et al. 1976b).

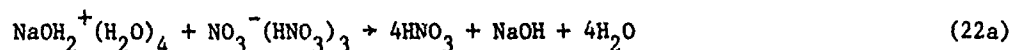
ION-ION RECOMBINATION: An interesting problem which has not yet been investigated in the laboratory is the nature of the neutral products of positive ion-negative ion recombination. This will lead to the net production of neutrals, e.g.  $\text{HNO}_3$  by



The numbers are not large,  $\sim 0.1 - 50 \text{ molecules cm}^{-3} \text{ s}^{-1}$ , depending on altitude, latitude and solar cycle.

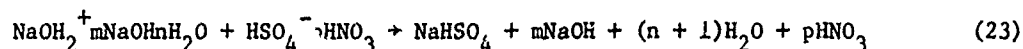
An interesting situation is that some of the ambient ions will be energetically unable to neutralize and separate into multiple species. For example in (21) for  $n+m > \sim 11$  the reaction is endothermic. With that extent of hydration the reverse reaction begins to approximate the solution (and ionization) of nitric acid, which of course is exothermic. The positive and negative ions will attract each other and stick together in a large cluster molecule containing all or most of the water molecules.

There are certainly cases involving observed stratospheric ions in which mutual neutralization is endothermic, e.g.



Channel (a) is  $45 \text{ kcal mol}^{-1}$  endothermic. Channel (b) is probably also endothermic.

The energetics of reactions such as



are uncertain because the thermochemistry of the species involved is not known.

The ions will of course still come together under the influence of the Coulomb attraction and form large dipolar ions, essentially microscopic ionized solution droplets. In the case of (23) for example, a solvated ion pair  $\text{Na}^+ \cdot \text{HSO}_4^- \cdot m\text{NaOH} \cdot \text{pHNO}_3 (n+1)\text{H}_2\text{O}$  will be produced, with

# FERGUSON

perhaps one or more of the neutral cluster molecules released during the association. An interesting possibility is that such microscopic solution droplets may serve as condensation nuclei.

## REFERENCES

- Aikin, A. C., Calcium Compounds as a Photoionization Source Below 70 km, EOS, 60, 336, 1979.
- Arijs, E., J. Ingels, D. Nevejans, Mass Spectrometric Measurements of the Positive Ion Composition of the Stratosphere, Nature, 271, 642, 1978.
- Arnold, F., H. Bohringer, G. Henschen, Composition Measurements of Stratospheric Positive Ions, Geophysical Research Letters, 5, 653, 1978.
- Arnold, F., G. Henschen, First Mass Analysis of Stratospheric Negative Ions, Nature, 275, 521, 1978.
- Arnold, F., R. Fabian, W. Joos, First Composition Measurements of Stratospheric negative ions, Geophysical Research Letters, in press 1980.
- Arnold, F., R. Fabian, First Measurements of Gas Phase Sulfuric Acid in the Stratosphere, Nature, submitted, 1980.
- Arnold, F., D. Krankowsky, K. H. Marien, First Mass Spectrometric Measurements of Positive Ions in the Stratosphere, Nature, 267, 30, 1977.
- Crutzen, P. J., I. S. A. Isaksen, G. C. Reid, Solar Proton Events: Stratospheric Sources of Nitric Oxide, Science, 189, 457, 1975.
- Davidson, J. A., A. A. Viggiano, C. J. Howard, I. Dotan, F. C. Fehsenfeld, D. L. Albritton, E. E. Ferguson, Rate Constants for the Reactions of  $O_2^+$ ,  $NO_2^+$ ,  $NO^+$ ,  $H_3O^+$ ,  $CO_3^+$ ,  $NO_2^+$ , and Halide Ions with  $N_2O_5$  at 300 K, Journal of Chemical Physics, 68, 2085, 1978.
- Dotan, I., J. A. Davidson, F. C. Fehsenfeld, D. L. Albritton, Reactions of  $O_2^+ \cdot O_2$  with  $CO_2$ ,  $O_3$  and  $CH_4$ , and  $O_2^+ \cdot O_3$  with  $H_2O$  and  $CH_4$ , and their role in stratospheric ion chemistry, Journal of Geophysical Research, 83, 4036, 1978.
- Fehsenfeld, F. C., E. E. Ferguson, Thermal Energy Positive Ion Reactions in a Wet Atmosphere Containing Ammonia, Journal of Chemical Physics, 59, 6272, 1973.
- Fehsenfeld, F. C., C. J. Howard, A. L. Schmeltekopf, Gas Phase Ion Chemistry of  $HNO_3$ , Journal of Chemical Physics, 63, 2835, 1975.
- Fehsenfeld, F. C., E. E. Ferguson, Reactions of Atmospheric Negative Ions with  $N_2O$ , Journal of Chemical Physics, 64, 1853, 1976.
- Fehsenfeld, F. C., E. E. Ferguson, G. E. Streit, D. L. Albritton, Stratospheric Ion Chemistry and the 11-Year Variation in Polar Ozone, Science, 194, 544, 1976a.
- Fehsenfeld, F. C., P. J. Crutzen, A. L. Schmeltekopf, C. J. Howard, D. L. Albritton, E. E. Ferguson, J. A. Davidson, H. I. Schiff, Ion Chemistry of Chlorine Compounds in the Troposphere and Stratosphere, Journal of Geophysical Research, 81, 4454, 1976b.
- Fehsenfeld, F. C., I. Dotan, D. L. Albritton, C. J. Howard, E. E. Ferguson, Stratospheric Positive Ion Chemistry of Formaldehyde and Methanol, Journal of Geophysical Research, 83, 1333, 1978.
- Ferguson, E. E., Sodium Hydroxide Ions in the Stratosphere, Geophysical Research Letters, 5, 1035, 1978.
- JANAF Thermochemical Tables, 2nd Edition, D. R. Stull, H. Prophet, Project Directors, NSRDS-NBS 37, 1971.
- Kearle, P., Ion Thermochemistry and Solvation from Gas Phase Ion Chemistry, Annual Review of Physical Chemistry, 28, 445, 1977.
- Liu, S. C., G. C. Reid, Sodium and Other Minor Constituents of Meteoric Origin in the Atmosphere, Geophysical Research Letters, 6, 283, 1979.
- Megie, G., F. Bos, J. E. Blamont, M. L. Chanin, Simultaneous Nighttime Lidar Measurements of Atmospheric Sodium and Potassium, Planetary and Space Science, 26, 27, 1978.
- Neher, H. V. Cosmic-Ray Particles That Changed from 1954 to 1958 to 1965, Journal of Geophysical Research, 72, 1527, 1967.
- Reid, G. C. The Middle Atmosphere, NASA CP-2090, report Middle Atmosphere Electrodynamics, Nelson Maynard, ed. 1979, p. 27.
- Ruderman, M. A., H. M. Foley, J. W. Chamberlain, Eleven-Year Variation in Polar Ozone and Stratospheric Ion Chemistry, Science, 192, 555, 1976.
- Smith, D., M. J. Church, Ion-Ion Recombination Rates in the Earth's Atmosphere, Planetary and Space Science, 25, 433, 1977.
- Smith, D. E., B. Munson, Proton Affinities of Some Sulfur-Oxygen Compounds, Journal of the American Chemical Society, 100, 497, 1978.
- Turco, R. P., P. Hamill, O. B. Toon, R. C. Whitten, C. S. Kiang, A One-Dimensional Model Describing Aerosol Formation and Evolution in the Stratosphere. I. Physical Processes and Mathematical Analogues., Journal of Atmospheric Science, 36, 699, 1979.
- Viggiano, A. A., R. A. Perry, D. L. Albritton, E. E. Ferguson, F. C. Fehsenfeld, The Role of  $H_2SO_4$  in Stratospheric Negative-Ion Chemistry, Journal of Geophysical Research, in press, 1979.



# OBSERVATION OF THE SOLAR ULTRAVIOLET RADIATION

Paul C. SIMON

Institut d'Aéronomie Spatiale de Belgique  
3, Avenue Circulaire, B-1180 Bruxelles, Belgique.

## Abstract

Ultraviolet solar irradiance observations at Lyman  $\alpha$  and between 175 and 400 nm are reviewed and discussed. The uncertainties between the different measurements are pointed out and the discrepancies are discussed in terms of solar variability showing the needs of new observations in order to determine accurately the absolute value of solar ultraviolet irradiation fluxes and their possible variations with the 11-year solar cycle.

## I. INTRODUCTION

The photodissociation processes of atmospheric constituents in the stratosphere and in the mesosphere are initiated by the solar radiation of wavelengths greater than 175 nm. As discussed extensively by Nicolet (1979), the penetration of solar irradiances in this wavelength range is driven by the absorption of molecular oxygen and of ozone, and by the Rayleigh scattering of light. Radiations of wavelengths below 175 nm are absorbed in the thermosphere, except for the Lyman  $\alpha$  emission line which penetrates deeply into the mesosphere, leading to the formation of the ionospheric D-region, and for the X-rays of wavelengths less than 1 nm. In order to determine the most reliable solar irradiation flux values to be used in photochemical models of the middle atmosphere, an accurate knowledge of the solar irradiances in the ultraviolet is required. Consequently, the available measurements must be critically discussed and compared.

Only full disc observation are pertinent for aeronomic purposes. Observations made with a spatial resolution on the solar disc cannot be considered because of the center-to-limb variation of the solar radiation. For instance, flux measurements made at the center of the disc for wavelengths beyond 152 nm represent only an upper limit for the

corresponding irradiance values because of the limb-darkening occurring in this part of the solar spectrum (Samain et al, 1975).

Among the most serious difficulties in determining the correct value of the solar irradiance are the uncertainties associated with each observation and the lack of inter-comparison of the calibration techniques used by the different experimenters. On the other hand, when comparing different sets of data, the possible variability of the solar fluxes with the 27-day rotation period of the sun and with the 11-year activity cycle must be taken into account. Variation related to solar flares can be neglected in the considered wavelength range, except for the Lyman  $\alpha$  emission line for which an enhancement of the order of 16% has been observed by Heath (1969) for a 3B flare and confirmed by Hall (1971) for other flare observations.

The purpose of this work is to present the recent ultraviolet solar irradiance measurements related to the middle atmosphere aeronomy, including the Lyman  $\alpha$  solar line. The uncertainties associated with the different experimental techniques of observation will be pointed out and the discrepancies between the data will be tentatively discussed in terms of solar variability.

## II. OBSERVATIONAL DATA

### The Lyman $\alpha$ emission line

The first measurement of Lyman  $\alpha$  irradiance was performed in 1949 by Friedman et al., (1951) using a rocket-borne photon counter and yield only an order of magnitude, between  $3.7 \times 10^{10}$  and  $3.7 \times 10^{11}$   $\text{hv} \cdot \text{sec}^{-1} \cdot \text{cm}^{-2}$ , for the intensity of this very strong chromospheric line. Since that time, many measurements, using various observational techniques, and leading to a conventional value of  $3 \times 10^{11}$   $\text{hv} \cdot \text{sec}^{-1} \cdot \text{cm}^{-2}$  have been made. For most of the observations, the quoted accuracy is of the order of  $\pm 30\%$ . That means that the irradiance of Lyman  $\alpha$  should be included between  $2.1$  and  $3.9 \times 10^{11}$   $\text{hv} \cdot \text{sec}^{-1} \cdot \text{cm}^{-2}$ .

Variations of this solar line with the 11-year cycle and with the 27-day rotational period of the sun, have to be considered and seem confirmed by observations performed during the solar cycles 19 and 20. But such variations are of the same order as the absolute accuracy claimed by the different experimenters. Hence, a main problem is to determine if these observed variations are due to calibration uncertainties, instrumental degradation or correspond to a real physical change of the solar output at this wavelength. The results obtained during the solar cycle 19 are summarized in table 1. These show a decrease from solar maximum conditions in 1960 to 1963, except for the value of Hinteregger (1961) which appears to be rather low in comparison with the other observations. During the same solar cycle, Weeks (1967) made an analysis of the results obtained by means of ion chambers over the interval between 1955 and 1966. His conclusion is that the variation of the Lyman  $\alpha$  irradiance appears to be of the order of 40% over the 11-year solar cycle.

Figure 1 shows the results of measurements performed during solar cycle 20. The most reliable measurements of Lyman  $\alpha$  variation are those obtained by means of the OSO 5 satellite (Vidal-Madjar, 1975). The experiment, which exhibits an instrumental sensitivity degradation of only 10% per year, leads to a variation of the order of 40%. Empirical relations relating the variability of Lyman  $\alpha$  irradiance with the 10.7 cm solar flux have been proposed by Vidal-Madjar (1975).

Variations related to the 27-day rotational period of the sun were measured for the first time by Kreplin et al. (1962) who deduced from SR 1 satellite observations, variations less than 18% in July 1960. Since that time, a maximum of solar variability of the order of 30% has been proposed on the basis of the observations of Hall and Hinteregger (1970), Heath (1973), Woodgate et al. (1973) and Vidal-Madjar (1975).

Nevertheless, due to calibration and instrumental problems, any quantitative conclusion concerning the solar Lyman  $\alpha$  variations may be subject to doubt. Table 2 presents a comparison of the OSO 5 data with rocket flight observations, showing that

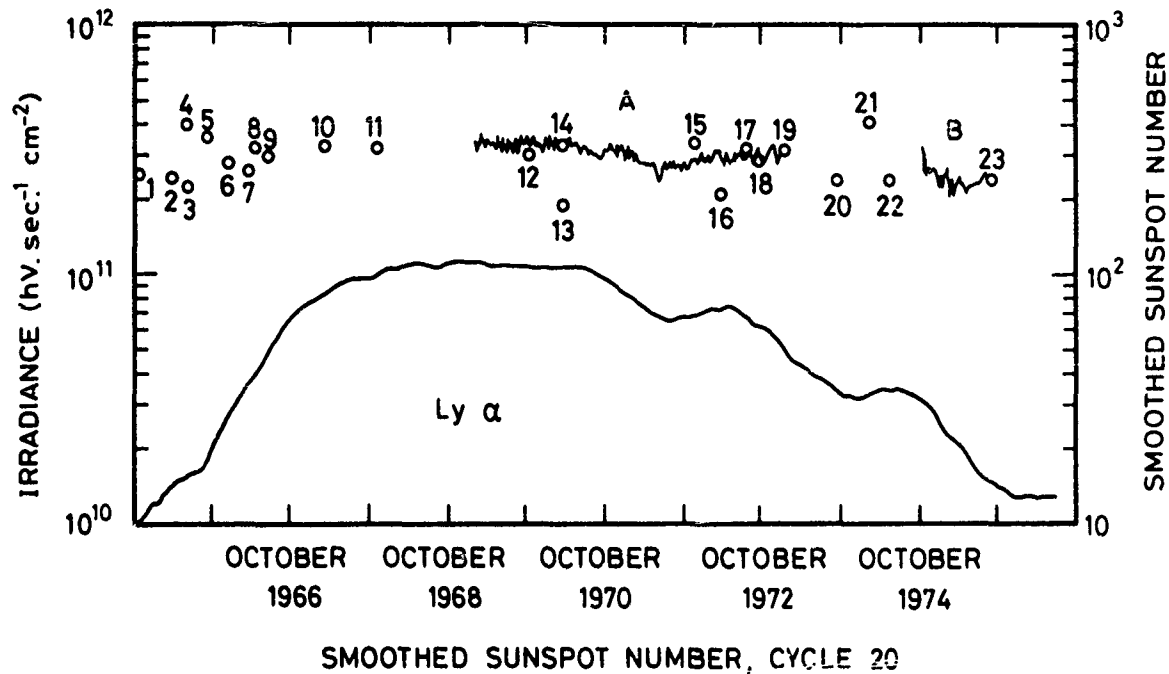


Fig. 1.- Comparison of Lyman  $\alpha$  solar irradiation flux measurements during the solar cycle 20. The smoothed sunspot numbers are also shown. References: 1, 2, 3, 4, 5, 6 and 9, Weeks (1967); 7, Fossi et al. (1969); 8, Bruner and Parker (1969); 10, Hinteregger (1970); 11, Bruner (private communication); 12, Woodgate et al. (1973); 13, Smith (1972); 14, Dickinson (1972); 15, Higgins (1976); 16, Ackerman and Simon (1973); 17, Prinz (1974); 18, Heroux et al. (1974); 19 and 20, Rottman (1974); 21, Oshio (private communication); 22, Heroux (private communication); 23, Rottman (private communication); A, Vidal-Madjar (1975); B, Vidal-Madjar (private communication) (after Delaboudinière et al., 1977).

## SIMON

TABLE 1.- Observation of the Lyman alpha irradiance during solar cycle 19.

Date	$10^{11} \text{ h sec}^{-1} \text{ cm}^{-2}$	Instrumentation	Reference
Oct 18, 1955	3,5	Ion Chamber	<u>Byram et al</u> (1956)
Oct 21, 1955	2,4	Ion Chamber	Id.
Nov 4, 1955	5,5	Ion Chamber	Id.
Dec 13, 1955	1,8	Spectrograph	<u>Miller et al</u> (1956)
Jul 20, 1956	3,7	Ion Chamber	<u>Chubb et al</u> (1957)
Jul 25, 1956	4,1	Ion Chamber	Id.
Jul 20, 1957	3,7	Ion Chamber	<u>Byram et al</u> unpu- blished data
Aug 6, 1957	2,1	Spectrograph	<u>Aboud et al</u> (1959)
Mar 23, 1958	3,9	Ion Chamber	<u>Byram et al</u> unpu- blished data
Jul 21, 1959	3,7	Ion Chamber	<u>Purcell and</u> <u>Tousey</u> (1960)
Jan 19, 1960	3,7	Ion Chamber	<u>Hinteregger</u> (1960)
Apr 19, 1960	3,7	Ion Chamber	<u>Detwiler et al</u> (1961)
Aug 20, 1960	3,4	Photoelectric	<u>Efremov et al</u> (1962)
Aug 23, 1960	2,0	Monochromator	<u>Hinteregger</u> (1961)
Aug 23, 1961	3,1	Monochromator	<u>Hall et al</u> (1963)
Dec 12, 1963	2,7	Monochromator	<u>Hall et al</u> (1965)

## SIMON

TABLE 2.- Lyman alpha irradiance : comparison of the OSO 5 data with  
 rocket flight observations (after Vidal-Madjar, 1977)

	OSO 5 ( $10^{11} \text{ h} \cdot \text{sec}^{-1} \cdot \text{cm}^{-2}$ )	Rocket data	Reference for rocket data
Mar 7, 1970	4,41	- 6%	<u>Dickinson</u> (1972)
Nov 9, 1971	~ 2,8	+ 26%	<u>Higgins</u> (1976)
Feb 28, 1972	~ 3,0	- 30%	<u>Ackerman and</u> <u>Simon</u> (1973)
Jul 10, 1972	3,1	+ 8%	<u>Prinz</u> (1974)
Aug 23, 1972	2,99	- 3%	<u>Heroux et al</u> (1974)
Dec 13, 1972	2,88	+ 10%	<u>Rottman</u> (1974)

most of the data from rocket measurements are in good agreement with the OSO 5 results (less than 10%). Consequently, the 30% variation with the 27-day rotational period of the sun and the factor of 2 variation with the 11-year cycle deduced from the OSO 5 satellite, should be realistic but need experimental confirmation during the following solar cycles.

#### The 175-240 nm wavelength interval

This wavelength interval is mainly related to the photodissociation of molecular oxygen in the mesosphere and in the upper stratosphere.

The source of the solar spectrum in this wavelength interval lies in a transition region of the solar atmosphere, between the photosphere and the chromosphere. Absorption lines which dominate the solar spectrum in the visible and in the near ultraviolet disappear progressively in the vacuum ultraviolet range in which emission lines of chromospheric origin become predominant around 150 nm. This is illustrated in figures 1 and 2 published by Samain and Simon (1976).

Unfortunately, the solar irradiation fluxes are not sufficiently well known, especially between 175 and 200 nm, corresponding to the Schumann-Runge absorption band system of molecular oxygen. The first measurement of solar irradiance in this wavelength interval were made by Detwiler et al. (1961) in 1960 by means of a rocket-borne spectrograph, but their results appear too high, by a factor of 3, in comparison with the more recent observations. The only measurements covering all the 175-200 nm wavelength interval are those of Samain and Simon (1976) and those of Brueckner et al. (1976). They measured, respectively, the solar radiance at the center of the disk and at a selected area of the quiet sun using photographic recording techniques. These radiances were converted into solar irradiance using the center-to-limb variations measured by Samain and Simon (1976). Other values covering, partially, the same wavelength range have been obtained by Rottman (1974), Simon (1974) and Heroux and Swirbalus (1976). All this results are given in figure 2 for comparison. The agreement between these authors is good at 175 nm but beyond this wavelength, disagreement, reaching a factor of two, can occur for given wavelengths. The agreement becomes better, within 20%, around 200 nm for the observations of Simon (1974), Samain and Simon (1976) and Brueckner et al. (1976). It should be pointed out that solar irradiances determined by Samain and Simon (1976) and by Brueckner et al. (1976) are not direct measurements of the full disc. They used limb-darkening data in order to determine irradiance values from radiance data based on photographic spectra for which calibration procedures are more complicated. This method introduces certain additional errors, leading to less accurate results. On the other hand, both instruments used by Rottman (1974) and by Heroux and Swirbalus (1976) have photoelectric detectors with a solar blind CsI photocathode for which the quantum yield exhibits a rapid decay for wavelengths greater than 185 nm. This is illustrated in figure 1 published by Heroux and Swirbalus (1976). Thus, accuracies of solar irradiation flux measurements beyond this wavelength are not as good as those at lower wavelengths because the laboratory determination of the spectral sensitivity could have more important experimental uncertainties. In conclusion, one may consider that, between 180 and 190 nm, the data of Samain and Simon (1976) represent the upper limit for the solar irradiance while the data of Heroux and Swirbalus (1976) could give a lower limit. Consequently, the solar irradiation flux is only known with a precision of  $\pm 25\%$  in this wavelength range and a mean value between the different observations should be introduced in the photodissociation calculations.

Beyond 200 nm, the recently published measurements of Broadfoot (1972), Simon (1974) and Simon et al. (1980) should be only considered in deducing the solar irradiation flux values. They are given in figure 3 and 4 for comparison. The previous observations of Ackerman et al. (1971), obtained by means of a balloon-borne spectrometer, are 40% higher than those obtained by Simon (1974) who used a spectrometer integrated in a stabilized gondola. This allowing direct pointing of the instrument toward the sun.

The measurement of solar irradiation fluxes from balloon-based platforms must, obviously, be corrected for the residual absorption by molecular oxygen and ozone because of the floating altitude, of the order of 40 km, reached by a stratospheric

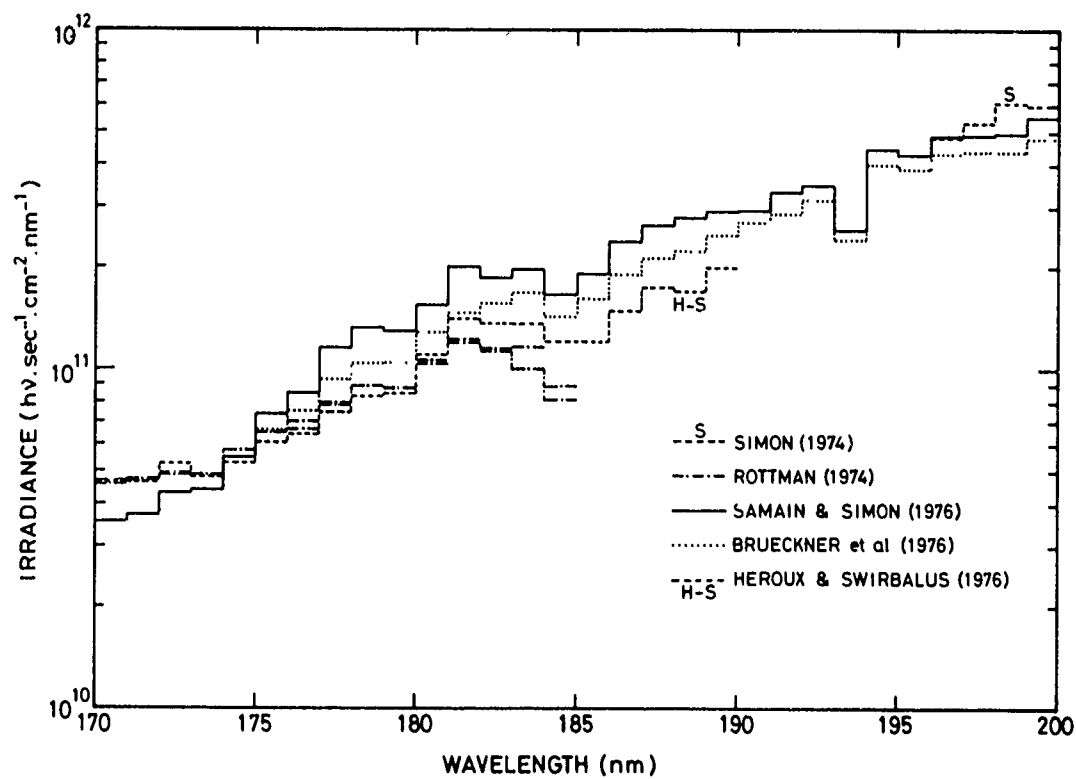


Fig. 2.- Comparison of ultraviolet solar irradiation fluxes reported by various experimenters from 170 to 200 nm.

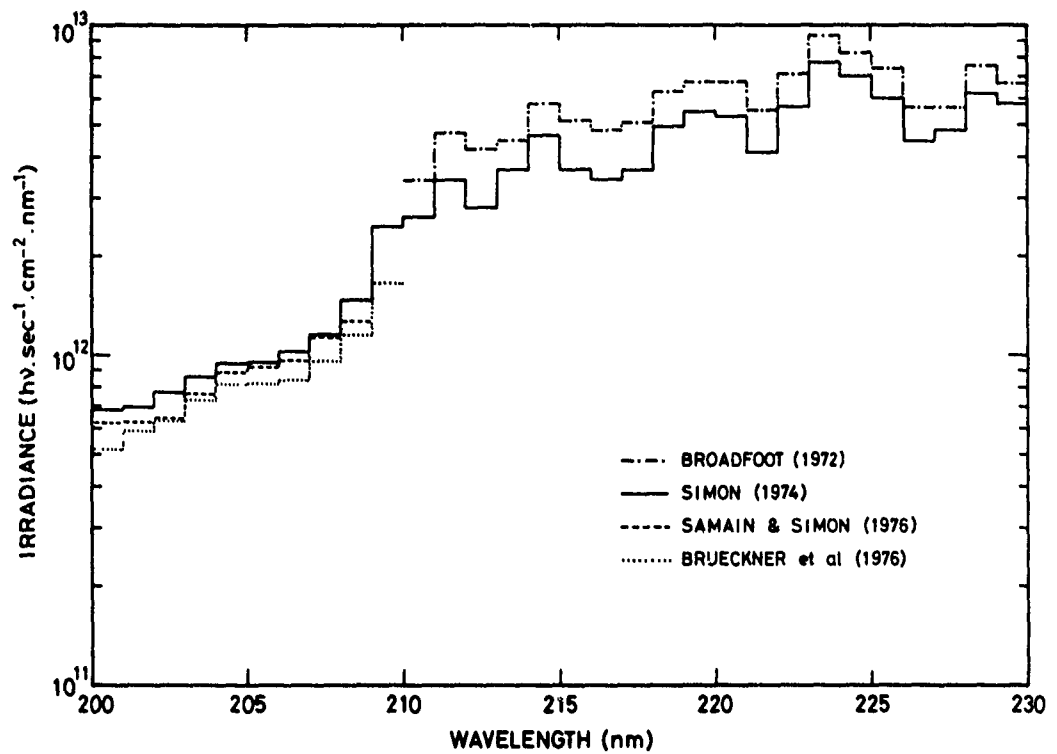


Fig. 3.- Comparison of ultraviolet solar irradiation fluxes reported by various experimenters from 200 to 230 nm. The measurements made by Ackerman et al (1971) and Simon et al. (1980) are not represented here for the sake of clarity.



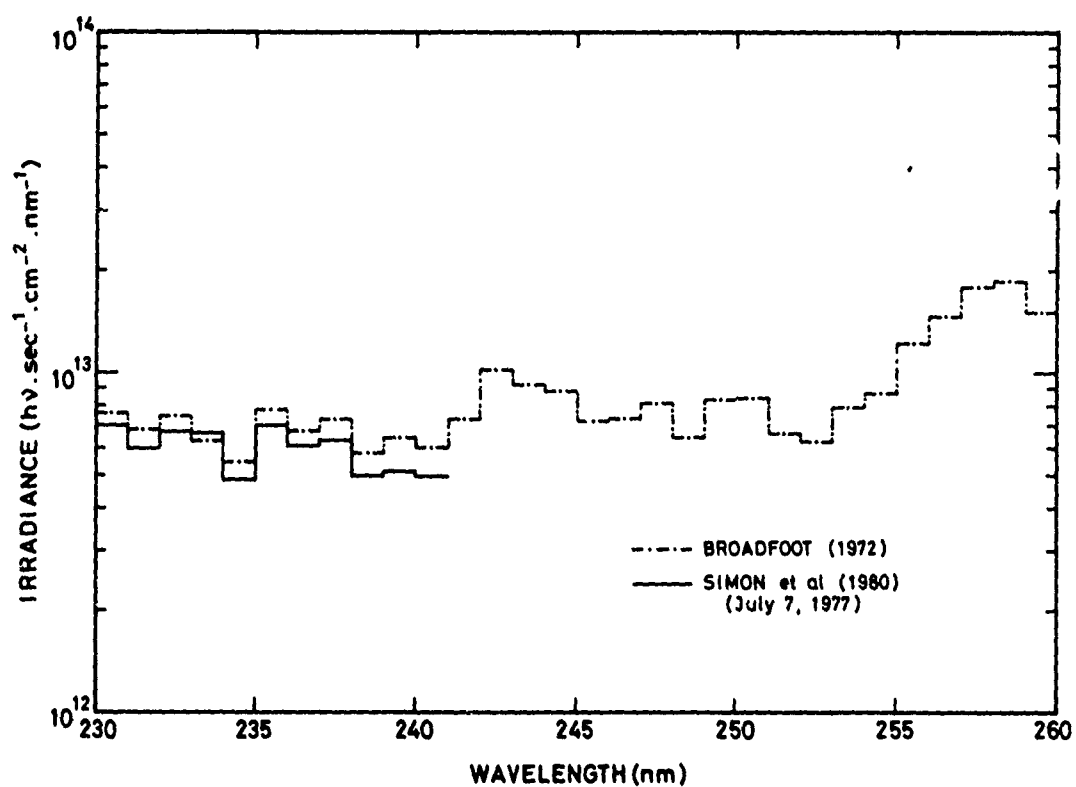


Fig. 4.- Comparison of ultraviolet solar irradiation fluxes reported by various experimenters from 230 to 260 nm.

balloon. Observations are made for different solar zenith angles and extraterrestrial solar irradiances can be deduced by extrapolation of measured solar fluxes to zero air mass. This can be done only if the floating altitude of the balloon is held rigorously constant in order to keep, for all recorded spectra, the same column content for molecular oxygen and ozone above the gondola. A second method consists for correcting the observed spectra by taking into account the real stratospheric absorption. For this purpose, accurate determination of molecular oxygen and ozone concentration should be carried out during the solar flux observations, on the same gondola. Both reduction methods have been used for the data obtained in 1973 by Simon (1974), giving a good agreement, within  $\pm 5\%$ , between the results obtained through these two different ways. This except for wavelengths beyond 225 nm where the influence of the altitude variation is very important on solar irradiance values deduced by extrapolation to zero air mass, due to the higher ozone absorption cross section above 225 nm. Molecular oxygen content was determined through pressure measurements and ozone column density was measured by means of the solar spectra recorded between 270 and 285 nm by the same solar spectrometer.

New balloon observations have been performed in 1976 and in 1977, giving solar irradiance values between 210 and 240 nm with an accuracy of  $\pm 15\%$  (Simon et al., 1980). The comparison with the previous balloon observations published by Simon (1974) and with the rocket measurement published by Broadfoot (1972) is shown on figure 5. The two recent balloon observations are, in general, in very good agreement, better than  $\pm 5\%$ , except beyond 235 nm. They give higher values than those published in 1974, with a maximum discrepancy of 9% for the 1976's flight and of 5% for the 1977's flight, over the 210-235 nm wavelength interval. Broadfoot's results, given with an accuracy of  $\pm 10\%$ , are systematically higher by a factor varying from 23% to 12% for wavelengths increasing from 200 to 240 nm. Such disagreement could be due to different calibration techniques or could be interpreted in terms of solar variability with the 11-year cycle and will be discussed later.

#### The 240 - 400 nm wavelength interval

This wavelength interval mainly related to the photodissociation of ozone has been investigated by many observers involving rocket borne spectrometers measuring solar irradiance between 210 and 320 nm (Broadfoot, 1972), satellite measurements at 12 discrete wavelengths between 255 and 340 nm (Heath, 1973), balloon-borne observation between 270 and 350 nm (Simon, 1975 and Simon et al., 1980), aircraft measurements performed by Arvesen et al. (1969) from 300 nm up to the infrared and ground-based observations by Labs and Neckel (1970) between 330 nm and 1250 nm. The only measurement covering the wavelength range between 240 and 280 nm was published by Broadfoot (1972) who quoted a calibration accuracy of  $\pm 10\%$ . The agreement with results of Heath (1973) as rather good. These latter measurements of solar irradiances have been made with a double ultraviolet spectrometer on board the Nimbus 4 satellite, launch in April 1970. The final accuracy is limited by the accuracy of the standard source used, namely  $\pm 8\%$  at 250 nm,  $\pm 4\%$  at 290 and  $\pm 3\%$  beyond 300 nm.

Figure 6, 7 and 8 presents measurements available beyond 280 nm. Discrepancies of the order of 25%, but reaching 40% at given wavelengths, appears in the 300-320 nm wavelength interval between Broadfoot (1972) and Arvesen et al. (1969). It should be pointed out that Broadfoot (1972) claimed an error larger than  $\pm 10\%$  for only wavelengths beyond 300 nm while Arvesen et al. (1969) estimate their error to be  $\pm 25\%$  at 300 nm,  $\pm 6\%$  at 320 nm and  $\pm 3.2\%$  at 400 nm. Consequently, data between 300 and 320 nm, taken from these two observations, should be considered very carefully. On the other hand, the absolute radiometric scale used for calibration by Arvesen et al. (1969) suffers from uncertainties due to changes in the spectral irradiance scale of the National Bureau of Standards in 1973 (Kostrowski, 1974). For all these reasons, data published by Simon (1975), which are in good agreement with Broadfoot (1972) below 300 nm give useful solar irradiance in this wavelength region. In addition, new balloon observations performed in 1976 and 1977 (Simon et al., 1980) give solar irradiance within  $\pm 10\%$ , in agreement with the results obtained in 1972 and 1973 (figure 9). The absolute accuracy is of the order of  $\pm 10\%$  and the good reproducibility of the different balloon experiments allows to conclude that the solar irradiance around 300 nm is actually known within 10%.

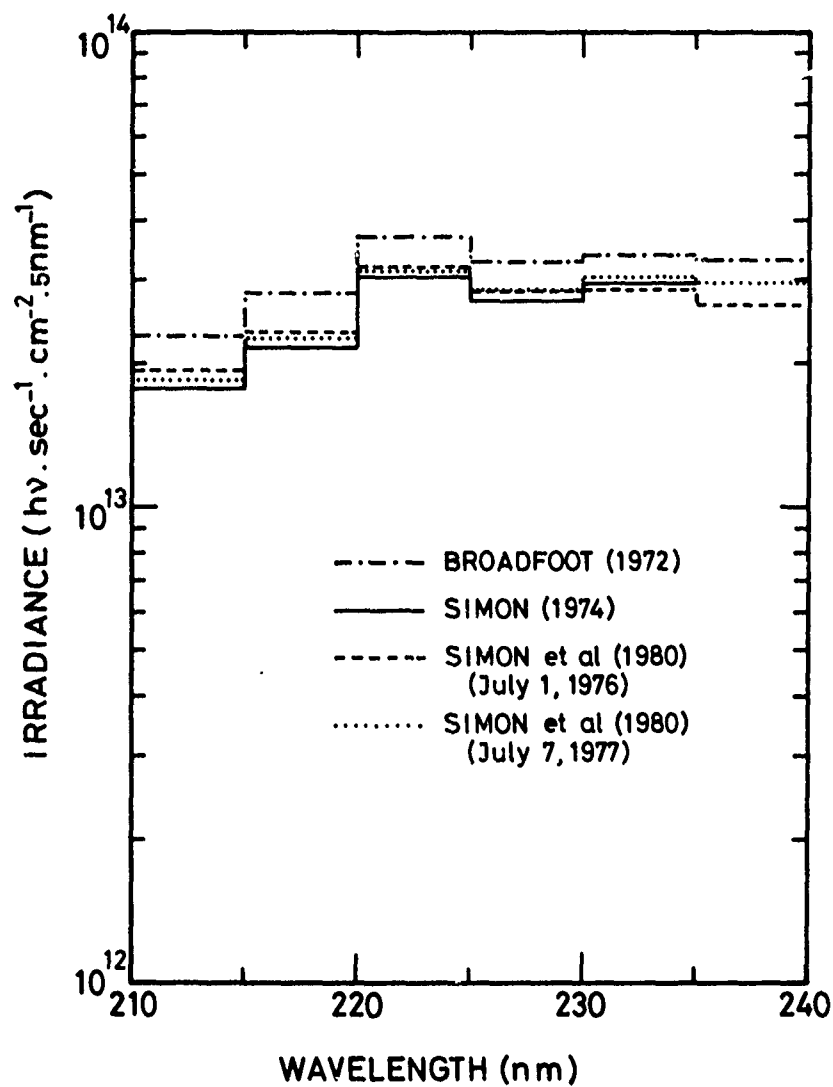


Fig. 5.- Comparison of ultraviolet solar irradiation flux integrated over 5 nm, obtained by balloon and rocket experiments between 210 and 240 nm.

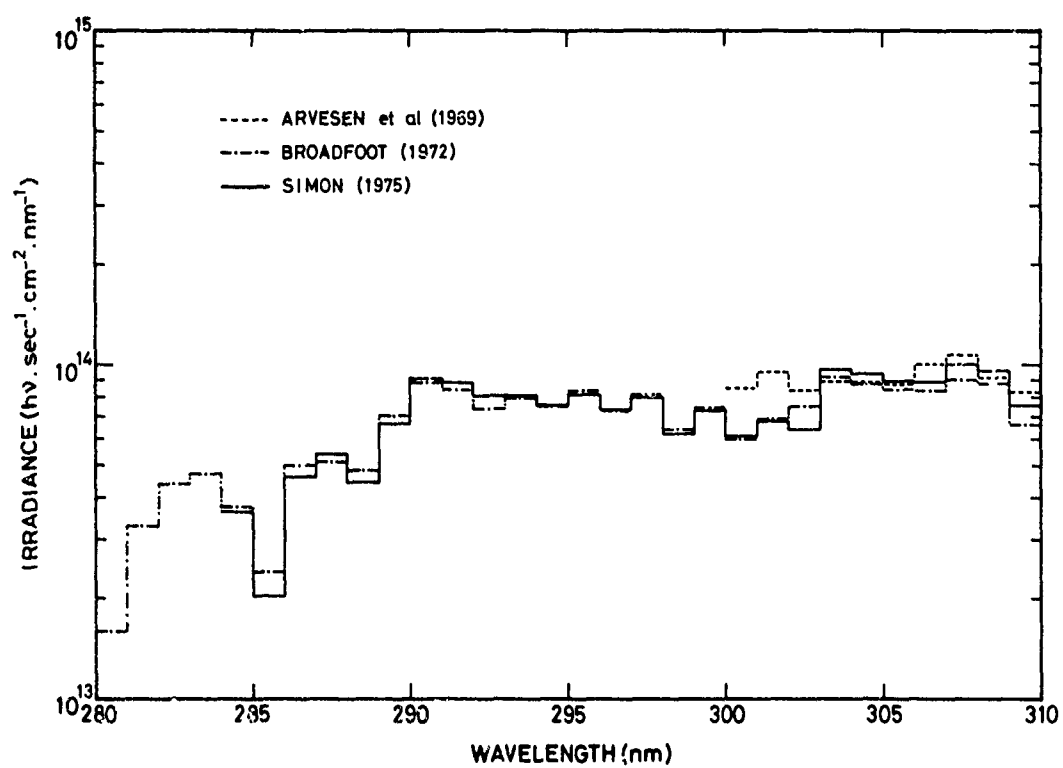


Fig. 6.- Comparison of ultraviolet solar irradiation fluxes reported by various experimenters from 280 to 310 nm.

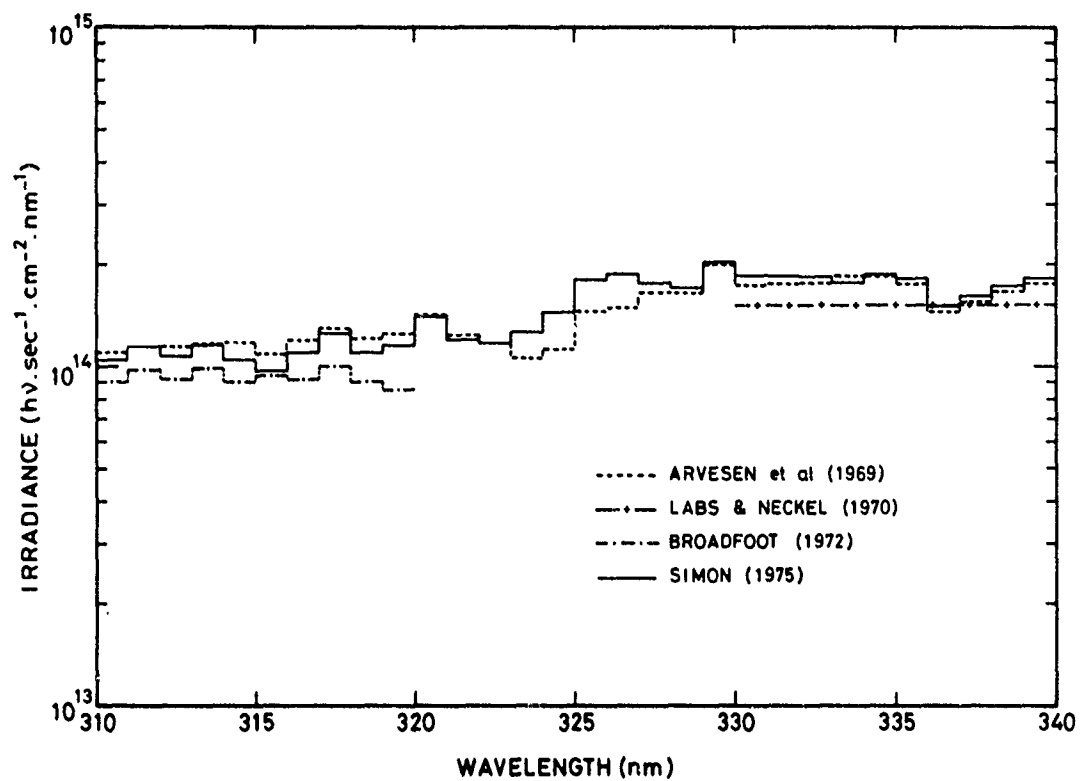


Fig. 7.- Comparison of ultraviolet solar irradiation fluxes reported by various experimenters from 310 to 340 nm.

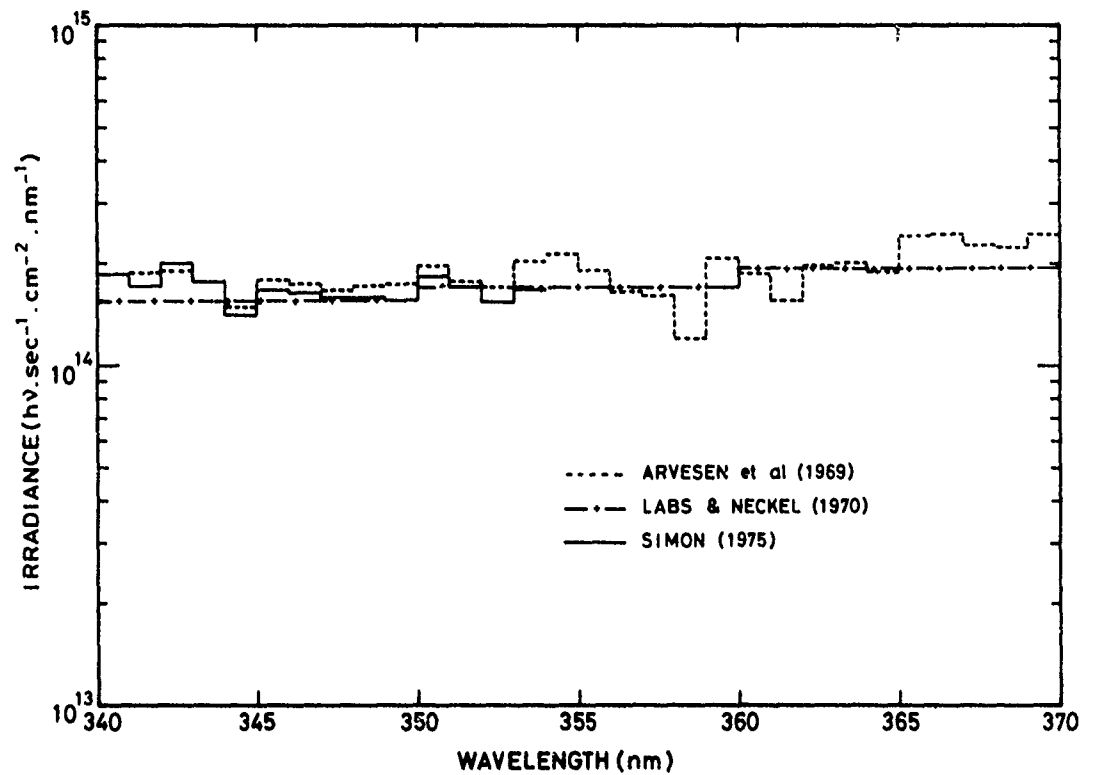


Fig. 8.- Comparison of ultraviolet solar irradiation fluxes reported by various experimenters from 340 to 370 nm.

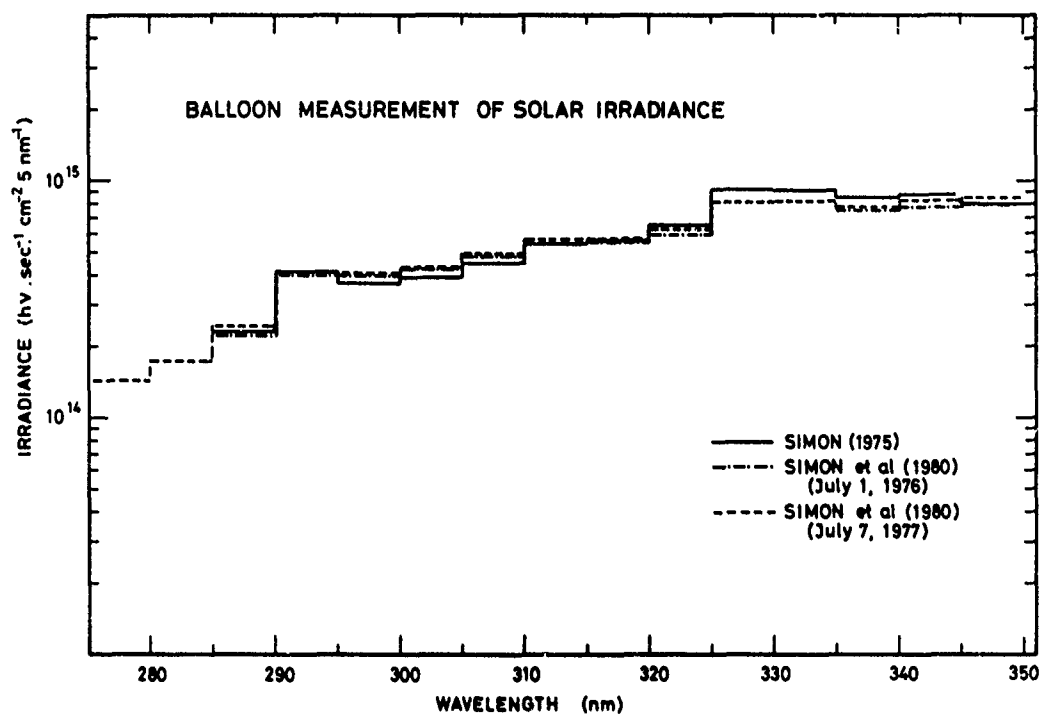


Fig. 9.- Comparison of ultraviolet solar irradiation flux integrated over 5 nm, obtained by balloon experiments between 280 and 350 nm.

Other observations have been performed from a Convair Jet aircraft belonging to NASA by Thekaekara et al. (1969). The published irradiance values, integrated over 5 nm, are, in fact, an average between data coming from four different instruments. These are : a single and a double monochromator, a filter radiometer and an interferometer. Other irradiance values beyond 300 nm, with the wavelength interval of 0.1 nm, have also been published by Thekaekara (1974) but, unfortunately, an error in the wavelength scale makes it difficult to make a correct comparison with the other measurements (Simon, 1975).

Very accurate ground-based observations have been carried out by Labs and Neckel (1970) from a high mountain observatory for wavelengths beyond 330 nm. Irradiance values were deduced from radiance measurements near the disc center and converted into irradiation fluxes using the limb-darkening data of David and Elste (1962). Absolute calibration was referenced to the International Practical Temperature Scale-1968. The near ultraviolet and visible irradiance values given by Labs and Neckel (1970) for 10 nm intervals could be used in order to adjust the data of Arvesen et al. (1969), obtained with a higher resolution, into a correct radiometric scale for wavelength above 330. Nevertheless, it should be taken into account that the data of Labs and Neckel (1970), which extends up to 1250 nm, leads to a solar constant value of  $1358 \text{ W.cm}^{-2}$  which is 0.9% lower than the recent solar constant measurements obtained by Willson and Hickey (1977), giving a value of  $1370 \text{ W.m}^{-2}$ .

#### Variability with the 27-day rotational period

Except in the case of the Lyman- $\alpha$  emission line, already discussed, very few investigations on this subject have been made experimentally. Only two reliable observations are available : firstly those published by Heath (1973) based on broad-band sensors on board of the satellites Nimbus 3 and 4, which were launched, respectively, in April 1969 and April 1970, and, secondly, those published by Hinteregger et al. (1977) who observed ultraviolet flux variations during the 1974-1976 period by means of a spectrometer on board of the satellite Atmospheric Explorer C. An additional observation has been performed by Prag and Morse (1970) but results have been obtained for only one solar rotation, leading to a variation of more than 50% for the broad wavelength interval 160-210 nm. This value seems too high by comparison with data obtained by Heath (1973) and Hinteregger et al. (1977) given in figure 10. For these authors, the irradiance variation beyond 175 nm, related to the 27-day rotational period, is less than 10% and are decreasing with increasing wavelength to be of the order of 1% around 300 nm. The value for wavelengths between 175 and 210 nm is also confirmed by Brueckner et al. (1976) on the basis of plage radiance measurements. Consequently, it appears that solar variation around 200 nm with its 27-day rotational period is of the same order of magnitude as the variability due to the semi-annual change of the sun-earth distance, corresponding to a  $\pm 3.3\%$  variation for the total solar irradiance.

#### Variability with the 11-year cycle

The solar irradiation flux variability with the 11-year cycle is very poorly known for all the solar spectrum. Long-term variability of the extreme ultraviolet flux with the solar cycle is quite evident but, even in this wavelength range, the data available do not suffice to determine, quantitatively, any variations during the last solar cycle (Schmidtke, 1978). The situation is worse in the wavelength range related to the middle atmosphere photodissociation processes. The inadequate time coverage of reliable data during the solar cycle 20 and the errors associated with each available measurement do not permit quantitative conclusions of solar variability with the 11-year cycle as it was stated by Simon (1978) and Delaboudiniere et al. (1978). This is illustrated by figures 11 and 12.

Nevertheless, quantitative variation of the solar irradiance between 175 and 380 nm has been proposed recently by Heath and Thekaekara (1977) on the basis of broad-band photometric observations by the Monitor of Ultraviolet Solar Energy experiment (MUSE) from a rocket flight in August 1966 and from satellites Nimbus 3 and 4 in April 1969 and April 1970, respectively. Another data were obtained with the double spectrometer on board of Nimbus 4 and Explorer 55 satellites, the latter launched in November 1975. The



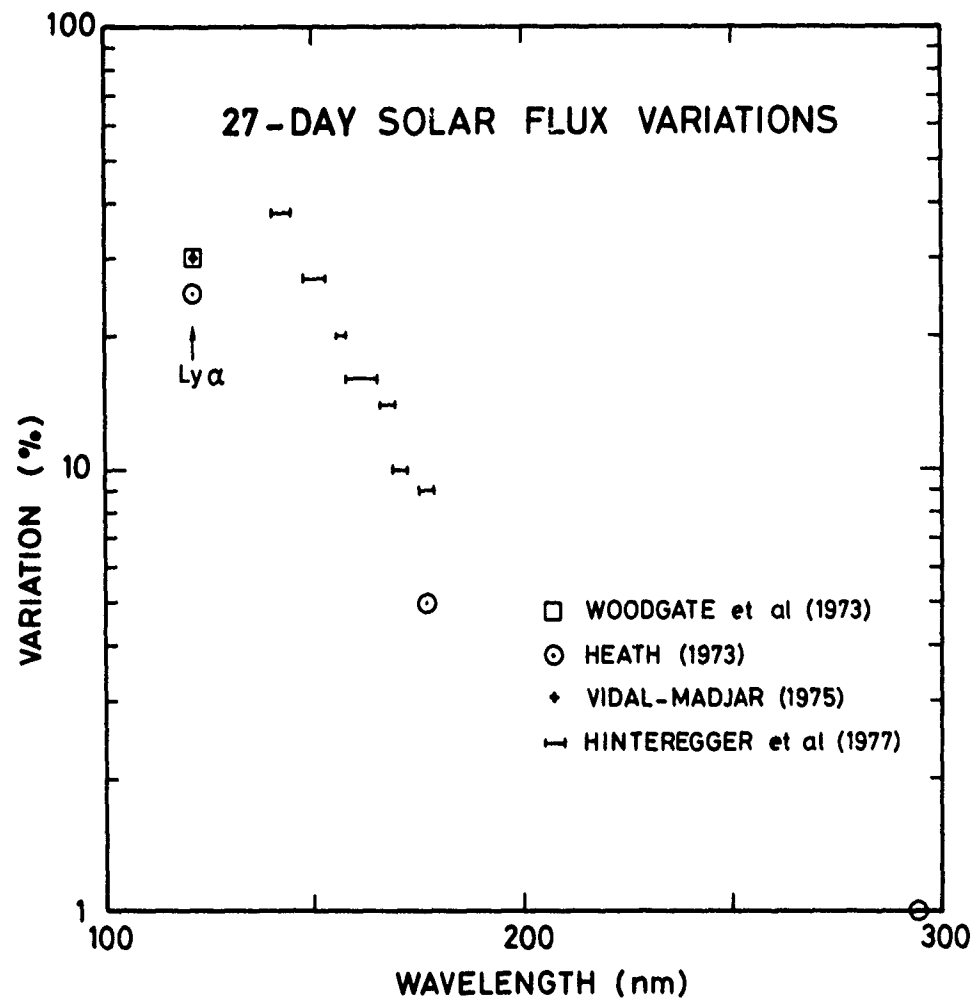


Fig. 10.- Solar flux variations related to the solar rotational period from Lyman  $\alpha$  to 300 nm. The values of Hinteregger et al. (1977) correspond to the Carrington rotation n° 1615 (June 1974).

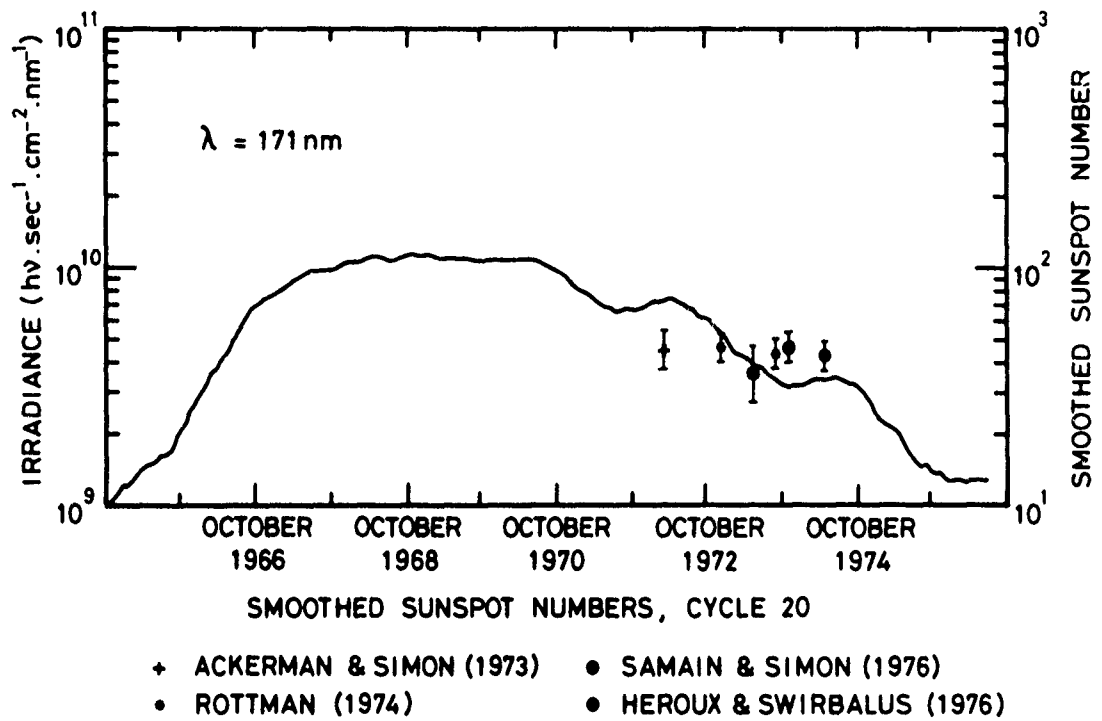


Fig. 11.- Comparison of solar irradiation flux measurements at 171 nm during the solar cycle 20. The smoothed sunspot numbers are also shown.

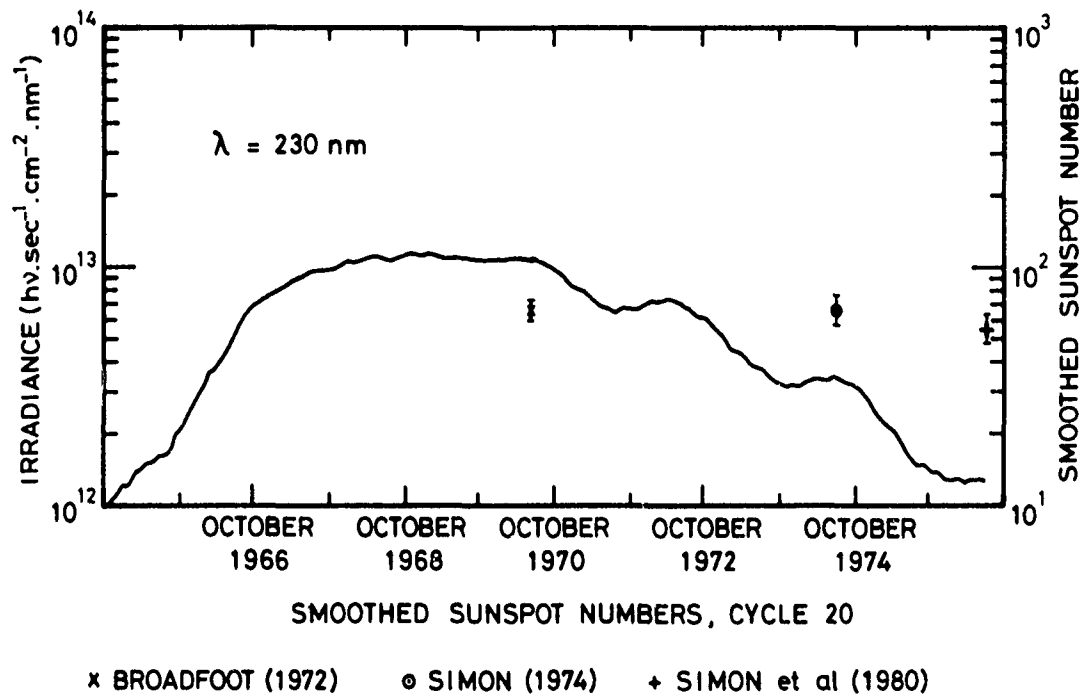


Fig. 12.- Comparison of solar irradiation flux measurements at 230 nm during the solar cycle 20. The smoothed sunspot numbers are also shown.

results are shown by figure 13 based on NASA (1977) and giving the ratio of solar irradiance measured at solar minimum to that at solar maximum. The solid curve represents the proposed solar variability during the cycle 20 for wavelengths between 170 and 340 nm. The accuracies of the data obtained by the broad-band sensors are, respectively,  $\pm 15\%$  and  $\pm 30\%$  for the shorter and the longer wavelength detector and between  $\pm 8\%$  and  $\pm 3\%$  for the double monochromator. Only two different ratios are available around 180 nm and the other values obtained around 290 nm with the double monochromator are higher by a factor of 15-20% than those obtained from the broad-band detectors at the same wavelength. A linear regression calculation is illustrated by the dashed lines for each type of measurements. Extrapolation to 320 nm of the solar irradiance ratio, obtained from the broad-band detectors data, give a variability ratio of 25% which disagrees with the variability ratio of 5% at the same wavelength based on the double monochromator measurements. In addition, extrapolation of these latter observation to 200 nm leads to a variability ratio of only 0.68 but there is no experimental evidence for either a linear dependance or for other functions of the solar variability dependance with the wavelength. Taking into account the possible experimental errors on the irradiance observations and the lack of data related to the solar activity, the validity of this curve needs to be confirmed by new measurements during solar cycle 21, with accurate cross-calibration making possible the intercomparison between the new data. The factor of 2 of variability claimed by Heath and Thekaekara (1977) seems also too high because there is no astrophysical reasons leading to variations with the 11-year cycle at 200 nm comparable to those observed for the Lyman  $\alpha$  chromospheric line. This represents the maximum possible long-term variability in the extreme-ultraviolet wavelength range.

These comments seem to be confirmed by the new observations made by means of a balloon-borne spectrometer in 1976 and 1977 already mentioned (Simon et al, 1980) and corresponding to a period of solar minimum activity. Comparing these data with those of Broadfoot (1972), obtained for solar maximum activity, variations between 210 and 240 nm could be included between 23% and 12%, the ratio decreasing with increasing wavelength, if the differences between these authors are interpreted as only variability of the solar output and not as experimental uncertainties which are of the order of  $\pm 15\%$ . Such a variation range shows the need of new measurements with both better accuracy and precision between 175 and 240 nm in order to deduce correct quantitative variabilities in this wavelength interval. Around 300 nm, there is no more conclusive evidence of variabilities of the order of 15%, due also to the uncertainties associated with each available measurement. Around 400 nm and in the visible range new observations of solar irradiance performed by Shaw and Fröhlich (1979) by means of a filter radiometer located at the Mauna Loa observatory in Hawaii do not cover a sufficiently large period of time: only 6 months of results were published and do not allow quantitative long-term variation determinations in this part of the solar spectrum.

### III. CONCLUSION

The ultraviolet solar irradiation flux observations related to the middle atmosphere have been extensively described and the current position of the accuracies and of the discrepancies between the different measurements is summarized in table 3. Uncertainties of laboratory radiometric standard sources and specific requirements for the future observations are also given.

The discrepancies are rather large and cannot be unambiguously interpreted as being caused by solar variabilities, due to the experimental errors associated with each measurement, to the inadequate time coverage during solar cycle 20, and to the lack of intercomparison of the calibration results of the instruments. The laboratory radiometric standards have a smaller uncertainty than the present measurement, and future observation accuracy requirements could be fulfilled :

- i) if a carefully calibration in the laboratory is made, allowing the transfer of the standard source accuracy to the instrument with little degradation, and
- ii) if the errors introduced by the measurements on the sun itself, in space environment, are reduced by appropriate techniques eliminating the degradation of the calibration accuracy.

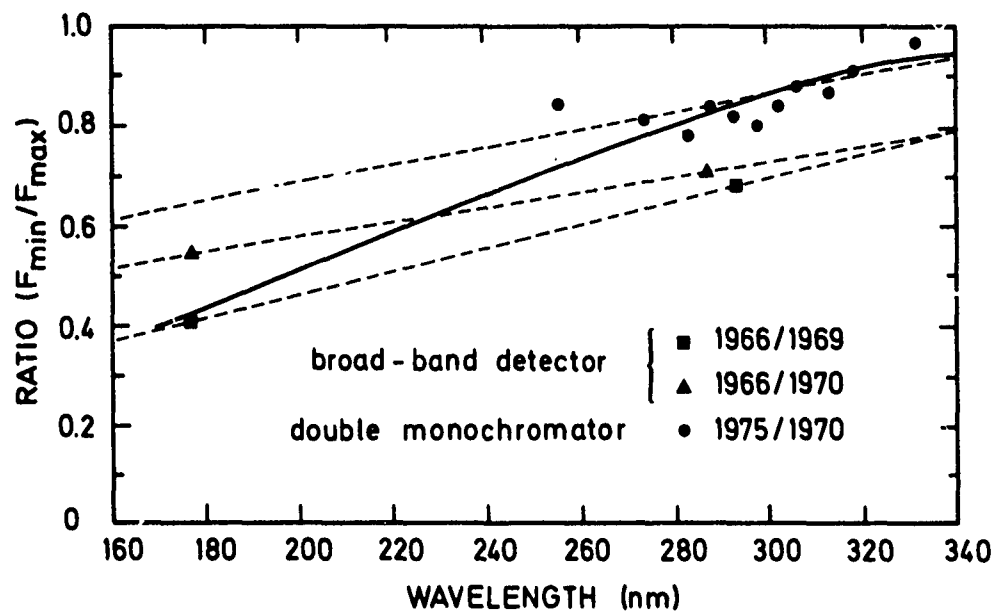


Fig. 13.- Ratio of solar flux measured near solar-cycle minimum to that measured near solar-cycle maximum versus wavelength (see text for explanations).

TABLE 3.- Uncertainties on solar ultraviolet irradiance measurements and  
 future needs

$\Delta\lambda(\text{nm})$	Ly $\alpha$	175 - 210	210 - 240	240 - 330	330 - 400
Quoted accuracy	$\pm 30\%$	$\pm 30\% - \pm 20\%$	$\pm 20\% - \pm 10\%$	$\pm 10\% - \pm 4\%$	$\pm 10\% - \pm 4\%$
Discrepancies between relevant observations	100%	50%	30%	25%	15%
Uncertainties on available standard sources	5%	5%	5%	3%	2%
Required accuracy	10%	5%	5%	5 to 2%	1 to 0.3%
Required precision	5%	1%	1%		

The cleanliness of the experiment is certainly an important factor to improve the validity of the future observations (Madden, 1978). A different method consists to measure directly the aging of the instrument sensitivity during the preflight storage, the measuring mode in space and after the flight. This implies that the instrument includes an in-flight calibration source and will be recoverable after the solar observation. The Space Shuttle, having a relatively short mission in space, without any severe limitation in weight and in power supply, seems a promising method since it allows the control of the ground calibration validity during and after the space observations. In addition, it could be now conceivable to recover a free-flyer instrument after a long survey of the sun and to measure in the laboratory its degradation in order to see which components are really aging in space environment, improving our knowledge on the proper choice of the materials.

Moreover, observations with different experimental techniques are required to eliminate the systematic errors. However intercomparison of calibration results for the various instruments should be performed before the flights to ensure a proper intercomparison of irradiance results after the flights.

The question of variability of the solar irradiance could be solved if new observations are performed with a correct time sampling, by means of repeated measurements with a very high precision. Variability measurements made from satellites will be only useful if the aging of the instrument sensitivity is checked by means of cross-calibrated observations with balloon, rocket or shuttle-borne instruments.

Such a measurement strategy for the near future could be applied to the "Solar ultraviolet Spectral Irradiance Measurement" and the "Solar Spectrum" experiments both on board the Space Shuttle, to the ultraviolet spectrometer on board the satellite "Solar Mesospheric Explorer", and to the rocket and the balloon observations performed during the same period by various laboratories.

## REFERENCES

- ABOUD, A., W.E. BERGING, W.A. RENSE, Emission-line intensities in the solar ultraviolet, Astrophys. J., 130, 381, 1959.
- ACKERMAN, M., P.C. SIMON, Rocket measurements of solar fluxes at 1216, 1450, and 1710 A, Solar Phys., 30, 345, 1973.
- ACKERMAN, M., D. FRIMOUT, R. PASTIELS, New ultraviolet solar flux measurements at 2000 A using a balloon borne instrument, New techniques in space astronomy, (Eds. Labuhn and Lüst), p. 251, D. Reidel, Dordrecht, Holland, 1971.
- ARVESEN, J.C., R.N. GRIFFIN Jr., B.D. PEARSON, Jr., Determination of extraterrestrial solar spectral irradiance from a research aircraft., Appl. Optics, 8, 2215, 1969.
- BROADFOOT, A.L., The solar spectrum 2100-3200 A, Astrophys. J., 173, 881, 1972.
- BRUECKNER, G.E., J.D.F. BARTOE, O. KJEDSETH MOE, M.E. HOOSIER, Absolute solar ultraviolet intensities and their variations with solar activity part 1 : the wavelength region 1750-2100 A, Astrophys. J., 209, 935, 1976.
- BRUNER, E.C., R.W. PARKER, Hydrogen geocorona and solar Lyman  $\alpha$  line, J. Geophys. Res., 74, 107, 1969.
- BYRAM, E.T., T.A. CHUBB, H. FRIEDMAN, N. GAILAR, Observations of the intensity of solar Lyman-alpha, Astrophys. J., 124, 480, 1956.
- CHUBB, T.A., H. FRIEDMAN, R.W. KREPLIN, J.E. KUPPERIAN, Jr., Lyman-alpha and X-ray emissions during a small solar flare, J. Geophys. Res., 62, 389, 1957.
- DAVID, K.H., G. ELSTE, Effect on scattered light on the photometry of the solar surface, Z. Astrophys., 54, 12, 1962.
- DELABOUDINIÈRE, J.P., R.F. DONNELLY, H. HINTEREGGER, G. SCHMIDTKE, P.C. SIMON, Inter-comparison / compilation of relevant solar flux data related to aeronomy, COSPAR Technique Manual No 7, 1978.
- DETWILER, C.R., D.L. GARRETT, J.D. PURCELL, R. TOUSEY, The intensity distribution in the ultraviolet solar spectrum, Ann. Geophys., 17, 9, 1961.
- DICKINSON, P.H., Measurements of solar Lyman  $\alpha$  radiation during the eclipse of 7 March 1970, J. Atmos. terr. Phys., 34, 621, 1972.
- EFREMOV, A.I., A.L. PODMOSHENSKIL, O.N. EFIMOV, A.A. LEBEDEV, The investigation of the sun's short - wave radiation, Planet. Space Sci., 9, 969, 1962.
- FOSSI, M.R., G. POLETO, G.L. TAGLIAFERRI, An outstanding Lyman  $\alpha$  event., Solar Phys., 10, 196, 1969.
- FRIEDMAN, J., S.W. LICHTMAN, E.T. BYRAM, Photon counter measurements of solar X-rays and EUV light, Phys. Rev., 83, 1025, 1951.
- HALL, L.A., Solar flares in the EUV, Solar Phys., 21, 167, 1971.
- HALL, L.A., K.R. DAMON, H.E. HINTEREGGER, Solar EUV photon flux measurements in the upper atmosphere of August 1961, Space Res., III, 745, 1963.
- HALL, L.A., W. SCHWEITZER, H.E. HINTEREGGER, Long-term variation of solar EUV fluxes, J. Geophys. Res., 70, 241, 1965.
- HALL, L.A., H.E. HINTEREGGER, Solar radiation in the EUV and its variation with solar rotation, J. Geophys. Res., 75, 6959, 1970.
- HEATH, D.F., Observations of the intensity and variability of the near solar flux from the Nimbus III satellite, J. Atmos. Sci., 26, 1157, 1969.
- HEATH, D.F., Space observations of the variability of solar irradiance in the near and far ultraviolet, J. Geophys. Res., 78, 2779, 1973.
- HEATH, D.F., M.P. THEKAEKARA, The solar spectrum between 1200 and 3000 A in : The solar output and its variation (Ed. White), p. 193, Colo. Ass. Univ. Press. Boulder, USA, 1977.
- HEROUX, L., R.A. SWIRLABUS, Full-disk solar fluxes between 1230 and 1940 A, J. Geophys. Res., 81, 436, 1976.
- HEROUX, L., L. COHEN, J.E. HIGGINS, Electron densities between 110 and 300 km derived from solar EUV fluxes of August 23, J. Geophys. Res., 79, 5237, 1974.
- HIGGINS, J.E., The solar EUV flux between 230 and 1220 A on 9 November 1971, J. Geophys. Res., 81, 1301, 1976.
- HINTEREGGER, H.E., Interplanetary ionization by solar EUV radiation, Astrophys. J., 132, 800, 1960.
- HINTEREGGER, H.E., Preliminary data on solar EUV radiation in the upper atmosphere, J. Geophys. Res., 66, 2367, 1961.
- HINTEREGGER, H.E., The EUV solar spectrum and its variation during a solar cycle, Ann. Geophys., 26, 547, 1970.



# SIMON

- HINTEREGGER, H.E., D.E. BEDO, J.E. MANSON, EUV flux variations with solar rotation observed during 1974-1976 from AE-C satellite, Space Res., XVII, 533, 1977.
- KREPLIN, R.W., T.A. CHUBB, H. FRIEDMAN, X-ray and Lyman  $\alpha$  emission from the sun as measured from the NRL SR-1 satellite, J. Geophys. Res., 67, 2231, 1962.
- KOSTHOWSKI, H.J., Spectral irradiance scale change, Opt. Rad. News, N.B.S., 3, 5, 1974.
- LABS, D., H. NECKEL, Transformation of the absolute solar radiation data into the "International Practical Temperature Scale of 1968", Solar Phys., 15, 79, 1970.
- MADDEN, R.P., Status of VUV radiometric calibration of space experiments Space Res., XVIII, 103, 1978.
- MILLER, Jr., S.C., R. MERCURE, W.A. RENSE, Lyman- $\alpha$  intensity and solar limb darkening from rocket spectrograms, Astrophys. J., 124, 580, 1956.
- National Aeronautics and Space Administration, Chlorofluoromethanes and the stratosphere, NASA - Reference Publication 1010, 1977.
- NICOLET, M., Solar radiation and its stratospheric and mesospheric absorption, in : Proceedings of the NATO Advanced Study Institute on Atmospheric Ozone, Portugal, 1979.
- PRAG, A.B., F.A. MORSE, Variation in the solar ultraviolet flux from 13 July to 9 August, 1968, J. Geophys. Res., 73, 4613, 1970.
- PRINZ, D.K., The spatial distribution of Lyman- $\alpha$  on the sun, Astrophys. J., 187, 369, 1974.
- PURCELL, J.D., R. TOUSEY, The profile of solar hydrogen Lyman  $\alpha$ , J. Geophys. Res., 65, 370, 1960.
- ROTTMAN, G.L., Disc value of the solar ultraviolet flux. 1150-1850 A, Trans. Ann. Geophys. Un., 56, 1157, 1974.
- SAMAIN, D., P.C. SIMON, Solar flux determination in the spectral range 150-210 nm., Solar Phys., 49, 33, 1976.
- SAMAIN, D., R.M. BONNET, R. GAYET, C. LIZAMBERT, Stigmatic spectra of the sun between 1200 and 2100 A, Astrophys. J., 39, 71, 1975.
- SHAW, G.E., G. FROHLICH, The variability and absolute magnitude of solar spectral irradiance, in : Solar - Terrestrial influences on weather and climate, (Ed. Mc. Cormac and Seliga) p. 69, D. Reidel, Dordrecht, Holland, 1979.
- SCHMIDTKE, G., Today's knowledge of the solar EUV output and the future needs for more accurate measurements for aeronomy, Planet. Space Sci., 26, 347, 1978.
- SIMON, P.C., Balloon measurements of solar fluxes between 1960 and 2300 A, in : Proceedings of the third conference on the climatic impact assessment Program (Eds. Broderick and Hard), P. 137, DOT-TSC-OST-74-15, 1974.
- SIMON, P.C., Nouvelles mesures de l'ultraviolet solaire dans la stratosphère, Bull. Acad. r. Belg. Cl. Sci., 61, 399, 1975.
- SIMON, P.C., Irradiation solar flux measurements between 120 and 400 nm. Current position and futures needs, Planet. Space Sci., 26, 355, 1978.
- SIMON, P.C., R. PASTIELS, D. NEVEJANS, to be published, 1980.
- SMITH, L.G., Rocket observations of solar ultraviolet radiation during the eclipse of 7 March 1970, J. Atm. Terr. Phys., 34, 601, 1972.
- THEKAEKARA, M.P., Extraterrestrial solar spectrum 3000-6100 A at 1-A intervals, Appl. Opt., 13, 518, 1974.
- THEKAEKARA, M.P., P. KRUGER, C.H. DUNCAN, Solar irradiance measurements from a research aircraft, App. Opt., 8, 1713, 1969.
- WEEKS, L.H., Lyman- $\alpha$  emission from the sun near solar minimum Astrophys. J., 147, 1203, 1967.
- VIDAL-MAJAR, A., Evolution of the solar Lyman  $\alpha$  flux during four consecutive years, Solar Phys., 40, 69, 1975.
- VIDAL-MAJAR, A., The solar spectrum at Lyman  $\alpha$ , in : The solar output and its variation (Ed. White) p. 213, Colo. Ass. Univ. Press. Boulder, USA, 1977.
- WILLSON, R.C., J.R. HICKEY, Rocket measurements of the solar constant and their implications for variation in the solar output in cycle 20, in : The solar output and its variation, (Ed. White) p. 111, Colo. Ass. Univ. Press. Boulder, USA, 1977.
- WOODGATE, B.E., D.E. KNIGHT, R. URIBE, P. SHEATER, J. BOWLES, R. NETTLESHIP, EUV line intensities from the sun. Proc. R. Soc. Lond., A332, 291, 1973.

# INFLUENCE OF DIFFUSE SOLAR RADIATION ON STRATOSPHERIC CHEMISTRY

G.Fiocco

Istituto di Fisica, Università di Roma, Roma, Italy

## Abstract

The diffuse component of solar radiation has important effects on stratospheric structure and composition because of photodissociation and heating. In the lecture the basic relevant aspects of radiative transfer theory are introduced. Recent analyses and calculations concerning the photodissociation and heating rates, which include the effects of the diffuse field, and their application to atmospheric models are reviewed. The results indicate that molecular multiple scattering should always be included in photodissociation calculations if accuracies of the order of a few percent are desired. The variable part of the diffuse field due to surface albedo, clouds and aerosols can be responsible for large fluctuations in the thermal structure and composition of the stratosphere.

## Contents

Introduction
Photodissociation coefficients
The direct fluxes
The equation of radiative transfer
The effect of molecular multiple scattering and surface reflection on the fluxes
The effect of molecular multiple scattering and surface reflection on the photodissociation coefficients of $O_3$
The effect of scattering by aerosols
Daytime integration
Results for other species
Results of including molecular scattering and surface reflections into photochemical models
Changes in chemistry induced by diffuse radiation via heating of the atmosphere
Conclusion
Acknowledgement
References

INTRODUCTION: Progress in the correlative analysis of experimental results and in the simulation by numerical models has focussed interest on mechanisms previously neglected in studies of the stratospheric structure and composition as being of secondary importance.

We shall presently consider the influence of the radiative field on the stratospheric composition taking into account the modifying effects of non-conservative scattering by small particles and reflection by the surface. Such effects are manifested through the photodissociation and heating rates.

Quantitative estimates of these rates were, in earlier analyses, based on considering the direct solar field only, with molecular absorption as the only mechanism of attenuation. In reality, however, scattering by atmospheric constituents, namely molecules and aerosols, determines additional extinction of the direct beam, while the radiative energy subtracted to the direct field is redistributed in all directions thus contributing to a diffuse component of the field distinct from the direct one.

Other contributions to the diffuse field come from the radiation scattered by the underlying surface and by clouds; and, in a wider sense, the diffuse field also includes the planetary radiation of thermal origin.

As a result the total field, sum of the direct and diffuse components, has a behaviour which depends on a number of variables and parameters, namely the size distribution and the physical and chemical characteristics of the aerosols, i.e. their composition and in particular their refractive index, the diffuse reflectivity or albedo of the surface, and also the concentration of certain gaseous species, in particular ozone. Of primary importance, but difficult to assess precisely, is the role of clouds, with their great variety of characteristics and geometries: for simplicity they are often assumed to be a surface effect and their diffuse reflectivity incorporated into the surface albedo.

All these quantities may change as a function of time and space, and their variability is reflected in the ensuing phenomenology. They may induce interactions and be vehicles for feedback effects. As regards strictly the effect of the molecular or Rayleigh scattering, on the other hand, it should be pointed out that while this is a term of major importance which cannot be disregarded in the analysis for any precise simulation, the atmospheric molecular number density does not change substantially as a function of either time or space. Thus its inclusion represents an important refinement in the computation: once introduced, it will not in itself be subject to large changes.

The diffuse field influences the stratospheric composition primarily because it affects the photodissociation coefficient; secondarily because it affects atmospheric heating, thus acting on the reaction rate coefficients through a change in the atmospheric temperature.

If the aim of the analysis is strictly to consider the photodissociation of those gaseous species which are important for the ozone chemistry, the spectral regions of interest should be limited to the ultraviolet and the visible, and the planetary field can be disregarded. If, on the other hand, consideration is extended to the effects that the diffuse solar field has on the thermal structure of the atmosphere, thus influencing the rate coefficients of the various gaseous reactions, or the existence of aerosols and aggregates with a low bond-energy, then the analysis should be more complete and include the infrared spectrum.

Several authors have worked at these problems: in the following a certainly incomplete list of various contributions is given. Callis (1974), Luther (1975), Luther and Gelinas (1976) and Sundararaman (1976) called attention to the modifications induced by molecular scattering and ground reflection on the photodissociation rates. Parameterizations of the Rayleigh scattering effects on the fluxes and on the resulting photodissociation rates have been considered and included in 1-D models by Callis et al. (1976), Ashby (1976), Kurzeja (1977) and Isaksen et al. (1978). Luther, Wuebbles, Duewer and Chang (1978) have carried out sensitivity studies with a 1-D photochemical model with transport by including in detail the effects of Rayleigh scattering on photodissociation rates. Fiocco, Mugnai and Forlizzi (1978), Mugnai, Petroncelli and Fiocco (1979), Petroncelli, Fiocco and Mugnai (1980) have extended these studies by including the effects of aerosols on the photodissociation of ozone and related species. The influence of the diffuse field on the heating rates was taken into account by Lacis and Hansen (1974) who considered extreme values of the ground albedo in a model including multiple scattering to calculate  $O_3$  heating rates. Fiocco, Grams and Visconti (1976), Fiocco, Grams and Mugnai (1976 and 1977) and Mugnai, Grams and Fiocco (1978) have considered the heating rates induced by the presence in situ of aerosols, taking surface reflectivity into account. Visconti, Pitari and Cunnold (1980) have included a simplified calculation of Rayleigh scattering (Pitari and Visconti, 1978) in a 2-D photochemical model considering realistic values of the ground reflectivities and have obtained latitudinal distributions of the main species for different seasons.

It should be pointed out that earlier work on the interaction of diffuse radiation with the ozone layer was directed to the development of measurement techniques, rather than to estimating the effects on structure and composition. This followed a suggestion by Singer and Wentworth (1957) for determining the vertical distribution of  $O_3$  by making spectral measurements from a satellite of the ultraviolet radiation backscattered from the Earth's atmosphere, later developed in the BUUV method (Heath et al., 1973). Several authors contributed in developing the radiative transfer formalism: Sekera and Dave (1961), Dave and Mateer (1967), Jozenas (1968), Herman and Yarger (1969), Yarger (1970) and others.

In these notes we shall be concerned mostly with the effects of the diffuse field on photodissociation, and in a minor way with the effects on heating. The presentation is biased towards the work with which I have been involved and for this an apology is due.

**PHOTODISSOCIATION COEFFICIENTS:** The quantity of primary interest in these analyses is the photodissociation coefficient

$$J_1(z, \lambda, \delta\lambda) = q(z, \lambda, \delta\lambda) C_{i,d}(\lambda) \quad (1)$$

which gives the probability that a molecule of species  $i$  is photodissociated in a unit time by the photon flux  $q$  available in the spectral interval  $\delta\lambda$  around the wavelength  $\lambda$  at a height  $z$  in the atmosphere.  $C_{i,d}(\lambda)$  is the cross section for photodissociation which can be written as

$$C_{i,d}(\lambda) = \alpha_i(\lambda) C_{i,a}(\lambda) \quad (2)$$

where  $C_{i,a}(\lambda)$  is the absorption cross section and  $\alpha$  is the quantum yield for the photolytic reaction under consideration. It is assumed that  $C_{i,d}(\lambda)$  has a constant value throughout the spectral interval  $\delta\lambda$ .  $q(\lambda, \delta\lambda)$  is the average number of photons per unit time in the interval  $\delta\lambda$  around  $\lambda$  entering a sphere of unit section. It can be written:

$$q(z, \lambda, \delta\lambda) = F(z, \lambda, \delta\lambda) \lambda/hc \quad (3)$$

where  $h$  and  $c$  are Planck's constant and the speed of light respectively and  $F$  is the radiant flux.

The total field can be split into a direct and a diffuse component

$$F_{\text{tot}}(z, \lambda, \delta\lambda) = F_{\text{dir}}(z, \lambda, \delta\lambda) + F_{\text{dif}}(z, \lambda, \delta\lambda) . \quad (4)$$

Consequently the photodissociation coefficients can be split into direct and diffuse components as follows

$$J_{\text{tot}}(z, \lambda, \delta\lambda) = J_{\text{dir}}(z, \lambda, \delta\lambda) + J_{\text{dif}}(z, \lambda, \delta\lambda) . \quad (5)$$

THE DIRECT FLUXES: The attenuation of a monochromatic pencil beam of intensity  $I(\lambda)$  is obtained by integrating the simple relationship

$$\begin{aligned} dI(z, \lambda) &= I(z, \lambda) k_e(\lambda, z) \rho(z) ds \\ &= I(z, \lambda) k_e(\lambda, z) \rho(z) dz \sec \theta . \end{aligned} \quad (6)$$

through the propagation path;  $\theta$  is the angle that the local direction of propagation  $\underline{s}$  makes with the vertical.  $k_e$  is the extinction coefficient for unit mass of air, and  $\rho$  is the air density. We can write

$$k_e = k_a + k_s \quad (7)$$

where  $k_a$  and  $k_s$  are the coefficients per unit mass for absorption and scattering, respectively.

Introducing the cross section for absorption and scattering,  $C_{i,a}$  and  $C_{i,s}$  respectively, and the number density,  $n_i$ , for the particles of species  $i$ , one can write equivalently:

$$k_a = \frac{1}{\rho} \sum_i C_{i,a} n_i , \quad k_s = \frac{1}{\rho} \sum_i C_{i,s} n_i \quad (8)$$

Then the optical depths can be defined

$$\begin{aligned} \tau &\equiv \tau_e \equiv \tau_a + \tau_s = \\ &= \int_z^\infty dz \sum_i C_{i,a} n_i \sec \theta + \int_z^\infty dz \sum_i C_{i,s} n_i \sec \theta \end{aligned} \quad (9)$$

For a plane-parallel atmosphere, eq. 6 can be simply integrated, to obtain Beer's law of exponential attenuation

$$\mu I(z, \lambda) = I(\infty, \lambda) \exp(-\tau_\perp / \mu) \quad (10)$$

where  $\mu = \cos \theta$ ;  $\tau_\perp$  is the optical depth for vertical propagation, and  $I(\infty, \lambda)$  is the monochromatic intensity outside the atmosphere.

Extending exp. 10 and more general forms of the equation of radiation transfer to large

spectral intervals involves some difficulties. In principle one could proceed doing line-by-line computations, with a considerable expenditure of computing effort, provided one had the fine grain description of the spectrum.

At the other extreme in terms of computing effort there are parameterization schemes such as those proposed by Lacis and Hansen (1974) which take into account the entire spectrum at once or possibly in only few sections. A compromise is to consider frequency intervals  $\delta\lambda$  small enough to resolve the quantities slowly varying with frequency, but large compared to individual line widths, and introduce extinction coefficients which are representative averages over those intervals. For this purpose it is worth mentioning here an approximation known as "the exponential - sum fitting of transmissions (ESFT) method" (Hunt and Grant, 1969; Yamamoto et al., 1970; Wiscombe and Evans, 1977). It is based on assuming that the average transmission function over an interval  $\delta\lambda$ , due to an absorber of scaled amount  $u$ , defined as

$$T(u, \lambda, \delta\lambda) = \frac{1}{\delta\lambda} \int_{\delta\lambda} \exp[-K(\lambda)u/\mu] d\lambda \quad (11)$$

can be approximated by a finite sum of exponentials, as follows

$$T(u, \lambda, \delta\lambda) \approx \sum_{l=1}^M a_l \exp(-K_l u/\mu) \quad (12)$$

$$\sum_{l=1}^M a_l = 1$$

This procedure leads to determining a series of coefficients  $a_l$  and absorption coefficients  $K_l$  since the transmissions are known experimentally. The  $a_l$  can be interpreted as that fraction of the interval occupied by the band with absorption coefficient near  $K_l$ . Examples of this computation are given by Fiocco et al. (1978).

In conclusion, for the direct solar flux one may write

$$\mu_S F_{dir}(z, \lambda, \delta\lambda) = F_S(\infty, \lambda, \delta\lambda) \exp[-\tau(z, \lambda, \delta\lambda)/\mu_S] \quad (13)$$

where  $\mu_S = \cos \chi$ ,  $\chi$  being the solar zenith angle.  $F_S(\infty, \lambda, \delta\lambda)$  is the flux outside the Earth's atmosphere.

It is worth mentioning that the assumption of a plane parallel atmosphere is a standard one for the difficulty of including a spherical geometry in the radiative transfer problem and specially so for the diffuse field. This assumption may be inadequate for high latitudes and for the winter months when a considerable fraction of the solar flux through the day impinges on the atmosphere at large zenith angles.

The spectroscopy of the important gaseous species and the resulting atmospheric transmission will not be discussed here in detail. Reference is made to Hudson (1977) and to other lectures of this Institute, in particular those of profs. Nicolet and Molina.

In this regard the spectral region of present concern for the effects of diffuse radiation on photodissociation extends approximately from 200 nm to 700 nm. This region is dominated by the absorption of  $O_2$  and  $O_3$  and, in a lesser way, by that of  $NO_2$ .

As a result of gaseous absorption, there is virtually no radiation transmitted to the lower atmosphere for  $\lambda < 290$  nm and there is a gradual transition to virtually complete transmission for  $\lambda > 330$  nm. This consideration dominates the basic aspect of our

problem. Most of the diffuse radiation in the stratosphere comes from the underlying troposphere and surface, where clouds and most of the atmospheric mass reside.

Thus the effects of diffuse radiation will be particularly evident for those species that photolyze for  $\lambda > 300$  nm. In addition to  $O_3$  and  $NO_2$ , whose presence as mentioned has an important effect on the radiative spectrum, other species such as  $H_2O_2$ ,  $HNO_3$ ,  $NO_3$ ,  $CH_3O$ ,  $ClONO_2$ ,  $HOCl$  photodissociate in that spectral region, although their presence does not substantially modify the spectrum.

The photodissociation coefficient  $J_0$  due to the direct solar flux for a purely absorbing molecular atmosphere in the absence of scattering is a useful reference quantity. Fig. 1 gives the vertical profiles of  $J_0$  for  $O_3$ ,  $NO_2$ ,  $NO_3$ ,  $HNO_3$ ,  $H_2O_2$ , at different values of the solar zenith angle  $\chi$ . Additional curves (from Luther and Gelinas, 1976) showing the contribution  $J(O_3)$  of the two photodissociation reactions of  $O_3$  leading respectively to  $O(^1P)$  and  $O(^1D)$  are given in Fig. 4 a,b.

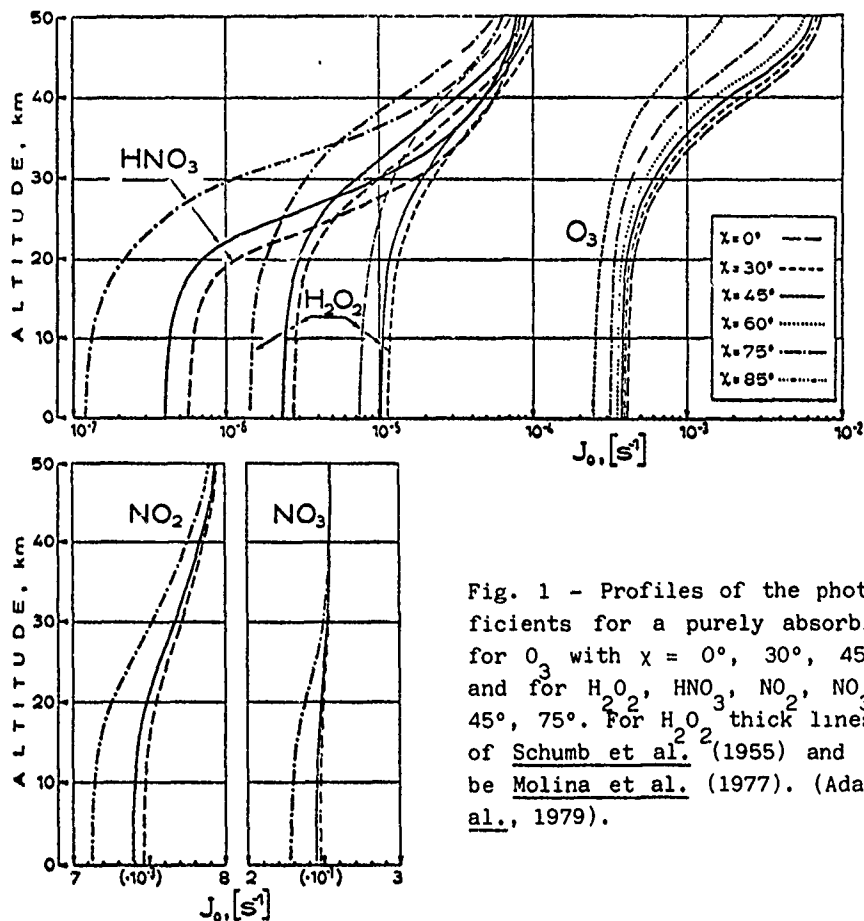


Fig. 1 - Profiles of the photodissociation coefficients for a purely absorbing atmosphere,  $J_0$ , for  $O_3$  with  $\chi = 0^\circ, 30^\circ, 45^\circ, 60^\circ, 75^\circ, 85^\circ$ , and for  $H_2O_2$ ,  $HNO_3$ ,  $NO_2$ ,  $NO_3$  with  $\chi = 0^\circ, 45^\circ, 75^\circ$ . For  $H_2O_2$  thick lines refer to the data of Schumb et al. (1955) and thin lines to those by Molina et al. (1977). (Adapted from Mugnai et al., 1979).

The different shape of the  $J_0$  profiles obtained for the five species is due to the different behaviour of absorption throughout the spectrum.  $NO_3$ , which is mainly photolyzed by visible radiation, is least sensitive to the variation in  $z$  and  $\chi$ . On the other hand, the large overall variation of  $J_0$  with altitude and solar zenith angle for  $H_2O_2$  and  $HNO_3$  is a result of the fact that the cross sections for these species increase in the UV portion of the spectrum, where the largest variation of the incoming flux with altitude is obtained.

SCATTERING AND THE EQUATION OF RADIATIVE TRANSFER: Introducing the effect of Rayleigh

scattering in the extinction of the direct beam, Fig. 2 from Callis et al. (1975) gives the variation of the normal optical depth of the entire atmosphere as a function of wavelength, separately due to molecular scattering and absorption. The graphs indicate that for  $200 \text{ nm} < \lambda < 730 \text{ nm}$  molecular scattering contributes in a non-negligible part to the total optical depth of the atmosphere, the minimum relative contribution occurring at 255 nm.

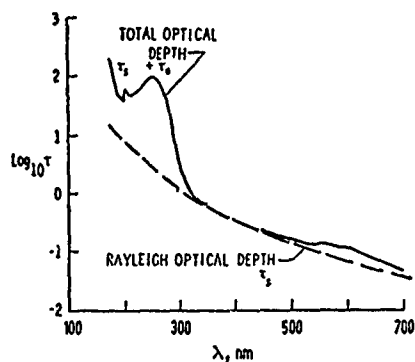


Fig. 2 - The total optical depth of the atmosphere and its Rayleigh molecular component (adapted from Callis et al., 1975).

We shall summarize now some aspects of the problem of the transfer of radiation through an optically dense atmosphere. For details the reader is referred to comprehensive works such as Paltridge and Platt (1976) and for the scattering theory to the book by Kerker (1969).

We have already considered the extinction of a pencil beam which leads to writing the Beer's law of exponential attenuation. In this way the scattering processes intervene only in attenuating the beam and no account is taken of the radiation which is subtracted to the beam but restituted to the field with a different direction of propagation. No account is taken also of the thermal emission or other sources present in the medium.

If we consider a beam  $I(\theta, \phi)$  which propagates in the direction  $\underline{s}$  characterized by the angles  $\theta, \phi$  and consider the contribution of pure scattering only we can write the equation:

$$dI_{\lambda}(\theta, \phi) = -k_{e, \lambda} \rho I_{\lambda}(\theta, \phi) ds + \frac{k_{s, \lambda} \rho}{4\pi} \int_0^{\pi} \int_0^{2\pi} \tilde{P}_{\lambda}(\theta, \phi; \theta', \phi') I_{\lambda}(\theta', \phi') \sin \theta' d\theta' d\phi' ds. \quad (14)$$

The two terms on the l.h.s. represent respectively the attenuation of the beam due to extinction and the contribution due to scattering of radiation from the direction  $\underline{s}'$  into the direction of  $\underline{s}$ .

The "phase function"  $\tilde{P}(\theta, \phi; \theta', \phi')$  divided by  $4\pi$  gives the fraction of the intensity  $I(\theta', \phi')$  which is scattered in the direction  $\underline{s}(\theta, \phi)$ .

The equation of radiative transfer can be concisely written, introducing the optical thickness:

$$dI_{\lambda}/d\tau = -I_{\lambda} + \sigma_{\lambda} \quad (15)$$

where  $\sigma_{\lambda}$  is the "source function".

The source function takes the following form in the case of pure scattering with no



absorption:

$$\sigma_{\lambda} = \frac{1}{4\pi} \int_{\phi'=0}^{2\pi} \int_{\theta'=0}^{\pi} \tilde{P}_{\lambda}(\theta, \phi; \theta', \phi') I_{\lambda}(\theta', \phi') \sin \theta' d\theta' d\phi' . \quad (16)$$

For the case of thermal equilibrium with no scattering it is:

$$\sigma_{\lambda} = B_{\lambda}(T) . \quad (17)$$

When both scattering and absorption are simultaneously present we can write:

$$\sigma_{\lambda} = \frac{\tilde{\omega}_0}{4\pi} \int_{\phi'=0}^{2\pi} \int_{\theta'=0}^{\pi} \tilde{P}_{\lambda}(\theta, \phi; \theta', \phi') I_{\lambda}(\theta', \phi') \sin \theta' d\theta' d\phi' + (1 - \tilde{\omega}_0) B_{\lambda}(T) . \quad (18)$$

$\omega_0$  is the "single scattering albedo" which represents the ratio between scattering and extinction in the infinitesimal volume:

$$\tilde{\omega}_0(\tau_{\lambda}) = d\tau_s / d\tau_e . \quad (19)$$

If there is no absorption,  $\omega_0 = 1$ . In (18) we have assumed  $\omega_0$  independent of direction. The phase function of particles much smaller than the wavelength of light (Rayleigh scatter) for unpolarized light is simply

$$\tilde{P}(\psi) = \frac{3}{4} (1 + \cos^2 \psi) . \quad (20)$$

where  $\psi$  is the scattering angle.

Aerosol particles are generally assumed to behave like spheres, characterized by radius,  $r$ , and complex refractive index,  $n = n' - i n''$ . For the sphere, exact solutions to the scattering problem are given by the Mie theory in the form of series expansions. The number of terms in the series necessary to adequately represent the scattered field is proportional to the ratio  $\alpha = 2\pi r/\lambda$ : thus for large values of  $\alpha$  and when a variety of sizes are considered the size of the computation may grow conspicuously

To make use of the radiative transfer equation it is necessary to introduce simplifications in the geometry, considering for example a plane-parallel stratified atmosphere, as well as in the analytic form, taking into account only a finite number of directions for  $\underline{s}$ , in the limit only two, and simplified forms for the phase function. Finally universal use of numerical computation is made.

The dilemma is between rather accurate but computationally slow methods of solution and faster methods whose accuracy is sometime difficult to assess, but which generally decays with the amount of detail required. We shall not be able to enter into this question but point out the necessity of comparing results obtained with different techniques.

Certain procedures are of universal use to account for multiple scattering. For a plane-parallel geometry one considers the atmosphere divided in a number of homogeneous layers, for instance of 1 km thickness. Since each layer may be optically thick, it is subdivided in a number possibly quite large of thin sub-layers, all of the same characteristics and such that the extinction in a sub-layer is correctly described by the hypothesis of single scattering. Knowing the characteristics of transmissivity and reflectivity for one sub-layer it is easy to sum them up with those of an adjacent layer. Obtained thus the characteristics of a double layer, it is now possible to sum them with those of an adjacent double layer and so on. These procedures of "adding" and "doubling"

permit to expedite computations considerably (in its present form the technique has been introduced by van de Hulst, 1963).

Of the various methods in existence to compute fluxes and their variants we mention those based on the work of Grant and Hunt (1967) which in principle permit a very high accuracy since the integration over the various variables are carried out in detail, and those based on the work of Lacis and Hansen (1974) where the major absorption processes over the entire spectrum are parameterized, although multiple scattering is accounted for in an accurate way by "adding" and "doubling" procedures.

THE EFFECT OF MOLECULAR MULTIPLE SCATTERING AND SURFACE REFLECTION ON THE FLUXES: Since the photodissociation coefficient results from integrating exp. 1 where both the flux and the cross section are functions of wavelength, it will be of help preliminarily to consider how the flux changes because of diffusion as a function of the different variables.

Fig. 3a-d, from Luther and Gelinas (1976), shows the effect of molecular multiple scattering and surface albedo on the flux. The curves give the ratio  $F_{\text{tot}}/F_0$  as a function of wavelength, for different heights and values of the albedo.  $F_0$  is the direct flux for a purely absorbing atmosphere. The solar zenith angle is fixed,  $\chi=60^\circ$ , and selected values of the surface albedo,  $A = 0.00, 0.25, 0.50, 0.75, 1.00$ , are used. The results are given for the altitudes  $z = 40 \text{ km}, 20 \text{ km}, 10 \text{ km}, 0 \text{ km}$ .

At an altitude of 40 km for  $\lambda < 290 \text{ nm}$  there is little change in the flux ratio, which is very close to unity, and there is no dependence on ground albedo since no radiation at those wavelengths reaches the ground. The effect of the molecular multiple scattering alone is given by the curves for  $A = 0.00$ ; its importance is maximum at  $\lambda \sim 330 \text{ nm}$ . At wavelengths greater than 300 nm there is a strong dependence on ground albedo: for a surface albedo  $A = 0.3$ , which is the approximate global mean, the flux is increased between 30% and 60% for  $\lambda > 330 \text{ nm}$ . At lower heights, down to 20 km, the flux ratio for  $\lambda > 300 \text{ nm}$  does not change substantially in comparison with the 40 km case. At shorter wavelengths however the ratio changes conspicuously since large values of the optical thickness are obtained. This, however, has a modest significance in view of the negligible amount of flux available for photodissociation at those heights and wavelengths.

Below 10 km, where most of the atmospheric is, the multiple scattering flux changes substantially as one moves close to ground in view of the progressive reduction of the underlying atmosphere available for scattering: the ground albedo, however, has a restoring effect and the flux ratio is close to 2 throughout the visible regions of the spectrum for  $A = 1.0$ .

THE EFFECTS OF MOLECULAR MULTIPLE SCATTERING AND SURFACE REFLECTION ON THE PHOTODISSOCIATION COEFFICIENTS OF  $\text{O}_3$ : By using the previously calculated values of the flux where the effects of molecular multiple scattering and surface albedo are introduced, Luther and Gelinas (1976) have calculated the photodissociation coefficients of  $\text{O}_3$  versus height shown in Fig. 4a,b for the two reactions  $\text{O}_3 + h\nu \rightarrow \text{O}(\text{P}) + \text{O}_2$  and  $\text{O}_3 + h\nu \rightarrow \text{O}(\text{D}) + \text{O}_2$ . The different curves refer to the pure absorption case and to various values of surface albedo.

Fig. 5 from Fiocco et al. (1978) gives similar results for  $\chi=45^\circ$  and for  $A = 0, 0.3$ , separately showing the contributions from different spectral regions.

In practice at all heights below approx 35 km photodissociation is mainly due to the contribution of the visible region of the spectrum while above 35 km it is mainly due to the Hartley  $\text{D}$  band. A full discussion of these results is postponed to a later section.

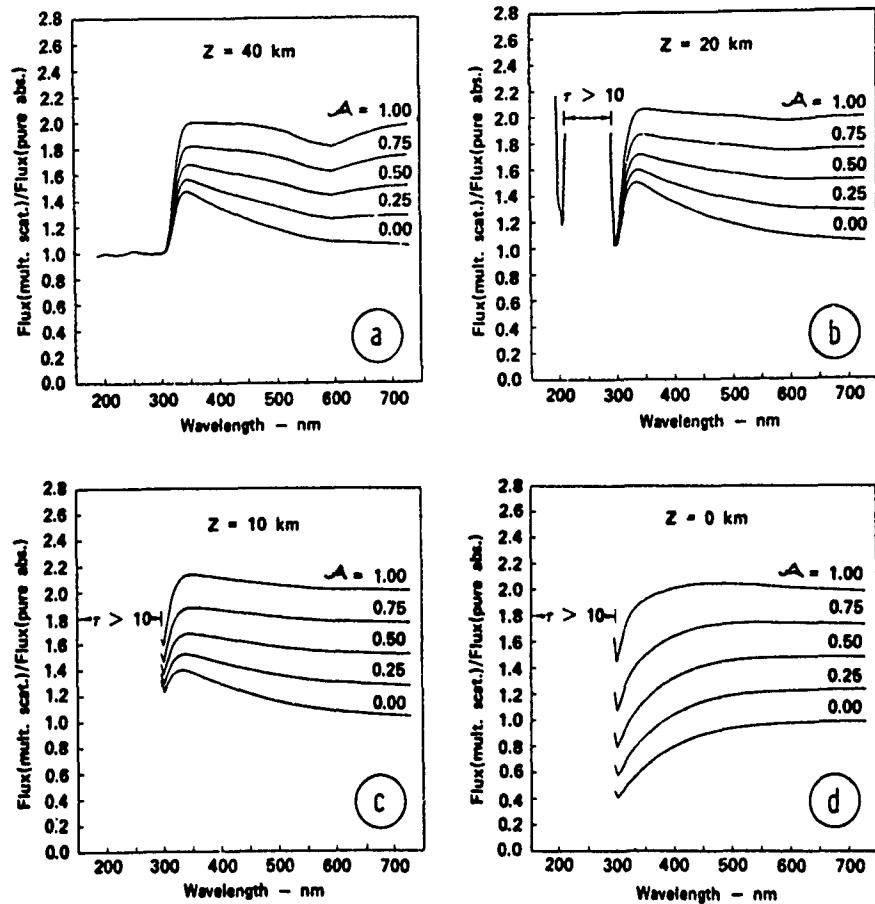


Fig. 3 - Effect of molecular multiple scattering and surface reflectivity on the fluxes at heights  $z = 40, 20, 10, 0$  km and  $A = 1.00, 0.75, 0.25, 0.00$  (adapted from Luther and Gelinas, 1976).

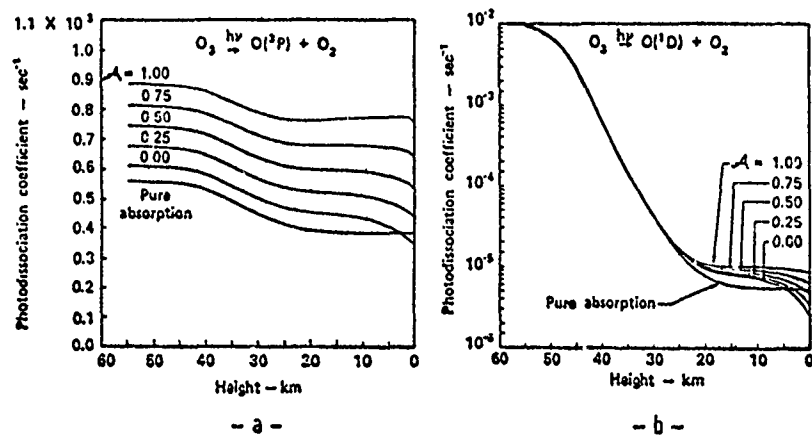


Fig. 4 - Profiles of the photodissociation coefficients of  $O_3$  for the pure absorption case,  $J_0$ , and for the multiple scattering case,  $J_m$ , with different values of the ground albedo and photolytic reactions: (a)  $O_3 + h\nu \rightarrow O(^3P) + O_2$  and (b)  $O_3 + h\nu \rightarrow O(^1D) + O_2$ . (Adapted from Luther and Gelinas, 1976).

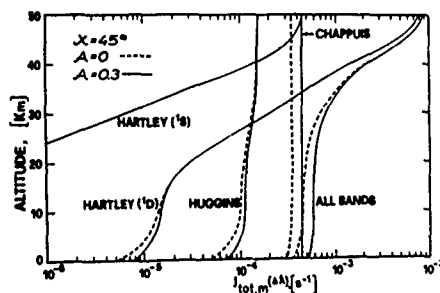


Fig. 5 - Profiles of the photodissociation coefficient of  $O_3$ , for a molecular atmosphere,  $J_{tot,m}(\lambda)$ , for albedo  $A = 0, 0.3$  at  $\lambda = 45^\circ$  and for the following spectral bands (after Fiocco et al., 1978): Hartley  $S$ ,  $\Delta\lambda = 200 - 236$  nm; Hartley  $D$ ,  $\Delta\lambda = 236 - 310$  nm; Huggins  $\Delta\lambda = 310 - 360$  nm; Chappuis  $\Delta\lambda = 410 - 730$  nm.

THE EFFECT OF SCATTERING BY AEROSOLS: The effects of aerosol loads on photodissociation have been considered by Fiocco et al. (1978), Mugnai et al. (1979) and Petroncelli et al. (1979) in a series of papers. To characterize the aerosol load they considered a few typical cases, which differ from each other in the vertical concentration profiles (Fig. 6). The attenuation data from Elterman (1968) was taken as indicative of an average situation (case a). As an example of heavy stratospheric load (case b) they considered the distribution existing 300 days after the Mt. Agung 1963 volcanic eruption at the latitude  $0^\circ N$  (Cadle, Kiang and Louis, 1976), while maintaining the Elterman's profile in the troposphere.

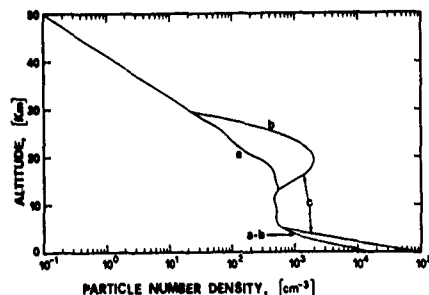


Fig. 6 - Reference aerosol concentration profiles, (a) average concentration (Elterman, 1968) at all heights; (b) average concentration in troposphere and Mt. Agung,  $0^\circ N$  in stratosphere (Cadle et al., 1976); (c) hazy concentration (McClatchey et al., 1970) in troposphere and Mt. Agung  $0^\circ N$  in stratosphere (after Fiocco et al., 1978).

It should be said that in view of the large latitudinal dependence of the Mt. Agung aerosol distribution, they examined also the  $45^\circ N$  profile, but found it to be not very different from the Elterman's profile. Finally a heavy atmospheric aerosol load at all heights (case c) was considered by utilizing in addition to the stratospheric Mt. Agung aerosol concentration the tropospheric profile obtained from the "hazy" attenuation case of McClatchey et al. (1970).

In all cases, the aerosol size distribution curve was assumed to follow a power law,  $dN/dr = Cr^{-3}$ , between the radius limits  $r_1 = 0.03 \mu m$  and  $r_2 = 3 \mu m$ .

The composition of the particles was allowed to change with altitude: the composition was taken to consist of dust in the troposphere and of a mixture of dust and impure sulphuric acid droplets with a mass ratio 1 to 2 in the stratosphere.

The dust composition and refractive index  $n = n' - in''$ , were taken according to the synthetic model of Ivlev and Popova (1973), i.e.  $n' = 1.65$  and  $n'' = 0.005$ . To represent the sulphuric acid droplets they used the experimental data reported by Palmer and Williams (1975) for the complex refractive index of a mixture of 75% sulphuric acid and 25% water, the proportions suggested by a number of investigators (e.g. Toon and Pollack, 1973; Russell et al., 1976). Since absorption of sulphuric acid droplets is expected to depend on the amount of impurities present in the particles, they considered different

values for the imaginary part of the refractive index of  $\text{H}_2\text{SO}_4$ . Most computations however were carried out for the value  $n''(\text{H}_2\text{SO}_4) = 0.001$ : it should be noted that this value fits well an analysis of the heating rates induced by the aerosol on the ambient gas (Fiocco, Grams and Mugnai, 1977), to be considered later in this review.

Table I summarizes, and Fig. 6 shows the different concentration profiles in the analysis: the quantity shown as a function of altitude is an equivalent number density (particles  $\text{cm}^{-3}$ ) which was computed from the attenuation profiles of Elterman (1968) and McClatchey (1976) and the mass concentration profiles of Cadle et al. (1976).

TABLE I

CASE	TROPOSPHERE	STRATOSPHERE
m		no aerosol
a		average
b	average *	heavy, Mt. Agung 0°N
c	hazy +	heavy, Mt. Agung 0°N

\* Elterman (1968); Cadle, Kiang and Louis (1976);  
McClatchey et al. (1970).

Figure 7 shows the percentage deviation of the total photodissociation coefficient,  $J_{\text{tot},x}$ , for the cases  $x = a, b, c$  in Table I with respect to the total photodissociation coefficient for a purely molecular atmosphere,  $J_{\text{tot},m}$ , integrated over the entire wavelength spectrum,

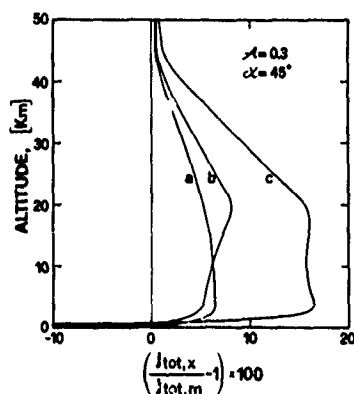


Fig. 7 - Percentage deviation of the photodissociation coefficient of  $\text{O}_3$ ,  $J_{\text{tot},x}$ , for the different aerosol loads shown in Fig. 1 ( $x = a, b, c$ ), with respect to the photodissociation coefficient for a molecular atmosphere,  $J_{\text{tot},m}$ , as a function of height (after Fiocco et al., 1978).

These curves show the relative importance of scattering and absorption by the aerosols. An increase in the aerosol loads always leads to enhanced photodissociation in the upper regions, while the effect of extinction leads to reduced rates in the lower regions.

In the 20 km region differences in the coefficients are in excess of 15% for heavy loads such as those of case c. However, even in the case a, which refers to an average aerosol load, the presence of the aerosol leads to an increase of  $J_{\text{tot}}$  of approximately 5%.

To strengthen this point further, Figs. 8 and 9 refer to the photodissociation rate, that is to the product  $n(\text{O}_3)J$  as a function of height. The profile for  $n(\text{O}_3)$ , utilized in the

# FIOCCO

analysis (US Standard Atmosphere Suppl. 1966) is shown in one of the curves of Fig. 8: also shown is the corresponding photodissociation rate  $n(O_3)J_{tot,m}$ . The effects of aerosol on such rate are displayed in Fig. 9 as the deviation  $n(O_3)(J_{tot,x} - J_{tot,m})$ , as a function of height. Such curves confirm that the effect of an increase in the aerosol load is to produce an enhancement in the photolysis at all heights except near the ground where the opposite occurs.

These results may provide an explanation for the negative correlation between the fluctuations of stratospheric aerosols and ozone found in a study of the effects of the Mt. Agung eruption (Grams and Fiocco, 1967). Computations, whose results are not displayed here, were also carried out assuming an extremely large load in the stratosphere obtained by multiplying by a factor of 10 the already large stratospheric aerosol concentrations of case b. The results show that, in that case, at heights below approximately 20 km, the effect of extinction is so large that a reduction in the J's would be obtained, compared to the molecular atmosphere. Thus, in such cases, positive correlations between ozone amounts might be obtained. In view however of the large preponderance of the effect in the upper stratosphere, it is expected that even in those cases the correlation between aerosol loads and total column amounts of  $O_3$  should be negative.

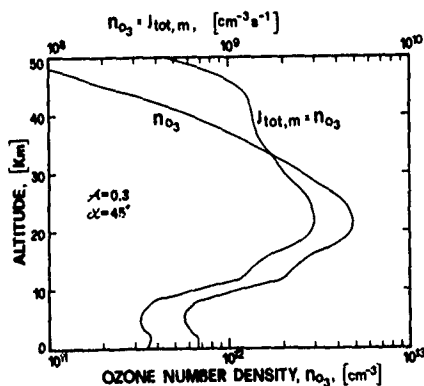


Fig. 8 - Concentration profile of  $O_3$  (US Standard Atmosphere Suppl. 1966) and photodissociation rate  $n(O_3)J_{tot,m}$ , for a molecular atmosphere (after Fiocco et al., 1978).

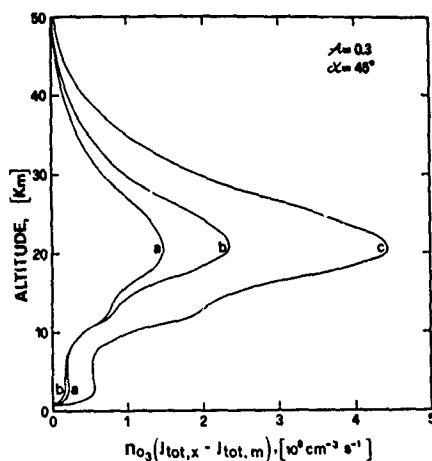


Fig. 9 - Deviation,  $n(O_3)(J_{tot,x} - J_{tot,m})$ , of the photodissociation rate for three aerosol loads ( $x = a, b, c$ ) and for  $\chi = 45^\circ$ ,  $A = 0.3$  (after Fiocco et al., 1978).

So far all computations have been referred to a solar zenith angle  $\chi = 45^\circ$ . Figure 10 shows the value of  $J_{\text{tot},m}$  for different values of the zenith angle  $\chi$  and for the two extreme cases of aerosol load, i.e.  $x = m$  and  $x = c$ , respectively.

For the same aerosol loads, Fig. 11 shows the variable importance of the diffuse to the total field at different values of  $\chi$ . Note, however, that in all computations the albedo value was  $A = 0.3$ ; the radiation diffused by the surface is a large fraction of the diffuse field at small zenith angles and it is small at large values of  $\chi$ . While for a molecular atmosphere (case m) an increase in the value of  $\chi$  corresponds to a reduction of the relative importance of the diffuse field, mainly due to the effects of albedo, for large aerosol loads (case c) an increase of  $\chi$  determines a reduction in the relative importance of the diffuse fields in the upper troposphere and in the stratosphere and an increase in the lower troposphere.

From the curves in Figs. 10 and 11 it is possible to infer the evolution of the direct and diffuse fields as a function of the zenith angle and therefore of the time of the day. This problem will be taken up in detail in the following section.

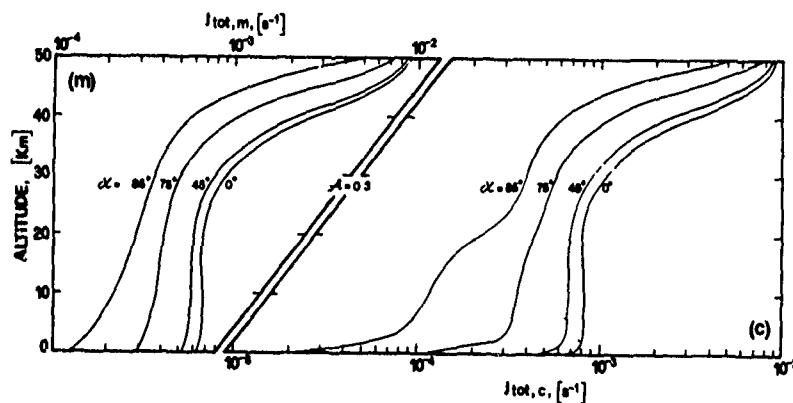


Fig. 10 - Effect of changing the solar zenith angle on the photodissociation coefficient for the two extreme cases of aerosol load ( $x = m, c$ ) (after Fiocco et al., 1978).

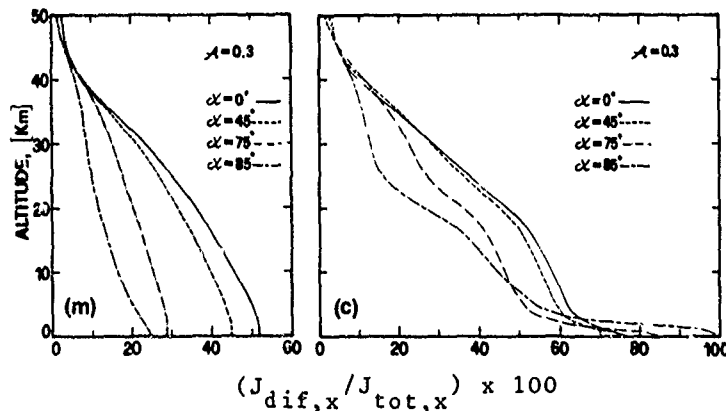


Fig. 11 - Percentage ratio of the photodissociation due to the diffuse field to that due to the total field, at different values of the zenith angle  $\chi$ , for the two extreme cases of aerosol load ( $x = m, c$ ) (after Fiocco et al., 1978).

**DAYTIME INTEGRATION:** The results shown so far indicate that the solar zenith angle is an important variable, at large angles the effects of extinction being conspicuously enhanced.

Fig. 12 shows, as a function of the hour of the day, the variation of the photodissociation coefficient for the cases o, m, c, at the two heights of 15 km and 30 km for  $\tau = 0.3$ .

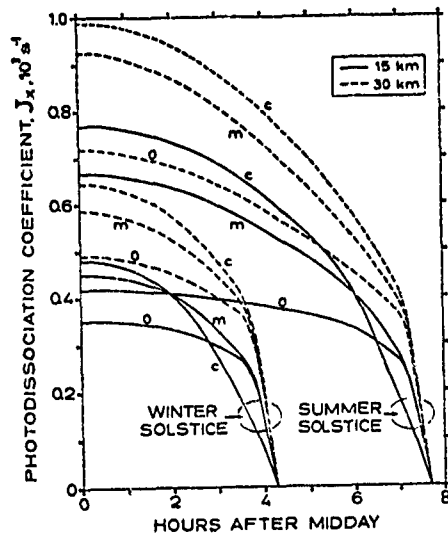


Fig. 12 - Daytime variation of the photodissociation coefficient vs time after midday, at 15 and 30 km and for the winter and summer solstices at  $45^\circ$  lat and  $A = 0.3$ ; case o is for pure absorption, case m for molecular multiple scattering and case c for heavy aerosol load (see Table 1); (after Petroncelli et al., 1980).

From Fig. 12 it is apparent that a different choice of the atmospheric conditions leads to a quite different behaviour of the  $J$ 's during the day, thus indicating the necessity of performing accurate numerical time-integrations over the length of the day in order to obtain realistic values of the daily-integrated photodissociation coefficients.

Petroncelli et al. (1980) have performed time integrations of the photodissociation coefficients  $J_o$ ,  $J_m$ ,  $J_x$  over a 24 hour interval taking into account the time variation of the solar zenith angle  $\chi(t)$ . What follows is taken almost verbatim from their paper. The daily integrated value is

$$L_{o,m,x}(D) = \epsilon(D) \int_{1\text{day}} J_{o,m,x}[\chi(D,t)] dt \quad (21)$$

where  $D$  indicates the particular day of the year ( $D = 0$  corresponds to January 1 and  $D = 364$  to December 31) and  $\epsilon(D)$  is a coefficient accounting for the variation of the Sun-Earth distance.

A yearly averaged value for the  $L$ 's has been also computed as follows:

$$\bar{L}_{o,m,x} = \frac{1}{365} \sum_{D=0}^{364} L_{o,m,x}(D) \quad (22)$$

To single out the effects of atmospheric scattering and ground diffuse reflectivity and further separate the contributions of the aerosol load from those of the molecular atmosphere, results are shown separately for  $L_o$  and for the ratios  $L_m/L_o$  and  $L_x/L_m$ , so that  $L_x$  may be obtained by the product:

$$L_x = L_o \cdot \frac{L_m}{L_o} \cdot \frac{L_x}{L_m} \quad (23)$$

Introducing now the results of the integrations, Fig. 13 gives, for reference the values



$L_m(D)$  at five specific heights. Fig. 14 depicts, in a three-dimensional presentation the  $L_m^o(z,D)/L_o^o(z,D)$  ratios for different values of the ground albedo ( $A = 0, 0.3, 0.7$ ).

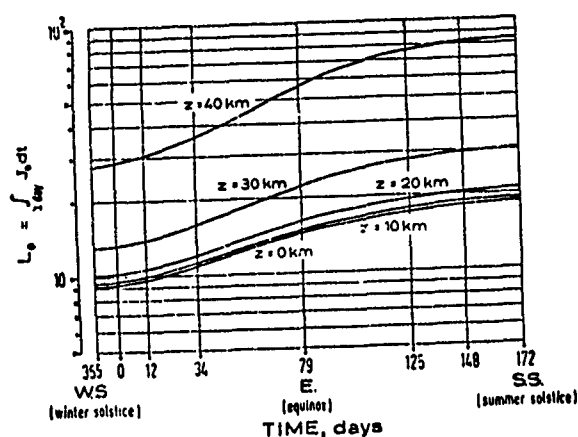


Fig. 13 - Annual variation of the daily integrated value,  $L_o$ , of the photodissociation coefficient for pure absorption,  $J_o$ , (after Petroncelli et al., 1980).

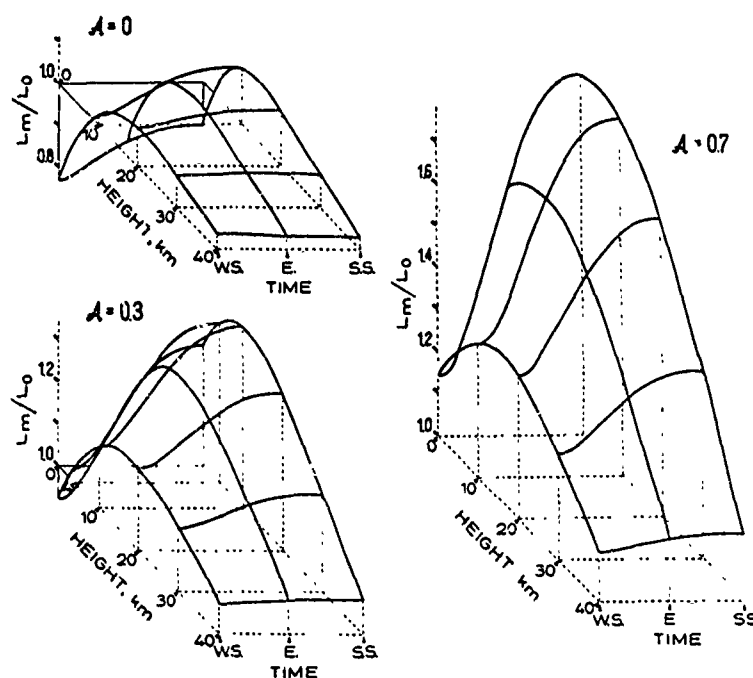


Fig. 14 - Ratio,  $L_m/L_o$ , between the daily integrated values of  $J_m$  and  $J_o$  as a function of height and time of the year at  $45^\circ$  lat. and for  $A = 0, 0.3, 0.7$ ; WS=winter solstice, E = equinox SS=summer solstice (after Petroncelli et al., 1980).

For  $A = 0$ , the inclusion of scattering involves a reduction of the photodissociation in the lower troposphere because of extinction, but in the upper troposphere and throughout the stratosphere, where the effects of photodissociation are most important,  $L$  increases due to the contribution by the solar radiation scattered by molecules in the lower troposphere, where most of the atmospheric mass is located. When the ground albedo increases, the overall effect is always positive, since the ground diffuse reflectivity does not contribute to  $L$ ; in particular, for  $A = 0.7$  the increase in the  $L$  is about 90% at ground level and exceeds 40% at 30 km during summer.

The increase in photodissociation because of the solar radiation diffused by the ground and by atmospheric molecules is almost always higher in summer than in winter; moreover, the effects of changes in albedo are felt less strongly in winter than in summer. In fact, in winter, due to the large values of the zenith angle, the direct solar radiation is considerably depleted before reaching the lower troposphere because of molecular scattering, thus diminishing also the contribution to the solar diffused field by surface reflectivity and by the molecular scattering by low-altitude atmospheric layers.

At a fixed height the greater the surface albedo the greater the seasonal variation in the ratio  $L$ ; however, the ratio becomes less and less dependent on the season at increasing heights. This is because the Hartley J component, where it is of importance, does not practically depend on scattering processes, since the strong absorption makes both the local attenuation by scattering and the contribution of the upcoming diffuse radiation negligible. Therefore this component in the case m is practically the same as in the case o. On the other hand, in the Huggins and Chappuis bands the attenuation due to either absorption or scattering is very weak in the upper stratosphere. As a consequence, above about 30 km the photolytic contribution of the upcoming diffuse field, the value of which increases by increasing  $A$  and decreasing  $\chi$ , is almost constant with respect to height and, furthermore, the contribution of the direct field is practically the same in the case m as in the case o. The latter contribution depends weakly on the  $\chi$  angle, while the former is more sensitive to variations in that parameter, because of the already mentioned conspicuous attenuation by the scattering at lower atmospheric levels. Therefore, the more important is the contribution to the  $J_m$  by the diffuse part of the Huggins-Chappuis J component, the greater is the difference in the behaviour of  $J_m$  and  $J_o$  when varying the angle  $\chi$ ; consequently the seasonal variability of the ratio  $L_m/L_o$  is larger. As shown, the importance of such contribution decreases at increasing heights and for low values of the albedo.

Fig. 15 is a composite, three-dimensional representation of the ratios  $L_x/L_o$  for the two aerosol cases  $x = a, c$  and for the three values of albedo  $A = 0, 0.3, 0.7$ . The ratio  $L_x/L_o$  is a correcting factor that can be applied to the previous values of the photodissociation coefficient, obtained for a molecular atmosphere, to account for the presence of an aerosol load. Let us point out that now both terms of this ratio depend effectively on the albedo.

The case a, representing the average condition of Elterman, leads to a ratio  $L_a/L_o$  which is larger than unity throughout the stratosphere, with the exception of the case  $m = 0.7$  in summer when it is slightly less than 1. The representative surfaces show a deep minimum down to 0.6 at the winter solstice below approximately 4 km; however, at the summer solstice this extinction effect of the aerosols in the lower troposphere is much less noticeable. The effect of the atmospheric particles on the ozone photodissociation are much more intense when a heavy aerosol distribution according to case c is considered, as shown in the inserts c in Fig. 15, again for the three albedo values  $A = 0, 0.3, 0.7$ .

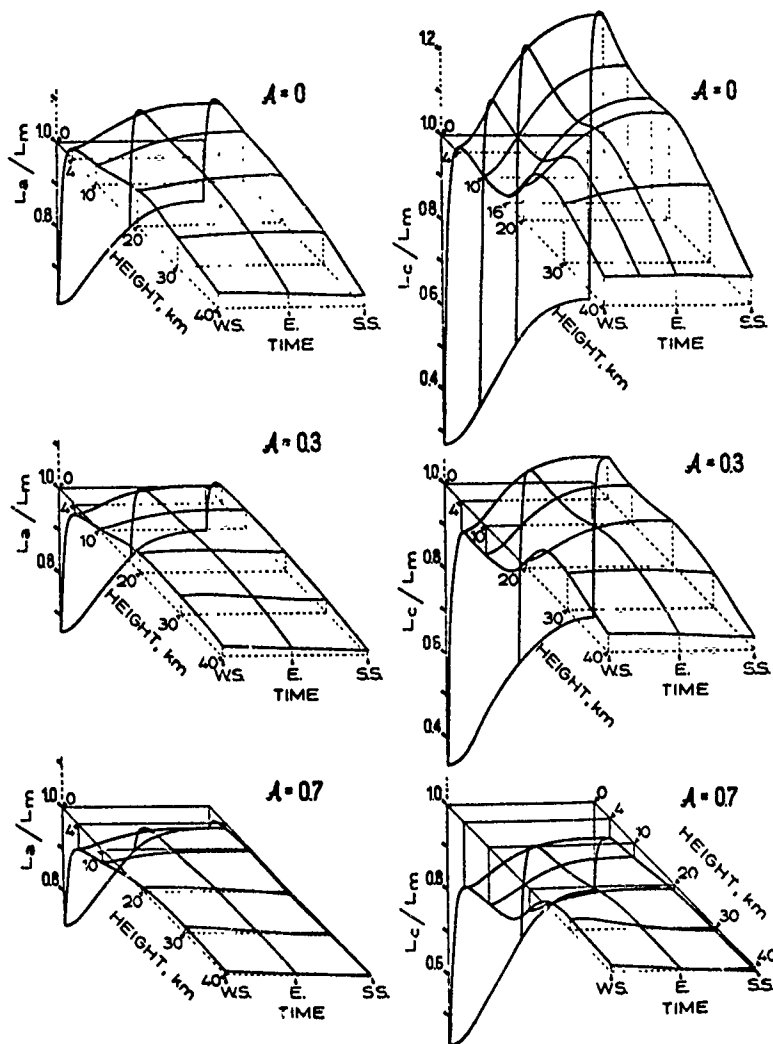


Fig. 15 - Ratios,  $L/L_m$  and  $L_c/L_m$ , between the daily integrated values of  $J_m^{a,c}$  for two different aerosol loads, a and c in Table I, and the daily integrated value of  $J_m^a$  at  $45^\circ$  lat. and for  $A = 0, 0.3, 0.7$ , as a function of height and time of the year; WS = winter solstice, E = equinox, SS = summer solstice (after Petroncelli et al., 1980).

In both case a and case c the particles are mainly concentrated in two regions: one near the ground and the other in the lower stratosphere. The aerosol layer near the ground, insofar as its effects on the stratosphere are concerned, determines a change of the albedo of the ground-troposphere system. This albedo increases, because of scattering by atmospheric particles, when the surface albedo is low, whereas it decreases, because of the extinction of the radiation going to and coming from the ground, when the surface albedo is high. In any case, such aerosol layer is quite effective when the flux of radiation reaching the lower troposphere is high: thus, for low values of the ground albedo the enhancement of photodissociation in the stratosphere is higher in summer than in winter, whereas increasing the ground albedo produces the ratios  $L/L_m$  to decrease more in summer than winter.

The effects of the stratospheric aerosol layer are quite evident in the reduction of the ratios  $L_x/L_m$  inside the layer and below it, with a strong seasonal dependence particularly for the very heavy load represented by case c. Above the stratospheric layer there is generally an increase of the photodissociation coefficient, the ratios  $L_x/L_m$  remaining however approximately constant as a function of the day of the year.

In order to ascertain whether the inclusion of scattering leads to an overall increase or a decrease of the photodissociation of ozone, yearly averages have been carried out. Fig. 16 shows the ratio of the yearly averages of  $L_m$  and  $L_o$ ,  $\bar{L}_m/\bar{L}_o$ , in the form of percentage variations: the effect of molecular scattering on the photodissociation is always strongly positive in the ozone layer region.

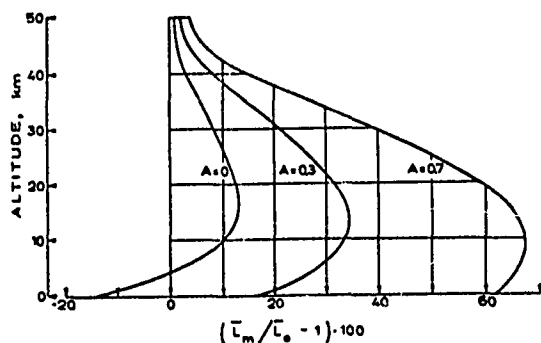


Fig. 16 - Vertical profiles of the percentage deviation  $(\bar{L}_m/\bar{L}_o - 1)100$  for three different values of the surface albedo;  $L_x/L_m$  are the yearly averages of the photodissociation coefficients for molecular scattering  $J_x$ , and pure absorption  $J_o$  (after Petroncelli et al., 1980).

More complex are the curves for the  $L_x/L_m$  and  $L_c/L_m$  ratios, shown in Fig. 17 again in the form of percentage deviations: the effect of the aerosols on the photodissociation of  $O_3$  is generally positive, but for large values of the ground albedo can be negative.

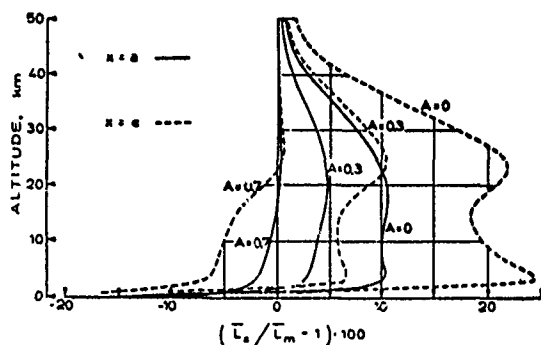


Fig. 17 - Vertical profiles of the percentage deviation  $(\bar{L}_x/\bar{L}_m - 1)100$  for three values of the surface albedo.  $\bar{L}_x$  and  $\bar{L}_m$  are the yearly averages of  $J_x$  and  $J_m$ ; cases x = a, c represent an average and a heavy aerosol load respectively (after Petroncelli et al., 1980).

**RESULTS FOR OTHER SPECIES:** We are presently going to consider other gaseous constituents, namely  $NO_2$ ,  $NO_3$ ,  $H_2O_2$  and  $HNO_3$ . Already in a previous section we have shown the reference photodissociation coefficient  $J_o$  obtained for these species in the pure absorption case.

Two sets of results are presented for each specie. The first set indicates the variation in the photodissociation coefficient, with respect to the pure absorption case, when the effects of molecular scattering and ground albedo both in the direct and diffuse field are included. The next set further extends the analysis by taking into account the effects of the molecules, of the aerosol load (x = a, b, c) and of the ground albedo.

The set of curves in Fig. 18 shows the variation of the ratio  $J_{tot,m}/J_o$  with height, for

the various species.  $J_{\text{tot},m}$  is the total photodissociation coefficient for a purely molecular atmosphere (case m). Profiles are given for different values of the albedo  $A = 0, 0.3, 0.7$  and of the zenith angle ( $\chi = 0^\circ, 45^\circ, 75^\circ$ ).

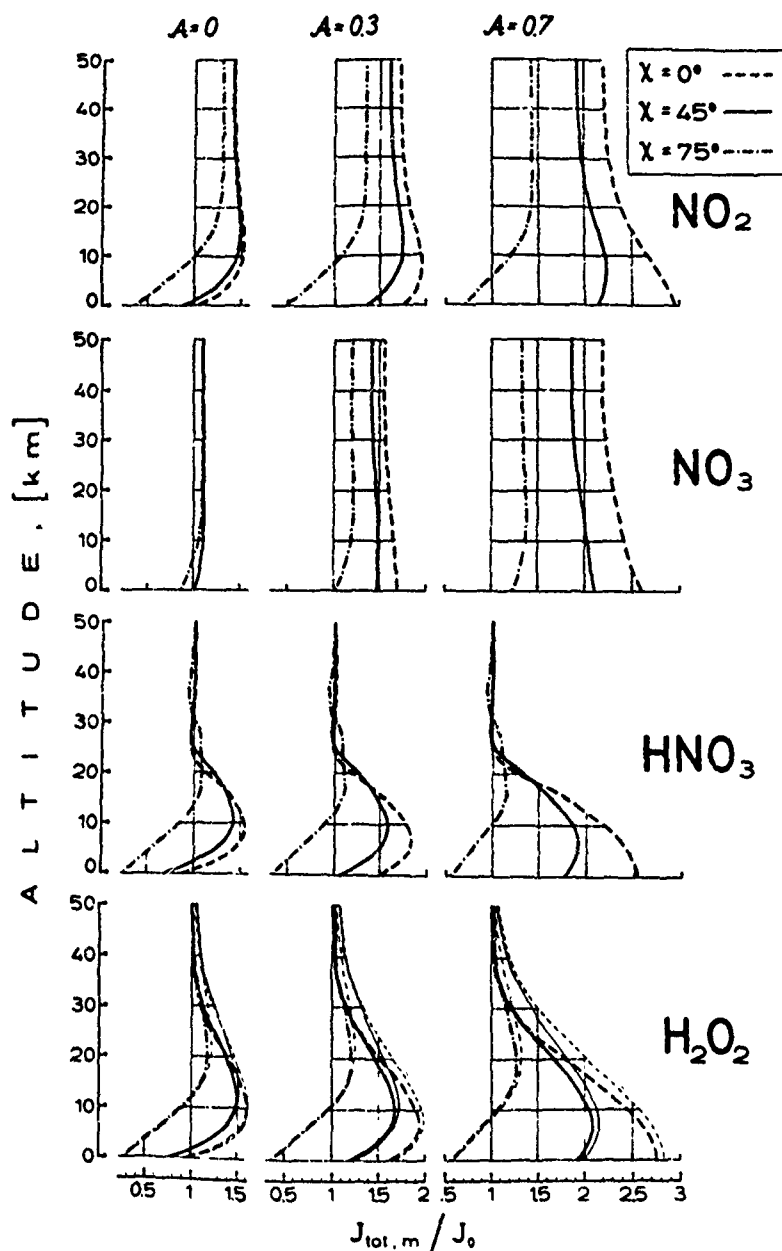


Fig. 18 - Vertical profiles of the ratios  $J_{\text{tot},m} / J_0$  for the various species and for different values of the albedo and of the solar zenith angle  $\chi$ .  $J_{\text{tot},m}$  is the total photodissociation coefficient which includes the effects of molecular scattering and of ground reflectivity. For  $\text{H}_2\text{O}_2$  thick lines refer to the data by Schumb et al. (1955) while thin lines refer to the data by Molina et al. (1977) (after Mugnai et al., 1979).

As for the previously considered photolysis of  $O_3$  these curves indicate the relative importance of the Rayleigh scattering in the two competing mechanisms of removing energy from the direct field and redistributing it into the diffuse field. The case  $A = 0$  helps in isolating the effects of the ground. The inclusion of molecular scattering always leads to an increase of the photodissociation, with the exception of the large zenith angles at tropospheric heights. This effect is quite evident for  $NO_2$ ,  $HNO_3$  and  $H_2O_2$ , but less important for  $NO_3$  which is photolysed mainly by visible radiation.

The results also show that the changes in the photodissociation obtained by the inclusion of molecular scattering are usually large and a sensitive function of the ground albedo, excepting  $HNO_3$  and  $H_2O_2$  in the upper stratosphere where these compounds are photolysed mainly by UV radiation.

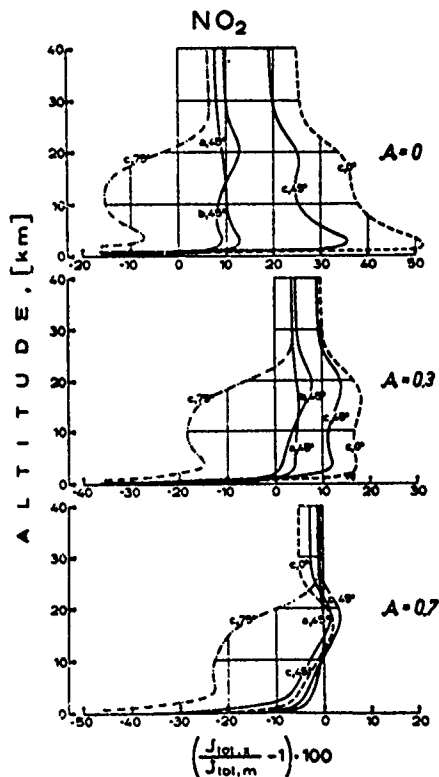


Fig. 19 - Vertical profiles of the percentage deviation  $(\frac{J_{tot,x}}{J_{tot,m}} - 1) \times 100$  of  $NO_2$  for different values of the albedo and for various aerosol loads ( $x = a, b, c$ ) at  $\chi = 45^\circ$ . For the heaviest load (case c) results corresponding to the two extreme values of the solar zenith angle ( $\chi = 0^\circ, 75^\circ$ ) are also shown (after Mugnai et al., 1979).

Fig. 19 displays the percentage deviation

$$\left( \frac{J_{tot,x}}{J_{tot,m}} - 1 \right) \times 100$$

for  $NO_2$ . As before,  $J_{tot,x}$  is the total photodissociation coefficient obtained for an aerosol load  $x$ . Profiles are given for different values of the albedo ( $A = 0, 0.3, 0.7$ ) and for the three aerosol loads ( $x = a, b, c$ ) at  $\chi = 45^\circ$ . For the heaviest load (case c) the results corresponding to the two extreme values for the zenith angle ( $\chi = 0^\circ, 75^\circ$ ) are also shown.

In conclusion, reassuming what has already been said, the main physical mechanism which

is explored by these computations results from the coupling of two factors, i.e. the ground reflectivity and the scattering and absorption by the overlaying aerosol structure. At low values of the ground albedo the presence of the aerosols generally leads, because of scattering, to an increase of the total radiation field in the upper troposphere and stratosphere, thus enhancing photodissociation. On the other hand, at large values of the albedo the main effect of the aerosols is to attenuate the radiation going into and coming from the ground and thus reducing the field and the resulting photodissociation. Although easily understood in principle, the mechanism depends in detail on many variable and it cannot be parameterized in a simple fashion; the interplay is essentially based on the relative importance of absorption and scattering by the aerosol.

The figures shows a large variation of the effect of the aerosols on the photodissociation coefficients with the solar zenith angle and therefore with the time of the day. At some heights, even a reversal in the sign of the effect can occur; increased photolysis at small zenith angles, reduced photolysis at large zenith angles. When the results are averaged over the length of the day, increased photodissociation should be obtained in summer and at the low latitudes; the opposite effect should be obtained in winter and at the high latitudes. In general only an integration over the length of the day as carried out for the case of  $O_3$ , utilizing realistic values of the aerosol loads vs latitude, will be able to ascertain the overall effect.

A point should be made regarding the photodissociation of  $O_2$  yielding  $O(^3P)$  ( $175 \text{ nm} < \lambda < 242 \text{ nm}$ ). In this case the radiation is strongly absorbed in the lower atmosphere and no effects due to surface albedo should be felt. However Rayleigh scattering is important at a height level where photolysis of  $O_2$  is relevant. Fig. 20 adopted from Callis et al. (1975) gives the ratios  $J/J_0$  for the photodissociation rate of  $O_2$  for two values of the solar zenith angle. Rayleigh scattering leads to a displacement of the height level where the process occurs when compared to estimates based on pure absorption.

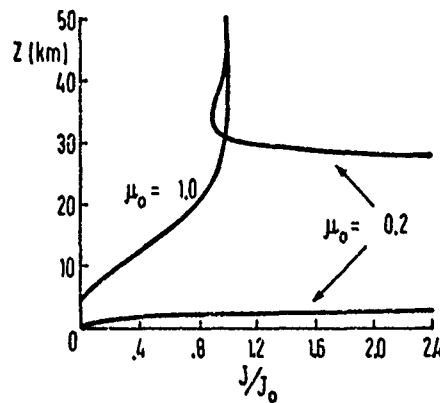


Fig. 20 - Ratios  $J/J_0$  for the photodissociation rate of  $O_2$  and two values of the solar zenith angle (adapted from Callis et al., 1975).

RESULTS OF INCLUDING MOLECULAR SCATTERING AND SURFACE REFLECTION INTO PHOTOCHEMICAL MODELS: In this section we mention briefly the results of including Rayleigh scattering and surface reflectance in photochemical models and various suggestions related to the use of simplified methods to account for diffuse radiation.

The question of the diurnal variation of the minor constituents in the stratosphere was studied by Kurzeja (1975), showing that non linearities in the destructions terms can have an important effect on the ozone concentration. In a subsequent paper Kurzeja (1977)

has included the effect of scattering on dissociation by employing the parameterization of Lacis and Hansen (1974). He has integrated the coupled set of photochemical reactions for 17 species neglecting transport. In his paper Kurzeja has also proposed a simple technique to include the effects of scattering and reflection in photochemical calculations.

A simplified method to account for molecular scattering and reflection has been proposed by Isaksen et al. (1977). The scattering is accounted for by assuming that one half of the radiation proceeds in the direction of the direct beam, the other half goes in the opposite direction. This computationally simple and relatively inexpensive method is claimed to approximate radiative fluxes within a few percent accuracy for virtually all conditions in the stratosphere. These authors compute dissociation rates for the gases  $O_3$ ,  $CH_2O$ ,  $H_2O_2$ ,  $NO_3$ ,  $HNO_3$ ,  $N_2O_5$ ,  $N_2O$  and  $ClONO$  as a function of height and solar zenith angle.

Luther et al. (1978) have incorporated the effects of multiple Rayleigh scattering into a one-dimensional model and have carried out sensitivity studies on the ozone chemistry. Their models considers a total of 83 reactions and is divided into 44 layers. Fig. 21 shows the change in concentration of various species in the,  $O$ ,  $HO$ ,  $NO$  families and containing chlorine, when Rayleigh scattering is included with a surface albedo  $\alpha = 0.25$  for a fixed zenith angle ( $\chi = 45^\circ$ ). Changes in  $[O(^1D)]$  and  $[OH]$  are as high as 60%, while those in  $[Cl]$  and  $[NO]$  are as high as 80% and 120% respectively, with related reductions in  $[O_3]$ ,  $[H_2O_2]$ ,  $[NO_2]$ ,  $[ClONO_2]$ ,  $[ClO]$ .

Visconti, Pitari and Cunnold (1980) have included Rayleigh scattering in the two-dimensional model of the stratosphere by Prinn et al. (1975). The 2-D model uses only two groups of seasons (North spring-South fall; North summer-South winter) and has a prescribed concentration of  $O_3$  at all latitudes. To evaluate photodissociation rates they have used the method proposed by Pitari and Visconti (1979) which is inspired by the work of Lacis and Hansen. Broad-band seasonally averaged albedo values which are a function of latitude (Raschke et al., 1973) have been utilized. Their calculation utilizes updated values of the reaction rates, including  $K(NO + HO_2)$ .

Fig. 22,a-f, shows the concentration of six important species as a function of latitude and height, for the Spring Fall case, with or without the inclusion of the diffuse field. An important point is the overall increase at all latitudes of  $O(^1D)$ ; as consequence the concentrations of both  $OH$  and  $HO_2$  increases due to the  $O(^1D)$  dissociation reaction with  $H_2O$ . A contribution to this increase is given also by the enhanced  $H_2O_2$  photolysis. The increase in  $OH$ , however, is not enough to compensate for the increase in  $HNO_3$  photodissociation so that there is a slight decrease of the  $HNO_3$  mixing ratio at all levels.

The higher  $O(^1D)$  concentration has the effect of increasing the  $NO$  mixing ratio ( $NO = NO + HNO_3$ ).  $NO$  ( $NO = NO + NO_2 + NO_3$ ) is totally responsible for this increase. Within the  $NO$  family the balance is increased drastically towards  $NO$  at all levels and latitudes. Specially the large variations in  $NO$  and  $H_2O_2$  indicate that a realistic simulation of stratospheric chemistry should include scattering effects.

CHANGES IN CHEMISTRY INDUCED BY DIFFUSE RADIATION VIA HEATING OF THE ATMOSPHERE: The other effect of diffuse radiation to be considered is the change in chemistry induced by heating. The gas temperature depends on the amount of energy absorbed by the atmospheric constituent and the reaction rates depend on such temperature.

Again, the variables of primary relevance are the diffuse reflectivities of surface, clouds, aerosol layers. From the point of view of modelling, of course, the average contributions of these elements of the radiative budget enter into the average temperatu-



re profiles which are used in the computations. On the other hand, spatial and temporal fluctuations of the radiative fields may induce recognizable changes in the reaction rates, depending on the thermal relaxation rates, and on the permanence of the gas in the changed condition. If  $Q$  is the amount of heat radiatively exchanged by a unit volume of gas the heating rate is defined as

$$\partial T / \partial t = Q / \rho c_p \quad (24)$$

where  $\rho$  and  $c_p$  are the density and the specific heat at constant pressure of air.

The dependence of a reaction rate coefficient

$$K = a \exp(b/T) \quad (25)$$

on the temperature  $T$ , can be written as

$$c = \frac{1}{K} \frac{\partial K}{\partial T} = - \frac{b}{T^2} \quad (26)$$

Values of the coefficients  $a$ ,  $b$  and the resulting values of  $c$  are shown in Table II for temperature sensitive reactions: it appears that changes up to 5% per degree  $^{\circ}\text{K}$  are possible.

TABLE II - Sensitivity of some reaction rates to changes in temperature, for  $T = 220^{\circ}\text{K}$ .

Reaction	$a$	$b, ^{\circ}\text{K}$	$c, ^{\circ}\text{K}^{-1}$
$\text{O} + \text{O}_2 + \text{M} \rightarrow \text{O}_3 + \text{M}$	$1.1 \times 10^{-34}$	500	$-0.10 \times 10^{-2}$
$\text{O}_3 + \text{O} \rightarrow \text{O}_2 + \text{O}_2$	$1.9 \times 10^{-11}$	-2300	$4.75 \times 10^{-2}$
$\text{O}_3 + \text{OH} \rightarrow \text{HO}_2 + \text{O}_2$	$1.6 \times 10^{-12}$	-1000	$2.07 \times 10^{-2}$
$\text{H}_2 + \text{OH} \rightarrow \text{H} + \text{H}_2\text{O}$	$2.3 \times 10^{-11}$	-2450	$5.06 \times 10^{-2}$
$\text{O}_3 + \text{NO} \rightarrow \text{NO}_2 + \text{O}_2$	$2.3 \times 10^{-12}$	-1450	$2.99 \times 10^{-2}$
$\text{Cl} + \text{OH} \rightarrow \text{HCl} + \text{O}$	$1.0 \times 10^{-11}$	-2970	$6.14 \times 10^{-2}$

We shall show the results of two different analyses. The first, which will not be considered in detail, refers to the change in the heating rate due to the absorption of solar radiation by ozone when different values of the ground albedo for a purely molecular atmosphere are considered. The second analysis refers to the heating rate

induced by the presence of aerosol in the stratosphere: this too is affected by changes in the ground albedo.

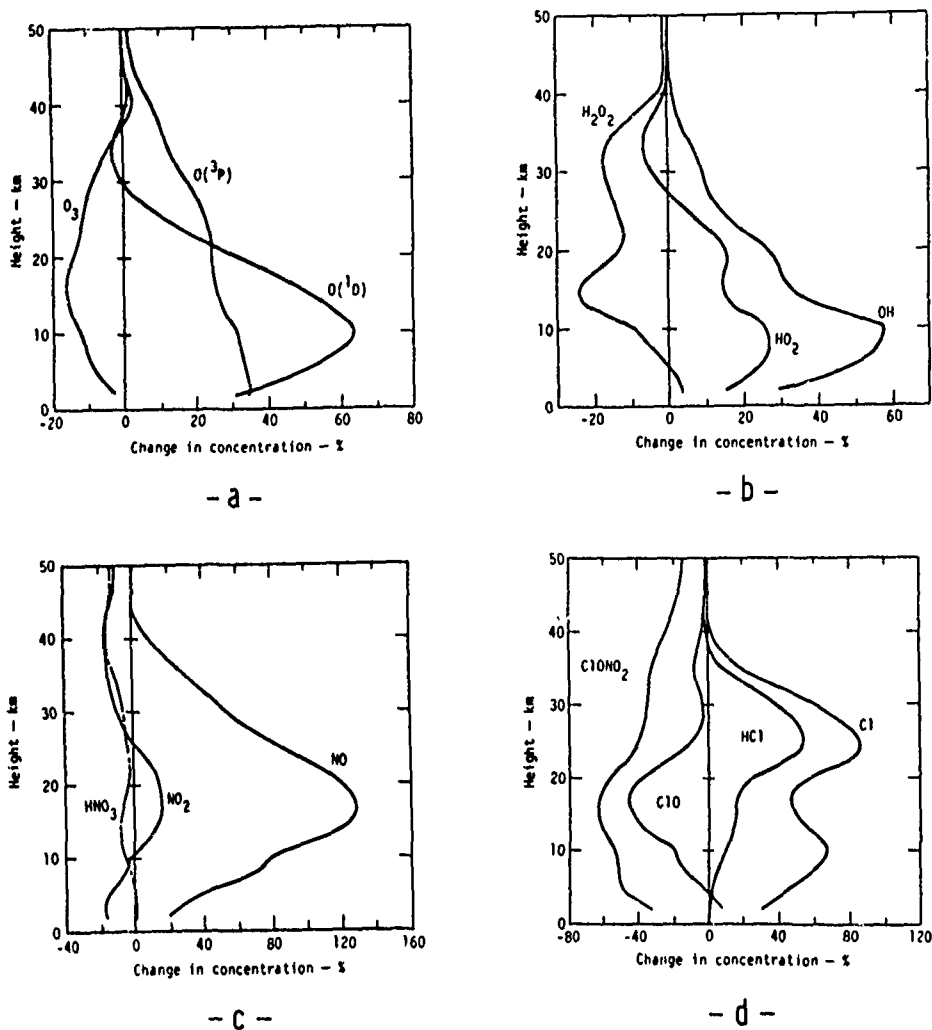


Fig. 21,a-d - Changes in the concentration of several species due to multiple scattering for  $A = 0.25$ , and a fixed zenith angle,  $\chi=45^\circ$  (adapted from Luther et al., 1978).

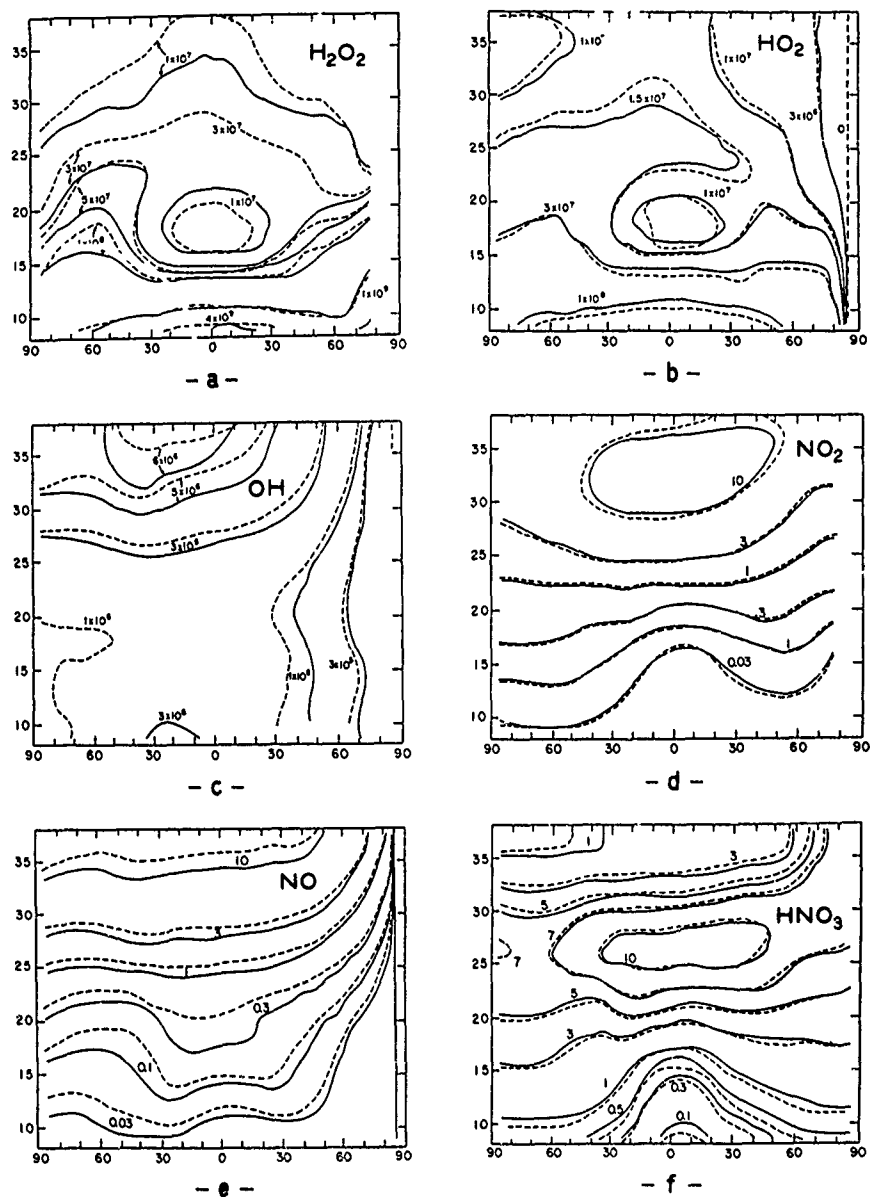


Fig. 22, - Effects of Rayleigh scattering and surface reflectivity on model calculation for six species, as a function of latitude and height for spring-fall: solid line, including molecular scattering and surface albedo, dashed line, for pure absorption. Spring is in on the left side: (a-c) concentrations of  $\text{H}_2\text{O}_2$ ,  $\text{HO}_2$ ,  $\text{OH}$  in  $\text{cm}^{-3}$ ; (d-f) mixing ratios of  $\text{NO}_2$ ,  $\text{NO}$ ,  $\text{HNO}_3$  in ppbv (adapted from Visconti et al., 1980).

As regards the first case, Lacis and Hansen (1974) in introducing their parameterized model have carried out heating rate calculations that show the effect of a change in diffuse radiation. Fig. 23 gives vertical profiles of the heating rate due to the absorption of solar radiation by ozone computed for three values of the zenith angle and two values of the ground albedo ( $A = 0, 1$ ). The heating rate in their curves is not a daily average, but an instantaneous value. A change in ground albedo from zero to unity determines a change in heating rate which can be as large as 4% at 50 km and 40% at 30 km.

Strobel (1978) has suggested the use of a much simplified expression for diffuse radiative heating which takes into account surface albedo: this formula is claimed to agree to within 10% with the results of Lacis and Hansen (1974).

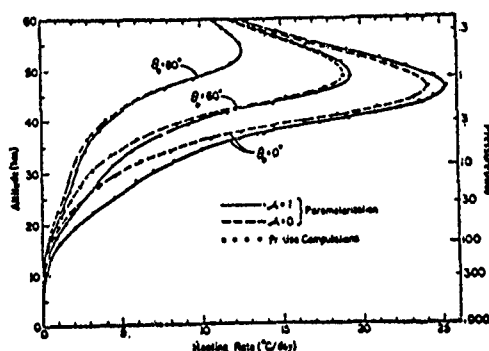


Fig. 23 - Vertical profiles of the heating rate of  $O_3$  computed including molecular scattering for three values of the solar zenith angle and two values of the albedo,  $A = 0, 1$  (adapted from Lacis and Hansen, 1974).

Fig. 24a,b shows daily averaged values of the ozone heating rate computed with the detailed methods utilized by Petroncelli et al. (1980) for two typical winter and summer days at latitude  $45^\circ$ . On the left hand side Fig. 24a shows the heating rates for a surface albedo  $A = 0$ . On the right hand side, Fig. 24b gives the difference in heating rate between the case  $A = 0.7$  and the case  $A = 0$ . The ozone profile is fixed (US Standard Atmosphere 1966). The change in albedo may produce a variation in heating rate as high as  $0.3 \text{ K/day}$ . Considering the relaxation rates, temperature increases of several degrees and a correspondingly high change in the reaction rates are involved.

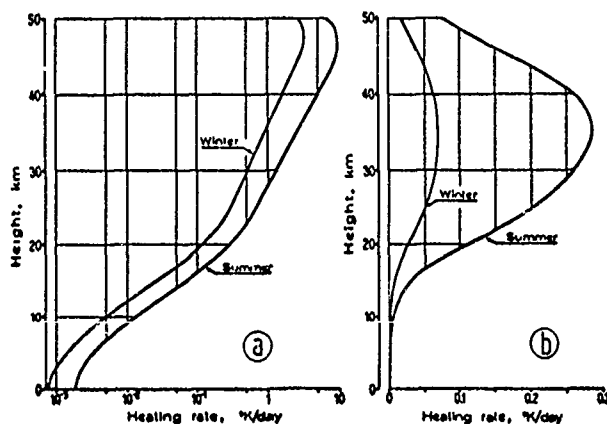


Fig. 24 - a) Profiles of the daily averaged values of the  $O_3$  heating rate at lat  $45^\circ$  for 15 January and 15 July including multiple molecular scattering for ground albedo  $A = 0$ ; the  $O_3$  profile is from US Stand. Atmos. Suppl. 1966. b) Increase in the values of (a) for  $= 0.7$ .

To stress this point further we shall consider in some more detail the heating induced by in-situ aerosols and how this quantity may change as a function of the albedo of the underlying surface-atmosphere system. Aerosols absorb radiation from the radiative field and, in part, transfer the absorbed energy into the ambient gas by way of collisions. Therefore spatial and temporal variation of the diffuse field are reflected in similar variations of the heating rate. The problem has been treated in detail by Fiocco, Grams and Visconti (1975); Fiocco, Grams and Mugnai (1976 and 1977); Mugnai, Grams and Fiocco (1978).

These analyses are based on establishing the equilibrium condition for a spherical aerosol particle of radius  $r$ ,

$$P_{a,S} + P_{a,pla} - P_r - P_c = 0 \quad (27)$$

where  $P_{a,S}$  is the solar radiation power absorbed by the particle,  $P_{a,pla}$  is the planetary radiation power absorbed by the particle,  $P_r$  is the thermal power radiated by the particle, and  $P_c$  is the power lost by the particle because of collisions with the ambient gas. In the equilibrium calculations, it is assumed that particles do not change size or state.

The solar radiation power absorbed can be expressed as

$$P_{a,S} = \pi r^2 (1 + 2 \cos \chi) \int_0^\infty Q_a(\lambda) F_S(\lambda) d\lambda \quad (28)$$

$Q$  is the efficiency factor for absorption, computed by using Mie theory; and  $F_S(\lambda)$  is the solar spectral flux. Here the analysis of the diffuse solar flux is quite simplified, only the contribution from a surface albedo independent of wavelength being taken into account; absorption and multiple scattering are neglected.

The absorbed planetary radiation power,  $P_{a,pla}$  is expressed as

$$P_{a,pla} = \pi r^2 \int_0^\infty Q_a(\lambda) F_{pla}(\lambda) d\lambda \quad (29)$$

where  $F_{pla}(\lambda)$  is the spectral flux of planetary radiation incident on the particle due to emission from the planetary surface and to atmospheric absorption and emission.

The thermal power radiated by the particle is

$$P_r = 4\pi r^2 \int_0^\infty Q_a F_\lambda(T_r) d\lambda \quad (30)$$

where  $F_\lambda(T)$  represents the Planck function in flux units at the temperature of the particle  $T_p$ .

The power collisionally exchanged with the ambient gas is

$$P_c = 2n_g r^2 \sqrt{2\pi K_B T_g / m_g} a(C_v m_g + \frac{1}{2} K_B)(T_r - T_g) \quad (31)$$

where  $a$  is the accommodation coefficient;  $c_v$  is the atmospheric specific heat at constant volume;  $n$ ,  $m$ , and  $T$  are, respectively, the number density, the mass, and the temperature of the ambient atmospheric molecules; and  $K_B$  is Boltzmann's constant.

Values of  $P_c$  at each particle size are then used to calculate the heating rates  $dT/dt$ . In the cited references the dependence on size and altitude of  $T_p$ ,  $P_c$  and  $dT/dt$  for different aerosol materials, latitudes and seasons, times of day, and for different values of the planetary albedo were studied. Also the hour-by-hour values of the heating rate were integrated to obtain the corresponding daily average heating rates. These

average values were also integrated over various particle size distribution to study the effect of the aerosol layer on the energy budget of the stratosphere and, in particular, those due to the emission of volcanic dust into the Earth's stratosphere after the Mt. Agung eruption of 1963. Following the eruption, anomalous increases in the stratospheric temperature were attributed to the presence of volcanic dust (e.g. Newell, 1971). One figure from Newell's paper is reproduced as Fig. 26a: it shows the difference in stratospheric temperature between January 1963 and January 1964, as a function of geographical location at an altitude of about 19 km. A large temperature increase is evident in the latitude strip between 0° and 20° S, with maxima around central Africa and New Guinea, and less pronounced over South America.

The effect can be explained by taking into account the geographical variations of the Earth's albedo. In this case, the heating rate induced by the aerosol on the ambient gas can be locally increased.

Figure 25 shows the results of applying the previous analysis to particles of different composition and refractive index. In particular Fig. 25a refers to the impure sulphuric acid particles and Fig. 25b to the dust particles, both previously considered. The curves give the heating rates at the 19 km level for particles having a size-number distribution according to the power law  $dN/d \log r = Cr^{-3}$ , for the radius interval  $0.03 \mu m < r < 3 \mu m$ ; the particle mass mixing ratio is  $v = 1$  ppb. For each particle composition, heating rates are presented for albedo values  $A = 0.1$  and  $A = 0.7$ . Notice that the heating rates thus computed take into account only the sensible heat exchanged between the particles and the gas by collisions, and does not take into account the fact that, in part, infrared emission radiated by the aerosol is absorbed by the ambient gas. At the height of 19 km, this contribution would be small, but it would essentially add to the heating rates specified.

Figure 26b shows the mean wintertime (December, January and February) values of the planetary albedo as a function of latitude and longitude obtained from satellite observations (Vonder Haar and Ellis, 1974). As already mentioned the general characteristics of the albedo patterns show relatively high values over land and lower values over the oceans which fit the longitudinal patterns observed in the temperature differences of Fig. 26a.

In calculating the heating rates as a function of latitude and longitude the data on the geographical variation of aerosol concentration at the 19 km level were from Cadle, Kiang and Louis (1976). The calculations utilized their results for 300 days after the Agung eruption, to establish the amount of fine-ash and impure sulfuric-acid. Then the results presented in Fig. 25 were combined to establish the contributions of impure sulfuric-acid droplets and fine-ash particles. The result of adding the heating rates for these two components of the stratospheric aerosol layer is shown in Fig. 26c. A very high degree of correlation between the temperature differences in Fig. 26a and the heating rates in Fig. 26c is evident. Maximum heating rates of about  $0.4 \text{ K day}^{-1}$  are associated with temperature differences of about 8 K. We thereby infer radiative relaxation time constants on the order of 20 days at the 19 km level, which agree well with the estimates of Sasamori and London (1966).

This result is interesting because it shows that by stationing for a sufficiently long time over geographical areas with different albedo air masses may acquire a different chemical characterization. This consideration applies in particular to the tropical belt, where zonal circulation is slow.

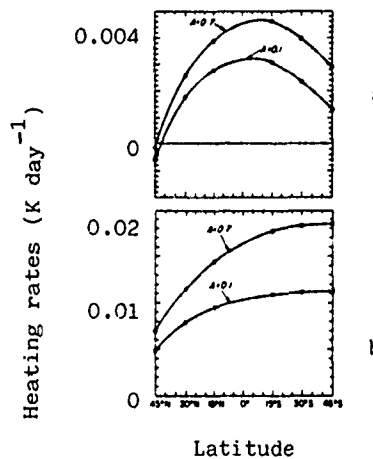


Fig. 25 - Heating rates,  $K \text{ day}^{-1}$ , at 19 km as a function of latitude and planetary albedo. Calculations refer to aerosol particles with a mass mixing ratio of 1 ppb and the Junge size-number distribution function. (a) impure sulfuric-acid droplets, (b) fine-ash particles (after Fiocco et al., 1977).

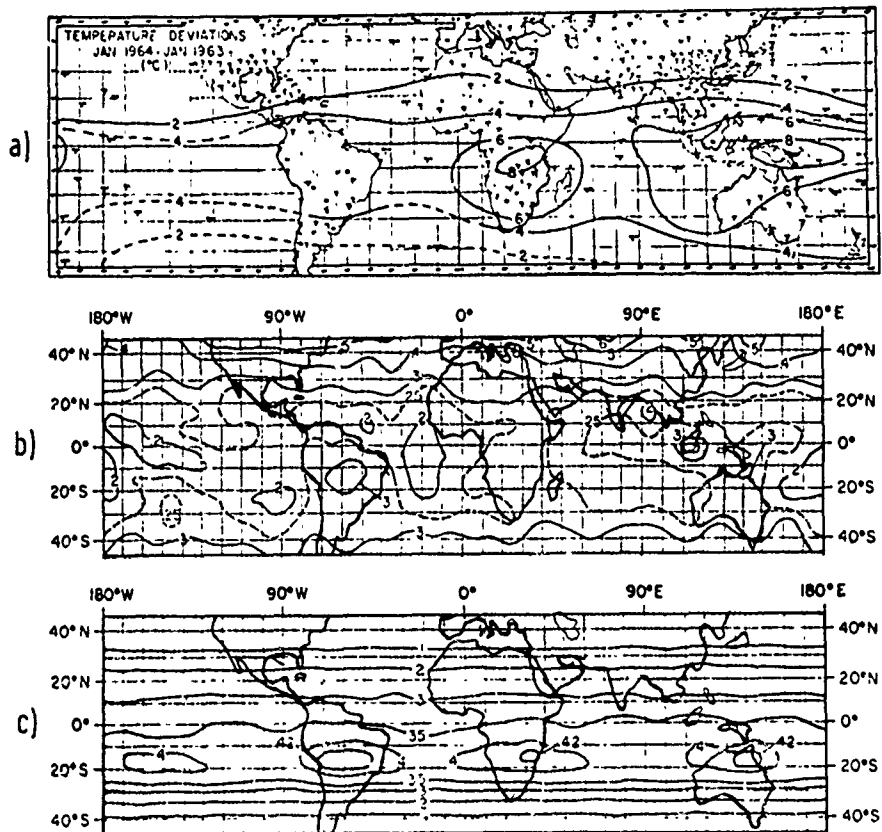


Fig. 26 - (a) Difference in stratospheric temperature between Jan 64 and Jan 63 (after Newell, 1971); (b) Mean values of planetary albedo (after Vonder Haar and Ellis, 1974); (c) estimated heating rate due to stratospheric aerosols with albedo as in fig. (b) (after Fiocco et al., 1977).

CONCLUSION: The importance of these results is various. On the one hand models should incorporate an adequate treatment of the radiation field for realistic simulations: the inclusion of the diffuse field leads to an overall substantial increase in precision. Also, experiments to measure the concentration of certain species should also include measurements of either the diffuse flux or the photolysis rate. On the other hand, the physical and chemical behaviour of the atmosphere depends strongly on these interacting effects and the fluctuating behaviour of the concentrations of some species to a large extent may depend on interactions dominated by the radiation field.

Since heating or photolysis effects depend on exposure time, it is reasonable to expect that the fluctuations in the concentrations of certain species can be partially explained by reconstructing the past history of the radiation exposure of an air mass.

These can be due, as already said, to motions over areas of different albedo, and also to the presence, in the air mass, of a large aerosol content that locally modifies the diffuse field. An example of a possible interaction of this type is shown by the negative correlations found between dust and ozone in a study of the stratosphere aerosol larger during 1963 and 1964 (Grams and Fiocco, 1967).

These mechanisms play an important role not only on the chemistry as explored here, but in the more general area of climate.

ACKNOWLEDGEMENT: This work was carried out at the Laboratorio Plasma Spazio, CNR, Frascati with partial support from "Progetto Finalizzato Ambiente, CNR" and from the Commission of European Communities.

#### REFERENCES

- Ashby, R.W., A numerical study of the chemical composition of the stratosphere, Ph.D. Thesis, microfilm 76-20653, Univ. of Wisconsin Madison, 1976.
- Cadle, R.D., C.S. Kiang, and J.F. Louis, The global scale dispersion of the eruption clouds from major volcanic eruptions, J. Geophys. Res., **81**, 3125-3132, 1976.
- Callis, L.B., The importance of Rayleigh scattering in photochemical processes in the stratosphere, 1974 AGU Fall Meeting, EOS **55**, 1124, 1974.
- Callis, L.B., V. Ramanathan, R.E. Boughner and B.R. Barkstrom, The stratosphere: scattering effects, a coupled 1-D model, and thermal balance effects, Proc. 4th Conf. on CIAP, DOT-TSC-OST- 75-38, (T.M. Hard and A.J. Broderick eds.), 224-233, 1976.
- Dave, J.V. and C.L. Mateer, A preliminary study of the possibility of estimating total atmospheric ozone from satellite measurements, J. Atmos. Sci., **24**, 414-427, 1967.
- Elterman, L., UV, visible and IR attenuation for altitudes up to 50 km, AFCRL Report 68-0153, Environmental Research Paper No. 285, Bedford, Mass, 1968.
- Fiocco, G., G. Grams and A. Mugnai, Energy exchange and temperature of aerosols in the Earth's atmosphere (0-60 km), J. Atmos. Sci., **33**, 2415-2424, 1976.
- Fiocco, G., G. Grams and A. Mugnai, Energy exchange and equilibrium temperature of aerosols in the Earth's atmosphere, Proceedings of the Symposium on Radiation in the Atmosphere, H.J. Bolle ed., Science Press, Princeton, New Jersey, 74-78, 1977.
- Fiocco, G., G. Grams and G. Visconti, Equilibrium temperature of small particles in the Earth's upper atmosphere (50-110 km), J. Atmos. Terr. Phys., **37**, 1327-1337, 1975.
- Fiocco, G., A. Mugnai and W. Forlizzi, Effects of radiation scattered by aerosols on the photodissociation of ozone, J. Atmos. Terr. Phys., **40**, 949-961, 1978.
- Grams, G. and G. Fiocco, The stratospheric aerosol layer during 1964 and 1965, J. Geophys. Res., **72**, 3253-3542, 1967.
- Grant, I.P. and G.E. Hunt, Discrete space theory of radiative transfer. I. Fundamentals, Proc. Roy. Soc. Lond. A **313**, 183-197, 1969.
- Heath, D.F., A.J. Krueger and L.C. Mateer, The Nimbus-4 backscatter ultraviolet (BUV) atmospheric ozone experiment, Pure Appl. Geophys., **106-108**, 1238-1253, 1973.



- Herman, B. and D.N. Yager, Estimating the vertical atmospheric ozone distribution inverting the radiative transfer equation for pure molecular scattering, J. Atmos. Sci., 26, 153-162, 1969.
- Hudson, R.D., Chlorofluoromethanes and the stratosphere, NASA RP 1010, Natl. Tech. In Serv., Springfield, Virginia, 1977.
- Hunt, G.E. and I.P. Grant, Discrete space theory of radiative transfer and its application to problems in planetary atmosphere, J. Atmos. Sci., 26, 963-972, 1969.
- Isaksen, I.S.A., K.H. Midtbo, J. Sunde and P.J. Crutzen, A simplified method to include molecular scattering and reflection in calculations of photon fluxes and photodissociation rates, Geophys. Norv. 31, 11-26, 1977.
- Jozenas, V.A., Determining the vertical ozone distribution in the upper atmospheric layers from satellite measurements of ultraviolet solar radiation scattered by the Earth's atmosphere, Geomag. Aeron. 8, 403-407, 1968.
- Kerker, M., The scattering of light and other electromagnetic radiation, Academic Press: New York & London, 1969.
- Kurzeja, R.J., The diurnal variation of minor constituents in the stratosphere and its effect on the ozone concentration, J. Atmos. Sci., 32, 899-909, 1975.
- Kurzeja, R., Effects of diurnal variations and scattering on ozone in the stratosphere for present-day and predicted future chlorine concentrations, J. Atmos. Sci., 34, 1120-1129, 1977.
- Lacis, A.A. and J.E. Hansen, A parameterization for the absorption of solar radiation in the Earth's atmosphere, J. Atmos. Sci. 31, 118-133, 1974.
- Luther, F.M., Results from recent solar radiation calculations, 4th Conf. on CIAP eds. 242-253, 1975.
- Luther, F.M. and R.J. Gelinas, Effect of molecular multiple scattering and surface albedo on atmospheric photodissociation rates, J. Geophys. Res. 81, 1125-1132, 1976.
- Luther, F.M., D.J. Wuebbles, W.H. Dwyer and J.C. Chang, Effect of multiple scattering on species concentrations and model sensitivity, J. Geophys. Res. 83, 3563-3570, 1978.
- McClatchey, R.A., R.W. Fenn, J.E.A. Selby, J.S. Garing and F.E. Volz, Optical properties of the atmosphere, AFCRL Report 70-0527, Environmental Research paper No. 331 Bedford, Mass, 1970.
- Molina, L.T., S.D. Schinke and M.J. Molina, Ultraviolet absorption spectrum of hydrogen peroxide vapor, Geophys. Res. Lett. 4, 580-582, 1977.
- Mugnai, A., G. Fiocco and G. Grams, Effects of aerosol optical properties and size distributions on heating rates induced by stratospheric aerosols, Q. J. Roy. Met. Soc. 104, 783-796, 1978.
- Mugnai, A., P. Petroncelli and G. Fiocco, Sensitivity of the photodissociation of  $\text{NO}_2$ ,  $\text{NO}_3$ ,  $\text{HNO}_3$  and  $\text{H}_2\text{O}_2$  to the solar radiation diffused by the ground and by atmospheric particles, J. Atmos. Terr. Phys. 41, 351-359, 1979.
- Newell, R.E., The global circulation of atmospheric pollutants, Sci. Am., 224, 32-42, 1971.
- Palmer, K.F. and D. Williams, Optical constants of sulfuric acid; application to the clouds of Venus? Appl. Opt., 14, 208-219, 1975.
- Paltridge, G.W. and C.M.R. Platt, Radiative processes in meteorology and climatology, Elsevier Sci. Publ. Co., Amsterdam, 1976.
- Petroncelli, P., G. Fiocco and A. Mugnai, Annual variation of the effects of diffuse radiation on the photodissociation of ozone, Pure Appl. Geophys., to appear 1980.
- Pitari, G. and G. Visconti, A simple method to account for Rayleigh scattering effects on photodissociation rates, J. Atmos. Sci., to appear 1980.
- Raschke, E., T.H. Vonder Haar, W.R. Bandeen and M. Pasternak, The annual radiation balance of the earth-atmosphere system during 1969-70 from Nimbus-3 measurements, J. Atmos. Sci., 30, 341-354, 1973.

FIOCCO

- Russell, P.B., W. Viezee, R.D. Hake, Jr. and R.T.H. Collis, Lidar observations of the stratospheric aerosol: California, October 1972 to March 1974, J. Roy. Met. Soc., 102, 675-695, 1976.
- Sasamori, T. and J. London, The decay of small temperature perturbations by thermal radiation in the atmosphere, J. Atmos. Sci., 23, 543-554, 1966.
- Schumb, W.C., C.N. Satterfield and R.L. Wentworth, Hydrogen Peroxide, Reinhold, New York, 1955.
- Sekera, Z. and J.V. Dave, Determination of the vertical distribution of ozone from the measurement of diffusely reflected ultraviolet solar radiation, Planetary Space Sci., 5, 122-136, 1961.
- Singer, S.F. and R.C. Wentworth, A method for the determination of the vertical ozone distribution from a satellite, J. Geophys. Res., 62, 299-308, 1957.
- Strobel, D.F., Parameterization of the atmospheric heating rate from 15 to 120 km due to  $O_2$  and  $O_3$  absorption of solar radiation, J. Geophys. Res., 83, 6225-6230, 1978.
- Sundararaman, N., The UV radiation field in the stratosphere, Proc. 4th Conf. on CIAP, (T.M. Hard and A.J. Broderick, eds.), 234-241, 1975.
- Toon, O.B. and J.P. Pollack, Physical properties of the stratospheric aerosols, J. Geophys. Res., 78, 7051-7056, 1973.
- Van de Hulst, H.C., Asymptotic fitting, a method for solving anisotropic transfer problems in thick layers, J. Comp. Phys., 3, 291-306, 1968.
- Visconti, G., G. Pitari and D. Cunnold, A two-dimensional photodissociation chemical model of the stratosphere with Rayleigh scattering, Pure Appl. Geophys., to appear 1980.
- Vonder Haar, T.H. and J.S. Ellis, Atlas of radiation budget measurements from satellites (1962-1970), Atmospheric Science Paper No. 231, Dept. of Atmospheric Science, Colorado State Univ., Fort Collins, Colorado, 1974.
- Yamamoto, G., M. Tanaka and S. Asano, Radiative transfer in water clouds in the infrared region, J. Atmos. Sci., 27, 282-292, 1970.
- Yager, D.N., An evolution of some methods of estimating the vertical atmospheric ozone distribution from the inversion of spectral ultraviolet radiation, J. Appl. Meteor., 9, 921-928, 1970.
- Wiscombe, W.J. and J.W. Evans, Exponential-sum fitting of radiative transmission functions, J. Comp. Phys., 24, 416-444, 1977.

## LABORATORY MEASUREMENTS OF ABSORPTION CROSS SECTIONS

Mario J. Molina

Dept. of Chemistry, University of California, Irvine, CA 92717

### Abstract

The UV spectra of a few selected molecules of importance in stratospheric photochemistry as well as some of the laboratory techniques employed for their study are described, and the general features of these spectra which determine the experimental requirements for UV absorption cross section measurements are discussed.

INTRODUCTION: For atmospheric work the extent of absorption of UV and visible light is expressed usually in terms of cross sections defined by the following expression of Beer's law:

$$I = I_0 \exp(-\sigma cl)$$

where

$I_0$ ,  $I$ : incident and transmitted light intensity  
 $\sigma$ : absorption cross section,  $\text{cm}^2 \text{ molecule}^{-1}$   
 $c$ : concentration,  $\text{molecule cm}^{-3}$   
 $l$ : path length, cm

The conversion factor between the common molar extinction coefficient (expressed in  $\text{dm}^3 \text{ mol}^{-1} \text{ cm}^{-1}$ , base 10) and absorption cross sections is  $3.82 \times 10^{-21}$ .

The ultraviolet absorption cross sections of  $\text{O}_2$  and  $\text{O}_3$  determine the extent of penetration of solar radiation into the stratosphere and troposphere, as discussed by Professor Nicolet in another paper in this series. For other atmospheric trace species the cross sections, as well as the quantum yields are needed to estimate their solar photodissociation rates.

There are several critical reviews which describe in a systematic way UV absorption cross sections and quantum yields of importance for stratospheric processes. The NASA Panel for Data Evaluation [1979] is currently updating its reports--which include a discussion of cross sections--approximately every nine months; also, an earlier review by Hudson [1971] presents a very careful discussion of sources of experimental errors, of effects of line shapes and instrumental slit widths on the measurements, etc. The present paper is limited to a discussion of some general features of UV spectra which

are pertinent to atmospheric photochemistry, using a few selected molecules as examples. For this purpose it is convenient to classify atmospheric trace species in three groups: (1) source species, (2) radicals, and (3) non-radical species which are generated in the atmosphere. Source species (e.g.,  $N_2O$ ,  $H_2O$ ,  $CF_2Cl_2$ ) are released into the troposphere and diffuse into the stratosphere where they decompose producing radicals (e.g.,  $NO$ ,  $OH$ ,  $Cl$ ), a radical being defined as a species possessing an odd number of electrons. The radicals react producing either other radicals (e.g.,  $NO_2$ ,  $HO_2$ ,  $ClO$ ) or molecules containing an even number of electrons (e.g.,  $HONO_2$ ,  $HCl$ ,  $ClONO_2$ ,  $CF_2O$ ).

**SOLAR FLUX:** The wavelength range where solar photolysis occurs depends on the characteristics of the uv spectrum of the species in question as well as on the relative intensity of solar radiation at the various wavelengths. Figure 1 shows this intensity as calculated by Wuebbles and Chang [1978], taking backscattering into account. As can be seen in the figure, there are two important spectral regions for stratospheric photolysis: (1) the 185-225 nm atmospheric "window" where solar radiation penetrates relatively deeply into the stratosphere (because the combined  $O_2$  and  $O_3$  UV absorption is weaker in this range than for any other wavelengths shorter than  $\sim 280$  nm); and (2) the region with wavelengths longer than 290 nm--the ozone "cutoff"--where UV and visible radiation penetrate all the way to the earth's surface.

**DISCUSSION OF UV SPECTRA:** Some general characteristics of the spectra of a few molecules pertaining to each of the three groups mentioned above is presented next.

**SOURCE SPECIES:** Nitrous Oxide,  $N_2O$ . The importance of weak absorptions in the spectral region beyond 290 nm for source species is clearly borne out by this example: the dominant sink for  $N_2O$  was believed to be solar photolysis in the troposphere until Johnston and Selwyn [1976] measured the cross sections shown in Figure 2; the figure also shows for comparison the long wavelength absorption tail that had previously been attributed to  $N_2O$  (in an unpublished paper cited by Bates and Hayes [1970]).

There is little difficulty in handling source species in the laboratory--they are by definition very stable--and furthermore, very weak absorptions can be measured reliably using long path absorption cells coupled to sensitive spectrophotometers; however, the samples have to be carefully purified to eliminate all traces of strongly absorbing impurities.

The  $N_2O$  absorption cross sections are temperature dependent [Selwyn et al., 1971], an effect which can be explained with the assumption that the cross sections differ among the various accessible vibrational states of the molecule. A few direct measurements of UV spectra of vibrationally excited species have been carried out [see, for example, Zittel and Little, 1979] and show that indeed the cross sections may be very significantly affected by vibrational excitation.

**Halocarbons.** The species  $CF_2Cl_2$ ,  $CFCl_3$  and  $CCl_4$  are similar in many respects to  $N_2O$ : their UV spectrum is continuous, they do not absorb in the  $\lambda > 290$  nm region, they photolyze in the stratosphere through absorption in the 190-210 nm window and their cross sections in this wavelength region are temperature dependent. This latter effect turns out to have relatively little consequence for atmospheric calculations involving source species.

Figure 3 shows the cross sections determined in our laboratory for various halocarbons [Rowland and Molina, 1975; Chou et al., 1978], together with solar flux values at various altitudes. As the number of chlorine atoms bonded to each carbon atom decreases--with a corresponding increase in the number of fluorine atoms--the spectra shift towards shorter wavelengths and photodissociation in the stratosphere occurs at higher altitudes. Similarly, replacement of chlorine atoms by bromine atoms red-shifts the spectra. This

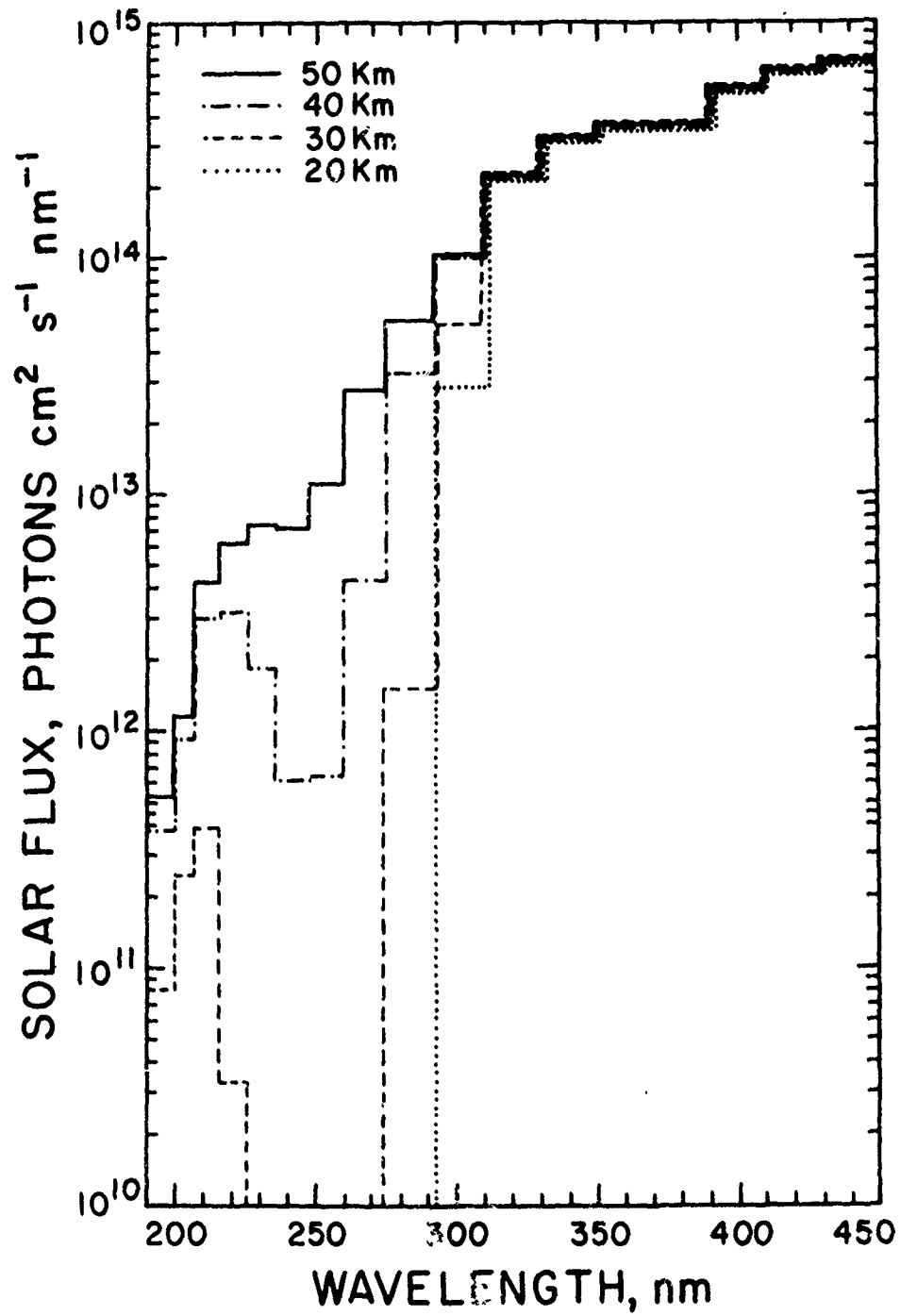


Figure 1. Flux of solar photons as a function of wavelength and altitude.

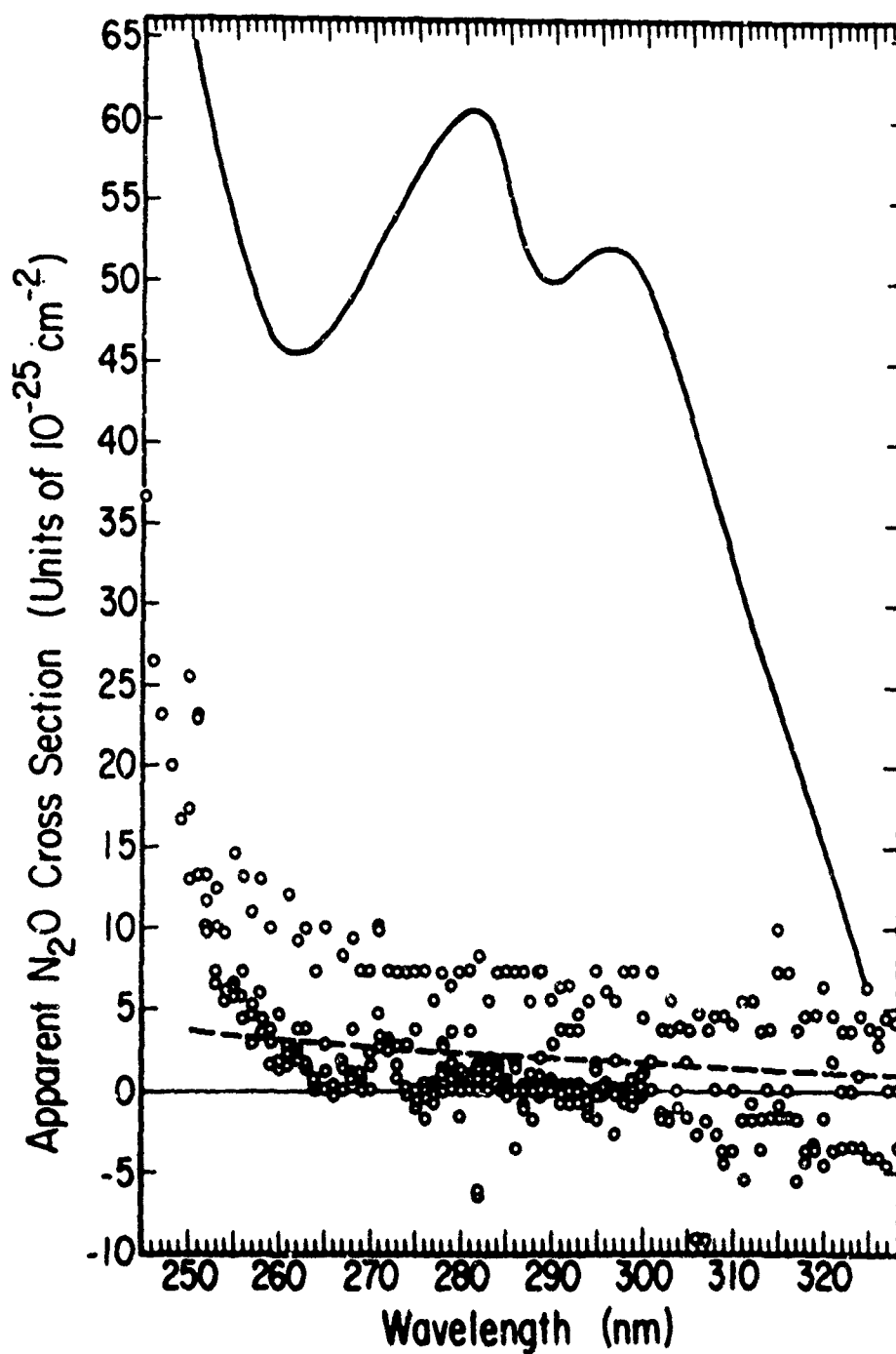


Figure 2. Observed, apparent absorption cross sections for nitrous oxide. Circles: Johnston and Selwyn [1975]; solid line: Bates and Hayes [1967]; dashed line: Rayleigh scattering.

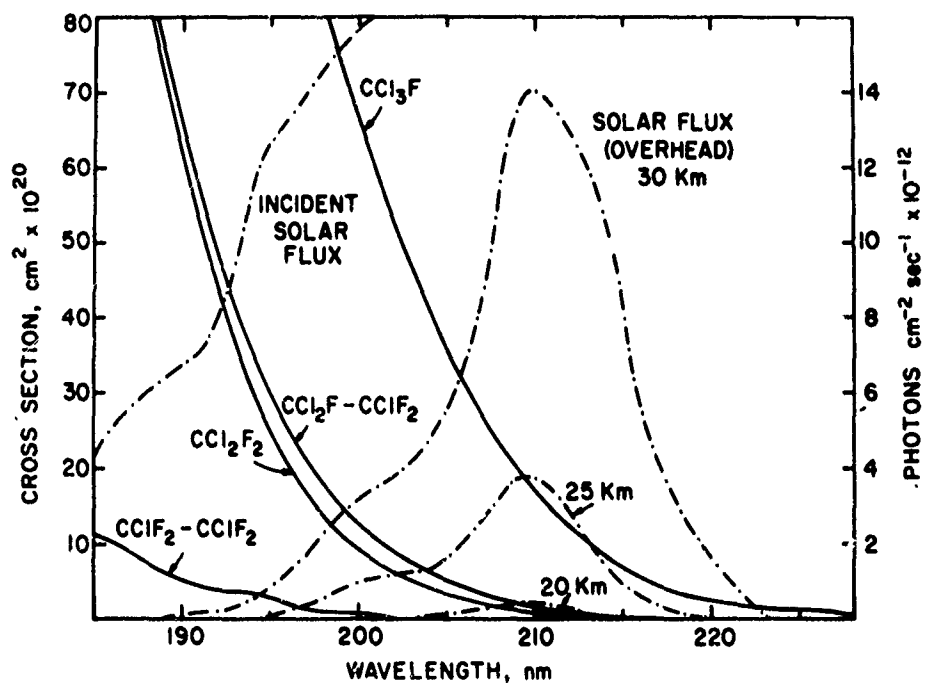


Figure 3. Absorption spectra of several saturated chlorofluorocarbon compounds (solid lines). The dashed lines represent the flux of solar photons.

trend is to be expected considering the nature of the electronic transition responsible for the absorption, namely an  $n-\sigma^*$  transition which involves excitation to a repulsive state that immediately dissociates by breaking the carbon-halogen bond.

The quantum yields for photo-decomposition have been established to be unity for  $\text{CF}_2\text{Cl}_2$  and for  $\text{CFCl}_3$  [Milstein and Rowland, 1975; Rebbert and Ausloos, 1975]. In fact, there are no known examples of atmospheric trace species with a continuous spectrum whose quantum yield for dissociation is not unity. In contrast, a highly structured spectrum indicates that the quantum yield is likely to be smaller than one.

Because of the importance of potential tropospheric sinks for  $\text{CCl}_4$ ,  $\text{CFCl}_3$ , and  $\text{CF}_2\text{Cl}_2$  the possibility of very small absorptions for wavelengths longer than 290 nm has been investigated rather thoroughly. The smallest photo-absorption cross sections that can be measured with a spectrophotometer are of the order of  $10^{-26} \text{ cm}^2$  (smaller values would be masked by Rayleigh scattering, as shown in Figure 1). In order to measure even smaller values Rebbert and Ausloos [1976/77] used gas chromatographic techniques to detect traces of photolysis products; in this fashion they established an upper limit to the  $\text{CCl}_4$  cross section at 313 nm of  $3 \times 10^{-26} \text{ cm}^2$ . The corresponding cross sections of  $\text{CFCl}_3$  and  $\text{CF}_2\text{Cl}_2$  must be even smaller since replacement of Cl by F in halocarbons shifts the spectrum towards shorter wavelengths, as described above.

**RADICALS:** In contrast to source species, radicals may undergo rapid chemical reactions in the atmosphere so that with a few notable exceptions photodissociation can be neglected in comparison with other atmospheric loss processes. From the point of view of laboratory measurements free radicals can be divided in two classes: those that react irreversibly with themselves and those that do not. The latter ones can usually be prepared in appreciable concentrations as pure compounds, and thus their absorption cross sections can be measured relatively easily; examples are  $\text{NO}_2$  and  $\text{OCIO}$ . However, most radicals can only be prepared as transients in the presence of a large excess of other compounds, and cross section measurements are quite difficult for this class of radicals. An example is  $\text{BrO}$ : due to its large absorption cross sections at wavelengths longer than 300 nm solar photodissociation turns out to be significant, as has been shown by Yung et al. [1979]. The  $\text{BrO}$  spectrum has been studied by Durie and Ramsay [1958] by means of a flash-photolytic technique, and by Clyne and Cruse [1970] using a discharge flow system.

A further complicating factor with radicals is that they often have highly structured UV and visible spectra and consequently their photodissociation quantum yields need to be determined in addition to their cross sections. The most important example is  $\text{NO}_2$ : its absorption cross sections can be measured in a relatively straight forward manner although instrumental resolution is an important factor and also the presence of the dimer  $\text{N}_2\text{O}_4$ , which also absorbs in the UV, has to be taken into account [Bass et al., 1976]. The quantum yield for production of oxygen atoms is wavelength and temperature dependent, and it does not appear to increase smoothly with decreasing wavelength, as shown recently by Harker et al. [1977] and by Davenport [1978].

**NON-RADICAL SPECIES:** There are two important species in this group whose photochemical behavior is discussed elsewhere in this series of papers:  $\text{O}_3$ , by Dr. Moortgat, and formaldehyde,  $\text{CH}_2\text{O}$ , by Professor Calvert. Here we will single out a particular subset of species belonging to this group, namely those that are formed in the atmosphere by reaction between two radicals. This type of compound often has one rather weak chemical bond; in the stratosphere the species might be thermally stable and it might react only very slowly with other atmospheric trace species, but in the laboratory it can be quite difficult to handle due to the occurrence of surface reactions. We will discuss two compounds belonging to this class: chlorine nitrate, and hypochlorous acid.

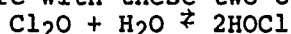


Chlorine nitrate.  $\text{ClONO}_2$  is formed by the recombination of  $\text{NO}_2$  and  $\text{ClO}$  radicals, and it is destroyed predominantly by solar photolysis. The UV spectrum measured in our laboratory is shown in Figure 4 [Molina and Molina, 1978]; for comparison, our earlier measurements [Rowland et al., 1976] carried out under conditions of somewhat lesser sensitivity are also shown in the figure. The cross sections in the 300-350 nm wavelength range are approximately four orders of magnitude smaller than the cross sections around 200 nm, and yet photolysis occurs predominantly at 300-350 nm for altitudes below about 30 km due to the strong attenuation of solar radiation at the lower altitudes (see Figure 1). It is now well established that the rather small cross sections around 350 nm are not due to the presence of impurities, since the cross section values are not changed by repeated purifications or by using different synthetic methods for the preparation of  $\text{ClONO}_2$ . Furthermore, the agreement between our measurements and those of Glasgow et al. [1976] is quite satisfactory.

The  $\text{ClONO}_2$  cross sections are weakly temperature dependent between 200 and 350 nm: the maximum effect occurs around 310 nm, where the room temperature cross section is about 30% larger than the cross section at 258 K. As mentioned above, the temperature effect can usually be attributed to transitions originating from vibrationally excited molecules, and is largest at the wings of an absorption band, e.g., for  $\text{N}_2\text{O}$  the 296 K cross section at 230 nm is a factor of 3 larger than the value at 225 K [Selwyn et al., 1971]. The rather small effect of temperature on  $\text{ClONO}_2$  cross sections indicates that the 320-450 nm shoulder which appears in the spectrum is actually due to an electronic transition other than the one responsible for the maximum around 220 nm [see Molina and Molina, 1979].

Hypochlorous acid. The photochemical behavior of hypochlorous acid,  $\text{HOCl}$ , is important since it is a potential inert reservoir for stratospheric chlorine. There are some theoretical calculations [Jaffe and Langhoff, 1978] which indicate negligible  $\text{HOCl}$  cross sections in the 300-350 nm range; if this is the case  $\text{HOCl}$  would be the predominant Cl-containing species throughout most of the stratosphere [Glasgow et al., 1979]. However, there are several laboratory measurements which point towards much larger cross sections in that same wavelength range, and there are little if any precedents to establish the validity of the *ab-initio* calculations of UV spectra of the type that Jaffe and Langhoff carried out.

The laboratory measurements involving  $\text{HOCl}$  are complicated by the fact that this species cannot be prepared as a pure compound since it disproportionates very readily yielding  $\text{Cl}_2\text{O}$  and  $\text{H}_2\text{O}$ . Usually,  $\text{HOCl}$  is handled in the laboratory in an equilibrium mixture with these two compounds:



By measuring the absorbances of these equilibrium mixtures and by taking into account the absorption due to  $\text{Cl}_2\text{O}$  it is possible to infer the  $\text{HOCl}$  cross sections; this has been done by two groups [Molina and Molina, 1978; and Knauth et al., 1979]. The results indicate that the  $\text{HOCl}$  cross sections in the 300-320 nm range are of the order of  $10^{-19}$ - $10^{-20}$   $\text{cm}^2$ , implying a stratospheric lifetime of about one hour. We have recently reinvestigated in our laboratory the  $\text{HOCl}$  spectrum around 310 nm by means of an entirely different technique: the amount of OH produced by laser photolysis of  $\text{HOCl}$  was measured directly using laser induced fluorescence, the  $\text{HOCl}$  being generated by the  $\text{Cl}_2\text{O} + \text{H}_2\text{O}$  as well as by the  $\text{HCl} + \text{Cl}_2\text{O}$  reactions. In this fashion the complications due to the presence of  $\text{Cl}_2\text{O}$  could be avoided; furthermore, the short time scale of the pulsed laser measurement insured that the OH was a primary photolysis product. The results are in good agreement with those obtained by the absorption technique, so that it is now reasonably well established that  $\text{HOCl}$  will photodissociate quite rapidly in the stratosphere.

In summary, there is no single laboratory technique which is suitable for all UV absorption cross section measurements of stratospherically important species, and thus the appropriate experiments have to be designed on a case-by-case basis.

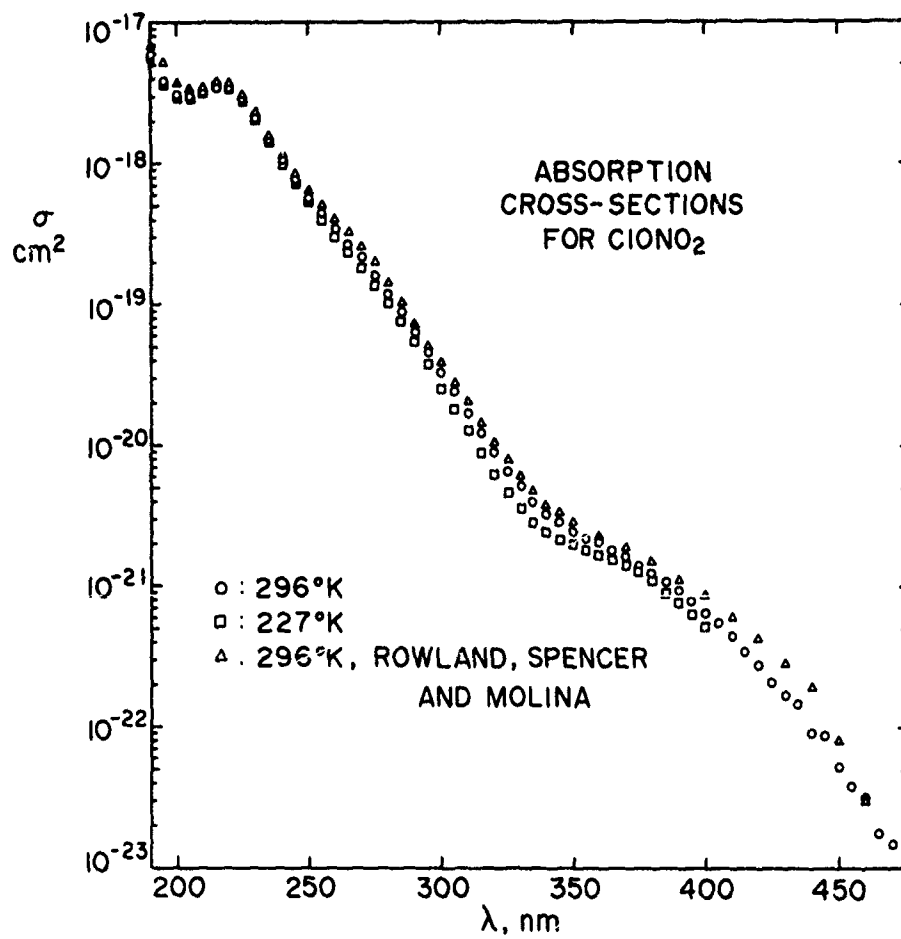


Figure 4. Absorption spectrum of  $\text{ClONO}_2$ , taken from Molina and Molina [1979], and Rowland et al., [1976].

## REFERENCES

- Bass, A.M., A.E. Ledford, and A.H. Laufer, Extinction Coefficients of NO<sub>2</sub> and N<sub>2</sub>O<sub>4</sub>, J. Research NBS, **80A**, 143-166, 1976.
- Bates, D.R., and P.B. Hayes, Atmospheric Nitrous Oxide, Planet Space Sci., **15**, 189-197, 1967.
- Clyne, M.A.A., and H.W. Cruse, Rates of Elementary Reactions Involving the BrO (x<sup>2</sup>II) Radicals and IO (x<sup>2</sup>II) Radicals: Part 1 - Formation and Decay of the BrO Radical, Trans. Faraday Soc., **66**, 2214-2226, 1970.
- Chou, C.C., R.J. Milstein, W.S. Smith, H. Vera-Ruiz, M.J. Molina, and F.S. Rowland, Stratospheric Photodissociation of Several Saturated Perhalo Chlorofluorocarbon Compounds in Current Technological Use (Fluorocarbons -13, -113, -114, and -115), J. Phys. Chem., **82**, 1-7, 1978.
- Davenport, J.E., Determination of NO<sub>2</sub> Photolysis Parameters for Stratospheric Modeling, Report No. FAA-EQ-78-14, 1978.
- Durie, R.A., and D.A. Ramsay, Absorption Spectra of the Halogen Monoxides, Can. J. Phys., **36**, 35-53, 1958.
- Glasgow, L.C., and J.P. Jesson, Photodissociation Rates of ClONO<sub>2</sub>, ClNO<sub>2</sub> and Cl<sub>2</sub>O, 12th Informal Photochemistry Conference, June 28-July 1, 1976.
- Glasgow, L.C., J.P. Jesson, D.L. Filkin, and C. Miller, The Stratospheric Abundance of Hypochlorous Acid (HOCl), Planet. Space Sci., **27**, 1047-1054, 1979.
- Harker, A.B., W. Ho, and J.J. Ratto, Photodissociation Quantum Yield of NO<sub>2</sub> in the Region 375 to 420 nm, Chem. Phys. Lett., **50**, 394-397, 1977.
- Hudson, R.D., Critical Review of Ultraviolet Photoabsorption Cross Sections for Molecules of Astrophysical and Aeronomic Interest, Rev. Geophys. Space Phys., **9**, 305-406, 1971.
- Jaffe, R.L., and S.R. Langhoff, Theoretical Study of the Photodissociation of HOCl, J. Chem. Phys., **68**, 1638-1648, 1978.
- Johnston, H.S., and G.S. Selwyn, New Cross Sections for the Absorption of Near Ultraviolet Radiation by Nitrous Oxide (N<sub>2</sub>O), Geophys. Res. Lett., **2**, 549-551, 1975.
- Knauth, H.D., H. Alberti, and H. Clausen, Equilibrium Constant of the Gas Reaction Cl<sub>2</sub>O + H<sub>2</sub>O = 2HOCl and the Ultraviolet Spectrum of HOCl, J. Phys. Chem., **83**, 1604-1619, 1979.
- Milstein, R., and F.S. Rowland, Quantum Yield for the Photolysis of CF<sub>2</sub>Cl<sub>2</sub> in O<sub>2</sub>, J. Phys. Chem., **79**, 669-670, 1975.
- Molina, L.T., and M.J. Molina, Ultraviolet Spectrum of HOCl, J. Phys. Chem., **82**, 2410-2414, 1978.
- Molina, L.T., and M.J. Molina, Chlorine Nitrate Ultraviolet Absorption Spectrum at Stratospheric Temperatures, J. Photochem., **11**, 139-144, 1979.
- NASA Panel for Data Evaluation, Chemical Kinetic and Photochemical Data for Use in Stratospheric Modeling, Evaluation No. 2, JPL Publication 79-27, 1979.
- Rebert, R.E., and P.J. Ausloos, Photodecomposition of CFCl<sub>3</sub> and CF<sub>2</sub>Cl<sub>2</sub>, J. Photochem., **4**, 419-434, 1975.
- Rebert, R.E., and P.J. Ausloos, Gas-Phase Photodecomposition of Carbon Tetrachloride, J. Photochem., **6**, 265-276, 1976/77.
- Rowland, F.S., and M.J. Molina, Chlorofluoromethanes in the Environment, Rev. of Geophys. and Space Phys., **13**, 1-35, 1975.
- Rowland, F.S., J.E. Spencer, and M.J. Molina, Stratospheric Formation and Photolysis of Chlorine Nitrate, J. Phys. Chem., **80**, 2711-2712, 1976.
- Selwyn, G., J. Podolske, and H.S. Johnston, Nitrous Oxide Ultraviolet Absorption Spectrum at Stratospheric Temperatures, Geophys. Res. Lett., **4**, 427-430, 1977.
- Wuebbles, D.J., and J.S. Chang, personal communication, 1978.
- Yung, Y.L., J.P. Pinto, R.T. Watson, and S.P. Sander, Atmospheric Bromine and Ozone Perturbations in the Lower Stratosphere, Contribution No. 3215 of the Div. of Geol. and Planet. Sciences, Cal. Inst. of Tech., Pasadena, California, 1979.
- Zittel, P.F., and D.D. Little, Photodissociation of Vibrationally Excited Hydrogen Bromide, J. Chem. Phys., **71**, 713-722, 1979.

O(<sup>1</sup>D) QUANTUM YIELDS FROM O<sub>3</sub> PHOTODISSOCIATION  
AND O(<sup>1</sup>D) REACTIONS WITH ATMOSPHERIC CONSTITUENTS.

Geert Karel Moortgat

Max Planck Institut für Chemie (Otto-Hahn Institut)  
Saarstrasse 23, D 6500 MAINZ, F.G.R.

Abstract

The ultraviolet photolysis of ozone is the main source of O(<sup>1</sup>D) in the atmosphere:  $O_3 \longrightarrow O(^1D) + O_2(^1\Delta_g)$ . Below 300 nm, the O(<sup>1</sup>D) is produced with "near unity" quantum yield. At 310 nm, the process is no longer energetically possible. Consequently, the O(<sup>1</sup>D) quantum yield drops to near zero at 320 nm. The exact shape of the O(<sup>1</sup>D) fall-off curve from the ozone photolysis in the near 295-325 nm range is important for aeronomical calculations. In the first part, numerous measurements of the relative and absolute O(<sup>1</sup>D) quantum yields, obtained at different wavelengths and temperatures, are reviewed and evaluated. The second part deals with the O(<sup>1</sup>D) reactions with atmospheric constituents such as N<sub>2</sub>, O<sub>2</sub>, CO<sub>2</sub>, CO, H<sub>2</sub>O, CH<sub>4</sub>, H<sub>2</sub>, N<sub>2</sub>O, NH<sub>3</sub>, HCl, and halocarbons. Recently measured reaction rate constants are reviewed and compared; the product channels (physical deactivation or/and chemical reaction) are discussed.

I) INTRODUCTION

The photolysis of ozone is one of the most important photochemical processes in the atmosphere, and the ozone photodissociation is generally the starting process for most photochemical models in the troposphere and the stratosphere. Indeed the primary products arising from the photolysis of ozone are the reactive initiators of many chemical reactions. One of the most important aspects of the ozone photolysis is the generation of excited

oxygen atoms,  $O(2^1D_2)$ , (or  $O(^1D)$  in short). They possess about 45 kcal/mole more energy than the ground electronic state  $O(2^3P_2)$ , ( $O(^3P)$  in short). The radiative transition from the  $O(^1D)$  to the  $O(^3P)$  state with emission at 630 nm is strongly forbidden, and consequently the radiative lifetime is very long ( $\sim 140$  s.)

In the atmosphere, most of the  $O(^1D)$  atoms lose their excess energy by collisions with air molecules. To a smaller extent,  $O(^1D)$  atoms, react with trace gases, such as  $H_2O$ ,  $H_2$ , and  $CH_4$  to produce OH radicals, and with  $N_2O$  to produce NO. It is now established that both OH and NO enter into the natural catalytic cycle of ozone destruction, and thus control the ozone budget in the stratosphere. The OH radical is also one of the most important oxidizing agents in the troposphere and controls the chemistry of many trace gases.

It would be appropriate to present the main features of the ozone photochemistry and briefly review the various primary processes in the different regions of the ozone absorption spectrum. For more detailed information, see the excellent reviews on photolytic studies, by Wayne [1972], Schiff [1972] and Welge [1974].

ABSORPTION SPECTRUM. At wavelengths larger than 200 nm, the absorption spectrum exhibits the Hartley bands and continuum (200 - 300 nm), the Huggins bands (300 - 360 nm) (Fig. 1.) and further to the red the weak Chappuis bands (450 - 800 nm). The absorption coefficients have been measured by several groups, and have recently been reviewed by Hudson [1974]. The absorption cross sections measured by Griggs [1968] and Vigroux [1969] are in excellent agreement with earlier work by Inn and Tanaka [1953] and Vigroux [1953]. It is worthy to note that Vigroux [1953] and Simons et al. [1973] observed a temperature dependence of the absorption spectrum in the Huggins region, as shown in Fig. 1, where spectra taken at 200 and 300 K are compared. The minima correspond to absorption by high rotational levels, and show a stronger temperature dependence than the maxima. The temperature effect is not negligible for the calculation of the upper tropospheric, and lower stratospheric  $O_3$  photodissociation rates, for which only solar radiation above 300 nm is available.

PRIMARY PROCESSES. The complexity of the ozone photolysis is due to the low bond strength of  $O_3$  ( $24.3 \pm 0.4$  kcal/mole) [Stull and Prophet, 1971], its large absorption coefficient in the ultra violet, and the possibility of producing not only ground state, but also several excited oxygen atoms and molecules. Atomic and molecular oxygen possess electronically excited states

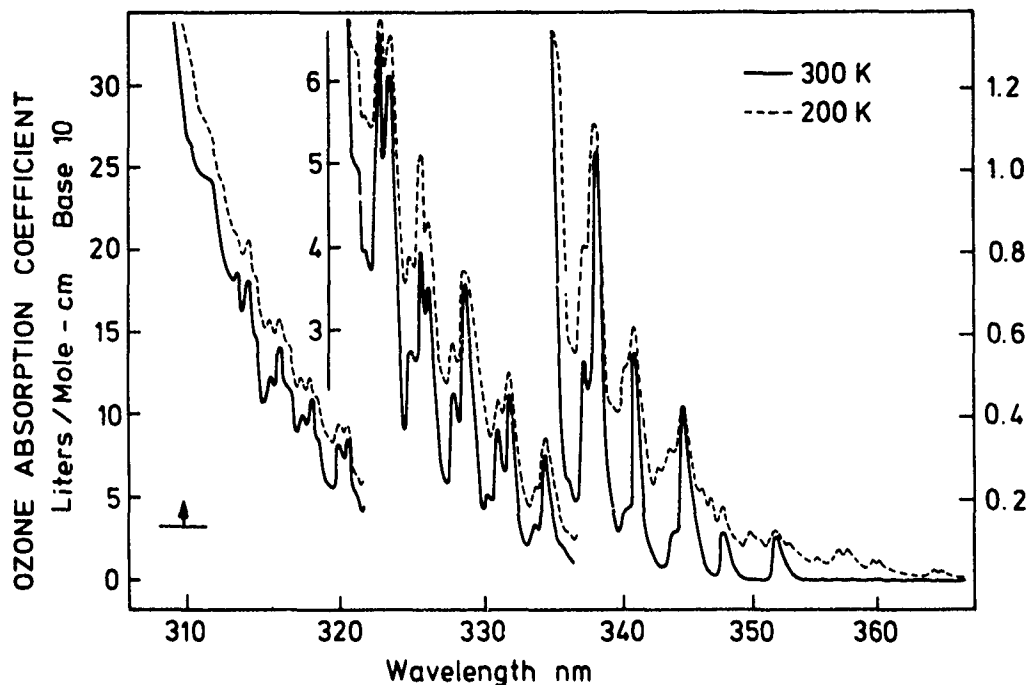
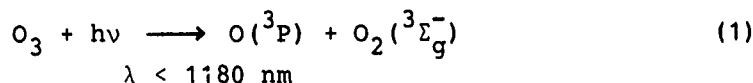


Fig. 1. Ozone absorption spectrum in the Huggins region at 200 and 300 K, after Simons, et al., [1973]. The arrow at the low left corresponds to the dissociation energy of 92.1 kcal/mole.

which are both relatively low lying, and are easily accessible upon photolysis of  $O_3$ . Table 1 shows the longest wavelength at which various products become energetically accessible.

In the weak region of the absorption spectrum (Chappuis region), ozone dissociates to ground state products with unity quantum yield:



Although the production of  $O_2(^1\Delta_g)$  is energetically possible below 611 nm (see Table 1) by a spin forbidden process, there is no evidence that  $O_2(^1\Delta_g)$  is produced. Process (1) is the main photolytic source of atomic oxygen below 30 nm.

In the strong ultraviolet absorption region of the Hartley continuum ( $1^1A_1 \longrightarrow 1^1B_2$  transition), ozone photodissociates to electronically excited products:

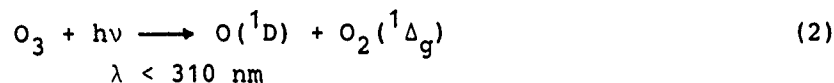
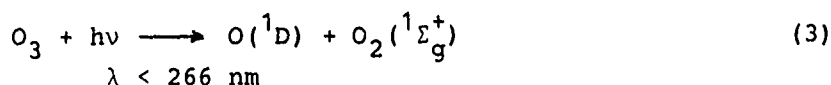


Table 1

Long wavelength limits (nm) for  $O_3$  photodissociation processes and energies (kcal/mole) of O and  $O_2$  species.

	O	$O_2$	$x^3\Sigma_g^-$	$a^1\Delta_g$	$b^1\Sigma_g^+$
			0	22.54	37.51
$^3P_2$		0	1180	(611)	(463)
$^1D_2$		45.23	(411)	310	266
$^1S_0$		96.71	(237)	199	179

Parentheses indicate spin forbidden fragment combinations.

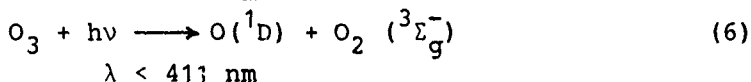
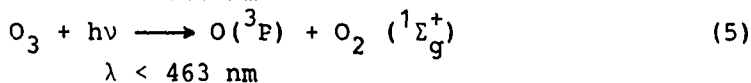
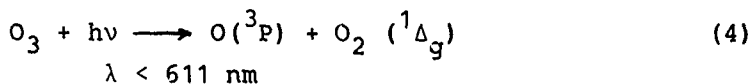


Because of the strong absorption, it was generally assumed that the photodissociation via the spin allowed processes (2) and (3) occurred with unity quantum yield, and that consequently the quantum yield for  $O(^1D)$  is unity below 310 nm. The nature of the molecular species appears to have been established. In a flash photolysis study of pure  $O_3$ , Gilpin et al. [1971], using time resolved emission spectroscopy, observed that the production of  $O_2(^1\Sigma_g^+)$  is not more than 5 %, in contradiction with earlier assumptions [Wallace and Hunten, 1968]. Also, Gauthier and Snelling [1971] and Jones and Wayne [1971] detected the direct infrared emission band at 1270 nm of  $O_2(^1\Delta_g)$  during the photolysis of  $O_3$  at 253.7 nm. It is thus safe to assume that  $O_2(^1\Delta_g)$  is the predominant molecular species in the photolysis of ozone between 310 and 240 nm, and that the photodissociation process (2) is the main atmospheric process responsible for the production of  $O(^1D)$ .

The exact wavelength limit of process (2) can be determined from basic thermodynamic properties of  $O_3(^1A)$ ,  $O(^1D)$  and  $O_2(^1\Delta_g)$ . However the dissociation energy of ozone is not sufficiently well known to derive the exact threshold wavelength for this process. Using the electronic excitation ener-

gy at 298 K of 45.23 kcal/mole for  $O(^1D)$  and 22.54 kcal/mole for  $O_2(^1\Delta_g)$  [Hampson and Garvin, 1978] and the bond dissociation energy of  $22.54 \pm 0.4$  kcal/mole for  $O_3$  [Stull and Prophet, 1971] the calculated limit for process (2) is  $92.1 \pm 0.4$  kcal/mole, which corresponds to  $310.1 \pm 1.3$  nm.

Above this threshold value, photodissociation in the Huggins region is energetically possible according to the spin forbidden processes:



The formation of  $O(^1D)$  at wavelengths larger than 310 nm is energetically still possible via process (6), but since spin is not conserved (the molecular product is ground state molecular  $O_2$ ) it is believed to be of minor importance. The quantum yield of  $O(^1D)$  formation should therefore decrease considerably. The range 300-320 nm is designed as the fall-off region for the  $O(^1D)$  production.

Below 234 nm, it is energetically possible to produce  $O(^1S)$ , however, it is not known whether  $O(^1S)$  is generated in the stratosphere.

#### AERONOMIC SIGNIFICANCE

The exact determination of the variation of the  $O(^1D)$  quantum yield with wavelength has an enormous aeronomic significance for the photochemistry of the lower stratosphere and troposphere. The individual parameters determining the rate of  $O(^1D)$  production,  $J_{O(^1D)}$ , are the  $O_3$  absorption cross section  $\sigma(\lambda)$ , the  $O(^1D)$  quantum yield  $\phi(\lambda)$ , and the solar actinic irradiance  $I(\lambda)$ ,

$$J_{O(^1D)} = \int_{\lambda_1}^{\lambda_2} \sigma(\lambda) \cdot \phi(\lambda) \cdot I(\lambda) \cdot d\lambda \quad (i)$$

The ozone layer in the mid-stratosphere very efficiently absorbs the solar radiation below 300 nm, and thus shields the earth surface against lethal ultraviolet light, below 295 nm. The intensity of solar radiation penetrating to the lower atmosphere increases rapidly at wavelengths greater than 300 nm, and in the same wavelength region, both the  $O(^1D)$  quantum yield and the ozone absorption cross section decrease to zero. The wavelength dependence of these parameters, as well as that of the  $O(^1D)$  production rate is shown in Fig. 2, in order to illustrate the narrow range of the effective



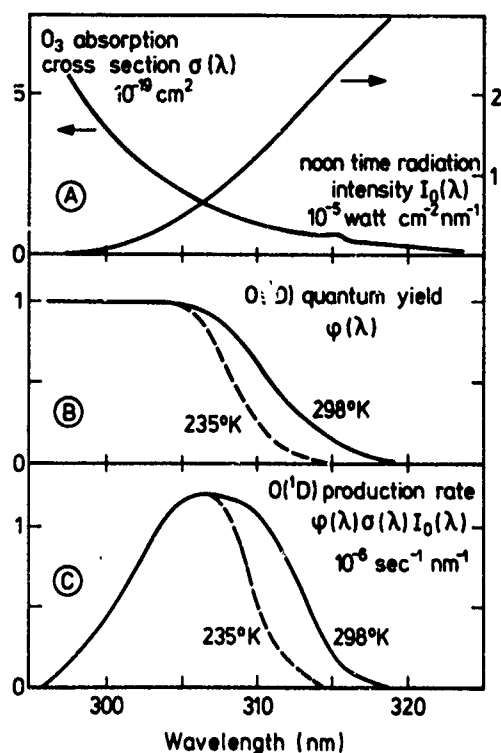


Fig. 2. Parameters determining the rate of  $O(^1D)$  formation from ozone as a function of wavelength. Top:  $O_3$  absorption cross sections and radiation intensities (noontime,  $30^\circ\text{N}$ , spring); middle  $O(^1D)$  quantum yields; bottom: product of above parameters. (after Warneck, [1977])

wavelength in the solar spectrum. From Fig. 2 C, it is apparent that two quantum yield determinations give different values for  $J_{O(^1D)}$ . Because of the importance of calculating the OH radical concentrations in the lower atmosphere, extensive investigations have been performed in the past in order to termine the exact course of the  $O(^1D)$  fall-off curve.

The first part of the present paper will confine itself to a review and evaluation of all the  $O(^1D)$  quantum yield measurements. The second part will deal with the  $O(^1D)$  reactions with the main atmospheric constituents considering recent rate constant data and product channels.

## II) $O(^1D)$ QUANTUM YIELD MEASUREMENTS

The exact shape of the fall-off curve has been subject to many controversies

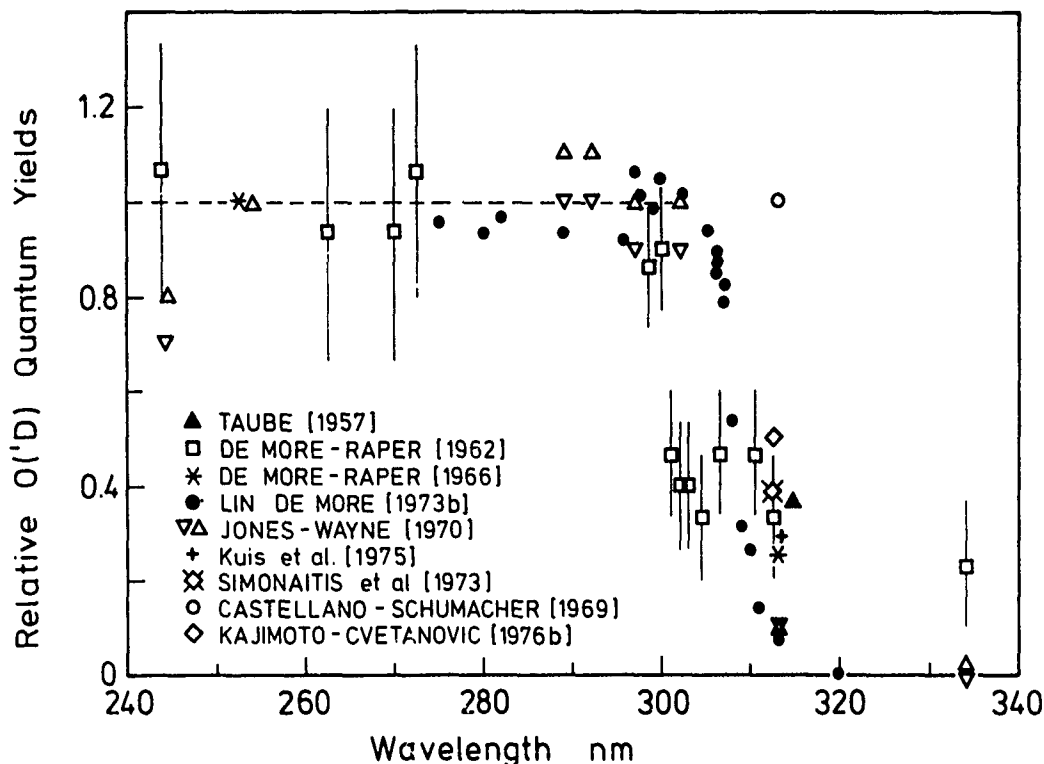


Fig. 3. Relative  $O(^1D)$  quantum measurements at various wavelengths, in the period 1957 - 1975.

between the various measurements in the last years. Most  $O(^1D)$  quantum yield measurements in the fall-off region (300 - 320 nm) are determined relative to  $O(^1D)$  quantum yield measurements below 300 nm. The quantum yield of process (2) in the Hartley absorption band below 300 nm is often cited as unity, although recent absolute  $O(^1D)$  quantum yield measurements rather suggest a value "close to unity". The author will therefore first chronologically report on the progress in the evaluation of the RELATIVE quantum yields, based on the quantum yield unity below 300 nm, and then briefly discuss recent ABSOLUTE quantum yield measurements.

#### RELATIVE QUANTUM YIELDS.

##### a) LIQUID AND SOLID PHASE PHOTOLYSIS

The first measurements on the  $O(^1D)$  quantum yields were performed in liquid and condensed phase. Taube [1957] photolysed  $O_3$  in acidified solutions, and determined the disappearance of  $O_3$  at 254 and 313 nm, from which the relative quantum yield  $\phi_{313} / \phi_{254} = 0.37$  was determined. DeMore and Raper [1962] photolysed dilute solutions of  $O_3$  in liquid  $N_2$  at several wavelengths

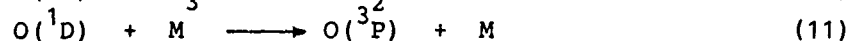
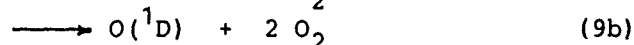
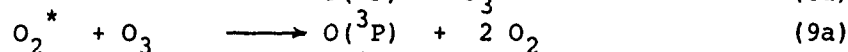
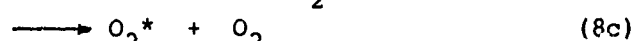
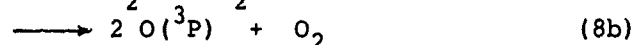
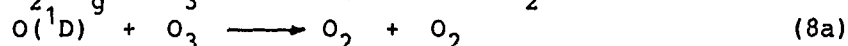
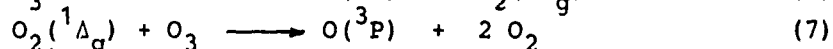
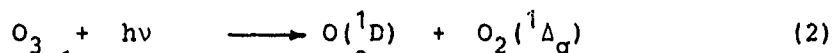
between 248 and 334 nm, and measured the formation of  $N_2O$ , which is formed by reaction of  $O(^1D)$  with the  $N_2$  solvent with extremely low efficiency. From the constancy of the  $N_2O$  yield between 248 and 300 nm, it was concluded that the  $O(^1D)$  yield was unity. The drop in the quantum yield between 300 and 325 nm from 1 to 0.4 instead of zero, as is shown in Fig. 3 remained unexplained.

A few years later, DeMore and Raper [1966] photolysed  $O_3$  in liquid Argon at 87 K, and measured the quantum yield of  $O_3$  consumption,  $\phi(-O_3)$  at 253.7 and 313.3 nm, as a function of  $O_3$  pressure. From the intercept of the plots of the inverse yields  $1/\phi(-O_3)$  versus pressure, the authors recommended  $\phi_{254} = 0.93$  and  $\phi_{313} = 0.4 \pm 1.5$ . A later evaluation of the data by Schiff [1972] and Welge [1974] suggested that the relative ratio of the yields be more accurate and recommended  $\phi_{313} / \phi_{254} = 0.27$ .

#### b) $O_3$ DISAPPEARANCE RATES IN GAS-PHASE PHOTOLYSIS

In the mid-sixties and early seventies, data on the  $O(^1D)$  quantum yield in the gas phase were derived from the photolysis of dry ozone, in the absence and presence of quenchers. By measuring the quantum yield of ozone destruction,  $\phi(-O_3)$ , at various wavelengths, one is able to derive the quantum yields of the primary products, provided the nature of the fragments is known, which occur in the secondary reactions.

The postulated mechanism of the ozone photolysis is listed below:



where  $O_2^*$  is an excited molecule in an unspecified state.

In the photolysis of ozone in the Hartley band, predominantly at 253.7 nm, various  $\phi(-O_3)$  were obtained. However, the resulting interpretations differed essentially in their choice of the products of the reaction  $O(^1D) + O_3$  via (8a), (8b) or (8c) and the succeeding reactions (9a) or (9b), and (10). Large values of  $\phi(-O_3)$  up to 16 were obtained by Norrish and coworkers, and

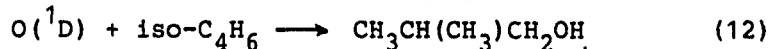
Wayne and coworkers [McGrath and Norrish, 1958; McGrath and Norrish, 1960; Norrish and Wayne, 1965a; Norrish and Wayne, 1965b; Jones and Wayne, 1970] and proposed the chain mechanism with chain carrier  $O_2^*$  and  $O(^1D)$  via reactions (8c) and (9b). Wayne and coworkers [Norrish and Wayne, 1965a; Jones and Wayne, 1970; Jones, Kaczmar and Wayne, 1970] found that  $\phi(-O_3)$  increased with  $O_3$  pressure. They extrapolated  $\phi(-O_3)$  to 4 at zero pressure  $O_3$ , which was explained by the quenching of  $O_2^*$ .

In contrast to the measurements by Wayne, Ellenrieder et al. [1971] obtained a quantum yield  $\phi(-O_3) = 6$  over a much larger pressure range (10 - 100 torr), and Lissi and Heicklen [1972] measured  $\phi(-O_3) = 5.5 \pm 0.5$  at  $O_3$  pressures near 1 torr. A quantum yield of  $\phi(-O_3) = 6.1 \pm 0.2$  was recently measured by Arnold and Comes [1979]. By addition of an effective quencher for  $O(^1D)$  such as  $N_2$  or  $CO_2$ , the  $\phi(-O_3)$  quantum yield dropped by two units, which suggests that the products of reaction (8) lead to the destruction of 2 more  $O_3$  molecules/hv. Two mechanisms were proposed at that time to be compatible with  $\phi(-O_3) = 6 : 1$  the sequence (2), (7), (8c), (9a) and 2 x (10); 2) the sequence (2), (7), (8b) and 3 x (10). It is not clear yet whether or not the chain mechanism proposed by Wayne and coworkers is dependent on experimental conditions such as the presence of impurities ( $H_2O$ ), since there is little evidence that reaction (9b) is participating.

Measurements in the Huggins bands at 313 nm done by Castellano and Schumacher [1969] resulted in  $\phi(-O_3) = 6$ , which suggests a quantum yield for  $O(^1D)$ , as was observed in the ultraviolet region. At 334 nm, they found  $\phi(-O_3) = 4$ . Jones and Wayne [1970] also measured  $\phi(-O_3)$  at 297/302, 313 and 334 nm, and extrapolated  $\phi(-O_3)$  to 4 at zero  $O_3$  pressure. Those results are hard to explain, if the onset for  $O(^1D)$  formation is believed to be at 310 nm. The discrepancies in the measurements of  $\phi(-O_3)$  and the resulting lack of precise knowledge of the mechanism of reaction (8) prevented the exact determination of the absolute  $O(^1D)$  quantum yield in the primary step (2). (The current status on reaction of  $O(^1D) + O_3$  will be discussed in the second section of this report.) However, the data by Jones and Wayne [1970] may be used to determine the relative  $O(^1D)$  quantum yields relative to their measurements at 253.7 nm. The decreasing dependence of  $\phi(-O_3)$  on  $O_3$  pressure at longer wavelengths indicates a decrease of the primary quantum yield for  $O(^1D)$  formation with increasing photoexcitation wavelength. The  $O(^1D)$  quantum yield remained essential unity below 300 nm; at 313 nm  $\phi = 0.1$  and at 334 nm  $\phi = 0$ . The data are entered in Fig. 3. A  $\phi(-O_3) = 4$  at 334 nm indicates that, according to reactions (4) or (5), an excited oxygen molecule is generated and a ground state atomic oxygen.

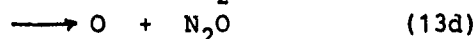
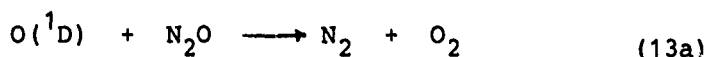
## c) CHEMICAL REACTIONS: ISOBUTANE AND NITROUS OXIDE

A substantial improvement in the accuracy of data on the wavelength dependence of the  $O(^1D)$  quantum yield was achieved by the work of Lin and deMore [1973b]. They measured the  $O(^1D)$  quantum yield from 275 to 334 nm by photolysing  $O_3$ /isobutane mixtures by monitoring the isobutanol produced by means of the selective insertion reaction (12).



Their data, which were obtained at  $-40^\circ\text{C}$ , are entered in Fig. 3. They indicate that  $\phi$  remained essential constant below 302 nm, but show a very sharp fall-off centered at 308 nm. At 313 nm, they obtained 0.08, which is in agreement with the data by Jones and Wayne [1970].

One of the most effective methods of measuring the  $O(^1D)$  quantum yields consists in measuring the products of the photolysis of mixtures of  $O_3$  with excess  $N_2O$ . This technique, which has been employed since 1972, warrants some description. Besides the initial primary reactions (2) and (7), the generated  $O(^1D)$  atoms react mainly with excess  $N_2O$  according to reaction (13):



In a recent study of the reaction mechanism by Davidson et al. [1979], it was shown that channels (13a) and (13b) contribute more than 96.3 % to the overall reaction, and that the ratio  $k_{13a}/k_{13b} = 0.79$  at  $25^\circ\text{C}$ . One method of measuring the  $O(^1D)$  quantum yield results in determining the  $N_2$  production in reaction (13a) after the photolysis at a selected wavelength. The method of measuring the quantum yield of  $N_2$  has been used by Simonaitis et al. [1973] in a photolysis study at 313 nm. In this case, the absolute  $O(^1D)$  quantum yield is given by the following equation (ii)

$$\phi_{O(^1D)} = \phi_{N_2} \frac{k_{13}}{k_{13a}} \left[ 1 + \frac{k_8}{k_{13}} \frac{[O_3]}{[N_2O]} \right] \quad (ii)$$

where  $k_x$  are the reaction rate constants and  $O_3$  and  $N_2O$  the concentrations of the reactants. This necessitates the exact knowledge of the contribution of channel (13a) to the overall reaction, a value which was not known accurately at the time of the investigation. Using  $k_8/k_{13} = 4$  and  $k_{13}/k_{13a} = 2.1$ , Simonaitis et al. [1973] derived  $\phi_{313} = 0.50 \pm 0.03$ . However in a later paper Kuis et al. [1975] revised this value to  $\phi_{313} = 0.35 \pm 0.08$ , by correcting for

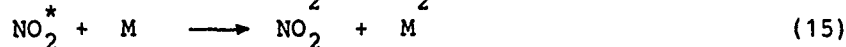
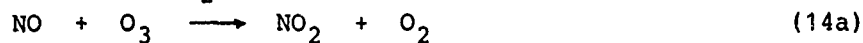
incomplete filtering of the 302 Hg line. Using the latest recommended values [NASA-2 1979] for  $k_{13a}/k_{13b}$  (0.79) with  $(k_{13a} + k_{13b})$  96.3 % accounting for contribution,  $k_{13}/k_{13a} = 2.35$  and accordingly  $\phi_{313} = 0.39 \pm 0.08$ . Repeating the photolysis of  $O_3$  with excess  $N_2O$  and  $O_2$  ( $O_2$  was added to minimize the net decomposition of  $O_3$  by scavenging  $O(^3P)$  to generate  $O_3$ ), Kuis et al. [1975] determined  $\phi_{313} = 0.29 \pm 0.02$  (after correction  $\phi_{313} = 0.31 \pm 0.02$ ). Since Simonaitis et al. [1973] and Kuis et al. [1975] performed an actinometric calibration for the quantum yield of  $N_2$ , the quantum yield data could be considered as absolute values at 313 nm.

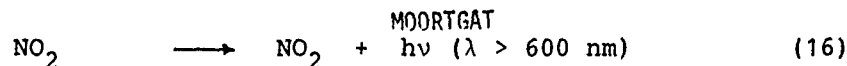
A similar determination of the  $N_2$ -quantum yield was performed by Kajimoto and Cvetanovic [1976b] at 313 and 245 nm. Using  $k_{13}/k_{13a} = 2$  and  $k_8/k_{13} = 2.5$ , they obtained  $\phi_{313} = 0.34$  and  $\phi_{245} = 0.65$  at 40°C. Although actinometry has been performed, they felt that the rate constants were not known accurately enough to derive absolute quantum yields for  $O(^1D)$ , and favored a relative quantum yield  $\phi_{313}/\phi_{254} = 0.53$ . Only slight corrections are made when the recommended rate constants [NASA 2, 1979] are employed:  $\phi_{313} = 0.37$  and  $\phi_{254} = 0.71$ , which does not resolve the discrepancy between the measurements of Simonaitis et al. [1973] and Kuis et al. [1975]. The cited data are also entered in Figure 3.

Figure 3 thus reflects the status of the relative  $O(^1D)$  quantum yields measurements at the end of 1975. It is to be noted that at 313 nm  $O(^1D)$  varied between 1 and 0.08. However an exact wavelength dependence was not deducible, since the low value of  $\phi_{313} = 0.08$  obtained by Lin and DeMore [1973b] fell below the bulk of the measurements. It is to be noted that a temperature dependence of the  $O(^1D)$  quantum yield at 313 nm was observed by Kuis et al. [1973], who obtained  $\phi = 0.22$  at 258 K and  $\phi = 0.11$  at 221 K, and by Kajimoto and Cvetanovic [1976b] with  $\phi = 0.37, 0.29$  and  $0.21$  at 273, 234 and 198 K, respectively. Since Lin and DeMore [1973b] obtained their  $O(^1D)$  wavelength dependence at 233 K, it was speculated that their low values in the fall-off region were caused by this temperature dependence.

#### d) CHEMILUMINESCENCE

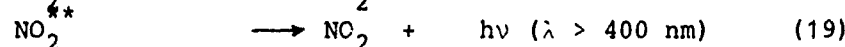
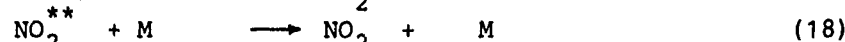
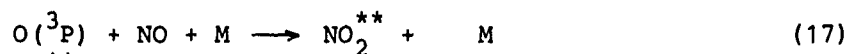
These discrepancies gave rise to the development of a more elegant method to measure the  $O(^1D)$  quantum yield at various wavelengths, by monitoring the  $NO_2^*$  chemiluminescence which occurs when  $O_3 / N_2O$  mixtures are irradiated.  $NO$  produced in reaction (13b) reacts with  $O_3$  present in the system to generate in part  $NO_2^*$ :





Only a portion of the  $\text{NO}_2$  is electronically excited [Clough and Thrush, 1967] as indicated by the asteric, and not all of the  $\text{NO}_2^*$  molecules emit their energy as radiation, because a fraction undergoes collisional quenching. The advantage over the  $\text{N}_2$ -method, is that the  $\text{NO}_2^*$  chemiluminescence is directly proportional to the  $\text{O}(^1\text{D})$  produced in reaction (2). This enables one to determine  $\text{O}(^1\text{D})$  quantum yields relative to the known quantum yields at a fixed wavelength, for example at 300 nm where it is assumed that  $\phi = 1$ .

$\text{O}(^3\text{P})$ , also present in the system, can react to produce electronically excited  $\text{NO}_2^{**}$  in the following manner:



Although the contribution of the  $\text{O}(^3\text{P})$  is very small, the  $\text{NO}_2^{**}$  emission (which occurs predominately between 400 and 600 nm) can be avoided by appropriate filtering.

The quantum yield as a function of wavelength  $\lambda$  is given by the expression (iii):

$$\phi(\lambda) = \frac{E(\lambda)}{\alpha \cdot C \cdot I_{\text{abs}}(\lambda)} \quad (iii)$$

where  $E(\lambda)$  is the intensity of chemiluminescence produced by the postulated reaction mechanism;  $\alpha$  is the factor considering all the influences of the geometry of the cell and the efficiency of the detecting system;  $C$  is given by the rates of the different contributing reactions in equation (iv)

$$C = \frac{2 k_{13b} [\text{N}_2\text{O}]}{k_{13} [\text{N}_2\text{O}] + k_8 [\text{O}_3]} \cdot \frac{k_{14b}}{k_{14}} \cdot \frac{k_{15}}{k_{15} + k_{16} ([\text{N}_2\text{O}] + [\text{O}_3])} \quad (iv)$$

the first term is the fraction that reacts to form 2 NO molecules, the second term is the fraction of the resulting NO that becomes electronically excited and the third term is the fraction of  $\text{NO}_2^*$  that emits photons.  $I_{\text{abs}}$  is the number of photons absorbed by  $\text{O}_3$  in the viewing angle of the photomultiplier. This  $\text{O}_3/\text{N}_2\text{O}$  - chemiluminescent technique was used by Moortgat and Warneck [1975], Martin et al. [1974], Moortgat et al. [1977], Arnold et al. [1977], Philen et al. [1977] and Brock and Watson [1979a].

Initially Moortgat and Warneck [1975] used a high intensity Xe arc photolysis lamp, combined with a monochromator to select the wavelength of the incident radiation, and monitored the  $\text{NO}_2^*$  emission perpendicular to the incident radiation. Since a bandwidth of 3.5 nm was chosen for intensity reasons, a correction was made to compensate for the finite resolution of the employed monochromator. Fig. 4 shows the resulting smoothed  $\text{O}(^1\text{D})$  quantum yield fall-off curve in the range 297 - 300 nm, which was obtained from seven profiles, after normalizing to unity at 300 nm, averaging, and

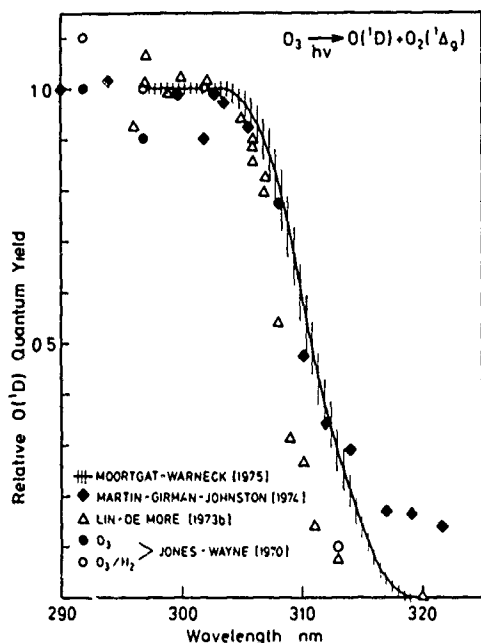


Fig. 4

Comparison between the  $\text{O}(^1\text{D})$  quantum yields curves obtained with a CW-lamp (Fig. 4) and Laser (Fig. 5) light source.

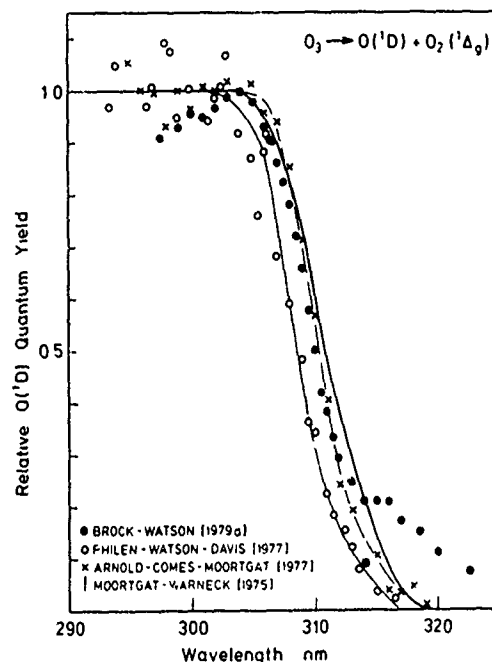


Fig. 5

correction for finite resolution. Below 305 nm, the relative  $\text{O}(^1\text{D})$  quantum yield is unity, but the fall-off region seems to be in conflict with the previously determined  $\phi$  curve by Lin and DeMore [1973b], also entered in Fig. 4. Although the onset of both curves are in agreement, the latter  $\phi$  curve is much steeper as the one measured by Moortgat and Warneck [1975]. As will be discussed later, the apparent disagreement was attributed to the different temperatures at which the experiments were executed. A similar  $\text{O}_3/\text{N}_2\text{O}$  photolysis study, using a Xe lamp /monochromator combination and  $\text{NO}_2^*$  chemiluminescence detection was performed by Martin et al [1974]. Their re-



lative  $O(^1D)$  quantum yield curve essentially agreed with the fall-off curve of Moortgat and Warneck [1975], shown in Fig. 4. However, they observed a more pronounced tail at wavelengths larger than 314 nm.

Concerned that the bandwidth employed was too broad to accurately resolve the rapid drop in  $\phi$  at increasing wavelengths, Arnold et al. [1977] initiated a laser flash photolysis study. For the photolysis between 295 and 320 nm, a frequency doubled-tunable dye laser was used and operated in repetitive mode to establish accumulation of the data during the laser pulse. The relative quantum yields were obtained from normalized plots of the integrator laser intensity versus total photocounted chemiluminescent emission at various wavelengths. Fig. 5 compares the results of the  $O(^1D)$  quantum yields, measured, with the laser flash - photolysis method, and the data obtained by Moortgat and Warneck [1975] with the CW Xe lamp. There is excellent agreement up to 308 nm, yet the observed wavelength dependence is somewhat steeper, as was to be expected from the small bandwidth.

Simultaneously, a flash-photolysis experiment was carried out by Philen et al. [1977], employing the same chemical  $O_3/N_2O$  system, analysis scheme, and a similar experimental laser set-up as Arnold et al. [1977]. The resulting  $O(^1D)$  fall-off curve showed the same curve-shape as Arnold's, yet there is an absolute wavelength shift by 2 nm toward the shorter wavelength. This significant disagreement between the measurements of Moortgat and Warneck [1975] and Arnold et al. [1977] and the data of Philen et al. [1977] is shown in Fig. 5. Their data are in close agreement with the results of Lin and DeMore [1973b].

#### e) TEMPERATURE DEPENDENCE OF THE $O(^1D)$ QUANTUM YIELDS.

At this point, it would be appropriate to report on the temperature dependence of the  $O(^1D)$  quantum yield. Indeed Moortgat et al. [1977] extended their  $O(^1D)$  measurements at 230, 263 and 320 K, and observed a shift of the  $O(^1D)$  fall-off curve towards shorter wavelengths, as the temperature was reduced. At 230 K, there is complete agreement with the data of Lin and DeMore [1973b] as can be seen in Fig. 6, alleviating the apparent discrepancy between both studies.

As reported earlier, Kuis et al. [1975] and Kajimoto and Cvetanović [1976b] studied the temperature dependence of the  $O(^1D)$  quantum yield at 313 nm. Both groups used identical analytical procedures, by photolysing  $O_3/N_2O$  mixtures and calculating the  $O(^1D)$  quantum yield according to equation (ii). The temperature variation of the  $O(^1D)$  quantum yield at 313 nm is shown in Fig. 7; within the experimental limits, there is excellent agreement

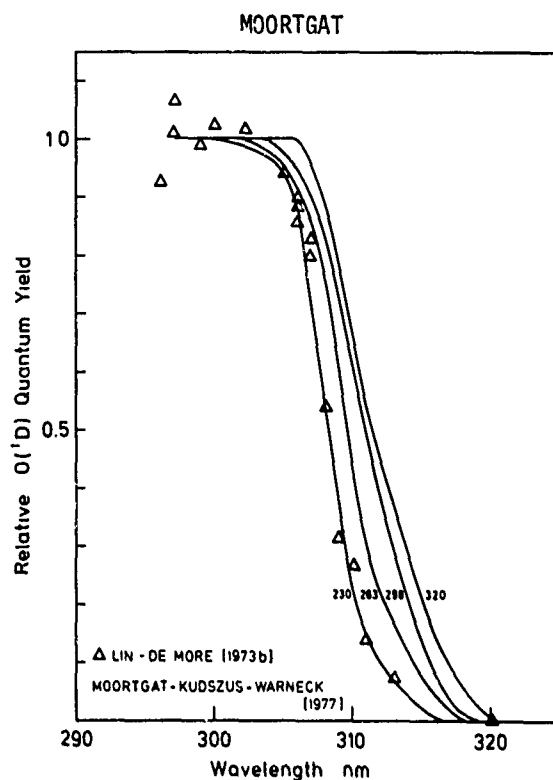


Fig. 6 Temperature dependence of the  $O(^1D)$  quantum yield. The data of Moortgat et al. [1977] are compared with those of Lin and DeMore [1973b] at 233 K.

between the data of Kuis et al. [1975] and Moortgat et al. [1977]. The data of Kajimoto et al. [1976b] are much higher, but exhibit a similar dependence on temperature.

The observed temperature dependence of the  $O(^1D)$  quantum yield implies the importance of thermal excitation in the energy budget of the photodissociating  $O_3$  molecule. The excitation of both vibrational and rotational levels contribute to the internal energy. However the contribution of excited vibrational levels compared to vibrational ground state is only a few %, so that the thermal energy of ground state ozone is found mainly in rotational energy. Kuis et al. [1975] and Kajimoto and Cvetanović [1976b] calculated the fraction of molecules which possess vibrational and rotational energy needed, to surpass the energy requirement for the  $O(^1D) + O_2(^1\Delta_g)$  production at 313 nm. The best fit to their experimental data Kuis et al. [1975] obtained in a quantum mechanical calculation in which it is assumed that only two degrees of rotational freedom are available to overcome the energy barrier because of the conservation of angular momentum in the dissociation process. The best fitted data are 0.26 (0.29), 0.20 (0.22) and 0.15 (0.11) at 293, 258 and 211 K, respectively, (the values in brackets are

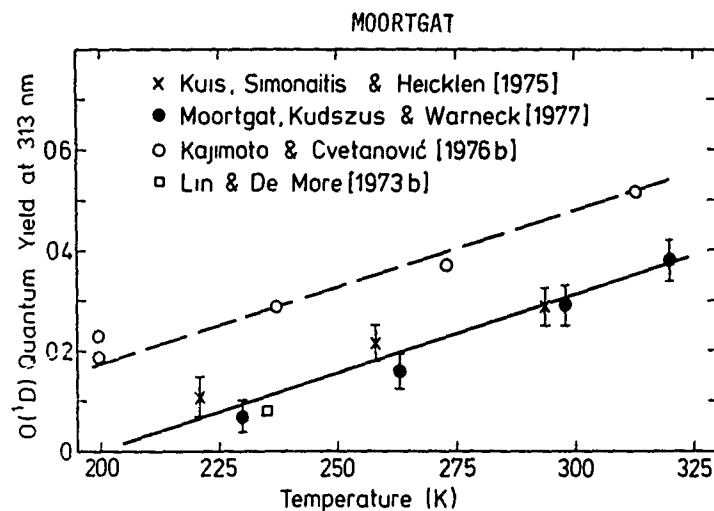


Fig. 7. Temperature variation of the  $O(^1D)$  quantum yield at 313 nm. The solid and broken lines representing the observed temperature are approximately parallel.

the experimental results), resulting in a deficiency energy of 0.86 kcal/mole between the exciting energy of 91.36 kcal/mole at 313 nm and the  $O(^1D)$  threshold energy at  $310.1 \pm 1.4$  nm. This would correspond to a value of 24.32 kcal/mole for the dissociation enthalpy at 0 K, provided that there were no barrier height for dissociation crossover from the excited  $^1B_2$  electronic state of  $O_3$ . It is believed that process (2) probably involves a vertical transition from  $O_3(^1A_1)$  ground state to the  $^1B_2$  bound state [Hay et al., 1973], which correlates to  $O(^1D) + O_2(^1\Delta_g)$  while process (4) or (5) involves the same vertical transition followed by curve crossing to a repulsive potential surface.

In a similar but classical calculation, Kajimoto and Cvetanović [1976b] calculated the equilibrium fraction of the molecules which possess vibrational and rotational energy in excess of the energy deficit of 0.9 kcal/mole for the photolysis at 313 nm. They assumed that all rotational energy was available for overcoming any barrier to dissociation and that  $\phi(^1D)$  had a value of unity at the thermodynamic energy limit. They calculated that the quantum yield to overcome the energy barrier was 0.44 (0.53), 0.37 (0.37), 0.29 (0.29), and 0.21 (0.20) at 313, 273, 234 and 198 K respectively. (experimental values are in brackets). In the 230 - 280 nm region, the relative  $O(^1D)$  quantum yield (unity) remained constant in the temperature range 313 - 198 K.

Moortgat et al. [1977] calculated the rotational population distribution to determine the fraction  $f_R$  of  $O_3$  molecules which possess rotational energy sufficient to contribute to the dissociation process at wavenumbers below the  $O(^1D)$  dissociation limit. Results of such calculation are shown in

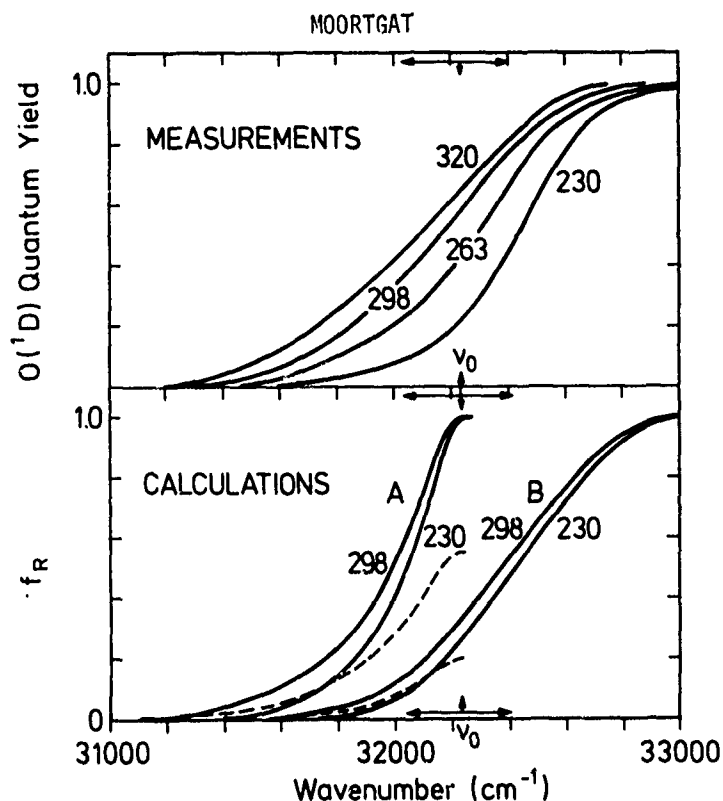


Fig. 8. Comparison of the  $O(^1D)$  quantum yields at the given temperatures, plotted versus the wavenumber of absorbed radiation, with the calculated fraction  $f_R(\nu)$  of ozone molecules endowed with rotational energy sufficient to contribute to the dissociation process, at the dissociation limit  $\nu_0$  (case A), and at  $\nu_0 + 800 \text{ cm}^{-1}$  (case B).

Fig. 8b, and compared with the experimental results expressed in wavenumbers Fig. 8a. In the first case A, it was assumed that at the threshold energy  $\nu_0$  (arrow), the  $O(^1D)$  quantum yield be unity. Calculation at 298 and 230 K showed little variation of  $f_R$  with energy. In order to match the observed  $\phi$  curve at 298 K, Moortgat et al. [1977] concluded that only 57 % of all transitions lead to the production of  $O(^1D)$ , and 20% at 230 K as indicated by the dotted lines. On the other hand, if the threshold energy was taken  $800 \text{ cm}^{-1}$  higher than  $\nu_0$ , it was possible to match  $f_R$  at 230 K, but not at 298 K (case B). The experimental curve at 298 can only be fitted if the threshold energy is  $\nu_0 + 350 \text{ cm}^{-1}$ . From these calculations it is apparent that the thermal energy, available in rotation, is by itself insufficient to explain the observed temperature effect. Moortgat et al. [1977] suggested that an additional dependence exists for the  $O(^1D)$  production efficiency above the dissociation limit, which may be ascribed to predissociation and the interaction of rotational levels in this process.

Table 2. Experimental and Calculated  $\phi(^1D)$  Quantum Yields\*

(nm)	230 K		263 K		298 K		320 K	
	$\phi_E$	$\phi_C$	$\phi_E$	$\phi_C$	$\phi_E$	$\phi_C$	$\phi_E$	$\phi_C$
300	1.00 + 0.03	1.00	1.00 + 0.02	1.00	1.00 + 0.01	1.00	1.00 + 0.02	1.00
301	0.995 $\pm$ 0.03	1.00	1.00 + 0.02	1.00	1.00 + 0.01	1.00	1.00 + 0.02	1.00
302	0.99 + 0.035	0.997	1.00 + 0.02	1.00	1.00 + 0.01	1.00	1.00 + 0.02	1.00
303	0.98 + 0.079	0.979	0.99 + 0.03	1.00	1.00 + 0.01	1.00	1.00 + 0.02	1.00
304	0.97 + 0.045	0.953	0.98 + 0.035	0.979	1.00 + 0.015	1.00	1.00 + 0.02	1.00
305	0.94 + 0.05	0.914	0.96 + 0.04	0.949	0.98 + 0.02	0.983	1.00 + 0.025	1.00
306	0.87 + 0.06	0.851	0.91 + 0.045	0.907	0.95 + 0.03	0.942	0.997 $\pm$ 0.03	0.991
307	0.72 + 0.7	0.741	0.87 + 0.05	0.847	0.90 + 0.04	0.889	0.96 + 0.035	0.932
308	0.55 + 0.07	0.560	0.76 + 0.055	0.756	0.83 + 0.05	0.819	0.89 + 0.04	0.861
309	0.36 + 0.06	0.359	0.61 + 0.06	0.626	0.73 + 0.06	0.729	0.78 + 0.045	0.774
310	0.23 + 0.05	0.222	0.45 + 0.05	0.468	0.60 + 0.055	0.619	0.66 + 0.05	0.674
311	0.15 + 0.04	0.143	0.34 + 0.05	0.326	0.49 + 0.05	0.497	0.53 + 0.05	0.566
312	0.10 + 0.04	0.097	0.22 + 0.04	0.223	0.38 + 0.05	0.378	0.44 + 0.055	0.458
313	0.07 + 0.03	0.067	0.16 + 0.035	0.153	0.29 + 0.04	0.277	0.38 + 0.06	0.359
314	0.046 $\pm$ 0.02	0.046	0.12 + 0.03	0.107	0.21 + 0.03	0.197	0.30 + 0.055	0.274
315	0.026 $\pm$ 0.02	0.031	0.08 + 0.025	0.074	0.14 + 0.02	0.136	0.22 + 0.05	0.204
316	0.00	0.019	0.052 $\pm$ 0.02	0.049	0.078 + 0.015	0.089	0.14 + 0.04	0.147
317	0.00	0.010	0.015 $\pm$ 0.02	0.031	0.037 + 0.01	0.052	0.095 $\pm$ 0.03	0.101
318	0.00	0.003	0.00	0.017	0.011 + 0.01	0.024	0.055 $\pm$ 0.02	0.064
319	0.00	0.00	0.00	0.005	0.0005 $\pm$ 0.0008	0.0007	0.032 $\pm$ 0.02	0.033
320	0.00	0.00	0.00	0.00	0.00	0.00	0.005 $\pm$ 0.02	0.007
321	0.00	0.00	0.00	0.00	0.00	0.00	0.00	0.00

\* From Moortgat and Kudszus [1978].  
 $\phi_E$  refers to the data obtained with the Xe-arc lamp/monochromator [Moortgat et al., 1977]  
 $\phi_C$  are the calculated quantum yields using the cited formula (see text).

## f) MATHEMATICAL EXPRESSION

The data obtained by Moortgat and Warneck [1975] and Moortgat et al. [1977] have been used to derive a mathematical expression, developed by Moortgat and Kudzus [1978]:

$$\phi_C(\lambda, T) = A(\tau) \arctan \left[ B(\tau) (\lambda - \lambda_O(\tau)) \right] + C(\tau) \quad (v)$$

where  $\tau = T - 230$  is a temperature function with T given Kelvin,  $\lambda$  is expressed in nm, and arctan in radians.

In the limits where  $\phi_C(\lambda, T) > 1$ , the quantum yield is set  $\phi_C = 1$ , and similarly for  $\phi_C(\lambda, T) < 0$ , the quantum yield is set  $\phi_C = 0$ .

The coefficients  $A(\tau)$ ,  $B(\tau)$ ,  $\lambda_O(\tau)$  and  $C(\tau)$  are expressed as interpolation polynomials of the third order:

$$\begin{aligned} A(\tau) &= 0.369 + 2.85 \times 10^{-4} \tau + 1.28 \times 10^{-5} \tau^2 + 2.57 \times 10^{-8} \tau^3 \\ B(\tau) &= -0.575 + 5.59 \times 10^{-3} \tau - 1.439 \times 10^{-5} \tau^2 - 3.27 \times 10^{-8} \tau^3 \\ \lambda_O(\tau) &= 308.20 + 4.4871 \times 10^{-2} \tau + 6.9380 \times 10^{-5} \tau^2 - 2.5452 \times 10^{-6} \tau^3 \\ C(\tau) &= 0.518 + 9.87 \times 10^{-4} \tau - 3.94 \times 10^{-5} \tau^2 + 3.91 \times 10^{-7} \tau^3. \end{aligned}$$

Equation (v) enables the calculation of the  $O(^1D)$  quantum yield at any wavelength and temperature in the range 230 - 320 K. The quantum yields,  $\phi_C$ , calculated using this equation are entered in Table 2 for comparison with the experimental data.

## g) INCONSISTENCIES IN THE FALL-OFF CURVE DETERMINATIONS

The temperature dependence of the  $O(^1D)$  quantum yields resolved some discrepancies between the measurements of Lin and DeMore [1973b] and Moortgat et al. [1977]. Nevertheless the two laser flash photolysis measurements by Arnold et al. [1977] and Philen et al. [1977] gave rise to inconsistencies among aeronomic modellers. For stratospheric modelling, the low temperature data from Lin and DeMore [1973b] and Moortgat et al. [1977] agree numerically with the data of Philen et al. [1977] and do not affect the  $O(^1D)$  production yield in the atmospheric regions where temperature is near 230 K. However in the calculation of  $O(^1D)$  the production yield in the troposphere, the disagreement caused a variation of up to 30 %, depending on the chosen value. The dilemma which curve to choose for tropospheric model calculations is evident from Fig. 9, where  $O(^1D)$  production rates are computed, using the data from Moortgat and Warneck [1975], Arnold et al. [1977] and Philen et al. [1977] for various solar zenith angles at ground level.

## h) RECENT MEASUREMENT OF THE FALL-OFF CURVE.

A very recent  $O_3$  flash photolysis study by Brock and Watson [1979a] resolved this dilemma. Employing a similar experimental set-up as Arnold et al. [1977] and Philen et al. [1977], they used the  $NO_2^*$  chemiluminescent techni-

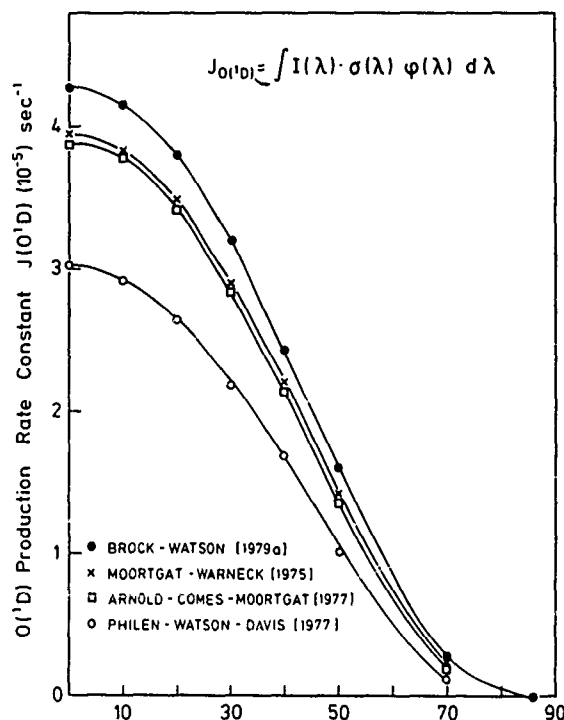


Fig. 9. Variation of the O(<sup>1</sup>D) production rate constant J(O<sup>1</sup>D) with solar zenith angle at ground level. The actinic irradiances of Peterson [1976] and the various O(<sup>1</sup>D) quantum yields (as indicated) were used for the calculation.

que for the determination of the relative O(<sup>1</sup>D) quantum yields at 298 K. The results are also entered in Fig. 5. For wavelengths shorter than 312 nm, there is now complete agreement among the laser measurements of Arnold et al. [1977] and the previous CW Xe lamp data by Moortgat and Warneck [1975] for 298 K. The authors admit that previous data by Philen and Watson [1977] are erroneous, probably due to the incorrect calibration of their excitation laser light source.

Interestingly, at longer wavelengths, Brock and Watson [1977a] observe a tail not reported in previous laser studies, however, observed by Martin et al. [1974] (see Fig. 4) and DeMore and Raper [1962] (see Fig. 5). Careful measurements of background intensities and the fact that NO<sub>2</sub><sup>\*</sup> chemiluminescence is present when both reactants (O<sub>3</sub> and N<sub>2</sub>O) are present in the cell, suggest that the pronounced tail in their O(<sup>1</sup>D) quantum yield curve is not an artefact. A possible explanation for the tail region would suggest a weak contribution of the spin forbidden processes (6). For the O(<sup>1</sup>D) production rate calculations, the tail region is making only a minor contribution at zenith angles below 50°. However it becomes increasingly important at higher zenith

Table 3

Summary of  $O(^1D)$  Quantum Yields at 313 nm

Investigator	$O(^1D)$	Temp °K	Technique	Photolytic Source
Taube [1957]	0.37	277	Decrease in $O_3$ , acidif. solution	CW Lamp
Raper, De More [1962]	$0.45 \pm 0.2$	87	$O_3$ , liquid $N_2$ , increase in $N_2O$	CW Lamp
Raper, De More [1966]	$0.40 \pm 15$	87	$O_3$ , liquid Ar, decrease in $O_3$	CW Lamp
Castellano, Schumacher [1969]	0.75	248	$O_3$ ;	CW Lamp
Jones, Wayne [1970]	1.0	298	Decrease in $O_3$ pressure	CW Lamp
Simonaitis, et al. [1973]	0.1	298	Decrease in $O_3$	Chem. Filter/CW
Lin, De More [1973]	$0.35 \pm 0.08$	298	$O_3, N_2$ ; increase in $N_2$	CW Lamp
Martin, et al. [1974]	0.08	235	$O_3$ , Isobutane	CW Lamp
Kuis, et al. [1975]	0.32	298	$O_3, N_2O$ ; $N_2O$ chemiluminescence	CW Lamp
	$0.29 \pm 0.04$	293	$O_3, O_2, N_2O$ ; Increase in $N_2$	CW/Chem. Filter
	$0.22 \pm 0.04$	258		
	$0.11 \pm 0.04$	221		
Moortgat, Warneck [1975]	$0.29 \pm 0.04$	298	$O_3, N_2O$ ; $NO_2$ chemiluminescence	CW Lamp
Moortgat et al. [1977]	$0.38 \pm 0.06$	320		
	$0.16 \pm 0.035$	262		
	$0.07 \pm 0.03$	230		
Kajimoto, Cvetanović [1976]	0.53	313	$O_3, N_2O$ ; Increase in $N_2$	CW Lamp
	$0.37 \pm 0.23$			Chemical Filter
	$0.29 \pm 0.234$			
	$0.21 \pm 0.198$			
Philen, et al. [1977]	$0.12 \pm 0.03$	298	$O_3, N_2O$ ; $NO_2$ chemiluminescence	Pulsed Dye Laser
Arnold, et al. [1977]	$0.19 \pm 0.01$	298	$O_3, N_2O$ ; $NO_2$ chemiluminescence	Pulsed Dye Laser
Brock, Watson [1979a]	$0.26 \pm 0.04$	298	$O_3, N_2O$ ; $NO_2$ chemiluminescence	Pulsed Dye Laser



angles, because the increased atmospheric path shifts the actinic irradiance reaching the lower atmosphere toward longer wavelengths.

Conclusively, if the data obtained by Philen et al. [1977] are considered to be erroneous, then there is complete agreement between the fall-off curves obtained in the CW lamp studies and the laser studies. The mathematical expression ( $\nu$ ) of the  $O(^1D)$  quantum yields as function of wavelength and temperature developed by Moortgat and Kudszus [1978] is sufficient accurate to be used by photochemical modellers for the determination of the vertical profile of the  $O(^1D)$  production rate coefficient. A summary of the determination of  $O(^1D)$  at 313 nm is made in Table 3. The value of  $\phi_{313} = 0.29 \pm 0.05$  at 298 nm is in agreement with the experimental limits of most investigations. The determinations of Jones and Wayne [1970] and Castellano and Schumacher [1969] are probably in error.

#### 1) $O(^1D)$ QUANTUM YIELDS BELOW 300 nm.

It has been generally assumed that the  $O(^1D)$  quantum yield is unity below 300 nm. A recent determination of the relative  $O(^1D)$  quantum yield in the region 250 - 300 nm by Fairchild and Lee [1978] confirms, at least partly, this assumption. Their results, obtained with the Xe arc lamp/monochromator -  $NO_2^*$  chemiluminescence method, are shown in Fig. 10. The data between 250

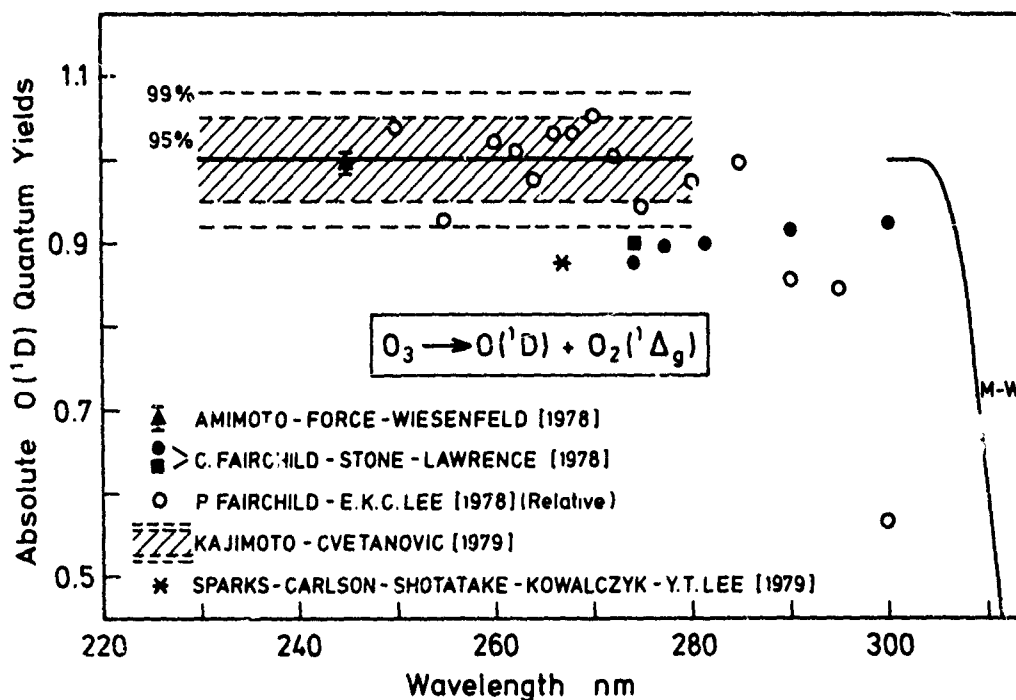


Fig. 10. Absolute quantum yields of  $O(^1D)$  formation in the ozone photolysis below 300 nm. MW = Moortgat and Warneck [1975].

and 285 nm show a continuity in the relative  $O(^1D)$  quantum yields within the experimental error ( $\pm 4\%$ ). They show, however, a drop of 15 % in the range 290 - 295, and a value of 0.58 at 300 nm. Earlier measurements by Lin and DeMore [1973b] in the range 275 - 300 nm (see Fig. 3) indicate that the relative  $O(^1D)$  quantum yield is constant. They do not show the discontinuity observed by Fairchild and Lee [1978] at wavelengths larger than 285 nm. The latter authors admit, that their data for 300 nm is too low, and could be unreliable for 290 - 295 nm, but give no explanation for these results. Only when the latter data (285 - 300 nm range) are discarded, the relative  $O(^1D)$  quantum yield in the 250 - 300 nm range, considering the measurements by Fairchild and Lee [1978], complemented with the data of Lin and DeMore [1973b], may be taken to be constant.

#### ABSOLUTE $O(^1D)$ QUANTUM YIELDS BELOW 300 NM.

All of the previously discussed  $O(^1D)$  quantum yield measurements were normalized to the quantum yield below 300 nm, which has been assumed to be unity, although reliable measurements were performed. There have recently been two independent molecular beam measurements, which indicate that a small fraction of  $O(^3P)$  is produced upon  $O_3$  ultraviolet photolysis at wavelengths below 300 nm.

Indeed, Fairchild et al. [1978] observed both  $O(^1D)$  and  $O(^3P)$  fragments in the molecular beam photofragment spectroscopy of  $O_3$  in the Hartley absorption region 270 - 300 nm. The oxygen atoms photofragments were detected by a gas-phase chemi-ionisation process ( $Sm + O \rightarrow SmO^+ + e^-$ ) by which their kinetic energies are determined using a time of flight technique. The product energy distribution provides information on the state distribution. The quantum yield for  $O(^3P)$  was determined to be 0.1 at 274 nm, and the dissociation partner is  $O_2(^3\Sigma_g^-)$ . The other channel yields as expected,  $O(^1D)$  and  $O_2(^1\Delta_g)$ . If the same detector-sensitivity is assumed, the contribution of  $O(^3P)$  in the range 273 to 300 nm decreases from 10 % to 6 %, as is depicted in Fig. 10. Similar high resolution molecular beam measurements of the translational energy distribution of the primary photolysis products of ozone were done by Sparks et al. [1979]. At 266 nm, they measured 12 % contribution of the  $O(^3P) + O_2(^3\Sigma_g^-)$  channel. In addition they obtained relative yields of the vibrational states of  $O_2(^1\Delta_g)$  : 57 %  $v = 0$ , 24 %  $v = 1$ , 12 %  $v = 2$ , and 7 %  $v = 3$ .

The results of the molecular beam experiments were contradicted by two recent measurements which indicated that  $O(^3P)$  is not a product. Amimoto et al. [1978] measured the rise time of the  $O(^3P)$  concentration after photolysis of ozone with a pulsed KrF laser at 248 nm. The relative quantum yields of oxy-

gen in the ground and electronically excited states may be directly determined by comparison of the  $O(^3P)$  resonance radiation immediately following the laser pulse with that arising from relaxation of  $O(^1D)$  to  $O(^3P)$ . The absolute value obtained for  $\phi O(^1D)$  was  $0.99 \pm 0.01$  at 248 nm. The other recent determination of the absolute quantum yield of  $O(^1D)$  in the photolysis of  $O_3$  in the Hartley band was done by Kajimoto and Cvetanović [1979] between 230 and 280 nm. Using the isotope exchange reaction between  $C^{16}O_2$  and  $O^{18}(^1D)$ , they photolysed  $^{18}O_3$  in the presence of large excess  $C^{16}O_2$ ; the  $^{18}O(^1D_2)$  atoms formed in the photolysis of  $^{18}O_3$  undergo rapid isotopic exchange with the excess  $C^{16}O_2$  releasing  $^{16}O(^3P)$  atoms in the amount 2/3 of the number of  $^{18}O(^1D)$  atoms consumed in the reaction with  $C^{16}O_2$  [Yamazaki and Cvetanović, 1964]. The  $^{16}O(^3P)$  atoms are trapped as  $O^{16}O^{18}$  by rapid exchange between  $^{16}O$  and  $^{18}O_2$ . The  $O(^1D)$  quantum yield is determined from the amount  $O^{16}O^{18}$  formed. Kajimoto and Cvetanović [1979] obtained a value of  $1.00 \pm 0.05$  with in 95 % confidence limit. For 99 % confidence limit the value of  $\phi$  would be  $1.00 \pm 0.08$  as shown in Fig. 10. These results confirm the quasi-unity quantum yield of Amimoto et al. [1978].

More work is needed to ascertain whether or not  $O(^3P)$  is produced directly in the photolysis of  $O_3$  at wavelengths below 300 nm.

### III) THE REACTION OF $O(^1D)$ WITH ATMOSPHERIC CONSTITUENTS.

As mentioned in the introduction, nearly all of the  $O(^1D)$  atoms formed are deactivated to the ground state upon collision with the molecules of the main atmospheric constituents  $N_2$ ,  $O_2$ ,  $CO_2$  and Ar. Only a small fraction reacts with atmospheric trace gases. Table 4. summarises typical concentrations of various species found at the tropopause and the corresponding recommended  $O(^1D)$  reaction rate constants at 220 K; also shown is the type of reaction which these species undergo upon interaction with  $O(^1D)$ : physical quenching (Q) and / or chemical reaction (R). As indicated in Table 4, at the tropopause 99.997 % of the reactions undergo collisional deactivation. That means that only 30 collisions in a million undergo chemical reaction with  $O(^1D)$ , predominantly with  $H_2O$ ,  $CH_4$ ,  $H_2$  and  $N_2O$ . the fluorochlorocarbons containing two or more Cl atoms will mainly be removed by photolytic action; as the number of Cl atoms decrease, reactions with  $O(^1D)$  (and with OH radicals) will become the most important removal processes above 30 km [Atkinson et al., 1976].

The second section of this paper will review the presently measured reaction rate constants with each of the chemical species listed in Table 4, and discusses the current status on the products evolving from those reactions.

Table 4

Reactions involving $O(^1D)$ in the atmosphere.					
Reactant		Concentration ppm at tropopause		k (220°K)	% Reactivity
N	*)	$7.81 \times 10^5$	Q	$3.26 \times 10^{-11}$	75.3
O <sub>2</sub>	*)	$2.1 \times 10^5$	Q	$3.94 \times 10^{-11}$	24.5
Ar	*)	$9.3 \times 10^3$	Q	$5 \times 10^{-13}$	0.0138
CO <sub>2</sub>	*)	325	Q	$1.16 \times 10^{-10}$	0.117
Ne		18	Q	$6.5 \times 10^{-15}$	$3.5 \times 10^{-7}$
He		5.2	Q	$1 \times 10^{-16}$	$1.5 \times 10^{-9}$
H <sub>2</sub> O		3	R	$2.3 \times 10^{-10}$	$2.04 \times 10^{-3}$
CH <sub>4</sub>		1.6	R	$1.4 \times 10^{-10}$	$6.64 \times 10^{-4}$
H <sub>2</sub>		0.55	R	$0.99 \times 10^{-10}$	$1.61 \times 10^{-4}$
N <sub>2</sub> O		0.320	R	$1.1 \times 10^{-10}$	$1.04 \times 10^{-4}$
CO		0.12	Q	$6.27 \times 10^{-11}$	$2.2 \times 10^{-5}$
NH <sub>3</sub>		$7.00 \times 10^{-4}$	R	$2.5 \times 10^{-10}$	$5.2 \times 10^{-7}$
HCl		$2.0 \times 10^{-4}$	R	$1.4 \times 10^{-10}$	$8.3 \times 10^{-8}$
CF <sub>2</sub> Cl <sub>2</sub>		$2.6 \times 10^{-4}$	R	$1.45 \times 10^{-10}$	$1.1 \times 10^{-7}$
CFC1 <sub>3</sub>		$1.5 \times 10^{-4}$	R	$2.2 \times 10^{-10}$	$9.8 \times 10^{-8}$
CCl <sub>4</sub>		$1.45 \times 10^{-4}$	R	$3.1 \times 10^{-10}$	$1.3 \times 10^{-7}$
$\% \text{ Reactivity} = \frac{[X] \cdot k_x \cdot 100\%}{\sum_i [X] \cdot k_x}$ <div style="display: flex; justify-content: space-between; align-items: flex-start;"> <div>Q = Physical Quenching R = Chemical Reaction <math>\Sigma^* = 99,9970 \%</math></div> </div>					

## REACTION RATE CONSTANTS.

Earlier determinations of the rate constants have been based on indirect (competitive) measurements, which provided relative rate constants; an excellent review of the relative  $O(^1D)$  rate constants measured prior 1974 was made by Cvetanovic [1974]. By the advent of signal averaging techniques, two different direct methods have been used for the determination of absolute reaction rate constants:

- a) the time-resolved  $O(^1D)$  630 nm "forbidden" emission technique used at the NOAA laboratories in Boulder, Colorado [Davidson et al., 1976 to 1979 Streit et al., 1976]. Following the laser uv flash photolysis of O<sub>3</sub>, the  $O(^1D)$  emission decay is analysed in order to determine the desired bimolecular reaction rate constant in the presence and absence of the reactant.
- b) the time-resolved atomic resonance absorption technique in the vacuum ultraviolet, used by Husain and coworkers at Cambridge, GB, [Heidner et al.

Table 5 Absolute O( <sup>1</sup> D) rate constants at 298 K. Units in 10 <sup>-10</sup> cm <sup>3</sup> /molecule. sec.						
Interactant	NOAA	Arimoto et al.* Brock-Watson **)	Husain et al. γ=0.41	Cvetanović [1974]	Schofield [1978]	NOAA-2 [1979]
O <sub>2</sub>	0.41 ± 0.05 a) 0.37 ± 0.07 b)	0.42 ± 0.02 *) 0.39 ± 0.04 **) 0.40 ± 0.06 ***)	0.70 ± 0.05 c) 0.53 ± 0.06 d)	0.74 ± 0.15	0.37 ± 0.3	0.36
O <sub>3</sub>	2.4 ± 0.1 a) 2.4 ± 0.5 b)	2.41 ± 0.11 e) 2.5 ± 0.5 **)	2.7 ± 0.2 c)	5.3 ± 2.6	2.3 ± 0.3	2.4
N <sub>2</sub>	0.30 ± 0.01 a) 0.28 ± 0.06 b)	0.24 ± 0.01 *) 0.27 ± 0.05 **)	0.69 ± 0.06 c)	0.54 ± 0.15	0.28 ± 0.03	0.29
N <sub>2</sub> O	1.4 ± 0.1 a) 1.1 ± 0.2 b)	1.20 ± 0.1 *)	2.2 ± 0.2 f)	2.2 ± 0.4	1.2 ± 0.15	1.1
NH <sub>3</sub>	3.4 ± 0.3 a) 2.5 ± 0.5 b)		6.3 ± 0.7 g)	4	2.7 ± 0.4	2.5
CO	0.58 ± 0.12 h)		0.73 ± 0.07 c)	0.77 ± 0.15	0.36 ± 0.05	
CO <sub>2</sub>	1.2 ± 0.09 a) 1.0 ± 0.2 b)	1.28 ± 0.07 *) 1.00 ± 0.1 **)	2.1 ± 0.2 c) 1.7 ± 0.2 d)	1.8 ± 0.3	1.0 ± 0.2	1.0
H <sub>2</sub>	1.3 ± 0.05 a) 0.99 ± 0.3 b)		2.7 ± 0.3 f)	2.9 ± 0.5	1.25 ± 0.25	0.99
H <sub>2</sub> O	2.1 ± 0.1 a) 2.3 ± 0.4 b)	1.95 ± 0.3 *)	3.0 ± 0.3 c)	3.5 ± 0.6	2.0 ± 0.3	2.3
CH <sub>4</sub>	1.3 ± 0.3 a)	1.57 ± 0.13 *)	3.1 ± 0.4 f)	4.0 ± 0.9	1.5 ± 0.3	1.4
HCl	1.4 ± 0.3 a) 1.4 ± 0.4 b)				1.3 ± 0.3	1.4
CFCl <sub>3</sub>	2.2 ± 0.7 i)		5.5 ± 0.3 d)		3.0 ± 0.6	2.2
CF <sub>2</sub> Cl <sub>2</sub>	1.45 ± 0.5 i)		4.8 ± 0.5 d)		2.6 ± 0.5	1.4
CCl <sub>4</sub>	3.1 ± 0.9 i)		8.5 ± 1.1 d)		3.4 ± 0.7	1.9
CF <sub>2</sub> ClCFCl <sub>2</sub>	2.0 ± 0.6 i)		5.3 ± 0.6 d)		1.35 ± 0.4	
NO			0.85 ± 0.10 f)	1.7 ± 0.9	0.4 ± 0.1	
NO <sub>2</sub>			2.3 ± 0.2 f)	2.8 ± 0.5	1.4 ± 0.3	

\*) Amimoto et al. [1979]; \*\*) Brock and Watson [1979b]; \*\*\*) Lee and Slanger [1978]; a) Davidson et al. [1976]; b) Davidson et al.; [1977]; c) Heidner et al. [1973]; d) Fletscher and Husain [1976a]; e) Amimoto et al. [1978]; f) Heidner and Husain [1973]; g) Fletcher and Husain [1976b]; h) Davidson et al. [1978a]; i) Davidson et al. [1978b].

\*) Arimoto et al. [1979]; \*\*) Brock and Watson [1979b]; \*\*\*) Lee and Slanger [1978]; a) Davidson et al. [1976]; b) Davidson et al. [1977]; c) Heidner et al. [1973]; d) Fletscher and Husain [1976a]; e) Arimoto et al. [1978]; f) Heidner and Husain [1973]; g) Fletcher and Husain [1976b]; h) Davidson et al. [1978a]; i) Davidson et al. [1978b].

1973; Heidner and Husain, 1973 and 1974, Fletcher and Husain, 1976 a and b]. They observe the attenuation of the resonance radiation  $O(3^1D_2 \leftarrow 2^1D_2)$  at 115.2 nm in the presence and absence of the reactant. The absorption appears to be best described by the modified Lambert-Beer law expression

$$I = I_0 \exp(-\epsilon(c)^\gamma) \quad (vi)$$

with the empirical constant  $\gamma = 0.41$ . The rate constant is proportional to  $\gamma^{-1}$ .

The absolute results obtained by emission and absorption techniques, however, differ by a factor of about 2.2, which posed a dilemma for the atmospheric modelers. Philipps [1976] calculated that absorption parameters should slightly deviate from Beer's law and suggested that a value  $\gamma = 0.9$  is more appropriate.

A new direct method has recently been developed by Amimoto et al. [1978 and 1979] who monitored the  $O(3P)$  atoms time profile by atomic resonance absorption technique. A direct relationship between atomic density and absorbance is given by this method. By monitoring the attenuation of the atomic resonance radiation, it is possible to distinguish between  $O(3P)$  arising from  $O(^1D)$  quenching or/and from chemical reaction. The data from Amimoto et al. [1979] agree very well with the emission measurements of the NOAA group.

Very recently Brock and Watson [1979b] used the time-resolved resonance fluorescence technique to monitor the rate of production of  $O(^3P)$  in the flash photolysis of  $O_3$  at 266 nm, and obtained preliminary results for the absolute reaction rate constants of  $O(^1D)$  with  $O_3$ ,  $N_2$ ,  $O_2$ , and  $CO_2$ , which are also in excellent agreement with the NOAA group and Amimoto et al.

Table 5 summarizes the  $O(^1D)$  absolute reaction rate constants obtained by the NOAA group, Amimoto et al. [1979], Brock and Watson [1979b] and Husain and coworkers. Since the review by Cvetanovic [1974], several evaluations of the rate constants have been published: Hampson and Garvin [1975]; NASA-1 [1977]; Hampson and Garvin [1978]; Schofield [1978]; NASA-2 [1979]. In order to indicate the enormous changes in the recommended rate constants, Table 5 also includes the data from the review of Cvetanović [1974] and the latest evaluations by Schofield [1978] and NASA-2 [1979]. It is to be noted that the values reported in the review of Cvetanović [1974] were based on the absolute data from Husain and coworkers, which are probably too high by a factor of 2. The recommended data of the NASA-2 report (with uncertainty factor of 1.3) are based on the NOAA measurements.

Streit et al. [1976] and Davidson et al. [1978 a,b] have measured the tempe-

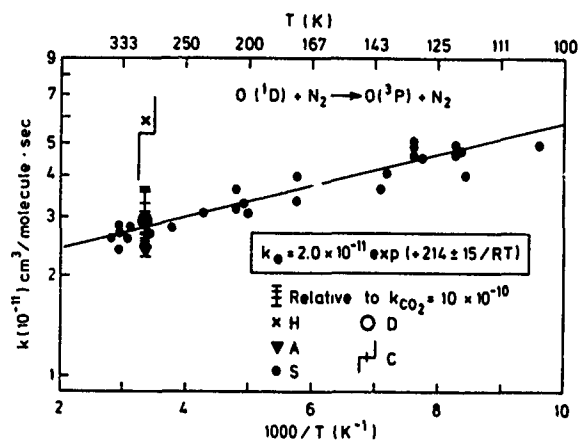


Fig. 11

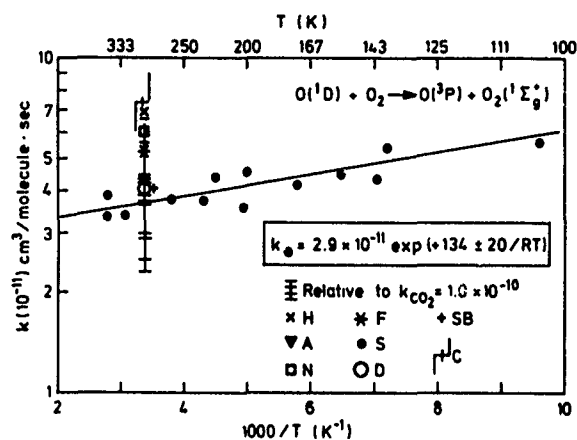


Fig. 12

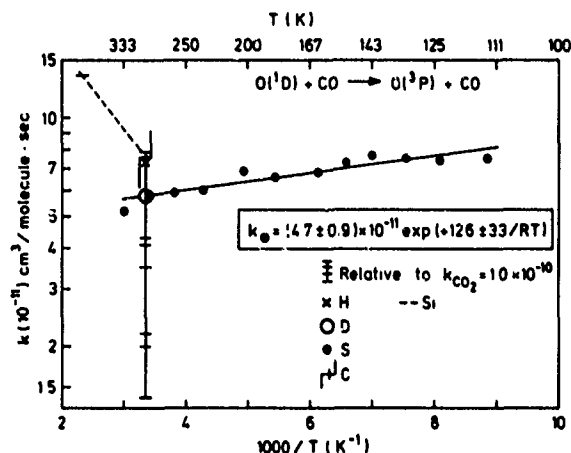


Fig. 13

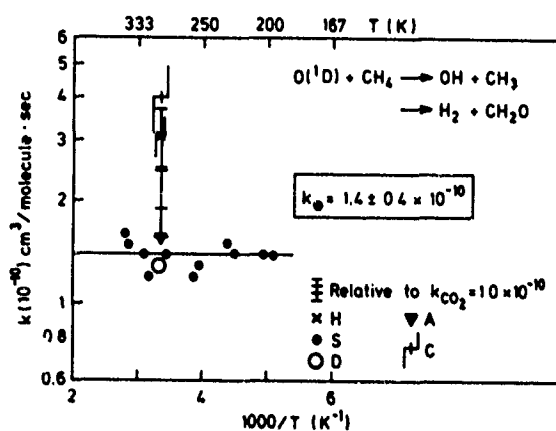


Fig. 14

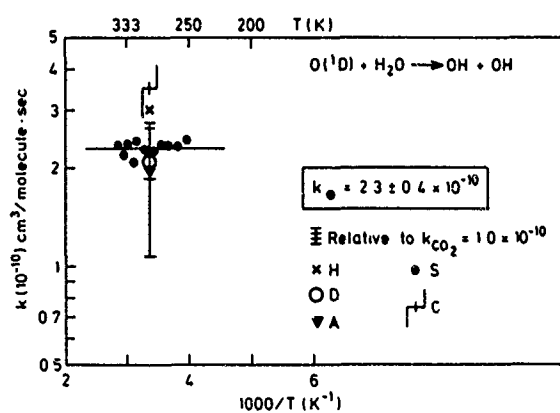


Fig. 15

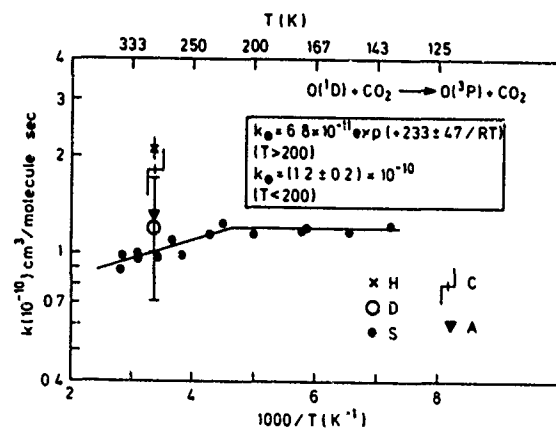


Fig. 16

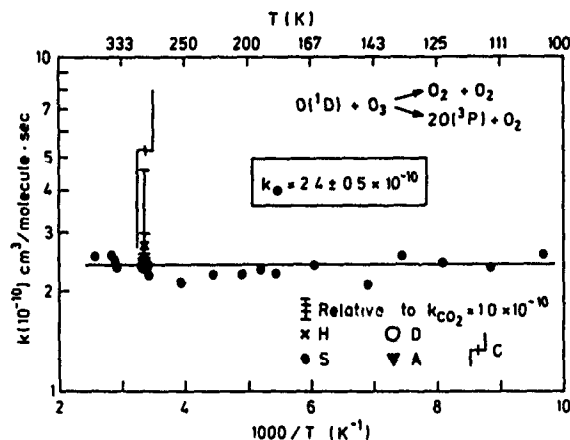


Fig. 17

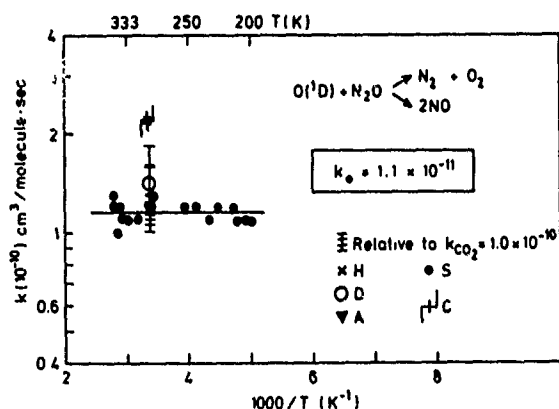


Fig. 18

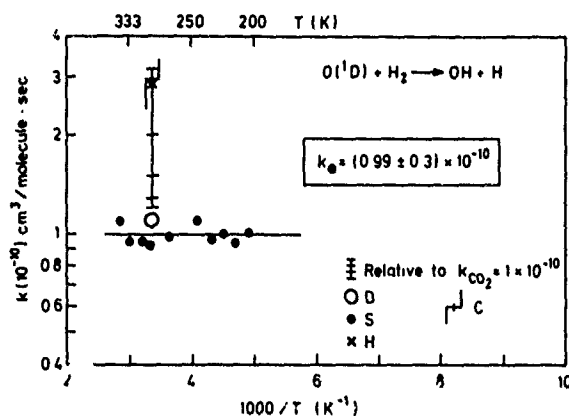


Fig. 19

Figures 11 - 19. Summary of the reaction rate constants of  $O(^1D)$  with  $N_2$ ,  $O_2$ ,  $CO_2$ ,  $CO$ ,  $H_2O$ ,  $CH_4$ ,  $N_2O$ ,  $O_3$  and  $H_2$  as a function of temperature. x H: Heidner et al. [1973], and Heidner and Husain [1973]; ▼ A: Amimoto et al. [1978 and 1979]; • S: Streit et al. [1976]; o D: Davidson et al. [1976, 1977 and 1978a]; ▽ C: Cvetanović [1974]; \* F: Fletcher and Husain [1976a]; □ N: Noxon [1970]; + JB: Lee and Slanger [1978]; ← B: Brock and Watson [1979b]; ±: from review of Cvetanović [1974]: each horizontal bar represents one measurement, which has been normalized relative to  $k_{CO_2} = 1.0 \times 10^{-10} \text{ cm}^3/\text{mole}\cdot\text{sec}$ ;  $k_0$  represents the actual recommended rate constant after the NASA-2 [1979] evaluation.



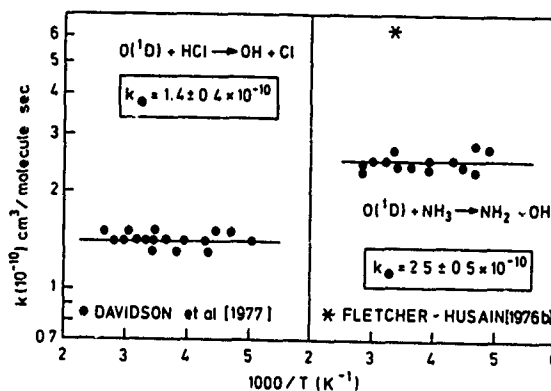


Fig. 20

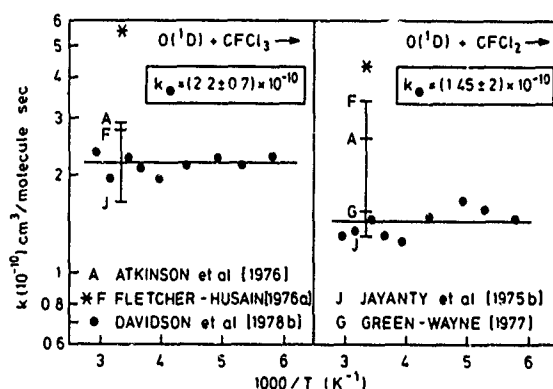


Fig. 21

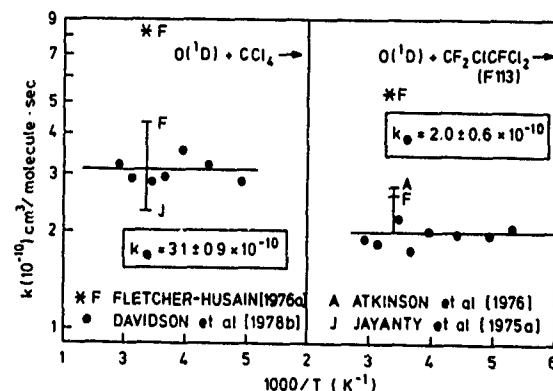


Fig. 22

Figures 20 to 22 : Summary of the reaction rate constants of  $O(^1D)$  with  $HCl$ ,  $NH_3$ ,  $CCl_4$ ,  $CF_2ClCFCl_2$ ,  $CFCl_3$  and  $CF_2Cl_2$ , as a function of temperature. The references are given in the figure.  $k$  represents the actual recommended rate constant after the NASA-2 [1979] evaluation.

temperature dependence of the reaction rate constants of  $O(^1D)$  with most atmospheric constituents. It was observed that gases which quench  $O(^1D)$  such as  $O_2$ ,  $N_2$ ,  $CO_2$  and  $CO$  display a small negative temperature dependence. The absolute and relative reaction rate constants (relative to  $k_{CO_2} = 1.0 \times 10^{-10} \text{ cm}^3/\text{molecules} \cdot \text{sec}$ ) and the temperature dependence data are shown in Figures 11 to 22 for the various atmospheric constituents.

The release of the halocarbons in the atmosphere and the possible depletion of the  $O_3$  layer is of current interest. A possible sink for the halocarbons is the reaction with  $O(^1D)$  atoms [Sandoval et al., 1974]. There have been several measurements of the reaction rate constants for various halocarbons, and are summarized in Table 6. As is shown in Figures 20 and 21, Davidson et al., [1978] observed no temperature dependence of the reaction rate constants. They also derived an expression which can accurately predict  $O(^1D)$

Table 6. Absolute reaction rate constants of the reaction of  $O(^1D)$  with halocarbons at 298 K.

Halocarbon	ABSOLUTE DATA				RELATIVE TO $k_{CO_2} = 1.0 \times 10^{-10}$				Calc. from form.f)
	Fletcher and Husain $\gamma = 0.41$	$\gamma = 1.0$	Davidson et al.[1978]	Jayanty et al.	Atkinson et al.[1976]	Green Wayne [1977]			
CF <sub>4</sub>	0.30 ± 0.04 a)	0.12 ± 0.01			0.11		0.12		
CF <sub>3</sub> Cl	2.5 ± 0.3 a)	1.0 ± 0.1					0.83		
CF <sub>2</sub> Cl <sub>2</sub>	4.8 ± 0.5 a)	2.0 ± 0.2	1.45 ± 0.5	0.57 c)	2.6 ± 0.3	1.54	1.5		
CFCl <sub>3</sub>	5.5 ± 0.7 a)	2.3 ± 0.2	2.2 ± 0.7	1.2 c)	2.9 ± 0.4		2.3		
CCl <sub>4</sub>	8.5 ± 1.1 a)	3.5 ± 0.3	3.1 ± 0.9	1.7 c)	3.3		3.0		
CHF <sub>3</sub>	0.98 ± 0.12 a)	0.40 ± 0.03		2.3 d)			0.41		
CHF <sub>2</sub> Cl	2.4 ± 0.3 a)	0.98 ± 0.1	0.95 ± 0.3		1.8 ± 0.2	0.9	1.1		
CHFC1 <sub>2</sub>	4.8 ± 0.5 a)	2.0 ± 0.2	1.9 ± 0.6				1.8		
CF <sub>2</sub> ClCF <sub>2</sub> Cl	3.7 ± 0.4 a)	1.5 ± 0.1			1.65 ± 0.2		1.6		
CF <sub>2</sub> ClCFCl <sub>2</sub>	5.3 ± 0.6 a)	2.2 ± 0.1	2.0 ± 0.6		2.75 ± 0.3		2.3		
COCl <sub>2</sub>	7.1 ± 0.9 b)	2.9 ± 0.3		1.7 e)					
COFCl	3.7 ± 0.4 b)	1.5 ± 0.1		1.1 e)	3.1 ± 0.4				
COF <sub>2</sub>	4.6 ± 0.4 b)	1.9 ± 0.1		0.45 e)	0.32 ± 0.04				

a) Fletcher and Husain [1976]; b) Fletcher and Husain [1978]; c) Jayanty et al. [1975a]; d) Jayanty et al. [1975b]; e) Jayanty et al. [1976]; f) Formula after Davidson et al. [1978], see text.  
All values are given in units: cm<sup>3</sup>/molecule.sec.

a) Fletcher and Husain [1976]; b) Fletcher and Husain [1978]; c) Jayanty et al. [1975a]; d) Jayanty et al. [1975b]; e) Jayanty et al. [1976]; f) Formula after Davidson et al. [1978], see text.

All values are given in units:  $cm^3 / molecule \cdot sec$ .

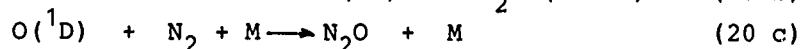
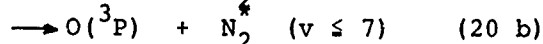
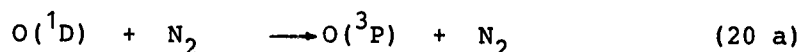
rate constants with methane and ethane molecules containing hydrogen, fluorine and chlorine:

$$k(C_n H_a F_b Cl_c) = 0.32 a + 0.03 b + 0.74 c \text{ in units } 10^{-10} \text{ cm}^3/\text{molec. sec}$$

The calculated rate constants are also entered in Table 6.

# PRODUCTS OF THE REACTIONS OF $O(^1D)$ WITH ATMOSPHERIC CONSTITUENTS

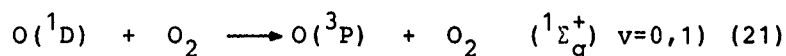
## A) $N_2$ .



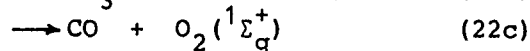
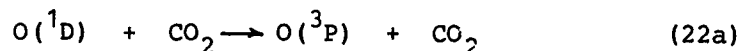
The process (20 a+b) quenches  $O(^1D)$  to  $O(^3P)$  with great efficiency and is accompanied by significant energy transfer. Slanger and Black [1974] have found that electronic to vibrational energy transfer occurs with 33 % efficiency (as vibrational energy) in  $N_2^*$  ( $v \leq 7$ ).

$N_2O$  is a product in the condensed phase reaction ( $N_2O = 0.015$ ) [De More and Raper, 1962]. Kajimoto and Cvetanović [1976a] measured at high pressure the quantum yield of  $N_2O$  formation of reaction (20 c) and deduced that in the gas phase  $N_2O = 3 \times 10^{-7}$  at 1 atm. This value is preferred over the data of Gaedtke et al. [1972], who observed a  $N_2O$  quantum yield two orders of magnitude larger. The rate constant for the termolecular reaction is  $k_{20c} = 6.5 \times 10^{-37} \text{ cm}^6/\text{molecule}^2 \cdot \text{sec.}$ , which is an order of magnitude smaller than the upper limit estimated by Simonaitis et al. [1972].

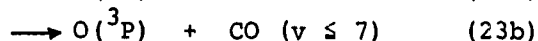
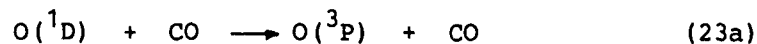
## B) $O_2$



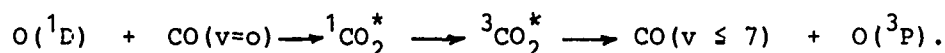
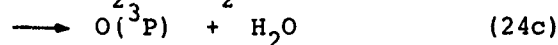
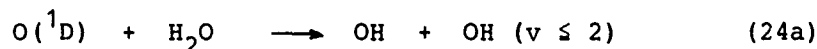
Process (21) is the major source of  $O_2(^1\Sigma_g^+)$  in the atmosphere. The reaction predominantly quenches  $O(^1D)$  to  $O(^3P)$  and produces an electronic excited oxygen molecule by electronic energy transfer with at least  $80 \pm 20$  % efficiency: Young and Black [1967] and Clark [1970] near 100 % eff.; Snelling and Gauthier [1971] 85 % eff.; Snelling [1974]  $75 \pm 20$  % eff.; Lee and Slanger [1978]  $77 \pm 20$  % eff. The latter group observed that only levels  $v = 0$  and 1 are produced in  $O_2(^1\Sigma_g^+)$  in a ratio  $k_1/k_0 \approx 0.7$ .  $O_2(^1\Sigma_g^+)_{v=1}$  is quenched very rapidly by  $O_2$  ( $k = 2.2 \times 10^{-11}$ ); this is 6 orders of magnitude faster than the  $O_2$  quenching of  $O_2(^1\Sigma_g^+)_{v=0}$  ( $k = 4 \times 10^{-17}$ ) and accounts for the weakness of the emission from the  $v = 1$  level in the terrestrial glow.

C)  $\underline{\text{CO}_2}$ 

The reaction of  $\text{O}(^1\text{D})$  with  $\text{CO}_2$  used to be the subject of some controversy, not only about the efficiency of  $\text{CO}_2$  as  $\text{O}(^1\text{D})$  quencher [Noxon, 1970] but also about the question whether the quenching was purely physical or produced a long-lived intermediate  $\text{CO}_3$  molecule [Clerc and Reiffsteck, 1968]. There is now enough evidence that the fate of  $\text{O}(^1\text{D})$  in the presence of  $\text{CO}_2$  is physical quenching [Young et al. 1968; Donovan et al. 1971; Black and Slanger, 1972], and that no CO [Felder et al., 1971] nor  $\text{CO}_3$  is formed [Paraskevopoulos and Cvetanović, 1969] in the gas phase under atmospheric conditions. The recent measurement of Amimoto et al. [1979] agrees with the concept of total quenching ( $0.99 \pm 0.03$ ) and the exclusion of any chemical reaction.

D)  $\underline{\text{CO}}$ 

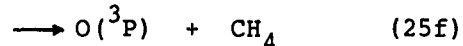
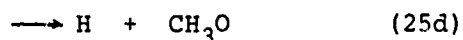
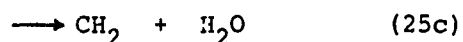
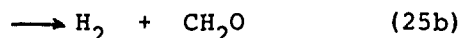
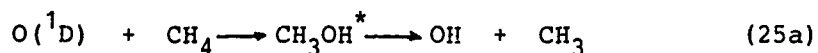
Paraskevopoulos and Cvetanović [1969] and Slanger and Black [1970] have shown that CO does not remove  $\text{O}(^1\text{D})$  chemically, but deactivates it quantitatively to an equivalent amount of  $\text{O}(^3\text{P})$ . During the  $\text{O}(^1\text{D}) + \text{CO}$  interaction, the CO molecule is vibrationally excited to  $v \leq 7$ , and the efficiency of the electronic to vibrational energy transfer was estimated to be  $40 \pm 8\%$  [Slanger and Black, 1974]. Shortridge and Lin [1976] have indicated that the quenching takes place via a complex mechanism, which involves a singlet-triplet system crossing process:

E)  $\underline{\text{H}_2\text{O}}$ 

It has been established that reaction (24a) is the primary source of OH radicals in the troposphere and in the lower stratosphere [Levy, 1974; Warneck, 1975]. Reaction (24a) is sufficiently exothermic to produce OH ( $v \leq 2$ ) [Basco and Norrish, 1961; Biedenkapp et al., 1970]. The branching ratio of path (24a) and (24b) was measured by Wagner [1979] to  $k_{24\text{b}}/k_{24\text{a}} = 0.01 (+0.005 / -0.01)$ . Therefore, reaction (24b) is not an important source of  $\text{H}_2$  in the stratosphere or troposphere. In a competitive study, Paraskevopoulos and

Cvetanović [1971] showed that, initially, all reactive collisions result in the formation of OH radicals, and that the contribution of the collisional deactivation (24c) is not more than 2 %. However, recent measurements of Amimoto et al. [1979] suggest a  $14 \pm 4$  % contribution of quenching.

F) CH<sub>4</sub>



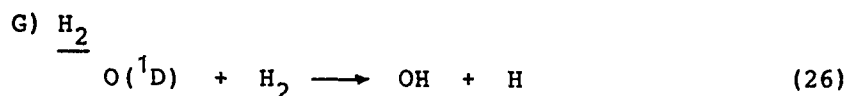
This reaction is an important oxidation process in the upper atmosphere. Table 7 summarises the contributions of the different channels. According to Lin and De More [1973a] and Jayanty et al. [1976b], the major channel (25a) involves the abstraction of an H atom to nearly 90 %, and a direct molecular elimination of H<sub>2</sub> via (25b) occurs to the extent of 10 %. Lin and De More [1973a] added O<sub>2</sub> as H atom scavenger in order to distinguish between H<sub>2</sub> formed in reaction (25b) and H<sub>2</sub> formed in a secondary reaction of H atoms, which are produced in reaction (25d). Since they found no change in the H<sub>2</sub> production, they assumed that H<sub>2</sub> was formed via reaction channel (25b). In a recent cross beam experiment, Lee [1979] found that CH<sub>3</sub>O + H is the next

Table 7 Product channels of the reaction  $\text{O}(^1\text{D}) + \text{CH}_4$

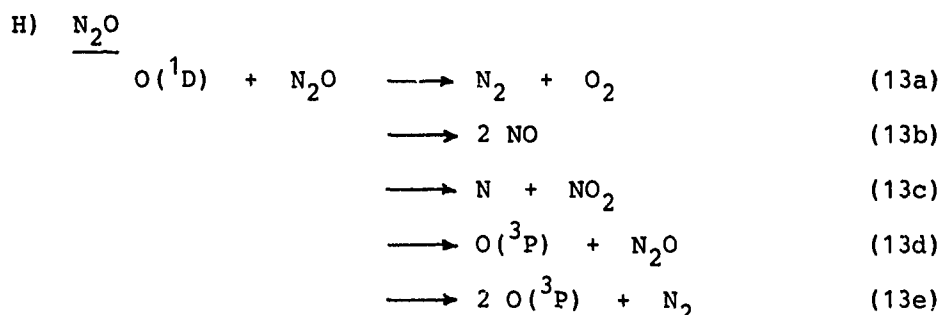
Products	PC	GH	LD	JSH	AFGW
OH + CH <sub>3</sub>	0.97	$0.95 \pm 0.05$	0.91	$0.89 \pm 0.02$	0.80
H <sub>2</sub> + CH <sub>2</sub> O		<0.002	0.09	$0.11 \pm 0.01$	0.08
CH <sub>2</sub> + H <sub>2</sub> O		<0.03		<0.01	
CH <sub>3</sub> OH		<0.01		<0.01	
CH <sub>4</sub> + O(^3P)	<0.03	$0.05 \pm 0.05$		<0.03	0.12

PC = Paraskevopoulos and Cvetanović, [1969]; GH = Greenberg and Heicklen, [1972]; LD = Lin and DeMore, [1973a]; JSH = Jayanty et al. [1976b]; AFGW = Amimoto et al., [1979].

important channel, and found no evidence for the reaction channel  $\text{CH}_2\text{O} + \text{H}_2$ . Although Paraskevopoulos and Cvetanović [1969] found little evidence for  $\text{O}(^1\text{D})$  deactivation by  $\text{CH}_4$ , Amimoto et al. [1979] accounted a  $12 \pm 4\%$  contribution to quenching. The origin of the  $\text{H}_2$ , and the possible contribution of collisional quenching thus remains still uncertain.



Paraskevopoulos and Cvetanović [1969] established that the reaction of  $\text{O}(^1\text{D})$  with  $\text{H}_2$  proceeds through a hydrogen abstraction, and found no evidence for collisional deactivation. Basco and Norrish [1961] have detected vibrationally excited  $\text{OH}$  ( $v \leq 2$ ) in reaction (26).



Reaction (13b) is believed to be the main source of  $\text{NO}$  in the stratosphere, and thus plays a dominant role in controlling the ozone budget. Many studies have been made in the past for the determination of the efficiency of each of the 5 exothermic reactions. Most studies however agree that channel (13a and 13b) contribute to the majority of the products.  $\text{NO}$  and  $\text{N}_2$  are produced in their ground electronic states; there is, however, sufficient energy to produce electronically excited oxygen molecules (favored because of spin conservation) [Wiesenfeld, 1977].

The branching ratio,  $R = k_{13a}/k_{13b}$  as given up to 1970 [Greenberg and Heicklen, 1970] varied between 1.56 and 0.5. Simonaitis et al. [1972a] related the difference in  $R$  to the thermalization of the originally hot  $\text{O}(^1\text{D})$  products in the photolysis. Table 8 summarizes the results obtained after 1970. Simonaitis et al., [1972a], Pirkle et al. [1977] and Davidson et al., [1979] observed that the ratio  $R$  is sensitive to the presence of Helium and increases from  $R = 0.68$  in pure  $\text{N}_2\text{O}$  to a value ranging between  $R = 0.80$  and  $0.90$  (Helium is added to remove excess kinetic energy.) On the contrary, Marx et al. [1979] studied the branching ratio as function of kinetic energy and found no variation of  $R (= 0.62 \pm 0.08)$  upon addition of 2000 torr Helium.

Table 8 Branching ratio of product channels of  $O(^1D) + N_2O \rightleftharpoons N_2 + O_2$   
 $R = k_{13a} / k_{13b}$

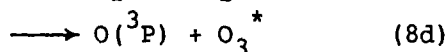
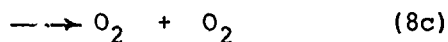
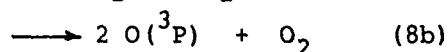
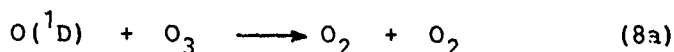
R hot $O(^1D)$	R Thermalized	Photolysis mixture	Technique	References
$0.59 \pm 0.01$		$N_2O$	$\phi N_2$	Greenberg-Heicklen [1970]
$0.59 \pm 0.08$		$N_2O$	$\phi N_2$	Goldmann et al. [1971]
	$1.08 \pm 0.19$	$N_2O$	$\phi N_2$	Scott et al. [1971]
	$1.01 \pm 0.06$	$NO_2/N_2O$	$\phi NO$ and $\phi N_2$	" "
	$0.99 \pm 0.06$	$N_2O/O_3$	$\phi N_2 / \phi N_2O$	" "
$0.65 \pm 0.07$	$0.83 \pm 0.06$	$N_2O/He$	$\phi O_2, \phi N_2$	Simonaitis et al. [1972a]
$0.70 \pm 0.02$		$O_3/N_2O/O_2$	$NO_2$ appear. rate	Ghormley et al [1973]
$1.0 \pm 0.17$	$1.0 \pm 0.17$	$N_2O (He)$	$N_2/NO$	Wiebe and Paraskevopoulos [1974]
$0.73 \pm 0.11$	$0.92 \pm 0.10$	$N_2O (He)$	$NO/NO_2$ chemi- lum	Pirkle et al. [1977]
$0.68 \pm 0.018$	$0.80 \pm 0.05$	$N_2O (He)$	Flowing after- + $N_2O$ glow	Davidson et al. [1979]
$0.62 \pm 0.04$	$0.62 \pm 0.04$	$N_2O (He)$	$\phi N_2, \phi O_2$ $\phi NO$ Chemilum.	Marx et al. [1979]

Scott et al. [1971] and Wiebe and Paraskevopoulos [1974], also reported that R is unaffected by the presence of Helium. Davidson et al. [1979] reported that the ratio R decreases slowly with increasing temperature over the range 170-434 K. Their data are fitted by the expression (vii)

$$\frac{k_{13a}}{k_{13b}} = (0.72 \pm 0.11) + \frac{21.6 \pm 7.0}{T} \quad (vii)$$

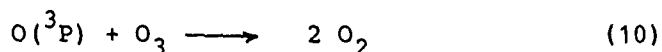
In addition, Davidson et al. [1979] showed that  $\frac{k_{13c} + k_{13d} + k_{13e}}{k_{13a} + k_{13b}} \leq 0.038$  in agreement with Scott et al. [1971], who measured  $k_{13c}/k_{13a} \leq 0.05$  and Greenberg and Heicklen [1970], who found  $\frac{k_{13d} + k_{13e}}{k_{13a} + k_{13b}} \leq 0.02$

However, Amimoto et al. [1979], using time resolved  $O(^3P)$  resonance spectroscopy, measured that the deactivation reaction (13c) contributes  $12 \pm 3 \%$ , which is not negligible. Further studies are advisable in order to clarify this discrepancy.

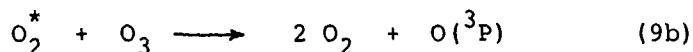
I)  $O_3$ 

where  $O_2^*$  is an excited oxygen in an unspecified state.

The mechanism of the reaction of  $O(^1D)$  with  $O_3$  has been controversial since the beginning of the  $O_3$  photolysis studies [Schiff, 1972; Wayne, 1972; Welge, 1974]. Different reaction schemes were proposed to explain the overall quantum yield of  $O_3$  consumption,  $\phi(-O_3)$ , of 6 in the ultra-violet photolysis of pure  $O_3$ , and of 4 in the presence of quenchers such as  $N_2$  and  $CO_2$ . Earlier measurements have indicated that neither  $O_2(^1\Delta_g)$  nor  $O_2(^1\Sigma_g^+)$  corresponded to  $O_2^*$  [Gauthier and Snelling, 1970; Webster and Bair, 1970; Gilpin et al., 1971; Ellis et al., 1971]. Although Baiamonte et al. [1971] found evidence by absorption spectroscopy that vibrational excited ground state  $O_2$  molecules up to  $v \leq 30$  were formed, they observed that large amounts of  $O_2$  ( $v \leq 17$ ) were generated in the reaction (10)



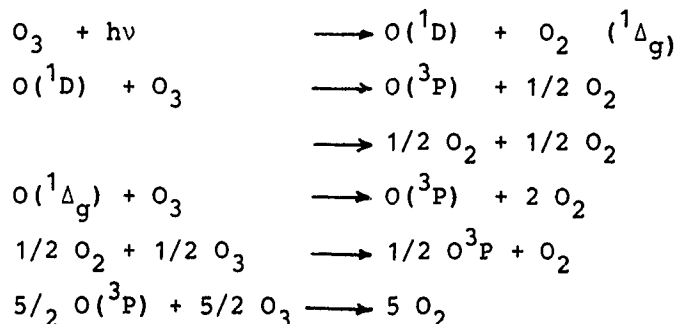
Using resonance fluorescence, the number of  $O(^3P)$  formed during the fast reactions (8) in the  $O_3$  uv flash photolysis was measured to be 0.7 [Giarchiardi and Wayne, 1972] and  $1.0 \pm 0.08$  [Davenport et al., 1972]. The latter value suggests that reaction channels (8a) and (8b) occurs with equal probability. Using time resolved absorption of  $O(^3P)$  atoms, Amimoto et al. [1978] also found that the removal of one excited  $O(^1D)$  atom is associated with the production of  $(1.01 \pm 0.05)$  ground state  $O(^3P)$  atom. They claim that  $k_{8a} = k_{8b}$  is fortuitous, and suggest that the reaction channel (8d) (physical quenching) may be responsible for the collisional deactivation of  $O(^1D)$ . This would lead to a  $\phi(-O_3) = 4$  in pure  $O_3$ . In a recent investigation, Arnold and Comes [1979] compared  $O(^3P)$  time-resolved absorption profiles in the 300 and 600 nm photolysis of  $O_3$  and deduced a  $\phi(-O_3) = 6.1 \pm 0.2$  in pure  $O_3$  and  $4.1 \pm 0.3$  in  $O_3/N_2$  mixtures. They confirmed that the number of fast  $O(^3P)$  is unity but must include reaction (8c) followed by (9b)



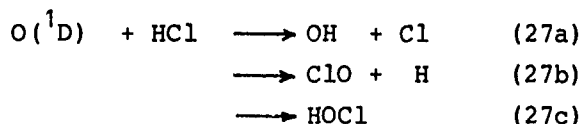
in order to simulate their  $O(^3P)$  time profiles. They concluded that reactions (8b) and (8c) participate with 50 % efficiency and also



deduced  $k_{9b} = 2.8 \pm 0.3 \times 10^{-15} \text{ cm}^3/\text{molecule} \cdot \text{sec}$ . Arnold and Comes [1979] proposed the following  $\text{O}_3$  photolysis mechanism:

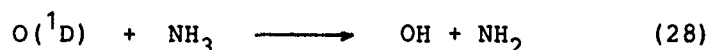


J) HCl



HCl is the major sink for  $\text{ClO}_x$  species in the stratosphere. Addison et al. [1976] have shown that process (27a) is the only reaction channel, as is predicted from theoretical expectation based on correlation diagrams. They suggest that the reaction could proceed through the formation of a HOCl complex, however of very short lifetime. Davidson et al. [1976] observed a "second emission at 630 nm, which could be associated with vibrational excited OH ( $v \leq 4$ ) formed in reaction (27a).

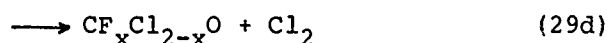
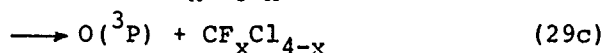
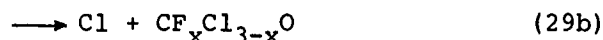
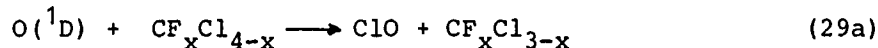
K)  $\text{NH}_3$



The reaction is believed to produce uniquely OH and  $\text{NH}_2$  radicals. Davidson et al. [1976] also have observed secondary emission at 630 nm which they attributed to vibrational excited OH.

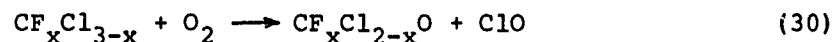
L) HALOCARBONS

There exists still controversies about the products of the reactions of  $\text{O}(^1\text{D})$  with halocarbons:





Gillespie and Donovan [1976] and Gillespie et al. [1977] have measured the direct yield of ClO from channel (29a) as 0.39, 0.47, 0.39, 0.27 and 0.36 for the halocarbons  $\text{CF}_3\text{Cl}$ ,  $\text{CF}_2\text{Cl}_2$ ,  $\text{CFCl}_3$ ,  $\text{CF}_2\text{HCl}$  and  $\text{CFHCl}_2$  respectively. On the other hand, Pitts et al. [1974] have observed, by infrared absorption spectroscopy, that  $\text{COF}_2$  is an endproduct from the reaction of  $\text{O}(^1\text{D})$  with  $\text{CHF}_2\text{Cl}$  and  $\text{CF}_2\text{Cl}_2$  with respectively  $0.5 \pm 0.1$  and  $0.8 \pm 0.1$  efficiency. Also  $\text{COFCl}$  was detected as endproduct from the reaction  $\text{O}(^1\text{D}) + \text{CFCl}_3$ . Since this study was performed in the competitive photolysis of  $\text{N}_2\text{O}$ /halocarbon mixture,  $\text{O}_2$  was present in the system. Hence it is not clear whether  $\text{COF}_2$  is formed in the primary reaction (29d), or as product of the secondary reaction



Also, participation of physical quenching (29c) is not to be excluded. Further study of these systems is clearly warranted.

#### ACKNOWLEDGEMENTS

This work was performed within the programme of the Sonderforschungsbereich 73 "Atmospheric Trace Components" and has received in part financial support from the Deutsche Forschungsgemeinschaft.

#### REFERENCES

- Addison, M. C., R. J. Donovan and H. M. Gillespie, Reaction of  $\text{O}(2^1\text{D}_2)$  with  $\text{HCl}$ , Chem. Phys. Lett., **44**, 602, 1976.
- Amimoto, S. T., A. P. Force, R. J. Gulotty and J. R. Wiesenfeld, Collisional deactivation of  $\text{O}(^1\text{D}_2)$  by atmospheric gases, to be published, 1979.
- Amimoto, S. T., A. P. Force and J. R. Wiesenfeld, Ozone Photochemistry: production and deactivation of  $\text{O}(2^1\text{D}_2)$  following photolysis at 248 nm, Chem. Phys. Lett., **60**, 40, 1978.
- Arnold, I. and F. J. Comes, Photolysis of ozone in the ultraviolet region, to be published, 1979.
- Arnold, I., F. J. Comes and G. K. Moortgat, Laser flash photolysis: quantum yield of  $\text{O}(^1\text{D})$  formation from ozone, Chem. Phys., **24**, 211, 1977.
- Atkinson, R., G. M. Breuer, J. N. Pitts, Jr and H. L. Sandoval, Tropospheric and stratospheric sinks for halocarbons: photooxidation,  $\text{O}(^1\text{D})$  atom, and OH radical reactions, J. Geophys. Res., **81**, 5765, 1976.

- Briamonte, V. D., L. G. Hartshorn and E. J. Bair, Ozone ultraviolet photolysis, III; disposition of vibrational energy, J. Chem. Phys., **55**, 3617, 1971.
- Basco, N. and R. G. W. Morrish, The production of vibrationally excited hydroxyl radicals under isothermal conditions by flash photolysis, Proc. Roy. Soc. London, A **260**, 293, 1961.
- Biedenkapp, D. and E. J. Bair, Ozone ultraviolet photolysis, I; the effect of molecular oxygen, J. Chem. Phys., **52**, 6119, 1970.
- Black, G., T. Slinger and B. J. Wood, Kinetics of  $O(^3P) + CO + M$  recombination, J. Chem. Phys., **57**, 233, 1972.
- Brock, J. C. and R. T. Watson, Laser flash photolysis of ozone:  $O(^1D)$  quantum yields in the fall-off region 297-325 nm, Nato Advanced Studies Institute on Atmospheric Ozone, Aldeia das Açoteias, Algarve Portugal, October, 1979 a.
- Brock, J. C. and R. T. Watson, Absolute  $O(^1D)$  rate constants. Nato Advanced Studies Institute on Atmospheric Ozone, Aldeia das Açoteias, Algarve, Portugal, October, 1979b.
- Castellano, E. and H. J. Schumacher, Die Kinetik und der Mechanismus des photochemischen Ozonzerfalles im Licht der Wellenlänge 313 nm, Z. physik. Chem. Neue Folge, **65**, 62, 1969.
- Clark, I. D., Energy transfer from  $O(^1D)$  to  $O_2$ , Chem. Phys. Lett., **5**, 317, 1970.
- Clerc, M. and A. Reiffsteck, Determination of the rate constant of the gas-phase reaction between  $O(^1D)$  and  $CO_2$ , J. Chem. Phys., **48**, 2799, 1968.
- Clough, P. N., and B. A. Thrush, Mechanism of chemiluminescent reaction between nitric oxide and ozone, Trans. Faraday Soc., **63**, 915, 1967.
- Cvetanović, R. J. Excited state chemistry in the stratosphere, Can. J. Chem., **52**, 1452, 1974 .
- Davenport, J., B. Ridley, H. I. Schiff and K. H. Welge, Communication to "Reactions of small molecules in excited states", Chem. Soc. Faraday Disc., **53**, 230, 1972.
- Davidson, J. A., C. J. Howard, H. I. Schiff and F. C. Fehsenfeld, Measurement of the branching ratios for the reaction of  $O(^1D_2)$  with  $N_2O$ , J. Chem. Phys., **70**, 1697, 1979 .
- Davidson, J. A., C. M. Sadowski, H. I. Schiff, G. E. Streit, C. J. Howard, D. A. Jennings and A. L. Schmeltekopf, Absolute rate constant determination for the deactivation of  $O(^1D)$  by time resolved decay of  $O(^1D) \rightarrow O(^3P)$  emission, J. Chem. Phys., **64**, 57, 1976.
- Davidson, J. A., H. I. Schiff, T. J. Brown and C. J. Howard, Temperature dependence of the deactivation of  $O(^1D)$  by CO from 113-333 K, J. Chem. Phys., **69**, 1216, 1978 a.

- Davidson, J. A., H. I. Schiff, T. J. Brown and C. J. Howard, Temperature dependence of the rate constants for reactions of  $O(^1D)$  atoms with a number of halocarbons, J. Chem. Phys., **69**, 4277, 1978 b.
- Davidson, J. A., H. I. Schiff, T. J. Brown, G. C. Streit, and C. J. Howard, Rate constants for the deactivation of  $O(^1D)$  by Xe, Kr, and Ar over the range 110 - 330 K., J. Chem. Phys., **69**, 1213, 1978 c.
- Davidson, J. A., H. I. Schiff, G. E. Streit, J. R. McAfee, A. L. Schmeltekopf and C. J. Howard, Temperature dependence of  $O(^1D)$  rate constants for reactions with  $H_2O$ ,  $H_2$ ,  $CH_4$ ,  $HCl$  and  $NH_3$ , J. Chem. Phys., **67**, 5021, 1977.
- DeMore, W. B. and O. F. Raper, Reaction of  $O(^1D)$  with nitrogen, J. Chem. Phys., **37**, 2048, 1962 .
- DeMore, W. B. and O. F. Raper, Primary processes in ozone photolysis, J. Chem. Phys., **44**, 1780, 1966 .
- Donovan, R. J., D. Husain and L. J. Kirsch, Reactions of oxygen atoms, Part 3: Reactions of  $O(2^3P_j)$  and  $O(2^1D_2)$  with  $CO$  and  $CO_2$ , Trans. Faraday Soc., **67**, 375, 1971 .
- Ellenrieder, G., E. Castellano and H. J. Schumacher, The kinetics and the mechanism of the photochemical decomposition of ozone with light of 2537 Å wavelength, Chem. Phys. Lett., **9**, 152, 1971.
- Ellis, D. M., J. J. Garvey and W. D. McGrath, Reaction of  $O(^3P)$  atoms with ozone, Nature, **229**, 153, 1971 .
- Fairchild, P. W. and E. K. C. Lee, Relative quantum yields of  $O(^1D)$  in ozone photolysis in the region between 250 and 300 nm, Chem. Phys. Lett., **60**, 36, 1978 .
- Fairchild, C. E., E. J. Stone and G. M. Lawrence, Photofragment spectroscopy of ozone in the uv region 270-310 nm and at 600 nm, J. Chem. Phys., **69**, 3632, 1978.
- Felder, W., W. Morrow and R. A. Young, Experimental test of the reaction  $O(^1D) + CO_2 \rightarrow CO + O_2$ , J. Chem. Phys., **54**, 2949, 1971.
- Fletcher, I. S. and D. Husain, Absolute reaction rates of oxygen ( $2^1D_2$ ) with halogenated paraffins by atomic absorption spectroscopy in the vacuum ultraviolet, J. Phys. Chem., **80**, 1837, 1976 a.
- Fletcher, I. S. and D. Husain, The collisional quenching of electronically excited oxygen atoms  $O(2^1D_2)$  by the gases  $NH_3$ ,  $H_2O_2$ ,  $C_2H_6$ ,  $C_3H_8$  and  $(CCl_3)_4$  using time resolved attenuation of atomic resonance radiation, Can. J. Chem., **54**, 1765, 1976 b.
- Fletcher, I. S. and D. Husain, The collisional quenching of  $O(2^1D_2)$  by  $COCl_2$ ,  $COFCl$  and  $COF_2$  using atomic absorption spectroscopy in the vacuum ultraviolet, J. Photochem., **8**, 355, 1978.
- Gaedtke, H., H. Hippler and J. Troe, Untersuchung der Photolyse von Ozon bei 2600 Å bei hohen Trägergasdrucken, Ber. Bunsenges. Phys. Chem., **76**, 1101, 1972 .

- Gauthier, M., and D. R. Snelling, Formation of singlet molecular oxygen from the ozone photochemical system, Chem. Phys. Lett., **5**, 93, 1970 .
- Gauthier, M. and D. R. Snelling, Mechanism of singlet molecular oxygen formation from photolysis of ozone at 2537 Å, J. Chem. Phys., **54**, 4317, 1971 .
- Ghormley, J.A., R. L. Ellsworth and C. J. Hochanadel, Reaction of excited oxygen atoms with nitrous oxide. Rate constants for reaction of ozone with nitric oxide and with nitrogen dioxide, J. Chem. Phys., **77**, 1341, 1973.
- Giachardi, D. J. and R. P. Wayne, The photolysis of ozone by ultraviolet radiation VI; reactions of  $O(^1D)$ , Proc. Roy. Soc. London, **A330**, 131, 1972 .
- Gillespie, H. M. and R. J. Donovan, Reaction of  $O(2^1D_2)$  atoms with chloro-fluoromethanes: formation of ClO, Chem. Phys. Lett., **37**, 468, 1976 .
- Gillespie, H. M., J. Garraway and R. J. Donovan, Reaction of  $O(^1D)$  with halomethanes, J. Photochem., **7**, 29, 1977.
- Gilpin, R., H. I. Schiff and K. H. Welge, Photodissociation of  $O_3$  in the Hartley Band: reaction of  $O(^1D)$  and  $O_2(^1\Sigma_g^+)$  with  $O_3$  and  $O_2$ , J. Chem. Phys., **55**, 1087, 1971 .
- Goldman, C. S., R. I. Greenberg and J. Heicklen, The reaction of  $O(^1D)$  with ozone and nitrous oxide, Intern. Chem. Kinetics, **3**, 501, 1971.
- Green, R. G. and R. P. Wayne, Relative rate constants for the reaction of  $O(^1D)$  atoms with fluorocarbons and with  $N_2O$ , J. Photochem., **6**, 381, 1975.
- Greenberg, R. I. and J. Heicklen, Reaction of  $O(^1D)$  with  $N_2O$ , Intern. J. Chem. Kinetics, **2**, 185, 1970 .
- Greenberg, R. I. and J. Heicklen, The reaction of  $O(^1D)$  with  $CH_4$ , Intern. J. Chem. Kinetics, **4**, 417, 1972 .
- Griggs, M., Absorption coefficients of ozone in the ultraviolet and visible regions, J. Chem. Phys., **49**, 857, 1958.
- Hampson, R. F. Jr. and D. Garvin, Chemical Kinetics and Photochemical data for modelling atmospheric chemistry, NBS Technical Note 866, National Bureau of Standards, Washington, D.C., 1975.
- Hampson, R. F. Jr. and D. Garvin, Reaction rate and photochemical data for atmospheric chemistry- 1977, NBS - Publication 513, National Bureau of Standards, Washington D. C., 1978.
- Hay, P. J., T. H. Dunning, Jr. and W. Goddard, III, Theoretical evidence for bound electronic excited states of ozone, Chem. Phys. Lett., **23**, 457, 1973.
- Heidner, R. F. III and D. Husain, Electronically excited oxygen atoms,  $O(2^1D_2)$ ; a time-resolved study of the collisional quenching by the gases  $H_2$ ,  $D_2$ ,  $NO$ ,  $N_2O$ ,  $NO_2$ ,  $CH_4$  and  $C_3O_2$  using atomic absorption spectroscopy in the ultraviolet, Intern. J. Chem. Kinetics, **5**, 819, 1973.

- Heidner, R. F. III, D. Husain and J. R. Wiesenfeld, Kinetic investigation of electronically excited oxygen atoms,  $O(2^1D_2)$ , by time-resolved attenuation of atomic resonance radiation in the vacuum ultraviolet; part 2: collisional quenching by the atmospheric gases  $N_2$ ,  $O_2$ ,  $CO$ ,  $CO_2$ ,  $H_2O$  and  $O_3$ , J. Chem. Soc. Faraday Trans. II, **69**, 927, 1973.
- Heidner, H. F. III and D. Husain, A study of the collisional quenching of  $O(2^1D_2)$  by the noble gases employing time-resolved attenuation of atomic resonance radiation in the vacuum ultraviolet, Intern. J. Chem. Kinetics, **6**, 77, 1974.
- Hudson, R. D., Absorption cross sections of stratospheric molecules, Can. J. Chem., **52**, 1465, 1974.
- Inn, E. C. Y. and Y. Tanaka, Absorption coefficient of ozone in the ultraviolet and visible regions, J. Opt. Soc. Am., **43**, 870, 1953.
- Jayanty, R. K. M., R. Simonaitis and J. Heicklen, The photolysis of  $CCl_4$  in the presence of  $O_2$  or  $O_3$  at 213.9 nm, and the reaction of  $O(^1D) + CCl_4$ , J. Photochem., **4**, 207, 1975a.
- Jayanty, R. K. M., R. Simonaitis and J. Heicklen, The photolysis of chlorofluoromethane in the presence of  $O_2$  or  $O_3$  at 213.9 nm, and their reactions with  $O(^1D)$ , J. Photochem., **4**, 381, 1975b.
- Jayanty, R. K. M., R. Simonaitis and J. Heicklen, The reaction of atomic oxygen  $O(^1D)$  with carbonic dichloride, carbonic fluoride chloride and carbonic difluoride, J. Photochem., **5**, 217, 1976a.
- Jayanty, R. K. M., R. Simonaitis and J. Heicklen,  $H_2$  formation in the reaction of  $O(^1D)$  with  $CH_4$ , Intern. J. Chem. Kinetics, **8**, 107, 1976b.
- Jones, I. T. N., U. B. Kaczmar and R. P. Wayne, The photolysis of dry ozone/oxygen mixtures at low pressures in a flow system, Proc. Roy. Soc. London, **A316**, 431, 1970.
- Jones, I. T. N. and R. P. Wayne, The photolysis of ozone by ultraviolet radiation IV; effect of photolysis wavelength on primary step, Proc. Roy. Soc. London, **A 319**, 273, 1970.
- Jones, I. T. N. and R. P. Wayne, The photolysis of ozone by ultraviolet radiation V; photochemical formation of  $O_2(^1\Delta_g)$ , Proc. Roy. Soc. London, **A321**, 409, 1971.
- Kajimoto, O. and R. J. Cvetanović, Formation of nitrous oxide in the reaction of  $O(^1D_2)$  atoms with nitrogen, J. Chem. Phys., **64**, 1005, 1976 a.
- Kajimoto, O. and R. J. Cvetanović, Temperature dependence of  $O(^1D_2)$  production in the photolysis of ozone at 315 nm, Chem. Phys. Lett., **37**, 533, 1976 b.
- Kajimoto, O. and R. J. Cvetanović, Absolute quantum yields of  $O(^1D_2)$  in the photolysis of ozone in the Hartley band, Intern. J. Chem. Kinetics, **11**, 605, 1979.

- Kuis, S. R. Simonaitis and J. Heicklen, Temperature dependence of the photolysis of ozone at 3130 Å, J. Geophys. Res., 80, 1328, 1975.
- Lee, L. C. and T. G. Slanger, Observations on  $O(^1D \rightarrow ^3P)$  and  $O_2(b^1\Sigma_g^+ \rightarrow X^3\Delta_g^-)$  following  $O_2$  photodissociation, J. Chem. Phys., 69, 4053, 1978.
- Lee, Y. T., Private communication, 1979.
- Levy, H., Photochemistry of the troposphere, Adv. Photochem., 9, 369, 1974.
- Lin, C. L. and W. B. DeMore, Reactions of  $O(^1D)$  with methane and ethane, J. Chem. Phys., 77, 863, 1973 a.
- Lin, C. L. and W. B. DeMore,  $O(^1D)$  production in ozone photolysis near 3100 Å, J. Photochem., 2, 161, 1973 b.
- Lissi, E. and J. Heicklen, The photolysis of ozone, J. Photochem., 1, 39, 1972.
- Martin, D., J. Girman, and H. S. Johnston,  $O(^1D)$  quantum yields from ozone photolysis at 290 - 325 nm, 167 th ACS National meeting, Los Angeles (1974).
- Marx, M., F. Bahe and U. Schurath, The yield of  $O(^1D) + N_2O$  as function of Kinetic Energy, Ber. Bunsenges. Phys. Chem., 83, 225, 1979.
- McGrath, W. D. and R. G. W. Norrish, The influence of water on the photolytic decomposition of ozone, Nature, 182, 235, 1958.
- McGrath, W. D. and R. G. W. Norrish, Studies of the reactions of excited oxygen atoms and molecules produced in the flash photolysis of ozone, Proc. Roy. Soc. London, A254, 317, 1960.
- Moortgat, G. K. and E. Kudzusz, Mathematical expression for the  $O(^1D)$  quantum yields from the  $O_3$  photolysis as a function of temperature (230-320 K) and wavelength (295-320 nm), Geophys. Res. Lett., 5, 191, 1978.
- Moortgat, G. K., E. Kudzusz and P. Warneck, Temperature dependence of  $O(^1D)$  formation in the near uv photolysis of ozone, J. Chem. Soc., Faraday Trans. II, 73, 1216, 1977.
- Moortgat, G. K. and P. Warneck, Relative  $O(^1D)$  quantum yields in the near uv photolysis of ozone at 298 K, Z. Naturforsch., 30 A, 835, 1975.
- NASA-1, National Aeronautics and Space Administration, Chlorofluoromethanes and the stratosphere, NASA Reference Publication 1010, 1977.
- NASA-2, National Aeronautics and Space Administration, Chemical Kinetic and photochemical data for use in stratospheric modelling, Evaluation Number 2, Jet Propulsion Laboratory, Pasadena, California, JPL Publication 79-27, 1979 .
- Norrish, R. G. W. and R. P. Wayne, The photolysis of ozone by ultraviolet radiation I; the photolysis of pure, dry ozone, Proc. Roy. Soc. London, A 288, 200, 1965 a.
- Norrish, R. G. W. and R. P. Wayne, The photolysis of ozone by ultraviolet radiation II; the photolysis of ozone mixed with certain hydrogen-con-

- taining substances, Proc. Roy. Soc. London, **A 288**, 361, 1965 b.
- Noxon, J. F., Optical emission from  $O(^1D)$  and  $O_2(^1\Sigma_g^+)$  in the ultraviolet photolysis of  $O_2$  and  $CO_2$ , J. Chem. Phys., **52**, 1852, 1970.
- Paraskevopoulos, G. and R. J. Cvetanović, Competitive reactions of the excited oxygen atoms  $O(^1D)$ , J. Am. Chem. Soc., **91**, 7572, 1969.
- Paraskevopoulos, G. and R. J. Cvetanović, Reactive rate of reactions of  $O(^1D)$  with  $H_2O$ , Chem. Phys. Lett., **9**, 603, 1971.
- Peterson, J. L., Calculated actinic fluxes (290-700 nm) for air pollution photochemistry applications. Report EPA-600/4-76-002, Environmental Protection Agency, Research Triangle Park. N.C. June 1976.
- Philen, D. E., R. T. Watson and D. D. Davis, A quantum yield determination of  $O(^1D)$  production from ozone via laser flash photolysis, J. Chem. Phys., **67**, 3316, 1977.
- Phillips, L. F., Theoretical curves of growth for  $O(^1D)$  absorption at 115.2 nm, Chem. Phys. Lett., **37**, 421, 1976.
- Pirkle, R. J., H. N. Volltrauer, W. Felder, and A. Fontijn, Measurements on  $O(^1D)/N_2O$  and  $HNO_2/O_3$  Kinetics, FAA-AEQ-77-10, 1977, Report prepared for High Altitude Pollution Program, U. S. Department of Transportation, Washington, D. C. , June 1977.
- Pitts, J. N. Jr., H. L. Sandoval and R. Atkinson, Relative rate constants for the reaction of  $O(^1D)$  atoms with fluorocarbons and  $N_2O$ , Chem. Phys. Lett., **29**, 31, 1974.
- Sandoval, H. L., R. Atkinson, and J. N. Pitts, Jr., Reactions of electronically excited  $O(^1D)$  atoms with fluorocarbons, J. Photochem., **3**, 325, 1973/74.
- Schiff, H. I., Laboratory measurements of reactions related to the ozone photochemistry, Ann. Géophys., **28**, 67, 1972.
- Schofield, K., Rate constants for the gaseous interactions of  $O(2^1D_2)$  and  $O(2^1S_0)$ ; a critical evaluation, J. Photochem., **9**, 55, 1978.
- Scott, P. M., K. F. Preston, R. J. Anderson and R. J. Cvetanović, The reaction of the electronically excited oxygen atom  $O(^1D_2)$  with nitrous oxide, Can. J. Chem., **49**, 1808, 1971.
- Shortridge, R. G. and M. C. Lin, The dynamics of the  $O(^1D) + CO(X^1\Sigma, ^1v = 0,)$  reaction, J. Chem. Phys., **64**, 4076, 1976.
- Simonaitis, R., S. Braslavsky, J. Heicklen and M. Nicolet, Photolysis of  $O_3$  at 3130 Å, Chem. Phys. Lett., **19**, 601, 1973.
- Simonaitis, R., R. I. Greenberg and J. Heicklen, The photolysis of  $N_2O$  at 2139 Å and 1849 Å, Intern. J. Chem. Kinetics, **4**, 497, 1972a.
- Simonaitis, R. and J. Heicklen, The reaction of OH with  $NO_2$  and the deactivation of  $O(^1D)$  by CO, Intern. J. Chem. Kinetics, **4**, 529, 1972.
- Simonaitis, R., E. Lissi and J. Heicklen, On the production of  $N_2O$  from reaction of  $O(^1D)$  with  $N_2$ , J. Geophys. Res., **77**, 4248, 1972b.



- Simons, J. W., R. J. Paur, H. A. Webster III and E. J. Bair, Ozone ultra-violet photolysis, VI; the ultraviolet spectrum, J. Chem. Phys., **59**, 1203, 1973.
- Slanger, T. G. and G. Black, Reaction rate measurements of  $O(^3P)$  atoms by resonance fluorescence, II;  $O(^3P) + CO + M \rightarrow CO_2 + M$ ,  $M = He, Ar, N_2$ , J. Chem. Phys., **53**, 3722, 1970.
- Slanger, T. G., and G. Black, The  $CO_2$  photolysis problem, J. Chem. Phys., **54**, 1889, 1971.
- Slanger, T. G. and G. Black, Electronic - to - vibrational energy transfer efficiency in the  $O(^1D) - N_2$  and  $O(^1D) - CO$  systems, J. Chem. Phys., **60**, 468, 1974.
- Snelling, D.R., The ultraviolet flash photolysis of ozone and the reactions of  $O(^1D)$  and  $O_2(^1\Sigma_g^+)$ , Can. J. Chem., **52**, 257, 1974.
- Snelling, D. R. and M. Gauthier, Efficiency of  $O_2(^1\Sigma_g^+)$  formation by  $O(^1D) + O_2$ , Chem. Phys. Lett., **9**, 254, 1971.
- Sparks, R. K., L. R. Carlson, K. Shobatake, M. L. Kowalczyk and Y. T. Lee, Ozone photolysis: a determination of the electronic and vibrational state distribution of primary products Lawrence Berkeley Laboratory, N<sup>o</sup> 9555, University of California, Berkeley, 1979.
- Streit, G. E., C. J. Howard, A. L. Schmeltekopf, J. A. Davidson and H. I. Schiff, Temperature dependence of  $O(^1D)$  rate constants for reactions with  $O_2$ ,  $N_2$ ,  $CO_2$ ,  $O_3$  and  $H_2O$ , J. Chem Phys., **65**, 4761, 1976.
- Stull, D. R. and H. Prophet, JANAF Thermochemical Tables, 2nd ed. NSRDS-NBS-37, 1971.
- Taube, H., Photochemical reactions of ozone in solution, Trans. Faraday Soc., **53**, 657, 1957.
- Vigroux, E., Contribution à l' étude expérimentale de l' absorption de l' ozone, Ann. Phys., **8**, 709, 1953.
- Vigroux, E., Coefficients d' absorption de l' ozone dans la bande de Hartley, Ann. Géophys., **25**, 169, 1969.
- Wagner, G., Blitzlicht Photolyse Untersuchungen zur Kinetik der Reaktionen  $OH + OH$ ,  $OH + OH + N_2$ ,  $OH + O_3$ , sowie zu den Produktkanälen der Reaktion  $O(^1D) + H_2O$ , Dissertation, Univ. Göttingen, 1979.
- Wallace, L. and D. M. Hunten, Dayglow of the oxygen A Band, J. Geophys. Res., **73**, 4813, 1968.
- Warneck, P., OH production rates in the troposphere, Planet. Space Sci., **23**, 1507, 1975.
- Warneck, The role of chemical reactions in the cycle of atmospheric trace gases, especially  $CH_4$ , Microbial Production and Utilization of Gases ( $H_2$ ,  $CH_4$ ,  $CO$ ), p. 53, Ed. Hans G. Schlehel, Gerhard Gottschalk and Norbert Pfennig; E. Glotze KG, Göttingen, 1976.
- Wayne, R. P., Reactions of excited species in the photolysis of ozone,

- Disc. Faraday Soc., 53, 172, 1972.
- Webster, H. and E. J. Bair, Ozone photolysis II: quantum yields at low ozone concentrations, J. Chem. Phys., 53, 4532, 1970.
- Welge, K. H., Photolysis of  $O_x$ ,  $HO_x$ ,  $CO_x$  and  $SO_x$  compounds, Can. J. Chem., 52, 1424, 1974.
- Wiebe, H. A. and G. Paraskevopoulos, The effect of the excess kinetic energy of the  $O(^1D)$  atoms from the flash photolysis of  $N_2O$  on their reaction with  $N_2O$ , Can. J. Chem., 52, 2165, 1974.
- Wiesenfeld, J. R., Effect of diabatic correlation on the reactions of  $O(2^3P, 2^1D)$  with  $N_2O$  and  $CO_2$ , Chem. Phys. Lett., 45, 384, 1977.
- Yamazaki, H. and R. J. Cvetanović, Isotope exchange of the excited oxygen atoms with  $CO_2^{18}$  and their collisional deactivation, J. Chem. Phys., 40, 582, 1964.
- Young, R. A. and G. Black, Deactivation of  $O(^1D)$ , J. Chem. Phys., 47, 2311, 1967.
- Young, R. A., G. Black and T. G. Slanger, Reaction and deactivation of  $O(^1D)$ , J. Chem. Phys., 68, 989, 1968.

# THE MESOSPHERIC AND STRATOSPHERIC ABSORPTION

## OF THE SOLAR ULTRAVIOLET RADIATION

Marcel Nicolet

External Geophysics, Brussels University, 1180 Brussels, Belgium

### Abstract

Solar radiation at Lyman-alpha (121,6 nm) and at wavelengths greater than 175 nm is absorbed in the mesosphere and stratosphere by molecular oxygen and ozone. A description is given of the photodissociation processes resulting from absorption in the Schumann-Runge bands and Herzberg continuum of molecular oxygen and also in the Hartley, Huggins and Chappuis bands of ozone. Special consideration is given to differences between the stratospheric and mesospheric problems related to the absorption processes.

INTRODUCTION: In order to study the photochemical action of solar radiation on stratospheric and mesospheric constituents, the solar spectrum must be divided in special ranges related to the molecular oxygen and ozone absorptions. The radiation of wavelengths less than 100 nm is absorbed by nitrogen and oxygen in the thermosphere; it leads, essentially, to ionization processes and is, therefore, not considered here. Only X-rays of wavelengths less than 1 nm (Figure 1) can penetrate into the atmosphere below 100 km, and lead indirectly to the dissociation of molecular constituents. Figures 2 and 3, which are graphs of absorption cross sections versus wavelengths, show that the values vary from about  $10^{-19} \text{ cm}^2$  at 1 nm to less than  $10^{-25} \text{ cm}^2$  at 0.001 nm. Absorption of X-rays by  $\text{N}_2$  and  $\text{O}_2$  (air) is an indication of the ultraviolet absorption possibilities. Figure 4 illustrates the X-ray absorption between 10 and 1 nm, i.e., the absorption cross section behavior which leads, for values greater than  $10^{-19} \text{ cm}^2$ , to an atmospheric absorption above 100 km.

The radiation of wavelengths less than 242 nm is absorbed by molecular oxygen and leads to its photodissociation. However, the principal photodissociation continuum ( $\text{O}_2$  Schumann-Runge continuum) at wavelengths less than 175 nm with an absorption cross section greater than  $10^{-19} \text{ cm}^2$  is absorbed in the thermosphere and can be neglected in the study of the mesosphere and stratosphere. But, at shorter wavelengths, an important solar line, Lyman-alpha at 121,6 nm, is situated in a so-called atmospheric window where the  $\text{O}_2$  absorption cross section is only of the order of  $10^{-20} \text{ cm}^2$ . Such a radiation is absorbed in the mesosphere and can, therefore, play a role in the photodissociation processes.

The second important spectral range, between 200 nm and 175 nm, is related to the  $\text{O}_2$  Schumann-Runge band system which includes 18 bands, (2-0) to 19-0), subject to the predissociation process. In this spectral region, the mean absorption cross sections are a function of the temperature and number of  $\text{O}_2$  absorbing molecules. The absorption, which is essentially a mesospheric process, also plays a role in various stratospheric photodissociations.

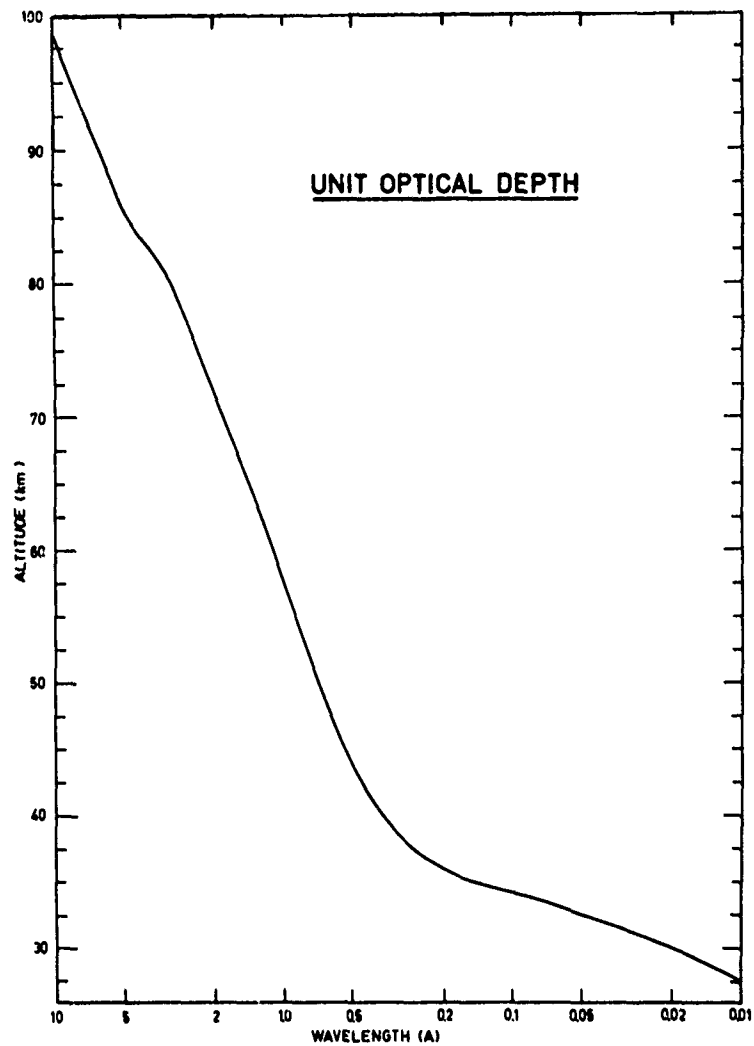


Figure 1. - Penetration of radiation of wavelengths less than 1 nm as represented by the absorption unit optical depth in a vertical column versus height.

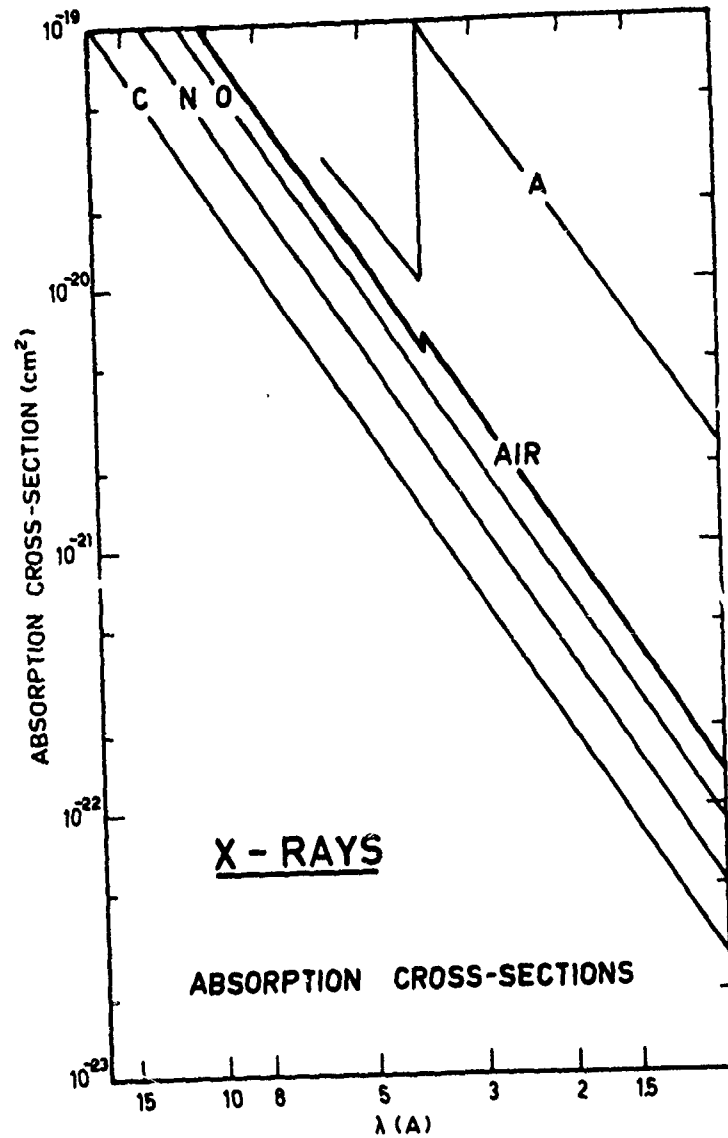


Figure 2. - X-ray absorption cross sections between 1.5 nm and 0.1 nm. Such cross sections lead essentially to a mesospheric absorption for wavelengths between 0.5 and 0.1 nm.

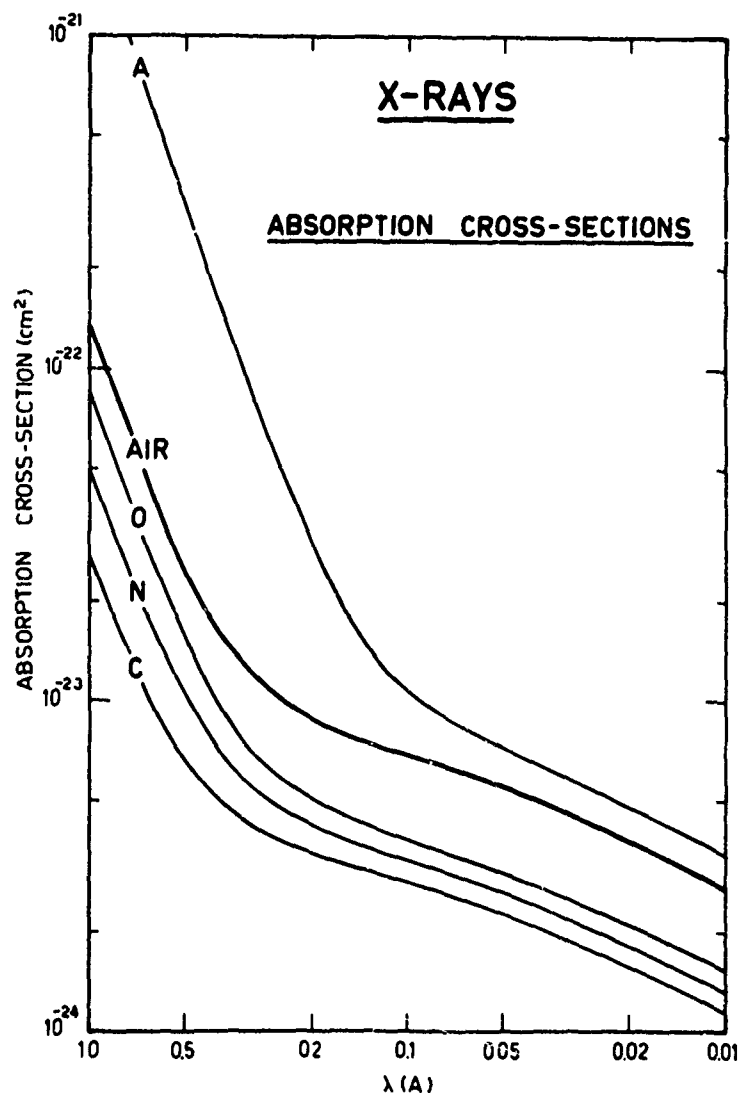


Figure 3. - X-ray absorption cross sections for wavelengths less than 0.1 nm. Such cross sections lead to a stratospheric absorption for an overhead radiation.

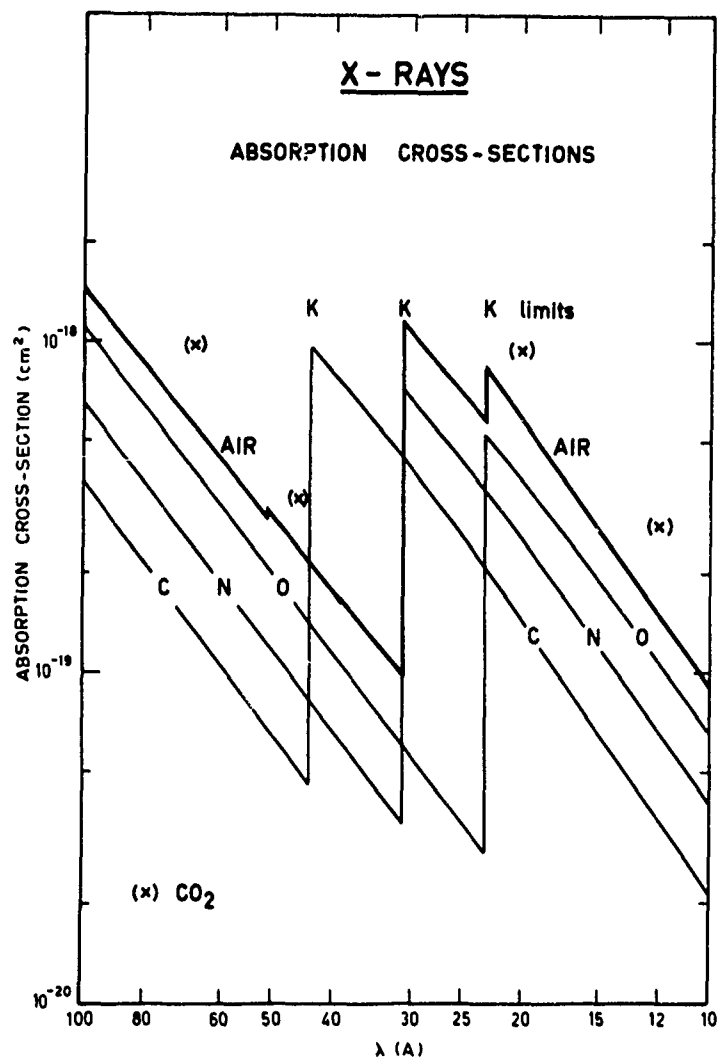


Figure 4. - X-ray absorption cross sections between 10 nm and 1 nm.  
Such cross sections lead to an absorption above 100 km.

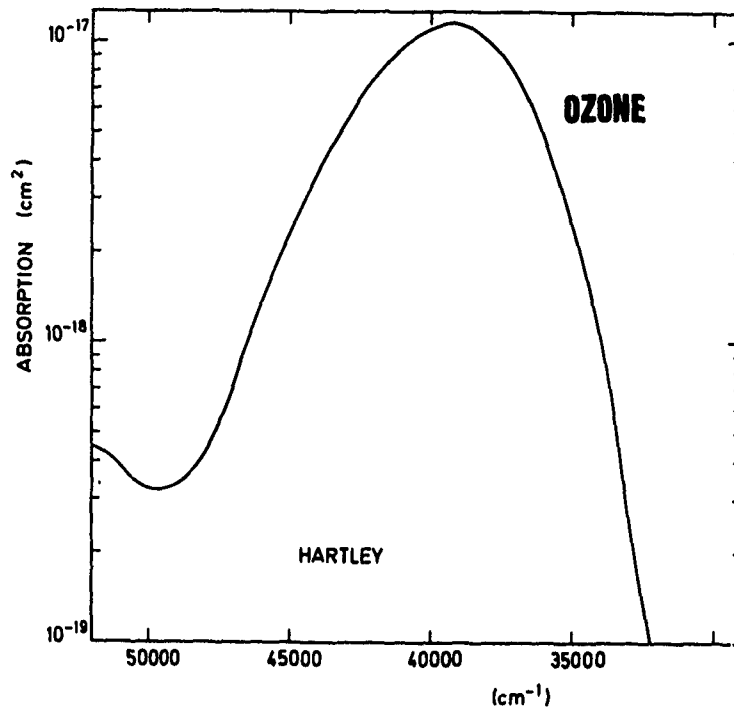


Figure 5: - Ozone absorption cross sections at wavelengths greater than 200 nm with a peak of the order of  $10^{-17}$  cm<sup>2</sup> near 250 nm.

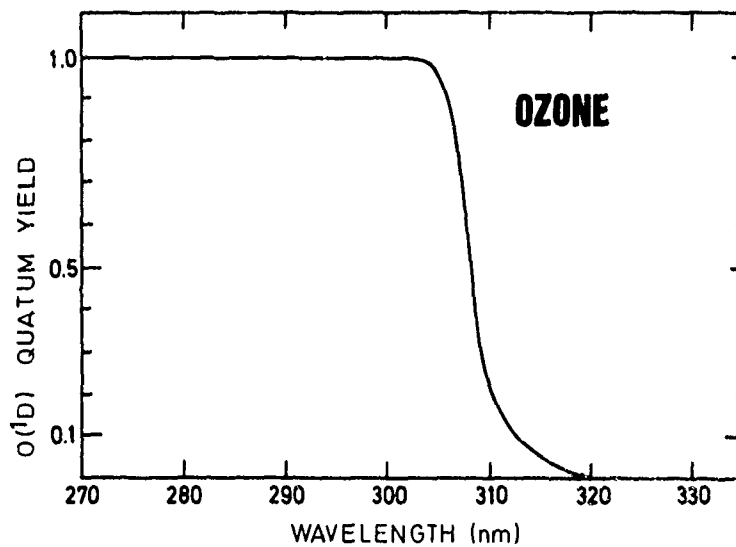


Figure 6. - Production of O(<sup>1</sup>D) atoms by ozone photodissociation at wavelengths less than 320 nm in the Hartley band.



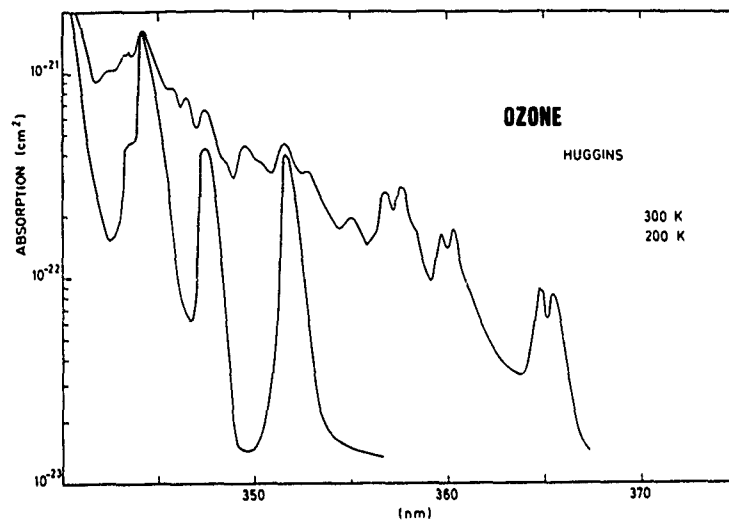


Figure 7. - Absorption cross section in the  $O_3$  Huggins bands at two temperatures. The upper curve at 300 K, and lower curve at 200 K, illustrate the temperature effect on the absorption cross section.

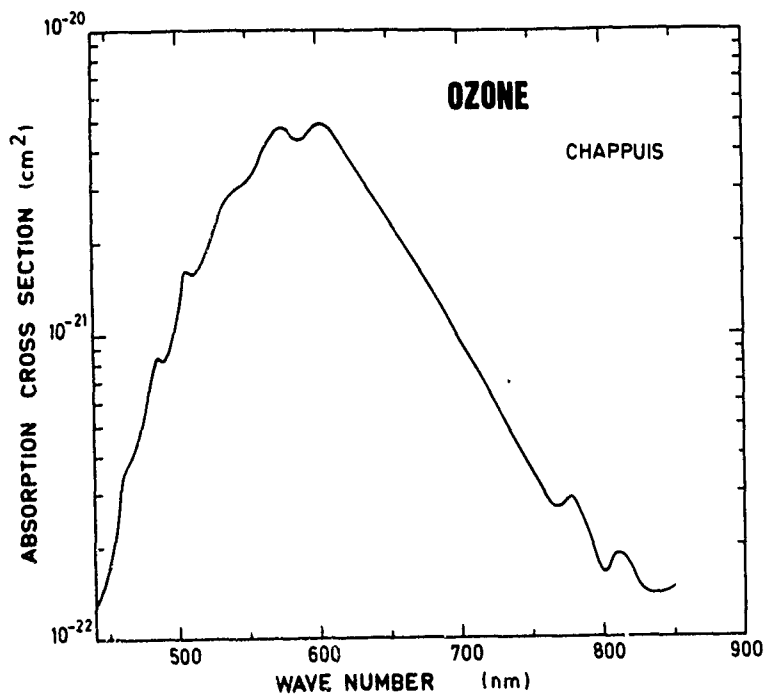
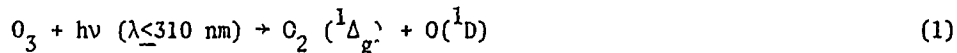


Figure 8. - Absorption cross section of the  $O_3$  Chappuis band in the visible part of the spectrum.

From 200 to 242 nm, the  $O_2$  absorption, which is related to the Herzberg continuum with low absorption cross sections from  $10^{-24}$  to  $10^{-25}$  cm<sup>2</sup>, occurs in the stratosphere (Figure 3). In addition, the ozone absorption must be introduced since the spectral region belongs to the spectral range of the  $O_3$  Hartley band with high values of the absorption cross sections (Figure 5). The simultaneous absorption by  $O_2$  and  $O_3$  must be considered in the stratosphere. In the mesosphere, the  $O_3$  absorption is practically negligible since the total number of ozone molecules is very small for low solar zenith angles.

At wavelengths less than 310 nm, corresponding to the  $O_3$  Hartley band, the ozone molecule has its principal absorption which occurs in the stratosphere. Its limit near 310 nm must be determined with precision, since the photodissociation process in the Hartley band, which is, (Figure 6),



leads to the production of  $O(^1D)$  atoms responsible, particularly below 50 km, for the production of OH from  $H_2O$ ,  $CH_4$  and  $H_2$  and also of NO from  $N_2O$ .

At wavelengths greater than 310 nm, the  $O_3$  Huggins bands (Figure 7) correspond to the limit of its ultraviolet absorption. The spectral range to be considered should be between 310 nm and 400 nm since it also corresponds to various limits of the absorption spectrum of  $H_2O_2$ ,  $H_2CO$ ,  $NO_2$ ,  $N_2O_5$ ,  $HNO_2$ ,  $HNO_3$ ,  $ClONO_2$ ,  $HOCl$ , ...

In the visible region (410-850 nm), the Chappuis bands (Figure 8) play an important role leading to the  $O_3$  photodissociation in the lower part of the atmosphere, troposphere and lower stratosphere.

At wavelengths greater than 300 nm, various effects such as the Rayleigh scattering and the albedo must be introduced. In particular, the photodissociation rates of  $O_3$ , ratio  $n(O)/n(O_3)$ , of  $NO_2$ , ratio  $n(NO_2)/n(NO)$ , and the absolute concentration of the other constituents absorbing in that spectral region are strongly affected by the Rayleigh scattering and albedo effects.

Thus, the photodissociation problem is related to a knowledge of the solar flux and its possible variations in certain spectral regions, the exact determination of the vertical distribution of the atmospheric optical depth of  $O_2$  and  $O_3$ , the measurement of the absorption cross-sections and photodissociation quantum yields for each constituent, and the introduction of the atmospheric conditions related to the radiation scattering and albedo.

THE SOLAR FLUX. In the spectral range of wavelengths greater than 175 nm, which is involved in mesospheric, stratospheric and tropospheric photodissociation processes, it has not yet been possible to identify solar flux variations associated with specific solar activity phenomena, if we consider the rocket and balloon observations published before 1979.

First, fluctuations of the solar constant  $S = 137 \pm 1 \text{ mW cm}^{-2}$  have not been established by direct absolute measurements; only a few atmospheric phenomena have been associated with the bi-annual variation of 6.6% in flux due to the variations of the earth-to-sun distance variation (Figure 9).

The maximum solar flux occurs in the first week of January while the minimum occurs 6 months later in the first week of July. The value at the mean earth-to-sun distance is equivalent to an effective temperature of  $5785 \pm 15 \text{ K}$  for the solar photosphere. This temperature is the absolute temperature  $T_s$  of a black body derived from the Stefan-Boltzman equation corresponding to the case in which Planck's law is applied to the entire spectrum with a dilution factor,  $\beta_s$ , of

$$\beta_s = R^2 / 4 r^2 = 5.4 \times 10^{-6} \quad (2)$$

where R represents the solar radius and  $r$  denotes the mean earth-to-sun distance. With the variation of that distance,  $\beta_S = 5.59 \times 10^{-6}$  in January and  $\beta_S = 5.23 \times 10^{-6}$  in July.

The solar radiation which reaches the upper atmosphere corresponds to the whole solar disk which is characterized in the visible region by a strong center to limb darkening (Figure 10). At the center of the disk the brightness temperature of the solar continuum is of the order of 7000 K while the mean solar brightness (at 550 nm) is of the order of 6000 K (Figure 10). However, the brightness temperature decreases in the infrared and in the ultra-violet as it is illustrated by the black body curves at 6000, 5800 and 5000 K. The variation with wavelength of the brightness temperature depends strongly on the opacity due to absorption lines of various solar constituents.

Figure 11 which is the result of an analysis made by Vernazza, Avrett and Loeser (1976), illustrates the variation of the brightness temperature associated with the variation with wavelength of the opacity. The various contributions to the photospheric opacity correspond not only to the different solar atoms with their different lines but also, in the region of wavelengths greater than 300 nm, to the band-free absorption of negative ion of hydrogen,  $H^-$ . The bound-free absorption of SiII plays a role at wavelengths less than 170 nm. Magnesium and aluminum with their band-free absorption are prominent at wavelengths less than 250 nm and 210 nm, respectively. In addition to these various contributions to the solar opacity, all atomic lines must be considered particularly in the spectral range between 200 nm and 450 nm.

Thus, it is not easy to predict the effect of active regions (solar plages) in the spectral ranges of the AlI and MgI edges and, therefore, the possible variations of the solar flux with solar activity for wavelengths greater than 175 nm. For these reasons, the spectral flux distributions, which have been obtained in various spectral regions, must be regarded as approximate values. In other words, the variability with solar cycle associated with differences in the absolute solar fluxes is within the observational errors for the spectrum of wavelengths greater than 175 nm, i.e., for the solar radiation absorbed in the mesosphere and stratosphere.

If we consider a variation of the effective solar temperature, there will be a variation of the solar constant S. A variation of the order of +15 K leads to  $S = 137 \pm 1 \text{ mW cm}^{-2}$ , corresponding to about +1%; but a variation of +50 K would correspond to about +3.5%. However, such a variation (Figure 12) would lead to differences of +20% in the solar flux at 175 nm, +10% at 250 nm and +5% at 350 nm. Unfortunately, since one still commonly finds differences (Figure 13) that are as large as 20% in comparing observational results from different experimenters, it is not possible to determine the accuracy of absolute calibration, the precision in each spectral range and the real fluctuations due to solar activity.

LYMAN-ALPHA. Only Lyman-alpha at 121.6 nm shows a clear evidence of an association of its intensity with solar activity controlled by identified chromospheric plages; see Vidal-Madjar, 1975, 1977. It is evident that a more precise absolute calibration of the total Lyman-alpha line flux is still required. On the other hand, the profile measurements (Tousely, 1963; Bruner and Parker, 1969; Bruner and Rense, 1969; Lemaire et al., 1978; Artzner, 1978) indicate that the solar global profile is a variable average profile whose form is determined by various solar features between the center and the limb. These are influenced by solar activity.

Hence, a mean value of  $3 \times 10^{11} \text{ photons cm}^{-2} \text{ sec}^{-1}$  for the Lyman-alpha solar flux at the mean earth-to-sun distance is almost a conventional value, since its accuracy cannot be better than +25%. If we write, at the top of the earth's atmosphere,

$$q (\text{Lyman-alpha}) = (3 \pm 1) \times 10^{11} \text{ photons cm}^{-2} \text{ sec}^{-1} \quad (3)$$

we may consider  $3 \times 10^{11} \text{ photons cm}^{-2} \text{ sec}^{-1}$  as a minimum working value and  $9 \times 10^{11} \text{ photons cm}^{-2} \text{ sec}^{-1}$  as an acceptable maximum value corresponding to quiet sun and active solar conditions, respectively. There is, therefore, a minimum variation of a factor of the order of 2 to 3 over a solar cycle. As far as the variations of the Lyman-alpha intensity associated with short-term fluctuations (27 day., for example) are concerned, it seems reasonable to use as an indication the preliminary empirical relations established by Vidal-Madjar (1975).

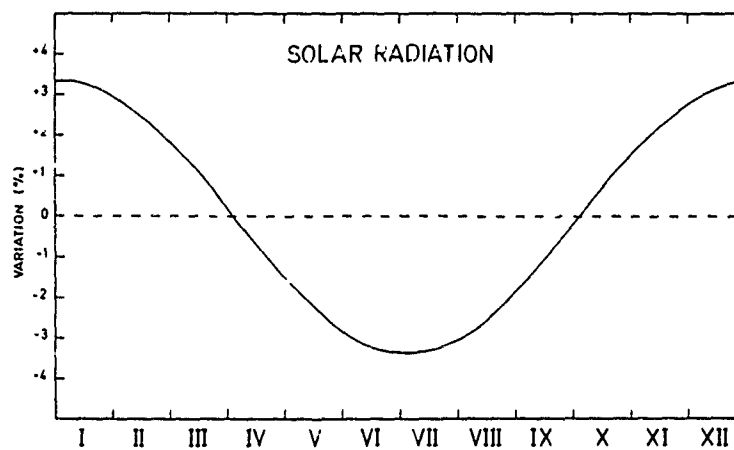


Figure 9. - Variations of the solar flux with the earth-to-sun distance variation. Maximum variation 6.6% in six months.

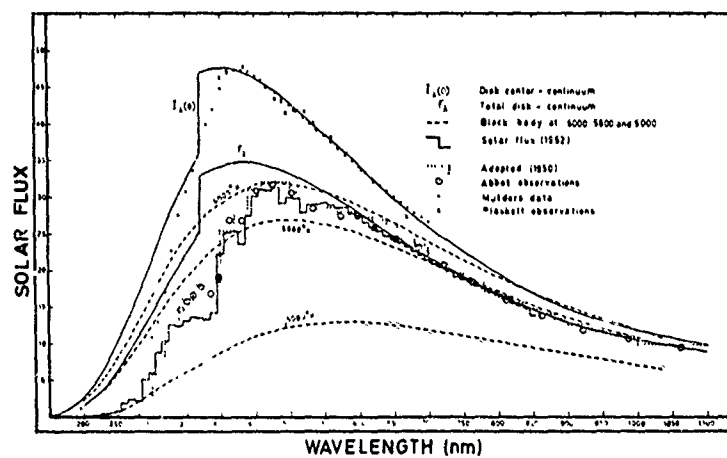


Figure 10. - Solar radiation at the center of the solar disk (continuum spectrum), for the total disk (continuum), and with the effect of solar absorption lines. Black body curves at 6000, 5800 and 5000 K for comparison with the observed fluxes.

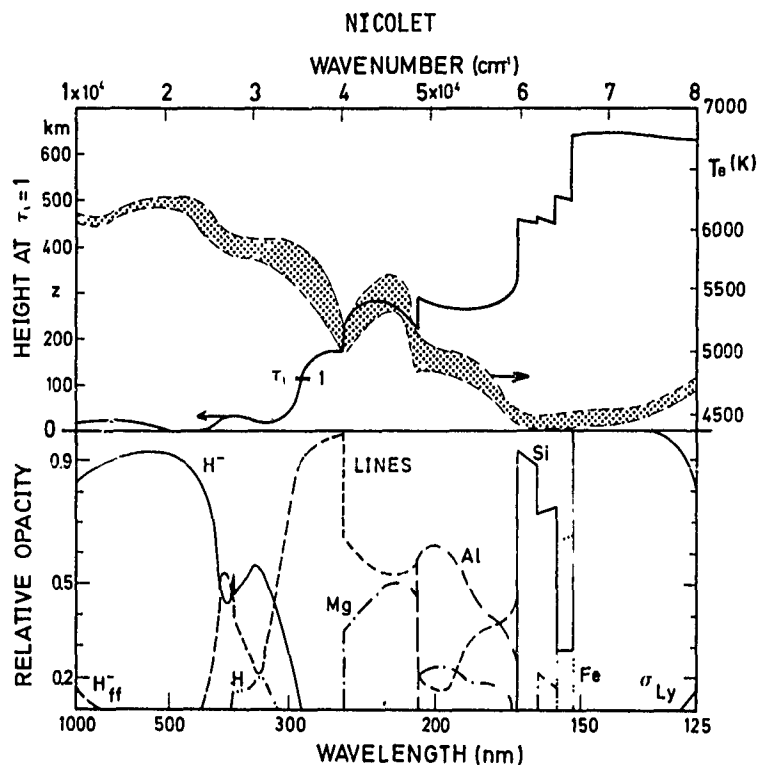


Figure 11. - Continuum brightness temperatures (lower and upper limits) at the disk center with the height of the unit optical depth (0 km for 500 nm). Relative opacities due to the H, Si, Al, Mg and Fe neutral atom bound face absorptions. Lines correspond to the effect of lines opacity.

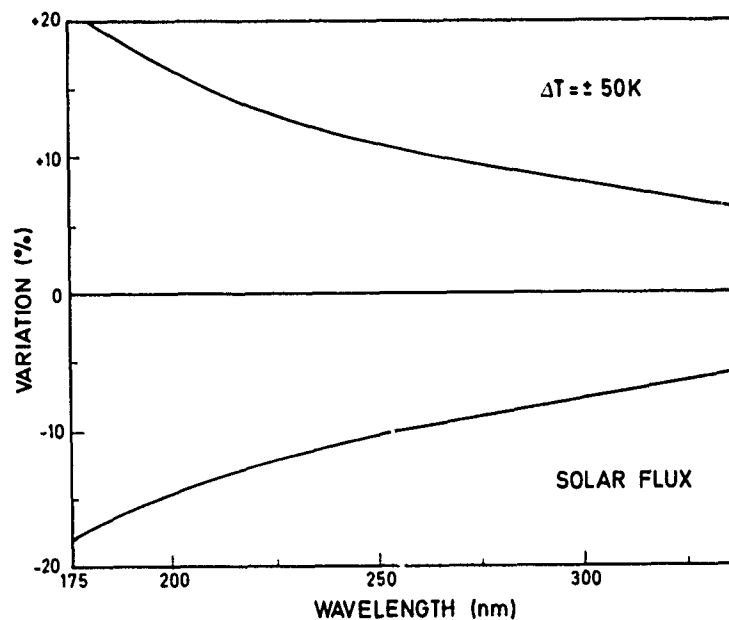


Figure 12. - Determination of the variation of the number of the solar photons versus wavelength for a hypothetical variation of 50 K of the radiation solar temperatures. Variations of about +20% at 175 nm to +5% at 350 nm and 3,5% for the solar constant.

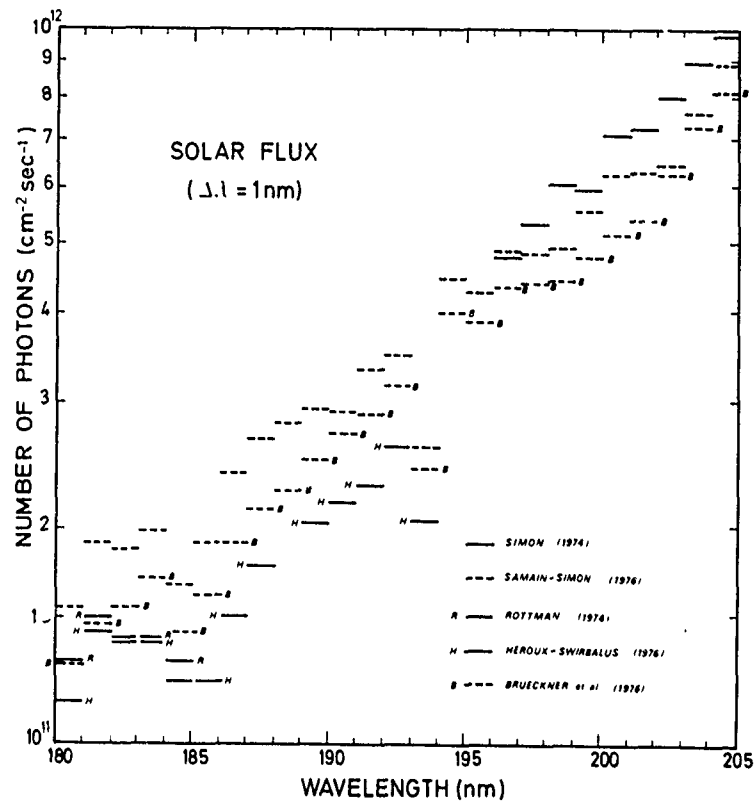


Figure 13. - Mean values of the solar flux for spectral ranges of 1 nm between 205 nm and 180 nm absorbed in the terrestrial atmosphere by the  $\text{O}_2$  Schumann-Runge bands.

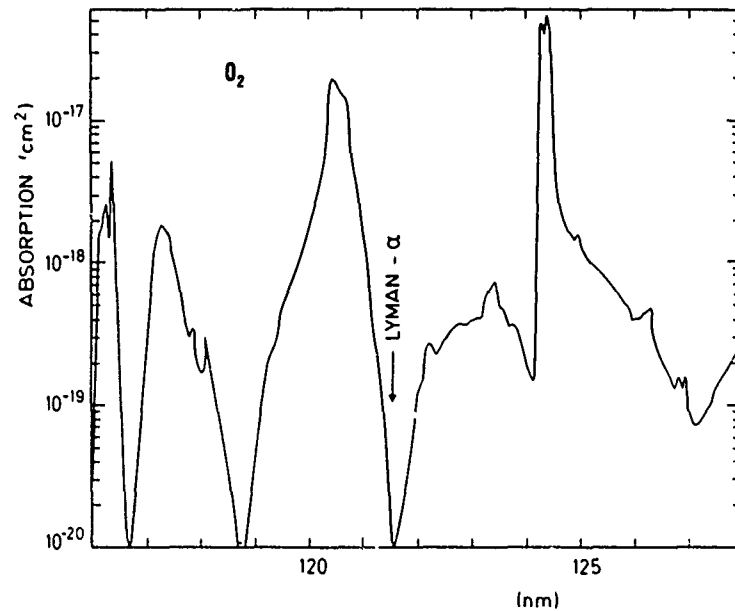


Figure 14. - Absorption of Lyman-alpha by molecular oxygen.

Lyman-alpha, which is absorbed in the atmosphere by molecular oxygen with a low cross section of the order of  $10^{-20} \text{ cm}^2$  (Figure 14), can penetrate into the mesosphere. But its absorption between two absorption bands depends on the temperature as illustrated by Figure 15, showing the laboratory results obtained by Carver et al., (1977). Adopting an average temperature of 190 K, it is possible to deduce an atmospheric absorption cross section related to the total number of  $\text{O}_2$  molecules (Figure 16) and also to deduce a simple formula for the absorption cross section and the optical depth. It is possible to write

$$\tau_{\text{L}\alpha}(\text{O}_2) = 4.17 \times 10^{-19} N(\text{O}_2)^{0.917} \quad (4)$$

corresponding to a varying cross section

$$\sigma_{\text{L}\alpha}(\text{O}_2) = 4.17 \times 10^{-19} N^{-0.083} \quad (5)$$

for  $N(\text{O}_2) > 1 \times 10^{19} \text{ cm}^{-2}$ .

For  $N(\text{O}_2) \leq 10^{19} \text{ cm}^{-2}$ , the conventional formula

$$J = \sigma q_{\infty} e^{-\tau} \quad (6)$$

can be adopted with

$$\sigma_{\text{L}\alpha}(\text{O}_2) = 1 \times 10^{-20} \text{ cm}^2 \quad (7)$$

For  $N(\text{O}_2) > 1 \times 10^{19} \text{ cm}^2$ , we write, therefore,

$$J_2(\text{L}\alpha) = q_{\infty} 4.17 \times 10^{-19} N^{-0.083} e^{-4.17 \times 10^{-19} N^{0.917}} \quad (8)$$

where  $q_{\infty}$  is the number of photons ( $\text{cm}^{-2} \text{ sec}^{-1}$ ) available at the top of the earth's atmosphere and  $N = N(\text{O}_2) \text{ cm}^{-2}$ , the total number of absorbing molecules.

The action of Lyman-alpha is particularly important for the photodissociation of  $\text{H}_2\text{O}$  and of  $\text{CO}_2$ . For these two molecules the Lyman-alpha photodissociation rate (Figure 17) corresponds to more than 70% of the total rate for  $N(\text{O}_2) \leq 2.5 \times 10^{19} \text{ cm}^{-2}$  (Nicolet, 1979) and must be considered as the principal contributor to their mesospheric dissociation, which will depend strongly on solar activity.

Even for molecular oxygen, Lyman-alpha leads to an important effect in addition to the dissociation processes resulting from absorption in the  $\text{O}_2$  Schumann-Runge band and Herzberg continuum ranges. Table I indicates that above 70 km, for an overhead sun, Lyman-alpha increases the  $\text{O}_2$  photodissociation rate by about 30% under average conditions. This percentage will vary with solar activity which will introduce variations of the  $\text{O}_2$  photodissociation in the upper mesosphere.

We consider, therefore, that the Lyman-alpha flux variations with solar activity are the maximum possible differences that can occur in the solar flux at wavelengths greater than 100 nm. Furthermore, there is no other astrophysical phenomena leading to such variations at wavelengths greater than 175 nm, except for a few emission lines of relatively low intensity which may be associated with solar plagues. A relatively recent review by Heath and Thekaekara (1977), which describes various observational results obtained between 1964 and 1975, would indicate the possibility of a variation of a factor of the order of 2 at 200 nm and not less than +10% at 300 nm. On the other hand, Simon (1978) and Delaboudinière et al. (1978) do not reach the conclusion that there is any such variability during the 11 year cycle. The new full-disk solar spectral irradiances at high solar activity (June 1979) obtained by Mount, Rottoman and Timothy (to be published, 1980) indicate a small increase of about 20% near 180 nm and no increase within their measurement errors (+15%) at 200 nm.

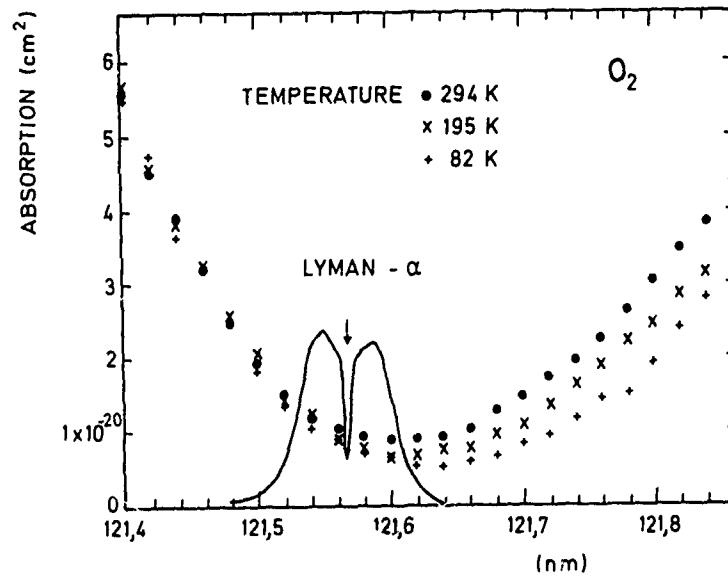


Figure 15. - Temperature effect on the  $O_2$  absorption cross section in the spectral region of solar Lyman-alpha.

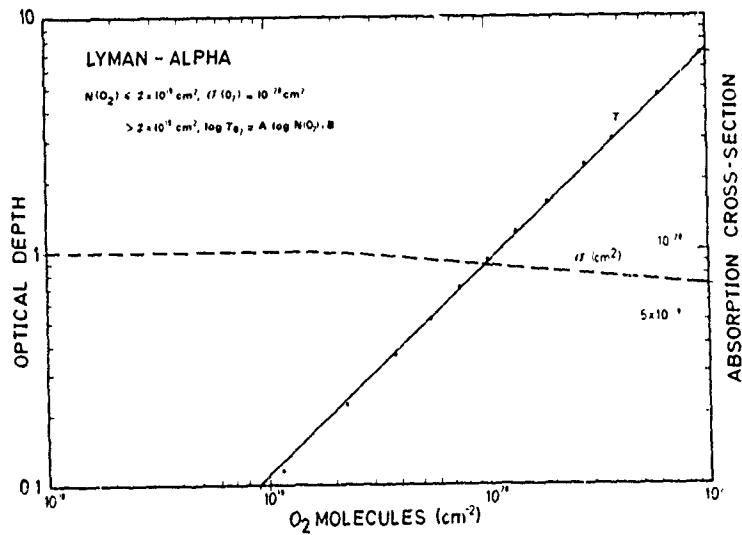


Figure 16. - Variation of the  $O_2$  optical depth and absorption cross section at Lyman-alpha.



TABLE I. - Effect of the Lyman-alpha radiation on the  $O_2$  photodissociation rate

$N(O_2)$	$J(\text{Lyman-alpha})^{(*)}$ ( $\text{sec}^{-1}$ )	$J_2(\text{total})^{(*)}$ ( $\text{sec}^{-1}$ )
$1.0 \times 10^{19}$	$2.72 \times 10^{-9}$	$1.80 \times 10^{-8}$
2.5	2.33	1.12
5.0	1.82	$7.44 \times 10^{-9}$
7.5	1.41	5.79
$1.0 \times 10^{20}$	1.10	4.80
2.5	$7.0 \times 10^{-10}$	2.97
5.0	$4.5 \times 10^{-11}$	1.75
7.5	$8.0 \times 10^{-12}$	1.41

(\*) only examples, since variations with solar activity

In fact, if we examine the observational results obtained in the ultraviolet region from the first rocket measurements to the latest observational results, we can see that there is a systematic decrease over the years in the published values of this solar ultraviolet flux.

TABLE II. - Solar flux at the top of the earth's atmosphere in the spectral range of the  $O_2$  Schumann-Runge bands

$O_2$ Band	$\text{Photons}(\text{cm}^{-2}\text{sec}^{-1})$		$O_2$ Band	$\text{Photons}(\text{cm}^{-2}\text{sec}^{-1})$	
	Minimum	Maximum		Minimum	Maximum (1979)
19-0	$2.47 \times 10^{10}$	$3.17 \times 10^{10}$	10-0	$3.15 \times 10^{11}$	$3.39 \times 10^{11}$
18-0	3.09	3.60	9-0	3.45	3.52
17-0	4.45	5.21	8-0	3.40	3.67
16-0	5.46	6.96	7-0	4.75	4.99
15-0	7.59	9.20	6-0	5.40	5.87
14-0	$1.05 \times 10^{11}$	$1.23 \times 10^{11}$	5-0	6.73	6.46
13-0	1.27	1.61	4-0	7.89	7.13
12-0	1.45	1.88	3-0	$1.13 \times 10^{12}$	$1.06 \times 10^{12}$
11-0	2.03	2.54	2-0	1.35	1.25

Furthermore, if we consider only the more recent observational data (Figure 13) in the spectral range of the  $O_2$  Schumann-Runge band system (Rottman, 1974; Simon, 1975; Samain and Simon, 1976; Heroux and Swirbalus, 1976; Brueckner et al., 1976), it is clear that the estimated precision in the flux measurement is of the order of +20%. Thus, any mean value adopted for this spectral region reflects the lack of accuracy resulting from the dubious character of absolute calibrations, and also from the limited precision due to various uncertainties in laboratory and atmospheric measurements in this spectral region.

Consequently, it must be conceded that any solar activity effect leading to a possible variation of the solar flux cannot as yet be distinguished from differences between various observations, even if they have been analyzed after discussion between observers. There is no clear indication leading to an accurate choice for mean or specific values of the solar flux in this spectral region leading to the  $O_2$  photodissociation. The adopted numerical values given in Table II are deduced from more recent rocket observations by Mount, Rottman and Timothy (to be published, 1980) for relatively quiet conditions and high solar activity (June 1979). There is a clear indication that the general solar activity effect is not important near 200 nm but begins in the spectral range of the Schumann-Runge bands which are absorbed in the mesosphere.

Several atmospheric measurements have been made (see Simon, 1978) in the region of the  $O_2$  Herzberg continuum at wavelengths less than 242 nm. The values adopted in 1978 are based essentially on data published by Broadfoot (1972) and Simon (1975) and are given in Table III for 500  $\text{cm}^{-1}$  spectral ranges. But the recent values obtained in June 1979 by Mount, Rottman and Timothy (1980) are systemically lower by an average factor of about 1.5. It is important to note (see Figure 18) that there is a remarkable discontinuity near 210 nm due to the Aluminium I ionization threshold, corresponding to a variation in the average radiation temperature of more than 200 K. The temperature increases from about 4700 K near 200 nm to about 5100 K near 210 nm, i.e., an increase of the order of a factor of 5 in the solar flux.

NICOLET

TABLE III. - Mean values of solar flux (photons  $\text{cm}^{-2}\text{sec}^{-1}$ ) at the top of the earth's atmosphere in the spectral range of the  $\text{O}_2$  Herzberg continuum. Average wavelength in  $\text{\AA}$  for a  $\pm 250 \text{ cm}^{-1}$  spectral range

Wavelength	Photons	New Data	Wavelength	Photons	New Data
2010	$1.44 \times 10^{12}$	$1.23 \times 10^{12}$	2209	$1.22 \times 10^{13}$	$7.46 \times 10^{12}$
2030	1.80	1.46	2234	1.77	$1.71 \times 10^{13}$
2051	2.08	1.71	2259	1.60	$9.62 \times 10^{12}$
2072	2.45	2.18	2286	1.96	$1.03 \times 10^{13}$
2094	5.09	3.67	2312	1.97	1.20
2116	7.12	5.84	2339	1.70	1.02
2139	9.23	6.29	2367	2.00	1.20
2162	8.42	6.31	2395	1.77	1.02
2186	$1.20 \times 10^{13}$	8.01	2424	1/2 (2.56)	$7.59 \times 10^{12}$

In order to avoid certain discrepancies between various observational data, particularly in the spectral region 300-400 nm (see DeLuigi, 1975; Simon, 1978), we have adopted, in the spectral region covered by the Hartley band from 242 nm to 310 nm, rocket data by Broadfoot (1972) with the values obtained by balloon measurements (Simon, 1975) at wavelengths greater than 284 nm. These values (Nicolet, 1975) are given in Table IV for  $500 \text{ cm}^{-1}$  spectral ranges. They are also illustrated in Figure 19 which shows radiation temperatures between 4800 and 5500 K.

TABLE IV. - Solar flux (photons  $\text{cm}^{-2}\text{sec}^{-1}$ ) at the top of the earth's atmosphere in the spectral range of the  $\text{O}_3$  Hartley band. Average wavelength in  $\text{\AA}$  for a  $\pm 250 \text{ cm}^{-1}$  spectral range

Wavelength	Photons	New Data	Wavelength	Photons
2424	$2.58 \times 10^{13}$	$1.64 \times 10^{13}$	2721	$1.17 \times 10^{14}$
2454	2.35	1.60	2759	1.11
2484	2.38	1.61	2797	$7.85 \times 10^{13}$
2516	2.28	1.35	2837	$1.50 \times 10^{14}$
2547	3.24		2877	2.12
2580	5.83		2919	3.56
2614	4.89		2963	3.33
2649	$1.19 \times 10^{14}$		3007	3.08
2684	1.29		3053	4.39

Furthermore, in the ultraviolet region, corresponding to the Huggins bands, it is necessary to introduce in the numerical values a smooth transition from about 300 nm, in the range of the spectral limit of observational data obtained by Broadfoot (1972), to 400 nm where the solar flux data obtained by Arvesen et al., (1969) can be accepted if the published values are reduced to a lower solar constant value (Nicolet, 1975). Such data for spectral ranges of 5 nm are given in Table V and illustrated in Figure 20. New measurements of the solar flux between 300 nm and 400 nm would be useful in helping to improve the accuracy of absolute values.

TABLE V. - Solar flux (photons  $\text{cm}^{-2}\text{sec}^{-1}$ ) at the top of the earth's atmosphere in the spectral range of the  $\text{O}_3$  Huggins bands and  $\text{NO}_2$  absorption. Average wavelengths in A for a  $\pm 2.5$  nm spectral range

Wavelength	Photons	Wavelength	Photons
3100	$4.95 \times 10^{14}$	3600	$8.23 \times 10^{14}$
3150	5.83	3650	$1.07 \times 10^{15}$
3200	6.22	3700	1.08
3250	6.96	3750	9.72
3300	8.61	3800	1.11
3350	8.15	3850	8.98
3400	8.94	3900	1.18
3450	8.44	3950	9.34
3500	8.69	4000	1.69
3550	9.14	4050	1.70

Finally, the solar flux, which is adopted in the visible region, corresponds to the numerical values adjusted to the present value of the solar constant (Nicolet, 1975) and deduced also from observational data published by Arvesen et al., (1969). They are given in TABLE VI for spectral ranges of 5 nm and are of the order of  $2 \times 10^{15}$  photons  $\text{cm}^{-2}\text{sec}^{-1}$ .

TABLE VI. - Solar flux (photons  $\text{cm}^{-2}\text{sec}^{-1}$ ) at the top of the earth's atmosphere in the spectral range of the  $\text{O}_3$  Chappuis bands. Average wavelength in A for a  $\pm 2.5$  nm spectral range

Wavelength	Photons	Wavelength	Photons	Wavelength	Photons
400	$1.69 \times 10^{15}$	550	$2.53 \times 10^{15}$	700	$2.58 \times 10^{15}$
405	1.70	555	2.54	705	2.52
410	1.84	560	2.50	710	2.51
415	1.97	565	2.57	715	2.48
420	1.95	570	2.58	720	2.45
425	1.81	575	2.67	725	2.48
430	1.67	580	2.67	730	2.45
435	1.98	585	2.70	735	2.44
440	2.02	590	2.62	740	2.39
445	2.18	595	2.69	745	2.40
450	2.36	600	2.63	750	2.41
455	2.31	605	2.68	755	2.40
460	2.39	610	2.66	760	2.38
465	2.38	615	2.59	765	2.34
470	2.39	620	2.69	770	2.32
475	2.44	625	2.61	775	2.30
480	2.51	630	2.62	780	2.33
485	2.30	635	2.62	785	2.34
490	2.39	640	2.63	790	2.29
495	2.48	645	2.60	795	2.29
500	2.40	650	2.55	800	2.27
505	2.46	655	2.48	805	2.27
510	2.49	660	2.57	810	2.20
515	2.32	665	2.61	815	2.22
520	2.39	670	2.61	820	2.18
525	2.42	675	2.62	825	2.20
530	2.55	680	2.62	830	2.14
535	2.51	685	2.57	835	2.14
540	2.49	690	2.52	840	2.13
545	2.55	695	2.60	845	2.09
				850	2.05

**MOLECULAR OXYGEN ABSORPTION.** The absorption cross-section (Figure 21) in the Herzberg continuum is known with an accuracy of less than 20% (Nicolet, 1979). At wavelengths greater than 230 nm, the  $O_2$  cross-section is not known with sufficient precision. But since the ozone absorption is maximum in this part of the ultraviolet spectrum, the numerical error is reduced for the value of the total  $O_2$  photodissociation rate. Table VII shows the values that we have adopted for the mean absorption cross section. These are based on the experimental data of Ditchburn and Young (1962), Ogawa (1971), Hasson and Nicholls (1971) and Shardanand and Rao (1977). They increase from about  $10^{-24} \text{ cm}^2$  at 240 nm to  $1.5 \times 10^{-23} \text{ cm}^2$  at 200 nm, but this last value involves the 0-0 and 0-1 Schumann-Runge band absorption. The resulting  $O_2$  photodissociation coefficient from identical energy spectral ranges ( $500 \text{ cm}^{-1}$ ) shows a rapid increase from 240 nm to 230 nm (Table VII) and also a decrease at wavelengths less than 210 nm as it is illustrated in Figure 22 in which values should be decreased by about 1.5.

**TABLE VII.** -  $O_2$  photodissociation coefficients ( $\text{sec}^{-1}$ ) at the top of the earth's atmosphere with the absorption cross sections ( $\text{cm}^2$ ) adopted for spectral ranges of  $500 \text{ cm}^{-1}$ . Average wavelength in Å for  $+250 \text{ cm}^{-1}$ .

Wavelength	Absorption	Dissociation	Wavelength	Absorption	Dissociation
2010	$1.50 \times 10^{-23}$	$1.84 \times 10^{-11}$	2209	$5.50 \times 10^{-24}$	$4.10 \times 10^{-11}$
2030	1.25	1.83	2234	4.75	5.75
2051	1.00	1.71	2259	4.05	3.90
2071	$9.80 \times 10^{-24}$	2.14	2286	3.35	3.45
2094	9.20	3.38	2312	2.70	3.24
2116	8.50	4.96	2339	2.20	2.24
2139	7.85	4.94	2367	1.6	1.98
2162	7.05	4.45	2395	1.20	1.22
2186	6.15	4.93	2424	0.75	$5.69 \times 10^{-12}$

The problem of the  $O_2$  photodissociation in the Schumann-Runge band spectral range, as well as its atmospheric absorption, has not yet attained a final solution. This is due to the fact that its rotational structure depends on the temperature and the average cross section also depends strongly on the number of  $O_2$  absorbing molecules. (Figure 23 and 24). After various applications of the first experimental results to the atmosphere (Hudson, Carter, Freig, 1969; Kockarts, 1971, 1976; Hudson and Mahle, 1972; Fang, Wofsy and Dalgarno, 1974; Park, 1974; Muramatsu, 1975; Shimazaki, Ogawa and Farrell, 1977), new experimental and theoretical results (Lewis, Carver, Hobbs, McCoy and Gies, 1978, 1979; Frederick and Hudson, 1979; Nicole and Peetermans, 1979) show that still more attention should be given to the accuracy problem.

There is general agreement on the molecular constants used for the  $O_2$  Schumann-Runge bands (see Fang, Wofsy and Dalgarno, 1974) as known from the experimental data obtained by Ackerman and Biamé (1970) and by Brix and Herzberg (1954). These have been analyzed for the fine structure of the upper level by Bergeman and Wofsy (1972). Additional measurements with still higher resolution would be useful. But precise oscillator strengths and linewidths associated with exact line positions are an absolute necessity for accurate determination of the photodissociation processes, particularly in the mesosphere.

From a comparative analysis (Nicolet and Peetermans, 1979) of the various parameters involved in the atmospheric  $O_2$  absorption, it can be concluded that there is no important direct effect of the Schumann-Runge band absorption on the total  $J_2$  value in the stratosphere. If the ratio (Figure 25) of the photodissociation rate  $J_{\text{SRB}}$ , which results from the Schumann-Runge band spectral range to the total photodissociation rate  $J_{\text{SRB-HERC}}$ , also resulting from the Herzberg continuum spectral region, is greater than 80% for a total number of  $O_2$  absorbing molecules  $N(O_2)$  greater than  $10^{10} \text{ cm}^{-2}$ ; it is only between 10 and 15% in the major part of the stratosphere. Furthermore, the essential fraction of this low percentage is due to bands corresponding to  $v_1'$  less than 10. The (2-0), (3-0), (4-0), (5-0), (6-0) and (7-0) bands lead for  $N(O_2) = 5 \times 10^{11} \text{ cm}^{-2}$  (stratopause neighbourhood) to about 3, 3, 2.5, 1.5 and 1.5%; respectively. Thus the total error due to incorrect parameters in the Schumann-Runge band system cannot account for the importance of the stratospheric  $J_2$  value. On the other hand, any solar activity effect which might be introduced in the calculation of these  $J_2$  values for wavelengths less than 200 nm could play only a minor role, corresponding to its 15% contribution, to the stratospheric photodissociation of molecular oxygen.

In the mesosphere, all Schumann-Runge bands between (2-0) and (19-0) must be considered. As an example, for  $N(O_2)=10^{20} \text{ cm}^{-2}$ , at and above 75 km, the (7-0) band corresponds to the maximum of the order of 10% while (2-0) and (15-0) have a less significant role, only between 1 and 2%.

In order to keep the same type of formula for the photodissociation of all constituents, we write for a molecule XY ( $O_2$  or  $H_2O$ , for example)

$$J_{XY} = \sum j_{XY} = \sum q_{\infty XY} e^{-\tau(O_2)} e^{-\tau(O_3)} \quad (9)$$

where  $q_{\infty}$  is the average number of photons ( $\text{cm}^{-2} \text{ sec}^{-1}$ ) at the top of the earth's atmosphere for the spectral range being considered,  $\sigma_{XY}$  is the photodissociation cross section adapted to such a spectral range. This can be a mean value for certain constituents but may depend on the temperature and number of molecules ( $O_2$  and NO for example);  $\tau(O_2)$  and  $\tau(O_3)$  are the optical depths for  $O_2$  and  $O_3$ , respectively. The ozone optical depth is related to a mean absorption cross section  $\sigma(O_3)$  which does not play a significant role in the mesosphere since the total number of  $O_3$  molecules is too small. The molecular oxygen optical depth involves an absorption cross section depending on the temperature and number of absorbing molecules. Thus, the first problem is the determination of the  $O_2$  absorption behavior which can lead to general numerical mean values of the optical depth.

We write for a mean optical depth adapted to a Schumann-Runge band

$$e^{-\tau(O_2)} = \frac{1}{n} \sum_{i=1}^n \exp[-\tau_i(O_2)] = \frac{1}{n} \sum_{i=1}^n \exp[-\sigma_i(T) N(O_2)] \quad (10)$$

which gives mean values,  $\overline{\tau(O_2)}$  and  $\overline{\sigma(O_2)}$ , which depend on the temperature and total number of  $O_2$  absorbing molecules. Formula (10) leads to a maximum average value

$$\sigma_M(T) = \frac{1}{n} \sum_{i=1}^n \sigma_i(T) \quad (11)$$

when  $N(O_2) \rightarrow 0$ , and to a minimum value

$$\sigma_m(T) = [\sigma_i(T)]_{\text{minimum}} \quad (12)$$

which corresponds to the smallest value of  $\sigma_i$  in the adopted spectral range, when  $N(O_2) \rightarrow \infty$  (TABLE VIII).

TABLE VIII. - Mean absorption cross section for  $O_2$  Schumann-Runge bands for  $T=230 \text{ K}$ . Maximum and minimum values (and ratios) corresponding to formulas 11 and 12; respectively

Band	Maximum	Minimum	Ratio
19-0	$7.52 \times 10^{-20}$	$1.02 \times 10^{-21}$	$7.3880 \times 10^1$
18-0	$1.41 \times 10^{-19}$	7.16	1.9728
17-0	1.72	4.13	4.1529
16-0	1.64	3.40	4.8345
15-0	1.44	1.37	$1.0523 \times 10^2$
14-0	1.28	$4.60 \times 10^{-22}$	2.7870
13-0	$9.91 \times 10^{-20}$	3.43	2.8864
12-0	7.14	6.01	1.1881
11-0	4.91	4.40	1.1177
10-0	3.17	1.01	3.1472
9-0	2.02	$8.81 \times 10^{-23}$	2.2935
8-0	1.17	8.27	1.4100
7-0	$6.06 \times 10^{-21}$	3.12	1.9402
6-0	2.86	1.82	1.5684
5-0	1.16	1.51	$7.6922 \times 10^1$
4-0	$4.05 \times 10^{-22}$	1.42	2.8497
3-0	1.29	1.31	$9.8410 \times 10^0$
2-0	$3.88 \times 10^{-23}$	1.25	3.1069

Formula 11 can be used, since it gives an average value without any atmospheric absorption to make a comparison between various computations. Differences observed, Nicolet and Peetermans (1979), correspond to differences in experimental parameters (linewidth and oscillator strength) and also in the formulation for the representation of the  $O_2$  optical depth. It is, therefore, clear that the errors will not diminish with increasing optical depths. Their importance may be limited not only through the compensating effect of positive and negative differences of all bands but also by a neutralizing action resulting from the weight of other spectral ranges in the value of the total photodissociation rate.

To determine the  $O_2$  photodissociation with formula (9), Nicolet and Peetermans (1979) first made a complete computation for each  $O_2$  Schumann-Runge band by integrating a cross section with  $0.5 \text{ cm}^{-1}$  resolution and using a Voigt profile at  $T = 190 \text{ K}$ ,  $230 \text{ K}$ ,  $270 \text{ K}$  and  $300 \text{ K}$ . The detailed results have been analyzed in order to give the mean value of  $\sigma(O_2)$  represented by  $\sigma_{xy}$  in formula (9), and also a different value ( $O_2$ ) used for the mean optical depth  $\tau(O_2)$ . With these definitions, we write for each band

$$\overline{\sigma(O_2)} = \Sigma \sigma(O_2) e^{-\tau(O_2)} / \Sigma e^{-\tau(O_2)} \quad (13)$$

and

$$\overline{\sigma(O_2)} = - \frac{1}{N(O_2)} \ln e^{-\tau(O_2)} \quad (14)$$

We can express the variation of  $\overline{\sigma(O_2)} \equiv \sigma_e(O_2)$  with  $T$  and  $N(O_2)$  by the following formula

$$\sigma_e(O_2) = \sigma_m [\sigma_M / \sigma_m]^{1 + \frac{1}{p}} \quad (15)$$

where  $\sigma_M$  and  $\sigma_m$  are the maximum and minimum photodissociation cross sections defined in (11) and (12), respectively;  $p$  is an expression given by the polynomial function

$$p = \Sigma P_i [\ln N(O_2)]^i \quad (16)$$

A simple formula with only 2 terms

$$p_2 = p_{2,0} + p_{2,1} \ln N(O_2) \quad (17)$$

can be used for the atmospheric calculations. In any case, a precise determination has been obtained with a formula with six terms.

Similarly, the transmission related to the mean optical depth  $\overline{\tau(O_2)}$  is defined as follows:

$$\exp [-\tau(O_2)] = \exp [-e^{+d}] \quad (18)$$

where  $d$  is given by another polynomial function

$$d = \sum_0^n d_i (\ln N)^i \quad (19)$$

leading to  $\overline{\tau(O_2)}$ , with two terms, to the simple form

$$\ln \tau(O_2) = d_2 \equiv d_{2,0} + d_{2,1} \ln N(O_2) \quad (20)$$

The numerical values of all these parameters are listed in Table IX for 230K and each Schumann-Runge band. Examples of the final results are given in Table X and illustrated in Figure 26. It is clear that the distribution of the photodissociation among the various bands is a direct function of the altitude, i.e., of the total number of absorbing  $O_2$  molecules. The principal bands, which play the leading role ( $v' \leq 8$ ) in the stratospheric absorptions related to all photodissociation processes, must be studied with the best values which are now available, and the  $O_2$  stratospheric photodissociation coefficients are certainly less affected by systematic errors than constituents for which the total photodissociation rate is almost equally subdivided between the spectral ranges of wavelengths less or greater than

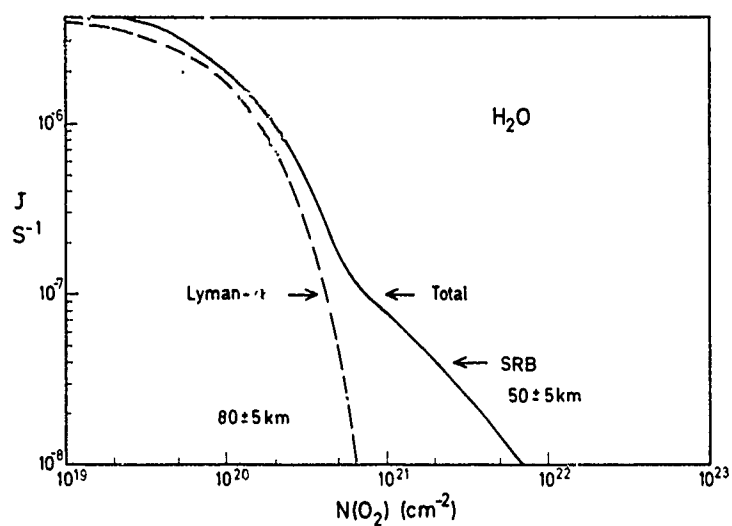


Figure 17. - Photodissociation of  $\text{H}_2\text{O}$  mainly due in the upper mesosphere to the Lyman-alpha absorption process.

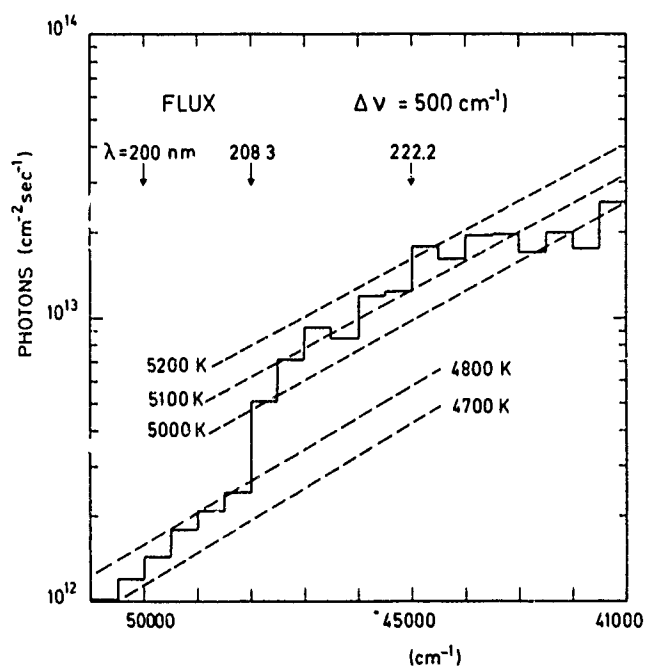


Figure 18. - Solar flux in the spectral range of the  $\text{O}_2$  Herzberg continuum.

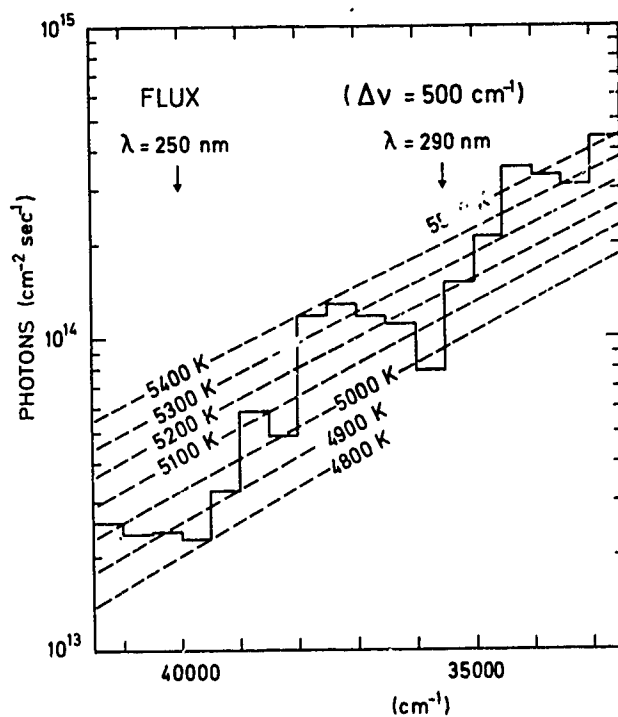


Figure 19. - Solar Flux in the spectral range of the  $O_3$  Hartley band.

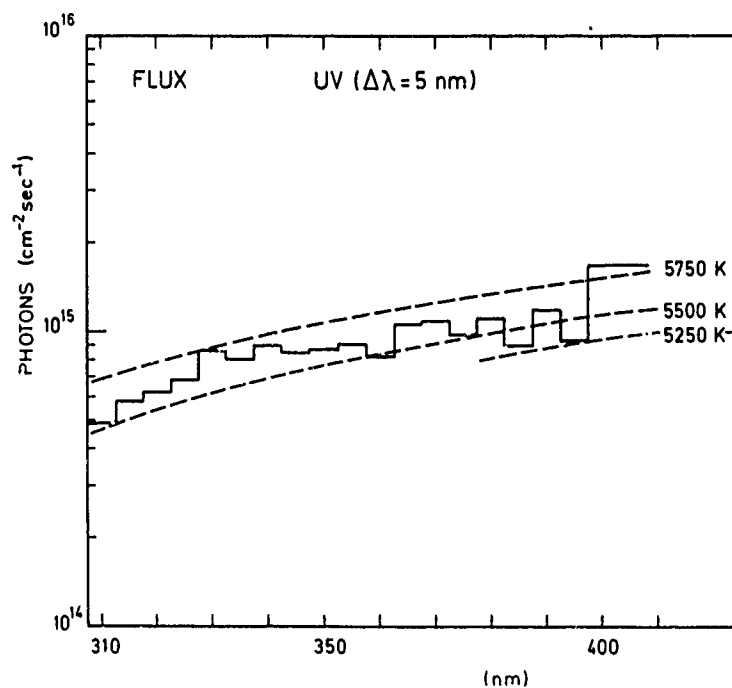


Figure 20. - Solar flux in the ultraviolet region of the spectrum reaching ground level.



TABLE IX. - Parameters for the calculation of the optical depth and photodissociation rates of molecular oxygen in the Schumann-Runge spectral range.

Band	$P_{2,0}$	$P_{2,1}$	$d_{2,0}$	$d_{2,1}$
19-0	-27.3660	0.5977	-20.511	0.4552
18-0	-31.1405	0.7022	-27.0032	0.6070
17-0	-31.5985	0.7086	-21.5692	0.4874
16-0	-28.2548	0.6337	-22.9975	0.5160
15-0	-27.0726	0.6043	-21.2109	0.4684
14-0	-19.5698	0.4363	-22.3230	0.4808
13-0	-18.5631	0.4154	-26.4881	0.5608
12-0	-23.3420	0.5187	-25.4172	0.5442
11-0	-27.2023	0.5917	-21.9458	0.4739
10-0	-20.3744	0.4415	-24.1133	0.5009
9-0	-22.6718	0.4876	-23.2161	0.4803
8-0	-25.3106	0.5374	-23.4269	0.4848
7-0	-25.6943	0.5381	-24.7619	0.5012
6-0	-24.8725	0.5169	-25.3433	0.5042
5-0	-27.1231	0.5570	-30.5188	0.6000
4-0	-34.5348	0.7014	-33.6523	0.6549
3-0	-34.1537	0.6929	-40.7366	0.7827
2-0	-30.5893	0.6222	-48.8488	0.9304

200 nm. It can be seen from the data listed in Table XI that the simple formulas with the parameters given in Table IX lead to a satisfactory agreement with the results of the complete and detailed calculation.

TABLE X. -  $O_2$  photodissociation rates. Effect of the Schumann-Runge band system. Total percentage; percentage for (2-0), (5-0), (10-0) and (15-0) bands from 175 to 200 nm and from 175 to 242 nm, respectively.

$N(O_2)$ ( $cm^{-2}$ )	J(SRB) $J_{SRB-HERC}$	Band (2-0)	Band (5-0)	Band (10-0)	Band (15-0)
$10^{18}$	98	0.1	1.6	9.3	8.7
$10^{19}$	95	0.1	1.6	9.3	8.7
$10^{20}$	79	0.4	4.5	8.4	5.7
$2.5 \times 10^{20}$	66	0.4	4.2	8.0	5.4
$5 \times 10^{20}$	33	1.9	10.7	8.4	2.3
$10^{21}$	39	1.5	8.5	6.6	1.8
$2.5 \times 10^{21}$	23	3.7	12.2	7.9	1.3
$5 \times 10^{21}$	16	2.5	8.0	5.2	0.8
$10^{22}$	14	5.3	13.0	7.3	0.7
$2.5 \times 10^{22}$	12	2.8	6.8	3.8	0.4
$5 \times 10^{22}$	12	8.0	13.8	6.4	0.3
$10^{23}$	12	3.1	5.3	2.5	0.1
$2.5 \times 10^{23}$	12	13.3	14.9	4.8	--
$5 \times 10^{23}$	12	3.1	3.5	1.1	--
$10^{24}$	1	18.8	15.0	3.1	--
		3.0	2.4	0.3	--
		26.5	13.9	1.4	--
		3.5	1.9	0.2	--
		38.4	10.4	0.2	--
		4.8	1.3	--	--
		48.9	6.9	--	--
		6.0	0.8	--	--
		59.7	3.6	--	--
		7.2	0.4	--	--
		86.7	--	--	--
		0.7	--	--	--

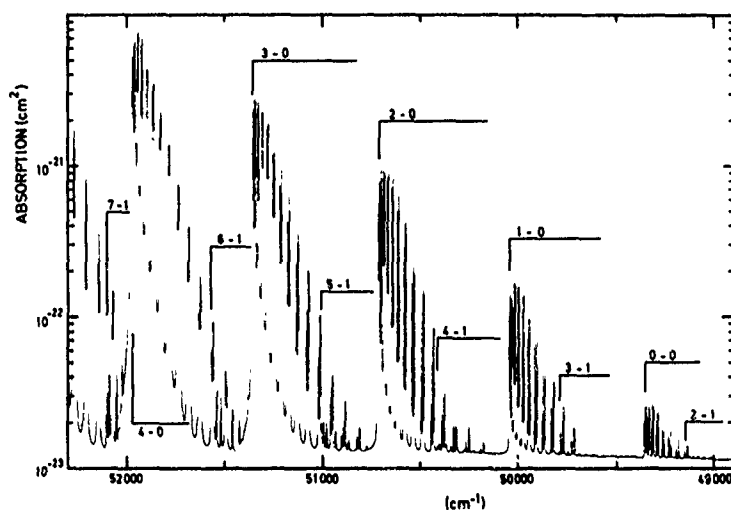


Figure 23. - Rotational structure of the  $O_2$  Schumann-Runge bands (From Biauomé's thesis).

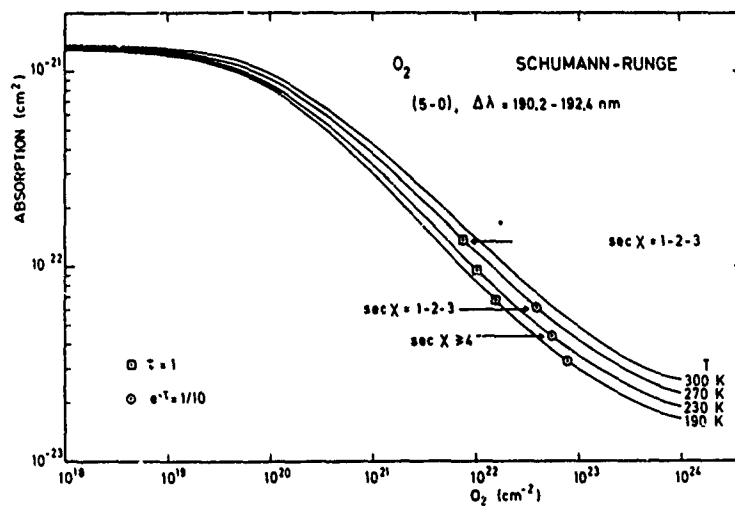


Figure 24. - Variation of the mean absorption cross sections for the (5-0) band of the  $O_2$  Schumann-Runge system with temperature (190 K to 300 K) and the total number of  $O_2$  molecules ( $10^{18}$  to  $10^{19} \text{ cm}^{-2}$ ).

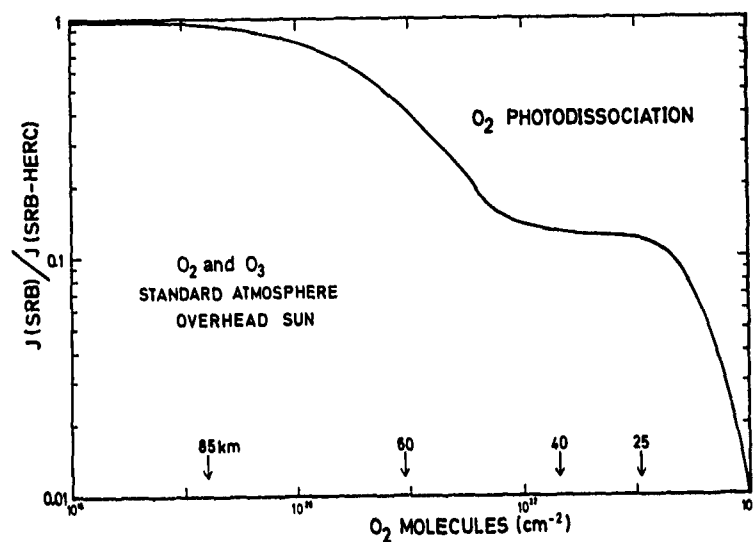


Figure 25. - Ratio of the  $O_2$  photodissociation rates in the atmosphere for spectral ranges corresponding to the Schumann-Runge bands (less than 200 nm) and to the Schumann-Runge bands and Herzberg continuum (less than 242 nm).

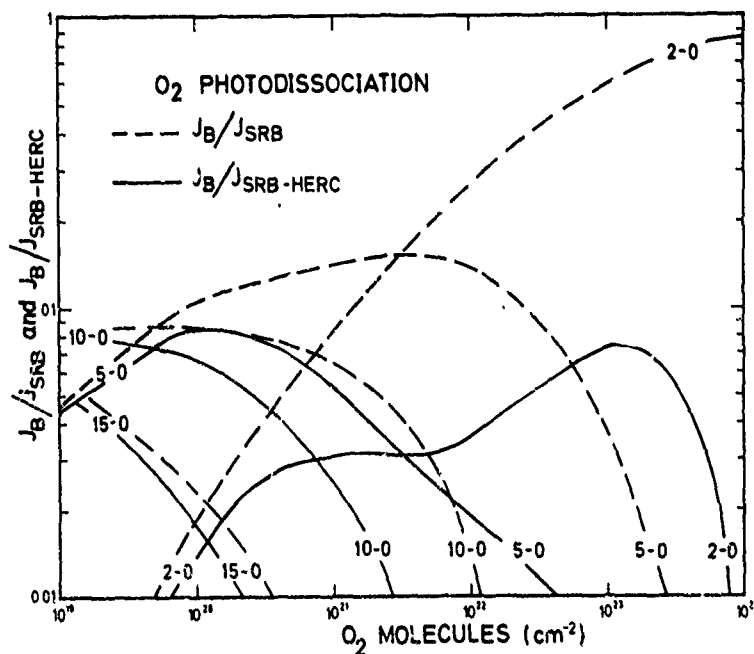


Figure 26. - Variation of the photodissociation coefficient of a Schumann-Runge band compared with the total photodissociation coefficient of the Schumann-Runge band system and of the Herzberg continuum with the Schumann-Runge band system, respectively.

TABLE XI. - Photodissociation rates of molecular oxygen for T = 230 K

N(O <sub>2</sub> ) (cm <sup>-2</sup> )	Detailed Calculation			Formula: 2 terms	
	Herzberg Continuum*	Schumann- Runge Bands	Total J(sec <sup>-1</sup> )	Schumann- Runge Bands	Total
1.0x10 <sup>19</sup>	8.38x10 <sup>-10</sup>	1.45x10 <sup>-8</sup>	1.53x10 <sup>-8</sup>	1.46x10 <sup>-8</sup>	1.54x10 <sup>-8</sup>
2.5	8.38	7.94x10 <sup>-9</sup>	8.78x10 <sup>-9</sup>	8.41x10 <sup>-9</sup>	9.25x10 <sup>-9</sup>
5.0	8.38	4.78	5.62	5.29	6.12
7.5	8.38	3.54	4.58	3.97	4.81
1.0x10 <sup>20</sup>	8.37	2.86	3.70	3.22	4.06
2.5	8.36	1.43	2.27	1.62	2.46
5.0	8.34	8.19x10 <sup>-10</sup>	1.65	9.40x10 <sup>-10</sup>	1.77
7.5	8.30	5.83	1.41	6.78	1.57
1.0x10 <sup>21</sup>	8.27	4.57	1.28	5.36	1.36
2.5	7.95	2.09	1.00	2.51	1.05
5.0	7.20	1.17	8.37x10 <sup>-10</sup>	1.41	8.62x10 <sup>-10</sup>
7.5	6.20	0.84	7.04	1.00	7.21
1.0x10 <sup>22</sup>	4.71	0.64	5.35	7.58x10 <sup>-11</sup>	5.46
2.5	2.16	0.27	2.43	3.02	2.47
5.0	8.35x10 <sup>-11</sup>	1.10x10 <sup>-11</sup>	9.45x10 <sup>-11</sup>	1.14	9.49x10 <sup>-11</sup>
7.5	4.17	0.54	4.71	5.38x10 <sup>-12</sup>	4.71
1.0x10 <sup>23</sup>	1.90	0.25	2.15	2.47	2.15
2.5	1.20x10 <sup>-12</sup>	0.11x10 <sup>-12</sup>	1.31x10 <sup>-12</sup>	1.11x10 <sup>-13</sup>	1.31x10 <sup>-12</sup>
5.0	4.61x10 <sup>-14</sup>	0.20x10 <sup>-14</sup>	4.81x10 <sup>-14</sup>	2.46x10 <sup>-15</sup>	4.85x10 <sup>-14</sup>
7.5	3.12x10 <sup>-15</sup>	0.06x10 <sup>-15</sup>	3.18x10 <sup>-15</sup>	1.02x10 <sup>-16</sup>	3.22x10 <sup>-15</sup>
1.0x10 <sup>24</sup>	2.50x10 <sup>-16</sup>	0.02x10 <sup>-16</sup>	2.52x10 <sup>-16</sup>	5.07x10 <sup>-17</sup>	2.56x10 <sup>-16</sup>

\*Effect of O<sub>3</sub> absorption introduced by the conventional model. These values must be decreased by the factor 1.5. The Herzberg continuum leads to  $J_{\infty}(O_2) = 5.7 \times 10^{-10} \text{ sec}^{-1}$ .

**OZONE PHOTODISSOCIATION:** The decrease of the ozone concentration with altitude is such that it is possible to neglect, for the determination of its photodissociation rate, the effect of the radiation absorption at wavelengths less than 200 nm. In the spectral region of the Hartley band, at wavelengths less than 310 nm, the absorption cross section as given by Ackerman (1971) and used by Nicolet (1975) can be adopted with the solar flux values listed in Tables III and IV. They are given in Table XII and the spectral distribution of the O<sub>3</sub> Hartley photodissociation rate at the top of the earth's atmosphere is illustrated in Figure 27. This shows the increase of the photodissociation with decreasing wavelength from 310 nm to 250 nm. But, there is again a problem in the determination of the photodissociation rate of ozone in the Herzberg continuum. A comparison (see Table XII) between the 1978 results and the new data obtained by Mount, Rottoman and Timothy in June 1979 from 200 nm to 250 nm leads to  $J_{\infty}(O_3) = 1.7 \times 10^{-3} \text{ sec}^{-1}$  and  $1.06 \times 10^{-3} \text{ sec}^{-1}$ , respectively. More full-disk solar spectral irradiance observations are needed between 200 and 300 nm.

The Huggins bands (Figure 28) play only a small part in the total O<sub>3</sub> photodissociation, but have, however, an important role in the absorption of solar absorption in the troposphere at wavelengths greater than 210 nm. It must be noted that the absolute absorption cross section depends on the temperature and the values of the parameters listed in Table XIII are not very precise. New laboratory determinations are needed.

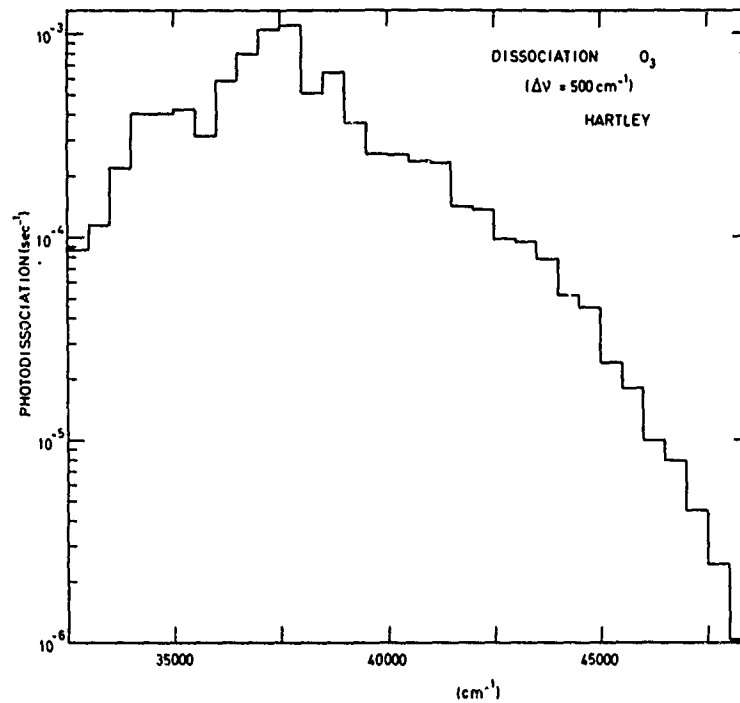


Figure 27. - O<sub>3</sub> photodissociation rates at the top of the earth's atmosphere for the mean earth-to-sun distance. Spectral ranges of 500 cm<sup>-1</sup> in the Hartley band.

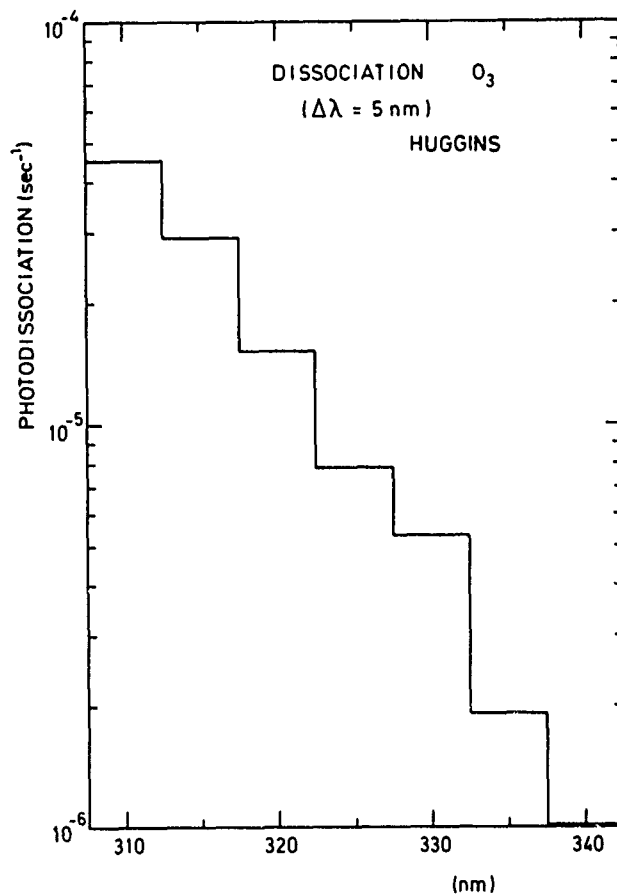


Figure 28. -  $O_3$  photodissociation rates at the top of the earth's atmosphere for the mean earth-to-sun distance. Spectral ranges of 5 nm in the Huggins bands.

NICOLET

**TABLE XII.** - Average cross section ( $\text{cm}^2$  for  $500 \text{ cm}^{-1}$ ) and  $\text{O}_3$  photodissociation coefficients ( $\text{sec}^{-1}$ ) at the top of the earth's atmosphere in the spectral ranges of the  $\text{O}_2$  Herzberg continuum and  $\text{O}_3$  Hartley band.

<u>Wavelength</u>	<u>Absorption</u>	<u>Dissociation</u>	<u>(New)</u>	<u>Wavelength</u>	<u>Absorption</u>	<u>Dissociation</u>	<u>(New)</u>
2010	3.26-19	4.69-07	4.01-07	2454	1.00-17	2.35-04	1.60-04
2030	3.26-19	5.87-07	4.76	2485	1.07-17	2.55-04	1.72
2051	3.51-19	7.30-07	6.00	2516	1.11-17	2.53-04	1.50
2072	4.11-19	1.01-06	8.96	2547	1.12-17	3.63-04	
2094	4.84-19	2.46-06	1.78-06	2580	1.11-17	6.46-04	
2116	6.26-19	4.46-06	3.66	2614	1.03-17	5.04-04	
2139	8.57-19	7.91-06	5.39	2649	9.43-18	1.12-03	
2162	1.17-18	9.85-06	7.38	2684	8.23-18	1.06-03	
2186	1.52-18	1.82-05	1.22-06	2721	6.81-18	7.97-04	
2209	1.97-18	2.40-05	1.47	2759	5.31-18	5.89-04	
2234	2.55-18	4.51-05	3.09	2797	3.99-18	3.13-04	
2259	3.24-18	5.18-05	3.12	2837	2.84-18	4.26-04	
2286	4.00-18	7.84-05	4.12	2877	1.92-18	4.07-04	
2312	4.83-18	9.52-05	5.80	2919	1.14-18	4.06-04	
2339	5.79-18	9.84-05	5.91	2963	6.60-19	2.20-04	
2367	6.86-18	1.37-04	8.23	3007	3.69-19	1.14-04	
2395	7.97-18	1.41-04	8.13	3053	1.97-19	8.65-05	
2424	9.00-18	2.32-04	1.48-04				

**TABLE XIII.** - Average cross section ( $\text{cm}^2$  for 5 nm) and  $\text{O}_3$  photodissociation coefficient ( $\text{sec}^{-1}$ ) in the spectral range of the  $\text{O}_3$  Huggins bands.

<u>Wavelength</u>	<u>Absorption</u>	<u>Dissociation</u>	<u>Wavelength</u>	<u>Absorption</u>	<u>Dissociation</u>
3100	1.05-19	5.20-05	3400	1.71-21	1.53-06
3150	5.23-20	3.05-05	3450	7.46-22	6.30-07
3200	2.91-20	1.81-05	3500	2.66-22	2.31-07
3250	1.50-20	1.04-05	3550	1.09-22	9.96-08
3300	7.78-21	6/70-06	3600	5.49-23	4.52-08
3350	3.72-21	3.03-06			

Finally, the Chappuis bands (Figure 29) in the visible part of the spectrum at wavelengths greater than 400 nm play an important part in the  $\text{O}_3$  photodissociation in the lower stratosphere and troposphere. Its total photodissociation rate of  $3.4 \times 10^{-4} \text{ sec}^{-1}$ , at the top of the earth's atmosphere is increased by the simultaneous effect of the Rayleigh scattering (10% for an overhead sun) and albedo (+35% for albedo = 0.25). The photodissociation rates for spectral ranges of 5 nm at the top of the earth's atmosphere are listed in Table XIV.

TABLE XIV.- Solar flux ( $q$  photons  $\text{cm}^{-2} \text{sec}^{-1}$ ) for spectral range of 5 nm  $\text{O}_3$  photodissociation coefficient ( $j$ ,  $\text{sec}^{-1}$ ) in the spectral range of the Chappuis bands.

nm	q	j	nm	q	j
400+25	$1.69 \times 10^{15}$		630+25	$2.62 \times 10^{15}$	$8.99 \times 10^{-6}$
405	1.70		635	2.62	8.31
410	1.84	$5.35 \times 10^{-8}$	640	2.63	7.21
415	1.97	6.19	645	2.60	6.79
420	1.95	7.78	650	2.55	6.17
425	1.81	$1.18 \times 10^{-7}$	655	2.48	5.46
430	1.67	1.14	660	2.57	5.19
435	1.98	1.71	665	2.61	4.83
440	2.02	2.25	670	2.61	4.36
445	2.18	3.25	675	2.62	4.03
450	2.36	4.04	680	2.62	3.72
455	2.31	4.90	685	2.57	3.21
460	2.39	8.53	690	2.52	2.82
465	2.38	8.76	695	2.60	2.65
470	2.39	9.70	700	2.58	2.37
475	2.44	$1.19 \times 10^{-6}$	705	2.52	2.12
480	2.51	1.78	710	2.51	1.93
485	2.30	1.94	715	2.48	1.73
490	2.39	1.98	720	2.45	1.54
495	2.48	2.25	725	2.48	1.41
500	2.40	2.93	730	2.45	1.29
505	2.46	3.99	735	2.44	1.16
510	2.49	3.93	740	2.39	1.07
515	2.32	3.71	745	2.40	1.01
520	2.39	4.25	750	2.41	$9.04 \times 10^{-7}$
525	2.42	5.01	755	2.40	7.80
530	2.55	6.50	760	2.38	6.95
535	2.51	6.88	765	2.34	6.46
540	2.49	7.17	770	2.32	6.26
545	2.55	7.83	775	2.30	6.44
550	2.53	8.02	780	2.33	6.64
555	2.54	8.53	785	2.34	2.90
560	2.50	9.70	790	2.29	5.04
565	2.57	$1.11 \times 10^{-5}$	795	2.29	4.17
570	2.58	1.20	800	2.27	3.70
575	2.67	1.27	805	2.27	3.97
580	2.67	1.21	810	2.20	4.18
585	2.70	1.17	815	2.22	4.11
590	2.62	1.16	820	2.18	3.71
595	2.69	1.24	825	2.20	3.34
600	2.63	1.29	830	2.14	3.04
605	2.68	1.30	835	2.14	3.00
610	2.66	1.21	840	2.13	2.98
615	2.59	1.10	845	2.09	2.97
620	2.69	1.05	850	2.05	2.97
625	2.61	$9.40 \times 10^{-6}$			



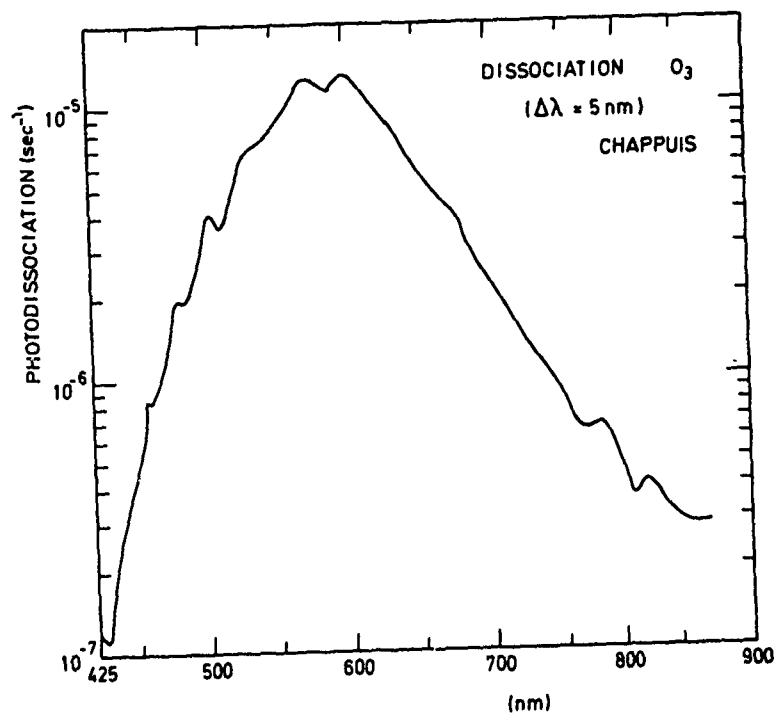


Figure 29. -  $O_3$  photodissociation rates at the top of the earth's atmosphere for the mean earth-to-sun distance. Spectral ranges of  $500\text{ cm}^{-1}$  in the Chappuis bands.

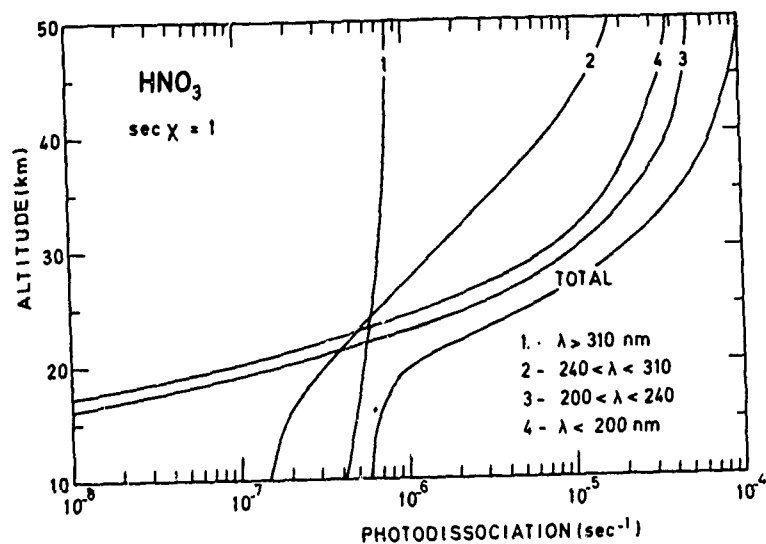


Figure 30. -  $HNO_3$  photodissociation in various spectral ranges corresponding to  $O_2$  and  $O_3$  absorption for overhead sun conditions.

In concluding this analysis of the absorption and dissociation of molecular oxygen and ozone, it must be noted that the photodissociation of all other constituents will depend on the absorption behavior of  $O_2$  and  $O_3$ . An example is illustrated in Figure 30. This shows the photodissociation rate of nitric acid in spectral ranges related to the  $O_2$  Schumann-Runge band system spectral range, the  $O_2$  Herzberg continuum and the  $O_3$  Hartley continuum. The spectral region of wavelengths greater than 310 nm will be subject to the effect of the Rayleigh scattering and albedo while the region of wavelengths less than 210 nm will depend only on the  $O_2$  and  $O_3$  absorption.  $HNO_3$  is a good example showing that all spectral ranges are involved in its stratospheric photodissociation with a variation of a factor of more than 100, between the stratopause and tropopause, of the photodissociation rate; i.e., from  $10^{-4}$  to less than  $10^{-6} \text{ sec}^{-1}$ .

$NO_2$  is an example showing that the absolute value of its photodissociation rate is related to atmospheric conditions since the absorption leading to its dissociation extends to 400 nm (Figure 31). The photodissociation coefficient at the top of the earth's atmosphere is  $0.75 \times 10^{-2} \text{ sec}^{-1}$ , but the Rayleigh scattering effect for overhead sun conditions leads, at 50 km and the whole atmosphere, to the value of  $1.1 \times 10^{-2} \text{ sec}^{-1}$ . This increases to  $1.25 \times 10^{-2} \text{ sec}^{-1}$  for an albedo of 0.25 and up to  $1.5 \times 10^{-2} \text{ sec}^{-1}$  for an albedo of 0.5. These values decrease, however, with the solar zenith angle. At  $60^\circ$ , the preceding values become  $1.0 \times 10^{-4}$ ,  $1.10 \times 10^{-4}$  and  $1.2 \times 10^{-4}$ , respectively. There is, therefore, an effect of the solar zenith angle on the photodissociation rates of constituents which absorb predominantly in the spectral region of wavelengths greater than 300 nm. This must be introduced in the atmospheric model calculations and is particularly important in the determination of the ratios  $n(O_3)/n(O)$  and  $n(NO_2)/n(NO)$  which depend on photodissociation conditions. It must also be kept in mind when comparisons are made between observations made under various conditions between noon and sunset or sunrise.

As previously mentioned, another part of the ultraviolet spectrum which requires a particular attention is Lyman alpha since it varies strongly with solar activity. The  $H_2O$  photodissociation illustrated in Figure 17 shows how the action of Lyman alpha plays the leading role in the upper mesosphere. The photodissociation of carbon dioxide is also strongly related to the Lyman alpha emission. For many other constituents, the spectral region of the  $O_2$  Schumann-Runge bands is of great importance, which varies according to the number of solar photons available in each band. Figure 32 illustrates the stratospheric behavior of the bands which are involved in the absorption of solar radiation.

The photodissociation of constituents such as nitrous oxide (Figure 33), and chlorofluorocarbons (Figures 34 and 35) depends on this absorption associated with the  $O_2$  absorption in the Herzberg continuum. The photodissociation of these various constituents in the upper stratosphere may be related to possibly different solar conditions in these two spectral regions. In any case, the results based on detailed and complete calculations and on the use of simplified formulas (18 to 20) have been verified and lead to the conclusion that formula (20) and parameters of Table IX can be adopted for numerical applications in the stratospheric models. The author has more detailed formulas (Nicolet and Peetermans, 1979) with six terms which can be applied for large optical depths.

But, the accuracy of any calculation depends primarily on the accuracy of the values of the solar flux and of the spectroscopic constants (oscillator strengths and line widths) of the  $O_2$  molecule. This is particularly important in the mesosphere where the Schumann-Runge bands play the leading role. Very recently, Cicerone and McCrumb (1979) have introduced the possible effect of the photodissociation of the isotope  $O^{18}O^{16}$ . They consider that the photodissociation rates at 80 km for overhead sun conditions are about  $3 \times 10^{-7} \text{ sec}^{-1}$  for  $J^{16-18}$  and not more than  $9 \times 10^{-9} \text{ sec}^{-1}$  for  $J^{16-16}$ , i.e., a ratio of the order of 30. Since the ratio  $O^{16-18}$  and  $O^{16-16}$  is of the order of  $4 \times 10^{-3}$ , an additional effect of about 10% could be introduced near the mesopause level; it would reach about 40% near 65 km and about 20% at the stratopause. Such a result increases the uncertainty in the determination of the photodissociation of molecular oxygen in the mesosphere.

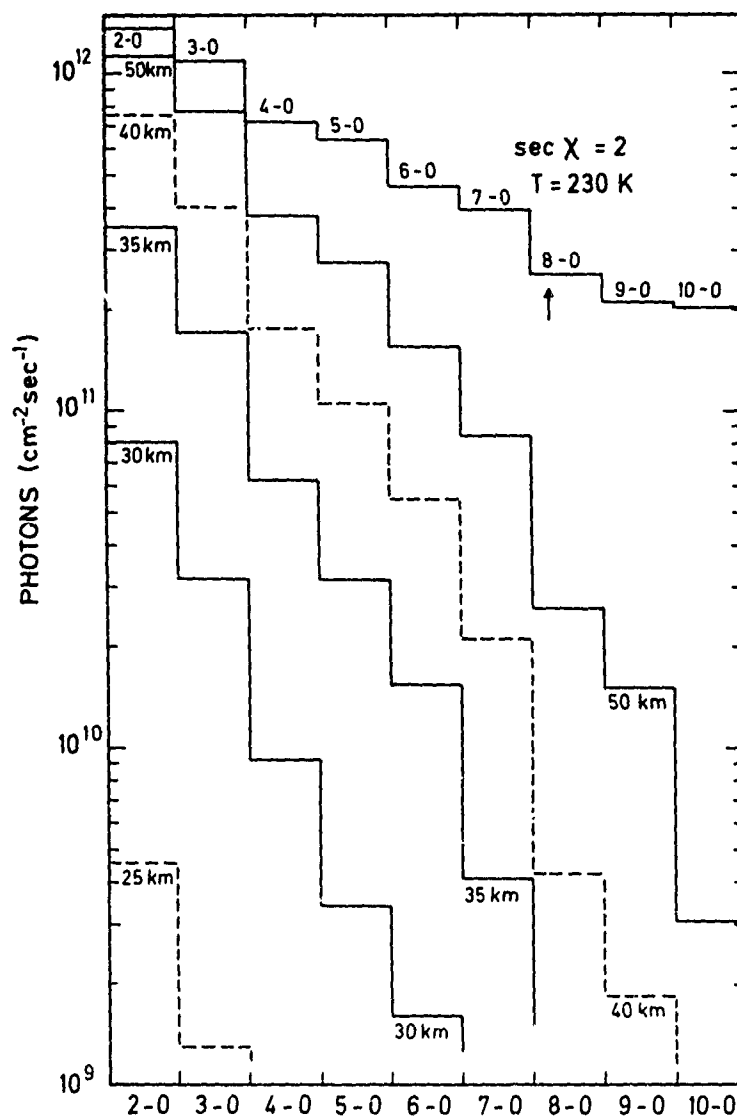


Figure 31. - Number of solar photons available at various heights in the spectral range of Schumann-Runge bands for a solar zenith angle of 60°. Upper curve corresponding to no atmospheric absorption.

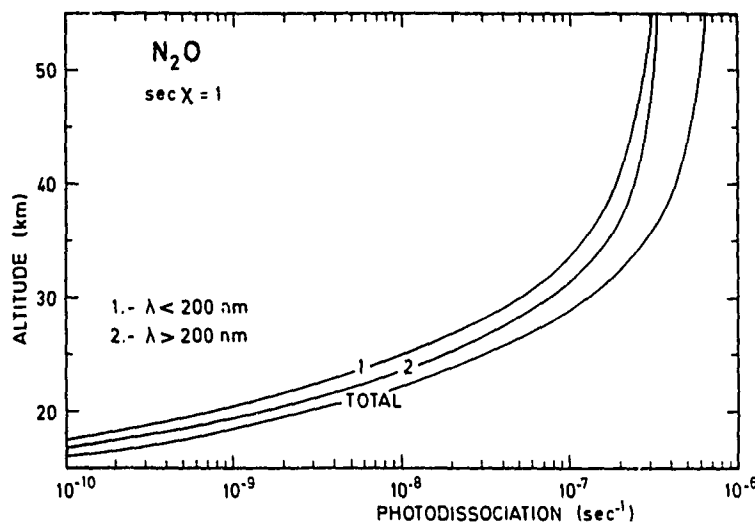


Figure 32. - N<sub>2</sub>O photodissociation coefficient for overhead sun conditions in the spectral ranges of the O<sub>2</sub> Schumann-Runge bands and Herzberg continuum.

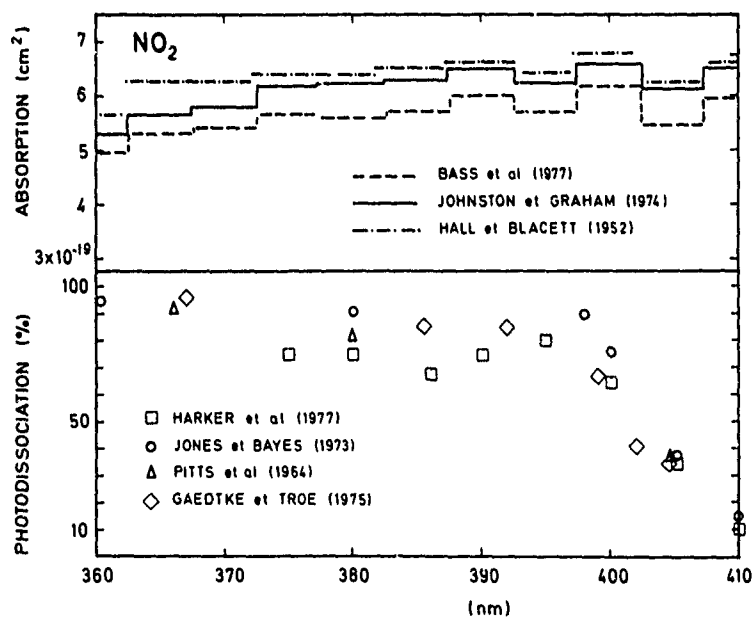


Figure 33. - NO<sub>2</sub> photodissociation coefficient at the top of the earth's atmosphere without scattering and albedo effects. Variation of the quantum yield at wavelengths greater than 360 nm.

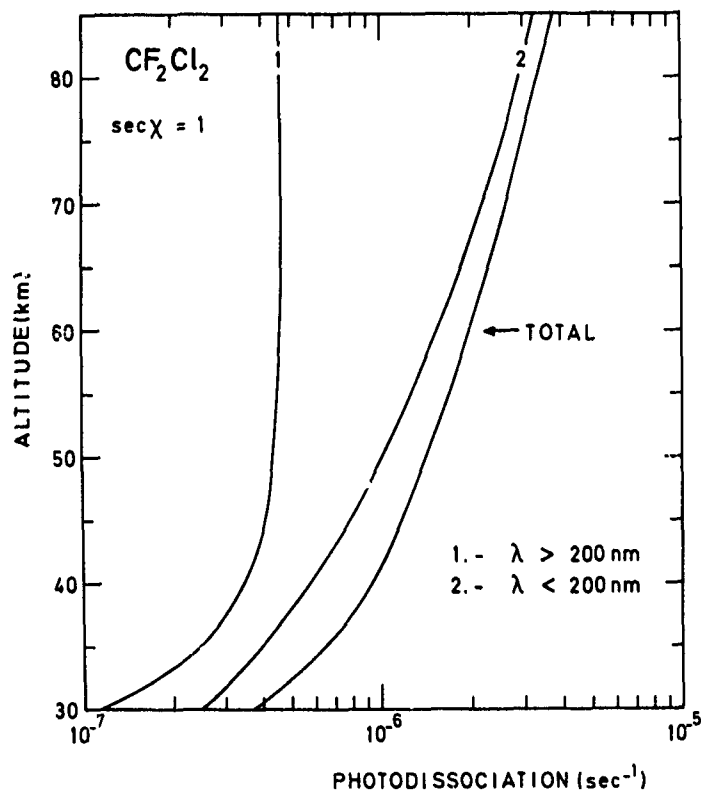


Figure 34. -  $\text{CF}_2\text{Cl}_2$  photodissociation coefficient for overhead sun conditions.

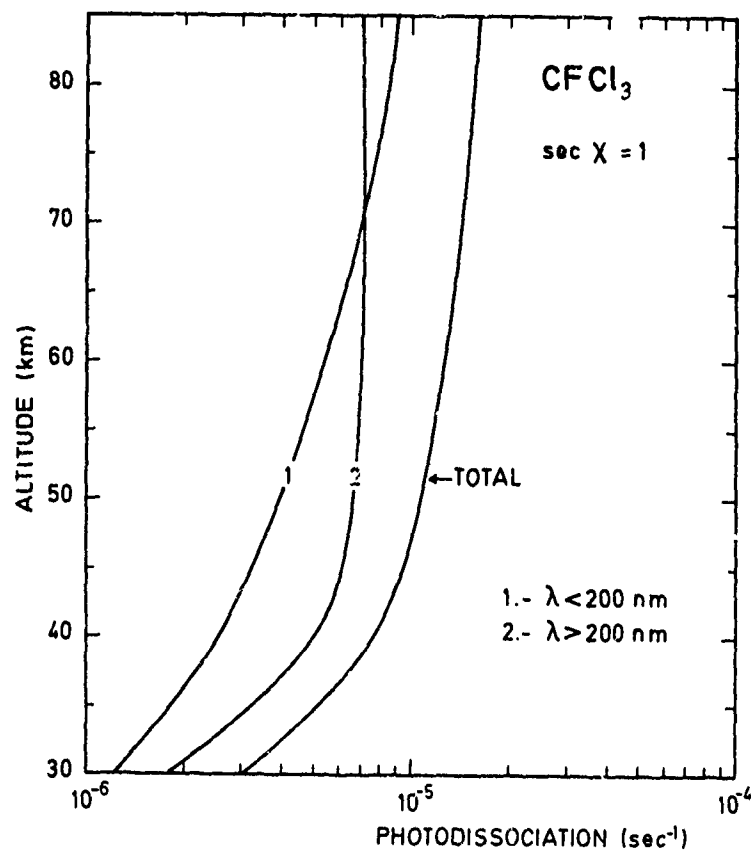


Figure 35. -  $\text{CFCl}_3$  photodissociation coefficient for overhead sun conditions.

Finally, a few words must be added concerning nitric oxide for which a detailed calculation is required since its photodissociation is due to rotational line predissociation. In fact, in two recent papers (Frederick and Hudson, 1979; Nicolet and Cieslik, 1979), the predissociation in the  $\delta(0-0)$  and  $\delta(1-0)$  bands of nitric oxide in the mesosphere and stratosphere has been studied in great detail. The differences (about 20%) in the unattenuated photodissociation between the two studies are essentially due to the different values which are used for the solar flux. An analysis made for temperatures between 175 and 300 K leads to the determination of simple empirical expressions which can be used for mesospheric and stratospheric calculations, and particularly for a direct calculation of the NO photodissociation rate.

The photodissociation rate at zero optical depth

$$J(\text{NO}) = 4.75 \times 10^{-6} \text{ sec}^{-1}$$

is an average value with a precision of +5% for  $T = 225 \pm 25$  K or of +10% for  $T = 225 \pm 50$  K. However, the accuracy is certainly not better than 25% (Nicolet, 1979) and an absolute error greater than 30% cannot be rejected. Therefore, it is convenient to represent the equivalent optical depth, by an equation identical to (20).

Numerical applications, between  $N(\text{O}_2) = 2 \times 10^{19} \text{ cm}^{-2}$  (85 km for an overhead sun) and  $N(\text{O}_2) = 5 \times 10^{22} \text{ cm}^{-2}$  (35 km for an overhead sun), lead to the following values of the equivalent optical depth depending on T and  $N \equiv N(\text{O}_2)$

$$T = 175 \text{ K} \quad \tau_{\text{NO}}(\text{O}_2) = 0.825 \times 10^{-8} N^{0.38} \quad (21a)$$

$$200 \text{ K}, \quad = 0.90 \times 10^{-8} N^{0.38} \quad (21b)$$

$$225 \text{ K}, \quad = 0.95 \times 10^{-8} N^{0.38} \quad (21c)$$

$$250 \text{ K}, \quad = 1.00 \times 10^{-8} N^{0.38} \quad (21d)$$

$$\text{and} \quad 275 \text{ K}, \quad = 1.125 \times 10^{-8} N^{0.38} \quad (21e)$$

For  $N(\text{O}_2) \leq 2 \times 10^{19} \text{ cm}^{-2}$ , i.e., above the mesopause, the following formula can be adopted:

$$J(\text{NO}) = J_{\infty}(\text{NO}) \exp(-1.5 \times 10^{-20} N) \quad (21)$$

Furthermore, if we accept that the precision cannot be better than +20%, every simple formula can be used for a direct application to mesospheric and stratospheric conditioning, i.e., formula (21d).

This leads to

$$J_{250\text{K}}(\text{NO}) = J_{\text{NO}} = 4.55 \times 10^{-6} \exp(-10^{-8} N^{0.38}) \quad (22)$$

corresponding to average conditions at  $T = 250$  K. To illustrate the use of (22), Table XV lists the numerical results obtained for  $J_{\text{NO}}$  with formula (22) between 85 km and 25 km for an overhead sun. In the same Table, the correction factors due to the ozone absorption and the de-excitation by  $N_2$  are introduced in order to determine the final photodissociation rate. It must be recognized that the  $J_{\text{NO}}$  values below  $10^{-8} \text{ sec}^{-1}$  are far from correct, but neglected in the computation of stratospheric models.

Finally, it can be shown that it is possible to use expression (21c) with  $J = 4.75 \times 10^{-6}$ , with a precision of +10% in the whole mesosphere

$$J_{225\text{K}}(\text{NO}) = 4.75 \times 10^{-6} \exp(-0.95 \times 10^{-8} N^{0.38}) \quad (23)$$

NICOLET

TABLE XV. - Photodissociation rate ( $\text{sec}^{-1}$ ) of nitric oxide for overhead sun conditions based on formula (22)

<u>Altitude</u>	<u>J(NO)</u>	<u>Altitude</u>	<u>J(NO)</u>
85 km	$3.70 \times 10^{-6} \text{sec}^{-1}$	65 km	$2.16 \times 10^{-6} \text{sec}^{-1}$
80	3.38	60	1.74
75	3.00	55	1.33
70	2.59	50	$9.61 \times 10^{-7}$

STRATOSPHERE

<u>Altitude</u>	<u>J<sub>NO</sub></u>	<u>Ozone</u> <u>Absorption*</u>	<u>N<sub>2</sub></u> <u>Effect</u>	<u>J<sub>NO</sub></u> <u>(Final)</u>
50 km	$9.61 \times 10^{-7}$	0.98	0.98	$9.22 \times 10^{-7}$
45	6.33	0.95	0.97	5.83
40	3.62	0.87	0.95	2.99
35	1.70	0.68	0.90	1.04
30	$5.90 \times 10^{-8}$	0.42	0.80	$1.98 \times 10^{-8}$
25	$(1.38 \times 10^{-8})$	0.18	0.64	$1.59 \times 10^{-9}$

\*O<sub>3</sub> absorption cross section, average value  $5 \times 10^{-19} \text{cm}^2$ .



NICOLET  
REFERENCES

- Ackerman, M., Ultraviolet solar radiation related to mesospheric processes, in Mesospheric Models and Related Experiments, Ed. G. Fiocco, Reidel Publ. Cy., Dordrecht, Holland, pp. 149-159, 1971.
- Ackerman, M. and F. Biaumé, Structure of the Schumann-Runge bands from the 0-0 to the 13-0 band, J. Mol. Spectr., **35**, 73, 1970.
- Arvesen, J. C., R. N. Griffin, Jr. and B. D. Pearson, Jr., Determination of extraterrestrial solar spectral irradiance from a research aircraft, Appl. Optics, **8**, 2215, 1969.
- Artzner, G., The solar H-Lyman-alpha line: Wavelength and profile measurement, Astron. Astrophys., **70**, LII, 1978.
- Bass, A. M., A. E. Ledford and A. H. Laufer, Extinction coefficients of  $\text{NO}_2$  and  $\text{N}_2\text{O}_4$ , J. Res. NBS, **80A**, 143, 1976.
- Bergeman, T. H. and S. C. Wofsy, The fine structure of  $\text{O}_2$  ( $\text{B}^3\Sigma_u^-$ ), Chem. Phys. Lett., **15**, 104, 1972.
- Brix, P. and G. Herzberg, Fine structure of the Schumann-Runge bands near the convergence limit and the dissociation energy of the oxygen molecule, Canad. J. Phys., **32**, 110, 1954.
- Broadfoot, A. L., The solar spectrum 2100-2900A, Astrophys. J., **173**, 681, 1972.
- Brueckner, G. E., J. D. F. Bartoe, O. K. Moe and M. E. Vanhoosier, Absolute solar ultraviolet intensities and their variations with solar activity. Part I: The wavelength region 1750A-2100A, Astrophys. J., **209**, 935, 1976.
- Bruner, E. C., Jr. and R. W. Parker, Hydrogen geocorona and solar Lyman-alpha line 1. Rocket measurement of the solar line profile, J. Geophys. Res., **74**, 107, 1969.
- Bruner, E. C., Jr. and W. A. Rense, Rocket observations of profiles of solar ultraviolet emission lines, Astrophys. J., **157**, 417, 1969.
- Carver, J. H., H. P. Gies, T. I. Hobbs, B. R. Lewis and D. G. McCoy, Temperature dependence of the molecular oxygen photoabsorption cross section near H Lyman alpha line, J. Geophys. Res., **82**, 1955, 1977.
- Cicerone, R. J. and J. L. McCrumb, Photodissociation or isotopically  $\text{O}_2$  as a source of atmospheric  $\text{O}_3$ , Geophys. Res. Lett., **6**, to be published, 1979.
- Delaboudinière, J. P., R. F. Donnelly, H. E. Hinteregger, G. Schmidtke and P. C. Simon, Intercomparison/compilation of relevant solar flux data related to aeronomy, COSPAR Technique Manual n° 7, 1978.
- DeLuise, J. J., Measurements of the extraterrestrial solar radiant flux from 2981 to 4000A and its transmission through the earth's atmosphere as it is affected by dust and ozone, J. Geophys. Res., **80**, 345, 1975.
- Ditchburn, R. W. and P. A. Young, The absorption of molecular oxygen between 1850 and 2500A, J. Atm. Terr. Phys., **24**, 127, 1962.
- Fang, T. M., S. C. Wofsy and A. Dalgarno, Opacity distribution functions and absorption in Schumann-Runge bands of molecular oxygen, Planet. Space Sci., **22**, 413, 1974.
- Frederick, J. E. and R. D. Hudson, Predissociation line widths and oscillator strengths for the (2-0) to (13-0) Schumann-Runge bands of  $\text{O}_2$ , J. Molec. Spectrosc., **74**, 247, 1979a.
- Frederick, J. E. and R. D. Hudson, Predissociation of nitric oxide in the mesosphere and stratosphere, J. Atmosph. Sci., **36**, 737, 1979.
- Gaedtke, H. and J. Troe, primary processes in the photolysis of  $\text{NO}_2$ , Ber. Bunsengesel. Phys. Chem., **79**, 184, 1975.
- Hall, T. C. and F. E. Blacett, Separation of the absorption spectra of  $\text{NO}_2$  and  $\text{N}_2\text{O}_4$  in the range of 2400-5000A, J. Chem. Phys., **20**, 1745, 1952.
- Harker, A. B., W. Ho and J. J. Ratto, Photodissociation quantum yield of  $\text{NO}_2$  in the region 375 to 420 nm, Chem. Phys. Lett., **50**, 394, 1977.
- Hasson, V. and R. W. Nicholls, Absolute spectral absorption measurements on molecular oxygen from 2640-1920A: II Continuum measurements 2430-1920A, J. Phys. B. Atomic. Molec. Phys., **4**, 1789, 1971.
- Heroux, L. and R. A. Swirbalus, Full-disk solar fluxes between 1230 and 1940A, J. Geophys. Res., **81**, 436, 1976.
- Heath, D. F. and M. P. Tekakara, The solar spectrum between 1200 and 3000A, in The Solar Output and its Variation, ed. O. R. White, Colorado Assoc. Univ. Press, Boulder, pp. 193-212, 1977.
- Hudson, R. D., V. L. Carter and E. L. Breig, Predissociation in the Schumann-Runge band system of  $\text{O}_2$ : Laboratory measurements and atmospheric effects, J. Geophys. Res., **74**, 4079, 1969.

- Hudson, R. D. and S. H. Mahle, Photodissociation rates of molecular oxygen in the mesosphere and lower thermosphere, J. Geophys. Res., 77, 2902, 1972.
- Johnston, H. S. and R. A. Graham, Photochemistry of  $\text{NO}_2$  and  $\text{HNO}_x$  compounds, Canad. J. Chem., 52, 1415, 1974.
- Jones, I. T. N. and K. D. Bayes, Photolysis of nitrogen dioxide, J. Chem. Phys., 59, 4836, 1973b.
- Kockarts, G., Penetration of solar radiation in the Schumann-Runge bands of molecular oxygen, in Mesospheric Models and Related Experiments, Ed. G. Fiocco, Reidel Publ. Cy., Dordrecht-Holland, pp. 160-176, 1971.
- Kockarts, G., Absorption and photodissociation in the Schumann-Runge bands of molecular oxygen in the terrestrial atmosphere, Planet. Space Sci., 24, 589, 1976.
- Lemaire, P. et al., Calibrated full disk solar HI Lyman-alpha and Lyman-beta profiles, Astrophys. J., 223, L55, 1978.
- Lewis, B. R., J. H. Carver, T. I. Hobbs, D. G. McCoy and H. P. F. Gies, Experimentally determined oscillator strengths and linewidths for the Schumann-Runge band system of molecular oxygen I. The (6-0) - (14-0) bands, J. Quant. Spectrosc. Radiat. Transfer, 20, 191, 1978.
- Lewis, B. R., J. H. Carver, T. I. Hobbs, D. G. McCoy and H. P. F. Gies, Experimentally determined oscillator strengths and linewidths for the Schumann-Runge and system of molecular oxygen II. The (2-0) to (5-0) bands, J. Quant. Spectrosc. Radiat. Transfer, 21, 213, 1979.
- Muramatzu, H., Dissociation rates of oxygen and ozone molecules in the stratosphere and mesosphere, Papers in Met. Geophys., 26, 219, 1975.
- Nicolet, M., Stratospheric ozone: An introduction to its study, Rev. Geophys. Space Phys., 13, 593, 1975.
- Nicolet, M., Solar UV radiation and its absorption in the mesosphere and stratosphere, Pure and Appl. Geophys., 108, to be published, 1979.
- Nicolet, M. and S. Cieslik, The photodissociation of nitric oxide in the mesosphere and stratosphere, Planet. Space Sci., 27, to be published, 1979.
- Nicolet, M. and W. Peetermans, Atmospheric absorption in the  $\text{O}_2$  Schumann-Runge band spectral range and photodissociation rates in the stratosphere and mesosphere, Planet. Space Sci., 27, to be published, 1979.
- Ogawa, M., Absorption cross sections of  $\text{O}_2$  and  $\text{CO}_2$  continua in the Schumann and far UV regions, J. Chem. Phys., 54, 2550, 1971.
- Park, J. H., The equivalent mean absorption cross sections for the  $\text{O}_2$  Schumann-Runge bands: Application to the  $\text{H}_2\text{O}$  and NO photodissociation rates, J. Atm. Sci., 31, 1893, 1974.
- Pitts, J. N., J. H. Sharp and S. I. Chan, Effects of wavelength and temperature on primary processes in the photolysis of nitrogen dioxide and a spectroscopic-photochemical determination of the dissociation energy, J. Chem. Phys., 40, 3655, 1964.
- Rottman, G. L., Disc values of the solar u.v. flux 1150-1850A. Trans. Am. Geophys. EOS, 56, 1157, 1974.
- Samain, D. and P. C. Simon, Solar flux determination in the spectral range 150-210 nm, Solar Phys., 49, 33, 1976.
- Shardanand and A. D. Prasad Rao, Collision-induced absorption of  $\text{O}_2$  in the Herzberg continuum, J. Quant. Spectrosc. Radiat. Transfer, 17, 433, 1977.
- Shimazaki, T., T. Ogawa and B. C. Farrell, Simplified methods for calculating photodissociation rates of various molecules in the Schumann-Runge band systems in the upper atmosphere, NASA Tech. Note TN D-8399, March 1977.
- Simon, P. C., Nouvelles mesures de l'u.v. solaire dans la stratosphère, Bull. Acad. r. Belg., Cl. Sci., 61, 399, 1975.
- Simon, P. C., Irradiation solar flux measurements between 120 and 400 nm, Current position and future needs, Planet. Space Sci., 26, 355, 1978.
- Tousey, R., The extreme ultraviolet spectrum of the sun, Space Sci. Rev., 2, 3, 1963.
- Vernazza, J. E., E. H. Avrett and R. Loeser, Structure of the solar chromosphere II. The underlying photosphere and temperature minimum region, Astrophys. J., Suppl. Ser., 30, 1, 1971.
- Vidal-Madjar, A., Evolution of the solar Lyman alpha flux during four consecutive years, Sol. Phys., 40, 69, 1975.

AN INTRODUCTION TO STUDIES OF THE GENERAL CHARACTERISTICS  
OF THE STRATOSPHERE AND MESOSPHERE

R.J. Murgatroyd

Meteorological Office, Bracknell, U.K.

Abstract

After a brief description of their principal observed features a short introduction is given to studies of the temperature and wind fields of the stratosphere and mesosphere using the dynamical equations. In particular the application of these equations when zonally averaged to investigations of equator to pole transports of heat, momentum and trace substances is described together with a consideration of the relationships between the mean cellular and eddy components of the motions. Finally the respective roles of the radiation fields and the dynamical factors in establishing the general structure and energetics of these regions are briefly discussed.

**INTRODUCTION:** Up to the past few years the stratosphere has been regarded as a well bounded and somewhat quiescent layer of the atmosphere, substantially in radiative equilibrium with temperatures that remained constant or increased with height everywhere, rather steady winds and no important synoptic systems. Consequently it was thought that the main features of the distribution of its constituents could be well explained in terms of oxygen-ozone chemistry as modified by the effects of various minor or trace species in the upper and middle stratosphere, plus a rather simple redistribution by the winds in the lower stratosphere. Given the distributions of the radiatively important constituents, principally that of ozone in absorbing solar ultra violet radiation and carbon dioxide, ozone and water vapour in emitting atmospheric radiation, a reasonable estimate could be made of the net radiative flux divergences. Hence, allowing for convection in the troposphere, distributions of radiative equilibrium temperature could be calculated from the tropopause to at least the stratopause and probably as far as the mesopause above. These were consistent with the familiar profiles of high temperatures near the surface, low temperatures near the tropopause, high temperatures near the stratopause and low temperatures above around the mesopause. Alternatively, by using available temperature observations, radiative calculations could be used to estimate the distributions of the primary heating sources and sinks. These provided a guide to the basic meridional (south-north) heat transports required from the general circulation in the stratosphere and mesosphere which could also transport the atmospheric constituents. At the same time it was expected and broadly confirmed by observations that the observed zonal (west-east) wind component fields would be linked directly to the temperature fields by the thermal wind equation, expressing broadly hydrostatic and geostrophic balance throughout most of the region.

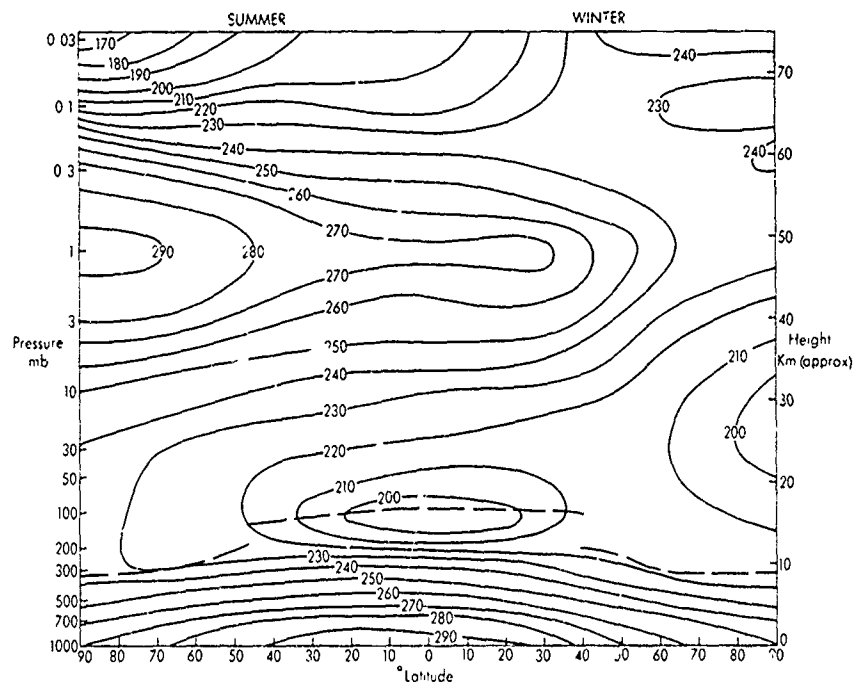
This picture although forming a useful background to modern studies is clearly not adequate to explain many of the detailed observations now available for example of tropopause and mesopause structures, constituent transfers, high resolution profiles, sudden warmings, quasi-biennial and other well-established oscillations. In addition it does not provide a sufficiently comprehensive theoretical basis for atmospheric modelling, particularly transports of constituents, which are still simulated in simple models by empirical or semi-empirical methods using inadequate diffusion theory. It has, however, the merit that it includes a number of the interactions between the various physical-chemical processes of importance. The distribution of the constituents depends on temperature dependent chemical kinetic processes and on transport mechanisms, the temperature depends on radiative processes, which in turn are dependent on the composition, and the wind distributions depend on the temperature fields. One major factor which has not been included in the above outline is the role of the motions in establishing the temperature structure. A second is inter-level transfers particularly the role of tropospheric processes in determining many features of the stratosphere- its composition, radiative fluxes, temperatures, mean winds and eddies. Their inclusion will require a consideration in some detail of the existence and propagation of all scales of motion within the general circulation at all levels. In this paper and no doubt in other papers in this Section on Dynamical Processes more extensive discussion will be presented of the various features which appear to be important in determining the observed characteristics of the Middle Atmosphere which are briefly described in the following sections and which must be incorporated properly in realistic models.

**AVERAGE CROSS-SECTIONS OF TEMPERATURE AND WIND COMPONENTS:** The mean variations of temperature and zonal wind component from winter to summer and with latitude in the Northern Hemisphere are illustrated in the 'back to back' cross-sections shown in Figs.1 and 2 Murgatroyd, 1969. Conditions in the Southern Hemisphere are broadly similar and the differences may be largely accounted for in terms of effects due to the different topography of the two hemispheres. It will be noted that the temperature patterns are irregular and could not be inferred without a considerable understanding of the dominant atmospheric processes. As expected the temperatures in the troposphere are highest in equatorial regions and lowest near the winter pole but in the lower stratosphere the temperatures are lowest in equatorial regions. Around the stratopause, the temperature is highest near the summer pole and lowest at high latitudes in winter whereas the reverse is the case near the mesopause. It should be remarked that in addition to the major changes with height, latitude and season there are other sources of variability of temperature in the form of oscillations and wave motions. This variability is evident in the standard deviations of temperature shown in the lower part of Fig.1 which have large values in the extratropical winter hemisphere particularly in the middle and upper stratosphere with comparatively small values in the summer hemisphere particularly at stratospheric levels.

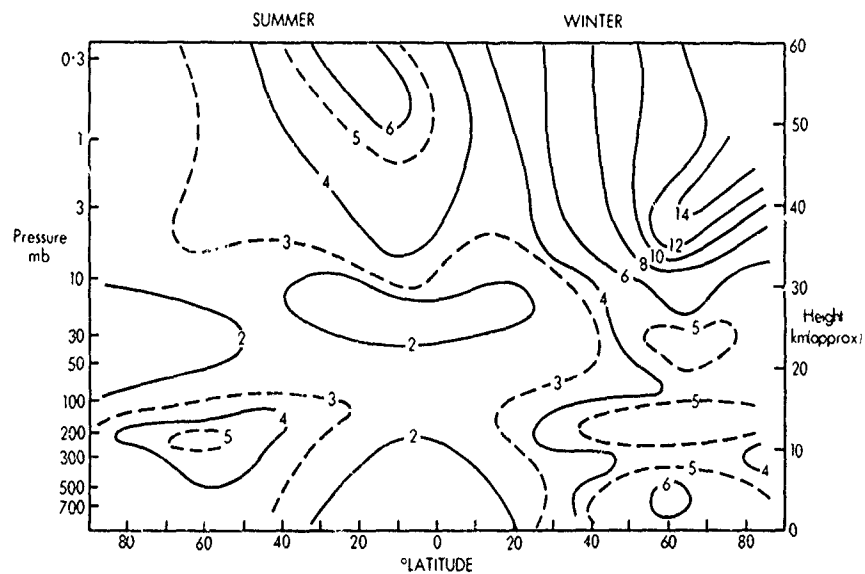
The zonal wind components in the troposphere are mainly easterly at low latitudes but the principal extratropical means are westerlies increasing with height to a maximum in the main tropopause gap area between the tropical and polar tropopause at 10 to 12 km in the lower middle latitudes. Values are greatest and the maximum nearest the equator in the Northern Hemisphere winter. The westerlies then become weaker in the lower stratosphere where the horizontal temperature gradient reverses. At greater heights winds become easterly in summer and westerly in winter increasing with height in both seasons to very strong maxima at about 65 km. At higher levels they decrease again with height. It will again be seen that the standard deviations are very small in summer but large in winter in the middle stratosphere.

The average meridional and vertical components which comprise the mean cells are more difficult to specify than the mean west-east components because the mean south-north component generally is found as an average of larger opposing values at the different longitudes. It is generally of the order of  $1 \text{ msec}^{-1}$  or less compared with the zonal mean component values of at least an order greater shown in Fig.2. To satisfy mass continuity the vertical component rarely exceeds about  $1 \text{ mm sec}^{-1}$ . Consequently in the stratosphere and above where the global wind data are relatively sparse the cellular components have to be inferred indirectly from estimations of the momentum and heat balances or from model results. The inferred distributions vary somewhat with the data used by different authors but there is general agreement that, extending from the top of the Hadley cell, there is a broad region

# MIRGATROYD

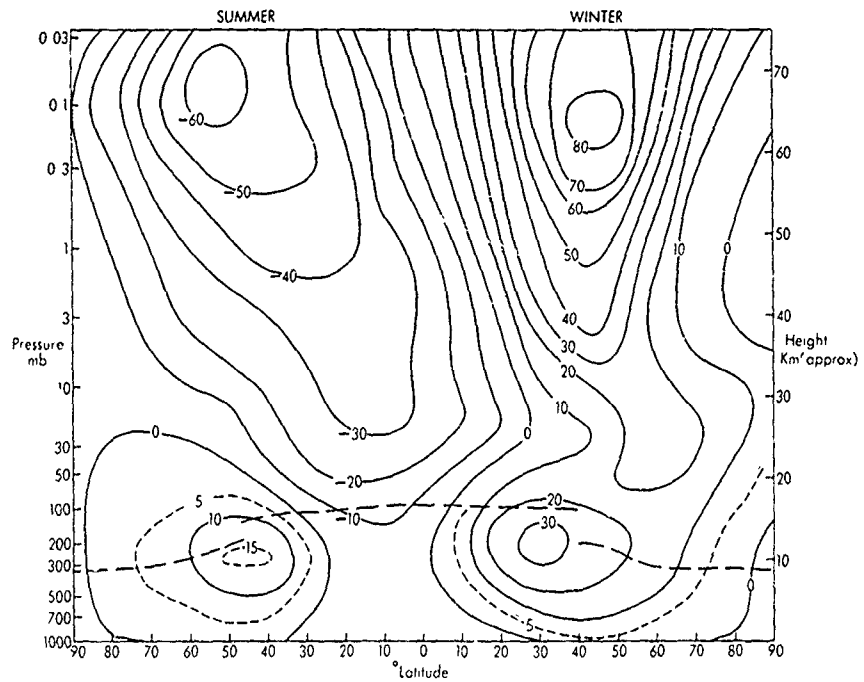


(a) Representative latitudinal mean cross section of temperatures, K, for the solstices. Heavy dashed lines represent the tropopause

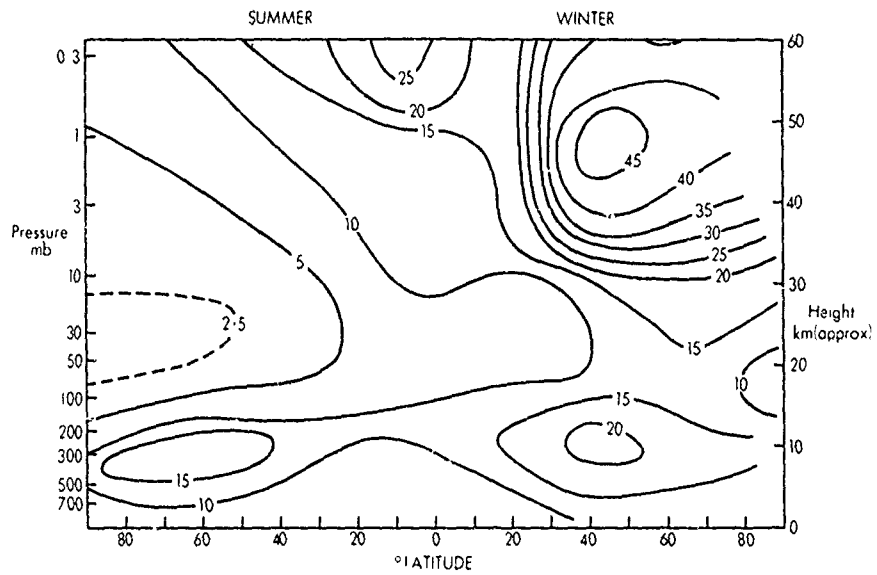


(b) Rough estimates of standard deviation of temperature, K, at the solstices

Figure 1 Zonal Temperature and Temperature Field Variance at the Solstices



(a) Representative latitudinal mean cross section of zonal wind speeds, in  $\text{m sec}^{-1}$ . West to east components are positive



(b) Rough estimates of standard vector deviations of wind, in  $\text{m sec}^{-1}$ , corresponding to winds in (a)

Figure 2 Zonal Wind and Wind Field Variance at the Solstices

transfer across the equator to the winter hemisphere followed by descent there in middle latitudes down to the main tropopause gap region. Usually there is a second cell at higher latitudes with rising motions over the poles but at times the stratosphere may have a three-cell distribution in winter similar to that of the troposphere.

Knowledge is sparse regarding the mean circulation in the mesosphere but the simplest models show mainly ascent in the summer hemisphere, transfer across the equator and descent in the winter hemisphere. At all Middle Atmosphere levels a seasonal reversal takes place probably giving largely symmetrical circulations in the two hemispheres during the transition period.

Although all the main features described above are generally reproduced from year to year changes in the detailed behaviour both in the means and in the observed systems below are possible.

**PRINCIPAL OSCILLATIONS, WAVE MOTIONS AND SYNOPTIC SYSTEMS:** As well as the major changes shown in Fig.1 there is an annual temperature variation near the equator which results in lowest temperatures in the lower stratosphere and a maximum equatorial tropopause height in January. In addition well-marked semi-annual oscillations in temperature are observed with maxima at the equinoxes at about 40 km over the equator and 30 km over the poles. Maxima of zonal wind components of about 30 msec<sup>-1</sup> westerly at the equinoxes and easterly at the solstices are observed at about 50 km over the equator and also found in the mesosphere at high latitudes.

There is also a well documented Quasi-Biennial ( $\sim 26$  month period Oscillation) in the temperature, motion and ozone fields. It has a maximum in zonal wind speed of about 20 msec<sup>-1</sup> at 25 to 30 km in the tropics where it is observed in the form of bands of mean easterly and westerly zonal components descending in succession in the stratosphere at about 1 km/month. Secondary maxima have also been found at high latitudes in the stratosphere and there is also evidence of its presence in the mesosphere (and in the troposphere). Its cause has been linked with the transference of momentum from eastward propagating Kelvin waves and westward propagating mixed Rossby-gravity waves of very long wavelength propagating upwards from the troposphere in tropical latitudes.

Extra-tropical tropospheric synoptic systems generally decrease in intensity and die out in the lowest few kms of the stratosphere. There appear to be no large scale synoptic systems at higher levels in the summer hemisphere with the result that the contours on pressure surfaces in the stratosphere are then broadly west-east in direction presenting a 'dart-board' appearance on a polar chart. In the winter hemisphere and near the equinoxes very long waves of wavenumbers 1 (which displace the vortex centre away from the pole) and 2 (which shows two 'highs' and two 'lows' on a global contour chart) penetrate substantially upwards from the troposphere into the Middle Atmosphere. The development and movements of these waves are the main cause of the large standard deviations of temperature and zonal wind component values in winter shown in Figs. 1(b) and 2(b) and are also responsible for the major 'sudden warming' phenomena which occur during the late winter, particularly in the Northern Hemisphere.

Synoptic scale wave motions are not generally generated in situ in the stratosphere as occurs in the troposphere but there is some limited evidence of short period transients in the stratopause region and possibly in the mesosphere. It also appears that any systems in the mesosphere will probably decrease in intensity and die out in the mesopause region although there are again little observational data as yet to support this.

Tidal wave motions (which are mainly of diurnal and semi-diurnal solar periods) have small (1-2 msec<sup>-1</sup>) amplitudes in the lower stratosphere but these increase with height until they become important contributors to the motion field in the mesosphere and are dominant in the motion field above about the 100 km level.

Shallow motion systems, very persistent for gravity waves, appear to exist at most levels. Gravity wave dissipation is often linked with intermittent clear air turbulence in the lower stratosphere and also gravity waves have been shown to be of major importance in

the upper mesosphere and lower thermosphere where their break up is thought to be an important source of turbulence and energy dissipation.

**SOME CURRENT PROBLEMS:** The above observations and also those of the radiation and composition fields raise many problems. Some of the most important are

(i) **Composition:** Global ozone distributions have been discussed in extenso in previous specialised papers and it will only be remarked here that photochemical theory alone requires maximum total ozone concentrations in low latitudes whereas they are observed to be a maximum at high latitudes (in spring) and to differ substantially between hemispheres. It is likely that other substances with long photochemical lifetimes in the lower stratosphere will exhibit similar patterns and they are also apparent in natural and artificially produced radioactive substances. Better quantitative knowledge is required of the transport processes involved. On the large-scale of planetary waves (wavenumbers 1-4) considerable variability occurs particularly during sudden warmings. Associations with synoptic systems in the troposphere are reasonably well established but not at present fully understood. Small scale ( $\sim 1$  km depth) irregularities also appear to occur in the ozone profiles at all latitudes in the lower stratosphere and are not well accounted for and frequently ignored.

The explanation of the distribution of the next best observed stratospheric minor constituent, water vapour, also presents difficulties. Humidity is very low in the lower stratosphere at all latitudes precluding any possible cloud formation except at extremely low temperatures (associated for example with mother of pearl clouds at high latitudes in winter) and its full explanation requires improved understanding of troposphere-stratosphere transfer. In addition the highest humidity at this level appears to occur in the lower latitudes and further explanation of this is required.

Clearly transport processes and their underlying dynamics require a great deal more study in order to understand in more detail the processes determining atmospheric composition and to decide how they can best be modelled.

(ii) **Temperature:** It might have been expected that, since the tropics receive solar radiation at low zenith angles throughout the year, the temperatures at low latitudes would generally be higher than those at middle and high latitudes, at least in winter. The equatorial tropopause level is, however, very cold and in winter the mid-latitudes in the lower stratosphere are warmer than either the tropics or the high latitudes. Moreover it might also be expected that the changeover from the typical tropospheric temperature profile (lapse rate) to that of the stratosphere at the tropopause would vary smoothly with latitude. In fact the tropopause exhibits a major break in mid-latitudes between the equatorial tropopause (at 15-18 km) and the polar tropopause (at 11-13 km) and other more transient breaks associated with different air masses and jet streams in higher latitudes. Similarly it might be expected that, since the summer pole is continually illuminated, its temperature at the mesopause would be higher than at the winter pole whereas the opposite is observed to be the case.

The strong absorption of solar ultra-violet radiation by ozone leads to the high temperature region around the stratopause. The net result of this heating and the cooling due to emission of atmospheric radiation by radiatively important constituents is to produce a heat source over the summer pole where the temperatures are highest and a sink over the low temperature winter pole. The resultant positive correlation results in a generation of available potential energy to drive the circulation and a need for heat transfer between summer and winter hemispheres at this level. However in the lower stratosphere the radiative conditions are such that there is net heating at low latitudes mainly due to convergence of the atmospheric radiative flux. Since this is a low temperature region, this can only be balanced by some cooling mechanism exporting energy out of this region. Evidently the energy transfers in the lower stratosphere are very different from those in both the upper stratosphere and in the troposphere and an energy cycle has to be constructed which will account for these differences. The mesopause region also has similar features to explain since its summer pole region appears to be associated with a radiative heat source and yet remains cold compared with the winter high latitude region, which seems to be a radiative sink although it is much warmer.



(iii) Winds: The main features of the wind fields in the lower stratosphere are that they generally decrease rapidly with height in mean zonal (west - east) speeds from their tropospheric values and also the tropospheric synoptic systems likewise die out in intensity in this region. Much of the polewards transport of constituents in the lower stratosphere is associated with these systems but so far it has not yet been possible to quantify it satisfactorily in terms of the meteorological parameters for use in one or two dimensional models. All of the other motion systems mentioned in the preceding sections contribute to the transport of constituents both 'natural' and artificially produced and means are required to understand and evaluate their separate contributions and incorporate them in models. In order to analyse the circulation processes in more detail particularly with reference to their transport mechanisms it is convenient to subdivide the primary wind components, temperatures, and constituent mixing ratios into their mean zonal (averages round latitude circles) and eddy (deviations at different longitudes from these means) components. If required any eddy parameters can also be Fourier analysed to study the contributions of motions of various scales. Such an approach has been widely used in diagnostic studies, mechanistic models, and also two (and one) dimensional models of the atmosphere. Before the impact of some of its results on understanding the features outlined above can be assessed, however, it is necessary to appreciate the basic laws which determine the temperature structure and the general circulation.

THE PHYSICAL LAWS, DYNAMICAL EQUATIONS AND ZONAL AVERAGING: The basic laws of interest here include the continuity equation (1) for each chemical species (and for the total mass), the momentum (2) and energy continuity equations (3). These are respectively:-

$$\frac{\partial R_i}{\partial t} + \underline{V} \cdot \nabla R_i = \frac{1}{n} (P_i - L_i) \quad \dots(1)$$

where  $R_i$  is the mixing ratio of the  $i$ th species,  $P_i$  and  $L_i$  its photochemical and other source and sink terms,  $\underline{V}$  the wind vector,  $t$  time and  $n$  the air number density,

$$\frac{d\underline{V}}{dt} = -2\underline{\Omega} \times \underline{V} - \frac{1}{\rho} \nabla p + \underline{g} + \underline{F} \quad \dots(2)$$

where  $\underline{\Omega}$  is the earth's angular velocity,  $\rho$  density,  $p$  pressure,  $\underline{g}$  gravity vector and  $\underline{F}$  friction force and

$$C_p \frac{dT}{dt} = \frac{1}{\rho} \frac{dp}{dt} + \dot{Q} \quad \dots(3)$$

where  $\dot{Q}$  is the net heating rate per unit mass due to solar and atmospheric radiation,  $C_p$  the specific heat at constant pressure and

$$\frac{d}{dt} ( ) = \frac{\partial}{\partial t} ( ) + \underline{V} \cdot \nabla ( ) \quad \dots(4)$$

If averaging round latitude circles is denoted by

$$\overline{( )} = \frac{1}{2\pi} \int_0^{2\pi} ( ) d\lambda \quad \dots(5)$$

and

$$( ) = \overline{( )} + ( )' \quad \dots(6)$$

where  $( )'$  denotes the local deviation at any longitude  $\lambda$  from the zonal mean at the latitude  $\phi$  it may be shown that the corresponding zonally averaged equations with  $p$  as the vertical coordinate and  $\omega = \frac{dp}{dt}$  as the vertical component of motion are

$$\frac{1}{a \cos \phi} \frac{\partial}{\partial \phi} \bar{v} \cos \phi + \frac{\partial \bar{w}}{\partial p} = 0 \quad \dots(7)$$

for mass continuity,

$$\frac{\partial \bar{R}_L}{\partial t} + \left( \frac{\bar{v}}{a} \frac{\partial \bar{R}_L}{\partial \phi} + \bar{w} \frac{\partial \bar{R}_L}{\partial p} \right) + \left( \frac{1}{a \cos \phi} \frac{\partial}{\partial \phi} \bar{v}' R_L' \cos \phi + \frac{\partial}{\partial p} \bar{w}' R_L' \right) = \frac{1}{n} (\bar{P}_L - \bar{L}_L) \quad \dots(8)$$

for continuity of each chemical species,

$$\frac{\partial \bar{u}}{\partial t} + \left( \frac{\bar{v}}{a \cos \phi} \frac{\partial \bar{u} \cos \phi}{\partial \phi} + \bar{w} \frac{\partial \bar{u}}{\partial p} \right) + \left( \frac{1}{a \cos \phi} \frac{\partial}{\partial \phi} \bar{u}' v' \cos \phi + \frac{\partial}{\partial p} \bar{u}' w' \right) = f \bar{v} \quad \dots(9)$$

from Newton's second law (momentum equation) assuming hydrostatic balance, no friction,  $f = 2\Omega \sin \phi$ ; ( $u, v$ ) the zonal and meridional wind components; and  $a$  is the earth's radius,

$$\frac{\partial \bar{T}}{\partial t} + \left( \frac{\bar{v}}{a} \frac{\partial \bar{T}}{\partial \phi} + \bar{w} \left( \frac{\partial \bar{T}}{\partial p} - \frac{R}{C_p} \frac{\bar{T}}{p} \right) \right) + \left( \frac{1}{a \cos \phi} \frac{\partial}{\partial \phi} \bar{v}' T' \cos \phi + \frac{\partial}{\partial p} \bar{w}' T' - \frac{R}{C_p} \frac{\bar{w}' T'}{p} \right) = \frac{\bar{Q}}{C_p} \quad \dots(10)$$

from the energy continuity (thermodynamic) equation, where  $R$  is the gas constant for air.

Eq.(7) with appropriate boundary conditions allows  $\bar{w}$  or  $\bar{v}$  to be calculated once the field of the other has been established. Eqs. (8), (9) and (10) allow the rate of change of  $\bar{R}_L$ ,  $\bar{u}$  and  $\bar{T}$  to be estimated from a knowledge of their fluxes due to the mean circulations and eddy motions (terms in the second and third brackets on their left hand sides respectively) and their effective source function on the right-hand side. It will be noted that in the treatment of the source terms in Eq. (8) problems will arise in the formation of any means of products terms included in their right hand sides, since products of primes i.e. 'eddy terms' (which are usually ignored) as well as products of mean values will be produced.

The integration of Eq. (8) which is of primary interest in studies of composition requires, in addition to knowledge of the mean meridional circulation ( $\bar{v}, \bar{w}$ ) and the (temperature dependent) source-sink terms, a means of expressing the eddy flux divergence terms as a function of  $\bar{R}_L$ . This is the central problem in the proper incorporation of the dynamics and so far has only been treated empirically or by use of 'K' theory writing for example

$$\begin{aligned} \bar{v}' R_L' &= -K_{yy} \frac{\partial \bar{R}_L}{\partial y} - K_{yp} \frac{\partial \bar{R}_L}{\partial p} \\ \bar{w}' R_L' &= -K_{py} \frac{\partial \bar{R}_L}{\partial y} - K_{pp} \frac{\partial \bar{R}_L}{\partial p} \end{aligned} \quad \dots(11)$$

which is of dubious applicability to the large-scale systems represented by these terms. The further averaging of Eq. (8) with respect to latitude removes all the terms except the vertical eddy flux and the source-sink terms in a one-dimensional formulation but the problem of expressing the eddy contribution as a function of the mean field remains. Unless this problem is properly solved the only realistic treatment based on this type of formulation will have to involve the full three-dimensional formulation of Eqs. (1), (2) and (3). There is, however, some hope of progress using models based on Lagrangian equations rather than the above Euler equations. These have the advantage of directly showing particle movements although they have other complications as yet unresolved as regards convergencies of trajectories and representations of sources in practical use. Eqs. (9) and (10) have been used extensively in studies of the role of their major terms in establishing the basic stratospheric dynamics. It has been shown by scaling arguments and also in diagnostic calculations and from model results that they usually give approxi-

mate balance in the steady state (with  $\frac{\partial}{\partial t}$  ( ) terms omitted). Moreover it appears that the contributions of the vertical component of the eddy terms are comparatively small and can be neglected for most purposes. The corresponding  $\frac{\partial}{\partial t} \bar{v}$  equation to Eq. (9) reduces at the same time for most applications to the geostrophic equation

$$f\bar{u} + \bar{u}^2 \frac{\tan \phi}{a} = - \frac{\partial \bar{\Phi}}{a \partial \phi} \quad ..(12)$$

where  $\bar{\Phi}$  is the geopotential.

The  $\bar{u}'v'$  (horizontal eddy momentum flux) and  $\bar{v}'T'$  (horizontal heat flux) terms can readily be evaluated from global (u, v, T) observed data. Either Eq. (9) or Eq. (10) can then be used in conjunction with Eq. (7) to infer the small but important mean meridional circulation parameters ( $\bar{v}$ ,  $\bar{w}$ ) and also check the consistency of the  $\bar{Q}$  calculations from the radiative transfer equations. Knowing the values of these eddy fluxes and the mean u and T fields it is then possible to carry out many basic studies of the general circulation processes. For example it can readily be checked whether the eddy fluxes are down-gradient. The directions of transfer between the basic energy forms (zonal and eddy kinetic energy, and zonal and eddy available potential energy) may also be inferred directly. Moreover, by eliminating the time dependent terms in Eqs. (9) and (10) (by differentiating the former with respect to  $p$  and the latter with respect to  $y$  ( $=a\phi$ ) and applying the balance condition of Eq. (12) it may be investigated how the mean circulation is driven by its eddy heat and momentum fluxes and its diabatic heating terms (see e.g. [Holton, 1972]). The general form of the results of this manipulation (neglecting curvature and smaller terms for convenience) gives for a stream function  $\chi$  of  $\bar{v}$  and  $\bar{w}$ , with vertical motion downwards at the lower latitudes (strictly a linear operator  $\mathcal{L}(\chi)$ ):-

$$\mathcal{L}(\chi) \propto \chi = \frac{\partial}{\partial y} \frac{\bar{Q}}{f} - \frac{\partial^2}{\partial y^2} \bar{v}'T' + f(p) \frac{\partial}{\partial p} \frac{\partial}{\partial y} \bar{u}'v' \quad ..(13)$$

The intimate linkage of the mean circulation with both the radiation field and the eddies is thus apparent. For example, it appears, in the Northern Hemisphere winter in the lower stratosphere that:-

(i) Since  $\bar{Q}$  is positive in low latitudes and negative in high latitudes  $\frac{\partial}{\partial y} \bar{Q}$  will generally be negative and hence this term will tend to produce upward motions in low latitudes and downward in high latitudes

(ii)  $\frac{\partial}{\partial y^2} \bar{v}'T'$  there is observed to be a maximum around 60°N except in summer. The resulting  $\frac{\partial}{\partial y^2} \bar{v}'T'$  term tends to produce a downward component in mid-latitudes and upward in both equatorial and polar latitudes

(iii) In the stratosphere  $\bar{u}'v'$  is also observed to be a maximum in middle latitudes in the Northern Hemisphere. Hence  $\frac{\partial}{\partial p} \frac{\partial}{\partial y} \bar{u}'v'$  will be positive in low latitudes and negative in high latitudes. If  $\bar{u}'v'$  increases with height as usually will be the case in winter in the extratropical middle stratosphere the  $\frac{\partial}{\partial p} \frac{\partial}{\partial y} \bar{u}'v'$  term will then tend to produce negative  $\chi$  at low latitudes and positive  $\chi$  at high latitudes i.e. vertical motion upwards near the equator and near the poles and downwards in middle latitudes. This pattern has been found in many diagnostic studies and model analyses and indicates the importance of eddy momentum as well as heat transfer. In summer the eddy forcing will change and consequently the mean circulation will also change becoming weaker generally and losing its markedly two cell character. In the Southern Hemisphere where the eddies, particularly the standing wave-number one component, are weaker the mean circulation tends to have more of a three cell than a two cell pattern and the balance is more complicated. The mean circulation appears to be largely responsible for the warm midlatitude region in the lower stratosphere in winter and also appears to be associated with the main tropopause break in this region. It is not possible to infer the corresponding mesospheric mean circulations with confidence since the nature of the heat sources and heat and momentum fluxes are not sufficiently well established. However a means of dynamically cooling the summer pole region e.g. by general ascent and equatorwards horizontal heat transfer and warming the winter pole region e.g. by subsidence appear to be demanded by the thermal fields.

The basic equations (1) to (3) also provide the tools for other studies. They can be used directly in finite difference or spectral three-dimensional models for example and manipulated for many other investigations such as the assessment of the energy conversion that takes place in the atmosphere as discussed in the next section. The main difficulty in their use is that being non-linear partial differential equations they are not in general amenable to analytical solutions. A good deal of progress in stratospheric studies is, however, being made using perturbation techniques (starting with equations for the eddy components obtained as differences between the  $(\frac{du}{dt}, \frac{dv}{dt}, \frac{dT}{dt})$  equations derived from Eqs. (2) and (3) and the  $(\frac{du}{dt}, \frac{dv}{dt}, \frac{dT}{dt})$  Eqs. (9), (12) and (10) respectively), linearising and investigating possible wave solutions. For some purposes it may be advantageous to study changes of vorticity or potential vorticity rather than  $u$  and  $v$  directly. Mechanistic models based on this approach have contributed greatly to subjects such as the vertical propagation of waves, effects of critical levels, generation of sudden warmings etc. which are beyond the scope of the present paper but hopefully will receive further discussion during this seminar. (See also [Holton, 1975] for further detailed information on these topics.

**ENERGY CONSIDERATIONS:** The previous sections have shown that in order to study stratospheric and mesospheric composition and thermal structure in detail both eddy motions and mean circulations have to be considered and these motions are interlinked. In addition there is good observational evidence that, although the typical systems of the troposphere of wavenumbers 3 to 9 decrease rapidly in intensity in the lower stratosphere, those of the very low wavenumbers particularly 1 and 2 may readily propagate to higher altitudes if the mean stratospheric winds are westerly but not if they are easterly (e.g. [Charney and Drazin, 1961]). It may be shown by multiplying the zonal ( $u$ ) and meridional ( $v$ ) component equations of Eq. (2) by  $u$  and  $v$  respectively, adding the result to  $C_p \times$  Eq. (3) and then integrating over the mass  $M$  of the stratosphere that

$$\frac{d}{dt} \int_M \left( \frac{u^2 + v^2}{2} + C_p T \right) dm = \int_M \dot{Q} dm + \int_A \left[ \left( \frac{u^2 + v^2}{2} + C_p T + \Phi \right) \frac{\omega}{g} \right] dA \quad \text{..(14)}$$

$P = P_T$

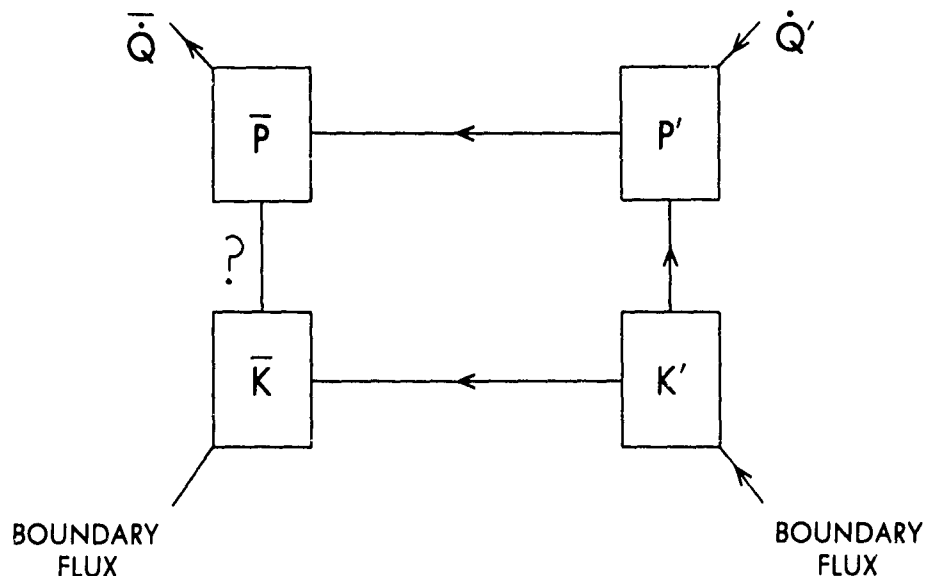
This equation indicates that the rate of change of total energy (kinetic plus total potential) in the Middle Atmosphere (neglecting transfer through its upper boundary) equals the rate of generation by radiative heating plus the flux of mechanical and total potential energy through the global surface  $A$  of the tropopause at pressure  $P_T$ . This rate of energy import when partitioned between mean and eddy components is found to be dominated by the eddy 'pressure interaction' term  $\omega \Phi$ . Accordingly many investigations have been made particularly in relation to 'sudden warming' phenomena attempting to relate this quantity (or its value at the low wavenumbers 1, 2 etc) to the behaviour of the stratospheric circulation. These studies first require the derivation of  $\omega$  fields which can be obtained by a number of well known techniques involving the use of the thermodynamic equation (3) or by the mass continuity equation directly or manipulations of the equations of motion (2) in the form of the vorticity or 'omega' equations. So far, however, the results of these investigations have not been particularly promising at least in the sense of producing a quantitative relationship between the size of the pressure interaction term and the magnitude of an ensuing sudden warming.

Within the stratosphere it is necessary to study the way the circulation exchanges between its kinetic energy  $K$  and available potential energy  $P$  components, both of which are again partitioned into their mean zonal ( $\bar{K}$ ,  $\bar{P}$ ) and eddy ( $K'$ ,  $P'$ ) forms. (Since the circulation arises because of the differences of potential energy between different localities it is these differences rather than their total potential energies which are important in deriving the budget of energy 'available' to drive and produce the kinetic energy of the circulation). It will be seen that, if an air column is relatively warm compared to another air column, further relative heating of the former will increase the available potential energy whereas if it were cooled their differences would decrease. Since it has been calculated that the cold equatorial tropopause region is a radiative heat source and the warmer polar region a heat sink, the stratosphere is losing available potential energy and in face of this its circulation is maintained by the eddy kinetic energy it receives through the tropopause. Similar statements can be made regarding the mesopause region which also requires an energy

## Lorenz Cycles of Energy Conversions.

Boxes indicate energy types ( $\text{K J m}^{-2}$ ) and connecting lines conversions ( $\text{mwm}^{-2}$ ) with arrows in direction of conversions.

(a) Lower Stratosphere and Upper Mesosphere (Refrigerator type).



(b) Troposphere, Upper Stratosphere and Lower Mesosphere (Heat Engine type).

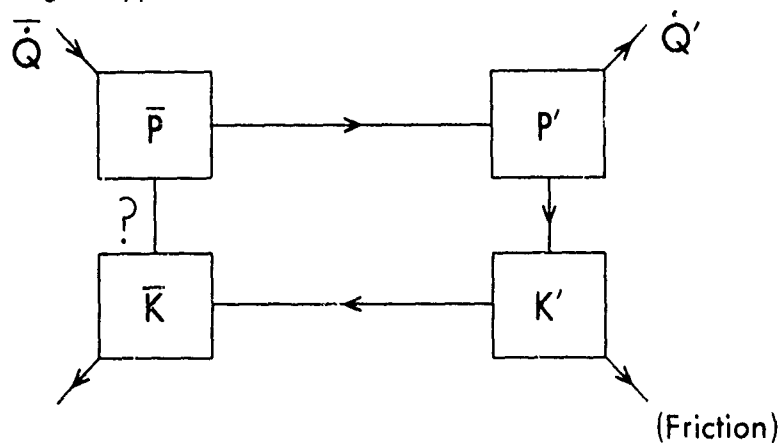


Figure 3

supply from below. It has also been found from diagnostic studies [Oort, 1964] that in the 100-30 mb layer the horizontal eddy heat flux is polewards against the mean temperature gradient (except at high latitudes in winter where it is downgradient) i.e.  $\overline{v' \frac{\partial T}{\partial y}}$  is positive which can be shown to represent a transfer from eddy to zonal available potential energy. Moreover the term  $\overline{u' \frac{\partial u}{\partial x}}$  in this layer is also positive in low latitudes representing a transfer from eddy to zonal kinetic energy. The eddy kinetic energy is also converted to eddy available potential energy which is generated when relatively warm air sinks within the eddies which, except at the very low wavenumbers in winter, rapidly become less intense as they penetrate upwards into the stratosphere. The above energy transfers may be regarded as 'refrigerator' cycles in the lower stratosphere and also the upper mesosphere and 'heat engine' cycles in the troposphere and upper stratosphere (where the radiation sources and high temperatures broadly occur in the same localities thus creating available potential energy). Fig. 3 shows a comparison of the two types of energy transfer sequences using the representation of [Lorenz, 1960]. It should be noted that these give broad annual averages for the whole of the Northern Hemisphere and details will vary somewhat with season and level. (See [Dopplack, 1971]).

**CONCLUSION:** Diagnostic studies and general circulation models based on Eqs. (1) to (3) together with radiation calculations have confirmed most of the general ideas mentioned in the Introduction as regards the overall nature and characteristics of the stratosphere, yet at the same time have demonstrated that its dynamics are of major importance in understanding and assessing the processes that take place (or may take place if it is perturbed in any way). In general it has high static stability due principally to the effects of heating by the ozone layer's absorption of solar ultraviolet radiation and this will limit unstable development. Thus it will not generally produce synoptic systems as in the troposphere. Moreover since the major means of transfer of tropospheric air to the stratosphere is apparently through the 'cold trap' of the low temperature tropical tropopause, its relative humidity is very low and cloudy 'weather' cannot generally be produced as in the troposphere. Energetically the lower stratosphere as a basically passive lid at the top of the active and denser troposphere has its circulation driven from below. This could be regarded as only an upward not very significant 'overshoot' or leakage of energy from the troposphere but, depending on the activity below and the wave propagation conditions, the stratospheric response can be major. This includes not only sudden warmings but the regular quasi-biennial oscillation. Some aspects of the climatological atmospheric structure such as the mid-latitude tropopause gaps and the latitudinal temperature distributions in the lower stratosphere are primarily due to the effects of the motions.

It is evident that conditions in the stratosphere as well as being strongly affected on the average by tropospheric characteristics will be varied by them on a short term basis. Seasonal changes, hemispheric differences and transient as well as standing wave activity in the troposphere are all contributors to stratospheric variability. In addition the conditions for upward propagation of wave energy from troposphere to middle stratosphere or above depend on the wind structure at all intermediate levels. Finally the amount of absorption of this propagated wave energy and the height at which it mainly occurs depends on conditions in the stratosphere itself e.g. the presence of critical levels, radiative and photochemical damping. Variations that take place in the eddy activity will also lead to variations in the mean circulation and to the fluxes of species between troposphere and stratosphere. It will be expected and indeed it is known that the fields of the various long-lived constituents will have small scale distributions determined by the synoptic systems, and just as waves are associated with given motion and temperature distributions they are likely to have similar relations with constituent distributions. Further detailed studies and a wider appreciation of the importance of tropospheric as well as stratospheric dynamics seem essential for future progress in understanding and modelling the behaviour of constituents.

It is not possible as yet to make statements regarding the characteristics of the mesosphere with as much confidence as for the stratosphere but hopefully the data to be obtained in the next few years will greatly improve that position. However present indications are that dynamical systems are also of great importance in determining its structure and energetically the mesopause region has many features that are similar to that of the tropopause region.

## REFERENCES

- Charney, J.G., P.G. Drazin, Propagation of Planetary Scale Disturbances from the Lower into the Upper Atmosphere, Journal of Geophysical Research, 66, 83-109, 1961.
- Dopplack, T.G., The Energetics of the Lower Stratosphere Including Radiative Effects, Quarterly Journal of the Royal Meteorological Society, 97, 209-237, 1971.
- Holton, J.R., An Introduction to Dynamic Meteorology, New York, Academic Press, 319, 1972.
- Holton, J.R., The Dynamic Meteorology of the Stratosphere and Mesosphere, Meteorological Monograph, 15, No. 37 American Meteorological Society, 218, 1975.
- Lorenz, E.N., Energy and Numerical Weather Prediction, Tellus, 12, 364-373, 1960.
- Murgatroyd, R.J., The Structure and Dynamics of the Stratosphere, The Global Circulation of the Atmosphere, G.A. Corby, Ed., London, Royal Meteorological Society, 159-195, 1969.
- Oort, A.H., On the Energetics of the Mean and Eddy Circulations in the Lower Stratosphere, Tellus, 16, 309-327, 1964.

# RADIATIVE ENERGY SOURCES AND SINKS IN THE

## STRATOSPHERE AND MESOSPHERE

Julius London

Dept. of Astro-Geophysics, University of Colorado  
Boulder, Colorado

### Abstract

Individual components for the seasonal net radiative heating and cooling distributions are presented as functions of latitude and height in the middle atmosphere (20-100 km). The principal gases involved in the radiative budget in this region are molecular oxygen and ozone (heating), and carbon dioxide and ozone (cooling). In addition, other radiatively active gases such as nitrogen dioxide and water vapor provide minor contributions to radiative energy sources and sinks for these levels. Approximate radiative equilibrium obtains in the lower stratosphere but at high latitudes in the upper stratosphere, mesosphere and lower thermosphere (40-100 km) there is strong net heating during the summer and net cooling during the winter seasons.

**INTRODUCTION:** The thermal structure and dominant wind fields in the stratosphere, mesosphere and lower thermosphere are largely functions of the chemical composition and strengths of the radiative energy sources and sinks of that region. At these levels the concentration of trace gases (and their variations) result from interactions in a non-linear system that involves atmospheric transport, both horizontal and vertical, and temperature dependent chemical kinetics. In turn the distribution of the trace gases affect the net radiative absorption and emission patterns that produce the circulation fields.

The lower and middle stratosphere is in approximate radiative equilibrium and its circulation is forced mainly by the vertical transport of mechanical energy from below (e.g., Louis et al., 1974; Holton, 1975). In the upper stratosphere and mesosphere, on the other hand, strong radiative imbalances exist that act to produce a direct circulation pattern with rising motion in polar regions during the summer and subsidence in polar regions during the winter (e.g., Murgatroyd, 1971; Park and London, 1974). Radiative processes at these levels help maintain strong quasi-horizontal meridional transport in the winter hemisphere. The driving mechanism for the circulation in the lower thermosphere is, by analogy, somewhat similar to that of the lower stratosphere in that the energy for its motions is derived from below, to effect a forced thermodynamically indirect (refrigerator type) circulation. The large scale dynamics of the middle atmosphere acts in one way or another as a response to the distribution of sources and sinks of radiative energy. We will review what is presently known of the radiative heating and cooling patterns in the region 20-100 km.



# LONDON

The zonally averaged temperature distribution in the middle atmosphere is shown in Fig. 1 and represents mainly summer and winter conditions in the Northern Hemisphere. The values are based on radiosonde observations (0-30 km), observations from the Meteorological Rocket Network (30-55 km) and indirect temperature measurements (above 55 km), as summarized by Groves (1971); Cole and Kantor (1975); Kantor and Cole (1975); Cole and Kantor (1977). Recent satellite derived temperature data for the stratosphere, mesosphere and lower temperature generally support the patterns obtained from the rocket measurements (Barnett et al., 1975; Houghton, 1979).

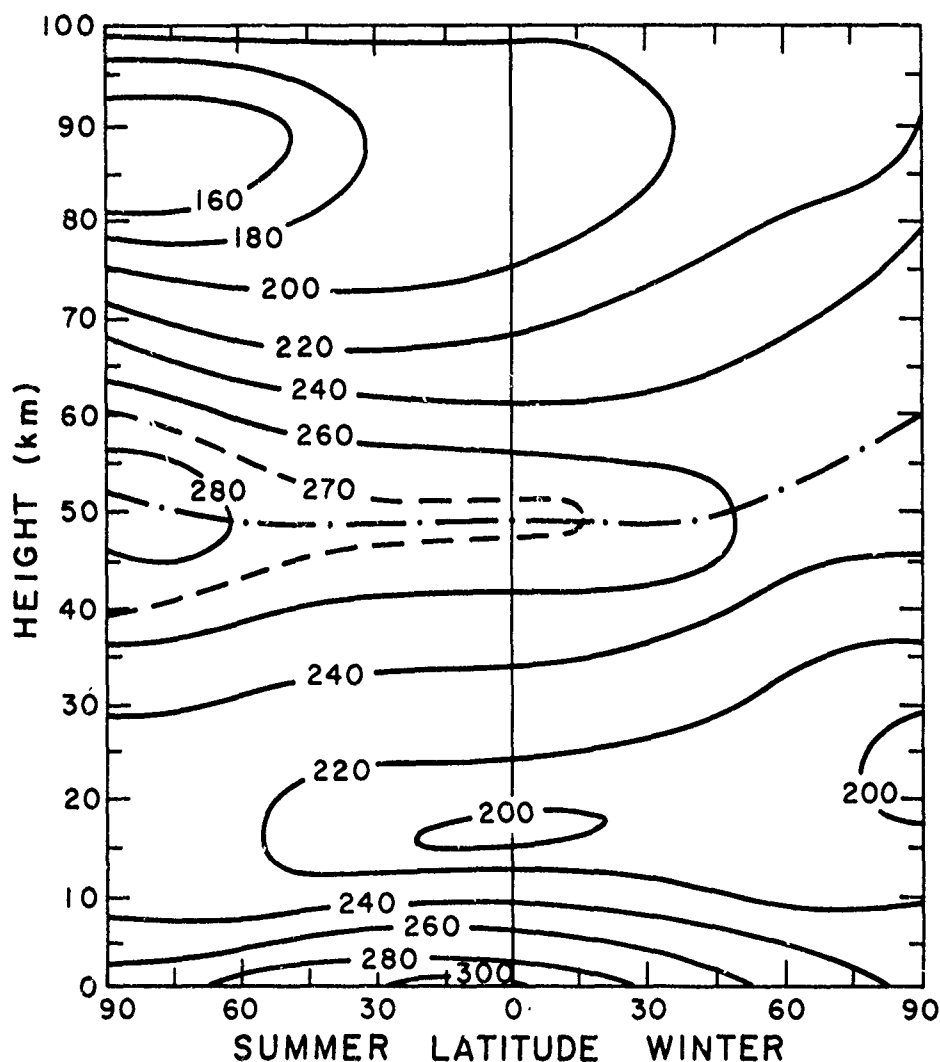


Fig. 1. The zonally averaged temperature distribution for summer and winter seasons, based mainly on Northern Hemisphere data.

The main features of the average observed temperature distribution can be summarized as follows:

1. A cold tropical tropopause ( $T < 200\text{K}$ ) and, in winter, a cold polar lower and middle stratosphere ( $T \sim 200\text{K}$ ).

## LONDON

2. A slight upward slope (with latitude) of the stratopause from the summer hemisphere ( $\sim 50$  km) to the winter polar regions ( $\sim 60$  km) with a positive latitudinal temperature gradient at these levels.  $T \sim 255$ K at the winter pole, and  $T \sim 285$ K at the summer pole.
3. A temperature minimum at polar and equatorial regions at the summer mesopause at a height of about 85 km ( $T \sim 160$ K at the summer pole) and a broad temperature minimum at the winter polar mesopause centered at a height of about 90 km ( $T \sim 210$ K).

The stratosphere is thermally stratified (temperature inversion) but less so at high latitudes during the winter than during the summer. In the mesosphere there is a marked seasonal variation in the vertical temperature gradient. The average lapse rate between the polar stratopause and mesopause is about  $3\text{ K km}^{-1}$  during the summer and just over  $1\text{ K km}^{-1}$  during the winter. The larger summer lapse rate results from the interaction of radiative and dynamical processes in the mesosphere (e.g., Holton, 1975) and helps to produce and maintain the sharp, cold polar mesopause during the summer.

The thermal structure of the lower stratosphere was first explained by Humphreys (1909) based on the assumption that the stratosphere was in radiative equilibrium with the underlying atmosphere which itself was in radiative equilibrium with solar irradiance. For a planetary albedo of 0.3, the effective radiative temperature of the underlying atmosphere is 254K and that of the stratosphere is then 214K, a value close to the present adopted standard temperature of the lower stratosphere.

It was later suggested by Lindemann and Dobson (1923) that the indirectly observed maximum at about 50-60 km resulted from absorption of solar ultraviolet radiation by ozone. This suggestion led to the first non-gray calculations to determine the temperature distribution of the stratosphere (11-55 km) under conditions of radiative equilibrium (Gowan, 1928, 1947). His computed equilibrium temperature at the stratopause was much too high mostly as a result of the high assumed solar ultraviolet irradiance and neglect of  $\text{CO}_2$  infrared emission at levels above 30 km.

More realistic radiative equilibrium temperature distributions were calculated by Manabe and Moller (1961) and Manabe and Strickler (1964) for the troposphere and lower stratosphere. A self consistent photochemical/radiative equilibrium ozone and temperature distribution in the upper stratosphere and mesosphere was derived by Leovy (1964). He considered an active photochemical system limited to oxygen allotropes, absorption of solar ultraviolet radiation by  $\text{O}_2$  and  $\text{O}_3$  and infrared emissions due to  $\text{CO}_2$  and  $\text{O}_3$ .

According to Leovy's results the radiative equilibrium temperature at 20 km is about 210K and is a maximum of about 305K at the summer polar stratopause at about 50 km. The equilibrium temperature then decreases to a minimum at a height of 70 km to less than 150K at the winter pole. The difference between the calculated radiative equilibrium temperature,  $T_r$ , and the observed temperature,  $T_o$ , indicates a local radiative energy source or sink. In the absence of other energy sources (i.e., latent heat, chemical heat, viscous dissipation) the radiative excess or deficit needs to be balanced by heat transport by the atmospheric circulation system (e.g., Dickinson, 1975).

At the earth's surface the radiative equilibrium temperature is everywhere higher than the observed temperature except in polar regions during the winter. The radiative excess at the surface is largest in equatorial and tropical regions. Radiative processes produce an energy sink in the troposphere. The distribution of net radiative heating and cooling in the atmospheric layer 0-15 km provides the direct potential energy source that powers the tropospheric circulation. A qualitative comparison of the radiative equilibrium and the observed temperature for the middle atmosphere is given in Table 1.

The importance of the radiative energy sources and sinks for the middle atmosphere can be seen in a comparison of the radiative and dynamic relaxation times. Large scale heat transport by atmospheric motions has a characteristic time of the order of 5-10 days in the troposphere (Van Mieghem, 1978) and 20-30 days in the stratosphere (Murgatroyd, 1971). The relaxation time for radiative cooling, on the other hand, varies from about 20 days in the troposphere and lower stratosphere (Manabe and Strickler, 1964; Sasamori and London, 1966; Hering et al., 1967) to a minimum of about 4-5 days at the stratopause and then increases

Table 1. Comparison of Approximate Radiative Equilibrium and Observed Temperature in the Middle Atmosphere

Height	Latitude	$T_r$ ( $^{\circ}\text{K}$ )	$T_o$ ( $^{\circ}\text{K}$ )	Radiative Energy Source/Sink
20 km	60° summer	215	225	Weak sink
	Equator	215	210	Weak source
	60° winter	205	215	Weak source
50 km	60° summer	305	275	Strong source
	Equator	285	265	Source
	60° winter	250	255	Weak sink
80 km	60° summer	235	185	Strong source
	Equator	225	190	Source
	60° winter	190	210	Sink

slightly through the mesosphere to about 10-20 days at 70 km (Dickinson, 1973; Alimandi and Visconti, 1979). Satellite observations at high latitudes during the winter indicate a time constant for radiative cooling at 42 km of about 6 days (Houghton, 1978). Photochemical coupling with the radiation field in the presence of solar radiation will shorten the radiative relaxation time in the upper stratosphere and mesosphere by about a factor of 2 (Blake and Lindzen, 1973; Strobel, 1978; Hartmann, 1978; Alimandi and Visconti, 1979). These faster time constants have also been inferred from satellite observations near the stratopause (Ghazi et al., 1979). As a result, radiative processes generally play a larger role in determining the thermal structure of the middle atmosphere than of the troposphere.

**RADIATION IN THE MIDDLE ATMOSPHERE:** In principle, the radiative transfer equation can be solved to yield the net radiative heating or cooling for a unit volume element in the atmosphere (see, for instance, Goody, 1964). The solution involves integration of the differential equation over:

- spherical geometry of the radiation field;
- all frequencies for which the extinction coefficients (absorption and scattering) are non-zero;
- the relevant range of optical depths for all significant absorbing and or scattering components in the atmosphere.

In practice, however, the equations can be solved analytically only in a few cases with rather limiting assumptions. Full numerical solutions require a priori information of:

- the temperature distribution and absorbing gas concentrations as functions of pressure in the atmosphere;
- the vertical distribution of aerosol concentrations;
- radiative boundary conditions. For the upper boundary, this involves the solar spectral irradiance; for the lower boundary the upwelling reflectance and thermal emittance characteristics are needed.

Some of the basic problems involved in calculations of radiative heating and cooling in the stratosphere and mesosphere are briefly summarized below. These problems have been discussed by Rodgers and Walshaw (1966). More recent discussions are contained in Ramanathan and Coakley, 1978; Tiwari, 1978, and others.

## LONDON

Hemispheric integration of the upward or downward directed radiance is usually simplified with relatively little loss in accuracy by the use of a 'diffusivity' factor of 5/3. For a collimated radiation beam (solar radiance) the assumption of a plane parallel atmosphere is not valid for high zenith angles and a correction is needed for the slant path of the incoming radiation (e.g., Chapman function -- see, for instance, Craig, 1965) particularly for levels above about 55 km.

Since the line positions, strengths and profiles of the major radiatively active gases in the middle atmosphere are reasonably well known, frequency integration of the transfer equation can generally be performed in a fairly straightforward manner providing that sufficiently large computing facilities are available. For practical purposes, however, it is necessary to average the radiative transmittances over different spectral intervals within an absorption band or in some cases over several bands. Simple averaging procedures for the absorption of solar radiation have been discussed by Lacis and Hansen, 1974; Chou and Arking, 1979, and others. More complicated band averaging models have been compared and discussed by Tiwari, 1978. In some cases, as for instance, absorption and emission of near infrared and infrared radiation by  $\text{CO}_2$  in the stratosphere and mesosphere it is important to consider spectral bands other than the fundamental bands and bands other than those of the principal gas isotope.

Spectral line shapes for  $\text{H}_2\text{O}$ ,  $\text{CO}_2$  and  $\text{O}_3$  are determined by pressure (Lorentz) broadening in the troposphere and lower stratosphere, and by thermal (Doppler) broadening in the upper mesosphere and thermosphere respectively. Between 30 and 70 km the line profiles are of mixed (Voigt) form. Lorentz and Doppler half widths are equal for the molecular lines of these gases in the middle stratosphere (25-35 km). For individual nonoverlapping lines (weak and widely spaced) the integration takes place over the entire line and is independent of the line profile. However, for calculations applied to the stratosphere and mesosphere, an equivalent width given by a Voigt profile is generally most appropriate.

Integration of the transfer equation with respect to optical depth involves integration over a vertical path along which pressure, temperature and the absorbing gas concentrations vary. As a result, suitable approximations need to be made for the equivalent line shape and temperature sensitive line or band strength as applied to each optical depth interval in the computed integration. It is usual and sufficiently accurate to apply a Curtis-Godson mass weighted approximation for most middle atmosphere calculations (see, for instance, Tiwari, 1978). An important exception, however, is the case of the  $9.6\mu\text{m}$  ozone band where a correction to the Curtis-Godson approximation needs to be applied (see, for instance, Yamamoto et al., 1972).

Additional problems arise in consideration of absorption and emission processes in the upper mesosphere and thermosphere. These involve retardation of direct heating by absorption of solar radiation by molecular oxygen due to photochemical relaxation and by carbon dioxide due to radiative relaxation (Park and London, 1974; Williams, 1971). Although assumptions of local thermodynamic equilibrium for the infrared bands of ozone and water vapor are valid for all levels for which these gases contribute significantly to the total radiative cooling, there are important deviations from a Planckian source function for carbon dioxide emission above about 75 km (see, for instance, Kuhn and London, 1969; Shved, 1974).

**GLOBAL AVERAGE COMPONENTS OF RADIATIVE HEATING AND COOLING:** Calculations of global average radiative heating and cooling components at various levels in the atmosphere up to 100 km have been made by Manabe and Möller (1961); Yamamoto (1962); Manabe and Strickler (1964); Houghton (1965); Dopplack (1972); Alimandi and Visconti (1979), and others. A composite of the calculated distributions for different atmospheric gases is shown in Fig. 2. The global average net radiative temperature change is shown in Fig. 3.

The most important radiatively active gases in the atmosphere, up to a height of about 100 km, are molecular oxygen, ozone, carbon dioxide and water vapor. Absorption of solar ultraviolet radiation by molecular oxygen and ozone are responsible for strong radiative heating in the thermosphere and in the region of the stratopause. This is balanced, in part, by infrared cooling by carbon dioxide and to a lesser extent by ozone. Radiative cooling in the troposphere due mainly to infrared emission by water vapor, is partially offset by

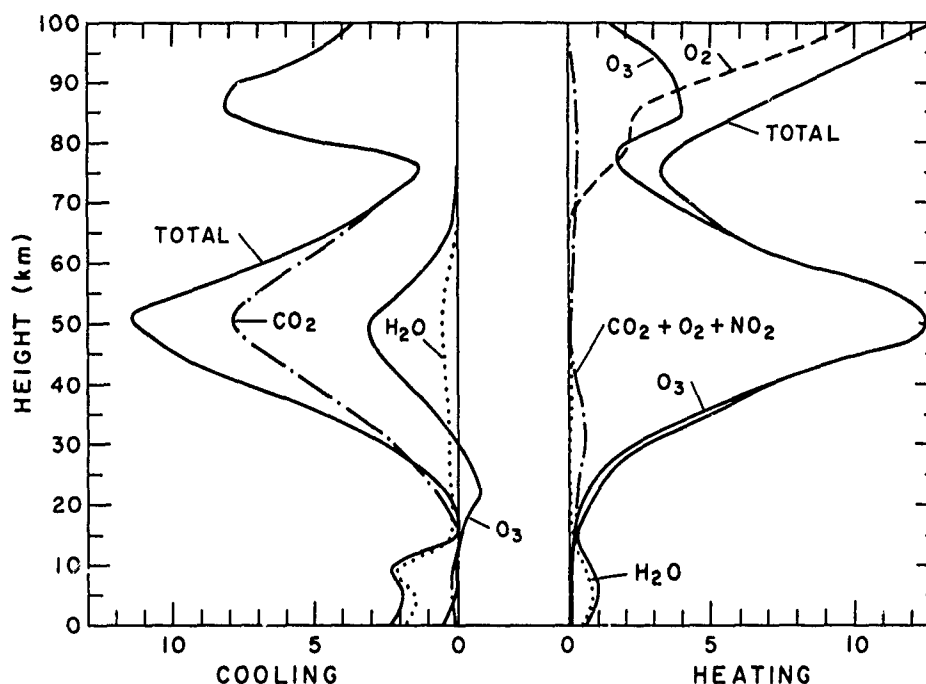


Fig. 2. Components of the global average radiative heating and cooling (0-100 km) ( $^{\circ}\text{K day}^{-1}$ ).

absorption of solar radiation in the near infrared. Radiative temperature changes involving carbon dioxide or ozone in the troposphere are relatively minor.

The troposphere is radiatively cooled (about  $1\text{K day}^{-1}$ ) and the lower stratosphere is heated slightly (about  $0.5\text{K day}^{-1}$ ). The latter results from infrared exchange between the cold lower stratosphere and the relatively warm earth's surface. The middle stratosphere and mesosphere is, on the average, in radiative equilibrium. But the upper stratosphere and mesosphere is warmed radiatively ( $1\text{-}2\text{K day}^{-1}$ ) as a result of net excess heating by ozone absorption. Absorption by molecular oxygen is chiefly responsible for the increased net heating in the lower thermosphere. The average summer and winter latitudinal distribution of radiative heating and cooling rates for the middle atmosphere (200-100 km) are discussed below.

**ABSORPTION OF SOLAR RADIATION:** 1. Molecular Oxygen - Heating of the high latitude thermosphere, below 100 km, during the summer is due mostly to absorption of solar ultraviolet radiation by molecular oxygen in the Schumann-Runge bands. The absorbed energy dissociates  $\text{O}_2$  producing two  $\text{O}(^3\text{P})$  oxygen atoms and, where recombination is sufficiently fast, is directly available for thermal heating. For a relatively long chemical relaxation time for atomic oxygen ( $\sim 1$  day) the absorbed energy is partially stored (temporarily) as chemical energy until reconverted to thermal energy at a later time and different place. This process is analogous to that involving water vapor evaporation and condensation, a process of major importance for the energy cycle in the troposphere. Net heating rate calculations due to  $\text{O}_2$  absorption in the thermosphere have been discussed by Park and London (1974) and Stroebel (1978). Above about 80 km the photochemical relaxation time for  $\text{O}(^3\text{P})$  becomes much longer than 1 day (e.g., Park and London, 1974) and local chemical storage must be considered.

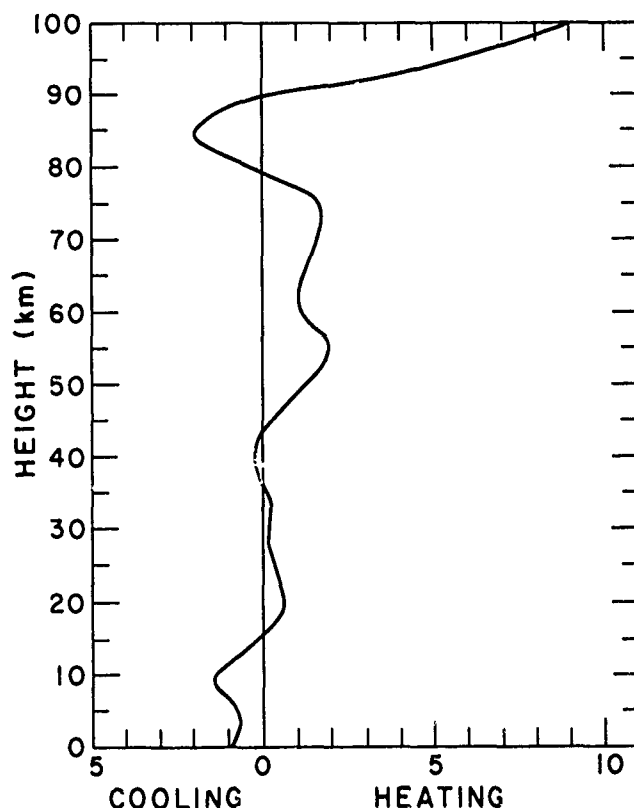


Fig. 3. Global average net heating/cooling due to radiative processes ( $^{\circ}\text{K day}^{-1}$ ).

As a result of horizontal and vertical transport, the energy released by atomic oxygen recombination is ultimately used for thermal heating at high latitudes in the thermosphere during the winter.

Recent discussions of the parameters involved in evaluation of the Schumann-Range band cross sections of  $\text{O}_2$  indicate some need for adjustments to the calculated heating rates at these levels (e.g., Kockarts, 1976; Hudson and Reed, 1979).

Absorption of solar radiation by  $\text{O}_2$  in the Herzberg continuum ( $\lambda < 242.4\text{nm}$ ) is important only in the stratosphere. But even in that spectral region, the absorption is overshadowed by stratospheric heating due to ozone absorption in the Hartley band (see, for instance, Strobel, 1978). Molecular oxygen absorption in the near infrared contributes slightly to the total heating in the lower stratosphere (see, for instance, Yamamoto, 1962; Houghton, 1963; Dopplnick, 1972). A parameterized expression for this absorption is given by Sasamori et al. (1972).

2. Ozone - Direct radiative heating of the upper stratosphere and mesosphere and the subsequent high temperature at the stratopause is a result of ozone absorption of solar radiation in the Hartley-Huggins bands (220-360nm). Calculations of the height and latitude distribution of this radiative heating have been discussed by Murgatroyd and Goody (1958), Park and London (1974) and many others. Parameterization of radiative heating rates in the stratosphere and mesosphere as functions of the ozone concentration and solar zenith angle

have been discussed by Lindzen and Will (1974), Lacis and Hansen (1974), and Strobel (1978). It should be noted that representative daily heating rates generally require diurnal averaging of the parametrically derived values.

Absorption by ozone in the Huggins (320-360nm) and the Chappuis (460-760nm) bands also contributes to radiative heating in the lower stratosphere. In the latter case, absorption of upwelling scattered solar radiation in the visible augments the direct heating by approximately 30 percent as originally suggested by Craig (1951) and recently confirmed by Strobel (1978) and Fiocco (1979).

The net heating due to absorption of solar radiation by ozone and molecular oxygen is shown in Fig. 4. The values are patterned after Park and London (1974) for levels above 30 km and after Dopplack (1972) for the lower stratosphere. The latter included the effects of the underlying albedo on the ozone absorption.

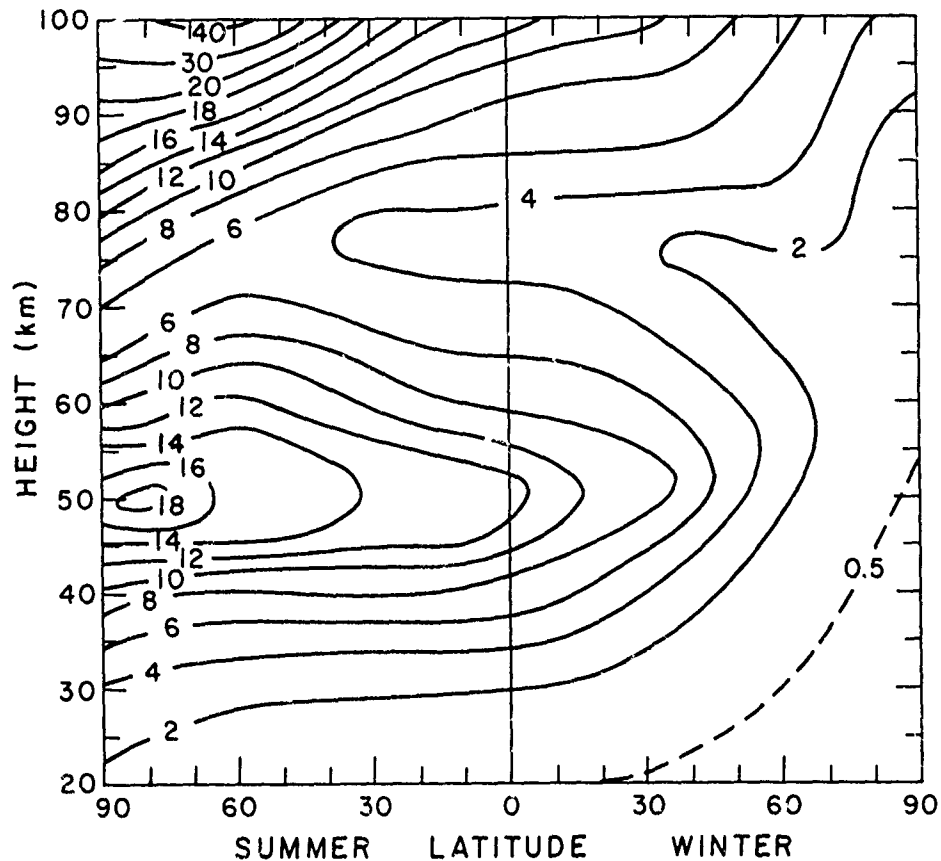


Fig. 4. Net heating due to absorption of solar radiation by  $O_3$  and  $O_2$  ( $^{\circ}K \text{ day}^{-1}$ ).

Ozone heating is very small, less than  $1K \text{ day}^{-1}$ , in the lower stratosphere but increases to a maximum of about  $18K \text{ day}^{-1}$  at high latitudes during the summer. The maximum ozone absorption takes place just above the peak ozone concentration (25-30 km). However, the absorption per unit mass (heating rate) occurs at about 50 km and the height of the strato-pause is determined by this level of maximum heating rate. The ultraviolet and visible solar energy absorbed by ozone in the stratosphere and mesosphere is sensitive to the

observed variations of the ozone concentration. Increased ozone will result in slightly increased absorption in the Huggins and Chappuis bands and thus increased heating of the lower and middle stratosphere. In the upper stratosphere, where the large optical depth for ozone is due to Hartley band absorption, increased ozone will lift the stratopause (i.e., the level of maximum heating) and will increase the heating rate at this level thereby increasing the lapse rate in the summer mesosphere.

The ozone mixing ratio and the heating rate decrease with height in the mesosphere up to about 75 km. At this level absorption by molecular oxygen becomes important. Although absorption in the Schumann-Runge bands accounts for less than  $10^{-4}$  of the total solar irradiance at the top of the atmosphere, the absorbed energy results in net heating (absorption minus energy used for molecular oxygen dissociation) of the lower thermosphere at high latitudes during the summer at a rate of about  $20\text{--}40\text{K day}^{-1}$ . The small heating in the lower thermosphere during the winter results from recombination of ground state atomic oxygen rather than direct absorption of solar ultraviolet radiation.

Absorption of solar radiation by molecular oxygen in the visible bands at  $0.76\text{ }\mu\text{m}$  contributes slightly to the total heating at about 20 km. These small effects were considered by Yamamoto (1962) and Doplick (1972) in their calculations and have been included in Fig. 5.

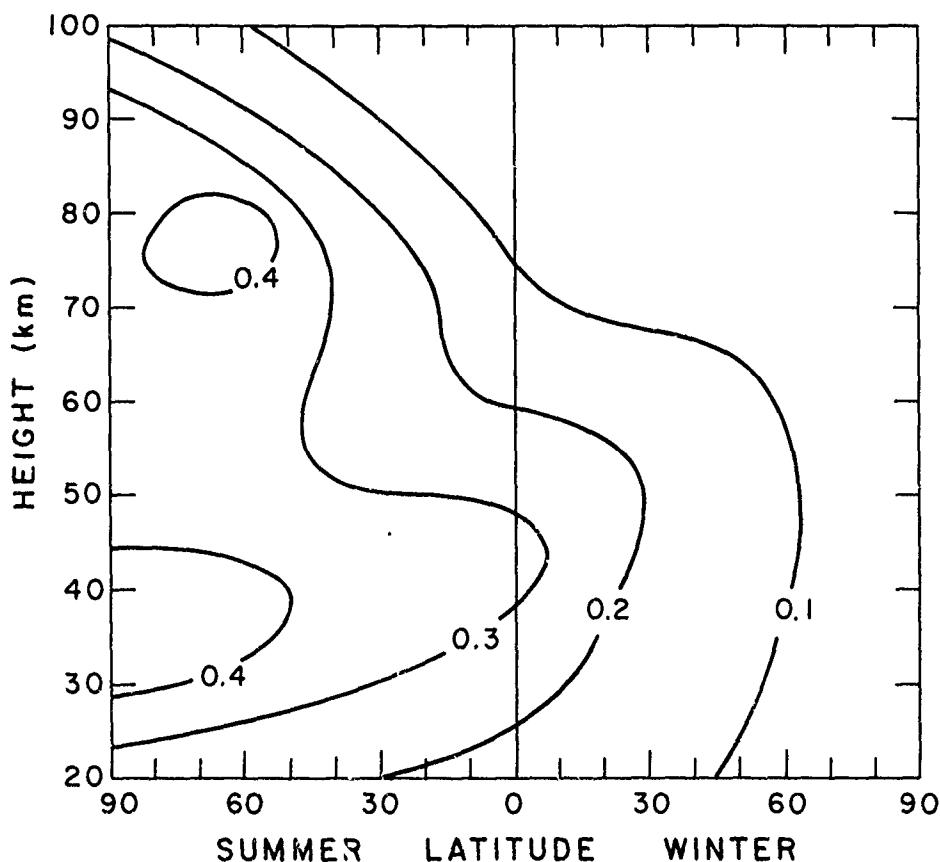


Fig. 5. Heating due to absorption of visible and near infrared solar radiation by  $\text{CO}_2$ ,  $\text{H}_2\text{O}$  and  $\text{O}_2$  ( $^{\circ}\text{K day}^{-1}$ ).



3. Carbon Dioxide - Absorption of solar radiation by near infrared bands of carbon dioxide was suggested by Kaplan (1966) to constitute a possible non-negligible radiative heat source in the summertime mesosphere. The two important  $\text{CO}_2$  absorption bands at these levels are at  $4.3 \mu\text{m}$  and  $2.7 \mu\text{m}$ . Although the  $4.3 \mu\text{m}$  band is the stronger of the two, as pointed out by Kaplan, the larger available solar energy at  $2.7 \mu\text{m}$  more than makes up the difference, particularly at high solar zenith angles. In the mesosphere, however, not all of the absorbed energy is immediately realized as kinetic (thermal) energy. At these levels vibrational relaxation is long enough so that much of the absorbed energy is reradiated in the  $15 \mu\text{m}$   $\text{CO}_2$  band. The collisional relaxation for the  $4.3 \mu\text{m}$  band has been discussed by Houghton (1967; 1969) who suggested a relaxation time of the order of  $7 \times 10^{-6}$  sec (STP) calculation of heating rates in the mesosphere by absorption of solar radiation in the  $2.7 \mu\text{m}$  and  $4.3 \mu\text{m}$  bands have been shown by Williams (1971) to be a maximum of about  $0.5^\circ\text{C day}^{-1}$  at about 80 km. In the stratosphere collisional de-excitation is rapid enough so that all of the absorbed energy is immediately realized as thermal heating. Calculation of the latitudinal and seasonal distributions of heating due to absorption in the near infrared  $\text{CO}_2$  bands have been carried out by Yamamoto (1962); Houghton (1963); Dopplnick (1972); and others. The results are generally quite consistent and are discussed below.

4. Water Vapor - Absorption of solar ultraviolet radiation at wavelengths below 195 nm by water vapor in the mesosphere and lower thermosphere result in photodissociation of the water molecule and contributes significantly to catalytic destruction of ozone at these levels. The amount of water vapor, however, is too small to influence the net radiative heating rates in the upper mesosphere and lower thermosphere. In addition, absorption of solar radiation at these wavelengths is effectively screened out by molecular oxygen absorption as discussed above.

Water vapor has a series of relatively weak absorption bands in the visible ( $0.55 \mu\text{m}$  -  $0.85 \mu\text{m}$ ) and a set of six rather strong bands in the near infrared ( $0.9 \mu\text{m}$  -  $1.9 \mu\text{m}$ ). In addition, the bands at  $2.7 \mu\text{m}$  and  $3.2 \mu\text{m}$  account for a small amount of absorbed solar radiation (Goody, 1964). Since the water vapor mixing ratio in the stratosphere and mesosphere is fairly low ( $\sim 3$ -4 ppm) absorption at altitudes above about 15 km is minor. In the troposphere, however, water vapor absorption is by far the most important radiative energy source and can account for midtropospheric heating of as much as  $1^\circ\text{K day}^{-1}$ .

The distribution of heating due to combined absorption of visible and near infrared solar radiation by  $\text{CO}_2$ ,  $\text{H}_2\text{O}$  and  $\text{O}_2$  is given in Fig. 5. The values are summarized from the results of Yamamoto (1962), Williams (1971), and Dopplnick (1972). Some adjustments to these heating rates have been suggested by Dopplnick (1979) but they do not affect the values shown here for the lower stratosphere. The heating rates are in general quite small and the heating is pretty much confined to the summer hemisphere. The maximum heating of  $0.5\text{K day}^{-1}$  at about 80 km is due to net absorption by  $\text{CO}_2$  at  $2.7 \mu\text{m}$ . In the stratosphere the heating results from absorption of solar radiation in the  $4.3 \mu\text{m}$  band of  $\text{CO}_2$ . As discussed above, heating due to absorption in the near infrared water vapor bands is negligible in the stratosphere and mesosphere because of the low water vapor concentrations at these levels.

5. Nitrogen Dioxide - Absorption of solar radiation by nitrogen dioxide in the stratosphere occurs in the near ultraviolet and visible spectral regions, from about 280 nm to 700 nm. Although  $\text{NO}_2$  is photodissociated at  $\lambda < 398$  nm, recombination with stratospheric ozone is fast and it can be assumed that all solar energy absorbed by  $\text{NO}_2$  is directly thermalized. At wavelengths below 300 nm the  $\text{NO}_2$  cross sections are significantly smaller than those for  $\text{O}_3$  and above about 600 nm the absorption is quite weak. The absorption peaks at about 410 nm and the spectral interval 300-600 nm needs to be considered for  $\text{NO}_2$  stratospheric heating calculation.

The earth/atmosphere system has an albedo in the near UV and visible slightly larger than 30 percent. The origin of this upwelling backscattered solar radiation lies mainly in the troposphere below the major region of  $\text{NO}_2$  absorption (middle stratosphere) and, as in the case of  $\text{O}_3$  absorption in the Chappuis (visible) bands, heating calculations for  $\text{NO}_2$  need to include the influence of this additional solar irradiance. The latitudinal distribution of radiative heating due to  $\text{NO}_2$  absorption has been discussed by Hesstvedt and Isaksen (1974) who incorporated the effects of both  $\text{NO}_2$  -  $\text{O}_3$  overlap and upwelling scattered visible

radiation in their computations.

Recent measurements in the spectral region below 420 nm indicate that the  $\text{NO}_2$  absorption cross sections used by Hesstvedt and Isaksen may have been about 10-15 percent too high (Johnson and Graham, 1974; Bass et al., 1976). Also, Hesstvedt and Isaksen assumed in their computations a column density above the tropopause of  $6 \times 10^{15} \text{ cm}^{-2}$ , a value somewhat larger than that observed (Noxon et al., 1979). Inclusion of these adjustments would not alter their computed heating rates significantly.

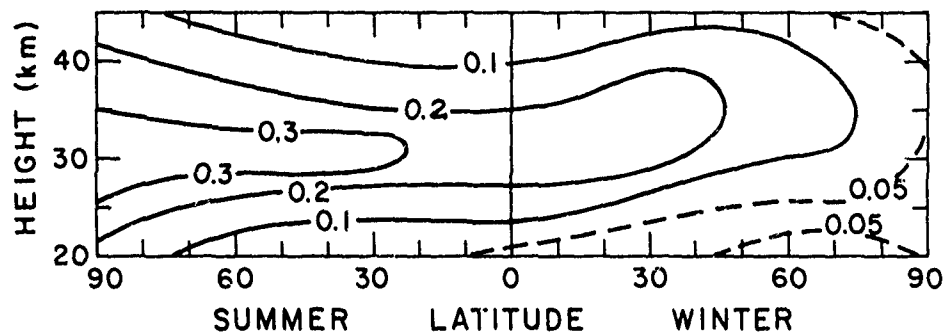


Fig. 6. Heating due to absorption of solar radiation by  $\text{NO}_2$  ( $^{\circ}\text{K day}^{-1}$ ).

The distribution of heating due to  $\text{NO}_2$  absorption as shown in Fig. 6 was patterned after the calculations of Hesstvedt and Isaksen. The  $\text{NO}_2$  radiative heating is a maximum in the summer hemisphere just above 30 km, close to the level of maximum  $\text{NO}_2$  mixing ratio. Although relatively small (only about 10 percent of the heating due to  $\text{O}_3$  absorption), it is comparable to the radiative input due to  $\text{CO}_2$  and  $\text{H}_2\text{O}$  in the middle stratosphere.

Additional absorption of solar radiation by  $\text{CH}_4$  ( $3.3 \mu\text{m}$ );  $\text{N}_2\text{O}$  ( $4.5 \mu\text{m}$ );  $\text{CO}$  ( $4.7 \mu\text{m}$ ) represent only very minor contributions to the lower stratospheric radiation budget as pointed out by Houghton (1963).

**INFRARED EMISSION.** 1. Carbon Dioxide - Infrared cooling in the stratosphere, mesosphere and lower thermosphere occurs mainly through radiative transfer in the  $15 \mu\text{m}$  band of  $\text{CO}_2$ . Early results of calculations for the stratosphere and mesosphere (Plass, 1965a; Ohring, 1958) indicated maximum cooling near the height of the temperature maximum (stratopause). In the region 30-75 km the cooling rate is sensitive to the temperature distribution as has been shown by Williams and Rodgers (1972). Relatively simple and fast approximate methods have been developed to calculate  $\text{CO}_2$  cooling as a function of the temperature (or temperature perturbation) at these heights (e.g., Dickinson, 1973). The level of equivalence for vibrational and radiational relaxation for the  $15 \mu\text{m}$   $\text{CO}_2$  band is about 75 km and computations by Murgatroyd and Goody (1958) and Kuhn and London (1969) included a non-local thermodynamic equilibrium source function in the transfer equation for application to their radiative cooling calculations above 70 km.

In addition to the dominant species, various isotopes constitute about 1.5 percent of the  $\text{CO}_2$  concentration in the atmosphere. Cooling rate calculations that include the fundamental and 'hot' bands for the most abundant and minor isotopes have been discussed by Williams and Rodgers (1972); Dickinson (1973); Alimandi and Visconti (1979) and others. The latitude/

# LONDON

height calculations of Williams and Rodgers (1972) are based on the earlier results of Kuhn and London (1969) with the addition of the extra radiative sources as mentioned above. The value assumed by them for collisional relaxation for the  $15\ \mu\text{m}$   $\text{CO}_2$  band of  $2 \times 10^{-5}$  (STP) is reasonably appropriate as recently suggested by Houghton (1978). The results of Williams and Rodgers indicate that significant contributions (of the order of  $\sim 2\text{K day}^{-1}$ ) to radiative cooling in the upper stratosphere and mesosphere can be made by the isotopic and 'hot' bands of  $\text{CO}_2$ . The distribution of infrared cooling due to  $\text{CO}_2$  shown in Fig. 7 is patterned after Kuhn and London (1969) and Dopplack (1972) in the lower and middle stratosphere (20-35 km), and Williams and Rodgers (1972) for the upper stratosphere, mesosphere and lower thermosphere (35-100 km).

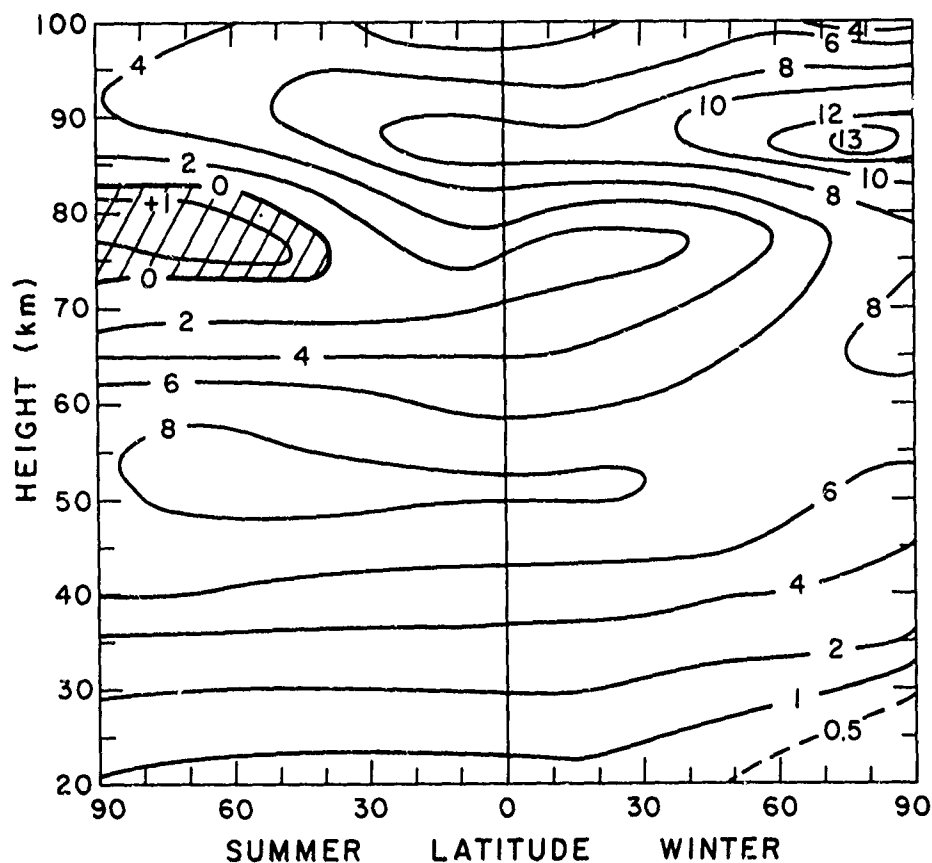


Fig. 7. Infrared cooling due to  $\text{CO}_2$  ( $^{\circ}\text{K day}^{-1}$ ).

Radiative cooling is very small in the troposphere and is less than  $1\text{K day}^{-1}$  up to about 20 km. The cooling, however, increases through the stratosphere. A strong radiative energy sink (cooling) is found at the summer stratopause ( $\sim 8\text{K day}^{-1}$ ) and at the winter mesopause ( $\sim 13\text{K day}^{-1}$ ) associated with the relatively warm temperatures in those regions. Radiative convergence leading to slight heating occurs in the regions of strong temperature minima--near the summer high latitude mesopause (cross hatched area) and the tropical tropopause (Dopplack, 1972, also, see Fig. 2). The values shown here are consistent in pattern with the results of Kuhn and London (1979) but with a  $1\text{-}2\text{K day}^{-1}$  increased cooling rate due to inclusion of the fundamental bands of four important isotopic species of  $\text{CO}_2$  and three higher level bands of the dominant isotope ( $\text{C}^{12}\text{O}_2^{16}$ ).

Calculations based on the temperature distribution shown in Fig. 1 would probably result in slightly increased cooling at the stratopause and decreased cooling in the lower thermosphere. The values shown here for the region above 80 km need to be regarded as tentative until the temperature dependence of the various band strengths and the vibrational relaxation time for the  $15\text{ }\mu\text{m}$   $\text{CO}_2$  band are better known. Also, the temperature distribution itself at these altitudes needs to be better documented.

2. Ozone - Approximately 25 percent of the total radiative cooling in the upper stratosphere is accounted for by infrared emission in the  $9.6\text{ }\mu\text{m}$  band of  $\text{O}_3$ . Calculations by Plass (1956b) and Kuhn and London (1969) show that a large part of this cooling is confined to a rather thin layer ( $\sim 10\text{ km}$ ) near the stratopause above which the temperature decreases and the ozone concentration falls off rapidly.

In the lower stratosphere, just below the average maximum ozone concentration, radiative transfer at  $9.6\text{ }\mu\text{m}$  leads to heating as first pointed out by Dobson et al. (1946). Since the  $9.6\text{ }\mu\text{m}$   $\text{O}_3$  band is in a spectral interval of principal atmospheric transparency, the lower part of the ozone layer can absorb a significant fraction of the energy emitted at this wavelength from the relatively warm earth's surface.

The distribution of infrared cooling in the stratosphere and mesosphere as shown in Fig. 8 is taken from Kuhn and London (1969) for the region above 30 km, and from Dopplack (1972) for the layer 20-30 km. Local thermodynamic equilibrium was assumed for the  $9.6\text{ }\mu\text{m}$   $\text{O}_3$  band since there is very little ozone present at heights for which a non-LTE source function is appropriate. As indicated in Fig. 8, there may be some very slight infrared ozone heating at about

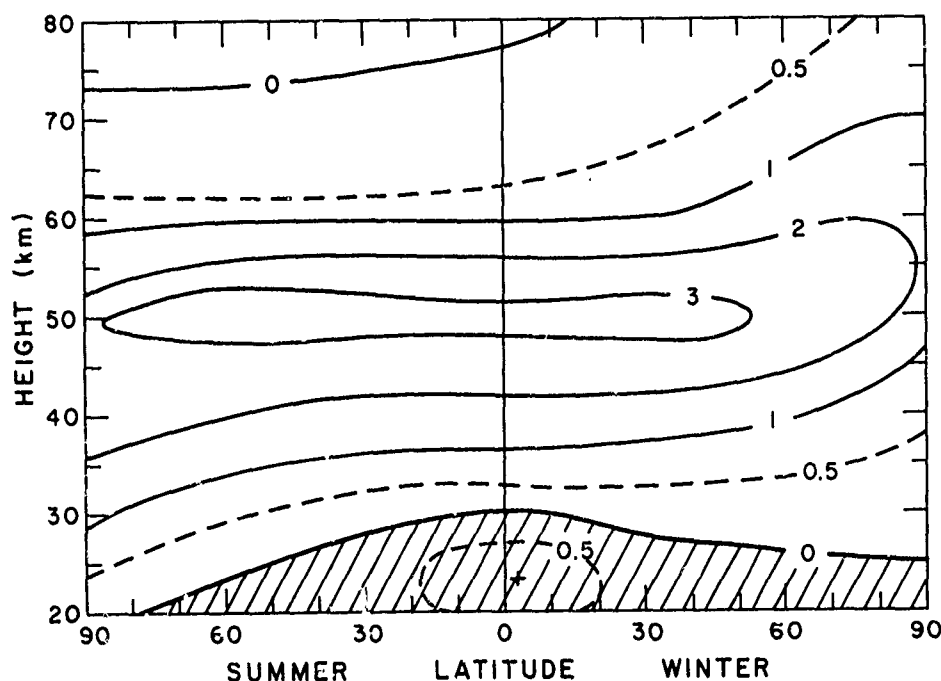


Fig. 8. Infrared cooling by  $\text{O}_3$  ( $^{\circ}\text{K day}^{-1}$ ).

80 km during the summer. Recent results of  $\text{O}_3$  cooling in this region published by Alimandi and Visconti (1979) are in general agreement with the values shown in Fig. 8.

3. Water Vapor - Infrared absorption and emission by water vapor in the  $6.3\ \mu\text{m}$  band controls the radiative energy loss in the troposphere. In the stratosphere and mesosphere, however, because of the generally lower temperature at these heights, the effective radiative cooling due to water vapor occurs through emission in the  $80\ \mu\text{m}$  rotation band. The water vapor mixing ratio above the tropopause is quite small ( $\sim 3\text{--}4\ \text{ppmm}$ ) and its contribution to the total radiative cooling is relatively minor (Rodgers and Walshaw, 1966; Kuhn and London, 1969).

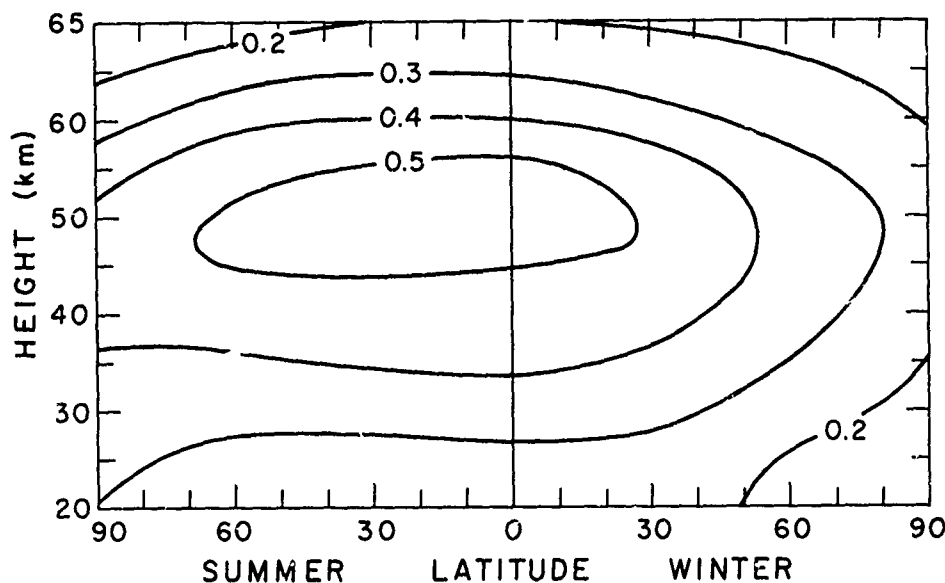


Fig. 9. Infrared cooling due to  $\text{H}_2\text{O}$  ( $^{\circ}\text{K day}^{-1}$ ).

The distribution of infrared radiative cooling due to water vapor in the stratosphere are shown in Fig. 9. The values were derived from the results of Kuhn and London (1969) and Dopplack (1972) and are consistent with those of Rodgers and Walshaw (1966) who included both the  $6.3\ \mu\text{m}$  and  $80\ \mu\text{m}$  bands in their computations. The maximum cooling at the stratosphere ( $\sim 0.5\text{K day}^{-1}$ ) represents less than five percent of the total infrared cooling at this level.

#### NET RADIATIVE ENERGY SOURCES AND SINKS IN THE STRATOSPHERE, MESOSPHERE AND LOWER THERMOSPHERE:

The atmospheric structure above 20 km is developed and maintained by a combination of radiative, mechanical and chemical energy sources and sinks. However, it is the initial input of absorbed solar radiation and ultimate infrared emission that is responsible for the overall temperature distribution, and the net imbalance of the radiation field (i.e., departures from radiative equilibrium) that provides the means by which atmospheric motions are activated to transport mechanical energy as part of the complete energy cycle. In this discussion we have summarized the individual radiative components that initiate the cycle. A composite of the average latitude and height distribution of net radiative heating and cooling for the summer and winter seasons is given in Fig. 10.

As a consequence of including the radiative contributions of additional isotopic species of  $\text{CO}_2$  (these additional isotopes account for approximately 1.5 percent of the total  $\text{CO}_2$  abundance--see, for instance, Alimandi and Visconti, 1979), and of the various 'hot' bands of the total  $15\ \mu\text{m}$  band system, infrared cooling in the stratosphere and mesosphere is significantly larger than that originally calculated by Murgatroyd and Goody (1958) and Kuhn and

# LONDON

London (1979). Thus, although the general pattern of radiative heating and cooling shown in Fig. 10 is very similar to that discussed by Park and London, the net global mean radiative budget for the stratosphere and mesosphere no longer indicates an energy excess. That is, on the average radiative heating during the summer is largely balanced by cooling during the winter. The overall balance, however, does not hold in detail and the horizontal (latitudinal) and vertical motions respond to adjust this detailed radiative imbalance.

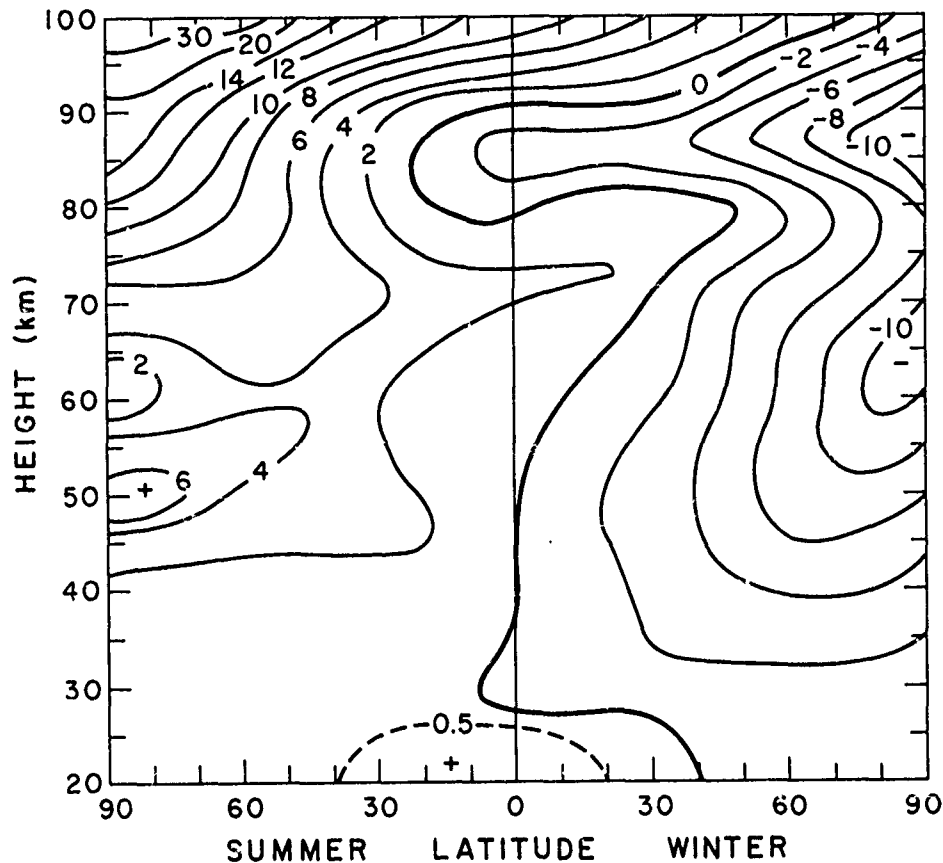


Fig. 10. Net radiative heating and cooling in the stratosphere, mesosphere and lower thermosphere ( $^{\circ}\text{K day}^{-1}$ ).

In the lower tropical stratosphere there is a weak net radiative energy source ( $+0.5\text{K day}^{-1}$ ) produced by infrared heating by ozone and, to a small extent, by carbon dioxide. The net heating at the summer stratopause ( $+6\text{K day}^{-1}$ ) represents the major radiative energy source for the stratosphere and mesosphere and, of course, is produced by the strong heating by ozone Hartley band absorption at these levels. The summertime net heating of the lower thermosphere indicates the importance of absorption in the Schumann-Runge bands by molecular oxygen. However, the heating at these levels may be somewhat too high since a temperature dependence of the mean absorption cross sections (e.g., Kockarts, 1976), particularly applicable for the extremely low temperatures at the summer mesopause, was not accounted for.

Although there is near radiative equilibrium in equatorial and tropical regions in the layer 25-50 km, the apparent net weak heating at 70 km combined with weak cooling at 85 km helps to

## LONDON

maintain the large vertical temperature lapse rate in the summer hemisphere. The major radiative energy sink is in the winter mesosphere and lower thermosphere. The net cooling seems to be concentrated in polar regions at about 65 km and 85 km ( $\sim -10\text{K day}^{-1}$ ).

In view of the strong heat source at the summer polar upper mesosphere and lower thermosphere, the very cold temperatures observed in that region must be maintained by dynamical processes if the heating and cooling patterns shown in Fig. 10 are reasonably correct. The relatively high temperatures observed in the winter polar mesosphere and lower thermosphere are presumably maintained by dissipation of hydrodynamic wave energy transported from below, large scale subsidence, and the release of stored chemical energy. Some recent dynamical studies (e.g., Schoeberl and Strobel, 1978) have addressed the problem of the mechanisms for transformation of the potential energy generated by the distribution of radiative energy sources and sinks to the motion field in the middle atmosphere and how the observed temperature distribution can be maintained.

ACKNOWLEDGEMENTS: Preparation of the manuscript was supported by the National Aeronautics and Space Administration under Research Grant NSG 5153. Technical assistance provided by Rose Gustafson and Mary Sable is gratefully acknowledged.

### REFERENCES:

- Alimandi, G. and G. Visconti, Thermal structure and relaxation rates of the perturbed radiative convection model, *Il Nuovo Cimento*, 2, 187-208, 1979.
- Barnett, J. J., R. S. Harwood, J. T. Houghton, C. G. Morgan, C. D. Rodgers and E. J. Williamson, Comparison between radiosonde, rocketsonde and satellite observations of atmospheric temperatures, *Quart. J. R. Met. Soc.*, 101, 423-436, 1975.
- Bass, Arnold M., Albert E. Ledford, Jr., and Allan H. Laufer, Extinction coefficients of  $\text{NO}_2$  and  $\text{N}_2\text{O}_4$ , *J. Research Nat. Bur. of Standards*, 80A, 143-166, 1976.
- Blake, Donna and Richard S. Lindzen, Effect of photochemical models on calculated equilibrium and cooling rates in the stratosphere, *Mon. Wea. Rev.*, 101, 783-802, 1973.
- Chou, Ming-Day and Albert Arking, A fast but accurate method for computing solar heating rates due to water, NASA Techn. Memo., TM 80254, 33pp., Apr. 1979.
- Cole, Allen E., and Arthur J. Kantor, Tropical atmospheres, 0 to 90 km, AFCRL-TR-0527, Env. Res. Pap., No. 536, 1975.
- Cole, Allen E., and Arthur J. Kantor, Arctic and subarctic atmospheres, 0 to 90 km, AFGL-TR-77-0046, Air Force Surveys in Geophys., No. 363, 11 Feb. 1977.
- Craig, R. A., Radiative temperature changes in the ozone layer, *Compend. of Met. Am. Met. Soc.*, 292-302, 1951.
- Craig, R. A., The upper atmosphere, *Internat. Geophys. Ser.*, 8, Academic Press, New York, 1965.
- Dickinson, Robert E., Method of parameterization for infrared cooling between altitudes of 30 and 70 kilometers, *J. Geophys. Res.*, 78, 4451-4457, 1973.
- Dickinson, Robert E., Energetics of the stratosphere, *J. Atmos. and Terr. Phys.*, 37, 855-864, 1975.
- Dobson, G. M. B., A. W. Brewer and B. M. Cwilog, Meteorology of the lower stratosphere, *Proc. Roy. Soc., London*, 185, 144-153, 1946.
- Dopplick, Thomas G., Radiative heating of the global atmosphere, *J. Atmos. Sci.*, 29, 1278-1294, 1972.

# LONDON

- Fiocco, G., Effects of scattering absorption and reflection of the solar flux in the stratosphere and troposphere, paper presented at the NATO Advanced Study Institute (to be published by the U. S. Federal Aviation Administration) 3 October 1979.
- Ghazi, A., V. Ramanathan and R. E. Dickinson, Acceleration of upper stratospheric radiative damping: observing evidence, *Geophys. Res. Lett.*, 6, 437-440, 1979.
- Goody, R. M., *Atmospheric radiation, theoretical basis*, Clarendon Press, Oxford, 1964.
- Gowan, E. H., The effect of ozone on the temperature of the upper atmosphere, *Proc. Roy. Soc.*, A120, 655-669, 1928.
- Gowan, E. H., Ozonosphere temperatures under radiation equilibrium, *Proc. Roy. Soc.*, A190, 219-226, 1947.
- Groves, G. V., Atmospheric structure and its variations in the region from 25 to 120 km, Air Force Systems Command, Rep. AFRCL-71-0410, No. 368, 1971.
- Hartmann, Dennis L., A note concerning the effect of varying extinction on radiative-photochemical relaxation, *J. Atmos. Sci.*, 35, 1125-1130, 1978.
- Hering, Wayne S., C. N. Touart and Thomas R. Borden, Jr., Ozone heating and radiative equilibrium in the lower stratosphere, *J. Atmos. Sci.*, 24, 402-413, 1967.
- Hesstvedt, Eigel and Ivar S. A. Isaksen, On NO<sub>2</sub> absorption of solar radiation and its role in the heat budget of the lower atmosphere, Institute Report Series, Univ. of Oslo, 6, 1-16, 1974.
- Holton, James R., The dynamic meteorology of the stratosphere and mesosphere, *Mnt. Mono.* 15, *Am. Met. Soc.*, 1975.
- Houghton, J. T., The absorption of solar infrared radiation by the lower stratosphere, *Quart. J. R. Met. Soc.*, 89, 319-331, 1963.
- Houghton, J. T., Infrared emission from the stratosphere and mesosphere, *Proc. Roy. Soc.*, A288, 545-555, 1965.
- Houghton, J. T., Fluorescence from the V<sub>3</sub> vibration of carbon dioxide, *Proc. Roy. Soc.*, 91, 439-448, 1967.
- Houghton, J. T., Absorption and emission by carbon dioxide in the mesosphere, *Quart. J. R. Met. Soc.*, 95, 1-20, 1969.
- Houghton, J. T., The stratosphere and mesosphere, *Quart. J. R. Met. Soc.*, 104, 1-29, 1979.
- Hudson, R. D. and E. I. Reed, The stratosphere: present and future, NASA Ref. Publ. 1049, 1979.
- Humphreys, W. J., Vertical temperature gradients of the atmosphere, especially in the region of the upper inversion, *Astrophys. J.*, 29, 14-32, 1909.
- Johnston, Harold S., and Richard Graham, Photochemistry of NO<sub>x</sub> and HNO<sub>x</sub> compounds, *Can. J. Chem.*, 52, 1415-1423, 1974.
- Kantor, Arthur J. and Allen E. Cole, Monthly midlatitude atmospheres, surface to 90 km, AFGL-TR-76-0140, Env. Res. Pap., No. 572, 1976.
- Kaplan, L. D., The absorption of solar radiation by CO<sub>2</sub>, *Les Problèmes Meteorologiques de la Stratosphere e' de la Mesosphere*, Centre National D'Etudes Spatiales, 307-312, 1966.
- Kockarts, G., Absorption and photodissociation in the Schumann-Runge bands of molecular oxygen in the terrestrial atmosphere, *Planet. Space Sci.*, 24, 589-604, Pergamon Press, 1976.



- Kuhn, W. R., and J. London, Infrared radiative cooling in the middle atmosphere (30-110 km), *J. Atmos. Sci.*, 26, 189-204, 1969.
- Lacis, Andrew A., and James E. Hansen, A parameterization for the absorption of solar radiation in the earth's atmosphere, *J. Atmos. Sci.*, 31, 118-133, 1974.
- Leovy, Conway, Radiative equilibrium of the mesosphere, *J. Atmos. Sci.*, 21, 238-248, 1964.
- Lindemann, F. A., and G. M. B. Dobson, Theory of meteors and density and temperatures of the outer atmosphere to which it leads, *Proc. Roy. Soc. London*, A102, 411-437, 1923.
- Lindzen, Richard S., and Douglas I. Will, An analytic formula for heating due to ozone absorption, *J. Atmos. Sci.*, 30, 513-515, 1973.
- Louis, Jean-Francois, A two-dimensional transport model of the atmosphere, PhD thesis, Dept. of Astro-Geophysics, Univ. of Colorado, 1974.
- Louis, Jean-Francois, Julius London and Edwin F. Danielson, The interaction of radiation and the meridional circulation in the stratosphere, *Proc. Int. Conf. on Struc., Melbourne, Australia*, 2, 1205-1214, 1974.
- Manabe, Syukuro, and Fritz Möller, On the radiative equilibrium and heat balance of the atmosphere, *Mon. Wea. Rev.*, 89, 503-532, 1961.
- Manabe, Syukuro, and R. F. Strickler, Thermal equilibrium of the atmosphere with a convection adjustment, *J. Atmos. Sci.*, 21, 361-385, 1964.
- Murgatroyd, R. J., and R. M. Goody, Sources and sinks of radiative energy from 30 to 90 km., *Quart. J. R. Met. Soc.*, 84, 225-234, 1958.
- Murgatroyd, R. J., Dynamical modelling of the stratosphere and mesosphere in mesospheric models and related experiments, Fiocco, ed., *Reidel Publ.*, 104-121, 1971.
- Noxon, J. F., E. C. Whipple, Jr., and R. S. Hyde, Stratospheric NO<sub>2</sub> -- observational behavior at mid-latitude, *J. Geophys. Res.*, 84, 5047-5065, 1979.
- Ohring, G., The radiation budget of the stratosphere, *J. Meteor.*, 15, 440-451, 1958.
- Park, J. H., and J. London, Ozone photochemistry and radiative heating of the middle atmosphere, *J. Atmos. Sci.*, 31, 1898-1916, 1974.
- Plass, G. N., The influence of the 15 $\mu$  carbon dioxide band on the atmospheric infrared cooling rate, *Quart. J. R. Met. Soc.*, 82, 310-324, 1956a.
- Plass, G. N., The influence of the 9.6 $\mu$  ozone band on the atmospheric infrared cooling rate, *Quart. J. R. Met. Soc.*, 82, 30-44, 1956b.
- Ramanathan, V., and J. A. Coakley, Jr., Climate modeling through radiative and convective models, *Rev. of Geophys. and Sp. Phys.*, 16, 465-489, 1978.
- Rodgers, C. D., and C. D. Walshaw, The computation of infrared cooling rate in planetary atmospheres, *Quart. J. R. Met. Soc.*, 92, 67-92, 1966.
- Sasamori, Takashi, and Julius London, The decay of small temperature perturbations by thermal radiation in the atmosphere, *J. Atmos. Sci.*, 23, 543-554, 1966.
- Sasamori, Takashi, Julius London and Douglas V. Hoyt, Radiation budget of the southern hemisphere, *Meteorological Monographs*, 13, 9-23, 1972.
- Schoeberl, M. R., and D. F. Strobel, The zonally averaged circulation of the middle atmosphere, *J. Atmos. Sci.*, 35, 577-591, 1978.

LONDON

- Shevd, G. M., Non-LTE radiative transfer in the vibration-rotation bands of linear molecules, *Sov. Astron.*, 18, 499-504, 1975.
- Strobel, Darrell F., Parameterization of the atmospheric heating rate from 15 to 120 km due to O<sub>2</sub> and O<sub>3</sub> absorption of solar radiation, *J. Geophys. Res.*, 83, 6225-6330, 1978.
- Tiwari, Surenda N., Models for infrared atmospheric radiation, *Adv. in Geophys.*, 20, 1-85, Academic Press, 1978.
- Van Mieghem, J., Scale analysis of large atmospheric motion systems in all latitudes, *Adv. in Geophys.*, 20, 87-130. Academic Press, 1978.
- Williams, A. P., Relaxation of the 2.7 $\mu$  and 4.3 $\mu$  bands of carbon dioxide. *Mesospheric Models and Related Experiments*, G. Fiocco, ed., Dordrecht, Holland, Reidel, 177-187, 1971.
- Williams, A. P., and C. D. Rodgers, Radiative transfer by the 15 $\mu$  CO<sub>2</sub> band in the mesosphere, *Proceedings of the International Radiation Symposium, Sendai, Japan, 253-260, 26 May - 2 June 1972.*
- Yamamoto, Giichi, Direct absorption of solar radiation by atmospheric water vapor, carbon dioxide and molecular oxygen, *J. Atmos. Sci.*, 19, 182-188, 1962.

## DYNAMICAL PROCESSES IN THE STRATOSPHERE:

### WAVE MOTIONS

Alan O'Neill †

U.K. Meteorological Office, London Road,  
Bracknell, Berks.

#### Abstract

Extra-tropical planetary waves generated in the troposphere exert a profound influence on the stratospheric circulation in winter. A brief account of the properties of these waves is given and the factors determining their associated fluxes of momentum, heat and energy are outlined. The conditions under which such waves may induce changes in the mean circulation are also described. Brief reference is made to the role of planetary-scale gravity waves in the circulation of the tropical stratosphere.

#### 1. Introduction

Dr. Murgatroyd, in a previous lecture, has outlined the principal dynamical processes determining the thermal structure and overall circulation of the stratosphere. In summary, stratospheric circulation patterns are produced primarily by a combination of mechanical forcing from the troposphere below and the local distribution of energy sources and sinks. As described by Dr. London, the latter results mainly from the absorption of solar energy by a layer of ozone molecules centered at about 50 km, together with the emission of infrared, thermal radiation by the  $15\mu$  bands of carbon dioxide and, to a lesser extent, by the  $9.6\mu$  band of ozone. The resulting net radiative heating has strong meridional and seasonal variations, with maximum heating at the summer pole and maximum cooling at the winter pole in the upper stratosphere, and provides the underlying drive for the seasonal wind reversals in the stratosphere.

As regards mechanical forcing from the troposphere, there is now a considerable body of evidence [see Holton, 1975, for a review] that upward-propagating, planetary-scale waves generated in the troposphere exert a profound influence on the stratospheric circulation in the winter hemisphere. A knowledge of these wave motions is often necessary in reliable studies of chemical processes in the stratosphere, since they act to redistribute trace gases within the stratosphere which consequently encounter different environmental conditions and various possibilities for photochemical interactions.

It is the purpose of the present lecture to describe these wave motions and to elucidate the principal theoretical advances that have led to progress in their understanding. Emphasis will be placed here on the properties of extra-tropical planetary waves and the factors which determine their structure, the directions of their associated fluxes of momentum, heat and energy, and the conditions under which they may induce changes in the mean circulation. Such

† Presently on secondment at the Joint Institute for the Study of the Atmosphere and Ocean, University of Washington, Seattle, Washington, 98195.

motions account for most of the eddy kinetic energy in the stratosphere. This description will serve as background for my subsequent lecture where the synoptic and dynamical features of stratospheric warmings will be described. In these warmings, extra-tropical planetary waves form an essential dynamical ingredient.

In addition, brief reference will be made to planetary-scale, gravity-wave modes in the equatorial stratosphere. These are also apparently excited in the troposphere and are believed to account for the quasi-biennial oscillation of the zonal wind in the equatorial stratosphere. Atmospheric tidal oscillations and gravity waves (other than those referred to above) will not be discussed because the waves have insufficient amplitude at stratospheric heights to influence significantly stratospheric dynamics or structure.

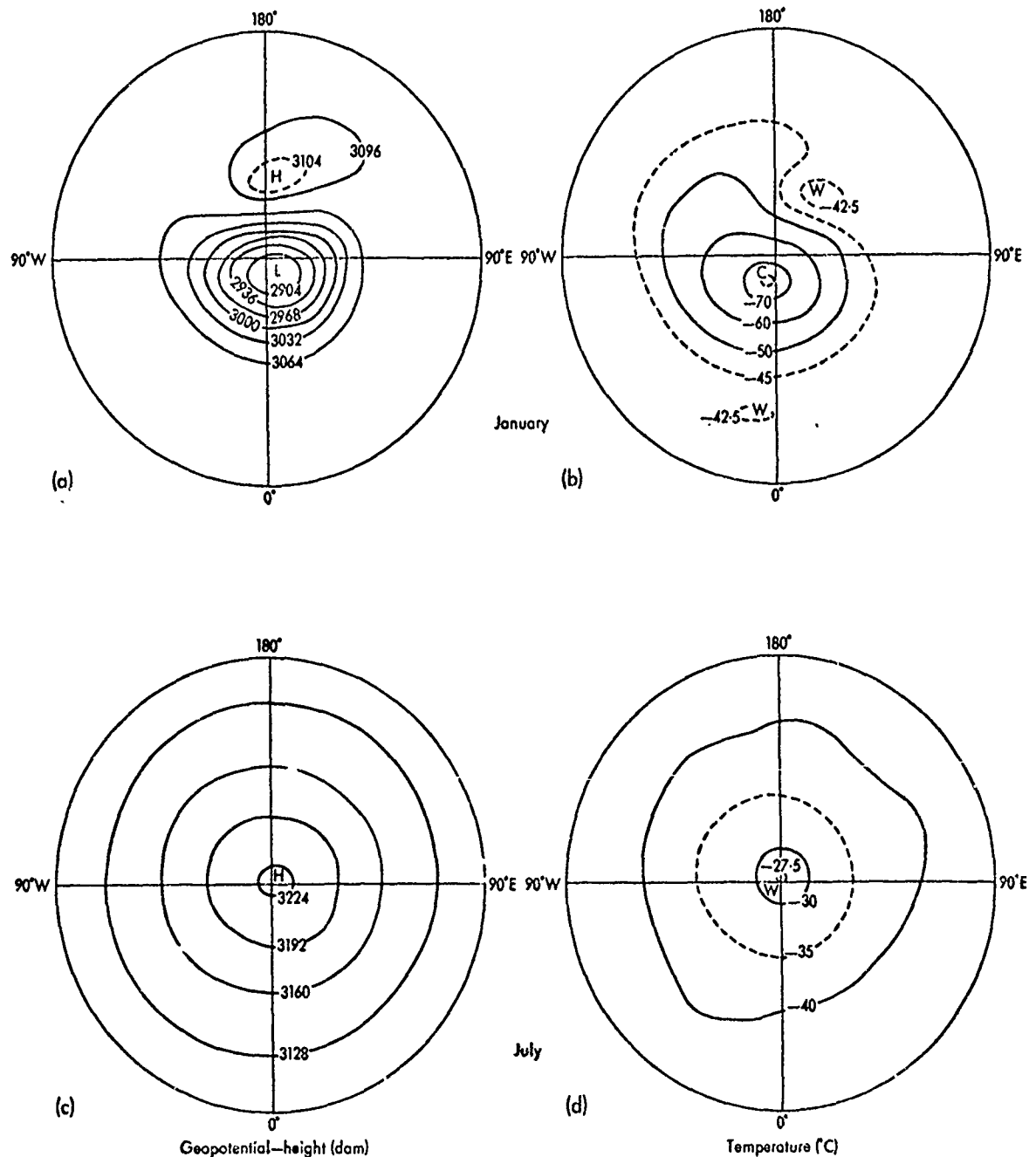


Fig. 1 Fields of geopotential-height (1 dam = 10m) and temperature at 10 mb for the Northern Hemisphere in winter and summer.

## 2. Wave structure in the stratosphere: observational basis.

A striking feature of the stratospheric circulation is its apparent simplicity as compared with that of the troposphere. Referring to Fig. 1, in summer the stratospheric flow is almost completely zonal with easterly winds around a warm anticyclone, approximately concentric with the pole. The winter mean circulation of the extra-tropical stratosphere above 100 mb in the Northern Hemisphere consists mainly of planetary waves of zonal wavenumbers (number of waves along a latitude circle) 1 and 2 superimposed on a zonal westerly flow around a cold polar vortex. These waves are quasi-stationary in phase (by which is meant that the geographical locations of the ridges and troughs remain approximately fixed) and tend to constructively interfere in the Northern Hemisphere winter stratosphere to produce the stationary anticyclone in the Aleutian sector, although they are subject to large-amplitude fluctuations. In the Southern Hemisphere winter stratosphere, the situation is broadly similar except that the wave perturbations are far less pronounced. Note that in Fig. 1, geopotential-height contours may be taken to approximate contours of geometric height, i.e., the actual height of the pressure surface above the ground.

Planetary-waves 1 and 2 have been shown to account for much of the variance in the stratospheric geopotential-height field during winter. This is clearly illustrated by Fig. 2, taken from Hare and Boville [1965], which highlights the pronounced difference in wave activity from winter to summer and shows that periods of relatively weak zonal wind in the winter stratosphere are well correlated with periods of enhanced wave activity, principally in wavenumber 1.

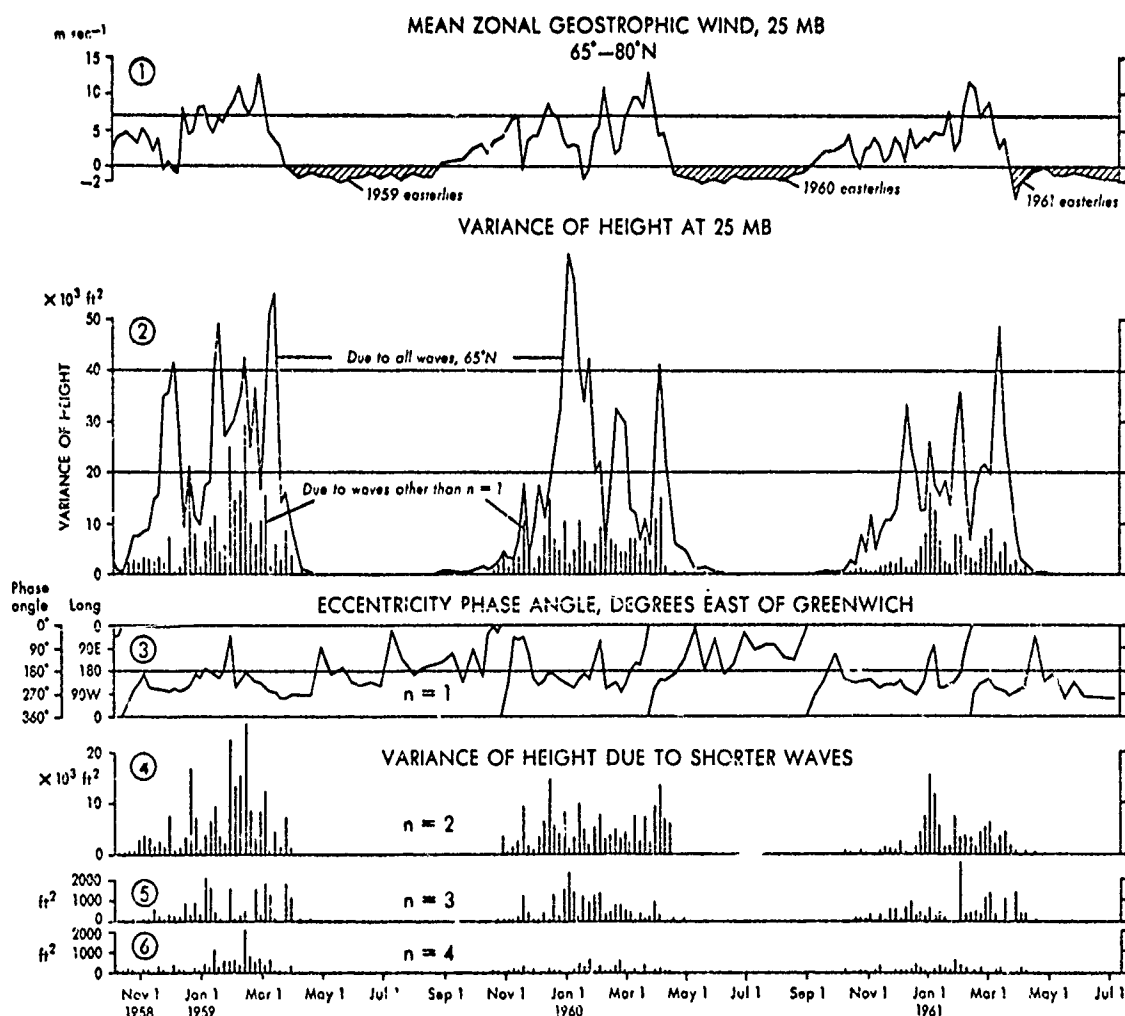


Fig. 2 Seasonal variability of the Northern Hemisphere stratosphere. Taken from Hare and Boville [1965].

Planetary-wave motions are often classified into stationary and travelling components, the former being usually defined as planetary waves with periods greater than 30 days, and thus appearing on monthly-mean charts, while the latter are considered as wave disturbances, travelling or otherwise, having a shorter time period. (Note, however, that the term "stationary" is also taken simply to mean zonal harmonic waves of zero phase speed relative to the ground, while "wave-transience" is a term frequently used to denote waves of fluctuating amplitude; these usages are adopted in Section 3). An important feature of the Northern Hemisphere winter stratosphere is that the stationary components of planetary-waves 1 and 2 are predominant. The vertical structures of these modes, as obtained by van Loon et al. [1973], are shown in Fig. 3, where contours of wave phase denote the location of the nearest wave ridge to the Greenwich meridian.

It may be seen that wavenumber 1 increases in amplitude with height at northerly latitudes and has a meridional structure which exhibits a westward vertical tilt of the trough/ridge axis with height, and a horizontal tilt of this axis from S.W. to N.E. in the middle stratosphere. Wave 2 behaves similarly but its amplitude increases much less rapidly with height

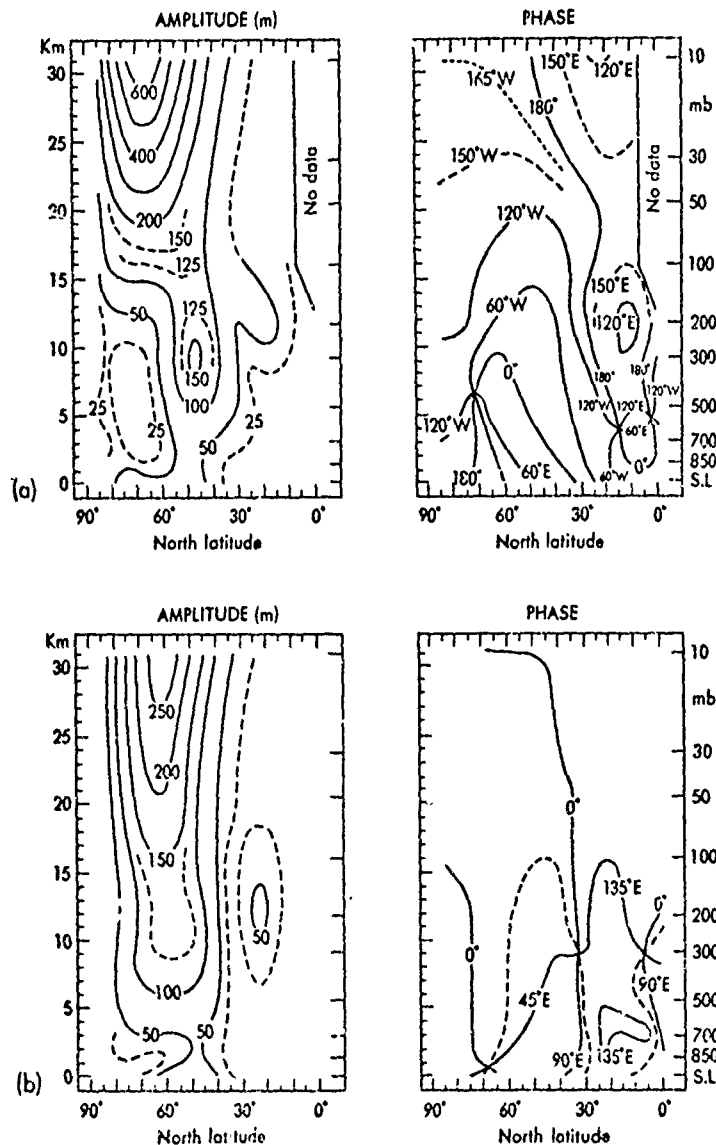


Fig. 3 Vertical structure of stationary waves in the Northern Hemisphere winter; (a) wave 1, (b) wave 2. Taken from van Loon et al. [1973].

than wave 1 (consistent with the dominance of a wave-1 pattern in the winter stratosphere exhibited in Fig. 1), and has relatively little vertical or meridional tilt in the stratosphere. Wave 3 and those waves of higher wavenumbers are essentially confined to the troposphere and contribute, in the mean, little to the overall structure of the stratospheric circulation patterns.

As may be seen by comparing Fig. 3 with the cross-section of zonal wind shown by Dr. Murgatroyd in his lecture, the meridional distribution of the wave disturbances has a close relation to that of the zonal wind. Namely the maximum amplitude of the wave is located at higher latitudes, corresponding to the presence of strong polar-night westerlies. This

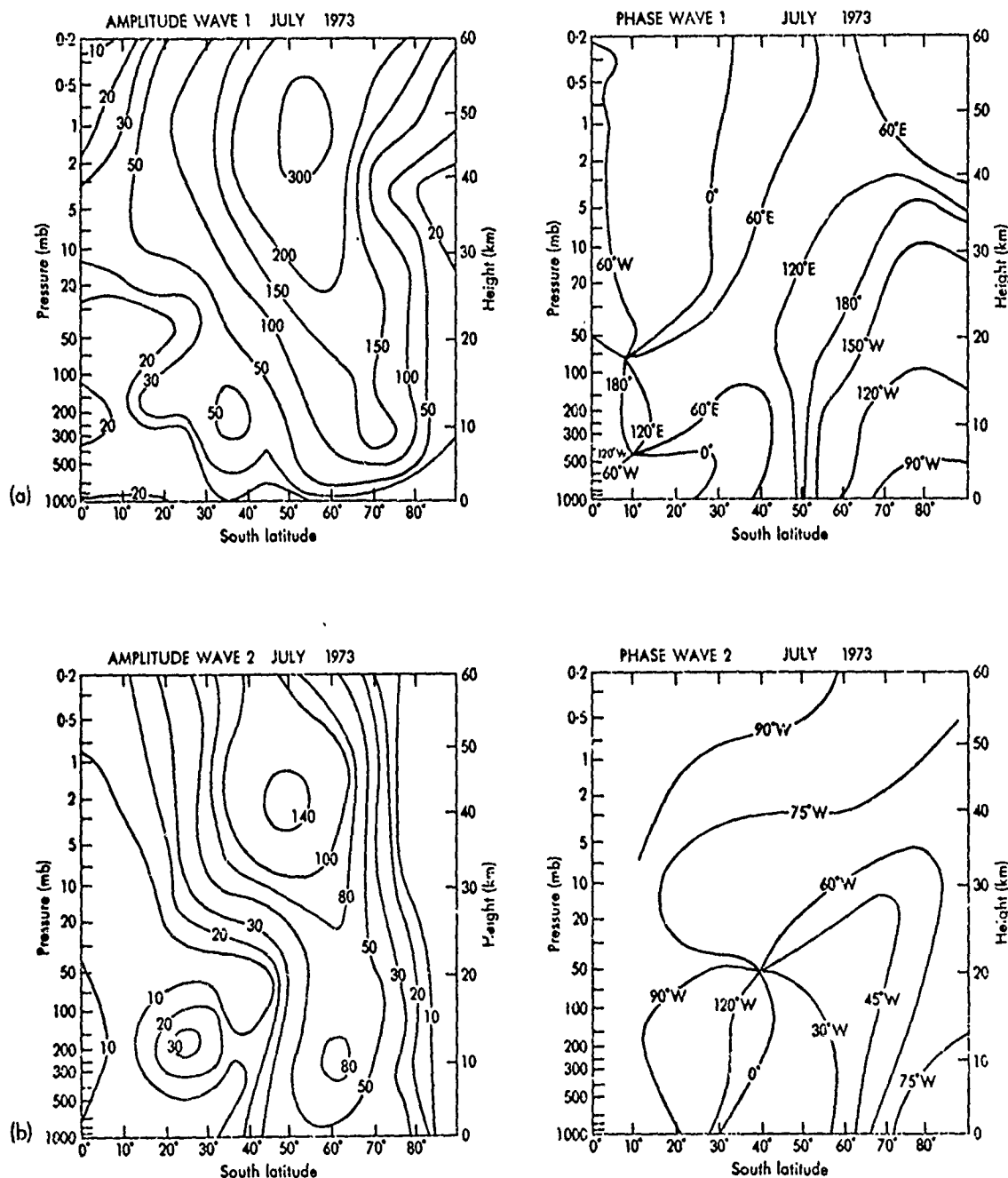


Fig. 4 Vertical structure of stationary waves in the Southern Hemisphere winter; (a) wave 1, (b) wave 2. Taken from Hartmann [1977].

"guiding" of the stationary planetary-wave disturbances into the region of strong mean zonal winds is a particularly important feature of the dynamics of the winter stratosphere which must be reproduced by any theory attempting to explain the presence of these wave motions in the stratosphere.

In the Southern Hemisphere winter stratosphere, similar quasi-stationary waves are found, as shown in Fig. 4, which is taken from Hartmann [1977]; note the change in scale along the ordinate as compared with Fig. 3. However, the disturbances are of much lower amplitude in the middle stratosphere than the corresponding waves in the Northern Hemisphere. In addition, no marked westward tilt with height is exhibited in the troposphere, which is likely to be a consequence of differences in continentality between the hemispheres.

As regards transient waves, comprising travelling waves and stationary waves of time-varying amplitude, while it has been noted that such waves are typically of much smaller amplitude than the stationary waves in the Northern Hemisphere stratosphere, in that of the Southern Hemisphere Deland [1973], Harwood [1975] and Hartmann [1975] have found prominent zonally-propagating components, particularly an eastward-propagating wave 2.

For zonal waves 1 and 2, this second type of transient behavior is of special importance to the dynamics of the winter stratosphere in the Northern Hemisphere. Muench [1965], Hirota and Sato [1969], and others have demonstrated that the amplitudes of these planetary waves vary daily on a time-scale of the order of two weeks. There is a similar variability in the vertical energy fluxes associated with these wave motions, which turns out to be linked to the most spectacular transient feature observed in the stratosphere—the sudden warming.

Fig. 5 shows that the observed vertical structure of planetary wave 1 in the stratosphere during summer is markedly different from that in winter, with comparatively very small amplitudes for the wave; this also applies to wave 2. Consequently, they have little impact on the general circulation and will not be described further.

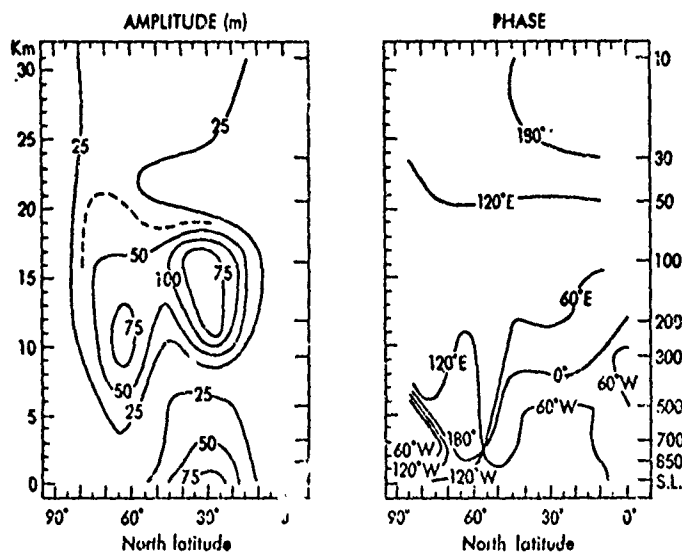


Fig. 5 Vertical structure of stationary wave 1 for the Northern Hemisphere in summer. Taken from van Loon et al. [1973].

### 3. Wave structure in the stratosphere: theoretical basis

It is now believed that the principal processes in the troposphere which lead to the upward propagation of planetary waves into the winter stratosphere are orographic forcing and differential heating associated with land/sea contrasts. These forcing mechanisms therefore excite primarily quasi-stationary wave modes—hence the dominance of these modes in the stratosphere. In addition, there may be some long-wave generation in the troposphere as a result of non-linear (wave-wave) interactions between waves on a smaller spatial scale produced by baroclinic instability in the troposphere.



In view of the above, it is reasonable to suppose that interhemispheric differences in stratospheric circulation characteristics are related to different conditions between hemispheres in the troposphere. This is supported by detailed studies involving general circulation models of the troposphere and stratosphere [e.g. Manabe and Mahlman, 1976]. In particular, numerical experiments by Kasahara et al. [1973] and Manabe and Terpstra [1974] have suggested that the large-scale mountain ranges in the Northern Hemisphere, such as the Tibetan Plateau and the Rocky Mountains, are chiefly responsible for maintaining the quasi-stationary waves in the troposphere.

For the theoretical analysis of the wave motions thus generated, dynamical meteorologists have made use of the fact that the stratospheric flow patterns are well described in terms of waves of low wavenumber superimposed on a background zonal flow, and have frequently resorted to perturbation techniques in their numerical analyses. This involves a linearisation of the equations of motion, requiring the assumption of smallness of wave amplitude in some sense. Charney and Drazin [1961] adopted this approach and were the first to show that the spatial distribution of the mean zonal wind exerted a controlling influence on the vertical structure of the waves. In order to obtain analytical solutions to their problem, they considered initially the simplest case of a zonal wind distribution independent of height and latitude, assuming that the waves were excited in the troposphere. For the dominant stationary wave component (zonal phase speed equal to zero), they found that vertical propagation could only occur in the presence of westerly winds weaker than a critical value which depended on the horizontal scale of the waves, in the sense that only the longest waves may propagate vertically into a region of strong westerly winds. Thus, the strong westerlies of the stratospheric polar-night jet may be considered to act as a selective filter, accounting for the dominance of planetary waves over synoptic scale waves in the stratosphere. This effect is confirmed by more detailed calculations, cited below, which are based on more realistic zonal wind profiles. In summer, when stratospheric zonal winds are easterly, the CD analysis predicted a trapping of the planetary waves in the troposphere; this accounts for the marked seasonal differences in stratospheric synoptic charts noted above.

According to the CD analysis, stationary planetary wavenumber 1 should propagate vertically only in the presence of westerly winds less than about  $40\text{ms}^{-1}$ . Thus, their simple theory predicted that planetary waves would be present in the upper atmosphere only during the equinoxes, whereas observations show maximum amplitudes in winter. Dickinson [1968, 1969a] helped resolve this point by showing that when the calculations were performed using spherical geometry, as opposed to the simplified (beta-plane) geometry employed by CD, the cut-off velocity for vertical propagation was greatly increased. Furthermore, he showed that radiative and photochemical damping strongly attenuates vertically-propagating planetary waves in the presence of only weak westerly winds.

Subsequent studies revealed that the latitudinal variation of zonal winds, not included in the CD theory, must also be considered [Matsuno, 1970; Simmons, 1974a]. Matsuno's analysis showed that wave propagation was governed by a two-dimensional wave equation in which a quantity appeared which could be interpreted as an index of refraction squared for the waves. Using the analogy of electromagnetic waves, Matsuno accounted qualitatively for the channeling along the axis of maximum basic winds, exhibited in both his observed and computed fields of wave amplitude, by suggesting that the upward-propagating waves were "refracted" into the region of high refractive index formed along the axis of the westerly jet. Moreover, Simmons [1974a] showed that wave disturbances having meridional structures similar to that of the zonal wind should penetrate to a greater height than other modes of disturbance. Consequently, far enough above the forcing level, the meridional distribution of wave amplitude should tend to follow that of the zonal wind, a feature noted earlier in reference to Fig. 3.

If dissipation is neglected in the linear calculations of Dickinson and Matsuno, a singularity occurs in the analysis for stationary waves along a line where the zonal wind speed is zero. This line is called a critical line (or critical level) and one exists in the equatorial stratosphere separating the summer and winter circulation regimes. Its influence on planetary-wave dynamics has been the subject of a number of investigations. On the basis of linear theory, Dickinson [1968] found that the planetary waves propagating meridionally towards the equatorial critical line should be absorbed there. Thus the energy flux associated with these waves, as quantified by the so-called pressure interaction terms (the left-hand sides of Eqs. [1] and [2] below), should be directed upward from the tropospheric source region for the waves and equatorward towards their energy sink. This finding is consistent with observations.

4. Eddy fluxes of momentum and heat in the stratosphere and the mean meridional circulation. From the expected directions of the planetary-wave energy fluxes arrived at above, the directions of the meridional eddy fluxes of heat and momentum may be inferred under steady conditions in the stratosphere from some useful relations derived by Eliassen and Palm [1961]:

$$\overline{\omega'z'} = \left\{ \frac{\partial \bar{\theta}}{\partial p} \right\}^{-1} \bar{u} \frac{f}{g} \overline{v'\theta'} \quad (1)$$

$$\overline{v'z'} = -\frac{\bar{u}}{g} \overline{u'v'} \quad (2)$$

In these equations, symbols have their customary meaning as defined in the Appendix; over-bars denote a zonal average and primes a departure from that average. The quantity  $\overline{\omega'z'}$  represents the vertical eddy energy flux, and is negative for upward-directed fluxes, while  $\overline{v'z'}$  represents the horizontal component of the flux (positive for poleward fluxes). Bearing in mind that  $\{\partial \bar{\theta} / \partial p\}$  is negative in the stratosphere, poleward eddy fluxes of heat and momentum may be deduced when the zonal winds are westerly. These are the typically observed directions for these fluxes in the winter stratosphere.

For extra-tropical, quasi-geostrophic waves of the type considered here, these results have implications for the structure to be expected of the stratospheric synoptic patterns. In the Northern Hemisphere, a northward eddy momentum flux is produced when the planetary waves have their troughs and ridges aligned in a S.W.-N.E. direction, while a northward eddy heat flux occurs when the troughs and ridges of the thermal wave lie westward of those of the geopotential-height wave. From the hydrostatic approximation, this second point implies a westward slope with height for the trough and ridge positions of the planetary waves. Thus, the above considerations are consistent with the observations presented earlier.

Vertical fluxes of eddy momentum and heat for those modes (i.e., the terms  $\overline{u'\omega'}$  and  $\overline{\omega'T'}$ ) are found, both observationally and by scale-analysis, to be usually an order of magnitude smaller than their horizontal counterparts in the winter stratosphere of the Northern Hemisphere. Such fluxes thus play a comparatively minor role in the dynamics of the stratosphere.

With this simplification and neglecting some additional terms which are also found to be comparatively small, the zonally-averaged momentum and thermodynamic equations presented by Dr. Murgatroyd earlier reduce to the following simple form:

$$\frac{\partial \bar{u}}{\partial t} = f\bar{v} - \frac{1}{a \cos^2 \phi} \frac{\partial}{\partial \phi} (\overline{u'v'} \cos^2 \phi) \quad (3)$$

$$\frac{\partial \bar{T}}{\partial t} = \bar{Q}/c_p - \bar{\omega} \bar{T} \frac{\partial (\ln \bar{\theta})}{\partial p} - \frac{1}{a \cos \phi} \frac{\partial}{\partial \phi} (\overline{v'T'} \cos \phi) \quad (4)$$

These are linked by the zonally-averaged continuity equation

$$\frac{1}{a \cos \phi} \frac{\partial}{\partial \phi} (\bar{v} \cos \phi) + \frac{\partial \bar{\omega}}{\partial p} = 0 \quad (5)$$

For the lower and middle stratosphere in the Northern Hemisphere winter, terms on the right of Eqs. (3) and (4) are plotted in Fig. 6 which was prepared using the computations of Vincent [1968]. It is seen that the momentum budget can be adequately described in terms of the competing effects of eddy momentum flux convergence, or divergence, and zonal wind accel-

JANUARY 1964

30-10 mb

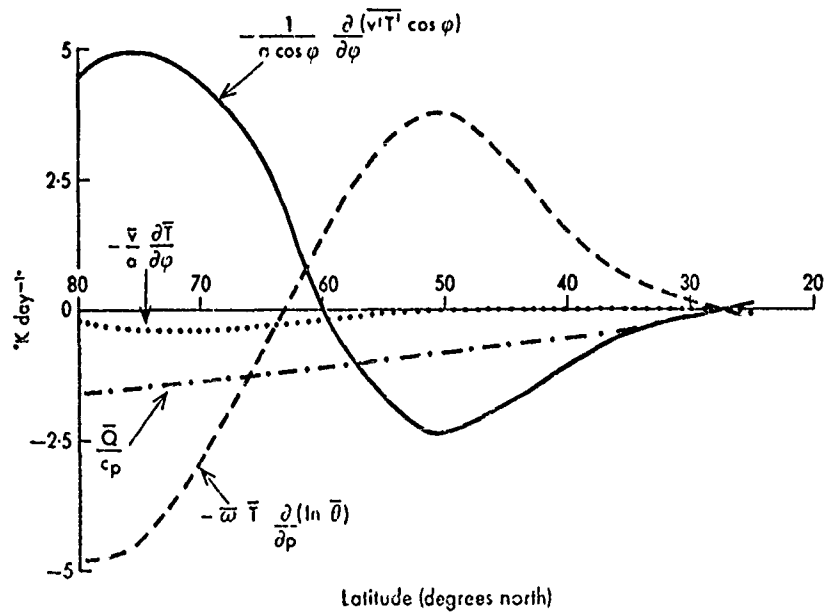
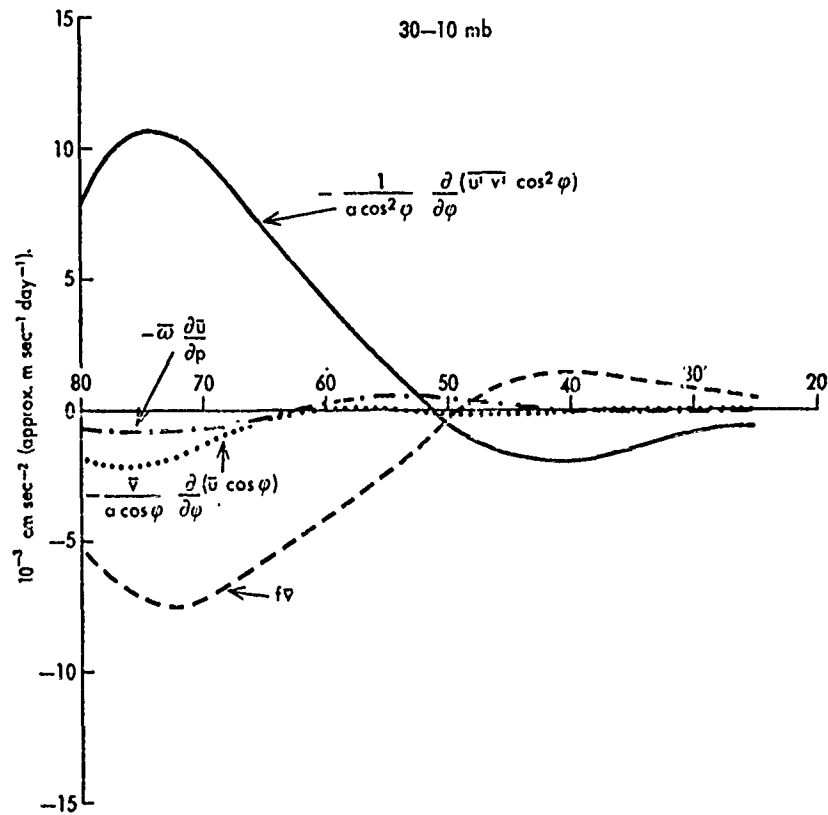


Fig. 6 Latitudinal distribution of terms in the momentum and heat budgets for the Northern Hemisphere stratosphere in winter. Curves plotted from the data of Vincent [1968].

erations due to Coriolis torques acting on the induced mean meridional circulation. Similarly, near compensation occurs between eddy heat flux convergence (divergence) and adiabatic cooling (warming) accompanying the zonal mean vertical motions; these terms individually dominating the effect of radiative cooling in the polar night.

An important point to bear in mind with regard to the interpretation of Fig. 6 is that it is incomplete, for example, to consider the effects of the eddy momentum fluxes purely within the context of the momentum budget, just because momentum flux is the "obvious" wave property which influences the zonal flow. Rather, through its effect on the mean meridional circulation (see Dr. Murgatroyd's lecture), momentum transports must be important in determining the thermodynamic state of the atmosphere. This point is important for the appreciation of some recent findings regarding the dynamics of sudden warmings, as discussed in my next lecture.

From Fig. 6, a mean meridional circulation may be inferred for the Northern Hemisphere winter stratosphere comprising two cells. This is illustrated schematically in Fig. 7, which shows, in addition, the well-known three-cell pattern of the winter troposphere. The lower-latitude cell in the stratosphere appears as the upward extension of the tropospheric Hadley

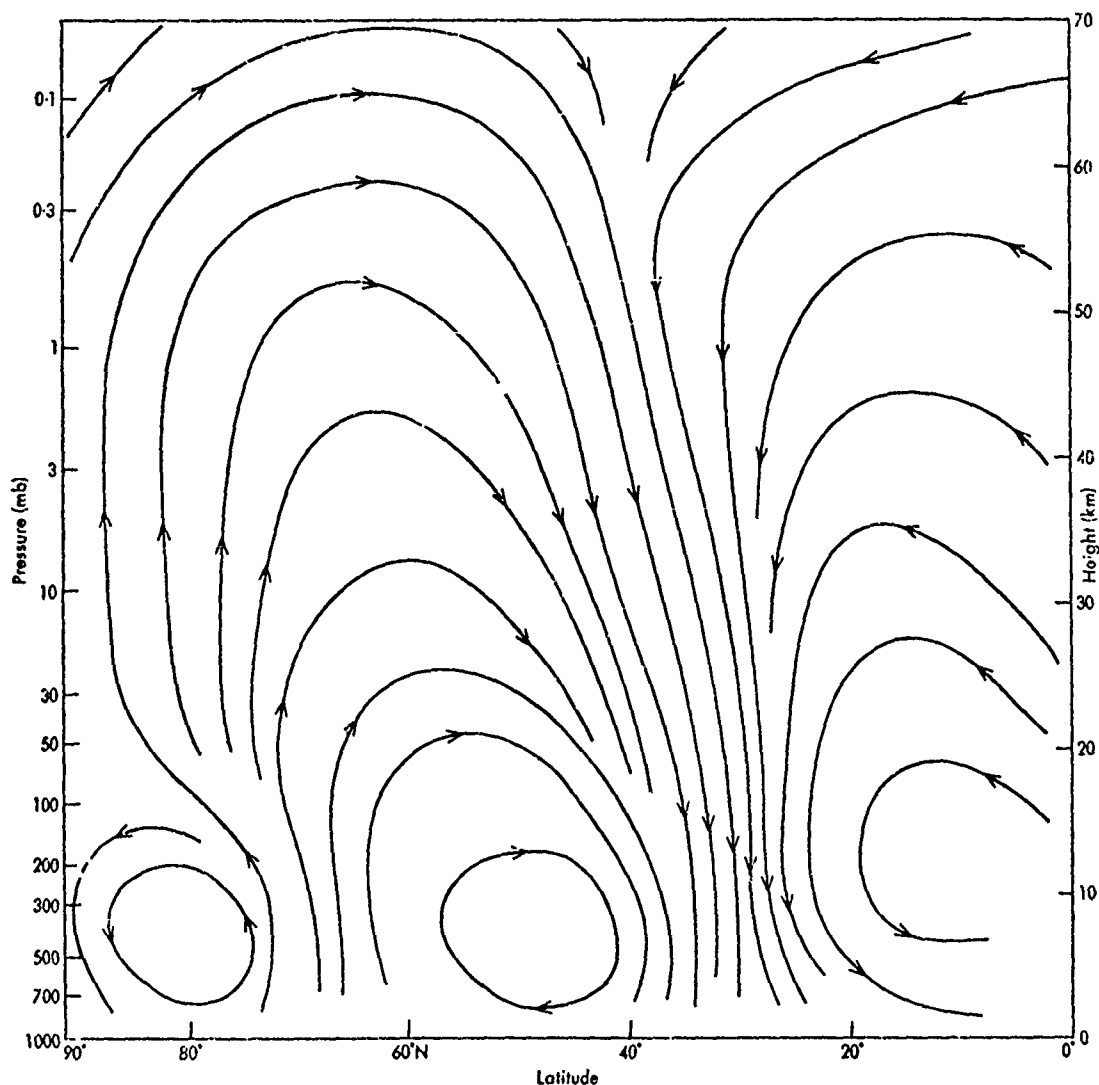


Fig. 7 Schematic mean meridional circulation for the Northern Hemisphere in winter. Contours represent stream-lines for the zonally-averaged meridional flow.

cell, while the cell at higher latitudes circulates in the same sense as the tropospheric Ferrel cell, in opposition to the sense of circulation expected from the field of net radiative heating alone.

The picture in the Southern Hemisphere winter stratosphere is broadly similar [Hartmann, 1976], although the meridional circulations are weaker. Adler [1975] found evidence for subsidence over the south pole during periods of weak eddy activity.

During summer in both hemispheres, the meridional circulations are weak and not apparently well organised. With the virtual absence of eddy activity in the stratosphere, the Murgatroyd and Singleton [1961] picture of a single cell with ascent over the pole and equatorward movement of air in the zonal mean is broadly applicable.

It may be noted in passing that both the planetary-scale eddies and the mean-meridional circulation in the winter stratosphere play a comparable role in the transport of trace substances. The virtual compensation between the effects of these aspects of the flow, noted in the momentum and heat budgets of Fig. 6, also occurs in the transport of tracers.

#### 5. Wave-mean flow interactions

The above discussion has emphasized the factors determining the structure of planetary waves in the stratosphere and their associated fluxes of energy, momentum and heat under steady conditions. However, it should be realized that the mere presence of wave disturbances does not guarantee that the concomitant eddy fluxes of momentum and heat will lead to changes in the mean circulation; as has been previously remarked, eddy fluxes are to a large extent offset by the mean meridional circulation which they induce. It is therefore important to determine the conditions under which complete compensation will not occur in order that phenomena such as the stratospheric sudden warming may be understood.

Charney and Drazin [1961], using a linearized form of the equations of motion in which dissipation was neglected, found that for a perturbation consisting of a single, zonally-propagating harmonic wave of constant amplitude and phase speed, and in the absence of a critical line where the phase speed equalled that of the zonal wind, the zonal flow was independent of time up to second order in the wave amplitude. This result is sometimes referred to as the Charney-Drazin non-acceleration theorem.

When critical lines exist somewhere, e.g. near the equator for quasi-stationary waves, the CD theorem can no longer be expected to be applicable, except that their results are likely to be a close approximation to reality in regions of the atmosphere well removed from any critical lines—provided wave transience and dissipation can be neglected.

Dickinson [1969b] has shown that such considerations also apply to small-amplitude transient waves, provided that their time-averaged eddy fluxes are steady or slowly varying in time. Holton [1974] extended these studies to include equatorial waves with the same results being obtained. The same problem was considered by Andrews and McIntyre [1976, 1978] and Boyd [1976] who removed some of the restrictive assumptions of the earlier works.

It may be concluded from these studies that only through the effects of wave transience, dissipation or critical-line interaction can vertically-propagating planetary waves account for the mean-circulation changes which are observed in the stratosphere, e.g. during sudden warmings.

#### 6. Hydrodynamic instability in the stratosphere

It was at one time thought that internal hydrodynamic instability in the stratosphere of either a baroclinic or barotropic type might be a contributory factor in the development of stratospheric disturbances, e.g., during sudden warmings. These types of instability are associated respectively with the development of strong zonal wind shears in the vertical and meridional directions. Under these conditions, wave disturbances may develop at the expense of the kinetic and potential energies of the zonal flow. The associated eddy momentum and heat fluxes tend to relax the zonal flow conditions that led to their generation.

Unfortunately, analytical studies of the stability of realistic zonal wind profiles is extremely difficult and therefore the question of instability in the winter stratosphere has not been finally resolved. Analyses of the stability of the stratosphere to the growth of

baroclinic disturbances have been made by Murray [1960], McIntyre [1970, 1972], and Simmons [1974b] using idealized zonal wind distributions. The overall view is that changes of vertical wind shear and static stability near the tropopause and stratopause may excite weak, shallow baroclinic disturbances near these levels, but they would not be likely to influence the stratospheric circulation on a large-scale. Numerical studies of the purely barotropic stability problem have been made by Nitta and Yanai [1969] and Dickinson and Clare [1973]. Again it was found that any unstable modes would not be of an appropriate scale to account for the disturbances observed in the stratosphere.

As regards the role of instability in warmings, the success of Matsuno's [1971] numerical simulation of a warming demonstrates that the sudden enhancement of tropospheric planetary waves is the causative factor, rather than internal instability.

#### 7. Equatorial waves

In addition to the extra-tropical disturbances discussed above, the stratosphere exhibits variability at tropical latitudes. Observations indicate that most of the large-scale variability can be accounted for by two wave modes: the Kelvin wave and the mixed Rossby-gravity wave [see Wallace, 1973].

The Kelvin wave is an eastward-propagating mode, primarily observed in wavenumbers 1 and 2 and having periods in the range 10–20 days and vertical wavelength of 6–12 km. The mixed Rossby-gravity wave is a westward-propagating mode with periods in the range 3–5 days, zonal wavelengths of about 10,000 km and vertical wavelengths of the order 4–8 km. The modes are believed to be generated in the troposphere by a variety of processes, which are not known in any detail, but latent heat release in convective storms appears to be their most likely source. The waves propagate vertically into the stratosphere where they are dissipated by radiative damping and mechanical processes.

These modes are believed to account for a particularly fascinating phenomenon exhibiting wave-mean flow interactions: the quasi-biennial oscillation (QBO). The QBO is revealed most dramatically in time-height sections of the zonal wind component near the equator. An alternating pattern of downward-propagating easterly and westerly wind regimes is observed, which repeats with an average period of 26 months and with maximum amplitude of oscillation at the equator. The necessary westerly acceleration of the zonal wind is believed to be provided by the dissipation of Kelvin waves in the stratosphere, these waves transporting westerly momentum upward. The easterly accelerations are thought to be provided by dissipation of the mixed Rossby-gravity wave. An elegant account of the dynamical processes involved in the QBO has been provided by Holton [1979].

The Kelvin waves are also believed to play a dynamical role in producing the westerly acceleration of the semi-annual oscillation of zonal wind [see Holton, 1975, for details]. The source of the easterly acceleration was previously attributed to absorption at the equatorial critical line of waves propagating meridionally from higher latitudes in the winter hemisphere. Recently, however, a numerical model developed by Holton and Wehrbein [1979] has indicated that advection of the mean zonal flow by the mean meridional wind can cause the required easterly acceleration during the solstice seasons.

#### 8. Summary

In conclusion, extra-tropical planetary waves play an essential role in determining the stratospheric circulation in winter. These waves are believed to be generated in the troposphere, not as the result of internal hydrodynamic instability in the stratosphere. The polar-night jet acts as a selective filter to these upward-propagating waves, leading to the dominance of planetary waves 1 and 2 at stratospheric levels. In summer, easterly zonal winds act to confine these modes essentially to the troposphere. Horizontal eddy momentum and heat fluxes associated with the disturbances induce mean meridional circulations which largely offset the effects of the fluxes on the mean state of the atmosphere, except in the presence of wave dissipation, transience or critical lines.

In the equatorial stratosphere, the principal planetary-wave modes are the Kelvin and mixed Rossby-gravity modes. These combine to produce the quasi-biennial oscillation of zonal wind while the Kelvin waves also contribute to driving the semi-annual oscillation.

## References

- Adler, R.F. Mean meridional circulation in the Southern Hemisphere stratosphere based on satellite information. J. Atmos. Sci., 32, 893-898, 1975.
- Andrews, D.G. and M.E. McIntyre. Planetary waves in horizontal and vertical shear: The generalized Eliassen-Palm relation and the mean zonal acceleration. J. Atmos. Sci., 33, 2031-2048, 1976.
- \_\_\_\_\_ An exact theory of nonlinear waves on a Lagrangian-mean flow. J. Fluid Mech., 89, 609-646, 1978.
- Boyd, J. The noninteraction of waves with the zonally-averaged flow on a spherical earth and the interrelationships of eddy fluxes of energy, heat and momentum. J. Atmos. Sci., 33, 2285-2291, 1976.
- Charney, J.G. and P.G. Drazin. Propagation of planetary-scale disturbances from the lower into the upper atmosphere. J. Geophys. Res., 66, 83-109, 1961.
- Deland, R.J. Analysis of Nimbus 3 SIRS radiance data: Traveling planetary-scale waves in the stratospheric temperature field. Mon. Wea. Rev., 101, 132-140, 1973.
- Dickinson, R.E. Planetary Rossby waves propagating vertically through weak westerly wind wave guides. J. Atmos. Sci., 25, 984-1002, 1968.
- \_\_\_\_\_ Vertical propagation of planetary waves through an atmosphere with Newtonian cooling. J. Geophys. Res., 74, 929-938, 1969a.
- \_\_\_\_\_ Theory of planetary wave-zonal flow interaction. J. Atmos. Sci., 26, 73-81, 1969b.
- Dickinson, R.E. and F.J. Clare. Numerical study of the unstable modes of a hyperbolic-tangent barotropic shear flow. J. Atmos. Sci., 30, 1035-1049, 1973.
- Eliassen, A. and E. Palm. On the transfer of energy in stationary mountain waves. Geofys. Publ., 22, No. 3, 1-23, 1961.
- Hare, F.K. and B.W. Boville. The polar circulation, Technical Note 70, World Meteorological Organisation, Geneva, pp. 43-78, 1965.
- Hartmann, D.L. The structure and dynamics of the Southern Hemisphere stratosphere during late winter, 1973. Ph.D. thesis, Geophysical Fluid Dynamics Program, Princeton University, 261 pp., 1975.
- \_\_\_\_\_ The dynamical climatology of the stratosphere in the Southern Hemisphere during late winter, 1973. J. Atmos. Sci., 33, 1789-1802, 1976.
- \_\_\_\_\_ Stationary planetary waves in the Southern Hemisphere. J. Geophys. Res., 82, 4930-4934, 1977.
- Harwood, R.S. The temperature structure of the Southern Hemisphere stratosphere, August-October, 1971. Quart. J. Roy. Meteorol. Soc., 101, 75-92, 1975.
- Hirota, I. and Y. Sato. Periodic variation of the winter circulation and intermittent vertical propagation of planetary waves. J. Meteor. Soc. Japan, 47, 390-402, 1969.
- Holton, J.R. Forcing of mean flows by stationary waves. J. Atmos. Sci., 31, 942-945, 1974.
- \_\_\_\_\_ The Dynamic Meteorology of the Stratosphere and Mesosphere, Meteor. Monogr., No. 37. Amer. Meteor. Soc., 216 pp., 1975.
- \_\_\_\_\_ Wave propagation and transport in the middle atmosphere. Proc. Roy. Soc. London (in press), 1979.
- Holton, J.R. and W.H. Wehrbein. A numerical model of the zonal mean circulation of the middle atmosphere. Pure and Appl. Geophys. (in press), 1979.
- Kasahara, A., T. Sasamori, and W.M. Washington. Simulation experiments with a 12-layer stratospheric global circulation model. I. Dynamical effect of the earth's orography and thermal influence of continentality. J. Atmos. Sci., 30, 1229-1251, 1973.
- Manabe, S. and J.D. Mahlman. Simulation of seasonal and interhemispheric variations in the stratospheric circulation. J. Atmos. Sci., 33, 2185-2217, 1976.

- Manabe, S. and T.B. Terpstra. The effects of mountains on the general circulation of the atmosphere as identified by numerical experiments. J. Atmos. Sci., 31, 3-42, 1974.
- Matsuno, T. Vertical propagation of stationary planetary waves in the winter Northern Hemisphere. J. Atmos. Sci., 27, 871-883, 1970.
- \_\_\_\_\_. A dynamical model of the stratospheric sudden warming. J. Atmos. Sci., 28, 1479-1494, 1971.
- McIntyre, M.E. On the nonseparable baroclinic parallel-flow instability problem. J. Fluid Mech., 40, 273-306, 1970.
- \_\_\_\_\_. Baroclinic instability of an idealized model of the polar-night jet. Quart. J. Roy. Meteorol. Soc., 98, 165-174, 1972.
- Muench, H.S. On the dynamics of the winter stratosphere circulation. J. Atmos. Sci., 22, 349-360, 1965.
- Murgatroyd, R.J. and F. Singleton. Possible meridional circulations in the stratosphere and mesosphere. Quart. J. Roy. Meteorol. Soc., 87, 125-135, 1961.
- Murray, F.W. Dynamic stability in the stratosphere. J. Geophys. Res., 65, 3273-3305, 1960.
- Nitta, T. and M. Yanai. A note on barotropic instability of the tropical easterly current. J. Meteor. Soc. Japan, 47, 183-197, 1969.
- Simmons, A.J. Planetary scale disturbances in the polar winter stratosphere. Quart. J. Roy. Meteorol. Soc., 100, 76-108, 1974a.
- \_\_\_\_\_. Baroclinic instability at the winter stratopause. Quart. J. Roy. Meteorol. Soc., 100, 531-540, 1974b.
- van Loon, H., R.L. Jenne and K. Labitzke. Zonal harmonic standing waves. J. Geophys. Res., 78, 4463-4471, 1973.
- Vincent, D.G. Mean meridional circulation in the Northern Hemisphere lower stratosphere during 1964 and 1965. Quart. J. Roy. Meteorol. Soc., 94, 333-349, 1968.
- Wallace, J.M. General circulation in the tropical lower stratosphere. Rev. Geophys. and Space Phys., 11, 191-222, 1973.



Appendix  
Symbols included in the text

a	radius of the Earth
$c_p$	specific heat capacity of dry air at constant pressure
f	Coriolis parameter
g	acceleration due to gravity
p	pressure
Q	adiabatic heating rate per unit mass of air
t	time
T	temperature
u	westerly wind component
v	southerly wind component
z	geopotential-height
$\theta$	potential temperature
$\lambda$	longitude
$\phi$	latitude
$\omega$	vertical velocity in pressure coordinates
$\{ \bar{\quad} \}$	$= \{ \frac{1}{2\pi} \} \int_0^{2\pi} \{ \quad \} d\lambda$ , zonal averaging operator on constant pressure surface
$\{ \quad \}'$	$= \{ \quad \} - \{ \bar{\quad} \}$ , departure from zonal average
$\{ \overline{a'b'} \}$	eddy fluxes of momentum, heat or energy for appropriate a and b

## STRATOSPHERIC SUDDEN WARMINGS

Alan O'Neill †

U.K. Meteorological Office, London Road,  
Bracknell, Berks.

### Abstract

The synoptic and dynamical features of stratospheric sudden warmings are presented and a brief account is given of dynamical theories that have been proposed to explain the observed characteristics of these events. Reference is also made to the accompanying circulation changes in the troposphere which are believed to be essential in driving the developments above.

### 1. Introduction

In my previous lecture, emphasis was placed on the dynamical role of upward-propagating, extra-tropical planetary waves in the stratosphere and the factors determining their structure and associated eddy fluxes of energy, momentum and heat. It was stressed that only under certain conditions could the waves induce changes in the stratospheric mean state to produce phenomena such as the sudden warming.

In this lecture, the synoptic and dynamical characteristics of sudden warmings will be outlined. The currently-favoured theoretical mechanism for warmings proposed by Matsuno is discussed, and will be appraised in the light of some recent findings derived from an observational study and an investigation using a numerical model. Some ideas regarding the accompanying circulation changes in the troposphere will also be presented.

### 2. The synoptic characteristics of stratospheric sudden warmings

The stratospheric warming phenomenon was discovered by Scherhag [1952] through high-altitude observations over Berlin during the winter 1951-1952. Since then, many further examples have been documented using data obtained from balloon- and rocket-sounding devices and satellite-borne remote sensors.

The "breakdown of the polar-night vortex is usually considered to be the chief characteristic of stratospheric warmings in the Northern Hemisphere. They are commonly categorized as being "major" or "minor", depending on whether the perturbation was of sufficient magnitude to cause circulation reversals (the appearance of zonal-mean easterlies) down to the 10 mb level. It should be noted, however, that major and minor warmings have many synoptic and dynamical features in common and a rigid separation is not desirable. Also, there is a need to distinguish between the normal warming, associated with the return of solar radiative heating to the upper

† Presently on secondment at the Joint Institute for the Study of the Atmosphere and Ocean, University of Washington, Seattle, Washington, 98195.

atmosphere during spring (i.e. "final warmings"), and these mid-winter events from which the winter westerly circulation at least partially recovers.

During stratospheric warmings, large thermal disturbances develop on a planetary scale through a significant depth of the atmosphere, and are accompanied by rapid temperature increases at some localities of often as much as  $40^{\circ}$ – $50^{\circ}\text{C}$  in a matter of days. During major warmings, circulation reversals at upper levels must be preceded by a reversal of the normal temperature-gradient at lower levels (cold pole, warmer mid latitudes) to satisfy the requirements of thermal wind balance.

The patterns observed in several major warmings since 1969 have been reviewed by Quiroz [1975]. Two principal types of development are indicated:

(i) a mode in which warm air moves poleward in an apparent wavenumber-1 pattern (e.g. January 1970).

(ii) a mode in which the thermal systems, one over the N. Atlantic and the other over E. Siberia, move poleward to form a pronounced wave-2 pattern (e.g. January–February 1963).

These modes are illustrated schematically in Fig. 1, while Fig. 2 shows 10 mb charts taken at the peak of the wave disturbances for the examples quoted in (i) and (ii).

Major warmings are not observed during every Northern Hemisphere winter. Polar warmings in the upper stratosphere, without a circulation reversal near 10 mb, occur quite commonly in both hemispheres during winter. These warming pulses appear as a subset of the repeating oscillations in stratospheric winter structure which recur at about 15-day intervals [e.g. Hirota and Sato, 1969].

The domain of the warming and the frequently observed compensating cooling in other regions extends well into the mesosphere. For example, Houghton [1975] has shown evidence of higher level cooling coinciding with periods of stratospheric warming during the Northern Hemisphere winter of 1976–77, while satellite data analyzed by Fritz and Soules [1972] and Barnett [1975] have indicated a degree of interhemispheric coupling during major warmings. The data also indicate a typical vertical wavelength of 45 km.

With regard to the vertical propagation of the warming, most recent work (Section 4) has emphasized that upward-propagating planetary waves are vital for the dynamical development. However, it should be realized that this does not preclude the downward phase propagation of the temperature waves. Thus, upward or downward propagation of warming may sometimes be observed as the thermal system moves over a fixed location.

In the above, reference to the Northern Hemisphere has been implicit as only rather incomplete descriptions of mid-winter events have been presented for the Southern Hemisphere, due to the relative lack of radiosonde data above 50 mb. Nevertheless, warming pulses have been observed in the Antarctic winter stratosphere which appear quite similar in structure to those studied in the Northern Hemisphere. The main difference between hemispheres is the much weaker stationary-wave component in the Southern Hemisphere; consequently, the superposition of stationary and transient modes leads to warmings of a less explosive nature than those observed in the Northern Hemisphere. Indeed, major warmings have not yet been observed in the Southern Hemisphere, the difference between hemispheres probably being related to differences in topographic forcing.

### 3. Synoptic conditions in the troposphere during stratospheric warmings

In view of the role of upward-propagating planetary waves in generating warmings, to be elucidated below, it is important to try to identify concomitant circulation changes in the troposphere. This is difficult because of the masking effect of waves of higher wavenumber than those prevailing in the stratosphere; also, tropospheric features typically have smaller amplitudes.

It has been noted by a number of investigators [e.g. Julian and Labitzke, 1965] that stratospheric warmings can occur in association with a rise in the pressure surfaces in the middle and upper troposphere, especially in the region of the North Atlantic. This, in association with other synoptic features (e.g. the extensive "low" over East Siberia), leads to enhanced wave-1 and/or -2 amplitudes in the troposphere. A significant rise in tropospheric pressure

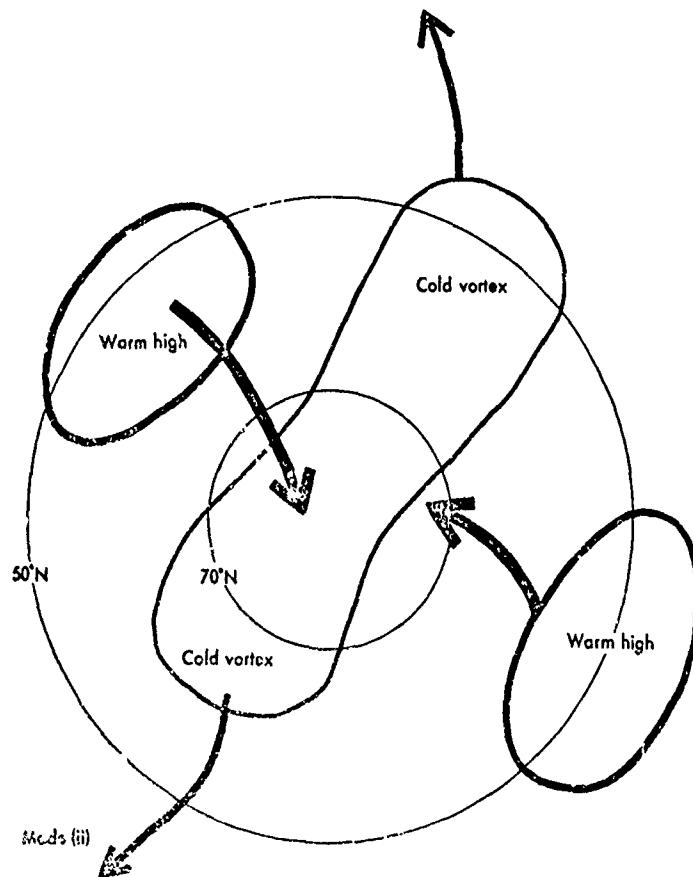
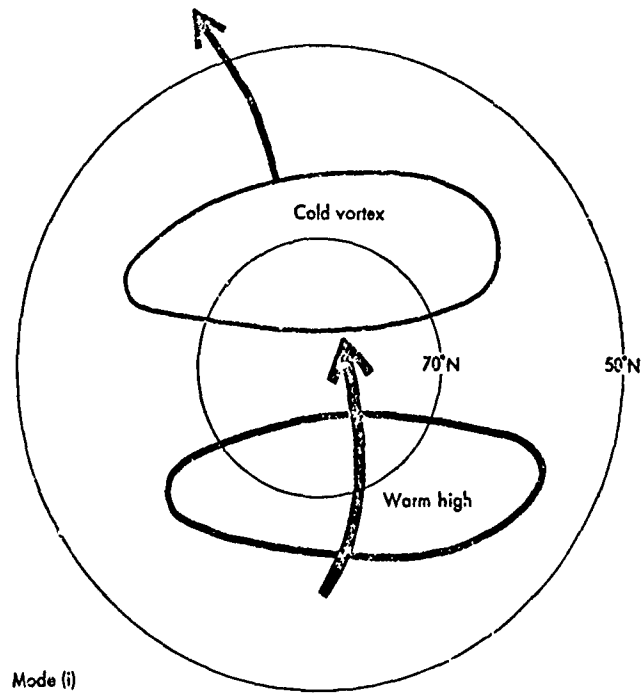


Fig. 1 Schematic illustration of the principal types of warming development: mode (i), wave-1 type; mode (ii), wave-2 type. Heavy lines represent contours of geopotential-height.

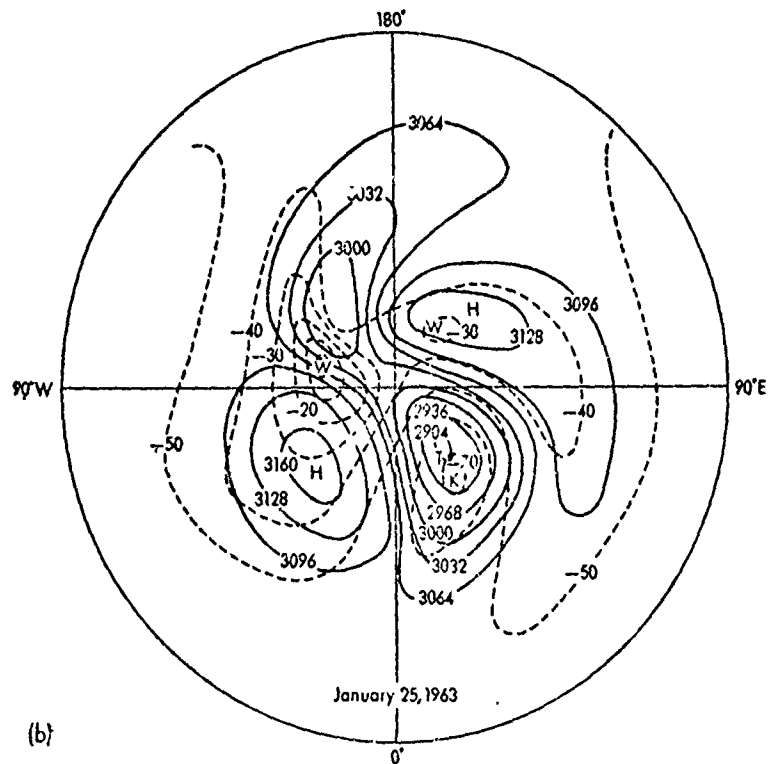
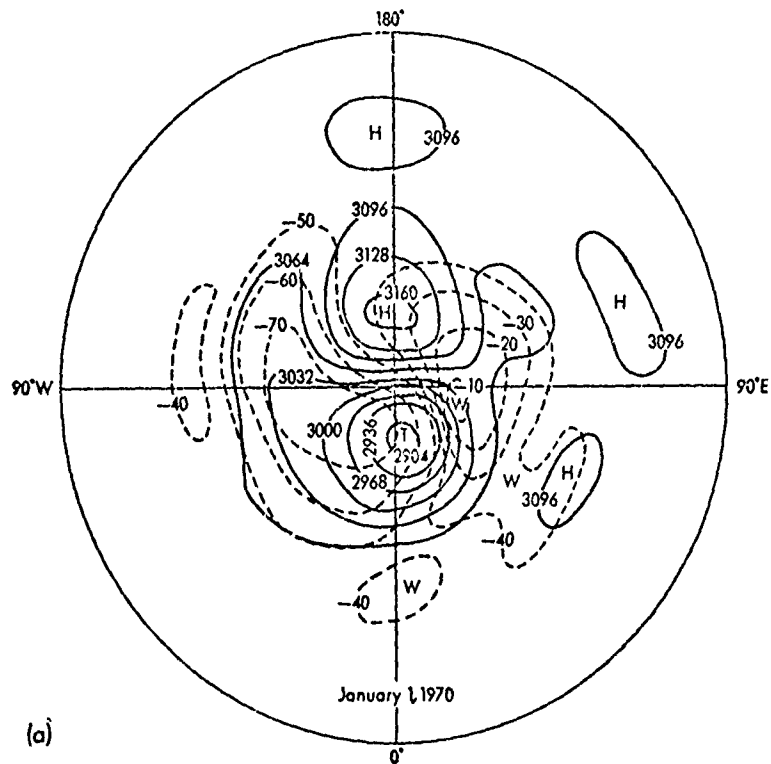


Fig. 2 Actual examples of the principal warming types in the Northern Hemisphere stratosphere at 10 mb: (a) wave 1; (b) wave 2. Solid lines are contours of geopotential-height (units: dam, where 1 dam = 10m), dashed lines are isotherms (units: °C).

may be exhibited in the form of "blocking"—a state of circulation, characterized by persistent high pressure in some preferred location (e.g. 50°W–20°E), in which basically zonal flow is interrupted by persistent meridional flow. The degree of blocking may be quantified by a "zonal index," which provides a crude measure of the average geostrophic flow between specified latitudes. Quiroz [1969] showed oscillations of this index at 700 mb which were in phase with oscillations in the upward geopotential flux through 100 mb (namely the quantity  $-\overline{w'z'}$  referred to in my earlier lecture), in the sense that weak winds in the troposphere occurred simultaneously with large values of the upward-directed flux.

#### 4. The dynamical characteristics of stratospheric sudden warmings

The contrasting behavior of the warming phenomena in the Northern and Southern Hemispheres and their differing topography point to the possibility that topographical influences transmitted upward from the troposphere might be an important influence on the dynamical evolution of warmings. Studies by Reed et al. [1963], Muench [1965], Perry [1967], and others of the energetics of the stratosphere during warming periods have all indicated that the rapid growth of planetary waves in the stratosphere, which occurs during warmings, is associated with an enhanced upward eddy energy flux from the troposphere; the weakening of the polar-night jet cannot be attributed solely to internal energy conversions in the stratosphere.

As a result of these observations, Matsuno [1971] postulated a mechanism for the sudden warming phenomenon based on the likely effects on the winter stratosphere of a sudden increase in planetary-wave activity in the troposphere. He then attempted to verify the validity of this mechanism by numerical calculation. Matsuno's theory involves two fundamental features of the dynamical interaction between waves and the mean zonal flow: the deceleration of the mean zonal flow which can occur as upward-propagating, growing waves extract energy from it, and the absorption of waves which occurs at a critical level (which for quasi-stationary waves is a level separating zonal mean easterlies from zonal mean westerlies). He argued that these processes could combine to produce stratospheric warmings as follows:

As mentioned in my previous lecture, quasi-stationary waves (generated in the troposphere) do not propagate vertically in easterly zonal winds; so, should they reach a critical level where the zonal wind speed is zero with easterlies above, the wave amplitude would decrease rapidly with height and the vertical energy flux would vanish. If the level were approximately horizontal, the meridional heat transfer by the waves would fall to zero at the critical level. Moreover, the convergence at high latitudes and divergence at low latitudes of the poleward eddy fluxes below the critical level would be, to a large extent, balanced by adiabatic cooling and warming due to mean vertical motion (a consequence of the Charney-Drazin [1961] non-acceleration theorem). Therefore, the jump in the heat fluxes would also induce a large mean meridional flow from high to low latitudes, in the vicinity of the critical level, in order that mass continuity is satisfied. The Coriolis torque acting on this southward flow creates strong easterly accelerations on the mean zonal wind, so that the zero-wind line moves downward as wave energy is absorbed at ever lower levels, and mean easterlies gradually replace westerlies in the winter stratosphere. This process might be expected to continue until the tropospheric energy supply diminishes or a level is reached where eddy transports are insufficient to reverse the prevailing zonal winds.

These processes are illustrated in Fig. 3. From Fig. 3(a) it may be seen that the temperature changes result from the balance between the heating due to the horizontal eddy fluxes and the effect of the mean vertical motions. Below the critical level, the former effect dominates and hence warming occurs at polar latitudes. Above this level, only vertical motion causes temperature changes and thus adiabatic cooling results above the levels of warming. This prediction is consistent with observations [e.g. Houghton, 1978]. At atmospheric levels far removed from the critical level, temperature and zonal wind changes are very small, as implied by the Charney-Drazin theorem (Fig. 3(b)).

Broadly the same argument applies to transient, growing waves even in the initial absence of a critical level. In the above account no statement was made as to how the extra-tropical critical level was formed initially. The idea is that planetary waves "turned on" in the troposphere will, at any given time, only have penetrated to a limited extent into the stratosphere. Above this, both the wave amplitude and eddy heat flux decrease rapidly with height, and therefore the previous argument pertains, albeit that in this case the effect is spread out over a finite depth of the atmosphere—as would be the case for critical levels if damping effects were included in the theory.

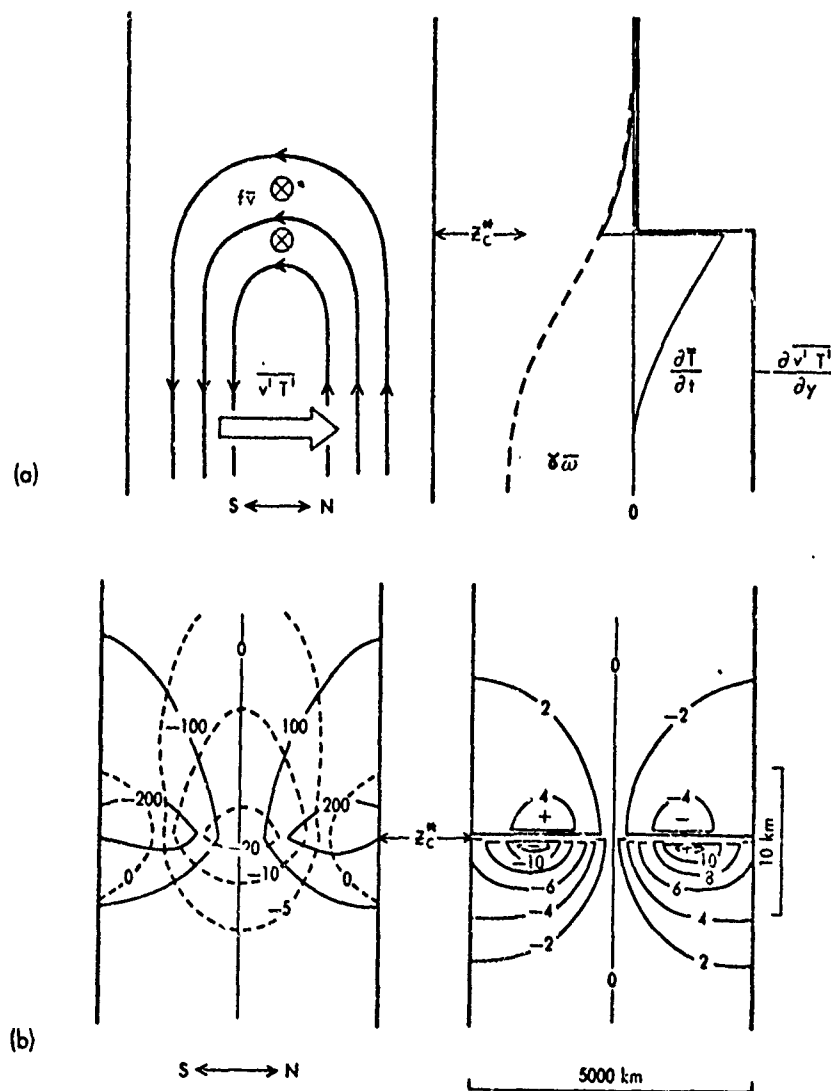


Fig. 3 Schematic illustration of Matsuno's conjectured mechanism for the stratospheric sudden warming [after Matsuno, 1971]. (a) left: mean-meridional circulation of the high-latitude cell driven by the northward eddy heat flux. (a) right: vertical profile near the pole of principal terms in heat budget equation ( $\gamma$  represents static stability).  $z_c^*$  denotes the critical level. (b) left: changes in the isobaric heights (solid lines,  $\text{m day}^{-1}$ ) and change in the mean zonal wind (dashed lines,  $\text{ms}^{-1}\text{day}^{-1}$ ). (b) right: temperature changes ( $^{\circ}\text{C day}^{-1}$ ). Amplitude of wave incident on critical level assumed to be 500 m.

Matsuno then developed a numerical model to test his ideas by attempting to simulate various aspects of the warming phenomenon. He used a linearized version of the quasi-geostrophic equations of motion, with the lower boundary of the model atmosphere chosen to correspond to the tropopause. At this level, the time evolution of perturbation wave amplitude was specified to be one of an initial rapid increase in amplitude up to a steady value which was subsequently maintained. This behaviour was in reasonable accord with the early temporal development of wave amplitude at 300 mb during the 1963 winter warming in the Northern Hemisphere. The system of equations was then numerically integrated forward in time, subject to the specified boundary conditions.

The numerical results thus obtained showed close similarities to those found in a diagnostic analysis of the observed warming of 1963, although Matsuno noted some discrepancies between the observed and simulated cases. Consequently, it is reasonable to conclude that the sudden warming can be explained essentially in terms of the vertical propagation of growing planetary waves forced in the troposphere and their interaction with the zonal flow. However, some recent studies, outlined below, show that the warming mechanism described above may be incomplete in an important respect, at least for some warming events.

#### 5. Dynamical developments in the troposphere during stratospheric sudden warmings

The central question to be answered with regard to the tropospheric development during stratospheric sudden warmings is: Why do certain large-scale waves amplify rapidly on occasions during winter? It is such transient behaviour of the waves that enables them to decelerate the mean flow as they propagate upwards into the stratosphere; i.e. the breakdown of the CD non-acceleration theorem during warmings is believed to be primarily a consequence of wave transience initiated in the troposphere.

Recently, Tung and Lindzen [1979] and Tung [1979] have advanced a theory to account for the rapid temporal development of the planetary waves in the troposphere. The basis of their idea is that these waves are waves at resonance with the topographic forcing and land/sea differential heating.

The zonal phase speed of a free-travelling Rossby planetary wave depends on the zonal wind speed. Therefore, to be resonant the wind condition in the atmosphere has to be such that the phase speed of the wave is reduced to zero with respect to the ground, and thus also to the topographic forcing and differential heating. The consequent amplification with time of the pressure ridges associated with the wave may be manifested in the form of a blocking pattern on tropospheric synoptic charts—hence the link between stratospheric warmings and tropospheric blockings, according to their theory.

For the resonance condition to be met in the Tung-Lindzen theory, the wave energy must be mostly contained and not dissipated. However, there is still some uncertainty as to the degree to which the equatorial zero-wind (critical) line dissipates energy associated with quasi-stationary waves or, under certain circumstances, reflects the energy incident on it. The presence of a significantly-absorbing critical line would not favour resonance conditions and would limit the applicability of their theory.

#### 6. Some recent dynamical studies of sudden warmings

In his proposed mechanism for the stratospheric sudden warming outlined above, Matsuno paid particular attention to the likely effect on the zonal circulation in the winter stratosphere of a sudden enhancement of poleward eddy heat fluxes associated with the upward-propagating waves. He did not consider explicitly the possible effects of changes in horizontal eddy momentum transport and no evidence was presented that this was not an important element in his actual simulation. In fact, Holton [1976] conducted a similar experiment using a primitive-equation model and noted that the zonal flow deceleration during the simulated warming was a small residual between the opposing effects of convergence of poleward eddy momentum flux and Coriolis torques acting on the induced mean-meridional circulation. This suggests that the mechanism for the zonal flow change may be more subtle than that proposed by Matsuno.

Additional evidence that horizontal eddy momentum fluxes can play a fundamental role in the evolution of some stratospheric warmings comes from the investigation by O'Neill and Taylor [1979] who analyzed the major warming which occurred in the Northern Hemisphere during the period December 1976 to January 1977. The warming was remarkable in that the reversal of the



zonal westerly wind field, which is a feature of major stratospheric warmings, was on this occasion also observed in the troposphere. Thus, in mid January, zonal mean easterlies were present north of 60°N from the surface up to at least the 10 mb layer.

They found that the dynamics of the event could not be satisfactorily explained within the terms of the Matsuno mechanism. One of the main findings of their study was that a reversal of wave-1 momentum flux at mid latitudes from its normal poleward direction in winter to an equatorward direction led to eddy momentum flux divergence at polar latitudes and was crucial in effecting a zonal wind reversal in both the stratosphere and the troposphere in that region.

The same conclusion was reached by O'Neill [1979] in a dynamical investigation of a stratospheric warming simulated by a general circulation model of the troposphere and stratosphere, although in this case the circulation reversal was confined to the model's middle stratosphere. Several warming events were generated spontaneously during the course of integration with a number of versions of the model, and not as a result of external specification of conditions at a lower boundary as occurs in the simplified mechanistic models of the type developed by Matsuno and Holton. The model warmings were also instigated by enhanced planetary-wave activity in the troposphere, and the establishment of equatorward eddy momentum fluxes in the winter stratosphere at mid latitudes was again a primary causative factor in decelerating the zonal jet at high latitudes.

The thermodynamic consequences of an eddy momentum flux reversal in the stratosphere may be understood by considering its effect on the mean meridional circulation. As may be determined from the dynamical equations presented earlier by Dr. Murgatroyd, equatorward eddy momentum fluxes with largest (negative) values at mid latitudes and increasing with height act with a tendency to drive a mean meridional circulation with subsidence over the pole. However, zonal-mean ascent over the pole would be required to offset the warming effect of eddy heat flux convergence at polar latitudes. Consequently, the stratospheric mean meridional circulation is unable to compensate simultaneously for oppositely directed eddy fluxes of momentum and heat, and the Charney-Drazin non-acceleration theorem cannot apply; i.e. changes in the zonal circulation must occur.

There is some additional observational evidence that eddy momentum flux reversals occur during other major stratospheric warmings [Arpe, 1976; Klinker, 1977a and b]. Nevertheless, it should not be expected that all warmings occur in conjunction with eddy momentum flux reversals, although it seems reasonable to suppose from the simplified dynamical argument presented above that such an occurrence would be associated with the most dramatic events.

The outstanding question yet to be resolved is the nature of the mechanism that can account for such a flux reversal. What is required is that the quasi-geostrophic planetary waves change their meridional structure from one in which the trough/ridge axes lie S.W. - N.E. (as usual) to one in which they lie S.E. - N.W. O'Neill and Taylor [1979] proposed that the re-orientation in the stratosphere could be forced by a similar circumstance in the troposphere; they noted that this could occur during the development and subsequent decay of tropospheric blocking patterns. However, the nature of the driving mechanism in the troposphere was not specified. Recently, O'Neill [1979] has suggested that the restructuring of the waves in the stratosphere may be a consequence of the effect on the waves of the evolving zonal wind field during the warming development, since it is known that this field affects the wave-propagation dynamics. Details of the argument will not be presented here, but it should be noted that the proposed mechanism is speculative and in need of validation.

## 7. Summary

Stratospheric sudden warmings are generated in the winter stratosphere by enhanced planetary-wave activity in the troposphere. Associated with the upward-propagating waves are eddy fluxes of momentum and heat. Matsuno's mechanism accounts for the polar warming in terms of increased eddy heat flux convergence at high latitudes, the zonal wind deceleration required to maintain thermal-wind balance being provided by Coriolis torques acting on the mean-meridional circulation. Recent studies using observational data and data provided as output of integrations with a general circulation model indicate that this dynamical picture is incomplete; the effect of horizontal eddy momentum fluxes must also be taken into account, particularly a reversal in the direction of these fluxes. The mechanism for such a reversal remains to be firmly established and more observational studies are required to determine whether these reversals commonly occur during major stratospheric warmings.

## References

- Arpe, K. Energetics of the stratosphere; a comparison between one winter without and two winters with major warmings. Beitr. Phys. Atmos., 49, 189-211, 1976.
- Barnett, J.J. Hemispheric coupling—evidence of a cross-equatorial planetary wave—guide in the stratosphere. Quart. J. Roy. Meteorol. Soc., 101, 835-845, 1975.
- Charney, J.G. and P.G. Drazin. Propagation of planetary-scale disturbances from the lower into the upper atmosphere. J. Geophys. Res., 66, 83-109, 1961.
- Fritz, S. and S.D. Soules. Planetary variations of stratospheric temperatures. Mon. Wea. Rev., 100, 582-589, 1972.
- Hirota, I. and Y. Sato. Periodic variation of the winter circulation and intermittent vertical propagation of planetary waves. J. Meteor. Soc. Japan, 47, 390-402, 1969.
- Holton, J.R. A semi-spectral model for wave-mean flow interactions in the stratosphere: Application to sudden stratospheric warmings. J. Atmos. Sci., 33, 1639-1649, 1976.
- Houghton, J.T. The stratosphere and mesosphere. Quart. J. Roy. Meteorol. Soc., 104, 1-29, 1978.
- Julian, P.R. and K.B. Labitzke. A study of atmospheric energetics during the January-February 1963 stratospheric warming. J. Atmos. Sci., 22, 597-610, 1965.
- Klinker, E. The energetics of the stratosphere during the winter warmings of 1970/71 and 1974/75. COSPAR Space Res., Vol. XVII, 89-101, 1977a.
- \_\_\_\_\_ Energetics of major and minor warmings. Collection of extended summaries of contributions presented at CMUA sessions, IAGA/IAMAP joint assembly, Seattle, Washington, paper 54, 1977b.
- Matsuno, T. A dynamical model of the stratospheric sudden warming. J. Atmos. Sci., 28, 1479-1494, 1971.
- Muench, H.S. On the dynamics of the wintertime stratospheric circulation. J. Atmos. Sci., 22, 349-360, 1965.
- O'Neill, A. The dynamics of stratospheric warmings generated by a general circulation model of the troposphere and stratosphere, submitted to Quart. J. Roy. Meteorol. Soc., 1979.
- \_\_\_\_\_ and B.F. Taylor. A study of the major stratospheric warming of 1976/77. Quart. J. Roy. Meteorol. Soc., 105, 71-92, 1979.
- Perry, J.S. Long wave energy processes in the 1963 sudden stratospheric warming. J. Atmos. Sci., 24, 537-550, 1967.
- Quiroz, R.S. The warming of the upper stratosphere in February 1966 and the associated structure of the mesosphere. Mon. Wea. Rev., 97, 541-552, 1969.
- \_\_\_\_\_ The stratospheric evolution of sudden warmings in 1969-74 determined from measured infra-red radiation fields. J. Atmos. Sci., 32, 211-224, 1975.
- Reed, R.J., J. Wolfe and H. Nishimoto. A spectral analysis of the energetics of the stratospheric sudden warming of early 1957. J. Atmos. Sci., 20, 256-275, 1963.
- Scherhag, R. Die explosionsartigen stratosphärischen Warmungen des Spät winters 1951-1952. Ber. Deut. Wetterd., 6, 51-63, 1952.
- Tung, K.K. A theory of stationary long waves. Part III: Quasi-normal modes in a singular wave-guide. Mon. Wea. Rev., 107, 751-774, 1979.
- \_\_\_\_\_ and R.S. Lindzen. A theory of stationary long waves. Part I: A simple theory of blocking. Mon. Wea. Rev., 107, 714-734, 1979.
- \_\_\_\_\_ and \_\_\_\_\_ A theory of stationary long waves. Part II: Resonant Rossby waves in the presence of realistic vertical shears. Mon. Wea. Rev., 107, 735-750, 1979.

# ONE-DIMENSIONAL COUPLED TRANSPORT AND CHEMICAL KINETICS MODELS OF THE STRATOSPHERE

Julius S. Chang and Donald J. Wuebbles

Lawrence Livermore Laboratory, University of California  
Livermore, California 94550 U.S.A.

## Abstract

One-dimensional coupled transport and chemical kinetics models have been one of the basic research tools in theoretical studies of the stratosphere in recent years. In fact, much of the current knowledge about the chemical structure of the stratosphere and the processes governing it have been derived with the help of one-dimensional model calculations. In addition, analyses of man's potential influence on stratospheric ozone have been primarily done with the aid of one-dimensional models (Grobeck, et al., 1974; Hudson, 1977, 1979; National Research Council, 1976, 1979). In this paper, we will analyze and describe the one-dimensional coupled transport and kinetics model and its components; examine its basis and the concepts that led to its development; and discuss its capabilities and limitations.

**INTRODUCTION:** One-dimensional coupled transport and chemical kinetics models have been one of the basic research tools in theoretical studies of the stratosphere in recent years. In fact, much of the current knowledge about the chemical structure of the stratosphere and the processes governing it have been derived with the help of one-dimensional model calculations. In addition, analyses of man's potential influence on stratospheric ozone have been primarily done with the aid of one-dimensional models (Grobeck, et al., 1974; Hudson, 1977, 1979; National Research Council, 1976, 1979).

These models are designed to simulate the vertical distribution of atmospheric trace species. They include a detailed representation of atmospheric chemical interactions and radiation processes. The one-dimensional models describe in a simplified way the effect of atmospheric transport. Only the average net vertical transport is considered by a phenomenologically constructed transport parameter. One-dimensional models can describe the essential features of atmospheric chemistry without excessive demands on computer time. Early attempts at calculating trace species distributions in the atmosphere included photochemical and chemical interactions only. In the 1960's, realization of the importance of including the effect of dynamical processes led to the development of the first one-dimensional coupled transport and chemical kinetics models. These models were first applied to studying chemical processes in the mesosphere and thermosphere (Colegrove et al., 1965, 1966; Shimazaki, 1967, 1968; Nicolet, 1968; Hesstvedt, 1968a, 1970; Hesstvedt and Jansson, 1969; Keneshea and Zimmerman, 1970; Strobel et al., 1970; Shimazaki and Laird, 1970, 1972; Strobel, 1971).

The first applications of one-dimensional model calculations to the stratosphere were concerned with explaining observations or with suggesting important chemical processes that influence the concentration of ozone and other stratospheric minor constituents such as  $H_2$ ,  $CH_4$ ,  $N_2O$ ,  $NO$ ,  $NO_2$ ,  $HNO_3$ , etc. (Hesstvedt, 1968b, 1971; Nicolet, 1971; McElroy and McConnell, 1971; Crutzen, 1971, 1972; Wofsy et al., 1972; McElroy, 1972; Junge et al., 1971; Warneck, 1972). Numerous later studies with one-dimensional models have continued towards improving our understanding of the processes important to stratospheric chemistry. Other studies have attempted to examine diurnal (Whitten and Turco, 1974; Wuebbles and Chang, 1975; Logan et al., 1978, 1979) and other natural temporal variations in trace species concentrations such as from solar flux variability (Penner and Chang, 1978, 1979; Callis and Nealy, 1978) and from solar eclipses (Wuebbles and Chang, 1979).

One-dimensional models have also been used to study the possible effects of events such as volcanic eruptions (Stolarski and Cicerone, 1974) and nuclear tests (Chang and Duewer, 1973; National Research Council, 1975; Chang et al., 1979) on the stratosphere.

Recognition that possible anthropogenic activities may cause changes in stratospheric ozone have led to a demand for prognostic applications of one-dimensional models. The possibility that oxides of nitrogen emitted by aircraft (Johnston, 1971; Crutzen, 1971) might catalytically destroy stratospheric ozone led to a number of one-dimensional model studies of the potential effect of aircraft emissions on stratospheric chemistry (CIAP Monograph III, 1975; National Research Council, 1975a; Poppoff et al., 1978; Luther et al., 1979). In 1974, Molina and Rowland proposed that chlorofluoromethanes released at the earth's surface may also deplete stratospheric ozone catalytically once the chlorofluoromethanes dissociate in the upper stratosphere (Molina and Rowland, 1974). Again, prognostic studies with one-dimensional models have followed to analyze this problem (Cicerone et al., 1974; Wofsy et al., 1975a; National Research Council, 1976; Hudson, 1977, 1979). Other recent studies have examined possible effects on stratospheric ozone caused by increased production of nitrous oxide (Logan et al., 1978), from bromine compounds (Wofsy et al., 1975b), from  $CO_2$  (Luther et al., 1977), and from increased  $CO$  and  $CH_4$  in the troposphere (Chameides et al., 1977; Sze, 1977).

Sensitivity and uncertainty analyses (Duewer et al., 1977; Stolarski et al., 1978) with one-dimensional models have been used to determine the effect of uncertainties in our understanding of atmospheric chemistry on calculations determining natural and perturbed species concentrations in the atmosphere.

In this paper, we will analyze and describe the one-dimensional coupled transport and kinetics model and its components; examine its basis and the concepts that led to its development; and discuss its capabilities and limitations.

**STRUCTURE OF THE ONE-DIMENSIONAL MODEL:** As shown in Fig. 1, the local concentration of trace species in an air parcel are determined by the chemical and photochemical processes and other sources and sinks occurring within the parcel, plus by the transport and radiative fluxes into and out of the parcel. These physical processes can be represented in mathematical form by the continuity equation,

$$\frac{\partial c_i}{\partial t} + \nabla \cdot \underline{F}_i(c_i, \underline{x}, t) = P_i(c, J(\underline{x}, t, c), k(T(\underline{x}, t), \rho)) - L_i(c, J(\underline{x}, t, c), k(T(\underline{x}, t), \rho))c_i + S_i(\underline{x}, t) \quad (1)$$

where  $c_i = c_i(\underline{x}, t)$  is the concentration of the  $i$ th chemical constituent;  $c$  is the general representation for all constituents;  $\underline{F}_i$  is the transport flux of  $c_i$ ;  $P_i$  and  $L_i c_i$  are respectively the chemical and photochemical production and loss rates of  $c_i$ ;  $S_i$  represents any other possible sources or sinks for  $c_i$ ;  $T$  is the ambient air temperature;  $\rho$  is the ambient air density;  $J$  represents photodissociation coefficients;  $k$  represents chemical reaction rate coefficients; and all of these variables are defined at a given spatial position  $\underline{x} = \underline{x}(x, y, z)$  at time  $t$ .

In one-dimensional models of the stratosphere, a longitudinal and latitudinal global

average of the transport flux is assumed. The resulting net vertical transport flux,  $F_i(z)$ , of any minor constituent  $c_i$  is represented through a diffusion approximation in which  $F_i(z)$  is assumed to be proportional to the gradient of the mixing ratio of that trace species:

$$F_i(z) = -K_z \rho \frac{\partial}{\partial z}(c_i/\rho) \quad (2)$$

where  $z$  is the altitude and  $K_z$  is the one-dimensional vertical diffusion coefficient (generally assumed to be independent of  $c_i$ ). One of the major assumptions in applying this equation to a one-dimensional representation of the atmosphere is that the effect of global averaged net vertical transport can indeed be approximated by a diffusive process.

It should also be noted that an approximation is introduced in the use of spatially and temporally averaged concentrations to calculate the nonlinear chemical terms in Eq. (1). Most of the reactions are bimolecular with rates of reaction of the form  $k_{ij}c_i c_j$ , where  $k_{ij}$  is the rate constant for reaction of species  $i$  with species  $j$ . The approximation arises because one does not obtain the same average rate by (a) first averaging the concentrations in different volumes and then multiplying, as one would find by (b) first multiplying then averaging. The latter, (b), gives the correct result, but it is not theoretically achievable even with higher dimensional models. The former case, (a), is a simplifying approximation that can be handled with the one-dimensional model. The effect of this approximation can potentially be quite large (Hilst, 1972). However, there is no very satisfactory method of estimating useful bounds for the errors they may induce.

**TRANSPORT PARAMETERIZATION:** The transport of atmospheric trace constituents in the 1-D model, as represented by equation (2), is an empirical representation not utilizing observed atmospheric motion directly but rather is based on observations of the temporal and spatial distributions of select trace species. Chemical tracers such as  $\text{CH}_4$  and  $\text{N}_2\text{O}$  and radionuclides from past atmospheric nuclear tests ( $^{14}\text{C}$ ,  $^{90}\text{Sr}$ ,  $^{95}\text{Zr}$  and  $^{185}\text{W}$ ) have been used as source data for deriving and testing the diffusion coefficient,  $K_z$ . For such tracers, it is assumed that the value of  $K_z$  determined is a function of only the transporting motion field, and within the scope of 1-D models is independent of both the details of the tracer field and the specific structure of the tracer sources and sinks distributions. In practice, however, the representation of transport in the 1-D model is limited by the lack of well-determined globally averaged data for the tracers and by uncertainties in understanding of the balances among sources, sinks and transport processes affecting the trace species distribution.

For any particular tracer  $c_i$ , assuming equation (1) and (2) are applicable and that the production and loss processes are known, then given an adequate globally averaged data base for the vertical profile of  $c_i$ , equation (1) can be inverted to determine  $K_z$  as a function of altitude. An example of how measurements of methane,  $\text{CH}_4$ , may be used to derive a  $K_z$  profile is shown in Figure 2. The only known significant sources of methane are at the surface and its primary loss in the atmosphere comes through reaction with  $\text{OH}$ ,  $\text{O}(^1\text{D})$  and  $\text{Cl}$ . It is assumed that equation (1) as used in Figure 2 can be represented by its time independent form for  $\text{CH}_4$ . Values for the concentration of methane, the air density  $\rho$ , and the reaction rates  $k_1$ ,  $k_2$ ,  $k_3$  as a function of altitude are assumed to be known from measurements. Because only a few, if any, measurements exist for the species  $\text{O}(^1\text{D})$ ,  $\text{OH}$ , and  $\text{Cl}$ , it is necessary to determine concentration profiles for these species from theoretical model calculations or other considerations. The resulting uncertainty will feed back on the  $K_z$  profile determined.

Nitrous oxide,  $\text{N}_2\text{O}$ , has also been extensively used to determine  $K_z$  profiles for the 1-D model. Nitrous oxide has less uncertainties as a tracer than methane because its primary loss comes from photolysis, and is not dependent to a large extent on the distribution of any other species. However, as with methane, the lack of global-averaged measurements and the lack of consideration in using global-averaged photolytic loss rates in the analyses contribute to uncertainty in determining the  $K_z$  profile from this species.

Because of these and other uncertainties, the choice of  $K_z$  profile is not unique.

However, there are similarities in the  $K_z$  profiles derived from various data bases and used in various one-dimensional models. Figure 3 shows two  $K_z$  profiles currently in use. In general, these and other profiles have large values in the troposphere, on the order of  $10^5$  cm<sup>2</sup>/sec, a much lower value in the region of the tropopause, and gradually increasing larger values in the upper stratosphere.

Figures 4 and 5 compares measurements of CH<sub>4</sub> and N<sub>2</sub>O with model-derived species profiles using LLL  $K_z$  in Figure 3 in the current LLL model (Luther et al., 1979). The chemistry used in the model is that recommended by the NASA Panel on Laboratory Measurements in Hudson (1979). Model calculations compare well with the measurements of Ehhalt et al. (1975) and Ackerman et al. (1978). More recent measurements of Ehhalt (1979) agree well with the earlier measurements. In general, the model-derived profile for N<sub>2</sub>O also agrees well with the measurements by Goldman et al. (1979). However, in the upper stratosphere, above 30 km, the measured N<sub>2</sub>O concentrations appear to fall off more rapidly than those derived with the model. A similar result is found in comparison of model calculation with measurements for other long-lived species such as CF<sub>2</sub>Cl<sub>2</sub> and CFC1<sub>3</sub> whose primary sinks are not directly dependent upon other species distributions. Changing the  $K_z$  profile to improve the comparison for N<sub>2</sub>O, CF<sub>2</sub>Cl<sub>2</sub> and CFC1<sub>3</sub> would reduce the agreement with CH<sub>4</sub>. However, the agreement with methane depends on comparison with limited available data above 40 km, which is basically two rocket measurements by Ehhalt. Assuming these measurements were accurate, then changing the transport coefficient would require that some mechanism be found that reduces the OH concentration, since reaction with OH is the primary sink for methane, in the 20-30 km region, but such mechanisms are only speculative at present.

Since there are intrinsic weaknesses in all available profiles of  $K_z$  and because  $K_z$  is such an important input parameter to the one-dimensional model, it is necessary to analyze model sensitivity to its variations in every application. For example, if we compare model calculations, using the LLL  $K_z$  in Figure 3 and a  $K_z$  (Hunten, 1975) qualitatively similar to the  $K_z$  labelled Harvard in Figure 3 except that the values above the tropopause are approximately a factor of two smaller we would find the following results. Because of the large minimum in the region of the tropopause, the Hunten  $K_z$  results in slower transport between the middle stratosphere and the troposphere. For the ambient atmosphere, this implies much smaller concentrations in the middle to upper atmosphere for those species having their sources in the troposphere and sinks in the lower or middle stratosphere. Because of the slower transport, stratospheric chemical and photochemical sinks have more time to act. For example, the concentration of CH<sub>4</sub> is calculated to be 42% smaller at 35 km and 71% smaller at 45 km and the concentration of N<sub>2</sub>O is 45% smaller at 35 km and 79% smaller at 45 km relative to the model with the LLL  $K_z$ . For those species produced in the stratosphere for which transport to and loss in the troposphere is an important process, much larger concentrations in the lower stratosphere and corresponding decreases in concentrations of the troposphere result when the Hunten  $K_z$  is used relative to the LLL  $K_z$ . Such species as HNO<sub>3</sub>, NO<sub>2</sub>, N<sub>2</sub>O<sub>5</sub>, and ClONO<sub>2</sub> result in 100% or higher increases in concentration in the lower stratosphere when the Hunten  $K_z$  is used. Given the variability of observed distributions of these species it is not obvious which  $K_z$  is necessarily more preferable.

But for perturbation studies, again because of slower transport between stratosphere and troposphere, there is a larger build-up of emitted species from the perturbation for the Hunten  $K_z$  than with the LLL  $K_z$ . This could lead to very significantly different results. For example, the Hunten  $K_z$  results in a reduction of total ozone of -21.8% at steady state for constant production of CF<sub>2</sub>Cl<sub>2</sub> and CFC1<sub>3</sub> at 1976 levels in the current LLL 1-D model as compared to -13.8% when the LLL  $K_z$  is used. Consequently in assessing the significance of 1-D model predictions we must analyze and take into consideration the model sensitivities to  $K_z$  uncertainties.

**CHEMICAL KINETICS SYSTEM:** Of all models that contain some type of transport process, one-dimensional models are generally the most detailed and complete in considering photochemical processes. All 1-D models now include the Chapman reactions, the NO<sub>x</sub>, HO<sub>x</sub> and ClO<sub>x</sub> catalytic cycles, and many of the transfer reactions among these basic cycles. In addition, essentially all 1-D models contain reactions for the species resulting from methane oxidation, and many have included bromine and sulfur chemistry in their calculations. Some even treat aerosol formation and loss.

The number of reactions included in present 1-D models range from approximately 60 to 400 chemical and photochemical reactions involving approximately 24 to 60 species whose concentrations are calculated. As an example, the LLL model presently contains 134 reactions to determine the distributions of 39 species.

The more extensive reaction sets used in some models include many minor reactions, but a comparison of representative models indicates that the chemical kinetics systems in current use are in essential agreement. However, as a result of new laboratory measurements and as the evolution of our understanding of the chemistry of the atmosphere continue, there is a continuous effort in updating reaction rate coefficients and introduction of additional reactions.

A detailed discussion of the chemical system warrants a separate paper, and will not be attempted here. Currently many models are using similar chemistries based on the recommendations of Hudson, 1979.

**RADIATIVE PROCESSES:** Photodissociation processes in the atmosphere are often extremely important mechanisms for the production and destruction of chemical species. The photodissociation rate, at altitude  $z$  for a species  $i$  to give a product  $j$  is defined by

$$J_{i \rightarrow j} = \int_{\text{all } \lambda} Q_{\lambda, i} \sigma_{\lambda, i} F_{\lambda}(\infty) e^{-\tau_{\lambda}} d\lambda \quad (3)$$

where  $Q_{\lambda, i} = Q_{\lambda, i(i \rightarrow j)}$  is the quantum yield for photodissociation of species  $i$  to result in production of species  $j$ ,  $\sigma_{\lambda, i}$  is the photoabsorption cross section,  $F_{\lambda}(\infty)$  is the solar flux at the top of the atmosphere.  $\tau_{\lambda}$  is the optical depth defined by

$$\tau_{\lambda} = \int_z^{\infty} \left( \sum_A N_A \sigma_{\lambda, A} \sec \chi \right) dz \quad (4)$$

The summation of species  $A$  includes all atmospheric absorbers each having number density  $N_A$  and a total absorption cross section  $\sigma_{\lambda, A}$ . The angle  $\chi$  is the solar zenith angle. In the troposphere and stratosphere the optical depth is primarily determined by  $O_2$ ,  $O_3$ , and  $NO_2$  absorption. The optical depth, and thus the photodissociation rate, is calculated as a function of altitude within the 1-D model.

The absorption of solar radiation as it is affected by the optical depth is calculated in a self-consistent manner from the concentration profiles of trace species predicted by the model. As such, 1-D models satisfy the minimum requirement for simulating photochemical processes in the atmosphere by calculating the attenuation of sunlight as a function of altitude. The external parameters affecting the calculated photodissociation rate are the wavelength dependence of the quantum yield and absorption cross-sections, which are based on laboratory measurements; the solar flux at the top of the atmosphere and the total column of absorptive species above the top of the model, which are based on atmospheric measurements; and the solar zenith angle which is determined by the season and time of day.

The importance of molecular multiple scattering and the surface albedo in determining atmospheric photodissociation rates is now well recognized (Luther and Gelinas, 1976; Callis et al., 1976; Kurzeja, 1976; Luther et al., 1978). To account for multiple scattering, the calculation of optical depth, equation (4), must be modified to include a term for Rayleigh scattering,

$$\tau_{\lambda} = \int_z^{\infty} \left( \sum_A N_A \sigma_{\lambda, A} \sec \chi \right) dz + \int_z^{\infty} \left( \sum_{\ell} N_{\ell} \sigma_{R, \lambda, \ell} \sec \chi \right) dz \quad (5)$$

In (5), the summation on  $\ell$  includes all atmospheric species, and  $\sigma_{R, \lambda, \ell}$  is the Rayleigh scattering cross-section for species  $\ell$ . In addition, the photodissociation coefficient must be further modified to include dependence on the scattered or diffuse radiation,

$$J_{i \rightarrow j} = \int_{\text{all } \lambda} Q_{\lambda, i} \sigma_{\lambda, i} \left\{ F_{\lambda}(\infty) e^{-\tau_{\lambda}} + \int_{4\pi} I_{\lambda} d\omega \right\} d\lambda \quad (6)$$

where  $I_{\lambda}$  is the specific intensity of the diffuse radiation and  $\omega$  is the solid angle.

The effect of including multiple scattering on several individual photodissociation rates is shown in Table 1. For these reactions, the calculated rates are significantly larger when multiple scattering is included as compared to the case of pure absorption only. In these calculations, a zenith angle of  $30^\circ$  and a planetary albedo of .25 were assumed. Similar effects also hold for many other reactions (Luther et al., 1978).

Changes in stratospheric composition can affect the stratospheric temperature profile via the solar and long-wave radiation balance. Changes in temperature affect chemical reaction rates, which in turn feed back on composition. This temperature feedback mechanism has been included in recent 1-D model calculations (McElroy et al., 1974; Luther et al., 1977; Tuck, 1977; Boughner, 1978). In these calculations the stratospheric temperature profile is calculated by using a radiative transfer model that includes solar absorption and long-wave interaction of the radiatively important stratospheric species (i.e.,  $O_3$ ,  $NO_2$ ,  $H_2O$ ,  $CO_2$ ).

The distribution of the radiatively important stratospheric species derived by the one-dimensional coupled transport and chemical kinetics model is used as input to the radiative transfer model, which then derives a new stratospheric temperature distribution. These temperatures are then used in determining chemical and photochemical reaction rates for the next calculation of species distributions in the 1-D model. This methodology is shown in figure 6. Because radiative equilibrium is generally assumed in these calculations at stratospheric altitudes, it is important to recognize that temperature feedback is generally more theoretically useful for time-independent or steady-state calculations than for time-dependent evaluations.

An example of the potential importance and the need for completeness of temperature feedback processes is provided by studying the impact on stratospheric ozone from doubling the  $N_2O$  concentration at the earth's surface. Without temperature feedback (i.e. fixed stratospheric temperature) the LLL 1-D model calculates a -2.2% change in the vertical ozone column due to doubling the  $N_2O$  surface concentration from 324 ppbv to 648 ppbv. If we include the effect of ozone changes on temperature, then the same model would only predict a -1.2% change in total ozone, i.e. only half of the previous result. The decrease in stratospheric ozone results in a decrease in temperature and a decrease in the catalytic efficiency of the major chemical cycles destroying ozone. However, for this special problem, the increase in  $NO_2$  resulting from the doubling of  $N_2O$  can provide enough absorption and heating to offset the decrease in ozone heating. The complete temperature feedback calculation (including both  $O_3$  and  $NO_2$  changes) results in a near cancellation of all temperature feedback effects, i.e. a -2.4% change in ozone column is calculated. Similar complexity in temperature feedback mechanisms is also present in other studies (Luther et al., 1977; Penner and Chang, 1978, 1979; NAS, 1979). Clearly, careful consideration of all temperature feedback processes in 1-D models must be developed.

**OTHER PHYSICAL DATA:** Altitude distributions of major constituents such as  $N_2$  and  $O_2$  are generally fixed in the calculations with concentrations based on a source such as the U.S. Standard Atmosphere (1976). In addition, some models do not calculate the distributions of some trace constituents, but rather fix their distributions based on atmospheric measurements. Because of the difficulty with treating water vapor in the troposphere, many models fix the concentration of water vapor in the troposphere, while calculating its concentration in the stratosphere. Unless temperature feedback effects are included, the temperature profile is usually based on a standard reference such as the U.S. Standard Atmosphere (1976).

**PHYSICAL DOMAIN AND BOUNDARY CONDITIONS:** The choice of spatial domain depends on the chemical species of interest and the level of detail desired. For each individual species either boundary concentrations or fluxes must be prescribed. Because atmospheric measurements of many chemical species are inadequate, it is difficult to construct reliable boundary conditions for some species. In practice, an iteration between estimated boundary conditions, model simulation results, and appropriate comparisons with available atmospheric data must be carried out. In models primarily designed to study global scale tropospheric and stratospheric chemistry, it is generally sufficient to assume zero flux at the earth's surface for the free radicals. The choice of fixed concentration or



surface flux must be carefully made for species with long chemical lifetimes. If a model's lower boundary is at the tropopause, careful consideration of boundary fluxes must be given to each species. Both fixed fluxes and fixed concentrations may be too restricting to a model whose lower boundary is at the tropopause. Except for perhaps a few species, zero flux can be assumed for the top boundary at the stratopause or above. For the few exceptions, i.e. NO we need to study the effect of the potentially significant fluxes into or out of the region of interest.

The need for accurate boundary conditions can be reduced by extending the physical domain beyond the minimum required by the problem at hand. Moving the boundary beyond a buffer zone serves to reduce the model sensitivity to uncertainties in boundary conditions. It is necessary also to include in the physical domain any region which may have feedbacks important to the region of interest. One should therefore include the effect of tropospheric feedbacks in models studying stratospheric chemistry. For many one-dimensional models the physical domain extends over the region from the earth's surface to or above the stratopause.

**SOLVING THE CONTINUITY EQUATION:** Once parameterizations of the relevant physical variables have been determined, the system of partial differential equations resulting from there being a continuity equation (1) for each species in the model is to be solved. This system of equations will have the form

$$\frac{\partial}{\partial t} \begin{bmatrix} c_1 \\ c_2 \\ \vdots \\ c_n \end{bmatrix} = \frac{\partial}{\partial z} (K_z \rho \frac{\partial}{\partial z} \begin{bmatrix} c_{1/\rho} \\ c_{2/\rho} \\ \vdots \\ c_{n/\rho} \end{bmatrix}) + \begin{bmatrix} P_1 - L_1 c_1 \\ P_2 - L_2 c_2 \\ \vdots \\ P_n - L_n c_n \end{bmatrix} + \begin{bmatrix} S_1 \\ S_2 \\ \vdots \\ S_n \end{bmatrix} \quad (7)$$

with  $n$  equal to the number of species. By solving this system of equations simultaneously, the distribution of the constituents computed in the model can be found in a totally self-consistent manner. This self-consistency is an important aspect of the models, for in general, any change made to a 1-D model, for example to improve comparison of a particular species distribution with observations, would also affect other species within the model. For physical reasons, the system of equations (7) is expected to have real positive solutions although no general mathematical proofs are available.

Because the chemical production and loss terms are often nonlinear functions of multiplied species concentrations, the system of equations (7) is nonlinear. This nonlinearity and the large number of equations to be solved makes it convenient to seek numerical solutions. To ready the system of equations (7) to be solved numerically, central finite differencing is generally used and altitude increments of the physical domain are established such that the choice of grid spacing will not affect the accuracy of the solution within the constraints of the problem to be solved.

It has long been recognized that differential equations arising from chemical kinetics interactions are often difficult to solve numerically. This difficulty is generally a result of the phenomenon of "stiffness". A mathematical system is stiff if it contains closely coupled eigenstates with greatly differing time constants. A unique computational dilemma results when the desired solution contains closely coupled eigenstates with greatly differing time constants, such that in order to obtain the solution at late time one must compute accurately at all times the evolution of the already decayed eigenstates, which in fact contribute little to the solution of interest. For traditional explicit and implicit numerical techniques, this implies computationally unstable solutions unless the time step is comparable to the smallest time constant. Fortunately, very powerful numerical techniques have been developed for stiff ordinary differential equations (Gear, 1971; Lapidus and Seinfeld, 1971; Hindmarsh, 1979) and can be adapted to the solution of equation (7) (Chang et al, 1974).

Although these direct methods of solution are both accurate and reasonably convenient for one-dimensional models, they require considerable computer memory and execution time. Another approach used is to identify closely coupled chemical species that can be summed into families, thereby providing a reduced set of equations to be solved (Logan et al,

1978; Turco and Whitten, 1977; Rundel et al, 1978; Liu et al, 1976). Once the equations are solved, each family of chemical species is partitioned into its components. The advantage of this method is a large reduction in the computation time. Transport in these models is done on the family, rather than on the individual species. The final partitioning can only be achieved with a heavy dose of physical intuition. Without additional physically based constraints, the system of mathematical equations representing the partitioning operation is under-determined; hence, possible unphysical solutions must be eliminated. The choice of family groupings for this method is nonunique and often changes as the problem progresses. In contrast to the direct solution technique, this prevents the development of a generally applicable computational model. Nevertheless for current problems of interest, one-dimensional models using this solution technique have compared well with those using direct solution methods (Hudson, 1977, 1979).

For some applications, it is possible to make simplifications in the equations to be solved in the model. For a few species, the chemical lifetimes are so short that at timescales of interest the transport term and the time derivative can be neglected in determining the concentration for these species. The concentration of these species can then be determined algebraically without including them in the system of equations to be solved numerically.

For simplicity and computational economy, steady-state solutions of the system of equation (7) are often useful and desirable. In general, though, fully time dependent models are more useful both diagnostically and prognostically, although their solutions are considerably more complicated and computationally expensive. For the analysis of atmospheric data on most chemically active species, time-dependent models and, in particular, diurnal models must be used.

**TEMPORAL VARIATIONS:** For many model applications, it is necessary to calculate the diurnal solar effect on trace species concentrations in the atmosphere. In the one-dimensional model, this effect is included by allowing the solar zenith angle to change as a function of time using the expression:

$$\cos \chi = \sin \theta \sin \delta + \cos \theta \cos \delta \cos \left( \frac{2\pi t}{8.64 \times 10^4} \right) \quad (8)$$

where  $\theta$  is the latitude,  $\delta$  is the solar declination angle, and  $t$  is the time in seconds relative to noon. Some models also have recently included the effect of the sphericity of the earth when computing sunrise and sunset as a function of altitude. For  $\chi > 90^\circ$ , photodissociation rates are assumed to be zero. The effect of sphericity plus the effect of the long solar path on both the direct and scattered beam should be included at sunrise and sunset in order to accurately calculate the detailed diurnal change in species concentration in the troposphere and stratosphere, although this has not yet been done.

Those atmospheric species whose chemical lifetimes are less than a day would be expected to show significant diurnal variation. An example of the diurnal variations at 30 km altitude for the species  $\text{NO}$ ,  $\text{NO}_2$ ,  $\text{NO}_3$  and  $\text{N}_2\text{O}_5$  as calculated in the LLL one-dimensional model are shown in Figure 7. As seen in Figure 7, there is a wide range of diurnal behaviors even within a set of closely coupled species as these. This occurs primarily because of the changing relative importance of several reactions as the solar intensity changes. Many other important species, especially the free radicals, are expected to have significant diurnal variations that need experimental confirmation which then serves as validations of the theory. Other trace species such as  $\text{N}_2\text{O}$ ,  $\text{CH}_4$ ,  $\text{CF}_2\text{Cl}_2$  and  $\text{CFCl}_3$  have much longer chemical lifetimes and would not be expected to have significant diurnal variations.

The direct approach of integrating the model equations with a time step small enough to properly reproduce the essential diurnal effects are expensive because of the approximately 3-4 years of model time necessary for achieving cyclic behavior of species concentrations from a steady state starting point (Wuebbles and Chang, 1975; Hudson, 1977). This and the need for long model integrating time for prognostic studies has led to the development of diurnal averaging techniques (Hudson, 1977; Luther, 1977; Turco and Whitten, 1978). Diurnal averaging is a procedure that permits chemical and photochemical

kinetic rates to be modified, generally by a multiplier constant, so that the long-term behavior of a constant zenith angle calculation is the same as the true diurnal average of the long time integration of the fully time-dependent calculation. Such techniques have greatly improved model self consistency as compared to the previously used constant sun or constant solar zenith angle approximation (CIAP Monograph III, 1975). Diurnal averaging processes are particularly important in calculating the concentrations for such species as  $\text{N}_2\text{O}_5$  and  $\text{ClONO}_2$  whose concentrations would be grossly underpredicted or overpredicted unless diurnal averaging is included. A comparison between the rates of reaction calculated using diurnal averaging or using constant sun, in which noon photolytic rates are divided by 2, is shown in Table 2 for a few sample reactions. In each of the 7 reactions shown, there is a large effect at some altitudes due to the diurnal effect.

Seasonal variations in trace constituent distributions cannot be adequately produced in one-dimensional models unless special constraints are specified. Since horizontal transport is neglected in the one-dimensional model, the seasonal effects of horizontal transport on such species as ozone are not included. Highly reactive chemical species interact strongly with the odd-oxygen species and in the one-dimensional model, the concentration of odd-oxygen, primarily determined by  $\text{O}_3$ , is directly related to the incident solar flux intensity. This results in seasonal distribution of vertical ozone that are positively correlated with solar flux intensity contrary to observation (see Figure 8). Only by using measured profiles of those species having significant seasonal horizontal transport effects can seasonal variations for highly reactive species (radicals) be determined. Thus, such quantities as the  $\text{O}_3$  distribution, total odd-nitrogen and total odd chlorine need to be fixed in seasonal calculations using 1-D models.

**INTERPRETATION AND LIMITATIONS:** Because the vertical transport parameterization is based on globally averaged values of vertical distributions of long-lived species such as  $\text{CH}_4$  and  $\text{N}_2\text{O}$ , for similar compounds, one-dimensional models should be viewed as approximately global averaged models. For short-lived species in near local photochemical equilibrium, it is necessary to realize that in the detailed representation of photolysis processes only local variables such as solar flux intensity and temperature can be used. This greatly complicates the interpretation of model results. Since a primary concern is the vertical distribution of ozone, one-dimensional models seem to represent best the conditions at  $30^\circ\text{N}$  latitude near the fall equinox.

By using measured ozone profiles and/or other chemical species data (e.g., total odd-nitrogen, total odd chlorine, etc) and the appropriate local conditions, one-dimensional models can be used to analyze the detailed chemical balances at other latitudes and/or seasons. The smoothness of the  $K_z$  profiles used and the nature of using a diffusion approximation results in species profiles being relatively smooth. Because of this and because of the averaging approach taken in developing the model, the one-dimensional model can account for natural variability and local structure in only a limited manner.

Dynamical feedbacks with radiatively important species such as ozone are neglected in the one-dimensional model. This severely impacts on the interpretation of large predicted perturbations to ozone when resulting temperature changes would be expected to feed back on atmospheric dynamics. Because of the mixed global and local representation, one-dimensional models must be applied with care in consideration of the intrinsic compatibility of the model and its intended use. However, at a minimum, one-dimensional models provide highly useful qualitative analyses of the intercoupling of chemical processes in the stratosphere. Limited comparison with available results from higher dimensional models indicate that in many applications quantitative results from one-dimensional models are no less reliable (CIAP Monograph III, 1975; Hudson, 1977, 1979).

Two- and three-dimensional models will likely play an ever increasing role in future diagnostic and prognostic studies of the atmosphere because of their improved capabilities in treating global dynamic and latitudinal effects. Nonetheless, one-dimensional calculations involving chemistry and a parameterized treatment of net vertical transport will continue to be useful. One dimensional models are particularly well suited to study the potential impact of newly suggested chemical and physical processes, to answer chemical balance questions, to study chemical uncertainties and model sensitivity, and to provide guidance to more complex model studies. One-dimensional models will contribute to the

development of higher dimensional models by developing the parameterized chemistry essential to such models. Thus while one-dimensional coupled transport and chemical kinetics models have been the dominant tool in diagnostic and prognostic studies in the last ten years, they will continue to play an important although less central role in future studies attempting to improve our understanding of chemical processes in the stratosphere.

**ACKNOWLEDGMENTS:** This work was performed under the auspices of the U.S. Department of Energy by the Lawrence Livermore Laboratory under contract No. W-7405-Eng-48, and supported in part by the High Altitude Pollution Program of the Department of Transportation, Federal Aviation Administration. The authors wish to acknowledge their appreciation of the continuing collaboration with our colleagues at Livermore: W. H. Duewer, H. W. Ellsaesser, F. M. Luther, J. E. Penner and R. L. Tarp.

#### NOTICE

This report was prepared as an account of work sponsored by the United States Government. Neither the United States nor the United States Department of Energy, nor any of their employees, nor any of their contractors, subcontractors, or their employees, makes any warranty, express or implied, or assumes any legal liability or responsibility for the accuracy, completeness or usefulness of any information, apparatus, product or process disclosed, or represents that its use would not infringe privately-owned rights

Reference to a company or product name does not imply approval or recommendation of the product by the University of California or the U.S. Department of Energy to the exclusion of others that may be suitable.

## REFERENCES

- Ackerman, M., D. Frimout, C. Muller and D. J. Wuebbles, "Stratospheric Methane Measurements and Predictions," Pageoph, 117, 367-380, 1978.
- Boughner, R. G., "The Effect of Increased Carbon Dioxide Concentrations in Stratospheric Ozone," J. Geophys. Res., 83, 1326-1332, 1978.
- Callis, L. B., R. E. Boughner, V. Ramanathan, and J. E. Nealy, "Ozone: Effect of UV Variability and Stratospheric Coupling Mechanisms," paper presented at the International Joint Symposium on Atmospheric Ozone, Int. Comm. on Atmos. Ozone and Int. Comm. on Atmos. Chem. and Global Pollut., Dresden, East Germany, Aug. 9-17, 1976.
- Callis, L. B. and J. E. Nealy, "Solar UV Variability and its Effect on Stratospheric Thermal Structure and Trace Constituents," Geophys. Res. Lett., 5, 249-252, 1978.
- Chameides, W. L., S. C. Liu and R. J. Cicerone, "Possible Variations in Atmospheric Methane," J. Geophys. Res., 82, 1795-1798, 1977.
- Chang, J. S. and W. H. Duewer, "On the Possible Effect of  $\text{NO}_x$  Injection in the Stratosphere Due to Past Atmospheric Nuclear Weapons Tests," paper presented at the AIAA/AMS Meeting, Amer. Inst. of Aeronaut. and Astronaut., Denver, Colo., June 1973. (Also Rep. UCRL-74480, Lawrence Livermore Laboratory, Livermore, California 94550, 1973.)
- Chang, J. S., W. H. Duewer and D. J. Wuebbles, "The Atmospheric Nuclear Tests of the 1950's and 1960's: A Possible Test of Ozone Depletion Theories," J. Geophys. Res., 84, 1755-1965, 1979.
- Chang, J. S., A. C. Hindmarsh, and N. K. Madsen, "Simulation of Chemical Kinetics Transport in the Stratosphere", in Stiff Differential Systems, ed. R. A. Willoughby, Plenum-New York, pp. 51-65, 1974.
- CIAP Monograph III, "The Stratosphere Perturbed by Propulsion Effluents," Department of Transportation Report, DOT-TST-75-53, 1975.
- Cicerone, R. J., R. S. Stolarski and S. Walters, "Stratospheric Ozone Destruction by Man-Made Chlorofluoromethanes," Science, 185, 1165-1166, 1974.
- Colegrove, F. D., W. B. Hanson and F. S. Johnson, "Eddy Diffusion and Oxygen Transport in the Lower Thermosphere," J. Geophys. Res., 70, 4931, 1965.
- Colegrove, F. D., F. S. Johnson and W. B. Hanson, "Atmospheric Composition in the Lower Thermosphere," J. Geophys. Res., 71, 2227-2236, 1966.
- Crutzen, P. J., "Ozone Production Rates in an Oxygen-Hydrogen - Nitrogen Oxide Atmosphere" J. Geophys. Res., 76, 7311-7327, 1971.
- Crutzen, P. J., "The Photochemistry of the Stratosphere with Special Attention Given to the Effects of  $\text{NO}_x$  Emitted by Supersonic Aircraft," Proceedings of the Survey Conference, U.S. Dept. of Transportation, DOT-TSC-OST-72-13, 1972.
- Duewer, W. H., D. J. Wuebbles, H. W. Ellsaesser and J. S. Chang, " $\text{NO}_x$  Catalytic Ozone Destruction: Sensitivity to Rate Coefficients," J. Geophys. Res., 82, 935-942, 1977.
- Ehhalt, D. H., L. E. Heidt, R. H. Lueb and W. Pollock, "The Vertical Distribution of Trace Gases in the Stratosphere," Pageoph, 113, 389-402, 1975.
- Ehhalt, D., "Hydrogen and Carbon Compounds and  $\text{N}_2\text{O}$ ,  $\text{CFCl}_3$ ,  $\text{CF}_2\text{Cl}_2$  in the Stratosphere," presented at NATO Advanced Study Institute on Atmospheric Ozone: Its Variation and Human Influences, 1979.
- Gear, C. W., "Numerical Initial Value Problems in Ordinary Differential Equations", Prentice-Hall, Englewood Cliffs, N.J., 1971.
- Goldan, P. D., W. C. Kuster, D. L. Albritton and A. L. Schmeltekopf, " $\text{CFCl}_3$ ,  $\text{CF}_2\text{Cl}_2$  and  $\text{N}_2\text{O}$  Height-Profile Measurements at Several Latitudes, preprint, 1979.
- Grobecker, A. J., S. C. Coroniti and R. H. Cannon, Jr., "Report of Findings," U.S. Department of Transportation, Washington, D.C., DOT-TSC-75-50, 1974.
- Hesstvedt, E., "On the Effect of Vertical Eddy Transport on Atmospheric Composition in the Mesosphere and Lower Thermosphere," Geophys. Norv., 27, 1-35, 1968a.
- Hesstvedt, E., "On the Photochemistry of Ozone in the Ozone Layer," Geofis. Publ., 27, No. 5, 16, 1968b.
- Hesstvedt, E., "A Theoretical Study of the Diurnal Variation of Hydroxyl Emission," J. Geophys. Res., 75, 2337-40, 1970.
- Hesstvedt, E. and U. B. Jansson, "On the Effect of Vertical Eddy Transport on the Distribution of Neutral Nitrogen Components in the D Region," in Meteorological and Chemical Factors in D-Region Aeronomy - Record of the Third Aeronomy Conference, University of Illinois Aeronomy Report 32, 190, 1969.
- Hesstvedt, E., "A Meridional Model of the Oxygen-Hydrogen Atmosphere," in Mesospheric Models and Related Experiments, G. Fiocco, ed., Reidel Publ., Dordrecht, Neth., 1971.

- Hilst, G. R., "Solution of the Chemical Kinetic Equations for Initially Inhomogeneous Mixtures," Proceedings of the Second Conference on the Climatic Impact Assessment Program, Department of Transportation, Washington, DC DOT-TSC-OST-73-4, 1972.
- Hindmarsh, A. C., "A Collection of Software for Ordinary Differential Equations", Proceeding of the American Nuclear Society, National Topical Meeting on Computational Methods in Nuclear Engineering, Williamsburg, Virginia, April, 1979.
- Hudson, R. D., editor, "Chlorofluoromethanes and the Stratosphere," NASA RP-1010, 1977.
- Hudson, R. D., editor, "The Stratosphere: Present and Future," NASA RP-1049, 1979.
- Hunten, D. M., "Vertical Transport in Atmospheres," in Atmospheres of Earth and the Planets, B. M. McCormac, ed., Reidel Publishing, Dordrecht, Neth., 1975.
- Johnston, H., "Reduction of Stratospheric Ozone by Nitrogen Oxide Catalysts from Supersonic Transport Exhaust," Science, **173**, 517-522, 1971.
- Junge, C., W. Seiler and P. Warneck, "The Atmospheric  $^{12}\text{CO}$  and  $^{14}\text{CO}$  Budget," J. Geophys. Res., **76**, 2866-2879, 1971.
- Keneshea, T. J., and S. P. Zimmerman, "The Effect of Mixing Upon Atomic and Molecular Oxygen in the 70-170 km Region of the Atmosphere," J. Atmos. Sci., **27**, 831-840, 1970.
- Kurzeja, R. J., "The Production and Transport of Ozone and Other Minor Constituents in the Stratosphere," Ph.D. thesis, Microfilm 76-28636, Fla. State Univ., Tallahassee, 1976.
- Lapidus, L. and J. H. Seinfeld, "Numerical Solution of Ordinary Differential Equations", Academic Press, New York, 1971.
- Liu, S. C., T. M. Donahue, R. J. Cicerone and W. L. Chameides, "Effect of Water Vapor on The Destruction of Ozone in the Stratosphere Perturbed by  $\text{Cl}_x$  or  $\text{NO}_x$  Pollutants," J. Geophys. Res., **81**, 3111-18, 1976.
- Logan, J. A., M. J. Prather, S. C. Wofsy and M. B. McElroy, "Atmospheric Chemistry: Response to Human Influence," Philosophical Transactions of the Royal Society of London A. Mathematical and Physical Sciences, **290**, 187-234, 1978.
- Luther, F. M. and R. J. Gelinas, "Effect of Molecular Multiple Scattering and Surface Albedo on Atmospheric Photodissociation Rates," J. Geophys. Res., **81**, 1125-1132, 1976.
- Luther, F. M., D. J. Wuebbles and J. S. Chang, "Temperature Feedback in a Stratospheric Model," J. Geophys. Res., **82**, 4935-4942, 1977.
- Luther, F. M., "Annual Report of Lawrence Livermore Laboratory to the High Altitude Pollution Program-1977," Lawrence Livermore Laboratory Report UCRL-50042-77, 1977.
- Luther, F. M., D. J. Wuebbles, W. H. Duewer and J. S. Chang, "Effect of Multiple Scattering on Species Concentration and Model Sensitivity," J. Geophys. Res., **83**, 3563-3570, 1978.
- Luther, F. M., J. S. Chang, W. H. Duewer, J. E. Penner, R. L. Tarp and D. J. Wuebbles, "Potential Environmental Effects of Aircraft Emissions," Lawrence Livermore Laboratory Report UCRL-52861, 1979.
- McElroy, M. B., "Conference Summary," Proceedings of the Survey Conference, Department of Transportation Report DOT-TSC-OST-72-13, 1972.
- McElroy, M. B. and J. C. McConnell, "Nitrous Oxide: A Natural Source of Stratospheric  $\text{NO}$ ," J. Atmos. Sci., **28**, 1095-1098, 1971.
- McElroy, M. B., S. C. Wofsy, J. E. Penner and J. C. McConnell, "Atmospheric Ozone: Possible Impact of Stratospheric Aviation," J. Atmos. Sci., **31**, 287-303, 1974.
- Molina, M. J. and F. S. Rowland, "Stratospheric Sink for Chlorofluoromethanes: Chlorine Atom Catalyzed Destruction of Ozone," Nature, **249**, 810-812, 1974.
- National Research Council, "Environmental Impact of Stratospheric Flight," National Academy of Sciences, Washington, D.C., 1975a.
- National Research Council, "Long-Term Worldwide Effects of Multiple Nuclear Weapons," National Academy of Sciences, Washington, D.C., 1975b.
- National Research Council, "Halocarbons: Effects on Atmospheric Ozone," National Academy of Sciences, Washington, D.C., 1976.
- National Research Council, "Stratospheric Ozone Depletion by Halocarbons: Chemistry and Transport," National Academy of Sciences, Washington, D.C., 1979.
- Nicolet, M., "On the Thermal-Diffusion Effect in the Thermosphere," Geophys. J. Royal Atomic Soc., **15**, 157-161, 1968.
- Nicolet, M., "Aeronomical Reactions of Hydrogen and Ozone," in Mesospheric Models and Related Experiments, G. Fiocco, ed. Reidel Publ., Dordrecht, Neth., 1971.
- Penner, J. E. and J. S. Chang, "Possible Variations in Atmospheric Ozone Related to the Eleven Year Solar Cycle," Geophys. Res. Lett., **5**, 817, 1978.
- Penner, J. E. and J. S. Chang, "The Relation Between Atmospheric Trace Species Variabilities and Solar UV Variability," Lawrence Livermore Laboratory Report UCRL-83029, 1979.

- Poppoff, I. G., R. C. Whitten, R. P. Turco and L. A. Capone, "An Assessment of the Effect of Supersonic Aircraft Operation on the Stratospheric Ozone Content," NASA R.P. -1026, 1978.
- Rundel, R. D., D. M. Butler and R. S. Stolarski, "Uncertainty Propagation in a Stratospheric Model, 1, Development of a Concise Stratospheric Model," J. Geophys. Res., **83**, 3063-73, 1978.
- Shimazaki, T., "Dynamic Effects on Atomic and Molecular Oxygen Density Distributions in the Upper Atmosphere: A Numerical Solution to Equations of Motion and Continuity," J. Atmos. Terr. Phys., **29**, 723, 1967.
- Shimazaki, T., "Dynamic Effects on Height Distributions of Neutral Constituents in the Earth's Upper Atmosphere: A Calculation of Atmospheric Model Between 70 km and 500 km," J. Atmos. Terr. Phys., **30**, 1279-1292, 1968.
- Shimazaki, T., and A. R. Laird, "A Model Calculation of the Diurnal Variation in Minor Neutral Constituents in the Mesosphere and Lower Thermosphere Including Transport Effects," J. Geophys. Res., **72**, 3221-3235, 1970.
- Shimazaki, T. and A. R. Laird, "Seasonal Effects on Distributions of Minor Neutral Constituents in the Mesosphere and Lower Thermosphere," Radio Sci., **7**(1), 23-43, 1972.
- Stolarski, R. S. and R. J. Cicerone, "Stratospheric Chlorine: A Possible Sink for Ozone," Can. J. Chem., **52**, 1610-1615, 1974.
- Stolarski, R. S., D. M. Butler and R. D. Rundel, "Uncertainty Propagation in Stratospheric Model, 2, Monte Carlo Analysis of Impressions Due to Reaction Rates," J. Geophys. Res., **83**, 3074-3078, 1978.
- Strobel, D. F., D. M. Hunten and M. B. McElroy, "Production and Diffusion of Nitric Oxide," J. Geophys. Res., **75**, 4307-4321, 1970.
- Strobel, D. F., "The Diurnal Variation in Nitric Oxide in the Upper Atmosphere," J. Geophys. Res., **76**, 2441-2452, 1971.
- Sze, N. D. "Anthropogenic CO Emissions: Implications for Atmospheric CO-OH-CH<sub>4</sub> Cycle," Science, **195**, 673-675, 1977.
- Tuck, A. F., "Numerical Model Studies of the Effect of Injected Nitrogen Oxides on Stratospheric Ozone," Proc. R. Soc. Lond. A., **355**, 267-299, 1977.
- Turco, R. P. and R. C. Whitten, "The NASA-Ames Research Center Stratospheric Models, I. The One-Dimensional Model," NASA Tech. Paper 1002, NTIS, Springfield, Va., Sept. 1977.
- Turco, R. P. and R. C. Whitten, "A Note on the Diurnal Averaging of Aeronomical Models," J. Atmos. Terr. Phys., **40**(1), pp 13-20, 1978.
- U. S. Standard Atmosphere, 1976, NOAA-S/T 76-1562, U. S. Government Printing Office, Washington, D.C.
- Warneck, P., "Cosmic Radiation as a Source of Odd Nitrogen in the Stratosphere," J. Geophys. Res., **77**, 6589-6591, 1972.
- Whitten, R. C. and R. P. Turco, "Diurnal Variations of HO<sub>x</sub> and NO<sub>x</sub> in the Stratosphere," J. Geophys. Res., **79**, 1302-1304, 1974.
- Wofsy, S. C., J. C. McConnell and M. B. McElroy, "Atmospheric CH<sub>4</sub>, CO and CO<sub>2</sub>," J. Geophys. Res., **77**, 4477-4493, 1972.
- Wofsy, S. C., M. B. McElroy and N. D. Sze, "Freon Consumption: Implications for Atmospheric Ozone," Science, **187**, 535-537, 1975a.
- Wofsy, S. C., M. B. McElroy and Y. L. Yung, "The Chemistry of Atmospheric Bromine," Geophys. Res. Lett., **2**, 215-218, 1975b.
- Wuebbles, D. J. and J. S. Chang, "Sensitivity of Time-Varying Parameters in Stratospheric Modeling," J. Geophys. Res., **80**, 2637-2642, 1975.
- Wuebbles, D. J. and J. S. Chang, "A Theoretical Study of Stratospheric Trace Species Variation During a Solar Eclipse," GRL, **6**, 179-182, 1979.

Table 1. Comparison of photodissociation rates calculated with and without multiple scattering effect included.

Altitude, km	$J_{\text{Pure Absorption}}, s^{-1}$	$J_{\text{Multiple Scattering}}, s^{-1}$	$J_{\text{MS}}/J_{\text{PA}}$
$O_3 + h\nu \rightarrow O(^3P) + O_2$			
40	$4.59 \times 10^{-4}$	$6.41 \times 10^{-4}$	1.40
30	$4.54 \times 10^{-4}$	$6.41 \times 10^{-4}$	1.41
20	$4.19 \times 10^{-4}$	$6.24 \times 10^{-4}$	1.49
10	$4.08 \times 10^{-4}$	$6.13 \times 10^{-4}$	1.50
$O_3 + h\nu \rightarrow O(^1D) + O_2$			
40	$2.28 \times 10^{-3}$	$2.28 \times 10^{-3}$	1.00
30	$2.06 \times 10^{-4}$	$2.09 \times 10^{-4}$	1.01
20	$3.14 \times 10^{-5}$	$3.94 \times 10^{-5}$	1.25
10	$2.22 \times 10^{-5}$	$3.47 \times 10^{-5}$	1.56
$NO_2 + h\nu \rightarrow NO + O$			
40	$7.95 \times 10^{-5}$	$1.27 \times 10^{-2}$	1.60
30	$7.75 \times 10^{-3}$	$1.25 \times 10^{-2}$	1.61
20	$7.56 \times 10^{-3}$	$1.24 \times 10^{-2}$	1.64
10	$7.52 \times 10^{-3}$	$1.22 \times 10^{-2}$	1.62
$H_2O_2 + h\nu \rightarrow 2OH$			
40	$6.07 \times 10^{-5}$	$6.67 \times 10^{-5}$	1.10
30	$1.90 \times 10^{-5}$	$2.51 \times 10^{-5}$	1.32
20	$1.14 \times 10^{-5}$	$1.85 \times 10^{-5}$	1.62
10	$1.07 \times 10^{-5}$	$1.79 \times 10^{-5}$	1.67



Table 2. The ratio of rates of reactions including the effect of diurnal averaging as compared to using the constant sun approximation.

<u>Reaction</u>	Ratio of reaction rates (diurnal averaging/constant sun)		
	<u>20 km</u>	<u>30 km</u>	<u>40 km</u>
$\text{NO} + \text{O}_3 \rightarrow \text{NO}_2 + \text{O}_2$	0.65	0.56	0.56
$\text{NO}_2 + \text{O} \rightarrow \text{NO} + \text{O}_2$	0.60	0.45	0.50
$\text{NO} + \text{ClO} \rightarrow \text{NO}_2 + \text{Cl}$	0.73	1.00	0.44
$\text{NO} + \text{HO}_2 \rightarrow \text{NO}_2 + \text{OH}$	0.75	0.55	0.56
$\text{ClO} + \text{NO}_2 + \text{M} \rightarrow \text{ClONO}_2 + \text{M}$	0.40	0.51	0.80
$\text{OH} + \text{HCl} \rightarrow \text{H}_2\text{O} + \text{Cl}$	0.79	1.31	0.68
$\text{NO}_2 + \text{NO}_3 + \text{M} \rightarrow \text{N}_2\text{O}_5 + \text{M}$	10.3	12.7	> 100

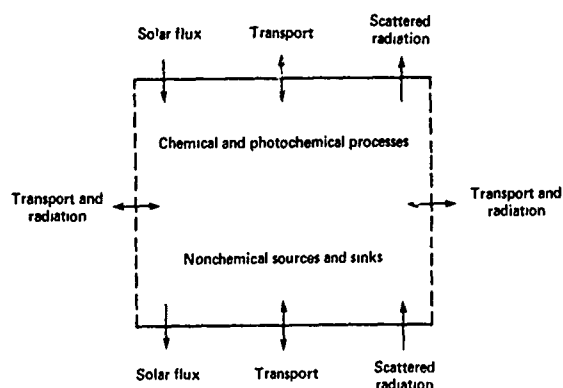


Fig. 1. Physical processes affecting the local concentrations of trace species.

$$\frac{\partial}{\partial z} K_z \rho \frac{\partial}{\partial z} \left( \frac{CH_4}{\rho} \right) - k_1 [O(^1D)] [CH_4] - k_2 [HO] [CH_4] - k_3 [Cl] [CH_4] = 0$$

Known variables from measurements

$$CH_4, \rho, k_1, k_2, k_3$$

Derived variables

$$[O(^1D)], [HO], [Cl]$$

Solve for  $K_z$

Fig. 2. Inversion technique for determining  $K_z$  profile from measurements of  $CH_4$ .

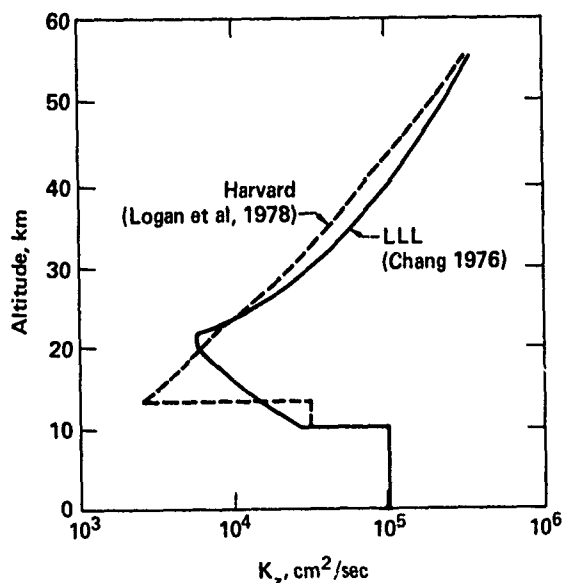


Fig. 3. Examples of  $K_z$  profiles used in recent 1-D model calculations.

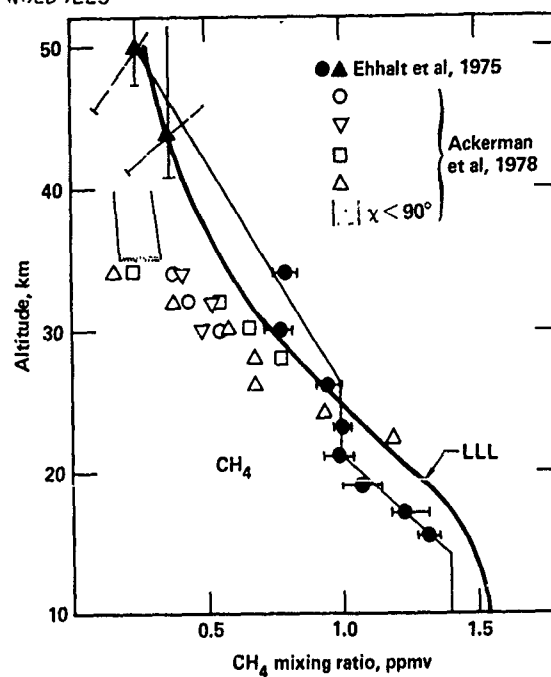


Fig. 4. Comparison between measured and model derived vertical distribution of methane,  $CH_4$ .

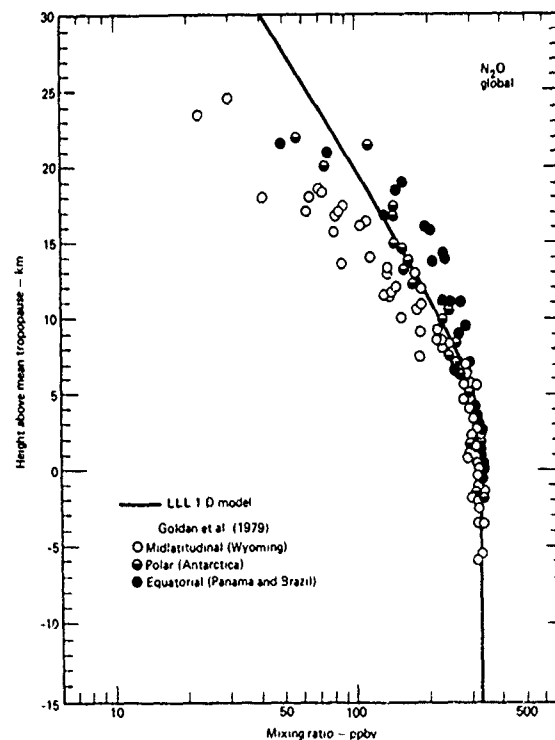


Fig. 5. Comparison between measured and model derived vertical distribution of nitrous oxide,  $N_2O$ .

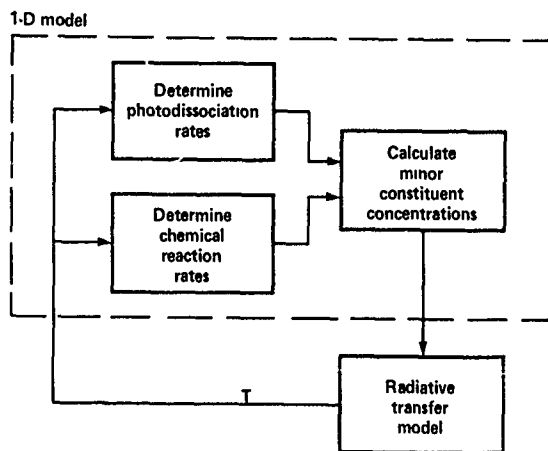


Fig. 6. Methodology for calculating temperature feedback effects with the one-dimensional model.

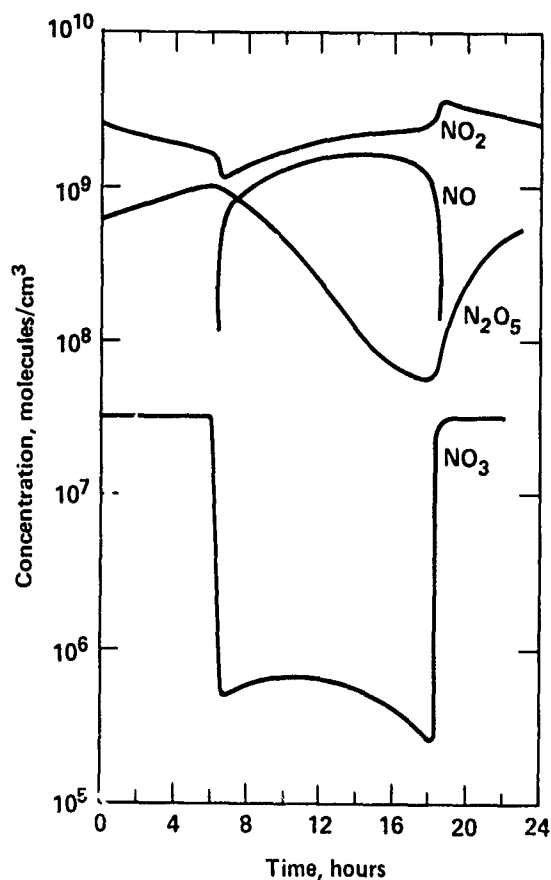


Fig. 7. One-dimensional model calculated diurnal variation of NO, NO<sub>2</sub>, NO<sub>3</sub> and N<sub>2</sub>O<sub>5</sub> at 30 km altitude.

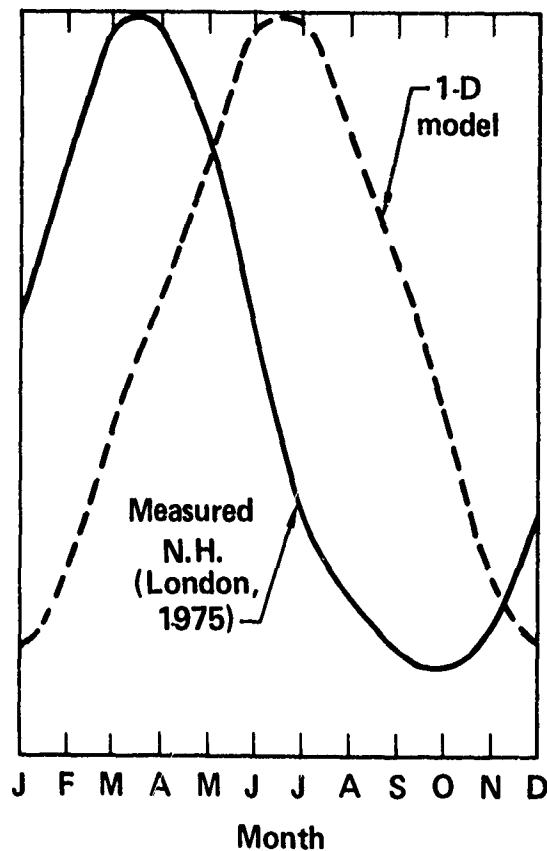


Fig. 8. Comparison of observed ozone seasonal variation for the Northern Hemisphere with the seasonal variation calculated by a one-dimensional model.

# ON EDDY DIFFUSION COEFFICIENTS

Guy BRASSEUR (\*)

Institut d'Aéronomie Spatiale  
3, Avenue Circulaire  
B-1180 Bruxelles, Belgium.

## Abstract

This paper presents a review concerning the transport by eddies in the stratosphere and its parameterization in atmospheric models. The eddy diffusion concept is very convenient for aeronomical calculations since it leads to satisfactory distributions of minor constituents but it is not theoretically demonstrated. Therefore the eddy diffusion coefficients are usually deduced from the distribution of several trace species and have to be considered as phenomenological parameters.

1. INTRODUCTION: The behavior of minor constituents in the atmosphere is determined by a combination of chemical and photochemical reactions and transport processes. The relative importance of these two effects varies considerably from one species to another and for each of them is a function of the altitude, latitude and time. When the residence time characterising a region of the atmosphere becomes of the same order of magnitude or smaller, than the chemical half time of a constituent its transport has to be taken into account.

Gaseous and particulate trace species suspended in the atmosphere are transported quasi-horizontally by motion systems of widely varying space and time scales. In fact, the transport of atmospheric trace substances can be represented by mean motions associated with the zonal and meridional circulation and by a broad spectrum of

---

(\*) Aspirant au Fonds National de la Recherche Scientifique.

wave motions. These include in particular the tropospheric systems of wavenumbers about 3 to 9 which die out in the lower stratosphere and the large wavenumbers 1-2 which may increase in amplitude with height in winter in the middle stratosphere.

In most two-dimensional stratospheric models, the transport of minor constituents will be parametrized by a combination of mean and turbulent motions. If one considers a small volume of particles suspended in the atmosphere, mean motions will displace the center of mass of the volume without deforming it and without modifying the particle concentrations; turbulent motions will distort the volume and the particles will be spread out. Therefore, from a macroscopic point of view, the eddy motions act very much as diffusion processes.

The purpose of this paper is to survey how the fluctuating component of the atmospheric dynamics can be mathematically modeled in the homosphere (below 100 km). The problem of assessing mean motions in relation to the thermal structure of the atmosphere is treated in other lectures of this Advanced Study Institute (see Murgatroyd, 1979; Pyle, 1979). It should be noted, however, that the distinction between mean motion and eddy diffusion is not unique and will, thus, depend upon the model. Therefore, in most cases, when both types of data are not consistent, the methods used to derive exchange coefficients (also called eddy diffusion coefficients) will lead to approximate values which will have to be tested and adjusted by making numerical experiments. Also, when deriving a transport model, a distinction should be made between two-dimensional models, where meridional exchanges are considered, and one-dimensional representations where horizontal stratification is assumed and only vertical transport is considered. In both cases, however, the definition of eddy diffusion coefficients for the transport of heat or minor constituents, such as ozone and water vapor, cannot be fully justified by fluid dynamics theory. However, since it leads to results (heat or particle concentration, fluxes,...) in rather good agreement with observation and since the formalism of such complicated mechanisms is rather simple, these coefficients are readily used by aeronomers while their use is widely criticised by meteorologists.

2. MEAN MOTIONS AND FLUCTUATIONS: Since many sporadic phenomena appear in the atmosphere, one assumes that the general circulation can be described by the average value of atmospheric quantities and by correlations between the fluctuations of these quantities about their average. Therefore, one introduces the temporal local mean

$$\bar{\chi}(T) = \frac{1}{T} \int_0^T \chi(t) dt \quad (1)$$

of any atmospheric quantity  $\chi(t)$  (e.g. the concentration, the temperature or the wind velocity), so that

$$\chi(t) = \bar{\chi} + \chi'(t) \quad (2)$$

where  $\chi'(t)$  represents the departure of  $\chi$  from  $\bar{\chi}$ . The time interval  $T$  is generally chosen so that the mean motion can be considered as stationary. Zonal means  $[\chi]$  i.e. averages round latitude circles can also be introduced and are of particular interest in two-dimensional models. If  $\lambda$  represents the longitude, one writes

$$[\chi] = \frac{1}{2\pi} \int_0^{2\pi} \chi(\lambda) d\lambda \quad (3)$$

and any atmospheric variable can be expressed as

$$\chi(\lambda) = [\chi] + \chi^*(\lambda) \quad (4)$$

where  $\chi^*(\lambda)$  is the departure of  $\chi$  from its zonal average.

Further mean quantities can be defined, for example averages over all longitudes and latitudes which are useful in one-dimensional (vertical) models. Finally, one can also introduce an average both in time and longitude called  $[\bar{\chi}]$  and write for any quantity varying with longitude and time

$$\chi(\lambda, t) = [\bar{\chi}] + [\chi'] + \bar{\chi}^* + \chi'^* \quad (5)$$

Here the first term  $[\bar{\chi}]$  refers to the zonal-time mean, the second  $[\chi']$  is the time fluctuation averaged over latitudinal circles, the third  $\bar{\chi}^*$  is the departure from the zonal mean averaged over a period of time and the last term  $\chi'^*$  is the residual. If one now considers the product of two fluctuating quantities (e.g. the concentration and the meridional wind component), the mean value of this product can be written following the example of Newell (1966)

$$\overline{n\vec{v}} = \bar{n} \cdot \bar{\vec{v}} + \overline{n'\vec{v}'} \quad (6a)$$

$$[n\vec{v}] = [n] \cdot [\vec{v}] + [n^*\vec{v}^*] \quad (6b)$$

$$[\overline{n\vec{v}}] = [\bar{n}] \cdot [\bar{\vec{v}}] + [\bar{n}^* \cdot \bar{\vec{v}}^*] + [\overline{n'\vec{v}'}] \quad (6c)$$

The last expression shows that the mean south to north over the time T transport of a quantity (here the concentration) in the meridional plane can be represented by the sum of :

- (i) a mean motion component  $[\bar{n}] \cdot [\bar{\vec{v}}]$
- (ii) a standing eddies component (expressed as the correlation between  $\bar{n}^*$  and  $\bar{\vec{v}}^*$  around the latitude circles)
- (iii) A transient eddy component (expressed as the zonal average of the time correlation of  $n'$  and  $\vec{v}'$ ).

Atmospheric motions of all scales contribute with different weights to the correlations between the fluctuations. The presence of these scale effects leads to serious difficulties in the treatment and interpretation of the equations of atmospheric dynamics.

3. CONTINUITY EQUATION AND TURBULENT TRANSPORT OF TRACE SPECIES: The instantaneous concentration  $n(t)$  of a trace constituent in the atmosphere can be derived, in the homosphere, from the continuity equation

$$\frac{\partial n}{\partial t} + \vec{\nabla} \cdot (n \cdot \vec{v}) = P - L \quad (7)$$

where P and L are, respectively, the local production and destruction rate of the species (e.g. chemical or photochemical reactions) and  $\vec{v}$  the instantaneous wind velocity vector. If one wishes to derive the mean local concentration  $\bar{n}$ , one has to solve the following equation

$$\frac{\partial \bar{n}}{\partial t} + \vec{\nabla} \cdot (\bar{n} \cdot \bar{\vec{v}} + \overline{n'\vec{v}'}) = \bar{P} - \bar{L} \quad (8)$$

while, if the zonal and time average concentration  $[n]$  is required, the continuity equation

$$\frac{\partial [\bar{n}]}{\partial t} + \vec{\nabla} \cdot ([\bar{n}] \cdot [\bar{\vec{v}}] + [\bar{n}^* \cdot \bar{\vec{v}}^*] + [\overline{n'\vec{v}'}]) = [\bar{P}] - [\bar{L}] \quad (9)$$

It should be noted that the determination of the mean value of P and L generally requires the calculation of time/space correlation products between the concentration of different species (and also reaction rates which may vary with temperature) and, therefore, depends on the turbulent state of the atmosphere. However, in most models this effect is usually neglected and will not be considered here.

Even if the mean circulation  $[\bar{\vec{v}}]$  is known, or is derived from other dynamical equations, equation (9) still needs a supplementary condition before it can be solved, namely an equation relating the turbulent and the mean motions terms. The K-theory provides the simplest turbulence closure approximation available for this purpose. It

assumes that the eddy fluxes are proportional to the negative gradient of the mixing ratio  $\bar{f} = n/n(M)$ , where  $n(M)$  is the total atmospheric concentration. If one defines the time and zonal mean of the meridional ( $y$ ) and vertical ( $z$ ) turbulent flux components by

$$[\overline{\phi_y}] = [\overline{n^* v^*}] + [\overline{n' v'}] \quad (10a)$$

$$[\overline{\phi_z}] = [\overline{n^* w^*}] + [\overline{n' w'}] \quad (10b)$$

where  $v$  and  $w$  refer respectively to the meridional and vertical components of the wind velocity  $\vec{v}$ , the simplest assumption leads to the Fickian law

$$[\overline{\phi_y}] = -K_y n(M) \frac{\partial f}{\partial y} \quad (11a)$$

$$[\overline{\phi_z}] = -K_z n(M) \frac{\partial f}{\partial z} \quad (11b)$$

where  $K_y$  and  $K_z$  are (positive) exchange coefficients.

These expressions have been used by Machta and List (1959), Prabhakara (1963) and Jessen (1973) but it has been recognized, after an analysis of heat fluxes (White, 1954; Murakami, 1962 and Peng, 1963) and ozone transport (Newell, 1961; Hering and Borden, 1964), that horizontal eddy fluxes could clearly be countergradient above the tropopause. In his study on heat transport in the lower stratosphere, White (1954) points out that "up to the 200 mb level (12 km), the eddy flux of sensible heat is poleward from regions of high to regions of low temperature as might normally be expected. At and above this level, the reverse is true". White notes that "above the tropopause level, the eddy processes are acting to build up rather than dissipate the existing temperature gradient". Newell (1964) has given a physical explanation for such an horizontal countergradient flux. He considers (figure 1) an air parcel A in the lower stratosphere moving poleward and downward at a slope exceeding that of the potential temperature. Such trajectories are common as shown by dispersion studies of radioactive tracers. Arriving in A', the air parcel will be warmer than its environment. Consequently it will be buoyant and tend to go back up unless forces are available to keep this from happening. Newell suggests that the kinetic energy of the motions themselves can do this, provided that the energy is replaced by upward transport from the lower portions of the westerly wind core. Figure 2 illustrates the slope of the maximum concentration level associated with various tracers injected into the stratosphere and shows that the inclination is steeper than the slopes of the isentropic surfaces. It can be seen that the motion AA' is up the horizontal gradient although it is down the vertical gradient.

4. THE CLASSICAL THEORY OF LARGE SCALE MERIDIONAL EDDY DIFFUSION: Demazure and Saïssac (1962) and Reed and German (1965) have developed a concept in 2 dimensions for eddy diffusion of conservative trace constituents taking into account possible countergradient transport in the meridional plane. The authors approach is based on the mixing length concept of the turbulence theory. For reasons of simplicity, transient and standing eddies are not distinguished and the flux is given by the following expressions

$$\phi_y = \overline{n' v'} \quad (12a)$$

$$\phi_z = \overline{n' w'} \quad (12b)$$

In this theory, it is assumed (figure 3) that an air parcel located at  $P_1$  and representative of its local environment, moves a distance  $\vec{l}(l_y, l_z)$ , called the displacement vector or the mixing length, before it mixes suddenly and completely with its new environmental air at  $P_2$ . It is also assumed that during the displacement the mixing ratio  $f$  in the air parcel is conserved. If the vector  $\vec{l}$  is allowed to have any orientation in space, the deviation of the conservative quantity  $f$  is given, to a first order approximation, by

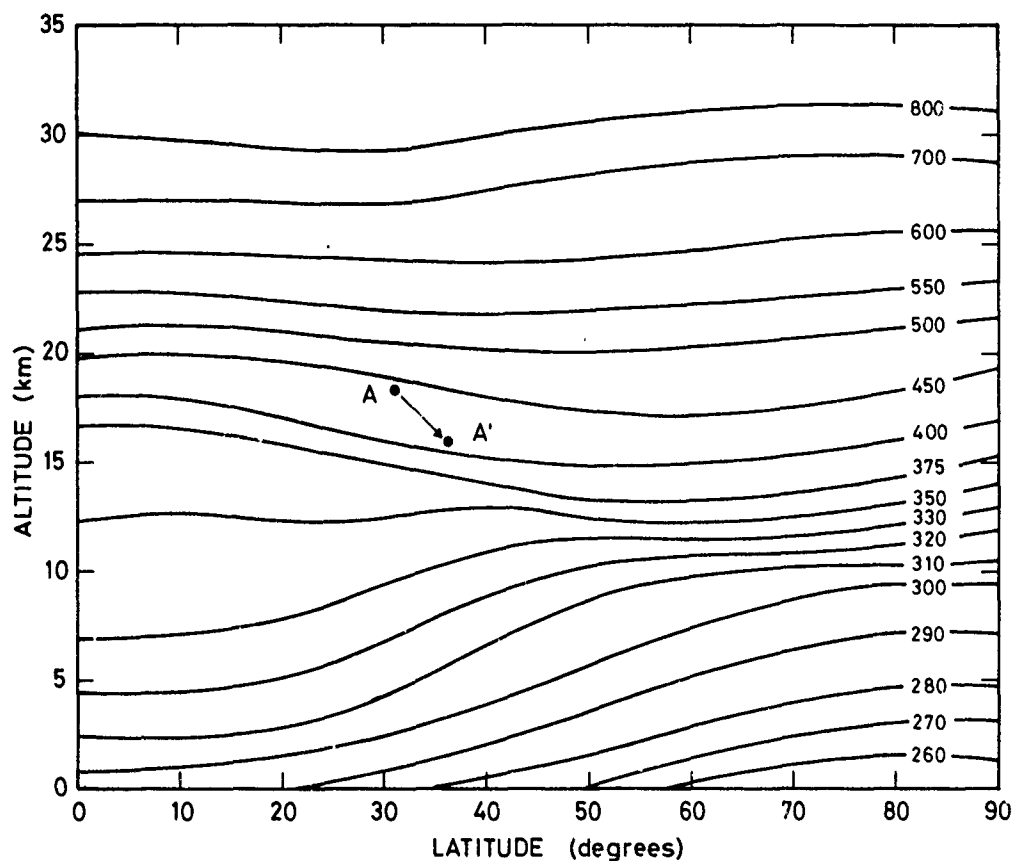


Fig. 1.- Potential temperature surfaces shown for one hemisphere in late winter. Temperature is given in degrees. Kelvin. In the lower stratosphere, poleward-moving parcels (A,A') descend more steeply than the potential temperature surfaces do. After Newell (1964).



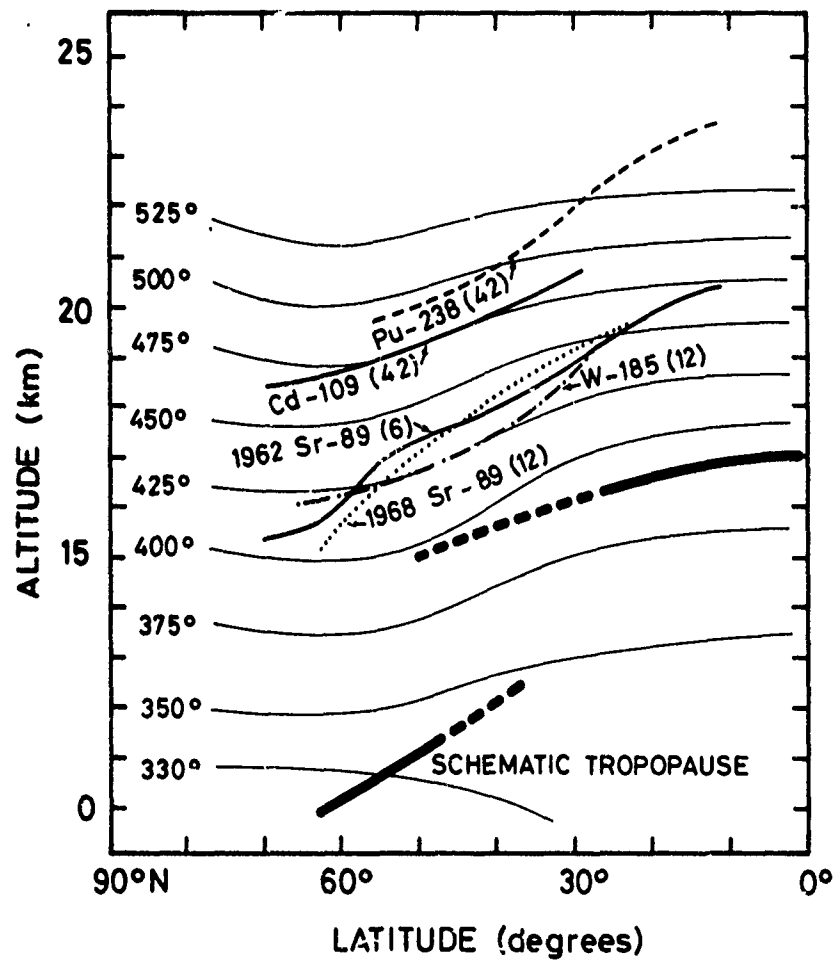


Fig. 2.- Altitude of the maximum concentration level versus latitude associated with various tracers injected into the stratosphere by the explosion of thermonuclear weapons in the early 60's. Potential temperature surfaces are also shown.

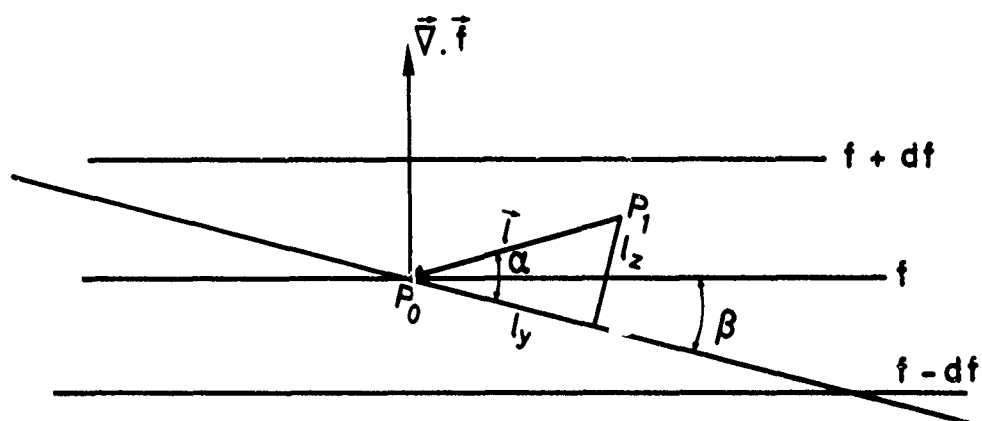


Fig. 3.- Model for the eddy flux of a property by exchange along a sloping mixing path. After Reed and German (1965).

$$f' = f_{P_1} - f_{P_0} = - \vec{l} \cdot \vec{\nabla} f = - (l_y \frac{\partial f}{\partial y} + l_z \frac{\partial f}{\partial z}) \quad (13)$$

Considering all the various parcel displacements to  $P_0$  during the time  $T$  substitution of (13) into (12a and b) leads to the time average flux components ( $f$  represents the mean mixing ratio)

$$\phi_y = - n(M) [K_{yy} \frac{\partial f}{\partial y} + K_{yz} \frac{\partial f}{\partial z}] \quad (14a)$$

$$\phi_z = - n(M) [K_{zy} \frac{\partial f}{\partial y} + K_{zz} \frac{\partial f}{\partial z}] \quad (14b)$$

where the  $K_{ij}$  coefficients are correlation products between the displacement and the velocity components :

$$K_{yy} = \overline{l_y v'} \quad (15a)$$

$$K_{yz} = \overline{l_z v'} \quad (15b)$$

$$K_{zy} = \overline{l_y w'} \quad (15c)$$

$$K_{zz} = \overline{l_z w'} \quad (15d)$$

Equations (14a and b) are reduced to the classical Fickian law (11a and b) only when the covariences between  $l_z$  and  $v'$  and  $l_y$  and  $w'$  are equal to zero. However, this is not the case since, as shown before, sinking motions in the stratosphere on the average coincide with polewards transport while rising motions are most frequently equatorwards. This was already established by Molla and Loisel in 1962. Accordingly, the introduction of  $K_{yz}$  and  $K_{zy}$  allows for the countergradient fluxes in the atmosphere.

Assuming that the mixing length  $\ell$  ( $\sim 100$  km) is small compared to the eddy sizes involved in the large scale mixing processes ( $\sim 1000$  km), Reed and German have made the hypothesis that the velocity  $\vec{V}$  and the displacement vector  $\vec{\ell}$  are in the same direction. If  $\alpha$  is the angle between  $\vec{\ell}$  and the horizontal axis, one can write, since for large scale motions this angle is very small ( $< 1/1000$ ),

$$v' = V \cos \alpha \cong V \quad (16a)$$

$$l_y = \ell \cos \alpha \cong \ell \quad (16b)$$

$$w' = V \sin \alpha \cong V\alpha \quad (16c)$$

$$l_z = \ell \sin \alpha \cong \ell\alpha \quad (16d)$$

Therefore, if  $\alpha$  is divided into its mean value  $\bar{\alpha}$  and its departure  $\alpha'$  and if  $\bar{\alpha}$  and  $\overline{\alpha'^2}$  are assumed to be independent of  $V$  and  $\ell$ , one obtains the relations

$$K_{yz} = K_{zy} = \bar{\alpha} K_{yy} \quad (17)$$

$$K_{zz} = (\bar{\alpha}^2 + \overline{\alpha'^2}) K_{yy} \quad (18)$$

Expression (17) shows that the diffusion matrix  $K_{ij}$  can be considered as symmetrical since the off diagonal terms  $K_{yz}$  and  $K_{zy}$  have the same value in this theory. Also, it appears that  $K_{yy}$  and  $K_{zz}$  necessarily have the same sign (positive) while the sign of  $K_{yz}$  is determined by that of the angle  $\alpha$ .

Introducing now the slope of the mixing ratio surface

$$\bar{\beta} \approx \tan \bar{\beta} = - \frac{\partial f / \partial y}{\partial f / \partial z} \quad (19)$$

the following expressions are obtained

$$\phi_y = - n(M) K_{yy} \left(1 - \frac{\bar{\alpha}}{\bar{\beta}}\right) \frac{\partial f}{\partial y} \quad (20a)$$

$$\phi_z = - n(M) K_{zz} \left(1 - \frac{\bar{\alpha}\bar{\beta}}{\bar{\alpha}^2 + \bar{\alpha}'^2}\right) \frac{\partial f}{\partial z} \quad (20b)$$

These equations show that the meridional flux of trace species becomes countergradient if

$$\bar{\alpha} > \bar{\beta} \quad (21)$$

that is when the slope of the preferred mixing surface becomes larger than the slope of the mixing ratio surface. This condition applies in the lower stratosphere but not in the extratropical troposphere where, according to Eady (1949),  $\alpha \approx \beta/2$ .

The same type of argument can be presented for heat transport. In this case, the heat flux components are written in the form

$$F_y = - n(M) \left[ K_{yy} \frac{\partial \bar{\theta}}{\partial y} + K_{yz} \frac{\partial \bar{\theta}}{\partial z} \right] \quad (22a)$$

$$F_z = - n(M) \left[ K_{zy} \frac{\partial \bar{\theta}}{\partial y} + K_{zz} \frac{\partial \bar{\theta}}{\partial z} \right] \quad (22b)$$

with  $K_{yz} = K_{zy}$ . Countergradient transport appears when the slope  $\bar{\alpha}$  becomes larger than that of the isentropic surfaces.

Adopting expressions (14a and b) and (9), the continuity/ transport equation becomes

$$\begin{aligned} n(M) \frac{\partial f}{\partial t} - \frac{\partial}{\partial y} \left( K_{yy}^* \frac{\partial f}{\partial y} \right) - \frac{\partial}{\partial y} \left( K_{yz}^* \frac{\partial f}{\partial z} \right) - \frac{\partial}{\partial z} \left( K_{zy}^* \frac{\partial f}{\partial y} \right) \\ - \frac{\partial}{\partial z} \left( K_{zz}^* \frac{\partial f}{\partial z} \right) + \left( v^* + \frac{K_{yy}^* \tan \varphi}{a} \right) \frac{\partial f}{\partial y} + \left( w^* + \frac{K_{yz}^* \tan \varphi}{a} \right) \frac{\partial f}{\partial z} \\ = P - L \end{aligned} \quad (23)$$

where  $K_{ij}^* = n(M) \cdot K_{ij}$ ,  $\bar{v}^* = n(M) \cdot \bar{v}$ ,  $\bar{w}^* = n(M) \cdot \bar{w}$ , and  $\bar{v}$  and  $\bar{w}$  are the mean wind components.<sup>13</sup> The numerical solution of this equation will provide the distribution of the mixing ratio (or concentration) of the trace species under consideration if all the parameters are known and if suitable boundary conditions are specified. In particular, the values of the exchange coefficients have to be established in the whole physical domain. The ellipticity condition associated with equation (23) implies that

$$K_{yz}^2 \leq K_{yy} K_{zz} \quad (24)$$

which is always verified as shown when expressions (17) and (18) are introduced in (24).

Since the diffusion tensor (or matrix) is symmetrical, it is possible to rotate (by an angle  $\gamma$ ) the (y,z) axis such that the new axes (Y,Z) become principal axes in which the off-diagonal elements  $K_{yz} = K_{zy}$  are eliminated. Reed and German show that the matrix in the principal axis system is given by

$$\begin{bmatrix} K_Y & 0 \\ 0 & K_Z \end{bmatrix} = \begin{bmatrix} K_{yy} \cos^2 \gamma + K_{yz} \sin 2\gamma + K_{zz} \sin^2 \gamma & \frac{K_{zz} - K_{yy}}{2} \sin 2\gamma + K_{yz} \cos 2\gamma \\ \frac{K_{zz} - K_{yy}}{2} \sin 2\gamma + K_{yz} \cos 2\gamma & K_{yy} \sin^2 \gamma - K_{yz} \sin 2\gamma + K_{zz} \cos^2 \gamma \end{bmatrix}$$

The angle  $\gamma$  corresponding to a principal axis system is thus given by

$$\frac{K_{zz} - K_{yy}}{2} \sin 2\gamma + K_{yz} \cos 2\gamma = 0 \quad (25)$$

or, since  $\bar{\alpha}$  is small,

$$\gamma = \bar{\alpha} \quad (26)$$

In other words, the inclination of the principal axis and the slope of the preferred mixing surface are identical.

Since the values of  $K_{ij}$  depend on the adopted axes and their inclination upon the direction of preferred mixing, it is sometimes convenient to use the following expressions which relate  $K_{ij}$  and the principal eddy diffusion components :

$$K_{yy} = K_Y \cos^2 \alpha + K_Z \sin^2 \alpha, \quad (27)$$

$$K_{yz} = K_{zy} = (K_Y - K_Z) \sin \alpha \cos \alpha, \quad (28)$$

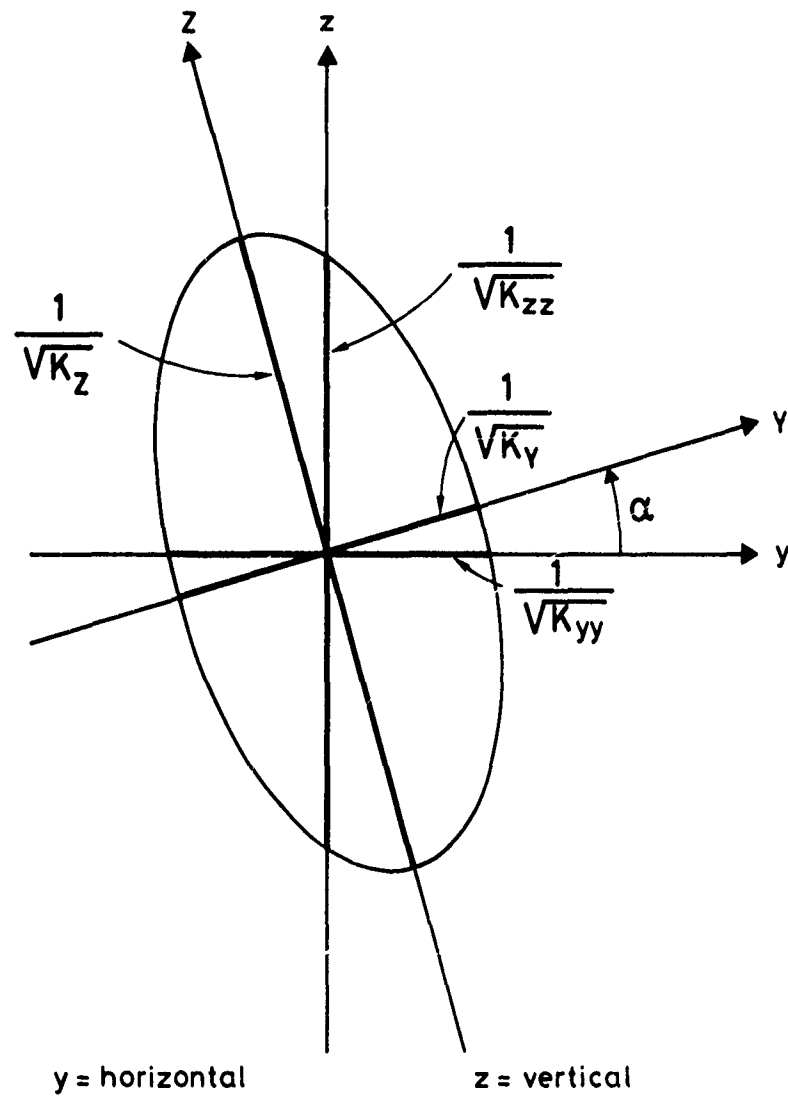
$$K_{zz} = K_Y \sin^2 \alpha + K_Z \cos^2 \alpha.$$

A geometrical representation is given by the diffusion ellipse (figure 4)

$$K_Y Y^2 + K_Z Z^2 = 1 \quad (30)$$

whose principal axes have a lengths respectively, of  $1/\sqrt{K_Y}$  and  $1/\sqrt{K_Z}$ . The magnitude of an eddy diffusion in a direction characterized by an angle  $\gamma$  can be derived from such a geometry (see fig. 4).

5. EVALUATION OF THE 2-D EXCHANGE COEFFICIENTS VALUES: The magnitude of the eddy diffusion coefficients vary with the scales of space-time averaging from a lower limit of molecular diffusion to an upper limit of global atmospheric mixing. This dependence of the K's versus space and time scales can be derived from a dispersion distance



$Y$  and  $Z$  principal diffusion axes

Fig. 4.- Diffusion ellipse.

(expressed by mean cloud width) as illustrated in figure 5. The lower limit on  $K_{yy}$  and  $K_{zz}$  (molecular diffusivity) decreases with height. The graph refers to a pressure of 100 mb. At these small scales, the turbulence is approximately isotropic and homogeneous. The global scale is characterized by anisotropy and by the presence of off-diagonal terms. In the intermediate range, the turbulence is intermittent and localized. The curve refers to average values which can be several orders of magnitude smaller than the values observed locally. In the following paragraphs, we will confine our attention on large scale eddy diffusion only.

A procedure for evaluating the  $K$  coefficients has been given by Reed and German (1965). The authors have derived the  $K_{yy}$  component in the baroclinically active troposphere from the heat flux data ( $F_y$ ) and the temperature distribution (Peixoto, 1960). In other atmospheric regions, they have computed  $K_{yy}$  by assuming that it is proportional to the variance of the meridional wind component as given by Buch (1954), Murakami (1962) and Peng (1963). The angle  $\bar{\alpha}$  has then been obtained from expression (20.a) introducing the values of the heat flux and the temperature compiled by Oort (1963).  $K_{zz}$  has then been computed with equation (17). Since, for symmetry reasons,  $\bar{\alpha} = 0$  at the equator, relation (18) provides  $\alpha'^2 = K_{zz}/K_{yy}$  in these regions. Adopting  $K_{zz} = 10^3 \text{ cm}^2 \text{ s}^{-1}$  in the equatorial zone, as suggested by the study of the vertical spread of tungsten 185,  $\alpha'^2$  has been calculated and assumed to remain constant at all other latitudes. Equation (18) was then employed to estimate  $K_{zz}$  in the whole domain.

Davidson, Friend and Seitz (1966) have developed a numerical model of diffusion and rain out of stratospheric radioactive material using a fairly simple distribution of  $K$ 's.  $K_{yy}$  varies smoothly from  $10^8 \text{ cm}^2 \text{ s}^{-1}$  at the pole to  $10^{10} \text{ cm}^2 \text{ s}^{-1}$  at the equator while  $K_{zz}$  is equal to  $10^3 \text{ cm}^2 \text{ s}^{-1}$  in the stratosphere and about  $4 \times 10^4 \text{ cm}^2 \text{ s}^{-1}$  in the troposphere with a transition region near the tropopause.

Gudiksen, Fairhall and Reed (1968) have considered simultaneously, mean motions and large scale eddy diffusion to model the dispersion of tungsten 185 released in the atmosphere during nuclear weapons tests. They extended the work of Reed and German to derive seasonal values of the  $K$ 's up to 27 km. The exchange coefficients obtained by Reed and German were reduced by a factor of 7-10 for  $K_{yy}$  and a factor of 2 for equatorial  $K_{zz}$ . The discrepancy between the two sets of data was, mainly, attributed to the fact that the coefficients derived from heat flux data by Reed and German may not be quantitatively applicable to the transport of particulate debris. In fact, the potential temperature may not behave as conservatively as tungsten 185 in the lower stratosphere while the transport of the gaseous species may physically differ from the transport of solid particulates.

Seitz, Davidson, Friend and Feely (1968) also extended their previous work by introducing the complementary effects of mean and turbulent motions. These authors were able to simulate relatively well the evolution of several different tracers with the same transport coefficients, showing that large scale diffusion could be described with  $K$ 's which are almost independent of the tracers.

Luther (1973) in a new investigation of the problem computed the values of  $K_{yy}$ ,  $K_{zz}$  and  $K_{yz}$  between 0 and 50 km using the method of Reed and German but adopting the heat flux associated with standing and transient eddies and the temperature and the wind variance as compiled by Oort and Rasmussen (1971) for the 1958-1963 period. Values in regions where observational data were not available were derived by Luther (1973) by extrapolation using the results of Woisy and McElroy (1973) and Newell et al. (1966).

Different attempts to establish more accurate distributions of the  $K$ 's have been carried out in the past years especially because of the demand by chemical modelers studying the stability of ozone in the stratosphere. Values have been proposed by Louis (1974), Kao, Obrasinski and Lordi (1978) and others. Moreover, Nastrom and Brown (1978) have recently derived exchange coefficients from 30 to 60 km altitude where the meridional component  $K_{yy}$  has been obtained using G.I. Taylor's theorem

$$K_{yy} = \int_0^\infty \overline{v'(t) v'(t+\tau)} d\tau = \overline{v'^2} \int_0^\infty R_{vv}(\tau) d\tau \quad (31)$$

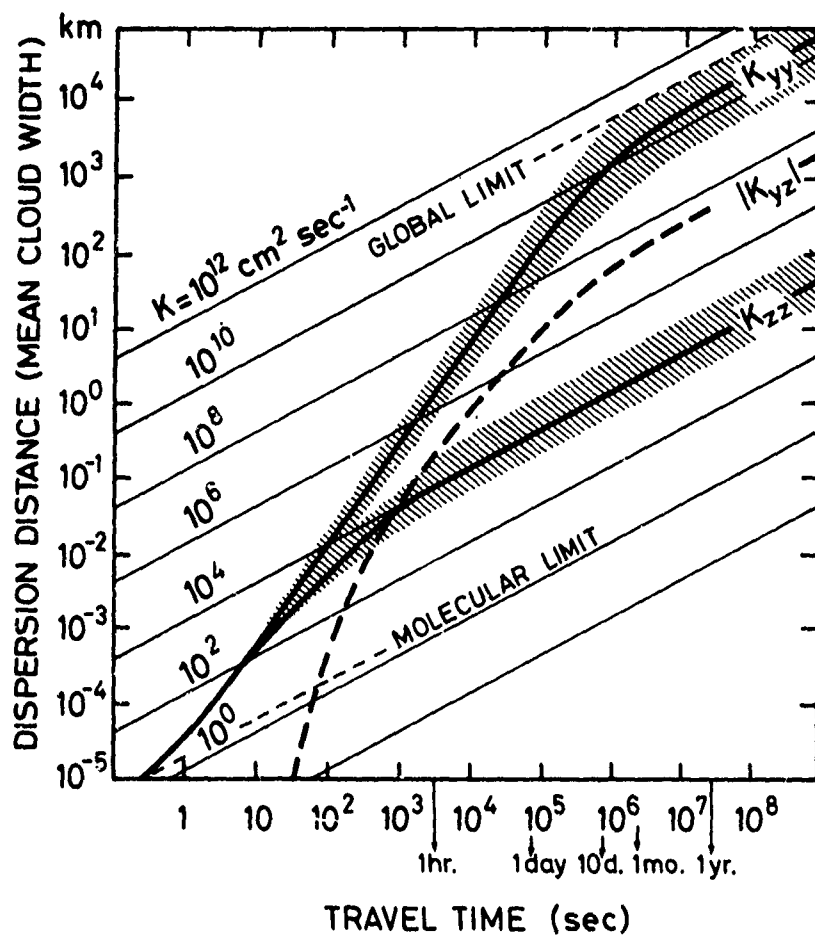


Fig. 5.- Stratospheric exchange coefficients as a function of dispersion distance and travel time. The range in values for a given travel time is given by the toned area. The dashed line represents the upper bound for  $|K_{yz}|$ . After Reiter *et al.* (1975).



where  $v'(t)$  is the meridional wind fluctuation,  $v'^2$  its variance and

$$R_{vv}(\tau) = \frac{\overline{v'(t) v'(t+\tau)}}{v'^2} \quad (32)$$

the autocorrelation coefficient of the meridional wind. This approach has been previously used by Murgatroyd (1969) who adopted for the autocorrelation coefficient a damped cosine function

$$R_{vv}(\tau) = e^{-p\tau} \cos q \tau \quad (33)$$

with  $p$  and  $q$  being obtained from wind trajectory data. The technique used by Nastrom and Brown to derive  $K_{yz}$  is based on that of Reed and German while the determination of the  $K_{zz}$  value follows a method suggested by Hines (1970). This author has assumed that the normal growth of gravity wave amplitude with height arising from decreasing density will be offset by energy lost to turbulence so that the wave amplitude is constant with altitude. Zimmerman (1974) has argued that no amplitude growth is a poor approximation and balancing the vertical gradient of the specific wave energy with an effective turbulent viscosity he derived the following expression

$$K_{zz} = \left( \frac{\lambda_z}{4\pi^2 T} \right) \left\{ \frac{1}{H} - \frac{1}{z} \ln \frac{V^2}{V_0^2} \right\} \quad (34)$$

where  $\lambda_z$  is the vertical wavelength of the upward propagating gravity wave responsible for turbulence,  $T$  is its period,  $V$  and  $V_0$  the perturbation velocity, respectively, at level  $z$  and at a reference level.

Figure 6a, b and c represents the exchange coefficients  $K_{yy}$ ,  $K_{yz}$  and  $K_{zz}$  adopted by Reed and German (1965), Gudiksen et al. (1968) and Luther (1974) versus latitude at two different levels, namely 100 mb (14 km) and 50 mb (20 km), and for two seasons (winter and summer). The shape of the latitudinal variation is generally the same but the magnitude of the data sometimes varies considerably. All of the three authors agree on the fact that  $K_{yy}$  increases from the equator to the pole during the winter period while it varies only slightly and remains small during the summer. The off-diagonal term  $K_{yz}$  which is negative in the Northern hemisphere (in standard spherical coordinates) is also larger during the winter than during the summer. Its value is almost zero at the equator and at the poles (for symmetry reasons) and peaks in the mid-latitude regions. The vertical exchange coefficient  $K_{zz}$  seems also to reach its maximum value between 30 and 50 degrees latitude with the most pronounced values during the winter. Similar data have been adopted in two-dimensional models of stratospheric minor constituents (Brasseur, 1978; Crutzen, 1975; Prinn, 1973; Pyle, 1978; Rao-Vupputuri, 1973; Widhopf, 1975; etc...) but they have been adjusted by a "trial and error" method to give the best agreement between observed and calculated distributions of trace species such as ozone or water vapor. Figure 7 shows and compares the values of  $K_{yy}$  at 20 km adopted by various authors. It should be noted, however, that these values have been adjusted for different distributions of the mean wind components (see e.g. Cunnold et al., 1974; Louis 1974).

The meridional distribution of eddy diffusion coefficients determined by Luther between the ground and the stratopause is illustrated in figures 8, 9 and 10 while the same coefficients provided by Nastrom and Brown between 30 and 60 km are reproduced in tables 1, 2 and 3. In both cases,  $K_{yy}$  appears to increase with latitude in the winter period and also with height above 30 km. The values derived during the winter are about a factor of ten larger than the data obtained during the summer. The chart representing  $K_{yz}$  shows that the sign of this coefficient changes from one hemisphere to the other and also when crossing the tropopause. The values are the highest in the winter mid-latitude region. Hence, the countergradient flux becomes greatest mostly during the winter season. The  $K_{zz}$  coefficient has a high value in the troposphere but the its magnitude

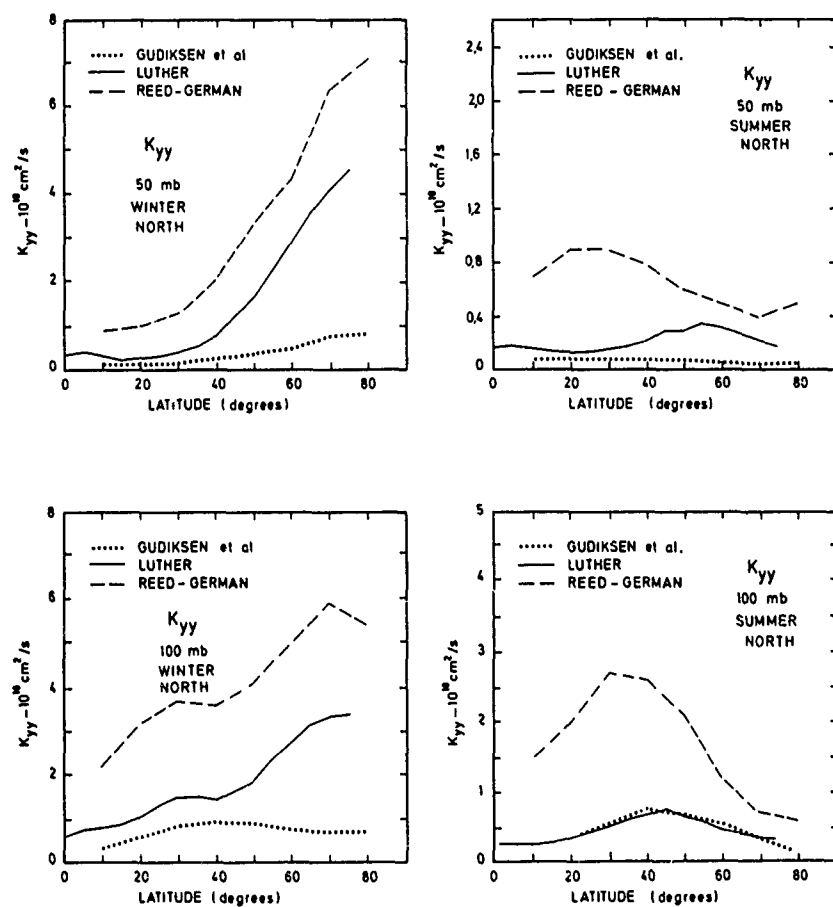


Fig. 6a.- Latitudinal distribution of the exchange coefficient  $K_{yy}$  according to different authors. The values are given for winter and summer conditions and for 50 and 100 mb levels.

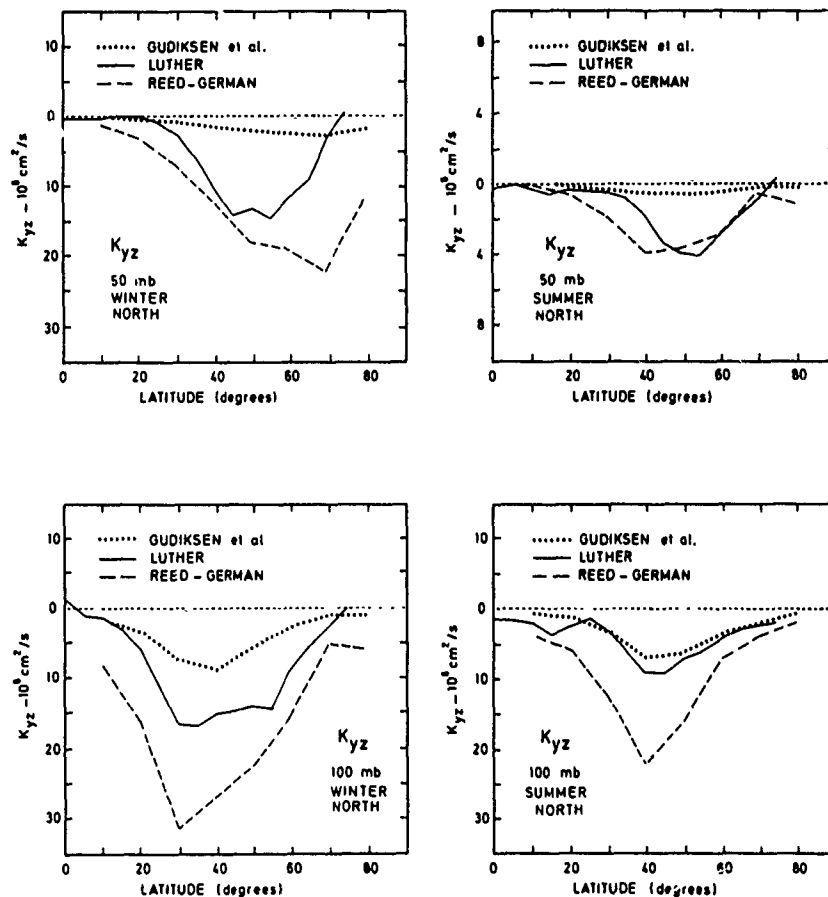


Fig. 6b.- Latitudinal distribution of the exchange coefficient  $K_{yz}$  according to different authors. The values are given for winter and summer conditions and for 50 and 100 mb levels.

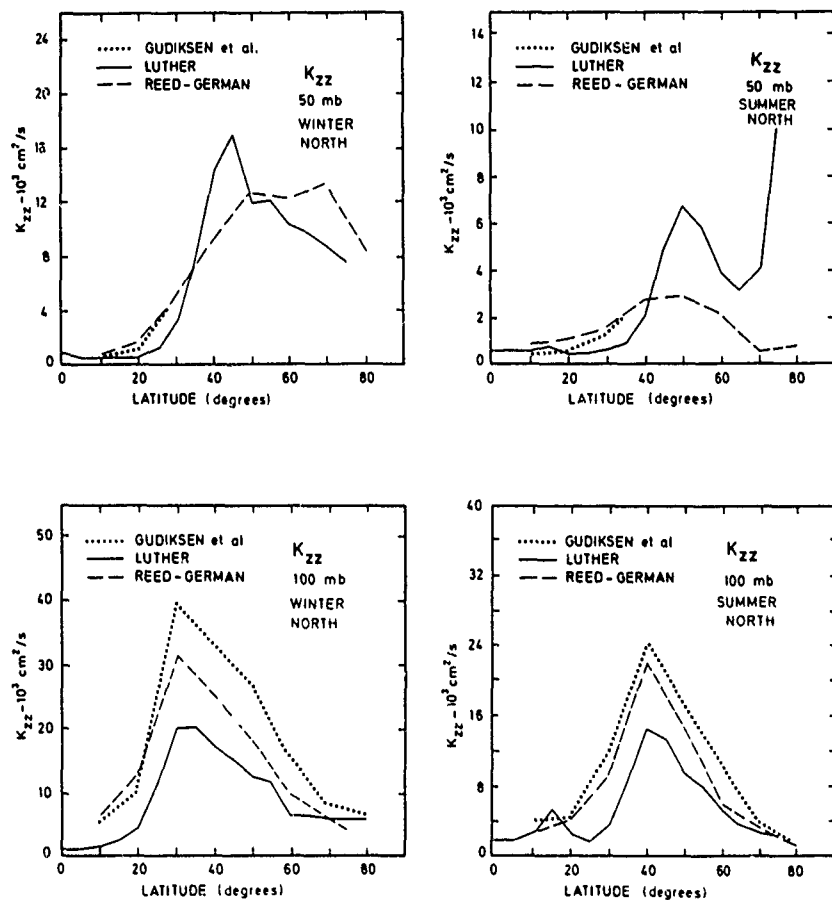


Fig. 6c.- Latitudinal distribution of the exchange coefficient  $K_{zz}$  according to different authors. The values are given for winter and summer conditions and for 50 and 100 mb levels.

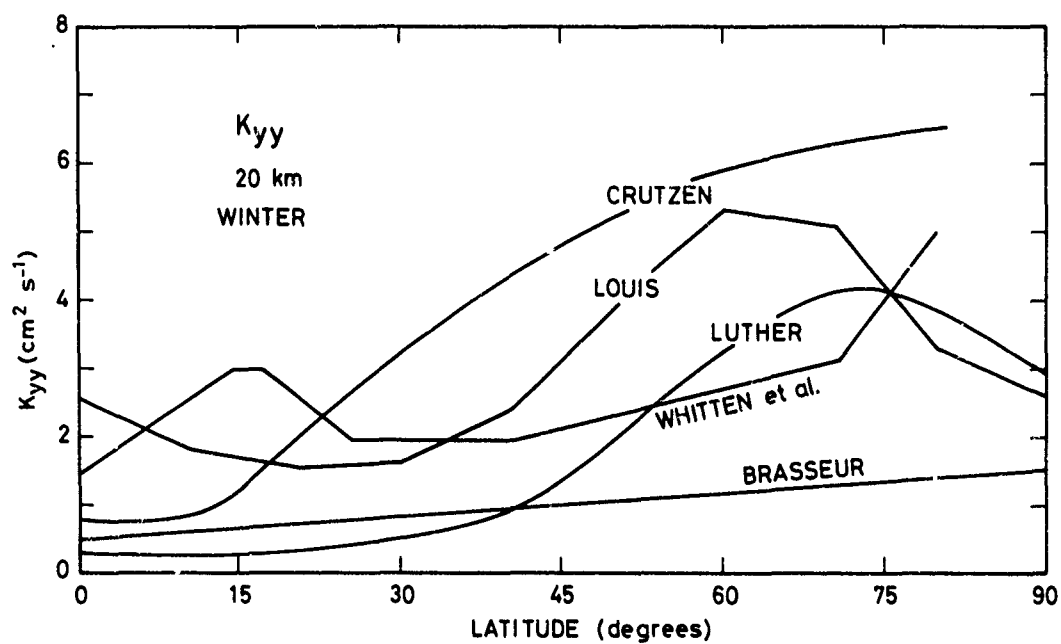


Fig. 7.- Latitudinal distribution of  $K_{yy}$  at 20 km adopted during the winter season in various stratospheric models.

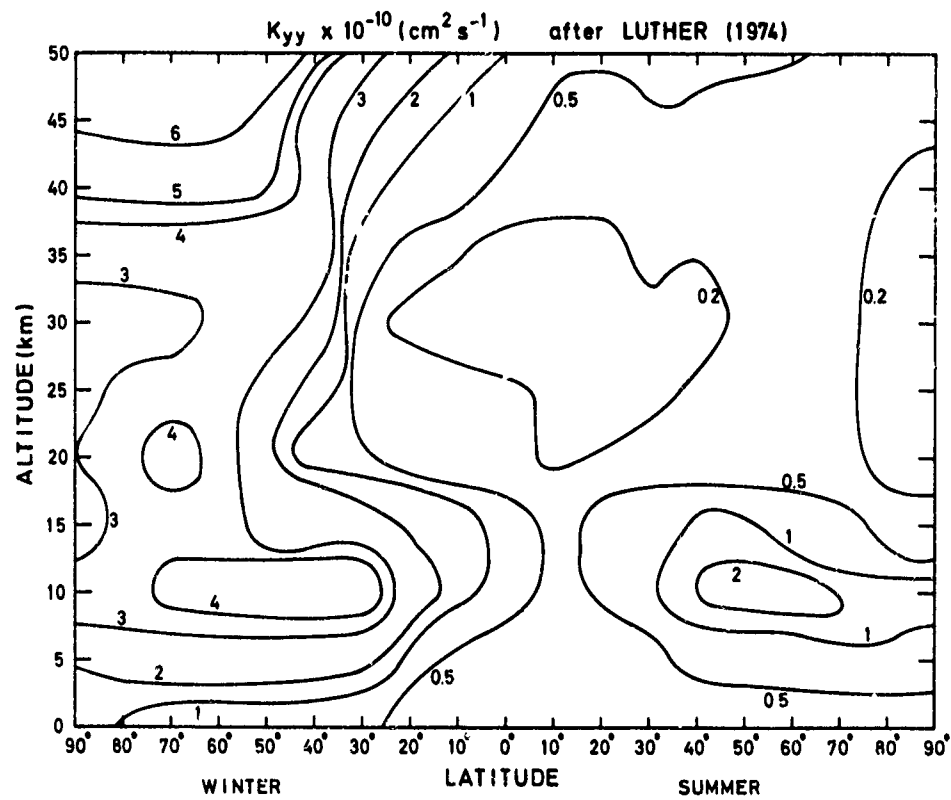


Fig. 8.- Meridional distribution of  $K_{yy}$  determined by Luther (1974).

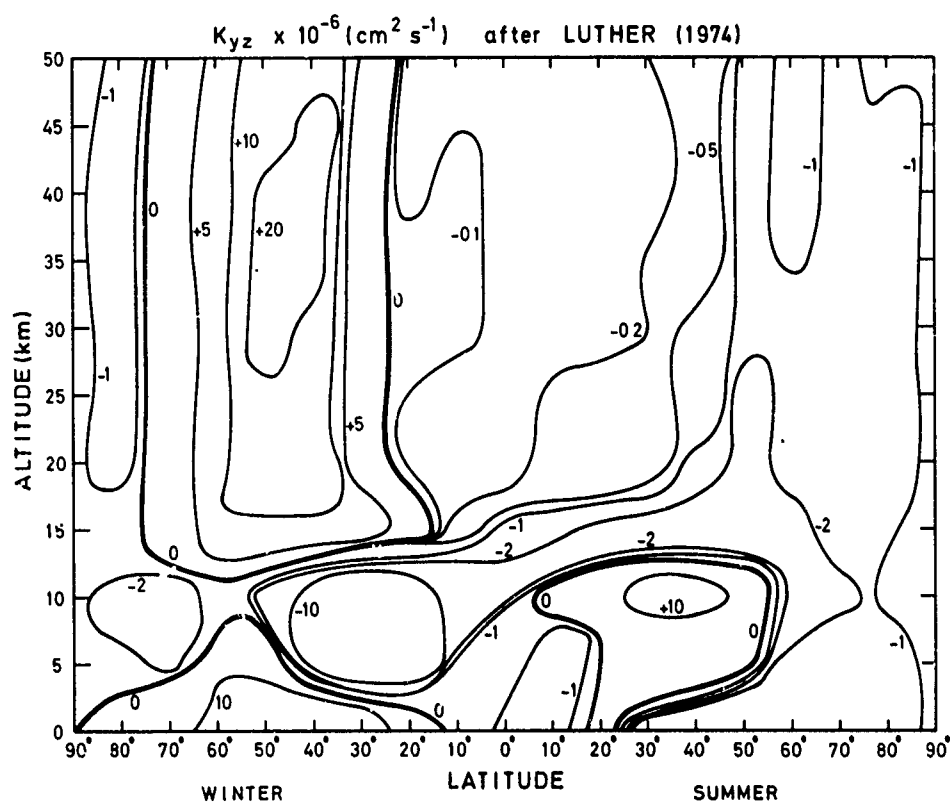


Fig. 9.- Meridional distribution of  $K_{yz}$  determined by Luther (1974). The sign of  $K_{yz}$  has been chosen so that the corresponding eddy flux is positive when it is directed from the North (winter) pole to the South (summer) pole.

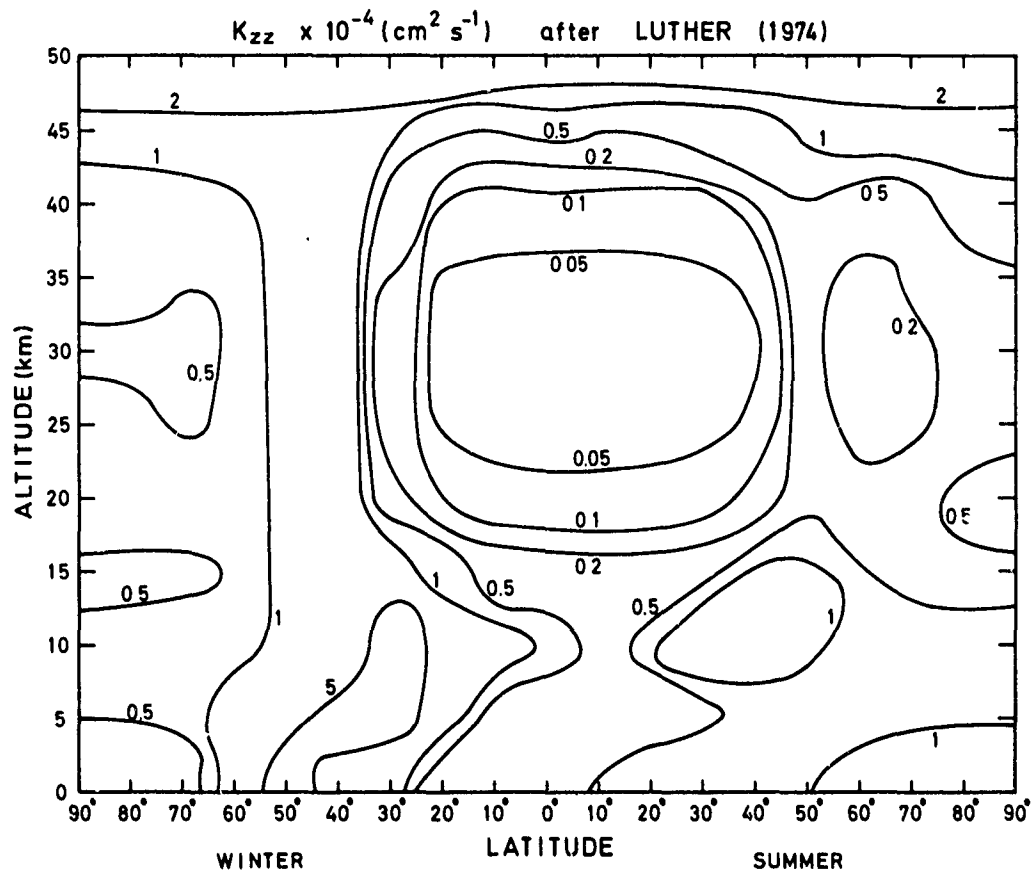


Fig. 10.- Meridional distribution of  $K_{zz}$  determined by Luther (1974).



## BRASSEUR

TABLE 1.- Seasonal values of  $K_{yy}$  ( $10^4 \text{ m}^2 \text{ sec}^{-1}$ ) after Nastrom and Brown (1978).

LATITUDE	75	70	65	60	55	50	45	40	35	30	25	20	15	10	5	0	-5
Winter																	
60.0 KM	884	741	566	445	322	220	194	173	223	165	132	131	123	119	100	105	115
57.5	759	681	562	487	395	302	251	219	236	170	137	135	123	126	116	117	112
55.0	634	622	558	529	468	385	307	264	250	174	143	139	123	132	131	129	110
52.5	500	515	513	513	476	405	325	268	233	151	114	113	112	121	101	98	89
50.0	365	409	469	498	484	425	344	272	215	128	86	88	101	110	70	68	68
47.5	312	360	453	446	409	347	279	229	196	127	82	72	79	80	56	54	54
45.0	258	310	438	395	334	269	215	187	177	125	78	57	57	50	41	40	41
42.5	360	399	469	408	330	254	191	153	139	106	76	57	48	40	36	35	33
40.0	462	487	500	420	327	238	165	118	100	88	74	56	39	30	30	29	25
37.5	415	475	469	403	313	219	140	92	78	67	52	40	35	28	26	23	20
35.0	367	462	438	386	298	201	115	65	55	46	31	24	31	26	22	17	15
32.5	258	346	339	299	231	156	91	50	41	38	29	22	24	20	13	10	10
30.0	149	230	239	211	163	111	66	36	26	30	26	20	18	13	4	2	5
Spring																	
60.0 KM	270	223	209	159	116	89	85	105	128	90	79	90	100	127	174	167	140
57.5	296	231	179	141	109	89	81	90	101	73	62	71	84	93	115	106	91
55.0	322	238	149	123	103	88	78	75	74	56	45	53	69	58	56	46	42
52.5	235	199	144	120	97	77	64	60	64	53	48	51	56	52	52	46	41
50.0	148	160	139	118	91	66	50	47	53	50	50	50	42	45	48	47	41
47.5	131	135	132	108	82	61	49	47	54	50	50	48	38	38	41	40	36
45.0	113	110	124	98	74	57	48	49	54	50	49	45	33	30	33	33	31
42.5	109	103	106	85	64	49	40	39	44	44	46	42	29	25	26	26	25
40.0	104	96	88	72	55	41	32	30	33	37	42	39	25	19	19	20	20
37.5	100	95	79	67	53	40	31	27	28	29	29	27	21	18	22	21	19
35.0	96	93	71	62	51	39	29	23	22	22	17	15	17	18	25	23	19
32.5	72	81	70	64	53	38	26	19	18	16	15	13	13	14	20	19	16
30.0	48	70	69	66	54	38	23	14	14	11	12	12	9	10	15	15	12
Summer																	
60.0 KM	193	137	79	61	59	70	87	99	100	96	96	95	102	143	240	232	185
57.5	110	93	65	59	59	63	72	83	90	83	78	74	74	101	165	160	133
55.0	43	49	51	58	58	56	56	66	80	69	59	53	47	60	85	88	81
52.5	35	40	41	46	47	45	45	50	59	54	47	43	43	53	76	77	70
50.0	26	30	31	34	35	34	33	35	39	39	35	34	39	46	68	66	59
47.5	22	24	24	26	26	25	25	27	32	36	35	33	37	42	53	54	52
45.0	18	19	18	18	17	16	16	19	26	34	35	33	33	37	39	42	44
42.5	15	16	14	14	13	12	13	16	22	26	27	26	24	27	33	37	39
40.0	12	13	10	11	10	8	9	13	19	19	20	20	16	17	28	32	34
37.5	12	13	9	10	10	8	7	10	15	15	15	15	13	16	26	28	28
35.0	12	13	9	10	9	7	6	7	11	10	10	10	10	14	23	24	21
32.5	11	10	7	7	6	5	4	6	9	8	9	9	8	12	22	22	20
30.0	9	8	6	4	3	2	2	4	7	7	8	8	6	9	20	21	18
Autumn																	
60.0 KM	792	628	501	334	202	124	99	119	154	135	121	103	87	159	359	332	229
57.5	635	528	442	315	208	141	114	124	147	124	110	101	88	117	222	202	144
55.0	479	428	384	295	214	158	129	129	140	113	100	98	89	76	86	71	58
52.5	393	374	355	276	194	132	101	110	140	106	94	79	68	52	54	46	44
50.0	307	320	325	257	175	106	72	92	141	97	68	60	47	29	21	21	30
47.5	300	293	297	236	170	117	87	89	111	89	67	55	43	29	25	25	29
45.0	292	265	270	216	166	128	102	86	81	80	66	49	40	29	29	28	28
42.5	258	252	244	199	151	110	81	67	67	66	55	41	32	25	25	25	25
40.0	224	238	218	181	136	93	61	47	52	52	44	34	25	20	21	22	22
37.5	196	217	205	168	122	79	48	37	43	39	33	26	19	16	19	19	19
35.0	168	195	191	155	109	66	36	26	33	25	21	19	13	12	17	16	15
32.5	140	162	161	131	92	57	31	22	25	21	17	15	11	10	13	14	14
30.0	111	128	130	105	76	48	27	17	18	17	13	9	9	9	10	11	12

## BRASSEUR

TABLE 2.- Seasonal values of  $K_{yz}$  ( $10^1 \text{ m}^2 \text{ sec}^{-1}$ ) after Nastrom and Brown 1978

LATITUDE	75	70	65	60	55	50	45	40	35	30	25	20	15	10	5	0	-5
Winter																	
60.0 KM	-188	-165	-58	-27	188	340	317	474	381	-88	-238	345	182	-71	-31	3	-32
57.5	-225	-188	-55	-24	184	397	351	622	386	-112	-214	213	117	-62	-24	4	-28
55.0	-261	-211	-52	-21	180	454	675	770	391	-135	-189	80	52	-52	-17	4	-23
52.5	-218	-181	-31	-12	112	314	497	578	326	-78	-128	54	31	-48	-10	3	-17
50.0	-174	-152	-11	-3	44	174	319	386	261	-20	-66	27	9	-43	-4	2	-12
47.5	-168	-145	0	2	-11	24	103	206	154	-22	-26	26	14	-21	-3	0	-6
45.0	-162	-139	12	8	-67	-125	-111	25	48	-25	12	24	18	0	-2	0	0
42.5	-239	-193	1	7	-76	-144	-124	4	33	-27	-2	22	14	0	-1	0	0
40.0	-317	-246	-9	7	-86	-164	-137	-16	18	-28	-17	20	9	0	0	0	0
37.5	-259	-215	-21	4	-76	-143	-109	-11	8	-22	-9	12	4	-1	0	0	0
35.0	-201	-184	-32	2	-66	-122	-81	-7	-1	-16	0	4	0	-3	0	0	0
32.5	-129	-125	-27	0	-44	-81	-47	7	-7	-23	-2	1	1	0	0	0	0
30.0	-56	-66	-22	0	-22	-40	-13	22	-13	-30	-3	-1	2	2	0	0	0
Spring																	
60.0 KM	67	-1	5	-172	-205	-143	-185	-240	-275	-61	60	-660	-536	604	350	-103	-230
57.5	-97	-136	-64	-163	-180	-143	-183	-215	-212	-4	64	-422	-382	375	196	-70	-144
55.0	-262	-272	-135	-155	-156	-144	-181	-191	-148	52	68	-184	-228	146	43	-36	-57
52.5	-139	-153	-87	-127	-133	-112	-131	-138	-122	33	77	-134	-133	103	30	-30	-46
50.0	-16	-35	-39	-99	-110	-81	-81	-85	-95	14	85	-84	-39	60	18	-23	-34
47.5	8	0	13	-33	-60	-51	-57	-66	-91	-4	78	-56	-15	56	18	-15	-25
45.0	32	36	66	32	-9	-21	-34	-48	-87	-23	70	-78	9	53	18	-7	-16
42.5	-12	-10	50	44	17	0	-14	-34	-66	-15	59	-4	19	45	15	-4	-11
40.0	-57	-57	34	56	43	19	4	-21	-45	-6	48	0	29	38	12	-1	-6
37.5	-98	-105	-8	31	43	26	15	-7	-26	4	35	-8	7	29	11	-2	-6
35.0	-139	-154	-50	6	42	33	25	7	-7	16	21	-15	-13	19	11	-3	-6
32.5	-114	-155	-72	-18	29	27	20	7	1	17	15	-12	-12	7	5	0	-1
30.0	-89	-155	-94	-43	16	21	15	7	10	17	15	-9	-11	-5	0	3	3
Summer																	
60.0 KM	0	0	-3	-10	-18	-24	-9	41	43	15	11	-28	114	156	27	17	137
57.5	0	0	-3	-8	-14	-18	-9	23	25	18	29	-17	64	96	17	10	88
55.0	0	0	-3	-7	-10	-11	-8	5	6	22	46	-6	14	36	8	4	39
52.5	0	0	-2	-4	-6	-6	-5	2	0	15	36	-9	11	35	8	2	29
50.0	0	0	-1	-2	-2	-2	-1	-1	-7	8	25	-11	8	35	8	1	19
47.5	0	0	0	-1	-1	-1	0	0	-7	5	25	-9	6	27	6	1	15
45.0	0	0	0	0	0	0	0	0	-6	2	25	-6	5	20	4	0	11
42.5	0	0	0	0	0	0	0	0	-4	1	14	-3	4	12	2	0	6
40.0	0	0	0	0	0	0	0	0	-1	0	4	0	3	4	1	0	2
37.5	0	0	0	0	0	0	0	0	-1	0	2	0	1	2	0	0	0
35.0	0	0	0	0	0	0	0	0	0	1	1	0	0	0	0	0	-1
32.5	0	0	3	0	0	0	0	0	0	1	2	0	0	0	0	0	0
30.0	0	0	0	0	0	0	0	0	0	0	3	-1	0	0	0	0	0
Autumn																	
60.0 KM	10	296	200	210	182	162	112	99	67	0	36	-90	-135	278	186	-351	-641
57.5	8	245	191	207	172	154	106	88	51	0	26	-69	-97	161	100	-207	-377
55.0	5	194	182	204	161	146	101	76	35	0	17	-48	-60	45	13	-64	-114
52.5	4	140	133	147	109	95	65	52	25	0	9	-29	-33	27	8	-36	-71
50.0	2	86	85	91	57	44	28	27	16	0	2	-11	-6	9	4	-8	-29
47.5	1	61	52	46	18	11	12	17	8	0	3	-7	-1	14	9	-10	-32
45.0	1	36	20	1	-20	-21	-3	8	1	0	5	-2	3	19	13	-12	-35
42.5	0	30	18	-2	-28	-28	-7	4	0	0	4	1	6	16	9	-5	-20
40.0	0	23	17	-7	-36	-35	-11	0	0	0	3	5	9	12	5	0	-4
37.5	0	19	18	-2	-29	-30	-10	-1	-1	0	3	3	6	10	5	0	-6
35.0	0	16	19	1	-23	-25	-8	-2	-1	0	2	0	3	8	5	-2	-8
32.5	0	10	14	2	-15	-18	-7	-2	-1	0	1	0	2	5	3	-1	-6
30.0	0	4	9	3	-7	-11	-4	-3	-1	0	1	0	1	2	1	0	-3

## BRASSEUR

TABLE 3.- Seasonal values of  $K_{zz}$  ( $10^3 \text{ cm}^2 \text{ sec}^{-1}$ ) after Nastrom and Brown 1978

LATITUDE	75	70	65	60	55	50	45	40	35	30	25	20	15	10	5	0	-5
Winter																	
60.0	1050	1000	1419	1575	1600	1550	1475	1375	1150	1100	1050	1125	1375	1641	2100	2300	2450
57.5	800	760	1161	1313	1413	1333	1280	1200	1050	975	913	963	1125	1329	1575	1750	1875
55.0	550	520	903	1050	1225	1115	1085	1025	950	850	775	800	875	976	1050	1200	1300
52.5	450	415	650	763	875	845	825	773	708	643	605	615	663	724	775	850	950
50.0	350	310	396	475	525	575	565	520	465	415	435	430	450	470	460	500	600
47.5	310	280	321	378	410	448	423	383	325	310	315	328	345	367	375	390	425
45.0	270	250	245	280	295	320	280	245	185	145	195	225	240	263	290	280	250
42.5	210	190	173	205	225	225	180	150	113	115	135	163	175	183	195	185	165
40.0	150	130	100	130	155	130	80	55	40	45	75	100	110	103	100	90	80
37.5	110	96	69	83	104	84	52	37	27	31	51	67	81	76	65	60	57
35.0	70	62	39	36	51	37	24	14	13	17	26	33	51	49	30	30	33
32.5	51	45	31	24	34	26	19	17	15	18	21	24	36	34	20	22	24
30.0	32	28	23	20	17	15	13	15	17	19	16	14	20	10	10	14	18
Spring																	
60.0	450	600	456	395	390	410	495	580	700	814	1000	975	775	649	700	900	1050
57.5	550	485	366	318	330	363	443	528	638	748	893	825	650	564	585	750	950
55.0	450	370	275	240	270	315	390	475	575	700	785	675	525	459	470	600	850
52.5	380	325	256	233	255	298	355	418	503	595	633	543	438	415	450	540	680
50.0	310	280	236	225	240	280	320	360	430	490	480	410	350	370	430	480	520
47.5	205	255	210	195	205	233	270	308	358	393	385	333	290	311	365	385	410
45.0	260	230	184	165	170	185	220	255	285	295	290	255	230	253	300	240	300
42.5	200	180	154	140	140	148	165	185	203	205	213	195	178	166	165	185	205
40.0	140	130	124	115	110	110	110	115	120	115	135	135	125	79	30	80	110
37.5	91	87	88	77	71	75	76	76	76	76	93	95	83	56	25	51	70
35.0	41	43	50	38	32	40	41	34	31	36	51	55	40	33	20	22	30
32.5	31	30	35	25	21	25	26	24	24	24	38	40	31	27	20	21	24
30.0	20	17	20	12	10	10	10	13	17	20	24	23	22	20	14	20	25
Summer																	
60.0	550	480	431	425	475	515	480	455	685	1120	1330	1525	1500	1338	1300	2000	2150
57.5	485	440	385	395	424	430	390	365	488	755	1010	1170	1163	1047	975	1550	1975
55.0	420	400	339	265	380	345	300	275	290	390	490	815	825	756	650	1100	1800
52.5	385	365	298	310	330	303	255	225	256	328	418	625	620	559	475	800	1350
50.0	350	330	256	255	280	260	210	175	225	265	445	435	415	361	300	500	900
47.5	285	295	228	214	238	205	153	128	183	235	290	343	300	265	200	335	625
45.0	220	260	199	175	195	150	95	80	140	205	235	250	185	169	100	170	350
42.5	145	190	150	135	145	113	70	78	128	163	170	168	133	124	75	125	225
40.0	110	120	101	95	95	75	45	75	115	120	105	85	80	78	60	80	100
37.5	71	78	73	73	75	61	44	61	78	77	67	57	57	57	37	54	67
35.0	31	35	43	50	53	46	43	47	41	34	29	28	34	35	24	28	33
32.5	25	28	33	37	38	31	27	30	31	27	25	25	29	30	23	23	23
30.0	19	20	22	21	23	16	11	13	20	20	20	23	24	25	21	17	11
Autumn																	
60.0	570	590	960	1110	1040	915	835	825	925	1075	1175	1525	1300	1500	2100	1800	1450
57.5	535	540	848	945	880	800	723	658	695	825	1138	1300	1193	1377	1900	1650	1250
55.0	500	490	735	780	720	685	610	490	465	575	900	1075	1085	1254	1700	1500	1050
52.5	410	410	594	628	588	570	510	438	423	488	490	875	910	1024	1350	1175	825
50.0	320	330	451	475	455	455	410	385	380	400	480	675	735	794	1000	850	600
47.5	250	265	318	328	320	330	330	325	315	333	385	500	570	612	750	645	465
45.0	180	200	185	140	185	205	250	255	250	265	290	325	405	429	500	440	330
42.5	150	160	140	128	128	145	190	200	185	190	210	243	295	314	350	300	230
40.0	120	120	94	75	70	85	130	135	120	115	130	160	185	199	200	160	130
37.5	105	95	75	58	56	66	88	92	86	80	90	110	126	133	132	107	88
35.0	90	70	56	40	42	46	46	48	52	44	49	60	65	66	44	53	45
32.5	58	47	40	30	30	31	32	34	37	34	36	42	45	46	46	38	31
30.0	25	24	25	14	14	16	17	20	23	23	22	23	25	27	28	22	17

increases with height above 30 km. One also notes a latitudinal variation below 45 km but, as shown also in the Nastrom and Brown data, the patterns of the K's tend to be more or less horizontal in the upper stratosphere and lower mesosphere. The cross sections represented here refer to zonal mean values. However, as shown by Nastrom and Brown and illustrated in figure 11, the values of the exchange coefficients may be quite different at two separate longitudes.

6. EDDY DIFFUSION AND OZONE TRANSPORT: In order to test the effect of each eddy diffusion component on the distribution of an atmospheric trace gas, such as ozone, different computations have been carried out with a two-dimensional numerical model. The full description of this model - including the chemical scheme - with its two versions has been given by Brasseur (1976; 1978). Firstly, one considers a steady state approach with a very simple transport parametrization. The action of the mean circulation is neglected and the dynamics is described only by the three eddy diffusion coefficients. In order to oversimplify the conditions, the following constant and uniform values are adopted:  $K_{yy} = 10^{10} \text{ cm}^2 \text{ s}^{-1}$  and  $K_{zz} = 10^4 \text{ cm}^2 \text{ s}^{-1}$ . Moreover,  $K_{yz}$  is adjusted in the winter and summer hemisphere until the calculated ozone distribution becomes compatible with the observations.

Figure 12 shows the meridional cross section of the ozone concentration when photochemical equilibrium conditions are prescribed (all K's are put equal to zero). In this case, the maximum concentration is located in the equatorial and tropical regions and almost no ozone is present below 10 km or at high latitudes. This is in contradiction with the reality.

When the vertical coefficient  $K_{zz} = 10^4 \text{ cm}^2 \text{ s}^{-1}$  is introduced while the other K's remain equal to zero (figure 13), ozone is present in the lower stratosphere (and troposphere) but its concentration remains insignificant at high latitudes. When the computation is performed with  $K_{yy} = 10^{10} \text{ cm}^2 \text{ s}^{-1}$  and  $K_{zz} = 10^4 \text{ cm}^2 \text{ s}^{-1}$  (figure 14) a horizontal flux appears and ozone penetrates in the high latitude regions. However, the maximum concentration still occurs in the equatorial zone where  $\text{O}_3$  is produced photochemically, which is in contradiction with the observation.

The existence of a countergradient flux becomes possible only with the introduction of the off-diagonal component  $K_{yz}$ . Fig. 15 shows the latitudinal variation of total ozone obtained for different values of  $K_{yz}$ . It clearly shows that the ozone distribution is very sensitive to  $K_{yz}$ , particularly at high latitudes. Therefore, it should be determined with a very high precision. Because of the high sensitivity of the distribution of ozone to  $K_{yz}$  and because of the rather large uncertainty on  $K_{yz}$ , it is most necessary to "tune" this coefficient with care until the distribution of trace species and/or temperature comes into agreement with the observation. It should be noted, however, that the solution is not unique and the results depend on the other parameters which are adopted, and especially the mean motion and the other K's. Further, it is not proven, but only assumed by most modellers, that the same K's may be used for all the different trace species of the atmosphere. This is only a first order approximation since the theory by Reed and German has its own limitations and assumes that the physical processes governing the transport are the same for all of the different atmospheric species. Adopting the latitudinal distribution of  $K_{yz}$  shown in figure 16, the meridional distribution of  $\text{O}_3$  as illustrated in figure 17 is obtained.

In order to give a crude estimation of the relative effect of the mean and turbulent transport of ozone, we now consider a second and more elaborate version of the 2-D model. The mean circulation as computed by Cunnold et al. (1974) is now introduced in the model while the eddy diffusion coefficients are adjusted at all latitudes and altitudes. Figure 18 gives some information concerning the distributions of these K's. In order to visualize the action of both types of transport, figure 19, 20 and 21 present, respectively, the mean, turbulent and total transport derived with the model calculation and show that the poleward ozone flux in winter is only possible if the horizontal (countergradient) transport by eddies is taken into account. In fact according to these calculations, horizontal mean motions play a significant role in the equatorial and polar regions while large scale turbulent transport is clearly dominant in the mid-latitude zone. Vertical winds in the Hadley cell near the equatorial tropopause prevent ozone from diffusing downward.

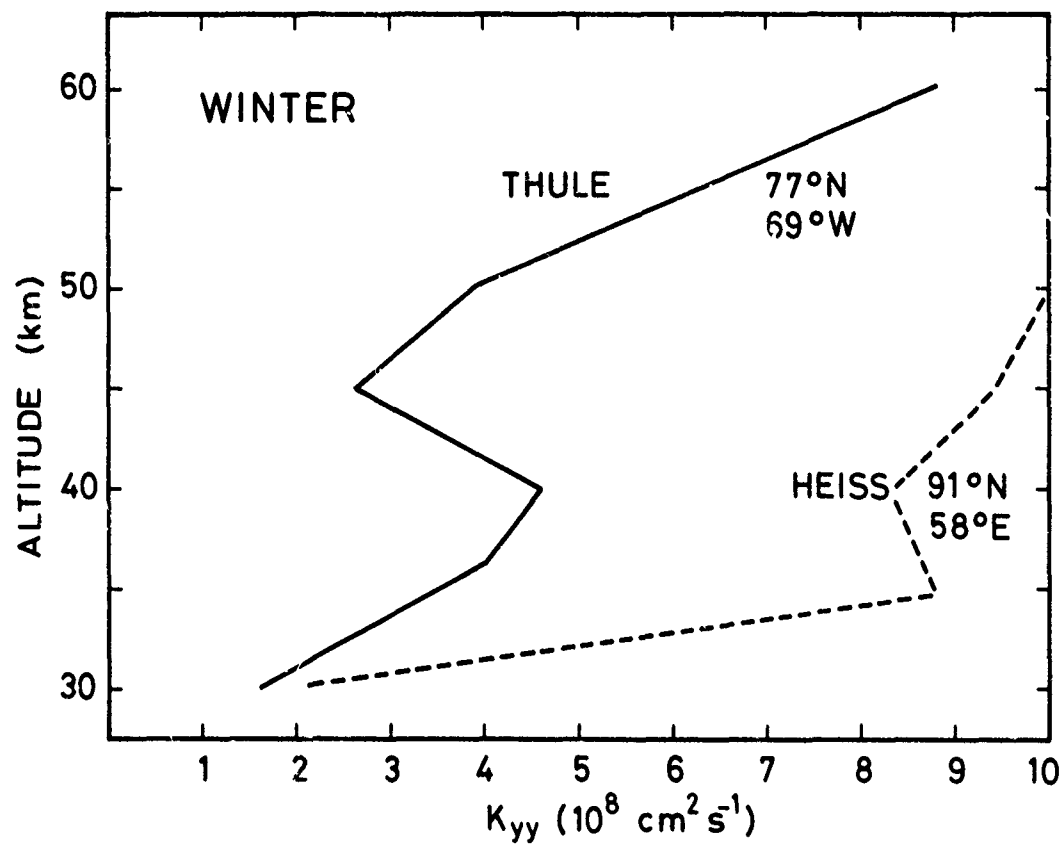


Fig. 11.- Comparison of  $K_{yy}$  during winter at Thule and Heiss. From Nastrom and Brown (1978).

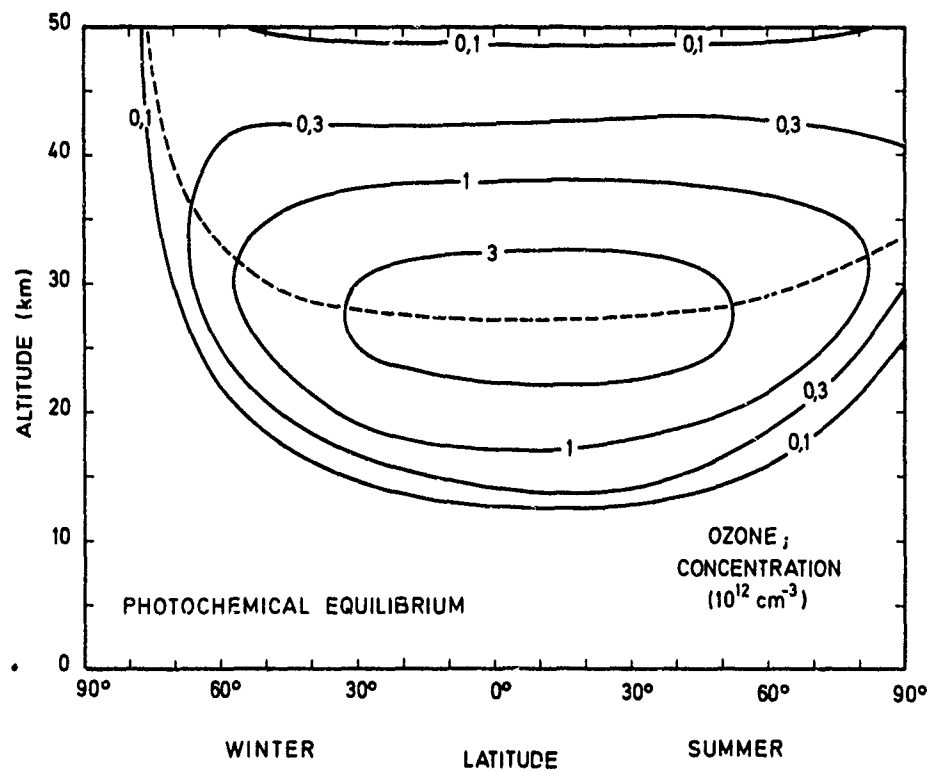


Fig. 12.- Meridional distribution of the ozone concentration assuming photochemical equilibrium conditions.

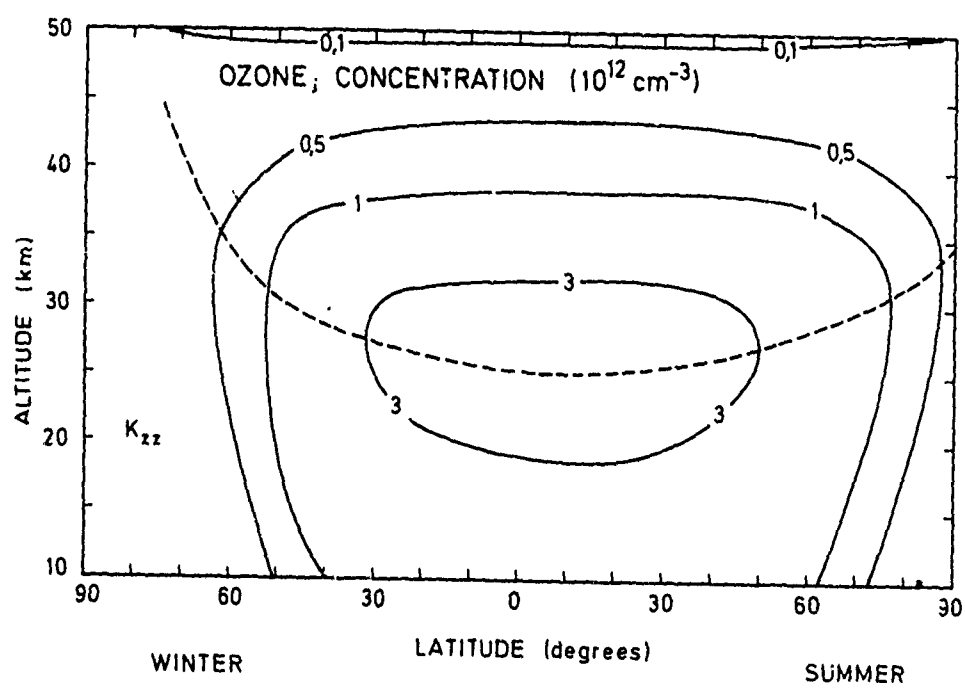


Fig. 13.- Meridional distribution of the ozone concentration when vertical exchange by diffusion is only taken into account.

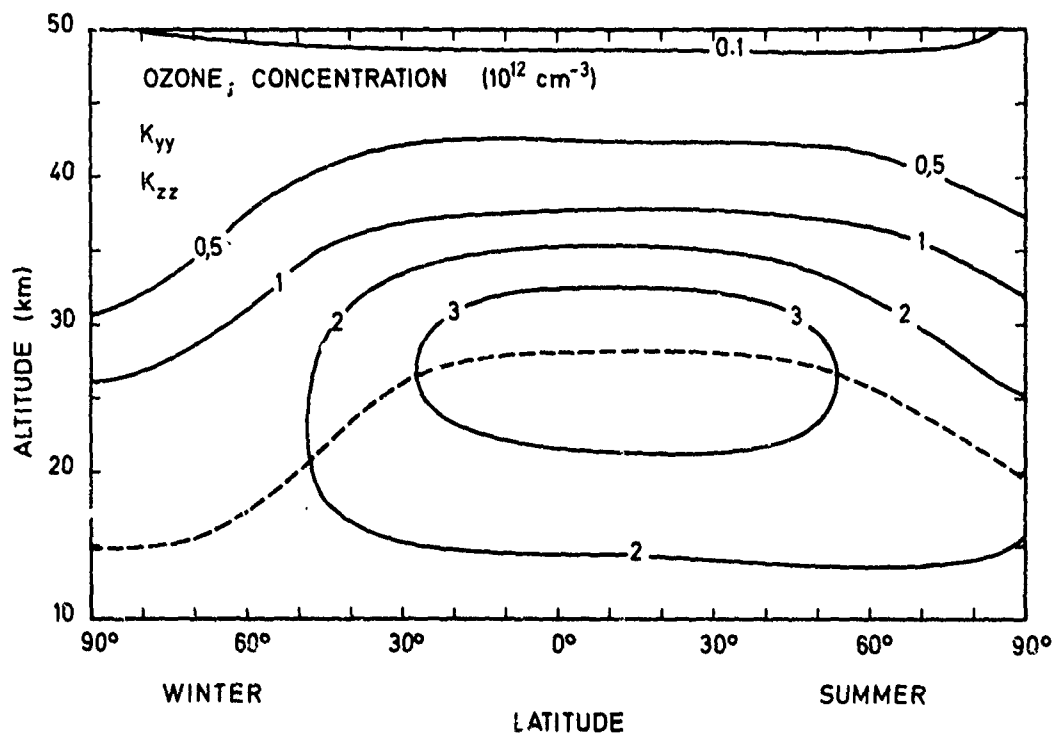


Fig. 14.- Meridional distribution of the ozone concentration when vertical and horizontal transport are taken into account, and are parameterized by  $K_{yy}$  and  $K_{zz}$  only.



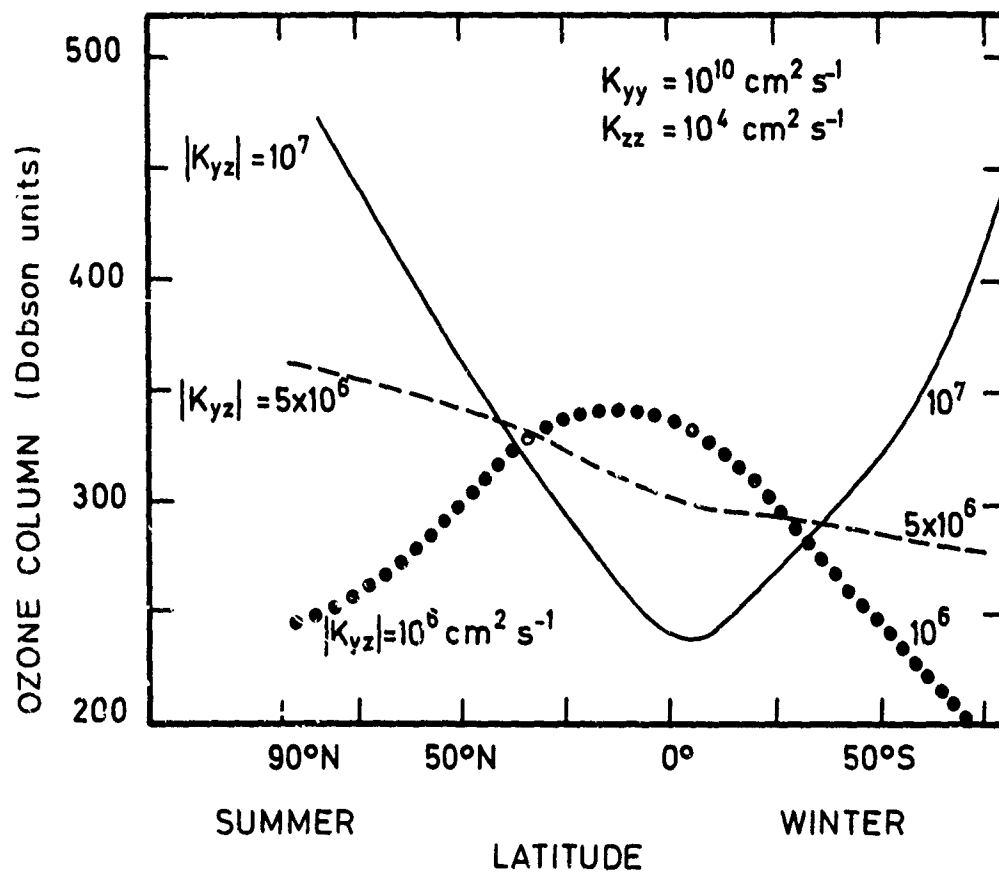


Fig. 15.- Effect of the anisotropic component  $K_{yz}$  on the latitudinal distribution of total ozone.

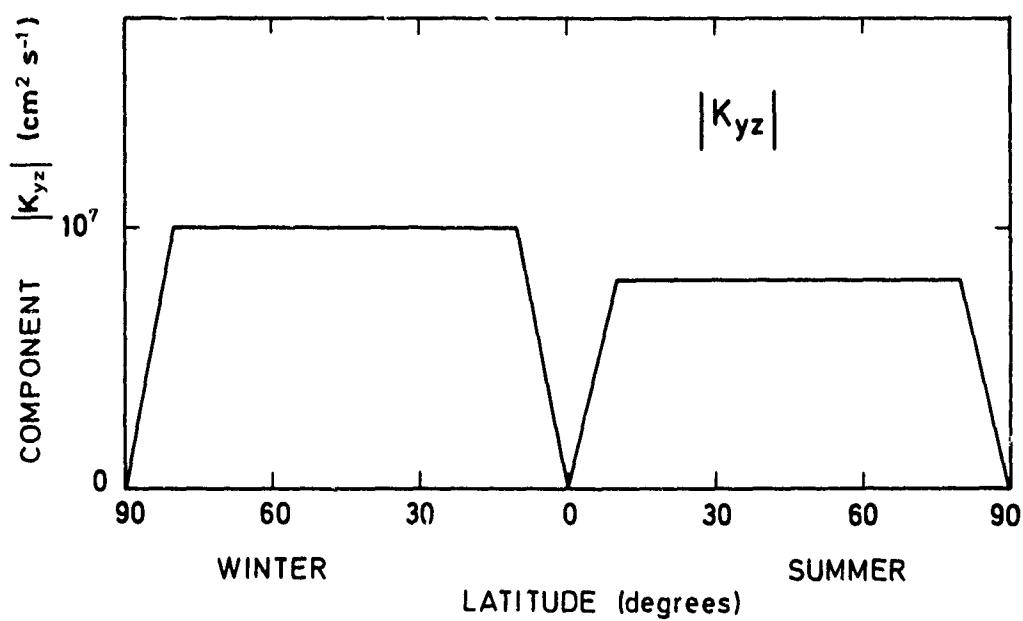


Fig. 16.- Example of a simple latitudinal distribution of  $|K_{yz}|$  in the stratosphere.

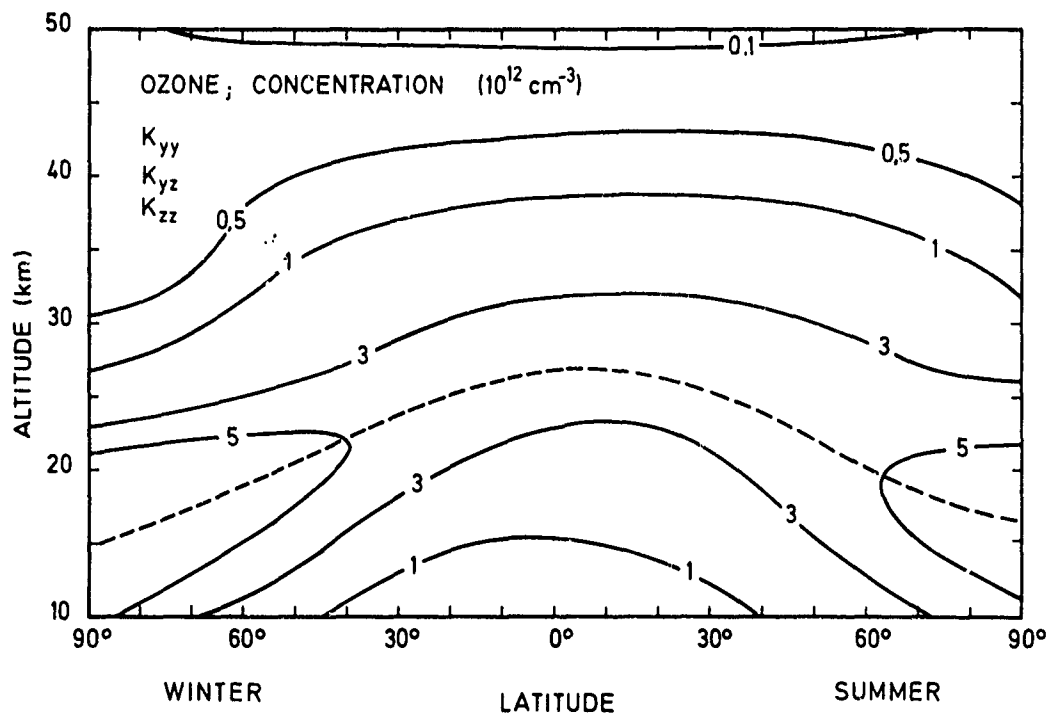


Fig. 17.- Meridional distribution of the ozone concentration when the transport  
 is parameterized by the three components  $K_{yy}$ ,  $K_{yz}$  and  $K_{zz}$ .

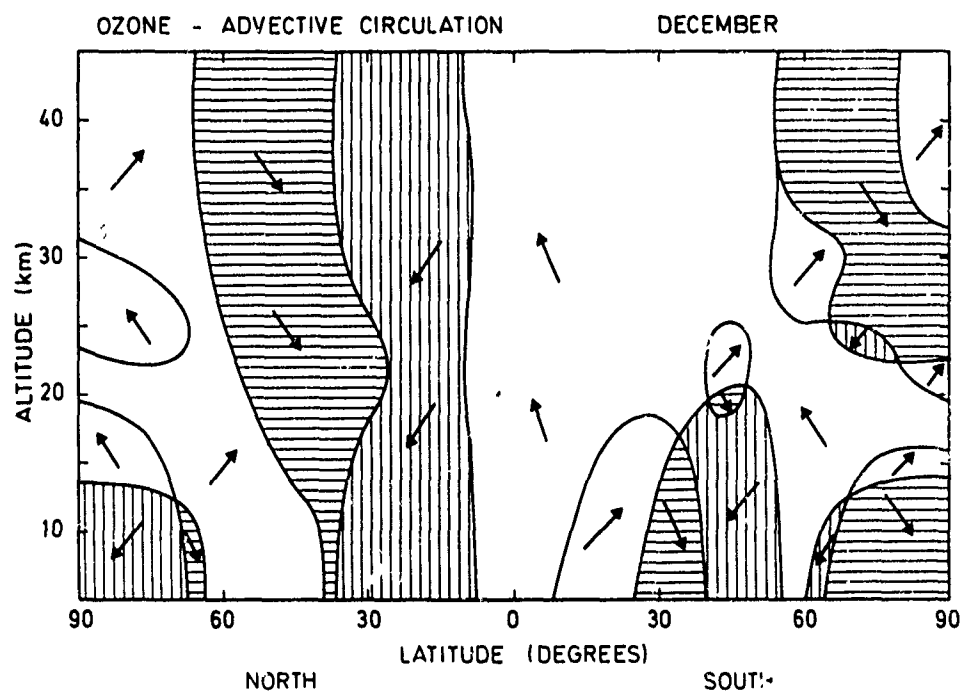


Fig. 19.- Representation of the circulation of ozone by mean motions ( $v$ ,  $w$ ).

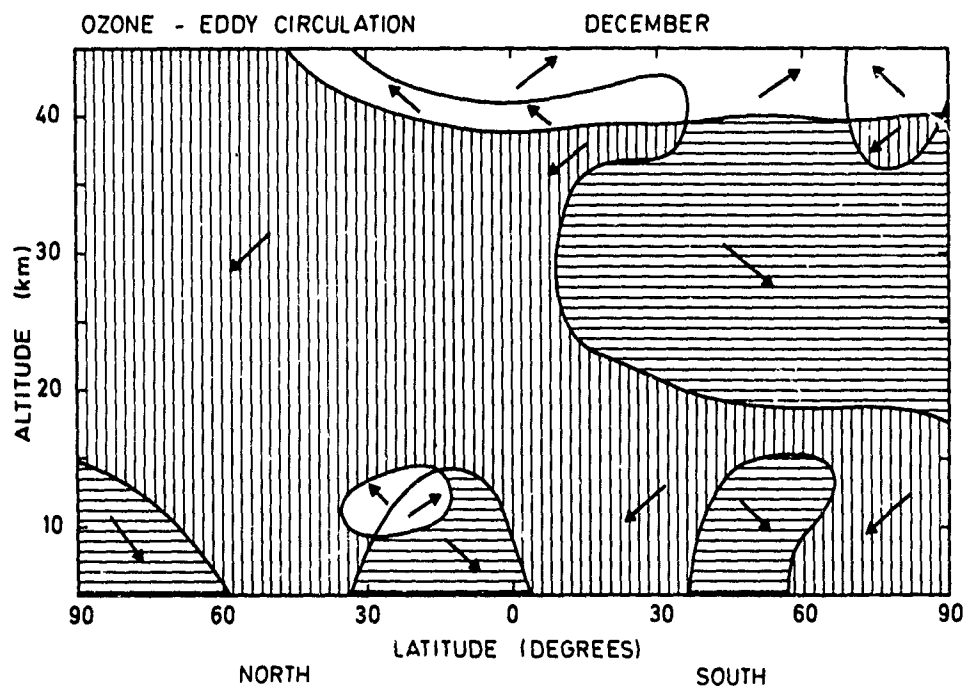


Fig. 20.- Representation of the circulation of ozone by large scale eddy diffusion ( $K_{yy}$ ,  $K_{yz}$ ,  $K_{zz}$ ).

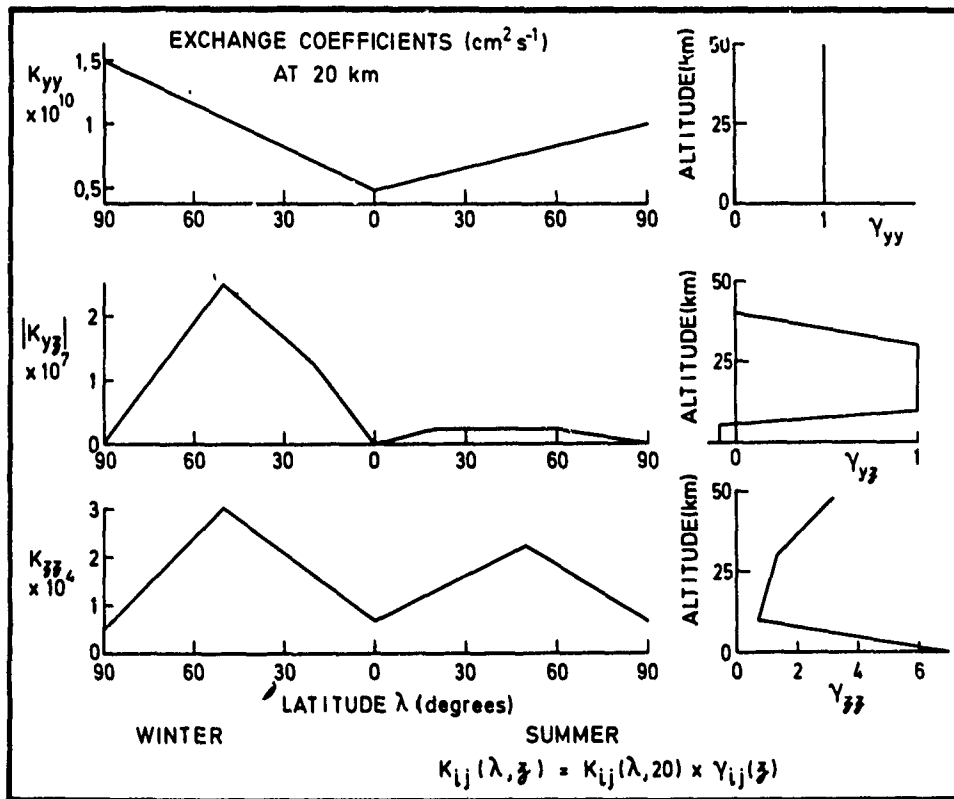


Fig. 18.- Distribution with latitude and altitude of the exchange coefficients adopted in the 2-D model used in this work.

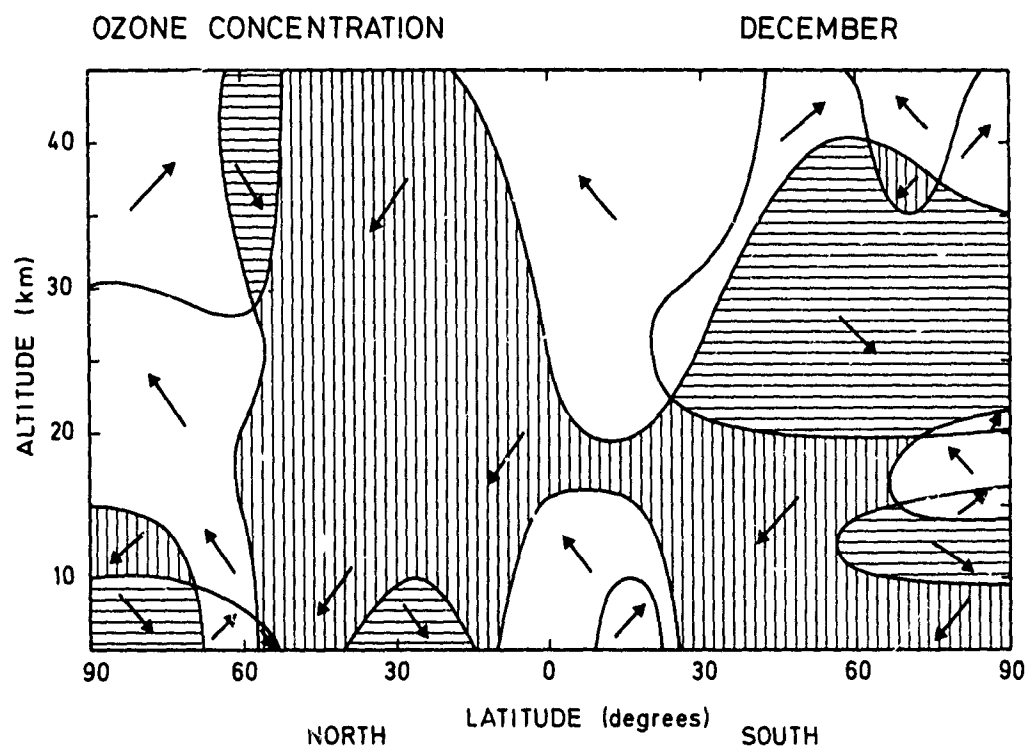


Fig. 21.- Representation of the global circulation of ozone by mean motions and eddy diffusion.

# BRASSEUR

7. VERTICAL 1-D TRANSPORT IN THE ATMOSPHERE: In many aeronomic studies, the problem of the behavior of minor constituents is treated by assuming average conditions over all latitudes and longitudes. In one-dimensional models, which are useful in the estimation of the dominant chemical and photochemical processes as a function of the altitude, the continuity equation becomes

$$\frac{\partial n}{\partial t} + \frac{\partial \phi}{\partial z} = P - L \quad (35)$$

where it is now assumed that all the quantities are averaged over the entire globe. In this equation, the contribution to the flux is due to large scale eddy mixing; the mean circulation does not appear since, for continuity reasons, the average vertical wind must be equal to zero. Again, the continuity equation (35) requires a closure condition and one assumes that a vertical flux of any minor constituent takes place when the distribution of this species departs from constant mixing ratio. The following equation, indicating that the net vertical flux is proportionnal to the negative gradient of the mixing ratio,

$$\phi = -K n(M) \frac{\partial f}{\partial z} \quad (36)$$

is adopted since it requires that the constituent moves from regions where it has a high mixing ratio to regions where it is low. In this expression,  $K$  is a vertical exchange coefficient which refers to global conditions (average over all latitudes and longitudes). This formalism for vertical 1-D transport has been introduced by Lettau (1951) and adopted by Colegrove *et al.* (1966) to study the transport of oxygen in the lower thermosphere. The vertical flux can also be written in the alternative forms

$$\phi = -K \left[ \frac{\partial n}{\partial z} + \frac{n}{H} + \frac{n}{T} \frac{\partial T}{\partial z} \right] \quad (37)$$

or

$$\phi = -K n \left[ \frac{1}{H} - \frac{1}{H_1} \right] \quad (38)$$

where  $T$  is the temperature,  $H$  the atmospheric scale height and  $H_1$  the scale height of the species being considered.

It should be noted that, while the form of these flux representations can be intuitively understood from the Prandtl's mixing length theory, there is no complete and fundamental theoretical explanation for an expression such as (36). There has been much confusion in the past in the interpretation of the physical sense of the  $K$  coefficient when it has been attempted to derive its absolute value from turbulence measurements. In fact, the vertical eddy-mixing coefficient is generally obtained without any explicit reference to the motions and it must be considered as a pure phenomenological parameter.  $K$  is simply a proportionality factor relating the flux to the gradient of the mixing ratio.

Studies of the dispersion processes in the mesosphere and the lower thermosphere have been undertaken by different methods, namely using radio meteor trails (e.g. Roper and Elford, 1963; Roper, 1966; Zimmerman, 1973; 1974; Cunnold, 1975) or chemical release observation (e.g. Blamont and de Jager, 1961; Zimmerman and Champion, 1963; Justus, 1969; Zimmerman and Trowbridge, 1973). Values for a diffusion coefficient have been derived in several cases. A profile of the coefficient for the vertical eddy diffusion of heat (which is of the same order of magnitude as the exchange coefficient of trace species) for the region between 50 and 100 km has been deduced by Johnson and Wilkins (1965) based upon the downward flux required to maintain the thermal structure of this



atmospheric region. These results were questioned, however, by Hunten (1974) since they did not take into account the heat input associated with the turbulence itself. Estimates of  $K$  due to small scale motions and, in particular, to internal gravity waves have been undertaken by Hodges (1969) and Hines (1970) while Justus (1973) has used Hines' theory in conjunction with wind observations to derive the profile of  $K$ . Lindzen (1971) has proposed values of  $K$  associated with atmospheric tides and Zimmerman (1973; 1974) has analyzed wind observations. Finally, exchange coefficient profiles have been deduced from the vertical distribution of long lived chemical species such as atomic oxygen in the 90-100 km region (Colegrove *et al*, 1965; da Mata, 1974). Adjustments of the  $K$  profiles have been made in most models when studying species such as NO (Strobel, 1971; Brasseur and Nicolet, 1973); CO (Hays and Olivero, 1970). Figure 22 illustrates different distributions of exchange coefficients in the mesosphere and lower thermosphere.

In the stratosphere and the troposphere where the pattern of vertical transport appears essentially to be determined by the meridional motions, the 1-D  $K$  profile should be, in principle, derived from elaborate circulation models (see e.g. Mahlman, 1975). However, an order of magnitude profile can be deduced from residence time ( $\tau$ ) considerations since it can be derived from the diffusion equations that

$$K \cong \frac{H^2}{\tau} \quad (39)$$

where  $H$  is a typical length, here the atmospheric scale height. Studies concerning the decay of radioactive debris from nuclear explosions have shown that the residence time is of the order of 2 years in the stratosphere while it is of the order of 1 month in the troposphere (see e.g. Reiter *et al*, 1975). Therefore, typical values for  $K$  are  $2 \times 10^5 \text{ cm}^2 \text{ s}^{-1}$  below the tropopause and between  $10^3$  and  $10^4 \text{ cm}^2 \text{ s}^{-1}$  above this transition region.

The vertical distribution of the exchange coefficient in the stratosphere can in principle be obtained by inverting the continuity/ transport equation (derived from 35 and 36). If the distribution of the production, the loss rates and the concentration of a tracer are known, it is possible to determine a corresponding  $K$  profile. Since the exchange coefficient characterizes a physical state of the atmosphere, it is usually assumed to be independent of particular choices of the species. Also, to make sense the different parameters adopted for the inversion (concentration, etc...) must be globally averaged values. Constituents with horizontal stratification are thus very useful for this type of calculation.

Two types of atmospheric tracers have been used to derive vertical profiles of  $K$ : chemically reactive gases such as  $\text{N}_2\text{O}$  or  $\text{CH}_4$  or chemically inert radionuclides introduced in the stratosphere by nuclear explosions.

a.  $\text{CH}_4$  and  $\text{N}_2\text{O}$  satisfy the conditions for applicability of one-dimensional eddy treatment since they are rather uniformly distributed in the horizontal and since their chemical loss mechanisms are relatively simple. Moreover, these two constituents are only produced at ground level and, therefore, the exchange coefficient profile is given by

$$K(z) = \frac{-\phi}{n(M) \frac{df}{dz}} = \frac{-\int_z^\infty L \, dz}{n(M) \frac{df}{dz}} \quad (40)$$

where  $\phi$  is the vertical flux,  $L$  the atmospheric destruction rate,  $f$  the volume mixing ratio and  $n(M)$  the total concentration.

Since, in general, large uncertainties remain in the determination of the global mixing ratio and the integrated loss rate,  $K$  cannot be derived without significant errors. Moreover, in the lower stratosphere and in the troposphere where  $n(M)$  becomes large and  $df/dz$  small for constituents such as  $\text{CH}_4$  and  $\text{N}_2\text{O}$ , this formula can no longer be applied. Hunten (1975) has used the methane data obtained by Ehhalt *et al*. (1972) to determine a

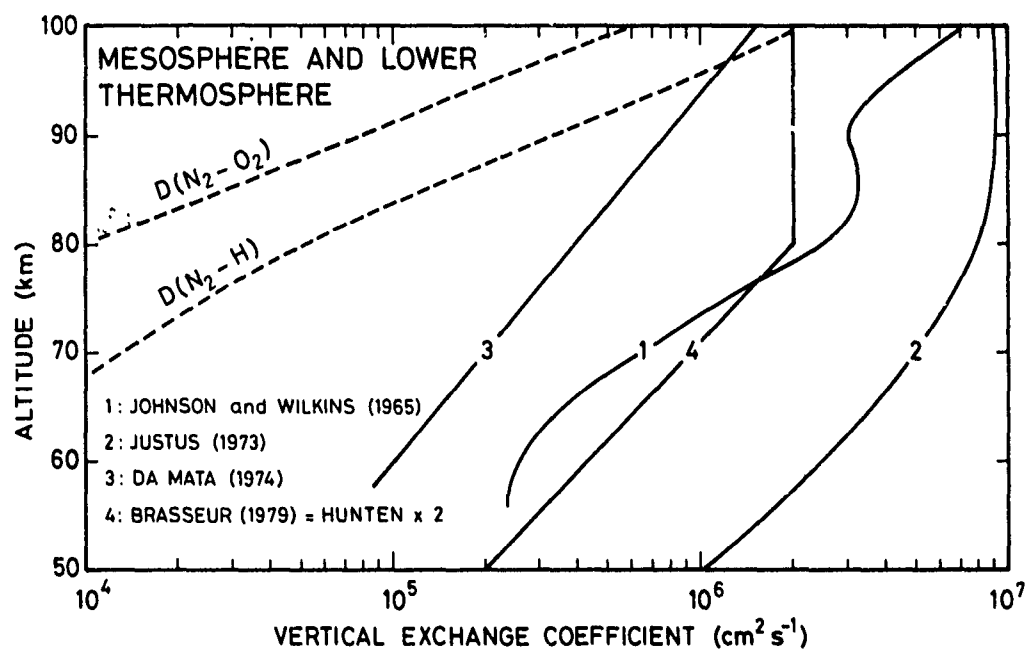


Fig. 22.- Vertical distribution of 1-D exchange coefficients  $K$  adopted in different mesospheric models. For comparison purposes, several molecular diffusion coefficients  $D$  are also shown.

K profile (figure 23) and has revised an earlier study by Wofsy and McElroy (1973). Dickinson (1976) has carefully analyzed the variability in the K profiles arising from differences in data interpretations. Other profiles have been suggested by various modelers (Liu and Cicerone, 1976; Crutzen and Isaksen, 1978; etc...) but recently, NASA (1977) has suggested consideration of whether to adopt an average of the Dickinson's results or the distribution given by Hunten but multiplied by a factor of 2. This last correction was introduced because the original Hunten's profile did not produce a chemical loss rate of  $\text{CH}_4$  which is consistent with that used in its derivation.

b. Tracers injected by nuclear explosions as fine particles (e.g.  $\text{Sr}^{90}$ ,  $\text{W}^{185}$ ,  $\text{Rh}^{102}$ ,  $\text{Cd}^{109}$  and  $\text{Zr}^{95}$ ) or as a true gas ( $\text{C}^{14}$ ) will provide useful information on stratospheric transport since they are not associated with any chemical source or sink (except the well understood radioactive decay). However such tracers are not uniformly distributed and because of the uncertainties in the meridional distributions (obtained by particle sampling) and due to the difficulties caused by the transient nature of the removal from the stratosphere and by the sedimentation of these particles, this method, which has been analyzed by Chang (1975), raises serious questions and does not provide more feasible results than those associated with chemically active species.

Figure 24 illustrates several profiles of exchange coefficients. Significant differences still occur which limit the validity of 1-D model calculations. To estimate the effect of transport uncertainties on chemical model results, figure 25 (Nicolet and Peetermans, 1972) shows the vertically integrated NO production rate in the stratosphere as a function of the vertically uniform eddy mixing coefficient K used in the calculation. Variations of about a factor of 10 occur. Also, figure 26 (NAS report, 1976) illustrates the different responses in the total ozone concentration to constant release of chlorofluoromethanes in the atmosphere until 1978 when release is suddenly and completely stopped. Again the results calculated with different K profiles differ significantly.

Finally, it should be clear that since the 1-D profile refers to globally average conditions, it cannot satisfactorily represent physical processes related to the details of the atmospheric dynamics, e.g. the formation of tropopause structure or the slope of the mixing surfaces in the lower stratosphere. Also, properties associated with the time variability of the atmospheric conditions are smoothed out by such 1-D approaches. For example, the vertical distribution of water vapor with the discontinuity in its scale height at the tropopause cannot be adequately represented in any 1-D model. Also, as explained by Newell (1977), carbon monoxide distributions can apparently be explained without invoking the 1-D model results that predict large sources from methane. Finally, the ozone distribution and budget can not be adequately described unless one adopts at least a 2-D representation.

8. SUMMARY: The so-called eddy diffusion coefficients are purely phenomenological but useful empirical parameters relating the mean flux to the gradient of the mixing ratio. When treating the transport of minor constituents in chemical models, the K-theory is very convenient but not theoretically verifiable. However, it leads to rather satisfactory results which should be considered as first approximations. More work is required to improve this parametrization and to introduce a more elaborate - but still handy - treatment of all scales of motions based on dynamical considerations. In the mean time, the K coefficients have to be deduced from the best known distributions of trace species and assumed to be independent of the choice of the minor constituents.

ACKNOWLEDGMENTS: The author wishes to extend special thanks to Prof. M. NICOLET for his kind invitation to present this paper at the Ozone Conference which has been held in Albufeiras (Portugal). Also, he is indebted to Dr. R. MURGATROYD and Prof. WAYNICK for their many comments and suggestions concerning this review paper.

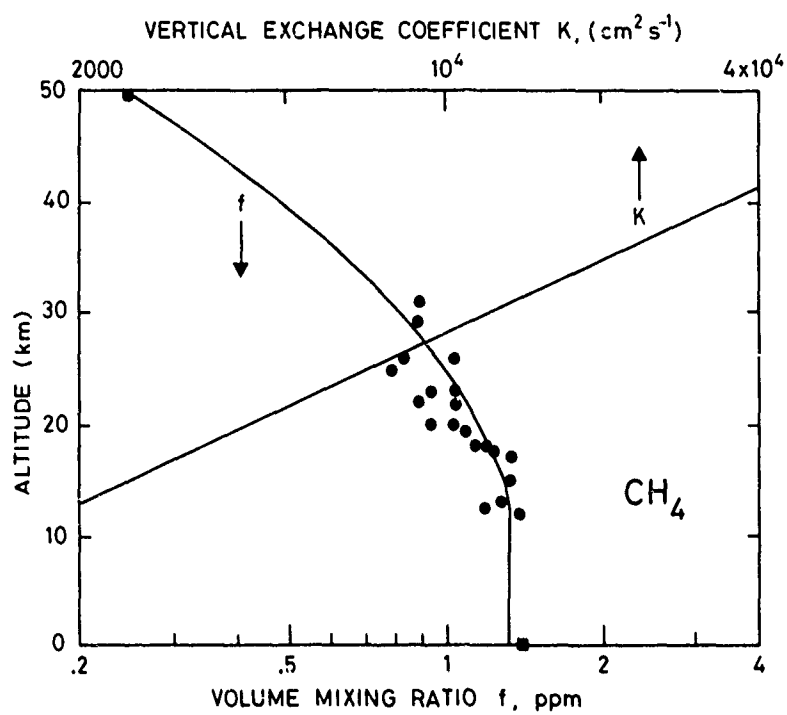


Fig. 23.- Stratospheric exchange coefficient profile derived  
by Hunten (1975) from methane data.

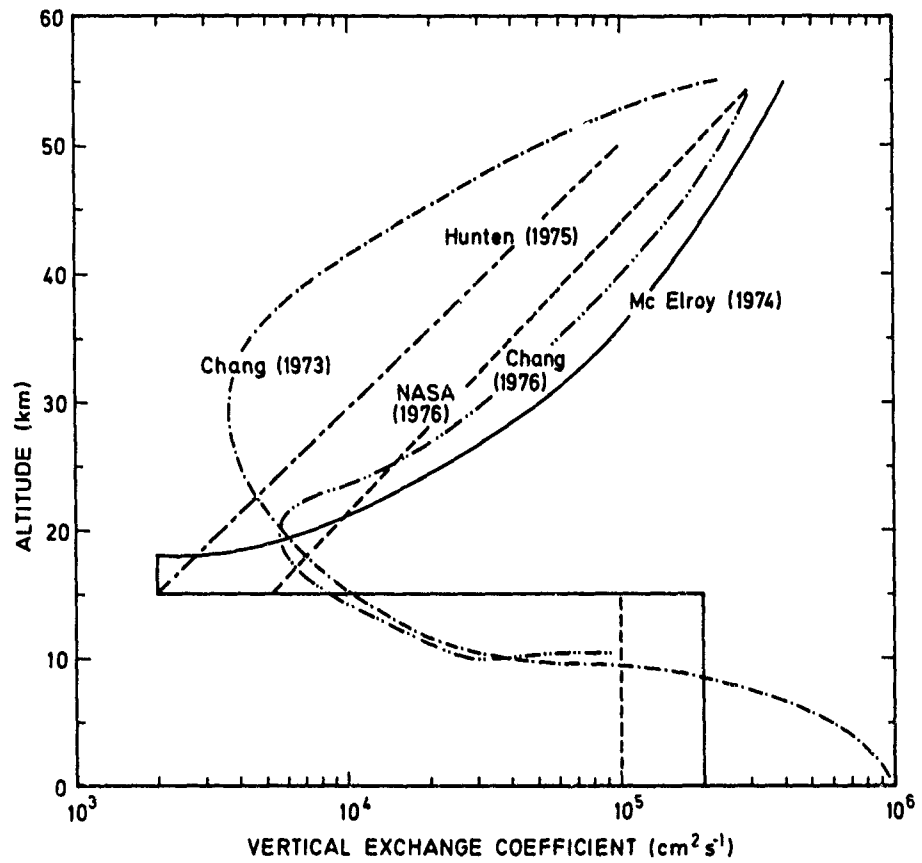


Fig. 24.- Exchange coefficients used in several stratospheric 1-D models.

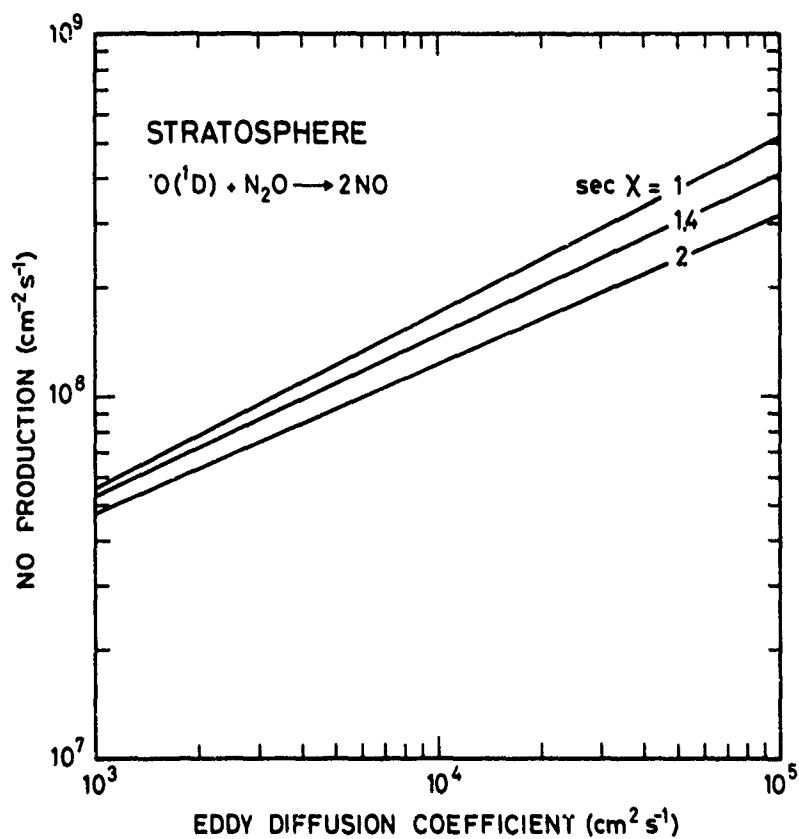


Fig. 25.- Integrated production rate of nitric oxide in the stratosphere as a function of the exchange coefficient  $K$  which is chosen constant with altitude. After Nicolet and Peetermans (1972).

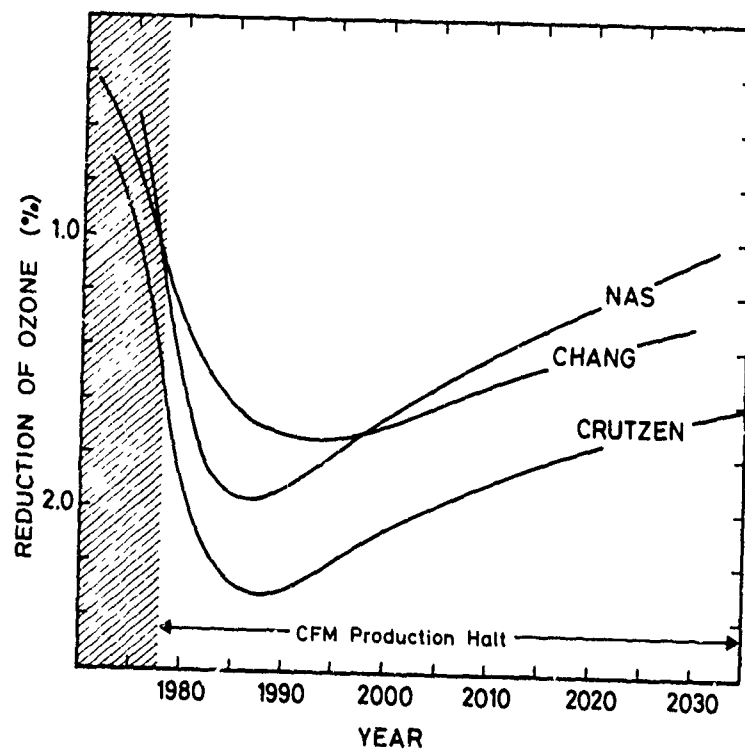


Fig. 26.- Behavior of total ozone when a constant release of chlorofluoromethanes in the atmosphere is completely stopped in 1978. Calculations with different exchange coefficients. After NAS (1976).

## REFERENCES

- BLAMONT, J.E. and C. deJAGER, Upper Atmospheric Turbulence near the 100 km level, *Ann. Geophys.*, **17**, 134, 1961.
- BRASSEUR, G. and M. NICOLET, Chemospheric processes of nitric oxide in the mesosphere and stratosphere, *Planet. Space Sci.*, **21**, 939, 1973.
- BRASSEUR G., L'action des oxydes d'azote sur l'ozone dans la stratosphère, Thèse de doctorat, Université Libre de Bruxelles, 1976.
- BRASSEUR, G., Un modèle bidimensionnel du comportement de l'ozone dans la stratosphère, *Planet. Space Sci.*, **26**, 139, 1978.
- BUSCH, H.S., Hemispheric wind conditions during the year 1950, Final report, part 2, contract No. AF 19-122-853, MIT, 1954.
- CHANG, J.S.; Uncertainties in the validation of parametrized transport in 1-D models of the stratosphere, Proceedings of the 4th CIAP conference, DOT-TSC-OST-75-38, 175, 1975.
- COLEGROVE, F.D., F.S. JOHNSON and W.B. HANSON, Atmospheric composition in the lower thermosphere, *J. Geophys. Res.*, **71**, 2227, 1966.
- COLEGROVE, F.D., W. HANSON and F. JOHNSON, Eddy diffusion and oxygen transport in the lower thermosphere, *J. Geophys. Res.*, **70**, 4931, 1965.
- CRUTZEN, P.J., A two-dimensional photochemical model of the stratosphere below 55 km: Estimates of natural and man-caused ozone perturbations due to  $\text{NO}_x$ , Proceedings of the 4th CIAP Conference, DOT-TSC-OST-75-38, 264, 1975.
- CRUTZEN, P.J. and I.S.A. ISAKSEN, The impact of the chlorocarbon industry on the ozone layer, *J. Geophys. Res.*, **83**, 345, 1978.
- CUNNOLD, D.M., F.N. ALEA, N.A. PHILLIPS and R.G. PRINN, A general circulation model of stratospheric ozone, Proceedings of the international conference on structure, composition and general circulation of the upper and lower atmospheres and possible anthropogenic perturbations, Melbourne, Australia, 1974.
- CUNNOLD, D.M., Vertical transport coefficients in the mesosphere obtained from radar observations, *J. Atm. Sci.*, **32**, 2191, 1975.
- DAVIDSON, B., J.P. FRIEND and H. SEITZ, Numerical models of diffusion and rainout of stratospheric radioactive materials, *Tellus XVIII*, **2**, 301, 1966.
- daMATA, L., La transition de l'homosphère à l'hétérosphère de l'atmosphère terrestre, Thèse de doctorat, Université Libre de Bruxelles, 1974.
- DEMAZURE, M. and J. SAISSAC, Généralisation de l'équation classique de diffusion, Note de l'Etablissement d'études et de recherches météorologiques No. 115, Paris 1962.
- DICKINSON, R., in Halocarbons; Effects on stratospheric ozone, National Academy of Sciences, Washington, D-C., USA, 1976.
- EADY, E.T., Long waves and cyclones waves, *Tellus*, **1**, 33, 1949.
- EHHALT, D.H., L.E. HEIDT and E.A. MARTELL, The concentration of atmospheric methane between 44 and 62 kilometers altitude, *J. Geophys. Res.*, **77**, 2193, 1972.
- GUDIKSEN, P.H., A.W. FAIRHALL and R.J. REED, Roles of mean meridional circulation and eddy diffusion in the transport of trace substances in the lower stratosphere, *J. Geophys. Res.*, **73**, 4461, 1968.
- HAYS, P. and J. OLIVERO, Carbon dioxide and monoxide above the troposphere, *Planet. Space Sci.*, **18**, 1792, 1970.
- HERING, W.S. and T.R. BORDEN, Jr., An analysis of the seasonal and synoptic-scale variations in the vertical ozone distribution, International Atmospheric Ozone Symposium, Albuquerque, N. Mex., 1964.
- HINES, C., Eddy diffusion coefficients due to instabilities in internal gravity waves, *J. Geophys. Res.*, **75**, 3937, 1970.
- HODGES, R., Eddy diffusion coefficients due to instabilities in internal gravity waves, *J. Geophys. Res.*, **74**, 4087, 1969.
- HUNTEN, D.M., Energetics of thermospheric eddy transport, *J. Geophys. Res.*, **79**, 2533, 1974.
- HUNTEN, D.M., Vertical transport in atmospheres, in McCormac (ed.) *Atmospheres of Earth and the Planets*, Reidel Cy, 1975.
- JESSEN, W., Ein Pchnenmodell zur Beschreibung des stratosphärischen Ozonkreislaufs, *Mitteilungen aus dem Max-Planck-Institut für Aeronomie*, **50**, Springer Verlag, 1973.
- JOHNSON, F.S. and E.M. WILKINS, Thermal upper limit on eddy diffusion in the mesosphere and lower thermosphere, *J. Geophys. Res.*, **70**, 1281, 1965.



## BRASSEUR

- JUSTUS, C.G., Dissipation and diffusion by turbulence and irregular winds near 100 km, J. Atmos. Sci., 25, 1137, 1969.
- JUSTUS, C.G., Upper atmospheric mixing by gravity waves, AIAA/AMS paper No. 73-495, 1973.
- KAO, S.K., R.J. OBRASINSKI and N.J. LORDI, Horizontal eddy diffusivities in the Northern Hemispheric stratosphere and lower mesosphere, NASA-CR-3006, 75th, 1978.
- LETTAU, H., Diffusion in the upper atmosphere, Compendium of meteorology, (T.F. Malone), American Meteorological Society, New York, 1951.
- LINDZEN, R.S., Tides and gravity waves in the upper atmosphere in Mesospheric Models and Related Experiments, 122, 1971.
- LIU, S.C. and R.J. CICERONE, Private communication to the US Academy of Sciences, 1976.
- LOUIS, J., A two-dimensional transport model of the atmosphere, Ph. D. thesis, University of Colorado, 150 pp., 1974.
- LUTHER, F.M., Monthly mean values of eddy diffusion coefficients in the lower stratosphere, AIAA paper No. 73-498, 1973.
- LUTHER, F.M., private communication.
- MACHTA, L. and R.J. LIST, Stratospheric Radioactivity Measurements, American Meteorological Society conference on Stratospheric Meteorology, Minneapolis, Minn. 1959.
- MAHLMAN, J.D., Some fundamental limitations of simplified transport models as implied by results from a three-dimensional general circulation/tracer model, Fourth Conference on CIAP, DOT-TSC-OST-75-38, 132, 1975.
- MURAKAMI, T., Stratospheric wind, temperature and isobaric height conditions during the IGY period - Part 1, Report No. 5, Contract No. AT (30-1) 2241, MIT, 1962.
- MURGATROYD, R.J., Estimation from geostrophic trajectories of horizontal diffusivity in the mid-latitude troposphere and lower stratosphere, J. of the R.M.S., 95, 40, 1969.
- MURGATROYD, R.J., Paper presented at the NATO Advanced Study Institute on atmospheric ozone, Albufeiras, Portugal, 1979.
- NASA, Reference publication 1010 : Chlorofluoromethanes and the stratosphere, R.D. Hudson, editor, 1977.
- NAS Report : Halocarbons : Effects on stratospheric ozone, National Academy of Sciences Washington D.C., 1976.
- NASTROM, G.D. and D.E. BROWN, Eddy diffusion coefficients and wind statistics, 30-60 km, Final report, Contract NAS 2-9578, Research and advanced design lab., Control Data Corporation, Minneapolis, 1978.
- NEWELL, R.E., The transport of trace substances in the atmosphere and their implications for the general circulation of the stratosphere, Geofis. Pura Appl., 49, 137, 1961.
- NEWELL, R.E., The circulation of the upper atmosphere, Scientific American, 210, 62, 1964.
- NEWELL, R.E., A Review of studies of eddy fluxes in the stratosphere and mesosphere, in Les problèmes météorologiques de la stratosphère et de la mésosphère, CNES, Presses universitaires de France, Paris, 1966.
- NEWELL, R.E., One-Dimensional Models : A critical comment and their application to carbon monoxide, J. Geophys. Res., 82, 1449, 1977.
- NICOLET, M. and W. PEETERMANS, The production of nitric oxide in the stratosphere by oxidation of nitrous oxide, Ann. Geophys., 28, 751, 1972.
- OORT, A.H., On the energy cycle in the lower stratosphere, Report No. 9, Contract AT (30-1), 2241, MIT, 1963.
- OORT, A.H. and D.M. RASSMUSSEN, Atmospheric circulation statistics, NOAA Professional Paper No. 5, 1971.
- PEIXOTO, J.P., Hemispheric temperature conditions during the year 1950, Scientific Report No. AF 19(604) - 6108, MIT, 1960.
- PENG, L., Stratospheric wind, temperature, and isobaric height conditions during the IGY period - Part II, Report No. 10, Contract AT (30-1), 2241, MIT, 1963.
- PRABHAKARA, C., Effects of Non-photochemical processes on the meridional distribution and total amount of ozone in the atmosphere, Mon. Wea. Rev., 91, 411, 1963.
- PRINN, R.G., F.N. ALEJA, D.M. CUNNOLD and A. KATZ, The distributions of odd nitrogen and odd hydrogen in the natural and perturbed stratosphere, Proceedings of the second international conference on the environmental impact of aerospace operations in the high atmosphere, American Meteorological Society, 1974.

# BRASSEUR

- PYLE, J.A., A zonal mean model of the stratosphere including feedback between chemistry, radiation and dynamics, Proceedings of the WMO symposium on the geophysical aspects and consequences of changes in the composition of the stratosphere, Toronto, 1978.
- PYLE, J.A., Paper presented at the NATO Advanced Study Institute on atmospheric ozone, Albufeiras, Portugal.
- RAO-VUPPUTURI, K., Numerical experiments on the steady state meridional structure and ozone distribution in the stratosphere, Mon. Wea. Rev., 101, 510, 1973.
- REED, R.J. and K.E. GERMAN, Contribution to the problem of stratospheric diffusion by large scale mixing, Mon. Wea. Rev., 93, 313, 1965.
- REITER, E.R., E. BAUER and S.C. CORONITI, The natural stratosphere of 1974, CIAP monograph 1, Dept. of Transportation, USA, 1975.
- ROPER, R.G. and W.G. ELFORD, Seasonal variation of turbulence in the upper atmosphere, Nature, 197, 963, 1963.
- ROPER, R.G., Atmospheric turbulence in the meteor region, J. Geophys. Res., 71, 5785, 1966.
- SEITZ, H., B. DAVIDSON, J.P. FRIEND and H.W. FEELY, Final report on project STREAK, Numerical models of transport, diffusion and fallout of stratospheric radioactive material, Report No. NYO - 3654-4, Isotopes, Inc., 1968.
- STROBEL, D., Odd nitrogen in the mesosphere, J. Geophys. Res., 76, 8384, 1971.
- WHITE, R.M., The counter-gradient flux of sensible heat in the lower stratosphere, Tellus, VI, 2, 177, 1954.
- WIDHOPF, G.F., A two-dimensional photochemical model of the stratosphere including initial results of inert-tracer studies, Proceedings of the 4th CIAP Conference, DOT-TSC-OST-75-38, 316, 1975.
- WOFSY, S. and M.B. McELROY, On vertical mixing in the upper stratosphere and mesosphere, J. Geophys. Res., 78, 2619, 1973.
- ZIMMERMAN, S.P. and K.S.W. CHAMPION, Transport processes in the upper atmosphere, J. Geophys. Res., 68, 3049, 1963.
- ZIMMERMAN, S.P., Meteor trails and atmospheric turbulence, J. Geophys. Res., 78, 3927, 1973.
- ZIMMERMAN, S.P. and C.A. TROWBRIDGE, The measurement of turbulent spectra and diffusion coefficients in the altitude region 95 to 110 km, Space Res. XIII, 203, 1973.
- ZIMMERMAN, S.P., The effective vertical turbulent viscosity as measured from radio meteor trails, J. Geophys. Res., 79, 1095, 1974.

# TRANSPORT PROCESSES

J. A. Pyle and C. F. Rogers

Department of Atmospheric Physics,  
Clarendon Laboratory, Oxford.

## Abstract

The current treatment of eddy transports in two-dimensional models is reviewed. Recent advances, including Lagrangian approaches, are discussed. A method of calculating K fields within a two-dimensional framework is presented.

INTRODUCTION: There has been considerable interest in recent years in the possible modification of the ozone layer due to man's activities. Numerical models of the atmosphere have been one of the major research tools to investigate the effect of high flying supersonic aircraft, of fertilizers, and of certain fluorocarbons on stratospheric ozone. While the aim should be to build models in which all the major processes, meteorological, radiative and photochemical, are treated in detail, limitations of computer resources have generally lead to attempts to simplify the problems. In particular what is in reality a three-dimensional problem has generally been reduced to either one (height only) or two (height and latitude) dimensions. The variation with longitude of the elements of interest is ignored.

In this short paper the treatment of transport processes in two-dimensional models is discussed. The problems of current models will be mentioned. Finally, some new approaches to the treatment of eddy transport, in particular, are discussed.

TWO-DIMENSIONAL MODELS. If we consider a co-ordinate system with  $x$ ,  $y$  and  $p$ , the eastward and northward co-ordinates and pressure respectively with velocity components  $u$ ,  $v$  and  $\omega$ , then the zonal mean continuity equation for some species of mixing ratio,  $R$ , may be written

$$\frac{\partial \bar{R}}{\partial t} + \bar{v} \frac{\partial \bar{R}}{\partial \phi} + \bar{\omega} \frac{\partial \bar{R}}{\partial p} = \bar{S} - \frac{1}{a \cos \phi} \frac{\partial}{\partial \phi} \overline{v' R'} - \frac{\partial}{\partial p} \overline{\omega' R'} \quad (1)$$

where  $(\bar{\phantom{x}})$  represents the zonal mean of a quantity (i.e.  $\bar{R} = \frac{1}{2\pi} \int_0^{2\pi} R d\lambda$ ,  $\lambda$  = longitude) and  $(\phantom{x})'$  represents a departure from the zonal mean (i.e.  $R' = R - \bar{R}$ ).  $a$  is the radius of the earth and  $\phi$  the latitude.  $S$  represents the sum of all sources and sinks. Notice that  $S$  can contain products of the perturbation quantities (see Tuck 1979) which can be significant, although they are generally ignored.

The main problem in two-dimensional modelling is the treatment of the final two terms on the right hand side of equation (1). These terms represent the eddy transport of  $R$ , the transport by a variety of atmospheric waves. The mean fluxes on the left hand side can be treated easily either using a climatological mean meridional circulation or by calculating the zonal mean circulation in the model (see Vupputuri, 1973; Harwood and Pyle, 1975). It is with the eddy transport that this paper will deal.

Reed and German (1965) applied a mixing length approach to the problem of the eddy transport of a quasi-conservative tracer. The horizontal and vertical fluxes of  $R$  are written in terms of mean gradients:

$$\begin{aligned} \overline{v'R'} &= -K_{yy} \frac{\partial \bar{R}}{\partial y} - K_{yp} \frac{\partial \bar{R}}{\partial p} \\ \overline{\omega'R'} &= -K_{py} \frac{\partial \bar{R}}{\partial y} - K_{pp} \frac{\partial \bar{R}}{\partial p} \end{aligned} \quad (2)$$

Thus if the  $K$ -coefficients are known equation (1) is easily solved. The  $K$ s are generally obtained from observations of the flux of some long-lived atmospheric traces, usually potential temperature, and this set of  $K$ s is then used for all transported species. Reed and German, for instance, showed that the  $K$ s calculated from heat flux data could be used to model the spread of stratospheric radioactive tracer quite satisfactorily.

Clearly to calculate  $K$ s, using equation 2, from just one set of flux data requires a number of approximations to be made. In particular Reed and German made the two approximations

$$\begin{aligned} K_{yp} &= K_{py} \\ K_{yp} &= \frac{\overline{\omega'R'}}{\overline{v'R'}} \cdot K_{yy} \end{aligned} \quad (3)$$

given some credence by an appeal to mixing length arguments.

While two-dimensional  $K$ -theory has been used with some success, a number of limitations have long been evident. Mahlman (1975), for instance, showed from three-dimensional model calculations that the nett flux of a tracer is not always down the nett zonal mean gradient, as implied by equation (2). In other words, the representation of the fluxes given in equation (2) sometimes fails.

A second problem is that specifying fixed  $K$  coefficients does not allow for an interactive calculation. It is well known that the propagation of planetary waves depends on the zonal mean wind structure (see e.g. Schoeberl and Geller 1976) and hence it is expected that the  $K$ s should vary with the wind structure. Thus there is a potentially important feedback loop which links

changes in ozone and consequent changes in the absorption of solar radiation with changes in the mean temperature and wind structure of the stratosphere and, therefore, with changes in the eddy transport of ozone (and other trace gases). This feedback has, however, not yet been included in any two-dimensional models. Indeed, unless the  $K$  coefficients can be computed from the model state, this will not be possible.

Finally, two related questions can be asked. Firstly, to what extent can the same set of  $K$  coefficients be used for all species? Secondly, remembering that Reed and German's approach treats a quasi-conservative tracer, to what extent might the  $K$ s vary for those species with significant photochemical sources and sinks?

In the next two sections some of these objections and questions relating to  $K$  theory will be considered.

**LAGRANGIAN MEAN IDEAS.** The previous section considered atmospheric motions within a Eulerian framework with the averaging performed round latitude circles at fixed heights and latitudes. Recent work, particularly that of Andrews and McIntyre (1978) on the wave-mean flow interaction, has made use of generalized Lagrangian means in which the averaging,  $(\bar{\quad})^L$ , is performed over thin material tubes, or groups of particles. The continuity equation for some conservative species  $R$  then becomes

$$\left( \frac{\partial}{\partial t} + \bar{v}^L \frac{\partial}{\partial y} + \bar{\omega}^L \frac{\partial}{\partial p} \right) \bar{R}^L = 0 \quad (4)$$

Thus in a Lagrangian framework the problem of the treatment of eddy transports does not arise: no eddy terms appear in equation (4). Another problem in Eulerian models is the non-cancellation of the eddy and mean transport terms (Hunt and Menage 1968, Harwood and Pyle 1977) and the subsequent calculation of the small residual. This problem, too, is circumvented.

The difficulty in this particular approach comes in the calculation of the Lagrangian mean circulation. A first attempt has been made by Dunkerton (1979) who identified the circulation with that driven by the Eulerian diabatic heating. Thus the circulation responsible for the transport of the centre of mass of a group of particles is similar to that calculated by Murgatroyd and Singleton (1961) and has a single cell structure like the Brewer-Dobson circulation, originally proposed to explain the stratospheric behaviour of ozone and water vapour.

Dunkerton's work provides an important insight into stratospheric transport processes but contains a number of approximations which need to be improved before Lagrangian models can be developed. For instance, the Eulerian rather than the Lagrangian mean heating rates were used. Similarly, in a photochemical model the Lagrangian mean sources and sinks would be required. McIntyre (1980) has spelt out in detail some of the practical problems which need to be overcome before the further development of Lagrangian models. It seems possible, then, that the most immediate use of Lagrangian ideas will be in diagnostic studies of stratospheric transport, where they have already proved to be a very powerful tool.

SOME NEW THOUGHTS ON K-THEORY. The interest shown in problems of stratospheric composition during recent years has prompted a re-examination of the K-theory approach to the treatment of eddy transport and improvements have been suggested by the work of Clark and Rogers (1978), Matsuno (1980), Plumb (1979) and Pyle and Rogers (1980). This new work offers the possibility of a K-theory approach on a firmer physical basis than that used hitherto.

Pyle and Rogers (1980) have combined Matsuno's (1970) calculation of the vertical propagation of stationary planetary waves, which allows determinations of the eddy velocities  $v' \cos \phi$  and  $w'$ , with solutions of the perturbation form of the species continuity equation, which provides  $R'$ . Thus the eddy correlations  $\overline{v'R'}$  and  $\overline{w'R'}$  can be found and the K-theory approach examined.

The perturbation continuity equation for any species can be found simply by subtracting equation (1) from the full continuity equation, and applying scaling arguments appropriate to planetary scale waves:

$$\left( \frac{\partial}{\partial t} + \bar{u} \frac{\partial}{\partial x} \right) R' - S' = -v' \frac{\partial \bar{R}}{\partial y} - w' \frac{\partial \bar{R}}{\partial z} \quad (5)$$

in an x, y, z co-ordinate system, where  $S'$  is the perturbation source/sink term. For the particular case of a photochemical scheme coupling  $O_3$  and  $NO_x$  then equation (5) becomes

$$\left( \frac{\partial}{\partial t} + \bar{u} \frac{\partial}{\partial x} \right) [O_3]' - A_{11}[O_3]' - A_{12}[NO_x]' = -v' \frac{\partial [\bar{O}_3]}{\partial y} - w' \frac{\partial [\bar{O}_3]}{\partial z} \quad (6)$$

$$\left( \frac{\partial}{\partial t} + \bar{u} \frac{\partial}{\partial x} \right) [NO_x]' - A_{21}[O_3]' - A_{22}[NO_x]' = -v' \frac{\partial [\bar{NO}_x]}{\partial y} - w' \frac{\partial [\bar{NO}_x]}{\partial z}$$

where  $[ ]$  represents concentration and the  $A$ s are products of reaction rate coefficients and zonal mean concentrations (see Pyle and Rogers (1980) for details). The off-diagonal elements of the matrix  $A$  couple  $O_3$  and  $NO_x$ . The solution of equation 6 for  $[O_3]'$  (and hence  $v'O_3'$ ) depends not just on the meteorological fields and the ozone concentration but also on  $[NO_x]'$ .

The zonal dependence of equation 5 can be removed by Fourier analysis. Thus

$$R'_i = R_e \sum r_i^m e^{im\lambda}$$

for a chemical scheme comprising  $i$  components. If the Fourier components of  $v'$  and  $w'$  are written as  $q^m$  and  $p^m$ , respectively, then equation 5 becomes:

$$\left( \frac{\partial}{\partial t} + i\bar{\omega} m \right) r_i^m + \sum_j A_{ij} r_j^m = -q^m \frac{\partial \bar{R}_i}{\partial y} - p^m \frac{\partial \bar{R}_i}{\partial z} \quad (7)$$

where  $\bar{\omega} = \bar{u}/a \cos \phi$ .

The stationary case solution of equation 7 is

$$\underline{f}^m = (\underline{Q}^m)^{-1} \left( -q^m \frac{\partial \bar{R}}{\partial y} - p^m \frac{\partial \bar{R}}{\partial z} \right) \quad (8)$$

for  $\det \underline{Q}^m \neq 0$

and the complex matrix  $\underline{Q}_{ij}^m = A_{ij} + \delta_{ij} i\omega m$

Thus the constituent vector eddy fluxes can be written

$$\begin{aligned} \overline{R'v'} &= -\frac{1}{2} \sum_m |q^m|^2 \operatorname{Re} \{ (\underline{Q}^m)^{-1} \} \frac{\partial \bar{R}}{\partial y} \\ &\quad - \frac{1}{2} \sum_m \operatorname{Re} \{ p^m q^{m*} (\underline{Q}^m)^{-1} \} \frac{\partial \bar{R}}{\partial z} \end{aligned} \quad (9)$$

and

$$\begin{aligned} \overline{R'w'} &= -\frac{1}{2} \sum_m |p^m|^2 \operatorname{Re} \{ (\underline{Q}^m)^{-1} \} \frac{\partial \bar{R}}{\partial z} \\ &\quad - \frac{1}{2} \sum_m \operatorname{Re} \{ p^{m*} q^m (\underline{Q}^m)^{-1} \} \frac{\partial \bar{R}}{\partial y} \end{aligned}$$

We see immediately that the form of equations (9) and (2) are similar and that we may define  $K$ s for the case of a stationary planetary wave. (See Plumb (1979) for a consideration of the role of transience.) Notice, however, that as a consequence of the coupling between the chemical species in equation 6 the  $K$ s are now matrices. The northward flux of  $O_3$  would, for example, be written

$$\overline{O_3'v'} = -K_{yy}^{(O_3)} \frac{\partial \bar{O}_3}{\partial y} - K_{yz}^{(O_3)} \frac{\partial \bar{O}_3}{\partial z} - K_{yy}^{(O_3)} \frac{\partial \bar{NO}_x}{\partial y} - K_{yz}^{(O_3)} \frac{\partial \bar{NO}_x}{\partial z} \quad (10)$$

The importance of this coupling is discussed in Pyle and Rogers (1980). Here we will concentrate on an uncoupled photochemical scheme. Then the  $K$ s take the following form:

$$\begin{aligned} K_{yy}^{(i)} &= \frac{1}{2} \sum_m |q^m|^2 \frac{A_{ii}}{(\omega^2 m^2 + A_{ii}^2)} \\ K_{yz}^{(i)} &= \frac{1}{2} \sum_m |p^m|^2 \frac{A_{ii}}{(\omega^2 m^2 + A_{ii}^2)} \\ K_{yz}^{(i)} &= \frac{1}{2} \sum_m \operatorname{Re} \{ q^{m*} p^m \frac{(A_{ii} - i\omega m)}{(\omega^2 m^2 + A_{ii}^2)} \} \end{aligned} \quad (11)$$

$$K_{zy} = \frac{1}{2} \sum_n \operatorname{Re} \left\{ p^{-n} q^n \frac{(A_{ii} - i n \bar{\omega})}{(\bar{\omega}^2 + A_{ii}^2)} \right\}$$

It is immediately obvious from equation (11) that different species will have different  $K$ s owing to their different chemistry (and, hence, different photochemical lifetimes,  $A_{ii}^{-1}$ ). The use of one set of  $K$ s for all species, commonly employed in one- and two-dimensional models, is not necessarily valid.

For an inert tracer  $A_{ii}$  is zero and the following interesting results follow:

$$K_{zy} = K_{zz} = 0$$

(12)

$$\text{and } K_{yz} = -K_{zy}$$

The latter expression is in disagreement with the assumptions of Reed and German (1965) who took  $K_{yz} = K_{zy}$ . The consequence of equation (12) is that the horizontal eddy transport of an inert tracer is proportional to its vertical gradient, and vice versa, a result already obtained by Clark and Rogers (1978), Holton (1980), Matsuno (1980) and Plumb (1979). When photochemistry dominates, however,  $A_{ii} \gg n \bar{\omega}$  and then  $K_{yz} = K_{zy}$ . The intermediate region between photochemical and dynamical control is also of interest (Hartmann and Garcia (1978)). It is here, for instance, that the fluxes of ozone tend to be largest.

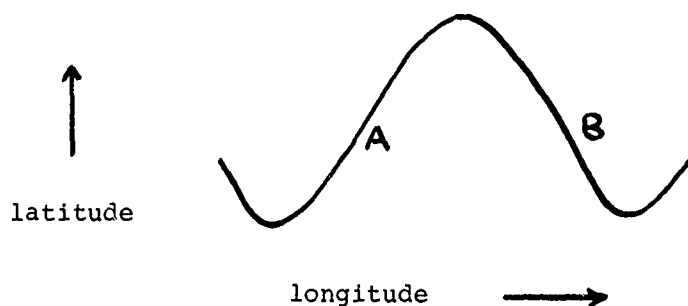


Figure 1: A schematic diagram of a north-south meander in a planetary scale wave.

It is instructive to consider these results in the light of figure 1. Figure 1 shows a schematic view of a north-south meander in a planetary scale wave.  $n \bar{\omega}$  is some measure of the speed with which a tracer element will move in the zonal direction. For a steady, non-dissipating wave, meridional transport can be accomplished if, for example, there are eddy sources and sinks of the tracer at A and B respectively. In this case the poleward flow is correlated with eddy production and the equatorward flow with eddy destruction, producing enhanced transport northwards and reduced transport to the south. Thus a net poleward flux which depends on the chemistry of the



tracer is induced. (Since the flux depends on the chemistry it is reasonable that the Ks should vary from species to species.) It should be remembered that this argument applies to eddy sources and sinks and that in the zonal mean the particular latitude will be either a net source or sink.

Clearly, the distribution of the eddy sources and sinks of ozone depends in part on the distribution of the nitrogen oxides. Thus, the ozone transport will also depend to some extent on the  $\text{NO}_x$  distribution. Furthermore, the distribution of  $\text{NO}_x$  is dependent on the ozone distribution since its production depends on the reaction of  $\text{N}_2\text{O}$  with  $\text{O}(\text{'D})$ . Clearly the fluxes of  $\text{O}_3$  and  $\text{NO}_x$  are coupled, with the flux equation of the form of equations 9 and 10.

These recent developments in the investigation of K-theory have removed some of the problems inherent in Reed and German's approach. It is desirable that these improvements should be incorporated into two-dimensional models of the stratosphere. Furthermore, the fact that the two-dimensional Ks vary from species to species should prompt a re-examination of the K-theory approach currently employed by one-dimensional modellers.

#### REFERENCES

- Andrew, D.G., M.E. McIntyre. An exact theory of nonlinear waves on a Lagrangian mean flow, J.Fluid Mech., **89**, 609, 1978.
- Clark, J.H.E., T.G. Rogers, The transport of conservative trace gases by planetary waves, J.Atmos.Sci., **35**, 2232, 1978.
- Dunkerton, T., On the mean meridional mass motions of the stratosphere and mesosphere, J.Atmos. Sci., **35**, 2325, 1978.
- Hartmann, D.L., R.R. Garcia, A mechanistic model of ozone transport by planetary waves in the stratosphere, J.Atmos.Sci., **36**, 350, 1978.
- Harwood, R.S., J.A. Pyle, Studies of the ozone budget using a zonal mean circulation model and linearized photochemistry. Quart.J.R.Met.Soc., **103**, 319, 1977.
- Holton, J.R., Wave propagation and transport in the middle atmosphere, Phil.Trans.R.Soc.Lond. (Middle Atmosphere Issue), in press, 1980.
- Hunt, B.G., S. Manabe, Experiments with a stratospheric general circulation model. II. Large-scale diffusion of tracers in the stratosphere, Mon.Wea.Rev., **96**, 503, 1968.
- Mahlman, J.D., Some fundamental limitations of simplified transport models as implied by results from a three-dimensional general-circulation/tracer model, Proceedings of the Fourth CIAP conference, 132, 1975.
- Matsuno, T., Vertical propagation of stationary planetary waves in the winter northern hemisphere, J.Atmos.Sci., **24**, 871, 1970.
- Matsuno, T., Lagrangian motion of air particles in the stratosphere in the presence of planetary waves, Pure and Applied Geophys., in press, 1980.
- McIntyre, M.E., Towards a Lagrangian-mean description of stratospheric circulations and chemical transports, Phil.Trans.R.Soc.Lond. (Middle Atmosphere Issue) in press, 1980.
- Murgatroyd, R.J., F. Singleton, Possible meridional circulations in the stratosphere and mesosphere, Quart.J.R.Met.Soc., **87**, 125, 1961.
- Plumb, R.A., Eddy fluxes of conserved quantities by small-amplitude waves, J.Atmos.Sci., **36**, 1699, 1979.
- Pyle, J.A., C.F. Rogers, Stratospheric transport by stationary planetary waves - the importance of chemical processes, Quart.J.R.Met.Soc., in press, 1980.
- Reed, R.J., K.E. German, A contribution to the problem of stratospheric diffusion by large-scale mixing, Mon.Wea.Rev., **93**, 313, 1965.
- Schoeberl, M.R., M.A. Geller, The structure of stationary planetary waves in winter in relation to the polar night jet intensity, Geophys.Res.Letts., **3**, 177, 1976.
- Tuck, A.F., A comparison of one-, two- and three-dimensional model representations of stratospheric gases, Phil.Trans.R.Soc.Lond., **A290**, 477, 1979.

## THE CHEMICAL EQUATIONS OF STRATOSPHERIC AND MESOSPHERIC OZONE

Marcel Nicolet

External Geophysics, Brussels University, 1180 Brussels, Belgium

### ABSTRACT

An analysis is made of the various parameters which may play a role in the atmospheric chemistry of ozone by using the chemical equations in their general form. After considering the production and destruction of ozone and atomic oxygen with their transports in an oxygen atmosphere, a general equation is written where all production and destruction terms due to the action of hydrogen, nitrogen and halogen compounds are included.

In the mesosphere, where the atomic oxygen concentration,  $n(O)$ , is greater than the ozone concentration,  $n(O_3)$ , the transport conditions of water vapor, molecular hydrogen, and also atomic hydrogen at the upper boundary must be introduced in the governing equation of the atomic oxygen concentration. Photochemical equilibrium can be adopted in the lower mesosphere.

In the stratosphere, where  $n(O_3)$  is always greater than  $n(O)$ , the chemical and photochemical equilibrium conditions are introduced particularly for the determination of the concentration ratios of  $OH$  and  $HO_2$ ,  $NO$  and  $NO_2$ ,  $Cl$  and  $ClO$ ,  $Br$  and  $BrO$ . After introducing these various ratios, the governing equation of ozone becomes a continuity equation which includes the transport terms of  $H_2O$ ,  $CO$ ,  $HNO_3$ , . . . The transport of water vapor is always included in the  $O$  and  $O_3$  general equation, while the transports terms of nitric acid and carbon monoxide cannot be neglected without due consideration of the lower stratosphere conditions. Furthermore, the effects of the transport terms of  $HNO_3$ ,  $HCl$  and  $HBr$  on the ratio of the  $OH$  and  $HO_2$  concentrations and their absolute values may be neglected only after due consideration of their numerical values in the lower stratosphere. Interchange reactions such as  $NO + HO_2$  or  $NO + CH_3O_2$  or disturbing terms corresponding to reactions such as  $ClO + OH$  or  $ClO + HO_2$  must be taken into consideration in the study of the cooperative action of chemical processes and atmospheric motions in the lower stratosphere. But to determine a reliable ozone distribution, the sources must be known with sufficient accuracy.

**INTRODUCTION:** The ozone chemistry in the stratosphere and mesosphere is complex because of interactions that occur between the various trace gas constituents. Even in the region where ozone is controlled only by photochemical processes, an overly simplified analysis may lead to deficiencies in the understanding of the ozone behavior. However, since important aspects may be neglected in a quantitative mathematical analysis, it is essential to know not only the most important parameters but also the basis of the chemistry of the atmosphere. Specifically, it is necessary to write the general equations and then to introduce adequate simplifications related to experimental or observational results or mathematical treatments. In this paper an attempt is made to present the chemical equations based on general considerations that may lead to different perceptions of various aspects of the ozone problem.

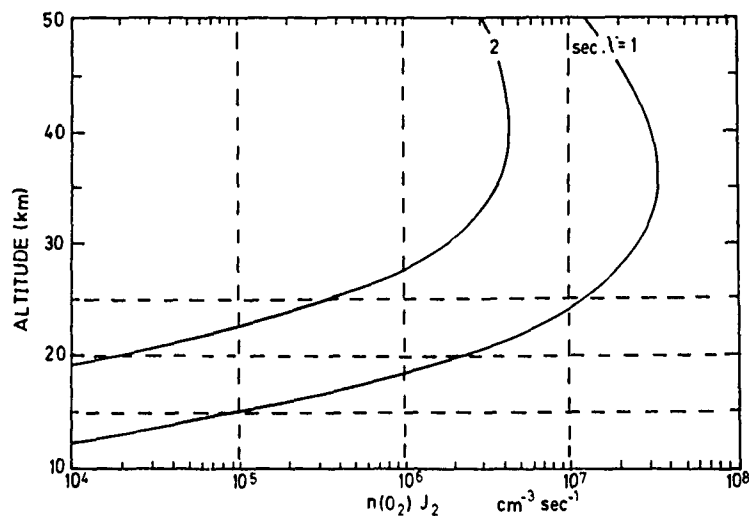


Fig. 1. - Photodissociation of  $O_2$  ( $cm^3 sec^{-1}$ ) for overhead sun conditions ( $sec \chi = 1$ ) and for a  $60^\circ$  zenith angle,  $sec \chi = 2$ . Standard conditions.

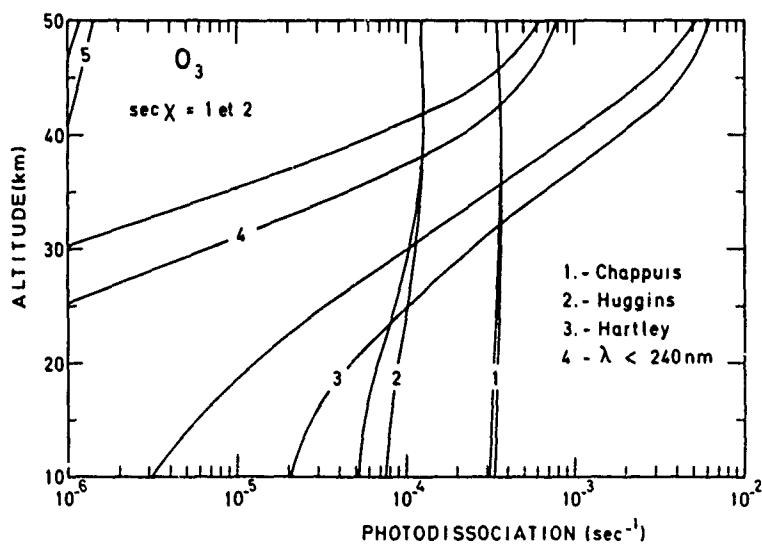


Fig. 2a. - Stratospheric photodissociation of  $O_3$  ( $sec^{-1}$ ) in its various spectral absorption bands for standard conditions without any albedo or scattering effects.

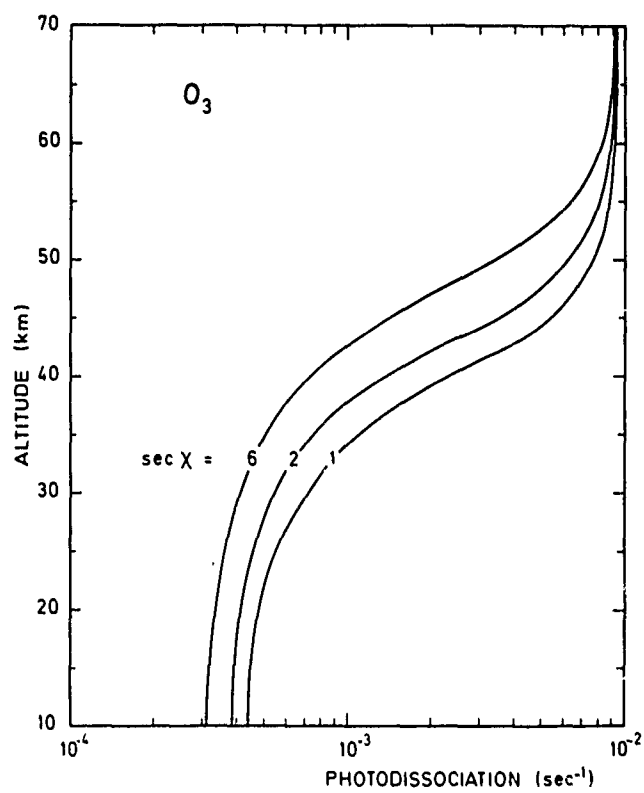


Fig. 2b. — Photodissociation rates of  $O_3$  for various solar zenith angles in the stratosphere and mesosphere. No albedo or scattering effects.

**THE PURE OXYGEN ATMOSPHERE:** In order to introduce the atmospheric problem in its specific aspects, it is useful to begin the study with the photodissociation of molecular oxygen, and its subsequent reactions, in an oxygen atmosphere without any active chemical action on the part of other constituents.

The radiation of wavelengths less than 242 nm absorbed by molecular oxygen leads to its photodissociation

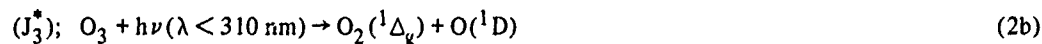


The principal photodissociation process in the Schumann-Runge continuum ( $\lambda < 175 \text{ nm}$ ) occurs in the thermosphere and plays no role in mesospheric and stratospheric chemistry. In fact, three spectral ranges must be considered for the  $\text{O}_2$  absorption; namely, Lyman- $\alpha$  at 1216 nm, only in the mesosphere, the Schumann-Runge band system ( $\lambda < 200 \text{ nm}$ ) in the mesosphere and partly in the stratosphere where the Hertzberg continuum between 242 – 200 nm plays a role which is controlled by the ozone absorption in its Hartley band. The peak of the  $\text{O}_2$  photodissociation occurs in the stratosphere (near 35 km for an overhead sun) where the total number of  $\text{O}_2$  molecules photodissociated is of the order of  $10^7 \text{ cm}^{-3} \text{ sec}^{-1}$  (Figure 1). Below the ozone peak ( $< 25 \text{ km}$ ) the photodissociation rate decreases rapidly; particularly when the solar zenith angle increases. At 20 km, there is a difference of a factor of 100 (Figure 1) between 0 and  $60^\circ$ .

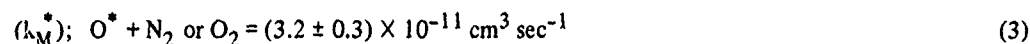
The ozone photodissociation occurs due to its absorption of solar radiation in the visible and the ultraviolet.



But at  $\lambda < 310 \text{ nm}$ , the  $\text{O}_3$  photodissociation leads to



where the excited oxygen atom  $\text{O}(^1\text{D}) \equiv \text{O}^*$  can react with atmospheric constituents even if the quenching effect of  $\text{O}_2$  and  $\text{N}_2$  is important,



In addition to the important Hartley band absorption,  $\text{O}_3$  also absorbs at  $\lambda > 310 \text{ nm}$  (Huggins bands) and in the visible (Chappuis bands).

Thus, the  $\text{O}_3$  photodissociation corresponds to the total photodissociation coefficients  $J_3$  of the order of  $10^{-2} \text{ sec}^{-1}$  in the mesosphere and to  $3 \cdot 10^{-4} \text{ sec}^{-1}$  in the stratosphere (Figure 2).

The recombination of atomic oxygen in the presence of a third body ( $\text{N}_2, \text{O}_2$ )



cannot be neglected in the mesosphere above 70 km, but plays no practical role in the study of stratospheric processes. The reaction which does play a role at all altitudes is the association of oxygen atoms with oxygen molecules



which leads to the formation of ozone.

Finally, ozone molecules and oxygen atoms react together



and lead to the re-formation of oxygen molecules and the final destruction of ozone.

Thus, the equations governing the rate of change of the concentrations of ozone,  $n(O_3)$ , and of atomic oxygen,  $n(O)$ , are

$$\begin{aligned} \frac{\partial n(O)}{\partial t} + \text{div} [n(O)w(O)] + 2k_1 n(M)n^2(O) \\ + k_2 n(M)n(O_2)n(O) + k_3 n(O_3)n(O) = 2n(O_2)J_2 + n(O_3)J_3 \end{aligned} \quad (7)$$

and

$$\frac{\partial n(O_3)}{\partial t} + \text{div} [n(O_3)w(O_3)] + n(O_3)J_3 + k_3 n(O)n(O_3) = k_2 n(M)n(O_2)n(O) \quad (8)$$

where  $\text{div} [nw]$  is the transport term which must be introduced when atmospheric exchanges are more significant than chemical processes.

It is known that, above a certain altitude in the mesosphere  $n(O) > n(O_3)$ , and also that  $O_3$  is in photochemical equilibrium in the solar radiation field. The equations (7) and (8) lead, therefore, to

$$\frac{\partial n(O)}{\partial t} + \text{div} [n(O)w(O)] + 2k_1 n(M)n^2(O) + 2k_3 n(O_3)n(O) = 2n(O_2)J_2 \quad (9)$$

with the equilibrium value of  $n(O_3) \equiv n_*(O_3)$

$$n_*(O_3)/n(O) = k_2 n(M)n(O_2)/J_3 + k_3 n(O) \quad (10)$$

It is also known that, in the middle mesosphere ( $\leq 70$  km), there is a region where photochemical equilibrium conditions can be introduced, and (9) becomes

$$k_{1M} n^2(O) + k_3 n(O_3)n(O) = n(O_2)J_2 \quad (11)$$

which leads to

$$n_*^2(O) = n(O_2)J_2 / k_{1M} \left[ \frac{1 + k_2 k_3 n(O_2)}{k_1 J_3} \right] \quad (12)$$

with

$$n_*(O_3)/n_*(O) = k_2 n(M)n(O_2)/J_3 \quad (13)$$

if  $J_3 > k_3 n(O)$ .

In the stratosphere,  $n(O) n(O_3)$  and atomic oxygen is always in photoequilibrium in the solar radiation field. Instead of (9), the general equation becomes

$$\frac{\partial n(O_3)}{\partial t} + \text{div} [n(O_3)w(O_3)] + 2k_3 n(O)n(O_3) = 2n(O_2)J_2 \quad (14)$$

Since

$$n_*(O) = \frac{n(O_3)J_3 + 2n(O_2)J_2}{k_2 n(M)n(O_2) + k_3 n(O_3)} \quad (15)$$

the rate of change of  $n(O_3)$  in a pure oxygen atmosphere becomes

$$\begin{aligned} \frac{\partial n(O_3)}{\partial t} + \text{div} [n(O_3)w(O_3)] + 2n^2(O_3) \frac{J_3 k_3}{k_2 n(M)n(O_2) + k_3 n(O_3)} \\ = 2n(O_2)J_2 \frac{k_2 n(M)n(O_2) - k_3 n(O_3)}{k_2 n(M)n(O_2) + k_3 n(O_3)} \end{aligned} \quad (16)$$

It can be shown that, under atmospheric conditions,

$$k_3 n(O_3) < k_2 n(M)n(O_3) \quad (17)$$

and is always correct in the stratosphere since the limiting value  $n_1(O_3)$ , which depends on the number of oxygen atoms which are available

$$n_1(O_3) = k_2 n(M)n(O_2)/k_3, \quad (18)$$

can never be reached. The practical equation is, therefore, with (16) and (17),

$$\frac{\partial n(O_3)}{\partial t} + \text{div} [n(O_3)w(O_3)] + 2 n^2(O_3) \frac{k_3 J_3}{k_2 n(M)n(O_2)} = 2n(O_2)J_2 \quad (19)$$

which is the conventional form of the ozone equation used in a pure oxygen stratosphere.

At the stratopause level and its neighborhood ( $\pm 10$  km) photochemical equilibrium conditions apply, and the ozone concentration  $n_*(O_3)$  is

$$n_*(O_3) = \frac{n(O_2)J_2}{n(O_3)J_3 + n(O_2)J_2} n(M)n(O_2) \frac{k_2}{k_3} \quad (20)$$

$$\text{with } n_*(O) = \frac{n(O_3)J_3 + n(O_2)J_2}{k_2 n(M)n(O_2)} \quad (21)$$

which becomes, with the application of the following atmospheric condition,

$$n(O_3)J_3 > n(O_2)J_2 \quad (22)$$

$$n_*^2(O_3) = \frac{J_2}{J_3} n(M)n^2(O_2) \frac{k_2}{k_3} \quad (23)$$

and

$$n_*(O) = \frac{n(O_3)J_3}{k_2 n(M)n(O_2)} \quad (24)$$

These two equations are the conventional equations of ozone and atomic oxygen in an oxygen atmosphere where other constituents play no chemical role.

**THE GENERAL EQUATION:** In order to write a general equation, we must introduce, simultaneously all processes involving hydrogen, nitrogen and halogen trace constituents; namely H, OH, HO<sub>2</sub>, H<sub>2</sub>O<sub>2</sub>, H<sub>2</sub>, H<sub>2</sub>O, CH<sub>4</sub> and CO<sub>2</sub>, N, NO, NO<sub>2</sub>, NO<sub>3</sub>, and N<sub>2</sub>O, Cl, ClO, HCl, ClONO<sub>2</sub>, and HOCl, Br, BrO, HBr, BrONO<sub>2</sub> and BrOCl, . . . which can produce or destroy O<sub>3</sub> and O. We use the following symbols for the reaction coefficients: k for O and O<sub>3</sub>, J for photodissociation, a for hydrogen, b for nitrogen, c for carbon, d for chlorine, e for bromine (and f for fluorine which will not be introduced here). The corresponding reactions are shown in Tables I to VII in the appendix. The numerical values are obtained from DeMore et al. "Chemical Kinetic and Photochemical Data for use in Stratospheric Modeling" JPL Publication 79-27, 1979 and from data given at the NATO Ozone Institute, October 1979.

Atomic oxygen and ozone concentrations are, therefore, governed by

$$\begin{aligned} \frac{\partial n(O)}{\partial t} + \frac{\partial n(O_3)}{\partial t} + \text{div} [n(O)w(O)] + \text{div} [n(O_3)w(O_3)] \\ + 2k_{1M}n^2(O) + 2k_3n(O)n(O_3) + n(O_3) [a_2n(H) + a_6n(OH) + a_{6c}n(HO_2) \\ + b_8n(N) + b_4n(NO) + b_9n(NO_2) + d_2n(Cl) + e_2n(Br)] \\ + n(O) [a_5n(OH) + a_7n(HO_2) + a_{24}n(H_2) + c_9n(H_2CO) \\ + b_1n(N) + b_2n(NO) + \{b_3 + b_{10M}\}n(NO_2) \\ + d_3n(ClO) + d_{12}n(HCl) + e_3n(BrO) + e_{12}n(HBr)] \\ + n(O^*) [a_{H_2O}^*n(H_2O) + a_{H_2}^*n(H_2) + \{c_{1a}^* + c_{1b}^*\}n(CH_4) + b_{N_2O}^*n(N_2O)] \\ = 2n(O_2)J_2 + n(H_2O)J_{H_2O} + n(HO_2)J_{HO_2} + a_{16}n^2(OH) \\ + n(H) [a_{20}n(HO_2) + a_{22}n(OH)] + n(CO_2)J_{CO_2} \end{aligned}$$



$$\begin{aligned}
 & + n(\text{NO})J_{\text{NO}} + n(\text{NO}_2)J_{\text{NO}_2} + n(\text{NO}_3)J_{\text{NO}_2-\text{O}} + n(\text{N}) [b_5 n(\text{NO}_2) + b_6 n(\text{NO}) + b_7 n(\text{NO}_2)] \\
 & + n(\text{ClO}) [J_{\text{ClO}} + c_{15b} n(\text{HO}_2)] + n(\text{ClONO}_2)J_{\text{ClONO}-\text{O}} + n(\text{HOCl})J_{\text{HCl}-\text{O}} \\
 & + n(\text{BrO})J_{\text{BrO}} + n(\text{BrONO}_2)J_{\text{BrONO}-\text{O}} + n(\text{HOBr})J_{\text{HBr}-\text{O}}
 \end{aligned} \tag{25}$$

In this equation several terms are negligible, particularly, as an example, those involving atomic nitrogen which does not exist, as a practical matter, in the stratosphere and mesosphere under normal conditions. Photoequilibrium conditions have been immediately adopted for the excited oxygen atom,  $\text{O}(^1\text{D}) \equiv \text{O}^*$ .

In order to simplify the study of this general equation, analyses must be first restricted to the mesosphere, or to the stratosphere, in consideration of possible application of photochemical equilibrium conditions. In the mesosphere, only the reactions involving hydrogen constituents need be dealt with, and all additional terms to  $2n(\text{O}_2)J_2$  can be neglected. Thus, the general mesospheric equation for atomic oxygen becomes

$$\begin{aligned}
 & \frac{\partial n(\text{O})}{\partial t} + \text{div} [n(\text{O})w(\text{O})] + 2k_{1M}n^2(\text{O}) \\
 & + n(\text{O}_3) [2k_3 n(\text{O}) + a_2 n(\text{H}) + a_6 n(\text{OH}) + a_{6c} n(\text{HO}_2)] \\
 & + n(\text{O}) [a_5 n(\text{OH}) + a_7 n(\text{HO}_2) + a_{24} n(\text{H}_2)] \\
 & + n(\text{O}^*) \left[ a_{\text{H}_2\text{O}}^* n(\text{H}_2\text{O}) + a_{\text{H}_2}^* n(\text{H}_2) + \{c_{1a}^* + c_{1b}^*\} n(\text{CH}_4) \right] \\
 & = 2n(\text{O}_2)J_2 + n(\text{H}_2\text{O})J_{\text{H}_2-\text{O}} + n(\text{HO}_2)J_{\text{HO}_2} + a_{16}n^2(\text{OH}) \\
 & + n(\text{H}) [a_{20}n(\text{HO}_2) + a_{22}n(\text{OH})] + n(\text{CO}_2)J_{\text{CO}_2}
 \end{aligned} \tag{26}$$

Several terms may be neglected later, but they must, initially, be kept before combining this equation with other equations governing  $\text{H}_2\text{O}$ ,  $\text{H}_2$ ,  $\text{H}$ ,  $\text{OH}$  and  $\text{HO}_2$ .

In the lower mesosphere, an immediate simplification corresponds to the neglect of the term  $\partial n(\text{O})/\partial t + \text{div} [n(\text{O})w(\text{O})] + 2k_{1M}n^2(\text{O})$ . The other terms, except those corresponding to very low reactions, must be retained in order to determine the final equation in its exact form.

**THE HYDROGEN CONSTITUENTS:** The principal hydrogen constituent is the water vapor whose the relative concentration (volume mixing ratio) is between  $10^{-6}$  and  $10^{-5}$  in the stratosphere (see Figure 3) and mesosphere. Its general equation is written as follows:

$$\begin{aligned}
 & \frac{\partial n(\text{H}_2\text{O})}{\partial t} + \text{div} [n(\text{H}_2\text{O})w(\text{H}_2\text{O})] + n(\text{H}_2\text{O}) [J_{\text{OH}-\text{H}} + J_{\text{H}_2-\text{O}} + a_{\text{H}_2\text{O}}^* n(\text{O}^*)] \\
 & = a_{20}n(\text{H})n(\text{HO}_2) \\
 & + n(\text{OH}) [a_{16}n(\text{OH}) + a_{17}n(\text{HO}_2) + a_{19}n(\text{H}_2) + a_{30}n(\text{H}_2\text{O}_2)]
 \end{aligned}$$

$$\begin{aligned}
 &+ c_2 n(\text{CH}_4) + c_7 n(\text{CH}_3\text{O}_2\text{H}) + c_8 n(\text{H}_2\text{CO}) \\
 &+ b_{25} n(\text{HNO}_2) + b_{27} n(\text{HNO}_3) + d_{11} n(\text{HCl}) + e_{11} n(\text{HBr})] \quad (27)
 \end{aligned}$$

The water vapor photodissociation can be described in the mesosphere by  $J_{\text{OH-H}}$  and  $J_{\text{H}_2\text{-O}}$  and its dissociation in the stratosphere by the term  $a_{\text{H}_2\text{O}}^* n(\text{O}^*)$ . Since these three terms are small, there is no chemical equilibrium and  $\text{H}_2\text{O}$  is subject to a permanent transport throughout the stratosphere and mesosphere. If the scatter among the observed profiles (Figure 3) indicates a real variability of the  $\text{H}_2\text{O}$  mixing ratio in the atmosphere, it is clear that the transport term shall be introduced in the analysis of the water vapor effect in models of stratospheric chemistry, and, in any case, cannot be neglected without due consideration.

The effect of methane must be introduced in the above equation. This constituent, with the conventional value of  $1.5 \times 10^{-6}$  for its relative concentration at the tropopause, cannot be re-formed when it is dissociated in the atmosphere. The general equation

$$\begin{aligned}
 &\frac{\partial n(\text{CH}_4)}{\partial t} + \text{div} [n(\text{CH}_4)w(\text{CH}_4)] + n(\text{CH}_4)J_{\text{CH}_2\text{-H}_2} \\
 &+ n(\text{CH}_4) \left[ \left\{ c_{1a}^* + c_{1b}^* \right\} n(\text{O}^*) + c_2 n(\text{OH}) + d_5 n(\text{Cl}) \right] = 0 \quad (28)
 \end{aligned}$$

shows that there is a permanent upward transport with complete transformation of  $\text{CH}_4$  to  $\text{H}_2$ ,  $\text{H}_2\text{O}$  and  $\text{CO}$ . The  $\text{CH}_4$  photodissociation due to Lyman alpha occurs only in the upper mesosphere, and the destruction processes in the stratosphere are due to its reaction with  $\text{O}^*$  and  $\text{OH}$ . The reaction of  $\text{Cl}$  with  $\text{CH}_4$  must be considered since it has an important effect on the formation of stratospheric  $\text{HCl}$ .

Several intermediate processes occur before reaching the complete destruction of  $\text{CH}_4$ : formation of  $\text{CH}_3$ ,  $\text{CH}_3\text{O}_2$ ,  $\text{H}_2\text{CO}$ ,  $\text{HCO}$ ,  $\text{CH}_3\text{O}$ ,  $\text{CH}_3\text{O}_2\text{H}$ , ...

Chemical equilibrium conditions can be introduced for a certain number of constituents since their lifetime is short enough, and we write

$$n(\text{CH}_3)c_{4M}n(\text{O}_2) = [c_{1a}^*n(\text{O}^*) + c_2n(\text{OH}) + d_5n(\text{Cl})]n(\text{CH}_4) \quad (29)$$

$$\begin{aligned}
 n(\text{CH}_3\text{O}_2)[c_5n(\text{N}) + c_7n(\text{HO}_2)] &= c_{17}n(\text{CH}_3\text{O}_2\text{H})n(\text{OH}) + c_{4M}n(\text{CH}_3)n(\text{O}_2) \\
 &= c_{17}n(\text{CH}_3\text{O}_2\text{H})n(\text{OH}) + [c_{1a}^*n(\text{O}^*) + c_2n(\text{OH}) + d_5n(\text{Cl})]n(\text{CH}_4) \quad (30)
 \end{aligned}$$

$$n(\text{CH}_3\text{O})c_{15}n(\text{O}_2) = c_5n(\text{NO})n(\text{CH}_3\text{O}_2) + n(\text{CH}_3\text{O}_2\text{H})J_{\text{CH}_3\text{O-OH}} \quad (31)$$

$$n(\text{HCO})[J_{\text{H-CO}} + c_{12}n(\text{O}_2)] = n(\text{H}_2\text{CO})[J_{\text{H-HCO}} + c_8n(\text{OH}) + c_9n(\text{O}) + d_{10}n(\text{Cl})] \quad (32)$$

There is sufficient indication of the absorption of  $\text{CH}_3\text{O}_2\text{H}$  to adopt, for general conditions photochemical conditions, and, therefore, to write

$$n(\text{CH}_3\text{O}_2\text{H})[J_{\text{CH}_3\text{O-OH}} + c_{17}n(\text{OH})] = c_7n(\text{CH}_3\text{O}_2)n(\text{HO}_2) \quad (33)$$

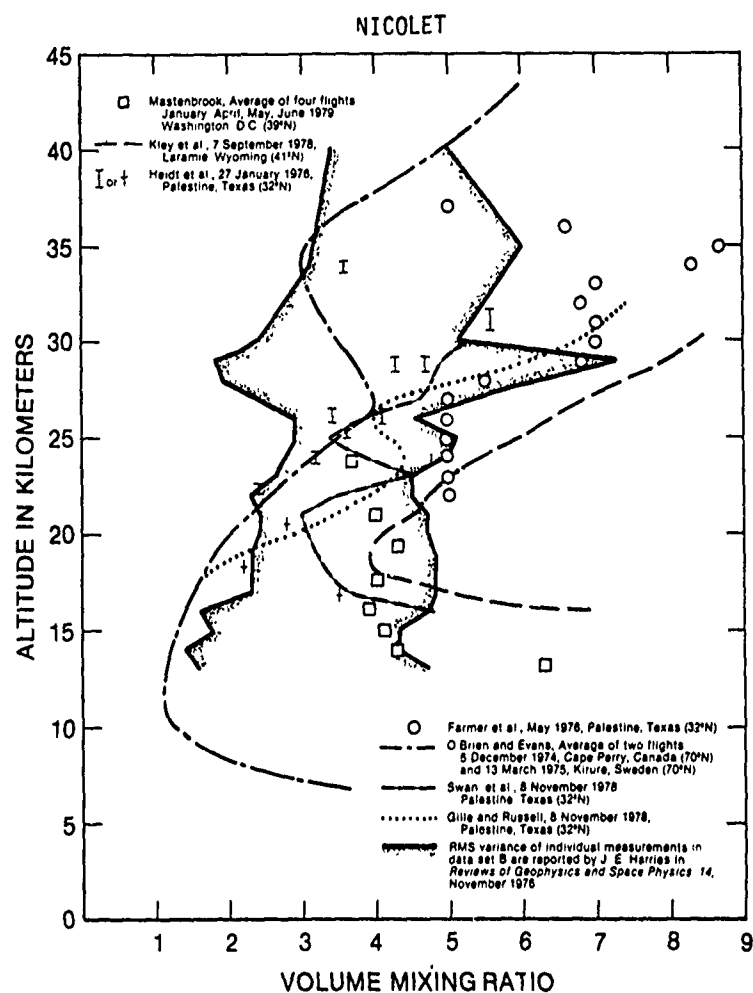


Fig. 3. — Relative concentration of water vapor in the stratosphere. These stratospheric water vapor profiles are a reproduction of a figure given in the Upper Atmospheric Programs Bulletin, No. 79-3, June 1979, published jointly by the Federal Aviation Administration and the National Aeronautics and Space Administration.

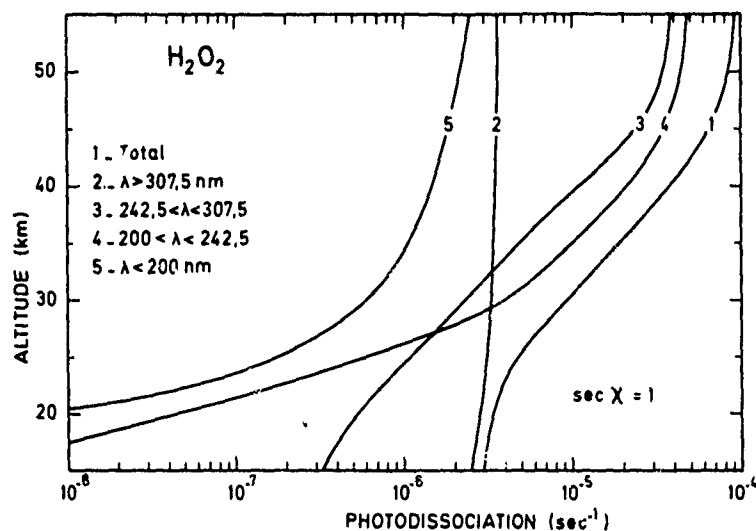


Fig. 4. — Photodissociation rates of  $H_2O_2$  in various spectral ranges for standard conditions without any albedo or scattering effects.

even if the effect of the solar zenith angle is important to lead to a diurnal variation. Finally, the formaldehyde molecule which plays an important role in the transformation of methane leads to the following equation

$$\begin{aligned}
 \frac{dn(\text{H}_2\text{CO})}{dt} + n(\text{H}_2\text{CO}) [J_{\text{H}-\text{HCO}} + J_{\text{H}_2-\text{CO}} + c_8 n(\text{OH}) + c_9 n(\text{O}) + d_{10} n(\text{Cl})] \\
 = c_{1b}^* n(\text{CH}_4) n(\text{O}^*) + c_{15} n(\text{CH}_3\text{O}) n(\text{O}_2) \\
 = n(\text{H}_2\text{CO}) J_{\text{H}_2-\text{CO}} + n(\text{HCO}) [J_{\text{HCO}} + c_{12} n(\text{O}_2)] \\
 = n(\text{CH}_4) \left[ \left\{ c_{1a}^* + c_{1b}^* \right\} n(\text{O}^*) + c_2 n(\text{OH}) + d_5 n(\text{Cl}) \right]
 \end{aligned} \quad (34)$$

However, since  $J_{\text{H}_2\text{CO}}$  is of the order of  $10^{-4} \text{ sec}^{-1}$  in the stratosphere, photochemical equilibrium conditions in (34) can be introduced in a general analysis. The result is that the carbon monoxide equation becomes

$$\begin{aligned}
 \frac{\partial n(\text{CO})}{\partial t} + \text{div} [n(\text{CO})w(\text{CO})] + n(\text{CO})c_{20} n(\text{OH}) \\
 = n(\text{CO}_2) J_{\text{CO}_2} + n(\text{CH}_4) \left[ \left\{ c_{1a}^* + c_{1b}^* \right\} n(\text{O}^*) + c_2 n(\text{OH}) + d_5 n(\text{Cl}) \right] \\
 = n(\text{CO}_2) J_{\text{CO}_2} + \frac{\partial n(\text{CH}_4)}{\partial t} + \text{div} [n(\text{CH}_4)w(\text{CH}_4)]
 \end{aligned} \quad (35)$$

The photodissociation of carbon dioxide is a mesospheric process compared to the  $\text{CH}_4$  oxidation which is a stratospheric process.

The other molecule, which must be introduced in this study, is  $\text{H}_2$ , for which the rate of change of its concentration is

$$\begin{aligned}
 \frac{\partial n(\text{H}_2)}{\partial t} + \text{div} [n(\text{H}_2)w(\text{H}_2)] \\
 + n(\text{H}_2) [a_{19} n(\text{OH}) + a_{24} n(\text{O}) + a_{\text{H}_2}^* n(\text{O}^*) + d_6 n(\text{Cl})] \\
 = n(\text{H}_2\text{O}) J_{\text{H}_2-\text{O}} + n(\text{H}) [a_{22} n(\text{OH}) + a_{23} n(\text{HO}_2)] \\
 + c_{1b}^* n(\text{O}^*) n(\text{CH}_4) + n(\text{H}_2\text{CO}) J_{\text{H}_2-\text{CO}}
 \end{aligned} \quad (36)$$

The  $\text{H}_2$  behavior is completely different in the stratosphere and in the mesosphere. In the latter region, the production terms correspond to the reaction of H with  $\text{HO}_2$  and the photodissociation of  $\text{H}_2\text{O}$  in  $\text{H}_2$  and O products while the stratospheric production is the photodissociation of formaldehyde and the reaction of an excited oxygen atom with methane. The stratospheric destruction, represented essentially by the term  $a_{\text{H}_2}^* n(\text{O}^*)$ , is very slow and it can be said that  $\text{H}_2$  is produced by different processes in two atmospheric layers; namely the mesosphere and stratosphere. Since its relative concentration at the tropopause level is of the order of  $0.5 \times 10^{-6}$ , it cannot be neglected in a precise stratospheric analysis and it must be introduced for its important role in the mesospheric processes related to atomic hydrogen and hydroxyl radicals.

If we return to the general equation (27), leading to the reformation of water vapor, we can see that, in addition to  $\text{CH}_4$  and  $\text{H}_2$ , there are possible additional effects due to nitrous and nitric acids and hydrogen chloride and bromide. Such effects may only play a role in the lower stratosphere; particularly for nitric acid which is an important minor constituent. In any case, the action of the OH radical on all these constituents is significant for dealing with the nitrogen and halogen problems in the stratosphere.

In order to study the behavior of the hydrogen constituents all reactions of H, OH,  $\text{HO}_2$  and  $\text{H}_2\text{O}_2$  must be known. The hydrogen peroxy concentration can be represented by

$$\begin{aligned} \frac{dn(\text{H}_2\text{O}_2)}{dt} + n(\text{H}_2\text{O}) [J_{\text{H}_2\text{O}_2} + a_{30}n(\text{OH}) + d_8n(\text{Cl}) + e_8n(\text{Br})] \\ = a_{27}n^2(\text{HO}_2) + a_{16M}n^2(\text{OH}) \end{aligned} \quad (37)$$

In this equation the photodissociation must be considered as an essential process. Since  $J_{\text{H}_2\text{O}_2}$  varies from about  $10^{-5} \text{ sec}^{-1}$  in the lower stratosphere to about  $10^{-4} \text{ sec}^{-1}$  near the stratopause, transport is not included in equation (37), and, in a general analysis, it is convenient to accept photochemical equilibrium conditions (Fig. 4).

If a numerical analysis of the various reactions of H, OH and  $\text{HO}_2$  is made, it is found that it is appropriate to adopt, for general conditions in the solar radiation field, chemical equilibrium conditions.

Thus, we write for atomic hydrogen

$$\begin{aligned} n(\text{H}) \left[ a_1 n(\text{M})n(\text{O}_2) + \{ a_2 + a_3 \} n(\text{O}_3) + a_{22}n(\text{OH}) + \{ a_{15} + a_{20} + a_{23} \} n(\text{HO}_2) \right] \\ = n(\text{OH}) [a_5 n(\text{O}) + a_{19}n(\text{H}_2) + c_{20}n(\text{CO})] \\ + n(\text{H}_2) [a_{24}n(\text{O}) + a_{24}^*n(\text{O}^*) + d_6n(\text{Cl})] \\ + n(\text{H}_2\text{O})J_{\text{H-OH}} + n(\text{H}_2\text{CO})J_{\text{H-HCO}} + n(\text{HCO})J_{\text{H-CO}} \\ + n(\text{HCl})J_{\text{H-Cl}} + n(\text{HBr})J_{\text{H-Br}} + n(\text{HOCl})J_{\text{H-ClO}} + n(\text{HOBr})J_{\text{H-BrO}} \end{aligned} \quad (38)$$

In this equation the photodissociation of the various halogen constituents may be neglected compared with the other terms. In fact, in a simplified version of (38), the principal terms are  $a_1 n(\text{M})n(\text{O}_2)$  and  $a_2 n(\text{O}_3)$  in the first member with  $a_5 n(\text{O})$  and  $c_{20}n(\text{CO})$  in the second member. Nevertheless, for a comprehensive review, all terms must be kept.

The associated  $\text{HO}_2$  radical leads to the following equation

$$\begin{aligned} n(\text{HO}_2) \left[ a_{6c}n(\text{O}_3) + a_7n(\text{O}) + a_{17}n(\text{OH}) + 2a_{27}n(\text{HO}_2) \right. \\ \left. + J_{\text{HO}_2} + \{ a_{15} + a_{20} + a_{23} \} n(\text{H}) + c_7n(\text{CH}_3\text{O}_2) \right. \\ \left. + b_{28M}n(\text{NO}_2) + b_{29}n(\text{NO}) \right] \end{aligned}$$

$$\begin{aligned}
 & + d_7 n(\text{Cl}) + d_{15} n(\text{ClO}) + e_7 n(\text{Br}) + e_{15} n(\text{BrO}) \Big] \\
 = & n(\text{H}) [a_1 n(\text{M})n(\text{O}_2) + a_3 n(\text{O}_3) \\
 & + n(\text{OH}) [a_6 n(\text{O}_3) + a_{30} n(\text{H}_2\text{O}_2) + d_{4b_1} n(\text{ClO}) + e_{4b_1} n(\text{BrO})] \\
 & + c_{12} n(\text{HCO})n(\text{O}_2) + c_{15} n(\text{O}_2) n(\text{CH}_3\text{O}) \\
 & + n(\text{HO}_2\text{NO}_2)J_{\text{HO}_2-\text{NO}_2} + n(\text{H}_2\text{O}_2) [d_8 n(\text{Cl}) + c_8 n(\text{Br})]
 \end{aligned} \tag{39}$$

The equivalent equation for the hydroxyl radical is

$$\begin{aligned}
 & n(\text{OH}) [a_5 n(\text{O}) + a_6 n(\text{O}_3) + 2a_{16} n(\text{OH}) + 2a_{16M} n(\text{OH}) + a_{17} n(\text{HO}_2) + a_{19} n(\text{H}_2) \\
 & + a_{22} n(\text{H}) + a_{30} n(\text{H}_2\text{O}_2) + c_{20} n(\text{CO}) + c_2 n(\text{CH}_4) + c_8 n(\text{H}_2\text{CO}) + c_{17} n(\text{CH}_3\text{O}_2\text{H}) \\
 & + b_{21M} n(\text{NO}) + b_{22M} n(\text{NO}_2) + b_{25} n(\text{HNO}_2) + b_{27} n(\text{HNO}_3) \\
 & + d_{4b} n(\text{ClO}) + d_{11} n(\text{HCl}) + e_{4b} n(\text{BrO}) + e_{11} n(\text{HBr})] \\
 = & n(\text{H}) [a_2 n(\text{O}_3) + 2a_{15} n(\text{HO}_2)] + n(\text{HO}_2) [a_6 n(\text{O}_3) + a_7 n(\text{O}) + J_{\text{HO}_2} + b_{29} n(\text{NO})] \\
 & + n(\text{H}_2) [a_{24} n(\text{O}) + a_{H_2}^* n(\text{O}^*)] + n(\text{H}_2\text{O}) [J_{\text{OH-H}} + 2a_{H_2\text{O}}^* n(\text{O}^*)] + 2n(\text{H}_2\text{O}_2)J_{\text{H}_2\text{O}_2} \\
 & + n(\text{CH}_4)c_{1a}^* n(\text{O}^*) + n(\text{CH}_3\text{O}_2\text{H})J_{\text{CH}_3\text{OOH}} + c_9 n(\text{H}_2\text{CO})n(\text{O}) \\
 & + n(\text{HNO}_2)J_{\text{HNO}_2} + n(\text{HNO}_3)J_{\text{HNO}_3} + n(\text{HO}_2\text{NO}_2)J_{\text{OH-NO}_3} \\
 & + n(\text{HOCl})J_{\text{OH-Cl}} + d_{12} n(\text{O})n(\text{HCl}) + n(\text{HOBr})J_{\text{OH-Br}} + e_{12} n(\text{O})n(\text{HBr})
 \end{aligned} \tag{40}$$

From the last four equations (37) to (40) is derived an expression determining the OH concentration

$$\begin{aligned}
 & 2n(\text{H}) \left[ a_3 n(\text{O}_3) + \left\{ a_{20} + a_{23} \right\} n(\text{HO}_2) \right] \\
 & + 2n(\text{OH}) [a_{16} n(\text{OH}) + a_{17} n(\text{HO}_2) + a_{22} n(\text{H}) + a_{30} n(\text{H}_2\text{O}_2) + c_{17} n(\text{CH}_3\text{O}_2\text{H}) \\
 & + b_{25} n(\text{HNO}_2) + b_{27} n(\text{HNO}_3) + d_{11} n(\text{HCl}) + e_{11} n(\text{HBr})]
 \end{aligned}$$

$$\begin{aligned}
 &= 2n(\text{H}_2\text{O}) [J_{\text{H-OH}} + a_{\text{H}_2\text{O}}^* n(\text{O}^*)] + 2n(\text{H}_2) [a_{24} n(\text{O}) + a_{\text{H}_2}^* n(\text{O}) + a_6 n(\text{Cl})] \\
 &+ 2n(\text{CH}_4) \left[ \left\{ c_{1a}^* n(\text{O}) + d_5 n(\text{Cl}) \right\} \left\{ \frac{1}{2} + \frac{1}{1+R_1} \right\} + \left\{ c_{1b}^* n(\text{O}^*) + c_2 n(\text{OH}) \right\} \frac{1}{1+R_1} \right] \\
 &+ \left\{ n(\text{HNO}_3) [J_{\text{HNO}_3} + b_{27} n(\text{OH}) + d_9 n(\text{Cl})] - b_{22M} n(\text{NO}_2) n(\text{OH}) \right\} \\
 &+ \left\{ n(\text{HO}_2\text{NO}_2) J_{\text{HO}_2\text{NO}_2} - b_{28M} n(\text{NO}_2) n(\text{HO}_2) \right\} \\
 &+ \left\{ n(\text{HNO}_2) [J_{\text{HNO}_2} + b_{25} n(\text{OH})] - b_{21M} n(\text{NO}) n(\text{OH}) \right\} \\
 &+ \left\{ n(\text{HCl}) [J_{\text{HCl}} + d_{11} n(\text{OH}) + d_{12} n(\text{O})] - d_{4b_2} n(\text{OH}) n(\text{ClO}) \right\} \\
 &- n(\text{Cl}) [d_5 n(\text{CH}_4) + d_6 n(\text{H}_2) + d_7 n(\text{HO}_2) + d_8 n(\text{H}_2\text{O}_2) + d_9 n(\text{HNO}_3) + d_{10} n(\text{H}_2\text{CO})] \\
 &+ \left\{ n(\text{HOCl}) J_{\text{HOCl}} - d_{15} n(\text{HO}_2) n(\text{ClO}) \right\} \\
 &+ \left\{ n(\text{HBr}) [J_{\text{HBr}} + e_{11} n(\text{OH}) + e_{12} n(\text{O})] - n(\text{Br}) e_7 n(\text{HO}_2) \right\} \\
 &+ \left\{ n(\text{HOBr}) J_{\text{HOBr}} - e_{15} n(\text{BrO}) n(\text{HO}_2) \right\} \quad (41a)
 \end{aligned}$$

where

$$R_1 = J_{\text{H}_2-\text{CO}} + c_8 n(\text{OH}) + \frac{1}{2} d_{10} n(\text{Cl}) / J_{\text{H-HCO}} + c_9 n(\text{O}) + \frac{1}{2} d_{10} n(\text{HCl}) \quad (41a_1)$$

shows the importance of an exact knowledge of the photodissociation quantum yields of  $\text{H}_2\text{CO}$ .

The term  $n(\text{H}) \{a_{20} + a_{23}\} n(\text{HO}_2)$  is a mesospheric term which is neglected in the stratosphere since the atomic hydrogen concentration is small compared with that of OH and  $\text{HO}_2$ . Among the various processes involving the destruction of OH, the principal action is due to its reaction with  $\text{HO}_2$ . However, particularly in the lower stratosphere, the actions of  $\text{HNO}_3$  and HCl cannot be neglected without due consideration.

The production terms are given by the various dissociation processes of  $\text{H}_2\text{O}$ ,  $\text{H}_2$  and  $\text{CH}_4$ . The action of  $\text{CH}_4$  is limited by the production of  $\text{H}_2$  through the photodissociation of formaldehyde in  $\text{H}_2 + \text{CO}$  which is indicated by  $R_1$  given by (42). All terms, which are written between braces from the sixth line to the last line in the above expression (41a) correspond to equations of photoequilibrium conditions of  $\text{HNO}_3$ ,  $\text{HO}_2\text{NO}_2$ ,  $\text{HNO}_2$ , HCl, HOCl, Hbr and HOBr, respectively. If we impose the following notation

$$\{ \text{HNO}_3 \} \equiv \left\{ n(\text{HNO}_3) [J_{\text{HNO}_3} + b_{27} n(\text{OH}) + d_9 n(\text{Cl})] - b_{22M} n(\text{NO}_2) n(\text{OH}) \right\}$$

to represent the photochemical equilibrium conditions, it will improve the general notation if the substitution is made in (41a). Furthermore, an additional improvement can be made if we write the general continuity equation

$$\frac{\partial n(XY)}{\partial t} + \text{div} [n(XY)w(XY)] + (P - L) = 0$$

where P and L denote the production and loss terms, respectively, by

$$\langle XY \rangle + \{XY\} = 0$$

i.e. for  $\text{HNO}_3$

$$\langle \text{HNO}_3 \rangle = -\{ \text{HNO}_3 \}$$

Hence, the equation (42a) is written as follows

$$\begin{aligned} & 2n(\text{H}) \{ a_{20} + a_{23} \} n(\text{HO}_2) + 2n(\text{OH}) [a_{16}n(\text{OH}) + a_{17}n(\text{HO}_2) + a_{22}n(\text{H}) \\ & + a_{30}n(\text{H}_2\text{O}_2) + c_{17}n(\text{CH}_3\text{O}_2\text{H}) + b_{25}n(\text{HNO}_2) + b_{27}n(\text{HNO}_3) \\ & + d_{11}n(\text{HCl}) + e_{11}n(\text{HBr})] + \langle \text{HNO}_3 \rangle + \langle \text{HCl} \rangle + \langle \text{HBr} \rangle \\ & = 2n(\text{H}_2\text{O}) [J_{\text{H-OH}} + a_{\text{H}_2\text{O}}^* n(\text{O}^*)] + 2n(\text{H}_2) [a_{24}n(\text{O}) + a_{\text{H}_2}^* n(\text{O}^*) + d_6n(\text{Cl})] \\ & + 2n(\text{CH}_4) \left[ \{ c_{1a}^* n(\text{O}^*) + d_5n(\text{Cl}) \} \left\{ 1 + \frac{1}{1+R_1} \right\} \right. \\ & + \left. \{ c_{1b}^* n(\text{O}^*) + c_2^* n(\text{OH}) \} \frac{1}{1+R_1} \right] + \{ \text{HO}_2\text{NO}_2 \} + \{ \text{HNO}_2 \} \\ & + \{ \text{HOCl} \} + \{ \text{HOBr} \} \end{aligned} \quad (41b)$$

where  $\langle XY \rangle$  denotes a possible departure from photochemical equilibrium conditions in the lower stratosphere. It will be shown later that  $\text{HNO}_3$  and  $\text{HCl}$  are not in chemical equilibrium conditions in the lower stratosphere, but that all other molecules are completely photochemically controlled.

In any case, it is necessary to start from equation (41) to determine the OH concentration in the stratosphere and mesosphere; in any simplified or general version  $a_{17}n(\text{OH})n(\text{HO}_2)$  must be considered as the first reaction. It is, therefore, required to determine the ratio  $n(\text{HO}_2)/n(\text{OH})$  which must be deduced from equations (37) to (40). Its general form is given by the following equation

$$\begin{aligned} & 2n(\text{H}) \{ a_2 + a_3 \} n(\text{O}_3) \\ & + 2n(\text{HO}_2) \left[ J_{\text{HO}_2} + a_{6c}n(\text{O}_3) + a_7n(\text{O}) + 2 \{ a_{15} + a_{20} + a_{23} \} n(\text{H}) \right. \\ & + \left. 2a_{27} n(\text{HO}_2) + c_7n(\text{CH}_3\text{O}_2) + b_{29}n(\text{NO}_2) + d_{15}n(\text{ClO}) + e_{15}n(\text{BrO}) \right] \end{aligned}$$



$$\begin{aligned}
 & + 2n(\text{H}_2\text{O}_2) J_{\text{H}_2\text{O}_2} + a_{\text{H}_2\text{O}}^* n(\text{H}_2\text{O}) n(\text{O}^*) + n(\text{HO}_2\text{NO}_2) J_{\text{OH-NO}_2} \\
 & + n(\text{O}) [d_{12} n(\text{HCl}) + e_{12} n(\text{HBr})] \\
 & + \langle \text{HCl} \rangle + \langle \text{HBr} \rangle \\
 & + \{ \text{HNO}_2 \} + \{ \text{HOCl} \} + \{ \text{HOBr} \} \\
 = & 2n(\text{OH}) \left[ a_5 n(\text{O}) + a_6 n(\text{O}_3) + a_{16} n(\text{OH}) + a_{19} n(\text{H}_2) + 2a_{30} n(\text{H}_2\text{O}_2) \right. \\
 & + \left\{ c_{20} n(\text{CO}) + c_2 n(\text{CH}_4) \right\} \left\{ 1 + \frac{1}{2} \cdot \frac{1 - R_2}{1 + R_2} \right\} + c_{17} n(\text{CH}_3\text{O}_2\text{H}) \Big] \\
 & + n(\text{CH}_4) \left[ \left\{ c_{1a}^* + c_{1b}^* \right\} n(\text{O}^*) + d_5 n(\text{Cl}) \right] \frac{1 - R_2}{1 + R_2} \\
 & + 2n(\text{OH}) [b_{25} n(\text{HNO}_2) + b_{27} n(\text{HNO}_3) + d_{4b} n(\text{ClO}) + e_{4b} n(\text{BrO})] \\
 & + \{ \text{HO}_2\text{NO}_2 \} + \langle \text{HNO}_3 \rangle
 \end{aligned} \tag{42a}$$

where  $R_2$  represents the effect of the  $\text{H}_2\text{CO}$  photodissociation

$$R_2 = J_{\text{H}_2-\text{CO}} + c_9 n(\text{O}) + \frac{1}{2} d_{10} n(\text{Cl}) \quad J_{\text{H}-\text{HCO}} + c_8 n(\text{OH}) + \frac{1}{2} d_{10} n(\text{Cl}) \tag{42a_1}$$

In this expression for the determination of  $n(\text{OH})/n(\text{HO}_2)$ , photochemical conditions can be generally applied except for  $\text{HNO}_3$  and  $\text{HCl}$  in the lower stratosphere. Numerical values of the transport terms must be considered before neglecting their departure from photochemical equilibrium conditions.

The principal terms of (42) may be written for a determination of stratospheric conditions as follows:

$$\begin{aligned}
 n(\text{H}) \left\{ a_2 + a_3 \right\} n(\text{O}_3) + n(\text{HO}_2) [a_{6c} n(\text{O}_3) + a_7 n(\text{O}) + b_{29} n(\text{NO}_2)] \\
 = n(\text{OH}) [a_5 n(\text{O}) + a_6 n(\text{O}_3) + c_{20} n(\text{CO})]
 \end{aligned} \tag{42b}$$

the term involving atomic hydrogen may be neglected in a preliminary calculation and this simplified form must be considered as the initial equation; a certain number of other terms must be introduced as possible perturbations in the exact determination of the daytime ratio  $n(\text{HO}_2)/n(\text{OH})$ .

At the stratopause level, we may write

$$n(\text{H}) \left\{ a_2 + a_3 \right\} n(\text{O}_3) + n(\text{HO}_2) a_7 n(\text{O}) = n(\text{OH}) a_5 n(\text{O}) \tag{42c_1}$$

and at the tropopause level, when the transport terms are not considered,

$$n(\text{HO}_2) [a_{6c}n(\text{O}_3) + b_{29}n(\text{NO}_2)] = n(\text{OH}) [a_6n(\text{O}_3) + c_{20}n(\text{CO})] \quad (42c_2)$$

Another form which may be used for the determination of the ratio  $n(\text{HO}_2)/n(\text{OH})$  is to introduce directly the equation for rate of change of  $n(\text{H}_2\text{O})$  in the OH equation. Instead of the equation (42a) we then write

$$\begin{aligned} & N(\text{H}) [a_2n(\text{O}_3) + 2a_{15}n(\text{HO}_2) + a_{20}n(\text{HO}_2)] \\ & + n(\text{HO}_2) [a_6n(\text{O}_3) + a_7n(\text{O}) + J_{\text{HO}_2} + b_{29}n(\text{NO})] \\ & + n(\text{H}_2) [a_{24}n(\text{O}) + a_{\text{H}_2}^* n(\text{O}^*)] + n(\text{H}_2\text{O}) a_{\text{H}_2\text{O}}^* n(\text{O}^*) + 2n(\text{H}_2\text{O}_2) J_{\text{H}_2\text{O}_2} \\ & + n(\text{CH}_4) c_{1a}^* n(\text{O}^*) + n(\text{CH}_3\text{O}_2\text{H}) J_{\text{CH}_3\text{O}_2\text{H}} + c_9 n(\text{H}_2\text{CO}) n(\text{O}) \\ & + n(\text{HO}_2\text{NO}_2) J_{\text{OH-NO}_3} + \left\{ \text{HNO}_2 \right\} + n(\text{HOCl}) J_{\text{OH-Cl}} + n(\text{HOBr}) J_{\text{OH-Br}} \\ & + n(\text{O}) [d_{12}n(\text{HCl}) + e_{12}n(\text{HBr})] \\ & = n(\text{OH}) [a_5n(\text{O}) + a_6n(\text{O}_3) + a_{16}n(\text{OH}) + 2a_{16M}n(\text{OH}) + a_{22}n(\text{H}) + c_{20}n(\text{CO}) \\ & + b_{25}n(\text{HNO}_2) + b_{27}n(\text{HNO}_3) + d_{4b}n(\text{ClO}) + e_{4b}n(\text{BrO})] \\ & + \frac{\partial n(\text{H}_2\text{O})}{\partial t} + \text{div} [n(\text{H}_2\text{O})w(\text{H}_2\text{O})] + n(\text{H}_2\text{O}) J_{\text{H}_2\text{O}-\text{O}} \\ & + \frac{\partial n(\text{HNO}_3)}{\partial t} + \text{div} [n(\text{HNO}_3)w(\text{HNO}_3)] + n(\text{HNO}_3) d_9 n(\text{Cl}) \end{aligned} \quad (42d)$$

From this equation, it is seen that certain terms neglected in (42b) may play a certain role. It is recommended that this be verified directly by the use of numerical values of the laboratory rate constants and observed atmospheric concentrations.

These last two general equations, (41) and (42), will be used in the determination of the equation governing the rate of change of the ozone concentration.

**THE NITROGEN CONSTITUENTS:** In the study of nitrogen compounds related to the stratospheric chemistry several polyatomic molecules such as  $\text{HNO}_3$ ,  $\text{HNO}_2$ ,  $\text{HO}_2\text{NO}_2$ ,  $\text{NO}_3$ , . . . must be introduced.

The most important polyatomic molecule in the stratosphere is nitric acid. It is represented by the equation

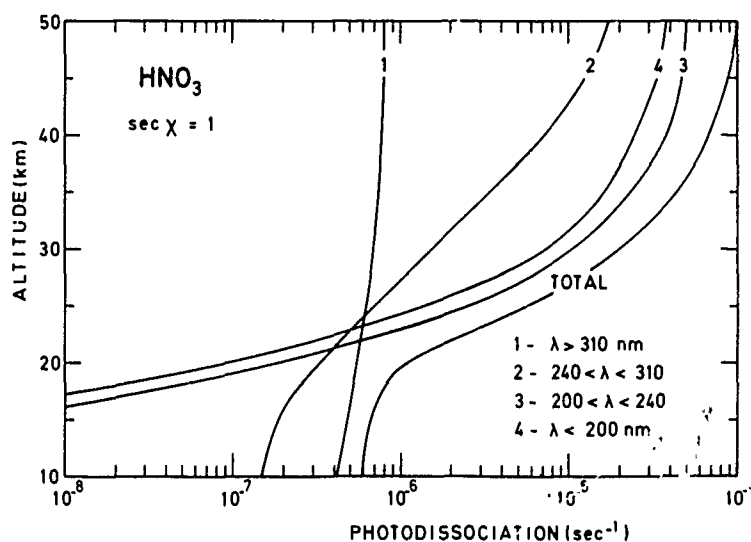


Fig. 5. — Photodissociation rates of nitric acid in various spectral ranges for standard conditions without any albedo or scattering effects.

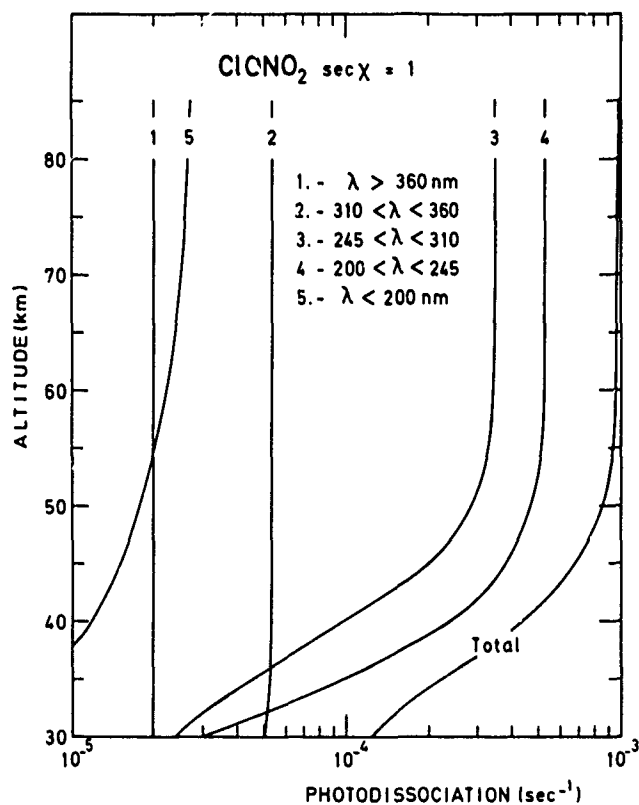


Fig. 6. — Photodissociation rates of  $\text{ClONO}_2$  in various spectral ranges for standard conditions with no scattering or albedo effects.

$$\frac{\partial n(\text{HNO}_3)}{\partial t} + \text{div} [n(\text{HNO}_3)w(\text{HNO}_3)] + n(\text{HNO}_3) [J_{\text{HNO}_3} + b_{27}n(\text{OH}) + d_9n(\text{Cl})] = b_{22M}n(\text{OH})n(\text{NO}_2) \quad (43)$$

Since  $J_{\text{HNO}_3}$  varies from  $10^{-4} \text{ sec}^{-1}$  in the neighborhood of the stratopause to  $5 \times 10^{-7}$  in the lower stratosphere (Figure 5), the long life time of  $\text{HNO}_3$  in the solar radiation field at low stratospheric levels leads to the possibility of atmospheric transport. It is for this reason that the transport terms cannot be neglected in (41) and (42), except in the middle and upper stratosphere where photochemical equilibrium conditions are rapidly reached. Thus, the lower boundary conditions in the stratosphere must play an important role on the behavior of  $\text{HNO}_3$  and, therefore, on its action in the ozone chemistry.

The equations for  $\text{HO}_2\text{NO}_2$  and  $\text{HNO}_2$  correspond to photochemical equilibrium equations since their photodissociation is sufficiently rapid. Hence,

$$n(\text{HNO}_2) [J_{\text{OH-NO}} + b_{25}n(\text{OH})] = b_{21M}n(\text{OH})n(\text{O}) \quad (44)$$

$$n(\text{HO}_2\text{NO}_2) [J_{\text{OH-NO}_3} + J_{\text{HO}_2\text{-NO}_2}] = b_{28M}n(\text{HO}_2)n(\text{NO}_2) \quad (45)$$

indicate that these two molecules cannot play a role identical to  $\text{HNO}_3$ ; their photodissociation rates lead to relative short lifetimes in the stratospheric solar radiation field.

The  $\text{NO}_3$  molecule, which has a very short lifetime of not more than 100 sec, is always in photochemical equilibrium, and its equation can be written

$$\begin{aligned} n(\text{NO}_3) [J_{\text{NO}_2\text{-O}} + J_{\text{NO-O}_2} + b_{11}n(\text{NO})] \\ = n(\text{NO}_2) [b_9n(\text{O}_3) + b_{10M}n(\text{O})] + b_{27}n(\text{OH})n(\text{HNO}_3) \\ + n(\text{HO}_2\text{NO}_2)J_{\text{OH-NO}_3} + n(\text{NO}_2) [b_9n(\text{O}_3) + b_{10M}n(\text{O})] \\ + n(\text{ClONO}_2)J_{\text{Cl-NO}_3} + d_9n(\text{Cl})n(\text{HNO}_3) + n(\text{BrONO}_2)J_{\text{Br-NO}_3} \end{aligned} \quad (46)$$

In this equation, the terms corresponding to the photoequilibrium equation of  $\text{N}_2\text{O}_5$ , have not been introduced. This molecule has the following form

$$\frac{dn(\text{N}_2\text{O}_5)}{dt} + n(\text{N}_2\text{O}_5) [J_{\text{N}_2\text{O}_5} + b_{12c}n(\text{M})] = b_{12M}n(\text{NO}_2)n(\text{NO}_3) \quad (47)$$

Since  $J_{\text{N}_2\text{O}_5}$  cannot be greater than  $5 \times 10^{-5} \text{ sec}^{-1}$ , the photoequilibrium equation can be used for general conditions, but not for an analysis of a diurnal variation.

Finally, the ozone chemistry in the stratosphere will depend on the behavior of  $\text{NO}$  and  $\text{NO}_2$  which are related as it is shown by their chemical and photochemical equilibrium equations, respectively

$$\begin{aligned}
 n(\text{NO}) [J_{\text{NO}} + b_2 n(\text{O}) + b_4 n(\text{O}_3) + b_6 n(\text{N}) + b_{11} n(\text{NO}_3) \\
 + b_{21\text{M}} n(\text{OH}) + b_{29} n(\text{HO}_2) + c_5 n(\text{CH}_3\text{O}_2) + d_{4\text{a}} n(\text{ClO}) + e_{4\text{a}} n(\text{BrO})] \\
 = n(\text{NO}_2) [J_{\text{NO}_2} + b_3 n(\text{O})] + n(\text{NO}_3) J_{\text{NO-O}_2} + n(\text{HNO}_2) J_{\text{OH-NO}} \\
 + P(\text{NO}) + 2b_{\text{NO}}^* n(\text{O}^*) n(\text{N}_2\text{O}) + n(\text{N}) [b_{1\text{M}} n(\text{O}) + b_7 n(\text{O}_2) + b_8 n(\text{O}_3)]
 \end{aligned} \quad (48)$$

and

$$\begin{aligned}
 n(\text{NO}_2) [J_{\text{NO}_2} + b_3 n(\text{O}) + b_5 n(\text{N}) + b_9 n(\text{O}_3) + b_{10\text{M}} n(\text{O}) \\
 + b_{22\text{M}} n(\text{OH}) + b_{28\text{M}} n(\text{HO}_2) + d_{13\text{M}} n(\text{ClO}) + e_{13\text{M}} n(\text{BrO})] \\
 = n(\text{NO}) [b_2 n(\text{NO}) + b_4 n(\text{O}_3) + 2b_{11} n(\text{NO}_3) + b_{29} n(\text{HO}_2) + c_5 n(\text{CH}_3\text{O}_2) + d_{4\text{a}} n(\text{ClO})] \\
 + n(\text{NO}_3) J_{\text{NO}_2-\text{O}} + n(\text{HNO}_3) J_{\text{HNO}_3} + b_{25} n(\text{OH}) n(\text{HNO}_2) + n(\text{HO}_2\text{NO}_2) J_{\text{HO}_2-\text{NO}_2} \\
 + \left\{ n(\text{N}_2\text{O}_5) [J_{\text{N}_2\text{O}_5} + b_{12\text{c}} n(\text{M})] = b_{12\text{M}} n(\text{NO}_3) n(\text{NO}_2) \right\}
 \end{aligned} \quad (49)$$

To complete this study of the principal reactions of the nitrogen oxide chemistry, the equation of atomic nitrogen must be also written; it is

$$n(\text{N}) [b_{1\text{M}} n(\text{O}) + b_5 n(\text{NO}_2) + b_6 n(\text{NO}) + b_7 n(\text{O}_2) + b_8 n(\text{O}_3)] = n(\text{NO}) J_{\text{NO}} + P(\text{N}) \quad (50)$$

In these two last equations,  $P(\text{NO})$  and  $P(\text{N})$  may represent natural or artificial production processes corresponding to a perturbation.

The conventional ratio  $n(\text{NO}_2)/n(\text{NO})$

$$n(\text{NO}_2)/n(\text{NO}) = b_4 n(\text{O}_3)/J_{\text{NO}_2} \quad (51\text{a})$$

which was generally used a few years ago in stratospheric chemistry must now be written, according to (48), as follows

$$\begin{aligned}
 n(\text{NO}) [b_4 n(\text{O}_3) + b_{29} n(\text{HO}_2) + c_5 n(\text{CH}_3\text{O}_2) + d_{4\text{a}} n(\text{ClO}) + e_{4\text{a}} n(\text{BrO})] \\
 = n(\text{NO}_2) [J_{\text{NO}_2} + b_3 n(\text{O})]
 \end{aligned} \quad (51\text{b})$$

in order to indicate clearly the possible action of hydrogen and halogen compounds on the numerical value of the ratio  $n(\text{NO}_2)/n(\text{NO})$ .

THE HALOGENED CONSTITUENTS: The behavior of chlorine, bromine and fluorine in the stratosphere is different since the reactions of the halogen atoms Cl, Br and F with  $\text{CH}_4$  and  $\text{H}_2$  and of HCl, HBr and HF with OH, are different; Cl reacts slowly with  $\text{CH}_4$ , F reacts rapidly, and Br does not react; HF does not react with OH when HCl and HBr react. Nevertheless, the stratospheric chemistry of the principal halogen compounds is characterized by photodissociation processes leading to the production of halogen atoms which react rapidly with ozone and form halogen monoxides

The chlorine atoms are always in chemical equilibrium, and

$$\begin{aligned} n(\text{Cl}) [d_2 n(\text{O}_3) + d_5 n(\text{CH}_4) + d_6 n(\text{H}_2) + d_7 n(\text{HO}_2) + d_8 n(\text{H}_2\text{O}_2) \\ + d_9 n(\text{HNO}_3) + d_{10} n(\text{H}_2\text{CO})] \\ = n(\text{HCl}) [J_{\text{HCl}} + d_{11} n(\text{OH}) + d_{12} n(\text{O})] + n(\text{ClONO}_2) J_{\text{Cl-NO}_3} + n(\text{HOCl}) J_{\text{OH-Cl}} \\ + n(\text{C}_x\text{Cl}_y \dots) J_{\text{C}_x\text{Cl}_y} + n(\text{ClO}) [d_3 n(\text{O}) + d_{4a} n(\text{NO}) + d_{4b} n(\text{OH}) + e_5 n(\text{BrO})] \end{aligned} \quad (52)$$

in which  $\text{C}_x\text{Cl}_y$  represent all possible halocarbons leading to chlorine atoms by photodissociation. This equation is the basic atmospheric equation which must be used to determine the concentration of chlorine atoms determining the ClO and HCl concentrations.

The chlorine monoxide can be also considered in chemical equilibrium, and

$$\begin{aligned} n(\text{ClO}) [J_{\text{ClO}} + d_3 n(\text{O}) + d_{4a} n(\text{NO}) + d_{4b} n(\text{OH}) \\ + d_{13M} n(\text{NO}_2) + d_{15} n(\text{HO}_2) + e_5 n(\text{BrO})] \\ = d_2 n(\text{Cl}) n(\text{O}_3) \end{aligned} \quad (53)$$

In this equation the photodissociation of  $\text{ClONO}_2$  to ClO and  $\text{NO}_2$  is neglected and the reactions of HOCl and  $\text{ClONO}_2$  with OH and O have not been introduced.

In the stratosphere, HCl is not always in chemical equilibrium, and the general equation must be written

$$\begin{aligned} \frac{\partial n(\text{HCl})}{\partial t} + \text{div} [n(\text{HCl})w(\text{HCl})] + n(\text{HCl}) [J_{\text{HCl}} + d_{11} n(\text{OH}) + d_{12} n(\text{O})] \\ = n(\text{Cl}) [d_5 n(\text{CH}_4) + d_6 n(\text{H}_2) + d_7 n(\text{HO}_2) + d_8 n(\text{H}_2\text{O}_2) + d_9 n(\text{HNO}_3) + d_{10} n(\text{H}_2\text{CO})] \\ + [d_{4b2} n(\text{OH}) + d_{15b} n(\text{HO}_2)] n(\text{ClO}) + n(\text{HOCl}) J_{\text{O-HCl}} \end{aligned} \quad (54)$$

The photodissociation of HCl is very slow, less than  $10^{-7} \text{ sec}^{-1}$  in the stratosphere. Its reaction with OH leads to a lifetime which may be more than  $10^6 \text{ sec}$  in the lower stratosphere and reaches about  $10^5 \text{ sec}$  near the stratopause.

$\text{ClONO}_2$  and HOCl must be introduced in the stratospheric chlorine chemistry, and their equations have the following forms

$$\frac{dn(\text{ClONO}_2)}{dt} + n(\text{ClONO}_2)J_{\text{ClONO}_2} = d_{13M}n(\text{ClO})n(\text{NO}_2) \quad (55)$$

and

$$\frac{dn(\text{HOCl})}{dt} + n(\text{HOCl})J_{\text{HOCl}} = d_{15}n(\text{ClO})n(\text{HO}_2) \quad (56)$$

In (55),  $J_{\text{ClONO}_2}$  may correspond to  $J_{\text{Cl-NO}_3} + J_{\text{ClONO-O}} + J_{\text{ClO-NO}_2}$  with Cl and  $\text{NO}_3$  as principal products; its lifetime is relatively short (Figure 6). The reactions of  $\text{ClONO}_2$  with OH and O have not been written here.

In (56),  $J_{\text{HOCl}}$  may correspond to  $J_{\text{OH-Cl}} + J_{\text{HCl-O}} + J_{\text{ClO-H}}$ , with OH and Cl as principal products; other reactions are neglected. HOCl, and particularly  $\text{ClONO}_2$ , may be considered in photochemical equilibrium conditions for a general analysis of stratospheric conditions.

If we compare the atmospheric bromine chemistry with that of chlorine, we note differences which gives the following equation for atomic bromine

$$\begin{aligned} n(\text{Br}) [e_2 n(\text{O}_3) + e_7 n(\text{HO}_2)] \\ = n(\text{HBr}) [J_{\text{HBr}} + e_{11} n(\text{OH}) + e_{12} n(\text{O})] + n(\text{BrONO}_2)J_{\text{Br-NO}_3} + n(\text{HOBr})J_{\text{OH-Br}} \\ + n(\text{C}_x\text{Br}_y)J_{\text{C}_x\text{Br}_y} \dots \\ + n(\text{BrO}) [e_3 n(\text{O}) + e_{4a} n(\text{NO}) + e_{4b} n(\text{OH}) + e_5 n(\text{ClO}) + 2e_6 n(\text{BrO})] \end{aligned} \quad (57)$$

The bromine monoxide equation takes the form

$$\begin{aligned} n(\text{BrO}) [J_{\text{BrO}} + e_3 n(\text{O}) + e_{4a} n(\text{NO}) + e_{4b} n(\text{OH}) + e_5 n(\text{ClO}) \\ + 2e_6 n(\text{BrO}) + e_{13M} n(\text{NO}_2) + e_{15} n(\text{HO}_2)] \\ = e_2 n(\text{Br})n(\text{O}_3) \end{aligned} \quad (58)$$

The bromine hydroxide is not in chemical equilibrium at all altitudes and, therefore,

$$\begin{aligned} \frac{\partial n(\text{HBr})}{\partial t} + \text{div} [n(\text{HBr})w(\text{HBr})] \\ + n(\text{HBr}) [J_{\text{HBr}} + e_{11} n(\text{OH}) + e_{12} n(\text{O})] = n(\text{Br})d_7 n(\text{HO}_2) + \dots \end{aligned} \quad (59)$$

In these equations, the effects of  $\text{CH}_4$  and  $\text{H}_2$  do not exist, and reactions between BrO with BrO and ClO are introduced

In addition to (57), (58) and (59),  $\text{BrONO}_2$  and  $\text{HOBr}$  must be also considered, and

$$\frac{dn(\text{BrONO}_2)}{dt} + n(\text{BrONO}_2)J_{\text{BrNO}_3} = e_{13M}n(\text{NO}_2)n(\text{BrO}) \quad (60)$$

and

$$\frac{dn(\text{HOBr})}{dt} + n(\text{HOBr})J_{\text{HOBr}} = e_{15}n(\text{HO}_2)n(\text{BrO}) \quad (61)$$

in which  $J_{\text{BrNO}_3}$  and  $J_{\text{HOBr}}$  may represent all possible photodissociation products. Reactions of  $\text{BrONO}_2$  and  $\text{HOBr}$  with other constituents have been neglected, but could be introduced without modifying our analysis.

The fluorine compounds will not be considered here since F and FO concentrations must be very small; however they should be discussed in a more general analysis of the stratospheric ozone chemistry.

**EFFECT OF HALOGEN COMPOUNDS AND NITROGEN OXIDES:** If we consider only the terms corresponding to chlorine and bromine in the general equation (25), we may write

$$\begin{aligned} \frac{\partial n(\text{O}_3)}{\partial t} + \dots + n(\text{O}) [2d_3n(\text{ClO}) + d_{12}n(\text{HCl}) + 2e_3n(\text{BrO}) + e_{12}n(\text{HBr})] \\ + n(\text{ClO}) [d_{4a}n(\text{NO}) + d_{4b}n(\text{OH}) + d_{13M}n(\text{NO}_2) + d_{15a}n(\text{HO}_2) + 2e_5n(\text{BrO})] \\ + n(\text{BrO}) [e_{4a}n(\text{NO}) + e_{4b}n(\text{OH}) + 2e_6n(\text{BrO}) + e_{13M}n(\text{NO}_2) + e_{15}n(\text{HO}_2)] \\ = \dots + n(\text{ClONO}_2)J_{\text{ClONO-O}} + n(\text{BrONO}_2)J_{\text{BrONO-O}} \\ + n(\text{HOCl})J_{\text{HCl-O}} + n(\text{HOBr})J_{\text{HBr-O}} \end{aligned} \quad (62)$$

In this expression, the chemical equilibrium equations (53) for ClO and (58) for BrO have been introduced without any simplification.

If we consider, also in the general equation (25), only the terms related to nitrogen oxides with the introduction of the chemical equilibrium conditions for nitric oxide given by (48) and also for nitrogen trioxide given by (46), the general equation takes the form

$$\begin{aligned} \frac{\partial n(\text{O}_3)}{\partial t} + \dots + 2b_3n(\text{O})n(\text{NO}_2) + P(\text{NO}) + 2n(\text{NO})J_{\text{NO-O}_2} + 2b_{N_2O}^*n(\text{O}^*)n(\text{N}_2\text{O}) \\ = n(\text{NO}) [2J_{\text{NO}} + b_{29}n(\text{HO}_2) + c_5n(\text{CH}_3\text{O}_2) + d_{4a}n(\text{ClO}) + e_{4a}n(\text{BrO})] \\ + n(\text{HO}_2\text{NO}_2)J_{\text{OH-NO}_3} + b_{27}n(\text{OH})n(\text{HNO}_3) + b_{25}n(\text{OH})n(\text{HNO}_2) \\ + \left\{ b_{21}n(\text{OH})n(\text{NO}) - n(\text{HNO}_2) [J_{\text{HNO}_2} + b_{25}n(\text{OH})] \right\} \end{aligned}$$



$$\begin{aligned}
 & + \left\{ n(\text{N}_2\text{O}_5) [J_{\text{N}_2\text{O}_5} + b_{12c}n(\text{M})] - b_{12M}n(\text{NO}_2)n(\text{NO}_3) \right\} \\
 & + 2n(\text{N}) [b_6n(\text{NO}) + b_5n(\text{NO}_2) - b_{1M}n(\text{NO}) - b_8n(\text{O}_3)] \\
 & + n(\text{ClONO}_2)J_{\text{Cl-NO}_3} + d_9n(\text{Cl})n(\text{HNO}_3) + n(\text{BrONO}_2)J_{\text{Br-NO}_3}
 \end{aligned} \tag{63}$$

The simultaneous effect of nitrogen oxides and halogen compounds is obtained by the addition of (62) and (63)

$$\begin{aligned}
 & \frac{\partial n(\text{O}_3)}{\partial t} + \dots \\
 & + n(\text{O}) [2b_3n(\text{NO}_2) + 2d_3n(\text{ClO}) + 2e_3n(\text{BrO}) + d_{12}n(\text{HCl}) + e_{12}n(\text{HBr})] \\
 & + P(\text{NO}) + 2b_{\text{N}_2\text{O}}^* n(\text{O}^*)n(\text{N}_2\text{O}) + 2n(\text{NO}_3)J_{\text{NO-O}_2} \\
 & + n(\text{ClO}) [d_{4b}n(\text{OH}) + 2e_5n(\text{BrO})] \\
 & + n(\text{BrO}) [e_{4b}n(\text{OH}) + 2e_6n(\text{BrO})] \\
 & = n(\text{NO}) [2J_{\text{NO}} + b_{29}n(\text{HO}_2) + c_5n(\text{CH}_3\text{O}_2)] \\
 & + n(\text{HO}_2\text{NO}_2)J_{\text{OH-NO}_3} + n(\text{OH}) [b_{25}n(\text{NO}) + b_{27}n(\text{NO}_2) + d_9n(\text{Cl})n(\text{HNO}_3)] \\
 & + 2n(\text{N}) [b_6n(\text{NO}) + b_5n(\text{NO}_2) - b_{1M}n(\text{NO}) - b_8n(\text{NO}_3)] \\
 & + \left\{ \text{HNO}_2 \right\} + \left\{ \text{N}_2\text{O}_5 \right\} + \left\{ \text{ClONO}_2 \right\} + \left\{ \text{BrONO}_2 \right\} \\
 & + [n(\text{HOCl})J_{\text{HCl-O}} - d_{15}n(\text{HO}_2)n(\text{ClO})] \\
 & + [n(\text{HOBr})J_{\text{HBr-O}} - e_{15}n(\text{HO}_2)n(\text{BrO})]
 \end{aligned} \tag{64}$$

In this expression, we may notice the characteristic terms  $2b_3n(\text{NO}_2)$ ,  $2d_3n(\text{ClO})$  and  $2e_3n(\text{BrO})$  and the perturbations terms introduced by the reactions of ClO and BrO with OH and BrO. Among the production terms we note the reaction of NO with  $\text{HO}_2$ . The braced terms involving  $\text{HNO}_2$ ,  $\text{N}_2\text{O}_5$ ,  $\text{ClONO}_2$  and  $\text{BrONO}_2$  represent equations for photochemical equilibrium conditions.

**EFFECT OF HYDROGEN COMPOUNDS:** In order to complete the general equation (25) modified by the effect of nitrogen oxides and halogen compounds represented by (64), it is necessary to introduce the effect of hydrogen compounds. On substituting the value of the OH concentration given by (40), the general stratospheric equation becomes

$$\begin{aligned}
 & \frac{\partial n(O_3)}{\partial t} + \text{div} [n(O_3)w(O_3)] \\
 & + 2 [k_3 n(O) + a_6 n(OH)] n(O_3) \\
 & + 2 [a_5 n(OH) + b_3 n(NO_2) + d_3 n(ClO) + e_3 n(BrO)] n(O) \\
 & + n(OH) [a_{16} n(OH) + 2a_{16M} n(OH) + a_{17} n(HO_2) + a_{19} n(H_2) + a_{30} n(H_2O_2)] \\
 & + c_2 n(CH_4) + c_8 n(H_2CO) + c_{17} n(CH_3O_2H) + c_{20} n(CO) \\
 & + b_{25} n(HNO_2) + b_{27} n(HNO_3) + d_{11} n(HCl) + e_{11} n(HBr)] \\
 & + 2n(ClO) [d_{4b} n(OH) + e_5 n(BrO)] + 2n(BrO) [e_{4b} n(OH) + e_6 n(BrO)] \\
 & + P(NO) + 2b_{NO}^* n(O^*) n(N_2O) + 2n(NO_3) J_{NO-O_2} \\
 = & 2n(O_2) J_2 + 2n(HO_2) J_{HO_2} + 2n(H_2O_2) J_{H_2O_2} \\
 & + n(H_2O) [J_{H-OH} + J_{H_2-O} + a_{H_2O}^* n(H_2O)] \\
 & + n(H) \{ a_{20} + 2a_{15} \} n(HO_2) \\
 & + n(CO_2) J_{CO_2} + n(CH_3O_2H) J_{CH_3OOH} + n(N_2O) J_{N_2O} \\
 & + 2n(HO_2NO_2) J_{OH-NO_3} + 2n(N) [b_6 n(NO) + b_5 n(O_3) - b_{1M} n(NO) - b_8 n(O_3)] \\
 & + n(NO) [2J_{NO} + 2b_{29} n(HO_2) + c_5 n(CH_3O_2)] \\
 & + \{ HNO_3 \} + \{ N_2O_5 \} + \{ ClONO_2 \} + \{ HOCl \} + \{ BrONO_2 \} + \{ HOBr \} \quad (65)
 \end{aligned}$$

THE STRATOSPHERIC OZONE EQUATION. If equation (27) governing the rate of change of the water vapor concentration is introduced in the final equation (65), the stratospheric ozone equation becomes

$$\begin{aligned}
 & \frac{\partial n(O_3)}{\partial t} + \text{div} [n(O_3)w(O_3)] + 2 [k_3 n(O) + a_6 n(OH)] n(O_3) \\
 & + 2 [a_5 n(OH) + b_3 n(NO_2) + d_3 n(ClO) + e_4 n(BrO)] n(O) \\
 & + 2 [d_{4b} n(OH) + e_5 n(BrO)] n(ClO) + 2 [e_{4b} n(OH) + e_6 n(BrO)] n(BrO)
 \end{aligned}$$

$$\begin{aligned}
 & + \frac{\partial n(\text{H}_2\text{O})}{\partial t} + \text{div} [n(\text{H}_2\text{O})w(\text{H}_2\text{O})] \\
 & + \frac{\partial n(\text{CO})}{\partial t} + \text{div} [n(\text{CO})w(\text{CO})] \\
 & + \frac{\partial n(\text{HNO}_3)}{\partial t} + \text{div} [n(\text{HNO}_3)w(\text{HNO}_3)] \\
 & + \frac{\partial n(\text{N}_2\text{O}_5)}{\partial t} + \text{div} [n(\text{N}_2\text{O}_5)w(\text{N}_2\text{O}_5)] \\
 & + \frac{\partial n(\text{ClONO}_2)}{\partial t} + \text{div} [n(\text{ClONO}_2)w(\text{ClONO}_2)] \\
 & + \frac{\partial n(\text{HOCl})}{\partial t} + \text{div} [n(\text{HOCl})w(\text{HOCl})] \\
 & + \frac{\partial n(\text{BrONO}_2)}{\partial t} + \text{div} [n(\text{BrONO}_2)w(\text{BrONO}_2)] \\
 & + \frac{\partial n(\text{HOBr})}{\partial t} + \text{div} [n(\text{HOBr})w(\text{HOBr})] \\
 & = 2n(\text{O}_2J_2) \\
 & + 2 \left\{ n(\text{H}_2\text{O}_2)J_{\text{H}_2\text{O}_2} + n(\text{HO}_2) \left[ J_{\text{HO}_2} + \{a_{15} + a_{20}\} n(\text{H}) \right] - a_{16}M n^2(\text{OH}) \right\} \\
 & + 2 \left\{ n(\text{NO}) [J_{\text{NO}} + b_{29}n(\text{HO}_2)] + n(\text{HO}_2\text{NO}_2)J_{\text{OH-NO}_3} + n(\text{N}) [\text{neglected}] \right\} \\
 & + \left\{ n(\text{N}_2\text{O}) [J_{\text{N}_2\text{O}} - b_{\text{N}_2\text{O}}^* n(\text{O}^*)] - P(\text{NO}) - 2n(\text{NO}_3)J_{\text{NO-O}_2} \right\} \quad (66)
 \end{aligned}$$

This equation shows that there are several processes of destruction of ozone: directly by 2 reactions of  $\text{O}_3$  with  $\text{O}$  and  $\text{OH}$ , by 4 reactions of  $\text{O}$  with  $\text{OH}$ ,  $\text{NO}$ ,  $\text{ClO}$  and  $\text{BrO}$  and, indirectly, by perturbations resulting from reactions of  $\text{ClO}$  and  $\text{BrO}$  with  $\text{OH}$  and  $\text{BrO}$ . As far as the actions of  $\text{ClO}$  (or  $\text{BrO}$ ) reaction with  $\text{OH}$  and  $\text{BrO}$  are concerned, they should be compared with the reactions of  $\text{OH}$  with  $\text{O}$  and of  $\text{ClO}$  with  $\text{O}$ , respectively, to determine the importance of their perturbation.

The ozone behavior may depend on the transport of several constituents. However, the effects of  $\text{HOBr}$ ,  $\text{BrONO}_2$ ,  $\text{HOCl}$ ,  $\text{ClONO}_2$  and  $\text{N}_2\text{O}_5$  can be neglected since photoequilibrium conditions can be used in a general analysis. The permanent transport of water vapor must be less than  $10^5$  to  $10^4$   $\text{H}_2\text{O}$  molecules  $\text{cm}^{-3} \text{sec}^{-1}$  in the lower stratosphere and less than  $10^6 \text{cm}^{-3} \text{sec}^{-1}$  (less than 10%) in the middle stratosphere in order to be neglected. As far as  $\text{CO}$  and  $\text{HNO}_3$  are concerned, their possible effect, only in the lower stratosphere, cannot be neglected without due consideration.

The production terms must be compared with the normal production term  $2n(\text{O}_2)J_2$  which decreases rapidly below 25 km. Terms which may reach values between  $10^6$  and  $10^5 \text{ cm}^{-3} \text{ sec}^{-1}$  below 20 km play an important role since  $n(\text{O}_2)J_2$  reaches, for an overhead sun,  $10^5 \text{ cm}^{-3} \text{ sec}^{-1}$  at 15 km, about  $10^6 \text{ cm}^{-3} \text{ sec}^{-1}$  at 20 km and about  $10^7$  at 25 km. For a solar zenith angle  $\chi$  corresponding to  $\sec \chi = 2$ , the corresponding values of  $n(\text{O}_2)J_2$  are only about  $10^4$  near 20 km and  $10^6$  between 25 and 30 km (see Figure 1).

If we consider the three braced groups of the second member of (66), we may conclude that very few terms may play a role. In the first group, terms involving OH and  $\text{HO}_2$  can be neglected and only  $n(\text{H}_2\text{O}_2)J_{\text{H}_2\text{O}_2}$  could be kept only to show that such a term is a production term.

In the second braced group,  $J_{\text{NO}}$  is negligible compared with  $b_{29}n(\text{HO}_2)$ ; which plays a role as a production term since  $b_{29}n(\text{HO}_2)n(\text{NO})$  can be greater than  $10^5 \text{ cm}^{-3} \text{ sec}^{-1}$ . The photodissociation of  $\text{HO}_2\text{NO}_2$  is shown as a production term if  $\text{HO}_2\text{NO}_2$  leads to  $\text{OH} + \text{NO}_3$ . This group also involves atomic nitrogen which is neglected under normal conditions. Finally, the third braced group involving  $\text{N}_2\text{O}$ , NO and  $\text{NO}_3$  does not play any role as production terms of oxygen atoms compared with other processes and  $n(\text{N}_2\text{O})J_{\text{N}_2\text{O}}$  is more important, under normal conditions, than the other (negative) terms.

Since, the effect of the reaction of  $\text{HO}_2$  with NO must be introduced in the lower stratosphere, as a production term in addition to the photodissociation of molecular oxygen it may be desired to remove this production term  $b_{29}n(\text{HO}_2)n(\text{NO})$  from equation (66). On taking the ratio  $n(\text{HO}_2)/n(\text{OH})$ , the corresponding equation for the rate of change of the stratospheric ozone concentration can be written

$$\begin{aligned} & \frac{\partial n(\text{O}_3)}{\partial t} + \text{div} [n(\text{O}_3)w(\text{O}_3)] + 2a_{15}n(\text{H})n(\text{HO}_2) \\ & + 2n(\text{O}_3) \left[ k_3n(\text{O}) + \left\{ a_2 + a_3 \right\} n(\text{H}) + a_{6c}n(\text{HO}_2) \right] \\ & + 2n(\text{O}) [a_7n(\text{HO}_2) + a_{24}n(\text{H}_2) + c_9n(\text{H}_2\text{CO}) + b_3n(\text{NO}_2) \\ & + d_3n(\text{ClO}) + d_{12}n(\text{HCl}) + e_3n(\text{BrO}) + e_{12}n(\text{HBr})] \\ & + 2n(\text{O}^*) [a_{\text{H}_2\text{O}}^* n(\text{H}_2\text{O}) + a_{\text{H}_2}^* n(\text{H}_2) + c_{1a}^* n(\text{CH}_4)] + 2n(\text{H}_2\text{O}_2)J_{\text{H}_2\text{O}_2} \\ & + 2n(\text{ClO})d_{15}n(\text{HO}_2) + 2n(\text{HOCl})J_{\text{HCl-O}} + 2n(\text{HOBr})J_{\text{HBr-O}} \\ & + 2n(\text{BrO}) [e_{15}n(\text{HO}_2) + e_5n(\text{ClO}) + e_6n(\text{BrO})] \\ & + 2 \left\{ \text{HNO}_2 \right\} + \left\{ \text{HOCl} \right\} + \left\{ \text{HOBr} \right\} \\ & + \frac{\partial n(\text{CO})}{\partial t} + \text{div} [n(\text{CO})w(\text{CO})] \\ & = 2n(\text{O}_2)J_2 + 2n(\text{H}_2\text{O})J_{\text{H}_2\text{-O}} + \frac{\partial n(\text{H}_2\text{O})}{\partial t} + \text{div} [n(\text{H}_2\text{O})w(\text{H}_2\text{O})] \\ & + 2n(\text{OH}) \left[ \left\{ a_{16} + a_{16M} \right\} n(\text{OH}) + a_{22}n(\text{H}) + b_{25}n(\text{HNO}_2) + b_{27}n(\text{HNO}_3) \right] \end{aligned}$$

$$+ 2n(\text{NO}) [J_{\text{NO}} + c_5 n(\text{CH}_3\text{O}_2)] + 2n(\text{CO}_2) J_{\text{CO}_2}$$

$$+ \frac{\partial n(\text{HNO}_3)}{\partial t} + \text{div} [n(\text{HNO}_3)w(\text{HNO}_3)]$$

$$+ \left\{ n(\text{N}_2\text{O}) [J_{\text{N}_2\text{O}} - b_{\text{N}_2\text{O}}^* n(\text{O}^*)] - P(\text{NO}) - 2n(\text{NO}_3) J_{\text{NO-O}_2} \right\}$$

$$+ 2d_9 n(\text{Cl})n(\text{HNO}_3) + \left\{ \text{N}_2\text{O}_5 \right\} + \left\{ \text{ClONO}_2 \right\} + \left\{ \text{BrONO}_2 \right\} \quad (67)$$

A detailed comparison between (66) and (67) indicates that the substitution of OH by HO<sub>2</sub> does not simplify the general discussion. In each equation the transport terms remain and it is notable that other terms occur in (67). By properly introducing numerical values of rate constants, and the concentrations, the principal perturbation terms should be recognized before finalizing the practical equations adapted to the different stratospheric regions; from the stratosphere with its photoequilibrium conditions to the tropopause with its varying lower boundary conditions.

**THE MESOSPHERIC PROBLEM:** It is convenient to consider the mesospheric conditions as an oxygen-hydrogen atmosphere. Hence, equation (26) can be considered as the most complete equation for a detailed analysis.

Since the ozone concentration is less than the atomic oxygen concentration the photochemical conditions can be considered

$$\frac{\partial n(\text{O}_3)}{\partial t} + \text{div} [n(\text{O}_3)w(\text{O}_3)] = 0 \quad (68)$$

and

$$\begin{aligned} n(\text{O}_3) \left[ J_3 + k_3 n(\text{O}) + \left\{ a_2 + a_3 \right\} n(\text{H}) + a_6 n(\text{OH}) + a_{6c} n(\text{HO}_2) \right] \\ = k_{24} n(\text{O}_2) n(\text{O}) \end{aligned} \quad (69)$$

The equation governing the rate of change of the concentration of atomic oxygen is, therefore, written

$$\begin{aligned} \frac{\partial n(\text{O})}{\partial t} + \text{div} [n(\text{O})w(\text{O})] + 2k_{1M} n^2(\text{O}) + k_{2M} n(\text{O}_2) n(\text{O}) \\ + n(\text{O}) [k_3 n(\text{O}_3) + a_5 n(\text{OH}) + a_7 n(\text{HO}_2) + a_{24} n(\text{H}_2)] \\ + n(\text{O}^*) [a_{\text{H}_2\text{O}}^* n(\text{H}_2\text{O}) + a_{\text{H}_2}^* n(\text{H}_2)] \\ = 2n(\text{O}_2) J_2 + n(\text{O}_3) [J_3 + a_2 n(\text{H})] + n(\text{H}_2\text{O}) J_{\text{H}_2-\text{O}} + n(\text{HO}_2) J_{\text{HO}_2} \\ + a_{16} n^2(\text{OH}) + a_{20} n(\text{H}) n(\text{HO}_2) + a_{22} n(\text{H}) n(\text{OH}) + n(\text{CO}_2) J_{\text{CO}_2} \end{aligned} \quad (70)$$

If we introduce the  $O_3$  photoequilibrium concentration (69) in equation (70), the general  $O$  concentration value is found to be

$$\begin{aligned}
 & \frac{\partial n(O)}{\partial t} + \text{div} [n(O)w(O)] + 2k_{1M}n^2(O) \\
 & + n(O_3) [2k_3n(O) + a_2n(H) + a_6n(OH) + a_{6c}n(OH)] \\
 & + n(O) [a_5n(OH) + a_7n(HO_2) + a_{24}n(H_2)] \\
 & + n(O^*) [a_{H_2O}^*n(O^*) + a_{H_2}^*n(H_2)] \\
 & = 2n(O_2)J_2 + n(H_2O)J_{H_2-O} + n(HO_2)J_{HO_2} + a_{20}n(H)n(HO_2) + a_{22}n(H)n(OH)
 \end{aligned} \quad (71)$$

The corresponding equations for  $HO_2$ ,  $OH$ ,  $H_2O_2$ ,  $H$ ,  $H_2$  and  $H_2O$  may be written with chemical equilibrium conditions for  $HO_2$ ,  $OH$  and  $H_2O_2$  and with transport conditions for  $H$ ,  $H_2$  and  $H_2O$ . Below a certain altitude atomic hydrogen is also in chemical equilibrium. Finally, photoequilibrium conditions can be adopted for atomic oxygen in the lower mesosphere, and are, in fact, introduced as lower boundary conditions at the stratopause level in a sunlit atmosphere.

From the preceding general expressions we readily find that

$$\begin{aligned}
 & n(HO_2) \left[ J_{HO_2} + a_{6c}n(O_3) + a_7n(O) + \left\{ a_{15} + a_{20} + a_{23} \right\} n(H) + a_{17}n(OH) \right. \\
 & \quad \left. + 2a_{27}n(HO_2) \right] \\
 & = n(H) [a_1n(M)n(O_2) + a_3n(O_3)] + n(OH) [a_6n(O_3) + a_{30}n(H_2O_2)]
 \end{aligned} \quad (72)$$

and

$$\begin{aligned}
 & n(OH) [a_5n(O) + a_6n(O_3) + a_{22}n(H) + 2a_{16}n(OH) + 2a_{16M}n(OH) \\
 & \quad + a_{17}n(HO_2) + a_{19}n(H_2) + a_{30}n(H_2O_2)] \\
 & = n(H) [a_2n(O_3) + 2a_{15}n(HO_2)] + n(HO_2) [J_{HO_2} + a_{6c}n(O_3) + a_7n(O)] \\
 & \quad + n(H_2) [a_{24}n(O) + a_{24}^*n(O^*)] + n(H_2O) [J_{H-OH} + 2a_{H_2O}^*n(O^*)] \\
 & \quad + 2n(H_2O_2)J_{H_2O_2}
 \end{aligned} \quad (73)$$

Hydrogen peroxide is also in photoequilibrium, and

$$n(H_2O_2) [J_{H_2O_2} + a_{30}n(OH)] = a_{27}n^2(HO_2) + a_{16M}n^2(OH) \quad (74)$$

Above the mesopause, where we must introduce the upper boundary conditions for atomic hydrogen, the transport conditions must be considered.

Hence

$$\begin{aligned}
 & \frac{\partial n(H)}{\partial t} + \text{div} [N(H)w(H)] \\
 & + n(H) \left[ a_1 n(M)n(O_2) + \{a_2 + a_3\} n(O_3) + a_{22}n(OH) + \{a_{15} + a_{20} + a_{23}\} n(HO_2) \right. \\
 & \left. = n(H_2O)J_{OH-H} + [a_5 n(O) + a_{19}n(H_2)] n(OH) + n(H_2) [a_{24}n(O) + a_{H_2}^* n(O^*)] \right] \quad (75)
 \end{aligned}$$

As far as  $H_2$  and  $H_2O$  are concerned, they are never in chemical equilibrium, and we must write the general mesospheric equations

$$\begin{aligned}
 & \frac{\partial n(H_2)}{\partial t} + \text{div} [n(H_2)w(H_2)] \\
 & + n(H_2) [a_{19}n(OH) + a_{24}n(O) + a_{H_2}^* n(O^*)] \\
 & = n(H) [a_{22}n(OH) + a_{23}n(HO_2) + n(H_2O)J_{H_2-O}] \quad (76)
 \end{aligned}$$

and

$$\begin{aligned}
 & \frac{\partial n(H_2O)}{\partial t} + \text{div} [n(H_2O)w(H_2O)] \\
 & + n(H_2O) [J_{OH-H} + J_{H_2O} + a_{H_2O}^* n(O^*)] \\
 & = n(H)a_{20}n(HO_2) + n(OH) [a_{16}n(OH) + a_{17}n(HO_2) + a_{19}n(H_2) + a_{30}n(H_2O_2)] \quad (77)
 \end{aligned}$$

The last three equations lead, of course, to

$$\begin{aligned}
 & \frac{\partial n(H)}{\partial t} + \text{div} [n(H)w(H)] + \frac{2 \partial n(H_2O)}{\partial t} + \text{div} [n(H_2O)w(H_2O)] \\
 & + \frac{2 \partial n(H_2)}{\partial t} + 2 \text{div} [n(H_2)w(H_2)] = 0 \quad (78)
 \end{aligned}$$

Equations (72) and (75) may be used to determine the value of the OH concentration. These equations reduce to

$$\frac{1}{2} \frac{\partial n(H)}{\partial t} + \frac{1}{2} \text{div} [n(H)w(H)]$$

$$\begin{aligned}
 & + n(H)a_{20}n(HO_2) + n(OH) [a_{16}n(OH) + a_{17}n(HO_2) + a_{27}n(H) + a_{30}n(H_2O_2)] \\
 & = n(H_2O) [J_{H-OH} + a_{H_2O}^* n(O^*)] + n(H_2) [a_{24}n(O) + a_{H_2}^* n(O^*)]
 \end{aligned} \tag{79}$$

This equation may be used in a very simplified form where atomic hydrogen is in chemical equilibrium. With this simplification, equation (79) reduces to

$$\begin{aligned}
 & n(HO_2) [a_{20}n(H) + a_{17}n(OH)] \\
 & = n(H_2O) [J_{H-OH} + a_{H_2O}^* n(O^*)] + n(H_2) [a_{24}n(O) + a_{H_2}^* n(O^*)]
 \end{aligned} \tag{80}$$

when the two slow reactions are neglected compared with the reaction of  $HO_2$  with H and OH.

Equations (72) to (79) may also be used to determine the ratio  $n(HO_2)/n(OH)$ . The general form is

$$\begin{aligned}
 & \frac{1}{2} \frac{\partial n(H)}{\partial t} + \frac{1}{2} \text{div} [n(H)w(H)] + n(H) \left\{ a_2 + a_3 \right\} n(O_3) \\
 & + n(HO_2) \left[ J_{HO_2} + a_{6c}n(O_3) + a_7n(O) + 2 \left\{ a_{15} + a_{20} + a_{23} \right\} n(H) \right. \\
 & \left. + 2a_{27}n(HO_2) \right] + n(H_2O)a_{H_2O}^* n(O^*) \\
 & = n(OH) [a_5n(O) + a_6n(O_3) + a_{16}n(OH) + a_{19}n(H_2) + 2a_{30}n(H_2O_2)]
 \end{aligned} \tag{81}$$

In simplified forms, where H is in chemical equilibrium, equation (81) becomes

$$n(H) \left\{ a_2 + a_3 \right\} n(O_3) + n(HO_2)a_7n(O) = n(OH)a_5n(O) \tag{82}$$

and equation (75),

$$n(H) \left[ a_1 n(M)n(O_2) + \left\{ a_2 + a_3 \right\} n(O_3) \right] = n(OH)a_5n(O) \tag{83}$$

After this general analysis, we may examine what type of simple formulas may be written instead of the general form (71). After eliminating reactions with atomic hydrogen, it is found that

$$\begin{aligned}
 & \frac{\partial n(O)}{\partial t} + \text{div} [n(O)w(O)] + 2k_{1M}n^2(O) + 2n(O_3) [k_3n(O) + a_6n(OH)] \\
 & + 2n(OH) [a_5n(O) + a_{16M}n(OH)] + \frac{\partial n(H_2O)}{\partial t} + \text{div} [n(H_2O)w(H_2O)] \\
 & = 2n(O_2)J_2 + 2n(H_2O_2)J_{H_2O_2} + 2n(HO_2)J_{HO_2} + 2 \left\{ a_{15} + a_{20} \right\} n(HO_2)n(H) \\
 & + n(CO_2)J_{CO_2}
 \end{aligned} \tag{84}$$



We can conveniently consider that

$$a_6 n(\text{OH}) < k_3 n(\text{O})$$

$$a_{16M} n(\text{OH}) < a_5 n(\text{O})$$

and also that

$$n(\text{O}_2) J_2 > 10^5 \text{ cm}^{-3} \text{ sec}^{-1} > n(\text{H}_2\text{O}_2) J_{\text{H}_2\text{O}_2} + n(\text{HO}_2) J_{\text{HO}_2} + \{a_{15} + a_{20}\} n(\text{H}) n(\text{HO}_2)$$

Hence, equation (84) is written in the simplified form

$$\begin{aligned} \frac{\partial n(\text{O})}{\partial t} + \text{div} [n(\text{O})w(\text{O})] + 2 \left[ k_{1M} + \frac{k_3 k_{2M}}{J_{3M}} \right] n^2(\text{O}) \\ + a_5 n(\text{OH}) n(\text{O}) + \frac{\partial n(\text{H}_2\text{O})}{\partial t} + \text{div} [n(\text{H}_2\text{O})w(\text{H}_2\text{O})] = 2n(\text{O}_2) J_2 \end{aligned} \quad (85)$$

if  $J_{3M}$  denotes, equation (69),

$$J_{3M} \equiv J_3 + k_{31} n(\text{O}) + \{a_2 + a_3\} n(\text{H}) + a_6 n(\text{OH}) + a_{6c} n(\text{HO}_2) \simeq J_3 + \{a_2 + a_3\} n(\text{H}) \quad (86)$$

Another form can be obtained instead of (84) if we keep the reactions of atomic hydrogen. We obtain

$$\begin{aligned} \frac{\partial n(\text{O})}{\partial t} + \text{div} [n(\text{O})w(\text{O})] + 2k_{1M} n^2(\text{O}) \\ + 2n(\text{O}_2) [k_3 n(\text{O}) + a_2 n(\text{H}) + a_6 n(\text{OH})] \\ + 2n(\text{H}) a_{1M} n(\text{O}_2) + \frac{\partial n(\text{H})}{\partial t} + \text{div} [n(\text{H})w(\text{H})] \\ = 2n(\text{O}_2) J_2 + 2n(\text{H}_2\text{O}_2) J_{\text{H}_2\text{O}_2} + 2n(\text{HO}_2) J_{\text{HO}_2} \\ + \frac{\partial n(\text{H}_2\text{O})}{\partial t} + \text{div} [n(\text{H}_2\text{O})w(\text{H}_2\text{O})] + 2n(\text{H}_2\text{O}) [J_{\text{OH-H}} + J_{\text{H}_2-\text{O}}] \end{aligned} \quad (87)$$

If we neglect the slow reactions, we may also write a simplified form corresponding to (86) to evaluate the importance of atomic hydrogen and its transport with the  $\text{H}_2\text{O}$  transport.

A final remark should be made concerning the reaction of  $\text{O}_3$  with  $\text{O}$ . If the reaction  $\text{O} + \text{O} + \text{O}_2 + \text{M} \rightarrow \text{O}_2^* + \text{M}$  leads to an excited molecule  $\text{O}_2^*$ , it is necessary to determine the various processes which are involved: photodissociation, reaction with atomic hydrogen, deactivation by collision, infrared emission and reaction with atomic oxygen. Since a

deactivation by collision is certainly important, an exact determination is required in order to find whether  $2k_3^*n(O)n(O_3^*)$  is negligible or can compare with  $2k_3n(O)n(O_3)$ .

Finally, the mesospheric chemistry is also different from the stratospheric chemistry since the  $O_2$  photodissociation also depends on the solar radiation absorbed at Lyman alpha and in the spectral range of the  $O_2$  Schumann-Runge bands; which play a minor role in the stratosphere.

## SUMMARY AND CONCLUSION

The general stratospheric equation (69) shows that the behavior of the stratospheric ozone depends not only on its own transport (in the lower stratosphere) but also on the transport conditions of  $H_2O$ , which is never in chemical equilibrium, and of CO and  $HNO_3$ , which are not in chemical or photochemical equilibrium in the lower part of the stratosphere.

In a simplified form equation (69) can be

$$\begin{aligned}
 & \frac{\partial n(O_3)}{\partial t} + \text{div} [n(O_3)w(O_3)] + 2 [k_3n(O) + a_6n(OH)] n(O_3) \\
 & + 2 [a_5n(OH) + b_3n(NO_2) + d_3n(ClO) + e_4n(BrO)] n(O) \\
 & + 2 [d_{4b}n(OH) + e_5n(BrO)] n(ClO) + 2 [e_{4b}n(OH) + e_6n(BrO)] n(BrO) \\
 & + \frac{\partial n(H_2O)}{\partial t} + \text{div} [n(H_2O)w(H_2O)] \\
 & + \frac{\partial n(CO)}{\partial t} + \text{div} [n(CO)w(CO)] \\
 & + \frac{\partial n(HNO_3)}{\partial t} + \text{div} [n(HNO_3)w(HNO_3)] \\
 & = 2n(O_2)J_2 + 2n(NO)b_{29}n(HO_2) + 2n(H_2O_2)J_{H_2O_2}
 \end{aligned} \tag{88}$$

With equation (88) we, thus, have a general convenient expression for the rate of change of stratospheric ozone concentration in which the action of hydrogen, nitrogen and halogen compounds are represented by OH,  $NO_2$ , ClO and BrO; respectively.

The OH concentration is related to its production from  $H_2O$ ,  $CH_4$  and  $H_2$  by an expression (41) in which the values of the  $HO_2$  and H concentrations must be introduced. The effect of atomic hydrogen may be considered only in the upper stratosphere. On the other hand, the ratio  $n(HO_2)/n(OH)$  varies from a very simple form  $n(HO_2)/n(OH) \sim 1$  near the stratopause to a very complicated formula in the lower stratosphere near the tropopause. Equations (42) can be regarded as expressions showing how the ratio  $n(HO_2)/n(OH)$  is sensitive to atmospheric conditions; particularly in the lower stratosphere below the ozone peak.

The nitrogen dioxide concentration cannot be determined without the knowledge of the nitric oxide concentration. In virtue of equations (48) or (49), the convenient expression (51) indicates that, not only the exact photodissociation rate of  $NO_2$ , but also the production of NO must be known in order to obtain an absolute value for the  $NO_2$  concentration. The normal production of nitric oxide, which is due to the oxydation of  $N_2O$  by the excited oxygen atom  $O(^1D)$ , requires knowing the vertical distribution of  $N_2O$ , i.e. the solution of the following equation

$$\frac{\partial n(\text{N}_2\text{O})}{\partial t} + \text{div} [n(\text{N}_2\text{O})w(\text{N}_2\text{O})] + n(\text{N}_2\text{O}) [J_{\text{N}_2-\text{O}} + b_{\text{N}_2\text{O}}^* n(\text{O}^*)] = 0 \quad (89)$$

As far as the halogen monoxides ClO and BrO are concerned, the use of the ratios  $n(\text{Cl})/n(\text{ClO})$  and  $n(\text{Br})/n(\text{BrO})$  requires the knowledge of all production processes of atomic chlorine and bromine, i.e. the exact distribution of the sources of these two atoms (photodissociation processes and subsequent products) in the stratosphere.

The effect of the reaction of  $\text{HO}_2$  with NO must be introduced as an effective production in addition to the photodissociation of molecular oxygen below the ozone peak.

NICOLET  
APPENDIX

TABLE I. — Ozone and atomic oxygen reactions

SYMBOL	REACTION	REMARK
$k_1$	$O + O + M \rightarrow O_2 + M$	Mesosphere
$k_2$	$O + O_2 + M \rightarrow O_3 + M$	50 km, $7 \times 10^{-3} \text{ sec}^{-1}$ ; 15 km, $4 \times 10^3$
$k_3$	$O + O_3 \rightarrow 2O_2$	50 km, $4 \times 10^{-15} \text{ cm}^3 \text{ sec}^{-1}$ ; 15 km, $5 \times 10^{-16}$

TABLE II. — Hydrogen reactions

SYMBOL	REACTION	REMARKS
a <sub>1</sub>	$\text{H} + \text{O}_2 + \text{M} \rightarrow \text{HO}_2$	50 km, $6 \text{ sec}^{-1}$ ; 15 km, $3 \times 10^5$
a <sub>2</sub>	$\text{O}_3 + \text{H} \rightarrow \text{O}_2 + \text{OH}^*$	85 km, $1 \times 10^{-11} \text{ cm}^3 \text{ sec}^{-1}$ ; 50 km, $2.5 \times 10^{-11}$
a <sub>3</sub>	$\text{O}_3 + \text{H} \rightarrow \text{O} + \text{HO}_2$	Less than $0.03 a_2$
a <sub>4</sub>	$\text{OH} + \text{O} + \text{M} \rightarrow \text{M} + \text{HO}_2$	neglected
a <sub>5</sub>	$\text{O} + \text{OH} \rightarrow \text{O}_2 + \text{H}$	$4 \times 10^{-11} \text{ cm}^3 \text{ sec}^{-1}$
a <sub>6</sub>	$\text{OH} + \text{O}_3 \rightarrow \text{HO}_2 + \text{O}_2$	50 km, $5 \times 10^{-14} \text{ cm}^3 \text{ sec}^{-1}$ ; 15 km, $2 \times 10^{-14}$
a <sub>6c</sub>	$\text{HO}_2 + \text{O}_3 \rightarrow \text{OH} + 2\text{O}_2$	50 km, $1 \times 10^{-15} \text{ cm}^3 \text{ sec}^{-1}$ ; 15 km, $6 \times 10^{-16}$
a <sub>7</sub>	$\text{O} + \text{HO}_2 \rightarrow \text{O}_2 + \text{OH}^*$	$4 \times 10^{-11} \text{ cm}^3 \text{ sec}^{-1}$
a <sub>8</sub>	$\text{OH} + h\nu \rightarrow \text{O} + \text{H}$	neglected
a <sub>9</sub>	$\text{HO}_2 + h\nu \rightarrow \text{OH} + \text{O}$	known, small effect
a <sub>10</sub>	$\text{HO}_2 + h\nu \rightarrow \text{H} + \text{O}_2$	neglected
a <sub>11</sub>	$\text{H}_2\text{O} + h\nu \rightarrow \text{H}_2 + \text{O}(^1\text{D})$	mesosphere
a <sub>12</sub>	$\text{O}(^1\text{D}) + \text{H}_2\text{O} \rightarrow 2\text{OH}$	$2.3 \times 10^{-10} \text{ cm}^3 \text{ sec}^{-1}$
a <sub>13</sub>	$\text{H}_2\text{O} + h\nu \rightarrow \text{OH} + \text{H}$	mesosphere
a <sub>14</sub>	$\text{H} + \text{OH} + \text{M} \rightarrow \text{H}_2\text{O} + \text{M}$	neglected
a <sub>15</sub>	$\text{H} + \text{HO}_2 \rightarrow \text{OH} + \text{OH}$	$4 \times 10^{-11} \text{ cm}^3 \text{ sec}^{-1}$
a <sub>16</sub>	$\text{OH} + \text{OH} \rightarrow \text{H}_2\text{O} + \text{O}$	$2 \times 10^{-12} \text{ cm}^3 \text{ sec}^{-1}$
a <sub>16M</sub>	$\text{OH} + \text{OH} + \text{M} \rightarrow \text{H}_2\text{O}_2 + \text{M}$	$2.5 \times 10^{-31} n(\text{M}) \rightarrow 3 \times 10^{-11} \text{ cm}^3 \text{ sec}^{-1}$
a <sub>17</sub>	$\text{OH} + \text{HO}_2 \rightarrow \text{H}_2\text{O} + \text{O}$	$(4 \pm 2) \times 10^{-11} \text{ cm}^3 \text{ sec}^{-1}$
a <sub>18</sub>	$\text{H}_2 + \text{O} + \text{M} \rightarrow \text{H}_2\text{O} + \text{M}$	neglected
a <sub>19</sub>	$\text{OH} + \text{H}_2 \rightarrow \text{H}_2\text{O} + \text{H}$	50 km, $4 \times 10^{-15} \text{ cm}^3 \text{ sec}^{-1}$ ; 15 km, $5 \times 10^{-16}$
a <sub>20</sub>	$\text{H} + \text{HO}_2 \rightarrow \text{H}_2\text{O} + \text{O}$	$10^{-12} \text{ cm}^3 \text{ sec}^{-1}$
a <sub>21</sub>	$\text{H} + \text{H} + \text{M} \rightarrow \text{H}_2 + \text{M}$	neglected
a <sub>22</sub>	$\text{H} + \text{OH} \rightarrow \text{H}_2 + \text{O}$	to be neglected
a <sub>23</sub>	$\text{H} + \text{HO}_2 \rightarrow \text{H}_2 + \text{O}_2$	$2 \times 10^{-11} \text{ cm}^3 \text{ sec}^{-1}$
a <sub>24</sub>	$\text{H}_2 + \text{O} \rightarrow \text{OH} + \text{H}$	50 km, $6 \times 10^{-19} \text{ cm}^3 \text{ sec}^{-1}$ ; 15 km, $10^{-20}$
a <sub>24</sub> <sup>*</sup>	$\text{H}_2 + \text{O}(^1\text{D}) \rightarrow \text{OH} + \text{H}$	$1 \times 10^{-11} \text{ cm}^3 \text{ sec}^{-1}$
a <sub>25</sub>	$\text{CO} + \text{OH} \rightarrow \text{H} + \text{CO}_2$	sec c <sub>20</sub>
a <sub>26</sub>	$\text{HO}_2 + \text{NO} \rightarrow \text{NO}_2 + \text{OH}$	sec b <sub>29</sub>
a <sub>27</sub>	$\text{HO}_2 + \text{HO}_2 \rightarrow \text{H}_2\text{O}_2 + \text{O}_2$	50 km, $4 \times 10^{-12} \text{ cm}^3 \text{ sec}^{-1}$ ; 15 km, $1 \times 10^{-11}$
a <sub>28</sub>	$\text{H}_2\text{O}_2 + h\nu \rightarrow 2\text{OH}$	stratosphere and mesosphere
a <sub>29</sub>	$\text{H} + \text{H}_2\text{O}_2 \rightarrow \text{products}$	neglected
a <sub>30</sub>	$\text{OH} + \text{H}_2\text{O}_2 \rightarrow \text{H}_2\text{O} + \text{HO}_2$	50 km, $3 \times 10^{-12} \text{ cm}^3 \text{ sec}^{-1}$ ; $1 \times 10^{-12}$
a <sub>31</sub>	$\text{O} + \text{H}_2\text{O}_2 \rightarrow \text{products}$	neglected

TABLE III. -- Nitrogen reactions

SYMBOL	REACTION	REMARKS
$b_{H_2O}^*$	$O(^1D) + N_2O \rightarrow N_2 + O_2$ $\rightarrow NO + NO$	$5 \times 10^{-11} \text{ cm}^3 \text{ sec}^{-1}$ $6 \times 10^{-11} \text{ cm}^3 \text{ sec}^{-1}$
$b_1$	$O + N + M \rightarrow M + NO$	neglected
$b_2$	$O + NO + M \rightarrow NO_2 + M$	$10^{-31} (300/T)^2 n(M) \text{ cm}^3 \text{ sec}^{-1} \rightarrow 3 \times 10^{-11}$
$b_3$	$O + NO_2 \rightarrow NO + O_2$	$9 \times 10^{-12} \text{ cm}^3 \text{ sec}^{-1}$
$b_4$	$O_3 + NO \rightarrow NO_2 + O_2$	50 km, $10^{-14} \text{ cm}^3 \text{ sec}^{-1}$ ; 15 km, $2.5 \times 10^{-15}$
$b_5$	$NO_2 + h\nu \rightarrow NO + O$	about $10^{-2} \text{ sec}^{-1}$
$b_6$	$N + NO \rightarrow O_2 + N_2$	$3.5 \times 10^{-11} \text{ cm}^3 \text{ sec}^{-1}$
$b_7$	$N + O_2 \rightarrow NO + O$	50 km, $4 \times 10^{-17} \text{ cm}^3 \text{ sec}^{-1}$ ; 15 km, $2 \times 10^{-18}$
$b_7^*$	$N(^2D) + O_2 \rightarrow NO + O$	$6 \times 10^{-12} \text{ cm}^3 \text{ sec}^{-1}$
$b_8$	$N + O_3 \rightarrow NO + O_2$	less than $10^{-15} \text{ cm}^3 \text{ sec}^{-1}$
$b_9$	$NO_2 + O_3 \rightarrow NO_3 + O$	50 km, $1.5 \times 10^{-17} \text{ cm}^3 \text{ sec}^{-1}$ ; 15 km, $1.5 \times 10^{-18}$
$b_{10}$	$O + NO_2 + M \rightarrow NO_3 + M$	$10^{-31} n(N_2)(300/T)^2 \text{ cm}^3 \text{ sec}^{-1} \rightarrow 2 \times 10^{-11}$
$b_{11}$	$NO_3 + NO \rightarrow 2NO_2$	$1 \times 10^{-11} \text{ cm}^3 \text{ sec}^{-1}$
$b_{12}$	$NO_3 + NO_2 + M \rightarrow N_2O_5 + M$	$1.5 \times 10^{-30} n(M)(300/T)^3 \text{ cm}^3 \text{ sec}^{-1} \rightarrow 10^{-12}$
$b_{12c}$	$N_2O_5 + M \rightarrow NO_2 + NO_3 + M$ $N_2O_5 + h\nu \rightarrow NO_2 + NO_3$	about $10^{-5} \text{ sec}^{-1}$
$b_{13}$	$NO_3 + NO_2 \rightarrow NO_2 + O_2 + NO$	neglected
$b_{14}$	$NO_3 + NO_3 \rightarrow 2NO_2 + O_2$	neglected
$b_{15}$	$O + NO_3 \rightarrow NO_2 + O_2$	$10^{-11} \text{ cm}^3 \text{ sec}^{-1}$
$b_{16}$	$H + NO \rightarrow HNO + h\nu$	neglected
$b_{17}$	$H + NO + M \rightarrow HNO + M$	neglected
$b_{18}$	$H + HNO \rightarrow NO + H_2$	neglected
$b_{19}$	$OH + HNO \rightarrow NO + H_2O$	neglected
$b_{20}$	$H + NO_2 \rightarrow OH + NO$	neglected
$b_{20M}$	$H + NO_2 + M \rightarrow HNO_2 + M$	neglected
$b_{21}$	$NO + OH + M \rightarrow HNO_2 + M$	$6 \times 10^{-31} n(M)(300/T)^{5/2} \text{ cm}^3 \text{ sec}^{-1} \rightarrow 10^{-11}$
$b_{22}$	$NO_2 + OH + M \rightarrow HNO_3 + M$	$2.5 \times 10^{-30} n(M)(300/T)^3 \text{ cm}^3 \text{ sec}^{-1} \rightarrow 2.5 \times 10^{-11}$
$b_{23}$	$NO + HO_2 + M \rightarrow HNO_3 + M$	not observed

SYMBOL	REACTION	REMARKS
b <sub>24</sub>	$\text{H} + \text{HNO}_2 \rightarrow \text{H}_2 + \text{NO}_2$	neglected
b <sub>25</sub>	$\text{OH} + \text{HNO}_2 \rightarrow \text{H}_2\text{O} + \text{NO}_2$	$6 \times 10^{-12} \text{ cm}^3 \text{ sec}^{-1}$
b <sub>26</sub>	$\text{H} + \text{HNO}_3 \rightarrow \text{H}_2\text{O} + \text{NO}_2$	neglected, small
b <sub>27</sub>	$\text{OH} + \text{HNO}_3 \rightarrow \text{H}_2\text{O} + \text{NO}_3$	$0.9 \times 10^{-13} \text{ cm}^3 \text{ sec}^{-1}$
b <sub>28</sub>	$\text{HO}_2 + \text{NO}_2 + \text{M} \rightarrow \text{HO}_2\text{NO}_2 + \text{M}$	$2 \times 10^{-31} n(\text{M})(300/\text{T})^5 \text{ cm}^3 \text{ sec}^{-1}$ $6 \times 10^{-12}$
b <sub>29</sub>	$\text{NO} + \text{HO}_2 \rightarrow \text{OH} + \text{NO}_2$	50 km, $8 \times 10^{-12}$ ; 15 km, $1 \times 10^{-11} \text{ cm}^3 \text{ sec}^{-1}$
b <sub>30</sub>	$\text{NO} + \text{H}_2\text{O}_2 \rightarrow \text{HNO}_2 + \text{OH}$	less than $5 \times 10^{-20} \text{ cm}^3 \text{ sec}^{-1}$ , neglected
J <sub>NO</sub>	$\text{NO} + h\nu \rightarrow \text{N} + \text{O}$	mesosphere, 190 nm
J <sub>NO<sub>3</sub></sub>	$\text{NO}_3 + h\nu \rightarrow \text{NO}_2 + \text{O}$ $\rightarrow \text{NO} + \text{O}_2$	$10^{-1} \text{ sec}^{-1}$
J <sub>HNO<sub>2</sub></sub>	$\text{HNO}_2 + h\nu \rightarrow \text{OH} + \text{NO}$	rapid
J <sub>HNO<sub>3</sub></sub>	$\text{HNO}_3 + h\nu \rightarrow \text{OH} + \text{NO}$	stratosphere
J <sub>HO<sub>2</sub>NO<sub>2</sub></sub>	$\text{HO}_2\text{NO}_2 + h\nu \rightarrow \text{HO}_2 + \text{NO}_2$ $\rightarrow \text{OH} + \text{NO}_3$	at 300 - 350 nm

TABLE IV. - Methane reactions

SYMBOL	REACTION	REMARKS
$c_1$	$O(^3P) + CH_4 \rightarrow CH_3 + OH$	50 km, $1.5 \times 10^{-18} \text{ cm}^3 \text{ sec}^{-1}$ ; 15 km, $6 \times 10^{-21}$
$c_{1a}^*$	$O(^1D) + CH_4 \rightarrow CH_3 + OH$	$1.3 \times 10^{-10} \text{ cm}^3 \text{ sec}^{-1}$
$c_{1b}^*$	$\rightarrow H_2 + H_2CO$	$1.4 \times 10^{-11} \text{ cm}^3 \text{ sec}^{-1}$
$c_2$	$OH + CH_4 \rightarrow CH_3 + H_2O$	50 km, $5 \times 10^{-15} \text{ cm}^3 \text{ sec}^{-1}$ ; 15 km, $2.5 \times 10^{-15}$
$c_3$	$O + CH_3 \rightarrow H + H_2CO$	$1 \times 10^{-10} \text{ cm}^3 \text{ sec}^{-1}$
$c_4$	$CH_3 + O_2 + M \rightarrow CH_3O_2 + M$	$2.2 \times 10^{-31} n(M)(300/T)^2 \text{ cm}^3 \text{ sec}^{-1} \rightarrow 2 \times 10^{-12}$
$c_5$	$CH_3O_2 + NO \rightarrow CH_3O + NO_2$	$7 \times 10^{-12} \text{ cm}^3 \text{ sec}^{-1}$
$c_6$	$CH_3O_2 + NO_2 + M \rightarrow CH_3O_2NO_2 + M$	$2 \times 10^{-30} n(M)(T/300)^4 \text{ cm}^3 \text{ sec}^{-1} \rightarrow 6 \times 10^{-12}$
$c_7$	$CH_3O_2 + HO_2 \rightarrow CH_3OOH + O_2$	$6 \times 10^{-12} \text{ cm}^3 \text{ sec}^{-1}$
$c_8$	$OH + H_2CO \rightarrow HCO + H_2O$	$c_8 = 10^{-11} \text{ cm}^3 \text{ sec}^{-1}$
$c_9$	$O + H_2CO \rightarrow OH + HCO$	50 km, $10^{-13} \text{ cm}^3 \text{ sec}^{-1}$ ; 15 km, $2 \times 10^{-14}$
$c_{10}$	$H + H_2CO \rightarrow H_2 + HCO$	neglected
$c_{11}$	$HCO + h\nu \rightarrow CO + H$	greater than $10^{-2} \text{ sec}^{-1}$
$c_{12}$	$HCO + O_2 \rightarrow CO + HO_2$	$5 \times 10^{-12} \text{ cm}^3 \text{ sec}^{-1}$
$c_{13}$	$HCO + OH \rightarrow H_2O + CO$	$1.5 \times 10^{-11} \text{ cm}^3 \text{ sec}^{-1}$
$c_{14}$	$CH_3O_2 + CH_3O_2 \rightarrow \text{products}$	$4 \times 10^{-13} \text{ cm}^3 \text{ sec}^{-1}$ , $c_5$ and $c_7$ more important
$c_{15}$	$CH_3O + O_2 \rightarrow HO_2 + H_2CO$	50 km, $1.4 \text{ sec}^{-1}$ ; 15 km, $4 \times 10^2 \text{ sec}^{-1}$
$c_{16}$	$CH_3O_2H \rightarrow H_2CO + OH$	absorption at 300 nm
$c_{17}$	$CH_3O_2H + OH \rightarrow H_2O_2 + CH_3O_2$	50 km, $6 \times 10^{-13} \text{ cm}^3 \text{ sec}^{-1}$ ; 15 km, $3 \times 10^{-13}$
$c_{18}$	$O_3 + H_2CO \rightarrow \text{products}$	less than $10^{-24} \text{ cm}^3 \text{ sec}^{-1}$ ; neglected
$c_{19}$	$O_3 + CH_3O_2 \rightarrow \text{products}$	less than $2 \times 10^{-17} \text{ cm}^3 \text{ sec}^{-1}$ ; neglected
$c_{20}$	$CO + OH \rightarrow CO_2 + H$	$1.35 \times 10^{-13} \text{ cm}^3 \text{ sec}^{-1}$
$(J_{CO_2})$	$CO_2 + h\nu \rightarrow CO + O$	particularly in mesosphere
$J_{H_2-CO}$	$H_2CO + h\nu \rightarrow H_2 + CO$	at 300 - 350 nm
$J_{H-HCO}$	$\rightarrow H + HCO$	



TABLE V. — Chlorine reactions

SYMBOL	REACTION	REMARKS
d <sub>1</sub>	$\text{XCl}_x + h\nu \rightarrow \text{XCl}_{x-1} + \text{Cl}$	Photodissociation
d <sub>2</sub>	$\text{Cl} + \text{O}_3 \rightarrow \text{ClO} + \text{O}_2$	50 km, $1 \times 10^{-11} \text{ cm}^3 \text{ sec}^{-1}$ ; 15 km, $6 \times 10^{-12}$
d <sub>3</sub>	$\text{ClO} + \text{O} \rightarrow \text{Cl} + \text{O}_2$	$5 \times 10^{-11} \text{ cm}^3 \text{ sec}^{-1}$
d <sub>4a</sub>	$\text{ClO} + \text{NO} \rightarrow \text{Cl} + \text{NO}_2$	50 km, $2 \times 10^{-11} \text{ cm}^3 \text{ sec}^{-1}$ ; 15 km, $3.5 \times 10^{-11} \text{ cm}^3 \text{ sec}^{-1}$
d <sub>4b1</sub>	$\text{ClO} + \text{OH} \rightarrow \text{Cl} + \text{HO}_2$	$1 \times 10^{-11} \text{ cm}^3 \text{ sec}^{-1}$
d <sub>4b2</sub>	$\rightarrow \text{O}_2 + \text{HCl}$	$d_{4b2} < 0.35 d_{4b}$
d <sub>5</sub>	$\text{Cl} + \text{CH}_4 \rightarrow \text{CH}_3 + \text{HCl}$	50 km, $7 \times 10^{-14} \text{ cm}^3 \text{ sec}^{-1}$ ; 15 km, $2 \times 10^{-14}$
d <sub>6</sub>	$\text{Cl} + \text{H}_2 \rightarrow \text{H} + \text{HCl}$	50 km, $7 \times 10^{-15} \text{ cm}^3 \text{ sec}^{-1}$ ; 15 km, $9 \times 10^{-16}$
d <sub>7</sub>	$\text{Cl} + \text{HO}_2 \rightarrow \text{O}_2 + \text{HCl}$	$4.5 \times 10^{-11} \text{ cm}^3 \text{ sec}^{-1}$
d <sub>8</sub>	$\text{Cl} + \text{H}_2\text{O}_2 \rightarrow \text{HO}_2 + \text{HCl}$	50 km, $3 \times 10^{-12} \text{ cm}^3 \text{ sec}^{-1}$ ; 15 km, $4 \times 10^{-13}$
d <sub>9</sub>	$\text{Cl} + \text{HNO}_3 \rightarrow \text{NO}_3 + \text{HCl}$	less than $5 \times 10^{-15} \text{ cm}^3 \text{ sec}^{-1}$
d <sub>10</sub>	$\text{Cl} + \text{H}_2\text{CO} \rightarrow \text{HCO} + \text{HCl}$	$7.5 \times 10^{-11} \text{ cm}^3 \text{ sec}^{-1}$
d <sub>11</sub>	$\text{HCl} + \text{OH} \rightarrow \text{Cl} + \text{H}_2\text{O}$	50 km, $6 \times 10^{-13} \text{ cm}^3 \text{ sec}^{-1}$ ; 15 km, $2 \times 10^{-13}$
d <sub>12</sub>	$\text{HCl} + \text{O} \rightarrow \text{Cl} + \text{OH}$	less than $10^{-16} \text{ cm}^3 \text{ sec}^{-1}$ , neglected
d <sub>13</sub>	$\text{ClO} + \text{NO}_2 + \text{M} \rightarrow \text{ClONO}_2 + \text{M}$	$1.5 \times 10^{-31} n(\text{M})(300/\text{T})^3 \text{ cm}^3 \text{ sec}^{-1}$ $1.5 \times 10^{-11}$
d <sub>14a</sub>	$\text{ClONO}_2 + h\nu \rightarrow \text{Cl} + \text{NO}_3$ $\rightarrow \text{ClONO}_2 + \text{O}$ $\rightarrow \text{Cl} + \text{NO}_2$	$J_{\text{ClONO}_2} \sim 10^{-3} \text{ cm}^3 \text{ sec}^{-1}$
d <sub>14b</sub>	$\text{ClONO}_2 + \text{OH} \rightarrow \text{products}$	50 km, $3.5 \times 10^{-13} \text{ cm}^3 \text{ sec}^{-1}$ ; 15 km, $2.5 \times 10^{-13}$
d <sub>14c</sub>	$\text{ClONO}_2 + \text{O}_2 \rightarrow \text{products}$	50 km, $1.5 \times 10^{-13} \text{ cm}^3 \text{ sec}^{-1}$ ; 15 km, $7.5 \times 10^{-14}$
d <sub>15a</sub>	$\text{ClO} + \text{HO}_2 \rightarrow \text{HOCl} + \text{O}_2$	50 km, $8 \times 10^{-12} \text{ cm}^3 \text{ sec}^{-1}$ ; 15 km, $2 \times 10^{-11}$
d <sub>15b</sub>	$\rightarrow \text{HCl} + \text{O}_3$	$d_{15b} < 0.03 d_{15}$
d <sub>16a</sub>	$\text{HOCl} + h\nu \rightarrow \text{OH} + \text{Cl}$ $\rightarrow \text{O} + \text{HCl}$	at 300 – 350 nm?
d <sub>16b</sub>	$\text{HOCl} + \text{OH} \rightarrow \text{H}_2\text{O} + \text{ClO}$	50 km, $1.5 \times 10^{-13} \text{ cm}^3 \text{ sec}^{-1}$ ; 15 km, $7 \times 10^{-14}$
d <sub>16c</sub>	$\text{HOCl} + \text{O} \rightarrow \text{OH} + \text{ClO}$	neglected

TABLE VI. — Bromine reactions

SYMBOL	REACTION	REMARKS
$e_1$	$XBr_x + h\nu \rightarrow XBr_{x-1} + Br$	Atom production
$e_2$	$Br + O_3 \rightarrow O_2 + BrO$	50 km, $10^{-12} \text{ cm}^3 \text{ sec}^{-1}$ ; 15 km, $5 \times 10^{-13}$
$e_3$	$BrO + O \rightarrow O_2 + Br$	$3 \times 10^{-11} \text{ cm}^3 \text{ sec}^{-1}$
$e_{4a}$	$BrO + NO \rightarrow NO_2 + Br$	50 km, $2.5 \times 10^{-11} \text{ cm}^3 \text{ sec}^{-1}$ ; 15 km, $3 \times 10^{-11}$
$e_{4b}$	$BrO + OH \rightarrow HO_2 + Br$	$5 \times 10^{-12} \text{ cm}^3 \text{ sec}^{-1}$
$e_5$	$BrO + ClO \rightarrow Br + Cl + O_2$	$1.5 \times 10^{-11} \text{ cm}^3 \text{ sec}^{-1}$
$e_6$	$BrO + BrO \rightarrow 2Br + O_2$	50 km, $6 \times 10^{-12} \text{ cm}^3 \text{ sec}^{-1}$ ; 15 km, $8 \times 10^{-12}$
$e_7$	$Br + HO_2 \rightarrow O_2 + HBr$	$2 \times 10^{-11} \text{ cm}^3 \text{ sec}^{-1}$
$e_8$	$Br + H_2O_2 \rightarrow HO_2 + HBr$	less than $10^{-14} \text{ cm}^3 \text{ sec}^{-1}$
$e_{11}$	$OH + HBr \rightarrow O_2 + HBr$	$8.5 \times 10^{-12} \text{ cm}^3 \text{ sec}^{-1}$
$e_{12}$	$O + HBr \rightarrow Br + OH$	neglected
$e_{13}$	$BrO + NO_2 + M \rightarrow BrONO_2 + M$	$5.5 \times 10^{-31} n(M) \text{ cm}^3 \text{ sec}^{-1} \rightarrow 10^{-11}$
$e_{14}$	$BrONO_2 + h\nu \rightarrow Br + NO_3$	see $ClONO_2$
$e_{15}$	$BrO + HO_2 \rightarrow O_2 + HOBr$	$5 \times 10^{-12} \text{ cm}^3 \text{ sec}^{-1}$
$e_{16}$	$HOBr + h\nu \rightarrow OH + Br$	see $HOCl$

TABLE VII. — Fluorine reactions

NICOLET

SYMBOL	REACTION	REMARKS
$f_1$	$\text{XF}_x + h\nu \rightarrow \text{XF}_{x-1} + \text{F}$	Photodissociation
$f_2$	$\text{F} + \text{O}_3 \rightarrow \text{FO} + \text{O}_2$	50 km, $1.2 \times 10^{-11} \text{ cm}^3 \text{ sec}^{-1}$ ; 15 km, $10^{-11}$
$f_3$	$\text{FO} + \text{O} \rightarrow \text{O}_2 + \text{F}$	$5 \times 10^{-11} \text{ cm}^3 \text{ sec}^{-1}$
$f_4$	$\text{FO} + \text{NO} \rightarrow \text{NO}_2 + \text{F}$	$2 \times 10^{-11} \text{ cm}^3 \text{ sec}^{-1}$
$f_5$	$\text{F} + \text{CH}_4 \rightarrow \text{CH}_3 + \text{HF}$	50 km, $7 \times 10^{-11} \text{ cm}^3 \text{ sec}^{-1}$ ; $4.5 \times 10^{-11}$
$f_6$	$\text{F} + \text{H}_2 \rightarrow \text{H} + \text{HF}$	50 km, $2 \times 10^{-11} \text{ cm}^3 \text{ sec}^{-1}$ ; $1 \times 10^{-11} \text{ cm}^3 \text{ sec}^{-1}$
$f_7$	$\text{F} + \text{H}_2\text{O} \rightarrow \text{OH} + \text{HF}$	$1 \times 10^{-11} \text{ cm}^3 \text{ sec}^{-1}$
$f_8$	$\text{F} + \text{O}_2 + \text{M} \rightarrow \text{FO}_2 + \text{M}$	$1 \times 10^{-32} n(\text{M})(300/\text{T})^{1.75} \text{ cm}^3 \text{ sec}^{-1}$
$f_9$	$\text{FO}_2 + \text{O} \rightarrow \text{FO} + \text{O}_2$	$5 \times 10^{-11} \text{ cm}^3 \text{ sec}^{-1}$
$f_{11}$	$\text{OH} + \text{HF}$	no reaction
$f_{13}$	$\text{FO} + \text{NO}_2 + \text{M} \rightarrow \text{FNO}_3 + \text{M}$	$8 \times 10^{-31} n(\text{M})(300/\text{T})^{3/4} \text{ cm}^3 \text{ sec}^{-1} \rightarrow 2 \times 10^{-11}$

# UNCERTAINTY AND SENSITIVITY STUDIES OF STRATOSPHERIC PHOTOCHEMISTRY

R. S. Stolarski  
National Aeronautics and Space Administration  
Laboratory for Planetary Atmospheres, Goddard Space Flight Center  
Greenbelt, MD 20771

## ABSTRACT

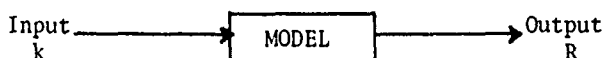
In the study of the potential effects of man-made pollutants on the earth's ozone layer, computer models of the stratosphere have been used extensively to provide quantitative predictions of ozone depletion. These models utilize as inputs experimentally determined transport coefficients, boundary conditions, chemical reaction rate coefficients and photodissociation cross sections and produce as outputs the concentrations of various chemical species as a function of altitude. In order to make an intelligent assessment of the impact of stratospheric pollution, it is necessary to know not only the predicted ozone depletion but also the precision of this prediction. A number of techniques have been developed for the study of uncertainty propagation. Amongst these are the sensitivity tests and Monte-Carlo simulations. The philosophy behind these techniques and their development and use on a variety of problems is described.

## I. Introduction

The subject of uncertainty in the calculations of atmospheric photochemical models is one in which little work has been done. Most of the work has been driven by the necessity to quantify uncertainty bounds on predictions of potential perturbations of ozone layer due to human activities. The major problem in such evaluations is the existence of two kinds of uncertainties which can be roughly thought of as analogous to precision and accuracy in an experiment. The precision in a model calculation is the result of the propagation of input parameter uncertainties through the model calculation. If the uncertainties in the input parameters can be estimated then the output uncertainty due to these sources is quantifiable. More difficult to evaluate is the problem of accuracy, or what has been left out of the model or is in error in the model because of incorrect assumptions. This type of uncertainty is, of course, unquantifiable. The problem then becomes one of determining the confidence that the model properly represents the physical and chemical processes occurring in the atmosphere by comparing results with well-defined field experiments. The balance of this paper will discuss first the techniques which have been used to propagate uncertainties in relatively well-known input parameters through a photochemical model calculation, and second the problems associated with determining the model accuracy.

## II. Sensitivity Technique

Consider a model of the stratosphere as a black box which has an input denoted by  $k$  and an output denoted by  $R$ . This situation is described by the simple diagram:



The input might represent a reaction rate coefficient, cross section, quantum yield, solar intensity, boundary condition, or transport coefficient while the output may be an ambient species concentration, perturbed concentration or column abundance. All of these are inputs or outputs, respectively, of typical stratospheric models. The crux of the sensitivity method is to isolate a single output variable  $R$  and study its response to a single input variable  $k$  assuming all other inputs constant. Thus the sensitivity can be defined as

$$S \equiv \frac{\text{fractional change in output}}{\text{fractional change in input}}$$

which can be rewritten as

$$S = \frac{dR/R}{dk/k} = \frac{d(\ln R)}{d(\ln k)}$$

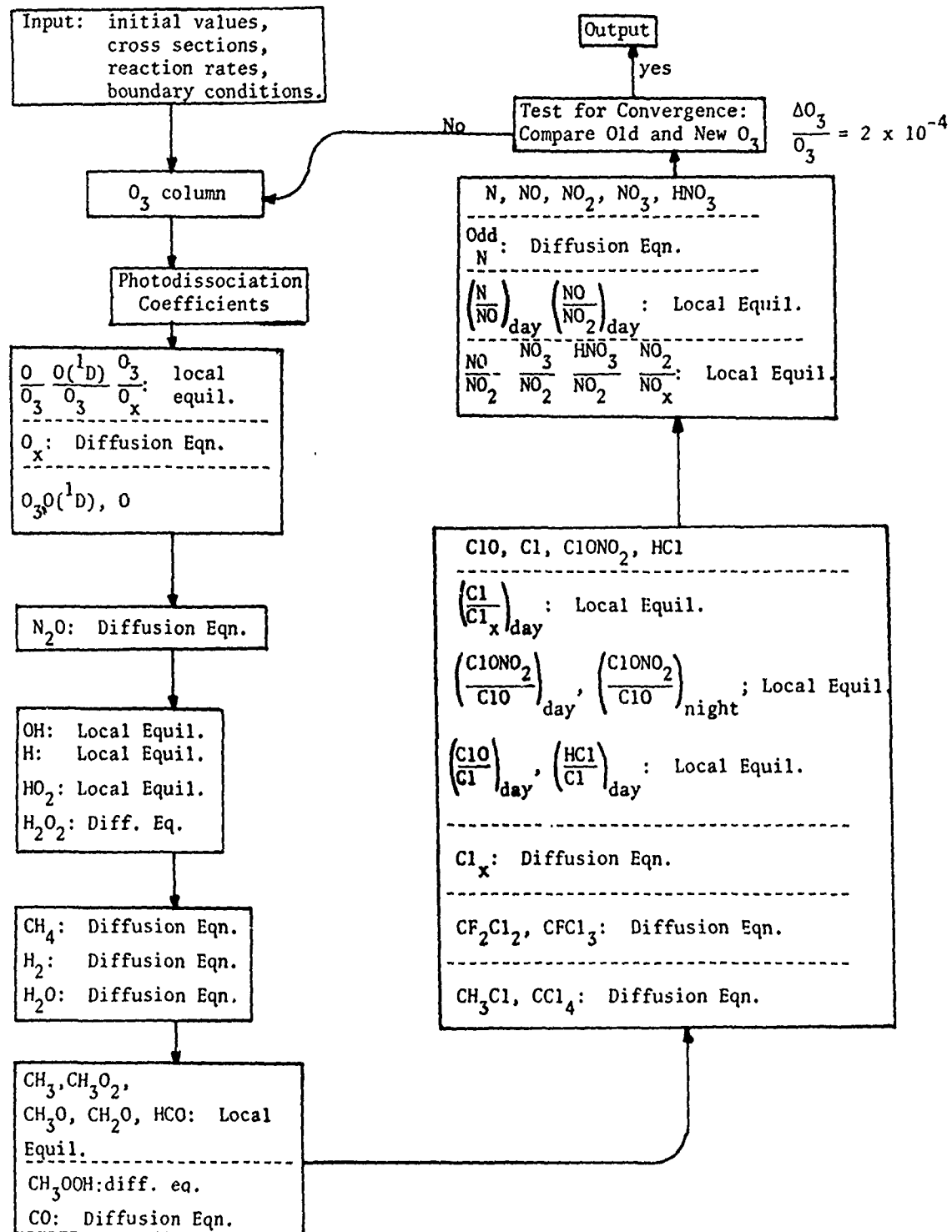


FIGURE 1: Logic diagram of steady-state model.

To evaluate a sensitivity  $S$  of an output parameter  $R$  to an input parameter  $k$  a model is required. Ideally the best possible model of stratospheric photochemistry should be used, but the large number of possible input and output parameters to be examined makes this approach too expensive. A much simpler model which takes much less computer time but retains the essential processes which determine atmospheric photochemical behavior is necessary. One possible realization of such a model is the one developed by our group at Goddard (see Rundel et al., 1978 and Butler, 1979). This model is one-dimensional, solves only for the steady-state, and assumes vertical transport in the diffusion approximation. Liberal use is made of the so-called "family approximation" transporting odd oxygen ( $O$ ,  $O_3$ ) odd nitrogen ( $N$ ,  $NO$ ,  $NO_2$ ,  $NO_3$ ,  $HNO_3$ ), and odd chlorine, or  $ClX$  ( $Cl$ ,  $ClO$ ,  $ClONO_2$ ,  $HCl$ ) as if each were a single species. Correlations of day to night variations are corrected for in  $ClO$ ,  $ClONO_2$ ,  $NO$ ,  $NO_2$ ,  $OH$  and  $HO_2$ . Figure 1 is a flow-chart, slightly modified to represent updates in the model, from Rundel et al. (1978) describing the logic of the model. The strategy to accomplish a relatively complete sensitivity study is then to use such a simplified model to investigate which output parameters show significant sensitivity to which input parameters. Then a more detailed model can be used to test the most significant sensitivities for comparison.

Examples of the type of results that can be obtained are shown in figure 2 from Butler (1979). All cases shown are the response of the change in the ozone column for a steady

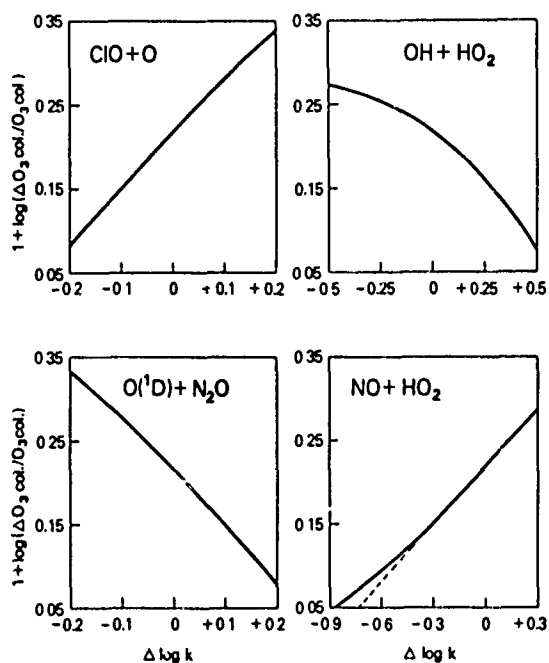


Figure 2: Calculated CFM-induced ozone perturbation vs. reaction rate coefficient with all other parameters held constant.

addition of fluorocarbons 11 and 12 at their 1975 release rates to changes in each of 4 reaction rate coefficients. The plots actually show one plus the log of the ozone column change versus  $\Delta \ln k$ , which is  $\ln k - \ln k_0$ . Since  $k_0$  is the assumed central value for the rate constant the slope of the plotted curve is the sensitivity  $d(\ln R)/d(\ln k)$  where  $R$  is the computed ozone column change for the given injection rate of fluorocarbons 11 and 12. As can be seen the sensitivity of chlorine-induced column ozone change to the rate coefficients for reaction of  $O$  with  $ClO$  and  $O(^1D)$  with  $N_2O$  proved to be remarkably constant over the range shown, which corresponds to the estimated  $\pm 2\sigma$  uncertainty limits. The magnitudes of the sensitivities deduced from these graphs are both about .65, one positive and one

negative. These were the results presented by Butler at the August 1977 IAGA-IAMAP meeting in Seattle. More recent results for these same sensitivities which will be given later in this paper are slightly over .4 in magnitude for each of these reactions. This illustrates one of the major difficulties in all uncertainty analyses; when one or more input parameters or model approximation changes, then the sensitivities to each of the input change as well as the basic centerline values of the outputs. Thus, while an input parameter change may require the rerunning of several model cases to determine new best values for perturbations, the same input parameter change may necessitate the complete rerunning of a sensitivity analysis which can be several hundred runs. In this case the major difference between the earlier results of Butler (1979) and the later results of Butler, Guthrie and Stolarski (some of which are published in the U.S. National Academy of Sciences report, 1979 and all of which are published in NASA RP 1049, Hudson and Reed, eds., 1980) is the improvement in model resolution from 5 Km to 1 1/4 km and the addition of temperature dependence on the rate coefficient for  $\text{NO} + \text{HO}_2$  to further increase its value and importance.

Also shown in figure 2 is the response of the ozone column change for a ClX perturbation to the rate coefficients for the reactions of OH with  $\text{HO}_2$  and NO with  $\text{HO}_2$ . These both show curvature illustrating the non-constancy of the sensitivity to a rate coefficient even when only that rate coefficient is changed. In both cases as the rate coefficient becomes small the sensitivity approaches zero as the reaction becomes completely insignificant compared to various competing reactions. The  $\text{NO} + \text{HO}_2$  reaction is a good illustration of the limitation of sensitivity and uncertainty studies such as those described in this paper. Prior to 1977 the reaction rate coefficient in most common use for this reaction was more than 10 times smaller than the presently used rate, based on Howard and Evenson (1978). The value used corresponded to a point well off the left-hand side of the graph and thus a very small slope and low sensitivity. An uncertainty study done at that time would probably not have assigned a large enough uncertainty to the rate coefficient of  $\text{NO} + \text{HO}_2$  to produce a significant uncertainty in the result and it would likely have been dismissed as a significant contributor to the overall uncertainty.

#### Relationship of Sensitivity to Uncertainty

The ultimate goal of the above sensitivity computations is to evaluate how they combine to lead to an overall uncertainty in an output parameter due to the uncertainties in all of the input parameters. The technique outlined below follows very closely that described in the U.S. National Academy of Sciences Report (1976) and subsequently by Butler (1979). To obtain total uncertainty consider first the uncertainty in an output parameter R due to only one input parameter k. Let U be the fractional uncertainty; then

$$U = dR/R = d(\ln R)$$

or by using the definition of sensitivity

$$U = S d(\ln k) = S (\ln k - \ln k_0)$$

Defining  $f = k/k_0$  gives

$$U = S \ln f$$

To obtain the cumulative uncertainty due to all input parameters let  $U_i$  be the uncertainty in the output R due to uncertainty in the input parameter  $k_i$ . Then the overall uncertainty is most readily represented by a root-mean-square sum, i.e.,

$$U_{\text{TOTAL}} = \sum_i U_i^2 = \sum_i (S_i \ln f_i)^2$$

Implicit in this technique is the assumption of normal distributions for the  $\ln k_i$  or  $\ln f_i$ . To convert  $U_{TOTAL}$  to the factors by which the centerline or "best" answer is to be multiplied to obtain the uncertainty limits, the exponential  $\exp(+U_{TOTAL})$  is taken. The upper uncertainty limit is  $\exp(+U_{TOTAL})$  times the centerline value while the lower uncertainty limit is  $\exp(-U_{TOTAL})$  times the centerline value. Whether these limits correspond to  $1\sigma$ ,  $2\sigma$  or some other uncertainty value depends on the input assumptions for the  $f_i$ .

The question of input uncertainties and what to assume for them is the biggest stumbling block in performing uncertainty analyses and is especially troublesome for the interpretation of results. Just as model results for ambient and perturbed concentration are entirely dependent upon assumed chemical reaction rates, boundary conditions, etc., the evaluations of output uncertainties are equally dependent on the assumed uncertainties in those input parameters. Fortunately, for the evaluation of "best" calculated values for ambient and perturbed concentrations, measured values are available for most crucial input parameters. Unfortunately for the purpose of the uncertainty analyses described here the input uncertainty is not really a measureable quantity. In fact it is not easy to agree on what is meant by the input uncertainty. The difficulty arises because of the two possible kinds of uncertainty in a measured value of, for instance, a rate coefficient. There is the precision, or reproducibility of a measurement which is frequently the experimental uncertainty which is quoted. But there is also the question of accuracy. If there is a known bias in an experiment it is usually corrected, but these corrections along with the other computations involved in analyzing the raw experimental data propagate uncertainties which can be estimated from the known precision of the measurement of system parameters to produce an estimate of the accuracy of a measurement. Many, but not all, experimenters include an estimate of accuracy in their quoted uncertainty limits. By far the greatest difficulty is the question of whether or not a particular laboratory measurement contains an unsuspected error leading to a grossly incorrect value whose uncertainty cannot be evaluated in any reasonable way. One form this problem frequently takes is the measurement, by two or more different groups using different techniques, of values that differ by significantly more than the stated uncertainty limits. Despite these difficulties the situation for reaction rate coefficients has improved to the point where with a few notable exceptions it is relatively easy to assign estimated uncertainties to the rates. This has been done by at least two groups of experts in reaction rate measurements and evaluations; Hampson and Garvin in their National Bureau of Standards monograph (NBS, 1978) and by a panel chaired by W. B. Demore (DeMore, 1979). In all the studies done by our group the evaluations of the DeMore committee have been taken at face value as the input uncertainties for rate coefficients. These are shown in the left column of Table 1 (from Butler et al. as published in NASA RP-1049, Hudson and Reed, eds., 1980) along with the estimates for boundary conditions, solar flux and cross-sections. The remaining 6 columns are the model computed sensitivities and uncertainties for the low side (difference in output for central value of input from that for minus  $2\sigma$  value of input), high side ( $+2\sigma$  minus central) and central ( $+1\sigma$  minus  $-1\sigma$ ) respectively. Variances in these values for a specific input parameter are an indication of nonlinearity and of possible growing or diminishing importance of a reaction as its rate coefficient is increased or decreased. Again it must be remembered that these are sensitivities of the chlorofluorocarbon induced ozone change to each of the inputs. If the sensitivity of say the ambient computed concentration of OH in the lower stratosphere were desired a completely different set of sensitivities would be obtained.

In order to focus the discussion table I will be taken as a specific example and only the central values considered. For emphasis the largest ten sensitivities have been enclosed in boxes while the largest ten uncertainties have been circled. Several interesting manipulations can be made with this data to illustrate how changes in the degree of knowledge concerning various rates will affect predictions of the overall uncertainty in an ozone perturbation. First the overall uncertainty may be computed from the r.m.s. sum, i.e., using only the first ten terms:

$$\begin{aligned} (U_{TOTAL})^2 &= (.257)^2 + (.233)^2 + (.207)^2 + (.204)^2 + (.166)^2 \\ &\quad + (.115)^2 + (.114)^2 + (.107)^2 + (.098)^2 = .315 \end{aligned}$$



giving  $U_{\text{TOTAL}} = .56$  and a factor uncertainty of  $\exp(U_{\text{TOTAL}})$  or 1.75 and 1/1.75. If all of the terms are used instead of only the first ten then  $(U_{\text{TOTAL}})^2 = .442$ ;  $U_{\text{TOTAL}} = .66$ , and the factors of uncertainty are 1.94 and 1/1.94. Thus, the accumulation of a number of very small uncertainty contributions can add up to a relatively significant impact. On the other hand, consider the case of the single largest uncertainty and for the sake of argument assume that it suddenly became zero while all of the others remained unchanged. Then  $(U_{\text{TOTAL}})^2 = .442 - .066 = .376$ ,  $U_{\text{TOTAL}} = .61$  and the factors of uncertainty are 1.84 and 1/1.84. Thus, improvement in a single rate coefficient or input parameter, even the most uncertain one has a less significant impact on the overall uncertainty than the combined effects of many small uncertainties. Finally, the important question must be asked; how much better can the answer be expected to be if all of the rate coefficients, boundary conditions, etc. were determined to  $\pm 10\%$  at the  $2\sigma$  level. This is equivalent to assuming all of the  $f_{2\sigma}$ 's to be 1.1 and then the  $U_i$ 's are all approximately .1 times the sensitivity. Thus,  $(U_{\text{TOTAL}})^2 = (.047)^2 + (.044)^2 + \dots = .014$  and  $U_{\text{TOTAL}} = .12$  yielding uncertainty factors of 1.13 and 1/1.13. The numbers presented in my talk were larger than this due to an arithmetic error on my part. These corrected values show that the expected best uncertainty in a prediction which can be achieved is not very much larger than the assumed uncertainty in the inputs and represents a significant improvement over the present situation (less than 15% vs. almost a factor of 2).

### III. Monte-Carlo Technique

The sensitivity technique described above is very useful for evaluation of the role of specific input parameter uncertainty effects but is subject to criticism on the grounds of not necessarily representing the combination of input uncertainties properly. This problem can be tested and overcome in a straight-forward manner by the application of a Monte-Carlo technique. Our group has attempted to carry out such a study for the ambient atmosphere concentrations and for a steady-state CFM scenario. Figure 3 is a logical flow diagram indicating how this particular study was designed. (See Stolarski et al., 1978; NASA RP-1010, Hudson, ed., 1977; NAS Panel on Stratospheric Chemistry and Transport, 1979; and NASA RP-1049, Hudson and Reed, eds., 1979). First, a "best" set of reaction rates must be chosen from which a centerline case for the ambient and perturbed atmosphere can be run. This is equivalent to what any modeler does when running a specific case to give an estimate of either an ambient concentration to compare with measurements or of a projected perturbation and provides a point of comparison for the distributions generated by the Monte-Carlo run. The next step involves the crucial additional assumption necessary to the Monte-Carlo analysis; that is, what input uncertainty distributions to use. At first glance it is tempting to use a normal distribution. For a well measured rate such as  $O + NO_2$  this might not be an unreasonable assumption. The rate coefficient has been measured to have virtually the same value by three separate investigators (Slanger et al., 1973; Davis et al., 1973; and Bemand et al., 1974) who reported over 60 individual measurements. The distribution of these measurements does indeed fit a normal distribution with a standard deviation of 7.8% which is slightly less than the overall uncertainty estimate given by the DeMore committee (JPL Publication 79-27, 1979) of a factor of 1.1. Because this rate coefficient is measured to have little or no temperature dependence there is little extra uncertainty in extrapolating to stratospheric temperatures.

More poorly known rate coefficients may be expected to have probability distributions that differ significantly from the normal distribution. A rate coefficient that is estimated to be uncertain by more than a factor of two on the high side cannot vary by the same linear magnitude on the low side because it would then become negative. The most natural assumption is to take the same factor for the low side uncertainty which is equivalent to assuming a linear uncertainty in the log of the input. Thus, a log-normal distribution might reasonably represent this case. For small uncertainties such as the  $O + NO_2$  example given above, the normal and log-normal distributions are virtually identical. Thus, the log-normal distribution is a possible distribution to describe the behavior of both small and large uncertainty and has been assumed as input, with distribution widths corresponding to a rate constant review such as that by the DeMore committee or Hampson and Garvin (1978),

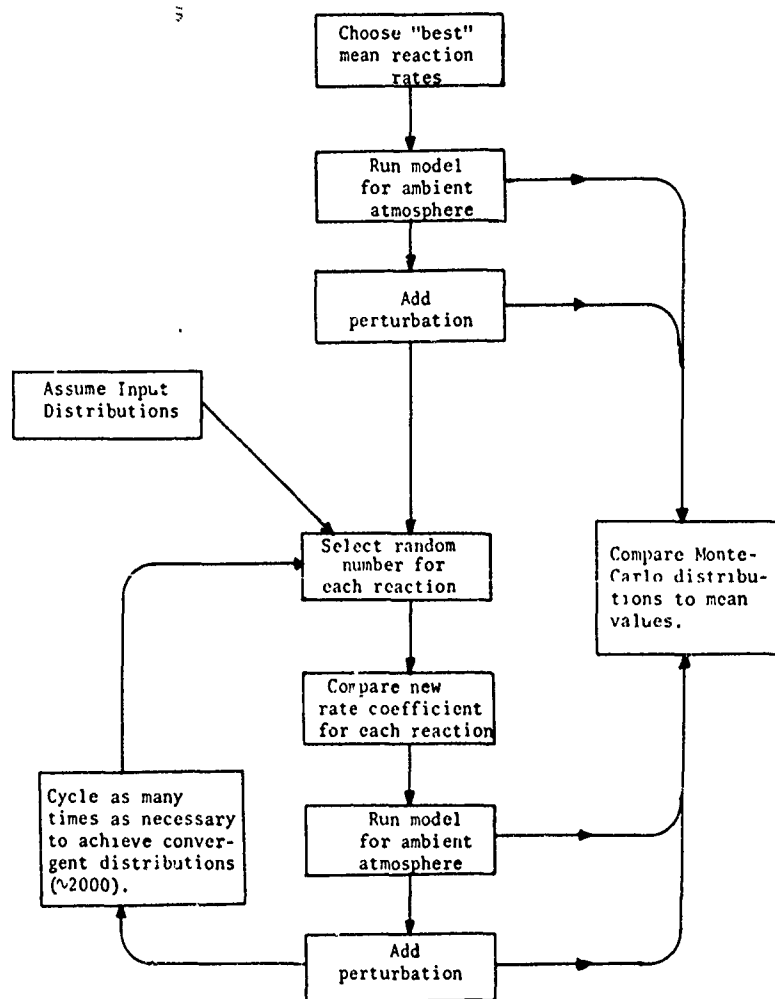


Figure 3: Logic diagram for Monte-Carlo uncertainty model.

in all of our group's studies. Another approach to the distributions has been taken by Smith (1978) and Duewer (personal communication). They both considered the historical accuracy of rate coefficient review panels as judged by how much evaluated coefficients changed in subsequent reviews. Both concluded that large changes from previous evaluations occurred more frequently than would have been expected on the basis of a log-normal distribution, i.e., a distribution much more like a Lorentzian which possesses a long tail would be more appropriate. No Monte-Carlo studies have been done using such a distribution. Such a study would probably consume significantly more computer time because of the increased frequency of hard to converge cases where an input parameter was significantly changed from its expected value.

Returning to figure 3, a random number is selected for each reaction which when combined with the assumed probability distribution determines a new value for the rate coefficient. The variation of each rate coefficient thus follows its assumed probability distribution but is independent of the values for all other rate coefficients or other input parameters being varied. Rate coefficients could be tied to one another, as when they are determined by ratio measurements, by simply using one random number to generate more than one new rate. The one simple experiment we did of this type was to tie together the  $\text{HO}_2$  reactions with a single varying random number. No significant difference in overall uncertainty was observed.

With each set of new reaction rate coefficients and other input parameters the model is then run for the ambient atmosphere and perturbation. These results are stored and the model is recycled to a new set of random numbers as many times as is needed to achieve convergent distributions of the output parameters. The convergence obtained in 500 Monte-Carlo iterations is not unreasonable. By 1000-1200 iterations the convergence is quite good and by 2000 essentially complete convergence has been obtained as determined by the variation in the running cumulative mean. These numbers are not unexpected because the sensitivity study shows significant uncertainty due to the order of 10 reactions. Thus, the space of significant variations in a column ozone perturbation due to CFM injection is spanned by about  $2^{11}$  or approximately 2000 iterations.

Application of this technique to a CFM-like perturbation yielded overall uncertainties (actually imprecision is a somewhat more descriptive term) for ozone depletion in approximate agreement with the sensitivity study (see e.g., Butler, 1979). This and the previously reported Monte-Carlo study (Stolarski et al., 1978) assumed that the output distributions were best fitted by log-normal curves on either side of the central value. Reanalysis of the distributions by Ehhalt et al., 1980 indicates that in fact linear normal curves provide a better fit. The distribution of column ozone change from a CFM perturbation was a linear normal form centered about a mean which was below the centerline case (15% to 16.5% column ozone depletion).

#### IV. Accuracy of a Model Representation

All of the above uncertainty propagation techniques and discussion has explicitly assumed that all of the uncertainties being dealt with were in known parameters and were quantifiable. The major additional problem is whether or not the model contains the correct mechanisms to describe the manner in which the atmosphere will respond to a perturbation. Put another way the computations described are an evaluation of the uncertainty of the model's response. The ultimately desired quantity is the uncertainty in the atmosphere's response to a perturbation. Three major categories of possible inaccuracies in a model's representation of the effects of a perturbation exist. These are:

1. Missing chemistry - are all of the important chemical interferences, storage mechanisms and removal processes included? This is, and will continue to be an unanswered question which can never be proven to have a positive answer. All that can be done is to demonstrate through careful experimentation, in the laboratory and in the field, that each alternative chemical possibility is unimportant. Of course some of the time, newly thought of processes turn out to be important. Then all of the models are rerun to evaluate the perturbations of interest including the new process, obtaining a different answer. In

general after such a change a reevaluation of the uncertainties yields a distribution as wide or wider than before but shifted to the new central value. Thus the uncertainty or imprecision of the model calculation may not improve; in fact because of the new process included the perception of the uncertainty may actually increase. But at the same time the confidence in the accuracy of the model's representation of the atmosphere has presumably increased. As more and more experimental facts concerning the atmosphere are found the latitude for alternative representations is reduced until eventually a consensus model representation of atmospheric chemistry will be obtained.

2. Feedbacks - is the temperature and dynamical response of the atmosphere properly included? The answer is, of course, no. The one-dimensional model which has been the major evaluation tool up to this time contains only a gross simplification of the transport due to dynamical processes that cannot respond to chemical perturbations. Thus, dynamical responses are ignored. Evaluation of the possibility of dynamical feedbacks on chemical perturbations is going to be a very difficult problem. Figure 4 is a schematic of the major types of processes occurring in the stratosphere. The chemistry or composition of

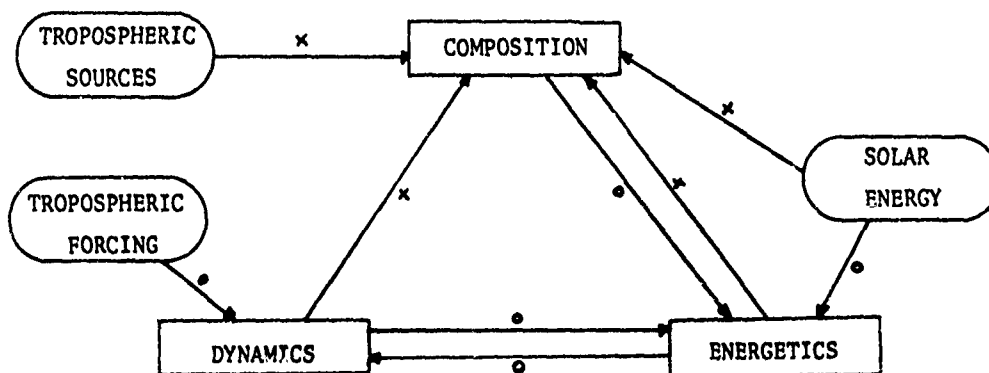


Figure 4: Logic diagram of upper atmospheric coupled radiative-chemical-dynamical system. x's and o's are explained in text.

the stratosphere is determined by a variety of processes; tropospheric sources provide stable molecules such as  $N_2O$ ,  $CH_4$ ,  $CH_3Cl$  etc. which are transported by dynamical processes to the stratosphere where solar radiation dissociates them into more reactive species such as the oxides  $NO$ ,  $ClO$ ,  $HO$  which are further transported from place to place by dynamical processes and eventually back out of the stratosphere as soluble species such as  $HNO_2$  and  $HCl$ . But the chemistry of these molecules is determined by the temperature through temperature dependent reaction rates while the temperature is a result of the overall energetics of radiative transfer which depends on the composition through both the uv absorption and IR emission processes. And further it is the energetics together with tropospheric forcing which drive stratospheric dynamical processes. The system of the composition, energetics, and dynamics of the stratosphere is closely coupled and a perturbation in any one element has the potential for affecting all of the others in non-simple ways. As an illustration of where the modeling field stands today on the modeling of this complex problem the x's in figure 4 indicate the processes that are typically computed explicitly or simply parameterized in a 1D photochemical model, while the o's indicate the processes typically accounted for in a general circulation model. The two are mutually exclusive and indicate an important current frontier of research in the field: that is how to begin to couple chemical and dynamical processes in a physically realistic way within both computer restrictions and our present limited experimental and theoretical understanding.

3. Other perturbations - how will other natural and anthropogenic changes affect any evaluation of a perturbing influence? Most model calculations of the effect of a perturbation consider that perturbation in isolation from all other possible influences on atmospheric ozone. While this is a legitimate procedure for isolating a specific effect for detailed study the application to the actual atmosphere is complicated by the interference of other mechanisms which also may affect ozone, but more importantly by the possible non-linear interactions between say  $\text{NO}_x$  and  $\text{ClO}_x$  perturbations (see e.g., Logan et al., 1978). Thus, the study of the budgets of all of the important stratospheric species is necessary for eventual improved evaluations.

## V. Summary

This paper has described some of the types of quantitative studies that have been done on uncertainty propagation for perturbation predictions and has attempted to stress some of the unquantifiable questions of model accuracy. These studies are in their infancy and have been mainly used in the practical process of attempting to give input to discussions of possible governmental regulations concerning perturbations of the ozone layer and to provide some guidance on program directions relative to the sensitivity of results to various rate coefficients and other input parameters. These analyses may prove more useful scientifically when they are applied to a model of a specific experiment such as species concentration ratios to determine the significance of a discrepancy from the expected ratio computed using measurements of other key parameters.

## References

- Bemand, P.P., M.A.A. Clyne and R.T. Watson, Atomic resonance fluorescence and mass spectrometry for measurements of the rate constants for elementary reactions:  $\text{O}(^3\text{P}) + \text{NO}_2 \rightarrow \text{NO}_2 + \text{O}_2$  and  $\text{NO} + \text{O}_3 \rightarrow \text{NO}_2 + \text{O}_2$ , J. Chem. Soc., Faraday Trans. 11, **70**, 564-576, 1974.
- Butler, D.M., Input sensitivity study of a stratospheric photochemistry model, PAGEOPH, **117**, 430-435, 1979.
- Davis, D.D., J.T. Herron and R.E. Huie, Absolute rate constants for the reaction  $\text{O}(^3\text{P}) + \text{NO}_2 \rightarrow \text{NO} + \text{O}_2$  over the temperature range 230-339K, J. Chem. Phys., **58**, 530-535, 1973.
- DeMore, W.B., ed., Chemical kinetic and photochemical data for use in stratospheric modeling, NASA/Jet Propulsion Laboratory Publication 79-27, 1979.
- Ehhalt, D.H., J.S. Chang and D.M. Butler, The probability distribution of the predicted DFM-induced ozone depletion, J. Geophys. Res., **84**, 7889-7894, 1979.
- Howard, Carleton J. and K.M. Evenson, Kinetics of the reaction of  $\text{HO}_2$  with  $\text{NO}$ , Geophys. Res. Letters, **4**, 437-440, 1977.
- Hudson, R.D., editor, Chlorofluoromethanes and the stratosphere, NASA RP-1010, 1977.
- Logan, J.A., M.J. Prather, S.C. Wofsy and M.B. McElroy, Atmospheric chemistry: Response to human influence, Phil. Trans. Royal Soc., (London), **290A**, 187-233, 1978.
- National Academy of Sciences, Halocarbons: Effects on stratospheric ozone, National Academy of Sciences, Washington, DC, 1976.
- National Academy of Sciences, Stratospheric ozone depletion by halocarbons: Chemistry and transport, National Academy of Sciences, Washington, DC, 1979.
- NASA RP-1049, R.D. Hudson and E.I. Reed eds., The stratosphere: Present and future, National Aeronautics and Space Administration, 1979.
- NBS (R.F. Hampson, Jr. and D. Garvin, eds.), Reaction rate and photochemical data for atmospheric chemistry-1977, U.S. Department of Commerce/National Bureau of Standards Special Publication 513, 1978.
- Rundel, R.D., D.M. Butler, and R.S. Stolarski, Uncertainty propagation in a stratospheric model I. Development of a concise stratospheric model, J. Geophys. Res., **83**, 3063-3073, 1978.
- Slanger, T.G., B.J. Wood and G. Black, Investigation of the rate coefficient for  $\text{O}(^3\text{P}) + \text{NO}_2 \rightarrow \text{O}_2 + \text{NO}$ , Int. J. Chem. Kinet., **5**, 615-620, 1973.
- Smith, W.S., Jr., Uncertainties in evaluated atmospheric rate constants, Proceedings of the WMO Symposium on the Geophysical Aspects and Consequences of Changes in the Composition of the Stratosphere, WMO-NO. 511, pp. 37-46, 1978.
- Stolarski, R.S., D.M. Butler and R.D. Rundel, Uncertainty Propagation in a Stratospheric Model: II. Monte-Carlo Analysis of Imprecisions Due to Reaction Rates, J. Geophys. Res., **83**, 3074-3078, 1978.

TABLE I

Input	$r_{20}$	S-	U-	S+	U+	Sc	Uc
$N_2O + O(^1D) \rightarrow NO + NO$	1.58	-0.338	-0.179	-0.488	-0.225	-0.429	-0.198
$O + O_2 + M \rightarrow O_3 + M$	1.38	-0.142	-0.046	-0.147	-0.047	-0.145	-0.047
$NO + HO_2 \rightarrow NO_2 + OH$	5.01 (-) 3.47 (+) 4.17 (c)	0.166	0.268	0.175	0.218	0.180	0.257
$O + O_3 \rightarrow O_2 + O_2$	1.58	-0.059	-0.027	-0.087	-0.040	-0.072	-0.033
$H_2O + O(^1D) \rightarrow OH + OH$	1.58	0.132	0.061	0.104	0.048	0.119	0.055
$OH + HO_2 \rightarrow H_2O + O_2$	3.16	-0.126	-0.145	-0.252	-0.290	-0.180	-0.207
$OH + O \rightarrow H + O_2$	2.00	-	-	-0.019	-0.013	-0.014	-
$OH + O_3 \rightarrow HO_2 + O_2$	2.00	-0.279	-0.193	-0.372	-0.257	-0.323	-0.223
$HO_2 + O_3 \rightarrow OH + O_2 + O_2$	1.58 (-) 3.98 (+) 7.94 (c)	0.056	0.155	0.085	0.118	0.080	0.166
$O(^1D) + M \rightarrow O + M$	1.38	0.275	0.075	0.275	0.095	0.295	0.075
$NO + O_3 \rightarrow NO_2 + O_2$	1.45	-0.170	-0.070	-0.186	-0.068	-0.170	-0.070
$NO_2 + O \rightarrow NO + O_2$	1.15	-0.175	-0.027	-0.206	-0.028	-0.200	-0.027
$NO_2 + OH + M \rightarrow HNO_3 + M$	1.58	0.264	0.122	0.228	0.105	0.247	0.114
$HNO_3 + OH \rightarrow NO_3 + H_2O$	1.26	-0.013	-	-0.030	-	-0.020	-
$CH_4 + OH \rightarrow CH_3 + H_2O$	1.58	0.092	0.043	0.093	0.043	0.093	0.043
$OH + CH_3Cl \rightarrow CH_2Cl + H_2O$	1.58	0.023	0.011	0.017	-	0.020	-
$CH_3O_2 + HO_2 \rightarrow CH_3OOH + O_2$	100.00	-	-	-	0.013	-	-
$N + NO \rightarrow N_2 + O$	1.58	0.032	0.015	0.039	0.018	0.036	0.017
$N + O_2 \rightarrow NO + O$	1.58	-0.035	-0.016	-0.031	-0.014	-0.033	-0.015
$H_2CO + OH \rightarrow HCO + H_2O$	2.51	-0.058	-0.054	-0.061	-0.056	-0.061	-0.056
$Cl + HO_2 \rightarrow HCl + O_2$	3.98	-0.022	-0.031	-0.091	-0.126	-0.047	-0.065
$Cl + O_3 \rightarrow ClO + O_2$	1.32	0.184	0.051	0.156	0.043	0.170	0.047
$ClO + O \rightarrow Cl + O_2$	1.58	0.477	0.220	0.405	0.186	0.442	0.204
$Cl + CH_4 \rightarrow HCl + CH_3$	2.29 (-) 1.32 (+) 1.74 (c)	-0.101	-0.084	-0.117	-0.032	-0.110	-0.061
$HCl + OH \rightarrow H_2 + Cl$	1.26	0.288	0.066	0.233	0.054	0.259	0.060
$ClO + NO \rightarrow NO_2 + Cl$	2.00	-0.105	-0.073	-0.119	-0.082	-0.112	-0.078
$OH + H_2O_2 \rightarrow HO_2 + H_2O$	2.00	-0.021	-0.015	-0.031	-0.022	-0.026	-0.018
$ClO + NO_2 + M \rightarrow ClONO_2 + M$	1.23 (-) 2.00 (+) 1.62 (c)	-	-0.041	-0.193	-0.133	-0.168	-0.081
$HNO_3 + O \rightarrow OH + NO_2$	(-) 100 (+) 2. (c) 14.1	-	-0.014	-0.019	-0.013	-	-0.018

\*All quantities with absolute values less than 0.010 have been suppressed

TABLE I: Sensitivities and uncertainties for CFM-induced ozone depletion.

TABLE I  
(Continued)

Input	$f_{2\sigma}$	S-	U-	S+	U+	Sc	Uc
N <sub>2</sub> O Flux (lower b.c.)	1.26	-0.437	-0.101	-0.513	-0.118	-0.472	-0.107
CH <sub>4</sub> Flux (lower b.c.)	1.45	-0.127	-0.047	-0.150	-0.055	-0.137	-0.051
H <sub>2</sub> O MR (lower b.c.)	1.45	0.087	0.032	0.089	0.033	0.087	0.033
Odd N Velocity (lower b.c.)	2.51	0.029	0.027	0.011	0.010	0.018	0.016
Odd Cl Velocity (lower b.c.)	2.00	-0.048	-0.033	-0.024	-0.016	-0.034	-0.024
CH <sub>3</sub> Cl Flux (lower b.c.)	2.00	-0.012	-	-0.028	-0.019	-0.019	-0.013
Odd N Velocity (Upper b.c.)	2.00	0.014	-	0.015	0.010	0.016	0.011
Odd O <sub>2</sub> Velocity (lower b.c.)	2.00	0.013	-	0.014	-	0.014	-
O( <sup>1</sup> D) quantum yield	1.11	-0.296	-0.030	-0.294	-0.030	-0.297	-0.030
O( <sup>1</sup> D) relative yield 300-305 nm	1.10	-0.034	-	-	-	-0.026	-
O( <sup>1</sup> D) relative yield 305-310 nm	1.69	-0.028	-0.015	-0.038	-0.020	-0.033	-0.018
$\lambda > 3200 \text{ \AA}$	1.10	0.393	0.036	0.394	0.036	0.393	0.036
1900-2000 $\text{\AA}$	1.45	0.087	0.032	0.109	0.040	0.096	0.036
2000-2050 $\text{\AA}$	1.45	0.048	0.018	0.060	0.022	0.053	0.020
2100-2150 $\text{\AA}$	1.45	-0.056	-0.021	-0.062	-0.023	-0.059	-0.022
2150-2200 $\text{\AA}$	1.45	-0.020	-	-0.025	-	-0.022	-
2600-2700 $\text{\AA}$	1.10	-0.016	-	-0.013	-	-0.013	-
2700-2800 $\text{\AA}$	1.10	-0.020	-	-0.022	-	-0.019	-
2800-2900 $\text{\AA}$	1.10	-0.038	-	-0.039	-	-0.037	-
2900-2950 $\text{\AA}$	1.10	-0.035	-	-0.036	-	-0.038	-
2950-3000 $\text{\AA}$	1.10	-0.033	-	-0.033	-	-0.034	-
3000-3050 $\text{\AA}$	1.10	-0.046	-	-0.045	-	-0.047	-
3050-3100 $\text{\AA}$	1.10	-0.046	-	-0.045	-	-0.045	-
$\sigma(\text{O}_2)$	1.20	0.276	0.051	0.257	0.047	0.266	0.049
$\sigma(\text{O}_2) \lambda > 2000 \text{ \AA}$	1.32	0.443	0.122	0.390	0.108	0.418	0.115
$\sigma(\text{O}_2) \text{SRB} (\lambda < 2000 \text{ \AA})$	1.74	0.054	0.030	-0.105	-0.058	-0.055	-0.030
$\sigma(\text{HNO}_3)$	1.20	-0.176	-0.036	-0.206	-0.038	-0.200	-0.037
$\sigma(\text{H}_2\text{CO} - \text{CO})$	1.45	0.069	0.025	0.071	0.026	0.070	0.026
$\sigma(\text{ClONO}_2)$	1.32	0.188	0.052	0.164	0.045	0.176	0.049
$\sigma(\text{H}_2\text{O}_2)$	1.74	0.035	0.020	0.026	0.014	0.031	0.017
$\sigma(\text{N}_2\text{O})$	1.32	0.373	0.103	0.340	0.094	0.355	0.098
$\sigma(\text{CFCl}_3)$	1.10	-0.051	-	-0.050	-	-0.052	-
$\sigma(\text{CF}_2\text{Cl}_2)$	1.15	-0.024	-	-0.024	-	-0.024	-
$\sigma(\text{NO}_2)$	1.45	0.125	0.046	0.140	0.052	0.133	0.049
$\sigma(\text{NO})$	2.29	0.031	0.025	0.042	0.035	0.037	0.031

\*All quantities with absolute values less than 0.010 have been suppressed.

Note: The first column labeled  $f_{2\sigma}$  is the estimated factor by which the input parameter should be multiplied and divided to give the 95% confidence limits. The remaining six columns are the model computed sensitivities and uncertainties determined in the following way: model runs at the central value,  $\pm 1\sigma$ , and  $\pm 2\sigma$  are made. Column 6 is the central sensitivity obtained from the difference of the  $+1\sigma$  and  $-1\sigma$  runs. Column 7 is the corresponding uncertainty, i.e. the sensitivity times  $\ln f_{2\sigma}$ . Columns 2 and 3 are the low side sensitivities and uncertainties obtained from the  $-2\sigma$  and central model runs while columns 4 and 5 are the corresponding high side values.

### THREE-DIMENSIONAL MODELS AND THEIR APPLICATION TO THE OZONE PROBLEM

D.M. Cunnold, F.N. Alyea, Atmospheric Sciences Program, Georgia Inst. of Technology, Atlanta,

Ga., and R.G. Prinn, Dept. of Meteorology, Mass. Inst. of Technology, Cambridge, Mass.

The status of three-dimensional modeling for estimating the effects of anthropogenically-produced chemicals on the atmospheric ozone distribution is described. In contrast to models of lower dimensionality, it is the aim of such models to realistically simulate the wave phase relationships and transience responsible for atmospheric transport. At this time these models possess certain limitations in their ability to simulate the climatology of dynamical variables and ozone. Even these models utilize a series of approximations and it is difficult to quantify the effects of either these approximations or the inadequacies in simulation. We thus believe that further development of these models including the addition of more chemistry and horizontal and vertical resolution is necessary before the models should form a basis for decisions concerning the potential atmospheric effects of anthropogenic species.

**INTRODUCTION:** Three-dimensional models of the stratosphere utilize the equations of motion and thermodynamics in order to derive motion and temperature fields (including non-linear transports) which are internally consistent at each time step. Forcing in these models is produced by the absorption of solar radiation; principally because of different exchange rates for radiation and water vapor between the land and sea surfaces and the atmosphere, this distribution of heating in the atmosphere possesses longitudinal as well as latitudinal asymmetries. In response to this forcing the models generate a spectrum of planetary waves (including a zonal mean circulation) and allow a continuous exchange of energy between individual wave components as a result of non-linear interactions. Energy is also continuously interchanged between its several forms - kinetic, potential and internal. In principle the models may be started from rest by turning on the sun; in practice, however, computation time is saved by using more dynamically realistic initial distributions of wind and temperature.

The numerical models of the stratosphere are still in their early stages of development and have, so far, been applied to the transport of only a limited number of chemical constituents. The three-dimensional models are, however, expected to make a unique contribution to stratospheric research through their ability to include the physical processes necessary to describe stratospheric transport. The transport should thus be dependent on day to day variability in dynamical conditions and species distribution. At the current time, certain deficiencies exist in the ability of these models to simulate the transport of heat and momentum in the stratosphere resulting in certain unrealistic features being produced in the seasonal-mean zonal-mean wind and temperature fields. Current efforts have concentrated on improving the simulation of these observationally well-documented, dynamically-related features of the models rather than the addition of more chemistry. Future efforts, however, will include the simulation of the transport of additional chemical species and the intro-



duction of additional photochemistry. The species to be included must be carefully chosen so as to minimize computation time while preserving the physics necessary to ensure a proper simulation of transport. Progress in numerical modeling is likely to be limited by both the tremendous computational requirements of the models and by the difficulties inherent in obtaining the global stratospheric data needed to test them.

A major problem with one- and two-dimensional models is that the development of three-dimensional models, and our understanding of atmospheric transport, has not progressed to the point that we can estimate the uncertainties resulting from the parameterizations introduced into the models having reduced dimensionality. Moreover, there is currently no way to estimate the effect of the inadequate simulation of certain dynamical features in three-dimensional models on their ability to simulate the transport of species. We thus encounter substantial difficulty in assigning error bars, at this time, to predictions of the atmospheric effects of anthropogenically produced chemicals. In this review of three-dimensional models, we emphasize that as we seek to eliminate the need for a parameterization of atmospheric transport, for which in one-dimensional models, for example, a single height-dependent parameter is used, we are forced by computational limitations to make a series of approximations. We are optimistic that none of these approximations will alter the nature of atmospheric transport or its inherent dependence on the species distributions. However, we shall only be able to test the validity of this statement when models capable of reproducing the principal observed dynamical features of the stratosphere have been produced.

2. Equations Utilized: The equations of motion and thermodynamics in the atmosphere in a frame of reference moving at the rotation rate of the earth are

$$\frac{d\mathbf{u}}{dt} = -2\mathbf{\Omega} \times \mathbf{u} - \frac{1}{\rho} \nabla p + \mathbf{g} + \mathbf{F} \quad (2.1)$$

$$\frac{dp}{dt} = -\rho \nabla \cdot \mathbf{u} \quad (2.2)$$

$$\frac{dT}{dt} = -(\gamma - 1) T \nabla \cdot \mathbf{u} + \frac{Q}{c_v} \quad (2.3)$$

$$\text{and } p = \rho RT \quad (2.4)$$

where  $\frac{d}{dt}$  = derivative in a frame of reference moving at velocity  $\mathbf{u}$ ,

$\mathbf{u}$  = velocity

$\mathbf{\Omega}$  = vector of earth's rotation

$p$  = local pressure

$\rho$  = density

$\mathbf{g}$  = earth's gravitational attraction

$\mathbf{F}$  = frictional force

$T$  = temperature

$\gamma$  = ratio of specific heats,  $\frac{c_p}{c_v}$

$Q$  = heating rate due both to radiative transfer in the stratosphere and conduction and frictional dissipation

$R$  = gas constant

These so-called exact equations are not used in numerical prediction because they allow

short period acoustic oscillations and would thus necessitate numerically a ridiculously small time step. The acoustic oscillations are unimportant for the general circulation of the stratosphere and are filtered out by replacing the vertical equation of motion by the hydrostatic assumption:

$$\frac{\partial p}{\partial z} = -\rho g \quad (2.5)$$

Just as in chemistry we sometimes assume instantaneous adjustment to photochemical equilibrium, we are assuming here that the pressure instantaneously adjusts to any vertical acceleration tendency. The vertical motion field is then that field which compensates for the effects of horizontal motions and maintains the pressure and density fields in hydrostatic equilibrium.

Because numerical models are used in long term prediction, it is highly desirable that the total energy (and angular momentum) of the model be conserved. This, in fact, provides one of the most important constraints for checking out the numerics of such a model. In order to preserve kinetic energy using the hydrostatic assumption, we neglect the vertical kinetic energy of the motion.

The dynamical equations utilizing the hydrostatic assumption are referred to in meteorology as the primitive equations. They are often expressed using pressure instead of height as the vertical coordinate: we then have

$$\frac{d\mathbf{U}}{dt} = f \mathbf{k} \times \mathbf{U} - g \nabla Z + \mathbf{F} \quad (2.6)$$

$$\nabla \cdot \mathbf{U} + \frac{\partial \omega}{\partial p} = 0 \quad (2.7)$$

$$\frac{dT}{dt} = \kappa T \frac{\omega}{p} + \frac{Q}{c_p} \quad (2.8)$$

$$\frac{\partial Z}{\partial p} = - \frac{RT}{gp} \quad (2.9)$$

where  $\nabla$  is the horizontal gradient operator evaluated on an isobaric surface

$\mathbf{U}$  is the velocity on this surface

$Z$  is the local height on the pressure surface

$f$  is the Coriolis parameter ( $= -2\Omega \sin \theta$  where  $\theta$  = latitude)

$\mathbf{k}$  is the vertical unit vector

$\omega$  is the vertical "velocity" on the isobaric surface ( $= \frac{dp}{dt}$ )

$\kappa = R/c_p$ .

The primitive equations with the addition of a prognostic equation for water vapor (which contributes to heating primarily through the release of latent heat) are used in all general circulation models. Some of these models have been extended to include several levels in the stratosphere (Manabe and Hunt, 1968; Kasahara, et al., 1973; Newson, 1974; Schlesinger and Mintz, 1979; Manabe and Mahlman, 1976). These models are, however, tremendous consumers of computer resources and consequently allow little flexibility in the addition of chemistry. Thus the stratosphere is often studied using the next order of approximation in the dynamical equations.

Although acoustic waves have been filtered out of the primitive equations, gravity waves having periods of order 1 hour remain. The restoring force due to gravity leads to Kelvin waves in the equatorial region but may be of negligible importance to the general circulation of the atmosphere. In order to take longer time steps and reduce computation time

gravity waves may be filtered out of the equation by using the quasi-geostrophic assumption. In this approximation, rather than replace the horizontal velocity by the geostrophic velocity ( $= \frac{g}{f} \mathbf{k} \times \nabla Z$ ) which would produce some energetically unreasonable assumptions, we allow the divergent part of the wind field to instantaneously adjust so that the vertical component of vorticity remains that due to the rotational part of the wind field - that is to say, vorticity changes are geostrophic. The set of equations then reduces to (after eliminating  $Z$ ):

$$\nabla \cdot (f \nabla \frac{\partial \psi}{\partial p}) = - \frac{R}{p} \nabla^2 T \quad (2.10)$$

$$\frac{\partial}{\partial t} (\nabla^2 \psi) = - \nabla \psi \cdot \nabla (f + \nabla^2 \psi) \times \mathbf{k} + \nabla \cdot (f \nabla \chi) + \nabla \cdot (F \times \mathbf{k}) \quad (2.11)$$

$$\frac{\partial T}{\partial t} = - \nabla \psi \cdot \nabla T \times \mathbf{k} + \nabla T \cdot \nabla \chi + \omega \left( - \frac{\partial T}{\partial p} + \kappa \frac{T}{p} \right) + \frac{Q}{c_p} \quad (2.12)$$

$$\text{and} \quad \nabla^2 \chi = \frac{\partial \omega}{\partial p} \quad (2.13)$$

where the horizontal wind field has been expressed as a sum of irrotational and rotational components,  $\mathbf{U} = \mathbf{k} \times \nabla \psi - \nabla \chi$ . This so-called quasi-geostrophic approximation essentially assumes that the rotational part of the wind field is much larger than the divergent part and that the rotational part of the wind field is essentially in geostrophic balance with the horizontal pressure gradient. It should be particularly noted that the balance condition (2.10) does not possess a singularity at the equator. These equations can thus be applied to global modeling. Although the quasi-geostrophic approximation can be shown by scale analysis to break down at the equator, and such a model may therefore be inadequate for describing transport there, we know of no reason why such a model should not adequately describe the global transport of trace constituents.

In the quasi-geostrophic system of equations the kinetic energy is just the kinetic energy of the rotational part of the horizontal wind field. Computationally in order to solve this set of equations the balance equation (2.10) must be expressed as an equation for  $\omega$  which is accomplished by taking the derivative of the balance condition with respect to time and using equations (2.11) and (2.12). The  $\omega$  equation contains spatial derivatives and its solution involves matrix inversion and is computationally complicated.

All quasi-geostrophic models which have so far been applied to the stratosphere (Peng, 1965; Clark, 1970; Trenberth, 1973; Cunnold, et al., 1975; and Ramanathan and Grose, 1978) have adopted an additional approximation in order to reduce computation time. In these models the horizontal advection is limited to just that due to the rotational part of the wind field. To obtain consistency in the model energetics this requires that the global mean temperature and static stability ( $-\partial T/\partial p + \kappa T/p$ ) be invariant with time (Lorenz, 1960). There is then no dynamical contribution to the global mean temperature and the latter is not predicted in such models. Possible ways around this problem do exist; for example, the global mean temperature in the stratosphere could be updated using the radiative equilibrium assumption or equations (2.10) to (2.13), which include horizontal advection of heat by the divergent part of the wind field, could be utilized. The latter approach would add an additional non-linear term and adds substantial complication to the solution of the  $\omega$  equation so that the model computation time would be more than doubled.

For additional details on the derivation of these equations the reader is referred to Lorenz (1967) and Holton (1975). For a discussion of the quasi-geostrophic assumption, see Phillips (1963). The limitations on our ability to simulate the physical processes in the stratosphere imposed by the assumption of quasi-geostrophy have not yet been fully evaluated. Eventually a comparison between primitive and quasi-geostrophic equation models and observations of the stratosphere should permit such an evaluation to be made.

**3. Modeling Atmospheric Heating:** All models are internally forced by heating. Heating due to the absorption of solar ultraviolet radiation by ozone (or by molecular oxygen in the mesosphere) presents no particular problem computationally (heating caused by the absorption of solar ultraviolet radiation by  $\text{NO}_2$  has not generally been included but in principle may be

included without difficulty). For example, a direct evaluation of the absorption of ultraviolet radiation in the form

$$Q(N \sec \psi) = \frac{\chi_{O_3}}{m} \int \alpha I \epsilon e^{-\alpha N \sec \psi} d\lambda \quad (3.1)$$

where  $Q$  is the atmospheric heating rate due to the absorption of ultraviolet radiation by ozone

$N$  is the vertically integrated ozone column above pressure  $p$

$\psi$  is the solar zenith angle at time  $t$

$\chi_{O_3}$  is the ozone mixing ratio

$m$  is the mass of an average air molecule

$\alpha$  is the absorption coefficient of ozone at wavelength  $\lambda$

$I$  is the solar flux incident on the stratosphere at wavelength  $\lambda$

$\epsilon$  is the energy of a photon of wavelength  $\lambda$ ,

can be made without severe requirements on computation speed. The ozone absorption is broad band, the contribution of the atmospheric albedo at ultraviolet wavelengths is negligible, and the contribution due to visible wavelengths in the Chappuis band need only be included to first order accuracy. Faster procedures of evaluating equation (3.1) are, however, generally used. Linear table interpolations as a function of the ozone column density have been utilized by Cunnold, *et al.* (1975) and Schlesinger and Mintz (1979) with the ozone column being obtained as a sum over model layers. Models now under construction by Alyea, *et al.* and Mahlman utilize a direct evaluation of equation (3.1) for the zonal mean ozone but use an exponential interpolation procedure for determining the heating rate around a latitude circle. Equation (3.1) may be also approximated quite accurately as a sum of just a few exponentials whose exponents include  $N \sec \psi$  (Lindzen and Will, 1973; Lacis and Hansen, 1974).

Several models, including all quasi-geostrophic models, filter out diurnal variations (eg., Cunnold, *et al.*, 1975; Manabe and Mahlman, 1976) and in that case equation (3.1) must be diurnally averaged. This is easily accomplished, for example, by using the approximation

$$Q(N; \text{latitude, time of year}) = \frac{H}{2.05\pi} [Q(N \sec \zeta_1) + Q(N \sec \zeta_2)]$$

where  $\zeta_1$  and  $\zeta_2$  are the zenith angles at the solar hour angle corresponding to local noon +  $H/4$  and local noon +  $3H/4$  and  $H$  is the hour angle of sunset. The factor 2.05 has been determined empirically to eliminate a slight bias in this expression. This approximation has been found to possess an accuracy of 5% (see, for example, Cogley and Borucki, 1976).

The transfer of infrared radiation in the atmosphere is much more difficult to represent in a computationally efficient manner. It is most simply included in the models by using the expression

$$Q_I = h(p) c_p (\bar{T} - T) \quad (3.2)$$

This is referred to as the Newtonian cooling approximation and permits no transfer of infrared radiation between models levels. Values of  $h(p)$  have been calculated, for example, by Dickinson (1973) based upon an accurate calculation of the transfer of infrared radiation by  $CO_2$  and  $O_3$  for a standard global mean temperature profile. Local perturbances of temperature by 0.1°K allow a determination of  $h(p)$ .

We should expect that cooling would be less than that given by equation (3.2) at high latitudes in winter, for example, where temperatures are quite low. Ramanathan (1976) has developed a procedure for including the transfer of infrared radiation between model levels and the dependence of  $h(p)$  on local temperature. This has been incorporated into a quasi-geostrophic model similar to that of Trenberth (1973) (see Ramanathan and Grose, 1978). Even more accurate infrared transfer schemes have been included in general circulation models in order to simulate heat transfer in the troposphere.

Heating in the troposphere involves not only the transfer of infrared radiation but also latent heat release. The latter is allowed to feed back to the dynamics in general circulation models through the prognostic equation for water vapor. Quasi-geostrophic models cannot adequately represent this process and therefore represent tropospheric forcing by a term

$$Q = h(p)c_p(T^*-T)$$

where  $T^*$  is calculated from climatologically determined distributions of  $T$  and  $Q$  (see, for example, Newell, et al., 1972) and  $h(p)$  is prescribed based on radiation calculations by Manabe and Strickler (1964), for example, and from experience with general circulation model calculations.  $T^*$  determined in this way possesses both zonal and non-zonal components and implicitly depends on land-sea differences as well as orography. Where climatological data is lacking (eg., the Southern Hemisphere) attempts are being made to base  $T^*$  on results obtained with general circulation models. Note that there are fewer feedbacks to the tropospheric generation of the stationary planetary waves, which play a significant role in stratospheric dynamics, in quasi-geostrophic models than in general circulation models.

At the current time only a few models have allowed a feedback between ozone and atmospheric heating - that is, the ozone distribution has generally been prescribed and allowed to vary at most seasonally. However, the quasi-geostrophic model of Cunnold, et al., (1975) and the general circulation model of Schlesinger and Mintz (1979) have included a prediction equation for ozone in which the relevant photodissociation rates have been determined using an expression similar to (3.1) and the distribution of species responsible for ozone distribution have been prescribed.

**4. Boundary Conditions:** The vertical velocity at the top and bottom of the atmosphere are specified in all models. General circulation models must also allow for the transport of heat and water vapor into the atmosphere at the surface. If any chemical constituents such as ozone are predicted, fluxes at the top and bottom of the stratosphere must also be prescribed.

At the top of the atmosphere, most models set  $\omega = 0$ . This prevents energy from radiating out of the model atmosphere and forces any energy incident on the upper surface to be reflected. This produces an energetically closed system. Moreover, since upward propagating wave energy is dissipated, energy reflected from the upper boundary should have a negligible effect at some large distance from that boundary. Physically it might be more desirable if energy incident on the upper surface of the model could be absorbed (corresponding to radiation to space). This has been attempted in the model of Schlesinger and Mintz (1979); however, it is not easily accomplished satisfactorily because large gradients in viscosity close to the upper boundary can produce anomalous reflections. For the present, results of three-dimensional models should only be used far enough from the upper boundary that the reflected energy is small compared with the energy incident from below.

At the surface the vertical velocity must satisfy

$$w(z_0) = \frac{dh}{dt} \approx \underline{k} \times \underline{\nabla} \psi(z_0) \cdot \underline{\nabla} h$$

in order for the air to remain in contact with the surface (where  $h$  is the orographic height). We approximate  $\omega(p_0)$  assuming  $p_0$  and  $z_0$  are coincident surfaces in a quasi-geostrophic system (ie., ignoring surface pressure variations) and assume

$$\omega(p_0) = \frac{dp}{dt} = -\rho g w(z_0).$$

5. Friction and subgrid-scale parameterizations: The frictional drag of the surface is simply represented by

$$\underline{F} = \frac{1}{\rho} k_d \frac{\partial \underline{V}}{\partial z} = \frac{1}{\rho} k_d \frac{\partial}{\partial z} \nabla \psi$$

and represents the transfer of momentum to the surface. The value of  $k_d$  is determined using our knowledge of the turning (the Ekman spiral) of horizontal velocity in the boundary layer.

At interior levels of the models  $\underline{F}$  includes a representation of the momentum transfer, and  $\underline{Q}$  includes a representation of heating, by subgrid scale motions. These processes depend on the resolution of the model and are thus model dependent. There must always exist some transfer of energy and momentum downscale from the resolved motions to the molecular scale where dissipation ultimately occurs. How to represent this process is, however, one of the most studied and difficult aspects of three-dimensional modeling. Ideally we should like the truncation limits to be far enough away from the modes which contain the maximum energy that the transfer of energy across the spectral truncation boundary will be insignificant. This would occur, for example, if model-resolved radiative processes were to be more important for dissipating energy than were subgrid scale processes. Unfortunately, in the troposphere the spectrum of oscillations is fairly broad (see Figure 1) and we would thus need a high resolution model to resolve the most important scales of motion. In the stratosphere, however, the spectrum appears to be peaked at wavenumbers 1 and 2 and appears to fall off rapidly with increasing wavenumber. Transport by large scale motions may thus dominate over subgrid scale mixing in establishing the distributions of stratospheric species.

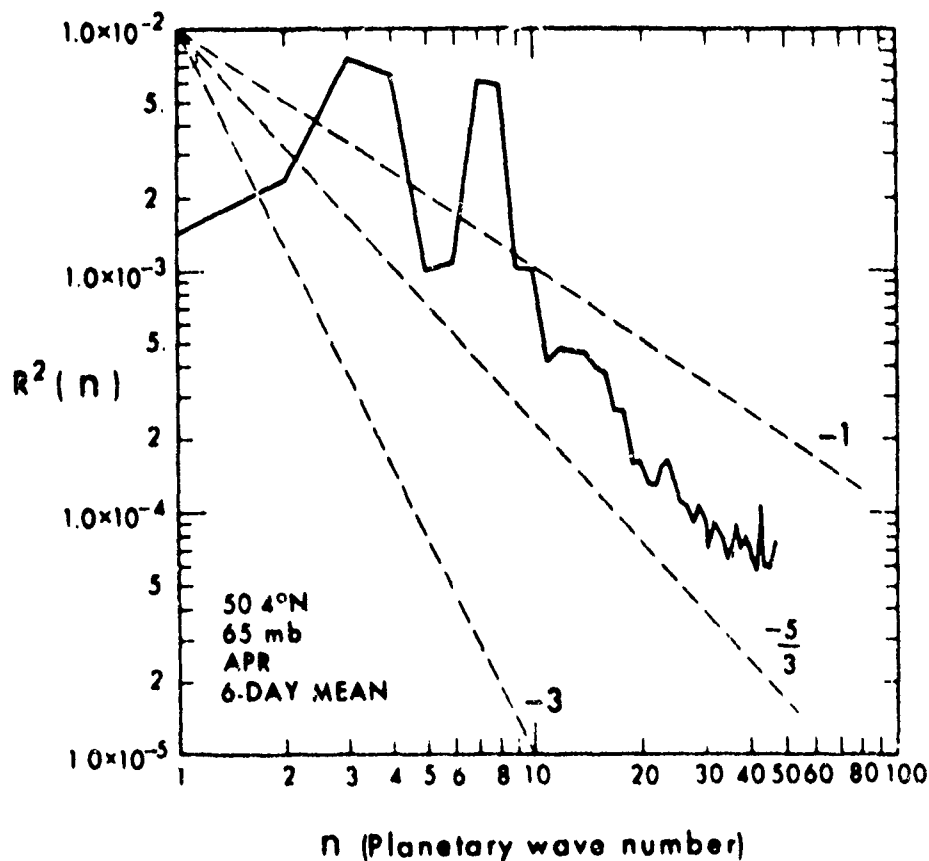


Figure 1. Zonal spectra of tracer mixing ratio squared ( $R^2$ ) as a function of planetary wavenumber ( $n$ ). Data are taken from the "Vertical Stratification" experiment of Mahlman (1973) at 50.4°N and 65 mb for the first six days of April (9th month of experiment). (from Mahlman, 1975).

Various attempts at establishing a realistic representation of subgrid-scale mixing in terms of an eddy diffusion coefficient have been made. A discussion concerning the scale dependence of this coefficient for the representation of tracers is given in Mahlman and Moxim (1978) who suggest a diffusion coefficient having a  $\nabla^2$  type form. Such a form tends to dissipate irregularities close to the truncation limit (where irregularities would otherwise tend to accumulate) but only weakly affects the largest scales of motion.

Difficulties in the representation of subgrid scale mixing can be illustrated for the case of ozone which has a source in the tropics of the lower stratosphere and sinks at high latitudes and at the ground. The small scale mixing out of a parcel of air containing ozone as it travels polewards and downwards from the source region is small and may have a negligible effect on the establishment of the mean ozone gradient as evidenced by the ability of a limited resolution model, containing very little diffusion, to simulate seasonal and latitudinal variations in columnar ozone (see Cunnold, *et al.*, 1980). The horizontal gradient is essentially established by the rate of transport from the equator to the polar regions where ozone is chemically destroyed. On the other hand, in a 6-wave model vertical motions apparently provide an inadequate downward transport of ozone through the tropopause. It is in principle possible to compensate for this deficiency by increasing the vertical diffusion coefficient. However, such an ad-hoc procedure has the disadvantage that it will also dissipate the ozone irregularities as they travel polewards and will thus tend to reduce the horizontal ozone gradient. It is thus difficult to compensate for any deficiencies in model resolution by using a parameterization of the subgrid-scale motions.

6. Time Stepping: The time stepping in these models must be consistent with the phase propagation speed of the shortest resolvable disturbances. In general circulation models, which have a horizontal resolution of a few hundred kilometers, time steps of order 10 minutes are utilized. In the quasi-geostrophic models time steps of approximately one hour have so far been used.

Aliasing or the introduction of spurious modes beyond the model resolution are a potential problem in numerical models. These numerical errors can grow quite rapidly. A scale dependent diffusion coefficient can be utilized to selectively destroy these modes. However, a more physically appealing procedure is to represent the fields in terms of their spatial spectra using Fourier transform techniques. Subgrid-scale motions introduced by non-linearities are then immediately eliminated and the tendency for energy transfer to the subgrid scale can be controlled using a prescribed diffusion coefficient. The representation of fields in terms of spherical harmonics is often used in three-dimensional models (and in fact has been used in all quasi-geostrophic models which have been applied to the stratosphere).

#### 7. Selected success and failures in the simulation of the stratosphere:

(a) Dynamics. Many of the stratospheric models' dynamical successes and failures can be illustrated by comparisons of the model-derived zonal-mean temperature structure with observation. An example taken from the model of Cunnold, *et al.*, (1975) illustrates the results of many of the stratospheric models (see Figure 2). In the lower stratosphere in winter, temperatures increase polewards from the equator. This region of the stratosphere acts like a refrigerator, as was first simulated in the general circulation model of Smagorinsky, *et al.*, (1963), in that it is forced from below by an upward flux of planetary wave energy and destroys this energy ultimately by heating where it is cool and cooling where it is warm. An interesting feature of the observed stratosphere is that this temperature gradient reverses poleward of mid-latitudes. This result has proved to be fairly difficult to simulate in the numerical models. Associated with this feature through the thermal wind equation, the polar night jet, which possesses a horizontal momentum which increases with altitude, begins to make its presence felt. In Figure 2 we note that in the model of Cunnold, *et al.*, (1975) the polar night jet is almost non-existent in this region and the temperature gradient does not reverse. If the energetics of this model are compared with an analysis of observations, we find that the energy diagram for the 10-100 mb region is consistent with that for 30-150 mb region by Oort (1964) but not with that of the analysis of the 10-100 mb region by Dopplack (1971). That is, wave kinetic energy exported by the troposphere is converted to internal energy of the waves ( $A_1$ ) and then to zonal energy ( $A_2$ ) through the large poleward upgradient flux of heat by the waves. What is apparently lacking is a large forcing of zonal kinetic energy by the pressure work term acting at the 100 mb level and the absorption of wave energy by the zonal mean flow ( $K_E + K_Z$ ). In this model this is almost certainly

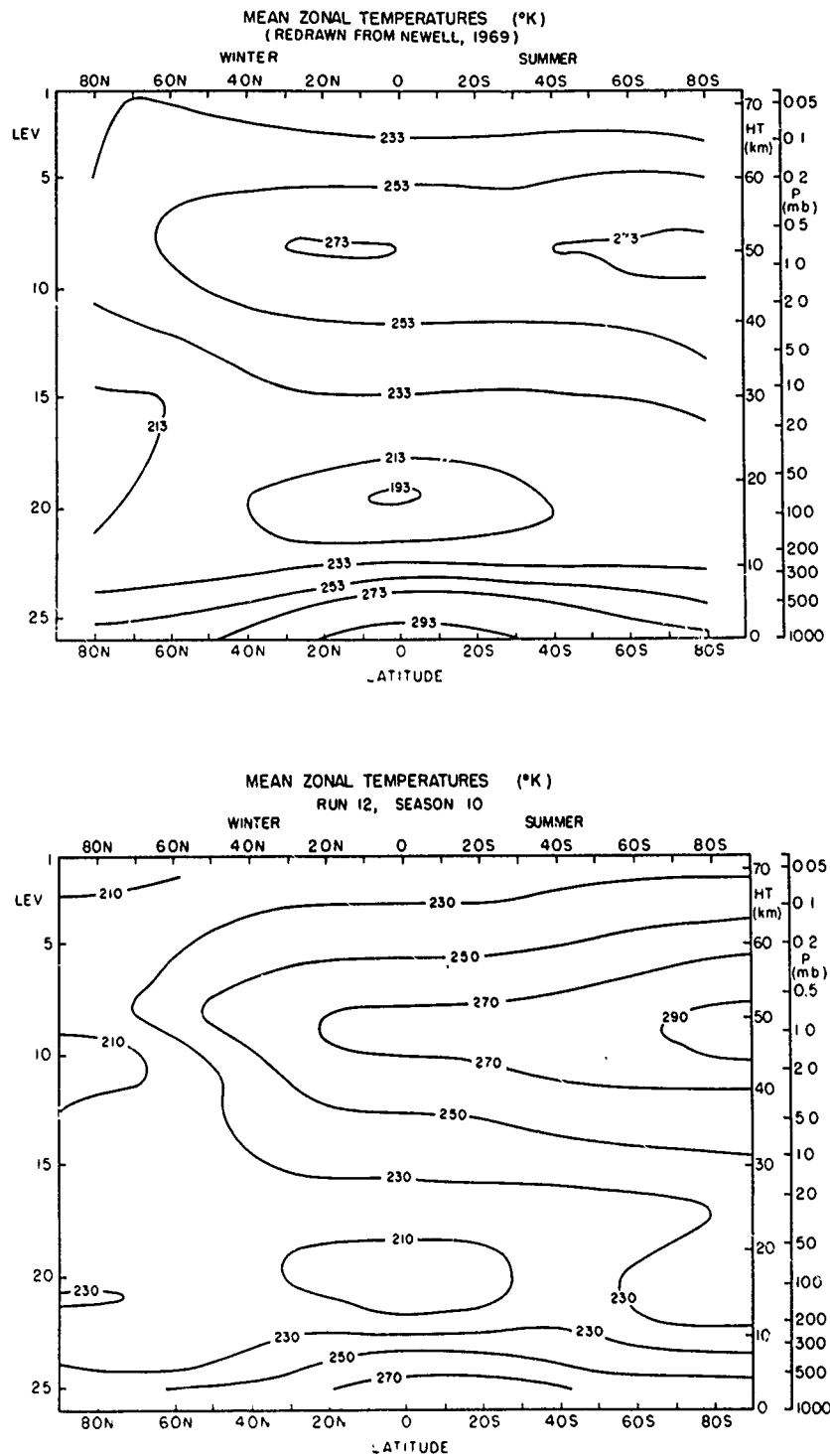


Figure 2. The atmospheric temperature distribution obtained for season 10 compared against the observed atmospheric temperature distribution for summer and winter according to Newell (1969). (From Cunnold, et al., 1975).



caused by the tropospheric jet stream being located too close to the equator (probably because of the model truncation which prevents the generation of higher wavenumber baroclinic eddies which are known to be mainly responsible for transporting momentum to mid-latitudes in the troposphere). A similar problem in the representation of the temperature distribution exists in the Langley model where probably for similar reasons the tropospheric jet stream (and, in that case, the indirect circulation) is too weak.

This problem does not, however, exist in higher resolution models, for example, the general circulation model of Manabe and Mahlman. In that particular case, however, while the tropospheric jet stream is much better represented, the polar night jet is much too strong and the polar temperatures between 30 and 10 mb are much too cold. Their poleward heat flux is almost certainly too small or even upgradient (away from the pole) and it is likely that forcing the vertical velocity to zero at 10 mb is weakening the stratospheric indirect circulation and the conversion from  $K_z$  and  $A_z$ .

This limitation of the dynamical models (ie., a cold winter pole and an excessively large polar night jet in the vicinity of the upper boundary) has existed in all models reported to date. In most cases the upper boundary condition in which  $\omega$  is set to zero probably contributes to this result by reducing the conversion between zonal kinetic and zonal available energy. For example, in Figure 2, an excessively cold pole is evident throughout the region above 5 mb. The energetics analysis of this case (Chen, *et al.*, 1980) indicates that a further problem in the 10-2 mb region is that the kinetic energy of the waves forced by the troposphere is being destroyed in the 100-10 mb region and insufficient wave energy is reaching 10 mb. Associated with inadequate wave activity there appears to be insufficient conversion from zonal to eddy available potential energy. The cold pole in the winter stratosphere has also been noted in the models of Schlesinger and Mintz (1979), Newson (1974), and Ramanathan and Grose (1978) and it has been suggested that inadequate wave energy reaching the upper stratosphere in winter may be a problem common to all such models (Schlesinger and Mintz, 1979).

Apart from this particular limitation of the three-dimensional models, most models appear to simulate the important atmosphere energy cycles of the various regions of the stratosphere quite well. The cold temperatures of the tropical tropopause region are well-simulated as is the temperature distribution throughout the stratosphere in summer (and hence also the easterly flow in summer). Moreover, all model lower stratospheres are driven by the import of energy from the troposphere, while in situ forcing significantly contributes to producing the temperature distribution in the upper stratosphere.

(b) Chemical constituents. Although three-dimensional models have not yet included much chemistry, their potential and some of their most exciting applications can be illustrated from results already obtained concerning the transport of ozone and tracers. The equation for any chemical specie can be written

$$\frac{dx_i}{dt} = \frac{1}{n_m} (P_i - L_i) + D_i \quad (7.1)$$

where  $d/dt$  is the total derivative following the motion,  $n_m$  is the local neutral density,  $x_i$  is the volume mixing ratio of species  $i$ ,  $P_i$  and  $L_i$  are the chemical production and destruction rates for species  $i$ , and  $D_i$  represents the subgrid scale mixing which tends to destroy irregularities as they are transported by the resolved motions.  $D_i$  is usually represented as a diffusion process. It is often convenient to split the advection term into components due to the zonal mean motion and due to the planetary waves. Thus for example, we can represent the zonal mean advection as

$$[\underline{u} \cdot \nabla x_i] = [\underline{u}] \cdot \nabla [x_i] + \underline{u}^* \cdot \nabla x_i^*$$

where  $[\ ]$  indicates zonal averaging and  $*$  indicates deviations from the zonal mean (ie., the planetary waves).

Many situations exist in the atmosphere in which the transport terms in equation 7.1 are much larger than the chemical production and loss terms (and  $D_i$  is small in a successful model). We are then considering a relatively inert tracer. Then if the tracer distribution

is changing only slowly, the mean and eddy contributions to advection must be approximately equal and opposite. This has been noted in many of the numerical model results for inert tracers and ozone in the lower stratosphere (e.g., Hunt and Manabe, 1963; Mahlman, 1973; Mahlman and Moxim, 1978; Cunnold, *et al.*, 1980). It is evident, for example, in the calculated budget of zonal mean column-integrated ozone shown in Figure 3 and especially in the contributions to the local budget of zonal-mean ozone in the lower stratosphere shown in Figures 4 and 5. Figure 5 also indicates a different situation, about which we shall have further comments, exists for ozone in the middle stratosphere, namely that the horizontal advection by planetary waves is no longer offset by the mean circulation and chemistry plays a more intrinsic role in controlling transport.

## CONTRIBUTIONS TO HEIGHT INTEGRATED OZONE CHANGE

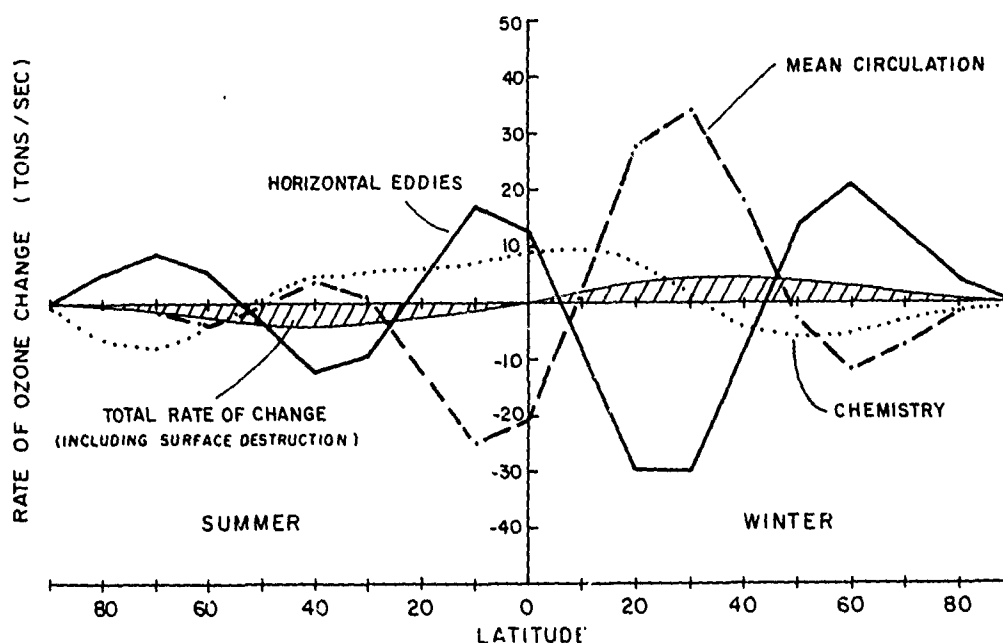


Figure 3. The calculated hemispheric budget of ozone in  $10^\circ$  latitude intervals (integrated longitudinally) during the summer and winter. (From Cunnold, *et al.*, 1980).

Let us illustrate the potential of the models by considering the physical nature of ozone transport in the lower stratosphere. From Figure 3 we note that at mid-latitudes the planetary waves are responsible for transporting ozone from the chemical source region at low latitudes to the chemical loss region at high latitudes. The wave phase relationships which appear to be responsible for this transport (in the lower stratosphere) are shown in Figure 6. Ozone irregularities are created in this altitude range by vertical motions acting on the underlying vertical ozone gradient (which is the result of both chemistry and dynamics). We thus should expect that ozone irregularities will lag the vertical velocity fluctuations by approximately  $\pi/2$  radians -- differences from  $\pi/2$  radians will be produced by the small chemical terms and because the horizontal advection is not exactly in phase with vertical advection. Because of the phase difference between vertical and horizontal motions the irregularities produced by vertical motions will possess a non-zero (poleward) horizontal velocity. Thus the zonal-mean horizontal gradient tendency resulting from chemistry will be modulated by horizontal advection. The horizontal advection will be a function of the planetary wave phase relationships of the dynamical variables and of the magnitude of the zonal mean gradients.

In the lower stratosphere poleward and downward motions are positively correlated and the ozone and temperature perturbations are in phase (the latter being created adiabatically by

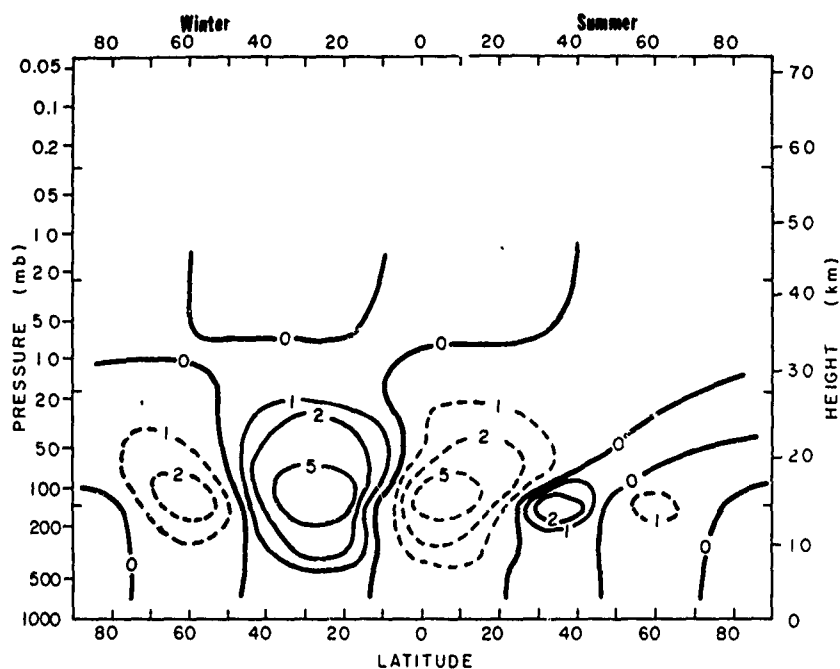


Figure 4. The calculated contribution to the seasonally-averaged ozone tendency resulting from horizontal and vertical transport by the mean circulation. Values have been weighted by the volume  $10^\circ$  latitude by  $360^\circ$  longitude by approximately 2.8 km ( $\nabla Z = 0.40574$ ), and are expressed in tons/sec. (From Cunnold, *et al.*, 1980).

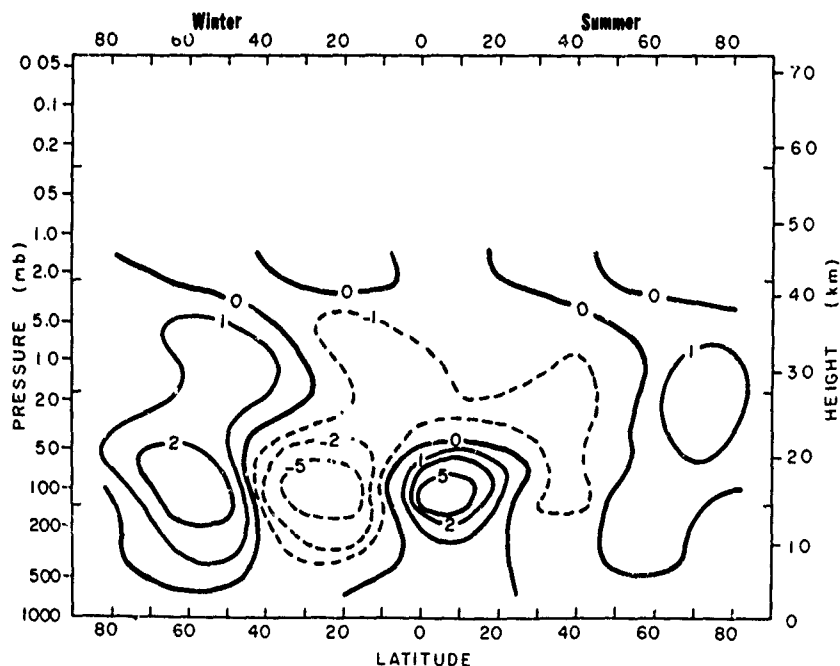


Figure 5. The calculated contribution to the seasonally-averaged ozone tendency resulting from horizontal advection by planetary waves. Values have been weighted by the volume  $10^\circ$  latitude by  $360^\circ$  longitude by approximately 2.8 km ( $\nabla Z = 0.40574$ ), and are expressed in tons/sec. (From Cunnold, *et al.*, 1980).

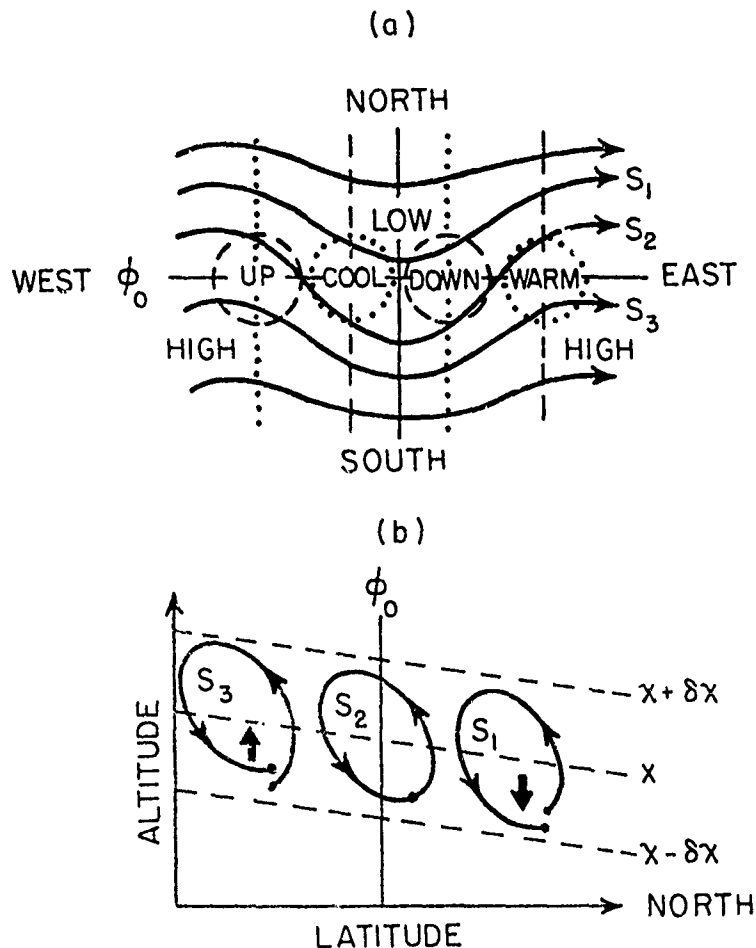


Figure 6. (a) Phase relationships believed to exist in the lower stratosphere above 100 mb. Ozone maxima are expected to coincide with warm air and minima with cold air. Trajectories  $S_1$ ,  $S_2$ ,  $S_3$  will produce polewards and downwards transport due to Stokes' drift as shown in (b). (From Prinn, Cunnold, and Alyea, manuscript in preparation, 1979).

downward motion) and maximize to the East of troughs and the maximum downward motion. Under these phase relationships (see Figure 6), air parcels traveling on the trajectory  $S_1$  tend to sink (due to Stoke's drift) while parcels on trajectory  $S_3$  will rise. Since planetary waves also tend to tilt Westward with height, air parcels to the North of the trough will also tend to move Northward as they sink across the downward sloping isentropes. It is the positive correlation between Northward and downward motion which tends to maintain the counter-gradient Northward flux of ozone. The justification for this picture of ozone transport is given in Prinn, Cunnold and Alyea (manuscript in preparation, 1979). We note, however, that analysis of observations by many researchers tend to support this picture. For example, Martin and Brewer (1959) found significant correlations between vertical motions, temperature, and vorticity at 100 mb and total ozone. Since ozone mixing ratio and potential temperature increase with height in the lower stratosphere and motions are apparently adiabatic, downward moving air parcels should be rich in ozone and potential temperature. Thus, a poleward transport of heat and ozone is expected when northward-moving air parcels tend to descend. Green (1960) demonstrated that this is indeed a feature of baroclinic waves in the lower stratosphere. Newell (1961) has provided observational evidence for a strong positive correlation between meridional velocity, temperature in the lower stratosphere, and columnar ozone. Hunt and Manabe (1968) analyzed the synoptic structure of ozone at 65 mb in their

mode" calculations. They also noted that the local maxima of tracer seemed to be located Eastward of planetary wave troughs.

This schematic picture of mid-latitude ozone transport has to be modified in the upper troposphere where poleward motion tends to be correlated with upward motion (rather than downward motion, as in the lower stratosphere). The transition between these two correlations seems to occur somewhere between 100 and 200 mb. A significant proportion of the horizontal transport of ozone seems to occur below this region. Thus, two schematic pictures may be necessary to completely describe ozone transport; at the lower elevations, a second picture has been proposed by Wallace (1978). In that picture, downward motions, warm temperatures, and high ozone concentrations are depicted as being shifted Westward by approximately  $\pi/2$  radians, compared with those given in Figure 6 and the poleward ozone flux is maintained by geostrophic motions.

These schematic pictures of tracer (eg., ozone) transport must be viewed in the context of the strong cancellation between mean circulation and planetary wave transports (Fjortoff, 1951). Net transport of tracers occurs only because of diabatic effects and non-linear interactions. These dissipative processes produce not only phase shifts of the wave variables but also wave damping. Net transport of tracers in the atmosphere may actually be the result of a series of transient events produced by strong temporal variability in the non-linear interactions. For example, Mahlman, *et al.*, (1979) have found that wave transience is particularly important for transport at mid-latitudes in winter. Mahlman and Moxim (1978) also found in their tracer studies that the mean and eddy cancellation for tracer change in the lower stratosphere is incomplete, particularly during the spring as planetary scale disturbances weaken and when the zonal mean flow in the stratosphere is weak. They attribute the latter effect to the absorption of planetary waves (and hence, alteration of the mean flow) at singular lines on which the speed of the mean flow equals the phase speed of a planetary wave. We note from Figure 3 that the cancellation in the lower stratosphere in our model is weaker in summer (when planetary waves are weaker because of stronger absorption) than in winter. Thus, while strong cancellation between mean and eddy motions appears to exist on the average, there may be many occasions when the previously described wave phase relationships result in substantial net transport.

Above 25 km altitude the nature of ozone transport changes because the photochemical and dynamical time constants become comparable. As we saw in Figure 5, the mean circulation contribution to advection no longer tends to be equal and opposite to that due to planetary waves. In fact, ozone irregularities are probably primarily generated photochemically in large part as a result of temperature inhomogeneities. Based on results from a three-dimensional model we find (Cunnold, *et al.*, 1980) that the correlation between ozone and temperature changes from being positive in the lower stratosphere to negative in the upper stratosphere. Observations supporting the former correlation having already been noted while observations supporting the latter relationship have been documented by Barnett, *et al.*, (1975). At approximately 35 km the correlation is zero. Since the phase relationships of large scale planetary waves are such that temperature is approximately  $\pi/2$  radians out of phase with north-south and vertical motions, we might expect that ozone perturbations would be in phase with these motions and substantial fluxes would be produced at approximately 35 km altitude (Hartmann and Garcia, 1979).

In order to understand ozone transport in this altitude region of the atmosphere, a chemical-dynamical model is needed because of the anticipated role of chemistry in establishing the phase relationships responsible for ozone transport by planetary waves. We find, in fact, that while significant fluxes do appear to be present as illustrated in Figure 5, these only result in relatively minor modifications of the zonal mean ozone distribution (excluding the polar night) at that altitude (Cunnold, *et al.*, 1980). This is probably because the amplitude of ozone irregularities is locally small because of the zero correlation with the temperature inhomogeneities creating the ozone irregularities. This result must, however, be regarded as preliminary in the absence of the inclusion of the transport of those long-lived chemical species which determine ozone destruction.

8. **Conclusions:** We have discussed the status and approximations involved in the application of three-dimensional models to the ozone problem and have noted that three-dimensional models are needed to fully evaluate the potential atmospheric effects of changes in ozone. Such models do appear to be capable of incorporating the most important chemical and dynamical

feedbacks. At the present time, however, they do not seem to provide an adequate simulation of stratospheric dynamics or include sufficient chemistry. Any predictions of potential atmospheric effects must allow for these uncertainties; moreover, our understanding has not progressed sufficiently that we are able to quantify these uncertainties.

Further progress in modeling is expected to result from the use of both improved horizontal and vertical resolution and additional chemistry. We hope that the former improvement will produce a more realistic penetration of planetary wave energy into the stratosphere and hence a more realistic polar night jet. This limitation in the current models has significant chemical implications because of the unrealistically cold temperatures produced over a significant proportion of the globe. Additional chemistry must be added to the models in order to simulate the transport of ozone particularly where the ozone chemical time constant is comparable with the dynamical time constant and where chemistry thus significantly modifies the phase relationships responsible for ozone transport. The addition of chemistry is also needed to evaluate the long term accumulation of anthropogenically-produced chemicals in the atmosphere. These modifications to the models should be undertaken simultaneously with additional measurements of long-lived species in the stratosphere and with carefully-planned experiments to simultaneously measure families of chemically-interactive species. These experiments are expected to aid our understanding of the phase relationships responsible for the transport of chemicals in the stratosphere.

### Acknowledgements

This work was supported by the National Aeronautics and Space Administration under NASA Grant NSG-2010 to the Massachusetts Institute of Technology. Computer time for the calculations was provided by Goddard Institute for Space Studies under Grant NGR-22-009-729.

### References

- Barnett, J.J., J.T. Houghton, and J.A. Pyle, The temperature dependence of the ozone concentration near the stratosphere, Quart. J. Roy. Met. Soc., 101, 245-257, 1975.
- Chen, T.C., D.M. Cunnold, F.N. Alyea, and R.G. Prinn, Manuscript in preparation on the energetics of a photochemical-dynamical model of the stratospheric circulation, 1980.
- Clark, J., A quasi-geostrophic model of the winter stratospheric circulation, Mon. Wea. Rev., 98, 443-461, 1970.
- Cogley, A.C., and W.J. Borucki, Exponential approximation for daily average solar heating or photolysis, J. Atmos. Sci., 33, 1347-1356, 1976.
- Cunnold, D.M., F.N. Alyea, N. Phillips, and R.G. Prinn, A three-dimensional dynamical-chemical model of atmospheric ozone, J. Atmos. Sci., 32, 170-194, 1975.
- Cunnold, D.M., F.N. Alyea, and R.G. Prinn, Preliminary calculations concerning the maintenance of the zonal mean ozone distribution in the Northern Hemisphere. To appear in Pure Appl. Geophys., 1980.
- Dickinson, R., A method of parameterization for infra-red cooling between altitudes of 30 and 70 km, J. Geophys. Res., 78, 4451-4457, 1973.
- Dopplack, T.G., The energetics of the lower stratosphere including radiative effects, Quart. J. Roy. Met. Soc., 97, 209-237, 1971.
- Fjortoft, R., Stability properties of large-scale atmospheric disturbances, in Compendium of Meteorology, T. Malone, ed., p. 454, Boston Amer. Met. Soc., 1334 pp., 1951.
- Green, J., A problem in baroclinic stability, Quart. J. Roy. Met. Soc., 86, 237-251, 1960.
- Hartmann, D., and R. Garcia, A mechanistic model of ozone transport by planetary waves in the stratosphere, J. Atmos. Sci., 36, 350-364, 1979.
- Holton, J.R., The dynamic meteorology of the stratosphere and mesosphere, Monogr., No. 37, Amer. Meteor. Soc., 216 pp., 1975.
- Hunt, B., and S. Manabe, Experiments with a stratospheric general circulation model, 2: Large scale diffusion of tracers in the stratosphere, Mon. Wea. Rev., 96, 503-539, 1968.
- Kasahara, A., T. Sasamori and W.M. Washington, Simulation experiments with a 12-layer stratospheric global circulation. I. Dynamic effect of the earth's orography and thermal influence of continentality, J. Atmos. Sci., 30, 1229-1251, 1973.
- Lacis, A.A., and J.E. Hansen, A parameterization for the absorption of solar radiation in the earth's stratosphere, J. Atmos. Sci., 31, 118-133, 1974.
- Lindzen, R.S., and D.I. Will, An analytic formula for heating due to ozone absorption, J. Atmos. Sci., 30, 513-515, 1973.

- Lorenz, E., Energy and numerical weather prediction, Tellus, 12, 364-373, 1960.
- Lorenz, E., The nature and theory of the general circulation of the atmosphere, World Meteorological Organization, 218, TP. 115, 161 pp., 1967.
- Mahlman, J.D., Preliminary results from a three-dimensional general circulation/tracer model, Proc. Second Conf. Climatic Impact Assessment Program, A.J. Broderick, Ed., 321-377 (DOT-TSC-OST-73-4), 1973.
- Mahlman, J.D., Some fundamental limitations of simplified-transport models as implied by results from a three-dimensional general circulation/tracer model, Proc. Fourth Conf. Climatic Impact Assessment Program, T.M. Hard and A.J. Broderick, Ed., 132-146 (DOT-TSC-OST-75-38), 1975.
- Mahlman, J.D., and W.J. Moxim, Tracer simulation using a global general circulation model: Results from a mid-latitude instantaneous source experiment, J. Atmos. Sci., 35, 1340-1374, 1978.
- Mahlman, J.D., H. Levy II, and W.J. Moxim, Three-dimensional tracer structure and behavior as simulated in two ozone precursor experiments, submitted to J. Atmos. Sci., May, 1979.
- Manabe, S., and R. Strickler, Thermal equilibrium of the atmosphere with a convective adjustment, J. Atmos. Sci., 21, 361-385, 1964.
- Manabe, S., and B.G. Hunt, Experiments with a stratospheric general circulation model. I. Radiative and dynamic aspects, Mon. Wea. Rev., 96, 477-502, 1968.
- Manabe, S., and J.D. Mahlman, Simulation of seasonal and interhemispheric variables in the stratospheric circulation, J. Atmos. Sci., 33, 2185-2217, 1976.
- Martin, D., and A. Brewer, A synoptic study of day-to-day changes of ozone over the British Isles, Quart. J. Roy. Met. Soc., 85, 393-403, 1959.
- Newell, R., The transport of trace substances in the atmosphere and their implications for the general circulation of the stratosphere, Geofs. Pura e Appl., 49, 137-158, 1961.
- Newell, R., D. Vincent, T. Dopplack, D. Ferruzza and J. Kidson, The energy balance of the global atmosphere, The Global Circulation of the Atmosphere, G.A. Corby, Ed., Roy. Meteor. Soc., 42-90, 1972.
- Newson, R.L., An experiment with a tropospheric and stratospheric three-dimensional general-circulation model Proc. Third Conf. Climatic Impact Assessment Program, U.S. Dept. of Trans., Rep. No. DOT-TX-OST-74-15, 461-473, 1974.
- Oort, A.H., On the energetics of the mean and eddy circulations in the lower stratosphere, Tellus, 16, 309-327, 1964.
- Phillips, N.W., Geostrophic motion, Rev. of Geophys., 1, 123-176, 1963.
- Peng, L., A simple numerical experiment concerning the general circulation in the lower stratosphere, Pure Appl. Geophys., 61, 191-218, 1965.
- Ramanathan, V., Radiative transfer within the earth's troposphere and stratosphere: A simplified radiative-convective model, J. Atmos. Sci., 33, 1330-1346, 1976.
- Ramanathan, V., and W.L. Grose, A numerical simulation of seasonal stratospheric climate. Part I. Zonal thermal and dynamical structure, J. Atmos. Sci., 35, 600-614, 1978.
- Schlesinger, M.E., and Y. Mintz, Numerical simulation of ozone production, transport and distribution with a global atmospheric general circulation model, J. Atmos. Sci., 36, 1325-1361, 1979.
- Smagorinsky, J., General circulation experiments with the primitive equations. I. The basic experiment, Mon. Wea. Rev., 91, 99-164, 1963.
- Trenberth, K., Global model of the general circulation of the atmosphere below 75 kilometers with an annual heating cycle, Mon. Wea. Rev., 101, 287-305, 1973.
- Wallace, J., Trajectory slopes, countergradient heat fluxes, and mixing by lower stratospheric waves, J. Atmos. Sci., 35, 554-560, 1978.

## MODELING TROPOSPHERIC $N_2O$

Hiram Levy II and J. D. Mahlman

Geophysical Fluid Dynamics Laboratory/NOAA  
Princeton University, P. O. Box 308  
Princeton, New Jersey 08540

Following a brief review, a series of numerical experiments utilizing a global three-dimensional  $N_2O$  model are discussed. In all three cases the  $N_2O$  loss path is stratospheric destruction which produces an  $N_2O$  atmospheric lifetime of 150 years. Three different surface source prescriptions are used: a uniform source with a global strength of  $10 \text{ tg N yr}^{-1}$ ; a highly non-uniform land source with the same global strength; and an experiment with the source removed. We find that the small surface source appropriate to a 150 year lifetime is sufficient to produce local relative standard deviations in the surface layer  $>0.5\%$  for a uniform source and  $>2\%$  for a non-uniform source. The mixing ratio and variability fields in the middle troposphere are essentially independent of the boundary layer and the nature of the surface source, but are indirectly influenced by the atmospheric lifetime ( $\tau$ ). In the boundary layer the source distribution and local source strength dominate the structure of these fields while  $\tau$  has little impact. The one exception may be regions far from local sources which have uniformly low variability and may be sensitive to  $\tau$ . These conclusions, while specific to  $N_2O$  in this paper, are in fact quite general and applicable to any long-lived tracer with a surface source and stratospheric sink.

### INTRODUCTION AND REVIEW

$N_2O$ , first observed in the earth's atmosphere by Adel (1939), was thought to have a bacterial source in the soil (Adel, 1951). Oxidation of  $N_2O$  by metastable atomic oxygen  $O(^1D)$ , provides the major natural source of stratospheric  $NO$  (McElroy and McConnell, 1971) which in turn drives the dominant destruction cycle for stratospheric  $O_3$  (Crutzen, 1970). Following Congressional testimony by McElroy (1974), there was considerable speculation about the impact of nitrogen fertilizers (Liu et al., 1976; Crutzen, 1976; McElroy et al., 1977) on atmospheric levels of  $N_2O$  and, indirectly, on stratospheric  $O_3$ .  $N_2O$  was also observed in power plant plumes (Weiss and Craig, 1976; Pierotti and Rasmussen, 1976) where it appeared to be an incomplete oxidation product of fuel nitrogen. The potential impact of both these direct and indirect anthropogenic sources of  $N_2O$  on the stratospheric mixing ratio of  $N_2O$ , and ultimately on  $O_3$ , is quite complex. Both the time scale and ultimate magnitude of the  $N_2O$  increase and  $O_3$  reduction are very sensitive to the size and distribution of the tropospheric sources and sinks of  $N_2O$  as well as its atmospheric lifetime.

At the time of the initial concern about possible reductions in the ozone layer due to man's direct or indirect production of  $N_2O$ , there was no clear understanding of atmospheric  $N_2O$ . Bates and Hayes (1967), using a 1-D eddy diffusion model with a surface source (Adel, 1951; Bates and Witherspoon, 1952) and a photodissociation sink in the stratosphere, had predicted that  $N_2O$  was well mixed in the troposphere with lifetime of approximately 70 years. Based on early measurements of tropospheric  $N_2O$  which were quite variable in space and time (Lahue, Pate, and Lodge, 1970; Goody, 1969; Schutz et al., 1970), Junge (1974) estimated an  $N_2O$  atmospheric lifetime of 8 years which required sources and sinks much larger than those



proposed by Bates and Hayes (1967). Extrapolating measurements of  $N_2O$  supersaturation in the north Atlantic to the world oceans, Hahn (1974) calculated an ocean  $N_2O$  source of  $85 \text{ tg (N) yr}^{-1}$ . Using much the same data with different assumptions, McElroy et al. (1976) estimated an ocean  $N_2O$  sink of up to  $40 \text{ tg (N) yr}^{-1}$ . To further confuse the situation, Johnston and Selwyn (1975) reported new measurements of  $N_2O$  photodissociation coefficients which reduced the estimated  $N_2O$  stratospheric sink to  $10 \text{ tg (N) yr}^{-1}$  and Blackman and Bremner (1976) reported that soil acted more effectively as a sink than as a source. These conflicting views regarding tropospheric  $N_2O$  were represented in a review by Hahn and Junge (1977) which supported the large tropospheric source, short lifetime position, and in a paper by Liu et al., (1977) which concluded that nothing regarding tropospheric sources, sinks, and lifetimes of  $N_2O$  was certain.

Using the GFDL general circulation/tracer model, we constructed a global model of  $N_2O$  based on a small surface source which balanced stratospheric destruction. With such a model it was possible to generate a global data set and to calculate the small but important spatial and temporal variabilities in the tropospheric  $N_2O$  fields. Given the uncertain nature of the  $N_2O$  source distribution and strength, we designed a series of numerical experiments to determine the level of tropospheric variability supported by such a small source and long lifetime and to identify the causes of this variability. We suspected that, as measurement techniques and instrumentation improved, the observed  $N_2O$  variability would decrease. Measurements by Weiss (private communication, 1976) suggested just that. It was also suspected that the Junge relationship between variability and lifetime was not appropriate for a trace gas with a 150 year lifetime and a vertical gradient in the stratosphere. Preliminary results of these experiments have already been published (Levy, Mahlman, and Moxim, 1979).

Between the start of these experiments in 1976 and their completion (Levy, Mahlman, and Moxim, 1980), a great deal of new data on tropospheric  $N_2O$  has emerged. Recent measurements have confirmed its low tropospheric variability and support a relatively long lifetime. Cicerone et al. (1978) reported a mean mixing ratio,  $R(N_2O)$ , of 330 ppbv with a relative standard deviation (V) of 1%; Pierotti and Rasmussen (1977) and Pierotti, Rasmussen, and Chatfield (1979) reported  $R(N_2O) \approx 330 \text{ ppbv}$  and, for a 3 month time series in the state of Washington,  $V = .3\%$ ; Singh, Salas, and Sigeishi (1979) reported  $R(N_2O) = 311 \text{ ppbv}$  with no variability observed outside their experimental error; Goldern et al., (1978) reported  $R(N_2O) = 326$  and  $V = 1.1\%$ ; Roy (1979) reported  $R(N_2O) \sim 340 \text{ ppbv}$  with no variability observed outside their experimental error; and Weiss (private communication, 1980) reported  $R(N_2O) = 300$  with  $V = .3-.5\%$  for a large number of measurements in the Pacific and Atlantic atmospheric boundary layer.

Cohen and Gorden (1979), using recent measurements of  $N_2O$  saturation and  $NO_3^-$  content in sea water, have estimated a global oceanic  $N_2O$  source of  $4-10 \text{ tg (N) yr}^{-1}$ . Pierotti and Rasmussen (1980) have inferred an  $N_2O$  source strength of  $7 \times 10^{10} \text{ molecules cm}^{-2} \text{ sec}^{-1}$  in the eastern tropical Pacific.

Earlier observations of a large decrease in  $R(N_2O)$  in air coming from the Sahara (Schutz et al., 1970), which suggested a dust or sand sink for  $N_2O$ , gained some credibility from laboratory observations of the disappearance of  $N_2O$  in glass flasks containing sand (Rebber and Ausloos, 1978). The disappearance took place in both the light and the dark but was greatly inhibited by moisture. While recent measurements of  $N_2O$  in dusty air by Pierotti, Rasmussen, and Rasmussen (1978) found a small reduction ( $<1\%$ ) which might have been significant, Weiss (private communication, 1979) was not able to observe a similar reduction near the Cape Verde Islands and over the Red Sea. The existence of a dust or sand heterogeneous sink for  $N_2O$  is possible, though not certain. Alyea, Cunnold, and Prinn (1978) demonstrated that the sink, if it existed, could be important. However, the recent atmospheric measurements mentioned above, while not definitive, do not support the existence of a large sink in the Sahara region.

The question of the role of soil appears to have been resolved in favor of a soil source (Freney, Denmead, and Simpson, 1978; Mathias, Blackmer, and Bremner, 1979). However it now appears that bacterial activity during nitrification in soil (Bremner and Blackmer, 1979; Breitenbeck, Blackmer, and Bremner, 1979), in fresh water (Elkins et al., 1978) and in the ocean (Cohen and Gorden, 1979) is the important mechanism of  $N_2O$  production, rather than during denitrification as previously assumed.

The recent determination of temperature-dependent  $N_2O$  dissociation cross sections (Selwyn, Podolske and Johnston, 1977) has resulted in a further reduction in the calculated stratospheric destruction rate. The resulting  $N_2O$  lifetime estimate has increased from 150 to 175 years (Johnston, Serang, and Podolske, 1979).

The current view of tropospheric  $N_2O$  could be summarized as low variability (1% or less), a variety of small natural soil and water sources which should be sufficient to balance stratospheric destruction, and the possibility of dust and sand surface destruction. With the exception of a dust or sand sink this would appear to be in harmony with the model we proposed in 1976. The three experiments we will now discuss should help determine if a stratospheric sink balanced by a small surface source is sufficient to explain the global structure and variability of  $N_2O$  as we now understand it. If the natural source of  $N_2O$  is that small, an anthropogenic contribution such as combustion may have considerable influence on the global budget of  $N_2O$  and ultimately its concentration in the stratosphere (Levy, Mahlman, and Moxim, 1979). The observations by Weiss and Craig (1976) that the tropospheric  $N_2O$  mixing ratio is increasing at a rate of .15% yr<sup>-1</sup> is consistent, as they suggest, with a significant combustion source.

#### MODEL DESCRIPTION

The numerical study of  $N_2O$  employed the GFDL 3-D general circulation/tracer model which has already been used to simulate the global dispersion and rainout of radioactive debris from nuclear weapons tests (Mahlman and Moxim, 1978) and the 3-D structure and behaviour of a simplified ozone tracer (Mahlman, Levy, and Moxim, 1980). This model has 11 terrain following ( $\sigma$ ) surfaces in the vertical with standard heights of 31.4, 22.3, 18.8, 15.5, 12.0, 8.7, 5.5, 3.1, 1.5, 0.5 and 0.1 km and a horizontal grid dimension of approximately 265 km. The model solves, by the method of finite differences, the continuity equation for the mixing ratio of  $N_2O$ . This equation, in  $\sigma$  coordinates, is given by

$$\frac{\partial R(N_2O)p_*}{\partial t} = - \nabla_{\sigma} \cdot \vec{V}_2 p_* R(N_2O) - \frac{\partial}{\partial \sigma} \dot{\sigma} p_* R(N_2O) + SO + \text{DIFFUSION} - S1 R(N_2O) \quad (\text{Eq. 1})$$

where  $p_*$  is surface pressure,  $\vec{V}_2$  is the horizontal wind vector,  $\dot{\sigma}$  is the vertical motion in  $\sigma$  coordinates,  $SO$  is the source, and  $S1$  is the destruction rate coefficient (sec<sup>-1</sup>). The contribution from DIFFUSION, consisting of sub-grid scale vertical and horizontal diffusion, is discussed elsewhere (see Levy, Mahlman, and Moxim, 1980).

The wind fields used in Eq. 1 are the 6 hour mean wind fields generated by a GFDL general circulation model. The preparation of the input data, the relevant features of the general circulation model providing it, and the numerical techniques used to integrate Eq. 1 have all been described previously (Mahlman, 1973; Mahlman and Moxim, 1978).

Photodissociation and oxidation by  $O(^1D)$  provide the stratospheric sink for  $N_2O$ . They act only in the top two model layers and lead to an  $N_2O$  atmospheric lifetime (global mass of  $N_2O$ /global  $N_2O$  destruction rate) of about 150 years. The rate coefficients for  $O(^1D)$  are taken from a compilation by Hampson and Garvin (1975) and the quantum yields from Levy (1974). The photodissociation calculation use the absorption coefficients measured by Johnston and Selwyn (1975), the solar flux data compiled by Ackerman (1971) and Simon (1974), the  $O_2$  and  $O_3$  absorption coefficients tabulated by Ackerman (1971), and annual mean  $O_3$  profiles constructed from observed data (Fels, Mahlman, Schwarzkopf, and Sinclair, 1980). Recent calculations by Johnston, Serang, and Podolske (1979) find an increase in the  $N_2O$  lifetime from 150 years to 175 years. While the exact  $N_2O$  lifetime is not yet known, the current uncertainty does not significantly effect the conclusions of this tropospheric study.

The first experiment ("Uniform Source") has a constant surface source of  $1.3 \times 10^9$  molecules cm<sup>-2</sup> sec<sup>-1</sup> over the globe and is designed to be a minimum variability experiment. This particular global source strength balances the stratospheric destruction with an  $N_2O$  field having a tropospheric value of approximately 300 ppbv. For the second experiment ("No Source"), we shut off the source and determine the tropospheric structure and variability after 13 month's integration. In the third experiment ("Swamp Source"), while the global source

strength is not changed from the first experiment, the distribution is highly non-uniform with a strength of  $2.00 \times 10^{10}$  molecules  $\text{cm}^{-2} \text{sec}^{-1}$  in those surface land boxes with a simulated annual rainfall exceeding an arbitrary minimum of 50 inches (127 cm). A map of the source distribution is given in Figure 1.

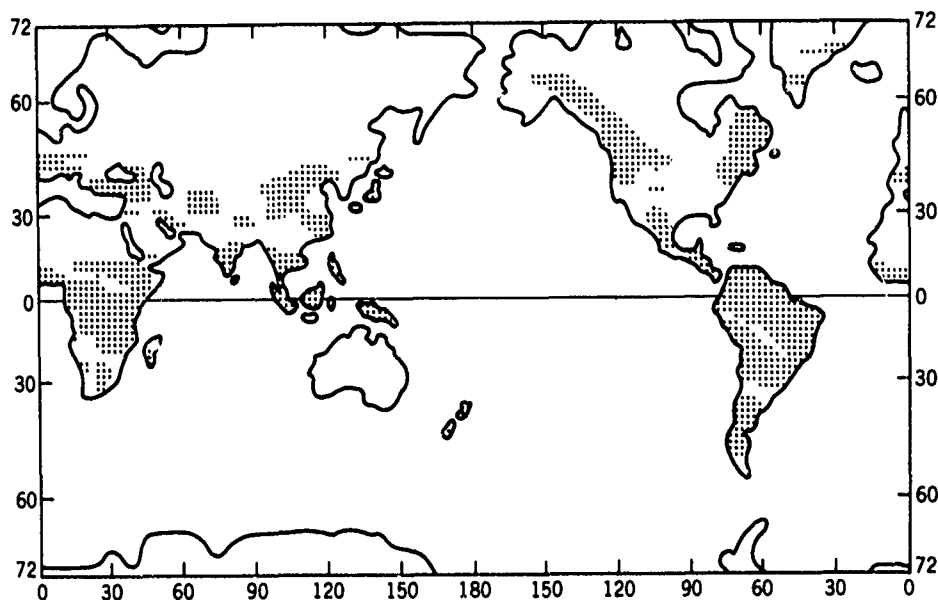


Fig. 1. Dotted areas are source regions for "Swamp Source"  $\text{N}_2\text{O}$ .

#### EXPERIMENTAL DESIGN

Given the uncertain state of knowledge regarding tropospheric sources and sinks for  $\text{N}_2\text{O}$  in 1976, it was not possible to include the correct tropospheric structure of  $\text{N}_2\text{O}$  sources. Rather, we sought, with this series of idealized source experiments, to establish bounds for the size and variability of the net tropospheric source, the need, if any, for large competing tropospheric sources and sinks, and the relationship between observed variability and atmospheric lifetime. We also hoped to determine the causes of  $\text{N}_2\text{O}$  tropospheric variability and the impact of source size and distribution on it.

##### "Uniform Source"

The first experiment is designed as a minimum variability experiment compatible with the quantitatively known stratospheric destruction rate. The surface  $\text{N}_2\text{O}$  source is constant in space and time. This choice removes source variability as a cause of mixing ratio variability and permits us to focus on the role of large scale motions. The "Uniform Source" experiment provides, in a global sense, a lower bound for tropospheric  $\text{N}_2\text{O}$  variability, and, if sufficient, demonstrates that large sources and sinks are not needed in the troposphere. The experiment, using an efficient updating technique involving successive re-initializations (Levy, Mahlman, and Moxim, 1980), has been integrated to both chemical and transport statistical equilibrium such that the yearly global destruction rate is within .3% of the final equilibrium value.

##### "No Source"

In the second experiment, ("No Source"  $\text{N}_2\text{O}$ ), we started with the equilibrated "Uniform Source"  $\text{N}_2\text{O}$  field and shut off the surface source. This experiment was then integrated for 13 months. The main goal is to examine the role of the surface source in tropospheric variability.

"Swamp Source"

We next wished to examine the effect of source distribution on both tropospheric structure and variability. We would have preferred to run the "correct"  $N_2O$  source experiment but the true nature of the  $N_2O$  source was still not clear in 1978 when this experiment began and remains so at this time. By 1978 it appeared that, while the role of the oceans was smaller than previously thought, the range of potential land sources and sinks was still quite wide. We chose, as our non-uniform source, a land based source that required high yearly rainfall. This experiment, "Swamp Source"  $N_2O$ , had a highly non-uniform source which was concentrated at low latitudes with a slight northern hemisphere bias (see Figure 1). It now appears that the actual  $N_2O$  sources include not only wet denitrifying soil regions, but agricultural areas, nitrate-rich fresh water lakes and rivers, and certain regions in the ocean. While "Swamp Source" is not designed to duplicate the "correct" source distribution, it is highly dispersed spatially. Together with "Uniform Source"  $N_2O$ , it explores the range of tropospheric variability and structure expected for tropospheric  $N_2O$  with a stratospheric sink balanced by a surface source. "Swamp Source"  $N_2O$  was started from the equilibrated "Uniform Source"  $N_2O$  field and integrated for 18 months. This was sufficient to produce an equilibrated tropospheric distribution.

## MODEL RESULTS

The  $R(N_2O)$  fields for the uniform and non-uniform source experiments have a global average surface mixing ratio of 293 ppbv. This value is a result of the three-dimensional equilibrium between an atmospheric lifetime of 150 years and an arbitrary global source of  $10 \text{ tg N yr}^{-1}$ . Rather than adjusting the source strength to generate the currently accepted surface mixing ratio, which still ranges between 300 ppbv and 330 ppbv, we kept the original choice. To convert the model field to a particular preferred surface value of  $R(N_2O)$ , one need only scale the data by a constant factor. Conclusions reached about tropospheric  $N_2O$  are independent of such a factor. If the higher of the current measured values (330 ppbv) is correct, the global source strength would be  $11 \text{ tg N yr}^{-1}$ .

The zonal mean  $N_2O$  mixing ratio and longitudinal relative standard deviation fields,  $V_\lambda$ , have already been discussed for "Uniform Source"  $N_2O$  (see Figure 1 in Levy, Mahlman, and Moxim, 1979). Their structure in the middle troposphere is no different for the other two experiments. While the meridional gradient in the boundary layer is influenced by the source distribution (Levy, Mahlman, and Moxim, 1980), the latitude-longitude cross sections that will be discussed are more useful for comparison with the type of atmospheric data normally gathered.

This discussion is divided into two sections. The first examines results from the model's 500 mb surface, and the second considers results from the model's surface or boundary layer.

## A. Middle Troposphere - 500 mb

The 500 mb January mean  $R(N_2O)$  latitude-longitude cross section for "Swamp Source"  $N_2O$  is shown in Figure 2.

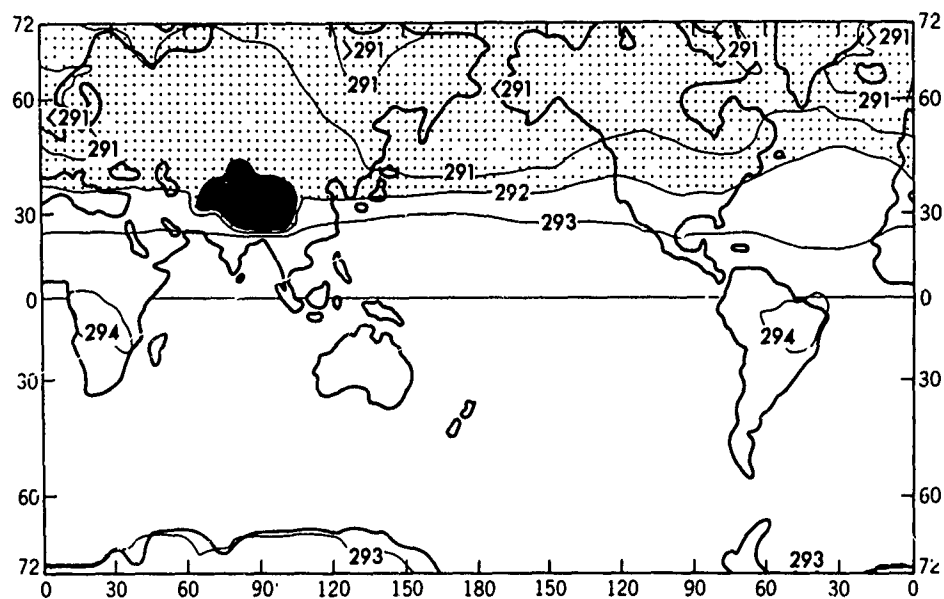


Fig. 2. January mean  $R(N_2O)$  at 500 mb for "Swamp Source"  $N_2O$ . Dotted area has  $R(N_2O) < 292$  ppbv.

The 500 mb fields for the other experiments are almost the same, except that the slight maxima located over strong local source regions in Brazil and Southern Africa are missing. In general the field is quite zonal with an essentially uniform distribution in the southern hemisphere. There is a slight gradient in the northern hemisphere and one non-zonal feature, the 291 ppbv contour line, which drops southward over the Pacific and North America. This is a result of the strong wintertime downward transport of  $N_2O$  poor stratospheric air (Mahlman, Levy, and Moxim, 1980) in the vicinity of the Aleutian low.

The January latitude-longitude cross section of local relative standard deviation,  $V_t$ , at 500 mb is given in Figure 3, where

$$V_t = \frac{100}{\overline{R}^t} \left[ \sum_{i=1}^D \frac{(R(N_2O)_i - \overline{R(N_2O)}^t)^2}{D} \right]^{1/2} \quad (\text{Eq. 2})$$

$\overline{R(N_2O)}^t$  is the monthly mean  $R(N_2O)$  for a given box and  $i$  is summed over the number of days in the month,  $D$ .

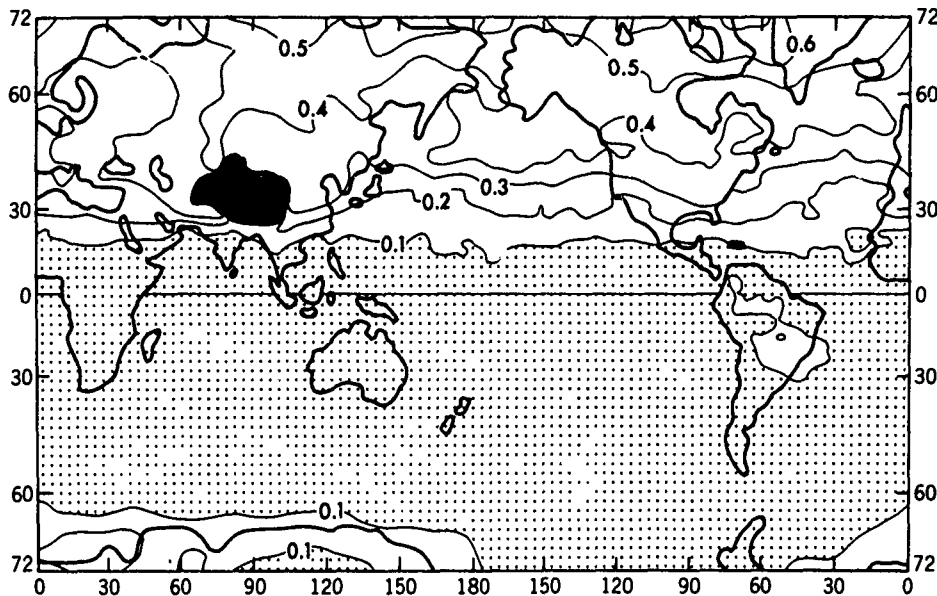


Fig. 3. January  $V_t$  at 500 mb for "Uniform Source"  $N_2O$ .  
Dotted area has  $V_t < .1\%$ .

Only the "Uniform  $N_2O$ " field is shown because  $V_t$  in the middle troposphere is also not influenced by the source distribution. The tropics and most of the southern hemisphere have  $V_t < .1\%$ . There is a large maximum exceeding .4% in the northern mid- and high-latitudes which shows up in the same region that was bounded by the 291 contour. The maximum in  $V_t$  is the result of fluctuations in  $R(N_2O)$  induced by the action of transient cyclonic waves on the  $R(N_2O)$  vertical gradients in that region of the middle troposphere. The local temporal variability in the middle troposphere is independent of the surface source's distribution and local strength. However, it should be sensitive to the atmospheric lifetime through its indirect dependence on the vertical gradients in the stratosphere which themselves depend on the atmospheric destruction rate.

#### B. Boundary Layer - 80 m Above the Surface

In this region the tracer distribution and variability are strongly influenced by both the model's large-scale resolved motions and sub-grid scale processes such as vertical diffusion and convection.

#### $R(N_2O)$ Fields

Latitude-longitude cross sections of boundary layer  $R(N_2O)$  for January are given in Figure 4.

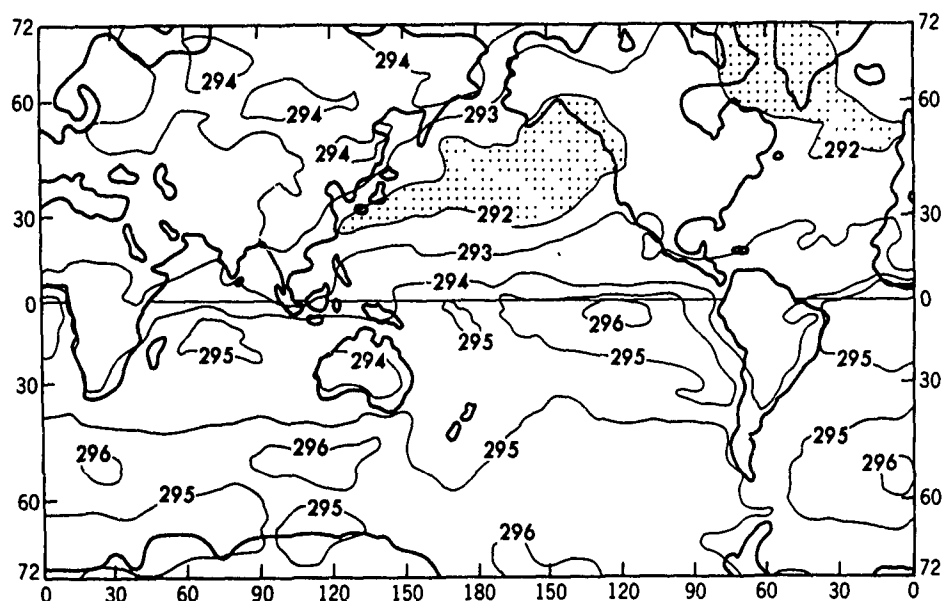


Fig. 4a. January mean  $R(N_2O)$  for "Uniform Source"  $N_2O$  80 m above the surface. Dotted areas have  $R(N_2O) \leq 292$  ppbv.

While the surface  $\overline{R(N_2O)}^t$  map for "Uniform Source" retains the hemispheric asymmetry observed in the zonal field, a great deal of non-zonal structure is present. In the equatorial region a mixing ratio maximum forms just south of the ITCZ. This maximum moves north and south with the ITCZ and spreads across the Pacific in the summer just as the ITCZ does. The slowly subsiding air behind the ITCZ results in an accumulation of  $N_2O$  in the boundary layer. In the southern hemisphere the continents have uniformly low  $\overline{R(N_2O)}^t$  relative to the oceans as a result of higher convective activity over land. In the northern hemisphere we find mixing ratio minimums at mid-latitudes over the Pacific and at high-latitudes over the Atlantic while local maximums are present over the Soviet Union.

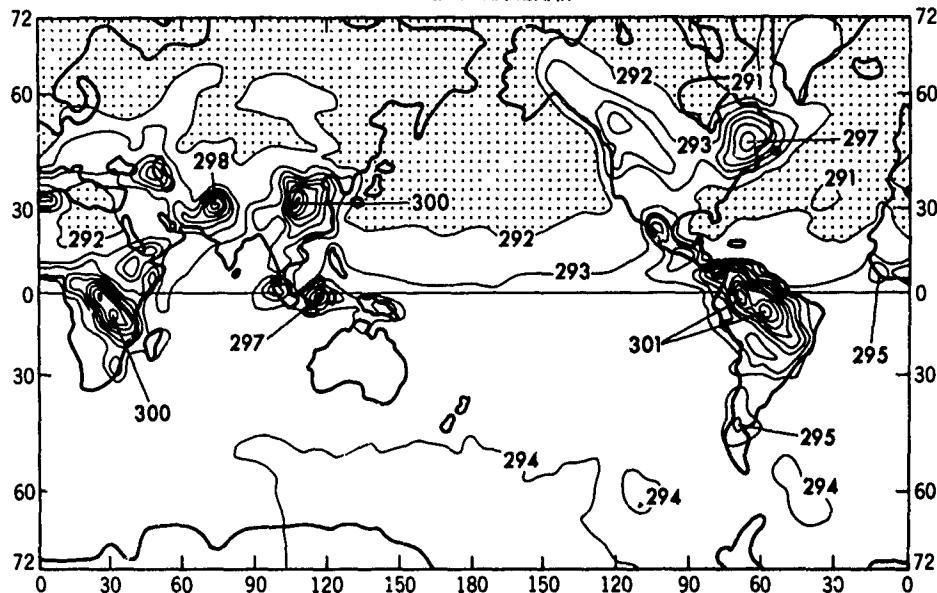


Fig. 4b. January mean  $R(N_2O)$  for "Swamp Source"  $N_2O$  80 m above the surface. Dotted areas have  $R(N_2O) \leq 292$  ppbv.

The most obvious feature of the "Swamp Source"  $N_2O$  boundary layer is the accumulation of  $R(N_2O)$  in the source regions. In the mean, increases of 2.5% over background (300 ppbv vs 293 ppbv) are common in the source region. The local accumulations are diluted, before they can spread horizontally, by vertical transport due to both resolved motions and subgrid scale diffusion. The steep north-south gradient observed in the Pacific for "Uniform Source"  $N_2O$  is moderated considerably when the ocean source is removed.

From these two experiments we see that non-uniform local sources lead to significant excess  $R(N_2O)$  in the source regions of the boundary layer relative to the global mean, and that the north-south gradient over the oceans is strongly influenced by the presence of a surface ocean source. Furthermore, the mixing ratio field is quite non-zonal, even for a uniform source distribution.

#### $V_t$ Fields

For a more sensitive signal we turn to the January longitude-latitude cross sections of  $V_t$  in Figure 5.



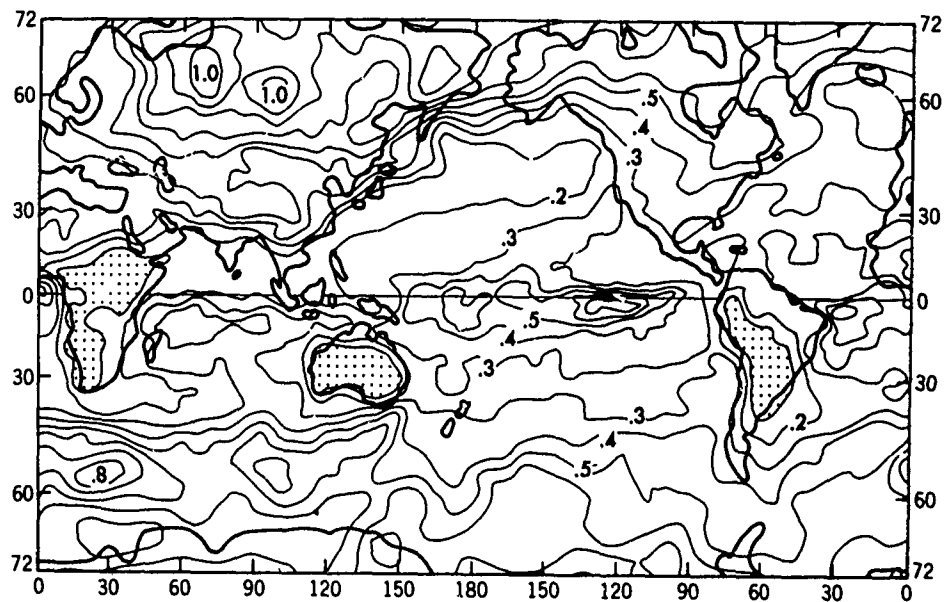


Fig. 5a. January  $V_t$  for "Uniform Source"  $N_2O$  80 m above the surface. Dotted areas have  $V_t \leq .1\%$ .

For "Uniform Source"  $N_2O$  we find January  $V_t > .4\%$  over most of the continental northern hemisphere above  $30^\circ N$  with the exception of Western Europe and the western United States. The Pacific south of  $40^\circ S$  which had high  $R(N_2O)_t$  also has  $V_t > .5\%$ . The one other region of high  $V_t$  is the region south of the ITCZ where there is  $R(N_2O)_t$  accumulation. The southern hemisphere continents which have low  $R(N_2O)_t$  due to summertime convective mixing also have low variability,  $V_t < .1\%$ .

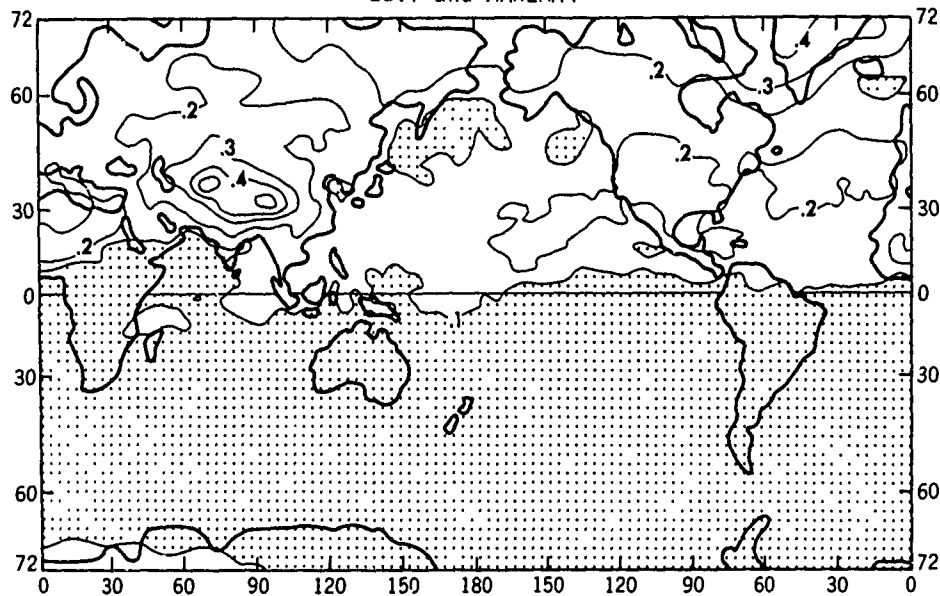


Fig. 5b. January  $V_t$  for "No Source"  $N_2O$  80 m above the surface.  
Dotted areas have  $V_t \leq 0.1\%$ .

The "No Source"  $N_2O$  experiment produces a much more uniform  $V_t$  field. The southern hemisphere  $V_t$  drops to  $<0.1\%$  and the only regions in the northern hemisphere with  $V_t > 0.2\%$  are over the Himalayan Plateau, Canada, and the central Atlantic. It is clear that the presence of a surface source, though not necessarily a large one, is needed to produce the gradients which result in variability in the boundary layer. The exceptions to this are the mid- and high-latitude regions which derive a significant fraction of their variability from the transient downward transport of  $N_2O$  poor air from the lower stratosphere.

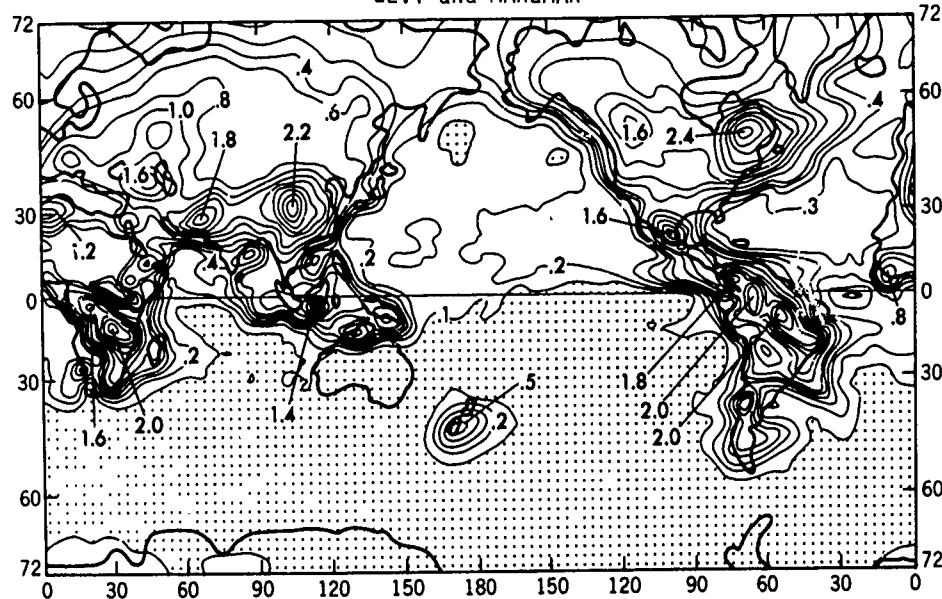


Fig. 5c. January  $V_t$  for "Swamp Source"  $N_2O$  80 m above the surface. Dotted areas have  $V_t < .1\%$ . Above .6%, the contour intervals change from .1% to .2%.

The  $V_t$  field from "Swamp Source"  $N_2O$  is quite interesting. The regions of high variability are located over the regions of high  $R(N_2O)_t$  which in turn are located over the model sources (Figure 1). It is common to find  $V_t > 2.0\%$  in these regions. On the other hand, most of the southern hemispheric ocean boundary layer where there is no source has  $V_t < 0.1\%$ . One could get a good qualitative representation of the "Swamp Source"  $V_t$  field by superimposing the source distribution in Figure 1 on the "No Source"  $V_t$  field.

In general, we can conclude that, in boundary layer regions where there is no nearby surface source, there will be very low variability ( $V_t < .1\%$ ), while in the source regions  $V_t$  will be proportional to the source strength. It is clear from the "Uniform Source" experiment that boundary layer values of  $V_t > .5\%$  are easily generated in the presence of a very small surface source. Proper measurements of  $R(N_2O)$  time series should be an important tool for determining the presence and strength of local sources. While  $R(N_2O)$  time series in regions far from sources will give no information about the nature of the tropospheric source, the residual  $V_t$  that does exist is mainly a result of the large scale motions acting on vertical gradients and thus may contain information about the atmospheric lifetime. It is clear from the wide range of  $V_t$  values possible for even the most uniform of sources, that it is not possible to relate local variability to global properties of  $N_2O$ .

#### SUMMARY AND CONCLUSIONS

Outside the model boundary layer we find that  $\overline{R(N_2O)_t}$  is relatively well mixed with a range of 1% or less. The  $\overline{R(N_2O)_t}$  structure in the middle troposphere, except for a few small regions with a combination of a strong surface source and strong convection, is independent of the surface source strength and distribution. In the middle troposphere, variability is also independent of the surface source strength and distribution.  $V_t$  does show meridional structure with  $V_t < .1\%$  from the northern subtropics to the southern polar regions and  $> .4\%$  in the northern mid- and high-latitudes. This is the result of large scale tropospheric and lower stratospheric motions acting on horizontal and vertical tracer gradients which are themselves determined by the atmospheric lifetime. Therefore, in the middle troposphere both the structure and magnitude of  $V_t$  and the  $\overline{R(N_2O)_t}$  meridional structure will be sensitive to  $\tau$ , though not to the surface source distribution.

In the boundary layer  $R(N_2O)^t$  is influenced by source strength and distribution. For the "Swamp Source" experiment we find  $R(N_2O)^t$  in source regions exceeding the global boundary layer mean by as much as 2.5%. In the area of a local non-uniform source,  $R(N_2O)^t$  should exceed the global boundary layer mean by an amount that increases with the local source strength.

In the boundary layer, even for "Uniform Source",  $V_t$  is quite variable. The distribution of  $V_t$  in January is far from zonal with the southern hemisphere continents having  $V_t < .1\%$  while  $V_t > .6\%$  in the eastern equatorial Pacific. When we consider highly non-uniform sources such as those given in "Swamp Source", the  $V_t$  boundary layer field becomes much more complex. Regions far from source regions have  $V_t < .1\%$ , while in the source region we have  $V_t$  reaching 1-2% for a global source that is still small enough to balance an atmospheric lifetime of 150 years.

In the boundary layer, the structure and magnitude of the  $R(N_2O)$  and  $V_t$  fields are controlled by the source distribution and local source strength. The  $N_2O$  atmospheric lifetime has little impact. The one exception would be regions far from local sources which have a small residual  $V_t$  that may be sensitive to lifetime. These conclusions, while specific to  $N_2O$  in this study, are quite general and apply to any long lived tracer with a surface source and stratospheric destruction.

#### ACKNOWLEDGMENT

We are deeply indebted to W. J. Moxim for his contribution to this work.

#### REFERENCES

- Ackerman, M., Ultraviolet solar radiation related to mesospheric processes, Mesospheric Models and Related Experiments, 149-159, D. Reidel, Dordrecht, 1971.
- Adel, A., Note on the atmospheric oxides of nitrogen, Astrophys. J., **90**, 627, 1939.
- Adel, A., Atmospheric nitrous oxide and the nitrogen cycle, Science, **113**, 624-625, 1951.
- Alyea, F. N., D. M. Cunnold, and R. G. Prinn, Meteorological constraints on tropospheric halocarbon and nitrous oxide destructions by siliceous land surfaces, Atmos. Environ., **12**, 1009-1011, 1978.
- Bates, D. R., and P. B. Hayes, Atmospheric nitrous oxide, Planet. Space Sci., **15**, 189-197, 1967.
- Bates, D. R., and A. E. Witherspoon, The photochemistry of some minor constituents of the earth's atmosphere ( $CO_2$ ,  $CO$ ,  $CH_4$ ,  $N_2O$ ), Mon. Nat. R. Astr. Soc., **112**, 101-124, 1952.
- Blackmer, A. M., and J. M. Bremner, Potential of soil as a sink for atmospheric nitrous oxide, Geophys. Res. Lett., **3**, 739-742, 1976.
- Breitenbeck, G. A., A. M. Blackmer, and J. M. Bremner, Effects of different nitrogen fertilizers on emission of nitrous oxide from soil, Geophys. Res. Lett., **7**, 85-88, 1980.
- Bremner, J. M., and A. M. Blackmer, Effects of acetylene and soil water content on emission of nitrous oxide from soils, Nature, **280**, 380-381, 1979.
- Cicerone, R. J., J. D. Shetter, D. H. Stedman, T. J. Kelly, and S. C. Liu, Atmospheric  $N_2O$ : Measurements to determine its sources, sinks, and variations, J. Geophys. Res., **83**, 3042-3050, 1978.
- Cohen, Y., and L. I. Gordon, Nitrous oxide production in the ocean, J. Geophys. Res., **84**, 347-353, 1979.
- Crutzen, P. J., The influence of nitrogen oxides on the atmospheric ozone content, Quart. J. R. Met. Soc., **96**, 320-325, 1970.
- Crutzen, P. J., Upper limits on atmospheric ozone reductions following increased application of fixed nitrogen to the soil, Geophys. Res. Lett., **3**, 169-172, 1976.
- Elkins, J. W., S. Wofsy, M. B. McElroy, C. E. Kolb, and W. A. Kaplan, Aquatic sources and sinks for nitrous oxide, Nature, **275**, 602-606, 1978.

- Fels, S. B., J. D. Mahlman, M. D. Schwarzkopf, and R. W. Sinclair, Stratospheric sensitivity to perturbations in ozone and carbon dioxide: radiative and dynamical response, J. Atmos. Sci., to be published 1980.
- Freney, J. R., O. T. Denmead, and J. R. Simpson, Soil as a source or sink for atmospheric nitrous oxide, Nature, 273, 530-532, 1978.
- Goldan, P. D., Y. A. Bush, F. C. Fehsenfeld, D. L. Albritton, P. J. Crutzen, A. L. Schmeltekopf, and E. E. Ferguson, Tropospheric  $N_2O$  mixing ratio measurements, J. Geophys. Res., 83, 935-939, 1978.
- Goody, R. M., Time variations in tropospheric  $N_2O$  in eastern Massachusetts, Planet. Spa. Sci., 17, 1319-1320, 1969.
- Hahn, J., The North Atlantic ocean as a source of atmospheric  $N_2O$ , Tellus, 26, 160-168, 1974.
- Hahn, J., and C. Junge, Atmospheric nitrous oxide: A critical review, Z. Naturforsch., 32a, 190-214, 1977.
- Hampson, R. F., and D. Garvin, Chemical kinetic and photochemical data for modelling atmospheric chemistry, Tech. Note 866, 113 pp. Nat. Bur. of Stand., Washington, D.C., 1975.
- Johnston, H. S., and G. Selwyn, New cross section for the absorption of near ultra-violet radiation by nitrous oxide ( $N_2O$ ), Geophys. Res. Lett., 2, 549-551, 1975.
- Johnston, H. S., O. Serang, and J. Podolske, Instantaneous global nitrous oxide photochemical rates, J. Geophys. Res., 84, 5077-5082, 1979.
- Junge, C., E. Residence time and variability of tropospheric trace gases, Tellus, 26, 477-488, 1974.
- LaHue, M. D., J. B. Pate, and J. P. Lodge, Jr., Atmospheric nitrous oxide concentrations in the humid tropics, J. Geophys. Res., 75, 2922-2926, 1970.
- Levy II, H., Photochemistry of the troposphere, Advances in Photochemistry, J. N. Pitts, Jr., G. S. Hammond and K. Gollnick, Eds. p. 448, J. Wiley and Sons, 1974.
- Levy II, H., J. D. Mahlman, and W. J. Moxim, A preliminary report on the numerical simulation of the three-dimensional structure and variability of atmospheric  $N_2O$ , Geophys. Res. Lett., 6, 155-158, 1979.
- Levy II, H., J. D. Mahlman, and W. J. Moxim, A 3-D numerical study of tropospheric  $N_2O$ , submitted to J. Geophys. Res., 1980.
- Liu, S. C., R. J. Cicerone, T. M. Donahue, and W. L. Chameides, Limitation of fertilizer-induced ozone reduction by the long lifetime of the reservoir of fixed nitrogen, Geophys. Res. Lett., 3, 157-160, 1976.
- Liu, S. C., R. J. Cicerone, T. M. Donahue, and W. L. Chameides, Sources and sinks of atmospheric  $N_2O$  and the possible ozone reduction due to industrial fixed nitrogen fertilizers, Tellus, 29, 251-263, 1977.
- Mahlman, J. D., Preliminary results from a three-dimensional general-circulation/tracer model, Proc. Second Conf. Climatic Impact Assessment Program, A. J. Broderick, Ed., 321-337, (DOT-TSC-OCT-73-4), 1973.
- Mahlman, J. D., H. Levy II, and W. J. Moxim, Three-dimensional tracer structure and behavior as simulated in two ozone precursor experiments, J. Atmos. Sci., 37, 655-685, 1980.
- Mahlman, J. D., and W. J. Moxim, Tracer simulation using a global general circulation model: Results from a midlatitude instantaneous source experiment, J. Atmos. Sci., 35, 1340-1374, 1978.
- Matthias, A. D., A. M. Blackmer, and S. M. Bremner, Diurnal variability of the concentration of  $N_2O$  in surface air, Geophys. Res. Lett., 6, 441-443, 1979.
- McElroy, M. B., Testimony presented to the Committee on Interstate and Foreign Commerce, U.S. House of Representatives, Washington, D.C., Dec. 11, 1974.
- McElroy, M. B., J. W. Elkins, S. C. Wofsy, and Y. L. Yung, Sources and sinks for atmospheric  $N_2O$ , Rev. Geophys. Space Phys., 14, 143-150, 1976.

- McElroy, M. B., and J. C. McConnell, Nitrous oxide: A natural source of stratospheric NO, J. Atmos. Sci., 28, 1095-1098, 1971.
- McElroy, M. B., S. C. Wofsy, and Y. L. Yung, The nitrogen cycle: Perturbations due to man and their impact on atmospheric N<sub>2</sub>O and O<sub>3</sub>, Phil. Trans. Roy. Soc., (London) 277, 159-181, 1977.
- Pierotti, D., and R. A. Rasmussen, Combustion as a source of nitrous oxide in the atmosphere, J. Geophys. Res., 3, 265-267, 1976.
- Pierotti, D., and R. A. Rasmussen, The atmospheric distribution of nitrous oxide, J. Geophys. Res., 82, 5823-5832, 1977.
- Pierotti, D., and R. A. Rasmussen, Nitrous oxide measurements in the eastern tropical Pacific, Tellus, 32, 56-72, 1980.
- Pierotti, D., R. A. Rasmussen, and R. Chatfield, Continuous measurements of nitrous oxide in the troposphere, Nature, 274, 574-576, 1978.
- Pierotti, D., L. E. Rasmussen, and R. A. Rasmussen, The Sahara as a possible sink for trace gases, Geophys. Res. Lett., 5, 1001-1004, 1978.
- Rebert, R. E., and P. Ausloos, Decomposition of N<sub>2</sub>O over particulate matter, Geophys. Res. Lett., 5, 761-764, 1978.
- Roy, C. R., Atmospheric nitrous oxide in mid-latitudes of the southern hemisphere, J. Geophys. Res., 84, 3711-3718, 1979.
- Schutz, K., C. Junge, R. Beck, and B. Albrecht, Studies of Atmospheric N<sub>2</sub>O, J. Geophys. Res., 75, 2230-2246, 1970.
- Selwyn, G., J. Podolske, and H. S. Johnston, Nitrous oxide ultraviolet absorption spectrum at stratospheric temperatures, Geophys. Res. Lett., 4, 427-430, 1977.
- Simon, P., Balloon measurements of solar fluxes between 1960Å and 2300Å, Proc. Third Conf. Climatic Impact Assessment Program, A. J. Broderick and T. Hard, Eds., 137-142, (DOT-TSC-OST-74-15), 1974.
- Singh, H. B., L. Salas, and H. Sigeishi, The distribution of N<sub>2</sub>O in the global atmosphere and the Pacific Ocean, Tellus, 1979.
- Weiss, R. F., and H. Craig, Production of atmospheric nitrous oxide by combustion, Geophys. Res. Lett., 3, 751-753, 1976.

# EFFECT OF PAST ATMOSPHERIC NUCLEAR EXPLOSIONS

## ON TOTAL OZONE\*

Ernest Bauer

Institute for Defense Analyses  
Arlington, Virginia, U.S.A.

Atmospheric thermonuclear explosions inject large quantities of oxides of nitrogen into the lower stratosphere, and thus might be expected to affect the ozone. This paper reviews the ozone record and predicted effects. On a global average basis, the predicted effects lie within the random variability of the data, and it is not apparent that any local or regional effects can be seen in the record.

**INTRODUCTION:** In 1972, Foley and Ruderman asked a question in the then-current context of the effects of supersonic transports on stratospheric ozone. At that time the principal threat to the ozone layer was considered to be provided by oxides of nitrogen ( $\text{NO}_x = \text{NO} + \text{NO}_2$ ) emitted from the engines, produced by heating of air above 2000-2500 °K which makes some NO that then "freezes-in" as the air cools. Foley and Ruderman pointed out that a large anthropogenic injection of NO into the stratosphere was provided by atmospheric nuclear testing, in particular by the very extensive Soviet and US test series of 1961 and 1962, in which some 340 Mt of nuclear weapons were exploded in the atmosphere. The NO injection was of the order of the ambient stratospheric burden of  $\text{NO}_x$  and this should--in terms of the qualitative understanding of 1972--have led to an observable reduction in total ozone. No such effect is apparent in the very noisy data.

Here the ozone data are reviewed, as are the changes in interpretation of the effect that was predicted between 1973 and 1979.

**THE OZONE RECORD:** The ozone column at any given point varies diurnally and also seasonally (Fig. 1). There is also a variation with latitude and some hints of a long-time variation with the 11-year solar cycle (Fig. 2). However, while the data in Fig. 2 do show a long-term trend, it should be noted that before 1955-1958 the data mostly come from just one station (Arosa, Switzerland) or, at most, three stations in Europe. Figure 2 has been used to argue that the 1961-1962 nuclear test series did deplete the ozone column and this explains the lack of a maximum in the early 1960s. A more detailed

---

\*This work has been supported by the High Altitude Pollution Program of the Federal Aviation Administration (FAA) under Contract DOT-FA77-WA-3965. The views expressed herein are those of the author only. Publication of this paper does not indicate endorsement by the FAA or by the Institute for Defense Analyses.

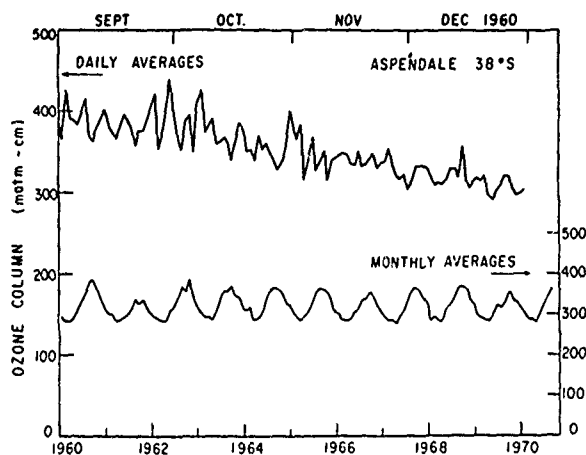
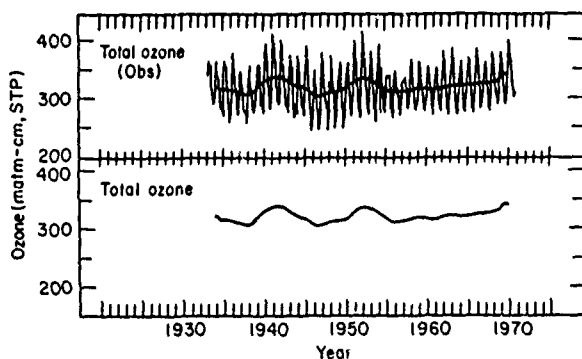


Fig. 1. Total ozone column at Aspendale, Australia, showing daily fluctuations and seasonal variations.

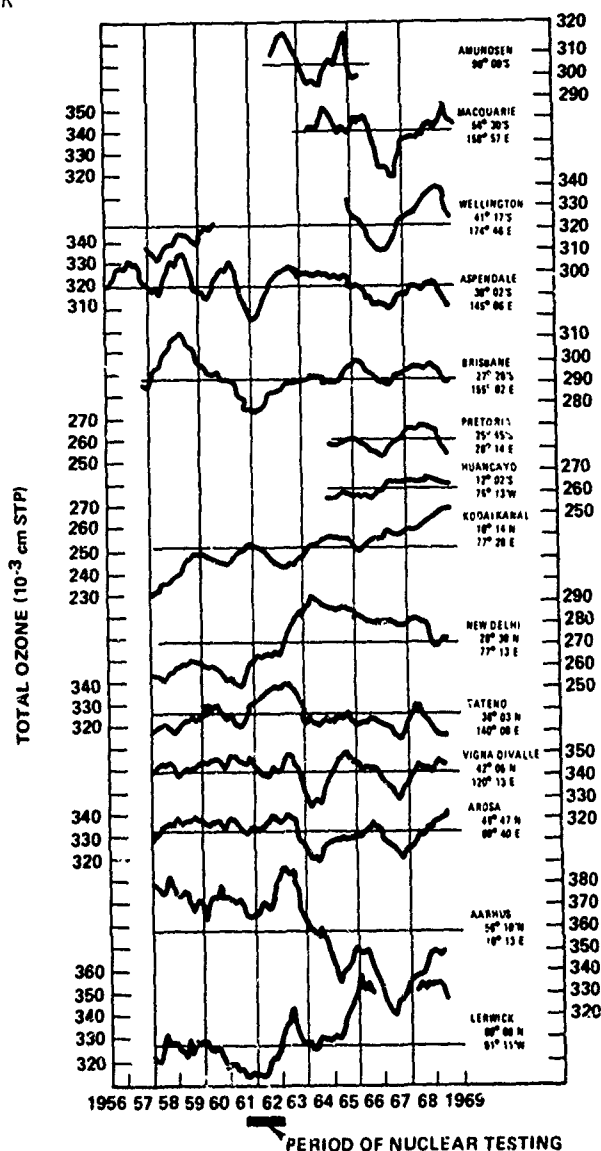


Source: National Academy of Sciences, 1975

Fig. 2. Long-term variations in total ozone in the Northern Hemisphere. The sharp seasonal variations are shown in the top panel. An 11-year running mean is inscribed in the top panel and repeated in the bottom panel. A possible 11-year cycle is indicated before 1960. An increasing trend is indicated for 1960-1970, but the high value is still less than high values before 1960. It is generally recognized that the data base before 1960 is too sparse to offer firm support to these suggested long-term trends.

plot of the record at several different ozone stations is shown in Fig. 3, where the annual variability shown in Figs. 1 and 2 has been removed by taking a 12-month running mean.

Angel<sup>1</sup> and Korshover [1973, 1976, 1978] and other authors who have looked at the total ozone data in detail have been unable to find any definite effect they can ascribe to the bombs.

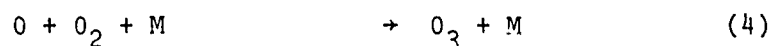
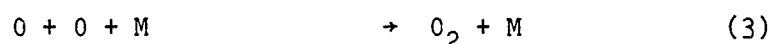
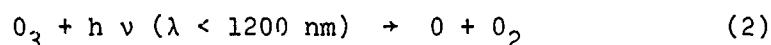
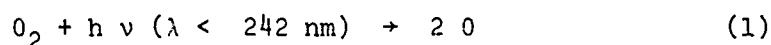


Source: Newell, 1972

Fig. 3. Twelve-month running mean of total ozone. During the period from mid-1961 to late 1962 there was massive nuclear testing in the atmosphere, but no unambiguous effect of this on ozone can be seen in the Fig.

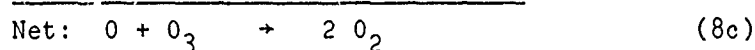
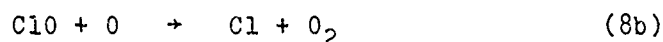
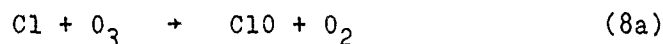
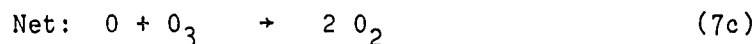
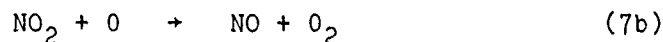
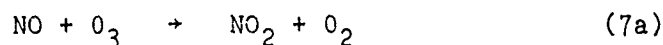
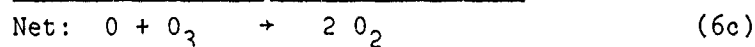
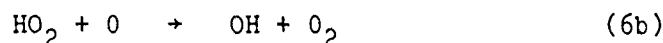
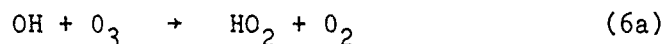


SOME CURRENT THEORIES: Chapman suggested in 1930 that the stratospheric ozone layer is produced by the photolysis of  $O_2$  and  $O_3$  coupled with recombination reactions:

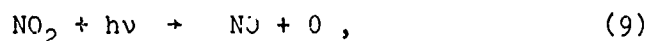


It is now thought that to explain the existing level of stratospheric ozone the reactions of oxides of hydrogen ( $HO_x = OH + HO_2$ ), oxides of nitrogen ( $NO_x = NO + NO_2 + \dots$ ), and chlorine ( $ClO_x = Cl + ClO + \dots$ ) with odd oxygen ( $O + O_3$ ) and with one another must also be considered.

The reactions to be considered may be represented as three cycles which tend to amplify the effective rate of reaction (5)\*:



There is also the photolysis of  $NO_2$



which in conjunction with reactions (7a) and (4), gives rise to a "null cycle" i.e., leads to no net change in odd oxygen,  $O + O_3$ .

A number of other reactions between the  $NO_x$ ,  $HO_x$ , and  $ClO_x$  species lead to the formation of  $HCl$  and  $HNO_3$ , which act as quasi-inert reservoirs of the reactive species  $HO_x$ ,  $NO_x$ , and  $ClO_x$  and which are eventually rained out in the troposphere.

The current picture is that injection of  $NO_x$  at altitude above about 30 km, where the  $O$ -atom concentration is high, leads to a net destruction of ozone, while at lower altitudes an  $NO_x$  injection leads to net ozone enhancement.

---

\*There are also more complex schemes, including some which produce the effect  $2O_3 \rightarrow 3O_2$ .

# BAUER

It has been suggested by Heath and Thekaekara [1977] that solar UV radiation below 250-300 nm varies with the 11-year solar cycle, with a maximum UV level at solar maximum. From their analysis of data taken (with different instruments) between 1964 and 1974, they suggest a 50 percent variability at 200 nm, less at longer and more at shorter wavelengths. Indeed, a factor 2 variability at H-Lyman  $\alpha$  (102.6 nm) is generally accepted Vidal-Madjar [1977]. Many workers in the field consider that the estimate of Heath and Thekaekara presents an upper bound for the possible variability. In any case, the experimental record on which estimates of long-term solar UV variability are based is so short that no definite estimate can yet be made.

More solar UV with  $\lambda < 240$  nm leads to more photolysis and more odd oxygen,  $O + O_3$ . The magnitude (but not the time variation) of ozone changes during the 1955-75 period can be explained very roughly in terms of Heath and Thekaekara's model-see Callis and Nealy [1978] and Penner and Chang [1978]. However, Angell and Korshover [1973, 1976, 1978] do not find the kind of variability of total ozone data with solar activity which models such as those of Callis and Nealy and Penner and Crang, imply.

**BOMB-INDUCED  $NO_x$  INJECTIONS:** An atmospheric nuclear explosion produces a large "fireball" of heated air. Roughly 106 tons of air/Mt of yield is heated above 2000-2500 K, and some 2000-8000 tons  $NO/Mt$  are produced and "freeze in" as the air cools. There are several specific mechanisms for producing  $NO$  which are outlined in Table 1, together with the best current estimate for total  $NO$  production per Mt, which is  $(0.4 - 1.5) \times 10^{32}$   $NO$  molecules per Mt. Thus, the total injection during the 1961-1962 test series was in the range  $(1.4 - 5) \times 10^{34}$   $NO$  molecules, which may be compared with the ambient global  $NO_y$  burden ( $NO_y = NO_x + HNO_3 = NO + NO_2 + HNO_3 + \dots$ ) of  $(4 - 15) \times 10^{34}$   $NO_y$  molecules see e.g., Bauer [1978, Appendix A].

TABLE 1 CALCULATED  $NO$  PRODUCTION FROM  
ATMOSPHERIC NUCLEAR EXPLOSIONS

Source: Gilmore [1975] where references to earlier work are given.  
See also Bauer and Gilmore [1975]

A. <u>Principal Mechanisms for <math>NO</math> Productions</u>	<u>Range of <math>NO</math> Production (tons <math>NO/Mt</math> yield)</u>
1. Shock heating and subsequent quick cooling of air:	3500
2. Fireball heating of air and slower cooling by radiation, expansion, and mixing in of cold air:	-1500 to +4000
3. Bombardment of air by ionizing radiation (betas, gammas, neutrons):	<500 (less important than other mechanisms)
B. <u>Total <math>NO</math> Production per Mt Yield:</u>	2000-8000
C. <u>Detrainment?</u> Various authors have suggested that a significant fraction of the $NO$ produced in the fireball is "detrained", or deposited below the stabilization height in the stratosphere. There seems no definite evidence for this, and so the effect is neglected See <u>Bauer [1978]</u> , Appendix B.	

#### BAUER

Since  $\text{NO}_x$  plays an important part in controlling the stratospheric ozone burden, one would certainly expect to see an effect. (Note that the stratospheric ozone burden is about  $4 \times 10^{37}$  molecules, or 290 m atm-cm: see, e.g. Penndorf [1978, p. S-4].)

As the discussion in the Section titled "Some Current Theories" points out, we believe that  $\text{NO}_x$  injections at 20 km and below produce ozone through the "smog" reactions, while at altitudes of 30 km and above  $\text{NO}_x$  injections produce a net destruction of odd oxygen ( $\text{O} + \text{O}_3$ ) through the catalytic cycle of Eqs. (7). For a detailed discussion, see Chang et al [1979], especially p. 1752.

It is thus very important to know how high the bomb clouds rose, and that would depend on both yield and latitude of injection. Figure 4 shows the available data (vertical lines) and some models (curves) on cloud rise height as a function of yield at different latitudes. It also shows the altitude distribution of ozone at representative latitudes, which indicates that bombs of megaton yield rise to heights corresponding to the maximum in the ozone distribution. From the figure one can see how very poor our knowledge of rise height is, especially at the high-yield, high-latitude bound which corresponds to the biggest total  $\text{NO}$  injection. The curve labeled "Polar Base, Seitz" probably gives a fairly reliable estimate for this quantity as it is based on relatively good observations, but we do not know how high the cloud tops went for the Soviet (high latitude) tests. On the one hand, the record of  $^{90}\text{Sr}$  measurements and excess  $^{14}\text{C}$  measurements [Telegadas, 1968, 1971], based mainly on aircraft observations below 20 km supplemented by high-altitude balloon flights at 32°N latitude shows no evidence that large quantities of these tracers rose above 25-30 km. An analysis of the time-decay of stratospheric  $^{90}\text{Sr}$  and excess  $^{14}\text{C}$  following the 1961-1962 test series also calls for a relatively low injection height (less than 25 km), see Bauer [1979]. On the other hand, after the October 1961 explosions of a 25 Mt and a 58 Mt device there was an enhancement in the lithium airglow [Sullivan and Hunten, 1964] which suggests that at least some of the material rose to very high altitudes (above 35-40 km).\*

The curves "Peterson, equatorial" are based on observations from U.S. tests at tropical latitudes and are, presumably, relatively well based for yields below 10-15 Mt; the curves "Foley-Ruderman" are shown merely to indicate an upper bound for cloud height which has been used in calculations (see the Section titled "Predicted Long-Term (> Months) Effects on Ozone Due to Atmospheric Nuclear Tests."

Table 2 gives a chronology of past atmospheric nuclear test series which shows that in 1961-1962 some 90 percent of total yield came from the Soviet (high latitude) series, so that the injection height of these high-yield, high-latitude injections is very important.

Atmospheric nuclear explosions also inject other materials into the stratosphere--typically 0.3 to 3  $\text{H}_2\text{O}$  molecules and up to 4  $\text{O}_3$  molecules for each  $\text{NO}$  molecule injected--see e.g., Bauer [1978] p. B-15ff. However, as the ambient levels of water and ozone are of order 1000 times larger than those of  $\text{NO}_x$ , these injections are not as important as those of  $\text{NO}$ .

SHORT-TERM (< 1 WEEK) OBSERVATIONS OF NUCLEAR CLOUDS: It is known that nuclear clouds are reddish-brown due to  $\text{NO}_2$ --see e.g., Glasstone and Dolan [1977] p. 29 and Telegadas [1979]. Three attempts have been made to look for the effect on ozone:

\*The observed airglow enhancement can be explained as due to several grams of additional Li. As the bombs must have injected some tens of kilograms of Li into the atmosphere, this provides no evidence that a significant fraction of the debris rose to high altitudes.

TABLE 2. CHRONOLOGY OF ATMOSPHERIC NUCLEAR TEST SERIES

<u>Time</u>	<u>Country/Location</u>	<u>Total Yield, Mt</u>	
1952-54	USA (Tropical)	59	60
	USSR (Mid-High Latitude)	1	
1955-56	USA (Tropical)	19	28
	USSR (Mid-High Latitude)	9	
1957-58	USA (Tropical)	30	85
	UK (Tropical)	7	
	USSR (Mid-High Latitude)	48	
1959-60	Moratorium: No Atmospheric Testing		
1961-62	USA (Tropical)	37	340
	USSR (High Latitude)	300	
1963	Partial Test Ban Treaty: No Atmospheric Testing		
1967-68	France (Tropical)	4	10
	China (Mid-Latitude)	6	
1969-70	France (Tropical)	2	8
	China (Mid-Latitude)	6	
1971	France (Tropical)	1	1
1973	China (Mid-Latitude)	2-3	2-3
1976	China (Mid-Latitude)	4	4

1. Miller et al [1974] analyzed ozone records from Nimbus IV of the cloud of the French 1 Mt tropical explosion of 30 May 1970, some 3 hours after the detonation observed a possible small (5 percent) reduction in ozone, a feature that was not observed the day before or the day after the relevant pass. They were able to identify the BUV signal because of a simultaneous sighting of the cloud in the visible channel. If the effect was real, it could be interpreted as due to reaction (7a), see [Bauer and Gilmore, 1975].
2. Christie [1974] tried to use Nimbus IV BUV data to look for the debris cloud from the French explosion of 3 July 1970, but he could find no evidence, perhaps because he did not have a visual sighting as Miller et al had.
3. McGhan et al [1979] attempted an in-situ probe of the cloud for the 4 Mt Chinese explosion of 17 November 1976 over the USA, some 7 days after the event. While the cloud was brown [Telegadas, 1979] they observed no enhancement in NO (they did not measure NO<sub>2</sub>), but some local enhancement in ozone. Apparently, they flew below the major portion of the cloud and thus their sampling was probably not representative.

In conclusion, it is surprising that no NO enhancement was seen in case 3 above, but the sampling was inadequate. Other than that, the short-term observations would tend to demonstrate the effects perhaps of reaction (7a), but not the long-term cycle (7c), etc.

PREDICTED LONG-TERM ( $\geq$  MONTHS) EFFECTS ON OZONE DUE TO ATMOSPHERIC NUCLEAR TESTS: The most careful and extensive calculations have been made by Chang, Duewer, and Wuebbles at Lawrence Livermore Laboratory using a 1-D code. They have repeated the calculations, as models for the chemical reaction set to be used have changed. Table 3 summarizes their results. The 1973 and 1974 chemistry did not include any ClX reactions, while the 1976 set included a number of reactions which couple the O<sub>x</sub>, NO<sub>x</sub>, HO<sub>x</sub>, and ClX cycles to one another.

## BAUER

TABLE 3. CHANGES IN PREDICTIONS OF MAXIMUM OZONE REDUCTION  
DUE TO 1961-1962 NUCLEAR TESTS

Chemistry	Stabilization Altitude*	Transport**	$10^{32}$ NO/Mt	Other	$O_3$ max	Reference
73	Hi	Fast	0.5	-	-4.8%	Chang et al. (1979)
73	Hi	Slow	0.5	-	-5.3%	Chang et al. (1979)
74	Hi	Fast	0.67	-	-8.2%	Chang et al. (1979)
76	Hi	Fast	0.67	diurnal average	-6.8%	Chang et al. (1979)
76	Lo	Fast	0.67	diurnal average	-5.1%	Chang et al. (1979)
76	Hi	Fast	0.67	no diurnal average	-5.0%	Chang et al. (1979)
76	Hi	Slow	0.67	no diurnal average	-4.3%	Chang et al. (1979)
77	Hi	Fast	0.67	diurnal average	-4.2%	Chang et al. (1979)
77	Lo	Fast	0.67	diurnal average	-1.9%	Chang et al. (1979)
77	Lo	Slow	0.67	diurnal average	-1.8%	Chang et al. (1979)
79	Hi	Fast	0.67	diurnal average	-3.0%	Duewer, private communication, 9/79
79	Lo	Fast	0.67	diurnal average	-0.9%	Duewer, private communication, 9/79

\*Hi = Foley-Ruderman model of Fig. 4 (used in Figs. 5 and 6).

Lo = "Seitz points (not curve) of Fig. 4 (used in Fig. 6).

\*\*Fast transport (Chang, Dickinson-Chang) moves material out of the stratosphere much more rapidly than does Slow transport (Hunten).

The 1977 rates which come from the NASA evaluation, [Hudson, 1977] include, most significantly, a large value for the rate constant of the reaction



[Howard and Evenson, 1977] which differs by a factor of 40 from the earlier values. The 1979 chemistry corresponds to NASA/JPL (1979) and differs from the earlier sets in that  $HOCl$ ,  $HO_2NO_2$ , and methane oxidation chemistries are all taken into account. Note that as time has passed the predicted sensitivity of total ozone to  $NO_x$  injection has decreased. This effect has been noted for aircraft injections-see e.g., Broderick [1978].

The other variations are the following:

1. Note the  $NO_x$  injection rate/Mt assumed; values in the range of  $(0.4-1.5) \times 10^{32}$  molecules/Mt are possible, with the ozone depletion being roughly linear with yield over this range.
2. There is a certain difference in transport coefficients in the two situations. Since the Soviet injections, which produced most of the effect in 1961-1962 (90 percent of total injections) occurred in fall/-winter, the model of fast transport is more appropriate-see Bauer [1979].

3. As was pointed out in the Section titled "Bomb-Induced NO<sub>x</sub> Injections," with particular reference to Fig. 4, our knowledge of the injection height of debris from the Soviet (high latitude) bombs is not good. I believe that the low estimate, either the curves shown in Fig. 4 at "Polar Base & Top, Seitz" or the low estimate of Chang et al [1979] is best in accord with the data.

Some representative results from Lawrence Livermore Laboratory are shown in Table 4 and Fig. 5. Table 4 indicates how a given NO<sub>x</sub> injection increases ozone at 20 km and below, and decreases it at 30 km and above, using 1977 chemistry. Figure 5 gives the effects of cloud rise height on total ozone, using the latest (1979) chemistry.

From Fig. 5 and Table 3 we see that using current (1979) chemistry, the low (Seitz) rise height estimate predicts a maximum ozone decrease of 0.9 percent, while the high (Foley-Ruderman) estimate predicts a maximum ozone decrease of 3 percent. In view of the discussion of the Section titled "Bomb-Induced NO<sub>x</sub> Injections" and item 3 above, I consider the best estimate with current chemistry to be a maximum hemispheric decrease of approximately 1 percent.

PROBLEMS WITH A 1-D MODEL: The calculations reported above use a one-dimensional, hemispheric average model. Thus, the atmospheric composition, transport, radiation, and chemistry are all annual averages. The Soviet tests, which put most of the NO<sub>x</sub> into the stratosphere, occurred at high latitude (75°N) in fall and winter, which certainly does not correspond to the global and annual average conditions that are simulated by a 1-D model.

Physically, what must have happened is that when the NO<sub>x</sub> was injected there was an immediate transformation from NO to NO<sub>2</sub> by reaction (7a). There is so little sunlight at high latitudes in late fall and winter that the photochemistry of reactions (7) and (9) simply would not be active until spring. The rapid winter circulation tends to remove a significant portion of the injected material from the lower stratosphere, so that the net effect on ozone would be less than might be expected from the total injection.

Thus, we see that to predict the effect on ozone due to these impulsive injections at a specific latitude and season by using an averaged 1-D model is very difficult because of the interaction of these different factors, which simply cannot be treated in such a 1-D model. The problem should be treated in three dimensions, or at least with a two-dimensional model which parameterizes both the radiation and the transport in terms of latitude and season.

MIGHT THE EFFECT ON TOTAL OZONE DUE TO THE BOMBS HAVE BEEN DETECTABLE? As was pointed out in the previous section, a 1-D model is not appropriate for a problem of this type. Nevertheless, one may try to extend the results of the Livermore Laboratory group to the situation at hand. The maximum conceivable effect on the average ozone column is a 3 percent reduction on a hemispheric basis (see Table 3). Chang et al [1979] point out that this is less than the standard error in global mean ozone, as indicated by Angell and Korshover [1978] so that one would not expect to be able to detect the effect on a global average basis. However, could something perhaps have been detected on a local or regional basis?

Purely for talking purposes we can hypothesize a maximum ozone reduction of order 10 percent in the Arctic region. (This corresponds to a 3 percent hemispheric average ozone reduction and the fact that the polar cap amounts to one fifth of the surface area of the hemisphere, so that if all the ozone reduction occurred at latitudes in excess of 60-65°, a  $(3/0.2) \sim 15$  percent ozone reduction might be conceivable in the Arctic.)

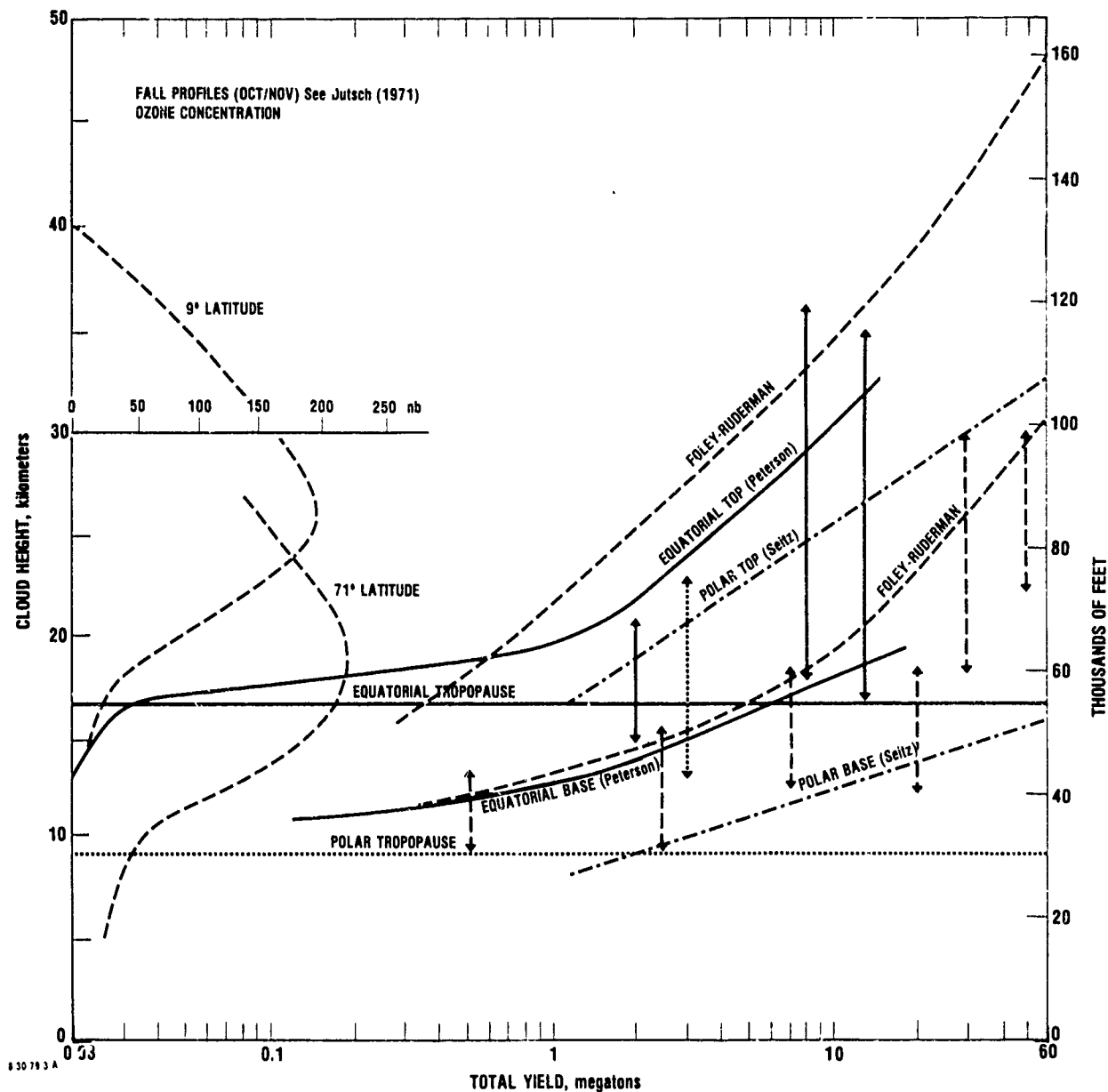


Fig. 4. Nuclear cloud rise height as a function of yield for different latitudes.

Data: Solid vertical lines correspond to US tests in the tropics (2-17°N), dotted to Chinese mid-latitude tests (40°N), and dashed to Soviet high latitude tests (75°N)-see Seitz et al [1968] Telegadas [1977]. (Some representative ozone profiles are also shown.)

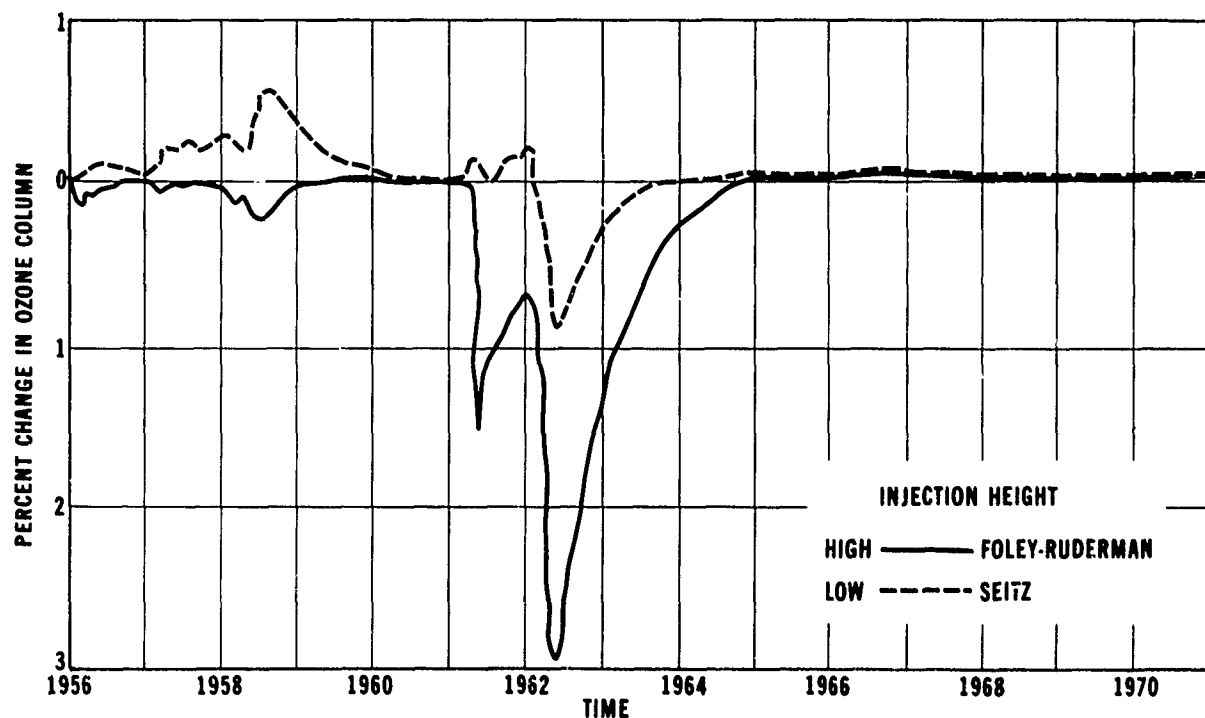
Cloud Rise Models: Peterson's [1970] equatorial model corresponds to US tests. The curves labeled "Polar (Seitz)" have been drawn through the Polar data points and the curves labeled "Foley-Ruderman" represent a global average--see Chang et al [1979].

Representative Ozone Profiles are also shown.

TABLE 4. CALCULATED MAXIMUM CHANGE IN LOCAL OZONE CONCENTRATION AT DIFFERENT HEIGHTS DUE TO ATMOSPHERIC NUCLEAR TESTS

Height, km	Maximum Change in Ozone Concentration, $10^{11}$ mol.s./cc
10	+0.4
20	+1.8
30	-2.4
40	-0.8

Source: Chang et al. [1979]. Figure 5. 1977 chemistry, high stabilization altitude, fast transport



9 18 79 5

Fig. 5. Percent change in column ozone due to atmospheric nuclear tests versus time: 1979 chemistry

Source: Duewer [September 1979] private communication



London et al. [1979] in Table 6.3.1, suggests that for a Dobson spectrometer the random error for zenith sky observations under average conditions is  $\pm 5$  percent or less under good conditions. However, conditions in fall/winter at high latitudes are presumably not as good as average because of cloudiness, the low solar zenith angle, and the fact that the closest observations to the injection would have been made with the M-83 instrument, which is not as accurate as the Dobson.

Thus, it appears that even if the effect was as large as the upper bound predicted by W. H. Duewer, the quality of observing conditions could have been so bad that the effect might not have been detected. On the other hand, if these upper-bound estimates were too big by a factor of 2-3, (which I believe to be the case--see e.g., Bauer [1979]) the signal would almost certainly have been within the noise.

CONCLUSIONS: During the 1961-1962 atmospheric nuclear test series there was a very large injection of  $\text{NO}_x$  into the stratosphere over an extended period. The injection height is not well known, and estimates of ozone reduction have only been made using 1-D models which are not well-suited for this kind of prediction. Explicitly, on a global or hemispheric average basis, the predicted effect on total ozone lies within the random errors in the total ozone record. Careful examination of the local and regional ozone record by Angell and Korshover [1978] and others shows no definite effect that can be attributed to the nuclear test series, other than the missing maximum in the early 1960s which is suggested by Fig. 2.

To round out the study of this effect, it is urged that the effect of atmospheric nuclear explosions should be calculated with a 2-D or 3-D photochemical model which reproduces the correct variation of insolation and transport with latitude and season.

The example demonstrates that to conduct an atmospheric experiment on a large scale, using a "target of opportunity" may be very difficult, and indeed in this instance the stratosphere appears to be surprisingly resilient or insensitive to a very large perturbation in oxides of nitrogen,  $\text{NO}_x$ .

#### REFERENCES

- Angell, J. K. and J. Korshover, "Quasi-Biennial and Long-Term Fluctuations in Total Ozone," *Mon. Weather Review*, **101**, 426, 1973.
- Angell, J. K. and J. Korshover, "Global Analysis of Recent Total Ozone Fluctuations," *Mon. Weather Review*, **104**, 63, 1976.
- Angell, J. K. and J. Korshover, "Global Ozone Variations: An Update Into 1976," *Mon. Weather Review*, **106**, 725, 1978.
- Bauer, E., "A Catalog of Perturbing Influences on Stratospheric Ozone, 1955-1975," Federal Aviation Administration Report No. FAA-EQ-78-20, (IDA Paper P-1340), September 1978. See also *J. Geophys. Res.*, in publication.
- Bauer, E., "A Study of Stratosphere-to-Troposphere Transfer, Using Radioactive Tracer Data in a 1-D Parameterization," ms, September 1979.
- Bauer, E. and F. R. Gilmore, "Effect of Atmospheric Nuclear Explosions on Total Ozone," *Rev. Geophys. Space Phys.*, **13**, 451, 1975.
- Broderick, A. J., "Stratospheric Effects from Aviation," *J. Air*, **15**, 643, 1978.
- Callis, L. B. and J. E. Nealy, "Solar UV Variability and Its Effect on Stratospheric Thermal Structure and Trace Constituents," *Geophys. Res. Lett.*, **5**, 249, 1978.
- Chang, J. S., W. H. Duewer, and D. J. Wuebbles, "The Atmospheric Nuclear Tests of the 50's and 60's: A Possible Test of Ozone Depletion," *J. Geophys. Res.*, **84**, 1755, 1979.
- Christie, A. D., "The Use of UV Satellite Observations to Study Ozone Depletion Processes," paper presented at the International Conference on Structure, Composition and General Circulation of the Upper and Lower Atmospheres and Possible Anthropogenic Perturbations, Int. Union of Geod. and Geophys., Melbourne, Australia, January 1974.

- Dütsch, H. U., "Photochemistry of Atmospheric Ozone," Advan. in Geophys., 15, 291-322, 1971.
- Gilmore, F. R., The Production of Nitrogen Oxides by Low-Altitude Nuclear Explosions, IDA Paper P-986, 1974. See also J. Geophys. Res., 80, 4553, 1975.
- Glasstone, S. and P. J. Dolan, Eds., The Effects of Nuclear Weapons, Department of Defense and Department of Energy, 3rd Ed., 1977.
- Heath, D. F. and M. P. Thekaekara, "The Solar Spectrum Between 1200 and 300 Å" in White, p. 193 ff, 1977.
- Hudson, R. D., Ed., "Chlorofluoromethanes and the Stratosphere," NASA Reference Publication, 1010, August 1977.
- London, J., Chairman, "Long-Term Trends of Stratospheric Parameters," Chapter 6, presented at NASA Workshop on the Stratosphere held at Harpers Ferry, West Virginia, June 1979.
- McGhan, M., A. Shaw, W. Sedlacek, and L. R. Megill, "Measurements of Nitric Oxides after a Nuclear Burst," ms, July 1979.
- Miller, A. J., A. J. Krueger, C. Prabhakara, and E. Hilsenrath, "Nuclear Weapons Tests and Short-Term Effects on Atmospheric Ozone," paper presented at the Second International Conference on the Environmental Impact of Aerospace Operations in the High Atmosphere, Amer. Inst. of Aeronaut. and Astronaut./Amer. Meteorol. Soc., San Diego, California, July 1974.
- National Academy of Sciences, Environmental Impact of Stratospheric Flight: Biological and Climatic Effects of Aircraft Emissions in the Stratosphere, Washington, D.C., 1975.
- Newell, R. E., "Climatology of the Stratosphere from Observations," Proceedings of the Survey Conference, DOT-TSC-OST-72-13, U.S. Dept. of Transportation, Washington, D.C., pp. 165-185, September 1972.
- Penndorf, R., "Analysis of Ozone and Water Vapor Field Measurement Data," FAA-EE-78-29, High Altitude Pollution Program, Federal Aviation Administration, Washington, D.C., November 1978.
- Penner, J. E., and J. S. Chang, "Possible Variations in Atmospheric Ozone Related to the 11-Year Solar Cycle," Geophys. Res. Lett., 5, 817, 1978.
- Peterson, K. R., "An Empirical Model for Estimating World-Wide Deposition from Atmospheric Nuclear Detonation," Health Physics, 18, 357-378, 1970.
- Seitz, H., et al., "Final Report on Project Streak: Numerical Models of Transport, Diffusion and Fallout of Stratospheric Radioactive Material," Report NYO-3654-4, Isotopes, Inc., prepared for AEC/DBER, 31 May 1968.
- Sullivan, H. M. and D. M. Hunten, "Lithium, Sodium, and Potassium in the Twilight Airglow," Can. J. Phys., 42, 937, 1964.
- Telegadas, K., "The Seasonal Stratospheric Distribution of Cd-109, Pu-238, and Sr-90," Department of Energy Report HASL-184, I-53, January 1968.
- Telegadas, K., "The Seasonal Stratospheric Distribution and Circulation of Excess C-14 from March 1955 to July 1969," Department of Energy Report HASL-243, I-3, July 1971.
- Telegadas, K., An Estimate of Maximum Credible Atmospheric Radioactivity Concentrations from Nuclear Tests, Department of Energy Report HASL-328, I-39, October 1977.
- Telegadas, K., "Estimation of Maximum Credible Atmospheric Radioactivity Concentration Dose Rates from Nuclear Tests," Atmos. Environ., 13, 327, 1979.
- Vidal-Madjar, A., "The Solar Spectrum at Lyman-Alpha, 1216 Å," in The Solar Output and Its Variations, in White, p. 213 f, 1977.
- White, O. R., Ed., The Solar Output and Its Variation, Colorado Associated University Press, Boulder, Colorado, 1977.

EFFECTS ON ATMOSPHERIC OZONE OF EMISSIONS FROM CRUISE AIRCRAFT:  
HISTORY AND CURRENT STATUS\*

R. C. Oliver

Institute for Defense Analyses  
400 Army-Navy Drive, Arlington, Virginia

ABSTRACT

The history of computed effects of aircraft engine emissions (principally the nitrogen oxides and water vapor components) on atmospheric ozone is presented, showing how predicted effects have been extremely sensitive to changes in the understanding of atmospheric chemistry. Current model evaluations are given; these models now indicate that the net effect of emissions from both subsonic and supersonic aircraft in plausible numbers will be an increase in the ozone column, but a resulting redistribution of ozone with altitude may be of concern. The question of the *predictive* validity of ozone models to postulated perturbations is discussed; history has shown repeatedly that the ability to model the existing atmosphere in terms of certain trace species concentrations, etc., providing an apparent *descriptive* validity, does not insure predictive validity. Such models are needed, however, for policy purposes; their development, and efforts toward demonstration of predictive validity, must continue.

INTRODUCTION

The effects that aircraft engine emissions may have on atmospheric (particularly stratospheric) ozone have now been intensively discussed and actively studied for about a decade. Much has transpired in this period as the science has progressed. Here I review these developments, using a historical approach, hoping thereby to put current evaluations, which I also provide, into context. This paper complements, brings up to date, and expands in certain particulars on a comprehensive review prepared by Broderick [1978]. I make no attempt to review the many details of the science of ozone nor of the many trace species involved; detailed treatments [e.g., Nicolet, 1975; Reiter et al., 1975] and topical reviews, with extensive bibliographies [Hudson, 1977; Hudson, 1979], are available elsewhere.

---

\* This work has been supported by the High Altitude Pollution Program of the Federal Aviation Administration (FAA) under Contract DOT-FA77-WA-3965. The views expressed herein are those of the author only. Publication of this paper does not indicate endorsement by the FAA or by the Institute for Defense Analyses.

## OLIVER

The stimulus for concerns about aircraft effects on stratospheric ozone was provided (inadvertently) by the U.S. supersonic transport (SST) development program. The projected vehicle, the "Boeing 2707", was to cruise near 20 km altitude, far higher than previous commercial aircraft, and well into the stratosphere, where vertical mixing is known to be slow and wherein the bulk of the earth's protective ozone shield lies. Large numbers of such vehicles were postulated in justifying development costs. These same large numbers implied large amounts of aircraft effluents being deposited in a region only somewhat below the region of maximum ozone concentration; the components of principal concern were water vapor initially and the nitrogen oxides later. This development program, for a variety of reasons, was halted by Congress in March 1971. The environmental issues were deemed to merit additional evaluation, at least in part because of ongoing SST developments elsewhere (the British-French Concorde and the Soviet TU-144). The U.S. SST program cancellation was thus followed shortly by initiation of a major research program, the Climatic Impact Assessment Program (CIAP) sponsored by the U.S. Department of Transportation, and by parallel studies by the U.S. National Academy of Sciences and by groups outside the U.S., particularly in the United Kingdom and France. CIAP was concerned primarily with SST effects on the stratosphere, but subsonic aircraft, rockets, and the space shuttle were also examined; the work included effects on climate as well as ozone, and was extended to biologic and economic effects. I restrict this paper to the ozone question.

The CIAP program was effectively completed, as planned, in December 1974. As shall be shown, new data have since made questionable many of the conclusions [Grobecker et al., 1978; National Academy of Sciences, 1975; COMESA, 1975; COVOS, 1976] drawn in these studies. In retrospect, the specific results found in these studies were of much less significance than was the fact of these studies, for the programs provided a major stimulus to the somewhat neglected field of the science of middle atmosphere. Major advances, particularly in atmospheric chemistry, have since followed, and new threats to the ozone shield (particularly the halocarbons) have since been identified. Each of these advances has had an impact--in some cases a dramatic one--on the predicted effects of aircraft exhaust.

In this paper, I discuss these predicted aircraft effects on ozone, primarily from nitrogen oxide and water vapor emissions, as they have varied with time. In using this historical data I note at several points that the apparent ability to *model* an existing atmosphere evidently provides but little confidence that the model can correctly predict effects of *perturbations* to that atmosphere; this point will be used, not to argue for inaction in the face of an environmental threat, but rather to emphasize the continuing need for maximum attention to any events or phenomena which may serve for validation of such models as a *predictive*, as opposed to *descriptive*, tool.

As necessary background for considering aircraft effects, some discussion of projected aircraft emissions and flight altitudes is first necessary. Following this treatment, I review early SST concerns, and note how these concerns have varied with the corresponding understanding of ozone chemistry. The broader questions of the effects of aircraft exhaust at different altitudes and in different projected atmospheres will then be discussed. In general, I shall not attempt to review atmospheric trace species measurements as compared to model estimates, but certain outstanding problems will be noted. Finally, some concluding comments will be offered.

### AIRCRAFT EMISSIONS, FLIGHT ALTITUDES AND THE ATMOSPHERE

Flight Altitudes: Figure 1 illustrates how aircraft flight altitudes generally increase with increasing mach number, and that supersonic aircraft operate well above the mean tropopause, at altitudes approaching those at which ozone density is a maximum; at such altitudes, aircraft exhaust disperses into air containing appreciable ozone. Subsonic aircraft operate in the 6 to 14 km

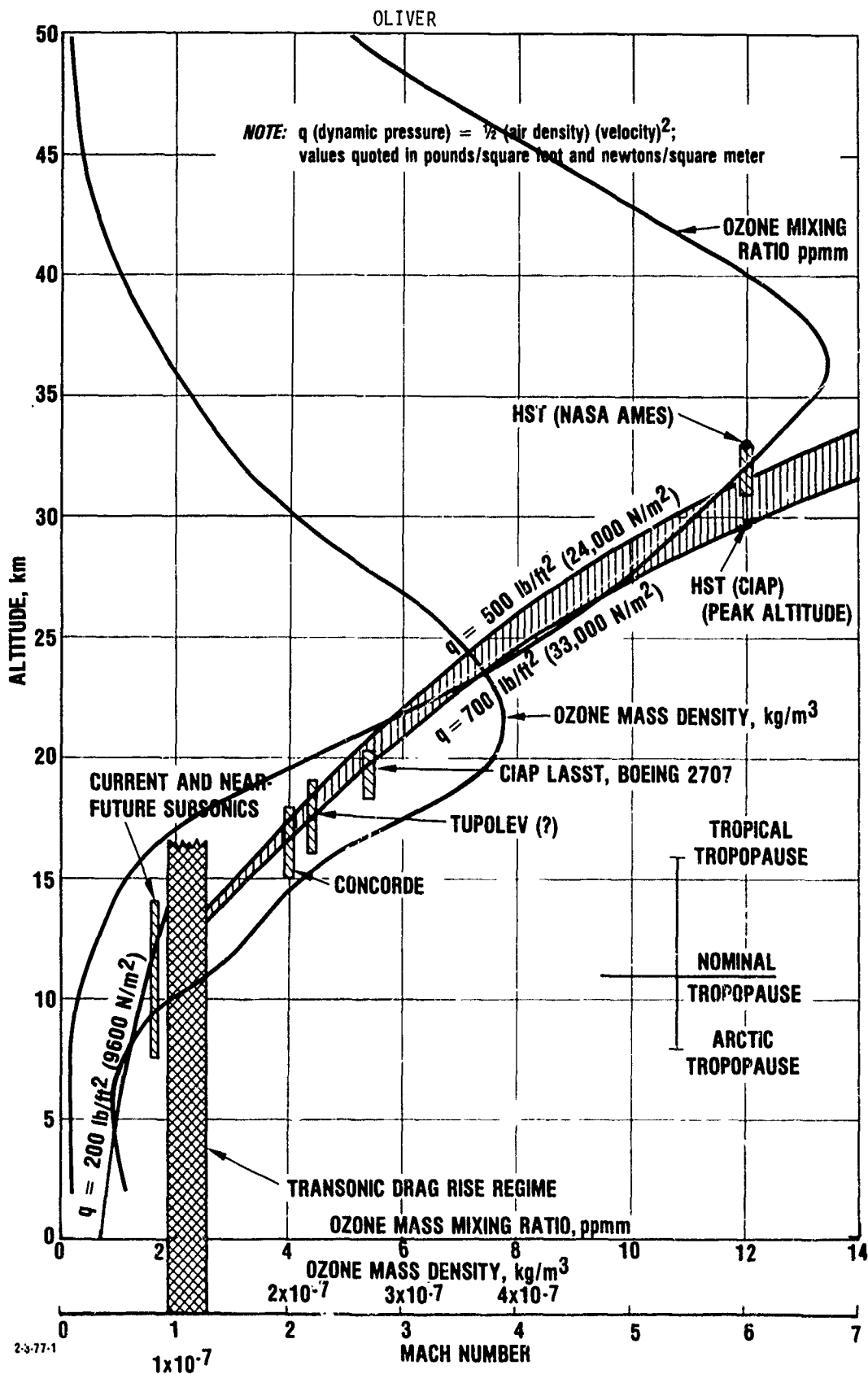


Fig. 1. Aircraft cruise altitudes and ozone data

region, sometimes above and sometimes below the tropopause, in regions of lower ozone density. As noted earlier, operation above the tropopause implies operation in a region of substantially reduced vertical transport, with corresponding increase in the loading, at steady state, of emission products from repetitive flights of aircraft. Of course, Figure 1 is essentially one-dimensional; ozone maxima, as well as tropopause heights, vary with latitude, longitude, and season. More detail on this latter point is provided in a later section.

Emissions: Commercial jet aircraft burn straight run kerosene-type fuels (Jet A or Jet A-1); some Jet-B, a naphtha-kerosene blend may also still be in use. These fuels produce the usual products of combustion,  $\text{CO}_2$  and  $\text{H}_2\text{O}$ , and minor amounts of other materials, such as nitrogen oxides, sulfur oxides, carbon monoxide, and particulates. Combustion efficiencies at cruise conditions are very high (~99.9 percent). Exhaust products, such as nitric oxide, are quoted in terms of their emission indices, in units of grams per kilogram of fuel (or lb/1000 lb, etc.). Typical emission index values follow in Table 1 [English et al., 1975].

TABLE 1. Typical Jet Engine Emission Indices at Cruise Altitudes. (English et al., 1975)

Exhaust Species	Emission Index, gm/kg
$\text{CO}_2$	3220
$\text{H}_2\text{O}$	1250
$\text{NO}_x$ (as $\text{NO}_2$ )*	6-30
CO	4
$\text{SO}_x$ (as $\text{SO}_2$ )	1.0
Hydrocarbon (as $\text{CH}_2$ )	0.1-0.2
Soot (as carbon)	0.1
Lubricating Oil	0.1
Trace Elements	0.01

\*" $\text{NO}_x$  (as  $\text{NO}_2$ )" is used to indicate the molecular sum of NO and  $\text{NO}_2$  emissions, calculated on a weight basis as though all such molecules were  $\text{NO}_2$ . The predominant nitrogen oxide species exhausted is NO.

The  $\text{CO}_2$  and  $\text{H}_2\text{O}$  emission indices are set by the fuel composition.  $\text{NO}_x$  is formed from the air itself; its emission index is determined by the combustion conditions and increase with pressure, inlet temperature, and residence time in the combustor. Much lower  $\text{NO}_x$  emission indices than those shown above have been achieved by use of lean premixed combustion techniques, but such combustion techniques are a long way from application; in fact, advanced techniques may be necessary in the future simply to maintain current emission levels as inlet pressures and temperatures are raised in an effort to minimize fuel consumption. A quoted value at cruise for the Concorde engine is 18 gm  $\text{NO}_x$  (as  $\text{NO}_2$ )/kg; somewhat higher values are given by Beadle [1977]. High values, such as the value of 30 shown above, are associated with high pressure ratio subsonic engines at take-off conditions. Much higher values have been reported using spectroscopic techniques, but these have not been confirmed by other investigators [Few et al., 1979; Oliver et al., 1978; Dodge et al., 1979].

Moisture in the air reduces peak combustion temperature and  $\text{NO}_x$  emissions. CO is produced by incomplete combustion. Sulfur oxides (mostly  $\text{SO}_2$ ) come from combustion of sulfur in the fuel; the emission index shown corresponds to 0.05 percent sulfur. Sulfur contents can be reduced by hydro-desulfurization of the fuel at relatively modest cost (approximately 1 cent per gallon, roughly updating figures quoted in Grobecker et al., [1974]).

The exhaust ingredients considered in depth in CIAP were  $\text{NO}_x$ ,  $\text{H}_2\text{O}$ , and  $\text{SO}_2$ ,  $\text{SO}_2$  being treated in a climatic, rather than ozone, context. All these are trace species in the stratosphere, with concentrations which could (as shown below) be significantly altered by emissions from large aircraft fleets.  $\text{CO}_2$  is present in a relatively massive quantity in the atmosphere, and little affected by aircraft sources. Note that for given fuels  $\text{H}_2\text{O}$  is the only one of the  $\text{NO}_x$ ,  $\text{H}_2\text{O}$ , and  $\text{SO}_2$  group for which the emission index cannot be altered by technology; any limitations in water emissions could be achieved only by limitations in fuel consumption.

Emission indices must be coupled with fuel consumption projections as well as with flight altitude (and latitude and season) data and used in a coupled chemical-dynamic model of the atmosphere to estimate effects on ozone.

Detailed projections of fuel flows as a function of latitude, longitude, and altitude have been prepared [Grobecker et al., 1974; English et al., 1975; Oliver et al., 1977 and 1978; Athens et al., 1976]. The three-dimensional projections have not yet been used; instead, models have called for projections reduced to two-dimensions, latitude and altitude, and one dimension, altitude only. While details of these traffic projections seem inappropriate for inclusion here, a few order-of-magnitude numbers may be of interest, as discussed below.

A nominal advanced SST fleet fuel consumption used in CIAP for modeling purposes, was  $10^{11}$  kg/year, yielding (at 18 gm  $\text{NO}_x$ , 1 gm  $\text{SO}_2$ , and 1250 gm  $\text{H}_2\text{O}/\text{kg}$ )  $1.8 \times 10^8$  kg/yr of  $\text{NO}_x$  (as  $\text{NO}_2$ ),  $10^8$  kg  $\text{SO}_2$ , and  $1.25 \times 10^{11}$  kg water per year. These numbers were sometimes interpreted as corresponding to a fleet of 500 Boeing 2707 SSTs; the  $10^{11}$  kg number was, in fact, an arbitrary round number, with the corresponding number of aircraft depending on the fuel flow per aircraft, number of hours such aircraft were assumed to operate per day, etc. (By CIAP figures,  $10^{11}$  kg fuel/year corresponds to 1170 Boeing aircraft or 1587 "advanced" SSTs; by National Academy of Sciences 1975 figures,  $10^{11}$  kg/year of fuel would be used by 1095 "advanced" SSTs). An SST fuel flow of this magnitude was to be reached about the year 2000, according to a CIAP "upper-bound" projection. For comparison, the total global stratospheric burden of  $\text{NO} + \text{NO}_2 + \text{HNO}_3$  (as  $\text{NO}_2$ ) is about  $(3 \text{ to } 11) \times 10^9$  kg [or  $(4 \text{ to } 15) \times 10^{34}$  molecules] [Bauer, 1978]; the global stratospheric water burden is about  $2 \times 10^{12}$  kg, so that, assuming a 2-year residence time, a fuel flow of this magnitude represents a severe ( $\text{NO}_x$ ) or significant ( $\text{H}_2\text{O}$ ) perturbation of the stratosphere. The  $\text{SO}_2$  perturbation level was less clear, because of a highly variable background. The postulated aircraft  $\text{SO}_2$  perturbation would be significant relative to a stratosphere long unperturbed by volcanic injections but trivial relative to periods following large eruptions, which may inject  $50 \times 10^8$  kg in a single event [Bauer, 1978]. A more recent, [Athens et al., 1976; Oliver et al., 1977] but still "optimistic" projection for SST fuel consumption (requiring about 142 Concorde-type SSTs) above 6 km is  $7.9 \times 10^9$  kg/yr in 1990 with  $\text{NO}_x$  (assuming current technology) emissions being  $1.2 \times 10^8$  kg/yr. Appended tables give a 2-D breakdown for fuel flow,  $\text{H}_2\text{O}$ , and  $\text{NO}_x$  (again, current technology) emissions from the full "optimistic" (high growth) 1990 fleet. The SST fleet contributes most of the emissions above 14 km.

The current nine-Concorde SST fleet has been estimated [by Beadle, 1977; Oliver et al., 1978] to use  $8.44 \times 10^6$  kg/week (takeoff to landing) or  $4.4 \times 10^8$  kg/year, of which 74.7 percent, or  $3.3 \times 10^8$  kg/year is burned above 11 km. The  $\text{NO}_x$  (as  $\text{NO}_2$ ) injected above 11 km, using the CIAP  $\text{NO}_x$  emission index of 18 gm/kg is  $6 \times 10^6$  kg/year. Beadle [1977] gives a detailed breakdown; his estimates for  $\text{NO}_x$  emission indices at cruise are 25 to 50 percent higher than those used in CIAP. At any rate, this fuel flow corresponds to 0.0033 times that nominally used in CIAP.

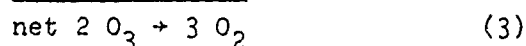
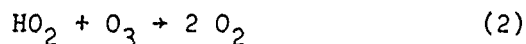
Subsonic fleets have grown in recent years, and growth continues. A.D. Little estimates [Athens et al., 1976; Oliver et al., 1977] indicated  $4.5 \times 10^{10}$  kg/year of fuel was consumed above 6 km by the subsonic fleet in 1975, a figure which would roughly double by 1985, with further increases to 1990. The A.D. Little "low" estimate for fuel consumption for 1990 was  $1.05 \times 10^{11}$  kg/yr, and the high estimate  $1.66 \times 10^{11}$  kg/yr. Note that the difference between  $1.74 \times 10^{11}$  kg/yr shown as total fuel flow in the Appendix example and  $1.66 \times 10^{11}$  represents the SST fuel flow ( $7.9 \times 10^9$  kg/yr fuel was quoted above).

Subsonic aircraft have trended in recent years to higher maximum cruise altitudes, with the 747SP being certified to 45,000 feet (13.7 km) and some business jets operating to 51,000 feet (15.5 km). The 747SP is an unusually long-range aircraft and reaches maximum altitude (if desired) only after much of the fuel is consumed. The business jets use a very small part of the total jet fuel. These altitude trends may be misleading; mean operating altitudes for subsonic aircraft have probably not increased much in recent years.

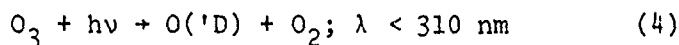
Subsonic aircraft, as indicated earlier in Figure 1, operate in regions near the tropopause. On average, their exhaust products spend far less time in the atmosphere than would those from an advanced SST at 20 km, or the Concorde at 17 km. Projected fuel flows for the 1985-1990 period are of the same order of magnitude as the nominal  $10^{11}$  kg/year fuel flow used in CIAP SST modeling, and thus (even allowing for reduced residence times) need examination for effects on the ozone column. This will be done later herein.

#### EARLY (PRE-CIAP) VIEWS OF OZONE CHEMISTRY AND SST EFFECTS

The first SST emittant proposed to deplete stratospheric ozone was water vapor [Hampson, 1964; 1966]. The role of H, OH, and  $\text{HO}_2$  ( $\text{HO}_x$ ) had been suggested by Bates and Nicolet [1950] as an extension to the classical Chapman [1930] explanation of stratospheric ozone formation and destruction, which involved O,  $\text{O}_2$ , and  $\text{O}_3$  ( $\text{O}_x$ ) species. In subsequent years [See Hunt, 1966a; Leovy, 1969; and Crutzen, 1971], it became evident that the classic Chapman model failed to provide adequate destruction pathways for  $\text{O}_3$ , and other pathways were sought. The first candidate system involved the  $\text{HO}_x$  radicals noted by Bates and Nicolet [1950]. A number of pathways were suggested. Hunt [1966b] modeled ozone destruction by  $\text{HO}_x$ , emphasizing the cycle:



The OH is provided by the reactions:



So that an increase in  $\text{H}_2\text{O}$  would increase OH and (by this model) thus the rate of the ozone destruction cycle.

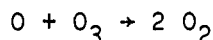
Hunt found that an  $\text{O}_3$  balance could be achieved with this cycle if Reaction 2 proceeded at a rate of  $10^{-14}$  cm<sup>3</sup>/sec-molecule; no measured rate was available. It was this cycle--using a model-required rate constant--which led to concerns about  $\text{O}_3$  destruction by SSTs due to water vapor emissions. The issue was discussed in the July 1970 "Study of Critical Environmental Problems" [SCEP, 1970], with calculations reported by London and Park [see SCEP, 1970]; these authors reported that an SST fleet would increase global average stratospheric water content from 3.0 to 3.2 ppm, and might locally increase  $\text{H}_2\text{O}$  from 3 to 5 ppm. For the first case, the decrease in ozone column was estimated to be 0.002 cm, and for the second 0.02 cm (from a base near 0.250 cm), or 0.8 to 8 percent. The authors warned that the results were provisional as some rates were poorly known. Other authors carried out similar calculations. Thus, Harrison [1970] compared Leovy's model [1969], to more detailed calculations which he carried out. He noted that, according to Leovy's model

$$\frac{\delta[\text{O}_3]}{[\text{O}_3]} = -\frac{1}{3} \frac{\delta[\text{H}_2\text{O}]}{\text{H}_2\text{O}} \quad .$$

Using this relationship, an assumed fleet of 500 U.S. and 350 non-U.S. SSTs, and additional assumptions as to fuel flow (13.4 and 9 kg/sec), residence times (1.5 year), traffic distribution (80 percent in Northern Hemisphere) and utilization (25 percent at cruise altitudes--presumably 6 hours per day), he estimated  $\delta[\text{H}_2\text{O}]$  to be 0.6 ppm/3.0 ppm, or 0.2, for a 7 percent reduction in  $[\text{H}_2\text{O}]$  ozone column by Leovy's model. He then carried out more detailed calculations, including thermal feedback effects, and found, for what he considered to be an extreme case (constant water concentration one scale height thick centered at 20 km), a much smaller column of -3.8 percent.

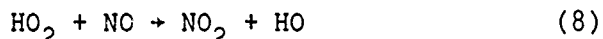


About this time, Nicolet [1970] argued on theoretical grounds that Reaction (2) must be very slow, much less than  $10^{-14}$  cm<sup>3</sup>/sec as found to be necessary by Hunt [1966b] and as used in the modeling just described. Crutzen [1971], in a study in which the then newly recognized importance of nitrogen oxide species was examined at length, noted Nicolet's [1970] argument as the  $\text{HO}_2 + \text{O}_3$  rate, and proceeded with his  $\text{NO}_x$  modeling work in which he set this rate to zero. (In a note added in proof, he remarked that a then-recently-measured value  $\leq 10^{-16}$ , made this reaction unimportant below 45 km.) He noted uncertainties in certain rates in the  $\text{O}_x - \text{HO}_x - \text{NO}_x$  system. His approach was to compute  $\text{NO} + \text{NO}_2$  concentrations necessary to balance ozone production, assuming the following catalytic cycle provided the necessary balance:



and found values which were not unreasonable in light of limited observations. The  $\text{NO}$  in the natural stratosphere comes from biologically-produced  $\text{N}_2\text{O}$  via reaction with  $\text{O}(\text{'D})$ . This  $\text{NO}_x$  catalytic cycle became all-important in the SST effects work, as calculated by Crutzen [1971], Johnston [1971], and later in CIAP.

Crutzen [1971], in view of the plausibility of this cycle, found that the  $\text{HO}_x$  reactions could contribute, at most, 10 percent of the total destruction of ozone. Crutzen [1971] also noted that  $\text{NO}_x$  from SSTs would lead to ozone depletion, but argued initially that the problem was very complex and gave no estimates, although he gave such estimates in a later paper [Crutzen, 1972]. An ironic aspect of this early modeling is that Crutzen [1971] recognized that the reaction



could take place, but in the absence of kinetic data, excluded it from his work. This reaction has since been found to be surprisingly fast [Howard, 1977] and of extreme importance.

Effects of  $\text{NO}_x$  injections by SSTs were estimated in detail by Johnston [1971], who emphasized the role of the  $\text{NO}_x$  catalytic cycle (Reactions 6 and 7) in controlling stratospheric ozone; and the fact that very small amounts of  $\text{NO}_x$  ( $< 0.1$  percent that of  $\text{O}_3$ ) were sufficient. Water ( $\text{HO}_x$ ) in this model served only as a modifier of the cycle, tying up some  $\text{NO}_x$  as  $\text{HNO}_3$ . Johnston's calculations (which considered but did not include  $\text{HNO}_3$ ) suggested that a 500-SST fleet at 20 km could lead to a 3 to 50 percent destruction of stratospheric ozone, depending on the vertical and horizontal dispersal of the exhaust. He emphasized that for  $\text{NO}_x$  buildups as postulated by the SCEP [1970] report (between 6.8 and 68 ppbv), the ozone column would be reduced by about a factor of 2. (The SCEP report considered  $\text{NO}$  emissions to be less important photochemically than water.) Johnston [1971] like Crutzen [1971], did not include the  $\text{HO}_2 + \text{O}_3$  reaction [Reaction (2)], and considered the  $\text{HO}_2 + \text{NO}$  (Reaction 8) to be unimportant.

The foregoing treatment is necessarily foreshortened, with much important work not noted. Two reports, one by the Australian Academy of Sciences [1972] and another by the U.S. Department of Commerce [1972], provide additional interesting information and background.

An important issue, somewhat aside from the central topic of this paper, should also be noted, which relates to the impact of ozone depletions. This is the

observation by McDonald [1971] that decreases in stratospheric ozone could lead to an increase in nonmelanoma skin cancer\*, an observation now widely accepted. McDonald's concerns were stimulated by models showing water-vapor-caused depletions of ozone. The physical aspects of this problem are discussed in Cutchis [1974].

Returning to direct effects of aircraft emissions, the effects of  $\text{NO}_x$  injections into the stratosphere became the core issue on which CIAP proceeded. Some aspects of this program will now be discussed.

#### THE CIAP YEARS 1972-1974\*\*

The Climatic Impact Assessment Program, sponsored by the U.S. Department of Transportation, was a \$23 million (approximate total) effort to assess the impacts of future stratospheric vehicles, including SSTs (on which emphasis was placed), subsonic aircraft, rockets, and the space shuttle. As noted earlier, the assessment considered effects on both stratospheric ozone and on climate, and attempted to evaluate biological and economic aspects. (A program history is given by Mormino et al., 1975.) Concurrent studies were undertaken by the British [COMESA, 1975] and by the French in cooperation with Belgium [COVOS, see Bertin et al., 1976] with other studies elsewhere [Canada, Canadian Meteorological Society, 1976; Belgium; Soviet Union, Budyko and Karol, 1976 and Budyko, 1977]. A major portion of the CIAP effort went into stratospheric measurements of trace species. Atmospheric models were developed, some in one dimension (1-D, a "global" average, altitude only), some in two dimensions (2-D, altitude and latitude, a "zonal" average) and one in three dimensions. A relatively small portion of the effort (about \$1 million or less) went into measurement of chemical reaction kinetics; in large measure, the chemistry employed was thus pre-CIAP [as in Johnston, 1971; Crutzen, 1971] but with refinements (as e.g., to include  $\text{HNO}_3$  in the modeling) which reduced effects some two-fold. A significant attempt was made to estimate uncertainties, but the true uncertainties (now evident) remained unappreciated.

More specifically, the chemistry set employed in CIAP was that of the  $\text{O}_x - \text{HO}_x$   $\text{NO}_x$  system. In this set, with the rate constants employed, the  $\text{NO}_x$  catalytic cycle provided the most important sink for ozone in the natural stratosphere [the  $\text{NO}_x$  as noted coming from  $\text{N}_2\text{O}$  via  $\text{O}(^1\text{D})$ ], so that  $\text{NO}_x$  additions necessarily led to a decrease in total ozone. The  $\text{CH}_4$  oxidation reactions, which were shown by Johnston [1974] to be capable of producing ozone with  $\text{NO}_x$  additions (by "smog" reactions), and which he found to lead to a crossover in ozone effect at about 13 km (depletion above, enhancement below), were not included in the models,† even when the models were used to evaluate effects of subsonic aircraft at 9 to 12 km.†† With this possible exception, the chemistry set was

\*The tie between decreases in ozone and skin cancer rates had been noted earlier and used in a science fiction story which appeared in 1946 [Latham, 1946]. "Philip Latham" is a pseudonym which was used by R.S. Richardson of Mt. Wilson and Palomar Observatories (per Arthur C. Clarke, ed., Time Probe: The Sciences in Science Fiction, 1966).

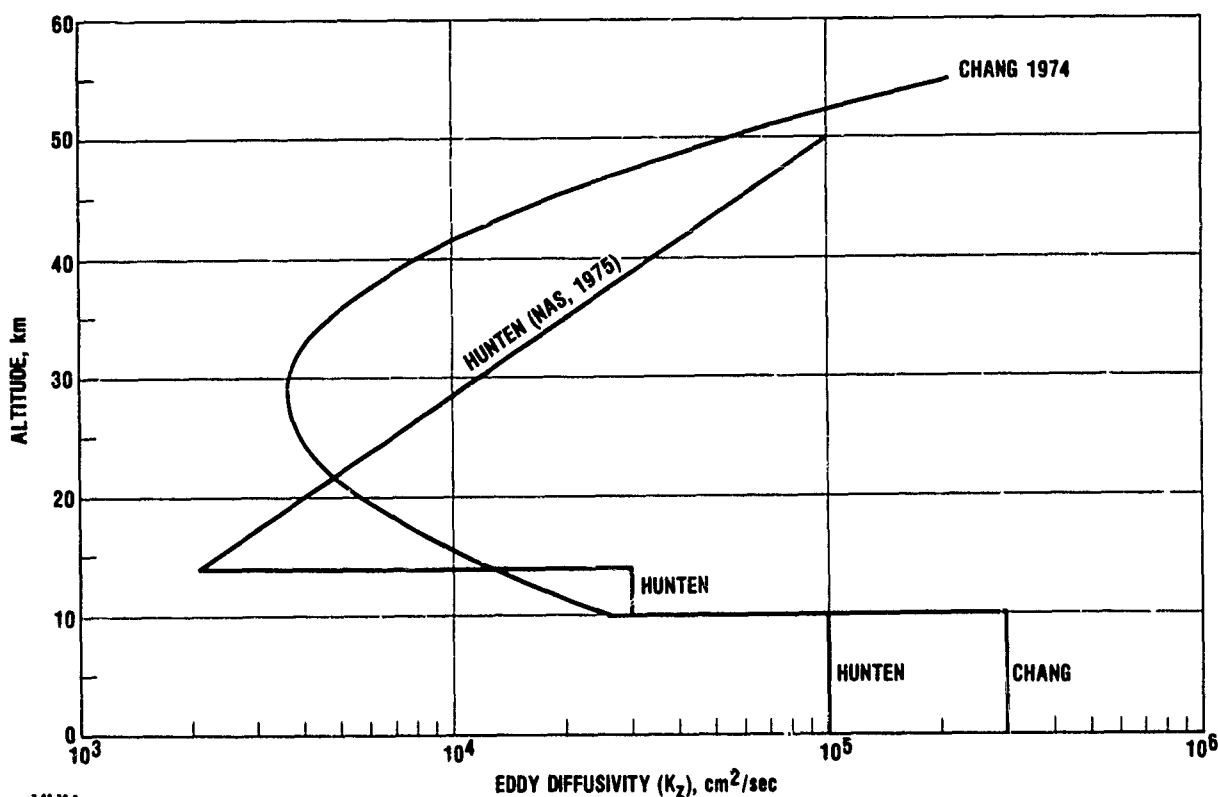
\*\*These were the years of peak activity. Some preparatory work was done in 1971 and some (primarily report preparation) was completed in 1975. The Report of Findings [Grobecker et al., 1974] is dated December 1974. A concurrent study by the National Academy of Sciences [1975] which interacted somewhat with the CIAP efforts, was published in early 1975.

†Some authors argued that the  $\text{CH}_4$  "smog" reactions are too poorly known to be included.

††The COMESA group included the  $\text{CH}_4$  reactions in the early phases of their study (and showed some enhancements for  $\text{NO}_x$  injections from subsonics) but the reactions were deleted in a later model to reduce computer time.

intended to be the best available, being examined and reexamined by a committee of experts and the National Bureau of Standards. Modelers were asked to use the data set recommended by this group in order to provide comparability: this approach, of course, tended to provide uniform answers, varying primarily with model representations of transport processes.

The CIAP conclusions (as well as the National Academy of Sciences, 1975, results) were based principally on 1-D models, with some adjustments based on 2-D results.\* In 1-D models, vertical transport is treated as a diffusion process, with transport proportional to a mixing ratio gradient times local density (molecules/cm<sup>3</sup>) and an "eddy diffusivity" ( $K_z$ ), which varies with altitude. Two important early examples of  $K_z$  profiles are shown in Figure 2.



Note: Mid-latitude sources are adjusted upward 2 km in National Academy of Sciences [1975] Hunten model.

Fig. 2. 1-D Eddy diffusivity ( $K_z$ ) profiles as used in Grobecker et al. [1974]

$K_z$  profiles for the stratosphere are generated from data on a tracer, such as CH<sub>4</sub> or N<sub>2</sub>O, which falls off in mixing ratio with height and is assumed to be at steady state, and for which chemical or photochemical loss processes are thought to be known. In principle, a great deal of such data is needed (at various latitudes and times, etc.; see Schmeltekopf et al., 1977); in practice, only limited data were available. Changes in understanding of loss processes change  $K_z$  profiles so derived.  $K_z$  profiles, in principle, also differ with model solar zenith angle and other modeling details.

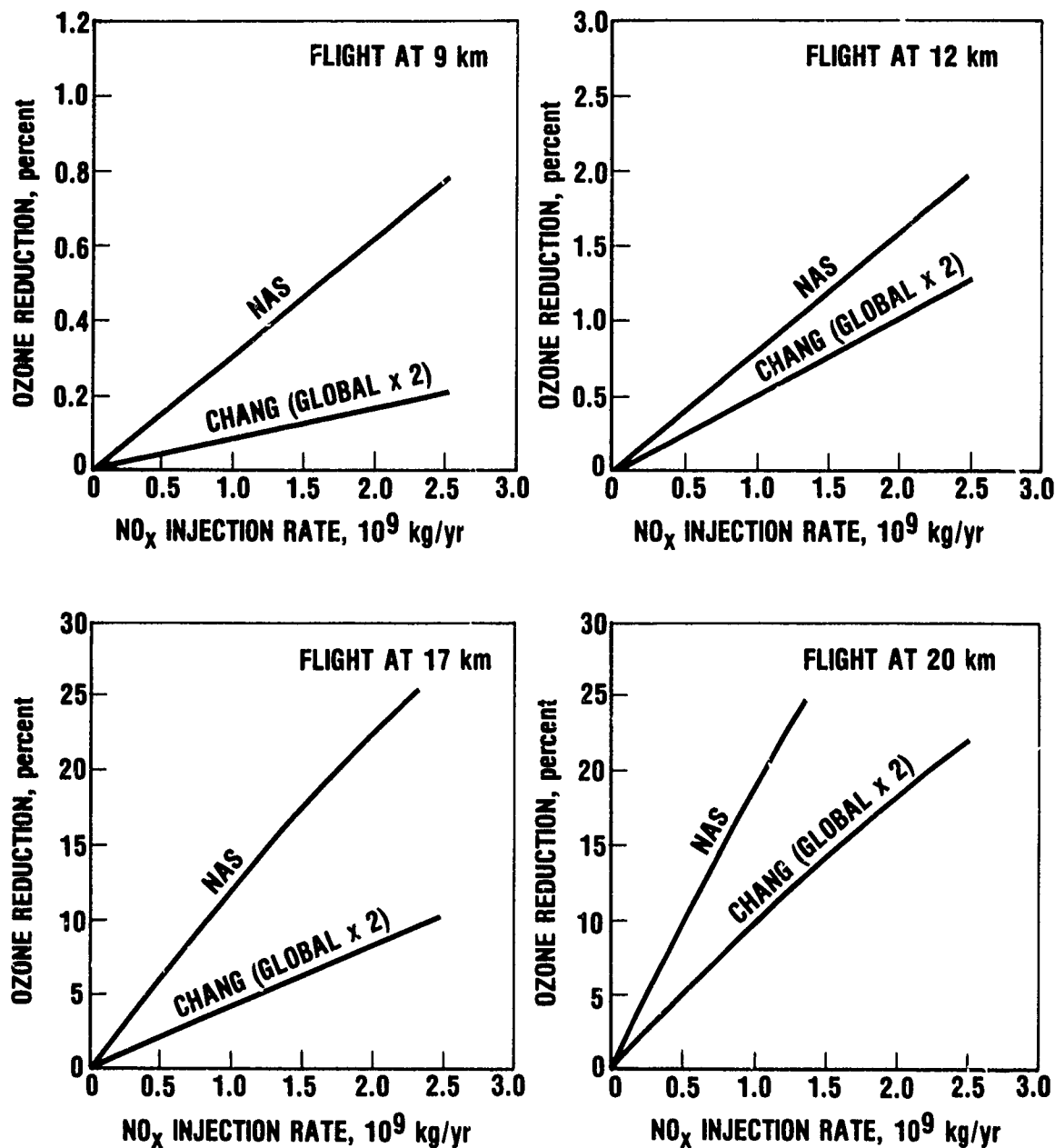
\* The 3-D model results were not considered reliable in terms of longitude, so were reduced to two dimensions. [Cunnold et al., 1975, 1977].

The lower portion of the  $K_z$  curves must be developed by different procedures; residence time data from injections of gaseous or particulate (usually radioactive) tracers have been used. The lower portions of the curves, which involve great uncertainty, and some conceptual difficulties\* are of considerable significance to the aircraft problem. [The Chang profile (Figure 2) does not show a conventional tropopause minimum.] The minimum  $K_z$  value, as in the Hunten profile, acts as a diffusion barrier upward if flight is below the model tropopause, and as a barrier downward for flight above the tropopause. The model values chosen for the tropopause height and minimum  $K_z$  are somewhat arbitrary, but are obviously important in computing effects of subsonic aircraft; an aircraft at a given altitude might be above a model tropopause but below a true tropopause. The Hunten profile shown provided better duplications of data on gaseous radioactive tracer (excess C-14) than did the Chang profile [National Academy of Sciences, 1975] but the various aspects of the treatment were debated [Chang, 1975].

The choice of  $K_z$  profile in CIAP was of considerable significance in a quantitative, and thus potentially in a regulatory, sense. With the chemistry employed,  $\text{NO}_x$  injections at all altitudes led to ozone depletion, as shown in Figure 3; these results implied that some depletion of ozone due to aircraft was inevitable. It was suggested [Grobecker et al., 1974], as a working postulate, based on a detectability argument, that 0.5 percent depletion of the ozone column might be acceptable. The corresponding permissible number of aircraft then depended on the operating hours at altitude per year per aircraft, the operating altitude, the fuel flow, and the  $\text{NO}_x$  emission index. Water vapor was of no concern in the CIAP ozone calculations; in fact, Crutzen [1973], using CIAP chemistry, showed that increases in water vapor alone, by reducing the effectiveness of the  $\text{NO}_x$  cycle, led to a slight increase in total ozone (a doubling of water vapor led to 1.5 percent increase in ozone). With given fleet projections, the 0.5 percent depletion figure would thus be reached at different times by different models, but inevitably would be reached as aircraft (particularly SST) traffic grew, unless the  $\text{NO}_x$  emission could be reduced by presumably costly means: The  $\text{NO}_x$  emission index is a function of combustor operating conditions for conventional combustors, as noted in an earlier section, but techniques are known (lean premixed prevaporized homogeneous or catalytic combustor systems) by which the  $\text{NO}_x$  emission index can be greatly reduced [English et al., 1975]. Problems were evident with these techniques, but a committee set up under NASA sponsorship (at CIAP request) suggested some possible goals. These were interpreted by the CIAP office as being 6-fold or 60-fold stepwise reduction goals, to be introduced prior to the time when the total ozone depletion would otherwise have been 0.5 percent [see Grobecker et al., 1974]. (It might be added that these goals now seem less easily attainable.)

While CIAP models all showed ozone depletions with  $\text{NO}_x$  injections, a nagging uncertainty was introduced by Foley and Ruderman [1972, 1973]. These authors pointed out that very large injections of  $\text{NO}_x$  into the stratosphere had occurred during the period of intensive nuclear testing in 1958-1962 which should by then-current models have led to substantial ozone depletion in the Northern Hemisphere. Ozone records for this period, however, showed no unambiguous evidence of ozone depletion. Extended arguments followed thereafter about "detectability" and the validity of the ozone data results. Perhaps the best argument for evidence of depletion was the one reported in National Academy of Sciences [1975, p. 101] in which a "missing peak" in a cyclic ozone record was noted as occurring about the time of the tests and thereafter.

\* The question is whether the so-parameterized transport processes relate in the proper way to the transport processes (meridional and zonal) which bring reactive species together in the real atmosphere. This problem is believed to be more severe in the lower stratosphere, where chemical lifetimes are long and vertical transport is slow, than in the upper stratosphere, where lifetimes are short and vertical transport is more rapid. See Newell, 1977.



7-23-79-3

Fig. 3. Ozone reduction estimates from CIAP period,  $\text{NO}_x$  is as  $\text{NO}_2$ . The National Academy of Sciences model is a hemispheric model; the Chang model is a global model. Hence, Chang model global averages have been doubled. The CIAP Report of Findings used an average of these two, assigning the result to depletions at  $30^\circ$  to  $60^\circ$  N. [See National Academy of Sciences, 1975 pp 116-119; Grobecker et al. 1974, Appendix B]

As CIAP neared an end, with Concorde SST sales lagging, with the Concorde production line approaching shutdown, and with the Soviet SST development moving slowly, the SST threat to ozone began to seem more remote. However, the subsonic question began to be of greater concern. Thus, the National Academy of Sciences [1975] report stated that advanced subsonics (such as the 747SP) cruising at 12 to 15 km altitude, would reduce Northern Hemisphere ozone by 0.16 percent per 100 aircraft. Only 300 such aircraft would thus give 0.5 percent ozone depletion. CIAP, (and English et al., [1975]) type projections suggested that this number might be reached within a few years, certainly before a radically new combustor technology could be available. It was clear that subsonics had to be given more detailed attention.

Summarizing, the CIAP period ozone studies yielded results which bore out, using much the same chemistry, prior contentions as to SST ozone depletion due to  $\text{NO}_x$  additions. The models were developed for SSTs for altitudes where other reactions (e.g.,  $\text{CH}_4$  oxidation) were believed to be insignificant, but were applied more broadly. Water vapor additions by SSTs, at least in one model run reported, by tying up  $\text{NO}_x$  as  $\text{HNO}_3$ , tended with this chemistry to slightly increase model ozone rather than to deplete it, as had been postulated earlier.

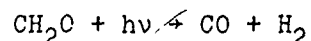
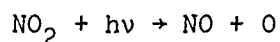
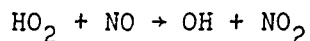
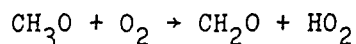
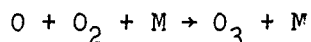
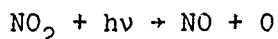
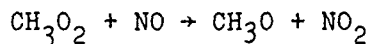
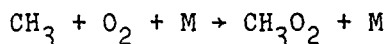
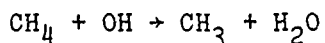
#### THE YEARS 1975-1976. $\text{CH}_4$ OXIDATION EFFECTS, UNCERTAINTIES, AND HALOCARBON EFFECTS

The two-year period following delivery of the CIAP Report of Findings [Gro-becker et al., 1974] in December 1974 involved three developments which were particularly significant to the calculation of aircraft effects. The first, in terms of its implication to the aircraft industry, was a further study of subsonic aircraft effects, including the methane oxidation reactions which had not been included in CIAP. The results, which are described below, showed small ozone enhancements rather than significant ozone depletions; the nature of any potential regulatory problem was thus totally altered. The second of these was a study by Duewer et al. [1977, 1977a] which focused on uncertainties in the modeling of the  $\text{O}_x - \text{HO}_x - \text{NO}_x$  atmosphere and in the effects of perturbations to it; the results showed that  $\text{NO}_x$  from SSTs at 17 to 20 km could increase the ozone column within the uncertainties of the chemical kinetics or could cause much more severe effects than previously thought. A third development, one of obviously more significance in an environmental and economic sense, was the recognition of the potential impact of chlorofluorocarbons. Another issue, much discussed at the time, had to do with the potential impact of man-made fertilizers, through nitrous oxide, on the ozone layer; this problem, however, had less impact on the aircraft effects question although it, like all other phenomena which affect the atmosphere, involves related phenomena.

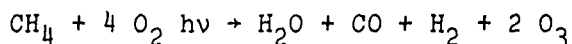
Revised fleet projections, in greater detail, on a 2-D basis, were also prepared in this time frame [Pozdena, 1976; Athens et al., 1976]. A 1990 "High Estimate" based on this work, is appended, as noted earlier. This projection assumed only mach 2 class SSTs would be in operation, and was considered by the authors [Pozdena et al., 1976] to be very much on the high side, at least for SSTs.

The Subsonic Question; the  $\text{CH}_4$  Oxidation Reactions: As discussed in the previous section, the National Academy of Sciences [1975] report (and less so, the CIAP Report) implied a substantial threat to the ozone column as the fleet of subsonic aircraft grows; if correct, large expenditures for combustor modification, modified flight paths, or other means would be needed to prevent this effect. It was thus of considerable interest to carry out modeling studies which included the known (actually poorly known) ozone-producing reactions associated with  $\text{CH}_4$  oxidation in the presence of  $\text{NO}_x$  injections. Fortunately, a 2-D model developed by P. Crutzen at the National Center for Atmospheric Research was available which included these reactions. The set of reactions is of the class [Hidalgo and Crutzen, 1977].

OLIVER



which together yielded the balance:

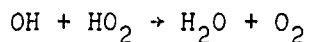


It was noted that the CO produced can go through a similar sequence, which combining with the above, yields overall

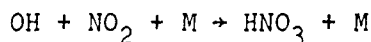


These reactions, particularly when taken as a global sum are, and were, known to involve a number of uncertainties, both in rates and in products. For example formaldehyde ( $\text{CH}_2\text{O}$ ) may go on photolysis to  $\text{CO} + 2\text{H}$ , rather than  $\text{CO} + \text{H}_2$ , with the H atoms then reacting with  $\text{O}_2$  to form  $\text{HO}_2$ . As a result, the actual production of  $\text{O}_3$  per  $\text{CH}_4$  destroyed is probably not as indicated in the overall reactions. Nevertheless, the reactions shown, at least the individual ones (the global sum reactions were not used as such), provided a plausible sequence, and were included in the then-available (but considered preliminary) model.

The studies were conducted with the Crutzen 2-D model, using  $\text{NO}_x$  distributed by latitude according to English et al., [1975] [Hidalgo and Crutzen, 1977]. The atmosphere chemistry used was largely that used in CIAP (during which time the model was built) but with certain then-current changes. E.g., the reaction rate for



was taken as  $6 \times 10^{-11} \text{ cm}^3/\text{sec}$  rather than  $2 \times 10^{-10}$  as used in CIAP. A fast rate for reaction (9) (as for any reaction which rapidly consumes OH) tends to decrease the amount of  $\text{NO}_2$  tied up as  $\text{HNO}_3$  according to



and to increase the ozone destruction by  $\text{NO}_x$ . An even slower value,  $3 \times 10^{-11}$  was later recommended by Hudson, [1977].

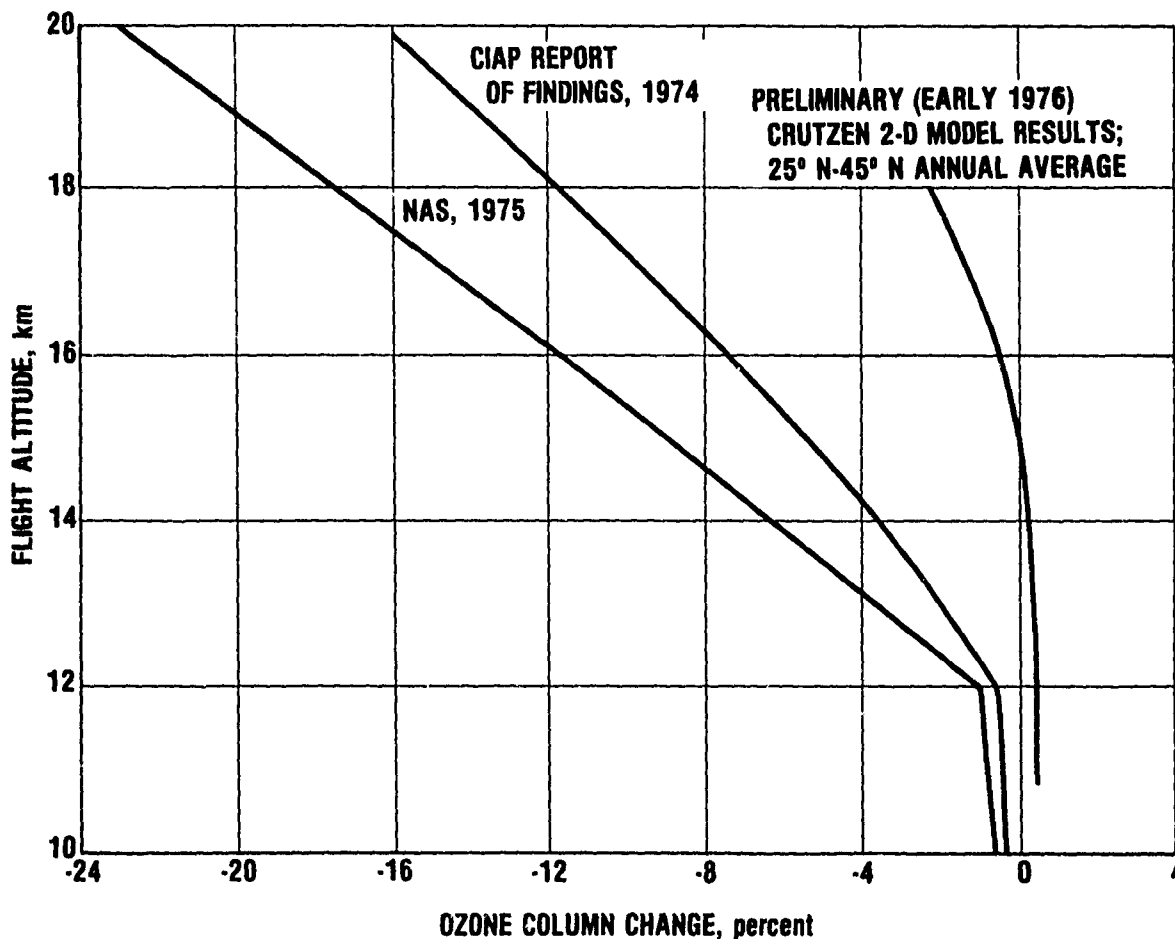
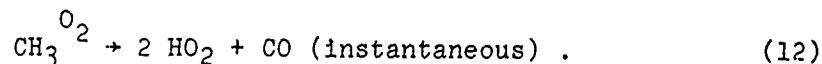
Results of this work were reported in detail in Hidalgo and Crutzen [1977] and in Oliver et al. [1977]. It was found, in general that ozone column changes were positive for low-altitude injections, and negative above 15 km, but much smaller, in general, than implied by earlier modeling, as shown by the comparison plot in Figure 4. Figure 5 gives latitudinal effects at various altitudes of injection from this work [Hidalgo and Crutzen, 1977]. Some smoothing was employed in these plots; changes of 0.04 percent are probably in the noise.

The "1990-High" fleet (Appendix) was also run by Widhopf, (1976), [also Oliver et al., (1977)] using much the same chemistry. Results showed ozone enhancements (Northern Hemisphere average) of the order of 0.8 percent. In this model, the ozone enhancement effects of the subsonics clearly outweighed the depletion effects of the relatively small (142 Concorde class) SST fleet.

Fully comparable 1-D runs (i.e., with the same chemistry) were not made. However, runs were made at Lawrence Livermore Laboratory with a simplified methane oxidation pathway in which the reaction



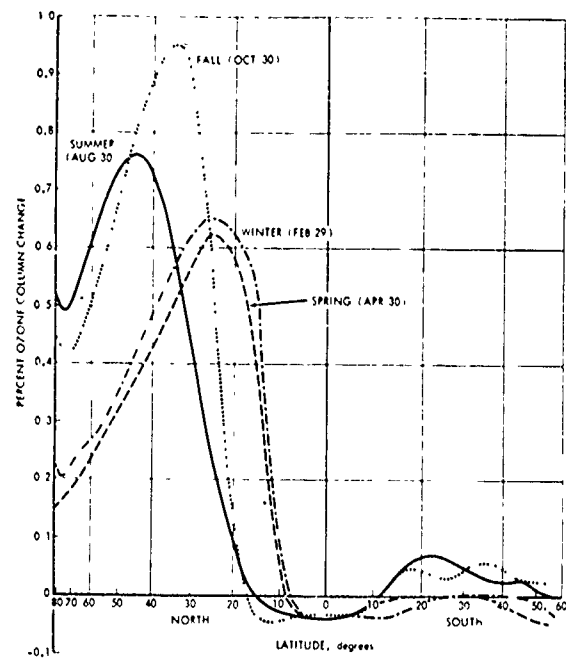
was, for model purposes, followed by:



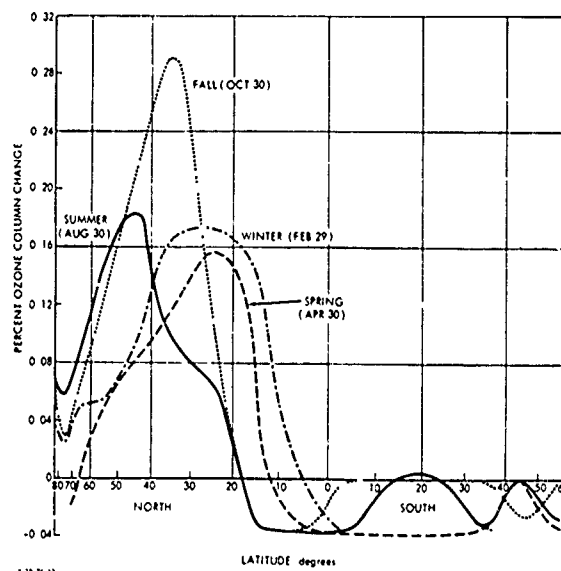
3-11-71

Fig. 4. Ozone column change results by various models. The injection rate assumed at each altitude is  $1.23 \times 10^9$  kg  $\text{NO}_x$  (as  $\text{NO}_2$ ) per year into a hemisphere. The National Academy of Sciences and CIAP curves are based on 1-D model results adjusted to correspond to changes to be expected in the "Hemisphere" (National Academy of Sciences) or "Corridor (30° to 60° N)" (CIAP). The curve at the right represents annually averaged results for 25° N to 45° N from runs with the Crutzen 2-D model adjusted, assuming linearity, to the same total input rate, as for the other curves, but distributed by latitude according to CIAP traffic estimates. The Crutzen results are after 6 model years.

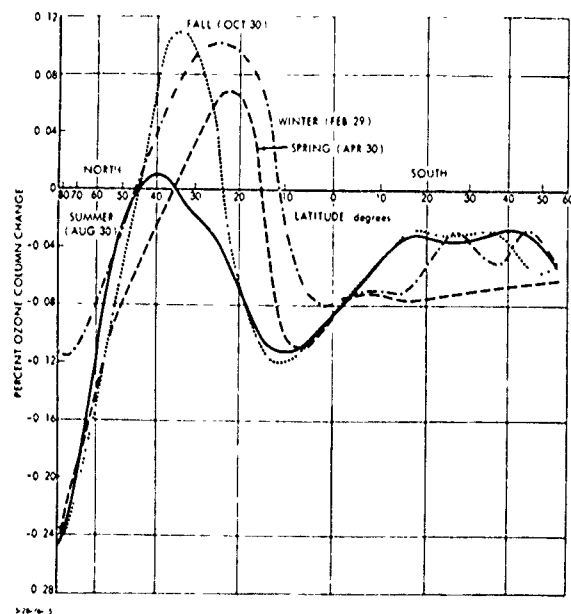




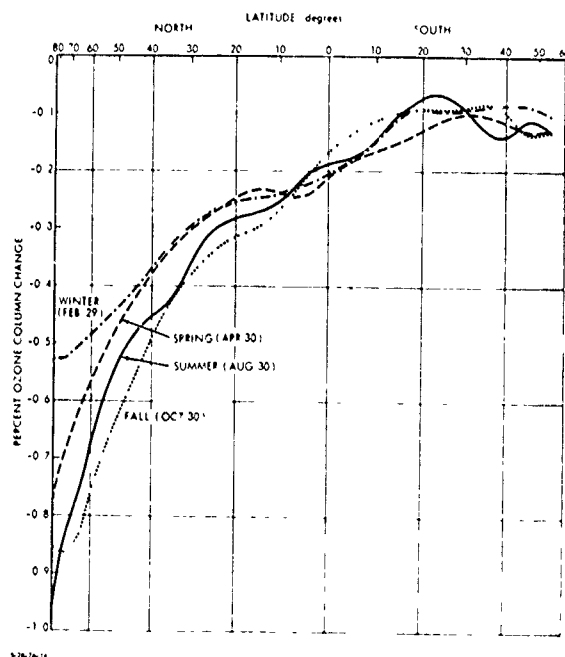
(a) 10.8 km injection,  $2.06 \times 10^9$  kg/yr  $\text{NO}_x$  (as  $\text{NO}_2$ )



(b) 12.7 km injection,  $0.455 \times 10^9$  kg/yr  $\text{NO}_x$  (as  $\text{NO}_2$ )



(c) 14.5 km injection,  $0.455 \times 10^9$  kg/yr  $\text{NO}_x$  (as  $\text{NO}_2$ )



(d) 18 km injection,  $0.226 \times 10^9$  kg/yr  $\text{NO}_x$  (as  $\text{NO}_2$ )

Source: Hidalgo and Crutzen [1977]

Fig. 5. Ozone column changes after 6 model years calculated with Crutzen's 2-D model (1976 chemistry). Note differing scales, input rates, and altitudes.

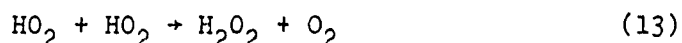
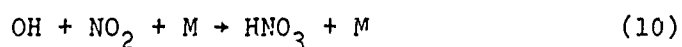
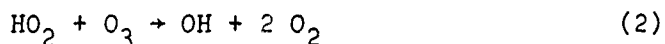
# OLIVER

HO<sub>2</sub> reacts (in one pathway) with NO to give NO<sub>2</sub>, which can then be photolyzed to give ozone.

Results [see Oliver et al., 1977] showed ozone column enhancements of the order of 0.04 percent or less for both Chang (1974) and Hunten (1975) K<sub>2</sub> profiles; the Hunten K<sub>2</sub> profile gave slightly larger values in line with slower vertical transport.

Uncertainties in the O<sub>x</sub> - HO<sub>x</sub> - NO<sub>x</sub> Atmosphere: Each reaction rate in a photochemical model has associated with it an estimated uncertainty. These estimated uncertainties have been found at times (as shown here, see also Smith, [1978]) to be seriously underestimated; also, no guarantee exists that all pertinent reactions have been included. (Thus, the uncertainty analysis is itself highly uncertain). Various procedures to estimate uncertainty have been used, but the one which appears to have given the most insight is the one adopted by Lawrence Livermore Laboratory in examining uncertainties in the O<sub>x</sub> - HC<sub>x</sub> - NO<sub>x</sub> model atmosphere. The procedure used was to simultaneously vary a number of key reaction rates, within the stated uncertainties, towards or away from ozone sensitivity to NO<sub>x</sub> (Duewer et al. [1977], [1977a]; reporting on work done in 1976).

Five reactions were found by Duewer et al. to be of particular significance. They are



Without going into extensive detail, it was found, as noted earlier, that ozone changes with NO<sub>x</sub> injections at SST altitudes could vary widely, ranging from relatively large negative values to slight positive values. With all rates maximized or minimized (with regard to NO<sub>x</sub> destruction of O<sub>3</sub>), the values shown in Table 2 were obtained.

TABLE 2. Ozone Column Changes in a 1-D Model (O<sub>x</sub>-HO<sub>x</sub>-NO<sub>x</sub> Atmosphere). Sensitivity to Rate Coefficients.  
Chang 1974 K<sub>2</sub> Profile  
NO<sub>x</sub> 2.46 x 10<sup>9</sup> kg/yr (as NO<sub>2</sub>)  
Duewer et al., [1977]

Injection Altitude, km	MAX	MIN	CIAP
17	-8.06	+2.22	-4.34
20	-15.92	+2.64	-9.79
35	-25.11	-6.42	-17.24
1.1 x H <sub>2</sub> O	+0.15	-0.54	+0.3

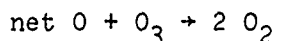
It was found that a change to one uncertainty limit in as few as 4 reactions could lead to ozone enhancements by SSTs. Note that in these results water injection effects on ozone go oppositely to NO<sub>x</sub> injection effects: if NO<sub>x</sub> increases O<sub>3</sub>, water decreases it, and conversely; this is now a commonly observed result. The water effect proved to be small but clearly was in need of more study. This work proved to be particularly farsighted.

# OLIVER

Chlorofluorocarbons: CIAP, in considering potential perturbations to stratospheric ozone, sponsored a small study effort on the space shuttle. The space shuttle is boosted into orbit by a combination of two large, separable, solid-propellant booster rockets and by hydrogen-oxygen engines in the orbiter itself. The solid-propellant rockets drop off at about 45 km. The solid-propellant rocket exhaust contains considerable HCl, which, it was recognized, could destroy ozone according to:



and the catalytic cycle



The various reactions were investigated by Stolarski and Cicerone [1974]; the cycle indicated, at equivalent concentrations, is much faster than the NO<sub>x</sub> cycle. Other less important chlorine catalytic cycles were also suggested. These authors considered various natural chlorine sources, suggesting the principal sources to be probably volcanic. At 1 ppb of ClO<sub>x</sub>\*, these cycles result in ozone destruction about equal to that in the Chapman cycle. At about that time, however, Farmer [1974], gave an upper limit for HCl in the lower stratosphere as about 0.18 ppb (which appears to have been misleading in light of later data). At that time it was not obvious that ClO<sub>x</sub> species were of particular significance in the natural stratosphere, except perhaps following volcanic eruptions. Stolarski and Cicerone pointed out that interactions would be present between the NO<sub>x</sub> and ClO<sub>x</sub> cycles. Crutzen [1974] and Wofsy and McElroy [1974] also discussed ClO<sub>x</sub> reactions in papers published at the same time.

The chlorine cycle thus at first seemed to be of minor interest in terms of the natural atmosphere, primarily a matter of concern to NASA and the space shuttle. The picture changed dramatically with publication in *Nature* of the article by Molina and Rowland [1974], pointing out the potential effects of chlorofluorocarbons, particularly CFC1<sub>3</sub> and CF<sub>2</sub>Cl<sub>2</sub>, usage (and release) of which had grown dramatically through widespread use as propellants in aerosol spray cans and refrigerants, etc. The only significant sink for these materials appeared (and still appears to be) photolysis in the stratosphere; the materials had been detected and measured on a worldwide basis by Lovelock [1973]. Hearings were held in December 1974 [Hearings, 1974]. The issue obviously had the potential for large economic impact as a total of some 800 million pounds of these two compounds had been produced in the U.S. alone in 1973. Studies by the National Academy of Sciences [National Academy of Sciences, 1976 and 1976a] resulted, with conclusions released in late 1976, and discussed [Kaufman, 1976] in a conference in September 1976. Large depletions of ozone (2 to 20 percent) were forecast even at 1973 release rates, requiring perhaps 50 years to equilibrate; with, of course, greater depletions if releases continued to grow.

The halocarbon work stimulated much new research, a large part of which is outside the topic of this paper. However, the aircraft NO<sub>x</sub> problem was affected, as it became clear with further stratospheric measurements that naturally occurring and man-made ClX species are and will be important in the stratosphere, and as noted earlier, that these will interact with previously known NO<sub>x</sub> (e.g., ClO + NO<sub>2</sub> + M → ClONO<sub>2</sub> + M); and HO<sub>x</sub> (possibly as HOCl) cycles.

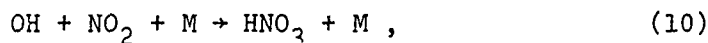
\*The terms ClO<sub>x</sub> and ClX are stated in Hudson [1977] to imply for ClO<sub>x</sub>, the sum of Cl, ClO, and higher chlorine oxides, and for ClX, the sum of all Cl-containing species produced from photooxidation and subsequent reactions of organic chlorine containing compounds, i.e. Cl + ClO + ClONO<sub>2</sub> + HCl + any other inorganic Cl-containing species.

# OLIVER

During the work, various reaction rates were reexamined. One reaction already discussed,



was particularly significant to both aircraft effects and to the halocarbon question. This is because in the  $\text{NO}_x$  cycle, OH ties up reactant  $\text{NO}_2$ , according to



whereas in the  $\text{ClO}_x$  cycle, OH reactivates material (Cl) otherwise in a reservoir (HCl), according to



As noted earlier, the rate used in most CIAP modeling for the  $\text{OH} + \text{HO}_2$  reaction was a very fast one ( $2 \times 10^{-10} \text{ cm}^3/\text{sec}$ ) which tended to maximize  $\text{NO}_x$  effects. In the halocarbon work, Reaction 9 was reexamined and a much slower rate ( $2 \times 10^{-11}$ ) taken as the preferred value. [National Academy of Sciences, 1976a, p. 143] This change, when applied to the  $\text{NO}_x$  problem, reduced calculated ozone depletions by nearly a factor of two. [See Eroderick, 1978].

The substance chlorine nitrate ( $\text{ClONO}_2$ ), introduced late in the deliberations on effects of halocarbon injections, once again demonstrated the sensitivity of these models to new species or rates. The first modeling studies which included this compound assumed  $\text{ClONO}_2$ , as one possibility, to be relatively stable in the stratosphere; the results showed that chlorine injections could thereby *increase* ozone, rather than cause serious depletion of ozone. [Eggleton et al., 1976]. More detailed studies however, including diurnal effects, showed that the compound, while significant, reduced the effects of chlorine injections perhaps 2-fold but not to the point of enhancing ozone. [National Academy of Sciences, 1976, 1976a].

Aircraft effects in a chlorine-containing atmosphere were later shown to be sensitive to the amount of chlorine present;  $\text{NO}_x$  has less effect as  $\text{ClX}$  content is increased, in some case, even with 1977 chemistry, going positive. As an example, in calculations performed at Lawrence Livermore Laboratory in 1976 [See Figure 3.26, Oliver et al., 1977] a large ( $2.46 \times 10^9 \text{ kg/yr}$ ) injection at 17 km of  $\text{NO}_x$  led to a 1.2 percent depletion of ozone at zero  $\text{ClX}$  but a 0.3 percent increase at 4 ppb  $\text{ClX}$ . Water injections in a  $\text{ClX}$  atmosphere were found to decrease ozone, but thermal feedback effects become important, as shown later herein.

Summarizing, at the end of 1976, the subsonic  $\text{NO}_x$  effect on ozone has been reversed from that found in CIAP; calculated effects of SSTs were smaller, uncertainties in SST effects were greater, and interaction with more current threats were evident.

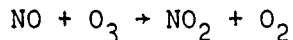
## THE KINETICS REVOLUTION (THE HOWARD BOMBSHELLS) 1977-1978

The reactions discussed by Duewer et al. [1977] in their uncertainty analysis included several involving the  $\text{HO}_2$  radical. The effects of a rate change in one of these ( $\text{HO}_2 + \text{OH} \rightarrow \text{H}_2\text{O} + \text{O}_2$ ) has already been noted. In general, during the CIAP period, rates for these reactions had been derived indirectly from measurements made at relatively high total pressures ( $\sim 1 \text{ atm}$ ). In 1977, however, Howard and Evenson [1977] utilized a laser-magnetic resonance procedure, but at low total pressures as described in Howard and Evenson [1974], to follow the decay of  $\text{HO}_2$  in the presence of  $\text{NO}$ . They found that, at 296 K and 140 to 220 Pascals (1 to 1.6 Torr; 0.0014 to 0.002 atm), the reaction



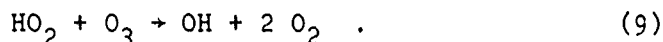
proceeds with a rate constant of  $(8.1 \pm 1.5) \times 10^{-12}$  cm<sup>3</sup>/mol-sec. This reaction, during CIAP, had been given [Reiter et al., 1975, p. 5-227] a preferred value of  $2 \times 10^{-13}$  cm<sup>3</sup>/sec (with an uncertainty factor of 3). The Howard and Evenson measured rate was thus some 40-fold times the prior preferred value. It should be noted that the measurements were at much lower-than-stratospheric pressures. The large change in rate from the previous value, and certain subsequent anomalous temperature dependence data, have led to speculation that the reaction (as well as other HO<sub>2</sub> reactions) may be pressure-dependent, possibly through formation of an intermediate unstable compound. The high rate apparently has been accepted by most groups.\*

Use of the Howard and Evenson [1977] rate for Reaction 8 leads to significant changes in the computed effects of NO<sub>x</sub> injections on ozone. This is because the high rate "short-circuits" the NO catalytic cycle by providing a second path, which does not destroy ozone, to NO<sub>2</sub>:



NO<sub>2</sub>, of course, continues to react with O atoms in the catalytic cycle to form NO, but an increased NO<sub>2</sub> concentration (relative to that in a model using a slow rate) also provides, by photolysis, a pathway which forms ozone; also the increased OH tends to tie up more NO<sub>2</sub> as inactive HNO<sub>3</sub>. The high rate for reaction (8), coupled with the reduced rate for HO<sub>2</sub> + OH → H<sub>2</sub>O + O<sub>2</sub> (and other less significant changes) tended to increase the model natural atmosphere ozone column above that measured [Oliver et al., 1978], creating doubts about model validity. It also implied that SST NO<sub>x</sub> injections, except at very high injection rates, would increase the ozone column through enhancements of ozone in the lower stratosphere.

Crutzen and Howard [1978]\*\* pointed out that to compute ozone enhancements in the stratosphere with NO<sub>x</sub> injections, a fast rate is also required for the reaction



The argument is a bit subtle, inasmuch as a fast rate for this reaction clearly destroys ozone. The issue, however, relates to NO<sub>x</sub> injections into a model atmosphere. The fast rate decreases the model atmosphere ozone (a needed effect as noted above), but NO<sub>x</sub> injections, if (9) is fast, *reduce the reduction*, leading to an ozone enhancement relative to the model atmosphere, by reactions such as



If reaction (9) is slow, this mode of O<sub>3</sub> destruction is less important, and SST NO<sub>x</sub> injections may deplete ozone (depending on choice of reaction rates).

This issue was resolved (at least temporarily) in Spring 1978 when the rate for (9) was measured by Zahniser and Howard [1978], again using a laser magnetic resonance technique at low pressure, who found the rate to be much *faster* than expected, it being

\*Significant pressure effects have been found for the HO<sub>2</sub> + HO<sub>2</sub> rates [B.A. Thrush and J.P.T. Wilkinson, "Pressure Dependence of the Rate of Reaction Between HO<sub>2</sub> Radicals," data presented at this symposium] and are suspected when negative activation energies (as in the HO<sub>2</sub> + NO rate) are found.

\*\* The model used did not include a troposphere.

$$\text{OLIVER} \\ (1.4 \pm 0.4) \times 10^{-14} e^{-(580 \pm 100)/T} .$$

At 230 K, the central value from this expression is  $1.1 \times 10^{-15} \text{ cm}^3/\text{sec}$ . This is to be compared with the rate from Hudson [1977] [ $7.3 \times 10^{-14} e^{-1275/T}$  or  $2.9 \times 10^{-16}$  at 230 K] or the value from CIAP [ $1 \times 10^{-13} e^{-1250/T}$  or  $4.4 \times 10^{-16}$  at 230 K]. A slow rate (at stratospheric temperature) has also been recommended in a 1977 NASA workshop [see Crutzen and Howard, 1978], i.e.,  $1 \times 10^{-13} e^{-1525/T}$  or  $1.3 \times 10^{-16}$  at 230 K.

These developments in reaction rates have had a profound effect on the understanding of ozone, both stratospheric and tropospheric, raising a number of questions in the process.  $\text{NO}_x$  injections in the various models, with this chemistry, except at very high rates, whether from SSTs or subsonics, increase the ozone column. Water effects, which now tend to reduce ozone, have generally been increased by these rate changes (as have  $\text{ClX}$  effects). Results follow.

#### CURRENT STATUS OF COMPUTED AIRCRAFT EFFECTS ON OZONE

As understanding of the many species and processes controlling ozone has grown, and models have become more complex, it has become necessary to be more precise in describing a model result and the model reference atmosphere when reporting the computed effect of a perturbation to that atmosphere. The time-dependent aspects, for example, can be troublesome, because stratospheric  $\text{ClX}$ ,  $\text{CO}_2$ , and  $\text{NO}_x$  (from  $\text{N}_2\text{O}$ ) and other species all will change with time; a model computation may (without necessarily so stating) be of a year 2000 perturbation in a 1978 atmosphere, or a 1978 perturbation in a halocarbon-equilibrated 2050 atmosphere. Groves and Tuck [1979], for example, have shown that an increase to 600 ppmv of  $\text{CO}_2$ , which might occur by about 2020, reduces the chlorofluoromethane effect at steady state on ozone by about 30 percent.  $\text{H}_2\text{O}$  and  $\text{NO}_2$  effects are sensitive to  $\text{ClX}$  content. Many other details also have a strong influence on results; inclusion or exclusion of thermal feedback effects, for example, has strong effect on computed water effects on ozone, as will be illustrated. Similarly, inclusion or exclusion of the troposphere in a model may affect the sign of a computed change in an ozone column. Any given model results must be examined and carefully evaluated in some detail.

SST Effects: Available model results (not all of which provide enough detail to be examined in terms of the foregoing) include the model predictions from a number of groups provided at June 1979 NASA Harper's Ferry Workshop (unpublished at the time of this paper's preparation), and a recently (but unfortunately already outdated by changes in chemistry) published 1-D assessment from NASA-Ames [Popoff et al., 1978], and later in 1-D results from the same group [Turco et al., 1978]. Some other results are also included which are not fully up to date, but which illustrate points still believed to be valid.

One part of the Harper's Ferry Workshop involved in comparison of models, using in the case of interest here a single  $\text{NO}_x$  perturbation. Results which, being from a draft report, should be considered preliminary\*, are given in Table 3. Details are not provided as to the reference atmospheres. The results are reasonably consistent, presumably reflecting the modeler's use of the same chemistry (JPL-79).

The Lawrence Livermore Laboratory results (W. Duewer, private communication, July 13, 1979) are for an atmosphere containing 2 ppb  $\text{ClX}$ . The model has 4.5 ppmv  $\text{H}_2\text{O}$  prescribed at 13 km, with water calculated above 13 km. The Chang 1976  $K_z$  profile was used.\*\* (Details of the other models were not sought). Note

\* This is probably true of all the position papers for the Harper's Ferry Workshop, others of which are also cited herein.

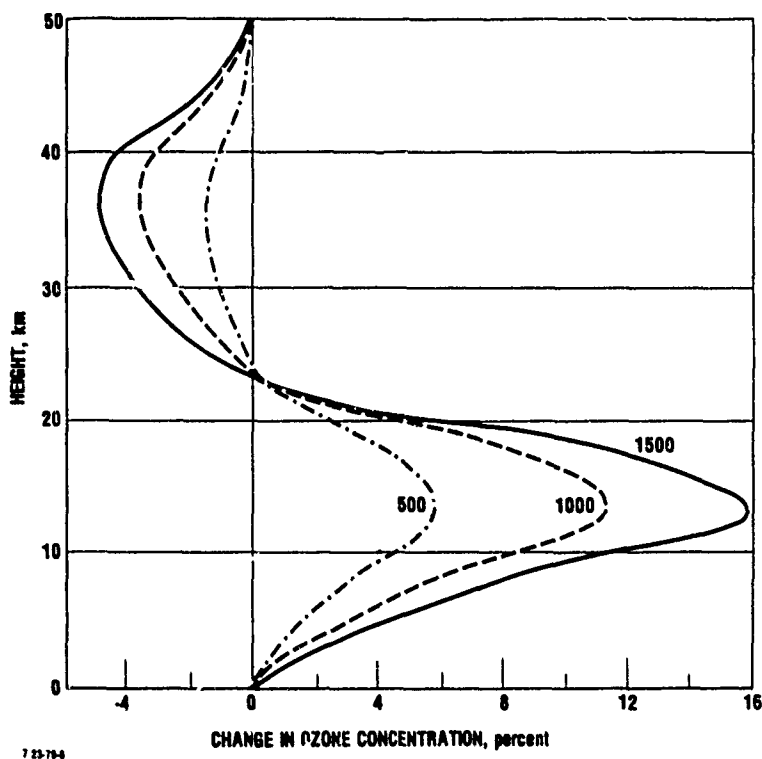
\*\* This profile differs significantly from the Chang/1974 profile given in Figure 2. See NAS [1976]. See also Appendix D in Oliver et al. [1977] for a compendium of  $K_z$  profiles.

TABLE 3. Steady-State Ozone Perturbations for an  $\text{NO}_x$  Injection  
Rate of  $1 \times 10^8$   $\text{NO}$  Molecules/ $\text{cm}^2$ -sec, or  $1.23 \times 10^9$   
 $\text{kg NO}_2/\text{yr}$  Over the Globe.

Source: Stolarski and Butler [Draft, 1979]

Modeling Group	17-18 km Injection			20 km Injection		
	$\Delta\text{O}_3(\text{col})$	$\Delta[\text{O}_3] \text{ (40 km)}$	$\Delta[\text{O}_3] \text{ (20 km)}$	$\Delta\text{O}_3(\text{col})$	$\Delta[\text{O}_3] \text{ (40 km)}$	$\Delta[\text{O}_3] \text{ (20 km)}$
Lawrence Livermore Laboratories	+1.4	-1.9	+5.0	+1.3		
DuPont	+2.6	-1.2	+5.1	+2.9	-1.9	+7.7
R&D Associates	+2.6	-1.5	+6.0	+2.4	-2.0	+6.3
California Institute of Technology	+2.2	-1.4	+5.1			
NOAA	+1.3	-1.0	+2.0	+1.2	-2.3	+3.0
Goddard Space Flight Center (Butler)	+1.5	-1.1	+4.4	+2.2		

that all models show ozone column enhancement for the specified (large) injection rates of  $\text{NO}_x$ . This column enhancement is made up of an enhancement in the lower stratosphere and a depletion in the upper stratosphere, as illustrated in Figure 6, which is from an earlier computation. The enhancement and

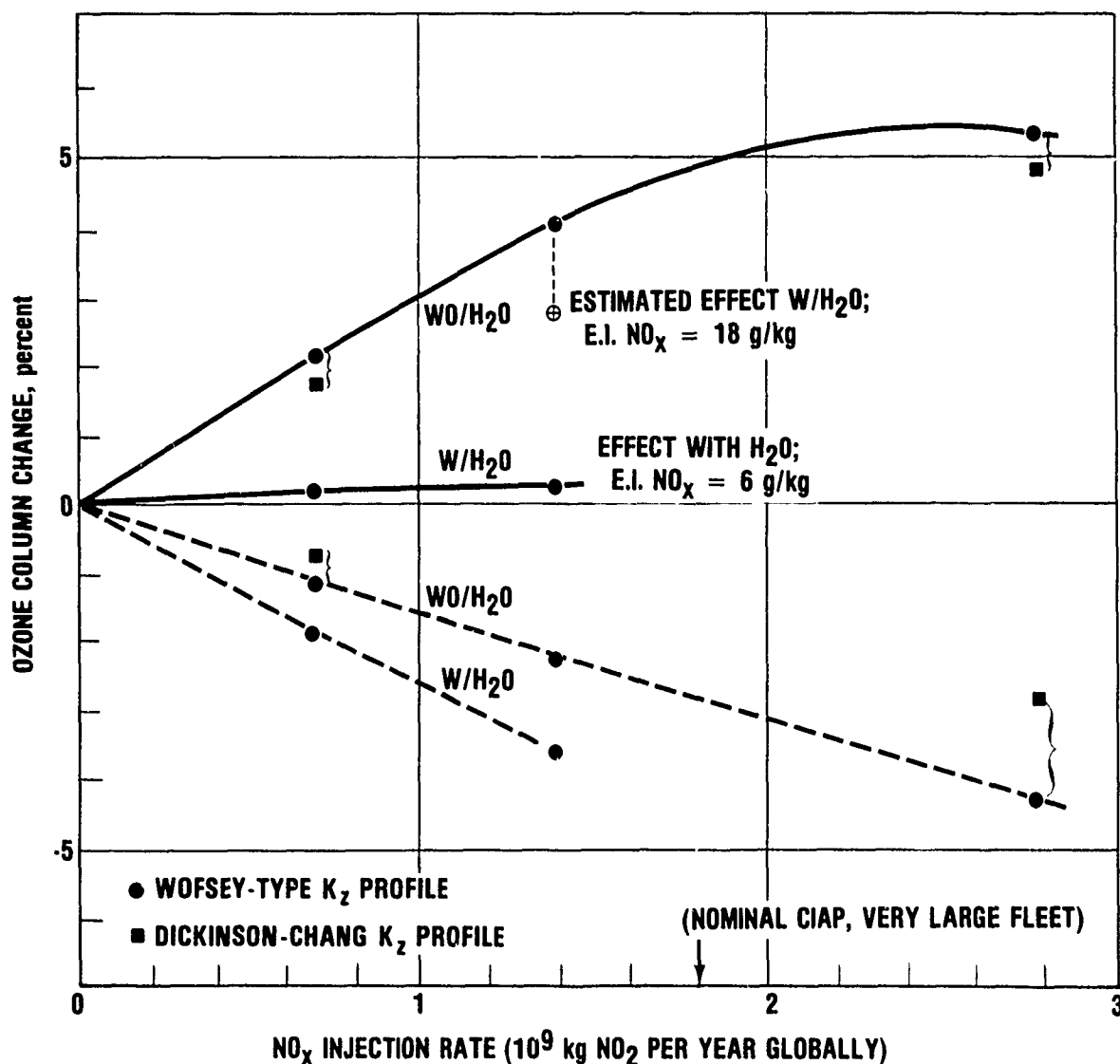


Source: Lawrence Livermore Laboratory (1978)

Fig. 6. Percentage changes in ozone vs. altitude for three injection rates of  $\text{NO}_x$  at 20 km. The rates shown are in molecules/ $\text{cm}^2$  sec over a 1-km band, and correspond to global injection rates of 0.62, 1.23, and  $1.85 \times 10^9$   $\text{kg NO}_x$  (as  $\text{NO}_2$ ) per year. Chang/1976  $\text{K}_2$  profile

depletion regions will vary with injection altitude  $K_7$  profile, feedback effects, chemistry used, with whether or not a troposphere is included in the model, etc.

Aircraft, of course, emit water (and other materials) as well as  $\text{NO}_x$ . With current chemistry, water additions tend to decrease ozone, and the effects on  $\text{O}_3$  are necessarily the combined, perhaps interactive, effect of these various emissions. Results on ozone for a specified  $\text{H}_2\text{O}/\text{NO}_x$  mass ratio (217:1, based on an assumed 6 gm  $\text{NO}_2$ /kg fuel and 1.3 kg  $\text{H}_2\text{O}$ /kg fuel), and ignoring thermal feedback are given in Figure 7. [Turco et al., 1978]. The distribution of effects by altitude is shown in Figure 8. Note that for the column above 10



7-23-79-4

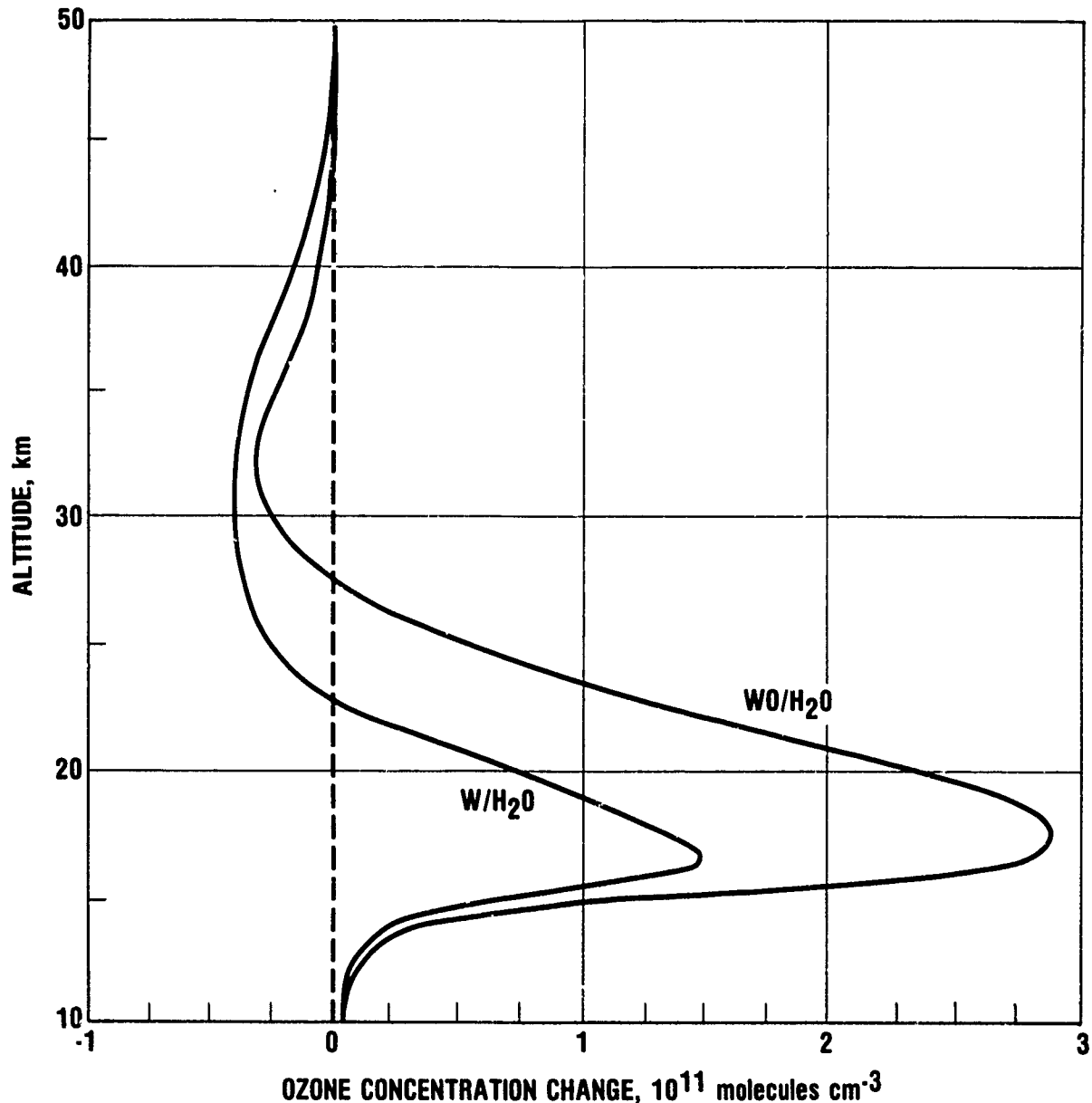
Source: Turco et al. [1978]

Fig. 7. Steady-state perturbations of the vertical ozone column above 10 km (solid line) and 30 km (dashed line) as a function of the rate of a steady  $\text{NO}_x$  injection at 20 km. Results are shown both with (W/H<sub>2</sub>O) and without (WO/H<sub>2</sub>O) simultaneous water vapor release. ●, values computed using a Wofsey-type diffusion coefficient; ■, values computed with a Dickinson-Chang diffusion profile. The point ⊕ has been added by this author, as have the notes. Thermal feedback effects have not been included



km, the water effect (at this ratio) about cancels the  $\text{NO}_x$  effect. The cancellation is not uniform with altitude, as shown in Figure 8. The model does not have a troposphere, so that changes at the model boundary at 10 km are minimal.

Results in Figures 7 and 8 imply use of advanced combustors, emitting about 1/3 the  $\text{NO}_x/\text{kg}$  fuel that present SST aircraft do. If linearity as to  $\text{H}_2\text{O}$  effect is assumed, the interpolated result marked  $\oplus$  at  $1.4 \times 10^9$  kg  $\text{NO}_x/\text{year}$ , is obtained. The net increase in ozone is greater, as would be the perturbation to the altitude-distribution of ozone. Note that the ozone increase is surprisingly



7-23-79 5

Source: Turco et al. [1978]

Fig. 8. Calculated steady-state stratospheric ozone concentration changes due to an  $\text{NO}_x$  injection of  $7 \times 10^8$  kg  $\text{NO}_2 \text{ yr}^{-1}$  (globally averaged) both with associated water vapor emissions ( $1.5 \times 10^9$  kg  $\text{H}_2\text{O}/\text{yr}$ ) and without  $\text{H}_2\text{O}$  injection

large-by extrapolation, over 3 percent--at the nominal  $1.8 \times 10^9$  kg/yr of  $\text{NO}_x$  often used in the CIAP calculations for which the water would have been 1/3 as great as that used by Turco et al. [1978].

The importance of thermal feedback in computing water effects on ozone is illustrated in Figure 9. These results are not based on fully up-to-date chemistry, but the trends shown should be valid. Note that with thermal feedback, the  $\text{H}_2\text{O}$ -alone effect on ozone is nearly negligible. If this effect is accepted, the near-cancellation of ozone column effects shown in Figure 8 cannot be achieved.\*

Note in Figure 7 that effects of  $\text{NO}_x$  injections on the ozone column are not linear with  $\text{NO}_x$  additions; at large enough  $\text{NO}_x$  emissions, even without water effects, the ozone column will be reduced. The amount of  $\text{NO}_x$  required will vary with  $K_z$  and with altitude; with present chemistry, the amounts tend to be very large indeed. Note that the nominal CIAP injection of  $1/8 \times 10^8$  kg/year, at an annual  $\text{NO}_x$  emission of  $5.7 \times 10^5$  kg  $\text{NO}_2$ /year-aircraft would correspond to 3160 SSTs, a number far beyond any current imagining.

The latest results from Lawrence Livermore Laboratory for  $\text{NO}_x$  injections (no  $\text{H}_2\text{O}$ , no thermal feedback, 2 ppb  $\text{ClX}$ ) are as given in Table 4.

TABLE 4. Ozone Column Changes Due to  $\text{NO}_x$  Injections. 1-D Model, Lawrence Livermore Laboratory Results (1979).<sup>a</sup>

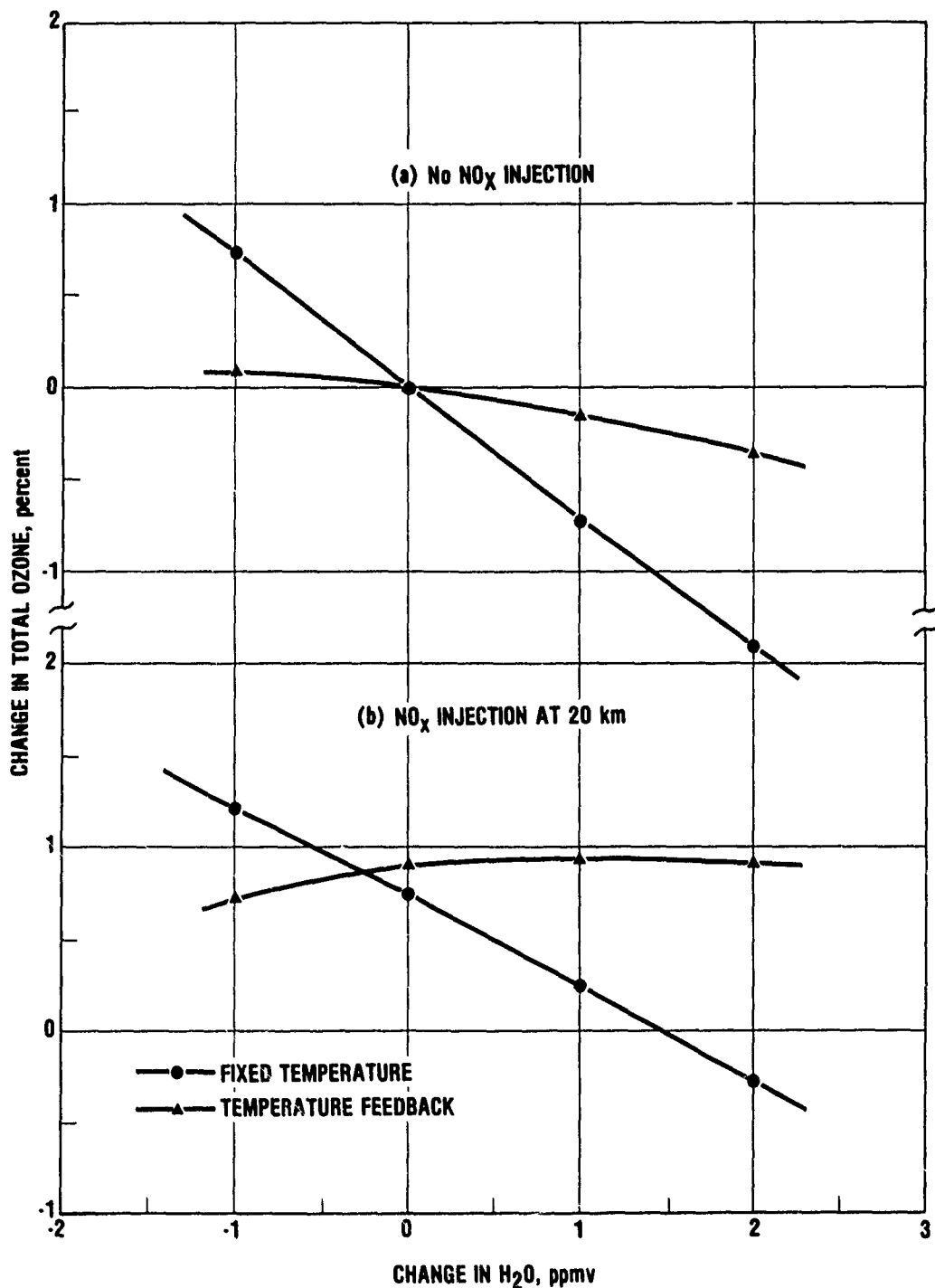
Altitude	Source Strength kg $\text{NO}_x$ /year ( $\text{NO}_2$ )	$\Delta\text{O}_3/\text{O}_3$
17	$1.22 \times 10^9$	1.25
20	$1.22 \times 10^9$	1.14

<sup>a</sup>. Duewer, W.H., private communication; November 1979.

These results do not show the increase in ozone column with increase in injection altitude found by some other modelers in Table 3, but the difference with altitude is small. This insensitivity to injection altitude apparently comes about from a combination of residence time (increase  $\text{NO}_x$  burden) and chemical effects:  $\text{NO}_x$  which reaches high altitudes and which (see Figure 8) depletes ozone, is increased; the increased  $\text{NO}_x$  burden at lower altitudes may more than compensate. For higher-altitude injections, e.g., 30 km,  $\text{NO}_x$  injections would be expected to lead to an ozone column decrease. Current results at higher injection altitudes are not available. It is evident that a model altitude exists which would maximize ozone column enhancement: the altitude would vary with  $K_z$  profile.

2-D Results: Recent results are available from Whitten [1979] and from Widhopf and Glatt [1979]. Whitten [1979] gives 2-D results for  $\text{NO}_x$ ,  $\text{H}_2\text{O}$ , and other

\*Note that the coupling of "globally-averaged" thermal feedback to "globally-averaged" transport and chemistry introduces additional uncertainties as to interpretation. Also, results become sensitive to activation energies, which may be poorly established. Possible pressure effects, as on  $\text{HO}_2$  reactions, would also affect results. Thermal feedback, if it affects tropical tropopause temperatures, would also affect stratospheric water content and chemistry. All such results must thus be viewed with caution.



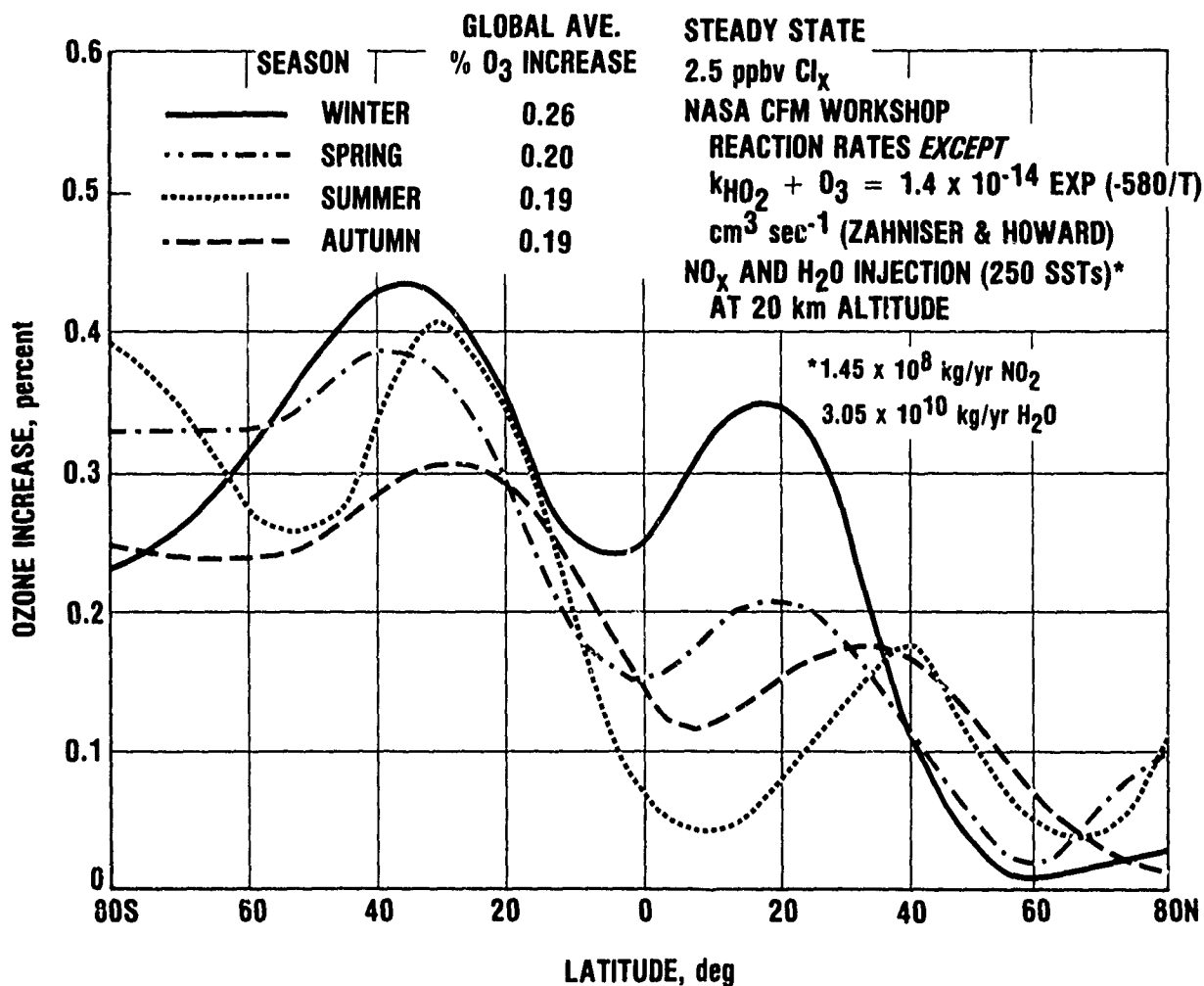
7-23 79 6

Fig. 9. Lawrence Livermore Laboratory modeling results (1978) illustrating water effects on the ozone column with and without consideration of thermal feedback effects. Chang/1976  $K_z$  profile.  $\text{NO}_x$  injection rate  $1000 \text{ mol/cm}^3\text{-sec}$  over 1 km. Critical rates include (in  $\text{cm}^3/\text{molecule-sec}$ )  $8.0 \times 10^{-12}$  for  $\text{H}_2\text{O} + \text{NO}$ ,  $3 \times 10^{-11}$  for  $\text{H}_2\text{O} + \text{OH}$ , and  $7.3 \times 10^{-14} \exp(-1225 \text{ K})$  for  $\text{H}_2\text{O} + \text{O}_3$ . Presumably, the results would change somewhat with use of latest reaction rates, but the effects illustrated should hold.

perturbations, using up-to-date chemistry. The model includes 2.5 ppbv of  $\text{Cl}_x$ . The model treats injected water from aircraft in much the same fashion (in terms of transport and sinks) as it does injected  $\text{NO}_x$ .

The particular calculation presented by Whitten [1979] is for an assumed fleet of 250 SSTs, each cruising 7 hr/day at 20 km and each burning fuel at the rate of 37,800 kg/hr, and emitting  $\text{NO}_x$  (as  $\text{NO}_2$ ) at 6 gm/kg fuel, or 227 kg/hr per aircraft. Water is emitted at the rate of 540 molecules per  $\text{NO}_x$  molecule, or 47,920 kg  $\text{H}_2\text{O}$ /hr/aircraft. The corresponding figures, for 250 aircraft are  $1.45 \times 10^8$  kg  $\text{NO}_x$  (as  $\text{NO}_2$ )/year and  $3.06 \times 10^{10}$  kg  $\text{H}_2\text{O}$ /year. The emission index taken for  $\text{NO}_x$  is for "long term" technology, and, again, is not representative of current engines. Most of the traffic is in the 30 to 60 deg N region.

Whitten's steady state results for this fleet are given in Figures 10 and 11. Note that the model gives greater net effects in the Southern than in the Northern

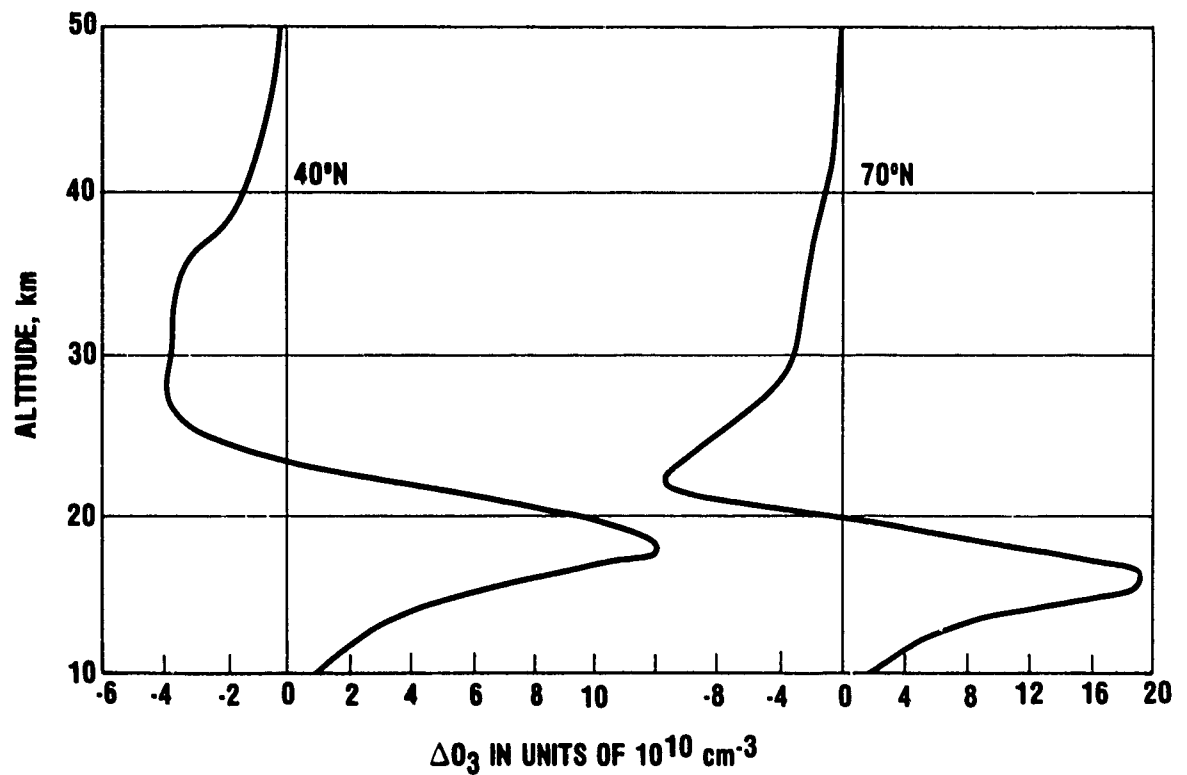
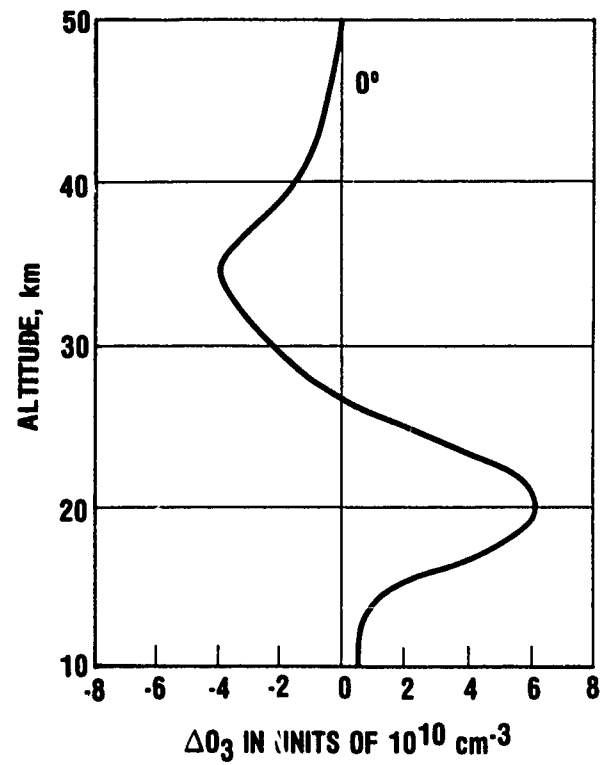


7-23-79-7

Source: Whitten [1979]

Fig. 10. Ozone column changes due to 250 advanced SSTs, including both  $\text{H}_2\text{O}$  and  $\text{NO}_x$  effects

SUMMER 20 km INJECTION  
STEADY-STATE

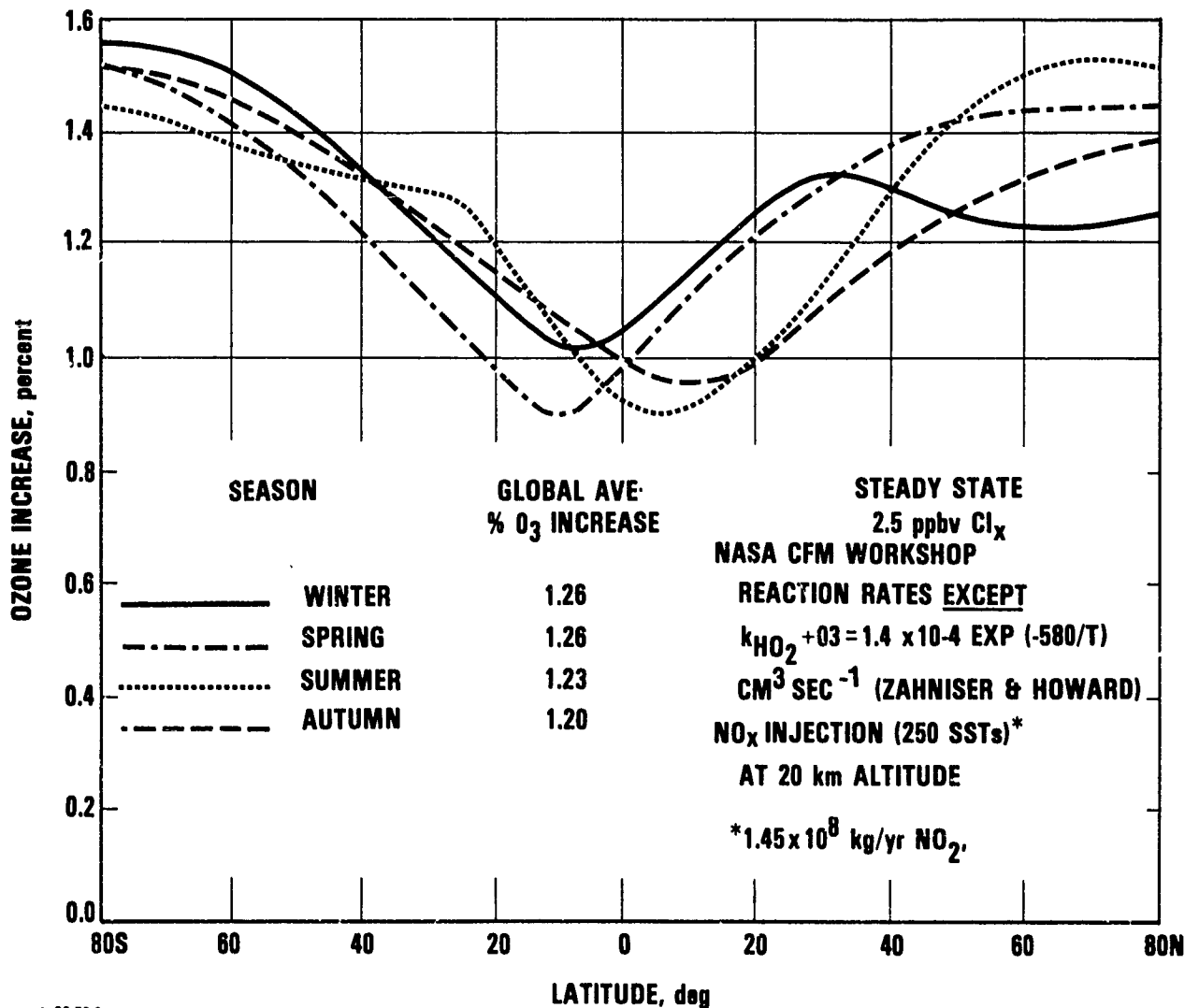


7-23-79-10

Source: Whitten [1979]

Fig. 11. Ozone changes at various latitudes due to 250 advanced SSTs

Hemisphere, a result which is somewhat difficult to accept, but apparently the result of non-linearities in the combined effects of  $H_2O$  and  $NO_x$ . Results in terms of altitude distribution of ozone changes are given in Figure 11. As with 1-D models, note the ozone enhancement at lower altitudes compensated by depletions at higher altitudes. Whitten also gives results for  $NO_x$  injections alone in Figure 12; note the greater enhancement at flight latitudes in the absence of water emissions, and the minimal overall effect of latitude. Water additions are clearly an important aspect of the problem; Whitten [1979] points out, however, that these results do not include thermal feedback effects, and thus overstate the effects of water on ozone.

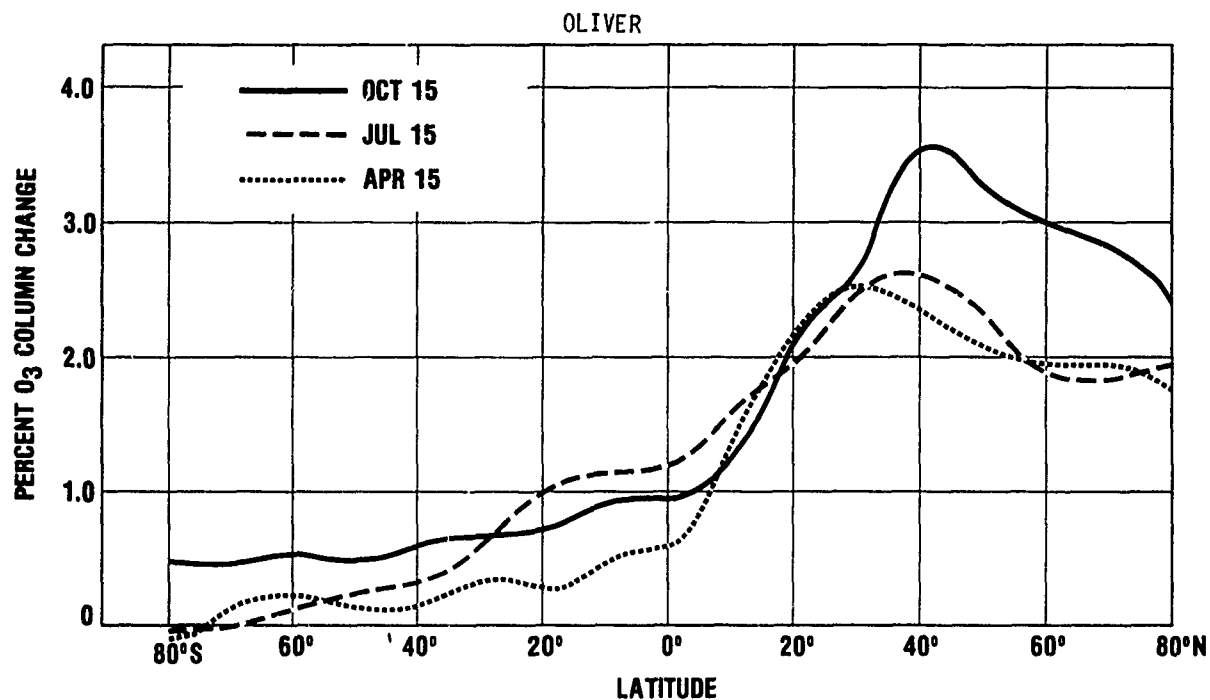


7-23-79-9

Source: Whitten [1979]

Fig. 12. Ozone column changes due to 250 advanced SSTs, including only the  $NO_x$  effects

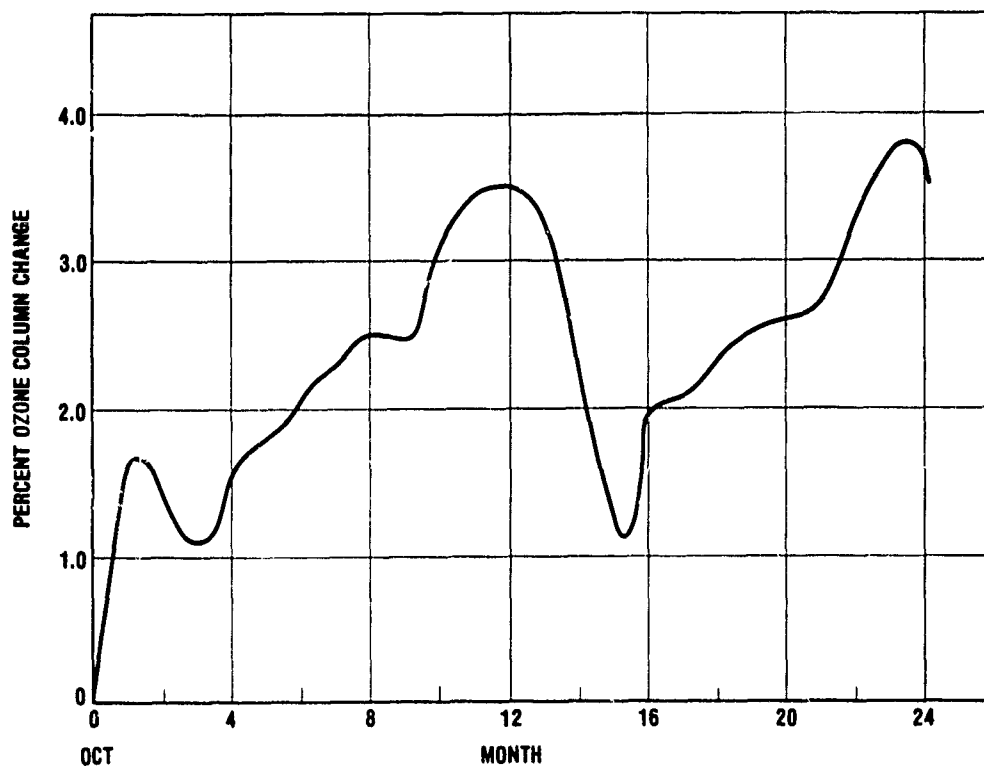
Widhopf and Glatt [1979], describe their model in detail. Results of particular interest here are given in Figures 13, 14, and 15, which are for the "1990-High" fleet, as appended. The atmosphere included 2 ppbv Cl<sub>x</sub> (Cl + ClO + ClONO<sub>2</sub> + HCl). Active water modeling was incorporated, assuming  $H_2O$  to be injected at 73.5 times the  $NO_x$  rates on a mass basis, an average value taken for subsonic and supersonic fleets. Thermal feedback was not included. Results shown in



10-23-79-7

Source: Widhopf and Glatt [1979]

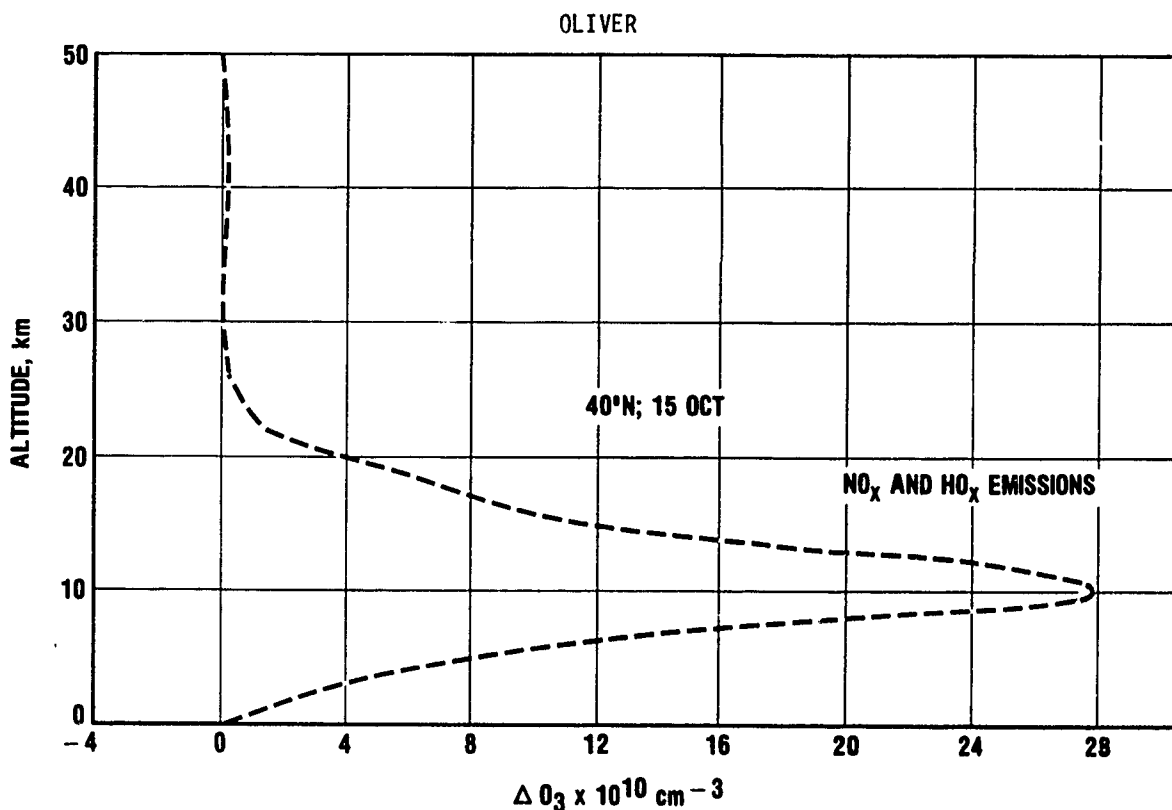
Fig. 13. O<sub>3</sub> column change resulting from NO<sub>x</sub> and HO<sub>x</sub> emissions from a combined fleet of subsonic and supersonic aircraft (NO<sub>x</sub> as appended; H<sub>2</sub>O 73.5 times NO<sub>x</sub> (as NO<sub>2</sub>); 2 ppbv C<sub>2</sub>X.)



10-23-79-8

Source: Widhopf and Glatt [1979]

Fig. 14. O<sub>3</sub> column change as a function of model time. Fleet and C<sub>2</sub>X as in Fig. 13.



10-23 79 8

Source: Widhopf and Glatt [1979]

Fig. 15. Vertical change in ozone concentration at 40° N during October. Fleet and  $ClX$  as in Fig. 13.

Figure 13 are for the second model year, which showed a modestly higher peak ozone enhancement than did the results at the end of the first model year, as shown in Figure 14, and thus may not have reached steady state. (The Hidalgo and Crutzen [1977] results were after 6 model years). However, previous work incorporated in Widhopf and Glatt [1979] had shown negligible changes after 2 model years. Figure 15 gives the change in  $O_3$  as a function of altitude.

The ozone concentration increase at 10 km of  $2.8 \times 10^{11}/\text{cm}^3$  corresponds to a large (142 percentage increase in model ozone at this altitude, partly due to the fact that the model underpredicts ozone in the upper troposphere. The increase ( $2.8 \times 10^{11}/\text{cm}^3$ ) relative to measurements as given by Widhopf (his figure 5a) is 50 to 100 percent, depending on the ozone data used.

The increase in  $O_3$  in terms of mixing ratio, assuming an atmospheric density at 10 km of  $9 \times 10^{18}/\text{cm}^3$ , is 31 ppbv, which is substantial and much larger than implied with older chemistry and a different model by Hidalgo and Crutzen [1977]. Widhopf and Glatt also give results, ignoring the water emissions, which for the altitude and time indicated give only a slightly larger increase in local  $O_3$  (145 percent vs 142 percent). These large increases come about because of a large increase in local  $NO$  and  $NO_2$  (726 percent and 744 percent in the perturbed model atmosphere). The results are troubling in terms of magnitude but are clearly sensitive to model vertical transport. The model representation of water vapor and ozone near the tropopause in the natural atmosphere (see Widhopf and Glatt [1979]) is such that these results (as well as other 2-D and 1-D results in this region) should be viewed with some caution. Additional discussion follows.



Subsonic Effects: Computations for large SST fleet effects are interesting from a historical point of view, and may again be of interest at some undefined future time. Of more practical near-term interest is the effect that subsonic aircraft emissions may have or be having on the upper troposphere and very low stratosphere. This is a particularly difficult region to model, as conventional meteorology has strong effects on the transport processes. Available results [Widhopf and Glatt, 1979; Hidalgo and Crutzen, 1977] just discussed, imply that there may be cause for concern, especially if ozone generated in the upper troposphere affects ground level ozone.

Before discussing subsonic effects further, it may be well to recall the true three-dimensional aspects of this problem. These aircraft typically cruise at altitudes of 6 to 14 km, with most of the fuel consumption being at about 11 km, as shown in Table 5, data for which are prior to advent of the 747SP

TABLE 5. Subsonic Aircraft Flight Altitudes (1972).  
Source: Broderick et al. [1975]

Altitude, ft	Percentage of Total Distance Flown at Specified Altitudes	
	American Airlines	United Airlines
41,000	0.7	2.0
39,000	25.2	20.3
37,000	46.0	30.4
35,000	8.2	36.0
33,000	0.6	6.8
31,000	2.4	3.5
29,000	-	0.2
28,000	4.2	0.4
27,000	-	0.1
26,000	12.7	0.1
Note: The American Airlines' sample consisted of 1,186,000 miles (~1.91 million km) flown during the winter of 1972-1973. The United Airlines' sample consisted of 342,000 miles (~0.55 million km) flown during the winter of 1973-1974.		

but otherwise believed to still be typical [Broderick et al., 1975]. Depending on its flight path, the aircraft may or may not be in the stratosphere, as shown by the tropopause distribution data in Figure 16. Winds, of course, also vary in direction and strength with flight altitude and season; west-to-east travel tends to be in the jet stream, if possible; east-to-west travel tends to avoid these regions for obvious reasons. Traffic is heavily concentrated over the United States, the North Atlantic, and Europe. Wind speeds and residence times (above the clouds) of 10 to 100 days are long enough so that emitted material can be spread around the world [see Oliver et al., 1977];

the purest air would probably be over the Pacific, but depending on atmospheric cleansing rates, the "pure" air at say 12 km altitude *may* (speculating) have as much as 1/3 or 1/2 the contaminant concentration over the heavily trafficked routes; this point clearly needs more investigation in a 3-D model. Emissions put into the stratosphere may, interestingly enough, move at times in quite different directions from those put in at slightly lower altitudes below the tropopause, since wind directions can change rapidly with altitude.

Unless current chemistry is completely erroneous, the  $\text{NO}_x$  emissions from subsonic aircraft should result in some increases in ozone concentration at flight altitudes and in slight increases in the ozone column. In this author's opinion, a slight increase in the ozone column is not of much environmental concern, recognizing that other, now-unavoidable, man-induced effects are tending (by current models) to decrease the ozone column by a larger amount. As indicated earlier, what may be of concern--and here no reliable estimates are available--is whether ozone generated in the lower stratosphere or upper troposphere can, during periods of tropopause folding or at other times, increase the ozone concentration at ground level in populated regions of the globe. Ozone sources and sinks in the troposphere (or into and out of the troposphere) have been much discussed in recent years, but little is unequivocally established.

This issue will require considerably more study before any confident assessment of subsonic aircraft effects can be made. Some indication of the seriousness of the problem may be gained from examination of the Hidalgo-Crutzen [1977] results and the Widhopf-Glatt [1979] results. These showed, respectively, enhancement for a large ( $2.06 \times 10^9$  kg/yr  $\text{NO}_2$ ) fleet at 10.8 km, of about 8 ppbv and about 31 ppbv at 10 km for a distributed fleet (apparently with  $2.8 \times 10^9$  kg/yr  $\text{NO}_x$ ). If such increments in ozone are diluted to the same degree as is the ozone in a typical tropopause folding event, a factor of 3 to 5\* being a minimum



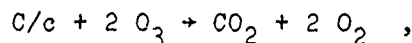
Source: English et al. [1975]

Fig. 16. Frequency distribution of tropopause heights (1 mbar = 100 N/m<sup>2</sup>; 1 ft = 0.3048 m)

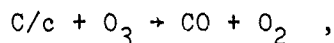
\* Dutkiewicz and Husain [1979] quote an approximate ten-fold dilution (presumably an average) for stratospheric air masses reaching the ground level.

(in the center line of the air mass reaching the ground), [Danielsen, 1977; see also Reiter, 1978], then the maximum incremental ozone at the ground, in these cases, would be 1.6 to 2.7 ppbv for the Hidalgo-Crutzen results and 6 to 10 ppbv for the Widhopf-Glatt results. Both of these can be compared to a Federal standard of 120 ppbv, which could well be violated naturally in such tropopause folding events by stratospheric ozone reaching the ground. Current (late 1979) emissions are probably about 40 percent of those shown in the Appendix. The average effect on ground-level ozone would be smaller than the figures illustrated. Again, the numbers cited are crude and preliminary estimates at best, but do suggest the need for further study. The problem involves transport on a global scale, and the need for better understanding of tropospheric ozone.

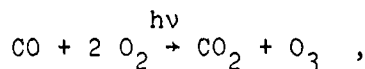
Effects of Other Exhaust Species: Aircraft emit a number of species or materials other than water or  $\text{NO}_x$ . A number of these can reasonably be dismissed. Thus,  $\text{CO}_2$ , because of its very long residence time, its thorough mixing through the atmosphere, and its massive (500 ppm) content, is affected by aircraft only proportionately to all other sources.  $\text{CO}_2$  changes (not due to aircraft alone) do affect (cool) stratospheric temperatures and thereby increase ozone slightly [Haigh and Pyle, 1979] and are increasing with time.  $\text{CH}_4$  and CO emitted by aircraft contribute to the background and, perhaps inefficiently, form small amounts of ozone. Soot may destroy some ozone, perhaps by some series of reactions leading to



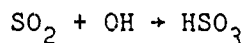
or more likely,



However, by a series of photochemical reactions, CO can react with  $\text{O}_2$ , the outcome being



so that no net effect may result. A number of authors have examined heterogeneous ozone destruction (for example from vanadium present in jet fuel) but reaction rates appear to be too slow to be of significance [Reiter et al., 1975]. This leaves  $\text{SO}_2$ , which is typically emitted at the rate of about 1 gm/kg fuel (unless the fuel is desulfurized).  $\text{SO}_2$  reacts with OH:



and by unidentified continuing reactions, forms  $\text{H}_2\text{SO}_4$ . Any substance reducing OH tends to increase the ozone destruction efficiency of the  $\text{NO}_x$  cycle. The  $\text{SO}_2$  oxidation process is poorly established, but model runs are needed to give some perspective to the potential effects (other than climatic as in CIAP) of this ingredient on ozone. [See Davis et al., 1979.]

#### VALIDITY QUESTIONS

Attempts to Establish Predictive Validity: Previous sections have shown that dramatic changes in computed effects of perturbations to the stratosphere have resulted as new reactions, new rates, and new species have been introduced. Yet, at each stage in this process (with minor exception, when too much ozone was produced by the revised  $\text{HO}_2 + \text{NO}$  rate constant) the models have appeared to duplicate reasonably well the ozone profile and many of the always-scattered measurements of trace species. These observations, coupled together, demonstrate the point made in the introduction that, while a model must duplicate reasonably a natural atmosphere in various particulars, history shows that it may be totally incorrect when used as a predictive tool. For this reason, observations of effects following known perturbations are invaluable and must

always be critically examined; unfortunately, as was the case with the nuclear test injections of  $\text{NO}_x$  [Foley-Ruderman, 1972; National Academy of Sciences, 1975, etc.] such observations tend to involve many ambiguities.

Before proceeding, it should be noted that various categories of validation can be described. Thus, a prediction of a change in the concentration of a trace species with altitude, later supported by measurement, provides an obvious, if partial, form of model validation. Ratios of reactive species in a region of photochemical equilibrium, if enough species can be measured simultaneously, also can provide extremely useful information and, should anomalies appear in concentration ratios, etc., provide even more useful information as the model undergoes critical examination for possible missing reactions, improper treatment of transport processes, etc. (Some examples of these anomalies will be given in the next section.) These partial validation efforts must proceed, but "global" tests of the models, if such can be found, would obviously be of more interest.

Several "global" (or at least quasi global) tests of the models can be noted. These come about from the nuclear weapons tests of the 1958 to 1962 period, the solar proton event of August 1972, solar variability (of ultraviolet output) over the 11-year cycle, and from Umkehr measurements of ozone at altitudes where theory says  $\text{ClX}$  species should be causing a decrease in ozone with time. Each of these is discussed briefly.

The first of these, the nuclear injections of  $\text{NO}_x$ , has been examined in detail by a number of authors [Foley and Ruderman, 1972; Chang, 1972; Johnston et al., 1972; Bauer and Gilmore, 1975; Chang et al., 1979]. Early computations (1973), based on 1-D models, suggested hemispheric ozone depletions of the order of 4 to 8 percent [Chang et al., 1979], which were not observed (nor necessarily observable). Significant uncertainties clearly existed in terms of injection heights,  $\text{NO}$  yield per megaton, etc. The issue was reexamined recently [Chang et al., 1979] using more current (1977) chemistry (in particular, the Howard and Evenson  $\text{HO}_2 + \text{NO}$  rate), again in a 1-D model, incorporating 1.1 to 1.3 ppb of  $\text{ClX}$  in the model atmosphere. Results showed little sensitivity to  $\text{K}_z$  profile, (except for recovery time, as expected), but showed considerable sensitivity to chemistry and injection heights. Details are given in Chang et al. [1979]; peak computed effects on Northern Hemisphere average ozone dropped from about 8 percent to 2 percent. The authors note that the fast rate for the  $\text{HO}_2 + \text{O}_3$  reaction was not included in these calculations, with which small enhancements in ozone might result. Bauer [1978] points out, in addition, that 1-D global average transport for far north winter injection may underestimate removal rates in the first few months, calling for use of 2-D models. In any event, the lack of observed effect of stratospheric ozone now seems far more compatible with model prediction than was the case in 1973 or 1974.

Perhaps the most dramatic model validation "test" was provided by the solar proton event of 4 August 1972. This event, the largest in 25 years, produced large quantities of  $\text{NO}_x$  and  $\text{HO}_x$  above 10 mbar in the polar regions (above about 55 deg latitude). Nimbus 4 provided data showing a sudden drop thereafter in the ozone column above 4 mbar, in which region most of the energy was deposited [Heath et al., 1977]. Crutzen, using a 2-D model and 1974 chemistry, showed that the local peak depletion should have been near 2 mbar and calculated that the local depletion at 2 mbar should have been about 16 percent 28 days after the event; this was smaller than the observed depletion (by about 30 percent, at 19 days); the peak reduction was at the same approximate altitude.  $\text{HO}_x$  effects were not included in the calculations. The calculated effect on the total ozone column was small (1.3 percent of the total) and could not have been detected. The model, however, showed effects at lower latitudes which were not found by the satellite. Boracki et al. [1978] (unpublished) examined the same event, again in a 2-D model, using later chemistry. Their results, while confirming certain aspects of prior modeling at 35 km (the altitude of peak percentage depletion) showed less effect in general and poor reproduction of the observations at lower altitudes. At 25 km, at 75 to 80 deg N, 19 days

after the event their model results showed very slight  $O_3$  enhancement, whereas the Nimbus 4 data showed a maximum absolute (in molecules/cm<sup>3</sup>) decrease at this altitude.

The August 1972 event has also been examined by Fabian et al. [1979], using a 2-D, time-dependent  $O_x - HO_x - NO_x$  model. The  $NO$  production estimate of Crutzen was increased by a factor of 1.7, based on an estimate by Arnold [1978] as quoted by Fabian. Good agreement between the BUV data and model predictions were found (using the 1.7 factor on  $NO$  production), for total ozone above 3 mbar at 70 to 80 deg N for the 30-day period after the event; the model, however overestimated the recovery at 30 days. Recovery was faster than suggested by the model at 55 to 65 deg N. Southern Hemisphere data were confounded by a stratospheric warming. The authors note that lower  $NO$  production rates have been estimated by Porter et al. [1978]. Furthermore, Jackman et al. [1979] in a later communication, argue that the increased  $NO$  production figures used by Fabian [1979] do not apply at altitudes near 4 mbar, although they may apply in the thermosphere.

Results from the SPE observation-modeling comparison thus remain somewhat ambiguous. Note that even perfect confirmation at 35 km would, since different reactions differ in importance with altitudes, again have provided only limited or partial validation of the model if applied to SST injections at 17 to 20 km.

The third solar UV variability effect, which while perhaps the weakest of all in terms of the input perturbation data base, may be of greatest long-term interest. The effects have been computed by Penner and Chang [1978] and by Callis et al. [1979] using the extreme variability estimates of Heath and Thekaekara [1977]. Using this input, variations in ozone of 8 to 10 percent have been computed between solar minimum and solar maximum. The model predictions and the ozone records have been compared by these authors. A number of periods are evident in which predicted effects seem to coincide with the measurements; other portions of the record are less supportive of the models. The great uncertainty here is in actual solar ultraviolet output over the solar cycle. The importance of this variation is shown by these modeling exercises; it is clear that the solar cycle effects *could* mask effects of other perturbations, such as nuclear weapons tests.

Another poorly established model validity question arises from Umkehr observations of ozone. Current halocarbon models indicate that a significant reduction in ozone at 35 to 40 km should have occurred due to halocarbons in the 1970 to 1978 time frame. Umkehr data, admittedly imperfect, showed no evidence of this effect [Angell, 1978], the ozone has instead increased about 8 percent.

It might also be noted that volcanic eruptions provide a potentially pulsed source of pollutants ( $HCl$ ,  $SO_2$ ,  $H_2O$ ) which could affect stratospheric ozone. Past ozone records have been examined, as for example, following Agung in 1963. Source data for most past tests are lacking; some data have been collected on some smaller recent events. A meaningful test in the future would require careful planning and elaborate sampling to determine the input parameters and also careful tracking of the dispersing cloud. In addition, a better understanding of  $SO_2$  chemistry (presently poorly established beyond  $OH + SO_2 \rightarrow HSO_3$ ) would be required.

#### ANOMALIES AND DEBATABLE MODELING QUESTIONS

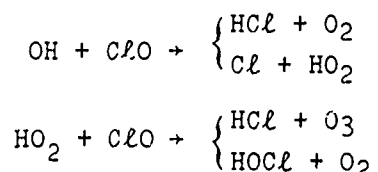
A number of current questions exist, which merit continued investigation:

1. *Stratospheric OH uncertainty, the  $HNO_3/NO_2$  ratio, and the  $NO/NO_2$  ratio.* Turco [1979] cites various measurements on  $OH$  and on the  $HNO_3/NO_2$  ratio; Evans et al. [1978] discusses the  $NO/NO_2$  ratio. The various data imply at least a factor of 2 uncertainty in  $OH$  concentrations and imply there is less  $OH$  in the real stratosphere than is currently computed by the models. The point is important, because reduced  $OH$  would increase ozone destruction by  $NO_x$  (SSTs) and

reduce ozone destruction by halogens. Various questions of the measurements and models are involved, as are possible pressure effects on HO<sub>2</sub> reaction rates.

2. *Stratospheric Cl and ClO* [Anderson et al., 1979]. Measured ClO value in the stratosphere have shown wide variations, which fact alone provides evidence of poor horizontal mixedness of the stratosphere, a fundamental postulate of 1-D models. A more important problem is that measured values have exceeded maximum predicted model values, based on known sources and sinks of chlorine, in one case by a factor of 7 or so [Anderson, 1977]. And finally, where the ClO was measured to be very high, the ozone concentration seemed not abnormal. A number of possible explanations have been offered; one possibility however [Anderson et al., 1979] is that an odd oxygen production mechanism exists which is not presently in the chlorine model chemistry.

3. *Missing Reactions*. Reactions about which nothing is known are necessarily left out of models or used as adjustable parameters to fit a postulate. For example, the HO<sub>2</sub> + NO reaction was noted by Crutzen [1970] but left out because no information on it existed. Similarly, the HO<sub>2</sub> + O<sub>3</sub> rate used in the early (1966 to 1970) water effects work was one found to be necessary to adjust the ozone distribution to observations. These facts were carefully reported, but the caveats tended to be lost when applying model results. Current questions relate to the significance of possible reactions between OH and ClO and HO<sub>2</sub> and ClO which may go according to



or, in both cases, to other products.

These reactions were not included in the original halocarbon modeling. The OH + ClO reaction has recently been shown to be fast, with the majority (> 65 percent) of the reaction going according to the second path [Leu and Lin, 1979]. If 35 percent (a maximum) goes by the first path, in which two reactive radicals are destroyed, a two-fold reduction in halocarbon effect results. The HO<sub>2</sub> + ClO reaction pathway question is at least equally important [see Fox, 1979] the HCl pathway, again, reducing chlorine effects on ozone. Computed aircraft effects would be altered by changes in the modeling of these reactions, but no computations have been reported.

Bromine and, to a much lesser extent, fluorine reactions may also affect the sensitivity of ozone to chlorine and NO<sub>x</sub> species. [See Turco, 1979].

4. *Erroneous Reaction Products*. Reaction rates have often been determined by following the disappearance of a given species, assuming products to be known. The rate so found may be entirely valid, but if the assumed product is wrong, as noted above, obviously the model result will be wrong.

5. *Multiple Solutions: A Modeling Problem*. Prather et al. [1979] have shown that current models may yield more than one set of solutions and suggest that such multiple solutions may have physical validity. Widely varying species

measurements with latitude may be the result of such phenomena. This observation, if confirmed, offers an entirely new class of model validation problem.

6. *Transport Uncertainties.* This paper has emphasized changes in chemistry with time, which have caused the most dramatic changes in results. It must be kept in mind, however, that significant questions (potentially far more important than implied by its treatment here) exist in stratospheric transport of even the "simple" tracer  $H_2O$ , and that corresponding uncertainties exist in the fate of materials injected into the lower stratosphere, as by aircraft in mid-latitudes. Robinson [1979] has explored one interesting possibility which would suggest that aircraft below 100 mbar in mid-latitudes would contaminate the global stratosphere only if the pollutants could survive passage into the troposphere and then upward through the tropical tropopause.

#### CONCLUDING COMMENTS

Predicted effects of  $NO_x$  and  $H_2O$  on stratospheric ozone have gone through wide changes in the last decade as understanding has grown. Currently,  $NO_x$  additions by plausible aircraft fleets at all plausible altitudes tends to increase the ozone column modestly; water, if thermal feedback effects are ignored, tends to decrease ozone. The net effect for realistic  $NO_x$  emission indices is one of small increases in the ozone column. The net combined effects of aircraft with halocarbons and  $CO_2$  changes on a time-dependent basis is not available, but interactions are unavoidable. Halocarbon ozone depletion effects would probably dominate, at least over the near term.

Aircraft effects on the ozone column now would seem to be of relatively little concern. However, questions and uncertainties persist. Effects on the distribution of ozone with height, a much more subtle question, may be of significance; these changes would have climatic consequences and need study in light of other potential aircraft climatic effects related to water vapor and sulfur dioxide emissions. Pressure effects on certain critical reaction rates (particularly  $HO_2 + OH$  and  $HO_2 + NO$ ) would alter, and could conceivably reverse these results, at least at advanced SST (20 km) altitudes. Thermal feedback effects, which reduce ozone distribution by  $H_2O$ , could change as better activation energy data become available.

Ozone generation by subsonic and/or supersonic aircraft needs to be carefully examined in terms of its possible impacts. It is true that such ozone will, at altitude, act to absorb some of the increased UV-B, which by current models will result even from present levels of halocarbons in the atmosphere; it is also true that it may be transported and increase ozone levels at the ground. The transport and fate of such ozone needs to be established clearly, and will require 3-D modeling and improvements in understanding of the dynamic and ozone chemistry of the troposphere.

The *predictive* capability of models of atmospheric ozone, as opposed to their *descriptive* capability, is not yet demonstrated. No alternative yet exists to the use of such models in formulating policy; their development, along with measurements of various kinds which provide the necessary supporting data, must be continued.

#### REFERENCES

- Anderson, J.G., H.J. Grassl, R.E. Shetter, and J.J. Margitan, "Stratospheric Free Chlorine Measured by Balloon-Borne In Situ Resonance Fluorescence," position paper prepared for NASA Stratospheric Workshop, Harpers Ferry, West Virginia, June 4-8, 1979.
- Anderson, J.G., J.J. Margitan, D.H. Stedman, "Atomic Chlorine and the Chlorine Monoxide Radical in the Stratosphere: Three In-Situ Observations," Science, Vol. 198, pp. 501-503, November 4, 1977.

- Angell, J.K. and J. Korshover, "Recent Trends in Total Ozone in the 32-46 km Layer," presented at the World Meteorological Organization Symposium on the Geophysical Aspects and Consequences of Changes in the Composition of the Stratosphere, WMO No. 511, Toronto, Canada, pp. 107-114, June 26-30, 1978.
- Arnold, F., paper presented during AEP Spring Meeting of German Physical Society, Munich, Germany, 1978.
- Athens, P., P. Gott, P. O'Farrell, and B. Huckins, Stratospheric Emissions Due to Current and Projected Aircraft Operations, Arthur D. Little, Inc., Cambridge, Massachusetts, DOT-FA76WAI-603, August 1976.
- Australian Academy of Sciences, Atmospheric Effects of Supersonic Aircraft, Report of the Australian Academy of Science, No. 15, February 1972.
- Bates, D.R. and M. Nicolet, "The Photochemistry of Atmospheric Water Vapour," J. Geophys. Res., Vol 55, p. 301, 1950.
- Bauer, E., A Catalog of Perturbing Influences on Stratospheric Ozone, 1955-1975, IDA Paper P-1340, September 1978.
- Bauer, E. and F.R. Gilmore, "Effect of Atmospheric Nuclear Explosions on Total Ozone," Revs. Geophys. Space Phys., Vol 13, No. 4, pp. 451-458, August 1975.
- Beadle, P.C., Concorde Fuel Usage and Emissions, Latitudinal and Seasonal Variation for Atmospheric Modelling, An Analysis of Current and Probable British Airways and Air France Route Networks, Environmental Sciences Group, Commercial Aircraft Division, British Aircraft Corp. Ltd., B30/PCB/479, July 1977.
- Bertin, M., R. Borghi, G. Brasseur, R. Joatton, and M. Maignan, Modeles Mathematiques de la Stratosphere, COVOS Report No. 6A, Paris, France, October 14, 1976.
- Borucki, W.J., D.S. Colburn, R.C. Whitten, L.A. Capone, and M. Covert, Model Analysis of the Ozone Depletion Due to the August 1972 Solar Proton Event, paper presented at AGU Meeting, Miami Beach, Florida, April 1978.
- Broderick, A.J., "Stratospheric Effects from Aviation," J. Aircraft, Vol. 15, No. 10, pp. 643-653, October 1978.
- Broderick, A.J., C.S. Downie, and R.C. Oliver, "Aircraft Engine Emissions at Altitude," in Propulsion Effluents in the Stratosphere, CIAP Monograph 2, Chapter 7, Department of Transportation, Washington, D.C., 1975.
- Budkyo, M.I., "On Present-Day Climatic Changes," Tellus, Vol. 29, pp. 193-204, 1977.
- Budkyo, M.I. and I.L. Karol, "Review of the Climatic Impact Assessment Program's Research," (Translated for HAPP, Department of Transportation-FAA), Moscow Meteorologiya i Gidrologiya in Russian No. 9, pp. 103-111, September 1976.
- Callis, L.B., M. Natarajan, and J.E. Nealy, "Ozone and Temperature Trends Associated with the 11-Year Solar Cycle," Science, Vol 204, No. 4399, pp. 1303-1306, 22 June 1979.
- Callis, L.B. and J.E. Nealy, Geophys. Res. Lett., 5, p. 249, paper presented at the 18th Meeting of the Committee on Space Research, Tel Aviv, June 1977, published 1978.
- Canadian Meteorological Society, "Stratospheric Pollution Issue," Atmosphere, Vol. 14, No. 3, 1976.
- Chang, J.S., "Uncertainties in the Validation of Parameterized Transport in 1-D Models of the Stratosphere," Proceedings, Fourth Conference on CIAP, pp. 175-182, February 1975.
- Chang, J.S., "Comments on the Possible Effect of NO<sub>x</sub> Injection Into the Stratosphere by Atmospheric Nuclear Weapons Tests," Proceedings of the Second Conference on the Climatic Impact Assessment Program, November 14-17, 1972, A.J. Broderick ed., held at Cambridge, Massachusetts, April 1973.
- Chang, J.S., W.H. Dwyer, and D.J. Wuebbles, "The Atmospheric Nuclear Tests of the 50's and 60's: A Possible Test of Ozone Depletion Theories," J. Geophys. Res., No. C4, pp. 1755-1765, April 20, 1979.
- Chapman, S., "A Theory of Upper Atmospheric Ozone," R. Meteorol. Soc. Quart. J., Vol. 3, pp. 103-125, 1930.
- COMESA, The Report of the Committee on Meteorological Effects of Stratospheric Aircraft 1972-1975, U.K. Meteorological Office, 1975.
- Crutzen, P.J., "A Discussion of the Chemistry of Some Minor Constituents in the Stratosphere and Troposphere," Pure and Appl. Geophys., Vol. 106-108, 1973.



- Crutzen, P., "A Review of Upper Atmospheric Photochemistry," International Association of Geomagnetism and Aeronomy Symposium, Kyoto, Japan, September 10-12, 1973a.
- Crutzen, P.J., "SSTs--A Threat to the Earth's Ozone Shield," Ambio, 1, pp. 41-51, 1972.
- Crutzen, P.J., "Ozone Production Rates in an Oxygen-Hydrogen-Nitrogen Oxide Atmosphere," J. Geophys. Res., Vol. 76, No. 30, pp. 7311-7327, October 20, 1971.
- Crutzen, P.J. and C.J. Howard, "The Effects of the  $\text{HO}_2 + \text{NO}$  Reaction Rate Constant on One-Dimensional Model Calculations of Stratospheric Ozone Perturbations," PAGEOPH, Vol. 116, Birkhauser Verlag, Basel, pp. 497-510, 1978.
- Crutzen, P.J., I.S.A. Isaksen, G.C. Field, "Solar Proton Events: Stratospheric Sources of Nitric Oxide," Science, Vol. 189, pp. 457-459, August 8, 1975.
- Cunnold, D.M., F. Alyea, and R. Prinn, "Relative Effects on Atmospheric Ozone of Latitude and Altitude of Supersonic Aircraft," AIAA Journal, Vol. 15, No. 3, pp. 337-345, March 1977.
- Cunnold, D., F. Alyea, N. Phillips, and R. Prinn, "A Three-Dimensional Dynamical-Chemical Model of Atmospheric Ozone," J. Atmos. Sci., Vol. 32, No. 1, pp. 170-194, 1975.
- Cutcher, P., "Stratospheric Ozone Depletion and Solar Ultraviolet Radiation on Earth," Science, Vol. 184, April 5, 1974.
- Danielsen, E.F. and V.A. Mohnen, "Project Dustorm Report: Ozone Measurements and Meteorological Analyses of Tropopause Folding," Symposium of the American Geophysical Union and the American Meteorological Society, Hollywood, Florida, November 10-12, 1976.
- Danielsen, E.G. and V.A. Mohnen, "Project Dustorm Report: Ozone Transport, in Situ Measurements, and Meteorological Analyses of Tropopause Folding," J. Geophys. Res., Vol. 82, No. 37, pp. 5867-5877, December 20, 1977.
- Davis, D.D., A.R. Ravishankara, and S. Fischer, " $\text{SO}_2$  Oxidation via the Hydroxyl Radical: Atmospheric Fate of  $\text{HSO}_x$  Radicals," Geophys. Res. Lett., Vol. 6, No. 2, pp. 113-116, February 1979.
- Dodge, L.G., M.B. Colket, III, M.F. Zabielski, J. Dusek, and D.J. Seery, Nitric Oxide Measurement Study: Optical Calibration, Task I Report, United Technologies Research Centre, East Hartford, Connecticut, DOT-FAA77WA-4081, June 1979.
- Duewer, W.H., D.J. Wuebbles, H.W. Ellsaesser, and J.S. Chang, " $\text{NO}_x$  Catalytic Ozone Destruction: Sensitivity to Rate Coefficients," J. Geophys. Res., Vol. 82, No. 6, pp. 935-942, February 20, 1977.
- Duewer, W.H., D.J. Wuebbles, H.W. Ellsaesser, and J.S. Chang, "Reply," J. Geophys. Res., Vol. 82, No. 18, pp. 2599-2605, June 20, 1977a.
- Dutkiewicz, V.A. and L. Husain, "Determination of Stratospheric Ozone at Ground Level Using  $^{70}\text{Be}$ /Ozone Ratios," Geophys. Res. Lett., Vol. 6, No. 3, pp. 171-174, March 1979.
- Eggleston, A., R.A. Cox, and R.G. Derwent, "Will Chlorofluorocarbons Really Affect the Ozone Shield?," New Scientist, pp. 402-403, May 20, 1976.
- English, J.M., R.C. Oliver, and A.K. Forney; CIAP Monograph 2, Propulsion Effluents in the Stratosphere, U.S. Department of Transportation Climatic Impact Assessment Program, DOT-TST-75-52, September 1975.
- Environmental Aspects of the Supersonic Transport, Report of the Panel on Supersonic Transport Environmental Research, U.S. Department of Commerce, May 1972.
- Evans, W.F.J., H. Fast, J.B. Kerr, C.T. McElroy, R.S. O'Brien, and D.I. Wardle, "Stratospheric Constituent Measurements from Project Stratoprobe," presented at the World Meteorological Organization Symposium on the Geophysical Aspects and Consequences of Changes in the Composition of the Stratosphere, Toronto, Canada, p. 55, June 26-30, 1978.
- Fabian, P. J.A. Pyle, and R.J. Wells, "The August 1972 Solar Proton Event and the Atmospheric Ozone Layer," Nature, Vol. 277, pp. 458-460, February 8, 1979.
- Farmer, C.B., "Infrared Measurements of Stratospheric Composition," paper presented at the International Association of Geomagnetism and Aeronomy Symposium, September 10-12, 1973, Kyoto, Japan, Can. J. Chem., Vol. 52, No. 8, 1974.

- Few, J.D., R.J. Bryson, and H.S. Lowry, III, Optical In Situ Versus Probe Measurements of Nitric Oxide Concentration as a Function of Axial Position in a Combustor Exhaust, Arnold Engineering Development Center, Tennessee, AEDC-TR-78-32, 21 July-27 August 1979.
- Foley, H.M. and M.S. Ruderman, "Stratospheric NO Production from Past Nuclear Explosions," J. Geophys. Res., Vol. 78, pp. 4441-4450, 1973.
- Foley, H.M. and M.A. Ruderman, Stratospheric Nitric Oxide Production from Past Nuclear Explosions and its Relevance to Projected SST Pollution, IDA Paper P-894, August 1972.
- Fox, L., "Atmospheric Ozone Issue Looms Again," Chemical & Engineering News, pp. 25-35, October 15, 1979.
- Grobecker, A.J., S.C. Coroniti, and R.H. Cannon, Jr., Report of Findings - The Effects of Stratospheric Pollution by Aircraft, DOT-TST-75-50, prepared by Department of Transportation, CIAP, December 1974.
- Groves, K.S. and A.F. Tuck, "Simultaneous Effects of CO<sub>2</sub> and Chlorofluoromethanes on Stratospheric Ozone," Nature, Vol. 280, pp. 127-129, July 12, 1979.
- Haigh, J.D. and J.A. Pyle, "A Two-Dimensional Calculation Including Atmospheric Carbon Dioxide and Stratospheric Ozone," Nature, Vol. 279, pp. 222-224, May 1979.
- Hampson, J., "Chemiluminescent Emissions Observed in the Stratosphere and Mesosphere," Les Problemes Meteorologiques de la Stratosphere et de la Mesosphere, edited by Centre National d'Etudes Spatiales, Presses Universitaires de France, Paris, 1966. (Cited in SCEP, 1970.) See also C.A.R.D.E. Technical Note 1738, 1966 and Science, Vol. 120, November 13, 1970.
- Hampson, J., "Photochemical Behaviour of the Ozone Layer," Canadian Armament Research Division Establishment Technical Note #1627, Val Cartier, Quebec: C.A.R.D.E., 1964. (Cited in SCEP, 1970, q.v.)
- Harrison, H., "Stratospheric Ozone with Added Water Vapor: Influence of High-Altitude Aircraft," Science, Vol. 170, pp. 734-736, August 17, 1970.
- Hearings Before the Subcommittee on Public Health and Environment of the Committee on Interstate and Foreign Commerce, Fluorocarbons-Impact on Health and Environment, House of Representatives, 93rd Congress, Second Session on H.R. 17577 and H.R. 17545, Serial No. 93-110, December 11-12, 1974.
- Heath, D.F., A.J. Krueger, and P.J. Crutzen, "Solar Proton Event: Influence on Stratospheric Ozone," Science, Vol. 197, No. 4306, pp. 886-888, August 26, 1977.
- Heath, D. and M. Thekaekara, NASA Tech. Mem. X-71172, 1976.
- Hidalgo, H., Status of Representative Two-Dimensional Models of the Stratosphere and Troposphere as of Mid-1978, IDA Paper P-1341, October 1978.
- Hidalgo, H. and P.J. Crutzen, "The Tropospheric and Stratospheric Composition Perturbed by NO<sub>x</sub> Emission of High Altitude Aircraft," J. Geophys. Res., Vol. 82, No. 37, pp. 5833-5866, December 20, 1977.
- Howard, C.J., "Kinetics of the Reaction of HO<sub>2</sub> with NO," Geophys. Res. Lett., Vol. 4, No. 10, pp. 437-440, October 1977.
- Howard, C.J. and K.M. Evenson, "Kinetics of the Reaction of HO<sub>2</sub> with NO," Geophys. Res. Lett., Vol. 4, No. 10, pp. 437-440, October 1977.
- Howard, C.J. and K.M. Evenson, "Laser Magnetic Resonance Study of the Gas Phase Reactions of OH with CO, NO, and NO<sub>2</sub>," J. Chem. Phys., 61, pp. 1943-1952, 1974.
- Hudson, R.D., "Minor Constituents in the Stratosphere and Mesosphere," Rev. of Geophys. and Space Physics, Vol. 17, No. 4, pp. 467-477, June 1979.
- Hudson, R.D., "Chlorofluoromethanes and the Stratosphere," NASA Reference Publication 1010, 1977.
- Hunt, B.G., "The Need for a Modified Photochemical Theory of the Ozonosphere," J. Atmos. Sci., Vol. 23, pp. 88-95, 1966a.
- Hunt, B.G., "Photochemistry of Ozone in a Moist Atmosphere," J. Geophys. Res., Vol. 71, pp. 1385-1398, 1966b.
- Jackman, C.H., H.S. Porter, and J.E. Frederick, "Upper Limits on Production Rate of NO per Ion Pair," Nature, Vol. 280, p. 170, 12 July 1979.
- Jet Propulsion Laboratory, "Chemical Kinetic and Photochemical Data for Use in Stratospheric Modelling: Evaluation Number 2," NASA Panel for Data Evaluation, JPL Publication 79-27, prepared for National Aeronautics and Space Administration, April 15, 1979.

- Johnston, H.S., "Reduction of Stratospheric Ozone by Nitrogen Oxide Catalysts from Supersonic Transport Exhaust," Science, Vol. 173, pp. 517-522, August 6, 1971.
- Johnston, H.S., D. Kattenhorn, and G. Whitten, "Use of Excess Carbon-14 Data to Calibrate Models of Stratospheric Ozone Depletion by Supersonic Transports," J. Geophys. Res., Vol. 81, No. 3, pp. 368-380, 1976.
- Johnston, H.S. and E. Quitevis, "The Oxides of Nitrogen with Respect to Urban Smog, Supersonic Transports, and Global Methane," paper presented to the International Congress of Radiation Research, Seattle, Washington, July 14-20, 1974.
- Johnston, et al., "The Effect of Nuclear Explosions on Stratospheric Nitric Oxide and Ozone," Proceedings of the Second Conference on the Climatic Impact Assessment Program, November 14-17, 1972, A.J. Broderick, ed., held at Cambridge, Massachusetts, April 1973.
- Kaufman, Frederick, "Halocarbons: Effects on Stratospheric Ozone," Summary of Findings presented to the Panel of the National Research Council at the International Conference on Problems Related to the Stratosphere, held at Utah State University, September 15-17, 1976, National Academy of Sciences, Washington, D.C.
- Krueger, A.J. and R.A. Minzner, "A Mid-Latitude Ozone Model for the 1976 U.S. Standard Atmosphere," J. Geophys. Res., Vol. 81, No. 24, August 20, 1976.
- Latham, P., "The Blindness," Astounding Science Fiction, p. 84, Street & Smith, July 1946.
- Leovy, C.B., "Atmospheric Ozone: An Analytic Model for Photochemistry in the Presence of Water Vapor," J. Geophys. Res., Vol. 74, No. 2, pp. 417-426, January 15, 1969.
- Leu, M.T. and C.L. Lin, "Rate Constants for the Reactions of OH with  $\text{ClO}$ ,  $\text{Cl}_2$ , and  $\text{Cl}_2\text{O}$  at 298K," Geophys. Res. Lett., Vol. 6, No. 6, pp. 425-428, June 1979.
- Lovelock, J.E., R.J. Maggs, and R.J. Wade, "Halogenated Hydrocarbons In and Over the Atlantic," Nature, Vol. 241, pp. 194-196, 1973.
- McDonald, J.E., Hearings before a Subcommittee of the Committee on Appropriations, House of Representatives, Civil Supersonic Aircraft Development. (SST), 1971.
- Molina, M.J. and F.S. Rowland, "Stratospheric Sink for Chlorofluoromethanes: Chlorine Atom Catalyzed Destruction of Ozone," Nature, Vol. 249, pp. 810-812, 1974.
- Mormino, J., D. Sola, and C. Patten, Climatic Impact Assessment Program: Development and Accomplishments 1971-1975, final report, prepared for the Department of Transportation, Contract No. DOT-TST-76-41, Washington, D.C., December 1975.
- National Academy of Sciences, Halocarbons: Effects on Stratospheric Ozone, Panel on Atmospheric Chemistry, National Research Council, 1976.
- National Academy of Sciences, Halocarbons Environmental Effects of Chlorofluoromethane Release, Committee on Impacts of Stratospheric Change, National Research Council, 1976a.
- National Academy of Sciences, Halocarbons: Effects on Stratospheric Flight: Biological and Climatic Effects of Aircraft Emissions in the Stratosphere, 1975.
- Newell, R.E., "One-Dimensional Models: A Critical Comment, and Their Application to Carbon Monoxide," J. Geophys. Res., Vol. 82, No. 9, pp. 1449-1450, March 20, 1977.
- Nicolet, M., "Stratospheric Ozone: An Introduction to Its Study," Rev. Geophys. and Space Phys., Vol. 13, No. 5, pp. 593-636, November 1975.
- Nicolet, M., "Ozone and Hydrogen Reactions," Ann. Geophys., Vol. 26, p. 531, 1970.
- Oliver, R.C., E. Bauer, and W. Wasylkiwskyj, Recent Developments in the Estimation of Potential Effects of High Altitude Aircraft Emissions on Ozone and Climate, IDA Paper P-1343, October 1978.
- Oliver, R.C., E. Bauer, H. Hidalgo, K.A. Gardner, W. Wasylkiwskyj, Aircraft Emissions: Potential Effects on Ozone and Climate, prepared for High Altitude Pollution Program, FAA-EQ-77-3, U.S. Department of Transportation, Federal Aviation Administration, Washington, D.C., March 1977.

- Penner, J.E. and J.S. Chang, "Possible Variations in Atmospheric Ozone Related to the Eleven-Year Solar Cycle," Geophys. Res. Lett., Vol. 5, No. 10, pp. 817-820, October 1978.
- Poppoff, I.G., R.C. Whitten, R.P. Turco, and L.A. Capone, An Assessment of the Effect of Supersonic Aircraft Operations on the Stratospheric Ozone Content, NASA Reference Publication 1026, August 1978.
- Porter, H.S., C.H. Jackman, and A.E.S. Green, "Efficiencies for Production of Atomic Nitrogen and Oxygen by Relativistic Proton Impact in Air," J. Chem. Phys., Vol. 65, pp. 154-167, 1976.
- Pozdena, R. Forecasts of Aircraft Activity by Altitude, World Region and Aircraft Type, Stanford Research Institute, FAA-AVP-76-18, November 1976.
- Prather, M.J., M.B. McElroy, S.C. Wofsy, and J.A. Logan, "Stratospheric Chemistry: Multiple Solutions," Geophys. Res. Lett., Vol. 6, No. 3, pp. 163-164, March 1979.
- Reiter, E.R., "Impact of Stratospheric Ozone on Tropospheric Concentrations," in Air Quality Meteorology and Atmospheric Ozone, A.L. Morris and R.C. Barras, eds., American Society for Testing and Materials, Philadelphia, Pennsylvania, October 1978.
- Reiter, E.R., E. Bauer, S.C. Coroniti, CIAP Monograph 1, The Natural Stratosphere of 1974, U.S. Department of Transportation, Climatic Impact Assessment Program, DOT-TST-75-51, September 1975.
- Robinson, G.D., "The Transport of Minor Atmospheric Constituents Between Troposphere and Stratosphere," (unpublished), 1979.
- Robinson, G.D., H. Hidalgo, and R. Greenstone, CIAP Monograph 3, The Stratosphere Perturbed by Propulsion Effluents, U.S. Department of Transportation, Climatic Impact Assessment Program, DOT-TST-75-53, September 1975.
- SCEP, Man's Impact on the Global Environment, Report of the Study of Critical Environmental Problems, MIT Press, Cambridge, Massachusetts, 1970.
- Schiff, H.I., "Aeronomy of the Stratosphere and Mesosphere," International Association of Geomagnetism and Aeronomy Symposium held in Kyoto, Japan, September 10-12, 1973, Vol. 52, pp. 1381-1634, April 15, 1974.
- Schmeltekopf, A.L., D.L. Albritton, P.J. Crutzen, P.D. Goldan, W.J. Harrop, W.R. Henderson, J.R. McAfee, M. McFarland, H.I. Schiff, T.L. Thompson, (NOAA), D.J. Hoffman, and N.T. Kjome (Univ. of Wyoming), "Stratospheric Nitrous Oxide Altitude Profiles at Various Altitudes," J. Atmos. Sci., Vol. 34, pp. 729-736, 1977.
- Smith, W.S., Jr., "Uncertainties in Evaluated Atmospheric Rate Constants," presented at World Meteorological Organization Symposium on the Geophysical Aspects and Consequences of Changes in the Composition of the Stratosphere, Toronto, Canada, pp. 36-45, 26-30 June 1978.
- Stolarski, R.S. and D.M. Butler, "Model Predictions," (draft) intended for presentation at NASA Stratospheric Workshop, Harpers Ferry, West Virginia, June 4-8, 1979.
- Stolarski, R.S. and R.J. Cicerone, "Stratospheric Chlorine: a Possible Sink for Ozone," International Association of Geomagnetism and Aeronomy Symposium, Kyoto, Japan, September 10-12, 1973.
- Turco, R.P., "Atmospheric Halogens: The Status of Current Model Predictions," position paper prepared for the NASA Stratospheric Workshop, Harpers Ferry, West Virginia, June 4-8, 1979.
- Turco, R.P., R.C. Whitten, I.G. Poppoff, and L.A. Capone, "SSTs, Nitrogen Fertilizer and Stratospheric Ozone," Nature, Vol. 276, pp. 805-807, December 1978.
- U.S. Department of Commerce, Environmental Aspects of the Supersonic Transport, a Recommended Program for Research and Measurement, May 1972.
- Whitten, R.C., "Latitudinal Effects," position paper prepared for the NASA Stratospheric Workshop, Harpers Ferry, West Virginia, June 4-8, 1979.
- Widhopf, G.F., L. Glatt, and R.F. Kramer, "Potential Ozone Column Increase Resulting from Subsonic and Supersonic Aircraft NO<sub>x</sub> Emissions," AIAAJ., Vol. 15, No. 9, pp. 1322-1330, September 1977.
- Widhopf, G.F. and L. Glatt, "Numerical Modeling of Atmospheric Pollution," presented at the Sixth International Conference on Numerical Methods in Fluid Dynamics, Tbilisi, USSR, June 20-25, 1978.

OLIVER

- Widhopf, G.F. and L. Glatt, "Two-Dimensional Description of the Natural Atmosphere Including Active Water Vapor Modeling and Potential Perturbations Due to  $\text{NO}_x$  and  $\text{HO}_x$  Aircraft Emissions," prepared for the High Altitude Pollution Program, FAA-EE-79-07, U.S. Department of Transportation, Federal Aviation Administration, Washington, D.C., April 15, 1979.
- Wofsy, S.C. and M.B. McElroy, " $\text{HO}_x$ ,  $\text{NO}_x$ , and  $\text{ClO}_x$ : Their Role in Atmospheric Photochemistry," International Association of Geomagnetism and Aeronomy Symposium, Kyoto, Japan, September 10-12, 1973.
- Zahniser, M.S. and C.J. Howard, "A Direct Measurement of the Temperature Dependence of the Rate Constant for the Reaction  $\text{HO}_2 + \text{O}_3 \rightarrow \text{OH} + 2 \text{O}_2$ ," presented at the World Meteorological Organization Symposium on the Geophysical Aspects and Consequences of Changes in the Composition of the Stratosphere, Toronto, Canada, June 26-30, 1978.

## APPENDIX

1990 WORLDWIDE AIRCRAFT NO<sub>x</sub> EMISSIONS, HIGH ESTIMATE, ADJUSTED<sup>1,2</sup>; kg/yr

Altitude	6-8	8-2	2-10	10-11	11-12	12-13	13-14	14-15	15-16	16-17	17-18	18-19	Total
N 60+	3.35E6	3.03E6	1.47E7	1.31E7	1.46E7	1.31E6	9.99E5	4.06E5	1.72E6	2.59E6	2.10E6	1.43E6	5.89E7
50-	2.15E7	2.59E7	9.44E7	1.06E8	9.09E7	8.26E6	3.72E6	2.12E6	6.57E6	1.03E7	8.06E6	3.71E6	3.81E8
40-	7.60E7	8.70E7	1.79E8	2.79E8	1.62E8	2.48E7	4.59E6	2.09E6	4.17E6	6.96E6	5.46E6	2.36E6	8.33E8
30-	7.74E7	9.20E7	1.67E8	3.09E8	1.72E8	2.97E7	3.11E6	1.74E6	1.30E6	2.73E6	2.07E6	8.63E5	8.58E8
20-	2.61E7	2.83E7	6.74E7	1.02E8	6.92E7	8.73E6	1.55E6	1.20E6	8.06E5	1.90E6	1.71E6	4.67E5	3.09E8
10-	1.11E7	1.18E7	2.65E7	4.20E7	3.99E7	3.67E6	4.74E5	1.54E5	3.24E5	5.38E5	4.22E5	1.71E5	1.37E8
0-	4.80E6	5.14E6	1.50E7	1.82E7	1.36E7	1.26E6	1.73E5	0	2.91E5	4.08E5	3.44E5	1.63E5	5.93E7
0-	3.31E6	3.77E6	1.22E7	1.38E7	1.09E7	8.65E5	1.38E5	0	3.01E5	4.22E5	3.56E5	1.65E5	4.62E7
10-	2.74E6	3.21E6	1.14E7	1.52E7	1.15E7	1.11E6	3.15E5	1.32E5	1.10E5	2.19E5	1.58E5	7.52E4	4.61E7
20-	3.67E6	4.01E6	9.47E6	1.37E7	8.66E6	9.31E5	5.10E4	0	9.85E4	1.38E5	1.16E5	6.63E4	4.09E7
30-	4.01E6	4.63E6	6.62E6	1.10E7	6.14E6	1.21E6	8.64E4	5.16E4	1.56E4	4.47E4	2.84E4	6.22E3	3.46E7
40-	2.36E5	3.05E5	3.19E5	8.28E5	4.46E5	9.29E4	1.5E4	0	0	0	0	0	2.22E6
50-	4.77E4	3.79E4	2.99E4	2.52E4	1.04E4	1.45E3	0.97	0	0	0	0	0	1.52E5
S 60+	0	0	0	0	0	0	0	0	0	0	0	0	0
Total	2.34E8	2.69E8	6.03E8	9.25E8	5.99E8	8.19E7	1.52E7	7.89E6	1.77E7	2.62E7	2.08E7	9.47E6	2.81E9

Reference: Athens et al [1976]. (A.D. Little)

<sup>1</sup>To make all "CP-6" aircraft have same emission indices as "JT-9D" aircraft. Current technology assumed throughout.<sup>2</sup>To distribute SST emissions in the 15-18 km band more closely to prior estimates. The A.D. Little estimates for 17-18 km were shifted to 15-16 km, and 15-16 and 16-17 estimates each moved up one km. [See Oliver et al., 1977]

1990 WORLDWIDE AIRCRAFT WATER EMISSIONS, HIGH ESTIMATE, ADJUSTED;<sup>1</sup> kg/yr

ALT (KM)	6-8	8-9	9-10	10-11	11-12	12-13	13-14	14-15	15-16	16-17	17-18	18-19
N POLE	2.46E	0.8	1.05E	0.9	1.25E	0.9	1.31E	0.7	1.20E	0.8	1.46E	0.8
50 TO 60	1.65E	0.9	1.32E	0.9	1.32E	0.9	1.32E	0.8	1.32E	0.8	1.46E	0.8
40 TO 50	4.49E	0.9	1.32E	0.9	1.32E	0.9	1.32E	0.8	1.32E	0.8	1.46E	0.8
30 TO 40	1.52E	0.9	1.32E	0.9	1.32E	0.9	1.32E	0.8	1.32E	0.8	1.46E	0.8
20 TO 30	6.46E	0.8	1.32E	0.9	1.32E	0.9	1.32E	0.8	1.32E	0.8	1.46E	0.8
10 TO 20	2.87E	0.8	1.32E	0.9	1.32E	0.9	1.32E	0.8	1.32E	0.8	1.46E	0.8
0 TO 10	2.21E	0.8	1.32E	0.9	1.32E	0.9	1.32E	0.8	1.32E	0.8	1.46E	0.8
-10 TO 0	1.76E	0.8	1.32E	0.9	1.32E	0.9	1.32E	0.8	1.32E	0.8	1.46E	0.8
-20 TO -10	2.28E	0.8	1.32E	0.9	1.32E	0.9	1.32E	0.8	1.32E	0.8	1.46E	0.8
-30 TO -20	2.35E	0.8	1.32E	0.9	1.32E	0.9	1.32E	0.8	1.32E	0.8	1.46E	0.8
-40 TO -30	1.59E	0.7	1.32E	0.9	1.32E	0.9	1.32E	0.8	1.32E	0.8	1.46E	0.8
-50 TO -40	2.61E	0.6	1.32E	0.9	1.32E	0.9	1.32E	0.8	1.32E	0.8	1.46E	0.8
-60 TO -50	0.0	0.0	0.0	0.0	0.0	0.0	0.0	0.0	0.0	0.0	0.0	0.0
S POLE	0.0	0.0	0.0	0.0	0.0	0.0	0.0	0.0	0.0	0.0	0.0	0.0

TOTAL CF ALL H2O = 2.37572E 11 (KILOGRAMS/YEAR)

1990 WORLDWIDE AIRCRAFT FUEL CONSUMPTION, HIGH ESTIMATE, ADJUSTED;<sup>1</sup> kg/yr

## 1990 WORLDWIDE AIRCRAFT EMISSIONS-HIGH ESTIMATE

## TOTAL EMISSIONS FOR ALL AIRCRAFT BY POLLUTANT (KILOGRAMS/YEAR)

ALT (KM)	6-8	8-9	9-10	10-11	11-12	12-13	13-14	14-15	15-16	16-17	17-18	18-19
N POLE	1.97E	0.8	1.94E	0.8	1.94E	0.8	1.94E	0.7	1.94E	0.7	1.94E	0.7
50 TO 60	1.32E	0.9	1.32E	0.9	1.32E	0.9	1.32E	0.8	1.32E	0.8	1.32E	0.8
40 TO 50	3.59E	0.9	1.32E	0.9	1.32E	0.9	1.32E	0.8	1.32E	0.8	1.32E	0.8
30 TO 40	1.22E	0.9	1.32E	0.9	1.32E	0.9	1.32E	0.8	1.32E	0.8	1.32E	0.8
20 TO 30	5.16E	0.8	1.32E	0.9	1.32E	0.9	1.32E	0.8	1.32E	0.8	1.32E	0.8
10 TO 20	2.29E	0.8	1.32E	0.9	1.32E	0.9	1.32E	0.8	1.32E	0.8	1.32E	0.8
0 TO 10	1.77E	0.8	1.32E	0.9	1.32E	0.9	1.32E	0.8	1.32E	0.8	1.32E	0.8
-10 TO 0	1.41E	0.8	1.32E	0.9	1.32E	0.9	1.32E	0.8	1.32E	0.8	1.32E	0.8
-20 TO -10	1.82E	0.8	1.32E	0.9	1.32E	0.9	1.32E	0.8	1.32E	0.8	1.32E	0.8
-30 TO -20	1.89E	0.8	1.32E	0.9	1.32E	0.9	1.32E	0.8	1.32E	0.8	1.32E	0.8
-40 TO -30	1.27E	0.7	1.32E	0.9	1.32E	0.9	1.32E	0.8	1.32E	0.8	1.32E	0.8
-50 TO -40	2.09E	0.6	1.32E	0.9	1.32E	0.9	1.32E	0.8	1.32E	0.8	1.32E	0.8
-60 TO -50	0.0	0.0	0.0	0.0	0.0	0.0	0.0	0.0	0.0	0.0	0.0	0.0
S POLE	0.0	0.0	0.0	0.0	0.0	0.0	0.0	0.0	0.0	0.0	0.0	0.0

TOTAL OF ALL FUEL = 1.75666E 11 (KILOGRAMS/YEAR)

Reference: Athens et al. [1976]

<sup>1</sup>See footnote 2, previous page.

SUMMARY OF THE U.S. NATIONAL ACADEMY OF SCIENCES

REPORT: STRATOSPHERIC OZONE DEPLETION BY HALOCARBONS: CHEMISTRY AND TRANSPORT

H.I. SCHIFF

CHEMISTRY DEPARTMENT, YORK UNIVERSITY, DOWNSVIEW, ONTARIO, CANADA, M3J 1P3

The 1979 report of the U.S. National Academy of Sciences agreed with previous reports that continued release of halocarbons into the atmosphere will result in a decrease in stratospheric ozone. The most probable value calculated for the eventual ozone depletion due to continued release of F-11 and F-12 at the 19.79 level is 16.5%. This value is obtained from the value of 18.6% calculated from the computer model by allowing for possible tropospheric sinks and for the effects of the halocarbon greenhouse effect on stratospheric chemistry. Although there are a few exceptions, the comparison between models and measurements is considered to be satisfactory. The uncertainties in the chemical rate coefficients, in atmospheric transport and in the use of 1-D models have been combined to give an overall uncertainty range of a factor of 6 within the 95% confidence limit. It is unlikely that direct measurements of the average global ozone amount would permit detection of a decrease of less than 5% attributable to human activity. If the rapidly increasing use of F-22 and  $\text{CH}_3\text{CCl}_3$  continues unabated, the release rates and atmospheric behavior of these compounds will require careful attention.

REITERATION OF THE PROBLEM: The importance of the relatively small amount of ozone in the earth's atmosphere lies mainly in its ability to absorb the biologically harmful ultraviolet radiation from the sun and to prevent most of it from reaching the surface. In addition, ozone plays an important role in determining the climate of this planet.

Most of the ozone is located in the stratosphere, a region of the atmosphere located between 10 and 50 km above the surface. Its concentration is determined by a balance between photochemical processes that produce it and others that destroy it and never reaches more than a few ten-thousandths of a percent. The natural processes that destroy ozone are believed to involve substances that are normally present in trace amounts, thousands of times less than that of ozone itself. These include chemical compounds that contain hydrogen ( $\text{HO}_x$ ), nitrogen ( $\text{NO}_x$ ), and chlorine ( $\text{ClO}_x$ ). These compounds enter into catalytic chain reactions in which one molecule can destroy many ozone molecules before being removed by some competing process. The concern is that human activities can appreciably alter the amounts of these catalytic substances in the stratosphere.



## SCHIFF

A number of such activities have been identified, including the use of high-flying aircraft, halocarbons, nuclear weapons, and nitrogen fertilizers. There may be others not yet identified. The "Clean Air Amendment of 1977" requires that all possibilities be evaluated. However, since the release of halocarbons appears to be the greatest and most immediate threat, the present report confines itself to evaluating the possible effects on stratospheric ozone of continued release of halocarbons.

**PREVIOUS EVALUATIONS:** The National Academy of Sciences (NAS) released a report in September 1976 entitled *Halocarbons: Effects on Stratospheric Ozone*.<sup>\*</sup> The study focused attention on chlorofluoromethanes (CFMs). Two of these,  $\text{CFC}_{13}$  (F-11) and  $\text{CF}_2\text{Cl}_2$  (F-12), were of greatest concern. They were being produced and released in large and increasing quantities. They were not removed, to our knowledge, in the troposphere (the region between the surface and the stratosphere), and so the same large quantities could enter the stratosphere. Here they could be dissociated by ultraviolet radiation into  $\text{ClO}_x$  fragments capable of destroying ozone. The main conclusion of that report was that "their continued release at the 1973 production rates would cause the ozone to decrease steadily until a probable reduction of about 6 to 7.5 percent is reached, with an uncertainty range of at least 2 to 20 percent using what are believed to be roughly 95 percent confidence limits. The time required for the reduction to attain half of this steady-state value (3 to 3.75 percent) would be 40 to 50 years."

The uncertainty range is determined by uncertainties in the rates at which these substances are released into the atmosphere, by uncertainties in the rate constants that determine the speeds of seven of the most important chemical reactions, and by the use of one-dimensional computer models to represent the distribution and transport of chemical species. Uncertainties in the rate constants made the largest contributions to the overall uncertainty. The 6 to 7.5 percent range for the most probable reduction allowed for the possibility of some CFM removal in the troposphere.

In August 1977, the National Aeronautics and Space Administration (NASA) released a report entitled *Chlorofluoromethanes and the Stratosphere*.<sup>†</sup> Eight modeling groups evaluated the ultimate ozone reduction resulting from continued release of these two substances at the 1975 rates. Their predictions of the most likely value ranged from 10.8 to 16.5 percent. This spread in most likely values is due to differences between the eight models and should not be confused with the uncertainty range given above for the NAS report. It will be noted that the most probable values predicted for ozone reduction in the NASA, 1977 report are close to a factor of 2 larger than, although still within the uncertainty range of, that of the NAS, 1976 report. The reason is that, in the period between these two reports, the rate constant for an important chemical reaction ( $\text{NO} + \text{HO}_2$ ) had been remeasured, using improved techniques, and found to be substantially different from the value used in the earlier report.

### PRESENT FINDINGS

*Chlorofluoromethanes:* Since the release of these two reports, there have been continuing improvements in the computer models and in the measurements used as inputs to these models. There has also been a considerable increase in the number and the quality of atmospheric measurements that can be used to check the validity of the models. These activities have not altered the principal conclusion reached in the previous reports that continued release of halocarbons into the atmosphere will result in a significant decrease in the amount of stratospheric ozone. For comparison purposes with the previous reports, the present study estimates an eventual decrease of 18.6 percent in the total amount of ozone for continued release of F-11 and F-12 at the 1977\*\* rates, which we call Case A.

Other considerations, to be discussed below, but not included in the previous reports, have led us to reduce the "best estimate" for the eventual ozone decrease to a value of 16.5 percent. Our estimate of uncertainty is such that there is a 95 percent probability that the true value of the ozone reduction lies between 5 percent and 28 percent, i.e., a range of a factor of 6. Ozone reduction to half the eventual value, to about 8 percent if the eventual value were 16.5 percent, would occur in about 30 years.

---

\*Subsequently referred to as the NAS, 1976 report.

†Subsequently referred to as the NASA, 1977 report.

\*\*The NAS, 1976 report used 1973 release rates; the NASA, 1977 report used 1975 release rates. These, and the 1977 release rates, are all within 5 percent of each other.

Although several countries have taken action to reduce the amount of CFMs that they are releasing into the atmosphere, release rates in other countries are increasing. It is therefore not possible to anticipate future, global release rates with any high degree of confidence. We have therefore chosen three additional scenarios to span the likely range. In Case B we assume the 1977 release rate until 1983, followed by a 25 percent reduction at that time, and then continuation at that reduced level. Case C is similar to Case B, except that an additional reduction of 25 percent is assumed to occur in 1988 with constant release thereafter at half the 1977 level. Cases B and C both tacitly presume further regulation to limit release. Case D has been suggested to us by the National Research Council Committee on Alternatives for the Reduction of CFC Emissions to reflect the increasing release rate in other industrial countries. It assumes a constant release rate at the 1977 level until 1980, a 7 percent per annum growth rate until 2000, and a constant release rate at the year 2000 level beyond that date.

The projected steady-state values for Cases B and C are 13.2 percent and 9.4 percent, respectively, with the same sixfold uncertainty range at the 95 percent confidence level. Case D leads to an ozone reduction of 25 percent in the year 2025 and an eventual steady-state reduction of 56.7 percent. High reliance cannot be placed on the steady-state value since, at large levels of ozone reduction, changes in the dynamics and temperature structure of the stratosphere are expected that would invalidate the model's treatment of transport. It is highly probable that the steady-state reduction for Case D would be at least 30 percent.

It is interesting to note that the model and error analysis also shows that a  $(2.1 \pm 1.5)$  percent reduction in  $O_3$  should have occurred and that by the year 2000 the reduction will be  $(5 \pm 3.5)$  percent, almost independent of which of the four cases is considered. Although there is no likelihood of it happening, immediately stopping all release worldwide would still produce roughly one and a half times the present reduction in about 15 years, after which the ozone level could gradually recover.

*Other Halocarbons:* Although the production of F-11 and F-12 has not been increasing significantly during the past four years, there has been a dramatic increase in the production of two other halocarbons capable of affecting stratospheric ozone. The use of F-22 ( $CHClF_2$ ), largely in refrigeration, has increased 25 percent in the past two years, and the production of methyl chloroform ( $CH_3CCl_3$ ) is now doubling every five years. Atmospheric measurements indicate that methyl chloroform is now contributing between a quarter to half as many chlorine atoms to the stratosphere as either F-11 or F-12. If it gains increased usage, as a substitute for other solvents in degreasing and coating operations, it may well become the largest source of stratospheric chlorine.\*

#### ESTIMATES OF UNCERTAINTIES

*Uncertainties Due to Chemistry:* To estimate the effect on stratospheric ozone of any scenario of halocarbon release rate, it is necessary to know the detailed chemistry of all substances that may be involved and the rates at which chemical species are transported into and out of the stratosphere.

In the model calculations, it is assumed that there are no processes that remove F-11 and F-12 in the troposphere and thereby prevent them from affecting stratospheric ozone. In our previous report we considered all such "inactive" removal processes that had been suggested and put upper limits on the degree to which each of them might reduce the predicted ozone depletion. Only three of these had upper limits that could have reduced the predictions by as much as 10 percent of the most probable value. The limits of two of these, removal by chemical reaction by gaseous ions and photodecomposition in the troposphere by sunlight, were based on the failure to observe these processes in laboratory experiments and an estimate of the detection limits in these experiments. Subsequent consideration has indicated that these processes are unlikely to be of any significance. The limit of the third process, removal by oceans, was based on very sparse measurements of the concentrations of F-11 in surface waters. Subsequent measurements have suggested that this process is also unimportant. One new removal process has been suggested, photodecomposition of the halocarbons when in contact with desert sand. This suggestion is based on laboratory studies that reveal that halocarbons, when in contact with sandlike materials, can be

\*Once methyl chloroform reaches the stratosphere, its effectiveness in destroying ozone is not identical to that of CFMs because of differences in the chemistry of these compounds. But, to a first approximation, these differences may be ignored.

decomposed by light of wavelengths that do not otherwise decompose them. These studies are at present not definitive enough to permit a reliable estimate of how much change, if any, is likely to result from this process. Nevertheless we have reduced our estimate from 18.6 percent to 17.4 percent for the most likely ozone reduction for Case A to take into account this and other possible "inactive" removal processes.

A more direct way to determine whether such processes do, in fact, exist would be to compare the amount of fluorocarbons released into the atmosphere minus the amount that has been calculated to have been dissociated in the stratosphere, with the amount still remaining in the entire atmosphere. Any difference between these two quantities could then be ascribed to inactive removal in the troposphere. Our previous study indicated that the uncertainties in the calculations based on the total amount now present in the atmosphere were too large to reach meaningful conclusions. Despite considerable improvement in the number and quality of the measurements that situation still obtains. It has been suggested that a more definitive answer to the problem may be achieved by measuring the rate at which the amount of fluorocarbons in the atmosphere increases with time. An experiment to make such measurements has been initiated.

All other halocarbons that are being released into the atmosphere in appreciable quantities contain either hydrogen atoms or double bonds and therefore are removed, to some extent, in the troposphere by reaction with HO radicals. This removal is virtually complete for most of these substances, so that they do not pose a threat to stratospheric ozone. Tropospheric removal by reaction with HO is, however, not complete for three of these halocarbons, methyl chloride, methyl chloroform, and F-22, so that appreciable fractions of these substances do reach the stratosphere and contribute to ozone destruction. Methyl chloride is mainly produced by natural processes and is therefore present in the natural atmosphere in essentially unchanging amounts. By contrast, F-22, and, to a large extent, methyl chloroform, are man-made chemicals that are being produced in rapidly accelerating amounts. The fraction of these chemicals that reaches the stratosphere depends on the HO concentrations in the troposphere, which are only poorly known.

For these reasons we have not undertaken an estimate of the magnitude of the threat to stratospheric ozone posed by increasing use of these chemicals, although there are sufficient grounds for concern. There is a need for increased measurements, in the troposphere, particularly of HO concentration. There is also a need for increased research efforts to improve our understanding of tropospheric chemistry.

Our understanding of stratospheric chemistry has improved considerably since our last report. Stratospheric measurements have supported the basic chemical postulates. Halocarbons do reach the stratosphere; they do photodissociate into fragments that can catalyze the destruction of ozone, and these fragments do, in fact, react with ozone. But there are still limitations to our knowledge of stratospheric chemistry that introduce uncertainties in our estimate of the magnitude of the expected ozone reduction. There has been considerable improvement in the accuracy with which the rate constants are known for the chemical reactions that are believed to occur in the stratosphere. But since the number of these reactions is large, at least 125, the cumulative uncertainty is also large and is unlikely to show rapid improvement in the near future. Measurements of several reactions have been made by more reliable, direct methods and have led to large changes in their rate constants compared with the values (deduced by indirect methods) that were used in our earlier report. These new values, particularly that for the reaction of  $\text{HO}_2$  with NO, have resulted in an increase in the predicted impact by halocarbons on ozone. In addition, they have forced us to recognize a much greater interaction among the various chemical families that affect stratospheric ozone; e.g., a change in the amount of  $\text{NO}_x$  or  $\text{HO}_x$  in the stratosphere has a marked effect on the ozone reduction caused by halocarbons. It is felt that large changes in the adopted values of rate constants are unlikely to occur in the future because direct methods are now generally used to measure these quantities. There is, however, a need to measure rate constants over the range of pressures that exist in the stratosphere, since there is reason to believe that some of them may be pressure-dependent. Moreover, many of the measurements have been made without confirming that the products of the reactions are the ones assumed. Efforts should be made to define all the products of each chemical reaction.

SECRET

In any description of a chemical system there is always the possibility that an important process has been overlooked or dismissed as being unimportant. This happened just before the completion of the NAS, 1976 report when it was learned that chlorine nitrate ( $\text{ClONO}_2$ ) was more stable than previously believed. The inclusion of the new information caused a reduction of the predicted ozone depletion by a factor of about 1.85. More recently, it has been suggested that hypochlorous acid,  $\text{HOCl}$ , might play a similar role. However, most of the laboratory studies on this compound indicate that it will be broken up relatively rapidly by sunlight and therefore will not provide a significant holding tank for stratospheric chlorine.

Two additional reactions that may affect the impact of halocarbons on stratospheric ozone have come to our attention too late to be incorporated into our model calculations. One of these, the reaction of  $\text{Cl}$  atoms with formaldehyde ( $\text{CH}_2\text{O}$ ), has the effect of decreasing the ozone depletion by roughly 7 percent of the calculated value. The other reaction, between  $\text{ClO}$  and  $\text{BrO}$ , increases the impact of halocarbons on stratospheric ozone by approximately the same factor. Since the effects of these two reactions operate in opposite directions, are somewhat speculative, and are not large, we do not believe their omission in our model produces significant errors in our projections.

In assessing the uncertainty in our prediction caused by the uncertainties in rate constants we have used an error analysis similar to that used in the NASA, 1977 report, which we consider to be an improvement over the method used in our 1976 report. This analysis gives a cumulative uncertainty for the predicted ozone change of a range of a factor of 4 at the 95 percent confidence limit.\* This can be compared with the fivefold range of uncertainty in our 1976 report in which only seven key reactions were considered. The lower range we obtain using all (~125) reactions in the analysis is a measure of the improvement that has been achieved in the laboratory measurements.

*Uncertainty Due to Transport:* The predictions of this and previous reports have been made using the so-called one-dimensional (1-D) model. This type of model considers only vertical motions of chemical substances. But air, of course, moves in three dimensions. The justification for this approximation is that, when all the motions are summed over all latitudes and longitudes, the effects of horizontal motions of substances largely cancel and the vertical movements dominate. These models therefore represent some form of global average over both distance and time. The speed with which these substances enter or leave the stratosphere as a result of these vertical movements is characterized by an "eddy-diffusion" coefficient  $K(z)$ , the value of which depends on altitude. The values of  $K(z)$  are usually determined by measuring the change with height of the concentration of some trace substances whose chemistry is believed to be well understood. Methane ( $\text{CH}_4$ ) and nitrous oxide ( $\text{N}_2\text{O}$ ) have often been used for this purpose.

The analysis of these data by the method used in the NAS, 1976 report indicates a somewhat wider possible variability than that given in our earlier report.

However, a second approach (described in Chapter 4), has, in fact, resulted in a decrease in our uncertainty estimate. This approach involves fitting simple analytic expressions to the vertical distributions of the concentrations of trace species. Data on three species were used, the measured  $\text{N}_2\text{O}$  data, global ozone data, and the distribution of an inert tracer generated by a three-dimensional model. This method showed remarkable self-consistency among the three tracers used and agreed with the results for  $\text{N}_2\text{O}$  in the first method. It is felt that the uncertainty in the eddy-diffusion coefficient at a given altitude is about a factor of 2, although it is admitted that this uncertainty estimate is somewhat subjective. Fortunately, the prediction of ozone depletion from halocarbon injection is not too sensitive to the choice of eddy-diffusion coefficient. Slower transport would permit a greater buildup of the chlorine compounds ( $\text{ClO}_x$ ) that destroy ozone but would also increase the concentration of nitrogen compounds ( $\text{NO}_x$ ). Because of chemical coupling processes, the increased  $\text{NO}_x$  would, in turn, decrease the effect of the chlorine compounds.

---

\*More specifically, for the most probable value of 16.5 percent for steady-state ozone reduction in Case A, there is 1 chance in 40 that, because of this particular error, it could be lower than 6.3 percent and 1 chance in 40 that it could be higher than 26 percent. The uncertainty range of a factor of 4 is equivalent to a  $\pm 60$  percent uncertainty in the predicted value, i.e.,  $(1 + 0.6)/(1 - 0.6) = 4$ .

*We estimate an uncertainty in the projections due to the use of the 1-D method of characterising transport to be a range of a factor of 2 within the 95 percent confidence level. This can be compared with the threefold range of our earlier report.*

*Other uncertainties Inherent in the 1-D Model:* We have seen that the 1-D model represents the vertical distribution of different chemicals averaged over the entire globe and over all seasons. Thus chemical reactions are represented as occurring between the average concentrations of each chemical species at a given altitude. In the real world, the reactions occur between chemicals having their instantaneous, local concentration. The global average of the products of these concentrations, which determine the chemical rates, is not necessarily the same as the product of their averages, which is used in 1-D models.

Moreover, there are feedback effects involving temperature changes resulting from ozone changes. A decrease in ozone due to halocarbons would result in a decrease in the stratospheric temperature that affects the rates of many of the chemical reactions. This temperature feedback is calculated to lower the predicted ozone reduction by 1.8 percent, for Case A at steady state.

The amount of water vapor in the stratosphere is believed to be governed mainly by the temperature of the tropical tropopause, by the boundary between the tropical troposphere and the tropical stratosphere, and by stratospheric methane. Stratospheric temperature will probably decrease as a result of halocarbon injection. Tropospheric temperature, in contrast, will increase because of the enhanced greenhouse effect caused by the halocarbons. The net effect is believed to be an increase in tropopause temperature, which would permit more water to enter the stratosphere. Increased water content results in ozone decrease. This feedback effect is estimated to increase ozone depletion for Case A at steady state by 0.9 percent. Temperature changes will also affect the transport to some extent.

*All these effects, the use of the 1-D approximation in treating the chemistry, and the temperature feedback effects just mentioned have their own uncertainties. We estimate that together they introduce an uncertainty in our projections of a range of a factor of 2.3 at the 95 percent confidence level.*

**VALIDATION OF THE 1-D MODELS:** There has been considerable refinement in the 1-D models. All models include methods for treating the diurnal (day and night) changes in solar intensity. Some are also capable of calculating the temperature changes that occur if the composition of the atmosphere changes. The quality of the data used as inputs to the models has also improved as a result of more and better atmospheric measurements.

The validity of the models can be checked by comparing calculated concentrations of minor constituents against measurements, particularly the way these concentrations change with height. There are, however, severe limitations to these comparisons. The 1-D models can, of course, only provide globally averaged values of these height profiles for long-lived trace species. Although the number of measurements and their geographic coverage have both increased considerably, they are still far from providing true global averages. However, the comparison can be considered satisfactory for most substances within these limitations and the uncertainties of the measurements. There are, however, some notable exceptions. One of the ClO measurement experiments has given high values for the concentrations, which are totally inconsistent with the models and our understanding of the chlorine budget. There are also some other disturbing inconsistencies between models and measurements, such as the shapes of the vertical profiles of ClO, HCl, and HF. Some of these may be the result of horizontal transport, which is excluded in the concept of 1-D models. Some early calculations made with two-dimensional (2-D) models do appear to account for some of the discrepancies. Two-dimensional models are under active development by several groups and may well provide us with improved projections in the near future. One of the interesting results already achieved with these models is an indication that the ozone changes resulting from halocarbon releases will be greater at mid and high latitudes than in the tropics and that, at these higher latitudes, the changes are largest in late winter and smallest in late summer. Three-dimensional (3-D) models would, in principle, be the most realistic for making predictions, and attempts are being made to incorporate chemistry in existing 3-D, general circulation models. But the cost and complexity make it unlikely that 3-D models will provide useful projections of ozone depletion in the near future. They are, however, making useful contributions in examining some of the feedback processes, and

their continued development should be encouraged.

In summary, 1-D models have probably reached their maximum potential. Despite their limitations, we believe that they provide projections for ozone depletion that have validity within the stated uncertainty ranges.

**OTHER EFFECTS:** We have become increasingly aware of the fact that the atmosphere is a closely coupled system. Changes in the tropospheric chemistry cause changes in the stratospheric chemistry. Changes in the amounts of  $\text{HO}_x$  and  $\text{NO}_x$  in the stratosphere will affect the impact of changing the amount of  $\text{ClO}_x$ . It is therefore difficult to project accurately the effect of increased halocarbon release when the release of other man-made pollutants may also be increasing in an undetermined way.

A moderate increase in stratospheric  $\text{NO}_x$  resulting, for example, from increased use of nitrogen fertilizers, would reduce the effect of halocarbons on ozone because of the coupling between  $\text{ClO}_x$  and  $\text{NO}_x$  chemistry and would increase the ozone amount at lower altitudes.

The amount of carbon dioxide ( $\text{CO}_2$ ) in our atmosphere is increasing rapidly as a result of the increased use of fossil fuels. It is probably also increasing because of the continuing removal of tropical rain forests, which are believed to play an important role in determining the  $\text{CO}_2$  balance. An increase in  $\text{CO}_2$  would warm the troposphere but cool the stratosphere. A decrease in stratospheric temperature would result in an increase in stratospheric ozone, thus offsetting to a small degree the decrease caused by halocarbon release.

An even more complex set of reactions can occur as a result of increased anthropogenic release of carbon monoxide (CO). Increased CO decreases the amount of HO in the troposphere. A decrease in HO concentration would permit a larger fraction of certain halocarbons such as methyl chloride (from natural sources) and methyl chloroform and F-22 (from human sources) to reach the stratosphere and thereby decrease stratospheric ozone. At the same time, through a set of complex reactions, involving  $\text{HO}_x$  and  $\text{NO}_x$ , there is likely to be an increase in the amount of ozone in the troposphere so that the net change in total ozone due to changes in CO is uncertain.

Even if we had reasonable scenarios for the increase in these other pollutants, our knowledge of tropospheric chemistry is still too incomplete to allow meaningful predictions to be made on the net ozone change that they would produce. This is an additional reason for increased research efforts in tropospheric chemistry.

**OZONE MONITORING AS AN EARLY WARNING SYSTEM:** The uncertainties inherent in the use of atmospheric models have prompted the suggestion that monitoring the total amount of global ozone might provide a direct way of detecting whether ozone depletion due to human activity is indeed occurring and, if such changes were detected could provide the basis for implementing regulation against that activity.

We have seen that stopping halocarbon releases will not immediately result in ozone returning to its former level. There is a time delay between halocarbon release and ozone destruction; the maximum ozone decrease actually occurs some 15 years after all release has stopped. Therefore, to be effective, an *early warning system* must be capable of detecting changes due to human activity in time to prevent the eventual maximum ozone decrease being greater than acceptable levels.

Most of the ozone measurements are now made with Dobson instruments located at a number of ground-based stations. There are a number of problems involved in using the data from this Dobson network to provide total global ozone amounts and trends. There are short- and long-term natural variations in the amount of ozone above any given station due to seasonal and other factors, many of which are unknown. Our study shows that there is an inherent statistical error due to these variations, which would limit the detection of a trend caused by human activity to at least 1.5 percent almost independent of the number of stations used for the analysis. In addition to these statistical errors, other long-term (5- to 100-year) changes may occur, which could lead to misinterpretation. The Dobson instruments may have long-term calibration and drift errors. Most of the Dobson stations are located on land; changes in meteorological patterns could move relatively high ozone amounts from sea to land or vice versa. Long-term changes in atmospheric aerosols, clouds,

and temperature could also lead to incorrect interpretation as ozone trends. Finally, there could be long-term changes in ozone due, for example, to changes in solar flux and changes in atmospheric substances resulting from natural or human causes not directly related to CFM releases. We therefore conclude that it is unlikely that a Dobson network would, within the next decade, be able to identify a reduction in global ozone attributable to CFM releases of less than 4 to 5 percent. The model predicts that such an ozone change will occur by about 1995. Total cessation of CFM release at that point would result in a decrease in ozone of about 7 percent some 15 years later.

Model calculations have shown that the decrease in ozone concentration due to CFM release is twice as great at 40 km as is the decrease in total ozone. There are also reasons for believing that natural variability is smaller at that altitude. Monitoring ozone concentrations at this altitude should therefore provide a more sensitive early warning system. This region of the stratosphere is best monitored by satellite. A number of satellites are currently measuring ozone by several techniques. The time period for which data are available is short, and some of the data still require verification. At the time of writing, the satellites do not provide a superior system for trend analysis to the Dobson network but should be able to do so in the near future.

#### CONCLUSIONS

*Effects of CFM Releases:* We find ourselves in agreement with the principal conclusion reached in our earlier report, viz.: that it is inevitable that CFMs released into the atmosphere do destroy ozone. In fact, the laboratory and atmospheric measurements, made in the interim between these two reports, have tended to strengthen this conclusion.

*The value of the ozone depletion caused by continuing release of F-11 and F-12 at the 1977 (similar to 1973) rates obtained by our 1-D model calculations is 18.6 percent. This can be compared with the most probable value of 7.5 percent of our previous report. The difference between these values is mainly the result of new, more reliable, measurements of the rate constants of several key chemical reactions.*

Destruction of ozone by halocarbons also changes the temperature profile in the stratosphere, which, in turn, changes the rates at which a number of chemical reactions occur. The temperature change in the stratosphere and the temperature change in the troposphere resulting from the increased greenhouse effect due to the halocarbons also alter the amount of water vapor that reaches the stratosphere. This, in turn, changes the amount of ozone destruction. *These feedbacks were not considered quantitatively in our previous report but are evaluated in the present report. They result in a reduction of the most probable value of ozone reduction to 17.7 percent.*

Although there is no compelling reason to believe that a "sink" exists that removes a significant portion of CFMs in the troposphere, we recognize that such a possibility exists. Removal by photodestruction in the presence of desert sand is one such possibility. *To make provision for possible tropospheric sinks we have, somewhat arbitrarily, reduced the most probable value to 16.5 percent.*

An improved error analysis has been used to estimate the uncertainty range due to uncertainties in all the rate constants. At the 95 percent confidence level, this source of uncertainty amounts to a range of a factor of 4, and remains the largest source of uncertainty.

Somewhat more subjectively, we estimate the uncertainty due to the approximation used to represent transport to be a range of a factor of 1.9.

The combination of these two sources of error gives a total uncertainty of a range of a factor of 5, which can be compared with the range of a factor of 10 estimated for these two sources of errors in the previous report. This improvement of the uncertainty range reflects the improvements in both laboratory and atmospheric measurements.

We have also estimated the error due to the feedback effects mentioned above and made an even more subjective estimate of the uncertainty resulting from the approximation inherent in treating rates of chemical reactions by the average concentrations of the 1-D models. These sources of uncertainties are estimated to amount to a range of a factor of 2.3.

*Combination of all these sources of error amounts to a range of a factor of 6. Thus our best estimate is that for continued CFM values at 1977 level, there is 1 chance in 40 that ozone depletion will be less than 5 percent and 1 chance in 40 that it will be greater than 28 percent.*

There are two possible sources of errors that, inherently, cannot be quantified. One is that some important chemical reaction has been overlooked. The other is that some systematic error exists in the chemistry, such as the existence of pressure dependence on the reaction rates, or that other product channels exist for some of the reactions. It is obviously impossible to estimate the unknown with any precision. Nevertheless, our experience of the past has prompted us to hazard a rough estimate of the probability. Inclusion of this subjective estimate obviously broadens the uncertainty limits. For example, with steady CFM release at the 1977 level, there is a 3 out of 4 chance that the ozone depletion will reach a steady-state value between 10 to 23 percent without including the uncertainty estimate due to these unknown effects; inclusion of this estimate extends the range to 9 to 24 percent.

*Release of Other Halocarbons:* We have not attempted to evaluate the ozone depletion due to halocarbons that contain hydrogen largely because our lack of knowledge of tropospheric chemistry introduces a large uncertainty in the fraction of these compounds that reach the stratosphere. However, if current trends in the rapidly increasing use of F-22 and methyl chloroform continue unabated, the release rates and atmospheric behavior of these compounds will require careful attention.



HIGH ALTITUDE POLLUTION PROGRAM  
OF THE  
U.S. FEDERAL AVIATION ADMINISTRATION

N. SUNDARARAMAN  
Manager, High Altitude Pollution Program

Federal Aviation Administration  
Washington, D.C. 20591

Abstract

The objective, program elements and the current status of the findings of the High Altitude Pollution Program of the U. S. Federal Aviation Administration are reviewed.

The Federal Aviation Administration (FAA) of the U.S. Department of Transportation (DOT) established the High Altitude Pollution Program (HAPP) in 1976 following the completion of DOI's Climatic Impact Assessment Program (CIAP). The CIAP findings had led to the conclusion that unrestricted growth of aircraft fleets could well pose an environmental threat by depleting stratospheric ozone. This view was more clearly affirmed by an independent study conducted by the Climatic Impact Committee (CIC) of the U.S. National Academies of Sciences and Engineering. The uncertainties in these investigations were large enough for the FAA to undertake HAPP in order "to quantitatively determine the requirements for reduced cruise-altitude exhaust emissions and, in conjunction with the Environmental Protection Agency (EPA) and the International Civil Aviation Organization (ICAO), to ensure that, if necessary, appropriate regulatory action is taken to avoid environmental degradation." The underlying philosophy of HAPP, then, is prevention rather than cure.

The organizational elements of HAPP are shown in the accompanying figure. The emphases in these program elements are mentioned below.

(1) Engines and Fuels.

- . Determine the emission characteristics for current and planned aircraft engines, under cruise conditions.
- . Consider the impact of alternative fuels.
- . Forecast world-wide emissions for future flight scenarios.

(2) Laboratory Measurements.

- . Continue critical evaluation of laboratory kinetics data.
- . Develop new techniques.
- . Identify and investigate chemical/photochemical reactions of stratospheric and upper tropospheric importance including rainout/washout processes.

(3) Field Measurements.

- . Obtain and analyze data on ozone, water vapor and stratospheric trace species, especially nitrogen-containing and hydrogen-containing species.
- . Work closely with National Aeronautics and Space Administration (NASA) and/or with National Oceanic and Atmospheric Administration (NOAA) in stratospheric measurements with satellites, aircraft, rockets, balloons and ground-based instruments.
- . Encourage and support development of new instrumentation and intercomparison of measurement techniques/instruments.

(4) Models.

- . Continue diagnostic and prognostic studies of one and two dimensional models.
- . Refine and improve one and two dimensional models.
- . Improve transport parameterization in the upper troposphere and lower stratosphere, a region of interest for aircraft operations.
- . Conduct studies on possible climate changes due to aircraft operations.

(5) Monitoring.

- . Work closely with NASA and NOAA to ensure that the FAA requirements are met within the national and international monitoring efforts.

(6) Assessment.

- . Perform uncertainty analyses.
- . Coordinate activities with appropriate national and international organizations.

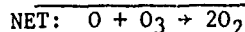
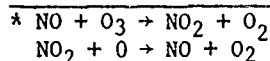
(7) Regulatory Policy.

- . Determine the immediacy of, the need for, and the type of regulations to protect the environment from possible harmful cruise-altitude emissions.

The interdependence among the program elements is indicated by the arrows in the figure.

Studies conducted under HAPP to-date lead us to believe that commercial aircraft operations (both subsonic and supersonic) in the foreseeable future would result in a slight increase in total columnar ozone rather than a decrease, in contrast to the earlier findings. This inference is based upon calculations of one dimensional chemical kinetics - transport models which have been refined and improved, since CIAP, by including chlorine and simplified methane oxidation chemistries and new determinations of chemical rate constants (e.g.,  $\text{HO}_2 + \text{NO}$ ). These models indicate that the nitrogen oxides ( $\text{NO}$  and  $\text{NO}_2$ ) in the aircraft exhaust generate ozone through smog-like mechanisms up to lower stratospheric levels and deplete it through the classical catalytic cycle\* at higher altitudes. The net result at present is a slight overall increase in total ozone.

The uncertainty associated with this calculation cannot yet be ascertained because calculations with plausible values for a number of yet-to-be-determined parameters (e.g.,  $\text{OH} + \text{HO}_2\text{NO}_2$ ,  $\text{OH} + \text{HNO}_3$ ,  $\text{HO}_2\text{NO}_2 + \text{hv}$ ) lead to an inference of possible overall ozone decreases.



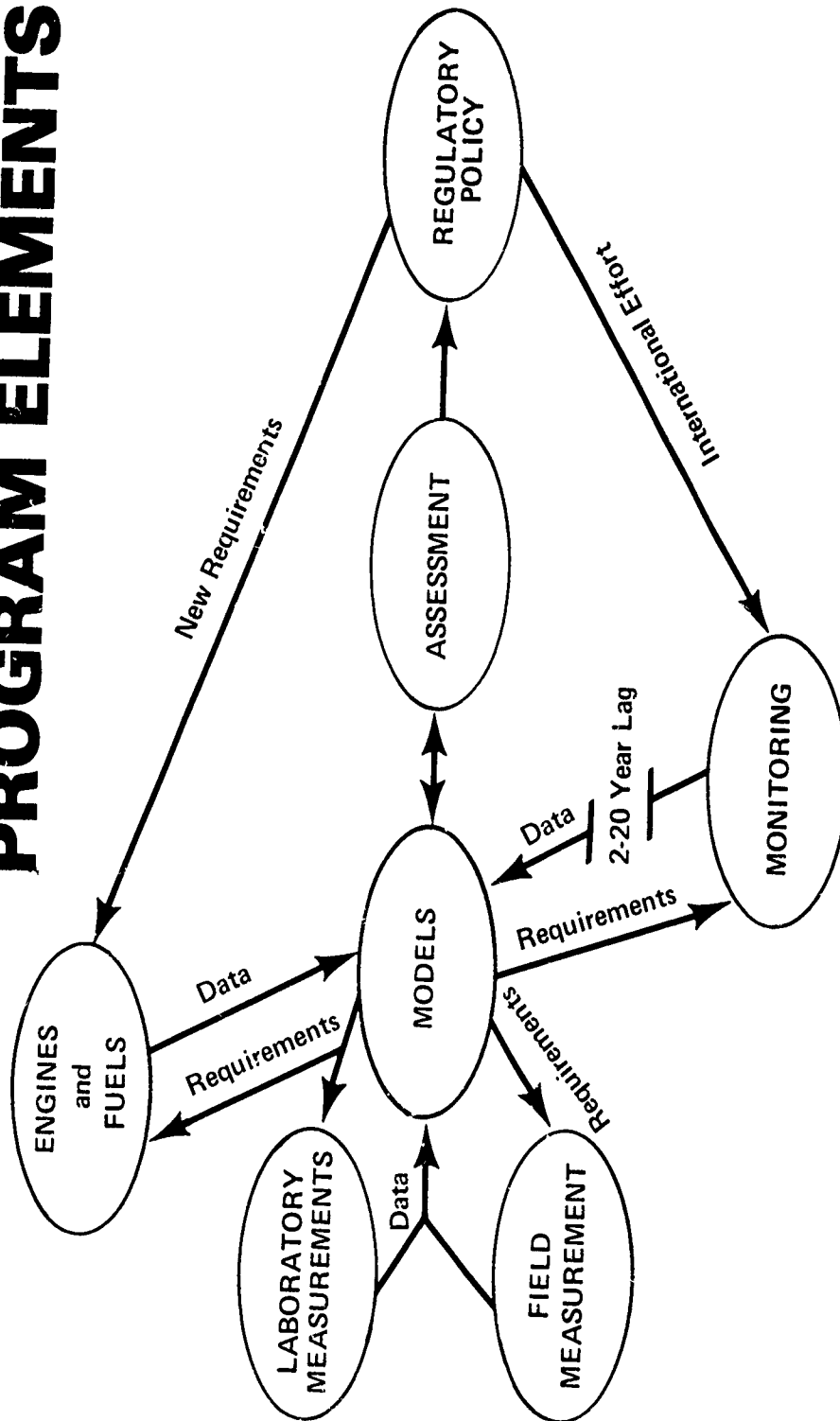
#### SUNDARARAMAN

Moreover, the redistribution of ozone in the vertical has climatic implications, especially if a warming of the tropopause should result, followed by greater transport of tropospheric water vapor into the stratosphere. Further, possible increases in upper tropospheric ozone, should it diffuse downward, would have air quality implications; and possible increases in upper tropospheric nitrogen oxides would raise questions about the role of aircraft emissions in the formation of acid rain.

A future direction of FAA's work in the environmental area may well be in addressing some of these issues.

To help review, evaluate, and guide HAPP, the FAA has established the High Altitude Pollution Program Scientific Advisory Committee (HAPPSAC) which meets once every ten months or so. The membership of HAPPSAC appears in the attached table.

FIGURE  
**PROGRAM ELEMENTS**



## TABLE

MEMBERS OF HIGH ALTITUDE POLLUTION PROGRAM  
SCIENTIFIC ADVISORY COMMITTEENational Members

1. Dr. F. Sherwood Rowland, Chairman  
University of California  
Irvine, California 92717
2. Dr. Julius S. Chang  
Lawrence Livermore Laboratory  
Livermore, California 92093
3. Dr. Ralph J. Cicerone  
Scripps Institute of Oceanography  
La Jolla, California 92093
4. Dr. Edwin F. Danielsen  
NASA Ames Research Center  
Moffett Field, California 94035
5. Dr. Harold S. Johnston  
University of California  
Berkeley, California 94720
6. Mr. George D. Kittredge  
U.S. Environmental Protection Agency  
Washington, D.C. 20460
7. Dr. Jerry D. Mahlman  
Geophysical Fluid Dynamics Laboratory  
Princeton, New Jersey 08540
8. Dr. Randall E. Murphy  
Air Force Geophysics Laboratory  
Bedford, Massachusetts 01731
9. Dr. Robert C. Oliver  
Institute for Defense Analyses  
Arlington, Virginia 22202
10. Dr. James N. Pitts, Jr.  
University of California  
Riverside, California 92521
11. Dr. Robert W. Rummel  
Robert W. Rummel Associates, Inc.,  
Mesa, Arizona 85206
12. Dr. Arthur L. Schmeltekopf  
National Oceanic and Atmospheric Admin.  
Boulder, Colorado 80303
13. Dr. Shelby G. Tilford  
National Aeronautics and Space Admin.  
Washington, D.C. 20546

Foreign Members

1. Dr. Marcel E. H. Ackerman  
Institut d'Aeronomie Spatiale  
de Belgique  
B-1180 Brussels, Belgium
2. Dr. Rumen D. Bojkov  
World Meteorological Organization  
Geneva 20, Switzerland
3. Dr. Paul Crutzen  
National Center for Atmospheric Research  
Boulder, Colorado 80307 USA
4. Dr. Dieter H. Ehhalt  
Max-Planck Institute  
517 Julich, Federal Republic of Germany
5. Dr. James E. Lovelock  
Coombe Mill, St. Giles-on-the-Heath  
Launceston, Cornwall, England
6. Dr. Robert J. Murgatroyd  
Meteorological Office  
Bracknell, England RG 12 2SZ
7. Dr. A. B. Pittock  
Commonwealth Science and Industrial  
Research Organization  
Mordialloc, Victoria 3195 Australia
8. Dr. George D. Robinson  
Center for Environment and Man, Inc.,  
Hartford, Connecticut, 06120 USA
9. Dr. Harold I. Schiff  
York University  
Downsview, Ontario  
Canada M3J 1P3
10. Dr. Adelin Villevieille  
Etablissement d'Etudes et  
Recherches Meteorologiques  
92106 Boulogne France
11. Air Commodore Sir Frank Whittle  
Columbia, Maryland 21044  
USA

## NASA'S ATMOSPHERIC RESEARCH PROGRAM

Shelby G. Tilford

National Aeronautics and Space Administration  
Washington, D.C. 20546

The NASA atmospheric research program was described and shown to have major elements in the Office of Space Science, e.g., Planetary Atmospheres and Plasma Physics, and in the Office of Space and Terrestrial Applications, e.g., Atmospheric Processes Branch. The overall program was shown to consist of Applications Research and Data Analysis (AR and DA); platform support for field measurement experiments; i.e., aircraft, balloons and rockets; free flying satellites, both research and operational; and Spacelab payloads, both principal investigators and multi-user type investigations.

The AR and DA part of the program was outlined, illustrating that the major components are laboratory studies, field measurements, and theoretical studies. The NASA satellite system, past, present and planned, was described showing the development from satellites carrying simple payloads with limited scientific return, e.g., ozone (Nimbus 4) to today's satellites which study one aspect of the atmosphere in some detail, e.g., chemical composition (Nimbus 7); to the planned satellites of tomorrow, e.g., SME and UARS, which would make measurements that emphasize the coupling between energy input, chemical composition, and dynamics. Developed Spacelab payloads, e.g., ATMOS (Atmospheric Trace Molecules Observed by Spectroscopy) and MAPS (Mapping Atmospheric Pollutants from Space) were described in addition to those recently approved, e.g., MLS (Microwave Limb Sounder) and HRDI (High Resolution Doppler Imager).

SUMMARY OF THE COMMISSION OF THE EUROPEAN COMMUNITIES REPORT:

CHLOROFLUOROCARBONS AND THEIR EFFECT ON STRATOSPHERIC OZONE

R. J. MURGATROYD

METEOROLOGICAL OFFICE, BRACKNELL, UNITED KINGDOM

Studies of the possible effects of chlorofluorocarbons on stratospheric ozone are being made in several countries in Europe and an integrated report on this work is being produced under the auspices of the Commission of the European Communities. It is hoped that this report will be completed in 1980 and comprise sections on (a) Modelling (b) Photochemical Data and (c) Measurements. Drafting of the Modelling Section is now well advanced and will contain, in addition to scientific reviews, descriptions and results from the modelling work in Belgium, Denmark, France, Italy, West Germany and the United Kingdom.

The British Government's Department of the Environment has recently published a report (1) which contains as well as an overall assessment a comprehensive account of the work of the UK modelling groups on this subject.

Reference:

- (1) Chlorofluorocarbons and their effect on Stratospheric Ozone, Pollution Paper N° 15, Department of the Environment, London, Her Majesty's Stationary Office, 1979.

# LIST OF PARTICIPANTS

Mr. Hamish Adam  
Dept. of Atmospheric Physics  
Clarendon Laboratory  
Oxford University  
Parks Road  
Oxford OX1-3PU  
UNITED KINGDOM

Dr. Arthur Aikin  
Code 964  
NASA Goddard Space Flight Center  
Greenbelt, MD 20771  
USA

Monsieur Patrick Aïmedieu  
Service d'Aéronomie du CNRS  
B.P. No. 3  
F-91370 Verrières-le-Buisson  
FRANCE

Mrs. Gail Anderson  
National Center for Atmospheric Research  
P. O. Box 3000  
Boulder, CO 80307  
USA

Prof. James Anderson  
Center for Earth and Planetary Physics  
Harvard University  
20 Oxford Street  
Cambridge, MA 02138  
USA

Mr. Ignaz J. Arnold  
Inst. für Phys. Chemie  
der Universität Frankfurt  
Robert Mayer Strasse 11  
D-6000 Frankfurt am Main  
WEST GERMANY

Mr. John Austin  
Meteorological Office  
London Road  
Bracknell Berks  
UNITED KINGDOM

Prof. Knut Bachmann  
Technische Hochschule Darmstadt  
Fachbereich Anorganische Chemie  
und Kernchemie  
Hochschulstrasse 4  
D-6100 Darmstadt  
WEST GERMANY

Dr. Alan Baldwin  
SRI International  
333 Ravenswood Avenue  
Menlo Park, CA 94025  
USA

Dr. Alain Barbe  
Faculté des Sciences de Reims  
Laboratoire de Physique  
Moléculaire  
B.P. 347  
F-51062 Reims Cedex  
FRANCE

Dr. Arnold Bass  
Gas and Particulate Science  
Division  
National Bureau of Standards  
Chemistry B162  
Washington, DC 20234  
USA

Dr. Ernest Bauer  
Institute for Defense Analyses  
400 Army-Navy Drive  
Arlington, VA 22202  
USA

Prof. Jacques Blamont  
Service d'Aéronomie du CNRS  
B.P. No. 3  
F-91370 Verrières-le-Buisson  
FRANCE

Dr. Roger Bonnet  
LPSP du CNRS  
B.P. No. 10  
F-91370 Verrières-le-Buisson  
FRANCE

Dr. Guy Brasseur  
Institut D'Aéronomie Spatiale  
de Belgique  
3, Avenue Circulaire  
B-1180 Brussels  
BELGIUM

Dr. John Brock  
Jet Propulsion Laboratory  
M.S. 183-901  
4800 Oak Grove Drive  
Pasadena, CA 91103  
USA



Mr. Gustavo Brose  
Institut für Geophysik und  
Meteorologie Der Universität  
zu Köln  
Albertus-Magnus-Platz  
D-5 Köln 41  
WEST GERMANY

Dr. John Burrows  
A.E.R.E. Harwell  
Environmental and Medical  
Sciences Division  
Oxfordshire OXII ORA  
UNITED KINGDOM

Dr. Jack Calvert  
Chemistry Department  
The Ohio State University  
140 West 18th Avenue  
Columbus, OH 43210  
USA

Mr. Daniel Cariolle  
Météorologie Nationale Etablissement  
d'Etudes et de Recherches Météo.  
77, Rue de Sevres  
F-92106 Boulogne Cedex  
FRANCE

Dr. Maria Joao de Carvalho  
Instituto Geofísico  
D. Luis (Fac. de Ciencias)  
Rua da Escola Politécnica No. 58  
Lisboa  
PORTUGAL

Dr. Dipak Chakrabarty  
Room No. 773  
Physical Research Laboratory  
Ahmedabad 380 009  
INDIA

Dr. William Chameides  
Dept. of Physics  
University of Florida  
Gainesville, FL 32611  
USA

Dr. Julius Chang  
Lawrence Livermore Laboratory  
University of California  
P. O. Box 808  
Livermore, CA 94550  
USA

Dr. Robert Chatfield  
National Center for Atmospheric Research  
Boulder, CO 80307  
USA

Mr. Juan Cisneros  
Instituto Nacional de  
Técnica Aeroespacial  
Paseo del Pintor Rosales 34  
Madrid 8  
SPAIN

Dr. Derek Cunnold  
Georgia Institute of Technology  
Atmospheric Sciences  
114 Baker Building  
Atlanta, GA 30332  
USA

Dr. Dirk De Muer  
Institut Royal Météorologique  
de Belgique  
3, Avenue Circulaire  
B-1180 Brussels  
BELGIUM

Mr. Taner Derbentli  
Teknik Universite  
Müh. Mim. Fakültesi  
İsi Teknigi Kursusu  
Macka Istanbul  
TURKEY

Dr. Thomas Donahue  
Dept. of Atmospheric & Oceanic Sciences  
University of Michigan  
2455 Hayward Street  
Ann Arbor, MI 48109  
USA

Dr. Richard Donnelly  
Space Environment Laboratory  
1-2119  
NOAA ERL  
Boulder, CO 80303  
USA

Dr. Gustav During  
National Defense Research Institute  
S-10450 Stockholm 80  
SWEDEN

Prof. Hans Dutsch  
Laboratory for Atmospheric Physics  
ETH  
Hönggerberg HPP  
CH-8093 Zurich  
SWITZERLAND

Dr. Dieter Ehhalt  
Kernforschungsanlage Julich  
Postfach 1913  
D-5170 Julich  
WEST GERMANY

Dr. Hugh Ellsaesser  
L-262  
Lawrence Livermore Laboratory  
P. O. Box 808  
Livermore, CA 94550  
USA

Mr. Christopher England  
Laboratory for Planetary Atmospheres  
Dept. of Physics and Astronomy  
University College London  
Gower Street  
London WC1E 6BT  
UNITED KINGDOM

Dr. Wayne Evans  
Atmospheric Environment Service  
4905 Dufferin Street  
Downsview, Ontario M3H 5T4  
CANADA

Dr. Eldon Ferguson  
Aeronomy Laboratory  
R44 NOAA  
325 S. Broadway  
Boulder, CO 80303  
USA

Dr. Mario Figuerira  
Instituto Nacional de  
Meteorologia e Geofisica  
Rua C - Aeroporto de Lisboa  
1700 Lisboa  
PORTUGAL

Dr. Giorgio Fiocco  
Istituto di Fisica  
Universita di Roma  
Citta Universitaria  
1-Roma  
ITALY

Mr. Rolando Garcia  
National Center for Atmospheric Research  
P. O. Box 3000  
Boulder, CO 80307  
USA

Mr. Brian Gardiner  
British Antarctic Survey  
Madingley Road  
Cambridge CB3 0ET  
UNITED KINGDOM

Dr. Anver Ghazi  
Institut fur Geophysik und  
Meteorologie Der Universitat  
zu Koln  
D-5 Koln 41  
WEST GERMANY

Dr. John Gille  
National Center for Atmospheric Research  
P. O. Box 3000  
Boulder, CO 80307  
USA

Dr. William Grose  
NASA Langley Research Center  
Mail Stop 401B  
Hampton, VA 23665  
USA

Dr. Hans Gusten  
Kernforschungszentrum Karlsruhe  
Institut fur Radiochemie  
D-7500 Karlsruhe  
WEST GERMANY

Miss Joanna Haigh  
Oxford University  
Dept. of Atmospheric Physics  
Clarendon Laboratory  
Parks Road  
Oxford OX1-3PU  
UNITED KINGDOM

Dr. Donald Heath  
Code 963  
NASA Goddard Space Flight Center  
Greenbelt, MD 20771  
USA

Dr. Michael Hebden  
Dept. of Environment  
Room 632-Becket House  
1 Lambeth Palace Road  
London SE1 7ER  
UNITED KINGDOM

Dr. Horst Hippler  
Institut für Physikalische Chemie  
Universität Göttingen  
Tammannstrasse 6  
D-3400 Göttingen  
WEST GERMANY

Dr. Carleton Howard  
NOAA - ERL  
USA Department of Commerce  
3522 Radio Building  
Boulder, CO 80303  
USA

Mr. Gerhard Hubler  
KFA Jülich GmbH/ICH 3  
Institut für Chemie 3  
P. O. Box 1913  
D-5170 Jülich  
WEST GERMANY

Dr. Robert Hudson  
Code 963  
NASA Goddard Space Flight Center  
Greenbelt, MD 20771  
USA

Dr. J. Peter Jesson  
DuPont Company  
DuPont Experimental Station E  
356/301  
Wilmington, DE 19898  
USA

Mr. Rod Jones  
Dept. of Atmospheric Physics  
Clarendon Laboratory  
Oxford University  
Parks Road  
Oxford OX1-3PU  
UNITED KINGDOM

Mr. Klaus Kaselau  
Institute for Geophysics  
University of Cologne  
Albertus-Magnus-Platz  
D-5000 Köln 41  
WEST GERMANY

Dr. Frederick Kaufman  
Dept. of Chemistry  
University of Pittsburgh  
Pittsburgh, PA 15260  
USA

Dr. Dieter Kley  
NOAA  
Aeronomy Laboratory  
Mail Code R448  
Boulder, CO 80303  
USA

Dr. Hans Knauth  
Institut für Physikalische Chemie  
Universität  
Hasseerstrasse 73  
D-73 Kiel  
WEST GERMANY

Mr. William J. Kohri  
National Center for Atmospheric Research  
P. O. Box 3000  
Boulder, CO 80307  
USA

Mr. Joseph Krasnec  
National Center for Atmospheric Research  
P. O. Box 3000  
Boulder, CO 80307  
USA

Dr. Olga Lado-Bordowsky  
Laboratoire de Spectroscopie  
Moléculaire  
Tour 13 - 3<sup>ème</sup> étage  
4, Place Jussieu  
F-75230 Paris Cedex 05  
FRANCE

Dr. Arunachalam Lakshmi  
1516 May Area Blvd. #B10  
Houston, TX 77058  
USA

Dr. Christiane Lalo-Kourilsky  
CIRS ERS7/ESPCI  
10, Rue Vauquelin  
F-75231 Paris Cedex 05  
FRANCE

Dr. Soren Larsen  
Institute of Physics  
University of Oslo  
P. O. Box 1048  
Blindern-Oslo 3  
NORWAY

Mr. Augusto Latas  
Instituto Nacional de Meteorologia  
e Geofisica  
Rua C - Aeroporto de Lisboa  
1700 Lisboa  
PORTUGAL

Dr. Georges Le Bras  
CNRS - CRCHT  
1C Avenue de la Recherche Scientifique  
F-45045 Orleans Cedex  
FRANCE

Dr. Ming-Taun Leu  
Jet Propulsion Laboratory  
4800 Oak Grove Drive  
Pasadena, CA 91011  
USA

Dr. H. Levy  
NOAA Geophysical Fluid  
Dynamics Laboratory  
P. O. Box 308  
Princeton University  
Princeton, NJ 08540  
USA

Dr. Jennifer Logan  
Harvard University  
108 Pierce Hall  
29 Oxford Street  
Cambridge, MA 02138  
USA

Prof. Julius London  
Dept. of Astro-Geophysics  
University of Colorado  
Mail Code 391  
Boulder, CO 80309  
USA

Dr. Heio Lopes  
Rua Montepio Geral 20,  
20, -Dt  
1500 Lisboa  
PORTUGAL

Madame Nicole Louisnard  
ONERA  
Avenue de la Division Leclerc  
F-92320 Chatillon/Bagneux  
FRANCE

Mr. David Lowe  
KFA Julich GmbH  
Institut fur Chemie III  
P. O. Box 1913  
D-5170 Julich  
WEST GERMANY

Dr. Robert Lowe  
Dept. of Physics  
University of Western Ontario  
London N6A 3K7  
CANADA

Dr. Ole Manscher  
Department of General and Organic Chemistry  
The H.C. Ørsted Institute  
University of Copenhagen  
Universitetsparken 5  
DK-2100 Ø Copenhagen  
DENMARK

Mr. Pierre Marche  
Faculte des Sciences de Reims  
Laboratoire de Physique Moleculaire  
B.P. 347  
F-51062 Reims Cedex  
FRANCE

Dr. James Margitan  
Space Physics Research Lab  
University of Michigan  
2455 Hayward Street  
Ann Arbor, MI 48109  
USA

Dr. Carlos Marques  
Instituto Geofisico  
D. Luis (Fac. de Ciencias)  
Rua da Escola Politecnica No. 58  
Lisboa  
PORTUGAL

Mr. Jose Marques  
Instituto Nacional de Meteorologia  
e Geofisica  
Rua C - Aeroporto de Lisboa  
1700 Lisboa  
PORTUGAL

Dr. Luis Mata  
Instituto Nacional de Meteorologia  
e Geofisica  
Rua C - Aeroporto de Lisboa  
1700 Lisboa  
PORTUGAL

Dr. Andrew Matthews  
Max-Planck Institute  
für Aeronomie  
P.O. Box 20  
D-3411 Katlenburg - Lindau 3  
WEST GERMANY

Dr. Michael McElroy  
Harvard University  
20 Oxford Street  
Cambridge, MA 02138  
USA

Dr. Gerard Megie  
Service d'Aeronomie du CNRS  
B.P. No. 3  
F-91370 Verrieres-le-Buisson  
FRANCE

Prof. Alfredo Mendes  
Instituto Nacional de Meteorologia  
e Geofisica  
Rua C - Aeroporto de Lisboa  
1700 Lisboa  
PORTUGAL

Dr. Joe Michael  
Code 691  
NASA Goddard Space Flight Center  
Greenbelt, MD 20771  
USA

Dr. Mario Molina  
University of California  
Dept. of Chemistry  
Irvine, CA 92717  
USA

Melle Nicole Monnanteuil  
Laboratoire de Spectroscopie Hertzienne  
U.E.R. de Physique  
Universite des Sciences et Techniques  
de Lille  
F-59655 Villeneuve D'ASCQ Cedex  
FRANCE

Dr. Derek Montague  
c/o Dr. F. S. Rowland  
Dept. of Chemistry  
University of California  
Irvine, CA 92717  
USA

Dr. Geert Moortgat  
Max-Planck Institut für  
Chemie-Otto-Hahn Institut  
Saarstrasse 23  
D-6500 Mainz  
WEST GERMANY

Dr. P. N. Moorthy  
Scientific Officer SF  
Chemistry Division  
Bhabha Atomic Research Centre  
Trombay, Bombay-400085  
INDIA

Dr. Alberto Mugnai  
Laboratorio Plasma - Spazio  
Via G. Galilei  
C.P. 27  
I - 00044 Frascati  
ITALY

Dr. David Murcay  
Dept. of Physics  
University of Denver  
Denver, CO 80208  
USA

Dr. Robert Murgatroyd  
Meteorological Office  
London Road  
Bracknell, Berkshire  
UNITED KINGDOM

Mr. Jean-Pierre Naudet  
Observatoire de Geneve  
CH - 1290 Sauverny  
SWITZERLAND

Dr. Marcel Nicolet  
External Geophysics  
Brussels University  
B-1180 Brussels  
BELGIUM

Mr. Francis Nouyrigat  
P.C.U.K.  
Direction de l'Innovation  
Tour Manhattan - Cedex 21  
F-92037 Paris La Defense 2  
FRANCE

Dr. Alan O'Neill  
Met. 0.20  
Meteorological Office  
London Road  
Bracknell Berkshire  
UNITED KINGDOM

Dr. Robert Oliver  
Institute for Defense Analyses  
400 Army-Navy Drive  
Arlington, VA 22202  
USA

Dr. John Olivero  
Penn. State University  
Ionosphere Research Laboratory  
Dept. of Meteorology  
509 Walker Building  
University Park, PA 16802  
USA

Dr. Hans Paetzold  
Inst. for Geophysics and  
Meteorology - University of  
Cologne  
Zuelpicherstrasse 49  
D-Koln  
WEST GERMANY

Mr. Roger Patrick  
Oxford University  
Dept. of Physical Chemistry  
South Parks Road  
Oxford OX1 3PU  
UNITED KINGDOM

Mr. William Peetermans  
Institut D'Aeronomie Spatiale  
de Belgique  
3, Avenue Circulaire  
B-1180 Brussels  
BELGIUM

Dr. Joyce Penner  
Lawrence Livermore Laboratory  
P. O. Box 808, L-71  
Livermore, CA 94550  
USA

Mr. Gian Paolo Petroncelli  
c/o Laboratorio Plasma-Spazio  
Via G. Galilei  
C.P. 27  
I - 00044 Frascati  
ITALY

Dr. Charles Philbrick  
Air Force Geophysics Laboratory  
LKB  
Hanscom AFB, MA 01731  
USA

Dr. Jean-Pierre Pommereau  
Service d'Aeronomie du CNRS  
B.P. No. 3  
F-91370 Verrieres-le-Buisson  
FRANCE

Dr. Gilles Poulet  
CNRS - CRCCHT  
F-45045 Orleans Cedex  
FRANCE

Dr. John Pyle  
Dept. of Atmospheric Physics  
Clarendon Laboratory  
Oxford University  
Parks Road  
Oxford OX1 3PU  
UNITED KINGDOM

Dr. Asit Rakshit  
Max-Planck Institut fur Chemie  
DOB 3060  
D-6500 Mainz  
WEST GERMANY

Dr. R. A. Rasmussen  
Oregon Graduate Center  
19600 N.W. Walker Road  
Beaverton, OR 97006  
USA

Dr. Pierre Rigaud  
Station Scientifique du Val Joyeux  
F-78450 Villepreux  
FRANCE

Dr. Clive Rodgers  
Dept. of Atmospheric Physics  
Clarendon Laboratory  
Oxford University  
Parks Road  
Oxford OX1 3PU  
UNITED KINGDOM

Dr. Bento Monteiro Rodrigues  
Instituto Nacional de Meteorologia  
e Geofisica  
Rua C - Aeroporto de Lisboa  
1700 Lisboa  
PORTUGAL

Dr. Ernest Roeth  
Inst. fur Chemie 3 der KFA  
Postfach 1913  
D-5170 Julich  
WEST GERMANY

Dr. Howard Roscoe  
Department of Atmospheric Physics  
Clarendon Laboratory  
Oxford University  
Park Road  
Oxford OX1 3PU  
UNITED KINGDOM

Dr. F. S. Rowland  
Dept. of Chemistry  
University of California  
Irvine, CA 92717  
USA

Mr. Joao Sampaio  
Instituto Nacional de Meteorologia  
e Geofisica  
Rua C - Aeroporto de Lisboa  
1700 Lisboa  
PORTUGAL

Dr. Harold Schiff  
Department of Chemistry  
York University  
4700 Keele Street  
Downsview, Ontario M3J 1P3  
CANADA

Dr. Manfred Schmidt  
Max-Planck Institute  
für Aeronomy  
P. O. Box 20  
D-3411 Katlenburg - Lindau 3  
WEST GERMANY

Dr. Ulrich Schmidt  
KFA Jülich GmbH  
Institut für Chemie III  
P. O. Box 1913  
D-5170 Jülich  
WEST GERMANY

Mr. Gunther Schonle  
Institute für Physikalische Chemie  
Universität Kiel  
Olshausenstrasse 40-60  
D-2300 Kiel  
WEST GERMANY

Dr. Ulrich Schurath  
University of Bonn  
Institut für Physikalische Chemie  
Wegelerstrasse 12  
D-5300 Bonn  
WEST GERMANY

Dr. William Sedlacek  
Los Alamos Scientific Laboratory  
University of California  
M.S. 514, P.O. Box 1663  
Los Alamos, NM 87545  
USA

Dr. Dhanwant Sethi  
University of Bridgeport  
Chemistry Department  
Bridgeport, CT 06602  
USA

Dr. John Shaw  
Dept. of Physics  
Ohio State University  
Columbus, OH 43210  
USA

Mr. Algirdas Silnickas  
Dept. of Physical Chemistry  
University of Cambridge  
5, Gledhow Mount  
Leeds LS8 5EW  
UNITED KINGDOM

Dr. Paul Simon  
Institute D'Aeronomie Spatiale  
de Belgique  
3, Avenue Circulaire  
B-1180 Brussels  
BELGIUM

Dr. R. Simcnaitis  
Ionosphere Research Laboratory  
The Pennsylvania State University  
University Park, PA 16802  
USA

Dr. Turan Soylemez  
c/o Institut für Strahlenchemie  
im Max-Planck Institut  
Stifstrasse 34  
D-4330 Mulheim a.d. Ruhr  
WEST GERMANY

Dr. Louis Stief  
Code 691  
NASA Goddard Space Flight Center  
Greenbelt, MD 20771  
USA

Dr. Richard S. Stolarski  
Code 964  
NASA Goddard Space Flight Center  
Greenbelt, MD 20771  
USA

Dr. Narasimhan Sundararaman  
Manager  
High Altitude Pollution Program  
Federal Aviation Administration  
AEE 300  
800 Independence Ave., S.W.  
Washington, DC 20591  
USA

Mr. Dexter Sutherland  
Los Alamos Scientific Laboratory  
P. O. Box 1663  
Los Alamos, NM 87545  
USA

Dr. William Swider  
LKD  
Air Force Geophysics Laboratory  
Hanscom AFB, MA 01731  
USA

Dr. Shelby Tilford  
Code EBT-8  
NASA Headquarters  
Washington, DC 20546  
USA

Dr. Stanley Tyler  
Dept. of Chemistry  
University of California  
Irvine, CA 92717  
USA

Mr. Geoffrey Tyndall  
Dept. of Physical Chemistry  
University of Cambridge  
Lensfield Road  
Cambridge CB2 1EP  
UNITED KINGDOM

Dr. Carlo Ulivieri  
Centro Ricerche Aerospaziali (CRA)  
Via Salaria 851  
I - 00199 Roma  
ITALY

Dr. Bernard Veyret  
Laboratoire de Chimie Physique A  
Bordeaux I  
F-33405 Talence  
FRANCE

Mr. Michael Wale  
Dept. of Atmospheric Physics  
Clarendon Laboratory  
Oxford University  
Parks Road  
Oxford OX1 3PU  
UNITED KINGDOM

Dr. Andrew Watson  
Dept. of Atmospheric & Oceanic Science  
University of Michigan  
2455 Hayward Street  
Ann Arbor, MI 48109  
USA

Dr. Robert Watson  
Building 183-601  
Jet Propulsion Laboratory  
4800 Oak Grove Drive  
Pasadena, CA 91103  
USA

Dr. Arthur Waynick  
Ionosphere Research Laboratory  
318 Electrical Engineering East  
The Pennsylvania State University  
University Park, PA 16802  
USA

Mr. Jeremy Wilkinson  
Dept. of Physical Chemistry  
Cambridge University  
Lensfield Road  
Cambridge  
UNITED KINGDOM

Dr. Donald Wuebbles  
Lawrence Livermore Laboratory  
P. O. Box 808  
L-262  
Livermore, CA 94550  
USA

Mr. Jean-Marc Zucconi  
Observatoire de Besancon  
41bis, Avenue de l'Observatoire  
F-25000 Besancon  
FRANCE



# AUTHOR INDEX

<u>Author</u>	<u>Paper</u>	<u>Page</u>
Addison, M.C., Burrows, J.P., Cox, R.A.	"Kinetic Studies of Atmospheric Free Radicals". . . . .	483
Aikin, A.C., Herman, J.R., Maier, E.J.	"Ethane and Ethylene Behavior in the Atmosphere". . . . .	191
Alyea, F.N., Cunnold, D.M., Prinn, R.G.	"Three-Dimensional Models and Their Application to the Ozone Problem". . . . .	877
Anderson, J.G.	"Free Radicals in the Earth's Stratosphere: A Review of Recent Results". . . . .	235
Bass, A.M., Glasgow, L.C., Miller, C., Jesson, J.P., Filkin, D.L.	"Temperature Dependent Absorption Cross Sections for Formaldehyde (CH <sub>2</sub> O): The Effect of Formaldehyde on Stratospheric Chlorine Chemistry". . . . .	467
Bauer, Ernest	"Effect of Past Atmospheric Nuclear Explosions on Total Ozone" . . . . .	909
Brasseur, Guy	"On Eddy Diffusion Coefficients". . . . .	767
Burrows, J.P., Cox, R.A., Addison, M.C.	"Kinetic Studies of Atmospheric Free Radicals". . . . .	483
Calvert, Jack G.	"The Homogeneous Chemistry of Formaldehyde Generation and Destruction within the Atmosphere". . . . .	153
Chakrabarty, D.K., Chakrabarty, Purobi	"Ozone Results from Indian Stations Using Dobson Instruments". . . . .	123
Chakrabarty, Purobi, Chakrabarty, D.K.	"Ozone Results from Indian Stations Using Dobson Instruments". . . . .	123
Chameides, W.L., Davis, D.D.	"The Photochemistry of Tropospheric Iodine" . . . . .	281
Chang, Julius S., Wuebbles, Donald J.	"One-Dimensional Coupled Transport and Chemical Kinetics Models of the Stratosphere" . . . . .	749
Combourieu, J., LeBras, G., Foon, R., Foulet, G.	"EPR Kinetic Study of the Reactions of H <sub>2</sub> CO with F, Cl and Br Atoms and ClO Radical" . . . . .	497
Cox, R.A., Burrows, J.P., Addison, M.C.	"Kinetic Studies of Atmospheric Free Radicals". . . . .	483

<u>Author</u>	<u>Paper</u>	<u>Page</u>
Cunnold, D.M., Alyea, F.N., Prinn, R.G.	"Three-Dimensional Models and Their Application to the Ozone Problem" . . . . .	877
Davis, D.D., Chameides, W.L.	"The Photochemistry of Tropospheric Iodine". . . . .	281
Donahue, Thomas M.	"The Atmospheric CH <sub>4</sub> Budget" . . . . .	301
Dutsch, H.U.	"Vertical Ozone Distribution and Tropospheric Ozone" . . . . .	7
Ehhalt, D.H., Tonniben, A.	"Hydrogen and Carbon Compounds in the Stratosphere" . . . . .	129
Ellsaesser, Hugh W.	"Sources and Sinks of Stratospheric Water Vapor". . . . .	283
Ferguson, Eldon E.	"Stratospheric Ion Chemistry Related to Neutral Trace Composition" . . . . .	517
Filkin, D.L., Bass, A.M., Glasgow, L.C. Miller, C., Jesson, J.P.	"Temperature Dependent Absorption Cross Sections for Formaldehyde (CH <sub>2</sub> O): The Effect of Formaldehyde on Stratospheric Chlorine Chemistry" . . . . .	457
Flocco, G.	"Influence of Diffuse Solar Radiation on Stratospheric Chemistry". . . . .	555
Foon, R., LeBras, G., Poulet, G., Combournieu, J.	"EPR Kinetic Study of the Reactions of H <sub>2</sub> CO with F, Cl and Br Atoms and ClO Radical" . . . . .	497
Gandrud, B.W., Sedlacek, W.A., Lazrus, A.L.	"Measurements of Stratospheric Bromine". . . . .	273
Gille, John C.	"Ozone Distributions by Infrared Limb Scanning: Preliminary Results from the LRIR" . . . . .	103
Glasgow, L.C., Bass, A.M., Miller, C., Jesson, J.P., Filkin, D.L.	"Temperature Dependent Absorption Cross Sections for Formaldehyde (CH <sub>2</sub> O): The Effect of Formaldehyde on Stratospheric Chlorine Chemistry" . . . . .	467
Heath, Donald F.	"Spatial and Temporal Variability of Ozone as Seen from Space" . . . . .	45
Herman, J.R., Aikin, A.C. Maier, E.J.	"Ethane and Ethylene Behavior in the Atmosphere" . . . . .	191

<u>Author</u>	<u>Paper</u>	<u>Page</u>
Howard, Carleton J.	"Laboratory Studies of Reactions of Odd Hydrogen Species of Atmospheric Interest" . . . . .	409
Jesson, J.P.	"Release of Industrial Halocarbons and Tropospheric Budget". . . . .	373
Jesson, J.P., Bass, A.M., Glasgow, L.C., Miller, C., Filkin, D.L.	"Temperature Dependent Absorption Cross Sections for Formaldehyde (CH <sub>2</sub> O): The Effect of Formaldehyde on Stratospheric Chlorine Chemistry" . . . . .	467
Kaufman, Fredrick	"Elementary Atmospheric Reactions: Laboratory Measurements and Their Interpretation". . . . .	397
Khalil, M.A.K., Rasmussen, R.A.	"Atmospheric Halocarbons: Measurements and Analyses of Selected Trace Gases" . . . . .	209
Kulessa, G., Schmidt, U., Roth, E.P.	"The Atmospheric H <sub>2</sub> Cycle" . . . . .	307
Lazrus, A.L., Sedlacek, W.A., Gandrud, B.W.	"Measurements of Stratospheric Bromine". . . . .	273
LeBras, G., Foon, R., Poulet, G., Combournieu, J.	"EPR Kinetic Study of the Reactions of H <sub>2</sub> CO with F, Cl and Br Atoms and ClO Radical" . . . . .	497
Levy, Hiram II, Mahlman, J.D.	"Modeling Tropospheric N <sub>2</sub> O". . . . .	893
Logan, Jennifer A.	"Sources and Sinks for Carbon Monoxide". . . . .	323
London, Julius	"Radiative Energy Sources and Sinks in the Stratosphere and Mesosphere" . . . . .	703
London, Julius	"The Observed Distribution and Variations of Total Ozone" . . . . .	31
Lovelock, J.E., Watson, Andrew J., Stedman, D.H.	"The Problem of Atmospheric Methyl Chloride" . . . . .	365
Mahlman, J.D., Levy, Hiram II	"Modeling Tropospheric N <sub>2</sub> O". . . . .	893
Maier, E.J., Aikin, A.C., Herman, J.R.	"Ethane and Ethylene Behavior in the Atmosphere" . . . . .	191
McElroy, Michael B.	"Sources and Sinks for Nitrous Oxide". . . . .	345
Michael, J.V., Stief, L.J., Nava, D.F., Payne, W.A.	"Absolute Rate of the Reaction OH + H <sub>2</sub> CO at Stratospheric Temperatures" . . . . .	479

<u>Author</u>	<u>Paper</u>	<u>Page</u>
Miller, C., Bass, A.M., Glasgow, L.C., Jesson, J.P., Filkin, D.L.	"Temperature Dependent Absorption Cross Sections for Formaldehyde (CH <sub>2</sub> O): The Effect of Formaldehyde on Stratospheric Chloride Chemistry" . . . . .	467
Molina, Mario J.	"Laboratory Measurements of Absorption Cross Sections" . . . . .	589
Moortgat, Geert Karel	"O( <sup>1</sup> D) Quantum Yields from O <sub>3</sub> Photodissociation and O( <sup>1</sup> D) Reactions with Atmospheric Constituents". . . .	599
Murcray, D.G.	"Observations of Odd Nitrogen Compounds in the Stratosphere" . . . . .	253
Murgatroyd, R.J.	"An Introduction to Studies of the General Characteristics of the Stratosphere and Mesosphere" . . . . .	689
Murgatroyd, R.J.	"Summary of the Commission of the European Communities Report: Chlorofluorocarbons and Their Effect on Stratospheric Ozone". . . . .	985
Nava, D.F., Stief, L.J., Payne, W.A., Michael, J.V.	"Absolute Rate of the Reaction OH + H <sub>2</sub> CO at Stratospheric Temperatures" . . . . .	479
Nicolet, Marcel	"The Chemical Equations of Stratospheric and Mesospheric Ozone". . . . .	823
Nicolet, Marcel	"The First Years of the Study of Atmospheric Ozone". . . . .	1
Nicolet, Marcel	"The Mesospheric and Stratospheric Absorption of the Solar Ultraviolet Radiation" . . . . .	647
Oliver, R.C.	"Effects on Atmospheric Ozone of Emissions from Cruise Aircraft: History and Current Status" . . . . .	921
O'Neill, Alan	"Dynamical Processes in the Stratosphere: Wave Motion" . . . . .	723
O'Neill, Alan	"Stratospheric Sudden Warmings". . . . .	739
Payne, W.A., Stief, L.J., Nava, D.F., Michael, J.V.	"Absolute Rate of the Reaction OH + H <sub>2</sub> CO at Stratospheric Temperatures" . . . . .	479
Poulet, G., LeBras, G., Foon, R., Combourieu, J.	"EPR Kinetic Study of the Reactions of H <sub>2</sub> CO with F, Cl and Br Atoms and ClO Radical" . . . . .	497

<u>Authors</u>	<u>Paper</u>	<u>Page</u>
Prinn, R.G., Cunnold, D.M., Altyea, F.N.	"Three-Dimensional Models and Their Application to the Ozone Problem" . . . . .	877
Pyle, J.A., Rogers, C.F.	"Transport Processes". . . . .	815
Rasmussen, R.A., Khalil, M.A.K.	"Atmospheric Halocarbons: Measurements and Analyses of Selected Trace Gases" . . . . .	209
Rogers, C.F., Pyle, J.A.	"Transport Processes". . . . .	815
Roth, E.P., Schmidt, U., Kulesa, G.	"The Atmospheric H <sub>2</sub> Cycle" . . . . .	307
Schiff, H.I.	"Summary of the U. S. National Academy of Sciences Report: Stratospheric Ozone Depletion by Halocarbons: Chemistry and Transport". . . . .	967
Schmidt, U., Kulesa, G., Roth, E.P.	"The Atmospheric H <sub>2</sub> Cycle" . . . . .	307
Sedlacek, W.A., Lazrus, A.L., Gandrud, B.W.	"Measurements of Stratospheric Bromine". . . . .	273
Simon, Paul C.	"Observation of the Solar Ultraviolet Radiation". . . . .	529
Simonaitis, R.	"Oxidation of the CH <sub>3</sub> Radical and Some Halomethyl and Haloethyl Radicals of Atmospheric Interest" . . . . .	501
Stedman, D.H., Watson, Andrew J., Lovelock, J.E.	"The Problem of Atmospheric Methyl Chloride" . . . . .	365
Stief, L.J., Nava, D.F., Payne, W.A., Michael, J.V.	"Absolute Rate of the Reaction OH + H <sub>2</sub> CO at Stratospheric Temperatures" . . . . .	479
Stolarski, R.S.	"Uncertainty and Sensitivity Studies of Stratospheric Photochemistry" . . . . .	865
Sundararaman, N.	"High Altitude Pollution Program of the U. S. Federal Aviation Administration". . . . .	977
Swider, William	"Nitric Oxide in the Upper Stratosphere and Mesosphere" . . . . .	263

<u>Author</u>	<u>Paper</u>	<u>Page</u>
Tilford, Shelby G.	"NASA's Atmospheric Research Program" . . . . .	983
Tonniben, A., Ehhalt, D.H.	"Hydrogen and Carbon Compounds in the Stratosphere" . . . . .	129
Watson, Andrew J., Lovelock, J.E., Stedman, D.H.	"The Problem of Atmospheric Methyl Chloride" . . . . .	365
Watson, R.T.	"Laboratory Studies of Halogen Compounds of Atmospheric Interest". . . . .	429
Wuebbles, Donald J., Chang, Julius S.	"One-Dimensional Coupled Transport and Chemical Kinetics Models of the Stratosphere" . . . . .	749

U.S. GOVERNMENT PRINTING OFFICE 1980 -O- 626-924/2258